PROCEEDINGS OF THE OCEAN DRILLING PROGRAM

INITIAL REPORTS

117

DRILLING LOCATIONS

LEG	LOCATION	SITES
101	Bahamas	626–636
102	Bermuda Rise	418
103	Galicia Margin	637–641
104	Norwegian Sea	642–644
105	Baffin Bay-Labrador Sea	645–647
106	Mid-Atlantic Ridge	648–649
107	Tyrrhenian Sea	650–656
108	Eastern Tropical Atlantic	657–668
109	Mid-Atlantic Ridge	669–670,395,648
110	Northern Barbados Ridge	671–676
111	Costa Rica Rift	677–678,504B
112	Peru Continental Margin	679–688
113	Weddell Sea, Antarctica	689–697
114	Subantarctic South Atlantic	698–704
115	Mascarene Plateau	705–716
116	Distal Bengal Fan	717–719
117	Oman Margin	720–731

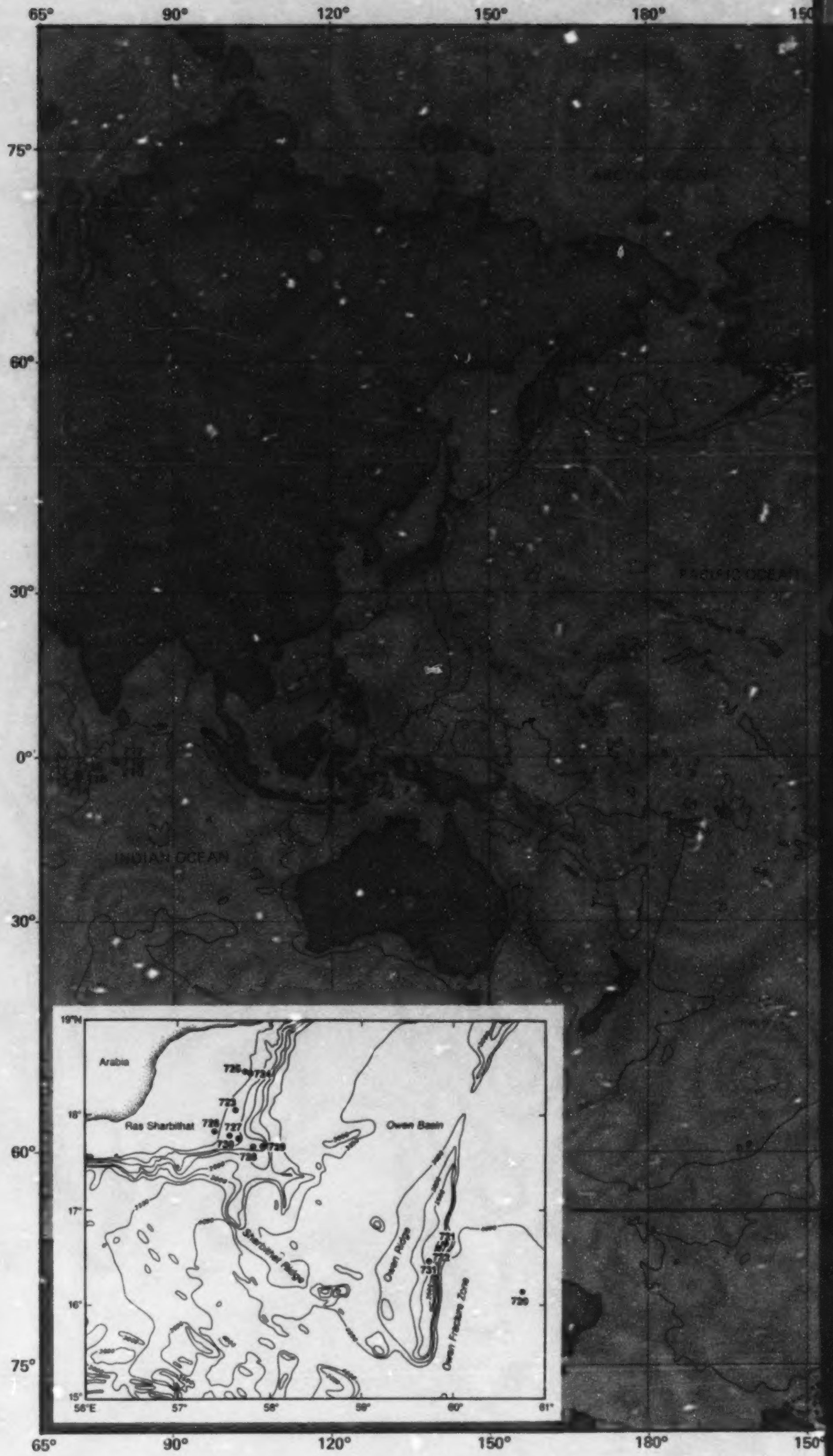
65°
90°
120°
150°
180°
150°
75°
60°
30°
0°
30°
60°
75°
ARCTIC OCEAN
PACIFIC OCEAN
INDIAN OCEAN
19°N
18°
17°
16°
15°
56°E
57°
58°
59°
60°
61°
Arabia
Ras Sharbithat
Owen Basin
Sharbithat Ridge
Owen Ridge
Owen Fracture Zone
725
724
723
726
727
730
729
728
731
721
722
720

NS 1.38/2:

OCEAN DRIL

120°
90°
60°
30°
0°
30°
60°
75°
60°
30°
0°
30°
60°
75°
GREENLAND
NORTH AMERICA
EUROPE
ATLANTIC OCEAN
ANTARCTICA
120°
90°
60°
30°
0°
30°
60°

ILLING PROGRAM

120°
90°
60°
30°
0°
30°
60°
75°
60°
30°
0°
30°
60°
75°
150°
120°
90°
60°
30°
0°
30°
60°
ANTARCTICA

ILLING PROGRAM

PROCEEDINGS OF THE OCEAN DRILLING PROGRAM

VOLUME 117
INITIAL REPORTS

OMAN MARGIN/NEOGENE PACKAGE

Covering Leg 117 of the cruises of the Drilling Vessel *JOIDES Resolution*,
Port Louis, Mauritius, to Port Louis, Mauritius, Sites 720–731,
19 August 1987–17 October 1987

Warren L. Prell, Nobuaki Niitsuma, Kay-Christian Emeis, Zaher Khalid Al-Sulaiman,
Ahmed Nasser Khalfan Al-Tobbah, David M. Anderson, Ross O. Barnes, Roman A. Bilak,
Jan Bloemendal, Cynthia J. Bray, William H. Busch, Steven C. Clemens, Peter de Menocal,
Pierre Debrabant, Akira Hayashida, J. Otto R. Hermelin, Richard D. Jarrard,
Lawrence A. Krissek, Dick Kroon, David W. Murray, Catherine A. Nigrini,
Thomas F. Pedersen, Werner Ricken, Graham B. Shimmield, Stacia A. Spaulding,
Toshiaki Takayama, H. Lo ten Haven, Graham P. Weedon
Participating Scientists

Kay-C. Emeis
Shipboard Staff Scientist

Prepared by the
OCEAN DRILLING PROGRAM
Texas A&M University

Norman J. Stewart
Volume Editor

in cooperation with the
NATIONAL SCIENCE FOUNDATION
and
JOINT OCEANOGRAPHIC INSTITUTIONS, INC.

This publication was prepared by the Ocean Drilling Program, Texas A&M University, as an account of work performed under the international Ocean Drilling Program, which is managed by Joint Oceanographic Institutions, Inc., under contract with the National Science Foundation. Funding for the program was provided by the following agencies at the time of this cruise:

Department of Energy, Mines and Resources (Canada)

Deutsche Forschungsgemeinschaft (Federal Republic of Germany)

Institut Français de Recherche pour l'Exploitation de la Mer (France)

National Science Foundation (United States)

Natural Environment Research Council (United Kingdom)

University of Tokyo, Ocean Research Institute (Japan)

Any opinions, findings, and conclusions or recommendations expressed in this publication are those of the author(s) and do not necessarily reflect the views of the National Science Foundation, the participating agencies, Joint Oceanographic Institutions, Inc., Texas A&M University, or Texas A&M Research Foundation.

It is recommended that reference to the whole or to part of this volume be made in one of the following forms, as appropriate:

Prell, W. L., Niitsuma N., et al., 1989. *Proc. ODP, Init. Repts.*, 117: College Station, TX (Ocean Drilling Program).

Mountain, G. S., and Prell, W. L., 1989. Geophysical reconnaissance for ODP Leg 117 in the northwest Indian Ocean. *In* Prell, W. L., Niitsuma, N., et al., *Proc. ODP, Init. Repts.*, 117: College Station, TX (Ocean Drilling Program), – .

Shipboard Scientific Party, 1989. Site 722. *In* Prell, W. L., Niitsuma, N., et al., *Proc. ODP, Init. Repts.*, 117: College Station, TX (Ocean Drilling Program), – .

Effective Publication Dates of ODP *Proceedings*

According to the International Code of Zoological Nomenclature, the date of publication of a work and of a contained name or statement affecting nomenclature is the date on which the publication was mailed to subscribers, placed on sale, or when the whole edition is distributed free of charge, mailed to institutions and individuals to whom free copies are distributed. The mailing date, *not the printed date*, is the correct one.

The mailing dates of recent *Proceedings of the Ocean Drilling Program* are as follows:

Volume 113 (*Initial Reports*): September 1988
Volume 114 (*Initial Reports*): November 1988
Volume 115 (*Initial Reports*): November 1988
Volume 116 (*Initial Reports*): January 1989
Volume 101/102 (*Scientific Results*): December 1988
Volume 103 (*Scientific Results*): December 1988

Distribution

Copies of this publication may be obtained from Publications Distribution Center, Ocean Drilling Program, 1000 Discovery Drive, College Station, Texas 77840. Orders for copies will require advance payment. See current ODP publication list for price and availability of this publication.

Printed May 1989

ISSN 0884-5883

The paper used in this publication meets the minimum requirements of American National Standard for Information Sciences—Permanence of Paper for Printed Library Materials, ANSI Z39.48-1984 ∞

Foreword

By the National Science Foundation

The scientists of the Ocean Drilling Program (ODP) have embarked on what could prove to be one of the most important earth science initiatives of the decade—an initiative rivaling in scope and impact the exploration of the frontiers of outer space. The program explores our planet's last frontier—the Earth's structure and history as it is revealed beneath the oceans. The scope of the program's scientific goals excites the imagination, challenges the intellect, and enhances the spirit of cooperation among peoples in countries around the world.

Between 1872 and 1876, HMS *Challenger* undertook the world's first major oceanographic expedition. That expedition greatly expanded man's knowledge of the world's oceans and revolutionized our ideas about planet Earth. From 1968 to 1983, another ship named *Challenger* logged more than 375,000 miles on 96 voyages across every ocean for the Deep Sea Drilling Project (DSDP), operated by Scripps Institution of Oceanography. Among the project's many remarkable discoveries were the confirmation of seafloor spreading and the establishment of the relative youth of the seafloor, thus verifying the dynamic and changing nature of the Earth's crust.

Today, the Ocean Drilling Program, which began in 1983, brings new resources to bear on scientific ocean drilling. A new drillship is in operation—the *JOIDES Resolution*—one of the world's most modern and best equipped drillships with enhanced capability for drilling and coring in polar areas and rough weather, expanded laboratory space, facilities for more scientists, and a major drill-hole logging program. The name of the ship was derived from the international scientific partnership that directs the program—the Joint Oceanographic Institutions for Deep Earth Sampling (JOIDES)—and from the flagship of Captain Cook's second voyage to the Pacific Ocean in the late 18th century. Texas A&M University is responsible for science operations in the program, and Lamont-Doherty Geological Observatory is responsible for the logging program.

The Ocean Drilling Program truly has international participation. In 1975, the International Phase of Ocean Drilling began with member nations—the U.S.A., U.S.S.R., the Federal Republic of Germany, Japan, the United Kingdom, and France—all providing funds and scientific guidance for the project. Today, ODP partners include the U.S.A., Canada, France, the Federal Republic of Germany, Japan, the United Kingdom, and the European Science Foundation, which represents Sweden, Finland, Norway, Iceland, Denmark, Belgium, the Netherlands, Spain, Switzerland, Italy, Greece, and Turkey. The National Science Foundation, with funds contributed by the United States and international partners, supports the scientific operations and planning for the ODP through a contract with Joint Oceanographic Institutions, Inc. (JOI).

The information gained by the program leads to a better understanding of the Earth and its dynamic processes. Drilled sediment cores and logs reveal clues to past climatic history and tie into parallel studies of paleoclimates from glacial ice cores drilled on the continents. Understanding these sediment cores will enable scientists to complete the map of major geologically active regions of the Earth, and to identify processes that lead to dynamic change such as earthquakes, volcanic eruptions, and mountain and continental growth. We are far from being able to predict such changes accurately now; but with the new tools and understanding, the accuracy of such predictions can be improved. This better understanding of the Earth's system(s) will allow us to identify regions of potential mineral and energy resource development, an issue of worldwide human interest. The Ocean Drilling Program is not in itself aimed at finding resources, but the knowledge of the Earth's processes that is gained through such a basic research program will inevitably provide pieces of information required for such resource discovery and exploitation.

The program is fully under way in its aim to further the understanding of the Earth's dynamic systems. People of our planet will benefit directly and indirectly from this research in both their daily living and work activities. This multinational endeavor will perhaps foster other cooperative efforts in science or among societies. The Ocean Drilling Program has distinguished ancestors in the original *Resolution* and *Challenger* expeditions and the Deep Sea Drilling Project. The National Science Foundation is proud to be playing a leading role in this program, and we are looking forward to significant and innovative science for many years to come.

Erich Bloch
Director
National Science Foundation

Washington, D.C.

Foreword

By Joint Oceanographic Institutions, Inc.

This volume presents results from the Ocean Drilling Program (ODP), where scientists use a specially equipped ocean drilling ship to sample and measure the properties of the submerged part of the Earth's crust. These data are then synthesized with other information to yield new insights into earth processes.

These results address the scientific goals of the program, which include providing a global description of geological and geophysical structures and materials, studying in detail areas of major geophysical activity such as mid-ocean ridges and the associated hydrothermal circulations, and studying passive and active continental margins. In addition, the ODP data support the study of sea-level and ocean-circulation changes, the effects of the Earth's orbital variations on climate, and the study of processes and mechanisms of evolution from the biological records in the cores which are recovered from drilling.

The Ocean Drilling Program is a partnership of scientists and governments. Overall scientific policy and management guidance is provided by Joint Oceanographic Institutions for Deep Earth Sampling (JOIDES), which consists of committees and panels made up of representatives of the participating institutions and other scientific and engineering experts. The JOIDES Executive Committee (EXCOM) provides general oversight; the JOIDES Planning Committee (PCOM) is the focal point for all scientific planning for the ODP and is key to the scientific success of the program.

The PCOM has a network of panels and working groups which screen drilling proposals, evaluate instrumentation and measurement techniques, and assess geophysical survey data and other safety and siting information. PCOM uses the recommendations of these panels and committees to select drilling targets, to specify the major scientific objectives of each two-month drilling segment or leg, and to provide the science operator with nominations for co-chief scientists. The science operator, Texas A&M University, in turn is responsible for planning the detailed ship's operations, actual drilling schedules, and final scientific rosters, which are developed in close cooperation with PCOM and the cognizant panels.

Many of the scientific goals can be met only with new technology. Thus the program has identified engineering goals, which include the ability to start a hole and to core on bare rock at mid-ocean ridge sites, to drill in high-temperature and corrosive regions typical of hydrothermal areas, and to core in high latitudes with minimum interference from high seas and sea ice. To meet these needs, the program operates a specially equipped drillship, the *JOIDES Resolution*, which contains laboratories and equipment that are state-of-the-art, and carries a major new logging program.

The ship, registered as SEDCO/BP 471 after her owners and her length in feet (144 meters), is 70 feet (21 meters) wide, and has a displacement of 16,595 long tons. Her derrick towers 200 feet (61 meters) above the waterline, and a computer-controlled dynamic-positioning system stabilizes the ship over a specific location while drilling in water depths up to 27,000 feet (8230 meters). The drilling system collects cores from beneath the seafloor with a derrick and drawworks that can handle 30,000 feet (9144 meters) of drill pipe. More than 12,000 square feet (1115 square meters) of space distributed throughout the ship is devoted to scientific laboratories and equipment. The ship sails with a scientific and technical crew of 50 and a ship's crew of 65.

Logging is a major part of the overall operation. The program provides a full suite of geochemical and geophysical measurements for every hole deeper than 1300 feet (400 meters). For each such hole, there are lowerings of basic oil-industry tools: nuclear, sonic, and electrical. In addition, a borehole televiewer is available for imaging the well-bore wall, a 12-channel logging tool provides accurate velocity and elastic property measurements as well as sonic waveforms for spectral analysis of energy propagation near the well bore, and a vertical seismic profiler records reflectors from below the total depth of the hole.

Texas A&M University serves as science operator for the Ocean Drilling Program. In this capacity, they operate and staff the drillship to collect cores from JOIDES-designated sites from around the world. The science operator also ensures that adequate scientific analyses are performed on the cores by maintaining the shipboard scientific laboratories and by providing logistical and technical support for shipboard scientific teams. Onshore, Texas A&M manages scientific activities after each leg, is curator for the cores, distributes samples, and coordinates the editing and publication of the scientific results. Lamont-Doherty Geological Observatory (LDGO) of Columbia University manages the program's logging operations, which include processing the data and provision of assistance to scientists in data analysis. The ODP Data Bank, a repository for geophysical data, is also managed by LDGO. Core samples from ODP and the previous Deep Sea Drilling Project are stored for future investigation at three sites: ODP Pacific and Indian Ocean cores at Texas A&M University, ODP and DSDP Atlantic and Antarctic cores at Lamont-Doherty Geological Observatory, and DSDP Pacific and Indian Ocean cores at Scripps Institution of Oceanography.

International oversight and coordination are provided by the ODP Council, a governmental consultative body of partner country representatives, chaired by the United States, which periodically reviews the general progress of the program and discusses financial plans and other management issues. Joint Oceanographic Institutions, Inc., a nonprofit consortium of U.S. oceanographic institutions, serves as the National Science Foundation's prime contractor and manages the ODP. JOI is responsible for seeing that the scientific objectives and plans are translated into scientific operations consistent with JOIDES recommendations and budgetary constraints.

Scientific achievements of the ODP already include new data on early seafloor spreading and how continents separate and their margins evolve. We have new insight into glacial cycles and the fluctuations of currents throughout geological time. Technical achievements include the first bare-rock coring, and logging data more accurate and complete than ever before. JOI is pleased to have played a facilitating role in the Ocean Drilling Program.

D James Baker

D. James Baker
President
Joint Oceanographic Institutions, Inc.

Washington, D.C.

OCEAN DRILLING PROGRAM

MEMBER ORGANIZATIONS OF THE JOINT OCEANOGRAPHIC INSTITUTIONS FOR DEEP EARTH SAMPLING (JOIDES):[1]

University of California at San Diego, Scripps Institution of Oceanography

Columbia University, Lamont-Doherty Geological Observatory

University of Hawaii, Hawaii Institute of Geophysics

University of Miami, Rosenstiel School of Marine and Atmospheric Science

Oregon State University, College of Oceanography

University of Rhode Island, Graduate School of Oceanography

Texas A&M University, College of Geosciences

University of Texas at Austin, Institute for Geophysics

University of Washington, College of Ocean and Fishery Sciences

Woods Hole Oceanographic Institution

Canada/Australia Consortium for the Ocean Drilling Program, Department of Energy, Mines and Resources (Canada) and Department of Primary Industries and Energy (Australia)

European Science Foundation Consortium for Ocean Drilling (ECOD), Belgium, Denmark, Finland, Iceland, Italy, Greece, the Netherlands, Norway, Spain, Sweden, Switzerland, and Turkey

Federal Republic of Germany, Bundesanstalt für Geowissenschaften und Rohstoffe

France, Institut Français de Recherche pour l'Exploitation de la Mer

Japan, University of Tokyo, Ocean Research Institute

United Kingdom, Natural Environment Research Council

PRIME CONTRACTOR

Joint Oceanographic Institutions, Inc.
Washington, D.C.

Thomas E. Pyle
Director, Ocean Drilling Programs

OPERATING INSTITUTION

College of Geosciences
Texas A&M University
College Station, Texas

Melvin Friedman, Principal Investigator

OCEAN DRILLING PROGRAM

Philip D. Rabinowitz
Director

Louis E. Garrison
Deputy Director

Sylvia Cecile DeVoge
Administrator

Audrey W. Meyer, Manager
Science Operations

Barry Harding, Manager
Engineering and Drilling Operations

Russell B. Merrill, Curator and Manager
Science Services

Robert E. Olivas, Manager
Technical and Logistics Support

LOGGING OPERATOR

Borehole Research Group
Lamont-Doherty Geological Observatory
Columbia University
Palisades, New York

Roger N. Anderson, Head

---

[1] Includes member organizations during time of cruise.

PARTICIPANTS ABOARD *JOIDES RESOLUTION* FOR LEG 117

Warren L. Prell
Co-Chief Scientist
Department of Geological Sciences
Brown University
Providence, Rhode Island 02912-1846

Nobuaki Niitsuma
Co-Chief Scientist
Institute of Geosciences
Shizuoka University
Oya 836, Shizuoka 422
Japan

Kay-Christian Emeis
ODP Staff Scientist/Organic Geochemist
Ocean Drilling Program
Texas A&M Research Park
1000 Discovery Drive
College Station, Texas 77840
(currently at:
c/o C. Wyatt
P.O. Box 363
E. Falmouth, Massachusetts 02536)

Zaher Khalid Al-Sulaiman
Sedimentologist
Ministry of Petroleum and Minerals
P.O. Box 551
Muscat
Sultanate of Oman

Ahmed Nasser Khalfan Al-Tobbah
Sedimentologist
Ministry of Petroleum and Minerals
P.O. Box 551
Muscat
Sultanate of Oman

David M. Anderson
Sedimentologist
Department of Geological Sciences
Brown University
Providence, Rhode Island 02912-1846

Ross O. Barnes
Water Sampling Specialist/Inorganic Geochemist
Rosario Geoscience Associates
104 Harbor Lane
Anacortes, Washington 98221

Roman A. Bilak
Physical Properties Specialist
Department of Earth Sciences
University of Waterloo
Waterloo, Ontario N2L 3G1
Canada

Jan Bloemendal
Paleomagnetist
Graduate School of Oceanography
University of Rhode Island
Narragansett Bay Campus
Narragansett, Rhode Island 02882-1197

Cynthia J. Bray
Physical Properties Specialist
Department of Geological Sciences
Cornell University
Ithaca, New York 14853

William H. Busch
Physical Properties Specialist
Department of Geology and Geophysics
University of New Orleans
New Orleans, Louisiana 70148

Steven C. Clemens
Sedimentologist
Department of Geological Sciences
Brown University
Providence, Rhode Island 02912-1846

Peter de Menocal
Paleomagnetist/Logging Scientist
Lamont-Doherty Geological Observatory
Columbia University
Palisades, New York 10964

Pierre Debrabant
Sedimentologist
Département des Sciences de La Terre
Université de Lille I
B.P. 36
59655 Villeneuve d'Ascq Cedex
France

Akira Hayashida
Paleomagnetist
Laboratory of Earth Science
Doshisha University
Kyoto 602
Japan

J. Otto R. Hermelin
Paleontologist (foraminifers)
Department of Geology
University of Stockholm
S-10691 Stockholm
Sweden

Richard D. Jarrard
LDGO Logging Scientist
Lamont-Doherty Geological Observatory
Columbia University
Palisades, New York 10964

Lawrence A. Krissek
Sedimentologist
Department of Geology and Mineralogy
Ohio State University
Columbus, Ohio 43210-1398

Dick Kroon
Paleontologist (foraminifers)
Instituut v. Aardwetenschappen
Vrije Universiteit
P.O. Box 7161
NL-1007 MC Amsterdam
Netherlands

David W. Murray
Sedimentologist
Department of Geological Sciences
Brown University
Providence, Rhode Island 02912-1846

Catherine A. Nigrini
Paleontologist (radiolarians)
510 Papyrus Drive
La Habra Heights, California 90631

Thomas F. Pedersen
Inorganic Geochemist
Department of Oceanography
University of British Columbia
6270 University Boulevard
Vancouver, British Columbia VGT 1W5
Canada

Werner Ricken
Sedimentologist
Institut für Geologie und Paläontologie
Universität Tübingen
Sigwartstrasse 10
D-7400 Tübingen
Federal Republic of Germany

Graham B. Shimmield
Inorganic Geochemist
Grant Institute of Geology
University of Edinburgh
West Mains Road
Edinburgh EH9 3JW, Scotland
United Kingdom

Stacia A. Spaulding
Paleontologist (nannofossils)
Department of Geology
University of Nebraska
Lincoln, Nebraska 68588-0340

Toshiaki Takayama
Paleontologist (nannofossils)
Department of Geology
Kanazawa University
1-1, Marunouchi
Kanazawa City 920
Japan

H. Lo ten Haven
Organic Geochemist
Institute of Petroleum and Organic Geochemistry
KFA Jülich GmbH
P.O. Box 1913
D-5170 Jülich
Federal Republic of Germany

Graham P. Weedon
Sedimentologist
Department of Earth Sciences
Cambridge University
Downing Street
Cambridge CB2 3EQ
United Kingdom

SEDCO OFFICIALS

Captain Gerard Kuster
Master of the Drilling Vessel
Underseas Drilling, Inc.
707 Texas Avenue South, Suite 103D
College Station, Texas 77840-1917

Jack Tarbutton
Drilling Superintendent
Underseas Drilling, Inc.
707 Texas Avenue South, Suite 103D
College Station, Texas 77840-1917

ODP ENGINEERING AND OPERATIONS PERSONNEL

Lamar Hayes	Operations Superintendent
Alan Milton	Special Tools Engineer

ODP TECHNICAL AND LOGISTICS PERSONNEL

Larry Bernstein	System Manager
Dan Bontempo	Marine Technician
Jim Briggs	Electronics Technician
Brant Bullard	Marine Technician
Stacey Cervantes	Photographer
Linda Chatham	Marine Technician
Bettina Domeyer	X-ray Technician
Ferrell Johnson	Weather Observer
Brad Julson	Laboratory Officer
Khalid Mahmood	Marine Technician
Dwight E. Mossman	Electronics Technician
Mark ("Trapper") Neschleba	Marine Technician
Katie Sigler-Tauxe	Chemistry Technician
Greg Simmons	Marine Technician
John Tauxe	Marine Technician
John Weisbruch	Marine Technician
Bob Wilcox	Curatorial Representative
Dawn J. Wright	Yeoperson

Ocean Drilling Program Publications Staff

Publications Supervisor
William D. Rose

Chief Editor
Norman J. Stewart

Editors
Eva M. Barbu
Elsa Kapitan Mazzullo
Sondra K. Stewart
William R. Winkler

Chief Production Editor
Raymond F. Silk

Publications Coordinator
Lona Haskins Dearmont

Hole Summary Coordinator
Laura J. Young

Publications Distribution Specialist
Fabiola Muñoz Byrne

Senior Photographer
John W. Beck

Photographer
Roy T. Davis

Chief Illustrator
Karen O. Benson

Illustrators
Garnet D. Gaither
Larry R. Lewis
Pamela C. Vesterby
Christine L. Yokley

Compositor
Mary E. Betz

Production Assistants
Susan Collinsworth
Gigi Delgado
Jaime A. Gracia
Melynda S. Poët

TABLE OF CONTENTS

VOLUME 117—INITIAL REPORTS

ACKNOWLEDGMENTS 1

SECTION 1: INTRODUCTION

1. INTRODUCTION, BACKGROUND, AND MAJOR OBJECTIVES FOR ODP LEG 117 5
Shipboard Scientific Party

2. EXPLANATORY NOTES 11
Shipboard Scientific Party

3. BACKGROUND AND SUMMARY OF DRILLING RESULTS—OWEN RIDGE 35
Shipboard Scientific Party

4. BACKGROUND AND SUMMARY OF DRILLING RESULTS—OMAN MARGIN 43
Shipboard Scientific Party

5. GEOPHYSICAL RECONNAISSANCE SURVEY FOR ODP LEG 117 IN THE NORTHWEST INDIAN OCEAN 51
G. S. Mountain and W. L. Prell

6. UNDERWAY GEOPHYSICS 65
G. Simmons and Shipboard Scientific Party

7. *IN-SITU* PORE-WATER SAMPLING AND DOWNHOLE TEMPERATURE MEASUREMENTS 151
Shipboard Scientific Party

SECTION 2: SITE REPORTS

8. SITE 720 157
Shipboard Scientific Party

9. SITE 721 197
Shipboard Scientific Party

10. SITE 722 255
Shipboard Scientific Party

11. SITE 723 319
Shipboard Scientific Party

12. SITE 724 385
Shipboard Scientific Party

13. SITE 725 419
Shipboard Scientific Party

14. SITE 726 441
Shipboard Scientific Party

15. SITE 727 467
Shipboard Scientific Party

16. SITE 728 495
Shipboard Scientific Party

17. SITE 729 547
Shipboard Scientific Party

18. SITE 730 555
Shipboard Scientific Party

19. SITE 731 585
Shipboard Scientific Party

SECTION 3: CORES

Core description forms and core photographs for:

Site 720 655

Site 721 683

Site 722 749

Site 723 835

Site 724 911

Site 725 971

Site 726 993

Site 727 1011

Site 728 1035

Site 729 1109

Site 730 1115

Site 731 1159

SECTION 4: POLICY

JOIDES ADVISORY GROUPS 1229

SAMPLE-DISTRIBUTION POLICY 1235

BACK-POCKET FOLDOUTS

INITIAL REPORTS: VOLUME 117: CHAPTER 17: FIGURE 5. A. SELECTED STRIKE-AND-DIP-LINE WATER GUN REFLECTION PROFILES ACROSS OWEN RIDGE

INITIAL REPORTS: VOLUME 117: CHAPTER 17: FIGURE 5. B. SELECTED STRIKE-AND-DIP-LINE WATER GUN REFLECTION PROFILES ACROSS THE SOUTHEAST OMAN MARGIN

ACKNOWLEDGMENTS

Leg 117 (Colombo to Mauritius) recovered a record 4600 m of core, primarily using the HPC and XCB under the guidance of ODP Operations Superintendent Lamar Hayes. We dedicate this volume to the memory of Lamar, who was set on recovering more and better cores and who was an island of calm in the frantic shallow-water drilling operations offshore Oman. His ingenious and efficient way of orchestrating the drilling operations paved the way for the recovery of unprecedented 4600 m of high-quality core during the leg. Captain Gerard Kuster, SEDCO Drilling Superintendent Jack Tarbutton, and their crews cooperated most enthusiastically and efficiently with the scientists and helped immensely in making this cruise memorable and successful. The entire scientific crew greatly appreciated the professional and friendly help of ODP Laboratory Officer Brad Julson and the ODP technicians, who maintained great spirit and high working standards throughout the entire leg. We appreciate the help given by Carl Brenner in the ODP Data Bank, by Hole Summary Coordinator Debra Williams, as well as by editors and the art group of ODP during preparation of the volume. We would further like to acknowledge the assistance of the JOIDES advisory structure, in particular the endorsements of the Sediment and Ocean History Panel (SOHP) and the Indian Ocean Panel (IOP), as well as the tolerance of the Lithosphere Panel (LITHP) and the Tectonics Panel (TECP) in the planning phase.

Lastly, we thank Senator Claiborne Pell for interceding on our behalf to obtain permission to operate in the waters of the Sultanate of Oman, and we gratefully acknowledge the permission given by the Sultanate of Oman to conduct our scientific drilling program on the continental margin.

SECTION 1: INTRODUCTION

1. INTRODUCTION, BACKGROUND, AND MAJOR OBJECTIVES FOR ODP LEG 117 (WESTERN ARABIAN SEA) IN SEARCH OF ANCIENT MONSOONS[1]

Shipboard Scientific Party[2]

The primary goal of Leg 117 was to explore the origin, evolution, and variability of the Indian Ocean Monsoon and its effect on the oceanic environments of the western Arabian Sea and the paleoclimates of tropical Africa, Arabia, India, and Asia. Briefly, the monsoon is characterized by seasonal changes in precipitation and in the direction and strength of the low-level winds over the northwest Indian Ocean and the adjacent continents. During the summer monsoon (June through August), the winds are from the southwest, are quite strong (consistently >15 m/s), and are associated with maximum seasonal precipitation over much of India and southern Asia. The causes of the monsoon are complex and include interactions between marine and continental tectonics, atmospheric and oceanic circulation, and variations of solar radiation. These factors, which cause changes in monsoon circulation, vary on different time-scales to produce a complex monsoonal response. One goal of ODP Leg 117 was to define more clearly the roles of these factors as causes of the evolution and variability of the Indian Ocean Monsoon. This goal is feasible because the monsoon leaves an indelible imprint on the climatic and oceanographic history of the western Arabian Sea that is recorded in its marine sediments. Below we summarize the tectonic, oceanographic, and climatic framework of the western Arabian Sea to illustrate how they are related to the monsoon and to suggest how the sediment record can produce a reliable record of monsoonal history.

TECTONIC FRAMEWORK OF THE WESTERN ARABIAN SEA

The major tectonic and depositional features of the western Arabian Sea include the Indus Fan, the Owen Ridge, the Owen Basin, and the Arabian margin off Oman (see Figs. 1 and 2). All of these features reflect the long, complex tectonic history of the Northern Indian Ocean. In most plate reconstructions, the initial separation of India, Madagascar, and Antarctica from Africa is thought to have begun in the late Jurassic (about 160 Ma) and halted in Early Cretaceous (about 102 Ma) (Rabinowitz et al., 1983; Cochran, 1987, in press). Most workers assume that the ocean crust along the African and Arabian margins was formed during this interval of spreading, an inference that implies that the Oman margin has been passive since its breakup and that the age of the Owen Basin is Jurassic (Whitmarsh, 1979; Beydoun, 1982; Stein and Cochran, 1985; Larson et al., 1985). The separation of India from Madagascar occurred on a new spreading ridge in the Late Cretaceous (at about 90 Ma). During this phase of spreading, the Owen Ridge is thought to have been the major transform fault that connected the ridge between India and Arabia with the east-west trending spreading center located to the north of Arabia (McKenzie and Sclater, 1971; Whitmarsh, 1974, 1979; Norton and Sclater, 1979; Stein and Cochran, 1985). During the Late Cretaceous (about 89 to 75 Ma), the Semail ophiolites were emplaced on the northern Arabian margin (Coleman, 1981). Similar ophiolitic sequences, but with less well known ages, are found striking southwestward on the Masirah Island, indicating possible emplacement from the Owen Basin (Moseley and Abbotts, 1979). Recent survey of the Oman margin (Mountain and Prell, 1987, in press) suggests that its history is more complex than a simple passive margin model would indicate.

The continental collision of India with Asia is thought to have occurred in the Eocene (about 50 Ma) (Patriat and Achache, 1984). Continued subduction and crustal thickening began the uplift of Asia and reduced the convergence rate between India and Asia. In the middle to late Oligocene (about 30–25 Ma), a major reorganization of plate geometry occurred in the Indian Ocean (McKenzie and Sclater, 1971; Sclater and Fisher, 1974; Sclater et al., 1976; Johnson et al., 1976; Johnson et al., 1980; Norton and Sclater, 1979; Schlich, 1982). The present Carlsberg Ridge was formed and began its progression into the Gulf of Aden, where the first emplacement of true oceanic crust occurred about 10 Ma (Laughton et al., 1970; Cochran, 1981). During this Oligocene to Holocene spreading phase, the Owen Ridge has been uplifted due to a component of compression along the Owen transform (Whitmarsh, 1979) (See "Background and Summary of Drilling Results—Owen Ridge chapter," this volume, for details).

Previous DSDP drilling in the Owen Basin (Site 223) and on the Owen Ridge (Site 224) (see Fig. 2 for locations) established igneous basement(?) ages of Paleocene to Eocene (Site 223) and pre-early Eocene (Site 224) for this area. These ages are inconsistent with the proposed Jurassic age for the Owen Basin.

OCEANOGRAPHIC FRAMEWORK OF THE WESTERN ARABIAN SEA

The oceanography of the Arabian Sea is characterized by three major divisions: (1) a seasonally changing monsoonal gyre in the surface waters, (2) a high-salinity, oxygen-poor intermediate water, and (3) the Indian Deep Water. In the following, we briefly review the characteristics of these circulation systems as they relate to the formation or modification of the sediment record in the western Arabian Sea.

The western Arabian Sea is characterized by large seasonal variations in current direction, upwelling intensity, and mixed-layer properties such as temperature, nutrient content, and productivity (Wyrtki, 1971, 1973). These seasonal changes represent a unique oceanic response that is forced by the large-scale monsoonal winds, especially by the intense southwesterly monsoon winds (see monsoon disscussion below). Along the coasts of northeastern Africa (Kenya and Somalia) and the Arabian Peninsula (Oman) (Fig. 3), the strong southwesterly winds are nearly parallel to the coast and cause Ekman transport of surface waters away (offshore) from the coasts and thus cause intense centers of seasonal coastal upwelling (Currie et al., 1973; Bruce, 1974; Wyrtki, 1973; Hastenrath and Lamb, 1979). This seasonal upwelling brings nutrient-rich, oxygen-poor, and cold

---

[1] Prell, W. L., Niitsuma, N., et al., 1989. *Proc. ODP, Init. Repts.*, 117: College Station, TX (Ocean Drilling Program).

[2] Shipboard Scientific Party is as given in the list of Participants preceding the contents.

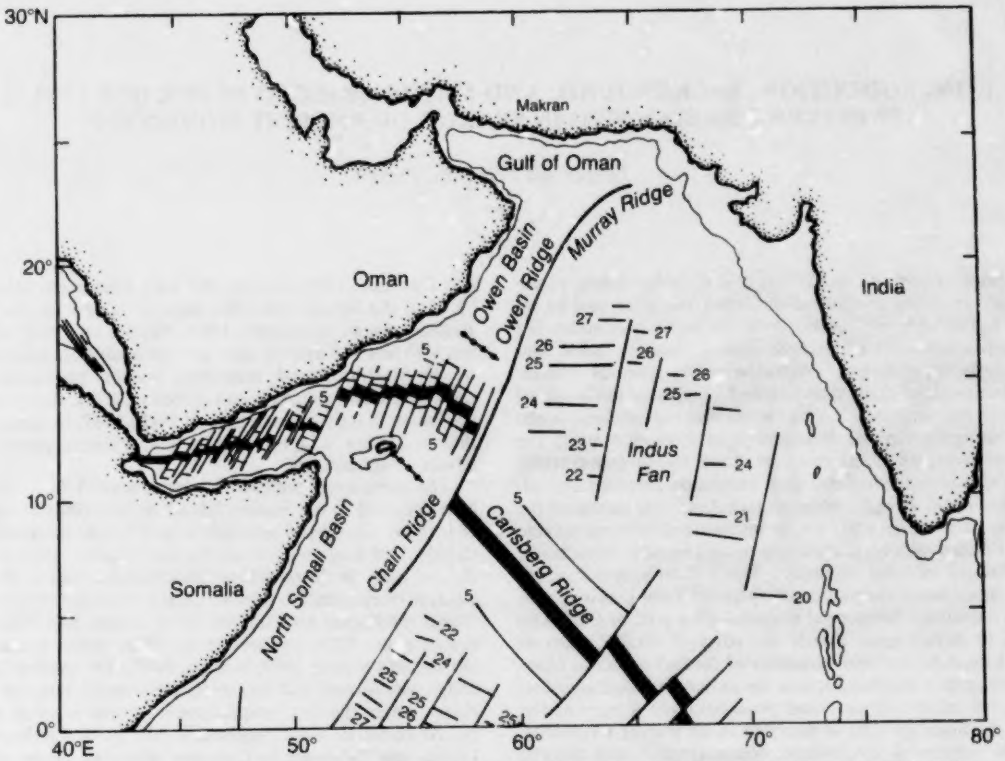

Figure 1. Tectonic features and magnetic anomalies in the northern Indian Ocean. Modified after Mountain and Prell (in press). Numbers = magnetic anomalies recognized on oceanic crust.

waters from several hundred meters depth to the surface and triggers high productivity in the euphotic zone (Krey and Babenerd, 1976). Since these upwelling events are largely driven by Ekman transport (Wyrtki, 1973; Prell and Streeter, 1982), their duration and intensity must reflect the intensity of the monsoonal winds. Thus, a direct and coherent link is established between monsoonal wind intensity, the intensity of coastal upwelling, biogenic productivity, and sediment input to underlying seafloor. This uniquely seasonal system differs sharply from other important upwelling systems such as off Peru and off the west coast of Africa, which are embedded in eastern boundary currents and are forced by large-scale, persistent atmospheric and oceanic circulation.

The intermediate waters of the Arabian Sea, named the North Indian Intermediate Water (NIIW) by Wyrtki (1973), are characterized by their high salinity, stability, and low oxygen concentrations. The source of the NIIW is the restricted marginal basins (Red Sea and Persian Gulf) adjacent to the Arabian Sea as well as the Gulf of Aden and the northern Arabian Sea. All of these sources produce relatively high salinity waters which combine to give the NIIW a density that is similar to the Antarctic Intermediate Water (Wyrtki, 1971, 1973). As a result, the meridional advective exchange with central Indian Ocean waters is restricted, and the NIIW in the Arabian Sea is relatively isolated and has a long residence time. This lack of advective recharge combined with the stability of the intermediate waters, and the high productivity of the surface waters (see below), results in extremely low oxygen concentrations (0.2 mL/L) between the depths of about 200 m and 1500 m. The NIIW thus forms a distinctive oxygen-minimum zone (OMZ) in the Arabian Sea and the entire northern Indian Ocean. Understanding the interactions of productivity and circulation on the OMZ and the effects of the OMZ on the sediments of the Oman margin are important goals for research associated with Leg 117.

The deep waters of the Arabian Sea are relatively homogeneous and are formed by elements of North Atlantic Deep Water (NADW), Circumpolar Deepwater (CD), and Antarctic Bottom Water (AABW). Global circulation of deep waters requires that some regional upwelling of deep water must occur in the northern Indian Ocean, but its influence on the intermediate waters is largely unknown. The deep waters of the Arabian Sea are saturated with carbonate above 3500 m (Broecker and Peng, 1982); thus they should have minimal influence on the dissolution of carbonate sediments on the crest of the Owen Ridge and the Oman margin.

MONSOONAL CLIMATE FRAMEWORK OF THE WESTERN ARABIAN SEA

The term "monsoon" is derived from the Arabic word "mausim," which means season and is usually applied to the seasonal reversals of wind direction around the Arabian Sea (Webster, 1987). The seasonal reversal of monsoonal winds strongly affects the Arabian Sea, and below we shall examine the fundamental boundary conditions that cause the monsoon and control its variability on geologic time scales.

The winter circulation of the northern Indian Ocean–Asian atmosphere is dominated by a high-pressure cell over the Tibetan Plateau, which is caused by cooling over Asia (Fig. 3). The resulting pressure gradient causes northeasterly winds to flow from the Asian continent over the Arabian Sea. These con-

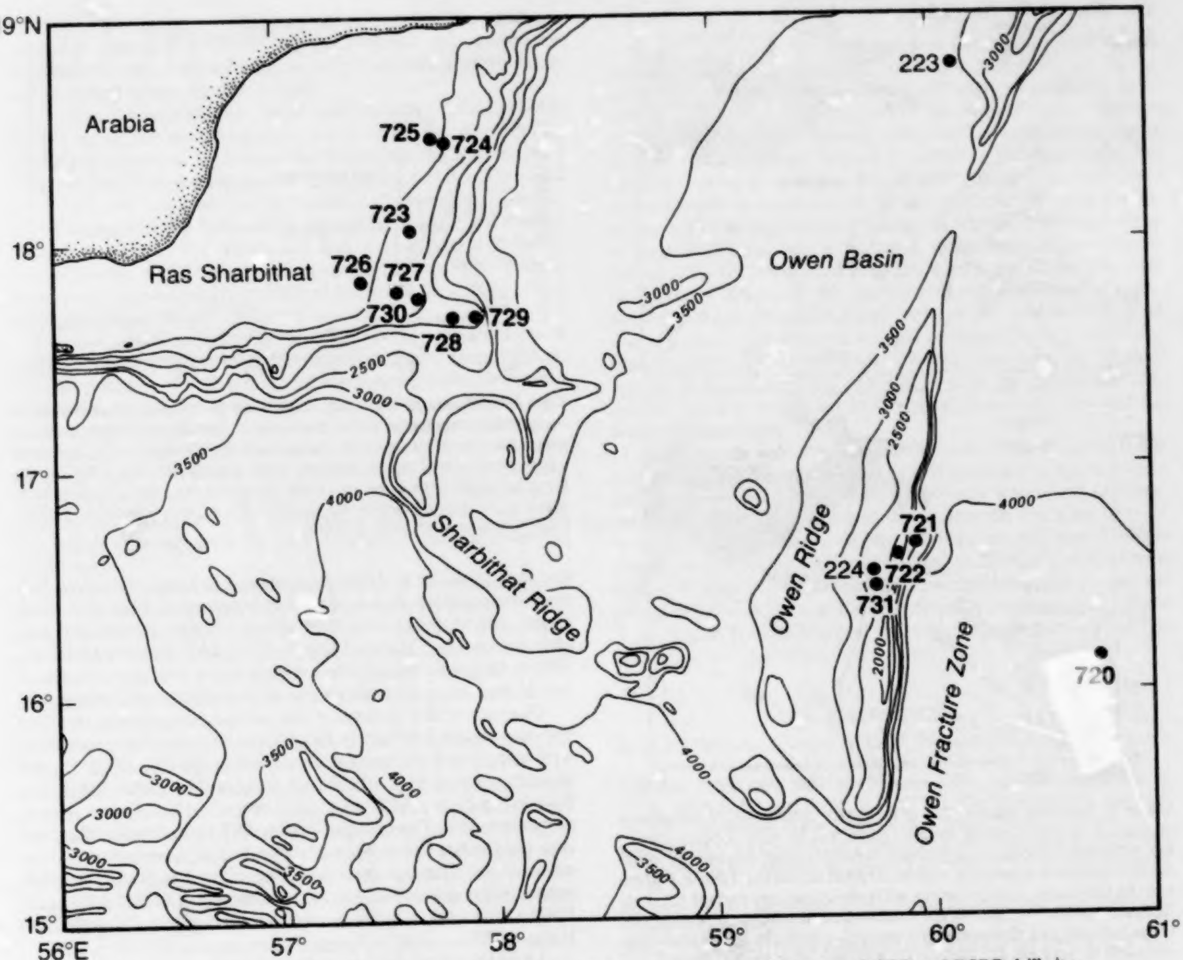

Figure 2. Simplified bathymetric map (contours in meters) of the Leg 117 operations area and location of ODP and DSDP drill sites.

tinental air masses tend to be dry and have relatively low wind speeds. During the northern hemisphere summer, seasonal solar heating of the Asian continent causes the ascent of air masses above the Tibetan Plateau and northern India. This heating, coupled with the release of latent heat from the ascending air masses, leads to the development of an intense low-pressure cell that is centered about 30°N (Figs. 3 and 4). The atmospheric pressure contrast between the Asian continent (low) and the cooler southern Indian Ocean (the Madagascar high) causes the strong low-level southwesterly winds that are characteristic of the summer monsoon in the western Indian Ocean. The convergence of these air masses over the Indian subcontinent and their uplift due to heating and orographic factors is the primary cause of the seasonal monsoon precipitation (Hastenrath, 1985; Fein and Stephens, 1987; Chang and Krishnamurti, 1987).

On the basis of this general mechanism of monsoonal circulation, climate model simulations and paleoclimatic reconstructions have identified four separate, but interrelated, factors that could potentially cause changes in the intensity of the monsoon. These are changes in the elevation of the Tibetan Plateau, the variation of northern hemisphere summer insolation, the albedo of Asia and the Tibetan Plateau, and the sea surface temperature of the west-central Indian Ocean.

The climatic effects of lower topography in Tibet and the Himalaya have been simulated by general circulation models (Hahn and Manabe, 1975). In general, higher elevation of the Tibet-Himalaya complex increases the effectiveness of sensible and latent heating of the upper troposphere over Asia and thus acts to increase the strength of the monsoon circulation (Fig. 4). Within the late Neogene, uplift rates of the Himalaya are thought to increase dramatically, especially in the Pliocene-Pleistocene (Mercier et al., 1987). Thus, if the "mountain" hypothesis and uplift estimates are correct, the monsoon should increase in intensity during this interval. If the monsoon response is not dependent on a "critical" elevation, one would expect the "uplift" trend to be long-term and relatively continuous.

Variations in the seasonal distribution of solar radiation due to changes in the earth's orbit (i.e., the Milankovitch mechanism) have long been thought to be an important factor in the cause and timing of the Ice Ages (for summaries see Berger et al., 1984). More recently, researchers have found that the Milankovitch mechanism also has strong effects on the hydrologic

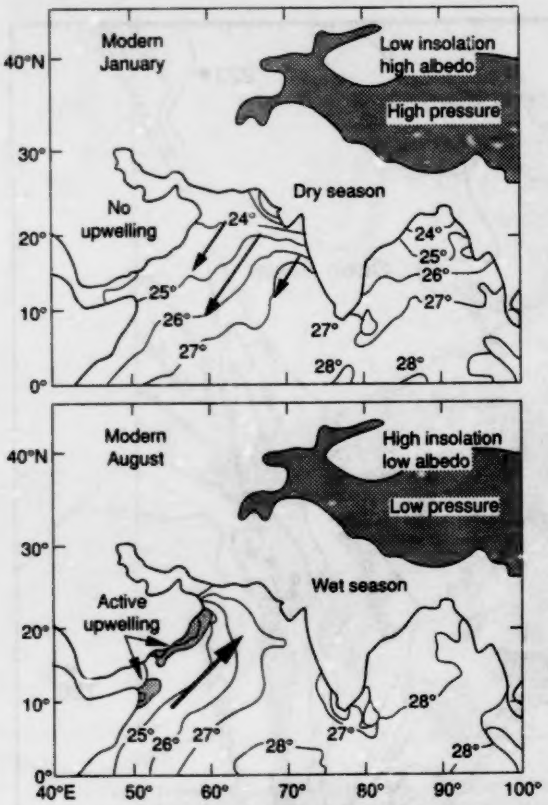

Figure 3. Seasonal changes in the boundary conditions of monsoonal circulation in the northern Indian Ocean and in Asia. Upper: During the northeastern monsoon in modern January. Lower: During the southwestern monsoon in modern August. Shaded area is the Tibetan Plateau and the Himalaya. Arrows denote wind directions; sea surface temperatures are given in °C. During the southwestern monsoon, upwelling offshore Somalia and Oman (shaded pattern) lowers the sea surface temperatures to between 22° and 24°C. Redrawn after Prell (1984a).

budgets and wind fields of the tropics and in particular on the Indian-African summer monsoon (Kutzbach, 1981; Prell, 1984a, 1984b; Kutzbach and Street-Perrott, 1985; Prell and Kutzbach, 1987). A combination of climate model simulations and paleoclimatic observations has established that increased summer radiation over Asia, especially changes associated with the precessional component of the earth's orbit, result in stronger monsoons. These radiation changes are induced by specific orbital components that have distinct periodicities (precession at 19 kyr and 23 kyr, tilt at 41 kyr, and eccentricity at 100 kyr and 414 kyr) that can be calculated over the past several million years. If these orbital-radiation components are important in forcing the monsoon response, then the temporal changes in the amplitude and timing of these components and their distinct spectral signatures should be reflected in the monsoon-related sediment record.

Changes in the albedo of the Asian continent (Fig. 4), especially due to increased extent or duration of snow and ice cover, have long been assumed to be important in determining the timing and strength of the modern monsoon (Blanford, 1884; Hahn and Shukla, 1976; Prell 1984a, 1984b). Although this mechanism is still somewhat controversial, increased albedo (i.e., more snow) is thought to delay the seasonal heating cycle over Asia and thus to retard and weaken the monsoon. During glacial periods, several researchers have inferred higher albedo and even ice-caps on the Tibetan Plateau (CLIMAP Project Members, 1981). Although this albedo increase is not well documented, it would lead to weaker monsoons during glacial conditions.

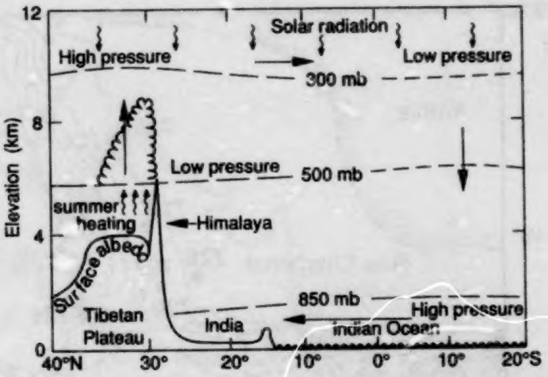

Figure 4. Schematic boundary conditions of monsoonal atmospheric and oceanic circulation in the northwest Indian Ocean during the summer monsoon. Heating of air masses over the highlands of Asia creates a low-pressure cell which induces intense southwesterly winds in the lower atmosphere over the northwest Indian Ocean. mb = atmospheric pressure surfaces (exaggerated) in millibars; arrows denote wind direction. Redrawn after Prell (1984a).

Changes in the pattern of sea surface temperature (SST) of the central and southern Indian Ocean have also been correlated with the strength of the monsoon (Fig. 4; Shukla, 1987). Glacial boundary conditions (CLIMAP Project Members, 1981) may have led to higher SST in the west-central Indian Ocean relative to modern SST. The effect of higher SST is to decrease the pressure gradient between Asia and the Indian Ocean and thus to decrease the monsoon response. This effect has been inferred in some studies of the last glacial maximum (Prell and Kutzbach, 1987) while others failed to find an SST effect (Manabe and Hahn, 1977).

All of the above factors vary on timescales from 10^3 to 10^6 yr and potentially affect the sediments deposited on the Owen Ridge and the Arabian margin. Below, we suggest how such changes might be observed in Neogene sediments of the Western Arabian Sea.

ENVIRONMENTAL EFFECTS OF THE MONSOON

The Indian Ocean monsoon imposes large seasonal variations, especially pronounced in the summer, on the environments of the western Arabian Sea. These variations include changes in current direction, upwelling intensity, depth of the mixed layer, structure of the OMZ, sea surface temperature, nutrient content, primary and secondary productivity, the composition of plankton assemblages, and in the concentration and source of eolian material. All of these phenomena respond to changes in the monsoon intensity; we recognize, however, that they are also affected by other oceanic and atmospheric processes.

On the basis of the above observations and rationale, past changes in the strength of the monsoonal circulation might be represented in the sediments of the western Arabian Sea by the following types of records:

Changes in productivity: Increased/decreased monsoonal winds might be expected to cause increased/decreased upwelling and hence productivity of the surface waters. Sedimentary records of a change in productivity could include changes in the following: organic carbon content, biogenic accumulation rates, and specific biotic indicator species.

Changes in faunal and floral assemblages: Increased/decreased upwelling would be expected to affect the distribution of plankton (such as Radiolaria vs. Foraminifera) and the relative abundance of species within those groups. Variations and trends between "tropical" versus "upwelling" assemblages should reflect changes in the monsoonal upwelling as well as of related oceanic processes. The amplitude and timing of cyclic variations of faunal and floral upwelling components may be quantitatively compared to the hypothetical record of monsoonal forcing to establish "causal" links.

Changes in eolian sediment components: Increased/decreased monsoonal winds might be expected to change the amount, size, and composition of eolian material transported into the western Indian Ocean. Those components that can be correlated with southwestern sources on the basis of mineralogy or pollen content could be interpreted in terms of strength of the southwestern monsoon. Components that are associated with more northern sources might reflect the winter monsoon. The usefulness of these eolian components in interpreting the monsoon patterns will largely depend upon the identification of distinct regional source areas.

Changes in pollen assemblages: Increased/decreased aridity and temperature on the adjacent continental land masses greatly affects the composition and amount of vegetation. The transport of pollen from these vegetational assemblages into the marine record offers the opportunity to directly compare the response of the terrestrial and marine environments to various climatic forcing mechanisms.

Changes in surface water temperature and chemistry: Increased/decreased upwelling would produce lower/higher SST and changes in the carbon budget of the surface waters. Such changes should be recorded by the oxygen and carbon isotopic composition of various species of planktonic foraminifera, as well as by temperature-dependent organic compounds and biomarkers, such as the ratios of unsaturated ketones from coccolithophorids. Estimates of SST from biotic data should also help to identify upwelling-related temperature changes.

Changes in the oxygen-minimum zone: Increased/decreased upwelling might be expected to change the structure and intensity of the OMZ. Two competing mechanisms that might modify the OMZ are: (1) increased/decreased productivity leading to increased/decreased oxygen demand, which would result in a stronger/weaker OMZ; and (2) increased/decreased vertical advection of deeper oxygen-rich waters below the OMZ is required by the upwelling and could lead to increased/decreased oxygen supply which would result in a weaker/stronger OMZ.

Some of the above measures have been useful in interpreting the environmental history of the western Arabian Sea. For example, the onset of upwelling in this area was suggested as having occurred at middle Miocene time on the basis of the increased abundance of siliceous microfossils (Whitmarsh, Weser, Ross, et al., 1974). Previous work on Owen Ridge sediments of late Quaternary age (Prell, 1984a; 1984b) has shown that planktonic foraminifer species can be used as indices of upwelling and that their abundance varies coherently with the 23-kyr precessional component of the earth's orbit, which is thought to be the solar radiation component forcing the monsoon. These studies show that the history of the monsoon can be reconstructed from the sediments and can be used to test hypotheses about the mechanisms that control the strength of the monsoon and cause changes in global climate.

GOALS AND DRILLING STRATEGY FOR LEG 117

Given the above observational and theoretical background, the major goal of Leg 117 was to sample a diversity of depositional environments that represent different atmospheric, oceanic, and sedimentologic regimes of the Indian Ocean monsoon system. Our sampling strategy was to drill on the Indus Fan to recover a clastic record related to uplift of the Himalayas and climatic/sea level changes. We drilled the crest of the Owen Ridge to recover a continuous section of upper Neogene pelagic sediments to establish both long-term tectonic and short-term Milankovitch variations in the biotic, sedimentologic, and chemical response to monsoonal changes. Lastly, we drilled the Arabian margin to recover the organic-rich sediments that accumulated rapidly in the zone of high productivity and detrital input and are associated with the oxygen minimum. These three distinct depositional environments allowed us to examine different aspects of the depositional response to changing monsoonal conditions that are embedded in changing global climates and sea levels.

Our interests in tectonic problems were focused on the uplift history of the Owen Ridge and how it is related to the reorganization of spreading centers and the growth of the Gulf of Aden. We also sought to understand the apparently complex tectonic and depositional history of the Arabian margin and how the timing of its tectonic features is related to the uplift of the Owen Ridge. Within the framework of these broad goals, we present the more detailed site-specific objectives for these areas in "Owen Ridge" and "Oman Margin" introductory chapters and in the respective site chapters (this volume).

REFERENCES

Berger, A., Imbrie, J., Hays, J., Kukla, G., and Saltzman, B., 1984. *Milankovitch and Climate*: Dordrecht (D. Reidel).

Beydoun, Z. R., 1982. The Gulf of Aden and northwest Arabian Sea. *In* Nairn, A.E.M., and Stehli, F. G. (Eds.), *The Ocean Basins and Margins: The Indian Ocean*: New York (Plenum Press), 253–313.

Blanford, H. F., 1884. On the connexion of the Himalaya snowfall with dry winds and seasons of droughts in India. *Proc. R. Soc. London*, 37:3.

Broecker, W. S., and Peng, T. H., 1982. Tracers in the Sea: Palisades, NY (Eldigio Press).

Bruce, J. G., 1974. Some details of upwelling off the Somali and Arabiann coasts. *J. Mar. Res.*, 32:419–423.

Chang, C.-P., and Krishnamurti, T. N. (Eds.), 1987. *Monsoon Meteorology*: New York (Oxford Univ. Press).

CLIMAP Project Members, 1981. Seasonal reconstructions in the earth's surface at the last glacial minimum. *Geol. Soc. Am. Map/Chart*, MC-36.

Cochran, J. R., 1981. The Gulf of Aden: structure and evolution of a young ocean basin and continental margin. *J. Geophys. Res.*, 86:263–288.

________, in press. The North Somali Basin, Chain Ridge, and the origin of the Somali Basin geoid/gravity low. *J. Geophys. Res.*

Coleman, R. G., 1981. Tectonic setting for ophiolite obduction in Oman. *J. Geophys. Res.*, 84:2497–2508.

Currie, R. I., Fisher, A. E., and Hargraves, P. M., 1973. Arabian Sea upwelling. *In* Zeitzschel, B., and Gerlach, S. A. (Eds.), *The Biology of the Indian Ocean*: New York (Springer-Verlag), 37–52.

Fein, J. S., and Stephens, P. L. (Eds.), 1987. *Monsoons*: New York (Wiley).

Hahn, D. G., and Manabe, S., 1975. The role of mountains in the South Asian monsoon circulation. *J. Atmos. Sci.*, 32:1515–1541.

Hahn, D. G., and Shukla, J., 1976. An apparent relationship between Eurasian snow cover and Indian monsoon rainfall. *J. Atmos. Sci.*, 33:2461–2463.

Hastenrath, S., 1985. *Climate and Circulation of the Tropics*: Boston (Reidel).

Hastenrath, S., and Lamb, P. J., 1979. *Climatic Atlas of the Indian Ocean*: Madison (Univ. Wisconsin Press).

Johnson, B. D., Powell, C. McA., and Veevers, J. J., 1976. Spreading history of the eastern Indian Ocean and greater India's northward flight from Antarctica and Australia. *Geol. Soc. Am. Bull.*, 87: 1560–1566.

________, 1980. Early spreading history of the Indian Ocean between Antarctica and Australia. *Earth Planet. Sci. Lett.*, 47:131–143.

Krey, J., and Babenerd, B., 1976. *Phytoplankton Production; Atlas of the International Indian Ocean Expedition*: Kiel (Institut für Meereskunde).

Kutzbach, J. E., 1981. Monsoon climate of the early Holocene: climate experiment with the earth's orbital parameters for 9000 years ago. *Science*, 214:59–61.

Kutzbach, J. E., and Street-Perrott, F. A., 1985. Milankovitch forcing of fluctuations in the level of tropical lakes from 18 to zero kyrBP. *Nature*, 317:130–134.

Larson, R. L., et al., 1985. *The Bedrock Geology of the World*: New York (W. H. Freeman).

Laughton, A. S., Whitmarsh, R. B., and Jones, M. T., 1970. The evolution of the Gulf of Aden. *Philos. Trans. R. Soc. London, A*, 267: 227–266.

McKenzie, D., and Sclater, J. G., 1971. The evolution of the Indian Ocean since the Late Cretaceous. *Geophys. J. R. Astron. Soc.*, 24: 437–528.

Manabe, S., and Hahn, D. G., 1977. Simulation of the tropical climate of an ice age. *J. Geophys. Res.*, 82:3889–3911.

Mercier, J.-T., Armijo, R., Tapponnier, P., Carey-Gailhardis, E., and Lin, H. T., 1987. Change from late Tertiary compression to Quaternary extension in Southern Tibet during the India-Asia collision. *Tectonics*, 6:275–304.

Mountain, G., and Prell, W. L., 1987. Leg 117 ODP site survey: a revised history of Owen Basin. *Eos, Trans. Am. Geophys. Union*, 68: 424.

________, in press. A multiphase plate tectonic history of the southeast continental margin of Oman. *In* Robertson, A.H.F., Searle, M. P., and Ries, A. C. (Eds.), *The Geology and Tectonics of the Oman Region*, Geol. Soc. Am. Spec. Publ.

Norton, I. O., and Sclater, J. G., 1979. A model for the evolution of the Indian Ocean and the breakup of Gondwanaland. *J. Geophys. Res.*, 84:12.

Patriat, P., and Achache, J., 1984. India-Eurasia collision chronology has implications for crustal shortening and driving mechanism of plates. *Nature*, 311:615–621.

Prell, W. L., 1984a. Variation of monsoonal upwelling: a response to changing solar radiation. *In* Hansen, J. E., and Takahashi, T. (Eds.), *Climatic Processes and Climate Sensitivity*: Washington (American Geophysical Union), Geophys. Monogr. 29, Maurice Ewing Series, 5:48–57.

________, 1984b. Monsoonal climate of the Arabian Sea during the late Quaternary: a response to changing solar radiation. *In* Berger, A., and Imbrie, J. (Eds.), *Milankovitch and Climate*: Dordrecht (D. Reidel), 349–366.

Prell, W. L., and Kutzbach, J. E., 1987. Monsoon variability over the past 150,000 years. *J. Geophys. Res.*, 92:8411–8425.

Prell, W. L., and Streeter, H. F., 1982. Temporal and spatial patterns of monsoonal upwelling along Arabia: a modern analogue for the interpretation of Quaternary SST anomalies. *J. Mar. Res.*, 40:143–155.

Rabinowitz, P. D., Coffin, M. F., and Falvey, D., 1983. The separation of Madagascar and Africa. *Science*, 220:67–69.

Schlich, R., 1982. The Indian Ocean: aseismic ridges, spreading centers, and oceanic basins. *In* Nairn, A.E.M., and Stehli, F. G. (Eds.), *The Ocean Basins and Margins, The Indian Ocean* (Vol. 6): New York (Plenum Press), 51–148.

Sclater, J. G., Luyendyls, B. P., and Meinke, L., 1976. Magnetic lineations in the southern part of the Central Indian Basin. *Geol. Soc. Am. Bull.* 87:371–376.

Sclater, J. G., and Fisher, R. L., 1974. The evolution of the east-central Indian Ocean, with emphasis on the tectonic setting of the Ninetyeast Ridge. *Geol. Soc. Am. Bull.* 85:683–702.

Shukla, J., 1987. Interannual variability of monsoons. *In* Fein, J. S., and Stephens, P. L. (Eds.), *Monsoons*: New York (Wiley), 399–463.

Stein, C. A., and Cochran, J. R., 1985. The transition between the Sheba Ridge and Owen Basin: rifting of old oceanic lithosphere. *Geophys. J. R. Astron. Soc.*, 81:47–74.

Webster, P. J., 1987. The elementary monsoon. *In* Fein, J. S., and Stephens, P. L. (Eds.), *Monsoons*: New York (Wiley), 3–32.

Whitmarsh, R. B., 1974. Some aspects of plate tectonics in the Arabian Sea. *In* Whitmarsh, R. B., Weser, O. E., Ross, D. A., et al., *Init. Repts. DSDP*, 23: Washington (U.S. Govt. Printing Office), 527–536.

________, 1979. The Owen Basin off the southeast margin of Arabia and the evolution of the Owen Fracture Zone. *Geophys. J. R. Astron. Soc.*, 58:441–470.

Whitmarsh, R. B., Weser, O. E., Ross, D. A., et al., 1974. *Init. Repts. DSDP*, 23: Washington (U.S. Govt. Printing Office).

Wyrtki, K., 1971. *Oceanographic Atlas of the International Ocean Expedition*: Washington (National Science Foundation).

________, 1973. Physical oceanography of the Indian Ocean. *In* Zeitschel, B., and Gerlach, S. A. (Eds.), *The Biology of the Indian Ocean*: New York (Springer-Verlag), 18–36.

Ms 117A:102

2. EXPLANATORY NOTES[1]

Shipboard Scientific Party[2]

Standard procedures for drilling operations and preliminary shipboard analysis of the material recovered have been regularly amended and upgraded since 1968 during investigations conducted by the Deep Sea Drilling Project (DSDP) and the Ocean Drilling Program (ODP). This chapter presents information to help the reader understand the data-gathering methods on which our preliminary conclusions are based and to help shore-based investigators select samples for further analysis. This information concerns primarily shipboard operations and analyses described in the Leg 117 site reports (this volume). Preliminary results from shipboard analysis of each individual site are given in the site chapters.

AUTHORSHIP OF SITE REPORTS

Authorship of the site reports is shared among the entire scientific party. The scientists responsible for a particular field also contributed for their specific area of study. Because of the heavy work load of the sedimentologists and biostratigraphers, a senior sedimentologist and senior biostratigrapher were responsible for compiling and editing the "Lithostratigraphy" and "Biostratigraphy" sections for each site chapter. The site chapters are organized as follows (authorship in parentheses):

Site Summary (Prell, Niitsuma, Emeis)
Background and Objectives (Prell, Niitsuma, Emeis)
Operations (Emeis)
Lithostratigraphy (Anderson, Clemens, Debrabant, Krissek, Murray, Niitsuma, Ricken, al Sulaimani, al Tobbah, Weedon)
Biostratigraphy (Hermelin, Kroon, Nigrini, Spaulding, Takayama)
Paleomagnetism (Bloemendal, Hayashida, de Menocal, al Tobbah)
Accumulation Rates (Murray, Niitsuma)
Interhole and Intersite Correlations (de Menocal, Niitsuma)
Physical Properties (Bilak, Bush, Bray)
Seismic Stratigraphy (Jarrard, Prell, Ricken)
Inorganic Geochemistry (Pedersen, Shimmield)
Organic Geochemistry (Emeis, ten Haven)
Downhole Measurements (Barnes, Jarrard)
Summary and Conclusions (Prell, Niitsuma)

Following the text are summaries ("barrel sheets") of the lithologic core descriptions and the biostratigraphic and magnetostratigraphic results and photographs of each core.

SURVEY AND DRILLING DATA

The survey data used to locate the site are discussed in the individual site chapters. En route between sites and upon arrival in the target areas, continuous observations were made of water depth and sub-bottom structure. Site surveys using a precision depth recorder (PDR) and seismic profiler were made aboard *JOIDES Resolution* before dropping the beacon. Equipment used and single-channel seismic-reflection data collected during Leg 117 are presented in the "Underway Geophysics" chapter (this volume).

Bathymetric data were obtained with both 3.5- and 12-kHz PDR echo-sounders, using a Raytheon PTR-105B transceiver and 12 Raytheon transducers for the 3.5-kHz data. Two Raytheon LSR-1807M recorders were used for display. Depths were read on the basis of an assumed 1463 m/s sound velocity. Water depth (in meters) at each site was corrected (1) according to the tables of Matthews (1939) and (2) for the depth of the hull transducer, 6 m below sea level. In addition, depths referred to the drilling platform are assumed to be 10.5 m above the water line.

DRILLING CHARACTERISTICS

Because water circulation down the hole is open, drill cuttings are lost onto the seafloor and cannot be recovered. The only information about characteristics of strata in uncored or unrecovered intervals, other than from seismic data or wireline-logging results, is from the rate of drilling penetration. Typically, the harder the layer, the slower and more difficult it is to penetrate. However, other factors that are not directly related to the hardness of the layers also determine the rate of penetration, including the parameters of bit weight, pump pressure, and revolutions per minute, all of which are noted on the drilling recorder.

DRILLING DEFORMATION

When cores are split, some show signs of significant sediment disturbance. Examples of this disturbance include the downward-concave bending of originally horizontal layers, the haphazard mixing of lumps of different lithologies, and the near-fluid state of some sediments recovered from tens to hundreds of meters below the seafloor. Core deformation probably occurs during one of three different steps: cutting, retrieval (with accompanying changes in pressure and temperature), and core handling.

SHIPBOARD SCIENTIFIC PROCEDURES

Numbering of Sites, Holes, Cores, and Samples

ODP drill sites are numbered consecutively from the first site drilled by *Glomar Challenger* in 1968. A site number refers to one or more holes drilled while the ship is positioned over a single acoustic beacon. Several holes may be drilled at a single site by pulling the drill pipe above the seafloor (out of one hole), moving the ship some distance from the previous hole, and then drilling another hole.

For all ODP drill sites, a letter suffix distinguishes each hole drilled at the same site. For example: the first hole takes the site number with suffix A, the second hole takes the site number with suffix B, and so forth. This procedure is different from that used by DSDP (Sites 1-624) but prevents ambiguity between site and hole number designations.

---

[1] Prell, W. L., Niitsuma, N., et al., 1989. *Proc. ODP, Init. Repts.*, 117: College Station, TX (Ocean Drilling Program).

[2] Shipboard Scientific Party is as given in the list of Participants preceding the contents.

All ODP core and sample identifiers indicate core type. The following abbreviations are used: R = rotary core barrel (RCB), H = advanced hydraulic piston core (APC), P = pressure core barrel, X = extended core barrel (XCB), B = drill-bit recovery, C = center-bit recovery, I = *in-situ* water sample, S = sidewall sample, W = wash core recovery, N = Navidrill core (used from Leg 104 on), and M = miscellaneous material. APC, XCB, RCB, I, and W were employed on Leg 117.

The cored interval is measured in meters below seafloor. The depth interval of an individual core is the depth below seafloor that the coring operation began to the depth that the coring operation ended. Each coring interval is as much as 9.7 m long, which is the maximum length of a core barrel. The coring interval may, however, be shorter. Cored intervals are not necessarily adjacent but may be separated by drilled intervals. In soft sediment, the drill string can be "washed ahead," keeping the core barrel in place but not recovering sediment, by pumping water down the pipe at high pressure to wash the sediment out of the way of the bit and up the annulus between the drill pipe and wall of the hole. However, if thin, hard rock layers are present, it is possible to get "spotty" sampling of these resistant layers within the washed interval.

Cores taken from a hole are numbered serially from the top of the hole downward (Fig. 1). Maximum full recovery from a single core is 9.7 m of sediment or rock in a plastic liner (6.6 cm inner diameter), plus a sample about 0.2 m long (without a plastic liner) in a core catcher (CC). The core catcher, a device at the bottom of the core barrel, prevents the core from sliding out when the barrel is retrieved from the hole. The sediment core, in the plastic liner, is cut into 1.5-m-long sections, which are numbered serially from the top of the core. With full recovery, the sections are numbered from 1 through 7, the last section being shorter than 1.5 m. For sediments and sedimentary rocks, the core-catcher sample is placed below the last section and treated as a separate section. For igneous and metamorphic rocks, material recovered in the core catcher is included at the bottom of the last section.

When recovery is less than 100%, whether or not the recovered material is contiguous, the recovered sediment is placed at the top of the cored interval, and then 1.5-m-long sections are numbered serially, starting with Section 1 at the top. There are as many sections as needed to accommodate the length of the core recovered. Sections are cut starting at the top of the recovered sediment, and the last section may be shorter than the normal 1.5-m length. If, after the core has been split, fragments that are separated by a void appear to have been contiguous *in situ*, a note is made in the description of the section. All voids, whether real or artificial, are curatorially preserved. We made an effort to compute depth below seafloor in cores with gas voids by collapsing the voids. Depths thus computed are given in the "Samples" column of the barrel sheets for Sites 723 and 724.

Sample locations are designated by distances in centimeters from the top of each section to the top and bottom of the sample. A full identification number for a sample consists of the following information: (1) leg, (2) site, (3) hole, (4) core number and type, (5) section, and (6) interval in centimeters. For example, the sample identification number "117-721A-3H-2, 98–100 cm" indicates that a sample was taken between 98 and 100 cm from the top of Section 2 of APC-drilled Core 3, from the first hole (A) drilled at Site 721 during Leg 117. A sample taken from between 8 and 9 cm in the core catcher of this core would be designated "117-721A-3H, CC (8–9 cm)." In the case of recovery less than or equal to 100%, the depth below seafloor of a given sample is calculated as follows: depth below seafloor of the top of the core (tabulated in the "Operations" section for each site) plus 1.5 m for each complete section plus the distance

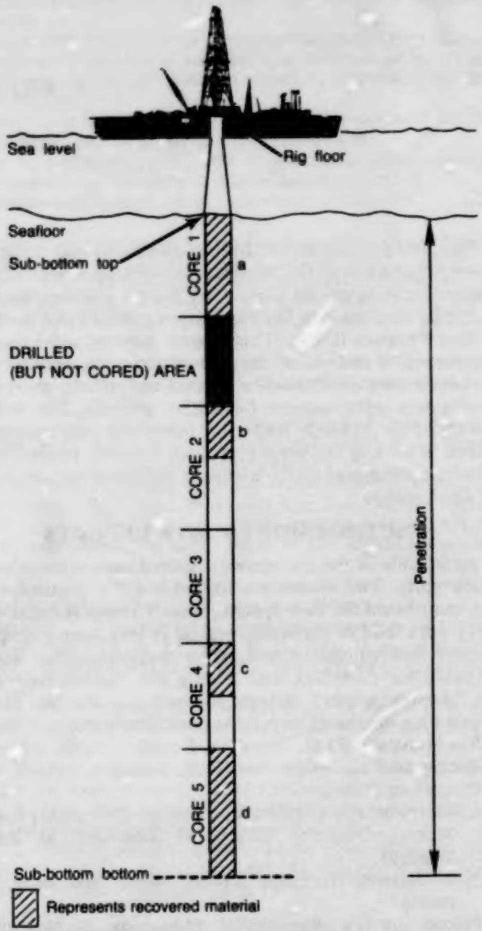

BOTTOM FELT: distance from rig floor to seafloor

TOTAL DEPTH: distance from rig floor to bottom of hole (sub-bottom bottom)

PENETRATION: distance from seafloor to bottom of hole (sub-bottom bottom)

NUMBER OF CORES: total of all cores recorded, including cores with no recovery

TOTAL LENGTH OF CORED SECTION: distance from sub-bottom top to sub-bottom bottom minus drilled (but not cored) areas in between

TOTAL CORE RECOVERED: total from adding a, b, c, and d in diagram

CORE RECOVERY (%): equals TOTAL CORE RECOVERED divided by TOTAL LENGTH OF CORED SECTION times 100

Figure 1. Numbering of core sections and terms used in coring operations and core recovery.

of the sample from the top of the sampled section. For example, the sub-bottom depth of Sample 117-721B-9H-5, 98–100 cm, is 83.38 m below seafloor (mbsf): 76.4 m (top of Core 117-721B-9H given in the Site 721 coring summary) plus 6.0 m (four complete (1.5-m) sections) plus 0.98 m (depth from top of Section 5). Sample depths given in this volume are given with two digits, even though such accuracy may be fictitious. Sample requests should refer to specific intervals, however, rather than to sub-bottom depths. Note that this assignment of subseafloor depth is an arbitrary convention; in the case of less than 100% recovery, the sample could have come from any interval within the cored interval.

Because of the gaseous nature of the organic-rich sediments of the Oman margin, core expansion resulting from decompression during core retrieval was a common phenomenon on Leg 117. Cores from Sites 723 and 724 in particular expanded significantly, giving rise to "recoveries" in excess of 110%, when voids separated sediment intervals. For example, Core 117-723A-35X drilled the interval from 321.5 to 326.3 mbsf (4.8 m), but voids developed in the core liner and pushed the sediment out of the liner. The voids were recorded in the barrel sheets so that the total length of the "recovered" section was 5.93 m, or 123% recovery. A uniform, though arbitrary, sub-bottom depth notation for samples from these expanded cores with a "recovered" section significantly longer than the cored interval (i.e., cores with greater than 105% recovery) is noted in the "Samples" column of the barrel sheets as collapsed depth in m below seafloor, following the subtraction of void space.

Core Handling

As soon as a core was retrieved on deck, a sample was taken from the core catcher and sent to the paleontological laboratory for an initial assessment of the age of the sample.

Next, the core was placed on the long horizontal rack on the catwalk, and gas samples were taken by piercing the core liner and withdrawing gas into a vacuum-tube sampler. Voids within the core were sought as sites for gas sampling. Most of the gas samples were analyzed immediately as part of the shipboard safety and pollution-prevention program. The core then was marked into section lengths; each section was labeled, and the core was cut into sections. Interstitial-water (IW) and organic geochemistry (OG) whole-round samples were taken as scheduled. Each section was sealed top and bottom with a plastic cap, blue to identify the top of a section and clear for the bottom. A yellow cap was placed on section ends from which a whole-round core sample had been removed. The caps were usually attached to the liner by coating the end of the liner and the inside rim of the end caps with acetone, though we elected to tape the end caps in place without acetone where geochemistry samples were taken on Leg 117.

The cores were then carried into the laboratory, and the complete identification was engraved on each section. The length of core in each section and the core-catcher sample was measured to the nearest centimeter; this information was logged into the shipboard core-log data base program.

Cores from some holes were allowed to warm to a stable temperature (approximately 3 hr) before splitting. During this time, the whole-round sections were run through the gamma ray attenuation porosity evaluator (GRAPE) device for estimating bulk density and porosity (see "Physical Properties" section, this chapter; Boyce, 1976), the *P*-wave logger (PWL), and the magnetic susceptibility apparatus. Owing to the large number of cores handled at some sites on Leg 117, it was not always possible to run every section through the GRAPE and PWL. After the temperature of the cores had reached equilibrium, thermal conductivity measurements were made immediately before splitting (see "Physical Properties" section, this chapter). Again, at "busy" sites, thermal conductivity could not be measured for every section. In this case, a measurement strategy was determined prior to each site.

Cores were split lengthwise into working and archive halves. The softer cores were split with a wire, and the harder ones with a band saw or diamond saw. In soft sediments, some smearing of material can occur. To minimize contamination, scientists avoided sampling the near-surface part of the split core.

The working half of the core was sampled for both shipboard and shore-based laboratory studies. Each extracted sample was logged in the sampling computer program by location and the name of the investigator receiving the sample. Records of all removed samples are kept by the ODP Curator at Texas A&M University. The extracted samples were sealed in plastic vials or bags and labeled with a computer-printed label.

The archive half was described visually. Smear slides were made from samples taken from the archive half, and thin sections were made from the working half. The archive half of each core was photographed after description with both black-and-white and color film.

Both halves were then put into labeled plastic tubes, sealed, and transferred to cold-storage space aboard the drilling vessel. Leg 117 cores were shipped from Mauritius in refrigerated containers to cold storage at the ODP Gulf Coast Repository at Texas A&M University, College Station, Texas.

At several sites on Leg 117, triple APC holes were drilled through the top 200 m of the sediment column to enable the implementation of extended whole-round sampling programs. The cores remaining after these samples were taken were not split (except where additional stratigraphic information was required) but were frozen and transported to the repository for ODP core preservation and aging studies. Unfortunately, they were accidentally thawed in port, which may limit their use as pristine samples for geochemical investigation.

SEDIMENT CORE DESCRIPTION FORMS ("BARREL SHEETS")

The core description forms (Fig. 2), or barrel sheets, summarize the data obtained during shipboard analysis of each core. The following discussion explains the ODP conventions used in compiling the data for each part of the core description form and exceptions from the standardized format necessitated by peculiarities of the sediments recovered during Leg 117.

Core Descriptions

Cores are designated using leg, site, hole, and core number and type as previously discussed (see "Numbering of Sites, Holes, Cores, and Samples," this chapter). In addition, the cored interval is specified in terms of meters below sea level (mbsl) and mbsf. Leg 117 mbsl depths are based on PDR measurements, whereas mbsf depths are drill-pipe measurements reported by the SEDCO Coring Technician and the ODP Operations Superintendent.

Age Data

Biostratigraphic zone assignments, as determined by shipboard paleontologists, appear on the core descriptions form under the heading "Biostratigraphic Zone/Fossil Character." Preservation and abundance of fossil groups are treated in the "Biostratigraphy" sections of the site chapters. An asterisk (*) denotes the location of samples taken from the core catcher or from the core. "Barren" signifies that no fossils of the particular group were recognized in the sample. Geologic age determined from the paleontological and/or paleomagnetic results noted in the "Time-Rock Unit" column. Detailed information on the zonations and terms used to report abundance and preservation appears in the "Biostratigraphy" section (this chapter).

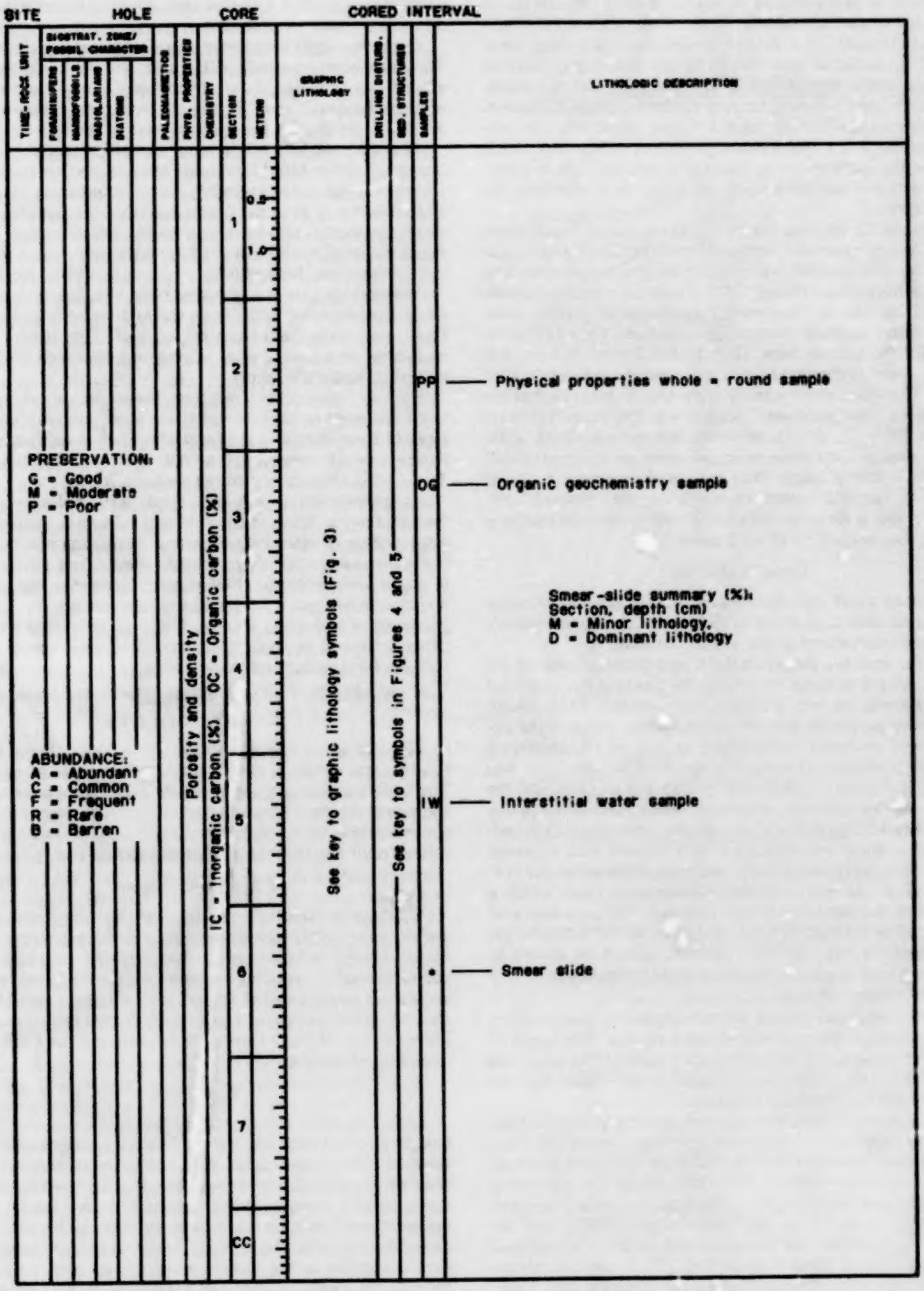
SITE
HOLE
CORE
CORED INTERVAL
TIME-ROCK UNIT
BIOSTRAT. ZONE/ FOSSIL CHARACTER
FORAMINIFERS
NANNOFOSSILS
RADIOLARIANS
DIATOMS
PALEOMAGNETICS
PHYS. PROPERTIES
CHEMISTRY
SECTION
METERS
GRAPHIC LITHOLOGY
DRILLING DISTURB.
SED. STRUCTURES
SAMPLES
LITHOLOGIC DESCRIPTION
0.5
1.0
1
2
3
4
5
6
7
CC
PRESERVATION:
G = Good
M = Moderate
P = Poor
ABUNDANCE:
A = Abundant
C = Common
F = Frequent
R = Rare
B = Barren
Porosity and density
IC = Inorganic carbon (%) OC = Organic carbon (%)
See key to graphic lithology symbols (Fig. 3)
See key to symbols in Figures 4 and 5
PP
Physical properties whole = round sample
OG
Organic geochemistry sample
Smear-slide summary (%):
Section, depth (cm)
M = Minor lithology,
D = Dominant lithology
IW
Interstitial water sample
•
Smear slide

Figure 2. Core description form (barrel sheet) used for sediments and sedimentary rocks.

Paleomagnetic, Physical Properties, and Chemical Data

Columns are provided on the core description form to record paleomagnetic results, location of the physical-properties samples, and shipboard results for undrained shear strength (γ) and porosity (ϕ), as well as results of inorganic carbon (IC) and organic carbon (OC) measurements on splits of squeezed sediments from interstitial-water or carbonate bomb samples. Information on shipboard procedures for collecting these types of data is in the "Physical Properties," "Paleomagnetics," and "Organic Geochemistry" sections of this chapter. Detailed results of these and other sample analyses are given in the respective sections for each site, as well as tabulated results of calcium carbonate concentrations in the "Lithostratigraphy" sections.

Graphic Lithology

Lithologies are shown on the core description form by one or more of the symbols shown in Figure 3. The symbols correspond to end-members of the sediment compositional range, such as nannofossil ooze (CB1) or diatom ooze (SB1). For sediments that are mixtures (e.g., clastic and biogenic sediments), the symbols for both constituents are shown divided by a dashed line. For interbedded sediments, the symbols are separated by a solid line. In each case, the abundance of each constituent approximately equals the percentage of the width of the graphic column that its symbol occupies. For example, if the left 20% of the column has a nannofossil ooze symbol (CB1) and the right 80% has a clay symbol (T1) separated by a dashed line, the sediment is a mixture of 80% clay and 20% calcareous nannofossils. A solid line separating the symbols would indicate that the lithology consists of interbedded clay and diatom ooze. Minor lithologies are noted in the "Lithologic Description" space but not in the "Graphic Lithology" column where they are less than 10 cm in thickness. At some sites, core expansion was severe and resulted in voids in the core liners. For these cases, the depth labels in the voids in the "Graphic Lithology" column of the core description form correspond to the depth below seafloor of the top of the following sediment interval with the void collapsed.

Drilling Disturbance

Recovered rocks and soft sediments may be slightly to extremely disturbed. The condition of disturbance is indicated in the "Drilling Disturbance" column on the core description forms. The symbols for the six disturbance categories used for soft and firm sediments are shown in Figure 4. The disturbance categories are defined as follows:

1. Slightly disturbed or fractured: Bedding contacts are slightly bent or disturbed by fractures.
2. Moderately disturbed or fractured: Bedding contacts have undergone extreme bowing, and firm sediment has been broken into drilling biscuits 5 to 10 cm in length.
3. Very disturbed or highly fragmented: Bedding is completely disturbed or homogenized by drilling, sometimes showing symmetrical diapirlike structure in softer sediments.
4. Soupy: Water-saturated intervals have lost all aspects of original bedding.
5. Brecciated: Indurated sediment broken into angular fragments by the drilling process, perhaps along preexisting fractures.

Sedimentary Structures

The locations and types of sedimentary structures in a core are shown by graphic symbols in the "Sedimentary Structures" column in the core description form. Figure 5 gives the key for these symbols. Horizontal dashed lines denote gradational boundaries between light and dark layers or subtle compositional changes. It should be noted, however, that in some cases (mostly in deeper sections) it is difficult to distinguish between natural structures and structures created by the drilling process.

Lithologic Description of Sediments

The sediment classification scheme that is used on Leg 117 is a modified version of the sediment classification system devised by the JOIDES Sedimentary Petrology and Physical Properties Panel (SP4) and adopted for use by the JOIDES Planning Committee in March, 1974. The classification scheme used on Leg 117 incorporates many of the suggestions and terminology of Dean et al. (1985). This classification scheme is descriptive rather than generic in nature—that is, the basic sediment types are defined on the basis of their texture and composition, rather than on the basis of their inferred origin. The texture and composition of sediment samples and the areal abundances of grain components were commonly estimated by the examination of smear slides with a petrographic microscope; thus, they may differ from more accurate measurements of texture and composition, especially for coarser grained sediments. The composition of some sediment samples was determined by more accurate methods, such as coulometer or X-ray diffraction analyses, in the shipboard laboratories.

General Rules of Classification

Every sample of sediment is assigned a main name that defines its sediment type, a major modifier(s) that describes the compositions and/or textures of grains present in abundances from 10% to 100%, and possibly a minor modifier(s) that describes the compositions and/or textures of grains that are present in abundances from 5% to 10%. Grains that are present in abundances from 0% to 5% are considered insignificant and are not included in this classification.

The minor modifiers are listed first in the string of terms that describes a sample and are attached to the suffix "-bearing," which distinguishes them from major modifiers. When two or more minor modifiers are employed, they are listed in order of increasing abundance. The major modifiers are always listed second in describing a sample, and they are listed in order of increasing abundance also. Some major modifiers are attached to the suffix "-rich", whereas others are not (e.g., diatomaceous vs. nannofossil-rich). The main name is the last term in the descriptive string.

The types of main names and modifiers that are employed in this classification scheme differ between the three basic sediment types (Table 1), and are described in the succeeding sections.

Color

Sediment colors are determined by comparison with the Geological Society of America Rock-Color Chart (Munsell Soil Color Charts, 1971). Colors were determined immediately after the cores were split and while they were still wet.

Smear Slide Summary

Smear slide/thin-section compositions and the section and centimeter intervals of all samples are listed below the core description. In addition, the sample locations in the cores are indicated by an asterisk in the "Samples" column on the core description forms.

BASIC SEDIMENT TYPES: DEFINITIONS

Three basic sediment types are defined on the basis of variations in the relative proportions of clastic, siliceous biogenic, and calcareous biogenic grains: clastic sediments, siliceous bio-

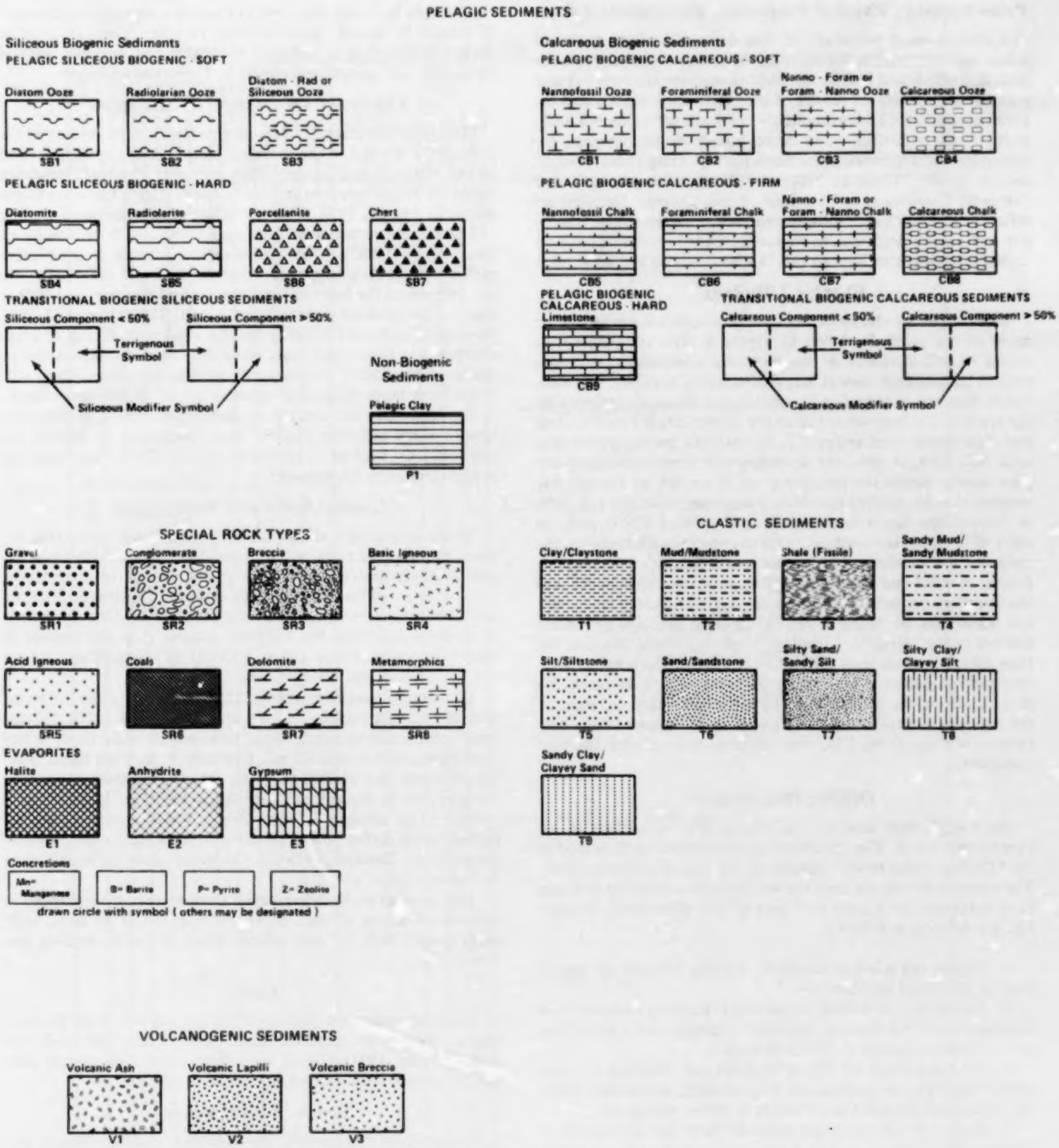
PELAGIC SEDIMENTS
Siliceous Biogenic Sediments
PELAGIC SILICEOUS BIOGENIC - SOFT
Diatom Ooze
Radiolarian Ooze
Diatom - Rad or Siliceous Ooze
SB1
SB2
SB3
PELAGIC SILICEOUS BIOGENIC - HARD
Diatomite
Radiolarite
Porcellanite
Chert
SB4
SB5
SB6
SB7
TRANSITIONAL BIOGENIC SILICEOUS SEDIMENTS
Siliceous Component < 50%
Siliceous Component > 50%
Terrigenous Symbol
Siliceous Modifier Symbol
Non-Biogenic Sediments
Pelagic Clay
P1
Calcareous Biogenic Sediments
PELAGIC BIOGENIC CALCAREOUS - SOFT
Nannofossil Ooze
Foraminiferal Ooze
Nanno - Foram or Foram - Nanno Ooze
Calcareous Ooze
CB1
CB2
CB3
CB4
PELAGIC BIOGENIC CALCAREOUS - FIRM
Nannofossil Chalk
Foraminiferal Chalk
Nanno - Foram or Foram - Nanno Chalk
Calcareous Chalk
CB5
CB6
CB7
CB8
PELAGIC BIOGENIC CALCAREOUS - HARD
Limestone
CB9
TRANSITIONAL BIOGENIC CALCAREOUS SEDIMENTS
Calcareous Component < 50%
Calcareous Component > 50%
Terrigenous Symbol
Calcareous Modifier Symbol
SPECIAL ROCK TYPES
Gravel
Conglomerate
Breccia
Basic Igneous
SR1
SR2
SR3
SR4
Acid Igneous
Coals
Dolomite
Metamorphics
SR5
SR6
SR7
SR8
EVAPORITES
Halite
Anhydrite
Gypsum
E1
E2
E3
Concretions
Mn= Manganese
B= Barite
P= Pyrite
Z= Zeolite
drawn circle with symbol (others may be designated)
CLASTIC SEDIMENTS
Clay/Claystone
Mud/Mudstone
Shale (Fissile)
Sandy Mud/ Sandy Mudstone
T1
T2
T3
T4
Silt/Siltstone
Sand/Sandstone
Silty Sand/ Sandy Silt
Silty Clay/ Clayey Silt
T5
T6
T7
T8
Sandy Clay/ Clayey Sand
T9
VOLCANOGENIC SEDIMENTS
Volcanic Ash
Volcanic Lapilli
Volcanic Breccia
V1
V2
V3

Figure 3. Graphic symbols corresponding to the lithologic visual core descriptions for sediments and sedimentary rocks.

genic sediments, and calcareous biogenic sediments (Fig. 3 and Table 1).

Clastic Sediments

Clastic (terrigenous) sediments are composed of greater than 30% terrigenous grains (i.e., rock and mineral fragments), less than 30% calcareous grains, and less than 10% siliceous biogenic and authigenic grains.

The main name for a clastic sediment describes the textures of the clastic grains and its degree of consolidation. The Wentworth (1922) grain-size scale (Table 2) is used to define the textural class names for clastic sediments. A single textural class name (e.g., "sand," "silt," or "clay") is used when one textural class is present in abundance exceeding 80%. When two or more textural classes are present in abundances greater than 20%, they are listed in order of increasing abundance (e.g., "silty

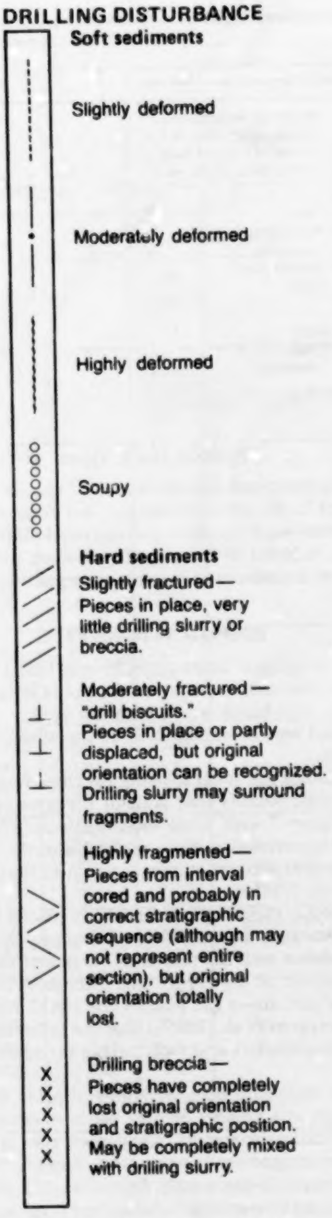
DRILLING DISTURBANCE
Soft sediments
Slightly deformed
Moderately deformed
Highly deformed
Soupy
Hard sediments
Slightly fractured—Pieces in place, very little drilling slurry or breccia.
Moderately fractured—"drill biscuits." Pieces in place or partly displaced, but original orientation can be recognized. Drilling slurry may surround fragments.
Highly fragmented—Pieces from interval cored and probably in correct stratigraphic sequence (although may not represent entire section), but original orientation totally lost.
Drilling breccia—Pieces have completely lost original orientation and stratigraphic position. May be completely mixed with drilling slurry.

Figure 4. Drilling disturbance symbols used on Leg 117 core description forms.

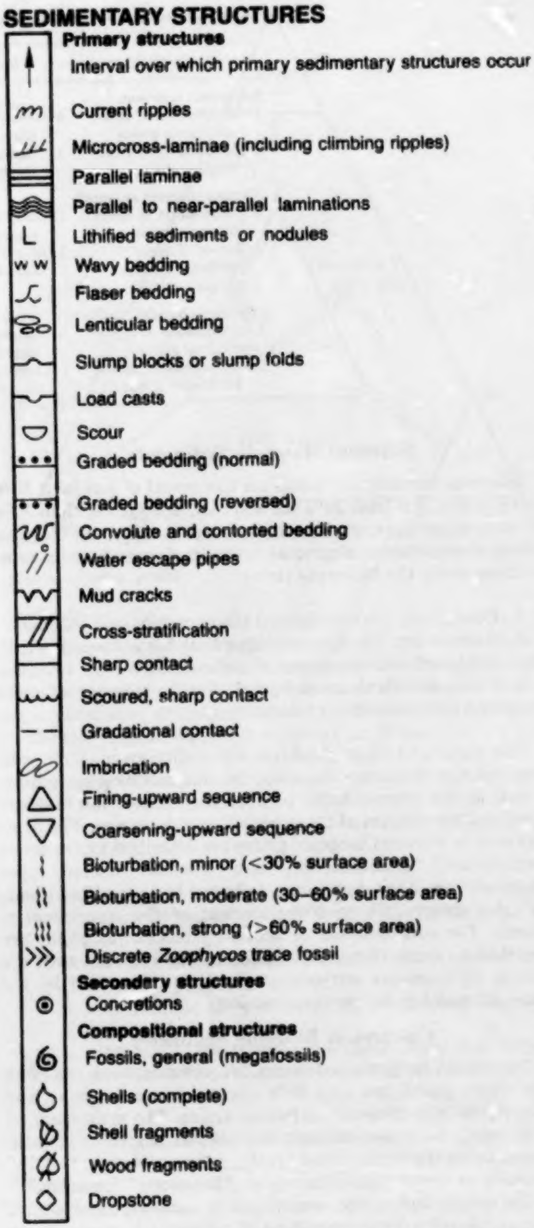
SEDIMENTARY STRUCTURES
Primary structures
Interval over which primary sedimentary structures occur
Current ripples
Microcross-laminae (including climbing ripples)
Parallel laminae
Parallel to near-parallel laminations
Lithified sediments or nodules
Wavy bedding
Flaser bedding
Lenticular bedding
Slump blocks or slump folds
Load casts
Scour
Graded bedding (normal)
Graded bedding (reversed)
Convolute and contorted bedding
Water escape pipes
Mud cracks
Cross-stratification
Sharp contact
Scoured, sharp contact
Gradational contact
Imbrication
Fining-upward sequence
Coarsening-upward sequence
Bioturbation, minor (<30% surface area)
Bioturbation, moderate (30–60% surface area)
Bioturbation, strong (>60% surface area)
Discrete Zoophycos trace fossil
Secondary structures
Concretions
Compositional structures
Fossils, general (megafossils)
Shells (complete)
Shell fragments
Wood fragments
Dropstone

Figure 5. Sedimentary structure symbols for sediments and sedimentary rocks.

sand" or "silty clay"). The term "mud" is restricted to mixtures of sand, silt, and clay, with greater than 20% and less that 60% of each textural class (Fig. 6).

The major and minor modifiers for a clastic sediment describe the compositions of the clastic grains as well as the compositions of accessory biogenic grains. The compositions of terrigenous grains can be described by terms such as "quartz," "feldspar," "glauconite," or "lithic" (for rock fragments). The major clastic components at all of the Leg 117 sites are clays and calcite of indeterminate, but not obviously biogenic, origin. This calcite is recorded as "inorganic calcite" in the smear slide analyses but is probably better described as "detrital." This detrital calcite is described by the major compositional modifier "calcitic." The modifier "calcareous" is restricted to describing biogenic calcareous components where component percentages are equivalent. The compositions of biogenic grains can be described by terms that are defined in the following sections.

Table 1. Summary of nomenclature of basic oceanic sediment types.

Minor modifiers	Major modifiers	Main name
Siliciclastic sediments		
1. Composition of minor siliciclastic grains 2. Composition of minor biogenic grains	1. Composition of major siliciclastic grains 2. Composition of minor biogenic grains	1. Texture of terrigenous grains (sand, silt, etc.) 2. Texture of volcaniclastic grains (ash, lapilli, etc.)
Siliceous biogenic sediments		
1. Composition of minor biogenic grains 2. Texture of minor siliciclastic grains	1. Composition of major biogenic grains 2. Texture of major siliciclastic grains	1. Ooze 2. Radiolarite 3. Diatomite 4. Porcellanite 5. Chert
Calcareous biogenic sediments		
1. Composition of minor biogenic grains 2. Composition of minor siliciclastic grains	1. Composition of major biogenic grains 2. Composition of major siliciclastic grains	1. Ooze 2. Chalk 3. Limestone

Siliceous Biogenic Sediments

Siliceous biogenic sediments are composed of less than 30% clastic grains, less than 30% silt and clay, and greater than 30% siliceous biogenic grains. The main name of a siliceous biogenic sediment describes its degree of consolidation and/or its composition, using the following terms:

1. Ooze: Soft, unconsolidated siliceous biogenic sediment.
2. Radiolarite: Hard, consolidated siliceous biogenic sediment composed predominantly of radiolarians.
3. Diatomite: Hard, consolidated siliceous biogenic sediment composed predominantly of diatoms.

The major and minor modifiers for a siliceous biogenic sediment describe the compositions of the siliceous biogenic grains, as well as the compositions of accessory calcareous biogenic grains and the textures of accessory siliciclastic grains. The compositions of siliceous biogenic grains are described by the terms "radiolarian," "diatomaceous," and "siliceous" if many types are present but none dominates, followed by the suffix "-bearing" if a minor (5% to 10%) amount of the component is present. The compositions of accessory calcareous grains are described by terms that are discussed in the following text; the textures of accessory terrigenous grains are described by the terms discussed in the previous section.

Calcareous Biogenic Sediments

Calcareous biogenic sediments are composed of less than 30% clastic grains, less than 30% siliceous-biogenic grains, and greater than 30% biogenic carbonate grains. The main name of a calcareous biogenic sediment describes its degree of consolidation, using the terms "ooze" (soft, unconsolidated), "chalk" (partially to firmly consolidated), or "limestone" (cemented).

The major and minor modifiers for a calcareous biogenic sediment describe the compositions of calcareous biogenic grains, as well as the compositions of accessory siliceous biogenic grains and the textures of accessory siliciclastic grains.

The compositions of calcareous biogenic grains are described by the terms "foraminifer," "nannofossil," or "calcareous" (for a combination thereof where none dominates), followed by the suffix "-rich" if the grain components are present in abundances of 10% to 25% and by the suffix "-bearing" if the grain components are present in minor (5% to 10%) amounts. The compositions of siliceous biogenic grains and the textures of siliciclastic grains are described by the terms previously discussed.

Special Rock Types

The definitions and nomenclatures of special rock types are not included in the previous section, but their description adheres as closely as possible to conventional ODP terminology. Rock types included in this category include phosphorite and shallow-water limestones (e.g., carbonate grainstones and packstones).

BIOSTRATIGRAPHY

Leg 117 shipboard biostratigraphy was based on planktonic foraminifers, calcareous nannofossils, and radiolarians. Age determinations were based on examination of the core-catcher assemblages and were refined with shore-based studies of intermediate samples.

Correlation of the zonal schemes for these fossil groups with the geomagnetic polarity time scale of Berggren et al. (1985b) is shown in Figure 7 with some modifications. These modifications make the correlation more applicable to the Leg 117 material and take into account studies made after the publication of Berggren et al. (1985b).

The Pliocene/Pleistocene boundary is placed at 1.66 Ma at the first appearance datum (FAD) of *Gephyrocapsa caribbeanica* in accordance with the results of studies of the Italian type section by Sato et al. (in press). The Miocene/Pliocene boundary is placed just above the base of the NN12 Zone in accordance with Berggren et al. (1985b). See the following sections on planktonic foraminifers and radiolarians for additional modifications.

Although shipboard determinations of paleomagnetic reversals were made at a number of sites, we have chosen to use previously published paleomagnetically derived ages in the site chapters (see "Paleomagnetism" section, this chapter). We have, however, used oxygen isotope data from Site 723 (Niitsuma and Oba, unpubl. data) to establish the ages of three late Pleistocene nannofossil events (FAD of *Emiliania huxleyi*, the last appearance datum (LAD) of *Pseudoemiliania lacunosa*, and the top of acme of *Reticulofenestra* sp. A).

Planktonic Foraminifers

A list of stratigraphically useful species events that were recognized in the Leg 117 material is presented in Table 3. Most ages were derived from Berggren et al. (1985b), except for the first occurrences (FOs) of *Sphaeroidinella dehiscens immatura* and *Neogloboquadrina acostaensis*. The *S. dehiscens immatura* appearance datum level (4.8 Ma) of van Gorsel and Troelstra

Table 2. Grain-size categories used for classification of terrigenous sediments (from Wentworth, 1922).

	MILLIMETERS	µm	PHI (Φ)	WENTWORTH SIZE CLASS	
			-20		
	4096		-12	Boulder (-8 to -12 Φ)	
	1024		-10		
	256		-8	Cobble (-6 to -8 Φ)	
	64		-6		GRAVEL
	16		-4	Pebble (-2 to -6 Φ)	
	4		-2		
	3.36		-1.75		
	2.83		-1.5	Granule	
	2.38		-1.25		
	2.00		-1.0		
	1.68		-0.75		
	1.41		-0.5	Very coarse sand	
	1.19		-0.25		
	1.00		0.0		
	0.84		0.25		
	0.71		0.5	Coarse sand	
	0.59		0.75		
1/2	0.50	500	1.0		
	0.42	420	1.25		
	0.35	350	1.5	Medium sand	SAND
	0.30	300	1.75		
1/4	0.25	250	2.0		
	0.210	210	2.25		
	0.177	177	2.5	Fine sand	
	0.149	149	2.75		
1/8	0.125	125	3.0		
	0.105	105	3.25		
	0.088	88	3.5	Very fine sand	
	0.074	74	3.75		
1/16	0.0625	63	4.0		
	0.053	53	4.25		
	0.044	44	4.5	Coarse silt	
	0.037	37	4.75		
1/32	0.031	31	5.0		
1/64	0.0156	15.6	6.0	Medium silt Fine silt	
1/128	0.0078	7.8	7.0	Very fine silt	
1/256	0.0039	3.9	8.0		MUD
	0.0020	2.0	9.0		
	0.00098	0.98	10.0	Clay	
	0.00049	0.49	11.0		
	0.00024	0.24	12.0		
	0.00012	0.12	13.0		
	0.00006	0.06	14.0		

(1981) was used, and the *N. acostaensis* FO (8.6 Ma) comes from Barron et al. (1985). These ages are in better correspondence to the calcareous nannofossil and radiolarian datum levels determined from Leg 117 material. During shipboard analysis it appeared that the zonal marker species for published Pleistocene-Pliocene zonal schemes are missing or show a highly scattered occurrence. For instance, the evolutionary series of *Globorotalia tosaensis* to *Globorotalia truncatulinoides* is missing in the upper Pliocene to lower Pleistocene. We approximated this boundary (N21/22) by using the extinction level of *Globigerinoides obliquus extremus* (1.8 Ma). In addition, subdivision of the Pliocene was difficult because of the scarcity of specimens of marker species such as *Globorotalia margaritae* and *Globigerinoides fistulosus*. Because published zonal schemes are difficult if not impossible to apply in this area, we have used the conventional zonation of Blow (1969) as closely as possible.

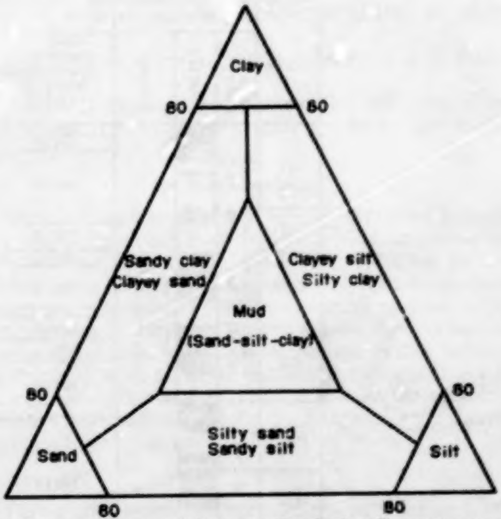

Figure 6. Ternary diagram defining the three basic sediment types on the basis of relative proportions of siliciclastic, siliceous biogenic, and calcareous biogenic grains.

Methods

Sediment samples of approximately 10 cm^3 from the core catchers were washed over a 45-µm-mesh sieve to extract sufficient foraminifers. The >125 µm fraction was studied, and the semiquantitative abundance of planktonic foraminiferal species of the total assemblage were estimated as follows:

R = rare (<1%)
F = few (1%-15%)
C = common (15%-30%)
A = abundant (>30%)

In addition, the 63-125-µm fraction was examined for planktonic foraminiferal markers if they were absent in the larger size fraction.

Three classes of foraminiferal preservation were employed:

P = poor (almost all specimens are broken and fragments dominate)
M = moderate (30%-90% of specimens show dissolution)
G = good (>90% of specimens are well preserved and unbroken)

Benthic Foraminifers

Methods

Sediment samples of approximately 10 cm^3 were processed for extraction of benthic foraminifers. The sediment samples were wet sieved over a 63-µm sieve, and the residue was dried under an infrared lamp. The benthic foraminifers were then extracted from the >125-µm fraction.

The abundance of benthic foraminifers in 10 cm^3 is defined as follows:

R = rare (<10 specimens)
P = poor (10-100 specimens)
C = common (101-500 specimens)
A = abundant (>500 specimens)

Preservation is determined by the degree of fragmentation and abrasion of the benthic tests:

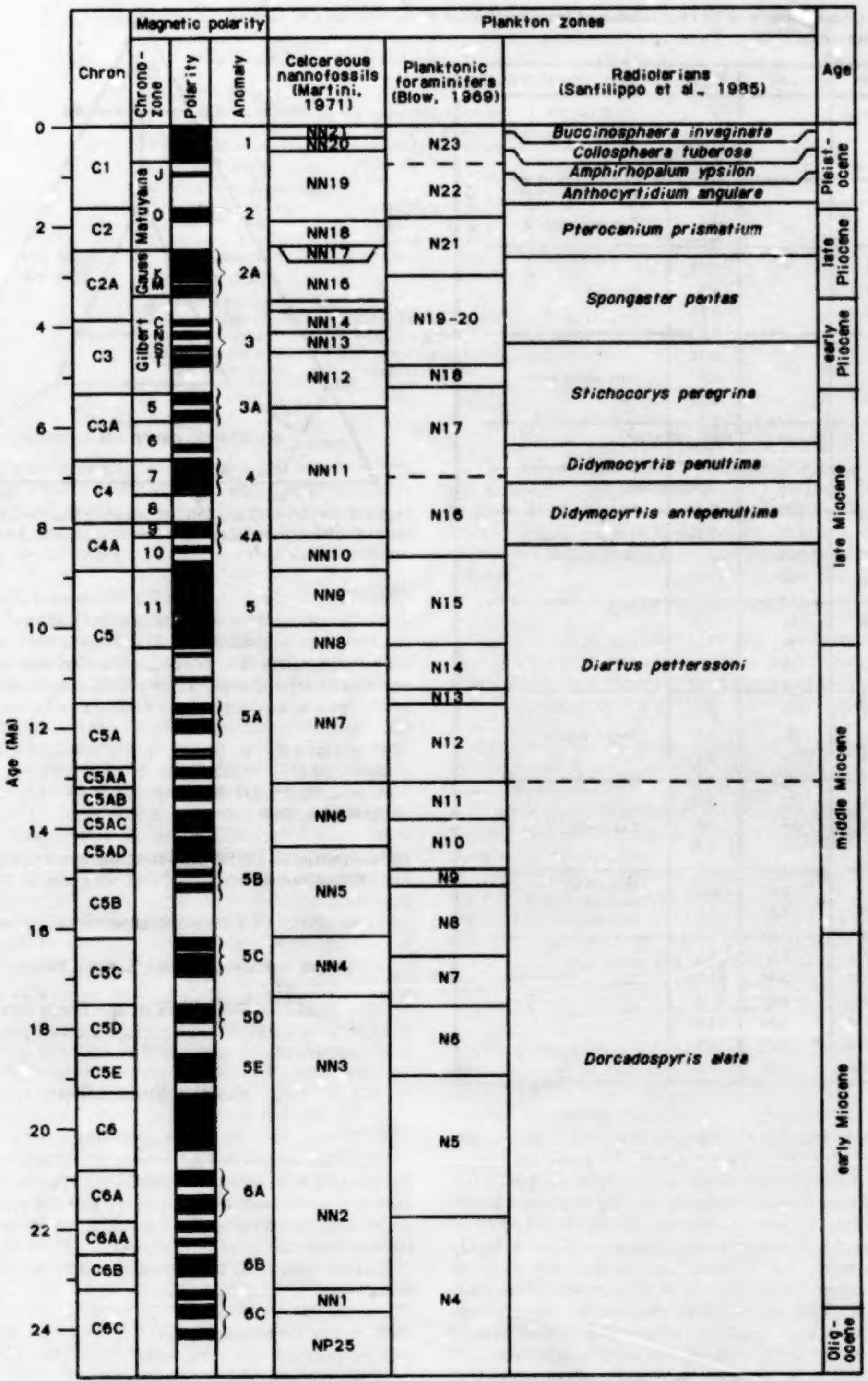

Magnetic polarity events: J = Jaramillo, O = Olduvai, K = Kaena, M = Mammoth,
C = Cochiti, N = Nunivak, S = Sidufjall, T = Thvera

Figure 7. Neogene geochronology modified from Berggren et al. (1985b) for Leg 117.

Table 3. Foraminiferal species events found in Leg 117 material.

Event	Species	Age (Ma)
LO	*Globigerinoides obliquus extremus*	1.8
LO	*Sphaeroidinellopsis* sp.	3.0
Coiling change of S/D *Pulleniatina*		3.8
FO	*Sphaeroidinella dehiscens immatura*	4.8
FO	*Globorotalia tumida tumida*	5.2
FO	*Pulleniatina primalis*	5.8
FO	*Neogloboquadrina acostaensis*	8.6
LO	*Globorotalia mayeri*	10.4
FO	*Globigerinoides nepenthes*	11.3
LO	*Globorotalia fohsi* s.l.	11.5
LO	*Globorotalia peripheronda*	14.6
FO	*Globorotalia peripheroacuta*	14.9
FO	*Orbulina universa*	15.2

Note: FO = first occurrence, LO = last occurrence. Ages are from Berggren et al. (1985b), except for: *Sphaeroidinella dehiscens immatura* (van Gorsel and Troelstra, 1981) and *Neogloboquadrina acostaensis* (Barron et al., 1985).

P = poor (mostly fragments and/or strongly etched specimens)
M = moderate (about 50% of the tests in an assemblage are broken or etched
G = good (most specimens are intact)

Planktonic/benthic ratios were determined in the >125-μm size fraction to reveal dissolution patterns or environmental conditions.

Calcareous Nannofossils

The zonal scheme established by Martini (1971) was employed on this leg. The biohorizons recognized in the Quaternary sequences in the North Atlantic on DSDP Leg 94 by Takayama and Sato (1987) were also used. The nannofossil zonation and the indication of estimated time relations are based on Takayama and Sato (1987) and Berggren et al. (1985b). Nannofossil datums used on Leg 117 are listed in Table 4.

Methods

Age determination made during Leg 117 was based on the study of each core-catcher sample and samples specially selected by the shipboard paleontologists. Shore-based studies are based on slides made from intermediate samples. Nannofossil slides were prepared from unprocessed sample material. These slides were examined under the binocular polarizing microscope at a magnification of 1250× with an oil-immersion objective.

Selective dissolution and overcalcification of calcareous nannofossils are important factors in species identification and species composition in deep-sea sediments, and as such, may have a considerable effect on biostratigraphic results. The overall preservation of the nannofossil assemblage was recorded using one of three letter designations:

G = good (little or no evidence of solution and/or overgrowth
M = moderate (some dissolution and/or overgrowth, but nearly all specimens can be identified
P = poor (dissolution and/or overgrowth on nearly every specimen, and many specimens cannot be identified)

Abundances were estimated semiquantitatively at 1250× magnification and tabulated according to a logarithmic scale as follows:

A = abundant (1 to 10 specimens of a taxon per field of view)
C = common (1 specimen of a taxon per 2 to 10 fields of view)
F = few (1 specimen of a taxon per 11 to 100 fields of view)
R = rare (1 specimen of a taxon per 101 to 1000 fields of view)

Radiolarians

The low-latitude zonations of Nigrini (1971) for the Quaternary and of Riedel and Sanfilippo (1978) and Sanfilippo et al. (1985) for the Tertiary were used on Leg 117 when the zonal markers could be found. *Pterocanium prismatium*, *Spongaster pentas*, and *Spongaster berminghami* are all very rare in Arabian Sea material. Hence, in some cases, other species had to be used to approximate certain zonal boundaries (see individual site chapters). Table 5 lists the radiolarian events used to establish a biochronology for Leg 117. Ages used are from previously published paleomagnetic data for the Indian Ocean (Johnson et al., in press; Johnson and Nigrini, 1985).

Methods

The recorded radiolarian abundance in each sample is based on qualitative examination of strewn slides of sieved acid residues. Consequently, there may be discrepancies between these observations and those in the lithology reports, which were based on smear slide observations. Estimates also reflect, in part, the amount of terrestrial input and nonradiolarian siliceous biota (mainly diatoms). Abundances are recorded as follows:

C = common (100 to 500 specimens in the noncalcareous fraction)
F = few (10 to 100 specimens)
R = rare (3 to 10 specimens)

The preservation of radiolarians in strewn slides is defined as follows:

G = good (no signs of dissolution)
M = moderate (dissolution observed, but minor)
P = poor (strong dissolution effect)

Samples preparation procedures used during this cruise are described in Sanfilippo et al. (1985). All samples were sieved with 63-μm mesh size.

PALEOMAGNETISM

Sampling and Magnetic Measurements

Soft sediments were sampled by pushing plastic cubes of 6 mL volume into the split-core face. For semilithified sediments we used a ceramic knife to cut out samples that were then inserted into the plastic cubes. For lithified sediments we used a diamond-tipped rotary drill to obtain minicores, which were then trimmed to a volume of about 10 mL. We routinely took two samples per 1.5-m core section from suitable (i.e., undisturbed) intervals; this sampling resolution was found to be adequate for resolving the magnetostratigraphy of the generally high accumulation rate sequences encountered on Leg 117. Usually, one of the samples from each section was demagnetized and measured aboard the ship, and the other was kept in its original condition for shore-based measurement.

The natural remanent magnetization (NRM) of the archive halves of cores was measured at 10-cm intervals using the 2G

Table 4. Calcareous nannofossil datums recognized on Leg 117.

Datum	Limit	Species	Age (Ma)	Source of age	Notes
1	T	*Helicosphaera inversa*	0.15	4	North Atlantic data
2	B	*Emiliania huxleyi*	0.19	3	
3	T	*Pseudoemiliania lacunosa*	0.49	3	
4	B	*Helicosphaera inversa*			
5	T	*Reticulofenestra* sp. A (acme)	0.82	3	
6	B	*Gephyrocapsa parallela*	0.89	4	North Atlantic data
7	T	*Gephyrocapsa* (large)	1.10	4	North Atlantic data
8	T	*Helicosphaera sellii*			May be diachronous
9	B	*Gephyrocapsa* (large)	1.36	4	North Atlantic data
10	T	*Calcidiscus macintyrei*	1.45	6	
10	B	*Gephyrocapsa oceanica*	1.57	4	North Atlantic data
	B	*Gephyrocapsa caribbeanica*	1.66	4, 8	North Atlantic age consistent with Italian-type section
	T	*Discoaster brouweri*	1.90	6	
	T	*Discoaster pentaradiatus*	2.40	6	
	T	*Discoaster surculus*	2.40	6	
	T	*Sphenolithus abies*	3.47	6	
	T	*Reticulofenestra pseudoumbilica*	3.50	6	
	B	*Discoaster tamalis*	3.8	6	Equatorial region only
	B	*Discoaster asymmetricus*	4.1	6	
	B	*Ceratolithus rugosus*	4.5	6	
	T	*Discoaster quinqueramus*	5.6	6	May be erroneous age
	B	*Discoaster quinqueramus*	8.2	6	
	T	*Discoaster hamatus*	8.85	6	
	B	*Discoaster hamatus*	10.0	6	
	B	*Catinaster coalitus*	10.8	6	
	B	*Discoaster kugleri*	ca. 13.1	6	
	T	*Sphenolithus heteromorphus*	14.4	6	
	T	*Sphenolithus belemnos*	17.4	6	

Note: T = upper limit and B = lower limit. Sources of ages are: 3 = oxygen isotope data for Site 723 (N. Niitsuma, unpubl. data); 4 = Takayama and Sato, 1987; 6 = Berggren et al., 1985b; and 8 = Sato et al., in press.

Enterprises pass-through cryogenic magnetometer; measurements were usually made after alternating field (AF) demagnetization at 5 or 9 mT with the pass-through demagnetizer. Pass-through NRM measurements were usually confined to APC cores; measurements obtained from XCB recovery were typically much more scattered. The NRM of discrete specimens was measured using the MINISPIN fluxgate spinner magnetometer and the Schonstedt AF demagnetizer. Where possible (depending on time constraints) one sample per core was subjected to stepwise AF demagnetization in order to select a suitable field for blanket demagnetization of the remaining samples from that core.

Most of the samples measured aboard ship were remeasured onshore with a ScT cryogenic magnetometer involving application of a higher peak AF (usually 15 mT) for demagnetization. Because the shore-based remeasurement generally confirmed the shipboard results, most of the magnetic polarity zone boundaries cited in the site chapters are those that were determined aboard ship. Resolution of some boundary horizons was, however, improved by the shore-based reanalysis. The volume magnetic susceptibility of whole cores was measured (usually at 5–10-cm intervals) using the Bartington Instruments MS1C sensor; the instrument was calibrated by calculating the volume susceptibility of a 30-cm length of core liner packed with MnO_2 as a standard.

Geomagnetic Polarity Time Scale

We use the geomagnetic polarity time scale (GPTS) of Berggren et al. (1985a). Our choice of chron nomenclature follows the marine magnetic anomaly-based system described in Cox (1983) with the addition of the prefix *C* (correlative). For convenience, in referring to chrons we include the traditional terminology used in chronostratigraphic unit in parentheses: e.g., chron C1N (Bruhnes chronozone) and chron C5N (chronozone 11). Using the depth and the age of our paleomagnetic polarity zone boundaries, we calculated interpolated ages for biostratigraphic datum levels. The paleomagnetic records from some sites, however, are incomplete, making accurate interpolation difficult. We could not find good records of relatively short polarity "events," such as C1r-1 (Jaramillo subchronozone) and C2N (Olduvai subchronozone) at the Owen Ridge sites and at Site 728 on the Oman margin. Furthermore, uncertainty exists as to whether the sedimentation rate was constant enough during a polarity chron. Therefore, we are reluctant, at this time, to accept the interpolated ages as reliable age estimates of biostratigraphic datums.

INTERHOLE AND INTERSITE CORRELATIONS

Because the recovery of several complete Neogene sequences was a primary objective of Leg 117 drilling, the ability to correlate between holes so that complete composite sequences could be constructed for a given site was of critical importance. As most of the sites are represented by two to three holes, the potential for constructing complete sequences is good. We applied two methods of correlation: visual comparison of the core photographs and correlation using whole-core magnetic susceptibility measurements.

For many of the sites, the dominant lithology consists of alternating layers of light, carbonate-rich intervals and darker, clay-rich intervals. Interhole comparison of core photographs indicated that these sedimentary layers could be visibly correlated between holes based on their color and thickness characteristics. Using the core photographs, the sedimentary layers could be correlated between holes to within 5–10 cm. For the Oman margin sites, and particularly for the Owen Ridge sites, several distinct and traceable layers were identified. Owen Ridge Hole 721A was the first hole for which these layers were observed and described, with the notation OR-a_0, a_1, . . ., a_n and OR-b_1, b_2, . . ., b_n. The OR-*a* indicates that the marker layer was first observed in Core 117-721A-1H, and the OR-*b* refers to layers observed in Core 117-721A-2H. The numbered subscripts identify the layer's sequence in a given core. Intersite correlation of these

Table 5. List of radiolarian events, their placement in the zonal scheme of Sanfilippo et al. (1985), and correlation with previously published paleomagnetically derived ages.

Radiolarian zone	Radiolarian event	Indian Ocean age (Ma)	Source of age	Notes
Buccinosphaera invaginata	**B *Buccinosphaera invaginata***	—		
Collosphaera tuberosa	T *Stylatractus universus*	0.37–0.47	1	
	B *Collosphaera tuberosa*	0.40–0.59	1	
Amphirhopalum ypsilon	T *Anthocyrtidium nosicaae*	0.66–0.76	1	
	B *Pterocorys hertwigii*	0.76–0.84	1	
	T *Anthocyrtidium angulare*	0.94–1.04	1	
Anthocyrtidium angulare	B *Lamprocyrtis nigriniae*	1.02–1.07	1	Possibly a diachronous event
	T *Lamprocyrtis neoheteroporos*	1.09–1.13	1	
	T *Pterocanium prismatium*	1.52–1.56	1	Rare in Leg 117 material
Pterocanium prismatium	B *Anthocyrtidium angulare*	1.52–1.64	1	
	B *Theocalyptra davisiana*	2.42–2.44	1	
	B *Lamprocyrtis neoheteroporos*	2.51–2.53	1	
	T *Stichocorys peregrina*	2.62–2.64	1	
Spongaster pentas	T *Phormostichoartus fistula*	3.26–3.28	1	
	T *Lychnodictyum audax*	3.33–3.35	1	
	T *Phormostichoartus doliolum*	3.53–3.55	1	
	B *Amphirhopalum ypsilon*	3.77–3.79	1	
	T *Spongaster pentas*	3.74–3.82	1	Not found in Leg 117 material
	B *Spongaster tetras tetras*	3.83–3.85	1	
	T *Spongaster berminghami*	3.85–3.87	1	Rare in Leg 117 material; possibly a diachronous event
	Spongaster berminghami* → *Spongaster pentas	4.3–4.4	2	Rate in Leg 117 material; possibly a diachronous event
Stichocorys peregrina	B *Spongaster pentas*	4.2–4.3	2	Rare in Leg 117 material; a diachronous event
	T *Solenosphaera omnitubus*	4.7–4.8	2	
	T *Spongodiscus ambus*	—		
	T *Botryostrobus bramlettei*	4.9–5.0	2	Not reliable in Leg 117 material
	T *Stichocorys delmontensis*	—		
	T *Siphostichartus corona*	5.0–5.1	2	
	T *Acrobotrys tritubus*	5.3–5.4	2	
	T *Stichocorys johnsoni*	5.7–5.8	2	*Eucyrtidium* cf. *diaphanes*
	B Spongodiscus ambus	—		
	Stichocorys delmontensis* → *Stichocorys peregrina	6.1–6.7	2	Possibly a diachronous event
Didymocyrtis penultima	T *Calocycletta caepa*	6.2–6.6	2	Age in west Pacific; possibly a diachronous event
	B *Solenosphaera omnitubus*	6.3–6.5	2	
	T *Diartus hughesi*	7.1–7.2	2	
Didymocyrtis antepenultima	B *Stichocorys peregrina*	—		
	T *Dictyocoryne ontongensis*	—		
	B *Acrobotrys tritubus*	7.7–7.78	2	Diachronous event
	T *Botryostrobus miralestensis*	8.1–8.2	2	Possibly a diachronous event
	T *Didymocyrtis laticonus*	—		
	T *Diartus pettersoni*	8.1–8.2	2	Possibly a diachronous event
	Diartus pettersoni* → *Diartus hughesi	8.3–8.5	2	Possibly a diachronous event
Diartus pettersoni	B *Spongaster berminghami*	7.9–8.0	2	Rare in Leg 117 material; possibly a diachronous event
	T *Stichocorys wolffii*	8.1–8.2	2	Age in west Pacific
	B *Botryostrobus bramlettei*	8.8–9.0	2	
	B *Diartus hughesi*	8.7–8.8	2	Diachronous event
	T *Cyrtocapsella japonica*	10.0–10.3	2	Possibly a diachronous event
	T *Lithopera thornburgi*	—		
	T *Cyrtocapsella cornuta*	11.6–11.9	2	

Note: T = upper morphotypic, B = lower morphotypic limit, and → = evolutionary transition. Events shown in bold face define zonal boundaries. Sources of ages are: 1 = Johnson et al., in press, and 2 = Johnson and Nigrini, 1985.

lithologic marker layers applies only to the Owen Ridge Sites 721, 722, and 731. The depths of the correlative horizons are listed in the respective site chapters.

Hole 723A was the first hole for which lithologic marker layers were identified for the Oman margin. As with the Owen Ridge sites, the marker layers were labeled OM-a_1, a_2, . . ., a_n and OM-b_1, b_2, . . ., b_n, with the *a* indicating that the layer occurs in Core 117-723A-1H and the numbered subscript identifying its sequence in that core.

These interhole correlations were confirmed using whole-core magnetic susceptibility measurements. The magnetic susceptibility of whole-core sections was measured at 5- to 10-cm intervals for all APC-recovered core material and most XCB- and RCB-recovered material. To the first order, downcore variations in magnetic susceptibility record reflect fluctuations in the concentration of magnetic materials, which are dominantly the ferrimagnetic minerals of the magnetite-titanomagnetite series for most marine sediments. In general, the darker, clay-rich intervals are identified by higher values of magnetic susceptibility. Compared to the lithologic datums, the susceptibility variations offer considerably more detail and character with which to construct correlations, and the data are quantitative (Fig. 8). By combining the lithologic and magnetic susceptibility correlation datums, it is possible to cross-validate proposed lithologic cor-

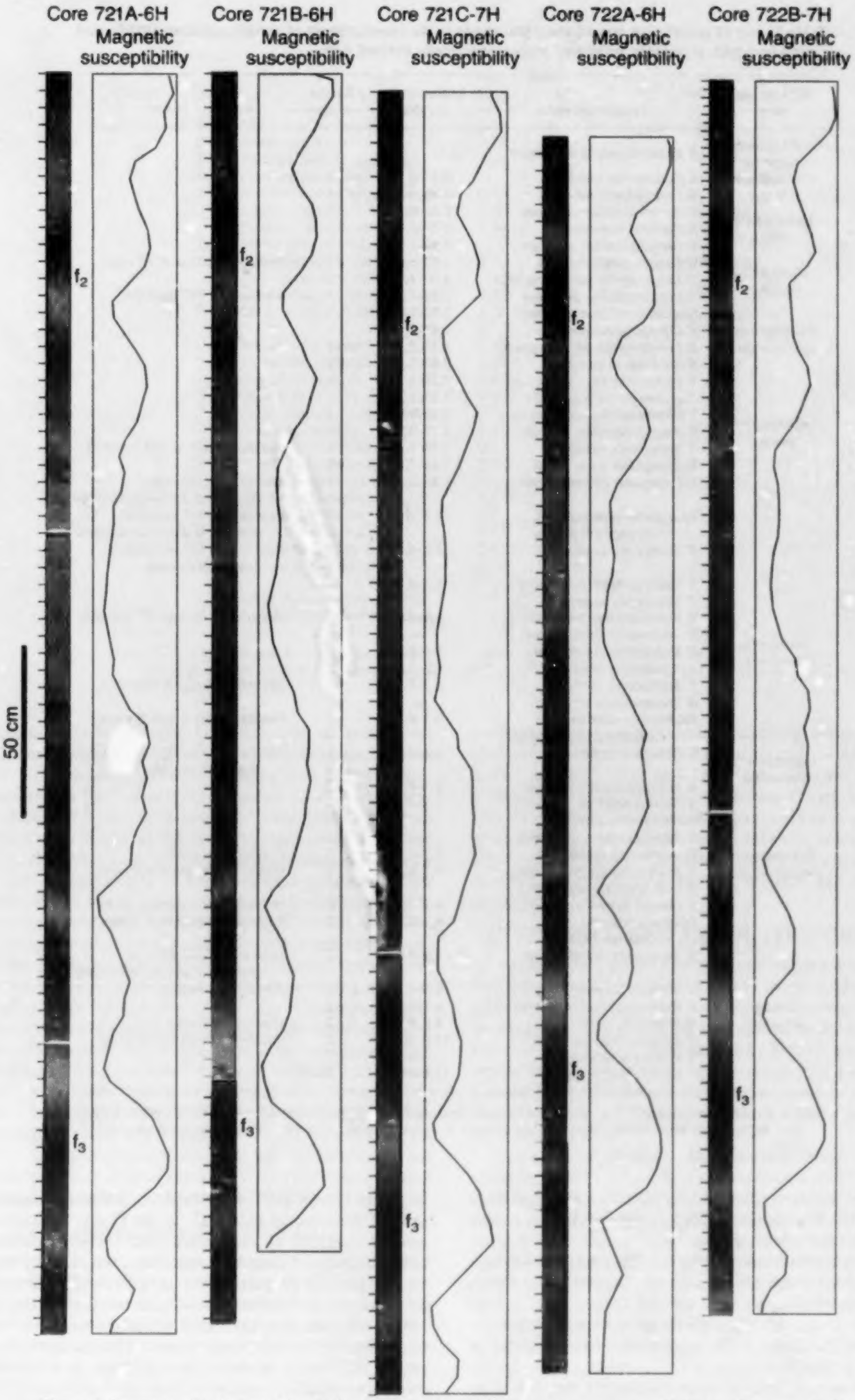

Figure 8. Example of sediment color and magnetic susceptibility measurements correlation used between hole and sites. See text for detailed explanation.

relations to obtain definitive correlation datums that are both detailed and accurate. For the Owen Ridge sites, the correlation accuracy is typically within ± 5 cm. The accuracy of the Oman margin correlations are comparable for the uppermost APC cores; however, correlations were typically not possible beyond ~ 50 mbsf because of the adverse effect of gas-expansion disturbances on both lithologic and magnetic datums.

Correlation datums given in the "Interhole and Intersite Correlations" sections of the "Site 721-724, 727, and 728" chapters are based on concordant lithologic and magnetic datums only. The intended application of these datums is to provide a series of connection points from which accurate interhole correlations can be made. The lithologic and magnetic susceptibility data from Owen Ridge Sites 721, 722, and 731 indicate that up to 1 to 2 m can be missing at APC core breaks; thus, the interhole correlation datums are necessary to compose complete sections around core breaks and voids (Fig. 9). For the ridge sites, the correlation datums allow a complete composite section to be constructed from the upper Pliocene upward. The margin sites have a wider range of sedimentation rates, but complete sections for some sites can be constructed for the upper Pliocene upward (Sites 727 and 728) and for the upper Pleistocene (Sites 723 and 724).

Intersite Correlations

Intersite correlations for the Owen Ridge sites and the Oman Margin sites are presented in the "Background and Objectives, Owen Ridge" and the "Background and Objectives, Oman Margin" chapters (this volume). As with the interhole correlations, the datums given in these chapters are based on concordant lithologic and magnetic susceptibility correlations. These correlations are generally accurate to within 10 cm. Between the Owen Ridge Sites 721, 722, and 731, intersite correlations are possible from the upper Pliocene upward. An example of correlation between cores of the three Owen Ridge sites is shown in Figure 8. Correlations between Owen margin Sites 727 and 728 are possible down to the upper Pliocene; correlations between margin Sites 723 and 724 are possible down to the upper Pleistocene only.

The combination of excellent Leg 117 sediment recovery and firm stratigraphic control allows the construction of complete composite sequences. Correlation datums provided in the site chapters have been confirmed using both lithologic and magnetic susceptibility datums. The detail of the interhole and intersite correlations is among the best reported for any drilled marine sequence recovered to date. Although the principal application of the correlation datums is to provide a means for composing complete sequences, they also serve to maximize sampling economy and diffuse future sampling intensity at any one hole.

PHYSICAL PROPERTIES

A thorough discussion of the equipment, methods, errors, and correction factors associated with the measurement of physical properties was presented by Boyce (1973, 1976). Only a brief review of the methods used on Leg 117 is presented here.

Gamma Ray Attenuation Porosity Evaluator (GRAPE)

The gamma ray attenuation porosity evaluator (GRAPE) consists of a drive device to move a gamma-ray source (^{133}Ba) and a shielded scintillation detector along the length of whole-round core sections. The attenuation of the gamma rays through the cores is directly correlated with the material's mass density, producing a continuous log of wet-bulk density. Details of the theory and operation of the GRAPE can be found in Boyce (1973, 1976). The GRAPE system was calibrated periodically with an aluminum standard; an error of 1.5% is estimated by Boyce (1976). The GRAPE density values were strongly affected by the degree to which the core material filled the core liners. On Leg 117 all coherent APC and XCB core sections more than 80 cm in length were run through the GRAPE.

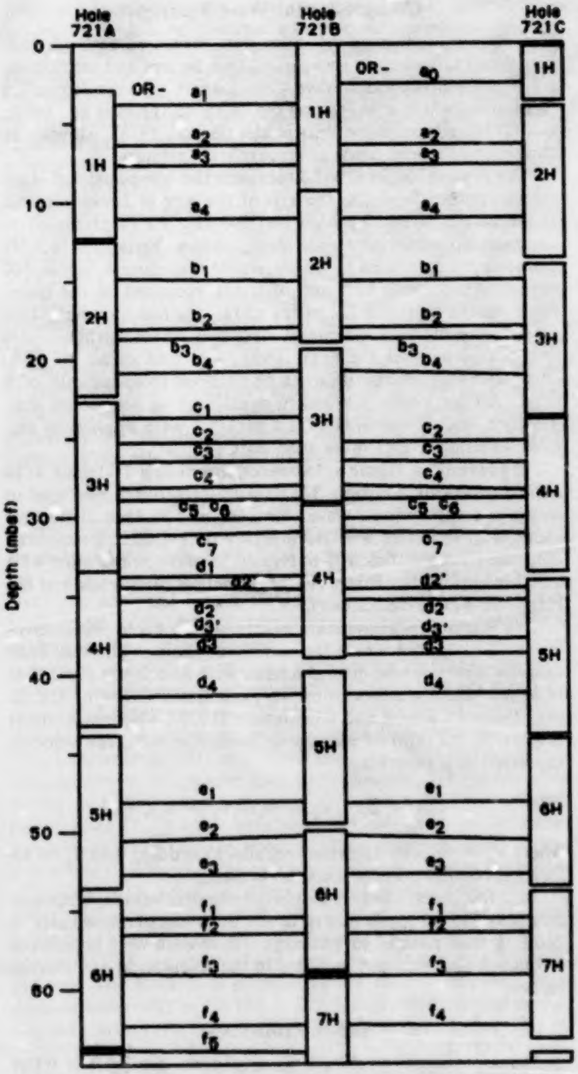

Figure 9. Correlation of sedimentary layers based on color and thickness (see text) for Holes 721A, -B, and -C, Cores 1-7.

In order to process the large volume of sediment recovered during Leg 117 it was necessary to modify the GRAPE software to increase the carriage speed by a factor of three to a rate of 0.76 cm/s. The duration of each gamma-ray count was not changed from the original 2-s count period followed by a 0.33 s break time between counts. Given this count interval and the new carriage speed, each gamma-ray count sampled a 1.5-cm-wide interval of core.

Two-minute GRAPE measurements on discrete samples were not routinely run on unlithified samples because of the large volume of sediment processed in the continuous mode. This technique, as described by Boyce (1976), was used, however, on samples of indurated sandstone.

Compressional-Wave Velocity

Compressional-wave velocities were measured through sediments and sedimentary rocks using two devices and techniques: (1) IOS Compressional-Wave Core Logger (*P*-wave logger), a continuous whole-core logging device (Schultheiss et al., 1988), and (2) Hamilton Frame Velocimeter (Boyce, 1973). All velocity measurements were made at atmospheric pressure.

The *P*-wave logger (PWL) measures the compressional-wave velocity perpendicular to the axis of the core at 2-mm intervals as the core is passed between two 500-kHz PZT4 piezoelectric compression-mode ultrasonic transponders. Variations in liner diameter are measured by displacement transducers, linear 1-K potentiometers with 12.5 mm of travel, mounted on the transducer blocks and coupled to the ultrasonic transponders. This apparatus provides good quality data only on undistrubed cores that completely fill the liner. Thus, it is best suited to APC cores, although reliable data can be obtained from suitable XCB cores. All cores were allowed to equilibrate to near room temperature, and corrections of 2.4 m/s/°C were applied to sections at temperatures other than 20°C.

The Hamilton Frame Velocimeter, linked to a Tektronix 5110 oscilloscope and Tektronix TM5006 counter/timer, was used to measure compressional-wave velocities at 500 kHz in discrete samples of sediment and sedimentary rock from all recovered cores that were sufficiently indurated to allow preparation of a suitable sample. See Boyce (1976) for details of operation of the Hamilton Frame Velocimeter.

The velocity measurements were primarily taken perpendicular to bedding, but where the sample conditions allowed, cube samples were cut and measurements were also taken parallel to bedding. Velocity anisotropies were calculated following the expressions of Carlson and Christensen (1979), where anisotropy is given as the ratio of velocity difference to the mean velocity, expressed as a percentage:

$$A = 200\,(V_n - V_v)/(V_n + V_v),$$

where V_n = velocity measured parallel to bedding and V_v = velocity measured perpendicular to bedding.

In a few cases, samples displayed negative velocity anisotropies (more rapid transmission in the direction perpendicular to bedding than parallel to bedding). These data were considered erroneous and were not included in the calculation of "average values."

Index Properties

Index properties (wet-bulk density, grain density, wet water content, and porosity) were routinely calculated from measurements of wet and dry weights and volumes. Samples of approximately 10 cm^3 were taken from every second core section or as sample quality permitted and placed in preweighed and numbered aluminum beakers. Sample weights were obtained to an accuracy of 0.01 g on a Scitech electronic balance. Sample volumes were measured with the shipboard Quantachrome Penta-Pycnometer, a helium-displacement pycnometer. The samples were oven dried at 105°C for 24 hr and allowed to cool in a desiccator prior to dry weight and volume determination. A salt correction (Hamilton, 1971) was applied to the density and porosity computations.

Vane Shear Strength

Shear-strength measurements were made using a Wykeham Farrance Laboratory vane apparatus according to the specifications of Boyce (1977). Approximately one measurement per core was taken on recovery of relatively undisturbed clay-rich sediments. All vanes were inserted parallel to bedding. Measurements were discontinued where cracking of the sediment was observed, indicating failure by fracture rather than by shear. Shear-strength measurements were not made on sediments that were disrupted by gas-induced expansion.

Thermal Conductivity

Thermal-conductivity measurements were made using the THERMCON-85 thermal conductivity instrument supplied to ODP by Woods Hole Oceanographic Institution. The needle probe technique employed by the THERMCON-85, developed by Von Herzen and Maxwell (1959), is described along with the operating procedures for the THERMCON by Pelletier and Von Herzen (unpubl. data). Measurements were taken on every other section of sediment from recovered core that was undisturbed and soft enough to allow insertion of the needle probes. All cores were allowed to equilibrate to room temperature for 3 hr or until temperature drift at the time of measurement was not greater than 0.04°C/min.

Downhole Temperature Measurements

All Leg 117 downhole temperature measurements were obtained using the combination water sampler-temperature-pressure (WSTP) tool first used on Leg 110 (Barnes, 1988). No multichannel data recorder was available for Leg 117; consequently, no fluid-pressure measurements were made. A single-channel data recorder (Yokota et al., 1980) was used to record temperatures measured by a thermistor, placed in a slightly tapered probe that extends 7.8 cm beyond a larger 6.03-cm-diameter filter probe. The larger filter probe extends 109 cm beyond the 8.89-cm diameter of the inner core barrel-WSTP tool assembly. A 10.16-cm-long cylindrical filter element at the bottom of the filter probe is approximately 12 to 22 cm above the thermistor. The lower 2.5 cm of the thermistor probe above the thermistor position has a uniform diameter of 1.27 cm (see Fig. 10).

The Leg 117 filter probe/thermistor probe assembly is an improved version of the probe design that has been used since DSDP Leg 69. The improvements include a larger filter surface area for increased pore fluid recovery, a larger diameter filter probe constructed of high-strength stainless steel, and a thermistor probe strengthened by tapering the upper section to a larger diameter than the previously uniform 1.27 cm. The new probe is 2.6 times stronger than the old probe, eliminating the need to use shortened probe lengths in stiff sediments. Probes shorter than 10.9 cm compromise the ability to obtain uncontaminated fluid samples and undisturbed temperature readings. The time constant of the thermistor probe is 2 to 3 min (Becker et al., 1983).

The Uyeda temperature recorder (Yokota et al., 1980) digitizes and stores up to 128 resistance values of a single thermistor in solid-state memory. The recording interval is 1 or 2 min. A 1-min recording interval was used during Leg 117. Resistance values are converted to temperature by the data reduction program, using the calibration curve for the thermistor in use. The nominal resolution is about 0.01° to 0.02°K over the temperature range of interest.

ORGANIC GEOCHEMISTRY

The following instrumentation and procedures were used on Leg 117 in order to determine the quantity and quality of sedimentary organic matter, to test the reproducibility of the Rock-Eval II apparatus, to measure the concentrations of hydrocarbon gases, and to calculate the ratio of diunsaturated and triunsaturated C_{37} alkenones (U^k_{37} index).

Inorganic and Organic Carbon

The mode of occurrence of carbon was determined by two CO_2 coulometers (Coulometrics Model 5011). Carbon from organic and inorganic sources was converted to CO_2, with the gas passed through a coulometer where it was quantitatively absorbed, reacting with monoethanolamine to form a titratable acid that causes a color indicator to change. The color change was monitored electronically. As the transmittance increased, the titration current was activated to stoichiometrically generate base at a rate proportional to the transmittance. The titration current was continually measured and integrated to provide a measure of CO_2.

The CO_2 coulometer serves as the detector for the Carbonate Carbon Apparatus (Coulometrics Model 5030) and the Total Carbon Apparatus (Coulometrics Model 5020). In the Carbonate Carbon Apparatus, CO_2 was generated by treatment of the sediment with HCl and gentle heating; the evolved CO_2 was transferred to the coulometer by a helium stream. Sample size varied between 15 and 75 mg of sediment. In the Total Carbon Apparatus, CO_2 was produced by the combustion of sediment at about 990°C in an oxygen atmosphere. Sample sizes ranged between 20 and 60 mg of sediment. Organic carbon was determined by the difference between total carbon and carbonate carbon. Pure calcite was used as an internal standard.

Type of Organic Matter

The character and maturity of organic matter was evaluated by means of the Delsi Rock-Eval II pyrolysis apparatus, following the process described by Espitalié et al. (1977). The Rock-Eval II is equipped with a TOC module, capable of measuring total organic carbon concentrations. However, these shipboard organic carbon values proved to be unreliable. The pyrolysis technique involved a graduated temperature program that first released volatile hydrocarbons at 300°C for 3 min and then released hydrocarbons from the thermal cracking of kerogen as the temperature increased by 25°C/min from 300° to 550°C. The total volatile (S1) and total pyrolytic (S2) hydrocarbons were measured by a flame ionization detector and are reported in mg of hydrocarbon per gram of sediment. The maximum temperature (T_{max}) value obtained corresponds to the temperature at which the kerogen yielded the maximum amount of hydrocarbons during the programmed pyrolysis. During the pyrolysis cycle, CO_2 produced from organic matter from 300° to 390°C was trapped by a molecular sieve and subsequently analyzed by a thermal conductivity detector (S3). The units of S3 are mg of CO_2 per gram of sediment. Sample size was typically 100 mg. The Rock-Eval parameters are used to calculate Production Index (PI) = S2/(S1 + S2), Petroleum Potential or Pyrolyzed Carbon (PC) = 0.8(S1 + S2), Hydrogen Index (HI) = 100(S2)/TOC, and Oxygen Index (OI) = 100(S3/TOC). Only the latter two indices are reported in the site chapter tables. Results of samples with organic carbon values below 0.25% are not reported here.

Standarization of the Rock Eval was done with the IFP "55000" standard, having the following pyrolytic characteristics: S2 = 8.62 ± 2.5%; S3 = 1.00 ± 8%; T_{max} = 419 ± 1°C, and TOC = 2.86 ± 3.5%. Calibration was checked with the internal "KFA" standard of the Institute of Petroleum and Organic Geochemistry (KFA, Jülich, FRG) with the following pyrolytic characteristics: S2 = 10.54, S3 = 0.54, T_{max} = 424°C, and TOC = 2.16%. Generally, the results of the internal standard were satisfactory. A test of the accuracy and precision of the standard (Table 6) showed that the variation of the S2 and S3 values is minor within one batch, but that the variations in the S2/S3 ratio and between different batches cannot be ignored, especially when one is dealing with samples characterized by low S3 values. Over 400 samples were analyzed with the Rock-Eval apparatus during Leg 117, and a surprisingly good correlation was observed between the organic carbon content (determined by difference) and the S2/S3 ratio. Within one

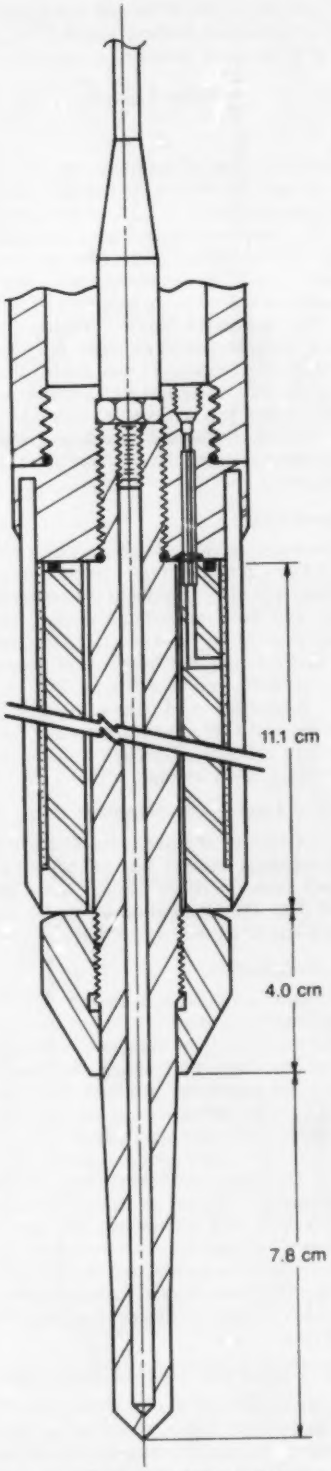

Figure 10. Cross section of the new WSTP tool filter probe/thermistor probe assembly.

Table 6. Rock-Eval pyrolysis characteristics of the "KEA" internal standard. Two batches were run on different days, each after standardization with the "55000" standard.

T_{max}	S_2	S_3	S_2/S_3
Batch 1			
430	11.07	0.35	31.62
425	11.41	0.41	27.82
432	10.85	0.45	24.11
429	11.88	0.49	24.24
428	11.98	0.38	31.52
429	11.46	0.52	22.03
Batch 2			
416	13.00	0.51	25.49
420	12.64	0.51	24.78
420	12.87	0.51	25.23
418	12.27	0.53	23.33
421	12.27	0.46	26.89
418	12.99	0.48	27.06
419	12.71	0.54	23.53
420	12.78	0.42	30.42
421	11.75	0.49	23.97

sample batch, correlation coefficients of over 0.9 were common. This seemed to be suspicious and, therefore, several experiments were carried out to be sure that we were not dealing with an artifact. The "55000" standard, the "KFA" standard, and a sample with a high S3 value were diluted with 25%, 50%, and 75% pure calcite, as well as with organic-matter-free sand. The S2 values showed the suspected proportional decrease, but the S3 values showed a decrease that was not proportional to the percentage of dilution, giving rise to lower S2/S3 ratios. The S2/S3 ratio of the diluted sample batch has a high correlation with the organic carbon content. Therefore, all the measured S3 values as well as the calculated oxygen indices as reported in the pertinent tables should be interpreted with extreme caution. After changing the molecular sieve, the same experiments were carried out once more with satisfactory results, i.e., the S2/S3 ratio remained constant. However, S3 values that dropped below 0.5 the analytical error of the Rock-Eval apparatus gave rise to unreliable results.

Hydrocarbon Gases

The compositions and concentrations of hydrocarbon gases in gas pockets, as well as those extracted from sediments, were measured on a Hach-Carle AGC Series 100 gas chromatograph (Model 211). Quantitative analyses of hydrocarbon gases, extracted from sediments, were performed with the so-called headspace procedure. A measured volume of sediment, usually 5 cm^3, was placed in a 22-cm^3 glass vial, sealed with a crimp cap. The vial was heated at 70°C for 45 min, and a portion of the gas inside the vial was analyzed by gas chromatography. A calibrated plunger was used to obtain a measured volume of sediment. The gas chromatograph was attached to a Hewlett-Packard Model 3393A Integrator, which permitted the single measurement of gas concentrations over six orders of magnitude after appropriate calibration. The HC instrument is designed to measure accurately and rapidly the concentrations of methane, ethane, and propane within 5 min. Sporadically, the HC was run for 16 min in order to determine qualitatively the presence of isobutane and butane. The HC is equipped with an 1.0 mL sample loop with column backflush and a column (1.8 m in length and 0.32-cm inner diameter) packed with 80% Poropak N + 20% Poropak Q (80/100 mesh) and flame ionization detector. The sample is run isothermally at 90°C with helium as carrier gas at 60 psi head pressure.

Lipid Analyses

Extraction

Wet sediment samples of approximately 10 cm^3 were lyophilized, homogenized in a mortar, and ultrasonically extracted for 10 min with approximately 20 mL dichloromethane. Following extraction, the sample was centrifuged, and the clear supernatant solution was pipetted off. The extraction was repeated with an additional 10 mL. The combined extract was evaporated by rotary evaporation and taken up in hexane. The hexane-soluble lipids were then transferred into a screw-top vial and concentrated under a gentle stream of nitrogen. No preseparation into different classes of compounds was made. Prior to use, all glassware was thoroughly washed with a soap solution, followed by three water rinses, two rinses with deionized water, and two rinses with dichloromethane. A blank procedure was run to check for contamination in the lab. but no major contaminations were observed.

Gas Chromatography

Gas chromatography was carried out with a Hewlett-Packard Model 5890A Gas Chromatograph equipped with a fused silica capillary column (25 m in length and 0.20-mm inner diameter), split injection, and flame ionization detection. Helium was used as carrier gas with 30 psi head pressure. Injector temperature was 250°C, and a multiramp temperature program (initial = 40°C for 3 min; 10°C/min to 220°C; 220°C for 1 min; 4°C/min to 300°C; isothermal = 15 min) was applied in order to obtain a separation of the long-chain alkenones. The detector temperature was kept at 300°C. Typically, 2 μL of hexane solution was injected with a 10-μL syringe.

Identification of Long-Chain Alkenones

The identification of diunsaturated and triunsaturated C_{37} alkenones in sediment extracts was established by coinjection with an extract from *Emiliania huxleyi*, available aboard ship since Leg 108 (Fig. 11). Calculation of the U^{k}_{37} ratio was made by peak height and hand-drawn base line.

Shipboard Contamination

Possible organic contaminants aboard *JOIDES Resolution* have been reported by Dunham (1987) and Kvenvolden and McDonald (1986). However, these authors overlooked the most obvious and most important contaminant, the acetone used on the catwalk to glue end caps to the core liner. The contamination of acetone in C_2–C_8 hydrocarbon studies was reported by Schaefer et al. (1983) and Schaefer and Leythaeuser (1984). The contamination was found to be more pronounced at the ends of a core section then in the middle. Fifteen milliliters of acetone, the approximate volume used to seal an end cap, was evaporated to dryness and taken up in 1 mL hexane. The gas chromatogram produced is shown in Figure 12. An unresolved complex mixture of high relative intensity is present and should be taken into consideration when observed in extracts from sediments. To minimize this contamination, organic geochemical samples should be taken in the middle of a section.

INORGANIC GEOCHEMISTRY

Interstitial-water samples were collected either by squeezing 5- or 10-cm whole-round sediment samples or with the Barnes *in-situ* pore-water sampler. Shipboard analyses included determinations of pH, alkalinity, salinity, magnesium, calcium, sulfate, chloride, phosphate, ammonia, and silica. Dissolved or-

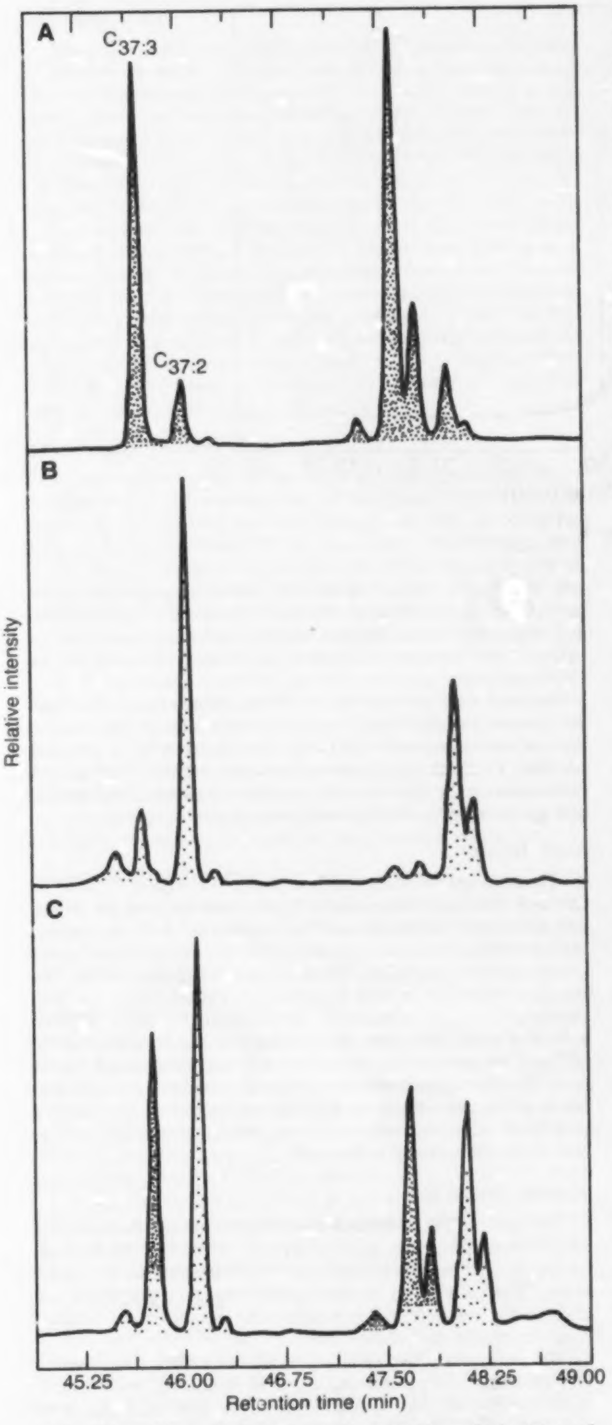

Figure 11. Partial gas chromatograms showing (A) standard mixture of long-chain unsaturated ketones extracted from *Emiliania huxleyi*, (B) extract from Hole 723B sediment sample, and (C) coinjection of A and B.

ganic carbon was measured at the Oman margin sites and at Site 731 on the Owen Ridge. Water was obtained by squeezing the samples in a stainless-steel press at a maximum pressure of 40,000 psi, collected in plastic syringes, and filtered through disposable 0.45-μm Gelman membrane filters. The primary standard used for the interstitial-water analyses was IAPSO standard seawater.

The pH and alkalinity were determined using a Metrohm 605 autotitrator pH meter coupled to a Hewlett-Packard microcomputer that automatically controlled the 0.1 M HCl titer and calculated the Gran function to determine alkalinity. The pH meter was calibrated with NBS standard buffer solutions with pH values of 4.01, 6.86, and 7.41. For alkalinity standardization, 2 to 5 mL of IAPSO standard seawater was used for each determination (see Table 7 for estimates of the relative precision of this method and the others described here).

Salinity values were determined from the refractive index of the water sample measured by a Reichert optical refractometer calibrated in g/kg units. The error on this method was approximately ±0.2 g/kg.

Sulfate concentrations were measured using the Dionex 2120i ion chromatograph, following dilution of 0.2 cm^3 of the sample to 100 cm^3 with deionized, low-conductivity water. Standardization was achieved using IAPSO standard seawater and artificial standards prepared by J. M. Gieskes.

Chloride, magnesium, and calcium concentrations were analyzed by microtitration using a Metrohm Dosimat titrator. Calcium was determined by the miniversion method of Tsunogai et al. (1968). Magnesium determinations were made after titrating against the total alkaline earths (Mg^{2+}, Ca^{2+}, and Sr^{2+}) and subtracting the Ca and Sr ions from the total. IAPSO standard seawater was used to calibrate the method and estimate precision.

Dissolved metabolites, phosphate, ammonia, silica, and organic carbon were determined by spectrophotometry. For all but the dissolved organic carbon, the procedure followed was as described in Gieskes and Peretsman (1986), together with their recommended standards. In interstitial waters containing dissolved HS the phosphate determination suffered from the precipitation of antimonyl sulfide, which imparted a brown color and precipitated to the reacting sample. This problem was alleviated by bubbling wet nitrogen through the sample for 30 min, which degassed the H_2S from the sample prior to analysis (the salinity was measured before and after to correct for any evaporation). Dissolved organic carbon ("gelbstoffe") was determined by measuring the absorbance of 1.5 mL of sample at 243.7 nm prior to the addition of the mixed phosphate reagent. This wavelength was determined by step-scanning the sample between 230 and 260 nm and calculating the wavelength of the peak of maximum absorbance.

DOWNHOLE MEASUREMENTS

Tool Strings

Downhole logging directly determines properties of *in-situ* formations adjacent to the borehole. After coring is completed at a hole, a tool string is lowered downhole on a 7-conductor cable, and each of several tools in the tool string continuously monitors some property of the adjacent borehole. Of the dozens of different tool strings commonly used in the petroleum industry, three were used on Leg 117: the seismic stratigraphic, lithoporosity, and geochemical combinations.

Two seismic stratigraphic combinations were used on Leg 117. A digital string, consisting of long-spaced sonic (LSS), natural gamma-ray tool (NGT) and phasor resistivity (DIT), was run at Site 720. An analog string, consisting of borehole com-

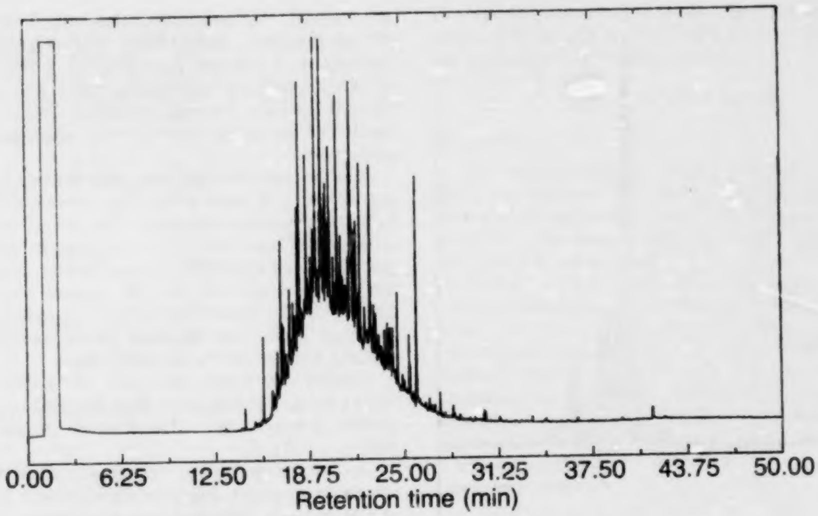

Figure 12. Gas chromatogram of an extract of acetone.

Table 7. Estimated precision (± 1 σ) of interstitial-water analyses.

Species	Number	%
Alkalinity	6	1.6
Cl^-	30	0.8
Ca^{2+}	18	0.5
Mg^{2+}	24	0.4
NH_4^+	6	1.7
PO_4^{3-}	6	2.0
Si	6	0.9

pensated sonic (BHC), gamma ray (GR), and resistivity (DIL), was run at the other logged sites.

The lithoporosity combination consists of the NGT, neutron porosity (CNT-G), and lithodensity (LDT). On Leg 117 this tool string also included an accelerometer and magnetometer tool (GPIT).

The geochemical combination normally includes the NGT, aluminum clay tool (ACT), and gamma spectrometry tool (GST). On Leg 117 this tool string also included the GPIT accelerometer. At Sites 728 and 731 a modified geochemical combination was run, using a CNT-G instead of the ACT.

Logs

A brief description of logging tools run during Leg 117 is given in the following. A detailed description of logging tool principles and applications is provided in Schlumberger (1972), Serra (1984), and Timur and Toksöz (1985).

Electrical Resistivity

The dual induction log (DIL) provides three different measurements of electrical resistivity, each one with a different depth of investigation. Two induction devices (deep and medium resistivity) send high-frequency alternating currents through transmitter coils, creating magnetic fields that induce secondary (Foucault) currents in the formation. These ground-loop currents produce new inductive signals, proportional to the conductivity of the formation, which are recorded by the receiving coils. A third device (spherically focused resistivity) measures the current necessary to maintain a constant voltage drop across a fixed interval, at near-dc frequencies. Vertical resolution is around 2 m for the medium and deep resistivity devices and about 1 m for the focused resistivity.

Water content and salinity are by far the most important factors controlling the electrical resistivity of rocks. To the first order, resistivity responds to the inverse square root of porosity (Archie, 1942). Other factors influencing resistivity include the concentration of hydrous and metallic minerals, vesicularity, and geometry of interconnected pore space.

Sonic Velocity

The long-spaced sonic (LSS) tool uses two acoustic transmitters and two receivers to measure the time required for sound waves to travel over source-receiver distances of 2.4, 3.0, and 3.6 m. The borehole compensated sonic (BHC) tool uses a different source-receiver geometry, with spacings of 0.9 and 1.5 m. The data are expressed as time required for a sound wave to travel through 0.31 m of formation. First arrivals for the individual source-receiver paths are used to calculate the velocities of the different waves traveling in the formation (compressional, shear, etc.). The vertical resolution of the tool is about 0.61 m. Compressional-wave velocity is dominantly controlled by porosity and lithification; decreases in porosity and increases in lithification cause the velocity to increase.

Natural Gamma Ray

The gamma-ray (GR) tool measures the natural radioactivity of the formation. Most gamma rays are emitted by the radioactive isotope K^{40} and by the radioactive elements of the U and Th series. The gamma-ray radiation originating in the formation close to the borehole wall is measured by a scintillation detector mounted inside the sonde.

Because radioactive elements tend to be most abundant in clay minerals, the gamma-ray curve is commonly used to estimate the clay or shale content. There are rock matrices, however, for which the radioactivity ranges from moderate to extremely high values, as a result of the presence of volcanic ash, potassic feldspar, or other radioactive minerals.

Lithodensity Tool

The lithodensity tool (LDT) uses a Ce^{137} gamma-ray source to measure the resulting flux at fixed distances from the source. Under the operating conditions, attenuation of gamma rays is chiefly caused by Compton scattering (Dewen, 1983); thus, the resultant count rates can be related to the formation bulk density. A photoelectric effect index is also provided. Photoelectric absorption occurs in the energy window below 150 keV and depends on the energy of the incident gamma ray, the atomic cross section, and the nature of the atom. Because this measurement is almost independent of porosity, it can be used directly as a matrix lithology indicator. The radioactive source and detector array is placed in a that which is pressed against the borehole wall by a strong spring. Excessive roughness of the hole will cause some drilling fluid to infiltrate between the skid and the formation. As a consequence, density readings can be artificially low. Corrections can be applied by using caliper data. The vertical resolution is about 0.30 m.

Compensated Neutron Porosity

A radioactive source mounted on the compensated neutron porosity tool (CNT) sonde emits fast neutrons (4 MeV) into the formation, where they are scattered and slowed by collisions with other nuclei. When the neutrons reach a low energy level (0.025 MeV) they are captured and absorbed by atomic nuclei such as hydrogen, chlorine, silicon, and boron. The scattering cross section is the quantity that describes the rate at which neutrons are slowed. Because the scattering cross section for hydrogen is about 100 times larger than for any other common element in the crust, most energy dissipation is caused by collisions with water molecules. Therefore, a change in the number of neutrons detected at a receiver can be related to porosity. In practice, an array of detectors is used to minimize borehole or drilling fluid effects. Porosity measurements made in presence of hydrous minerals are overestimates of the true porosity. The vertical resolution of the tool is theoretically about 0.25 m, but low signal-to-noise ratio degrades this potential resolution.

Natural Gamma-Ray Tool

The natural gamma-ray tool (NGT), also called the spectral gamma-ray tool, measures the three different components (K, Th, and U) of the natural gamma-ray spectrum by differentiating between gamma rays of different energies.

Gamma Spectrometry Tool

This induced spectral gamma-ray tool (GST) consists of a pulsed source of 14-MeV neutrons and a gamma-ray scintillation detector. A surface computer performs spectral analysis of gamma rays resulting from the interactions of neutrons emitted by the source with atomic nuclei in the formation (Hertzog, 1979). Characteristic sets of gamma rays from six elements dominate the spectrum, permitting calculation of six elemental yields: Ca, Si, Fe, Cl, H, and S. As their sum is always one, they do not reflect the actual elemental composition. Therefore, ratios of these yields are commonly used in interpreting the lithology, porosity, and salinity of the formation fluid.

Aluminum Clay Tool

Aluminum abundance as measured by the Aluminum Clay Tool (ACT) is determined by neutron-induced (Cf chemical source) late gamma-ray spectrometry. By placing NaI detectors both above and below the neutron source, contributions from natural gamma-ray activity can be removed. Calibration to elemental weight percent is performed by taking irradiated core samples of known volume and density and measuring their gamma-ray output while placed in a jig attached to the logging tool (generally after logging).

Log Data Quality

Log data quality may be seriously degraded in excessively large sections of the borehole or by rapid changes in the hole diameter. Resistivity and velocity measurements are less sensitive to borehole effects, whereas the nuclear measurements (neutron porosity and natural and induced spectral gamma ray) are most seriously impaired, because of the large attenuation by the borehole fluid. Corrections can be applied to the original data in order to reduce the effects of these conditions and, generally, any departure from the conditions under which the tool was calibrated.

Different logs may have small depth mismatches, caused by either cable stretch or ship heave during recording. Small errors in depth matching can impair the results in zones of rapidly varying lithology. To minimize such errors, a hydraulic heave compensator adjusts for rig motion in real time. The heave compensator performed poorly on Leg 117; fortunately, seas were generally calm. Precise depth matching of legs with cores is not obtainable in zones where core recovery is low because of the inherent ambiguity of placing the recovered section within the interval cored.

Log Analysis

During logging, incoming data were observed in real time on a monitor oscilloscope and simultaneously recorded on digital tape in the Schlumberger logging unit. After logging, this tape was copied from 800- to 1600-bpi on the shipboard VAX computer system. The 1600-bpi tape was then read by the Masscomp computer system in the downhole logging laboratory aboard ship and reformatted to a file format compatible with the Terralog log-interpretation software package. Rather than being a "black box," Terralog is an interactive system consisting of many log manipulation and plot options. Thus, the log analysis and interpretation varied in duration and procedure for each site. Most log interpretation was carried out aboard ship; further analysis and interpretation were undertaken after the cruise, using a companion system in the Borehole Research Laboratory of Lamont-Doherty Geological Observatory.

Reprocessing of Geochemical Logs

Raw GST logs for Leg 117 are shown following the barrel sheets for each site at which the GST was run (see chapters for Sites 723, 728, and 731). Raw count rates for six elements (Ca, Si, Fe, S, Cl, and H) are obtained in real time by the Schlumberger data acquisition software. These count rates commonly exhibit some inversion interference of chlorine with other elemental count rates, which is manifest as a strong but spurious correlation between chlorine and calcium, and weaker correlations with other elements measured by the tool. This interference, which is attributable to the dominance of the induced gamma spectrum by chlorine, is unavoidable in ODP holes because the minimum pipe diameter is too small to permit use of a boron sleeve for chlorine count suppression. Most of this interference effect was removed aboard ship by standardizing each count-rate log and then removing a first-degree regression with chlorine.

The shipboard correction was obviated by post-cruise reprocessing, using a Schlumberger Elite 1000 workstation and proprietary Schlumberger software. With a revised algorithm, the gamma spectrum at each depth is inverted for titanium, gadolinium, and potassium in addition to the six elements (Ca, Si, Fe, S, Cl, and H) in the shipboard inversion. Though gadolinium is present in concentrations of only a few parts per million, its neutron capture cross section is so large that gadolinium can account for 10%–30% of the total gamma spectrum. Inclusion of these additional elements improves the quality of the overall inversion, particularly improving the accuracy of calculated calcium abundance, by converting sources of unaccounted variance to signals. However, the determined potassium concentrations are less accurate than those from the NGT, and the hydrogen concentrations are less accurate than those from the neutron tool.

Data from the NGT were also reprocessed after the cruise with Schlumberger software. Shipboard real-time calculation of potassium, thorium, and uranium was based on all five recorded energy windows of the natural gamma spectrum. In the reprocessing, data from the lowest energy window are not used because this window has the highest noise level and is by far the most sensitivity to possible mud effects on the gamma spectrum. Every logged hole on Leg 117 was filled with mud.

All spectral gamma data from Leg 117 were reprocessed. In general, this reprocessing had little effect on the character of upcoming logs, but it increased estimated potassium and thorium concentrations significantly. The reprocessing degraded the quality of downgoing logs, as evidenced by an increase in log variance and decrease of replicability with upcoming logs. Apparently, with the faster logging speeds and reduced accuracy of count-rate statistics for downgoing logs, one cannot afford to discard a spectral window even if its signal-to-noise ratio is lower than that of the other four windows. Consequently, the downgoing spectral gamma logs shown in the "Downhole Measurements" sections of the site chapters are without reprocessing. The reprocessed upcoming logs shown in "Downhole Measurements" sections are in contrast to the raw upcoming logs following the barrel sheets of the site chapters.

Aluminum concentrations from the ACT require only one correction, an adjustment for variations in cable speed. Changes in logging speed affect the time lag between neutron irradiation of the formation and recording of the induced gamma spectrum because the number of induced gamma rays decreases rapidly with time. Post-cruise correction was made based on the cable speed recorded during logging. However, the small amount of ship heave during logging may make this correction less reliable in ODP holes than in land wells.

When all three Schlumberger tool strings are run, further reprocessing of geochemical logs is possible. The relative abundances of Ca, Si, Fe, Ti, Al, K, S, Th, U, and Gd are used to calculate a log of predicted photoelectric effect. The difference between this log and the actual log of photoelectric effect can be attributed to the only two major elements not directly measured, Mg and Na. Major elements are converted from volume percent to weight percent using logs of total porosity (bound water plus pore water) and density. Major elements are expressed in terms of oxide dry weight percent, based on the assumption that oxygen is 50% of the total dry weight. Site 723 was the only Leg 117 site where three-tool strings were run and, thus, for which these procedures were undertaken.

If GST data are available but not enough log types are run to permit complete solution for oxide weight percentage, one further processing step is made. Omitting chlorine and hydrogen, the yields of the other GST elements (Ca, Si, Fe, Ti, S, K, and Gd) are summed, and each is expressed as a fraction of this total yield. This procedure corrects for porosity and count rate variations. Although the absolute abundance of each element is not determined, downhole variations in relative abundance are indicated. This processing was conducted at Sites 722 and 731.

REFERENCES

Archie, G. E., 1942. The electrical resistivity log as an aid in determining some reservoir characteristics. *Pet. Technol.*, 5(1).

Barnes, R. O., 1987. ODP *in-situ* fluid sampling and measurement: a new wireline tool. *In* Mascle, A., Moore, J. C., et al., *Proc. ODP, Init. Repts.*, 110: College Station, TX (Ocean Drilling Program), 55–63.

Barron, J. A., Keller, G., and Dunn, D. A., 1985. A multiple microfossil biochronology for the Miocene. *In* Kennett, J. P. (Ed.), *The Miocene Ocean: Paleoceanography and Biogeography*: Mem. Geol. Soc. Am., 163:21–36.

Becker, K., Langseth, M. G., and Von Herzen, R. P., 1983. Deep crustal geothermal measurements, Hole 504B, Deep Sea Drilling Project Legs 69 and 70. *In* Cann, J. R., Langseth, M. G., Honnorez, J., Von Herzen, R. P., White, S. M., et al., *Init. Repts. DSDP*, 69: Washington (U.S. Govt. Printing Office), 223–235.

Berggren, W. A., Kent, D. V., Flynn, J. J., and Van Couvering, J. A., 1985a. Cenozoic geochronology. *Geol. Soc. Am. Bull.*, 96:1407–1418.

Berggren, W. A., Kent, D. V., and Van Couvering, J. A., 1985b. The Neogene: Part 2, Neogene geochronology and chronostratigraphy. *In* Snelling, N. J. (Ed.), *The Chronology of the Geological Record*: Geol. Soc. Mem. (London), 10:211–260.

Blow, W. H., 1969. Late middle Eocene to Recent planktonic foraminiferal biostratigraphy. *In* Bronnimann, P., and Renz, H. H. (Eds.), *Proceedings of the First International Conference Planktonic Microfossils, Geneva, 1967*: Leiden (E. J. Brill), 1:199–421.

Boyce, R. E., 1973. Appendix I. Physical property methods. *In* Edgar, N. T., Saunders, J. B., et al., *Init. Repts. DSDP*, 15: Washington (U.S. Govt. Printing Office), 1115–1128.

________, 1976. Definitions and laboratory techniques of compressional sound velocity parameters and wet-water content, wet-bulk density, and porosity parameters by gravimetric and gamma ray attenuation techniques. *In* Schlanger, S. O., Jackson, E. D., et al., *Init. Repts. DSDP*, 33: Washington (U.S. Govt. Printing Office), 931–958.

________, 1977. Deep-sea drilling procedures for shear strength measurements of clayey sediment using modified Wykeham Farrance Laboratory Vane Apparatus. *In* Barker, P., Dalziel, I.W.D., et al., *Init. Repts. DSDP*, 36: Washington (U.S. Govt. Printing Office), 1059–1068.

Carlson, R. L., and Christensen, N. L., 1979. Velocity anisotropy in semi-indurated calcareous deep-sea sediments. *J. Geophys. Res.*, 84:205–211.

Cox, A., 1983. Magnetic reversal time-scale. *In* Harland, W. B. (Ed.), *A Geologic Time-Scale*: Cambridge (Cambridge Univ. Press), 63–84.

Dean, W. E., Leinen, M., and Stow, D.A.V., 1985. Classification of deep-sea, fine-grained sediments. *J. Sediment. Petrol.*, 55:250–256.

Dewen, J. T., 1983. *Essentials of Modern Open Hole Log Interpretations*: Tulsa (Penwall).

Dunham, K. W., 1987. Potential organic geochemical contaminants on board the *JOIDES Resolution*. *In* Boillot, G., Winterer, E. L., et al., *Proc. ODP, Init. Repts.*, 103: College Station, TX (Ocean Drilling Program), 71–74.

Espitalié, J., Madec, M., and Tissot, B., 1977. Source rock charcterization method for petroleum exploration. *Proc. Annu. Offshore Technol. Conf.*, 9:399–404.

Gieskes, J. M., and Peretsman, G., 1986. Water chemistry procedures aboard *Joides Resolution*—some comments. *ODP Tech. Note*, 5:1–46.

Hamilton, E. L., 1971. Prediction of *in-situ* acoustic and elastic properties of marine sediments. *Geophysics*, 36:266–284.

Hertzog, R., 1979. Laboratory and field evaluation of an inelastic-neutron-scattering and capture gamma ray spectroscopy tool. *Soc. Pet. Eng. Pap.*, 7430.

Johnson, D. A., Nigrini, C., and Caulet, J. P., in press. Pliocene-Pleistocene radiolarian events and magnetostratigraphic calibrations for the tropical Indian Ocean. *Mar. Micropaleontol.*

Johnson, D. A., and Nigrini, C. A., 1985. Synchronous and time-transgressive Neogene radiolarian datum levels in the equatorial Indian and Pacific Oceans. *Mar. Micropaleontol.*, 9:489–523.

Kvenvolden, K. A., and McDonald, T. J., 1986. Organic geochemistry on the *JOIDES Resolution*—an assay. *ODP Tech. Note*, 6.

Martini, E., 1971. Standard Tertiary and Quaternary calcareous nannoplankton zonation. *In* Farinacci, A. (Ed.), *Proceedings of the Planktonic Conference, II, Roma, 1970*: Rome (Ed. Technoscienze), 2:739–785.

Matthews, D. J., 1939. *Tables of Velocity of Sound in Pore Water and in Seawater*: London (Admiralty, Hydrogr. Dept).

Munsell Soil Color Charts, 1971. Baltimore (Munsell Color).

Nigrini, C., 1971. Radiolarian zones in the Quaternary of the equatorial Pacific Ocean. *In* Funnell, B. M. and Riedel, W. R. (Eds.), *The Micropalaeontology of Oceans*: Cambridge (Cambridge Univ. Press), 442–461.

Riedel, W. R., and Sanfillipo, A., 1978. Stratigraphy and evolution of tropical Cenozoic radiolarians. *Micropaleontology*, 24:61–96.

Sanfillipo, A., Westberg-Smith, M. J., and Riedel, W. R., 1985. Cenozoic Radiolaria. *In* Bolli, H. M., Saunders, J. B., Perch-Nielsen, K. (Eds.), *Plankton Stratigraphy*: Cambridge (Cambridge Univ. Press), 631–712.

Sato, T., Takayama, T., Kato, M., Kudo, T., and Kameo, K., in press. Calcareous microfossil biostratigraphy of the uppermost Cenozoic formations distributed in the coast of the Japan Sea. Part 4: Conclusion. *Sekiyu Gijutsu Kyokaishi.*

Schaefer, R. G., and Leythaeuser, D., 1984. C_2–C_8 hydrocarbons in sediments from Deep Sea Drilling Project Leg 75, Holes 530A, Angola Basin, and 532, Walvis Ridge. *In* Hay, W. W., Sibuet, J.-C., et al., *Init. Repts. DSDP*, 75: Washington (U.S. Govt. Printing Office), 1055–1067.

Schaefer, R. G., von der Dick, H., and Leythaeuser, D., 1983. C_2–C_8 hydrocarbons from Deep Sea Drilling Project Leg 71, Site 511, Falkland Plateau, South Atlantic. *In* Ludwig, W. J., Krasheninnikov, V. A., et al., *Init. Repts DSDP*, 71: Washington (U.S. Govt. Printing Office), 1033–1044.

Schlumberger, Ltd., 1972. *Log Interpretation* (Vol. 1, Principles): New York (Schlumberger).

Schultheiss, P. J., Mienert, J., and Shipboard Scientific Party, 1988. Whole-core *P*-wave velocity and gamma ray attenuation logs from Leg 108. *In* Ruddiman, W., Sarnthein, M., et al., *Proc. ODP, Init. Repts.*, 108: College Station, TX (Ocean Drilling Program), 1015–1046.

Serra, O., 1984. *Fundamentals of Well Log Interpretation* (Vol. 1): *The Acquisition of Logging Data*: Amsterdam (Elsevier).

Takayama, T., and Sato, T., 1987. Coccolith biostratigraphy of the North Atlantic Ocean, Deep Sea Drilling Project Leg 94. *In* Ruddiman, W. F., Kidd, R. B., Thomas, E., et al., *Init. Repts. DSDP*, 94, Pt. 2: Washington (U.S. Govt. Printing Office), 651–702.

Timur, A., and Toksöz, M. N., 1985. Fundamentals of well log interpretation. *Ann. Rev. Earth Planet. Sci.*, 13:315–344.

Tsunogai, S., Nishimura, M., and Nakaya, S., 1968. Complexometric titration of calcium in the presence of large amounts of magnesium. *Talanta*, 15:385–390.

van Gorsel, J. T., and Troelstra, S. R., 1981. Late Neogene planktonic foraminiferal biostratigraphy and climatostratigraphy of the Solo River section (Java, Indonesia). *Mar. Micropaleontol.*, 6:183–209.

Wentworth, C. K., 1922. A scale of grade and class terms of clastic sediments. *J. Geol.*, 30:377–390.

Von Herzen, R. P., and Maxwell, A. E., 1959. The measurement of thermal conductivity of deep-sea sediments by a needle-probe method. *J. Geophys. Res.*, 64:1557–1563.

Yokota, T., Kinoshita, H., and Uyeda, S., 1980. New DSDP (Deep Sea Drilling Project) downhole temperature probe utilizing IC RAM (memory) elements. *Tokyo Daigaku Jishin Kenkyusho Iho*, 55:75–88.

Ms 117A-103

3. BACKGROUND AND SUMMARY OF DRILLING RESULTS—OWEN RIDGE[1]

Shipboard Scientific Party[2]

The Owen Ridge is an asymmetric, northeast-trending ridge that originates at about 15°30′N, 59°50′E, where the Sharbithat Ridge intersects the Owen Fracture Zone, and extends to about 20°N, 61°E, where it merges with the Murray Ridge (Figs. 1 and 2). The trend of the Owen Ridge is somewhat oblique to the Arabian continental margin and its distance from land is about 320 km in the south and about 200 km in the north. The Owen Basin, which lies between the Arabian margin and the Owen Ridge, is sediment filled and has depths of 3200–3500 m (Fig. 1).

The crest of the ridge varies from about 1900 m to 2100 m below sea level and has two distinct sediment caps that are formed of thick, smooth, subhorizontal pelagic sediments (Fig. 2). The eastern scarp of the ridge dips steeply (about 15°) to the east, where it abuts the Indus Fan at about 4000 m (Figs. 2 and 3). The Owen Fracture Zone bounds the base of the scarp and is observed as a deformation front in the Indus Fan sediments (Fig. 3, see also "Seismic Stratigraphy" section, "Site 720" chapter, this volume). The orientation of the eastern scarp and the character of deformation in the fan sediments changes at about 16°30′N (Fig. 2), where the ridge trends more northeastward and is associated with uplift and deformation of the adjacent fan sediments, as indicated by the eastward displacement of the 4000-m isobath. The western flank of the ridge dips more gently (about 4°) and merges into the Owen Basin at about 3500 m. The physiography of the western flank is extremely complex and is characterized by eastward-trending slump valleys and sediment ridges (Fig. 2). Much of the sediment in the valleys appears to be displaced and reworked, so that drill sites for Leg 117 were targeted only on the sediment ridges and caps near the crest of the ridge.

The origin of the Owen Ridge and the age of the underlying basement rock are connected to both the early separation of Madagascar and India and to the middle Tertiary reorganization of seafloor spreading in the Indian Ocean. Several authors (McKenzie and Sclater, 1971; Whitmarsh, 1974; Norton and Sclater, 1979; Whitmarsh, 1979; Stein and Cochran, 1985) postulate that the Owen Fracture Zone was the major transform between spreading centers to the north and south of the Arabian margin. This plate geometry places the Owen Ridge and Owen Basin on the passive Arabian margin and assigns them a Jurassic age. However, DSDP drilling in the easternmost Owen Basin (Site 223 is 30 km west of the Owen Fracture Zone) found a basal igneous unit (717–740 mbsf) of trachybasalt and hyaloclastic breccia overlain by late Paleocene tuffaceous claystone (Whitmarsh et al., 1974). DSDP drilling on the Owen Ridge (Site 224) recovered middle to lower Eocene sediments above lamprophyric igneous rocks (Site 224; Whitmarsh et al., 1974). Supporters of the Jurassic-Triassic age for the Owen Basin generally discount the Sites 223 and 224 igneous rocks as not representing true oceanic basement. Thus, questions still remain concerning the age and nature of igneous basement underlying the Owen Ridge and Basin.

The uplift history of the Owen Ridge has been interpreted on the basis of drilling results at DSDP Site 224 (Whitmarsh et al., 1974) and seismic reflection profiles (Whitmarsh et al., 1974; Whitmarsh, 1979) and Leg 117 site survey data (Mountain and Prell, this volume). The timing and amount of uplift is based on the presumption that the upper Oligocene to lower Miocene turbidite beds deposited at the site were originally flat lying and that they have been uplifted along the Owen Fracture Zone and tilted westward. The stratigraphy at Site 224 (Whitmarsh et al., 1974) indicates that the transition from turbidites to pelagic sediments occurred in late Oligocene to early Miocene time, but poor recovery precludes a more exact reconstruction of the uplift history. The cause of the uplift is attributed to compression along the Owen Fracture Zone caused by changes in spreading direction associated with the continued collision of India and Asia and the opening of the Gulf of Aden (Whitmarsh, 1979).

Following its uplift above the reach of turbidite deposition, the ridge crest has accumulated predominantly pelagic, carbonate-rich sediments during the late Neogene (Whitmarsh et al., 1974; Prell, 1984a; 1984b; Mountain and Prell, unpubl. site survey data). The crest of Owen Ridge lies more than 2000 m above the surface of the Indus Fan and about 1500 m above the Owen Basin, and thus acts as a platform for the accumulation of pelagic sediments. Most of the Owen Ridge and all of Leg 117 drilling sites except Site 720 are shallower than the Holocene carbonate lysocline at 3900–4000 m (Kolla et al., 1976) and the foraminiferal lysocline, which lies at about 3300 m (Cullen and Prell, 1984). Hence, the late Neogene sediments were expected to have good carbonate preservation, so that paleoenvironmental interpretations based on foraminifers and calcareous nannofossils would not be biased by dissolution.

The sediments typically range from 50% to 80% in carbonate content and have accumulation rates of 30–40 m/m.y. in the late Neogene. The pelagic carbonates of the ridge are diluted by terrigenous sediments that are transported to the ridge primarily by winds. Recent studies have shown that the concentrations of mineral aerosols over the Arabian Sea are among the highest recorded in the global marine environment (Savoie et al., 1987; Chester et al., 1985; Prodi et al., 1983). Other studies have documented agreement between the distribution of seafloor clay minerals and aerosol mineral concentrations (Chester et al., 1985) and between estimates of their flux based on mean aerosol concentrations and sediment data (Savoie et al., 1987). Mineralogical studies of modern seafloor sediments suggest that eolian components comprise a significant proportion of Arabian Sea sediments as a whole and are the dominant terrigenous component in the northwestern Arabian Sea (Goldberg and Griffin, 1970; Kolla and Biscaye, 1976; Kolla et al., 1981). These mineralogical studies also indicate that the Arabian and Somali peninsulas are major source areas for eolian palygorskite while the Iran-Pakistan region is a major source for eolian illite and chlorite. Mineral-specific source areas such as these offer the possibility of studying the relative influence of the winter and summer monsoon regimes in the geologic past. The record of eolian transport and deposition on the Owen Ridge should provide in-

---

[1] Prell, W. L., Niitsuma, N., et al., 1989. *Proc. ODP, Init. Repts.*, 117: College Station, TX (Ocean Drilling Program).

[2] Shipboard Scientific Party is as given in the list of Participants preceding the contents.

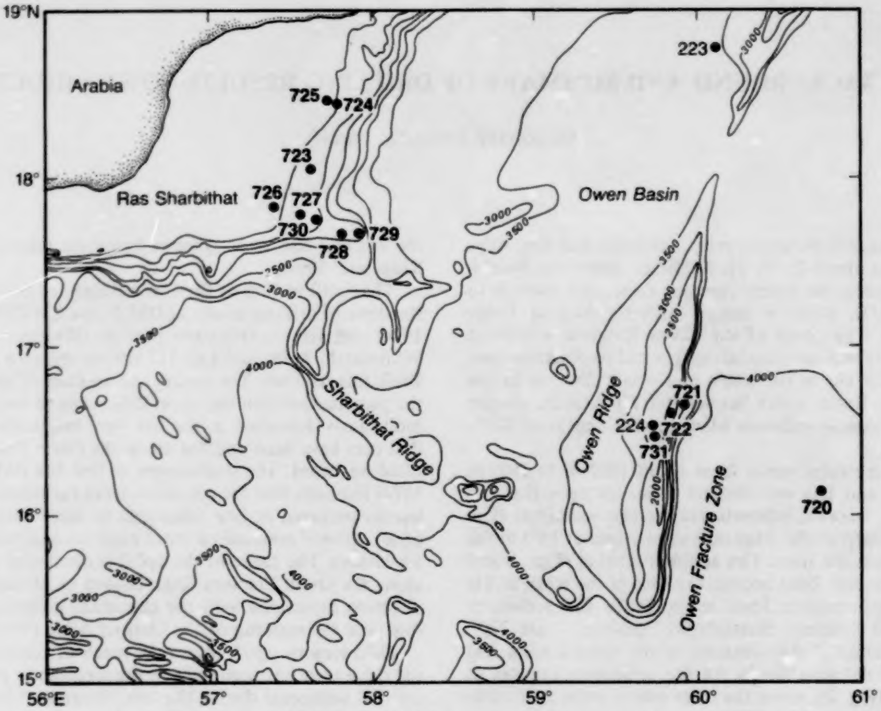

Figure 1. General bathymetry of the northwestern Indian Ocean and ODP Leg 117 study area with locations of ODP and DSDP drill sites.

formation about past monsoonal variability both in terms of the aridity of surrounding landmasses and the monsoon wind strength.

Opal is relatively sparse in the ridgecrest sediments, but does occur in the more interglacial intervals of the upper Quaternary sediments. The appearance of siliceous microfossils in the early to late Miocene of Sites 223 and 224 (Whitmarsh et al., 1974) has been interpreted to signify the onset of higher productivity associated with upwelling in the western Arabian Sea. The biotic signature of monsoonal upwelling is also recorded by other plankton groups. For example, the abundance of certain indicator species of planktonic foraminifers (such as *Globigerina bulloides*) has been used in modern plankton samples (Kroon, pers. comm., 1987) and in surface and Quaternary sediments (Prell, 1984a) as an index of monsoonal upwelling. Planktonic foraminiferal data indicate that in the late Quaternary, the intensity of the monsoonal upwelling underwent cyclic variations related to the orbitally induced changes in summer radiation in the northern hemisphere (see "Introduction" chapter, this volume).

In summary, the Owen Ridge is known to contain well-preserved late Neogene pelagic and eolian sediments that should record the past variations of monsoonal upwelling and climates.

DRILLING OBJECTIVES

Given this observational and theoretical background, which is further outlined in the "Introduction, Background, and Major Objectives for ODP Leg 117 (Western Arabian Sea) in Search of Ancient Monsoons" chapter (this volume), the specific objectives for drilling on the Owen Ridge were:

1. To recover a continuous upper Neogene section of pelagic sediments from the crest of the Owen Ridge that would contain both long-term (10^5–10^6 yr) variations, possibly related to Himalayan tectonics, and short-term (10^4–10^5 yr) variations in the biotic, sedimentologic, and chemical response to monsoonal circulation that are related to the Milankovitch mechanism of climate change (i.e., orbitally-induced changes in seasonal radiation).
2. To use these biotic and geologic records (time series) to test the hypotheses of orbital (by changes in solar radiation) and orographic (by uplift of mountains) forcing of monsoon intensity and to identify other nonorbital processes that affect the record of monsoonal variation.
3. To use the pelagic and eolian sediment record to identify the initiation and history of monsoonal upwelling and of pelagic carbonate deposition in the Arabian Sea.
4. To use the age and character of the terrigenous and pelagic sediments and the transition between them, and the preservation state of the pelagic carbonates to reconstruct the uplift history of the Owen Ridge.

SUMMARY OF DRILLING RESULTS

Leg 117 cored three sites (Sites 721, 722, and 731) on the Owen Ridge (Figs. 1 and 2). The major themes in the interpretation of the depositional history of these sites emphasize the lithologic facies and uplift of the Owen Ridge, the first occurrence and preservation of siliceous plankton microfossils and the appearance of distinct upwelling faunas, and the pattern of high-frequency variability in the abundance of various sedimentary

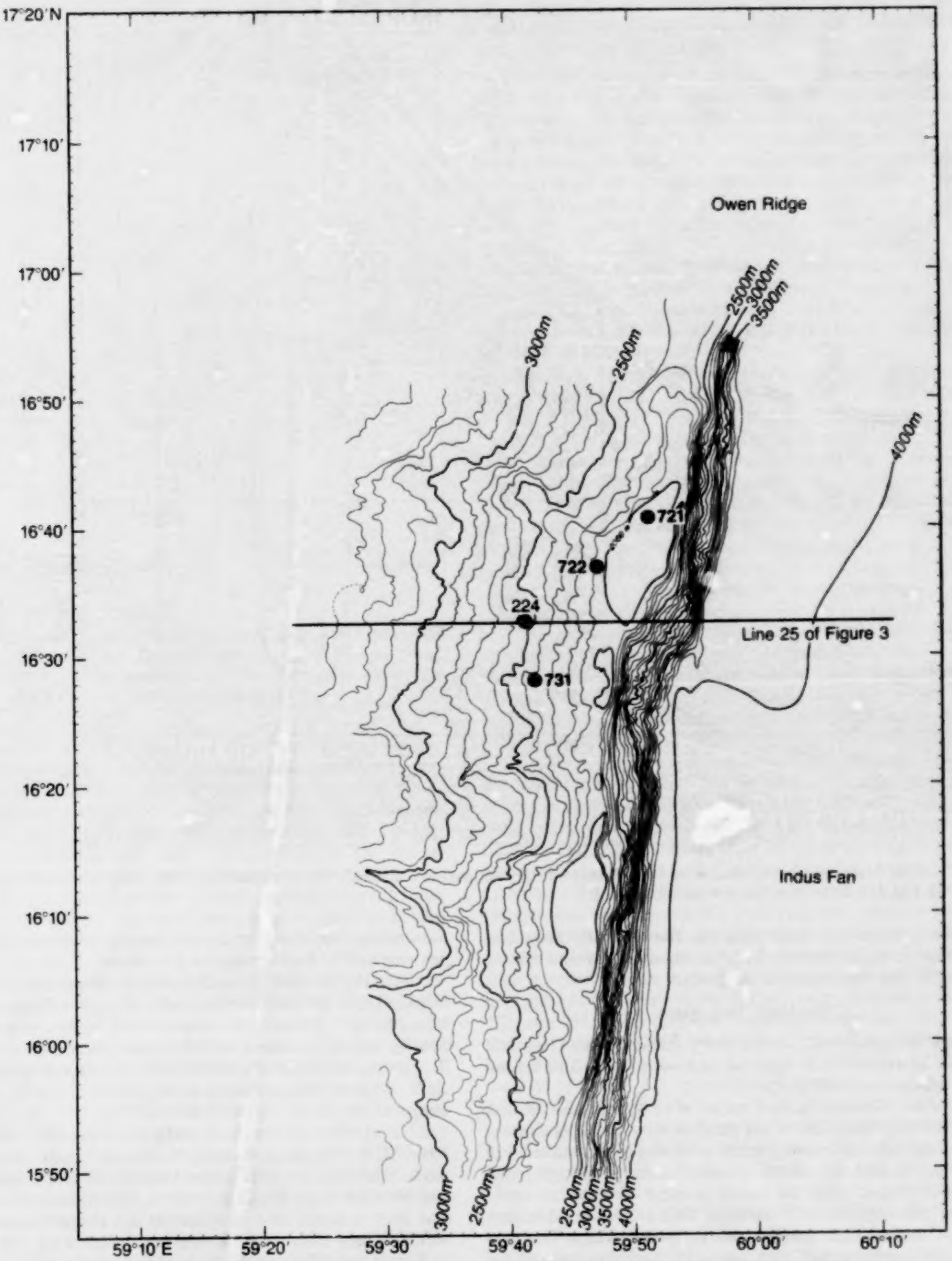
17°20'N
17°10'
17°00'
16°50'
16°40'
16°30'
16°20'
16°10'
16°00'
15°50'
59°10'E
59°20'
59°30'
59°40'
59°50'
60°00'
60°10'
Owen Ridge
Indus Fan
Line 25 of Figure 3
721
722
224
731
2500m
3000m
3500m
4000m

Figure 2. Bathymetry of the Owen Ridge according to results of site survey cruise RC2704 (Mountain and Prell, this volume). Locations of DSDP Sites 224, and Sites 721, 722, and 731 drilled during ODP Leg 117 are noted, as well as the location of RC2704 seismic Line 25 (see Fig. 3).

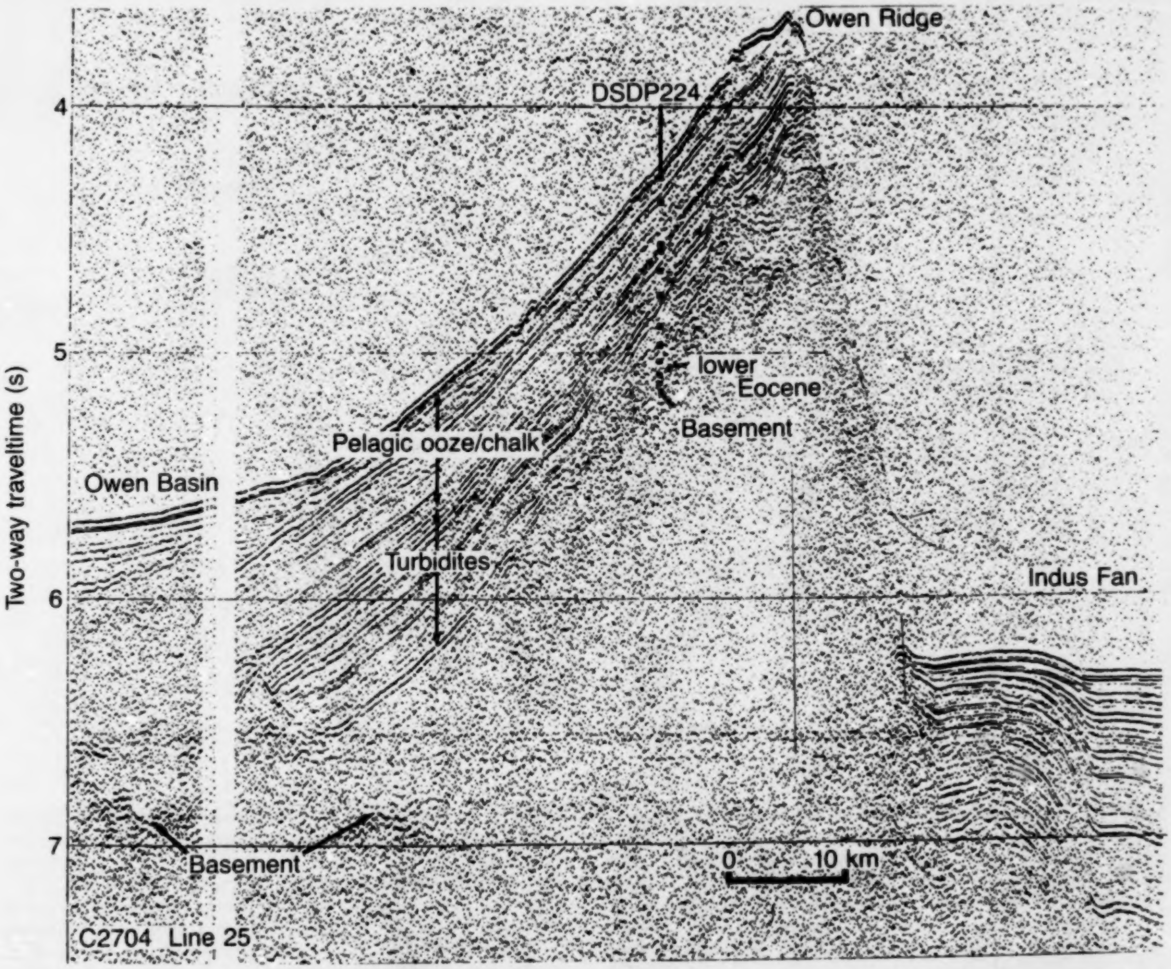

Figure 3. Seismic image and interpretation of Line 25 taken during site survey cruise RC2704 (Mountain and Prell, this volume) across the Owen Ridge in the Leg 117 study area (see text for discussion).

components. Below, we summarize our shipboard findings that are relevant to these themes. Specific observations and results are found in the respective site chapters.

Lithologic Sequence

The section penetrated on the Owen Ridge ranges from late Oligocene to Holocene in age and has been divided into four major lithologic units (Fig. 4).

The oldest lithologic unit, Unit IV with the thickest drilled section reaching from 320 to 994 mbsf in Hole 731C, is characterized by alternating coarse-grained sand and silt turbidites and mud turbidites with no overall large-scale fining-upward trend that were deposited from the late Oligocene(?) to the late early Miocene. The uppermost 70-80 m of Unit IV (lower Miocene) consist of interbedded fine-grained turbidites which fine upward and are interbedded with nannofossil chalks toward the top of this unit. The increase of pelagic deposits upsection is probably related to the uplift of the Owen Ridge out of the regime of turbidite deposition rather than to a decrease in turbidite deposition in the area. Preservation of planktonic calcareous and opaline tests is poor, and benthic foraminifers from upper and middle bathyal depths are absent.

Unit III (the thickest undisturbed section, 241-320 mbsf in Hole 731A) is composed of nannofossil chalk of early to middle Miocene age. The unit is characterized by low porosity, high density, and high seismic velocity. Silica preservation is poor in the carbonate-rich chalks (80%-90% $CaCO_3$). A hiatus, equivalent to about 45 m sediment (compared to Sites 731 and 722), occurs at the top of this unit at Site 721.

Unit II (the thickest undisturbed section, 221-343 mbsf in Hole 722B) comprises siliceous nannofossil chalk and ooze that grade upsection to foraminifer-nannofossil chalk and ooze of late Miocene age. Biogenic opal is an abundant component, and both diatoms and radiolarians are preserved in the sediments. These silica components are reflected by the low bulk and grain densities and the high porosity of Unit II. The gradients in physical properties give the chalk and siliceous units a distinctive seismic reflection signature that can be mapped over much of the Owen Ridge. At Site 721, the upper boundary of Unit II is marked by a compressed section, and sediments of the

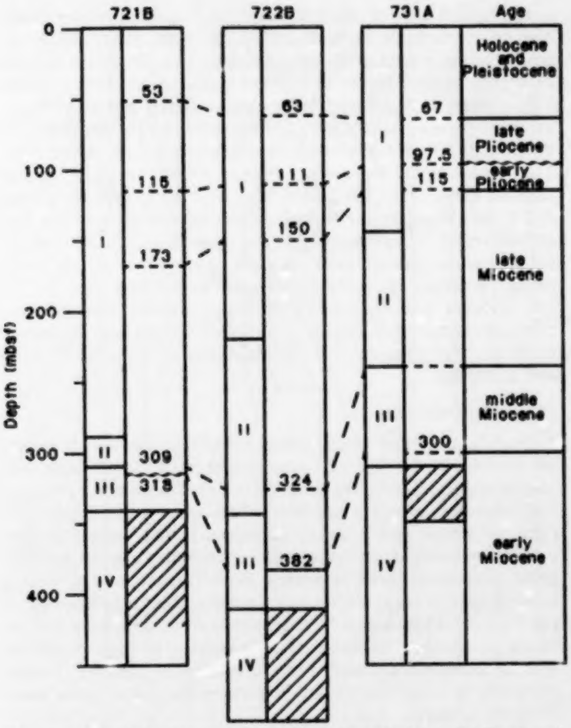

Figure 4. Synthesis diagram of lithologic boundaries (solid lines) and age boundaries (dashed lines) for Sites 721, 722, and 731 on the Owen Ridge. Hiatuses are shown as wavy lines. Patterned areas denote the transitional turbidite-pelagic facies discussed in the text.

lower half of the unit show evidence of soft-sediment deformation throughout, corresponding to a loss of about 100 m of section relative to Site 722. At Sites 722 and 731, the interval of siliceous sediments with the highest porosity and lowest density also displays distinctive sigmoidal vein structures that are perpendicular to bedding and occur preferentially in the darker opaline, organic carbon-rich bands. Similar structures have been observed in accretionary prisms (Lundberg and Leggett, 1986, and references therein) and have been ascribed both to hydrofracturing by dewatering mechanisms and to dilation as a result of applied deviatoric stresses. The significance of these structures is not clear, but we note their association with the low-density sediments that failed by slumping at Site 721. Possibly the slump event caused a decrease of lateral stress. However, the vein structures have only about 300 m of overburden at present and had less at the time of vein formation. These structural features may reflect tectonic processes that caused the uplift of Owen Ridge, but the specific relationship cannot be determined with our scant evidence. Microfossil assemblages in Unit II are characterized by the lack of typical tropical species and the dominance of cool-water assemblages. Sedimentation rates range from 20 to 50 m/m.y. over much of the interval of Units II but decrease near its upper boundary.

Unit I (the thickest undisturbed section, 0–221 mbsf in holes at Site 722) consists exclusively of alternating light and dark layers of foraminifer-bearing to foraminifer-nannofossil ooze, and nannofossil ooze of Holocene to late Miocene age. In contrast to Unit II, biogenic silica is sparse and poorly preserved in Unit I. The sediments of this unit reveal strong cyclicity that is indicated by changes in color, bulk density, carbonate content, and magnetic susceptibility on whole-round cores (see discussion below).

Uplift of Owen Ridge and Comparison of Sedimentary Sections

The uplift history of Owen Ridge is indicated by the gradational transition within lithologic Unit IV from turbiditic to pelagic facies in the late early Miocene and by phases of nondeposition and erosion. On the basis of mineralogy, we infer that the provenance of the turbiditic sediments on the Owen Ridge was probably the same source as for the Indus Fan. This inference is based on the presence of well-crystallized chlorite and the absence of kaolinite in turbiditic sediments from Site 722; this association is identical to the mineralogy of the Indus Fan deposits recovered at Site 720. The upper boundary of the turbiditic sequence is marked by a prominent seismic reflector (C) that onlaps onto a basement peak near Site 722 and can be mapped over much of the Owen Ridge and Basin (Fig. 3 and site survey chapter, this volume).

Preliminary examination of the sedimentary sections recovered at Sites 721, 722, and 731 during Leg 117, and at Site 224 during DSDP Leg 23 (Whitmarsh et al., 1974) provides some insights into the tectonic and depositional evolution of the Owen Ridge. Lithostratigraphic summaries of the Owen Ridge Sites (based on preliminary biostratigraphic data at Sites 721, 722, and 731) are compared in Figure 4. Water depths for these sites are 1945 m, 2028 m, and 2365 m, respectively. The oldest sediments recovered at Sites 722 and 731 are terrigenous turbidites of late Oligocene to early Miocene age; at Sites 722 and 731, these are conformably overlain by mixed turbidite-carbonate (i.e., "transitional") lithofacies of late early Miocene age. The oldest sediments recovered at Site 721 consist of this lower Miocene mixed turbidite-carbonate ("transitional") lithofacies.

Age control in the basal portions of these sites is limited by the scarcity of biostratigraphic datums, but ages for the tops of the "transitional" lithofacies have been estimated from available age-depth plots (see "Biostratigraphy" section in "Site 721," "Site 722," and "Site 731" chapters, this volume). These ages are approximately 15–16 Ma at each site, suggesting that all three locations were uplifted above the level of turbidite dominance at approximately the same time. Consistent onlap directions in seismic reflection profiles of the ridge suggest that shallower portions of the Owen Ridge (Site 721) began to be uplifted before deeper locations (Sites 722 and 731; see site survey chapter, this volume); such a pattern is not apparent from the recovered sediments with the age control presently available.

Thicknesses of the mixed turbidite-carbonate lithofacies do show a consistent variation across the study area, however, and may provide information about early rates of uplift at Sites 721, 722, and 731. As described above, the change from entirely terrigenous turbidites to a lithofacies of mixed turbidites and carbonate caps is interpreted as a record of uplift for the site above the level of turbidite-dominated sedimentation. In a similar manner, the change from the mixed turbidite-carbonate lithofacies to entirely pelagic carbonates can be interpreted as a record of uplift above the shallowest level of turbidite sedimentation. By assuming that the flux of turbidites to this area remained relatively constant through the early to middle Miocene, the thickness of the mixed turbidite-carbonate interval at each site can be used as rough indicator of the time required for that site to be uplifted through the zone of transitional deposition. Under those conditions, thicker mixed turbidite-carbonate intervals imply a longer residence time in the transition zone and slower rates of uplift. Of course, changes in the turbidite flux to the area and between sites cannot be ruled out at this time. The mixed turbidite-carbonate lithofacies at Site 721 is at least 80 m thick (its base was not recovered), and the same lithofacies at Sites 722 and 731 is 86 m and 40 m thick, respectively. The general pattern is that sites presently in shallower water have thicker transitional intervals. This pattern may indicate either that uplift of Owen Ridge accelerated after its initiation in the early Miocene, or that the Owen Ridge was not uplifted as a single coherent block. Although the general pattern and time of uplift of the Owen Ridge region is clear from the stratigraphic section, detailed biostratigraphic, sedimentologic, and seismic stratigraphic analyses must be integrated to adequately define the rates of uplift of the Owen Ridge.

The Onset of Upwelling Faunas and Opal Deposition

As summarized in the introduction, the western Arabian Sea experiences large seasonal or monsoonal variations in atmospheric and oceanic circulation that affect the upwelling, productivity, and species composition of the western Arabian Sea off the continental margin of Oman. Monsoonal variability also affects the climates of the surrounding lands and, thus, the composition and transport of eolian dust and pollen species to the marine environment. All of these environmental responses to past monsoonal variations must be recorded in the sediments of the Owen Ridge. Here, we summarize our preliminary observations on silica deposition, fossil plankton composition, and accumulation rates as they relate to the interpretation of monsoonal evolution and variability.

Middle Miocene

The first indication of enhanced productivity over the Owen Ridge, possibly associated with monsoonal upwelling, is a dramatic change in the sediment facies. Prior to the upper middle Miocene, biogenic opal was absent from the Unit III chalks, and carbonate was abundant but poorly preserved. The opaline microfossil abundances increase suddenly (between Cores 722A-36A and -37X) at the base of Unit II in the upper middle Miocene and remain abundant throughout Unit II (late Miocene). The siliceous microfossil assemblage is composed of radiolarians and diatoms that are tropical in nature according to our preliminary investigation. The associated planktonic foraminifer fauna also contains some species (rare, but well-preserved) that are indicative of higher productivity. Preliminary analyses indicate that this early phase of opal accumulation is associated with increasing accumulation rates relative to the chalk Unit III, but that the highest rates occur in the late Miocene. The upper middle and lower upper Miocene interval has average carbonate and noncarbonate (including opal) accumulation rates of 1–2 g/cm^2/k.y. (Fig. 5). Over this interval, organic carbon increases from les than 0.1% in Units III and IV to greater than 1.0% at the base of the opal-rich Unit II. Hence, the sediments of the upper middle Miocene exhibit the first evidence of higher surface water productivity, which may be associated with monsoon-induced upwelling in the western Arabian sea.

Late Miocene

The siliceous facies (Unit II) grades upward to foraminifer-nannofossil ooze and chalk (Unit I) within the late Miocene. During this interval, the different plankton groups undergo dramatic, but not simultaneous, changes. The first clear faunal indication of upwelling is the appearance of radiolarian assemblages that contain more robust, cool-water forms and lack many tropical forms. A distinctive upwelling planktonic foraminifer fauna appears in the early late Miocene near the boundary between lithologic Units II and I with the simultaneous appearance of *Globigerina bulloides*, *Globorotalia menardii*, and *G. tumida*, and the *Neogloboquadrina* lineage of *N. acostaensis* and *N. dutertrei*. The nannofossil floras of this interval are characterized by low diversity. Although not all of the biotic and sedimentologic indicators of high productivity are in accord, the latter half of the late Miocene was clearly an interval of higher pelagic influx to the sediments of the Owen Ridge. This pattern does not seem to be caused merely by better preservation, because changes in the preservation of foraminifers and nannofossils do not coincide with changes in accumulation rates. The remainder of the upper Miocene is characterized by high rates of carbonate (2–4 g/cm^2/k.y.) and noncarbonate (about 1–2 g/cm^2/k.y.) accumulation. Accumulation rates of organic carbon reach 70 mg/cm^2/k.y. in the uppermost Miocene, where the high accumulation rates are associated with abundant, well-preserved planktonic foraminifers and nannofossils (Fig. 5). The late Miocene sediments of Owen Ridge display clear sedimentary signatures, such as high accumulation rates and distinctive plankton assemblages, that are indicative of high productivity and upwelling.

Pliocene-Pleistocene

The Pliocene-Pleistocene sediments of the ridge are composed of foraminifer-bearing and foraminifer-nannofossil ooze with alternating light and dark bands (Unit I). This cyclic pattern of sedimentation is also a possible reflection of monsoonal influence on climate and is discussed below. In the lower Pliocene, cold-water forms of calcareous nannoplankton appear, but biogenic silica abundance decreases. Both tropical and upwelling assemblages of planktonic forams remain abundant throughout the Pliocene-Pleistocene. This sequence of assemblages may indicate an ecologic response to the evolution of monsoonal upwelling. However, detailed study of the faunal and floral variations will be needed to establish the oceanographic significance of biotic changes.

The high rates of carbonate accumulation in the late Miocene decrease to about 1–2 g/cm^2/k.y. in the Pliocene and the decrease appears independent of any change in carbonate preservation (Fig. 5). From the lower Pliocene toward the Holocene, both carbonate and noncarbonate accumulation rates appear to increase; the details of the trend vary from site to site. Two sites show a decrease in accumulation rates in the latest Pleistocene. In summary, the Pliocene to Holocene sediments on Owen Ridge indicate that upwelling has continued throughout this period, but that the ecologic response (carbonate rather than siliceous primary production) to the upwelling and the relative preservation of fossil groups has changed. We speculate that this change may reflect the evolution of the monsoon or of the circulation patterns of the western Arabian Sea during this time.

Although the broad pattern of increased productivity and composition of plankton assemblages is in accord with our premises of the monsoon-induced sedimentation, the verification of the causal relationship between different modes of monsoonal upwelling and sediment facies must be confirmed by establishing the exact relationship between the biotic assemblages, accumulation rates, and sedimentary responses to monsoonal upwelling and global climate.

Leg 117 results have shown that the onset of silica deposition, a possible indicator of monsoonal upwelling, occurred in the late middle Miocene. In the late Miocene, the high carbonate and carbon accumulation rates associated with the appearance of upwelling faunas clearly indicate that the monsoonal upwelling system was active. However, other areas of the world ocean also have high accumulation rates in the upper Miocene (Prell et al., 1982; Theyer et al., 1984). Thus, the question of global causes vs. regional causes of high productivity in the western Arabian Sea must be considered before the apparent upwelling phase of the late Miocene can be solely attributed to the relatively local monsoonal mechanism. The long-term increase in carbonate accumulation rates in the Pliocene and Pleis-

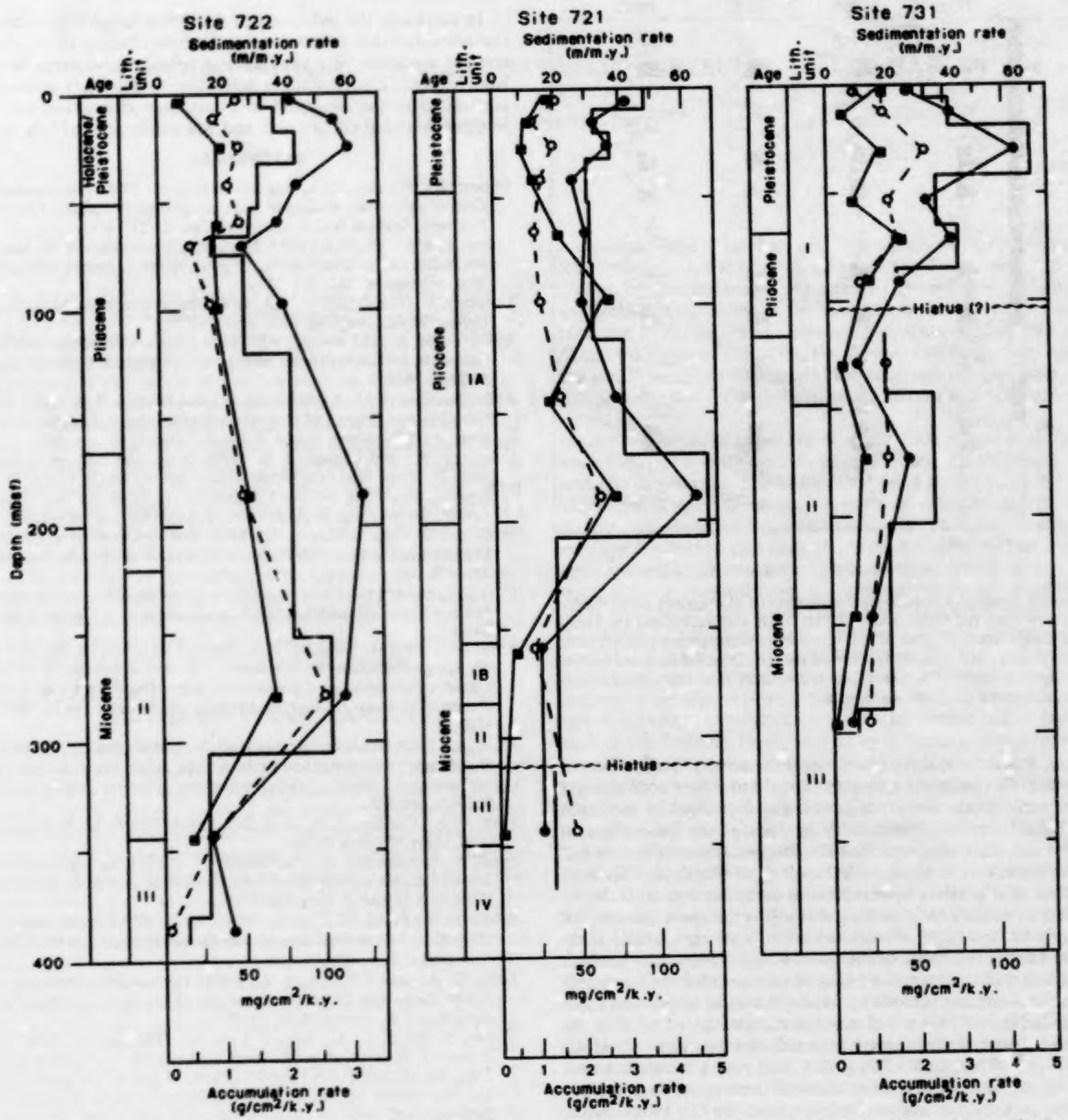

Figure 5. Summary of age, lithologic units, sedimentation (step-pattern) and accumulation rates of noncarbonate (circles), carbonate (dots), and organic carbon (squares) from Owen Ridge Sites 722, 721, and 731. Note the different scale for organic carbon inside the bottom line.

tocene may also reflect an increase in the intensity of monsoonal upwelling and eolian transport brought about by continued uplift of the Himalaya. This long-term trend would be consistent with the gradual modification of climatic boundary conditions due to tectonic mechanisms rather than with the short-term orbital insolation changes. The persistent abundance of upwelling faunas in the Pleistocene/Holocene support this speculation, but the lower rates of organic carbon accumulation raise questions about the association of upwelling with productivity. Alternatively, some of the intervals of low accumulation rate on the Owen Ridge may reflect changes in the depositional environment due to phases of local uplift.

In summary, the sediments of Owen Ridge give ample evidence of large changes in productivity and composition and abundance of upwelling-related faunas. The discrimination between regional vs. global causes, and the specific relationship between productivity and upwelling remain one aspect to be clarified during post-cruise research.

Short-term Variability and Sedimentary Cycles

The major characteristic of the Pliocene and Pleistocene sediments of the Owen Ridge is the continuous alternation of foraminifer-bearing, foraminifer-nannofossil, and nannofossil ooze, (Unit I). This alternation is revealed as a cyclicity in sediment

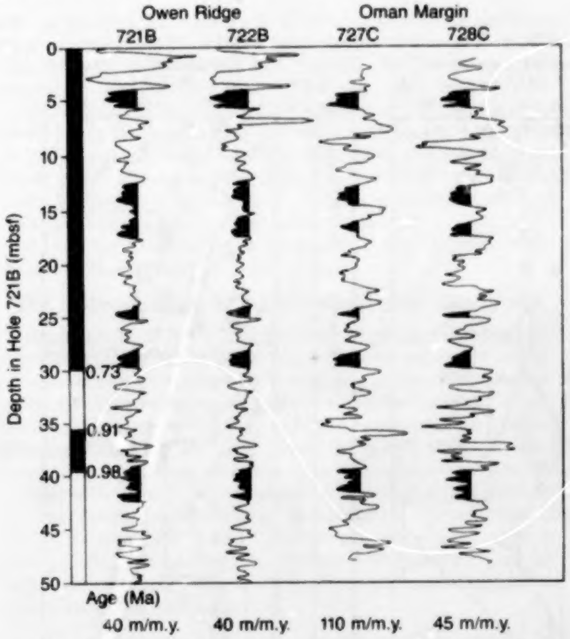

Figure 6. Examples of high-resolution records of magnetic susceptibility in cores from the Owen Ridge (Holes 721B and 722B) and the Oman margin (Holes 727C and 728C). Correlative intervals are shaded; magnetic polarity and reversal ages are on the left. Depth scale is normalized to depth of correlative interval in Hole 721B; note the different sedimentation rate for each site (bottom).

color, magnetic susceptibility, wet-bulk density, and carbonate content. The sediment cycles are thought to reflect both changes in oceanic productivity/preservation and changes in the input of eolian material. Preliminary analysis of the mineralogy of the clastic fraction reveals that the concentrations of quartz and dolomite covary in phase with the susceptibility data. This association of minerals is consistent with an eolian source. If the intensity of monsoonal upwelling and eolian transport is controlled largely by variations of solar radiation, a strong cyclicity is expected in the sediments of the Owen Ridge. Preliminary analysis of detailed (5-cm intervals) magnetic susceptibility measurements reveal a dominant periodicity of about 1 m in length and other periodicities of about 1-2 m, 3-4 m, and 12-14 m (Fig. 6). Power spectra of the magnetic susceptibility time series for Holes 721B (0-2.7 Ma) and 722A (0-2.6 Ma) gave periodicities near 19, 23, 41, and 400 k.y. Some intervals show power near 100 k.y. These periodicities match those expected for the Milankovitch mechanism, which is suspected to be a major cause of variations in monsoon intensity. A similar conclusion was reached at Site 721 by calculating the Walsh spectrum of sediment color changes that were classified as dark, medium, and light. Using a linear sedimentation rate over the past 2.95 m.y., we found the same periodicities that were observed in the magnetic susceptibility data. Here, we should note that these periodicities are not unique to the monsoon mechanism and that post-cruise research will focus on the distinction between global and monsoonal variability over these intervals.

SUMMARY

In summary, the sediments of the Owen Ridge exhibit many characteristics that reflect the tectonic uplift history of the ridge and the evolution of upwelling and pelagic ecosystems in the late Neogene. Understanding how these sedimentary responses are related to the evolution of monsoonal circulation and to changes in global climate was and is a major goal of Leg 117.

REFERENCES

Chester, R., Sharples, E. J., and Sanders, G. S., 1985. The concentrations of particulate aluminum and clay minerals in aerosols from the Northern Arabian Sea. *J. Sediment. Petrol.*, 55:37-41.

Cullen, J., and Prell, W. L., 1984. Planktonic foraminifera of the Northern Indian Ocean: distribution and preservation in surface sediments. *Mar. Micropaleontol.*, 9:1-52.

Goldberg, E. D., and Griffin, J. J., 1970. The sediments of the northern Indian Ocean. *Deep-Sea Res.*, 17:513-537.

Kolla, V., Be, A., and Biscaye, P.E., 1976. Calcium carbonate distribution in the surface sediments of the Indian Ocean. *J. Geophys. Res.*, 81:2605-2616.

Kolla, V., Kostecki, J. A., Robinson, F., and Biscaye, P. E., 1981. Distribution and origins of clay minerals and quartz in surface sediments of the Arabian Sea. *J. Sediment. Petrol.*, 61:563-569.

Lundberg, N., and Leggett, J. K., 1986. Structural features in cores from the slope landward of the Japan Trench, DSDP Leg 87B. *In* Kagami, H., Karig, D. E., Coulbourn, W. T., et al., *Init. Repts. DSDP*, 87: Washington (U.S. Govt. Printing Office), 809-826.

McKenzie, D., and Sclater, J. G., 1971. The evolution of the Indian Ocean since the Late Cretaceous. *Geophys. J. R. Astron. Soc.*, 24:437-528.

Norton, I. O., and Sclater, J. G., 1979. A model for the evolution of the Indian Ocean and the breakup of Gondwanaland. *J. Geophys. Res.*, 84:12.

Prell, W. L., 1984a. Variation of monsoonal upwelling: a response to changing solar radiation. *In* Hansen, J. E., and Takahashi, T. (Eds.), *Climatic Processes and Climate Sensitivity*: Washington (American Geophysical Union), Geophys. Monogr. 29, Maurice Ewing Series, 5:48-57.

________, 1984b. Monsoonal climate of the Arabian Sea during the late Quaternary: a response to changing solar radiation. *In* Berger, A., and Imbrie, J. (Eds.), *Milankovitch and Climate*: Dordrecht (D. Reidel), 349-366.

Prell, W. L., Gardner, J. V., et al. *Init. Repts. DSDP*, 68: Washington (U.S. Govt. Printing Office).

Prodi, F., Santachiara, G., and Oliosi, F., 1983. Characterization of aerosols marine environments (Mediterranean, Red Sea, and Indian Ocean). *J. Geophys. Res.*, 88:957-968.

Savoie, D. L., Prospero, J. M., and Nees, R. T., 1987. Nitrate, non-sea-salt sulfate, and mineral aerosol over the northwestern Indian Ocean. *J. Geophys. Res.*, 92:933-942.

Stein, C. A., and Cochran, J. R., 1985. The transition between the Sheba Ridge and Owen Basin: rifting of old oceanic lithosphere. *Geophys. J. R. Astron. Soc.*, 81:47-74.

Theyer, F., Mayer, L. A., Barron, J. A., and Thomas, E., 1984. The equatorial Pacific high-productivity belt: elements for a synthesis of Deep Sea Drilling Project Leg 85 results. *In* Mayer, L., Theyer, F. et al., *Init. Repts. DSDP*, 85: Washington (U.S. Govt. Printing Office), 971-985.

Whitmarsh, R. B., 1974. Some aspects of plate tectonics in the Arabian Sea. *In* Whitmarsh, R. B., Weser, O. E., Ross, D. A., et al., *Init. Repts. DSDP*, 23: Washington (U.S. Govt. Printing Office), 527-536.

________, 1979. The Owen basin off the southeast margin of Arabia and the evolution of the Owen Fracture Zone. *Geophys. J. R. Astron. Soc.*, 58:441-470.

Whitmarsh, R. B., Weser, O. E., Ross, D. A., et al., 1974. *Init. Repts. DSDP*, 23: Washington (U.S. Govt. Printing Office).

Ms 117A-105

4. BACKGROUND AND SUMMARY OF DRILLING RESULTS—OMAN MARGIN[1]

Shipboard Scientific Party[2]

INTRODUCTION

A major portion of Leg 117 was dedicated to the study of the Arabian continental margin between 17°30′N and 18°30′N offshore of Oman. Eight sites were drilled here in water depths ranging from 310 to 1430 m (Table 1, Fig. 1). The primary goal of drilling in this sector of the Arabian Sea was to understand the origin and variability of organic-carbon-rich sediments that result from the combined effects of monsoon-induced upwelling and the related oxygen-minimum zone (OMZ), which lies between 200 and 1200 m of water depth. The sites were selected to recover continuous and expanded sedimentary sections from zones of high biological productivity in order to establish the history of the depositional system. A secondary goal was to clarify the Neogene tectonic evolution of the Oman margin.

The majority of the margin sites have common objectives. Here, we summarize the geologic and oceanographic background for the margin sites, state the general objectives of drilling on the margin, and outline the principal results. Site-specific information is presented in the individual site chapters.

AGE, STRUCTURE, AND SEDIMENTS OF THE SOUTHEAST OMAN MARGIN

Most plate-tectonic reconstructions of the Indian Ocean infer that the Arabian margin and the adjacent Owen Basin are Jurassic in age, and that the margin is passive in character (Whitmarsh, 1979). Some aspects of the modern margin appear to be inconsistent with this interpretation (Mountain and Prell, in press). Much of the Oman margin is characterized by a narrow continental shelf bordered by an extremely steep continental slope, which is thought to be a megashear associated with the formation of the margin (Whitmarsh, 1979; Stein and Cochran, 1985). However, the embayment between Ras al Madrakah and Ras Sharbithat has a relatively wide continental shelf (about 75 km), which abuts the Sharbithat Ridge to the south and converges on the Ras al Madrakah headland to the north. The continental slope in this area is characterized by a series of linear, north-northeast-trending sediment terraces underlain by sedimentary basins. These terraces lie at water depths ranging from 500 to 1000 m in the upper basin and from 1400 to 1500 m in the lower basin, and thus accumulate sediments in the interval influenced by the intermediate-water OMZ (see below).

Seismic-reflection profiles of the margin reveal that the upper basin is bounded landward (west) by the steeply dipping Siquirah Fault (Mountain and Prell, in press) and seaward by a buried ridge of acoustic basement (Figs. 1 and 2). The upper basin shoals and narrows to the north. The southern part of the basin lies at about 1000 m and is about 15 km wide, whereas the northern part lies at about 600 m and is about 5 km wide. Seismic profiles show that the sediments in these basins are thick, acoustically highly layered, and structurally isolated from the sediments of adjacent basins by bounding faults, with the exception of the shallowest few hundred meters. The sediments are thickest in the center of the basin (more than 2000 m; Mountain and Prell, in press), forming a syncline-shaped deposit. Along the strike of the basin, the surface and subsurface layers dip gently to the southwest and are relatively conformable, although some deformational and slump-related structures are observed.

The deeper slope basin lies at about 1500 m and is about 8 km wide, but it only extends approximately 15 km along the strike of the margin. The basin is bounded on the south by the Sharbithat Ridge and on the north by an erosional scarp. The eastern and western boundaries are basement highs. The sediments of the basin onlap onto and have been deformed by movement relative to the adjacent basement structures. The shallow sediments dip seaward from the upper slope basin toward the lower constraining basement peak. Sediments are thickest near the center of the lower basin, forming a synclinal-shaped deposit that thins by pinch-out and onlap to the east and west.

The age and composition of acoustic basement along this portion of the margin is not directly known. The basement structure is complex, characterized as it is by several major faults, such as the Siquirah Fault, and by long, narrow ridges formed from basement peaks. Several lines of evidence support an interpretation, however, of the basement as landward-thrust oceanic crust (ophiolitic rocks). First, the seismic, gravity, and magnetic data collected during RC2704 (Mountain and Prell, this volume) did not identify anomalies that are characteristic of either salt or igneous intrusions. Second, the coastal geology of Oman includes ophiolites unconformably overlain by Eocene limestones, such as those on both Ras al Madrakah and Masirah Island, which are directly upstrike from our study area (Moseley and Abbotts, 1979). Third, industrial multichannel seismic data indicate that another major fault, the Masirah Fault, lies immediately landward of these exposed ophiolites, suggesting that the basement material seen in the study area is of similar origin and has been obducted onto the continental margin. Given these data, we infer that ophiolites underlie the outer shelf and slope basins. Testing this hypothesis was one of the objectives of drilling on the Oman margin.

Studies of box and piston cores from the upper slope basin indicate that Holocene accumulation rates range from 80 to 150 m/m.y., while carbonate and organic carbon contents range from 20 to 60 wt% and 4% to 8%, respectively (Shimmield et al., in press; Prell, unpubl. data). Accumulation rates in the lower basin are about 50–60 m/m.y. (about one-third of the rates in the upper basin). Carbonate and organic carbon contents range from 45 to 70 wt% and 2% to 4%, respectively. Most of the sediment on the margin is bioturbated, even though oxygen values in the bottom water on the margin are as low as 0.2 mL/L. Shimmield et al. (in press) report the occurrence of laminated sediments in small shelf basins within the OMZ; these laminated sediments also contain excess SiO_2 interpreted as diatomaceous opal. Diatom frustules contribute considerably to

---

[1] Prell, W. L., Niitsuma, N., et al., 1989. *Proc. ODP, Init. Repts.*, 117: College Station, TX (Ocean Drilling Program).

[2] Shipboard Scientific Party is as given in the list of Participants preceding the contents.

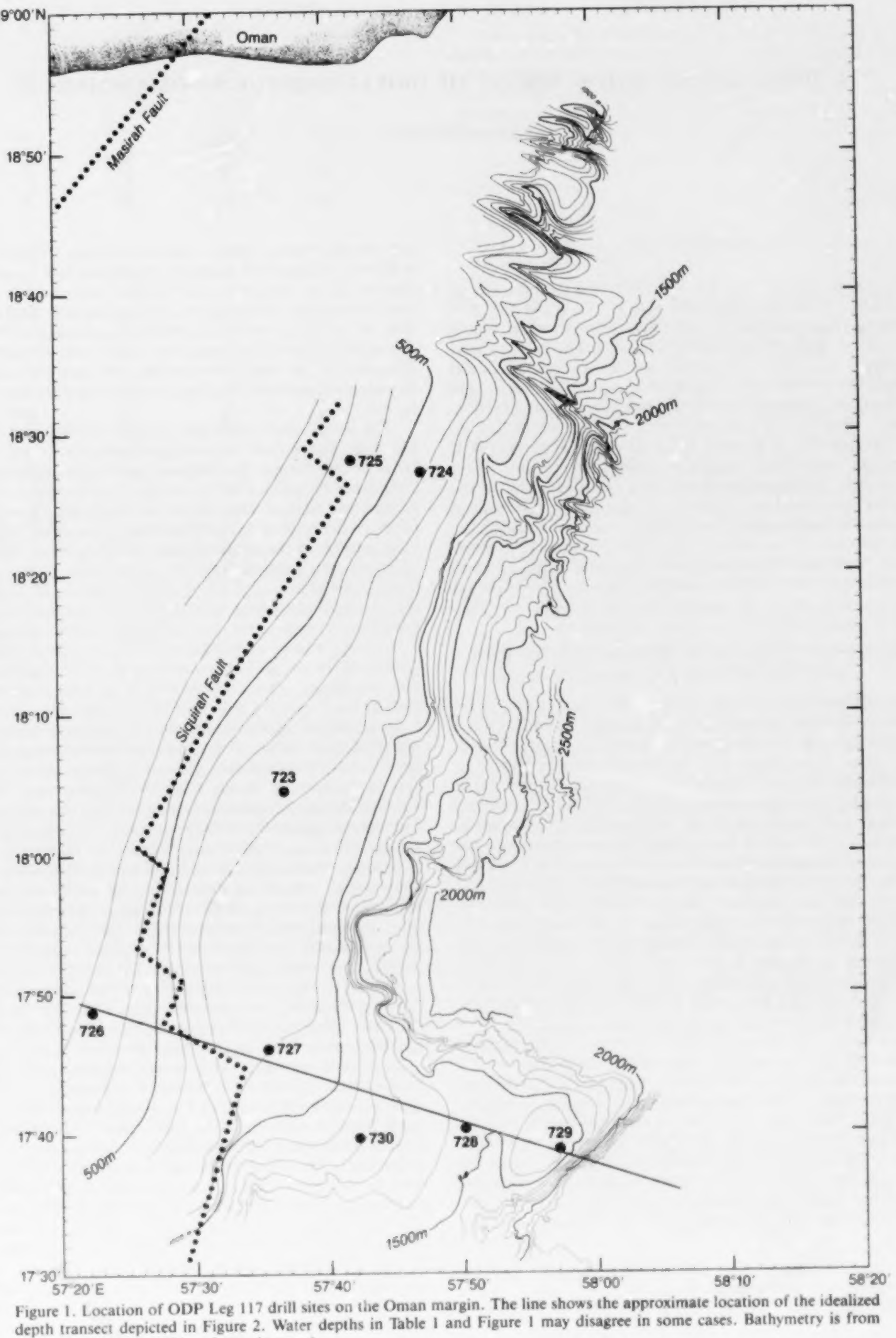
19°00'N
18°50'
18°40'
18°30'
18°20'
18°10'
18°00'
17°50'
17°40'
17°30'
57°20'E
57°30'
57°40'
57°50'
58°00'
58°10'
58°20'
Oman
Masirah Fault
Siquirah Fault
500m
1500m
2000m
2500m
725
724
723
726
727
730
728
729

Figure 1. Location of ODP Leg 117 drill sites on the Oman margin. The line shows the approximate location of the idealized depth transect depicted in Figure 2. Water depths in Table 1 and Figure 1 may disagree in some cases. Bathymetry is from Mountain and Press (this volume; in press).

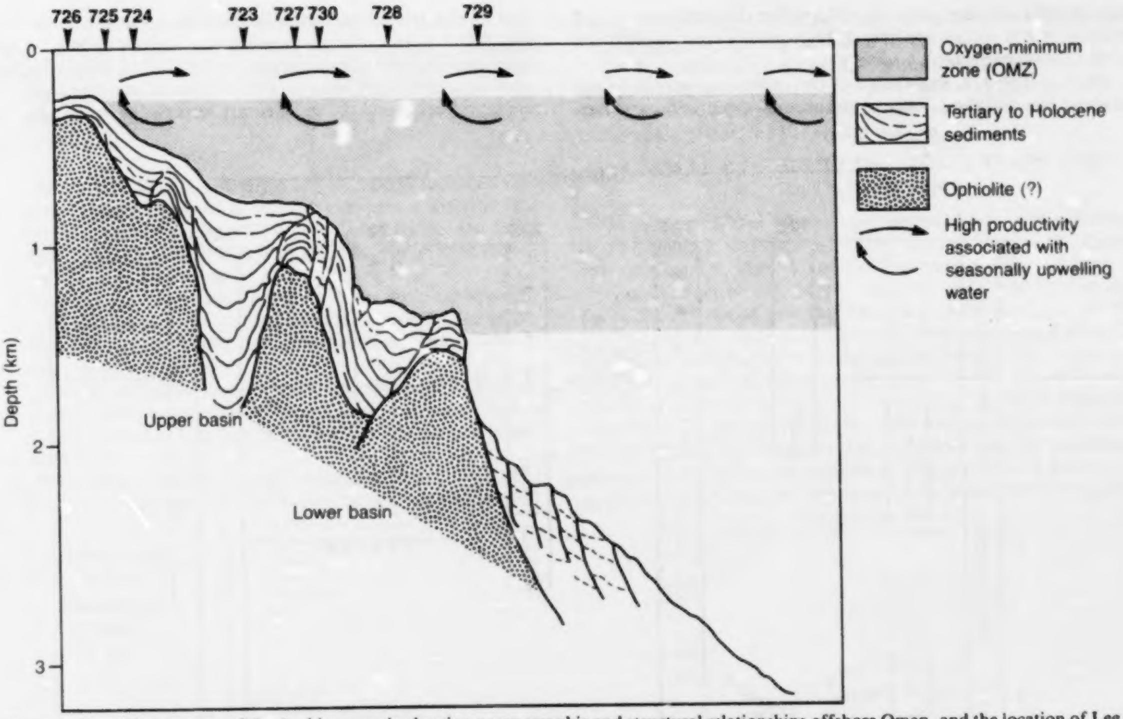
726
725
724
723
727
730
728
729
0
1
2
3
Depth (km)
Upper basin
Lower basin
Oxygen-minimum zone (OMZ)
Tertiary to Holocene sediments
Ophiolite (?)
High productivity associated with seasonally upwelling water

Figure 2. Simplified transect of the Arabian margin showing oceanographic and structural relationships offshore Oman, and the location of Leg 117 drill sites on this margin.

the total annual particulate flux in the upwelling areas of the northwest Indian Ocean (Krey, 1973), but they are not preserved in most surface sediments.

MODERN AND ANCIENT OCEANOGRAPHY OF THE SOUTHEAST OMAN MARGIN

The modern oceanography of the Arabian margin is characterized by seasonal monsoonal upwelling and a strong midwater OMZ. As outlined in the "Introduction" (this volume), strong, southwesterly, near-surface winds during the summer drive an offshore Ekman transport of surface waters, which are replaced by colder, nutrient-rich waters from several hundred meters deep. Sea-surface temperatures of less than 20°C occur over the shelf during the southwest monsoonal season (Currie et al., 1973). Nutrient concentrations at the surface during the southwest monsoon average >2 μmol/L for phosphate, >10 mmol/L for nitrate, and >10 μmol/L for silicate (Wyrtki, 1973; Krey and Babenerd, 1976). In contrast, surface-water concentrations are 0.4 μmol/L, <0.5 mmol/L, and >5 μmol/L, respectively, during the nonupwelling period from November to April.

In response to the richer nutrient supply, primary production in surface waters averages >500 mg C/m^2/day in May to October and drops to values as low as 150 mg C/m^2/day during November to April (Krey and Babenerd, 1976). Thus, wind speed and the duration of the monsoon control the strength and duration of upwelling, which in turn causes enhanced production of biogenic sedimentary components. By identifying the processes that control the production and preservation of various sedimentary components, the clastic and biogenic components deposited beneath the centers of upwelling can be used to interpret the history of monsoonal upwelling, including upwelling intensity, monsoon strength, and the oceanographic history of surface waters in the northwest Arabian Sea.

At present, the intermediate waters of the northwest Arabian Sea (200–1000 m of water depth) are characterized by high salinity, oxygen depletion between 200 and 1200 m water depth (<1 mL/L in all areas north of 3°N), and spatial and temporal stability. The sources of the intermediate waters are the Red Sea overflow, which spreads at about 800 m, and the Persian Gulf overflow, which spreads at about 300 m. Other sources of intermediate waters are the low-latitude regions of the Arabian Sea and the Gulf of Aden. These four sources combine to form North Indian Intermediate Water (NIIW), which has a uniform salinity of about 34.8 ‰ (Wyrtki, 1971, 1973) and occupies a depth of approximately 200–1200 m throughout the Arabian Sea. Limited horizontal advection of central Indian Ocean water, stable salinity and temperature stratification, and high chemical oxygen demand due to upwelling-related high productivity (>500 mg C/m^2/day) combine to form a stable zone of oxygen depletion, the OMZ. The OMZ presently occurs at depths from 200 to 1200 m, where values <0.2 mL/L O_2 are commonly found (Wyrtki, 1971; Spencer et al., 1982; Shimmield et al., in press). This oxygen-deficient layer is intercalated between the oxygen-rich and highly productive shallow mixed layer and the deeper layers originating from circumpolar and North Atlantic deep waters. The saline (34.84 ‰) and cold (2.2°C) deep waters reach the northern Indian Ocean with a moderate O_2 content (approximately 4 mL/L), and lie below the OMZ.

The OMZ of the Arabian Sea today thus reflects a combination of biochemical processes (productivity and bacterial oxygen consumption), stable stratification of the water masses, and sluggish subsurface circulation. Many of these influences may have changed in the past, either in response to climatic or oceanographic variability on time scales of glacial-interglacial cycles, or during Neogene sea-level fluctuations and tectonic events. We can expect such changes to be reflected in the sediments of the margin, which we can consider as high-quality records of the regional paleoceanographic history.

Prior to Leg 117, knowledge of the paleoceanography of the Arabian Sea and the history of monsoonal circulation was limited to numeric climate models and sedimentary records of the last 500 k.y. In order to improve our understanding of long-term climatic and ocean-circulation variability, longer high-resolution sedimentary records were needed to examine changes in climatic forcing and the sedimentary response over geologic time.

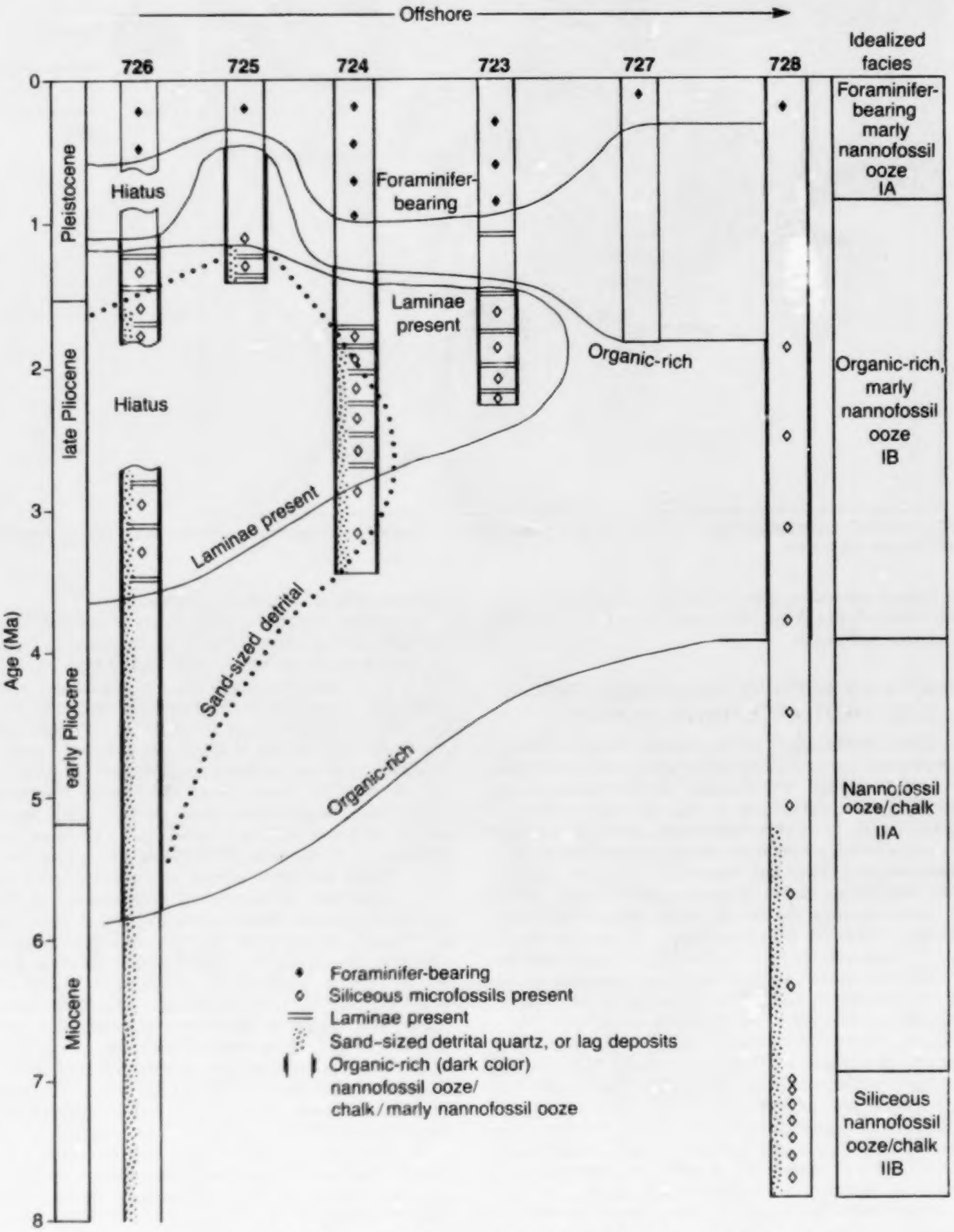
Offshore
726
725
724
723
727
728
Idealized facies
Age (Ma)
0
1
2
3
4
5
6
7
8
Pleistocene
late Pliocene
early Pliocene
Miocene
Hiatus
Hiatus
Foraminifer-bearing
Laminae present
Organic-rich
Laminae present
Sand-sized detrital
Organic-rich
Foraminifer-bearing marly nannofossil ooze IA
Organic-rich, marly nannofossil ooze IB
Nannofossil ooze/chalk IIA
Siliceous nannofossil ooze/chalk IIB
Foraminifer-bearing
Siliceous microfossils present
Laminae present
Sand-sized detrital quartz, or lag deposits
Organic-rich (dark color) nannofossil ooze/ chalk/marly nannofossil ooze

Figure 3. Schematic representation of sedimentary facies at margin sites through time. See text for discussion.

OBJECTIVES

The above summary of geologic and oceanographic information about the Oman margin raises a number of questions that can be addressed by drilling. The main objectives of drilling on the continental margin of Oman during Leg 117 can be summarized as follows:

1. To identify and characterize the proximal (coastal) upwelling facies on the margin in order to compare it with the distal upwelling records recovered from the Owen Ridge. Do these two areas show the same trends during the Neogene in response to climatic and tectonic events?
2. To define the depositional history of organic-carbon-rich sediments underlying a productive upwelling area and to relate variations in the constituents of sediments to differing climatic and oceanographic regimes.
3. To trace the influence of suboxic deposition and diagenesis in organic-carbon-rich sediments over a range of water depths and oxygen contents. Can variations of the OMZ be inferred from such data?
4. To determine whether margin sediments record changes in the water-mass structure of the northwest Indian Ocean and changes in the supply of water from the Red Sea and the Persian Gulf throughout the depositional history.
5. To investigate the age and nature of the acoustic basement and the tectonic history of shelf and slope basins, and to examine the relationship between uplift on the Owen Ridge and the tectonic history of the Oman margin.

SUMMARY OF DRILLING RESULTS ON THE OMAN MARGIN

More than 2600 m of core were recovered (at a mean recovery rate of 80%) at the eight sites (16 holes) drilled on the Oman margin (Table 1, Figs. 1 and 2). The water depths sampled at this transect across the margin ranged from 311 to 1428 m and bracketed the depth interval where the OMZ impinges on the modern margin. The oldest sediments recovered were Eocene (?) shallow-water foraminifer limestones. Unfortunately, we did not penetrate the acoustic basement at Sites 726 and 729, so we were unable to confirm our speculation that it is formed of ophiolitic rocks. The Eocene (?) limestones were overlain by upwelling-influenced sediments of Miocene to Holocene age. The upwelling-influenced sediments are dominated by green to olive calcareous oozes to clayey silts, are rich in organic carbon (2%–8%), and

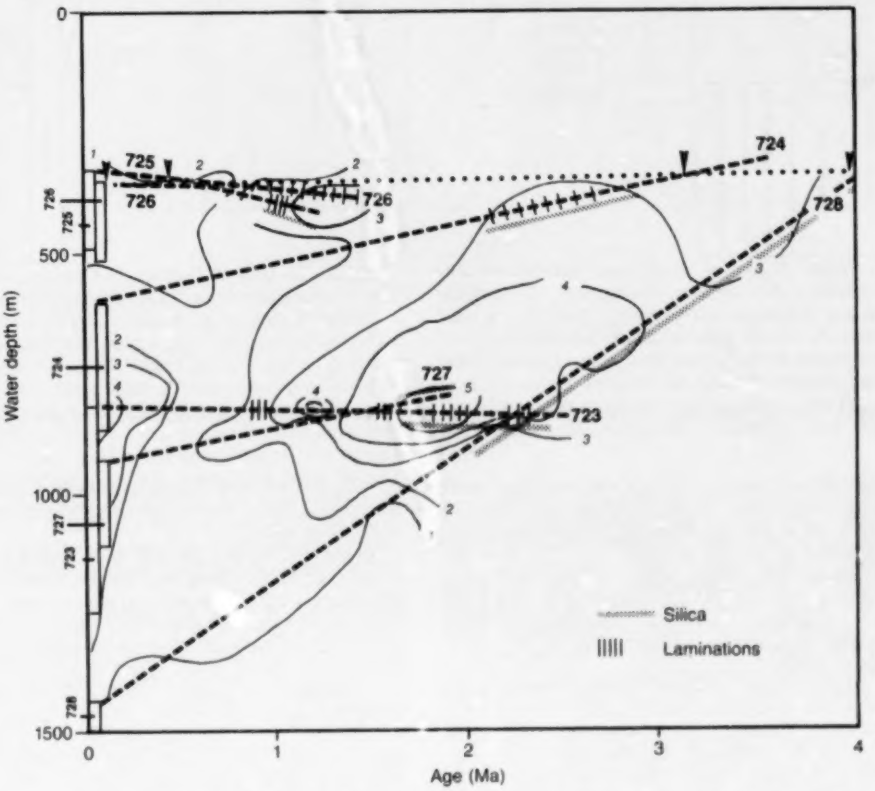

Figure 4. Age (in m.y.) vs. depth (m) of Oman margin Sites 723 through 728. Sediment sections recovered at individual sites are plotted to the left of the diagram according to their present water depth and the total depth drilled. The estimated depth of the sediment/water interface through time is indicated by the dashed line for each site and was reconstructed using the presence or absence of the benthic foraminifer *Ammonia beccarii*. The occurrence of this species is considered an indication of water depth shallower than 350 m. Arrows on the backtracking lines (dotted lines) for each site denote the transitions from <350 m to >350 m water depth based on this indicator. Isopleths of organic carbon concentrations of the paleosurface sediments are shown for the correct water depths and ages. Vertical lines in the backtracking curves denote laminated intervals, and occurrences of biogenic opal are indicated by dark shading.

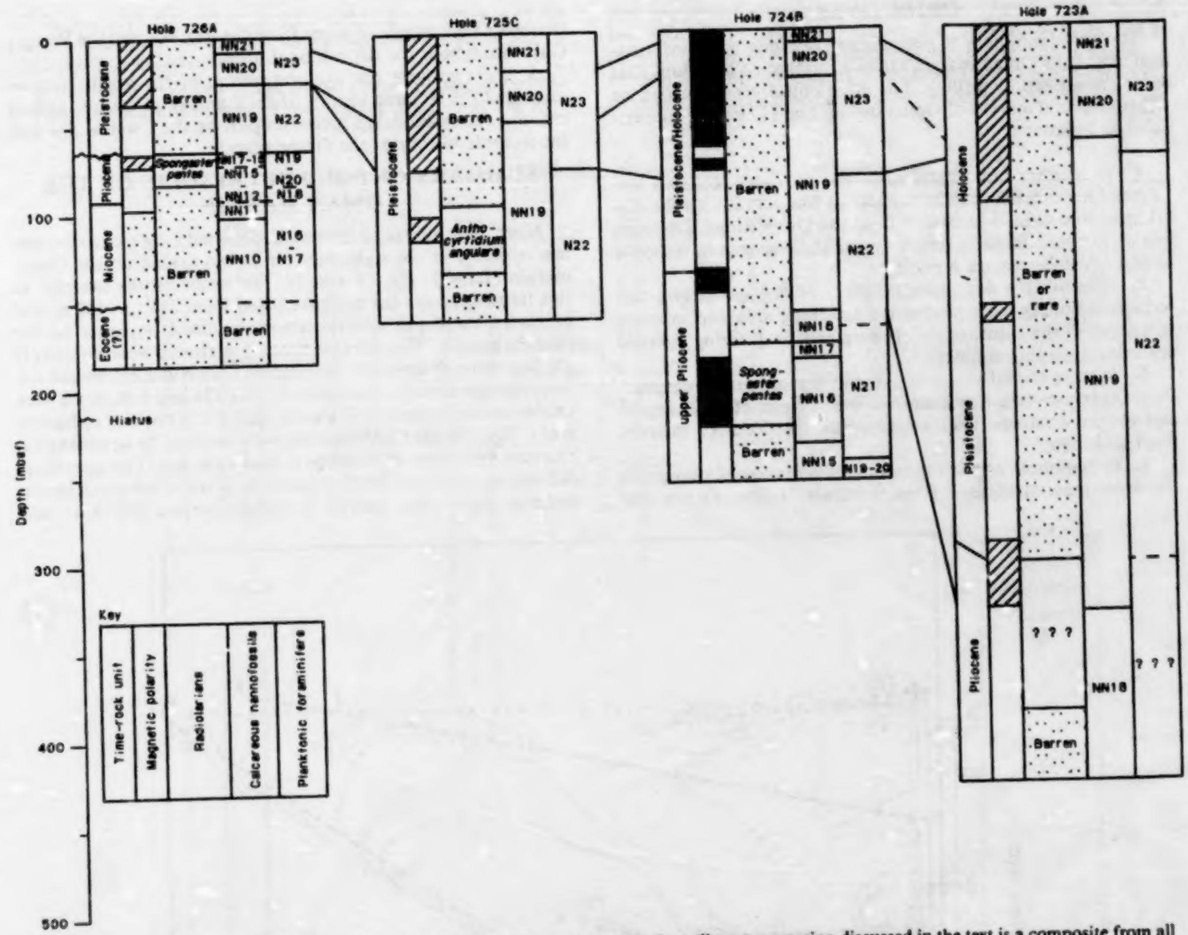

Figure 5. Correlation of margin sites based on stratigraphic evidence. Note that the sediment succession discussed in the text is a composite from all sites.

include laminated, diatom-bearing intervals rich in organic matter (>5%) at sites in the center of the upwelling zone (Site 724 at 600 m and Site 723 at 800 m). Intervals of abundant sand-sized detrital material at near-shore sites (726, 725, 724) are thought to indicate terrestrial input, while phosphorite-rich lag deposits at the shallowest site (726) are interpreted to record the effects of current winnowing. A schematic representation of the lateral and temporal variations in sediment facies on the Oman margin is shown in Figure 3.

The oldest coherent signal observed in these sections is the increased preservation of organic matter during the late Miocene to early Pliocene. The effect of an intensified OMZ on the sediments is seen in the laminated, organic-carbon-rich sediments that occur in the upper Pliocene and lower Pleistocene of the four landward sites. The preservation of laminae is paralleled to some extent by an increase in the abundance of sand-sized detrital material in nearshore Sites 724, 725, and 726. The increase in the abundance of coarse clastics may be a result of lower sea level or increased wind strength and enhanced eolian input. A further characteristic of the laminated and organic-carbon-rich sediments is the preservation of opaline microfossils. Upper Pleistocene sediments are uniform in fossil and organic carbon content at all sites, indicating that the significant climatic and sea-level fluctuations known from the late Pleistocene glacial phases did not affect sedimentation patterns to any noticeable extent.

In general, the margin sediments bear a continuous imprint of constant high-surface productivity, while facies changes signify changes in the depositional environment. The complex interaction between the tectonic evolution of the margin and slope basins and the deposition and preservation of organic-rich, opal-rich, and laminated facies results in patterns of deposition that are summarized in Figure 4. In this illustration the abundance of organic carbon in the sediments is contoured on a plot of paleodepth vs. time. The plot reveals a striking coincidence of organic-carbon-rich, opaline, and laminated facies near 800-m paleowater depth in the upper Pliocene and lower Pleistocene. The late Pliocene mode of deposition and preservation of laminated sediments may reflect an intensified and stable OMZ. Sediments of late Pleistocene and Holocene age also contain high organic-carbon concentrations, but these sediments are not laminated and lack opal.

The abundance of organic carbon in the Oman margin sediments leads to diagenetic changes in those sediments, and indications of microbial activity deep in the sediment column were pronounced. Biogenic methane gas was found in high concen-

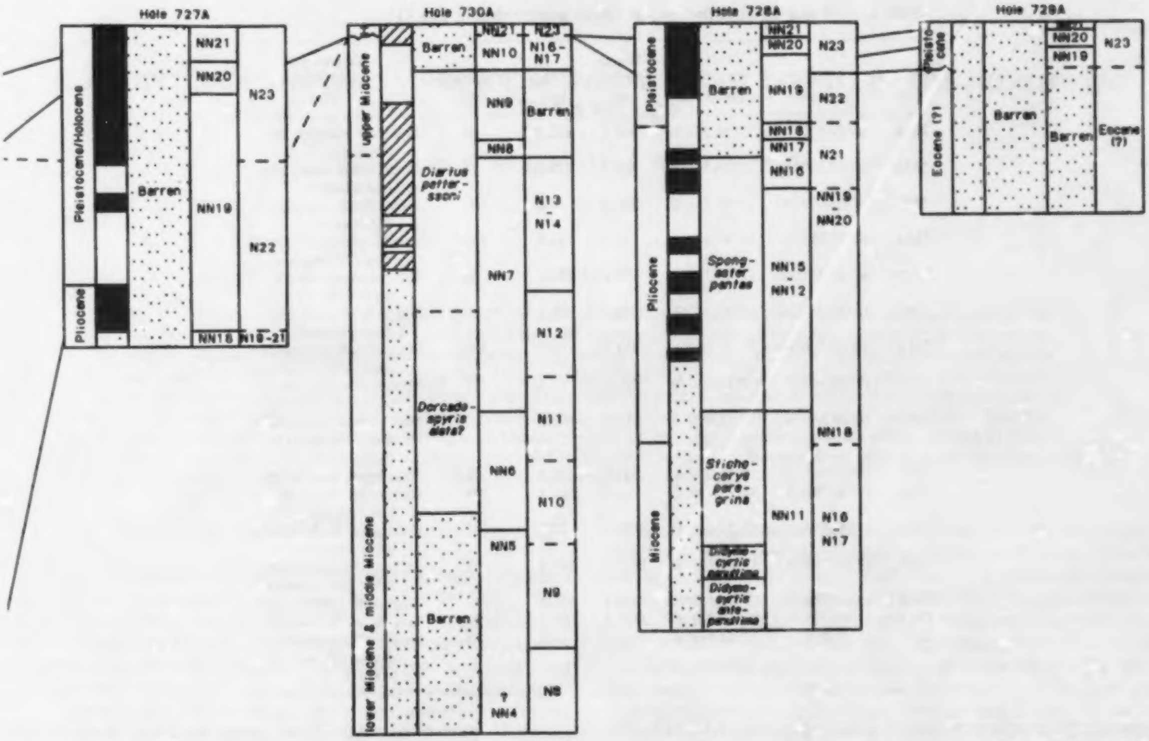
Hole 727A
Pleistocene/Holocene
Pliocene
Barren
NN21
NN20
NN19
NN18
N23
N22
N19-21
Hole 730A
upper Miocene
lower Miocene & middle Miocene
Barren
Diartus petterssoni
Dorcadospyris alata?
NN21
NN10
NN9
NN8
NN7
NN6
NN5
?
NN4
N23
N16-N17
Barren
N13-N14
N12
N11
N10
N9
N8
Hole 728A
Pleistocene
Pliocene
Miocene
Barren
Spongaster pentas
Stichocorys peregrina
Didymocyrtis penultima
Didymocyrtis antepenultima
NN21
NN20
NN19
NN18
NN17-NN16
NN15-NN12
NN11
N23
N22
N21
N19-N20
N18
N16-N17
Hole 729A
Pleistocene
Eocene (?)
Barren
NN20
NN19
Barren
N23
Eocene (?)

Figure 5 (continued).

trations at all sites and reached up to 0.29 L/L of sediment. High bottom-water temperatures and shallow water depths precluded the formation of gas hydrates at these sites. In addition to the high methane content, thermogenic gas was observed in low concentrations at Sites 723, 724, 725, 727, and 728. Interestingly, Sites 723 and 724 displayed pore-water profiles that suggest an advective supply of sulfate-bearing waters from some deep source, similar to the situation in the Peru slope basins (Suess, von Huene, et al., 1988). The additional supply of sulfate fuels microbial sulfate reduction beyond the range usually found in deep-sea sediments and creates very high concentrations of alkalinity (107 mmol/L) and ammonia (40 mmol/L) in pore waters. High alkalinity and interstitial calcium and magnesium ions combine to form diagenetic dolomites at depth at Site 723.

Biostratigraphic zonations showed that Sites 725 and 727 have expanded Pleistocene sections and that Sites 723 and 724 are expanded in the Pleistocene and upper Pliocene (Fig. 5). Calcareous nannofossils are abundant in most samples, but they exhibit low species diversity. Planktonic foraminifers are abundant in Pleistocene sediments, but their abundance and preservation declines near the Pliocene/Pleistocene boundary. Benthic foraminifers are abundant and highly diverse in the relatively shallow sites on the margin, and benthic assemblages reveal the subsidence history on the margin. This history is marked by rapid subsidence events from <300 m water depth in the middle Pliocene to >800 m at present. Radiolarian faunas were found in upper Miocene and Pliocene strata only. In general, the microfossil assemblages reveal a trend from more siliceous sediments in the Miocene and Pliocene to more calcareous sediments in the Pleistocene.

Intensities of natural remanent magnetization (NRM) in the margin sediments were commonly less than 1 mA/m and decreased with sediment depth, so that the use of paleomagnetic methods for stratigraphy was somewhat limited. These problems are partially offset by the unusually detailed correlation between holes and even sites using records of magnetic susceptibility measured with high resolution on whole cores.

In summary, some of the most important findings of ODP Leg 117 pertain to the tectonic history of the Oman margin and the evolution of monsoonal circulation since the middle Miocene:

1. Parts of the Arabian margin have subsided as much as 1000 m during the late Neogene. This can be deduced from unconformities, sedimentation rates, and benthic faunas.

2. The geometry of slope basins and the occurrence of shallow-water platform carbonates similar to those overlying the ophiolitic rocks in Masirah Island suggest that much of the margin is underlain by ophiolitic rocks. The occurrence of thermogenic gas and interstitial water sulfate profiles further suggest that advective subsurface flow and gas migration occurs from deep geologic structures, possibly from beneath the ophiolitic rocks.

3. The organic-carbon-rich margin sediments are dominantly calcareous mudstones that include eolian and diagenetic minerals but are poor in opal. This composition is unusual when compared with opal-rich sediments typical of other major upwelling systems.

4. Faunas and floras indicative of upwelling appear in the early middle Miocene on the margin; variations in the intensity of the monsoon during the Neogene were not immediately discernible from the microfossil data.

5. Laminated organic-carbon-rich sediments that contain siliceous microfossils are restricted to the upper Pliocene and lower Pleistocene, suggesting that during that time a different

Table 1. Sites and holes drilled on the Oman margin during Leg 117.

Site	Latitude	Longitude	Water depth (m)	Drilled (m)	Recovery (%)	Nature and age of oldest strata
723A	18°03.079′N	57°36.561′E	807.8	432.3	68	Dolomite biscuits; late Pliocene
723B	18°03.079′N	57°36.561′E	807.8	429.0	73	Nannofossil clayey silt; late Pliocene
723C	18°03.079′N	57°36.561′E	807.8	76.8	107	Nannofossil clayey silt; Pleistocene
724A	18°27.713′N	57°47.147′E	592.8	44.5	100	Foraminifer nannofossil ooze; Pleistocene
724B	18°27.713′N	57°47.147′E	592.8	257.7	83	Calcareous clayey silt; early Pliocene
724C	18°27.713′N	57°47.147′E	592.8	252.4	96	Calcareous clayey silt; early Pliocene
725A	18°29.200′N	57°42.080′E	311.5	4.5	100	Nannofossil-foraminifer sandy silt; Pleistocene
725B	18°29.200′N	57°42.080′E	311.5	93.8	11	Foraminifer-rich calcitic sandy silt; Pleistocene
725C	18°29.200′N	57°42.080′E	311.5	162.8	60	Nannofossil-rich calcitic sand, silt, and clay; Pleistocene
726A	17°48.965′N	57°22.290′E	330.8	186.3	59	Limestone; Eocene (?)
727A	17°46.096′N	57°35.216′E	914.8	182.2	103	Calcareous clayey silt; late Pliocene
727B	17°46.096′N	57°35.216′E	914.8	27.1	103	Calcareous clayey silt; late Pleistocene
728A	17°40.790′N	57°49.553′E	1427.8	346.4	99	Foraminifer-nannofossil ooze; late Miocene
728B	17°40.790′N	57°49.553′E	1427.8	347.7	100	Claystone; late Miocene
729A	17°38.715′N	57°57.221′E	1398.8	109.1	29	Limestone; Eocene (?)
730A	17°38.885′N	57°42.519′E	1065.8	403.9	80	Foraminifer-nannofossil chalk; late early Miocene

oceanographic regime produced a more pronounced OMZ. The absence of benthic macroorganisms in the suboxic/anoxic bottom waters of an intensified OMZ would explain the preservation of primary sedimentary features.

REFERENCES

Currie, R. I., Fisher, A. E., and Hargraves, P. M., 1973. Arabian Sea upwelling. *In* Zeitzschel, B., and Gerlach, S. A. (Eds.), *The Biology of the Indian Ocean*: New York (Springer-Verlag), 37–52.

Krey, J., 1973. Primary production in the Indian Ocean. *In* Zeitzschel, B., and Gerlach, S. A. (Eds.), *The Biology of the Indian Ocean*: New York (Springer-Verlag), 115–126.

Krey, J., and Babenerd, B., 1976. *Phytoplankton production; Atlas of the International Indian Ocean Expedition*: Kiel (Institut für Meereskunde).

Moseley, F., and Abbotts, I. L., 1979. The ophiolite melange of Masirah, Oman. *J. Geol. Soc. London*, 136: 713–724.

Mountain, G., and Prell, W., in press. A multiphase plate tectonic history of the southeast continental margin of Oman. *In* Robertson, A.H.F., Searle, M. P., and Ries, A. C. (Eds.), *The Geology and Tectonics of the Oman Region*. Geol. Soc. Am. Spec. Publ.

Shimmield, G. B., Price, N. B., and Pedersen, T. F., in press. The influence of hydrography, bathymetry, and productivity on sediment type and composition from the Oman margin and the northwest Arabian Sea. *In* Robertson, A.H.F., Searle, M. P., and Ries, A. C. (Eds.), *The Geology and Tectonics of the Oman Region*. Geol. Soc. Am. Spec. Publ.

Spencer, D., Broecker, W. S., Craig, H., and Weiss, R. F., 1982. *GEOSECS Indian Ocean Expedition, Sections and Profiles* (Vol. 6): Washington (National Science Foundation).

Stein, C. A., and Cochran, J. R., 1985. The transition between the Sheba Ridge and Owen Basin: rifting of old oceanic lithosphere. *Geophys. J. R. Astron. Soc*, 81:47–74.

Suess, E., von Huene, R., et al., 1988. *Proc. ODP, Init. Rept.*, 112: College Station, TX (Ocean Drilling Program).

Whitmarsh, R. B., 1979. The Owen Basin off the southeast margin of Arabia and the evolution of the Owen Fracture Zone. *Geophys. J. R. Astron. Soc.* 58: 441–470.

Wyrtki, K., 1971. *Oceanographic Atlas of the International Indian Ocean Expedition*: Washington (National Science Foundation).

———, 1973. Physical oceanography of the Indian Ocean. *In* Zeitzschel, B., and Gerlach, S. A. (Eds.), *The Biology of the Indian Ocean*: New York (Springer-Verlag), 18–36.

Ms 117A-109

5. GEOPHYSICAL RECONNAISSANCE SURVEY FOR ODP LEG 117 IN THE NORTHWEST INDIAN OCEAN[1]

Gregory S. Mountain[2] and Warren L. Prell[3]

ABSTRACT

Cruise 2704 of the *Robert D. Conrad* (RC2704) in the spring of 1986 acquired reconnaissance data necessary for the location and interpretation of ODP Leg 117 drill sites. In addition, three regions were examined in detail using underway geophysical techniques, and geologic and hydrologic samples were collected while on station. These regions include (1) a channel/levee complex of the Indus Fan, (2) the western flank of Owen Ridge, and (3) the southeastern margin of Oman. This report represents preliminary analysis of the underway geophysical data. The first of the three surveys adds to the growing knowledge of meandering channels recently discovered in other deep-sea fans. Tied to DSDP Site 224, the Owen Ridge survey documents the age and nature of uplift of the ridge. Speculations concerning the age of Owen Basin, integrated with survey data offshore Oman and published reports of onshore geology, provide a new hypothesis concerning the multiphase tectonic history of the northwest Indian Ocean.

INTRODUCTION

High wind stress of the summer monsoon strongly influences the regional oceanography of the northwest Indian Ocean, producing strong seasonal upwelling and high surface productivity. RC2704 of the *Robert D. Conrad* was designed to examine relationships between this seasonal climate pattern and long-term changes in productivity, hydrography, and sediment accumulation. The recovery of representative surficial sediments is essential to the accurate reconstruction of this record, and therefore, reconnaissance survey data were collected and examined prior to coring. A variety of underway and station data were gathered during the 37 days at sea. Continuous measurements of magnetics, gravity, Sea Beam bathymetry, and 3.5-kHz sonograms were collected along the 10,500 km of ship track out from and returning to Colombo, Sri Lanka (Fig. 1). In addition, 6600 km of digitally recorded water gun seismic-reflection profiles and seven sonobuoy measurements of sound velocity were acquired within and between the three survey grids. Station work acquired a total of 30 piston cores (3 to 15 m long), 22 giant gravity cores (4 in. diameter), six box cores, four plankton tows, three trigger gravity cores (1 in. diameter), and three hydrocasts (Table 1). Three areas were examined in detail: a channel/levee complex of the Indus Fan, the southern Owen Ridge, and the southeast Oman margin. The following is a summary of the results of this three-part survey.

INDUS FAN

Background

The Indus Fan is the second largest submarine fan in the world (Barnes and Normark, 1985). It is fed by sediments coming primarily from the Indus River, where until recently (before upstream damming) sediment discharge was comparable to that of the Mississippi River (Lisitzin, 1972). Fan sediments reach as far south as the flanks of the Carlsberg Ridge and extend from the Indian margin to the eastern escarpment of Owen Ridge (Fig. 1). Sediment thickness reaches a maximum of 6.0 s of reflection time near the main depocenter at 23°N; it decreases steadily southward with the exception of thin cover above the Chagos-Laccadive and Lakshmi ridges (Kolla and Coumes, 1987). Initial intercontinental collision between India and Asia dates from the middle Eocene (Molnar and Tapponnier, 1975; Patriat and Achache, 1984), and consequently it is assumed that the Indus Fan began to develop at this time. The underlying oceanic crust is post-middle Cretaceous in age (Norton and Sclater, 1979), implying that the preceding measurements of total sediment accumulation include some indeterminate amount of pre-fan sediment as well.

The grid surveyed in detail during RC2704 lies near the 4000-m contour of the Indus Fan, 100 km east of Owen Ridge (Fig. 1). The seafloor gradient in this region is 1:1055 (Kolla and Coumes, 1987). On the basis of gradient alone, the survey grid is placed at the uppermost part of the lower fan; on the basis of echo character, however, the grid is well within the lower fan (Kolla and Coumes, 1987). Ship crossings are too sparse to allow the many channels of this region to be traced between tracks. Nonetheless, Kolla and Coumes (1987) noted an especially large number of channels between the 4000- and 4400-m isobaths. Typical channel-to-levee heights are 30–40 m on the middle fan, whereas most heights on the lower fan are 20 m or less.

Bathymetry

Several tens of distributary channels of the Indus Fan were crossed during the outbound transit to the first survey area on Owen Ridge. Each channel is characterized by an axis from one to several kilometers wide, bounded by roughly symmetric levees that are tens of meters high. In most instances the channel axis is within a few meters of the water depth of the surrounding interchannel region. Most 3.5-kHz sonograms from between channel/levee complexes show a prolonged surface echo with few to no sub-bottom reflectors. This echo character implies that sand/silt beds roughly 5 to 10 cm thick comprise about 25% of the upper few tens of the sediment column (Kolla and Coumes, 1987). In contrast, internal acoustic structure can be seen on many levee crests, which are consequently interpreted as being composed of more uniformly fine-grained sediment.

An especially broad, symmetric channel/levee system that had been crossed on the outbound transit was chosen for a brief survey during the return to Colombo (Fig. 1). The elevated levee

---

[1] Prell, W. L., Niitsuma, N., et al., 1989. *Proc. ODP, Init. Repts.*, 117: College Station, TX (Ocean Drilling Program).

[2] Lamont-Doherty Geological Observatory, Palisades, NY 10964.

[3] Department of Geological Sciences, Brown University, Providence, RI 02912.

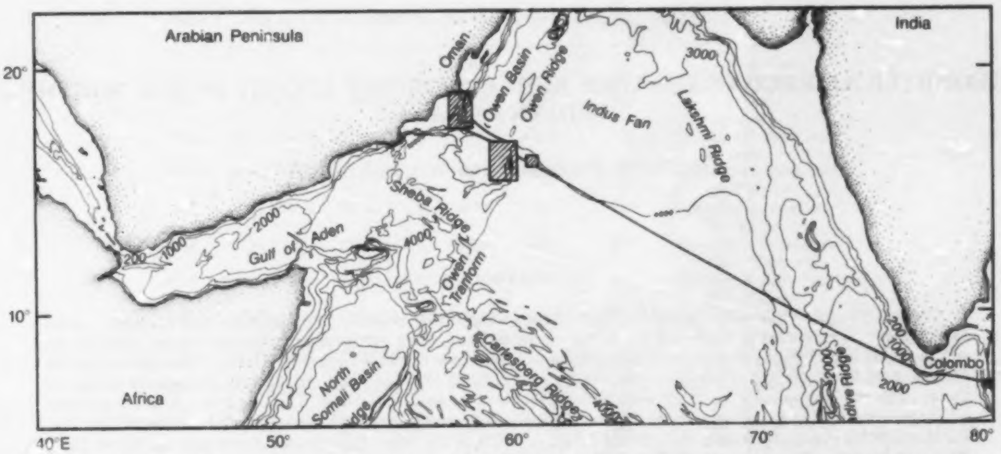

Figure 1. Bathymetry of the northwest Indian Ocean showing the ship track and three detailed surveys of RC2704.

system is roughly 40 km wide. As the ship approached the channel axis, it was possible to observe both levee flanks on the real-time Sea Beam contour plot, and guided by this image, the vessel was maneuvered so as to follow the channel axis as closely as possible. Whereas the channel deepens gradually and uniformly in the down-fan direction, levee crests vary in water depth and shape in small and irregular ways. Four of eight crossings of the channel show different levee heights; in three of these four, the western crest is higher by 3 to 5 m. The variable character of the levees probably resulted from localized slumping into the channel and/or evulsion of channelized flows and the development of crevasse splays (Damuth et al., 1983). The resulting bathymetric chart (Fig. 2) shows a meandering channel with the characteristics summarized in Table 2. Similar measurements from the Amazon Fan are listed for comparison.

The most notable feature of this Indus Fan channel is that it is unusually wide to be located in such deep water so far from the feeder channel. Several facts imply it is no longer an active conduit for turbidity currents: (1) the small channel gradient, (2) the irregular channel walls, (3) the variable levee heights, and (4) the channel axis roughly 10 m deeper than the surrounding interchannel region. The latter suggests other channel systems are delivering sands and silts to the survey area, and although the abandoned channel remains isolated, the interchannel regions are aggrading at present. In an effort to monitor accumulation rates, age, and sediment type, a single piston core was taken in the acoustically stratified levee.

Core RC27-62 (3997 m water depth; 11.8 m long) from the eastern levee (Fig. 2) reveals several sediment characteristics that are unusual for fan cores. First, it has an anomalously high carbonate content (about 45%) with an upward-increasing trend. Second, its carbonate stratigraphy can readily be correlated to cores on the Owen Ridge. This correlation indicates that the stratigraphic record is relatively continuous and extends back about 425,000 yr. The average accumulation rate for this interval is only about 2.7 cm/1000 yr, far below that of most fans. Third, the core has only a few of the discrete sand or silt beds that indicate turbidite or overbank deposition, even during glacial low stands of sea level. We infer from these observations that this western Indus Fan tributary-levee system has been inactive for almost 400,000 yr.

Seismic Profiling

Single-channel reflection profiles collected across the Indus Fan during RC2704 reveal more than 1 s of acoustically stratified sediment (Fig. 3). No high-amplitude reflectors such as those reported beneath meandering channels in both the Mississippi and Amazon fans as either real or acoustic artifacts (Kastens and Shor, 1985; Flood and Damuth, 1987; Flood, 1987) occur in the RC2704 survey area. Channel/levee complexes of the Indus Fan that are similar in dimension and acoustic character to those on the seafloor are observed down to 0.3-s sub-bottom reflection time (Fig. 3). Such structures are recognized by the onlap of horizontal or gently dipping reflectors onto a zone of weak, often irregular reflectors; the center of each of these zones of weak reflectors is usually chaotic, suggesting that slumping of channel walls accompanies the burial of channel axes. Several strong reflectors beneath the Indus Fan have moderately extensive continuity (several tens to a few a few hundred kilometers), indicating sand-rich deposits of former interlevee regions or unchannelized lower fan deposits now overstepped by the middle fan.

A sonobuoy deployed at the departure of the survey grid detected a strong reflector at 2.9-s sub-bottom traveltime. The graphically measured refraction velocity from beneath this surface measured 4.8 km/s, suggesting that it marks the top of oceanic crust. This burial depth is slightly more than the roughly 2.3 s of sediment reported for this region by Kolla and Coumes (1987).

OWEN RIDGE

Background

Owen Ridge is composed of elevated oceanic crust dividing the Indus Fan from Owen Basin. To the south it aligns with the Owen Transform Fault offsetting the Carlsberg and East Sheba ridges (Fig. 1; Matthews, 1966); to the north it curves east and merges with Murray Ridge (Barker, 1966). The generalized trend of Owen Ridge is slightly oblique to the southeast Oman margin; consequently the width of Owen Basin decreases northward from roughly 260 to 200 km. Considerable along-strike variability in depth occurs along the crest of Owen Ridge: a minimum of 1890 m was measured during RC2704, but elsewhere it stands only a few hundred meters above the approximately 3500-m water depths of the Owen Basin. In cross section, Owen Ridge is a dramatically asymmetric feature along much of its length. Within the study area its western flank is covered by about 1 km of sediment, and a fairly uniform seafloor dip of roughly 2° is maintained westward to Owen Basin. Its eastern flank is an especially steep (>15°) drop to the Indus Fan, with bare-rock outcrops and few interrupting terraces.

Table 1. Station summary, RC2704.

	Station[a]	Day/Time	Latitude (N)	Longitude (E)	Water depth (m)	Recovery[b] (m)
2	H-1	140/10:59	17°29.5′	58°02.8′	2020	8 BOT, 0–600
3	H-2	140/14:30	17°30.3′	58°03.5′	2092	8 BOT, 600–2000
4	C-2PC	145/06:34	17°41.6′	57°52.6′	1474	5.94
5	C-3GGC	145/08:17	17°40.5′	57°53.0′	1473	0.00
6	C-4PC	145/11:17	17°38.6′	57°43.9′	1276	5.93
7	C-5GGC	145/12:43	17°38.7′	57°42.9′	1275	0.00
8	C-6GGC	145/15:14	17°37.7′	57°43.0′	1275	0.28
9	C-7PC	145/17:43	17°42.9′	57°37.6′	965	10.10
10	C-8GGC	145/19:14	17°42.6′	57°37.3′	957	1.02
11	C-9PC	145/21:13	17°46.7′	57°37.3′	891	10.38
12	C-10GGC	145/22:23	17°45.8′	57°39.5′	889	1.23
13	C-11PC	146/00:43	17°53.7′	57°34.8′	861	11.04
14	C-12PC	146/04:09	18°03.8′	57°37.0′	788	11.63
15	C-13PC	146/07:25	18°14.6′	57°41.0′	689	10.34
16	C-14PC	146/12:12	18°15.2′	57°39.3′	590	10.92
17	C-15GGC	146/14:10	18°15.6′	57°39.2′	579	0.00
18	C-16PC	146/16:30	18°16.1′	57°37.8′	479	10.26
19	C-17PC	146/20:10	18°16.6′	57°37.6′	438	9.81
20	C-18GGC	146/21:57	18°17.8′	57°38.6′	452	0.59
21	C-19PC	146/23:51	18°17.4′	57°38.6′	459	5.77
22	C-20PC	147/02:31	18°16.1′	57°33.4′	296	5.43
23	C-21PC	147/05:41	18°06.6′	57°31.8′	569	12.03
24	C-22PC	147/11:44	18°04.2′	57°33.8′	749	11.25
25	C-23PC	147/15:16	17°59.7′	57°35.4′	815	10.83
26	C-24PC	147/19:40	17°43.1′	57°49.2′	1416	11.74
27	C-25PC	147/22:27	17°37.6′	57°39.9′	1347	10.50
28	C-26PC	148/00:52	17°40.7′	57°39.9′	1064	11.21
29	C-27BOX	148/08:04	17°54.5′	57°35.5′	860	0.56
30	C-28GGC	148/12:03	17°54.2′	57°35.4′	866	2.78
31	C-29BOX	148/14:43	17°53.1′	57°37.3′	868	0.00
32	C-30BOX	148/18:47	18°13.0′	57°41.0′	698	0.51
33	C-31GGC	148/20:09	18°12.8′	57°41.1′	707	2.68
34	C-32GGC	148/22:30	18°14.3′	57°38.7′	601	0.00
35	C-33BOX	148/23:35	18°13.5′	57°38.8′	630	0.49
36	H-3	149/01:10	18°12.6′	57°38.9′	688	8 BOT, 0–600
37	C-34GGC	149/03:45	18°13.9′	57°35.0′	509	0.00
38	C-35BOX	149/04:48	18°14.0′	57°35.9′	498	0.42
39	C-36TW	149/07:56	18°19.5′	57°30.1′	185	0.00
40	C-37TW	149/08:22	18°20.5′	57°31.2′	188	0.00
41	C-38TW	149/09:08	18°19.7′	57°33.5′	247	0.15
42	C-39GGC	156/07:48	16°37.2′	59°51.9′	1889	3.05
43 +	C-40PC	156/09:23	16°37.2′	59°52.1′	1890	11.40
44 +	C-41GGC	156/12:31	16°31.7′	59°47.3′	2052	2.01
45	C-42PC	156/13:55	16°31.1′	59°47.0′	2044	11.11
46	C-43GGC	156/16:49	16°36.2′	59°46.0′	2159	2.45
47	C-44PC	156/18:37	16°36.2′	59°46.0′	2159	11.75
48	C-45GGC	156/21:21	16°36.0′	59°40.8′	2406	2.88
49	C-46PC	156/23:37	16°38.8′	59°42.7′	2441	10.65
50	C-47GGC	157/02:13	16°38.2′	59°41.5′	2530	2.89
51	C-48PC	157/03:52	16°38.1′	59°41.3′	2545	11.79
52	C-49GGC	157/06:12	16°39.1′	59°39.1′	2686	2.94
53 +	C-50PC	157/08:04	16°40.2′	59°39.6′	2707	12.07
54	C-51GGC	157/11:22	16°42.2′	59°36.0′	2918	2.68
55	C-52PC	157/13:22	16°40.8′	59°35.9′	2985	11.89
56	C-53GGC	157/18:08	16°32.3′	58°27.3′	[c]3258	2.37
57	C-54PC	157/20:31	16°32.1′	59°27.3′	3275	11.76
58 +	C-55GGC	158/00:14	16°28.6′	59°21.2′	3392	2.72
59	C-56PC	158/02:47	16°29.0′	59°20.7′	3405	11.59
60	C-57GGC	158/06:20	16°20.9′	59°17.6′	3490	2.92
61	C-58PC	158/08:28	16°22.0′	59°11.2′	3484	11.84
62	C-59BOX	158/12:07	16°22.0′	59°10.9′	3488	0.00
63	C-60GGC	158/21:04	16°36.8′	59°51.5′	1887	0.93
64	C-61PC	159/06:08	16°39.5′	59°31.4′	1893	15.97
65	C-62PC	159/21:22	16°09.6′	60°40.8′	3997	11.78

[a] + = surface plankton tow; C = core; PC = piston core; GGC = giant gravity core; BOX = box core (Soutar); TW = trigger gravity core; H = hydrographic cast.

[b] All core lengths are corrected for voids and short sections; BOT = hydrographic sampling bottles.

[c] 3.5-kHz depth, wire out, and pinger depths do not agree.

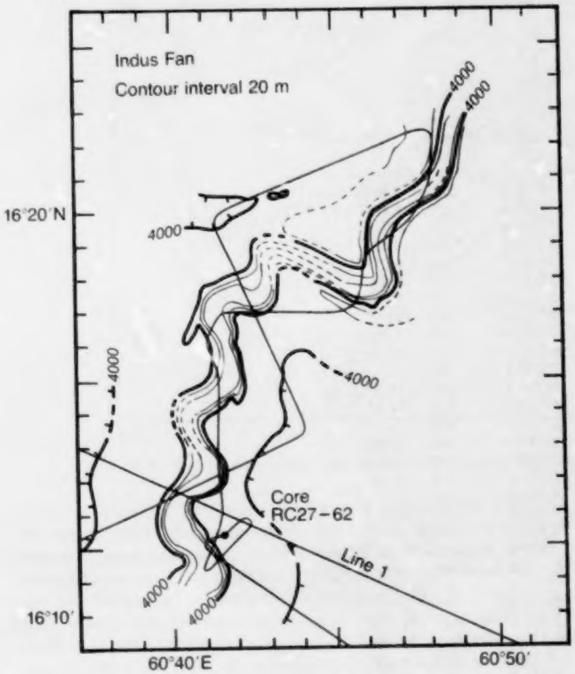

Figure 2. Bathymetry of a meandering channel of the Indus Fan contoured from Sea Beam swath-map soundings. Track-line control and location of piston Core 62 of RC2704 are shown. Single-channel seismic line 1 crosses the channel axis and is shown in Figure 3.

Owen Ridge was an elevated structure at least as far back in time as the middle Miocene. This fact is derived from Deep Sea Drilling Project (DSDP) Site 224 on the west flank of the Ridge, where lower Miocene turbidites were recovered several hundred meters above lateral equivalents traced in seismic profiles from Owen Basin (Whitmarsh, Weser, et al., 1974). The topographic relief maintained at present is consistent with (but not proof of) the role of Owen Ridge as a plate boundary. Many published maps portray Owen Ridge as a fracture zone between the Indian and Arabian plates (with or without transpressional motion at present), based on one or more of the following types of reasoning:

Table 2. Channel parameters, Indus and Amazon fans.

Parameter	Indus Fan	Amazon Fan
Channel to levee crest	48–71 m	10–30 m
Width between opposite levee crests	8 km	(Not available)
Width between steepest points of opposite channel walls	1.8–2.4 km	0.4 km
Channel gradient along axis	1:4600	1:550
Channel gradient in straight line	1:3800	1:280
Channel sinuousity	1.2	1.8

1. Seismic focal mechanisms imply right-lateral motion across the ridge (Sykes, 1968).
2. East Sheba Ridge is spreading slightly faster than Carlsberg Ridge. These segments are offset by the Owens Transform Fault, and if this contrast is maintained across Owen Ridge as well, 2–4 mm/yr of right-lateral motion is implied (DeMets and Gordon, 1987).
3. Global solutions for instantaneous rotation poles, yielding right-lateral motion between the Indian and Arabian plates. These, if taken up across Owen Ridge, result in slip rates and convergence rates between a few millimeters and 1–2 cm/yr (McKenzie and Sclater, 1971; Chase, 1978; Minster and Jordan, 1978; DeMets and Gordon, 1987, in press).
4. Contrasting marine magnetic anomaly patterns to either side of Owen Ridge demonstrate an early Cenozoic age for the crust beneath Indus Fan, but fail to reveal any identifiable anomalies within the adjacent Owen Basin (Whitmarsh, 1979; Larson et al., 1985).

Accepting Owen Ridge as the boundary between the Indian and Arabian plates has implications concerning the regional tectonic history. Most importantly, this predicts that the crust of Owen Basin is considerably older than that of the adjacent Indus Fan, and indeed, most maps of the area show Mesozoic crust within Owen Basin. This assumption is based on the ap-

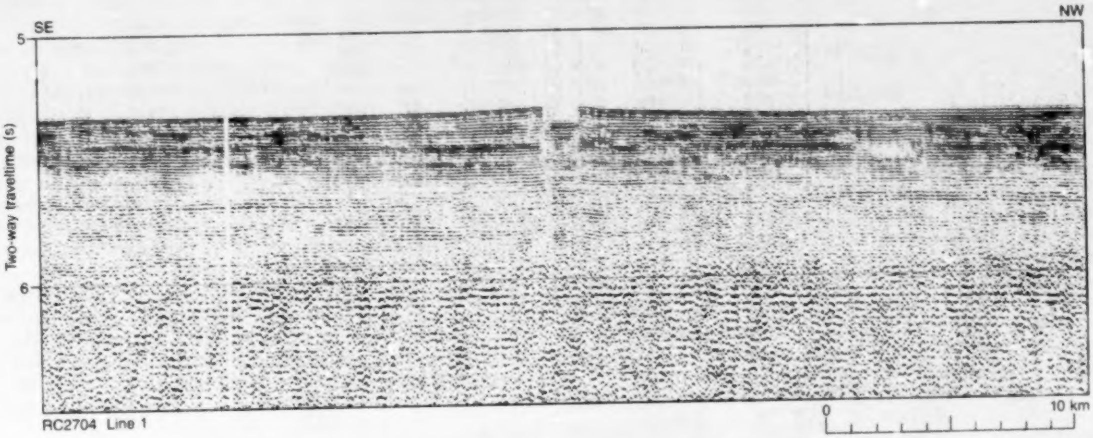

Figure 3. Single-channel seismic line 1 centered on the meandering channel axis mapped in Figure 2. The gently sloping, elevated levees to either side of the channel span the width of this display. Several buried channel axes can be seen down to at least 0.3 s sub-bottom.

parent similarities among the several basins of the western Indian Ocean (Owen, North Somali, West Somali, and Mozambique basins). Spreading anomalies within the latter two basins (Segoufin, 1978; Segoufin and Patriat, 1980; Rabinowitz et al., 1983) show conclusively that both formed as east and west Gondwanaland drifted apart in Middle to Late Jurassic time; it is generally assumed that the North Somali and Owen basins formed at this time by the same process (Whitmarsh, 1979; Cochran, 1981; Stein and Cochran, 1985). However, the lack of identifiable spreading anomalies, drill holes, and/or reconnaissance data within Owen Basin leave this history unproven.

The RC2704 survey grid on Owen Ridge was designed to locate suitable targets for bottom sampling. Upwelling that results from the southwest monsoon creates high surface productivity for part of each year in the northwest Indian Ocean; it was anticipated that time-series analysis of productivity patterns in sediment cores would reveal past changes in the monsoon system. The elevation of Owen Ridge above the carbonate compensation depth and the diluting turbidites of the Indus Fan make it ideal for this purpose. A totally unexpected outcome of this survey, however, was that it provided information that casts doubt on a Mesozoic origin for Owen Basin and the adjacent Oman margin.

Bathymetry

Most of the RC2704 survey lines across Owen Ridge were run in the north-south strike direction so as to minimize the chance of missing narrow features oriented downslope (slump scars, faults, etc.). The 3-km spacing between lines vs. the width of the Sea Beam swath resulted in roughly 75% bathymetric coverage at the foot of Owen Ridge and 50% coverage at the crest. The crest of Owen Ridge within the survey area consists of two broad, uniformly sedimented summits slightly shallower than 2000 m (at 16°40′N and 16°10′N; Fig. 4). These features are separated by a narrow saddle of irregular water depths that coincides with a slight change in trend of the Ridge. Slump scars begin immediately below 2000 m, where the seafloor gradient increases abruptly to about 2°. On the west flank these slump scars broaden downslope toward Owen Basin, and they comprise a significant majority of the seafloor area on this flank. The eastern flank is so precipitous (generally about 15°, and sporadically more than 20°) that little sediment cover is detectable on either 3.5-kHz sonograms or on seismic-reflection profiles. Most of the slump scars on the west flank are fairly wide and crudely U-shaped; typical values are several kilometers wide and one to several hundred meters deep. These contrast with active canyons typical of continental slopes. The latter are generally V-shaped, have steeper walls, show less downslope change in cross-section, and often have trellislike networks of tributary gullies (Twichell and Roberts, 1982; Farre et al., 1983) that are not detected on Owen Ridge.

Seismic Profiling

RC2704 reflection profiles on Owen Ridge reveal a history of deposition, uplift, and sediment redistribution. Several north-south and east-west lines (strike and dip, respectively) are shown in Figure 5 (in the back pocket of this volume) and their dominant features are described here. Along much of the west flank of the Ridge there is a weakly reflective unit (<0.2 s thick) separating the irregular reflectors of volcanic basement from the stratified, high-amplitude reflectors of overlying sedimentary units. Total sediment thickness increases from roughly 1.0 s at the crest to a maximum of 1.6 s within Owen Basin. However, this pattern varies considerably owing to local basement topography. Three aspects of basement fabric are especially noteworthy: (1) angular onlap onto basement highs (or the reflectorless veneer) shows that basement topography controlled the distribution of the oldest (presumably turbidite-rich) stratified units, (2) most of the basement highs are aligned roughly east-west, and (3) despite early infilling of basement topography, the locations of relatively recent slumps down the west flank continue to be influenced by underlying basement features.

We infer from these observations that topographic highs (inherited from either a roughly north-south or east-west spreading ridge) were first covered by a blanket of pelagic sediments and later were smoothed during a period of turbidite deposition (Fig. 6). Differential compaction within the sediment column has since enabled this basement topography to influence the redistribution of sediments. Little evidence suggests that the uplift of Owen Ridge occurred on the local level; to the contrary, it appears that the region covered by the survey grid was elevated rather uniformly, as a single unit. This elevation is revealed by the geometry of reflectors (Fig. 6). Apart from the basement onlap described previously, the most deeply buried sediments maintain uniform thickness up the west flank of Owen Ridge. Regional onlap of sedimentary units onto underlying sedimentary units indicates syndepositional uplift, and this process begins at the level marked with the deeper of the two dotted lines in Figure 5. The seismic interval between the dotted lines consists of numerous high-amplitude reflector units that thin toward the crest of Owen Ridge. These are interpreted as turbidites barely covering a slowly rising structure. The upper set of dots highlights a diachronous surface that is stratigraphically shallower (younger) at the foot of the Ridge than it is at the crest. It is identified in this way to emphasize the conclusion that Owen Ridge emerged from the turbidite plain from east to west. While turbidites (high-amplitude reflectors that converge eastward) were being deposited in Owen Basin, an increasingly larger area of the Ridge was being covered by pelagic sediments (low-amplitude, parallel reflectors.)

The onset of widespread slumping occurs at various stratigraphic levels along Owen Ridge. In the northern part of the survey area, irregular reflectors (slump deposits) showing various types of baselap occur a few tenths of a second above the turbidite/pelagic transition (the upper dotted line in Fig. 5). Along several profiles from the southern part of the survey, this same seismic facies rests directly on the turbidites. Because of the difficulty of tracing reflectors within this irregular and discontinuous unit of slumps, age comparisons between the slumps of the north and south cannot be inferred reliably. Slumping may have begun earlier in the south; alternatively, the process may have been more severe in the south, and more of the underlying pelagic unit was removed than it was in the north.

At the time of RC2704, age control of sediments on Owen Ridge was known only from the spot cores of DSDP Site 224 (Whitmarsh, Weser, et al., 1974; drill site located on line 35, Fig. 5). Approximate ages (Fig. 6) correlated to the seismic units described in this report are as follows. Lower Eocene to lower Oligocene nannofossil chalk rests as a draping unit on volcanic basement. Lower to "mid"-Oligocene turbidites infill this topography; within a few kilometers of Site 224 they are considerably older, perhaps middle or even lower Eocene. The beginning of Owen Ridge uplift (derived from RC2704 data and marked by the lower dotted line in Fig. 5) occurs in the 109-m gap between Cores 224-6 and 224-7, within the upper Oligocene. The turbidite/pelagic transition at Site 224 (the upper dotted line in Fig. 5) is near to the boundary between Cores 224-3 and 224-4, which marks an unconformable lower to middle Miocene contact at the drill site. Seismic profiles do not suggest a stratigraphic gap as large as the approximately 7 Ma hiatus reported at Site 224 (Whitmarsh, Weser, et al., 1974). The onset of widespread slumps, by contrast, is clearly associated with a seismic unconformity, but the spot coring at Site 224 prohibits an age assignment more accurate than late Miocene or younger.

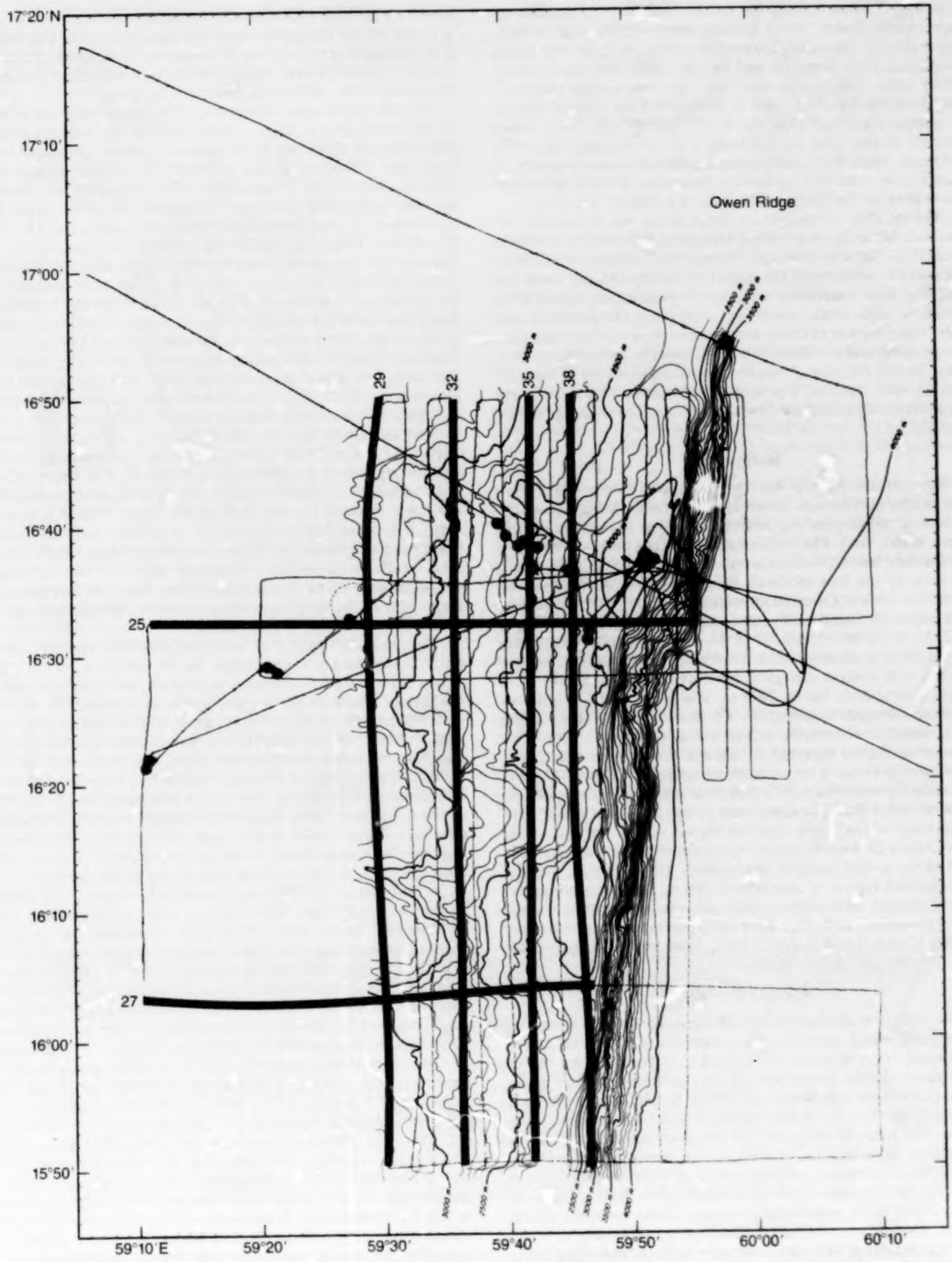
17°20'N
17°10'
17°00'
16°50'
16°40'
16°30'
16°20'
16°10'
16°00'
15°50'
59°10'E
59°20'
59°30'
59°40'
59°50'
60°00'
60°10'
Owen Ridge
25
27
29
32
35
38
2500 m
3000 m
3500 m
4000 m

Figure 4. Bathymetry of Owen Ridge contoured from Sea Beam soundings. Track control and piston cores taken on RC2704 are shown. Numbered, bold single-channel seismic profiles are shown in Figure 5 (back pocket).

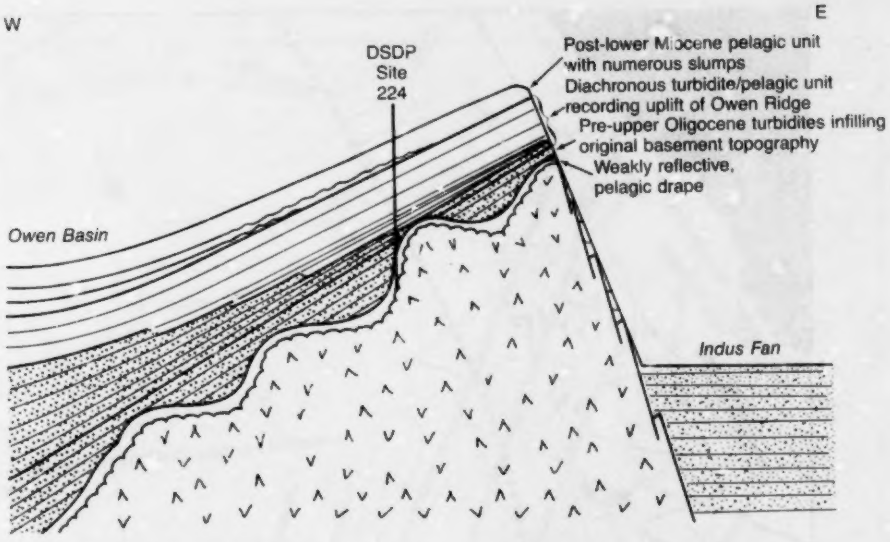
W
E
DSDP Site 224
Post-lower Miocene pelagic unit with numerous slumps
Diachronous turbidite/pelagic unit recording uplift of Owen Ridge
Pre-upper Oligocene turbidites infilling original basement topography
Weakly reflective, pelagic drape
Owen Basin
Indus Fan

Figure 6. Idealized dip-line profile across Owen Ridge (not to scale).

OMAN MARGIN

Background

Prior to RC2704, the topography, sediment character, and sub-bottom structures offshore southeast Oman were not known in detail. Surveys north of 19°N had found a narrow shelf and fairly steep slope with uniform northeast strike; gravity and seismic data revealed margin-parallel basins beneath the slope filled with several kilometers of sediment (Whitmarsh, 1979). The few geologic maps of the onshore region showed extensive Quaternary sand cover with outcrops restricted to (1) a window along Masirah Bay (Fig. 7) where pre-Cambrian dolomites, Paleozoic clastics, and Mesozoic marls and limestones crop out in a structurally complex terrain (Gorin et al., 1982) and (2) ophiolites of possible Late Cretaceous age on Masirah Island (Moseley and Abbotts, 1979) and on the headland comprising Ra's Madrakah (Fig. 7; Al-Marjeby and Nash, 1986). The lack of a widespread, encroaching Upper Cretaceous coastal plain, plus the occurrence of ophiolites along the margin raise questions about the accuracy of a Jurassic pull-apart history. This inconsistency is all the more apparent in that transcurrent, margin-parallel faults have appeared on generalized geologic maps for decades (Morton, 1959; Beydoun, 1982). One of these features, the Masirah Fault, cuts across Ra's Madrakah from Masirah Bay and into Siquirah Bay (Fig. 7; Gorin et al., 1982).

Few bottom samples from offshore southeast Oman have been reported in the literature. Based on inference from known patterns of surface productivity and hydrography, similarities to the western margin of India (Setty, 1983), and chemical profiles (Wyrtki, 1973) we expected that the bottom water between 500 and 1500 m along Oman is very low in dissolved oxygen, perhaps even anoxic. If true, then the scarcity or total lack of bioturbation in these surficial sediments could provide exceptional high-resolution stratigraphy. In anticipation of this opportunity, suitable coring targets were selected within a grid of bathymetric mapping, 3.5-kHz echo-sounding, and single-channel seismic profiles collected during RC2704. As along Owen Ridge, these data provided the necessary survey for bottom sampling, and furthermore, revealed conflicts with the prevailing tectonic history.

Bathymetry

Similar in design to the Oman Ridge survey, numerous strike-direction lines were run parallel to the Oman margin to identify the dominant downslope bathymetric and structural fabric. The survey extended from the 200-m isobath seaward to 2500 m. Sea Beam coverage was generally less than 25% of the seafloor area. At the landward edge of the grid, this coverage decreased to less than 5%, but bathymetric complexity in this region is generally simple enough to enable reliable contouring to be made between track lines (Fig. 8).

The bathymetry of the northern and southern extremes of the survey grid contrasts significantly. North of 18°30′N there are numerous submarine canyons resembling those typically found along passive continental margins. Most Oman canyons are incised several hundred meters into the slope. Canyon walls face inward with roughly 10° gradients, and there are at least several "tributary gullies" leading into the major canyons (Twichell and Roberts, 1982; Farre et al., 1983). All canyons have along-axis gradients of 3.5° to 3.75°; these axes are narrow and clear of debris, indicating recent activity.

That these canyons are restricted to the area adjacent to the narrowest part of the shelf, directly offshore of the headland of Ra's Madrakah, suggests a mechanism for their formation: currents parallel to the shoreline sweep sediment toward the headland and into canyon heads that have long been entrenched in the shelf break. Merely attributing the occurrence of these canyons to eustatic lowering or to times of vigorous fluvial runoff from Oman is insufficient; the density and complexity of the canyons argue for numerous events, meaning a significant period of time (at least hundreds of thousands of years) was required for their formation. Because of the high sedimentation rates of this productive margin (probably tens of centimeters per thousand years), these canyons would be filling up if there were no processes keeping them clear of pelagic and reworked intercanyon sediment. The most likely clearing processes are turbidity currents that result from shelf sediment constantly supplied to canyon heads.

Few canyons traverse the margin south of 18°30′N. Instead, this region is dominated by a broad, gently sloping (<0.5°)

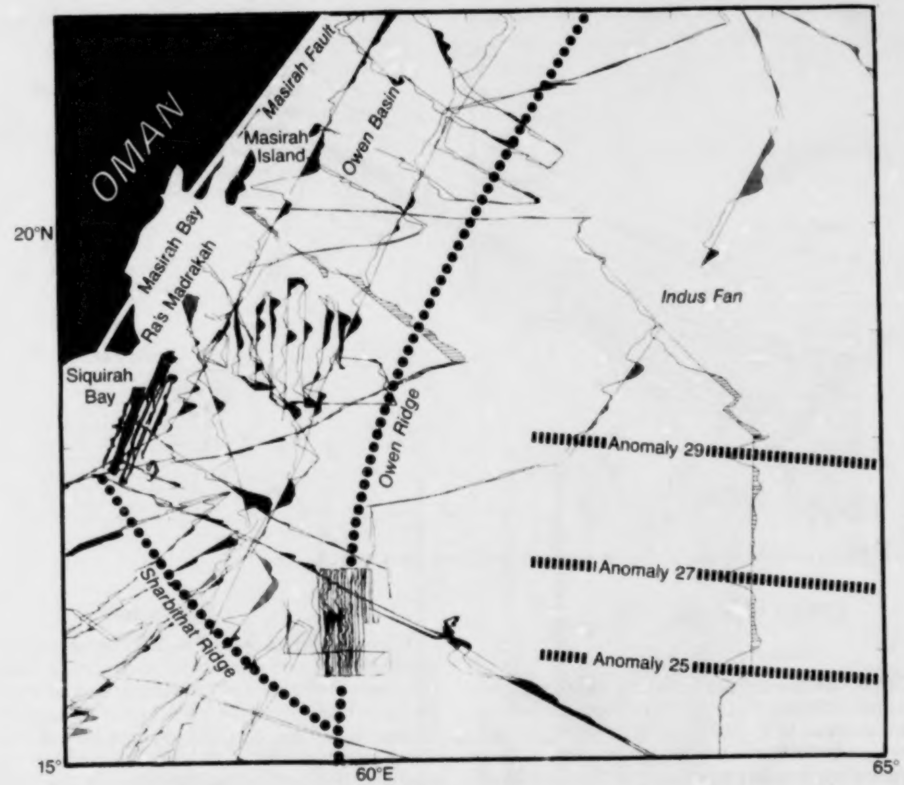

Figure 7. Bathymetry (Canadian Hydrographic Service 1975 GEBCO map series) and magnetic anomalies (up to and including results of RC2704) of Owen Basin and adjacent regions. Despite the west-southwest–east-northeast magnetic fabric in Owen Basin and along the southeast Oman margin (Whitmarsh, 1979), these features have not been correlated to any series of seafloor spreading anomalies. The RC2704 survey offshore Siquirah Bay was several tens of kilometers seaward of the margin-parallel, transcurrent Masirah Fault (Morton, 1959; Beydoun, 1982; Gorin et al., 1982).

"terrace" in a water depth between 700 and 1000 m. A smooth 3.5° to 3.75° slope devoid of canyons occurs landward of this area; only one exposed slump scar was identified (on both Sea Beam and 3.5-kHz records; Fig. 5), trending north-south and beginning at 18°23′N, 57°42′E. Beyond the 1000-m isobath is a steep (7° to 12°) drop-off and a few narrow incised canyons; generally, broad "amphitheater-type" features indent this part of the margin. Water depths steadily increase seaward of this region, with the exception of an offshore high near 17°40′N, 57°55′E. The seaward face of this latter structure is a particularly steep (18°) escarpment trending southwest-northeast, oblique to most other structural trends within the survey grid.

Seismic Profiling

The "stair-step" bathymetry in the central part of the survey grid is clearly controlled by two underlying lineations approximately beneath the 500- and 1000-m isobaths. The landward lineation is an abrupt, seaward-facing drop in acoustic basement named the Siquirah Fault (Mountain and Prell, in press); the second is a complex of steep-sided, sub-bottom structures that are not crystalline basement (see profiles in Fig. 5). Between these lineations is the gentle midslope "terrace," and in this region basement is too deep to be detected on water gun reflection profiles. Regionally low values of free-air gravity identify this thick depocenter (Fig. 9); two reversed sonobuoy experiments along the axis of this depocenter demonstrate that the sediments are 2.4 km thick. The landward boundary of this depocenter, the Siquirah Fault, does not follow a perfectly straight trace. Instead, there are several sharp discontinuities mapped here as orthogonal offsets (Fig. 9). The fault deviates landward toward the north and is not crossed in the northern third of the survey. Profiles of 3.5-kHz sonograms show several vertical offsets reach the seafloor immediately above the basement scarp, proving that faulting continues at present. Both the seismic and the gravity data indicate that the midslope depocenter gradually thins northward. The seaward boundary of the depocenter (the complex structures near the 1000-m isobath) can be followed into the northern part of the survey where many of these structures are dissected by slope canyons. As much as 1.0 s of acoustic stratification can be seen within these features, indicating sedimentary composition. Because of their narrow and complexly faulted character, the internal detail within many of these structures is commonly lost among diffractions, often giving them the misleading appearance of diapirs (e.g., line 15, Fig. 5). Dip-line 18 (Fig. 5) provides the clearest evidence that these structures are actually rotated blocks of comparatively parallel-stratified sediments; their upturned, landward sides terminate in abrupt faults. The onlapping pattern of reflectors along their landward sides demonstrates they are significantly older than most of the sediments comprising the midslope depocenter. That they do not

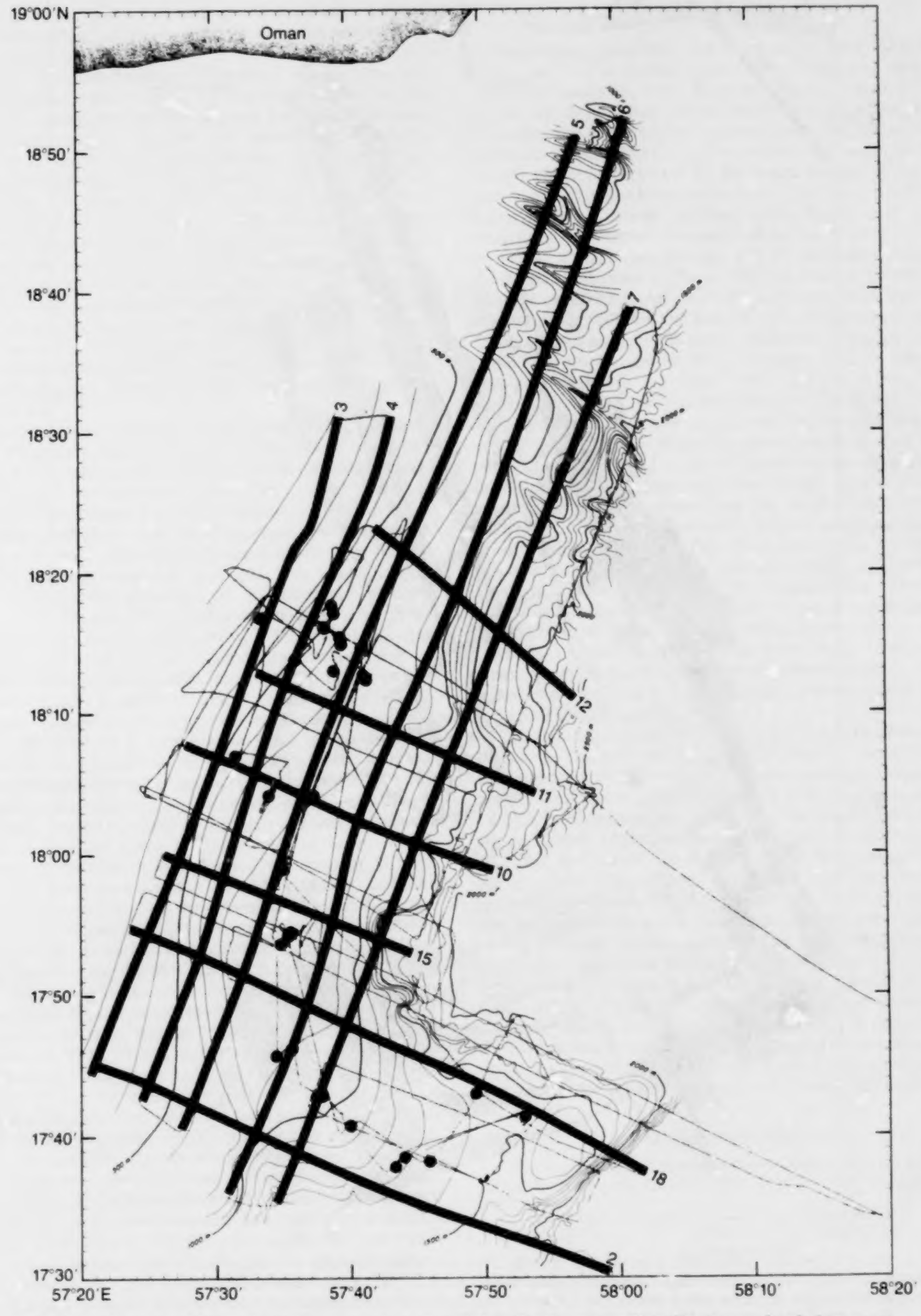
19°00′N
18°50′
18°40′
18°30′
18°20′
18°10′
18°00′
17°50′
17°40′
17°30′
57°20′E
57°30′
57°40′
57°50′
58°00′
58°10′
58°20′
Oman
2
3
4
5
6
7
10
11
12
15
18
2000 m

Figure 8. Bathymetry of the southeast Oman margin contoured from Sea Beam soundings. Track control and piston cores taken on RC2704 are shown. Numbered, bold lines are single-channel seismic profiles shown in Figure 5.

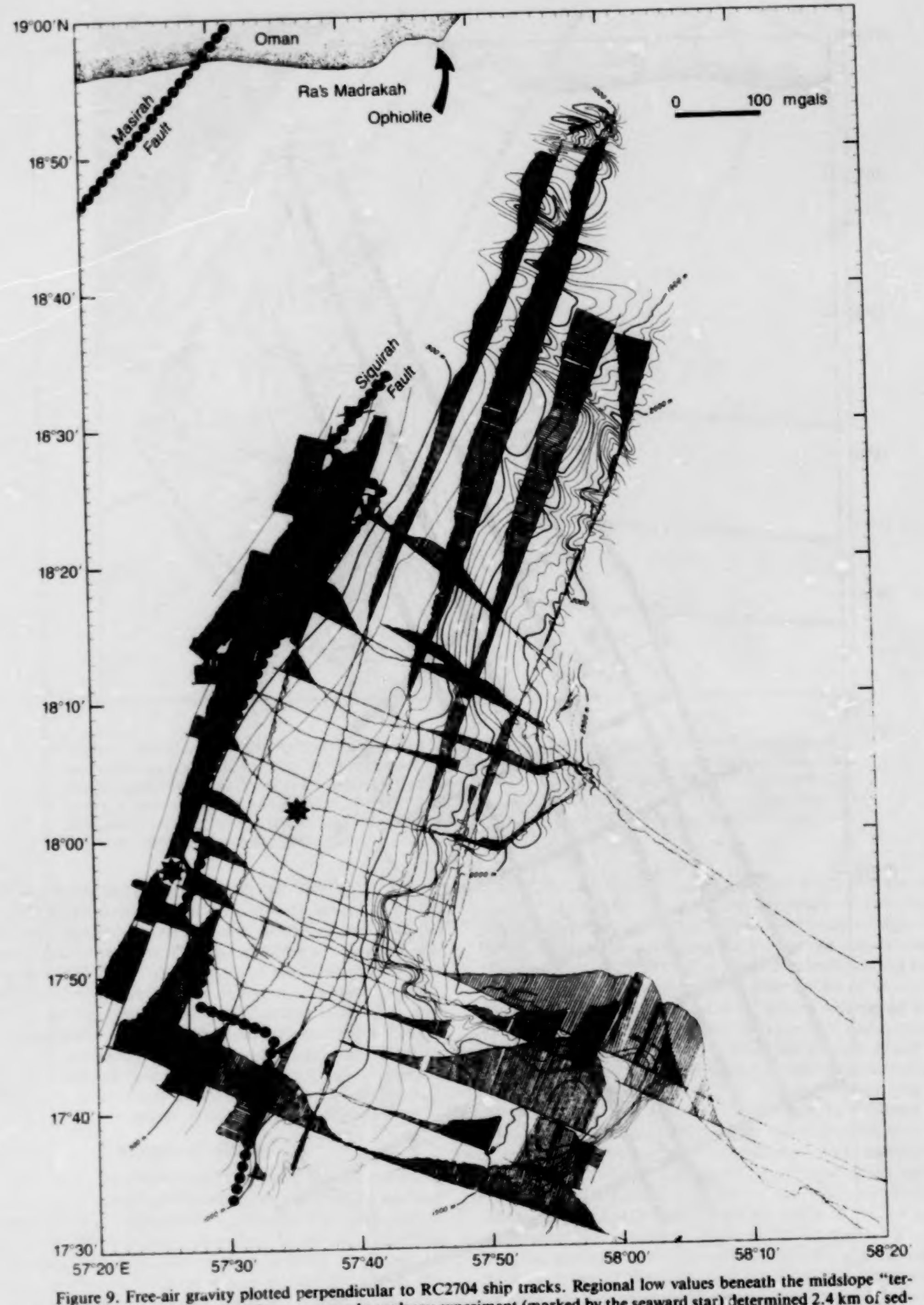
19°00'N
18°50'
18°40'
18°30'
18°20'
18°10'
18°00'
17°50'
17°40'
17°30'
57°20'E
57°30'
57°40'
57°50'
58°00'
58°10'
58°20'
Oman
Ra's Madrakah
Ophiolite
0
100 mgals
Masirah Fault
Siquirah Fault

Figure 9. Free-air gravity plotted perpendicular to RC2704 ship tracks. Regional low values beneath the midslope "terrace" outline a depocenter where a reversed sonobuoy experiment (marked by the seaward star) determined 2.4 km of sediment above a refractor with a velocity of 5.3 km/s. Another sonobuoy (star symbol landward of the Siquirah Fault) found thin sediments and a basement velocity of 4.8 km/s. The irregular trace of the Siquirah Fault (Mountain and Prell, in press) was determined with single-channel reflection profiles (see Fig. 5). The Masirah Fault, several tens of kilometers farther landward, was not crossed during RC2704. The northeast extension of the region between these faults intersects Ra's Madrakah and Masirah Island where ophiolites of probable Late Cretaceous–Paleogene age and origin are found (Moseley, 1969; Moseley and Abbotts, 1979; Gorin et al., 1982).

coincide with free-air gravity anomalies (Fig. 9) suggests basement is not structurally involved to a significant degree. Beyond these first-order observations, however, their exact origin is far from clear with available data.

In general, the term "acoustic basement" has no compositional significance; it simply indicates that deeper reflecting horizons cannot be detected. Refraction and magnetic data from RC2704, however, suggest that acoustic basement along southeast Oman is crystalline rock and in fact may be oceanic crust. Graphically-derived velocities from sonobuoys provide values of 4.6 and 5.3 km/s, as shown in Fig. 5. The slower value was measured landward of the Siquirah Fault, where the level and shallow nature of acoustic basement suggests it underwent subaerial erosion, and the relatively low refraction velocity is probably from a weathered surface. By contrast, the faster velocity from beneath the midslope depocenter is well within the range of values typical of oceanic Layer 2A. Reflections from acoustic basement are observed at this location with the 700-in.^{3} air gun used during sonobuoy experiments; these reflectors have the irregular to hyperbolic character associated with (but not unique to) the top of Layer 2A.

Amplitudes and wavelengths of magnetic anomalies along the Oman margin are clearly a function of depth to this acoustic basement. Where most sharply defined, these anomalies reveal an east-northeast–west-southwest grain that parallels the magnetic fabric of Owen Basin (Fig. 7; Whitmarsh, 1979). Although metamorphic continental crust could produce similar magnetic lineations, such close alignment with those of the deep basin is unlikely. As with the refraction velocities, this information is consistent with, but not diagnostic of, the occurrence of Layer 2A within the survey grid. The complex and recently active structures described here argue against a simple Jurassic rifted origin for the southeast Oman margin. The most significant discovery in this regard is the basement high interpreted to be subaerially eroded, magnetically lineated oceanic crust landward of the Siquirah Fault. Although the survey did not extend far enough landward to be certain, it is probable that this feature is bounded on the west by the Masirah Fault. Ophiolites of both Ra's Madrakah and Masirah Island farther north are exactly in line with this structure, and they, too, are bounded on the west by the Masirah Fault. We are virtually certain that the basement structure within the RC2704 survey area originated in the same manner as these exposed mafic complexes. Obduction of Masirah Island occurred sometime between the mid-Cretaceous and middle Eocene, although age of formation or the seafloor and direction of emplacement is unknown (Moseley and Abbotts, 1982). Until these age and directional uncertainties are resolved, it remains possible that the Masirah and Ra's Madrakah ophiolites, plus their submerged counterpart reported here, match the well-documented Semail ophiolites in age and tectonic process. These latter rocks were formed in what is now the Gulf of Oman at about 90 to 80 Ma, and 10 Ma later were obducted onto the Arabian Peninsula to form the Oman mountains (Coleman, 1981). The sedimentary blocks comprising the lineation beneath the 1000-m isobath may have been rotated, faulted, and emplaced during this same obduction, but this history is unlikely for two reasons: (1) free-air gravity suggests basement does not follow the structural form of these features and (2) if indeed analogous to the Masirah ophiolites and thrust landward 70 to 80 Ma ago, there is suspiciously little overlying sediment. Considering the evidence of recent offset along Siquirah Fault, plus the very rapid subsidence that led to the thick depocenter beneath the midslope "terrace," another and more recent process has probably affected this part of the margin. Supporting data for this argument are described in the following section.

OWEN BASIN AND A REVISED TECTONIC HISTORY

Well-defined magnetic anomalies in the West Somali Basin record the Middle Jurassic separation of east and west Gondwanaland (Segoufin, 1978; Rabinowitz et al., 1983). Drilling at DSDP Site 241 in West Somali Basin reached mid-Cretaceous sediment, and accumulation rates extrapolated downward to the basement reflection at 8.1 s corroborate a Jurassic age. The approach and departure lines of the Oman margin survey yielded data across the southern Owen Basin that demonstrate a distinctly different history to Owen Basin. Specifically, (1) magnetic lineations cannot be matched to the M-series, (2) basement is at a maximum of 6.5 s, and (3) seismic correlations of the deepest reflectors in Owen Basin to those at the bottom of Site 224 on Owen Ridge imply a Late Cretaceous age for this basement (Fig. 10). On the basis of these inferences from Owen Basin, as well as from the recent tectonism along the southeast Oman margin, a new model of regional tectonic history has been proposed (Mountain and Prell, 1987, in press). The previous interpretation maintained that Owen Basin, like West Somali Basin, was originally part of the African plate and formed during the roughly northwest-southeast separation of east and west Gondwanaland. During the Late Cretaceous spreading of India away from Madagascar, Owen Ridge developed as a very long transform fault connecting the roughly east-west proto-Carlsberg Ridge with an unknown Tethyan spreading ridge north of the Arabian Peninsula. This resulted in a great age discontinuity across Owen Ridge: Cenozoic crust of the Indian plate was adjacent to Mesozoic crust of the African plate. This ancient boundary became the locus of renewed plate interaction in the Oligocene to Miocene, when spreading in the Gulf of Aden resulted in compression and uplift of Owen Ridge. In this manner, Owen Basin became part of the new Arabian plate, but it retained the record of a Jurassic origin that it shared with the southeast Oman margin.

The data from RC2704 suggest a small but significant modification of this prevailing model. The relative "youth" of Owen Basin and the recent tectonism of the southeast Oman margin discovered from RC2704 data could both be explained if the Late Cretaceous transform connecting the proto-Carlsberg Ridge with a Tethyan equivalent developed along the southeast Oman coastline and not at the modern Owen Ridge (Fig. 11). This would predict that (1) Owen Basin is of Late Cretaceous age in the south, becoming younger toward the north; (2) the southeast coast of Oman was a transform margin in the Late Cretaceous; (3) Late Cretaceous lineaments along the margin very likely were reactivated as transpressional features in the Oligocene to Miocene opening of Aden that also resulted in uplift of Owen Ridge; and (4) the small amount of relative motion between the Indian and Arabian plates presently is shared between the eastern escarpment of Owen Ridge and the southeast Oman margin. Consequently, the abrupt normal faults and deep narrow basins along the margin probably involve transcurrent faulting as well.

ACKNOWLEDGMENTS

The acquisition and interpretation of data from RC2704 was supported by NSF grant OCE85-11571. This is LDGO contribution no. 4407.

REFERENCES

Al-Marjeby, A., and Nash, D., 1986. A summary of the geology and oil habitat of the eastern flank hydrocarbon province of South Oman. *Mar. Pet. Geol.*, 3:306–314.

Barker, P. F., 1966. A reconnaissance survey of the Murray Ridge. *Philos. Trans. R. Soc. London*, 259A:187–197.

Barnes, N. E., and Normark, W. R., 1985. Diagnostic parameters for comparing modern submarine fans and ancient turbidite systems. *In* Bouma, A., Normark, W., and Barnes, C. R. (Eds.), *Submarine Fans and Related Turbidite Systems*: New York (Springer-Verlag), 13–14.

Beydoun, Z. R., 1982. The Gulf of Aden and northwest Arabian Sea. *In* Nairn, A.E.M., and Stelhi, F. G. (Eds.), *The Ocean Basins and Margins: The Indian Ocean*: New York (Plenum), 253–313.

Chase, C. G., 1978. Plate kinematics: the Americas, East Africa, and the rest of the world. *Earth Planet. Sci. Lett.*, 37:355–368.

Cochran, J. R., 1981. The Gulf of Aden: structure and evolution of a young ocean basin and continental margin. *J. Geophys. Res. B*, 86: 263–288.

Coleman, R. G., 1981. Tectonic setting for ophiolite obduction in Oman. *J. Geophys. Res. B*, 86:2497–2508.

Damuth, J. E., Kolla, V., Follod, R. D., Kowsmannn, R. O., Monteiro, M. C., Gorini, M. A., Palma, J.J.C., and Belderson, R. H., 1983. Distributary channel meandering and bifurcation patterns on Amazon deep-sea fan as revealed by long-range side-scan sonar (GLORIA). *Geology*, 11:94–98.

DeMets, C., and Gordon, R. G., 1987. Limits on motion along the Owen Fracture Zone. *EOS, Trans. Am. Geophys. Union*, 68:1473.

Farre, J. A., MacGregor, B. A., Ryan, W.B.F., and Robb, J. M., 1983. Breaching the shelfbreak: passage from youthful to mature phase in submarine canyon evolution. *In* Stanley, D. J., and Moore, G. T. (Eds.), *The Shelfbreak: A Critical Interface on Continental Margins*: Spec. Publ. Soc. Econ. Paleontol. Mineral., 33:25–39.

Flood, R. D., 1987. Side echoes from a sinuous fan channel obscure the structure of submarine fan channel/levee systems, Amazon Fan. *Geo-Mar. Lett.*, 7:15–22.

Flood, R. D., and Damuth, J. E., 1987. Quantitative characteristics of sinuous distributary channels on the Amazon deep-sea fan. *Geol. Soc. Am. Bull.*, 98:728–738.

Gorin, G. E., Racz, L. G., and Walter, M. R., 1982. Late Precambrian-Cambrian sediments of Hugf Group, Sultanate of Oman. *AAPG Bull.*, 66:2609–2627.

Kastens, K. A., and Shor, A. N., 1985. Depositional processes of a meandering channel on Mississippi Fan. *AAPG Bull.*, 69:190–202.

Kolla, V., and Coumes, F., 1987. Morphology, internal structure, seismic stratigraphy, and sedimentation of Indus Fan. *AAPG Bull.*, 71: 650–677.

Larson, R. L., Pitman, W. C., Golovchenko, X., Cande, S. C., Dewey, J. F., Haxby, W. F., and LaBrecque, J. L., 1985. *The Bedrock Geology of the World*: New York (Freemont).

Lisitzin, A. P., 1972. *Sedimentation in the World Ocean, with Emphasis on the Nature, Distribution and Behavior of Marine Suspensions*: Spec. Publ. Soc. Econ. Paleontol. Mineral., 17.

Matthews, D. H., 1966. The Owen Fracture Zone and the northern end of the Carlsberg Ridge. *Philos. Trans. R. Soc. London*, 259A:172–186.

McKenzie, D., and Sclater, J. G., 1971. The evolution of the Indian Ocean since the Late Cretaceous. *Geophys. J. R. Astron. Soc.*, 24: 437–528.

Minster, J. B., and Jordan, T. H., 1978. Present-day plate motions. *J. Geophys. Res. B*, 83:5331–5354.

Molnar, P., and Tapponnier, P., 1975. Cenozoic tectonics of Asia: effects of a continental collision. *Science*, 189:419–425.

Morton, D. M., 1959. The geology of Oman. *Proc. World Pet. Congr., 5th*, 227–280.

Moseley, F., 1969. The Upper Cretaceous ophiolite complex of Masirah Island, Oman. *Geol. J.*, 6:293–306.

Moseley, F., and Abbotts, I. L., 1979. The Ophiolite mélange of Masirah, Oman. *J. Geol. Soc. (London)*, 136:713–724.

Mountain, G., and Prell, W., 1987. Leg 117 ODP site survey: a revised history of Owen Basin. *EOS, Trans. Am. Geophys. Union*, 68:424.

________, in press. A multiphase plate tectonic history of the southeast continental margin of Oman. *In* Robertson, A.H.F., Searle, M. P., Ries, A. C., and Smewing, J. D. (Eds.), *The Geology and Tectonic of the Oman Region*: Spec. Publ. Geol. Soc. London.

Norton, I. O., and Sclater, J. G., 1979. A model for the evolution of the Indian Ocean and the breakup of Gondwanaland. *J. Geophys. Res. B*, 84:6803–6830.

Patriat, P., and Achache, J., 1984. India-Eurasia collision chronology has implications for crustal shortening and driving mechanism of plates. *Nature*, 311:615–621.

Rabinowitz, P. D., Coffin, M. F., and Falvey, D., 1983. The separation of Madagascar and Africa. *Science*, 220:67–69.

Segoufin, J., 1978. Anomalies magnétiques mésozoiques dans le bassin de Mozambique. *C. R. Acad. Sci., Ser. 3*, 287:109–112.

Segoufin, J., and Patriat, P., 1980. Existence d'anomalies mésozoiques dans le basin de Somalie. Implications pour les relations Afrique-Antarctique-Madagascar. *C. R. Acad. Sci., Ser. 2*, 291:85–88.

Setty, M.G.A.P., 1983. Upwelling along the western Indian continental margin and its geological record: a summary. *In* Thiede, J., and Suess, E. (Eds.), *Coastal Upwelling, Its Sediment Record, Part B: Records of Ancient Coastal Upwelling*: NATO Conf. Ser. 4, 10B: 201–216.

Stein, C. A., and Cochran, J. R., 1985. The transition between the Sheba Ridge and Owen Basin: rifting of old oceanic lithosphere. *Geophys. J. R. Astron. Soc.*, 81:47–74.

Sykes, L. R., 1968. Seismological evidence for transform faults, seafloor spreading, and continental drift. *In* Phinney, R. A. (Ed.), *The History of the Earth's Crust*: Princeton, NJ (Princeton Univ. Press), 120–150.

Twichell, D. C., and Roberts, D. G., 1982. Morphology, distribution, and development of submarine canyons on the United States Atlantic continental slope between Hudson and Baltimore canyons. *Geology*, 10:408–412.

Whitmarsh, R. B., 1974. Some aspects of plate tectonics in the Arabian Sea. *In* Whitmarsh, R. B., Weser, O. E., Ross, D. A., et al., *Init. Repts. DSDP*, 23: Washington (U.S. Govt. Printing Office), 527–536.

________, 1979. The Owen Basin off the south-east margin of Arabia and the evolution of the Owen Fracture Zone. *Geophys. J. R. Astron. Soc.*, 58:441–470.

Whitmarsh, R. B., Weser, O. E., Ross, D. A., et al., 1974. *Init. Repts. DSDP*, 23: Washington (U.S. Govt. Printing Office).

Wyrtki, K., 1973. Physical oceanography of the Indian Ocean. *In* Zeitschel, B. (Ed.), *The Biology of the Indian Ocean*: New York (Springer-Verlag), 18–36.

Ms 117A-118

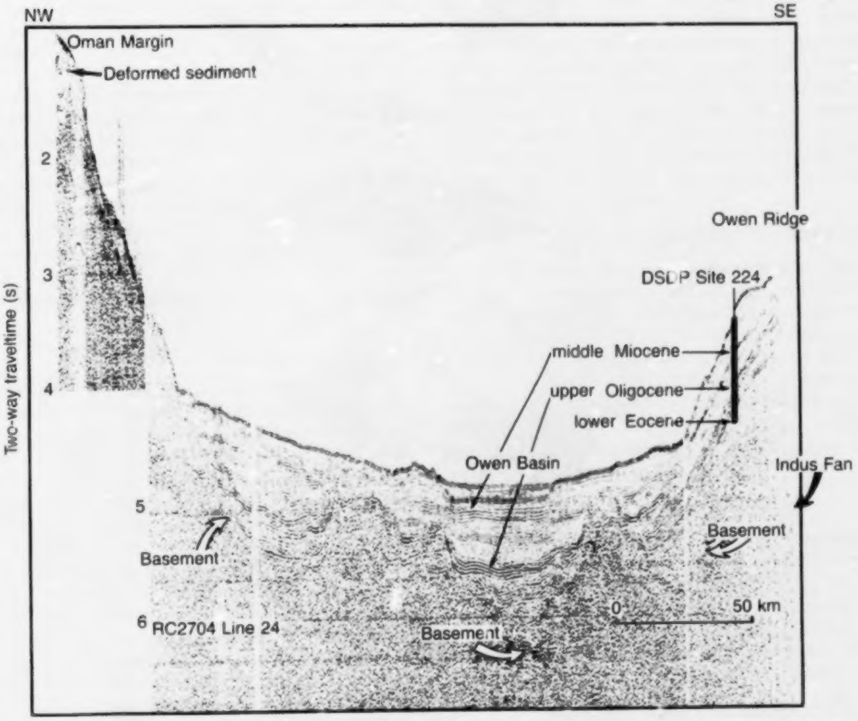

Figure 10. RC2704 line 24 across Owen Basin. Basal sediments at DSDP Site 224 are lower Eocene (Whitmarsh, Weser, et al., 1974), and tracing the corresponding seismic unit along this profile predicts that basement within Owen Basin cannot be much older than basal Paleocene.

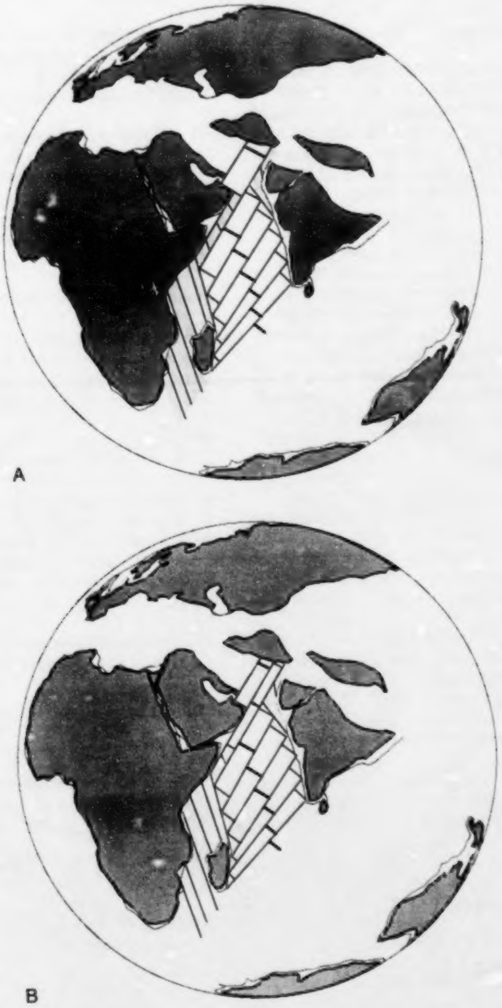

Figure 11. Reconstruction of the northwest Indian Ocean at 50 Ma (mapped by Terra Mobilis) with two possible spreading ridge/plate boundary arrangements sketched in. **A.** The generally accepted version places the African/Indian plate boundary at Owen Ridge, making the present Owen Basin a remnant of Jurassic to Early Cretaceous age seafloor, similar to other basins of the western Indian Ocean. **B.** Revised version shows a ridge-ridge transform along the southeast Oman margin (Mountain and Prell, 1987, in press) and predicts that Owen Basin formed during Late Cretaceous spreading of the proto-Carlsberg Ridge.

6. UNDERWAY GEOPHYSICS[1]

Gregory Simmons[2] and Shipboard Scientific Party[3]

INTRODUCTION

Geophysical data presented in this chapter were collected during Leg 117 of the Ocean Drilling Program (ODP). *JOIDES Resolution* was underway for 19 days of the 54.5 days at sea, traveling approximately 4310 nmi between Colombo, Sri Lanka, and Port Louis, Mauritius.

Shipboard geophysical instrumentation included two precision echo-sounders, a magnetometer, single channel seismic-reflection profilers, and satellite navigation systems. The instruments were maintained and operated by ODP marine technicians, in cooperation with the scientific party and the officers and crew of SEDCO-FOREX, Inc.

Navigation and bathymetric data, as well as magnetic data, were routinely collected while under way, with coverage in both categories consisting of approximately 91% of the total distance traveled. Seismic reflection data, on the other hand, were generally collected only during surveys while on approach to sites, with coverage consisting of approximately 7% of the total distance traveled.

NAVIGATION

Navigation data were recorded in the Underway Geophysics Lab by a Magnavox-1107 GPS Transit Satellite Receiver. The previous source of raw data, collected on the bridge by a Magnavox-702A-3 Transit Satellite Receiver, was relegated to backup use. The Global Positioning System (GPS) data are preferred over transit satellite and dead-reckoning positions because of the continually updated, higher-quality data available during a GPS "window." This "window" was a period of 4-5 hr each day when positioning data from three or more GPS satellites could be received. Routine collection of navigation data includes recording course and speed data by HIGHRES, the shipboard seismic data acquisition and processing software package.

A plot of the general navigation from Leg 117 is shown in Figure 1. This plot was generated from GPS transit satellite positions, course- and speed-change data, and on- and off-site information compiled from the bridge log, the underway geophysical log, and the HIGHRES tape headers. The Geological Data Center at Scripps Institution of Oceanography produced the navigation compilation (see Appendix). The final site locations are an average of all positions collected while on site.

Site approach surveys were generally carried out during GPS windows; therefore, the information used to reconstruct the ship's track around each drill site is generally GPS data. The sampling density depends on the nature of the survey, generally one fix per 15-30 min in the initial part of the survey, and increasing to one fix per 1-5 min in more critical parts of the survey. The ship's tracks were assumed to proceed from point to point unless suggested otherwise by course-change information listed in the HIGHRES tape headers. The density of points illustrated in the ship's track reconstructions does not necessarily conform with the amount of data collected, but is sufficient to ensure an accurate reconstruction of the ship's tracks. A number of problems with the Magnavox-1107 GPS Transit Satellite Receiver contributed to the collection of unreliable navigation data during several site approaches; in particular Line 1 on approach to Site 720, Line 3 on approach to Site 723, Line 4 on approach to Sites 724 and 725, Line 6 on approach to Site 727, and Line 8 on approach to Site 730. In these cases the ship's tracks were reconstructed, primarily using two sources of information, namely GPS and transit satellite positions listed on the bridge log, and course and speed information listed in the HIGHRES tape headers.

BATHYMETRIC DATA RECORDING

Bathymetric data were obtained with both 3.5-kHz (Raytheon recorder system) and 12-kHz (EDO-248C recorder system) echo-sounders. Unfortunately, because of poor transducer location, the quality of the recorded data was poor when the ship was traveling at speeds greater than 6 kt. Consequently, site surveys requiring detailed bathymetric data were conducted at speeds slower than 6 kt (see the site chapters, this volume). A total of 3927 nmi of bathymetric data were collected on Leg 117, and a generalized bathymetric profile, along with the magnetic profile, is presented in Figure 2.

MAGNETICS

A Geometrics-801 proton procession magnetometer was used to collect a total of 3910 nmi of magnetic data on Leg 117. A generalized magnetic record compiled by the Geological Data Center at Scripps Institution of Oceanography is presented in Figure 2. The magnetic values were retrieved at approximately 1-nmi spacing, and the regional field was removed using the 1985 International Geomagnetic Reference Field.

SEISMIC REFLECTION PROFILES

The seismic sources used aboard *JOIDES Resolution* during Leg 117 were two synchronized 80-in.^{3} Seismic System, Inc. water guns operated at approximately 1900 psi. One 100-m-long Teledyne streamer containing 60 active sections, combined to produce a single signal, was deployed from the fantail and towed about 500 m behind the vessel.

Seismic data were displayed in real time in analog format on two EDO-550 dry-paper recorders, using only streamers, amplifier, and band-pass filters (Table 1). Seismic data were also recorded using a Masscomp-561 computer, which functions as the central unit to record, process, and display the data. Data were processed and displayed in real time on a 15-in.-wide Printronix high-resolution graphic printer (160 dots/in.). Raw data were recorded on magnetic tapes, using a SEG-Y format and a density of 1600 bits/in. Seismic lines recorded with the Masscomp were reprocessed at ODP headquarters according to the parameters listed in Table 2. The final data were displayed on a 22-in.-wide Versatec plotter (200 dots/in.).

---

[1] Prell, W. L., Niitsuma, N., et al., 1989. *Proc. ODP, Init. Repts.*, 117: College Station, TX (Ocean Drilling Program).

[2] Ocean Drilling Program, Texas A&M University, College Station, TX 77843.

[3] Shipboard Scientific Party is as given in the list of Participants preceding the contents.

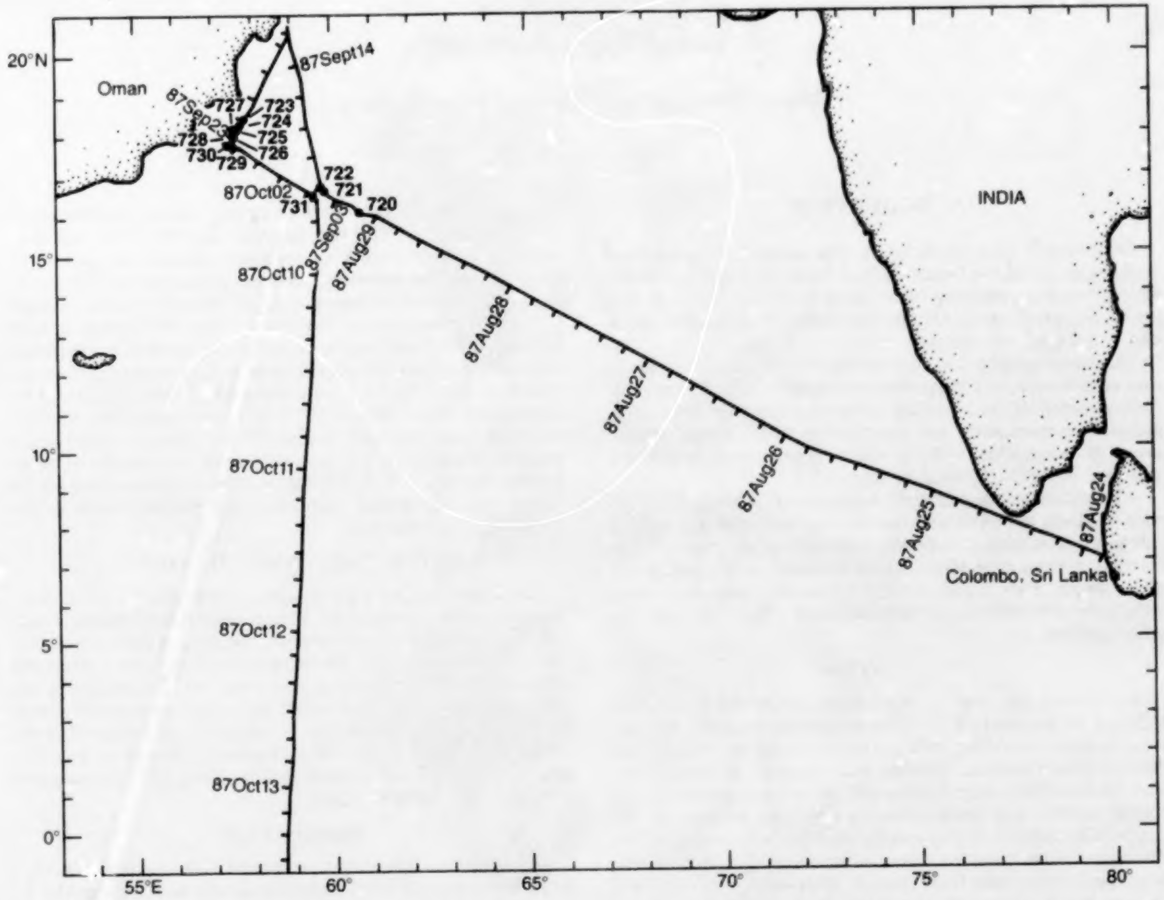

Figure 1. General navigation and site location plot for Leg 117, generated from satellite, course-, and speed-change data given in the Appendix. Detailed ship's tracks for seismic lines/site approaches are shown on Figures 3, 5, 8, 10, 12, 14, 16, 18, and 21.

We recorded nine seismic lines during Leg 117, covering approximately 290 nmi. These profiles are available from the ODP Data Base Supervisor.

1. Seismic line 1 was collected on the approach to Site 720 along the track shown in Figure 3. The processed digital seismic profile is shown in Figure 4 (from Julian Day 241/0241 UTC/shotpoint 4988 to Julian Day 241/0549 UTC/shotpoint 5928).

2. Seismic line 2 was collected en route to and on approach to Sites 721 and 722. While en route to the sites a problem was discovered in collection of digital data, and the line is therefore broken into three parts, line 2A consisting of the processed digital data collected before the problem occurred, line 2B consisting of the analog records collected during the absence of digital data, and line 2C consisting of the processed digital data collected after the problem was corrected. Lines 2A and 2B were collected en route to Sites 721 and 722 along the track shown in Figure 5. The processed digital and analog seismic profiles are shown in Figure 6 (from Julian Day 245/1736 UTC/shotpoint 100 to Julian Day 245/2016 UTC/shotpoint 900) and Figure 7 (from Julian Day 245/2016 UTC/shotpoint 900 to Julian Day 246/0212 UTC/shotpoint 2683), respectively. Line 2C was collected on approach to Sites 721 and 722 along the track shown in Figure 8. The processed digital seismic profile is shown in Figure 9 (from Julian Day 246/0212 UTC/shotpoint 2683 to Julian Day 246/0708 UTC/shotpoint 4160).

3. Seismic line 3 was collected on approach to Site 723 along the track shown in Figure 10. The processed digital seismic profile is shown in Figure 11 (from Julian Day 258/0356 UTC/shotpoint 1863 to Julian Day 258/0554 UTC/shotpoint 2636).

4. Seismic line 4 was collected en route to and on approach to Sites 724 and 725 along the track shown in Figure 12. The processed digital seismic profile is shown in Figure 13 (from Julian Day 262/2052 UTC/shotpoint 23 to Julian Day 263/0535 UTC/shotpoint 2635).

5. Seismic line 5 was collected en route to and on approach to Site 726 along the track shown in Figure 14. The processed digital seismic profile is shown in Figure 15 (from Julian Day 265/2040 UTC/shotpoint 1 to Julian Day 266/0438 UTC/shotpoint 2391).

6. Seismic line 6 was collected en route to and on approach to Site 727 along the track shown in Figure 16. The processed

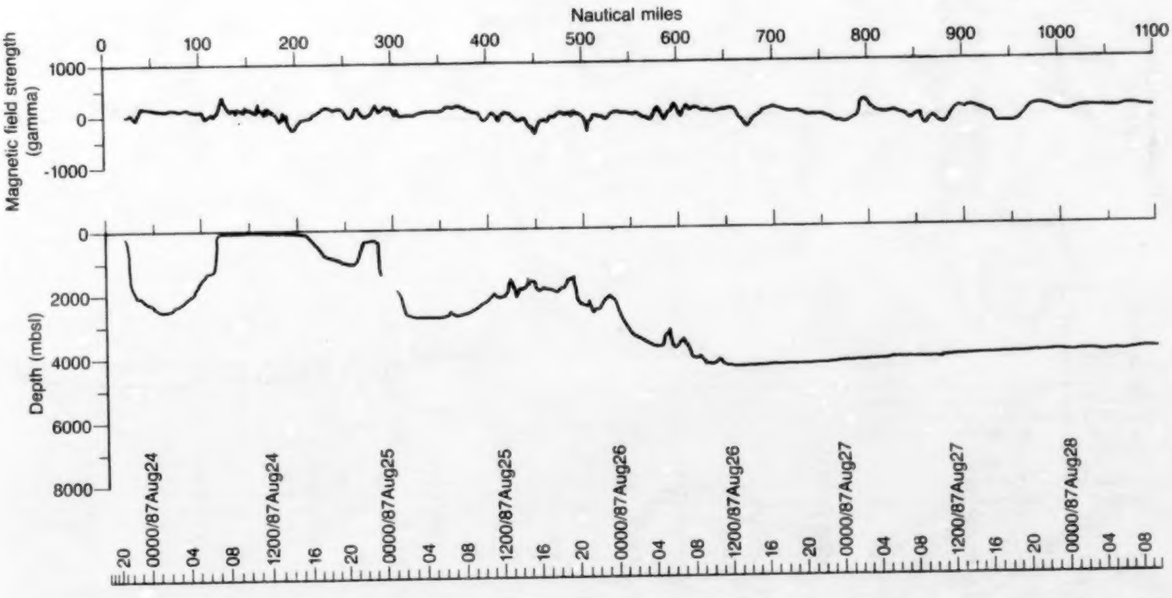

Figure 2. Records of magnetic and bathymetric profiles obtained during Leg 117. Solid bars indicate seismic-reflection coverage. Bottom horizontal scale indicates date and time in hours.

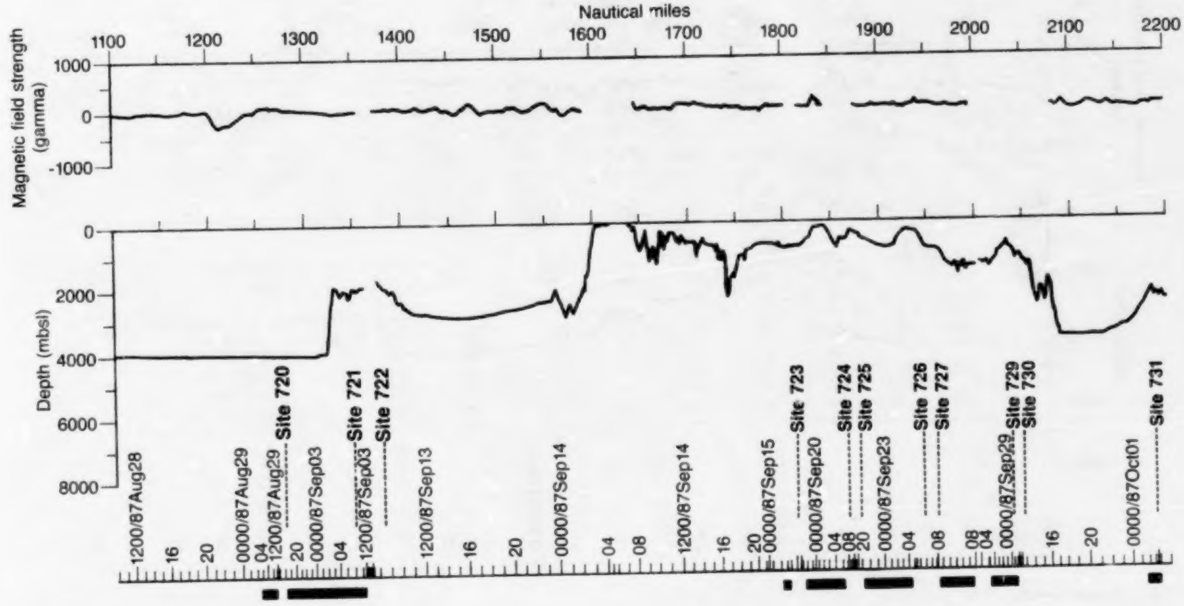

Figure 2 (continued).

digital seismic profile is shown in Figure 17 (from Julian Day 267/0448 UTC/shotpoint 1 to Julian Day 267/0730 UTC/shotpoint 812).

7. Seismic line 7 was collected en route to and on approach to Sites 728 and 729 along the track shown in Figure 18. Because of its close association, the track for line 8 is also shown in Figure 18. The processed digital seismic profile for line 7 is shown in Figure 19 (from Julian Day 268/0225 UTC/shotpoint 1 to Julian Day 268/0740 UTC/shotpoint 1579).

8. Seismic line 8 was collected en route to and on approach to Site 730 along one of the tracks shown in Figure 18. The processed digital seismic profile is shown in Figure 20 (from Julian

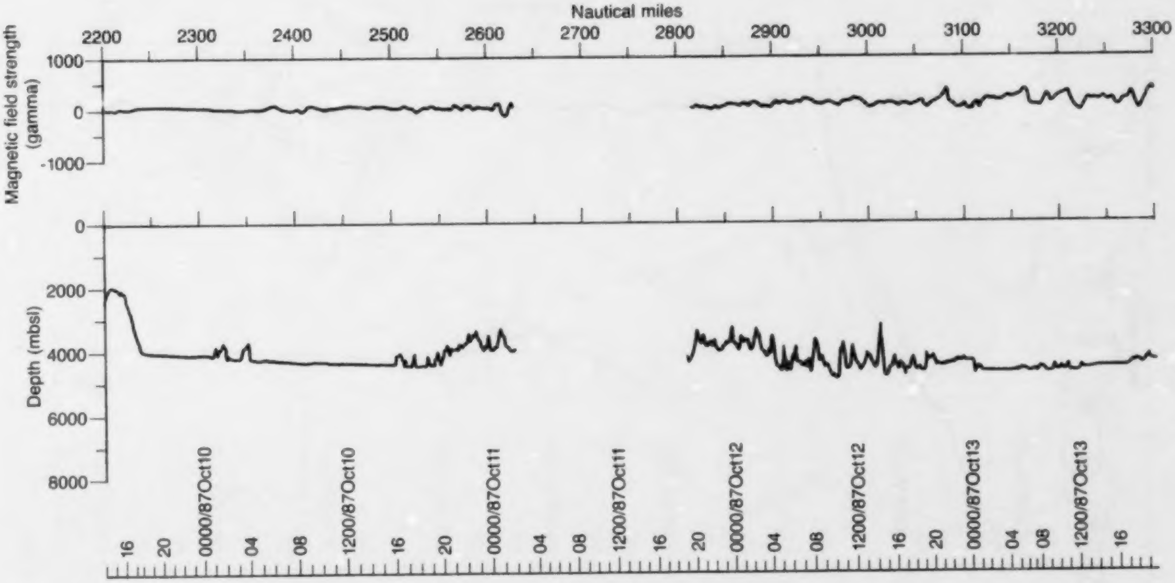

Figure 2 (continued).

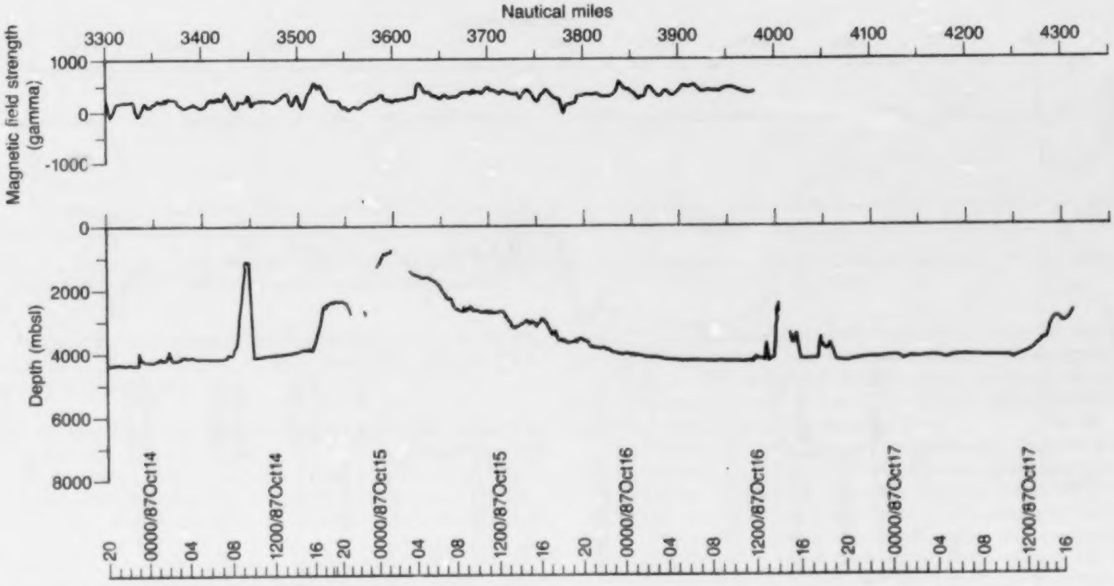

Figure 2 (continued).

Day 271/1855 UTC/shotpoint 1 to Julian Day 272/0208 UTC/shotpoint 2165).

9. Seismic line 9 was collected on approach to approach to Site 731 along the track shown in Figure 21. The processed digital seismic profile is shown in Figure 22 (from Julian Day 274/0148 UTC/shotpoint 595 to Julian Day 274/0337 UTC/shotpoint 1135).

Ms 117A-119

Table 1. Seismic-data real-time recording parameters.

	Line 1	Line 2	Line 3	Line 4	Line 5	Line 6	Line 7	Line 8	Line 9
Start at	16°03.71′N 60°49.86′E	Site 720	18°05.25′N 57°37.74′E	Site 723	Site 724/725	Site 726	Site 727	Site 728/729	16°28.39′N 59°39.04′N
End at	Site 720	Site 721/722	Site 723	Site 724/725	Site 726	Site 727	Site 728/729	Site 730	Site 731
Source	Two 80-in.^{3} water guns	Two 80-in.^{3} water guns	Two 80-in.^{3} water guns	Two 80-in.^{3} water guns	Two 80-in.^{3} water guns	Two 80-in.^{3} water guns	Two 80-in.^{3} water guns	Two 80-in.^{3} water guns	Two 80-in.^{3} water guns
Streamer	Port	Port	Port	Port	Port	Port	Port	Port	Port
EDO-1:									
High cut (Hz)	130	130	115	130	115	150	150	150	150
Low cut (Hz)	48	36	46	48	38	40	40	40	40
Gain:									
Amp (db)	90	90	90	90	90	90	90	90	90
EDO-2:									
High cut (Hz)	150	150	150	150	150	150	150	150	150
Low cut (Hz)	40	40	41	41	41	40	40	40	40
Gain:									
Amp (db)	90	90	90	90	90	90	90	90	90

Table 2. Seismic-data processing and reprocessing parameters.

	Line 1	Line 2A	Line 2C	Line 3	Line 4	Line 5	Line 6	Line 7	Line 8	Line 9
Data window (ms):										
From	5000	5200	2400	800	200	200	400	1000	800	2800
To	7000	7000	6400	4500	4200	4000	4200	4800	4700	6400
AGC:										
Response time (ms)	200	200	200	200	200	200	200	200	300	200
Start time (ms)	5000	5200	2400	800	200	200	400	1000	800	2800
Gain (%)	75	75	75	75	75	75	75	75	75	75
Zero-phase band-pass filter:										
High cut (Hz)	150	150	150	150	150	150	150	150	150	150
Taper width	12	12	12	12	12	12	12	12	12	12
Low cut (Hz)	30	30	30	30	30	30	30	30	30	30
Taper width	20	20	20	20	20	20	25	20	20	20
Seafloor mute applied	yes	yes	yes	yes	yes	yes	yes	yes	yes	

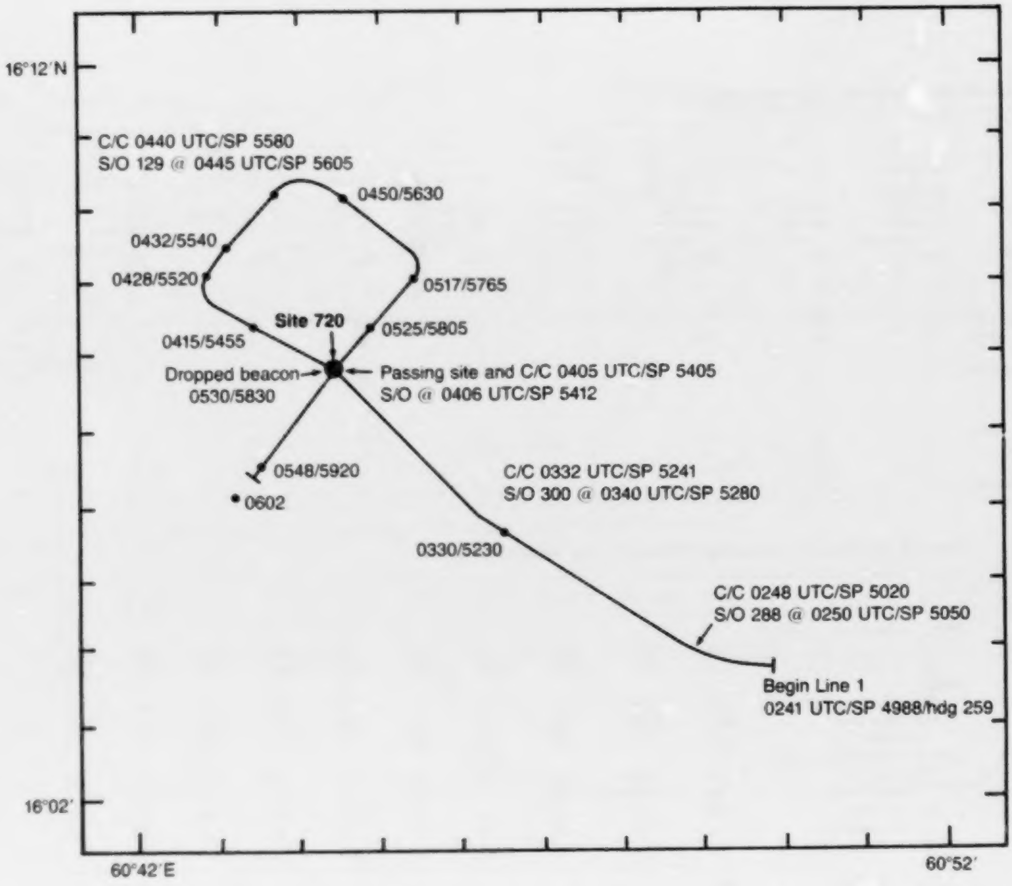
16°12′N
16°02′
60°42′E
60°52′
C/C 0440 UTC/SP 5580
S/O 129 @ 0445 UTC/SP 5605
0450/5630
0432/5540
0428/5520
0517/5765
Site 720
0415/5455
0525/5805
Dropped beacon
0530/5830
Passing site and C/C 0405 UTC/SP 5405
S/O @ 0406 UTC/SP 5412
0548/5920
0602
C/C 0332 UTC/SP 5241
S/O 300 @ 0340 UTC/SP 5280
0330/5230
C/C 0248 UTC/SP 5020
S/O 288 @ 0250 UTC/SP 5050
Begin Line 1
0241 UTC/SP 4988/hdg 259

Figure 3. Detailed ship's track for seismic line 1, on approach to Site 720. Satellite fixes are shown as points and are identified by UTC/shotpoint (SP). Extrapolated positions are shown as tick marks. The processed digital seismic profile is shown in Figure 4.

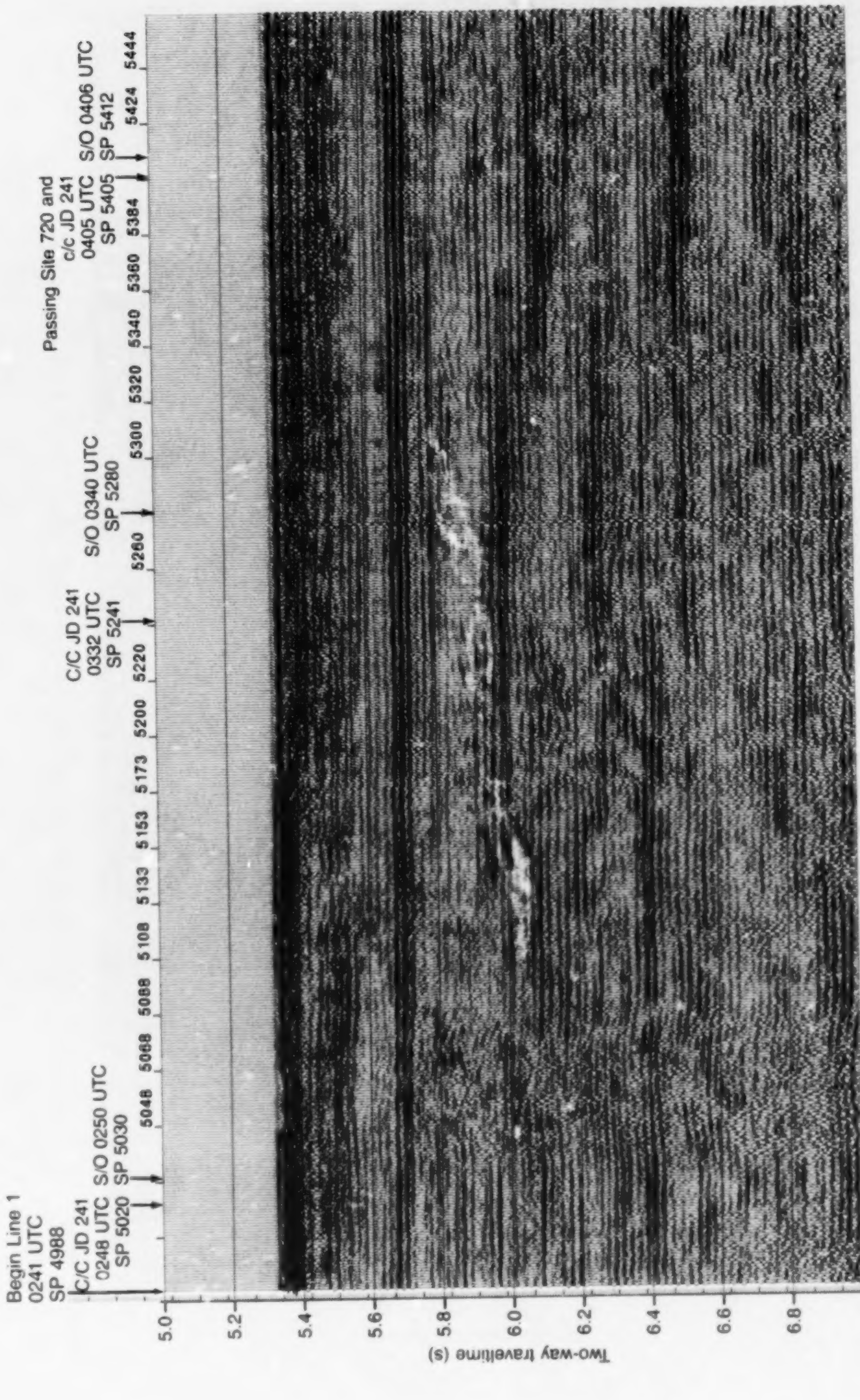

Figure 4. Processed digital seismic profile of line 1, collected on approach to Site 720. The profile was plotted on the Versatec plotter according to the processing parameters given in Table 2. The ship's track is shown in Figure 3.

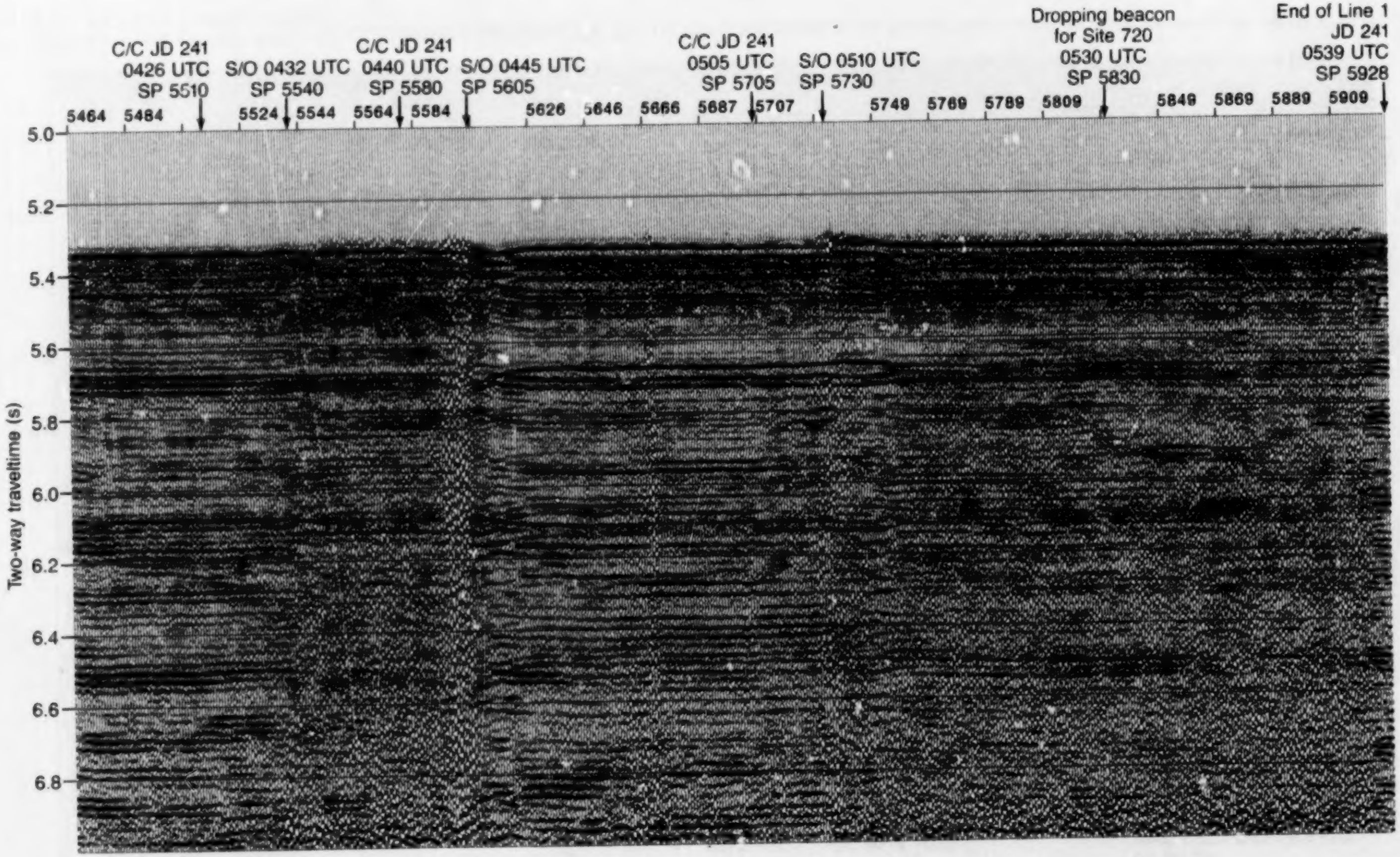

Figure 4 (continued).

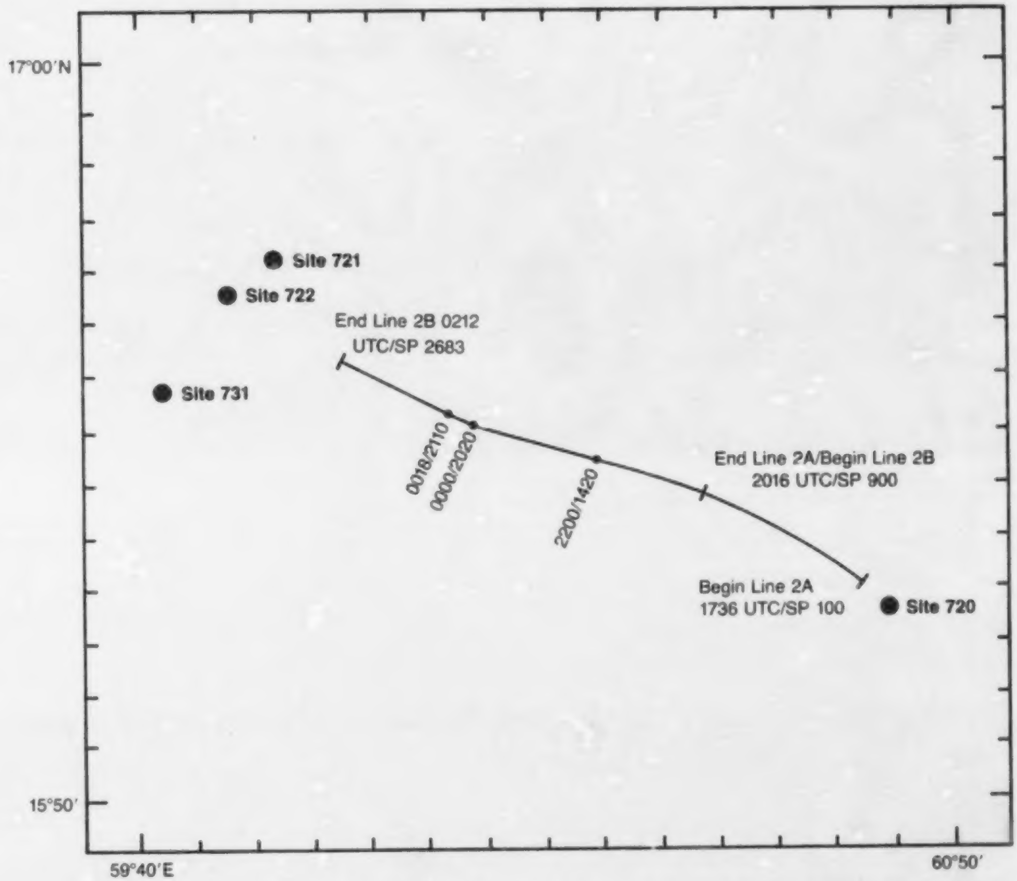
17°00′N
15°50′
59°40′E
60°50′
Site 721
Site 722
Site 731
Site 720
End Line 2B 0212
UTC/SP 2683
0018/2110
0000/2020
2200/1420
End Line 2A/Begin Line 2B
2016 UTC/SP 900
Begin Line 2A
1736 UTC/SP 100

Figure 5. Detailed ship's track for seismic lines 2A and 2B, en route to Sites 721 and 722. Satellite fixes are shown as points and are identified by UTC/shotpoint (SP). Extrapolated positions are shown as tick marks. Line 2B corresponds to the period over which a problem was discovered in the collection of digital data. The processed digital seismic profile for line 2A and the analog seismic profile for line 2B are shown in Figures 6 and 7, respectively.

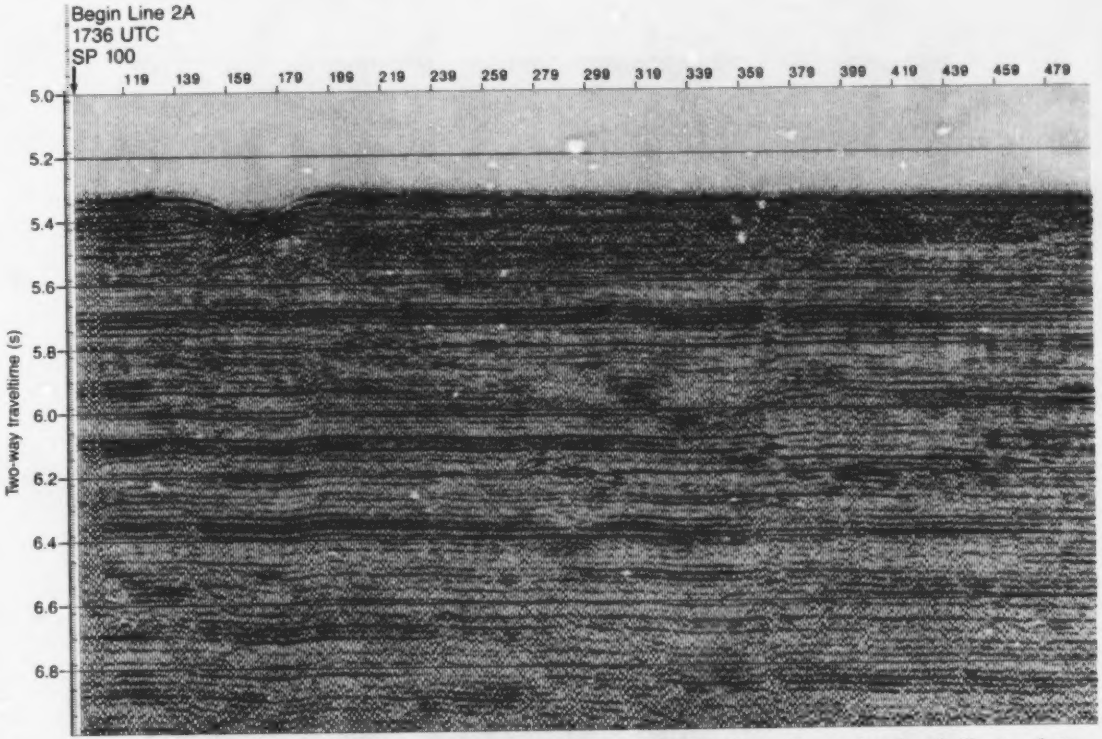

Figure 6. Processed digital seismic profile of line 2A, collected en route to Sites 721 and 722. The profile was plotted on the Versatec plotter according to the processing parameters given in Table 2. The ship's track is shown in Figure 5.

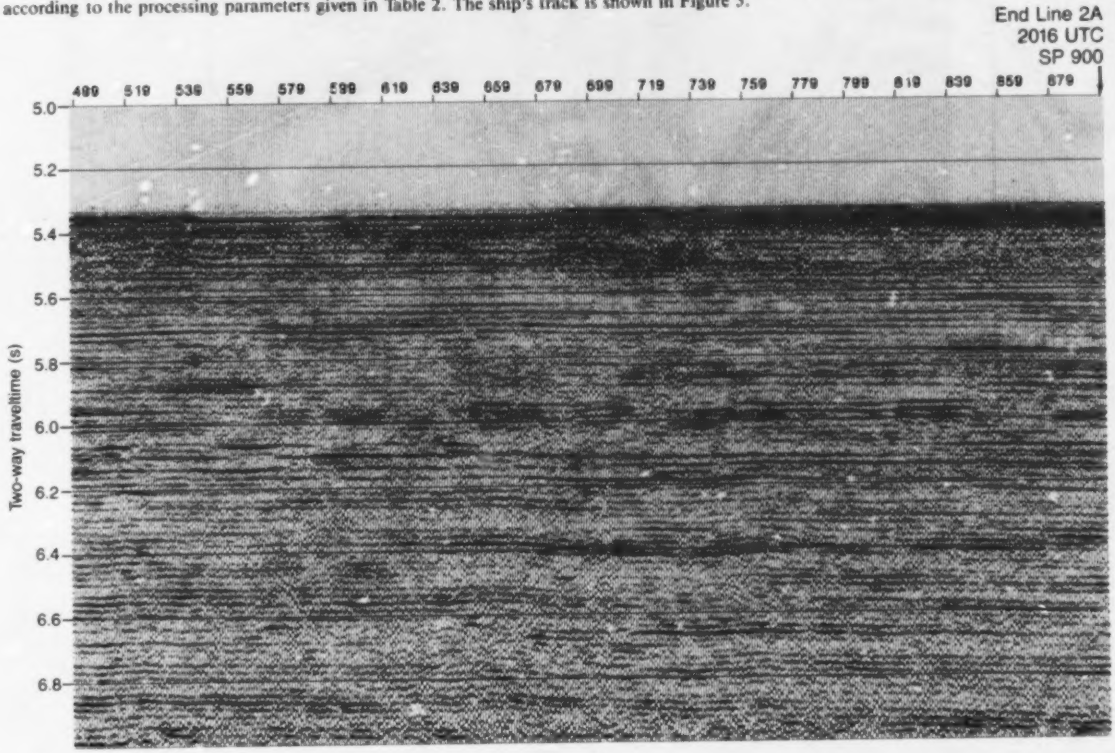

Figure 6 (continued).

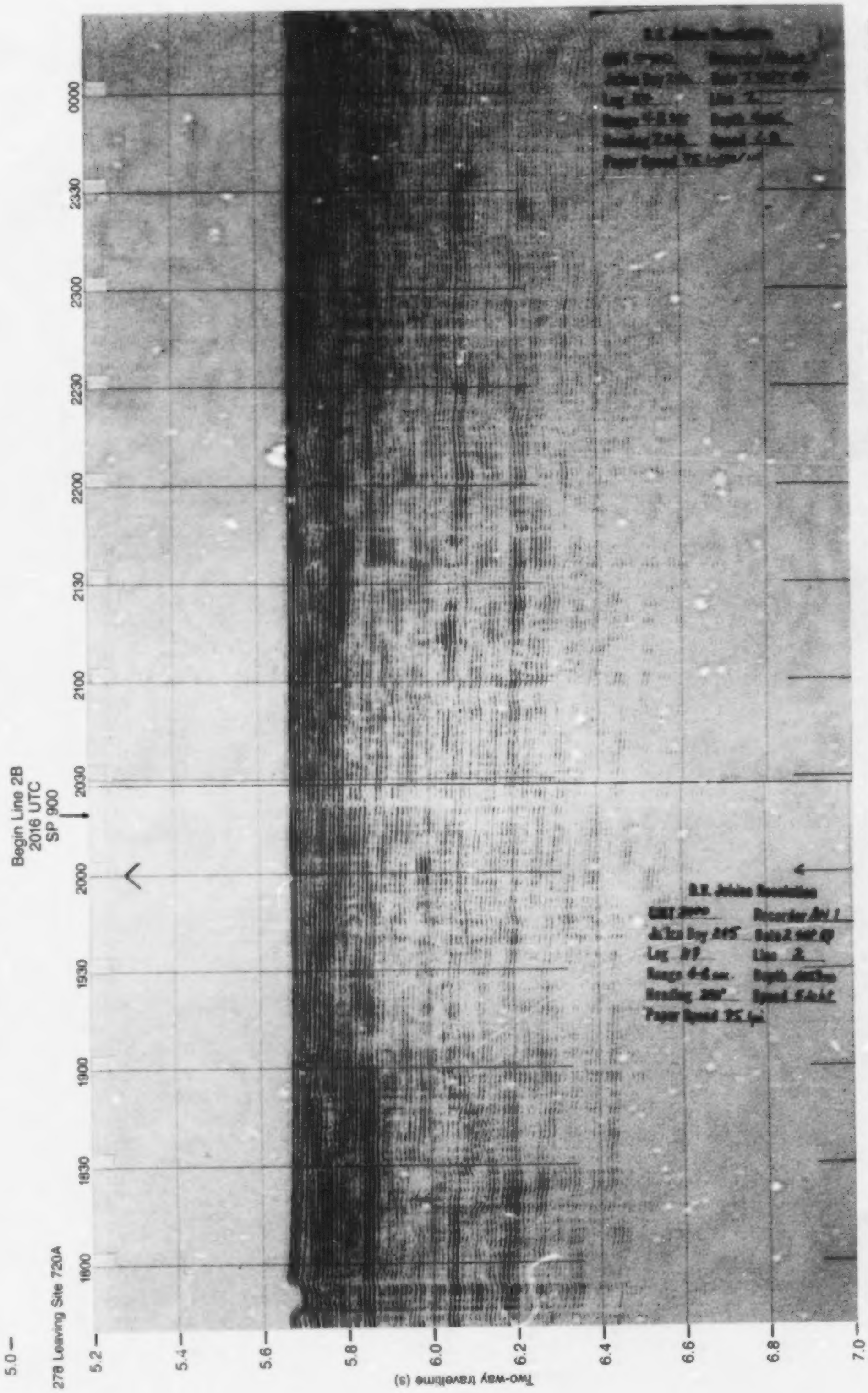

Figure 7. Analog seismic profile of line 2B, collected en route to Sites 721 and 722. The profile was recorded on an EDO-550 dry-paper recorder according to the parameters given in Table 2. The ship's track is shown in Figure 5.

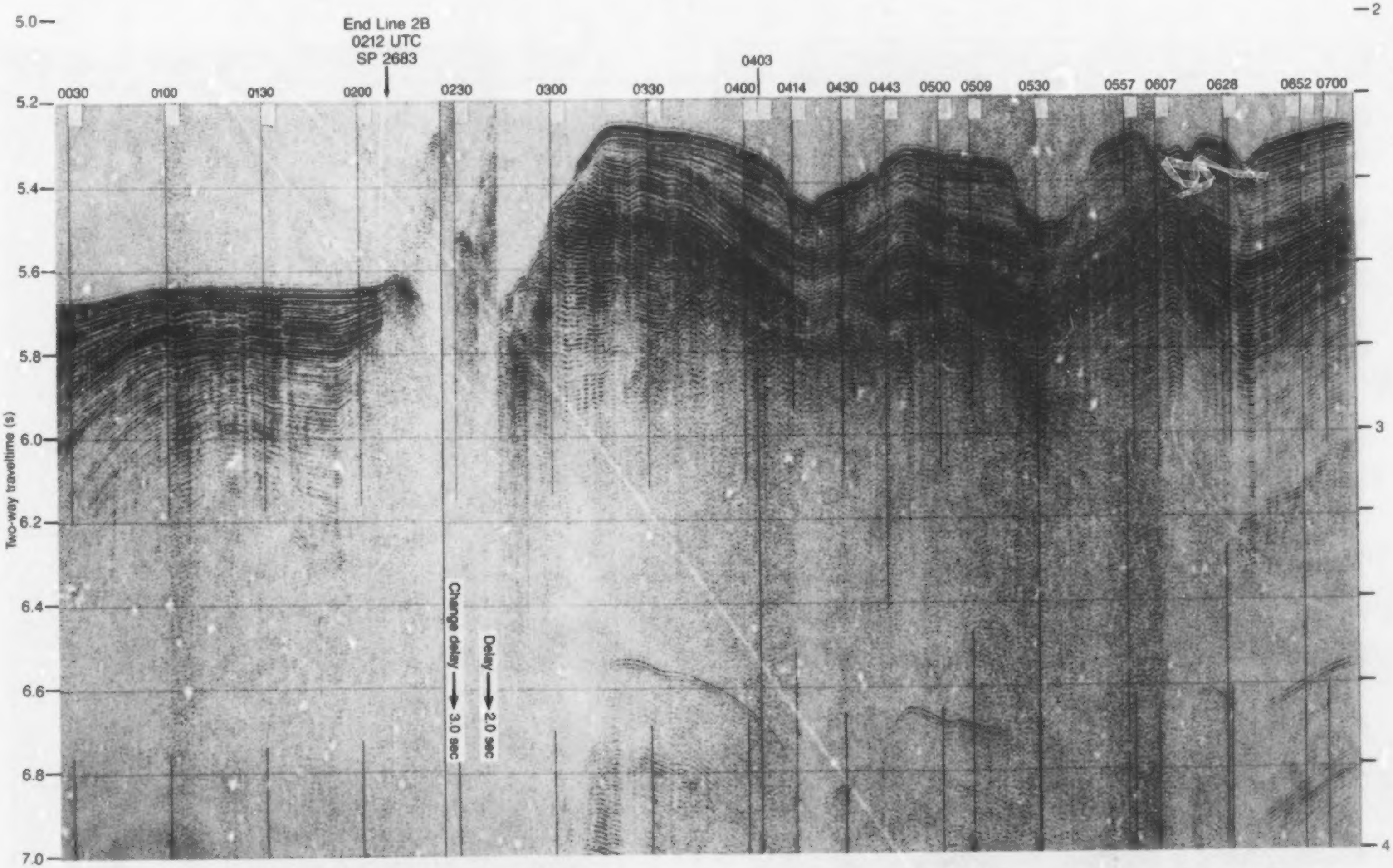

Figure 7 (continued).

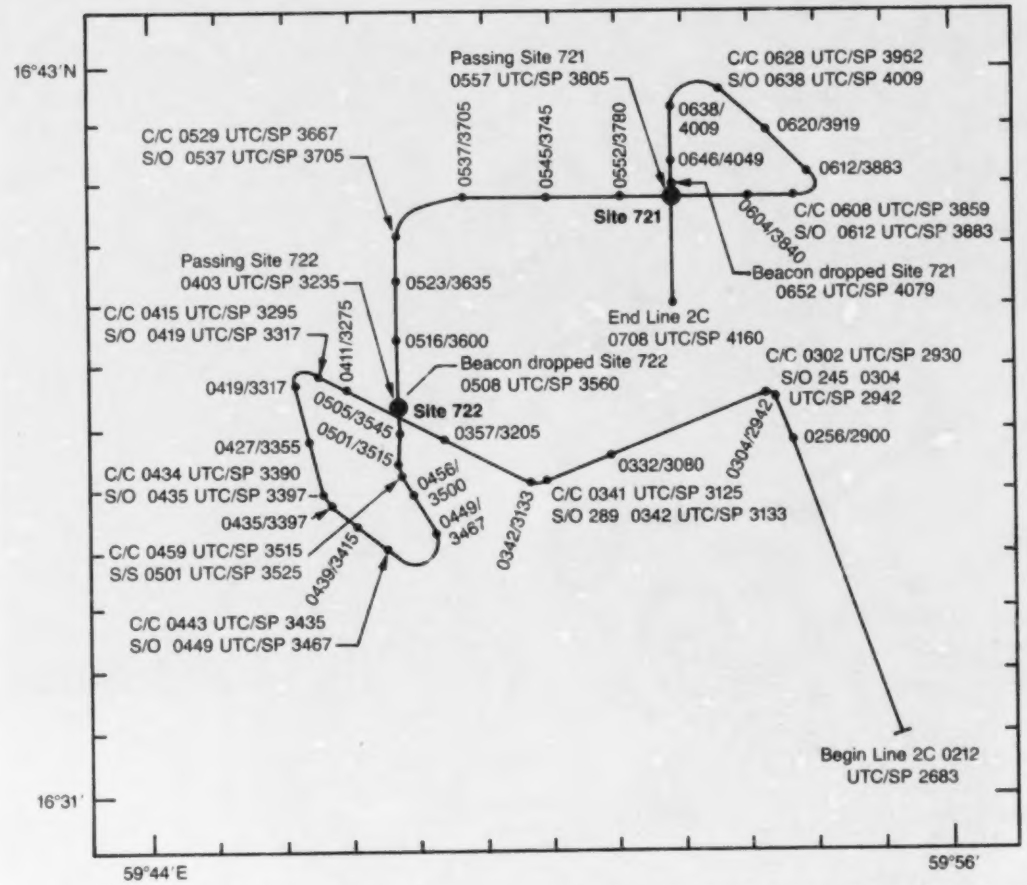
16°43′N
16°31′
59°44′E
59°56′
Passing Site 721
0557 UTC/SP 3805
C/C 0628 UTC/SP 3952
S/O 0638 UTC/SP 4009
0638/
4009
0620/3919
0646/4049
0612/3883
C/C 0529 UTC/SP 3667
S/O 0537 UTC/SP 3705
0537/3705
0545/3745
0552/3780
Site 721
C/C 0608 UTC/SP 3859
S/O 0612 UTC/SP 3883
0604/3840
Beacon dropped Site 721
0652 UTC/SP 4079
Passing Site 722
0403 UTC/SP 3235
0523/3635
C/C 0415 UTC/SP 3295
S/O 0419 UTC/SP 3317
0411/3275
0516/3600
End Line 2C
0708 UTC/SP 4160
Beacon dropped Site 722
0508 UTC/SP 3560
C/C 0302 UTC/SP 2930
S/O 245 0304
UTC/SP 2942
0419/3317
0505/3545
Site 722
0357/3205
0501/3515
0304/2942
0256/2900
0427/3355
0332/3080
C/C 0434 UTC/SP 3390
S/O 0435 UTC/SP 3397
0456/
3500
C/C 0341 UTC/SP 3125
S/O 289 0342 UTC/SP 3133
0342/3133
0435/3397
0449/
3467
C/C 0459 UTC/SP 3515
S/S 0501 UTC/SP 3525
0439/3415
C/C 0443 UTC/SP 3435
S/O 0449 UTC/SP 3467
Begin Line 2C 0212
UTC/SP 2683

Figure 8. Detailed ship's track for seismic line 2C, on approach to Sites 721 and 722. Satellite fixes are shown as points and are identified by UTC/shotpoint (SP). Extrapolated positions are shown as tick marks. The processed digital seismic profile is shown in Figure 9.

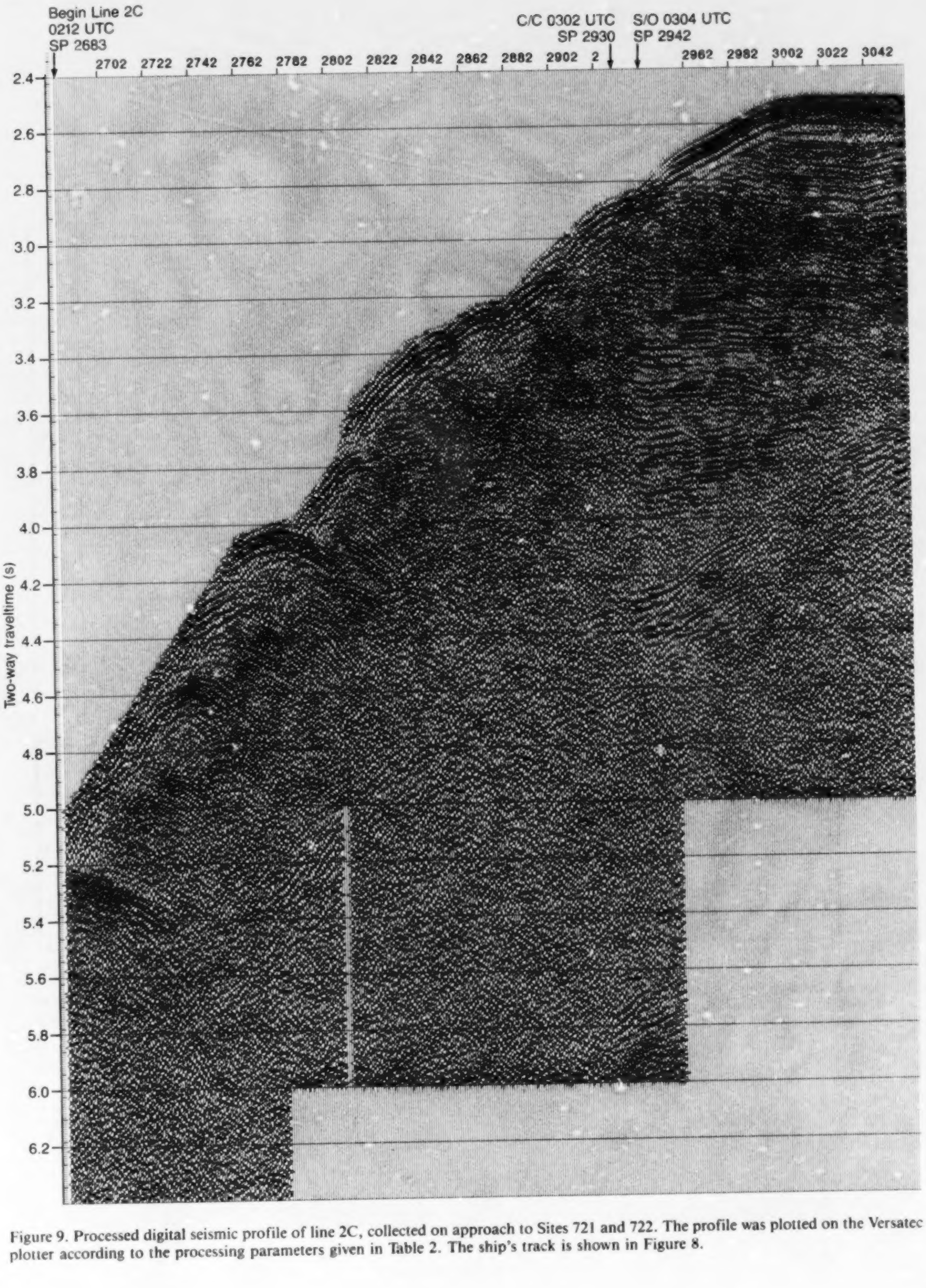

Figure 9. Processed digital seismic profile of line 2C, collected on approach to Sites 721 and 722. The profile was plotted on the Versatec plotter according to the processing parameters given in Table 2. The ship's track is shown in Figure 8.

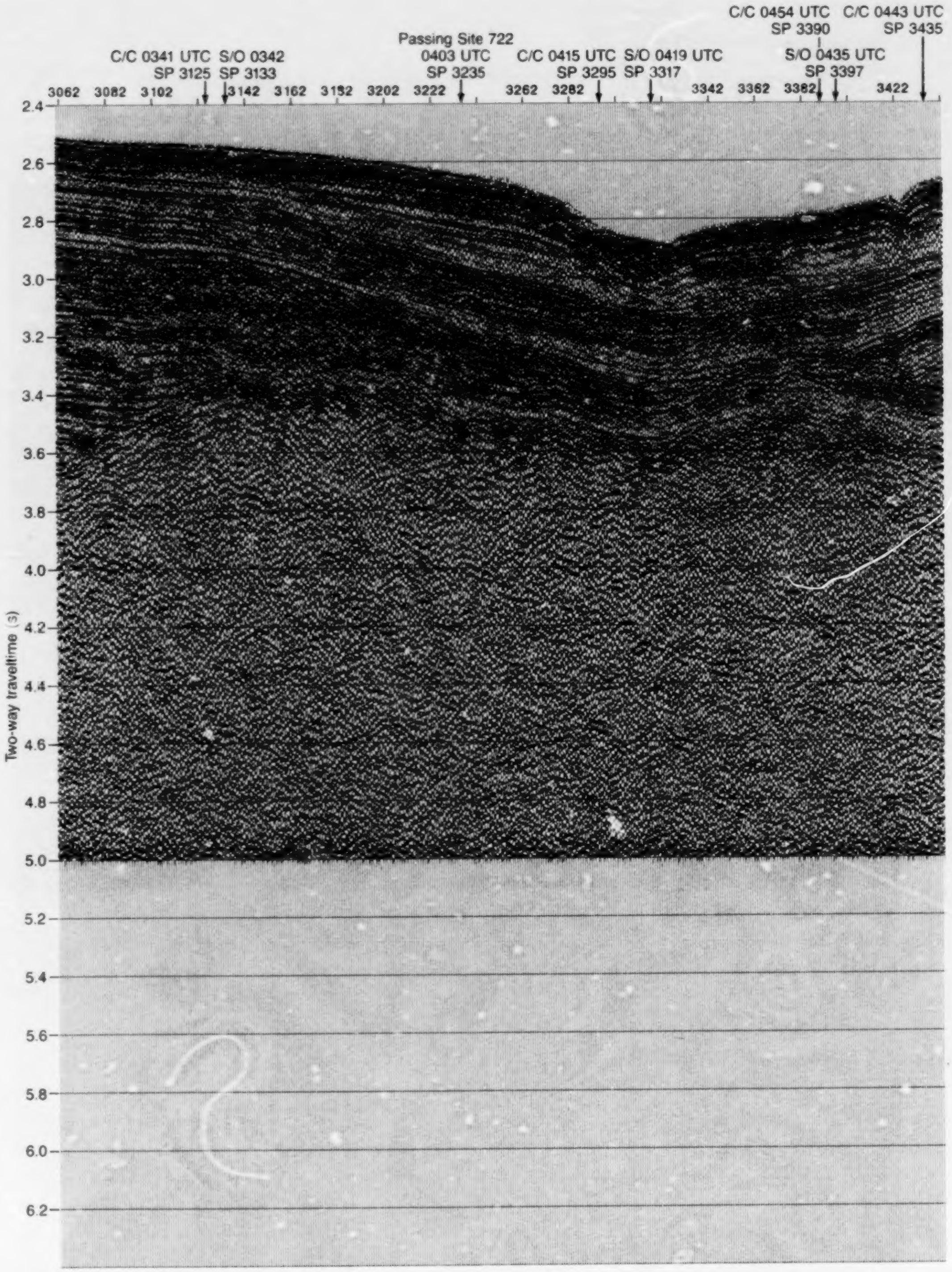

Figure 9 (continued).

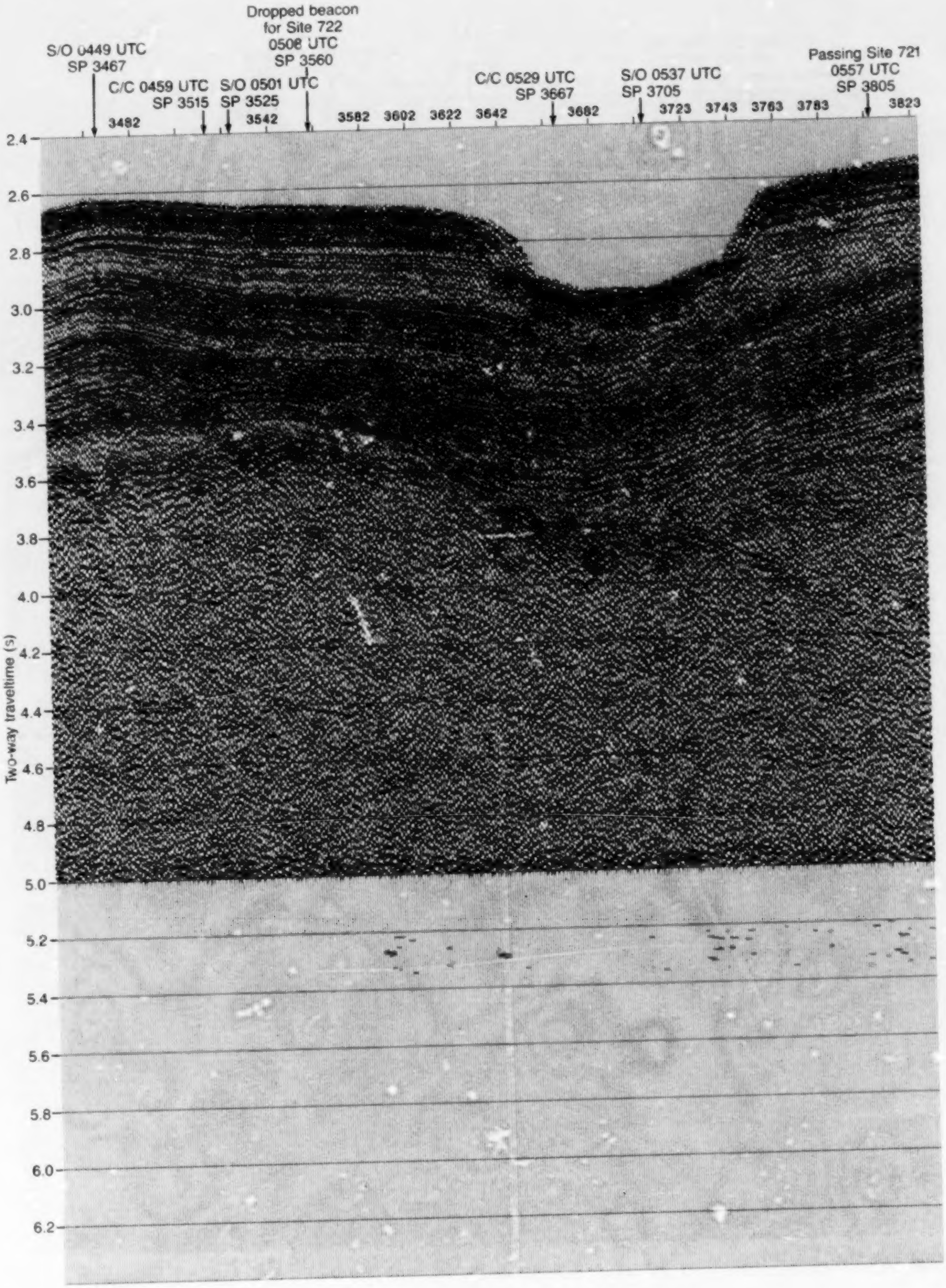

Figure 9 (continued).

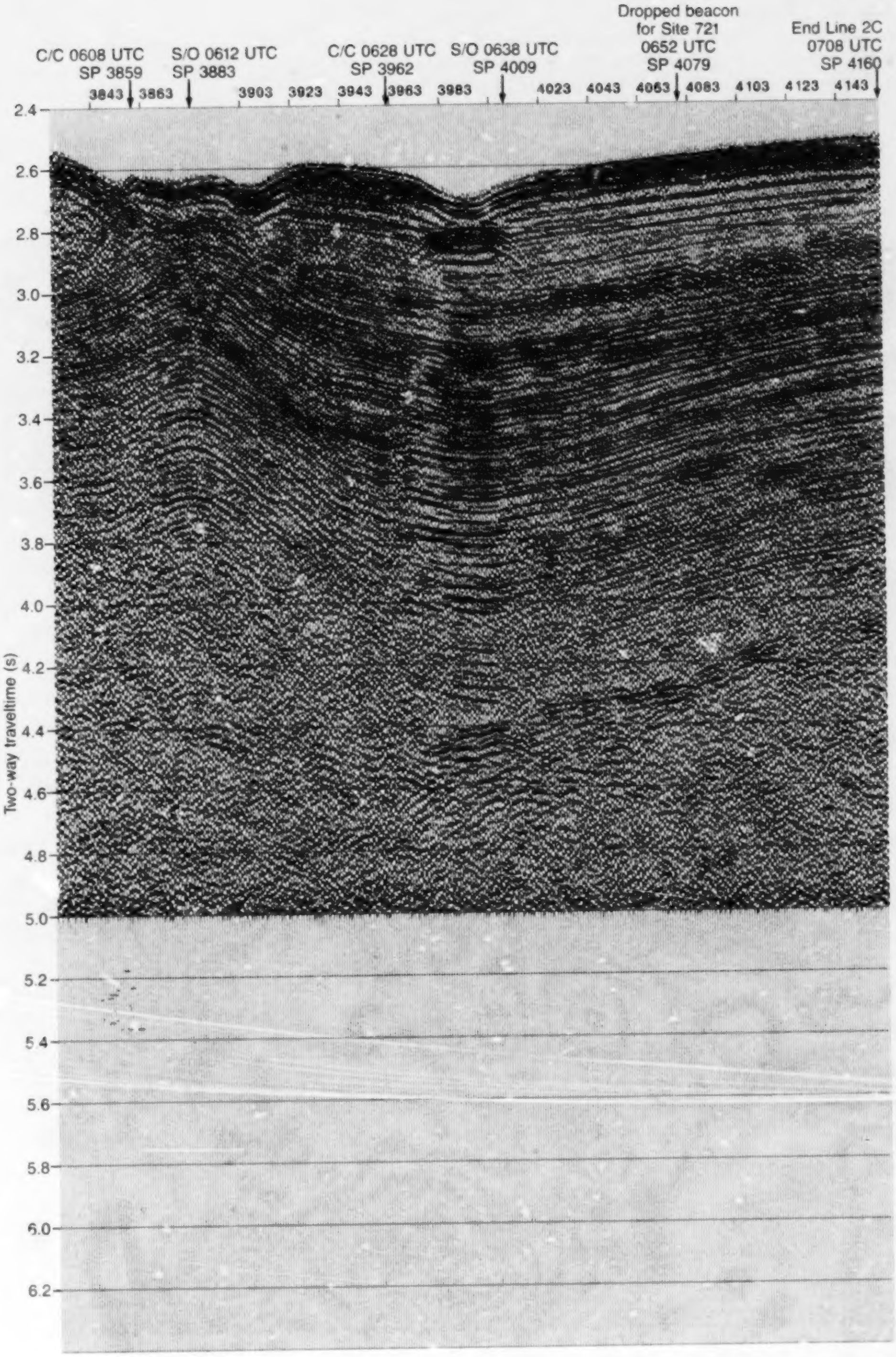

Figure 9 (continued).

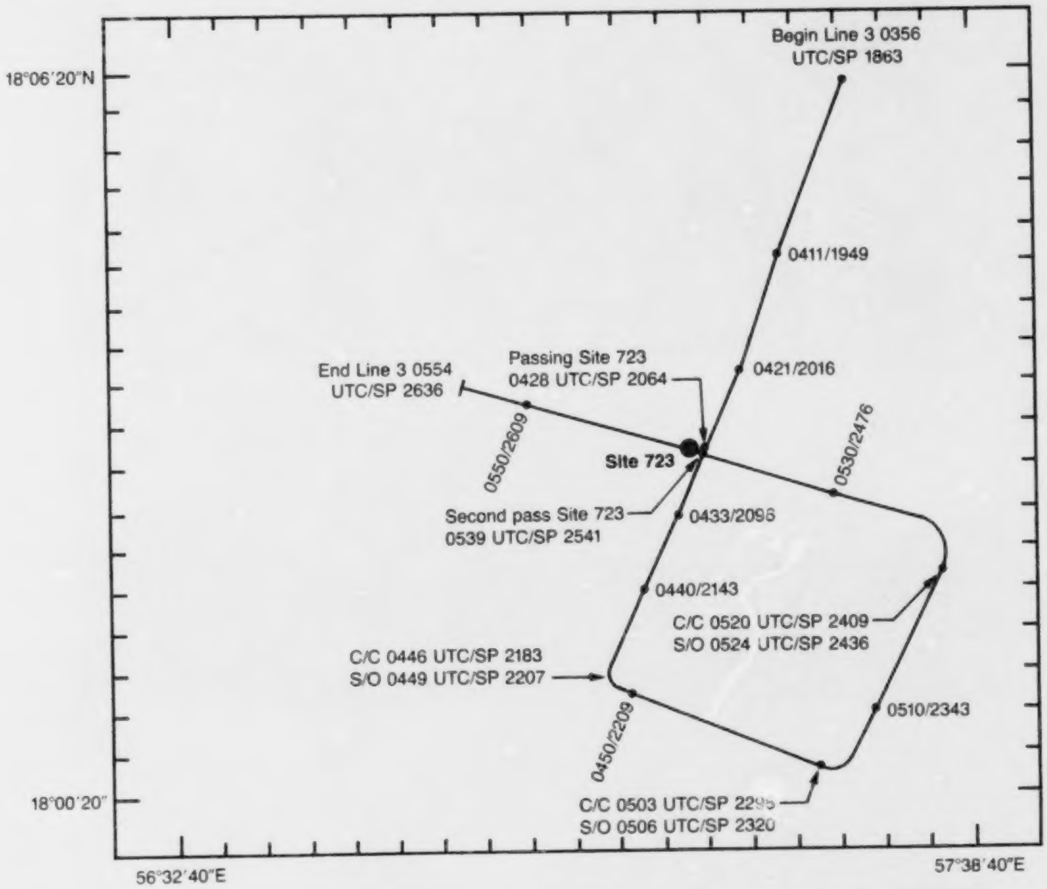
Begin Line 3 0356
UTC/SP 1863
18°06′20″N
0411/1949
0421/2016
End Line 3 0554
UTC/SP 2636
Passing Site 723
0428 UTC/SP 2064
0550/2609
Site 723
0530/2476
Second pass Site 723
0539 UTC/SP 2541
0433/2096
0440/2143
C/C 0520 UTC/SP 2409
S/O 0524 UTC/SP 2436
C/C 0446 UTC/SP 2183
S/O 0449 UTC/SP 2207
0450/2209
0510/2343
18°00′20″
C/C 0503 UTC/SP 2295
S/O 0506 UTC/SP 2320
56°32′40″E
57°38′40″E

Figure 10. Detailed ship's track for seismic line 3, on approach to Site 723. Satellite fixes are shown as points and are identified by UTC/shotpoint (SP). Extrapolated positions are shown as tick marks. The processed digital seismic profile is shown in Figure 11.

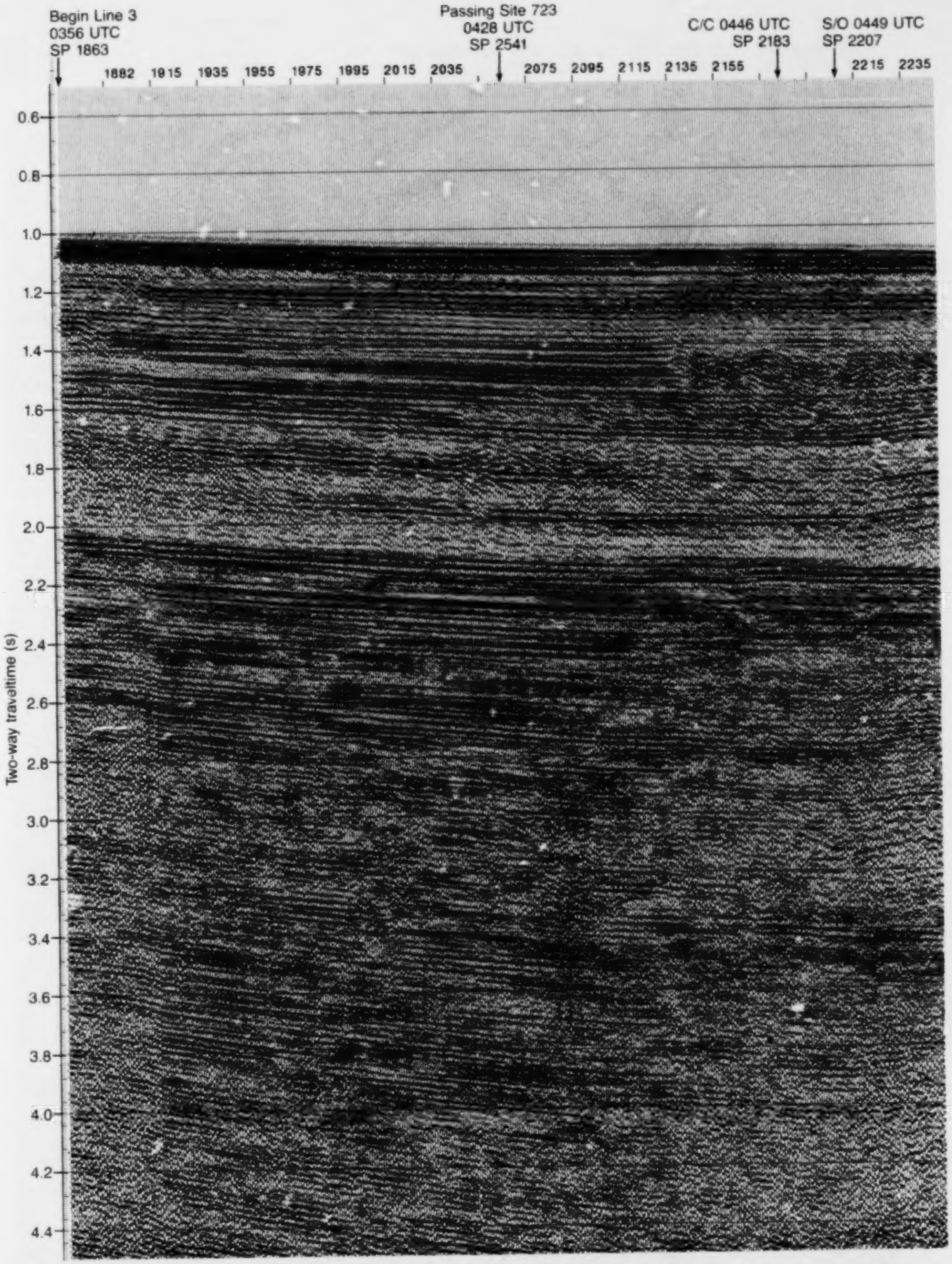

Figure 11. Processed digital seismic profile of line 3, collected on approach to Site 723. The profile was plotted on the Versatec plotter according to the processing parameters given in Table 2. The ship's track is shown in Figure 10.

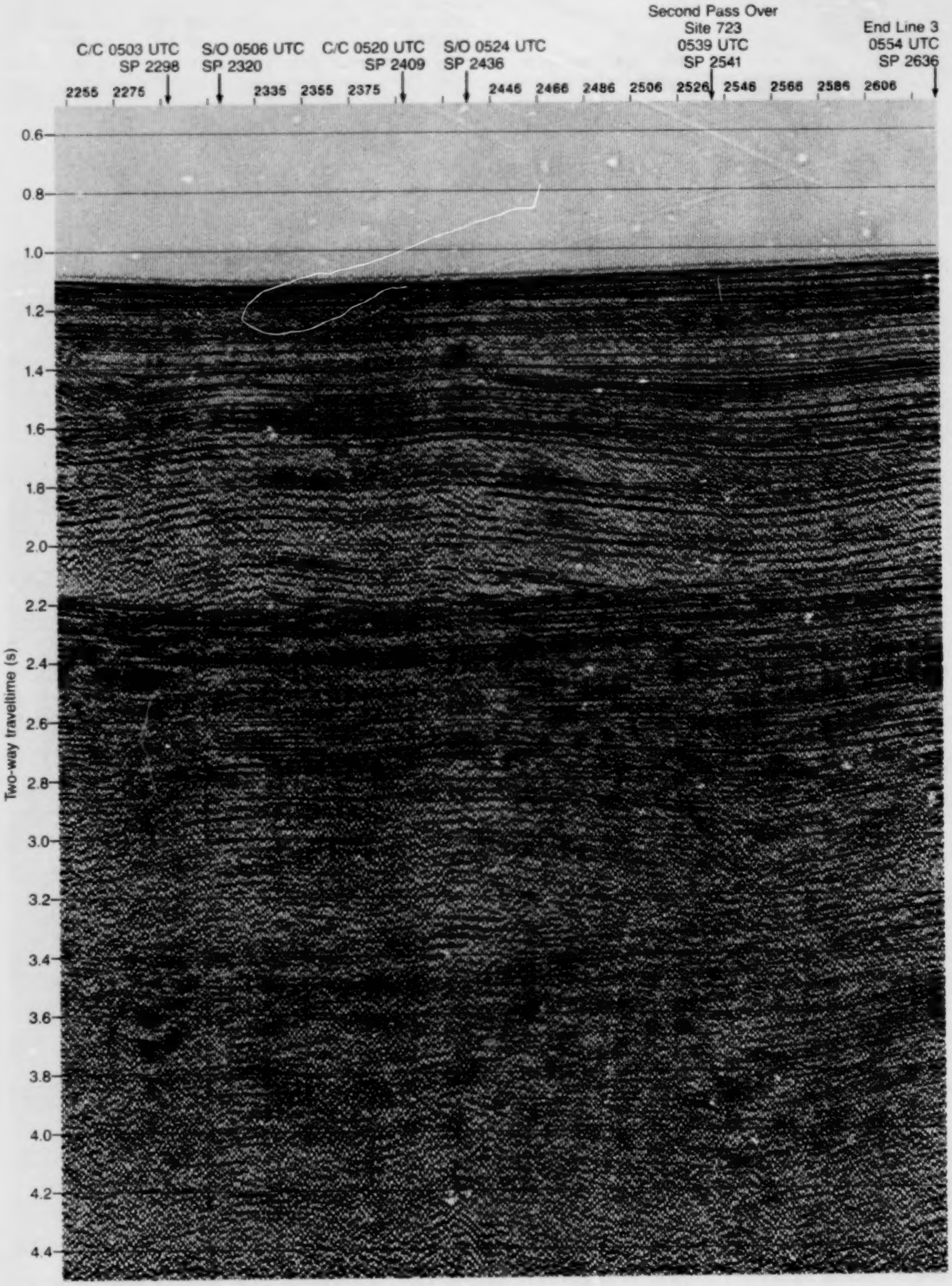

Figure 11 (continued).

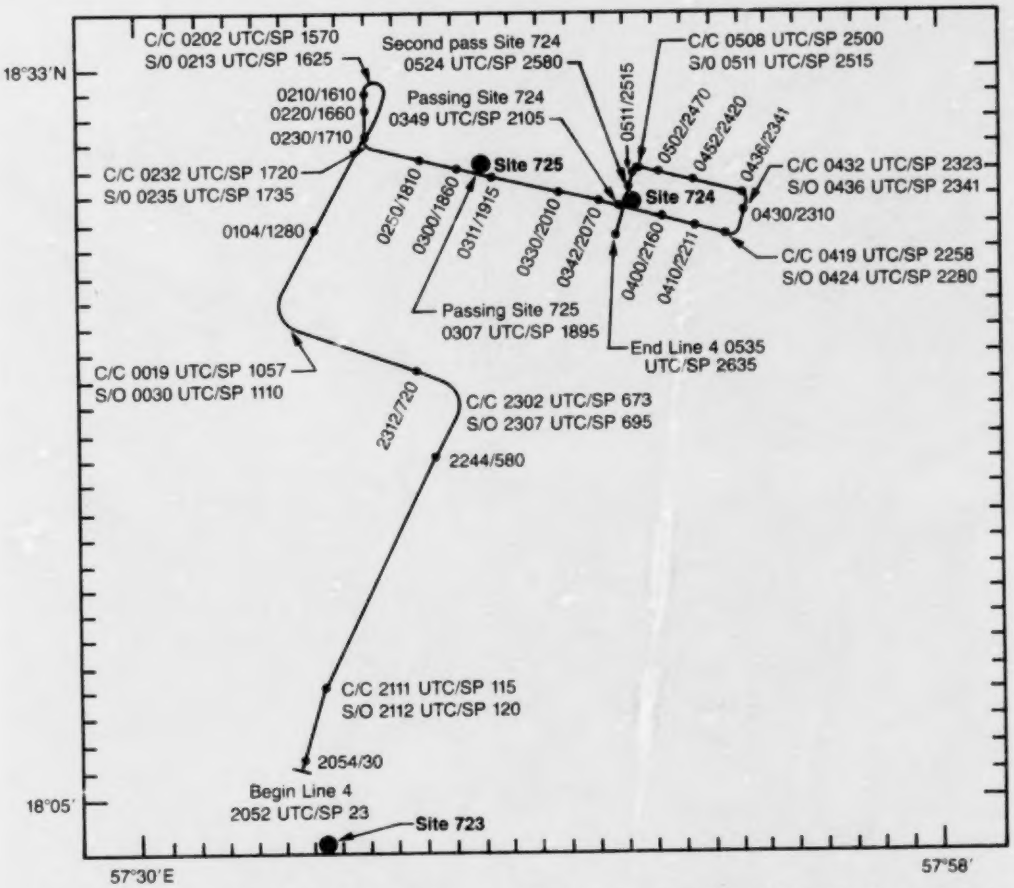
18°33′N
18°05′
57°30′E
57°58′
C/C 0202 UTC/SP 1570
S/0 0213 UTC/SP 1625
0210/1610
0220/1660
0230/1710
C/C 0232 UTC/SP 1720
S/0 0235 UTC/SP 1735
0104/1280
Second pass Site 724
0524 UTC/SP 2580
Passing Site 724
0349 UTC/SP 2105
Site 725
0250/1810
0300/1860
0311/1915
0330/2010
0342/2070
0511/2515
0502/2470
0452/2420
0436/2341
C/C 0508 UTC/SP 2500
S/0 0511 UTC/SP 2515
Site 724
C/C 0432 UTC/SP 2323
S/O 0436 UTC/SP 2341
0430/2310
C/C 0419 UTC/SP 2258
S/O 0424 UTC/SP 2280
0400/2160
0410/2211
Passing Site 725
0307 UTC/SP 1895
End Line 4 0535
UTC/SP 2635
C/C 0019 UTC/SP 1057
S/O 0030 UTC/SP 1110
2312/720
C/C 2302 UTC/SP 673
S/O 2307 UTC/SP 695
2244/580
C/C 2111 UTC/SP 115
S/O 2112 UTC/SP 120
2054/30
Begin Line 4
2052 UTC/SP 23
Site 723

Figure 12. Detailed ship's track for seismic line 4, en route to and on approach to Sites 724 and 725. Satellite fixes are shown as points and are identified by UTC/shotpoint (SP). Extrapolated positions are shown as tick marks. The processed digital seismic profile is shown in Figure 13.

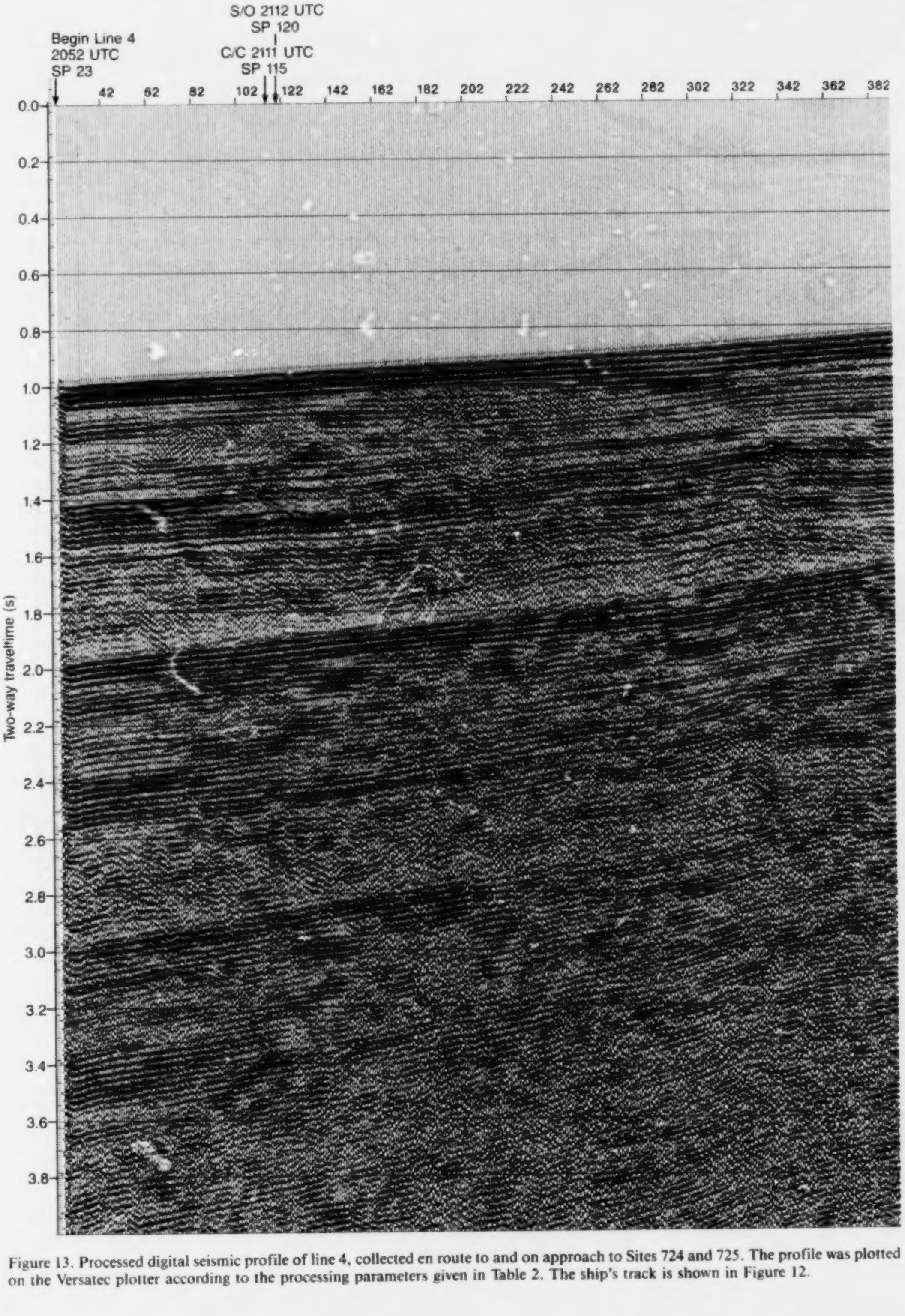

Figure 13. Processed digital seismic profile of line 4, collected en route to and on approach to Sites 724 and 725. The profile was plotted on the Versatec plotter according to the processing parameters given in Table 2. The ship's track is shown in Figure 12.

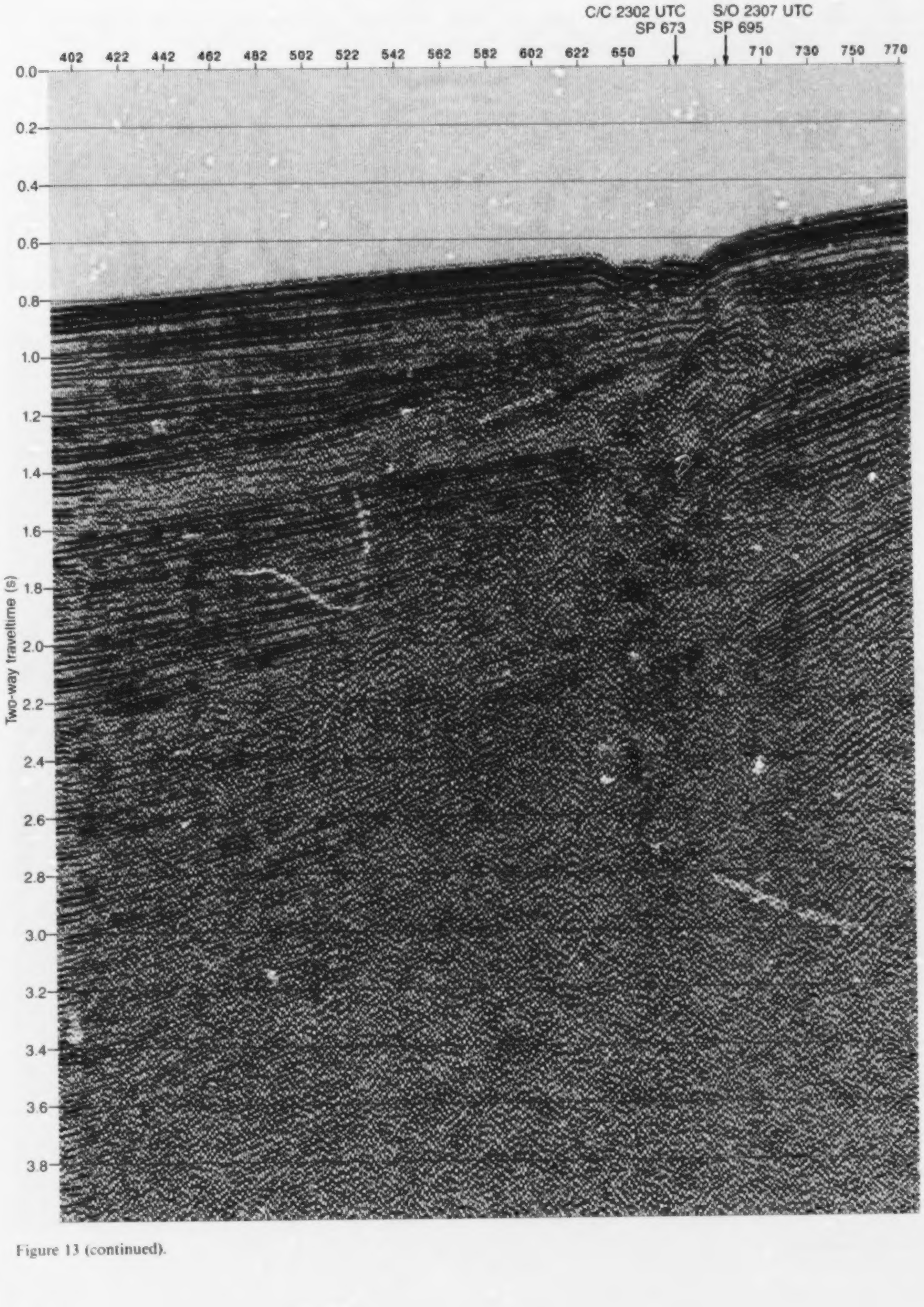

Figure 13 (continued).

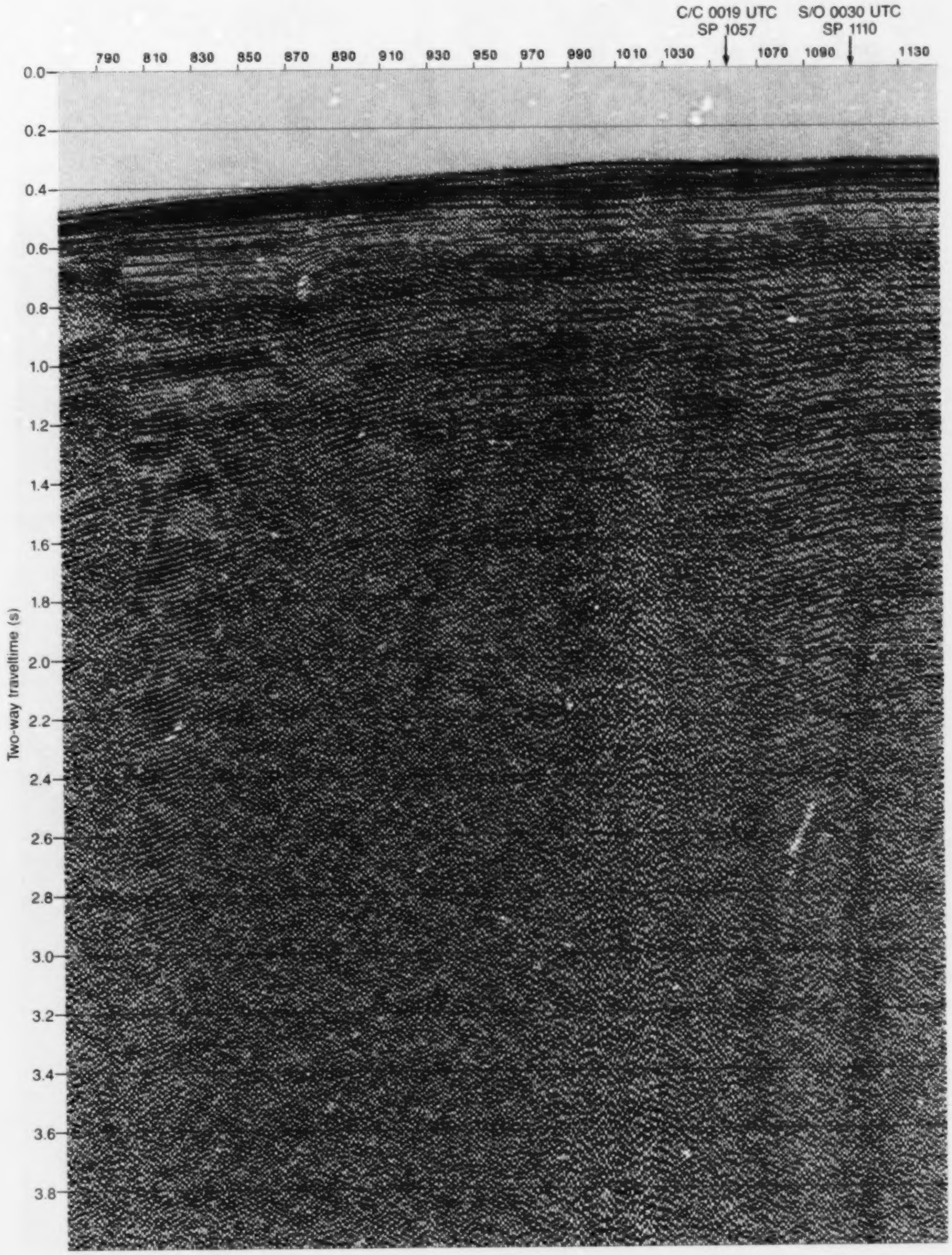

Figure 13 (continued).

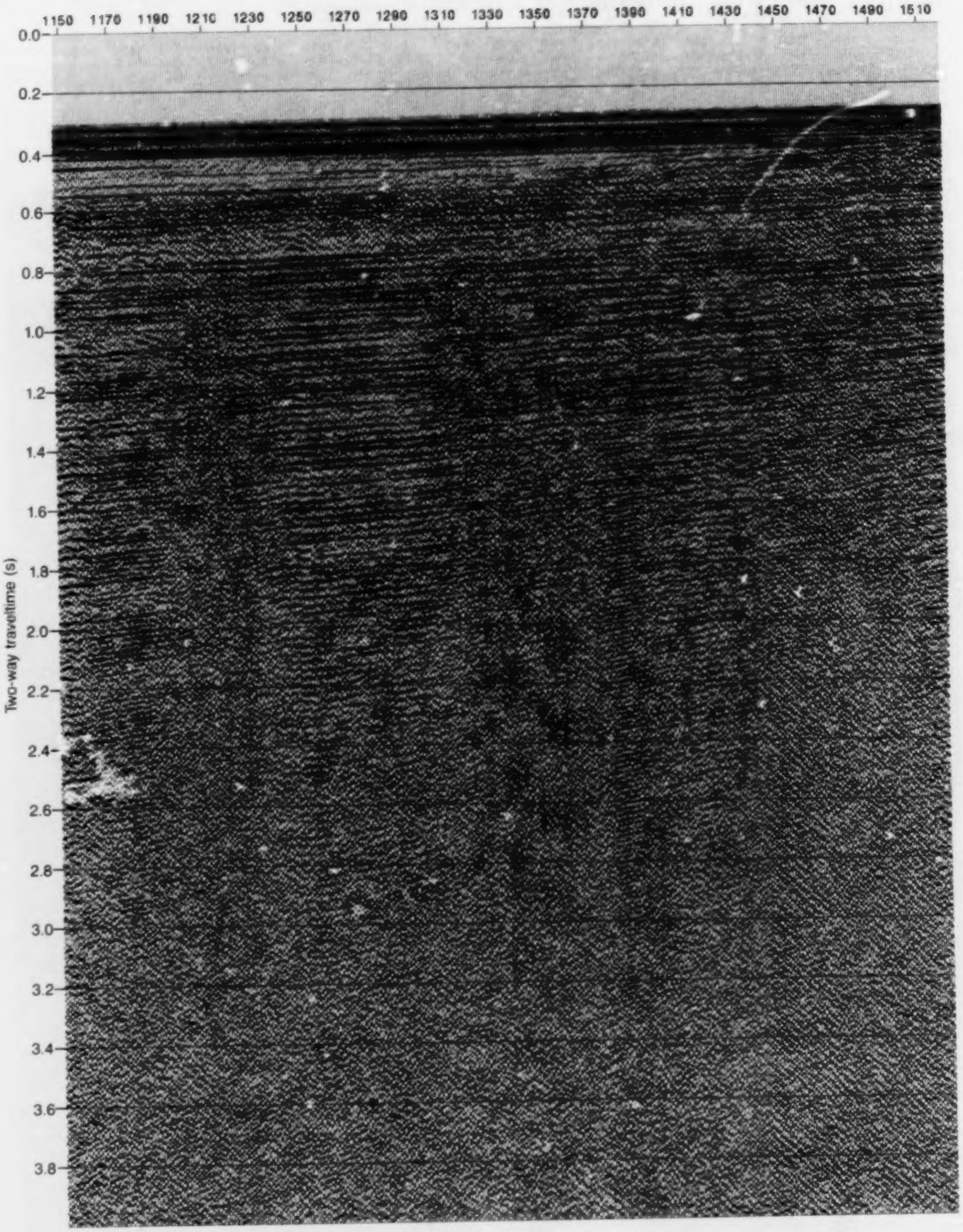

Figure 13 (continued).

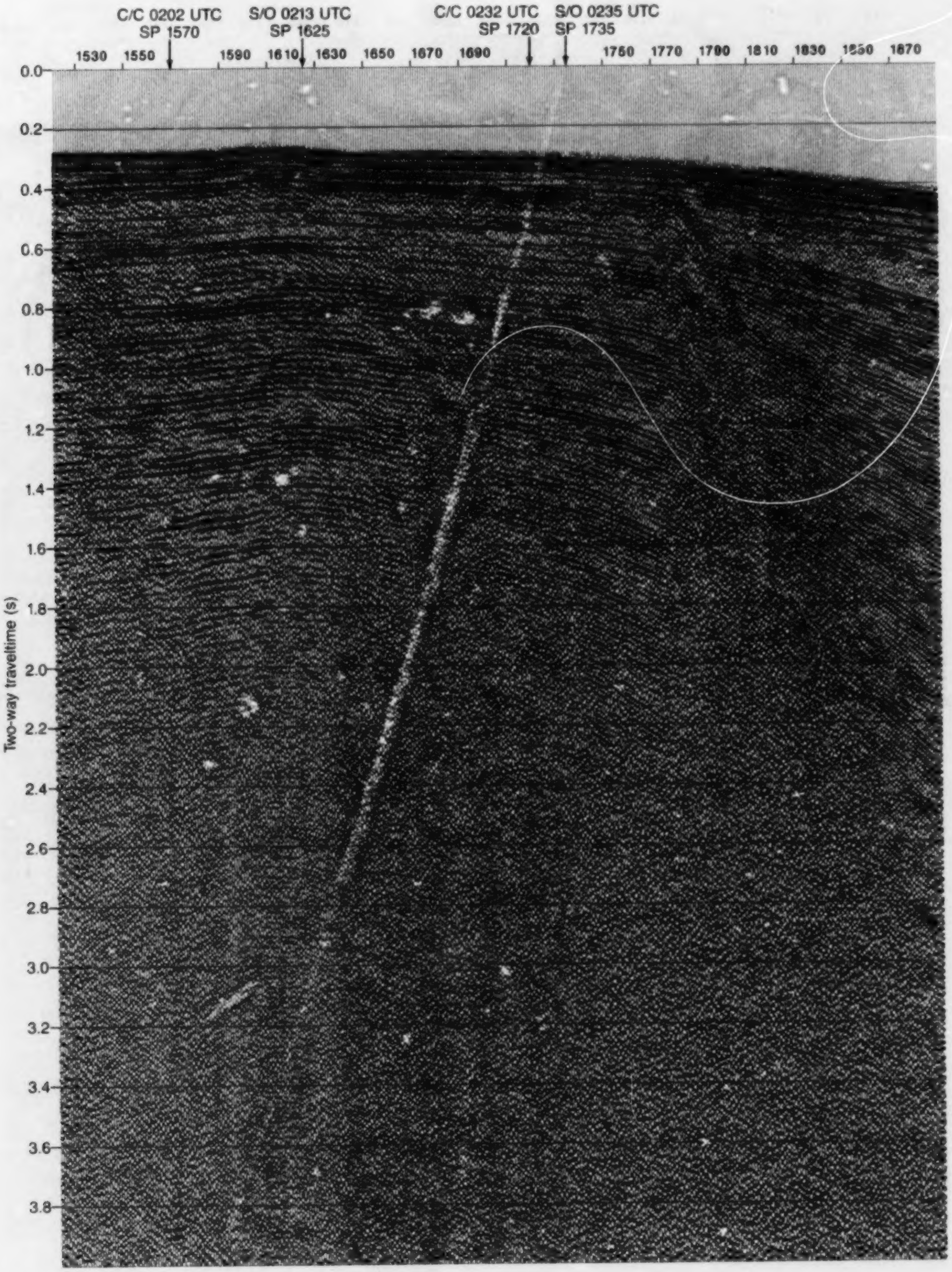

Figure 13 (continued).

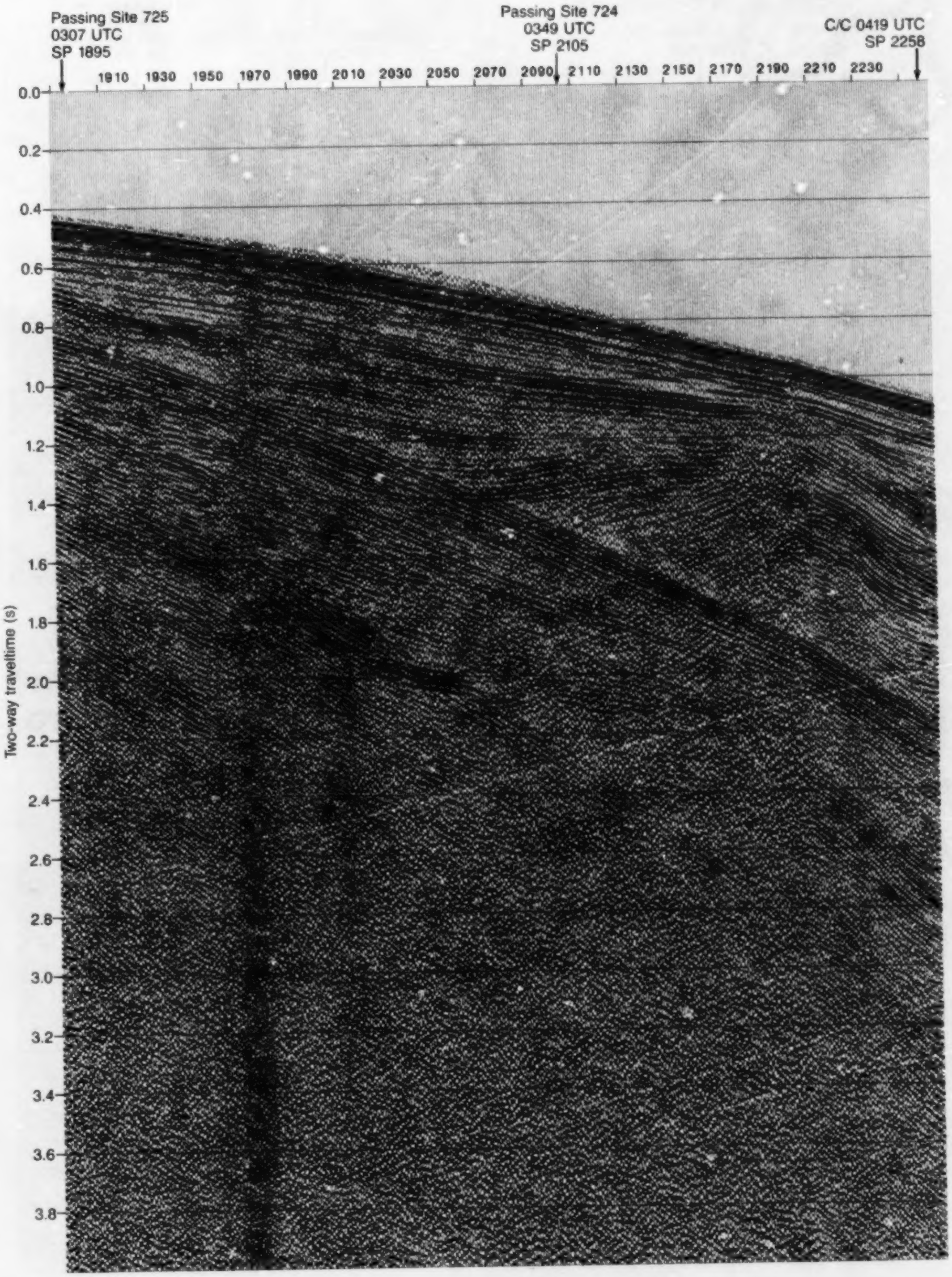

Figure 13 (continued).

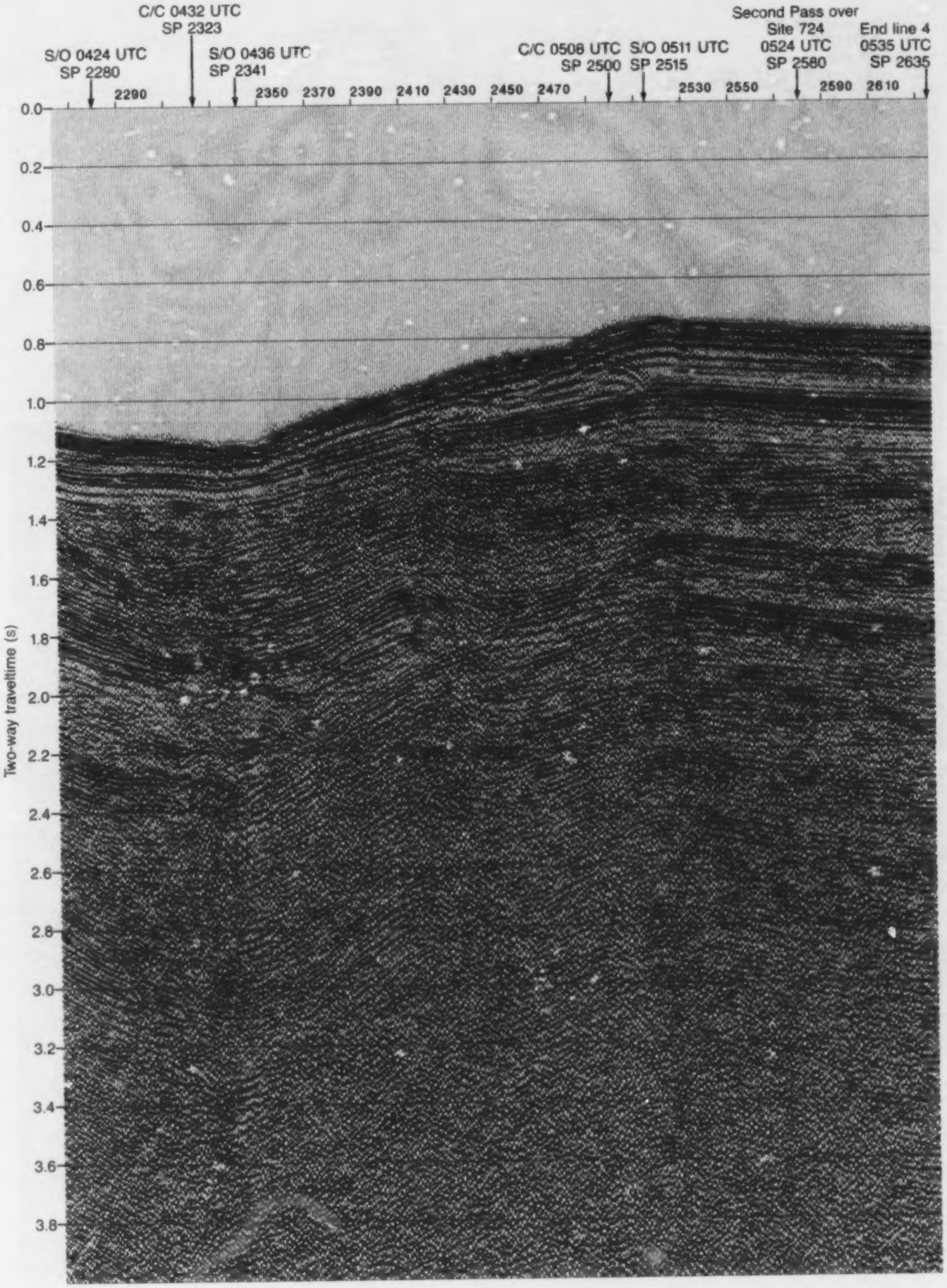

Figure 13 (continued).

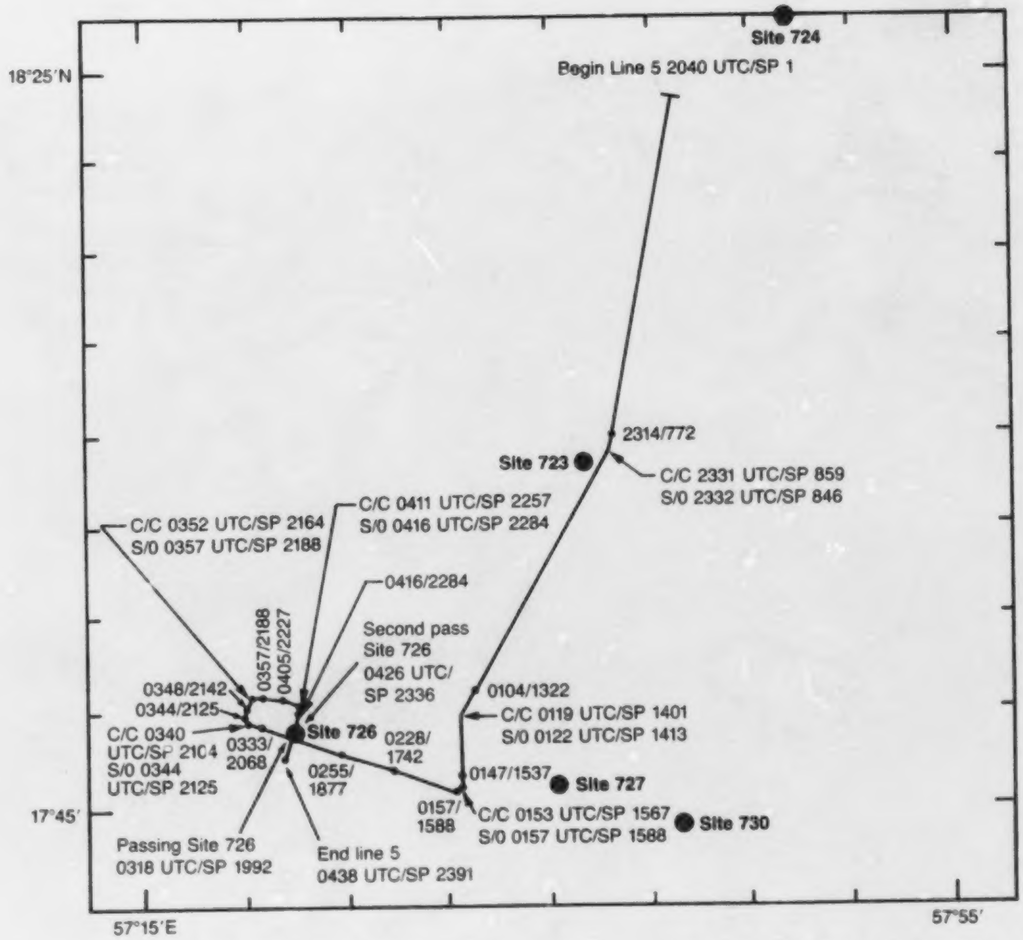
Site 724
18°25′N
Begin Line 5 2040 UTC/SP 1
2314/772
Site 723
C/C 2331 UTC/SP 859
S/0 2332 UTC/SP 846
C/C 0411 UTC/SP 2257
S/0 0416 UTC/SP 2284
C/C 0352 UTC/SP 2164
S/0 0357 UTC/SP 2188
0416/2284
0357/2188
0405/2227
Second pass
Site 726
0426 UTC/
SP 2336
0348/2142
0344/2125
0104/1322
C/C 0119 UTC/SP 1401
S/0 0122 UTC/SP 1413
C/C 0340
UTC/SP 2104
S/0 0344
UTC/SP 2125
0333/
2068
Site 726
0228/
1742
0255/
1877
0147/1537
Site 727
17°45′
0157/
1588
C/C 0153 UTC/SP 1567
S/0 0157 UTC/SP 1588
Site 730
Passing Site 726
0318 UTC/SP 1992
End line 5
0438 UTC/SP 2391
57°15′E
57°55′

Figure 14. Detailed ship's track for seismic line 5, en route to and on approach to Site 726. Satellite fixes are shown as points and are identified by UTC/shotpoint (SP). Extrapolated positions are shown as tick marks. The processed digital seismic profile is shown in Figure 15.

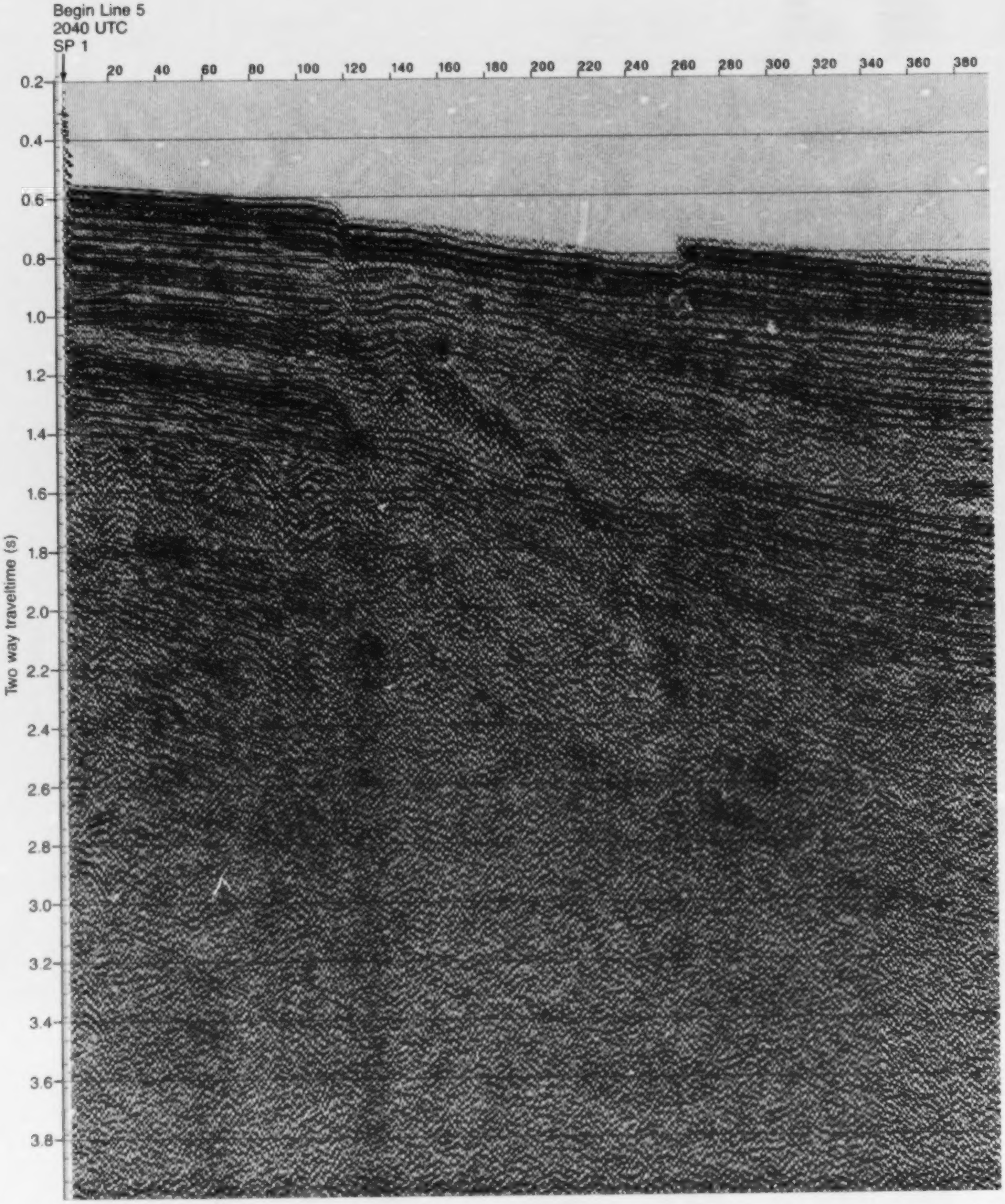

Figure 15. Processed digital seismic profile of line 5, collected en route to and on approach to Site 726. The profile was plotted on the Versatec plotter according to the processing parameters given in Table 2. The ship's track is shown in Figure 14.

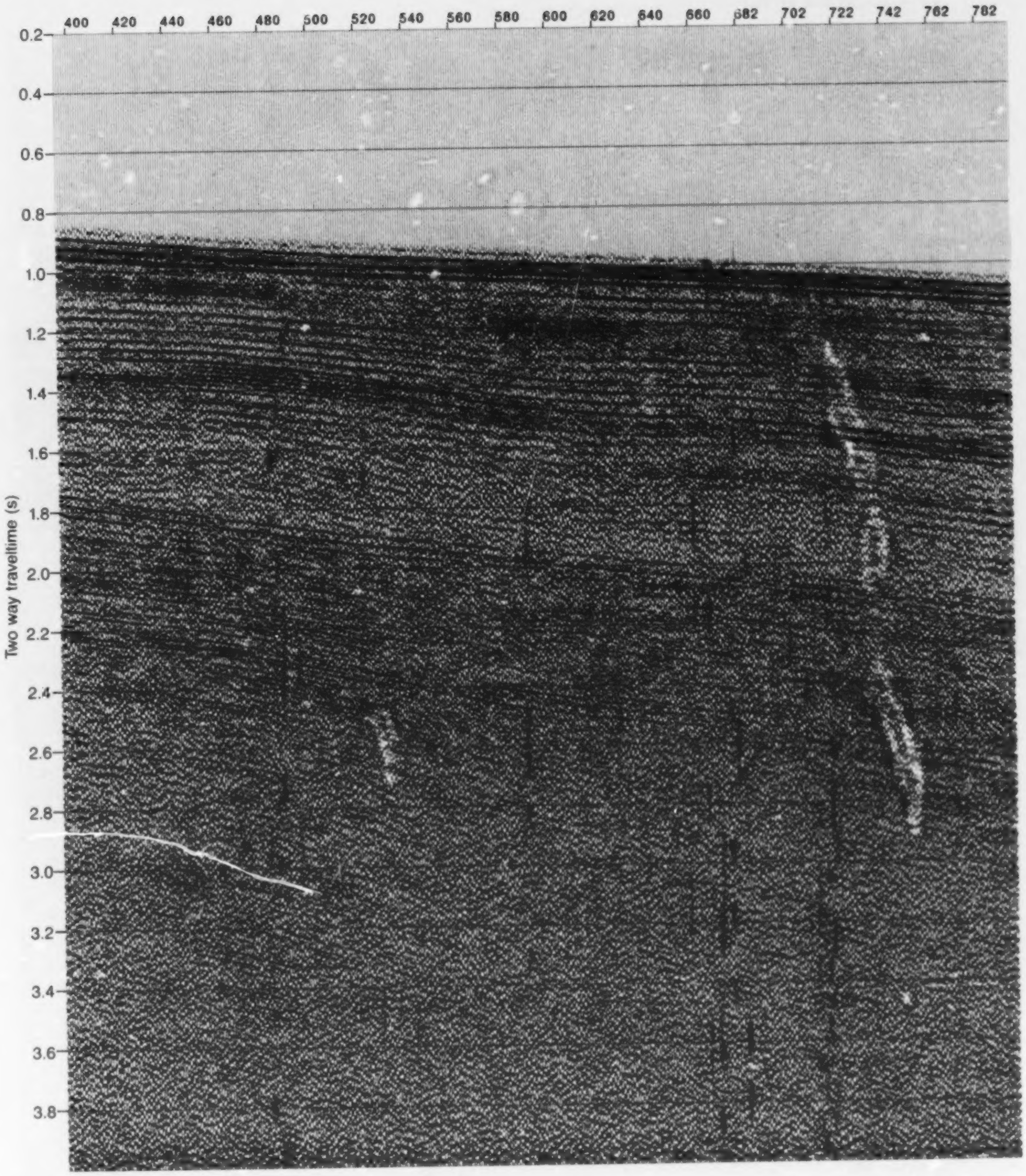

Figure 15 (continued).

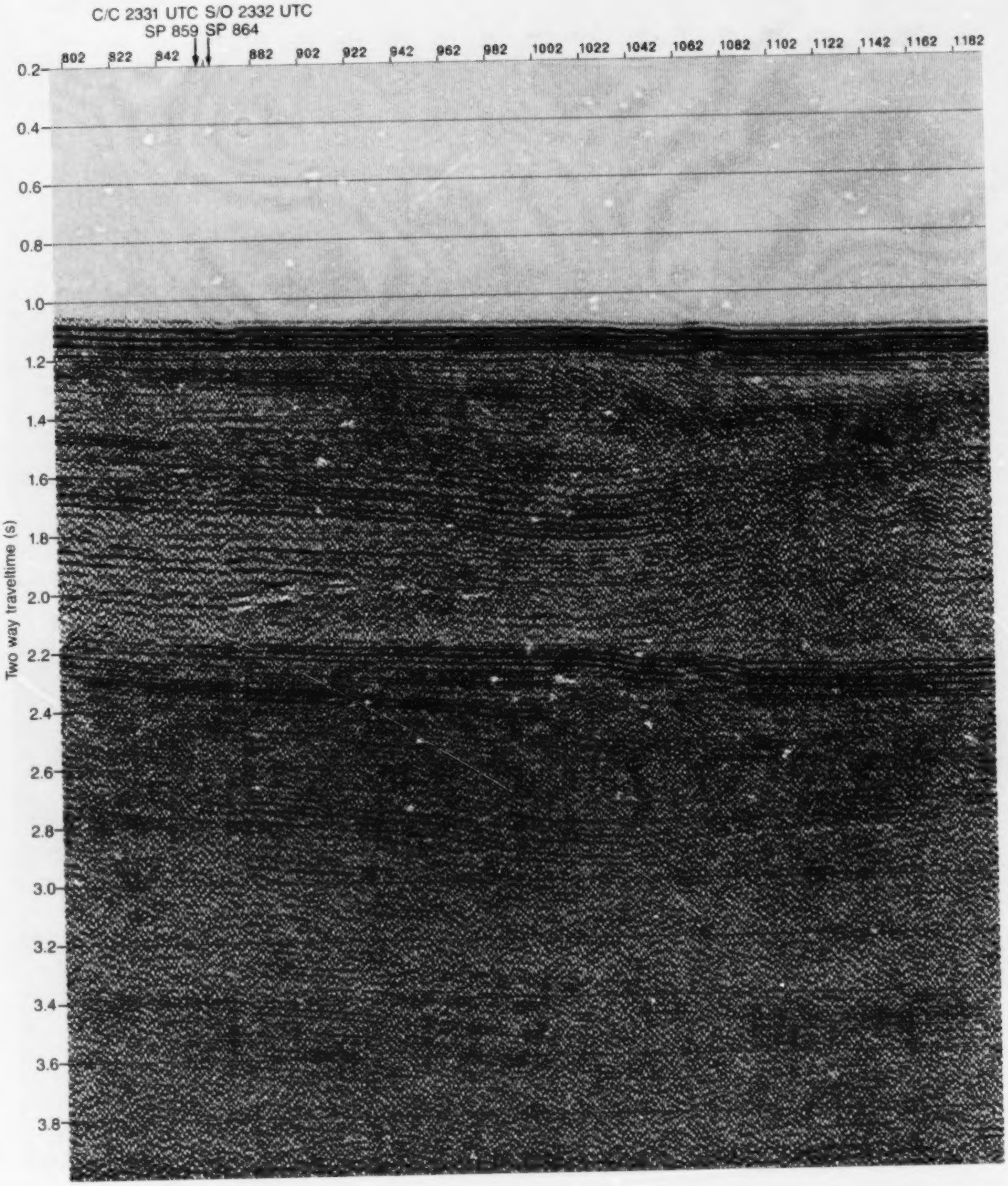

Figure 15 (continued).

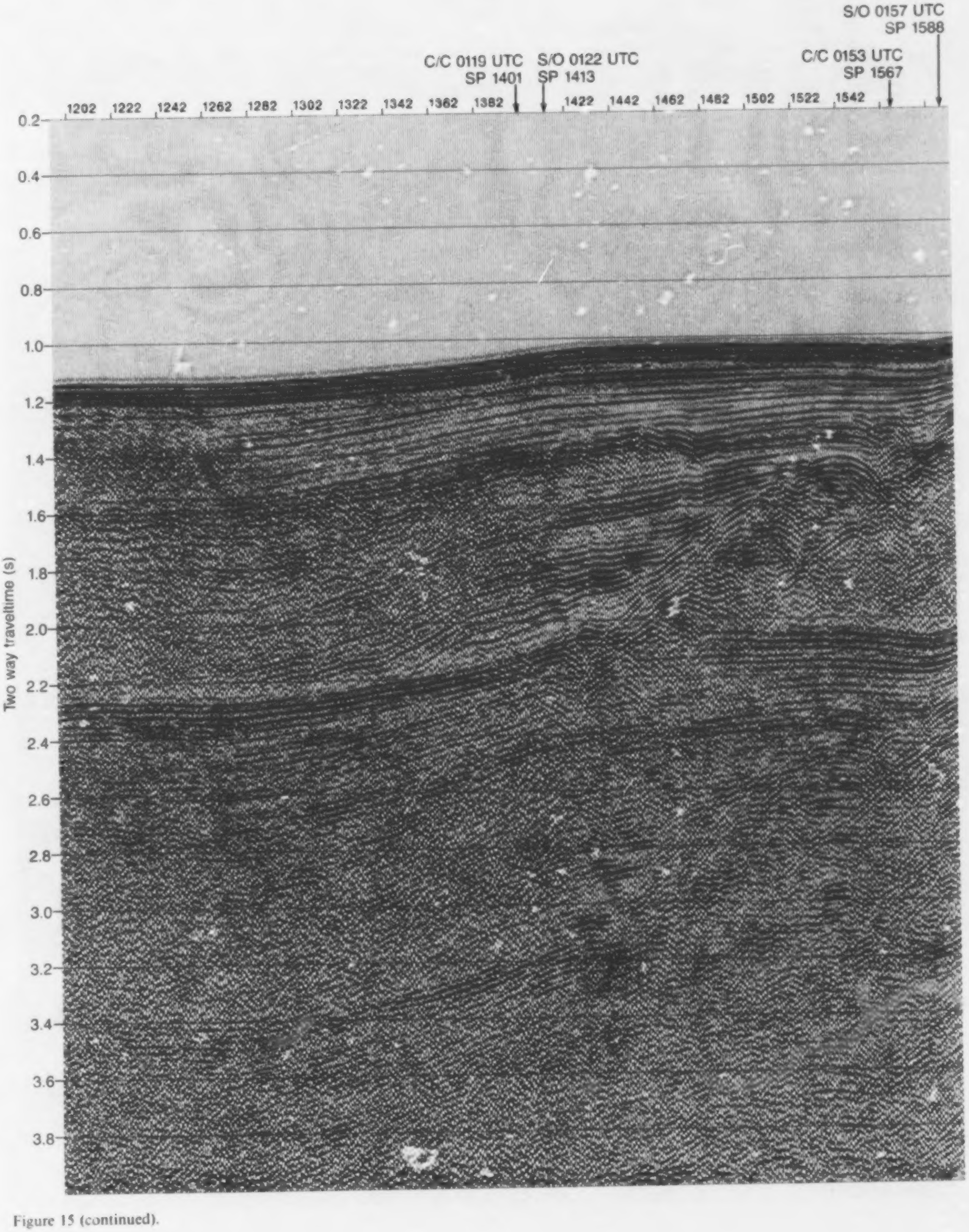

Figure 15 (continued).

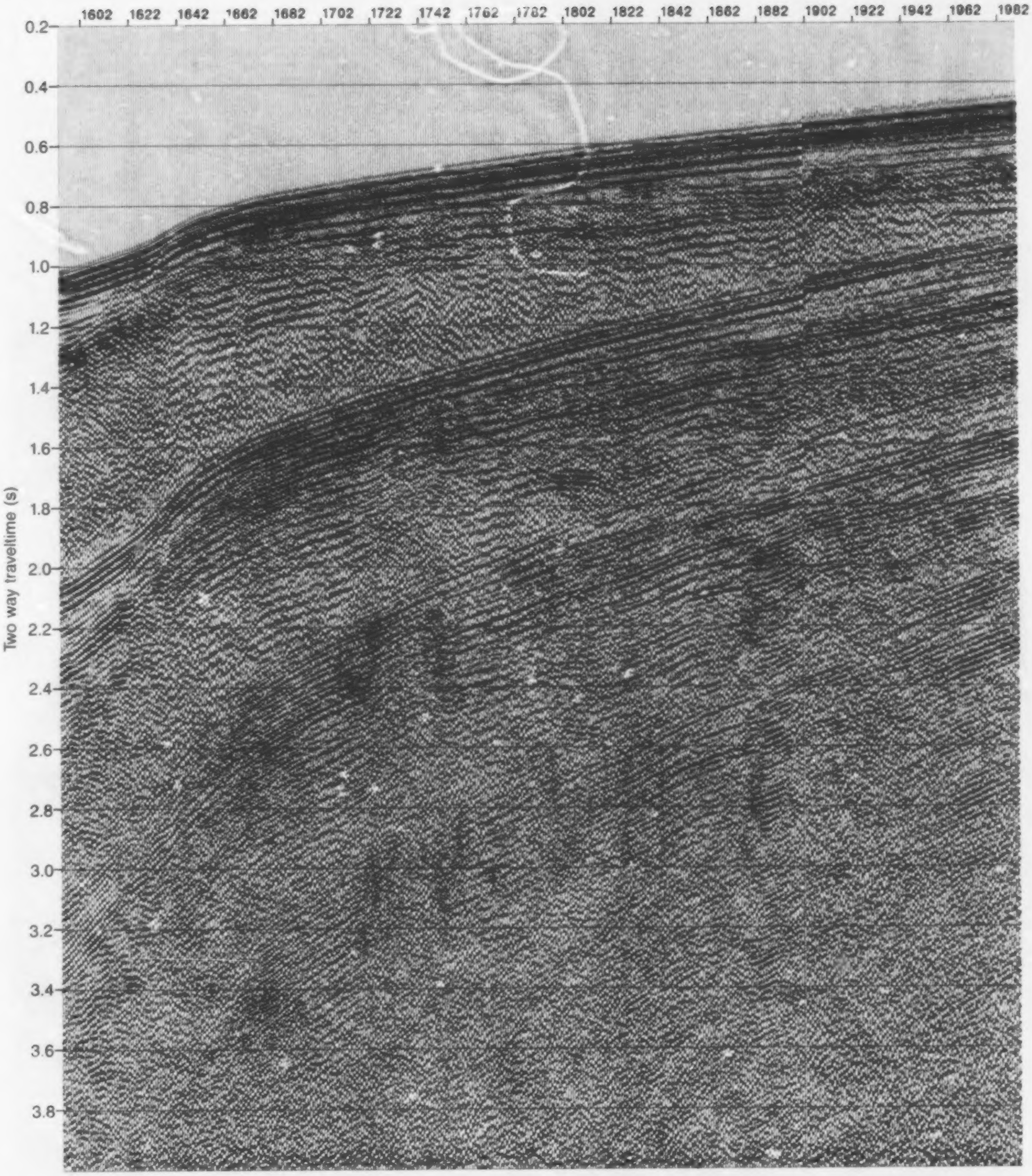

Figure 15 (continued).

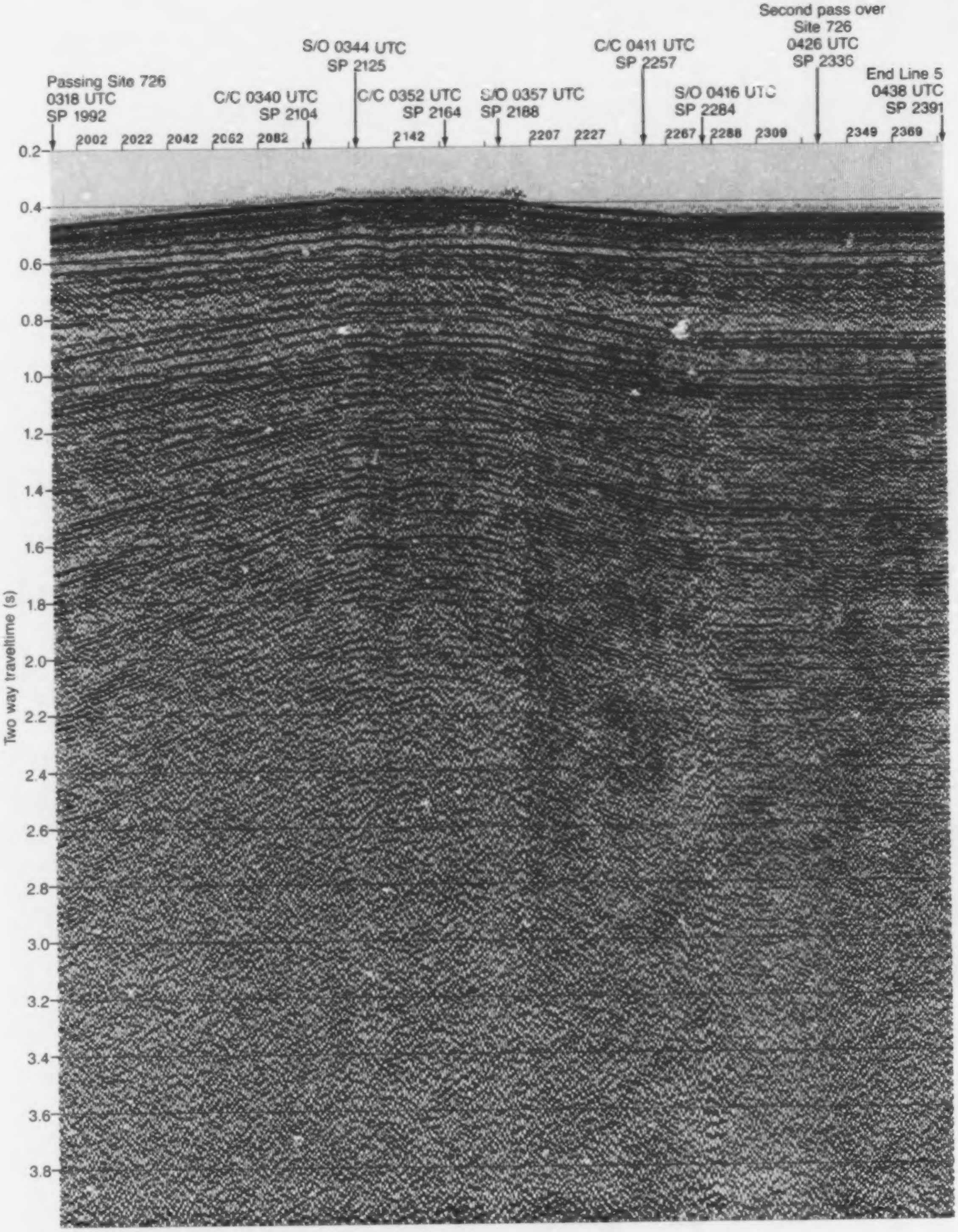

Figure 15 (continued).

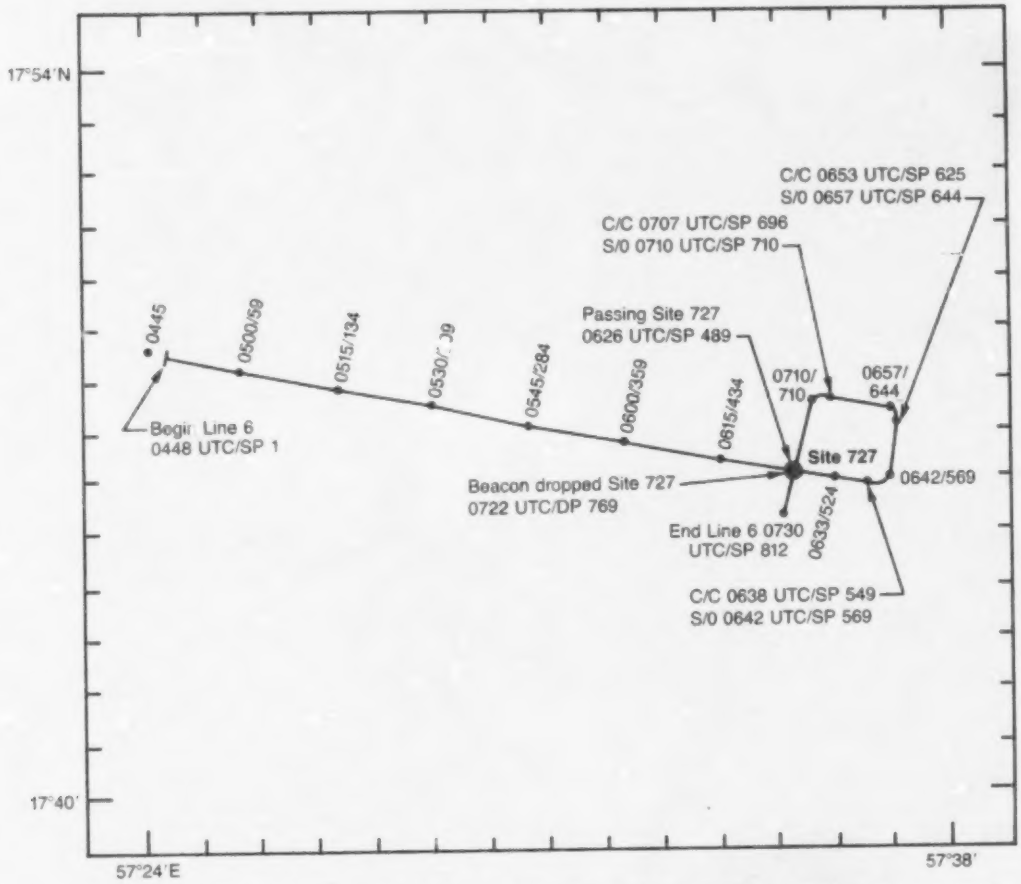
17°54′N
17°40′
57°24′E
57°38′
0445
0500/59
0515/134
0530/209
0545/284
0600/359
0815/434
Begin Line 6
0448 UTC/SP 1
Passing Site 727
0626 UTC/SP 489
C/C 0707 UTC/SP 696
S/0 0710 UTC/SP 710
C/C 0653 UTC/SP 625
S/0 0657 UTC/SP 644
0710/
710
0657/
644
Site 727
0642/569
Beacon dropped Site 727
0722 UTC/DP 769
End Line 6 0730
UTC/SP 812
0633/524
C/C 0638 UTC/SP 549
S/0 0642 UTC/SP 569

Figure 16. Detailed ship's track for seismic line 6, en route to and on approach to Site 727. Satellite fixes are shown as points and are identified by UTC/shotpoint (SP). Extrapolated positions are shown as tick marks. The processed digital seismic profile is shown in Figure 17.

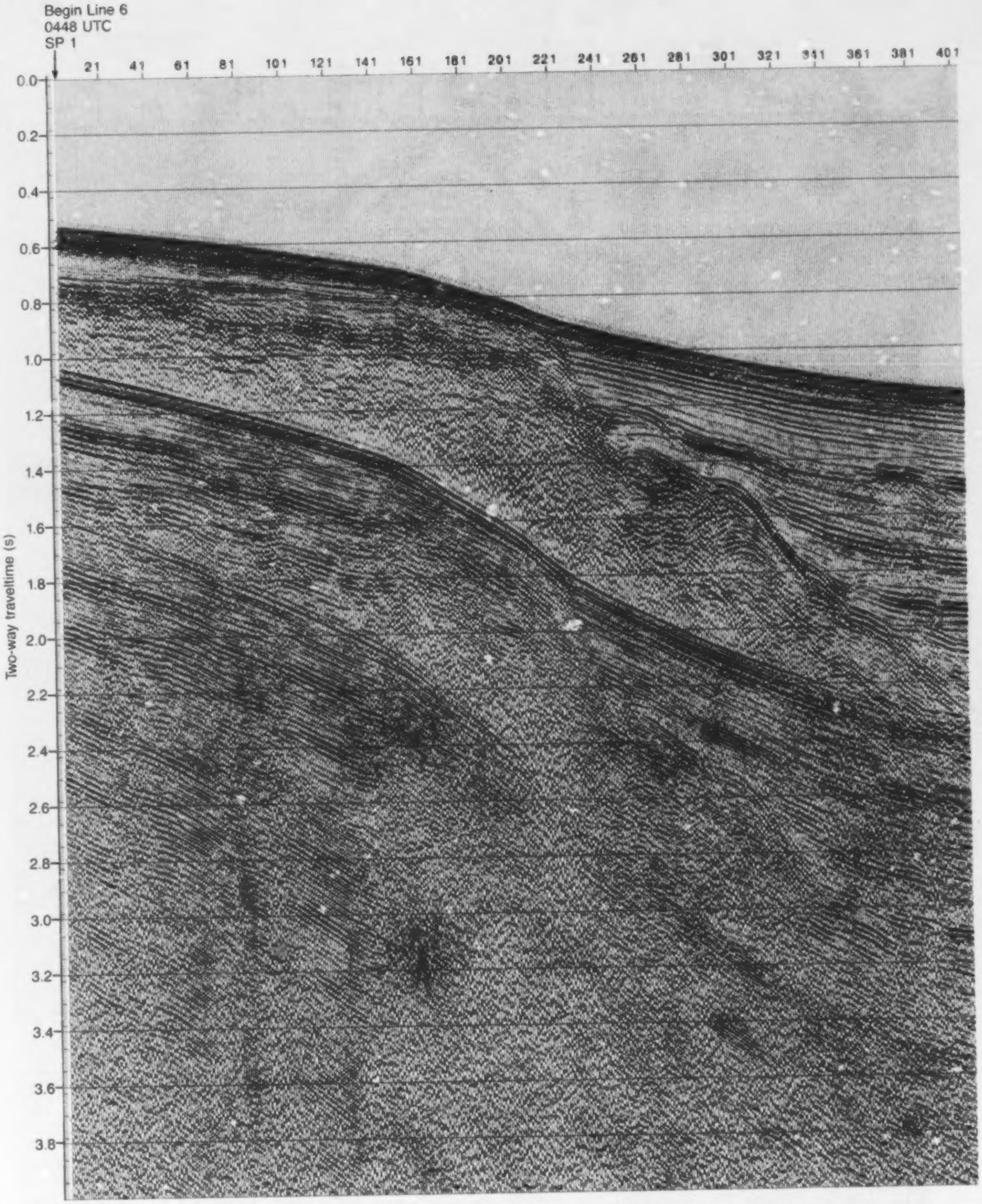

Figure 17. Processed digital seismic profile of line 6, collected en route to and on approach to Site 727. The profile was plotted on the Versatec plotter according to the processing parameters given in Table 2. The ship's track is shown in Figure 16.

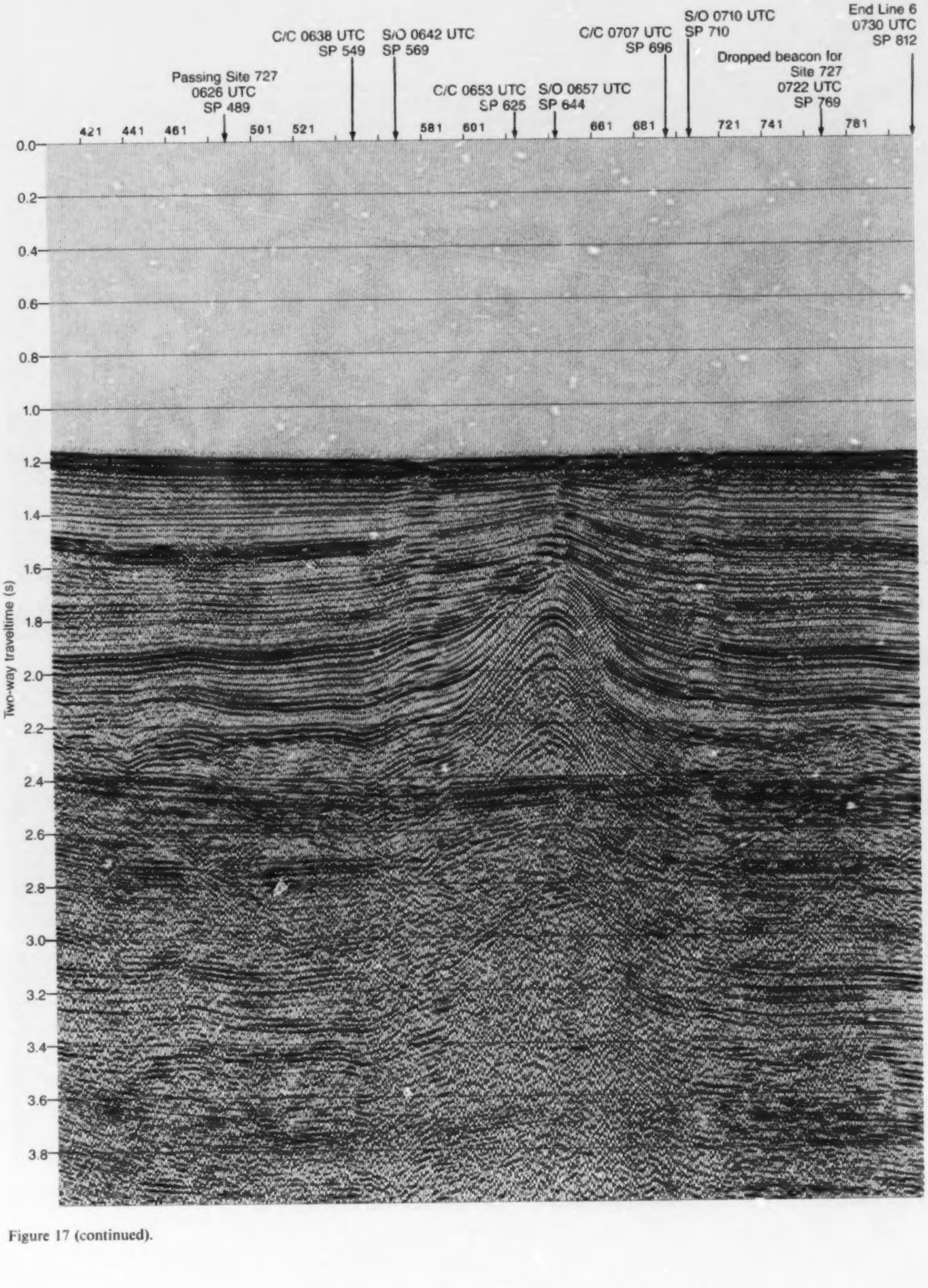

Figure 17 (continued).

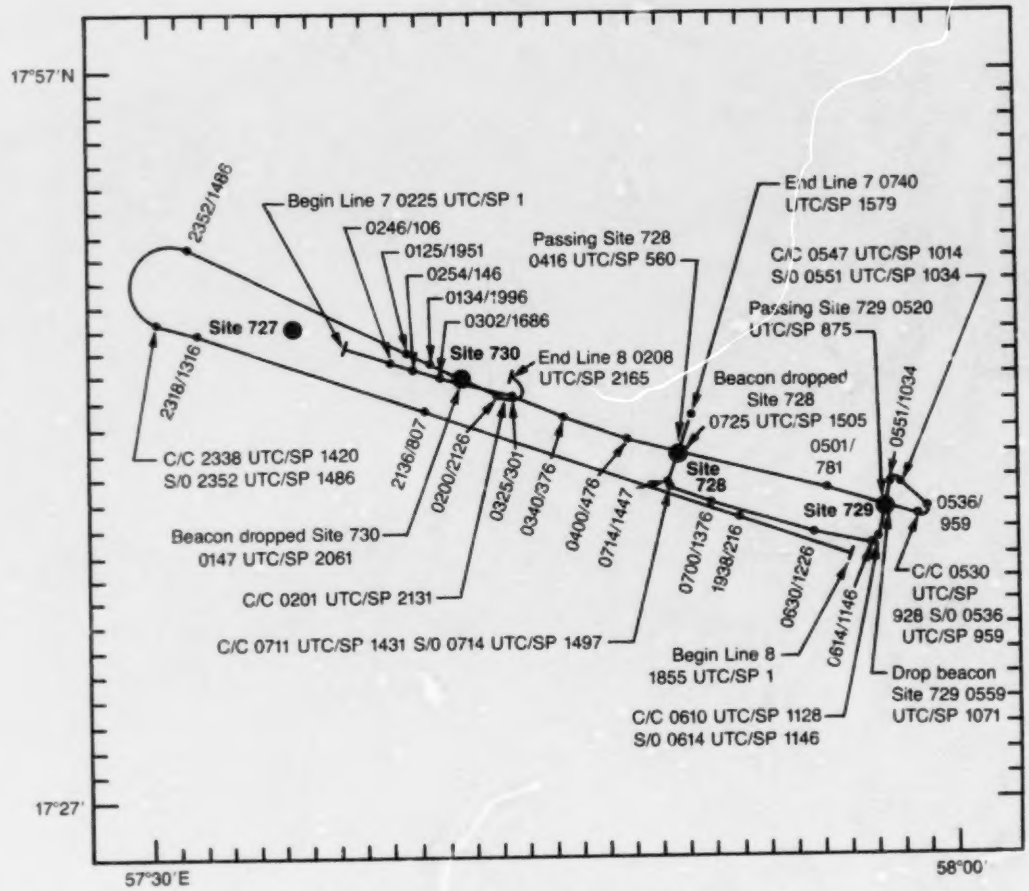
17°57'N
17°27'
57°30'E
58°00'
2352/1486
Begin Line 7 0225 UTC/SP 1
0246/106
0125/1951
0254/146
0134/1996
0302/1686
Site 727
Site 730
End Line 8 0208 UTC/SP 2165
Passing Site 728 0416 UTC/SP 560
End Line 7 0740 UTC/SP 1579
C/C 0547 UTC/SP 1014
S/0 0551 UTC/SP 1034
Passing Site 729 0520 UTC/SP 875
Beacon dropped Site 728 0725 UTC/SP 1505
0501/781
0551/1034
Site 728
Site 729
0536/959
2318/1316
C/C 2338 UTC/SP 1420
S/0 2352 UTC/SP 1486
2136/807
0200/2126
0325/301
0340/376
0400/476
0714/1447
0700/1376
1938/216
0630/1226
0614/1146
Beacon dropped Site 730 0147 UTC/SP 2061
C/C 0201 UTC/SP 2131
C/C 0711 UTC/SP 1431 S/0 0714 UTC/SP 1497
Begin Line 8 1855 UTC/SP 1
C/C 0610 UTC/SP 1128
S/0 0614 UTC/SP 1146
C/C 0530 UTC/SP 928 S/0 0536 UTC/SP 959
Drop beacon Site 729 0559 UTC/SP 1071

Figure 18. Detailed ship's tracks for seismic line 7, en route to and on approach to Sites 728 and 729, and for seismic line 8, en route to and on approach to Site 730. Satellite fixes are shown as points and are identified by UTC/shotpoint (SP). Extrapolated positions are shown as tick marks. The processed digital seismic profiles for lines 7 and 8 are shown in Figures 19 and 20, respectively.

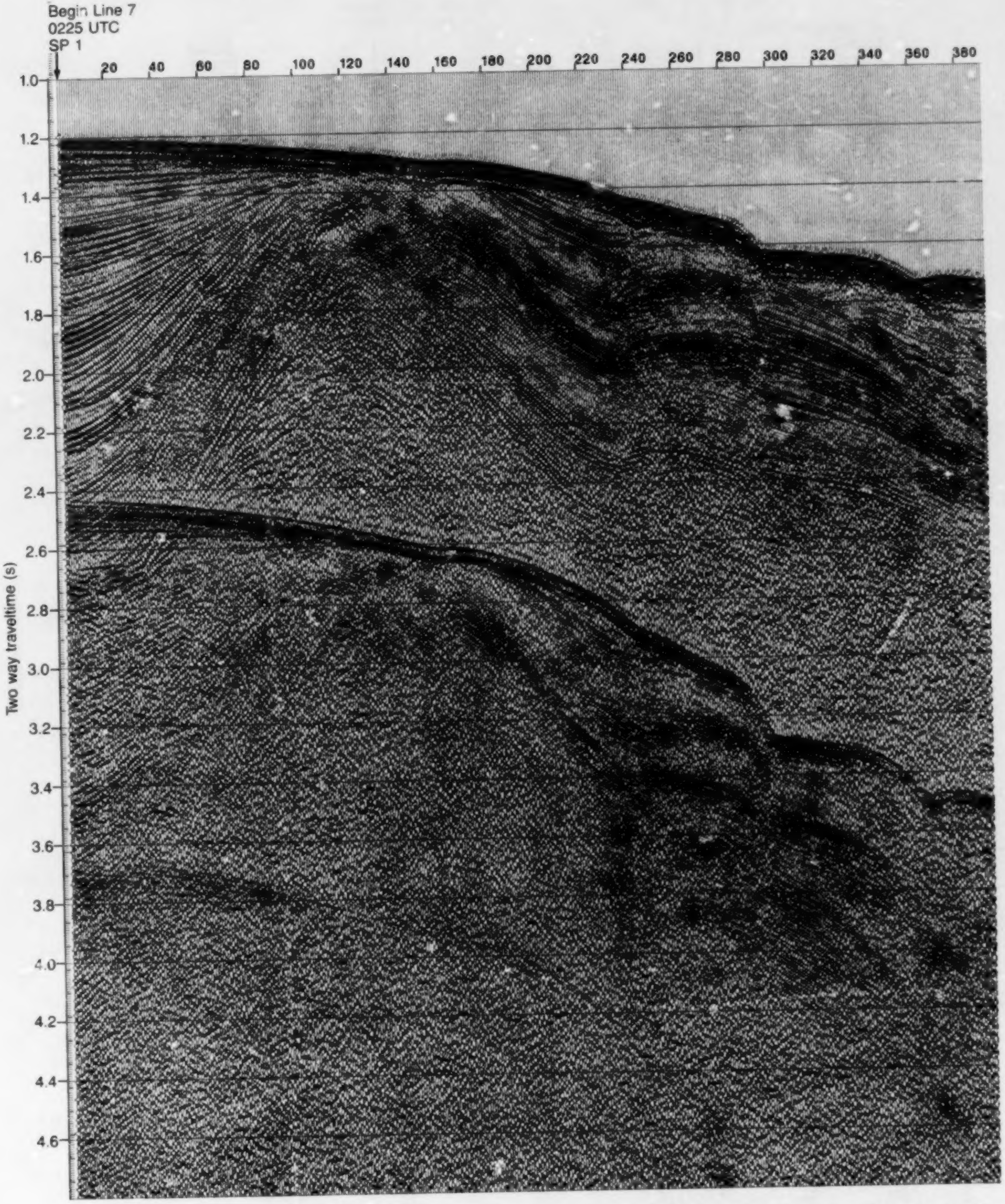

Figure 19. Processed digital seismic profile of line 7, collected en route to and on approach to Sites 728 and 729. The profile was plotted on the Versatec plotter according to the processing parameters given in Table 2. The ship's track is shown in Figure 18.

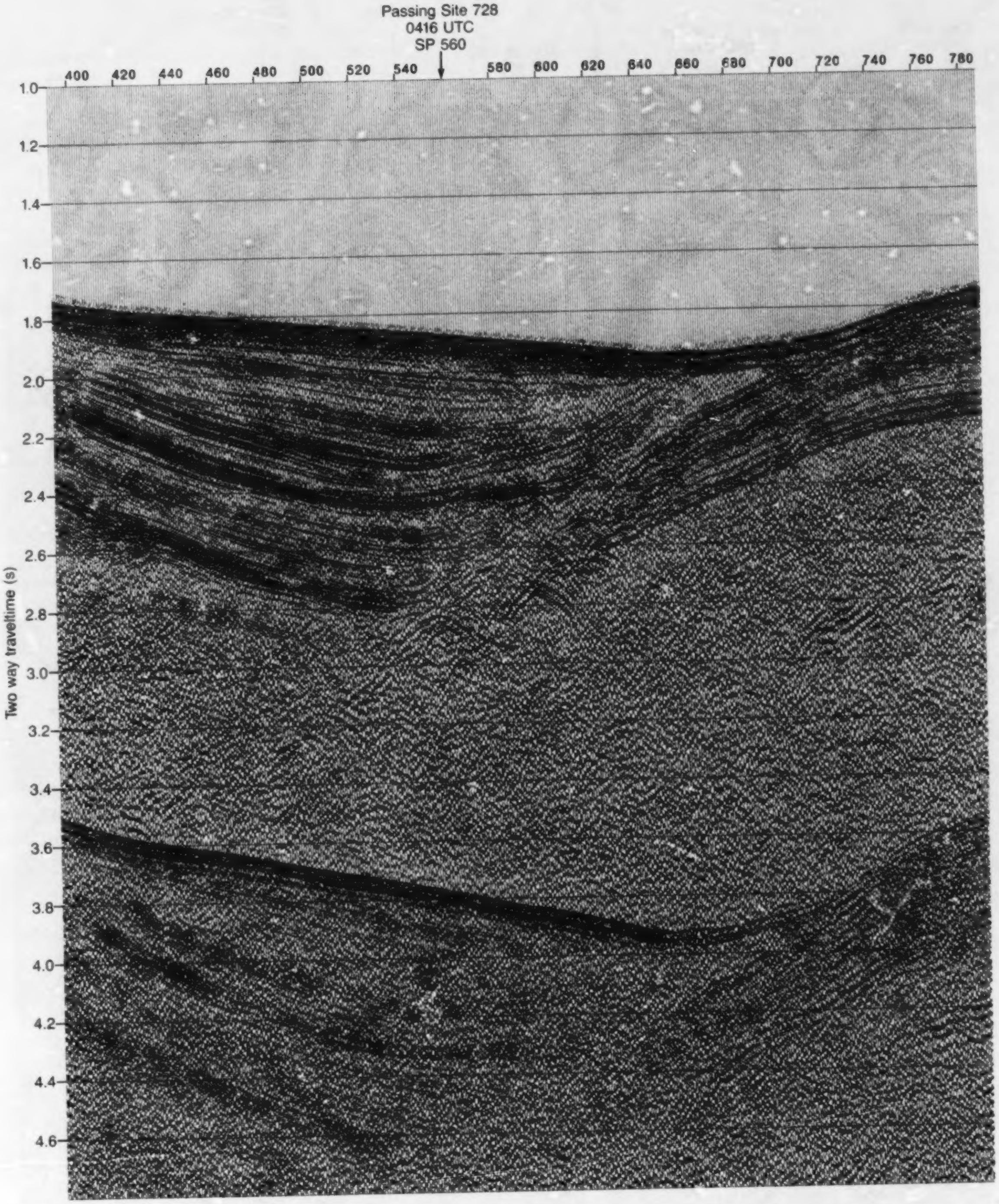

Figure 19 (continued).

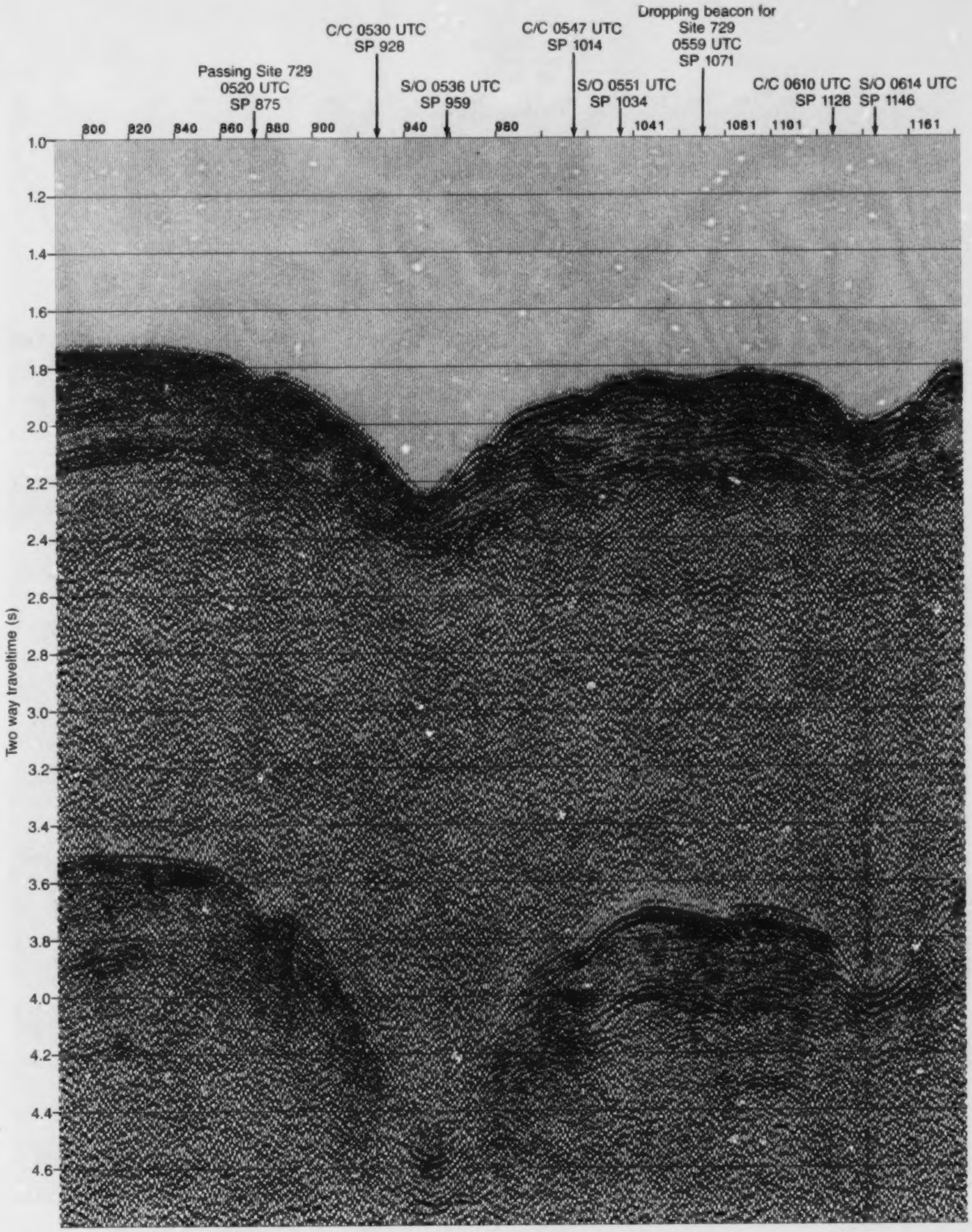

Figure 19 (continued).

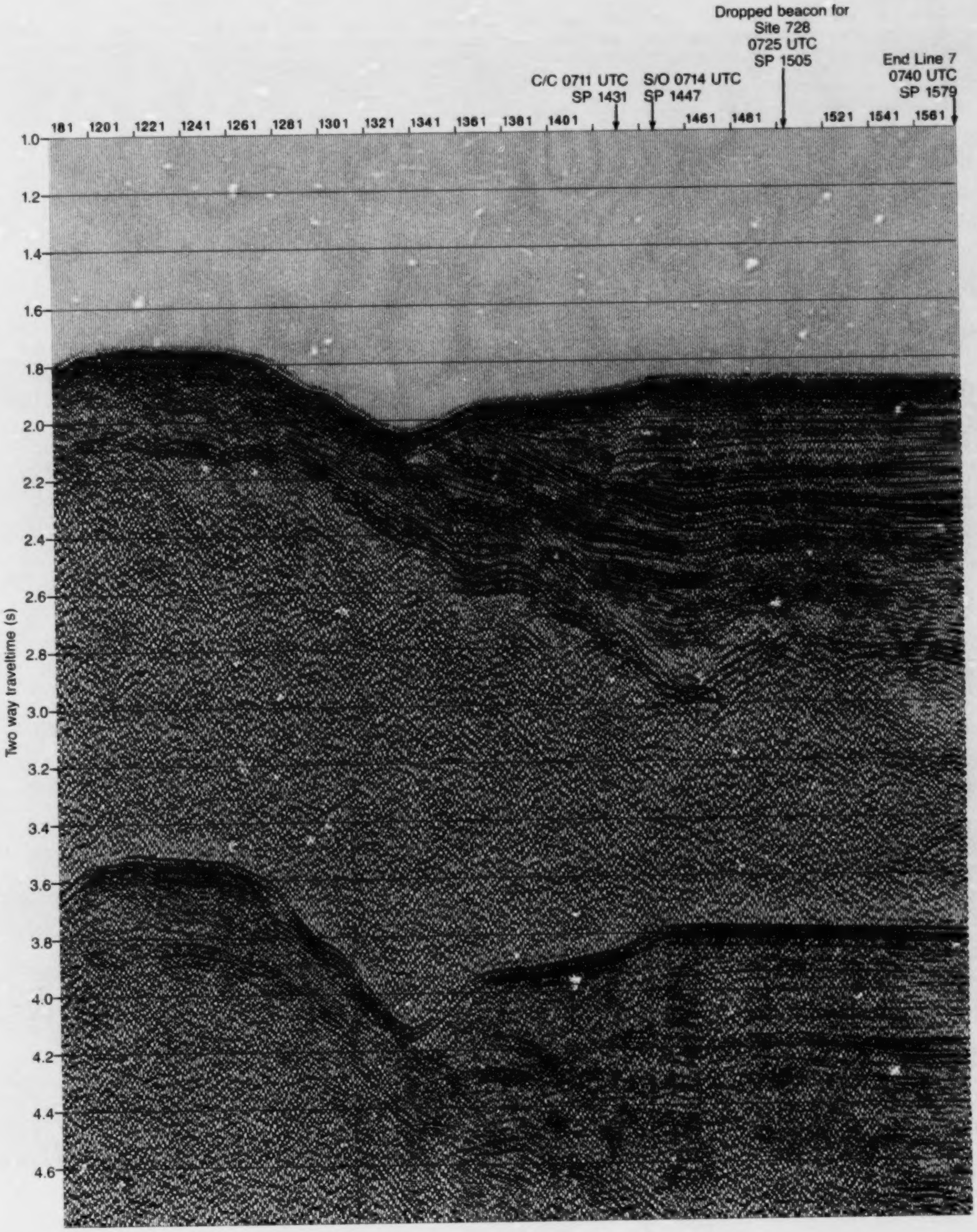

Figure 19 (continued).

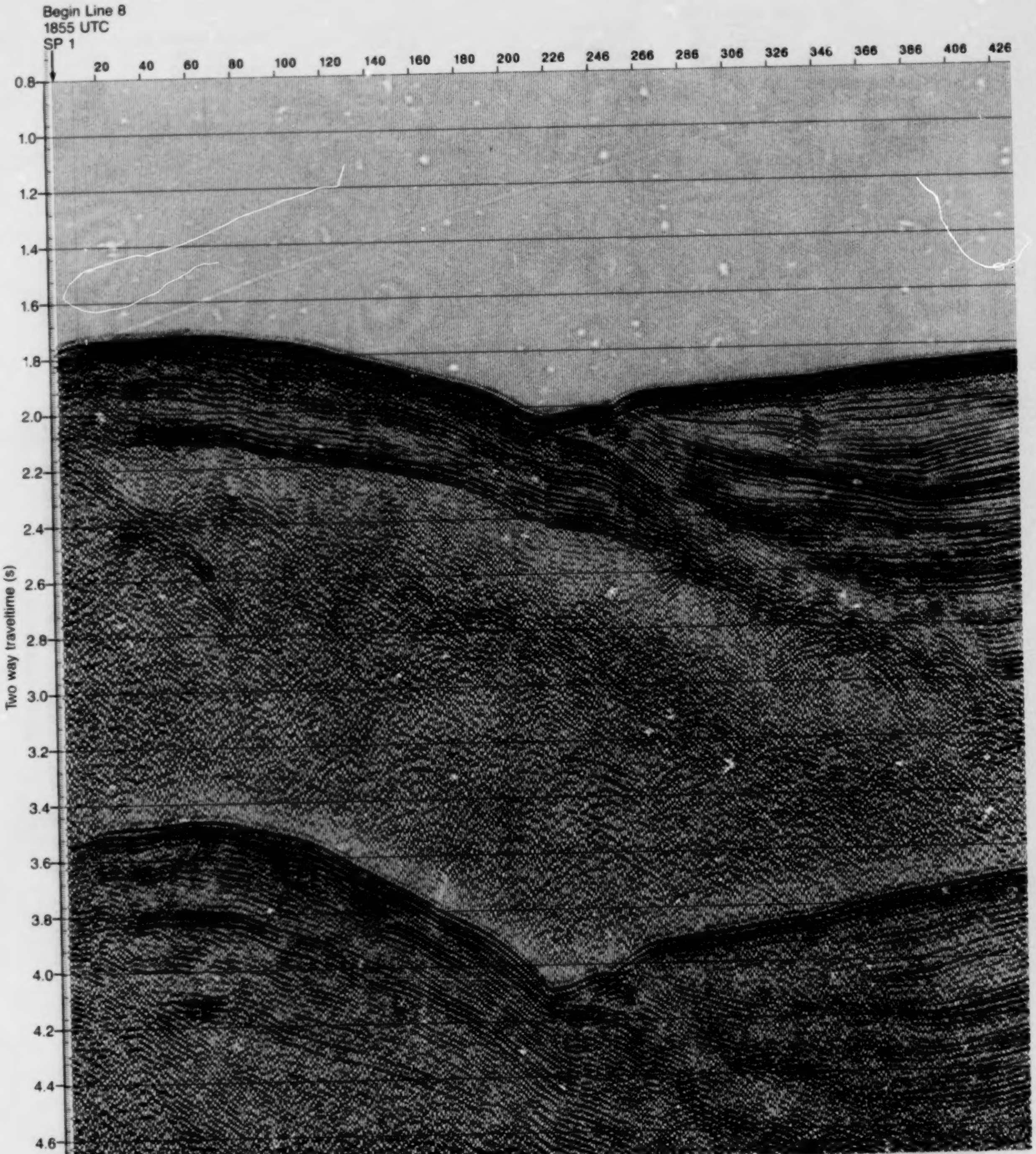

Figure 20. Processed digital seismic profile on line 8, collected en route to and on approach to Site 730. The profile was plotted on the Versatec plotter according to the processing parameters given in Table 2. The ship's track is shown in Figure 18.

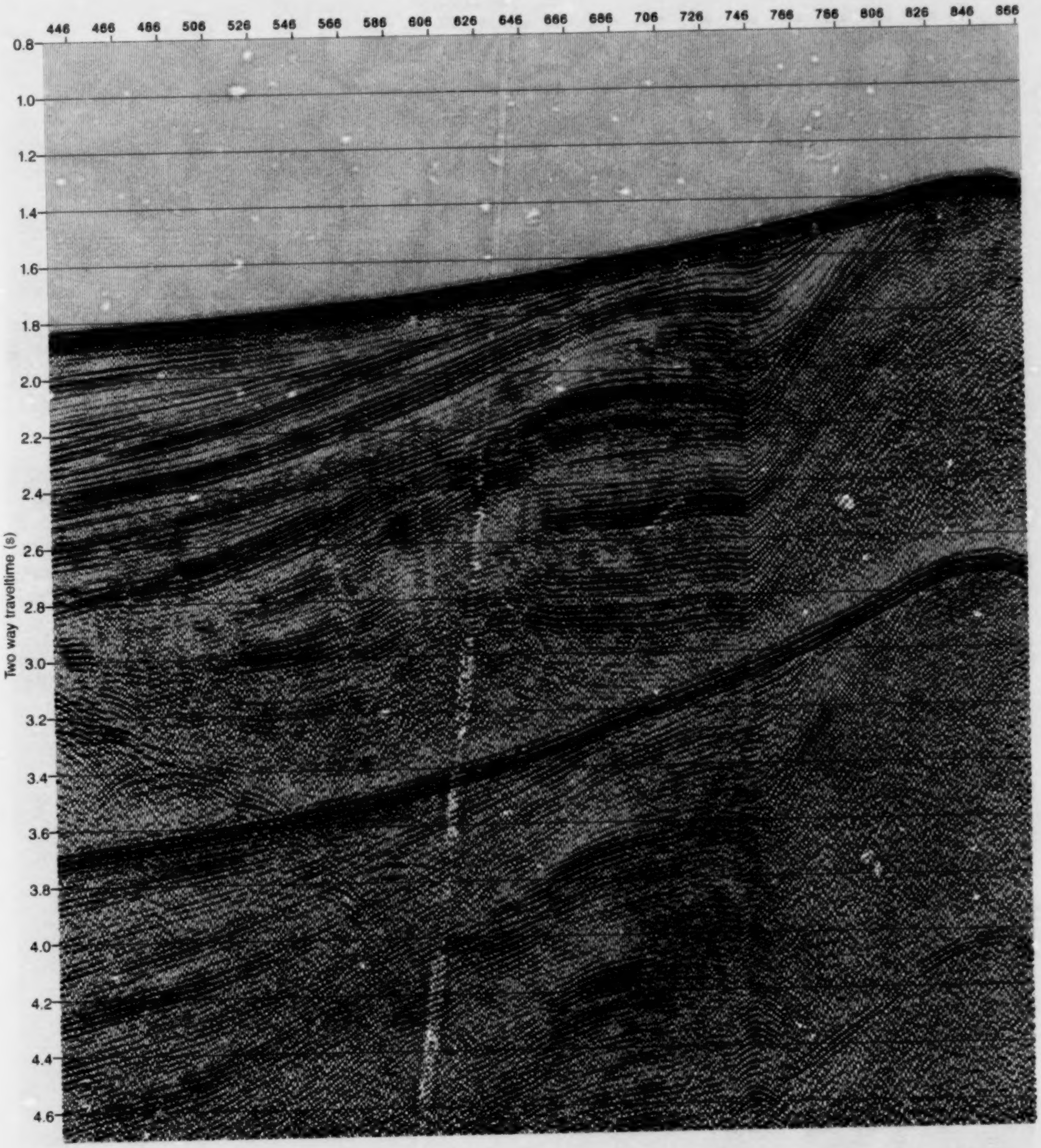

Figure 20 (continued).

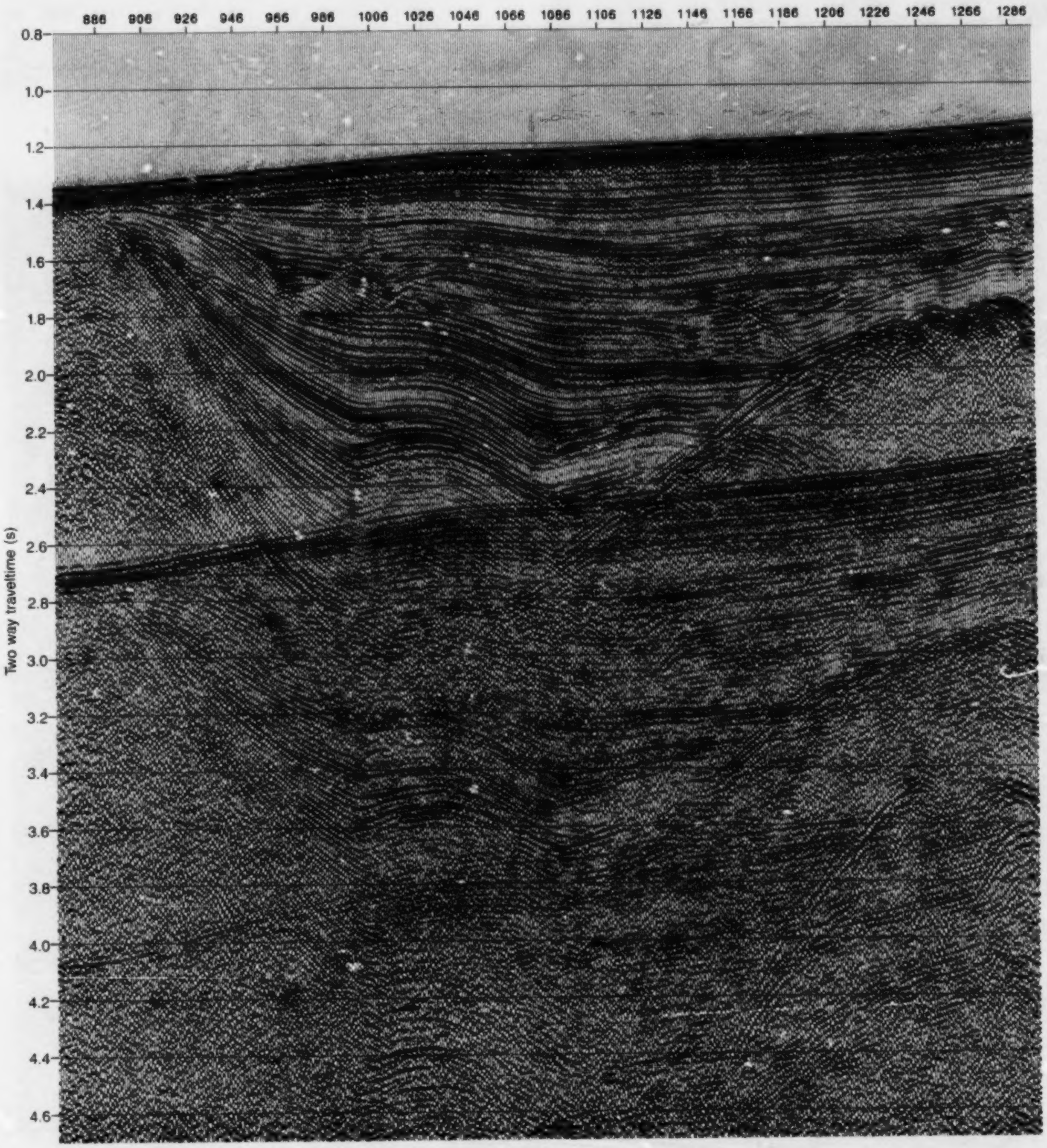

Figure 20 (continued).

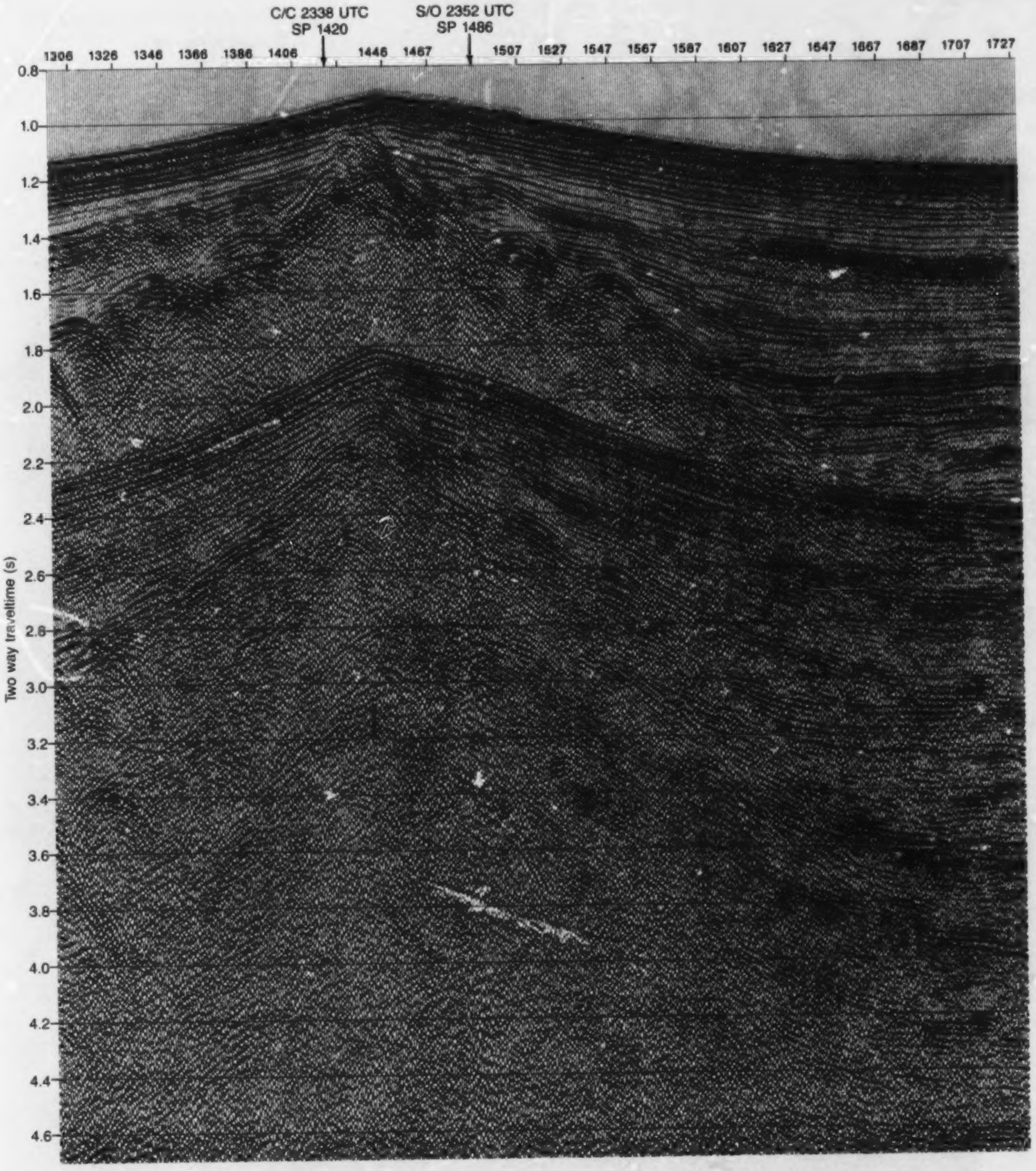

Figure 20 (continued).

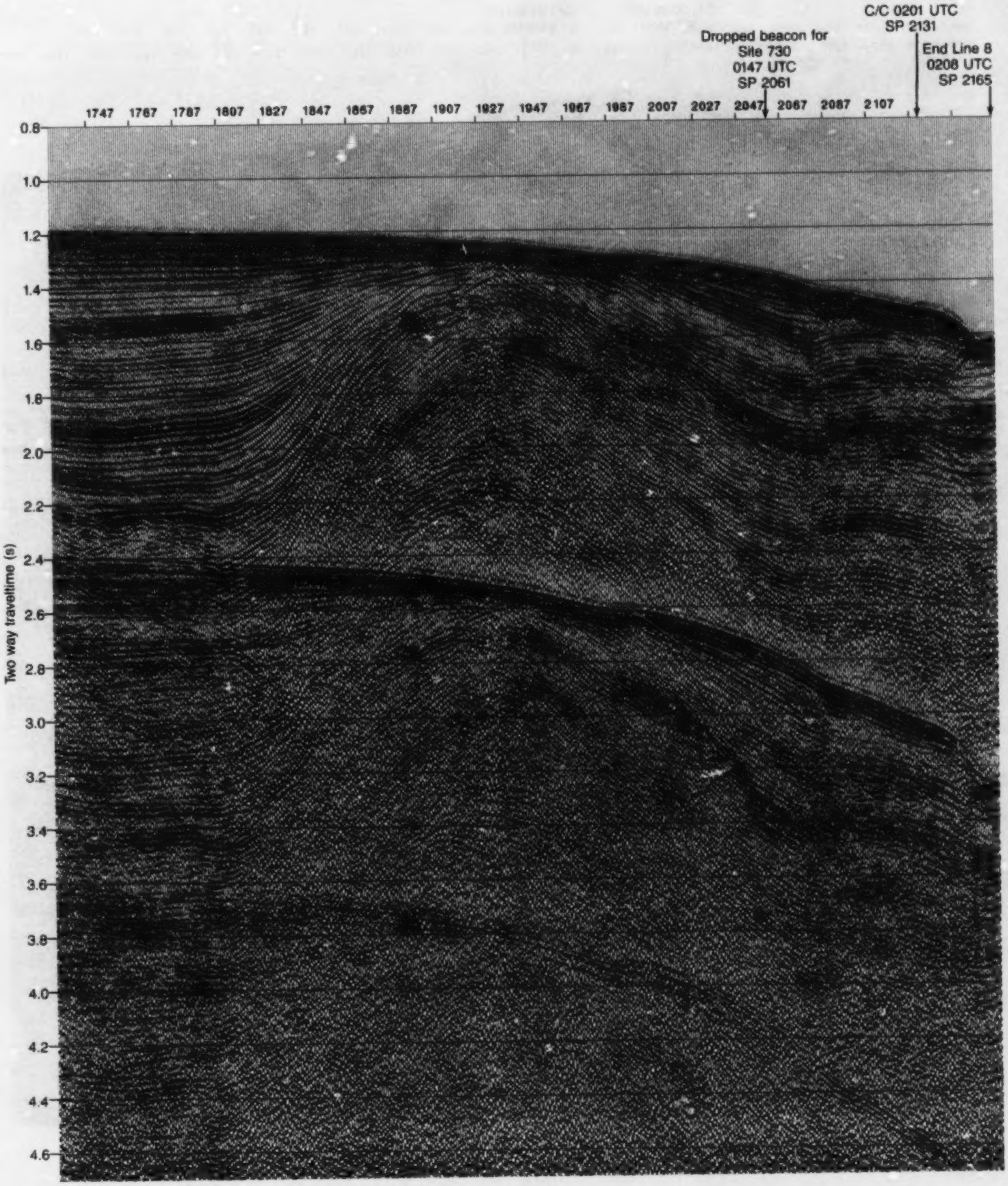

Figure 20 (continued).

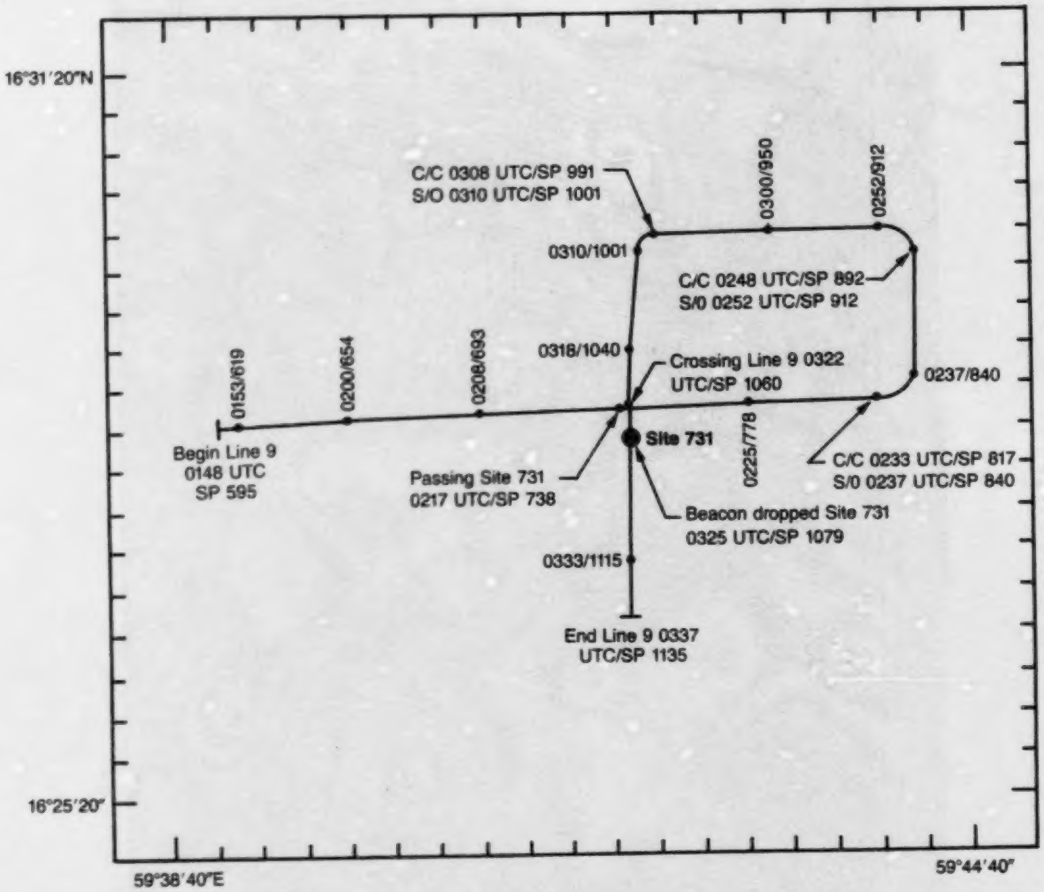
16°31′20″N
16°25′20″
59°38′40″E
59°44′40″
C/C 0308 UTC/SP 991
S/O 0310 UTC/SP 1001
0300/950
0252/912
0310/1001
C/C 0248 UTC/SP 892
S/0 0252 UTC/SP 912
0153/619
0200/654
0208/693
0318/1040
Crossing Line 9 0322
UTC/SP 1060
0237/840
Site 731
0225/778
Begin Line 9
0148 UTC
SP 595
Passing Site 731
0217 UTC/SP 738
C/C 0233 UTC/SP 817
S/0 0237 UTC/SP 840
Beacon dropped Site 731
0325 UTC/SP 1079
0333/1115
End Line 9 0337
UTC/SP 1135

Figure 21. Detailed ship's track for seismic line 9, on approach to Site 731. Satellite fixes are shown as points and are identified by UTC/shotpoint (SP). Extrapolated positions are shown as tick marks. The processed digital seismic profile is shown in Figure 22.

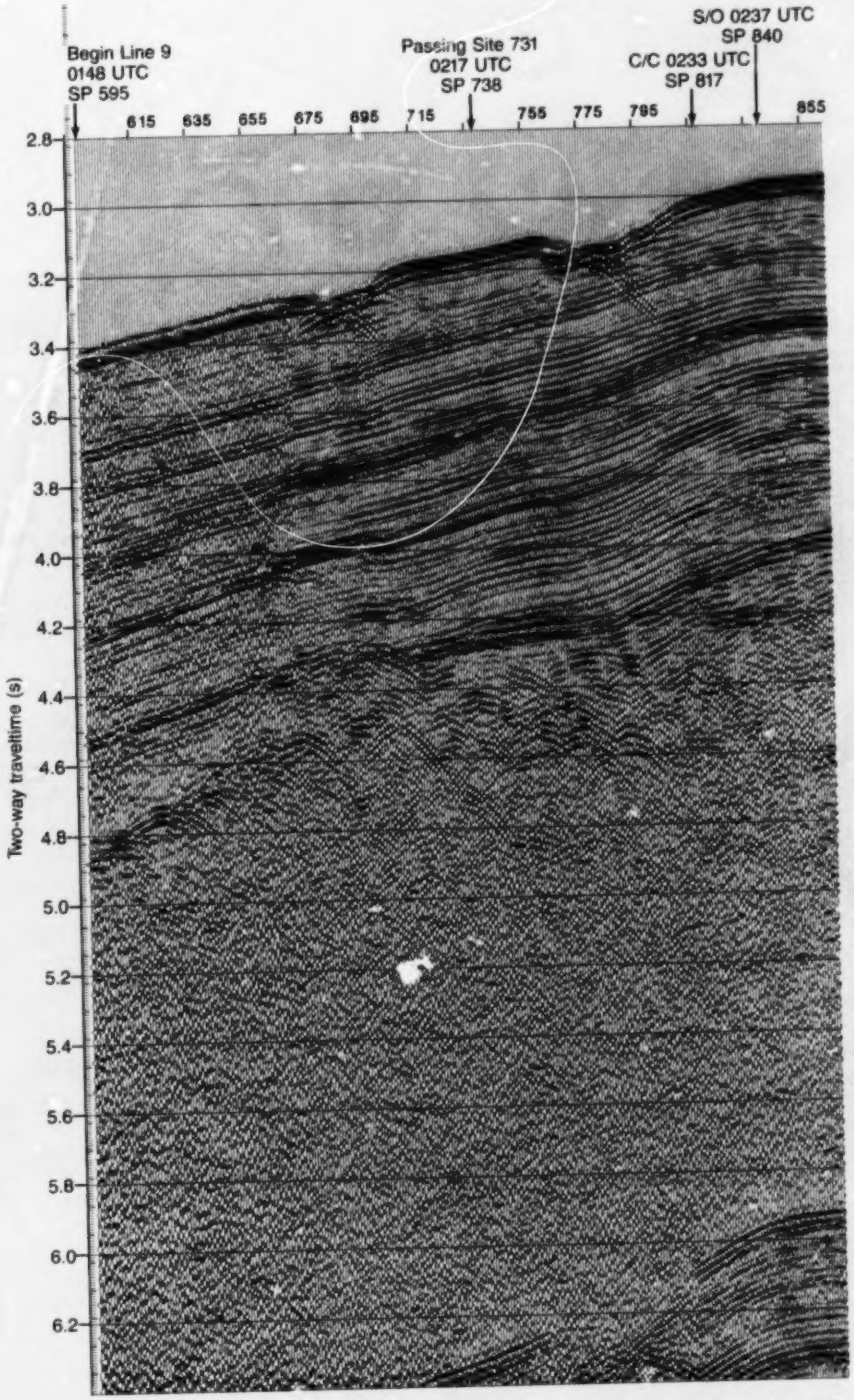

Figure 22. Processed digital seismic profile of line 9, collected on approach to Site 731. The profile was plotted on the Versatec plotter according to the processing parameters given in Table 2. The ship's track is shown in Figure 21.

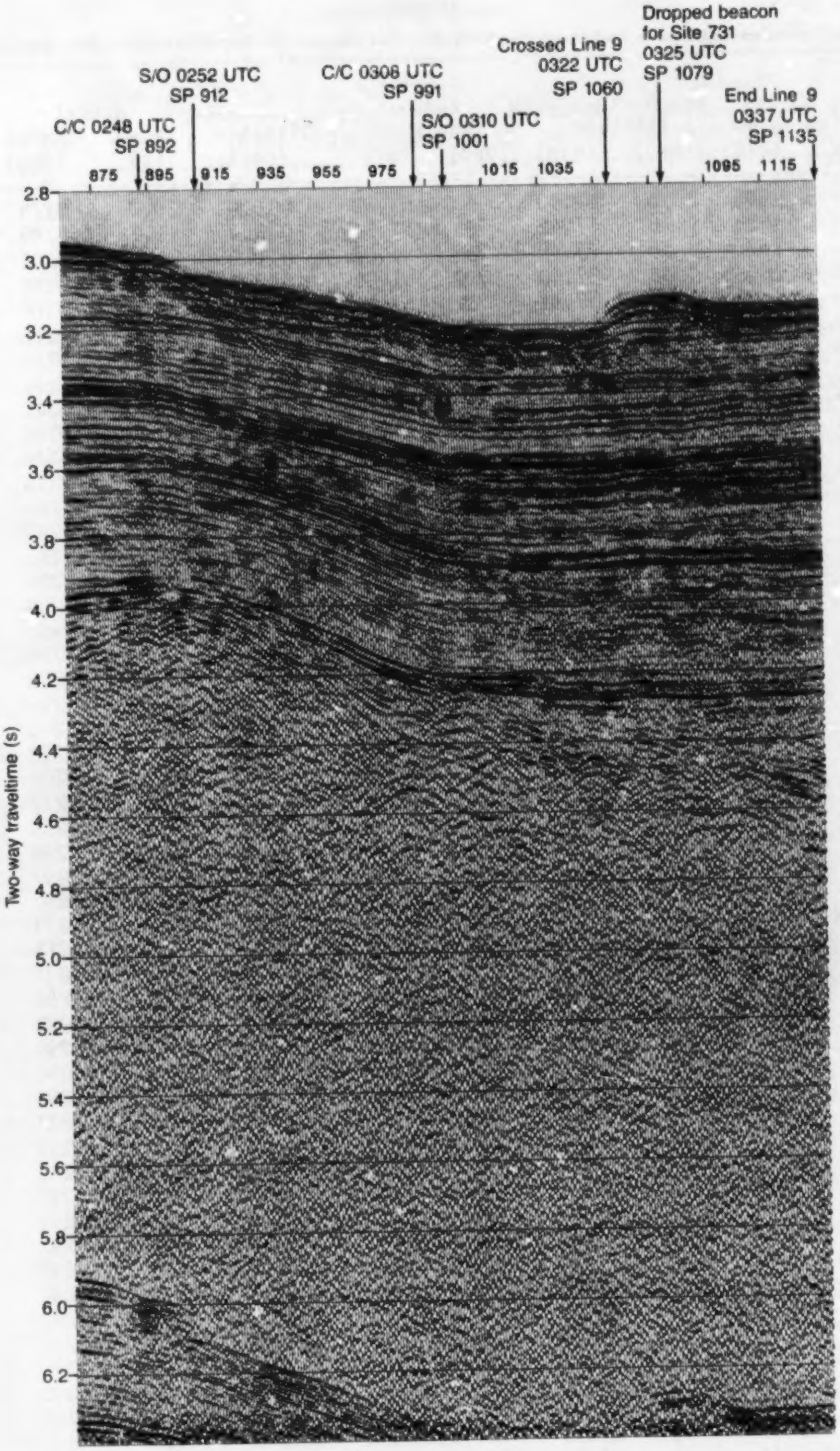

Figure 22 (continued).

APPENDIX

Satellite Navigation And Course- And Speed-change Data Used To Generate The Leg 117 Track-line Plots Shown in Figure 1.

			North latitude		East longitude			Actual		
Date (1987)	Julian day	Time (UTC)	(deg)	(min)	(deg)	(min)	Distance (nmi)	speed (kt)	course (deg)	Comments[a]
23 Aug	235	1605	6	57.43	79	51.32	0.0	0.0	225	GF
23	235	1635	6	57.42	79	51.31	0.0	1.7	43	GF
23	235	1635	6	57.40	79	51.30	0.0	1.1	301	c/cs
23	235	1638	6	57.40	79	51.30	0.1	2.3	185	c/cs
23	235	1639	6	57.41	79	51.26	0.1	4.2	200	SF
23	235	1641	6	57.30	79	51.20	0.2	4.3	216	c/cs
23	235	1646	6	57.00	79	51.00	0.6	2.1	255	c/cs
23	235	1648	6	57.00	79	50.90	0.7	0.9	285	c/cs
23	235	1651	6	57.00	79	50.90	0.7	1.8	345	c/cs
23	235	1654	6	57.10	79	50.90	0.8	5.9	346	c/cs
23	235	1656	6	57.30	79	50.80	1.0	8.2	346	c/cs
23	235	1658	6	57.50	79	50.70	1.3	9.2	315	c/cs
23	235	1659	6	57.60	79	50.60	1.4	8.6	289	c/cs
23	235	1700	6	57.68	79	50.50	1.6	8.6	293	GF
23	235	1701	6	57.70	79	50.40	1.7	6.2	293	c/cs
23	235	1704	6	57.90	79	50.10	2.0	5.1	296	c/cs
23	235	1711	6	58.10	79	49.50	2.6	6.5	296	c/cs
23	235	1714	6	58.30	79	49.30	2.9	2.8	283	c/cs
23	235	1719	6	58.30	79	49.00	3.2	2.4	299	c/cs
23	235	1742	6	58.80	79	48.20	4.1	4.6	299	c/cs
23	235	1754	6	59.20	79	47.40	5.0	4.8	299	c/cs
23	235	1810	6	59.80	79	46.30	6.3	4.3	273	c/cs
23	235	1812	6	59.80	79	46.10	6.4	3.1	228	c/cs
23	235	1815	6	59.70	79	46.00	6.6	2.6	208	c/cs
23	235	1830	6	59.10	79	45.70	7.2	2.1	212	c/cs
23	235	1833	6	59.10	79	45.60	7.4	1.8	255	c/cs
23	235	1837	6	59.00	79	45.50	7.5	3.1	296	c/cs
23	235	1841	6	59.10	79	45.30	7.7	4.5	297	c/cs
23	235	1850	6	59.40	79	44.70	8.4	4.9	297	c/cs
23	235	1903	6	59.90	79	43.80	9.4	4.5	297	c/cs
23	235	1925	7	0.70	79	42.30	11.1	4.7	295	c/cs
23	235	1949	7	1.50	79	40.60	13.0	4.3	297	c/cs
23	235	2004	7	1.90	79	39.60	14.0	4.7	295	c/cs
23	235	2027	7	2.70	79	37.90	15.9	4.8	295	c/cs
23	235	2047	7	3.40	79	36.50	17.5	4.7	296	c/cs
23	235	2105	7	4.00	79	35.20	18.9	5.0	296	c/cs
23	235	2123	7	4.70	79	33.90	20.4	6.8	295	c/cs
23	235	2130	7	5.00	79	33.10	21.2	7.3	294	c/cs
23	235	2143	7	5.70	79	31.70	22.7	8.8	292	c/cs
23	235	2151	7	6.10	79	30.60	23.9	9.3	292	c/cs
23	235	2208	7	7.10	79	28.10	26.5	9.5	292	c/cs
23	235	2229	7	8.30	79	25.00	29.9	9.9	292	c/cs
23	235	2249	7	9.60	79	21.90	33.2	10.1	292	c/cs
23	235	2309	7	10.90	79	18.80	36.5	10.1	292	c/cs
23	235	2340	7	12.80	79	13.90	41.7	9.9	292	c/cs
24 Aug	236	0000	7	14.10	79	10.90	45.1	9.9	292	c/cs
24	236	0007	7	14.50	79	9.80	46.2	10.2	293	c/cs
24	236	0032	7	16.20	79	5.80	50.5	10.3	293	c/cs
24	236	0043	7	16.90	79	4.10	52.3	10.6	293	c/cs
24	236	0058	7	17.90	79	1.60	55.0	10.4	293	c/cs
24	236	0109	7	18.70	78	59.90	56.9	10.6	293	c/cs
24	236	0116	7	19.20	78	58.70	58.1	10.3	293	c/cs
24	236	0126	7	19.90	78	57.10	59.8	10.6	293	c/cs

APPENDIX (continued).

Date (1987)	Julian day	Time (UTC)	North latitude (deg)	North latitude (min)	East longitude (deg)	East longitude (min)	Distance (nmi)	Actual speed (kt)	Actual course (deg)	Comments[a]
24	236	0136	7	20.50	78	55.50	61.6	10.9	293	c/cs
24	236	0142	7	21.00	78	54.50	62.7	10.9	293	c/cs
24	236	0151	7	21.60	78	53.00	64.3	10.7	293	c/cs
24	236	0159	7	22.20	78	51.70	65.7	10.7	293	c/cs
24	236	0202	7	22.40	78	51.20	66.3	10.7	293	c/cs
24	236	0217	7	23.40	78	48.70	68.9	10.2	292	c/cs
24	236	0222	7	23.70	78	47.90	69.8	10.7	292	c/cs
24	236	0227	7	24.10	78	47.10	70.7	9.6	292	c/cs
24	236	0230	7	24.30	78	46.60	71.2	10.7	292	c/cs
24	236	0239	7	24.90	78	45.10	72.8	10.6	292	c/cs
24	236	0255	7	25.90	78	42.50	75.6	10.2	292	c/cs
24	236	0315	7	27.20	78	39.30	79.0	10.2	292	c/cs
24	236	0336	7	28.60	78	35.90	82.6	10.6	293	c/cs
24	236	0341	7	28.90	78	35.10	83.5	10.2	292	c/cs
24	236	0353	7	29.70	78	33.20	85.5	10.6	292	c/cs
24	236	0359	7	30.10	78	32.20	86.6	10.2	291	c/cs
24	236	0411	7	30.80	78	30.30	88.6	10.5	290	c/cs
24	236	0436	7	32.30	78	26.20	93.0	10.1	290	c/cs
24	236	0454	7	33.30	78	23.30	96.0	10.1	290	c/cs
24	236	0514	7	34.50	78	20.10	99.4	9.9	290	c/cs
24	236	0535	7	35.69	78	16.82	102.8	10.3	287	GF
24	236	0542	7	36.00	78	15.70	104.0	10.3	287	c/cs
24	236	0550	7	36.50	78	14.30	105.4	10.4	287	c/cs
24	236	0555	7	36.70	78	13.50	106.3	10.0	287	c/cs
24	236	0600	7	36.95	78	12.70	107.1	10.7	287	GF
24	236	0603	7	37.10	78	12.20	107.6	10.9	287	c/cs
24	236	0621	7	38.10	78	9.00	110.9	10.9	292	c/cs
24	236	0628	7	38.60	78	7.80	112.2	10.4	292	c/cs
24	236	0635	7	39.00	78	6.70	113.4	9.7	291	GF
24	236	0636	7	39.10	78	6.50	113.6	10.2	291	c/cs
24	236	0646	7	39.70	78	4.90	115.3	9.9	291	c/cs
24	236	0700	7	40.50	78	2.76	117.6	10.8	292	GF
24	236	0704	7	40.80	78	2.10	118.3	11.1	292	c/cs
24	236	0714	7	41.50	78	0.40	120.2	11.1	292	c/cs
24	236	0729	7	42.50	77	57.80	122.9	11.7	292	c/cs
24	236	0735	7	42.96	77	56.66	124.1	10.4	294	GF
24	236	0757	7	44.50	77	53.10	127.9	9.9	295	c/cs
24	236	0800	7	44.69	77	52.67	128.4	10.6	296	GF
24	236	0812	7	45.60	77	50.70	130.6	10.9	295	c/cs
24	236	0818	7	46.10	77	49.70	131.7	10.6	295	c/cs
24	236	0828	7	46.90	77	48.10	133.4	11.0	295	c/cs
24	236	0845	7	48.20	77	45.30	136.5	10.8	293	c/cs
24	236	0900	7	49.25	77	42.79	139.2	10.8	293	GF
24	236	0924	7	50.90	77	38.80	143.6	10.8	292	c/cs
24	236	0944	7	52.30	77	35.40	147.2	10.7	292	c/cs
24	236	1000	7	53.39	77	32.75	150.0	10.9	292	GF
24	236	1002	7	53.50	77	32.40	150.4	11.0	293	c/cs
24	236	1024	7	55.10	77	28.70	154.4	11.1	292	c/cs
24	236	1035	7	55.82	77	26.74	156.4	10.8	292	GF
24	236	1044	7	56.40	77	25.20	158.1	10.6	293	c/cs
24	236	1052	7	57.00	77	23.90	159.5	10.5	293	c/cs
24	236	1057	7	57.30	77	23.10	160.3	10.8	293	c/cs
24	236	1100	7	57.50	77	22.58	160.9	11.5	293	GF
24	236	1108	7	58.10	77	21.10	162.4	11.1	292	c/cs

APPENDIX (continued).

Date (1987)	Julian day	Time (UTC)	North latitude		East longitude		Distance (nmi)	Actual		Comments[a]
			(deg)	(min)	(deg)	(min)		speed (kt)	course (deg)	
24	236	1117	7	58.70	77	19.60	164.1	11.4	292	c/cs
24	236	1133	7	59.80	77	16.70	167.1	11.3	292	c/cs
24	236	1135	7	59.97	77	16.38	167.5	11.0	291	GF
24	236	1148	8	0.80	77	14.10	169.9	10.9	292	c/cs
24	236	1155	8	1.30	77	12.90	171.2	11.0	292	c/cs
24	236	1200	8	1.67	77	12.09	172.1	11.7	293	GF
24	236	1219	8	3.10	77	8.60	175.8	11.7	293	c/cs
24	236	1235	8	4.30	77	5.73	178.9	11.4	293	GF
24	236	1249	8	5.30	77	3.30	181.6	11.8	293	c/cs
24	236	1300	8	6.18	77	1.26	183.7	11.4	292	GF
24	236	1301	8	6.30	77	1.10	183.9	11.4	292	c/cs
24	236	1309	8	6.80	76	59.70	185.4	11.5	292	c/cs
24	236	1319	8	7.50	76	57.90	187.3	11.1	291	c/cs
24	236	1348	8	9.45	76	52.81	192.7	10.4	289	GF
24	236	1349	8	9.50	76	52.60	192.9	9.7	290	c/cs
24	236	1355	8	9.80	76	51.70	193.8	10.2	289	c/cs
24	236	1400	8	10.12	76	50.91	194.7	11.5	287	GF
24	236	1405	8	10.40	76	50.00	195.7	10.9	288	c/cs
24	236	1418	8	11.14	76	47.73	198.0	9.8	290	GF
24	236	1420	8	11.30	76	47.40	198.3	10.2	289	c/cs
24	236	1428	8	11.70	76	46.10	199.7	9.8	289	c/cs
24	236	1451	8	12.90	76	42.50	203.5	10.1	290	c/cs
24	236	1500	8	13.40	76	41.08	205.0	8.5	297	GF
24	236	1504	8	13.70	76	40.60	205.5	8.5	297	c/cs
24	236	1518	8	14.54	76	38.78	207.5	9.5	289	GF
24	236	1526	8	15.00	76	37.60	208.8	9.2	289	c/cs
24	236	1532	8	15.30	76	36.70	209.7	9.3	292	c/cs
24	236	1542	8	15.80	76	35.20	211.2	9.1	293	c/cs
24	236	1549	8	16.20	76	34.20	212.3	8.8	293	c/cs
24	236	1559	8	16.80	76	32.90	213.8	9.1	293	c/cs
24	236	1619	8	18.00	76	30.10	216.8	9.2	292	c/cs
24	236	1630	8	18.63	76	28.48	218.5	9.6	292	GF
24	236	1645	8	19.50	76	26.20	220.9	10.1	292	c/cs
24	236	1658	8	20.30	76	24.20	223.1	9.7	293	c/cs
24	236	1707	8	20.90	76	22.80	224.5	9.9	293	c/cs
24	236	1715	8	21.43	76	21.59	225.9	9.7	296	GF
24	236	1718	8	21.60	76	21.20	226.3	9.0	296	c/cs
24	236	1723	8	22.00	76	20.50	227.1	9.7	296	c/cs
24	236	1731	8	22.50	76	19.30	228.4	9.3	295	c/cs
24	236	1747	8	23.60	76	17.00	230.9	9.6	296	c/cs
24	236	1759	8	24.40	76	15.30	232.8	9.6	296	c/cs
24	236	1816	8	25.60	76	12.80	235.5	9.5	296	c/cs
24	236	1829	8	26.50	76	10.90	237.6	9.2	293	c/cs
24	236	1839	8	27.10	76	9.50	239.1	9.0	293	c/cs
24	236	1844	8	27.40	76	8.80	239.9	9.5	293	c/cs
24	236	1905	8	28.70	76	5.70	243.2	9.7	293	c/cs
24	236	1922	8	29.80	76	3.20	245.9	9.0	293	c/cs
24	236	1932	8	30.40	76	1.80	247.4	9.5	293	c/cs
24	236	1938	8	30.80	76	0.90	248.4	9.0	293	c/cs
24	236	1950	8	31.50	75	59.20	250.2	9.3	293	c/cs
24	236	2006	8	32.50	75	56.90	252.7	9.5	293	c/cs
24	236	2020	8	33.30	75	54.80	254.9	9.8	293	c/cs
24	236	2043	8	34.80	75	51.40	258.6	10.0	293	c/cs
24	236	2049	8	35.20	75	50.40	259.6	10.1	292	c/cs

APPENDIX (continued).

Date (1987)	Julian day	Time (UTC)	North latitude (deg)	North latitude (min)	East longitude (deg)	East longitude (min)	Distance (nmi)	Actual speed (kt)	Actual course (deg)	Comments[a]
24	236	2102	8	36.00	75	48.40	261.8	9.7	293	c/cs
24	236	2116	8	36.90	75	46.30	264.1	9.8	293	c/cs
24	236	2135	8	38.10	75	43.40	267.2	9.4	293	c/cs
24	236	2142	8	38.50	75	42.40	268.2	9.8	293	c/cs
24	236	2147	8	38.86	75	41.64	269.1	10.4	295	SF
24	236	2157	8	39.60	75	40.00	270.8	10.5	294	c/cs
24	236	2208	8	40.40	75	38.30	272.7	10.7	291	c/cs
24	236	2213	8	40.70	75	37.40	273.6	10.3	292	c/cs
24	236	2223	8	41.30	75	35.80	275.3	10.0	292	c/cs
24	236	2228	8	41.60	75	35.00	276.2	10.1	292	c/cs
24	236	2248	8	42.90	75	31.80	279.5	9.3	293	c/cs
24	236	2251	8	43.10	75	31.40	280.0	10.1	292	c/cs
24	236	2314	8	44.50	75	27.80	283.9	10.4	293	c/cs
24	236	2319	8	44.80	75	27.00	284.8	9.6	293	c/cs
24	236	2323	8	45.10	75	26.40	285.4	10.4	292	c/cs
24	236	2341	8	46.20	75	23.40	288.5	10.6	292	c/cs
24	236	2356	8	47.20	75	21.00	291.1	10.2	292	c/cs
25 Aug	237	0000	8	47.50	75	20.30	291.8	10.2	292	c/cs
25	237	0007	8	47.90	75	19.20	293.0	9.6	293	c/cs
25	237	0012	8	48.20	75	18.50	293.8	10.3	292	c/cs
25	237	0027	8	49.20	75	16.00	296.4	10.6	292	c/cs
25	237	0039	8	50.00	75	14.00	298.5	10.4	293	c/cs
25	237	0044	8	50.30	75	13.20	299.4	10.2	292	c/cs
25	237	0053	8	50.90	75	11.80	300.9	10.0	292	c/cs
25	237	0105	8	51.60	75	9.90	302.9	10.5	292	c/cs
25	237	0123	8	52.80	75	7.00	306.1	10.3	292	c/cs
25	237	0133	8	53.40	75	5.40	307.8	10.7	291	c/cs
25	237	0143	8	54.10	75	3.70	309.6	10.4	291	c/cs
25	237	0156	8	54.90	75	1.50	311.8	10.0	291	c/cs
25	237	0201	8	55.20	75	0.80	312.6	10.8	291	c/cs
25	237	0216	8	56.10	74	58.20	315.3	10.5	290	c/cs
25	237	0223	8	56.50	74	57.00	316.6	10.7	291	c/cs
25	237	0229	8	56.90	74	56.00	317.6	10.2	291	c/cs
25	237	0244	8	57.80	74	53.60	320.2	10.3	290	c/cs
25	237	0254	8	58.40	74	52.00	321.9	10.2	291	c/cs
25	237	0301	8	58.80	74	50.90	323.1	10.7	291	c/cs
25	237	0307	8	59.20	74	49.90	324.1	10.5	291	c/cs
25	237	0327	9	0.50	74	46.50	327.6	10.6	290	c/cs
25	237	0340	9	1.30	74	44.40	329.9	10.2	290	c/cs
25	237	0355	9	2.10	74	41.90	332.5	10.1	290	c/cs
25	237	0413	9	3.20	74	39.10	335.5	10.5	291	c/cs
25	237	0423	9	3.80	74	37.40	337.2	10.4	290	c/cs
25	237	0451	9	5.40	74	32.80	342.1	10.3	291	c/cs
25	237	0501	9	6.00	74	31.20	343.8	10.1	291	c/cs
25	237	0506	9	6.30	74	30.40	344.6	10.6	290	c/cs
25	237	0519	9	7.10	74	28.20	347.0	10.4	291	c/cs
25	237	0524	9	7.40	74	27.40	347.8	10.3	290	c/cs
25	237	0530	9	7.79	74	26.39	348.8	10.2	290	GF
25	237	0532	9	7.90	74	26.10	349.2	9.7	292	c/cs
25	237	0547	9	8.80	74	23.80	351.6	10.6	293	c/cs
25	237	0549	9	8.94	74	23.45	352.0	10.3	292	GF
25	237	0600	9	9.63	74	21.68	353.8	10.2	289	GF
25	237	0605	9	9.90	74	20.90	354.7	10.2	289	c/cs
25	237	0619	9	10.70	74	18.60	357.1	9.8	290	GF

APPENDIX (continued).

Date (1987)	Julian day	Time (UTC)	North latitude		East longitude		Distance (nmi)	Actual		Comments[a]
			(deg)	(min)	(deg)	(min)		speed (kt)	course (deg)	
25	237	0628	9	11.20	74	17.20	358.5	9.2	290	c/cs
25	237	0630	9	11.31	74	16.91	358.8	9.5	291	GF
25	237	0640	9	11.90	74	15.40	360.4	10.0	291	c/cs
25	237	0649	9	12.41	74	13.99	361.9	9.8	291	GF
25	237	0653	9	12.60	74	13.40	362.6	10.2	291	c/cs
25	237	0658	9	12.90	74	12.60	363.4	11.0	291	c/cs
25	237	0700	9	13.07	74	12.22	363.8	11.0	292	GF
25	237	0701	9	13.10	74	12.00	364.0	10.4	292	c/cs
25	237	0716	9	14.10	74	9.60	366.6	10.8	291	c/cs
25	237	0728	9	14.90	74	7.50	368.8	10.1	291	c/cs
25	237	0730	9	14.99	74	7.23	369.1	10.3	291	GF
25	237	0741	9	15.70	74	5.40	371.0	10.6	291	c/cs
25	237	0746	9	16.00	74	4.60	371.9	10.0	292	c/cs
25	237	0749	9	16.19	74	4.14	372.4	9.8	291	GF
25	237	0800	9	16.82	74	2.44	374.2	9.9	290	GF
25	237	0804	9	17.00	74	1.80	374.8	10.9	290	C/CS
25	237	0822	9	18.20	73	58.70	378.1	10.5	291	C/CS
25	237	0829	9	18.60	73	57.50	379.3	10.3	290	C/CS
25	237	0830	9	18.65	73	57.35	379.5	10.4	291	GF
25	237	0849	9	19.82	73	54.22	382.8	10.3	290	GF
25	237	0855	9	20.20	73	53.20	383.8	10.5	291	C/CS
25	237	0900	9	20.49	73	52.42	384.7	10.3	292	GF
25	237	0900	9	20.50	73	52.40	384.7	9.8	291	C/CS
25	237	0918	9	21.50	73	49.60	387.7	10.0	291	C/CS
25	237	0930	9	22.24	73	47.73	389.7	10.2	290	GF
25	237	0930	9	22.20	73	47.70	389.7	10.0	291	C/CS
25	237	0933	9	22.40	73	47.30	390.1	10.5	291	C/CS
25	237	0937	9	22.70	73	46.60	390.9	9.9	290	C/CS
25	237	0949	9	23.36	73	44.72	392.8	9.8	291	GF
25	237	0956	9	23.80	73	43.60	394.0	10.2	291	C/CS
25	237	1000	9	24.00	73	43.00	394.6	10.2	290	GF
25	237	1011	9	24.60	73	41.20	396.5	9.9	291	C/CS
25	237	1024	9	25.40	73	39.20	398.7	9.8	290	C/CS
25	237	1030	9	25.72	73	38.25	399.6	9.8	289	GF
25	237	1036	9	26.00	73	37.30	400.6	10.1	290	C/CS
25	237	1100	9	27.43	73	33.44	404.7	10.2	290	GF
25	237	1102	9	27.50	73	33.10	405.0	9.9	290	C/CS
25	237	1114	9	28.20	73	31.20	407.0	10.3	289	C/CS
25	237	1119	9	28.48	73	30.41	407.8	9.8	289	GF
25	237	1122	9	28.60	73	29.90	408.3	9.5	289	C/CS
25	237	1130	9	29.05	73	28.73	409.6	9.8	289	GF
25	237	1132	9	29.20	73	28.40	409.9	9.4	290	C/CS
25	237	1153	9	30.30	73	25.30	413.2	9.5	290	C/CS
25	237	1200	9	30.65	73	24.22	414.3	9.7	290	GF
25	237	1202	9	30.80	73	23.90	414.6	9.6	289	C/CS
25	237	1215	9	31.40	73	21.90	416.7	9.3	289	C/CS
25	237	1219	9	31.65	73	21.33	417.3	9.0	289	GF
25	237	1220	9	31.70	73	21.20	417.5	9.6	289	c/cs
25	237	1226	9	32.00	73	20.30	418.4	9.2	289	c/cs
25	237	1230	9	32.20	73	19.68	419.1	9.4	288	GF
25	237	1238	9	32.60	73	18.50	420.3	9.7	289	c/cs
25	237	1251	9	33.30	73	16.40	422.4	9.9	288	c/cs
25	237	1300	9	33.71	73	15.02	423.9	9.9	288	GF
25	237	1306	9	34.00	73	14.10	424.9	9.7	288	c/cs

APPENDIX (continued).

Date (1987)	Julian day	Time (UTC)	North latitude (deg)	North latitude (min)	East longitude (deg)	East longitude (min)	Distance (nmi)	Actual speed (kt)	Actual course (deg)	Comments[a]
25	237	1316	9	34.50	73	12.50	426.5	9.9	288	c/cs
25	237	1319	9	34.65	73	12.03	427.0	9.7	288	GF
25	237	1329	9	35.10	73	10.50	428.6	9.9	288	c/cs
25	237	1341	9	35.70	73	8.60	430.6	10.1	290	c/cs
25	237	1349	9	36.20	73	7.27	431.9	9.7	289	GF
25	237	1400	9	36.79	73	5.57	433.7	9.8	289	GF
25	237	1402	9	36.90	73	5.30	434.0	9.6	289	c/cs
25	237	1414	9	37.50	73	3.40	436.0	9.7	288	c/cs
25	237	1425	9	38.10	73	1.70	437.7	9.7	289	c/cs
25	237	1430	9	38.32	73	0.92	438.5	10.0	290	GF
25	237	1430	9	38.30	73	0.90	438.5	9.3	290	c/cs
25	237	1448	9	39.30	72	58.30	441.3	10.0	292	c/cs
25	237	1457	9	39.80	72	56.90	442.8	9.7	291	c/cs
25	237	1500	9	40.01	72	56.41	443.3	9.8	290	GF
25	237	1528	9	41.60	72	52.00	447.9	10.7	291	c/cs
25	237	1531	9	41.80	72	51.50	448.4	9.7	291	c/cs
25	237	1536	9	42.10	72	50.80	449.2	10.0	290	c/cs
25	237	1549	9	42.80	72	48.70	451.4	9.8	290	c/cs
25	237	1600	9	43.40	72	47.00	453.2	10.1	291	GF
25	237	1604	9	43.60	72	46.40	453.9	10.4	291	c/cs
25	237	1617	9	44.50	72	44.20	456.1	9.8	290	c/cs
25	237	1619	9	44.57	72	43.92	456.4	9.5	290	GF
25	237	1624	9	44.80	72	43.20	457.2	9.7	291	c/cs
25	237	1630	9	45.19	72	42.25	458.2	10.1	292	GF
25	237	1654	9	46.70	72	38.50	462.2	9.7	293	c/cs
25	237	1702	9	47.20	72	37.30	463.5	10.3	292	c/cs
25	237	1714	9	48.00	72	35.30	465.6	10.3	292	c/cs
25	237	1725	9	48.70	72	33.60	467.4	10.4	292	c/cs
25	237	1738	9	49.50	72	31.40	469.7	10.0	293	c/cs
25	237	1750	9	50.30	72	29.60	471.7	10.2	291	c/cs
25	237	1803	9	51.10	72	27.50	473.9	9.8	292	c/cs
25	237	1813	9	51.70	72	26.00	475.5	10.3	291	c/cs
25	237	1821	9	52.20	72	24.70	476.9	10.0	291	c/cs
25	237	1836	9	53.10	72	22.30	479.4	9.8	292	c/cs
25	237	1841	9	53.40	72	21.50	480.2	9.9	292	c/cs
25	237	1907	9	55.00	72	17.50	484.5	10.3	292	c/cs
25	237	1919	9	55.80	72	15.50	486.6	9.6	292	c/cs
25	237	1924	9	56.10	72	14.80	487.4	10.3	292	c/cs
25	237	1929	9	56.40	72	14.00	488.3	9.7	292	c/cs
25	237	1935	9	56.80	72	13.00	489.2	10.2	292	c/cs
25	237	1942	9	57.30	72	11.90	490.4	9.7	293	c/cs
25	237	1950	9	57.80	72	10.70	491.7	10.2	292	c/cs
25	237	2005	9	58.70	72	8.30	494.3	9.8	297	c/cs
25	237	2023	10	0.00	72	5.60	497.2	10.0	297	c/cs
25	237	2033	10	0.80	72	4.10	498.9	9.6	297	c/cs
25	237	2046	10	1.70	72	2.20	501.0	10.1	296	c/cs
25	237	2100	10	2.80	72	0.10	503.3	10.2	297	c/cs
25	237	2105	10	3.20	71	59.30	504.2	10.1	297	c/cs
25	237	2116	10	4.00	71	57.60	506.0	9.9	298	c/cs
25	237	2124	10	4.61	71	56.46	507.3	9.8	300	SF
25	237	2136	10	5.60	71	54.70	509.3	10.0	299	c/cs
25	237	2144	10	6.20	71	53.50	510.6	9.8	300	c/cs
25	237	2152	10	6.90	71	52.40	511.9	10.1	299	c/cs
25	237	2159	10	7.40	71	51.30	513.1	10.1	299	c/cs

APPENDIX (continued).

Date (1987)	Julian day	Time (UTC)	North latitude (deg)	North latitude (min)	East longitude (deg)	East longitude (min)	Distance (nmi)	Actual speed (kt)	Actual course (deg)	Comments[a]
25	237	2212	10	8.50	71	49.40	515.3	9.5	299	c/cs
25	237	2229	10	9.80	71	47.00	518.0	10.0	299	c/cs
25	237	2245	10	11.10	71	44.60	520.7	10.2	299	c/cs
25	237	2252	10	11.60	71	43.60	521.8	9.6	299	c/cs
25	237	2315	10	13.40	71	40.30	525.5	9.9	300	c/cs
25	237	2333	10	14.90	71	37.70	528.5	9.9	301	c/cs
25	237	2338	10	15.30	71	36.90	529.3	9.4	301	c/cs
25	237	2343	10	15.70	71	36.20	530.1	9.7	301	c/cs
25	237	2350	10	16.30	71	35.30	531.2	10.0	301	c/cs
25	237	2356	10	16.80	71	34.40	532.2	9.9	301	c/cs
26 Aug	238	0000	10	17.10	71	33.80	532.9	9.9	301	c/cs
26	238	0014	10	18.30	71	31.80	535.2	9.3	301	c/cs
26	238	0021	10	18.80	71	30.80	536.3	9.6	301	c/cs
26	238	0036	10	20.10	71	28.80	538.7	10.1	301	c/cs
26	238	0047	10	21.00	71	27.14	540.5	10.3	300	SF
26	238	0057	10	21.90	71	25.60	542.2	9.7	300	c/cs
26	238	0110	10	22.90	71	23.80	544.3	10.1	299	c/cs
26	238	0119	10	23.70	71	22.40	545.9	10.3	299	c/cs
26	238	0123	10	24.00	71	21.83	546.6	10.3	301	SF
26	238	0132	10	24.80	71	20.50	548.1	10.1	302	c/cs
26	238	0200	10	27.30	71	16.40	552.8	9.9	301	c/cs
26	238	0208	10	27.90	71	15.30	554.1	10.3	301	c/cs
26	238	0221	10	29.10	71	13.30	556.3	9.9	302	c/cs
26	238	0228	10	29.70	71	12.30	557.5	10.2	301	c/cs
26	238	0241	10	30.80	71	10.40	559.7	10.4	302	c/cs
26	238	0253	10	31.90	71	8.60	561.8	10.2	301	c/cs
26	238	0311	10	33.40	71	5.90	564.8	10.0	302	c/cs
26	238	0322	10	34.40	71	4.30	566.7	9.5	302	c/cs
26	238	0334	10	35.40	71	2.60	568.6	9.3	302	c/cs
26	238	0344	10	36.20	71	1.30	570.1	9.9	301	c/cs
26	238	0349	10	36.60	71	0.60	571.0	10.5	302	c/cs
26	238	0355	10	37.20	70	59.70	572.0	10.3	301	c/cs
26	238	0404	10	38.00	70	58.30	573.6	10.4	301	c/cs
26	238	0412	10	38.70	70	57.10	574.9	9.8	301	c/cs
26	238	0422	10	39.50	70	55.70	576.6	10.1	301	c/cs
26	238	0438	10	40.90	70	53.30	579.3	10.8	301	c/cs
26	238	0445	10	41.50	70	52.20	580.5	10.0	301	c/cs
26	238	0450	10	41.90	70	51.50	581.3	10.2	302	c/cs
26	238	0455	10	42.40	70	50.80	582.2	10.2	301	c/cs
26	238	0516	10	44.20	70	47.70	585.8	10.8	301	c/cs
26	238	0526	10	45.10	70	46.10	587.6	10.2	301	c/cs
26	238	0530	10	45.49	70	45.49	588.2	10.2	302	GF
26	238	0600	10	48.15	70	41.08	593.3	10.0	299	GF
26	238	0626	10	50.30	70	37.20	597.6	10.0	298	c/cs
26	238	0630	10	50.58	70	36.65	598.3	10.3	299	GF
26	238	0632	10	50.70	70	36.30	598.7	10.5	298	c/cs
26	238	0649	10	52.15	70	33.67	601.6	9.7	298	GF
26	238	0654	10	52.50	70	32.90	602.4	9.9	298	c/cs
26	238	0715	10	54.20	70	29.90	605.9	9.9	303	c/cs
26	238	0728	10	55.30	70	28.00	608.0	9.7	304	c/cs
26	238	0730	10	55.51	70	27.74	608.4	9.8	302	GF
26	238	0735	10	55.90	70	27.00	609.2	10.1	302	c/cs
26	238	0748	10	57.10	70	25.10	611.4	10.0	302	c/cs
26	238	0756	10	57.80	70	24.00	612.7	10.0	302	c/cs

APPENDIX (continued).

Date (1987)	Julian day	Time (UTC)	North latitude (deg)	North latitude (min)	East longitude (deg)	East longitude (min)	Distance (nmi)	Actual speed (kt)	Actual course (deg)	Comments[a]
26	238	0806	10	58.70	70	22.50	614.4	9.9	302	c/cs
26	238	0830	11	0.77	70	19.14	618.3	9.7	302	GF
26	238	0834	11	1.10	70	18.60	619.0	10.2	302	c/cs
26	238	0844	11	2.00	70	17.10	620.6	9.9	302	c/cs
26	238	0852	11	2.70	70	16.00	622.0	9.9	303	c/cs
26	238	0857	11	3.20	70	15.30	622.8	9.5	302	c/cs
26	238	0900	11	3.44	70	14.89	623.3	9.9	301	GF
26	238	0902	11	3.60	70	14.60	623.6	10.4	301	c/cs
26	238	0912	11	4.50	70	13.10	625.3	10.1	301	c/cs
26	238	0919	11	5.12	70	12.06	626.5	9.2	301	GF
26	238	0930	11	5.99	70	10.59	628.2	9.6	301	GF
26	238	0932	11	6.20	70	10.30	628.5	9.6	301	c/cs
26	238	0940	11	6.80	70	9.20	629.8	9.8	301	c/cs
26	238	0947	11	7.40	70	8.20	630.9	9.8	301	c/cs
26	238	0958	11	8.30	70	6.60	632.7	10.0	301	c/cs
26	238	1000	11	8.51	70	6.36	633.0	9.9	302	GF
26	238	1018	11	10.10	70	3.80	636.0	9.8	302	c/cs
26	238	1028	11	11.00	70	2.40	637.7	9.6	302	c/cs
26	238	1030	11	11.12	70	2.10	638.0	9.8	302	GF
26	238	1048	11	12.70	69	59.60	640.9	10.2	302	c/cs
26	238	1100	11	13.79	69	57.80	643.0	10.0	302	GF
26	238	1119	11	15.47	69	55.05	646.1	9.1	302	GF
26	238	1130	11	16.35	69	53.61	647.8	10.0	301	GF
26	238	1133	11	16.60	69	53.20	648.3	9.8	301	c/cs
26	238	1209	11	19.70	69	48.00	654.2	9.7	301	c/cs
26	238	1223	11	20.80	69	46.10	656.4	9.4	301	c/cs
26	238	1230	11	21.41	69	45.13	657.5	10.1	300	GF
26	238	1246	11	22.70	69	42.70	660.2	10.2	300	c/cs
26	238	1249	11	23.00	69	42.29	660.7	9.0	300	GF
26	238	1259	11	23.70	69	41.00	662.2	9.1	300	c/cs
26	238	1300	11	23.82	69	40.83	662.4	9.8	300	GF
26	238	1310	11	24.60	69	39.40	664.0	9.8	300	c/cs
26	238	1329	11	26.20	69	36.70	667.1	9.8	300	c/cs
26	238	1330	11	26.27	69	36.52	667.3	9.8	302	GF
26	238	1337	11	26.90	69	35.50	668.4	9.4	302	c/cs
26	238	1350	11	27.90	69	33.80	670.5	9.5	301	c/cs
26	238	1400	11	28.74	69	32.37	672.0	10.0	301	GF
26	238	1400	11	28.70	69	32.40	672.0	9.7	301	c/cs
26	238	1407	11	29.30	69	31.40	673.2	10.3	301	c/cs
26	238	1419	11	30.39	69	29.58	675.2	9.3	301	GF
26	238	1426	11	30.90	69	28.60	676.3	9.1	301	c/cs
26	238	1430	11	31.26	69	28.10	676.9	10.0	302	GF
26	238	1453	11	33.30	69	24.80	680.8	10.0	302	c/cs
26	238	1503	11	34.10	69	23.30	682.4	9.6	301	c/cs
26	238	1519	11	35.50	69	21.10	685.0	10.0	301	c/cs
26	238	1527	11	36.14	69	19.89	686.3	9.6	301	SF
26	238	1532	11	36.60	69	19.20	687.1	9.0	301	c/cs
26	238	1539	11	37.10	69	18.30	688.2	9.3	301	c/cs
26	238	1552	11	38.10	69	16.50	690.2	9.3	301	c/cs
26	238	1555	11	38.40	69	16.10	690.7	9.8	301	c/cs
26	238	1559	11	38.70	69	15.50	691.3	9.9	301	c/cs
26	238	1600	11	38.80	69	15.39	691.5	10.6	300	SF
26	238	1602	11	39.00	69	15.10	691.8	9.6	299	c/cs
26	238	1610	11	39.60	69	13.90	693.1	10.1	299	c/cs

APPENDIX (continued).

Date (1987)	Julian day	Time (UTC)	North latitude		East longitude		Distance (nmi)	Actual		Comments[a]
			(deg)	(min)	(deg)	(min)		speed (kt)	course (deg)	
26	238	1630	11	41.20	69	10.90	696.5	9.7	300	GF
26	238	1637	11	41.80	69	9.90	697.6	9.8	300	c/cs
26	238	1643	11	42.30	69	9.00	698.6	10.5	300	c/cs
26	238	1648	11	42.70	69	8.30	699.5	9.7	300	c/cs
26	238	1701	11	43.70	69	6.40	701.6	10.6	300	c/cs
26	238	1703	11	43.90	69	6.10	701.9	9.7	300	c/cs
26	238	1716	11	45.00	69	4.20	704.0	9.8	300	c/cs
26	238	1728	11	45.90	69	2.50	706.0	9.9	299	c/cs
26	238	1759	11	48.40	68	57.90	711.1	10.0	299	c/cs
26	238	1804	11	48.80	68	57.20	711.9	10.7	300	c/cs
26	238	1807	11	49.10	68	56.70	712.5	9.8	300	c/cs
26	238	1817	11	49.90	68	55.30	714.1	9.4	300	c/cs
26	238	1827	11	50.70	68	53.90	715.7	10.0	300	c/cs
26	238	1840	11	51.70	68	51.90	717.8	9.9	299	c/cs
26	238	1845	11	52.10	68	51.20	718.7	10.3	299	c/cs
26	238	1852	11	52.70	68	50.10	719.9	9.8	299	c/cs
26	238	1905	11	53.80	68	48.20	722.0	10.3	299	c/cs
26	238	1907	11	53.90	68	47.90	722.3	9.5	299	c/cs
26	238	1913	11	54.40	68	47.10	723.3	10.0	299	c/cs
26	238	1925	11	55.30	68	45.30	725.3	9.9	300	c/cs
26	238	1933	11	56.00	68	44.10	726.6	10.1	300	c/cs
26	238	1943	11	56.80	68	42.60	728.3	10.1	300	c/cs
26	238	1951	11	57.50	68	41.40	729.6	9.7	299	c/cs
26	238	2006	11	58.70	68	39.30	732.0	9.9	299	c/cs
26	238	2016	11	59.50	68	37.80	733.7	9.5	300	c/cs
26	238	2019	11	59.70	68	37.40	734.2	10.1	300	c/cs
26	238	2039	12	1.40	68	34.40	737.5	9.7	300	c/cs
26	238	2049	12	2.20	68	33.00	739.1	10.0	300	c/cs
26	238	2057	12	2.90	68	31.80	740.5	10.3	299	c/cs
26	238	2104	12	3.40	68	30.70	741.7	10.3	299	c/cs
26	238	2125	12	5.20	68	27.50	745.3	10.4	300	c/cs
26	238	2134	12	6.00	68	26.10	746.8	9.8	300	c/cs
26	238	2155	12	7.70	68	23.00	750.3	10.2	300	c/cs
26	238	2208	12	8.80	68	21.10	752.5	9.7	300	c/cs
26	238	2223	12	10.00	68	18.90	754.9	10.1	300	c/cs
26	238	2235	12	11.00	68	17.20	756.9	9.2	299	c/cs
26	238	2243	12	11.60	68	16.10	758.1	9.4	300	c/cs
26	238	2248	12	12.00	68	15.40	758.9	9.6	300	c/cs
26	238	2304	12	13.20	68	13.10	761.5	9.9	300	c/cs
26	238	2314	12	14.10	68	11.60	763.1	9.2	300	c/cs
26	238	2319	12	14.40	68	11.00	763.9	9.9	300	c/cs
26	238	2333	12	15.60	68	8.90	766.2	9.5	300	c/cs
26	238	2346	12	16.60	68	7.10	768.3	9.5	300	c/cs
26	238	2354	12	17.20	68	6.00	769.5	9.7	300	c/cs
27 Aug	239	0000	12	17.70	68	5.10	770.5	9.7	300	c/cs
27	239	0012	12	18.70	68	3.40	772.4	9.8	299	c/cs
27	239	0013	12	18.78	68	3.23	772.6	9.7	300	SF
27	239	0025	12	19.70	68	1.50	774.5	9.4	301	c/cs
27	239	0032	12	20.30	68	0.50	775.6	9.6	301	c/cs
27	239	0050	12	21.80	67	58.00	778.5	9.8	301	c/cs
27	239	0103	12	22.90	67	56.10	780.6	9.9	301	c/cs
27	239	0125	12	24.70	67	53.00	784.3	9.9	300	c/cs
27	239	0140	12	26.00	67	50.80	786.7	9.6	300	c/cs
27	239	0154	12	27.10	67	48.80	789.0	9.6	301	c/cs

APPENDIX (continued).

Date (1987)	Julian day	Time (UTC)	North latitude		East longitude		Distance (nmi)	Actual speed (kt)	Actual course (deg)	Comments[a]
			(deg)	(min)	(deg)	(min)				
27	239	0159	12	27.50	67	48.10	789.8	9.8	300	c/cs
27	239	0209	12	28.30	67	46.60	791.4	9.7	301	c/cs
27	239	0224	12	29.60	67	44.50	793.8	9.4	300	c/cs
27	239	0232	12	30.20	67	43.40	795.1	9.5	301	c/cs
27	239	0237	12	30.60	67	42.70	795.9	9.9	300	c/cs
27	239	0254	12	32.00	67	40.20	798.7	9.9	301	c/cs
27	239	0320	12	34.20	67	36.40	803.0	10.0	301	c/cs
27	239	0343	12	36.10	67	33.10	806.8	9.7	301	c/cs
27	239	0353	12	37.00	67	31.60	808.4	9.9	300	c/cs
27	239	0408	12	38.20	67	29.40	810.9	9.7	300	c/cs
27	239	0434	12	40.30	67	25.70	815.1	9.9	301	c/cs
27	239	0451	12	41.70	67	23.20	817.9	9.2	301	c/cs
27	239	0459	12	42.30	67	22.20	819.1	9.9	300	c/cs
27	239	0509	12	43.20	67	20.70	820.7	9.7	299	c/cs
27	239	0513	12	43.47	67	20.12	821.4	9.6	298	SF
27	239	0519	12	43.90	67	19.20	822.4	9.8	297	c/cs
27	239	0536	12	45.20	67	16.70	825.1	9.8	298	c/cs
27	239	0548	12	46.10	67	14.90	827.1	10.1	298	c/cs
27	239	0557	12	46.80	67	13.60	828.6	9.8	297	c/cs
27	239	0612	12	47.90	67	11.30	831.1	9.9	297	c/cs
27	239	0630	12	49.28	67	8.63	834.0	10.0	296	GF
27	239	0638	12	49.90	67	7.40	835.4	9.7	296	c/cs
27	239	0644	12	50.28	67	6.50	836.3	9.6	296	GF
27	239	0658	12	51.30	67	4.40	838.6	10.0	296	c/cs
27	239	0700	12	51.42	67	4.13	838.9	10.0	296	GF
27	239	0706	12	51.90	67	3.20	839.9	9.8	296	c/cs
27	239	0714	12	52.45	67	2.01	841.2	9.6	297	GF
27	239	0724	12	53.20	67	0.50	842.8	9.7	298	c/cs
27	239	0730	12	53.63	66	59.67	843.8	9.7	297	GF
27	239	0731	12	53.70	66	59.50	843.9	9.3	297	c/cs
27	239	0739	12	54.30	66	58.40	845.2	10.1	297	c/cs
27	239	0749	12	55.00	66	56.90	846.9	9.9	297	c/cs
27	239	0800	12	55.85	66	55.19	848.7	9.9	298	GF
27	239	0804	12	56.20	66	54.60	849.3	10.0	297	c/cs
27	239	0812	12	56.80	66	53.40	850.7	9.3	298	c/cs
27	239	0824	12	57.60	66	51.70	852.5	9.6	297	c/cs
27	239	0830	12	58.05	66	50.80	853.5	9.8	297	GF
27	239	0832	12	58.20	66	50.50	853.8	9.9	298	c/cs
27	239	0844	12	59.12	66	48.71	855.8	9.6	298	GF
27	239	0854	12	59.90	66	47.30	857.4	9.6	299	c/cs
27	239	0900	13	0.34	66	46.40	858.4	9.8	298	GF
27	239	0920	13	1.90	66	43.50	861.6	9.8	298	c/cs
27	239	0930	13	2.67	66	41.99	863.2	9.8	298	GF
27	239	0931	13	2.70	66	41.80	863.4	9.6	298	c/cs
27	239	0941	13	3.50	66	40.40	865.0	10.1	298	c/cs
27	239	0958	13	4.90	66	37.80	867.9	9.5	298	c/cs
27	239	1000	13	5.00	66	37.53	868.2	9.5	298	GF
27	239	1001	13	5.10	66	37.40	868.3	10.2	298	c/cs
27	239	1004	13	5.30	66	36.90	868.8	9.6	298	c/cs
27	239	1009	13	5.70	66	36.20	869.6	9.7	298	c/cs
27	239	1024	13	6.90	66	34.00	872.1	9.7	298	c/cs
27	239	1030	13	7.32	66	33.13	873.0	9.9	299	GF
27	239	1041	13	8.20	66	31.50	874.8	10.1	299	c/cs
27	239	1044	13	8.45	66	31.06	875.4	9.8	300	GF

APPENDIX (continued).

Date (1987)	Julian day	Time (UTC)	North latitude (deg)	North latitude (min)	East longitude (deg)	East longitude (min)	Distance (nmi)	Actual speed (kt)	Actual course (deg)	Comments[a]
27	239	1057	13	9.50	66	29.20	877.5	9.7	299	c/cs
27	239	1100	13	9.73	66	28.72	878.0	9.8	299	GF
27	239	1114	13	10.80	66	26.70	880.2	9.8	300	c/cs
27	239	1125	13	11.70	66	25.10	882.0	9.5	300	c/cs
27	239	1130	13	12.14	66	24.38	882.8	9.6	300	GF
27	239	1132	13	12.30	66	24.10	883.2	10.0	299	c/cs
27	239	1144	13	13.28	66	22.31	885.1	9.7	300	GF
27	239	1150	13	13.80	66	21.40	886.1	9.8	300	c/cs
27	239	1200	13	14.58	66	19.99	887.8	10.0	300	GF
27	239	1214	13	15.75	66	17.92	890.1	9.6	300	GF
27	239	1215	13	15.80	66	17.80	890.2	9.6	300	c/cs
27	239	1230	13	17.02	66	15.65	892.6	9.9	300	GF
27	239	1243	13	18.10	66	13.70	894.8	10.0	300	c/cs
27	239	1259	13	19.40	66	11.40	897.4	10.2	299	c/cs
27	239	1300	13	19.49	66	11.21	897.6	10.2	299	GF
27	239	1308	13	20.10	66	10.00	899.0	9.9	298	c/cs
27	239	1319	13	21.00	66	8.30	900.8	10.0	299	c/cs
27	239	1330	13	21.89	66	6.70	902.6	10.3	299	GF
27	239	1337	13	22.50	66	5.60	903.8	10.0	300	c/cs
27	239	1344	13	23.05	66	4.58	905.0	9.4	300	GF
27	239	1349	13	23.40	66	3.90	905.8	9.9	300	c/cs
27	239	1400	13	24.33	66	2.27	907.6	10.0	299	GF
27	239	1405	13	24.70	66	1.50	908.4	9.7	299	c/cs
27	239	1430	13	26.72	65	57.89	912.4	9.8	300	GF
27	239	1433	13	27.00	65	57.50	912.9	9.8	300	c/cs
27	239	1442	13	27.70	65	56.10	914.4	9.6	300	c/cs
27	239	1450	13	28.30	65	55.00	915.7	10.1	300	c/cs
27	239	1458	13	29.00	65	53.80	917.0	10.0	300	c/cs
27	239	1513	13	30.20	65	51.50	919.6	10.3	300	c/cs
27	239	1518	13	30.70	65	50.80	920.4	9.8	299	c/cs
27	239	1539	13	32.30	65	47.70	923.8	10.0	299	c/cs
27	239	1553	13	33.40	65	45.60	926.2	10.0	299	c/cs
27	239	1559	13	33.90	65	44.70	927.2	9.5	299	c/cs
27	239	1612	13	34.90	65	42.80	929.2	10.1	299	c/cs
27	239	1617	13	35.30	65	42.00	930.1	9.5	298	c/cs
27	239	1621	13	35.60	65	41.50	930.7	9.6	299	c/cs
27	239	1634	13	36.60	65	39.60	932.8	10.1	299	c/cs
27	239	1650	13	37.90	65	37.20	935.5	9.8	299	c/cs
27	239	1704	13	39.00	65	35.10	937.8	10.0	299	c/cs
27	239	1715	13	39.90	65	33.50	939.6	9.8	300	c/cs
27	239	1735	13	41.50	65	30.50	942.9	9.6	300	c/cs
27	239	1740	13	41.90	65	29.80	943.7	9.8	300	c/cs
27	239	1804	13	43.86	65	26.29	947.6	9.6	301	GF
27	239	1808	13	44.20	65	25.70	948.3	9.4	300	c/cs
27	239	1816	13	44.80	65	24.60	949.5	9.8	301	c/cs
27	239	1821	13	45.30	65	23.90	950.3	9.4	300	c/cs
27	239	1826	13	45.60	65	23.20	951.1	9.8	301	c/cs
27	239	1854	13	48.00	65	19.20	955.7	9.9	301	c/cs
27	239	1912	13	49.60	65	16.50	958.7	9.7	301	c/cs
27	239	1930	13	51.10	65	14.00	961.6	10.0	301	c/cs
27	239	1935	13	51.50	65	13.30	962.4	9.7	301	c/cs
27	239	1945	13	52.30	65	11.80	964.0	9.7	301	c/cs
27	239	2000	13	53.60	65	9.70	966.5	9.5	301	c/cs
27	239	2005	13	54.00	65	9.00	967.2	10.0	300	c/cs

APPENDIX (continued).

Date (1987)	Julian day	Time (UTC)	North latitude (deg)	North latitude (min)	East longitude (deg)	East longitude (min)	Distance (nmi)	Actual speed (kt)	Actual course (deg)	Comments[a]
27	239	2010	13	54.40	65	8.30	968.1	9.6	300	c/cs
27	239	2022	13	55.40	65	6.50	970.0	9.8	299	c/cs
27	239	2036	13	56.50	65	4.50	972.3	9.5	300	c/cs
27	239	2041	13	56.90	65	3.60	973.1	9.8	299	c/cs
27	239	2101	13	58.50	65	0.80	976.4	9.5	299	c/cs
27	239	2119	13	59.90	64	58.30	979.2	9.9	299	c/cs
27	239	2142	14	1.70	64	54.90	983.0	9.8	299	c/cs
27	239	2156	14	2.90	64	52.80	985.3	9.9	299	c/cs
27	239	2225	14	5.20	64	48.50	990.1	10.1	299	c/cs
27	239	2228	14	5.44	64	48.05	990.6	10.0	298	SF
27	239	2248	14	7.00	64	45.00	993.9	9.6	298	c/cs
27	239	2312	14	8.80	64	41.50	997.7	9.7	298	c/cs
27	239	2326	14	9.90	64	39.50	1000.0	9.4	298	c/cs
27	239	2333	14	10.40	64	38.50	1001.1	9.6	298	c/cs
28 Aug	240	0000	14	12.50	64	34.50	1005.4	9.6	298	c/cs
28	240	0004	14	12.80	64	34.00	1006.1	9.6	298	c/cs
28	240	0014	14	13.54	64	32.50	1007.7	9.6	302	SF
28	240	0024	14	14.40	64	31.10	1009.3	9.7	302	c/cs
28	240	0102	14	17.60	64	25.70	1015.4	9.5	302	c/cs
28	240	0122	14	19.31	64	22.96	1018.6	9.5	302	SF
28	240	0124	14	19.50	64	22.70	1018.9	9.4	302	c/cs
28	240	0143	14	21.10	64	20.10	1021.9	9.6	300	c/cs
28	240	0155	14	22.00	64	18.30	1023.8	9.4	300	c/cs
28	240	0218	14	23.80	64	15.10	1027.4	9.8	300	c/cs
28	240	0220	14	24.00	64	14.80	1027.7	9.2	301	c/cs
28	240	0226	14	24.50	64	14.00	1028.7	9.5	300	c/cs
28	240	0244	14	25.90	64	11.50	1031.5	9.7	300	c/cs
28	240	0254	14	26.70	64	10.00	1033.1	10.0	300	c/cs
28	240	0329	14	29.50	64	4.80	1038.9	9.8	300	c/cs
28	240	0334	14	29.90	64	4.10	1039.7	9.3	300	c/cs
28	240	0352	14	31.30	64	1.60	1042.5	9.8	299	c/cs
28	240	0415	14	33.10	63	58.10	1046.3	9.9	299	c/cs
28	240	0428	14	34.20	63	56.20	1048.4	9.8	299	c/cs
28	240	0437	14	34.90	63	54.90	1049.9	9.9	299	c/cs
28	240	0448	14	35.70	63	53.20	1051.7	9.7	299	c/cs
28	240	0506	14	37.10	63	50.60	1054.6	9.6	297	c/cs
28	240	0515	14	37.80	63	49.30	1056.1	9.4	297	c/cs
28	240	0548	14	40.10	63	44.50	1061.2	9.3	297	c/cs
28	240	0558	14	40.79	63	43.07	1062.8	9.8	298	GF
28	240	0559	14	40.90	63	42.90	1062.9	9.6	298	c/cs
28	240	0604	14	41.20	63	42.20	1063.7	9.9	297	c/cs
28	240	0616	14	42.20	63	40.40	1065.7	9.7	295	c/cs
28	240	0628	14	42.99	63	38.55	1067.7	9.4	295	GF
28	240	0630	14	43.10	63	38.30	1068.0	9.5	295	c/cs
28	240	0639	14	43.70	63	36.90	1069.4	9.4	295	c/cs
28	240	0649	14	44.40	63	35.40	1071.0	9.3	295	c/cs
28	240	0700	14	45.09	63	33.85	1072.7	9.4	295	GF
28	240	0723	14	46.60	63	30.50	1076.3	9.4	295	c/cs
28	240	0730	14	47.07	63	29.44	1077.4	9.6	295	GF
28	240	0741	14	47.80	63	27.80	1079.1	9.6	295	c/cs
28	240	0753	14	48.60	63	26.00	1081.1	9.7	295	c/cs
28	240	0758	14	48.97	63	25.23	1081.9	9.5	294	GF
28	240	0809	14	49.70	63	23.60	1083.6	9.6	294	c/cs
28	240	0828	14	50.93	63	20.71	1086.7	9.3	294	GF

APPENDIX (continued).

Date (1987)	Julian day	Time (UTC)	North latitude (deg)	(min)	East longitude (deg)	(min)	Distance (nmi)	Actual speed (kt)	course (deg)	Comments[a]
28	240	0834	14	51.30	63	19.80	1087.6	9.8	296	c/cs
28	240	0836	14	51.50	63	19.50	1087.9	9.8	301	c/cs
28	240	0842	14	52.00	63	18.70	1088.9	9.6	299	c/cs
28	240	0851	14	52.70	63	17.40	1090.4	9.4	300	c/cs
28	240	0900	14	53.37	63	16.09	1091.8	9.5	299	GF
28	240	0904	14	53.70	63	15.50	1092.4	9.8	299	c/cs
28	240	0924	14	55.20	63	12.60	1095.6	9.6	299	c/cs
28	240	0930	14	55.70	63	11.69	1096.6	9.4	298	GF
28	240	0932	14	55.80	63	11.40	1096.9	9.0	298	c/cs
28	240	0937	14	56.20	63	10.70	1097.7	9.4	299	c/cs
28	240	0948	14	57.00	63	9.20	1099.4	9.7	301	c/cs
28	240	0958	14	57.90	63	7.70	1101.0	9.4	299	c/cs
28	240	1000	14	58.02	63	7.44	1101.3	9.4	298	GF
28	240	1015	14	59.10	63	5.30	1103.7	9.4	298	c/cs
28	240	1029	15	0.18	63	3.31	1105.9	9.3	299	GF
28	240	1041	15	1.10	63	1.60	1107.7	9.0	299	c/cs
28	240	1051	15	1.80	63	0.20	1109.2	9.2	299	c/cs
28	240	1100	15	2.46	62	58.99	1110.6	9.2	298	GF
28	240	1108	15	3.00	62	57.90	1111.8	9.5	298	c/cs
28	240	1114	15	3.50	62	57.00	1112.8	8.5	298	c/cs
28	240	1119	15	3.80	62	56.30	1113.5	9.0	298	c/cs
28	240	1129	15	4.51	62	54.98	1115.0	9.1	298	GF
28	240	1141	15	5.30	62	53.30	1116.8	9.1	297	c/cs
28	240	1157	15	6.50	62	51.10	1119.3	9.1	296	c/cs
28	240	1159	15	6.61	62	50.79	1119.6	9.1	295	GF
28	240	1212	15	7.40	62	48.90	1121.5	9.2	293	c/cs
28	240	1220	15	7.90	62	47.80	1122.8	8.7	295	c/cs
28	240	1225	15	8.20	62	47.10	1123.5	8.9	295	c/cs
28	240	1230	15	8.53	62	46.38	1124.2	8.8	295	GF
28	240	1245	15	9.50	62	44.30	1126.4	8.8	295	c/cs
28	240	1300	15	10.38	62	42.23	1128.6	8.8	295	GF
28	240	1305	15	10.70	62	41.50	1129.4	9.0	296	c/cs
28	240	1316	15	11.40	62	40.00	1131.0	9.2	296	c/cs
28	240	1326	15	12.10	62	38.60	1132.6	8.8	295	c/cs
28	240	1329	15	12.24	62	38.15	1133.0	9.8	294	GF
28	240	1335	15	12.60	62	37.20	1134.0	10.0	295	c/cs
28	240	1336	15	12.71	62	37.07	1134.1	9.1	296	SF
28	240	1351	15	13.70	62	35.00	1136.4	9.1	297	c/cs
28	240	1404	15	14.60	62	33.10	1138.4	9.0	299	c/cs
28	240	1419	15	15.70	62	31.10	1140.6	9.4	299	c/cs
28	240	1427	15	16.30	62	30.00	1141.9	9.2	298	c/cs
28	240	1449	15	17.90	62	26.90	1145.2	9.5	298	c/cs
28	240	1457	15	18.50	62	25.70	1146.5	9.6	300	c/cs
28	240	1504	15	19.10	62	24.70	1147.6	9.3	298	c/cs
28	240	1532	15	21.10	62	20.80	1152.0	9.2	299	c/cs
28	240	1545	15	22.10	62	19.00	1154.0	9.3	298	c/cs
28	240	1553	15	22.70	62	17.90	1155.2	9.2	298	c/cs
28	240	1626	15	25.11	62	13.22	1160.3	8.9	298	SN
28	240	1631	15	25.50	62	12.50	1161.0	8.8	300	c/cs
28	240	1654	15	27.10	62	9.50	1164.4	9.0	301	c/cs
28	240	1711	15	28.40	62	7.20	1166.9	9.2	301	c/cs
28	240	1716	15	28.82	62	6.54	1167.7	8.9	301	SN
28	240	1722	15	29.30	62	5.70	1168.6	8.9	301	c/cs
28	240	1734	15	30.20	62	4.20	1170.4	8.9	300	c/cs

APPENDIX (continued).

Date (1987)	Julian day	Time (UTC)	North latitude (deg)	North latitude (min)	East longitude (deg)	East longitude (min)	Distance (nmi)	Actual speed (kt)	Actual course (deg)	Comments[a]
28	240	1739	15	30.60	62	3.50	1171.1	8.6	302	c/cs
28	240	1744	15	31.00	62	2.90	1171.8	9.0	301	c/cs
28	240	1807	15	32.70	61	59.80	1175.3	8.8	301	c/cs
28	240	1816	15	33.42	61	58.64	1176.6	8.9	299	SN
28	240	1824	15	34.00	61	57.60	1177.8	9.1	299	c/cs
28	240	1846	15	35.62	61	54.55	1181.1	9.2	305	SN
28	240	1847	15	35.70	61	54.40	1181.3	9.3	303	c/cs
28	240	1903	15	37.10	61	52.30	1183.7	9.2	304	c/cs
28	240	1904	15	37.16	61	52.13	1183.9	9.2	300	SN
28	240	1911	15	37.70	61	51.20	1185.0	9.4	300	c/cs
28	240	1938	15	39.80	61	47.40	1189.2	9.6	299	c/cs
28	240	1946	15	40.50	61	46.20	1190.5	9.5	300	c/cs
28	240	2009	15	42.30	61	43.00	1194.1	9.3	300	c/cs
28	240	2037	15	44.50	61	39.00	1198.5	9.6	300	c/cs
28	240	2044	15	45.10	61	38.00	1199.6	9.4	300	c/cs
28	240	2120	15	47.90	61	33.00	1205.2	9.3	300	c/cs
28	240	2145	15	49.90	61	29.50	1209.1	9.4	300	c/cs
28	240	2204	15	51.37	61	26.84	1212.1	9.8	303	SN
28	240	2206	15	51.50	61	26.60	1212.4	9.8	302	c/cs
28	240	2226	15	53.30	61	23.70	1215.7	9.7	300	c/cs
28	240	2241	15	54.50	61	21.50	1218.1	9.7	300	c/cs
28	240	2301	15	56.10	61	18.50	1221.4	9.6	300	c/cs
28	240	2316	15	57.30	61	16.40	1223.8	9.9	300	c/cs
28	240	2330	15	58.40	61	14.30	1226.1	9.8	300	c/cs
28	240	2347	15	59.80	61	11.80	1228.9	9.9	300	c/cs
28	240	2353	16	0.28	61	10.88	1229.8	10.2	301	SF
29 Aug	241	0000	16	0.90	61	9.80	1231.0	10.2	301	c/cs
29	241	0007	16	1.50	61	8.70	1232.2	10.1	294	c/cs
29	241	0008	16	1.60	61	8.60	1232.4	9.1	281	c/cs
29	241	0013	16	1.70	61	7.80	1233.2	7.6	286	c/cs
29	241	0025	16	2.10	61	6.30	1234.7	7.6	288	c/cs
29	241	0028	16	2.30	61	5.90	1235.1	7.3	281	c/cs
29	241	0045	16	2.60	61	3.80	1237.1	7.0	282	c/cs
29	241	0056	16	2.90	61	2.50	1238.4	7.4	281	c/cs
29	241	0111	16	3.20	61	0.60	1240.3	7.4	281	c/cs
29	241	0119	16	3.40	60	59.60	1241.2	7.8	280	c/cs
29	241	0124	16	3.50	60	58.90	1241.9	7.5	281	c/cs
29	241	0127	16	3.61	60	58.55	1242.3	7.9	282	SF
29	241	0138	16	3.90	60	57.10	1243.7	7.4	271	c/cs
29	241	0208	16	4.00	60	53.20	1247.4	7.0	268	c/cs
29	241	0214	16	3.90	60	52.50	1248.1	5.1	269	c/cs
29	241	0217	16	3.90	60	52.20	1248.3	4.6	269	c/cs
29	241	0241	16	3.90	60	50.30	1250.2	4.3	271	c/cs
29	241	0248	16	3.90	60	49.80	1250.7	5.7	297	c/cs
29	241	0254	16	4.10	60	49.30	1251.3	5.7	299	c/cs
29	241	0300	16	4.40	60	48.70	1251.8	5.0	300	c/cs
29	241	0316	16	5.10	60	47.50	1253.2	4.9	301	c/cs
29	241	0330	16	5.67	60	46.53	1254.3	4.5	306	XX
29	241	0333	16	5.80	60	46.30	1254.5	4.9	313	c/cs
29	241	0347	16	6.60	60	45.50	1255.7	5.4	319	c/cs
29	241	0402	16	7.60	60	44.50	1257.0	5.5	319	c/cs
29	241	0407	16	8.00	60	44.20	1257.5	5.0	311	c/cs
29	241	0427	16	9.00	60	42.90	1259.2	5.4	328	c/cs
29	241	0428	16	9.12	60	42.87	1259.3	5.1	330	SF

APPENDIX (continued).

Date (1987)	Julian day	Time (UTC)	North latitude		East longitude		Distance (nmi)	Actual		Comments[a]
			(deg)	(min)	(deg)	(min)		speed (kt)	course (deg)	
29	241	0429	16	9.20	60	42.80	1259.3	6.0	3	c/cs
29	241	0430	16	9.30	60	42.80	1259.4	6.8	33	c/cs
29	241	0432	16	9.50	60	43.00	1259.7	8.3	42	c/cs
29	241	0441	16	10.40	60	43.80	1260.9	8.3	59	c/cs
29	241	0442	16	10.50	60	44.00	1261.0	7.3	77	c/cs
29	241	0443	16	10.50	60	44.10	1261.2	6.5	98	c/cs
29	241	0444	16	10.50	60	44.20	1261.3	4.8	125	c/cs
29	241	0450	16	10.21	60	44.60	1261.8	4.5	135	XX
29	241	0451	16	10.20	60	44.70	1261.8	4.8	135	c/cs
29	241	0503	16	9.50	60	45.40	1262.8	4.4	136	c/cs
29	241	0506	16	9.30	60	45.50	1263.0	3.2	169	c/cs
29	241	0508	16	9.20	60	45.50	1263.1	2.4	215	c/cs
29	241	0513	16	9.10	60	45.40	1263.3	4.6	217	c/cs
29	241	0516	16	8.90	60	45.30	1263.5	5.8	217	c/cs
29	241	0530	16	7.79	60	44.43	1264.9	6.2	215	XX
29	241	0531	16	7.70	60	44.40	1265.0	6.3	215	c/cs
29	241	0545	16	6.50	60	43.50	1266.5	0.5	66	c/cs
29	241	0548	16	6.52	60	43.52	1266.5	0.0	39	XX
2 Sept	245	1624	16	7.84	60	44.64	1268.2	1.0	27	720
2	245	1627	16	7.90	60	44.70	1268.2	1.0	21	c/cs
2	245	1648	16	8.20	60	44.80	1268.6	1.5	352	c/cs
2	245	1650	16	8.30	60	44.80	1268.7	2.6	317	c/cs
2	245	1652	16	8.30	60	44.70	1268.7	5.1	305	c/cs
2	245	1657	16	8.60	60	44.40	1269.2	5.6	307	c/cs
2	245	1705	16	9.00	60	43.70	1269.9	5.8	309	c/cs
2	245	1747	16	11.60	60	40.50	1274.0	5.9	310	c/cs
2	245	1817	16	13.50	60	38.10	1276.9	5.8	309	c/cs
2	245	1828	16	14.10	60	37.30	1278.0	5.6	299	c/cs
2	245	1858	16	15.50	60	34.70	1280.8	5.7	300	c/cs
2	245	1928	16	16.90	60	32.20	1283.6	5.6	299	c/cs
2	245	1958	16	18.30	60	29.60	1286.4	5.6	299	c/cs
2	245	2019	16	19.20	60	27.80	1288.4	5.1	288	c/cs
2	245	2037	16	19.70	60	26.30	1289.9	5.2	290	c/cs
2	245	2107	16	20.60	60	23.80	1292.5	5.1	289	c/cs
2	245	2134	16	21.30	60	21.50	1294.8	5.1	289	c/cs
2	245	2200	16	22.01	60	19.33	1297.0	4.7	289	SF
2	245	2204	16	22.10	60	19.00	1297.3	5.0	289	c/cs
2	245	2219	16	22.50	60	17.80	1298.5	5.6	289	c/cs
2	245	2249	16	23.40	60	15.00	1301.3	5.6	288	c/cs
2	245	2311	16	24.10	60	13.00	1303.4	5.5	289	c/cs
2	245	2335	16	24.80	60	10.80	1305.6	5.6	290	c/cs
2	245	2358	16	25.50	60	8.70	1307.7	6.7	297	c/cs
3 Sept	246	0000	16	25.60	60	8.50	1308.0	6.7	297	c/cs
3	246	0009	16	26.00	60	7.60	1309.0	6.9	299	c/cs
3	246	0018	16	26.52	60	6.63	1310.0	6.4	300	SF
3	246	0027	16	27.00	60	5.80	1311.0	5.9	299	c/cs
3	246	0038	16	27.50	60	4.80	1312.0	5.9	299	c/cs
3	246	0059	16	28.50	60	2.90	1314.1	6.6	299	c/cs
3	246	0111	16	29.20	60	1.70	1315.4	6.3	300	c/cs
3	246	0141	16	30.80	59	58.90	1318.5	6.3	301	c/cs
3	246	0207	16	32.20	59	56.40	1321.3	6.6	312	c/cs
3	246	0214	16	32.70	59	55.80	1322.1	6.8	319	c/cs
3	246	0219	16	33.10	59	55.40	1322.6	6.4	329	c/cs
3	246	0226	16	33.80	59	55.00	1323.4	6.5	332	c/cs

APPENDIX (continued).

Date (1987)	Julian day	Time (UTC)	North latitude (deg)	North latitude (min)	East longitude (deg)	East longitude (min)	Distance (nmi)	Actual speed (kt)	Actual course (deg)	Comments[a]
3	246	0243	16	35.40	59	54.10	1325.2	6.8	342	c/cs
3	246	0256	16	36.80	59	53.64	1326.7	7.3	341	GF
3	246	0257	16	36.90	59	53.60	1326.8	7.2	340	c/cs
3	246	0302	16	37.60	59	53.40	1327.4	6.2	311	c/cs
3	246	0303	16	37.50	59	53.30	1327.5	3.6	261	c/cs
3	246	0306	16	37.50	59	53.10	1327.7	4.1	253	c/cs
3	246	0310	16	37.44	59	52.85	1328.0	4.4	246	GF
3	246	0313	16	37.30	59	52.60	1328.2	5.7	247	c/cs
3	246	0320	16	37.09	59	52.00	1328.9	5.7	245	GF
3	246	0328	16	36.80	59	51.30	1329.6	6.2	245	c/cs
3	246	0330	16	36.69	59	51.09	1329.8	6.2	243	GF
3	246	0340	16	36.22	59	50.13	1330.9	6.0	242	GF
3	246	0341	16	36.20	59	50.00	1331.0	5.7	260	c/cs
3	246	0342	16	36.20	59	49.90	1331.1	6.2	293	c/cs
3	246	0349	16	36.40	59	49.20	1331.8	6.6	294	c/cs
3	246	0350	16	36.49	59	49.14	1331.9	6.7	296	GF
3	246	0400	16	36.99	59	48.09	1333.0	6.9	299	GF
3	246	0407	16	37.40	59	47.40	1333.8	7.1	299	c/cs
3	246	0410	16	37.55	59	47.03	1334.2	7.2	297	GF
3	246	0415	16	37.80	59	46.50	1334.8	5.9	275	c/cs
3	246	0416	16	37.80	59	46.40	1334.9	5.3	239	c/cs
3	246	0418	16	37.70	59	46.20	1335.1	4.9	210	c/cs
3	246	0419	16	37.70	59	46.20	1335.2	5.7	172	c/cs
3	246	0420	16	37.58	59	46.18	1335.2	7.1	168	GF
3	246	0425	16	37.00	59	46.30	1335.8	7.7	167	c/cs
3	246	0430	16	36.38	59	46.46	1336.5	7.3	164	GF
3	246	0434	16	35.90	59	46.60	1337.0	8.2	133	c/cs
3	246	0440	16	35.35	59	47.22	1337.8	8.5	130	GF
3	246	0441	16	35.30	59	47.30	1337.9	9.0	124	c/cs
3	246	0444	16	35.00	59	47.70	1338.4	9.6	102	c/cs
3	246	0445	16	35.00	59	47.90	1338.5	9.2	83	c/cs
3	246	0446	16	35.00	59	48.00	1338.7	9.0	60	c/cs
3	246	0447	16	35.10	59	48.20	1338.8	7.9	32	c/cs
3	246	0448	16	35.20	59	48.30	1339.0	5.7	358	c/cs
3	246	0450	16	35.37	59	48.25	1339.2	6.0	349	GF
3	246	0450	16	35.40	59	48.20	1339.2	6.4	329	c/cs
3	246	0457	16	36.00	59	47.90	1339.9	6.8	334	c/cs
3	246	0500	16	36.31	59	47.70	1340.2	7.0	332	GF
3	246	0500	16	36.30	59	47.70	1340.2	7.6	6	c/cs
3	246	0504	16	36.80	59	47.80	1340.7	7.8	355	c/cs
3	246	0510	16	37.59	59	47.69	1341.5	7.7	353	GF
3	246	0510	16	37.60	59	47.70	1341.5	8.3	360	c/cs
3	246	0520	16	38.98	59	47.68	1342.9	8.4	359	GF
3	246	0525	16	39.70	59	47.70	1343.6	8.5	5	c/cs
3	246	0530	16	40.38	59	47.73	1344.3	8.4	6	GF
3	246	0530	16	40.40	59	47.70	1344.3	7.5	43	c/cs
3	246	0531	16	40.50	59	47.80	1344.4	8.6	65	c/cs
3	246	0536	16	40.80	59	48.50	1345.2	8.9	86	c/cs
3	246	0540	16	40.81	59	49.11	1345.7	9.0	88	GF
3	246	0543	16	40.80	59	49.60	1346.2	9.2	90	c/cs
3	246	0549	16	40.80	59	50.50	1347.1	9.3	95	c/cs
3	246	0550	16	40.82	59	50.70	1347.3	9.4	90	GF
3	246	0600	16	40.81	59	52.33	1348.8	9.4	89	GF
3	246	0608	16	40.80	59	53.60	1350.1	9.6	69	c/cs

APPENDIX (continued).

Date (1987)	Julian day	Time (UTC)	North latitude		East longitude		Distance (nmi)	Actual		Comments[a]
			(deg)	(min)	(deg)	(min)		speed (kt)	course (deg)	
3	246	0609	16	40.90	59	53.80	1350.2	8.6	41	c/cs
3	246	0610	16	41.00	59	53.89	1350.4	7.8	40	GF
3	246	0610	16	41.00	59	53.90	1350.4	7.8	15	c/cs
3	246	0611	16	41.10	59	53.90	1350.5	7.3	348	c/cs
3	246	0612	16	41.20	59	53.90	1350.6	6.9	318	c/cs
3	246	0619	16	41.80	59	53.30	1351.4	7.4	318	c/cs
3	246	0620	16	41.93	59	53.25	1351.6	7.5	318	GF
3	246	0629	16	42.80	59	52.50	1352.7	6.9	293	c/cs
3	246	0630	16	42.81	59	52.35	1352.8	6.8	287	GF
3	246	0630	16	42.80	59	52.40	1352.8	5.5	246	c/cs
3	246	0633	16	42.70	59	52.10	1353.1	5.6	216	c/cs
3	246	0635	16	42.50	59	52.00	1353.3	5.8	202	c/cs
3	246	0638	16	42.30	59	51.90	1353.6	6.3	188	c/cs
3	246	0640	16	42.07	59	51.83	1353.8	6.1	184	GF
3	246	0642	16	41.90	59	51.80	1354.0	6.3	177	c/cs
3	246	0644	16	41.70	59	51.80	1354.2	6.3	177	c/cs
3	246	0647	16	41.30	59	51.80	1354.5	6.2	184	c/cs
3	246	0650	16	41.03	59	51.82	1354.8	6.3	179	GF
3	246	0655	16	40.50	59	51.80	1355.3	6.5	179	c/cs
3	246	0700	16	39.96	59	51.84	1355.9	6.8	179	GF
3	246	0705	16	39.40	59	51.80	1356.4	6.6	184	c/cs
3	246	0708	16	39.10	59	51.80	1356.8	6.6	183	c/cs
3	246	0710	16	38.85	59	51.81	1357.0	4.5	172	GF
3	246	0720	16	38.10	59	51.92	1357.7	6.2	195	GF
3	246	0735	16	36.60	59	51.50	1359.3	0.1	5	c/cs
3	246	1641	16	40.67	59	51.87	1363.4	0.9	230	721
6 Sept	249	2230	16	37.31	59	47.72	1368.6	0.0	90	722
6	249	0730	16	37.31	59	47.72	1368.6	4.2	3	722
13 Sept	256	0730	16	37.40	59	47.70	1368.7	6.4	354	c/cs
13	256	0732	16	37.70	59	47.70	1368.9	9.7	355	c/cs
13	256	0734	16	38.10	59	47.70	1369.4	12.1	354	c/cs
13	256	0737	16	39.70	59	47.50	1371.0	12.7	353	c/cs
13	256	0745	16	42.90	59	47.10	1374.2	12.2	351	GF
13	256	0800	16	47.90	59	46.20	1379.3	12.4	351	c/cs
13	256	0825	16	54.60	59	45.10	1386.1	12.5	351	c/cs
13	256	0858	16	55.04	59	45.03	1386.5	12.2	350	GF
13	256	0900	17	1.02	59	43.88	1392.6	11.9	350	GF
13	256	0930	17	4.30	59	43.30	1395.9	12.0	350	c/cs
13	256	0947	17	6.89	59	42.77	1398.5	11.9	349	GF
13	256	1000	17	10.80	59	42.00	1402.5	11.8	349	c/cs
13	256	1020	17	12.73	59	41.61	1404.5	11.8	349	GF
13	256	1030	17	14.10	59	41.30	1405.9	12.0	349	c/cs
13	256	1037	17	18.58	59	40.40	1410.4	12.1	348	GF
13	256	1100	17	23.70	59	39.30	1415.7	12.2	349	c/cs
13	256	1126	17	24.52	59	39.13	1416.5	12.2	350	GF
13	256	1130	17	29.30	59	38.20	1421.4	12.3	350	c/cs
13	256	1154	17	30.54	59	38.01	1422.6	12.0	351	GF
13	256	1200	17	34.30	59	37.40	1426.4	12.0	351	c/cs
13	256	1219	17	36.47	59	36.99	1428.6	11.3	347	GF
13	256	1230	17	38.10	59	36.60	1430.3	11.3	347	c/cs
13	256	1239	17	45.50	59	34.80	1437.9	11.5	346	c/cs
13	256	1319	17	48.10	59	34.10	1440.6	11.3	346	c/cs
13	256	1333	17	51.20	59	33.30	1443.8	11.2	346	c/cs
13	256	1350	17	55.40	59	32.20	1448.1	11.2	346	c/cs
13	256	1413								

APPENDIX (continued).

Date (1987)	Julian day	Time (UTC)	North latitude		East longitude		Distance (nmi)	Actual		Comments[a]
			(deg)	(min)	(deg)	(min)		speed (kt)	course (deg)	
13	256	1435	17	59.30	59	31.20	1452.2	11.3	346	c/cs
13	256	1504	18	4.60	59	29.80	1457.6	11.2	346	c/cs
13	256	1539	18	11.00	59	28.10	1464.2	11.3	346	c/cs
13	256	1607	18	16.10	59	26.80	1469.4	11.3	346	c/cs
13	256	1637	18	21.58	59	25.36	1475.1	11.6	351	SF
13	256	1648	18	23.70	59	25.00	1477.2	11.6	351	c/cs
13	256	1738	18	33.20	59	23.40	1486.9	11.6	351	c/cs
13	256	1756	18	36.60	59	22.90	1490.3	11.6	355	c/cs
13	256	1845	18	46.10	59	22.00	1499.8	11.6	355	c/cs
13	256	1908	18	50.60	59	21.60	1504.3	11.7	355	c/cs
13	256	1958	19	0.30	59	20.70	1514.1	11.8	355	c/cs
13	256	2019	19	4.40	59	20.30	1518.2	11.7	355	c/cs
13	256	2057	19	11.80	59	19.60	1525.6	11.7	355	c/cs
13	256	2125	19	17.26	59	19.08	1531.1	12.0	354	SF
13	256	2140	19	20.20	59	18.80	1534.1	12.1	350	c/cs
13	256	2228	19	29.80	59	17.00	1543.8	12.5	350	c/cs
13	256	2253	19	34.90	59	16.00	1549.0	12.3	342	c/cs
13	256	2332	19	42.50	59	13.40	1556.9	12.2	342	c/cs
14 Sept	257	0000	19	47.90	59	11.50	1562.6	12.2	342	c/cs
14	257	0002	19	48.30	59	11.40	1563.0	12.2	342	c/cs
14	257	0014	19	50.60	59	10.60	1565.5	12.3	340	c/cs
14	257	0038	19	55.20	59	8.80	1570.4	12.4	343	c/cs
14	257	0103	20	0.10	59	7.20	1575.5	12.4	343	c/cs
14	257	0113	20	2.10	59	6.50	1577.6	12.4	343	c/cs
14	257	0131	20	5.60	59	5.40	1581.3	12.6	343	c/cs
14	257	0139	20	7.20	59	4.80	1583.0	12.5	347	c/cs
14	257	0156	20	10.70	59	4.00	1586.5	12.6	349	c/cs
14	257	0206	20	12.70	59	3.50	1588.6	12.2	352	c/cs
14	257	0226	20	16.80	59	3.00	1592.7	12.1	351	c/cs
14	257	0230	20	17.56	59	2.83	1593.5	12.3	351	GF
14	257	0242	20	20.00	59	2.40	1596.0	12.4	350	c/cs
14	257	0300	20	23.64	59	1.70	1599.7	12.6	352	GF
14	257	0315	20	26.80	59	1.20	1602.8	12.7	352	c/cs
14	257	0330	20	29.89	59	0.72	1606.0	12.3	350	GF
14	257	0358	20	35.50	58	59.70	1611.7	12.2	351	c/cs
14	257	0400	20	35.94	58	59.62	1612.1	11.3	350	GF
14	257	0411	20	38.00	58	59.30	1614.2	10.8	350	c/cs
14	257	0418	20	39.20	58	59.00	1615.4	8.4	350	c/cs
14	257	0421	20	39.60	58	58.90	1615.9	6.6	351	c/cs
14	257	0424	20	40.00	58	58.90	1616.2	4.8	353	c/cs
14	257	0429	20	40.40	58	58.80	1616.6	3.5	336	c/cs
14	257	0430	20	40.41	58	58.80	1616.7	1.5	330	GF
14	257	0431	20	40.40	58	58.80	1616.7	0.3	77	c/cs
14	257	0500	20	40.47	58	58.96	1616.8	0.1	69	GF
14	257	0521	20	40.50	58	59.00	1616.9	0.1	20	c/cs
14	257	0529	20	40.50	58	59.00	1616.9	2.1	233	c/cs
14	257	0530	20	40.47	58	58.97	1616.9	4.3	198	GF
14	257	0530	20	40.50	58	59.00	1616.9	5.9	162	c/cs
14	257	0532	20	40.30	58	59.00	1617.1	8.7	167	c/cs
14	257	0534	20	40.00	58	59.10	1617.4	11.6	169	c/cs
14	257	0542	20	38.50	58	59.40	1619.0	12.0	169	c/cs
14	257	0555	20	35.90	58	59.90	1621.6	11.6	178	c/cs
14	257	0600	20	34.95	58	59.95	1622.5	11.1	180	GF
14	257	0608	20	33.50	58	59.90	1624.0	11.2	180	c/cs

APPENDIX (continued).

Date (1987)	Julian day	Time (UTC)	North latitude		East longitude		Distance (nmi)	Actual		Comments[a]
			(deg)	(min)	(deg)	(min)		speed (kt)	course (deg)	
14	257	0618	20	31.60	58	60.00	1625.9	10.4	190	c/cs
14	257	0620	20	31.30	58	59.90	1626.2	11.0	202	c/cs
14	257	0630	20	29.56	58	59.15	1628.1	10.8	208	GF
14	257	0653	20	25.90	58	57.10	1632.2	10.8	209	c/cs
14	257	0700	20	24.80	58	56.43	1633.5	11.1	209	GF
14	257	0721	20	21.40	58	54.40	1637.4	10.8	208	c/cs
14	257	0730	20	19.95	58	53.62	1639.0	11.0	207	GF
14	257	0739	20	18.50	58	52.80	1640.6	10.9	207	c/cs
14	257	0800	20	15.08	58	50.94	1644.5	10.8	209	GF
14	257	0802	20	14.80	58	50.80	1644.8	11.1	208	c/cs
14	257	0827	20	10.70	58	48.40	1649.5	11.1	208	c/cs
14	257	0830	20	10.19	58	48.15	1650.0	11.2	207	GF
14	257	0853	20	6.40	58	46.10	1654.3	11.2	208	c/cs
14	257	0900	20	5.21	58	45.41	1655.6	11.4	207	GF
14	257	0910	20	3.50	58	44.50	1657.5	11.3	207	c/cs
14	257	0930	20	0.18	58	42.63	1661.3	11.6	208	GF
14	257	1000	19	55.07	58	39.76	1667.1	11.7	209	GF
14	257	1001	19	54.90	58	39.70	1667.3	11.8	209	c/cs
14	257	1030	19	49.91	58	36.74	1673.0	11.8	207	GF
14	257	1032	19	49.60	58	36.50	1673.3	11.9	207	c/cs
14	257	1042	19	47.80	58	35.60	1675.3	11.8	204	c/cs
14	257	1100	19	44.57	58	34.05	1678.9	12.1	204	GF
14	257	1112	19	42.40	58	33.00	1681.3	12.2	205	c/cs
14	257	1119	19	41.10	58	32.40	1682.7	12.3	209	c/cs
14	257	1130	19	39.09	58	31.21	1685.0	12.1	211	GF
14	257	1135	19	38.20	58	30.70	1686.0	12.2	211	c/cs
14	257	1200	19	33.86	58	27.92	1691.0	11.1	210	GF
14	257	1200	19	33.90	58	27.90	1691.0	10.9	210	c/cs
14	257	1230	19	29.15	58	25.04	1696.5	10.7	208	GF
14	257	1236	19	28.20	58	24.50	1697.6	10.6	209	c/cs
14	257	1246	19	26.70	58	23.60	1699.3	10.6	207	c/cs
14	257	1303	19	24.00	58	22.20	1702.3	10.5	206	c/cs
14	257	1327	19	20.20	58	20.20	1706.5	10.7	206	c/cs
14	257	1336	19	18.70	58	19.50	1708.1	10.6	206	c/cs
14	257	1402	19	14.60	58	17.40	1712.7	10.5	206	c/cs
14	257	1412	19	13.00	58	16.60	1714.5	10.6	206	c/cs
14	257	1420	19	11.70	58	15.90	1715.9	10.4	205	c/cs
14	257	1505	19	4.70	58	12.40	1723.7	10.3	205	c/cs
14	257	1524	19	1.70	58	10.90	1727.0	10.4	205	c/cs
14	257	1525	19	1.57	58	10.82	1727.2	9.6	201	SF
14	257	1534	19	0.20	58	10.30	1728.6	9.4	202	c/cs
14	257	1553	18	57.50	58	9.10	1731.6	9.4	203	c/cs
14	257	1616	18	54.10	58	7.60	1735.2	9.3	203	c/cs
14	257	1627	18	52.60	58	6.90	1736.9	9.7	203	c/cs
14	257	1642	18	50.30	58	5.90	1739.3	9.5	203	c/cs
14	257	1700	18	47.70	58	4.80	1742.1	9.7	204	c/cs
14	257	1708	18	46.50	58	4.20	1743.4	9.4	206	c/cs
14	257	1712	18	45.98	58	3.93	1744.1	9.9	213	SF
14	257	1725	18	44.20	58	2.70	1745.2	10.2	213	c/cs
14	257	1735	18	42.70	58	1.80	1747.9	3.1	211	c/cs
14	257	1736	18	42.70	58	1.70	1747.9	10.2	213	c/cs
14	257	1748	18	41.00	58	0.60	1750.0	10.0	213	c/cs
14	257	1808	18	38.20	57	58.70	1753.3	9.9	213	c/cs
14	257	1834	18	34.60	57	56.20	1757.6	10.1	213	c/cs

APPENDIX (continued).

Date (1987)	Julian day	Time (UTC)	North latitude		East longitude		Distance (nmi)	Actual		Comments[a]
			(deg)	(min)	(deg)	(min)		speed (kt)	course (deg)	
14	257	1835	18	34.41	57	56.14	1757.8	8.6	215	SF
14	257	1844	18	33.40	57	55.40	1759.1	8.4	215	c/cs
14	257	1856	18	32.00	57	54.40	1760.8	8.3	214	c/cs
14	257	1907	18	30.70	57	53.50	1762.3	8.5	214	c/cs
14	257	1922	18	28.90	57	52.20	1764.4	8.4	214	c/cs
14	257	1945	18	26.30	57	50.30	1767.6	8.0	214	c/cs
14	257	1957	18	24.90	57	49.40	1769.2	8.3	214	c/cs
14	257	2018	18	22.50	57	47.70	1772.1	8.3	214	c/cs
14	257	2033	18	20.80	57	46.50	1774.2	8.4	214	c/cs
14	257	2106	18	17.00	57	43.80	1778.8	6.7	213	c/cs
14	257	2109	18	16.70	57	43.60	1779.1	4.4	222	c/cs
14	257	2114	18	16.40	57	43.30	1779.5	3.0	224	c/cs
14	257	2118	18	16.30	57	43.20	1779.7	1.3	232	c/cs
14	257	2124	18	16.20	57	43.10	1779.8	0.5	266	c/cs
14	257	2137	18	16.20	57	43.00	1779.9	0.4	305	c/cs
14	257	2227	18	16.40	57	42.70	1780.3	0.4	308	c/cs
14	257	2316	18	16.60	57	42.40	1780.6	0.4	311	c/cs
15 Sept	258	0000	18	16.80	57	42.20	1780.9	0.4	311	c/cs
15	258	0006	18	16.80	57	42.10	1780.9	0.4	310	c/cs
15	258	0047	18	17.00	57	41.90	1781.2	0.5	235	c/cs
15	258	0107	18	16.90	57	41.80	1781.4	0.6	221	c/cs
15	258	0156	18	16.50	57	41.40	1781.9	0.5	221	c/cs
15	258	0200	18	16.50	57	41.39	1781.9	2.8	216	GF
15	258	0234	18	15.20	57	40.40	1783.5	2.8	216	c/cs
15	258	0259	18	14.30	57	39.70	1784.7	3.9	208	c/cs
15	258	0300	18	14.20	57	39.64	1784.8	4.3	191	GF
15	258	0302	18	14.10	57	39.60	1784.9	7.3	191	c/cs
15	258	0304	18	13.80	57	39.60	1785.1	8.8	191	c/cs
15	258	0307	18	13.40	57	39.50	1785.6	10.5	191	c/cs
15	258	0314	18	12.18	57	39.24	1786.8	10.4	190	GF
15	258	0324	18	10.47	57	38.91	1788.5	10.4	190	GF
15	258	0334	18	8.76	57	38.58	1790.3	9.7	190	GF
15	258	0335	18	8.60	57	38.50	1790.4	9.3	192	c/cs
15	258	0340	18	7.80	57	38.40	1791.2	8.5	199	c/cs
15	258	0344	18	7.31	57	38.18	1791.8	6.2	202	GF
15	258	0352	18	6.50	57	37.90	1792.6	3.8	201	c/cs
15	258	0354	18	6.42	57	37.81	1792.7	6.1	200	GF
15	258	0404	18	5.46	57	37.44	1793.8	6.2	196	GF
15	258	0407	18	5.20	57	37.40	1794.1	6.2	196	c/cs
15	258	0414	18	4.47	57	37.14	1794.8	6.1	198	GF
15	258	0424	18	3.50	57	36.80	1795.8	6.0	200	GF
15	258	0424	18	3.50	57	36.80	1795.8	6.1	202	c/cs
15	258	0440	18	2.00	57	36.16	1797.4	6.1	199	XX
15	258	0446	18	1.40	57	36.00	1798.0	5.7	177	c/cs
15	258	0448	18	1.20	57	36.00	1798.2	5.2	136	c/cs
15	258	0450	18	1.11	57	36.09	1798.4	7.3	113	XX
15	258	0454	18	0.90	57	36.60	1798.9	8.2	111	c/cs
15	258	0504	18	0.40	57	37.90	1800.3	7.9	86	c/cs
15	258	0505	18	0.50	57	38.00	1800.4	6.5	63	c/cs
15	258	0507	18	0.50	57	38.20	1800.6	6.5	48	c/cs
15	258	0513	18	1.00	57	38.80	1801.3	7.0	47	c/cs
15	258	0521	18	1.60	57	39.50	1802.2	3.7	8	c/cs
15	258	0523	18	1.70	57	39.50	1802.3	1.8	288	c/cs
15	258	0535	18	1.80	57	39.10	1802.7	2.2	292	c/cs

APPENDIX (continued).

			North latitude		East longitude			Actual		
Date (1987)	Julian day	Time (UTC)	(deg)	(min)	(deg)	(min)	Distance (nmi)	speed (kt)	course (deg)	Comments[a]
15	258	0553	18	2.10	57	38.50	1803.4	2.4	296	c/cs
15	258	0555	18	2.10	57	38.40	1803.4	2.4	299	c/cs
15	258	0645	18	3.11	57	36.54	1805.5	5.4	290	723
15	258	0645	18	3.10	57	36.50	1805.5	0.0	90	c/cs
19 Sept	262	1157	18	3.11	57	36.54	1805.5	1.1	335	723
19	262	2048	18	12.00	57	32.20	1815.2	4.3	7	c/cs
19	262	2112	18	13.70	57	32.40	1816.9	4.5	12	c/cs
19	262	2141	18	15.80	57	32.90	1819.1	4.5	13	c/cs
19	262	2210	18	17.90	57	33.40	1821.3	5.7	15	c/cs
19	262	2225	18	19.30	57	33.80	1822.7	5.9	15	c/cs
19	262	2254	18	22.00	57	34.60	1825.6	5.9	15	c/cs
19	262	2303	18	22.90	57	34.80	1826.4	6.0	347	c/cs
19	262	2305	18	23.10	57	34.80	1826.6	5.2	308	c/cs
19	262	2308	18	23.30	57	34.50	1826.9	5.6	296	c/cs
19	262	2312	18	23.42	57	34.20	1827.3	3.8	314	XX
19	262	2321	18	23.80	57	33.80	1827.8	3.0	317	c/cs
19	262	2333	18	24.30	57	33.30	1828.5	2.6	320	c/cs
19	262	2355	18	25.00	57	32.70	1829.4	1.5	352	c/cs
20 Sept	263	0000	18	25.10	57	32.70	1829.5	1.5	352	c/cs
20	263	0003	18	25.20	57	32.70	1829.6	1.5	9	c/cs
20	263	0018	18	25.60	57	32.70	1830.0	1.8	356	c/cs
20	263	0023	18	25.70	57	32.70	1830.1	3.2	9	c/cs
20	263	0027	18	25.90	57	32.70	1830.3	4.3	35	c/cs
20	263	0031	18	26.10	57	32.90	1830.6	4.8	40	c/cs
20	263	0101	18	28.00	57	34.50	1833.1	4.9	40	c/cs
20	263	0123	18	29.40	57	35.80	1834.9	4.7	40	c/cs
20	263	0153	18	31.20	57	37.40	1837.2	4.7	40	c/cs
20	263	0203	18	31.80	57	37.90	1838.0	3.7	17	c/cs
20	263	0206	18	32.00	57	38.00	1838.2	1.5	348	c/cs
20	263	0209	18	32.10	57	37.90	1838.3	0.8	144	c/cs
20	263	0210	18	32.05	57	37.95	1838.3	3.3	192	XX
20	263	0212	18	31.90	57	37.90	1838.4	4.4	174	c/cs
20	263	0217	18	31.60	57	38.00	1838.8	5.5	175	c/cs
20	263	0220	18	31.30	57	37.99	1839.0	5.4	177	XX
20	263	0230	18	30.41	57	38.04	1839.9	5.0	154	XX
20	263	0233	18	30.20	57	38.20	1840.2	5.8	127	c/cs
20	263	0235	18	30.10	57	38.30	1840.4	6.3	113	c/cs
20	263	0245	18	29.70	57	39.30	1841.4	6.9	109	c/cs
20	263	0250	18	29.48	57	39.91	1842.0	7.4	106	XX
20	263	0300	18	29.14	57	41.16	1843.2	6.7	106	XX
20	263	0304	18	29.00	57	41.60	1843.7	6.7	106	c/cs
20	263	0311	18	28.80	57	42.41	1844.5	7.1	105	XX
20	263	0330	18	28.23	57	44.72	1846.7	7.1	104	XX
20	263	0342	18	27.88	57	46.17	1848.1	6.9	104	XX
20	263	0349	18	27.69	57	47.00	1849.0	7.0	106	XX
20	263	0400	18	27.33	57	48.29	1850.2	7.3	106	XX
20	263	0410	18	27.00	57	49.52	1851.4	6.8	106	XX
20	263	0419	18	26.71	57	50.56	1852.5	6.5	101	XX
20	263	0420	18	26.70	57	50.70	1852.6	6.3	30	c/cs
20	263	0430	18	27.60	57	51.22	1853.6	7.4	358	XX
20	263	0430	18	27.60	57	51.20	1853.6	7.3	0	c/cs
20	263	0435	18	28.20	57	51.20	1854.2	6.5	297	c/cs
20	263	0436	18	28.26	57	51.12	1854.3	6.2	281	GF
20	263	0446	18	28.45	57	50.05	1855.4	6.6	285	GF

APPENDIX (continued).

			North latitude		East longitude			Actual		
Date (1987)	Julian day	Time (UTC)	(deg)	(min)	(deg)	(min)	Distance (nmi)	speed (kt)	course (deg)	Comments[a]
20	263	0456	18	28.73	57	48.93	1856.5	7.2	290	GF
20	263	0505	18	29.10	57	47.90	1857.6	4.2	237	c/cs
20	263	0506	18	29.07	57	47.80	1857.6	4.3	228	GF
20	263	0516	18	28.59	57	47.24	1858.3	6.1	195	GF
20	263	0526	18	27.60	57	46.97	1859.4	6.1	195	GF
20	263	0536	18	26.62	57	46.70	1860.4	6.0	197	GF
20	263	0546	18	25.66	57	46.39	1861.4	8.4	0	GF
20	263	0556	18	27.06	57	46.39	1862.8	1.4	137	GF
20	263	0558	18	27.00	57	46.40	1862.8	10.8	16	c/cs
20	263	0600	18	27.40	57	46.50	1863.2	4.1	34	c/cs
20	263	0606	18	27.71	57	46.77	1863.6	1.2	128	GF
20	263	0616	18	27.59	57	46.93	1863.8	0.2	57	GF
20	263	0800	18	27.75	57	47.19	1864.1	0.0	90	724
21	264	1150	18	27.75	57	47.19	1864.1	0.0	7	724
21	264	1945	18	27.90	57	47.20	1864.3	2.3	273	c/cs
21	264	2030	18	28.00	57	45.40	1866.0	1.7	291	c/cs
21	264	2230	18	29.24	57	42.04	1869.4	1.7	290	725
21	264	2230	18	29.20	57	42.00	1869.4	0.0	90	c/cs
22	265	1810	18	29.24	57	42.04	1869.4	2.3	189	725
22	265	2039	18	23.50	57	41.10	1875.2	7.0	193	c/cs
22	265	2104	18	20.60	57	40.40	1878.2	8.1	193	c/cs
22	265	2114	18	19.30	57	40.00	1879.5	8.4	193	c/cs
22	265	2144	18	15.20	57	39.00	1883.7	8.4	193	c/cs
22	265	2214	18	11.10	57	38.00	1887.9	8.2	193	c/cs
22	265	2244	18	7.20	57	37.00	1892.0	8.1	193	c/cs
22	265	2314	18	3.20	57	36.00	1896.1	8.2	193	c/cs
22	265	2332	18	0.80	57	35.40	1898.5	6.9	201	c/cs
22	265	2342	17	59.70	57	35.00	1899.7	6.7	202	c/cs
23 Sept	266	0000	17	57.90	57	34.20	1901.7	6.7	202	c/cs
23	266	0012	17	56.60	57	33.70	1903.0	6.7	201	c/cs
23	266	0042	17	53.50	57	32.50	1906.4	6.8	201	c/cs
23	266	0110	17	50.50	57	31.30	1909.6	6.7	200	c/cs
23	266	0121	17	49.40	57	30.80	1910.8	6.3	185	c/cs
23	266	0146	17	46.70	57	30.60	1913.4	6.0	190	c/cs
23	266	0147	17	46.65	57	30.54	1913.5	5.7	190	GF
23	266	0154	17	46.00	57	30.40	1914.2	4.5	212	c/cs
23	266	0156	17	45.90	57	30.30	1914.4	3.7	245	c/cs
23	266	0157	17	45.84	57	30.28	1914.4	5.0	280	GF
23	266	0201	17	45.90	57	29.90	1914.8	5.8	286	c/cs
23	266	0207	17	46.06	57	29.35	1915.3	6.0	289	GF
23	266	0209	17	46.10	57	29.20	1915.5	6.4	292	c/cs
23	266	0217	17	46.45	57	28.32	1916.4	6.2	295	GF
23	266	0227	17	46.88	57	27.33	1917.4	5.9	295	GF
23	266	0237	17	47.30	57	26.39	1918.4	6.2	291	GF
23	266	0237	17	47.30	57	26.40	1918.4	6.2	289	c/cs
23	266	0247	17	47.64	57	25.37	1919.4	6.1	291	GF
23	266	0257	17	48.00	57	24.37	1920.5	6.1	290	GF
23	266	0307	17	48.35	57	23.36	1921.5	6.2	292	GF
23	266	0307	17	48.40	57	23.40	1921.5	6.3	289	c/cs
23	266	0317	17	48.70	57	22.32	1922.5	6.4	291	GF
23	266	0327	17	49.08	57	21.28	1923.6	6.2	293	GF
23	266	0337	17	49.48	57	20.28	1924.6	5.3	301	GF
23	266	0337	17	49.50	57	20.30	1924.6	5.3	303	c/cs
23	266	0342	17	49.70	57	19.90	1925.1	5.5	346	c/cs

APPENDIX (continued).

Date (1987)	Julian day	Time (UTC)	North latitude (deg)	North latitude (min)	East longitude (deg)	East longitude (min)	Distance (nmi)	Actual speed (kt)	Actual course (deg)	Comments[a]
23	266	0344	17	49.90	57	19.80	1925.3	6.4	12	c/cs
23	266	0347	17	50.21	57	19.91	1925.6	7.1	28	GF
23	266	0351	17	50.60	57	20.10	1926.0	7.3	35	c/cs
23	266	0354	17	50.90	57	20.40	1926.4	6.8	68	c/cs
23	266	0356	17	51.00	57	20.60	1926.6	6.2	94	c/cs
23	266	0357	17	51.00	57	20.70	1926.7	7.4	112	GF
23	266	0405	17	50.60	57	21.70	1927.7	7.7	114	c/cs
23	266	0407	17	50.52	57	21.90	1928.0	6.4	120	GF
23	266	0411	17	50.30	57	22.30	1928.4	5.9	142	c/cs
23	266	0413	17	50.20	57	22.40	1928.6	4.8	182	c/cs
23	266	0417	17	49.83	57	22.41	1928.9	6.0	191	GF
23	266	0417	17	49.80	57	22.40	1928.9	5.9	198	c/cs
23	266	0424	17	49.20	57	22.20	1929.6	6.2	194	c/cs
23	266	0427	17	48.87	57	22.10	1929.9	6.7	196	GF
23	266	0432	17	48.30	57	21.90	1930.5	6.6	197	c/cs
23	266	0437	17	47.81	57	21.77	1931.0	7.0	197	GF
23	266	0438	17	47.70	57	21.70	1931.2	6.9	197	c/cs
23	266	0447	17	46.71	57	21.41	1932.2	2.9	224	GF
23	266	0457	17	46.36	57	21.06	1932.7	9.7	23	GF
23	266	0507	17	47.85	57	21.71	1934.3	3.8	5	GF
23	266	0510	17	48.00	57	21.70	1934.5	7.7	15	c/cs
23	266	0517	17	48.90	57	21.97	1935.4	0.4	79	GF
23	266	0600	17	48.96	57	22.29	1935.7	0.0	90	726
24 Sept	267	0335	17	48.96	57	22.29	1935.7	0.6	77	726
24	267	0430	17	49.08	57	22.83	1936.2	0.6	156	GF
24	267	0430	17	49.10	57	22.80	1936.2	6.4	106	c/cs
24	267	0449	17	48.50	57	24.90	1938.2	4.7	112	c/cs
24	267	0500	17	48.19	57	25.72	1939.1	6.6	104	GF
24	267	0510	17	47.90	57	26.80	1940.2	6.6	102	c/cs
24	267	0515	17	47.80	57	27.40	1940.8	6.3	102	GF
24	267	0530	17	47.48	57	29.02	1942.3	6.5	102	GF
24	267	0540	17	47.30	57	30.10	1943.4	6.5	102	c/cs
24	267	0545	17	47.15	57	30.70	1944.0	6.4	103	GF
24	267	0600	17	46.80	57	32.34	1945.6	6.6	103	GF
24	267	0610	17	46.60	57	33.50	1946.7	6.6	101	c/cs
24	267	0615	17	46.45	57	34.03	1947.2	6.5	102	GF
24	267	0633	17	46.05	57	36.03	1949.2	6.1	99	GF
24	267	0639	17	45.90	57	36.70	1949.8	5.8	86	c/cs
24	267	0640	17	46.00	57	36.80	1949.9	5.0	54	c/cs
24	267	0642	17	46.10	57	36.90	1950.0	4.5	31	c/cs
24	267	0643	17	46.12	57	36.95	1950.1	5.8	8	GF
24	267	0649	17	46.70	57	37.00	1950.7	6.2	10	c/cs
24	267	0653	17	47.10	57	37.11	1951.1	5.2	354	GF
24	267	0654	17	47.20	57	37.10	1951.2	5.3	324	c/cs
24	267	0656	17	47.30	57	37.00	1951.4	5.0	290	c/cs
24	267	0701	17	47.50	57	36.60	1951.8	6.1	287	c/cs
24	267	0703	17	47.53	57	36.38	1952.0	6.3	271	GF
24	267	0708	17	47.50	57	35.80	1952.5	5.6	234	c/cs
24	267	0710	17	47.40	57	35.70	1952.7	5.6	211	c/cs
24	267	0713	17	47.19	57	35.52	1953.0	7.2	192	GF
24	267	0717	17	46.70	57	35.40	1953.4	7.4	192	c/cs
24	267	0723	17	46.00	57	35.25	1954.2	6.5	191	GF
24	267	0726	17	45.70	57	35.20	1954.5	5.1	191	c/cs
24	267	0730	17	45.40	57	35.10	1954.9	4.7	190	c/cs

APPENDIX (continued).

Date (1987)	Julian day	Time (UTC)	North latitude (deg)	North latitude (min)	East longitude (deg)	East longitude (min)	Distance (nmi)	Actual speed (kt)	Actual course (deg)	Comments[a]
24	267	0733	17	45.12	57	35.07	1955.1	6.9	193	GF
24	267	0734	17	45.00	57	35.00	1955.2	4.2	191	c/cs
24	267	0743	17	44.39	57	34.92	1955.8	4.1	4	GF
24	267	0754	17	45.14	57	34.97	1956.6	1.7	19	GF
24	267	0830	17	46.08	57	35.31	1957.6	0.0	90	727
25 Sept	268	0200	17	46.08	57	35.31	1957.6	2.8	110	727
25	268	0225	17	45.70	57	36.50	1958.7	6.9	111	c/cs
25	268	0247	17	44.80	57	38.90	1961.3	7.5	110	c/cs
25	268	0256	17	44.38	57	40.03	1962.4	6.9	111	GF
25	268	0306	17	43.97	57	41.16	1963.5	6.9	110	GF
25	268	0309	17	43.90	57	41.50	1963.9	7.4	110	c/cs
25	268	0316	17	43.56	57	42.35	1964.7	7.5	110	GF
25	268	0326	17	43.13	57	43.58	1966.0	7.5	111	GF
25	268	0336	17	42.68	57	44.80	1967.2	7.5	112	GF
25	268	0339	17	42.50	57	45.20	1967.6	7.5	112	c/cs
25	268	0346	17	42.22	57	46.02	1968.5	7.5	111	GF
25	268	0356	17	41.78	57	47.24	1969.7	7.3	111	GF
25	268	0406	17	41.35	57	48.43	1970.9	7.3	111	GF
25	268	0409	17	41.20	57	48.80	1971.3	7.4	110	c/cs
25	268	0416	17	40.92	57	49.64	1972.2	7.3	107	GF
25	268	0421	17	40.70	57	50.20	1972.8	7.3	106	c/cs
25	268	0426	17	40.57	57	50.86	1973.4	7.3	105	GF
25	268	0436	17	40.26	57	52.09	1974.6	7.3	106	GF
25	268	0446	17	39.93	57	53.31	1975.8	7.1	106	GF
25	268	0450	17	39.80	57	53.80	1976.3	7.2	109	c/cs
25	268	0456	17	39.57	57	54.50	1977.0	7.0	107	GF
25	268	0506	17	39.23	57	55.68	1978.2	7.2	106	GF
25	268	0517	17	38.86	57	57.00	1979.5	7.3	107	GF
25	268	0520	17	38.80	57	57.40	1979.8	7.2	106	c/cs
25	268	0527	17	38.52	57	58.22	1980.7	5.6	97	GF
25	268	0531	17	38.50	57	58.60	1981.1	5.8	67	c/cs
25	268	0533	17	38.50	57	58.80	1981.3	5.5	17	c/cs
25	268	0535	17	38.70	57	58.90	1981.4	4.5	328	c/cs
25	268	0537	17	38.85	57	58.77	1981.6	5.5	305	GF
25	268	0539	17	39.00	57	58.60	1981.8	6.0	302	c/cs
25	268	0548	17	39.40	57	57.80	1982.7	5.5	281	c/cs
25	268	0549	17	39.40	57	57.70	1982.8	4.3	245	c/cs
25	268	0551	17	39.40	57	57.60	1982.9	4.5	213	c/cs
25	268	0555	17	39.10	57	57.40	1983.2	5.1	206	c/cs
25	268	0557	17	38.98	57	57.32	1983.4	6.8	189	GF
25	268	0607	17	37.87	57	57.13	1984.5	6.0	205	GF
25	268	0611	17	37.50	57	57.00	1984.9	5.8	237	c/cs
25	268	0613	17	37.40	57	56.80	1985.1	5.9	271	c/cs
25	268	0617	17	37.41	57	56.37	1985.5	7.2	283	GF
25	268	0620	17	37.50	57	56.00	1985.9	7.8	286	c/cs
25	268	0627	17	37.74	57	55.08	1986.8	7.7	285	GF
25	268	0637	17	38.07	57	53.78	1988.1	7.8	287	GF
25	268	0647	17	38.45	57	52.47	1989.4	7.8	286	GF
25	268	0649	17	38.50	57	52.20	1989.6	7.8	287	c/cs
25	268	0657	17	38.83	57	51.16	1990.7	7.9	288	GF
25	268	0707	17	39.23	57	49.85	1992.0	6.5	295	GF
25	268	0712	17	39.50	57	49.30	1992.5	5.4	337	c/cs
25	268	0714	17	39.60	57	49.30	1992.7	6.0	5	c/cs
25	268	0718	17	40.02	57	49.30	1993.1	6.9	18	GF

APPENDIX (continued).

Date (1987)	Julian day	Time (UTC)	North latitude (deg)	North latitude (min)	East longitude (deg)	East longitude (min)	Distance (nmi)	Actual speed (kt)	Actual course (deg)	Comments[a]
25	268	0719	17	40.10	57	49.30	1993.2	7.3	22	c/cs
25	268	0728	17	41.15	57	49.76	1994.3	7.1	19	GF
25	268	0728	17	41.10	57	49.80	1994.3	7.0	14	c/cs
25	268	0735	17	41.90	57	50.00	1995.1	5.5	12	c/cs
25	268	0738	17	42.21	57	50.02	1995.4	4.6	12	GF
25	268	0740	17	42.40	57	50.10	1995.5	4.3	14	c/cs
25	268	0748	17	42.92	57	50.20	1996.1	1.6	44	GF
25	268	0758	17	43.11	57	50.39	1996.4	9.3	199	GF
25	268	0808	17	41.65	57	49.85	1997.9	3.5	23	GF
25	268	0841	17	43.40	57	50.60	1999.9	0.1	202	c/cs
27 Sept	270	1007	17	40.81	57	49.54	2002.7	0.0	90	728
27	270	2000	17	40.81	57	49.54	2002.7	0.1	107	728
28 Sept	271	0100	17	40.70	57	49.90	2003.0	6.8	106	c/cs
28	271	0200	17	38.80	57	56.80	2009.8	0.1	107	c/cs
28	271	0848	17	38.68	57	57.28	2010.3	0.0	90	729
28	271	1830	17	38.68	57	57.28	2010.3	0.8	294	729
28	271	1855	17	38.80	57	56.90	2010.7	4.5	285	c/cs
28	271	1925	17	39.40	57	54.70	2012.9	4.5	286	c/cs
28	271	1955	17	40.00	57	52.40	2015.2	4.5	286	c/cs
28	271	2025	17	40.60	57	50.10	2017.5	4.5	286	c/cs
28	271	2055	17	41.30	57	47.80	2019.7	4.5	286	c/cs
28	271	2125	17	41.90	57	45.50	2022.0	4.6	287	c/cs
28	271	2146	17	42.30	57	43.90	2023.6	4.7	291	c/cs
28	271	2216	17	43.20	57	41.60	2025.9	4.7	291	c/cs
28	271	2246	17	44.00	57	39.30	2028.3	4.7	291	c/cs
28	271	2313	17	44.70	57	37.30	2030.4	4.6	292	c/cs
28	271	2340	17	45.50	57	35.20	2032.4	4.6	318	c/cs
28	271	2342	17	45.60	57	35.10	2032.6	4.1	2	c/cs
28	271	2346	17	45.90	57	35.10	2032.9	4.4	11	c/cs
28	271	2349	17	46.10	57	35.20	2033.1	3.1	59	c/cs
28	271	2351	17	46.10	57	35.30	2033.2	3.2	109	c/cs
29 Sept	272	0000	17	46.00	57	35.80	2033.7	3.2	109	c/cs
29	272	0006	17	45.90	57	36.10	2034.0	3.4	107	c/cs
29	272	0036	17	45.40	57	37.80	2035.7	3.4	109	c/cs
29	272	0106	17	44.90	57	39.40	2037.4	3.3	110	c/cs
29	272	0120	17	44.60	57	40.20	2038.1	3.3	127	c/cs
29	272	0150	17	43.60	57	41.60	2039.8	3.4	125	c/cs
29	272	0202	17	43.20	57	42.20	2040.4	3.2	83	c/cs
29	272	0204	17	43.20	57	42.30	2040.6	3.6	22	c/cs
29	272	0206	17	43.30	57	42.30	2040.7	4.0	329	c/cs
29	272	0208	17	43.50	57	42.20	2040.8	4.2	304	c/cs
29	272	0220	17	43.92	57	41.51	2041.6	3.4	306	730
29	272	0220	17	43.90	57	41.50	2041.6	0.0	90	c/cs
30 Sept	273	0935	17	43.92	57	41.51	2041.6	1.2	123	730
30	273	1229	17	42.00	57	44.60	2045.1	5.7	123	c/cs
30	273	1232	17	41.90	57	44.80	2045.4	8.3	123	c/cs
30	273	1240	17	41.30	57	45.80	2046.5	8.9	122	c/cs
30	273	1303	17	39.50	57	48.90	2049.9	9.0	123	c/cs
30	273	1353	17	35.40	57	55.50	2057.4	9.1	123	c/cs
30	273	1359	17	34.90	57	56.30	2058.3	9.7	123	c/cs
30	273	1432	17	32.00	58	1.00	2063.7	9.7	122	c/cs
30	273	1500	17	29.59	58	4.98	2068.2	8.9	124	DR
30	273	1504	17	29.26	58	5.50	2068.8	8.4	124	DR
30	273	1505	17	29.20	58	5.60	2068.9	8.2	124	c/cs

APPENDIX (continued).

			North latitude		East longitude			Actual		
Date (1987)	Julian day	Time (UTC)	(deg)	(min)	(deg)	(min)	Distance (nmi)	speed (kt)	course (deg)	Comments[a]
30	273	1534	17	26.96	58	9.07	2072.9	8.2	124	DR
30	273	1555	17	25.40	58	11.60	2075.8	8.1	124	c/cs
30	273	1601	17	24.90	58	12.30	2076.6	8.0	124	c/cs
30	273	1604	17	24.69	58	12.64	2077.0	8.0	124	DR
30	273	1611	17	24.20	58	13.50	2077.9	8.3	124	c/cs
30	273	1634	17	22.37	58	16.21	2081.1	8.3	124	DR
30	273	1648	17	21.30	58	17.90	2083.1	8.4	125	c/cs
30	273	1704	17	19.98	58	19.80	2085.3	8.4	126	DR
30	273	1714	17	19.20	58	21.00	2086.7	8.5	126	c/cs
30	273	1730	17	17.80	58	22.90	2089.0	8.4	126	c/cs
30	273	1734	17	17.51	58	23.38	2089.5	8.4	126	DR
30	273	1804	17	15.06	58	26.95	2093.7	8.5	125	DR
30	273	1805	17	15.00	58	27.10	2093.9	8.5	126	c/cs
30	273	1834	17	12.55	58	30.54	2098.0	12.9	123	DR
30	273	1850	17	10.70	58	33.60	2101.4	13.0	123	c/cs
30	273	1908	17	8.60	58	37.00	2105.3	8.8	122	c/cs
30	273	1910	17	8.50	58	37.20	2105.6	12.6	123	c/cs
30	273	1941	17	4.90	58	43.00	2112.1	12.5	123	c/cs
30	273	2004	17	2.30	58	47.20	2116.9	12.6	123	c/cs
30	273	2014	17	1.20	58	49.10	2119.0	11.6	122	c/cs
30	273	2049	16	57.50	58	55.00	2125.8	11.6	122	c/cs
30	273	2125	16	53.80	59	1.20	2132.8	11.6	122	c/cs
30	273	2215	16	48.60	59	9.70	2142.4	11.6	122	c/cs
30	273	2233	16	46.80	59	12.80	2145.9	10.4	122	c/cs
30	273	2314	16	43.00	59	19.00	2153.0	10.2	122	c/cs
30	273	2332	16	41.40	59	21.80	2156.0	10.3	122	c/cs
1 Oct	274	0000	16	38.90	59	26.00	2160.8	10.3	122	c/cs
1	274	0005	16	38.40	59	26.80	2161.7	10.1	122	c/cs
1	274	0014	16	37.60	59	28.10	2163.2	10.0	122	c/cs
1	274	0022	16	36.90	59	29.30	2164.5	8.7	122	c/cs
1	274	0037	16	35.70	59	31.20	2166.7	8.6	122	c/cs
1	274	0106	16	33.50	59	34.90	2170.9	8.4	130	c/cs
1	274	0108	16	33.40	59	35.10	2171.1	7.7	143	c/cs
1	274	0111	16	33.10	59	35.40	2171.5	9.6	154	c/cs
1	274	0116	16	32.30	59	35.70	2172.3	9.4	162	c/cs
1	274	0128	16	30.50	59	36.30	2174.2	9.2	163	c/cs
1	274	0131	16	30.10	59	36.50	2174.7	8.6	130	c/cs
1	274	0146	16	28.70	59	38.20	2176.8	8.0	106	c/cs
1	274	0155	16	28.39	59	39.40	2178.0	6.9	91	GF
1	274	0156	16	28.40	59	39.50	2178.2	6.9	87	c/cs
1	274	0205	16	28.44	59	40.60	2179.2	7.0	88	GF
1	274	0215	16	28.48	59	41.81	2180.4	6.9	89	GF
1	274	0225	16	28.51	59	43.01	2181.5	6.7	87	GF
1	274	0226	16	28.50	59	43.10	2181.6	6.8	87	c/cs
1	274	0233	16	28.60	59	44.00	2182.4	6.1	65	c/cs
1	274	0235	16	28.64	59	44.15	2182.6	5.4	42	GF
1	274	0236	16	28.70	59	44.20	2182.7	5.1	12	c/cs
1	274	0242	16	29.20	59	44.30	2183.2	5.4	1	c/cs
1	274	0245	16	29.47	59	44.33	2183.5	5.1	345	GF
1	274	0248	16	29.70	59	44.30	2183.7	5.7	325	c/cs
1	274	0250	16	29.90	59	44.10	2183.9	5.2	298	c/cs
1	274	0252	16	29.90	59	44.00	2184.1	5.3	281	c/cs
1	274	0255	16	30.00	59	43.72	2184.4	6.1	270	GF
1	274	0303	16	30.00	59	42.90	2185.2	6.3	269	c/cs

APPENDIX (continued).

Date (1987)	Julian day	Time (UTC)	North latitude		East longitude		Distance (nmi)	Actual		Comments[a]
			(deg)	(min)	(deg)	(min)		speed (kt)	course (deg)	
1	274	0305	16	30.00	59	42.65	2185.4	5.2	253	GF
1	274	0308	16	29.90	59	42.40	2185.6	5.8	234	c/cs
1	274	0309	16	29.90	59	42.30	2185.7	5.5	199	c/cs
1	274	0311	16	29.70	59	42.20	2185.9	5.9	194	c/cs
1	274	0315	16	29.31	59	42.15	2186.3	6.3	183	GF
1	274	0319	16	28.90	59	42.10	2186.7	6.6	181	c/cs
1	274	0325	16	28.23	59	42.12	2187.4	4.8	192	731
1	274	0325	16	28.20	59	42.10	2187.4	0.0	90	c/cs
6 Oct	279	1000	16	28.23	59	42.12	2187.4	0.0	90	731
9 Oct	282	1245	16	28.23	59	42.12	2187.4	4.5	268	731
9	282	1245	16	28.20	59	42.10	2187.4	8.1	215	c/cs
9	282	1251	16	27.60	59	41.60	2188.2	7.5	219	c/cs
9	282	1254	16	27.30	59	41.40	2188.6	8.1	215	c/cs
9	282	1259	16	26.70	59	41.00	2189.3	9.2	211	c/cs
9	282	1304	16	26.06	59	40.57	2190.0	9.7	177	SATL
9	282	1309	16	25.30	59	40.60	2190.8	10.8	178	c/cs
9	282	1331	16	21.30	59	40.80	2194.8	10.9	178	c/cs
9	282	1347	16	18.40	59	40.90	2197.7	11.0	178	c/cs
9	262	1433	16	9.90	59	41.20	2206.2	11.1	178	c/cs
9	282	1506	16	3.80	59	41.40	2212.3	11.0	178	c/cs
9	282	1549	15	55.90	59	41.70	2220.2	10.4	178	c/cs
9	282	1604	15	53.40	59	41.80	2222.8	10.3	178	c/cs
9	282	1635	15	48.00	59	42.00	2228.1	10.3	178	c/cs
9	282	1652	15	45.10	59	42.10	2231.0	10.2	178	c/cs
9	282	1722	15	40.00	59	42.30	2236.1	9.6	171	c/cs
9	282	1723	15	39.90	59	42.30	2236.3	3.7	109	c/cs
9	282	1725	15	39.80	59	42.50	2236.4	1.5	146	c/cs
9	282	1730	15	39.70	59	42.50	2236.5	1.8	165	c/cs
9	282	1746	15	39.20	59	42.70	2237.0	4.5	211	c/cs
9	282	1748	15	39.10	59	42.60	2237.2	7.4	181	c/cs
9	282	1750	15	38.90	59	42.60	2237.4	10.3	178	c/cs
9	282	1755	15	38.00	59	42.60	2238.3	10.9	179	c/cs
9	282	1841	15	29.70	59	42.80	2246.6	11.0	179	c/cs
9	282	1902	15	25.80	59	42.90	2250.5	10.9	184	c/cs
9	282	1924	15	21.80	59	42.60	2254.5	10.9	184	c/cs
9	282	2003	15	14.70	59	42.10	2261.6	11.0	184	c/cs
9	282	2041	15	7.80	59	41.60	2268.5	10.9	185	c/cs
9	282	2131	14	58.80	59	40.80	2277.6	11.0	184	c/cs
9	282	2207	14	52.20	59	40.40	2284.2	10.9	184	c/cs
9	282	2240	14	46.20	59	40.00	2290.1	10.9	184	c/cs
9	282	2330	14	37.10	59	39.30	2299.2	11.0	184	c/cs
10 Oct	283	0000	14	31.70	59	38.90	2304.7	11.0	184	c/cs
10	283	0019	14	28.20	59	38.70	2308.2	11.0	184	c/cs
10	283	0035	14	25.27	59	38.49	2311.1	12.2	192	GPS
10	283	0041	14	24.10	59	38.20	2312.4	12.1	192	c/cs
10	283	0125	14	15.40	59	36.30	2321.2	12.1	192	c/cs
10	283	0200	14	8.49	59	34.78	2328.3	12.3	191	GPS
10	283	0201	14	8.30	59	34.70	2328.5	12.5	191	c/cs
10	283	0205	14	7.50	59	34.60	2329.4	12.3	185	c/cs
10	283	0254	13	57.40	59	33.60	2339.4	12.3	185	c/cs
10	283	0319	13	52.30	59	33.10	2344.6	12.4	185	c/cs
10	283	0350	13	46.00	59	32.60	2350.9	12.3	185	c/cs
10	283	0400	13	43.92	59	32.43	2353.0	12.4	183	GPS
10	283	0413	13	41.20	59	32.30	2355.7	12.4	183	c/cs

APPENDIX (continued).

Date (1987)	Julian day	Time (UTC)	North latitude (deg)	North latitude (min)	East longitude (deg)	East longitude (min)	Distance (nmi)	Actual speed (kt)	Actual course (deg)	Comments[a]
10	283	0453	13	33.00	59	31.90	2363.9	12.4	183	c/cs
10	283	0511	13	29.30	59	31.70	2367.7	12.4	183	c/cs
10	283	0552	13	20.80	59	31.20	2376.2	12.6	183	c/cs
10	283	0600	13	19.10	59	31.13	2377.8	12.7	181	GPS
10	283	0627	13	13.40	59	31.00	2383.6	12.7	181	c/cs
10	283	0702	13	6.00	59	30.90	2390.9	12.7	181	c/cs
10	283	0740	12	58.00	59	30.70	2399.0	12.7	181	c/cs
10	283	0800	12	53.73	59	30.59	2403.2	12.8	180	GPS
10	283	0804	12	52.90	59	30.60	2404.1	12.7	182	c/cs
10	283	0852	12	42.80	59	30.20	2414.2	12.7	182	c/cs
10	283	0900	12	41.06	59	30.11	2415.9	12.8	182	GPS
10	283	0930	12	34.70	59	29.90	2422.3	12.5	182	c/cs
10	283	0958	12	28.80	59	29.70	2428.1	12.6	183	c/cs
10	283	1000	12	28.42	59	29.67	2428.5	12.3	179	GPS
10	283	1011	12	26.20	59	29.70	2430.8	12.1	180	c/cs
10	283	1036	12	21.10	59	29.70	2435.9	12.0	181	c/cs
10	283	1054	12	17.50	59	29.60	2439.4	12.1	182	c/cs
10	283	1100	12	16.32	59	29.56	2440.6	12.9	186	GPS
10	283	1114	12	13.30	59	29.30	2443.7	13.0	185	c/cs
10	283	1134	12	9.01	59	28.88	2448.0	12.6	184	SATL
10	283	1142	12	7.30	59	28.80	2449.7	12.7	185	c/cs
10	283	1207	12	2.00	59	28.30	2455.0	12.8	185	c/cs
10	283	1233	11	56.50	59	27.80	2460.5	12.8	185	c/cs
10	283	1242	11	54.62	59	27.67	2462.4	12.6	185	SATL
10	283	1306	11	49.60	59	27.20	2467.4	12.5	185	c/cs
10	283	1356	11	39.20	59	26.30	2477.9	12.6	185	c/cs
10	283	1404	11	37.55	59	26.16	2479.6	12.6	185	SATL
10	283	1430	11	32.11	59	25.70	2485.0	12.5	187	SATL
10	283	1445	11	29.00	59	25.30	2488.2	12.5	187	c/cs
10	283	1506	11	24.65	59	24.81	2492.5	12.6	187	SATL
10	283	1522	11	21.30	59	24.40	2495.9	12.5	186	c/cs
10	283	1551	11	15.30	59	23.70	2502.0	12.3	186	c/cs
10	283	1608	11	11.80	59	23.40	2505.5	12.5	184	c/cs
10	283	1638	11	5.50	59	23.00	2511.7	12.6	184	c/cs
10	283	1648	11	3.45	59	22.83	2513.8	12.7	186	SATL
10	283	1659	11	1.10	59	22.60	2516.2	12.8	186	c/cs
10	283	1737	10	53.10	59	21.80	2524.2	12.7	186	c/cs
10	283	1823	10	43.40	59	20.80	2534.0	12.6	186	c/cs
10	283	1840	10	39.84	59	20.50	2537.5	12.4	185	SATL
10	283	1846	10	38.60	59	20.40	2538.8	12.1	185	c/cs
10	283	1853	10	37.20	59	20.30	2540.2	10.2	186	c/cs
10	283	1859	10	36.20	59	20.20	2541.2	9.9	185	c/cs
10	283	1918	10	33.10	59	19.90	2544.3	12.3	185	c/cs
10	283	1929	10	30.80	59	19.70	2546.6	12.5	185	c/cs
10	283	2001	10	24.20	59	19.10	2553.3	12.5	184	c/cs
10	283	2002	10	23.95	59	19.10	2553.5	12.8	185	SATL
10	283	2022	10	19.70	59	18.70	2557.8	12.7	185	c/cs
10	283	2040	10	15.90	59	18.30	2561.6	12.7	185	c/cs
10	283	2108	10	10.00	59	17.80	2567.5	12.8	185	c/cs
10	283	2134	10	4.49	59	17.27	2573.0	13.0	186	SATL
10	283	2143	10	2.60	59	17.10	2575.0	12.9	186	c/cs
10	283	2156	9	59.80	59	16.70	2577.8	12.9	185	c/cs
10	283	2246	9	49.10	59	15.80	2588.5	12.8	185	c/cs
10	283	2320	9	41.80	59	15.20	2595.8	13.1	185	c/cs

APPENDIX (continued).

Date (1987)	Julian day	Time (UTC)	North latitude		East longitude		Distance (nmi)	Actual		Comments[a]
			(deg)	(min)	(deg)	(min)		speed (kt)	course (deg)	
10	283	2324	9	40.96	59	15.10	2596.7	13.1	183	SATL
10	283	2335	9	38.60	59	15.00	2599.1	13.0	183	c/cs
11 Oct	284	0001	9	32.90	59	14.70	2604.7	12.9	183	c/cs
11	284	0026	9	27.60	59	14.40	2610.1	12.9	183	c/cs
11	284	0056	9	21.10	59	14.10	2616.6	12.8	183	c/cs
11	284	0100	9	20.24	59	14.08	2617.4	12.8	183	GPS
11	284	0137	9	12.40	59	13.70	2625.3	12.9	183	c/cs
11	284	0154	9	8.70	59	13.50	2628.9	12.8	184	c/cs
11	284	0200	9	7.45	59	13.38	2630.2	11.4	183	GPS
11	284	0400	8	44.70	59	12.29	2653.0	10.4	182	GPS
11	284	0600	8	24.00	59	11.51	2673.7	10.3	182	GPS
11	284	0800	8	3.40	59	10.67	2694.3	10.8	180	GPS
11	284	0900	7	52.60	59	10.63	2705.1	7.8	177	GPS
11	284	0912	7	51.04	59	10.70	2706.7	9.8	183	SATL
11	284	0936	7	47.12	59	10.47	2710.6	11.2	182	SATL
11	284	1000	7	42.63	59	10.31	2715.1	10.7	182	GPS
11	284	1100	7	31.90	59	9.86	2725.8	10.6	183	SATL
11	284	1542	6	42.23	59	7.32	2775.6	10.2	185	SATL
11	284	1935	6	2.80	59	3.80	2815.2	8.6	188	c/cs
11	284	1938	6	2.36	59	3.76	2815.6	9.6	183	SATL
11	284	2002	5	58.50	59	3.50	2819.5	9.9	182	c/cs
11	284	2033	5	53.40	59	3.40	2824.6	10.1	182	c/cs
11	284	2114	5	46.50	59	3.10	2831.5	10.2	183	c/cs
11	284	2141	5	41.90	59	2.90	2836.1	10.3	184	c/cs
11	284	2222	5	34.90	59	2.30	2843.1	10.3	184	c/cs
11	284	2246	5	30.75	59	2.08	2847.3	9.8	179	GPS
11	284	2250	5	30.10	59	2.10	2847.9	9.9	179	c/cs
11	284	2310	5	26.80	59	2.10	2851.2	9.9	179	c/cs
11	284	2341	5	21.70	59	2.20	2856.3	9.9	179	c/cs
12 Oct	285	0000	5	18.50	59	2.20	2859.5	9.9	179	c/cs
12	285	0019	5	15.40	59	2.20	2862.6	9.9	182	c/cs
12	285	0044	5	11.30	59	2.10	2866.8	9.9	182	c/cs
12	285	0100	5	8.63	59	1.99	2869.4	9.8	183	GPS
12	285	0125	5	4.50	59	1.80	2873.5	9.9	183	c/cs
12	285	0147	5	0.90	59	1.60	2877.1	10.0	183	c/cs
12	285	0200	4	58.74	59	1.48	2879.3	10.0	184	GPS
12	285	0216	4	56.10	59	1.30	2882.0	10.0	184	c/cs
12	285	0300	4	48.80	59	0.70	2889.3	10.3	185	GPS
12	285	0306	4	47.80	59	0.60	2890.3	10.1	184	c/cs
12	285	0341	4	41.90	59	0.20	2896.2	10.1	184	c/cs
12	285	0400	4	38.70	59	0.00	2899.4	10.1	185	GPS
12	285	0405	4	37.90	58	59.90	2900.2	10.0	185	c/cs
12	285	0430	4	33.70	58	59.60	2904.4	10.0	185	c/cs
12	285	0506	4	27.70	58	59.00	2910.4	10.9	185	c/cs
12	285	0534	4	22.70	58	58.60	2915.5	11.2	185	c/cs
12	285	0544	4	20.80	58	58.40	2917.3	11.0	183	c/cs
12	285	0607	4	16.60	58	58.20	2921.6	11.5	183	GPS
12	285	0607	4	16.60	58	58.20	2921.6	11.5	183	c/cs
12	285	0631	4	12.00	58	57.90	2926.2	11.6	183	c/cs
12	285	0700	4	6.40	58	57.60	2931.8	11.3	185	GPS
12	285	0709	4	4.70	58	57.40	2933.5	11.2	185	c/cs
12	285	0747	3	57.70	58	56.80	2940.6	11.4	185	c/cs
12	285	0800	3	55.20	58	56.57	2943.0	11.4	185	GPS

APPENDIX (continued).

Date (1987)	Julian day	Time (UTC)	North latitude		East longitude		Distance (nmi)	Actual		Comments[a]
			(deg)	(min)	(deg)	(min)		speed (kt)	course (deg)	
12	285	0815	3	52.40	58	56.30	2945.9	11.4	182	c/cs
12	285	0851	3	45.50	58	56.10	2952.7	11.5	182	c/cs
12	285	0912	3	41.53	58	55.89	2956.7	11.1	185	SATL
12	285	0913	3	41.30	58	55.90	2956.9	11.1	185	c/cs
12	285	0943	3	35.80	58	55.40	2962.4	11.1	185	c/cs
12	285	1000	3	32.72	58	55.18	2965.6	10.7	186	GPS
12	285	1002	3	32.40	58	55.10	2965.9	10.8	186	c/cs
12	285	1019	3	29.30	58	54.80	2969.0	10.7	186	c/cs
12	285	1026	3	28.08	58	54.66	2970.2	11.0	184	SATL
12	285	1047	3	24.20	58	54.40	2974.1	11.2	184	c/cs
12	285	1100	3	21.81	58	54.23	2976.5	10.8	182	GPS
12	285	1136	3	15.40	58	54.00	2983.0	10.7	182	c/cs
12	285	1226	3	6.40	58	53.80	2991.9	10.8	183	c/cs
12	285	1246	3	2.80	58	53.60	2995.5	10.8	183	c/cs
12	285	1319	2	56.90	58	53.30	3001.4	10.8	183	c/cs
12	285	1346	2	52.07	58	53.11	3006.3	10.0	179	SATL
12	285	1352	2	51.10	58	53.10	3007.3	9.9	179	c/cs
12	285	1441	2	43.00	58	53.30	3015.4	9.9	179	c/cs
12	285	1531	2	34.70	58	53.50	3023.7	9.9	179	c/cs
12	285	1552	2	31.20	58	53.60	3027.1	9.8	182	c/cs
12	285	1640	2	23.40	58	53.30	3035.0	9.8	182	c/cs
12	285	1708	2	18.80	58	53.22	3039.6	9.5	180	SATL
12	285	1726	2	16.00	58	53.20	3042.4	9.5	183	c/cs
12	285	1803	2	10.10	58	52.90	3048.2	9.6	183	c/cs
12	285	1845	2	3.40	58	52.50	3055.0	9.4	183	c/cs
12	285	1856	2	1.69	58	52.44	3056.7	9.7	186	SATL
12	285	1925	1	57.10	58	51.90	3061.4	9.7	186	c/cs
12	285	1953	1	52.50	58	51.40	3065.9	9.8	186	c/cs
12	285	2013	1	49.30	58	51.10	3069.2	9.7	186	c/cs
12	285	2036	1	45.60	58	50.70	3072.9	9.7	186	c/cs
12	285	2104	1	41.09	58	50.18	3077.4	10.1	186	SATL
12	285	2126	1	37.40	58	49.80	3081.1	10.0	186	c/cs
12	285	2210	1	30.10	58	49.10	3088.4	9.8	185	c/cs
12	285	2243	1	24.70	58	48.60	3093.8	9.9	185	c/cs
12	285	2308	1	20.60	58	48.20	3098.0	9.9	185	c/cs
12	285	2357	1	12.60	58	47.40	3106.0	9.9	185	c/cs
13 Oct	286	0000	1	12.09	58	47.40	3106.5	9.6	186	GPS
13	286	0000	1	12.10	58	47.40	3106.5	9.6	186	c/cs
13	286	0025	1	8.10	58	47.00	3110.5	9.7	187	c/cs
13	286	0050	1	4.10	58	46.40	3114.6	9.6	186	c/cs
13	286	0140	0	56.20	58	45.50	3122.6	9.7	187	c/cs
13	286	0158	0	53.30	58	45.20	3125.5	9.7	186	c/cs
13	286	0200	0	52.94	58	45.12	3125.8	10.4	185	GPS
13	286	0214	0	50.50	58	44.90	3128.2	10.2	180	c/cs
13	286	0231	0	47.60	58	44.90	3131.1	10.4	180	c/cs
13	286	0302	0	42.30	58	44.80	3136.5	10.4	180	c/cs
13	286	0348	0	34.30	58	44.80	3144.5	10.4	182	c/cs
13	286	0400	0	32.20	58	44.70	3146.6	10.2	183	GPS
13	286	0408	0	30.80	58	44.60	3147.9	10.2	183	c/cs
13	286	0426	0	27.80	58	44.50	3151.0	10.1	183	c/cs
13	286	0448	0	24.10	58	44.30	3154.7	9.9	182	c/cs
13	286	0509	0	20.60	58	44.20	3158.2	9.8	183	c/cs
13	286	0529	0	17.30	58	44.00	3161.5	9.2	183	c/cs
13	286	0539	0	15.80	58	43.90	3163.0	8.8	184	c/cs
13	286	0549	0	14.30	58	43.80	3164.5	7.9	184	c/cs

APPENDIX (continued).

Date (1987)	Julian day	Time (UTC)	North latitude (deg)	North latitude (min)	East longitude (deg)	East longitude (min)	Distance (nmi)	Actual speed (kt)	Actual course (deg)	Comments[a]
13	286	0600	0	12.90	58	43.73	3165.9	7.3	185	GPS
13	286	0607	0	12.00	58	43.70	3166.8	7.1	184	c/cs
13	286	0650	0	7.00	58	43.30	3171.8	7.1	185	c/cs
13	286	0711	0	4.50	58	43.10	3174.3	6.0	183	c/cs
13	286	0741	0	1.50	58	42.90	3177.3	6.1	182	c/cs
13	286	0756	0	0.00	58	42.90	3178.8	7.4	184	c/cs
13	286	0800	0	-0.50	58	42.82	3179.3	8.8	180	GPS
13	286	0808	0	-1.70	58	42.80	3180.5	9.9	180	c/cs
13	286	0834	0	-6.00	58	42.80	3184.8	10.3	181	c/cs
13	286	0840	0	-7.00	58	42.80	3185.8	10.9	180	c/cs
13	286	0848	0	-8.40	58	42.80	3187.3	10.8	180	c/cs
13	286	0850	0	-8.80	58	42.81	3187.6	9.2	186	SATL
13	286	0901	0	10.50	58	42.60	3189.3	9.1	175	c/cs
13	286	0910	0	11.80	58	42.80	3190.7	9.1	180	c/cs
13	286	0922	0	13.70	58	42.80	3192.5	9.3	184	c/cs
13	286	0938	0	16.10	58	42.60	3195.0	9.5	184	c/cs
13	286	0952	0	18.34	58	42.45	3197.2	10.6	179	SATL
13	286	1008	0	21.20	58	42.50	3200.0	10.6	179	c/cs
13	286	1026	0	24.40	58	42.50	3203.2	10.6	179	c/cs
13	286	1041	0	27.00	58	42.50	3205.9	10.6	179	c/cs
13	286	1051	0	28.80	58	42.60	3207.6	5.7	176	c/cs
13	286	1053	0	29.00	58	42.60	3207.8	10.7	179	c/cs
13	286	1101	0	30.40	58	42.60	3209.2	10.7	179	c/cs
13	286	1124	0	34.50	58	42.60	3213.3	10.7	179	c/cs
13	286	1207	0	42.10	58	42.70	3221.0	3.6	173	c/cs
13	286	1209	0	42.20	58	42.70	3221.1	10.7	179	c/cs
13	286	1237	0	47.20	58	42.80	3226.1	7.3	179	c/cs
13	286	1238	0	47.40	58	42.80	3226.2	10.5	179	c/cs
13	286	1251	0	49.60	58	42.80	3228.5	10.6	183	c/cs
13	286	1313	0	53.50	58	42.60	3232.4	7.1	182	c/cs
13	286	1315	0	53.70	58	42.60	3232.6	10.5	184	c/cs
13	286	1324	0	55.32	58	42.51	3234.2	10.4	187	SATL
13	286	1348	0	59.40	58	42.00	3238.4	10.5	187	c/cs
13	286	1407	-1	2.70	58	41.60	3241.7	10.5	187	c/cs
13	286	1440	-1	8.50	58	40.90	3247.5	10.4	187	c/cs
13	286	1508	-1	13.30	58	40.30	3252.3	10.4	187	c/cs
13	286	1540	-1	18.80	58	39.60	3257.8	10.4	187	c/cs
13	286	1556	-1	21.50	58	39.20	3260.6	10.3	187	c/cs
13	286	1644	-1	29.70	58	38.20	3268.8	10.1	187	c/cs
13	286	1656	-1	31.71	58	37.96	3270.9	10.0	186	SATL
13	286	1657	-1	31.90	58	37.90	3271.0	9.8	185	c/cs
13	286	1712	-1	34.30	58	37.70	3273.5	9.7	181	c/cs
13	286	1725	-1	36.40	58	37.70	3275.6	9.8	181	c/cs
13	286	1743	-1	39.30	58	37.70	3278.5	9.9	181	c/cs
13	286	1755	-1	41.30	58	37.60	3280.5	9.9	181	c/cs
13	286	1807	-1	43.30	58	37.60	3282.5	9.9	181	c/cs
13	286	1808	-1	43.47	58	37.62	3282.6	10.5	182	SATL
13	286	1831	-1	47.50	58	37.40	3286.7	10.5	182	c/cs
13	286	1846	-1	50.10	58	37.30	3289.3	10.7	182	c/cs
13	286	1911	-1	54.60	58	37.10	3293.7	10.6	182	c/cs
13	286	1932	-1	58.30	58	37.00	3297.4	10.8	182	c/cs
13	286	1937	-1	59.20	58	36.90	3298.3	6.2	184	c/cs
13	286	1939	-1	59.40	58	36.90	3298.6	10.6	182	c/cs
13	286	2007	-2	4.30	58	36.70	3303.5	8.4	183	c/cs

APPENDIX (continued).

Date (1987)	Julian day	Time (UTC)	North latitude		East longitude		Distance (nmi)	Actual		Comments[a]
			(deg)	(min)	(deg)	(min)		speed (kt)	course (deg)	
13	286	2009	-2	4.60	58	36.70	3303.8	10.6	182	c/cs
13	286	2014	-2	5.50	58	36.70	3304.7	4.4	183	c/cs
13	286	2015	-2	5.50	58	36.70	3304.7	10.5	182	c/cs
13	286	2040	-2	9.90	58	36.50	3309.1	10.5	182	c/cs
13	286	2106	-2	14.50	58	36.30	3313.6	10.5	182	c/cs
13	286	2116	-2	16.20	58	36.20	3315.4	8.0	183	c/cs
13	286	2118	-2	16.50	58	36.20	3315.7	10.4	182	c/cs
13	286	2138	-2	19.90	58	36.10	3319.1	6.3	184	c/cs
13	286	2139	-2	20.00	58	36.00	3319.2	10.3	182	c/cs
13	286	2154	-2	22.60	58	35.90	3321.8	10.2	182	c/cs
13	286	2204	-2	24.30	58	35.90	3323.5	10.4	182	c/cs
13	286	2217	-2	26.60	58	35.80	3325.8	10.6	182	c/cs
13	286	2237	-2	30.10	58	35.60	3329.3	10.5	182	c/cs
13	286	2257	-2	33.60	58	35.50	3332.8	10.7	182	c/cs
13	286	2300	-2	34.10	58	35.40	3333.3	8.3	183	c/cs
13	286	2302	-2	34.40	58	35.40	3333.6	10.5	183	c/cs
13	286	2313	-2	36.30	58	35.30	3335.6	10.6	182	c/cs
13	286	2322	-2	37.92	58	35.25	3337.1	10.7	182	SATL
14 Oct	287	0001	-2	44.90	58	35.00	3344.1	10.4	183	c/cs
14	287	0005	-2	45.60	58	35.00	3344.8	7.2	183	c/cs
14	287	0006	-2	45.70	58	35.00	3344.9	10.6	182	c/cs
14	287	0019	-2	48.00	58	34.90	3347.2	10.6	182	c/cs
14	287	0044	-2	52.40	58	34.70	3351.6	10.7	182	c/cs
14	287	0107	-2	56.50	58	34.50	3355.7	10.5	183	c/cs
14	287	0118	-2	58.42	58	34.45	3357.7	10.6	183	SATL
14	287	0132	-3	0.90	58	34.30	3360.1	10.6	183	c/cs
14	287	0145	-3	3.20	58	34.20	3362.4	10.9	183	c/cs
14	287	0220	-3	9.50	58	33.80	3368.8	10.8	183	c/cs
14	287	0233	-3	11.90	58	33.70	3371.1	10.9	183	c/cs
14	287	0250	-3	15.00	58	33.50	3374.2	11.1	183	c/cs
14	287	0256	-3	16.10	58	33.40	3375.3	4.9	184	c/cs
14	287	0258	-3	16.20	58	33.40	3375.5	10.9	183	c/cs
14	287	0305	-3	17.50	58	33.40	3376.8	6.4	184	c/cs
14	287	0306	-3	17.60	58	33.30	3376.9	10.9	183	c/cs
14	287	0354	-3	26.30	58	32.90	3385.6	10.9	183	c/cs
14	287	0400	-3	27.38	58	32.79	3386.7	11.2	183	GPS
14	287	0409	-3	29.10	58	32.70	3388.3	11.1	182	c/cs
14	287	0425	-3	32.00	58	32.60	3391.3	4.8	183	c/cs
14	287	0427	-3	32.20	58	32.60	3391.5	11.2	182	c/cs
14	287	0440	-3	34.60	58	32.50	3393.9	11.2	182	c/cs
14	287	0450	-3	36.50	58	32.40	3395.8	11.1	182	c/cs
14	287	0513	-3	40.70	58	32.30	3400.0	11.5	182	c/cs
14	287	0526	-3	43.20	58	32.20	3402.5	11.2	183	c/cs
14	287	0533	-3	44.50	58	32.10	3403.8	11.5	182	c/cs
14	287	0554	-3	48.50	58	31.90	3407.8	11.3	182	c/cs
14	287	0600	-3	49.64	58	31.90	3408.9	11.2	182	GPS
14	287	0614	-3	52.30	58	31.80	3411.6	11.3	182	c/cs
14	287	0632	-3	55.60	58	31.60	3414.9	11.5	182	c/cs
14	287	0707	-4	2.30	58	31.40	3421.6	11.0	189	c/cs
14	287	0710	-4	2.90	58	31.30	3422.2	11.1	192	c/cs
14	287	0712	-4	3.20	58	31.20	3422.6	11.3	183	c/cs
14	287	0737	-4	7.90	58	30.90	3427.3	4.2	184	c/cs
14	287	0738	-4	8.00	58	30.90	3427.3	11.4	183	c/cs
14	287	0800	-4	12.18	58	30.69	3431.5	11.2	181	GPS

APPENDIX (continued).

Date (1987)	Julian day	Time (UTC)	North latitude (deg)	North latitude (min)	East longitude (deg)	East longitude (min)	Distance (nmi)	Actual speed (kt)	Actual course (deg)	Comments[a]
14	287	0816	-4	15.20	58	30.60	3434.5	11.2	181	c/cs
14	287	0823	-4	16.50	58	30.60	3435.8	10.8	181	c/cs
14	287	0826	-4	17.00	58	30.60	3436.4	11.3	181	c/cs
14	287	0828	-4	17.39	58	30.57	3436.7	11.6	183	SATL
14	287	0833	-4	18.40	58	30.50	3437.7	5.9	183	c/cs
14	287	0835	-4	18.60	58	30.50	3437.9	11.5	183	c/cs
14	287	0900	-4	23.33	58	30.24	3442.7	11.4	181	GPS
14	287	0904	-4	24.10	58	30.20	3443.4	11.8	181	c/cs
14	287	0906	-4	24.50	58	30.20	3443.8	10.9	181	c/cs
14	287	0918	-4	26.67	58	30.18	3446.0	10.9	187	SATL
14	287	0924	-4	27.80	58	30.10	3447.1	11.1	187	c/cs
14	287	0929	-4	28.70	58	29.90	3448.0	5.4	191	c/cs
14	287	0931	-4	28.80	58	29.90	3448.2	11.2	187	c/cs
14	287	0945	-4	31.40	58	29.60	3450.8	11.3	187	c/cs
14	287	1000	-4	34.24	58	29.28	3453.6	11.1	180	GPS
14	287	1005	-4	35.20	58	29.30	3454.6	10.8	180	c/cs
14	287	1022	-4	38.20	58	29.30	3457.6	10.9	180	c/cs
14	287	1100	-4	45.13	58	29.25	3464.5	11.2	187	GPS
14	287	1106	-4	46.24	58	29.12	3465.7	11.0	183	SATL
14	287	1108	-4	46.60	58	29.10	3466.0	11.0	183	c/cs
14	287	1134	-4	51.40	58	28.80	3470.8	11.2	183	c/cs
14	287	1149	-4	54.20	58	28.70	3473.6	10.8	182	c/cs
14	287	1209	-4	57.80	58	28.50	3477.2	5.8	183	c/cs
14	287	1211	-4	58.00	58	28.50	3477.4	11.0	183	c/cs
14	287	1242	-5	3.60	58	28.20	3483.1	11.0	183	c/cs
14	287	1300	-5	6.90	58	28.00	3486.4	10.8	183	c/cs
14	287	1304	-5	7.63	58	27.98	3487.1	10.7	182	SATL
14	287	1310	-5	8.70	58	27.90	3488.1	10.8	182	c/cs
14	287	1325	-5	11.40	58	27.80	3490.8	11.0	182	c/cs
14	287	1346	-5	15.20	58	27.70	3494.7	10.8	182	c/cs
14	287	1405	-5	18.70	58	27.60	3498.1	10.7	182	c/cs
14	287	1424	-5	22.04	58	27.46	3501.5	10.4	180	SATL
14	287	1428	-5	22.70	58	27.50	3502.2	7.3	179	c/cs
14	287	1429	-5	22.90	58	27.50	3502.3	10.5	180	c/cs
14	287	1449	-5	26.40	58	27.50	3505.8	10.5	179	c/cs
14	287	1504	-5	29.00	58	27.50	3508.4	10.3	174	c/cs
14	287	1507	-5	29.50	58	27.60	3509.0	6.6	174	c/cs
14	287	1509	-5	29.70	58	27.60	3509.2	10.1	174	c/cs
14	287	1515	-5	30.70	58	27.70	3510.2	2.8	168	c/cs
14	287	1517	-5	30.80	58	27.70	3510.3	10.2	174	c/cs
14	287	1535	-5	33.90	58	28.00	3513.3	10.0	174	c/cs
14	287	1550	-5	36.30	58	28.30	3515.8	9.6	174	c/cs
14	287	1558	-5	37.60	58	28.50	3517.1	9.8	174	c/cs
14	287	1617	-5	40.70	58	28.80	3520.2	10.0	173	c/cs
14	287	1630	-5	42.80	58	29.10	3522.4	9.9	170	c/cs
14	287	1651	-5	46.20	58	29.70	3525.8	10.0	169	c/cs
14	287	1706	-5	48.70	58	30.20	3528.3	9.8	169	c/cs
14	287	1721	-5	51.10	58	30.70	3530.8	9.0	140	c/cs
14	287	1723	-5	51.30	58	30.90	3531.1	8.6	123	c/cs
14	287	1724	-5	51.40	58	31.00	3531.2	6.5	130	c/cs
14	287	1726	-5	51.50	58	31.10	3531.4	3.5	138	c/cs
14	287	1727	-5	51.60	58	31.20	3531.5	9.3	127	c/cs
14	287	1732	-5	52.10	58	31.80	3532.3	9.1	127	c/cs
14	287	1742	-5	53.00	58	33.00	3533.8	9.4	126	c/cs

APPENDIX (continued).

			North latitude		East longitude			Actual		
Date (1987)	Julian day	Time (UTC)	(deg)	(min)	(deg)	(min)	Distance (nmi)	speed (kt)	course (deg)	Comments[a]
14	287	1752	-5	53.90	58	34.30	3535.4	7.4	127	c/cs
14	287	1754	-5	54.00	58	34.50	3535.6	5.0	139	c/cs
14	287	1756	-5	54.20	58	34.60	3535.8	2.4	184	c/cs
14	287	1802	-5	54.40	58	34.60	3536.0	1.9	180	c/cs
14	287	1807	-5	54.60	58	34.60	3536.2	7.1	212	c/cs
14	287	1809	-5	54.80	58	34.50	3536.4	1.7	175	c/cs
14	287	1835	-5	55.50	58	34.50	3537.1	2.8	177	c/cs
14	287	1840	-5	55.70	58	34.50	3537.4	3.2	165	c/cs
14	287	1845	-5	56.00	58	34.60	3537.6	4.3	167	c/cs
14	287	1853	-5	56.50	58	34.70	3538.2	2.7	163	c/cs
14	287	1900	-5	56.80	58	34.80	3538.5	4.4	166	c/cs
14	287	1903	-5	57.10	58	34.90	3538.8	6.1	167	c/cs
14	287	1911	-5	57.90	58	35.10	3539.6	6.9	167	c/cs
14	287	1920	-5	58.90	58	35.30	3540.6	7.8	168	c/cs
14	287	1921	-5	59.00	58	35.30	3540.7	1.9	163	c/cs
14	287	1923	-5	59.10	58	35.30	3540.8	8.4	168	c/cs
14	287	1931	-6	0.10	58	35.60	3541.9	9.0	168	c/cs
14	287	1943	-6	1.90	58	36.00	3543.7	4.0	166	c/cs
14	287	1944	-6	2.00	58	36.00	3543.8	9.1	168	c/cs
14	287	1949	-6	2.70	58	36.20	3544.6	9.6	168	c/cs
14	287	2001	-6	4.60	58	36.60	3546.5	9.8	169	c/cs
14	287	2006	-6	5.40	58	36.70	3547.3	9.2	168	c/cs
14	287	2014	-6	6.60	58	37.00	3548.5	9.7	168	c/cs
14	287	2036	-6	10.10	58	37.70	3552.1	5.4	167	c/cs
14	287	2037	-6	10.20	58	37.80	3552.2	9.6	168	c/cs
14	287	2052	-6	12.50	58	38.30	3554.6	5.6	168	c/cs
14	287	2054	-6	12.70	58	38.30	3554.7	9.6	168	c/cs
14	287	2056	-6	13.00	58	38.37	3555.1	10.0	169	SATL
14	287	2107	-6	14.80	58	38.70	3556.9	9.7	169	c/cs
14	287	2138	-6	19.70	58	39.70	3561.9	9.7	169	c/cs
14	287	2145	-6	20.80	58	39.90	3563.0	9.7	169	c/cs
14	287	2158	-6	22.90	58	40.30	3565.1	9.8	169	c/cs
14	287	2216	-6	25.80	58	40.90	3568.1	10.1	169	c/cs
14	287	2233	-6	28.60	58	41.40	3570.9	9.6	169	c/cs
14	287	2244	-6	30.30	58	41.78	3572.7	9.3	172	SATL
14	287	2244	-6	30.30	58	41.80	3572.7	9.8	172	c/cs
14	287	2259	-6	32.70	58	42.10	3575.1	9.4	172	c/cs
14	287	2321	-6	36.10	58	42.60	3578.6	9.6	172	c/cs
14	287	2334	-6	38.20	58	43.00	3580.7	10.0	185	c/cs
15 Oct	288	0000	-6	42.50	58	42.60	3585.0	10.0	185	c/cs
15	288	0003	-6	43.00	58	42.60	3585.5	9.9	184	c/cs
15	288	0028	-6	47.10	58	42.30	3589.6	9.5	184	c/cs
15	288	0048	-6	50.30	58	42.00	3592.8	10.0	184	c/cs
15	288	0050	-6	50.62	58	42.02	3593.1	10.3	184	SATL
15	288	0106	-6	53.40	58	41.80	3595.9	10.3	184	c/cs
15	288	0156	-7	1.91	58	41.13	3604.5	10.1	184	SATL
15	288	0300	-7	12.60	58	40.40	3615.2	10.4	186	c/cs
15	288	0330	-7	17.80	58	39.80	3620.4	9.5	181	c/cs
15	288	0400	-7	22.52	58	39.77	3625.1	9.2	186	GPS
15	288	0400	-7	22.50	58	39.80	3625.1	9.5	181	c/cs
15	288	0500	-7	32.10	58	39.60	3634.7	10.5	190	c/cs
15	288	0600	-7	42.42	58	37.77	3645.2	10.7	190	GPS
15	288	0800	-8	3.53	58	34.09	3666.6	10.8	190	GPS
15	288	0848	-8	12.02	58	32.64	3675.2	11.3	188	SATL

APPENDIX (continued).

Date (1987)	Julian day	Time (UTC)	North latitude		East longitude		Distance (nmi)	Actual		Comments[a]
			(deg)	(min)	(deg)	(min)		speed (kt)	course (deg)	
15	288	1100	-8	36.68	58	29.20	3700.1	10.9	186	GPS
15	288	1242	-8	55.08	58	27.34	3718.6	10.7	187	SATL
15	288	1336	-9	4.62	58	26.13	3728.2	11.0	187	SATL
15	288	1430	-9	14.47	58	24.96	3738.1	11.0	186	SATL
15	288	1524	-9	24.29	58	23.98	3748.0	10.9	185	SATL
15	288	1628	-9	35.91	58	22.86	3759.7	10.7	188	SATL
15	288	1730	-9	46.90	58	21.40	3770.7	11.2	187	c/cs
15	288	1824	-9	56.88	58	20.22	3780.8	11.3	186	SATL
15	288	1950	-10	13.00	58	18.50	3797.0	11.0	184	SATL
15	288	2206	-10	37.95	58	16.65	3822.0	11.0	185	SATL
16 Oct	289	0000	-10	58.70	58	14.70	3842.9	11.5	186	c/cs
16	289	0026	-11	3.64	58	14.17	3847.8	11.2	185	SATL
16	289	0108	-11	11.45	58	13.41	3855.7	11.4	185	SATL
16	289	0400	-11	44.00	58	10.41	3888.4	10.6	188	GPS
16	289	0500	-11	54.53	58	8.91	3899.0	11.7	190	GPS
16	289	0600	-12	6.04	58	6.94	3910.7	11.9	189	GPS
16	289	0700	-12	17.80	58	5.14	3922.6	11.7	190	GPS
16	289	0800	-12	29.37	58	3.11	3934.3	11.3	187	GPS
16	289	0936	-12	47.38	58	0.90	3952.4	11.6	188	SATL
16	289	1100	-13	3.41	57	58.43	3968.6	11.9	188	GPS
16	289	1200	-13	15.18	57	56.88	3980.5	14.8	185	GPS
16	289	1220	-13	20.10	57	56.50	3985.4	10.9	184	c/cs
16	289	1400	-13	38.20	57	55.20	4003.6	13.9	185	c/cs
16	289	1408	-13	40.05	57	55.00	4005.4	12.1	185	SATL
16	289	1500	-13	50.50	57	54.00	4016.0	10.4	184	c/cs
16	289	1520	-13	53.98	57	53.78	4019.4	11.8	184	SATL
16	289	1706	-14	14.72	57	52.27	4040.2	11.9	184	SATL
16	289	1926	-14	42.31	57	50.42	4067.9	12.1	184	SATL
17 Oct	290	0100	-15	49.35	57	45.32	4135.1	11.4	185	GPS
17	290	0200	-16	0.69	57	44.30	4146.5	12.0	183	GPS
17	290	0400	-16	24.55	57	42.86	4170.4	11.9	184	GPS
17	290	0600	-16	48.33	57	41.25	4194.2	11.9	185	GPS
17	290	0800	-17	12.02	57	39.26	4218.0	11.9	182	GPS
17	290	0914	-17	26.68	57	38.67	4232.6	12.1	186	SATL
17	290	1000	-17	35.87	57	37.59	4241.9	12.2	186	GPS
17	290	1100	-17	48.00	57	36.19	4254.1	13.0	184	GPS
17	290	1110	-17	50.16	57	36.02	4256.3	9.6	186	SATL
17	290	1650	-18	44.17	57	30.28	4310.5	9.6	186	SATL

[a] GF = global fix; SF, SATL, SN = satellite navigation fixes; c/cs = change of course; DR = dead reckoning; XX = extra; 720, etc. = Site 720, etc.

7. *IN-SITU* PORE-WATER SAMPLING AND DOWNHOLE TEMPERATURE MEASUREMENTS[1]

Shipboard Scientific Party[2]

TEMPERATURE

This chapter is a discussion of sediment temperature measurements for all Leg 117 sites. The "Explanatory Notes" chapter (this volume) includes a description of the water sampler-temperature-pressure (WSTP) tool used during Leg 117. Temperature measurements were attempted at seven sites on Owen Ridge and the Oman margin. Temperatures were obtained at only five sites because of recorder malfunctions on five of the tool lowerings (see Table 1). The complete temperature records for each lowering are shown in Figures 1A–1K.

All runs except 117-723C-6I-1 and 117-726A-4I-6 provide excellent undisturbed records of sediment temperature. During these two runs, temperatures started to drift upward after the water-sampling valve opened and pore fluid began to flow into the sampler filter element, which is 12–22 cm above the thermistor. The valve open time is indicated on all of the records by an arrow. The 200–250 mL of pore fluids filtered on the two runs depicted in Figures 1A and 1C should not have significantly disturbed the sediment around the thermistor position in the tool. Indeed, no other temperature records show significant effects from fluid filtering except for a possible slight effect on run 117-727A-11I-1 (Fig. 1D).

Nevertheless, because of the apparent causal relationship between valve opening and temperature disturbance for runs 117-723C-6I-1 and 117-726A-4I-6, temperatures for these two runs were estimated from the record made prior to the valve opening. For the other runs listed in Table 1, temperatures were read from the end of the undisturbed (i.e., before the probe was pulled out of the mud) sediment record. Because the sediment temperature records are much longer than the 1–2-min time constant of the probe, no curve-fitting program was used to estimate equilibrium temperature.

We deployed the WSTP tool in the free-fall mode, which is possible during piston core/extended core barrel operations because the full diameter of the inner core barrel can extend through and beyond the drill bit. The temperature records displayed in Figure 1 show little, if any, disturbance caused by motion of the thermistor probe in the sediment; the one possible exception is run 1A-726A-4I-6 (Fig. 1C). These results contrast with the frequently disturbed records obtained in soft sediments when the sampler is latched into the drill string and the sampler probe is pushed into the sediment by the weight of the bottom-hole assembly (Uyeda and Horai, 1982; Shipley and Shephard, 1982; Becker et al., 1983).

Bottom Water Temperature

The temperature probe was dropped into the sediment at high velocity and raised immediately to the ship after pullout. No mud-line temperatures were obtained. Thus, bottom water temperatures must be estimated from local or regional hydrographic data. At the shallowest Site 726, bottom water temperature was measured directly by an expendable-bathythermograph cast. For the other sites, some uncertainty resides in the assigned bottom water temperatures (Table 1). Based on the hydrographic section across the Arabian Sea at 15°N latitude (Sastry and D'Souza, 1971), all Oman margin sites are situated in the significant temperature gradient below the thermocline. Additional uncertainty is introduced by current- and upwelling-induced fluctuations of the isotherms as they intersect the continental slope off Oman. Additional hydrographic data may improve the estimates of bottom water temperature.

Thermal Conductivity

Thermal-conductivity values were measured over the same depth interval as the temperature measurements at Sites 727, 728, and 731; in addition, thermal conductivity was measured at Site 720 on the Indus Fan where no temperature measurements were made. The Site 720 sediments are similar in composition to the deeper Owen Ridge sediments, so Site 720 thermal-conductivity values might be useful in extrapolating the Site 731 thermal gradient to deeper parts of the sediment column. The thermal-conductivity measurements are presented and discussed in the "Physical Properties" sections of the respective site chapters in this volume. Only averaged values are presented here in Table 2. Thermal conductivity was not measured on cores from Sites 723 and 726. Average thermal-conductivity values for these sites were estimated from the wet-bulk-density values for the respective sites and plots of wet-bulk density vs. thermal conductivity for the other Oman margin sites where thermal conductivity was measured (see "Physical Properties" sections, "Site 727" and "Site 728" chapters). The upper sediments at all margin sites are similar in composition.

Thermal Gradients and Heat Flow

Figure 2 plots the combined temperature profiles for Leg 117 sites. The dashed line on the Hole 728B profile is a straight-line extension of the gradient below 107 m below seafloor (mbsf). The lower thermal gradient at the top of Hole 728B and the higher thermal gradient in the 175–242 mbsf interval in Hole 731A can be correlated with respective increased and decreased thermal-conductivity values in these depth intervals (see "Physical Properties" sections, "Site 728" and "Site 731" chapters), which counter the general trend of increasing thermal conductivity with increasing depth. The calculated heat flow for the 0–50 mbsf and 107–233 mbsf depth intervals at Site 728 are similar (Table 2).

Table 2 lists the thermal gradients displayed in Figure 1, average thermal-conductivity values calculated from physical-property data, and the corresponding heat flow. Except for Site 726 (see the following discussion), the thermal gradient varies between 44 and 54 K/km and the heat flow from 56 to 65 mW/m².

Site 726

Site 726 is on the edge of the Oman continental shelf about 5 km landward of the sharp shelf/slope break. The edge of the

---

[1] Prell, W. L., Niitsuma, N., et al., 1989. *Proc. ODP, Init. Repts.*, 117: College Station, TX (Ocean Drilling Program).

[2] Shipboard Scientific Party is as given in the list of Participants preceding the contents.

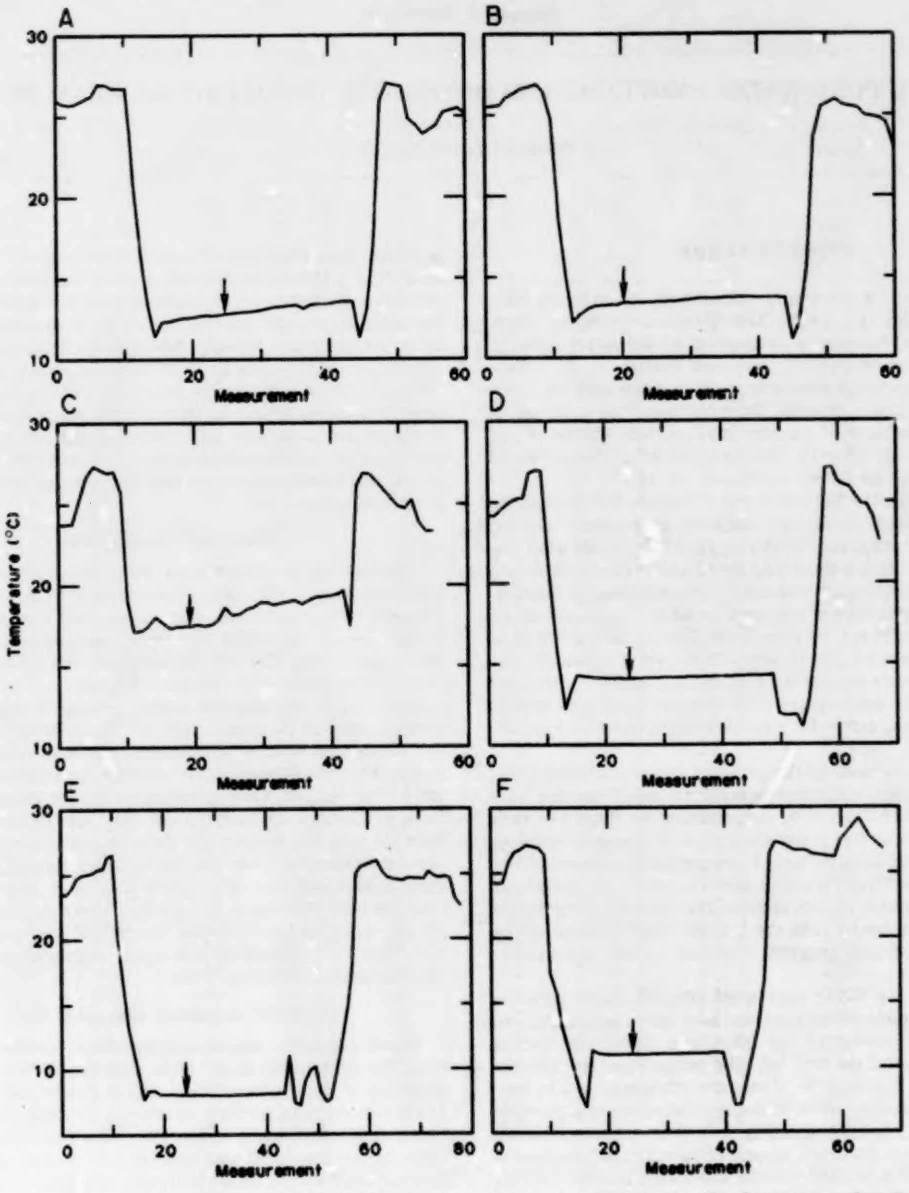

Figure 1. Downhole temperature records for WSTP tool runs. The arrows mark the time that the water sampler valve opened. **A.** Run 117-723C-6I-1, 49 mbsf. **B.** Run 117-723C-8I-1, 68.2 mbsf. **C.** Run 117-726A-4I-6, 36 mbsf. **D.** Run 117-727A-11I-1, 96.4 mbsf. **E.** Run 117-728B-7I-1, 49.5 mbsf. **F.** Run 117-728B-13I-1, 107 mbsf. **G.** Run 117-728B-18I-1, 155.4 mbsf. **H.** Run 117-728B-26I-1, 232.8 mbsf. **I.** Run 117-731A-7I-6, 66 mbsf. **J.** 117-731A-19I-1, 174.4 mbsf. **K.** 117-731A-26I-1, 242.3 mbsf.

shelf is underlain by block-faulted basement, thought to be an ophiolite complex (see "Background and Objectives" and "Summary and Conclusions" sections, "Site 726" chapter, this volume). The sediment section over basement is relatively thin, consisting of 131 m of hemipelagic sediments which is similar to other Oman margin sites that unconformably overlie porous shallow-water dolostones and limestones of Eocene age (see "Lithostratigraphy" section, "Site 726" chapter).

The high thermal gradient at this site suggests the possibility of significant hydrothermal convection. The permeable, lithified carbonates below 131 mbsf and the shallow basement high provide conditions conducive to fluid advection beneath the hemipelagic sediments. The single temperature measurement does not permit us to directly evaluate the possibility of vertical fluid flow through the thin hemipelagic cap. Fluids can be forced through sediments considerably thicker than those at Site 726

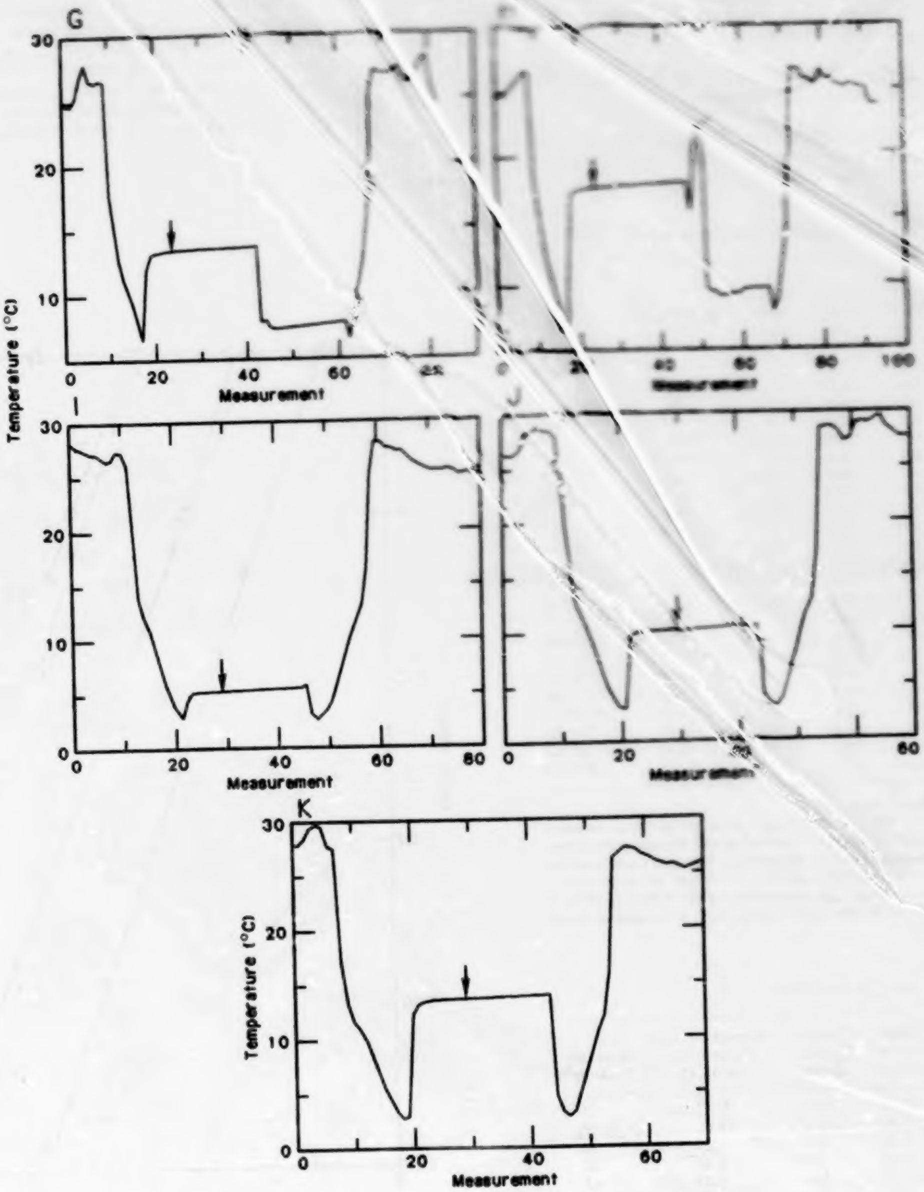

Figure 1 (continued).

when significant lateral hydraulic gradients exist at depth (Becker, Sakai, et al., 1988). However, the high thermal gradient to 36 mbsf could also reflect the upward movement of isotherms in response to upward fluid flow in the permeable rocks below the pelagic cap with little flow, if any, in the cap itself. Fluids could exit elsewhere, such as the block-faulted margin of the upper slope east of Site 726.

In contrast to other Oman margin sites, the pore-fluid chemistry at Site 726 also suggests the presence of a renewable pool of slightly hypersaline waters below the pelagic cap. These fluids are low in silica and only mildly affected by the diagenetic processes accompanying sulfate reduction (see "Inorganic Geochemistry" section, "Site 726" chapter). These fluids diffuse (and advect?) into the pelagic cap, limiting the response of the pore fluids in the cap to the anoxic metabolic processes occurring there.

REFERENCES

Becker, K., Von Herzen, R. P., and Karato, S., 1983. Geothermal measurements from drilling of sediments near the Galapagos Spreading

Center, 86°W, Deep Sea Drilling Project Leg 70. *In* Honnorez, J., Von Herzen, R. P., et al., *Init. Repts. DSDP*, 70: Washington (U.S. Govt. Printing Office), 445–458.

Becker, K., Sakai, H., et al., 1988. *Proc. ODP, Init. Repts.*, 111: College Station, TX (Ocean Drilling Program).

Sastry, J. S., and D'Souza, R. S., 1971. Oceanography of the Arabian Sea during southwest monsoon season, Part I: thermal structure. *Indian J. Meteorol. Geophys.*, 21:367–382.

Shipley, T. H., and Shephard, L. E., 1982. Temperature data from the Mexico drilling area: report on logging and inhole temperature experiments. *In* Watkins, J. S., Moore, J. C., et al., *Init. Repts. DSDP*, 66: Washington (U.S. Govt. Printing Office), 771–774.

Uyeda, S., and Horai, K., 1982. Heat flow measurements on Deep Sea Drilling Project Leg 60. *In* Hussong, D. M., Uyeda, S., et al., *Init. Repts. DSDP*, 60: Washington (U.S. Govt. Printing Office), 789–800.

Ms 117A-120

Table 1. Leg 117 downhole temperature measurements.

Hole	WSTP[a] run	Water depth (m)	Sub-bottom depth (mbsf)	Temperature[b] (°C)	Source[c]
721C	BW	1945	0	—	—
	12I-1	1945	100.5	NR	—
	16I-1	1945	139.0	NR	—
722A	BW	2028	0	—	—
	30I-1	2028	281.0	NR	—
723C	BW	808	0	(10.3)	HYDRO
	6I-1	808	49.0	*(12.83)	T-PROBE
	8I-1	808	68 2	13.73	T-PROBE
	9I-1	808	77.8	NR	—
726A	BW	331	0	14.00	XBT
	4I-6	331	36.0	#(17.6)	T-PROBE
727A	BW	915	0	(10.0)	HYDRO
	4I-6	915	35.0	NR	—
	11I-1	915	96.4	14.29	T-PROBE
728B	BW	1428	0	(6.0)	HYDRO
	7I-1	1428	49.5	8.19	T-PROBE
	13I-1	1428	107.0	11.13	T-PROBE
	18I-1	1428	155.4	13.70	T-PROBE
	26I-1	1428	232.8	17.93	T-PROBE
731A	BW	2366	0	(2.5)	HYDRO
	7I-6	2366	66.0	5.70	T-PROBE
	19I-1	2366	174.4	10.52	T-PROBE
	26I-1	2366	242.3	14.35	T-PROBE

[a] BW = bottom water.

[b] NR = no record; * = temperature drifts up, minimum sediment temperature; # = temperature drifts up and possible probe disturbance, minimum probable temperature. Values in parentheses indicate more than usual uncertainty — see text for explanation.

[c] HYDRO = regional hydrography (Sastry and D'Sousa, 1971); T-PROBE = WSTP thermistor probe; XBT = expendable bathythermograph.

Table 2. Leg 117 heat flow.

Hole	Depth interval (mbsf)	Thermal gradient (K/km)	Average thermal conductivity (W/m-K)	Heat flow (mW/m^2)
723C	0–68	50.0	[a]1.25	63
726A	0–36	[b](100.0)	[a]1.65	[b](165)
727A	0–96	44.5	1.25	56
728B	0–50	44.0	1.40	62
	107–233	54.0	1.20	65
731A	0–242	47.0	1.25	59

Note: Values in parentheses indicate more than usual uncertainty — see text for explanation.

[a] No thermal-conductivity measurements made at this hole. Value is estimated from wet-bulk density profile of this site and thermal conductivity vs. wet-bulk density plot for other Oman margin sites (727 and 728).

[b] Gradient possibly nonlinear, minimum total heat flow.

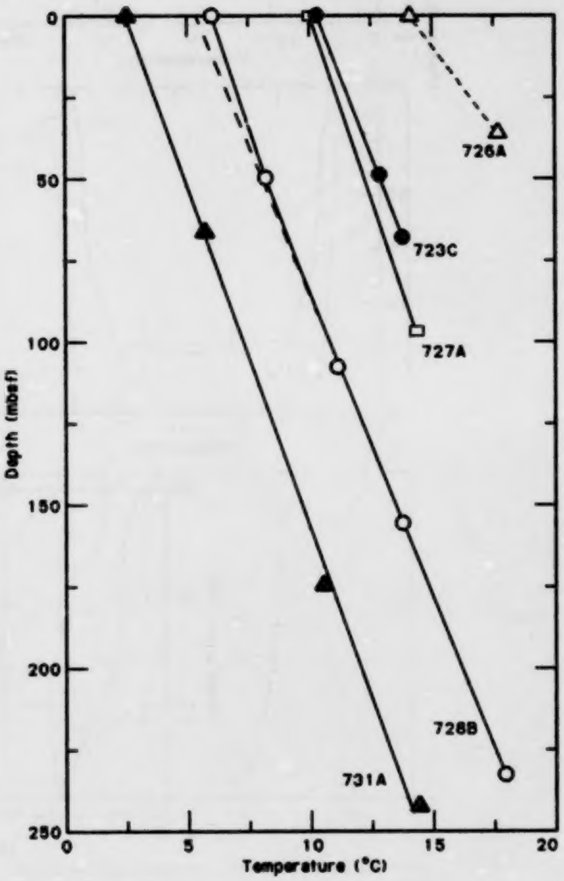

Figure 2. Leg 117 temperature profiles.

SECTION 2: SITE REPORTS

8. SITE 720[1]

Shipboard Scientific Party[2]

HOLE 720A

Date occupied: 29 August 1987

Date departed: 2 September 1987

Time on hole: 4 days, 11 hr, 30 min

Position: 16°07.796′N, 60°44.621′E

Water depth (sea level; corrected m, echo-sounding): 4037.5

Water depth (rig floor; corrected m, echo-sounding): 4048

Bottom felt (m, drill pipe): 4045.4

Penetration (m): 414.3

Number of cores: 43

Total length of cored section (m): 414.3

Total core recovered (m): 89.4

Core recovery (%): 21.6

Oldest sediment cored:
Depth sub-bottom (m): 414.3
Nature: turbiditic silt, sand, and mud
Age: Pleistocene (NN 19?)
Measured velocity (km/s): 1.9

Principal results: Site 720 is located on the westernmost part of the middle Indus Fan. The sediments drilled at Site 720 consist of turbiditic clastic sediments intercalated with pelagic nannofossil ooze; the entire sequence is Pleistocene in age (NN21 to NN19) and has been subdivided into two lithologic units.

Unit I: Nannofossil ooze from 0 to 17.2 mbsf (Holocene to upper Pleistocene) was deposited during a phase (about 0.5 Ma long) of pelagic deposition following abandonment of the major tubidite channel. Pelagic deposition persisted during several sea-level cycles of the late Quaternary. The nannofossil ooze has variable carbonate content and was deposited at a rate of approximately 32 m/m.y.

Unit II: Clastic sediments of turbiditic origin include silty clays, silty sands, sands, and clays and dominate the section from 17.2 mbsf to total depth of 414.3 mbsf. The turbidite sequence is intercalated with numerous thin nannofossil ooze layers (< 10 m thickness) observed in the cores and in downhole log data. They are thought to represent intervals of pelagic deposition related to changes in turbidite flux, which possibly is associated with sea-level changes and abandonment of channels with subsequent deposition on elevated levees. The rate of sedimentation of the turbidite sequence varies from 137 to 944 m/m.y.

BACKGROUND AND OBJECTIVES

Site 720 is located at 16°07.80′N and 60°44.62′E, on the westernmost part of the middle Indus Fan in a water depth of 4045 m. The Indus Fan is 1500 km long, 960 km across at its widest point, covers an area of over 1.1×10^6 km^2 and is the dominant physiographic feature of the Arabian Sea (Whitmarsh et al., 1974; Kolla and Coumes, 1984). The fan is primarily fed by the Indus River, which drains the Himalaya mountains and crosses the fluvial basins and lowlands of Pakistan.

Initiation of Indus Fan deposition is thought to have begun in Oligocene–early Miocene time as the result of collision between the Indian and Asian plates which caused major uplift of the Himalaya (Whitmarsh et al., 1974). A coincident lowering of sea level is also thought to have contributed to the onset of fan deposition (Kolla and Coumes, 1987). Sediments characteristic of the Indus drainage, which is illite-rich (Kolla et al., 1981a; Emeis, 1985), began to accumulate on the distal Indus Fan (DSDP Site 221) in the late Oligocene (Kolla and Coumes, 1987; Weser, 1974). Although major uplift of the Himalaya occurred during the early and middle Miocene, the most recent phase of accelerated uplift may have begun in the late Pliocene and has continued to the present (Mercier et al., 1987).

Previous drilling of the western Indus Fan (DSDP Site 222) penetrated 1300 m, and recovered alternating facies of gray carbonate-rich and green nannofossil-rich detrital silty clays (Whitmarsh et al., 1974). Sediment accumulation rates at Site 222 were very high (greater than 600 m/m.y.) in the late Miocene, and decreased in the early and late Pliocene (135–300 m/m.y.) and in the Pleistocene (40 to 50 m/m.y.). The entire Pleistocene section was dominated by a more pelagic (green) facies and has slower accumulation rates. Hence, the apparent increase in uplift rate of the Himalaya during the Pliocene-Pleistocene is not reflected in the accumulation rates at Site 222. The lower rates of deposition in the Pleistocene, however, may result from channel- and canyon-switching at the head of the fan (McHargue and Webb, 1986). Although deposition at Site 222 is related to sediment flux from the Indus, only about 10% of the recovered section is coarse-grained (Weser, 1974). The depositional processes responsible for these dominantly fine-grained facies are not clear, but Jipa and Kidd (1974) concluded that traditional turbidite mechanisms were not responsible for depositing such facies. Some of the sediment at Site 222 may have come from the Oman coast via downslope and eolian transport. Kolla and Coumes (1987) emphasized the roles of channel abandonment, channel avulsion, and overbank spilling in developing mud-rich deposits, although they did not directly consider the lithologic section from Site 222. On the basis of echo characteristics (Type I) and near-surface sediment samples, Kolla and Coumes (1987) devised a depositional model for the fan that predicts the sediments of the middle fan to lower fan transition should be primarily fine-grained muds with only a few sand-silt beds deposited by overbank flow.

Site 720 is located about 360 km south-southwest of Site 222, at a water depth of 4045 m (Fig. 1). The site lies on the western edge of the Indus Fan, near the boundary between the middle and the lower fan (Kolla and Coumes, 1987). Sediment thickness at Site 720 is greater than 2000 m (Leg 117 Site Survey; Kolla and Coumes, 1987). The site lies near magnetic anomaly 25 (Whitmarsh, 1974), which indicates a Paleocene basement age of about 60 Ma. The site is about 5 km east of a meandering channel that is about 1.5 km wide, 50 m deep, and has a levee elevation of about 30 m above the surrounding seafloor (Fig. 1B). This location was selected to avoid channel deposits,

---

[1] Prell, W. L., Niitsuma, N., et al., 1989. *Proc. ODP, Init. Repts.*, 117: College Station, TX (Ocean Drilling Program).

[2] Shipboard Scientific Party is as given in the list of Participants preceding the contents.

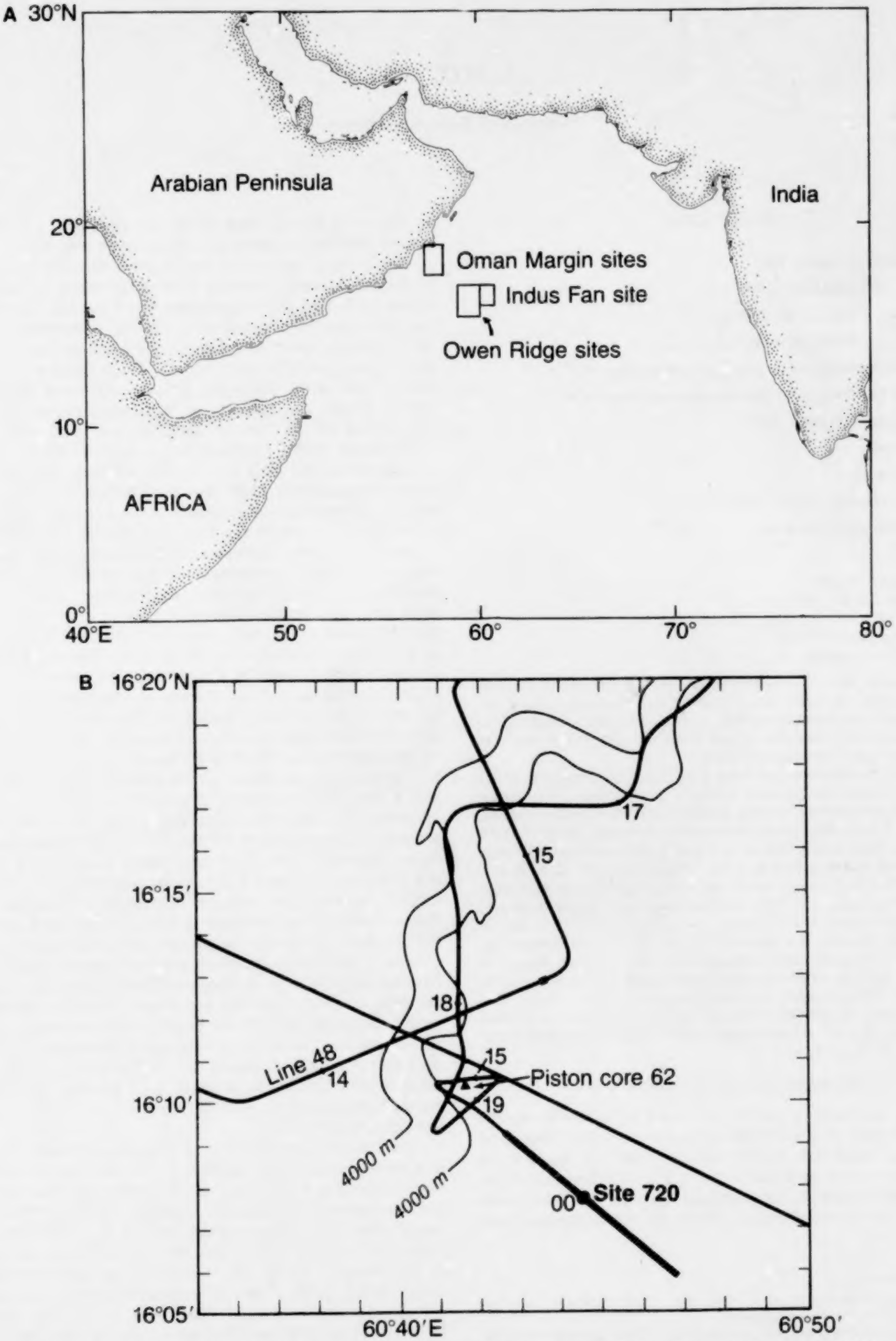
A
30°N
20°
10°
0°
40°E
50°
60°
70°
80°
Arabian Peninsula
India
AFRICA
Oman Margin sites
Indus Fan site
Owen Ridge sites
B
16°20′N
16°15′
16°10′
16°05′
60°40′E
60°50′
17
15
18
Line 48
14
15
Piston core 62
19
4000 m
4000 m
00
Site 720

Figure 1. A. Location of Site 720 and operation area of Leg 117 in the northwest Indian Ocean. B. Tracks of RC2704 seismic lines 48 and 49, location of piston core 62, and position of Site 720 in relation to channel. Thick line denotes part of seismic line 49 depicted in Figure 2.

thereby maximizing the opportunity to collect a relatively continuous depositional record that can be related to uplift and sea-level changes. Hence, the site was located on the middle fan in the western portion of the fan away from known depocenters of sand. The site was selected on the SCS (single channel seismic) track of RC2704 (Line 49, 6-09-86, 0000 hr; Fig. 2) on the basis of the uniformity of reflectors and the lack of strong acoustical facies associated with coarse channel fill. A 12-m piston core near the site (RC2762) revealed relatively high (30%-70%) carbonate content, no distinct turbidites, and mostly silty sediment with an average accumulation rate of about 25 m/m.y (Prell, W. L., unpubl. data).

Objectives

The principal objectives of Site 720 were: (1) to recover a continuous upper Neogene section of fine-grained overbank deposits from the middle fan region of the western Indus Fan; (2) to identify the depositional facies, their composition, and their accumulation rates for comparison to other Indus Fan and Ganges Fan (Leg 116) sites; and (3) to interpret the depositional history of the Indus Fan sediments in terms of uplift of the source region (Himalaya), changes in sea level, changes in climate, circulation, and weathering processes.

OPERATIONS

Leg 117 departed Colombo, Sri Lanka, on 23 August 1987 at 2200 hr and set out to transit for the first operational area on the middle Indus Fan at Site 720. During the transit of 1234 nmi and traveling at an average speed of 9.9 kt, continuous magnetometer and 3.5-kHz profiles were obtained. Upon approach to Site 720, the ship slowed down, seismic gear was deployed on 29 August at 0615, and the site was selected on the basis of a single-channel seismic profile obtained on the second pass (see Figs. 2 and 3).

The beacon was dropped at 0930, the seismic gear was retrieved, and the ship maneuvered back to the beacon. The Global Positioning Satellite (GPS) established the position of Site 720 as being 16°07.796′N and 60°44.621′E. Water depth recorded by the Precision Depth Recorder (PDR) was 4,048.3 m. Pipe was being tripped by 1115 hr and the mud line was established at 4045.3 m around 2400 on 29 August.

Three Advanced Hydraulic Piston Corer (APC) cores were recovered with excellent recovery of 99.4%, until 40,000 pounds of overpull in sands below Core 117-720A-3H made Extended Core Barrel (XCB) coring necessary. Recovery declined dramatically in silty sands and sands retrieved in Cores 117-720A-4X to -43X, and average recovery dropped to 15.7%. Overall rate of recovery of Hole 720A, drilled to a total depth of 414.3 mbsf with Core 117-720A-43X, was 21.6% (see Table 1).

In the light of poor recovery coring was terminated at 1130 hr on 1 September. The hole was conditioned for logging by sweeping with 30 bbls of gel and a wiper trip to 70 mbsf. Maximum overpull at this stage was 20,000 pounds. On 1 September at 2230 hr, the pipe was set at 70 mbsf and the three-string Schlumberger tool was rigged and lowered. After a very successful run with the DIT, LSS, and GR combination in the interval from 4,458 to 4,152 m below sea level, the tool became stuck on the way out by a bridge 20 m below the bottom-hole assembly (BHA). An attempt to crimp the tool and cut the logging wire to retrieve the tool with the pipe failed, and the tool was lost with about 2,600 m of logging wire. Hole 720A was cleared by 1430 hr on 2 September, and the ship was underway to Site 721 by 2100.

LITHOSTRATIGRAPHY

The stratigraphic sequence recovered at Site 720 is Quaternary in age and consists predominantly of interbedded silty clays, clayey silts, silts, and sandy silts, with lesser amounts of sand and nannofossil ooze. This sequence has been subdivided into lithologic units and lithologic facies on the basis of visual core description (color and physical and biological structures), sediment composition determined by smear slide analysis, and carbonate content. A more detailed discussion of the carbonate and organic carbon contents at this site is located in the "Organic Geochemistry" section (this chapter). Sediment residues from nine interstitial water samples were analyzed by X-ray diffractometry (XRD) on the shipboard Philips system, providing qualitative mineralogical information.

Lithologic Units

The stratigraphic sequence recovered at Site 720 has been subdivided into two lithologic units, as shown in Figure 4 and Table 2. Lithologic Unit I is relatively uniform, while lithologic Unit II is heterogenous. Because of this heterogeneity, three distinct facies have been recognized within Unit II. The characteristics and general occurrences of these units and facies are summarized in Table 2.

Unit I (Depth: 0-17.22 mbsf; Age: Holocene-Pleistocene)

Core 117-720A-1H to 117-720A-2H-6, 32 cm.

Lithologic Unit I is composed of nannofossil ooze and foraminifer-bearing nannofossil ooze, with colors of light olive gray (5Y 6/2) to gray (5Y 6/1) and light greenish-gray (5GY 7/1) to grayish-green (5G 5/2). Faint color banding on a scale of several centimeters is common throughout this interval, and the unit is slightly to moderately bioturbated.

Smear slide analyses indicate that Unit I contains 70%-85% nannofossils, 5%-20% foraminifers, 1%-5% radiolarians, trace diatoms, and 1%-5% each of quartz, volcanic glass, clays, and accessory minerals. The smear slide data do not indicate any consistent trends in composition through this interval. Carbonate content (Fig. 5 and Table 3) ranges from 35.5% to 68.4%, supporting the classification of these sediments as carbonate oozes. The residue of one interstitial-water sample from this interval (117-720A-1H-4, 145-150 cm) was analyzed by X-ray diffractometry. Calcite, quartz, and kaolinite peaks were identified on the diffractogram, with the calcite peaks dominant.

Unit II (Depth: 17.22-414.3 mbsf; Age: Pleistocene)

117-720A-2H-6, 32 cm, to Core 117-720A-43X.

Lithologic Unit II is dominated by interbedded silty clays, silts, silty sands, and sands, which form alternating bands of light and dark color, and minor occurrences of nannofossil ooze. A silty zone with abundant charcoal occurred at 117-720A-12X-2, 21-28 cm. The discontinuous recovery at Site 720 and the heterogeneous nature of this stratigraphic interval complicate the identification of stratigraphically-continuous and unique subunits. Three facies, however, can be identified, and their repeated occurrences characterize lithologic Unit II (Table 2).

Calcareous Facies

The calcareous facies is composed of nannofossil ooze, nannofossil-rich mud, and associated muds and clays, generally showing slight to moderate bioturbation. The calcareous facies ranges in color from light gray (5Y 7/1) to very dark gray (5Y 3/1) and greenish-gray (5GY 6/1) to dark greenish-gray (5GY 4/1). In its thickest occurrences, such as Core 117-720A-30X, the calcareous facies shows color banding on a scale of 20-30 cm.

The composition of the nannofossil oozes in the calcareous facies is similar to that of lithologic Unit I, although nannofossil abundances increase to as much as 90%, and detrital (inorganic) carbonate occurs at abundances up to 20%. The associated clays and muds contain 0%-10% nannofossils, 0%-5% radiolarians, 55%-95% clay, 10%-30% inorganic carbonate,

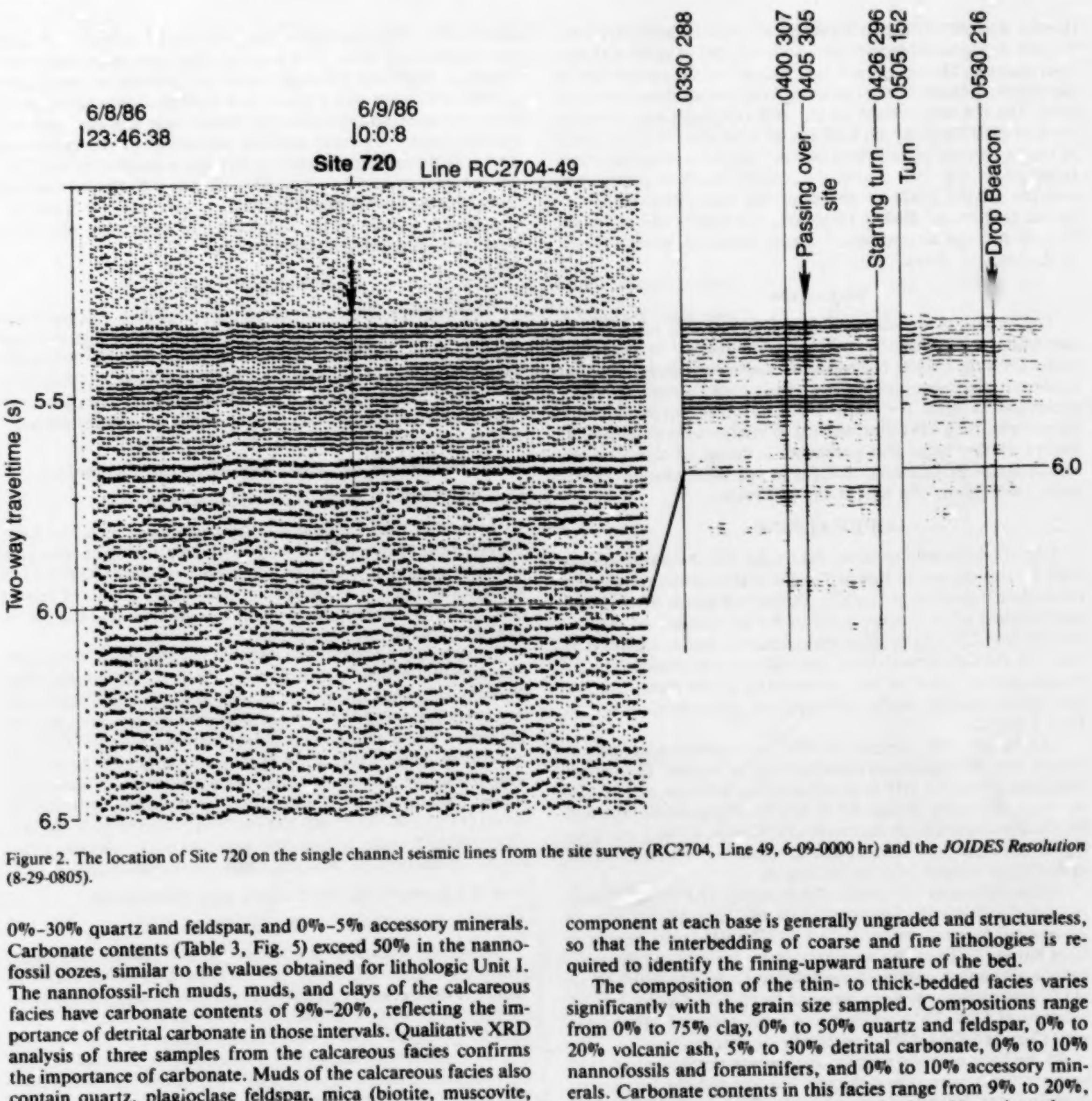

Figure 2. The location of Site 720 on the single channel seismic lines from the site survey (RC2704, Line 49, 6-09-0000 hr) and the *JOIDES Resolution* (8-29-0805).

0%–30% quartz and feldspar, and 0%–5% accessory minerals. Carbonate contents (Table 3, Fig. 5) exceed 50% in the nannofossil oozes, similar to the values obtained for lithologic Unit I. The nannofossil-rich muds, muds, and clays of the calcareous facies have carbonate contents of 9%–20%, reflecting the importance of detrital carbonate in those intervals. Qualitative XRD analysis of three samples from the calcareous facies confirms the importance of carbonate. Muds of the calcareous facies also contain quartz, plagioclase feldspar, mica (biotite, muscovite, illite), and kaolinite/chlorite (undifferentiated).

Thin- to Thick-bedded Facies

The thin- to thick-bedded facies is composed of silty clays, clayey silts, silty sands, and sands, with colors generally ranging from dark gray (5Y 4/1) and olive gray (5Y 4/2) to very dark gray (5Y 3/1) and black (5Y 2.5/1). Within the thin- to thick-bedded facies, these lithologies are characteristically combined to produce light/dark color alternations and fining-upward beds. The thin- to thick-bedded facies is defined by the presence of fining-upward beds with coarse-grained bases of variable thickness, ranging from < 1 to approximately 50 cm. These fining-upward beds generally have sharp bases, rarely with scour or load structures, and grade from a coarse component (sand or silt) at the base to clayey silts or silty clays at the top. The fine-grained tops generally show little or no bioturbation. The coarse component at each base is generally ungraded and structureless, so that the interbedding of coarse and fine lithologies is required to identify the fining-upward nature of the bed.

The composition of the thin- to thick-bedded facies varies significantly with the grain size sampled. Compositions range from 0% to 75% clay, 0% to 50% quartz and feldspar, 0% to 20% volcanic ash, 5% to 30% detrital carbonate, 0% to 10% nannofossils and foraminifers, and 0% to 10% accessory minerals. Carbonate contents in this facies range from 9% to 20%, indicating the presence of detrital and minor biogenic carbonate. XRD analyses of four samples from the thin- to thick-bedded facies indicate the presence of quartz, plagioclase feldspar, mica (biotite/muscovite/illite), calcite, chlorite, and kaolinite(?). Traces of dolomite and pyrite are also present. The pyrite is interpreted as authigenic, while the dolomite may have both detrital and authigenic sources (see "Inorganic Geochemistry" section, this chapter). No consistent downhole compositional trends are apparent from these data.

Thick-bedded Facies

The thick-bedded facies is compositionally similar to the thin- to thick-bedded facies, consisting of interbedded silty clays, clayey silts, silty sands, silts, and sands that form fining-upward beds with sharp lower contacts, uniform bases of silt or sand, and gradational fine-grained tops. The thick-bedded facies dif-

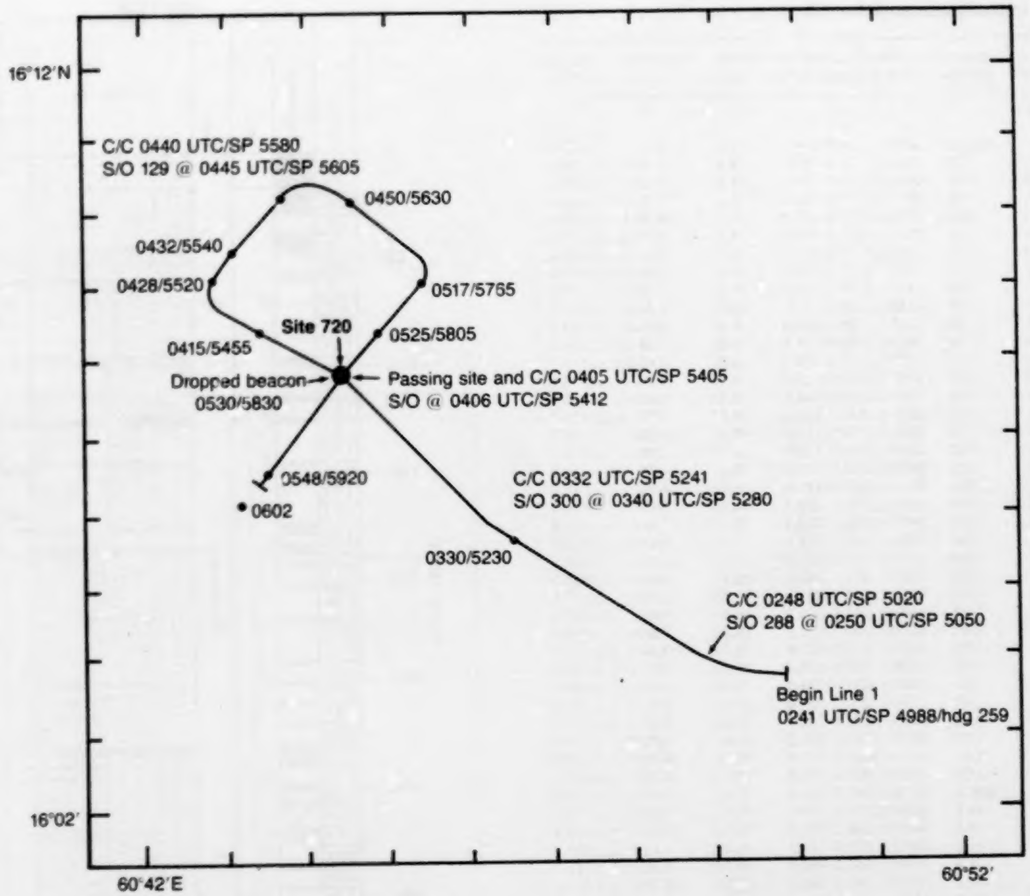
16°12′N
16°02′
60°42′E
60°52′
C/C 0440 UTC/SP 5580
S/O 129 @ 0445 UTC/SP 5605
0450/5630
0432/5540
0428/5520
0517/5765
Site 720
0525/5805
0415/5455
Dropped beacon
0530/5830
Passing site and C/C 0405 UTC/SP 5405
S/O @ 0406 UTC/SP 5412
0548/5920
0602
C/C 0332 UTC/SP 5241
S/O 300 @ 0340 UTC/SP 5280
0330/5230
C/C 0248 UTC/SP 5020
S/O 288 @ 0250 UTC/SP 5050
Begin Line 1
0241 UTC/SP 4988/hdg 259

Figure 3. Track chart of approach to Site 720.

fers from the thin- to thick-bedded facies, however, by only containing sequences with coarse-grained bases more than 5 cm thick. Colors range from dark gray (5Y 4/1) and olive gray (5Y 4/2) to very dark gray (5Y 3/1) and black (5Y 2.5/1).

Abundances of sedimentary components in the thick-bedded facies are generally similar to those of the thin- to thick-bedded facies. Carbonate contents in the thick-bedded facies range from 7% to approximately 17% (Table 3, Fig. 5). Qualitative XRD analysis of one sample from the thick-bedded facies indicates the presence of quartz, plagioclase feldspar, calcite, mica, chlorite, kaolinite(?), and dolomite. Mineralogical compositions are generally similar for the thin- to thick-bedded facies and the thick-bedded facies.

In summary, the stratigraphic section recovered at Site 720 has been divided into two lithologic units, with Unit II further subdivided into three facies. Lithologic Unit I and the calcareous facies of lithologic Unit II both contain biogenic and fine-grained terrigenous components, while the thin- to thick-bedded facies and the thick-bedded facies of lithologic Unit II are dominated by fining-upward beds of coarse to fine terrigenous material.

Discussion

The subdivisions of the stratigraphic sequence at Site 720 generally reflect variations in the relative importance of marine processes and terrigenous sediment supply. As such, these sediments may carry signals related to regional and hemispheric conditions, including surface water productivity, deep-water dissolution, continental uplift, regional tectonism, and climate. The recognition and interpretation of such records, however, is complicated by the poor recovery at this site, which directly influences the lithostratigraphic divisions presented here.

As summarized above, lithologic Unit I and the calcareous facies of lithologic Unit II are similar in composition, while the major difference between the thin- to thick-bedded facies and the thick-bedded facies in lithologic Unit II is the scale of the coarse basal intervals of the fining-upward sequences. Limited core recovery at this site, however, leaves open the question of how representative the recovered lithologies are of the entire stratigraphic section at Site 720. To assess this question, downhole logging data (see "Downhole Measurements" section, this chapter) were visually compared to the recovered intervals to establish log responses for different lithologies. Log data from the unrecovered intervals were then inspected for similar signatures. This inspection supports the following conclusions: (1) two possible occurrences of the calcareous facies in Unit II were not recovered, as indicated at approximately 150 and 170 mbsf in Figure 4; and (2) the other unrecovered intervals in Unit II are consistent with the log signatures of the thin- to thick-bedded facies and the thick-bedded facies. As a result, we interpret the entire

Table 1. Coring summary, Site 720.

Core no.	Date (1987)	Time	Depth (mbsf)	Cored (m)	Recovered (m)	Recovery (%)
117-720A-						
1H	Aug 30	0145	0.0-9.4	9.4	9.42	100.0
2H	30	0300	9.4-19.0	9.6	9.48	98.8
3H	30	0430	19.0-28.6	9.6	9.54	99.4
4X	30	0715	28.6-38.2	9.6	0.01	0.1
5X	30	0830	38.2-47.9	9.7	8.38	86.4
6X	30	0945	47.9-57.6	9.7	0.70	7.2
7X	30	1100	57.6-67.3	9.7	2.76	28.4
8X	30	1215	67.3-77.0	9.7	0.00	0.0
9X	30	1315	77.0-86.7	9.7	0.00	0.0
10X	30	1430	86.7-96.4	9.7	0.24	2.5
11X	30	1545	96.4-106.0	9.6	4.96	51.6
12X	30	1645	106.0-115.7	9.7	2.39	24.6
13X	30	1745	115.7-125.4	9.7	0.42	4.3
14X	30	1900	125.4-135.0	9.6	0.63	6.6
15X	30	2015	135.0-144.7	9.7	0.00	0.0
16X	30	2115	144.7-154.4	9.7	2.79	28.7
17X	30	2245	154.4-164.0	9.6	0.03	0.3
18X	30	2330	164.0-173.7	9.7	0.00	0.0
19X	31	0050	173.7-183.4	9.7	4.26	43.9
20X	31	0215	183.4-193.0	9.6	4.52	47.1
21X	31	0315	193.0-202.7	9.7	0.99	10.2
22X	31	0425	202.7-212.4	9.7	1.06	10.9
23X	31	0540	212.4-222.0	9.6	0.21	2.2
24X	31	0645	222.0-231.7	9.7	1.85	19.1
25X	31	0800	231.7-241.4	9.7	0.00	0.0
26X	31	0925	241.4-251.0	9.6	0.67	7.0
27X	31	1100	251.0-260.5	9.5	0.98	10.3
28X	31	1215	260.5-270.1	9.6	1.54	16.0
29X	31	1315	270.1-279.8	9.7	0.52	5.4
30X	31	1430	279.8-289.4	9.6	9.47	98.6
31X	31	1600	289.4-299.0	9.6	1.01	10.5
32X	31	1730	299.0-308.6	9.6	3.01	31.3
33X	31	1900	308.6-318.2	9.6	0.43	4.5
34X	31	2045	318.2-327.8	9.6	0.00	0.0
35X	31	2215	327.8-337.4	9.6	0.00	0.0
36X	31	2345	337.4-347.0	9.6	0.78	8.1
37X	Sep. 1	0115	347.0-356.6	9.6	0.57	5.9
38X	1	0250	356.6-366.2	9.6	0.30	3.1
39X	1	0415	366.2-375.9	9.7	0.66	6.8
40X	1	0540	375.9-385.2	9.3	2.17	23.3
41X	1	0730	385.2-394.9	9.7	1.10	11.3
42X	1	0935	394.9-404.6	9.7	0.35	3.6
43X	1	1130	404.6-414.3	9.7	1.18	12.1
				414.3	89.38	

stratigraphic section at Site 720 in terms of the lithostratigraphic divisions established above. Given their similarity, Unit I and the calcareous facies of Unit II are interpreted to indicate similar depositional conditions. The thin- to thick-bedded facies and the thick-bedded facies of Unit II are interpreted as recording one basic mechanism of deposition, with variations in scale.

Pelagic Deposits

The abundance of biogenic carbonate and the variety of microfossils in Unit I and the calcareous facies of Unit II indicate that these are pelagic deposits (Fig. 4), formed during periods of increased surface-water productivity and/or decreased clastic influx. The uniformity of Unit I and its age (~0.5 Ma at its base) indicate that the conditions controlling pelagic deposition have not changed drastically during late Pleistocene climatic fluctuations, although a more subtle record may be preserved by minor changes in clastic content and magnetic susceptibility (see "Paleomagnetism" section, this chapter). The linear sedimentation rate in Unit I is approximately 32 m/m.y. (see "Accumulation Rates" section, this chapter), suggesting that clastic influx was low during deposition of this ooze. The dominant control on clastic influx may be large-scale (i.e., climatic or tectonic) or more localized, such as depositional patterns on the upper (Kolla and Coumes, 1987), middle, or lower Indus Fan, or differential uplift/subsidence between the Owen Ridge and the western Indus Fan (see "Seismic Stratigraphy" section, this chapter). These controls must be examined by detailed shore-based studies to outline their effects more clearly.

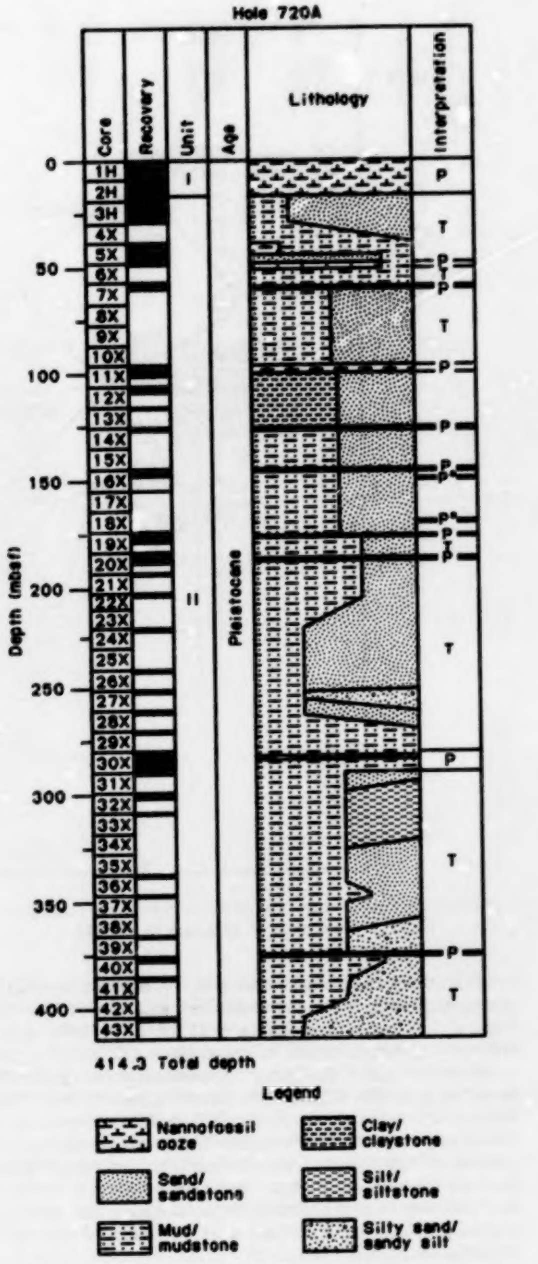
Hole 720A
Core
Recovery
Unit
Age
Lithology
Interpretation
Depth (mbsf)
0
50
100
150
200
250
300
350
400
1H
2H
3H
4X
5X
6X
7X
8X
9X
10X
11X
12X
13X
14X
15X
16X
17X
18X
19X
20X
21X
22X
23X
24X
25X
26X
27X
28X
29X
30X
31X
32X
33X
34X
35X
36X
37X
38X
39X
40X
41X
42X
43X
I
II
Pleistocene
P
T
P
T
P
T
P
P
P
P*
P*
P
T
P
T
P
T
P
T
414.3 Total depth
Legend
Nannofossil ooze
Clay/ claystone
Sand/ sandstone
Silt/ siltstone
Mud/ mudstone
Silty sand/ sandy silt

Figure 4. Lithostratigraphic summary, Site 720. Lithology is inferred between recovered intervals. T = turbidite section, P = pelagic section, and P* = possible pelagic section inferred from downhole logs.

Table 2. Lithostratigraphic summary, Site 720.

Lithologic Unit	Depth	Cores and section
I Nannofossil ooze	0.0–17.2	1H to 2H-6
II Silty clays, silts, sands, with minor nannofossil ooze	17.2–414.3	2H-6 to 43X

Facies	Best developed in core and section
Calcareous facies—Nannofossil ooze	6X, 11X-1 to 11X-3, and 30X-2
Thin- to thick-bedded facies—Interbedded silty clays, silts, and sands	3H, 11X-4 to 11X-CC, and 32X
Thick-bedded facies—Thickly-interbedded silty clays, silts, and sands	22X and 24X

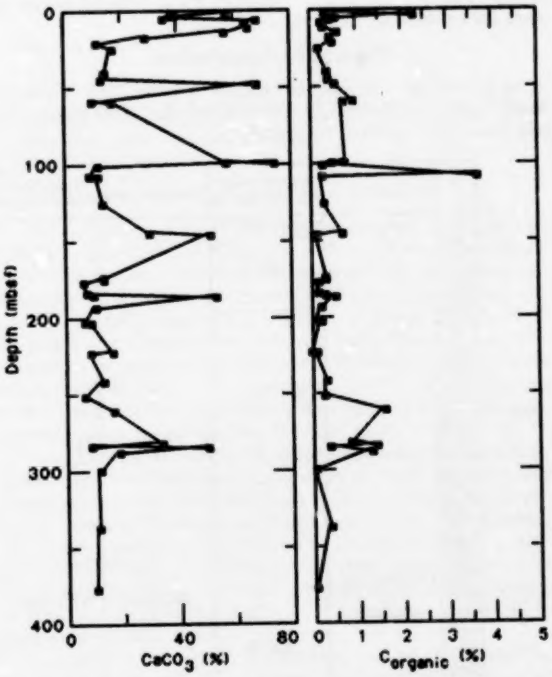

Figure 5. Carbonate and organic carbon profiles, Site 720.

Table 3. Carbonate and organic carbon abundances, Site 720.

Core, section interval (cm)	Depth (mbsf)	Total carbon (%)	Inorganic carbon (%)	Organic carbon (%)	$CaCO_3$ (%)
117-720A-					
1H-2, 40–42	1.90	7.24	6.91	0.33	57.6
1H-3, 34–35	3.34	6.90	4.60	2.30	38.3
1H-4, 40–42	4.90	4.84	4.26	0.58	35.5
1H-4, 144–145	5.94	8.67	8.21	0.46	68.4
1H-6, 40–42	7.90	7.98	7.73	0.25	64.4
2H-2, 40–42	11.30	8.16	7.86	0.30	65.5
2H-4, 40–42	14.30	7.45	6.84	0.61	57.0
2H-6, 40–42	17.30	3.95	3.51	0.44	29.2
3H-2, 24–26	20.74	1.95	1.44	0.51	12.0
3H-4, 144–145	24.94	2.31	2.11	0.20	17.6
5X-2, 36–38	40.06	2.14	1.76	0.38	14.7
5X-5, 85–87	45.05	2.02	1.61	0.41	13.4
6X-1, 16–18	48.06	8.80	8.25	0.55	68.7
7X-1, 144–145	59.04	2.20	1.24	0.96	10.3
7X-2, 49–51	59.59	2.79	2.05	0.74	17.1
11X-2, 109–111	98.99	7.71	6.93	0.78	57.7
11X-2, 144–145	99.34	9.47	8.97	0.50	74.7
11X-CC, 0–1	101.07	1.78	1.48	0.30	12.3
12X-2, 25–26	107.75	4.83	1.13	3.70	9.4
12X-2, 56–58	108.06	1.74	1.46	0.28	12.2
14X-1, 29–31	125.69	1.99	1.67	0.32	13.9
16X-1, 64–66	145.34	4.35	3.63	0.72	30.2
16X-1, 144–145	146.14	6.39	6.23	0.16	51.9
19X-1, 34–36	174.04	2.01	1.67	0.34	13.9
19X-1, 149–150	175.19	2.06	1.71	0.35	14.2
19X-3, 34–36	177.04	0.98	0.81	0.17	6.8
20X-1, 45–47	183.85	1.17	0.98	0.19	8.2
20X-2, 63–64	185.53	1.59	1.26	0.33	10.5
20X-3, 45–47	186.85	7.03	6.47	0.56	53.9
21X-1, 51–53	193.51	1.60	1.35	0.25	11.3
22X-1, 0–1	202.70	0.97	0.86	0.11	7.2
22X-1, 52–54	203.22	1.38	1.14	0.24	9.5
24X-1, 90–92	222.90	2.06	2.03	0.03	16.9
24X-1, 139–141	223.39	1.23	1.10	0.13	9.2
26X-1, 31–33	241.71	2.01	1.67	0.34	13.9
27X-1, 40–42	251.40	1.13	0.84	0.29	7.0
28X-1, 40–42	260.90	3.71	2.07	1.64	17.2
30X-2, 111–113	282.41	4.97	4.09	0.88	34.1
30X-4, 1-2	284.31	2.56	1.11	1.45	
30X-4, 98–100	285.28	6.52	6.10	0.42	50.8
30X-6, 100–102	288.30	3.65	2.31	1.34	19.2
32X-1, 77–78	299.77	1.58	1.48	0.10	12.3
32X-1, 93–95	299.93	1.70	1.34	0.36	11.2
33X-1, 25–27	308.85	1.15	1.00	0.15	8.3
36X-1, 0–1	337.40	1.80	1.39	0.41	11.6
36X-1, 60–62	338.00	1.89	1.62	0.27	13.5
37X-1, 19–21	347.19	1.90	1.62	0.28	13.5
39X-CC, 10–11	366.71	6.60	6.06	0.54	50.5
40X-1, 24–26	376.14	1.93	1.53	0.40	12.7
40X-1, 139–140	377.29	1.29	1.23	0.06	10.3
41X-1, 46–48	385.66	1.32	1.15	0.17	9.6
43X-1, 57–59	405.17	2.23	1.88	0.35	15.7

The presence of the calcareous facies within Unit II indicates that similar conditions of increased marine or decreased clastic importance were repeatedly established at Site 720 prior to 0.5 Ma. By including the two pelagic zones recognized on the downhole logs, a total of 11 such intervals are identified (Fig. 4). The pelagic units are distributed irregularly downcore, however, with 9 of the 11 located above 200 mbsf. By using the sedimentation rates presently available (see "Accumulation Rates" section, this chapter), these 9 pelagic intervals were deposited between 1.0 and 0.5 Ma, while only 2 pelagic layers were deposited prior to 1.0 Ma.

Several lines of evidence indicate that changes in terrigenous sedimentation on the Indus Fan were the major control on the lithologic variations observed in Unit II:

1. The dominance of terrigenous sediments in Unit II, their interpretation as turbidites (see below), and the high rate of sedimentation are all characteristic of a fan setting. The long-term importance of the terrigenous source is indicated by the presence of detrital illite and chlorite throughout Unit II, recording input from a Himalayan source during both clastic and carbonate deposition (Weser, 1974).

2. Seismic reflection records from the study area are interpreted (see "Seismic Stratigraphy" section, this chapter) as indicating that sedimentation on the western Indus Fan is controlled by channel migration. Near the Owen Ridge, channel migration may respond to differential tectonics, which creates depressions subject to rapid sedimentary infilling. Each phase of infilling ends with deposition of a major pelagic drape, while minor pelagic drapes are deposited during channel switching.

3. Pelagic units, similar in appearance and composition to those described here, were recognized at DSDP Site 222, also located on the deep Indus Fan (Whitmarsh et al., 1974). At that

site, an 80-m-thick pelagic unit of Pleistocene age was underlain by 1220 m of interbedded pelagic and terrigenous sediments of Pliocene to late Miocene age. The presence of a thinner Pleistocene pelagic unit at Site 222 and a thicker, terrigenous-dominated Pleistocene unit at Site 720 supports the hypothesis that deposition of the calcareous facies in Unit II at Site 720 was controlled by decreased clastic influx.

These data all suggest that variations in clastic supply controlled the deposition of Unit II more directly than changes in marine conditions. Further investigation will be required, however, to fully understand such controls.

Turbidites

The predominance of terrigenous components, their grain sizes, and the abundance of fining-upward sequences in the thin- to thick-bedded facies and the thick-bedded facies of lithologic Unit II support the interpretation of these facies as deposits of low-density mass-transport events. These sediments are interpreted as turbidites in a general sense, but vary somewhat from the idealized model of a complete turbidite (Bouma sequence): (1) the coarse basal zones generally do not show visible grading; (2) primary sedimentary structures are absent in the thicker basal sands; and (3) the upper portions of these sequences lack both a distinct interturbidite layer (Bouma E interval) and significant bioturbation. Explanations can be advanced for each of these differences. The absence of grading may reflect a uniform grain size of the coarse fraction in transport, perhaps because of the distal to middle fan location of Site 720. The absence of primary sedimentary structures could be caused by subtle coring disturbance of the sands. Some interturbidite layers may have been eroded by subsequent events, while others may be indistinguishable from the underlying, fine-grained turbidite tops.

The differences between these sequences and the idealized turbidite, however, may also record important variations in transport and deposition mechanisms. Jipa and Kidd (1974) used textural, compositional, and sedimentary structure data to investigate similar lithologies in the older clastic unit at DSDP Site 222. Some of the intervals considered at Site 222 also lacked basal grading, sedimentary structures, pelagic intervals, and bioturbation. Jipa and Kidd (1974) concluded that the classic model of fan construction, dominated by episodic sand deposition by turbidity flows, was inadequate for the Indus Fan. Instead, they concluded that several processes were active. Turbidity flows probably supplied coarse silt and fine sand episodically, while more semipermanent bottom-following turbidity flows deposited finer sediments derived from reworking on the shelf. Similar processes may also have influenced deposition at Site 720, although interpretations of seismic reflection data emphasize channel levee deposits in this area (see "Seismic Stratigraphy" section, this chapter).

Variations in turbidite-type deposits on the Indus Fan have also been discussed by Kolla and Coumes (1987), who use varying importance of channelized flow, unchannelized flow, channel avulsion, and overbank flow to account for changes in sediment character (see "Seismic Stratigraphy" section, this chapter). According to their model, the thin- to thick-bedded facies at Site 720 contains both overbank (thin, mud-dominated) and channelized to unchannelized (thicker, sand-dominated) deposits, while overbank deposits are absent in the thick-bedded facies. The poor recovery of both clastic facies in Unit II limits our ability to trace these depositional histories in detail, but further study may provide insight into these depositional sequences.

BIOSTRATIGRAPHY

Introduction

Hole 720A consisted of a short pelagic sequence in Cores 117-720A-1H and -2H, followed by a long sequence of turbidites interrupted by short pelagic intervals (e.g., Core 117-720A-30X). Calcareous fossils (planktonic and benthic foraminifers and nannofossils) are abundant, moderately well preserved, and fairly diverse in the upper pelagic sequence. Radiolarians are present, but rare, and show signs of dissolution. Within the turbidite sequence, radiolarians are absent while the calcareous fossils become increasingly impoverished, dissolved, and reworked with depth. In the pelagic sequence of Core 117-720A-30X (279.8–289.4 mbsf) a reasonable calcareous assemblage (mostly planktonic foraminifers and nannofossils) was found along with a robust radiolarian fauna. A correlation of microfossil zones for Site 720 is presented in Figure 6; for a detailed listing of these data points see Table 4.

Planktonic Foraminifers

In general the core catcher samples of Hole 720A contained poorly preserved planktonic foraminifers that show dissolution and have been reworked by turbidites.

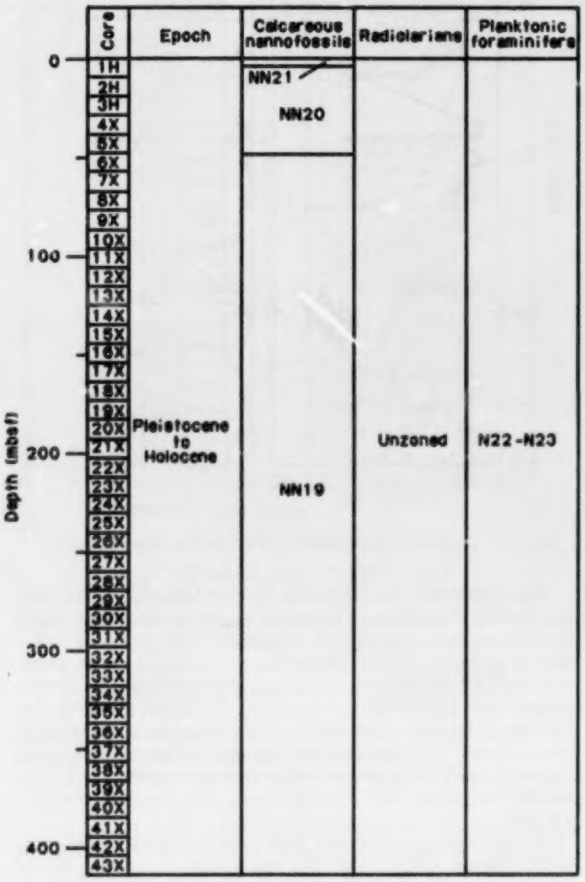

Figure 6. Correlation of biostratigraphic zones for Hole 720A. See Table 4 for a listing of events.

Table 4. Chronological listing of faunal events and paleomagnetic reversals for Hole 720A.

Event	Core, section interval (cm)	Depth (mbsf)	Age (Ma)	Source of age
B *Emiliania huxleyi*	1H-3, 100–101	4.00	0.19	3
	1H-5, 100–101	7.00		
T *Pseudoemiliania lacunosa*	5X-CC	46.56	0.49	3
	6X-1, 32–33	48.22		
Brunhes/Matuyama	7X-2, 68–70	59.78	0.73	6
	11X-1, 99–101	97.39		
T *Reticulofenestra* sp. A	17X-CC	154.42	0.82	3
	19X-2, 33–34	175.53		
B *Gephyrocapsa parallela*	19X-CC	177.94	0.89	4
	20X-2, 70–71	185.60		
T Jaramillo	20X-2, 96–98	185.86	0.91	6
	20X-3, 95–97	187.35		
B Jaramillo	22X-1, 48–50	203.18	0.98	6
	26X-1, 36–38	241.76		
T *Gephyrocapsa* "large"[a]	23X-CC	212.60	[b]1.10	4
	24X-CC	223.83		
T *Helicosphaera sellii*[c]	30X-3, 100–101	283.80		
	30X-5, 100–101	286.80		

Note: T = upper limit and B = lower limit. Sources of age: 3 = oxygen isotope data for Site 723 (N. Niitsuma, unpubl. data); 4 = Takayama and Sato, 1987; and 6 = Berggren et al., 1985.

[a] Long axis greater than 6 μm.

[b] North Atlantic data.

[c] No consistent ages recorded; event appears to be diachronous.

The calcareous pelagic part of the sequence (Sections 117-720A-1H, CC, and 117-720A-2H, CC) yields abundant planktonic foraminifers. *Globorotalia menardii* and *Neogloboquadrina dutertrei* dominate the foraminiferal assemblages along with *Globigerina bulloides, Globigerinoides trilobus, Globigerinoides ruber*, and *Globigerinita glutinata*. The presence of rare *Globorotalia truncatulinoides* indicates a Pleistocene age for these sediments (Zone N22). These pelagic oozes are late Pleistocene or Holocene (N23) as suggested by the occurrence of rare *Globigerinella calida calida* specimens (Blow, 1969).

From Section 117-720A-3H, CC, downhole, the planktonic foraminifers are diluted by terrigenous particles or are totally absent in the sandy turbidites thus making age assignments difficult. However, the occurrence of *Globorotalia truncatulinoides* in some samples (117-720A-13X, CC; 117-720A-14X, CC, and 117-720A-20X, CC) indicates that these sandy layers are of Pleistocene age (Zone N22). The presence of *Globorotalia tosaensis* in Section 117-720A-20X, CC, indicates that the sample is older than 0.6 Ma.

Core catcher Sections 117-720A-21X, CC, to 117-720A-43X, CC (202.7–414.30 mbsf), are essentially barren with only some reworked specimens present. This interval probably can also be referred to Zone N22 as no upper Pliocene species could be found.

Benthic Foraminifers

The benthic foraminiferal fauna of Hole 720A is for the most part sparse, poorly to moderately preserved, and shows signs of reworking from older and/or shallower sediments.

The upper part of the sequence, which consists of pelagic oozes (Samples 117-720A-1H-2, 52–54 cm, through -2H-2, 56–58 cm, 117-720A-2H-4, 56–58 cm), and the uppermost part of the turbidite sequence (Section 117-720A-2H, CC) yield an abundant, well-preserved, and relatively diverse benthic fauna. The number of benthic foraminifers per 10 cm^3 of wet unsieved sediment was approximately 300. Below Section 117-720A-2H-2, the abundance of benthic foraminifers decreases (0 to approximately 100 specimens per 10 cm^3 sediment) and the preservation is usually moderate to poor.

The most abundant species are *Chilostomella oolina, Cibicidoides wuellerstorfi, Epistominella exigua, Oridorsalis umbonatus*, and *Pullenia subcarinata* (relative abundance generally between 10% and 20%). Minor components are *Eggerella bradyi, Fissurina* spp., *Melonis* spp., *Pyrgo* spp., *Siphotextularia* spp., and *Uvigerina* spp. Sections 117-720A-11X, CC, 117-720A-12X, CC, 117-720A-22X, CC, 117-720A-24X, CC, 117-720A-26X, CC, 117-720A-27X, CC, 117-720A-30X, CC, 117-720A-33X, CC, 117-720A-38X, CC, 117-720A-41X, CC, and 117-720A-43X, CC, are completely barren.

The samples in the turbiditic section often contain poorly preserved specimens of *Ammonia beccarii* (a shallow-water form; Murray, 1976) and/or *Nuttallides truempyi* (with a stratigraphic range of Late Cretaceous to Eocene; van Morkhoven et al., 1986), which indicates reworking.

Calcareous Nannofossils

Coccoliths occur throughout Hole 720A and they range from abundant to rare. Pelagic oozes contain well-preserved, diverse assemblages of nannofossils. Unfortunately, most of the core catcher material recovered consisted of turbiditic sequences, in which the nannofossils were moderately to poorly preserved and present in low concentrations. Due to these circumstances age assignments for many samples have low confidence.

The general zonation used in this section is that of Martini (1971), and the Quaternary zonation of Takayama and Sato (1987) was used to further refine the biostratigraphy. The ages assigned fossil datums are derived from Berggren et al. (1985) and from Takayama and Sato (1987).

Emiliania huxleyi is present in Core 117-720A-1H down to Sample 117-720A-1H-3, 100–101 cm, but is not present in 117-720A-1H-5, 100–101 cm (4.0–7.0 mbsf). Therefore, its first occurrence at 0.19 Ma is located somewhere within this interval. The sediments containing *E. huxleyi* are assigned to Zone NN21. Sediments which contain neither *E. huxleyi* nor *Pseudoemiliania lacunosa* are assigned to Zone NN20. The last occurrence of *P. lacunosa*, at 0.49 Ma, is between Section 117-720A-5X, CC, and Sample 117-720A-6X-1, 32–33 cm (46.56–48.22 mbsf). All cores down to Section 117-720A-39X, CC, contain *Gephyrocapsa oceanica* and/or *G. caribbeanica*, which have their first occurrences at 1.57 Ma and 1.66 Ma within Zone NN19, respectively.

A trace of Cretaceous and Tertiary reworked specimens such as *Chiastozygus litterarius, Cretarhabdus* spp., *Eiffelithus turriseiffelii, Micula decussata, Prediscosphaera* spp., *Tranolithus phacelosus, Watznaueria barnesae, Dictyococcites bisecta, Discoaster barbadiensis, D. saipanensis, Ericsonia formosa, Cyclicargolithus floridanus*, and *Sphenolithus heteromorphus* also occur throughout the recovered section.

Radiolarians

At Site 720A, radiolarians were found only in Cores 117-720A-1H through 117-720A-3H (0–28.6 mbsf), in Section 117-720A-17X, CC (164.0 mbsf), and in Core 117-720A-30X (279.8–289.4 mbsf). In Cores 117-720A-1H through 117-720A-3H, radiolarians are generally rare and show signs of dissolution; both abundance and preservation decline with depth, and there is considerable masking by terrigenous material throughout. The fauna consists mainly of Spumellaria and age-diagnostic forms are sparse. *Pterocorys hertwigii* and *Lamprocyrtis nigriniae* were found in Section 117-720A-1H, CC, thus placing the sample in the upper Pleistocene. The Quaternary zonation of Nigrini (1971) could not be applied. A sparse, moderately well preserved fauna was found in Section 117-720A-17X, CC, but age-diagnostic taxa are lacking. Single specimens of *Eucyrtidium acuminatum* and *Pterocanium praetextum eucolpum* suggest a cool-water fauna.

The most robust and diverse radiolarian fauna found at this site occurred within two samples from pelagic layers within Core 117-720A-30X (117-720A-30X-2, 80-82 cm, and -30X-4, 74-76 cm). This fauna also suggests a cool-water fauna with very robust specimens of *Lamprocyrtis neoheteroporos* and *Eucyrtidium calvertense*. A single specimen of *Anthocyrtidium angulare* places Sample 117-720A-30X-4, 74-76 cm, in the *A. angulare* Zone of Nigrini (1971), while the presence of *L. neoheteroporos* means that the sample is older than 1.1 Ma, but younger than 1.5 Ma (Johnson et al., in press).

PALEOMAGNETISM

Introduction

Hole 720A was cored using the APC to 28.6 mbsf and then the XCB to 414.3 mbsf. The lithologies recovered included calcareous ooze and silt/sand turbidites. We measured the natural remanent magnetization (NRM) of the archive halves of the APC cores and of discrete samples obtained from the ooze and silt, in order to establish a paleomagnetic chronology for the Site 720 sediments.

Coring/Corer-Induced Remanence

Because of the very poor recovery, the high degree of core disturbance and the frequent occurrence of coarse-grained intervals, we concentrated our efforts on measuring discrete samples. However, we did use the pass-through cryogenic magnetometer to measure the NRM of the archive halves of all APC cores (117-720A-1H, -2H, -3H) and some XCB cores (117-720A-6X, -7X). This did not produce any significant magnetostratigraphic results but it did illustrate the remanence induced by APC coring described on previous legs, in particular on Legs 115 and 116. Figure 7 shows the results of pass-through measurements for Core 117-720A-2H at demagnetizing fields of 0, 5, and 9 mT. The undemagnetized inclination values generally are greater than 70°, greatly exceeding the expected axial dipole value (30°) for this latitude, and indicating the presence of a steep downward overprint which is only partially removed after alternating field (AF) cleaning at 5 and 9 mT. There is also some evidence of anhysteretic remanent magnetization acquisition in the upper 1 m of the core after the 9 mT step, shown by the increased intensity. The Zijderveldt plot for a discrete sample from Core 117-720A-2H (Fig. 8) also illustrates the effect of coring-induced magnetization, although in this case it appears to be removed completely at 5 mT. A strong, steep, low-coercivity overprint did not appear to be a feature of the XCB-recovered sediments at this site.

Previous shipboard paleomagnetists have attributed this steep overprint to an induced remanent magnetization (IRM) acquired from the stainless-steel APC barrel. We measured the magnetization of the core barrel after the Site 720 APC cores had been taken and found that it gave "off-scale" values on a crude portable magnetometer with a range of 2 mT. We learned subsequently that the procedure used for checking for flaws in the drill string involves magnetizing it, and that from Leg 115 onwards a much higher field (100 vs. 18 mT) has been used for this purpose. This undoubtedly has the effect of magnetizing the APC barrel. Demagnetization of the APC barrel can be performed onboard the ship; however, the Leg 116 paleomagnetist (see "Paleomagnetism" sections in Cochran, Stow, et al., in press) states that the barrel is quickly remagnetized in the drill string. The low maximum AF field of the cryogenic demagnetizer means that it may be difficult to obtain reliable results from whole APC cores. We recommend (1) that the drill string sections be demagnetized routinely after the flaw-checking procedure, and (2) that the demagnetizer power supply for the cryogenic magnetometer be enhanced as quickly as possible to give a peak AF of at least 15 mT.

Magnetostratigraphy

We measured a total of 49 discrete samples using the Minispin fluxgate magnetometer. We avoided sampling obviously disturbed and/or coarse-grained intervals. Low NRM intensities (mostly less than 5 mA/m) prevented our using the discrete sample measuring mode on the cryogenic magnetometer, since the noise level of the Z channel was high (about 10 mA/m). The noise level of the Minispin was much lower (about 0.02 mA/m). All of the samples were stepwise AF demagnetized and Figures 9-13 show Zijderveldt plots of some of the results, both for well-behaved (Figs. 9-11 and 13) and poorly-behaved samples (Fig. 12).

The stable magnetic directions of some of the better-behaved samples are listed in Table 5, and Figure 14 shows a histogram of the distribution of inclinations. Although the number of samples is small, there is a tendency to conform to the expected axial dipole value. Figure 15 shows the inclinations plotted against depth downhole, together with a tentative and partial correlation with the reversal time-scale. The location of the chron C1N/C1R (Brunhes/Matuyama chronozones) boundary between Samples 117-720A-7X-2, 68-70 cm, and 117-720A-11X-1, 99-101 cm (59.78-97.39 mbsf), is in good agreement with the nannofossil stratigraphy ("Biostratigraphy" section, this chapter). Our assignment of two samples to subchron C1R-1 (Jaramillo subchronozone) is more tentative, but again is in reasonable agreement with the nannofossil stratigraphy. If this correlation is correct then the C1R-1 upper boundary lies between Samples 117-720A-20X-2, 96-98 cm, and 117-720A-20X-3, 95-97 cm (185.86-187.35 mbsf). The lower boundary is not so well constrained, occurring between samples 117-720A-22X-1, 48-50 cm, and 117-720A-26X-1, 36-38 cm (203.18-241.76 mbsf), ignoring the anomalously steep normal sample at about 223 mbsf. Below about 300 mbsf a combination of too few stable samples and lack of biostratigraphic control prevents any reliable correlations with the reversal time scale.

Magnetic Susceptibility

The volume magnetic susceptibility of Hole 720A cores was measured using a Bartington Instruments susceptibility meter and M.S.1 sensor. The cores were measured at 5-cm intervals using the low-frequency (0.47-kHz) and high sensitivity (0.1) settings. Downcore susceptibility profiles can be interpreted as reflecting fluctuations in the volume concentration of magnetic particles. A total of 1475 measurements were made over the entire depth range of Hole 720A, although 571 of these were measured for the upper 30 m of core due to the good recovery of that interval. The measured values ranged from 25×10^{-6} to 75×10^{-4} SI units, over two decades of variation, which suggests that the susceptibility data are reflecting the dynamic depositional setting of the Indus fan. The susceptibility record from Hole 720A is best interpreted in two parts, the first part being shallower than 30 mbsf where recovery was good, and the second part below 30 mbsf where recovery was poor and only general observations are appropriate.

The upper 30 m of Hole 720A showed marked variations in susceptibility which could be generally related to varying lithologies (Fig. 16). Sections 117-720A-1H-1 through -5 contain an apparently pelagic unit with cyclic susceptibility variations. Comparison of the susceptibility values with the core descriptions indicates that the lower-valued susceptibility units are light gray in color, have higher percent carbonate content, and generally contain less clay than those units of relatively higher susceptibility which are commonly olive-green in color. An example of a high

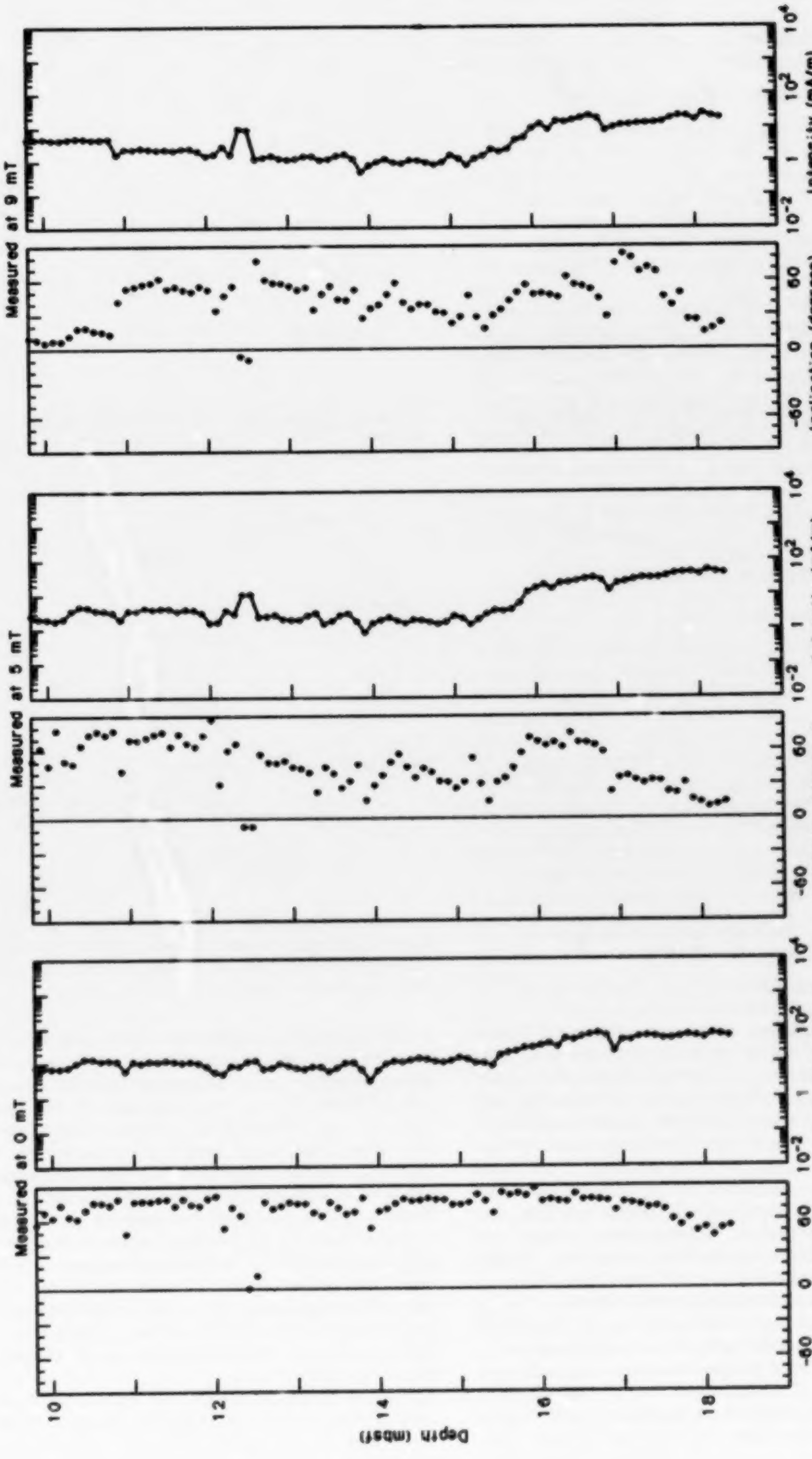

Figure 7. Plots of magnetic inclination and intensity of Core 117-720A-2H, measured on the pass-through cryogenic magnetometer after alternating field (AF) demagnetization at 0 mT (left pair), 5 mT (middle pair), and 9 mT (right pair).

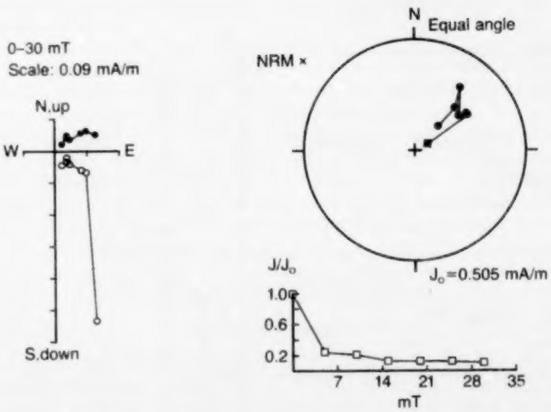

Figure 8. Results of stepwise alternating field (AF) demagnetization of Sample 117-720A-2H-1, 119–121 cm, plotted on a Zijderveld diagram and an equal-area projection.

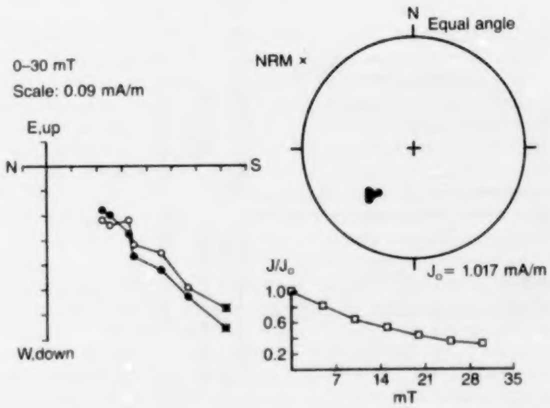

Figure 9. Results of stepwise alternating field (AF) demagnetization of Sample 117-720A-6X-1, 24–26 cm, plotted on a Zijderveld diagram and a equal-area projection.

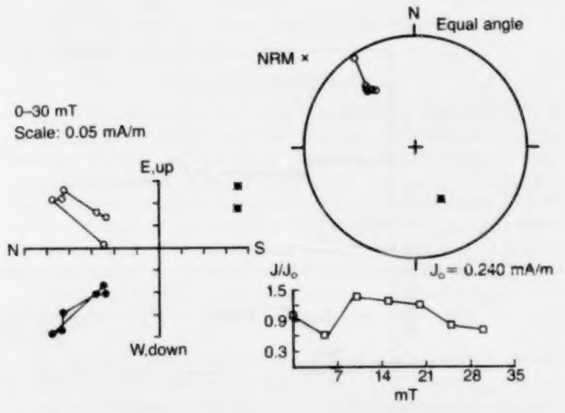

Figure 10. Results of stepwise alternating field (AF) demagnetization of Sample 117-720A-11X-1, 99–101 cm, plotted on a Zijderveld diagram and a equal-area projection.

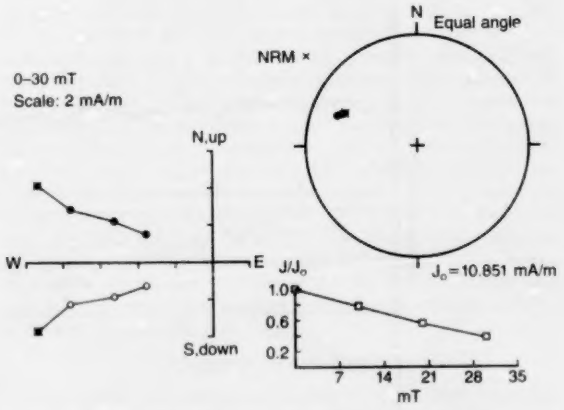

Figure 11. Results of stepwise alternating field (AF) demagnetization of Sample 117-720A-22X-1, 48–50 cm, plotted on a Zijderveld diagram and a equal-area projection.

susceptibility and low carbonate sequence is Section 117-720A-1H-4, 0–77 cm (4.50–5.27 mbsf); an example of the lower susceptibility, high carbonate unit is Section 117-720A-1H-4, 77–150 cm (5.27–6.00 mbsf; see "Lithostratigraphy" section, this chapter). Although the carbonate percentages were determined from smear slide analyses, an inverse correlation between susceptibility and carbonate is apparent for the upper 7.50 m of Hole 720A. A preliminary correlation of high susceptibility intervals with even (glacial) isotope stages (Niitsuma and Oba, unpubl. data) yields an age model for the first 600 k.y. that is consistent with the paleomagnetic and biostratigraphic data. We are uncertain whether this relation is due to dilution (from changing productivity) or magnetic mineral dissolution effects.

Underlying the pelagic unit below Section 117-720A-2H-5 (17.2 mbsf) is another unit composed of interbedded normally-graded clayey-silt sequences of variable thickness which extends to the base of Section 117-720A-3H-6 (28.4 mbsf; Fig. 17). Susceptibility values over this interval are generally much higher and are much more variable than the overlying pelagic unit. Given the depositional environment on the Indus fan and the graded appearance of the unit, these sediments are interpreted as turbidites. Recovery deteriorates below 117-720A-3H, which is almost certainly a consequence of the poorly consolidated nature of the turbidites. The progression of these clayey-silt units from 28.4 to 17.2 mbsf is from generally thick to thin units. This upward-thinning is apparent not only in the core descriptions (see "Lithostratigraphy" section, this chapter), but also can be seen in some of the susceptibility data as well (Fig. 17). Numerous thin (less than 1 m) graded units were encountered between 17.0 and 21.0 mbsf; below this, more massive units dominate (exceeding 2 m thickness). A general feature of all turbidites is that they show a strong susceptibility maximum at the base and gradually decline in susceptibility toward the top. Presumably, this is a reflection of the grading process, whereby the densest minerals and largest grains are concentrated at the basal part of the turbidite.

An interesting correlation was noted between the whole-core Gamma Ray Attenuation Porosity Evaluator (GRAPE) density values and the susceptibility data for the uppermost 30 m. The susceptibility data appear to correlate well with the GRAPE

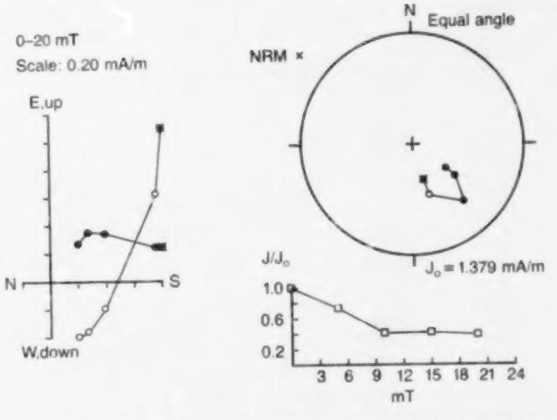

Figure 12. Results of stepwise alternating (AF) demagnetization of Sample 117-720A-29X-1, 10–12 cm, plotted on a Zijderveld diagram and a equal-area projection.

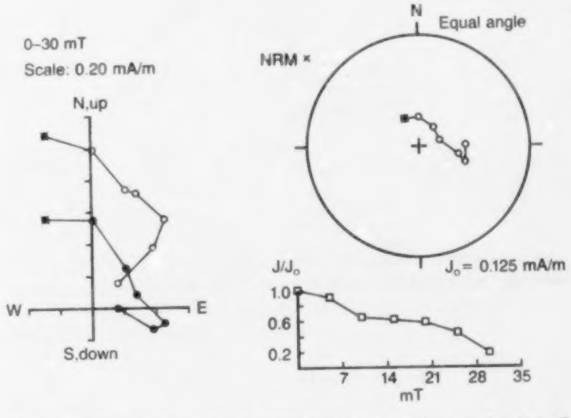

Figure 13. Results of stepwise alternating field (AF) demagnetization of Sample 117-720A-30X-3, 94–96 cm, plotted on a Zijderveld diagram and a equal-area projection.

density values, suggesting that there may be a causal link between the two parameters (Fig. 18). The highest densities and susceptibilities occur within the turbidite units, so that changes in grain size may be the common cause.

A final observation about the general trend of the data with respect to the susceptibility data from Holes 717C and 719A from the Bengal Fan region (Leg 116) suggests that the Indus and Bengal fan depositional histories may have differed over the past ~2.0 Ma. The Leg 116 susceptibility data (Cochran, Stow, et al., in press) indicate that the Bengal Fan experienced two episodes of increased magnetic particle influx at Holes 717C and 719A, ~0.9-3.5 Ma and ~5.0-5.6 Ma (Fig. 19), which the authors (S. Hall and W. Sager) tentatively interpret as reflecting increased influx of terrigenous material. Although the oldest sediment of Hole 720A was deposited at only ~1.5 Ma, a comparison of Indus and Bengal Fan sites suggests that the increased magnetic influx to the Bengal Fan sites from ~0.9-3.5 Ma did not occur at Site 720. Even though the data of Hole 720A are sparse, so that interpretation is at best tentative, we found no evidence for the very high susceptibilities seen at the Bengal Fan sites in the poorly-recovered coeval sediments of Site 720. The reasons for this may be geological (sediment diversion), diagenetic (Fe^{3+} reduction), or technical (poor turbidite recovery).

ACCUMULATION RATES

The sediment accumulation rates for Site 720 (Fig.20) are based on five calcareous nannofossil and three paleomagnetic datum levels (Table 4). The upper nannofossil ooze unit (0–17 mbsf) has a mean rate of 32 m/m.y. which is similar to recent pelagic deposits on the nearby Owen Ridge (see "Site 721," "Site 722," and "Site 731" chapters, this volume). This suggests that clastic influx to this site was low during the past 200,000 years.

The rate of sedimentation within the turbidite sequences averages more than a factor-of-ten higher than the pelagic deposits and ranges from 137 to 944 m/m.y. over the last million years. Because of poor recovery and a lack of diagnostic microfossils in the deeper cored interval (>225 mbsf), sedimentation rates could not be determined in sediments older than ~1 m.y. However, the older cored sections are dominantly turbidites (see "Lithostratigraphy" section, this chapter), and the rates calculated between 17 and 225 mbsf should be applicable to the base of the hole. Therefore, the oldest sediments cored at Site 720 are probably Pleistocene.

PHYSICAL PROPERTIES

Introduction

Physical properties measured on discrete samples of sediments recovered from Hole 720A include index properties, thermal conductivity, vane shear strength, and compressional-wave velocity (Table 6). The GRAPE and *P*-wave logger were used to measure wet-bulk density and compressional-wave velocity continuously in core sections that were 100 cm or more in length. All techniques and equipment used are described in the "Explanatory Notes" chapter (this volume).

All samples were taken from the least-disturbed, most-coherent intervals of the recovered core. Sampling frequency was limited by the poor recovery and drilling-induced disturbance. Gas expansion and accompanying cracking, particularly between 50 and 300 mbsf, further hampered sampling for physical properties.

Index Properties

The transition from the pelagic carbonate ooze of lithologic Unit I to the terrigenous turbidites of lithologic Unit II is reflected in the index properties (Fig. 21). Throughout Unit I, 0–17.2 mbsf, porosity is nearly constant at approximately 70%. Water content and wet-bulk density values are also nearly constant with sub-bottom depth, averaging 45% and 1.55 g/cm^3, respectively. Within the terrigenous sequence of Unit II, porosity decreases gradually from 60% at 17.3 mbsf to 46% at 376.1 mbsf (the last reliable measurement). The profiles of water content and bulk density both reflect the same gradual downsection consolidation of Unit II that is illustrated in the porosity profile. Water content decreases from 36% at the top of Unit II to 23% at 376.1 mbsf, while wet-bulk density increases from 1.70 g/cm^3 to 2.03 g/cm^3 over the same interval. The relatively high bulk densities and low porosities between 188 and 277 mbsf reflect the high sand content of thick-bedded turbidites that are characteristic of seismic units B-2 and B-3 (see "Seismic Stratigraphy" section, this chapter).

Grain densities of the sediments recovered from Site 720 average 2.70 g/cm^3 over the entire drilled sequence (Fig. 21). The

Table 5. Results of magnetic measurements of discrete samples, Hole 720A.

Core, section, interval (cm)	Depth (mbsf)	AFD (mT)	CSD (°)	Declination (°)	Inclination (°)	Intensity (mA/m)
117-720A-						
1H-1, 91	0.91	25	7.7	86.9	22.8	0.4213
1H-2, 26	1.76	20	12.4	116.0	17.2	1.3733
1H-3, 26	3.26	20	4.9	147.8	22.5	1.8383
1H-4, 11	4.61	20	7.2	195.8	28.9	0.7218
1H-5, 20	6.20	20	4.7	223.1	21.5	0.3908
2H-1, 119	10.59	5	14.6	57.4	30.9	0.1201
2H-2, 119	12.09	20	11.9	62.5	33.2	0.0914
2H-3, 119	13.59	20	4.5	84.1	29.3	0.2343
2H-4, 119	15.09	22	—	91.0	13.9	0.2807
2H-5, 119	16.59	20	2.4	85.9	38.2	4.9185
5X-6, 39	46.09	20	2.7	268.5	30.9	2.5914
6X-1, 24	48.14	10	5.4	222.3	29.5	0.6461
7X-1, 24	57.84	20	15.0	284.8	15.8	16.3038
7X-2, 68	59.78	15	5.2	356.7	22.7	3.7679
11X-1, 99	97.39	20	6.3	325.6	−26.6	0.2872
11X-2, 99	98.89	30	8.5	4.5	−11.2	0.2630
11X-3, 92	100.32	25	10.1	191.7	−14.8	1.6036
12X-1, 95	106.95	20	4.4	250.3	−10.1	1.2054
16X-1, 95	145.65	30	—	201.1	78.2	1.4484
16X-2, 38	146.58	20	12.5	255.8	64.6	2.5797
19X-1, 36	174.06	20	6.8	170.3	−36.0	6.6931
19X-2, 42	175.62	20	12.6	81.6	−22.2	3.8985
20X-2, 96	185.86	20	25.4	279.6	−68.3	0.1235
20X-3, 95	187.35	20	5.3	310.2	19.7	1.8479
21X-1, 35	193.35	20	4.0	179.3	5.7	6.5672
22X-1, 48	203.18	20	7.3	292.6	18.0	5.9603
24X-1, 124	223.24	20	7.6	339.1	85.0	0.8900
26X-1, 36	241.76	20	5.0	164.1	−58.5	1.5948
28X-1, 109	261.59	10	3.6	258.6	−30.1	1.4794
30X-3, 94	283.74	25	23.1	109.5	−42.8	0.0551
32X-2, 55	301.05	10	5.8	181.8	−39.0	0.6018
33X-1, 20	308.80	5	4.0	38.7	26.3	0.7397
36X-1, 20	337.60	20	3.7	240.8	38.5	3.0011
37X-1, 10	347.10	10	4.9	47.8	−61.4	0.8197
39X-1, 14	366.34	10	3.3	325.6	44.7	2.3075
40X-1, 93	376.83	20	54.8	194.4	−30.0	0.4797
41X-1, 48	385.68	10	12.1	4.1	−76.6	2.4173

only notable trend is a difference in degree of scatter of the data from the two lithologic units. Grain densities within Unit I quite consistently range from 2.65 to 2.75 g/cm³. Within Unit II the grain density values showed considerable scatter (2.54 to 2.90 g/cm³) but most values lie between 2.65 and 2.75 g/cm³.

Compressional Velocity Measurements

P-wave velocity measurements were limited by the condition of recovered sediment at Site 720. At depths less than 100 mbsf the sediments were too soft to allow determination of *P*-wave velocities in the Hamilton Frame Velocimeter. At depths greater than 100 mbsf, the gas expansion inhibited signal transmission through sediment samples. Only two measurements were made, both perpendicular to bedding (Fig. 22). The velocity at 7.8 mbsf, 1461 m/s, is less than that of seawater but is not unusual for seafloor sediments (Hamilton, 1974). At 60.1 mbsf, the measured velocity is unusually high, 1960 m/s, and is possibly not reliable.

Thermal Conductivity

Thermal conductivity of the sediments increases gradually from 1.20 W/m·K near the seafloor to 1.35 W/m·K at 400 mbsf (Fig. 22). The increase in thermal conductivity with depth tracks the increase in wet-bulk density with depth.

Vane Shear Strength

Drilling-induced core disturbance limited the number of vane shear strength determinations. Only three measurements are considered reliable because at depths greater than 105.5 mbsf (Core 117-720A-11X), failure occurred by fracturing rather than shearing of the sediment. The brittle behavior of the sediments is likely the result of gas expansion within the sediments. The maximum measured shear strength was 50 kPa at 99 mbsf (Fig. 22).

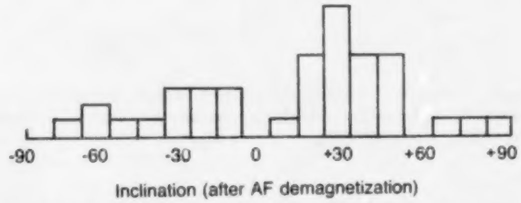

Figure 14. Histogram of inclination values of discrete samples after alternating field (AF) demagnetization. Values grouped in 10° steps.

GRAPE and P-Wave Logs

Reliable continuous records from the GRAPE and *P*-wave logging devices are limited to depths shallower than 30 mbsf. *P*-wave logs were not obtained for cores deeper than Core 117-720A-5X because of signal transmission failure resulting from incompletely filled cores and gas-expanded sediments. GRAPE data quality decreases below Core 117-720A-5X as a consequence of nonuniform core diameter. GRAPE logs for the interval 0–30 mbsf show the increase in wet-bulk density that marks the boundary between lithologic Units I and II (Fig. 23). Cyclic density

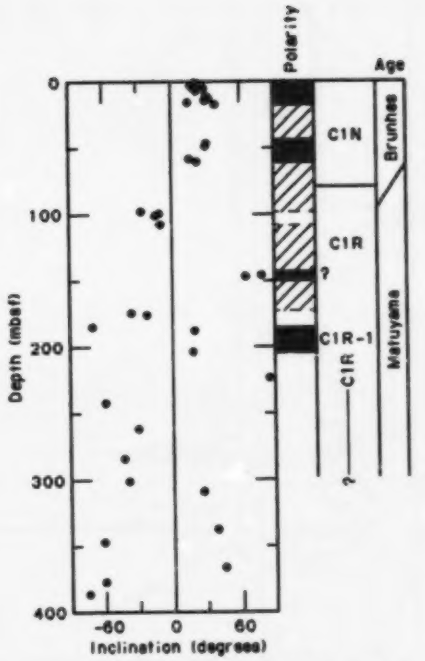

Figure 15. Plot of magnetic inclinations against sub-bottom depth. Magnetic polarity log (black = normal, white = reversed, hatched = undetermined) and its tentative assignment to the polarity time-scale are shown on the right.

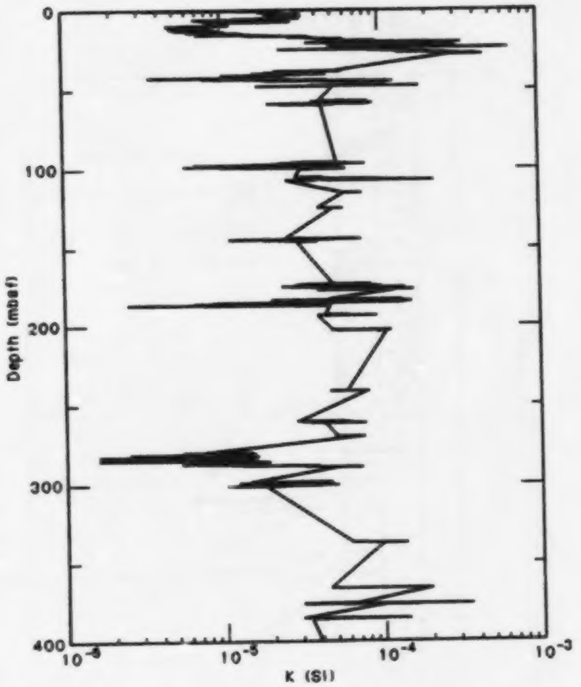

Figure 16. Log-normal plot of magnetic susceptibility as a function of sub-bottom depth. Note that the data range over two decades of variation in the upper 30 m.

variations in Unit I are in phase with variations of magnetic susceptibility interpreted to represent glacial-interglacial fluctuations in the supply of calcium carbonate and magnetic minerals (see "Paleomagnetism" section, this chapter).

SEISMIC STRATIGRAPHY

Introduction

Site 720 is located on the western margin of the Indus Fan near the transition from middle fan to lower fan (Kolla and Coumes, 1987). Based on modern depositional patterns on this fan (Kolla and Coumes, 1987), the lithology of Site 720 was expected to consist of: (1) sands and silts of channel levee deposits, (2) silty clays and mud turbidites of overbank deposits from more distant channels, (3) sand sheet deposits from unchannelized flows occurring at the terminations of channels, and (4) pelagic sediments from times when channels are so distant or inactive that no turbidites reach the site.

In this section we discuss the cored sequence at Site 720 in the context of regional seismic stratigraphy, in order to determine the lateral implications of observed downhole variations. Our approach is based on a sequence analysis of two *Robert Conrad* site survey lines which cross the Indus Fan in roughly northwest-southeast directions: RC 2704 Line 1, which is 3 km northward of Site 720, and RC 2704 Line 49, which crosses the site. We then compare the seismic sequences to core and log data, based on depth-to-time conversion through a synthetic seismogram.

Seismic Sequences

The surface morphology of the Indus Fan in the vicinity of Site 720 is characterized by several meandering channels (e.g., Fig. 1). Two major surface channels that are observed on seismic profiles or precision depth records are within 200 km of the site. The nearest surface channel is only 5 km northwest of the site. These channels are about 1.5 km wide, 50 m deep, and have levee elevations about 30 m above the surrounding fan surface. Thus, the surface of the fan has slight depth variations caused by the depositional levees and erosional channels. On the basis of the site survey data, the levees in the vicinity of the site have characteristic widths of 15–20 km.

The digitally recorded single-channel seismic data for this area show a variety of subsurface features that are most likely related to turbidite flux and levee building, channel migration, and abandonment. The subsurface levee/channel complexes are characterized by convexly inclined reflectors that converge and pinch out away from the central channel area that has diffuse, irregular reflectors. According to McHargue and Webb (1986) and Kolla and Coumes (1987), the inclined reflectors are interpreted as levee deposits and the diffuse patterns are thought to represent a mixture of channel sands, slumped levee deposits, and fine-grained channel fill accumulated after abandonment of the channel.

A study of the major regional sedimentary and tectonic processes on the lower part of the western Indus Fan was possible due to a long seismic line collected during the *Robert Conrad* site survey cruise in 1986 (Leg 2704, Fig. 24). Line 1 runs 3 km north of Site 720 in a roughly northwest-southeast direction and shows the major depositional patterns found at Site 270 in both the lithostratigraphic and downhole logging record. Tracing of laterally distinctive reflectors permits the identification of three major seismic sequences, which we refer to as A, B, and C (downsection).

Changes in the small-scale depositional patterns associated with channel migration can be tentatively identified on seismic

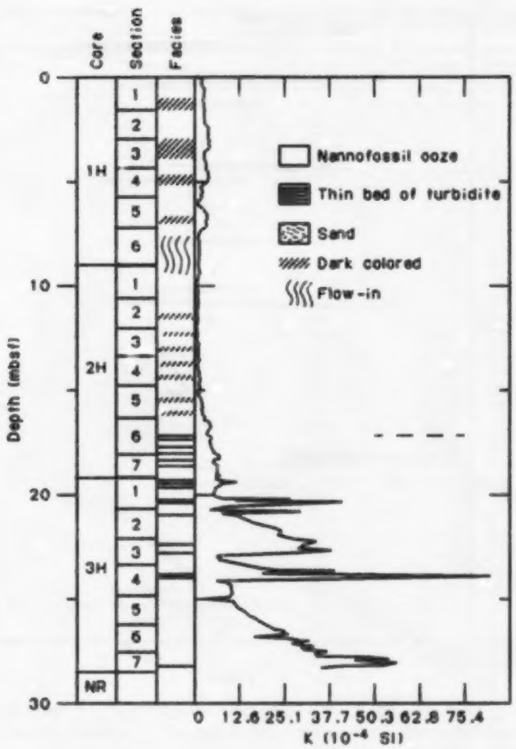

Figure 17. Plot of volume magnetic susceptibility as a function of depth for the upper ~30 mbsf of Hole 720A. Turbidite facies dominates the sediments between 18–30 mbsf, pelagic facies dominates the upper 18 mbsf.

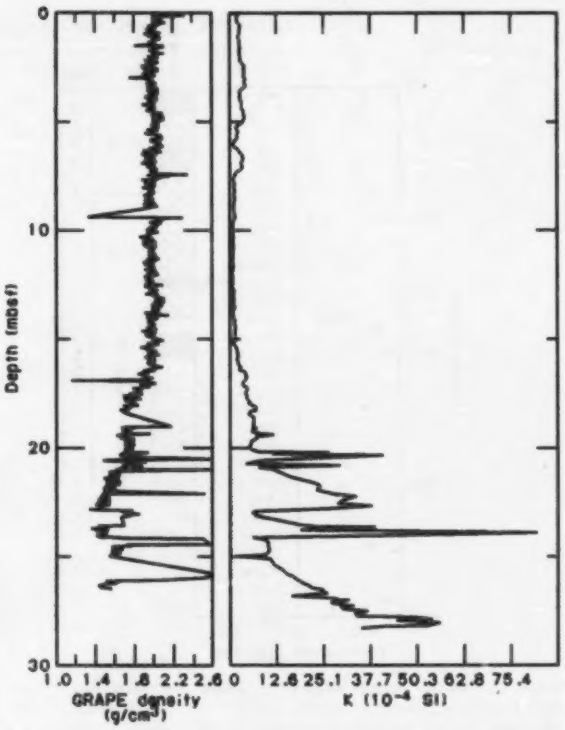

Figure 18. GRAPE bulk density estimates and magnetic susceptibility plotted as a function of depth for the upper 30 mbsf. Note the covariance of the two parameters.

line RC7204-49 (Fig. 25), based on the seismic sequence analysis techniques of Vail et al. (1977). In nearly flat-lying sequences such as these, the terms "onlap" and "downlap" are interchangeable; we use the term "downlap" here because of the assumed small initial downward slope away from each levee. Traveltimes to sequence boundaries discussed below refer to the sub-bottom two-way traveltime of these boundaries at Site 720. On the section across Site 720 (Fig. 25), we identify seven subunits of the three major seismic sequences found on Figure 24. The seismic processing used for Figure 25 is very different than that for Figure 24; the former is preferable for determining continuity of reflectors, while the latter is more appropriate for identifying variations in reflection strength and, indirectly, importance.

Sequence A is at the western margin of the Indus Fan, 75–200 m thick (102 m thick at Site 720), and has three subunits. Sequence A shows abundant development of medium and small channels which are spaced about 20 km apart. The sequence shows abundant channel switching, often with eastward migration of channels (see also McHargue and Webb, 1986; Kolla and Coumes, 1987), and also stable or intermittent positions of channels. Phases of channel switching are followed by well-established reflectors which drape the former channel and channel levee deposits (Fig. 25).

In Sequence A, the highest rates of deposition occur at the portion of the fan closest to Owen Ridge (Fig. 24) where young tectonic movements caused a 100–150 m relative uplift of the eastern margin of the Owen Ridge, accompanied by a relative downward movement of the western Indus Fan sediments. This uplift is inferred from the narrower spacing of the seismic reflectors above the Owen Ridge margin, the major increase in thickness of Sequence A between Site 720 and the margin of the uplift zone, and the concentration of buried channels within Sequence A just east of the uplift zone. A major tectonic episode occurred during the deposition of Sequence A (around 0.75 Ma, see below).

The newly accumulated sediment wedge of Sequence A is draped at the surface with a thin transparent layer, Subsequence A-1 (coincident with lithologic Unit I). This unit is too thin (0.02 s) to be detectable on the digital seismic lines, because of interference with the bottom reflector (0.07 s in duration). Subsequence A-1 is evident on the higher frequency 3.5-kHz records. Draping of the subunit over pre-existing topography indicates a recent period of inactivity which followed the period of rapid infill. This layer also drapes the uplifted part of Owen Ridge. A similar but much thicker pelagic layer caps the section penetrated at DSDP Site 222, on the portion of the Indus Fan west of Owen Ridge.

Subsequence A-2 (0.02–0.07 s) consists of generally parallel reflectors (Fig. 25), with some eastward downlap evident at the base of the subsequence just to the east of the site. The sequence exhibits a gradual decrease in traveltime width to the east, probably caused by an eastward thinning associated with pinch-outs of the lowest horizons. At Site 720 this subsequence is likely to consist of overbank deposits from the modern channel just to the left (west) of the seismic section of Figure 25.

Subsequence A-3 (0.07–0.10 s) is a thin unit of strongly progradational reflectors, clearly associated with a buried channel at 0.05–0.11 s sub-bottom. The sequence thickens substantially to the east (right on Fig. 25). The characteristic convex upward

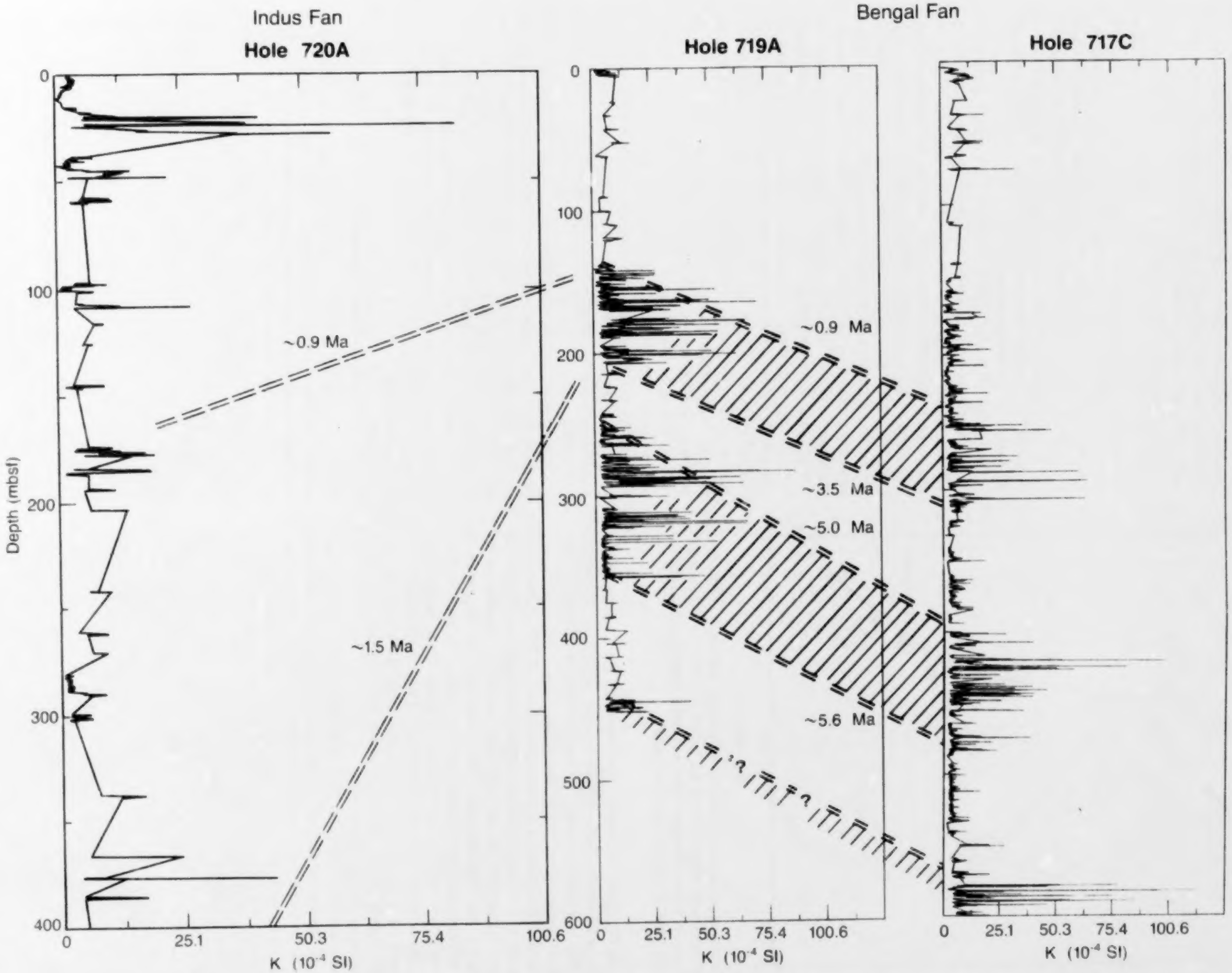

Figure 19. Magnetic susceptibility data for Hole 720A compared to Holes 717C and 719A from the Bengal fan. Tie lines indicate approximate time-correlative horizons. Note that Hole 720A does not display the high susceptibility values apparent in the Bengal fan sites during the 0.9–1.5 Ma interval.

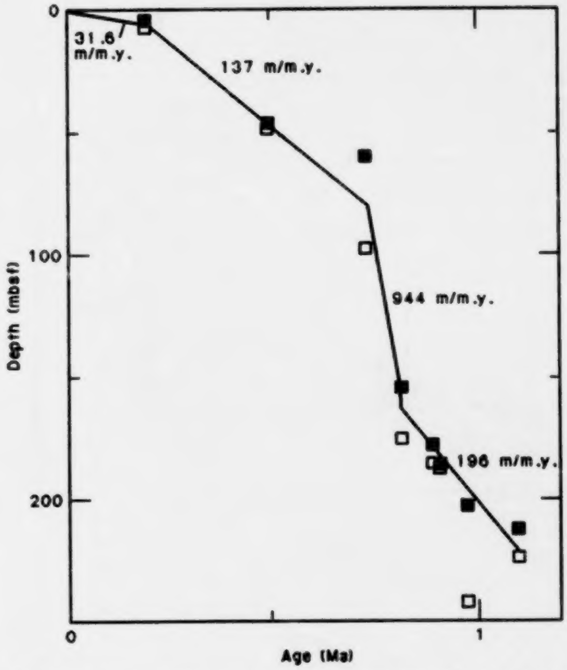

Figure 20. Sedimentation rate curve for the top 250 mbsf of Site 720. The indicated sedimentation rates are based on a best fit of the stratigraphic datum levels (Table 4). Filled and open boxes are the respective upper and lower depths of the datum levels.

shape of the levee is evident just west of the channel. Both downlap and toplap patterns are evident in this subsequence; the toplap is probably caused by later erosion or thinning of the levee beds toward the crest of the levees.

Sequence B displays a constant thickness of 180–200 m over a distance of 150 km, although some syndepositional uplift of the Owen Ridge may be inferred from the closer spacing of reflectors on the ridge margin. The lower part of Sequence B shows a rather uniform pattern with no major channel visible, while the upper half of this package displays three large channels within a lateral distance of 150 km. The top of Sequence B is defined by a nearly continuous reflector. Based on unconformities identified on seismic Line 49 near the site, we subdivide Sequence B into three units.

Subsequence B-1 (0.10–0.22 s) is a thick, fairly uniform sequence of mostly parallel reflectors. No pinchouts are visible at the top of the sequence. Gradual eastward downlap of basal horizons is seen, probably accounting for the slight thickening of the section to the west. A long-lived or volumetrically important channel is implied by the thickness and uniformity of the sequence. The downlap pattern and thickening to the west suggest that the channel was to the west; it gradually flattened out the initially substantial slope of the underlying B-2 levee system.

Subsequence B-2 (0.22–0.25 s) is a thin unit of reflectors prograding strongly to the west (Fig. 25). Its seismic signature is very similar to Subsequence A-3, and the corresponding buried channel is clearly evident at 0.2–0.25 s sub-bottom on Figure 25, almost immediately below the channel of Subsequence A-3. The levee of the channel's west bank appears to be visible beneath the A-3 channel. This "levee" could be an artifact and actually be "velocity pullup," caused by higher-velocity sediments in the channel of Subsequence A. If so, the levee deposits of A-3 would need to be more clay-rich and therefore have a higher velocity than the channel fill. Subsequence B-2 exhibits the same westward downlap and eastward toplap as Subsequence A-3. Again, the downlap is likely to be constructional (levee and overbank deposits), and the toplap is probably erosional or caused by wedge-shaped overbank beds. Subsequence B-2 thins to the west with increasing distance from the source channel.

Subsequence B-3 (0.25–0.36 s) is a fairly uniform sequence of parallel reflectors, with no toplap and almost no basal downlap. A single toplap pinchout may be present near the Subsequence B-2 channel, and possible downlaps may be present at and slightly east of Site 720. No significant thickness changes are evident within the portion of Subsequence B-3 shown in Figure 25. A source from the same channel as Subsequence B-2 is possible but the identification of a channel of Subsequence B-3 on Figure 25 is highly tentative.

Sequence C is about 300 m thick. The upper part of Sequence C shows only one well-developed, large channel along a 150-km section (Fig. 24). Levee deposits associated with this channel are more than 20 km wide, and the channel apparently remained active and stationary throughout the upper part of Sequence C. A distinctly developed reflector can be traced over the top of this channel and laterally for more than 200 km, suggesting a major draping period of pelagic sediments after a phase of rapid deposition. This prominent reflector, which crosses Site 720 at a sub-bottom time of 0.33 s, appears to be conformable with the upper portion of Sequence C. The reflector is well displayed on Figure 24 but much less prominent on the heavily clipped section of Figure 25. We pick the top of Sequence C at 0.36 seconds sub-bottom, which represents the top of the major channel which was responsible for much of the Sequence C deposition. Sequence C contains at least two units.

The top of Subsequence C-1 (0.36–0.42 s) is clearly associated with the top of a channel fill and its western levee system. One toplap pinchout and one downlap of the overlying unit is visible to the west of the channel. The bottom of the sequence is marked by a pinch-out (downlap) to the east and toplap of the underlying unit.

Subsequence C-2 (0.42–0.47 s) is the lowest seismic sequence likely to have been encountered at Site 720. This sequence has conformable bottom reflectors, overlying a deeper sequence whose top boundary is defined on the basis of toplap pinchouts to the west. The top of Subsequence C-2 is also marked by toplap of several horizons, but to the east. This toplap probably is caused by erosion associated with establishment of the nearby Subsequence C-1 channel. The channel source for Subsequence C-2 is uncertain.

Depth-to-time Conversion for Site 720

The velocity log at Site 720 provides a continuous and representative curve of velocity variations, which can be used to link core depth to seismic traveltime. We used the velocity log of Figure 32 and a pseudodensity log based on porosity to calculate a synthetic seismogram for the site. Density logs seldom have much effect on ODP synthetic seismograms, because both density and velocity are responding primarily to porosity changes. A possible exception to this generalization occurs at major lithologic boundaries such as between turbidites and pelagic clays. The velocity contrast between these two lithologies is relatively small in comparison to the porosity contrast, so the density contrast at these boundaries may be more effective in creating seismic reflectors than is the velocity contrast.

The synthetic seismogram was calculated using a convolutional model, with internal multiples. For calculation of a synthetic comparable to the site survey line of *Robert Conrad* across the site, we used a wavelet appropriate for the *Robert Conrad*. Rather than utilizing a near-field wavelet recorded by hydro-

Table 6. Physical properties summary for Site 720.

Core, section, interval (cm)	Depth (mbsf)	Wet-bulk density (g/cm^3)	Porosity (%)	Water content (%)	Grain density (g/cm^3)	Velocity[a] (m/sec)	Thermal conductivity (W/mK)	Vane shear strength (kPa)
117-720A-								
1H-2, 40–42	1.90	1.553	69.6	45.9	2.695		1.20	
1H-4, 40–42	4.90	1.514	74.1	50.1	2.713		1.12	7.1
1H-6, 35–38	7.85					1461		
1H-6, 40–42	7.90	1.553	68.6	45.3	2.647		1.21	
2H-2, 40–42	11.30	1.549	67.7	44.8	2.664		1.26	
2H-4, 40–42	14.30	1.554	70.1	46.2	2.684		1.22	9.6
2H-6, 40–42	17.30	1.704	60.5	36.4	2.747		1.39	
3H-2, 23–25	20.73	1.888	59.1	32.1	2.896			
3H-4, 40–42	23.90				2.845			
5X-2, 38–40	40.08	1.846	55.9	31.0	2.541		1.33	
5X-4, 40–40	43.10						1.46	
5X-5, 85–87	45.05	1.928	57.2	30.4	2.796			
7X-1, 48–48	58.08						1.36	
7X-1, 52-54								17.6
7X-2, 49–51	59.59	1.791	57.8	33.1	2.590		1.20	
7X-2, 106–108	60.06					1960		
11X-1, 110–110	97.50						1.23	
11X-2, 110–112	99.00	1.806	69.3	39.3	2.684		1.21	
11X-3, 98–100	100.38							50.3
11X-3, 110–110	100.50						1.35	
12X-1, 56–56	106.06						1.09	
12X-2, 56–58	108.06	1.984	45.0	23.2	2.539		1.41	
14X-1, 30–32	125.70	1.837	54.4	30.4	2.551		1.47	
16X-1, 64–66	145.34	1.842	55.6	30.9	2.598			
16X-2, 20–20							1.32	
19X-1, 34–36	174.04	1.883	52.5	28.6	2.639		1.01	
19X-1, 42–44	174.12							23.2
19X-3, 34–36	177.04				2.722		1.92	
20X-1, 45–47	183.85				2.733		1.40	
20X-3, 45–47	186.85	1.826	53.2	29.9	2.591		1.40	34.6
21X-1, 51–53	193.51	2.114	53.3	25.8	2.708			
21X-1, 58–60	193.58							22.8
22X-1, 34–34	203.04						1.35	
22X-1, 52–54	203.22				2.690			
24X-1, 90–92	222.90	2.029	46.6	23.5	2.738			
24X-1, 110–110	223.10						1.24	
26X-1, 31–33	241.71	1.974	50.3	26.1	2.778			
27X-1, 40–42	251.40				2.671			
28X-1, 40–42	260.90				2.719		1.22	
30X-2, 100–100							1.43	
30X-2, 112–114	282.42	1.841	54.4	30.3	2.750			
30X-4, 98–100	285.28	1.766	57.3	33.2	2.634		1.20	
30X-6, 100–102	288.30	1.781	53.4	30.7	2.544		1.34	
32X-1, 50–50	299.50						1.39	
32X-1, 93–95	299.93	1.889	50.4	27.3	2.691			
32X-2, 50–50	301.00						1.21	
33X-1, 25–27	308.85				2.703			
36X-1, 60–62	338.00	1.882	52.1	28.4	2.711			
37X-1, 19–21	347.19	1.938	48.3	25.5	2.691			
39X-CC, 11–13	366.72	1.897	48.4	26.2	2.589			
40X-1, 24–26	376.14	2.027	46.3	23.4	2.779		1.31	
41X-1, 46–48	385.66				2.677			
43X-1, 50–50	405.10						1.61	
43X-1, 57–59	405.17				2.731			

[a] Velocity measurements prependicular to bedding.

phone (which may differ from the actual far-field wavelet), we used an average of the seafloor returns obtained at shotpoint 540 on RC2704 Line 19 and shotpoint 1692 on RC2704 Line 35 (Fig. 26). Selection of these particular shotpoint numbers is not important; both are in regions of very stable seafloor returns over long intervals. examination of site survey lines suggests that these two line portions show both a high signal-to-noise ratio and, more significantly, no evidence of shallow sub-bottom reflections that could contaminate the wavelet estimate. The close similarity of the two wavelet estimates for 0–75 ms confirms the suitability of this wavelet estimate (Fig. 26).

Figure 27 shows the final synthetic seismogram for the portion of the hole between 78.8 and 412.4 mbsf. No synthetic seismogram was possible for the interval 0–78.8 mbsf, because the sonic log does not work through pipe in uncompacted sediments and because gas traces caused Hamilton Frame velocity measurements on cores to be unreliable (see "Physical Properties" section, this chapter).

In Figure 27, the synthetic seismogram is compared to a 10-trace average of the *Robert Conrad* seismic data at the site, as well as to a portion of the same line processed as in Figure 25. The latter is heavily clipped and shows only peaks (with troughs blanked); this processing is useful for regional seismic correlation but is of limited usefulness for comparison to the synthetic. In contrast, the composite seismic trace is unclipped and shows both peaks and troughs; this display is best for comparison to

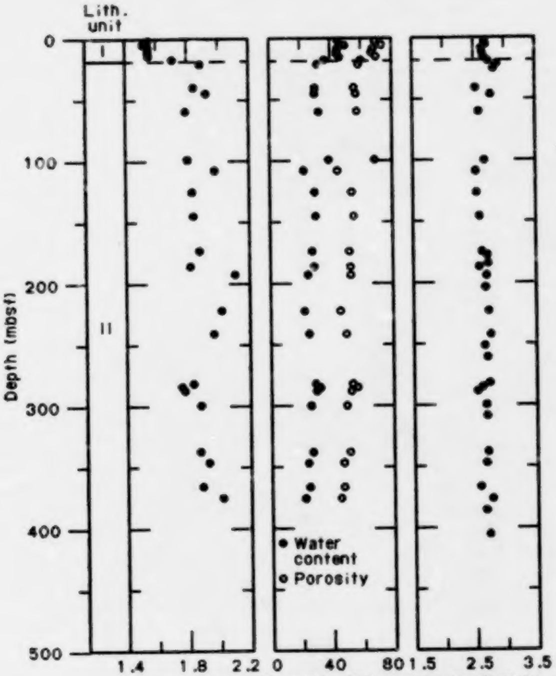

Figure 21. Index properties (wet-bulk density, porosity, water content, and grain density) at Site 720.

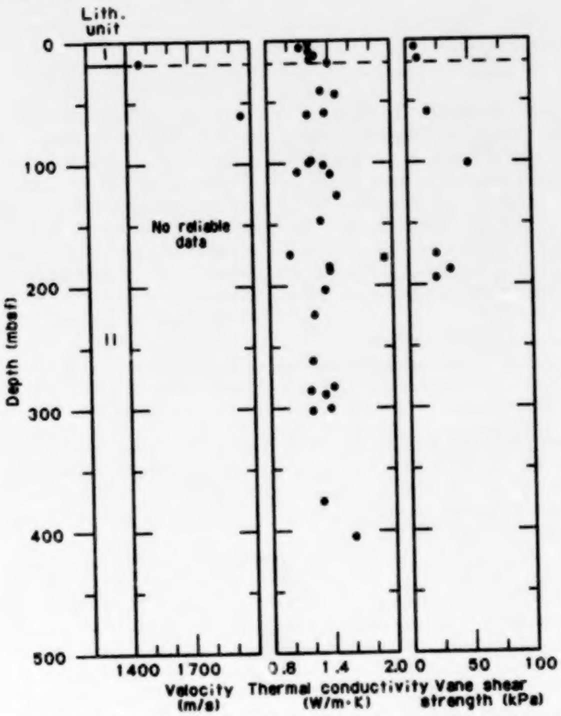

Figure 22. Compressional-wave velocity, thermal conductivity, and vane shear strength measured on discrete samples at Site 720.

the synthetic seismogram but provides no information on the lateral continuity of peaks and troughs, information essential to distinguishing signal from local noise.

Initial comparison of the synthetic seismogram to the seismic traces showed a fair correlation, but traveltimes between the few readily correlatable reflectors were about 8% longer on the seismic trace than on the synthetic. Therefore sonic traveltimes were increased by 8%, in spite of the high replicability found for sonic log data at this site. The revised synthetic shows not only a consistency with seismic traveltimes between reflectors, but also a much better character correlation with the composite seismic trace (Fig. 27). Small-scale features show only a moderate correlation, but major reflectors are readily identified. The peak/trough pair at 100 mbsf on the synthetic seismogram corresponds with a similar pair at 0.11–0.12 s sub-bottom on seismic, the packet of four peaks and central major trough at 213–247 mbsf corresponds with a similar packet at 0.25–0.29 s, and the large peak at 390 mbsf corresponds to a seismic peak at 0.46 s sub-bottom. The most significant mismatch is that the trough on the synthetic seismogram centered on the pelagic unit of 278–290 mbsf occurs in a featureless portion of the seismic trace. However, this trough is the largest sub-bottom reflector on Figure 24 so the composite seismic trace must be contaminated by noise at this location.

Table 7 shows the depths of sequence boundaries at Site 720, based on the correlation between seismic and synthetic seismogram in Figure 27. The A-1/-2 and A-2-/3 boundaries lie above the logged interval, so their depths are based on the assumption of a linear velocity increase between the seafloor and the start of the synthetic seismogram.

SYNTHESIS OF SEISMIC AND STRATIGRAPHIC SEQUENCES

The cored interval at Site 720 is divided into two units based on lithostratigraphy (see "Lithostratigraphy" section, this chapter). Lithologic Unit I, from 0 to 17.22 mbsf, is composed of pelagic nannofossil ooze, with a noncarbonate component of primarily quartz and clay minerals. Lithologic Unit II, from 17.22 mbsf to the bottom of the hole, includes some pelagic beds similar to Unit I but is dominated by turbidite facies: interbedded silty clays, silts, silty sands, and sands which commonly occur in fining-upward sequences on scales of <2 to >50 cm. Unit II has been further subdivided into at least four informal subunits based on downhole log responses (see "Downhole Measurements" section, this chapter).

In the synthesis that follows, an exact match of the estimated depths of sequence boundaries with log depths is not expected: most seismic reflectors are interference patterns that resulting from convolution of the 70-ms long wavelet with a depth interval of about 12 m. In comparing the approximate sequence boundaries with sedimentary facies interpretations from logs, we have used the logs to revise the depths of sequence boundaries by an average of 11 m (Table 7).

The most distinctive relationship between seismic sequences and the lithostratigraphy of Site 720 is in the occurrence of pelagic beds. Both Sequences A and B, as well as five or six of the eight subsequences, have pelagic units at their tops. The two thickest pelagic units in the logged interval (78.8–412.4 mbsf) are at the top of Sequences B and C (3 and 12 m thick, respectively). Subsequence A-1 is the pelagic drape of Subsequence A-2, whereas Subsequence A-3 may have a pelagic top, but limited core recovery precludes precise depth determination for the pelagic bed of Core 117-720A-7X. Only the tops of Subsequence C-1 and the strata below C-2 have no detected pelagic beds. Probably few if any of these sub-bottom pelagic beds are as laterally continuous as the modern sediments of Subsequence A-1. We often identified toplap of underlying beds by the initial ero-

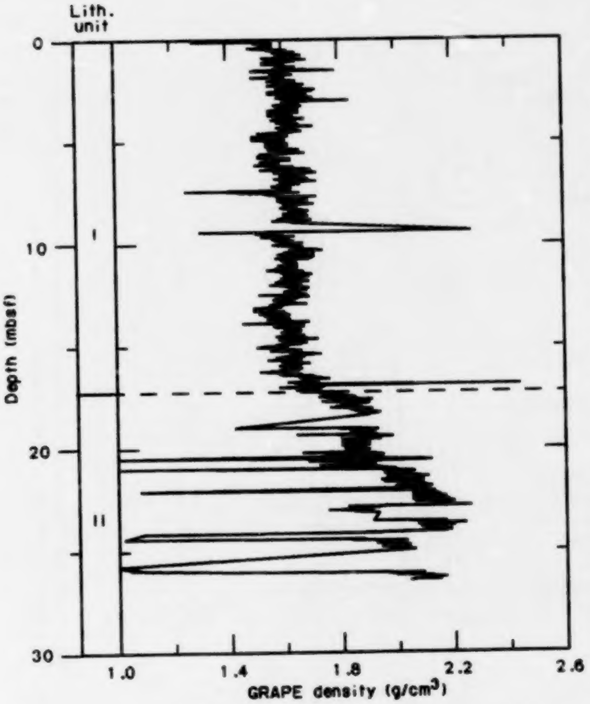

Figure 23. Wet-bulk density as measured by GRAPE for sediments recovered in the interval 0–30 mbsf.

sive stage of channel formation, or by lateral levee migration. Only at the boundary between Sequence B and C is the pelagic bed thick enough to create a prominent seismic reflector (Fig. 24). For the other sequence boundaries, the seismic reflector is created by the velocity contrast between the uppermost clay-rich turbidites of one sequence and the basal, sandy turbidites of the overlying strata.

The top portion of Sequence A (Subsequence A-1) is correlated with lithostratigraphic Unit I, a 17.2-m thick pelagic bed which is 0.5 Ma old. Unit I is the thickest of the many pelagic beds penetrated at Site 720. Its occurrence at Site 720 results from a major late Pleistocene eastward shift of active channel deposition on the Indus Fan (Kolla and Coumes, 1987). Sequence A is mainly composed of turbiditic channel-levee deposits with a high clay content. Since channel switching occurred rapidly, a suite of fining-upward sequences is expected. Due to the need to anchor the bottom-hole assembly during logging, only the lowermost part of Sequence A was logged. Paleontologic and magnetostratigraphic data indicate an age of roughly 0.75 Ma for the base of Sequence A. The most recent episode of substantial uplift of the western margin of Owen Ridge probably occurred between 0.75 and 0.5 Ma, based on the substantial subsidence and turbidite infilling in Subsequences A-2 and A-3 near Owen Ridge, and the lack of a modern seafloor slope toward the ridge in spite of pelagic sedimentation since 0.5 Ma. Two major channels supplied the sediments of Sequence A. The "modern" channel just west of the site formed Subsequence A-2, and a now-buried channel west of the site formed Subsequence A-3. Subsequence A-3 corresponds to an interval of virtually zero core recovery.

On the interpreted thorium log (Fig. 27), the upper part of Sequence B (Subsequence B-1) displays two suites of fining-upward sequences (25 and 60 m thick, respectively), which are composed entirely of small-scale, 5-m thick fining-upward sequences. The two large fining-upward sequences are interpreted to reflect the gradual build-up of levee deposits interrupted by a phase of channel switching, whereas the small-scale fining-upward sequences probably reflect activity periods in the channels. Seismic progradational patterns suggest that both channels were west of the site. The lower part of Sequence B shows large-scale fining- and coarsening-upward sequences on the thorium log, related to the build-up and retreat of unchannelized sheet sands associated to terminated channels (Kolla and Coumes, 1987).

Seven to nine pelagic beds in Sequence B have been identified from logs, and the presence of five has been confirmed in cores, in spite of the 18% average core recovery for Sequence B. Based on comparison of core lithology with logs from Sequence B, core recovery was about 80% for pelagic sediments and about 10% for turbidites. Generally, pelagic intervals may be related to two sources:

1. Major periods of channel switching which occurs after tectonically induced periods of rapid infill. An example is the pelagic Subsequence A-1, which comprises several glacial and interglacial times.
2. Pleistocene sea level variations which largely influence the sediment input to the fan (e.g., Shanmugam and Moiola, 1982). On seismic sections, draping of channel levee deposits occurs when the position of the channel is stable, indicating active and passive periods in channel deposition.

In the interpreted thorium log (Fig. 27), Sequence C exhibits a set of small-scale fining-upward sequences of turbiditic levee deposits. The consistent pattern of thorium log responses throughout the penetrated portion of Sequence C is most easily interpreted as related to a constant position of the nearby large channel. However, as previously discussed, the seismic data are ambiguous concerning the source channel for sediments of Subsequence C-2. No pelagic interbeds are detected in logs from Sequence C, however a single thin bed was identified in Core 117-720A-40X.

INORGANIC GEOCHEMISTRY

Introduction

The results from interstitial water analyses of nine samples from Hole 720A are summarized in Table 8 and displayed in Figure 28. No *in-situ* interstitial water samples were recovered at this site for analysis.

Salinity, Chloride, and pH

The concentration profiles of salinity and chloride in Hole 720A together with the measured pH are shown in Figure 28. Overall, a slight decrease in salinity from 34.3 to 30.6 g/kg to ~300 m was observed, with most of the decrease (about 2.5 g/kg) occurring in the top 50 mbsf. In contrast, the chloride content decreases over the same interval by only ~10 mmol/L (about 0.3 g/kg) from a value at 5.95 mbsf of 554 mmol/L. The salinity decrease can be accounted for by the loss of Mg^{2+} and SO_4^{2-} from solution; a roughly 25-mmol/L decrease in the Mg^{2+} concentration and total depletion of sulfate within the top 50 m at this site (see below) would reduce the salinity by roughly 3 g/kg which approximately accounts for the observed difference. Hole 720A has a mean pH value of 7.77 and displays little significant variation with depth.

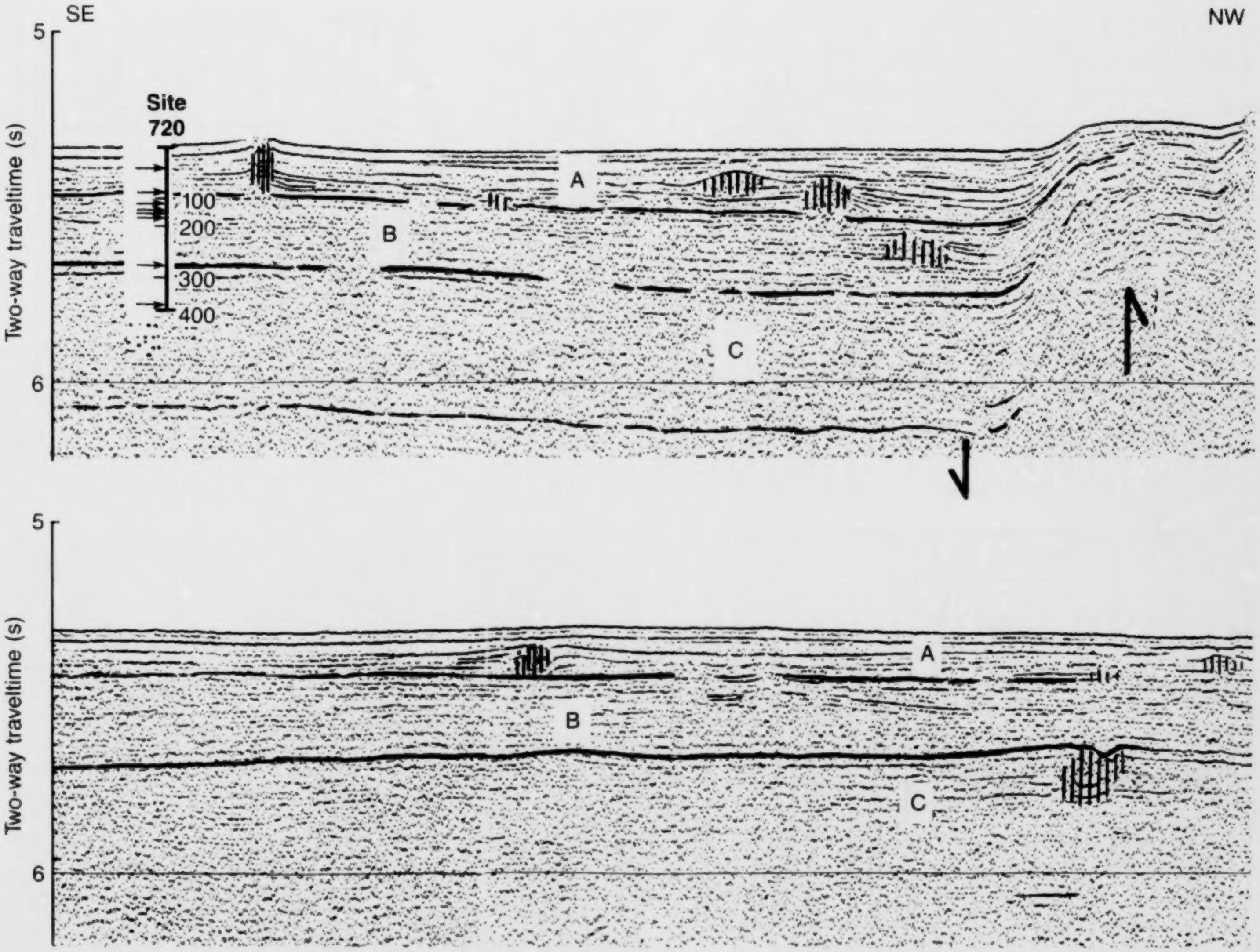
SE
NW
Site 720
100
200
300
400
A
B
C
5
6
Two-way traveltime (s)
5
6
Two-way traveltime (s)
A
B
C

Figure 24. Cross section through the western part of the Indus Fan and the eastern margin of Owen Ridge. A, B, and C tie to major depositional sequence boundaries. Arrows (->) on Site 720 section point to pelagic horizons as identified by the lithologic sequence recovered (from seismic line RC2704 Line 1, 1986). Section is 150 km long.

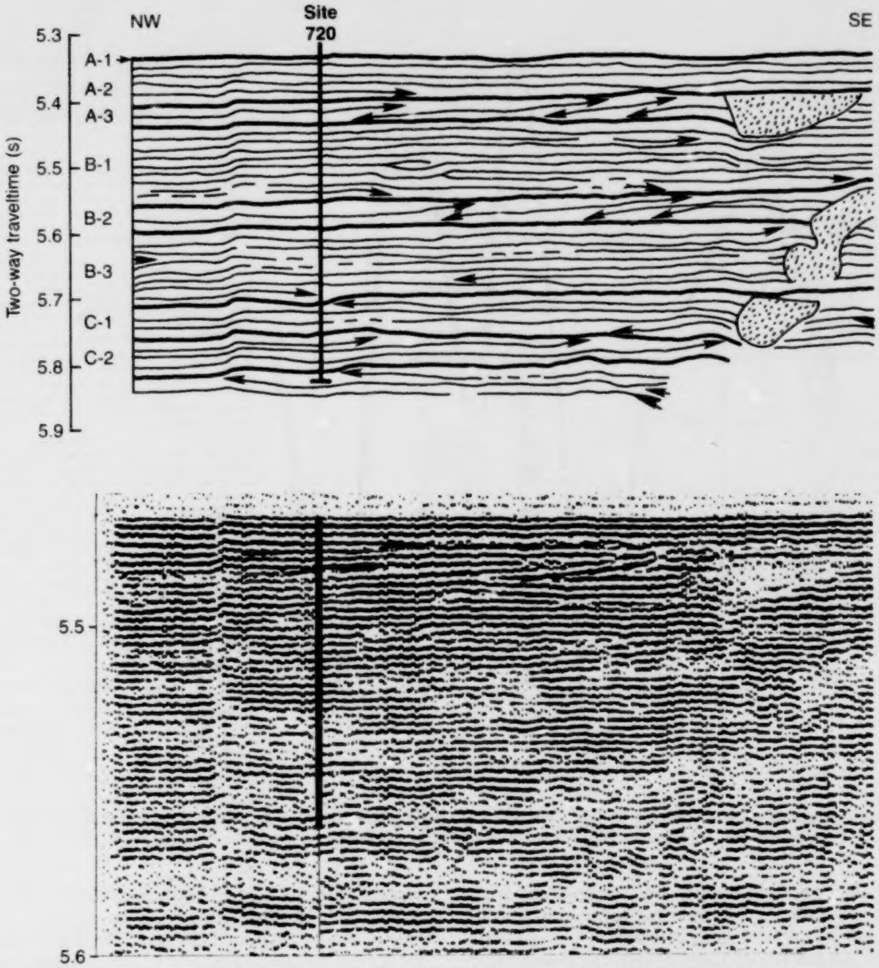

Figure 25. Interpretation of seismic section at Site 720 displays major depositional sequences (A, B, and C), which are divided into subsequences (from seismic line RC2704 Line 49, Leg 2704, 1986).

Sulfate and Alkalinity

Figure 28 indicates that sulfate reduction is complete by 59 mbsf. This is not surprising considering that the turbidites contain substantial organic matter (see "Organic Geochemistry" section, this chapter) and accumulate very rapidly (see "Biostratigraphy" section, this chapter). The amount of oxygen which can diffuse into the sediments to replenish that lost during bacterial degradation of the organic component is thus strongly limited, and sulfate is depleted as a consequence. The production of sulfide in these sediments and the associated reduction and removal of iron from clay minerals and oxide grain-coatings leads to the formation of pyrite (see below). Because no dissolved sulfide was present in the pore waters, an observation based entirely on the absence of the odor of H_2S, we infer that relatively large concentrations of iron must have been extracted from clay minerals or iron minerals and fixed as authigenic pyrite. Drever (1974) has suggested that Mg^{2+} replaces Fe^{3+} extracted diagenetically in this way. Such a reaction could account for some of the Mg^{2+} depletion observed at depth at this site.

Alkalinity, largely a measure of the HCO_3^- content, increases from 5.08 mmol/L at 6 m depth to 6.73 mmol/L at 23.5 mbsf (Fig. 28). Below this depth, the alkalinity decreases to a mid-hole minimum of 3.12 mmol/L at 146 mbsf. A local maximum of 5.68 mmol/L at 284 m depth (Core 117-720A-30X) coincides with the occurrence of a pelagic nannofossil ooze sequence which is enriched in organic carbon. Dissolved ammonia, phosphate, and silicate concentrations are also anomalously higher at this depth, indicating that the pelagic unit is (or was?) a locus of diagenetic activity within the drilled fan sequence. The low value (2.50 mmol/L) at the bottom of the hole suggests that authigenic carbonate minerals are precipitating near the base of the cored section.

Calcium and Magnesium

At Site 720 both Ca^{2+} and Mg^{2+} are depleted below seawater values (Fig. 28) in the topmost sample (7.9 and 50.3 mmol/L, respectively). However, while Mg^{2+} decreases asymptotically to a value of ~30 mmol/L, the Ca^{2+} concentration generally rises with depth below 25 mbsf reaching a maximum of 9.36 mmol/L at the bottom of the hole. This relationship is reflected by the decreasing Mg^{2+}/Ca^{2+} ratio (Fig. 28). Maximum curvature on the depth profiles of these two cations suggests that most of the

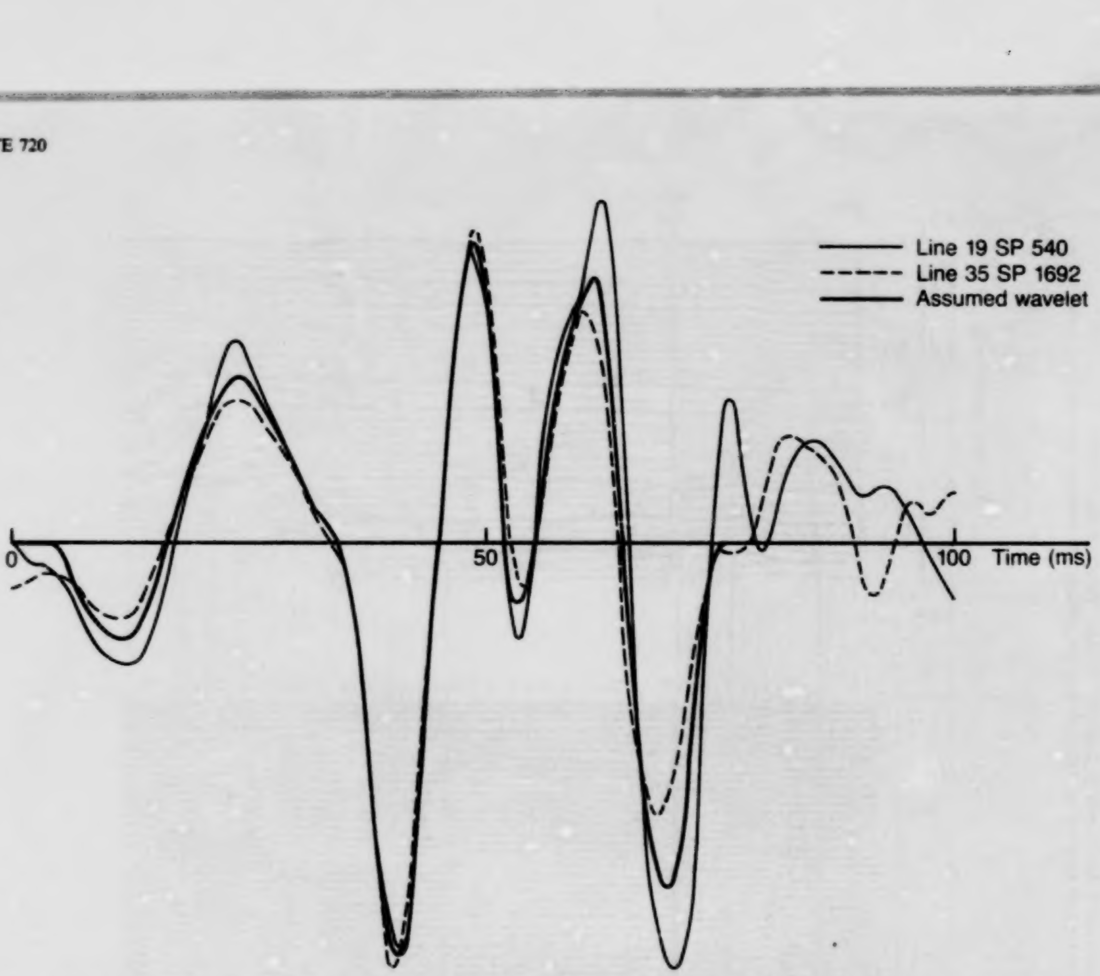

Figure 26. Greatly expanded seafloor portion of seismic traces from two regions surveyed by *Robert Conrad* for Leg 117 (RC2704). The heavy solid line is the wavelet used for the synthetic seismogram of Figure 27, based on averaging the two traces.

diagenetic reactions involving calcium and magnesium (e.g., ionic exchange in clay lattice sites such as replacement of iron by magnesium, and calcite and dolomite dissolution/precipitation reactions) occur in the top 100 m. Interestingly, the lowest Mg^{2+} and highest Ca^{2+} contents (26.3 and 9.4 mmol/L, respectively) occur in the deepest sample where the minimum alkalinity was observed. These observations are consistent with the contention that dolomite formation, perhaps by dolomitization of calcite, is occurring in this deep zone.

Ammonia, Phosphate and Silicate

Ammonia and phosphate distributions (Fig. 28) in the upper 100 m at the site are consistent with the addition of metabolites to pore water during the bacterially-mediated decomposition of organic matter. Ammonia concentrations increase from 0.58 mmol/L at 6 m depth to a relatively high maximum of 3.12 mmol/L at 284 mbsf. Although phosphate values reach a maximum of 13.9 μmol/L at 23 m depth, the extremely high ammonia/phosphate ratio and the decrease in concentration at greater depths suggests that phosphate is being removed from solution by the diagenetic precipitation of minor amounts of apatite (not detectable by XRD). The silicate concentration at 6 mbsf (626 μmol/L, Fig. 28) is much higher than the predicted bottom-water value (140 μmol/L; Broecker and Peng, 1982) indicating that opaline silica is dissolving in the pelagic nannofossil ooze. Below the uppermost sample, dissolved silicate levels decrease to ~150 μmol/L $\pm$100 μmol/L except for the sample at 284 m depth which contains the highest concentration (1014 μmol/L) measured in the hole. Relatively high levels of phosphate, ammonia, and alkalinity also occur at this depth which, as noted earlier, can be attributed to more pronounced diagenetic reactivity in the organic-carbon-rich nannofossil ooze sequence in Core 117-720A-30X. The high dissolved silica content reflects local dissolution of biogenic opal in this interval. The deficiency of dissolved silica in much of the rest of the hole may be attributed to a paucity of opal in the terrigenous turbidite facies. It is clear that interstitial waters at this site cannot be in diffusive steady state, which is a direct consequence of the extremely high sedimentation rates on the fan. Length scales for diffusion over a period of 1 Ma would be in the range of 60-90 m assuming a diffusion coefficient on the order of 10^{-6} cm^2s^{-1}.

Sediment Mineralogy

The mineralogy of the nine sediment residues remaining after extraction of interstitial waters was determined by X-ray diffractometry using the onboard Philips PW1729 diffractometer. Samples were lightly ground in a porcelain mortar and pestle and presented to the X-ray beam as pressed unoriented powders in aluminium holders. No pre- or post-diffraction treatments were performed.

The gross mineralogy of the bulk sediments varies predictably and in accord with the major lithological units: calcite dominates the pelagic nannofossil oozes and quartz the terrigenous clastics. Notable concentrations of calcite also occur in all samples comprised of terrigenous clastics which can be attributed to the presence of calcite of detrital origin in addition to biogenic

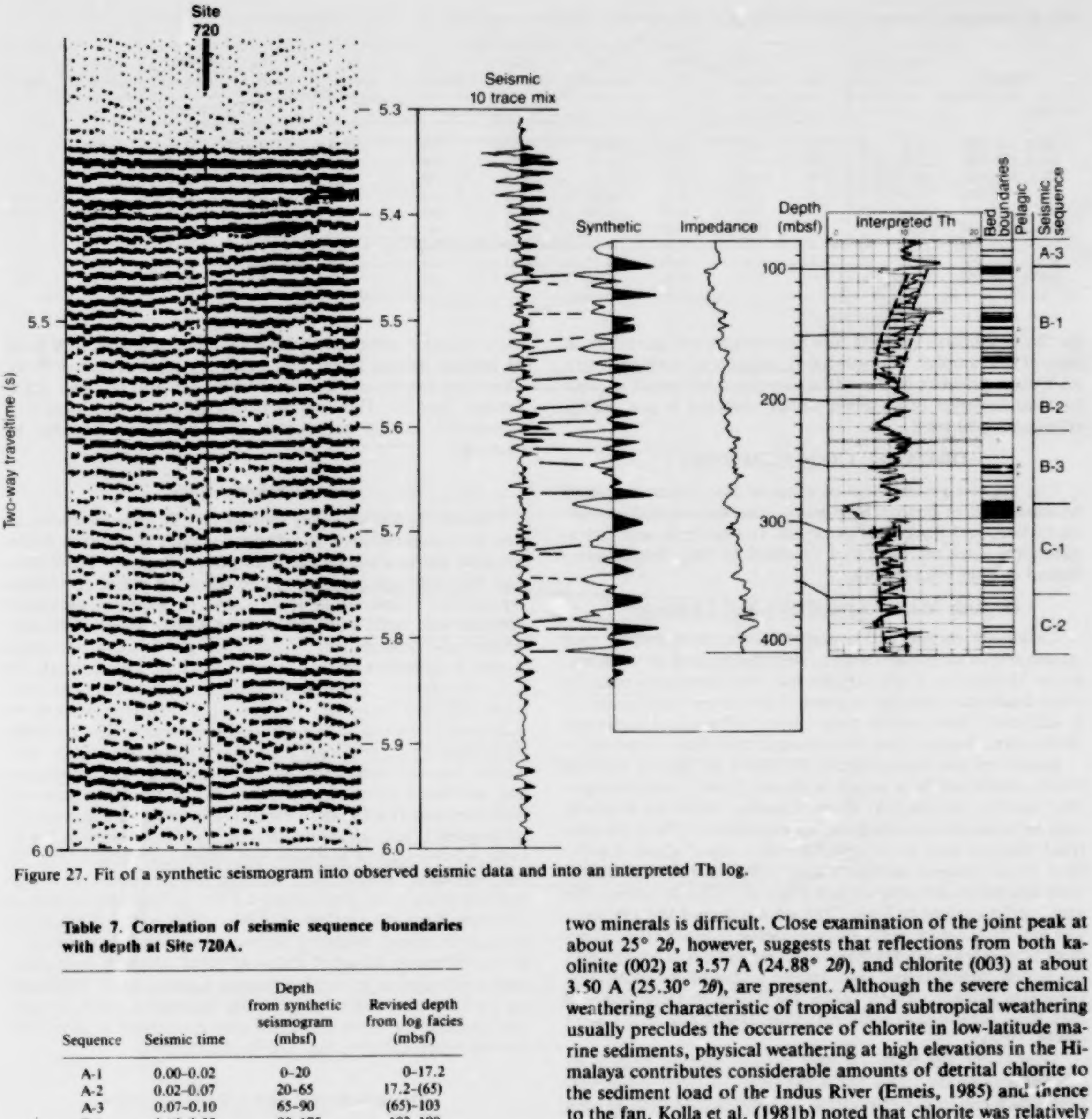

Figure 27. Fit of a synthetic seismogram into observed seismic data and into an interpreted Th log.

Table 7. Correlation of seismic sequence boundaries with depth at Site 720A.

Sequence	Seismic time	Depth from synthetic seismogram (mbsf)	Revised depth from log facies (mbsf)
A-1	0.00-0.02	0-20	0-17.2
A-2	0.02-0.07	20-65	17.2-(65)
A-3	0.07-0.10	65-90	(65)-103
B-1	0.10-0.22	90-175	103-190
B-2	0.22-0.25	175-205	190-222
B-3	0.25-0.36	205-300	222-290
C-1	0.36-0.42	300-355	290-347
C-2	0.42-0.47	355-400	347-391

$CaCO_3$. The former was observed by optical microscopy (see "Lithostratigraphy" section, this chapter). Micas and illite occur in significant amounts in the terrigenous detritus of both mud- and sand-dominated facies. Muscovite and biotite were identified in smear slides and are evident in all diffractograms with the exception of the calcareous ooze samples. A small but well-defined peak at about 12.5° 2θ is attributed to kaolinite plus chlorite. Because the kaolinite and chlorite diffraction spectra overlap to a considerable extent, differentiating between the two minerals is difficult. Close examination of the joint peak at about 25° 2θ, however, suggests that reflections from both kaolinite (002) at 3.57 A (24.88° 2θ), and chlorite (003) at about 3.50 A (25.30° 2θ), are present. Although the severe chemical weathering characteristic of tropical and subtropical weathering usually precludes the occurrence of chlorite in low-latitude marine sediments, physical weathering at high elevations in the Himalaya contributes considerable amounts of detrital chlorite to the sediment load of the Indus River (Emeis, 1985) and thence to the fan. Kolla et al. (1981b) noted that chlorite was relatively abundant in the clay fraction of surface sediments in the northern and central Arabian Sea and that kaolinite was uncommon in these areas.

The occurrence of two other minerals bears mention in this summary. Dolomite occurs in trace quantities in all samples with the exception of the terrigenous mud at 294 mbsf in which a significantly larger concentration (several percent) of the mineral is present. Although the Mg^{2+} and alkalinity depletions observed in the pore waters suggest, as described above, that authigenic dolomite is forming at depth in the sediments, authigenesis is unlikely to account for the significant presence of the mineral indicated by the diffractograms. Dolomite of apparent detrital origin was noted in the sedimentological descriptions (see "Lithostratigraphy" section, this chapter) and it is probable that a continental source may account for the presence of the mineral in

Table 8. Summary of interstitial water geochemical data for Hole 720A.

Sample	Depth (mbsf)	Vol. (mL)	pH	Alk. (mmol/L)	Sal. (g/kg)	Mg (mmol/L)	Ca (mmol/L)	Cl (mmol/L)	SO_4 (mmol/L)	PO_4 (μmol/L)	NH_4 (mmol/L)	SiO_2 (μmol/L)	Mg/Ca
117-720A-													
1H-4, 145-150	5.95	70	7.54	5.08	34.3	50.28	7.85	554	21.4	9.6	0.58	626	6.41
3H-3, 145-150	23.45	35	7.80	6.73	33.0	41.19	4.73	558	8.5	13.9	1.18	162	8.71
7X-1, 145-150	59.05	28	7.68	5.58	31.8	31.40	5.91	544	0.0	1.9	2.01	218	5.31
11X-2, 145-150	99.35	39	7.55	3.88	32.2	31.22	7.29	546	0.0	1.5	2.79	391	4.28
16X-1, 145-150	146.15	29	7.79	3.12	31.7	30.88	6.35	543	0.0	1.6	3.09	233	4.86
19X-2, 140-150	176.60	29	8.00	4.09	31.0	29.98	6.55	545	0.0	1.0	2.47	116	4.58
24X-1, 140-150	223.40	40	7.97	—	31.0	31.07	6.89	548	0.0	0.6	2.43	121	4.51
30X-3, 145-150	284.25	28	7.63	5.68	30.6	28.93	6.81	543	0.0	3.8	3.12	1014	4.25
40X-1, 140-150	377.30	30	7.96	2.50	31.8	26.32	9.36	547	0.0	<0.2	2.19	80	2.88

the fan sediments. Pyrite is also present in trace quantities in most of the samples. This mineral is certainly of authigenic origin and its presence in the diffraction traces is consistent with the total depletion of dissolved sulfate observed in pore waters below about 50 mbsf.

ORGANIC GEOCHEMISTRY

The organic geochemical program at Site 720 consisted of measurements of hydrocarbon gases, total carbon and carbonate carbon, and Rock-Eval pyrolysis. The methods and instrumentation used are described in detail in the "Explanatory Notes" chapter (this volume).

Organic Matter Abundance and Character

Carbonate carbon and organic carbon, measured as total carbon minus carbonate carbon, were determined by coulometry on 52 samples. These samples had been previously used for either headspace analyses or physical properties measurements. In addition, some samples were selected after visual inspection of the cores, because they were thought to contain charcoal.

Results of the measurements are listed in Table 3 and the $CaCO_3$ depth profile is shown in Figure 5 (see "Lithostratigraphy" section, this chapter). Organic carbon values are relatively high for open marine sediments; approximately 50% of the analyzed samples have an organic carbon content above 0.40%. Most pelagic marine sediments have organic carbon concentrations less than 0.2% (Degens and Mopper, 1976). In general, organic carbon values in Hole 720A do not exceed the 1% level. The terrestrial nature of the organic matter in Hole 720A, as evident from Rock-Eval pyrolysis measurements, is in accord with the largely turbiditic and land-derived nature of the sediments. Generally, organic carbon values are higher at ODP Site 720 than those measured in sediments from DSDP Site 222, Leg 23 (Bode, 1974).

Most likely, the relatively high organic carbon content of sediments from the Indus fan is the result of rapid sedimentation, which enhances preservation, in combination with an high input of terrigenous organic matter (see below). The sedimentary sink of continental-derived organic matter is normally in nearshore environments, but the major river systems of southeast Asia, such as the Indus, are known to have depositional centers extending several thousand kilometers offshore (Kolla et al., 1981b).

The Rock-Eval pyrolysis method was used to characterize the type and maturity of the organic matter. The results are listed in Table 9. The hydrogen index vs. the oxygen index (both calculated from the coulometric organic carbon data) of the organic matter are plotted in Figure 29. They show that oxygen-rich, cyclic, or refractory organic matter (kerogen type III) is the almost exclusive organic component in sediments of sedimentary Unit II, i.e., the turbiditic unit below 17.3 mbsf to total depth. The organic matter in sedimentary Unit I is immature, and, in spite of its marine pelagic facies, has relatively high oxygen indices. Therefore, the organic matter of Unit I can also be classified as kerogen Type III. This may be attributable to a contribution of oxygen-rich components which have not been degraded by bacteria.

Hydrocarbon Gases

During the routine safety monitoring program for hydrocarbon gas accumulations, 10 sediment samples were taken for interstitial gas analysis by the headspace technique. These samples were collected adjacent to interstitial water and geochemistry samples (Table 10) in Hole 720A. In addition, vacutainer samples were taken when gas pockets were observed. The overwhelmingly predominant hydrocarbon gas is methane, which occurs in quantities ranging from 27 μL/L of sediment to 0.375 L/L of sediment. The organic carbon concentrations are relatively high and the terrestrial origin of the organic matter in the sediments recovered at Site 720 (see below) classifies the turbiditic sequence of lithologic Unit II as a gas-prone source rock. *In-situ* thermal maturation has not produced any thermogenic gas, and hence ratios of methane to C_{2+} hydrocarbons are very high (between 31×10^3 and 19×10^3). The methane appears to be of biogenic origin, an assumption that is corroborated by the inverse relationship of methane and interstitial sulfate (Fig. 30; see "Inorganic Geochemistry" section, this chapter). Due to high sedimentation rates and closing of the sedimentary system to diffusion from the seafloor, the interstitial sulfate is exhausted by organic matter oxidation during microbial sulfate reduction at approximately 60 mbsf. Below 60 mbsf microbial remineralization of sedimentary organic matter appears to be dominated by methane production. A generally decreasing trend of methane abundances below 100 mbsf may be attributed to exhaustion of organic matter that can be metabolized.

DOWNHOLE MEASUREMENTS

Introduction

Three Schlumberger logging runs were planned at Site 720, i.e., the seismic stratigraphic, lithoporosity, and geochemical combinations. The tool strings and their applications are described in the "Explanatory Notes" chapter (this volume). The primary logging objectives at the site were: (1) turbidite bed delineation for study of variations in source region and depositional environment, (2) determination of the thickness and location of pelagic interbeds, (3) seismic/core tie through a synthetic seismogram, (4) detailed mineralogy, and (5) major element geochemistry. Only the first three objectives were fully achieved, due to loss of the seismic stratigraphic tool string downhole and consequent curtailment of logging operations.

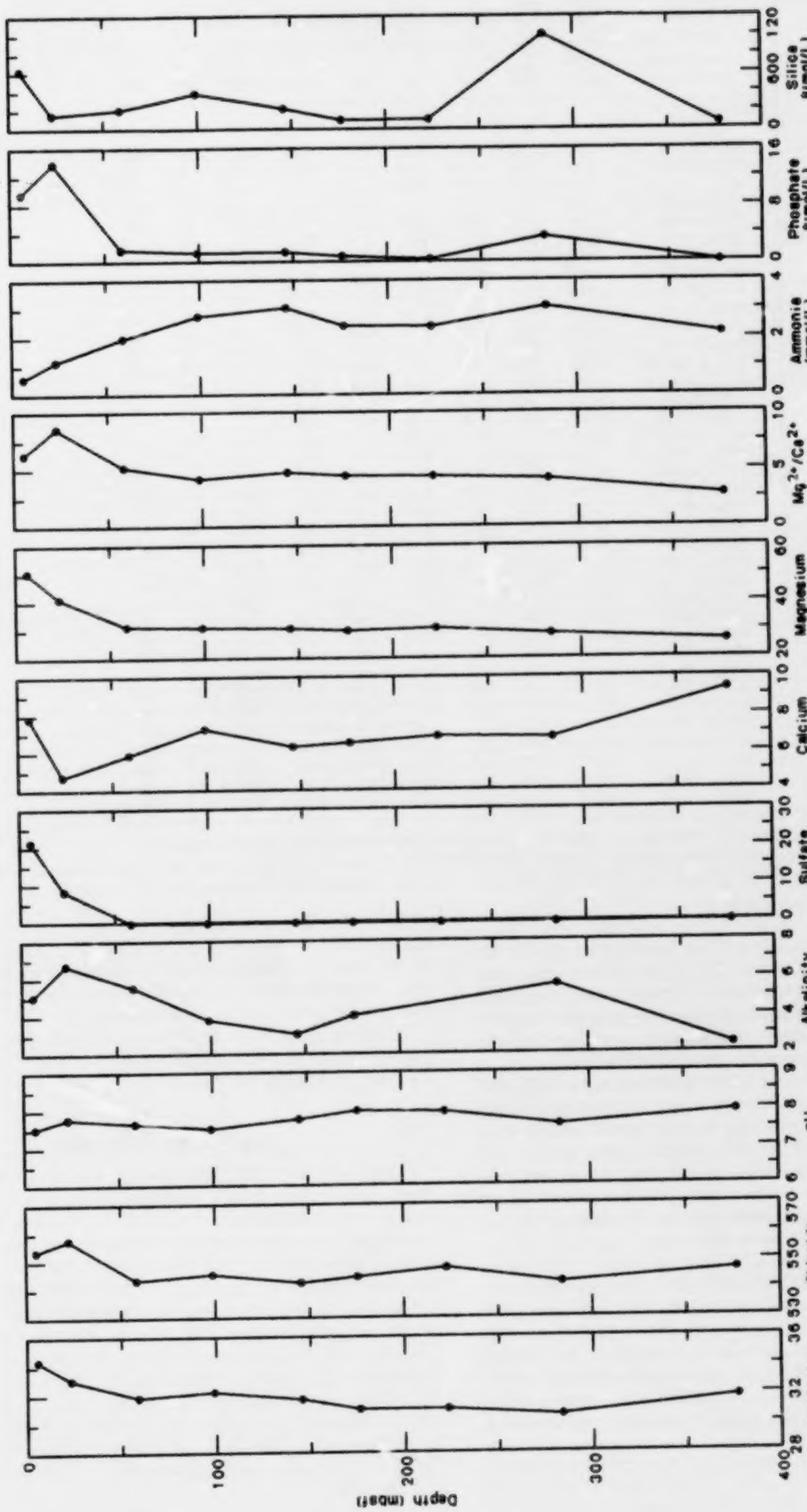

Figure 28. Concentrations profiles vs. depth for Hole 720A.

Table 9. Results of Rock-Eval pyrolysis of sediment samples from Hole 720A.

Core, section, interval (cm)	Depth (mbsf)	T_{max} (°C)	S_1	S_2	S_3	S_2/S_3	TOC	HI	OI
117-720A-									
1H-2, 40–42	1.90	395	0.09	0.13	0.62	0.20	0.53	40	188
1H-4, 40–42	4.90	393	0.15	0.30	0.68	0.44	0.58	52	117
1H-4, 144–145	5.94	404	0.37	0.42	0.81	0.51	0.46	91	176
1H-6, 40–42	7.90	396	0.11	0.23	0.56	0.41	0.25	92	224
2H-2, 40–42	11.30	395	0.10	0.18	0.54	0.33	0.30	60	180
2H-4, 40–42	14.30	407	0.15	0.45	0.70	0.64	0.61	74	115
3H-2, 24–26	20.74	590	0.04	0.09	0.47	0.19	0.51	18	92
5X-2, 36–38	40.06	475	0.15	0.06	0.39	0.15	0.38	16	103
5X-5, 85–87	45.05	379	0	0.06	1.35	0.04	0.41	15	329
6X-1, 16–18	48.06	419	0	0.57	1.84	0.30	0.55	104	335
7X-1, 144–145	59.04	393	0.23	0.43	0.25	1.72	0.96	45	26
7X-2, 49–51	59.59	403	0	0.17	1.30	0.13	0.74	23	176
11X-2, 144–150	99.34	415	0.19	0.54	0.69	0.78	0.50	108	138
11X-2, 109–111	98.99	418	0	0.59	2.04	0.28	0.78	76	261
11X CC, 0–1	101.07	393	0.15	0.07	0.18	0.38	0.30	23	60
12X-2, 25–26	107.75	366	1.48	2.66	0.92	2.89	3.70	72	[a]25
12X-2, 56–58	108.05	312	0	0.05	0.69	0.07	0.28	18	246
14X-1, 29–31	125.69	276	0	0.02	1.03	0.01	0.32	6	322
16X-1, 64–66	145.34	383	0	0.39	1.96	0.19	0.72	54	272
19X-1, 149–150	175.19	332	0.03	0.05	0.44	0.11	0.35	14	126
19X-1, 34–36	174.04	312	0	0.07	1.55	0.04	0.39	21	456
20X-2, 63–64	185.53	367	0.16	0.10	0.32	0.31	0.33	30	96
20X-3, 45–47	186.85	397	0	0.34	1.67	0.20	0.56	61	298
21X-1, 51–53	193.51	273	0	0.01	0.92	0.01	0.25	4	368
26X-1, 31–33	241.71	273	0	0.04	1.11	0.03	0.34	11	326
27X-1, 40–42	251.40	237	0	0	0.22	0	0.29	0	76
28X-1, 40–42	260.90	420	0	0.05	0.60	0.08	1.64	3	36
30X-2, 111–113	281.41	390	0	0.21	1.66	0.12	0.88	23	188
30X-4, 1–2	284.31	409	0	0.91	1.96	0.46	1.45	62	135
30X-4, 98–100	285.28	386	0	0.38	2.01	0.18	0.42	90	478
30X-6, 100–102	288.30	413	0	1.39	2.17	0.64	1.34	103	161
32X-1, 93–95	299.95	232	0	0.02	1.46	0.01	0.36	5	405
36X-1, 1–2	337.41	212	0	0.07	1.32	0.05	0.41	17	321
37X-1, 19–21	347.19	203	0	0.04	0.94	0.04	0.28	14	335
39X CC, 11–13	366.72	193	0	0.04	1.35	0.02	0.54	7	250
40X-1, 24–26	376.14	397	0	0.23	1.70	0.13	0.40	57	425
43X-1, 57–59	405.17	268	0	0.03	0.37	0.08	0.35	8	105

Note: HI = hydrogen index and OI = oxygen index. For a detailed description of parameters, see "Explanatory Notes" chapter (this volume).

[a] Sample suspected to contain charcoal.

Operations

Thirty eight hours were allotted for logging at Site 720, including time allotted for possible use of the sidewall entry sub (SES). The SES was not used, because drilling and hole conditioning showed good hole conditions, and because capillary suction time tests on three samples (pelagic clay, turbidite clay, and turbidite clayey silt) showed only minor clay swelling.

Hole conditioning began at 1440 on 1 September 1987 and concluded at 2245. This conditioning included sweeping the hole with 30 barrels of gel mud, a wiper trip, another 30 barrel sweep, bit release, displacing the hole with polymer mud, and pulling pipe to 70 mbsf for logging. Hole conditioning was slower than anticipated because of special projects (pressure testing of the Barnes tool and treating the sand line) and because gas shows required displacing the hole with mud.

Logging tool rigup began at 2245 and concluded 1.75 hr later. The digital seismic stratigraphic combination (long spaced sonic, spectral gamma ray, and phaser resistivity) obtained open-hole logs while running down to the bottom. Hole conditions were generally good, with only one bridge encountered and broken through at about 90 mbsf. Logging upward commenced at 0342 on 2 September. Nearly the entire interval was logged, before the tool was stopped and soon stuck in the reformed bridge at 97 mbsf.

In order to free the tool, a new cutter and crimper combination was sent down the pipe at 0810. The objective was to cut and clamp the logging cable in the BHA, lower pipe through the bridge to free the tool, then pull both pipe and logging tool out of the hole. However, the cutter/crimper fired at 1500 m below rig floor rather than 4050 m, and lowering the pipe apparently failed to break through all of the bridge and free the logging tool. When the BHA was pulled to the rig floor, 2600 m of cable and the tool string failed to accompany it.

Logging operations terminated at 1030 on 2 September, when pulling up of the drill string commenced. In all, 20 of the 38 hr allotted for logging were utilized.

Log Quality and Editing

Logs were obtained both during lowering of the tool string from pipe to total drilled depth and during raising of the tool string from total depth to the bridge at 97 mbsf. Less than 2 m of cavings were present at the bottom of the hole. A more significant data loss near the bottom of the hole results from the length of the tool string: resistivity is measured 1.8–2.9 m above the bottom of the tool, sonic response is measured 12.8–13.4 m above the tool bottom, and spectral gamma ray is measured 21.2 m above tool bottom. A 45-cm downward shift of resistivity curves was applied, as indicated by comparison of the depths of similar horizons on sonic and resistivity. A 2.6-m upward shift of downgoing logs was applied to depth-justify them with upcoming logs. The final log interval of live data was 78.8–390.9 mbsf for downgoing logs and 104.0–412.4 mbsf for upcoming logs.

Log quality was generally excellent for upcoming logs and very good for downgoing logs. Overlay of downgoing and up-

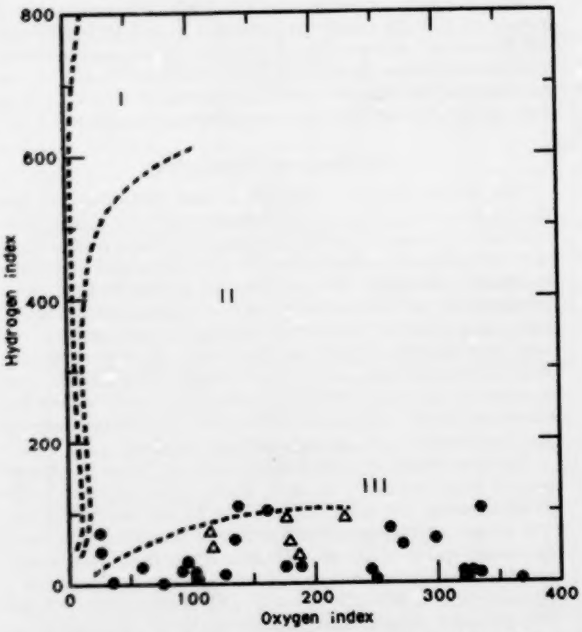

Figure 29. Oxygen vs. hydrogen indices of organic matter in Hole 720A, indicating that the organic matter is predominantly of kerogen type III. This type of diagram suggests that sediments are dominated by terrestrial and reworked residual material from erosion of the continent and transport of land-derived organic matter via turbidity currents. Explanation of symbols: triangle = Pelagic Unit 1; circle = Pelagic interval Core 30X; dot = Clastic Unit 2.

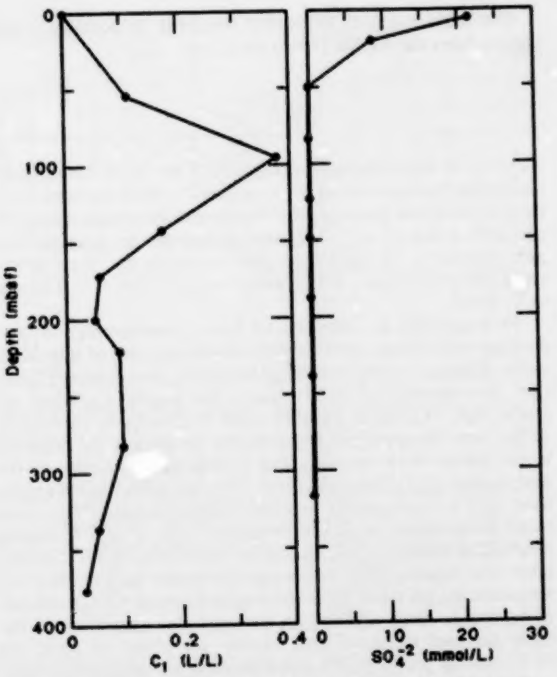

Figure 30. Methane abundances in sediments from Hole 720A. Sulfate concentrations, which determine the extent of organic matter oxidation and methane production, approach 0 mmol/L at approximately 60 mbsf. Below this depth, methane concentrations from bacterial processes rise significantly.

Table 10. Interstitial gas abundances and ratios of methane (C_1) to ethane (C_2) in samples of headspace gas from Hole 720A.

Core, section interval (cm)	Depth (mbsf)	C_1 (μL/L)	C_2 (μL/L)	C_1/C_2
117-720A-				
1H-4, 144-145	5.94	27		
7X-1, 144-145	59.04	110,418		
11X-2, 149-150	99.39	375,390	12	31,283
16X-1, 120-121	145.90	170,446	9	18,938
19X-1, 149-150	177.19	61,622		
22X-1, 0-1	202.70	52,364		
24X-1, 139-140	223.39	94,323	3	31,441
30X-4, 1-2	284.31	98,675	5	19,735
36X-1, 0-1	337.41	52,979		
40X-1, 139-140	377.29	27,245		

Note: Values are expressed in μL/L (volume gas/volume wet sediment). The very high ratios of C_1/C_2 show that gas is of biogenic origin.

coming logs shows that the two are virtually identical for resistivity and sonic logs. Gamma ray logs are quite similar but differ in finest-scale features, as expected from the poorer counting statistics for the spectral gamma tool at the high logging speed used for the downgoing log. This degradation of counting statistics makes the calculated abundances of potassium, thorium, and uranium substantially less accurate in the downgoing log than in the upcoming log. Post-cruise reprocessing of spectral gamma ray logs is possible but has not yet been done.

Because of the higher accuracy of the upcoming logs, we only use these in the interval for which they are available. We did not average downgoing and upcoming logs, because slight cable stretch between and within runs is likely to cause depth mismatches of up to 30 cm; averaging then would degrade vertical resolution without significantly improving signal-to-noise ratio. Downgoing logs for the interval 78.8-104.0 mbsf were merged with the upcoming logs available below that depth, in order to provide continuous logs over the interval 78.8-412.4 mbsf. Note, however, that the spectral gamma log obtained data only for the interval 78.8-394.3 mbsf, because of its higher position in the tool string.

The only unreliable data obtained were from the spherically focussed log (SFL). Nearly all of the SFL data are consistent with the other resistivity logs, but occasional very large resistivity spikes occur. These presumably are caused by either electrical or data telemetry problems. A similar phenomenon was noted on Leg 116. No problems were encountered in bench tests.

Porosity and Velocity

In deep-sea sediments, both the sonic and resistivity logs respond primarily to porosity variations. Resistivity is relatively insensitive to mineralogy (at least for the high-porosity sediments considered here), whereas sonic velocity is somewhat sensitive to mineralogy though dominantly sensitive to porosity. Furthermore, the relationship of velocity to porosity is poorly known for high-porosity sediments. Thus resistivity can be a superior tool for porosity determination.

The relationship of formation resistivity to porosity is well known from the Archie (1942) equation:

$$S_w^n = \frac{aR_w}{f^m R_t}$$

where S_w is water saturation (equal to 1 for these virtually hydrocarbon-free sediments), R_w is resistivity of the formation water, f is fractional porosity, R_t is measured formation resistivity, and both a and m are "constants" dependent on lithology and pore geometry. We calculated porosity using the Humble formula (Winsauer et al., 1952), which assumes that $a = 0.62$ and $m = 2.15$.

We calculated R_w based on its known relationships to temperature and salinity (Keller, 1982). Measurements of interstitial water salinities at this site (see "Inorganic Geochemistry" section, this chapter) are widely spaced but suggest a gradual decrease from 31 g/kg at about 70 mbsf to 29 g/kg at the bottom of the hole. Temperature of formation water near the borehole is not known with certainty, but it is probably similar to the temperature of the borehole fluid. Temperature within the resistivity tool is continuously measured during logging. This measured temperature gradually increased from 4°to 5°C during downgoing logging, and it decreased from 38°C to 37°C during upcoming logging. The substantial difference between the two temperature logs arises from the long delay time for the interior of the tool to reach equilibrium with ambient temperatures. Because the tool remained near bottom for about an hour, the 38°C reading probably is a good estimate of bottom-hole temperatures. We assumed a linear thermal gradient from 1°C at the seafloor to 38°C at 412 mbsf. This thermal gradient is consistent with the seafloor age and is identical to that measured at Site 646 (Arthur et al., in press), where both crustal age and sediment type are very similar to Site 720.

The resulting porosity log closely mimics the character of the measured resistivity log, while the overall trend of porosity values is controlled by the choice of a, m, and R_w. Calculated porosities were much lower than expected porosities for terrigenous sediments, probably because the values for a and m are inappropriate for these sediments. Unfortunately, these parameters have seldom been determined for high-porosity terrigenous sediments. Thus we are forced to calibrate our porosity log to either laboratory measurements on cores (see "Physical Properties" section, this chapter) or the empirical porosity/depth trend of Hamilton (1976). We used the core measurements for calibration, multiplying all calculated porosities by 1.5.

This final porosity curve (Fig. 31) may be incorrect by as much as 5% porosity, but the relative porosity changes are much more accurate, as they are controlled by measured resistivity rather than assumed values for a and m. The gradual and normal compaction profile is not evident in the resistivity log (Fig. 31), because the effect of gradual compaction on resistivity is obscured by the gradual downward decrease in fluid resistivity due to increasing temperature. The effect of the salinity correction is trivial.

Two velocity logs are measured during each logging run: a short-spaced log which measures the difference between traveltimes for receivers 2.44 and 3.05 m from the transmitter, and a long-spaced log which similarly uses 3.05- and 3.66-m spacings. Both logs are virtually identical throughout each run, and the the downgoing and upcoming logs are nearly identical. Figure 31 shows the long-spaced velocity log. Velocities increase gradually from 1.7 to 2.1 km/s over the logged interval due to compaction. Substantial variations from this average trend are observed, primarily due directly to porosity changes (Fig. 31) and indirectly to changes in clay mineral content. Velocities are generally slightly higher than the empirical velocity/depth trend of Hamilton (1979) for terrigenous sediments. This observation is consistent with the finding of lower core porosities (see "Physical Properties" section, this chapter) and lower core-calibrated log porosities than Hamilton's (1976) empirical trend, suggesting that the clay mineral content at Site 720 is somewhat lower than at the sites on which the empirical trends were based.

Lithology and Mineralogy

The logged interval at Site 720 is from lithologic Unit II, a dominantly terrigenous turbidite section with rare pelagic interbeds (see "Lithostratigraphy" section, this chapter). The turbidites are primarily clayey silts and silty clays, with rare clays. Dominant minerals in the turbidites are quartz, feldspar, detrital carbonate, and clay minerals, with occasional mica. Preliminary clay mineralogy studies (see "Inorganic Geochemistry" section, this chapter) indicate that illite is the dominant clay mineral, but chlorite also occurs. Most pelagic interbeds are a few centimeters to 2 m in thickness; a single bed greater than 9 m thick was found in Core 117-720A-30X. The pelagic intervals are composed of clay minerals and nannofossils.

The gamma-ray log, which responds to K, Th, and U that are usually found primarily in clays, shows a general trend of decreasing values downhole, from 85 to 70 API units (Fig. 32). The pelagic intervals are readily visible on the gamma-ray log as downward spikes of 20–30 API units below the turbidite average. Based on the gamma-ray response, pelagic interbeds probably occur at 101–103, 139, 155–156, 170, 188–190, 201–202, and 277–290 mbsf. Several other negative spikes of lower amplitude are probably thinner pelagic units that are near the 0.5-m vertical resolution limit of the log. Separately examining the K and Th contributions to the gamma ray log (Fig. 33), we see that both Th and K are lower in the pelagic intervals than in the turbidites. The Th/K ratio is only slightly lower in the pelagics than in the turbidites (Fig. 32). U/Th (not shown) exhibits extremely large positive spikes at the two pelagic intervals 188–190 and 277–290 mbsf, indicating U enrichment in addition to the Th depletion. U/Th spikes are often caused by enrichment of organic material (Fertl, 1979).

The pelagic intervals are also visible on the porosity log (Fig. 31) as high-porosity zones, but the porosity variability within the turbidites precludes identification of pelagic units from porosity alone. The higher porosity in pelagics than in turbidites is probably attributable to the much higher clay content in the former. The high porosity in the pelagics causes only slightly lower velocities, probably indicating that higher matrix velocity in the pelagics is reducing the velocity contrast associated with porosity.

Th/K ratio is often a useful indicator of clay type. The majority of the logged interval at this site has Th/K of $5\text{–}8 \times 10^{-4}$. This ratio indicates either an illite or montmorillonite dominance (Fertl, 1979). The potassium concentrations of about 1%–2% are more consistent with illite (3.5%–8.3% for pure illite) than with montmorillonite (0%–0.6%; Serra, 1987). Mica has a high potassium content (consistent with observed values) but too low a Th/K ratio ($<0.7 \times 10^{-4}$) to be the dominant mineral. Probably the log responses result from a mixture of dominant illite and subsidiary other clay minerals. In contrast, the pelagic clays have Th/K ratios that are slightly lower ($2.5\text{–}5 \times 10^{-4}$) and very low K and Th concentrations. These changes could be partly caused by a greater proportion of montmorillonite in the clays, but dilution associated with the 50%–80% nannofossils in the pelagic units also is partially responsible for the very low K and Th concentrations.

Th/K ratio exhibits a large number of spikes to 11 to 14×10^{-4} (Fig. 32). These spikes are present but less noticeable on

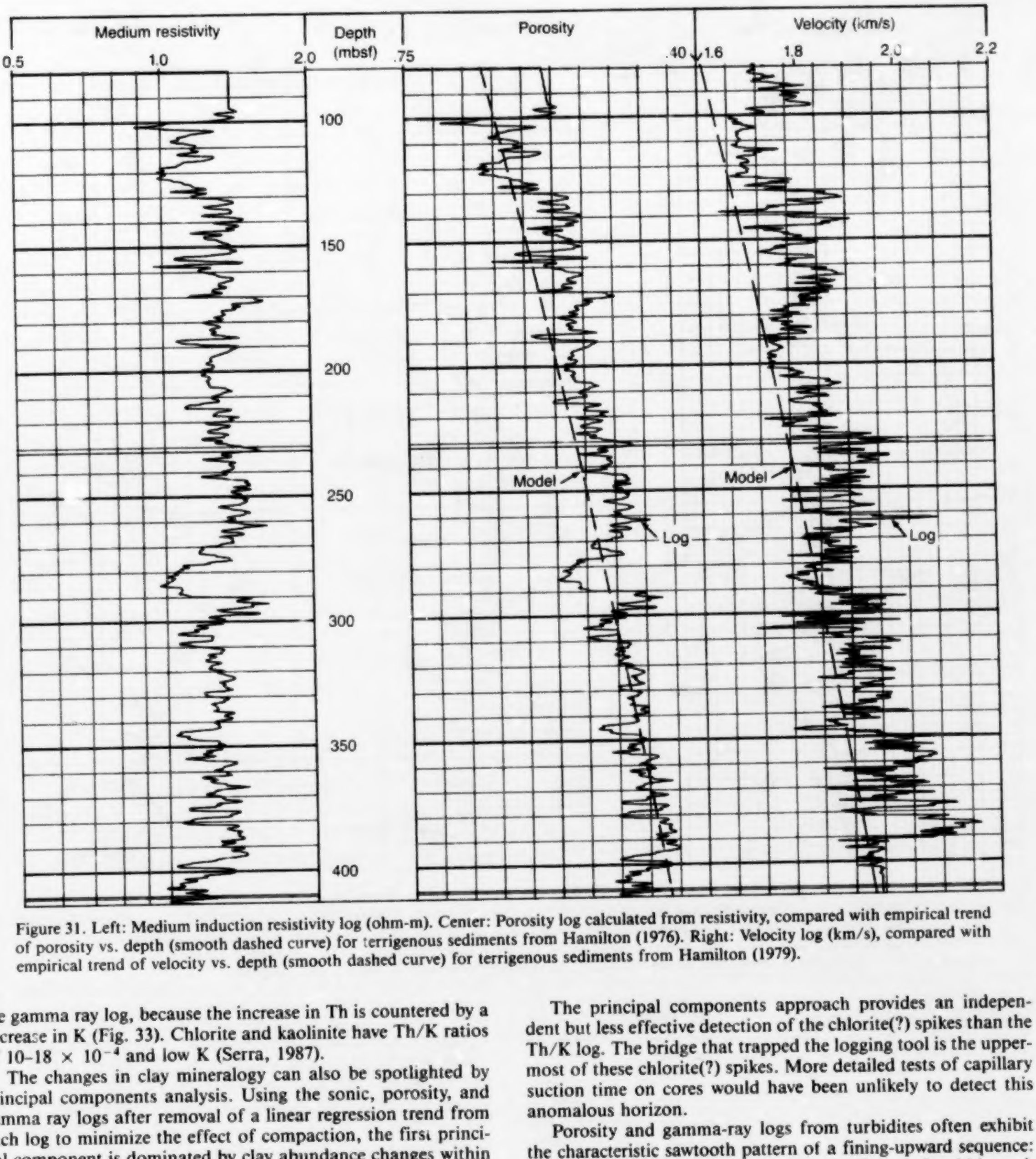

Figure 31. Left: Medium induction resistivity log (ohm-m). Center: Porosity log calculated from resistivity, compared with empirical trend of porosity vs. depth (smooth dashed curve) for terrigenous sediments from Hamilton (1976). Right: Velocity log (km/s), compared with empirical trend of velocity vs. depth (smooth dashed curve) for terrigenous sediments from Hamilton (1979).

the gamma ray log, because the increase in Th is countered by a decrease in K (Fig. 33). Chlorite and kaolinite have Th/K ratios of 10–18 × 10^{-4} and low K (Serra, 1987).

The changes in clay mineralogy can also be spotlighted by principal components analysis. Using the sonic, porosity, and gamma ray logs after removal of a linear regression trend from each log to minimize the effect of compaction, the first principal component is dominated by clay abundance changes within the turbidites. The second principal component (Fig. 32), accounting for 32% of the covariance, is dominated by the gamma ray term (0.9438) and includes a slight positive correlation with porosity (0.1073) and stronger inverse correlation with velocity (−0.3124). This component appears to respond primarily to clay type. The dominance of a single clay mineral (illite?) and occasional spikes of a second clay mineral (chlorite?) are evident throughout the turbidites, and the different mineralogy of the pelagic sediments is also evident.

The principal components approach provides an independent but less effective detection of the chlorite(?) spikes than the Th/K log. The bridge that trapped the logging tool is the uppermost of these chlorite(?) spikes. More detailed tests of capillary suction time on cores would have been unlikely to detect this anomalous horizon.

Porosity and gamma-ray logs from turbidites often exhibit the characteristic sawtooth pattern of a fining-upward sequence: clay content and porosity increase gradually uphole within each bed or group of beds. Such a pattern is rare at Site 720 (Figs. 31 and 32). Thick intervals of gradually increasing gamma ray response are evident at 104–129 and 190–221 mbsf. In contrast, the Th log does show the sawtooth pattern of gradual upward increase and sharp decrease. For example, the gamma ray unit at 104–129 mbsf is seen on the Th log to be composed of three subunits. This pattern probably indicates a fining-upward sequence, in which increasing clay mineral concentration causes

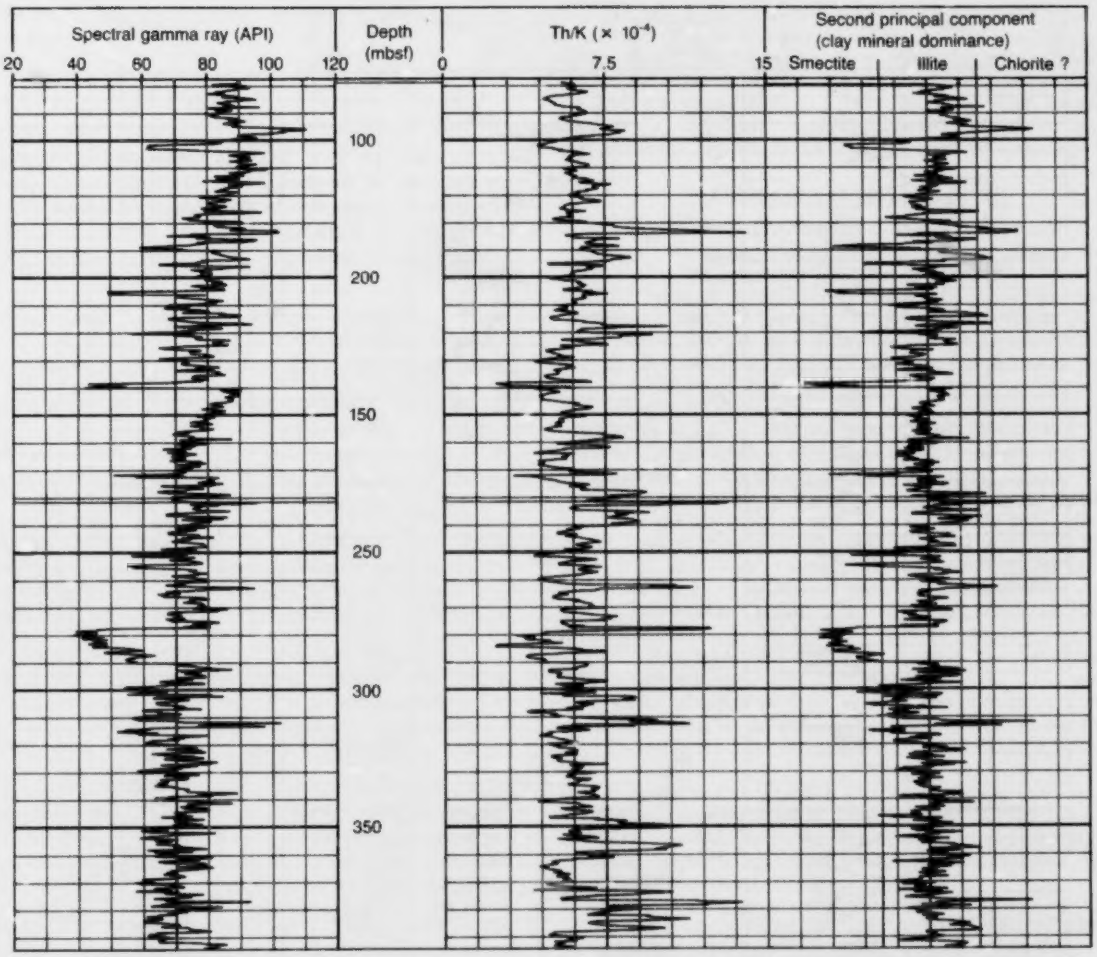

Figure 32. Left: Gamma-ray log (API units). Center: Th/K ratio ($\times 10^{-4}$). Right: Second principal component of porosity, velocity, and gamma-ray covariance. Note the pronounced gamma-ray and principal component spikes toward the left, marking the locations of pelagic beds. Also note the pronounced Th/K and principal component spikes toward the right, indicating turbidite horizons with a very different clay mineral composition (chlorite?). The minerals listed above the three zones on the principal-component log refer to the dominant clay mineral in that zone from the standpoint of log responses; actual clay mineralogy is much more complex.

increasing Th. However, Th is positively correlated with velocity at Site 720, the opposite of the usual pattern of clays being more porous and therefore lower in velocity than silts and sands.

In general, Th seems to be the most effective of the obtained logs for delineation of turbidite beds or packets. In addition to revealing fining-upward sequences, it often shows abrupt shifts to a different baseline value, indicating a significant compositional change. In Figure 33 an identification of the most obvious turbidite bed boundaries is attempted based on Th alone. Fining-upward and coarsening-upward beds are highlighted by heavy curves on the Th log, and long-term trends are highlighted by heavy dashed lines.

Depositional Environments

From near the bottom of the hole (383 mbsf) to 290 mbsf, a relatively uniform depositional environment of turbidites prevails (Fig. 33). Little change in average bed thickness, a predominance of fining-upward sequences, and two relatively well-defined limiting compositions of clayey silt and silty clay are evident. No pelagic interbeds are detected. Thin chlorite(?) beds top two of the fining-upward sequences, and several chlorite horizons may be present in the interval 373–388 mbsf (Fig. 33). Deposition was probably controlled by overflow from a stable, distant channel. A single major seismic reflector occurs just below this interval at 391 mbsf, associated with a sudden upward decrease in porosity (see "Seismic Stratigraphy" section, this chapter). Because the spectral gamma tool did not reach this depth, the cause of this porosity change cannot be determined from logs.

From 277 to 290 mbsf, a relatively thick pelagic clay interval was deposited. A facies change resulting from a sudden shift of the turbidite channel to a position far from Site 720 is implied. A small seismic reflector is associated with this pelagic unit in the synthetic seismogram (Fig. 27), but it is possible that the associated density drop is larger than assumed.

From 277 to 188 mbsf, the depositional environment at Site 720 was quite variable. Turbidite deposition resumed, interrupted by at least four thin pelagic intervals. Both fining- and coarsen-

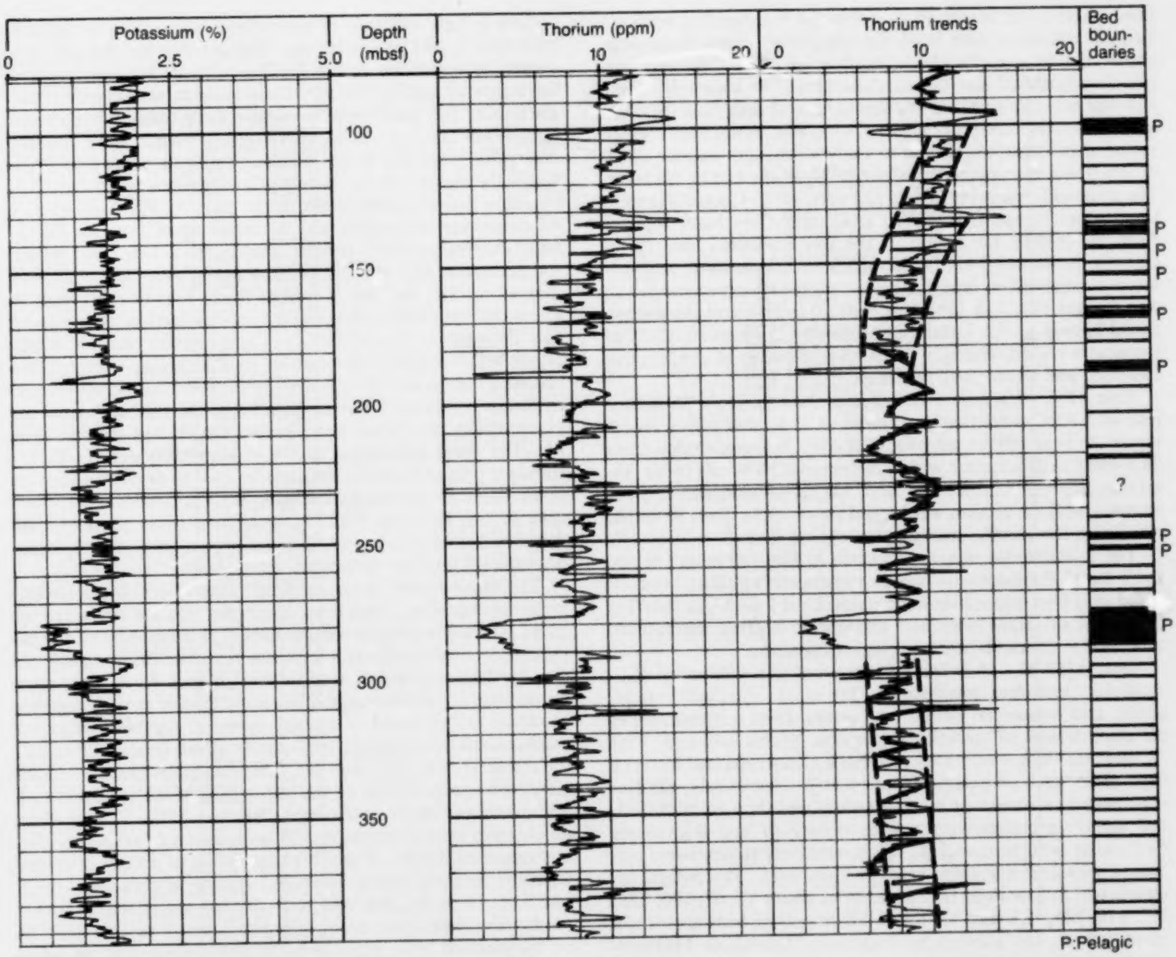

Figure 33. Left: Potassium log (weight percent). Center: Thorium log (ppm). Right: Thorium log with bold-line highlighting of interpreted patterns within a turbidite bed, and with dashed-line highlighting of interpreted long-period patterns. Far right: Probable locations of turbidite bed boundaries based on Th variations, and pelagic interbeds from Figure 32.

ing-upward sequences are present, at first similar in thickness to the lower sequence but later much thicker. Chlorite(?) interbeds occur occasionally, most notably as the first sedimentation after deposition of the pelagic unit and in the interval 226–240 mbsf. The unit is capped by a 32-m-thick claying-upward sequence (based on gamma-ray, Fig. 32) topped by a 2-m-thick pelagic unit, but the Th log shows that this sequence is more complex than a single thick turbidite.

From 188 to 103 mbsf, rhythmic turbidite deposition resumed, but with several characteristic differences from the somewhat similar interval 383–290 mbsf. Again, several thin chlorite(?) beds are present, bed thicknesses are 3–6 m, and fining-upward sequences are common. However, this entire interval shows a general trend toward increasing clay content, as indicated by the potassium and gamma ray logs. An exception is a single setback at 130 mbsf, as indicated by the Th log. The interval 188–130 mbsf, like the interval 220–190 mbsf, shows a smooth fining-upward sequence on the gamma-ray and several smaller fining-upward sequences on the Th log; both are topped by moderately thick pelagic units (2 and 3–4 m, respectively). Log responses for the entire unit from 188 to 103 mbsf may indicate a period of variable but gradually waning supply from a distant channel. The unit is topped by a pelagic/chlorite(?) pair (like 277–290 mbsf) that creates a seismic reflector.

SUMMARY AND CONCLUSIONS

Site 720 is located on the westernmost part of the Indus Fan, near the boundary between the middle and the lower fan sectors, in a water depth of 4048 m. The Indus Fan is 1500 km long, 960 km across at its widest point, covers an area of over 1.1×10^6 km^2, and is the dominant physiographic feature of the Arabian Sea. Initiation of Indus Fan deposition is thought to have begun in Oligocene to early Miocene time when the Indian and Asian plates collided and caused major uplift of the Himalayas.

Sediment thickness at Site 720, inferred from seismic reflection and refraction data, is greater than 2000 m. The site lies near magnetic anomaly 25, which indicates a Paleocene basement age of about 60 Ma. The site is about 5 km east of a meandering channel that is 1.5 km wide, 50 m deep, and has a levee elevation of about 30 m above the surrounding seafloor. Seismic reflection data from the site survey reveal levee complexes of similar size in the subsurface near Site 720 (see "Seismic Stratigraphy" section, this chapter). The location of Site 720 was selected to avoid channel deposits, and thus to maximize the opportunity to collect a relatively continuous depositional record that was related to sea-level changes and the uplift of the Indus Fan source areas in the Himalaya and in Pakistan. The principal objectives of Site 720 were: (1) to recover a continuous upper Neogene section of fine-grained overbank deposits from the middle fan region of the western Indus Fan; (2) to identify the depositional facies, sediment composition, and sediment accumulation rates for comparison with other Indus Fan and Ganges Fan (Leg 116) sites; and (3) to interpret the depositional history of the Indus Fan sediments in terms of uplift of the source region, changes in sea level, changes in climate, circulation, and weathering processes.

One APC/XCB hole was drilled at the site. Hole 720A consists of 3 APC cores that penetrated to 28.6 mbsf with a recovery of 28.44 m (99%), and 40 XCB cores that penetrated from 28.6 mbsf to 414.3 mbsf with a recovery of 60.94 m (16%). Total recovery was 21.6%. The hole was terminated due to poor recovery, and the section was logged successfully from 80 to 380 mbsf with the seismic stratigraphy logging tool.

The stratigraphic section recovered at Site 720 ranges in age from basal Pleistocene to upper Pleistocene and has been divided into two major lithologic units. Unit I (0–17.22 mbsf) is composed of nannofossil and foraminifer-bearing nannofossil ooze that is characteristic of pelagic deposition.

Unit II (17.22–414.3 mbsf) is composed of a wide range of lithologies, including interbedded silty clays, silts, silty sands, sands, and occasional nannofossil oozes; these sediment types are characteristic of turbiditic deposition. Within lithologic Unit II, three facies represent intervals that are characterized by: (1) a high abundance of pelagic (nannofossil) components; (2) fining-upward sequences of mud turbidites and thin- to thick-bedded sandy turbidites with a wide variety of bed thicknesses (<2 cm to >50 cm); and (3) sandy, relatively structureless turbidites with coarse-grained bases >5 cm thick. The pelagic intervals within lithologic Unit II occur at about 52, 62, 100, 125, 150, 179, 185, 285, and 375 mbsf. These pelagic beds are clearly identified on the gamma-ray logs (see "Downhole Measurements" section, this chapter), and some are observed in the seismic sections (see "Seismic Stratigraphy" section, this chapter). The downhole logging data also identify several pelagic intervals within Unit II that were not recovered. The logging results further indicate that most of the unrecovered section was of a turbiditic character.

Within lithologic Unit II, the fan sediments contain relatively high concentrations (average of about 0.4%) of organic carbon that is mostly derived from terrestrial sources as indicated by its pyrolysis character. The sediments are also characterized by complete sulfate reduction below 50 mbsf, its depth being largely a function of high sedimentation rates. Traces of dolomite occur throughout the sequence and are thought to reflect both detrital sources and *in-situ* precipitation. Sediments of Unit II contained 20% detrital calcite and 5% feldspar as observed in the smear slides.

Biostratigraphic and magnetostratigraphic data from the pelagic intervals indicate that the average rates of sedimentation range from 137 to 944 m/m.y. for the turbidite sequence and 32 m/m.y. for the pelagic intervals of Pleistocene age (Fig. 34). If we assume that the pelagic intervals interbedded within the turbidite sequence have the same sedimentation rate as the comparable sediments of lithologic Unit I, i.e., 20–30 m/m.y., then the plot of age vs. depth should have a steplike pattern (the dotted line in Fig. 34) indicating alternating phases of very rapid and slow sedimentation.

The pelagic intervals of nannofossil ooze, notably in lithologic Unit I, display cyclic color changes that are thought to be caused by variations in the $CaCO_3$ content. Measurements of the magnetic susceptibility of the sediments also detected a cyclic pattern that appears to correlate with calcium-carbonate content. Light-colored $CaCO_3$-rich layers generally have low susceptibility, while the darker sandy and silty turbidite layers have distinctly higher values. A transition between the pelagic and turbidite facies occurs in the lower part of lithologic Unit I, where susceptibility gradually decreases upsection (see Fig. 17 and "Paleomagnetism" section, this chapter). This trend reflects the decreasing turbidite dilution of the pelagic carbonate sedimentation. The decrease is evident from 28 to 14 mbsf and signifies decreasing turbidite activity in this section of the Indus Fan. Because the top of the ooze (light in color and low in susceptibility) probably corresponds to the last interglacial, low values in the upper 8 m of Hole 720A may be correlated with interglacial conditions. The amplitudes of the fluctuations in the susceptibility are rather large in this upper 8-m interval (Fig. 35). The good correlation of the susceptibility curve with the standard oxygen isotope curve can be used to develop a very detailed curve of sedimentation rates for the uppermost Pleistocene at Site 720 (Fig. 35). The upper and lower parts of sedimentary Unit I may have higher rates because of less compaction and dilution by turbidites, respectively.

The depositional history at Site 720 has been dominated by turbidite deposition with brief interludes that are characterized by an increase in pelagic components. The deposition of the pelagic beds clearly reflects a decrease in clastic influx to the site (see "Lithostratigraphy" section, this chapter, for a discussion) rather than an increase in pelagic sedimentation rate. A decrease in clastic influx could be caused by local, regional, or global mechanisms. For example, highstands of sea level could reduce the clastic flux to the entire fan. This pattern is observed in the Holocene age sediments of the Indus Fan, which are foraminiferal marls and oozes (Kolla and Coumes, 1987). This sea-level mechanism thus produces thin pelagic interbeds with great lateral extent on the fan. Therefore, the timing of pelagic interbeds within a generally clastic fan facies should be coincident with, and controlled by, sea-level and climate variations. Another mechanism that could produce predominantly pelagic deposits on the elevated levee deposits is the abandonment of an active channel. This mechanism would be local in extent (affecting only the active channel levee) and would allow pelagic sediments to accumulate over several sea-level cycles until the channel became active or another channel migrated into the area. The timing of channel switching and abandonment, although difficult to establish precisely, is also likely to be related to increased clastic influx during low or falling sea level. These mechanisms may act separately or in combination to produce the observed thickness and timing of the pelagic intervals observed at Site 720.

In this summary of Site 720, the term "bed" is used to refer to individual turbidites as observed in the lithologic logs. The term "sequence" refers to larger-scale trends, such as fining, that are observed in the downhole logging data and in the seismic data sections. Here, we combine the lithologic, logging, and seismic to interpret the evolution of depositional environments at Site 720.

The lower part of the section (390–290 mbsf, seismic Sequence C) is of early Pleistocene age and has no pelagic interbeds. It is mostly composed of thin- to thick-bedded muddy and sandy turbidites that form upward-fining sequences with relatively uniform thickness. This association is characteristic of active overbank deposition and minor channel migration over an extended period of time. A sharp transition to finer-grained and more pelagic deposition (Core 117-720A-30X, ∼277–290 mbsf) probably indicates a major shift in the distributary channel which may be related to differential tectonic motion between

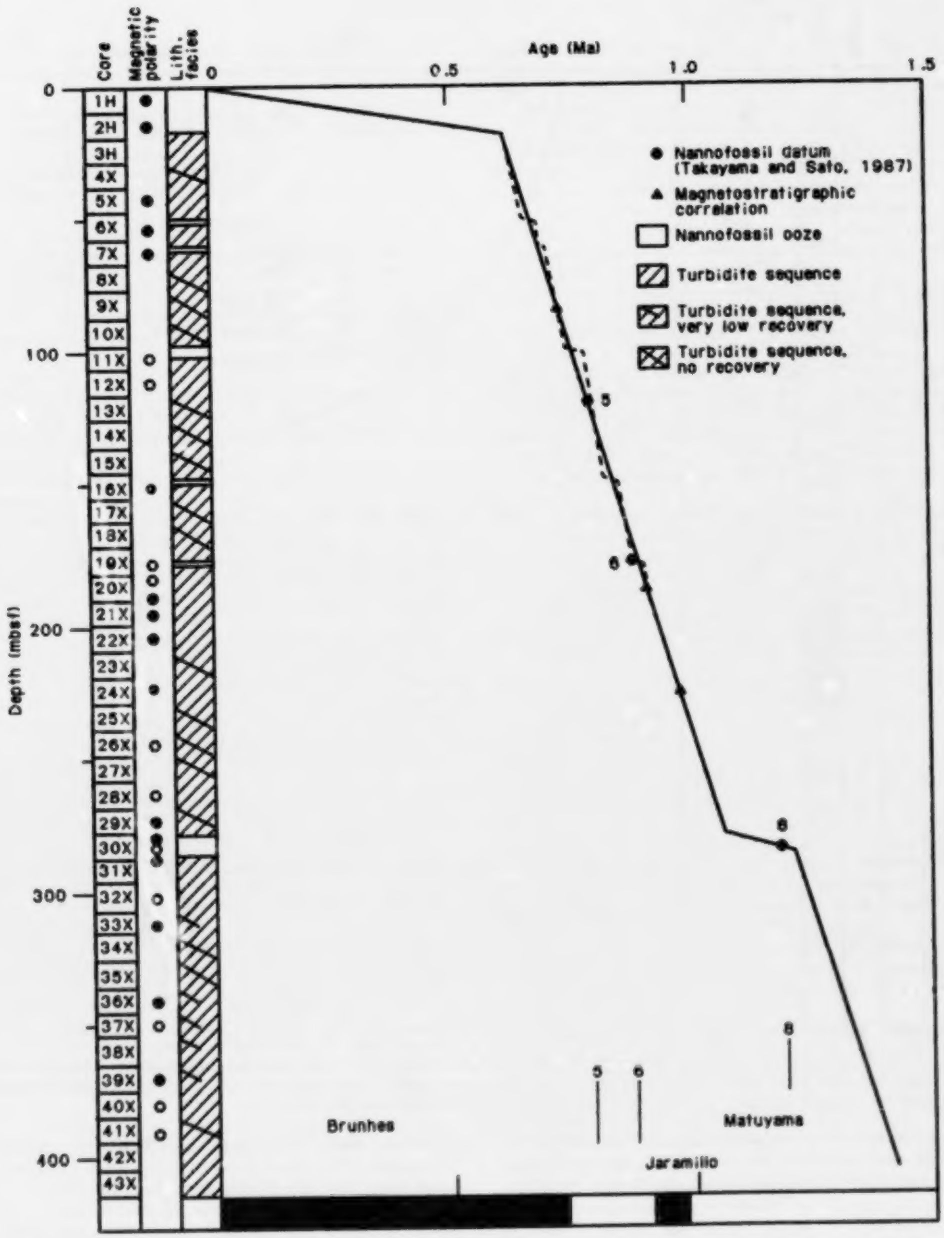

Figure 34. Depth-age diagram of Hole 720A. Vertical columns show core interval, magnetic polarity (solid circle: normal; open circle: reversed; half solid circle: intermediate) and lithologic facies. Bottom column shows standard magnetostratigraphic sequence. Numbers represent nannofossil datum number by Takayama and Sato (1987). Solid line shows average curve of sedimentation rate and dotted line shows changes inferred for pelagic intervals.

the Owen Ridge and the Indus Fan (see "Seismic Stratigraphy" section, this chapter). On the basis of sedimentation rates in similar sediments of lithologic Unit I, this quiescent interval of pelagic deposition may have lasted as long as 300,000 years.

The lower Pleistocene (~1.19 Ma) pelagic interval of Core 117-720A-30X is overlain by sandy thick-bedded turbidites that form both fining- and coarsening-upward sequences from about 277 to 188 mbsf in seismic Subsequence B-2 and B-3. The turbiditic interval is interrupted by at least four pelagic intervals; these are observed in the log data, but were not recovered in the cores. We interpret this interval to represent intermittent deposition by unchannelized sand sheets with occasional quiescent periods of pelagic deposition.

The interval from 188 to 103 mbsf of Susbequence B-1 is

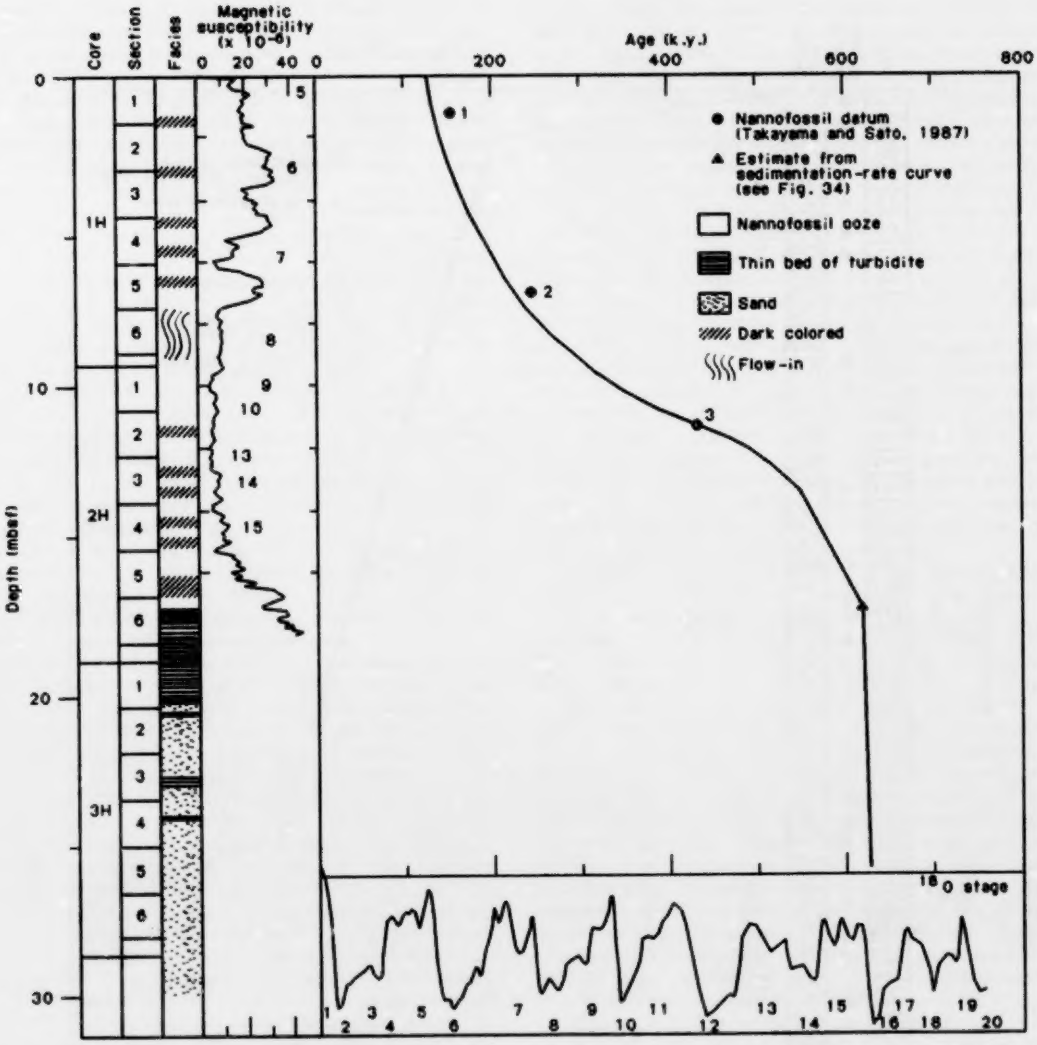

Figure 35. Depth-age diagram of the top part of Hole 720A. Vertical columns show core interval, section interval, lithologic facies, and magnetic susceptibility (number: correlative oxygen isotopic stage). Bottom column shows standard oxygen isotope stratigraphy. Numbers on the diagram represent nannofossil datum number by Takayama and Sato (1987).

characterized by turbidites of variable thickness, numerous thin pelagic intervals, and generally increasing clay content upsection. This interval forms the two large upward-fining sequences observed in the log data (see "Downhole Measurements" section, this chapter). The facies indicates that turbiditic deposition was dominated by large overbank events or sheet flow of thick sands, alternating with a normal overbank-levee environment that accumulated mud turbidites primarily. The upsection increase in clay content could alternatively indicate that the size and frequency of the turbidite events was decreasing.

The upper 100 mbsf at Site 720 (seismic Sequence A) is characterized by further channel switching and abandonment of active channels resulting in several pelagic intervals intercalated with turbiditic sediments. This seismic Sequence (A) thickens toward the Owen Ridge and has abundant buried channels that indicate a rapid infilling over the past 0.7 m.y. (Fig. 34 and "Seismic Stratigraphy" section, this chapter). The most recent transition from predominantly turbiditic to pelagic deposition (lithologic Unit I) occurs at about 0.5 Ma (17 mbsf). On most submarine fans, late Pleistocene rates of turbidite deposition are generally related to changes in sea level; higher rates are usually observed during low sea-level stands. However, pelagic Unit I of Site 720 does not contain turbidites. Therefore, the temporary lack of terrigenous influx to the site is probably related to switching of the distributary channel away from the site rather than to a general decrease in turbidite deposition on the Indus Fan.

The high rates (>500 m/m.y.) of Pleistocene turbidite deposition on the Indus Fan are more than twice the rates found by Leg 116 on the distal Ganges Fan. These high accumulation rates are consistent with accelerated uplift and erosion in the Indus source area. However, the lack of a longer record precludes any observations concerning longer-term relations between the rates of uplift and sedimentation on the Indus Fan at Site 720.

REFERENCES

Archie, G. E., 1942. The electrical resistivity log as an aid in determining some reservoir characteristics. *Trans. Am. Inst. Min. Eng.*, 146: 54–63.

Arthur, M. A., Srivastava, S., et al., 1987. Site 646. *In* Arthur, M. A., Srivastava, S., et al., *Proc. ODP, Init. Repts.*, 105: College Station, TX (Ocean Drilling Program), 419–674.

Barron, J. A., Keller, G., and Dunn, D. A., 1985. A multiple microfossil biochronology for the Miocene. *Geol. Soc. Am. Mem.*, 163:21–36.

Berggren, W. A., Kent, D. V., and Van Couvering, J.A., 1985. The Neogene: Part 2, Neogene geochronology and chronostratigraphy. *In* Snelling, N. J. (Ed.), *The Chronology of the Geological Record*: Geol. Soc. Mem. (London), 10:211–260.

Blow, W. H., 1969. Late Middle Eocene to Recent planktonic foraminiferal biostratigraphy. *In* Bronnimann, R. and Renz, H. H. (Eds.), *Proceedings of the International Conference on Planktonic Microfossils*: Leiden (E. J. Brill), 1:199–421.

Bode, G. W., 1974. Appendix II. Carbon and carbonate analyses, Leg 23. *In* Whitmarsh, R. B., Weser, O. E., Ross, D. A., et al., *Init. Repts. DSDP*, 23: Washington (U.S. Govt. Printing Office), 1131–1135.

Broecker, W. S., and Peng, T. L., 1982. *Tracers in the Sea*: New York (Eldigio Press).

Cochran, J. R., Stow, D.A.V., et al., in press. *Proc. ODP, Init. Repts.*, 116: College Station, TX (Ocean Drilling Program).

Degens, E. T., and Mopper, K., 1976. Factors controlling the distribution and early diagenesis of organic material in marine sediments. *In* Riley, J. P., and Chester, R. (Eds.), *Chemical Oceanography* (Vol. 6): New York (Academic Press), 59–113.

Drever, J. I., 1974. The magnesium problem. *In* Goldberg, E. D. (Ed.), *The Sea* (Vol. 5): New York (John Wiley Press), 337–357.

Emeis, K, 1985. Particulate suspended matter in major world rivers–II: Results on the rivers Indus, Waikato, Nile, St. Lawrence, Yangtse, Parana, Orinoco, Caroni, and Mackenzie. *SCOPE/UNEP Sonderband*, Mitt. Geol.-Paläont. Inst., Univ. Hamburg, Heft 58:593–617.

Fertl, H. H., 1979. *Gamma Ray Spectral Data Assists in Complex Formation Evaluation*: Dresser-Atlas.

Hamilton, E. L., 1974. Prediction of deep-sea sediment properties: state-of-the art. *In* Interbitzen, A. L., (Ed.), *Deep-Sea Sediments: Physical and Mechanical Properties*: New York (Plenum Press), 1–43.

_______, 1976. Variations of density and porosity with depth in deep-sea sediments. *J. Sediment. Petrol.*, 46:280–300.

_______, 1979. Sound velocity gradients in marine sediments. *J. Acoust. Soc. Am.*, 63:909–922.

Jipa, D., and Kidd, R. B., 1974. Sedimentation of coarser grained interbeds in the Arabian Sea and sedimentation processes of the Indus Cone. *In* Whitmarsh, R. B., Weser, O. E., Ross, D. A., et al., *Init. Repts. DSDP*, 23: Washington (U.S. Govt. Printing Office), 471–495.

Johnson, D. A., Nigrini, C., Caulet, J. P., Schneider, D., and Kent, D., in press. Pliocene-Pleistocene radiolarian events and magnetostratigraphic calibrations for the tropical Indian Ocean. *Mar. Micropaleontology.*

Johnson, D. A., and Nigrini, C. A., 1985. Synchronous and time transgressive Neogene radiolarian datum levels in the equatorial Indian and Pacific Oceans. *Mar. Micropaleontol.*, 9:489–523.

Keller, G. V., 1982. Electrical properties of rocks. *In* Carmichael, R. S. (Ed.), *Handbook of Physical Properties of Rocks* (Vol. 1): Boca Raton, FL (CRC Press), 217–293.

Kolla, V., Kostecki, J. A., Robinson, F., and Biscaye, P. E., 1981a. Distribution and origins of clay minerals and quartz in surface sediments of the Arabian Sea. *J. Sediment. Petrol.*, 51:563–569.

Kolla, V., Ray, P. K., and Kostecki, J. A., 1981b. Surficial sediments of the Arabian Sea. *Mar. Geol.*, 41:183–204.

Kolla, V., and Coumes, F., 1984. Morpho-acoustic and sedimentologic characteristics of the Indus fan. *Geomarine Lett.*, 3:133–139.

_______, 1987. Morphology, internal structure, seismic stratigraphy, and sedimentation of Indus fan. *AAPG Bull.*, 71(6):650–677.

McHargue, T. R., and Webb, J. E., 1986. Internal geometry, seismic facies, and petroleum potential of canyons and inner fan channels of the Indus submarine fan. *AAPG Bull.*, 70:161–180.

Martini, E., 1971. Standard Tertiary and Quaternary calcareous nannoplankton zonation. *In* Farinacci, A. (Ed.), *Proc. II Planktonic Conf.*: Roma (Ed. Technoscienza), 2:739–785.

Mercier, J.-L., Armijo, R., Tapponnier, P., Carey-Gailhardis, E., and Lin, H. T., 1987. Change from late Tertiary compression to Quaternary extension in Southern Tibet during the India-Asia collision. *Tectonics*, 6:275–304.

Murray, J. W., 1976. Comparative studies of living and dead benthic foraminiferal distributions. *In* Hedley, R. H., and Adams, C. G. (Eds.), *Foraminifera* (Vol. 2): London (Academic Press), 45–109.

Nigrini, C. A., 1971. Radiolarian zones in the Quaternary of the equatorial Pacific Ocean. *In* Funnell, B. M., and Riedel, W. R. (Eds.), *The Micropalaeontology of Oceans*: Cambridge (Cambridge Univ. Press), 443–461.

Sato, T., Takayama, T., Kato, M., Kudo, T., and Kameo, K., in press: Calcareous microfossil biostratigraphy of the uppermost Cenozoic formations distributed in the coast of the Japan Sea. Part 4: Conclusion. *Sekiyu Gijutsu Kyokaishi.*

Serra, O., 1987. *Fundamentals of Well-log Interpretation, (Vol. 2, Part 2; The Interpretation of Logging Data:* Amsterdam (Elsevier).

Shanmugam, G., and Moiola, R. J., 1982. Eustatic control of turbidites and winnowed turbidites. *Geology*, 10:231–235.

Takayama, T., and Sato, T., 1987. Coccolith biostratigraphy of the North Atlantic Ocean, Deep Sea Drilling Project Leg 94. *In* Ruddiman, W. F., Kidd, R. B., Thomas, E., et al., *Init. Repts. DSDP*, 94, Pt. 2: Washington (U.S. Govt. Printing Office), 651–702.

Vail, P. R., Mitchum, R. M., Todd, R. G., et. al., 1977. Seismic stratigraphy and global sealevel changes. *In* Payton, C. E. (Ed.), *Seismic Stratigraphy*, AAPG Mem., 26:49–212.

van Gorsel, J. T., and Troelstra, S. R., 1981. Late Neogene planktonic foraminiferal biostratigraphy and climatostratigraphy of the Salo River section (Java, Indonesia). *Mar. Micropaleontol.*, 6:183–209.

van Morkhoven, F. P., Berggren, W. A., and Edwards, A. S., 1986. Cenozoic cosmopolitan deep-water benthic foraminifera. *Bull. Cent. Rech. Explor.-Prod. Elf-Aquitaine*, Mem. 11.

Weser, O. E., 1974. Sedimentological aspects of strata encountered on Leg 23 in the Northern Arabian Sea. *In* Whitmarsh, R. B., Weser, O. E., Ross, D. A., et al., *Init. Repts. DSDP*, 23: Washington (U.S. Govt. Printing Office), 503–519.

Whitmarsh, R. B., 1974. Some aspects of plate tectonics in the Arabian Sea. *In* Whitmarsh, R. B., Weser, O. E., Ross, D. A., et al., *Init. Repts. DSDP*, 23: Washington (U.S. Govt. Printing Office), 527–535.

Whitmarsh, R. B., Weser, O. E., Ross, D. A., et al., 1974. *Init. Repts. DSDP*, 23: Washington (U.S. Govt. Printing Office).

Winsauer, W. O., Shearin, H. M., Jr., Masson, P. H., and Williams, M., 1952. Resistivity of brine saturated sands in relation to pore geometry. *AAPG Bull.*, 36:253–277.

Ms 113A-104

Summary Log for Hole 720A

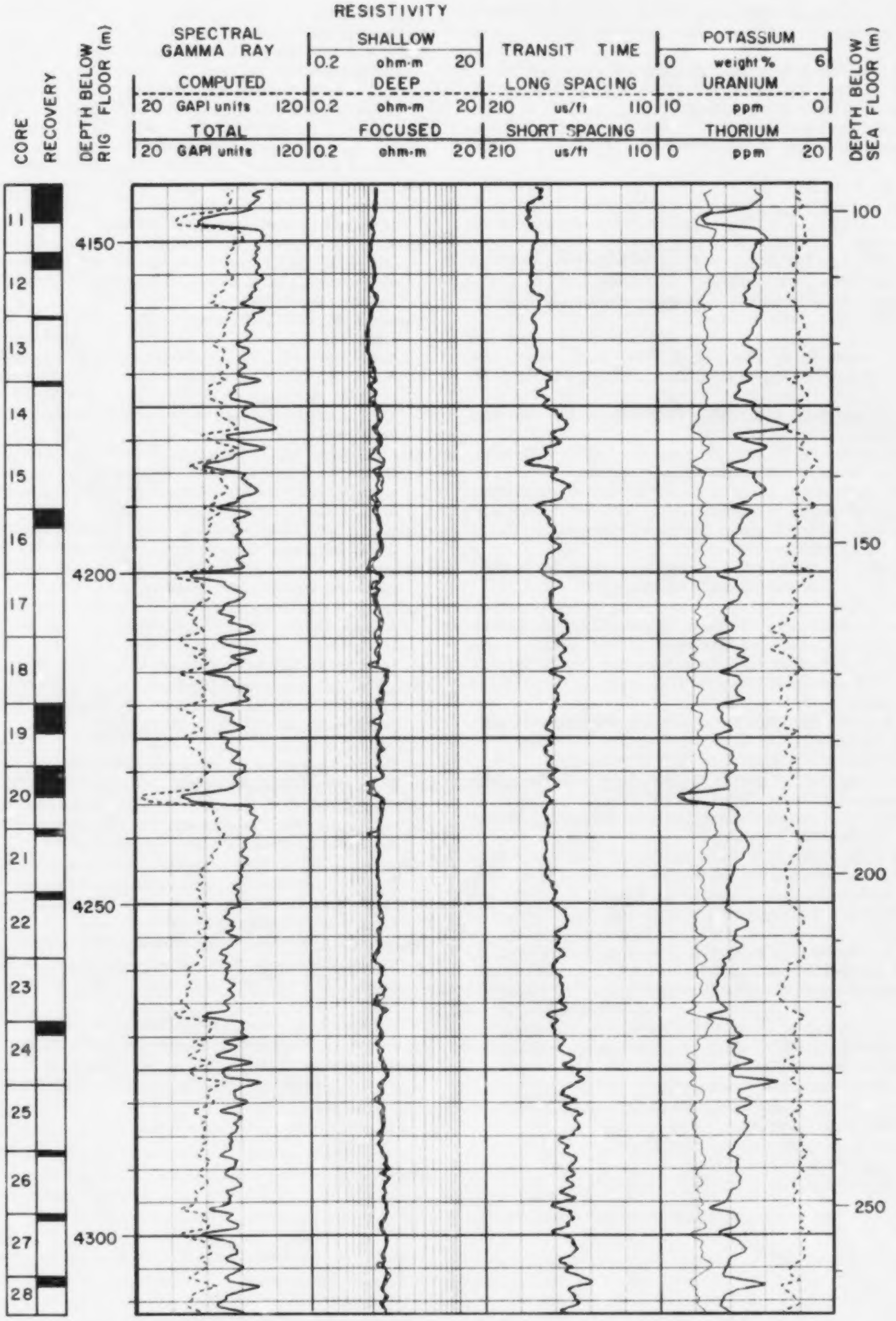

Summary Log for Hole 720A (continued)

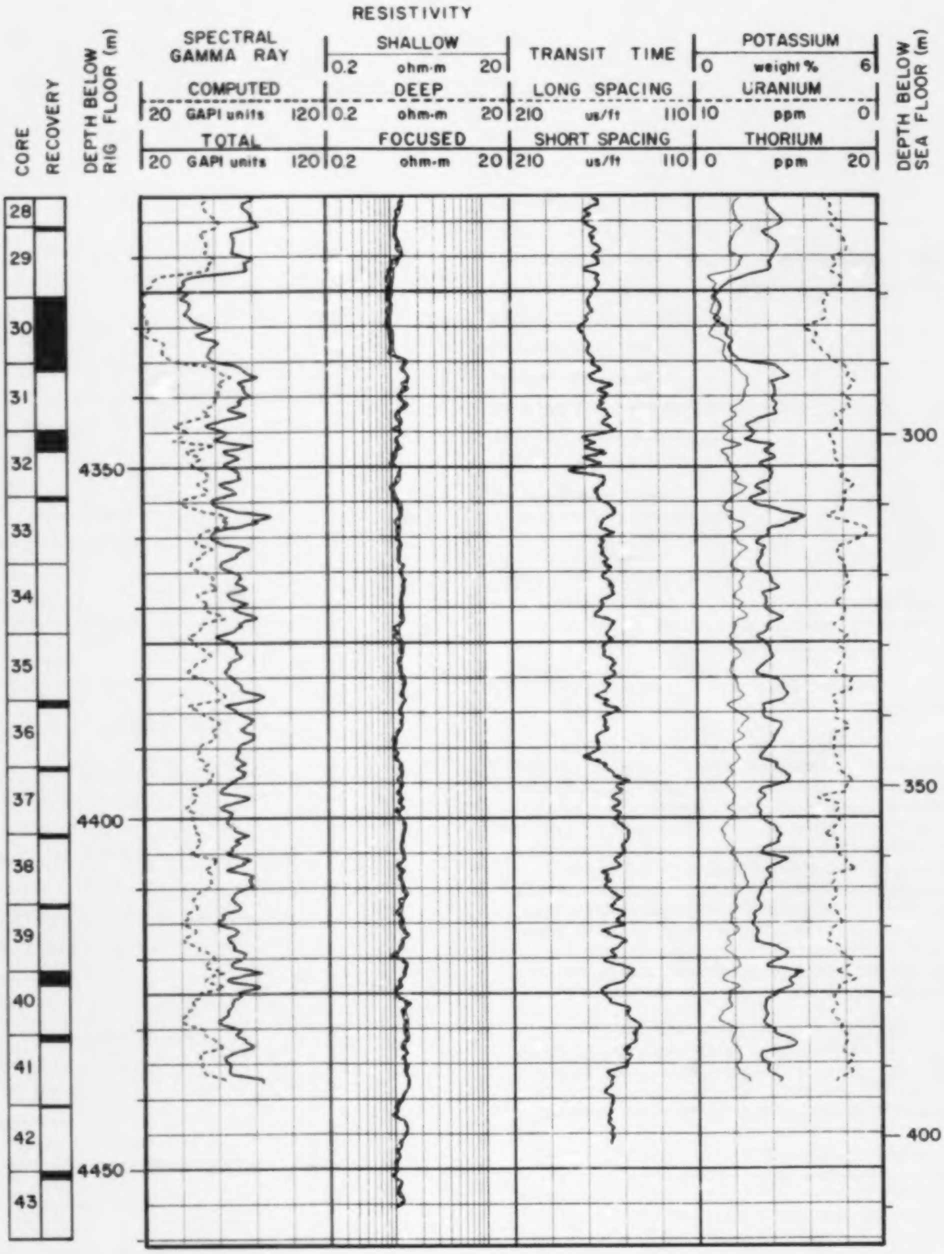

9. SITE 721[1]

Shipboard Scientific Party[2]

HOLE 721A

Date occupied: 3 September 1987

Date departed: 3 September 1987

Time on hole: 13 hr

Position: 16°40.636′N, 59°51.879′E

Water depth (sea level; corrected m, echo-sounding): 1944.8

Water depth (rig floor; corrected m, echo-sounding): 1955.3

Bottom felt (m, drill pipe): 1952.2

Penetration (m): 86.4

Number of cores: 9

Total length of cored section (m): 86.4

Total core recovered (m): 89.28

Core recovery (%): 103.3

Oldest sediment cored:
Depth sub-bottom (m): 86.4
Nature: nannofossil ooze
Age: late Pliocene
Measured velocity (km/s): 1.55

HOLE 721B

Date occupied: 4 September 1987

Date departed: 6 September 1987

Time on hole: 50 hr, 15 min

Position: 16°40.636′N, 59°51.879′E

Water depth (sea level; corrected m, echo-sounding): 1944.8

Water depth (rig floor; corrected m, echo-sounding): 1955.3

Bottom felt (m, drill pipe): 1949.0

Penetration (m): 424.2

Number of cores: 44

Total length of cored section (m): 424.2

Total core recovered (m): 342.8

Core recovery (%): 80.8

Oldest sediment cored:
Depth sub-bottom (m): 424.2
Nature: siltstone, claystone, and mudstone
Age: early Miocene
Measured velocity (km/s): 1.55

HOLE 721C

Date occupied: 6 September 1987

Date departed: 6 September 1987

Time on hole: 20 hr, 25 min

Position: 16°40.636′N, 59°51.879′E

Water depth (sea level; corrected m, echo-sounding): 1944.8

Water depth (rig floor; corrected m, echo-sounding): 1955.3

Bottom felt (m, drill pipe): 1949.1

Penetration (m): 138.0

Number of cores: 15

Total length of cored section (m): 138.0

Total core recovered (m): 133.8

Core recovery (%): 97

Oldest sediment cored:
Depth sub-bottom (m): 138.0
Nature: nannofossil ooze
Age: early Pliocene
Measured velocity (km/s): 1.55

Principal Results: Site 721 is located on the Owen Ridge in the western Arabian Sea. Its objective was to recover a continuous upper Neogene section of pelagic sediments that record changes in the monsoonal circulation system.

The section penetrated at Site 721 ranges from early Miocene to Holocene in age and has been divided into four major lithologic units.

Unit I (0.0–289.0 mbsf) consists exclusively of alternating light and dark layers of foraminifer-bearing to foraminifer-nannofossil ooze-chalk, and nannofossil ooze-chalk of Holocene to late Miocene age. The sediments of this unit reveal strong cyclicity that is indicated by changes in color, bulk density, carbonate content, and particularily well by magnetic susceptibility on whole-round cores.

Unit II (289.0–309.9 mbsf) is a siliceous-bearing nannofossil- to diatomaceous nannofossil chalk of early late Miocene age. Sediments of this unit show evidence of soft sediment deformation throughout. In contrast to Unit I, biogenic opal is an abundant component of Unit II, and both diatoms and radiolarians are preserved in the sediments. Microfossil assemblages in general are characterized by the lack of typical tropical species and the dominance of cool water assemblages.

Unit III (309.9–340.7 mbsf) is comprised of nannofossil chalk of middle Miocene age. Silica preservation is poor in the carbonate-rich chalks (which average about 77% $CaCO_3$). A hiatus (from Zone NN9 to NN5) occurs at the top of this unit (at about 310 mbsf), and as much as 150 m of the middle Miocene section may be missing.

Unit IV (340.7–424.2 mbsf) is characterized by turbiditic intercalations of silts and mud turbidites and contrasts from the dominantly pelagic facies of the overlying units. Clay-bearing nannofossil chalk grades downsection into calcareous silty clay and clayey siltstone of early Miocene age. Preservation of planktonic calcareous and opaline tests is poor and benthic foraminifers from the upper and middle bathyal depths are absent. The increase of pelagic deposits upsection is related to the uplift of the Owen Ridge out of the regime of turbidite deposition.

The sediments at Site 721 indicate that the monsoonal upwelling system of the northern Indian Ocean was active in the late Miocene. Turbidite deposition on the ridge ceased as the ridge rose over the surrounding seafloor during the early Miocene in the wake of tectonic reorganization of spreading centers and transform faults in the Indian Ocean.

---

[1] Prell, W. L., Niitsuma, N., et al., 1989. *Proc. ODP, Init. Repts.*, 117: College Station, TX (Ocean Drilling Program).

[2] Shipboard Scientific Party is as given in the List of Participants preceding the contents.

BACKGROUND AND OBJECTIVES

Site 721 is located near the crest of the Owen Ridge at 16°40.636′N and 59°51.879′E, at a water depth of 1944.8 m (Fig. 1). The site is positioned above the regional carbonate lysocline to avoid major dissolution changes in the calcareous deposits. The site was selected on Line 40 (2010 hr, 3 June 1986) of the *Robert Conrad* (Leg 27-04) site survey (Fig. 2). Total sediment thickness is about 1.62 s (about 1400 m), and the target depth is at 0.5 s (about 425 m). The upper part of the section (0.34 s, ~290 mbsf) has relatively smooth, low-amplitude parallel reflectors with some structure near 0.22 s (about 180 mbsf). A prominent seismic reflector (see "Seismic Stratigraphy" section, this chapter) with complex structure occurs at 0.34–0.38 s (~290–320 mbsf), and the top of a strongly reflective sequence occurs at 0.47 s (about 410 mbsf). Correlating the recovered section at DSDP Site 224 (Whitmarsh et al., 1974) with the seismic data from the site survey, the upper seismic reflector was thought to be of late Miocene age and the lower reflector to be of middle to early Miocene age. The strongly reflective sequence below the reflector at 0.47 s was interpreted as correlative with the terrigenous detrital clayey silty claystones observed in Site 224. The target depth of Site 721 was calculated to penetrate this terrigenous sequence at about 420 mbsf.

OPERATIONS

The vessel departed Site 720 at 2100 hr on 2 September for the area of the Owen Ridge Sites 721 and 722. Because of the

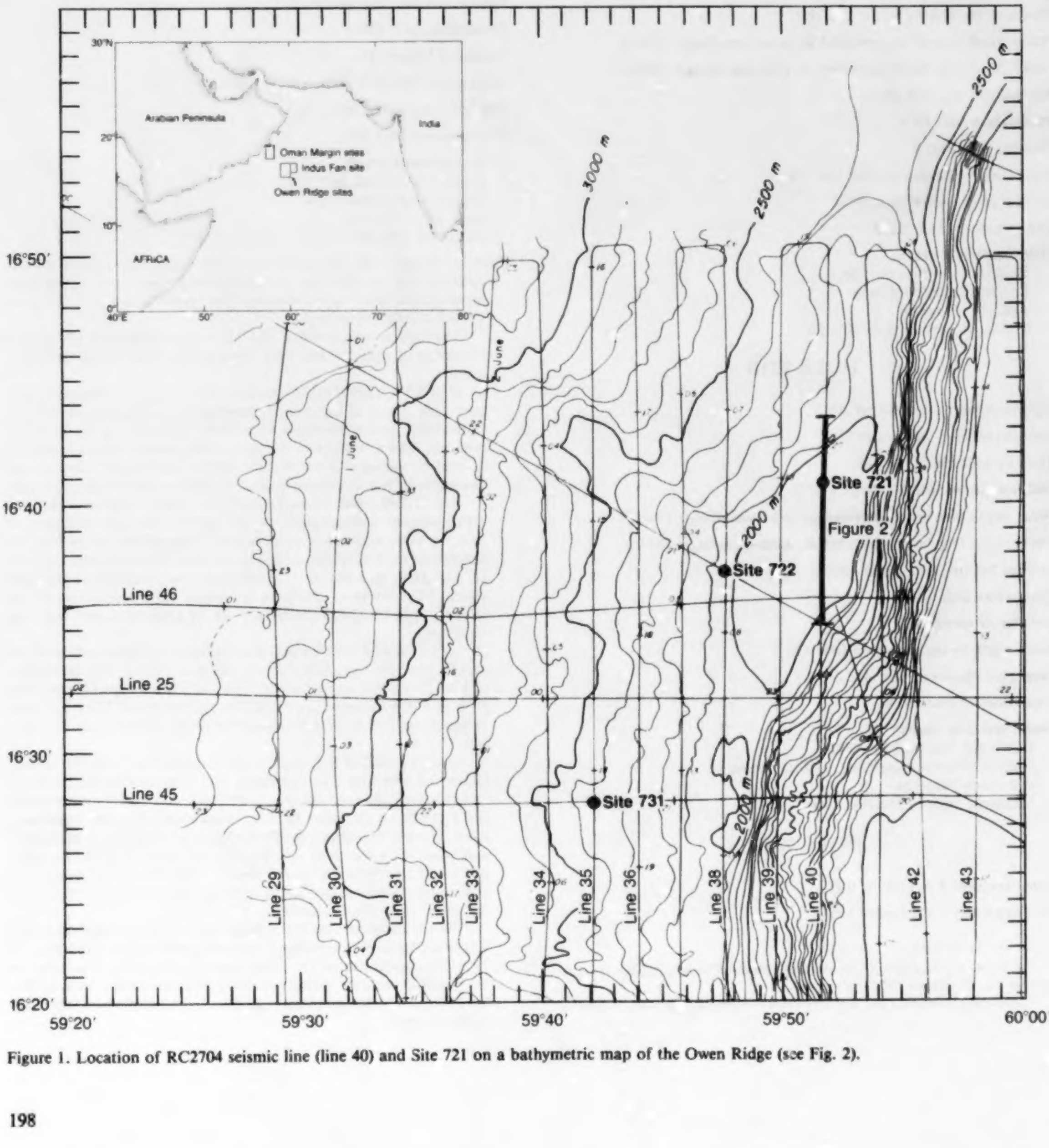

30°N
20°
10°
0°
40°E
50°
60°
70°
80°
Arabian Peninsula
India
AFRICA
Oman Margin sites
Indus Fan site
Owen Ridge sites
3000 m
2500 m
2500 m
2000 m
2000 m
June
1 June
Site 721
Figure 2
Site 722
Site 731
Line 46
Line 25
Line 45
Line 29
Line 30
Line 31
Line 32
Line 33
Line 34
Line 35
Line 36
Line 38
Line 39
Line 40
Line 42
Line 43
16°50′
16°40′
16°30′
16°20′
59°20′
59°30′
59°40′
59°50′
60°00′

Figure 1. Location of RC2704 seismic line (line 40) and Site 721 on a bathymetric map of the Owen Ridge (see Fig. 2).

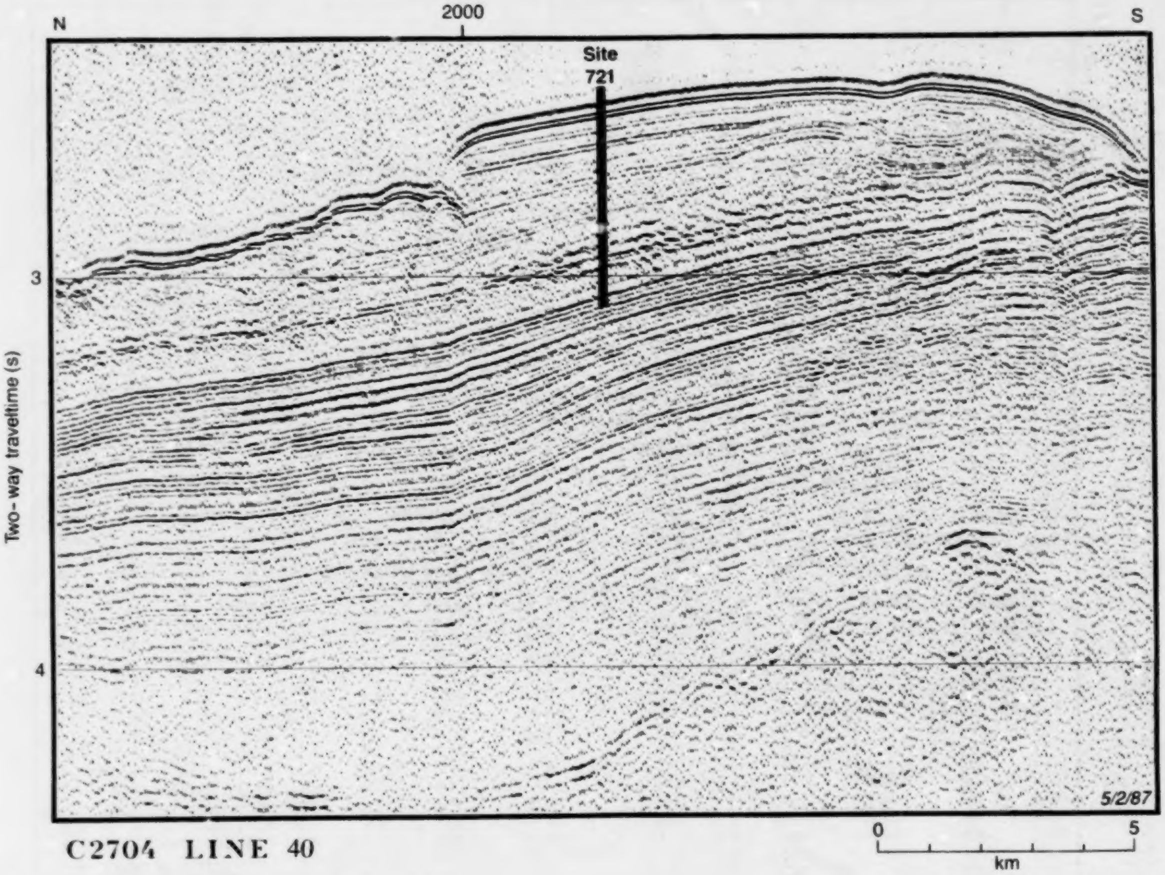

Figure 2. Seismic profile of Site 721 (Line RC2704-40).

proximity of the two sites, it was decided to survey both locations on approach to Site 721, and the seismic gear was deployed upon departure from Site 720. Good GPS coverage ensured accurate positioning throughout the survey and site approach, and a high-resolution positioning chart was obtained for the ship's track (Fig. 3). Upon passage of the target location of Site 722 at 0900 hr on 3 September, a beacon was dropped at the site, and the ship continued approach to Site 721, where the beacon was dropped at 1100 hr. The final position of Site 721 was established as 16°40.636′N and 59°51.879′E. The seismic gear was retrieved and the ship positioned, and the mud line of Hole 721A was established at 1952 m (bottom felt) at 1515 hr on 3 September.

Nine APC cores were drilled with a maximum overpull of 10,000 pounds with excellent recovery (>100%) to a total depth for Hole 721A of 86.4 mbsf (Table 1). Core 117-721A-10H stuck in a clay-rich interval, and the core barrel failed at 140,000 pounds overpull, so that Hole 721A had to be abandoned.

Hole 721B was spudded 20 m west of Hole 721A at 0017 hr on 4 September. Nine APC cores recovered >100% of the cored section to 86.0 mbsf. Because of an increase of overpull to 25,000 pounds, drilling mode was switched to XCB coring from Core 117-721B-10X. Forty-four cores were drilled to the target depth of 424.2 mbsf with an average recovery of 81%. After clearing the mud line, the ship positioned 20 m west of Hole 721B and spudded Hole 721C at 0335 hr on 6 September. Ten APC cores yielded >100% recovery to a depth of 89.9 mbsf, where a maximum overpull of 35,000 pounds necessitated a switch to XCB coring. Overall recovery was 97% in the 138.0 m total depth of Hole 721C. The *in-situ* pore-water sampler was deployed twice in Hole 721C. At 2230 hr on 6 September, the mud line was cleared and the ship relocated to Site 722 without pulling pipe.

LITHOSTRATIGRAPHY

Lithologic Units

Sediments recovered at Site 721 span the time interval from early Miocene to Holocene and are divided into four lithologic units (Table 2, Fig. 4). This subdivision is based on visual core descriptions, smear slide analysis, calcium carbonate content (Table 3, Fig. 5), and biostratigraphic data. Lithologic Unit I is further divided into two subunits.

Unit I (Depth: 0–289.0 mbsf; Age: Holocene to late Miocene)

Core 117-721A-1H to Section 117-721A-9H, CC; Cores 117-721B-1H to 117-721B-30X; Cores 117-721C-1H to 117-721C-15X. Bottom of Unit I not reached in Holes 721A and 721C.

Subunit IA (Depth: 0–261.2 mbsf)

Lithologic Subunit IA extends from 0 to 261.2 mbsf and consists of alternating light and dark layers of foraminifer-bear-

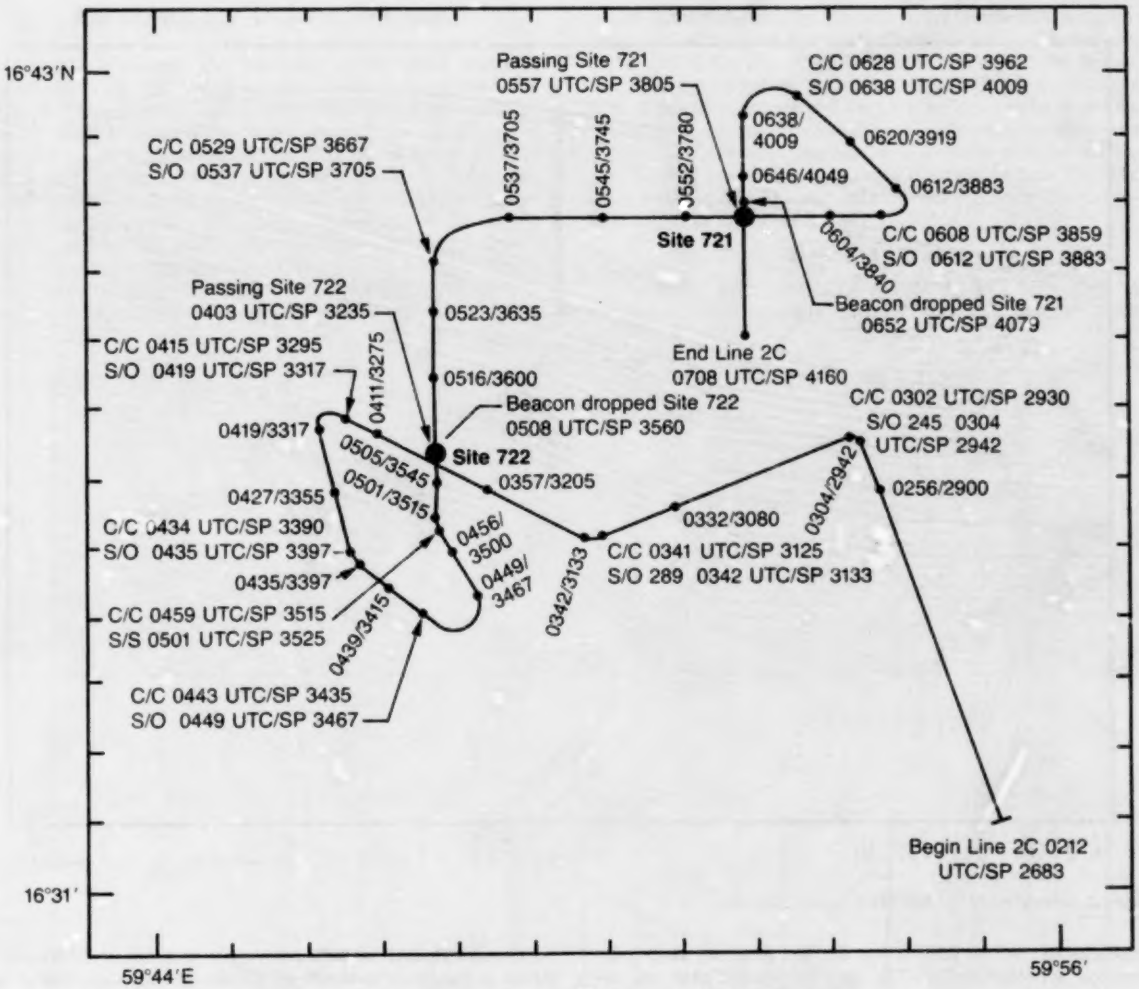
16°43′N
16°31′
59°44′E
59°56′
Passing Site 721
0557 UTC/SP 3805
C/C 0628 UTC/SP 3962
S/O 0638 UTC/SP 4009
0638/
4009
0620/3919
0646/4049
0612/3883
C/C 0529 UTC/SP 3667
S/O 0537 UTC/SP 3705
0537/3705
0545/3745
0552/3780
Site 721
0604/3840
C/C 0608 UTC/SP 3859
S/O 0612 UTC/SP 3883
Beacon dropped Site 721
0652 UTC/SP 4079
Passing Site 722
0403 UTC/SP 3235
0523/3635
C/C 0415 UTC/SP 3295
S/O 0419 UTC/SP 3317
0411/3275
0516/3600
End Line 2C
0708 UTC/SP 4160
Beacon dropped Site 722
0508 UTC/SP 3560
C/C 0302 UTC/SP 2930
S/O 245 0304
UTC/SP 2942
0419/3317
0505/3545
Site 722
0501/3515
0357/3205
0256/2900
0304/2942
0427/3355
0332/3080
C/C 0434 UTC/SP 3390
S/O 0435 UTC/SP 3397
0456/
3500
C/C 0341 UTC/SP 3125
S/O 289 0342 UTC/SP 3133
0342/3133
0435/3397
0449/
3467
C/C 0459 UTC/SP 3515
S/S 0501 UTC/SP 3525
0439/3415
C/C 0443 UTC/SP 3435
S/O 0449 UTC/SP 3467
Begin Line 2C 0212
UTC/SP 2683

Figure 3. Ship track during approach to Owen Ridge operational area and survey of Sites 721 and 722.

ing nannofossil oozes, foraminifer-nannofossil oozes, and nannofossil oozes, which grade to chalks by 155 mbsf. These beds are between 10 and 200 cm thick. Light beds range in color from light greenish gray (10Y 6/2-7/1) to light gray and light olive gray (5Y 6/2-7/1). Dark beds range from dark greenish gray (10Y 5/-4/) to olive, pale olive, and olive gray (5Y 6/3, 6/4, 5/1, 4/1), and dark beds generally contain 5%-20% more terrigenous silty clay and 5%-20% less biogenic calcium carbonate than do light beds. Generally, the boundaries between these beds are gradational and blurred by bioturbation (Figs. 6-8). Calcium carbonate concentrations range from 38% to 90%, with a mean of 66.0% (Fig. 5, Table 3). Based on smear slide analysis, nannofossils are the dominant sedimentary component. Foraminifers range from 10% to 35% in the first core of each hole to less than 10% for the remainder of lithologic Subunit IA, and biogenic silica rarely occurs in more than trace amounts. Inorganic calcite ranges from 0% to 20%, but is commonly less than 5%. Quartz, dolomite, mica, and accessory minerals are present in trace amounts. Further documentation of the mineralogy can be found in the "Inorganic Geochemistry" section of this chapter. The transition from oozes to chalks (top of Core 117-721B-17X) reflects a change to more indurated sediments downhole.

Drilling of Hole 721A was stopped below 86 mbsf (after coring of 117-721A-9H) because a stiff sediment layer could not be penetrated by the APC. In Holes 721B and 721C this level corresponds to the appearance of a dark olive gray (5Y 3/2) marly nannofossil ooze beginning at 117-721B-10X-1, 35 cm (86.35 mbsf), and 117-721C-10X-4, 20 cm (85 mbsf). The marly ooze is interbedded with nannofossil ooze beds over the next 5-10 m downhole. Based on smear slide analysis, the dark marly layer contains more than 30% terrigenous clay. Calcium carbonate values near 55% (Table 3, Fig. 5) are consistent with higher clay contents for these layers.

Subunit IB (Depth: 261.1-289.0 mbsf)

Subunit IB is composed of foraminifer-bearing nannofossil and nannofossil chalks and extends from 261.2 to 289.0 mbsf. Subunit IB contains microfaults and other disturbance structures not attributable to drilling, which distinguishes it from Subunit IA. The structures are thought to record the emplacement of material at this site by slumping. The material is com-

Table 1. Coring summary, Site 721.

Core no.	Date (Sept. 1987)	Time	Depth (mbsf)	Cored (m)	Recovered (m)	Recovery (%)
117-721A-						
1H	3	1630	0.0–9.8	9.8	9.84	100.0
2H	3	1700	9.8–19.5	9.7	9.84	101.0
3H	3	1735	19.5–29.2	9.7	10.11	104.2
4H	3	1800	29.2–38.9	9.7	10.09	104.0
5H	3	1845	38.9–48.5	9.6	9.45	98.4
6H	3	1915	48.5–57.8	9.3	10.08	108.4
7H	3	2000	57.8–67.3	9.5	9.98	105.0
8H	3	2030	67.3–76.8	9.5	10.04	105.7
9H	3	2115	76.8–86.4	9.6	9.85	102.0
				86.4	89.28	
117-721B-						
1H	4	0045	0.0–9.4	9.4	9.39	99.9
2H	4	0125	9.4–19.1	9.7	9.99	103.0
3H	4	0210	19.1–28.8	9.7	9.91	102.0
4H	4	0300	28.8–38.5	9.7	10.04	103.5
5H	4	0340	38.5–48.1	9.6	10.13	105.5
6H	4	0420	48.1–57.4	9.3	9.98	107.0
7H	4	0500	57.4–66.9	9.5	9.84	103.0
8H	4	0545	66.9–76.4	9.5	10.08	106.1
9H	4	0640	76.4–86.0	9.6	9.89	103.0
10X	4	0815	86.0–95.6	9.6	9.78	102.0
11X	4	0900	95.6–105.2	9.6	8.10	84.4
12X	4	0950	105.2–114.8	9.6	3.73	38.8
13X	4	1035	114.8–124.4	9.6	9.69	101.0
14X	4	1125	124.4–134.1	9.7	9.70	100.0
15X	4	1205	134.1–143.8	9.7	8.62	88.8
16X	4	1240	143.8–153.5	9.7	9.63	99.3
17X	4	1325	153.5–163.2	9.7	9.81	101.0
18X	4	1405	163.2–172.9	9.7	9.77	101.0
19X	4	1440	172.9–182.6	9.7	9.57	98.6
20X	4	1510	182.6–192.3	9.7	8.38	86.4
21X	4	1815	192.3–202.0	9.7	3.68	37.9
22X	4	1900	202.0–211.7	9.7	9.83	101.0
23X	4	1945	211.7–221.3	9.6	5.11	53.2
24X	4	2030	221.3–230.5	9.2	5.29	57.5
25X	4	2115	230.5–240.1	9.6	9.58	99.8
26X	4	2155	240.1–249.8	9.7	6.26	64.5
27X	4	2235	249.8–259.6	9.8	6.87	70.1
28X	4	2340	259.6–269.4	9.8	9.21	94.0
29X	5	0105	269.4–279.2	9.8	3.92	40.0
30X	5	0215	279.2–289.0	9.8	5.46	55.7
31X	5	0310	289.0–298.8	9.8	9.06	92.4
32X	5	0355	298.8–308.4	9.6	9.79	102.0
33X	5	0450	308.4–318.0	9.6	3.30	34.4
34X	5	0615	318.0–327.7	9.7	7.18	74.0
35X	5	0720	327.7–337.4	9.7	5.28	54.4
36X	5	0915	337.4–347.0	9.6	3.78	39.4
37X	5	1125	347.0–356.6	9.6	9.83	102.0
38X	5	1315	356.6–366.3	9.7	9.45	97.4
39X	5	1500	366.3–375.9	9.6	0.10	1.0
40X	5	1705	375.9–385.6	9.7	9.85	101.0
41X	5	1855	385.6–395.2	9.6	9.86	103.0
42X	5	2020	395.2–404.9	9.7	3.70	38.1
43X	5	2115	404.9–414.5	9.6	0.48	5.0
44X	5	2330	414.5–424.2	9.7	9.88	102.0
				424.2	342.78	
117-721C-						
1H	6	0345	0.0–3.6	3.6	3.63	101.0
2H	6	0420	3.6–13.3	9.7	9.95	102.0
3H	6	0455	13.3–23.0	9.7	9.91	102.0
4H	6	0525	23.0–32.7	9.7	9.78	101.0
5H	6	0555	32.7–42.4	9.7	9.57	98.6
6H	6	0635	42.4–52.0	9.6	9.99	104.0
7H	6	0715	52.0–61.3	9.3	10.01	107.6
8H	6	0755	61.3–70.8	9.5	9.91	104.0
9H	6	0840	70.8–80.3	9.5	9.98	105.0
10H	6	0920	80.3–89.9	9.6	10.01	104.3
11X	6	1045	89.9–99.5	9.6	7.40	77.1
12X	6	1240	99.5–109.1	9.6	9.49	98.8
13X	6	1315	109.1–118.7	9.6	7.21	75.1
14X	6	1355	118.7–128.3	9.6	7.19	74.9
15X	6	1435	128.3–138.0	9.7	9.76	100.0
				138.0	133.79	

Table 2. Lithostratigraphic summary, Site 721.

Lithologic unit	Depth (mbsf)	Cores	Age	CaCO$_3$ ($\bar{x}$ %)
IA Foraminifer-bearing nannofossil, foraminifer-nannofossil, and nannofossil ooze/chalk; alternating light and dark beds	0.0–261.2	721A-1H to -9H, CC 721B-1H to -30X, CC 721C-1H to -15X, CC	Holocene to late Miocene	66.0
IB Foraminifer-bearing nannofossil amd nannofossil chalk; alternating light and dark beds; disturbed beds	261.2–289.0	721B-28X-2, 10 cm to 721B-30X, CC	late Miocene	51.6
II Siliceous-bearing nannofossil, diatomaceous nannofossil, and nannofossil chalk; alternating light and dark beds; disturbed beds	289.0–309.9	721B-31X 721B-33X-2, 0 cm	early late Miocene	43.9
III Nannofossil chalk	309.9–340.7	721B-33X-2, 0 cm 721B-36X, CC, 30 cm	middle Miocene	76.6
IV Interbedded fine-grained turbidites and nannofossil chalk	340.7–424.2	721B-36X, CC, 30 cm 721B-44X, CC	middle to early Miocene	26.8

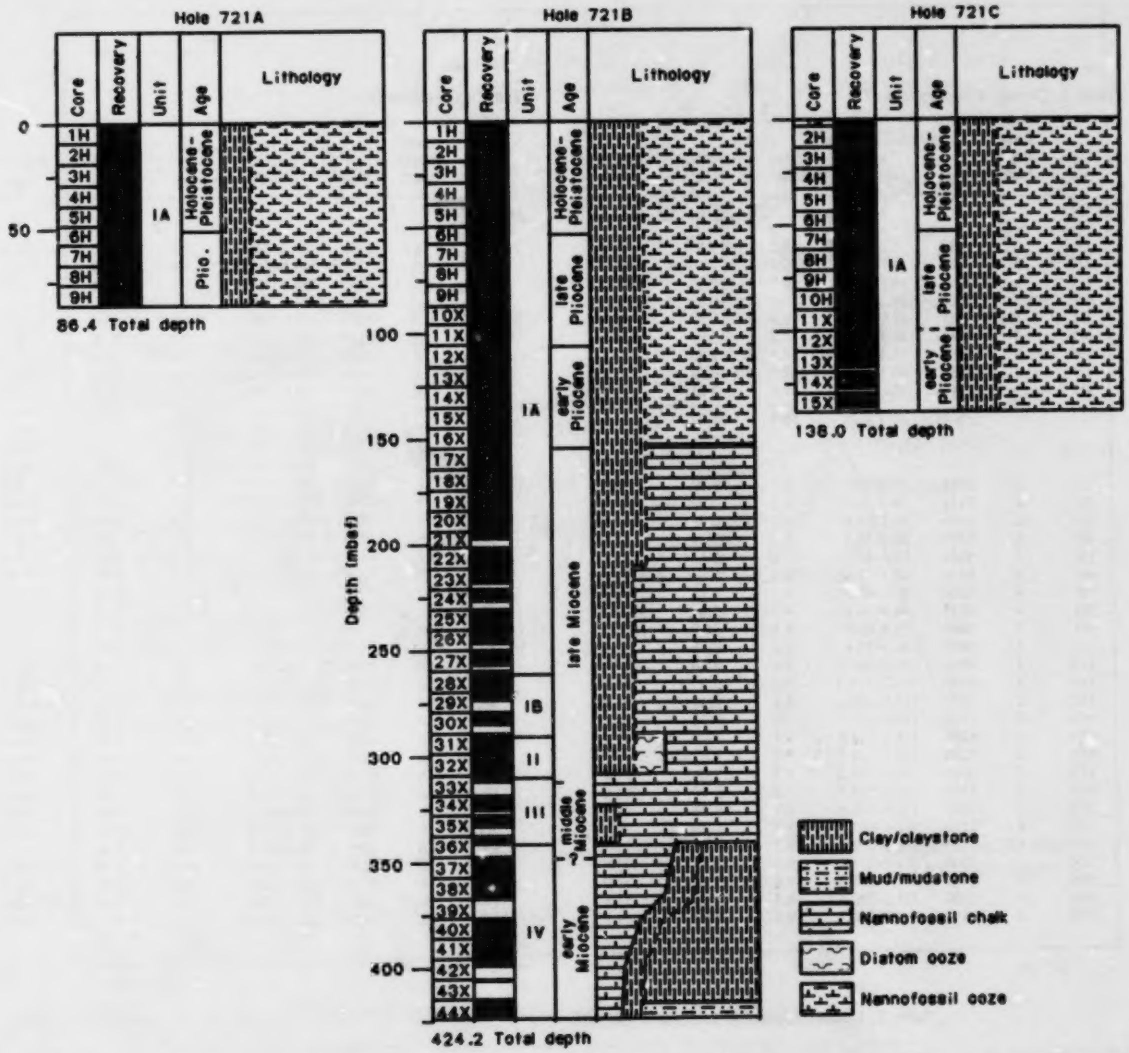
Hole 721A
Core
Recovery
Unit
Age
Lithology
0
50
1H
2H
3H
4H
5H
6H
7H
8H
9H
IA
Holocene-Pleistocene
Plio.
86.4 Total depth
Hole 721B
100
150
200
250
300
350
400
Depth (mbsf)
10X
11X
12X
13X
14X
15X
16X
17X
18X
19X
20X
21X
22X
23X
24X
25X
26X
27X
28X
29X
30X
31X
32X
33X
34X
35X
36X
37X
38X
39X
40X
41X
42X
43X
44X
IA
IB
II
III
IV
late Pliocene
early Pliocene
late Miocene
middle Miocene
?
early Miocene
424.2 Total depth
Hole 721C
10H
late Pliocene
early Pliocene
138.0 Total depth
Clay/claystone
Mud/mudstone
Nannofossil chalk
Diatom ooze
Nannofossil ooze

Figure 4. Lithostratigraphic summary, Site 721. Lithology is inferred between recovered intervals.

positionally different from the sediments above and below and the contacts are relatively sharp. The appearance of these features corresponds to an increase in reworked microfossils (see "Biostratigraphy" section, this chapter) which characterizes lithologic Subunit IB and Unit II. However, drilling disturbances are prevalent between 261.2 and 309.9, and it is difficult to distinguish natural disturbances from those caused by drilling.

Unit II (Depth: 289.0–309.9 mbsf; Age: early late Miocene)

Core 117-721B-31 to Section 117-721B-33X-2.

Lithologic Unit II, between 289 and 309.9 mbsf, consists of alternating light and dark layers of siliceous-bearing nannofossil, diatomaceous nannofossil, and nannofossil chalks. It can be distinguished from lithologic Units I and III by the consistent appearance of siliceous microfossils on smear slides. Nannofossils remain the dominant sediment component and smear slides from dark layers contain as much as 20% more siliceous microfossils and 10%–20% more terrigenous clay than do those of light layers. The mean calcium carbonate concentration in lithologic Unit II is lower than in Unit I (Table 2) and reflects the added siliceous component. Lithologic Unit II is characterized by microfaults and disturbance structures similar to those found in Subunit IB. Figure 9 shows one example of these microfaults.

Unit III (Depth: 309.9–340.7 mbsf; Age: middle Miocene)

Samples 117-721B-33X, CC, 10 cm, to 117-721B-36X, CC, 30 cm.

Unit III consists of a greenish gray and light greenish gray (5G 7/1-5G 5/1) to white (2.5Y 8/0) nannofossil chalk. Lithologic Unit III has the highest mean calcium carbonate concentration (76.6%) of the units recognized at Site 721. Slight to moderate bioturbation is evident throughout. The upper and lower boundaries of lithologic Unit III at Site 721 are sharp. The contact between Units IV and III is marked by a change from a grayish brown (2.5Y 5/2) calcareous silty claystone to a greenish gray (5BG 6/1) nannofossil chalk. The Unit III to Unit II contact is identified by a change from greenish gray nanno-

Table 3. Calcium carbonate and organic carbon abundances, Site 721. Asterisk (*) notes samples from Hole 721B not plotted in Figure 5. Depths reported for Hole 721A samples are not comparable to the reported depths for Hole 721B. See Table 17 for depth adjustments.

Hole, core, section, interval (cm)	Depth (mbsf)	Total carbon (%)	Inorganic carbon (%)	Organic carbon (%)	$CaCO_3$ (%)
721A-1H-1, 25-26	0.25	9.40	8.45	0.95	70.4
*721B-1H-1, 50-53	0.50	9.33	9.26	0.07	77.1
721A-1H-1, 75-76	0.75	7.28	6.81	0.47	56.7
721A-1H-1, 125-126	1.25		7.32		61.0
721A-1H-2, 25-26	1.75	9.05	8.04	1.01	67.0
*721B-1H-2, 100-103	2.50	9.07	7.78	1.29	64.8
721A-1H-2, 125-126	2.75		8.25		68.7
721A-1H-3, 25-26	3.25		8.10		67.5
721A-1H-3, 75-76	3.75		8.11		67.6
721A-1H-3, 125-126	4.25		7.15		59.6
721A-1H-4, 25-26	4.75		6.66		55.5
*721B-1H-4, 80-83	5.30	8.93	8.50	0.43	70.8
721A-1H-4, 125-126	5.75		7.70		64.1
*721B-1H-5, 24-27	6.24	9.07	7.86	1.21	65.5
721A-1H-5, 25-26	6.25		9.42		78.5
721A-1H-5, 75-76	6.75		9.46		78.8
721A-1H-5, 125-126	7.25	8.12	7.74	0.38	64.5
721A-1H-6, 25-26	7.75		7.88		65.6
721A-1H-6, 75-76	8.25		8.42		70.1
721A-1H-6, 125-126	8.75		8.19		68.2
721A-1H-6, 144-145	8.94	8.35	7.79	0.56	64.9
721A-1H-6, 145-150	8.95		7.57		63.1
721A-1H-7, 25-26	9.25		7.42		61.8
721A-2H-1, 25-26	10.05		8.98		74.8
*721B-2H-1, 87-90	10.27	9.83	9.37	0.46	78.1
721A-2H-1, 75-76	10.55		9.54		79.5
*721B-2H-2, 17-20	11.07	9.27	7.36	1.91	61.3
721A-2H-2, 25-26	11.55		8.19		68.2
721A-2H-2, 75-76	12.05	8.88	8.63	0.25	71.9
*721B-2H-3, 27-30	12.67	9.27	8.67	0.60	72.2
721A-2H-3, 75-76	13.55		9.42		78.5
721A-2H-3, 125-126	14.05		9.89		82.4
721A-2H-4, 25-26	14.55		7.99		66.6
721A-2H-4, 75-76	15.05		8.41		70.1
721A-2H-4, 125-126	15.55		8.53		71.1
721A-2H-5, 25-26	16.05		7.85		65.4
721A-2H-5, 75-76	16.55		8.73		72.7
721A-2H-5, 125-126	17.05		8.81		73.4
721A-2H-6, 75-76	18.05		8.44		70.3
721A-2H-6, 125-126	18.55		9.14		76.1
721A-2H-6, 149-150	18.79	8.69	8.31	0.38	69.2
721A-3H-1, 25-26	19.75	8.72	8.35	0.37	69.6
721A-3H-1, 125-126	20.75		7.54		62.8
721A-3H-2, 25-26	21.25		7.67		63.9
721A-3H-2, 75-76	21.75		8.38		69.8
*721B-3H-3, 10-13	22.20	8.48	7.74	0.74	64.5
721A-3H-2, 125-126	22.25		6.85		57.1
721A-3H-3, 25-26	22.75		8.73		72.7
721A-3H-3, 75-76	23.25		8.66		72.1
721A-3H-3, 125-126	23.75		8.68		72.3
721A-3H-4, 25-26	24.25		8.29		69.1
721A-3H-4, 75-76	24.75		7.91		65.9
721A-3H-4, 125-126	25.25	8.62	8.25	0.37	68.7
721A-3H-5, 25-26	25.75		8.95		74.6
721A-3H-5, 75-76	26.25		9.49		79.1
*721B-3H-5, 145-150	26.55		8.90		74.1
721A-3H-5, 125-126	26.75		9.32		77.6
721A-3H-6, 25-26	27.25		6.54		54.5
721A-3H-6, 116-117	28.16		6.96		58.0
721A-3H-6, 119-120	28.19	7.13	6.83	0.30	56.9
721A-3H-7, 25-26	28.75		8.41		70.1
721A-3H-7, 75-76	29.25		6.95		57.9
721A-4H-1, 25-26	29.45		7.26		60.5
721A-4H-1, 75-76	29.95		7.15		59.6
721A-4H-1, 125-126	30.45		7.63		63.6
721A-4H-2, 25-26	30.95		8.39		69.9
721A-4H-2, 75-76	31.45		8.44		70.3
721A-4H-2, 125-126	31.95		8.23		68.6
721A-4H-3, 25-26	32.45		7.96		66.3
721A-4H-3, 75-76	32.95		8.19		68.2
721A-4H-3, 125-126	33.45		7.41		61.7
721A-4H-4, 25-26	33.95		9.15		76.2
721A-4H-4, 75-76	34.45		8.79		73.2
721A-4H-4, 125-126	34.95		8.55		71.2
721A-4H-5, 0-1	35.20	8.75	8.09	0.66	67.4
721A-4H-5, 41-42	35.61		7.50		62.5
721A-4H-5, 75-76	35.95		6.25		52.1
721A-4H-5, 125-126	36.45		8.42		70.1
721A-4H-6, 25-26	36.95		8.70		72.5
721A-4H-6, 75-76	37.45		9.06		75.5
721A-4H-6, 125-126	37.95		8.36		69.6
721A-4H-7, 75-76	38.95		9.76		81.3
721A-5H-1, 25-26	39.15		7.61		63.4
721A-5H-1, 75-76	39.65		7.82		65.1
721A-5H-1, 125-126	40.15		7.45		62.1
721A-5H-2, 25-26	40.65		7.67		63.9
721A-5H-2, 75-76	41.15		9.27		77.2
721A-5H-2, 125-126	41.65		6.55		54.6
721A-5H-3, 25-26	42.15		6.57		54.7
721A-5H-3, 75-76	42.65		8.60		71.6
721A-5H-3, 125-126	43.15		8.01		66.7
721A-5H-4, 25-26	43.65		9.37		78.1
721A-5H-4, 75-76	44.15		7.13		59.4
721A-5H-4, 125-126	44.65		8.54		71.1
721A-5H-4, 149-150	44.89	7.78	6.74	1.04	56.1
721A-5H-5, 25-26	45.15		6.72		56.0
721A-5H-5, 75-76	45.65		8.07		67.2
721A-5H-5, 125-126	46.15		7.67		63.9
721A-5H-6, 25-26	46.65		7.00		58.3
721A-5H-6, 75-76	47.15		8.09		67.4
721A-5H-6, 125-126	47.65		7.04		58.6
721A-6H-1, 25-26	48.75		8.22		68.5
721A-6H-1, 75-76	49.25		6.62		55.1
721A-6H-1, 125-126	49.75		6.70		55.8
721A-6H-2, 25-26	50.25		4.86		40.5
721A-6H-2, 75-76	50.75		5.23		43.6
721A-6H-2, 125-126	51.25		8.24		68.6
721A-6H-3, 25-26	51.75		7.64		63.6
721A-6H-3, 75-76	52.25		4.64		38.7
721A-6H-3, 125-126	52.75		8.55		71.2
721A-6H-4, 25-26	53.25		5.39		44.9
721A-6H-4, 75-76	53.75		7.27		60.6
721A-6H-4, 125-126	54.25		5.65		47.1
721A-6H-5, 25-26	54.75		9.33		77.7
721A-6H-5, 75-76	55.25		5.83		48.6
721A-6H-5, 125-126	55.75		7.72		64.3
721A-6H-6, 25-26	56.25		8.34		69.5
721A-6H-6, 75-76	56.75		6.48		54.0
721A-6H-6, 119-120	57.19	9.61	8.73	0.88	72.7
721A-6H-6, 145-150	57.45		8.43		70.2
721A-6H-7, 25-26	57.75		8.41		70.1
721A-6H-7, 75-76	58.25		7.35		61.2
721A-7H-1, 75-76	58.55		6.00		50.0
721A-7H-1, 125-126	59.05		6.17		51.4
721A-7H-2, 25-26	59.55		5.81		48.4
721A-7H-2, 75-76	60.05		9.82		81.8
721A-7H-2, 125-126	60.55		8.58		71.5
721A-7H-3, 25-26	61.05		8.90		74.1
721A-7H-3, 75-76	61.55		8.57		71.4
721A-7H-3, 125-126	62.05		7.49		62.4
721A-7H-4, 25-26	62.55		7.58		63.1
721A-7H-4, 125-126	63.55		9.84		82.0
721A-7H-5, 25-26	64.05		7.92		66.0
721A-7H-5, 75-76	64.55		8.68		72.3
721A-7H-5, 125-126	65.05		8.57		71.4
721A-7H-5, 149-150	65.29	8.50	7.46	1.04	62.1
721A-7H-6, 25-26	65.55		9.00		75.0
721A-7H-6, 75-125	66.05		7.78		64.8
721A-7H-6, 125-126	66.55		7.95		66.2
721A-7H-7, 25-26	67.05		8.90		74.1
721A-7H-7, 70-71	67.50		9.26		77.1
721A-8H-1, 25-26	67.55		10.04		83.6
721A-8H-1, 75-76	68.05		9.44		78.6
721A-8H-1, 125-126	68.55		7.96		66.3
721A-8H-2, 25-26	69.05		7.82		65.1
721A-8H-2, 75-76	69.55		8.53		71.1
721A-8H-2, 125-126	70.05		8.38		69.8
721A-8H-3, 25-26	70.55		8.73		72.7
721A-8H-3, 75-76	71.05		8.50		70.8
721A-8H-3, 125-126	71.55		7.68		64.0
721A-8H-4, 25-26	72.05		6.90		57.5

Table 3 (continued).

Hole, core, section, interval (cm)	Depth (mbsf)	Total carbon (%)	Inorganic carbon (%)	Organic carbon (%)	$CaCO_3$ (%)
721A-8H-4, 75-76	72.55		8.16		68.0
721A-8H-4, 125-126	73.05		7.21		60.1
721A-8H-5, 25-26	73.55		9.34		77.8
721A-8H-5, 75-76	74.05		7.12		59.3
721A-8H-5, 125-126	74.55		7.98		66.5
721A-8H-5, 149-150	74.79	9.93	8.48	1.45	70.6
721A-8H-6, 25-26	75.05		8.28		69.0
721A-8H-6, 75-76	75.55		8.97		74.7
721A-8H-6, 125-126	76.05		8.85		73.7
721A-8H-7, 25-26	76.55		8.27		68.9
*721B-9H-1, 25-26	76.65		4.89		40.7
721A-9H-1, 25-26	77.05		7.79		64.9
*721B-9H-1, 75-76	77.15		7.03		58.6
721A-9H-1, 75-76	77.55		8.05		67.1
*721B-9H-1, 125-126	77.65		6.36		53.0
721A-9H-1, 125-126	78.05		8.23		68.6
*721B-9H-2, 25-26	78.15		9.00		75.0
721A-9H-2, 25-26	78.55		9.14		76.1
*721B-9H-2, 75-76	78.65		7.22		60.1
721A-9H-2, 75-76	79.05		8.35		69.6
*721B-9H-2, 125-126	79.15		7.57		63.1
*721B-9H-2, 144-145	79.34	9.95	8.00	1.95	66.6
721A-9H-2, 125-126	79.55		8.86		73.8
*721B-9H-3, 25-26	79.65		7.87		65.6
721A-9H-3, 25-26	80.05		7.61		63.4
721A-9H-3, 75-76	80.55		7.98		66.5
*721B-9H-3, 125-126	80.65		8.82		73.5
721A-9H-3, 125-126	81.05		7.53		62.7
*721B-9H-4, 25-26	81.15		9.34		77.8
721A-9H-4, 25-26	81.55		7.55		62.9
*721B-9H-4, 75-76	81.65		5.99		49.9
721A-9H-4, 75-76	82.05		5.48		45.7
*721B-9H-4, 125-126	82.15		8.54		71.1
*721B-9H-4, 145-150	82.35		8.03		66.9
721A-9H-4, 125-126	82.55		8.04		67.0
*721B-9H-5, 25-26	82.65		4.83		40.2
721A-9H-5, 25-26	83.05		8.87		73.9
*721B-9H-5, 75-76	83.15		7.28		60.6
721A-9H-5, 75-76	83.55		7.89		65.7
721A-9H-5, 125-126	84.05		7.63		63.6
*721B-9H-6, 25-26	84.15		8.50		70.8
721A-9H-6, 25-26	84.55		7.96		66.3
*721B-9H-6, 75-76	84.65		7.95		66.2
721A-9H-6, 75-76	85.05		7.39		61.6
*721B-9H-6, 125-126	85.15		8.58		71.5
721A-9H-6, 117-118	85.47		6.03		50.2
721A-9H-6, 119-120	85.49	9.95	6.27	3.68	52.2
*721B-9H-7, 25-26	85.65		7.94		66.1
721A-9H-6, 145-150	85.75		6.32		52.7
721A-9H-7, 25-26	86.05		7.86		65.5
*721B-10X-1, 25-26	86.25		8.09		67.4
*721B-10X-1, 75-76	86.75		6.89		57.4
*721B-10X-1, 125-126	87.25		5.89		49.1
*721B-10X-2, 25-26	87.75		8.86		73.8
*721B-10X-2, 75-76	88.25		8.13		67.7
*721B-10X-2, 125-126	88.75		6.52		54.3
*721B-10X-3, 25-26	89.25		8.88		74.0
*721B-10X-3, 75-76	89.75		7.05		58.7
*721B-10X-3, 125-126	90.25		7.28		60.6
*721B-10X-4, 75-76	91.25		8.39		69.9
721B-10X-4, 125-126	91.75		7.35		61.2
721B-10X-4, 149-150	91.99	10.58	9.62	0.96	80.1
721B-10X-5, 25-26	92.25		8.27		68.9
721B-10X-5, 75-76	92.75		7.55		62.9
721B-10X-5, 125-126	93.25		7.06		58.8
721B-10X-6, 25-26	93.75		8.63		71.9
721B-10X-6, 75-76	94.25		7.27		60.6
721B-10X-6, 125-126	94.75		8.42		70.1
721B-10X-7, 25-26	95.25		9.09		75.7
721B-11X-1, 25-26	95.85		7.95		66.2
721B-11X-1, 75-76	96.35		8.21		68.4
721B-11X-1, 125-126	96.85		9.02		75.1
721B-11X-2, 25-26	97.35		7.58		63.1
721B-11X-2, 75-76	97.85		8.36		69.6
721B-11X-2, 125-126	98.35		7.14		59.5
721B-11X-2, 149-150	98.59	9.95	6.88	3.07	57.3
721B-11X-3, 25-26	98.85		8.07		67.2
721B-11X-3, 75-76	99.35		8.07		67.2
721B-11X-3, 125-126	99.85		8.99		74.9
721B-11X-4, 25-26	100.35		6.66		55.5
721B-11X-4, 75-76	100.85		7.90		65.8
721B-11X-4, 125-126	101.35		9.27		77.2
721B-11X-5, 25-26	101.85		7.13		59.4
721B-11X-5, 75-76	102.35		9.60		80.0
721B-11X-5, 125-126	102.85		8.13		67.7
721B-11X-6, 23-24	103.33		8.88		74.0
721B-12X-1, 25-26	105.45		7.01		58.4
721B-12X-1, 75-76	105.95		7.35		61.2
721B-12X-1, 125-126	106.45		7.91		65.9
721B-12X-1, 144-145	106.64	9.94	8.38	1.56	69.8
721B-12X-1, 145-150	106.65		8.77		73.1
721B-12X-2, 25-26	106.95		8.23		68.6
721B-12X-2, 75-76	107.45		8.71		72.6
721B-12X-2, 125-126	107.95		8.84		73.6
721B-12X-CC, 25-26	108.70		9.32		77.6
721B-13X-1, 25-26	115.05		6.41		53.4
721B-13X-1, 75-76	115.55		6.12		51.0
721B-13X-1, 125-126	116.05		9.33		77.7
721B-13X-2, 25-26	116.55		5.53		46.1
721B-13X-2, 75-76	117.05		8.61		71.7
721B-13X-2, 125-126	117.55		6.91		57.6
721B-13X-3, 25-26	118.05		7.67		63.9
721B-13X-3, 75-76	118.55		6.66		55.5
721B-13X-3, 125-126	119.05		6.94		57.8
721B-13X-4, 25-26	119.55		7.56		63.0
721B-13X-4, 75-76	120.05		7.70		64.1
721B-13X-4, 125-126	120.55		7.13		59.4
721B-13X-4, 149-150	120.79	8.63	8.03	0.60	66.9
721B-13X-5, 25-26	121.05		8.87		73.9
721B-13X-5, 75-76	121.55		6.63		55.2
721B-13X-5, 125-126	122.05		6.99		58.2
721B-13X-6, 25-26	122.55		8.24		68.6
721B-13X-6, 75-76	123.05		8.44		70.3
721B-13X-6, 125-126	123.55		8.74		72.8
721B-14X-1, 25-26	124.65		7.56		63.0
721B-14X-1, 75-76	125.15		8.36		69.6
721B-14X-1, 125-126	125.65		8.44		70.3
721B-14X-1, 149-150	125.89	7.75	6.38	1.37	53.2
721B-14X-2, 25-26	126.15		6.89		57.4
721B-14X-2, 75-76	126.65		7.28		60.6
721B-14X-2, 125-126	127.15		6.61		55.1
721B-14X-3, 25-26	127.65		8.83		73.6
721B-14X-3, 75-76	128.15		4.87		40.6
721B-14X-3, 125-126	128.65		7.92		66.0
721B-14X-4, 25-26	129.15		9.84		82.0
721B-14X-4, 75-76	129.65		6.69		55.7
721B-14X-4, 125-126	130.15		7.71		64.2
721B-14X-5, 25-26	130.65		9.56		79.6
721B-14X-5, 75-76	131.15		6.34		52.8
721B-14X-5, 125-126	131.65		8.88		74.0
721B-14X-6, 25-26	132.15		8.77		73.1
721B-14X-6, 75-76	132.65		7.74		64.5
721B-14X-6, 125-126	133.15		7.63		63.6
721B-14X-7, 25-26	133.65		8.67		72.2
721B-15X-1, 25-26	134.35		8.87		73.9
721B-16X-1, 125-126	145.05		7.05		58.7
721B-16X-2, 25-26	145.55		8.07		67.2
721B-16X-2, 75-76	146.05		8.14		67.8
721B-16X-2, 125-126	146.55		7.81		65.1
721B-16X-3, 25-26	147.05		8.92		74.3
721B-16X-3, 75-76	147.55		7.56		63.0
721B-16X-3, 125-126	148.05		9.43		78.6
721B-16X-4, 25-26	148.55		9.65		80.4
721B-16X-4, 75-76	149.05		8.88		74.0
721B-16X-4, 125-126	149.55		8.60		71.6
721B-16X-5, 25-26	150.05		9.23		76.9
721B-16X-5, 75-76	150.55		8.81		73.4
721B-16X-5, 125-126	151.05		7.57		63.1
721B-16X-5, 149-150	151.29	8.48	7.78	0.70	64.8
721B-16X-6, 25-26	151.55		7.60		63.3
721B-16X-6, 75-76	152.05		8.08		67.3
721B-16X-6, 125-126	152.55		8.95		74.6
721B-16X-7, 25-26	153.05		7.73		64.4
721B-17X-1, 25-26	153.75		6.15		51.2
721B-17X-1, 75-76	154.25		9.46		78.8
721B-17X-1, 125-126	154.75		7.35		61.2

Table 3 (continued).

Hole, core, section, interval (cm)	Depth (mbsf)	Total carbon (%)	Inorganic carbon (%)	Organic carbon (%)	$CaCO_3$ (%)
721B-17X-2, 25–26	155.25		8.77		73.1
721B-17X-2, 75–76	155.75		6.62		55.1
721B-17X-2, 125–126	156.25		9.19		76.6
721B-17X-3, 25–26	156.75		6.81		56.7
721B-17X-3, 75–76	157.25		6.44		53.7
721B-17X-3, 125–126	157.75		7.86		65.5
721B-17X-4, 25–26	158.25		8.56		71.3
721B-17X-4, 75–76	158.75		9.11		75.9
721B-17X-4, 125–126	159.25		7.42		61.8
721B-17X-5, 25–26	159.75		6.70		55.8
721B-17X-5, 75–76	160.25		9.24		77.0
721B-17X-5, 125–126	160.75		6.59		54.9
721B-17X-5, 149–150	160.99	9.14	8.57	0.57	71.4
721B-17X-6, 75–76	161.75		8.39		69.9
721B-17X-6, 125–126	162.25		8.24		68.6
721B-17X-7, 25–26	162.75		10.44		87.0
721B-18X-1, 25–26	163.45		6.05		50.4
721B-18X-1, 75–76	163.95		9.57		79.7
721B-18X-1, 125–126	164.45		8.45		70.4
721B-18X-2, 25–26	164.95		5.60		46.7
721B-18X-2, 75–76	165.45		7.75		64.6
721B-18X-2, 125–126	165.95		6.84		57.0
721B-18X-3, 25–26	166.45		7.69		64.1
721B-18X-3, 75–76	166.95		7.81		65.1
721B-18X-3, 125–126	167.45		7.11		59.2
721B-18X-4, 25–26	167.95		6.75		56.2
721B-18X-4, 75–76	168.45		6.03		50.2
721B-18X-4, 125–126	168.95		7.82		65.1
721B-18X-5, 25–26	169.45		7.38		61.5
721B-18X-5, 75–76	169.95		7.77		64.7
721B-18X-5, 119–120	170.39	8.26	6.77	1.49	56.4
721B-18X-5, 145–150	170.65		9.67		80.6
721B-18X-6, 25–26	170.95		6.45		53.7
721B-18X-6, 75–76	171.45		8.93		74.4
721B-18X-6, 125–126	171.95		7.45		62.1
721B-18X-7, 25–26	172.45		7.01		58.4
721B-18X-CC, 25–26	172.78		8.03		66.9
721B-19X-1, 25–26	173.15		6.83		56.9
721B-19X-1, 75–76	173.65		8.30		69.0
721B-19X-1, 125–126	174.15		7.78		64.8
721B-19X-2, 25–26	174.65		8.68		72.3
721B-19X-2, 75–76	175.15		6.36		53.0
721B-19X-2, 125–126	175.65		7.88		65.6
721B-19X-3, 25–26	176.15		7.04		58.6
721B-19X-3, 75–76	176.65		7.46		62.1
721B-19X-3, 125–126	177.15		7.98		66.5
721B-19X-4, 25–26	177.65		5.73		47.7
721B-19X-4, 75–76	178.15		7.20		60.0
721B-19X-4, 125–126	178.65		7.73		64.4
721B-19X-5, 25–26	179.15		8.43		70.2
721B-19X-5, 75–76	179.65		7.13		59.4
721B-19X-5, 125–126	180.15		8.54		71.1
721B-19X-5, 149–150	180.39	9.23	7.26	1.97	60.5
721B-19X-6, 25–26	180.65		8.76		73.0
721B-19X-6, 75–76	181.15		8.98		74.8
721B-19X-6, 125–126	181.65		6.86		57.1
721B-20X-1, 25–26	182.85		6.93		57.7
721B-20X-1, 75–76	183.35		7.56		63.0
721B-20X-1, 125–126	183.85		8.65		72.1
721B-20X-2, 25–26	184.35		8.66		72.1
721B-20X-2, 75–76	184.85		9.52		79.3
721B-20X-2, 125–126	185.35		8.13		67.7
721B-20X-3, 25–26	185.85		9.39		78.2
721B-20X-3, 75–76	186.35		7.49		62.4
721B-20X-3, 125–126	186.85		8.93		74.4
721B-20X-4, 25–26	187.35		6.73		56.1
721B-20X-4, 75–76	187.85		7.55		62.9
721B-20X-4, 125–126	188.35		8.77		73.1
721B-20X-5, 25–26	188.85		8.32		69.3
721B-20X-5, 75–76	189.35		6.42		53.5
721B-20X-5, 125–126	189.85		8.60		71.6
721B-20X-5, 149–150	190.09	8.23	7.31	0.92	60.9
721B-20X-6, 25–26	190.35		6.72		56.0
721B-21X-1, 25–26	192.55		7.20		60.0
721B-21X-1, 75–76	193.05		6.70		55.8
721B-21X-1, 125–126	193.55		9.04		75.3
721B-21X-2, 0–1	193.80	8.91	8.63	0.28	71.9
721B-21X-2, 25–26	194.05		7.40		61.6

Table 3 (continued).

Hole, core, section, interval (cm)	Depth (mbsf)	Total carbon (%)	Inorganic carbon (%)	Organic carbon (%)	$CaCO_3$ (%)
721B-21X-2, 75–76	194.55		7.59		63.2
721B-21X-2, 125–126	195.05		6.33		52.7
721B-22X-1, 25–26	202.25		7.56		63.0
721B-22X-1, 75–76	202.75		7.27		60.6
721B-22X-1, 125–126	203.25		6.55		54.6
721B-22X-2, 25–26	203.75		10.09		84.1
721B-22X-2, 75–76	204.25		8.37		69.7
721B-22X-2, 125–126	204.75		8.58		71.5
721B-22X-3, 0–1	205.00	9.84	9.06	0.78	75.5
721B-22X-3, 25–26	205.25		6.60		55.0
721B-22X-3, 75–76	205.75		7.44		62.0
721B-22X-3, 125–126	206.25		9.53		79.4
721B-22X-4, 25–26	206.75		5.95		49.6
721B-22X-4, 75–76	207.25		10.28		85.6
721B-22X-4, 125–126	207.75		8.23		68.6
721B-22X-5, 25–26	208.25		7.92		66.0
721B-22X-5, 75–76	208.75		8.77		73.1
721B-22X-5, 119–120	209.19		7.30		60.8
721B-22X-5, 145–150	209.45		10.09		84.1
721B-22X-6, 25–26	209.75		9.40		78.3
721B-22X-6, 75–76	210.25		8.60		71.6
721B-22X-6, 125–126	210.75		7.09		59.1
721B-22X-7, 25–26	211.25		8.70		72.5
721B-23X-1, 25–26	211.95		7.83		65.2
721B-23X-1, 125–126	212.95		8.50		70.8
721B-23X-2, 25–26	213.45		6.36		53.0
721B-23X-2, 75–76	213.95		8.83		73.6
721B-23X-2, 125–126	214.45		7.89		65.7
721B-23X-3, 25–26	214.95		10.30		85.8
721B-23X-3, 75–76	215.45		6.95		57.9
721B-24X-1, 25–26	221.55		8.58		71.5
721B-24X-1, 75–76	222.05		10.80		90.0
721B-24X-1, 120–121	222.50		8.21		68.4
721B-24X-2, 25–26	223.05		6.11		50.9
721B-24X-2, 75–76	223.55		9.32		77.6
721B-24X-2, 112–113	223.92		8.98		74.8
721B-24X-2, 140–150	224.20		8.81		73.4
721B-24X-3, 0–1	224.30	8.69	8.13	0.56	67.0
721B-24X-3, 25–26	224.55		5.21		43.4
721B-24X-3, 75–76	225.05		6.11		50.9
721B-24X-3, 125–126	225.55		4.61		38.4
721B-24X-4, 25–26	226.05		8.40		70.0
721B-25X-1, 25–26	230.75		7.16		59.6
721B-25X-1, 75–76	231.25		7.19		59.9
721B-25X-1, 125–126	231.75		6.74		56.1
721B-25X-2, 25–26	232.25		9.05		75.4
721B-25X-2, 75–76	232.75		7.92		66.0
721B-25X-2, 122–123	233.22		8.54		71.1
721B-25X-3, 25–26	233.75		10.46		87.1
721B-25X-3, 75–76	234.25		8.94		74.5
721B-25X-3, 125–126	234.75		7.78		64.8
721B-25X-4, 25–26	235.25		8.72		72.6
721B-25X-4, 75–76	235.75		7.89		65.7
721B-25X-4, 125–126	236.25		8.16		68.0
721B-25X-5, 0–1	236.50	8.93	8.56	0.37	71.3
721B-25X-5, 25–26	236.75		8.41		70.1
721B-25X-5, 75–76	237.25		8.26		68.8
721B-25X-5, 125–126	237.75		8.37		69.7
721B-25X-6, 25–26	238.25		9.48		79.0
721B-25X-6, 75–76	238.75		8.12		67.6
721B-25X-6, 125–126	239.25		7.38		61.5
721B-26X-1, 25–26	240.35		8.46		70.5
721B-26X-1, 75–76	240.85		7.74		64.5
721B-26X-1, 125–126	241.35		7.68		64.0
721B-26X-2, 25–26	241.85		7.81		65.1
721B-26X-2, 75–76	242.35		9.53		79.4
721B-26X-2, 125–126	242.85		7.74		64.5
721B-26X-2, 125–126	242.85		7.74		64.5
721B-26X-3, 25–26	243.35		7.40		61.6
721B-26X-3, 75–76	243.85		8.74		72.8
721B-26X-3, 125–126	244.35		7.23		60.2
721B-26X-3, 149–150	244.59	6.02	5.80	0.22	48.3
721B-26X-4, 25–26	244.85		9.37		78.1
721B-26X-4, 75–76	245.35		6.16		51.3
721B-26X-4, 125–126	245.85		7.59		63.2
721B-26X-CC, 25–26	246.13		7.40		61.6
721B-27X-1, 75–76	250.55		6.37		53.1
721B-27X-1, 125–126	251.05		10.52		87.6

Table 3 (continued).

Hole, core, section, interval (cm)	Depth (mbsf)	Total carbon (%)	Inorganic carbon (%)	Organic carbon (%)	$CaCO_3$ (%)
721B-27X-2, 25–26	251.55		6.88		57.3
721B-27X-2, 75–76	252.05		6.53		54.4
721B-27X-2, 125–126	252.55		9.52		79.3
721B-27X-3, 25–26	253.05		8.76		73.0
721B-27X-3, 75–76	253.55		6.68		55.6
721B-27X-3, 117–118	253.97		10.36		86.3
721B-27X-3, 119–120	253.99	8.44	8.19	0.25	68.2
721B-27X-3, 145–150	254.25		10.80		90.0
721B-27X-4, 25–26	254.55		7.92		66.0
721B-27X-4, 75–76	255.05		7.37		61.4
721B-27X-4, 125–126	255.55		6.73		56.1
721B-27X-5, 25–26	256.05		8.77		73.1
721B-27X-CC, 25–26	256.48		7.88		65.6
721B-28X-1, 25–26	259.85		7.02		58.5
721B-28X-1, 75–76	260.35		8.04		67.0
721B-28X-1, 125–126	260.85		7.62		63.5
721B-28X-2, 25–26	261.35		6.54		54.5
721B-28X-2, 75–76	261.85		4.70		39.2
721B-28X-2, 125–126	262.35		7.68		64.0
721B-28X-3, 25–26	262.85		4.09		34.1
721B-28X-3, 75–76	263.35		5.25		43.7
721B-28X-4, 25–26	264.35		8.10		67.5
721B-28X-4, 75–76	264.85		5.61		46.7
721B-28X-4, 125–126	265.35		8.47		70.6
721B-28X-5, 0–1	265.60	7.43	6.63	0.80	55.2
721B-28X-5, 25–26	265.85		4.89		40.7
721B-28X-5, 125–126	266.85		5.60		46.7
721B-28X-6, 25–26	267.35		5.72		47.7
721B-28X-CC, 25–26	268.59		4.19		34.9
721B-29X-1, 25–26	269.65		8.68		72.3
721B-29X-1, 75–76	270.15		7.37		61.4
721B-29X-1, 125–126	270.65		4.48		37.3
721B-29X-2, 0–1	270.90	7.89	7.46	0.43	62.1
721B-29X-2, 25–26	271.15		5.82		48.5
721B-29X-2, 75–76	271.65		5.90		49.2
721B-29X-2, 125–126	272.15		6.83		56.9
721B-29X-3, 25–26	272.65		6.24		52.0
721B-29X-CC, 25–26	273.08		2.47		20.6
721B-30X-1, 25–26	279.45		6.50		54.2
721B-30X-1, 75–76	279.95		8.96		74.6
721B-30X-1, 125–126	280.45		9.21		76.7
721B-30X-2, 25–26	280.95		6.30		52.5
721B-30X-2, 75–76	281.45		5.71		47.6
721B-30X-2, 114–115	281.84	6.36	6.22	0.14	51.8
721B-30X-2, 140–150	282.10		11.26		93.8
721B-30X-3, 25–26	282.45		3.55		29.6
721B-30X-3, 75–76	282.95		3.59		29.9
721B-30X-3, 125–126	283.45		7.35		61.2
721B-30X-4, 25–26	283.95		3.29		27.4
721B-30X-CC, 25–26	284.52		5.97		49.7
721B-31X-1, 25–26	289.25		3.25		27.1
721B-31X-1, 75–76	289.75		6.68		55.6
721B-31X-1, 125–126	290.25		6.99		58.2
721B-31X-2, 28–29	290.78		3.32		27.7
721B-31X-2, 75–76	291.25		4.90		40.8
721B-31X-2, 125–126	291.75		7.64		63.6
721B-31X-3, 25–26	292.25		3.59		29.9
721B-31X-3, 125–126	293.25		2.76		23.0
721B-31X-3, 149–150	293.49	5.02	4.17	0.85	34.7
721B-31X-4, 25–26	293.75		8.63		71.9
721B-31X-4, 77–78	294.27		4.22		35.2
721B-31X-4, 125–126	294.75		7.70		64.1
721B-31X-5, 14–15	295.14		4.26		35.5
721B-31X-5, 75–76	295.75		4.45		37.1
721B-31X-5, 125–126	296.25		8.80		73.3
721B-31X-6, 25–26	296.75		1.39		11.6
721B-31X-6, 75–76	297.25		2.80		23.3
721B-32X-1, 25–26	299.05		6.13		51.1
721B-32X-1, 75–76	299.55		6.39		53.2
721B-32X-1, 125–126	300.05		6.29		52.4
721B-32X-2, 25–26	300.55		3.11		25.9
721B-32X-2, 75–76	301.05		7.81		65.1
721B-32X-2, 125–126	301.55		6.64		55.3
721B-32X-2, 149–150	301.79	5.06	3.59	1.47	29.9
721B-32X-3, 25–26	302.05		2.75		22.9
721B-32X-3, 75–76	302.55		7.76		64.6
721B-32X-3, 125–126	303.05		2.90		24.2
721B-32X-4, 25–26	303.55		8.13		67.7

Table 3 (continued).

Hole, core, section, interval (cm)	Depth (mbsf)	Total carbon (%)	Inorganic carbon (%)	Organic carbon (%)	$CaCO_3$ (%)
721B-32X-4, 75–76	304.05		3.58		29.8
721B-32X-4, 125–126	304.55		5.93		49.4
721B-32X-5, 25–26	305.05		7.89		65.7
721B-32X-5, 75–76	305.55		5.51		45.9
721B-32X-5, 125–126	306.05		4.63		38.6
721B-32X-6, 25–26	306.55		1.42		11.8
721B-32X-6, 75–76	307.05		7.18		59.8
721B-32X-6, 125–126	307.55		3.36		28.0
721B-32X-7, 25–26	308.05		4.19		34.9
721B-33X-1, 24–25	308.64		3.43		28.6
721B-33X-1, 75–76	309.15		7.02		58.5
721B-33X-1, 112–113	309.52		2.89		24.1
721B-33X-1, 114–115	309.54	4.66	3.06	1.60	25.5
721B-33X-1, 140–150	309.80		8.31		69.2
721B-33X-2, 24–25	310.14		5.76		48.0
721B-33X-2, 75–76	310.65		9.93		82.7
721B-33X-2, 124–125	311.14		6.04		50.3
721B-33X-CC, 24-25	311.49		10.82		90.1
721B-34X-1, 5–6	318.05		9.03		75.2
721B-34X-1, 54–55	318.54		10.50		87.5
721B-34X-1, 145–146	319.45		7.10		59.1
721B-34X-2, 5–6	319.55		7.53		62.7
721B-34X-2, 54–55	320.04		10.97		91.4
721B-34X-2, 126–128	320.76		9.78		81.5
721B-34X-3, 5–6	321.05		3.83		31.9
721B-34X-3, 70–71	321.70		10.83		90.2
721B-34X-3, 134–135	322.34		10.99		91.6
721B-34X-4, 0–1	322.50	10.81	10.81	0.00	90.1
721B-34X-4, 14–15	322.64		10.87		90.6
721B-34X-4, 71–72	323.21		10.75		89.6
721B-34X-4, 126–127	323.76		8.35		69.6
721B-34X-5, 10–11	324.10		10.44		87.0
721B-34X-5, 45–46	324.45		8.91		74.2
721B-35X-1, 25–26	327.95		10.79		89.9
721B-35X-1, 125–126	328.95		11.91		99.2
721B-35X-2, 25–26	329.45		7.37		61.4
721B-35X-2, 75–76	329.95		5.87		48.9
721B-35X-2, 125–126	330.45		11.07		92.2
721B-35X-2, 145–150	330.65	4.06	4.06	0.00	33.8
721B-35X-3, 25–26	330.95		9.05		75.4
721B-35X-3, 75–76	331.45		9.70		80.8
721B-36X-1, 25–26	337.65		10.13		84.4
721B-36X-1, 75–76	338.15		10.36		86.3
721B-36X-1, 114–115	338.54	10.92	10.55	0.37	87.9
721B-36X-1, 140–150	338.80		10.43		86.9
721B-36X-2, 25–26	339.15		10.58		88.1
721B-36X-2, 75–76	339.65		5.26		43.8
721B-36X-2, 125–126	340.15		8.80		73.3
721B-36X-3, 25–26	340.65		6.66		55.5
721B-37X-1, 25–26	347.25		0.91		7.6
721B-37X-1, 75–76	347.75		3.98		33.2
721B-37X-1, 125–126	348.25		5.53		46.1
721B-37X-2, 25–26	348.75		7.12		59.2
721B-37X-2, 75–76	349.25	1.47		12.3	
721B-37X-2, 125–126	349.75		6.89		57.4
721B-37X-3, 25–26	350.25		2.93		24.4
721B-37X-3, 125–126	351.25		4.21		35.1
721B-37X-3, 149–150	351.49	1.00	0.93	0.07	7.8
721B-37X-4, 25–26	351.75		2.44		20.3
721B-37X-4, 75–76	352.25		5.06		42.2
721B-37X-4, 125–126	352.75		6.57		54.7
721B-37X-5, 25–26	353.25		6.44		53.7
721B-37X-5, 125–126	354.25		5.43		45.2
721B-37X-6, 25–26	354.75		3.39		28.2
721B-37X-6, 25–26	354.75		3.39		28.2
721B-37X-6, 39–40	354.89	1.02	0.97	0.05	8.1
721B-37X-6, 40–42	354.90	1.11	1.10	0.01	9.2
721B-37X-6, 42–43	354.92	1.11	1.06	0.05	8.8
721B-37X-6, 46–47	354.96	6.45	6.43	0.02	53.6
721B-37X-6, 75–76	355.25	5.47		45.6	
721B-37X-6, 126–127	355.76		0.75		6.3
721B-40X-5, 114–115	383.04		0.66		5.5
721B-40X-5, 114–115	383.04	0.56	0.50	0.06	4.2
721B-41X-5, 114–115	392.74	0.56	0.50	0.06	4.2
721B-41X-5, 149–150	393.09	5.05	4.86	0.19	40.5
721B-42X-2, 149–150	398.19	2.69	2.57	0.12	21.4
721B-44X-5, 114–115	421.64	1.42	1.31	0.11	10.9
721B-44X-5, 140–150	421.90		1.24		10.3

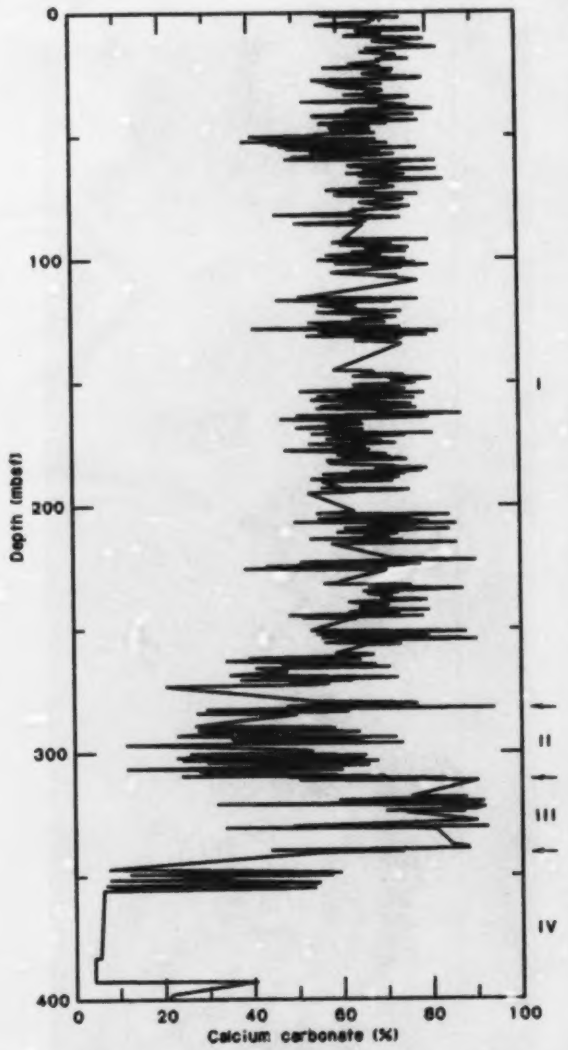

Figure 5. Calcium carbonate profile, Site 721. Hole 721A samples cover 0–86 mbsf, and Hole 721B samples correspond to the interval from 92–422 mbsf. Because the recorded depths in Hole 721A are 3–5 m shallower than corresponding depths in 721B, an artificial gap exists between 86 and 92 mbsf downhole. The arrows denote lithologic boundaries, and the numbers correspond to lithologic units.

fossil chalk to olive (5Y 4/3) siliceous bearing nannofossil chalk. These lithologic changes are evident on seismic reflection profiles (see "Seismic Stratigraphy" section, this chapter).

Unit IV (Depth: 340.7–424.2 mbsf; Age: middle Miocene to early Miocene)

Sample 117-721B-36X, CC, 30 cm, to Section 117-721B-44, CC.

Unit IV contains marly nannofossil and nannofossil chalks that overlie fining-upward turbidite sequences (5–300 cm thick) of clayey siltstones to silty claystones. The basal layers of the turbidites fine upward through Unit IV from mudstones in Core 117-721B-44X to silty claystones in Core 117-721B-36X. The deposits have low organic carbon and calcium carbonate values

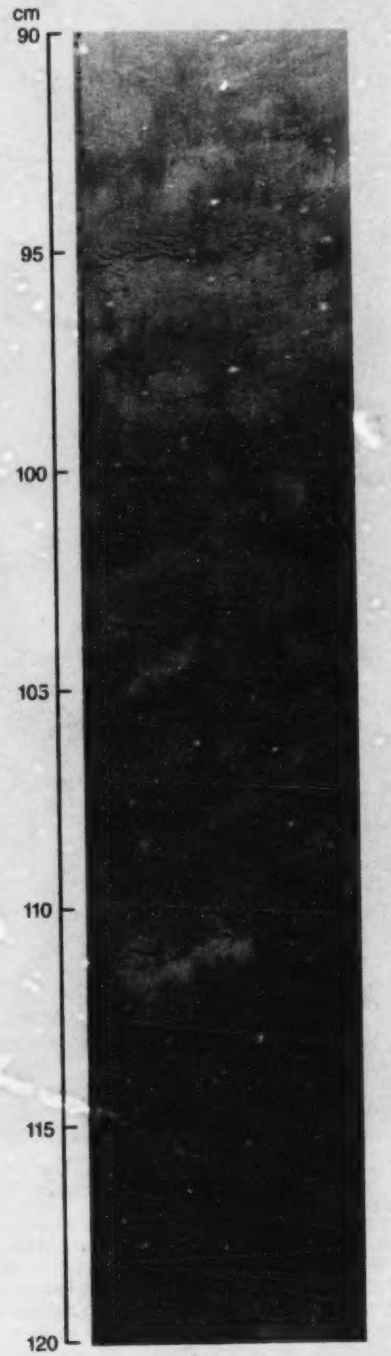

Figure 6. Burrow structures at boundary between light and dark layers in Unit I (Section 117-721B-17X-1, 90–120 cm). Note blurring of boundary by bioturbation.

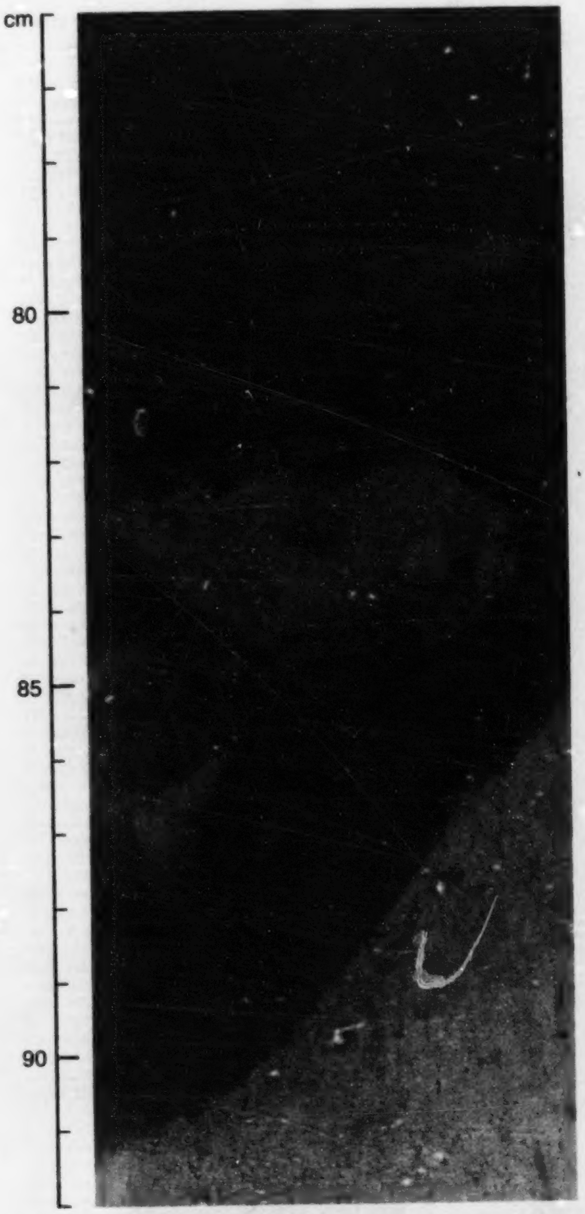

Figure 7. Transition between light and dark layers in Unit I (Section 117-721B-3H-6, 76–92 cm). Note mixing of dark material into light colored material by burrowing.

(Table 3) and some turbidites contain thin (0.1–2 mm) sand- to silt-sized pyrite bands (Fig. 10). These pyrite bands contain euhedral grains and framboids which imply an authigenic source. Because the grains are concentrated mostly in layers near the base of turbidites, we cannot discard the possibility that the bands result from winnowing of previously deposited sediments which contain pyrite as their sole coarse component.

The basal layers range from dark gray (N 4/0) and dark greenish gray (5G 4/1) to dark reddish gray (5YR 4/2). Above

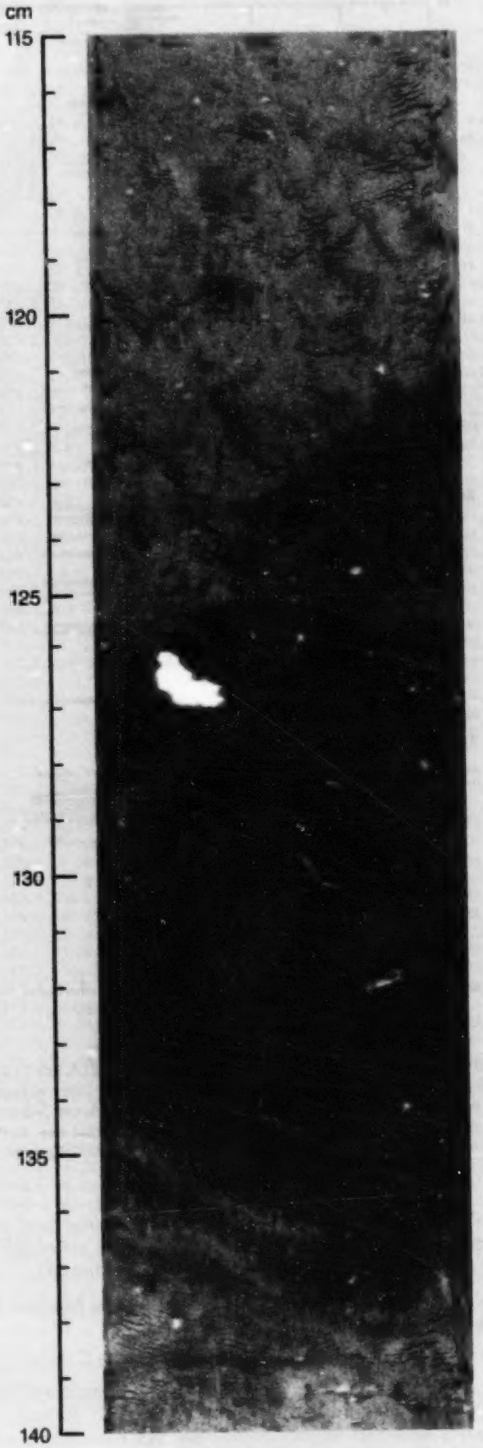

Figure 8. Inclined contact of dark material and light layer. Possible slump feature in Subunit IB (Section 117-721B-29X-2, 115–140 cm).

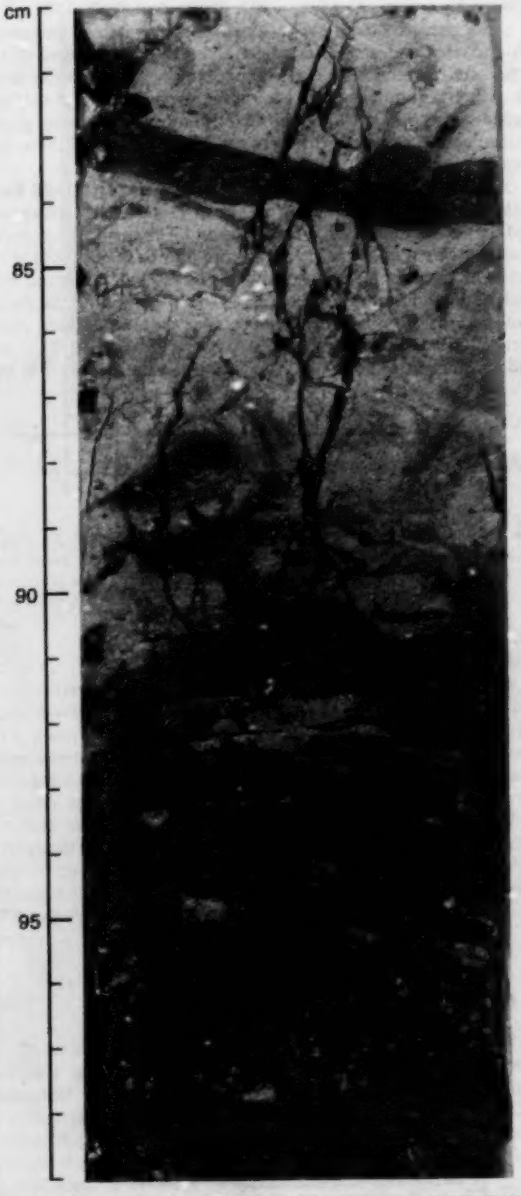

Figure 9. Disturbed section in lithologic Unit II (Section 117-721B-32X-6, 81–99 cm) showing microfault between 85 and 90 cm. Large fractures are attributed to coring disturbance.

the basal layers, olive (5Y 4/3), dark brown (10YR 3/3), and greenish brown (10YR 5/2) silty claystones and clayey siltstones predominate which in turn grade upward to greenish gray (5GY 5/1, 5BG 4/1, and 5BG 5/1) calcareous silty claystones. These claystones are frequently capped by olive (5Y 5/3), brown (10YR 5/3), and pale brown (10YR 6/2) marly nannofossil chalks and light gray (5Y 7/1) nannofossil chalks. The calcareous silty claystone and chalks are slightly to moderately bioturbated. The sharp contact which characterizes the change from pelagic deposition (nannofossil chalk) to the turbidites is shown in Figure 11.

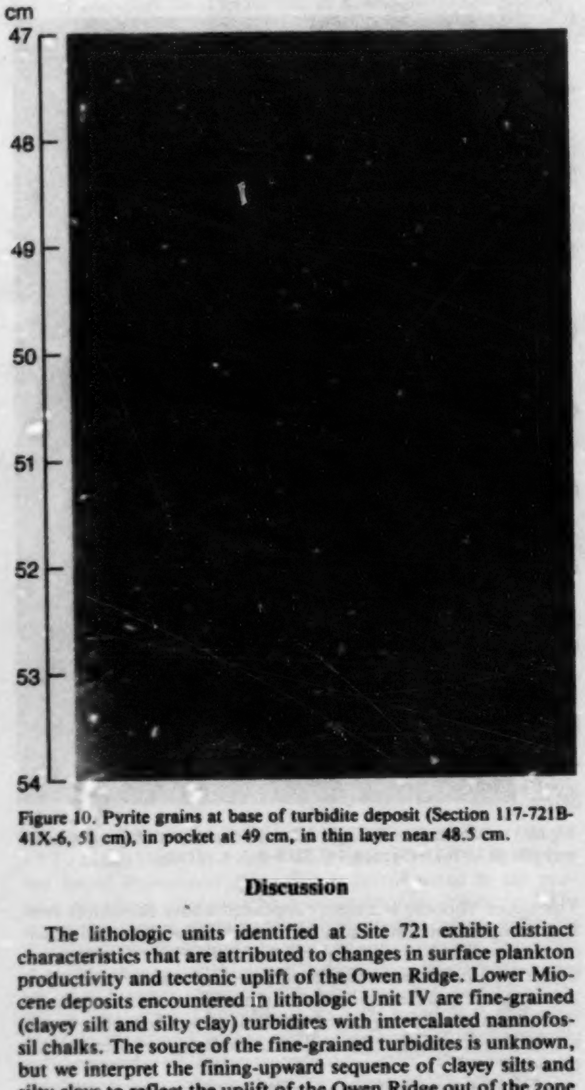

Figure 10. Pyrite grains at base of turbidite deposit (Section 117-721B-41X-6, 51 cm), in pocket at 49 cm, in thin layer near 48.5 cm.

Discussion

The lithologic units identified at Site 721 exhibit distinct characteristics that are attributed to changes in surface plankton productivity and tectonic uplift of the Owen Ridge. Lower Miocene deposits encountered in lithologic Unit IV are fine-grained (clayey silt and silty clay) turbidites with intercalated nannofossil chalks. The source of the fine-grained turbidites is unknown, but we interpret the fining-upward sequence of clayey silts and silty clays to reflect the uplift of the Owen Ridge out of the zone of turbidity current deposition. As the lower Miocene turbidite sequences below seismic reflector C (see "Seismic Stratigraphy" section, this chapter) were uplifted, the fine-grained turbidite deposits became more common in addition to thicker pelagic interbeds. This sequence is expected as the site is lifted above the zone of bedload transport. Seismic reflection profiles (see "Seismic Stratigraphy" section, this chapter) show the expected offlapping reflectors during this interval and the timing is consistent with early Miocene uplift of the Owen Ridge discussed by Whitmarsh et al. (1974) and Whitmarsh (1979). By middle Miocene, the site was elevated above the zone of turbidite deposition and Unit III, a nannofossil chalk, reflects pelagic deposition. Site 721 contains a record of much higher resolution of the lower Miocene uplift of the Owen Ridge than was available previously.

An unconformity at 310 mbsf separates Units II and III. This contact corresponds to a 5-m.y. hiatus in the sediment record (see "Biostratigraphy" section, this chapter) and separates nannofossil chalks from siliceous-bearing nannofossil chalks.

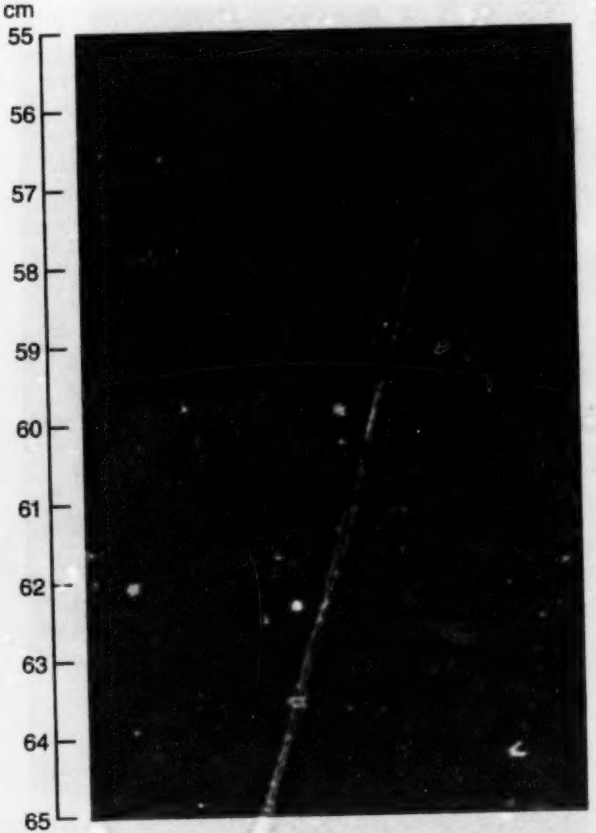

Figure 11. Contact between light colored pelagic nannofossil chalk and turbidite in Unit IV (Section 117-721B-41X-6, 60 cm).

The upper Miocene sediments deposited above the hiatus contain reworked microfossils in addition to microfault and possible slump-related structures (Figs. 8 and 9). These data are consistent with postdepositional disturbance of sediments in lithologic Unit II and Subunit IB. On the scale of seismic images, the reflectors which correspond to Unit II and Subunit IB also exhibit this disturbance (see "Seismic Stratigraphy" section, this chapter).

Upper Miocene sediments in Unit II represent a dramatic change in the plankton assemblage where, in addition to nannofossils, biogenic silica becomes abundant and both diatoms and radiolarians are preserved in the sediments. Unfortunately, the initiation of opaline sedimentation in the middle to late Miocene, which may reflect the onset of monsoonal upwelling (Whitmarsh et al., 1974), is not recorded in Hole 721B because of the unconformity between Units II and III. However, Hole 722B, in close proximity to Site 721, contains a more complete section that includes this interval and will be used to document this transition (see "Site 722" chapter, this volume).

Upper Miocene to Holocene deposits are dominantly alternating light and dark layers of foraminifer-bearing, foraminifer-nannofossil, and nannofossil oozes with a mean calcium carbonate content of 66% and a range from 40% to 90%. The color alternations in the upper Miocene to Holocene sediments reflect changes in calcium carbonate concentration and terrigenous clay abundance. Similar sediment cycles, which are evident from the Miocene to the Holocene, have been identified in other regions (i.e., Gardner, 1982; Pisias and Prell, 1985). The primary cause of these cycles has been attributed to carbonate productivity and/or preservation changes and changes in the eolian (terrigenous silty clay) input. However, post-cruise studies, which will quantify the accumulation of carbonate and terrigenous components and provide estimates of carbonate dissolution, are necessary to differentiate between each of these factors.

A preliminary analysis for cyclicity of the light and dark bedding was made on the top 100 m of Hole 721B. Colors, coded as +1 for light, 0 for medium, and −1 for dark, were assessed at 10 cm intervals from the core photos. The resulting series, which represents color changes (Fig. 12), was analyzed with Walsh spectral analysis (Weedon, 1986) to determine the dominant periods of variation. The spectra reveal well-defined peaks corresponding to cycles of 0.52, 0.64, 0.95, 1.51, 4.09, 7.87, and 17.06 m (Fig. 13). Assuming a constant sedimentation rate

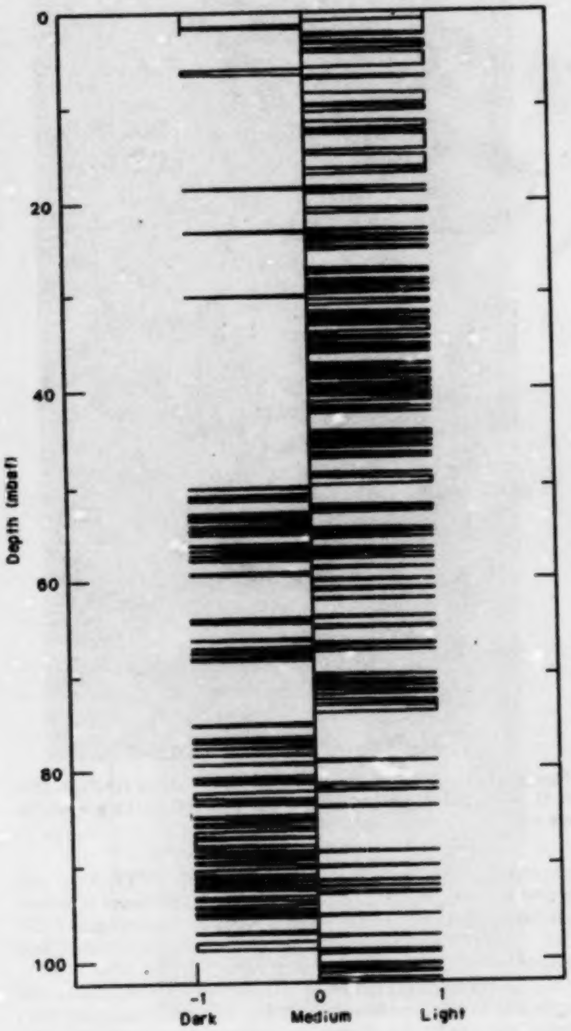

Figure 12. Diagram showing alternating light and dark layers at 10-cm intervals in the top 100 m of Hole 721B.

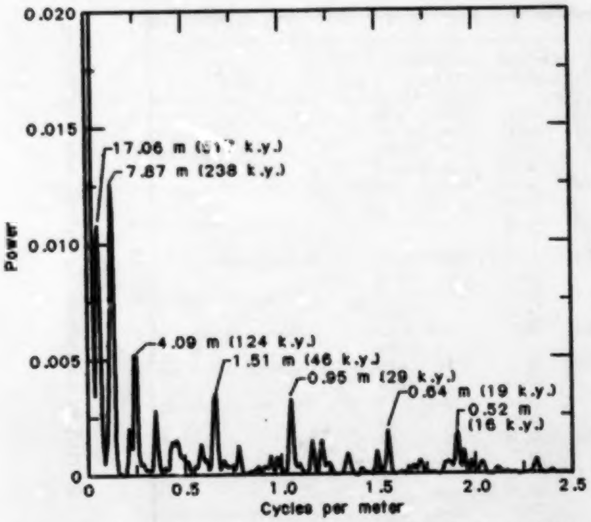

Figure 13. Walsh power spectrum of thickness variations in light and dark layers. Dominant periods are noted. Conversion to k.y. is based on a constant sedimentation rate of 33 m/m.y., and the plot represents the time since 3.10 Ma.

of 33 m/m.y. (see "Accumulation Rates" section, this chapter), these cycles correspond to 16, 19, 29, 46, 124, 238, and 517 k.y., respectively. The cycles with periods close to 410, 100, 40, and 21 k.y. correspond to the known variations in the earth's orbital parameters (Milankovitch frequencies). The high correspondence between orbital variations which influence climate and the sedimentary cycles implies that the compositional changes causing the light and dark layering may reflect climatic variations. These preliminary results are encouraging. Post-cruise studies will identify the components responsible for the color changes and their response to climatic fluctuations, and establish a high-resolution age model to document more precisely the periods of variation.

BIOSTRATIGRAPHY

Introduction

To investigate the evolution of monsoonal upwelling and the tectonic uplift history of the Owen Ridge, three holes were drilled at the top of the Owen Ridge at Site 721 to provide a partly overlapping and composite section down to the lower Miocene. A plot of faunal datum levels and paleomagnetic reversals vs. depth below the seafloor is presented in Figure 14; for a detailed listing of these data points, see Tables 4 and 5.

Planktonic foraminifers are abundant, highly diverse, and well-preserved in Hole 721A and the upper part of Hole 721B. The lower part of Hole 721B, however, contains low-diversity and sparse assemblages. Benthic foraminifers are abundant, highly diverse, and well-preserved throughout almost all of the cores. Calcareous nannofossils are abundant throughout the cores. However, below the top of lithologic Unit III (310 mbsf) the state of preservation of coccoliths is poor. Radiolarians are abundant and well-preserved in almost all samples down to the bottom of lithologic Unit II. Diatoms start to increase in number in the middle part of lithologic Subunit IA (around 125 mbsf) downhole and become abundant from the lower part of Subunit IA (around 220 mbsf).

The zonation of the various fossil groups is summarized in Figures 15, 16, and 17. A hiatus is inferred between lithologic Unit II and Unit III. The bottom of lithologic Unit II belongs to nannofossil Zone NN9 (upper middle Miocene to lower upper Miocene). The nannofossils in the uppermost part of lithologic Unit III belong to Zone NN5 (uppermost lower Miocene to middle Miocene). The planktonic foraminifers also show a similar hiatus between Zone N15 (middle to upper Miocene) at the bottom of lithologic Unit II and Zones N7 to N8 (uppermost lower Miocene) at the top of lithologic Unit III. Most of the middle Miocene sediments are not recorded.

The nannofossil flora and radiolarian fauna of Site 721 are characterized by the absence of some typical tropical species since the late Miocene. Remarkable changes in nannoflora occur at the top of the Miocene (around 140 mbsf) and in radiolarian fauna in the upper Miocene (around 220 mbsf). Planktonic foraminifers indicate an increased upwelling intensity from the lowermost upper Miocene (around 260 mbsf). Two horizons of faunal change are recognized; one is just above the unconformity (308 mbsf) in the middle Miocene and another is in the middle part of Unit I (around 135 mbsf) in the lowermost Pliocene. The faunal and floral events in combination with the observed increase in diatom abundance downhole represent strong environmental changes during the earliest late Miocene, which may be related to stronger upwelling intensity and/or global cooling events.

Planktonic Foraminifers

Hole 721A and the upper part of Hole 721B in general contain highly diverse, well-preserved foraminiferal faunas. The lower interval (Samples 117-721B-28X, CC, 269.4 mbsf, to 117-721B-44X, CC, 424.2 mbsf) yields low-diversity assemblages and only sparse specimens of planktonic foraminifers. The lowest concentrations are confined to a turbidite sequence (Samples 117-721B-37X, CC, 356.6 mbsf, to 117-721B-44X, CC, 424.2 mbsf), where only reworked specimens were found. Zonal boundaries are tentatively assigned based on shipboard analyses of the core-catcher samples. Samples were not investigated from Hole 721C.

In Cores 117-721A-1H to -7H and 117-721B-1H to -7H (0–67.3 mbsf in Hole 721A and 0–66.9 mbsf in Hole 721B) the faunas are of Pleistocene age, which is corroborated by the presence of sparse *Globorotalia truncatulinoides* specimens. The upper three cores contain rare *Globigerinella calida calida* and *Globigerinella digitata* specimens, and thus represent Zone N23. A coiling change in the tests of *Pulleniatina obliquiloculata* was observed between Cores 117-721A-3H and -4H, and 117-721B-3H and -4H (29.2–38.9 mbsf in Hole 721A and 28.8–38.5 mbsf in Hole 721B) and is thought to correlate with the Jaramillo subchronozone (0.9 Ma; Saito et al., 1975). Planktonic foraminifers were completely absent from Sample 117-721A-8H, CC (76.8 mbsf) and *Globorotalia truncatulinoides* could not be identified in Sample 117-721B-8H, CC (76.4 mbsf). The last appearance of *Globigerinoides obliquus* was observed in Sample 117-721A-8H, CC (76.8 mbsf) and in Sample 117-721B-8H, CC (76.4 mbsf).

Zone N21 could not be identified because of the absence of *Globorotalia tosaensis* in this interval of the hole. The first appearance of *Sphaeroidinella dehiscens*, which marks the N18/N19–20 zonal boundary, could not be assigned, because specimens of this species are absent or rare. The recognition of the N17/N18 and N16/N17 zonal boundaries are difficult because these boundaries are defined by transitional forms in the evolutionary morphological series of subspecies of *Globorotalia tumida*. However, the first appearance of *Globorotalia tumida tumida* (N17/N18 boundary) seems to lie approximately between Samples 117-721B-21X, CC (202.0 mbsf), and 117-721B-22X, CC (211.7 mbsf). This datum also defines the base of the Pliocene (Berggren et al., 1985a). The position of the N16/N17 boundary has been estimated to lie between Samples 117-721B-

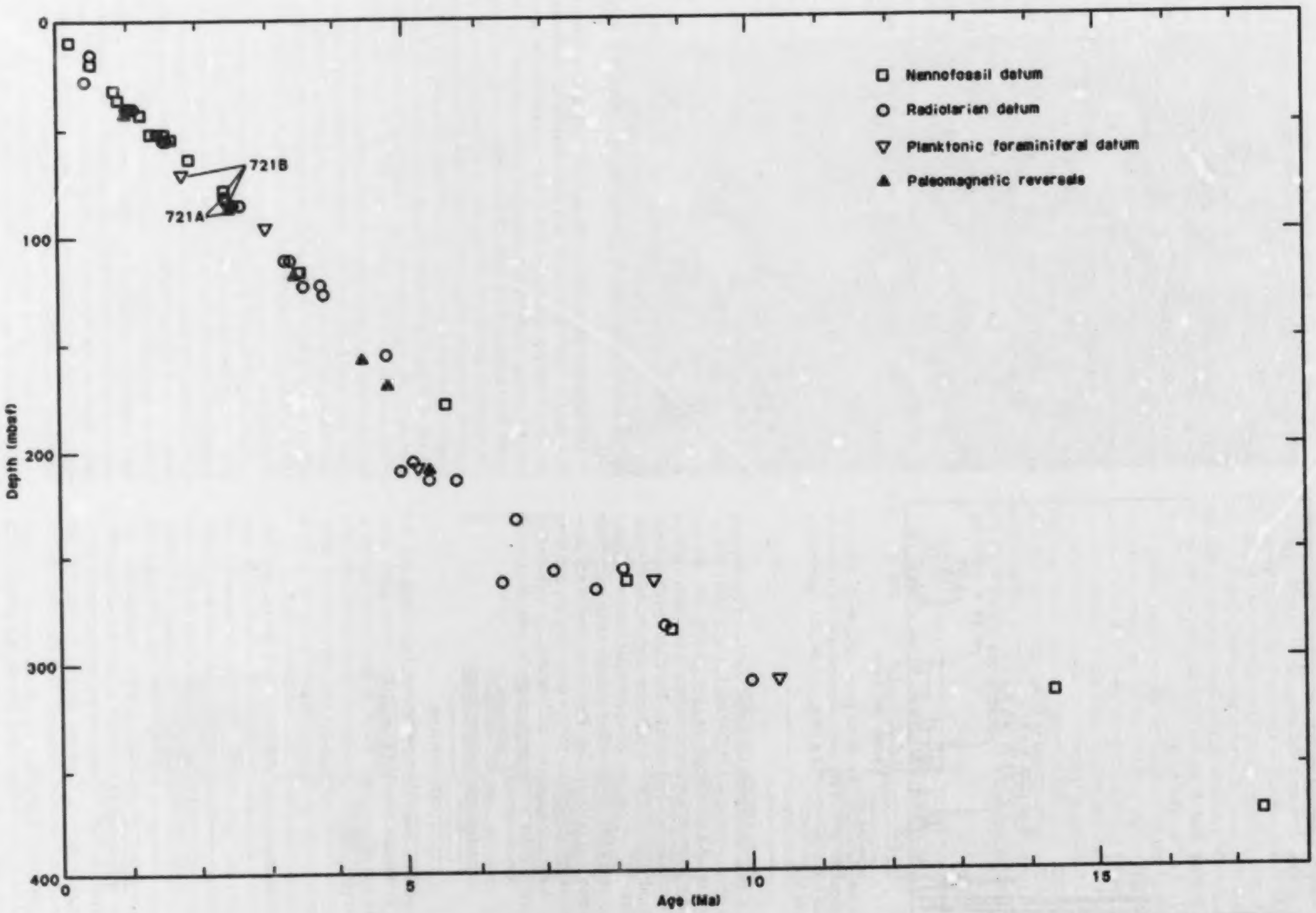

Figure 14. Stratigraphic datum vs. depth plot for Site 721. For the upper part, approximately above 80 mbsf, datum levels from Hole 721A are used, whereas datum levels from Hole 721B are used for the lower part below 80 mbsf. For a detailed listing of events, see Tables 4 and 5.

Table 4. Stratigraphic listing of faunal events and paleomagnetic reversals for Hole 721A.

Event	Core Level	Depth (mbsf)	Age (Ma)	Source of age	Notes
B *Emiliania huxleyi*	1H-4, 115–117 1H-5, 115–117	8.40 9.90	0.19	3	
B *Collosphaera tuberosa*	1H-CC 2H-4, 85–87	12.55 17.90	0.40–0.59	1	Cores MD81-369, RC14-22, and VM24-35; DSDP 214 data probably less accurate.
T *Pseudoemiliania lacunosa*	2H-4, 115–117 2H-5, 115–117	18.20 19.70	0.49	3	
T *Stylatractus universus*	2H-CC 3H-CC	22.25 31.95	0.37–0.47	1	
T *Reticulofenestra* sp. A (acme)	3H-6, 115–117 3H-CC	30.87 31.95	0.82	3	
B *Gephyrocapsa parallela*	4H-2, 115–117 4H-3, 115–117	34.60 36.10	[a]0.89	4	
T *Anthocyrtidium angulare*	4H-4, 85–87 4H-CC	37.30 41.65	0.94–1.04	1	
B *Lamprocyrtis nigriniae*	4H-4, 85–87 4H-CC	37.30 41.65	1.02–1.07	1	
T *Lamprocyrtis neoheteroporos*	4H-4, 85–87 4H-CC	37.30 41.65	1.09–1.13	1	
B Jaramillo	4H-7, 35–37 5H-1, 115–117	41.30 42.80	0.98	6	
T *Gephyrocapsa* "large"[b]	4H-CC 5H-1, 115–117	41.65 42.80	[a]1.10	4	
T *Helicosphaera sellii*	5H-5, 115–117 5H-6, 115–117	48.80 50.30			No good published age; event may be diachronous.
B *Gephyrocapsa* "large"[b]	5H-6, 115–117 5H-CC	50.30 51.25	[a]1.36	4	
T *Calcidiscus macintyrei*	5H-6, 115–117 5H-CC	50.30 51.25	1.45	6	
B *Gephyrocapsa oceanica*	5H-6, 115–117 5H-CC	50.30 51.25	[a]1.57	4	
T *Pterocanium prismatium*	5H-CC 6H-4, 85–87	52.25 56.60	1.52–1.56	1	
B *Anthocyrtidium angulare*	5H-CC 6H-4, 85–87	51.25 56.60	1.52–1.64	1	
B *Gephyrocapsa caribbeanica*	6H-1, 115–117 6H-2, 115–117	52.40 53.90	[c]1.66	4, 8	
T *Discoaster brouweri*	7H-1, 115–117 7H-2, 115–117	61.70 63.20	1.90	6	
T *Discoaster pentaradiatus*	8H-CC 9H-1, 115–117	79.55 80.70	2.40	6	
B *Theocalyptra davisiana*	8H-CC 9H-4, 85–87	79.55 84.90	2.42–2.44	1	
Matuyama/Gauss	9H-2, 146–148 9H-3, 35–37	82.51 82.90	2.47	6	

Note: Depths in Hole 721A reflect the addition of 2.75 m at the top of the hole to account for loss due to coring (see "Interhole Correlation" section, this chapter). T = upper limit and B = lower limit. Sources of ages are: 1 = Johnson et al., in press; 3 = oxygen isotope data for Site 723 (N. Niitsuma, unpubl. data); 4 = Takayama and Sato, 1987; 6 = Berggren et al., 1985b; 8 = Sato et al., in press.

[a] North Atlantic data.

[b] Long axis greater than 6 μm.

[c] North Atlantic age consistent with Italian-type section.

23X, CC (221.3 mbsf) and 117-721B-24X, CC (230.5 mbsf). The first appearance of *Neogloboquadrina acostaensis* defines the N15/N16 boundary which could be recognized in Sample 117-721B-27X, CC (259.6 mbsf). Because foraminifers are rare in this interval, this boundary is considered unreliable.

A sharp faunal break occurs between Zones N15 and N16, which is characterized by a dramatic increase in the abundance of *Globigerina bulloides*, *Globorotalia menardii*, and the appearance of the *Neogloboquadrina acostaensis-humerosa-dutertrei* group. This faunal event may represent an increased upwelling intensity during the earliest late Miocene, because the modern representatives are known to be upwelling indicators (Bé, 1977).

Samples 117-721B-28X, CC (269.4 mbsf), to 117-721B-30X, CC (289.0 mbsf), have tentatively been assigned to Zone N15, based on the absence of *Neogloboquadrina acostaensis*. No foraminifers were present in Sample 117-721B-31X, CC, and no zonal indicator could be found in Sample 117-721B-32X, CC. The co-occurrence of *Globorotalia birnageae* and *Globorotalia mayeri/siakensis* (Zones N7–8) in Samples 117-721B-33X, CC (318.0 mbsf), to 117-721B-36X, CC (347.0 mbsf), indicate a late early Miocene age; hence a discontinuity exists between Samples 117-721B-32X, CC (308.4 mbsf), and 117-721B-33X, CC (318.0 mbsf).

Planktonic foraminifers are absent in the remainder of the recovered section or are reworked.

Benthic Foraminifers

The benthic foraminiferal fauna (Corliss, 1979; Mead, 1985) was studied at Site 721 in the core-catcher samples of Hole 721A down to 86.4 mbsf (117-721A-1H, CC, through -9H, CC) and in the core-catcher samples of Hole 721B for the depths below 86.0 mbsf (117-721B-9H, CC, through -44X, CC). The abundance ranges from abundant to common in the uppermost interval (down to 240.1 mbsf). The interval from 249.8 to 347.0 mbsf contains few benthic foraminifers, whereas the lowermost interval (356.6–424.2 mbsf) contains few or no benthic foraminifers. The diversity is high in the upper part of the recovered se-

Table 5. Stratigraphic listing of faunal events and paleomagnetic reversals for Hole 721B.

Event	Core level	Depth (mbsf)	Age (Ma)	Source of age	Notes
T *Globigerinoides extremus*	7H-4, 65–67 8H-CC	63.21 76.40	[a]1.8	6	
T *Discoaster pentaradiatus*	8H-CC 9H-1, 115–117	76.97 77.55	2.40	6	
B *Lamprocyrtis neoheteroporos*	9H-4, 85–87 9H-CC	81.75 86.00	2.51–2.53	1	Cores MD81-369, RC14-22 and VM34-35; DSDP 214 data probably less accurate.
T *Stichocorys peregrina*	9H-4, 85–87 9H-CC	81.75 86.00	2.62–2.64	1	
Matuyama/Gauss	9H-6, 115–117 10X-1, 35–37	85.05 86.35	2.47	6	
T *Sphaeroidinellopsis* sp.	10X-4, 65–67 11X-2, 65–67	91.15 97.75	3.0	6	
T *Phormostichoartus fistula*	11X-CC 12X-CC	105.20 114.80	3.26–3.28	1	
T *Lychnodictyum audax*	11X-CC 12X-CC	105.20 114.80	3.33–3.35	1	
T *Sphenolithus abies*	12X-CC 13X-1, 115–117	114.80 115.95	3.47	6	
T *Reticulofenestra pseudoumbilica*	12X-CC 13X-1, 115–117	114.80 115.95	3.50	6	
Gauss/Gilbert	13X-2, 35–37 13X-2, 115–117	116.65 117.45	3.40	6	
T *Phormostichoartus doliolum*	13X-4, 85–87 13X-CC	120.15 124.40	3.53–3.55	1	
B *Amphirhopalum ypsilon*	13X-4, 85–87 13X-CC	120.15 124.40	3.77–3.79	1	
T *Spongodiscus ambus*	13X-4, 85–87 13X-CC	120.15 124.40			Irregular distribution at top of range.
B *Spongaster tetras tetras*	13X-CC 14X-4, 85–87	124.40 129.75	3.83–3.85	1	
T *Didymocyrtis penultima*	14X-4, 85–87 14X-CC	129.75 134.10			
T *Solenosphaera omnitubus*	16X-CC 17X-4, 85–87	153.50 158.85	4.7–4.8	2	
T Sidufjall	17X-2, 115–117 17X-4, 115–117	156.15 159.15	4.40	6	
T *Stichocorys delmontensis*	17X-CC 18X-4, 85–87	163.20 168.55			
B Thvera	18X-3, 115–117 18X-6, 115–117	167.35 171.85	4.77	6	
T *Discoaster quinqueramus*	19X-3, 115–117 19X-4, 115–117	177.05 178.55	5.6	6	Age appears to be erroneous.
T *Siphostichartus corona*	21X-CC 22X-4, 85–87	202.00 207.35	5.0–5.1	2	
B *Globorotalia tumida tumida*	22X-2, 65–67 22X-CC	204.15 211.70	5.2	6	

quence and deteriorates downhole. The preservation shows the same pattern as the diversity, with well-preserved fauna occurring in the upper part. Preservation becomes good further down, and below 385.6 mbsf the fauna is badly preserved and shows signs of reworking.

Eggerella bradyi, *Globocassidulina subglobosa*, *Melonis barleeanum*, and *Pullenia bulloides* are the only species that occur consistently in high relative abundances throughout the sequence; occurrences of other species are restricted to parts of the sequence. A slight faunal change in the benthic foraminiferal fauna appears to occur somewhere between Sample 117-721B-14X, CC (134.1 mbsf), and 117-721B-16X, CC (153.5 mbsf). The most abundant species in the uppermost part (above 76.8 mbsf) are *Cassidulina carinata* and *Uvigerina auberiana*, which together make up about 40% of the benthic foraminiferal fauna in these samples. Species like *Cassidulina carinata* and *Hoeglundina elegans* are not present below this interval.

The species *Sigmoilinopsis schlumbergeri* occurs consistently above 221.3 mbsf and is absent below.

A sharp faunal change occurs approximately at the level of Sample 117-721B-32X, CC (308.4 mbsf), or slightly above. *Cibicidoides wuellerstorfi*, *Melonis pompiloides*, *Uvigerina auberiana*, and *Uvigerina peregrina* do not occur below this level, whereas *Anomalinoides semicribratus* and *Vulvulina spinosa* occur with high relative abundances below this level; the former species has a known stratigraphic range from middle Eocene (P12) through middle Miocene (N12; van Morkhoven et al., 1986). *Ehrenbergina hystrix* disappears just above and *Globocassidulina decorata* just below this level. This faunal change coincides with the apparent break in sedimentation seen both in the planktonic foraminiferal and nannofossil records.

Calcareous Nannofossils

Abundant and well-preserved nannofossils are found throughout the Quaternary sequences in Holes 721A to 721C. Samples 117-721B-1H, CC (9.4 mbsf), and 117-721C-1H, CC (3.6 mbsf), contain *Emiliania huxleyi* and can be correlated with the upper Pleistocene to Holocene Zone NN21. Because *Emiliania huxleyi* and *Pseudoemiliania lacunosa* are absent in Sample 117-721A-1H-5, 115–117 cm, down to Sample 117-721A-2H-4, 115–117 cm (12.55–18.20 mbsf), and 117-721C-2H, CC (13.3 mbsf), they are assigned to the Pleistocene Zone NN20. The presence of *P. lacunosa* and the absence of discoasters place Samples 117-721A-2H, 115–117 cm, through 117-721A-7H-1, 115–117 cm (19.70–61.70 cm), and Samples 117-721B-2H, CC (19.1 mbsf), through 117-721B-7H, CC (66.9 mbsf), in Zone NN19. Within Zone NN19 the following calcareous nannofossil datums which were recognized in the North Atlantic Ocean (Perch-Nielsen,

Table 5 (continued).

Event	Core level	Depth (mbsf)	Age (Ma)	Source of age	Notes
Gilbert/Chronozone 5	22X-4, 115-117 22X-5, 35-37	207.65 208.35	5.35	6	
T *Botryostrobus bramlettei*	22X-4, 85-87 22X-CC	207.35 211.70	4.9-5.0	2	Should be higher.
T *Acrobotrys tritubus*	22X-CC 23X-C, 85-87	211.70 215.55	5.3-5.4	2	
T *Stichocorys johnsoni*	22X-CC 23X-3, 85-87	211.70 215.55	[b]5.7-5.8	2	
S. delmontensis *S. peregrina*	24X-CC 25X-4, 85-87	230.50 235.85	6.1-6.7	2	
B *Spongodiscus ambus*	25X-CC 26X-4, 85-87	240.10 245.45			
T *Diartus hughesi*	27X-4, 85-87 27X-CC	255.15 259.60	7.1-7.2	2	Considerable reworking of this species.
T *Diartus petterssoni*	27X-4, 85-87 27X-CC	255.15 259.60	8.1-8.2	2	Considerable reworking of this species.
B *Solenosphaera omnitubus*	27X-CC 28X-4, 85-87	259.60 264.95	6.3-6.5	2	
B *Stichocorys peregrina*	27X-CC 28X-4, 85-87	259.60 264.95			
B *Discoaster quinqueramus*	28X-1, 105-106 28X-2, 107-109	260.65 262.17	8.2	6	
B *Neogloboquadrina acostaensis*	28X-2, 65-67 28X-4, 65-67	261.75 264.75	8.6	6	
B *Acrobotrys tritubus*	28X-4, 85-87 28X-CC	264.95 269.40	7.7-7.8	2	Rare in Site 721.
B *Diartus hughesi*	29X-CC 30X-CC	279.20 289.00	8.7-8.8	2	
T *Discoaster hamatus*	30X-3, 115-117 30X-CC	283.37 289.00	8.85	6	
T *Globorotalia mayeri*	32X-CC 33X-2, 65-67	308.40 310.55	[c]10.4	6	
B *Discoaster hamatus*	33X-1, 115-116 33X-2, 115-116	309.55 311.05	10.0	6	
T *Sphenolithus heteromorphus*	33X-2, 115-116 33X-CC	311.05 318.00	14.4	6	
T *Sphenolithus belemnos*	38X-CC 39X-CC	366.30 375.90	17.4	6	

Note: T = upper limit of event and B = lower limit. Sources of ages are: 1 = Johnson et al., in press; 2 = Johnson and Nigrini, 1985; and 6 = Berggren et al., 1985b.

[a] *G. obliquus extremus* cited in Berggren et al., 1985b.

[b] *E.* cf. *diaphanes* cited in Johnson and Johnson and Nigrini, 1985.

[c] *G. siakensis* cited in Berggren et al., 1985.

1985; Takayama and Sato, 1987) are recognized in descending order in Holes 721B and 721C: (1) top of acme of *Reticulofenestra* sp. A, 0.83 Ma, 117-721B-3H, CC, 117-721A-3H, CC; (2) First Appearance Datum (FAD) *Gephyrocapsa parallela*, 0.89 Ma, 117-721C-4H, CC; (3) Last Appearance Datum (LAD) *Helicosphaera sellii*, 1.19 Ma, 117-721B-5H, CC;(4) FAD *Gephyrocapsa oceanica*, 1.57 Ma, 117-721B-6H, CC; (5) FAD *Gephyrocapsa caribbeanica*, 1.66 Ma, 117-721B-6H, CC.

The Pliocene/Pleistocene boundary, which is designated by the bottom of *Gephyrocapsa caribbeanica* is placed somewhere between Samples 117-721A-6H-1, 115-117 cm, and 117-721A-6H-2, 115-117 cm (52.40-53.90 mbsf), and Samples 117-721B-6H, CC, and 117-721B-7H, CC. The top of *Discoaster brouweri*, which marks the NN19/NN18 boundary occurs between Samples 117-721A-7H-1, 115-117 cm, and 117-721A-7H-2, 115-117 cm (61.70-63.20 mbsf). The top of *Discoaster pentaradiatus* occurs between 117-721A-8H, CC, and 117-721A-8H, CC, and 117-721A-9H-1, 115-117 cm. Samples below the top of *D. pentaradiatus* are assigned to Zone NN17. Sample 117-721B-8H, CC (76.4 mbsf), contains only one discoaster species, *D. brouweri*, and is therefore assigned to Zone NN18. The assemblages in Samples 117-721B-9H, CC (86.0 mbsf), through 117-721B-11X, CC (105.2 mbsf), are characterized by the occurrences of *D. brouweri* and *D. pentaradiatus*. Abundant occurrences of *Reticulofenestra pseudoumbilica* are first observed in Sample 117-721B-12X, CC (114.8 mbsf). Therefore, the samples mentioned above are placed in Zones NN17 to NN16. Notably, *Discoaster surculus* and *D. tamalis* are not found in these samples. In the absence of ceratoliths Samples 117-721B-12X, CC (114.8 mbsf), through 117-721B-14X, CC (134.1 mbsf), are tentatively placed in lower Pliocene Zones NN15 and NN14. The next two samples, 117-721B-15X, CC (143.8 mbsf), and 117-721B-16X, CC (153.5 mbsf) are assigned to Zones NN13 and NN12 (lower Pliocene to uppermost Miocene) because of the absence of both *Discoaster asymmetricus* and *D. quinqueramus*. As ceratoliths are rare, the distinction between the two zones is uncertain.

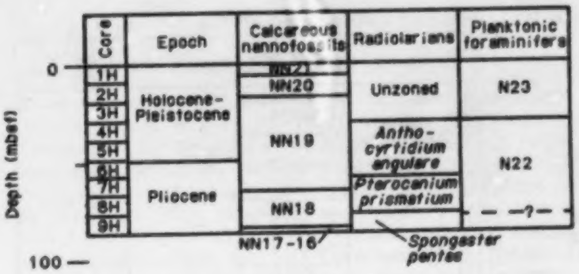

Figure 15. Correlation of planktonic microfossil zones in Hole 721A.

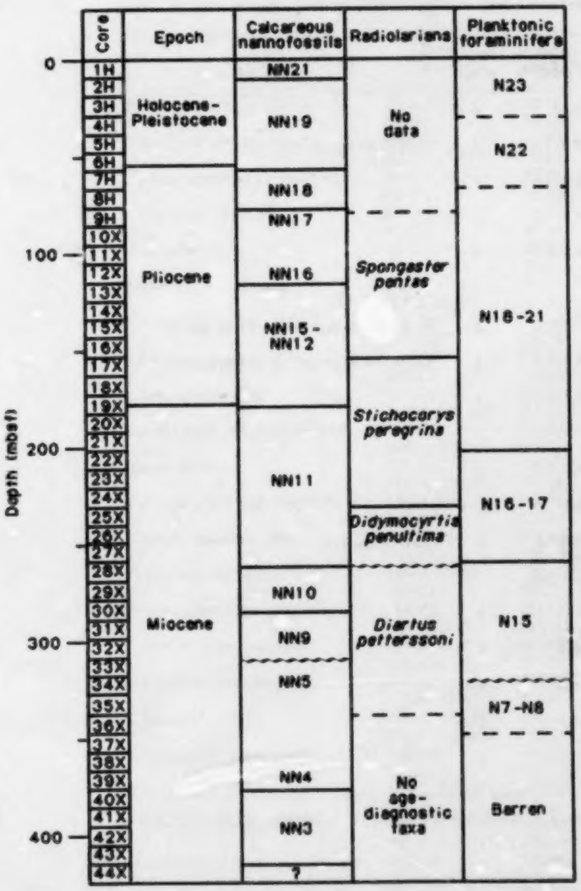

Figure 16. Correlation of planktonic microfossil zones in Hole 721B.

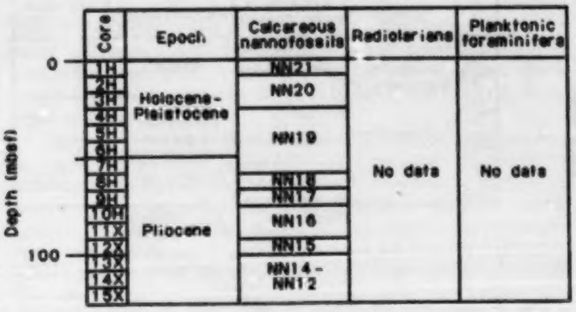

Figure 17. Correlation of planktonic microfossil zones in Hole 721C.

Sample 117-721B-17X, CC (163.2 mbsf), contains rare specimens of *Ceratolithus armatus* and can be assigned to Zone NN12. Below this core the nannoflora changes progressively with a gradual increase in the number of species and specimens of discoasters. The interval from Sample 117-721B-18X, CC (172.9 mbsf), down to 117-721B-27X, CC (259.6 mbsf), contains *Discoaster quinqueramus* together with *D. berggrenii*, *D. surculus*, *D. pentaradiatus*, and *D. variabilis* and belongs to the upper Miocene (Zone NN11). The occurrence of *Discoaster hamatus* suggests that Samples 117-721B-30X, CC (289.0 mbsf), through 117-721B-32X, CC (308.4 mbsf), can be correlated with Zone NN9. Therefore, Samples 117-721B-28X, CC (269.4 mbsf), and 117-721B-29X, CC (279.2 mbsf), belong to Zone NN10.

A remarkable change in species composition and the state of preservation of calcareous nannofossils occurs between Samples 117-721B-32X, CC (308.4 mbsf), and 117-721B-33X, CC (318.0 mbsf). In contrast to the previous samples, sediments below this horizon contain abundant *Cyclicargolithus floridanus*, and the preservation of coccoliths is poor. Though *Helicosphaera ampliaperta* is not found in this hole (it is known to be rare or absent in some regions of the South Atlantic and the Pacific; Perch-Nielsen, 1985), the occurrence of *Sphenolithus heteromorphus* suggests that Samples 117-721B-33X, CC, (318.0 mbsf), through 117-721B-40X, CC (385.6 mbsf), belong to lower and middle Miocene Zones NN5 and NN4. Therefore, Zones NN8 through NN6 are missing; a middle Miocene hiatus is inferred at this site. From Sample 117-721B-33X, CC (318.0 mbsf), down to the bottom of this hole, age-diagnostic species are absent, and no biostratigraphic age assignments can be made.

Nannofossil assemblages in Hole 721C are similar to those observed in Hole 721B. In this hole, however, sporadic occurrences of *Discoaster surculus* are recognized. Based on these occurrences of *D. surculus*, Samples 117-721C-10X, CC (89.9 mbsf), and 117-721C-11X, CC (99.5 mbsf), are assigned to the upper Pliocene (Zone NN16).

As mentioned above, asteroliths and ceratoliths are comparatively rare in the Pliocene sequences at this site. For example, *Discoaster surculus* is known to prefer warm waters (Aubry, 1984) and is extremely rare and *D. tamalis* is absent. *Ceratolithus cristatus*, *C. rugosus*, and *Amaurolithus tricorniculatus* are missing. In addition, *Coccolithus pelagicus*, which is the typical cold-water species, is dominant. Throughout the Quaternary section, *Pseudoemiliania lacunosa* and *Rhabdosphaera* are rare. The Pliocene and Quaternary flora may suggest an initiation of upwelling in this area at the end of Miocene.

Radiolarians

Shipboard analysis of radiolarians consisted of examination of all core-catcher samples from 721A and Samples 117-721B-9H, CC (86.0 mbsf), to 117-721B-44X, CC (424.2 mbsf). Additional intermediate samples were examined during shore-based studies. Radiolarians are abundant, robust, and well-preserved in all samples examined except for Samples 117-721A-2H, CC (19.5 mbsf), 117-721A-3H, CC (29.2 mbsf), and 117-721A-6H, CC (57.8 mbsf), where they are few and only moderately well-preserved. From 117-721B-33X, CC (318.0 mbsf), to 117-721B-44X, CC (424.2 mbsf), radiolarians are virtually absent. Most samples below 117-721A-7H, CC (67.3 mbsf), contain some reworked middle Miocene taxa. Samples from Hole 721A and the upper part of Hole 721B (down to about 117-721B-23X, CC, 221.3 mbsf) are particularly heavy-shelled and large and contain some forms not commonly found in tropical sediments; they may reflect a response to upwelling conditions. Conversely, some typically tropical forms are absent or very rare. Diatoms are noticeable in Sample 117-721B-13X, CC (124.4 mbsf), and gradually increase in abundance downhole until they become quite abundant in Sample 117-721B-23X, CC (221.3 mbsf).

Sample 117-721A-1H, CC (9.8 mbsf) probably belongs to the upper part of the *Collosphaera tuberosa* Zone. Samples 117-721A-2H, CC (19.5 mbsf), through 117-721A-4H-4, 85–87 cm (37.25 mbsf), belong to the *Amphirohopalum ypsilon* Zone. Samples 117-721A-4H, CC (38.9 mbsf), through 117-721A-6H, CC (57.8 mbsf), belong to the *Anthocyrtidium angulare* Zone. It follows that Sample 117-721A-6H-4, 85–87 cm (56.60 mbsf), belongs to the *Pterocanium prismatium* Zone, but this determination is based on only two specimens in the sample. *Pterocanium prismatium* is extremely rare in all other material examined from this site. A similar virtual absence of this species was noted by Nigrini (1974) at DSDP Site 223. Sample 117-721A-9H, CC (89.15 mbsf), belongs to the *Spongaster pentas* Zone.

Sample 117-721B-9H, CC (86.0 mbsf), also belongs to the *Spongaster pentas* Zone, and the zone persists through Sample 117-721B-16X, CC (153.3 mbsf). Samples 117-721B-17X, CC (163.2 mbsf), through 117-721B-24X, CC (230.5 mbsf), lie within the *Stichocorys peregrina* Zone. Since only a single specimen of *Spongaster pentas* was observed in the material from Sample 117-721B-15X, CC (143.8 mbsf), and *Spongaster berminghami* and *Pterocanium prismatium* are absent, the zonal boundary was approximated to the last appearance of *Solenosphaera omnitubus*. The transition from *Stichocorys delmontensis* to *Stichocorys peregrina*, marking the top of the *Didymocyrtis penultima* Zone, occurs between Samples 117-721B-24X, CC (230.5 mbsf) and 117-721B-25X-4, 85–87 cm, CC (235.85 mbsf). However, considerable reworking of *S. delmontensis* may have influenced the placement of this zonal boundary. Between Samples 117-721B-27X-4, 85–87 cm, and 117-721B-27X, there appears to be a hiatus, and the *Didymocyrtis antepenultima* Zone is entirely missing. The material from Sample 117-721B-27X, CC (259.6 mbsf), lies within the *Diartus petterssoni* Zone, which continues through Sample 117-721B-32X, CC (308.4 mbsf). The rest of the recovered material is virtually barren of radiolarians.

PALEOMAGNETISM

Magnetostratigraphy

Magnetostratigraphy of the Site 721 sediments was studied by measuring discrete samples on the MINISPIN spinner magnetometer. The samples were obtained from Cores 117-721A-1H to -9H, and Cores 117-721B-9H to -32X. We also measured additional samples from Cores 117-721B-4H and -5H to examine horizons of the Brunhes/Matuyama Chronozone boundary and the Jaramillo Subchronozone. Stepwise alternating field (AF) demagnetization was carried out on a pilot sample from most of the cores. Some results of the AF demagnetization tests are shown in Figures 18–20. These results show that several samples had soft magnetic components, which can be erased by AF demagnetization up to 5 mT. These components include coring-induced remanence, which showed steep inclination. The magnetization cleaned by peak AF of 10 or 15 mT tends to be decreased toward the origin of the Zijderveld diagram by subsequent demagnetization. The higher coercivity component was, therefore, assumed to represent characteristic magnetization of the sediments. Other samples were routinely demagnetized at peak AF of 10 or 15 mT. Magnetic intensities after the demagnetization ranges from 0.02 to 1.8 mA/m. Figure 21 shows a histogram of inclinations obtained after the routine demagnetization. While the inclination values are distributed in a relatively wide range, the modes of normal and reversed polarity are concordant with those expected from geocentric axial dipole field at the site (30.0°).

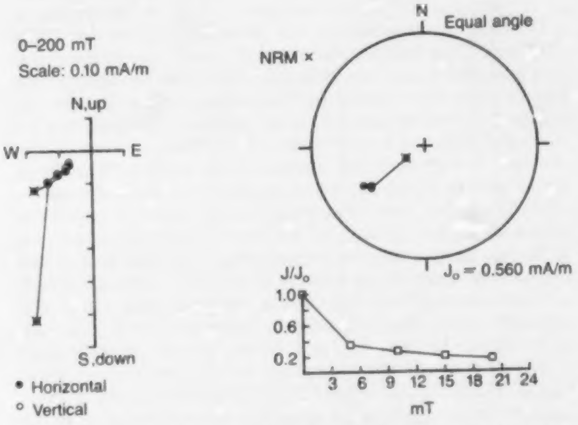

Figure 18. Result of stepwise AF demagnetization for Sample 117-721A-4H-1, 115–117 cm.

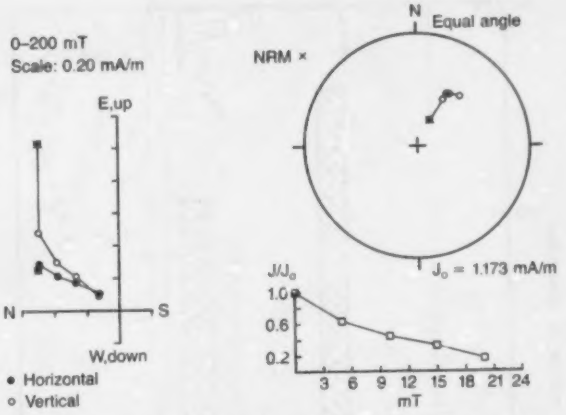

Figure 19. Result of stepwise AF demagnetization for Sample 117-721A-9H-1, 115–117 cm.

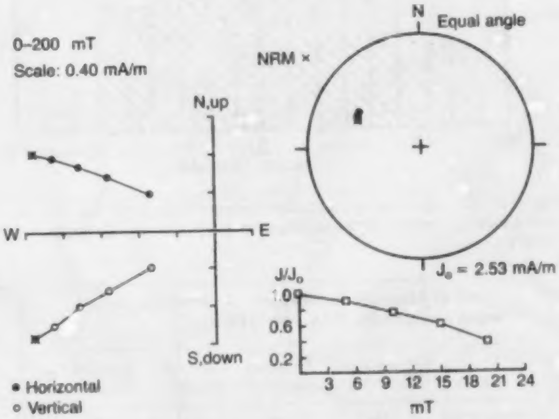

Figure 20. Result of stepwise AF demagnetization for Sample 117-721A-10X-1, 115–117 cm.

A total of 11 oriented cores were obtained from Site 721 by using a APC and a multishot core orientation tool (Cores 117-721A-5H to -10H and 117-721B-5H to -9H). The orientation data and mean magnetic declinations of discrete samples are listed in Table 6. Declination values estimated from the orientation data are widely scattered, and are generally inconsistent with the expected geomagnetic direction (0° or 180°). The reason for this deflection is not clear at present.

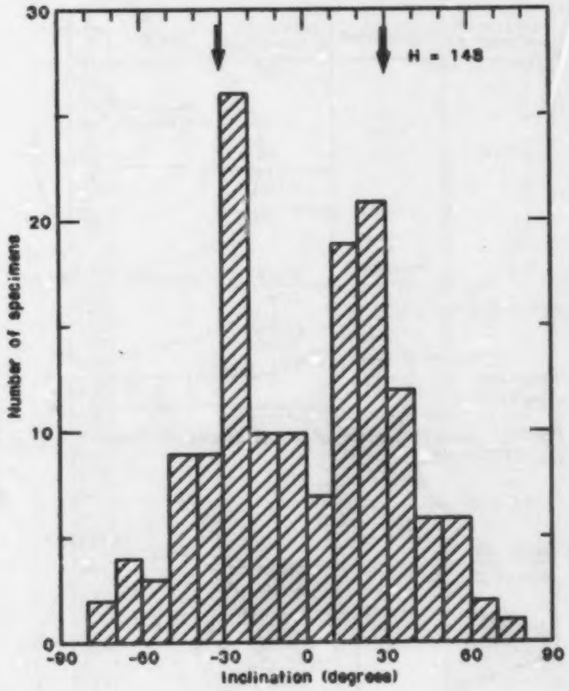

Figure 21. Histogram of magnetic inclination values from Site 721. Arrows shows the values expected from the geocentric axial dipole field (30.6°).

Table 6. Magnetic declinations of samples from oriented cores, Holes 721A and 721B.

Core	Orientation (degrees)	Measured (degrees)	Corrected (degrees)	Expected (degrees)
721A-5H	185	276 (R)	91	180
721A-6H	235	206 (R)	331	180
721A-7H	250	66 (R)	176	180
721A-8H	255	124 (R)	229	180
721A-9H	300	277 (R)	337	180
721B-5H	132	87 (N?)	315	0

Note: Orientation is azimuth of the double-line of a core tube measured from geomagnetic north by a multishot orientation tool. Measured declination is obtained as mean of paleomangetic declination relative to the double-line, and N and R indicate normal and reversed polarity estimated from inclination values. Corrected values are estimates of "true" declination of remanent magnetization, which are expected to be around 0° or 180°.

Figure 22 shows plots of directions and intensities of remanent magnetization of the samples from Hole 721A. The inclination plots in this figure show a reversed polarity zone existing between 39 and 80 mbsf of Hole 721A. Because a reversely magnetized sample was found at 36.35 mbsf, we assigned the polarity change at 39 mbsf to the beginning of the Jaramillo Subchronozone (C1r-1/C1r; 0.98 Ma). Results from the correlative horizons of Site 721B are shown in Figure 23. The polarity zone boundary at 80 mbsf of Hole 721A was also observed on the concordant horizon of Hole 721B (at 86 mbsf). Based on calcareous nannofossil data (see "Biostratigraphy" section, this chapter), this horizon is assigned to the Matuyama/Gauss boundary (C2r/C2A, 2.47 Ma). This interpretation implies that the Olduvai Subchronozone (C2) was not detected at Site 721.

Lack of records of short polarity interval records, such as Olduvai and Brunhes-Jaramillo, suggests a possibility that the Site 721 sediments have acquired remanent magnetization by averaging the geomagnetic field for intervals as long as 10^5 yr. This duration, corresponding to a thickness of about 3 m, is much longer than previously assumed as the interval of postdepositional detrital remanent magnetization (postdepositional DRM). A short hiatus in sedimentation or overprint of chemical remanent magnetization (CRM) may explain the deficiency of paleomagnetic record in some parts.

Results obtained from the Hole 721B sediments between 0 and 310 mbsf are shown in Figure 24. Using these results and additional data from the shore-based work, we determined horizons of magnetic polarity changes and assigned them to a magnetic polarity timescale as listed in Table 7. Most samples from the sections below about 250 mbsf had quite weak magnetization less than 0.04 mA/m. Their CSD (circular standard deviation) values are relatively high, suggesting difficulty of high-precision measurements of these samples. Magnetozones were therefore not identified in the lower part.

Magnetic Susceptibility

All recovered sections of Holes 721A, 721B, and 721C were measured at 5-cm intervals with a total of 1833, 6006, and 2490 measurements on Holes 721A, 721B, and 721C, respectively.

Paleomagnetic and biostratigraphic data of Hole 721A suggest that the oldest recovered sediments are late Pliocene in age (~2.5 Ma). The susceptibility data indicate lower values than observed at Site 720 (Fig. 25). The data generally vary between 25 and 125 X 10^{-6} volume S.I. units. Inspection of the data indicates cyclic fluctuations of susceptibility at a depth scale of ~1 m (Fig. 26). Using an approximate 3.5 cm/k.y. sedimentation rate for Hole 721A, this suggests a periodicity which is very close to the 23 k.y. and 19 k.y periods of precessional insolation fluctuations. Although this higher frequency variability appears to dominate the record, lower frequencies are apparent as well. Additional periodicities of ~1-2 m, ~3-4 m, and ~12-14 m suggest the presence of 41 k.y., 100 k.y., and 400 k.y. periodicities, tentatively correlated with orbital periodicities of obliquity and eccentricity. A possible cause of these cyclic variations in susceptibility is discussed below.

Paleomagnetic and biostratigraphic analyses indicate that the sequence recovered in Hole 721B extends to the early Miocene (~17 Ma) and that a hiatus between ~10-14 Ma occurs at ~310 mbsf. Comparison of the susceptibility data for Holes 721A and 721B indicate that the APC cores can be correlated on a point-for-point basis (Fig. 26). Note that the susceptibility data for each hole have virtually identical profiles. Detailed interhole correlations based on these data and lithologic marker layers are presented in the "Interhole Correlation" section (this chapter). The effect of rust contamination of the XCB core tops can be seen in Figure 27, which appears as ~10-m-spaced susceptibility spikes. Rust contamination was found to largely obliterate the upper ~1-2 m of the susceptibility record of each XCB core. Despite the rust contamination, the rapid and cyclical fluctuations apparent particularly in the APC cores are clearly present in many of the XCB cores as well to at least ~260 mbsf (upper Miocene). Below this depth, higher and less regular variations occur. In part, this may be due to the generally poor quality of the recovered sediments, which were often very disturbed. However, this change is coincident with a sharp lithologic boundary between the overlying nannofossil ooze (lithologic Subunit IA) and the underlying chalk sediments (lithologic Subunit IB; see "Lithostratigraphy" section, this chapter).

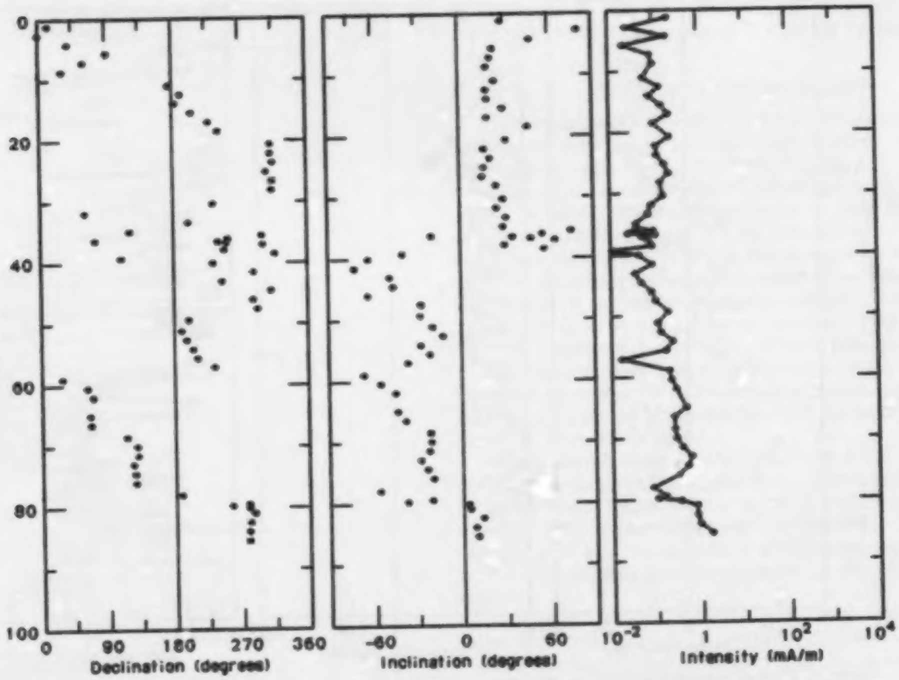

Figure 22. Plots of magnetic declination (relative values), inclination, and intensity against depth of Hole 721A, obtained after AF demagnetization.

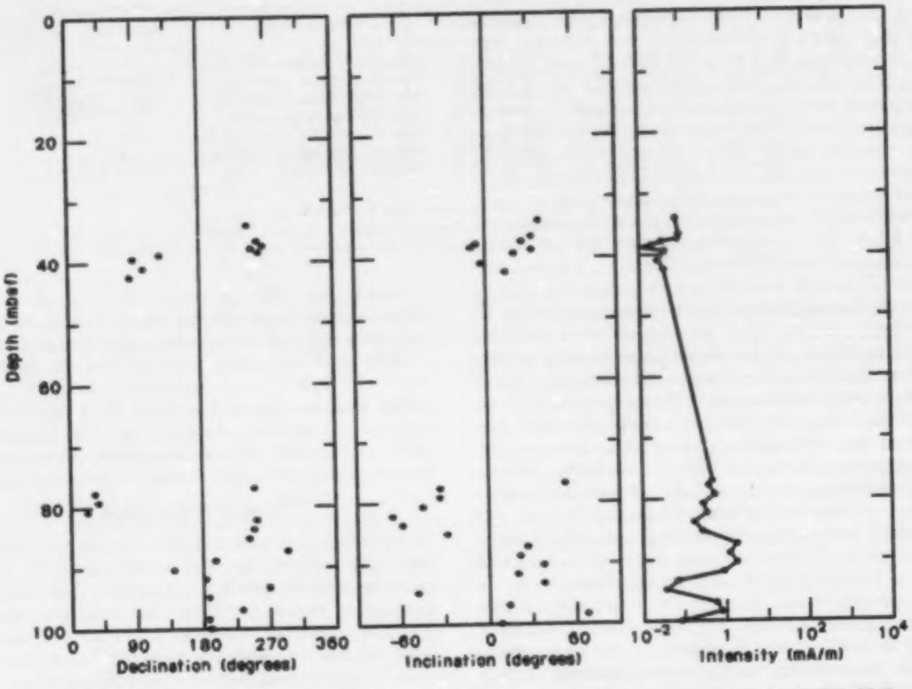

Figure 23. Plots of magnetic declination (relative values), inclination, and intensity against depth of Hole 721B, obtained after AF demagnetization.

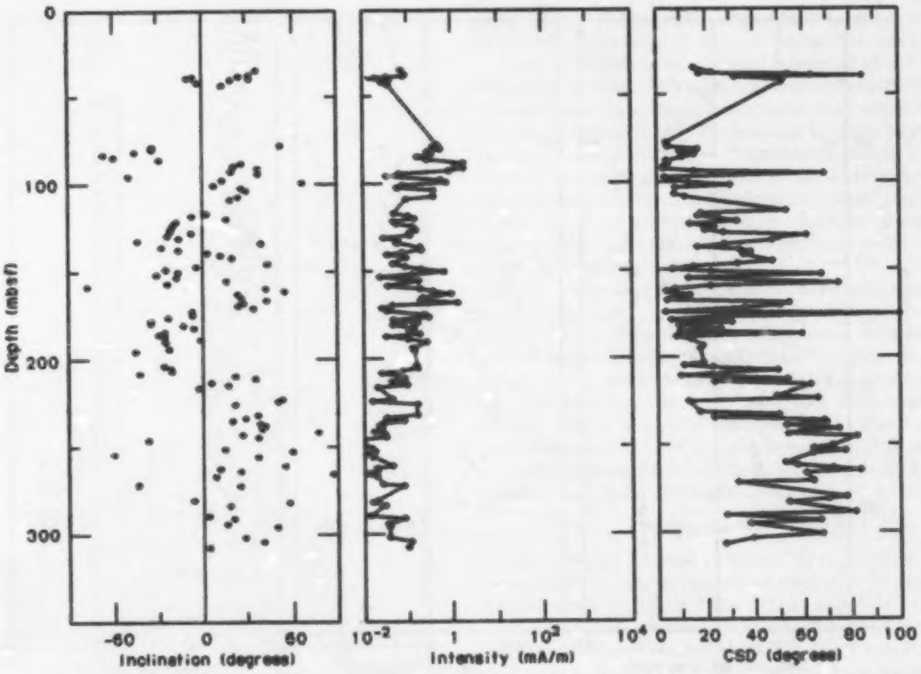

Figure 24. Plots of magnetic inclination, intensity, and CSD value against depth of Hole 721B between 0 and 310 mbsf, obtained after AF demagnetization.

Table 7. Magnetostratigraphic boundaries in Holes 721A and 721B.[a]

Hole, sample (cm)	Depth (mbsf)	Chronozone	Age (Ma)
721A-4H-7, 35 to 5H-1, 115	[b]38.55-40.05	Jaramillo/Matuyama (C1r-1/C1r)	0.98
721A-9H-2, 146 to 9H-3, 35	[b]79.76-80.15	Matuyama/Gauss (C2r/C2A)	2.47
721B-9H-6, 115 to 10X-1, 35	85.05-86.35	Matuyama/Gauss (C2r/C2A)	2.47
721B-13X-2, 35 to 13X-2, 115	116.65-117.45	Gauss/Gilbert (C2A/C2Ar)	3.40
721B-17X-2, 115 to 17X-4, 115	156.15-159.15	Top of Sidufjall (C3.2r/C3.2r1)	4.40
721B-18X-3, 115 to 18X-6, 115	167.35-171.85	Bottom of Thvera (C3A/C3Ar)	4.77
721B-22X-4, 115 to 22X-5, 35	207.65-208.35	Gilbert/5 (C3r/C3A)	5.35

[a] Based on the data with CSD less than 40. Boundary ages are after Berggren et al. (1985).

[b] Correlation with Hole 721B indicates that 2.75 m is missing from the top of Hole 721A. The corrected (true) sub-bottom depths for these events can be calculated by adding 2.75 m to the reported depths.

The shift from the carbonate sediments of lithologic Subunit IB to the more siliceous sediments of lithologic Unit II occurs at 289 mbsf, and is recorded as a significant decrease in the susceptibility data over the interval represented by lithologic Unit II (289-309.9 mbsf). A nannofossil chalk (lithologic Unit III) extends from 309.9 to ~341 mbsf and rests unconformably below lithologic Unit II (see "Biostratigraphy" section, this chapter). Other than a slight increase in the mean susceptibility, this hiatus and change in lithology is not identified in the susceptibility data. However, the boundary of Unit III and Unit IV at 341 mbsf, comprised of terrigenous, clay-bearing, nannofossil chalk, is dramatically indicated by an increase of nearly 2 decades of susceptibility. Visually, the cores of lithologic Unit IV were a reddish, buff color containing numerous mud turbidites, so the increase in susceptibility was not surprising. From ~412 mbsf to the base of Hole 721B, core descriptions indicate a significant increase in the sand-sized terrigenous component. This is consistent with the dramatic increase in susceptibility observed below ~412 mbsf, which may be due to both an increase in concentration and size of the ferrimagnetic grains.

Hole 721C was APC-cored to Core 117-721C-10H at 89.9 mbsf and XCB cored to termination at 138.0 mbsf. The fine-scale variations observed in Holes 721A and 721B are also apparent in Hole 721C (Figs. 26 and 28). Unfortunately, poor XCB recovery and rust contamination compromise these correlations below ~90 mbsf, despite the relatively good recovery.

X-Ray Diffraction Results

In an effort to understand what may be responsible for the cyclic fluctuations observed in the upper 90 m of the three holes, we took discrete 3.0-cm^3 samples from susceptibility maxima and minima over the 0.0-13.0 mbsf interval of Hole 721C. This was done to determine which sedimentary components may be covarying with the susceptibility record. The samples were freeze-dried and ground to a fine powder for X-ray-diffraction (XRD) and carbonate analyses, which were performed

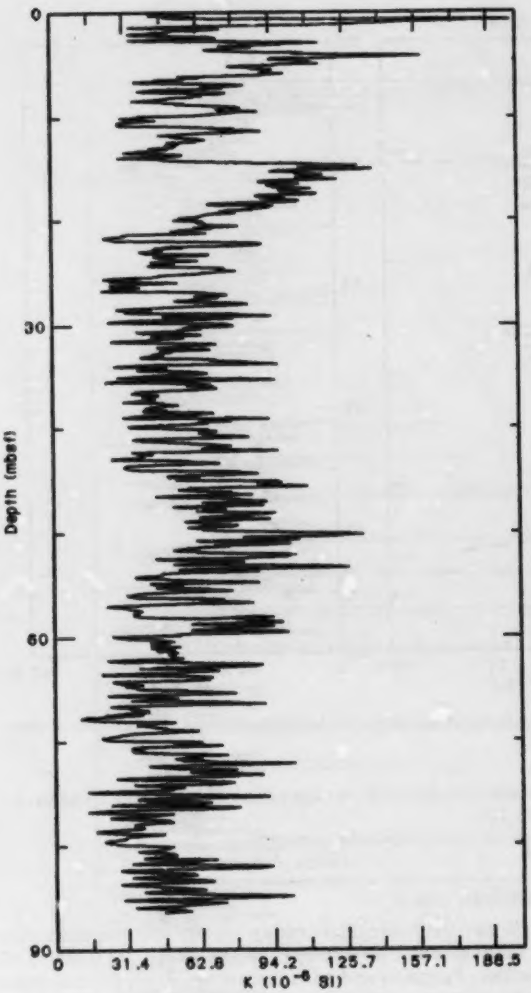

Figure 25. Volume magnetic susceptibility for Hole 721B.

by the shipboard geochemists. Once the XRD data were collected, the carbonate, quartz, dolomite, plagioclase feldspar, and combined kaolinite-chlorite peak areas (total counts) were extracted (Table 8). The carbonate percentages are also shown in Table 8.

Results from these analyses show a general inverse relationship between susceptibility and carbonate. Although this finding is common, the apparent cause of this relationship is interesting. Figure 29 shows plots of quartz, dolomite, plagioclase feldspar, and kaolinite-chlorite against susceptibility. In each case, a well-defined positive correlation exists, particularly for quartz and dolomite. This relation between quartz and dolomite was observed in other Site 721 samples as well (see "Inorganic Geochemistry" section, this chapter). If the mineral species are plotted against quartz a positive correlation emerges, suggesting that the increasing quartz brings with it increasing amounts of the other terrigenous minerals (Fig. 30). If the quartz and dolomite minerals can be interpreted as eolian tracers, then the inverse susceptibility-carbonate relation is most likely one of terrigenous (eolian) dilution of carbonate. However, in the absence of accumulation rate data, it is difficult to determine whether the susceptibility signal is one of terrigenous or carbonate dilution.

ACCUMULATION RATES

Sedimentation rates for Site 721 are based on the mean depth and age of magneto- and biostratigraphic datum levels identified in Holes 721A and 721B (Tables 4 and 5; Fig. 31). Because of uncertainties in the shipboard paleomagnetic data (see "Explanatory Notes" chapter, this volume), we favor the nannofossil biostratigraphic datums for the determination of the sedimentation rates at Leg 117 sites. For the interval from 0 to 3.5 m.y., we used seven nannofossil datums with ages based on oxygen isotope stratigraphy (Niitsuma, unpubl. data) and from Berggren et al. (1985) to determine variations in the mean sedimentation (Tables 4, 5, and 9). These same biohorizons are used to determine the mean sedimentation rate at other Leg 117 sites to permit the comparison of sediment accumulation of hemipelagic deposits on the Oman Margin and the more pelagic sediments on the Owen Ridge.

Four lithologic units are identified at Site 721 which reflect the changing depositional environment at the site due to the uplift of the Owen Ridge, and variations in surface plankton productivity (see "Lithostratigraphy" section, this chapter). Because of poor age control in the turbidite sequence of lithologic Unit IV, no estimate of sedimentation rate can be made at this time.

Lithologic Unit III, a nannofossil chalk deposited in the early to middle Miocene, is characterized by a relatively low mean sedimentation rate of 19 m/m.y. This low rate reflects pelagic sedimentation above the zone of turbidite deposition but still in waters corrosive to calcium carbonate (see "Lithostratigraphy" section, this chapter).

At Site 721, a hiatus spanning approximately 4 m.y. separates lithologic Units II and III. A more complete section representing the transition from Unit III to II in the late middle Miocene can be found in nearby Site 722 (see "Site 722" chapter, this volume). Sediments deposited between 261.2 and 309.9 mbsf at Site 721 (liothologic Units IB and II) at a mean rate of 21 m/m.y. appear disturbed and probably do not reflect continuous sediment accumulation (see "Lithostratigraphy" section, this chapter). The large scatter in age estimates for particular depths within this section, especially near 260 mbsf (Fig. 31), reflect this disturbance. The mean sedimentation rates calculated for comparable sections in nearby Site 722 are much higher than at Site 721 (42–54 m/m.y. vs. 21 m/m.y.) suggesting that Site 722 contains a more complete record of continuous sedimentation in ther middle to late Miocene than is found at Site 721.

Nannofossil oozes in the lower part of lithologic Unit I, which was deposited at the end of the Miocene and the beginning of the Pliocene (169–208 mbsf), are characterized by a high mean sedimentation rate (67 m/m.y.; Fig. 31). The high sedimentation rate may reflect an increase in particle flux associated with an increase in productivity and/or an increase in eolian input, an increase in calcite preservation at the site moves to less corrosive waters, or a change in the tectonic setting of the site such that more of the primary flux accumulated. The cause of this increase cannot be determined at this time.

During the last 3.5 m.y. (the upper part of lithologic Unit I), the mean sedimentation rate at Site 721 varied between 31 and 48 m/m.y. with an average of 33 m/m.y. (Fig. 31; Table 9). These are similar to the rates at Owen Ridge Sites 722 and 731 over this same time interval and of pelagic sedimentation in other areas, but are two to five times lower than rates during comparable time intervals from hemipelagic deposits on the Oman Margin (see "Site 723" through "Site 730" chapters, this volume).

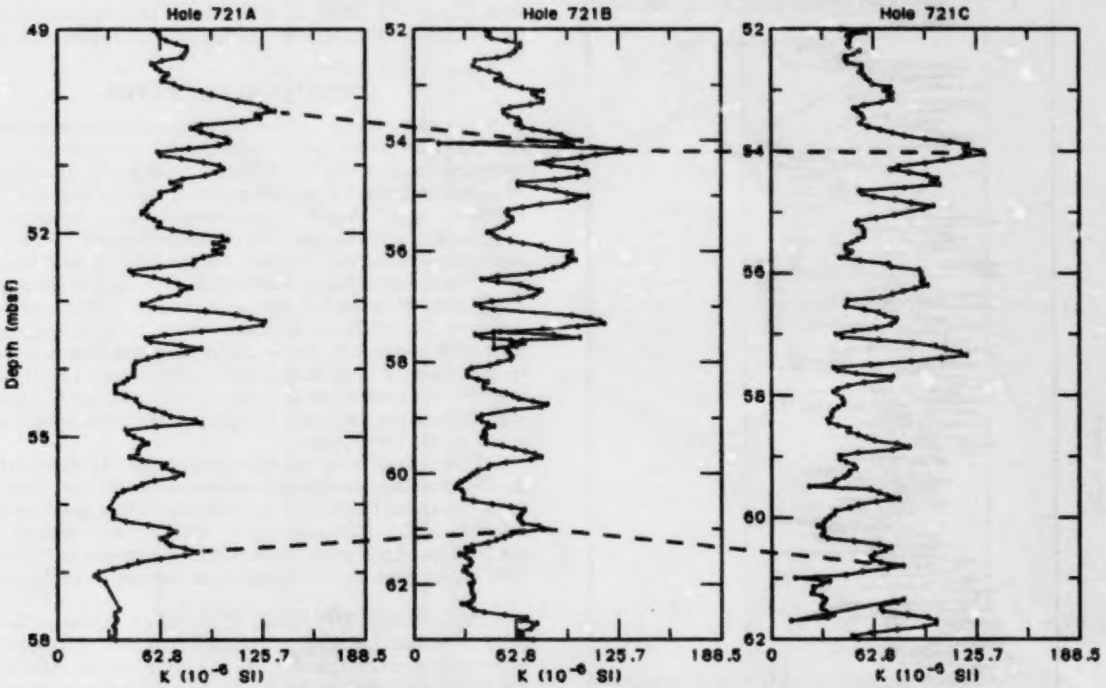

Figure 26. Comparisons of volume magnetic susceptibility of correlative ~1-m sections of Holes 721A, 721B, and 721C. Dashed lines denote correlative horizons.

The mass accumulation rates of calcium carbonate, noncarbonate (100 - $CaCO_3$). and organic carbon are calculated from the average values between selected datums (Table 9: Fig. 32). These data allowed an independent examination of the temporal variability in each component. The accumulation rates of calcium carbonate and noncarbonate at Site 721 mostly mirror the sedimentation rates, and calcium carbonate accumulation is generally twice that of noncarbonate in Pliocene-Pleistocene deposits. The present rate of calcite accumulation (~3 g/cm^2/k.y.) is 1.5 times lower than the mean annual flux of calcium carbonate measured in a sediment trap from the mid-water column in the Panama Basin, a comparable high-productivity region (Honjo, 1982). The high rate of calcium carbonate accumulation near the Miocene/Pliocene boundary equals present rates measured in the Panama Basin sediment traps. These rates are characteristic of areas having a high production of calcium carbonate shells of coccolithophores and foraminifers.

PHYSICAL PROPERTIES

Introduction

Physical properties measured on discrete samples of sediments recovered from Site 721 include index properties (wet-bulk density, porosity, water content, and grain density), compressional-wave velocity, and vane shear strength (Tables 10 and 11). Wet-bulk density and compressional-wave velocity were measured on all whole-round core sections that were at least 80 cm in length using the GRAPE and *P*-wave logging apparatus. All techniques and equipment used are described in the "Explanatory Notes" chapter, this volume.

Relatively high overall recovery rate allowed for a high sampling frequency at this site. With this large data set, transitions in the physical properties profiles clearly mark the boundaries between the four lithostratigraphic units that were recognized at Site 721.

Index Properties

Lithologic Unit I

Within the foraminifer-bearing nannofossil ooze and nannofossil ooze/chalk of lithologic Subunit IA (0–261.2 mbsf), the profiles of porosity and water content show very gradual monotonic decreases with depth, with the exception of two zones where the gradients are reversed (Fig. 33). Average values of porosity and water content measure 65% and 45%, respectively, near the seafloor and decrease to about 63% and 43%, respectively, at a depth of 90 mbsf. Between 90 and 110 mbsf a local porosity/water content maximum (and wet-bulk density minimum) was measured as a result of a 10%–15% increase in the concentration of clay minerals. Although this perturbation of the profiles is minimal on the profiles of discrete measurements (Fig. 33), it is a prominent feature on the wet-bulk-density profiles measured by the GRAPE (Fig. 34). Between 110 and 225 mbsf the porosity and water content profiles resume their gradual decreasing trends downhole. Below this level to the base of lithologic Subunit IA at 261.2 mbsf, porosity and water content increase slightly, perhaps in response to the general decrease in calcium carbonate content (see "Lithostratigraphy" section, this chapter; Fig. 5).

Porosity values determined from calcareous sediments (greater than 30% calcium carbonate) from several DSDP sites in the central Pacific (Hamilton, 1976) show a slightly more rapid decrease with depth than the gradient determined at Site 721. The principal deviation from Hamilton's curve occurs in the upper 150 m of lithologic Unit I. In this interval of similar lithofacies, Hamilton reports average porosities of 75%–65% (uncorrected

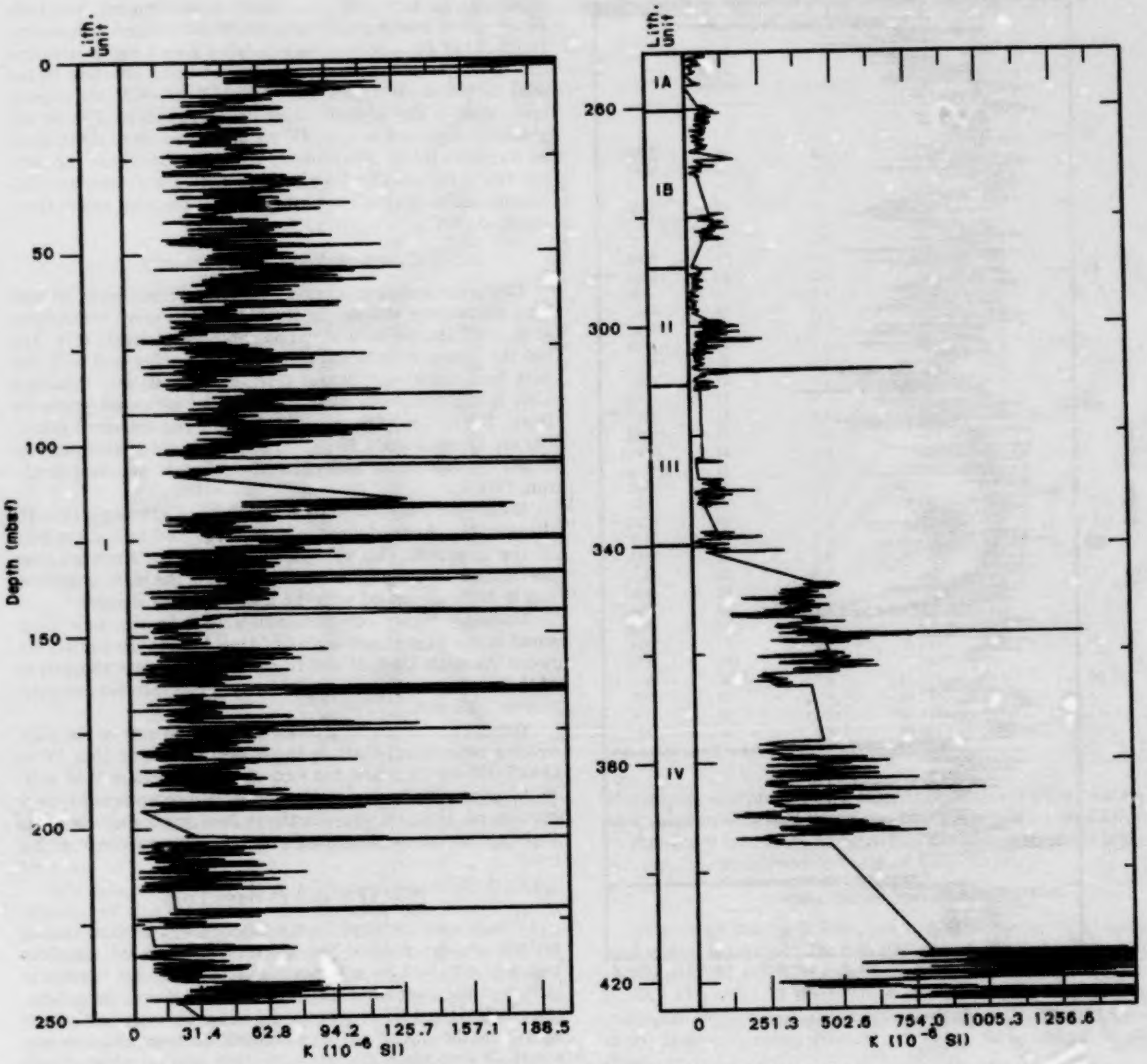

Figure 27. Volume magnetic susceptibility for Hole 721B. Note the susceptibility scale change at 250 mbsf.

for sediment expansion) as compared to the values of 65%–63% measured in the section at Site 721.

The grain densities throughout lithologic Subunit IA vary from a minimum of approximately 2.40 g/cm^3 to a maximum of 2.75 g/cm^3, but the values remain close to 2.60 g/cm^3 at all depths. Given the nearly constant average grain density of Subunit IA, changes in wet-bulk density primarily reflect changes in water content. Throughout Subunit IA, wet-bulk density increases slightly with depth from 1.65 g/cm^3 to 1.70 g/cm^3 at 225 mbsf as a result of increasing overburden pressure. As also noted in the porosity and water content profiles, the wet-bulk density profile reverses slope near 225 mbsf, and values decrease to 1.65 g/cm^3 at 261.2 mbsf. Within the foraminifer-bearing nannofossil ooze and chalk of Subunit IB (261.2–289.0 mbsf) the profiles of index properties display the normal gradient observed in the upper portions of Subunit IA (Fig. 33).

Lithologic Unit II

The siliceous-nannofossil chalk of Lithologic Unit II (289.0–309.9 mbsf) is markedly more porous than the adjacent sediments due to the increased abundance of diatoms frustules and the presence of radiolarians (see "Lithostratigraphy" section, this chapter). The structural attributes of the siliceous microfossils produce an open sediment fabric and higher porosity. Porosities vary from 66% to 75% with a corresponding variation in the water contents (44%–54%) that reflect the inherent high water content of this siliceous unit. The wet-bulk and grain densities show marked decreases to minima of 1.39 g/cm^3 and 2.16

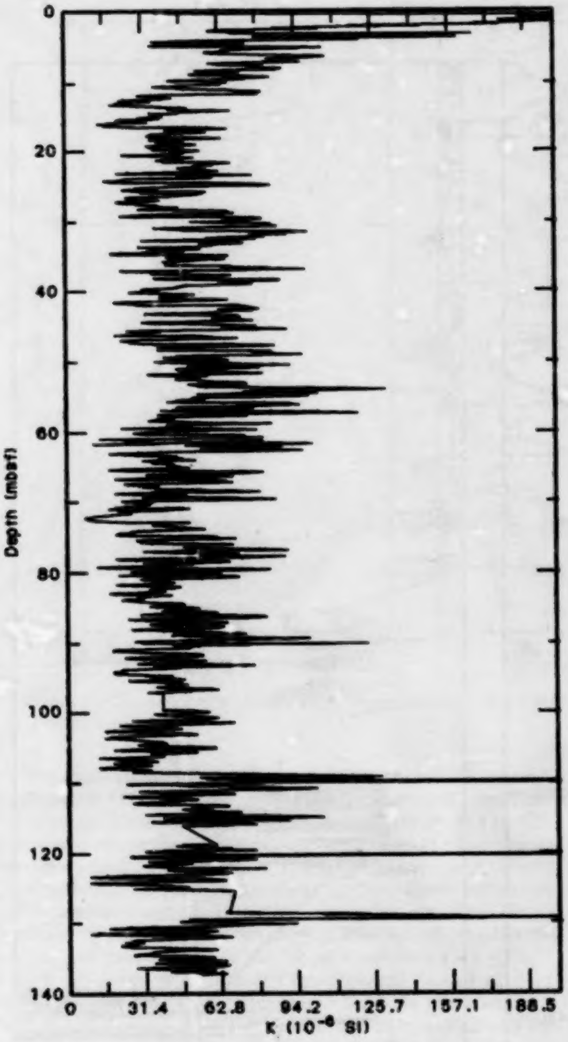

Figure 28. Volume magnetic susceptibility for Hole 721C.

g/cm^3, respectively. These decreases are attributed to the low grain density of the opal of the siliceous microfossils.

Lithologic Unit III

At the contact between Unit II and the underlying nannofossil chalk of lithologic Unit III (309.9 mbsf), the porosity and water content decrease abruptly in response to the disappearance of the siliceous microfossils. Coincident increases in wet-bulk and grain densities are also seen. Throughout lithologic Unit III (309.9–340.7 mbsf) the index properties profiles again resume the original gradients established in the nannofossil ooze of lithologic Unit I. Average porosity and water content values decrease from 52% to 49% and from 27% to 25%, respectively.

Lithologic Unit IV

As the section changes to a clay-bearing nannofossil chalk interbedded with mud turbidites in lithologic Unit IV (340.7–424.2 mbsf), the profiles of porosity, water content, and bulk density show similar gradients to those encountered in lithologic Unit I. They are, however, slightly offset toward higher densities and lower porosities. The porosity and water contents in the mud turbidites of Cores 117-721B-37X to -40X are slightly lower than in the adjacent more calcareous units. The overall gradients displayed in Unit IV are similar to those determined by Hamilton (1976). The porosity values are lower than the average values reported by Hamilton for both terrigenous and calcareous sediments but are in the range of reported values (Bryant et al., 1981).

Compressional-Wave Velocity

Compressional-wave velocities measured perpendicular to bedding on discrete samples in the Hamilton Frame Velocimeter show considerable variation at all sub-bottom depths (Fig. 35), but the values were found to match reasonably well with the data from the *P*-wave logger (Fig. 36). Throughout lithologic Unit I, the compressional-wave velocities increased gradually from 1500 m/s to 1560 m/s at 260 mbsf. The measured velocities are approximately 50 to 100 m/s lower than velocities predicted for calcareous sediments of equivalent density (Hamilton, 1978).

Within the siliceous nannofossil chalk of lithologic Unit II, the velocities dropped drastically to about 1530 m/s at the base of the sequence. This reversal in the velocity/depth gradient correlates with the gradient reversals seen in the index properties and is likely associated with the lower wet-bulk density.

Markedly higher compressional-wave velocities were measured in the nannofossil chalks of Unit III. At the contact between lithologic Units II and III, velocities increase abruptly to 1620 m/s. Within this unit the velocity values increase downsection to 1640 m/s.

Velocities continue to increase at a similar rate in the clay-bearing nannofossil chalk in the upper portion of Unit IV to (340.7–355 mbsf), where the velocity values average 1660 m/s. In the underlying terrigenous section, which comprises the lower portion of Unit IV, the velocity values apparently decrease slightly, but few measurements are available to confirm this trend.

GRAPE and *P*-Wave Logs

Overall, data collected by the GRAPE and *P*-wave logging systems are very good at Site 721 (Figs. 34 and 36). Excellent logs were obtained for sediments of lithologic Unit I, particularly over the interval cored with the APC. Cores from lithologic Units II and III commonly did not completely fill the core liners, and the lack of coupling between sediment and liner prevented *P*-wave signal transmission. Intervals for which the *P*-wave logs were not obtained should also be viewed as intervals in which the GRAPE underestimates the wet-bulk density. Full cores were more common for lithologic Unit IV, and moderately good GRAPE and *P*-wave logs were obtained. In all lithologic units a positive correlation exists between the GRAPE-determined wet-bulk density and the *P*-wave velocity.

The general pattern of density variation represented in the GRAPE records (Fig. 34) corresponds to that of wet-bulk density determined for discrete samples with two exceptions. The first discrepancy is in the interval 0–45 mbsf, where densities measured on discrete samples are approximately 0.10 g/cm^3 lower than the GRAPE density. Discrete-sample data in this interval display a large variation, and low values may be the product of sampling and measurement error or incorporation of water in the sediment during core splitting. The second feature of the GRAPE records that is not clearly evident in the discrete-sample data is the broad density minimum between 80 and 110 mbsf. This pattern is partially obscured in the discrete-sample

Table 8. XRD data from Hole 721C showing carbonate, quartz, dolomite, plagioclase feldspar, and combined kaolinite-chlorite peak areas extracted.

Core, section, interval (cm)	Depth (mbsf)	Kaolinite-chlorite	Quartz	Plagioclase feldspar	$CaCO_3$	Dolomite	Susceptibility	$CaCO_3$/ quartz	$CaCO_3$ (wt %)
117-721C-									
1H-1, 30	0.30	0	196	25	3493	20	3.0	17.821	79.1
1H-2, 70	2.20	13	484	50	2830	48	9.3	5.847	70.5
1H-2, 110	2.60	59	655	128	3114	77	8.3	4.754	62.9
1H-3, 10	3.10	30	437	88	2621	24	6.0	5.998	68.3
2H-1, 65	4.25	16	213	59	2841	29	5.9	13.338	72.5
2H-1, 85	4.45	13	246	58	2788	12	2.9	11.333	75.3
2H-1, 110	4.70	28	400	506	2992	40	5.9	7.480	52.7
2H-1, 140	5.00	0	137	86	2088	16	2.8	15.241	
2H-2, 15	5.25	18	372	85	2016	55	8.4	5.419	64.6
2H-2, 50	5.60	24	458	110	2314	40	5.4	5.052	67.0
2H-2, 95	6.05	23	454	52	2841	61	4.6	6.258	67.2
2H-2, 145	6.55	28	645	146	1936	45	8.5	3.002	59.9
2H-3, 35	6.95	30	484	119	1673	52	6.7	3.457	58.0
2H-3, 50	7.10	27	645	139	1521	77	7.6	2.358	54.6
2H-3, 95	7.55	25	365	85	2927	27	4.7	8.019	69.5
2H-3, 120	7.80	20	357	110	1325	25	6.5	3.711	61.7
2H-4, 15	8.25	38	538	177	2894	52	5.3	5.379	62.3
2H-4, 40	8.50	23	279	52	3564	18	4.9	12.774	73.1
2H-4, 70	8.80	17	272	62	3446	31	5.7	12.669	76.4
2H-4, 100	9.10	10	151	26	3125	11	4.1	20.695	80.1
2H-4, 135	9.45	38	524	156	2694	35	6.7	5.141	64.9
2H-5, 5	9.65	21	376	125	3283	41	5.2	8.731	70.1
2H-5, 35	9.95	12	204	28	3422	0	3.4	16.775	80.2
2H-5, 50	10.10	26	266	64	2314	36	5.3	8.699	68.6
2H-5, 100	10.60	17	392	62	2391	30	4.3	6.099	70.6
2H-5, 125	10.85	19	289	83	3047	27	2.9	10.543	70.6
2H-6, 15	11.25	38	790	128	2611	49	5.2	3.305	63.2
2H-6, 50	11.60	38	497	106	2725	44	6.3	5.483	61.5
2H-6, 80	11.90	0	392	77	3457	17	4.8	8.819	70.3
2H-6, 100	12.10	0	240	36	3434	17	2.4	14.308	73.3
2H-6, 130	12.40	29	286	67	3446	20	5.6	12.049	79.8
2H-7, 20	12.80	10	156	35	3204	17	1.8	20.538	81.4
2H-7, 35	12.95	30	286	36	3612	14	2.8	12.629	76.6
2H-7, 60	13.20	18	210	188	3881	0	1.8	10.481	80.1

record by the scatter of data at shallow depths. The density minimum roughly coincides with a darkening of sediment color and an increase in the clay mineral abundance in the 80–110 mbsf interval.

The *P*-wave log pattern (Fig. 36) follows that of the GRAPE-determined density. A velocity minimum coincides with the broad density minimum centered at 90 mbsf. The *P*-wave logger velocities correspond approximately to those measured with the Hamilton Frame Velocimeter, although the Hamilton Frame data are more widely varying than the *P*-wave logger data. At depths less than 35 mbsf the velocities measured for discrete samples are significantly lower than the *P*-wave logs. Difficulties in measuring velocities of soft sediments with the Hamilton Frame may account for this discrepancy.

In lithologic Unit I, GRAPE and *P*-wave records display patterns of cyclic variation on the scale of tens of centimeters to meters. This variation is typified by that in the 0–50 mbsf interval (Fig. 37). The scale of the variation corresponds to the scale of color change, but the relationship between sediment color and relative density is not consistent. The GRAPE and *P*-wave records were further compared with the results of shipboard carbonate measurements, and a consistent relationship between sediment density and velocity and percent calcium carbonate is not present either. The lack of such a correlation may be partly the product of comparing the closely spaced (approximately 2 cm) data of the GRAPE and *P*-wave logs with the data from the more widely spaced (50 cm) carbonate samples. The small-scale variation displayed in Figure 37 is well-developed in all three holes drilled at Site 721, and individual peaks in the records can be correlated between holes. The density and velocity variations also display a strong positive correlation with variation in magnetic susceptibility and thus must be regarded as an expression of changes in sediment characteristics over relatively short intervals (see "Paleomagnetism" section, this chapter).

Vane Shear Strength

Vane shear strengths were measured in the nine APC cores recovered from each of the two holes (Fig. 35). Shear strengths increased from 14.6 kPa near the surface to a maximum value of 97.7 kPa at 81.75 mbsf. Shear strength measurements were attempted in Cores 117-721B-10X through -20X, but the sediment developed radial fractures prior to shear failure in all cases.

SEISMIC STRATIGRAPHY

The Owen Ridge is an asymmetric, linear feature in the western Arabian Sea that trends northeastward and dips gently to the west (Fig. 38). The ridge is uplifted lamprophyric basement overlain by claystones, chalks, and turbiditic sequences of Eocene to Miocene age that are, in turn, capped by Miocene and younger pelagic sediments (Whitmarsh et al., 1974; Whitmarsh, 1979). The seismic stratigraphy of the ridge is complex and includes irregular basement features, large-scale onlap of turbidite and other facies, numerous slump scars and large slump(?) canyons, and several prominent sub-bottom reflectors. To interpret the seismic stratigraphy of Site 721 and companion Site 722, we have used several single-channel seismic (SCS) profiles from the Leg 117 site survey by the *Robert Conrad* (see Mountain and Prell, this volume), in combination with the drilling results from Sites 721 and 722 (see "Lithostratigraphy" section,

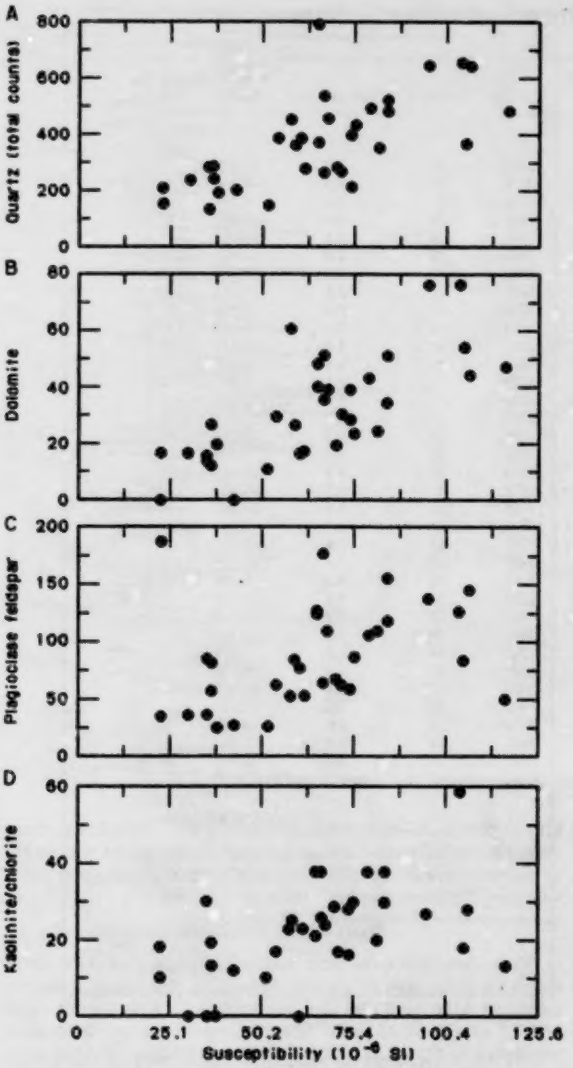

Figure 29. Plots of quartz, dolomite, plagioclase feldspar, and kaolinite-chlorite results from the X-ray-diffraction analyses of discrete samples taken from susceptibility maxima and minima of Hole 721C (0–~13 mbsf). Note the positive correlations of terrigenous components with susceptibility.

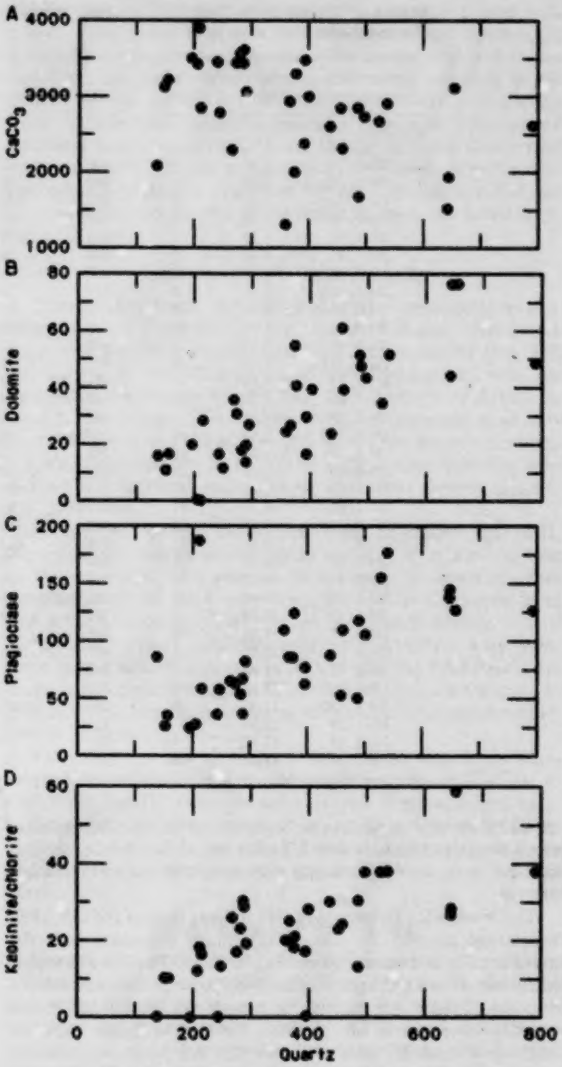

Figure 30. Plots of carbonate, dolomite, plagioclase feldspar, and kaolinite-chlorite vs. quartz as determined from the XRD analyses.

this chapter and "Site 722" chapter, this volume). Downhole logging data from Site 722 (see "Downhole Measurements" section, "Site 722" chapter, this volume), as well as the SCS data obtained during the site approaches by the *JOIDES Resolution* were also used for this synthesis. Figure 38 shows the location of the SCS tracks used in this discussion in relation to the bathymetry of the Owen Ridge (Sea Beam data from the site survey; Prell, unpubl. data).

The sedimentary sequence at Site 721 is complicated by several hiatuses and the seismic stratigraphy at this site must be compared to the more complete sedimentary and seismic section available at Site 722. Thus, we initially use SCS Line 38 and results of drilling and logging at Site 722 to associate reflector sequences with the lithologic section. Subsequently, we use RC2704 SCS lines 39 and 40 to project the reflector stratigraphy into the section recovered at Site 721. The detailed correlation of Site 722 with SCS profiles, lithology, logging data, and the synthetic seismogram are discussed in the "Seismic Stratigraphy" section, "Site 722" chapter (this volume). Here, we only summarize the identification and lithologic significance of the important reflectors within the cored section. The correlation of the major reflectors recognized at both Site 722 and Site 721 is shown in Figure 39. The reflectors are identified by an alpha-numeric code and are discussed in order of increasing depth.

Regional Seismic Stratigraphy

Reflector A is a high-amplitude return that is coincident with the top of the siliceous lithologic Unit II in Site 722. It can be easily traced through Line 39 to the the crest of the ridge (Line

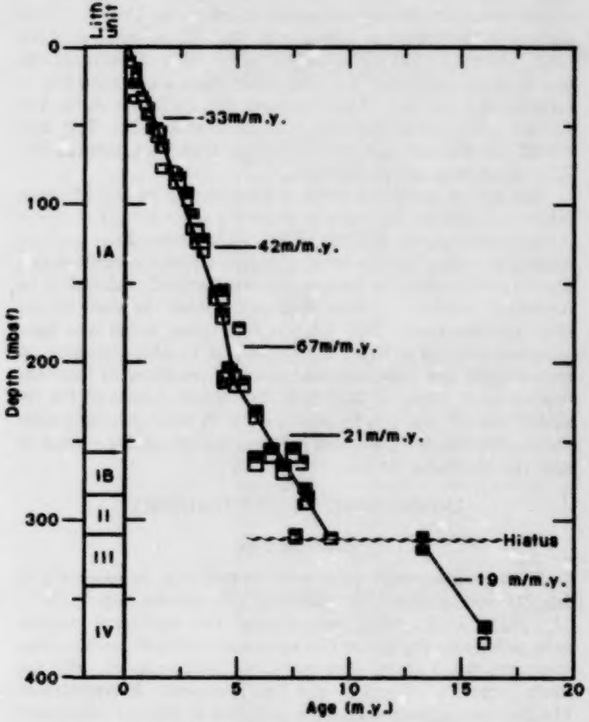

Figure 31. Age-depth plot of stratigraphic datums listed in Tables 4 and 5. The filled and open boxes are the upper and lower depths of each datum level, respectively. Indicated sedimentation rates are based on a best fit to all stratigraphic data. Sedimentation rates calculated between reliable nannofossil datum levels in the top 115 m are listed in Table 9 and shown in Figure 32.

40, Fig. 39). Reflector A cannot be traced directly into Site 721 (Line 40), but it is generally correlative with the irregular reflectors that mark the top of the siliceous facies in lithologic Unit II in Site 721 (see Fig. 40).

Reflector B is a series of reflectors that are associated with the siliceous and chalk units. B_1 marks the bottom of a package of four closely spaced conformable reflectors that have a distinctive pattern and are coincident with the lower part of siliceous lithologic Unit II in Site 722 (Fig. 39). B_1 is easily traced through Line 39 to the crest of the ridge (Line 40, Fig. 39), but B_1 is missing at Site 721 (Line 40, Fig. 39). B_2 is a low-amplitude reflector that correlates with the top of the chalks in the lower half of lithologic Unit III at Site 721. These chalks have higher velocity and higher density than the surrounding lithologies. B_2 becomes more reflective as it trends upslope through Line 39 to the crest of the ridge (Line 40) and to Site 721. The increase in amplitude between Site 722 and the crest of the ridge may be associated with the increased thickness of the lower chalk. The increased amplitude is probably related to the pronounced hiatus identified at this level in Site 721, which brings very-low-velocity siliceous sediments in contact with the much faster lower chalk unit. This hiatus and its corresponding high-amplitude reflector were not found at Site 722. Reflector B_3 has a variable amplitude and at Site 722 coincides with the boundary between the chalk (lithologic Unit III) and the turbiditic sediments of lithologic Unit IV (Fig. 39).

Reflector C is the uppermost strong return of a thick series of parallel reflectors that are generally correlated to turbidite deposits within lithologic Unit IV at both Sites 721 and 722 (Fig. 39). Reflector C is not, however, the top of lithologic Unit IV, which is marked by B_3.

Seismic Stratigraphy of Site 721

The relationship of the reflectors to the stratigraphic section at Site 721 is shown in a plot of traveltime (two-way) vs. depth (mbsf; Fig. 40). The correlation of traveltimes and lithologic features indicates average sediment velocities of 1.6–1.7 km/s. These average velocities are lower than the empirical time-depth relationships for carbonate-dominated sediments (Hamilton, 1979). Reflector C is clearly identified at about 0.48 s (Figs. 39 and 41) and is projected to be about 400 mbsf at Site 721. Reflectors B_3 and B_2 are observed at about 0.42 and 0.38 s, respectively, and are interpreted to represent the bottom and the top of the high-density chalk unit. Reflector B_2 also represents the base of a major hiatus that spans about 5 m.y. (from nannofossil Zone NN9 to NN5). Reflector B_1 is not observed at Site 721 as its associated sediments are missing within the hiatus. Identification of seismic reflector A is difficult at Site 721 because it is included in the slumped section. The time-depth relations (Fig. 40) indicate that both the top of the low-density siliceous facies and the top of the disturbed section (top of lithologic Unit II) are marked by reflectors at 0.365–0.350 s and 0.32 s, respectively. Alternatively, the deformed slump surface could be represented by the strong negative peak at about 0.33 s. The section above 0.32 s is characterized by conformable reflectors indicating a continuous pelagic deposition.

On a larger scale (about 20 km), seismic stratigraphy of the sediments capping the crest of the Owen Ridge reveals the origin of the hiatus found at Site 721. The sediment thickness at the Site 721 is about 1.62 s. The sediments overlie a strong irregular reflector that rises to the south and is interpreted as basement. Overlying basement is a zone of diffuse reflection from about

Table 9. Sedimentation and accumulation rate data for Site 721.

Depth interval (mbsf)	Age range (m.y.)	$CaCO_3$ ($\bar{x}$ %)	C_{org} ($\bar{x}$ %)	Dry-bulk density ($\bar{x}$ g/cm^3)	Sed. rate ($\bar{x}$ m/m.y.)	$CaCO_3$ acc. rate (g/cm^2/k.y.)	Non-$CaCO_3$ acc. rate (g/cm^2/k.y.)	C_{org} acc. rate (mg/cm^2/k.y.)
0-9.2	0-0.19	66.9	0.77	0.940	48.2	3.03	1.50	34.9
9.2-19.0	0.19-0.49	70.5	0.72	1.012	32.8	2.34	0.98	23.9
19.0-31.4	0.49-0.82	64.9	0.45	1.082	37.6	2.64	1.43	18.3
31.4-50.5	0.82-1.45	61.8	0.85	0.988	30.8	1.88	1.16	25.9
50.8-80.5	1.45-2.4	68.0	1.33	1.015	31.3	2.16	1.02	42.3
80.5-115.4	2.4-3.48	64.9	2.32	0.986	32.3	2.07	1.12	78.9
115.4-169.0	3.48-4.77	64.1	0.81	1.043	41.6	2.78	1.56	35.1
169.0-208.0	4.77-5.35	65.0	1.09	1.038	67.2	4.53	2.44	76.0
208.0-310.0	5.35-10.25	53.7	0.68	0.969	20.8	1.08	0.93	13.7
315.0-370.0	14.4-17.4	37.4	0.07	1.540	18.8	1.08	1.81	2.0

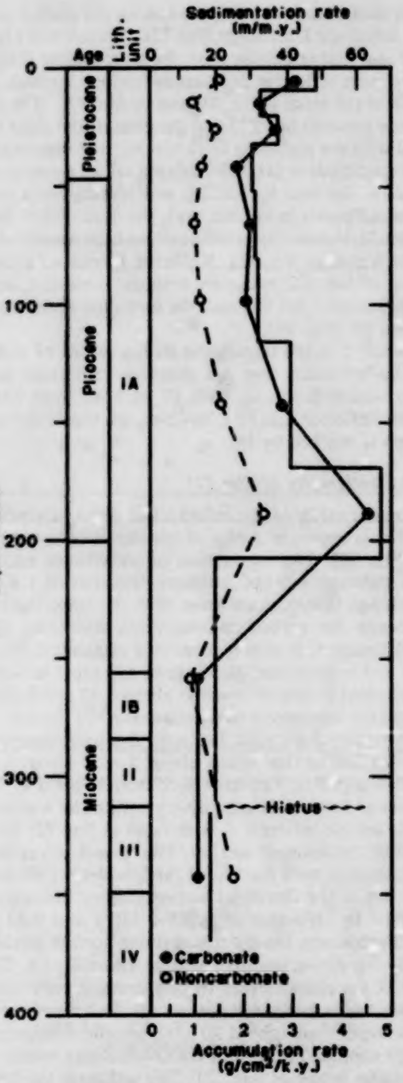

Figure 32. Sedimentation rate (m/m.y.; solid line), calcium carbonate accumulation rate (g/cm^2/k.y.; dots), and noncarbonate accumulation rate (g/cm^2/k.y.; circles) vs. depth at Site 721. Accumulation rates are plotted at the midpoint of the respective depth intervals.

1.62 to 1.26 sbsf. This diffuse zone is succeeded by a thick sequence of strongly reflective, largely conformable reflectors that are capped by seismic reflector C. This sequence is interpreted as the clastic-turbidite facies of Oligocene to Miocene age that was observed at DSDP Site 224 (Whitmarsh et al., 1974) and at the base of Site 721. The surface of the turbidite facies (reflector C) dips about 1° to the northwest. Near the crest of the ridge, about 5 km updip and south from Site 721, the stratigraphic section is relatively complete (Fig. 41) and almost identical to the section at Site 722 (Fig. 39). Below the crest, a slump fault cuts through the section and eliminates most of the sediments between seismic reflectors B_2 and A. The base of the slump coincides with the top of the chalk facies in lithologic Unit II at Site 721. The slump fault probably occurred in the siliceous low-density sediments of lithologic Unit II. Comparison of the seismic stratigraphy at Site 722, at the crest of the ridge, and at Site 721 indicates that about 90 m of sediment was lost by slumping at Site 721. The upper chalk (corresponding to reflector B_2) and top of the siliceous unit (reflector A) in Site 721 are 135 m thick, but only 51 m thick at Site 721. This estimated loss assumes that all of lithologic Unit I is present at Site 721, which may not be the case.

The age of the slump event is estimated to be late Miocene (about 7.7 Ma) on the basis of overlying sediments. The slump is clearly associated with the uplift, which created the inclined sediments, but it cannot be assigned to a specific uplift event. Conformable seismic reflectors below reflector C, inferred to be turbidites, exhibit a modest thickening from the crest of the ridge into the basin. They suggest that minor uplift may have occurred prior to reflector C time, about 17 Ma. However, no major uplift can have occurred prior to cessation of turbidite deposition at Sites 721 and 722. Post-cruise studies of the regional seismic stratigraphy combined with these drilling results should provide more detailed information about the timing of uplift of the Owen Ridge.

INORGANIC GEOCHEMISTRY

Introduction

Eighteen interstitial water samples collected by squeezing at Site 721 were analyzed for alkalinity, pH, salinity, Mg^{2+}, Ca^{2+}, Cl^-, SO_4^{2-}, PO_4^{3-}, NH_4^+, and silicate. Two additional samples were collected using the *in-situ* pore-water sampler; all the measurements listed above were made on these samples, with the single exception of sulfate and one phosphate determination. The first four squeezed samples collected at this site were taken from Hole 721A and the remainder from Hole 721B. The *in-situ* samples were taken from Hole 721C. The samples were obtained from different depths in the three holes, but because the stratigraphic correlation between the three was excellent, we have chosen to plot all the results on a common depth scale in Figure 42. All data are listed in Table 12.

Salinity, Chlorinity, and pH

The concentration profiles of chloride, salinity, and pH are shown in Figure 42. Although the distribution of chloride shows little variation with depth in the upper 300 m, the salinity decreases distinctly from about 34.3 g/kg in the topmost sample to ~32.2 g/kg at ~90 mbsf. This decrease reflects the loss of sulfate (and to some extent magnesium) from interstitial solution over this same depth interval. A slight, and apparently real, ~2% increase with depth of the chloride concentration occurs over the lowermost 110 m of the hole. The cause of this distribution is not clear but it may be related to uptake of water to the interlayer sites of clay minerals in the turbidites near the bottom of the hole. The slight increase in salinity and the presence of a small quantity of sulfate in the deepest sample (422 mbsf) are probably due to contamination with drill water; Core 117-721A-44X from which the sample was collected showed abundant evidence of drilling disturbance ("biscuiting").

The pH ranges between ~7.2 and ~8.0 over the cored section (Fig. 42). Lower values probably result from the production of H_2S which is abundant in the upper 300-350 m and dissociates to form HS^- and H^+. Because the carbonate oozes tend to be iron-depleted, sulfide precipitation is limited, allowing substantial H_2S to occur in the interstitial water. Of those pore waters collected by squeezing, the highest pH (7.94) was measured in the deepest sample which may have been contaminated with seawater. Both *in-situ* samples have slightly higher pH levels than the squeezed samples collected at similar depths (Table 12),

Table 10. Physical properties summary for Hole 721A.

Core, section, interval (cm)	Depth (mbsf)	Wet-bulk density (g/cm³)	Porosity (%)	Water content (%)	Grain density (g/cm³)	Dry-bulk density (g/cm³)	Velocity (m/s)	Vane shear strength (kPa)
117-721A-								
1H-2, 38–40	1.88	1.553	66.3	43.7	2.393	0.873		
1H-2, 49–49	1.99							14.6
1H-4, 40–42	4.90	1.635	61.2	38.3	2.504	1.008		
1H-6, 40–42	7.90	1.646	65.4	40.7	2.579	0.977		
2H-2, 50–52	11.80	1.624	63.1	39.8	2.621	0.978		
2H-4, 40–40	14.70							23.8
2H-4, 50–52	14.80	1.722	62.4	37.1	2.691	1.083		
2H-6, 50–52	17.80	1.671	62.1	38.1	2.750	1.035		
3H-2, 50–52	21.50	1.559	64.7	42.5	2.635	0.896		
3H-4, 50–52	24.50	1.590	59.3	38.2	2.595	0.983		
3H-5, 43–43	25.93							17.6
3H-5, 80–83	26.30						[a]1465	
3H-6, 50–52	27.50	1.646	63.8	39.7	2.539	0.992		
4H-2, 50–52	31.20	1.665	64.3	39.6	2.675	1.006		
4H-5, 43–43	34.13							23.6
4H-5, 50–52	34.20	1.564	64.0	41.9	2.491	0.908		
4H-5, 80–83	36.00						[a]1527	
4H-6, 50–52	37.20	1.644	63.1	39.3	2.659	0.997		
5H-2, 47–49	40.87	1.670	62.0	38.0	2.686	1.035		
5H-5, 47–49	43.87	1.587	65.9	42.5	2.635	0.912		
5H-5, 60–60	44.00							44.7
5H-5, 80–83	45.70						[a]1539	
5H-6, 47–49	46.87	1.693	62.5	37.8	2.591	1.053		
6H-2, 45–47	50.45	1.677	62.2	38.0	2.660	1.040		
6H-5, 45–47	53.45	1.688	60.0	36.5	2.626	1.072		62.3
6H-6, 41–44	56.41						[a]1350	
6H-6, 45–47	56.45	1.712	61.0	36.5	2.683	1.087		
7H-2, 45–47	59.75	1.671	64.0	39.2	2.630	1.015		
7H-5, 45–47	62.75	1.698	63.3	38.2	2.539	1.049		72.3
7H-6, 41–44	65.71						[a]1297	
7H-6, 45–47	65.75	1.714	65.4	39.1	2.480	1.044		
8H-2, 45–47	69.25	1.677	63.0	38.5	2.593	1.032		
8H-5, 60–62	72.40	1.693	58.9	35.6	2.580	1.090		56.1
8H-6, 45–47	75.25	1.697	58.9	35.6	2.548	1.093		
8H-6, 48–51	75.28						[a]1521	
9H-2, 45–47	78.75	1.625	64.3	40.5	2.596	0.967		
9H-5, 45–47	81.75	1.643	62.4	38.9	2.520	1.003		97.7
9H-6, 45–47	84.75	1.659	60.0	37.1	2.462	1.044		

[a] Velocity measurement perpendicular to bedding.

but it is not clear whether or not the difference is related to a sampling artifact.

Sulfate and Alkalinity

Sulfate reduction at this site is complete by about 100 mbsf, and is pronounced in the top several meters (Fig. 42). The deepest sample contains >4 mmol/L SO_4^{2-} which is thought to represent contamination (see above). The turbidites near the base of the cored section contained abundant macroscopic pyrite as both discrete grains and veinlets (see "Lithostratigraphy" section, this chapter).

Titration alkalinity increases from ~5.5 mmol/L at 9 mbsf depth to a distinct maximum near 90 mbsf before decreasing steadily toward the bottom of the hole (Fig. 42). Above the maximum the increase with depth can be attributed to the production of HCO_3^- during sulfate reduction; the decrease at greater depths presumably reflects carbonate precipitation reactions. The reduction of about 25 mmol/L of sulfate over the top 100 m should be mirrored by an increase in alkalinity of about 50 mmol/L, 40 mmol/L more than is observed. The missing alkalinity must be consumed during the precipitation of authigenic carbonate phases. However, 40 mmol/L of alkalinity is only sufficient to precipitate <1% of authigenic carbonate, assuming a porosity of 50% and a grain density of 2.75 g/cm³, neglecting additional supply via diffusion. It is unlikely that such a small change in mineralogy would be detected by lithological examination. The alkalinity measured in the upper *in-situ* pore-water sample (100 mbsf) is about 1 mmol lower than in the adjacent squeezed samples, which is well in excess of analytical uncertainty. The reason for the difference is not clear.

Calcium and Magnesium

Profiles of dissolved calcium and magnesium are shown in Figure 42. The calcium concentration decreases to a minimum of ~6 mmol/L at about 80 mbsf depth before increasing to ~12 mmol/L at the base of the hole. Mg^{2+} decreases relatively rapidly to about 31 mmol/L over the top 100 m and more gradually to a near-constant minimum of ~26 mmol/L in the lower 200 m. The curved segments of these profiles represent zones of production and consumption: precipitation of carbonate phases in the upper 100 m must be responsible for the Ca^{2+} and at least some of the Mg^{2+} decreases, while both carbonate precipitation and alteration reactions involving alumino-silicate phases can probably account for the addition of calcium to solution and magnesium uptake at greater depths. The extent of removal of Mg^{2+} from pore water in the upper 100 m greatly exceeds that observed for calcium. Although it is possible that Mg-rich calcite could be precipitating in this zone, such a reaction would be insufficient to account for the relative magnesium deficit. Therefore, Mg^{2+} is probably being adsorbed by clay minerals in addition to participating in carbonate authigenesis. Dolomitization of calcite would also consume Mg^{2+} and release Ca^{2+}, which would tend to reduce the net calcium depletion but enhance the removal of magnesium; this latter suggestion is consistent with

Table 11. Physical properties summary for Hole 721B.

Core, section, interval (cm)	Depth (mbsf)	Wet-bulk density (g/cm^3)	Porosity (%)	Water content (%)	Grain density (g/cm^3)	Dry-bulk density (g/cm^3)	Velocity (m/s)	Vane shear strength (kPa)
117-721B-								
1H-4, 48-52	4.98	1.578	62.2	40.4	2.604	0.940		15.0
2H-5, 68-70	16.08	1.648	62.1	38.6	2.601	1.012		19.5
2H-5, 72-75	16.12						[a]1466	
3H-2, 35-38	20.95						[a]1518	
3H-2, 41-43	21.01	1.714	61.7	36.9	2.740	1.082		25.2
5H-3, 47-50	41.97						[a]1528	
5H-3, 50-52	42.00	1.654	65.0	40.3	2.707	0.988		22.3
6H-3, 95-98	52.05						[a]1532	
6H-3, 104-106	52.14	1.649	63.3	39.3	2.600	1.001		20.0
7H-3, 70-72	61.10	1.599	63.4	40.6	2.464	0.950		70.8
7H-3, 72-75	61.12						[a]1517	
8H-4, 57-59	71.97						[a]1555	
8H-4, 60-62	72.00	1.694	58.8	35.6	2.543	1.092		43.8
9H-3, 70-72	80.10	1.663	63.2	39.0	2.634	1.015		67.3
10X-1, 70-72	86.70	1.632	63.1	39.6	2.519	0.986		
10X-3, 70-72	89.70	1.616	64.9	41.1	2.561	0.951		
10X-5, 66-69	92.66						[a]1546	
10X-5, 70-72	92.70	1.632	65.6	41.2	2.621	0.960		
11X-1, 70-72	96.30	1.779	71.0	40.9	2.698	1.052		
11X-3, 70-72	99.30	1.509	57.5	39.1	2.665	0.920		
11X-5, 68-71	102.28						[a]1476	
11X-5, 70-72	102.30	1.677	64.0	39.1	2.635	1.021		
12X-2, 40-42	107.10	1.652	62.4	38.7	2.549	1.013		
12X-2, 43-46	107.13						[a]1523	
13X-2, 40-42	116.70	1.699	62.1	37.4	2.654	1.064		
13X-4, 40-42	119.70	1.681	61.7	37.6	2.583	1.049		
13X-6, 40-42	122.70	1.726	62.0	36.8	2.719	1.091		
14X-2, 40-42	126.30	1.643	63.7	39.8	2.542	0.990		
14X-2, 44-47	126.34						[a]1526	
14X-4, 40-42	129.30	1.680	61.9	37.7	2.584	1.047		
14X-5, 40-42	130.80	1.720	61.7	36.7	2.584	1.088		
14X-5, 143-145	131.80							51.7
15X-2, 40-42	136.00	1.659	60.3	37.2	2.386	1.041		
15X-4, 40-42	139.00	1.759	60.4	35.2	2.748	1.141		
15X-6, 40-42	142.00	1.655	63.1	39.1	2.540	1.008		
16X-2, 40-42	145.70	1.719	61.1	36.4	2.541	1.093		
16X-4, 40-42	148.70	1.653	61.7	38.2	2.577	1.021		
16X-6, 40-42	151.70	1.680	63.5	38.7	2.552	1.030		
16X-6, 82-84	152.12							42.0
17X-2, 40-42	155.40	1.707	61.2	36.7	2.524	1.080		
17X-2, 44-47	155.44						[a]1454	
17X-4, 40-42	158.40	1.617	62.7	39.7	2.327	0.974		
17X-6, 40-42	161.40	1.629	64.8	40.8	2.427	0.965		
17X-6, 132-132	162.32							63.7
18X-2, 38-40	165.08	1.664	63.5	39.1	2.594	1.014		
18X-4, 46-48	168.16	1.679	63.3	38.6	2.638	1.030		
18X-6, 96-98	171.66	1.653	62.6	38.8	2.531	1.011		
19X-2, 40-42	174.80	1.621	63.4	40.0	2.495	0.972		
19X-4, 10-12	177.50	1.705	61.0	36.7	2.631	1.080		
19X-4, 19-21	177.59						[a]1562	
19X-6, 40-42	180.80	1.626	63.7	40.2	2.585	0.973		
20X-2, 40-42	184.50	1.703	61.6	37.0	2.631	1.072		
20X-4, 40-42	187.50	1.659	62.4	38.5	2.575	1.020		
20X-4, 50-53	187.60						[a]1531	
20X-6, 10-12	190.20	1.690	58.6	35.5	2.521	1.090		
21X-2, 52-54	194.32	1.656	61.1	37.8	2.556	1.030		
21X-4, 48-50	197.28						[a]1590	
22X-2, 40-42	203.90	1.692	63.2	38.3	2.676	1.045		

the substantially greater loss of Mg^{2+} from solution compared to calcium. Furthermore, reprecipitation as calcite of the Ca^{2+} released during dolomitization would consume dissolved bicarbonate, which would help to account for the missing alkalinity. Similar suites of reactions have been postulated to explain calcium and magnesium distributions observed at other sites where carbonate-rich hemipelagic sediments have been drilled (e.g., Gieskes, 1981).

Ammonia, Phosphate, and Silicate

As noted at Site 720, ammonia and phosphate are added to solution as products of the degradation of organic matter under anoxic conditions. Ammonia levels are relatively high, reaching a maximum of about 2.5 mmol/L at 180 mbsf; concentrations decrease to about 1 mmol/L toward the base of the cored section (Fig. 42). Ignoring the effect of methanogenesis, total depletion of sulfate as observed over the top 100 m at this site should be accompanied by the release to solution of about 4 mmol/L of ammonia if the initial organic substrate had a near-Redfield C:N ratio of 106:16. About half this predicted ammonia value is observed, indicating that the degrading organic matter is relatively nitrogen depleted or that ammonia has been removed from solution by ion exchange with clay minerals such as illite; with the limited information at hand, we cannot differentiate between these two possibilities.

Table 11 (continued).

Core, section, interval (cm)	Depth (mbsf)	Wet-bulk density (g/cm³)	Porosity (%)	Water content (%)	Grain density (g/cm³)	Dry-bulk density (g/cm³)	Velocity (m/s)	Vane shear strength (kPa)
117-721B-								
22X-4, 28-30	206.78						[a]1568	
22X-4, 40-42	206.90	1.718	61.7	36.8	2.669	1.086		
22X-6, 40-42	209.90	1.753	58.6	34.3	2.632	1.152		
23X-2, 32-35	213.52						[a]1538	
23X-2, 37-39	213.57	1.743	57.3	33.7	2.605	1.156		
24X-2, 38-40	223.18						[a]1558	
24X-2, 43-45	223.23	1.522	54.4	36.6	2.649	0.965		
24X-4, 4-6	225.84	1.890	69.5	37.6	2.638	1.179		
25X-2, 46-48	232.46	1.659	60.2	37.1	2.548	1.043		
25X-4, 48-50	235.48	1.713	59.6	35.6	2.562	1.103		
25X-6, 50-52	238.50						[a]1584	
25X-6, 48-50	238.48	1.746	61.3	36.0	2.723	1.117		
26X-2, 46-48	242.06	1.673	61.2	37.5	2.561	1.046		
26X-3, 112-113	244.22						[a]1507	
26X-4, 70-72	245.30	1.617	64.9	41.1	2.572	0.952		
27X-2, 45-47	251.75	1.579	65.3	42.3	2.400	0.911		
27X-4, 42-45	254.72						[a]1549	
27X-4, 45-47	254.75	1.607	60.6	38.6	2.555	0.986		
28X-2, 48-50	261.58	1.632	66.0	41.5	2.647	0.955		
28X-4, 35-37	264.45						[a]1587	
28X-4, 50-52	264.60	1.694	63.0	38.1	2.607	1.049		
28X-6, 77-79	267.87	1.730	58.3	34.5	2.579	1.133		
29X-2, 48-50	271.38						[a]1577	
29X-2, 58-60	271.48	1.683	61.9	37.7	2.625	1.049		
30X-2, 41-43	281.11	1.805	57.2	32.5	2.705	1.219		
30X-4, 33-34	284.03						[a]1534	
30X-4, 34-35	284.04	1.478	73.7	51.1	2.576	0.723		
31X-2, 40-42	290.90	1.567	68.1	44.5	2.608	0.869		
31X-4, 40-42	293.90	1.534	66.4	44.3	2.425	0.854		
31X-6, 40-42	296.90	1.464	72.6	50.8	2.367	0.721		
32X-2, 42-44	300.72	1.398	73.4	53.8	2.284	0.646		
32X-4, 62-64	303.92	1.435	75.0	53.5	2.167	0.667		
32X-6, 61-63	306.91	1.518	73.8	49.8	2.567	0.762	[a]1519	
33X-1, 4-6	308.44	1.569	68.1	44.5	2.451	0.872	[a]1542	
33X-CC, 41-43	311.66	1.988	49.4	25.5	2.722	1.481	[a]1653	
34X-4, 138-141	323.88	1.975	52.0	27.0	2.713	1.443	[a]1647	
34X-6, 21-24	325.71						[a]1553	
34X-CC, 21-24	324.95	1.928	50.7	26.9	2.578	1.409		
35X-2, 65-67	329.85	1.984	51.4	26.5	2.757	1.457	[a]1675	
35X-4, 2-4	332.22	1.966	49.5	25.8	2.747	1.459	[a]1634	
36X-CC, 28-30	341.01	2.098	47.6	23.3	2.732	1.610	[a]1648	
37X-1, 86-88	347.86	1.948	52.8	27.8	2.760	1.406		
37X-4, 39-41	351.89	2.088	44.4	21.8	2.774	1.633	[a]1674	
37X-5, 72-74	353.72	2.004	48.6	24.8	2.703	1.506	[a]1668	
38X-2, 60-62	358.70	1.976	50.7	26.3	2.831	1.457		
38X-4, 60-62	361.70	2.272	36.1	16.3	2.723	1.902		
38X-6, 60-62	364.70	2.081	41.6	20.5	2.642	1.654		
40X-2, 90-92	378.30	2.105	38.5	18.8	2.693	1.710	[a]1541	
40X-4, 90-92	381.30	2.056	43.4	21.6	2.708	1.612		
40X-6, 90-92	384.30	2.084	43.2	21.3	2.794	1.641		
41X-2, 60-62	387.70	2.085	50.4	24.7	2.861	1.569		
41X-4, 100-102	391.10	1.963	45.4	23.7	2.671	1.497		
41X-6, 90-92	394.00	2.006	45.7	23.4	2.686	1.537	[a]1584	
42X-2, 40-42	397.10	1.975	44.8	23.2	2.680	1.516		
44X-2, 51-53	416.51	1.966	45.8	23.9	2.674	1.496		
44X-4, 49-51	419.49	1.979	46.0	23.8	2.711	1.507		
44X-6, 45-46	422.45						[a]1630	
44X-6, 50-52	422.50	2.038	42.1	21.2	2.633	1.607		

[a] Velocity measurement perpendicular to bedding.

Similar reasoning indicates that a significant amount of phosphate has been removed from pore water at depth (Fig. 42). Decomposition of organic matter having a Redfield-type molar N:P ratio of 16 would yield about 50 μmol/L of dissolved phosphate per millimol of ammonia. Only about a tenth of this concentration is observed at this site (Table 12). Such a deficit is commonly observed in drill holes of DSDP and ODP and must be due to the precipitation of authigenic apatite phases. Calcite surfaces provide preferential nucleation sites for the precipitation of microcrystalline apatite (Stumm and Morgan, 1970).

The dissolved silica profile at Site 721 denotes two zones of reactivity (Fig. 42). Dissolution of biogenic opal in the nannofossil oozes which characterize the upper 300–350 m is almost certainly responsible for the high concentrations of silicate in pore water in this zone. However, the levels measured in interstitial waters collected from the turbidite sequence in the lower 50 m are lower by a factor of five, and the concentration in the deepest sample (51 μmol/L) is less than one-half that in present-day Arabian Sea bottom water. Because sedimentation rates just above the turbidites in the lower part of the hole (see "Accumu-

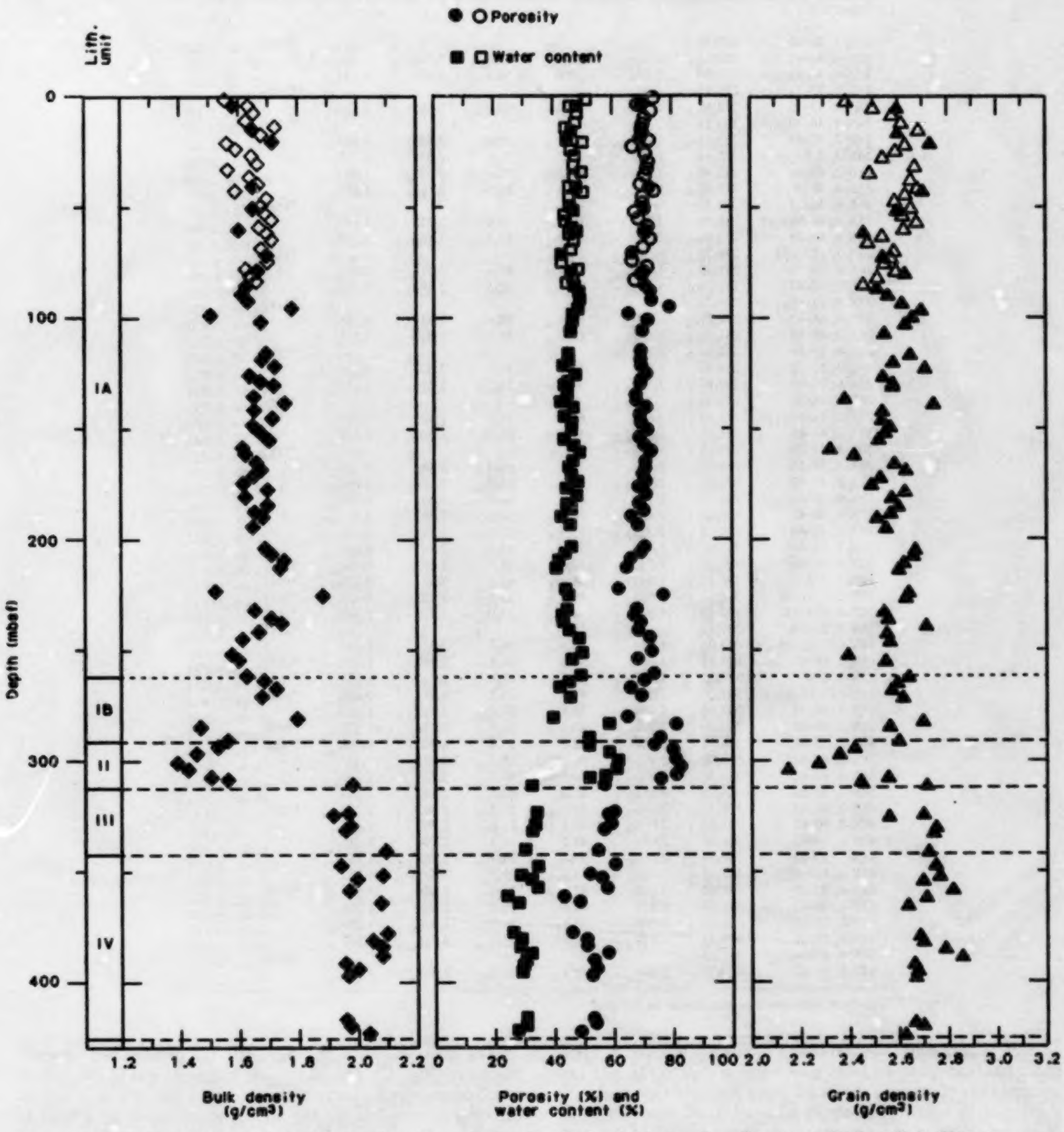

Figure 33. Index properties (wet-bulk density, porosity, water content, and grain density) measured on discrete samples from Holes 721A (open symbols) and 721B (solid symbols). Values are not corrected for sediment expansion.

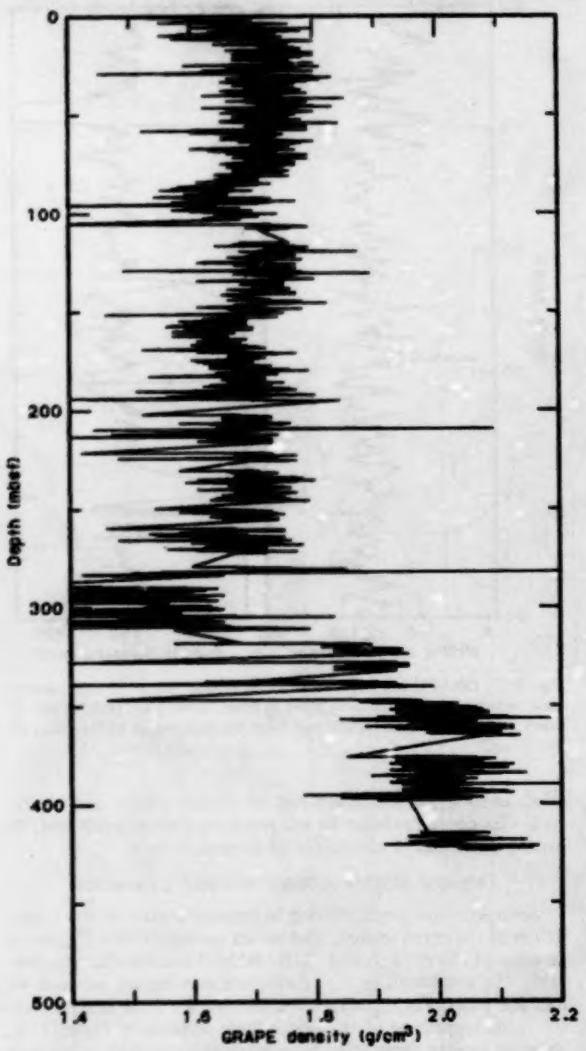

Figure 34. Wet-bulk density as measured by GRAPE for sediments in Hole 721B. The profile is based on 10-cm block averages of the data.

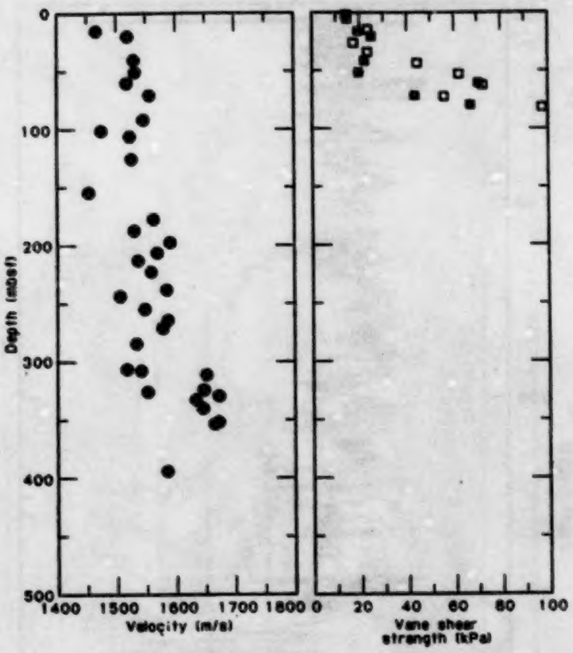

Figure 35. Compressional-wave velocity measured perpendicular to bedding in the Hamilton Frame Velocimeter and vane shear strength at Holes 721A (open symbols) and 721B (solid symbols).

lation Rates" section, this chapter) are about half the effective rate of diffusion of dissolved silica, the silica deficiency below 400 m depth must reflect SiO_2 precipitation rather than simply a paucity of dissolvable biogenic opal in the terrigenous deposits. Presumably, the dissolved silica distribution indicates that siliceous cementation is currently proceeding in the turbidite sequence. Indeed, both silica overgrowths on discoasters and replacement of discoaster calcite is observed in the turbidites (see "Lithostratigraphy" section, this chapter).

Sediment Mineralogy

The mineralogy of 16 sediment residues from Hole 721B remaining after interstitial water extraction was determined by X-ray diffractometry. Unoriented pressed-powder mounts were analyzed under standard operating conditions. No sample pretreatment was carried out. Relative abundances of illite, kaolinite, quartz, and dolomite (Fig. 43) were determined by correcting the net peak area counts for the effects of mineral mass absorption variation and changes in the calcite content (dilution)(MACC). The units expressed are therefore internally consistent among the four minerals, but have not been quantified with standards. The peak position used for the determination of illite may have a contribution from mica, and likewise chlorite may contribute to the kaolinite determination.

The general lithology of Site 721 is of pelagic nannofossil ooze overlying fine-grained muddy turbidites, with a sharp lithologic contrast between the two facies at 340 mbsf. Figure 43 suggests that both illite and kaolinite are abundant in the upper half of the core, with kaolinite being restricted to 110 mbsf. Over this interval kaolinite appears to be more abundant than illite. In contrast, quartz and dolomite occur throughout the cored section with quartz being apparently 2-3 times more abundant.

As indicated above, and in the "Lithostratigraphy" section (this chapter), the mineralogy of the nannofossil ooze is strikingly different from the fine-grained turbidites. In the latter, calcite is subordinate to quartz and significant concentrations of illite, chlorite, kaolinite, plagioclase feldspar, and pyrite were observed. Within the nannofossil ooze the proportion of terrigenous minerals per unit volume is controlled by variation in the terrigenous flux.

In order to assess the mode of occurrence of the dolomite at Site 721, the relative proportions of quartz and dolomite have been plotted together in Figure 44. A positive correlation is observed which argues in favor of a common source for the quartz and dolomite. If the dolomite was solely of authigenic origin, such a relationship would not be expected. A plausible source for both these minerals is the eolian transport of material to the Arabian Sea from adjacent landmasses.

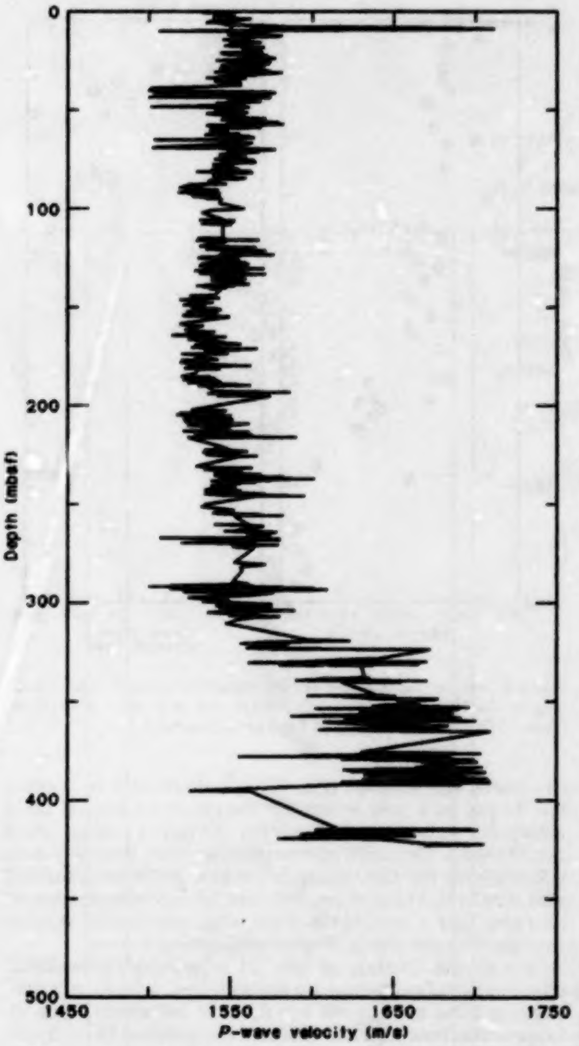

Figure 36. Compressional-wave velocity as the *P*-wave logger in Hole 721B. The profile is based on 5-cm block averages of the data.

Finally, four samples from Core 117-721B-18X (Samples 117-721B-18X-1, 150 cm; -1, 107 cm; -2, 20 cm; and -2, 61 cm) were examined in order to evaluate the mineralogical evidence for the high values of magnetic susceptibility (see "Paleomagnetism" section, this chapter). No unusual mineralogy was observed, and the main mineral was calcite.

ORGANIC GEOCHEMISTRY

The organic geochemical parameters routinely determined on sediments of Holes 721A and 721B were the abundance of organic carbon and pyrolysis characteristics. These parameters provide information on provenance of the organic matter and its maturity. Abundance of interstitial gas was determined in each core, and ratios of di- and triunsaturated C_{37} alkenones were measured in eight selected samples of Quaternary age to test their usefulness as indicators for variations in the sea-surface water temperatures. In general, organic matter is abundant in all levels of the cored interval of marine origin, and immature. Gas concentrations do not reach saturation levels and, as expected, the gas is exclusively of biogenic origin.

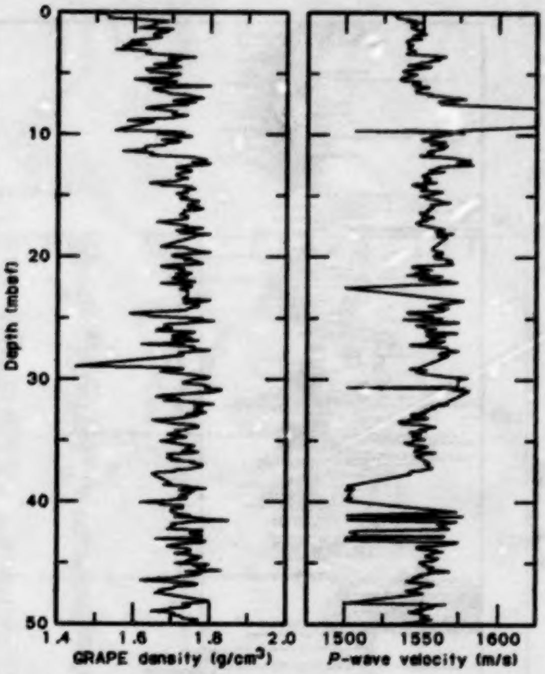

Figure 37. GRAPE wet-bulk density and *P*-wave logger compressional-wave velocity profiles for 0–50 mbsf in Hole 721B. The GRAPE and *P*-wave profiles are based on 10- and 5-cm block averages of the data, respectively.

Organic Matter Abundance and Character

Sediments are generally rich in organic matter in the upper 310 m of the cored section, and values average 0.74% C_{org} in all samples of Holes 721A and 721B (Tables 3 and 13; Fig. 45). Notably, the maximum in C_{org} concentrations occurs between 40 and 200 mbsf. The eight samples selected for lipid analysis, after visual inspection of the upper three sections of Hole 721B, show an inverse correlation between organic carbon values and carbonate content. Layers with high organic carbon contents have low carbonate values and vice versa (see Table 3). The overall correlation coefficient ($r = 0.20$; all samples), however, shows that the organic carbon concentration does not correlate significantly with $CaCO_3$ content.

The organic matter is immature as shown by the uniformly low temperatures of maximum pyrolysis release of hydrocarbons, $T_{max} < 435°C$ (Table 13). The extremely low values measured in samples below 340 mbsf should be considered erroneous. Most samples plot in the lower part of the field of immature marine organic matter on the hydrogen index/oxygen index diagram (Fig. 46), but show a considerable scatter. Possible sources of CO_2 are admixtures of inert organic matter from terrigenous sources, CO_2 from carbonates which break down at temperatures below 390°C, or instrumental artifact (see "Explanatory Notes" chapter, this volume). A possible indicator for the origin of organic matter is the hydrogen index (HI) (Fig. 45). The good correlation of C_{org} concentrations with the HI indicates that increases in organic carbon concentrations are due to enhanced burial of marine, lipid-rich organic matter. This is

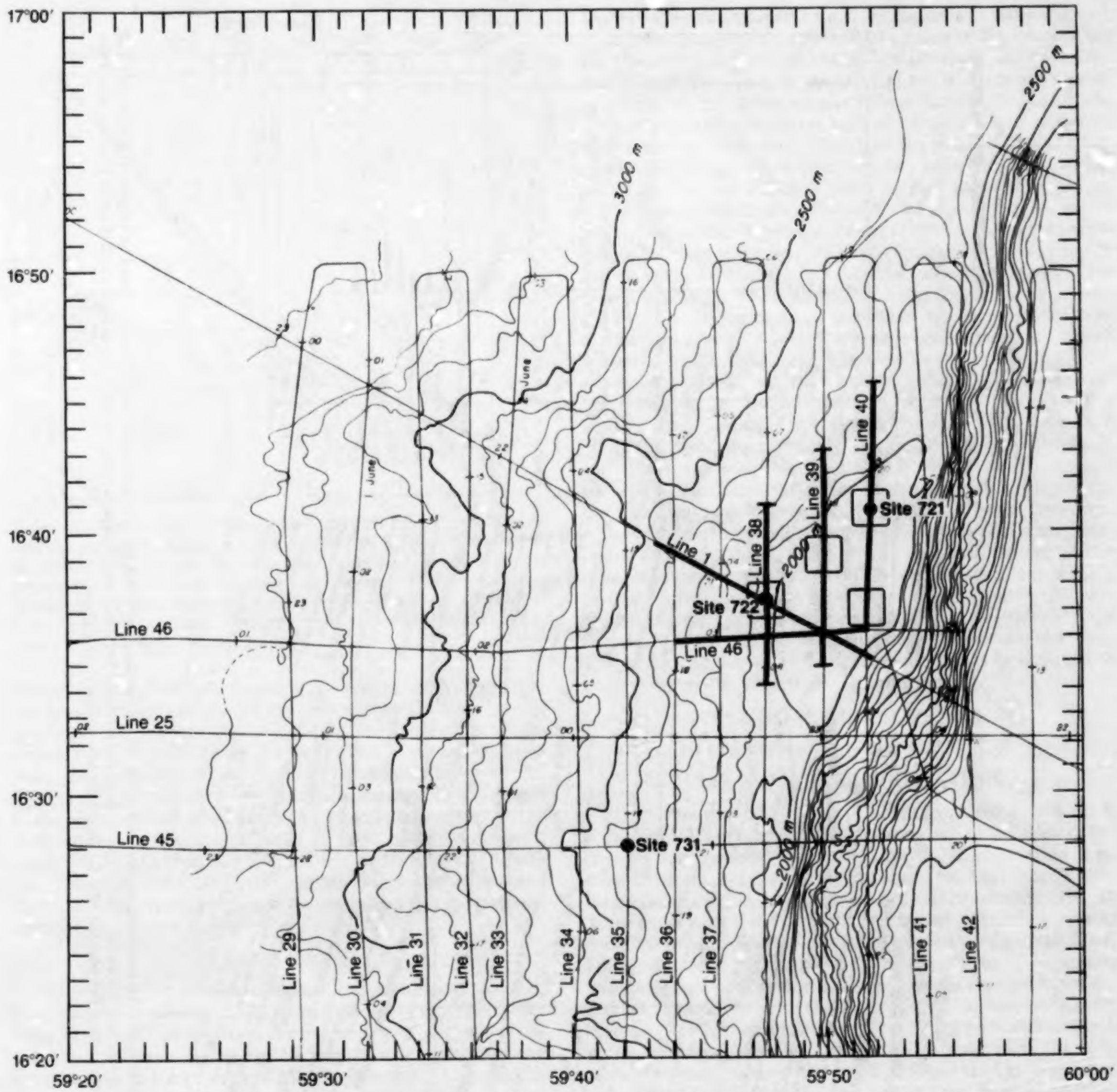
17°00′
16°50′
16°40′
16°30′
16°20′
59°20′
59°30′
59°40′
59°50′
60°00′
3000 m
2500 m
2500 m
2000 m
2000 m
June
1 June
Line 1
Line 38
Line 39
Line 40
Site 721
Site 722
Site 731
Line 46
Line 46
Line 25
Line 45
Line 29
Line 30
Line 31
Line 32
Line 33
Line 34
Line 35
Line 36
Line 37
Line 41
Line 42

Figure 38. The location of Sites 721 and 722 and the SCS tracks used to establish the seismic stratigraphy of the Owen Ridge. Intervals used are shown as heavy lines and the boxes indicate portions of the tracks shown in Figure 39. The bathymetry is based on Sea Beam data from the Leg 117 site survey (RC2704, 1986).

somewhat surprising, as lipid-rich organic matter is considered to be the preferred substrate for microbial remineralization. Furthermore, benthic remineralization is believed to be more effective during times of low sedimentation rates, while burial of organic matter is more effective at high sedimentation rates (Müller and Suess, 1979). We would, therefore, expect lower HI values ratios in the intervals of low sedimentation rates between 41 and 170 mbsf. This is not the case, however, and with the data presently available, we are unable to decide whether we are dealing with an input signal (higher productivity and/or different organic matter source within the marine primary producers) or an enhanced preservation effect.

Hydrocarbon Gases

Samples for interstitial gas analysis with the headspace method were taken in each core of Hole 721A, and each core of Hole 721B starting from Core 117-721A-9H. Results are given in Table 14 and are shown vs. depth in Figure 47. As is usually observed in marine sediments containing more than baseline values of organic carbon (>0.2%), methane is generated in considerable quantities below the depth of sulfate depletion (see "Inorganic Geochemistry" section, this chapter) at approximately 100 mbsf. Values of methane per liter of wet sediment reach a maximum of 156 mL/L at 393 mbsf. Variability in the

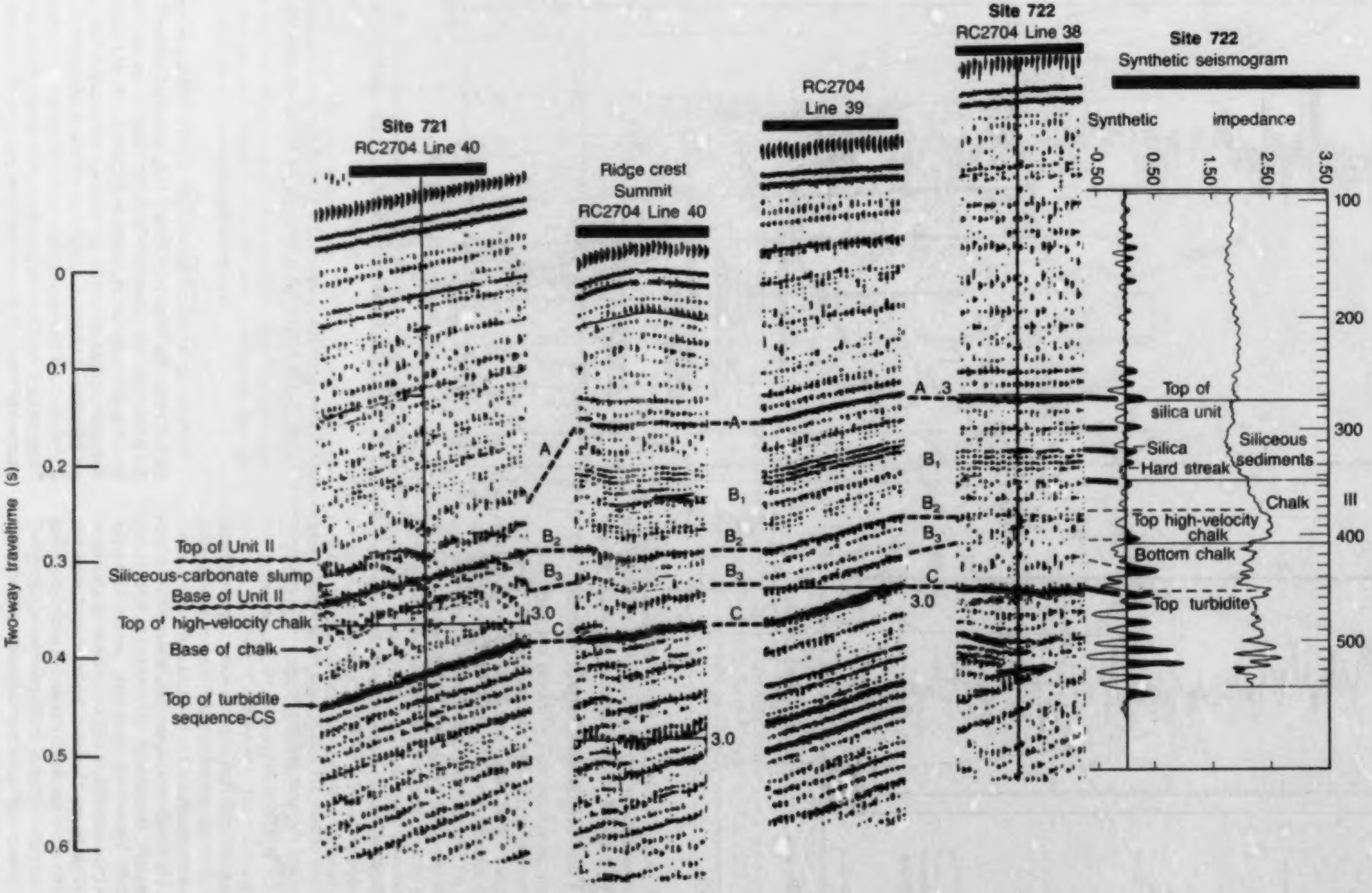

Figure 39. Correlation of reflectors (see text for discussion) between seismic profiles (see Fig. 38 for locations) and with the synthetic seismogram, which is based on logging data from Site 722 (see "Downhole Measurements" and "Seismic Stratigraphy" sections, "Site 722" chapter, this volume). Synthetic seismogram is scaled in mbsf and seismic profiles are in two-way traveltime (s). Profiles are aligned so that Reflector C is continuous; the position of 3.0 s below the sea surface is also shown.

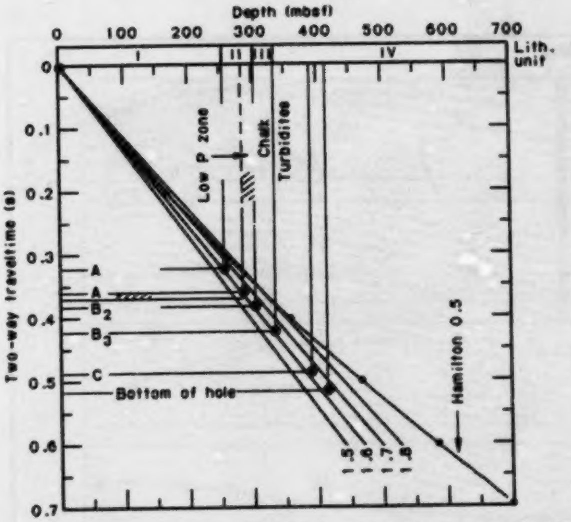

Figure 40. Plot of two-way traveltime (from SCS Line 40, see Figs. 39 and 41) and depth (mbsf) of lithologic features at Site 721. Reflectors are indicated on the traveltime axis and lithologic units and facies are shown on the depth axis. The wavy lines represent hiatuses. Diagonal straight lines correspond to time-depth curves for average velocities of 1.5, 1.6, 1.7, and 1.8 km/s. The slightly curved line is Hamilton's (1979) empirical curve for carbonate sediments.

concentrations downhole appear to be independent of organic matter abundance and quality (as expressed by the HI, Fig. 45), and below 200 mbsf the methane abundance levels out at values around 0.1 L/L. Insufficient gas was present in the sediments to cause the formation of gas pockets. The concentration of the C_{2+} gases is very low (only ethane could be detected) and attests to the immature nature of the organic matter in the Miocene to Holocene sediments cored at Site 721. Most likely the ethane is generated by microbial activity, and not by thermogenic cracking. Therefore, the C_1/C_2 ratios do not follow the exponential decrease with depth which one would expect by thermogenic cracking of kerogen (Claypool and Kaplan, 1974).

Lipid Analyses

An attempt was made to analyze the molecular distributions of extractable organic compounds in Quaternary sediments from Hole 721B, with emphasis on the occurrence of long-chain unsaturated ketones (alkenones). Variations in sea-surface water temperatures in the geological past are potentially recorded by these alkenones. Planktonic organisms that biosynthesize these compounds react to increasing water temperature with a decrease in the average degree of unsaturation (i.e., number of double bonds; Brassell et al., 1986; ten Haven et al., 1987). Brassell et al. (1986) defined an alkenone unsaturation index as:

$$U^{k}_{37} = \text{diunsaturated } C_{37} \text{ / diunsaturated + triunsaturated } C_{7} \text{ ketones}$$

This ratio can vary between 0 and 1, i.e., from cold to warm. Eight samples were selected from the upper three cores of Hole 721B. Depth, organic carbon and carbonate content of these samples are given in Table 15. The experimental procedure, as well as the gas chromatographic conditions are described in the "Explanatory Notes" chapter (this volume). The gas chromatograms of four sediment extracts are shown in Figure 48. The alkenones elute with retention times between 45 and 49 minutes. The first two eluting compounds are the di- and triunsaturated C_{37} ketones, respectively, followed by a group of C_{38} unsaturated ketones approximately 2 min later. Straight-chain alkanes are indicated with dots, and the numbers above the dots correspond to the number of carbon atoms of the molecules (the identification has been solely made on basis of retention times compared with a standard solution). The C_{17} straight-chain alkane (heptacosane) is the most prominent alkane, and abundances of C_{27} to C_{33} alkanes from cuticular waxes are low. These findings support a dominantly marine origin of the organic matter which has to be elucidated by shore-based investigation. An enlargement of the retention time range of alkenone elution is given in Fig. 49 for two extreme values, and the calculated U^{k}_{37} ratios are given in Table 15. The U^{k}_{37} ratios of sediments investigated here are high and in the range of data from the Sierra Leone Rise (0.88–0.97; Brassell et al., 1986). Our results point to "cool" sea-surface water temperatures in Samples 117-721B-1H-2, 100–103 cm. and 117-721B-2H-2, 17–20 cm, while higher sea-surface water temperatures are indicated in Sample 117-721B-2H-1, 87–90 cm. Using the calibration regression equation (U^{k}_{37} = 0.033T + 0.043) based on laboratory cultures (Prahl and Wakeham, 1987), absolute temperatures are 25.0°C and 28.5°C, respectively. The maximum difference in the U^{k}_{37} ratio (0.11) is the same as measured in samples of Leg 108 (offshore Morocco, Atlantic Ocean), covering a glacial/interglacial time span (Shipboard Scientific Party, 1988). In the Atlantic Ocean, glacial times are characterized by low $CaCO_3$ contents and high organic carbon contents, and vice versa for interglacial times. Surprisingly, a correlation seems to exist between the U^{k}_{37} ratio and the carbonate content of the sediments investigated from the Owen Ridge (Fig. 50). However, more samples need to be analyzed to prove whether this correlation is significant.

DOWNHOLE MEASUREMENTS

No logging was done at Site 721.

INTERHOLE CORRELATION

The upper part of lithologic Unit I recognized at Site 721 is characterized by cyclic changes in the nature of sediments. The changes can be detected not only by visual observation (i.e., color changes), but also by magnetic susceptibility (see "Paleomagnetism" section, this chapter) and $CaCO_3$ content (Fig. 5). Three holes were drilled by APC cores and collected sequences from the upper 100 mbsf within lithologic Unit I (Holes 721A, 721B, and 721C; Fig. 51). The correlation of the cycles among these holes provides valuable information on changes in the depositional environment and on gaps in the sections which are necessary for high-resolution studies. Uniformity and continuity of each layer gives information on differences in the sedimentation rates between the holes at Site 721. The essence of the interhole correlation process involves the determination of correlative lithologic marker layers which are then confirmed using the detailed whole-core magnetic susceptibility data; the process is summarized in the "Explanatory Notes" chapter (this volume).

The holes are located on the crest of the Owen Ridge and are aligned in a north-northeast direction. Hole 721B is 20 m west of Hole 721A, and Hole 721C lies 20 m south of Hole 721B. Hole 721A drilled to 86.4 mbsf with APC, and the recovery was almost perfect. Hole 721B is the deepest hole in Site 721 and reached 424.2 mbsf by APC and XCB drilling. Hole 721C was drilled by APC and XCB, and the bottom depth was 138.0 mbsf. The top of Hole 721C obtained the mud line, which was not recognized in Cores 117-721A-1H and 117-721B-1H, respectively.

Apart from visual correlation, physical and magnetic properties were used to correlate between the holes. The GRAPE

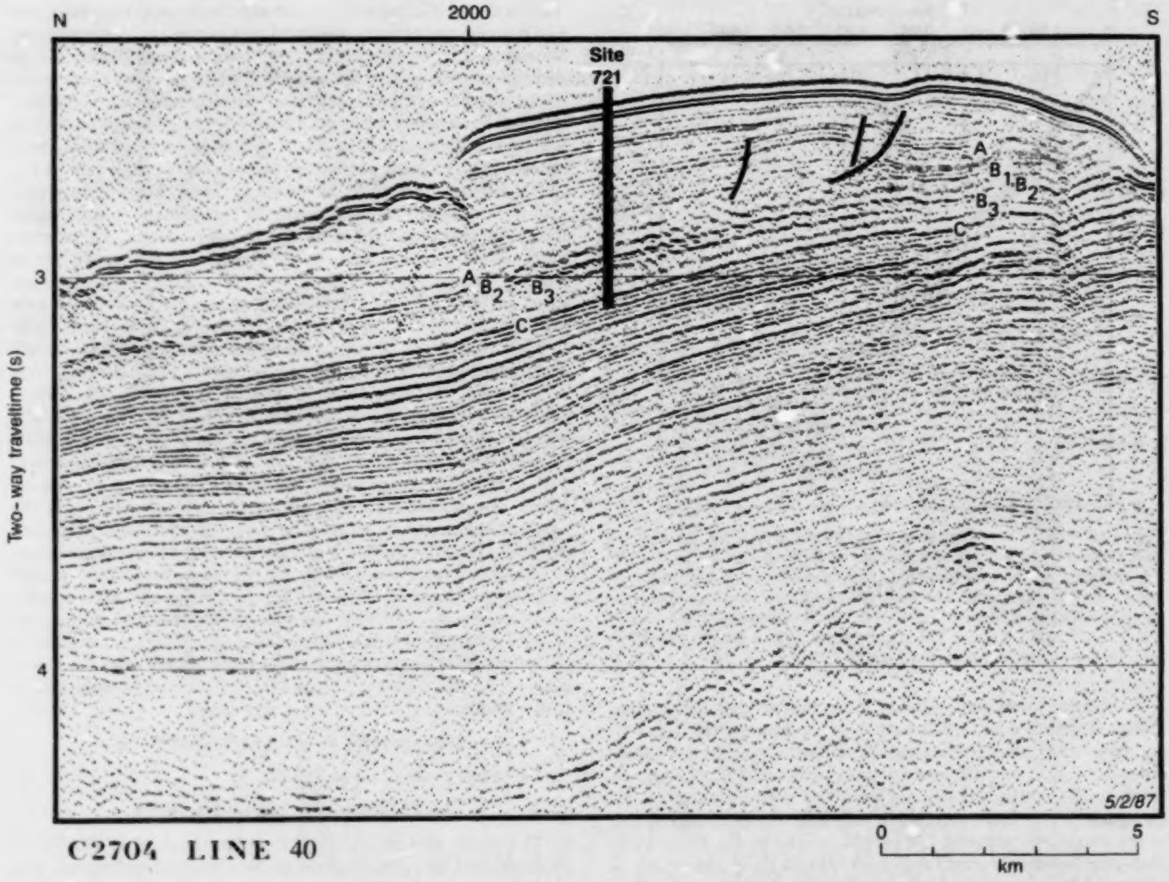

Figure 41. Seismic reflection profile (Line 40, see Fig. 38) across Site 721 to the crest of the Owen Ridge. The location and recovered interval of Site 721 are shown, along with the reflector identifications and interpreted faults.

density and magnetic susceptibility of the sediments were measured at 1.2- and 5-cm intervals before splitting the sections. Lithologic descriptions and photographs were obtained on the split sections.

Visual correlation of the cores relied on the core photographs. Several distinct and traceable layers were determined in each core and were notated as a_0, a_1, ·····, n_2, n_3 (Table 16). The marker layers were defined on the cored sediments of Hole 721A above 91.7 mbsf (i_4) and on Hole 721B below 94.25 mbsf (i_5).

Figure 52 shows an example of the correlations by visual and magnetic susceptibility methods. The figure shows the correlative interval with layer f_1 and f_2: Samples 117-721A-6H-1, 110 cm, to 117-721A-6H-2, 120 cm (49.70–51.20 mbsf); Samples 117-721B-6H-4, 100 cm to 117-721B-6H-5, 100 cm (53.60–55.10 mbsf); 117-721C-7H-2, 0–150 cm (53.50–55.00 mbsf). Visual lithologic correlations were based on the color pattern and bioturbation features. Light-colored intervals typically correspond to lower susceptibility while dark intervals correspond to higher susceptibility and lower $CaCO_3$ content. In this way the lithologic marker layer correlations were verified using the magnetic susceptibility data, which are quantitative.

The results of the layer-by-layer correlation allow us to calculate true thickness between these layers coinciding with and cut by core boundaries. Occasionally core tops were expanded by water uptake during drilling, and in such instances the apparent thickness of the sediment layer divided by the core boundary is assumed to be thicker than the original length. In some instances, the top part of the core was missing. In this case apparent thickness is assumed to be thinner than the original length. Fortunately, the three holes were staggered, so that they have different horizons at core boundaries as shown in Table 16. The original thickness of layers coinciding with core tops or bottoms can be obtained by comparing thickness of the correlative layer in the continuous section of the other holes. The differences in Hole 721B can be calculated by referring to Hole 721A and 721B. Unfortunately, the core boundaries in Hole 721A and 721C are located almost in the same horizons. The differences between these two were calculated by referring to the correlative intervals of Hole 721B. Table 17 shows the differences between the depth calculated by the ODP core log data and assigned depth, and depth calculated by the layer-by-layer correlation method. The reliability of this method to produce corrected depths is high; computation of corrected depths have errors less

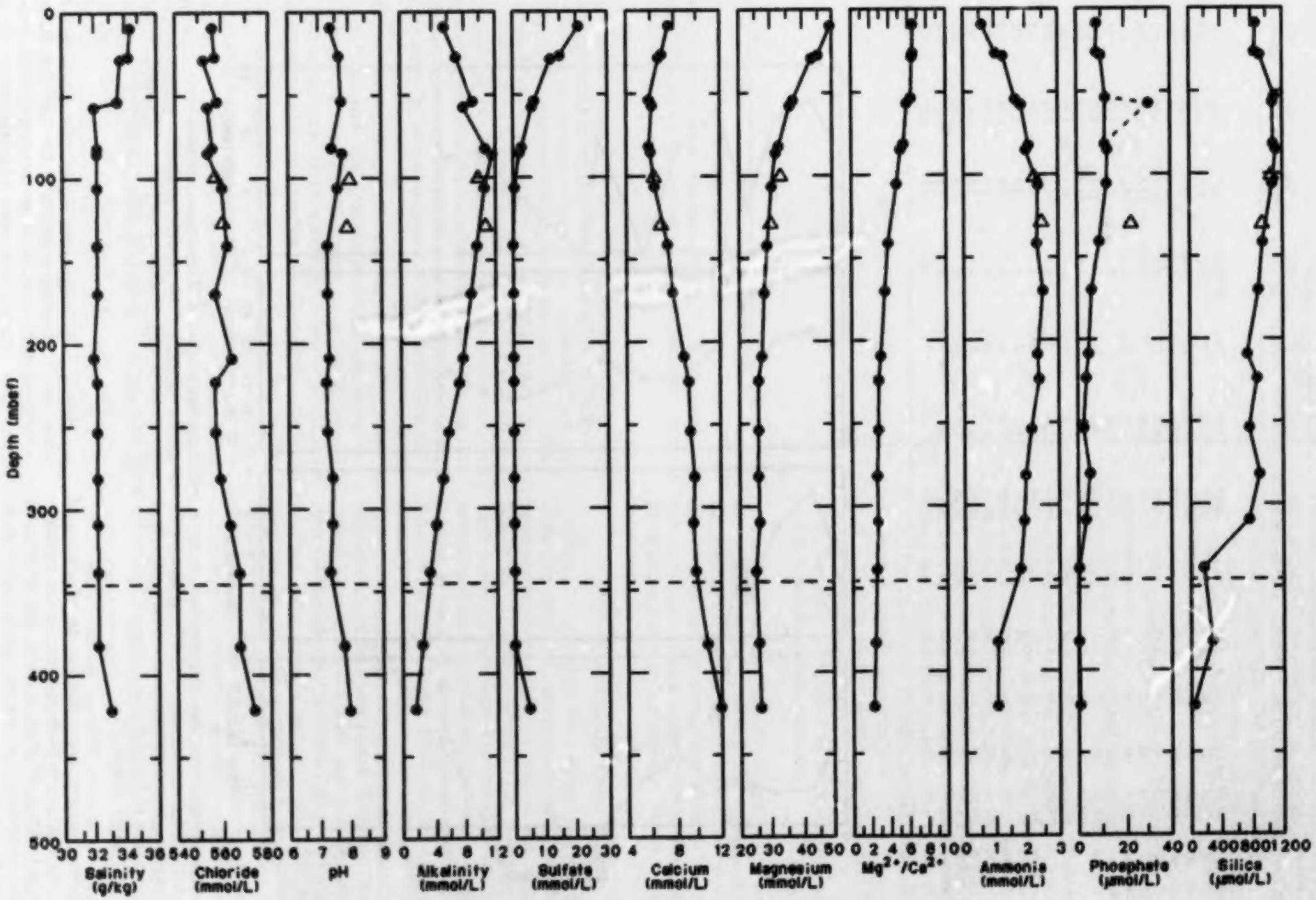

Figure 42. Concentration profiles vs. depth for Site 721. Dots = squeezed pore waters; triangles = *in-situ* pore-water samples obtained with the Barnes water sampler. The horizontal dashed line indicates the break in lithology between the biogenic ooze (Unit III) and the turbidites (Unit IV).

Table 12. Summary of interstitial water geochemical data for Holes 721A and 721B.

Hole, core, section (cm)	Depth (mbsf)	Vol. (mL)	pH	Alk. (mmol/L)	Sal. (g/kg)	Mg (mmol/L)	Ca (mmol/L)	Cl (mmol/L)	SO_4 (mmol/L)	PO_4 (µmol/L)	NH_4 (mmol/L)	SiO_2 (µmol/L)	Mg/Ca
117-													
721A-1H-6, 145-150	8.95	43	7.38	5.47	34.3	49.25	7.61	556	20.9	8.7	0.60	855	6.47
721B-3H-5, 145-150	26.55	45	7.66	6.99	34.2	45.35	7.01	557	15.0	8.6	1.03	846	6.47
721A-3H-6, 145-150	28.45	35	—	—	33.7	43.16	6.75	552	12.0	10.3	1.26	914	6.39
721B-6H-4, 145-150	54.05	55	7.74	9.02	33.5	37.42	5.94	558	6.8	12.4	1.66	1100	6.30
721A-6H-6, 145-150	57.45	40	—	7.88	32.0	36.29	6.20	554	6.1	30.7	1.84	1075	5.85
721B-9H-4, 145-150	82.35	48	7.42	10.72	32.2	32.77	5.93	556	2.75	12.0	2.07	1083	5.53
721A-9H-6, 145-150	85.75	48	7.76	11.56	32.2	31.81	6.10	554	2.01	13.2	1.99	1117	5.21
721C-12I-1, 0-1	100.00	15	8.02	9.75	32.3	33.39	6.08	556	0	—	2.19	1024	5.49
721B-12X-1, 145-150	106.65	40	7.61	10.55	32.2	30.54	6.42	560	0.5	12.9	2.37	1075	4.76
721C-15I-1, 0-1	129.00	15	7.84	10.57	31.7	30.37	6.92	559	0.0	23.2	2.48	948	4.39
721B-15X-5, 145-150	141.55	37	7.28	9.58	32.2	29.26	7.54	562	0	9.7	2.32	948	3.88
721B-18X-5, 145-150	170.65	32	7.28	8.87	32.2	28.18	7.99	557	0.2	6.3	2.51	889	3.53
721B-22X-5, 145-150	209.45	37	7.31	7.77	32.0	27.44	8.89	564	0	4.9	2.34	745	3.09
721B-24X-2, 140-150	224.20	73	7.23	7.36	32.2	26.31	9.31	557	0	3.8	2.39	872	2.83
721B-27X-3, 145-150	254.25	31	7.26	5.90	32.2	26.26	9.44	557	0	2.6	2.14	770	2.78
721B-30X-2, 140-150	282.10	50	7.42	5.20	32.2	26.14	9.79	559	0	5.3	1.96	897	2.67
721B-33X-1, 140-150	309.80	58	7.41	4.34	32.2	26.58	9.67	563	0	3.6	1.91	762	2.75
721B-36X-1, 140-150	338.80	30	7.33	3.60	32.2	25.49	9.89	567	0	0.5	1.79	178	2.58
721B-40X-5, 140-150	383.30	21	7.78	2.59	32.2	26.13	10.83	567	0	0.4	1.07	280	2.41
721B-44X-5, 140-150	421.90	30	7.94	1.63	33.0	26.74	11.96	573	4.6	0.8	1.06	51	2.24

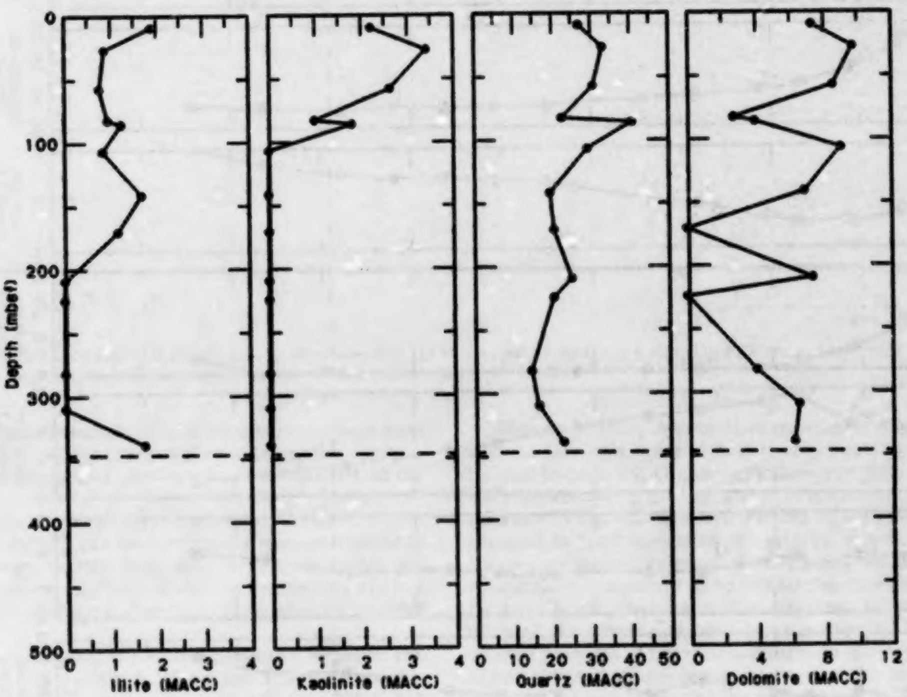

Figure 43. Qualitative distributions of illite, kaolinite, quartz, and dolomite in Site 721 sediments, corrected for dilution by calcium carbonate and differential mass absorption effects (MACC). Chlorite may contribute to the kaolinite peak. The abscissae show relative scales only and are not meant to imply absolute concentrations. The concentration of detrital clays and quartz in the turbidite facies greatly exceeds the levels in the nannofossil oozes and are thus not plotted.

than 20 cm. Using this correction offset for the calculation of true thickness, the thicknesses between a_2 and i_4 can be calculated as 87.95 m in 721A, 87.65 m in 721B, and 85.95 m in 721C. The sediments in Hole 721C are apparently 2.0 m thinner than in Hole 721A and 721B.

Hole 721C recovered the mud line in the first core. It appears that Hole 721B also has recovered the mud line, because the subsurface depth of a_0 is 10 cm deeper than Hole 721C. Hole 721A, however, missed the top 2.75 mbsf based on the correlation of horizon a_1. This estimate is substantiated by correlating

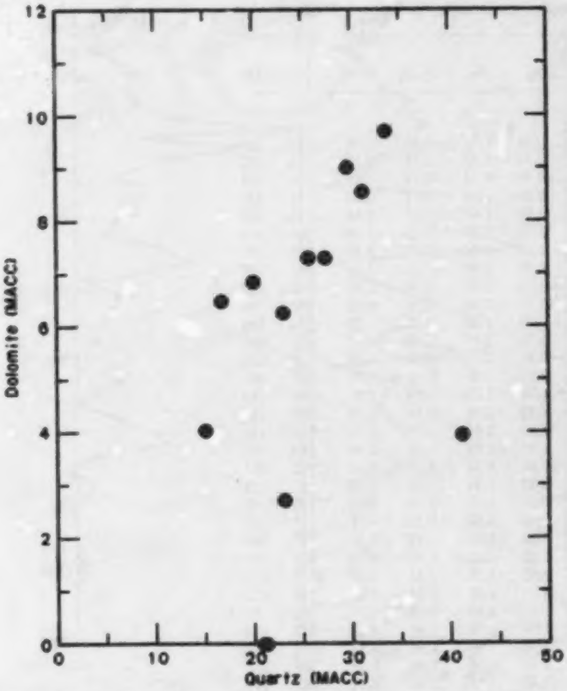

Figure 44. Correlation between the mass-absorption and carbonate-corrected (MACC) relative concentrations of dolomite and quartz in Site 721 sediments.

CaCO$_3$ data from Hole 721A and from a piston core (RC27-61) taken during the site survey (Fig. 53). Based on the calcium carbonate profile correlations, at least 2.25 m is missing from the top of 721A. A correlation of the piston core to trigger cores implies that 20 cm is missing from the top of RC27-61. Thus, the top of Hole 721A begins at least 2.45 m (2.25 ± 0.20 m) below the mud line. The 30-cm difference between the estimate of missing section based on the correlation to Hole 721B and the estimate based on carbonate profiles could be due to stretching of the sediments in the soupy section at the top of Core 117-721B-1H and differences in sedimentation rate between the two locations.

Hole 721B contains the most complete sediment record for the top 100 mbsf at Site 721. The correction factors in Table 17 are utilized to correct the ODP CORELOG data to provided a continuous sediment section for Site 721 (Table 18).

SUMMARY AND CONCLUSIONS

The primary reason for coring at Site 721 was to recover a continuous high-resolution section of pelagic sediments of late Neogene age from the crest of the Owen Ridge. These sediments have been deposited well above the carbonate lysocline and beyond the zone of lateral bottom transport from the continental margin. Study of this sedimentary sequence was expected to identify the initiation, and document the history, of monsoonal upwelling in the Arabian Sea (Kutzbach, 1981; Prell and Kutzbach, 1987). The detailed biotic, chemical, and sedimentologic records obtained from these sediments can provide data to test the hypothesis that much of the short-term variability (10^3 yr) of monsoonal upwelling is forced by changes in solar radiation related to cyclical variations in the earth's orbit (the Milankovitch mechanism). Long-term trends of the intensity of the monsoon related to the uplift of the Himalayas may also be imprinted on the long paleoenvironmental record from the ridge (Hahn and Manabe, 1975). In addition, the age and character of the sediments at Site 721 could be used to reconstruct the depositional and tectonic uplift history of the Owen Ridge.

The preliminary shipboard findings at Site 721 pertinent to the above objectives are summarized in Figure 54 and include the identification of:

1. The appearance of siliceous facies in the lower part of the upper Miocene.
2. The appearance of cold "upwelling" faunas in the middle upper Miocene.
3. Well-defined sedimentary cycles that are defined by changes in sediment color, magnetic susceptibility, and physical properties. The cycles have distinct periodicities, which are consistent with the Milankovitch frequencies, and individual cycles can be correlated in detail between holes.
4. High accumulation rates in the upper Miocene, which are followed by low rates in the lower Pliocene, and increasing rates during the Pliocene-Pleistocene.
5. The cessation of turbidite deposition on the ridge crest in the lower to middle Miocene.
6. The covariation of quartz and dolomite in the clastic fraction of the sediments.
7. Generally high values of marine-derived organic carbon and its relatively pristine character.

The major themes that are relevant to the interpretation of the depositional history of Site 721 combine such phenomena as the uplift of the Owen Ridge, the onset and preservation of siliceous fossils and the appearance of distinct upwelling faunas, and the pattern of high-frequency variability in the abundance of various sedimentary components. Below, we briefly address these themes.

Uplift of the Owen Ridge

The uplift history of Owen Ridge is indicated by variations in the lithofacies, i.e., by the gradation of turbiditic facies, and by phases of nondeposition or erosion. The lower Miocene section at Site 721 is characterized by silty turbidites that grade upward to muddy turbidites. The turbidites are typically low in organic carbon and carbonate, and frequently display concentrations of sand- to silt-sized pyrite (placers?) at their bases. Preservation of planktonic fossils is poor and opaline silica is sparse (Fig. 54). This sequence was laid down in an active deep-water turbidite depositional environment before the Owen Ridge was uplifted. In the upper part of lithologic Unit IV, the grain size of basal layers decreases, and finer-grained muddy turbidites are intercalated with pelagic nannofossil chalks. This trend of finer, more distal(?), and fewer turbiditic deposits is also shown in the decrease in magnetic susceptibility, bulk density (Fig. 54), and *P*-wave velocity. The source of the fine mud turbidites and their pyrite bed load is unknown. A shelf origin is assumed in spite of their low organic carbon content. We interpret the fining-upward sequence as an indicator of progressive uplift of the site above the surrounding seafloor. Thus, the coarser bed load of the turbidite flows would not reach the site. Seismic reflection profiles of the region indicate some onlap to the reflectors that are equivalent to the turbidites in Unit IV, so that some uplift probably occurred prior to the deposition of the deepest sediments recovered at Site 721. The upper limit of the turbiditic sequence is marked by a prominent seismic reflector (C) that can be mapped over much of the Owen Ridge and in the adjacent Owen Basin (Mountain and Prell, 1987).

The uppermost lower and middle Miocene deposits recovered at Site 721 were entirely composed of nannofossil chalk

Table 13. Results of Rock-Eval pyrolysis of samples from Holes 721A and 721B.

Hole, core, section, interval (cm)	Depth (mbsf)	T_{max} (°C)	S_1	S_2	S_3	S_2/S_3	TOC	HI	OI
117-									
721A-1H-6, 144–145	8.94	406	0.00	0.55	1.71	0.32	0.56	98	305
721A-2H-6, 149–150	18.79	411	0.00	0.51	1.38	0.36	0.38	134	363
721A-2H-7, 25–27	19.05	418	0.00	0.99	1.33	0.74	1.01	98	131
721A-3H-6, 119–120	28.19	390	0.00	0.20	1.31	0.15	0.30	66	436
721A-4H-5, 0–1	35.20	412	0.00	0.74	1.64	0.45	0.66	112	248
721A-5H-4, 149–150	44.89	417	0.00	2.11	1.83	1.15	1.04	203	176
721A-6H-6, 119–120	57.19	423	0.00	1.70	1.51	1.12	0.88	193	171
721A-7H-5, 149–150	65.29	419	0.00	2.77	1.80	1.53	1.04	266	173
721A-8H-5, 149–150	74.79	418	0.00	3.52	2.00	1.76	1.45	242	137
721A-9X-6, 119–120	85.48	416	0.00	14.72	3.36	4.38	3.68	400	91
721B-1H-2, 100–103	2.50	417	0.01	2.79	3.20	0.87	1.29	216	248
721B-1H-4, 80–83	5.30	405	0.02	0.78	2.11	0.36	0.43	181	490
721B-1H-5, 24–27	6.24	414	0.02	2.41	2.55	0.94	1.21	199	210
721B-2H-1, 87–90	10.27	407	0.02	0.91	2.04	0.44	0.46	197	443
721B-2H-2, 17–20	11.07	414	0.01	1.70	2.29	0.74	1.91	89	119
721B-3H-3, 10–13	22.20	417	0.02	1.52	1.98	0.76	0.74	205	267
721B-9H-4, 144–145	82.34	421	0.00	6.17	2.66	2.31	1.95	316	136
721B-10X-4, 149–150	91.99	419	0.00	1.82	1.73	1.05	0.96	189	180
721B-11X-2, 149–150	98.59	420	0.00	12.06	3.24	3.72	3.07	392	105
721B-12X-1, 144–145	106.64	422	0.00	2.93	1.91	1.53	1.56	187	122
721B-13X-4, 149–150	120.79	414	0.00	0.80	1.47	0.54	0.60	133	245
721B-14X-1, 149–150	125.89	396	0.00	0.46	1.88	0.24	1.37	33	137
721B-15X-2, 119–120	136.79	419	0.00	3.81	1.93	1.97	0.66	577	292
721B-16X-5, 149–150	151.29	422	0.00	1.92	1.65	1.16	0.70	274	235
721B-17X-5, 149–150	160.99	422	0.00	8.65	2.57	3.36	0.57	1517	450
721B-18X-5, 119–120	170.39	418	0.00	2.81	1.86	1.51	1.49	188	125
721B-19X-5, 149–150	180.39	418	0.00	1.11	1.60	0.69	1.97	56	81
721B-20X-5, 149–150	190.09	409	0.03	1.01	1.70	0.59	0.92	109	184
721B-21X-2, 0–1	193.80	420	0.00	3.74	1.90	1.96	0.28	1335	678
721B-22X-3, 0–1	205.00	420	0.00	2.55	1.65	1.54	0.78	326	211
721B-24X-3, 0–1	224.30	417	0.00	1.47	1.67	0.88	0.56	262	298
721B-25X-5, 0–1	236.50	413	0.00	0.62	1.75	0.35	0.37	167	472
721B-27X-3, 119–120	253.99	352	0.00	0.13	1.02	0.12	0.25	52	408
721B-28X-5, 0–1	265.60	415	0.02	1.80	1.70	1.05	0.80	225	212
721B-29X-2, 0–1	270.90	408	0.02	0.88	1.46	0.60	0.43	204	339
721B-31X-3, 149–150	293.49	411	0.04	1.74	1.62	1.07	0.85	204	190
721B-32X-2, 149–150	301.79	413	0.05	3.81	1.63	2.33	1.47	259	110
721B-33X-1, 114–115	309.54	418	0.07	4.46	2.02	2.20	1.60	278	126
721B-36X-1, 114–115	338.54	264	0.03	0.29	0.61	0.47	0.37	78	164

Note: Samples are mainly headspace residues. For a detailed description of parameters, see "Explanatory Notes" chapter (this volume).

(Unit III) that is characterized by high carbonate content (76%) and poor opal preservation (Fig. 54). Thus, by this time, the site had been uplifted well above the influence of turbidite deposition and was accumulating pelagic sediments. However, much of the middle Miocene section is missing. A significant hiatus (from nannofossil Zone NN9 to NN5) occurs at about 311 mbsf and correlates to seismic reflector B_2 (see "Seismic Stratigraphy," this chapter). Lithologic Unit II lies above the reflector B_2 and is composed of siliceous nannofossil oozes and chalks that are disturbed by slumping. The lower part of this unit is characterized by low bulk and grain densities and high porosities that reflect the greater biogenic silica content (Fig. 54). This stratigraphic interval appears to be the locus of the slump fault that removed most of the middle Miocene. The top of lithologic Unit II may also marked by a hiatus, but of much smaller extent than the basal hiatus. On the basis of biostratigraphy and comparison to other seismic sections on the Owen Ridge, we estimate that about 90 m of the middle Miocene is missing at Site 721. The slump of the sediments is, no doubt, related to the inclination caused by the uplift of the Owen Ridge, but the specific event cannot yet be attributed to a discrete uplift phase. Another phase of uplift, indicated by low accumulation rates (see below), may have occurred in the early Pliocene.

The Onset of Upwelling Faunas and Opal Deposition

If late Neogene uplift and orbital changes have affected the monsoon as outlined in the "Introduction, Background, and Major Objectives for Leg 117" chapter (this volume), the sediments at Site 721 should record both increased productivity and distinct faunas due to the upwelling. The sediments should also reflect increased eolian transport (although some of the transport may occur during the winter season). Furthermore, variations in source area of the eolian components may result in differing mineralogy and chemistry. Thus, the cyclic variations in sediment composition related to changes in solar radiation should have specific frequencies, the Milankovitch spectrum, that may be quantitatively identified in the sediments of Site 721.

The first indication of enhanced productivity at Site 721 is the appearance of the siliceous facies of lithologic Unit II in the upper Miocene (Fig. 54). Both radiolarians and diatoms appear at the base of this unit, but the species are tropical in nature. At the same time, organic carbon increases from less than 0.1% in Units III and IV to almost 2.0% in the base of the siliceous Unit II. As previously noted, this interval is also characterized by low bulk and grain densities and low velocities due to the admixture of siliceous fossils. Unfortunately, the base of the siliceous fa-

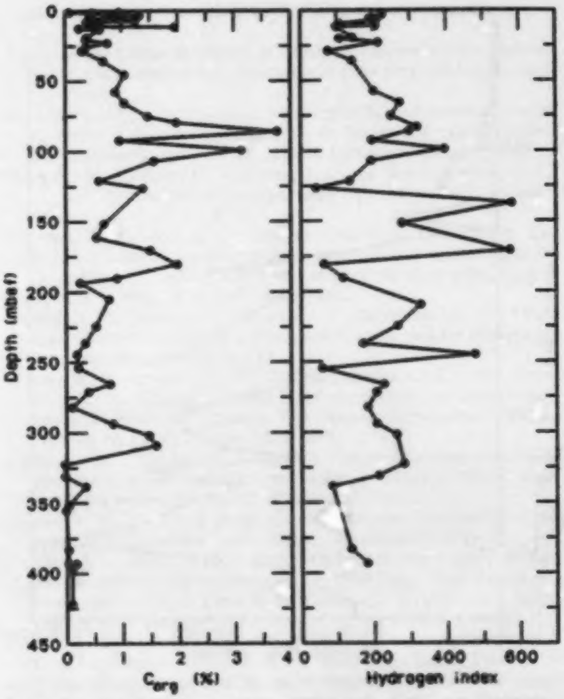

Figure 45. Downhole plots of C_{org} and hydrogen index values in Holes 721A and 721B. High values of HI are considered to be an attribute of lipid-rich, undegraded marine organic matter.

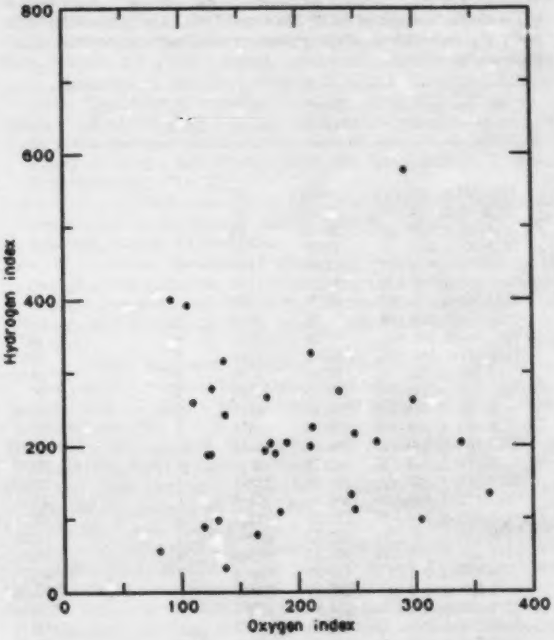

Figure 46. Plot of the hydrogen index vs. oxygen index (OI) of samples from Holes 721A and 721B. Samples plot mainly in the section for immature marine organic matter rich in relatively labile oxygen-rich functional groups.

cies (the boundary between lithologic Units II and III) corresponds to the basal hiatus of Unit II, so that the true age of the onset of siliceous deposition on the Owen Ridge is not recognized at Site 721. The siliceous facies (Unit II) grades upward to foraminifer-nannofossil ooze (chalk) with deformation and slump features (Unit II) and eventually to foraminifer-bearing and foraminifer-nannofossil ooze with alternating light and dark bands (Unit I). The different plankton assemblages undergo dramatic, but not simultaneous, changes in the upper Miocene. The first indication of upwelling is the appearance of a radiolarian fauna in the middle Miocene. This assemblage contains typical tropical species, but younger radiolarian faunas contain more robust, cool-water forms and lack many tropical forms. A distinctive upwelling planktonic foraminiferal fauna appears in the early late Miocene with the simultaneous appearance of *Globoratalia bulloides*, *Globoratalia menardii*, and *G. tumida*, and the *Neogloboguadrina* lineage of *N. acostaensis* and *N. dutertrei* at the boundary between lithologic Units II and I (Fig. 54). Finally, in the early Pliocene, cold-water forms of calcareous nannoplankton appear at Site 721. This sequence of assemblages may indicate an ecologic response to the evolution of monsoonal upwelling. However, detailed study of the faunal and floral variations will be needed to establish the oceanographic significance of this sequence.

Another possible indication of changes in monsoonal upwelling is the variation in accumulation rates, especially biogenic rates. The percent carbonate content of Unit I is relatively high (average about 60% with variations from 80% to 40%) and shows no long-term trends. However, the carbonate and noncarbonate accumulation rates show significant fourfold variations since the late Miocene. The carbonate accumulation rates increase from about 1 g/cm^2/k.y. to over 4 g/cm^2/k.y. in the middle of the upper Miocene and then decrease to about 2 g/cm^2/k.y. in the uppermost Miocene and lower Pliocene (Fig. 54). From the lower Pliocene to the present, both carbonate and noncarbonate accumulation rates show variability around a long-term increase. The accumulation of organic carbon shows a similar pattern in the upper Miocene and lower Pliocene, but is highest in the upper Pliocene and decreases toward the present.

The high carbonate and carbon accumulation rates associated with the appearance of upwelling faunas clearly indicate that the monsoonal upwelling system was active in the late Miocene. However, other areas of the world ocean also have high accumulation rates in the late Miocene (Prell et al., 1982; Theyer et al., 1985). Thus, the question of global vs. regional causes of high productivity in the western Arabian Sea must be considered before the apparent upwelling phase of the late Miocene can be solely attributed to the relatively local monsoonal mechanism. Even so, the onset of monsoonal upwelling may occur in the middle Miocene; an interval that is largely missing at Site 721. The long-term increase in carbonate accumulation rates from the late Pliocene to the present may also reflect an increase in the intensity of monsoonal upwelling and eolian transport brought about by continued uplift of the Himalaya (Mercier et al., 1987). This long-term trend would be consistent with the gradual modification of surface boundary conditions due to tectonic mechanisms rather than with the short-term orbital, Milankovitch mechanism. The persistent continued abundance of upwelling faunas support this speculation, but the decrease in organic carbon accumulation raises questions about the variability of upwelling productivity. Alternatively, some of the intervals of low accumulation rate on the Owen Ridge may reflect changes in the depositional environment due to phases of local

Table 14. Concentrations of methane (C_1) and ethane (C_2) per liter of wet sediment in cores of Holes 721A and 721B. Also given is the ratio of C_1/C_2, an indicator of gas provenance and maturation state of organic matter.

Hole, core, section, interval (cm)	Depth (mbsf)	C_1 (μL/L)	C_2 (μL/L)	C_3 (μL/L)	C_1/C_2
117-					
721A-1H-6, 149–150	8.99	19			
721A-2H-6, 149–150	18.49	25			
721A-3H-6, 119–120	28.19	60			
721A-4H-5, 0–1	35.20	80			
721A-5H-4, 149–150	44.89	195			
721A-6H-6, 119–120	57.19	832			
721A-7H-6, 149–150	66.79	1488			
721A-8H-5, 149–150	74.79	2940	3		1131
721A-9H-6, 119–120	85.49	5421	6		847
721B-9H-4, 144–145	82.34	3766	3		1107
721B-10X-5, 149–150	93.49	4694	3		1618
721B-11X-3, 149–150	100.09	5280	5		
721B-12X-1, 144–145	106.64	4886			16286
721B-13X-4, 149–150	120.79	17625	3		5334
721B-14X-3, 149–150	128.89	19434	4		4983
721B-15X-6, 119–120	142.79	10138	3		3620
721B-16X-5, 149–150	151.29	35094	1		70188
721B-17X-5, 149–150	160.99	6426	5		1338
721B-18X-5, 119–120	170.39	35334	5		7852
721B-19X-5, 149–150	180.39	60006	5		12501
721B-20X-5, 149–150	190.09	98506	10		10261
721B-21X-2, 0–1	193.80	72608	5		16135
721B-22X-6, 0–1	209.50	74096	5		16466
721B-24X-3, 0–1	224.30	85872	5		17174
721B-25X-5, 0–1	236.50	96243	5		17823
721B-26X-3, 149–150	244.59	96960	6		16160
721B-27X-3, 119–120	253.99	111981	6		19307
721B-29X-2, 0–1	270.90	62406	4		15602
721B-30X-2, 114–115	281.84	83380	4		20845
721B-31X-3, 149–150	293.49	106544	4		23676
721B-32X-2, 149–150	301.69	89502	5		15983
721B-33X-1, 114–115	309.54	106584	7		14024
721B-34X-4, 0–1	322.50	94345	3		29483
721B-35X-2, 149–150	330.69	68718			
721B-36X-1, 114–115	338.54	119994	3		39998
721B-37X-3, 149–150	351.49	92963			
721B-40X-5, 114–115	383.04	126298			
721B-41X-5, 149–150	393.09	156886			
721B-42X-2, 149–150	398.19	125027			
721B-44X-5, 114–115	421.64	45767	2		20803

Note: Values are expressed in μL/L (volume gas/volume wet sediment).

uplift. In summary, the record at Site 721 gives ample evidence of large changes in productivity and upwelling-related faunas. The discrimination between regional vs. global causes, and the specific relationship between productivity and upwelling remain subjects for post-cruise research.

Short-term Variability and Sedimentary Cycles

The major characteristic of the Pliocene and Pleistocene sediments at Site 721 is a strong cyclicity that is documented by changes in sediment color, magnetic susceptibility, wet-bulk density, and carbonate content. If the intensity of monsoonal upwelling and eolian transport is controlled largely by variations of solar radiation, a strong cyclicity is expected in the sediments of the Owen Ridge. Preliminary analysis of over 20,000 magnetic susceptibility measurements in three holes reveal a dominant periodicity of about 1 m in length, which represents about 25 k.y. Other periodicities of about 1–2 m, 3–4 m, and 12–14 m suggest the presence of periodicities near 41 k.y., 100 k.y., and 400 k.y., respectively. These periodicities match those expected for the Milankovitch mechanism and suggest that it is a major cause of variations in monsoon intensity. A similar conclusion was reached by calculating the Walsh spectrum of sediment color changes that were classified as dark, medium, and light. Using a linear sedimentation rate over the past 2.95 m.y., we found the same periodicities that were observed in the magnetic susceptibility data. Here, we should note that these periodicities are not unique to the monsoon mechanism and that much post-cruise research is needed to identify the true monsoon spectrum. However, the sediment cycles are thought to reflect both changes in oceanic productivity/preservation and changes in the input of eolian material. Preliminary analysis of the mineralogy of the clastic fraction reveals that the concentrations of quartz and dolomite covary and are in phase with the susceptibility data. This association of minerals is consistent with an eolian source. The subject of the exact origin of the susceptibility cycles, which have been used for detailed cross-correlation between cores, and their significance with respect to monsoonal climate changes will be the major focus of the post-cruise research.

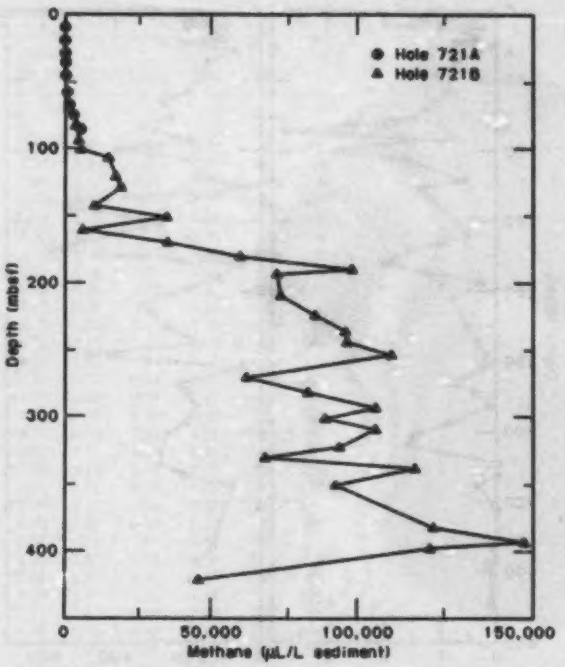

Figure 47. Downhole concentrations of methane in sediments from Holes 721A and 721B. The steep increase in concentrations below 100 mbsf coincides with the depletion of interstitial sulfate, which results in a predominance of fermentation reactions as the main mode of microbial organic matter degradation.

Table 15. Depth, organic carbon and $CaCO_3$ content, and U^k_{37} ratios of sediments from Hole 721B.

Core, section, interval (cm)	Depth (mbsf)	Organic carbon (%)	$CaCO_3$ (%)	U^k_{37}
117-721B-				
1H-1, 50–53	0.50	0.07	77.1	[a]n.k.
1H-2, 100–103	2.50	1.29	64.8	0.88
1H-4, 80–83	5.30	0.43	70.8	0.97
1H-5, 24–27	6.24	1.21	65.5	0.95
2H-1, 87–90	10.77	0.46	78.1	0.98
2H-2, 17–20	11.07	1.91	61.3	0.87
2H-3, 27–30	12.67	0.60	72.2	0.92
3H-3, 10–13	22.20	0.74	64.5	0.92

[a] n.k. = no ketones detected.

REFERENCES

Aubry, M.-P., 1984. *Handbook of Cenozoic Calcareous Nannoplankton, Book 1: Ortholithae (Discoasters)*: New York (Micropaleontology Press).

Bé, A.W.H., 1977. An ecological, zoogeographic and taxonomic review of Recent planktonic Foraminifera. *In* Ramsay, A. (Ed.), *Oceanic Micropalaeontology* (Vol. 1): London (Academic Press), 1-100.

Berggren, W. A., Kent, D. V., Flynn, J. J., and Van Couvering, J. A., 1985a. Cenozoic geochronology. *Geol. Soc. Am. Bull.*, 96:1407-1418.

Berggren, W. A., Kent, D. V., and Van Couvering, J. A., 1985b. The Neogene: Part 2, Neogene geochronology and chronostratigraphy. *In* Snelling, N. J. (Ed.), *The Chronology of the Geological Record*: Geol. Soc. Mem. (London), 10:211-260.

Brassell, S. C., Eglinton, G., Marlowe, I. T., Sarnthein, M., and Pflaumann, U., 1986. Molecular stratigraphy: a new tool for climatic assessment. *Nature*, 320:129-133.

Bryant, W. R., Bennett, R. H., and Katherman, C. E., 1981. Shear strength, consolidation, porosity, and permeability of oceanic sediments. *In* Emiliani, C. (Ed.), *The Oceanic Lithosphere*: *The Sea* (Vol. 7): New York (Wiley), 1555-1616.

Claypool, G. E., and Kaplan, I. R., 1974. The origin and distribution of methane in marine sediments. *In* Kaplan, I. R. (Ed.) *Natural Gases in Marine Sediments*: New York (Plenum), 94-129.

Corliss, B. H., 1979. Taxonomy of Recent deep-sea benthonic Foraminifera in the southeast Indian Ocean. *Micropaleontology*, 25:1-19.

Gardner, J. V., 1982. High-resolution carbonate and organic-carbon stratigraphies for the late Neogene and Quaternary from the eastern equatorial Pacific. *In* Prell, W. L., Gardner, J. V., et al., *Init. Repts. DSDP*, 68: Washington (U.S. Govt. Printing Office), 347-364.

Gieskes, J. M., 1981. Deep sea drilling interstitial water studies: implications for chemical alteration of the ocean crust, Layers I and II. *In* Warme, J. E., Douglas, R. C., and Winterer, E. L. (Eds.), *The Deep Sea Drilling Project: A Decade of Progress*, Soc. Econ. Paleontol. Mineral. Spec. Publ., 32:149-168.

Hahn, D. G., and Manabe, S., 1975. The role of mountains in the South Asian monsoon circulation. *J. Atmos. Sci.*, 32:1515-1541.

Hamilton, E. L., 1976. Variations of density and porosity with depth in deep-sea sediments. *J. Sediment. Petrol.*, 46:280-300.

________, 1978. Sound velocity-density relations in sea-floor sediments and rocks. *J. Acoust. Soc. Am.*, 63:366-377.

________, 1979. Sound velocity gradients in marine sediments. *J. Acoust. Soc. Am.*, 65:909-922.

Honjo, S., 1982. Seasonality and interaction of biogenic and lithogenic particulate flux at the Panama Basin. *Science*, 218:883-884.

Johnson, D. A., and Nigrini, C. A., 1985. Synchronous and time-transgressive Neogene radiolarian datum levels in the equatorial Indian and Pacific Oceans. *Mar. Micropaleontol.*, 9:489-523.

Johnson, D. A., Nigrini, C. A., Caulet, J.-P., Schneider, D., and Kent, D., in press. Pliocene-Pleistocene radiolarian events and magnetostratigraphic calibrations for the tropical Indian Ocean. *Mar. Micropaleontol.*

Kutzbach, J. E., 1981. Monsoon climate of the early Holocene: climate experiment with the earth's orbital parameters for 9000 years ago. *Science*, 214:59-61.

Mead, G. A., 1985. Recent benthic Foraminifera in the Polar Front region of the southwest Atlantic. *Micropaleontology*, 31:221-248.

Mercier, J.-T., Armijo, R., Tapponnier, P., Carey-Gailhardis, E., and Lin, H.T., 1987. Change from late Tertiary compression to Quaternary extension in Southern Tibet during the India-Asia collision. *Tectonics*, 6:275-304.

Mountain, G., and Prell, W. L., 1987. Leg 117 ODP site survey: a revised history of Owen Basin. *Eos, Trans. Am. Geophys. Union*, 68: 424.

Müller, P. J., and Suess, E., 1979. Productivity, sedimentation rate, and sedimentary organic matter in the oceans—I. Organic carbon preservation. *Deep-Sea Res.*, Part A, 26:1347-1362.

Nigrini, C. A., 1974. Cenozoic Radiolaria from the Arabian Sea, DSDP Leg 23. *In* Davies, T. A., Luyendyk, B. P., et al., *Init. Repts. DSDP*, 26: Washington (U. S. Govt. Printing Office), 1051-1121.

Perch-Nielsen, K., 1985. Cenozoic calcareous nannofossils. *In* Bolli, H., Saunders, J., and Perch-Nielsen, K. (Eds.), *Planktonic Stratigraphy*: Cambridge (Cambridge University Press), 427-554.

Pisias, N. G., and Prell, W. L., 1985. High resolution carbonate records from the hydraulic piston cored section of Site 572. *In* Mayer, L., Theyer, F., et al., *Init. Repts. DSDP*, 85: Washington (U.S. Govt. Printing Office), 711-722.

Prahl, F. G., and Wakeham, S. G., 1987. Calibration of unsaturation patterns in long-chain ketone compositions for paleotemperature assessment. *Nature*, 330:367-369.

Prell, W. L., 1984a. Variation of monsoonal upwelling: a response to changing solar radiation. *In* Hansen, J. E., and Takahashi, T. (Eds.), *Climatic Processes and Climate Sensitivity*: Washington (American Geophysical Union), Geophys. Monogr. 29, Maurice Ewing Series, 5:48-57.

________, 1984b. Monsoonal climate of the Arabian Sea during the late Quaternary: a response to changing solar radiation. *In* Berger, A., and Imbrie, J. (Eds.), *Milankovitch and Climate*: Dordrecht (D. Reidel), 349-366.

Prell, W. L., Gardner, J. V., et al., 1982. *Init. Repts. DSDP*, 68: Washington (U.S. Govt. Printing Office).

Prell, W. L., and Kutzbach, J. E., 1987. Monsoon variability over the past 150,000 years. *J. Geophys. Res.*, 92:8411-8425.

Saito, T., Burckle, L. H., and Hays, J. D., 1975. Late Miocene to Pleistocene biostratigraphy of equatorial Pacific sediments. *In* Saito, T., and Burckle L. H. (Eds.), *Late Neogene Epoch Boundaries*: New York (Micropaleontology Press), 226-244.

Sato, T., Takayama, T., Kato, M., Kudo, T., and Kameo, K., in press. Calcareous microfossil biostratigraphy of the uppermost Cenozoic formations distributed in the coast of the Japan Sea. Part 4: Conclusion. *Sekiyu Gijutsu Kyokaishi*.

Shipboard Scientific Party, 1988. Site 658. *In* Ruddiman, W., Sarntheim, M., et al., *Proc. ODP, Init. Repts.*, 108: College Station, TX (Ocean Drilling Program), 105-219.

Stumm, W., and Morgan, J. J., 1970. *Aquatic Chemistry*: New York (Wiley).

Takayama, T., and Sato, T., 1987. Coccolith biostratigraphy of the North Atlantic Ocean, Deep Sea Drilling Project Leg 94. *In* Ruddiman, W. E., Kidd, R. B., Thomas, E., et al., *Init. Repts. DSDP*, 94, Pt. 2: Washington (U.S. Govt. Printing Office), 651-702.

ten Haven, H. L., Baas, M., Kroot, M., de Leeuw, J. W., Schenck, P. A., and Ebbing, J., 1987. Late Quaternary Mediterranean sapropels: III. Assessment of source of input and palaeotemperature as derived from biological markers. *Geochim. Cosmochim. Acta*, 51: 803-810.

Theyer, F., Mayer, L. A., Barron, J. A., and Thomas, E., 1985. The equatorial Pacific high-productivity belt: elements for a synthesis of Deep Sea Drilling Project Leg 85 results. *In* Mayer, L., Theyer, F., et al., *Init. Repts. DSDP*, 85: Washington (U.S. Govt. Printing Office), 971-985.

van Morkhoven, F. P., Berggren, W. A., and Edwards, A. S., 1986. Cenozoic cosmopolitan deep-water benthic Foraminifera. *Bull. Cent. Rech. Explor.-Prod. Elf-Aquitaine, Mem.*, 11.

Weedon, G. P., 1986. Hemipelagic shelf sedimentation and climatic cycles: the basal Jurassic (Blue Lias) of South Britain. *Earth Planet. Sci. Lett.*, 76:321-325.

Whitmarsh, R. B., 1979. The Owen Basin off the southeast margin of Arabia and the evolution of the Owen Fracture Zone. *Geophys. J. R. Astron. Soc.*, 58:441-470.

Whitmarsh, R. B., Weser, O. E., Ross, D. A., et al., 1974. *Init. Repts. DSDP*, 23: Washington (U.S. Govt. Printing Office).

Ms 117A-106

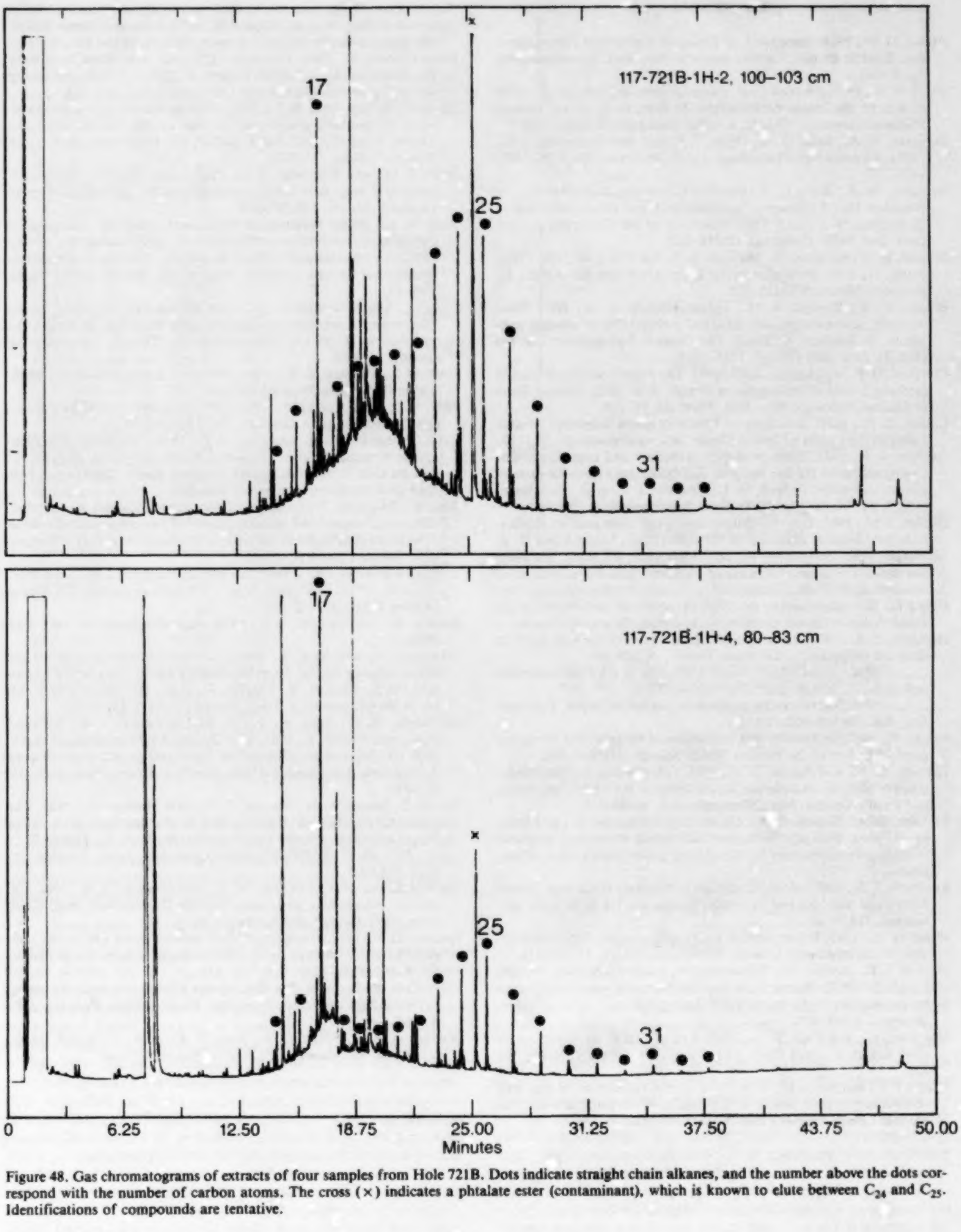

Figure 48. Gas chromatograms of extracts of four samples from Hole 721B. Dots indicate straight chain alkanes, and the number above the dots correspond with the number of carbon atoms. The cross (×) indicates a phtalate ester (contaminant), which is known to elute between C_{24} and C_{25}. Identifications of compounds are tentative.

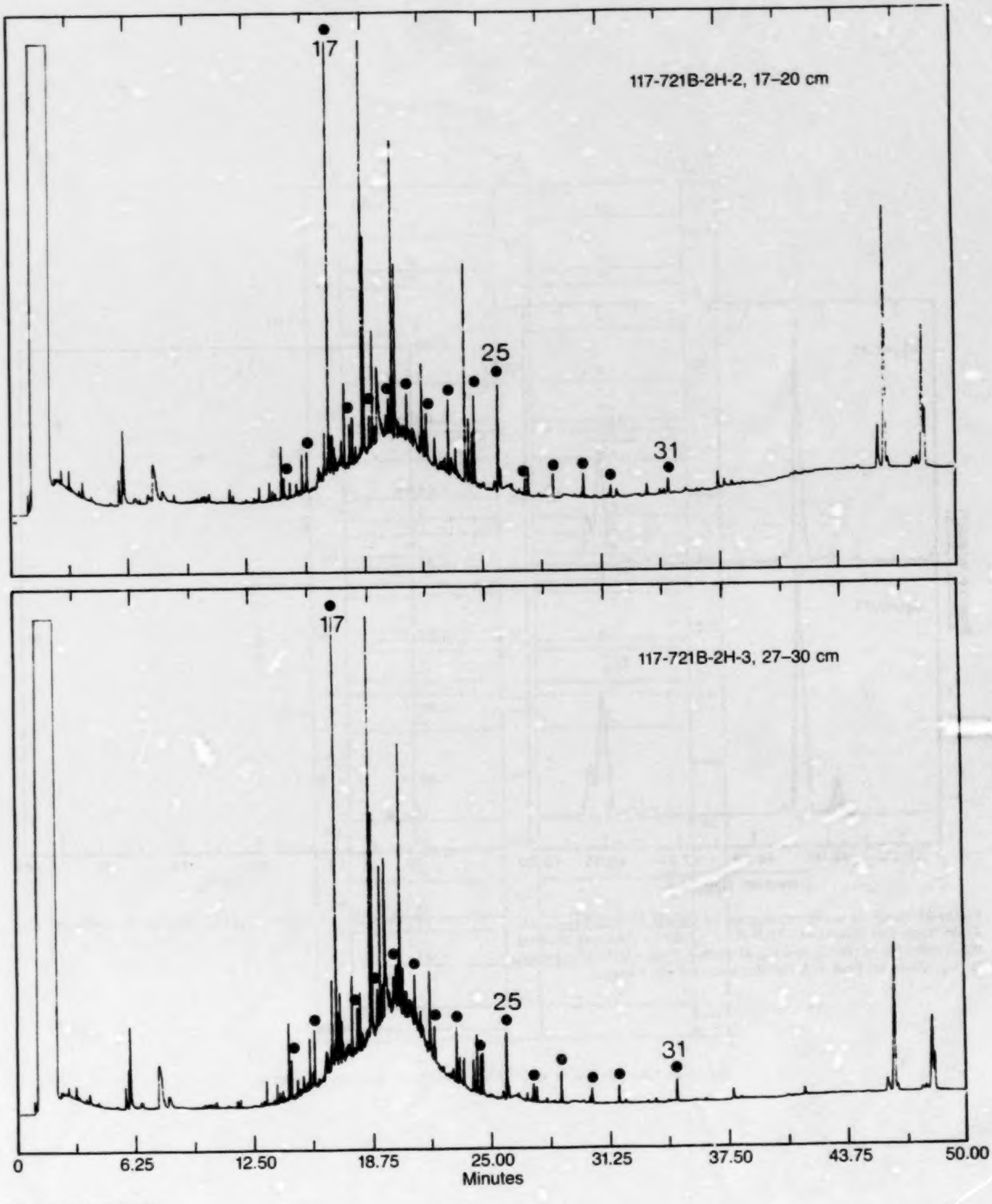

Figure 48 (continued).

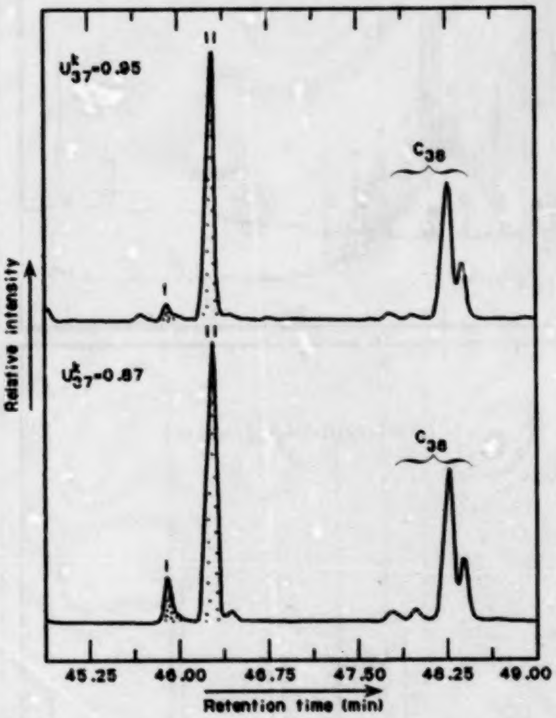

Figure 49. Detail of gas chromatogram of Sample 117-721B-1H-5, 24–27 cm (top), and Sample 117-721B-2H-2, 17–20 cm (bottom), showing the distribution of the C_{37} and C_{38} alkenones. Peak I is the triunsaturated C_{37} alkenone; Peak II is the diunsaturated C_{37} alkenone.

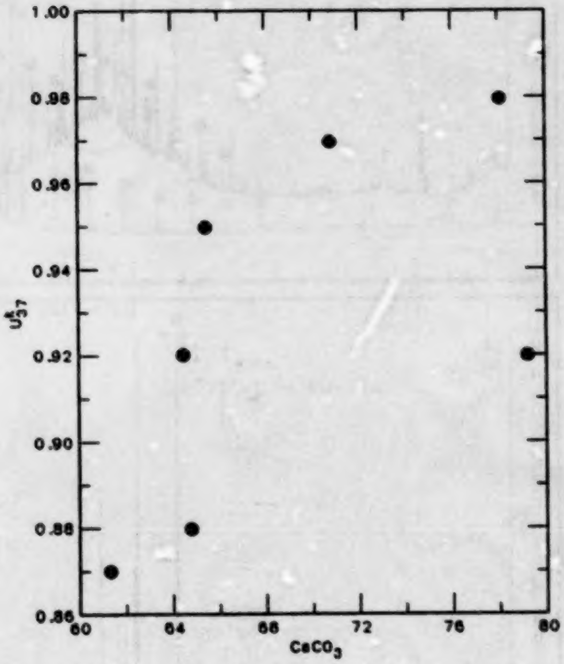

Figure 50. Crossplot of U^k_{37} vs. $CaCO_3$. Correlation coefficient r = 0.77.

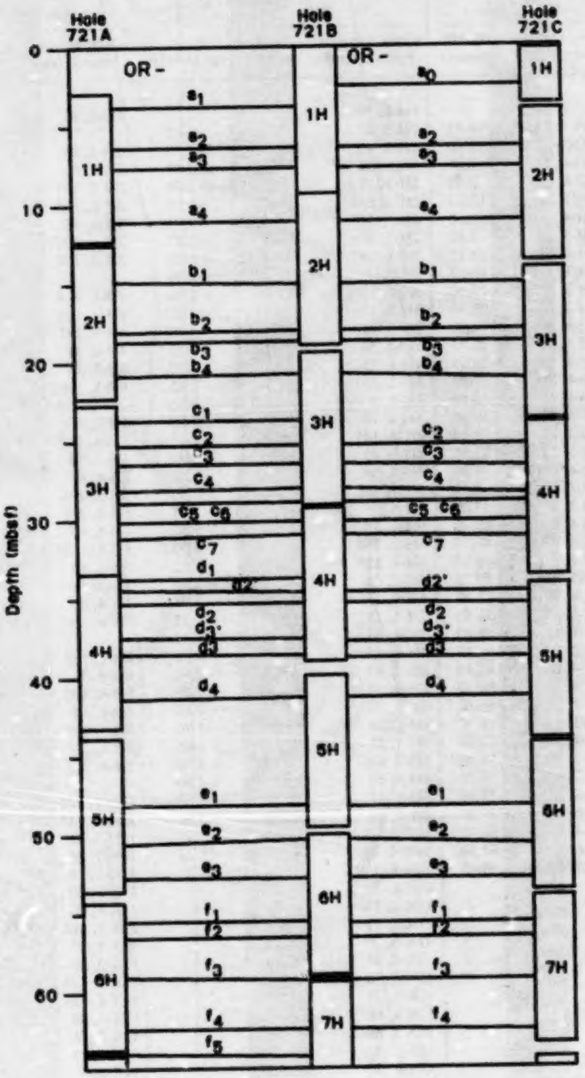
Hole 721A
Hole 721B
Hole 721C
Depth (mbsf)
0
10
20
30
40
50
60
OR -
OR -
1H
2H
3H
4H
5H
6H
7H
a0
a1
a2
a3
a4
b1
b2
b3
b4
c1
c2
c3
c4
c5
c6
c7
d1
d2'
d2
d3'
d3
d4
e1
e2
e3
f1
f2
f3
f4
f5

Figure 51. Correlation of Holes 721A, 721B, and 721C based on marker layers.

Table 16. Stratigraphic depths of the marker layers at Site 721.

	Hole 721A		Hole 721B			Hole 721C		
	Core, section, interval (cm)	Depth (mbsf)	Core, section, interval (cm)	Depth (mbsf)	Holes 721A–721B	Core, section, interval (cm)	Depth (mbsf)	Holes 721C–721B
117-721A-								
OR-a_0			1H-2, 105	2.55		1H-2, 95	2.45	−0.10
a_1	1H-1, 115	1.15	1H-3, 90	3.90	−2.75			
a_2	1H-3, 70	3.70	1H-5, 45	6.45	−2.75	2H-2, 95	6.05	−0.40
a_3	1H-4, 45	4.95	1H-6, 32	7.82	−2.87	2H-3, 65	7.25	−0.57
a_4	1H-6, 90	8.40	2H-2, 25	11.15	−2.75	2H-5, 105	10.65	−0.50
b_1	2H-2, 90	12.20	2H-4, 135	15.25	−3.05	3H-1, 100	14.30	−0.95
b_2	2H-4, 100	15.30	2H-6, 115	18.05	−2.75	3H-3, 95	17.25	−0.80
b_3	2H-5, 15	15.95	2H-7, 40	18.80	−2.85	3H-4, 20	18.00	−0.80
b_4	2H-6, 85	18.15	3H-1, 140	20.50	−2.35	3H-5, 100	20.30	−0.20
c_1	3H-1, 100	20.50	3H-3,130	23.40	−2.90			
c_2	3H-2, 100	22.00	3H-4, 130	24.90	−2.90	4H-1, 140	24.40	−0.50
c_3	3H-3, 80	23.30	3H-5, 105	26.15	−2.85	4H-2, 125	25.75	−0.40
c_4	3H-4, 90	24.90	3H-6, 110	27.70	−2.80	4H-3, 145	27.45	−0.25
c_5	3H-5, 25	25.75	3H-7, 50	28.60	−2.85	4H-4, 55	28.05	−0.55
c_6	3H-5, 135	26.85	4H-1, 75	29.55	−2.70	4H-5, 35	29.35	−0.20
c_7	3H-6, 85	27.85	4H-2, 20	30.50	−2.65	4H-5, 120	30.20	−0.30
d_1	4H-1, 40	29.60	4H-4, 0	33.30	−3.70			
$d_{2'}$	4H-1, 100	30.20	4H-4, 70	34.00	−3.80	5H-1, 50	33.20	−0.80
d_2	4H-2, 40	31.10	4H-4, 145	34.75	−3.65	5H-1, 130	34.00	−0.75
$d_{3'}$	4H-3, 105	33.25	4H-6, 85	37.15	−3.90	5H-3, 70	36.40	−0.75
d_3	4H-4, 60	34.30	4H-7, 30	38.10	−3.80	5H-4, 0	37.20	−0.90
d_4	4H-6, 45	37.15	5H-1, 125	39.75	−2.60	5H-5, 105	39.75	0.00
e_1	5H-3, 130	43.20	5H-6, 75	46.75	−3.55	6H-3, 110	46.50	−0.25
e_2	5H-5, 70	45.60	6H-1, 35	48.45	−2.85	6H-5, 60	49.00	−0.55
e_3	5H-6, 130	47.70	6H-2, 130	50.90	−3.20	6H-H 130	51.20	0.30
f_1	6H-1, 130	49.80	6H-4, 115	53.75	−3.95	7H-2, 15	53.65	−0.10
f_2	6H-2, 75	50.75	6H-5, 60	54.70	−3.95	7H-2, 110	54.60	−0.10
f_3	6H-4, 30	53.30	6H-7, 15	57.25	−3.95	7H-4, 80	57.30	0.05
f_4	6H-6, 60	56.60	7H-3, 45	60.85	−4.25	7H-6, 100	60.50	−0.35
f_5	6H-7, 70	58.20	7H-4, 65	62.55	−4.35			
g_1	7H-2, 25	59.55	7H-5, 45	63.85	−4.30	8H-1, 130	62.60	−1.25
g_2	7H-4, 65	62.95	8H-1, 85	67.75	−4.80	8H-4, 25	66.05	−1.70
g_3	7H-5, 30	64.10	8H-2, 50	68.90	−4.80	8H-4, 140	67.20	−1.70
g_4	7H-6, 50	65.80	8H-3, 70	70.60	−4.80	8H-6, 10	68.90	−1.70
h_1	8H-3, 140	71.70	8H-7, 50	76.40	−4.70	9H-4, 105	76.35	−0.05
h_2	8H-4, 50	72.30	9H-1, 35	76.75	−4.45	9H-5, 15	76.95	0.20
h_3	8H-5, 70	74.00	9H-2, 60	78.50	−4.50	9H-6, 25	78.55	0.05
h_4	8H-7, 50	76.80	9H-4, 40	81.30	−4.50			
i_1	9H-1, 45	77.25	9H-5, 45	82.85	−5.60	10H-1, 135	81.65	−1.20
i_2	9H-3, 40	80.20	9H-7, 40	85.80	−5.60	10H-3, 115	84.45	−1.35
i_*	9H-4, 140	82.70	10X-2, 50	88.00	−5.30	10H-5, 70	87.00	−1.00
i_3	9H-6, 100	85.30	10X-4, 25	90.75	−5.45	10H-7, 60	89.90	−0.85
i_4	9H-7, 65	86.45	10X-4, 120	91.70	−5.25	11X-1, 70	90.60	−1.10
i_5			10X-6, 75	94.25		11X-3, 40	93.30	−0.95
j_1			11X-1, 120	96.80		11X-4, 90	95.30	−1.50
j_2			11X-2, 130	98.40		11X-5, 100	96.90	−1.50
j_3			11X-3, 70	99.30		17X-1, 85	100.35	1.05
j_4			11X-4, 65	100.75		12X-2, 90	101.90	1.15
j_5			11X-5, 90	102.50		12X-3, 125	103.75	−1.25
k_1			12X-1, 55	105.75		12X-4, 130	105.30	−0.45
l_1			13X-1, 60	115.40		13X-1, 90	110.00	−5.40
l_2			13X-2, 60	116.90		13X-2, 55	111.15	−5.75
l_3			13X-4, 40	119.70		13X-4, 15	113.75	−5.95
l_4			13X-6, 30	122.30		14X-2,45	120.65	−1.65
m_1			14X-2, 115	127.05		14X-4, 40	123.60	−3.45
m_2			14X-3, 120	128.60		14X-5, 55	125.25	−3.35
m_3			14X-4, 70	129.60		15X-1, 60	128.90	−0.70
n_1			15X-1, 75	134.85		15X-4, 140	134.20	−0.65
n_2			15X-2, 135	136.95		15X-6, 45	136.25	−0.70
n_3			15X-3, 130	138.40				

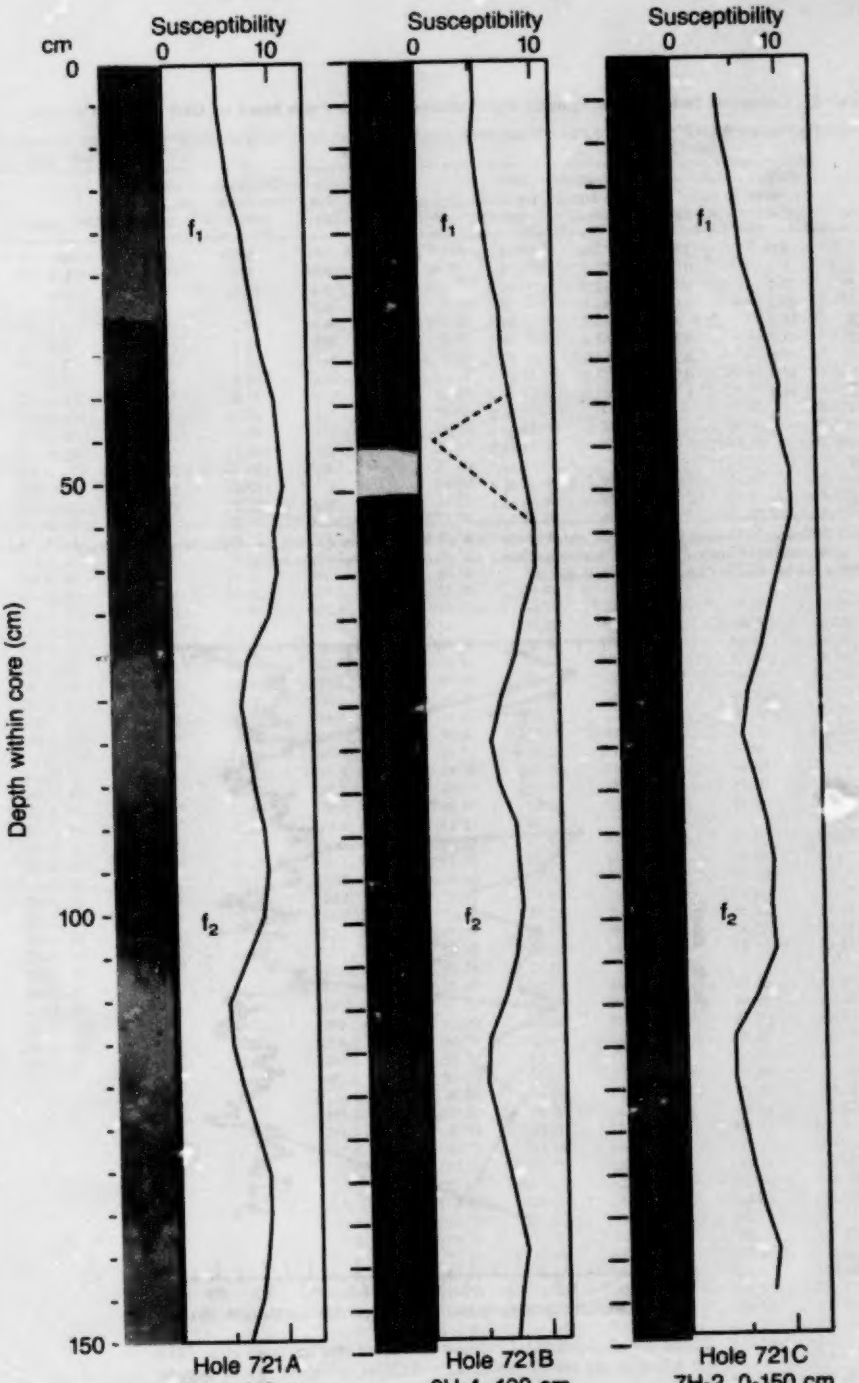

Figure 52. Example of the correlations by visual and magnetic susceptibility methods. The correlative interval corresponds to layer f_1 and f_2.

Table 17. Correction factor for stratigraphic depth calculation from depth based on ODP CORELOG data.

Core	Hole 721A ODP, top depth (mbsf)	Hole 721A Difference	Hole 721A Corrected top depth (mbsf)	Hole 721B ODP top depth (mbsf)	Hole 721B Difference	Hole 721B Offset (m)	Hole 721B Corrected top depth (mbsf)	Hole 721C ODP top depth (mbsf)	Hole 721C Difference	Hole 721C Corrected top depth (mbsf)
1	0.0	2.8	2.8	0.0	0.0		0.0	0.0	0.1	0.1
2	9.8	0.1	12.7	9.4	0.0	0.0	9.4	3.6	0.4	4.1
3	19.5	0.5	22.9	19.1	0.5	0.6	19.6	13.3	0.4	14.2
4	29.2	1.0	33.6	28.8	0.2	0.2	29.5	23.0	0.2	24.1
5	38.9	ᵃ1.0-0.3	44.0	38.5	ᵃ1.2-0.3	0.9	40.1	32.7	0.5	34.3
6	48.5	0.8	54.4	48.1	0.4	0.4	50.1	42.4	0.2	44.2
7	57.8	0.1	63.5	57.4	−0.3	−0.3	59.1	52.0	0.3	54.1
8	67.3	0.0	73.3	66.9	−0.5	−0.4	68.2	61.3	0.9	64.3
9	76.8	1.1	83.9	76.4	0.2	0.2	77.9	70.8	−1.7	72.1
10				86.0	0.3	0.3	87.8	80.3	1.5	83.1
11				95.6		−0.4	97.0	89.9	0.1	92.8
12				105.2		−1.7	104.9	99.5	−2.7	99.7
13				114.8		−5.7	109.1	109.1		109.1
14				124.4		−1.7	117.0	118.7	−4.0	114.7
15				134.1		0.0	126.7	128.3	−2.7	121.6

Note: Difference is between the depth calculated by the ODP CORELOG data and assigned depth, and depth calculated by the layer-by-layer correlation method. Offset = correction factor for stratigraphic depth calculation.

ᵃ Corrected for void at Core 721A-4H-5, 0–30 cm.

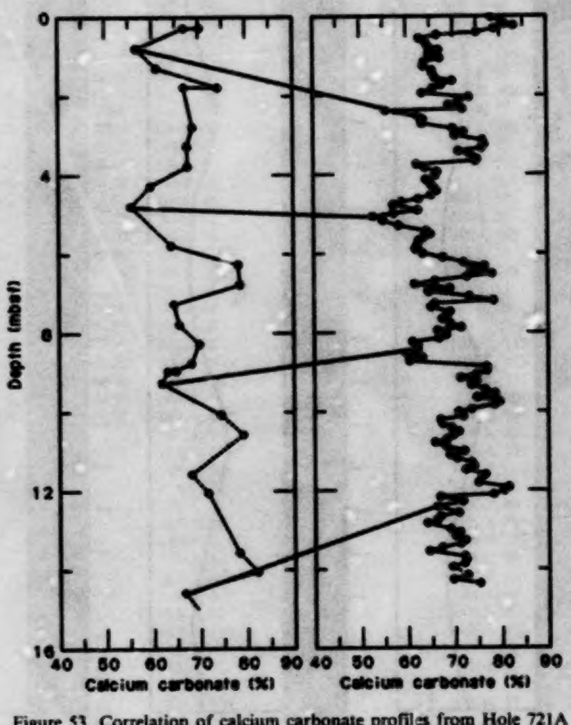

Figure 53. Correlation of calcium carbonate profiles from Hole 721A on left and site survey piston core RC2761 on right (Prell, unpubl. data).

Table 18. Depth of the marker layers in Hole 721B, based on the correction factor of Table 17. Depth based on ODP CORELOG data.

	Hole 721A			Hole 721B			Hole 721C		
	Core, section, interval (cm)	Curated depth (mbsf)	Corrected depth (m)	Core, section, interval (cm)	Curated depth (mbsf)	Corrected depth (m)	Core, section, interval (cm)	Curated depth (mbsf)	Corrected depth (m)
OR-a_0				1H-2, 105	2.55	2.55	1H-2, 95	2.45	2.55
a_1	1H-1, 115	1.15	3.95	1H-3, 90	3.90	3.90			
a_2	1H-3, 70	3.70	6.50	1H-5, 45	6.45	6.45	2H-2, 95	6.05	6.55
a_3	1H-4, 45	4.95	7.75	1H-6, 32	7.82	7.82	2H-3, 65	7.25	7.75
a_4	1H-6, 90	8.40	11.20	2H-2, 25	11.15	11.15	2H-5, 105	10.65	11.15
b_1	2H-2, 90	12.20	15.10	2H-4, 135	15.25	15.25	3H-1, 100	14.30	15.20
b_2	2H-4, 100	15.30	18.20	2H-6, 115	18.05	18.05	3H-3, 95	17.25	18.15
b_3	2H-5, 15	15.95	18.85	2H-7, 40	18.80	18.80	3H-4, 20	18.00	18.90
b_4	2H-6, 85	18.15	21.05	3H-1, 140	20.50	21.00	3H-5, 100	20.30	21.20
c_1	3H-1, 100	20.50	23.90	3H-3, 130	23.40	23.90			
c_2	3H-2, 100	22.00	25.40	3H-4, 130	24.90	25.40	4H-1, 140	24.40	25.50
c_3	3H-3, 80	23.30	26.70	3H-5, 105	26.15	26.65	4H-2, 125	25.75	26.85
c_4	3H-4, 90	24.90	28.30	3H-6, 110	27.70	28.20	4H-3, 145	27.45	28.55
c_5	3H-5, 25	25.75	29.15	3H-7, 50	28.60	29.10	4H-4, 55	28.05	29.15
c_6	3H-5, 135	26.85	30.25	4H-1, 75	29.55	30.25	4H-5, 35	29.35	30.45
c_7	3H-6, 85	27.85	31.25	4H-2, 20	30.50	31.20	4H-5, 120	30.20	31.30
d_1	4H-1, 40	29.60	34.00	4H-4, 0	33.30	34.00			
$d_{2'}$	4H-1, 100	30.20	34.60	4H-4, 70	34.00	34.70	5H-1, 50	33.20	34.80
d_2	4H-2, 40	31.10	35.50	4H-4, 145	34.75	35.45	5H-1, 130	34.00	35.60
$d_{3'}$	4H-3, 105	33.25	37.65	4H-6, 85	37.15	37.85	5H-3, 70	36.40	38.00
d_3	4H-4, 60	34.30	38.70	4H-7, 30	38.10	38.80	5H-4, 0	37.20	38.80
d_4	4H-6, 45	37.15	41.55	5H-1, 125	39.75	41.35	5H-5, 105	39.75	41.35
e_1	5H-3, 130	43.20	48.30	5H-6, 75	46.75	48.35	6H-3, 110	46.50	48.30
e_2	5H-5, 70	45.60	50.70	6H-1, 35	48.45	50.45	6H-5, 60	49.00	50.80
e_3	5H-6, 130	47.70	52.80	6H-2, 130	50.90	52.90	6H-6, 130	51.20	53.00
f_1	6H-1, 130	49.80	55.70	6H-4, 115	53.75	55.75	7H-2, 15	53.65	55.75
f_2	6H-2, 75	50.75	56.65	6H-5, 60	54.70	56.70	7H-2, 110	54.60	56.70
f_3	6H-4, 30	53.30	59.20	6H-7, 15	57.25	59.25	7H-4, 80	57.30	59.40
f_4	6H-6, 60	56.60	62.50	7H-3, 45	60.85	62.55	7H-6, 100	60.50	62.60
f_5	6H-7, 70	58.20	64.10	7H-4, 65	62.55	64.25			
g_1	7H-2, 25	59.55	65.55	7H-5, 45	63.85	65.55	8H-1, 130	62.60	65.60
g_2	7H-4, 65	62.95	68.95	8H-1, 85	67.75	69.05	8H-4, 25	66.05	69.05
g_3	7H-5, 30	64.10	70.10	8H-2, 50	68.90	70.20	8H-4, 140	67.20	70.20
g_4	7H-6, 50	65.80	71.80	8H-3, 70	70.60	71.90	8H-6, 10	68.90	71.90
h_1	8H-3, 140	71.70	77.70	8H-7, 50	76.40	77.70	9H-4, 105	76.35	77.65
h_2	8H-4, 50	72.30	78.30	9H-1, 35	76.75	78.25	9H-5, 15	76.95	78.25
h_3	8H-5, 70	74.00	80.00	9H-2, 60	78.50	80.00	9H-6, 25	78.55	79.85
h_4	8H-7, 50	76.80	82.80	9H-4, 40	81.30	82.80			
i_1	9H-1, 45	77.25	84.35	9H-5, 45	82.85	84.35	10H-1, 135	81.65	84.45
i_2	9H-3, 40	80.20	87.30	9H-7, 40	85.80	87.30	10H-3, 115	84.45	87.25
i*	9H-4, 140	82.70	89.80	10H-2, 50	88.00	89.80	10H-5, 70	87.00	89.80
i_3	9H-6, 100	85.30	92.40	10H-4, 25	90.75	92.55	10H-7, 60	89.90	92.70
i_4	9H-7, 65	86.45	93.55	10H-4, 120	91.70	93.50	11X-1, 70	90.60	93.50
i_5				10H-6, 75	94.25	96.05	11X-3, 40	93.30	96.20
j_1				11H-1, 120	96.80	98.20	11X-4, 90	95.30	98.20
j_2				11H-2, 130	98.40	99.80	11X-5, 100	96.90	99.80
j_3				11H-3, 70	99.30	100.70	12X-1, 85	100.35	100.55
j_4				11H-4, 65	100.75	102.15	12X-2, 90	101.90	102.10
j_5				11H-5, 90	102.50	103.90	12X-3, 125	103.75	103.95
k_1				12H-1, 55	105.75	105.45	12X-4, 130	105.30	105.50
l_1				13H-1, 60	115.40	109.70	13X-1, 90	110.00	110.00
l_2				13H-2, 60	116.90	111.20	13X-2, 55	111.15	111.15
l_3				13H-4, 40	119.70	114.00	13X-4, 15	113.75	113.75
l_4				13H-6, 30	122.30	116.90	14X-2, 45	120.65	116.65
m_1				14H-2, 115	127.05	119.65	14X-4, 40	123.60	119.60
m_2				14H-3, 120	128.60	121.20	14X-5, 55	125.25	121.25
m_3				14H-4, 70	129.60	122.20	15X-1, 60	128.90	122.20
n_1				15H-1, 75	134.85	127.45	15X-4, 140	134.20	127.50
n_2				15H-2, 135	136.95	129.55	15X-6, 45	136.25	129.55
n_3				15H-3, 130	138.40	131.00			

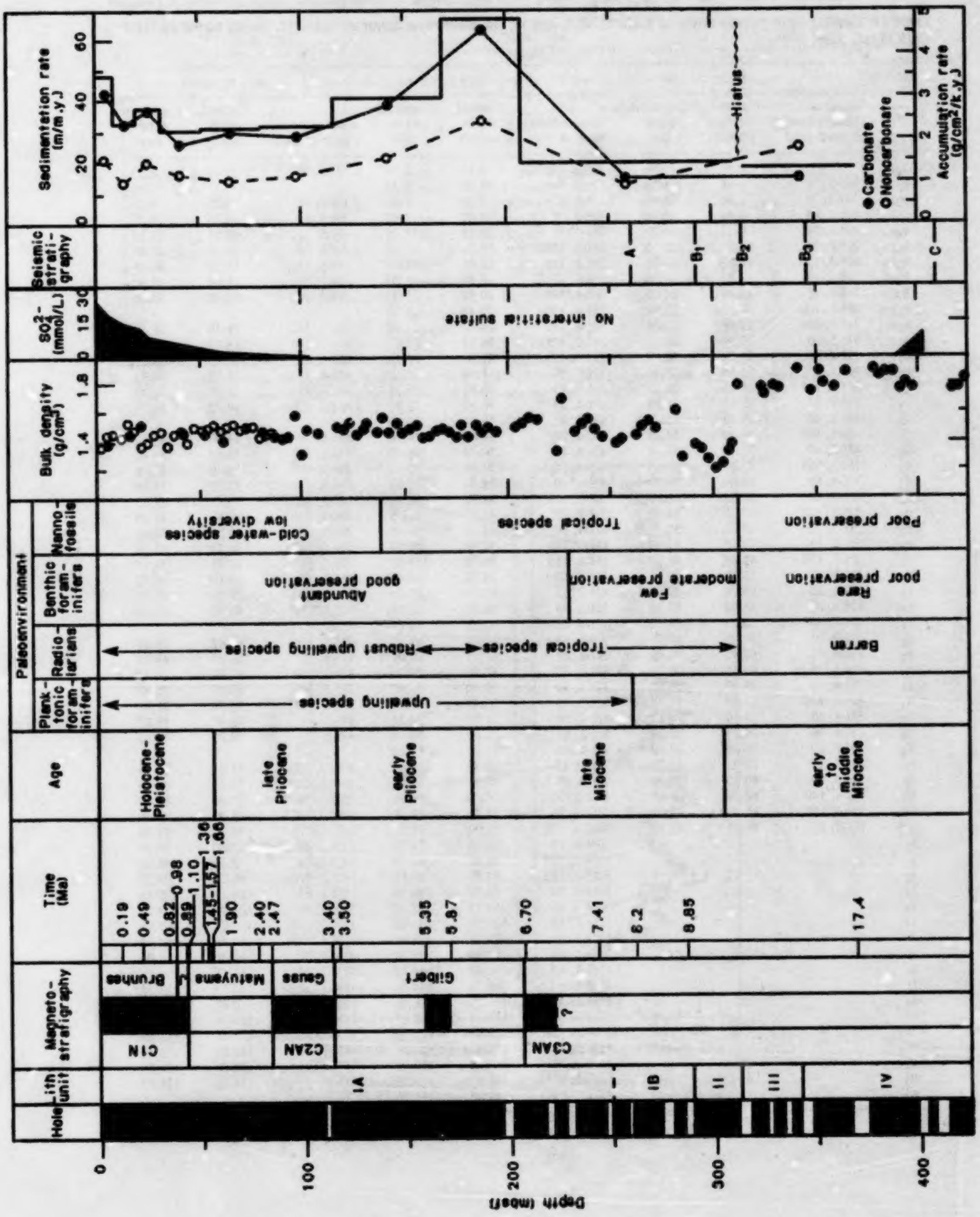

Figure 54. Summary chart outlining preliminary shipboard findings at Site 721.

10. SITE 722[1]

Shipboard Scientific Party[2]

HOLE 722A

Date occupied: 6 September 1987

Date departed: 8 September 1987

Time on hole: 37 hr

Position: 16°37.312'N, 59°47.755'E

Water depth (sea level; corrected m, echo-sounding): 2027.8

Water depth (rig floor; corrected m, echo-sounding): 2038.3

Bottom felt (m, drill pipe): 2034.0

Penetration (m): 280.0

Number of cores: 29

Total length of cored section (m): 280.0

Total core recovered (m): 225.96

Core recovery (%): 80.7

Oldest sediment cored:
Depth sub-bottom (m): 280.0
Nature: nannofossil ooze
Age: late Miocene
Measured velocity (km/s): 1.7

HOLE 722B

Date occupied: 8 September 1987

Date departed: 13 September 1987

Time on hole: 4 days, 23 hr

Position: 16°37.312'N, 59°47.755'E

Water depth (sea level; corrected m, echo-sounding): 2027.8

Water depth (rig floor; corrected m, echo-sounding): 2038.3

Bottom felt (m, drill pipe): 2033.2

Penetration (m): 565.6

Number of cores: 59

Total length of cored section (m): 565.6

Total core recovered (m): 385.9

Core recovery (%): 68.2

Oldest sediment cored:
Depth sub-bottom (m): 565.0
Nature: silty claystones
Age: early Miocene
Measured velocity (km/s): 2.21

Principal results: Site 722 is located in the Western Arabian Sea on the Owen Ridge and was drilled to recover a continuous upper Neogene sequence of pelagic sediments from an area of monsoonal upwelling.

The section penetrated at Site 722 ranges from early Miocene to Holocene in age and has been divided into four major lithologic units.

Unit I (0.0–221.5 mbsf) consists exclusively of alternating light and dark layers of foraminifer-bearing to foraminifer-nannofossil ooze and nannofossil ooze of Holocene to late Miocene age. Radiolarian and foraminiferal upwelling assemblages occur throughout this interval. The sediments of this unit reveal strong cyclicity that is indicated by changes in colors, bulk densities, carbonate content, and particularly well by magnetic susceptibility on whole-round cores. Sedimentation rates in lithologic Unit I range from 20 m/m.y. to about 45 m/m.y. and are lowest in the uppermost part of the upper Miocene and the lower Pliocene.

Unit II (221.5–343.4 mbsf) is composed of foraminifer-bearing, radiolarian-bearing, diatomaceous, and diatomaceous marly nannofossil chalks of late to middle Miocene age. Biogenic opal is an abundant component and its abundance is the major difference between lithologic Units I and II.

Unit III (343.4–411.1 mbsf) is primarily composed of white nannofossil chalk of middle Miocene age. Silica preservation is poor in the carbonate-rich chalks but increases dramatically at the boundary to lithologic Unit II in the uppermost part of the middle Miocene. The onset of silica preservation at this site coincides with the occurrence of upwelling faunas in the uppermost middle Miocene in Unit III.

Unit IV (411.1–565.6 mbsf) is early to middle Miocene in age. It is characterized by turbidite beds of silty clays capped by nannofossil chalks. The entire turbidite interval of early Miocene age becomes coarser downsection, where coarse basal layers with disseminated charcoal and pyrite are common in the silty clays. Preservation of planktonic calcareous and opaline tests is poor and the abundance of benthic foraminifers is low. The trend from turbiditic to increasingly pelagic deposition is related to the uplift of the Owen Ridge.

BACKGROUND AND OBJECTIVES

Site 722 is located near the crest of the Owen Ridge at 16°37.312'N and 59°47.755'E, at a water depth of 2028 m (Fig. 1). The site was selected at the intersection of two seismic lines collected on the site survey (RC2704). The site is located on Line 38 at 0745, 3 June 1986, and Line 1 at 2047, 19 May 1986 (Fig. 2).

Total sediment thickness (using Hamilton (1979) to convert two-way traveltime to thickness) at Site 722 is about 0.7 s (about 725 m) and the target depth is at 0.62 s (about 625 m). The upper part of the section (~290 mbsf) is characterized by relatively smooth, low-amplitude parallel reflectors that lie above a prominent but smooth reflector at 0.32 s (seismic reflector Owen Ridge A, OR-A). A second prominent reflector (Owen Ridge reflector B, OR-B) occurs at 0.53 s (about 520 mbsf). The interval between reflectors OR-A and OR-B is characterized by relatively flat lying, smooth, low-amplitude reflectors. The reflector sequence below OR-B has strongly dipping, high-amplitude reflectors lapping onto basement drape (reflectors conformable with acoustic basement) and an irregular surface thought to be a basement high. Correlation of the section at DSDP Site 224 with the seismic data from the site survey indicates that reflector OR-A is of late Miocene age and reflector OR-B is of middle to early Miocene age. The strongly reflective onlapping reflectors

---

[1] Prell, W. L., Niitsuma, N., et al., 1989. *Proc. ODP, Init. Repts.*, 117: College Station, TX (Ocean Drilling Program).

[2] Shipboard Scientific Party is as given in the list of Participants preceding the contents.

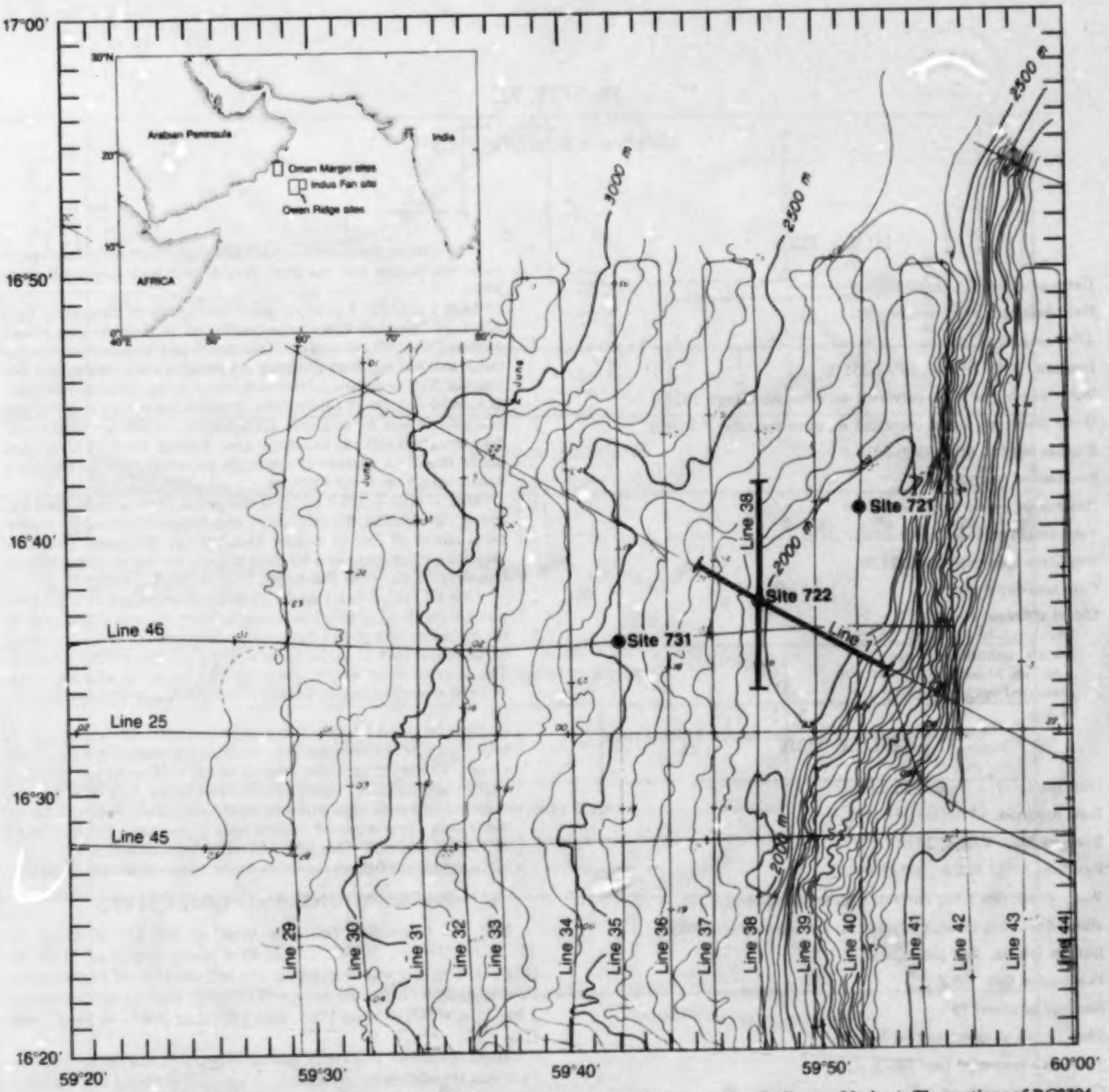
17°00'
16°50'
16°40'
16°30'
16°20'
59°20'
59°30'
59°40'
59°50'
60°00'
30°N
Arabian Peninsula
India
20°
Oman Margin sites
Indus Fan site
Owen Ridge sites
10°
AFRICA
40°E
50°
60°
70°
80°
3000 m
2500 m
2500 m
2000 m
2000 m
Site 721
Site 722
Site 731
Line 1
Line 38
Line 46
Line 25
Line 45
June
Line 29
Line 30
Line 31
Line 32
Line 33
Line 34
Line 35
Line 36
Line 37
Line 38
Line 39
Line 40
Line 41
Line 42
Line 43
Line 44

Figure 1. The location of Site 722 on the Owen Ridge. Bathymetry is from Sea Beam site survey data (Prell, unpubl. data). The portions of RC2704 seismic lines (Lines 1 and 38) (shown in Fig. 2) crossing Site 722 are indicated by the heavy lines.

of OR-B are thought to correlate to the detrital silts and claystones found in Site 224. The target depth in Site 722 is to penetrate these terrigenous sediments.

OPERATIONS

Moving the ship over 6 mi in dynamic positioning mode while tripping pipe, the rig relocated from Site 721 at 0230 on 07 September to the beacon dropped at Site 722 during the joint survey for Sites 721 and 722. The final position of Site 722 was established by Global Positioning System (GPS) as 16°37.312′N and 59°47.755′E. The first core was shot at 0455 in 2027.8 m water depth. For a plot of the ship's track during survey and positioning of the beacon, refer to "Operations" section, "Site 721" chapter (this volume).

Hole 722A was drilled by Advanced Piston Coring (APC) to Core 117-722A-9H (86.5 mbsf), when overpull rose to 50,000 pounds from previous 5,000 pounds and made deployment of the Extended Core Barrel (XCB) necessary. Cores 117-722A-5H to -9H were oriented. Recovery of the nine APC cores averaged 102%. Core 117-722A-29X was the last core to be cut in Hole 722A, which reached a total depth of 280.0 mbsf. Recovery in the XCB mode averaged 71%, so that overall recovery rate in Hole 722A averages 80.7%. The hole was terminated at this depth because the *in-situ* Pore-Water Sampler (PWS) became stuck in the flapper valve. The string had to be pulled up to retrieve the PWS and upon inspection of the Bottom-hole Assembly (BHA) the tool was found to be stuck at a flapper connection and was recovered on the rig floor. The ship offset 20 m to

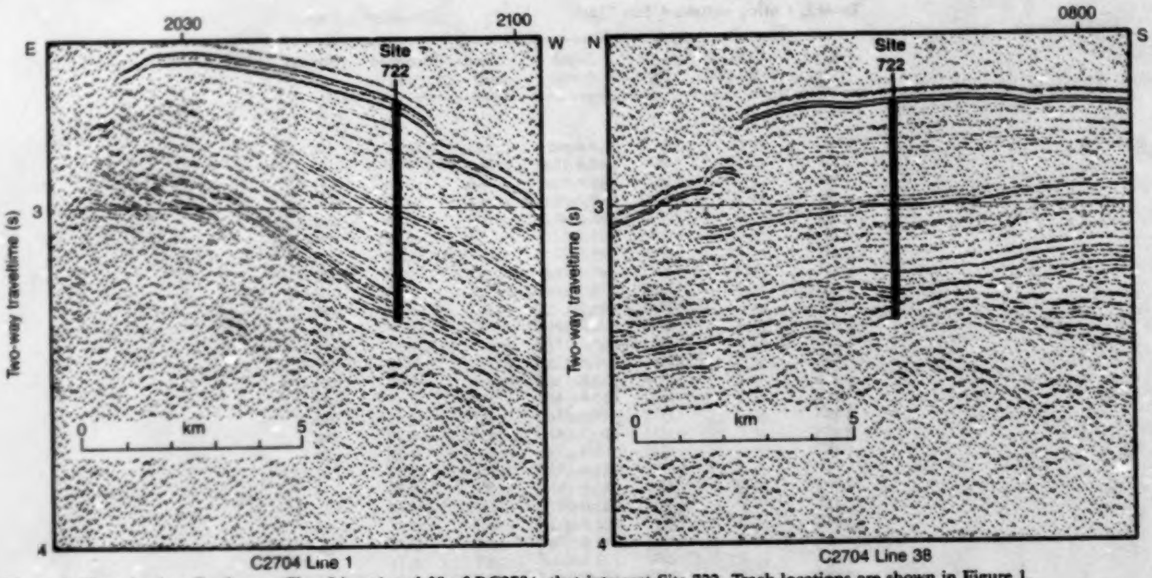

Figure 2. The seismic reflection profiles, Lines 1 and 38 of RC2704, that intersect Site 722. Track locations are shown in Figure 1.

the northwest, where Hole 722B was spudded at 1615 hr on 8 September.

In order to obtain the mud line and to overlap the cores of Holes 722A and 722B, the bit was positioned 5 m above the mud line when Core 117-722B-1H was shot. Ten APC cores with an average recovery of 103% were drilled to 91.9 mbsf, below which 25,000 pounds of overpull in Core 117-722B-10H made continuation by XCB necessary. Oriented cores were taken from Core 117-722B-7H to -10H. Total depth of 565.6 mbsf was reached with Core 117-722B-59X on 11 September (Table 1). The average recovery of XCB system was 61% and varied widely in response to variable lithology and sediment lithification. Overall recovery for Hole 722B was 68.3%.

Wiper trips to total depth and sweeping with polymer conditioned the hole for logging with the sidewall entry sub to facilitate removal of potential bridges. After two runs with the shifting tool to release the bit, the BHA was positioned 94.3 mbsf at the bottom of the section excellently recovered by APC. A string consisting of sonic, gamma ray, resistivity, and caliper tools was deployed first and obtained a good log from approximately 555.5 mbsf to the BHA at 94.3 mbsf in the first run. A second string with LD, CNL, and NGT tools was disabled by a short in the cable head, repaired, and deployed a second time. The run failed due to a defect in the swivel head of the tool, and it was decided to log without the SES after the hole conditions were established by running the pipe to the bottom of the hole. The third deployment of the second logging string was successful, and good logs were obtained from 71.4 mbsf to 550.9 mbsf (14 m above total depth).

Upon retrieval of the second logging string, the bowspring of the tool became stuck at the end of the BHA. 8,000 pounds of pull on the logging line failed to free the tool and a crimping tool was pumped down to crimp the logging line and subsequently cut it with a Kinley cutter. In order to be able to reenter the hole if the crimper had failed to hold the tool, a minicone was deployed before the drill string was pulled. The tool was found stuck in the BHA upon retrieval to the drill floor.

The ship was underway to Masirah Island at 1130 on 13 September to pick up two Omani shipboard participants before proceeding to the next target, Site 723 on the Oman margin.

LITHOSTRATIGRAPHY

Lithologic Units

Sediments recovered from Site 722 range from early Miocene to Holocene in age. The lithologies consist of nannofossil oozes and chalks, and fine-grained turbidites interbedded with nannofossil chalks. Site 722 sediments are divided into four lithologic units based on visual core descriptions, smear slide analysis, and calcium carbonate content (Table 2, Fig. 3). The lithologies at Site 722 are identical to those at Site 721, though Site 721 contains a hiatus between lithologic Units II and III. Thus, lithologic Units II and III are 100 and 40 m thicker, respectively, at Site 722 compared to Site 721. Further, lithologic Unit I at Site 721 contains disturbed (slumped) sediments which are not present at Site 722 (see "Lithostratigraphy" section, "Site 721" chapter, this volume).

Unit I (Depth: Hole 722A, 0–221.5 mbsf; Hole 722B, 0–221.5 mbsf; Age: Holocene to late Miocene)

Core 117-722A-1H to Section 117-722A-23X, CC, 2 cm; Core 117-722B-1H to Section 117-722B-24X-1, 72 cm.

Lithologic Unit I consists of alternating light and dark beds of foraminifer-bearing nannofossil ooze, nannofossil ooze/chalk, and marly nannofossil ooze/chalk. The beds range in thickness from 0.05 to 1.00 m. Bioturbation is minor to moderate throughout the unit; occasional pyrite-lined burrows were noted. Contacts between beds are generally gradational and mottled by burrows (Fig. 4). Light beds range in color from gray (5Y 6/1) to light olive gray (5Y 6/2), light gray (5Y 7/1, 7/2), and light greenish gray (5GY 7/1, 10Y 6/2). Darker beds range from pale olive (5Y 6/3) to olive gray (5Y 5/2), olive (5Y 4/3, 4/4, 5/3), and dark olive gray (5Y 3/2). Dark beds contain 10%–20% more silty clay than do the light beds. The average calcium carbonate content for this unit is 70%, ranging from 50% to 89% (Table 3, Fig. 5). The higher calcium carbonate values correspond to the lighter color beds.

Smear slide analysis indicates that nannofossils are the dominant sediment component throughout lithologic Unit I. Foraminifers range from 5% to 25% in the first four cores (roughly

Table 1. Coring summary, Site 722.

Core no.	Date (Sept. 1987)	Time	Depth (mbsf)	Cored (m)	Recovered (m)	Recovery (%)
117-722A-						
1H	7	0455	0.0-9.8	9.8	9.87	101.0
2H	7	0545	9.8-19.4	9.6	9.70	101.0
3H	7	0625	19.4-29.0	9.6	9.76	101.0
4H	7	0700	29.0-38.6	9.6	9.73	101.0
5H	7	0800	38.6-48.2	9.6	9.79	102.0
6H	7	0845	48.2-57.5	9.3	10.00	107.5
7H	7	0930	57.5-67.2	9.7	10.00	103.1
8H	7	1015	67.2-76.8	9.6	9.92	103.0
9H	7	1105	76.8-86.5	9.7	9.83	101.0
10X	7	1255	86.5-96.2	9.7	7.83	80.7
11X	7	1340	96.2-105.9	9.7	9.55	98.4
12X	7	1425	105.9-115.6	9.7	8.55	88.1
13X	7	1515	115.6-125.3	9.7	9.50	97.9
14X	7	1555	125.3-134.9	9.6	6.57	68.4
15X	7	1630	134.9-144.6	9.7	9.53	98.2
16X	7	1710	144.6-154.3	9.7	9.62	99.2
17X	7	1755	154.3-163.9	9.6	4.70	48.9
18X	7	1840	163.9-173.6	9.7	7.79	80.3
19X	7	1920	173.6-183.3	9.7	9.42	97.1
20X	7	2000	183.3-193.0	9.7	7.76	80.0
21X	7	2035	193.0-202.7	9.7	4.66	48.0
22X	7	2115	202.7-212.4	9.7	9.41	97.0
23X	7	2155	212.4-222.0	9.6	9.88	103.0
24X	7	2230	222.0-231.7	9.7	9.73	100.0
25X	7	2310	231.7-241.7	10.0	1.58	15.8
26X	7	2340	241.7-251.0	9.3	1.32	14.2
27X	8	0055	251.0-260.7	9.7	5.84	60.2
28X	8	0220	260.7-270.4	9.7	0.52	5.4
29X	8	0340	270.4-280.0	9.6	3.60	37.5
				280.0	225.96	
117-722B-						
1H	8	1700	0.0-5.5	5.5	5.53	100.0
2H	8	1730	5.5-15.1	9.6	9.56	99.6
3H	8	1810	15.1-24.7	9.6	10.08	105.0
4H	8	1840	24.7-34.3	9.6	9.89	103.0
5H	8	1910	34.3-43.9	9.6	9.79	102.0
6H	8	1950	43.9-53.2	9.3	9.94	107.0
7H	8	2025	53.2-62.9	9.7	10.10	104.1
8H	8	2100	62.9-72.5	9.6	9.84	102.5
9H	8	2155	72.5-82.2	9.7	10.04	103.5
10H	8	2235	82.7-91.9	9.2	10.05	109.2
11X	8	2325	91.9-101.5	9.6	6.06	63.1
12X	9	0005	101.5-111.2	9.7	4.59	47.3
13X	9	0045	111.2-120.9	9.7	4.44	45.8

0–40 mbsf), thereafter comprising from 0% to 5% of the sediment. Siliceous tests are present only in trace amounts within lithologic Unit I. Clays and inorganic calcite constitute the major terrigenous components. Clays range from 10% to 30%; the largest concentrations are found in the marly nannofossil oozes (darker beds) of cores 117-722A-6H to 117-722A-11X (roughly 45–100 mbsf). Inorganic calcite is found in amounts ranging from 5% to 10%. Other minerals (usually less than 5% of the sediment) include quartz, feldspar, mica, opaque minerals (pyrite?), and dolomite. Volcanic glass is also present in trace amounts.

Unit II (Depth: Hole 722A, 221.5–280.0 mbsf; Hole 722B, 221.5–343.4 mbsf; Age: late Miocene to middle Miocene)

Section 117-722A-23X-CC, 2 cm, to Section 117-722A-29X, CC, 12 cm; Section 117-722B-24X-1, 72 cm, to Section 117-722B-36X, CC, 45 cm.

Lithologic Unit II consists of alternating light and dark beds of nannofossil chalks, foraminifer-bearing nannofossil chalks, diatom-nannofossil chalks, radiolarian-bearing diatom-nannofossil chalks, and diatom-marly nannofossil chalks. Bioturbation is minor to moderate throughout the unit. Lighter beds range from white (10Y 8/1, 5Y 8/1) to light olive gray (5Y 6/2), light gray (5Y 7/1, 7/2), light greenish gray (10Y 7/1, 7/2), and gray (5Y 6/1). Darker beds range from pale olive (5Y 6/3) to olive gray (5Y 5/2, 4/2), olive (5Y 5/3, 5/4), dark greenish gray (10Y 5/2), and dark olive gray (5Y 3/2).

The major difference between lithologic Units I and II is the presence of diatoms and radiolarians in the darker beds of Unit II. Smear slide analysis indicates that the biogenic silica content (primarily diatoms) gradually increases with depth, from trace amounts at the bottom of lithologic Unit I to a maximum (as much as 20%) in Cores 117-722B-27X to -35X (roughly 245–330 mbsf). The biogenic silica content declines sharply to 0% at the top of lithologic Unit III. The gradual increase in silica downsection in lithologic Unit II is also evident in the down-hole logs (see "Downhole Measurements" section, this chapter). The overall increase in biogenic silica in this unit is coincident with a decrease in the average calcium carbonate content from 70% in lithologic Unit I to 51% in lithologic Unit II (Table 3, Fig. 5).

The increase in biogenic silica in lithologic Unit II is further indicated by low grain density and bulk density and high porosity and water content values (see "Physical Properties" section, this chapter). Lithologic Unit II also contains en echelon, subvertical dewatering(?) structures (Fig. 6). These structures are coeval with the slump features and missing section in nearby Site 721 and may be genetically related. Similar structures were

Table 1 (continued).

Core no.	Date (Sept. 1987)	Time	Depth (mbsf)	Cored (m)	Recovered (m)	Recovery (%)
117-722B-						
14X	9	0120	120.9–130.5	9.6	9.52	99.1
15X	9	0155	130.5–140.2	9.7	1.76	18.1
16X	9	0230	140.2–149.9	9.7	9.48	97.7
17X	9	0300	149.9–159.5	9.6	9.59	99.9
18X	9	0340	159.5–169.2	9.7	9.75	100.0
19X	9	0415	169.2–178.9	9.7	7.92	81.6
20X	9	0455	178.9–188.5	9.6	4.23	44.0
21X	9	0530	188.5–198.2	9.7	5.74	59.2
22X	9	0605	198.2–207.9	9.7	9.18	94.6
23X	9	0645	207.9–217.5	9.6	7.88	82.1
24X	9	0725	217.5–227.2	9.7	9.72	100.0
25X	9	0810	227.2–236.9	9.7	9.49	97.8
26X	9	0840	236.9–246.5	9.6	9.34	97.3
27X	9	0920	246.5–256.2	9.7	9.76	100.0
28X	9	1025	256.2–265.9	9.7	3.21	33.1
29X	9	1130	265.9–275.6	9.7	9.59	98.8
30X	9	1230	275.6–285.3	9.7	2.21	22.8
31X	9	1330	285.3–295.0	9.7	9.28	95.7
32X	9	1440	295.0–304.7	9.7	6.52	67.2
33X	9	1545	304.7–314.3	9.6	5.00	52.1
34X	9	1650	314.3–324.0	9.7	5.70	58.7
35X	9	1800	324.0–333.7	9.7	9.93	102.0
36X	9	1900	333.7–343.4	9.7	5.91	60.9
37X	9	2005	343.4–353.1	9.7	9.74	100.0
38X	9	2110	353.1–362.8	9.7	9.38	96.7
39X	10	0000	362.8–372.5	9.7	3.00	30.9
40X	10	0215	372.5–382.2	9.7	3.70	38.1
41X	10	0400	382.2–391.8	9.6	2.37	24.7
42X	10	0615	391.8–401.4	9.6	5.31	55.3
43X	10	0830	401.4–411.1	9.7	3.65	37.6
44X	10	1050	411.1–420.8	9.7	7.67	79.1
45X	10	1250	420.8–430.5	9.7	9.76	100.0
46X	10	1430	430.5–440.2	9.7	9.94	102.0
47X	10	1555	440.2–449.8	9.6	0.00	0.0
48X	10	1705	449.8–459.4	9.6	1.13	11.8
49X	10	1845	459.4–469.0	9.6	6.43	67.0
50X	10	2005	469.0–478.6	9.6	6.21	64.7
51X	10	2130	478.6–488.2	9.6	1.36	14.1
52X	10	2305	488.2–497.9	9.7	9.88	102.0
53X	11	0030	497.9–507.6	9.7	1.22	12.6
54X	11	0140	507.6–517.2	9.6	0.92	9.6
55X	11	0340	517.2–526.9	9.7	0.66	6.8
56X	11	0540	526.9–536.6	9.7	0.34	3.5
57X	11	0745	536.6–546.2	9.6	1.56	16.3
58X	11	1005	546.2–555.9	9.7	9.92	102.0
59X	11	1316	555.9–565.6	9.7	1.14	11.7
				565.6	385.91	

previously observed in opal-rich sediments at Site 681 off Peru and were attributed to volume loss due to conversion from opal A to opal CT (Suess, von Huene, et al., 1988). Additional characteristic features of sediments in this unit are concentric purple alteration halos around burrows (Fig. 7).

Unit III (Depth: 343.3–411.1 mbsf; Age: middle Miocene)

Section 117-722B-36X-CC, 45 cm, to Section 117-722B-43X, CC, 20 cm.

Lithologic Unit III consists of alternating light and dark beds of nannofossil chalks, foraminifer-bearing nannofossil chalks, and marly nannofossil chalks. Bioturbation is minor to moderate throughout the unit. The bed thickness ranges from 0.05 to 1.00 m. Light beds dominate and range in color from white (5Y 8/1, 2.5Y 8/1, N8/) to light gray (5Y 7/1, N7/), light greenish gray (10Y 7/1, 6/1, 6/2, 5G 7/1, 5BG 7/1), light olive gray (5Y 6/2), and gray (5Y 5/1, 6/1). Darker layers are olive gray (5Y 5/2, 4/2). The calcium carbonate content in lithologic Unit III ranges from 41% to 92% (Table 3, Fig. 5). Biogenic silica is found only in trace amounts in lithologic Unit III. Compared to lithologic Units I and II, lithologic Unit III sediments show a sharp increase in magnetic susceptibility and bulk density and a decrease in porosity and water content (see "Paleomagnetism" and "Physical Properties" sections, this chapter). The differences in the physical properties between lithologic Units II and III account for the well-developed seismic reflector correlated to the white chalks (Cores 117-722B-41X to -43X; 382–411 mbsf) in the lower half of lithologic Unit III (see "Seismic Stratigraphy" section, this chapter).

Unit IV (Depth: 411.1–565.6 mbsf; Age: middle Miocene to early Miocene)

Section 117-722B-43X, CC, 20 cm, to Section 117-722B-59X, CC, 25 cm.

The upper 87 m of lithologic Unit IV (roughly 410–497 mbsf) consists of interbedded greenish gray (5G 6/1, 5/1) silty claystones and nannofossil/marly nannofossil chalks (Fig. 8). The silty claystones contain millimeter- to centimeter-scale parallel laminae, have sharp basal contacts, and fine upward into the nannofossil chalks, forming repeated fine-grained turbidite sequences (20–50 cm thick) capped by gray and olive gray bioturbated nannofossil chalks. The silty clay intervals occasionally

Table 2. Lithologic summary, for Site 722.

	Lithologic unit	Depth (mbsf)	Cores	Age	$CaCO_3$ ($\bar{X}$ %)
I	Foraminifer-bearing nannofossil ooze and nannofossil and marly nannofossil ooze/chalk; alternating light and dark beds	0.0–221.5 0.0–221.5	722A-1H to -23X-CC, 2 cm 722B-1H to -24X-1, 72 cm	Holocene–late Miocene	70
II	Foraminifer-bearing nannofossil, nannofossil, diatomaceous-nannofossil, radiolarian-bearing diatomaceous nannofossil, and diatomaceous-marly nannofossil chalks; alternating light and dark beds	221.5–280.0 221.5–343.4	722A-23X-CC, 2 cm to -29X-CC, 12 cm 722B-24X-1, 72 cm to -36X-CC, 45 cm	late Miocene–middle Miocene	51
III	Nannofossil, foraminifer-bearing nannofossil, and marly nannofossil chalks	343.4–411.1	722B-36X-1, 45 cm to -43X-CC, 20 cm	middle Miocene	64
IV	Interbedded fine-grained turbidites and marly nannofossil chalk	411.1–565.6	722B-43X-CC, 20 cm to -59X-CC, 25 cm	middle Miocene–early Miocene	12

contain millimeter- to centimeter-scale charcoal-rich bands (Fig. 8, 84–85 cm), pyrite-rich bands, and biogenic carbonate turbidites. The nannofossil chalks and marly nannofossil chalks range in color from light gray (5Y 7/1, 10YR 7/2) to gray (5Y 6/1), greenish gray (5Y 5/1), olive gray (5Y 5/2, 4/3, 4/2), olive (5Y 6/2), yellowish brown (10YR 5/4), light brownish gray (10YR 6/2), pale brown (10YR 6/3), brown (10YR 5/3), and dark grayish brown (10YR 4/3). Smear slide analysis indicates little compositional difference between the nannofossil chalks found in lithologic Units I and III and those found in lithologic Unit IV. However, the nannofossil chalks found in lithologic Unit IV contain darker beds and are low in calcium carbonate content (Table 3, Fig. 5). No nannofossil chalks were recovered below Core 117-722B-52X (497.9 mbsf). Recovery was very poor (22%) below 497.9 mbsf; sediments recovered below this depth consist of micaceous sands, sandstones, and silty claystones which appear to be interbedded and fine upward into claystones (Core 117-722B-59X).

The basal turbidite layers of lithologic Unit IV coarsen from silty clay (Core 117-722B-44X) to clayey sand (Core 117-722B-52X), while the upper nannofossil chalks are replaced by silty clays (Cores 117-722B-53X to -58X) and clays (Cores 117-722B-58X to -59X) downhole. Based on our limited recovery, the overall trend for lithologic Unit IV is a downsection coarsening of basal layers and fining of upper layers within individual turbidites.

Discussion

The basal (coarsest) layers of the early to middle Miocene turbidite sequences (Unit IV) fine upsection from micaceous sands to silty clays, reflecting the early Miocene tectonic uplift of the Owen Ridge (Whitmarsh, 1974). This change may have occurred as the uplift of the Owen Ridge moved Site 722 above the level of turbidite bed-load (sand) deposition, allowing only the suspended portions of turbidity flows to reach the site. The upper layers of the turbidites, however, coarsen upsection from clay to silty clay through the early Miocene.

The coarsening-upward trend of the fine-grained turbidite tops requires either a coarsening of the suspended load of the individual turbidity flows or a change in the turbidite source during the early Miocene, possibly coincident with initial stages of Owen Ridge uplift. The two most likely terrigenous turbidite sources for Site 722 during the early Miocene were the Oman margin and the Indus Fan. The extent to which each actively supplied sediment to Site 722 was influenced by the history of glacio-eustatic sea-level fluctuations, the uplift history of the Owen Ridge, and, in the case of the Indus Fan, the history of channel migrations. Initial X-ray diffraction (XRD) investigations indicate that the Indus Fan is more likely to be the primary source of turbidite sediment throughout most of Unit IV (see "Inorganic Geochemistry" section, this chapter). During the late early Miocene, the Owen Ridge was uplifted above the realm of turbidite deposition, and the initiation of pelagic dominated sedimentation began.

By the middle Miocene, deposition at Site 722 consisted entirely of pelagic nannofossil ooze/chalk (lithologic Units I–III, 0–411.1 mbsf). With the cessation of turbidite deposition at Site 722, the major control on sedimentation became the relative production and preservation of biogenic calcium carbonate and silica, and the supply of terrigenous eolian sediment (Koila et al., 1981) from the surrounding landmasses. The relative input of these sedimentary components has varied both on tectonic time scales (millions of years) and on orbital and climatic time scales (Milankovitch frequencies and glacial-interglacial cycles).

The shift from turbidite sedimentation to pelagic sedimentation is thought to be a tectonically controlled change at Site 722 (Whitmarsh, 1974), while Milankovitch cyclicity (climatically controlled sedimentation variations) in Owen Ridge sediments has been documented in Pleistocene high-resolution pollen and planktonic foraminifer (*G. bulloides*) records. These pollen and foraminifer records, which are used as proxy monsoon-strength indicators, are highly correlated with the 22-k.y. precession periodicity (Prell and Van Campo, 1986). Preliminary low-resolution carbonate records and high-resolution magnetic susceptibility records from Site 722 indicate that these types of cyclicities may extend into the Tertiary (see Fig. 5 and "Paleomagnetism" section, this chapter). Thus, Site 722 sediments contain long-term signals (tectonic uplift) upon which higher frequency signals (Milankovitch cyclicities) are superimposed. Detailed resolution and interpretation of these signals and evaluation of the forcing mechanisms to which they respond await shore-based investigation.

BIOSTRATIGRAPHY

Introduction

Planktonic and benthic foraminifers, nannofossils, and radiolarians in the cored sediments at Site 722 have been analyzed in order to evaluate the effects of upwelling on sediments deposited on the Owen Ridge.

Biostratigraphic analysis of planktonic foraminifers, nannofossils, and radiolarians in the sediments of Site 722 show that

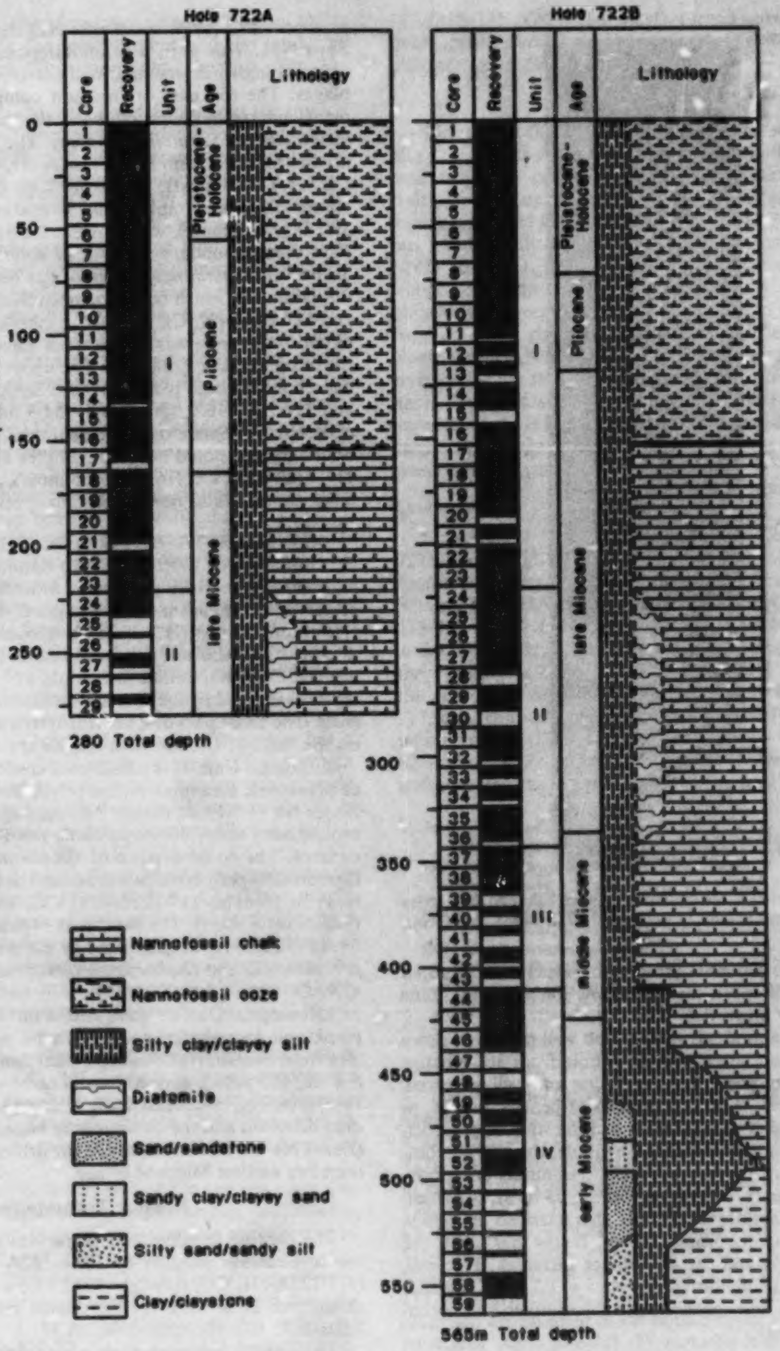
Hole 722A
Hole 722B
Core
Recovery
Unit
Age
Lithology
Depth (mbsf)
0
50
100
150
200
250
300
350
400
450
500
550
Pleistocene-Holocene
Pliocene
late Miocene
middle Miocene
early Miocene
I
II
III
IV
280 Total depth
565m Total depth
Nannofossil chalk
Nannofossil ooze
Silty clay/clayey silt
Diatomite
Sand/sandstone
Sandy clay/clayey sand
Silty sand/sandy silt
Clay/claystone

Figure 3. Lithologic summary, Site 722. Lithology is inferred between recovered intervals.

there has been more or less continuous sedimentation from early Miocene through Pleistocene (see Figs. 9 and 10). The Pliocene/Pleistocene boundary was recognized at approximately 55 mbsf. Nannofossils indicate that there is a hiatus between the uppermost Miocene and lowermost Pliocene. A plot of faunal datum levels and paleomagnetic reversals vs. sub-bottom depth is presented in Figure 11; for a detailed listing of these data points see Table 4.

Planktonic foraminifers are abundant, highly diverse, and well preserved in Hole 722A and in the upper part of Hole

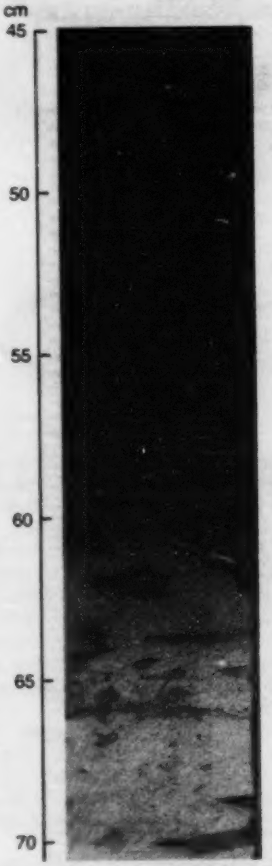

Figure 4. Burrow structures at the boundary between light and dark layers characteristic of sediments in Unit I (Section 117-722B-34X-3, 45–70 cm).

722B, down to about 230 mbsf (lithologic Units I and the upper part of II). Below 230 mbsf, the planktonic foraminiferal fauna is sparse and poorly preserved.

Radiolarians are abundant, robust, and well preserved down to about 360 mbsf, but are absent downhole from 360 mbsf.

The benthic foraminiferal fauna is diverse and well preserved, especially in the upper 77 m. The number of benthic species, as well as the total number of specimens and the state of preservation deteriorates downhole. Further downhole, the benthic foraminifers show signs of pyritization and occasionally are recrystallized. The lowest part of the hole, below 425 mbsf, is barren.

The calcareous nannofossil flora is characterized by its low diversity, especially in the upper 200 m. Below 200 mbsf, the preservation improves and the abundance increases. However, the preservation of the nannofossils below 411.1 mbsf is generally poor; asteroliths and sphenoliths are overgrown and coccoliths show dissolution.

Planktonic Foraminifers

Planktonic foraminifer faunas were analyzed in all core catchers of Hole 722A and Samples 117-722B-30X, CC, to 117-722B-59X, CC (285.5–565.5 mbsf), of Hole 722B.

Lithologic Unit I (see "Lithostratigraphy" section, this chapter) ranges from Pleistocene to upper Miocene, indicated by the presence of foraminiferal Zones N23 through the upper part of Zone N16. This unit, a foraminifer-bearing nannofossil ooze, contains highly diverse and well-preserved foraminiferal assemblages. The top part of this unit comprises Quaternary sediments marked by sparse *Globorotalia truncatulinoides* and *Globigerinella calida calida* specimens. The N23/N22 zonal boundary lies between Samples 117-722A-2H, CC, and 117-722A-3H, CC (19.4–29.0 mbsf). Below this level *Globorotalia truncatulinoides* disappears rapidly and is absent in Sample 117-722A-5H, CC (48.2 mbsf), which makes the position of the Pliocene/Pleistocene boundary difficult to determine. The last appearance of *Globigerinoides obliquus* has been used to approximate this boundary, which occurs between Samples 117-722A-6H, CC, and 117-722A-7H, CC (57.5–67.2 mbsf). The virtual absence of *Globorotalia tosaensis* in the upper Pliocene sequence hampers the recognition of Zone N21. The upper boundary of Zone N18 has tentatively been placed between Samples 117-722A-15X, CC, and 117-722A-16X, CC (144.6–154.3 mbsf), based on the first occurrence of *Sphaeroidinella dehiscens*. The Miocene/Pliocene boundary was noted between Samples 117-722A-17X, CC, and 117-722A-18X, CC (163.9–173.6 mbsf), as the robust, relatively large *Globorotalia tumida tumida* specimens disappear below this level.

Below Sample 117-722A-24X, CC (231.7 mbsf) the sediments are composed of partly opal-rich nannofossil chalks of lithologic Unit II, in which planktonic foraminifers occur rarely. The preservation remains moderate to good. The lower part of Zone N16 through Zone N13 could be recognized, which indicates a middle to late Miocene age for the entire unit. The zonal boundary N15/N16 was found in Sample 117-722A-30X, CC (285.3 mbsf) as defined by the first appearance of *Globorotalia acostaensis*. The basal part of Unit II is referred to Zones N13 to N14 on the basis of *Globorotalia mayeri* specimens.

Lithologic Unit III is nannofossil chalks with rare occurrences of planktonic foraminifers; the preservation of the tests is poor. Zones N9 to N13 of middle Miocene age are present, and the evolutionary series of *Globorotalia fohsi* subspecies can be recognized. The co-occurrence of *Globorotalia peripheronda* and *Globorotalia peripheroacuta* indicates the presence of Zones N10 to 11 in Samples 117-722B-40X, CC, and 117-722B-41X, CC (382.2–391.8 mbsf). The basal part of lithological Unit III is referred to Zone N9 as supported by the presence of *Globorotalia peripheronda* and *Globorotalia birnageae* in Sample 117-722B-42X, CC (401.4 mbsf).

Lithological Unit IV comprises a turbidite sequence, and no planktonic foraminifers could be found in the core-catcher samples from this interval. An additional Sample (117-722B-58X-5, 6–8 cm; 552 mbsf), derived from a carbonate-rich layer between two turbidites, contained some crushed specimens of *Catapsydrax dissimilis* and the *Globorotalia kugleri/peripheronda* series (Zones N4–5). The basal part of the drilled turbidite sequence is therefore earliest Miocene in age.

Benthic Foraminifers

The benthic foraminiferal fauna was studied at Site 722 in the core-catcher samples of Hole 722A down to 280.0 mbsf (117-722A-1H, CC, through -29X, CC) and in the core-catcher samples of Hole 722B for the depths below 265.9 mbsf (117-722B-28X, CC, through -59X, CC).

The abundance ranges from abundant to common in the uppermost interval (down to 202.7 mbsf in Hole 722A). The interval from 212.4 mbsf to 280.0 mbsf of Hole 722A and 265.9 mbsf to 285.3 mbsf of Hole 722B contains few benthic foraminifers, as does the interval down to 420.8 mbsf. The interval below 430.5 mbsf down to 565.6 mbsf is essentially barren. The diversity is high in the upper part of the recovered sequence and deteriorates downhole and becomes very poor below 430.5 mbsf.

This stepwise decrease in the abundance of benthic foraminifers corresponds well in both the total number and the timing to data from Site 721 (see "Biostratigraphy" section, Site 721 chapter).

The state of preservation is very good throughout the studied sequence, although a fair portion of the benthic foraminiferal population, as well as of the planktonic foraminifer population, has been pyritized. This pyritization seems to be most prominent below Sample 117-722A-24X, CC (231.7 mbsf), at the approximate level where the sedimentation changes from a siliceous nannofossil-bearing ooze (lithologic Unit II) to a foraminifer-bearing nannofossil ooze (lithologic Unit I). It becomes more distinct below this level. In some of the samples a distinct calcitic recrystallization can be recognized. Samples 117-722A-28X, CC (270.4 mbsf), 117-722B-41X, CC (391.8 mbsf), and 117-722B-42X, CC (401.4 mbsf) are strongly affected by recrystallization. The tests of planktonic foraminifers outnumber the tests of benthic foraminiferal species in most samples. However, in samples below Sample 117-722B-42X, CC (401.4 mbsf), that yielded benthic foraminifers, planktonic foraminifers had a very low percentage or were totally absent. This can be explained by selective preservation where the tests of planktonic foraminifers dissolves more easily than benthic foraminiferal tests.

Several species occur with varying relative abundance throughout the sequence studied. The most abundant are *Astrononion novozealandicum*, *Globocassidulina subglobosa*, *Epistominella exigua*, *Oridorsalis umbonatus*, *Pullenia bulloides*, and the arenaceous species *Eggerella bradyi*; minor species are *Melonis barleeanum* and *Pullenia subcarinata*. These abundant species are essentially the same as in Site 721. Occurrence of other species are restricted to certain intervals. *Bulimina aculeata* and *Chilostomella oolina* are only present in Samples 117-722A-1H, CC, through 117-722A-5H, CC (9.8–48.2 mbsf); the former has a known stratigraphic range from upper Miocene (N16) through Pleistocene (N23). *Bulimina exilis*, which has an stratigraphic range from lower Pliocene (N19) through Pleistocene (N23), is only found in three samples within the upper Pliocene (N21), i.e., Samples 117-722A-7H, CC, 117-722A-8H, CC, and 117-722A-9H, CC (67.2–86.5 mbsf). Tests of *Melonis pompiloides* are numerous below Sample 117-722A-16X, CC (154.3 mbsf), whereas they occur only sporadically above this level. The final peak in the relative abundance of *M. pompilioides* is concomitant with a peak in the relative abundance in *Ehrenbergina trigona* and slightly predates the appearance of *Cassidulina carinata*. The changes in *M. pompilioides* and *E. trigona* are coeval at Site 721 and Site 722.

The species *Uvigerina auberiana* appears for the first time in Sample 117-722B-31X, CC (295.0 mbsf), *Uvigerina peregrina* appears slightly above. They both occur throughout the sequence of Hole 722B and throughout all of Hole 722A. The order as well as the timing of these two occurrences corresponds well to the data from Site 721.

Species restricted to the lower part of the sequence are *Ehrenbergina hystrix*, *Anomalinoides semicribratus*, and *Globocassidulina decorata* with their last appearances encountered in Samples 117-722A-29X, CC, (280.0 mbsf), 117-722B-39X, CC (372.5 mbsf), and 117-722B-44X, CC (420.8 mbsf), respectively. The timing of these occurrences again agrees well with the data from Site 721. Species of the genera *Globobulimina* and *Nonionella* occur in Sample 117-722B-50X, CC (478.6 mbsf), from within the turbiditic sequence of lithologic Unit IV and they account for about 60% of the benthic foraminiferal fauna in that sample. These two species were not recognized at Site 721.

Not surprisingly, the benthic foraminiferal fauna of Site 722 is very similar to that of nearby Site 721. The interval missing at Site 721 is present at Site 722 and in some instances first and last appearances of some species at the approximate level of Sample 117-721B-33X, CC (318.0 mbsf), turned out to be caused by the interrupted sedimentary sequence when compared to the complete section at Site 722.

Calcareous Nannofossils

Nannofossil floras at Site 722 are similar to those observed at Site 721. At this site Holocene, Pleistocene, Pliocene, and Miocene sediments could be identified by calcareous nannofossil stratigraphy (Zones NN21–NN3), and all samples from lithologic Units I and II are characterized by fairly abundant calcareous nannofossils. Lithologic Unit I was found to range from NN21 to NN11, and the Pliocene/Pleistocene boundary was recognized in this unit. The species diversity, however, is comparatively low, especially in Quaternary and Pliocene sediments from the upper part of lithologic Unit I. The upper part of lithologic Unit III, a nannofossil chalk, has moderate to good preservation, while the lower part is poorly preserved. In general, nannofossils are abundant throughout Unit III. In samples from lower Miocene lithologic Unit IV, the abundance of calcareous nannofossil ranges from barren to abundant and the state of the preservation is generally poor.

Quaternary

Samples 117-722A-1H-4, 115–117 cm (5.65 mbsf), and 117-722B-1H, CC (5.5 mbsf), are assigned to Zone NN21. Because *Emiliania huxleyi* and *Pseudoemiliania lacunosa* are absent in Sample 117-722A-1H-5, 115–117 cm, through 117-722A-2H-5, 115–117 cm, (7.15–16.95 mbsf) 117-722B-2H, CC (15.1 mbsf), and 117-72B-3H, CC (24.7 mbsf), the samples are assigned to the Pleistocene Zone NN20. The presence of *P. lacunosa* and the absence of discoasters place Samples 117-722A-2H-6, 115–177 cm, through 117-722A-7H-4, 114–116 cm (18.46–63.14 mbsf), and 117-722B-4H, CC, through 117-722B-7H, CC (34.3–62.9 mbsf), in Zone NN19, where the following calcareous nannofossils datums are recognized in Hole 117-722B:

Top of acme of *Reticulofenestra* sp. A	0.83 Ma
117-722B-4H, CC (34.3 mbsf)/117-722B-5H, CC (43.9 mbsf)	
FAD *Gephyrocapsa parallela*	0.89 Ma
117-722B-4H, CC (34.3 mbsf)/117-722B-5H, CC (43.9 mbsf)	
LAD *Helicosphaera sellii*	1.19 Ma
117-722B-5H, CC (43.9 mbsf)/117-722B-6H, CC (53.2 mbsf)	
FAD *Gephyrocapsa oceanica*	1.57 Ma
117-722B-6H, CC (53.2 mbsf)/117-722B-7H, CC (62.9 mbsf)	
FAD *Gephyrocapsa caribbeanica*	1.66 Ma
117-722B-7H, CC (62.9 mbsf)/177-722B-8H, CC (72.5 mbsf)	

Neogene

The Pliocene/Pleistocene boundary was recognized between Samples 117-722A-6H-4, 115–117 cm (53.85 mbsf), and 117-722A-6H-5, 115–117 cm (55.35 mbsf), in Hole 722A and 117-722B-7H, CC (62.9 mbsf), and 117-722B-8H, CC (72.5 mbsf), in Hole 722B. The presence of *Discoaster brouweri* in Samples 117-722A-7H-5, 115–117 cm (64.65 mbsf), and 117-722B-8H, CC (72.5 mbsf), assigns them to Zone NN18. Samples 117-722A-8H-6, 115–117 cm, through 117-722A-11X, CC (75.85–105.61 mbsf), and 177-722B-9H, CC, through 117-722B-12X, CC (82.2–111.20 mbsf), contain *Discoaster pentaradiatus* but lack *D. surculus* and are assigned to the middle upper Pliocene (Zone NN17 to NN16). As at Site 721, *D. surculus* is not present in the uppermost part of its known range.

Ceratoliths are rare and amauroliths are absent at this site as they were at Site 721. The first samples with *R. pseudoumbilica* are 117-722A-12X-1, 116–118 cm (107.06 mbsf), and 117-722B-13X, CC (120.9 mbsf). These have been assigned to Zone NN15 because they occur below the samples of Zone NN16. Without *Amaurolithus tricorniculatus* and *Discoaster asymmetricus*, how-

Table 3. Calcium carbonate and organic carbon contents, Site 722.

Hole, core, section, interval (cm)	Depth (mbsf)	Total carbon (%)	Inorganic carbon (%)	Organic carbon (%)	$CaCO_3$ (%)
722A-1H-2, 52–54	2.02		8.29		69.1
722A-1H-4, 52–54	5.02		6.72		56.0
722A-1H-4, 144–145	5.94	7.93	7.58	0.35	63.1
722A-1H-6, 52–54	8.02		8.57		71.4
722A-2H-2, 50–52	11.80		9.43		78.6
722A-2H-4, 50–52	14.80		9.16		76.3
722A-2H-6, 50–52	17.80		7.95		66.2
722B-3H-3, 51–53	18.61	9.04	8.17	0.87	68.1
722A-3H-2, 50–52	21.40		9.01		75.1
722A-3H-4, 50–52	24.40		9.27		77.2
722A-3H-4, 114–115	25.04	9.22	8.39	0.83	69.9
722A-3H-6, 50–52	27.40		8.73		72.7
722A-4H-2, 50–52	31.00		7.23		60.2
722A-4H-4, 50–52	34.00		7.77		64.7
722A-4H-6, 50–52	37.00		8.33		69.4
722A-5H-2, 50–52	40.60		8.09		67.4
722A-5H-4, 50–52	43.60		6.92		57.6
722A-5H-6, 50–52	46.60		9.21		76.7
722A-6H-2, 50–52	50.20		7.35		61.2
722A-6H-4, 50–52	53.20		7.46		62.1
722A-6H-4, 114–115	53.84	7.89	6.76	1.13	56.3
722A-6H-6, 50–52	56.20		6.69		55.7
722A-7H-2, 50–52	59.50		7.02		58.5
722A-7H-4, 50–52	62.50		6.14		51.2
722A-7H-6, 50–52	65.50		8.59		71.6
722A-8H-2, 50–52	69.20		9.15		76.2
722A-8H-4, 50–52	72.20		8.01		66.7
722A-8H-6, 50–52	75.20		7.56		63.0
722A-9H-2, 50–52	78.80		6.03		50.2
722A-9H-4, 50–52	81.80		7.71		64.2
722A-9H-4, 119–120	82.49	10.43	8.33	2.10	69.4
722A-9H-6, 50–52	84.80		8.25		68.7
722A-10X-2, 50–52	88.50		7.58		63.1
722A-10X-4, 50–52	91.50		8.06		67.1
722A-11X-2, 50–52	98.20		8.90		74.1
722A-11X-4, 50–52	101.20		9.26		77.1
722A-11X-6, 50–52	104.20		9.04		75.3
722A-12X-2, 49–51	107.89		9.57		79.7
722A-12X-4, 49–51	110.89		8.13		67.7
722A-12X-4, 119–120	111.59	9.81	9.40	0.41	78.3
722A-12X-6, 49–51	113.89		8.45		70.4
722A-13X-2, 50–52	117.60		10.03		83.6
722A-13X-4, 50–52	120.60		8.09		67.4
722A-13X-6, 50–52	123.60		9.40		78.3
722A-14X-2, 50–52	127.30		9.88		82.3
722A-14X-4, 52–54	130.32		8.76		73.0
722A-15X-2, 60–62	137.00		8.30		69.1
722A-15X-4, 60–62	140.00		10.40		86.6
722A-15X-5, 145–150	142.35	10.66	10.45	0.21	87.1
722A-15X-6, 15–17	142.55		6.11		50.9
722A-16X-2, 20–21	146.30	10.07	10.42	0.00	86.8
722A-16X-2, 25–26	146.35	10.53	10.09	0.44	84.1
722A-16X-2, 29–30	146.39	10.37	9.79	0.58	81.6
722A-16X-2, 34–35	146.44	10.51	9.48	1.03	79.0
722A-16X-2, 39–40	146.49	10.21	8.55	1.66	71.2
722A-16X-2, 43–44	146.53	10.47	8.53	1.94	71.1
722A-16X-2, 48–49	146.58	9.99	8.06	1.93	67.1
722A-16X-2, 52–54	146.62		7.90		65.8
722A-16X-2, 56–57	146.66	9.28	7.35	1.93	61.2
722A-16X-2, 60–61	146.70	8.79	6.85	1.94	57.1
722A-16X-2, 65–66	146.75	8.62	6.74	1.88	56.1
722A-16X-2, 69–70	146.79	8.85	6.79	2.06	56.6
722A-16X-2, 75–76	146.85	9.62	6.65	2.97	55.4
722A-16X-2, 80–81	146.90	9.26	8.14	1.12	67.8
722A-16X-2, 85–86	146.95	9.56	8.62	0.94	71.8
722A-16X-2, 90–91	147.00	10.61	10.14	0.47	
722A-16X-2, 95–96	147.05	10.61	10.16	0.45	84.6
722A-16X-4, 53–55	149.63		8.07		67.2
722A-16X-6, 50–52	152.60		8.93		74.4
722A-17X-1, 108–110	155.38		10.13		84.4
722A-17X-3, 103–105	158.33		8.86		73.8
722A-18X-2, 58–60	165.98		8.39		69.9
722B-19X-1, 40–42	169.60		1.25		10.4
722A-18X-6, 58–60	170.20		10.40		86.6
722A-19X-2, 62–64	175.72		7.63		63.6
722A-19X-4, 59–61	178.69		10.45		87.1

Table 3 (continued).

Hole, core, section, interval (cm)	Depth (mbsf)	Total carbon (%)	Inorganic carbon (%)	Organic carbon (%)	$CaCO_3$ (%)
722A-19X-4, 119–120	179.29	8.58	7.27	1.31	60.6
722A-20X-2, 36–38	185.16		10.54		87.8
722A-20X-4, 60–62	188.40		7.94		66
722A-21X-1, 57–59	193.57		10.29		85.7
722A-21X-3, 60–62	196.60		7.66		63.8
722A-22X-2, 52–54	204.72		10.06		83.8
722A-22X-4, 52–54	207.72		9.86		82.1
722A-22X-4, 119–120	208.39	8.28	7.68	0.60	64.0
722A-22X-4, 119–120	208.39	8.28	7.68	0.60	64.0
722A-22X-6, 52–54	210.72		8.70		72.5
722A-23X-2, 50–52	214.40		8.72		72.6
722A-23X-4, 68–70	217.58		8.53		71.1
722A-23X-6, 38–40	220.28		8.02		66.8
722A-24X-2, 17–20	223.67		8.72		72.6
722A-24X-4, 50–52	227.00		6.46		53.8
722A-24X-6, 50–52	230.00		7.61		63.4
722A-25X-1, 50–52	232.20		10.71		89.2
722A-26X-1, 58–60	242.28		7.31		60.9
722B-27X-4, 114–115	252.14	9.30	9.09	0.21	75.7
722A-27X-2, 29–31	252.79		5.11		42.6
722A-27X-2, 114–115	253.64	9.64	9.54	0.10	79.5
722A-27X-4, 17–19	255.67		2.69		22.4
722B-28X-2, 47–49	258.17		10.54		87.8
722B-29X-3, 60–63	269.50		5.34		44.5
722B-29X-3, 113–114	270.03	9.54	9.38	0.16	78.1
722B-29X-3, 120–121	270.10	8.15	7.43	0.72	61.9
722B-29X-3, 125–126	270.15	7.78	5.99	1.79	49.9
722B-29X-3, 130–131	270.20	7.60	5.37	2.23	44.7
722B-29X-3, 135–136	270.25	7.56	5.34	2.22	44.5
722B-29X-3, 140–141	270.30	7.16	4.99	2.17	41.6
722B-29X-3, 145–146	270.35	6.95	4.69	2.26	39.1
722B-29X-3, 149–150	270.39	6.89	4.66	2.23	38.8
722B-29X-4, 5–6	270.45	6.15	4.31	1.84	35.9
722B-29X-4, 10–11	270.50	5.36	3.85	1.51	32.1
722B-29X-4, 15–16	270.55	3.90	3.77	0.13	31.4
722B-29X-4, 20–21	270.60	5.39	4.29	1.10	35.7
722B-29X-4, 25–26	270.65	4.98	4.01	0.97	33.4
722B-29X-4, 30–31	270.70	5.27	4.44	0.83	37.0
722B-29X-4, 35–36	270.75	6.21	5.41	0.80	45.1
722A-29X-1, 37–40	270.77		10.17		84.7
722B-29X-4, 40–41	270.80	7.94	7.45	0.49	62.1
722B-29X-4, 47–48	270.87	9.46	8.72	0.74	72.6
722B-29X-4, 52–53	270.92	9.53	9.25	0.28	77.1
722B-29X-4, 60–61	271.00	9.03	8.76	0.27	73.0
722A-29X-3, 39–40	273.79	6.36	2.20	4.16	18.3
722B-31X-2, 50–52	287.30		6.24		52.0
722B-31X-4, 50–52	290.30		9.55		79.6
722B-31X-4, 114–115	290.94	6.62	5.71	0.91	47.6
722B-31X-6, 50–52	293.30		9.33		77.7
722B-32X-2, 50–52	297.00		8.92		74.3
722B-32X-4, 50–52	300.00		5.47		45.6
722B-33X-2, 28–30	306.48		2.95		24.6
722B-34X-2, 80–82	316.60		3.34		27.8
722B-34X-2, 114–115	316.94	5.08	3.77	1.31	31.4
722B-34X-4, 40–42	319.20		4.87		40.6
722B-35X-2, 52–54	326.02		7.97		66.4
722B-35X-4, 51–53	329.01		3.22		26.8
722B-35X-6, 50–52	332.00		6.64		55.3
722B-36X-2, 48–50	335.68		6.11		50.9
722B-36X-4, 77–79	338.97		5.18		43.2
722B-37X-2, 51–53	345.41		8.99		74.9
722B-37X-4, 51–53	348.41		6.35		52.9
722B-37X-6, 50–52	351.40		9.91		82.6
722B-38X-2, 71–73	355.31		4.97		41.4
722B-38X-4, 83–85	358.43		8.48		70.6
722B-38X-6, 52–54	361.12		5.04		42.0
722B-39X-1, 12–14	362.92		8.52		71.0
722B-40X-3, 16–18	375.66		4.48		37.3
722B-41X-2, 29–31	383.99		11.09		92.4
722B-42X-1, 22–24	392.02		10.80		90.0
722B-42X-3, 33–35	395.13		6.30		52.5
722B-43X-1, 40–42	401.80		10.74		89.5
722B-43X-2, 114–115	404.04	7.01	6.83	0.18	56.9
722B-43X-3, 23–25	404.63		6.36		53.0
722B-44X-2, 38–40	412.98		6.32		52.7
722B-44X-4, 17–19	415.77		0.76		6.3

Table 3 (continued).

Hole, core, section, interval (cm)	Depth (mbsf)	Total carbon (%)	Inorganic carbon (%)	Organic carbon (%)	$CaCO_3$ (%)
722B-45X-2, 23–25	422.53		0.62		5.2
722B-45X-4, 27–29	425.57		3.00		25.0
722B-45X-6, 138–140	429.68		0.58		4.8
722B-46X-2, 1–3	432.01		1.31		10.9
722B-46X-4, 141–143	436.41		3.25		27.1
722B-46X-5, 114–115	437.64	0.89	0.78	0.11	6.5
722B-46X-6, 132–134	439.32		1.56		13.0
722B-48X-1, 33–35	450.13		1.14		9.5
722B-49X-1, 40–42	459.80		1.25		10.4
722B-49X-3, 114–115	463.54	1.76	1.49	0.27	12.4
722B-49X-4, 40–42	464.30		1.25		10.4
722B-50X-2, 39–41	470.89		1.26		10.5
722B-50X-4, 30–32	473.80		1.36		11.3
722B-51X-1, 69–71	479.29		1.42		11.8
722B-51X-CC, 0–0	479.39	41.91	0.10	41.81	0.8
722B-52X-2, 79–81	490.49		0.51		4.3
722B-52X-5, 54–56	494.74		1.17		9.8
722B-52X-7, 8–10	497.28		0.51		4.3
722B-53X-1, 41–43	498.31		1.74		14.5
722B-58X-1, 134–136	547.54		1.50		12.5
722B-58X-3, 74–76	549.94		1.28		10.7
722B-58X-4, 114–115	551.84	2.55	2.50	0.05	20.8
722B-59X-CC, 12–14	556.86		0.72		6.0

ever, we cannot be certain that this is the correct age assignment. As was the case with the above two samples, Samples down to 117-722A-17X, CC (158.63 mbsf), and 117-722B-14X, CC, through 117-722B-17X, CC (130.5–159.5 mbsf), may belong to Zone NN15–NN12. *D. quinqueramus* is present in Samples 117-722A-18X-1, 115–116 cm, through 117-722A-28X, CC (165.05–270.4 mbsf), and 117-722B-18X, CC, through 117-722B-29X, CC (169.2–275.6 mbsf). These samples generally contain a diverse assemblage of nannofossils which includes several species of discoasters. *D. berggrenii, D. pentaradiatus, D. brouweri, D. variabilis, D. pseudovariabilis, D. bellus, D. blackstockae, D. triradiatus, D. neohamatus, D. challengeri, D. loeblichii, D. neorectus, D. intercalaris, D. calcaris*, and *D. surculus* are found in this zone.

In Hole 722B Zone NN12 (upper Miocene to lowermost Pliocene) appears to be missing and the discontinuity is assumed between Samples 117-722B-17X, CC (159.5 mbsf), and 117-722B-18X, CC (169.2 mbsf). The same discontinuity may be present in Hole 722A but the lack of marker species in cores of the equivalent ages precludes the definite recognition of missing sediments. Because Samples 117-722A-29X-1, 114–116 cm (271.54 mbsf), the deepest sample from the bottom of Hole 722A, and 117-722B-30X, CC, through 117-722B-32X, CC (285.3–304.7 mbsf), contain neither *D. quinqueramus* nor *D. hamatus*, they are assigned to Zone NN10 (middle upper Miocene). *D. hamatus* is found in Samples 117-722B-33X-1, 115–116 cm, through 117-722B-34X, CC (305.85–324.0 mbsf), so that a zonal assignment of NN9 is given. *Catinaster coalitus* is not found in samples of this site and only the presence of *Discoaster kugleri* identifies Samples 117-722B-35X, CC, through 117-722B-40X-2, 110–111 cm (333.55–375.10 mbsf), as belonging to Zones NN8–NN7 (middle Miocene). Samples 117-722B-40X, CC (382.2 mbsf), through 117-722B-41X-1, 21–22 cm (382.41 mbsf), contains neither *D. kugleri* nor *Sphenolithus heteromorphus* and can be assigned to Zone NN6. *S. heteromorphus* is present in Samples 117-722B-41X, CC, through 117-722B-43X, CC (391.8–411.1 mbsf), that this interval has been included in NN4–NN5. The presence of *Helicosphaera ampliaperta* is used to divide Zones NN4 from NN5, but unfortunately *H. ampliaperta* is missing from the sediments of this site as was the case at Site 721.

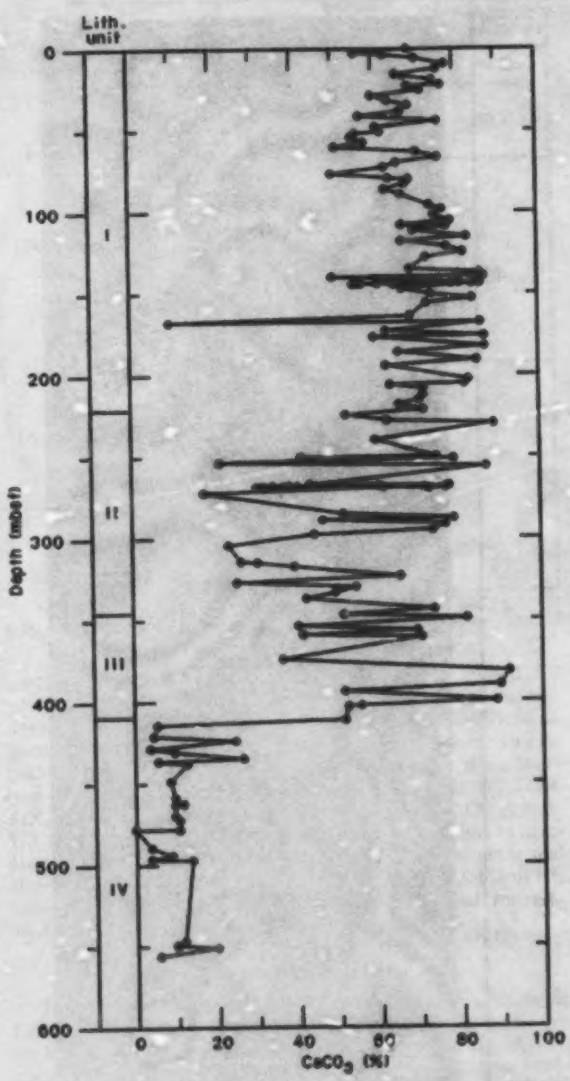

Figure 5. Calcium carbonate profile at Site 722. Samples from 0 to 255 mbsf are from Hole 722A and samples from 255 to 556 mbsf are from Hole 722B.

The preservation of nannofossils becomes poor in Sample 117-722B-42X, CC (401.4 mbsf), and remains poor to the bottom of the hole. Asteroliths and sphenoliths are heavily overgrown and the coccoliths have undergone varying degrees of dissolution. As a result, the biostratigraphy of this part of the hole is dubious. Samples 117-722B-49X, CC, through 117-722B-51X, CC (469.0–488.2 mbsf), are barren or have such small quantities of nannofossils that they should be considered barren. Samples 117-722B-53X, CC, through 117-722B-57X, CC (507.6–546.2 mbsf), contain no age-diagnostic species. Sample 117-722B-58X, CC (555.9 mbsf), from turbiditic sediments of lithologic Unit IV contains a mixed flora of Miocene, Oligocene, and Eocene age. Sample 117-722B-59X, CC (565.6 mbsf), contains *S. belemnos* and *D. druggii* and was assigned to Zone NN3 (lower Miocene).

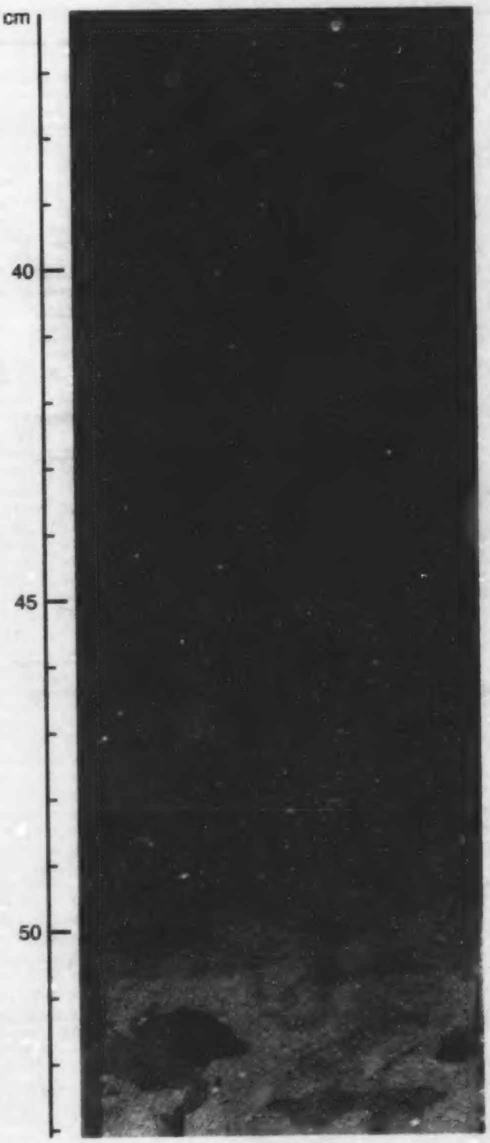

Figure 6. Subvertical, en echelon dewatering(?) structures characteristic of opal-rich sediments in Unit III (Section 117-722B-34X-1, 37–53 cm).

Radiolarians

Shipboard analysis included all core-catcher samples from Hole 722A and Samples 117-722B-28X, CC, through Sample 117-722B-38X, CC (265.9–362.8 mbsf). Intermediate samples were analyzed during subsequent shore-based studies. Radiolarians are abundant, robust, and well preserved throughout Hole 722A and in lithologic Units I and II of Hole 722B. Sample 117-722B-38X, CC (362.8 mbsf), contains few radiolarians, most of which are coated with pyrite. The remainder of Hole 722B below this sample is barren of radiolarians. Radiolarian zones from the Pleistocene to upper Miocene were identified in lithologic Unit I of Hole 722A. The uppermost Quaternary radiolarian zone, *Buccinosphaera invaginata*, is missing and Sample 117-722A-1H, CC (9.8 mbsf), probably belongs to the *Collosphaera tuberosa* Zone. Samples 117-722A-2H-4, 85–87 cm (15.15 mbsf), through 117-722A-6H-4, 85–87 cm (43.95 mbsf), belong to the *Amphirhopalum ypsilon* Zone, while Samples 117-722A-5H, CC, through 117-722A-6H-4, 85–87 cm (48.20–53.55 mbsf), are in the *Anthocyrtidium angulare* Zone. The top of the *Pterocanium prismatium* Zone has been placed at Sample 117-722A-6H, CC (57.5 mbsf), but this is based on the presence of only two specimens of *P. prismatium*, which seems to be very rare in this part of the Indian Ocean. The zone is present through Sample 117-722A-8H, CC (76.8 mbsf). Sample 117-722A-9H, CC (86.5 mbsf), contains the last common occurrence of *Stichocorys peregrina* and marks the top of the *Spongaster pentas* Zone, although few reworked specimens were found above this level. The lower limit of the *S. pentas* Zone is impossible to locate accurately, because it is based on the evolutionary transition of *Spongaster berminghami* to *Spongaster pentas*; the latter species seems to be absent or extremely rare in this area. Therefore, the *S. pentas*/*S. peregrina* boundary has been approximated to the last occurrence of *Solenosphaera omnitubus* in Sample 117-722A-16X, CC (154.3 mbsf). The lower limit of the *S. peregrina* Zone is also difficult to determine accurately because that boundary is defined by the evolutionary transition of *Stichocorys delmontensis* to *S. peregrina* and the samples contain considerable reworking of the ancestral species, as well as various Miocene species of *Didymocyrtis* and *Diartus*. The boundary between the *S. peregrina* and *Didymocyrtis penultima* Zone has been placed, with some misgivings, between Samples 117-722A-22X, CC, and 117-722A-23X-4, 85–87 cm (212.40–217.75 mbsf). Hence, the boundary between lithologic Units I and II is located in the *D. penultima* Zone. The top of the *Didymocyrtis*

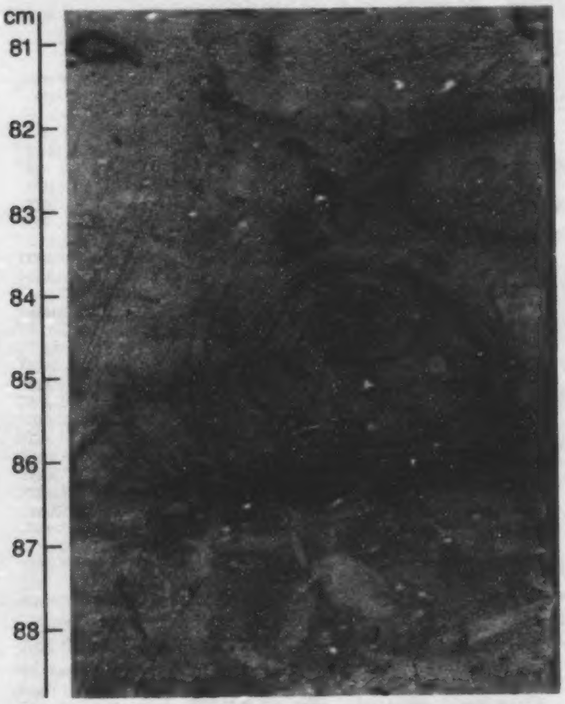

Figure 7. Concentric, purple alteration rings characteristic of sediments in Unit III (Section 117-722B-35X-5, 81–88 cm).

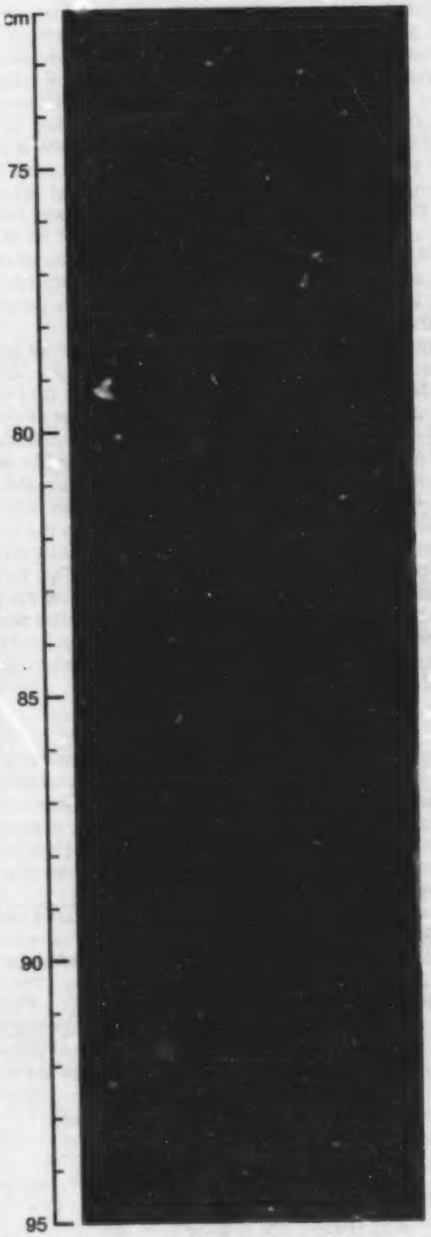

Figure 8. Silty claystone interbedded with silty clays and marly nannofossil chalks; representative of the upper 100 m of Unit IV. Note charcoal-rich bed from 84 to 85 cm. Downsection the silty claystone is replaced by micaceous sands and sandstones while the marly nannofossil chalks are replaced by silty clays (Section 117-722B-49X-2, 72–95 cm).

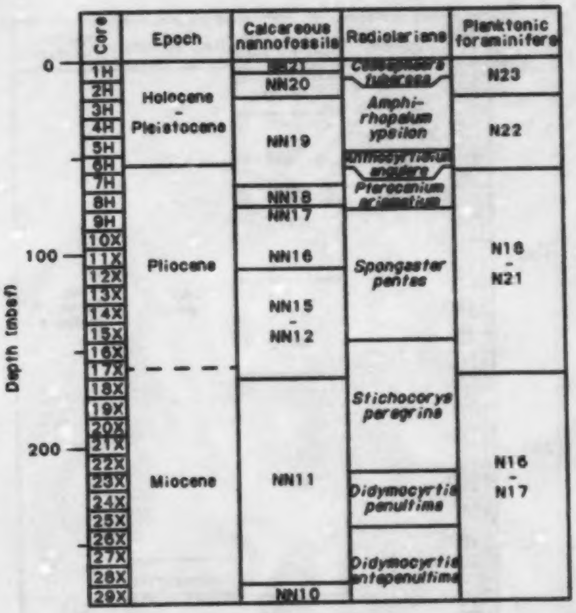

Figure 9. Correlation of planktonic microfossil zones in Hole 722A.

antepenultima Zone is defined by the last occurrence of *Diartus hughesi* in Sample 117-722A-26X, CC (251.0 mbsf), although reworking of *D. hughesi* presents some difficulties in defining the boundary. At this level diatoms also become quite common.

Analysis in Hole 722B began with Sample 117-722B-28X, CC, which was assigned to the *D. antepenultima* Zone; the zone continues through Sample 117-722B-30X, CC (265.9–285.3 mbsf). The remainder of the section lies within the *Diartus petterssoni* Zone. However, reworking again makes it difficult to locate a boundary which is dependent upon an evolutionary sequence (*D. petterssoni* to *D. hughesi* in this case). In the lower part of Unit II and upper part of Unit III (Sample 117-722B-31X, CC, and downhole to Sample 117-722B-37X, CC (295.0–353.1 mbsf), diatoms are abundant. The siliceous fauna in Sample 117-722B-37X, CC (353.1 mbsf), of Unit III is robust and diverse. In Sample 117-722B-38X, CC (362.8 mbsf), of Unit III, however, the fauna is much reduced and more than half the radiolarians have been pyritized; diatoms are absent.

Paleoenvironmental Implications

The preservation states of the calcareous tests of planktonic foraminifers and coccoliths are thought to be related to the uplift history of Owen Ridge and variations of the CCD and lysocline. The lower part of the sequence corresponding to lithologic Unit IV contains only badly preserved coccoliths and one pelagic calcareous interval with some planktonic foraminifer remains, which indicates deposition just above the CCD. In the lower upper Miocene to lower middle Miocene (lithologic Unit III) planktonic and benthic foraminifers are rare, but coccoliths are abundant. By this time Owen Ridge had been either at least partially uplifted or the lysocline had deepened. Improvement of preservation on Owen Ridge continued during the late Miocene, as is indicated by well-developed planktonic and benthic foraminiferal faunas in the upper sediments of lithological Unit II.

The increase of opal in the lower part of lithological Unit II (upper Miocene) indicates changing environmental conditions which may be related to changes in circulation, global cooling, and/or increased upwelling intensity. This cooling period may have enhanced bottom circulation and could have been responsible for a rise in the CCD in the Indian Ocean (Kennett, 1982). However, benthic foraminiferal data do not indicate that high-latitude water masses influenced the Arabian Sea. The Carls-

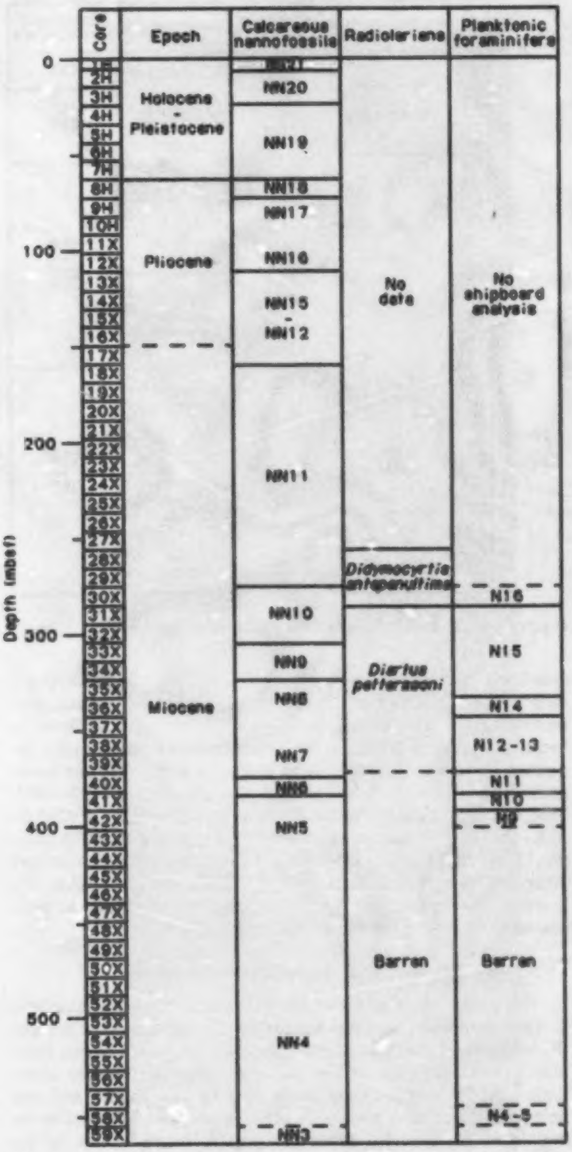
Core
Epoch
Calcareous nannofossils
Radiolarians
Planktonic foraminifers
Depth (mbsf)
0
100
200
300
400
500
1H
2H
3H
4H
5H
6H
7H
8H
9H
10H
11X
12X
13X
14X
15X
16X
17X
18X
19X
20X
21X
22X
23X
24X
25X
26X
27X
28X
29X
30X
31X
32X
33X
34X
35X
36X
37X
38X
39X
40X
41X
42X
43X
44X
45X
46X
47X
48X
49X
50X
51X
52X
53X
54X
55X
56X
57X
58X
59X
Holocene - Pleistocene
Pliocene
Miocene
NN21
NN20
NN19
NN18
NN17
NN16
NN15 - NN12
NN11
NN10
NN9
NN8
NN7
NN6
NN5
NN4
NN3
No data
Didymocyrtis antepenultima
Diartus petterssoni
Barren
No shipboard analysis
N16
N15
N14
N12-13
N11
N10
N9
N4-5
Barren

Figure 10. Correlation of planktonic microfossil zones in Hole 722B.

berg Ridge may have prevented these bottom currents from affecting this area.

PALEOMAGNETISM

Magnetic Measurements

We used the pass-through cryogenic magnetometer to measure the natural remanent magnetization (NRM) of the archive halves of Cores 117-722A-1H through 117-722A-9H, and the whole rounds and archive halves of Cores 117-722B-6H and 117-722B-7H. However, as at Sites 720 and 721, we were unable achieve reliable results; again this appeared to be the result of a coring/core-barrel-induced remanence, together with a possible anhysteretic remanent magnetization acquired from the pass-through alternating-field (AF) demagnetizer. Therefore, all our magnetostratigraphic results are based on measurements of discrete samples using the MINISPIN fluxgate spinner magnetometer and the Schonstedt AF demagnetizer. We measured 144 samples from Hole 722A and 150 samples from Hole 722B. Because of time constraints we did not routinely subject selected samples to stepwise alternating field demagnetization but instead demagnetized all samples at a blanket AF of either 10 or 15 mT. Our results from Site 721 (about 6 mi away from Site 722) suggested that for these sediments a field of 10–15 mT is sufficient to isolate the characteristic magnetization of most of the samples. More detailed shore-based demagnetization studies revealed that some samples change their magnetic polarity between 10 mT and 15 mT AF cleaning.

Figure 12 shows the discrete sample NRM results after AF demagnetization for the combined data from Holes 722A and 722B. The geometric mean intensity is very low: 0.13 mA/m. The circular standard deviation (CSD) is a measure of the reliability of each measurement, with higher values indicating decreasing reliability. In the nannofossil oozes and chalks of lithologic Units I to III (see "Lithostratigraphy" section, this chapter) the intensities after AF demagnetization are very weak (almost always less than 0.2 mA/m); higher values (up to about 20 mA/m) occur in lithologic Unit IV (predominantly silty claystones), beginning at 411.1 mbsf in Hole 722B. This pattern is paralleled in the magnetic susceptibility record (see discussion below), showing that the NRM intensity is controlled primarily by the concentration of magnetic minerals. A clear inverse relationship exists between the reliability of the measurements, as expressed by the CSD, and the NRM intensity.

Magnetostratigraphy

Figure 13 shows a histogram of the inclination values grouped into 10° classes; the arrows show the expected geocentric axial dipole inclination value (30.6°) for this latitude. Despite the low NRM intensities, the correspondence between the observed and expected inclination values is acceptable, which gives us some confidence in our magnetostratigraphic interpretations of a somewhat noisy data set.

We determined magnetic polarity zone boundaries of Holes 722A and 722B, based on inclination values of samples with CSD values of less than 40 together with results of shore-based measurements after 15 mT AF demagnetization. The depth within core and section of the reversal boundaries are given in Table 5. As at Site 721 the Chron C1/C1r (Brunhes/Matuyama Chronozone) boundary is absent or poorly defined (although it is indicated by a shallowing of inclination values between 30 and 40 mbsf), and we interpret the first clear normal to reversed transition at about 40 mbsf as the boundary between Subchron C1r-1 (Jaramillo Subchronozone) and Chron C1r (Matuyama Chronozone). As at Site 721, Chron C2 (Olduvai Subchronozone) cannot be identified. We place the upper and lower boundaries of Chron C2A (Gauss Chronozone) at about 85 mbsf and about 105 mbsf respectively, and the lower boundary of Chron C3.3 (Thvera) at about 150–155 mbsf. These assignments are in good agreement with biostratigraphic evidence (see "Biostratigraphy" section, this chapter). We place the upper boundary of Chron C3A (Chronozone 5) at about 180–185 mbsf. Because of the relatively small number of stable samples over this interval we are less confident in recognizing the lower boundary of Chron C3A (Chronozone 5), but place it at about 220 mbsf. Again, this agrees with biostratigraphic evidence.

The character of the polarity transitions at this site is of interest: as at Site 721 the interval of reattainment of the expected geocentric axial dipole inclination values across a transition ex-

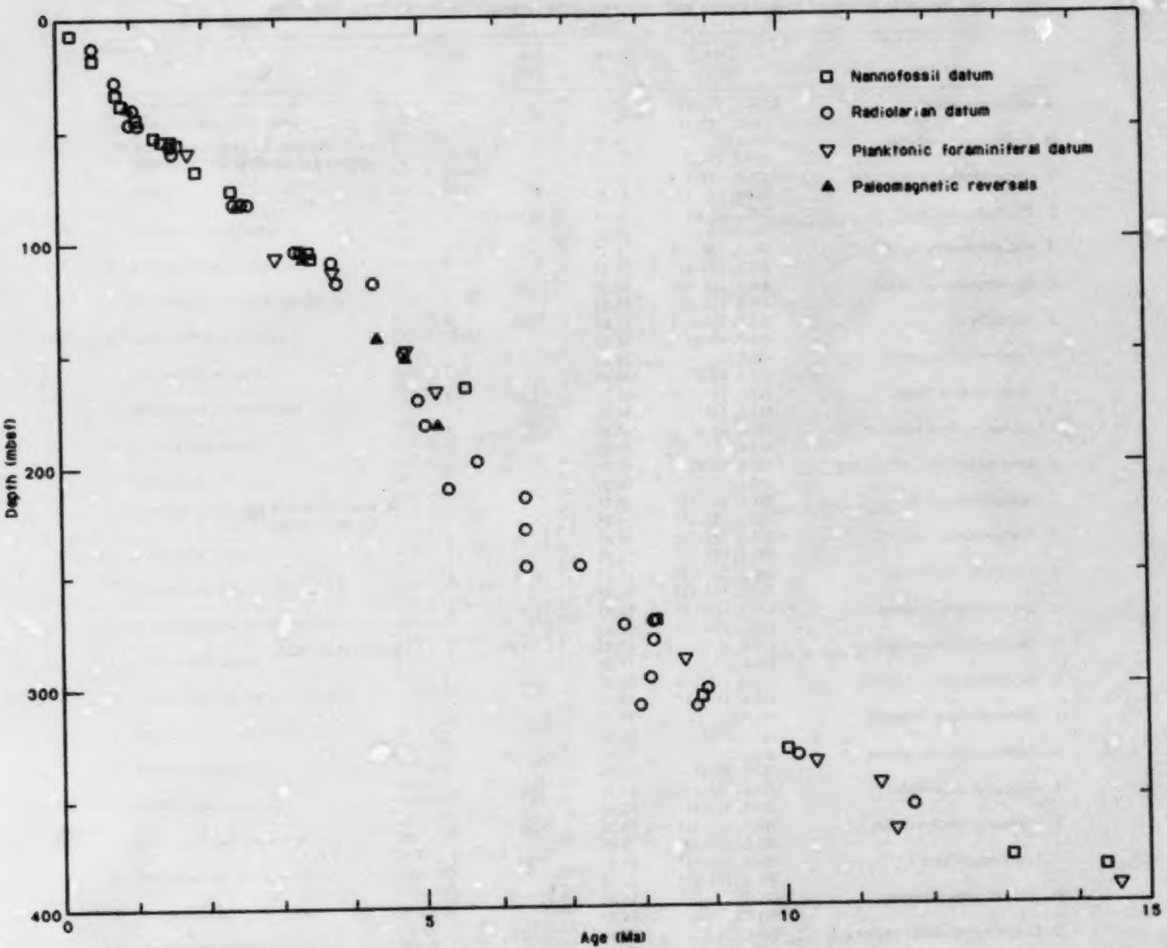

Figure 11. Age-depth plot for Site 722. For a detailed listing of the events see Table 4.

tends over several meters. With an average sediment accumulation rate of about 3 cm/k.y. at this site this represents a much longer period of time than the duration of an average polarity transition (about 5 k.y.). This suggests that the time required for the geomagnetic signal to be "locked in" is much longer than appears to be the case for some other deep-sea sediments. This inference is compatible with the apparent inability of the sediment sequences at Sites 721 and 722 to record polarity intervals of relatively short duration, such as the interval between the base of Chron C1 (Brunhes Chronozone) and the upper boundary of Subchron C1r-1 (Jaramillo Subchronozone), and Chron C2 (Olduvai Subchronozone). Intense bioturbation is a possible explanation; however, this would have to operate over a depth range of several meters to achieve the required effect, which seems unlikely. Moreover, the occurrence of susceptibility variations on a depth scale of 1 m and less (see discussion below) argues against bioturbation being the cause. Another possibility is that the NRM is of chemical origin, perhaps carried by authigenic ferrimagnetic iron sulfides, which could require relatively long intervals to form. Such an explanation is compatible with the highly reduced state of the sediments. Shore-based rock-magnetic and X-ray diffraction studies of magnetic concentrates could provide a way of testing this second possibility. At present both explanations are entirely speculative.

Core Orientation

Table 6 compares the orientation of Cores 117-722A-5H through -7H and Cores 117-722B-6H and -8H through -10H as estimated from the multishot device with the orientation as estimated from the measured average declination values of discrete samples from the cores. As at Site 721, there is complete disagreement between the two methods, which raises further doubt about the reliability of the multishot estimates.

Magnetic Susceptibility

The volume magnetic susceptibility of whole sections of Holes 722A and 722B was measured using the Bartington M.S. 1 whole-core sensor at the 0.1 sensitivity and low-frequency (0.47-kHz) settings. All cores from Hole 722A and Cores 117-722B-1H to -11X were measured at 5-cm intervals; Cores 117-722B-12X to -58X were measured at 10-cm intervals to speed up core processing. A total of 3914 and 4368 measurements were made for Holes 722A and 722B, respectively.

The susceptibility data from Hole 722A were very similar in character to those obtained from Site 721, which was located ~6 mi to the southwest (Fig. 14; see "Paleomagnetism" section, "Site 721" chapter, this volume). As with the Site 721 sediments, the susceptibility values are generally very low and the

Table 4. Stratigraphic listing of faunal events and paleomagnetic reversals for Holes 722A and 722B.

Event	Core level	Depth (mbsf)	Age (Ma)	Source of age	Notes
B *Emiliania huxleyi*	A1H-4, 115-117 1H-5, 115-117	5.65 7.15	0.19	3	
B *Collosphaera tuberosa*	1H-CC 2H-4, 85-87	9.80 15.15	0.40-0.59	1	Cores MD81-369, RC14-22 and VM34-35; DSDP 214 probably less accurate.
T *Pseudoemiliania lacunosa*	2H-5, 115-117 2H-6, 115-117	16.95 18.45	0.49	3	
B *Pterocorys hertwigii*	3H-4, 85-87 3H-CC	24.75 29.00	0.76-0.84	1	
T *Reticulofenestra* sp. A	4H-2, 118-119 4H-3, 115-117	31.68 33.15	0.82	3	
B *Gephyrocapsa parallela*	4H 5, 118-119 4H-6, 118-119	36.18 37.68	[a]0.89	4	
B Jaramillo	4H-6, 115-117 4H-7, 40-42	37.65 38.40	0.98	6	
B *Lamprocyrtis nigriniae*	4H-CC 5H-2, 85-87	38.60 40.95	1.02-1.07	1	
T *Gephyrocapsa* "large"[b]	5H-3, 115-117 5H-4, 115-117	42.75 44.25	[a]1.10	4	
T *Anthocyrtidium angulare*	5H-4, 85-87 5H-CC	43.95 48.20	0.94-1.04	1	
T *Lamprocyrtis neoheteroporos*	5H-4, 85 87 5H-CC	43.95 48.20	1.09-1.13	1	
T *Helicosphaera sellii*	6H-1, 115-117 6H-2, 115-117	49.35 50.85			No good published age; event appears to be diachronous.
B *Gephyrocapsa* "large"[b]	6H-2, 115-117 6H-3, 115-117	50.85 52.35	[a]1.36	4	
T *Calcidiscus macintyrei*	6H-3, 115-117 6H-4, 115-117	52.35 53.85	1.45	6	
B *Gephyrocapsa oceanica*	6H-3, 115-117 6H-4, 115-117	52.35 53.85	[a]1.57	4	
T *Pterocanium prismatium*	6H-4, 85-87 6H-CC	53.55 57.50	1.52-1.56	1	Rare in Hole 722A.
B *Gephyrocapsa caribbeanica*	6H-4, 115-117 6H-5, 115-117	53.85 55.35	[c]1.66	4,8	
T *Globigerinoides extermus*	6H-CC 7H-2, 65-67	57.50 59.65	[d]1.8	6	
B *Anthocyrtidium angulare*	6H-CC 7H-2, 85-87	57.50 59.85	1.52-1.64	1	
T *Discoaster brouweri*	7H-4, 114-116 7H-5, 115-117	63.14 69.65	1.90	6	
T *Discoaster pentaradiatus*	8H-5, 115-117 8H-6, 115-117	74.35 75.85	2.40	6	
Matuyama/Gauss	9H-4, 115-117 9H-5, 115-117	82.45 83.95	2.47	6	
B *Theocalyptra davisiana*	8H-CC 9H-CC	76.80 86.50	2.42-2.44	1	
B *Lamprocyrtis neoheteroporos*	8H-CC 9H-CC	76.80 86.50	2.51-2.53	1	
T *Stichocorys peregrina*	8H-CC 9H-CC	76.80 86.50	2.62-2.64	1	
T *Phormostichoartus fistula*	11X-4, 85-87 11X-CC	101.55 105.90	3.26-3.28	1	
T *Lychnodictyum audax*	11X-4, 85-87 11X-CC	101.55 105.90	3.33-3.35	1	
T *Sphenolithus abies*	11X-5, 115-117 11X-6, 115-117	103.35 104.85	3.47	6	
T *Reticulofenestra pseudoumbilica*	11X-CC 12X-1, 116-118	105.90 107.06	3.50	6	
T *Sphaeroidinellopsis* sp.	11X-CC 12X-2, 65-67	105.90 108.05	3.0	6	Rare in Hole 722A.
Gauss/Gilbert	11X-5, 115-117 12X-3, 115-117	103.35 110.05	3.40	6	
T *Phormostichoartus doliolum*	11X-CC 12X-4, 85-87	105.90 111.25	3.53-3.55	1	
B *Amphirhopalum ypsilon*	11X-CC 12X-4, 85-87	105.90 111.25	3.77-3.79	1	
coiling change in *Pulleniatina*	12X-4, 65-67 12X-CC	111.05 115.60	3.8	6	
B *Spongaster tetras tetras*	12X-CC 13X-4, 85-87	115.60 120.95	3.83-3.85	1	
S. berminghami to *S. pentas*[e]	12X-CC 13X-4, 85-87	115.60 120.95	4.3-4.44	2	? or lower.
T *Spongodiscus ambus*	14X-4, 85-87 14X-CC	130.65 134.90			
T *Didymocyrtis penultima*	14X-CC 15X-4, 85-87	134.90 140.25			
T Sidufjall	15X-5, 115-117 15X-6, 45-47	142.03 142.85	4.40	6	

Table 4 (continued).

Event	Core level	Depth (mbsf)	Age (Ma)	Source of age	Notes
T *Solenosphaera omnitubus*	15X-CC 16X-CC	144.60 154.30	4.7–4.8	2	
B *Sphaeroidinella dehiscens*	16X-2, 62–64 16X-4, 65–67	146.72 149.75	4.8	5	
B Thvera	16X-5, 40–42 16X-5, 123–125	151.00 151.83	4.77	6	
T *Discoaster quinqueramus*	17X-CC 18X-1, 115–116	163.90 165.05	5.6	6	Age appears to be erroneous.
T *Botryostrobus bramlettei*	18X-2, 85–87 18X-CC	166.25 173.60	4.9–5.0	2	
B *Globorotalia tumida tumida*	18X-2, 65–67 18X-4, 65–67	166.05 168.18	5.2	6	
T *Siphostichartus corona*	19X-4, 85–87 19X-CC	178.95 183.30	5.0–5.1	2	
Gilbert/Chronozone 5	19X-5, 113–115 19X-6, 115–117	180.73 182.25	5.35	6	
T *Stichocorys delmontensis*	19X-CC 20X-CC	183.30 193.00			
B *Pulleniatina primalis*	20X-4, 65–67 20X-CC	188.45 193.00	5.8	6	
T *Stichocorys johnsoni*	20X-CC 21X-CC	193.00 202.70	[f]5.7–5.8	2	
T *Acrobotrys tritubus*	22X-4, 85–87 22X-CC	208.05 212.40	5.3–5.4	2	Rare in Hole 722A.
B *Spongodiscus ambus*	22X-4, 85–87 22X-CC	208.05 212.40			
Chronozone 5/Chronozone 6	22X-6, 113–115 23X-6, 115–117	211.33 221.05	5.89	6	
S. delmontensis to *S. peregrina*[e]	22X-CC 23X-4, 85–87	212.40 217.75	6.1–6.7	2	
T *Calocycletta caepa*	24X-4, 85–87 24X-CC	227.35 231.70	6.2–6.6	2	Age in western Pacific.
T *Phormostichoartus marylandicus*	24X-CC 25X-CC	231.70 241.70			
B *Solenosphaera omnitubus*	25X-CC 26X-CC	241.70 251.00	6.3–6.5	2	
T *Diartus hughesi*	25X-CC 26X-CC	241.70 251.00	7.1–7.2	2	
B *Stichocorys peregrina*	26X-CC 27X-CC	251.00 260.70			
B *Discoaster quinqueramus*	28X-CC 29X-1, 114–116	270.40 271.54	8.2	6	
T *Dictyocoryne ontongensis*	28X-CC 29X-CC	270.40 280.00			
T *Botryostrobus miralestensis*	28X-CC 29X-2, 85–87	270.40 272.75	8.1–8.2	2	May be reworked.
B *Acrobotrys tritubus*	B29X-4, 85–87 29X-CC	271.25 275.60	7.7–7.8	2	Rare in Hole 722A.
T *Didymocyrtis laticonus*	29X-4, 85–87 29X-CC	271.25 275.60			
T *Diartus petterssoni*	29X-CC 30X-CC	275.60 285.30	8.1–8.2	2	
D. petterssoni to *D. hughesi*[e]	30X-CC 32X-CC	285.30 304.70	8.3–8.5	2	
B *Neogloboquadrina acostaensis*	31X-2, 65–67 31X-4, 65–67	287.45 290.45	8.6	7	
T *Stichocorys wolffii*	31X-CC 32X-4, 85–87	295.00 300.35	[g]8.0–8.2	2	
B *Botryostrobus bramlettei*	32X-4, 85–87 32X-CC	300.35 304.70	8.8–9.0	2	
T *Discoaster hamatus*	32X-CC 33X-1, 115–116	304.70 305.85	8.85	6	
B *Spongaster berminghami*	32X-CC 33X-CC	304.70 314.30	7.9–8.0	2	
B *Diartus hughesi*	32X-CC 33X-CC	304.70 314.30	8.7–8.8	2	
B *Discoaster hamatus*	34X-CC 35X-CC	324.00 333.70	10.0	6	
T *Cyrtocapsella japonica*	35X-4 35X-CC	329.35 333.70	10.0–10.3	2	
T *Globorotalia mayeri*	35X-CC 36X-2, 65–67	333.70 335.85	[h]10.4	6	
B *Globogerinoides nepenthes*	36X-CC 37X-4, 65–67	339.05 348.55	11.3	6	
T *Lithopera thornburgi*	37X-4, 85–87 37X-CC	348.75 353.10			
T *Cyrtocapsella cornuta*	37X-CC 38X-4, 85–87	353.10 358.45	11.6–11.9	2	

Table 4 (continued).

Event	Core level	Depth (mbsf)	Age (Ma)	Source of age	Notes
T *Globorotalia fohsi*	38X-4, 65–67 39X-CC	358.25 372.50	11.5	6	
B *Discoaster kugleri*	40X-2, 110–111 40X-CC	375.10 382.20	13.1	6	
T *Sphenolithus heteromorphus*	41X-1, 21–22 41X-2, 32–33	382.41 384.02	14.4	6	
T *Globorotalia peripheronda*	41X-CC 42X-2, 56–58	391.80 393.86	14.6	6	

Note: T = upper limit and B = lower limit. Sources of age are: 1 = Johnson et al., in press; 2 = Johnson and Nigrini, 1985; 3 = oxygen isotope data for Site 723 (N. Niitsuma, unpubl. data); 4 = Takayama and Sato, 1987; 5 = Barron et al., 1985; 6 = Berggren et al., 1985; 7 = van Gorsel and Troelstra, 1981; and 8 = Sato et al., in press.

[a] North Atlantic data.

[b] Long axis greater than 6 μm.

[c] North Atlantic age consistent with Italian-type section.

[d] *G. obliquus extremus* cited in Berggren et al., 1985.

[e] An evolutionary transition.

[f] *E.* cf. *diaphanes* cited in Johnson and Nigrini, 1985.

[g] Pacific Ocean data.

[h] *G. siakensis* cited in this source.

range of values is relatively narrow (~25 to 125 × 10^{-6} volume S.I. units). Hole 722A was APC-cored to 86.5 mbsf (Core 117-722A-9H), and recovery by drilling in XCB mode to 280.0 mbsf was generally very good. Occasionally, pipe-rust contamination of the XCB cores was so severe that many of the susceptibility features apparent in Holes 721B and 721C were obscured at Hole 722A. This condition generally prohibited intersite correlations below ~90 mbsf. However, within the common interval of APC recovery (above ~90 mbsf) susceptibility features between sites are correlatable to within the interval of measurement, or 5–10 cm (Fig. 15). Insufficient time was available at sea to create correlated composite sequences for Sites 721 and 722, this will be one of our main shore-based objectives.

Cyclicity in the susceptibility data of Holes 722A and 722B is apparent at ~1 m, 1–2 m, 3–4 m, and 12–14 m periods. Applying sedimentation rate of ~3.5 cm/k.y. obtained for Hole 722A, these periods correspond roughly to the 19–23 k.y., 41 k.y., 100 k.y., and ~400 k.y. periodicities of orbital insolation forcing. Below we discuss a preliminary analysis of the frequency spectra of the susceptibility data from Sites 721 and 722.

Hole 722B was APC-cored with full recovery to Core 117-722B-10H (91.9 mbsf), XCB-coring continued below this with generally good recovery to 565.6 mbsf (Fig. 16). As in Hole 722A, detailed intra- and intersite correlations are possible for the APC-cored sediments (Fig. 15). Detailed interhole correlations based on these data and lithologic marker layers are presented in the "Interhole Correlation" section (this chapter). The pipe-rust contamination seen in Hole 722A was less severe in Hole 722B, and this should permit some detailed correlations below the depth of APC recovery. Lithologic Unit I, a foraminifer-bearing nannofossil ooze extending to 221.5 mbsf, contains the low and cyclic susceptibility variations described previously (Fig. 16). Although Unit I contained couplets of alternating light greenish-grey and dark olive sediments within spacings of about 1 m, detailed comparison of these layers with the susceptibility data did not indicate a simple relationship between color and susceptibility. The siliceous nannofossil chalk facies of lithologic Unit II (221.5–343.4 mbsf) does not display any remarkable differences from lithologic Unit I in terms of the susceptibility data, except that the Unit II values are slightly higher. The cyclicity apparent in Unit I is also present in many of the less disturbed cores from Unit II. The cycles appear to have very regular ~1-m periods (Fig. 17). The susceptibility data representative of lithologic Unit III (nannofossil chalk; 343.4–411.1 mbsf) are sparse due to the very poor recovery of this interval. Slightly increased susceptibility values were observed for Unit III. The susceptibility cyclicity apparent in lithologic Units I and II is also present in some of the less disturbed sections of Unit III. Again, the predominant cyclicity is at ~1-m periods (Fig. 17). Lithologic Unit IV consists largely of silty claystone turbidites interbedded with pelagic nannofossil chalks. As in Hole 721B, this unit coincides with a dramatic increase in susceptibility of nearly two decades (Fig. 16). The data of Unit IV do not have the cyclic periodicities which were present in the previous lithologic units; the increase in values is most likely in response to the increased grain size and concentration of ferrimagnetic grains.

Spectral Analysis

Noting that the frequencies of susceptibility variation were roughly coincident with those predicted by Milankovitch orbital insolation anomalies, we analyzed the frequency spectra of two susceptibility records. Since core quality and recovery were best for the APC cores, the data from the first nine APC cores of Holes 721B (to 86.0 mbsf) and 722A (to 86.5 mbsf) were selected for spectral analysis. A principal constraint for our analyses, however, was the lack of detailed age-depth data. For both holes, the only firm datums available were the Jaramillo/Matuyama boundary (0.98 Ma) and the Matuyama/Gauss boundary (2.48 Ma). Depth tabulations of these datums for Hole 722A and 721B are shown in Table 5 (this chapter) and Table 7 of the "Paleomagnetism" section in the "Site 721" chapter (this volume). The susceptibility data for both holes were linearly interpolated to age, resampled to equal age increments of 1.5 k.y. and linearly detrended. The total time-series represented is 0 to ~2.7 Ma for Hole 721B, and 0 to ~2.6 Ma for Hole 722A.

The frequency spectra program used in this analysis uses a windowing procedure in which the data set is subdivided into a series of overlapping data subsets, or windows. Each window is one-quarter length of the entire data set (~0.68 Ma for Hole 721B, ~0.65 Ma for Hole 722A). The power spectrum is calculated for the first window, then the window position shifts downward to a level equal to one-eighth of the data-set length, and then the power spectrum of the second window is calculated. For a given data set, spectra are calculated for seven consecutive, overlapping windows.

The resulting frequency power spectra for Holes 721B and 722A are shown in Figure 18. Vertical lines are drawn to show the positions of the principal orbital periodicities of precession (19 k.y., 23 k.y.), obliquity (41 k.y.), and eccentricity (100 k.y., ~400 k.y.). Although the age models are crude, the calculated power spectra of both holes suggest that orbital periodicities are

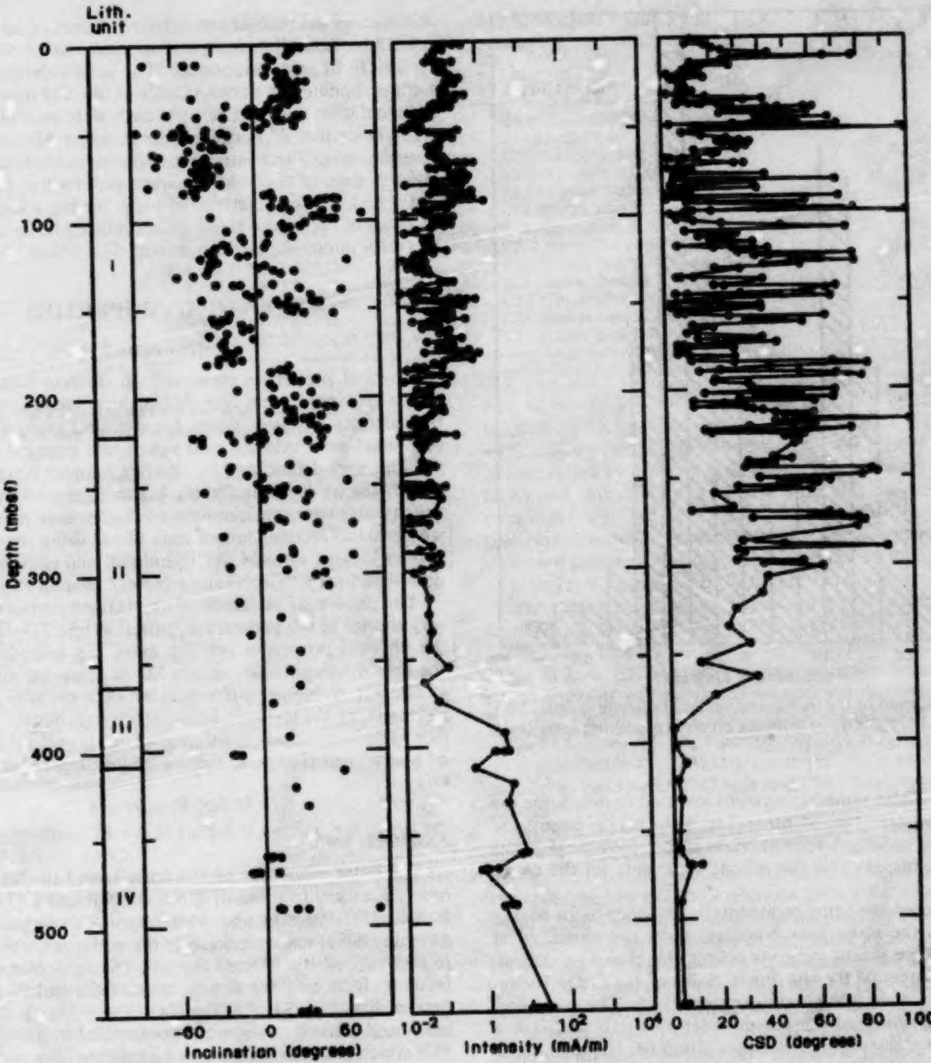

Figure 12. Inclination, intensity, and circular standard deviation (CSD) for the combined discrete sample sets from Holes 722A and 722B.

present in the susceptibility data. The windowing procedure illustrates two important aspects of the observed power spectra. First, the 23 k.y./19 k.y. precessional couplet can be seen to shift in unison toward slightly higher and lower frequencies than expected. This suggests that the orbital spectra are present but are displaced due to age model inadequacies. Second, the distribution of power among the 100 k.y., 41 k.y., 23 k.y., and 19 k.y frequencies is highly variable between windows. Although this may also be a consequence of crude age modeling, the general shift in both Holes 721B and 722A from high 100-k.y. power for the youngest windows (0–~1.0 Ma) to high 41 k.y. power for the oldest windows (~1.0–2.6 Ma) may be significant in terms of paleoclimate. This tentative interpretation is consistent with oxygen-isotope and sea-surface temperature data from the North Atlantic which indicate that the predominantly 41-k.y. periodicity of ice-sheet-induced climate variability during the late Pliocene to middle Pleistocene shifted to a predominantly 100-k.y. periodicity during the late Pleistocene (Pisias and Moore, 1981).

ACCUMULATION RATES

Sedimentation rates for Site 722 are based on the mean depth and age magneto- and biostratigraphic datum levels identified in Holes 722A and 722B (Table 4 and Fig. 19). Because of uncertainties in the shipboard paleomagnetic data (see "Explanatory Notes" section, this volume), we favor the nannofossil biostratigraphic datums for the determination of the sedimentation rates at Leg 117 sites. For the interval from 0 to 2.4 m.y., we used six nannofossil datums with ages based on oxygen isotope stratigraphy (Niitsuma, unpubl. data) and from Berggren et al. (1985) to determine variations in the mean sedimentation (Ta-

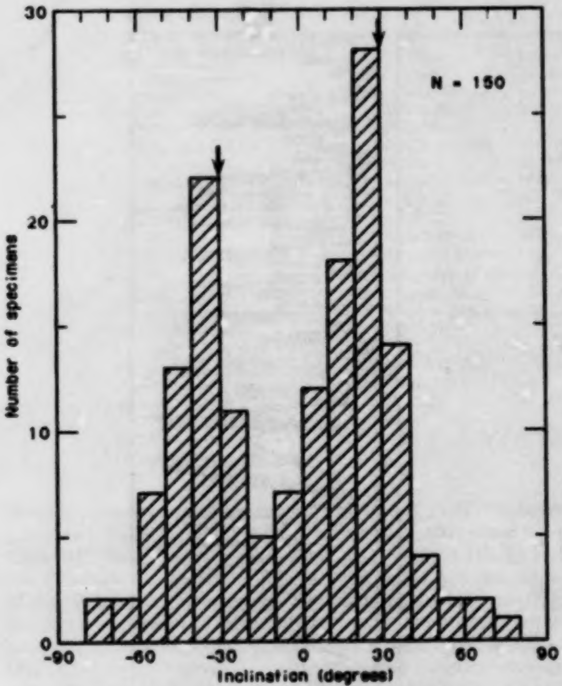

Figure 13. Histogram of the inclination values of discrete samples from Holes 722A and 722B. Arrows show the expected geocentric axial dipole inclination values for the site latitude.

bles 4 and 7). These same biohorizons are used to determine the mean sedimentation rate at other Leg 117 sites to permit the comparison of sediment accumulation of hemipelagic deposits on the Oman margin and the pelagic sediments on the Owen Ridge.

Site 722 cored the same sedimentary sequence as in nearby Site 721, and the same four lithologic units are identified at both sites. These lithologic units reflect the changing depositional environment of the site due to uplift of the Owen Ridge, and variations in surface plankton productivity. The cored section at Site 721 contains a hiatus between Units III and II and postdepositional disturbance of Units II and IB. However, these intervals appear complete and undisturbed in Site 722. Because of poor age control in the turbidite sequence of lithologic Unit IV, no estimate of sedimentation can be made at this time.

Lithologic Unit III, a nannofossil chalk deposited in the middle Miocene, is characterized by relatively low mean sedimentation rates of 8–15 m/m.y. These low rates reflect pelagic sedimentation above the zone of turbidite deposition but still in waters corrosive to calcium carbonate. The transition from Unit III to II is identified by an increase in opal and organic-carbon-rich sediments which characterize lithologic Unit II. High sedimentation rates which average 54 m/m.y. are associated with these upper Miocene opal-rich sediments (Fig. 20 and Table 7).

The nannofossil oozes/chalks of lithologic Unit I ranging from late Miocene to Holocene were deposited at rates of 17–45 m/m.y. (Fig. 20 and Table 7). These are similar to the rates at Owen Ridge Sites 721 and 731 over this same time interval and of pelagic sedimentation in other areas, but are two to five times lower than rates during comparable time intervals from hemipelagic deposits on the Oman margin.

The mass accumulation rates of calcium carbonate, noncarbonate (100 - $CaCO_3$), and organic carbon are calculated from the average values between selected datums (Table 7 and Fig. 20). These data allow independent examination of the temporal variability in each component. The accumulation rates of calcium carbonate and noncarbonate at Site 722 mostly mirror the sedimentation rate, and calcium carbonate accumulation is generally twice that of noncarbonate in upper Miocene to Pleistocene deposits. These rates are similar to those found at carbonate-rich sites in the eastern equatorial Pacific (Theyer et al., 1985) and are characteristic of areas having a high production of calcium carbonate shells of coccolithophores and foraminifers with minimal postdepositional dissolution.

PHYSICAL PROPERTIES

Introduction

Physical properties measured on discrete samples of sediments recovered from Site 722 include index properties (wet-bulk density, porosity, water content, and grain density), compressional-wave velocity, and vane-shear strength. The properties that were determined for discrete samples from Holes 722A and 722B are listed in Tables 8 and 9, respectively. Wet-bulk density and compressional-wave velocity were measured on all whole-round sections longer than 80 cm using the GRAPE and *P*-wave logging systems. All techniques and equipment used are described in the "Explanatory Notes" chapter (this volume).

The pattern of variation of physical properties at Site 722 is very similar to the pattern recognized at Site 721. Transitions in the physical properties profiles mark the boundaries between the four lithologic units at Site 722 in a manner similar to that at Site 721. Principal differences between the sites are a greater thickness of low-density, high-porosity sediments of the opal-rich nannofossil chalk in lithologic Unit II and a thicker interval of gradational change at the top of lithologic Unit III.

Index Properties

Lithologic Unit I

The index properties of lithologic Unit I (0–221.5 mbsf) are nearly identical to those of lithologic Subunit I (0–261.2 mbsf) at Site 721. Porosity and water content averages range from 64% and 40%, respectively, near the seafloor to 59% and 35%, respectively, at the base of the unit (Fig. 21). Wet-bulk density increases from 1.65 g/cm^3 near the seafloor to 1.74 g/cm^3 at the base of lithologic Unit I (Fig. 21). The wet-bulk density minimum and porosity maximum between 90 to 110 mbsf at Site 722, which coincide with an increase in the clay percentage, are also present at similar depths at Site 721.

Lithologic Unit II

Lithologic Unit II (221.5–343.4 mbsf) includes sediments with anomalously high porosity and water content and low grain and bulk densities (Fig. 21) in association with an increased abundance of siliceous microfossils. The maximum porosity within Unit II is 76%, and the minimum grain and wet-bulk densities are 2.30 g/cm^3 and 1.42 g/cm^3, respectively. Lithologic Unit II at Site 722 is approximately 72 m thicker than the corresponding interval at Site 721. The upper 60 m of the unit maintains the porosity and density trends of lithologic Unit I, but displays more widely varying properties than Unit I.

Lithologic Unit III

Lithologic Unit III (343.4–411.1 mbsf) contains an upper interval, 40 m thick, in which porosity rapidly decreases with depth from 60% to 45% and wet-bulk density increases from 1.74 to 2.02 g/cm^3 (Fig. 21). This interval of gradational change is not present at Site 721 where the top of lithologic Unit III (309.9–340.7 mbsf) is marked by an unconformity and an abrupt change

Table 5. Location and age or inferred polarity transitions at Site 722.

Hole, core, section, interval (cm)	Depth (mbsf)	Transition	Age (Ma)
722A-4H-6, 115/4H-7, 40	37.65/38.40	C1r-1 (Jaramillo) Bottom	0.98
722A-9H-4, 115/9H-5, 115	82.45/83.95	C2A (Gauss) Top	2.47
722A-11X-5, 115/12X-3, 115	103.95/110.05	C2A (Gauss) Bottom	3.40
722A-15X-5, 115/15X-6, 45	142.03/142.85	C3.2r-1 (Sidufjall) Top	4.40
722A-16X-5, 40/16X-5, 123	151.00/151.83	C3.3 (Thvera) Bottom	4.77
722A-19X-5, 113/19X-6, 115	180.73/182.25	C3A (Chronozone 5) Top	5.35
722A-22X-6, 113/23X-6, 115	211.33/221.05	C3A (Chronozone 5) Bottom	5.89
722B-5H-4, 100/5H-5, 30	39.80/40.60	C1r-1 (Jaramillo) Bottom	0.98
722B-10X-1, 110/10X-2, 100	83.80/85.20	C2A (Gauss) Top	2.47
722B-12X-2, 100/12X-3, 108	104.00/105.58	C2A (Gauss) Bottom	3.40
722B-17X-2, 100/17X-4, 100	152.40/155.40	C3.3 (Thvera) Bottom	4.77
722B-20X-2, 99/21X-1, 110	181.39/189.60	C3A (Chronozone 5) Top	5.35
722B-24X-1, 100/24X-3, 100	218.50/221.50	C3A (Chronozone 5) Bottom	5.89

Table 6. Core orientation data for Site 722: comparison of multishot and measured mean core declination estimates.

Hole and core	Multishot orientation (°)	Measured mean core declination (°)	Corrected mean core declination (°)
722A-5H	303	61 (N)	118
722A-6H	110	90 (R)	340
722A-7H	305	301 (R)	356
722B-6H	260	157 (R)	257
722B-8H	224	180 (R)	316
722B-9H	157	239 (R)	82
722B-10H	332	252 (R)	280

Note: N = normal polarity; and R = reversed polarity. Corrected mean core declination = measured mean core declination/multishot orientation. The resultant value should be 0° for normally magnetized cores and 180° for reversely magnetized cores.

in physical properties. Below 383 mbsf the index properties are nearly constant with depth.

Lithologic Unit IV

Lithologic Unit IV at Site 722 (411.1–565.6 mbsf) displays a uniform decrease in porosity and increase in wet-bulk density nearly identical to that of lithologic Unit IV at Site 721 (340.7–424.2 mbsf). Porosity decreases in Unit IV from 45% to 42%, and wet-bulk density increases from 1.95 to 2.05 g/cm^3 (Fig. 21). This unit was drilled to a greater depth at Site 722, and near the depth of maximum penetration, well-lithified sandstones were recovered in Cores 117-722B-55X (517 mbsf) and 117-722B-56X (527 mbsf). Index properties were only obtained from a sample from Core 117-722B-55X. The porosity and wet-bulk density of this sample are 12% and 2.71 g/cm^3, respectively.

Compressional-Wave Velocity

At Site 722 compressional-wave velocities were measured perpendicular to bedding (V_v) on discrete samples from all cores recovered from Holes 722A and 722B from which suitable samples could be prepared. Velocities were also measured parallel to bedding (V_h) on samples from Hole 722B that were sufficiently indurated to allow a cubic sample to be cut using a razor blade or rock saw. Variation in compressional-wave velocities measured in the sediments recovered from Site 722 is comparable to that found at Site 721 at all sub-bottom depths. In spite of the wide variation of the data, general trends, similar to those at Site 721, can be identified and correlated with index properties.

Within the nannofossil ooze of lithologic Unit I, V_v increases gradually with depth and with decreasing porosity (Fig. 22). Surficial values near 1500 m/s increase to about 1600 m/s at the base of lithologic Unit I (221.5 mbsf). In the upper portion of lithologic Unit II, the gradual decrease in bulk density associated with an increasing abundance of siliceous microfossils is accompanied by a decrease in compressional-wave velocity. Velocity and bulk density minima of 1520 m/s and 1.42 g/cm^3 are coincident near 315 mbsf. Near the base of lithologic Unit II, the sediments are sufficiently indurated to allow velocities to be measured parallel to bedding (Fig. 22). Within the basal sequence of Unit II, V_h averaged 2.1% higher than V_v.

The gradual reduction in abundance of the siliceous microfossils in the lower portions of lithologic Unit II is marked by an increase in velocity that continues throughout the nannofossil chalk of Unit III. Markedly higher velocities were measured in two samples of well-indurated nannofossil chalk from lithologic Unit III; Sample 117-722B-41X-1, 22–24 cm, and Sample 117-722B-43X-1, 40–42 cm, transmit compressional-waves perpendicular to bedding at 1944 m/s and 1902 m/s, respectively, and parallel to bedding at 2064 m/s and 2022 m/s, respectively (Fig. 22 and Table 9).

At Site 722, as at Site 721, velocities in lithologic Unit IV vary widely despite a relatively uniform increase in density with depth. Throughout this unit, velocities are 50 to 200 m/s less than predicted by empirical relations for similar lithofacies (Hamilton, 1978). Bedding-parallel velocities are comparably low.

Given the high variability of the velocity data at Site 722, velocity-density relations for these sediments are loosely defined (Fig. 23). The general trends displayed by the nannofossil ooze/chalk, diatomaceous-nannofossil chalk, and clay-rich turbidites are however distinct. Compressional-wave velocity increases more rapidly with density in the clay-rich units than in the more calcareous sequences. The diatomaceous-nannofossil chalks of lithologic Unit II show the weakest correlation between velocity and density, and the most gentle velocity-density gradient.

Anisotropy of the compressional-wave velocities for both the nannofossil ooze/chalk of lithologic Units I through III and the clay-rich sequences of Unit IV are displayed on a crossplot of V_v and V_h (Fig. 24). In the calcareous sediments, anisotropy tends to increase with density from an average of 2.4% in Cores 177-722B-34X to -40X to 58% in the indurated chalks of Core 117-722B-41X and -43X. It is also evident, however, as it has been to other investigators (e.g., Carlson et al., 1983), that anisotropy of calcareous sediment can vary significantly with density. In the clay-rich sequences, anisotropy shows no consistent relationship with density.

GRAPE and *P*-Wave Logs

GRAPE and *P*-wave logger records are of similar quality and character as those at Site 721. Large-scale features such as the density minimum between 90 and 110 mbsf and the transition interval at the top of lithologic Unit III are evident on the logs

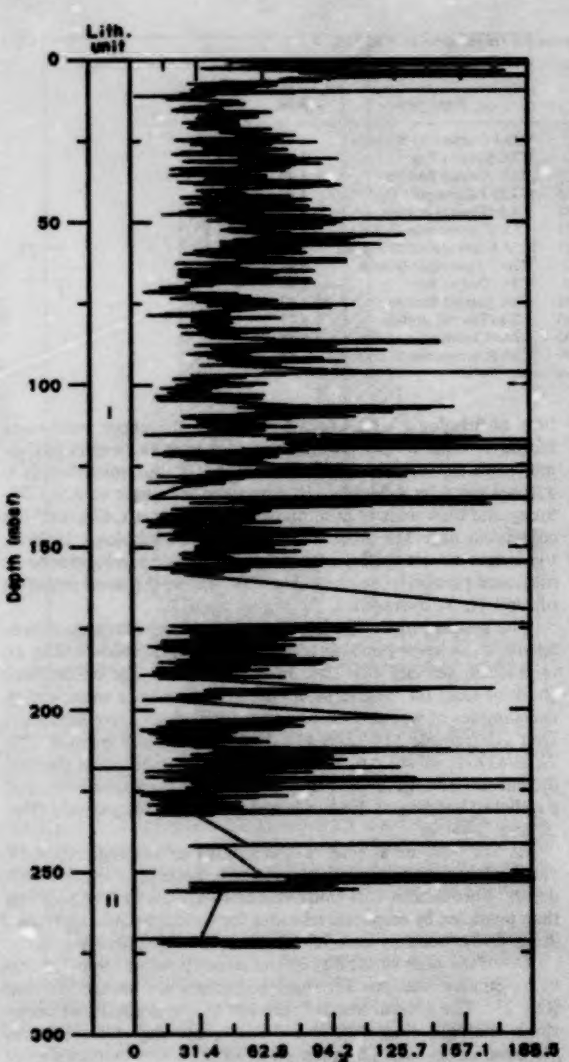

Figure 14. Hole 722A volume magnetic susceptibility data.

(Fig. 25). Smaller-scale cyclic variation, on the order of 1 m, is present in the GRAPE and *P*-wave records from lithologic Unit I. These features can be correlated between holes at Site 722 and between Site 722 and Site 721 (Fig. 26).

Vane Shear Strength

Vane shear strengths were measured in seven APC and one XCB cores from Hole 722A (Table 8). Shear strengths were comparable to those measured at Site 721, ranging from 19.1 kPa at 5.0 mbsf to 73.1 kPa at 62.5 mbsf.

SEISMIC STRATIGRAPHY

The Owen Ridge is an asymmetric linear feature in the western Arabian Sea that trends northeastward and dips gently to the west (see Fig. 1). At DSDP Site 224, the ridge is uplifted lamprophyre basement overlain by claystones, chalks, and turbiditic sequences of Eocene to Miocene that are in turn capped by Miocene and younger pelagic sediments (Whitmarsh et al., 1974; Whitmarsh, 1979).

The seismic stratigraphy of the ridge is complex and includes irregular basement features, large-scale onlap of turbidite and other facies, numerous slump scars and large slump(?) canyons, as well as several prominent sub-bottom reflectors. To interpret the seismic stratigraphy of Site 722, we have used several single channel seismic (SCS) profiles from the Leg 117 site survey by the *Robert Conrad* (RC2704), in combination with the drilling results from Site 722 (see "Lithostratigraphy" section, this chapter). Downhole logging data from Site 722 (see "Downhole Measurements" section, this chapter), as well as the SCS data obtained during the site approaches by the *JOIDES Resolution*, were also used for this synthesis. Figure 27 shows the location of the SCS tracks used in this discussion in relation to the bathymetry of the Owen Ridge (Sea Beam data from the site survey; Prell, unpubl. data).

The sedimentary sequence at Site 722 is relatively complete with no major hiatuses. Thus, we use the results of drilling and logging at Site 722 and SCS Line 38 to define the relationship between reflector sequences and the lithologic section of the northern Owen Ridge. Here we discuss the synthetic seismogram generated from the downhole logging data and summarize the identification and lithologic significance of the important reflectors within the seismic section at Site 722.

Synthetic Seismogram

Based on sonic and density logs obtained at Site 722, a synthetic seismogram was calculated. We used a convolutional model with interbed multiples. The wavelet utilized is an estimate of the water-gun source signature of *Robert Conrad* (see "Downhole Measurements" section, "Site 720" chapter, this volume). The synthetic seismogram begins at the first open-hole log data (93 mbsf) and extends to the deepest sonic data obtained (543 mbsf). The synthetic seismogram and the acoustic impedance log, on which the synthetic was based, are shown in Figure 28.

Site 722

Correlation of the major reflectors recognized in the seismic profile (Line 38, Figs. 27, 28, and 29) with the synthetic seismogram and lithologic units at Site 722 is shown in Figure 28. The traveltime-depth relationship of the lithologic units is shown in Figure 30. The reflectors are identified by an alpha-numeric code and are discussed in order of increasing depth below seafloor.

At Site 722, the upper 0.33 s of the seismic profile is characterized by parallel, conformable reflectors that represent the pelagic drape deposited on the Owen Ridge after the early Miocene.

Reflector A occurs at 0.33 s and is a high-amplitude return that is coincident with the top of the siliceous lithologic Unit II in Site 722 (Fig. 30). In the synthetic seismogram, the reflector corresponds to the largest peak in a triplet of peaks associated with the transition from lithologic Unit I to II (Fig. 28). It can be easily traced through Line 39 to the the crest of the ridge (Line 40, Fig. 39, "Seismic Stratigraphy" section, "Site 721" chapter, this volume).

Reflector B is a series of reflectors that are associated with the siliceous and chalk units at Site 722. B_1 marks the bottom of a package of four closely spaced conformable reflectors that have a distinctive pattern and are coincident with the lower part of siliceous lithologic Unit II in Site 722 (Figs. 28 and 30). The top of this package is also observed as a reflector and is associated with a hard streak in the drilling (Fig. 30). Reflector B_1 is observed in the synthetic as a small peak that coincides with the siliceous-chalk transition and the ramp of increasing impedance (Fig. 28). B_1 was selected as a key reflector because it corre-

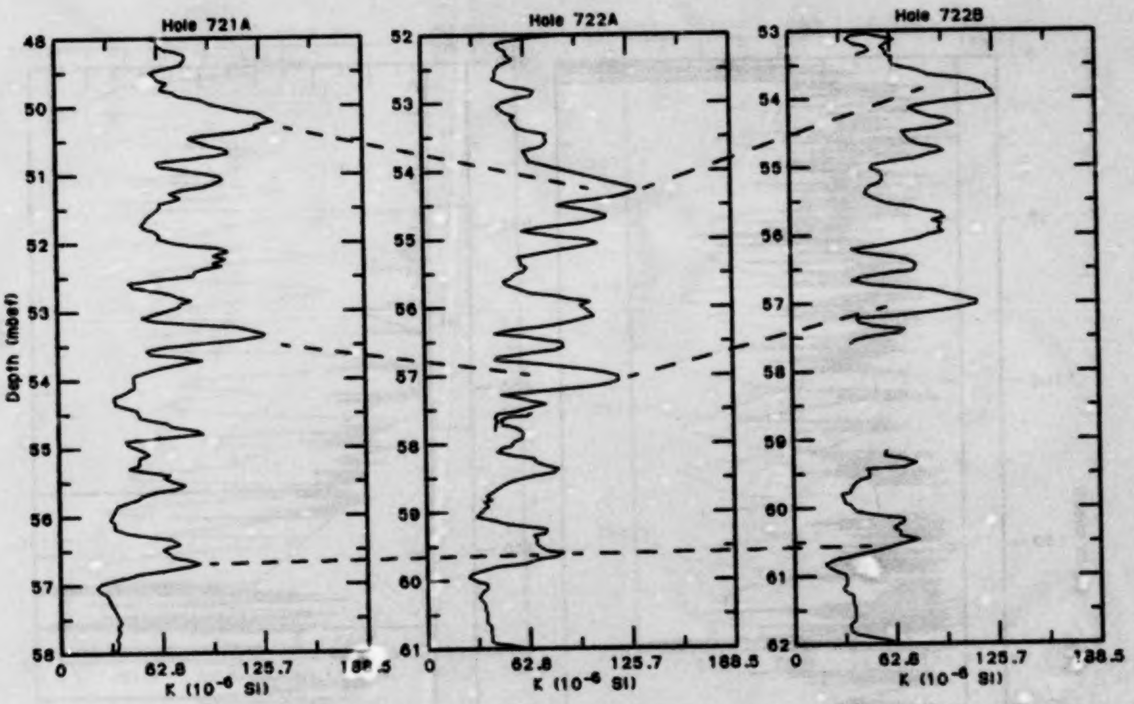

Figure 15. Intra- and intersite correlations between Holes 722A, 722B, and 721A using magnetic susceptibility.

sponds to a specific lithologic boundary. B_1 is easily traced to the crest of the ridge, but is missing at Site 721 ("Seismic Stratigraphy" section, "Site 721" chapter, this volume). B_2 is a low-amplitude reflector that correlates with the top of the chalks in the lower half of lithologic Unit III at Site 722 (Fig. 30). These chalks a have higher velocity and a higher density than the surrounding lithologies, but the synthetic shows only a small peak (Fig. 28), because the two-way traveltime through the high-velocity chalks is less than the duration of the wavelet. The amplitude of seismic reflector B_2 increases between Site 722 and the crest of the ridge and is probably related to the pronounced hiatus identified at this level in Site 721, which brings lower velocity siliceous sediments in contact with the much faster lower chalk unit. As Site 722 does not contain this hiatus, the corresponding high amplitude of reflector B_2 was not found at Site 722. Reflector B_3 coincides with the boundary between the chalk (lithologic Unit III) and the turbiditic sediments of lithologic Unit IV at Site 722 (Figs. 28 and 30). It appears in the synthetic seismogram as a distinct peak/trough pair that corresponds with a sharp drop in impedance across the chalk-turbidite transition.

Seismic reflector C is the uppermost strong return of a thick series of generally parallel reflectors that are generally correlated to turbidite deposits within lithologic Unit IV at Site 722 (Figs. 28 and 30). Reflector C is not, however, the top of lithologic Unit IV, which is marked by B_3. The synthetic seismogram shows one large peak between reflectors C and B_3 that is lower in amplitude on the seismic profile. About 0.05 s below C in the vicinity of Site 722, the reflector pattern is laterally heterogeneous, because of onlapping fill of a small topographic low.

Regional Seismic Stratigraphy

On a larger scale, the seismic stratigraphy of the sediments capping the crest of the Owen Ridge reveals that Site 722 overlies a basement high. The sediment thickness at Site 722 is about 0.82 s. The sediments overlie an irregular reflector, interpreted as basement, that dips to the west and is truncated against the eastward facing scarp of the Owen Ridge. Overlying portions of the basement (especially in the strike section, Line 38, Fig. 29) is a zone of diffuse reflections from about 0.82 to 0.67 sbsf. This diffuse zone thins and laps onto the basement peaks and is succeeded by a thick sequence of strongly reflective layers that lap onto the underlying sediments. This sequence is capped by reflector C and is interpreted as the clastic-turbidite facies of Oligocene to Miocene age that was observed at DSDP Site 224 (Whitmarsh et al., 1974) and at the base of Site 722. The surface of the turbidite facies (reflector C) dips only slightly to the north but about 4° to the west.

These new seismic data support the idea that the Owen Ridge is uplifted oceanic crust that was initially covered by flat-lying claystones and siltstones resulting from turbiditic and gravity deposition. These sediments lapped onto the basement highs and their drapes of older sediments to almost the level of the seafloor. No basement peaks are observed above reflector C. Uplift of the turbidite sequences (reflector C and below) probably began in early Miocene, because this is the last occurrence of turbidites in the sequence. However, some onlap can be observed prior to reflector C so that uplift may have begun earlier. Following the termination of the turbidite deposition, the ridge at Site 722 has been the locus of pelagic deposition since the late early Miocene. The reflectors within this pelagic cap largely reflect changes in the lithology of the pelagic sediments.

INORGANIC GEOCHEMISTRY

Introduction

Twenty interstitial water samples were collected throughout the four lithostratigraphic units at Site 722, nineteen by squeezing and one using the Barnes *in-situ* sampler. Samples were col-

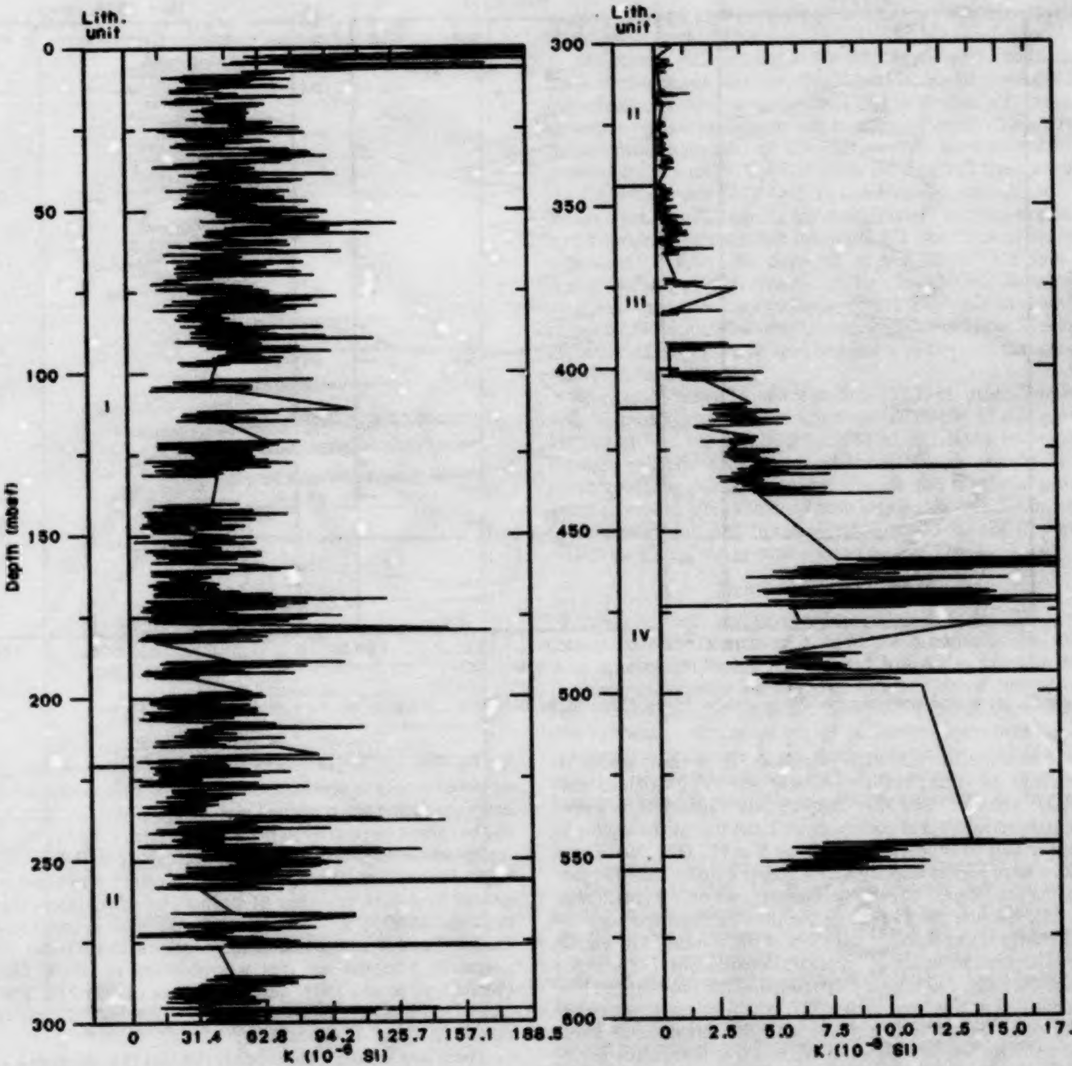

Figure 16. Hole 722B volume magnetic susceptibility data.

lected from Hole 722A down to 254 mbsf, and from the lower half of Hole 722B down to a total depth of 552 mbsf. All data are presented in Table 10, while Figure 31 combines analyses from both holes.

Salinity, Chlorinity, and pH

The concentration profiles of salinity, chloride and pH are shown in Figure 31. In comparison with Site 721, the salinity profile shows very little structure, and certainly no marked decrease over the top ~100 mbsf. In contrast, the chloride profile indicates an increase in concentration from 549 mmol/L in Core 117-722A-1H to ~570 mmol/L at 438 mbsf. This gradient of 0.048 mmol/L/m is approximately constant over lithostratigraphic Units I, II, and III. Within Unit IV (turbidites), the salinity decreases slightly, while a marked drop in interstitial chloride concentration (~20 mmol/L) indicates a very different pore water chemistry in this lithology (see discussion below). The chloride minimum at 464 mbsf is accompanied by a local minimum in salinity (Fig. 31). The reason for these relatively abrupt changes is unknown, but they do appear to be real and not analytical artifacts.

The pH ranges from 7.19 to 7.79 over the cored section and displays a vertical structure very similar to that in Hole 721. These values, which in all cases are lower than that of seawater, probably reflect release of H^+ during H_2S dissociation. The high pH value at 252 mbsf in Core 117-722B-27X-4 probably occurred as a sampling artifact as a delayed measurement allowed CO_2 to degas from the sample.

The *in-situ* sample at 276 mbsf was characterized by an anomalous salinity of 34.4 g/kg, a high magnesium level, slightly ele-

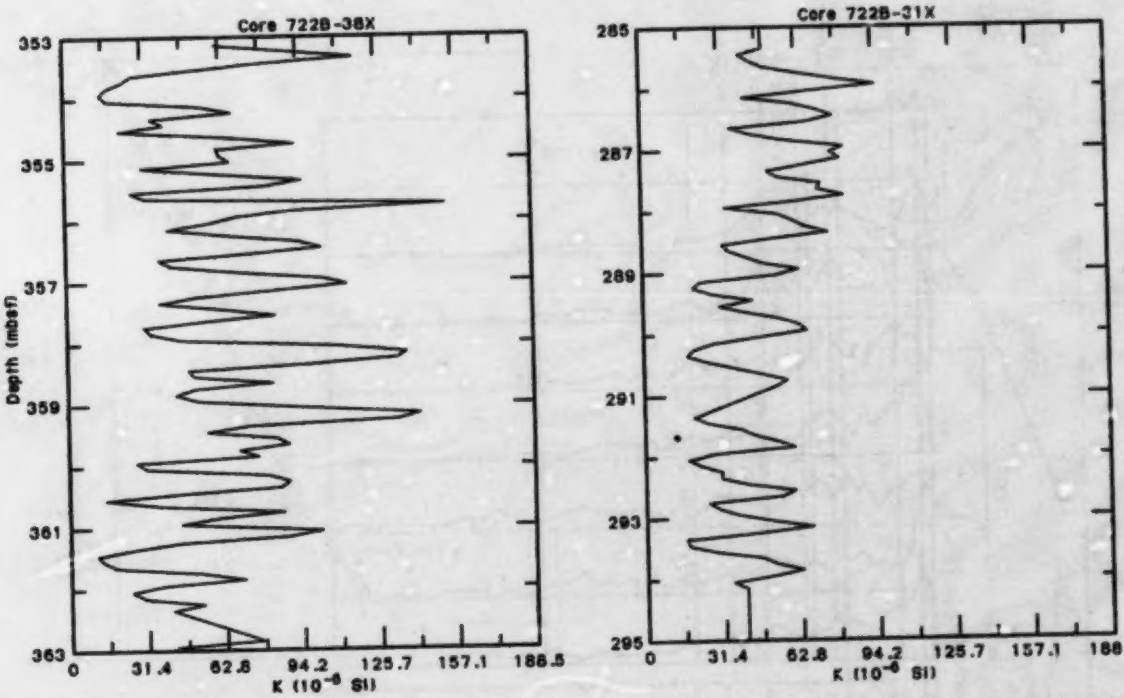

Figure 17. Susceptibility data from lithologic Unit III (Core 117-722B-38X) and lithologic Unit II (Core 117-722B-31X). Note that both lithologic units display cyclic susceptibility variations over less than 1 m. Measurement interval is 10 cm.

Table 7. Sedimentation and accumulation rate data for Site 722.

Depth interval (mbsf)	Age range (m.y.)	$CaCO_3$ ($\bar{x}$ %)	C_{org} ($\bar{x}$ %)	Dry-bulk density ($\bar{x}$ g/cm^3)	Sed. rate ($\bar{x}$ m/m.y.)	$CaCO_3$ acc. rate (g/cm^2/k.y.)	Non-$CaCO_3$ acc. rate (g/cm^2/k.y.)	C_{org} acc. rate (mg/cm^2/k.y.)
0–6.4	0–0.19	62.7	0.35	1.017	33.7	2.15	1.28	12.0
6.4–17.7	0.19–0.49	75.4	ND	0.991	37.7	2.82	0.92	ND
17.7–32.4	0.49–0.82	69.9	0.85	0.981	44.5	3.05	1.31	37.1
32.4–53.1	0.82–1.45	66.2	ND	1.029	32.9	2.24	1.14	ND
53.1–66.4	1.45–1.90	59.2	1.13	1.094	29.6	1.92	1.32	36.6
66.4–75.1	1.90–2.40	71.5	ND	1.091	17.4	1.36	0.54	ND
75.1–120.0	2.40–4.0	70.1	1.26	1.032	27.7	2.00	0.85	36.0
120.0–251.0	4.0–7.1	70.8	1.20	1.082	42.3	3.24	1.34	54.9
251.0–305.0	7.1–8.1	52.9	1.23	1.021	54.0	2.92	2.60	67.9
305.0–380.0	8.1–13.1	49.4	1.31	1.070	15.0	0.79	0.81	21.0
380.0–392.0	13.1–14.6	91.2	ND	1.541	8.0	1.12	0.11	ND

Note: ND = no data for the interval.

vated sulfate, and a lowered silicate concentration. We believe that this sample was at least partially contaminated with seawater during sampling.

Sulfate and Alkalinity

Sulfate reduction at Site 722 is pronounced over the top ~100 meters of the core, but is measurable down to a depth of 208 mbsf. Consumption of sulfate as an oxidant during degradation of organic matter results in an increase in HCO_3^- and hence in alkalinity from 5.0 mmol/L in Core 117-722A-1H to 9.1 mmol/L in Core 117-722A-9H at 83 mbsf. In a fashion similar to Site 721, the alkalinity deficit is probably due to authigenic carbonate precipitation. However, assuming that similar solubility controls exist at both sites, the deeper penetration of sulfate and lower maximum alkalinity value may indicate that the content of degradable organic matter is more limited at Site 722.

Below the maximum at 83 mbsf, alkalinity decreases linearly (0.023 mmol/L/m) to a depth of ~400 mbsf. Over the remaining ~150 m of Hole 722B the alkalinity is almost constant at 1.6–1.8 mmol/L. The break in gradient at 400 mbsf coincides with the depth at which SiO_2 is consumed in diagenetic reactions (see discussion below) in the marly nannofossil chalk of Unit III. Alkalinity is consistently <2 mmol/L throughout the turbidites of Unit IV. The lack of curvature in the profile at depth suggests that diagenetic reactions involving carbonate precipitation are limited.

The sulfate increase below 317 mbsf is somewhat of an enigma. Three possibilities for the occurrence of the sulfate may be advanced (we believe no artifacts were introduced in either the sample collection or analysis): (1) seawater became "trapped" during rapid turbidite emplacement and "sealed" with a pelagic clay drape; (2) the cored section has penetrated sulfate-rich

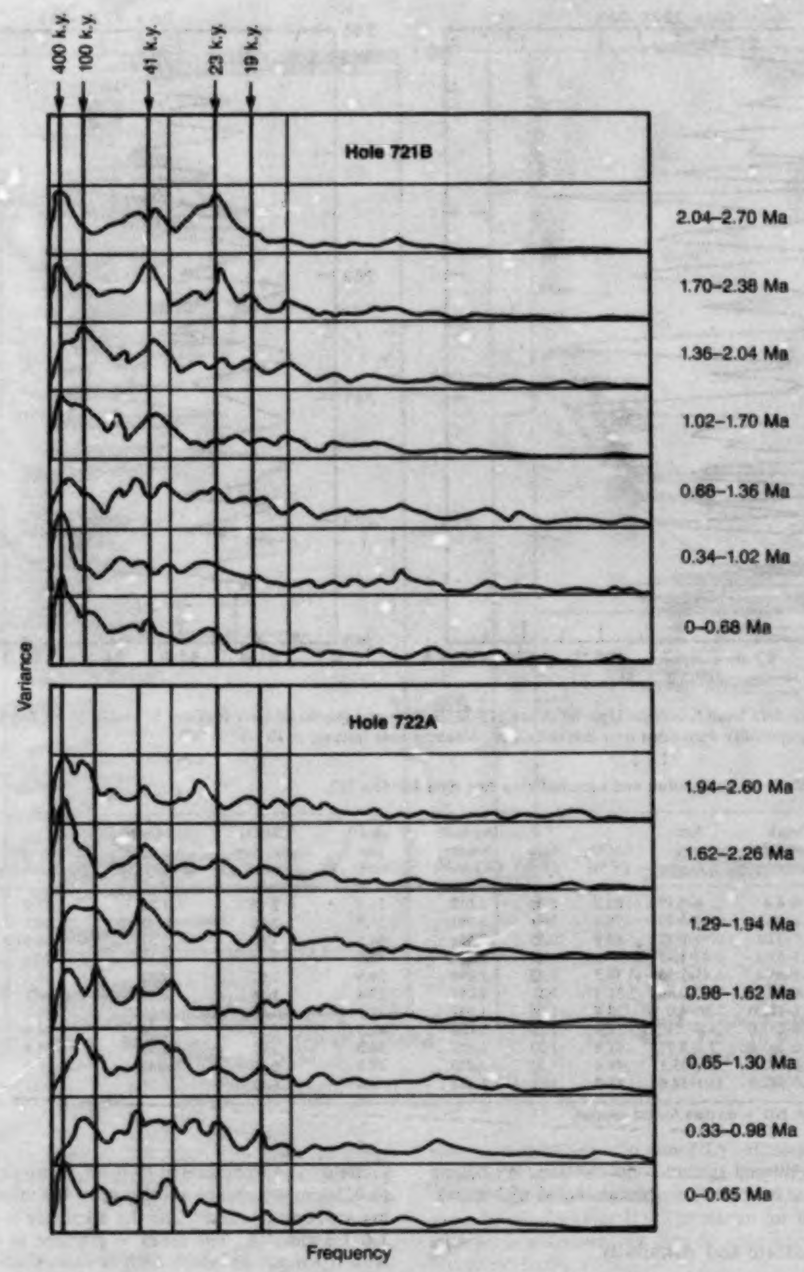

Figure 18. Spectral analysis results for Hole 721B (0–~2.7 Ma) and Hole 722A (0–~2.60 Ma) susceptibility data. Vertical lines indicate the positions of the orbital periodicities at ~400, ~100, 41, 23, and 19 k.y.

brines; or (3) dewatering during compaction and lithification of the sandstones has led to minor pyrite oxidation. Hypothesis (1) requires restricted diffusion of SO_4^{2-} over the last 15 Ma. With our present knowledge of SO_4^{2-} diffusivity and accumulation rates in Unit IV (>5 m/m.y.), the sulfate content of the trapped sea water is unlikely to be preserved (the diffusion path length would be on the order of 100 m/m.y.). The presence of brines is also unlikely because the increase in sulfate is not matched by salinity or chloride contents (Fig. 31). Sedimentological descriptions of cores from Unit II indicate the presence of many dewatering structures but these were not seen in Unit IV. However, expulsion of interlayer water from clays during compaction might be sufficient to partly oxidize some sulfide to ferric oxyhydroxide and sulfate if an oxygen source is present. We have no evi-

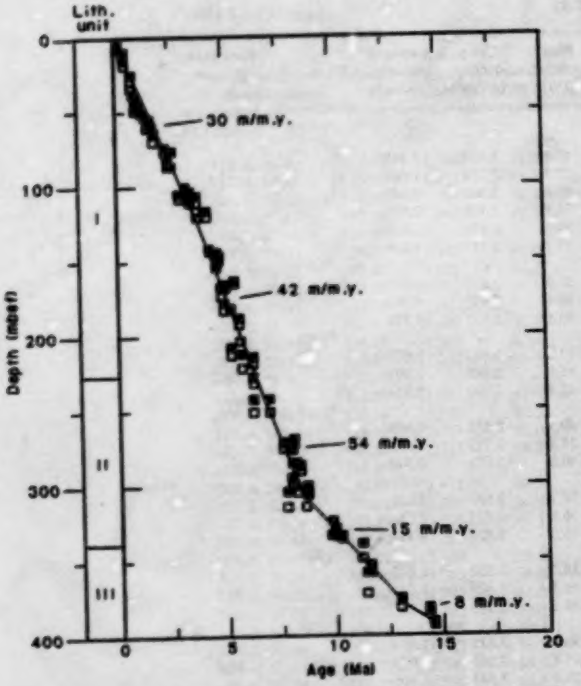

Figure 19. Age-depth plot of Site 722 stratigraphic datums listed in Table 4. The solid and open boxes are the upper and lower depths of each datum level, respectively. Indicated sedimentation rates are based on a best fit to all stratigraphic data. Sedimentation rates calculated between reliable nannofossil datum levels in the top 120 m are listed in Table 7.

dence to support this hypothesis. In addition, this reaction would tend to lower the pH of the interstitial water if the system were closed, which is not observed, and there is sedimentological evidence to support authigenic pyrite formation rather than oxidation. On balance, it would appear that the sulfate increase in depth in Units III and IV may reflect the last vestige of ongoing diffusion of sulfate from seawater originally trapped within the rapidly-accumulating, carbon-poor turbidites. It is clear that any interpretation of the sulfate increase at depth in Units III and IV is based largely on speculation.

Calcium and Magnesium

The profiles of dissolved calcium and magnesium at Site 722 are displayed in Figure 31. In all respects the decrease in Mg^{2+} and increase in Ca^{2+} are identical to Site 721, with precisely the same depth gradients. This is to be expected if the lithology of the substrate plays an important part in maintaining the mass balance of the major ions in the carbonate system. The deeper penetration of Hole 722B indicates that the concentration of Ca^{2+} is still increasing with depth while Mg^{2+} has reached an asymptote of ~29 mmol/L. We believe that the carbonate precipitation/dissolution reactions discussed in the Site 721 summary are equally applicable to Site 722.

Ammonia, Phosphate, and Silica

The distribution of these metabolites is displayed in Figure 31. Compared with Site 721, ammonia reaches a maximum concentration of 2.31 mmol/L at 142 mbsf, some 30 m shallower than at the previous site. This depth is consistent with the zone of near sulfate depletion. Below 142 mbsf ammonia removal occurs, possibly via clay adsorption reactions. Phosphate is rapidly released during organic matter degradation giving a maximum value of 6.49 μmol/L in Core 117-722A-3H at 25 mbsf. Sequestration of phosphate, which we attribute to apatite formation, occurs throughout the remainder of the hole.

The profile of dissolved silica is very interesting in that it appears to reflect sediment lithology extremely well. Rapid dissolution of biogenic tests occurs over the top 5 mbsf, followed by a more gradual increase to a uniform concentration of ~1000-1040 μmol/L for the remainder of Unit I. In Unit II the appearance of diatoms is matched by an increase in dissolved silica, which achieves a maximum of 1257 μmol/L at 291 mbsf. At the base of the diatom-rich pelagic ooze, silica concentrations rapidly fall to 167 μmol/L at 404 mbsf within the marly nannofos-

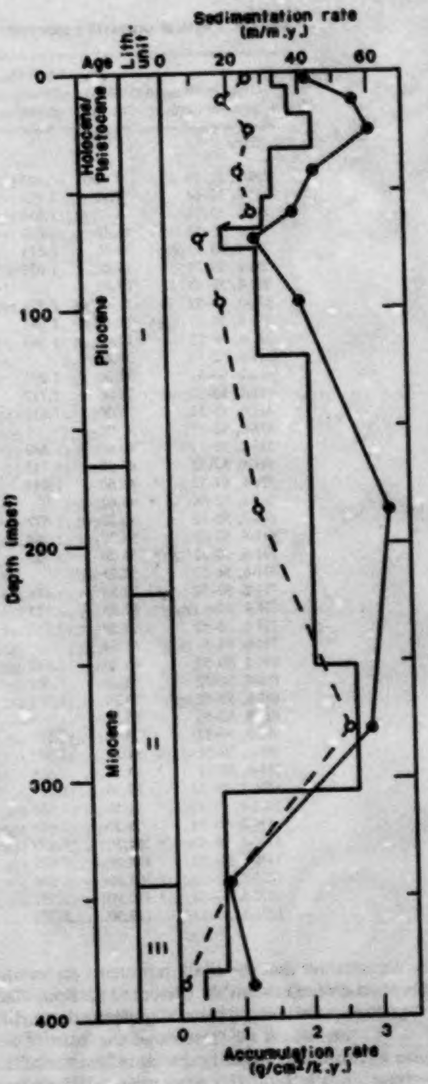

Figure 20. Sedimentation rate (m/m.y., solid line), calcium carbonate accumulation rate (g/cm²/k.y., dots), and noncarbonate accumulation rate (g/cm²/k.y., circles) vs. depth (mbsf) at Site 722. Accumulation rates are plotted at the midpoint of the respective depth intervals.

Table 8. Physical properties summary for Hole 722A.

Core, section, interval (cm)	Depth (mbsf)	Wet-bulk density (g/cm^3)	Porosity (%)	Water content (%)	Grain density (g/cm^3)	Dry-bulk density (g/cm^3)	Velocity^a (m/s)	Vane shear strength (kPa)
117-722A-								
1H-2, 52-54	2.02	1.625	66.0	41.6	2.670	0.948		
1H-4, 52-54	5.02	1.725	62.4	37.1	2.754	1.086		19.1
1H-6, 52-54	8.02	1.616	63.9	40.6	2.545	0.960		
2H-2, 50-52	11.80	1.623	61.7	38.9	2.703	0.991		
2H-4, 50-52	14.80	1.674	63.7	39.0	2.670	1.022		20.4
2H-6, 50-52	17.80	1.672	60.8	37.3	2.554	1.049		
2H-6, 52-55	17.82						^{a}1457	
3H-2, 50-52	21.40	1.589	65.6	42.3	2.670	0.917		
3H-4, 50-52	24.40	1.643	63.4	39.6	2.590	0.993		18.1
3H-6, 50-52	27.40	1.562	67.2	44.1	2.527	0.874		
3H-6, 52-55	27.42						^{a}1501	
4H-2, 50-52	31.00	1.697	61.3	37.0	2.695	1.070		
4H-4, 50-52	34.00	1.717	60.1	35.8	2.646	1.101		28.5
4H-6, 50-52	37.00	1.611	67.1	42.7	2.642	0.924		
4H-6, 52-55	37.02						^{a}1542	
5H-2, 50-52	40.60	1.649	64.5	40.1	2.653	0.988		
5H-4, 50-52	43.60	1.743	59.9	35.2	2.717	1.129		
5H-6, 50-52	46.60	1.649	64.3	40.0	2.633	0.990		
5H-6, 52-56	46.62						^{a}1501	
6H-2, 50-52	50.20	1.677	62.3	38.1	2.599	1.039		
6H-4, 50-52	53.20	1.684	60.7	36.9	2.525	1.062		
6H-6, 50-52	56.20	1.733	59.6	35.3	2.599	1.122		
6H-6, 54-57	56.24						^{a}1534	
7H-2, 50-52	59.50	1.686	60.1	36.5	2.532	1.070		
7H-4, 50-52	62.50	1.723	61.4	36.5	2.603	1.094		73.1
7H-6, 50-52	65.50	1.732	59.4	35.1	2.595	1.124		
7H-6, 54-57	65.54						^{a}1526	
8H-2, 50-52	69.20	1.692	60.3	36.5	2.625	1.074		
8H-4, 50-52	72.20	1.701	59.4	35.8	2.567	1.093		33.8
8H-6, 50-52	75.20	1.711	59.1	35.4	2.543	1.106		
8H-6, 52-55	75.22						^{a}1556	
9H-2, 50-52	78.80	1.617	65.7	41.7	2.553	0.943		
9H-4, 50-52	81.80	1.599	63.9	40.9	2.400	0.945		65.4
9H-6, 50-52	84.80	1.656	61.3	37.9	2.470	1.028		
10X-2, 50-52	88.50	1.597	64.3	41.2	2.479	0.938		
10X-4, 50-52	91.50	1.663	64.5	39.7	2.651	1.003		
11X-2, 50-52	98.20	1.661	62.7	38.7	2.503	1.019		
11X-4, 50-52	101.20	1.699	64.0	38.6	2.674	1.043		
11X-6, 50-52	104.20	1.697	61.7	37.3	2.616	1.064		
12X-2, 50-52	107.90	1.696	59.9	36.2	2.514	1.083		
12X-4, 50-52	110.90	1.751	61.5	36.0	2.654	1.121		
12X-6, 50-52	113.90	1.755	61.6	35.9	2.707	1.124		

sil chalk. We consider that the chalk represents an important locus of diagenetic reaction within the cored section. Below this depth silica concentrations increase slightly in the turbidites of Unit IV to 361 μmol/L at the bottom of the hole.

We have attempted to quantify the mass transfer of dissolved to solid-phase silica in Unit III. Assuming a diffusivity of 5 × 10^{-6} cm^2 s^{-1} and a path length of 50 m, about 1.9 mg cm^{-2} k.y.$^{-1}$ of SiO_2 could be supplied by steady state diffusion. Unit III accumulates at ~3 cm k.y.$^{-1}$ (see "Accumulation Rates" section, this chapter) giving a total sediment accumulation rate of ~3.6 g cm^{-2} k.y.$^{-1}$. Hence, precipitation of diagenetic silica within this unit accounts for a concentration increase of solid-phase SiO_2 of only 0.05 wt%.

Sediment Mineralogy

The mineralogy of 11 sediment residues from Holes 722A and 722B remaining after interstitial water extraction was determined by X-ray diffractometry. In all cases, $CaCO_3$ was removed with 10% HCl prior to analysis; the acid treatment was followed by two washes of the insoluble residue with deionized water. The calcium carbonate-free samples were then pipetted onto glass slides as a slurry in acetone and dried at low temperature on a hotplate. Two of the samples were subsequently exposed for several hours to ethylene glycol in a desiccator to check for the presence of expandable clays.

The noncarbonate fraction of the sediments at Site 722 is in general composed of the same suite of minerals found at the nearby Site 721: quartz, feldspar, chlorite (and kaolinite?), and illite and/or mica are common in all samples, while pyrite occurs in trace quantities in most, but not all, of the analyzed residues. The occurrence of pyrite in the sequence appears to be random as no clear patterns of distribution were observed. Dolomite is rare in the residues. We were unable to identify with certainty characteristic dolomite peaks in any of the insoluble residues; this is not the case for bulk carbonate-rich samples and probably reflects the destruction of finely-crystalline dolomite during the acid treatment.

The possible presence of smectite was evaluated by glycolation of samples from Core 117-722B-12X (foraminifer-bearing nannofossil ooze) and Core 117-722B-37X (marly nannofossil chalk). No shift of the ~14 Å peak was observed in the nannofossil ooze but a distinct shift of a portion of the 14 Å peak in the marly chalk to a d-spacing of ~17 Å indicated that some smectite is present in lithologic Unit III (see "Lithostratigraphy" section, this chapter). Well-crystallized chlorite, indicated by the presence of sharp peaks at 14, 7, 3.5, and ~2 Å, is abundant in Unit IV (sandy to silty claystones and turbidites interbedded with nannofossil chalk in the upper part of the sequence). An ultraslow scan of the 24°–26° portion of the diffraction spectrum of a sample of pale-green silty clay from 438 mbsf

Table 8 (continued).

Core, section, interval (cm)	Depth (mbsf)	Wet-bulk density (g/cm^3)	Porosity (%)	Water content (%)	Grain density (g/cm^3)	Dry-bulk density (g/cm^3)	Velocity^a (m/s)	Vane shear strength (kPa)
117-722A- (Cont.)								
13X-2, 50–52	117.60	1.706	61.7	37.0	2.682	1.074		
13X-4, 50–52	120.60	1.711	64.1	38.4	2.678	1.055		
13X-6, 50–52	123.60	1.724	58.4	34.7	2.443	1.125		
14X-2, 51–53	127.31	1.684	61.6	37.5	2.557	1.0531		
14X-3, 60–63	128.90						^{a}1497	
14X-4, 51–53	130.31	1.682	60.8	37.1	2.500	1.059		
15X-2, 60–62	137.00	1.691	62.5	37.8	2.634	1.052		
15X-4, 60–62	140.00	1.703	63.1	37.9	2.717	1.057		62.5
15X-6, 10–13	142.50						^{a}1561	
15X-6, 15–17	142.55	1.665	61.3	37.7	2.563	1.037		
16X-2, 52–54	146.62	1.639	62.1	38.8	2.556	1.002		
16X-4, 53–55	149.63	1.662	61.9	38.2	2.517	1.027		
16X-6, 39–42	152.49						^{a}1592	
16X-6, 50–52	152.60	1.717	61.4	36.6	2.643	1.088		
17X-1, 108–110	155.38	1.656	62.5	38.7	2.605	1.016		
17X-3, 103–105	158.33	1.713	62.0	37.1	2.727	1.077		
18X-2, 58–60	165.98	1.711	58.8	35.2	2.573	1.108		
18X-2, 60–62	166.00						^{a}1560	
18X-6, 58–60	170.20	1.671	63.5	39.0	2.567	1.020		
19X-2, 62–64	175.72	1.694	60.6	36.7	2.532	1.073		
19X-4, 59–61	178.69	1.700	63.1	38.0	2.684	1.053		
19X-6, 58–61	181.68						^{a}1607	
19X-6, 62–64	181.72	1.735	58.9	34.8	2.576	1.132		
20X-2, 36–38	185.16	1.703	58.8	35.4	2.559	1.077		
20X-4, 60–63	188.40	1.701	61.0	36.7	2.637	1.101	^{a}1608	
21X-1, 57–59	193.57	1.715	62.7	37.5	2.744	1.072		
21X-3, 60–63	196.60	1.690	59.5	36.1	2.543	1.080	^{a}1611	
22X-2, 52–54	204.72	1.727	59.3	35.2	2.590	1.120		
22X-4, 52–54	207.72	1.747	59.5	34.9	2.679	1.137		
22X-6, 52–54	210.72	1.790	59.8	34.2	2.767	1.178	^{a}1594	
23X-2, 50–52	214.40	1.702	52.4	31.5	2.647	1.165		
23X-4, 68–70	217.58	1.641	60.6	37.8	2.394	1.021		
23X-6, 38–40	220.28	1.721	58.3	34.7	2.523	1.124	^{a}1614	
24X-2, 17–19	223.67	1.740	59.1	34.8	2.631	1.135		
24X-4, 50–52	227.00	1.693	60.2	36.5	2.596	1.076		
24X-6, 50–52	230.00	1.742	58.6	34.5	2.605	1.142	^{a}1548	
25X-1, 50–52	232.20	1.760	58.6	34.1	2.705	1.160		
26X-1, 58–60	242.28	1.633	63.1	39.6	2.514	0.987	^{a}1570	
27X-2, 29–31	252.79	1.570	65.7	42.9	2.474	0.999		
27X-4, 17–19	255.67	1.662	64.8	39.9	2.574	0.897	^{a}1556	
29X-1, 37–40	270.77	1.781	59.5	34.3	2.709	1.171	^{a}1625	

^{a} Velocity measurement perpendicular to bedding.

showed no indication that kaolinite was present in the sample. The dearth of kaolinite and the high degree of crystallinity of the chlorite in the turbidites suggest that this clastic sequence has the same provenance as the mineralogically-similar Indus Fan deposits cored at Site 720. There is no indication from our data that the turbidites were derived from the Oman margin area.

In and above Core 117-722B-37X (corresponding to lithologic Units I and II), the sediments appear to contain some palygorskite. The diffraction pattern of this mineral is characterized by a principal reflection at about 8.4° two-theta (~10.5 Å), which has the effect of broadening the illite/mica 10 Å peak if both palygorskite and illite are present in the same sample. Most of the residues above and including that from Core 117-722B-37X show diffractograms with broadened 10 Å peaks compared to samples deeper in the hole, and we tentatively suggest that the difference can be attributed to the presence of palygorskite in lithologic Units I and II. This mineral is known to be a common constituent of soils of the Arabian Peninsula and Somali regions (Kolla et al., 1981) and indeed is common in modern sediments on the Oman margin (Kolla et al., 1981). Its apparent occurrence in Site 722 sediments may be due to eolian transport. A similar mechanism was proposed to explain the coexistence of dolomite and quartz at Site 721. The absence of palygorskite in the Unit IV turbidites, indicated by sharp, rather than broadened, 10 Å peaks, rules out the Oman margin as a significant source area for terrigenous detritus during the early to middle Miocene. This observation is consistent with the conclusions derived above based on the distribution of chlorite.

Illite and/or mica are relatively abundant in all residues studied. We have made no attempt to differentiate between illite, muscovite, and biotite (which have similar diffraction patterns) in this study, but it is clear from the examination of smear slides that both muscovite and biotite are present in at least some samples, notably from the turbidite sequence. Earlier studies (e.g., Kolla et al., 1981) have shown that illite is a major constituent of the clay-sized fraction in the north-central Arabian Sea. It is probable that the ubiquitous 10 Å peak in the diffractograms represents largely muscovite and biotite in lithologic Unit IV and illite in Units I to III.

ORGANIC GEOCHEMISTRY

The organic geochemical parameters routinely determined on sediments of Holes 722A and 722B were the abundance of organic carbon and pyrolysis characteristics of organic matter in headspace residues. In addition, closely spaced samples (spacing of about 5 cm) were taken across two examples of cyclic sedimentation in upper Miocene nannofossil oozes and muds typical of lithologic Units I and II. Color changes in these cycles

Table 9. Physical properties summary for Hole 722B.

Core, section, interval (cm)	Depth (mbsf)	Wet-bulk density (g/cm³)	Porosity (%)	Water content (%)	Grain density (g/cm³)	Dry-bulk density (g/cm³)	Velocity (m/s)
117-722-							
1H-3, 50-52	3.50	1.654	62.7	38.8	2.566	1.012	
2H-3, 50-52	9.00	1.552	70.6	46.6	2.675	0.829	
3H-3, 50-52	18.60	1.623	66.6	42.0	2.641	0.941	[a]1465
4H-3, 50-52	28.20	1.644	61.7	38.4	2.597	1.013	[a]1556
5H-3, 50-52	37.80	1.607	65.6	41.8	2.694	0.935	[a]1547
6H-3, 50-52	47.40	1.646	64.7	40.3	2.678	0.983	[a]1545
7H-3, 50-52	56.70	1.708	62.3	37.4	2.675	1.070	[a]1555
8H-3, 50-52	66.40	1.650	63.0	39.1	2.622	1.005	[a]1522
9H-3, 50-52	76.00	1.727	62.1	36.8	2.699	1.091	[a]1508
10H-3, 50-52	86.20	1.661	62.1	38.3	2.617	1.025	[a]1549
11X-3, 92-94	95.82	1.669	59.7	36.6	2.542	1.058	[a]1559
12X-3, 17-19	104.67	1.714	60.3	36.1	2.661	1.096	[a]1625
13X-3, 29-31	114.49	1.703	57.3	34.5	2.684	1.116	
14X-3, 46-48	124.36	1.707	60.2	36.1	2.583	1.091	[a]1592
16X-3, 50-52	143.70	1.668	61.0	37.5	2.480	1.043	
17X-3, 50-52	153.40	1.685	63.7	38.7	2.532	1.032	
18X-3, 52-54	163.02	1.719	61.2	36.5	2.656	1.093	[a]1604
19X-5, 112-114	176.32	1.762	59.6	34.6	2.680	1.152	[a]1612
20X-2, 74-76	181.14	1.731	59.4	35.1	2.528	1.123	[a]1625
21X-3, 66-68	192.16	1.692	60.7	36.8	2.521	1.070	[a]1626
22X-3, 51-54	201.71	1.688	59.9	36.4	2.522	1.074	[a]1616
23X-3, 45-48	211.35	1.730	59.7	35.4	2.546	1.118	[a]1535
24X-3, 50-53	221.00	1.754	60.5	35.3	2.682	1.135	[a]1529
25X-6, 43-47	235.13	1.750	58.4	34.2	2.589	1.152	[a]1597
26X-5, 21-23	243.11	1.665	64.1	39.5	2.646	1.008	[a]1601
27X-4, 40-42	251.40	1.756	61.0	35.6	2.703	1.131	[a]1571
28X-2, 47-49	258.17	1.699	60.5	36.5	2.624	1.079	
29X-3, 60-62	269.50	1.572	69.8	45.5	2.610	0.857	[a]1507
31X-2, 50-52	287.30	1.630	66.1	41.5	2.677	0.953	
31X-4, 50-52	290.30	1.670	60.5	37.1	2.506	1.051	[a]1535
31X-6, 50-52	293.30	1.730	62.0	36.7	2.696	1.095	
32X-2, 50-52	297.00	1.669	59.7	36 6	2.610	1.057	
32X-4, 50-52	300.00	1.609	64.7	41.2	2.528	0.946	
33X-2, 28-31	306.46	1.461	74.3	52.1	2.551	0.700	[a]1583
34X-2, 80-82	316.60	1.422	75.5	54.4	2.299	0.648	[a]1541
34X-2, 80-82	316.60						1614
34X-4, 40-42	319.20	1.439	70.5	50.2	2.354	0.717	
35X-2, 52-54	326.02	1.688	61.0	37.0	2.539	1.063	
35X-4, 51-53	329.01	1.568	69.1	45.2	2.722	0.860	[a]1587
35X-4, 51-53	329.01						1634
35X-6, 50-53	332.00	1.662	63.2	39.0	2.615	1.015	[a]1580
35X-6, 50-53	332.00						1611
36X-2, 48-50	335.68	1.720	62.9	37.5	2.742	1.075	[a]1600
36X-2, 48-50	335.68						1617
36X-4, 77-79	338.97	1.637	63.7	39.8	2.630	0.985	[a]1614
36X-4, 77-79	338.97						1653
37X-2, 51-53	345.41	1.796	55.9	31.9	2.747	1.224	[a]1616
37X-2, 51-53	345.41						1639
37X-4, 51-53	348.41	1.756	55.6	32.5	2.601	1.186	[a]1646
37X-4, 51-53	348.41						1710
37X-6, 50-52	351.40	1.790	58.2	33.3	2.732	1.194	[a]1605
37X-6, 50-52	351.40						1643
38X-2, 71-73	355.31	1.740	60.5	35.6	2.755	1.120	[a]1631
38X-2, 71-73	355.31						1668
38X-4, 83-85	358.43	1.781	56.0	32.2	2.648	1.207	
38X-6, 52-54	361.12	1.802	56.8	32.3	2.764	1.219	[a]1658
38X-6, 52-54	361.12						1696
39X-1, 12-14	362.92	1.855	54.2	29.9	2.762	1.300	[a]1676
39X-1, 12-14	362.92						1736
39X-CC, 8-10	365.45	1.821	53.6	30.2	2.723	1.272	[a]1673
39X-CC, 8-10	365.45						1734
40X-3, 16-18	375.66	1.912	49.6	26.6	2.737	1.404	[a]1637

(about 1 m thick) correlate with changes in abundance of major sediment components, as well as with variations in physical, magnetic, and chemical properties of the sediments (see "Lithostratigraphy," "Physical Properties," and "Paleomagnetism" sections, this chapter). By investigating detailed transects across two of these cycles, we hoped to shed light on variations in organic-matter abundance and origin, as well as on organic-matter diagenesis. Such detailed studies are a prerequisite for identifying characteristics of the cyclic sedimentation pattern, which is presumed to be the sedimentary expression of recurring changes in monsoonal induced upwelling.

Organic Carbon Abundance and Character

Sediments of lithologic Units I, II, and III are characterized by alternating sequences of organic-carbon-rich sediments and sediments with less organic carbon (about 2% and <0.5% organic carbon by weight, respectively; see Table 3). Organic-carbon-rich layers coincide with dark green coloration and lower

Table 9 (continued).

Core, section, interval (cm)	Depth (mbsf)	Wet-bulk density (g/cm^3)	Porosity (%)	Water content (%)	Grain density (g/cm^3)	Dry-bulk density (g/cm^3)	Velocity (m/s)
117-722- (Cont.)							
40X-3, 16–18	375.66						1649
41X-2, 29–31	383.99	2.023	44.6	22.6	2.710	1.566	[a]1943
41X-2, 29–31	383.99						2063
42X-1, 22–24	392.02	1.972	44.6	23.2	2.675	1.515	[a]1761
42X-1, 22–24	392.02						1859
42X-3, 33–35	395.13	1.920	48.3	25.8	2.803	1.425	[a]1627
42X-3, 33–35	395.13						1643
43X-1, 40–42	401.80	1.981	44.3	22.9	2.634	1.527	[a]1902
43X-1, 40–42	401.80						2022
43X-3, 23–25	404.63	1.847	44.8	24.8	2.723	1.388	[a]1648
43X-3, 23–25	404.63						1677
44X-2, 38–40	412.98	2.135	39.8	19.1	2.796	1.727	[a]1759
44X-2, 38–40	412.98						1768
44X-4, 17–19	415.77	1.862	38.2	21.0	2.832	1.470	[a]1701
44X-4, 17–19	415.77						1744
45X-2, 23–25	422.53	1.980	46.9	24.3	2.748	1.499	[a]1564
45X-2, 23–25	422.53						1577
45X-4, 27–29	425.57	2.003	45.3	23.2	2.683	1.538	[a]1713
45X-4, 27–29	425.57						1751
45X-6, 138–140	429.68	1.990	47.1	24.2	2.729	1.508	[a]1703
45X-6, 138–140	429.68	1.990					1706
46X-2, 2–4	432.02	1.970	42.8	22.3	2.735	1.531	[a]1748
46X-2, 2–4	432.02						1692
46X-4, 141–143	436.41	1.970	46.8	24.4	2.685	1.490	[a]1651
46X-4, 141–143	436.41						1688
46X-6, 132–134	439.32	2.002	57.1	29.2	2.624	1.417	[a]1771
46X-6, 132–134	439.32						1706
48X-1, 33–35	450.13	2.008	47.7	24.4	2.802	1.519	[a]1614
48X-1, 33–35	450.13						1633
49X-1, 40–43	459.80	1.957	48.7	25.5	2.753	1.458	[a]1598
49X-1, 40–43	459.80						1586
49X-4, 40–43	464.30	2.000	46.4	23.8	2.788	1.525	[a]1579
49X-4, 40–43	464.30						1577
50X-2, 39–41	470.89	1.884	43.3	23.6	2.781	1.440	[a]1589
50X-2, 39–41	470.89						1617
50X-4, 30–32	473.80	1.976	45.2	23.4	2.701	1.513	[a]1612
50X-4, 30–32	473.80						1635
51X-1, 68–70	479.28				2.793		
52X-2, 79–81	490.49	2.023	45.1	22.9	2.796	1.560	
52X-5, 54–56	494.74	1.793	36.7	21.0	2.719	1.417	[a]1647
52X-5, 54–56	494.74						1666
52X-7, 8–10	497.28	2.041	42.2	21.2	2.694	1.609	[a]1689
52X-7, 8–10	497.28						1810
53X-1, 41–43	498.31	2.049	43.8	21.9	2.752	1.600	[a]1609
53X-1, 41–43	498.31						1607
55X-1, 4–6	517.24	2.714	11.6	4.4	2.794	2.595	[a]3620
55X-1, 4–6	517.24						4093
56X-CC, 20–22	527.10						[a]3852
56X-CC, 20–22	527.10						4139
57X-1, 79–81	537.39	2.070	41.3	20.4	2.784	1.647	[a]1683
57X-1, 79–81	537.39						1699
58X-1, 134–136	547.54	2.090	38.1	18.7	2.663	1.700	[a]1743
58X-1, 134–136	547.54						1730
58X-3, 74–76	549.94	2.063	42.1	20.9	2.740	1.631	
58X-5, 76–78	552.96	2.009	43.9	22.4	2.683	1.560	[a]1697
58X-5, 76–78	552.95						1808
59X-CC, 12–14	556.86	2.042	42.4	21.3	2.691	1.607	[a]1676
59X-CC, 12–14	556.86						1723

[a] Velocity measurement perpendicular to bedding; others measured parallel to bedding

carbonate concentrations, even though direct correlation of $CaCO_3$ and organic carbon yields a statistically insignificant correlation coefficient of only −0.32. Average organic carbon concentration in the pelagic sediments of sedimentary Units I–III is 1.2% by weight, with a rather large standard deviation of about ± 0.9%. As will be shown below, these large variations occur within individual couplets of dark green and light sediments. Sediments from lithologic Unit IV are lean in organic carbon (average 0.15 with ± 0.1%), with the exception of a distinct coal layer in the core catcher of Core 117-722B-51X, an allochthonous component of a turbidite layer.

The organic matter is immature as shown by the uniformly low temperatures of maximum pyrolysis release of hydrocarbons, $T_{max} < 435°C$ (Table 11). Most samples plot in the field of immature marine organic matter on the hydrogen index/oxygen index diagram (Fig. 32), but show a considerable scatter. A similar kind of scatter was also noticed in Site 721. Samples with a low organic carbon content (< 0.5%) show unusually high oxygen indices (Table 11), which may either be an attribute of immature organic carbon with abundant oxygen-bearing functional groups, or, more likely, due to an artifact of calculating the index (see "Explanatory Notes" chapter, this volume). Even

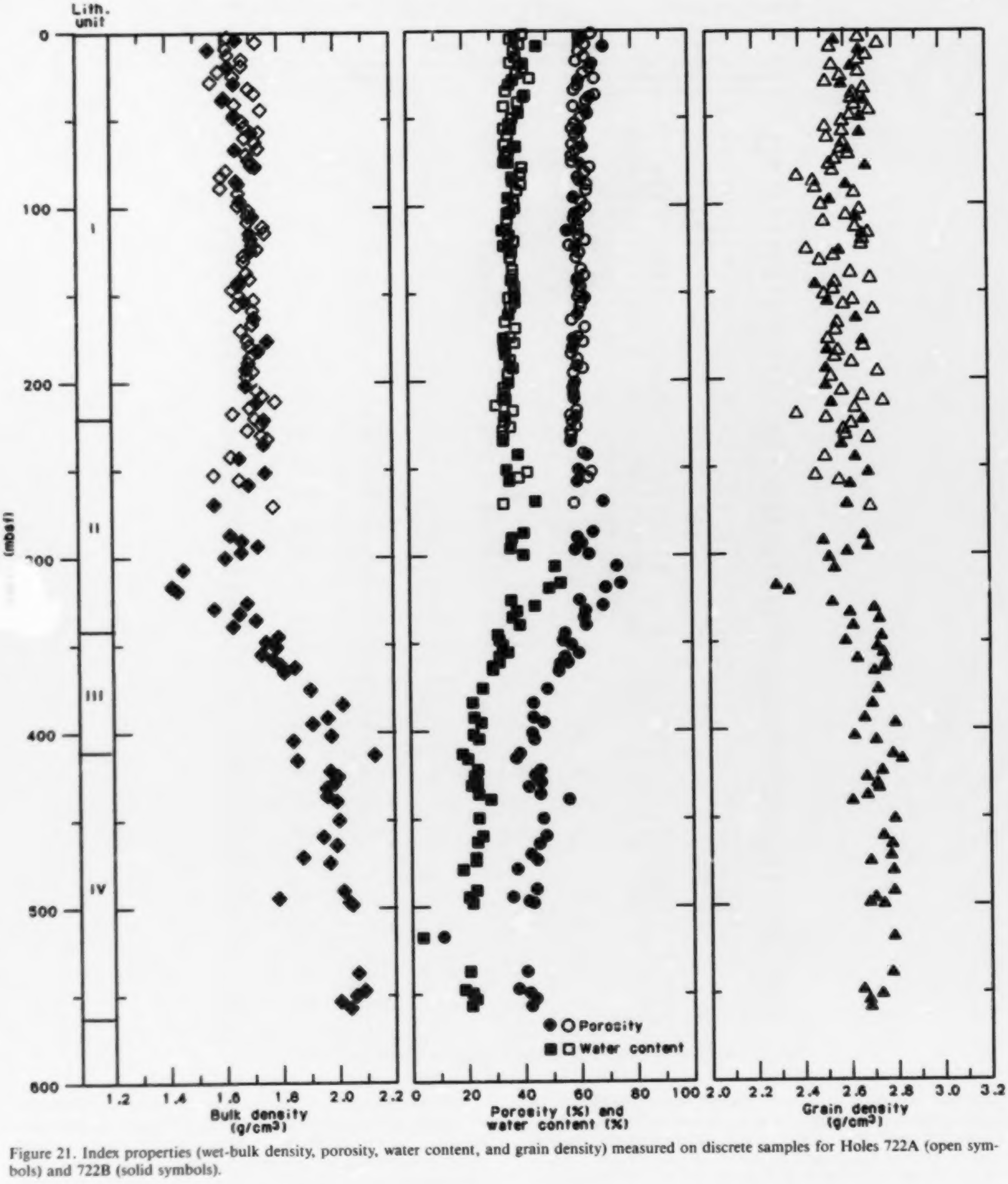

Figure 21. Index properties (wet-bulk density, porosity, water content, and grain density) measured on discrete samples for Holes 722A (open symbols) and 722B (solid symbols).

though we are aware that traditional evolutionary paths given in the van-Krevelen-type (Tissot and Welte, 1984) diagram depicted in Figure 32. do not apply for immature marine organic matter rich in lipids—they were established for kerogens of different provenance—results of S_2, S_3, and TOC as well as derived parameters may well be meaningful and are suitable to describe properties of immature and lipid-rich sedimentary organic matter.

If samples of Core 117-722A-16X and 117-722B-29X for instance are plotted on the HI/OI diagram (Fig. 32), they cluster

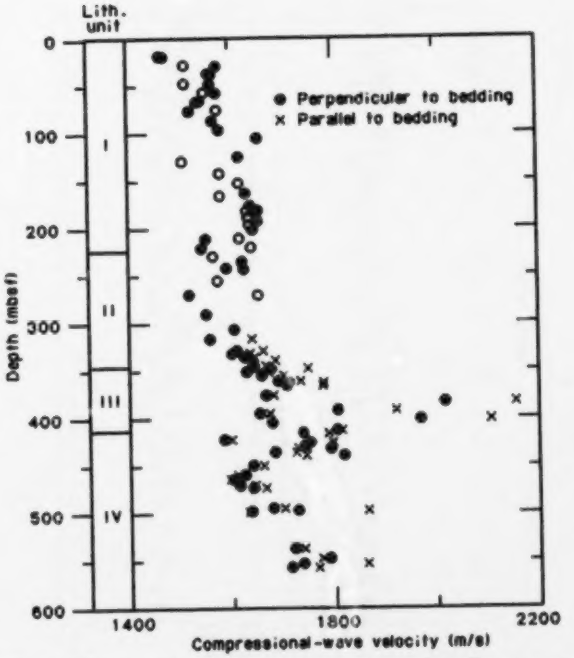

Figure 22. Compressional-wave velocity as measured on discrete samples in the Hamilton Frame Velocimeter in Holes 722A (open symbols) and 722B (solid symbols).

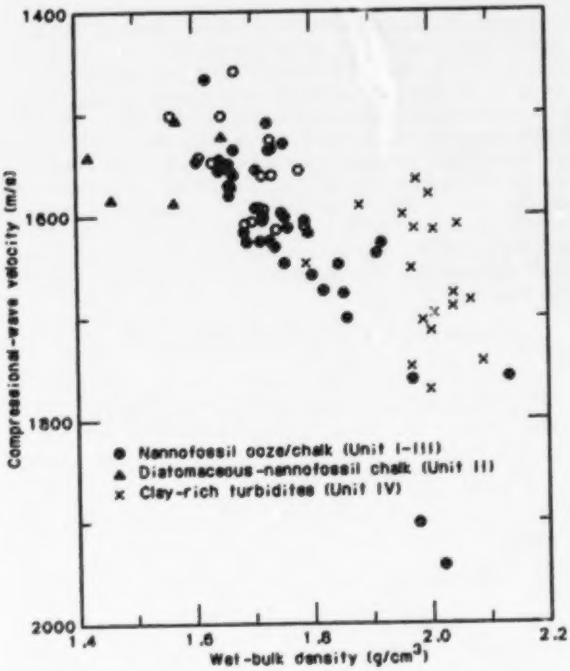

Figure 23. Wet-bulk density vs. compressional-wave velocity measured on discrete samples of nannofossil ooze/chalk, diatomaceous-nannofossil chalk, and clay-rich turbidites in Holes 722A (open symbols) and 722B (solid symbols).

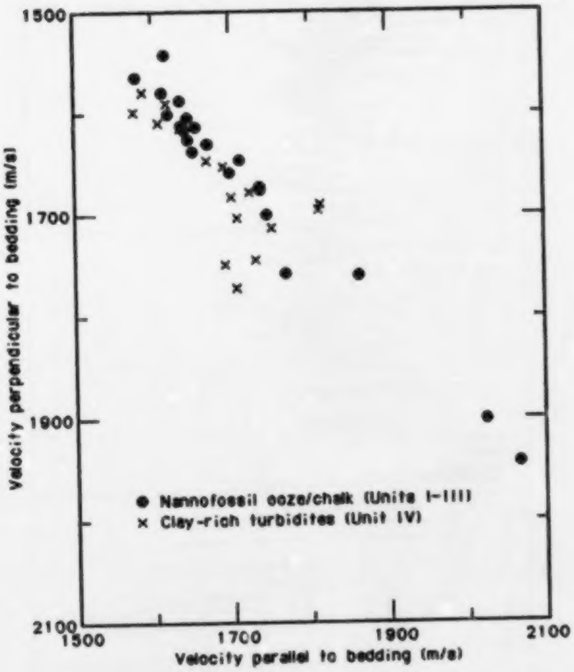

Figure 24. Crossplot of compressional-wave velocity measured perpendicular and parallel to bedding on discrete samples from Hole 722B.

in two distinct areas of the diagram. The only exception is a data point of Core 117-722A-16X that may be dubious because of an unusually high (and possibly false) organic carbon value (and therefore a low hydrogen and oxygen index). With increasing maturation—loss of functional groups and increasing polycondensation either by thermal or diagenetic processes—organic matter releases progressively less hydrocarbons (S_2) and CO_2 (S_3). It is conceivable that samples from Core 117-722A-16X, from approximately 150 mbsf and an age of approximately 6 Ma, contain more oxygenated compounds than those of Core 117-722A-29X at 270 mbsf and several million years older. In the older samples, diagenesis may be more advanced and may have stripped the organic matter of oxygenated components. Another explanation could be that the dominant type of input changed from more hydrogen-rich (proteins, lipids) to more oxygen-rich (sugars) material. In both cases, the organic matter is primarily of marine origin. Two analyses of the same coal sample from sedimentary Unit IV are denoted "C" in Figure 32.

Detailed Sample Series across Sections 117-722A-16X-2 and 117-722B-29X-3, -4

A strong negative correlation was observed for calcium carbonate vs. organic carbon abundances in the two detailed sample series (Figs. 33 and 34). While the two signals follow each other closely in Core 117-722A-16X (Fig. 33), they show a considerable time lag in Core 117-722B-29X (Fig. 34). In the case of samples from Core 117-722A-16X, the response of the carbonate preservation or production to a postulated change in the sedimentary environment appears to precede enhanced production or preservation of the organic matter (compare Figs. 33 and 34). A good correlation was observed between the organic carbon content and the HI of the organic matter in both sample suites. The absolute values of the HI, however, are slightly higher in Core 117-722B-29X as compared to Core 117-722A-16X.

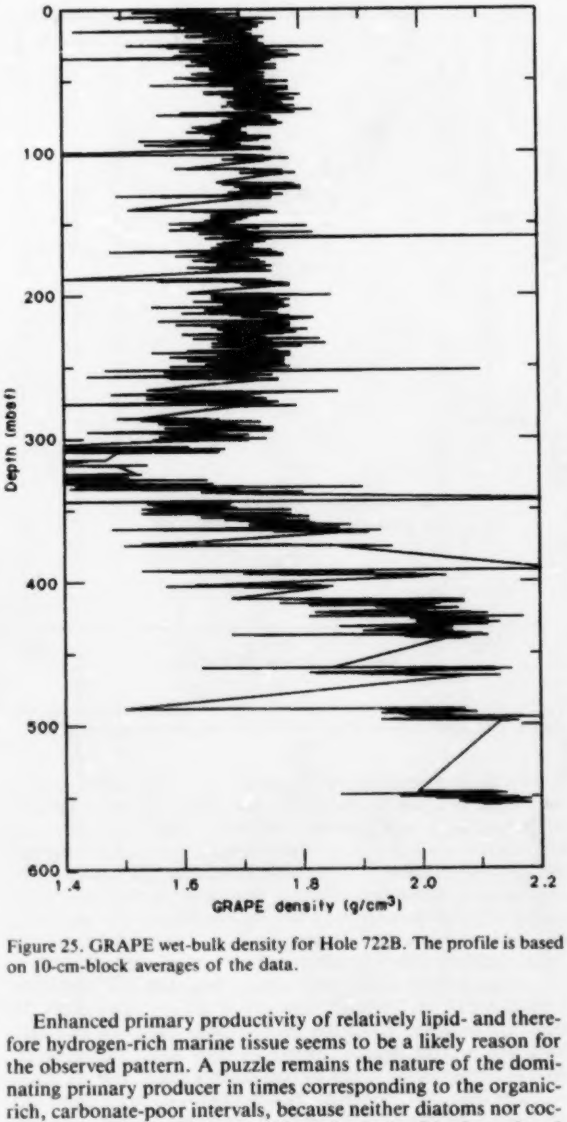

Figure 25. GRAPE wet-bulk density for Hole 722B. The profile is based on 10-cm-block averages of the data.

Enhanced primary productivity of relatively lipid- and therefore hydrogen-rich marine tissue seems to be a likely reason for the observed pattern. A puzzle remains the nature of the dominating primary producer in times corresponding to the organic-rich, carbonate-poor intervals, because neither diatoms nor coccolithophorids are likely candidates for lack of both opal and carbonate in the sediments. If input of organic carbon was constant and from the same source organisms, the higher HI in the deeper samples implies that preservation of organic matter was better during time of deposition.

Hydrocarbon Gases

Abundance of interstitial gas was determined in sediments adjacent to routine organic geochemical samples following the procedure outlined in the "Explanatory Notes" chapter (this volume). Gas concentrations, when compared to the previous site on the Owen Ridge, are extremely low ($< 800\ \mu L/L$ sediment). If the data are to be trusted, then biogenic methane is the dominating hydrocarbon gas, with only trace quantities of ethane ($< 5\ \mu L/L$ sediment) occurring in three samples (see Table 12). A viable reason for low rates of bacterial methane production may be the fact that interstitial sulfate, a limiting factor for bacterial methane production, is not completely depleted throughout most of the section. In the deepest samples (see "Inorganic Geochemistry" section, this chapter), sulfate concentrations even appear to increase. The persistent occurrence of sulfate, except in samples between approximately 250 and 290 mbsf, may thus be the reason for the abnormally low methane abundances. Thermal maturity of the organic matter in all sedimentary units is low, so that thermogenic gas was not expected. The occurrence of coal layers in sedimentary Unit IV, in particular of a thick seam in Section 117-722B-51X-CC, is attributable to the turbiditic nature of the sediments in this unit. The coal was most likely redeposited after exhumation from a nearshore or shelf sediment.

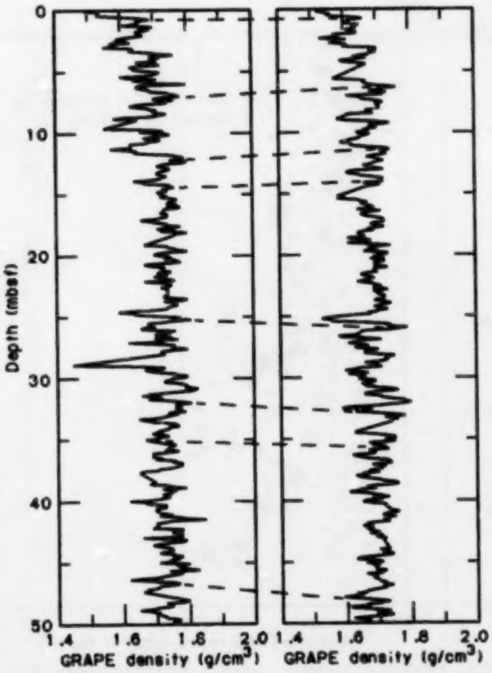

Figure 26. GRAPE wet-bulk density for 0-50 mbsf in Holes 721B (left) and 722B (right). The profiles are based on 10-cm-block averages of the data.

DOWNHOLE MEASUREMENTS

Operations

Logging operations at Hole 722B began at 1314 on 11 September, with a hole conditioning program similar to that used at Site 720. The Schlumberger seismic stratigraphic combination, wireline heave compensator, and sidewall entry sub (SES) were rigged up between 2215 and 0200 on September 12. The SES was used because tests of capillary suction time (CST) indicated a moderate to high potential for clay swelling in the bottom 150 m of the hole (CST values of 80 to 150 s for mud salinity of 29 g/kg). The drill-pipe heave compensator was used during logging to reduce the possibility of pipe bending.

The seismic stratigraphic combination was run between 0200 and 0545. At Site 722 this tool string consisted of the analog borehole-compensated sonic tool, gamma ray tool, and dual induction resistivity (see "Explanatory Notes" chapter, this volume). Logs were obtained both downgoing and upcoming, from

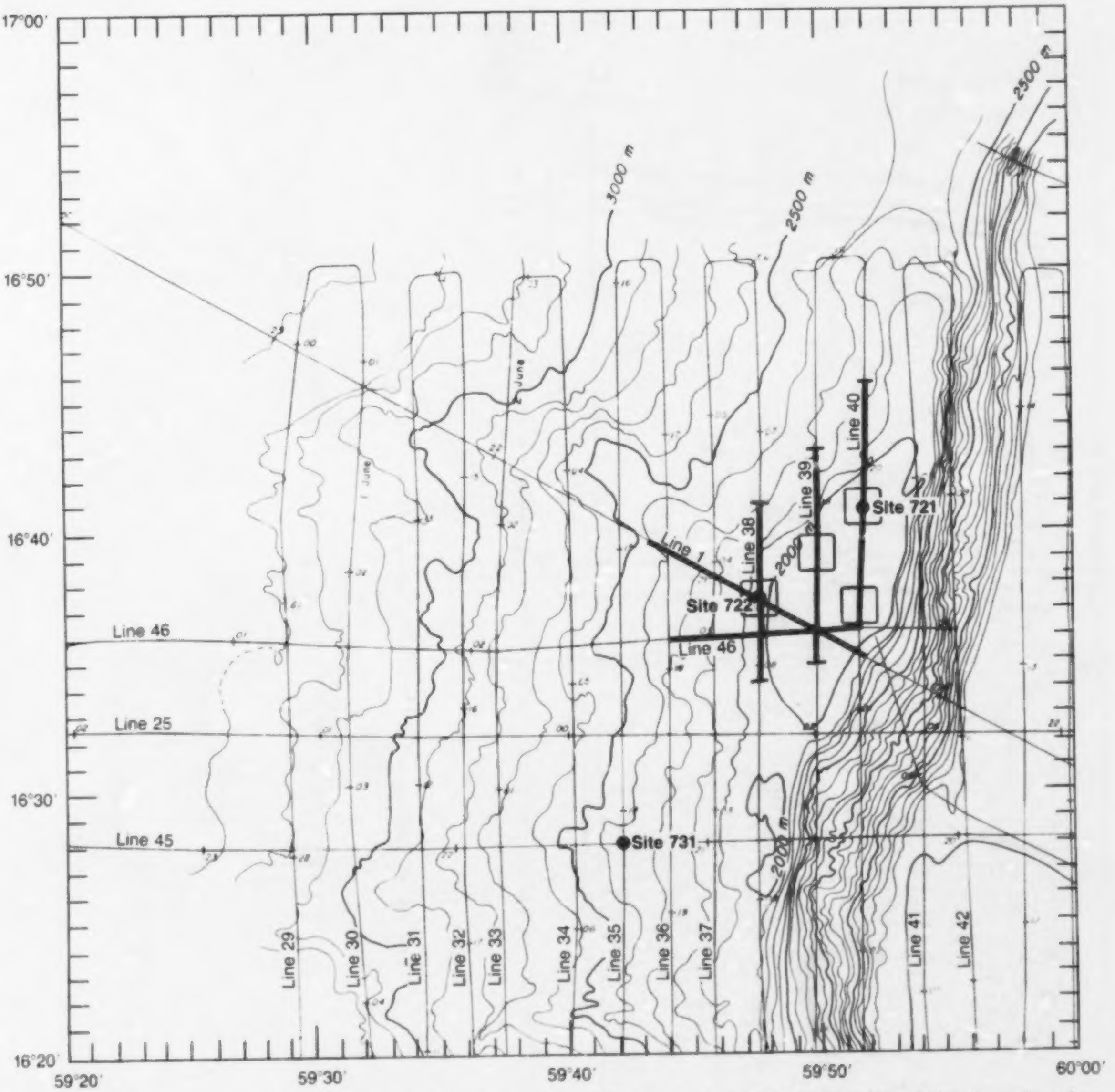
17°00′
16°50′
16°40′
16°30′
16°20′
59°20′
59°30′
59°40′
59°50′
60°00′
3000 m
2500 m
2500 m
2000 m
2000 m
Site 721
Site 722
Site 731
Line 1
Line 38
Line 39
Line 40
Line 46
Line 46
Line 25
Line 45
Line 29
Line 30
Line 31
Line 32
Line 33
Line 34
Line 35
Line 36
Line 37
Line 41
Line 42
1 June
1 June

Figure 27. The location of Sites 721 and 722 and the SCS tracks used to establish the seismic stratigraphy of the Owen Ridge. Intervals used are shown as heavy lines and the boxes indicate portions of the tracks shown in Figures 28 and 29. The bathymetry is based on Sea Beam data from the Leg 117 site survey (RC2704, 1986).

just beneath the base of pipe (94.3 mbsf) to 555.5 mbsf. Very little fill was found at the bottom of the hole (total drilled depth 565.1 mbsf), and no bridges were encountered. The wireline heave compensator failed and was shut off shortly after beginning logging up.

The second tool string run was the Schlumberger lithoporosity combination. At Site 722 this tool string consisted of the spectral gamma ray, neutron porosity, lithodensity, and GPIT accelerometer tools (see "Explanatory Notes" chapter, this volume). At 0915 this tool string started down for the first time, but the run was aborted because of an electrical short only 300 m below the ship. Upon rigdown, the cause of the short was found to be a badly twisted pigtail at the cable head. This twisting was caused by rotating the SES to connect it to pipe; the bowspring on the density tool prevented the tool string from rotating along with the SES. The pigtail was replaced, and a swivel was installed in the tool string to prevent a recurrence of the twisting problem. However, the second run of the tool string downhole failed at 700 m below the ship, due to a short in the swivel. The swivel was removed, the SES was rigged down, and a wiper trip was made to break up any possible bridges.

The third run of the lithoporosity combination, from 1900 to 2325, was much more successful. Nearly the entire open-hole interval (94.2–539.9 mbsf) was logged going down. While logging up, pipe was raised 20 m, so that open-hole logs were obtained between 71.4 and 550.9 mbsf. However, the upper bowspring on the density tool would not collapse sufficiently to enter the pipe. Therefore it was necessary to deploy the crimper and cutter

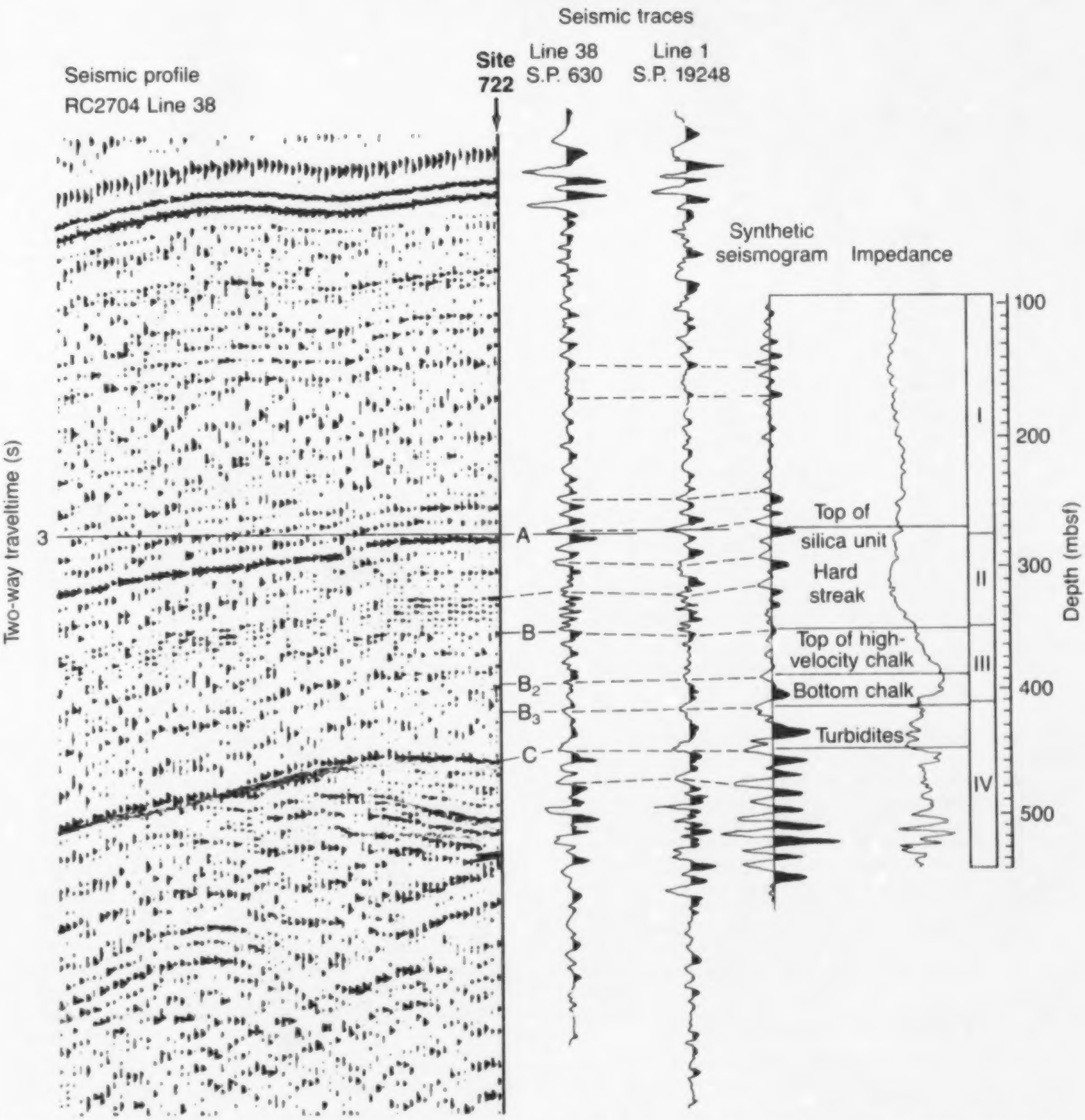

Figure 28. Correlation of reflectors (see text for discussion) between seismic profiles and with the synthetic seismogram, which is based on logging data from Site 722 (see "Downhole Measurements" section, this chapter). Synthetic seismogram is scaled in mbsf and seismic profiles are in two-way traveltime (s).

tools, to cut the wireline. A minicone was made up and dropped, to permit reentry and cementing of the hole in case the tool string was not retrieved. The crimper and cutter worked successfully; after the drill string was pulled, the tool string was retrieved with the bottom-hole assembly.

Log Quality and Editing

Several logs from Site 722 required a substantial amount of editing to improve their initially fair-to-poor quality. Editing or reprocessing was undertaken for sonic, resistivity, density, and gamma ray logs. After editing, the quality of nearly all logs was very good.

Sonic logging at Site 722 utilized a borehole compensated tool (BHC). This backup tool is less reliable in high-porosity sediments than the normal long-spaced sonic (LSS) because of its short source-receiver spacing. At each depth, two short-spaced (0.9 m) and two medium-spaced (1.5 m) source-receiver combinations are used. The upcoming log had only one cycle skip on one short-spaced pair, but this shift at 179 mbsf causes a substantial baseline shift in sonic transit times (Fig. 35). The down-

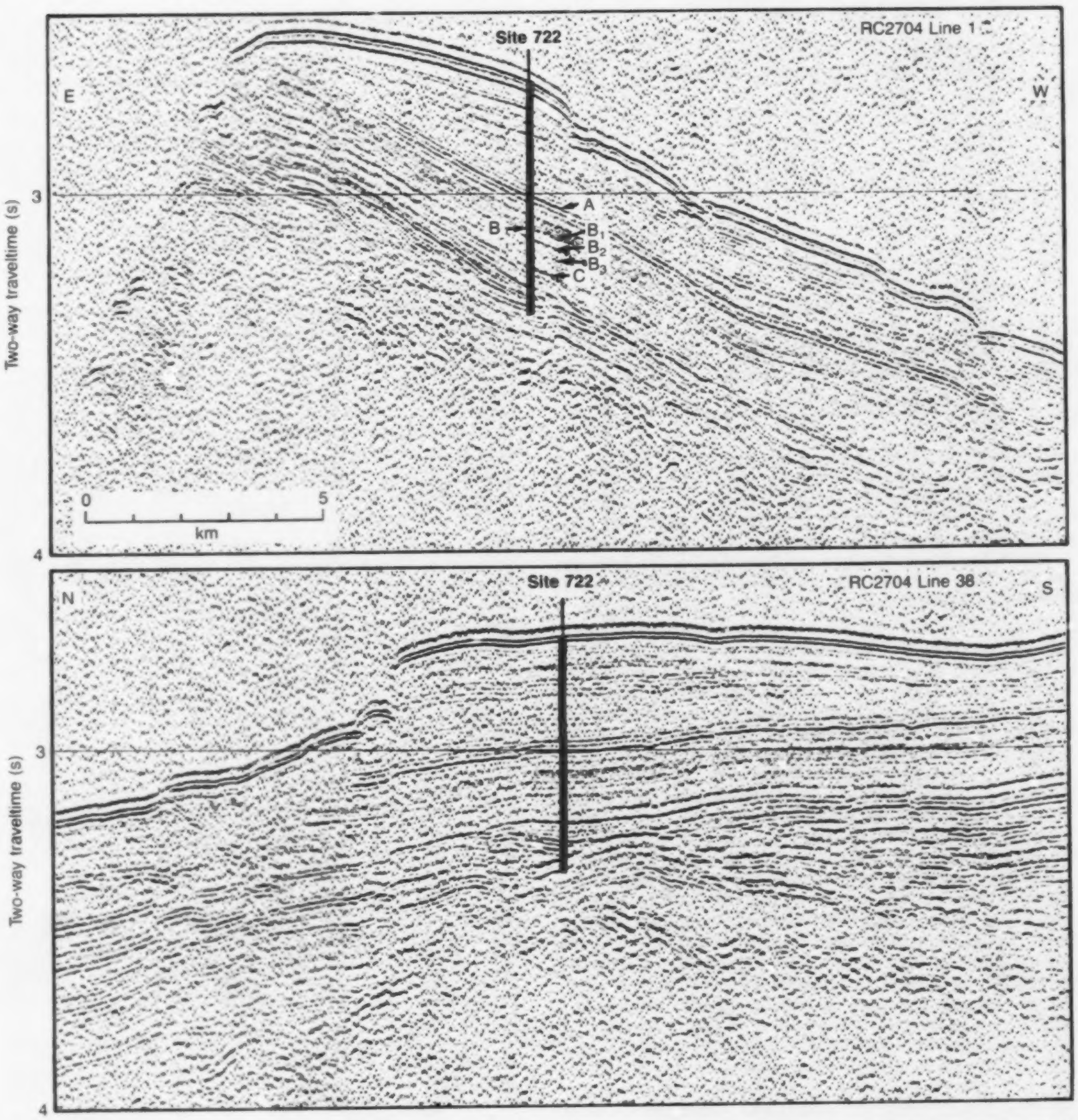

Figure 29. Seismic reflection profile (Lines 1 and 38, Fig. 27) across Site 722 to the crest of the Owen Ridge. The location and recovered interval of Site 722 are shown, along with the reflector identifications.

going log was much less reliable, with cycle skips on all channels, probably because of the much faster logging speed. Raw sonic transit times for the downgoing log are much slower than in water in the interval above 163 mbsf (Fig. 35). No cycle skipping is observed in either log below 275 mbsf.

Cycle skips were removed from both downgoing and upcoming source-receiver transit times, by simply removing all sudden baseline shifts. The edited transit times were then reprocessed, to increase vertical resolution to 0.6 m and exclude unreliable data according to an algorithm described by Shipboard Scientific Party (1987). Figure 35 shows an overlay of the downgoing and upcoming reprocessed sonic logs. The two agree quite well throughout the depth range. Comparing the reprocessed logs to the raw logs, very little change is observed below 275 mbsf, but the interval above this depth is substantially revised. In particular, the slowest values are now 193 μs/ft (1.58 km/s), in contrast to raw sonic values slower than 210 μs/ft (1.45 km/s). For comparison, an empirical curve of velocity as a function of depth for calcareous sediments predicts velocities of about 1.7 km/s at 100 mbsf (Hamilton, 1979).

Downhole resistivity log calibrations were poor prior to resistivity logging. Because of time constraints, resistivity logging

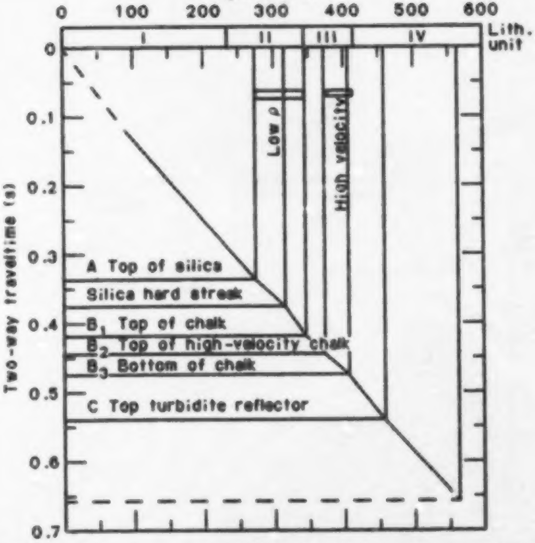

Figure 30. Plot of two-way traveltime (from SCS line 38, see Figs. 28 and 29) and depth (mbsf) of lithologic features at Site 722. Reflectors are indicated on the traveltime axis, and lithologic units and facies are shown on the depth axis.

was undertaken anyway. During downgoing logging, the gain of the spherically-focused resistivity was adjusted twice, and the gains of medium and deep resistivity logs were each adjusted once. At the conclusion of upcoming logging, the resistivity calibration was good. The gain adjustments apparently solved the calibration problem, while causing step-function changes in the downgoing logs which we have subsequently removed.

The upgoing and downgoing resistivity logs are very similar except in one aspect: the spherically-focused resistivity in the chalks (above 400 mbsf) is relatively constant as a function of depth in the downgoing log, but higher and increasing uphole in the upcoming log. We do not know why this log reads much higher than the two other resistivity logs in the chalks, yet similar to them in the turbidites. We suspect that the spherically-focused log is not properly calibrating in the chalks; at Site 731 this log agreed with the other resistivity logs in this same formation (see "Downhole Measurements" section, "Site 731" chapter, this volume). The higher variance in the spherically-focused log is expected, because it has both higher vertical resolution and lower signal-to-noise ratio than the deeper resistivity logs.

The only editing applied to the gamma ray log was the removal of pipe attenuation effects from the portion of downgoing log obtained through the bottom-hole assembly, 57–91 mbsf. Based on comparison of the mean gamma ray response for a 10-m interval inside pipe with a 10-m interval just below the gamma ray spike at 92–93 mbsf, a gain factor of 4.4 was applied to the through-pipe log (Fig. 36). Comparison of this edited log with the reprocessed spectral gamma ray log shows a fair agreement in the open-hole interval and poor match in the portion for which the gamma ray log was obtained through pipe. The assumption of similar true means above and below the gamma ray spike at 92 mbsf, though appropriate when editing a log independent of other logs, is shown to be invalid by the spectral gamma ray log. In the open-hole interval below 91 mbsf, a character match of large-scale features is found between gamma ray and spectral gamma ray, but the smallest-scale features are not replicated. The open-hole upcoming gamma ray log is similar to the other two logs, with greatest similarity of small-scale features to the spectral gamma ray log. In the interval for which gamma ray data were collected through pipe and spectral gamma ray data were collected in the open hole, no character match at all is found.

These differences between gamma ray logs are largely attributable to logging speeds. The downgoing gamma ray log was obtained at 1200 m/hr, the upcoming log at 550 m/hr, and the spectral gamma ray log at 300 m/hr. With faster logging speed, the counting statistics of natural gamma radiation decrease in accuracy. With the fastest logging speed, the accuracy is apparently about 2–5 API units, comparable in magnitude to the formation variations in signal strength for through-pipe logging at this site. Much higher replicability of repeat runs was obtained for gamma ray logs obtained at lower logging speeds in more radioactive formations at Site 723 (see "Downhole Measurements" section, "Site 723" chapter, this volume).

The density log for Site 722 was adversely affected by voltage fluctuations in the neutron tool. "Corrected" density values, based on the difference between signal strength at two receivers, were nearly all negative. However, after removal of the extremely large hole-size correction (DRHO) that had been applied by the acquisition software and removal of a 0.4-g/cm^3 baseline shift at 265 mbsf in the downgoing log, resulting density values exhibited reasonable replication of downgoing and upcoming runs (Fig. 37). An exception is the upper turbidite interval, 410–545 mbsf. In general, these density logs are consistent with laboratory measurements of density (see "Physical Properties" section, this chapter). Unfortunately, this omitted DRHO correction is normally useful in removing the adverse effects of variations in quality of tool padding against the borehole wall. Thus the "uncorrected" density log that we must use for Site 722 is sensitive to washouts, enlarged portions of the hole.

An extreme example of this sensitivity is shown in Figures 37 and 38. The upcoming density log exhibits low densities and a strong cyclicity in the interval 130–230 mbsf. This cyclicity is not found in any other log (Figs. 37 and 38), including the downgoing density log. Calculation of apparent matrix (or grain) density from the density and neutron logs yields excursions of matrix density to unrealistically low values of 2.0–2.2 in the cyclical density lows. In contrast, the cyclical density highs give matrix densities that are both more reasonable (2.6–2.7) and more similar to the flanking depth intervals. The cyclical density lows are unreliable, because of borehole enlargement. The periodicity of the density cycles is about 9.2 m, very close to the 9.4 m interval at which cores are taken. Further, the core breaks occur at the density minima (Fig. 38). These density lows are probably caused by the circulation that is used to pump the core barrel down the pipe, while the pipe is stationary. Below 230 mbsf the formation is apparently strong enough to prevent hole washout associated with this pumping. We do not know why this cyclical pattern of apparent density fluctuations is not evident on the downgoing density log.

Post-cruise reprocessing of the density logs yielded logs even less reliable than the corrected logs of Figure 37. Our best estimate of density variations at Site 722 is a composite log consisting of the downgoing log above 231 mbsf and upcoming log below that depth. The reliability of this log is judged to be fair.

A log of photoelectric effect was obtained from the same tool as the density log. This log was also severely affected by the invalid density "correction," and neither shipboard nor post-cruise reprocessing of this log has yielded any useful data.

Log Responses of Lithologic Units

Lithologic Unit I (0–221.5 mbsf) consists of nannofossil ooze and marly nannofossil ooze. Alternation of light and dark beds, associated with fluctuations in relative amounts of calcium car-

Table 10. Summary of interstitial water geochemical data, Site 722.

Hole, core, section, interval (cm)	Depth (mbsf)	Vol. (mL)	pH	Alk. (mmol/L)	Sal. (g/kg)	Mg (mmol/L)	Ca (mmol/L)	Cl (mmol/L)	SO_4 (mmol/L)	PO_4 (µmol/L)	NH_4 (mmol/L)	SiO_2 (µmol/L)	Mg/Ca
722A-1H-4, 145-150	5.95	68	7.48	5.00	33.0	49.90	8.22	549	23.0	7.2	0.51	678	6.07
722A-3H-4, 145-150	25.35	45	7.61	6.75	33.0	44.64	6.88	555	14.8	9.9	1.20	893	6.49
722A-6H-4, 145-150	54.15	50	7.73	8.05	32.5	37.04	6.10	554	8.1	8.8	1.82	1044	6.07
722A-9H-4, 145-150	82.75	56	7.79	9.11	32.3	34.36	6.18	556	3.5	7.8	1.92	1032	5.56
722A-12X-4, 145-150	111.85	39	7.61	7.94	32.2	30.81	7.15	555	1.0	7.4	2.14	1042	4.31
722A-15X-5, 145-150	142.35	42	7.56	6.91	32.0	28.99	7.48	559	0.7	4.5	2.31	1012	3.88
722A-19X-4, 145-150	179.55	41	7.49	6.25	32.0	29.17	8.71	556	0.7	3.2	2.13	916	3.35
722A-22X-4, 145-150	208.65	34	7.33	5.63	31.8	27.86	9.55	558	1.0	2.7	2.15	1014	2.92
722A-27X-2, 140-150	253.90	60	7.32	4.91	32.3	27.31	10.10	562	0.0	2.4	2.08	1190	2.7
722B-27X-4, 140-150	252.40	55	7.67	4.85	31.8	27.14	10.14	563	0.0	2.0	1.93	1190	2.68
722B-30X-1, 0-1	275.60	15	7.35	4.02	34.4	39.42	11.47	566	1.0	2.3	1.59	846	3.44
722B-31X-4, 140-150	291.20	67	7.38	4.16	32.0	27.26	11.21	565	0.0	1.5	1.92	1257	2.43
722B-34X-2, 140-150	317.20	95	7.48	3.68	32.5	29.21	11.98	563	1.0	1.5	1.56	1161	2.44
722B-37X-5, 140-150	350.80	56	7.19	3.02	32.4	27.15	12.88	566	1.0	0.7	1.51	1208	2.11
722B-40X-2, 140-150	375.40	33	7.44	2.11	32.6	27.70	13.41	568	2.4	0.7	1.19	646	2.07
722B-43X-2, 140-150	404.30	10	7.49	1.49	32.8	28.00	13.58	570	2.4	0.0	1.21	167	2.06
722B-46X-5, 140-150	437.90	42	7.53	1.83	33.0	29.20	15.48	569	3.5	0.9	0.63	320	1.89
722B-49X-1, 140-150	463.80	31	7.58	1.81	32.0	28.17	15.58	548	3.9	0.3	0.61	226	1.81
722B-52X-5, 140-150	495.60	27	7.66	1.62	32.8	29.08	17.15	558	4.6	0.3	0.43	322	1.70
722B-58X-4, 140-150	552.10	15	7.63	1.69	33.0	28.94	18.69	562	3.5	0.4	0.41	361	1.55

bonate and silty clay, is present on a scale of 0.05-1.0 m. Calcium carbonate ranges from 50% to 89% and clay content ranges from 10% to 30% (see "Lithostratigraphy" section, this chapter).

The fine-scale cyclicity is largely beyond the vertical resolution of the logs. However, it does cause a fine-scale variation in neutron porosity (Fig. 37), resistivity (Fig. 37), gamma ray (Fig. 36), potassium, thorium, and uranium (Fig. 39) that occasionally defines individual beds but more often looks like noise because of undersampling. Clay content, as indicated by K and Th logs (Fig. 39), shows little overall change in the portion of Unit I for which openhole logs are available (73-221.5 mbsf). The K and Th do suggest a subtle and gradual downhole decrease in clay from 63 to 130-160 mbsf, followed by a slight increase down to the base of Unit I. A similar pattern is more obvious in the neutron porosity (Fig. 37), but the apparent correlation of highest porosities with lowest clay in the interval 130-160 mbsf is the opposite of the expected effect of clay on porosity.

The largest log response in Unit I is a major uranium peak at 91-94 mbsf (Fig. 39). This peak dominates the gamma ray response for Unit I (Fig. 36). Two possible causes for this peak are: (1) precipitation of uranium at a redox front, probably associated with high organic matter, or (2) a phosphorite layer, probably associated with a hiatus. Log responses do not indicate clearly which explanation is more likely. Immediately below the uranium spike is a pronounced uranium minimum at 99-104 mbsf, possibly implying local uranium leaching. This minimum is a slightly clay-rich layer, based on Th and K. From 104 mbsf to the base of Unit I, uranium exhibits a substantial overall decrease, with high-frequency oscillations. This decrease is not echoed by K and Th decreases, and high-frequency variations in U are out of phase with K and Th variations. Thus the U is dominantly not in the clays but in a component that is richest in the low-clay layers. Nannofossils are very low in U, and the component carrying the U is not known.

Sonic velocities exhibit a single substantial change in the logged interval of Unit I: a sudden downhole velocity increase from 1.62 km/s to 1.75 km/s (slowness decrease from 188 to 174 µs/ft; Fig. 35) in the interval 150-159 mbsf. This change is not caused by a change in clay mineral content (Fig. 39) or porosity (Figs. 37 and 38).

Lithologic Unit II (221.5-343.4 mbsf) includes nannofossil chalks and marly nannofossil chalks similar to Unit I. Based on log responses, the top of Unit II is probably the 218 mbsf upward increase in uranium and decrease in thorium (Fig. 39). Unlike Unit I, diatoms are often abundant in Unit II. Based on examination of smear slides, biogenic silica component gradually increases downhole from trace amounts in basal Unit I to a maximum of 20% in the interval 245-330 mbsf. Between 330 mbsf and 343.4 mbsf, the biogenic silica component decreases rapidly to zero (see "Lithostratigraphy" section, this chapter).

Diatoms have a very large impact on many log responses, because even a small diatom content greatly increases porosity (e.g., Hamilton, 1976; Shipboard Scientific Party, 1987). The same overall pattern of diatom variations seen in smear slides is detected in log responses, but the log responses suggest some refinements to the depth distribution of diatoms in Unit II. From 221.5 mbsf to 298 mbsf, variations in relative abundance of diatoms and nannofossils undergo at least four major cycles, with a periodicity that fluctuates but averages about 15 m. This cyclicity is most obvious on the velocity log (Fig. 35), which is very sensitive to porosity variations at high porosities. The cyclicity is also present but is less obvious on density, neutron porosity resistivity (Fig. 37), and potassium (Fig. 39) logs. The log response to the diatom-rich intervals is a decrease in velocity, density, and resistivity, and an increase in neutron porosity. Potassium here is positively correlated with diatom abundance indications from other logs, indicating that the diatom-rich zones are also more clay-rich than the adjacent, presumably carbonate-rich, zones. Smaller-scale cycles, with periods of 3-4 m, are superimposed on the four large cycles.

Between 298 and 320 mbsf, diatom abundance is probably at a maximum, because this interval encompasses the lowest velocities, densities, grain densities, and resistivities, and highest neutron porosities of Unit II. Grain densities (calculated from density and neutron porosity) fluctuate between 2.0 and 2.4, very close to the 2.2 g/cm³ grain density of opal. This depth interval is consistent with smear slides but is much narrower than the 245-330 mbsf interval of maximum diatoms from smear slides. Almost the entire interval 248-341 mbsf is rich in diatoms based on log responses (exceptions are lows at 253-260, 268-275, and 332-336 mbsf), but the richest and most constant interval is 298-320 mbsf. Core recovery was unusually low in this short interval.

Both smear slides and logs indicate that the base of the diatom-rich zone is rather sharp. Velocity, density, grain density, and resistivity increase and porosity decreases through the interval 320-343 mbsf. A single cycle to high porosity and clay con-

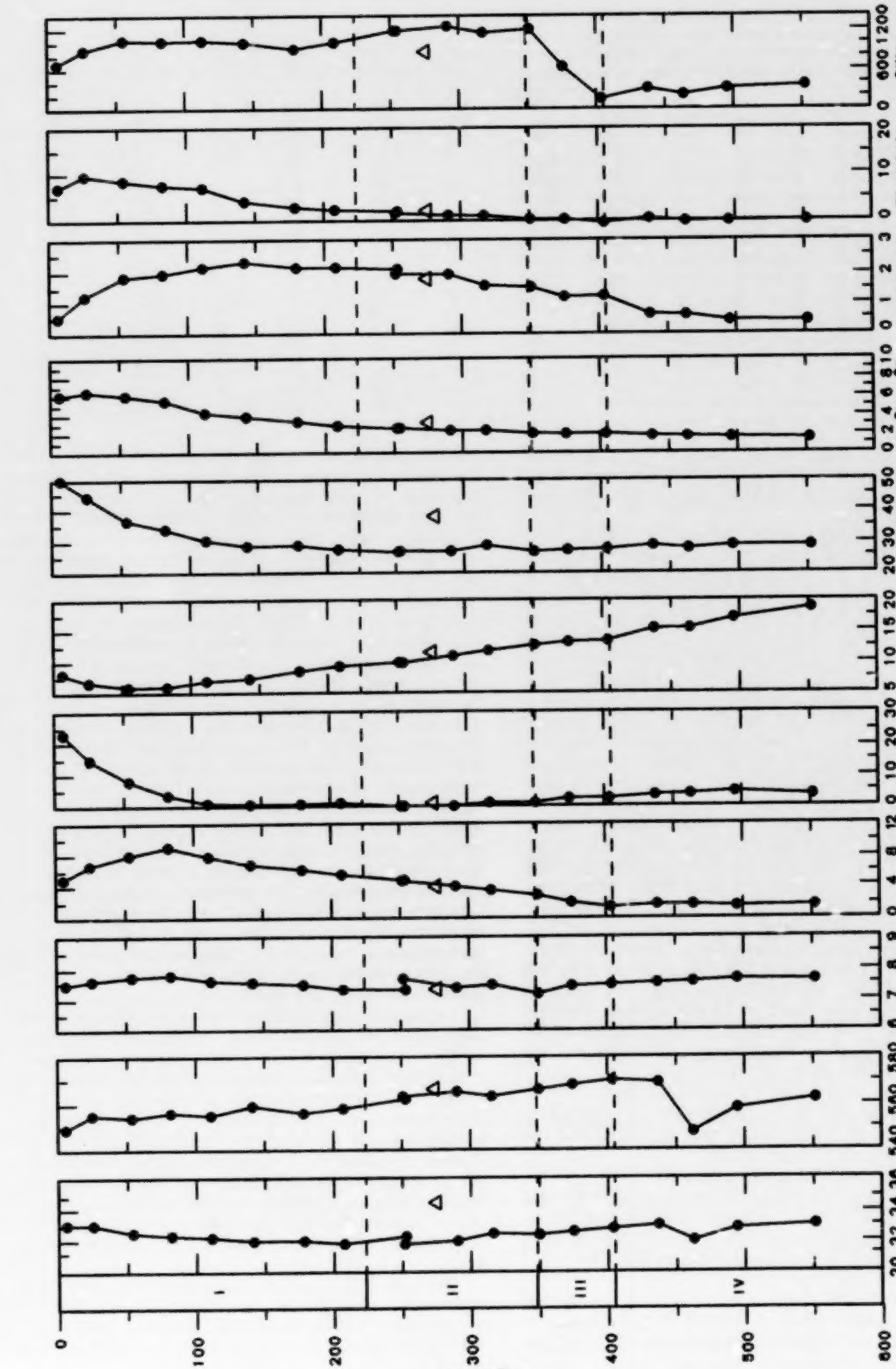

Figure 31. Concentration profiles vs. depth for Site 722. Dots = squeezed pore waters, triangles = *in-situ* pore-water samples. The dashed lines and numerals refer to the lithostratigraphic units.

Table 11. Results of Rock-Eval pyrolysis of samples from Holes 722A and 722B.

Core, section, interval (cm)	Depth (mbsf)	T_{max} (°C)	S_1	S_2	S_3	S_2/S_3	TOC	HI	OI
117-722A-									
1H-4, 144–145	5.94	421	0.21	0.78	4.54	0.17	0.35	222	1297
3H-4, 114–115	25.04	428	0.30	1.94	4.87	0.39	0.83	233	586
6H-4, 114–115	53.84	425	0.29	2.06	4.99	0.41	1.13	182	441
9H-4, 119–120	82.48	421	0.82	5.82	6.38	0.91	2.10	277	303
12X-4, 119–120	111.59	417	0.26	0.63	3.67	0.17	0.41	153	895
16X-2, 25–26	146.35	418	0.14	0.69	2.91	0.23	0.44	157	661
16X-2, 29–30	146.39	422	0.17	1.09	3.36	0.32	0.58	188	579
16X-2, 34–35	146.44	424	0.27	2.33	3.87	0.60	1.03	226	376
16X-2, 39–40	146.49	417	0.58	5.08	5.40	0.94	1.66	306	325
16X-2, 42–43	146.53	418	0.67	5.00	5.44	0.91	1.94	258	280
16X-2, 48–49	146.53	420	0.52	5.29	5.56	0.95	1.93	274	288
16X-2, 56–57	146.66	420	0.65	5.28	5.81	0.90	1.93	274	301
16X-2, 60–61	146.70	418	0.67	5.34	5.71	0.93	1.94	275	294
16X-2, 65–66	146.75	418	0.55	4.69	5.43	0.86	1.88	250	289
16X-2, 69–70	146.79	424	0.62	6.01	6.01	1.00	2.06	292	292
16X-2, 75–76	146.85	468	0.47	3.57	5.08	0.70	2.97	120	171
16X-2, 80–81	146.90	423	0.50	3.42	5.03	0.67	1.12	305	449
16X-2, 85–86	146.95	421	0.30	2.01	4.43	0.45	0.94	214	471
16X-2, 90–91	147.00	420	0.25	0.93	3.72	0.25	0.47	193	791
16X-2, 95–96	147.05	418	0.19	0.57	3.22	0.17	0.45	127	716
19X-4, 119–120	179.29	417	0.43	3.03	5.03	0.60	1.31	231	383
22X-4, 119–120	208.39	422	0.26	1.21	3.76	0.32	0.60	201	626
29X-3, 39–40	273.79	418	2.93	13.26	7.07	1.87	4.16	319	170
117-722B-									
29X-3, 120–121	270.10	442	0.27	2.03	1.86	1.09	0.72	282	258
29X-3, 125–126	270.15	412	0.70	5.25	2.57	2.04	1.79	293	144
29X-3, 130–131	270.20	417	1.20	7.49	2.93	2.55	2.23	336	131
29X-3, 135–136	270.25	409	1.05	7.44	2.93	2.53	2.22	335	132
29X-3, 140–141	270.30	413	0.98	8.00	3.00	2.66	2.17	369	138
29X-3, 145–146	270.35	418	1.16	8.37	2.95	2.83	2.26	370	131
29X-3, 149–150	270.39	412	1.00	7.84	2.97	2.63	2.23	362	133
29X-4, 5–6	270.45	416	0.77	6.35	2.62	2.42	1.84	345	142
29X-4, 10–11	270.50	413	0.62	4.34	2.50	1.73	1.51	287	166
29X-4, 15–16	270.55	411	0.47	3.07	2.47	1.24	1.30	235	190
29X-4, 20–21	270.60	416	0.31	2.82	2.31	1.22	1.10	256	210
29X-4, 25–26	270.65	410	0.35	1.78	2.12	0.83	0.97	184	219
29X-4, 30–31	270.70	410	0.23	1.31	2.06	0.63	0.83	158	248
29X-4, 35–36	270.75	403	0.28	0.98	2.29	0.42	0.80	123	286
29X-4, 40–41	270.80	403	0.39	0.84	2.06	0.40	0.49	171	420
29X-4, 47–48	270.87	408	0.20	0.44	1.48	0.29	0.74	58	200
29X-4, 52–53	270.92	403	0.10	0.29	1.38	0.21	0.28	103	493
29X-4, 60–61	271.00	421	0.17	0.54	1.52	0.35	0.27	200	562
31X-2, 114–115	290.94	422	0.46	2.94	4.84	0.60	0.91	323	531
51X-CC, 0–1	479.39	360	12.15	21.07	23.30	0.90	41.81	51	56
51X-CC, 2–3	479.40	354	13.86	29.77	17.12	1.73	53.78	55	31

Note: HI = hydrogen index and OI = oxygen index. For a detailed description of parameters, see "Explanatory Notes" chapter (this volume). The organic carbon data are measured by difference (total carbon minus inorganic carbon).

tent (and probably high diatoms) occurs within this interval at 337–339 mbsf, and much of the overall drop in diatoms probably occurs in the two short intervals 331–333 and 341–342 mbsf. Based on log responses, the base of Unit II is at 342 mbsf, very close to the 343.4 mbsf identification from lithostratigraphy.

Unit III (343.4–411.1 mbsf) consists of nannofossil chalk and marly nannofossil chalk, with only trace amounts of biogenic silica. Unit III is very similar to Unit I, except that porosities are much lower (see "Lithostratigraphy" and "Physical Properties" sections, this chapter).

Based on log responses, Unit III could be divided into two subunits. In the upper subunit (342–376 mbsf), both compaction and clay content gradually increase, based on increases in velocity, density, grain density, resistivity, potassium, and thorium, and decrease in neutron porosity. The lower subunit (376–405 mbsf) appears to be a relatively uniform chalk with low clay content, based on high velocity, density, and resistivity and low potassium, thorium, and porosity. The 50% neutron porosity of this interval is lower than any other pelagic interval at Site 722, but about 5% higher than core measurements (see "Physical Properties" section, this chapter) because of the bound water in clays.

Unit IV (411.1–565.6 mbsf) consists of turbidites. In the interval 411–506 mbsf, the turbidites fine upward from silty claystone to nannofossil chalk or marly nannofossil chalk. Carbonate content gradually decreases downhole, to near zero below 495 mbsf. The interval 506–565.6 mbsf appears to consist of micaceous sands fining upward into silty clays and clays, though core recovery was only 22% below 497.9 mbsf (see "Lithostratigraphy" section, this chapter).

The transition from Unit III to Unit IV is obvious on all of the logs, but it is most pronounced on the K and Th logs because both the terrigenous and biogenous turbidites are much higher in clay minerals and mica than are the pelagic units above. A complex log response results from the complex and variable mineralogy of the turbidites, and it is not possible to determine lithology unambiguously without a formal log inversion. For example, in the interval 407–448 mbsf, velocity increases down-

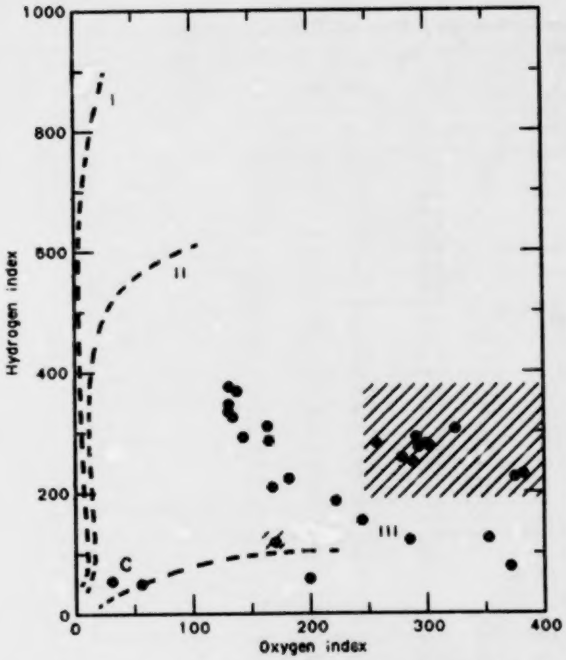

Figure 32. Plot of the hydrogen index vs. oxygen index of samples from Holes 722A and 722B. Samples plot mainly in the section for immature marine organic matter rich in relatively labile oxygen-rich functional groups. Samples from Core 117-722A-16X plot in the patterned area of the figure, while most samples from Core 117-722B-29X plot in the middle. C denotes two analyses of the coal sample.

hole, with a pronounced 10-m cyclicity that may represent variations in relative abundance of calcite and clay. However, the lowest-velocity intervals, which would normally be associated with clay, are lower in K and Th than the higher-velocity intervals. Further, mica in the sandier units can be higher in Th and K than the clays. This may explain the observation that most uranium variations are opposite in sign to K and Th variations, which requires that U be present in a different component than clay. These complexities can be unraveled by a quantitative log inversion for mineralogy; such a shore-based study is planned.

Borehole Deviation and Downhole Magnetometer

The GPIT accelerometer, which was included on the second logging run at Site 722, measures borehole deviation and magnetic moment. Because this run is padded against the borehole wall, neither measurement is adversely affected by the tool wobble which degrades the quality of GPIT logs run with free-swinging tools (e.g., "Downhole Measurements" section, "Site 723" chapter, this volume). The borehole deviation of Site 722 is a relatively constant 2.5° to the northeast (Fig. 40).

The GPIT uses three perpendicular fluxgate magnetometers to measure magnetic moment. The tool was designed for obtaining the azimuthal orientation of dipmeter logs, so no attempt was made to magnetically insulate the tool from the magnetic influence of the tool string itself. Tool-string magnetization is substantial: the measured inclination in the "nonmagnetic" chalks at Site 722 is 18.5°–19.0° (Fig. 40), in contrast to the inclination of about 30° for the earth's magnetic field at this latitude. Tool magnetization can be removed, as was done when this tool was used to log the magnetization of the oceanic crust at Hole 504B (Shipboard Scientific Party, 1988). However, this correction has not been applied yet at Site 722, because the tilt of the tool is relatively constant and has little effect on the character of the log record. To our knowledge, Site 722 is the first oceanic sediment section to be logged with a downhole magnetometer. Two logging runs were obtained, by recording during both logging down and logging up.

The total moment log exhibits long wavelength variations which are not reproduced in the two logging runs (Fig. 40). These gradual changes are probably caused by the high daily variation (Sq) at low latitudes. An approximate removal of daily variation effects is possible, based on average daily variation at this latitude or observatory records. However, a more reliable correction would require suspending a magnetometer beneath the ship, as was subsequently done at Sites 723 and 728 (see "Downhole Measurements" sections, "Site 723" and "Site 728" chapters, this volume). This daily variation has primarily a subtle long-term effect on the inclination logs (Fig. 40), perhaps causing the offset of upgoing and downgoing logs. However, some finer-scale effects are also present, such as the inclination low in the upcoming log at 263 mbsf and the inclination shift in the downgoing log at 451 mbsf. Thus only the inclination features which replicate well on two logging passes should be attributed to changes in formation magnetization, and even replication is not a fail-safe indicator of formation changes (e.g., the shifts in both inclination and moment for both downgoing and upcoming logs at 187 mbsf).

The inclination records in the chalks of Units I to III are relatively flat, with little coherent variation on the two logging runs. A baseline shift in inclination at 270–280 mbsf may indicate a real change in magnetic properties of the formation, but, in general, the magnetic log exhibits the lack of formation response that would be expected from the very low susceptibility and intensity of magnetization of these sediments (see "Paleomagnetism" section, this chapter). Even the increased susceptibility of Unit III, in comparison to Unit II (see "Paleomagnetism" section, this chapter), is subtle or absent in the inclination records.

In contrast to the chalks, the turbidites of Unit IV do have a detectable formation magnetization. Magnetic inclination increases from 391 mbsf, just above the top of Unit IV (411.1 mbsf), to 466 mbsf. Several of the fine-scale fluctuations in this interval of increase are present on both logs. Below 466 mbsf the two logs overlay very closely (Fig. 40).

The source of the changes in formation magnetization detected by the downhole magnetometer is probably susceptibility. Viscous magnetization and remanent magnetization also contribute to the magnetization, but their magnitudes are probably much lower.

INTERHOLE CORRELATION

At Site 722, the two holes are located west and slightly downdip of the crest of the Owen Ridge and are aligned in a north-northeast direction. Hole 722B is 20 m northwest of Hole 722A. Hole 722A was drilled to 86.5 mbsf with the APC and to 280.0 m with the XCB, while Hole 722B was drilled to 91.9 m with the APC and to 565.1 m with the XCB. The recovery of the APC was almost perfect in both holes. The top of Hole 722B obtained the mud line, which was not recognized in Core 117-722A-1H. The age range of the sedimentary sequence is Pleistocene to the early Miocene.

Here we provide detailed correlations within lithologic Unit I at Site 722. Lithologic Unit I has an age range from Pleistocene to the late Miocene, 0–7.5 Ma, and is characterized by cyclic changes in the nature of sediments that can be identified by visual observation and by variations of magnetic susceptibility and $CaCO_3$ content. Correlation of the sedimentary cycles of layers among these holes provides valuable information on the relative rate of sedimentation, which is necessary information for any

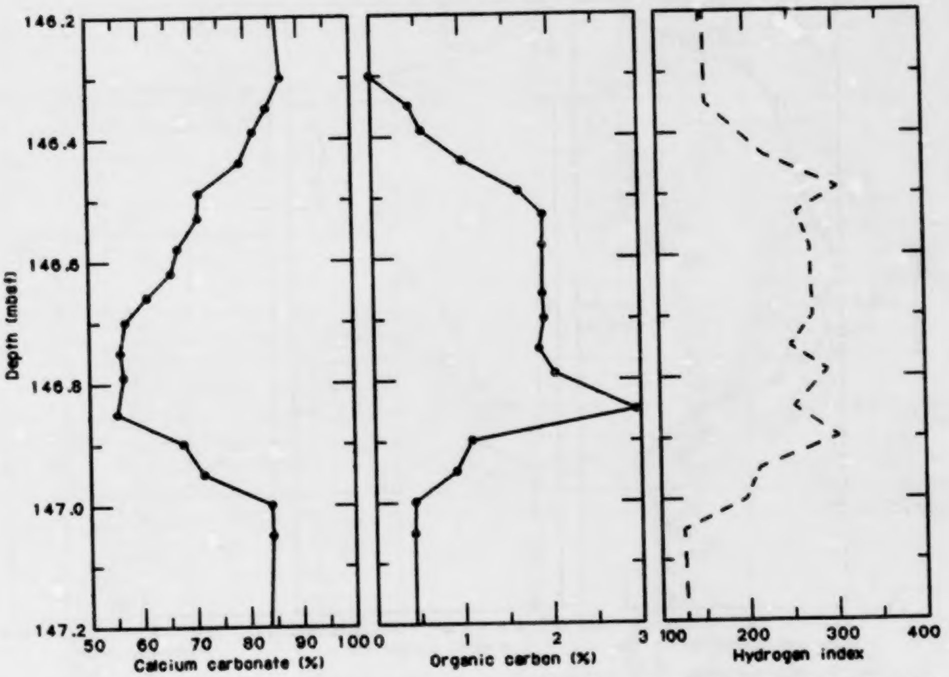

Figure 33. Downhole plot of the calcium carbonate and organic-carbon content and the hydrogen index in Section 117-722A-16X-2.

high-resolution study of depositional environments. The essence of the correlation procedure is discussed in the "Explanatory Notes" chapter (this volume).

Hole-to-hole correlations were made on the basis of visual identification of distinctive layers, as well as on physical and magnetic properties. The GRAPE density and magnetic susceptibility were measured continuously and at 5-cm intervals, respectively, on whole core sections. Lithologic descriptions and photographs were made on the split cores.

The visual correlation of the cores relied primarily on the core photographs. Several distinct and traceable layers have been determined in the upper 140 m interval of the correlatable sedimentary sequence at Site 721 and have been notated as a_0, a_1, ·····, n_2, and n_3, based on the correlation between Holes 721A, 721B, and 721C. The letter code (i.e., a, b, c, ··) refers to the sequence of cores, and the number code indicates the number of marker layers in each core. For example, the notation "a_3" corresponds to the third marker layer defined in Core 117-721A-1H, and "b_1" denotes the second marker layer in Core 117-721A-2H. The marker layers a_0 to i_4 were defined on the cored sediments of Hole 721A above 91.7 mbsf and i_5 to n_3 on Hole 721B below 94.25 mbsf. The criterion to define a marker layer is that the layer is distinct enough to trace it in the sedimentary sequence of the other holes and that the character does not change. The useful criteria for recognizing the marker are color boundaries, distinctly colored layers, shape of bioturbations, and sequence of color change in surrounding sediments. The marker layers were based mainly on the sedimentary sequence initially described at Hole 721B. Two new marker layers, k_2 and t_3, were defined in Hole 722A. Table 13 lists the depth of the marker layers in the two holes of Site 722.

Figure 41 shows the magnetic susceptibility curve and positions of individual, visually correlatable layers. The pattern of the susceptibility and the positions of layers match very well, not only among the two holes, but also between Sites 721 and 722. The stratigraphy of the magnetic susceptibility data and the visually identified layers are extremely consistent in that a particular visually characteristic layer always coincides in depth with a distinct feature in the magnetic susceptibility curve. In this way the lithologic correlations have been verified using the magnetic susceptibility data, which are quantitative. The reliability of any given correlation is bounded by the interval of susceptibility measurement, which is ± 5 cm.

The results of the layer-by-layer correlation allow us to calculate true thickness between the layers that coincide with and are separated by core boundaries. Occasionally core tops were expanded by water uptake during drilling. In this case, the apparent thickness of the disturbed sediment layer is observed to be thicker than the original thickness. In some instances, the top part of the core was missing; in this case apparent thickness is observed to be thinner than the original thickness. Fortunately, the two holes were staggered in depth, so that they have different horizons at core boundaries (Table 13). The original thickness of layers coinciding with core tops or bottoms can be obtained by comparing thickness of the correlative layer in the continuous section of the other holes. The calculation of the amount of the difference can be achieved by the differences in the depths of marker layers between the holes (last column in Table 13). The differences of marker layers a_0 and a_1 are −1.85 and −1.65 m. The differences were caused by the missing of the mudline in Hole 722A. The differences a_2, a_3 and a_4 are −1.40, −1.55, and −1.35 m, respectively, which are significantly different from that of a_0 and a_1. Marker layers a_0 to a_4 are identified within Core 117-722A-1H; however, they are separated into Cores 117-722B-2H and -3H. Because the core boundary of Cores 722B-1H to -2H is located between a_1 and a_2, the changes

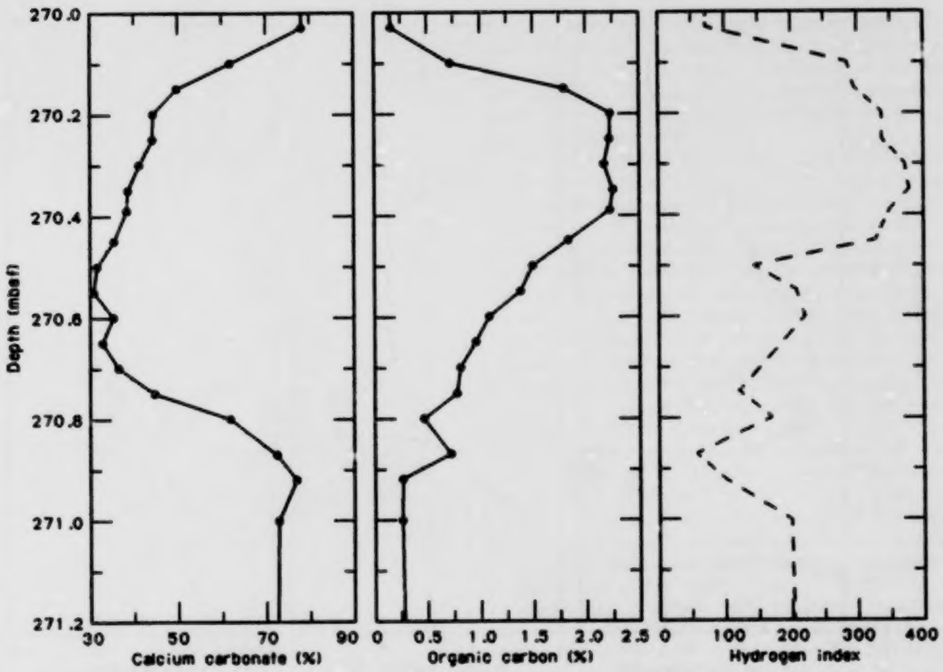

Figure 34. Downhole plot of the calcium carbonate and organic-carbon content and the hydrogen index in Sections 117-722B-29X-3 and -4.

Table 12. Concentrations of methane (C_1) and ethane (C_2) per liter of wet sediment in cores of Holes 722A and 722B.

Core, section, interval (cm)	Depth (mbsf)	C_1 (μL/L)	C_2 (μL/L)
117-722A-			
1H-4, 144–145	5.94	732	
3H-4, 119–120	25.09	76	
6H-4, 119–120	53.89	110	
9H-4, 119–120	82.49	95	2
12X-4, 119–120	111.59	246	3
27X-2, 114–115	253.64	94	
117-722B-			
27X-4, 114–115	252.14	107	
31X-4, 114–115	290.94	128	2
43X-2, 114–115	404.04	23	
46X-5, 114–115	437.64	17	
49X-3, 114–115	463.54	12	
58X-4, 114–115	551.84	13	

Note: Values are expressed in μL/L (volume gas/volume wet sediment).

in the depth differences can be explained by the lack of about 20 cm missing in Core 117-722B-3H. Table 14 gives the differences between the depth (mbsf) calculated by the ODP CORELOG computer program data and the corrected depth (mbsf) calculated by the layer-by-layer correlation method.

The layer-by-layer method on the double- or triple-cored sedimentary sequences gives us true stratigraphic thickness after the correction for core-boundary disturbance. Table 15 shows the stratigraphic thickness at Site 721, where most of the marker layers were defined, and Holes 722A and 722B. The corrected depths in Hole 722A and 722B agree well with each other. The intersite correlation of the marker layers shows clearly the existence of a hiatus at Site 722 in the interval from l_4 to n_1.

SUMMARY AND CONCLUSIONS

The primary reason for coring at Site 722 was to recover a continuous high-resolution section of pelagic sediments of late Neogene age from another area of the crest of the Owen Ridge to complement the records obtained at Site 721. The seismic stratigraphy at Site 722 revealed that it had a more complete section than did Site 721. The sediments on the ridge have been deposited well above the carbonate lysocline and beyond the zone of lateral bottom transport from the continental margin for much of the Neogene. Study of the sedimentary sequences obtained at Sites 721, 722, and 730 will provide information on the initiation, variability, and history of monsoonal upwelling in the Arabian Sea. The detailed biotic, chemical, and sedimentologic records obtained at this site also will provide data on monsoonal upwelling that, combined with data from the Oman margin Sites 723 to 730, will be used to test the hypothesis that much of the short-term variability (10^3 yr) of monsoonal upwelling is forced by changes in solar radiation related to variations in the shape of the earth's orbit (the Milankovitch mechanism). Long-term trends of the intensity of the monsoon related to the uplift of the Himalaya may also be imprinted on the long paleoenvironmental record from the ridge. The combined record of Sites 722 and 721 insures that a complete record of the upper Neogene sediments have been recovered from the Owen Ridge. In addition, the age and character of the sediments at Site 722 will be used to investigate the depositional and tectonic uplift history of the Owen Ridge.

The preliminary shipboard findings at Site 722 parallel the findings at Site 721. Here, we summarize the new information

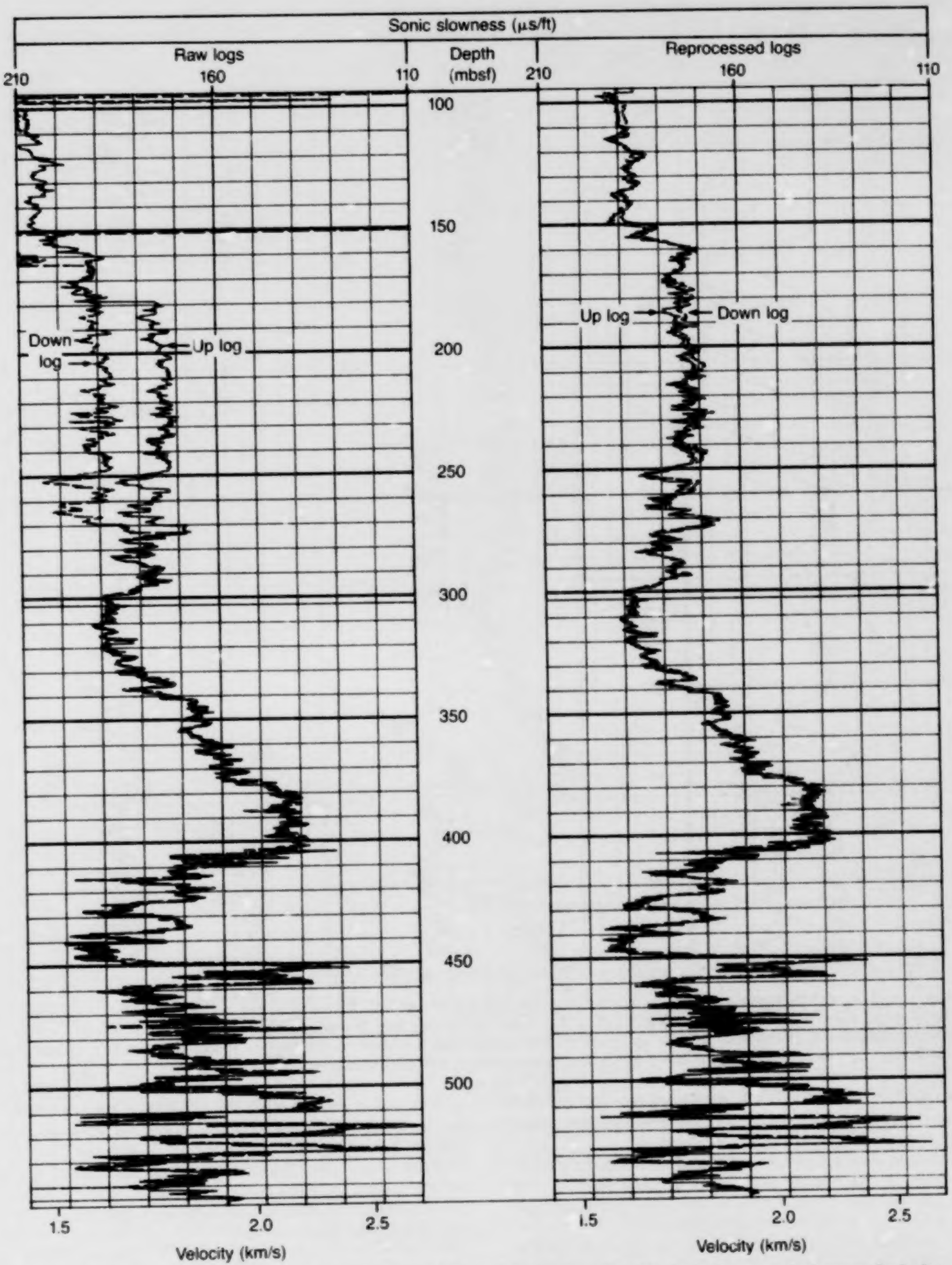

Figure 35. Comparison of the raw (left) and reprocessed (right) sonic logs from Site 722. Sonic slowness, the inverse of velocity, is in microseconds per foot. Both downgoing (dashed) and upcoming (solid) logs are shown.

pertinent to the above objectives (Fig. 42). These findings include the identification of:

1. A complete stratigraphic section from early Miocene to the Holocene.

2. The appearance of siliceous facies in the middle Miocene.

3. The sequential appearance of cold "upwelling" faunas in the upper Miocene and Pliocene.

4. Well-defined sedimentary cycles that are defined by changes in sediment color, magnetic susceptibility, and physical

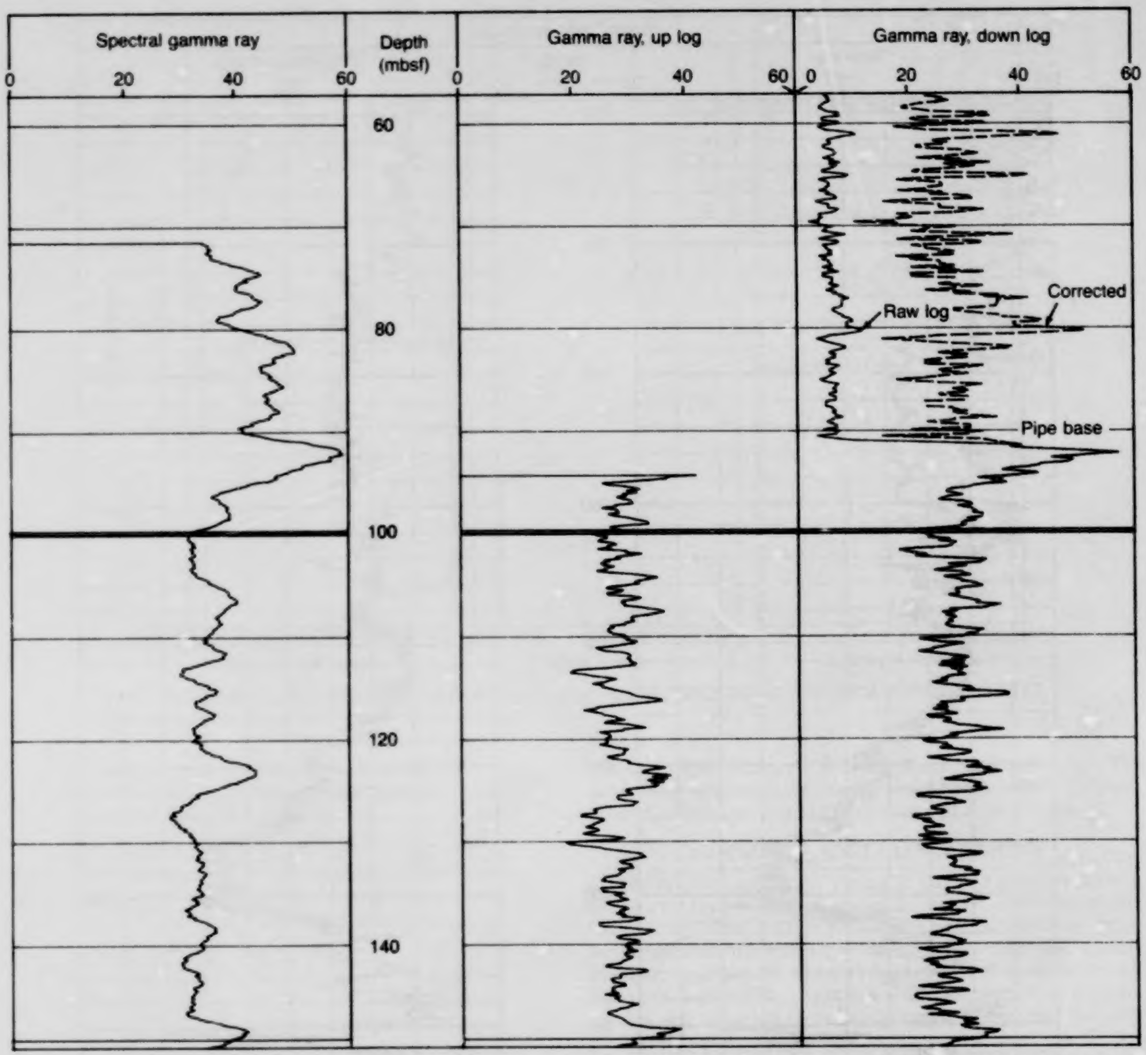

Figure 36. Comparison of three gamma ray logs for part of the upper portion of Site 722. The spectral gamma-ray log (left) was obtained from a different logging tool than the upcoming (center) and downgoing (right) gamma ray logs. Horizontal heavy lines indicate the varying depth of pipe for the different runs. The attenuation of gamma ray signal in through-pipe logs is evident on the downgoing log. An attempt to correct this portion of log (dashed line) by applying a gain factor yields results inconsistent with the spectral gamma ray log (left).

properties and that can be correlated between holes and between Sites 722 and 721. The cycles have distinct periodicities, which are consistent with the Milankovitch frequencies.

5. A threefold increase in carbonate and noncarbonate accumulation rates in the middle and lower upper Miocene. The high rates are followed by low rates in the lower Pliocene, and increasing rates during the Pliocene-Pleistocene.

6. The cessation of turbidite deposition on the ridge crest in the lower Miocene.

7. The occurrence of vein structures in the siliceous Unit II, which appears to be coincident with the slumped section in Site 721.

8. Generally high values of marine-derived organic carbon within phases of high sediment accumulation.

9. The presence of chlorite and absence of kaolinite in the noncarbonate mineral fraction, which was similar to the mineralogy of the Indus Fan Site 720.

The major themes that are relevant to the interpretation of the depositional history of Site 722 are the same as at Site 721 and emphasize the uplift of the Owen Ridge, the onset and preservation of siliceous fossils and the appearance of distinct upwelling faunas, and the pattern of high-frequency variability in the abundance of various sedimentary components. Below, we briefly address these themes.

Uplift of the Owen Ridge

The uplift history of Owen Ridge at Site 722 is indicated by the gradational transition from a turbiditic to a pelagic facies in the latest early Miocene, as was the case at Site 721. On the basis of mineralogy, we infer that the provenance of the the turbiditic sediments on the Owen Ridge was probably the same source as for the Indus Fan. This inference is based on the presence of well-crystallized chlorite and the absence of kaolinite; an associ-

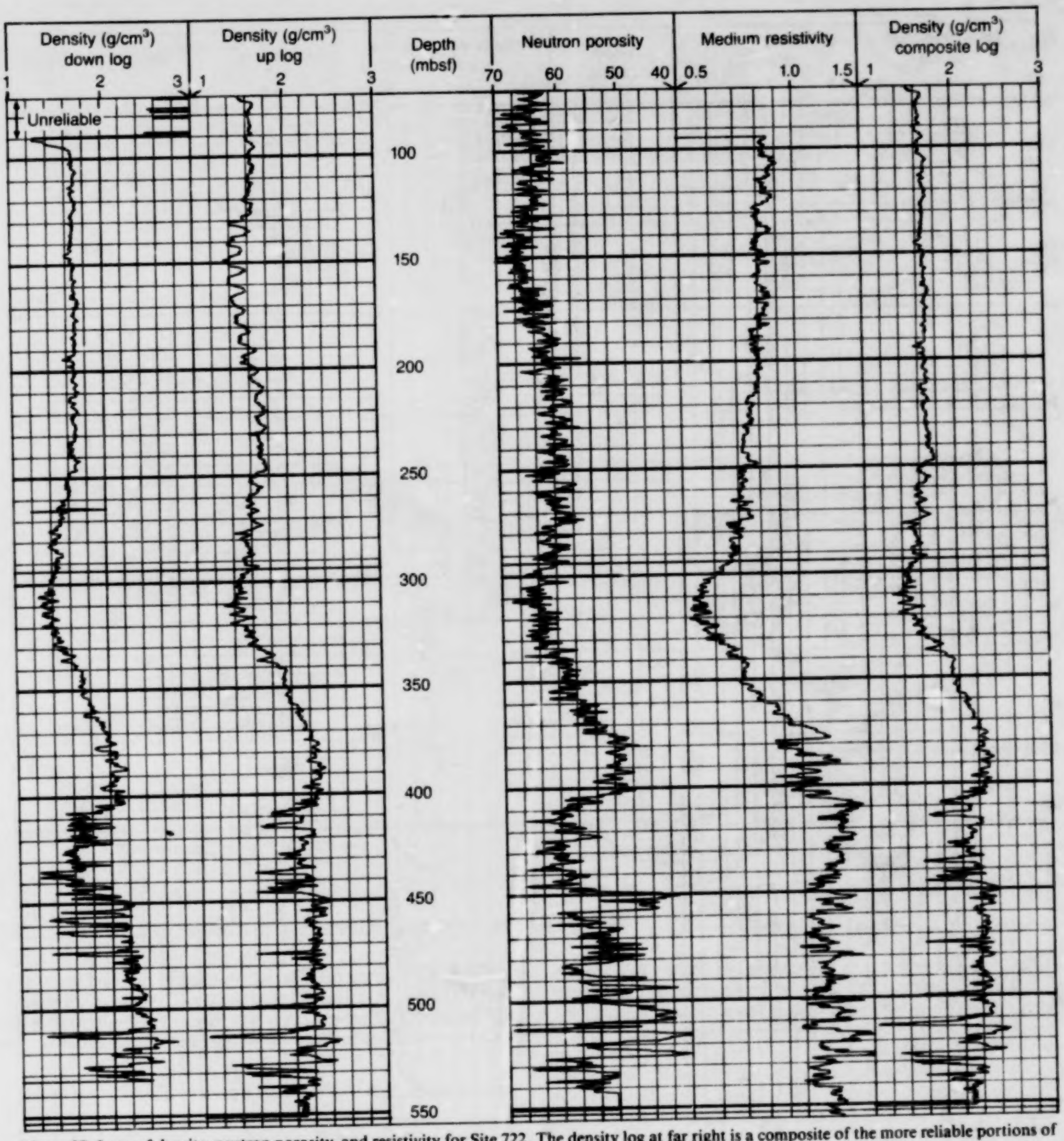

Figure 37. Logs of density, neutron porosity, and resistivity for Site 722. The density log at far right is a composite of the more reliable portions of the two density logs at far left.

ation that is identical to the mineralogy of the Indus Fan deposits recovered at Site 720. The upper boundary of the turbiditic sequence at Site 722 is marked by a prominent seismic reflector (C) that onlaps onto a basement peak near the site.

The lower Miocene turbidites at Site 722 are overlain by pelagic nannofossil chalks of lithologic Unit III that are middle Miocene in age (Fig. 42). The chalks are characterized by high carbonate content (76%) and poor opal preservation. The chalk unit is about 68 m thick and is succeeded by 122 m of siliceous nannofossil chalks of lithologic Unit II that are middle and late Miocene age. This sequence exhibits distinct trends in its physical properties as it grades from low porosity and high densities and velocity at the base of the chalk unit to high porosity and low density and velocity in the middle of the siliceous unit (Fig. 42). These gradients in physical properties give the chalk and siliceous units a distinctive seismic reflection signature that can be

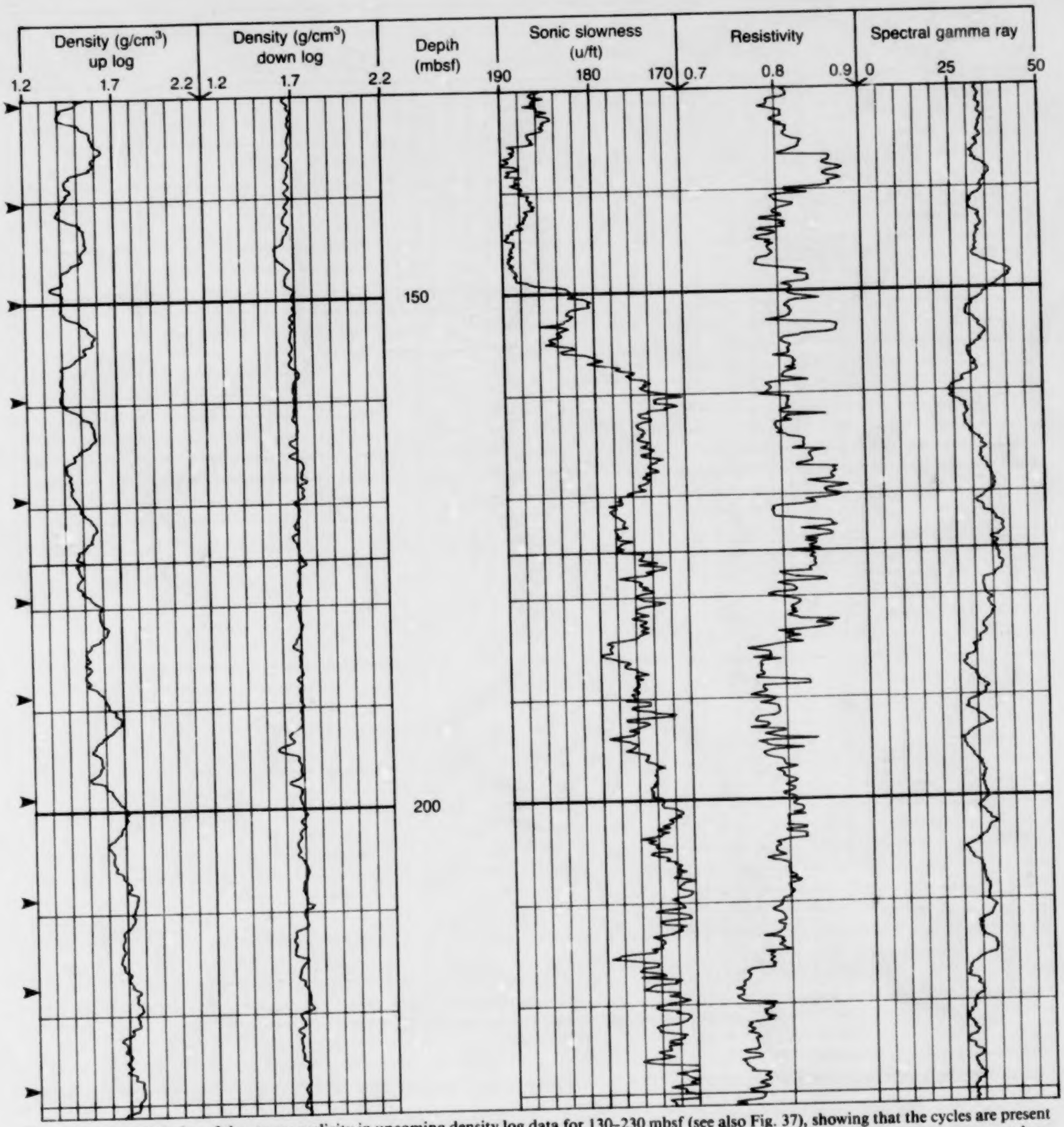

Figure 38. Expanded plot of the strong cyclicity in upcoming density log data for 130–230 mbsf (see also Fig. 37), showing that the cycles are present in sonic, resistivity, gamma-ray, or upcoming density logs. The cycles do correlate strongly with drill-pipe position at the times cores were taken; they are an artifact associated with the effects of circulating during coring on borehole diameter.

mapped over much of the Owen Ridge. The stratigraphic and seismic data indicate that much of this middle Miocene section is missing at Site 721. Comparison of the sections at Sites 721 and 722 indicate that about 30 m of the chalk unit and 90 m of the siliceous unit are missing at Site 721.

The interval of the siliceous sediments in lithologic Unit II with the highest porosity and lowest density also displays distinctive sigmoidal vein structures. The vein structures are perpendicular to bedding and occur preferentially in the darker bands. Similar structures have been observed in accretionary prisms (Suess, von Huene, et al., 1988) and have been ascribed to both hydrofracturing by dewatering mechanisms, and dilation as a result of applied deviatoric stresses. The significance of these structures at Site 722 is not clear, but we note their association with the low-density sediments that failed by slumping at Site 721. Possibly the slump event caused a decrease of lateral stress at Site 722, which is about 10 km away. However, the vein structures have only about 300 m of overburden at present and

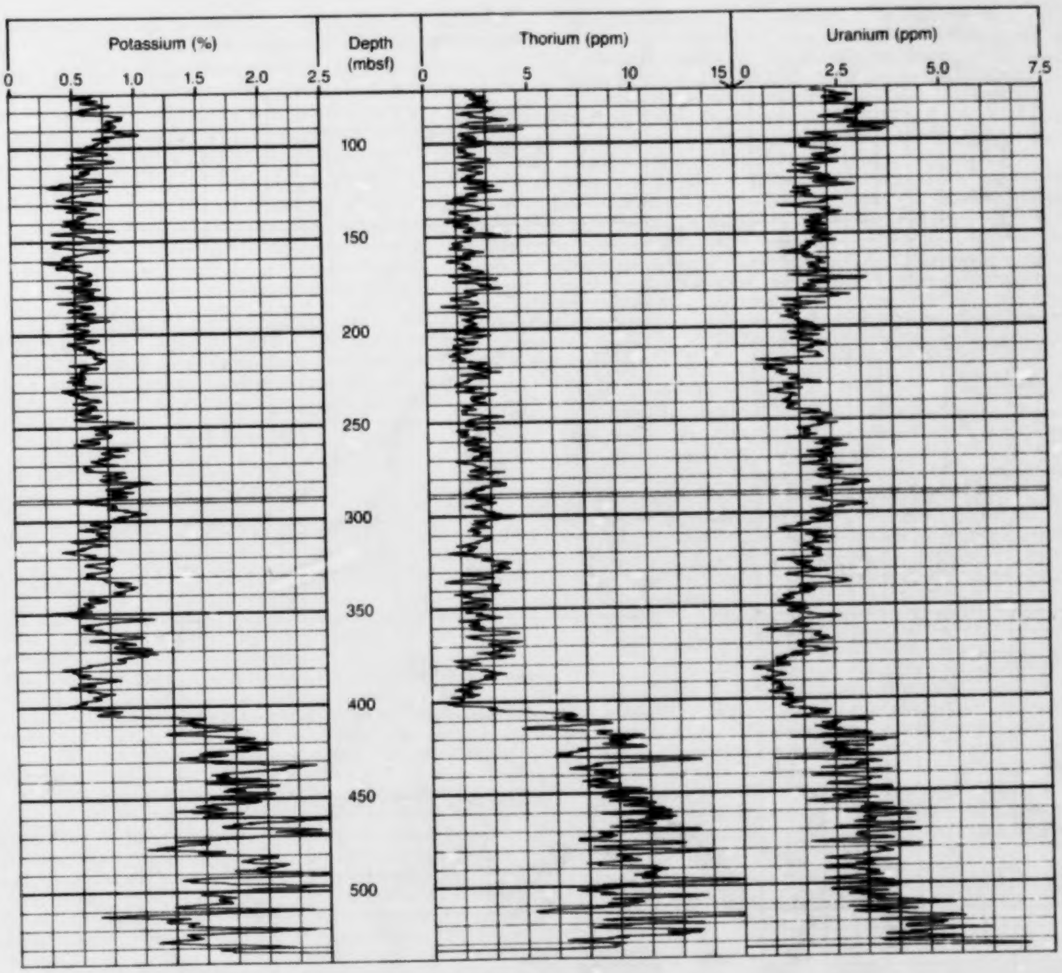

Figure 39. Reprocessed logs of potassium, thorium, and uranium at Site 722.

may have had less at the time of vein formation, which is unknown at this time. The structural features may reflect the tectonic processes that caused the uplift of the Owen Ridge, but the specific relationship cannot yet be identified.

The Onset of Upwelling Faunas and Opal Deposition

The western Arabian Sea is presently characterized by large seasonal or monsoonal variations in atmospheric and oceanic circulation. During the southwest summer monsoon (June-July-August), the winds blow strongly from the southwest and cause intense upwelling along the continental margin of Oman. This upwelling causes significant changes in the properties of the oceanic mixed-layer. For example, in the western Arabian Sea, sea-surface temperatures decrease, and nutrient content and productivity increase. In the modern and late Pleistocene ocean, these changes are recorded by the response of planktonic organisms to changing environments (i.e., carbonate and opal productivity and species composition), by the composition and input of eolian dust, and by the relative proportions of pollen species. On the basis of such paleoceanographic reconstructions, several hypotheses have been put forward concerning the mechanisms that control the strength of the monsoon and how it is related to changes in global climate. Two of the potential causes for changes in monsoonal intensity are changes in the topography of Tibet-Himalaya complex and variations in the seasonal distribution of solar radiation due to changes in the earth's orbit; i.e., the Milankovitch mechanism. Both higher elevations of the Tibet-Himalaya complex and increased summer solar radiation produce stronger monsoonal circulation.

If late Neogene uplift and orbital changes affect the intensity of the monsoon, the sediments at Site 722 should record both changes in productivity and variations in distinct biotic assemblages due to the variations of upwelling. The sediments should also reflect increased eolian transport, although much of the transport may occur during the winter season. Furthermore, variations in source area of the eolian components may result in differing mineralogy and chemistry. Thus, the cyclic variations in sediment composition related to changes in solar radiation should have specific frequencies, the "Milankovitch spectrum," that may be quantitatively identified in the sediments of Site 722.

At Site 722, we recognized a dramatic change in the sediment facies in the upper middle Miocene. Prior to this time, biogenic

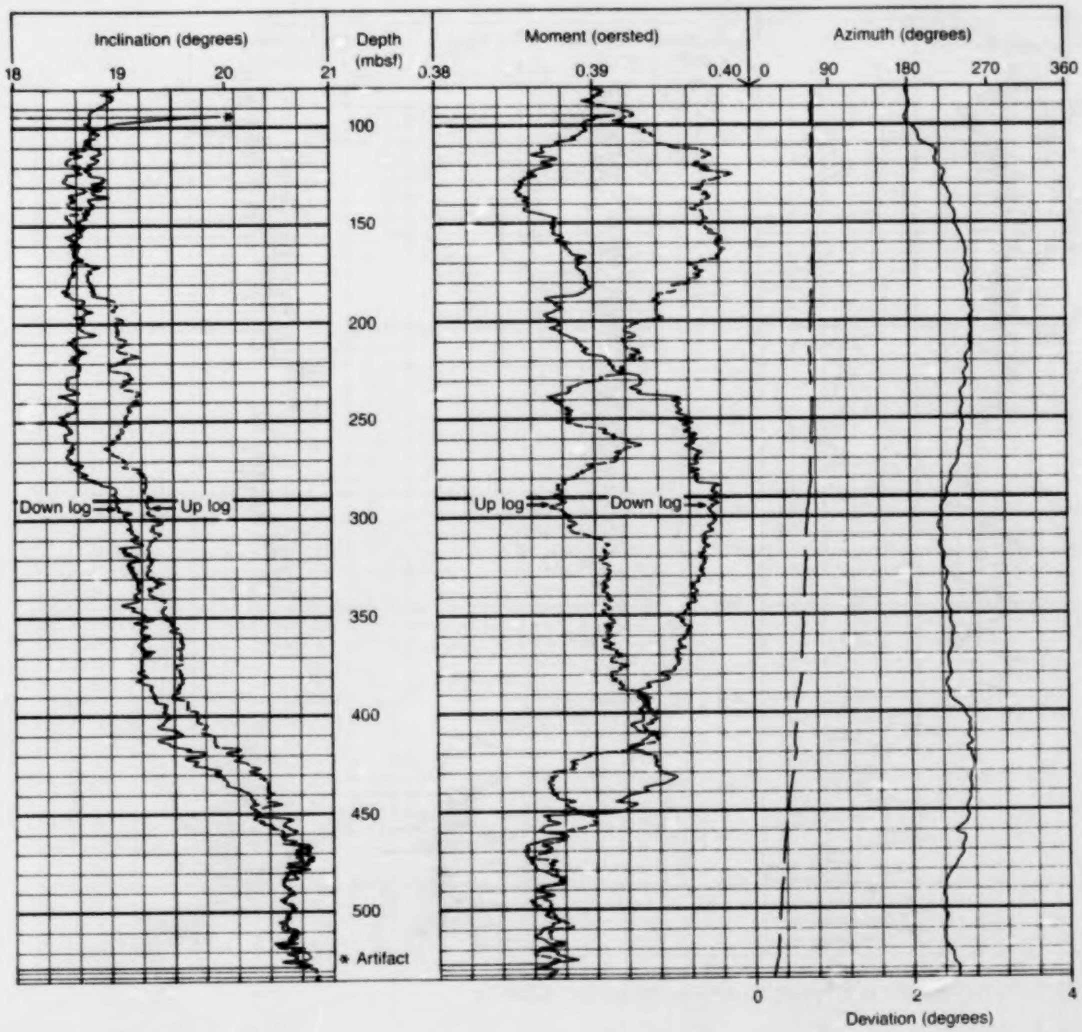

Figure 40. Logs of magnetic inclination (degrees), magnetic field strength (oersteds), borehole deviation (degrees), and deviation azimuth (degrees) at Site 722.

opal was absent from the sediments and carbonate was poorly preserved. The opal appears suddenly (between two cores) in the top of chalk Unit III in the upper middle Miocene (Fig. 42). Both radiolarians and diatoms are abundant and the species are tropical in nature. However, the associated planktonic foraminifer fauna contains species (rare, but well-preserved) that are indicative of upwelling. Preliminary analyses indicates that this early phase of opal accumulation on the ridge is not associated with particularly high accumulation rates. The upper middle and lower upper Miocene interval has carbonate and noncarbonate (including opal) accumulation rates of 1–3 g/cm^2/k.y. (Fig. 42). The remainder of the upper Miocene is characterized by high rates of carbonate (over 3 g/cm^2/k.y.) and moderate noncarbonate (about 1 g/cm^2/k.y.) accumulation. The radiolarian assemblage is a mix of tropical and upwelling species, while the nannofossil floras have low diversity (Fig. 42). Although not all of these biotic and sedimentologic indicators of high productivity are in accord, the latter half of the late Miocene was clearly an interval of higher pelagic influx to the sediments at Site 722. This pattern does not seem to be caused merely by better preservation, because changes in the preservation of foraminifers and nannofossils do not coincide with changes in rates.

The carbonate accumulation rate decreases to about 1.5 g/cm^2/k.y. in the lower Pliocene and the decrease appears independent of any change in carbonate preservation. From the upper Pliocene to the Present, both carbonate and noncarbonate accumulation rates show a continuous long-term increase (Fig. 42). The exact relationships between the biotic assemblages, accumulation rates, monsoonal upwelling, and global climate change will have to be clarified during post-cruise research.

Short-term Variability and Sedimentary Cycles

The cyclic character of the Pliocene and Pleistocene sediments at Site 722 is identical to that of Site 721. The alternation of foraminifer-bearing, foraminifer-nannofossil, and nannofossil ooze (Unit I) is paralleled by changes in sediment color, magnetic susceptibility, bulk density, and carbonate content. The strong cyclicity of these sediments is shown by detailed measurements of magnetic susceptibility that reveal a distinct and dominant periodicities. Using paleomagnetic boundaries for age control, power spectra of the magnetic susceptibility time series give periodicities near 19 k.y., 23 k.y., 41 k.y., and 400 k.y. Some intervals show power near 100 k.y. These periodicities match those expected for the Milankovitch mechanism, which is suspected to be a major cause of variations in monsoon intensity. The sediment cycles observed in Site 722 are thought to reflect changes in pelagic productivity, in the preservation of opal and carbonate, and in the input of eolian material. Again, we emphasize that these periodicities are not unique to the monsoon mechanism and that much post-cruise research is needed to identify the true monsoon signature and its spectrum.

REFERENCES

Barron, J. A., Keller, G., and Dunn. D. A., 1985. A multiple microfossil biochronology for the Miocene. *Geol. Soc. Am. Mem.*, 163:21–36.

Berggren, W. A., Kent, D. V., and Van Couvering, J. A., 1985. The Neogene: Part 2, Neogene geochronology and chronostratigraphy. *In* Snelling, N. J. (Ed.), *The Chronology of the Geological Record*: *Geol. Soc. Mem.* (London), 10:211–260.

Carlson, R. L., Schaftenaar, C. H., and Moore, R. P., 1979. Causes of compressional-wave anisotropy in calcareous sediments from the Rio Grand Rise. *In* Barker, P. F., Carlson, R. L., Johnson, D. A., et al., *Init. Repts. DSDP*, 72: Washington (U.S. Govt. Printing Office), 565–576.

Hamilton, E. L., 1976. Variations of density and porosity with depth in deep-sea sediments. *J. Sediment. Petrol.*, 46:280–300.

________, 1978. Sound velocity-density relations in sea-floor sediments and rocks. *J. Acoust. Soc. Am.*, 63:366–377.

________, 1979. Sound velocity gradients in marine sediments. *J. Acoust. Soc. Am.*, 65:909–922.

Johnson, D. A., and Nigrini, C. A., 1985. Synchronous and time-transgressive Neogene radiolarian datum levels in the equatorial Indian and Pacific Oceans. *Mar. Micropaleontol.*, 9:489–523.

Johnson, D. A., Nigrini, C. A., Caulet, J.-P., Schneider, D., and Kent, D., in press. Pliocene-Pleistocene radiolarian events and magnetostratigraphic calibrations for the tropical Indian Ocean. *Mar. Micropaleontol.*

Kennett, J. P., 1982. *Marine Geology*: Englewood Cliffs, N.J. (Prentice-Hall).

Kolla, V., Kostecki, J. A., Robinson, F., and Biscaye, P. E., 1981. Distribution and origins of clay minerals and quartz in surface sediments of the Arabian Sea. *J. Sediment. Petrol.*, 51:563–569.

Pisias, N. J., and Moore, T. C., 1981. The evolution of Pleistocene climate: a time-series approach. *Earth Planet. Sci. Lett.*, 52:450–458.

Prell, W. L., and Van Campo, E., 1986. Coherent response of Arabian Sea upwelling and pollen transport to late Quaternary monsoonal winds. *Nature*, 323:526–528.

Sato, T., Takayama, T., Kato, M., Kudo, T., and Kameo, K., in press. Calcareous microfossil biostratigraphy of the uppermost Cenozoic formations distributed in the coast of the Japan Sea. Part 4: Conclusion. *Sekiyu Gijutsu Kyokaishi.*

Shipboard Scientific Party, 1987. Site 645. *In* Srivastava, S., Arthur, M. A., et al., *Proc. ODP, Init. Repts.*, 105: College Station, TX (Ocean Drilling Program), 61–418.

________, 1988. Site 504. *In* Becker, K., Sakai, H., et al., *Proc. ODP, Init. Repts.*, 111: College Station, TX (Ocean Drilling Program), 35–251.

Suess, E., von Huene, R., et al., 1988. *Proc. ODP, Init. Repts.*, 112: College Station. TX (Ocean Drilling Program).

Takayama, T., and Sato, T., 1987. Coccolith biostratigraphy of the North Atlantic Ocean, Deep Sea Drilling Project Leg 94. *In* Ruddiman, W. F., Kidd, R. B., Thomas, E., et al., *Init. Repts. DSDP*, 94, Pt. 2: Washington (U.S. Govt. Printing Office), 651–702.

Theyer, F., Mayer, L. A., Barron, J. A., and Thomas, E., 1985. The equatorial Pacific high-productivity belt: elements for a synthesis of Deep Sea Drilling Project Leg 85 results. *In* Mayer, L., Theyer, F., et al., *Init. Repts. DSDP*, 85: Washington (U.S. Govt. Printing Office), 971–985.

Tissot, B. P., and Welte, D. H., 1984. *Petroleum Formation and Occurrence* (2nd Ed.): Berlin (Springer-Verlag).

van Gorsel, J. T., and Troelstra, S. R., 1981. Late Neogene planktonic foraminiferal biostratigraphy and climatostratigraphy of the Solo River section (Java, Indonesia). *Mar. Micropaleontol.*, 6:183–209.

Whitmarsh, R. B., 1974. Summary of general features of Arabian Sea and Red Sea Cenozoic history based on Leg 23 cores. *In* Whitmarsh, R. B., Weser, O. E., Ross, D. A., et al., *Init. Repts. DSDP*, 23: Washington (U.S. Govt. Printing Office), 1115–1123.

________, 1979. The Owen Basin off the southeast margin of Arabia and the evolution of the Owen Fracture Zone. *Geophys. J. R. Astron. Soc.*, 58:441–470.

Whitmarsh, R. B., Weser, O. E., Ross, D. A., et al., 1974. *Init. Repts. DSDP*, 23: Washington (U.S. Govt. Printing Office).

Ms 117A-107

Table 13. Stratigraphic depths of the marker layers at Site 722.

	Hole 722A		Hole 722B		
	Core, section, interval (cm)	Depth (mbsf)	Core, section interval (cm)	Depth (mbsf)	Holes 722A–722B
OR-a_0	1H-1, 50	0.50	1H-2, 85	2.35	−1.85
a_1	1H-2, 35	1.85	1H-3, 50	3.50	−1.65
a_2	1H-3, 135	4.35	2H-1, 25	5.75	−1.40
a_3	1H-4, 115	5.65	2H-2, 20	7.20	−1.55
a_4	1H-7, 30	9.30	2H-4, 65	10.65	−1.35
b_1	2H-3, 20	13.00			
b_2	2H-5, 95	16.75	3H-2, 105	17.65	−0.90
b_3	2H-6, 30	17.60	3H-3, 45	18.55	−0.95
b_4	3H-1, 60	20.00	3H-5, 10	21.20	−1.20
c_1	3H-3, 85	23.25	3H-7, 15	24.25	−1.00
c_2	3H-4, 115	25.05	4H-1, 85	25.55	−0.50
c_3	3H-5, 85	26.25	4H-2, 60	26.80	−0.55
c_4	3H-6, 100	27.90	4H-3, 85	28.55	−0.65
c_5	3H-7, 40	28.80	4H-4, 40	29.60	−0.80
c_6	4H-1, 30	29.30	4H-5, 5	30.75	−1.20
c_7	4H-1, 140	30.40	4H-5, 100	31.70	−1.30
$d_{1'}$	4H-3, 65	32.65	4H-6, 140	33.60	−0.90
d_1	4H-4, 5	33.35			
$d_{2'}$	4H-4, 65	33.95	5H-1, 70	35.00	−1.05
d_2	4H-4, 150	34.80	5H-2, 10	35.90	−1.10
$d_{3'}$	4H-6, 80	37.10	5H-3, 100	38.30	−1.20
d_3	4H-7, 25	38.05	5H-4, 30	39.10	−1.05
d_4	5H-1, 90	39.50	5H-5, 20	40.50	−1.00
e_1	5H-6, 115	47.25	6H-3, 130	48.20	−0.95
e_2	6H-1, 105	49.25	6H-5, 60	50.50	−1.25
e_3	6H-3, 40	51.60	6H-6, 130	52.70	−1.10
f_1	6H-4, 120	53.90	7H-1, 45	53.65	0.25
f_2	6H-5, 55	54.75	7H-1, 140	54.60	0.15
f_3	6H-6, 130	57.00	7H-3, 85	57.05	−0.05
f_4	7H-2, 45	59.45	7H-5, 100	60.20	−0.80
f_5	7H-3, 50	61.00	7H-6, 120	61.90	−0.90
g_1	7H-4, 40	62.40			
g_2	7H-6, 90	65.90	8H-3, 75	66.65	−0.75
g_3	8H-1, 30	67.50	8H-4, 120	68.60	−1.10
g_4	8H-2, 45	69.15	8H-5, 140	70.30	−1.15
h_1	8H-6, 60	75.30	9H-3, 50	76.00	−0.70
h_2	8H-6, 110	75.80	9H-3, 110	76.60	−0.80
h_3			9H-4, 110	78.10	
h_4			9H-6, 60	80.60	
i_1	9H-3, 90	80.70	9H-7, 50	82.00	−1.30
i_2	9H-4, 100	82.30	10H-2, 60	84.30	−2.00
$i_{2'}$	9H-5, 70	83.50	10H-3, 75	85.95	−2.45
i_3	10X-1, 5	86.55	10H-5, 40	88.60	−2.05
i_4	10X-1, 125	87.75	10H-5, 135	89.55	−1.80
i_5	10X-3, 25	89.75			
j_1	10X-4, 60	91.60	11X-2, 5	93.45	−1.85
j_2	10X-5, 60	93.10	11X-3, 35	95.25	−2.15
j_3	10X-5, 120	93.70	11X-3, 80	95.70	−2.00
OR-j_4	11X-1, 50	96.70	11X-4, 50	96.90	−0.20
j_5	11X-2, 95	98.65			
k_1	11X-3, 100	100.20			
k_2	11X-6, 100	104.70	12X-3, 45	104.95	−0.25
l_1	12X-1, 45	106.35			
l_2	12X-2, 45	107.85			
l_3	12X-4, 10	110.50	13X-1, 65	111.85	−1.35
l_4	12X-5, 115	113.05	13X-3, 45	114.65	−1.60
m_1	13X-1, 50	116.10			
m_2	13X-2, 90	118.00			
m_3	13X-3, 35	118.95			
n_1	13X-6, 95	124.05	14X-3, 90	124.80	−0.75
n_2			14X-4, 65	126.05	
n_3			14X-5, 20	127.10	
n_4	14X-3, 45	128.75	15X-1, 95	131.45	−2.70
o_1	14X-4, 100	130.80			
o_2	14X-5, 15	131.45			
p_1	15X-2, 120	137.60			
p_2	15X-3, 65	138.55			
p_3	15X-4, 45	139.85			
p_4	15X-5, 40	141.30	16X-2, 35	142.05	−0.75
p_5	15X-6, 70	143.10	16X-3, 75	143.95	−0.85
p_6	15X-7, 20	144.10	16X-4, 15	144.85	−0.75
q_1	16X-1, 65	145.25	16X-5, 35	146.55	−1.30
q_2	16X-2, 30	146.40	16X-5, 130	147.50	−1.10
q_3	16X-2, 110	147.20	16X-6, 60	148.30	−1.10
q_4	16X-3, 100	148.60			
q_5	16X-4, 30	149.40			
q_6	16X-5, 15	150.75	17X-2, 5	151.45	−0.70
r_1	17X-1, 125	155.55	17X-4, 145	155.85	−0.30
r_2	17X-2, 110	156.90	17X-5, 75	156.65	0.20
r_3			17X-C, 20	159.30	
r_4			18X-1, 125	160.75	
s_1			18X-4, 130	165.30	
s_2			18X-6, 50	167.50	
s_3			18X-7, 5	168.55	
s_4	19X-1, 75	174.35	19X-1, 90	170.10	4.25
t_1	19X-5, 30	179.90	19X-5, 90	176.10	3.80
t_2	19X-6, 95	182.05	20X-1, 110	180.00	2.05
u_1	20X-2, 65	185.45			
u_2	20X-3, 75	187.05			
v_1			21X-2, 40	190.40	
v_2	21X-1, 150	194.50	21X-3, 90	192.40	2.10
w_1	22X-3, 45	206.15	22X-6, 50	206.20	−0.05
w_2	22X-4, 120	208.40			
x_1			23X-3, 130	212.20	
x_2	23X-2, 120	215.10	23X-5, 45	214.35	0.75
y_1	23X-6, 55	220.45	24X-3, 45	220.95	−0.50
y_2	23X-C, 40	222.20	24X-4, 75	222.75	−0.55

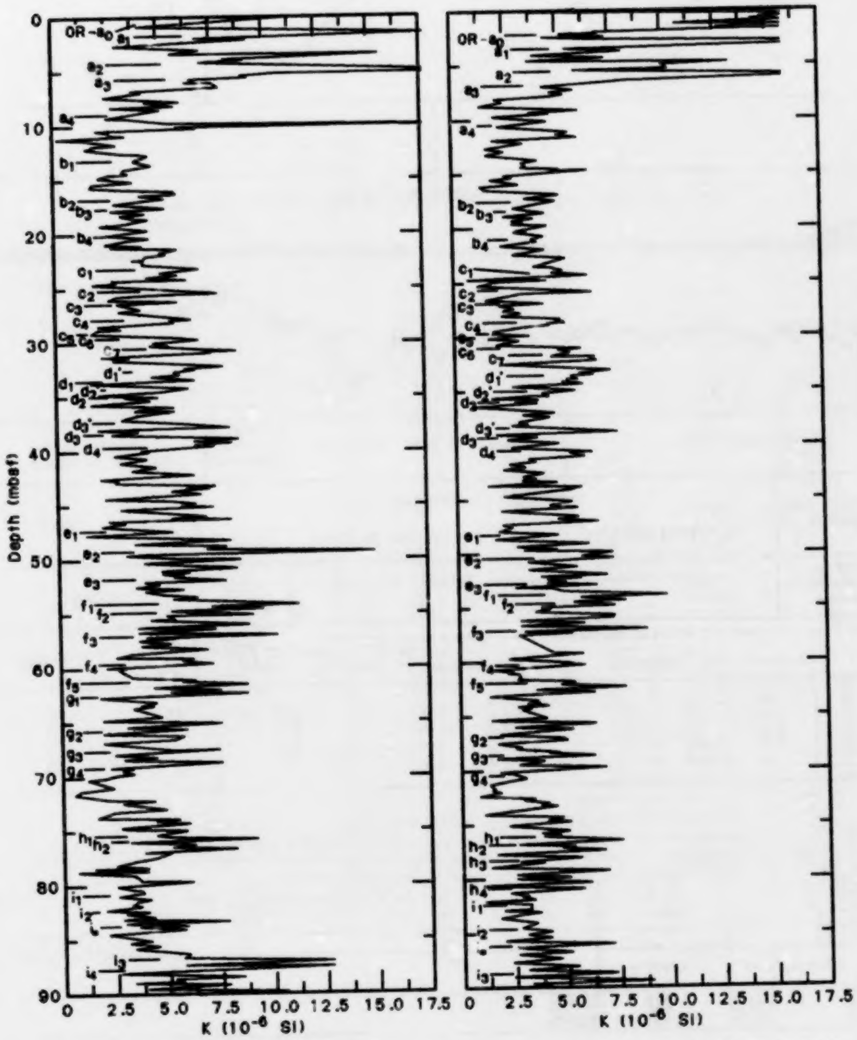

Figure 41. Volume magnetic susceptibility curve and positions of the marker layers in Hole 722A (left) and 722B (right).

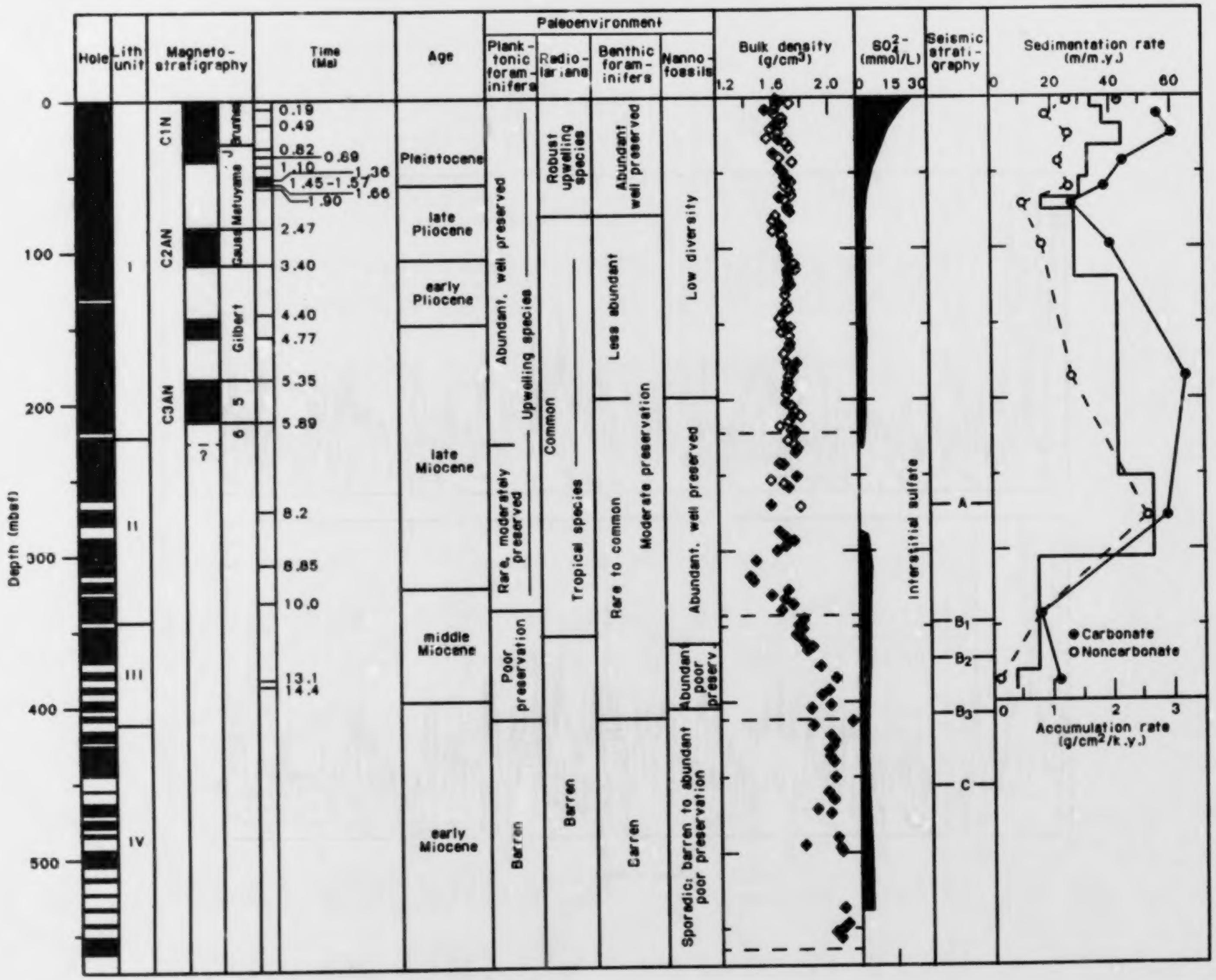

Figure 42. Summary chart outlining preliminary shipboard findings at Site 722.

Table 14. Corrected depth of core top for stratigraphic sub-bottom depth calculation.

	Hole 722A			Hole 722B		
Core	ODP top depth (mbsf)	Difference	Corrected top depth (mbsf)	ODP top depth (mbsf)	Difference	Corrected top depth (mbsf)
1	0.0	1.8	1.8	0.0	0.0	0.0
2	9.8	−0.6	11.0	5.5	0.3	5.8
3	19.4	0.2	20.8	15.1		15.4
4	29.0	0.7	31.1	24.7	0.5	25.5
5	38.6	−0.1	40.6	34.3	0.2	35.3
6	48.2	0.3	50.5	43.9	0.1	45.0
7	57.5	1.0	60.8	53.2	1.3	55.6
8	67.2	0.4	70.9	62.9	0.2	65.5
9	76.8	0.6	81.1	72.5	0.4	75.5
10	86.5	−0.1	90.7	82.2	−0.9	84.3
11	96.2	−1.8	98.6	91.9	0.1	94.1
12	105.9	1.2	109.5	101.5	−0.1	103.6
13	115.6	−0.7	118.5	111.2		113.3
14	125.3	1.8	129.1	120.9		123.0
15	134.9	−1.8	137.8	130.5		132.6
16	144.6	0.4	147.9	140.2		142.3
17	154.3	−0.6	157.0	149.9	0.5	152.5
18	163.9		166.6	159.5		162.1
19	173.6		176.3	169.2	4.1	175.9
20	183.3		186.0	178.9	−1.9	183.7
21	193.0		195.7	188.5		193.3
22	202.7	2.2	207.6	198.2		203.0
23	212.4	−0.8	216.5	207.9		212.7
24				217.5	−1.3	221.0

Note: ODP top depth = depth (mbsf) of core top calculated by the ODP CORELOG program data. Difference = difference in meters between the depth calculated by the ODP CORELOG data and the depth calculated by the layer-by-layer correlation method. Corrected top depth = depth (mbsf) of core top calculated by the layer-by-layer correlation method.

Table 15. Stratigraphic depths of the marker layers in Sites 722 and 721.

	Hole 721B		Hole 722A			Hole 722B		
	Core, section, interval (cm)	Corrected depth (mbsf)	Core, section, interval (cm)	ODP depth (mbsf)	Corrected depth (mbsf)	Core, section, interval (cm)	ODP depth (mbsf)	Corrected depth (mbsf)
OR-a_0	1H-2, 105	2.55	1H-1, 50	0.50	2.30	1H-2, 85	2.35	2.35
a_1	1H-3, 90	3.90	1H-2, 35	1.85	3.65	1H-3, 50	3.50	3.50
a_2	1H-5, 45	6.45	1H-3, 135	4.35	6.15	2H-1, 25	5.75	6.05
a_3	1H-6, 32	7.82	1H-4, 115	5.65	7.45	2H-2, 20	7.20	7.50
a_4	2H-2, 25	11.15	1H-7, 30	9.30	11.10	2H-4, 65	10.65	10.95
b_1	2H-4, 135	15.25	2H-3, 20	13.00	14.20			
b_2	2H-6, 115	18.05	2H-5, 95	16.75	17.95	3H-2, 105	17.65	17.95
b_3	2H-7, 40	18.80	2H-6, 30	17.60	18.80	3H-3, 45	18.55	18.85
b_4	3H-1, 140	21.00	3H-1, 60	20.00	21.40	3H-5, 10	21.20	21.50
c_1	3H-3, 130	23.90	3H-3, 85	23.25	24.65	3H-7, 15	24.25	24.55
c_2	3H-4, 130	25.40	3H-4, 115	25.05	26.45	4H-1, 85	25.55	26.35
c_3	3H-5, 105	26.65	3H-5, 85	26.25	27.65	4H-2, 60	26.80	27.60
c_4	3H-6, 110	28.20	3H-6, 100	27.90	29.30	4H-3, 85	28.55	29.35
c_5	3H-7, 50	29.10	3H-7, 40	28.80	30.20	4H-4, 40	29.60	30.40
c_6	4H-1, 75	30.25	4H-1, 30	29.30	31.40	4H-5, 5	30.75	31.55
c_7	4H-2, 20	31.20	4H-1, 140	30.40	32.50	4H-5, 100	31.70	32.50
$d_{1'}$	4H-3, 70	33.20	4H-3, 65	32.65	34.75	4H-6, 140	33.60	34.40
d_1	4H-4, 0	34.00	4H-4, 5	33.35	35.45			
$d_{2'}$	4H-4, 70	34.70	4H-4, 65	33.95	36.05	5H-1, 70	35.00	36.00
d_2	4H-4, 145	35.45	4H-4, 150	34.80	36.90	5H-2, 10	35.90	36.90
$d_{3'}$	4H-6, 85	37.85	4H-6, 80	37.10	39.20	5H-3, 100	38.30	39.30
d_3	4H-7, 30	38.80	4H-7, 25	38.05	40.15	5H-4, 30	39.10	40.10
d_4	5H-1, 125	41.35	5H-1, 90	39.50	41.50	5H-5, 20	40.50	41.50
e_1	5H-6, 75	48.35	5H-6, 115	47.25	49.25	6H-3, 130	48.20	49.30
e_2	6H-1, 35	50.45	6H-1, 105	49.25	51.55	6H-5, 60	50.50	51.60
e_3	6H-2, 130	52.90	6H-3, 40	51.60	53.90	6H-6, 130	52.70	53.80
f_1	6H-4, 115	55.75	6H-4, 120	53.90	56.20	7H-1 45	53.65	56.05
f_2	6H-5, 60	56.70	6H-5, 55	54.75	57.05	7H-1, 140	54.60	57.00
f_3	6H-7, 15	59.25	6H-6, 130	57.00	59.30	7H-3, 85	57.05	59.45
f_4	7H-3, 45	62.55	7H-2, 45	59.45	62.75	7H-5, 100	60.20	62.60
f_5	7H-4, 65	64.25	7H-3, 50	61.00	64.30	7H-6, 120	61.90	64.40
g_1	7H-5, 45	65.55	7H-4, 40	62.40	65.70			
g_2	8H-1, 85	69.05	7H-6, 90	65.90	69.20	8H-3, 75	66.65	69.25
g_3	8H-2, 50	70.20	8H-1, 30	67.50	71.20	8H-4, 120	68.60	71.20
g_4	8H-3, 70	71.90	8H-2, 45	69.15	72.85	8H-5, 140	70.30	72.90
h_1	8H-7, 50	77.70	8H-6, 60	75.30	79.00	9H-3, 50	76.00	79.00
h_2	9H-1, 35	78.25	8H-6, 110	75.80	79.50	9H-3, 110	76.60	79.60
h_3	9H-2, 60	80.00				9H-4, 110	78.10	81.10
h_4	9H-4, 40	82.80				9H-6, 60	80.60	83.60
i_1	9H-5, 45	84.35	9H-3, 90	80.70	85.00	9H-7, 50	82.00	85.00
i_2	9H-7, 40	87.30	9H-4, 100	82.30	86.60	10H-2, 60	84.30	86.40
i_*	10X-2, 50	89.80	9H-5, 70	83.50	87.80	10H-3, 75	85.95	88.05
i_3	10X-4, 25	92.55	10X-1, 5	86.55	90.75	10H-5, 40	88.60	90.70
i_4	10X-4, 120	93.50	10X-1, 125	87.75	91.95	10H-5, 135	89.55	91.65
i_5	10X-6, 75	96.05	10X-3, 25	89.75	93.95			
j_1	11X-1, 120	98.20	10X-4, 60	91.60	95.80	11X-2, 5	93.45	95.65
j_2	11X-2, 130	99.80	10X-5, 60	93.10	97.30	11X-3, 35	95.25	97.45
j_3	11X-3, 70	100.70	10X-5, 120	93.70	97.90	11X-3, 80	95.70	97.90
j_4	11X-4, 65	102.15	11X-1, 50	96.70	99.10	11X-4, 50	96.90	99.10

Table 15 (continued).

	Hole 721B		Hole 722A			Hole 722B		
	Core, section, interval (cm)	Corrected depth (mbsf)	Core, section, interval (cm)	ODP depth (mbsf)	Corrected depth (mbsf)	Core, section, interval (cm)	ODP depth (mbsf)	Corrected depth (mbsf)
OR-j_5	11X-5, 90	103.90	11X-2, 95	98.65	101.05			
k_1	12X-1, 55	105.45	11X-3, 100	100.20	102.60			
k_2			11X-6, 100	104.70	107.10	12X-3, 45	104.95	107.05
l_1	13X-1, 60	109.70	12X-1, 45	106.35	109.95			
l_2	13X-2, 60	111.20	12X-2, 45	107.85	111.45			
l_3	13X-4, 40	114.00	12X-4, 10	110.50	114.10	13X-1, 65	111.35	113.95
l_4	13X-6, 30	116.90	12X-5, 115	113.05	116.65	13X-3, 45	114.65	116.75
m_1	14X-2, 115	119.65	13X-1, 50	116.10	119.00			
m_2	14X-3, 120	121.20	13X-2, 90	118.00	120.90			
m_3	14X-4, 70	122.20	13X-3, 35	118.95	121.85			
n_1	15X-1, 75	127.45	13X-6, 95	124.05	126.95	14X-3, 90	124.80	126.90
n_2	15X-2, 135	129.55				14X-4, 65	126.05	128.15
n_3	15X-3, 130	131.00				14X-5, 20	127.10	129.20
n_4	15X-6, 15	134.35	14X-3, 45	128.75	132.55	15X-1, 95	131.45	133.55
o_1	16X-2, 70	138.60	14X-4, 100	130.80	134.60			
o_2	16X-3, 30	139.70	14X-5, 15	131.45	135.25			
p_1	17X-1, 95	147.00	15X-2, 120	137.60	140.50			
p_2	17X-2, 45	148.05	15X-3, 65	138.55	141.45			
p_3	17X-3, 90	150.00	15X-4, 45	139.85	142.75			
p_4	17X-4, 70	151.30	15X-5, 40	141.30	144.20	16X-2, 35	142.05	144.15
p_5	17X-5, 100	153.10	15X-6, 70	143.10	146.00	16X-3, 75	143.95	146.05
p_6	17X-6, 90	154.50	15X-7, 20	144.10	147.00	16X-4, 15	144.85	146.95
q_1	18X-1, 120	157.00	16X-1, 65	145.25	148.55	16X-5, 35	146.55	148.65
q_2	18X-2, 90	158.20	16X-2, 30	146.40	149.70	16X-5, 130	147.50	149.60
q_3	18X-3, 45	159.25	16X-2, 110	147.20	150.50	16X-6, 60	148.30	150.40
q_4	18X-4, 100	161.30	16X-3, 100	148.60	151.90			
q_5	18X-5, 70	162.20	16X-4, 30	149.40	152.70			
q_6	18X-6, 90	164.20	16X-5, 15	150.75	154.05	17X-2, 5	151.45	154.05
r_1	19X-1, 110	166.60	17X-1, 125	155.55	158.25	17X-4, 145	155.85	158.45
r_2	19X-2, 55	167.55	17X-2, 110	156.90	159.60	17X-5, 75	156.65	159.25
r_3	19X-4, 70	170.70				17X-C, 20	159.30	161.90
r_4	19X-5, 100	172.50				18X-1, 125	160.75	163.45
s_1	20X 2, 105	177.75				18X-4, 130	165.30	168.00
s_2	20X-3, 100	179.20				18X-6, 50	167.50	170.20
s_3	20X-4, 65	180.35				18X-7, 5	168.55	171.25
s_4	20X-4, 140	181.10	19X-1, 75	174.35	177.05	19X-1, 90	170.10	176.80
t_1	21X-1, 20	185.10	19X-5, 30	179.90	182.60	19X-5, 90	176.10	182.80
t_2	21X-2, 110	187.50	19X-6, 95	182.05	184.75	20X-1, 110	180.00	184.80
u_1	22X-3, 30	197.90	20X-2, 65	185.45	188.15			
u_2	22X-4, 65	199.75	20X-3, 75	187.05	189.75			
v_1	23X-2, 45	206.25				21X-2, 40	190.40	195.20
v_2	23X-3, 120	208.50	21X-1, 150	194.50	197.20	21X-3, 90	192.40	197.20
w_1	24X-2, 60	216.00	22X-3, 45	206.15	211.15	22X-6, 50	206.20	211.00
w_2	24X-3, 100	217.90	22X-4, 120	208.40	213.40			
x_1	25X-3, 125	227.35				23X-3, 130	212.20	217.00
x_2	25X-5, 65	229.75	23X-2, 120	215.10	219.20	23X-5, 45	214.35	219.15
y_1	26X-3, 50	236.20	23X-6, 55	220.45	224.55	24X-3, 45	220.95	224.45
y_2	26X-4, 90	238.10	23X-C, 40	222.20	226.30	24X-4, 75	222.75	226.25

Note: Depths are based on the correction factor of Table 14, which are based on ODP CORELOG data. Corrected depth = corrected depth for straigraphic thickness.

Summary Log for Hole 722B

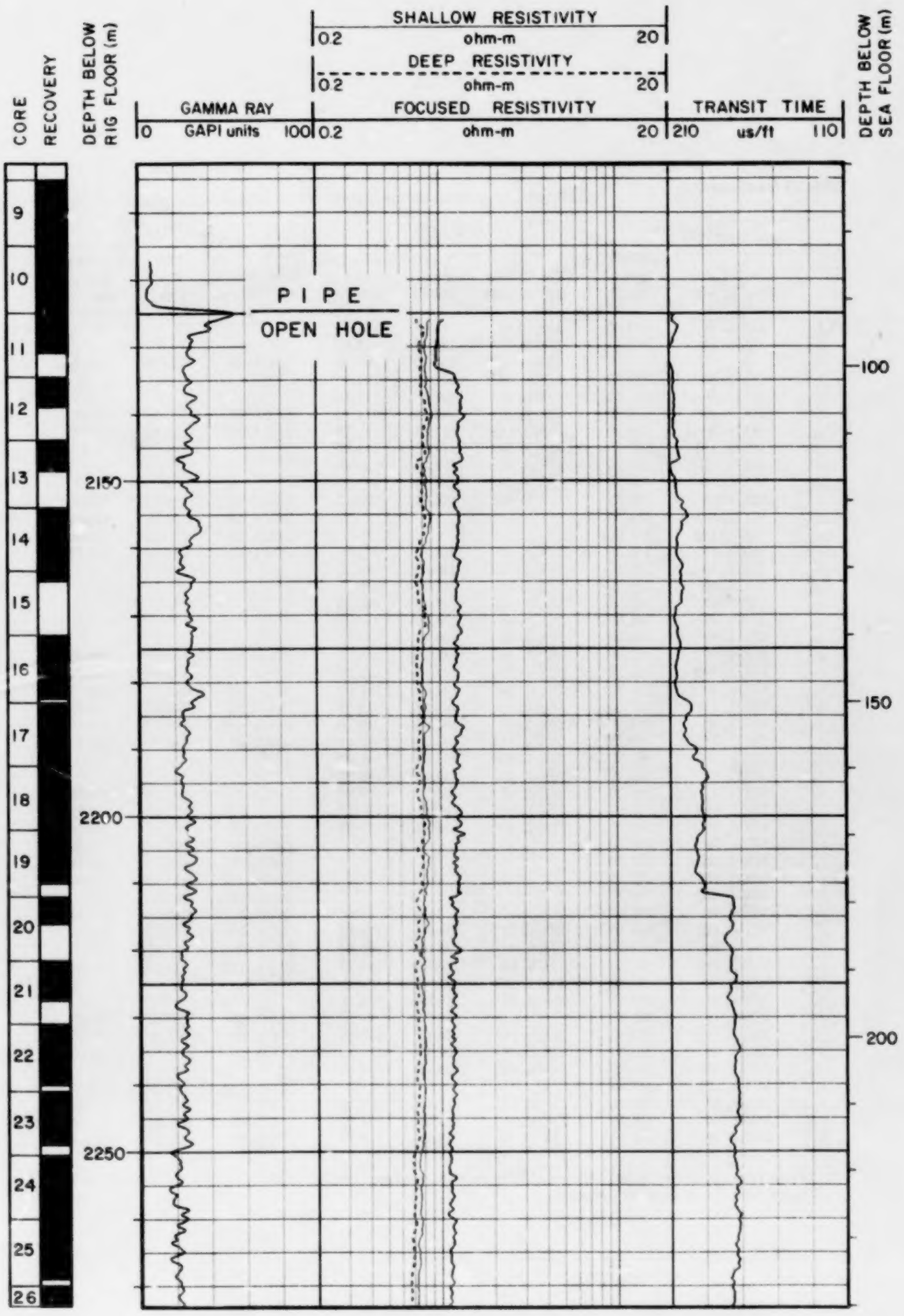

Summary Log for Hole 722B (continued)

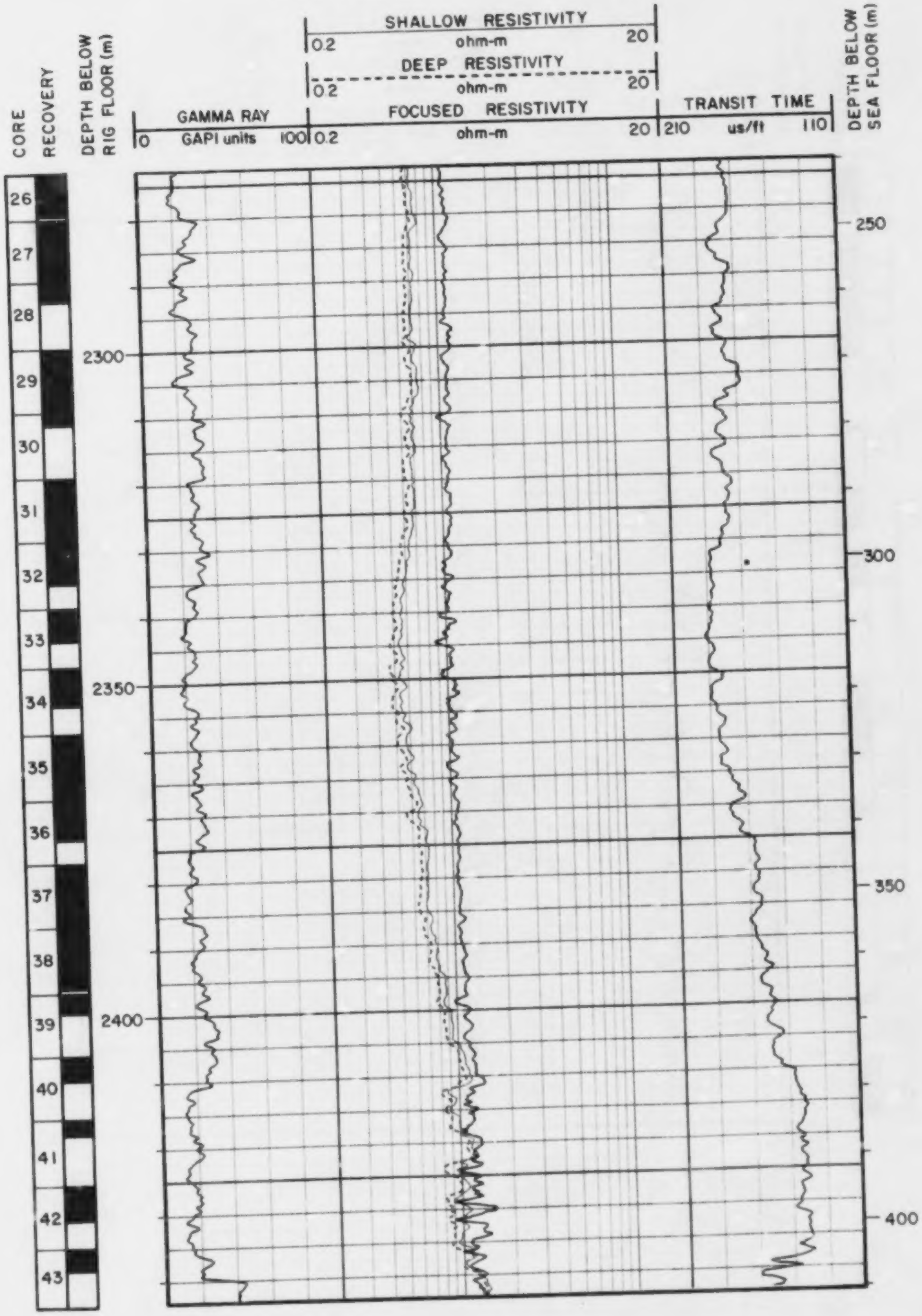

Summary Log for Hole 722B (continued)

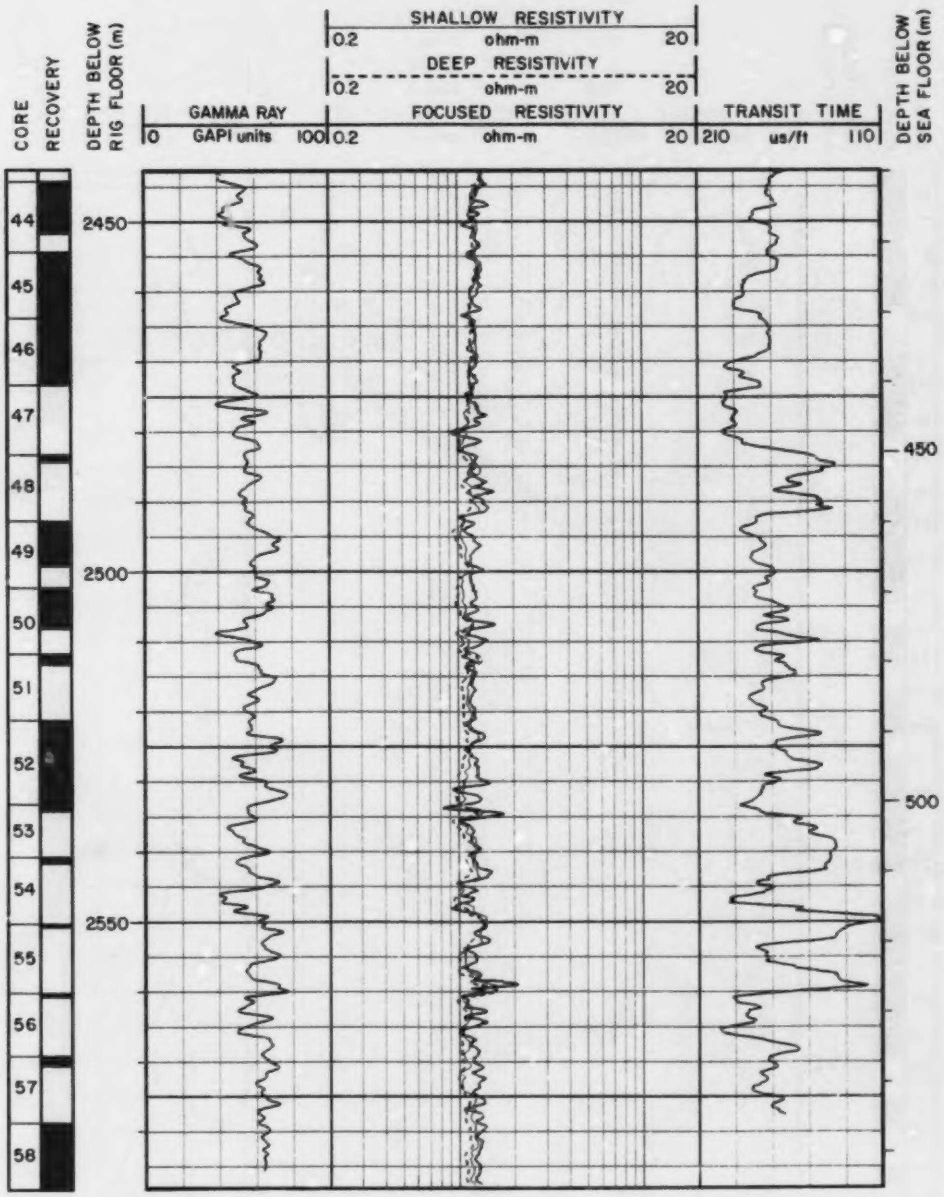

Summary Log for Hole 722B (continued)

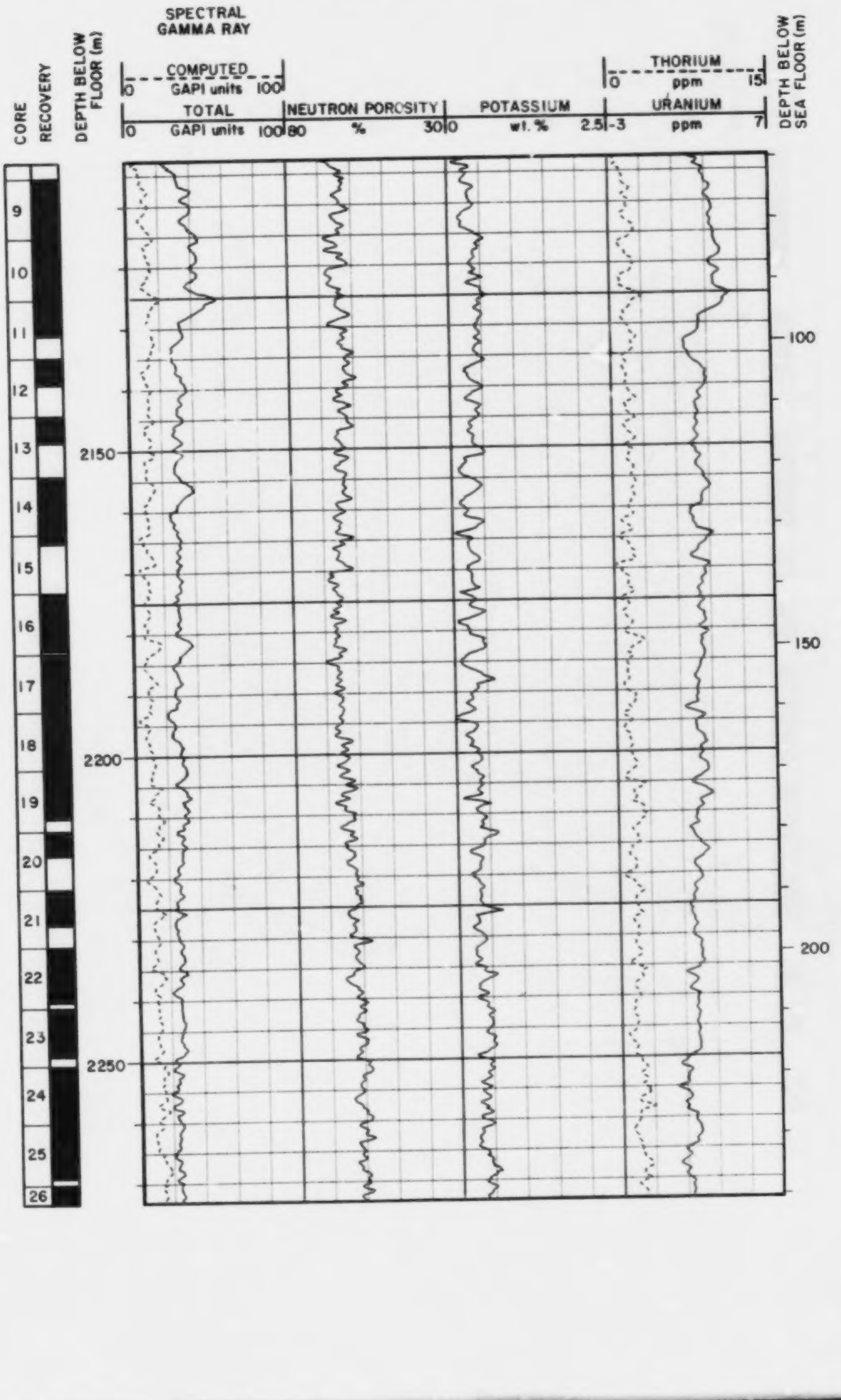

Summary Log for Hole 722B (continued)

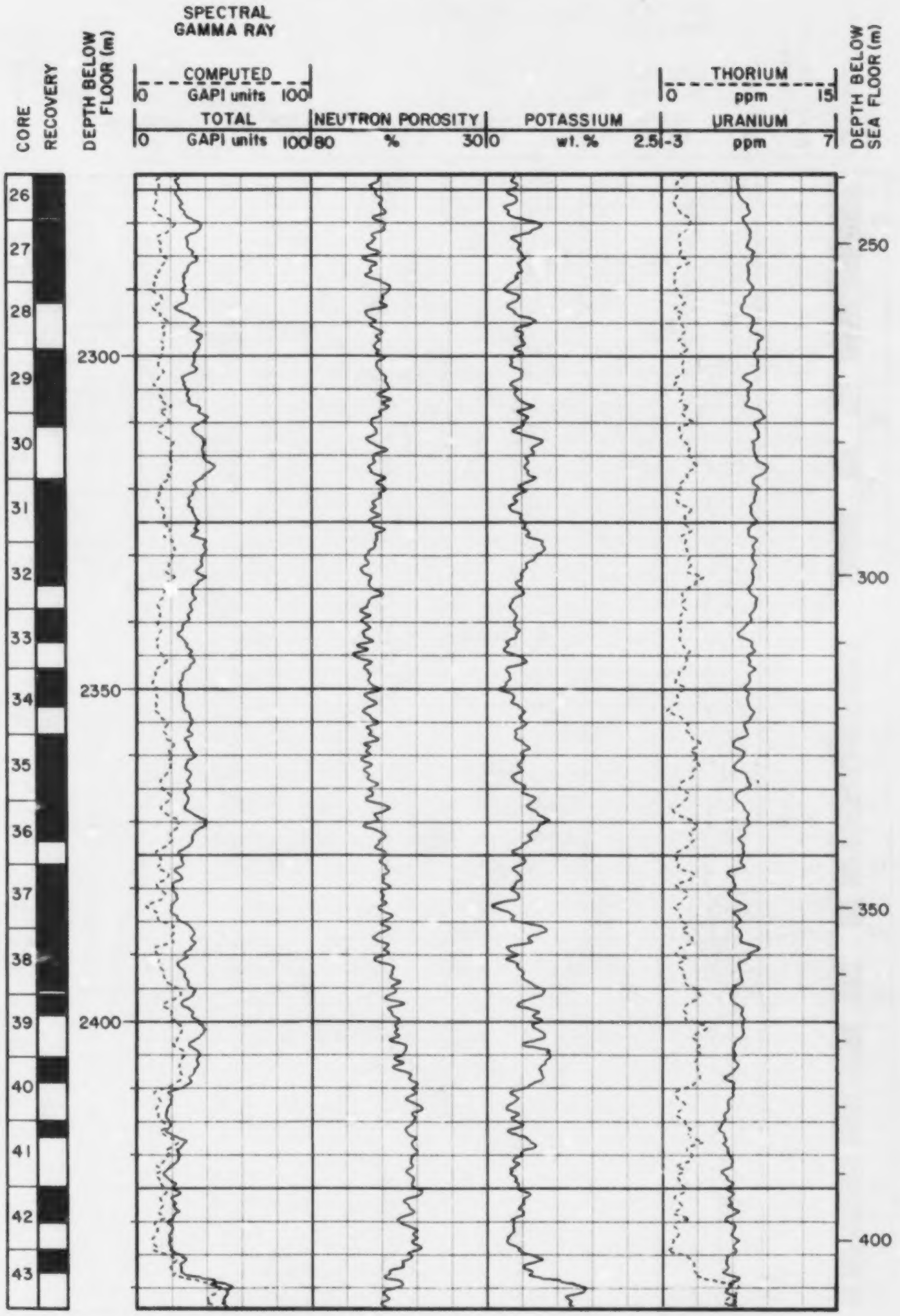

Summary Log for Hole 722B (continued)

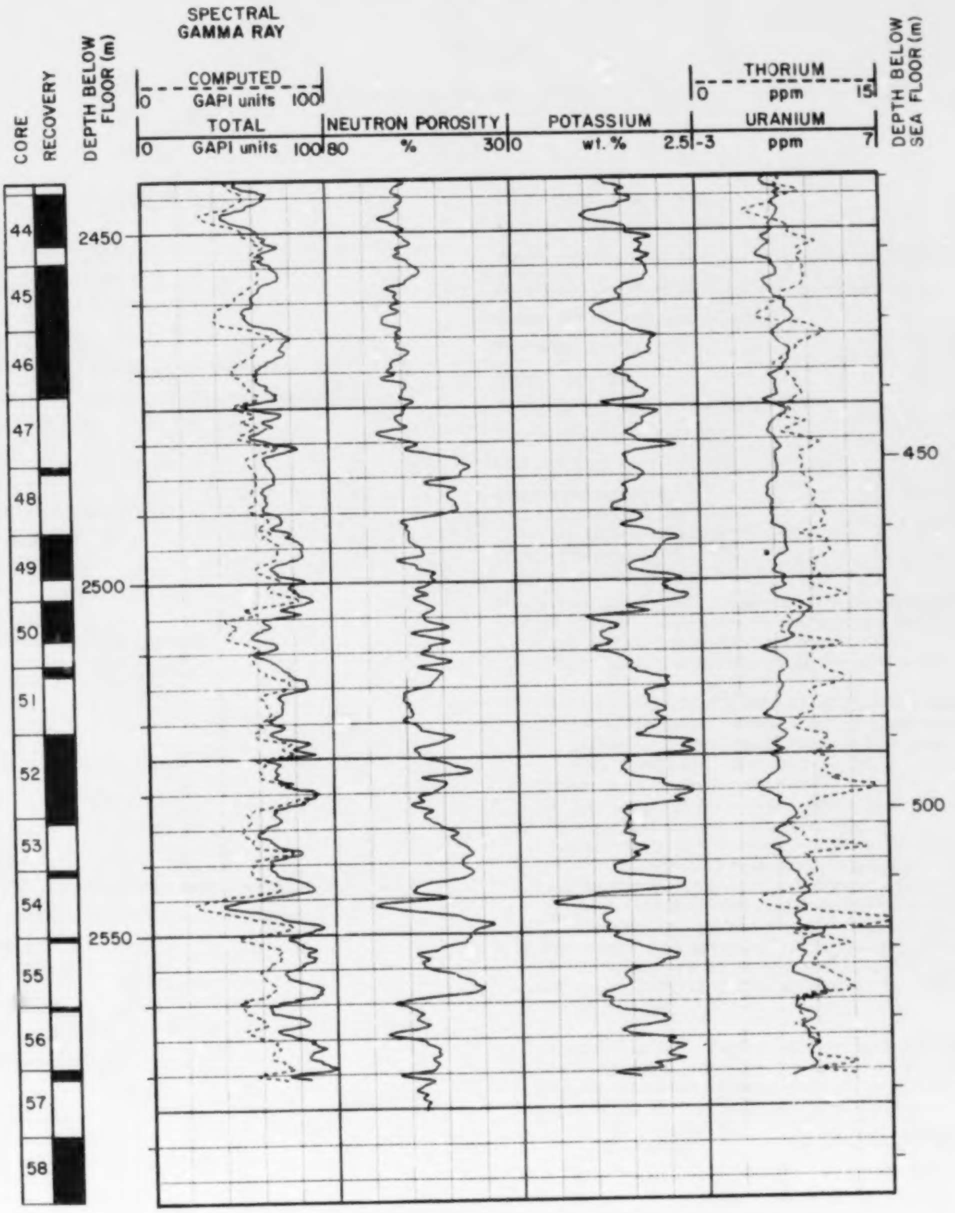

11. SITE 723[1]

Shipboard Scientific Party[2]

HOLE 723A

Date occupied: 15 September 1987

Date departed: 17 September 1987

Time on hole: 1 day, 16 hr, 30 min

Position: 18°03.079′N, 57°36.561′E

Water depth (sea level; corrected m, echo-sounding): 807.8

Water depth (rig floor; corrected m, echo-sounding): 818.3

Bottom felt (m, drill pipe): 816.2

Penetration (m): 432.3

Number of cores: 46

Total length of cored section (m): 432.3

Total core recovered (m): 298.2

Core recovery (%): 69

Oldest sediment cored:
Depth sub-bottom (m): 432.3
Nature: carbonate/limestone biscuits
Age: late Pliocene (NN18)
Measured velocity (km/s): 5.5

HOLE 723B

Date occupied: 17 September 1987

Date departed: 19 September 1987

Time on hole: 2 days, 10 hr, 45 min

Position: 18°03.079′N, 57°36.561′E

Water depth (sea level; corrected m, echo-sounding): 807.8

Water depth (rig floor; corrected m, echo-sounding): 818.3

Bottom felt (m, drill pipe): 816.7

Penetration (m): 429.0

Number of cores: 44

Total length of cored section (m): 400.1

Total core recovered (m): 295.4

Core recovery (%): 73.8

Oldest sediment cored:
Depth sub-bottom (m): 429.0
Nature: nannofossil clayey silt
Age: late Pliocene
Measured velocity (km/s): 1.7

HOLE 723C

Date occupied: 19 September 1987

Date departed: 19 September 1987

Time on hole: 8 hr, 45 min

Position: 18°03.079′N, 57°36.561′E

Water depth (sea level; corrected m, echo-sounding): 807.8

Water depth (rig floor; corrected m, echo-sounding): 818.3

Bottom felt (m, drill pipe): 815.8

Penetration (m): 76.8

Number of cores: 8

Total length of cored section (m): 76.8

Total core recovered (m): 82.17

Core recovery (%): 107

Oldest sediment cored:
Depth sub-bottom (m): 76.8
Nature: nannofossil clayey silt
Age: Pleistocene
Measured velocity (km/s): 1.6

Principal results: Site 723 corresponds to the central drilling target of a depth transect of sites across the Oman margin and is positioned in the center of the oxygen-minimum zone (OMZ).

Major findings at Site 723 include the identification of:

1. Laminated, opal-rich facies of late Pliocene and early Pleistocene age (the laminations indicate a lack of bioturbation);
2. Dolomite lenses within the hemipelagic sequence;
3. High accumulation rates (on average 175 m/m.y.) with detrital calcite as an important component;
4. High accumulation rates of marine organic carbon, especially in the upper Pliocene and lower Pleistocene;
5. Rapid and complete sulfate depletion by 50 mbsf, followed by an increase of interstitial sulfate from a subsurface source that fuels intense diagenetic reactions in the organic-rich sediments;
6. An increase in chloride near the base of the recovered section;
7. Abundant methane with traces of ethane and propane, which indicate thermogenic generation of hydrocarbons at depth;
8. Distinctive variations of magnetic susceptibility and physical properties which define specific periodicities that can be correlated to the Owen Ridge.

Overall, Site 723 provides a high-resolution sedimentary record of biotic, chemical, and sedimentologic variations associated with organic-rich sediments deposited under the influence of strong seasonal upwelling and generally low oxygen conditions.

BACKGROUND AND OBJECTIVES

Site 723 is located at 18°03.079′N and 57°36.561′E on the continental margin of Oman in water depths of 808 m. The position is near the center of the upper slope basin, where it shows the maximum sediment thickness. The location and depositional setting of Site 723 is shown in Figures 1 and 2; structural aspects of the site are shown in Figure 3.

At this location, the slope basin is about 15 km wide and is bounded on the west by a faulted block and on the east by a basement ridge. Both basement features are thought to be ophiolite complexes. The seismic reflection profiles of the basin sediments show numerous highly reflective layers that both onlap and drape the adjacent basement structures. The sediments are thickest in the center of the basin (>2000 m, based on sono-

---

[1] Prell, W. L., Niitsuma, N., et al., 1989. *Proc. ODP, Init. Repts.*, 117: College Station, TX (Ocean Drilling Program).

[2] Shipboard Scientific Party is as given in the list of Participants preceding the contents.

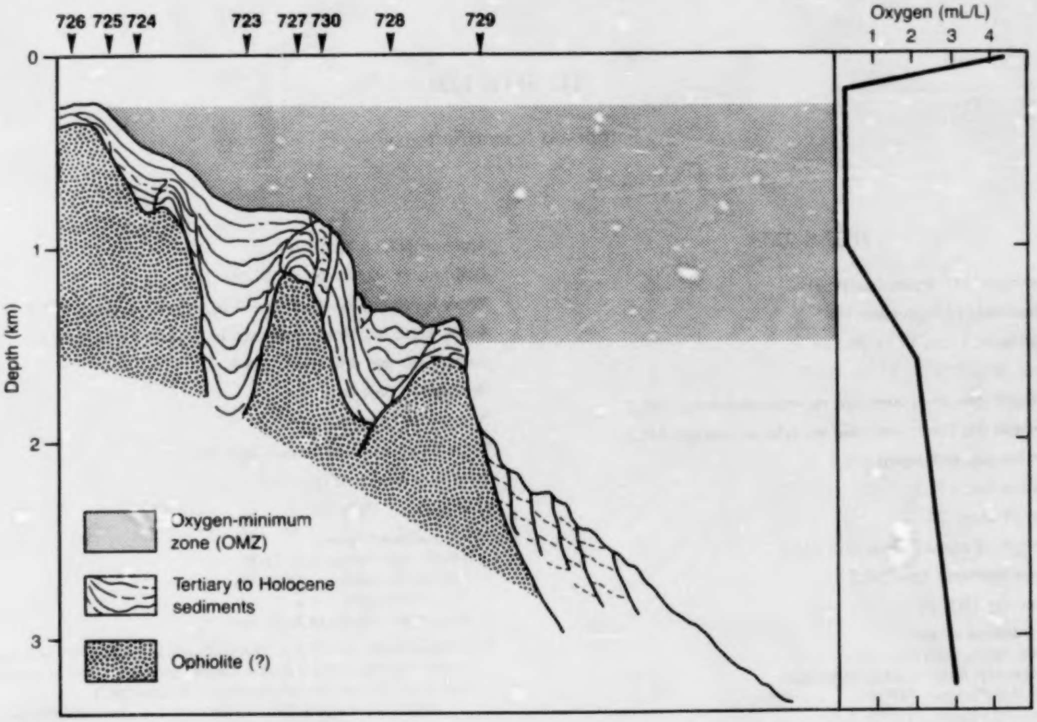

Figure 1. Structure of the Oman margin and the oxygen-minimum zone (OMZ). The schematic cross section of the margin shows the series of basement ophiolite blocks and the sedimentary basins between them. The concentration of oxygen in the water column (RC2704, unpublished data) defines the depth range of the OMZ and where it impinges on the margin.

buoy data; Mountain and Prell, this volume) and thus form a syncline-shaped deposit (Fig. 3). Along the strike of the basin, the surface and subsurface layers dip gently to the southwest and are relatively conformable, although some deformation and slump-related structures are observed (see "Seismic Stratigraphy" section, this chapter).

Site 723 was located within a zone of continuous reflectors (Fig. 3) that is bounded by two areas of irregular reflectors and diffuse seismic returns. The preliminary correlation of seismic reflectors within the basin indicates that the average accumulation rates increase from north to south and are highest near the location of Site 723. The site was selected to provide a high-resolution sedimentary record of the monsoonal upwelling during the Pliocene-Pleistocene.

Specific objectives for drilling at Site 723 were:

1. To obtain a high-resolution record of the sediments associated with the near-continent zone of the monsoonal upwelling system, in order to establish the changes in timing and intensity of the monsoon.
2. To examine the organic-rich sedimentary facies of the margin and establish their relationship to the oxygen-minimum zone (OMZ), and to document variations in the OMZ through time.
3. To document the diagenetic processes associated with the OMZ and the organic-rich sediments.
4. To search for evidence of changes in the structure of the intermediate-water masses of the Arabian Sea during the Pliocene-Pleistocene.

OPERATIONS

JOIDES Resolution departed Site 722 on 13 September 1987 en route for the island of Masirah (Oman) in order to pick up two Omani geologists who participated in the remainder of the leg. The rendezvous point was reached on 14 September at 0815 hours. By 0930 the helicopter had departed, and the ship set course for Site 723. On the approach to Site 723, the gear was streamed at 0700 on 15 September, and by 1145 the location of Site 723 had been chosen (Fig. 4). The first beacon was lowered on a taut wire in 808-m water depths. Erratic beacon signals necessitated deployment of two more beacons. The mud line of Hole 723A was shot at 1645 hours, and the final position of Site 723 was assessed as 18°03.079′N and 57°36.561′E by global positioning system (GPS).

Hole 723A was drilled to 85.1 mbsf using the advanced hydraulic piston corer (APC) mode (Cores 117-723A-1H to -9H) for an average recovery rate of 104%. Gas expansion and strong H_2S odors were noted throughout. An overpull of 80,000 lb during the retrieval of Core 117-723A-9H made the switch to extended core barrel (XCB) drilling necessary at this level. Coring was continued to Core 117-723A-46X (432.3 mbsf total depth [TD]). Recovery in the 347.2-m interval cored by XCB was 60%, so that the gross recovery of Hole 723A was 69%.

The rig was offset 10 m to the south on 16 September 1987, where the mud line of Hole 723B was cored at 0530 (Table 1). Nine APC cores were cored to a depth of 81.6 mbsf, for an average recovery rate of 104%, until a maximum overpull of 70,000 lb was reached. Drilling to 429.0 mbsf TD in the XCB mode re-

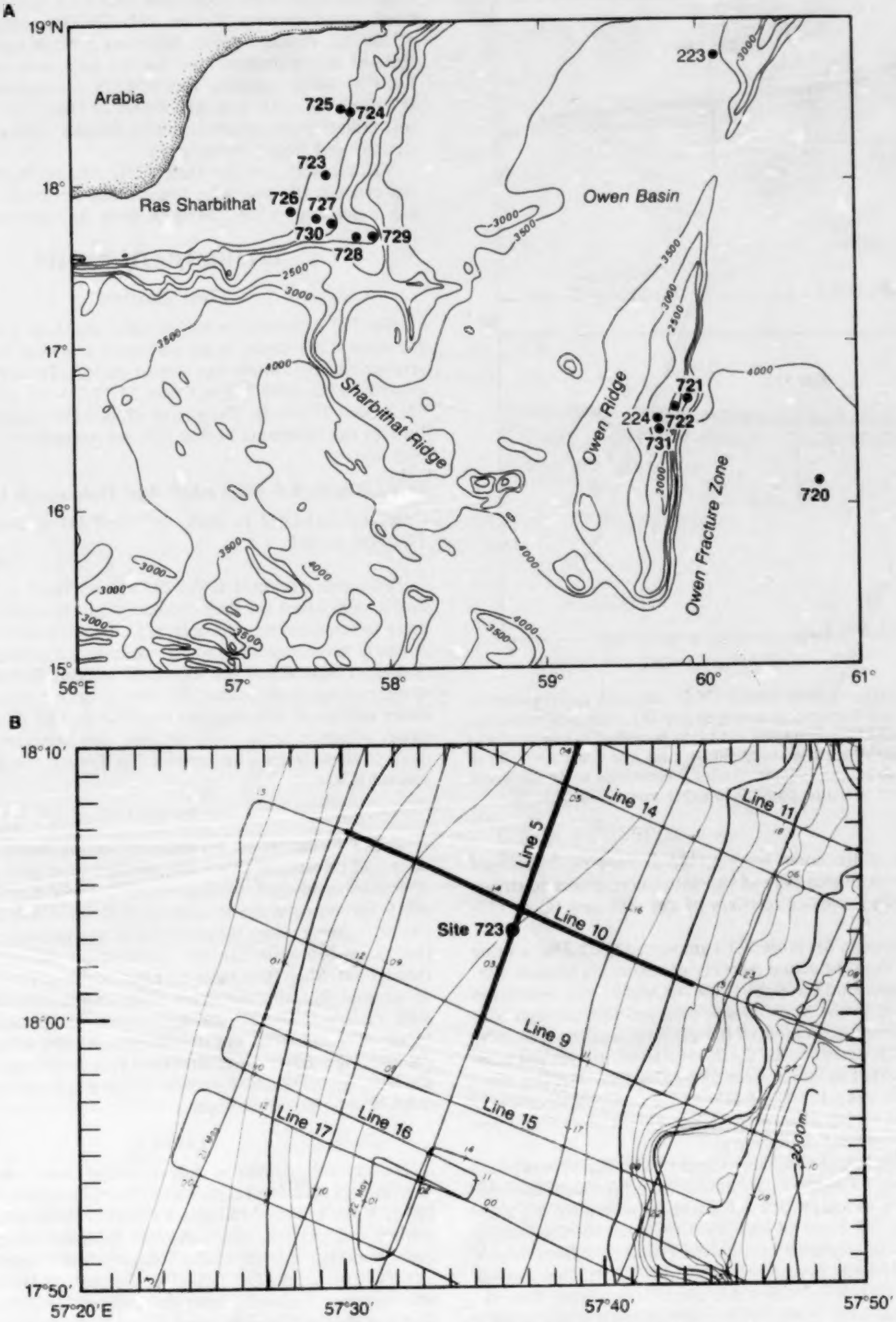
A
19°N
18°
17°
16°
15°
56°E
57°
58°
59°
60°
61°
Arabia
Ras Sharbithat
Owen Basin
Sharbithat Ridge
Owen Ridge
Owen Fracture Zone
223
725
724
723
726
727
730
728
729
721
224
722
731
720
2500
3000
3500
4000
2000
B
18°10′
18°00′
17°50′
57°20′E
57°30′
57°40′
57°50′
Line 5
Line 14
Line 11
Line 10
Line 9
Line 15
Line 16
Line 17
Site 723
2000m

Figure 2. A. Bathymetry of the Oman margin and the location of Site 723. B. Detailed location of Site 723 and the seismic profiles shown in Figure 3. Bathymetry and seismic data are from the site survey (RC2704, 1986).

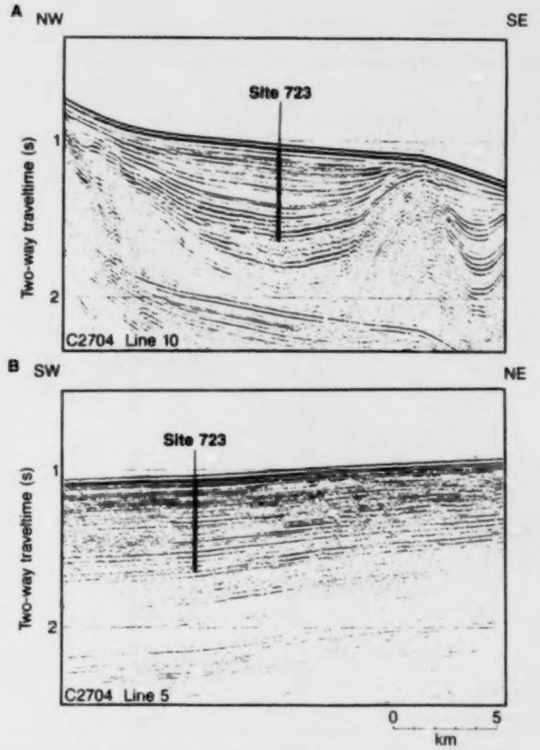

Figure 3. **A.** Single-channel seismic (SCS) reflection profiles showing the structural and depositional setting of Site 723. Line 10 is perpendicular to the trend of the basin and shows the bounding basement blocks and the synclinal-shaped sediment fill. **B.** Line 5 is along the strike of the basin and shows the sediment thickness decreasing to the northeast. Note the diffuse reflection patterns to either side of Site 723.

covered 66% of the cored section. We decided to drill ahead with a center bit in that part of the hole where dolomite stringers and nodules prevented recovery of any sediment (Core 117-723B-30X).

Average recovery for Hole 723B amounted to 73.8%, a value that is higher than the actual recovery of sediments because substantial gas expansion throughout the recovered cores resulted in abundant voids in the liners. Some core was lost through core expansion. Even though most of the gas pressure appeared to be due to high CO_2 pressure, the C_1:C_2 ratio in vacutainer gas samples had decreased to 800 in Core 117-723B-40X. The last sample taken from Core 117-723B-44X had a C_1:C_2 ratio of 1400. We terminated coring after we cut Core 117-723B-44X and noticed no improvement on recovery.

Prior to logging, the lockable flapper valve (LFV) was tested successfully with a dummy core barrel run on the sand line. After a wiper trip to total depth and sweeping with polymer, a go-devil was pumped down to lock the LFV open for the logging and the hole was displaced with polymer mud. The bottom-hole assembly (BHA) was positioned at 90 mbsf for the first logging run with the DIT/BHC/GR/CAL combination tool. The second string used LDT/CNL/NGT combinations, while string 3 employed GST/ACT tools. Except for slight hardware problems upon retrieval of the second run, all logs were of good quality and successfully completed. After completion, the BHA was pulled clear of Hole 723B by 1415 on 19 September 1987.

Hole 723C was spudded by 1430 hours without offsetting the ship, and eight APC cores were shot to a total depth of 76.8 mbsf. Upon retrieval of Core 117-723C-8H, constant overpull of 100,000 lb was needed. Shooting a ninth core, which was planned as the deepest core for the hole, was not attempted. The Pore-Water Sampling Tool (PWST) was deployed after Cores 117-723C-5H, -7H, and -8H. Cores of Hole 723C, a dedicated hole drilled to obtain geochemistry samples, were cut into 50-cm sections and frozen immediately.

The recovery rate for Hole 723C was 107%. The mud line was cleared, the taut-wire beacon was retrieved, and the ship was under way to Site 724 by 0030 on 20 September 1987.

LITHOSTRATIGRAPHY

Introduction

Site 723 is located in 808-m water depth near the center of the upper slope basin, at its maximum sediment thickness. The recovery in APC mode was almost perfect. However, severe gas expansion occurred below Cores 117-723A-4H and 117-723B-5H (about 35 mbsf). The top of Hole 723B obtained the mud line. In the sediments at Site 723, we recognized one sedimentary unit.

Unit I (Depth: 0.0–432.2 mbsf; Age: Holocene to late Pliocene)

Cores 117-723A-1H to -46X, 117-723B-1H to -44X, and 117-723C-1H to -8H.

Sediments recovered at Site 723 are described as a single lithologic unit based on their similarity of composition and primary sedimentary structures (Fig. 5). Three facies are identified. A marly nannofossil ooze with variable terrigenous content is dominant throughout the recovered section. Two minor facies occur intermittently below 240 mbsf in both holes: intervals of finely laminated siliceous and marly ooze, and dolomitic limestone, which in some cases displays fine laminae. The occurrence of these facies is summarized in Table 2; the facies are described below.

Facies I

Facies I consists of foraminifer-bearing marly nannofossil ooze and calcareous clayey silt, mottled olive gray (5Y 4/2, 5Y 4/3) grading to dark olive gray (5Y 3/1, 5Y 2.5/1) below 230 mbsf. Variations in the abundance of foraminifers and silt-sized calcite in smear slides explain most of the variation observed in this facies. Foraminifers are common on the split core face throughout. Shell fragments are most common in the upper half of the hole. Biogenic carbonate content varies between 30% and 50% on smear slides. The terrigenous component varies between 30% and 80%, but it is not specifically related to minor color changes observed at all scales. It is dominated by clay and silt-size detrital calcite. Euhedral dolomite rhombs are observed in trace amounts at all depths.

Facies II

Dolomitic limestone in thin cemented layers contains many components found in Facies I and III. Thin sections from Cores 117-723A-28X and -37X and Cores 117-723B-27X and -23X contain spar cement, clay, abundant foraminifers, traces of organic material, quartz, and siliceous skeletal debris. The thin section from Core 117-723A-45X, a cemented laminated interval, contains alternating layers of diatomaceous skeletal structure and darker clay-rich layers.

The diffraction pattern of a sample from Core 117-723A-45X indicates almost pure dolomite based on the d-spacing of the (211) reflection (see "Inorganic Geochemistry" section, this chapter). Depths where these layers occur are shown in Figure 5.

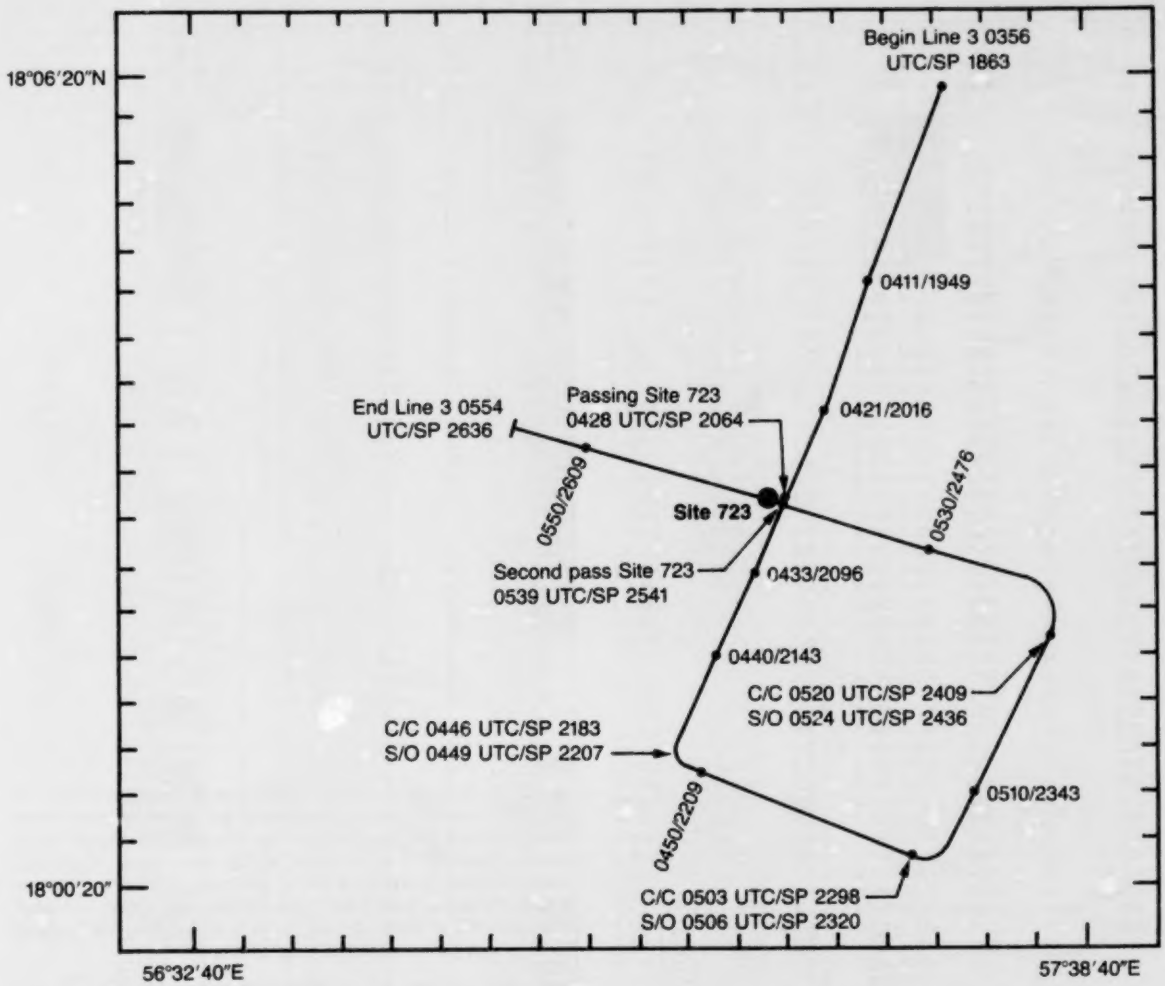
Begin Line 3 0356
UTC/SP 1863
18°06'20"N
0411/1949
Passing Site 723
0428 UTC/SP 2064
End Line 3 0554
UTC/SP 2636
0421/2016
0550/2609
Site 723
0530/2476
Second pass Site 723
0539 UTC/SP 2541
0433/2096
0440/2143
C/C 0520 UTC/SP 2409
S/O 0524 UTC/SP 2436
C/C 0446 UTC/SP 2183
S/O 0449 UTC/SP 2207
0510/2343
0450/2209
18°00'20"
C/C 0503 UTC/SP 2298
S/O 0506 UTC/SP 2320
56°32'40"E
57°38'40"E

Figure 4. Track of *JOIDES Resolution* on approach to Site 723.

Seven different layers are identified in Hole 723A or 723B, at 245, 262, 318, 336, 377, 403 and 420 mbsf (Table 2). Log data indicate the presence of nine layers (see "Downhole Measurements" section, this chapter), six of which correlate with the recovered intervals. Recovered thickness varies between 5 and 30 cm, and log data suggests a maximum thickness of 1 m for each interval.

Facies III

Light and dark laminae 0.1–1.0 mm thick (Fig. 6) comprise Facies III. Light layers are diatom ooze or diatomite often dominated by a single species. Radiolarians, silicoflagellates, and sponge spicules are present in trace amounts. Light laminae also contain variable amounts of detrital calcite and nannofossils. The dark laminae are composed of marly nannofossil ooze, similar in composition to Facies I, but they often contain traces of organic material which occurs as pellets or clay aggregates.

Laminated intervals are usually less than 10 cm thick, observed in hard drilling biscuits and indistinct in softer sediment. The upper and lower contacts are gradational with Facies I (marly ooze), and individual laminae are often indistinct and variable in thickness within laminated intervals. The longest continuously laminated interval observed is approximately 2 m thick. Although one interval is found in the lower Pleistocene (Core 117-723B-18X; 162 mbsf), the greatest frequency of laminated intervals occurs between 300 and 350 mbsf in the upper Pliocene (Table 2).

Disturbance

Gas expansion began to affect core recovery below 35 mbsf. Initially, the sediment separated into flakes and very small spaces (< 1 cm) which are not evaluated as void space in core descriptions but which do reduce the sediment density measured by GRAPE, magnetic susceptibility, and other whole-core sampling tools. This expansion gradually became localized in larger voids, probably related to increased cohesiveness of the sediment and to a change in core handling. When the voids became noticeable, the gas was released by puncturing the core liner.

Between 35 and 100 mbsf disturbance becomes more pronounced, as observed in physical properties data and in the core descriptions. In the upper cores the sediment appears continuous across these voids; deeper in the holes this stratigraphic con-

Table 1. Coring summary, Site 723.

Core no.	Date (Sept. 1987)	Time (local)	Depth (mbsf)	Cored (m)	Recovered (m)	Recovery (%)
117-723A-						
1H	15	1720	0–7.8	7.8	7.88	101.0
2H	15	1745	7.8–17.5	9.7	9.87	102.0
3H	15	1805	17.5–27.1	9.6	9.86	103.0
4H	15	1825	27.1–36.8	9.7	9.90	102.0
5H	15	1840	36.8–46.4	9.6	9.82	102.0
6H	15	1920	46.4–56.1	9.7	10.20	105.1
7H	15	1940	56.1–65.8	9.7	10.54	108.6
8H	15	2020	65.8–75.4	9.6	10.12	105.4
9H	15	2020	75.4–85.1	9.7	10.11	104.2
10X	15	2130	85.1–94.8	9.7	0	0
11X	15	2230	94.8–104.4	9.6	2.63	27.4
12X	15	2300	104.4–114.1	9.7	0	0
13X	15	2345	114.1–123.8	9.7	6.96	71.7
14X	16	0040	123.8–133.4	9.6	6.83	71.1
15X	16	0125	133.4–143.1	9.7	9.78	101.0
16X	16	0215	143.1–152.8	9.7	0	0
17X	16	0250	152.8–162.4	9.6	3.55	37.0
18X	16	0325	162.4–172.1	9.7	0	0
19X	16	0355	172.1–181.8	9.7	10.50	108.2
20X	16	0425	181.8–191.4	9.6	9.71	101.0
21X	16	0450	191.4–201.1	9.7	9.74	100.0
22X	16	0525	201.1–210.8	9.7	10.08	103.9
23X	16	0555	210.8–220.4	9.6	3.63	37.8
24X	16	0635	220.4–230.1	9.7	10.12	104.3
25X	16	0710	230.1–239.8	9.7	9.57	98.6
26X	16	0755	239.8–249.4	9.6	6.53	68.0
27X	16	0835	249.4–259.1	9.7	8.54	88.0
28X	16	0925	259.1–268.7	9.6	3.84	40.0
29X	16	1000	268.7–278.3	9.6	10.07	104.9
30X	16	1055	278.3–287.9	9.6	7.61	79.3
31X	16	1135	287.9–297.5	9.6	10.18	106.0
32X	16	1215	297.5–307.1	9.6	9.83	102.0
33X	16	1250	307.1–316.7	9.6	10.10	105.2
34X	16	1330	316.7–321.5	4.8	0.48	10.0
35X	16	1355	321.5–326.3	4.8	5.93	123.0
36X	16	1430	326.3–335.8	9.5	11.28	118.7
37X	16	1535	335.8–345.4	9.6	1.57	16.3
38X	16	1610	345.4–355.0	9.6	0	0
39X	16	1655	355.0–364.7	9.7	9.58	98.7
40X	16	1730	364.7–374.3	9.6	9.86	103.0
41X	16	1830	374.3–384.0	9.7	9.15	94.3
42X	16	1930	384.0–393.6	9.6	1.94	20.2
43X	16	2035	393.6–403.3	9.7	0	0
44X	16	2135	403.3–413.0	9.7	0.05	0.5
45X	16	2250	413.0–422.6	9.6	0.28	2.9
46X	16	2345	422.6–432.3	9.7	0	0
				432.3	298.22	
117-723B-						
1H	17	0605	0–4.3	4.3	4.29	99.7
2H	17	0630	4.3–14.0	9.7	9.93	102.0
3H	17	0650	14.0–23.6	9.6	9.97	104.0
4H	17	0715	23.6–33.3	9.7	9.83	101.0
5H	17	0735	33.3–42.9	9.6	10.00	104.1
6H	17	0805	42.9–52.6	9.7	10.36	106.8
7H	17	0840	52.6–62.3	9.7	10.45	107.7
8H	17	0910	62.3–71.9	9.6	10.25	106.8
9H	17	0940	71.9–81.6	9.7	10.21	105.2
10X	17	1055	81.6–91.2	9.6	9.53	99.3
11X	17	1115	91.2–100.7	9.5	9.87	104.0
12X	17	1205	100.7–110.3	9.6	8.83	92.0
13X	17	1245	110.3–119.9	9.6	8.45	88.0
14X	17	1315	119.9–129.6	9.7	9.39	96.8
15X	17	1350	129.6–139.2	9.6	9.29	96.8
16X	17	1420	139.2–148.9	9.7	4.74	48.8
17X	17	1445	148.9–158.6	9.7	9.65	99.5
18X	17	1510	158.6–168.2	9.6	9.72	101.0
19X	17	1540	168.2–177.9	9.7	10.37	106.9
20X	17	1600	177.9–187.6	9.7	10.13	104.4
21X	17	1625	187.6–197.3	9.7	10.03	103.4
22X	17	1650	197.3–206.9	9.6	9.43	98.2
23X	17	1715	206.9–216.5	9.6	9.89	103.0
24X	17	1800	216.5–226.2	9.7	10.59	109.2
25X	17	1830	226.2–235.9	9.7	10.13	104.4
26X	17	1900	235.9–245.6	9.7	9.39	96.8
27X	17	2000	245.6–247.2	1.6	1.88	117.5
28X	17	2040	247.2–255.0	7.8	0	0
29X	17	2155	255.0–264.7	9.7	0	0
30X	17	2230	264.7–274.4	9.7	0	0
31X	18	0045	293.7–303.3	9.6	9.54	99.4
32X	18	0155	303.3–313.0	9.7	0	0
33X	18	0300	313.0–317.4	4.4	4.17	94.8
34X	18	0345	317.4–322.7	5.3	0	0
35X	18	0430	322.7–332.5	9.8	3.33	34.0
36X	18	0545	332.5–342.2	9.7	1.59	16.4
37X	18	0625	342.2–351.9	9.7	0	0
38X	18	0710	351.9–361.6	9.7	3.31	34.1
39X	18	0755	361.6–371.3	9.7	9.60	98.9
40X	18	0900	371.3–381.0	9.7	5.57	57.4
41X	18	0950	381.0–390.7	9.7	6.71	69.2
42X	18	1140	400.3–409.8	9.5	5.01	52.7
43X	18	1235	409.8–419.4	9.6	0	0
44X	18	1400	419.4–429.0	9.6	0.22	2.3
				400.1	295.65	
117-723C-						
1H	19	1600	0–9.2	9.2	9.20	100.0
2H	19	1615	9.2–18.9	9.7	10.01	103.2
3H	19	1630	18.9–28.5	9.6	9.79	102.0
4H	19	1645	28.5–38.2	9.7	10.00	103.1
5H	19	1700	38.2–47.8	9.6	10.13	105.5
6H	19	1800	47.8–57.5	9.7	10.32	106.4
7H	19	1825	57.5–67.2	9.7	11.62	119.8
8H	19	2015	67.2–76.8	9.6	11.10	115.6
				76.8	82.17	

tinuity is difficult to assess. Voids where soupy sediment or structure suggests missing sediment are noted on the barrel sheets. Lithologic observations thus suggest that except where noted, sediment is continuous within each core. Therefore, where recovery is less than 100%, sediment is missing from the top or bottom of each core (Table 3). Recovery above 250 mbsf averaged 70% in Hole 723A and 85% in Hole 723B; this dropped to 45% and 31% below 250 mbsf (Table 1).

Discussion

The dominance of Facies I throughout the recovered interval suggests that a similar depositional environment has dominated the Pleistocene and late Pliocene. The absence of turbidites, erosional contacts, and massive gravity-flow structures suggests a relatively undisturbed sediment deposition, with varying terrigenous and biogenic sediment components. In contrast to Sites 725 and 726 closer to the shelf break (see "Site 725" and "Site 726" chapters, this volume), little sand-sized terrigenous material was transported to Site 723.

In smear slides nannofossils dominate the biogenic component even though foraminifers are abundant in sieved samples. Siliceous microfossils are present in the surface sample and in the downhole laminated intervals, but are rare in the remainder of the cored sections. The absence of opal below the surface sediment suggests that it is produced in the modern environment, but that the opal dissolves rapidly and is not preserved.

Sediments contain abundant silt-sized detrital calcite, presumably derived from the adjacent carbonate deserts. The flux of terrigenous sediment, primarily of clay and silt size, is greater than at sites on the Owen Ridge. Compared with Owen Ridge Sites 721 and 722, sedimentation rates are three to four times higher. The carbonate content is lower, which indicates dilution

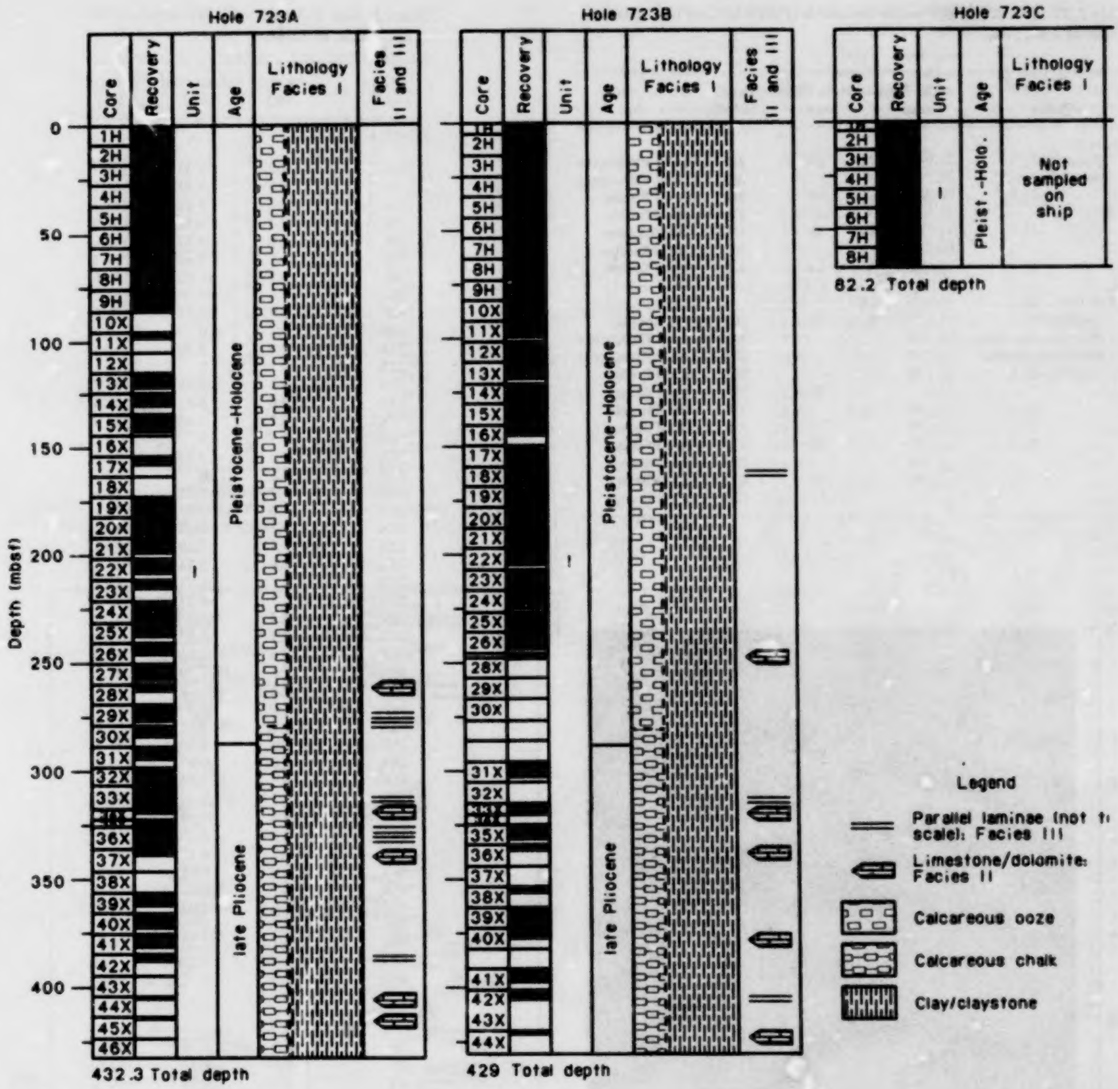
Hole 723A
Hole 723B
Hole 723C
Core
Recovery
Unit
Age
Lithology Facies I
Facies II and III
Depth (mbsf)
0
50
100
150
200
250
300
350
400
I
Pleistocene-Holocene
late Pliocene
Pleist.-Holo.
Not sampled on ship
432.3 Total depth
429 Total depth
82.2 Total depth
Legend
Parallel laminae (not to scale): Facies III
Limestone/dolomite: Facies II
Calcareous ooze
Calcareous chalk
Clay/claystone

Figure 5. Lithologic summary, Site 723.

by the terrigenous components. The variations in sediment composition on the margin reflect changes in the relative flux of terrigenous and biogenic components. Variable fluxes produce a facies which varies between a marly ooze with 30%-60% carbonate, and infrequent intervals where the carbonate content is <30%.

Variations in biogenic carbonate flux will be difficult to evaluate by analyses which combust both detrital and biogenic calcite; some means of identifying the terrigenous fraction of the carbonate must be employed. These two sources of carbonate partially explain the differences in carbonate stratigraphies between Site 723 and Sites 721 and 722 on the Owen Ridge. Figure 7 shows the carbonate and organic carbon record for Hole 723A sampled at 75-cm intervals (see also Table 4). These data show cyclicity at several scales, but the average value does not change significantly downhole (mean = 56.1% $CaCO_3$, SD = 8.04%, min = 29.4%, max = 71.6%).

The episodic, rather than the continuous, occurrence of laminated intervals suggests that in the late Pliocene through early Pleistocene conditions existed for short intervals of time which allowed the formation and preservation of laminated sediments. If the light layers represent annual upwelling seasons, then these conditions most often existed for tens to hundreds of years at a time. Typical sedimentation rates during intervals in Core 117-723B-32X are 80 and 130 cm/k.y. (assuming annual varves). Within the intervals the laminae are variable in thickness and lateral extent and the contact with Facies I is gradational. Conditions necessary for varve formation and preservation appear transient.

Facies II (dolomite layers) and Facies III are found adjacent, and in some cases the dolomite layers are laminated. Dolomite stringers were also found on Leg 112 in the organic-rich sediments of the Peru upwelling system (Suess, von Huene, et al., 1988). Organic-rich sediment is one prerequisite for the forma-

Table 2. Occurrence of dolomitic limestone (Facies II) and laminated intervals (Facies III).

Facies	Hole 723A core	Hole 723B core	Depth (mbsf)	Age
Facies II:				
Dolomitic		27	245	early Pleistocene
limestone	29		262	early Pleistocene
	34	33	318	late Pliocene
	37	36	336	late Pliocene
		40	377	late Pliocene
	44		403	late Pliocene
	45	44	420	late Pliocene
Facies III:				
Laminated		18	162	Pleistocene
diatomaceous ooze	29		273	early Pleistocene
and marly nanno-	30		278	early Pleistocene
fossil ooze	33		312	late Pliocene
		33	315	late Pliocene
	35		323	late Pliocene
	36		330	late Pliocene
	37	36	338	late Pliocene
	42		386	late Pliocene
	44	42	405	late Pliocene
		44	420	late Pliocene

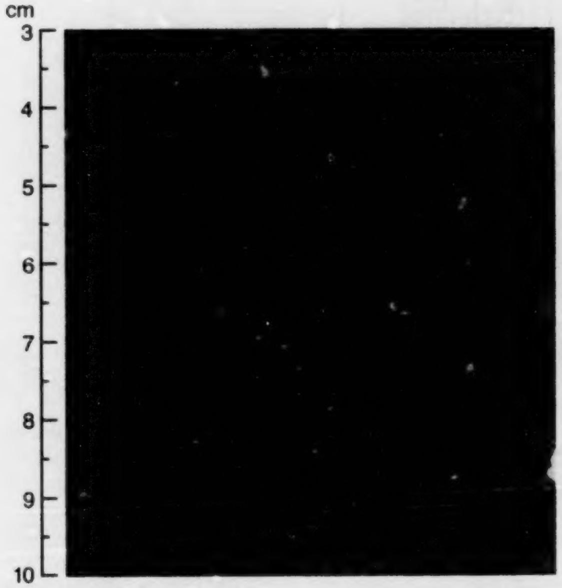

Figure 6. Laminated diatomite and marly nannofossil ooze (117-723A-29X-7, 3–10 cm).

tion of these layers, and their presence in the upper Pliocene and lower Pleistocene and absence in the upper Pleistocene is consistent with higher contents of organic material in this interval, which coincides approximately with the time when laminae were formed. The youngest dolomite is formed approximately 20 m above the limit of the intensely laminated zone.

Another necessary condition for the formation and preservation of laminae is the absence of bioturbation at the seafloor. On the face of split cores we see a decrease in burrow mottling and benthic shell fragments deeper in the section. A third indi-

Table 3. Site 723 core recovery adjusted for voids within sections.

Core no.	Length (m)	Recovered (m)	Percent (%)
117-723A-			
1H	7.8	7.81	100.1
2H	9.7	9.81	101.1
3H	9.6	9.81	102.2
4H	9.7	9.83	101.3
5H	9.6	9.83	102.0
6H	9.7	9.63	99.3
7H	9.7	11.02	113.6
8H	9.6	10.05	104.7
9H	9.7	9.95	102.6
10X	9.7	0	0
11X	9.6	2.60	27.1
12X	9.7	0	0
13X	9.7	6.18	63.7
14X	9.6	5.61	58.4
15X	9.7	7.66	79.0
16X	9.7	0	0
17X	9.6	3.32	34.6
18X	9.7	0	0
19X	9.7	9.21	94.9
20X	9.6	7.37	76.8
21X	9.7	6.13	63.2
22X	9.7	7.69	79.3
23X	9.6	2.74	28.5
24X	9.7	8.71	89.8
25X	9.7	5.07	52.3
26X	9.6	4.55	47.4
27X	9.7	6.93	71.4
28X	9.6	2.65	27.6
29X	9.6	7.79	81.1
30X	9.6	4.62	92.5
31X	9.6	6.5	67.7
32X	9.6	9.15	95.3
33X	9.6	8.17	85.1
34X	4.8	0.47	9.8
35X	4.8	4.44	92.5
36X	9.5	9.43	99.3
37X	9.6	1.58	16.5
38X	9.6	0	0
39X	9.7	6.13	63.2
40X	9.6	6.58	68.5
41X	9.7	5.82	60.0
42X	9.6	1.62	16.9
43X	9.7	0	0
44X	9.7	0.03	0.3
45X	9.6	0.28	2.9
46X	9.7	0	0
117-723B-			
1H	4.3	4.29	99.7
2H	9.7	9.93	102.0
3H	9.6	9.97	104.0
4H	9.7	9.83	101.0
5H	9.6	10.00	104.1
6H	9.7	10.36	106.8
7H	9.7	10.32	106.4
8H	9.6	9.72	101.3
9H	9.7	9.40	96.9
10X	9.6	7.89	82.2
11X	9.5	7.73	81.4
12X	9.6	8.73	90.9
13X	9.6	6.83	71.1
14X	9.7	8.24	84.9
15X	9.6	8.75	91.1
16X	9.7	4.05	41.8
17X	9.7	8.85	91.2
18X	9.6	8.61	89.7
19X	9.7	9.43	97.2
20X	9.7	8.15	84.0
21X	9.7	8.07	83.2
22X	9.6	7.25	75.5
23X	9.6	8.01	83.4
24X	9.7	8.55	88.1
25X	9.7	7.73	79.7
26X	9.7	7.61	78.5

Table 3 (continued).

Core no.	Length (m)	Recovered (m)	Percent (%)
117-723B-			
27X	1.6	1.68	105.0
28X	7.8	0	0
29X	9.7	0	0
30X	9.7	0	0
31X	9.6	6.91	72.0
32X	9.7	0	0
33X	4.4	3.45	78.4
34X	5.3	0	0
35X	9.8	2.61	26.7
36X	9.7	1.48	15.3
37X	9.7	0	0
38X	9.7	2.18	22.5
39X	9.7	7.10	73.2
40X	9.7	3.47	35.8
41X	9.7	5.33	54.9
42X	9.5	3.43	36.1
43X	9.6	0	0
44X	9.6	0.22	2.3

Note: This table was produced by subtracting all voids >1 cm from the original recovered length noted in the core recovery log.

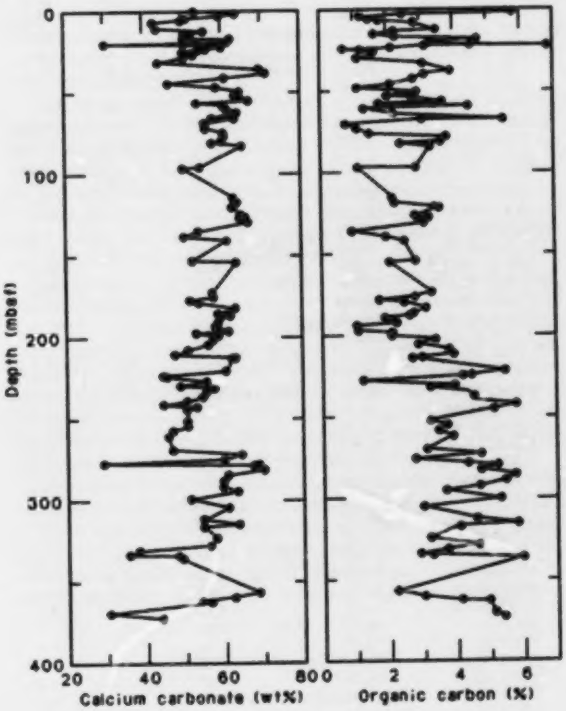

Figure 7. Downhole plot of calcium carbonate and organic carbon.

cator of decreased benthic activity may be the observed increase in organic carbon. Sediment accumulated faster than organic matter could be remineralized by benthic organisms. Cores below 230 mbsf (Core 117-723A-25X) are darker (dark olive gray 5Y 3/1, 5Y 2.5/1) than those above (olive 5Y 4/3, 5Y 4/2). This general change is also observed in the mean organic carbon content (Fig. 7 and Table 4). Lithologic observations thus suggest

Table 4. Calcium carbonate and organic carbon data for Hole 723A.

Core, section, interval (cm)	Depth (mbsf)	Total carbon (%)	Inorganic carbon (%)	Organic carbon (%)	$CaCO_3$ (wt%)
117-723A-					
1H-1, 43–44	0.43	12.25	6.45	5.80	53.7
1H-1, 113–114	1.13		7.22		60.1
1H-2, 43–44	1.93	10.18	7.67	2.51	63.9
1H-2, 110–114	2.60		7.52		62.6
1H-3, 43–44	3.43	8.42	7.17	1.25	59.7
1H-3, 113–114	4.13		6.64		55.3
1H-4, 43–44	4.93	7.68	6.19	1.49	51.6
1H-4, 110–114	5.60		6.14		51.2
1H-4, 144–145	5.94	7.82	6.02	1.80	50.2
1H-5, 113–114	7.13	8.03	5.17	2.86	43.1
2H-1, 113–114	8.93		6.89		57.4
2H-2, 113–114	10.43		5.20		43.3
2H-3, 43–44	11.23	8.84	5.28	3.56	44.0
2H-3, 113–114	11.93		6.51		54.2
2H-4, 43–44	12.73	8.95	6.70	2.25	55.8
2H-4, 113–114	13.43		6.37		53.1
2H-5, 43–44	14.23	7.82	6.14	1.68	51.2
2H-5, 113–114	14.93		5.85		48.7
2H-6, 43–44	15.73	8.59	6.32	2.27	52.7
2H-6, 113–114	16.43		7.30		60.8
2H-7, 43–44	17.23	10.91	6.14	4.77	51.2
3H-1, 43–44	17.93	11.12	7.53	3.59	62.7
3H-1, 113–114	18.63		7.46		62.1
3H-2, 43–44	19.43	10.84	7.46	3.38	62.1
3H-2, 113–114	20.13		6.48		54.0
3H-2, 127–128	20.27	10.70	6.12	4.58	51.0
3H-2, 138–139	20.38	10.52	3.69	6.83	30.7
3H-3, 43–44	20.93	9.76	6.56	3.20	54.6
3H-3, 113–114	21.63		8.31		69.2
3H-4, 43–44	22.43	9.41	7.23	2.18	60.2
3H-4, 113–114	23.13		6.79		56.6
3H-4, 144–145	23.44	7.48	6.77	0.71	56.4
3H-5, 43–44	23.93	7.81	6.58	1.23	54.8
3H-5, 113–114	24.63		5.88		49.0
3H-6, 43–44	25.43	7.76	6.10	1.66	50.8
3H-6, 113–114	26.13		5.53		46.1
3H-7, 43–44	26.93	8.01	6.41	1.60	53.4
4H-1, 43–44	27.53		6.51		54.2
4H-2, 43–44	29.03	7.23	6.11	1.12	50.9
4H-3, 43–44	30.53		6.04		50.3
4H-4, 43–44	32.03	8.49	5.33	3.16	44.4
4H-5, 43–44	33.53		6.42		53.5
4H-6, 43–44	35.03		4.57		38.1
4H-7, 43–44	36.53	12.40	8.42	3.98	70.1
5H-1, 33–34	37.13		7.24		60.3
5H-2, 43–44	38.73	11.78	8.59	3.19	71.6
5H-3, 43–44	40.23		7.10		59.1
5H-4, 43–44	41.73	10.18	7.33	2.85	61.1
5H-5, 46–47	43.26		6.68		55.6
5H-6, 43–44	44.73	7.78	5.62	2.16	46.8
5H-7, 43–44	46.23		6.34		52.8
6H-1, 43–44	46.83	8.17	7.05	1.12	58.7
6H-2, 43–44	48.33		6.99		58.2
6H-3, 43–44	49.83	10.76	7.81	2.95	65.1
6H-4, 43–44	51.33		7.77		64.7
6H-4, 144–145	52.34	9.71	7.67	2.04	63.9
6H-5, 43–44	52.83	10.58	7.79	2.79	64.9
6H-6, 43–44	54.33		7.42		61.8
6H-7, 43–44	55.83	11.80	8.08	3.72	67.3
7H-1, 38–39	56.48		7.53		62.7
7H-2, 43–44	56.94	8.30	6.48	1.82	54.0
7H-2, 149–150	58.00	11.76	7.26	4.50	60.5
7H-4, 43–44	59.94	8.69	7.37	1.32	61.4
7H-5, 43–44	61.44		7.60		63.3
7H-6, 43–44	62.94	9.94	7.72	2.22	64.3
7H-7, 43–44	64.44		7.73		64.4
7H-8, 43–44	65.94	12.46	6.95	5.51	57.9
7H, CC, 16–17	66.58		8.07		67.2
8H-1, 43–44	66.23	10.77	7.65	3.12	63.7
8H-2, 43–44	67.73		7.57		63.1
8H-3, 43–44	69.23	7.47	6.71	0.76	55.9
8H-4, 43–44	70.73		6.94		57.8
8H-4, 149–150	71.79	7.84	6.75	1.09	56.2
8H-5, 43–44	72.23	7.80	6.73	1.07	56.1
8H-6, 43–44	73.73		6.66		55.5
8H-7, 43–44	75.23	8.75	7.27	1.48	60.6

Table 4 (continued).

Core, section, interval (cm)	Depth (mbsf)	Total carbon (%)	Inorganic carbon (%)	Organic carbon (%)	$CaCO_3$ (wt%)
117-723A-					
9H-1, 46–47	75.86		7.19		59.9
9H-2, 43–44	77.33	11.14	7.29	3.85	60.7
9H-3, 43–44	78.83		7.29		60.7
9H-4, 43–44	80.33	10.91	7.23	3.68	60.2
9H-4, 144–145	81.34	9.36	6.94	2.42	57.8
9H-5, 39–40	81.79		7.18		59.8
9H-6, 43–44	83.33	11.23	7.86	3.37	65.5
9H-7, 43–44	84.83		7.22		60.1
11X-1, 107–108	95.87	9.46	6.55	2.91	54.6
11X-1, 149–150	96.29	7.14	6.05	1.09	50.4
11X-2, 46–47	96.76		5.31		44.2
13X-1, 43–44	114.53	9.75	7.56	2.19	63.0
13X-2, 43–44	116.03		7.48		62.3
13X-3, 43–44	117.53	9.94	7.70	2.24	64.1
13X-4, 46–47	119.06		7.45		62.1
13X-4, 119–120	119.79	11.09	7.60	3.49	63.3
13X-5, 43–44	120.53	11.14	7.53	3.61	62.7
14X-1, 43–44	124.23		8.02		66.8
14X-2, 43–44	125.73	10.72	7.84	2.88	65.3
14X-2, 149–150	126.79	11.25	7.97	3.28	66.4
14X-3, 70–71	127.50	10.76	7.79	2.97	64.9
14X-4, 43–44	128.73		7.54		62.8
14X-5, 20–21	130.00	11.14	8.01	3.13	66.7
15X-1, 40–41	133.80		6.52		54.3
15X-2, 43–44	135.33	7.41	6.49	0.92	54.1
15X-3, 70–71	137.10		6.39		53.2
15X-4, 43–44	138.33	7.99	6.04	1.95	50.3
15X-5, 70–71	140.10		7.06		58.8
15X-6, 0–1	140.90	9.85	7.34	2.51	61.1
15X-7, 20–21	142.60		7.05		58.7
17X-1, 43–44	153.23	9.16	6.30	2.86	52.5
17X-2, 0–1	154.30	9.68	7.62	2.06	63.5
17X-2, 43–44	154.73		7.52		62.6
19X-1, 42–43	172.52	10.22	6.87	3.35	57.2
19X-2, 30–31	173.90		6.78		56.5
19X-3, 42–43	175.52	9.72	6.92	2.80	57.6
19X-4, 42–43	177.02		6.49		54.1
19X-4, 64–65	177.24	7.97	6.21	1.76	51.7
19X-5, 42–43	178.52	8.94	6.47	2.47	53.9
19X-6, 30–31	179.90		6.47		53.9
19X-7, 42–43	181.52		6.85		57.1
20X-1, 40–41	182.20	10.77	7.60	3.17	63.3
20X-2, 40–41	183.70		7.20		60.0
20X-3, 40–41	185.20	9.82	7.04	2.78	58.6
20X-4, 30–31	186.60	10.08	7.43	2.65	61.9
20X-4, 40–41	186.70		7.45		62.1
20X-5, 40–41	188.20	9.05	7.12	1.93	59.3
20X-6, 50–51	189.80		6.68		55.6
20X-7, 40–41	191.20	9.32	7.06	2.26	58.8
21X-1, 27–28	191.67		6.72		56.0
21X-2, 27–28	193.17	8.02	6.98	1.04	58.1
21X-3, 27–28	194.67		7.04		58.6
21X-4, 33–34	196.23	8.46	7.37	1.09	61.4
21X-5, 0–1	197.40	8.50	6.38	2.12	53.2
21X-5, 27–28	197.67		6.34		52.8
21X-6, 45–46	199.35	9.17	7.06	2.11	58.8
21X, CC, 27–28	200.77		6.78		56.5
22X-1, 29–30	201.39	10.36	6.89	3.47	57.4
22X-2, 29–30	202.89		6.90		57.5
22X-3, 29–30	204.39	9.66	6.74	2.92	56.1
22X-4, 29–30	205.89		6.55		54.6
22X-5, 29–30	207.39	10.00	6.14	3.86	51.2
22X-6, 29–30	208.89		6.01		50.1
22X-7, 29–30	210.39	9.75	5.74	4.01	47.8
23X-1, 67–68	211.47		7.17		59.7
23X-2, 0–1	212.30	10.62	7.58	3.04	63.1
23X-2, 31–32	212.61	10.18	7.47	2.71	62.2
23X-3, 30–31	214.10		7.45		62.1
24X-1, 48–49	220.88	12.76	7.27	5.49	60.6
24X-2, 31–32	222.21		7.48		62.3
24X-3, 0–1	223.40	9.85	5.34	4.51	44.5
24X-3, 45–46	223.85	9.74	5.47	4.27	45.6
24X-4, 21–22	225.11		6.82		56.8
24X-5, 44–45	226.84	7.90	6.68	1.22	55.6
24X-6, 47–48	228.37		6.12		51.0
24X-7, 27–28	229.67	9.90	5.89	4.01	49.1
24X, CC, 44–45	230.27		7.23		60.2
25X-1, 72–73	230.82	10.19	6.90	3.29	57.5
25X-2, 72–73	232.32		6.82		56.8
25X-3, 19–20	233.29	11.07	6.68	4.39	55.6
25X-4, 43–44	235.03		6.64		55.3
25X-5, 43–44	236.53	11.18	6.58	4.60	54.8
25X-6, 43–44	238.03		6.22		51.8
25X-7, 20–21	239.30	10.70	6.07	4.63	50.6
26X-1, 24–25	240.04		5.81		48.4
26X-2, 24–25	241.54	11.20	5.35	5.85	44.6
26X-3, 0–1	242.80	11.99	6.39	5.60	53.2
26X-3, 24–25	243.04		5.83		48.6
26X-4, 24–25	244.54	11.28	6.09	5.19	50.7
26X-5, 24–25	246.04		6.51		54.2
27X-1, 43–44	249.83		6.21		51.7
27X-2, 43–44	251.33	9.30	6.09	3.21	50.7
27X-3, 43–44	252.83		6.12		51.0
27X-4, 43–44	254.33	9.95	6.11	3.84	50.9
27X-5, 43–44	255.83		6.33		52.7
27X-6, 43–44	257.33	9.15	5.63	3.52	46.9
28X-1, 48–49	259.58		6.37		53.1
28X-2, 48–49	261.08	9.43	5.47	3.96	45.6
28X-3, 21–22	262.31		4.97		41.4
29X-1, 43–44	269.13	8.79	5.63	3.16	46.9
29X-2, 43–44	270.63		5.45		45.4
29X-3, 43–44	272.13	12.54	7.75	4.79	64.6
29X-4, 43–44	273.63		5.85		48.7
29X-5, 43–44	275.13	9.98	7.18	2.80	59.8
29X-6, 43–44	276.63		5.65		47.1
29X-6, 119–120	277.39	7.92	3.53	4.39	29.4
30X-1, 0–1	278.30	13.18	8.28	4.90	69.0
30X-1, 62–63	278.92	13.38	8.12	5.26	67.6
30X-2, 24–25	280.04		8.77		73.1
30X-3, 43–44	281.73	13.20	8.40	4.80	70.0
30X-4, 49–50	283.29		6.46		53.8
30X-5, 47–48	284.77	13.09	7.31	5.78	60.9
30X, CC, 40–41	285.71		7.00		58.3
31X-1, 57–58	288.47	12.69	7.17	5.52	59.7
31X-2, 144–145	290.84		8.21		68.4
31X-3, 112–113	292.02	11.90	7.15	4.75	59.6
31X-4, 116–117	293.56		7.75		64.6
31X-5, 92–93	294.82	11.35	7.60	3.75	63.3
31X-6, 90–91	296.30		7.48		62.3
31X-8, 20–21	297.53	9.13	6.76	2.37	56.3
32X-1, 43–44	297.93		6.53		54.4
32X-2, 43–44	299.43	11.51	6.17	5.34	51.4
32X-3, 43–44	300.93		6.44		53.7
32X-4, 43–44	302.43		8.07		67.2
32X-5, 43–44	303.93		7.28		60.6
32X-5, 119–120	304.69	10.36	7.30	3.06	60.8
32X-6, 43–44	305.43		7.39		61.6
33X-1, 40–41	307.50		6.55		54.6
33X-2, 40–41	309.00		5.60		46.7
33X-3, 31–32	310.41		5.72		47.7
33X-4, 40–41	312.00	11.21	6.55	4.66	54.6
33X-5, 40–41	313.50		5.72		47.7
33X-6, 40–41	315.00	13.47	7.63	5.84	63.6
33X-7, 40–41	316.50		5.12		42.7
34X-1, 1–2	316.71	10.69	6.56	4.13	54.6
35X-1, 43–44	321.93		7.32		61.0
35X-2, 45–46	323.45	10.21	6.94	3.27	57.8
35X-3, 45–46	324.95		6.60		55.0
35X-4, 30–31	326.30		6.45		53.7
36X-2, 36–37	327.95	11.42	6.73	4.69	56.1
36X-3, 52–53	329.61		6.08		50.7
36X-4, 43–44	331.02	8.35	4.58	3.77	38.2
36X-5, 35–36	332.44		8.45		70.4
36X-6, 0–1	333.59	7.20	4.29	2.91	35.7
36X-6, 35–36	333.94	9.09	5.77	3.32	48.1
36X-7, 35–36	335.44		7.88		65.6
37X-1, 29–31	336.09	11.88	5.89	5.99	49.1
39X-1, 43–44	355.43		8.76		73.0
39X-2, 46–47	356.96	10.47	8.24	2.23	68.6
39X-3, 46–47	358.46		7.65		63.7
39X-4, 46–47	359.96	10.52	7.47	3.05	62.2
39X-5, 46–47	361.46		6.64		55.3

Table 4 (continued).

Core, section, interval (cm)	Depth (mbsf)	Total carbon (%)	Inorganic carbon (%)	Organic carbon (%)	$CaCO_3$ (wt%)
117-723A-					
39X-5, 119–120	362.19	10.66	6.49	4.17	54.1
39X-6, 46–47	362.96	11.76	6.75	5.01	56.2
40X-2, 83–84	367.03		8.81		73.4
40X-4, 43–44	369.63	8.85	3.68	5.17	30.7
40X-5, 44–45	371.14		7.26		60.5
40X-6, 45–46	372.65	10.71	5.26	5.45	43.8
40X-7, 28–29	373.98		5.88		49.0
40X, CC, 24–25	374.33	5.09			
41X-2, 1–10	375.81		8.35		69.6
41X-3, 44–45	377.74		7.41		61.7
41X-4, 59–60	379.39		3.55		29.6
41X-5, 45–46	380.75		3.91		32.6
41X-6, 45–46	382.25		6.31		52.6
41X, CC, 43–44	382.86		7.72		64.3
42X-1, 43–44	384.43		3.61		30.1

reduced bioturbation and greater organic content in sediments below 230 mbsf.

Silica is preserved in the laminated intervals, but siliceous microfossils only occur in minor abundance adjacent to laminae. High silica flux, rapid burial, and lack of bioturbation appear necessary for the formation of visible laminae at this site. The stratigraphic occurrence of laminae implies that the critical combination of these conditions was met episodically rather than continuously.

The mechanisms which enhance the preservation of silica and organic carbon may also explain the occurrence of laminae in the lower Pleistocene and upper Pliocene. More frequent anoxic conditions would reduce bioturbation, and the thickness of the sediment mixed layer in which silica dissolves would be small. This mechanism is not specifically limited to changes in local productivity and may imply changes in the general circulation and oceanography of the northwest Indian Ocean.

The intensity of the oxygen-minimum zone (OMZ) is controlled, among other things, by the flux of organic matter into the OMZ, the oxygen concentration of the north Indian Ocean deep water, by the lateral advection and diffusion (or lack thereof) of water masses which have a different oxygen content, and by the physical processes which control the stratification of the water column. Tracers of higher productivity, such as isotopic composition and faunal assemblages, may be used to differentiate local from regional productivity changes.

The Owen Ridge sites should record the same productivity signal caused by upwelling, but because they are situated in a different depositional environment, we may be able to distinguish local from regional effects. Thus, the organic-rich laminated facies produced on the Arabian margin reveal past environmental conditions that are strikingly different than modern conditions.

BIOSTRATIGRAPHY

Introduction

Site 723 was drilled on the margin of the western Arabian Sea in order to evaluate the history of the upwelling system in the monsoonal circulation system through time. Nutrient-rich waters injected into the euphotic zone appear to have enhanced blooming of distinctive opportunistic species of the various faunal and floral groups. As a consequence, determination of biostratigraphic zonations is difficult because age-diagnostic species are often lacking or show only scattered occurrences (Figs. 8 and 9). Radiolarians and planktonic foraminifers cannot be used for stratigraphic purposes at this site. Fortunately, age control is provided by the nannoflora.

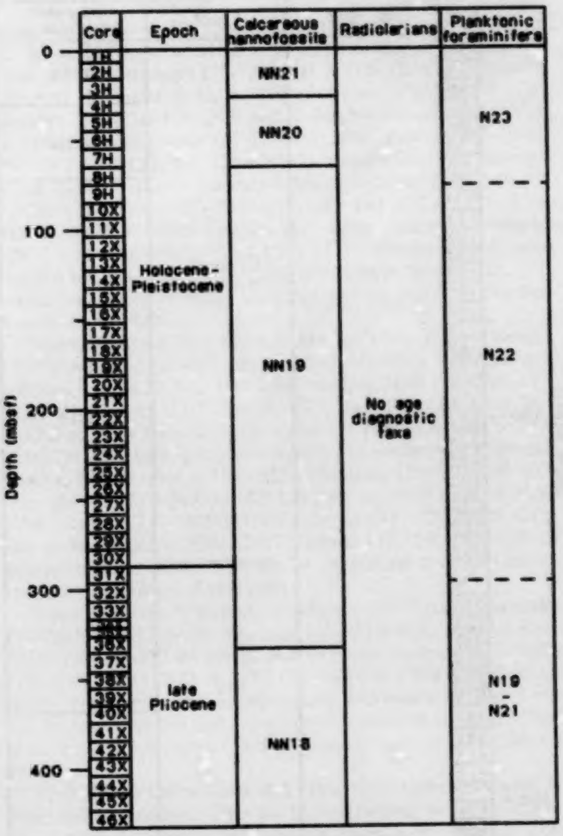

Figure 8. Correlation of planktonic microfossil zones in Hole 723A.

The Pliocene/Pleistocene boundary was recognized between Samples 117-723A-30X-5, 89–90 cm, and 117-723A-30X, CC (285.19–287.90 mbsf), and Samples 117-723B-30X, CC, and 117-723B-31X, CC (274.4–303.3 mbsf). A schematic correlation of nannofossil zones at Site 723 is depicted in Figure 10, and a plot of datum levels vs. depth below the seafloor is presented in Figure 11. For a detailed listing of these data points, see Table 5.

Calcareous nannofossils are abundant and well preserved throughout the entire section, whereas planktonic foraminifers are abundant only in the upper part of the sequence (Samples 117-723A-1H, CC, through 117-723A-31X, CC; 7.8–297.5 mbsf), and are sparse downhole. Although radiolarians show a highly scattered pattern, they are most abundant near the Pliocene-Pleistocene boundary. Benthic foraminifers are abundant, well preserved, and highly diverse throughout the sequence studied.

Planktonic Foraminifers

The sequence recovered at Site 723 contains upper Pliocene to Pleistocene foraminifer-bearing marly nannofossil oozes. Only the planktonic foraminifers in Hole 723A core-catcher samples were studied. Assemblages are highly diverse in the upper part of the section, and the preservation state of the calcareous tests is good (Samples 117-723A-1H, CC, to 117-723A-31X,

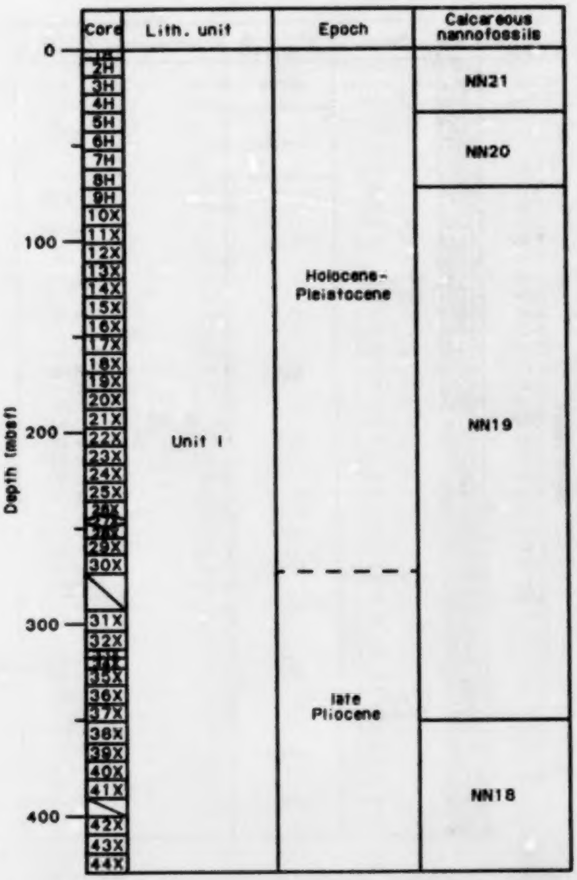
Core
Lith. unit
Epoch
Calcareous nannofossils
0
100
200
300
400
Depth (mbsf)
2H
3H
4H
5H
6H
7H
8H
9H
10X
11X
12X
13X
14X
15X
16X
17X
18X
19X
20X
21X
22X
23X
24X
25X
29X
30X
31X
32X
35X
36X
37X
38X
39X
40X
41X
42X
43X
44X
Unit I
Holocene-Pleistocene
late Pliocene
NN21
NN20
NN19
NN18

Figure 9. Correlation of planktonic microfossil zones in Hole 723B.

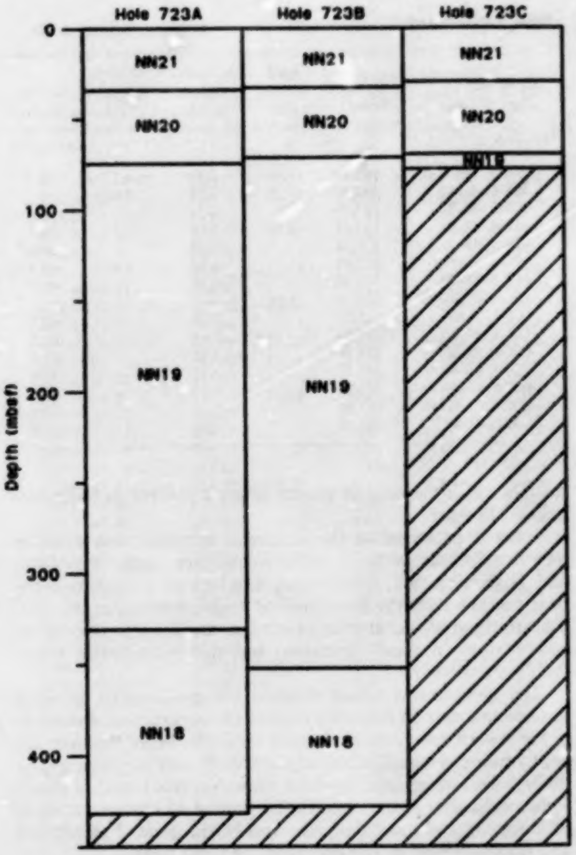
Hole 723A
Hole 723B
Hole 723C
0
100
200
300
400
Depth (mbsf)
NN21
NN20
NN19
NN18
NN21
NN20
NN19
NN18
NN21
NN20
NN19

Figure 10. Correlation of nannofossil zones in Holes 723A, 723B, and 723C.

CC; 7.8–297.5 mbsf). Below this level the planktonic foraminifers are sparse and moderately well preserved.

The top part of the Pleistocene sequence is referred to Zone N23 (Samples 117-723A-1H, CC, to 117-723A-8H, CC; 7.8–75.4 mbsf) as indicated by the presence of *Globigerinella calida calida*. Downhole Zone N22, marked by *Globorotalia truncatulinoides*, could be recognized and persists through Sample 117-723A-27X, CC (259.1 mbsf). The Pleistocene/Pliocene boundary could not be determined by using the evolution of this species from *Globorotalia tosaensis* because both species disappear rapidly below this level. Also, the sparse occurrences of other species do not allow accurate positioning of this boundary. A well-developed late Pliocene fauna is present in Sample 117-723A-39X, CC (364.7 mbsf), with abundant *Globorotalia acostaensis*, common *Globigerinoides obliquus*, and rare *Globorotalia limbata*, and can be assigned to Zones N19–N21. Pliocene Zones N19–N21 could not be subdivided because the zonal markers are missing. The remainder of the hole belongs to Zones N19–N21 as well.

The foraminiferal fauna in Hole 723A is characterized by high relative frequencies of *Globigerina bulloides*, *Neogloboquadrina dutertrei*, *Globorotalia menardii*, and *Globigerinita glutinata*. This indicates upwelling conditions throughout the Pleistocene and late Pliocene in this area. Shore-based counts of relative frequencies of key species will unravel the upwelling intensity through time as a response to changes in the monsoonal system.

Benthic Foraminifers

Benthic foraminiferal fauna were studied at Site 723 in the core-catcher samples of Hole 723A. Benthic foraminifers are abundant and well preserved throughout most of the cored sequence, although benthic foraminifers are absent below 393.6 mbsf. The diversity of the fauna is high and most species are present in all of the samples we studied.

The total number of benthic foraminiferal specimens per 10-cm^3 sediment is very high in the upper 230 m (Samples 117-723A-1H, CC, through -24X, CC; 7.8–230.1 mbsf), where it ranges from 4,000 to 13,000 specimens with an average of about 7,000. The average is slightly higher in the upper part. In the samples below 280 mbsf, the average is significantly lower (about 1,500).

The benthic foraminiferal fauna of Site 723 is dominated by *Bolivina pygmaea*, *B. ordinaria*, *Uvigerina auberiana*, and *U. peregrina*. Other species with high relative abundances are *Cassidulina carinata*, *Epistominella exigua*, and *Hyalinea baltica*. Species with lower relative abundance are *Florilus* spp. and *Plectofrondicularia* spp.

The only significant change in the benthic foraminiferal assemblage occurs at about 180 mbsf (Sample 117-723A-19X, CC).

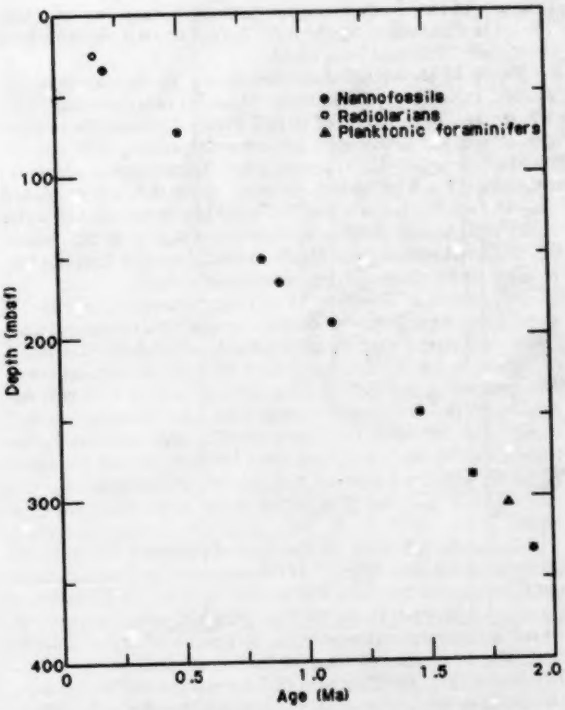

Figure 11. Age-depth plot for Hole 723A. For a detailed listing of datum levels, see Table 5.

Table 5. Chronologic listing of faunal events for Hole 723A.

Event	Core, section, interval (cm)	Depth (mbsf)	Age (Ma)	Source of age
T *Helicosphaera inversa*	117-723A-3H-5, 120–121	24.70	[a]0.15	4
	117-723A-3H, CC	27.10		
B *Emiliania huxleyi*	117-723A-4H-5, 120–121	34.30	0.19	3
	117-723A-4H, CC	36.80		
T *Pseudoemiliania lacunosa*	117-723A-8H-5, 120–121	73.00	0.49	3
	117-723A-8H, CC	75.40		
T *Reticulofenestra* sp. A	117-723A-16X, CC	152.80	0.82	3
	117-723A-17X-1, 90–91	153.70		
B *Gephyrocapsa parallela*	117-723A-17X, CC	162.40	[a]0.89	4
	117-723A-18X, CC	172.10		
T [b]*Gephyrocapsa* "large"	117-723A-20X, CC	191.40	[a]1.10	4
	117-723A-21X-1, 134–135	192.74		
T *Helicosphaera sellii*	117-723A-25X-1, 117–118	231.27	[c]—	—
	117-723A-25X-3, 5–6	233.15		
T *Calcidiscus macintyrei*	117-723A-26X-5, 7–8	245.87	1.45	6
	117-723A-26X, CC	249.40		
B *Gephyrocapsa caribbeanica*	117-723A-30X-5, 89–90	285.19	[d]1.66	4, 8
	117-723A-30X, CC	287.90		
T *Globigerinoides extremus*	117-723A-32X-4, 65–67	302.65	[e]1.80	6
	117-723A-32X, CC	307.10		
T *Discoaster brouweri*	117-723A-36X-3, 127–128	330.36	1.9	6
	117-723A-36X-5, 144–145	333.53		

Note: T = morphotypic top of range and B = bottom of range. Sources of ages are: 3 = oxygen isotope data for Site 723 (N. Niitsuma, unpubl. data); 4 = Takayama and Sato, 1987; 6 = Berggren et al., 1985; and 8 = Sato et al., in press.

[a] North Atlantic data.

[b] Long axis greater than 6μm.

[c] North Atlantic age consistent with Italian-type section.

[d] No good published age; event appears to be diachronous.

[e] *G. obliquus extremus* in Berggren et al., 1985.

At this level *Bulimina truncana*, *Epistominella exigua*, and *Plectofrondicularia* sp. *A* have their last occurrences at this site.

Calcareous Nannofossils

Three holes drilled at Site 723 (Fig. 10) provided a largely overlapping and complete composite section down to the upper Pliocene. Calcareous nannofossils are abundant and well preserved throughout, but species diversity is comparatively low.

Sediments down to 34.30 mbsf in Hole 723A (Samples 117-723A-1H, CC, through 117-723A-4H-5, 120–121 cm), sediments down to 33.3 mbsf in Hole 723B (Samples 117-723B-1H, CC, through 117-723B-4H, CC), and sediments down to 28.5 mbsf in Hole 723C (Samples 117-723C-1H, CC, through 117-723C-3H, CC) are assigned to Zone NN21 because they contain *Emiliania huxleyi*. Datum 1 occurs between Samples 177-723A-3H-5, 120–121 cm, and 117-723A-3H, CC, and in Core 117-723B-4H (23.6–33.3 mbsf) within this zone. Datum 2 is the NN21/NN20 boundary. Since most of the specimens of *E. huxleyi* are too small to identify under the light microscope, this boundary is hard to detect precisely. Datum 3 defines the bottom of Zone NN20.

Sediments from 34.4 to 73.0 mbsf in Hole 723A (Samples 117-723A-4H-5, 120–121 cm, to 117-723A-8H-5, 120–121 cm), sediments from 33.3 to 71.9 mbsf in Hole 723B (Samples 117-723B-4H, CC, to 117-723B-8H, CC), and sediments from 28.5 to 67.2 mbsf in Hole 723C (Samples 117-723C-3H, CC, to 117-723C-7H, CC) belong to Zone NN20. The underlying sediments down to 330.36 mbsf in Hole 723A (Samples 117-723A-8H, CC, through 117-723A-36X-3, 127–128 cm), to 342.2 mbsf in Hole 723B (Samples 117-723B-9H, CC, through 117-723B-36X, CC), and to 76.8 mbsf in Hole 723C (Sample 117-723C-8H, CC) all belong to Zone NN19. The top of *Discoaster brouweri* marks the lower boundary of this zone.

The Pleistocene/Pliocene boundary occurs between Samples 117-723A-30X-5, 89–90 cm, and 117-723A-30X, CC, in Hole 723A (285.19–287.90 mbsf) and between Samples 117-723B-27X, CC, and 117-723B-31X, CC, in Hole 723B (247.2–303.0 mbsf). Underlying sediments contain *Discoaster brouweri* but not *D. pentaradiatus* and are assigned, therefore, to Zone NN18 (Pliocene), which persists to the termination of Holes 723A and 723B.

Throughout Holes 723A and Hole 723B there are traces of reworked nannofossils from the Paleogene and Neogene. *Cyclicargolithus floridanus*, *Sphenolithus abies*, *S. moriformis*, *Discoaster saipanensis*, *D. barbadiensis*, *D. deflandrei*, *D. druggii*, *Reticulofenestra pseudoumbilica*, *Dictyococcites bisectus*, and *D. dictyodus* were encountered.

Samples 117-723A-27X, CC, through 117-723A-38X, CC (259.1–355.0 mbsf), and Sample 117-723B-33X, CC (317.4 mbsf), contain numerous specimens of *Coccolithus pelagicus*. One thin lamina (about 1 mm; Sample 117-723A-35X-3, 46 cm) consists of a bloom of *C. pelagicus* with a few specimens of *Discoaster brouweri*. *Coccolithus pelagicus* is known to be a cold-water species.

Many species of *Helicosphaera* are found more commonly in hemipelagic sediments; they are usually very rare or absent in pelagic sediments. The possibility exists that this genus is restricted to, or prefers, areas of upwelling (Perch-Nielsen, 1984). *Helicosphaera* species are especially numerous in Samples 117-723A-32X, CC (307.1 mbsf), 117-723A-33X, CC (316.7 mbsf), 117-723A-35X, CC (326.3 mbsf), and 117-723A-39X, CC (364.7 mbsf).

A single specimen of *Braarudosphaera bigelowi* was recovered from Sample 117-723B-35X, CC (332.5 mbsf). This is a typical shallow-water species (Martini, 1967; Takayama, 1972).

Radiolarians

We examined all core-catcher samples from Hole 723A for radiolarians; we did not study samples from Holes 723B and 723C. Radiolarian abundances vary from barren to common, with peak abundances ("common") in Samples 117-723A-5H, CC (46.4 mbsf), 117-723A-33X, CC, through 117-723A-37X, CC (316.7–345.4 mbsf), 117-723A-41X, CC (384.0 mbsf), and 117-723A-42X, CC (393.6 mbsf). The core-catcher samples from the following cores contained "few" radiolarians: 117-723A-15X (143.1 mbsf), 117-723A-22X (210.8 mbsf), 117-723A-24X (230.1 mbsf), 117-723A-29X (278.3 mbsf), 117-723A-32X (307.1 mbsf), and 117-723A-40X (374.3 mbsf).

In general, diatom abundances are in concert with radiolarian abundances. Considerable detrital material was found in all processed samples. Low radiolarian abundances could, therefore, reflect low-standing crops or masking by detritus or a combination of both conditions.

All the usual tropical Pleistocene and upper Pliocene zonal markers are absent. All elements of the *Lamprocyrtis heteroporos* to *Lamprocyrtis nigriniae* lineage are present, but their sporadic occurrences in this material provide unreliable datum levels.

The criteria described by Johnson and Nigrini (1982) for a modern Arabian Upwelling Assemblage were tested on the uppermost sample containing common radiolarians (i.e., Sample 117-732A-5H, CC). This assemblage is dependent upon the presence of their Recurrent Group D′ (*Collosphaera* cf. *huxleyi*, *Lamprocyclas maritalis ventricosa*, and *Lamprocyrtis nigriniae*) and the absence of a majority of the species belonging to their tropical Recurrent Group A′. Sample 117-723A-5H, CC, does contain the Arabian Upwelling Assemblage. In addition, two species (*Lithostrobus* cf. *hexagonalis* and *Acrosphaera murrayana*) associated with the Peru Current upwelling (Nigrini, 1968), but not included in Johnson and Nigrini's (1982) study, are consistently present in Hole 723A.

Paleoenvironmental Implications

Upwelling conditions are clearly indicated by the planktonic foraminifers, with well-known tropical upwelling species like *Globigerina bulloides* and *Neogloboquadrina dutertrei* dominating the fauna throughout the section. Also, numerous specimens of *Coccolithus pelagicus* (nannoflora) in Samples 117-723A-32X, CC, through 117-723A-39X, CC (316.7–364.7 mbsf) indicate relatively cold water. *Helicosphaera*, a genus thought to prefer upwelling areas, is abundant in some of these same cores as well. Counts of relative abundances are required to record upwelling intensity through time.

The presence of the hyaline benthic foraminifer, *Hyalinea baltica*, throughout the sequence is interesting since it is considered to be a species indicative of cool-water masses. If the relative abundance of *H. baltica* is dependent upon the temperature of the water mass, then Site 723 must have been located within this cool-water mass during at least the late Pliocene and Pleistocene.

PALEOMAGNETISM

Introduction

Site 723 is located at 18°03.079′N, 57°36.561′E, in water depths of about 800 m on the Oman margin. Holes 723A, 723B, and 723C were cored to depths of 432.3 mbsf, 400.1 mbsf, and 76.8 mbsf, respectively. The lithology consisted predominantly of marly nannofossil ooze and calcareous clayey silt.

Magnetic Measurements

We measured the archive halves of Cores 117-723A-1H through 117-723A-9H and Cores 117-723B-1H through 117-723B-9H using the whole-core, pass-through cryogenic magnetometer, after alternating-field (AF) demagnetization at 5 mT. On the basis of these results, the sediments appeared to be less severely affected by the coring-induced remanence seen at Sites 720–722 on the Owen Ridge. Moreover, the inclination values after AF demagnetization at 5 mT generally accorded with the expected geocentric axial dipole values for the site latitude. The failure to acquire a significant coring remanence appears to be an intrinsic property of the Oman margin sediments, because we only succeeded in demagnetizing the APC barrels to an acceptable level after Hole 723B had been cored.

Figure 12 shows the combined results of measurements of discrete samples on the Molspin Minispin magnetometer after AF demagnetization at 5 or 10 mT. Figure 13 shows the remainder of the same data set after removing points with circular standard deviation (CSD) values >40°. The intensities are weak, generally <1 mA/m (arithmetic mean = 0.6 mA/m). A marked drop in intensity below about 100 mbsf is accompanied by a rise in the CSD and an obvious increase in the scatter of the inclinations. The transition from higher to low intensities does not correspond to an obvious lithostratigraphic change.

The results of stepwise AF demagnetization (Figs. 14–17) show that sample behavior during demagnetization tends to become more erratic with increasing depth, which coincides with a reduction in the median destructive field of the natural remanent magnetization (NRM) from ~15–20 mT to <10 mT. According to the nannofossil stratigraphy (see "Biostratigraphy" section, this chapter), the Chron C1/C1r (Brunhes/Matuyama Chronozone) boundary should occur between 100 and 150 mbsf. However, with the exception of a few reversed samples over this interval, it is not clearly reflected in the inclination plot (Fig. 13).

Also, although most of the interval between 100 and 400 mbsf corresponds to Chron C1r (Matuyama Chronozone), there is an absence of reversely magnetized samples (an exception is the interval between about 200 and 250 mbsf, with consistent reversed inclinations corresponding to a zone of higher intensities). The histogram of the distribution of inclinations within 10° classes (Fig. 18) illustrates this normal magnetization bias. On the basis of the above, we concluded that the sediments at Site 723 are relatively poor geomagnetic field recorders and that little reliable magnetostratigraphic information can be obtained from the data set.

The only other feature of interest in the inclination record is the zone of shallow inclinations with two reversed specimens at about 80 mbsf. The interval above 100 mbsf in Figure 13 consists entirely of specimens from Hole 723A. This zone of shallow inclinations was also evident in the archive-half cryogenic results from Core 117-723A-9H. However, it was not evident in the archive-half cryogenic data from the same sub-bottom depth interval in Hole 723B, despite the fact that a comparison of the susceptibility records for Holes 723A and 723B suggests insignificant offset between the two holes. At present, we are unable to determine whether its origin is sedimentologic, geomagnetic, or a coring artifact.

A question arises regarding the reason for the drastic reduction in NRM intensity below 100 mbsf at this site. Figure 19 shows plots of NRM intensity, magnetic susceptibility, and the Königsberger ratio (Q = NRM/susceptibility). The susceptibility values are from the results of whole-core measurements. The NRM decrease is accompanied by a decrease in Q-ratio, which suggests a coarsening of the magnetic grain-size distribution. Several causes are possible: (1) a reduction in the flux (biogenic or detrital) of fine-grained magnetic material to the sediments; (2) destruction of fine magnetic grains by reduction diagenesis (Canfield and Berner, 1987); and/or (3) randomization of fine magnetic grains by gas expansion, which began to be evident below 70 mbsf at this site (in which case the NRM decrease would not necessarily reflect a reduction in the concentration of fine-grained magnetic material).

At present we are unable to decide which of the above factors is the most likely. The third cause can be tested by measurements of anhysteretic remanence across the interval. The second factor is well-documented in marine sediments with high concentrations of organic matter and active sulfate reduction (such

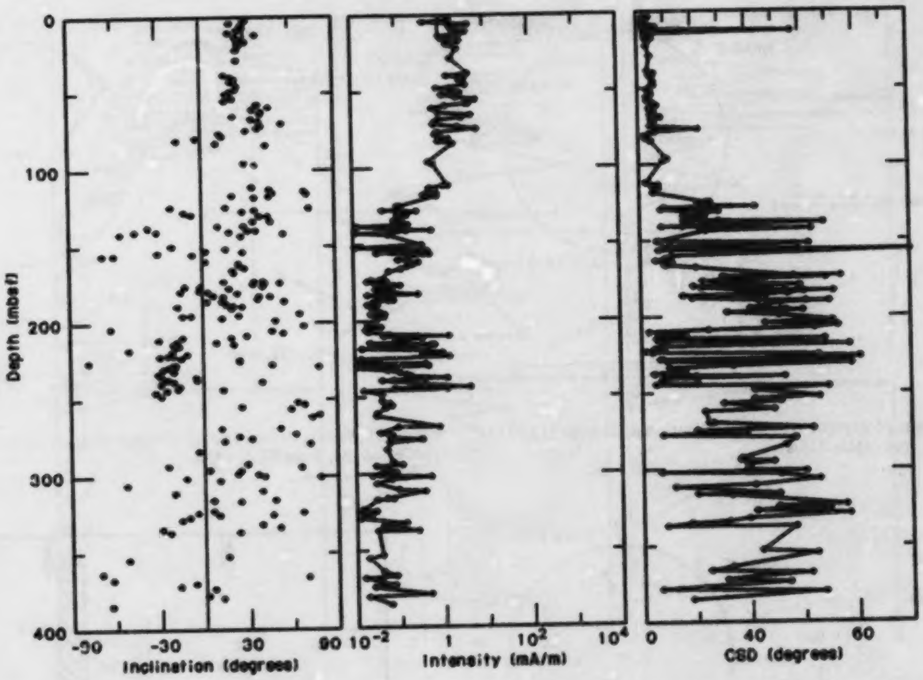

Figure 12. Inclination, natural-remanent-magnetization (NRM) intensity after 5- or 10-mT alternating field (AF) demagnetization, and circular standard deviation (CSD) for the combined discrete sample data from Holes 723A and 723B.

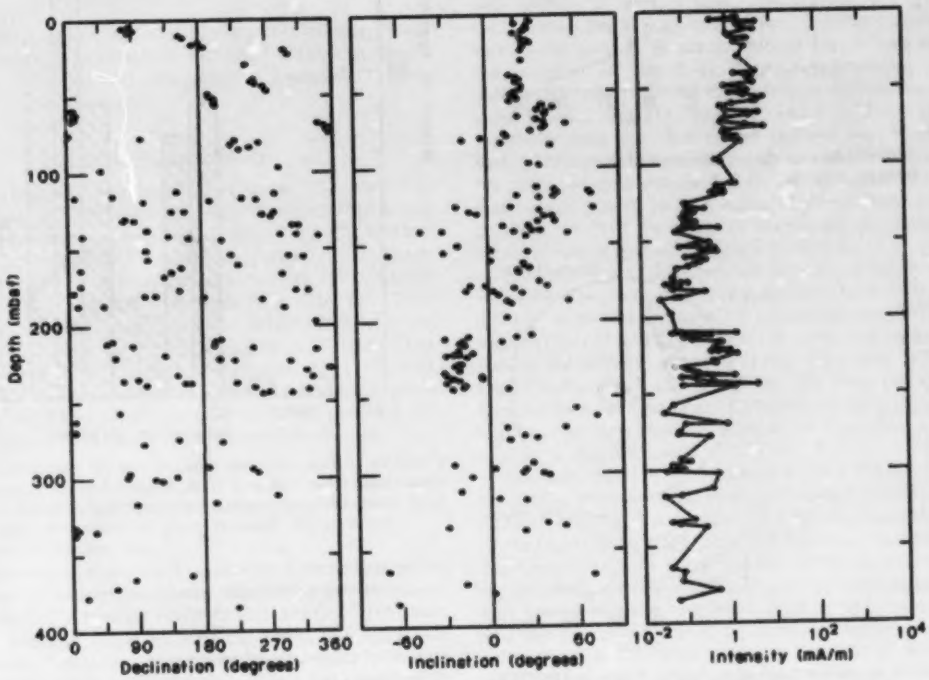

Figure 13. Declination, inclination, and NRM intensity after 5- or 10-mT AF demagnetization for the data set shown in Figure 12 after the removal of specimens with CSD values >40.

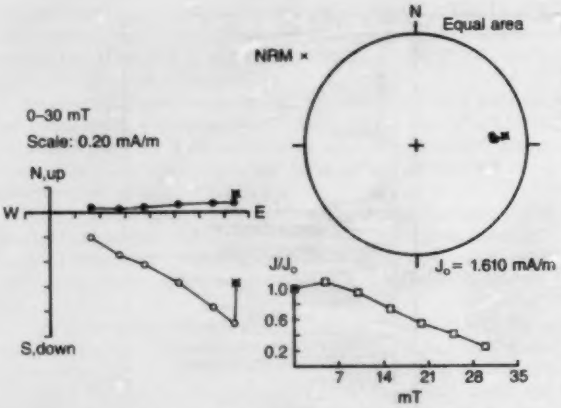

Figure 14. Results of stepwise AF demagnetization of Sample 117-723A-1H-2, 115 cm, from Hole 723A.

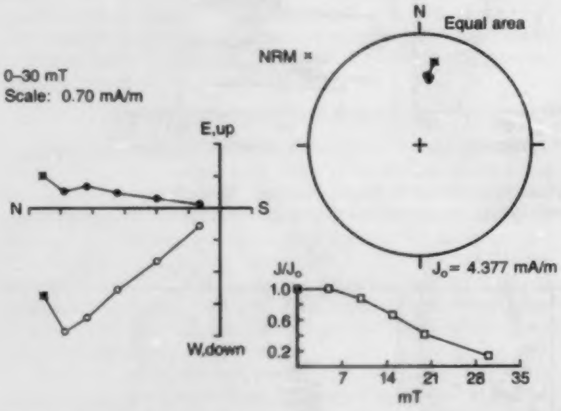

Figure 15. Results of stepwise AF demagnetization of Sample 117-723A-7H-2, 120 cm, from Hole 723A.

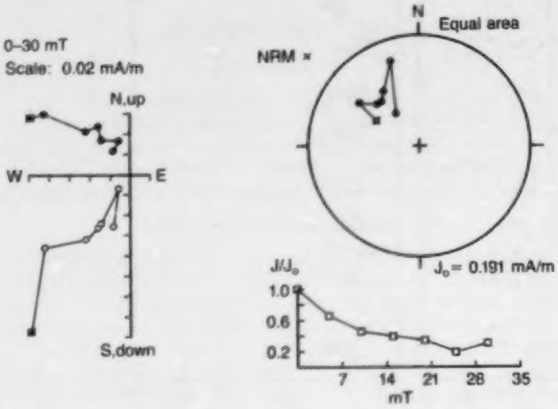

Figure 16. Results of stepwise AF demagnetization of Sample 117-723A-15X-1, 45 cm, from Hole 723A.

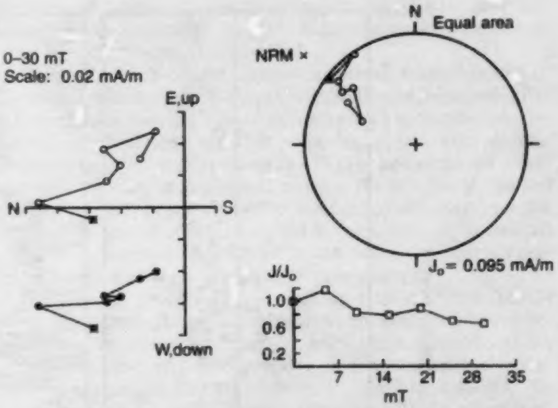

Figure 17. Results of stepwise AF demagnetization of Sample 117-723B-19X-6, 66 cm, from Hole 723B.

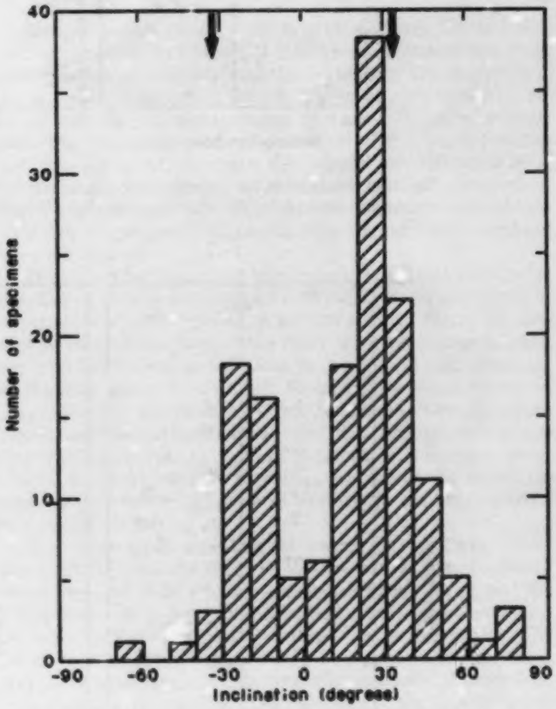

Figure 18. Inclination values grouped into 10° classes for discrete specimens from Holes 723A and 723B. Arrows show the expected geocentric axial dipole inclination values for the site latitude.

as the sediments at Site 723). However, it is interesting that the results of the pore-water geochemistry (see "Inorganic Geochemistry" section, this chapter) show that sulfate declines to low levels well above the zone of NRM decrease. In previous studies of the relationship between sulfate reduction, magnetite dissolution, and pyritization, the three phenomena have tended to occur concurrently (e.g., Canfield and Berner, 1987).

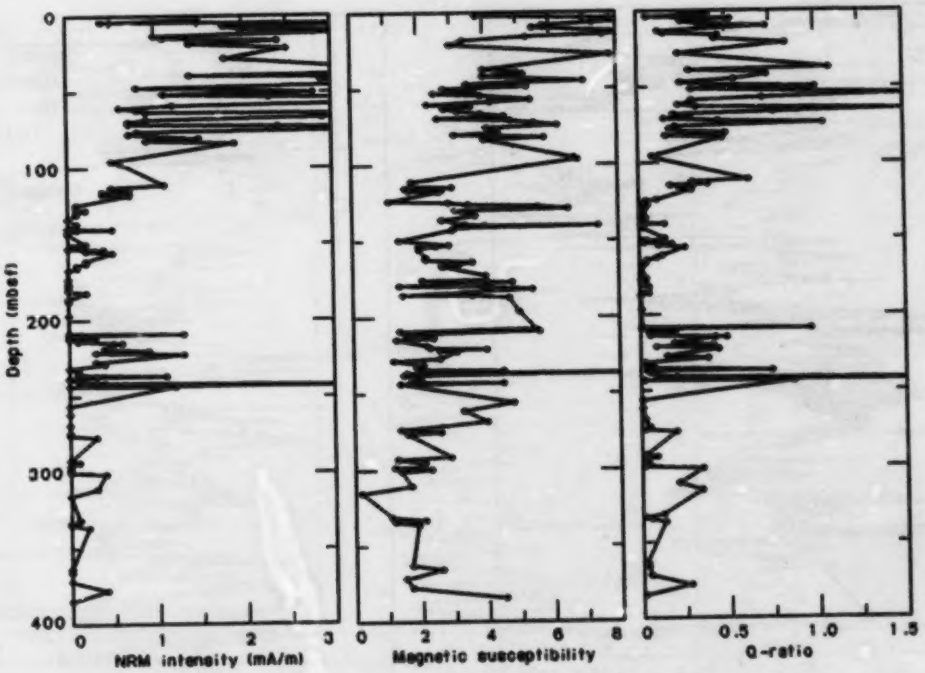

Figure 19. NRM intensity, magnetic susceptibility, and Q-ratio (NRM/susceptibility) for combined discrete samples from Holes 723A and 723B.

Core Orientation

Table 6 shows a comparison of multishot core orientation estimates with estimates obtained by averaging within-core declination values. As at previous sites, there is a notable discrepancy between the two estimates.

Magnetic Susceptibility

The volume magnetic susceptibility of Holes 723A and 723B was measured on a Bartington Magnetic Susceptibility Meter and MS1 sensor. The cores were measured at 5-cm intervals using the low-frequency (0.47 kHz) and high-sensitivity (0.1) settings. We cored Hole 723A with the APC to Core 117-723A-9H (85.1 mbsf) and drilled in the XCB mode from Core 117-723A-10X to -46X (432.3 mbsf). We cored Hole 723B with the APC to Core 117-723B-9H (81.6 mbsf) and with the XCB from Core 117-723B-10X to -44X (429.0 mbsf, core interval 400.1 m). Hole 723C was dedicated to pore-water analyses, so susceptibility was not measured. All cores were measured at 10-cm intervals because of the high accumulation rates expected at this site.

Table 6. Comparison of estimates of core orientation obtained from the multishot with estimates from mean within-core declination data.

Core	Multishot orientation (degrees)	Measured mean declination (degrees)	Corrected mean core declination (degrees)
117-723A-6H	224	199 (N)	335
117-723A-7H	233	10 (N)	137
117-723A-8H	25	354 (N)	329
117-723A-9H	346	239 (N)	253

The susceptibility records from both holes were generally well defined down to Cores 117-723A-6H and 117-723B-6H (~55 mbsf). Below this depth, however, gas expansion tended to disturb the record. To accommodate the shifting of sediment that occurred in these cores during core-splitting procedures, half-round sections rather than whole-round sections were measured below Cores 117-723A-27X and 117-723B-13X. The susceptibility data from half-round sections were multiplied by 2 during data processing so that they would be roughly comparable with the data obtained from whole-round sections. Ultimately, this proved to be a rather fruitless effort since gas expansion also had the effect of decreasing the volume of sediment measured by the susceptibility sensor.

For both holes, the susceptibility record below ~100 mbsf was generally too disturbed and discontinuous to be interpreted reliably, so only the uppermost 100 meters are presented in this report (Figs. 20 and 21). Above 100 mbsf, however, some correlations are possible between Holes 723A and 723B from the Oman margin with Holes 722 and 721 from the Owen Ridge. Detailed interhole correlations based on these data and lithologic marker layers are presented in the "Interhole Correlation" section of this chapter.

The uppermost ~100 meters of the Site 723 holes are roughly correlative with the uppermost ~25 meters of the holes in Sites 722 and 721 (Fig. 22). Despite the differing depositional regimes of the Owen Ridge site (722B) and the Oman margin site (Holes 723A and 723B), the major features of the susceptibility records are generally correlative. The degree of correlation is remarkable considering the fourfold difference in accumulation rates and the broadly different depositional settings. Susceptibility values for Site 723 ranged from ~25 to 100 X 10^{-6} volume SI units, which is somewhat lower than the range observed for the Owen Ridge sites. The lower values at Site 723 may reflect dilution by nonmagnetic terrigenous and/or biogenic components.

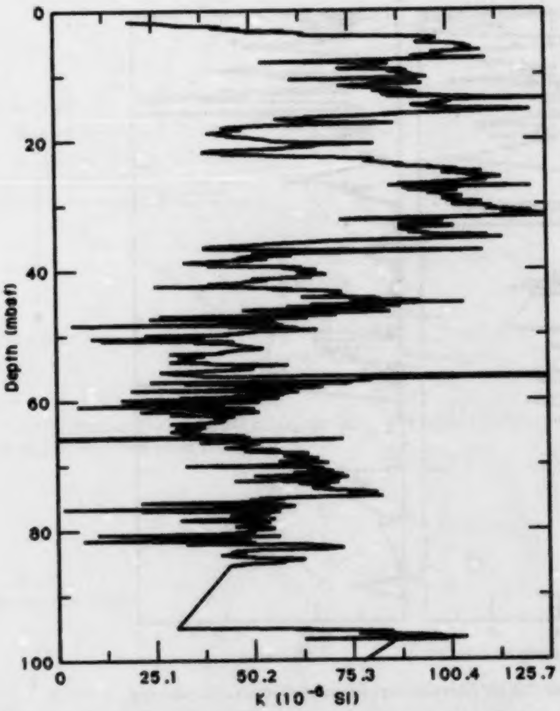

Figure 20. Whole-core magnetic susceptibility for 0 to 100 mbsf, Hole 723A.

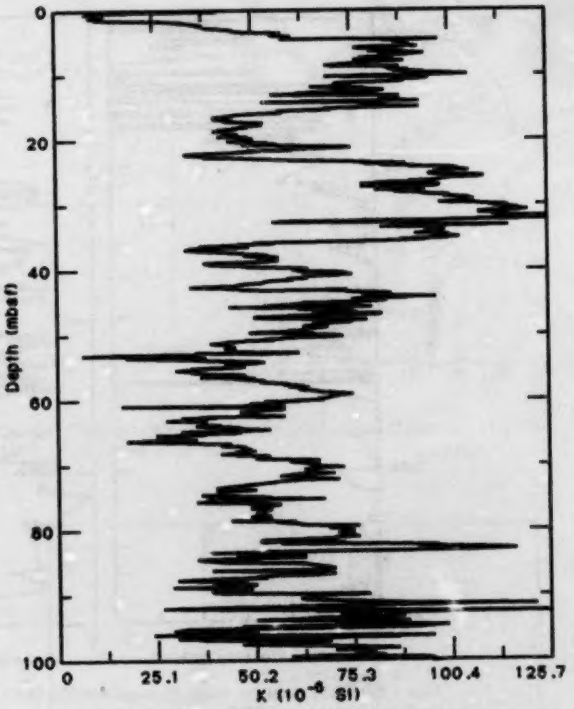

Figure 21. Whole-core magnetic susceptibility for 0 to 100 mbsf, Hole 723B.

It is interesting to consider the differences in susceptibility accumulation between the Owen Ridge and Oman margin sites. Since the susceptibility measurements are volumetrically based, the unit of measurement in SI units is dimensionless. Therefore, to calculate susceptibility accumulation, the data should be multiplied by the applicable sedimentation rates. The susceptibility accumulation rates presented here are calculated for the first major sub-bottom increase in susceptibility for Sites 720, 721, 722, and 723, which is roughly coincident with isotopic Stage 2 at ~18 k.y. For Holes 723A and 723B, this level occurs at ~5 mbsf. These data were compiled from the respective Leg 117 site reports and are shown in Table 7.

These preliminary results suggest that the Indus Fan Site 720 and the Owen Ridge Sites 721 and 722 have very similar susceptibility accumulation rates during this time, whereas the Oman margin Site 723 has nearly twice this rate for the same interval. These preliminary findings may suggest a local and possibly eolian supply of terrigenous ferrimagnetic particles, as was indicated from the X-ray diffraction data of Site 722 (see "Paleomagnetism" section, "Site 722" chapter, this volume). At present, however, the high susceptibility accumulation rate at Site 723 may be either the consequence of local sediment ponding of terrigenous sediments or increased proximity to an eolian source.

ACCUMULATION RATES

Sedimentation rates for Site 723 are based on biostratigraphic datum levels identified in Hole 723A (Table 5). Rates are determined between six datums which are assigned ages based on oxygen isotope stratigraphy (Niitsuma, unpubl. data) or from Berggren et al. (1985; Table 8 and Figs. 23 and 24). Sediments accumulated at Site 723 faster than at any other site cored during Leg 117, with rates ranging from 129 to 240 m/m.y. and a mean of 175 m/m.y. for the last 1.9 m.y. These values are typical of hemipelagic sedimentation and are about five times faster than pelagic accumulation on the Owen Ridge (see "Accumulation Rates" sections, "Site 721," "Site 722," and "Site 731" chapters, this volume).

The mass accumulation of calcium carbonate, organic carbon, and noncarbonate sediment components are calculated from average values between the datum levels (Table 8 and Fig. 24). Total accumulation averages 20 g/cm^2/k.y., with more than one half of this value attributed to calcium carbonate. Since significant detrital calcite was recognized in smear slides (see "Lithostratigraphy" section, this chapter), the accumulation of calcium carbonate has both detrital and pelagic components.

A general decrease in organic carbon accumulation is observed from the late Pliocene to the Holocene at Site 723. The maximum organic carbon accumulation near the Pliocene-Pleistocene boundary (~900 mg C/cm^2/k.y.; Table 8) is more than twice late Pleistocene levels and corresponds to a time when laminae and opaline microfossils were preserved at Site 723. These high values are 20-30 times the accumulation of organic carbon at the Owen Ridge sites.

PHYSICAL PROPERTIES

Introduction

The measurement of physical properties at Site 723 was severely hampered by the abundance of gas and the accompanying sediment expansion and disturbance. Discrete samples were taken from the least disturbed intervals for measurement of index properties (wet-bulk density, porosity, water content, and grain density). Vane shear strength measurements were limited to the APC cores. Compressional-wave velocity measurements

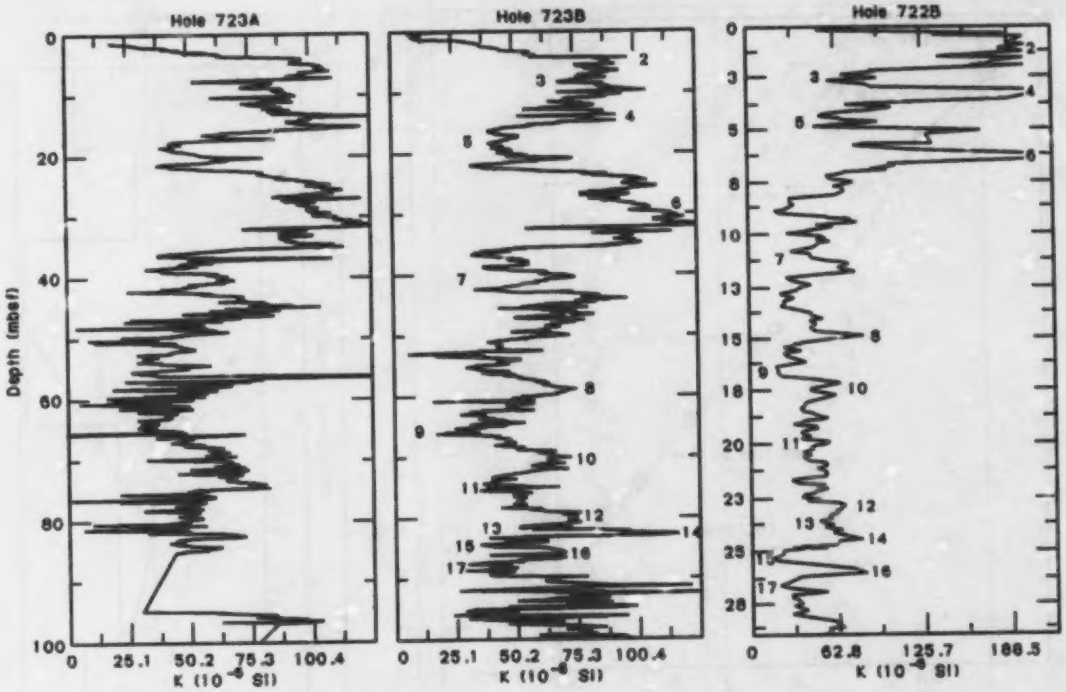

Figure 22. Preliminary correlations between the Oman margin (Holes 723A and 723B) and Owen Ridge (Hole 722B).

Table 7. Preliminary estimates of susceptibility flux, calculated as the product of accumulation rate and dimensionless susceptibility, for Sites 720, 721, 722, and 723.

Site	Accumulation rate (m/Ma)	"Stage 2" susceptibility	Flux
720	30.0	23.0	690
721	43.0	16.0	688
722	47.0	15.5	728
723	185.0	7.1	1313

Note: The Indus Fan (720) and Owen Ridge (721 and 722) sites have comparable susceptibility fluxes, whereas the Oman margin (723) site is more than twice this value.

in the Hamilton Frame were only successful in the indurated dolomites of Facies II.

Wet-bulk density and compressional-wave velocity were measured on the least disturbed, most coherent, whole-round core sections in the GRAPE and *P*-wave logging systems. Only those cores from the upper 50 m of each hole, however, yielded reliable data. All techniques and equipment used are described in the "Explanatory Notes" (this volume).

Index Properties

Throughout Holes 723A and 723B the index properties of the sediments display trends with depth that are controlled not only by increasing overburden pressures but also by changes in sediment composition (Fig. 25). The entire section at Site 723 is characterized by relatively low wet-bulk and grain densities because of the high organic carbon content that averages 2.5% in the upper 200 m of the section and 4.5% in the remainder of the drilled sequence.

In the uppermost portion of the foraminifer-bearing marly nannofossil ooze and calcareous clayey silts in Facies I, porosity and water content averages decrease relatively rapidly from 66% and 42%, respectively, near the seafloor to 56% and 30%, respectively, at 195 mbsf. The average wet-bulk density increases from 1.65 to 1.75 g/cm^3 over this interval, in response to the decreasing water content. The bulk densities also show considerable variation that is attributable to changes in grain density.

Table 8. Sedimentation and accumulation rate data for the top 330 m of Site 723.

Depth interval (mbsf)	Age range (m.y.)	$CaCO_3$ ($\overline{X}$%)	C_{org} ($\overline{X}$%)	Dry-bulk density ($\overline{X}$g/cm^3)	Sed. rate ($\overline{X}$m/m.y.)	$CaCO_3$ acc. rate (g/cm^2/k.y.)	Non-$CaCO_3$ acc. rate (g/cm^2/k.y.)	C_{org} acc. rate (mg/cm^2/k.y.)
0-35.6	0-0.19	52.6	2.76	0.924	187.4	9.11	8.21	477.9
35.6-74.2	0.19-0.49	61.1	2.57	1.035	128.7	8.14	5.18	342.3
74.2-153.3	0.49-0.82	60.2	2.68	1.064	239.7	15.35	10.15	683.5
153.3-247.6	0.92-1.45	55.6	3.27	1.143	149.7	9.51	7.60	559.5
247.6-286.5	1.45-1.66	55.2	4.2	1.106	185.2	11.31	9.18	860.3
286.5-331.9	1.66-1.9	56.3	4.43	1.089	189.2	11.60	9.00	912.8

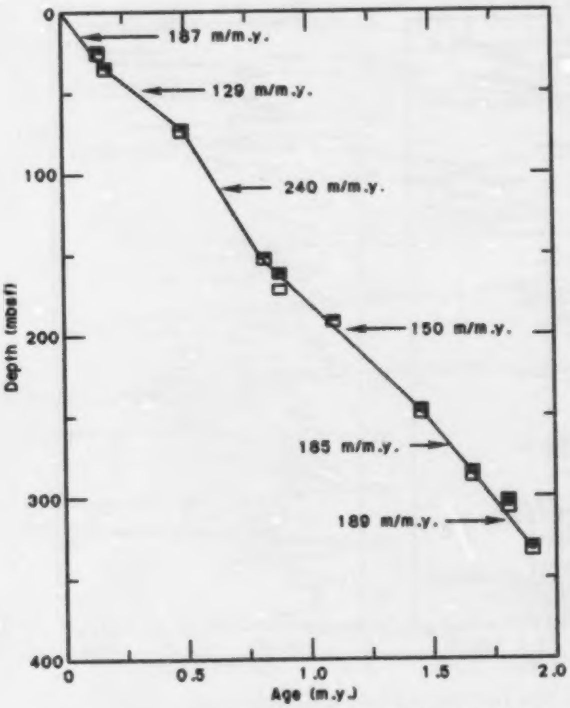

Figure 23. Age-depth plot of stratigraphic datums listed in Table 5. The filled and open boxes are the upper and lower depths of each datum level, respectively. Indicated sedimentation rates are calculated between reliable datum levels.

Grain densities vary from a minimum of 2.267 g/cm^3 in a diatom-rich layer (Facies II) in Core 117-723B-18X to a maximum of 2.648 g/cm^3 in Core 117-723A-4H, but they average 2.50 g/cm^3. Varying concentrations of calcium carbonate and organic carbon are most likely responsible for the variation in grain density through this interval (Fig. 26).

Between 195 and 270 mbsf calcium carbonate decreases and organic carbon increases in abundance, and the porosity and water content are relatively constant at 56% and 32%, respectively. Wet-bulk density decreases from 1.75 to 1.70 g/cm^3 over this interval in response to a continuous decrease in grain density from 2.60 to 2.40 g/cm^3 that is associated with an increase in the abundance of radiolarians and diatoms (see "Biostratigraphy" section, this chapter). This portion of the section also shows a distinctly higher average organic carbon content (4.5%) than the overlying sequence (2.5%).

In the interval from 270 to 340 mbsf, the average values of water content and porosity increase slightly with depth (i.e., from 54% to 62% and from 32% to 40%, respectively). Local maxima in porosity and water content of 63% and 40%, respectively, occur coincidently with an increase in calcium carbonate content to 70% near 280 mbsf (Figs. 25 and 26). Average values of wet-bulk density increase slightly from 270 to 340 mbsf, but individual values vary widely. Grain densities vary widely in response to fluctuations in the abundance of radiolarians and diatoms and are primarily responsible for controlling variations in bulk density.

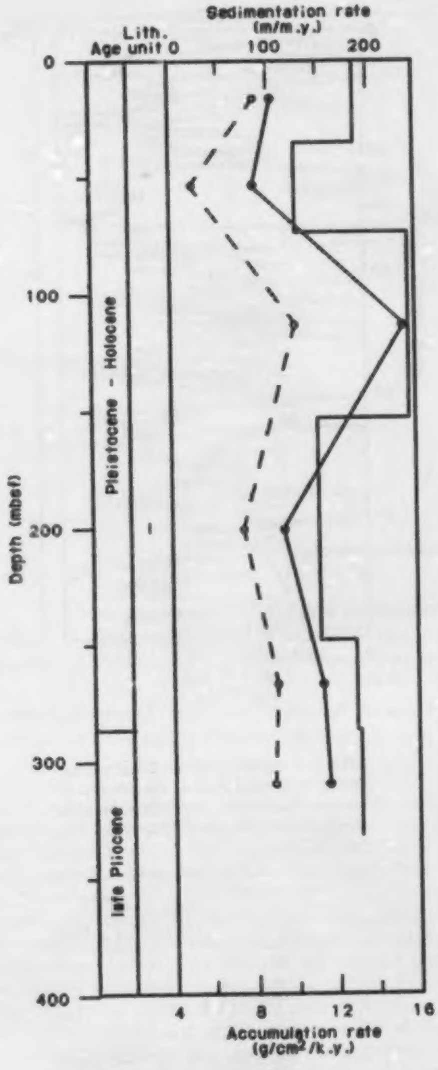

Figure 24. Sedimentation rate (m/m.y.; solid line), calcium carbonate accumulation rate (g/cm^2/k.y.; dots), and noncarbonate accumulation rate (g/cm^2/k.y.; circles) vs. depth (mbsf) at Site 723. Accumulation rates are plotted at the midpoint of the respective depth intervals.

Throughout the basal sequence (360–410 mbsf), continuous decreases in wet-bulk density (from 1.75 to 1.50 g/cm^3) and in grain density (from 2.55 to 2.20 g/cm^3) reflect a marked increase in the occurrence of radiolarians and diatoms. The gradual increase in porosity and water content throughout this interval can be attributed to the more open sediment fabric created by the occurrence of abundant siliceous microfossils.

The wet-bulk density of four samples of dolomites of Facies II from Holes 723A and 723B were measured using 2-min GRAPE counts (Table 9). Wet-bulk densities of these samples ranged from 2.71 to 2.77 g/cm^3.

Compressional-Wave Velocity

Compressional-wave velocities were measured on four dolomite samples from Holes 723A and 723B (Table 9). Velocities

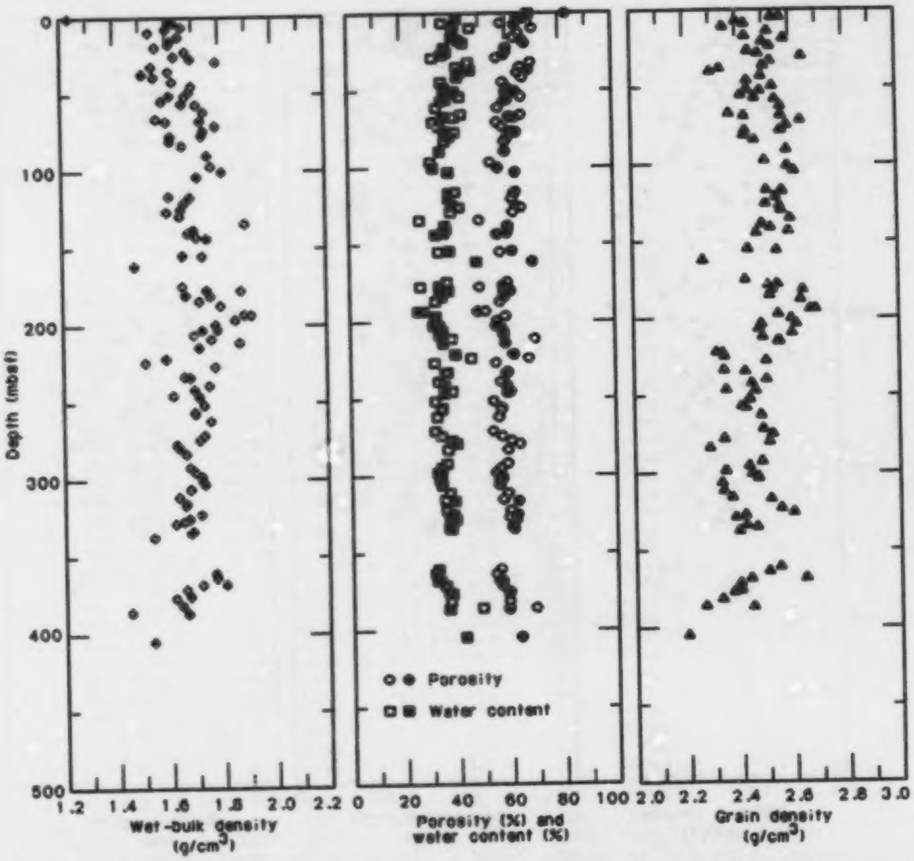

Figure 25. Index properties (wet-bulk density, porosity, water content, and grain density) measured on discrete samples from Holes 723A (open symbols) and 723B (solid symbols). Values are not corrected for sediment expansion.

perpendicular to bedding ranged from 4467 to 5383 m/s. Velocities parallel to bedding averaged 9% higher than those perpendicular to bedding, ranging from 4944 to 5560 m/s.

GRAPE and *P*-Wave Logs

Acquisition of continuous GRAPE and *P*-wave logs at Site 723 was limited by gas-induced sediment expansion. Useful GRAPE records were obtained for the intervals cored with the APC (Cores 117-723A-1H through -9H and Cores 117-723B-1H through -9H). Accurate wet-bulk-density determination by the GRAPE was limited to Cores 117-723A-1H to -4H (0–36.8 mbsf) and Cores 117-723B-1H to -5H (0–42.9 mbsf).

A comparison of GRAPE records and measurements on discrete samples indicates that below 36.8 mbsf in Hole 723A and below 42.9 mbsf in Hole 723B GRAPE density is less than the actual wet-bulk density (Fig. 27), probably as a consequence of small, expansion-related fractures. In the intervals where density is reduced by expansion, a high-frequency variation is superimposed on the records, but the overall character of the profiles remains the same. The pattern that is displayed in the profiles is a cyclic variation with cycles on the order of 5-m thick. This pattern is similar to that of GRAPE records at Sites 721 and 722, except that cycles of density variation at those sites are 1–2 m thick.

We obtained *P*-wave logs only for Cores 117-723A-1H through -3H (0–27.1 mbsf) and Cores 117-723B-1H through -4H (0–33.3 mbsf); these data are presented in Figure 28. Below these intervals, *P*-wave transmission through the cores was inhibited by the lack of coupling of the sediment and the core liner. The *P*-wave velocity is positively correlated to the density determined by the GRAPE, and the logs display a pattern of cyclic variation similar to that of the GRAPE data. The velocity determined by the *P*-wave logger ranges from 1535 to 1620 m/s. This range is comparable with velocities determined for sediments of equivalent depth at Owen Ridge, Sites 721 and 722.

Vane Shear Strength

The extreme sediment disturbance caused by expansion of gas during recovery rendered most of the sediments from Site 723 unsuitable for vane shear strength measurements. Six measurements were made in Cores 117-723A-1H through -9H (Table 9). No correlation is seen between sub-bottom depth and increasing shear strength, perhaps due to the gas-induced sediment disturbance.

In Hole 723B one vane measurement was taken in each of Cores 117-723B-1H through -6H (Table 9). Shear-strength values increased from 7.1 kPa in Core 117-723B-1H (3.60 mbsf) to 45.4 kPa in Core 117-723B-6H (50.90 mbsf).

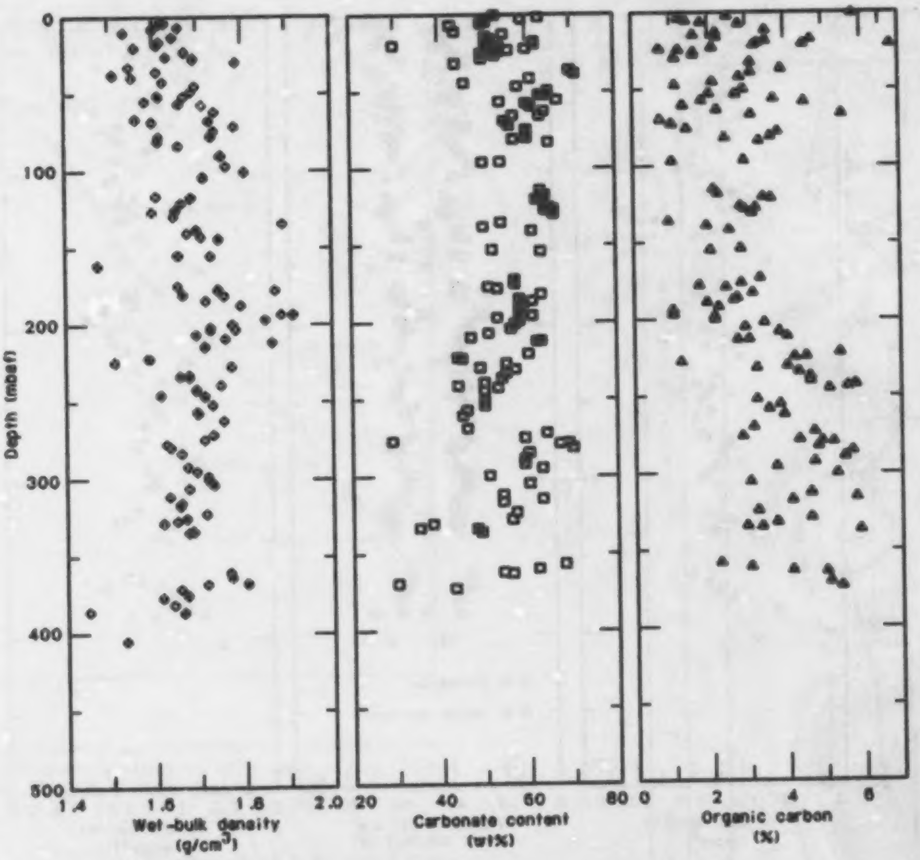

Figure 26. Wet-bulk density for Holes 723A (open symbols) and 723B (solid symbols), and calcium carbonate and organic carbon percentages for Hole 723A. All measurements were made on discrete samples.

SEISMIC STRATIGRAPHY

General Setting

Site 723 is located in the western slope basin of the Oman margin. This slope basin is not a basin from the standpoint of submarine topography, however. The continental slope dips seaward at an angle of 1°-2° throughout, and slopes are much steeper on the eastern flanks of the two basement highs that confine the slope basin (Fig. 29).

A seismic dip section across the slope basin shows a synclinal morphology of seismic horizons. This morphology arises from two sources: (1) normal faulting at boundary faults that separate the slope basin from the adjacent basement highs, and (2) a greater thickness of the seismic units in the center of the basin, with an onlap of seismic horizons toward both basement highs.

Based on lateral variations in traveltime between reflector pairs, the highest sedimentation rates have occurred very near the central axis of the slope basin down to at least 1 s sub-bottom traveltime, the limit of our seismic penetration.

As seen on a dip line, Site 723 is located on the central axis of the slope basin (Fig. 29). This location implies that the site has sampled the most continuous and highest sedimentation rates within the portion of the basin traversed by the dip line. On a strike line (Fig. 30), the site is also near the portion with the highest sedimentation rates; the visible section of the sub-basin thins substantially toward the northeast. Three other sites are located in the slope basin. Site 724 also is located along the central axis of the sub-basin, far to the northeast where average accumulation rates are about half those at Site 723. Site 725 is located near Site 724 but on the northwest flank of the sub-basin. Site 727 is located near the central axis of the sub-basin to the southwest of Site 723, where sedimentation rates are about 50% of those at Site 723.

Relative to the flanking basement highs, the western basin has been rapidly subsiding since at least 2 Ma. Sedimentation probably has kept up with subsidence and to some extent has isostatically driven this subsidence, so that the graben structure has maintained a seaward slope of the seafloor and has seldom, if ever, been topographically a basin during the last 2 m.y. This conclusion is based largely on the fact that seismic sequences thin but continue over the southeastern basement high. Some sudden truncation of reflectors against this basement high is possible, which would indicate that basement was occasionally a topographic high; however, such truncation, if present, is below the resolution of our seismic data.

If the southeast ridge was a topographic high for a significant period of time, then the location of thickest sediment accumulation might be expected to be near the ridge, at the downslope edge of the sub-basin. Instead, the currently deepest portion of each visible horizon deeper than the Site 723 penetration is immediately below Site 723. In contrast, from the base of Site 723 up to the seafloor, the axis of the depositional syncline mi-

Table 9. Physical properties summary for Holes 723A and 723B.

Core, sample, interval (cm)	Depth (mbsf)	Wet-bulk density (g/cm^3)	Porosity (%)	Water content (%)	Grain density (g/cm^3)	Dry-bulk density (g/cm^3)	Velocity (m/s)	Vane shear strength (kPa)
117-723-								
1H-1, 50-52	0.50	1.233	82.7	68.7	1.858	0.386		
1H-3, 50-52	3.50	1.628	66.8	42.0	2.568	0.944		
1H-5, 50-52	6.50	1.659	58.4	36.1	2.403	1.060		
1H-6, 5-7	7.55							15.2
2H-2, 50-52	9.80	1.536	70.0	46.7	2.353	0.819		
2H-4, 50-52	12.80	1.646	64.8	40.4	2.520	0.982		
2H-6, 50-52	15.80	1.616	63.0	39.9	2.436	0.971		
2H-7, 33-35	17.13							46.1
3H-2, 50-52	19.50	1.560	67.1	44.0	2.501	0.873		
3H-4, 50-52	22.50	1.673	60.2	36.9	2.529	1.056		
3H-6, 50-52	25.50	1.631	60.0	37.7	2.446	1.016		
3H-7, 15-17	26.65							21.9
4H-2, 50-52	29.10	1.788	56.6	32.4	2.648	1.208		
4H-4, 50-52	32.10	1.547	69.4	46.0	2.530	0.836		
4H-6, 50-52	35.10	1.609	65.3	41.5	2.504	0.941		
5H-2, 50-52	38.80	1.553	64.4	42.5	2.303	0.893		
5H-4, 50-52	41.80	1.623	66.2	41.8	2.495	0.945		
5H-6, 50-52	44.80	1.696	58.9	35.6	2.442	1.092		
6H-2, 50-52	48.40	1.686	60.3	36.6	2.536	1.069		
6H-4, 50-52	51.40	1.670	59.8	36.7	2.490	1.057		
6H-6, 50-52	54.40	1.582	65.4	42.4	2.418	0.912		
7H-2, 45-47	56.96	1.711	59.3	35.5	2.545	1.104		
7H-5, 50-52	61.51	1.739	56.8	33.5	2.565	1.157		
7H-8, 52-54	66.03	1.561	65.3	42.8	2.373	0.893		30.4
8H-2, 50-52	67.80	1.598	62.8	40.2	2.429	0.955		
8H-4, 50-52	70.80	1.783	56.3	32.3	2.640	1.207		
8H-6, 50-52	73.80	1.737	58.4	34.4	2.588	1.139		22.8
9H-2, 50-52	77.40	1.613	63.4	40.3	2.432	0.963		
9H-4, 50-52	80.40	1.611	60.3	38.4	2.425	0.993		
9H-6, 50-52	83.40	1.657	59.1	36.6	2.466	1.051		40.4
11X-2, 50-52	96.80	1.764	53.5	31.1	2.504	1.215		
13X-2, 50-52	116.10	1.606	63.0	40.2	2.509	0.960		
13X-5, 50-52	120.60	1.662	61.5	37.9	2.543	1.032		
14X-2, 91-93	126.21	1.596	64.9	41.7	2.558	0.930		
14X-4, 90-92	129.20	1.645	61.9	38.5	2.563	1.011		
15X-1, 88-90	134.28	1.891	49.2	26.7	2.597	1.386		
15X-5, 80-82	140.20	1.675	59.9	36.6	2.523	1.062		
15X-7, 28-30	142.68	1.707	59.5	35.7	2.590	1.097		
17X-2, 60-62	154.90	1.728	56.8	33.7	2.544	1.145		
19X-2, 78-80	174.38	1.653	59.4	36.8	2.426	1.045		
19X-4, 90-92	177.50	1.873	49.0	26.8	2.509	1.371		
19X-6, 127-129	180.87	1.757	58.2	34.0	2.642	1.160		
20X-2, 80-82	184.10	1.716	58.2	34.7	2.516	1.120		
20X-4, 80-82	187.10	1.795	56.6	32.3	2.633	1.214		
21X-2, 30-32	193.20	1.886	51.2	27.8	2.689	1.362		
21X-4, 65-67	196.55	1.850	58.7	32.5	2.548	1.249		
21X-6, 60-62	199.50	1.776	55.5	32.0	2.597	1.208		
22X-2, 20-22	202.80	1.783	55.0	31.6	2.615	1.219		
22X-4, 59-61	206.19	1.694	57.8	35.0	2.475	1.101		
22X-6, 16-18	208.76	1.760	57.9	33.7	2.599	1.167		
23X-3, 8					2.552			
23X-1, 50-52	211.30	1.866	69.5	38.2	2.488	1.154		
24X-1, 82-84	221.22	1.587	61.3	39.6	2.313	0.958		
24X-3, 37-39	223.77	1.510	67.2	45.6	2.342	0.822		
24X-5, 32-34	226.72	1.773	54.8	31.7	2.500	1.212		
25X-2, 127-129	232.87	1.657	59.3	36.6	2.341	1.050		
25X-6, 120-122	238.80	1.749	56.6	33.1	2.501	1.169		
26X-4, 97-99	245.27	1.613	60.1	38.2	2.349	0.997		
27X-2, 65-67	251.55	1.730	53.8	31.9	2.437	1.179		
27X-5, 67-69	256.07	1.695	56.9	34.4	2.407	1.112		
27X-6, 11-13	257.01	1.697	56.7	34.2	2.422	1.117		
28X-2, 124-126	261.84	1.755	55.7	32.5	2.479	1.185		
29X-2, 68-70	270.88	1.731	53.5	31.7	2.487	1.183		
29X-4, 98-100	274.18	1.711	56.8	34.0	2.521	1.129		
29X-6, 94-96	277.14	1.625	60.2	38.0	2.340	1.007		
30X-1, 91-93	279.21	1.635	63.4	39.8	2.508	0.985		
30X-4, 24-26	283.04	1.659	59.0	36.4	2.285	1.055		
31X-3, 94-96	291.84	1.673	58.8	36.0	2.481	1.071		
31X-5, 95-97	294.85	1.693	56.2	34.0	2.432	1.117		
31X, CC, 56-58	297.90	1.719	54.5	32.5	2.344	1.161		
32X-2, 98-100	299.98	1.719	56.6	33.7	2.441	1.139		
32X-4, 78-80	302.78	1.729	56.0	33.2	2.466	1.155		
32X-6, 78-80	305.78	1.675	55.6	34.0	2.329	1.105		
33X-3, 91-93	311.01	1.631	58.9	37.0	2.335	1.027		
33X-6, 64-66	315.24	1.658	57.0	35.2	2.367	1.073		
35X-1, 75-77	322.25	1.714	59.7	35.7	2.551	1.102		

Table 9 (continued).

Core, sample, interval (cm)	Depth (mbsf)	Wet-bulk density (g/cm^3)	Porosity (%)	Water content (%)	Grain density (g/cm^3)	Dry-bulk density (g/cm^3)	Velocity (m/s)	Vane shear strength (kPa)
117-723- (Cont.)								
35X-4, 72–74	326.72	1.648	59.3	36.9	2.416	1.040		
36X-2, 60–62	328.19	1.617	61.7	39.1	2.379	0.986		
36X-6, 69–71	334.28	1.674	60.9	37.3	2.459	1.050		
37X-1, 116–118	336.96	1.536	65.5	43.7	2.392	0.866		
39X-4, 75–77	360.25	1.767	55.7	32.3	2.545	1.197		
39X-6, 73–75	363.23	1.770	54.0	31.3	2.503	1.217		
40X-3, 4–6	367.74	1.715	55.1	32.9	2.434	1.150		
40X-5, 20–22	370.90	1.655	56.3	34.9	2.394	1.078		
41X-2, 76–78	376.56	1.614	58.7	37.3	2.369	1.013		
41X-5, 86–88	381.16	1.639	58.8	36.8	2.325	1.036		
42X-2, 3–5	385.53	1.448	68.9	48.8	2.263	0.742		
45X, CC, 10–12	413.10	2.766					^{a}5383	
45X, CC, 10–12	413.10						^{b}5560	
117-723B-								
1H-3, 60–62	3.60	1.616	64.5	40.9	2.537	0.956		7.1
2H-3, 50–52	7.80	1.601	63.5	40.6	2.434	0.950		18.2
3H-3, 60–62	17.60	1.611	66.2	42.1	2.582	0.932		20.0
4H-3, 50–52	27.10	1.692	59.3	35.9	2.485	1.085		18.5
5H-3, 60–62	36.90	1.509	68.5	46.5	2.340	0.807		25.4
6H-6, 50–52	50.90	1.612	63.5	40.4	2.442	0.961		45.4
7H-3, 50–52	56.10	1.658	60.3	37.2	2.469	1.041		
8H-4, 60–62	67.40	1.726	61.0	36.2	2.567	1.100		
9H-4, 50–52	76.90	1.731	62.2	36.8	2.566	1.094		
10X-6, 80–82	89.90	1.751	59.2	34.6	2.587	1.145		
11X-7, 30–32	100.50	1.805	56.4	32.0	2.590	1.228		
12X-3, 50–52	103.64	1.712	62.9	37.7	2.614	1.067		
13X-5, 60–62	116.90	1.685	62.3	37.9	2.568	1.046		
14X-4, 50–52	124.90	1.650	62.9	39.1	2.506	1.006		
15X-6, 90–92	138.00	1.697	50.0	36.2	2.492	1.083		
16X-3, 141–143	143.61	1.746	55.8	32.7	2.470	1.175		
17X-4, 100–102	154.40	1.654	61.3	37.9	2.438	1.026		
18X-2, 132–134	161.42	1.474	69.0	48.0	2.267	0.767		
19X-6, 134–136	177.04	1.744	57.8	33.9	2.546	1.152		
20X-2, 88–90	180.28	1.664	60.6	37.3	2.526	1.042		
21X-4, 137–139	193.47	1.912	48.3	25.9	2.670	1.417		
22X-4, 112–114	202.92	1.726	56.6	33.6	2.485	1.146		
23X-5, 123–125	214.13	1.713	58.4	34.9	2.545	1.115		
24X-4, 55–57	221.55	1.589	61.6	39.7	2.336	0.958		
25X-5, 133–135	233.53	1.678	58.7	35.8	2.421	1.077		
26X-4, 106–108	241.46	1.694	58.7	35.5	2.445	1.092		
27X-1, 50–52	246.10	1.712	59.2	35.4	2.459	1.106		
27X, CC, 16–18	247.16	2.771					^{a}5131	
27X, CC, 16–18	247.16						^{b}5541	
31X-6, 73–75	301.93	1.727	56.7	33.6	2.465	1.147		
33X-3, 22–24	316.22	1.655	62.6	38.8	2.512	1.014		
33X, CC, 28–30	317.10	2.712					^{a}4650	
33X, CC, 28–30	317.10						^{b}5285	
35X-2, 92–94	325.12	1.669	62.2	38.1	2.598	1.033		
36X-1, 76–78	333.26	1.683	60.3	36.7	2.419	1.066		
39X-5, 2–4	367.62	1.806	56.1	31.8	2.641	1.232		
40X-3, 80–82	375.10	1.670	58.9	36.1	2.396	1.067		
40X, CC, 31–33	376.79	2.726					^{a}4467	
40X, CC, 31–33	376.79						^{b}4944	
41X-4, 67–69	386.17	1.661	58.6	36.2	2.443	1.061		
42X-3, 115–117	404.45	1.531	63.2	42.3	2.196	0.883		

[a] Velocity measurement perpendicular to bedding.
[b] Velocity measurement parallel to bedding.

grates to a position about halfway between the site and the southeast basement high. This migration does not imply any change in the subsidence pattern. If future deposition continues to be highest in the center of the basin, the associated differential subsidence will cause the axis of the present upper portion of the syncline to migrate to the center of the basin, to a position concordant with the maximum sedimentation rate. From the seismic section across Site 723, we can infer only relative subsidence within the basin and with respect to flanking basement highs. We can draw no conclusions concerning the amount of absolute subsidence of the entire region.

On the seismic lines crossing Site 723 (Figs. 29 and 30), we can see that the sediment section is almost devoid of faults, except for the major normal faults on the flanks. These two faults are not imaged well on the unmigrated sections. A single small-offset reverse fault may be present just below Site 723. The reversed nature of this possible fault does not require horizontal compression; indeed, a strong dominance of horizontal extension is implied by the thinning of both faulted and overlying seismic sequences away from the axis of the depositional syncline. Instead, the reversed fault is probably caused by slight differential subsidence of the northwestern portion of the basin.

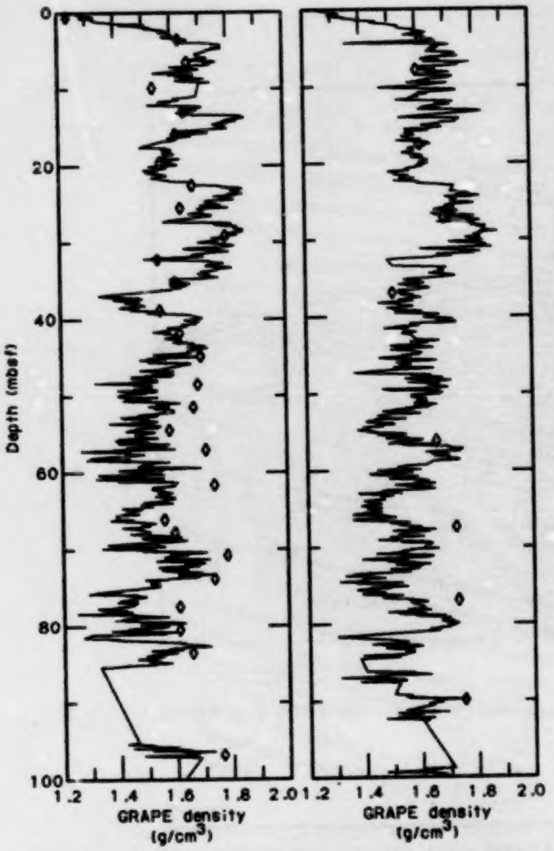

Figure 27. GRAPE wet-bulk density (solid line) and wet-bulk density from discrete samples (diamonds) for Holes 723A and 723B. GRAPE profile is based on 10-cm-block averages of the data.

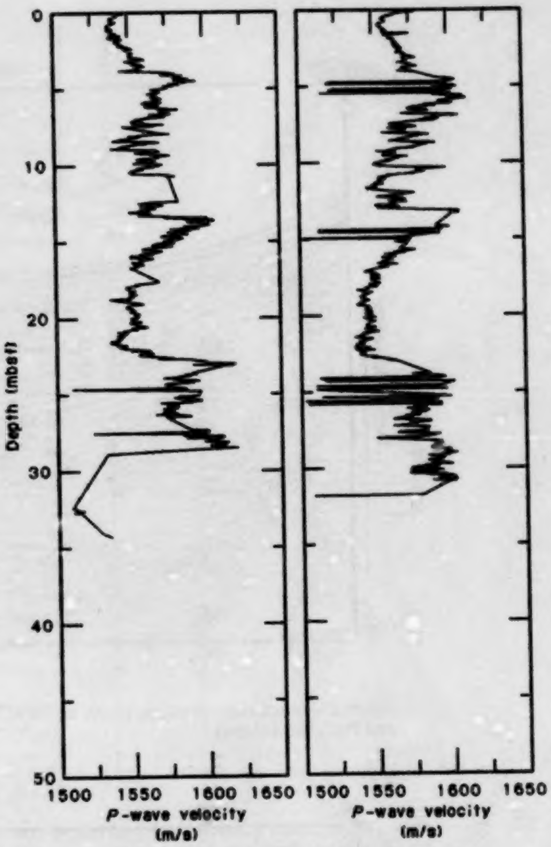

Figure 28. Compressional-wave velocity as measured by the *P*-wave logger in Cores 117-723A-1H to -3H and Cores 117-723B-1H to -4H.

The reversed fault dies out upsection just below the deepest portion of Site 723; it was active, therefore, ∼2.5 Ma. This fault is a possible conduit for the advecting fluids hypothesized on the basis of pore fluid geochemistry, hydrocarbon type, and downhole logging (see "Inorganic Geochemistry," "Organic Geochemistry," and "Downhole Measurements" sections, this chapter). However, the offset on this suspected fault is too small for confirmation of the fault's existence.

Relation of Seismic Traveltime to Core Depth

Both sonic velocity and density logs were obtained for Site 723. Reliable velocity log data extend from 97.5 to 413.8 mbsf; reliable density log data extend from 88.4 to 425.5 mbsf. We estimated sonic velocities for 413.8 to 424.4 mbsf, based on resistivity for this depth interval and a regression of sonic traveltime on resistivity ($r = -0.677$) from the overlying interval (372.0–413.8 mbsf).

Continuous sonic and density logs for the interval from 97.5 to 424.4 mbsf were used to calculate a synthetic seismogram for Site 723. A convolutional model with interbed multiples was used. The wavelet was estimated from *Conrad* profiles from the same site survey cruise as the profiles of Figures 29 and 30 (see "Site 720" chapter, this volume). A synthetic seismogram calculated with the sonic log and a constant-density assumption was almost identical to the one based on both sonic and density logs. No reliable velocity information is available from the top 88.4 m of Site 723. Thus, when comparing the synthetic seismogram to the seismic section, the starting time of the synthetic must be based on character correlation between seismic and synthetic.

Figure 31 compares the synthetic seismogram from Site 723 with a single expanded seismic trace and the portion of Figure 29 approaching the site. The single seismic trace is a 10-trace mix centered at the site. The single trace and seismic section are from the same *Conrad* seismic line. The single trace is more useful for a direct comparison to the synthetic seismogram because it includes both peaks and troughs. The adjacent seismic section provides complementary information concerning lateral variability of reflector strength. The amplitudes of the synthetic seismogram and seismic trace are individually scaled to the largest peak or trough. Thus, the much lower plot amplitudes in the correlated portion of the seismic section compared with the synthetic seismogram are not significant. This difference arises simply from the fact that only the seismic trace encompasses the very high-amplitude seafloor return. Relative amplitudes and character within each trace are unaffected by the scaling.

Pronounced spikes are evident on the relative impedance log of Figure 31. These spikes are much more obvious on the sonic and density logs (see below) because the latter logs are closely sampled at 0.15-m depth increments, while the impedance log is an integrated record more coarsely sampled at a 0.002-s incre-

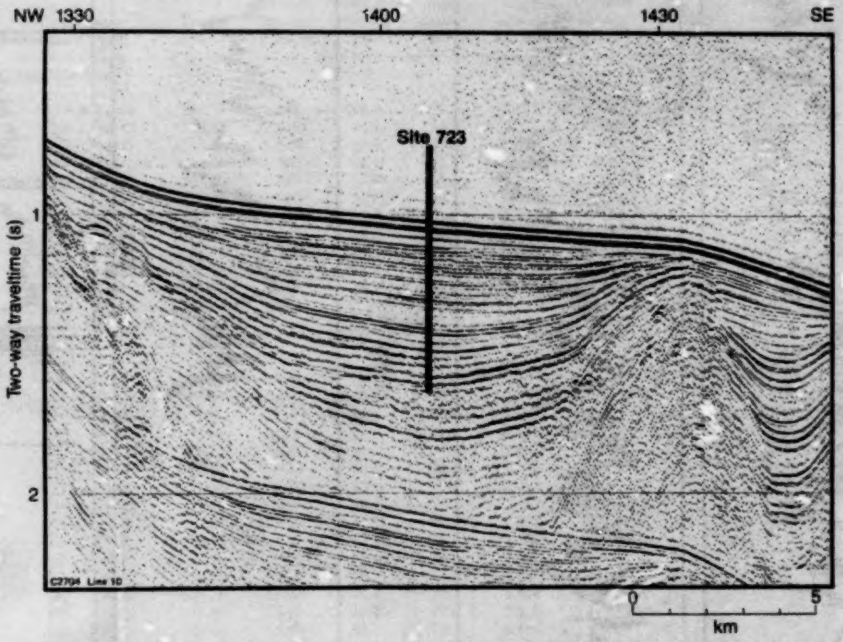

Figure 29. Seismic line 10 of site survey cruise RC2704, showing a dip section across Site 723 (Mountain and Prell, this volume).

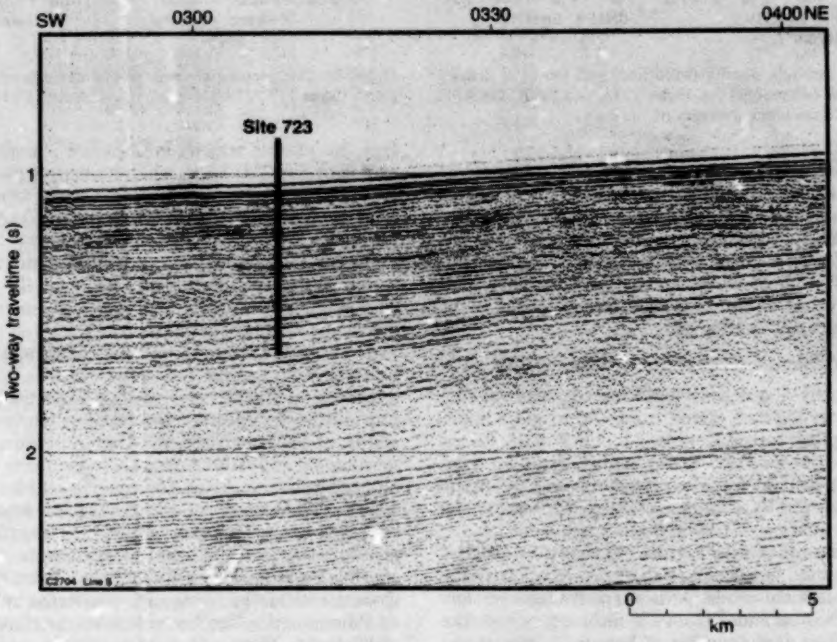

Figure 30. Seismic line 5 of *Robert Conrad* site survey cruise RC2704, showing a strike section across Site 723.

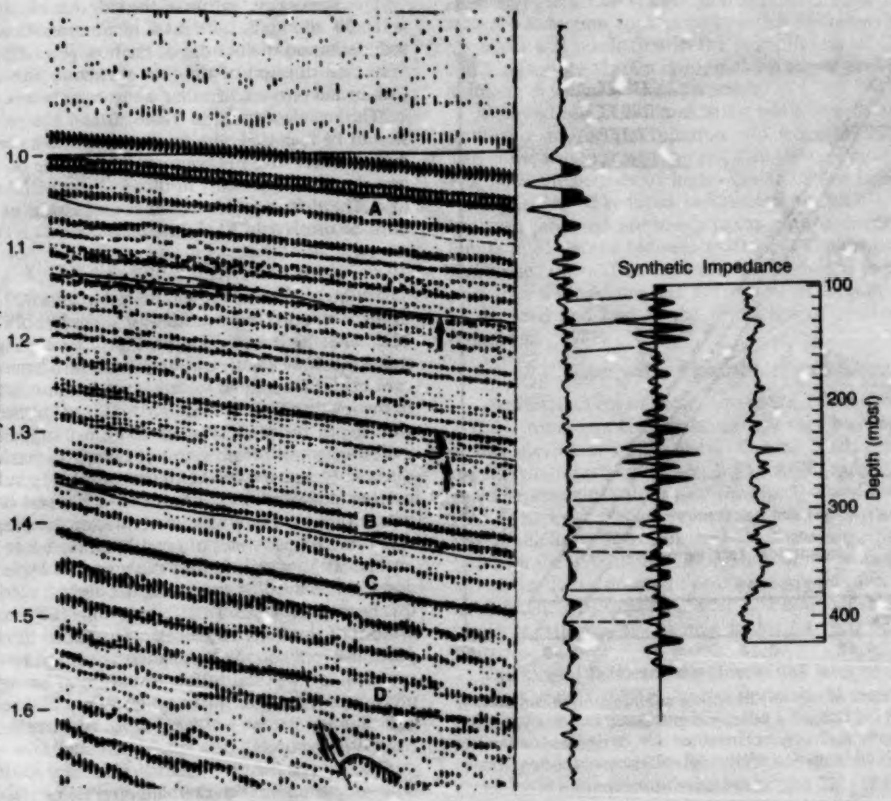

Figure 31. Synthetic seismogram for Site 723, based on sonic and density logs, and correlated with both the seismic trace nearest the site and seismic line 10. The vertical axis of all three is two-way traveltime; a depth scale for the site is shown at right.

ment. These thin spikes are 0.5–2.0-m-thick dolomite beds, with a much higher velocity and density than the surrounding sediments. The thinnest beds are invisible to seismic, because reflection coefficients at the top and bottom of each bed are nearly identical but opposite in sign, and the seismic traveltime between the two reflection coefficients is extremely short in comparison to the frequency of the wavelet.

Only the dolomite bed at 244 mbsf obviously produces a substantial seismic reflector, and this reflector is created as much by the possibly spurious 7-m-thick zone of increasing velocities toward the dolomite bed (Fig. 48) as by the dolomite bed itself. The correlative portion of the seismic trace has much lower relative amplitudes than does the synthetic, indicating that the 244-mbsf dolomite horizon is undetected or only faintly detected by the seismic line.

This difference probably has two causes:

1. The existence of a seismic Fresnel zone is not modeled in a 1-D synthetic seismogram, so the actual vertical resolution of seismic data is slightly lower than implied by a 1-D synthetic.
2. The dolomite beds may lack lateral continuity, based on their inconsistent detection in the A and B holes and on the lack of evidence for permeability barriers to compaction (see "Lithostratigraphy" and "Downhole Measurements" sections, this chapter).

With the exception of the 244-mbsf "reflector," a reasonably good character match exists between the synthetic seismogram and seismic trace.

Only in the bottom-most portion of the synthetic seismogram is the correlation with seismic tenuous. For most of the interval from 97.5 to 390 mbsf, core depths can be matched to seismic traveltime with moderate confidence.

The most distinctive seismic reflector peaks at Site 723 are at 1.18 s (122 mbsf), 1.42–1.43 s (312–330 mbsf), and 1.49 s (382 mbsf). The doublet of peaks at 1.42–1.43 s corresponds to the base of a laminated unit and to the top of a unit rich in siliceous material. This horizon can be traced to the northwest on Figure 29 and identified as approximately the first horizon deposited after abandonment of a small feeder channel once active at the base of the northwest basement high. The channel probably carried sediments from the shallower northeast part of the subbasin down along the base of the basement high. The peak at 1.18 s results from a porosity decrease and is not clearly related to any lithologic change. The peak at 1.49 s, along with the trough just above it, is associated with a zone from 352 to 395 mbsf of rapidly increasing porosity downhole, due to a high organic content and, in particular, to a high siliceous content.

The traveltime/depth relationship of Figure 31 is shown in crossplot form in Figure 32. Also shown is a similarly determined time/depth curve for Site 728, the only other Oman mar-

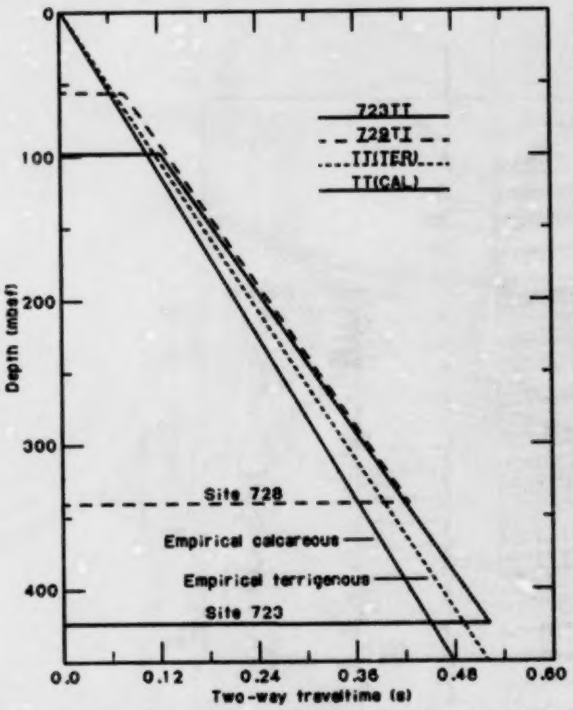

Figure 32. Four plots of two-way traveltime as a function of sub-bottom depth, based on the following velocity/depth functions: Site 723 sonic log, Site 728 sonic log, empirical relation for terrigenous sediments (Hamilton, 1979), and empirical relation for calcareous sediments (Hamilton, 1979).

gin site that was logged. The two curves are almost identical, and both indicate significantly slower velocities than the empirical trends for terrigenous and calcareous sediments of Hamilton (1979). However, some caution is needed when applying the Site 723 and 728 curves to other Oman margin sites. The Site 723 curve is slowed substantially with respect to empirical trends by the very high organic matter throughout the site, higher than at any of the other Oman margin sites. In contrast, the Site 728 curve is slowed by the presence of half as much organic matter as at Site 723, plus a substantial siliceous component below 85 mbsf. Thus, varying amounts of organic and siliceous matter at other sites would cause departures from the curves for Sites 723 and 728.

INORGANIC GEOCHEMISTRY

Introduction

At Site 723, we collected 33 interstitial water samples from Holes 723A and 723C, 30 by squeezing and 3 with the Barnes *in-situ* water sampler. All analytical results are listed in Tables 10 and 11 and presented in Figures 33 through 36.

Salinity, Chloride, and pH

The concentration profiles of salinity, chloride, and pH are shown in Figure 33. As at previous sites, the ~2‰ decrease in salinity over the top 60 m can be attributed mainly to the loss of sulfate and magnesium from solution. Salinities near 36‰ in the lowermost 100 m of the hole reflect the progressive addition of alkalinity to pore waters at depth.

One important feature of the chloride distribution at this site is the 30–40 mmol/L decrease in concentration between surface sediments and the bottom of the hole (Fig. 33). The profile suggests that dilution of the pore waters by the upward diffusion and/or advection of fresher water may be occurring.

The pH data listed in Table 10 and the profile in Figure 33 should be regarded with caution because a very strong upward drift of successive pH measurements made on the same sample was observed, especially in those waters with very high alkalinities. The drift was attributed to degassing of high concentrations of dissolved CO_2 in the laboratory.

Sulfate and Alkalinity

Sulfate depletion is pronounced at Site 723, with a gradient of ~0.5 mmol/L/m over the top 45 m in both Holes 723A and 723C. The high-resolution profile shown in Figure 34 indicates that the sulfate concentration falls to zero near 44 mbsf. Significant concentrations of sulfate up to 2.2 mmol/L were measured in the lower 200 m of Hole 723A (Fig. 33); the gradual increase with depth between 240 and 400 mbsf suggests that sulfate is diffusing upward from a source below the base of the cored sequence. Reduction of the upward-diffusing sulfate may be occurring at almost any depth between 200 and 400 mbsf. It is not possible given the available resolution to pinpoint more precisely the zone or zones of reaction in the lower half of the hole.

The titration alkalinities measured in Hole 723A (Table 10 and Figs. 33 and 34) are among the highest ever recorded during the history of ODP/DSDP, exceeding 100 mmol/L near the bottom of the hole. Higher concentrations have been measured previously only on the Peru margin during Leg 112. Because the reduction of the total sulfate inventory of buried seawater could produce a maximum of roughly 60 mmol/L of alkalinity, the higher levels below ~100 m depth must reflect contributions from other sources.

One source for the "excess" alkalinity must be the generation of ammonia via methane-producing fermentation reactions, which increases titration alkalinity by producing hydroxyl in the reaction $NH_3 + H_2O = NH_4^+ + OH^-$. In Hole 723A, ammonium concentrations increase with depth by about 20 mmol/L in the zone between ~60 and 200 m depth (Table 10 and Fig. 33) where no sulfate is present. This distribution probably reflects production of ammonia during methanogenesis. Between ~185 and 385 mbsf alkalinity increases by ~20 mmol/L (Table 10) while ammonia increases by only about 3 mmol/L. Presumably, the difference is due to the reduction of sulfate, which is diffusing upward from a deep-seated source and continuing to produce alkalinity, in this case largely as bicarbonate, below a depth of ~200 m. In addition, upward diffusion of bicarbonate could contribute to the observed distribution of alkalinity in the lowermost 200 m of the hole.

Such phenomena were observed on the Peru margin during Leg 112, where both chloride and sulfate profiles indicated that upward-diffusing brines were supplying sulfate to zones of reduction at depth in a number of holes (Suess, von Huene et al., 1988). A major difference between the Peru margin model and our observations here, however, is that the chloride concentration at Site 723 *decreases* with depth. We suggest that the only mechanism which can explain the observed trio of distributions (the chloride decrease and the alkalinity and sulfate increases with depth) is diffusion related to an underlying fluid which is sulfate enriched and chloride depleted. Such a fluid could be produced by the percolation of relatively fresh groundwater through gypsum or anhydrite beds. However, the location of such deposits is unknown.

If such a mechanism was active, one would expect calcium, in addition to sulfate, to be added to the percolating water. A small increase in the calcium concentration with depth is observed in the lower 100 m of Hole 723A (Fig. 33), which tends to support our suggestion. Therefore, a plausible explanation for the unusual pore-water chemistry at this site is the presence of a fluid of rather unique composition in the sediments below 400 mbsf. This conclusion is supported by logging results (see "Downhole Measurements" section, this chapter).

Calcium and Magnesium

Dissolved calcium and magnesium profiles are shown in Figures 33 and 34. The concentrations of both ions decrease with depth, with the exception of the calcium addition to solution below ~300 mbsf that was discussed above. The depletion of both elements is more severe than has been observed at either Sites 722, 724, or 725, which is probably related to the extremely high alkalinity below a depth of only ~50 mbsf. Presumably, precipitation of calcite is responsible for the increase in the magnesium/calcium ratio in the top 15 m of Hole 723C (Fig. 34). Immediately below this level, the magnesium concentration decreases quite markedly to ~37 mmol/L at 40 mbsf.

The downward concavity of the detailed profile suggests that dolomite is currently forming within the sulfate reduction zone between 20 and 40 mbsf (Fig. 34), and smear slide observations indicate that euhedral dolomite rhombs of apparent authigenic origin are indeed present in small amounts throughout the cored sequence. The magnesium concentration continues to decrease to the bottom of the hole, apparently linearly, which suggests that the postulated fluid at greater depths is magnesium depleted. Thus, Mg^{2+} is diffusing steadily downward, evidently without involvement in diagenetic reactions between ~100 mbsf and the bottom of the hole.

Carbonate mineral layers occur at several horizons between 250 mbsf and the bottom of Hole 723A and are occasionally associated spatially with laminated sediments. The X-ray diffraction results (see "Sediment Mineralogy," below) indicated that these layers consist of nearly 100% dolomite. Five such layers were observed in the recovered sediments (see "Lithostratigraphy" section, this chapter); nine were noted in the logging records for the hole (see "Downhole Measurements" section, this chapter). Dolomite can precipitate via a number of reactions in continental margin sediments, including the following (Baker and Burns, 1985):

(1) $2CaCO_3 + Mg^{2+} = CaMg(CO_3)_2 + Ca^{2+}$ (replacement of aragonite or calcite);

(2) $Ca^{2+} + Mg^{2+} + 4HCO_3^- = CaMg(CO_3)_2 + 2CO_2 + 2H_2O$ (direct precipitation from solution); and

(3) $CaCO_3 + Mg^{2+} + 2HCO_3^- = CaMg(CO_3)_2 + CO_2 + H_2O$ (addition of magnesium without Ca^{2+} release).

The layers recovered at Site 723 range up to nearly a meter thick. One view on their significance, which was favored by the shipboard geochemists, is that the layers could not have formed at any significant depth because it is physically impossible for vertical diffusion to supply much magnesium (and/or calcium) to precipitation loci at depth in rapidly accumulating sediments. Therefore, the formation of the dolomite layers must have commenced when those horizons were nearer the sediment-water interface. Because reactions (2) and (3) above would be more likely to proceed when the bicarbonate concentration is high, a high organic carbon accumulation rate, which would lead to high alkalinity in interstitial waters, would facilitate dolomite formation. Reaction (1) would also proceed more readily in the sulphate reduction zone in carbon-rich sediments because high alkalinity will result first in the precipitation of $CaCO_3$ which will increase the Mg/Ca ratio, making subsequent formation of dolomite chemically more favorable.

A slowed rate of sedimentation will also permit more Mg^{2+} to diffuse to the precipitation site from overlying seawater. Therefore, we tentatively suggest that the dolomite layers at Site 723 represent periods of high organic matter input coincident with episodes of reduced sedimentation. Such an association has been proposed previously to explain the distribution of dolomite in Holocene sediments off Baja California (Shimmield and Price, 1984). The depositional conditions required to support such a model are met at times of maximum transgression of sea level and lead to the formation of condensed sections (Haq et al., 1987).

Ammonia, Phosphate, and Silica

The distribution of these metabolites is shown in Figures 33 and 34. Ammonia concentrations are very high below 30 mbsf at this site, which is due to two factors. First, the sedimentary organic matter content is very high, which leads to the relatively rapid depletion of sulfate over the top 40 m and methanogenesis below this level. Sulfate reduction probably replaces fermentation in the lower 100 m of the hole as the principal mechanism by which the degradation of organic matter proceeds. Both bacterially mediated processes produce ammonia from the nitrogenous fraction of organic matter; the abundance of organic nitrogen is reflected by the high interstitial ammonia concentrations.

The second factor which governs the level of dissolved ammonia is uptake of NH_4^+ by clay minerals. In many organic-rich sediments, the exchange of NH_4^+ for K^+ and Na^+ is of a magnitude comparable to the concentration of ammonia produced (see, e.g., Moore and Gieskes, 1980), and it is possible that such exchange is an important reaction at Site 723. If so, then in the discussion above, a larger proportion of the "excess" alkalinity at depth should be credited to the protonation of NH_3 and a smaller proportion to the generation of HCO_3^-.

Dissolved phosphate concentrations are much lower than expected given the high ammonia levels and can be explained by the precipitation of fluorapatite, which is common throughout the section (see "Sediment Mineralogy," below). The disagreement between the high-resolution phosphate profile obtained from Hole 723C (Fig. 34) with the Hole 723A results between about 20 and 70 m depth is an analytical artifact caused by interference of sulfide during the analysis of samples from the latter hole. Large quantities of a brown precipitate, believed to be antimonyl sulfide, formed in the reaction cuvettes upon the addition of the potassium antimonyl tartrate reagent during the colorimetric analysis. The resulting turbidity gave spuriously high absorbances. To avoid this problem in subsequent determinations (including measurements on samples from Hole 723C), we bubbled N_2 through the pore-water samples for ~1 hr prior to the addition of the colorimetric reagents. The additional step reduced the dissolved sulfide concentration to very low values and effectively eliminated the interference.

The dissolved silica profile (Figs. 33 and 34) is similar to that seen previously. Dissolution of opal yields concentrations which approach an asymptotic value of ~1000 μmol/L near 40 m depth; the rather shallow gradient (~20 μmol/L/m) indicates that the sediments at this site are not rich in opal. The increase to 1400 μmol/L near the bottom of the hole suggests that an opal-rich horizon may exist near 400 mbsf. This observation agrees with the logging results (see "Downhole Measurements" section, this chapter), which indicate the occurrence of a low-density, high-porosity band at a similar depth.

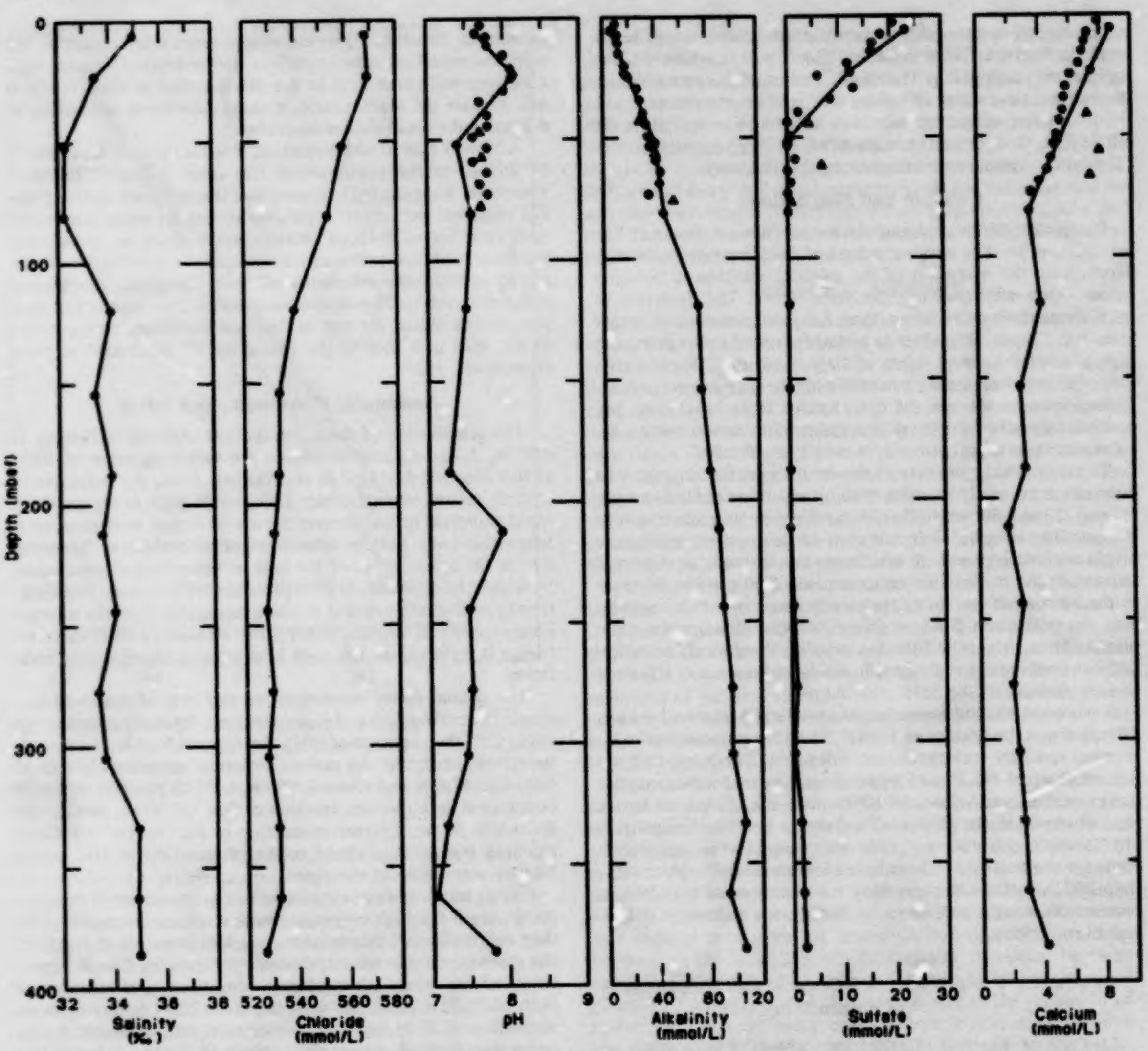

Figure 33. Concentrations vs. depth for Site 723. Dots = squeezed pore waters; triangles = *in-situ* pore-water samples obtained with the Barnes water sampler. The solid lines join data points from Hole 723A only. The other points represent measurements made on samples from Hole 723C.

Dissolved Organic Carbon

Relative concentrations of dissolved organic carbon (DOC) in the interstitial water samples were determined at this site by measuring the absorbance of the pore water at a wavelength of ~240 nm. The results are listed in Table 11 and plotted in Figures 35 and 36. Note that the data are given in absorbance units rather than as absolute values and are therefore useful only as a relative indication of DOC abundance. However, the measured absorbance is directly proportional to the DOC concentration (Krom, 1976).

In general, DOC at this site increases downhole to a maximum value at 385 mbsf which is about four times its concentration at shallow depths (Fig. 36). This profile reflects the general distribution of organic matter in the cored section (see "Organic Geochemistry" section, this chapter). The sharp increase in DOC at ~30 mbsf correlates well with inflections in the magnesium and alkalinity profiles and suggests that diagenetic activity is particularly pronounced at this depth. Such reactivity may be related to the local maximum in the organic carbon concentration evident between 25 and 35 mbsf (see "Organic Chemistry" section, this chapter).

In-Situ Samples

Three interstitial water samples were collected from Hole 723C using the Barnes downhole water sampler (DHWS). Analytical results are listed in Table 10 and are plotted as triangles on the previously discussed figures. With the exception of phosphate, the results are in reasonable agreement with the measurements made on the squeezed samples. The *in-situ* results for phosphate are highly variable and appear to be spurious; such variability is common for phosphate in *in-situ* samples and is thought to be due to contamination from the stainless steel coil in the Barnes sampler (R. Barnes, pers. comm.).

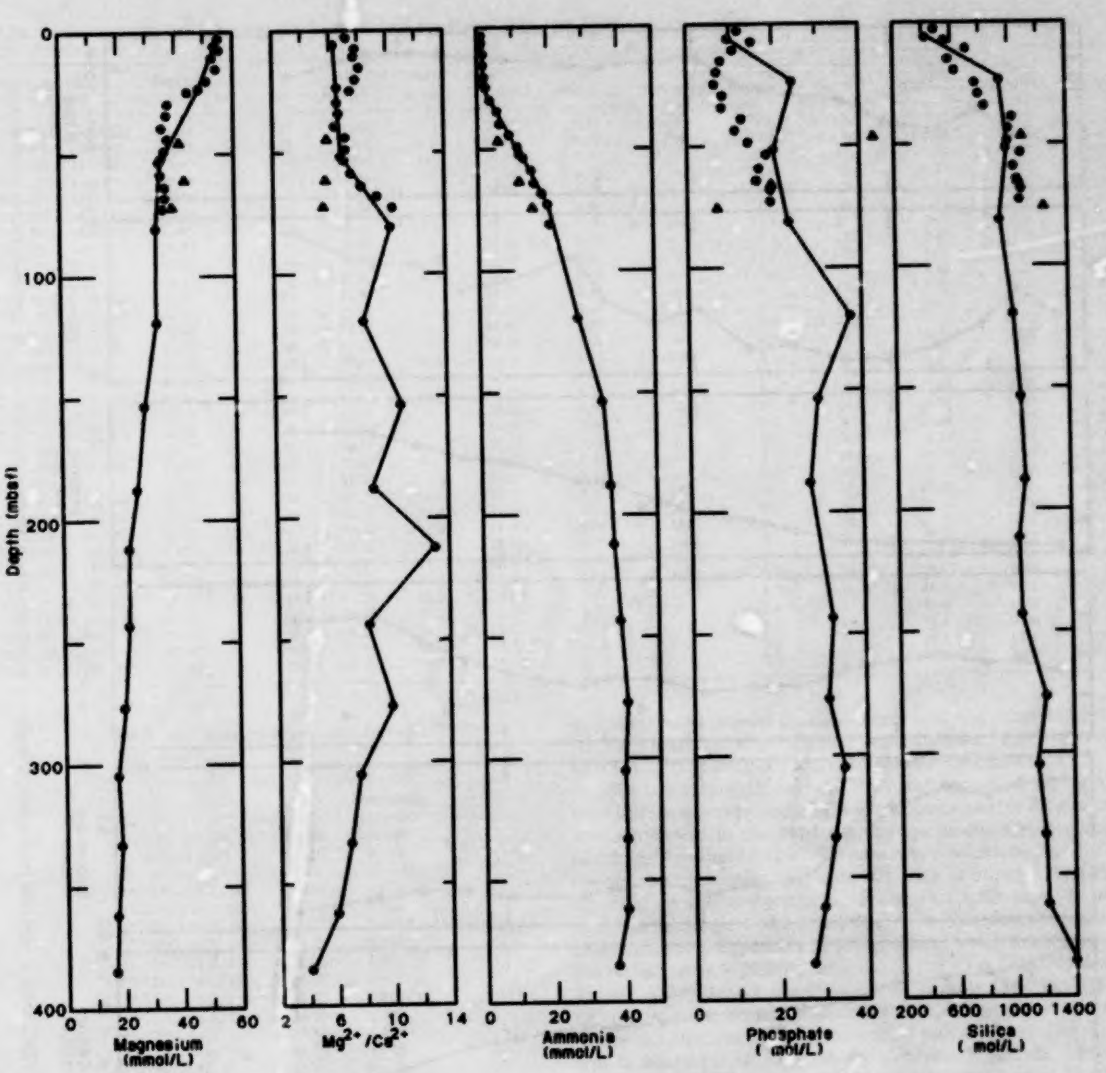

Figure 33 (continued).

Dissolved sulfate is higher than expected in the sample collected from Core 117-723C-8I (~66 mbsf), indicating some contamination with seawater. Concentrations of Ca^{2+} are also high compared with measurements made on squeezed samples from the same depths, suggesting that some $CaCO_3$ may have precipitated from the pore waters during core recovery. Based on the slight downward offset of the *in-situ* ammonia data, as compared with the regular sample (Fig. 33I; R. Barnes, pers. comm.), we believe that the *in-situ* samples may have been collected several meters higher than indicated by the driller.

Sediment Mineralogy

The mineralogy of 10 sediment residues from Hole 723A remaining after interstitial water extraction was determined by X-ray diffractometry. In all cases, $CaCO_3$ was removed with 10% HCl prior to analysis; the acid treatment was followed by two washes of the insoluble residue with deionized water. Diffractograms were also obtained for three additional samples thought to be apatite, aragonite, and dolomitic limestone, respectively. No glycolation was carried out at this site, but slow scans were made on three samples in an attempt to differentiate between overlapping pairs of clay mineral spectra.

The noncarbonate fraction of the sediments at Site 723 is composed largely of the same suite of minerals observed in the calcareous units on the Owen Ridge (Site 722). Quartz, feldspar, chlorite, and illite and/or mica are common to all samples. There appears to be no gross variation in the relative abundances of these minerals with depth throughout the Quaternary and late Pliocene, suggesting that source areas have not changed significantly during the last 2–3 m.y.

Pyrite occurs in significant quantities throughout the cored section at Site 723, in contrast to only traces observed in lithologic Units I, II, and III at Site 722. This difference can be attributed to the higher organic carbon content and concomitant severe sulfate depletion at Site 723.

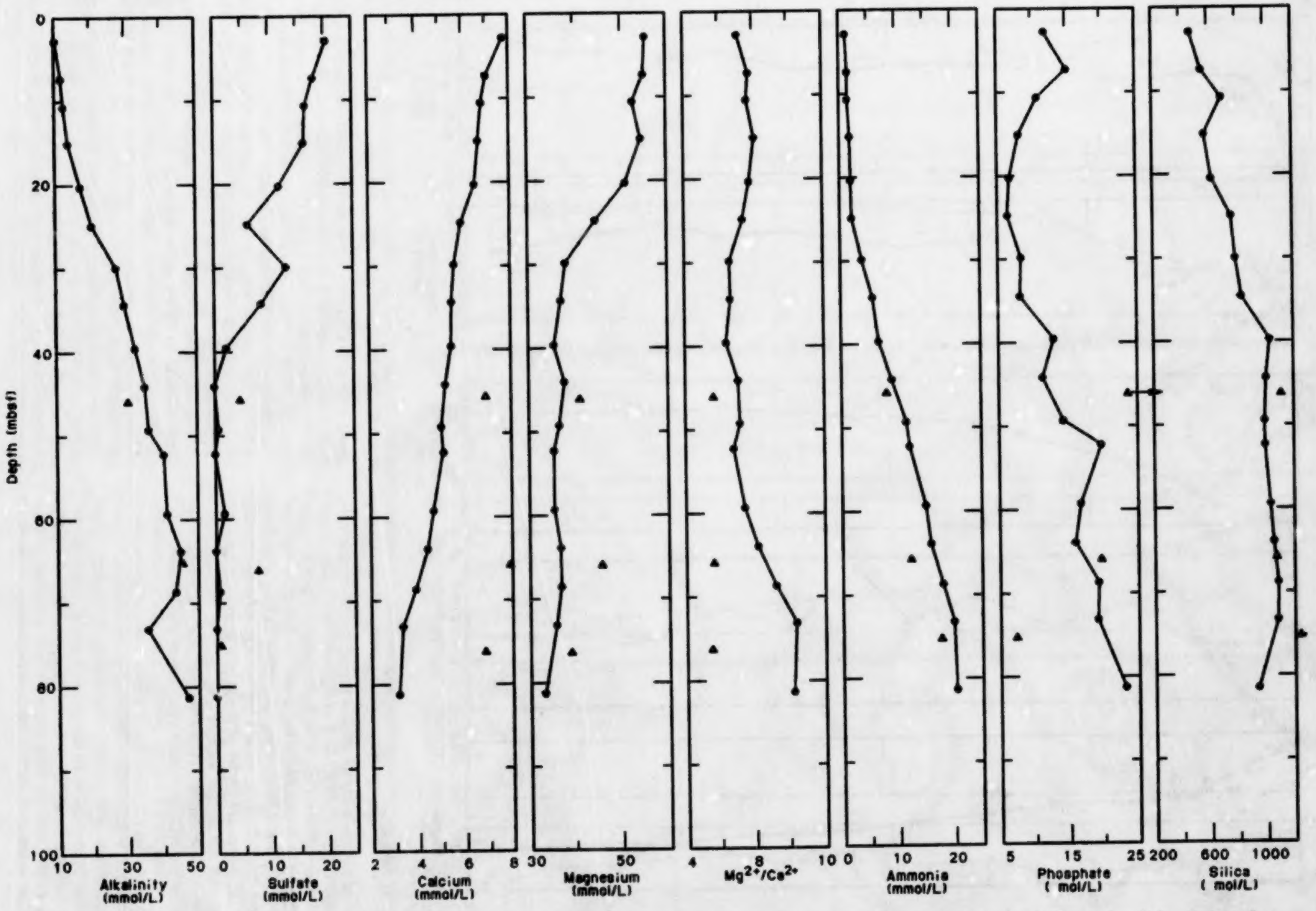

Figure 34. High-resolution profiles of samples from Hole 723C. Dots = squeezed pore waters; triangles = *in-situ* pore-water samples obtained with the Barnes downhole water sampler.

Table 10. Summary of interstitial water geochemical data for Holes 723A and 723C.

Core, sample, interval (cm)	Depth (mbsf)	Vol. (mL)	pH	Alk. (mmol/L)	Sal. (g/kg)	Mg (mmol/L)	Ca (mmol/L)	Cl (mmol/L)	SO_4 (mmol/L)	PO_4 (µmol/L)	NH_4 (mmol/L)	SiO_2 (µmol/L)	Mg/Ca
117-723C-1H-2, 145–150	2.95	59	7.70	10.45	—	55.66	7.77	—	20.6	12.0	1.20	477	7.16
117-723A-1H-4, 145–150	5.95	56	7.65	7.42	36.0	54.15	8.58	568	23.2	9.5	1.22	423	6.31
117-723C-1H-5, 145–150	7.45	57	7.80	12.04	—	55.09	7.07	—	18.1	15.2	1.40	562	7.79
117-723C-2H-2, 145–150	10.75	53	7.80	12.71	—	52.99	6.88	—	16.6	10.8	1.56	703	7.70
117-723C-2H-5, 145–150	15.25	58	8.00	13.99	—	54.69	6.76	—	16.3	8.1	1.81	580	8.09
117-723C-3H-2, 145–150	20.45	56	8.10	17.35	—	51.25	6.56	—	11.8	6.9	2.04	625	7.81
117-723A-3H-4, 145–150	23.45	38	8.14	18.40	35.0	48.28	7.26	569	12.2	24.6	2.51	937	6.65
117-723C-3H-5, 145–150	24.95	44	8.10	20.66	—	44.67	6.01	—	6.1	6.7	2.13	770	7.43
117-723C-4H-2, 145–150	30.05	36	8.00	27.39	—	37.99	5.72	—	13.0	8.4	3.89	799	6.64
117-723C-4H-5, 145–150	34.55	46	7.70	29.68	—	37.12	5.56	—	8.5	8.3	5.80	838	6.68
117-723C-5H-2, 145–150	39.75	37	7.80	32.50	—	35.57	5.53	—	2.2	13.0	6.91	1030	6.43
117-723C-5H-5, 145–150	44.25	53	7.80	35.26	—	37.71	5.29	—	0	11.4	9.13	1004	7.13
117-723I-6I-1, 0-1	46.40	10	7.70	30.17	—	41.40	7.36	—	4.6	43.6	7.77	1110	5.58
117-723C-6H-2, 145–150	49.35	32	7.60	36.28	—	36.56	5.09	—	0.7	14.4	11.69	991	7.18
117-723A-6H-4, 145–150	52.35	41	7.38	40.60	34.2	35.26	5.17	559	0	19.9	12.17	991	6.82
117-723C-6H-5, 145–150	53.85	30	7.80	36.47	—	34.92	4.91	—	0	18.2	12.96	1082	7.11
117-723C-7H-3, 145–150	59.46	35	7.60	41.45	—	35.33	4.74	—	1.6	16.7	15.09	1030	7.45
117-723C-7H-6, 145–150	63.96	39	7.80	45.33	—	36.62	4.48	—	0	16.0	16.06	1053	8.17
117-723I-8I-1, 0-1	65.80	10	7.60	43.96	—	43.96	7.99	—	7.3	19.4	13.08	1077	5.50
117-723C-8H-2, 145–150	68.75	48	7.70	43.85	—	36.79	3.99	—	0.7	19.4	18.14	1082	9.22
117-723C-8H-5, 145–150	73.25	42	7.80	35.67	—	35.67	3.45	—	0	19.2	20.03	1077	10.34
117-723I-9I-1, 0-1	75.40	10	7.70	58.91	—	38.61	7.32	—	0.7	6.8	17.77	1230	5.27
117-723A-9H-4, 145–150	81.35	36	7.58	47.20	34.2	33.12	3.25	553	0	23.2	20.46	941	10.19
117-723A-13X-4, 140–150	120.05	35	7.49	73.90	35.4	33.09	4.04	540	0	37.4	28.29	1020	8.19
117-723A-17X-1, 145–150	154.25	33	—	76.30	35.0	28.65	2.66	534	0	29.5	35.25	1062	10.77
117-723A-20X-4, 145–150	187.75	36	7.26	82.40	35.4	25.98	3.00	534	0	27.7	37.04	1085	8.66
117-723A-23X-1, 145–150	212.25	35	7.96	88.50	35.2	22.82	1.77	532	0	—	37.84	1042	12.89
117-723A-26X-3, 145–150	244.25	30	7.51	91.60	35.5	22.60	2.76	529	0.6	32.5	39.62	1052	8.19
117-723A-29X-6, 145–150	277.65	30	7.55	97.70	35.0	20.65	2.07	531	1.1	31.3	41.0	1211	9.98
117-723A-32X-5, 145–150	304.95	39	7.47	97.80	35.2	18.29	2.39	529	0.4	34.6	40.0	1144	7.65
117-723A-36X-5, 145–150	333.54	53	7.21	106.80	36.0	19.09	2.74	533	1.6	32.3	40.4	1196	6.97
117-723A-39X-5, 145–150	362.45	53	7.06	93.90	36.0	17.35	2.92	533	1.9	29.8	40.4	1211	5.94
117-723A-42X-1, 140–150	385.40	49	7.81	106.70	36.0	16.67	4.08	527	2.2	27.4	37.0	1401	4.09

Table 11. Dissolved organic carbon data, Site 723.

Core, sample, interval (cm)	Depth (mbsf)	Dissolved organic carbon (a.u.)
117-723C-1H-2, 145	2.95	0.602
117-723C-1H-5, 145	7.45	0.644
117-723C-2H-2, 145	10.75	0.660
117-723C-2H-5, 145	15.25	0.694
117-723C-3H-2, 145	20.45	1.004
117-723C-3H-5, 145	24.95	1.070
117-723C-4H-2, 145	30.05	2.366
117-723C-4H-5, 145	34.55	1.360
117-723C-5H-2, 145	39.37	1.215
117-723C-5H-5, 145	44.25	1.200
117-723C-6I-1, 1	46.60	1.449
117-723C-6H-2, 145	49.35	1.241
117-723C-6H-5, 145	52.35	1.216
117-723C-7H-3, 145	59.46	1.160
117-723C-7H-6, 145	63.96	1.267
117-723C-8I-1, 1	65.80	0.920
117-723C-8H-2, 145	68.75	1.230
117-723C-8H-5, 145	73.25	1.228
117-723C-9I-1, 1	75.00	0.993
117-723A-17X-1, 145	154.25	1.412
117-723A-20X-4, 145	187.75	1.360
117-723A-26X-3, 145	244.25	1.827
117-723A-29X-6, 145	244.25	2.004
117-723A-32X-5, 145	304.95	2.103
117-723A-36X-5, 145	333.45	2.031
117-723A-39X-4, 145	362.45	2.104
117-723A-42X-1, 145	385.40	2.166

Note: a.u. = absorbance unit.

Kaolinite is not present in the sediments at this site. Slow scans from 24°–26.5° of a pair of samples from Cores 117-723A-3H and -9H showed only a peak corresponding to the chlorite 003 reflection: the kaolinite 002 peak was absent in both cases. These observations agree with the results of Kolla et al. (1981), who showed that sediments near the coast of northern Oman are chlorite rich and kaolinite poor. Farther to the south, kaolinite becomes increasingly more abundant.

Illite is common throughout the cored sequence. We use the term illite in a generic sense here—muscovite and/or biotite may also be present in the sediments but yield diffraction spectra which overlap that of illite. We have made no attempt to differentiate these minerals. The illite 001 peak is broader than that observed in diffractograms of Indus Fan sediments, as was noted in lithologic Units I and II at Site 722. We attribute the broadening to the presence of palygorskite, which has its principal reflection at ~10.5 A, adjacent to the 10 A illite 001 peak. Indeed, a slow scan from 7° to 10° of Sample 117-723A-3H-4, 145 cm, showed a shallow but distinct separation between the two peaks confirming the presence of palygorskite. This mineral is abundant in soils on the Arabian Peninsula (Müller, 1961, cited in Kolla et al., 1981), and its occurrence at Site 723 probably reflects eolian transport from the adjacent landmass.

Fluorapatite occurs in trace concentrations throughout the hole as brown to golden fragments of fish bones and apparently authigenic aggregates having rough or knobby surface textures. This material was recovered from the >250 µm sieve fraction of four core-catcher samples spaced across the cored sequence. The bone fragments and aggregates tended to be very small, typically <1 mm in size. The occurrence of the apparently authigenic material in visible quantities at this site is consistent with the distribution of phosphate in interstitial water as discussed above.

A single sample of a whitish or cream-colored, partly fibrous aggregate about 1 cm in diameter was collected from Core 117-723B-24X and diffracted. The material was found to consist of a mixture of aragonite and calcite and was suspected to be a partly comminuted shell fragment in a matrix of nannofossil ooze.

A sample of one of the "limestone" layers from the lower half of Hole 723A was shown by diffractometry to be nearly pure dolomite. The spacing of the (211) reflection can be used

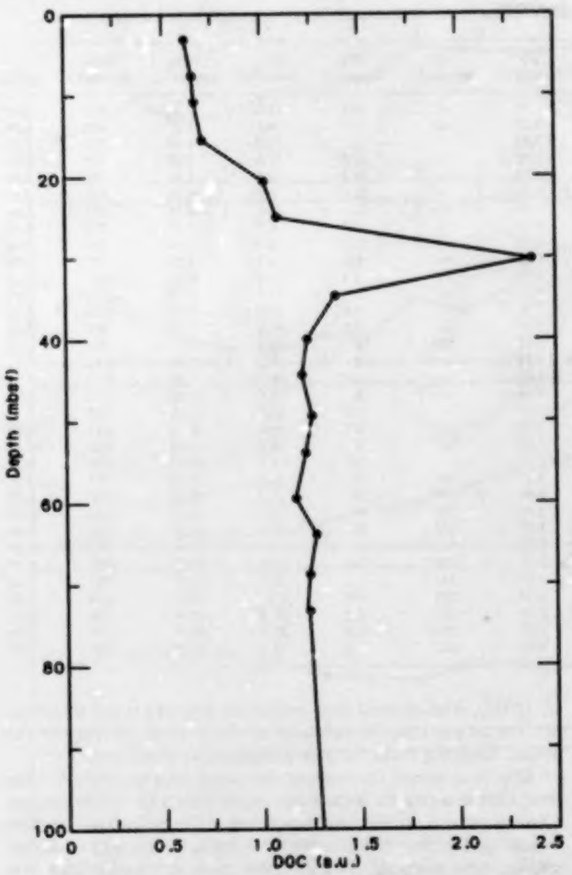

Figure 35. High-resolution dissolved organic carbon (DOC) profile, Hole 723C. Note that the data are plotted in terms of absorbance units (a.u.) and indicate relative concentration only.

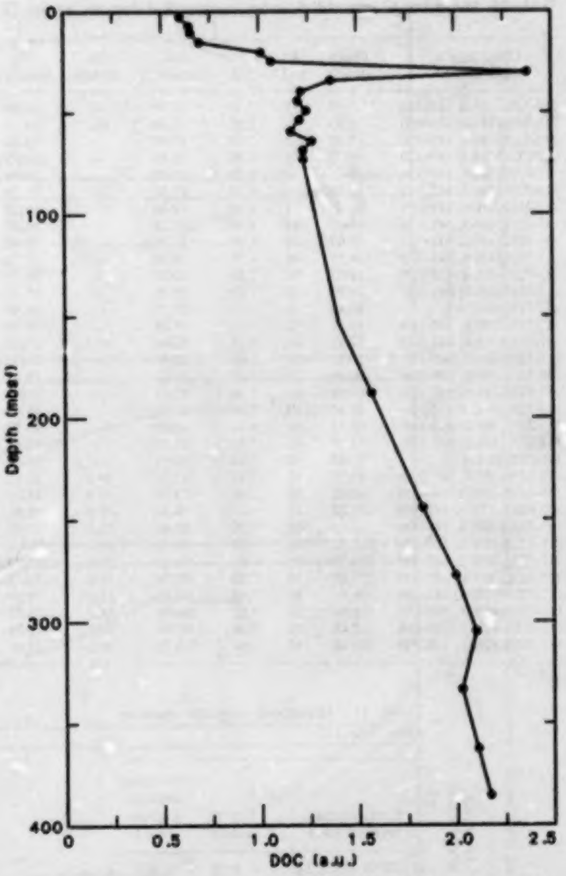

Figure 36. Stacked dissolved organic carbon (DOC) profile at Site 723 compiled from data from Holes 723A and 723C. Note that the data are plotted in terms of absorbance units (a.u.) and indicate relative concentration only.

as an indicator of the magnesium content; in this case, the spacing indicated that dolomite comprising the dolostone contained 52 mol% magnesium.

ORGANIC GEOCHEMISTRY

The organic carbon concentration in 125 Pleistocene to upper Pliocene sediment samples from Site 723 ranges from 0.71% to 6.83% (mean of 3.23%) and shows a slight increase with depth. Organic matter is immature and rich in marine-derived, lipid-rich material, which has not been noticeably degraded by diagenesis.

The influx of sulfate from the subsurface produces high alkalinity in pore waters while depleting interstitial methane or impeding biogenic fermentation reactions. Gas expansion throughout the recovered section thus appears to be due mainly to high partial pressures of CO_2 gas. The fairly steady increase of ethane and propane with depth points to a production of gas at greater depth by early thermogenic cracking of organic matter.

Variations in paleotemperatures of the sea-surface water, as recorded by the U^k_{37} index, are of the same magnitude as measured at Site 721 (Owen Ridge). The molecular index for relative temperatures shows, however, that water temperatures were colder over the margin when compared with the more distal Owen Ridge.

Organic Matter Abundance and Character

The Pleistocene to uppermost Pliocene sediments at Site 723 are rich in organic carbon. Values reach up to 6.83% and rarely fall below 1% (Fig. 37). A trend toward higher values at the base of the hole may indicate that the oldest sediments recovered are the richest organically, although the data may be biased by nonrepresentative sampling. Such high organic carbon values are most likely the result of high primary productivity in the monsoon-induced seasonal upwelling. Given the high sedimentation rates at this site and concomitant enhanced preservation, the Neogene sediments constitute ideal substrates for anaerobic remineralization at depth.

A subset of 88 samples was subjected to Rock-Eval pyrolysis in order to decipher the nature and maturity of the organic matter. The results are given in Table 12. The Rock-Eval apparatus is equipped with a module to analyze total organic carbon (TOC) and these results are listed as TOC^a in Table 12. A comparison of the Rock-Eval TOC values with the TOC values measured by difference (TOC^b in Table 12; see "Explanatory Notes,"

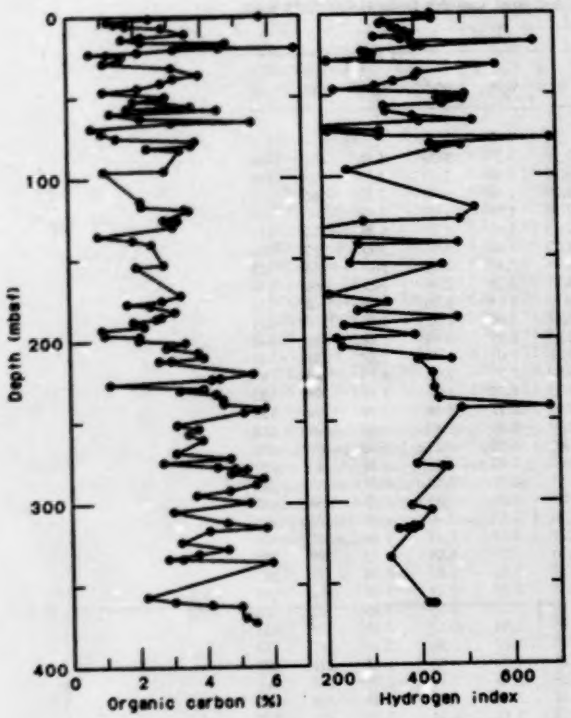

Figure 37. Downhole plots of organic carbon and the hydrogen index in Hole 723A.

this volume) shows that the Rock-Eval results are unreliable. Therefore, the hydrogen (HI) and oxygen indices (OI) were recalculated on the basis of the TOC^b data (Table 12). They are plotted in Figure 38, together with the results from Site 722.

Generally, samples from the margin sites are characterized by higher HI and lower OI values when compared with samples from Site 722 on the Owen Ridge. This can best be explained by a higher input of lipid-rich organic material at the margin sites due to increased primary productivity in combination with enhanced preservation conditions. The uniformly low temperatures of maximum pyrolysis (T_{max} <435°C) point to an immature character of the organic matter (Table 12).

The hydrogen and oxygen indices are measures of the amount of hydrocarbons and CO_2, respectively, liberated by pyrolysis and normalized to the organic carbon content of the sample. They should be constant if organic matter was produced by one type of primary producers and not altered by diagenesis. A plot of the HI and the OI vs. organic carbon of samples from Site 723 is shown in Figure 39. We can see that the HI appears to stabilize around 400 at a value of approximately 3% organic carbon, while the OI stabilizes at a value of around 100. It seems that with rapid burial of sediments containing 3% or more organic carbon, hydrogen-rich material is not further depleted.

Hydrocarbon Gases

Samples for interstitial gas analysis with the headspace method were taken in several cores from Hole 723A and 723B, and in Sections 2 and 5 from each core of Hole 723C. The results are given in Table 13 and are shown vs. depth in Figure 40. Methane concentrations are high in the uppermost 100 m of the sedimentary sequence and tend to level out at depth. This contrasts with the ethane and propane concentrations, which both show a steady increase with depth. Even though Whelan et al. (1982) reported the occurrence of trace amounts of volatile C_1–C_8 hydrocarbons in macroalgae, it is not clear whether any biogenic source can account for C_2–C_8 hydrocarbons in sediments. Therefore, we are inclined to ascribe the observed downhole increase of ethane and propane to early thermogenic cracking of organic matter at depth.

Production of biogenic methane in the deeper sediments is inhibited because an increase of interstitial sulfate was observed (see "Inorganic Geochemistry" section, this chapter). The expected concentrations of thermogenic methane in addition to ethane and propane are likely to be masked by traces of biogenic methane persisting throughout the section. Gas concentrations measured quantitatively in Holes 723A and 723C, while showing similar trends, do not agree well and suggest that the method of quantifying interstitial gas with the shipboard methodology is far from being truly quantitative.

Similar gas distribution profiles were compiled from measurements of vacutainer samples of gas pockets (Table 14 and Fig. 41). In addition to the aforementioned gases, butane and isobutane were observed to increase with depth, which corroborates the suggestion that the C_{2+} interstitial gas is thermogenic in origin.

Lipid Analyses

We analyzed 18 samples from the first three cores of Hole 723B for the relative abundance of di- and triunsaturated ketones (see "Explanatory Notes" and "Organic Geochemistry" section, "Site 721" chapter, this volume). The results, expressed as an alkenone unsaturation index U^{k}_{37}, together with the organic carbon and $CaCO_3$ content of these samples, are listed in Table 15 and are shown vs. depth in Figure 42.

The U^{k}_{37} ratio ranges from 0.80 to 0.91. This corresponds to sea-surface water temperatures of 23°C and 26.5°C, respectively. These values are significantly lower than those measured on sediments from Site 721, located on the Owen Ridge (U^{k}_{37} = 0.88–0.97). The shift to lower values is the expected result of upwelling of deep cold water near the margin. Of notable interest is that the interval between 9 and 13 mbsf is characterized by low U^{k}_{37} values, pointing to cold sea-surface water temperatures during the time of deposition, which might be related to an intensification of the upwelling. The organic carbon values of this interval are also slightly enhanced in comparison with the bounding sediments, but they never reach the value measured in the uppermost sample. This sample shows the highest U^{k}_{37} index and has thus been deposited under warm sea-surface water conditions.

DOWNHOLE MEASUREMENTS

Three logging runs of Schlumberger tool strings were conducted in Hole 723B. The seismic stratigraphic combination (BHC/DIT/GR/CALI; see "Explanatory Notes," this volume) was run in the openhole interval, logging downward from 92.2 to 415.0 mbsf, followed by logging upward from 429.0 to 100.9 mbsf. The lithoporosity combination (LDT/CNL/NGT/GPIT) was run through both pipe and openhole, logging downward from just above the seafloor to 410.8 mbsf, then logging upward from 426 mbsf to the seafloor. The geochemical combination (GST/ACT/GPIT) was run logging upward from 422.1 to 70.5 mbsf. Very little fill was encountered in the hole, so the bottom of the tool strings reached between 0 and 6 m of the 429 mbsf total depth on different runs.

Log Quality and Processing

Unedited original logs are shown following the barrel sheets. Log quality was generally very good. The major exception was that the caliper was unreliable; this is often true for ODP caliper

Table 12. Results of Rock-Eval pyrolysis of sediment samples from Holes 723A and 723B.

Core, sample, interval (cm)	Depth (mbsf)	S_1	S_2	S_3	S_2/S_3	TOC[a]	TOC[b]	HI	OI
117-723A-									
1H-1, 43–44	0.43	5.26	23.29	9.80	2.37	5.38	5.80	402	169
1H-2, 43–44	1.93	1.56	9.28	4.74	1.95	2.27	2.51	370	189
1H-3, 43–44	3.43	0.45	3.31	2.79	1.18	0.76	1.25	265	223
1H-4, 43–44	4.93	0.47	3.58	2.38	1.50	1.07	1.49	240	159
1H-4, 144–145	5.94	0.53	4.16	2.93	1.41	1.27	1.80	231	163
1H-5, 43–44	6.43	0.61	4.29	2.68	1.60	1.31	ND	327	[c]204
2H-1, 43–44	8.23	0.85	5.52	2.96	1.86	1.56	ND	353	[c]189
2H-2, 43–44	9.73	1.50	9.94	4.22	2.35	2.73	ND	364	[c]154
2H-3, 43–44	11.23	2.09	12.29	4.14	2.96	3.24	3.56	345	116
2H-4, 43–44	12.73	1.22	7.22	3.44	2.09	1.85	2.25	321	151
2H-5, 43–44	14.23	0.29	3.00	2.36	1.27	0.95	1.68	179	140
2H-6, 43–44	15.73	0.97	6.47	3.21	2.01	1.74	2.27	285	141
2H-7, 43–44	17.23	2.06	11.56	4.62	2.50	2.94	4.77	242	97
3H-1, 43–44	17.93	1.22	10.74	4.75	2.26	1.64	3.59	299	132
3H-2, 43–44	19.43	1.23	10.42	4.50	2.31	2.58	3.38	308	133
3H-2, 128–129	20.28	2.57	15.67	5.19	3.01	3.85	4.58	342	113
3H-2, 138–139	20.38	8.87	33.96	7.46	4.55	8.19	6.83	497	109
3H-3, 43–44	20.93	1.83	13.20	5.03	2.62	3.30	3.20	412	157
3H-4, 144–145	23.44	0.17	1.54	1.87	0.82	0.53	0.71	217	263
3H-5, 43–44	23.93	0.38	3.13	1.99	1.57	1.05	1.23	254	162
3H-6, 43–44	25.43	0.46	3.07	1.73	1.77	0.99	1.66	185	104
3H-7, 43–44	26.93	1.05	4.88	2.21	2.20	1.58	1.60	305	138
4H-2, 43–44	29.03	0.25	2.23	1.43	1.55	1.04	1.12	199	128
4H-4, 43–44	32.03	1.75	10.39	3.39	3.12	1.85	3.16	335	107
4H-7, 43–44	36.53	2.99	15.53	4.38	3.54	3.81	3.98	400	110
5H-2, 43–44	38.73	2.19	12.21	3.90	3.13	3.04	3.19	382	122
5H-4, 43–44	41.73	1.24	10.20	3.45	2.95	0.97	2.85	358	121
5H-6, 43–44	44.73	0.82	6.16	2.45	2.51	1.95	2.16	285	113
6H-1, 43–44	46.83	0.42	2.48	2.28	1.08	1.08	1.12	221	203
6H-3, 43–44	49.83	1.22	10.81	3.29	3.28	2.14	2.95	366	111
6H-4, 144–145	52.34	0.89	8.13	3.35	2.42	1.82	2.04	398	164
6H-5, 43–44	52.83	0.97	8.69	3.54	2.45	1.74	2.79	311	127
6H-7, 43–44	55.83	1.96	14.11	4.01	3.51	3.08	3.72	379	108
7H-2, 43–44	56.94	0.85	5.08	2.74	1.85	1.52	1.82	279	150
7H-4, 43–44	59.94	0.58	3.93	2.34	1.67	1.16	1.32	297	177
7H-6, 43–44	62.94	1.20	7.85	3.13	2.50	1.99	2.22	354	141
7H-8, 43–44	65.94	4.80	22.67	5.61	4.04	4.35	5.51	411	102
8H-1, 43–44	66.23	1.86	11.84	3.63	3.26	2.90	3.12	397	116
8H-3, 43–44	69.23	0.18	1.07	1.77	0.60	0.75	0.76	140	233
8H-4, 149–150	71.79	0.33	2.74	1.94	1.41	0.84	1.09	251	178
8H-5, 43–44	72.23	0.30	2.06	1.96	1.05	0.96	1.07	193	183
8H-7, 43–44	75.23	0.62	3.98	2.15	1.85	1.23	1.48	269	145
9H-2, 43–44	77.33	2.58	14.66	3.99	3.67	2.13	3.85	381	104
9H-4, 43–44	80.33	3.90	16.10	3.65	4.41	3.74	3.68	438	99
9H-4, 144–150	81.34	1.47	10.93	2.97	3.68	2.20	2.42	452	123
9H-6, 43–44	83.33	1.35	9.57	2.62	3.65	2.16	3.37	284	78
11X-1, 149–150	96.29	0.44	2.77	1.81	1.53	1.09	1.09	254	166
13X-4, 119–120	119.79	1.54	15.25	3.85	3.96	2.91	3.49	437	110
14X-2, 149–150	126.79	2.00	13.69	3.36	4.07	2.78	3.28	417	102
14X-3, 70–71	127.50	2.01	12.38	2.40	5.15	4.31	2.97	417	81
15X-2, 43–44	135.33	0.29	1.66	1.05	1.58	1.28	0.92	180	114
15X-6, 0–1	140.90	1.74	10.58	2.95	3.58	2.16	2.51	422	118
15X-6, 70–71	141.60	2.32	11.24	2.05	5.48	4.05	2.81	400	73
17X-1, 43–44	153.23	2.20	9.90	2.45	4.04	3.80	2.86	346	86
17X-2, 0–1	154.30	0.99	7.81	2.46	3.17	1.72	2.06	379	119
19X-1, 42–43	172.52	1.09	7.99	2.02	3.95	3.71	3.35	239	60
19X-4, 64–65	177.24	0.52	4.68	2.39	1.95	1.38	1.76	266	136
20X-1, 40–41	182.20	1.71	12.14	2.39	5.07	4.43	3.17	383	75
20X-4, 30–31	186.60	1.21	10.47	3.02	3.46	2.16	2.65	395	114
20X-7, 40–41	191.20	1.27	8.26	2.08	3.97	3.35	2.26	365	92
21X-5, 0–1	197.40	0.94	7.67	2.51	3.05	1.94	2.12	362	118
21X-6, 45–16	199.35	1.21	8.49	2.12	4.00	3.70	2.11	402	100
22X-3, 29–30	204.39	1.84	11.44	2.34	4.88	4.74	2.92	392	80
23X-2, 0–1	212.30	1.88	12.00	3.46	3.46	2.54	3.04	395	114
23X-2, 31–32	212.61	1.55	10.84	2.63	4.12	4.16	2.71	400	97
24X-1, 48–49	220.88	5.14	23.61	3.97	5.94	7.95	5.49	430	72
24X-7, 27–28	229.67	3.86	17.33	2.88	6.01	7.06	4.01	432	72
25X-5, 43–44	236.53	3.84	20.44	3.43	5.95	7.28	4.60	444	75
26X-2, 24–25	241.54	3.64	22.31	3.79	5.88	3.29	5.85	381	65
26X-3, 0–1	242.80	3.58	25.78	4.65	5.54	5.22	5.60	460	83
29X-6, 119–120	276.70	6.19	18.43	3.56	5.17	4.62	4.39	420	81
30X-1, 0–1	278.30	4.19	22.10	3.46	6.38	4.78	4.90	451	71
30X-1, 0–1	278.30	4.41	21.25	4.10	5.18	4.69	4.90	434	[d]84
32X-3, 119–120	301.69	1.82	11.94	3.28	3.64	3.10	ND	385	[c]105
32X-5, 119–120	304.69	1.70	12.30	2.69	4.57	2.89	3.06	402	88
33X-2, 78–79	315.28	6.00	18.33	3.50	5.23	4.62	ND	396	[c]75

Table 12 (continued).

Core, sample, interval (cm)	Depth (mbsf)	S_1	S_2	S_3	S_2/S_3	TOC[a]	TOC[b]	HI	OI
117-723A-									
33X-2, 88–89	315.38	3.67	11.07	3.11	3.55	2.85	ND	388	[c]109
33X-2, 98–99	315.48	5.00	16.92	3.38	5.00	4.21	ND	401	[c]80
33X-2, 118–119	315.68	4.91	15.45	4.10	3.76	3.93	ND	393	[c]104
33X-2, 128–129	315.78	3.88	11.99	3.98	3.01	3.12	ND	384	[c]127
33X-2, 138–139	315.88	4.21	12.18	3.75	3.24	3.25	ND	374	[c]115
33X-2, 148–149	315.98	4.11	13.23	3.98	3.32	3.59	ND	368	[c]110
33X-3, 8–9	316.08	3.65	15.15	4.42	3.42	3.90	ND	388	[c]113
33X-3, 20–21	316.20	4.23	15.23	3.71	4.10	4.07	ND	374	[c]91
33X-3, 28–29	316.28	2.44	11.20	3.67	3.05	3.17	ND	353	[c]115
33X-3, 38–39	316.38	1.99	10.48	3.27	3.20	2.91	2.91	360	112
33X-3, 48–49	316.48	3.19	12.87	3.30	3.90	3.32	3.32	387	99
36X-6, 0–1	333.59	3.12	11.60	3.23	3.59	3.44	2.91	399	111
36X-6, 0–1	333.59	3.75	12.09	3.52	3.43	3.57	2.91	415	[d]121
39X-5, 119–120	362.19	2.16	18.19	3.33	5.46	4.25	4.17	436	80
39X-5, 119–120	362.19	2.99	18.44	3.80	4.85	4.42	4.17	442	[d]91

Note: HI = hydrogen index and OI = oxygen index; the hydrogen and oxygen indices were calculated on the basis of the TOC[b] values. For a detailed description of parameters, see "Explanatory Notes" chapter (this volume). ND = not determined.

[a] Organic carbon measured by Rock-Eval.

[b] Organic carbon measured by difference.

[c] Hydrogen and oxygen values calculated from Rock-Eval organic carbon data.

[d] Duplicate analysis.

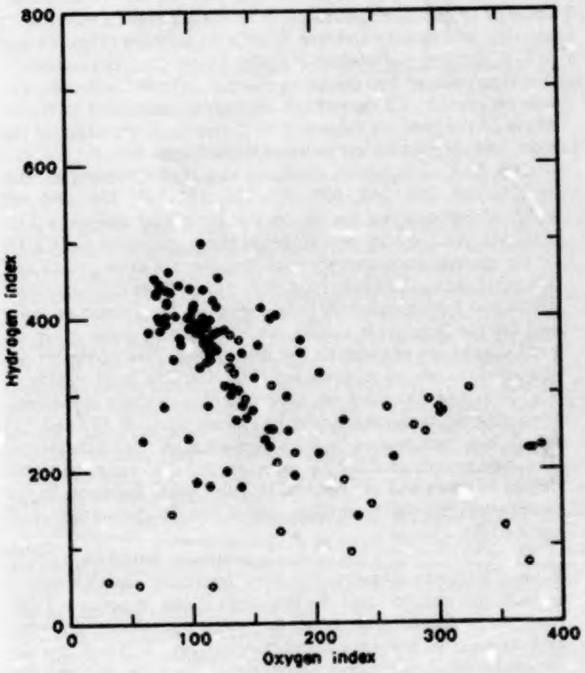

Figure 38. Plot of hydrogen index vs. oxygen index of samples from Holes 723A and 723B (dots) compared with samples from Hole 722 (circles).

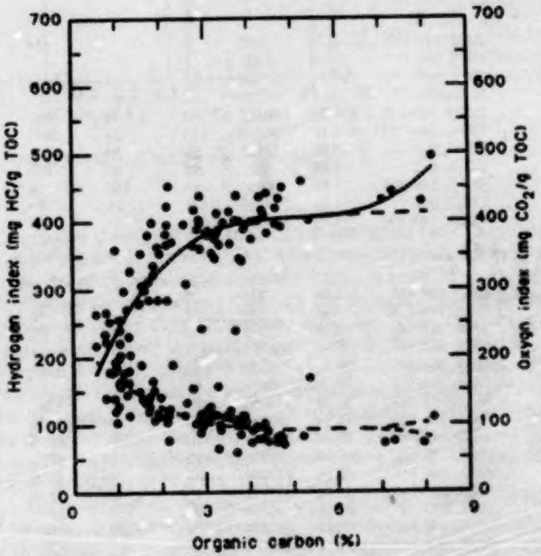

Figure 39. Cross plot of hydrogen index (dots) and oxygen index (circles) vs. organic carbon of samples from Hole 723A and 723B. Lines are polynomial least-squares regressions. TOC values are from the Rock-Eval instruments.

logs. A caliper was calculated from sonic traveltimes, but it indicated only a minimum size of 0.4 m for the borehole. The sonic log exhibited some cycle skipping, which was removed manually before reprocessing. Geochemical logs were reprocessed postcruise and converted to oxide dry weight percentages, as described in the "Explanatory Notes" chapter (this volume). Reproducibility of logs was generally excellent, based on a comparison of downgoing and upcoming logs for the first two tool strings. The lowest reproducibility was found for the hole deviation and magnetometer logs. Except for these logs, usually only the upcoming logs are shown in the figures.

Logs from the seismic stratigraphic combination were depth shifted downward by 2.4 m, and logs from the lithoporosity and geochemical combinations were depth shifted downward by 2.2 m. The amount of the depth adjustment was based on detection of three horizons in logs that were also measured during drilling: the base of pipe, a thin dolomite bed at 247.2 mbsf, and a thin dolomite bed at 317.3 mbsf. These two dolomite beds are

Table 13. Concentrations of methane (C_1), ethane (C_2), and propane (C_3) per liter of wet sediment in cores of Holes 723A, 723B, and 723C.

Core, sample, interval (cm)	Depth (mbsf)	C_1 (μL/L)	C_2 (μL/L)	C_3 (μL/L)	C_1:C_2
117-723A-					
1H-4, 144–145	5.94	346210	21	5	16486
3H-4, 144–145	23.44	165220	11	2	15020
6H-4, 144–145	52.34	106240	14	10	7589
7H-7, 149–150	65.50	123415	23	26	5366
8H-4, 140–141	71.70	13415	5	4	2683
9H-4, 144–145	81.34	117000	20	21	5850
11X-1, 149–150	96.29	55290	15	20	3686
13X-4, 119–120	119.79	42095	20	30	2104
14X-2, 149–150	126.79	24115	15	25	1608
15X-6, 0–1	140.90	5850	20	45	293
17X-2, 0–1	154.30	7380	12	24	607
19X-4, 149–150	178.09	41835	6	0	6972
20X-4, 30–31	186.60	160425	23	20	6975
21X-5, 0–1	197.40	6895	20	35	345
23X-2, 0–1	212.30	4440	30	55	15
24X-3, 0–1	223.40	5687	17	33	335
26X-3, 0–1	242.80	2457	30	67	82
29X-6, 119–120	277.39	4200	24	54	175
30X-1, 0–1	278.30	3550	35	70	101
32X-5, 119–120	304.69	2740	25	50	110
36X-6, 0–1	333.59	6335	25	55	253
39X-5, 119–120	362.19	2410	50	105	48
117-723B-					
2H-3, 149–150	8.79	4990	9		554
4H-3, 149–150	28.09	235			
5H-3, 149–150	37.79	188420	20	10	9421
10X-2, 0–1	83.10	535			
13X-4, 149–150	116.29	180520	40	50	4513
16X-2, 149–150	142.19	54710	15	25	3647
18X-5, 0–1	164.60	10515	20	30	526
22X-6, 0–1	204.80	6675	35	65	191
25X-5, 149–150	233.69	6655	85	140	78
33X-2, 0–1	314.50	1745	45	95	39
40X-3, 149–150	375.79	5950	10		595
117-723C-					
1H-2, 144–145	2.94	125	5		8
1H-5, 144–145	7.44	150	1		30
2H-2, 144–145	12.14	415	15	20	28
2H-5, 144–145	16.64	355	5		71
3H-2, 144–145	21.84	1330	15	10	89
3H-3, 144–145	23.34	1005	15		67
4H-2, 144–145	31.44	194055	25	5	7762
4H-5, 144–145	35.94	289880	30	10	9663
5H-2, 144–145	41.14	163505	10	5	16351
5H-5, 144–145	45.64	175775	20	10	8789
6H-2, 144–145	50.74	151880	25	20	6075
6H-5, 144–145	55.24	137815	25	15	5513
7H-3, 144–145	61.94	36490	10	10	3649
7H-5, 144–145	64.94	113800	30	30	3793
8H-2, 144–145	70.14	128531	52	65	2472
8H-5, 144–145	74.64	25955	10	15	2596

Note: Values are expressed in μL/L (volume gas/volume wet sediment).

the only dolomites with precisely known depths based on core recovery.

Only the spectral gamma-ray and neutron logs were run through pipe. Pipe attenuates the signal of both tools, but useful information is still present, though of lower quality than openhole logs. Figure 43 illustrates this conclusion with a comparison of upcoming and downgoing uranium logs. The through-pipe logs shown in Figure 43 are obtained after multiplying raw counts by an empirical gain model to correct for the attenuation of gamma rays by passage through pipe. The shape of this model (Fig. 43) is based on known variations in pipe thickness: the BHA is twice as thick as drill pipe, and drill pipe has increased thickness every 10 m at pipe joints.

The amplitude of the gain model is based on a comparison of the mean uranium reading for 15-m intervals immediately above and below pipe, which suggests that the BHA suppresses uranium counts by a factor of about 6; a similar suppression of the standard deviation was seen. This estimate is probably less accurate at Site 723 than at most sites because of the strong cyclicity and variability in the short intervals used for establishing the gain factor. Indeed, a gain of only 3 was estimated from a similar analysis at Site 728 (see "Site 728" chapter, this volume), and we know of no published research on pipe attenuation. The gain factor has only a small effect on the agreement between logs. Pipe was not set at exactly the same depth for both runs, and the small peak shown at 92–99 mbsf in the downgoing through-pipe log is confirmed by the upcoming openhole log (Fig. 43).

Character match between through-pipe logs is generally reasonable, though less than observed for the openhole logs (Fig. 43). The one marked disagreement between the two through-pipe logs is in the magnitude of the uranium peak at 36 mbsf. Small depth shifts between the two logs appear to be present, as evidenced by slight differences in the depths of peaks or troughs between runs.

Dolomite Layers

The most obvious feature of many of the logs is the occurrence of several thin spikes. These spikes are high in velocity, resistivity, and density and low in neutron porosity (Figs. 44 and 45). Within-log variability of spike amplitudes is probably a function more of bed thickness than of differences in composition or porosity of these hard streaks, or cemented intervals. Many of the beds are thinner than the vertical resolution of the logs, and amplitudes are reduced accordingly.

Based on log responses alone, we identified nine hard streaks: at 223, 247, 260, 268, 300, 317–318, 337–338, 374, and 408 mbsf. These nine are visible on the sonic and resistivity logs (Fig. 44). All are also detectable on the signal strength (CSIG) of the gamma spectrometry tool, but the horizons at 223 and 268 mbsf are too subtle to have been picked from this log alone. These two hard streaks are subtle also on the neutron porosity and density logs, as is the 30-mbsf horizon, but the other six hard streaks are obvious on the density log. Five of the six are also obvious on the neutron log (Fig. 45). The hard streaks at 223, 268, and 300 mbsf are probably thinner than the others. Even thinner hard streaks may be present (e.g., at 192 and 355 mbsf), but they cannot be identified as such with confidence. The most pronounced hard streaks are also detected at the same depths in cores and are marked by substantial decreases in the penetration rate on the drilling record (see "Lithostratigraphy" section, this chapter).

These hard streaks are probably dolomite, based on a single X-ray diffraction measurement (see "Inorganic Geochemistry" section, this chapter) and the similarity in log responses of different beds. Most log responses (e.g., density, velocity, porosity, and thorium/potassium natural radioactivity; Figs. 44 and 45) are consistent with either dolomite or calcite, with near-zero porosities. However, the photoelectric effect (Fig. 45) is much more consistent with dolomite (Pe = 3.14) than with calcite (Pe = 5.08). Most of the hard streaks are subtle or undetectable (Pe = 2.9–3.3) on the log of photoelectric effect, presumably because dolomite Pe is near the 2.5–3.5 range of most of the Pe log. In contrast, the low "background" Pe below 350 mbsf makes the hard streaks at 374 and 408 mbsf quite evident on the Pe log, with maximum Pe values of 3.1 and 3.5.

Geochemical logs (Fig. 46) indicate that the hard streaks are either dolomite or calcite plus dolomite. Calcium and magne-

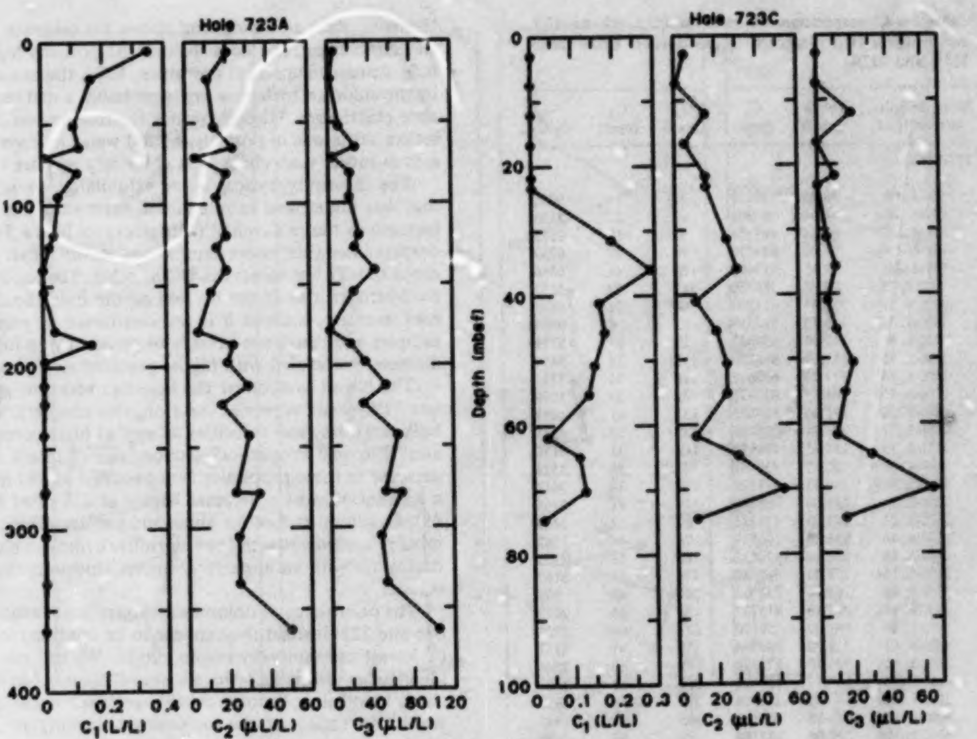

Figure 40. Downhole concentrations of methane (C_1), ethane (C_2), and propane (C_3) in headspace samples from Holes 723A and 723C.

sium spikes to high values invariably occur at the locations of hard streaks. Magnesium oxide never reaches a peak abundance greater than 12%, but the much higher concentrations of calcium oxide could be caused by the thin-bed effect rather than by a mixture of calcite and dolomite in the hard streaks. The hard streaks at 247 and 374 mbsf are particularly obvious on the geochemical logs (Fig. 46). Quartz depletion in the hard streaks is indicated by consistently low concentrations of SiO_2, falling to zero at 374 mbsf. Aluminum and potassium are usually low (a notable exception is the potassium peak at 300 mbsf), indicating low clay content. Other elements (iron, titanium, sulfur, gadolinium, thorium, and uranium) show a less consistent pattern at locations of the dolomite beds.

Diagenetic precipitation from advecting fluids is clearly the cause of the dolomite stringers. In general, geochemical log behavior in the dolomite stringers suggests that dolomite precipitation occurred preferentially in locations high in carbonate and low in clay (K_2O, thorium, Al_2O_3), quartz (SiO_2), and organic carbon (U). Uranium is often dissolved from calcite by circulating fluids; it is then concentrated at the depth of precipitation (e.g., Fertl, 1979; "Site 722" chapter, this volume) if this depth is adjacent to reducing sediments (e.g., an organic-rich horizon). Such a concentration is notably absent at Site 723.

The compaction pattern at Site 723, as revealed by the sonic, density, and neutron porosity logs, is unaffected by the presence of dolomite horizons. A significant density borehole correction (DRHO) usually occurs in the 2 m immediately below each dolomite bed, and both low density and high porosity are often logged in the 2 m immediately above each dolomite bed. However, these changes are probably washouts, caused by increased circulation during drilling of the hard horizons; the changes do not reflect actual porosity lows. The absence of shifts in the porosity baseline across the dolomite beds, in spite of their very low permeability, suggests that they are stringers lacking lateral continuity rather than widespread horizons. Thus, they do not significantly retard continuing compaction. This conclusion is supported by the comparison of a synthetic seismogram with the seismic line across the site, discussed in the "Seismic Stratigraphy" section (this chapter). This conclusion is also supported by the observation that only some of the dolomite horizons detected in cores and the drilling record at Hole 723B were also detected at 723A, only a few meters away.

The source of the magnesium in the dolomite stringers is not known with certainty. Magnesium in interstitial waters exhibits a rapid decrease with increasing depth, suggesting diffusion and depletion of seawater magnesium (see "Inorganic Geochemistry" section, this chapter). The geochemical logs (Fig. 46) indicate generally high magnesium oxide contents of 4%–9%. The magnesium oxide is inversely correlated with SiO_2, indicating that it is not residing primarily in clays. Magnesium oxide is very positively correlated with calcium oxide, suggesting that dolomite is present in significant quantities throughout the logged section. However, mineral identification from smear slides (see barrel sheets) detected only trace amounts of authigenic dolomite. Based on calcium oxide and magnesium oxide log responses, it is possible that about a third of the detrital carbonate identified in smear slides is actually detrital dolomite. Dissolution of part of this possible detrital dolomite could be a source of much of the magnesium incorporated in the dolomite beds.

Table 14. Concentrations of methane (C_1), ethane (C_2), and propane (C_3) measured in gas pockets from Holes 723A and 723B.

Core, sample, interval (cm)	Depth (mbsf)	C_1 (ppm)	C_2 (ppm)	C_3 (ppm)	C_1:C_2
117-723A-					
5H-2, 18	38.48	778327	84	14	9265
6H-5, 34	52.74	799301	93	20	8595
7H-4, 117	60.68	487234	51	12	9572
8H-4, 110	71.40	864514	99	27	8732
9H-4, 25	80.15	819498	125	43	6556
11X-2, 75	97.05	383750	118	62	3252
13X-4, 39	118.99	451209	68	21	6635
14X-3, 30	127.10	117515	12	4	9793
15X-6, 8	140.98	653047	113	34	5779
17X-2, 73	155.03	616270	113	33	5454
19X-4, 64	177.24	619615	118	35	5251
20X-2, 105	184.35	632353	124	34	5099
21X-5, 20	197.60	555827	137	41	4057
22X-5, 71	207.81	550780	130	35	4237
23X-2, 35	212.65	494590	119	33	4156
24X-4, 127	226.17	430408	122	38	3528
25X-3, 115	234.25	571509	158	39	3617
26X-2, 6	241.36	403730	146	41	2765
26X-3, 23	243.03	171725	69	22	2489
27X-4, 44	254.34	166538	108	44	1542
28X-2, 48	261.08	430532	183	53	2353
29X-4, 104	274.24	563682	178	51	3167
30X-4, 66	283.46	241637	247	96	978
31X-5, 146	295.36	413737	156	46	2652
32X-5, 20	303.70	559190	223	66	2508
33X-4, 62	312.22	386984	119	31	3252
35X-3, 120	325.70	272376	182	60	2046
36X-5, 50	332.59	429494	252	81	1704
39X-4, 120	360.70	488516	253	73	1930
40X-4, 149	370.69	440110	305	94	1443
41X-2, 120	377.00	288194	193	60	1493
117-723B-					
6H-3, 17	46.07	983462	91	16	10807
10X-4, 100	87.10	894868	121	40	7313
13X-4, 145	116.25	821589	125	50	6573
16X-2, 145	142.15	11466	1		11466
18X-5, 40	165.00	810462	123	35	6589
20X-5, 50	184.40	306936	49	13	6264
22X-4, 95	202.75	149635	22	7	6802
25X-5, 120	233.40	665682	150	39	4438
27X-1, 95	246.55	338439	179	49	1891
33X-1, 146	314.46	58354	104	44	561
35X-2, 38	324.58	109688	115	45	954
38X-2, 20	353.60	332627	177	55	1879
40X-3, 30	374.60	219835	257	94	855
41X-4, 50	386.00	263462	257	114	1025
42X-3, 59	403.89	411146	240	75	1700

Note: Values are expressed in μL/L (volume gas/volume wet sediment.

Chlorinity

Interstitial water analyses show that chlorinity decreases markedly between the seafloor and about 150 mbsf, decreases more subtly between 150 and 250 mbsf, and is relatively constant below that depth (see "Inorganic Geochemistry" section, this chapter). This pattern is also revealed by the chlorine/hydrogen count rate ratio from the gamma spectroscopy tool (Fig. 47). The chlorine/hydrogen ratio is low and relatively constant from 390 to 255 mbsf, then rises at an accelerating pace from 255 mbsf to the shallowest measurements at 70 mbsf.

The chlorine/hydrogen log has two ambiguities not present in the interstitial water analyses: (1) it does not distinguish between pore water and bound water in clays, so the pattern could be caused by a downhole increase in clay mineral abundance, or (2) the pattern could be caused by a downhole decrease in hole diameter, with a constant low chlorinity of interstitial waters. However, the gamma-ray log shows no evidence of downhole clay enrichment, nor does the neutron porosity log show an uphole increase in apparent porosities. Thus, the broad trend shown by the chlorine/hydrogen log is probably a real indicator of relative chlorinities. High-frequency fluctuations on Figure 47 may reflect variations in porosity, bound water in clays, and organic matter rather than changes in chlorinity of pore waters.

The chlorinity/hydrogen log exhibits one important feature that was undetected in interstitial water samples: a substantial increase in the chlorinity/hydrogen ratio below 390 mbsf. The deepest interstitial water sample was at 385 mbsf; core recovery drops to very low values below 387 mbsf. The log-based chlorinity/hydrogen rise at the bottom of the hole should be considered tentative, because it is not confirmed by interstitial water samples and could conceivably be caused by an increase in hole diameter associated with higher-porosity sediments.

The lowest portion of the hole has very low grain densities (see "Physical Properties" section, this chapter), wet- and dry-bulk densities, and velocities as well as high porosities (Fig. 48 and "Physical Properties" section, this chapter). However, the decrease in these properties is not sudden at 390 mbsf; instead, a gradual downhole decrease begins at 352 mbsf (Figs. 44 and 45). Uranium and sulfur show sudden decreases at about 390 mbsf in agreement with the chlorinity/hydrogen rise, suggesting that water with an apparently higher chlorinity/hydrogen ratio is oxic.

The occurrence of dolomite stringers is not random throughout Site 723; instead they appear to be confined to the interval of lowest chlorinity/hydrogen ratios. We did not confidently identify any dolomite stringers above 221 mbsf in the region of rising chlorinity. A dolomite stringer does occur at 407 mbsf, within the region of the increasing chlorinity/hydrogen ratio; but it occurs exactly on a chlorinity/hydrogen trough to low baseline values. However, the wide spacing of dolomite stringers and the narrowness (28 m) of the measured zone of apparently increasing chlorinity makes any speculation about a lower limit to stringer formation tenuous.

In general, no correlation between the chlorinity/hydrogen ratio and the location of modern dolomite stringers is found within the long interval of low chlorinity/hydrogen. This apparent association of low present chlorinity/hydrogen ratios with dolomite stringers may be coincidental. Magnesium in interstitial waters decreases with depth and is too low to support much modern dolomite precipitation in the depth range containing dolomite stringers (see "Inorganic Geochemistry" section, this chapter).

Uranium Concentrations

Uranium concentrations at Site 723 are an order of magnitude higher than in most deep-sea sediments. Normally, the gamma-ray log, which detects the natural radioactivity of potassium, thorium, and uranium, is dominated by potassium in clays. In contrast, uranium accounts for about 80% of the total gamma radioactivity at Site 723, and uranium concentrations are predominantly about 5–10 ppm. Potassium and thorium tend to be positively correlated with aluminum, as is commonly the case, because variations in clay mineral abundance are usually larger than variations in clay mineral composition. However, the positive correlation between uranium and both thorium and potassium is weaker at Site 723 than in most other regions, and this correlation is not present in some portions of the hole. Clay minerals probably carry most of the potassium and thorium, but the majority of uranium is in a different component.

The component associated with the anomalously high uranium concentrations is probably organic matter. Other conceivable components with high uranium concentrations (phosphorite, zircon, magnetite, and biotite) are absent at Site 723 or are

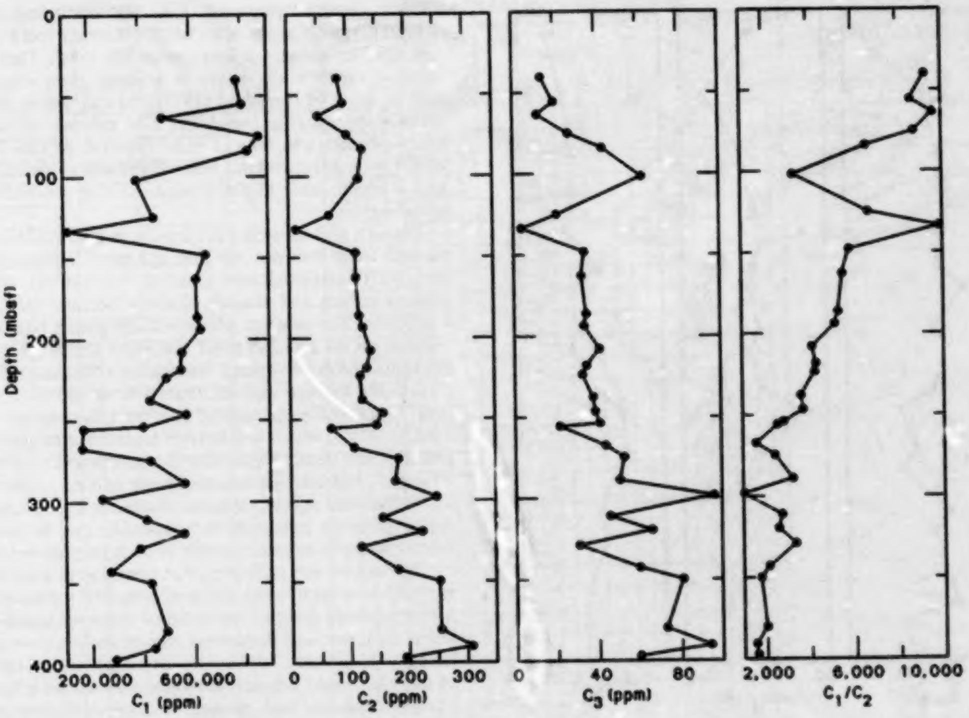

Figure 41. Downhole concentrations of methane (C_1), ethane (C_2), propane (C_3), and the C_1:C_2 ratio in gas pockets from Hole 723A.

Table 15. Organic carbon, $CaCO_3$, and U^k_{37} values of selected samples from Hole 723B.

Core, sample, interval (cm)	Depth (mbsf)	Organic carbon (%)	$CaCO_3$ (%)	U^k_{37}
117-723B-				
1H-1, 50-53	0.50	5.66	51.4	0.91
1H-2, 50-53	2.00	2.83	63.6	0.89
1H-3, 50-53	3.50	2.28	53.4	0.88
2H-1, 50-53	4.80	1.73	50.6	0.88
2H-1, 100-103	5.30	2.27	47.6	0.89
2H-2, 50-53	6.30	2.21	50.1	0.84
2H-2, 100-103	6.80	1.17	51.2	0.88
2H-3, 55-58	7.85	2.45	49.0	0.87
2H-3, 100-103	8.30	1.96	51.9	0.88
2H-4, 50-53	9.30	2.49	48.3	0.84
2H-4, 100-103	9.80	3.87	35.7	0.81
2H-5, 50-53	10.80	3.25	46.2	0.80
2H-5, 100-103	11.30	3.89	55.6	0.82
2H-6, 50-53	12.30	1.80	52.7	0.84
2H-6, 100-103	12.80	2.46	53.8	0.83
3H-1, 50-53	14.50	1.57	53.7	0.86
3H-1, 100-103	15.00	3.73	47.5	0.86
3H-2, 50-53	16.00	3.21	62.6	0.86

present in concentrations far too low to account for observed uranium concentrations. Phosphorite could be present in thin horizons in sufficient concentrations to affect the uranium log, but it is not pervasive enough to account for uranium variability. Uranium/thorium and uranium/potassium ratios are far too high for clay minerals.

In contrast, organic matter is very high at Site 723 (see "Organic Geochemistry" section, this chapter), and organic carbon is often found to be rich in uranium (Fertl, 1979). Figure 43 compares the core measurements of organic carbon percentages (see "Organic Geochemistry" section, this chapter) with the uranium logs. Considering the difficulty of correlating discrete measurements with a continuous log, the character correlation between the two data types is remarkably good.

It is surprising that the organic matter appears to be approximately constant in uranium concentrations, since the relationship between the two is not based on the primary uranium content of organic matter. Instead, it is based on preferential precipitation of uranium in the low-redox conditions associated with organic matter. The uranium spike at 18 mbsf, corresponding with the largest measured organic carbon percentage, occurs close to but not exactly at a 30-mbsf, very high spike in dissolved organic carbon. The peak in dissolved organic carbon is within the sulfate reduction zone (see "Inorganic Geochemistry" section, this chapter), and it is likely that the uranium concentration is still changing at these shallow depths.

In the interval from 100 to 175 mbsf, the uranium concentration exhibits a high-frequency oscillation, with a period of 5–10 m. This cyclical behavior has far too high a frequency to be detected with the discrete organic carbon measurements or correlated with these measurements. These uranium cycles are highly correlated with physical properties cycles (Figs. 44 and 49): uranium highs correspond to lows in bulk density, photoelectric effect, resistivity, and sonic velocity, and to highs in neutron porosity. This correlation is strongest in the interval from 100 to 150 mbsf, where uranium variations are largest, but a correlation between uranium and density clearly continues below 150

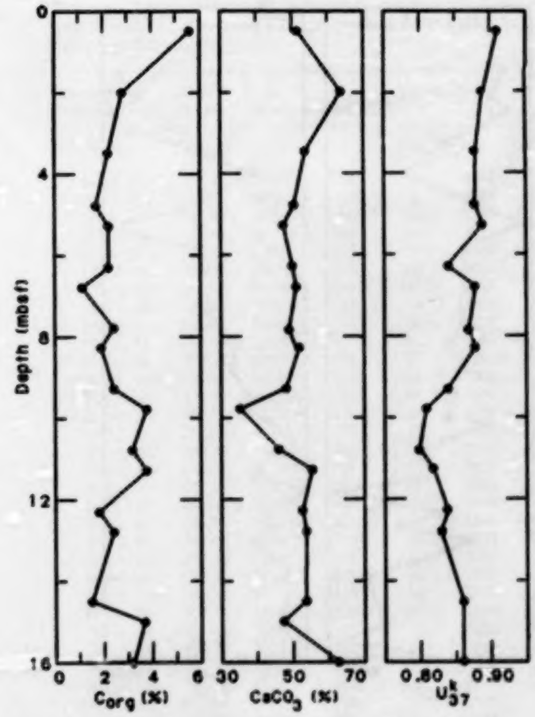

Figure 42. Downhole plot of organic carbon, $CaCO_3$, and the U^k_{37} index in sediment samples from Hole 723B.

mbsf. High organic matter accounts for both the anomalously low grain densities (see "Physical Properties" section, this chapter) and correlation of uranium with physical properties.

In contrast, clay content exhibits a poor correlation with both uranium and the physical properties logs above 145 mbsf, where the uranium fluctuations are highest in amplitude. Clay content often controls porosity variations and is indicated in Figure 49 by the potassium/thorium gamma-ray log. Only below 145 mbsf does the potassium/thorium log exhibit some correlation with uranium and physical properties. However, here too organic carbon fluctuations may be a more important source of physical property variations than is clay content. The correlation between potassium/thorium gamma ray and uranium in this lower interval of Figure 49 implies that the concentration of organic matter is higher in the clay-rich zones than in the carbonate-rich zones; this association is common also in other regions.

Although uranium variations at Site 723 are controlled primarily by variations in organic matter, a small amount of uranium must also be present in the clays. Based on typical uranium/potassium and uranium/thorium ratios for clay minerals (Fertl, 1979), about 1–3 ppm of uranium may be in the clays. As a result, the approximate doubling of average organic carbon concentrations below 200–220 mbsf is accompanied by an increase, but not a doubling, of uranium concentrations (Fig. 43).

Velocity, Density, and Porosity

The trends of velocity, density, and porosity with depth are anomalous in two respects: (1) lack of the normal compaction trends, and (2) velocity and density decrease below 352 mbsf. Of the three physical properties measured *in situ*, only velocity exhibits a compaction trend (Fig. 44). Excluding the dolomite stringers, velocities show an overall increase from 1.55 km/s at 100 mbsf to about 1.8 km/s near 350 mbsf. This compaction trend is substantially lower in velocity than empirical trends such as those of Hamilton (1979) and Carlson et al. (1986). Superimposed on this broad trend is substantial variability on scales of meters to tens of meters. Much of this velocity variability (Fig. 44) correlates well with uranium variations (Fig. 45) and is attributable to fluctuations in the concentration of organic matter.

Density and neutron porosity exhibit no evidence of a compaction trend between 100 and 352 mbsf. Except for fine-scale variability correlated with uranium fluctuations, density is virtually constant and neutron porosity actually increases slightly downhole. The neutron porosity undergoes a baseline shift upward at about 200–220 mbsf, the same depth interval at which organic carbon percentage undergoes a baseline shift to almost double the average amount from 100 to 200 mbsf (see Fig. 43 and "Organic Geochemistry" section, this chapter). The photoelectric effect, which is relatively insensitive to porosity, closely parallels the neutron porosity fluctuations (except in dolomite stringers), indicating a compositional control on neutron porosity variations. Again, organic matter is the likely cause: the higher neutron porosities are probably due as much to high bound water in organic matter as to high pore volume.

The lack of any evidence of compaction in porosity and density trends is both important and puzzling, particularly in light of the subdued compaction trend of the sonic log. Further, density is far lower, and porosity is higher, than is normal for any lithology (Hamilton, 1976). The very high rate of sedimentation at this site would account for some retardation of compaction, but porosities are high enough to imply sufficient permeability for some compaction.

To our knowledge, greatly undercompacted sequences are found in only two environments: deltas and accretionary prisms. In deltaic environments such as the U.S. Gulf Coast, the combination of extremely high sedimentation rates and high clay contents (relatively low permeability) results in underpressured zones. In these zones, overburden-related compaction is retarded at the lowest permeability zones, resulting in a sudden downward increase in porosity. In accretionary prisms, undercompacted sediments are caused by pervasive fluid flow from below associated with subduction (e.g., ODP Leg 110).

The undercompaction at Site 723 is more similar to the gradual porosity profiles of accretionary prisms than to the sudden porosity increases of overpressured deltaic sediments. Therefore, our preferred interpretation is that compaction is retarded by fluid replenishment. Unlike the replenishment from below that occurs in accretionary prisms, the flow at Site 723 may be from either below or subhorizontally. The geochemistry of pore fluids suggests a deeper source of sulfate-enriched and chloride-depleted sediments (see "Inorganic Geochemistry" section, this chapter). We cannot completely exclude the Gulf Coast analog, because clay variability is subtle and conceivably permeability is relatively uniform.

Below 355 mbsf, porosity increases and velocity, density, and resistivity decrease to very low values for such depths. This zone could be an overpressured zone. However, several observations suggest a different interpretation. First, chlorinities are higher than in the overlying sediments (Fig. 47); thus, this zone cannot be the source of hydraulically pumped brackish water or the cause of undercompaction in the overlying sediments. Second, the sharp top of this zone at 355 mbsf, though relatively high in density and low in porosity, corresponds with lows in Al_2O_3, K_2O, and thorium (Fig. 46) and is therefore unlikely to be an impermeable clay. The very high Pe of 3.3 is consistent with dolomite, but the neutron porosity of 70% would appear to pre-

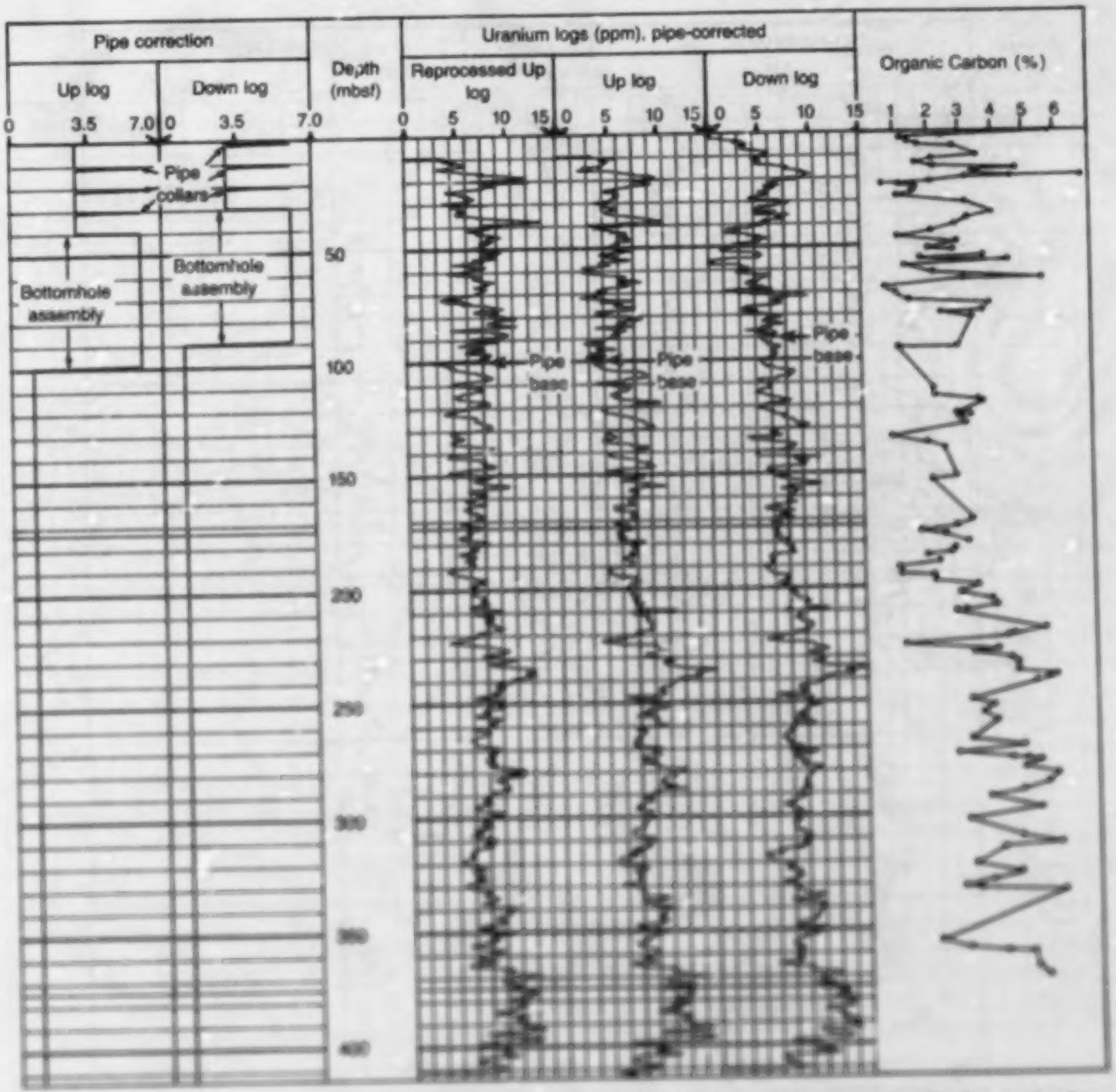

Figure 63. Comparison of organic carbon percentage measured on core samples with logs of uranium concentration. The three uranium logs shown are reprocessed upgoing (left), original upgoing (center), and original downgoing (right) logs.

clude impermeable dolomite. Third, Pe drops dramatically beneath 355 mbsf, indicating that this high-porosity zone is compositionally distinct from overlying sediments (except perhaps for the Pe peaks).

Siliceous microfossils are the most likely explanation of the high-porosity, low-velocity, low-density zone at the bottom of Site 723. Comparable low velocities and high porosities were observed in diatom oozes at shallower depths at ODP Site 647 (Arthur, Srivastava, et al., 1987). Core recovery below 387 mbsf is too low for quantitative estimation of representative siliceous microfossil abundance, and this recovery probably is heavily biased toward the more compacted clay interbeds. Of four cores recovered below 387 mbsf from Holes 723A and 723B, three are only a few centimeters long and are composed of clay or limestone, and one is 7 m long and composed of diatomaceous shale (see "Lithostratigraphy" section, this chapter).

Grain densities decrease substantially in this zone (see "Physical Properties" section, this chapter) to values consistent with that of opal. Further, Pe decreases to a value appropriate for pure opal in some portions of this zone. Very high levels of dissolved silica are present in the deepest interstitial water sample, at 383 mbsf (see "Inorganic Geochemistry" section, this chapter), but core recovery precluded interstitial water sampling below 387 mbsf. At about the depth of this water sample, a diatomaceous clay layer is identified in both Holes 723A and 723B (see "Lithostratigraphy" section, this chapter) and a siliceous bed is evident in log responses around 380–385 mbsf (Fig. 60).

Based on log responses, siliceous microfossil abundance is quite variable below 380 mbsf (Fig. 60). At the bottom of the hole, immediately below the lowest dolomite stringer, the log responses are quite sinusoidal, with a period of 5.5 m. This log response is not an artifact, as it is evident and correlatable in the

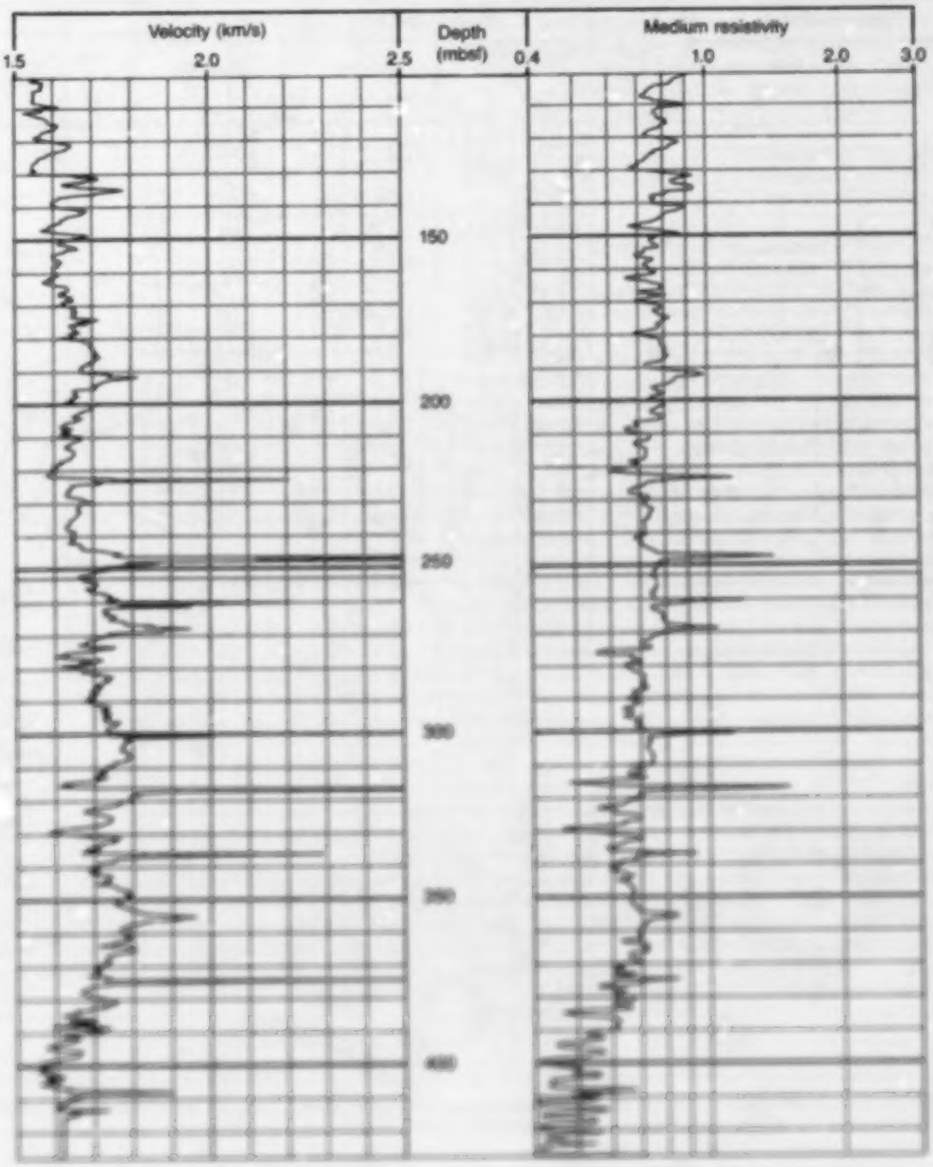

Figure 48. Velocity and resistivity logs. The spikes are interpreted to be dolomite stringers.

lowest logging tool of every logging run. Unfortunately, this zone is so near the bottom of the hole that the length of each tool string prevented all but the bottom tool from sampling this zone. Based on the very low density and Pe of 1.7 for the troughs in log response, the troughs are nearly pure siliceous ooze (Pe = 1.7).

The probable cause of the disappearance of core recovery below 307 mbsf is evident in Figure 48: very soupy sediments (except for the dolomite stringers), more appropriate for an APC core catcher than for an XCB. Neither core recovery nor the number of logs permits accurate determination of the mineralogy of the peaks below 411 mbsf (Fig. 46). The increases in Al_2O_3 and SiO_2 below 380 mbsf (Fig. 46), with Fe_2O_3 and K_2O, suggest that palygorskite may be the dominant clay mineral below 380 mbsf. Both palygorskite and opal may be indicators of high monsoon intensity.

Hole Deviation and Downhole Magnetics

The Schlumberger GPIT tool measures acceleration, hole deviation, and magnetic moment. At Site 723, this tool was included in two tool strings: the lithoporosity combination (Run #1) and the geochemical combination (Run #3). Because Run #2 obtained both downgoing and upcoming logs, a total of three openhole passes with the GPIT was obtained.

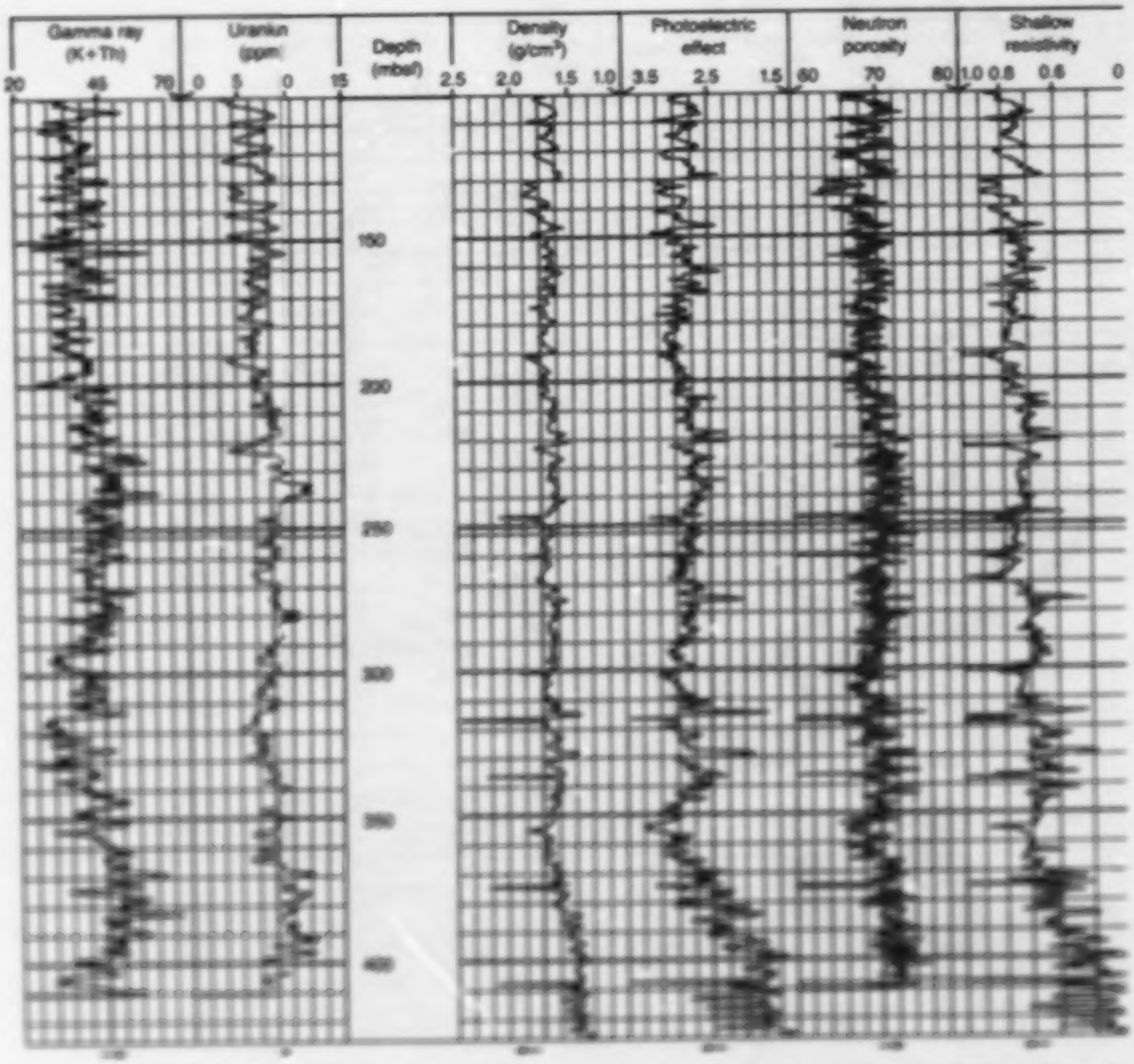

Figure 45. Comparison of physical-properties logs (density, photoelectric effect, neutron porosity and shallow (focused) resistivity) with two indicators of composition that can control these properties. Clay content, as indicated by the potassium + thorium (CGR) log, shows much lower correlation with physical properties in these [illegible] sediments, an indicator [illegible] of organic matter variations.

The two deviation surveys / Run #2 were quite consistent (Fig. 50). Borehole deviation ranges gradually from a 1° tilt to the southeast at 100 mbsf to a 2.5° tilt to the east at 400 mbsf. These deviations are too small to have a significant effect on any interpretations (including paleomagnetism) in this report. A slight difference between the downgoing and upcoming surveys of Run #1 occurs in the interval 210–310 mbsf (Fig. 50). In the downgoing log, a temporary 0.6° deviation excursion begins at the 230-mbsf [illegible] and in the upcoming log a similar 0.5° excursion begins the same point. These excursions are minor in their impact on the measurement of hole deviation, but they are more relevant for the subsequent interpretation of downhole magnets.

The Run #2 deviation [illegible] shows the gradual increase from 1° to 2.5°, but [illegible] is poor. Unlike Run #1, which is pressed against the borehole wall by bowsprings, Run #2 is free to wobble in the borehole. Temporary deviation excursions are common in this log, occurring when the GPIT portion of the toolstring is at or above a dolomite stringer (Fig. 50). This correlation can be seen by comparing locations of double-peaked excursions with locations of dolomite stringers, as indicated by the signal strength [illegible] log obtained on the same logging run.

The three perpendicular fluxgate magnetometers used for measuring azimuth of deviation can also be used to calculate total moment (its intensity and magnetic inclination). The three logs of total moment indicate that the magnetic field of the tool string is quite different for Run #2 than for Run #1. Furthermore, the hole-deviation excursions noted in Figure 50 are reflected by magnetic-moment excursions. This similarity indicates that

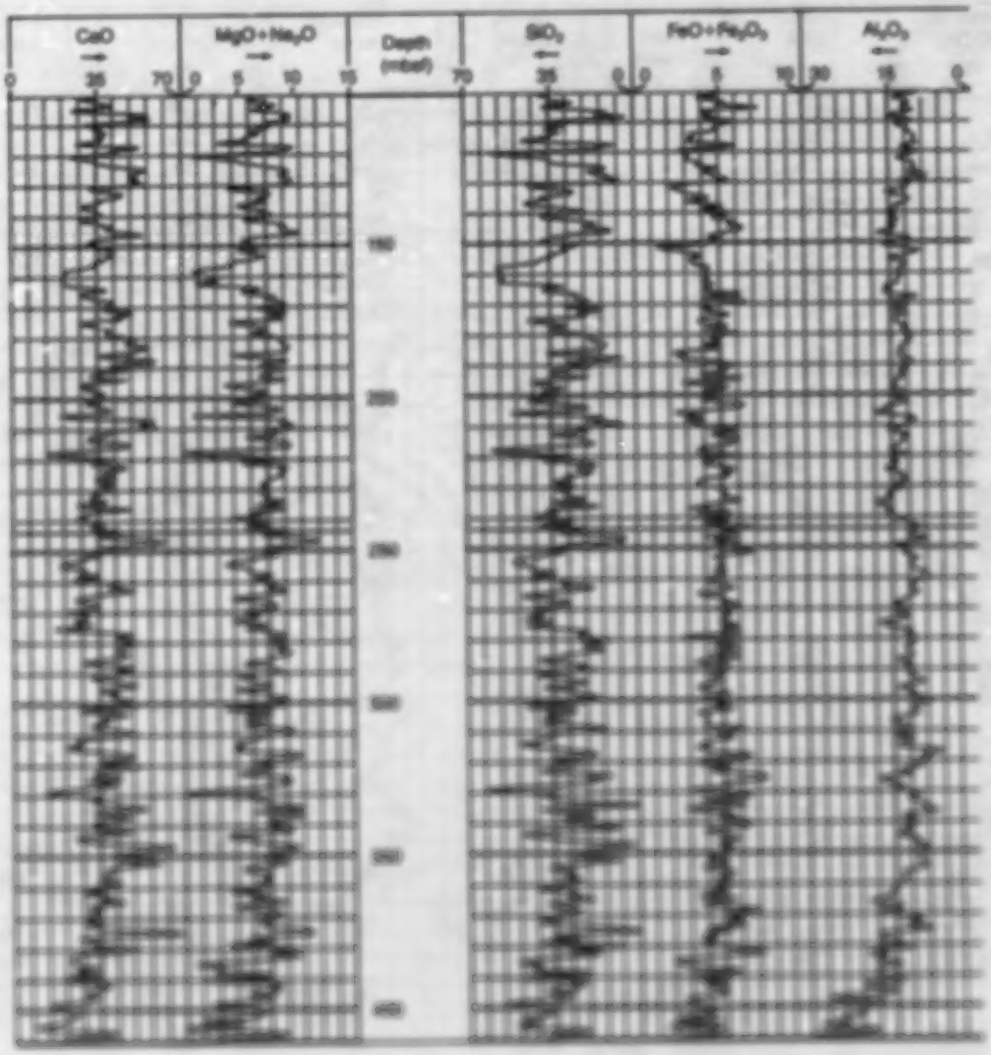

Figure [illegible]. Elemental concentration logs based on [illegible] of geochemical logs. [illegible] (CaO, $MgO + Na_2O$, SiO_2, [illegible]) are expressed as oxide (dry-weight percentages). [illegible]

although the total measured moment is usually a constant vector sum of the earth's magnetic field and logging tool, and this changes the magnitude of this vector sum.

Like total moment, magnetic inclination (Fig. [illegible]) is dominated by the vector sum of the earth's and tool's magnetic moments; thus, the horizontal scale in Figure [illegible] is different for Run [illegible] than for Run [illegible]. The character of the [illegible] inclination records is very similar, except for an obvious excursion at [illegible] mbsf in downgoing Run [illegible], associated with the same collision of the logging tool with a [illegible] stronger than [illegible] in Figure [illegible]. A second collision at the same horizon during the upcoming log is subtle in its magnetic effect, observable at [illegible] mbsf only by comparison with Run [illegible].

The depth-coherent character of the three logging runs strongly suggests that the variations in magnetic inclination are caused by variations in magnetization of the sediments. The sediment magnetization variations could be associated with induced magnetization, viscous remanent magnetization, or magnetic minerals. Although shipboard paleomagnetic analyses to date have not included estimates of the relative magnitudes of these three components, induced magnetization is always much larger than remanent magnetization in deep-sea sediments.

INTERHOLE CORRELATION

Here we provide detailed interhole correlations in the upper [illegible] m of the drilled sediments at Site 723. The upper interval has an age range from 0 to [illegible] Ma and is characterized by cyclic changes in the nature of sediments that can be identified by visual observation and by variations of magnetic susceptibility and $CaCO_3$ content. Correlation of the sedimentary cycles of layers among three holes provides valuable information on the relative rate of sedimentation, which is commonly [illegible]

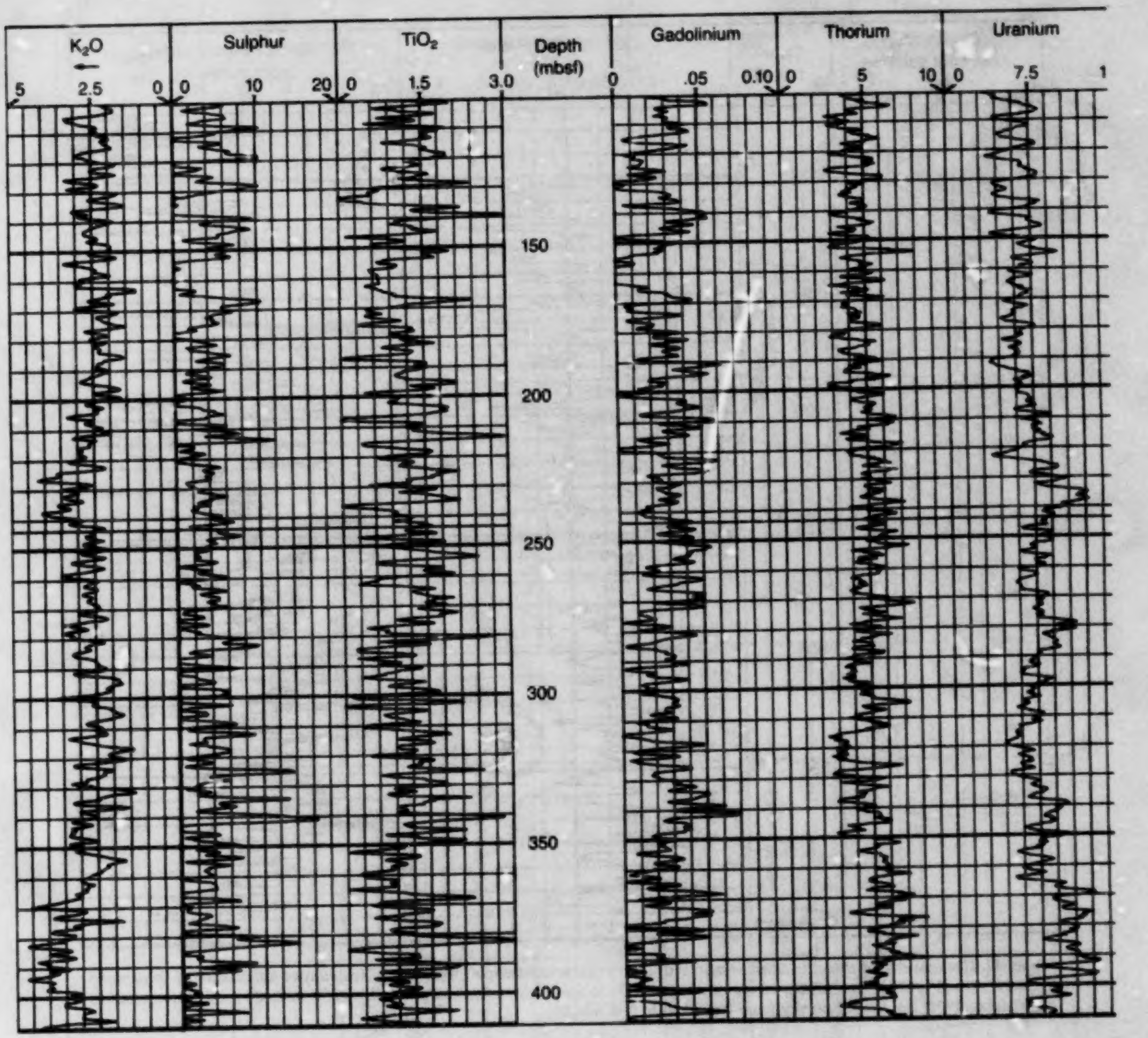

Figure 46 (continued).

high-resolution study of depositional environments. The essence of the correlation process is outlined in the "Explanatory Notes" chapter (this volume).

Hole-to-hole correlations were made on the basis of visual identification of distinctive layers, which were then verified using physical property and magnetic data. The magnetic susceptibility was measured at 10-cm intervals on whole-core sections. Photographs were then taken of the split cores.

The visual correlation of the cores relied primarily on the core photographs. We determined 23 distinct and traceable layers in the upper 80-m interval of the correlatable sedimentary sequence at Site 723 and notated them as OM-a_1, . . . , h_3, and h_4. The letter code (i.e., a, b, c, . . . , etc.) refers to the sequence of cores, and the number code indicates the number of marker layers in each core. For example, the notation "a_2" corresponds to the second marker layer defined in Core 117-723A-1H, and "b_1" denotes the first marker layer in Core 117-723A-2H. The marker layers a_1–h_4 were defined on the cored sediments of Hole 723A above 78.75 mbsf. In order for a marker layer to be defined as such it had to meet the following criteria: the layer must be distinct enough to trace in the sedimentary sequence of the other holes and its character must not change. Useful criteria for recognizing markers are color boundaries, distinctly colored layers, the shape of bioturbation, and the sequence of color changes in the surrounding sediments.

Figure 52 shows the magnetic susceptibility curve and positions of individual, visually correlatable layers. The pattern of the susceptibility and the positions of layers match very well. The stratigraphy of the magnetic susceptibility data and the visually identified layers are extremely consistent in that a particular visually characteristic layer always coincides in depth with a distinct feature in the magnetic susceptibility curve. In this way the lithologic correlations could be verified using the magnetic susceptibility data, which are quantitative. The reliability of the correlations is great; the accuracy of correlation is bounded by the magnetic susceptibility measurement interval (10 cm).

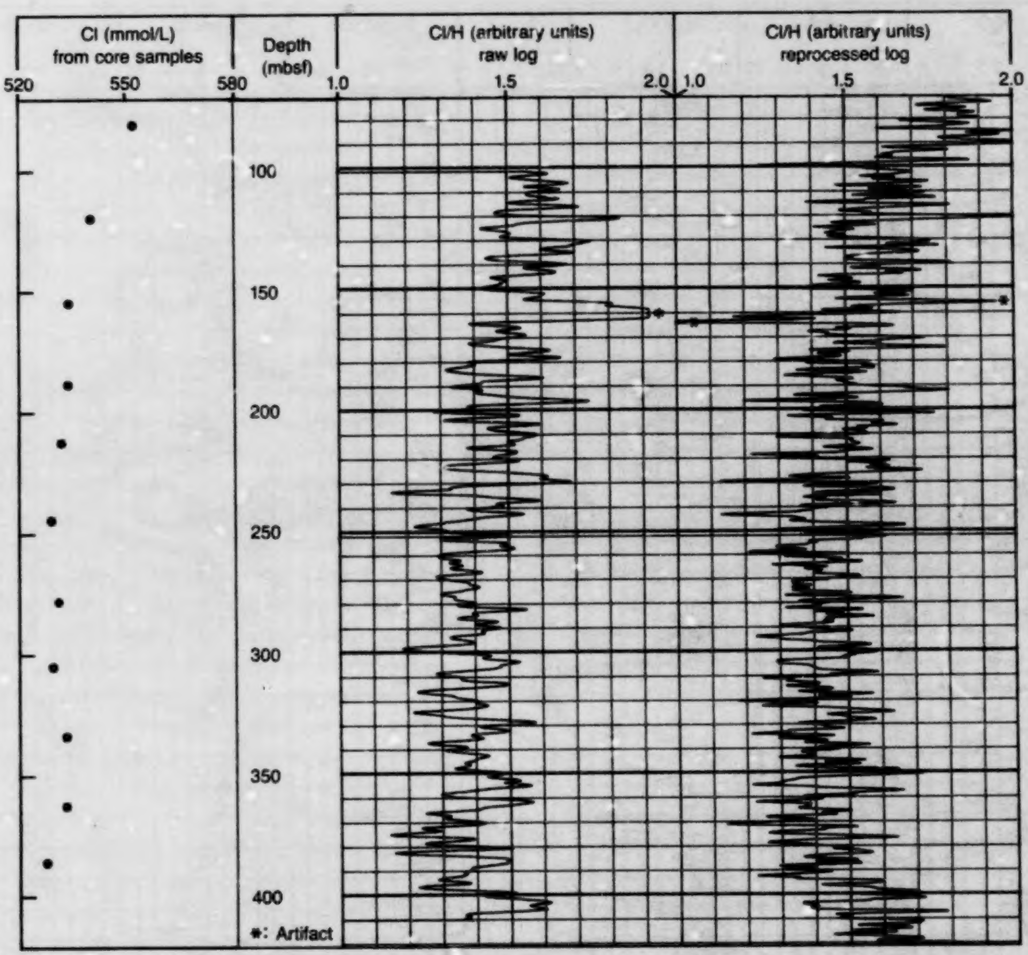

Figure 47. Comparison of chloride concentrations of interstitial water samples with logs of the relative abundance of chlorine to hydrogen. The log at left is reprocessed and the log at right is the original shipboard log. Asterisks indicate spikes interpreted to be artifacts. Note the low chlorinity zone from 150 to 390 mbsf.

The results of the layer-by-layer correlation allow us to calculate true thickness between the layers that coincide with and are separated by core boundaries (Fig. 53). Occasionally, core tops were expanded by water uptake during drilling. In this case, the apparent thickness of the disturbed sediment layer is observed to be thicker than the original thickness. In some instances, the top part of the core was missing; in this case apparent thickness is observed to be thinner than the original thickness. Fortunately, the two holes were staggered in depth, so that they have different horizons at core boundaries (Table 16).

The original thickness of layers coinciding with core tops or bottoms can be obtained by comparing the thicknesses of correlative layers in the continuous sections of other holes. The calculation of the amount of the difference can be achieved by the differences in the ODP depths of marker layers between holes ("723B - 723A ODP" in Table 16). Table 17 gives the differences between the depth (mbsf) calculated by the ODP CORELOG data and the corrected depth (mbsf) calculated by the layer-by-layer correlation method. This method can be applied for the cored sediments, which keep their original thickness within the cored interval. Because cored sediments at Site 723 do not keep their original thickness due to gas expansion below 35 mbsf, we cannot provide either the corrected depth or the precise thicknesses between the marker layers below the gas expansion horizon.

SUMMARY AND CONCLUSIONS

Site 723 is located in the northwest Arabian Sea on the continental margin of Oman and corresponds to the central drilling target of a depth transect of sites across the Oman margin. The transect brackets water depths ranging from 300 to 1500 m that correspond to the vertical extent of a pronounced mid-water oxygen-minimum zone. Site 723 is located in the center of a slope basin formed by a narrow halfgraben in what is presumed to be ophiolitic basement. Biogenic material produced by coastal upwelling and eolian detritus are deposited here at high rates (on average 175 m/m.y.). The sediments were expected to record

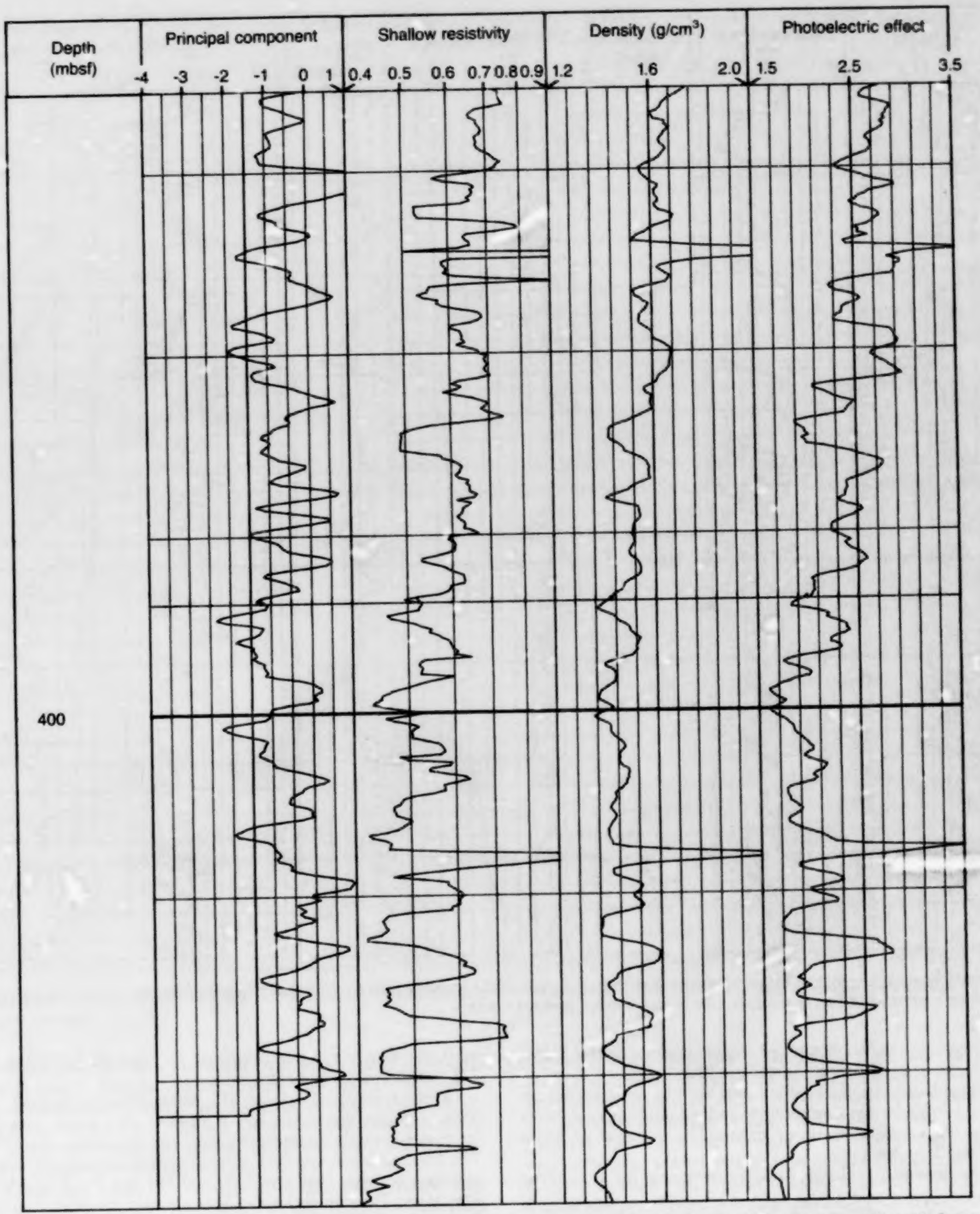

Figure 48. Four logs of the bottom portion of Site 723. The left log is the first principal component of the raw elemental counts from the gamma spectroscopy tool; deflections to the right correspond to high silicon and iron and low calcium.

changes in sedimentation and oceanographic/atmospheric circulation in considerable detail due to impeded benthic activity. The intention of Site 723 was to sample these continuous and expanded sections of upper Neogene to Holocene sediments.

Some of the major findings at Site 723 are summarized in Figure 54 and include the identification of:

1. Laminated, opal-rich facies of late Pliocene and early Pleistocene age. The laminations are interpreted to indicate a lack of bioturbation.
2. Dolomite stringers within the hemipelagic sequence.
3. High accumulation rates (175 m/m.y.) with detrital calcite as an important component.

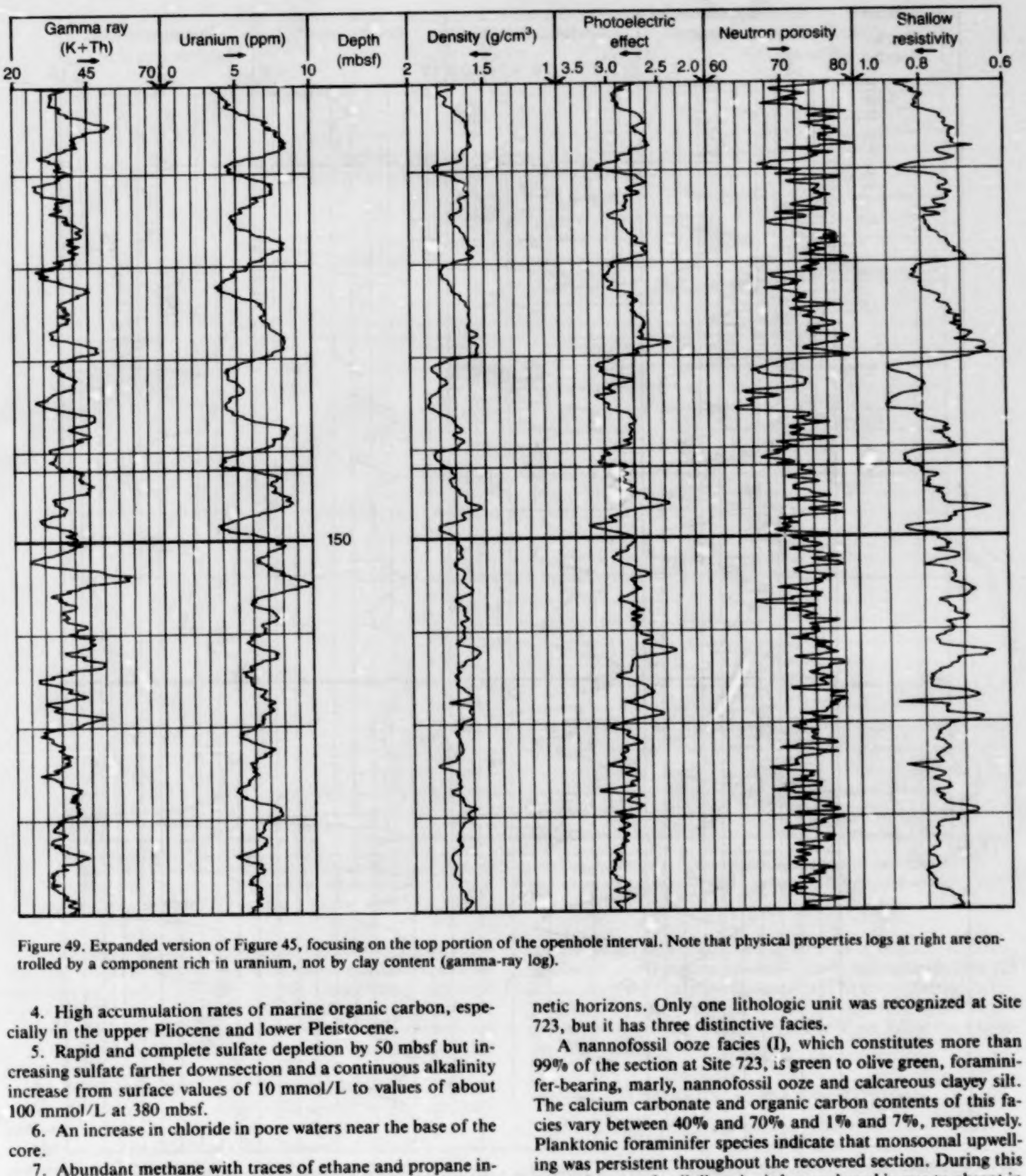

Figure 49. Expanded version of Figure 45, focusing on the top portion of the openhole interval. Note that physical properties logs at right are controlled by a component rich in uranium, not by clay content (gamma-ray log).

4. High accumulation rates of marine organic carbon, especially in the upper Pliocene and lower Pleistocene.

5. Rapid and complete sulfate depletion by 50 mbsf but increasing sulfate farther downsection and a continuous alkalinity increase from surface values of 10 mmol/L to values of about 100 mmol/L at 380 mbsf.

6. An increase in chloride in pore waters near the base of the core.

7. Abundant methane with traces of ethane and propane indicating thermogenic cracking at depth.

8. Distinctive variations of magnetic susceptibility and physical properties that define specific periodicities that can be correlated to the Owen Ridge.

The section penetrated at Site 723 ranges from upper Pliocene (NN18) to the Pleistocene and Holocene. Age control was achieved mainly from calcareous nannoplankton and paleomagnetic horizons. Only one lithologic unit was recognized at Site 723, but it has three distinctive facies.

A nannofossil ooze facies (I), which constitutes more than 99% of the section at Site 723, is green to olive green, foraminifer-bearing, marly, nannofossil ooze and calcareous clayey silt. The calcium carbonate and organic carbon contents of this facies vary between 40% and 70% and 1% and 7%, respectively. Planktonic foraminifer species indicate that monsoonal upwelling was persistent throughout the recovered section. During this interval, nannofossil diversity is low and opal is rare to absent in this facies (Fig. 54). Accumulation rates of carbonate and noncarbonate are consistently high, ranging from 5 to 15 g/cm²/k.y. (Fig. 24), but they are greatest in the upper Pliocene and lower Pleistocene. The rates of accumulation of organic carbon are likewise high, ranging from over 900 mg/cm²/k.y. in the upper Pliocene and lower Pleistocene to an average of about 500 mg/cm²/k.y. in the middle and upper Pleistocene. Both mag-

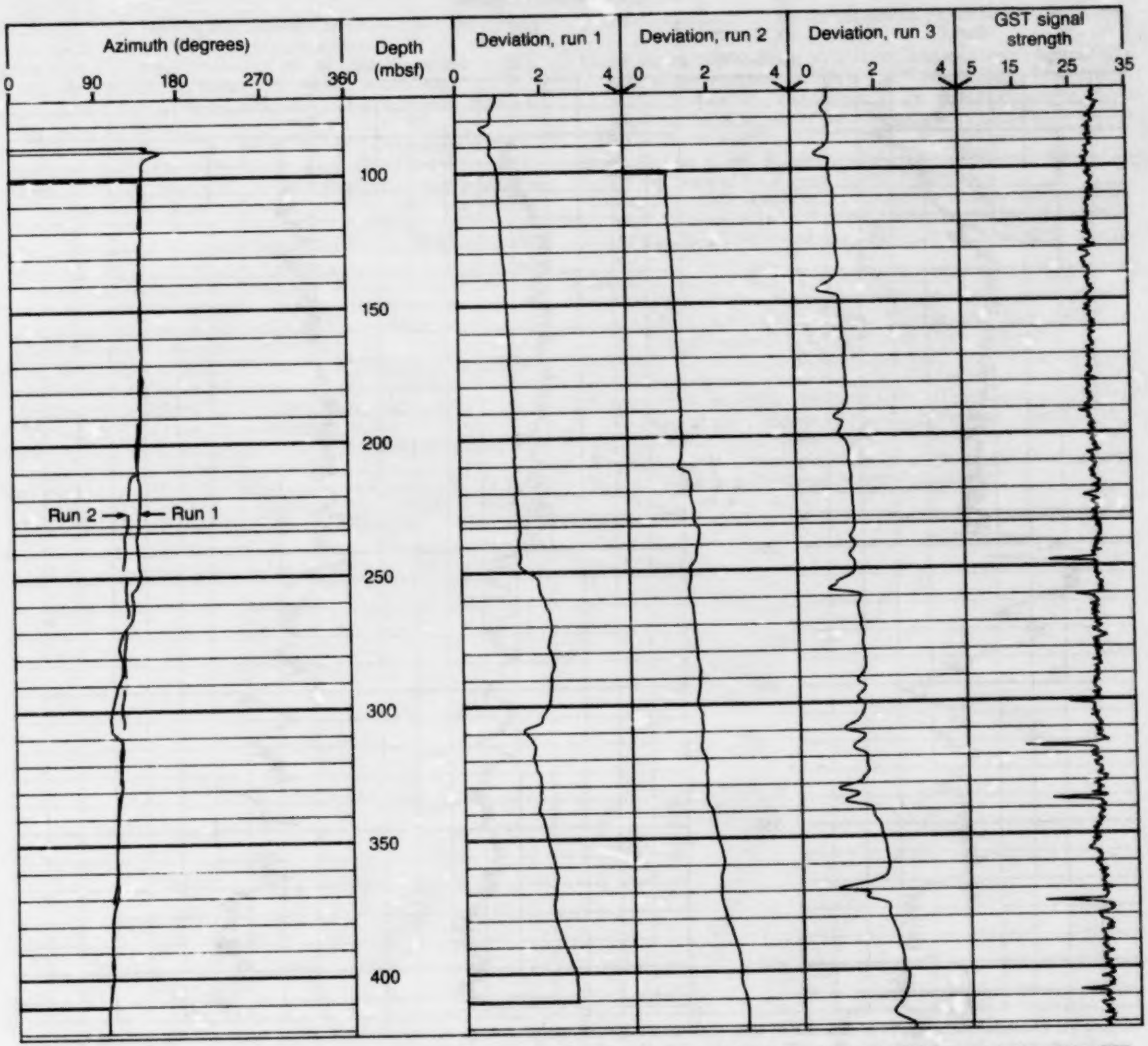

Figure 50. Replicate logs of borehole deviation from vertical and of deviation azimuth, and location of dolomite stringers as indicated by GST signal strength.

netic susceptibility and downhole logs show cyclic variability that probably reflects climate-related changes in the depositional system dominated by upwelling and eolian input. This facies is the hemipelagic background at Site 723, and its rate of accumulation reflects the subsidence of the slope basin as well as the pelagic and terrigenous input.

A dolomite facies (II) consists of occasional cemented beds and stringers of almost pure dolomite that range in color from pale green to olive green. The beds contain foraminifer molds and tests and preserve soft-sediment burrows and primary laminations. Seven dolomite layers, ranging from 5 to 30 cm in thickness, were recovered between 260 and 420 mbsf and two more were identified in the downhole logs. Several of the dolomite layers preserve fine-scale laminations.

A laminated facies (III) consists of beds of parallel laminae which individually are 0.1–1 mm thick. This facies is most frequent in the upper Pliocene, but it is rarely observed in beds exceeding a few centimeters in thickness. Light-colored laminae are accumulations of nannofossils or diatoms and dark-colored layers are organic-rich clayey silt. The occurrence of opal at Site 723 is largely coincident with the laminated facies. The nannofossils in this interval are thought to be indicative of cold water and upwelling. Monospecific assemblages of nannofossils and diatoms in some light laminae suggest that they were produced during blooms of relatively short duration (< 1 yr) and that bioturbation was inhibited, possibly due to complete oxygen depletion in the deeper-water column. High accumulation rates of organic carbon are characteristic of, but not limited to, the laminated facies (Fig. 54). In addition, the laminated facies often occurs in close association with the dolomite facies (Fig. 54).

The chemical composition of the interstitial waters and gas supports the notion that diagenetic cementation of dolomites is related to an unusual hydrologic regime in the subsurface of the slope basin penetrated at Site 723. Alkalinity reached a maxi-

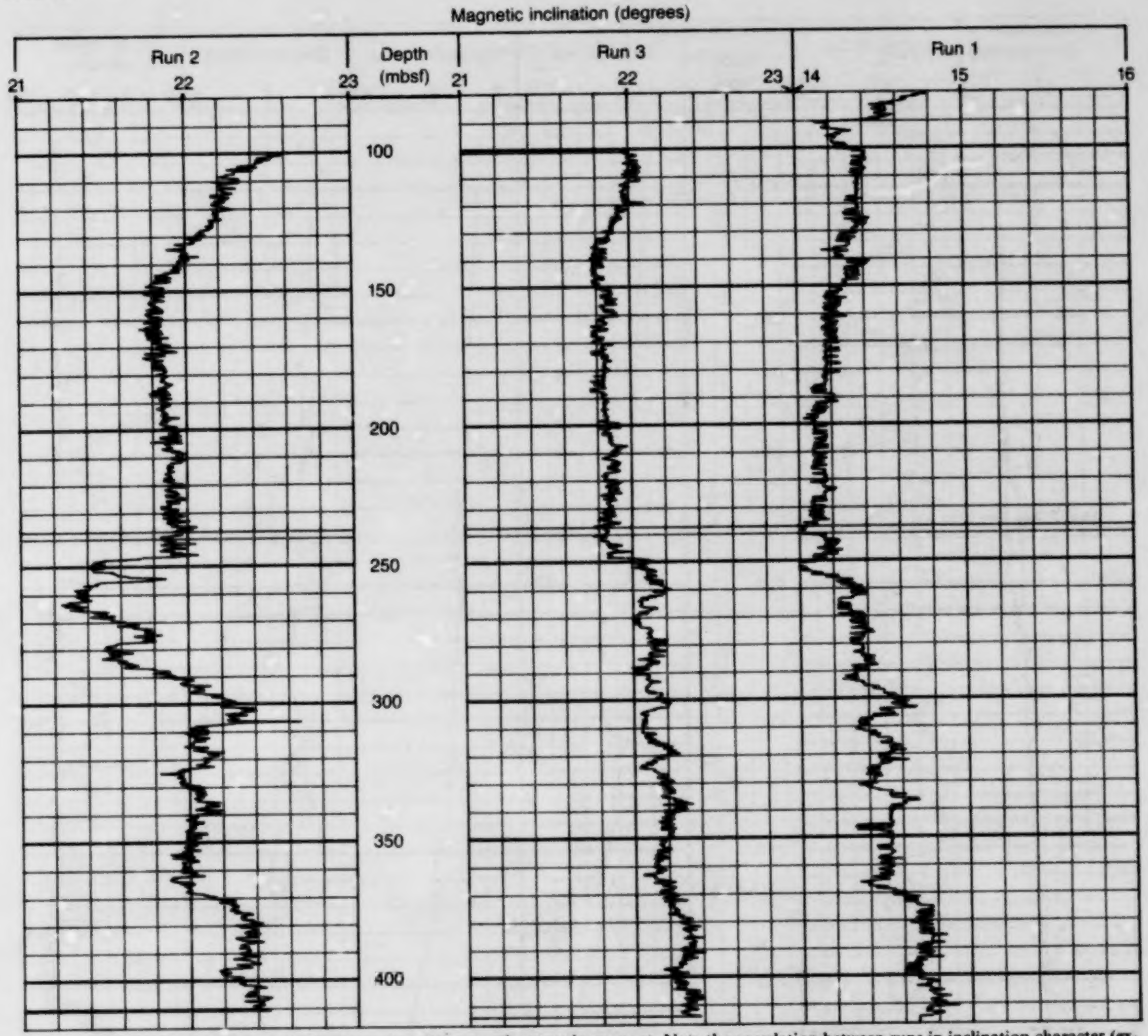

Figure 51. Three replicate logs of inclination of total measured magnetic moment. Note the correlation between runs in inclination character (except for the excursion in downgoing Run #2), indicating detection of sediment magnetization.

mum of >100 mmol/L at total depth (Fig. 54), which appears to be associated with severe degassing (apparently of CO_2) and core expansion, while chlorinity decreased by 30 mmol/L. The reason for the unusually high and persistent increase in alkalinity and for dolomite precipitation below 260 mbsf is a concomitant increase in sulfate below the zone of sulfate depletion (Fig. 54). Profiles of sulfate, chloride, and calcium, as well as magnesium, are attributed to advective flow of fresh water that dissolved gypsum and anhydrite from an evaporitic source. The traces of ethane and propane also indicate that some thermogenic cracking must have occurred within the deeper parts of the margin, possibly below the suspected ophiolite thrusts.

Overall, Site 723 provides a high-resolution record of biotic, chemical, and sedimentologic variations associated with organic-rich sediments deposited under the influence of strong seasonal upwelling and generally low oxygen conditions.

REFERENCES

Arthur, M. A., Srivastava, S., et al., 1987. Site 647. *In* Arthur, M. A., Srivastava, S., et al., *Proc. ODP, Init. Repts.*, 105: College Station, TX (Ocean Drilling Program), 645–907.

Baker, P. A., and Burns, S. J., 1985. Occurrence and formation of dolomite in organic-rich continental margin sediments. *Am. Assoc. Petrol. Geol. Bull.*, 69:1917–1930.

Berggren, W. A., Kent, D. V., and Van Couvering, J. A., 1985. The Neogene: Part 2, Neogene geochronology and chronostratigraphy. *In* Snelling, N. J. (Ed.), *The Chronology of the Geological Record*, Geol. Soc. Mem. (London), 10:211–260.

Canfield, D. E., and Berner, R. A, 1987. Dissolution and pyritization of magnetite in anoxic marine sediments. *Geochem. Cosmochim. Acta*, 51:645–659.

Carlson, R. L., Gangi, A. F., and Snow, K. R., 1986. Empirical reflection travel time versus depth and velocity versus depth functions for the deep-sea sediment column. *J. Geophys. Res.*, 91:8249–8266.

Fertl, H. H., 1979. *Gamma Ray Spectral Data Assists in Complex Formation Evaluation*: Houston (Dresser-Atlas).

Hamilton, E. L., 1976. Variations of density and porosity with depth in deep-sea sediments. *J. Sedimentol. Petrol.*, 46:280–300.

________, 1979. Sound velocity gradients in marine sediments. *J. Acoust. Soc. Am.*, 65:909–922.

Haq, B. U., Hardenbol, J., and Vail, P. R., 1987. Chronology of fluctuating sea levels since the Triassic. *Science*, 235:1156–1167.

Johnson, D. A., and Nigrini, C. A. 1982. Radiolarian biogeography in surface sediments of the eastern Indian Ocean. *Mar. Micropaleontol.*, 7:237–281.

Kolla, V., Kostecki, J. A., Robinson, F., and Biscaye, P. E., 1981. Distribution and origins of clay minerals and quartz in surface sediments of the Arabian Sea. *J. Sedimentol. Petrol.*, 51:563–569.

Martini, E., 1967. Nannoplankton und Umlagerungserscheinungen im Persischen Golf und im nördlichen Arabischen Meer. *Neues Jahrb. Geol. Palaeontol., Monatsh.*, 10:597–607.

Moore, G. W., and Gieskes, J. M., 1980. Interactions between sediment and interstitial water near the Japan Trench, Leg 57, Deep Sea Drilling Project. *In* Scientific Party, *Init. Repts. DSDP*, 56, 57, Pt. 2: Washington (U.S. Govt. Printing Office), 1269–1275.

Nigrini, C. A., 1968. Radiolaria from eastern tropical Pacific sediments. *Micropaleontology*, 14:51–63.

Perch-Nielsen, K., 1984. Cenozoic calcareous nannofossils. *In* Bolli, H., Saunders, J., and Perch-Nielsen, K. (Eds.) *Plankton Stratigraphy*: Cambridge (Cambridge Univ. Press), 427–554.

Sato, T., Takayama, T., Kato, M., Kudo, T., and Kameo, K., in press. Calcareous microfossil biostratigraphy of the uppermost Cenozoic formations distributed in the coast of the Japan Sea. Part 4: Conclusion. *Sekiyu Gijutsu Kyokaishi.*

Shimmield, G. B., and Price, N. B., 1984. Recent dolomite formation in hemipelagic sediments off Baja California, Mexico, *In* Garrison, R. E., Kastner, M., and Zenger, D. H. (Eds.), *Dolomites of the Monterey Formation and Other Organic-Rich Units*, Pacific Section S.E.P.M., 41:5–18.

Suess, E., von Huene, R., et al., 1988. *Proc. ODP, Init. Repts.*, 112: College Station, TX (Ocean Drilling Program).

Takayama, T., 1972. A note on the distribution of *Braarudosphaera bigelowi* (Gran and Braarud) Deflandre in the bottom sediments of Sendai Bay, Japan. *Paleontol. Soc. Japan, Trans. Proc. N. S.*, 87:429–435.

Takayama, T., and Sato, T., 1987. Coccolith biostratigraphy of the North Atlantic Ocean, Deep Sea Drilling Project, Leg 94. *In* Ruddiman, W. E., Kidd, R. B., Thomas, E., et al., *Init. Repts. DSDP*, 94, Pt. 2: Washington (U.S. Govt. Printing Office), 651–702.

Whelan, J. K., Tarafa, M. E., and Hunt, J. M., 1982. Volatile C_1-C_8 organic compounds in macroalgae. *Nature*, 299:50–52.

Whitmarsh, R. B., 1979. The Owen Basin off the southeast margin of Arabia and the evolution of the Owen Fracture Zone. *Geophys. J. R. Astron. Soc.*, 58:441–470.

Wyrtki, K., 1971. *Oceanographic Atlas of the Indian Ocean Expedition:* Washington (National Science Foundation).

Ms 117A-110

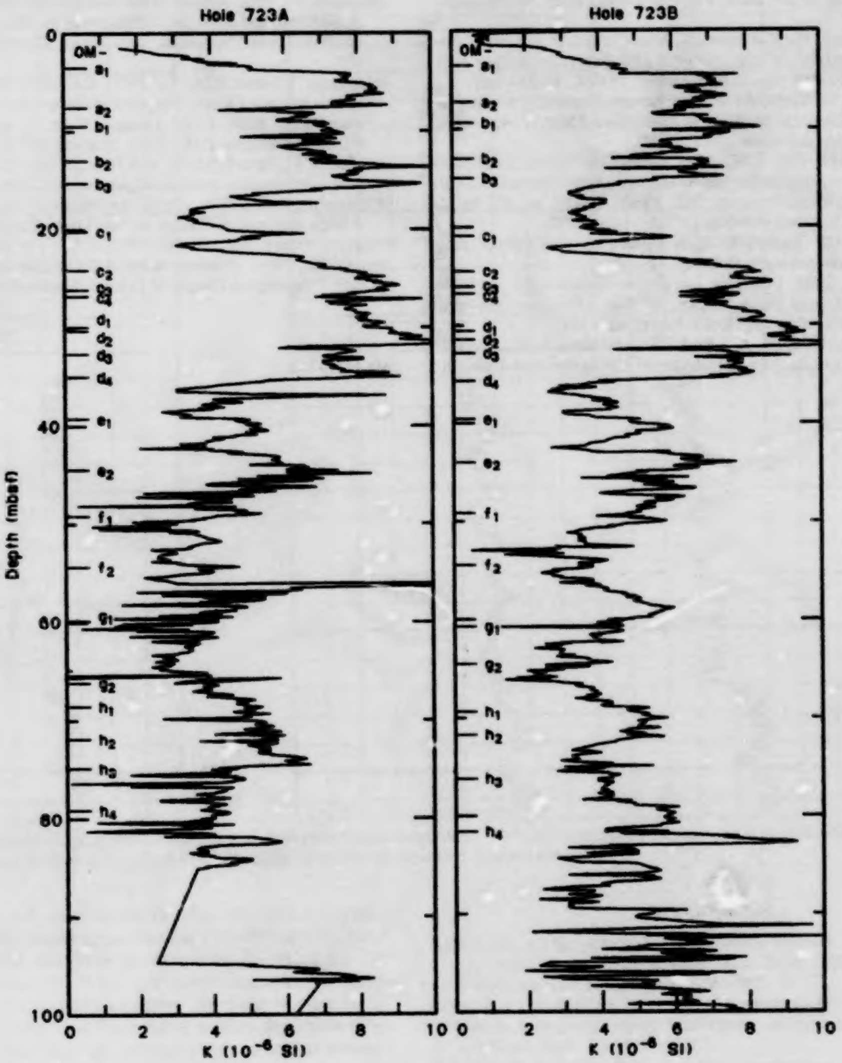

Figure 52. Magnetic susceptibility and positions of marker layers at Holes 723A and 723B.

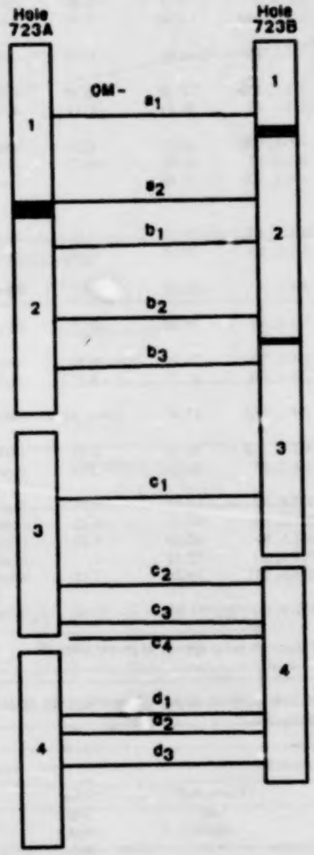
Hole 723A
Hole 723B
OM-
a1
a2
b1
b2
b3
c1
c2
c3
c4
d1
d2
d3
1
2
3
4
1
2
3
4

Figure 53. Correlation of Holes 723A and 723B based on marker layers.

Table 16. Stratigraphic depths and descriptions of the marker layers at Site 723 for layer-by-layer correlation in the Oman margin.

	Hole 723A		Hole 723B			
Layer	Core, sample, interval (cm)	Depth (mbsf)	Core, sample, interval (cm)	Depth (mbsf)	Holes 723B – 723A	Remarks[a]
OM-a_1	1H-3, 20	3.20	1H-3, 35	3.35	0.15	top of white later (10)
a_2	1H-5, 125	7.25	2H-3, 20	7.50	0.25	base of dark layer (10 horizontal)
b_1	2H-2, 55	9.85	2H-4, 65	9.45	−0.40	central band of 3 very black bands (30)
b_2	2H-4, 90	13.20	2H-6, 110	12.90	−0.30	base of dark band in dark layer overlying light layer
b_3	2H-6, 10	15.40	3H-1, 95	14.95	−0.45	very black layer in dark zone (5–10 semi-horizontal)
c_1	3H-3, 10	20.60	3H-5, 110	21.10	0.50	very black layer (20 horizontal mottled)
c_2	3H-5, 110	24.60	4H-1, 85	24.45	−0.15	dark layer in basal part of white layer; top of centimeter-scale lamination
c_3	3H-6, 130	26.30	4H-2, 100	26.10	−0.20	laminated top light band in dark interval
c_4	3H-7, 45	26.95	4H-3, 15	26.75	−0.20	dark band overlying light layer
c_5	—	—	4H-3, 100	27.60	—	lower dark thin band (50 mm) of 3 bands in light layer (present in Hole 723B only; upper band noted as OM-c_4)
d_1	4H-2, 135	29.95	4H-5, 70	30.30	0.35	dark band overlying light layer (20–30)
d_2	4H-3, 70	30.80	4H-6, 10	31.20	0.40	dark layer overlying light layer with sharp contact
d_3	4H-4, 65	32.25	4H-7, 5	32.65	0.40	basal boundary of dark layer (10 semihorizontal)
d_4	4H-6, 45	35.05	5H-2, 50	35.30	0.25	very black band in middle part of dark layer
e_1	5H-2, 90	39.20	5H-5, 20	39.50	0.30	white layer overlain by dark layer (10)
e_2	5H-6, 35	44.65	6H-1, 90	43.80	−0.85	dark band in lower part of light layer (20 vertical)
e_3	—	—	6H-3, 150	47.40	—	dark band in dark layer overlying on light layer (present in Hole 723B only)
f_1	6H-2, 115	49.05	6H-5, 120	50.10	1.05	dark band in dark layer (20–30 vertical)
f_2	6H-6, 70	54.60	7H-2, 15	54.25	−0.35	base of black layer overlying light interval (horizontal 10)
g_1	7H-3, 75	59.85	7H-6, 30	60.40	0.55	dark band in dark layer
g_2	7H-8, 5	66.65	8H-2, 60	64.40	−2.25	center of black layer (20–30 vertical)
h_1	8H-2, 80	68.10	8H-5, 90	69.20	1.10	top of white layer (20 semivertical)
h_2	8H-5, 30	72.10	9H-1, 20	72.10	0	base of dark band in light interval
h_3	8H-6, 140	74.70	9H-3, 135	76.25	1.55	boundary between dark layer and light layer (30 vertical)
h_4	9H-3, 35	78.75	9H-7, 95	81.85	3.10	light band in dark layer

[a] Description of bioturbation and size of layer (in mm) appear in parentheses.

Table 17. Correlated sub-bottom depth of core-top for stratigraphic sub-bottom depth calculation.

	Hole 723A				Hole 723B		
Core	ODP top depth (mbsf)	Difference	Corrected top depth (mbsf)	Core	ODP top depth (mbsf)	Difference	Corrected top depth (mbsf)
1H	0	0	0	1H	0	0	0
2H	7.8	−0.6	7.2	2H	4.3	−0.3	4.0
3H	17.5	0.9	17.8	3H	14.0	0.1	13.8
4H	27.1	0.5	27.6	4H	23.6	0.7	24.1

Note: ODP top depth = sub-bottom depth of core top calculated by the ODP CORELOG data; Difference = the difference between the depth calculated by the ODP CORELOG data and the depth calculated by the layer-by-layer correlation method; Corrected top depth = sub-bottom depth of core top calculated by the layer-by-layer correlation method.

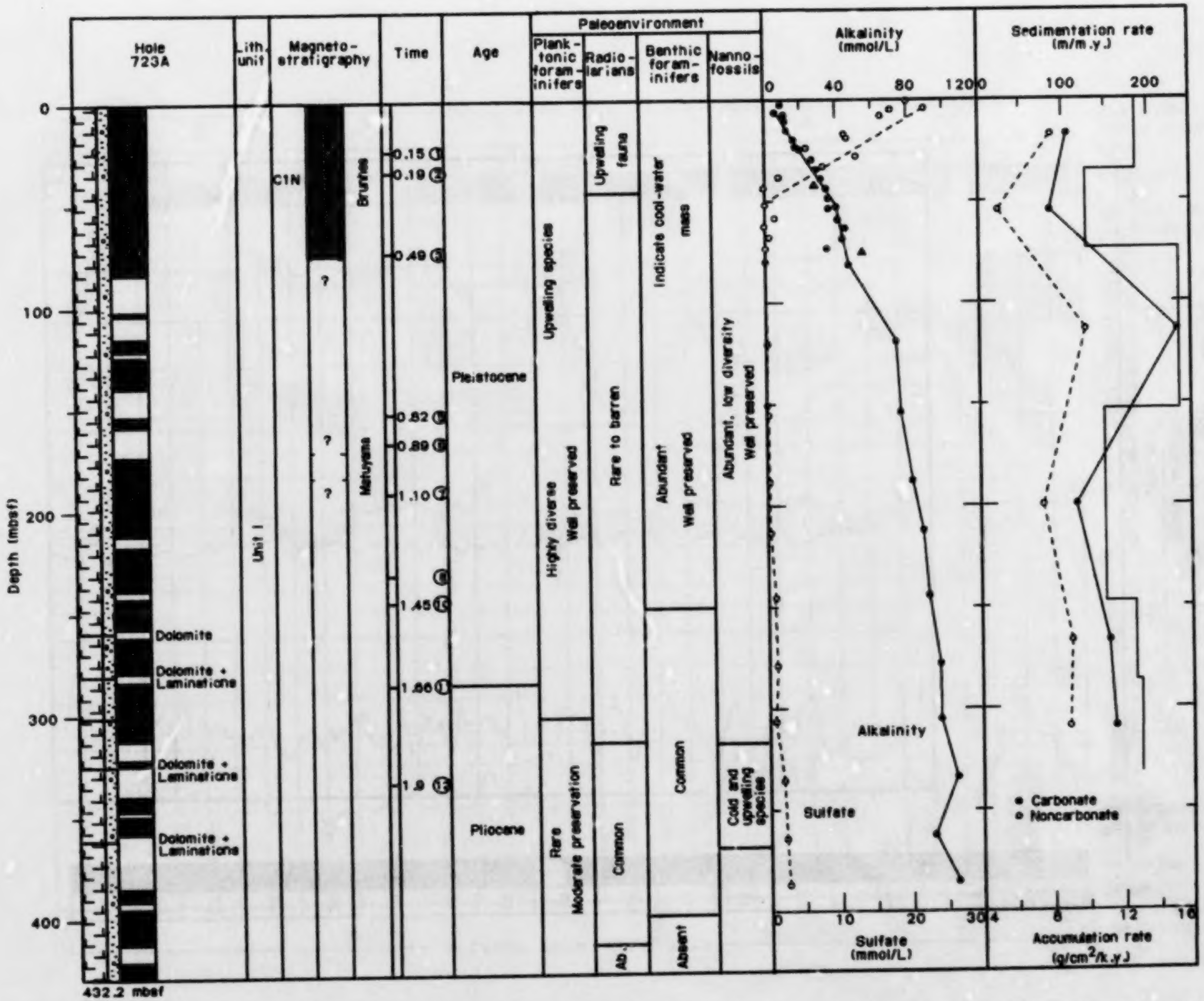

Figure 54. Summary chart outlining preliminary shipboard findings at Site 723. Numbers in circles under "Time" correspond to nannofossil datum levels (see "Biostratigraphy" section, this volume).

Summary Log for Hole 723B

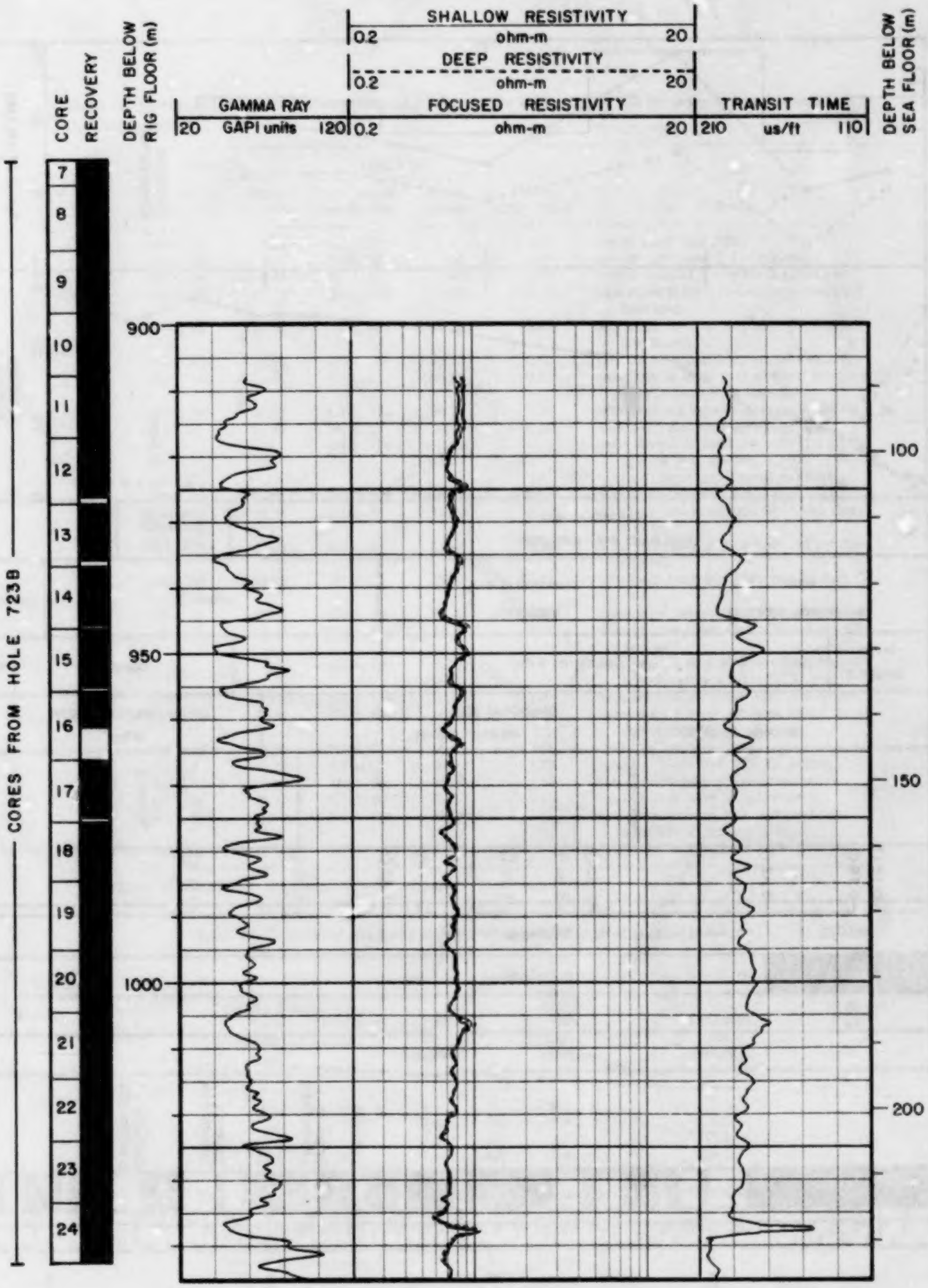

Summary Log for Hole 723B (continued)

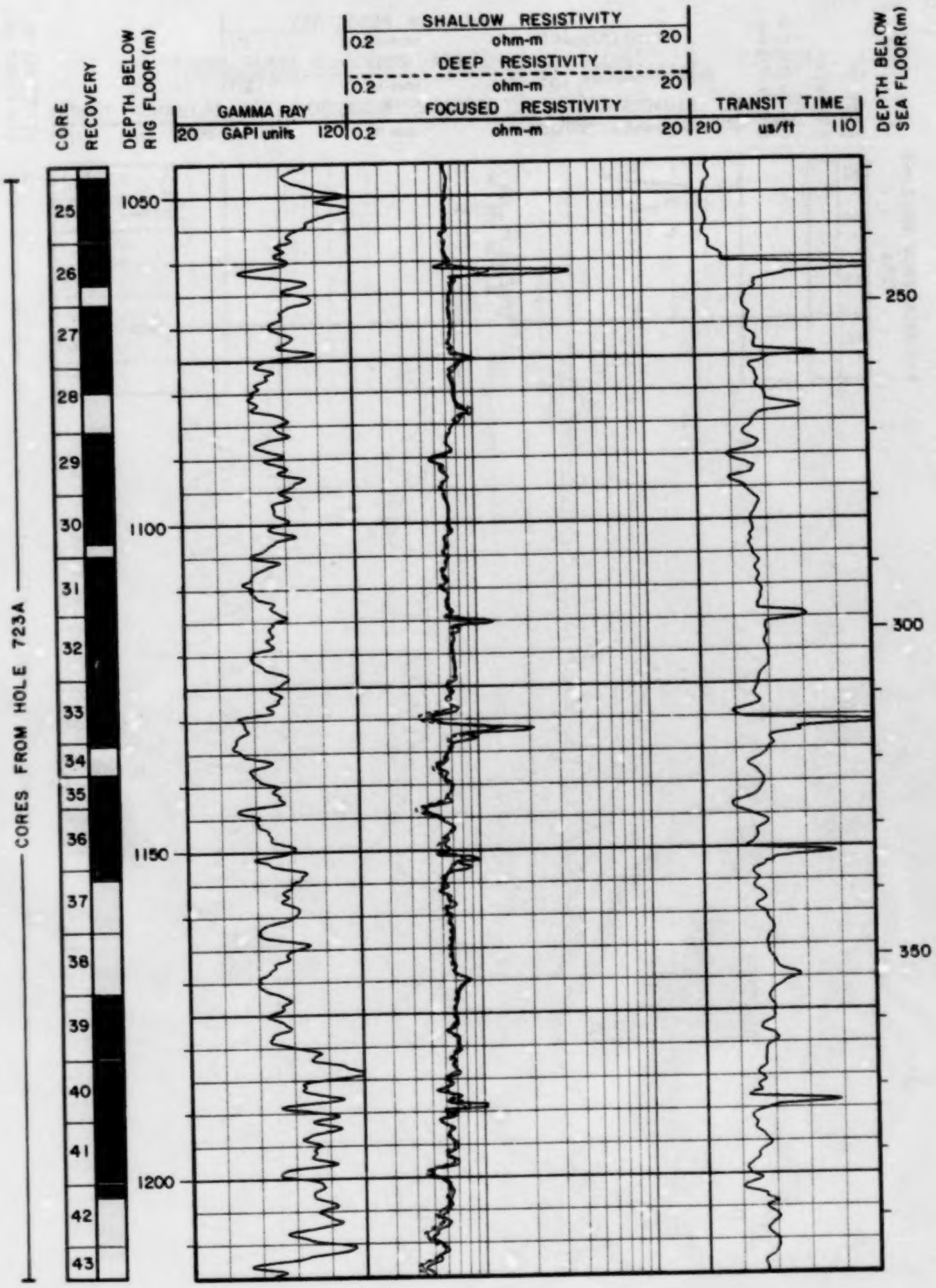

Summary Log for Hole 723B (continued)

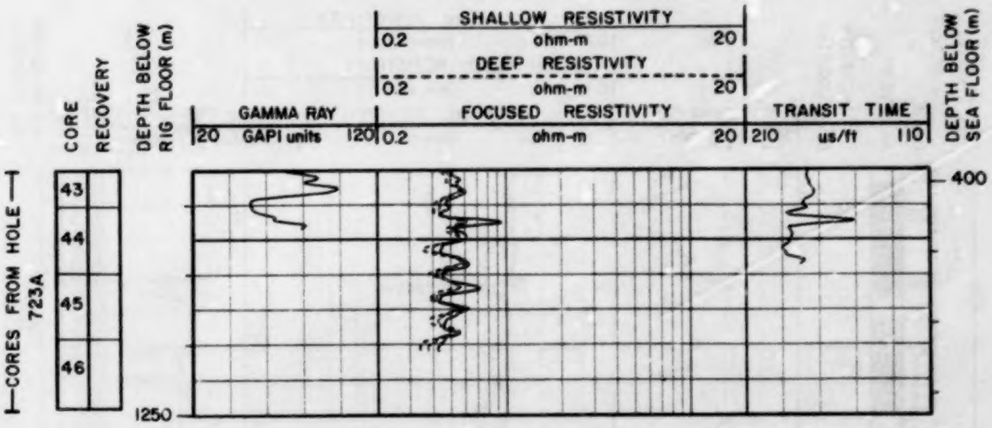

Summary Log for Hole 723B (continued)

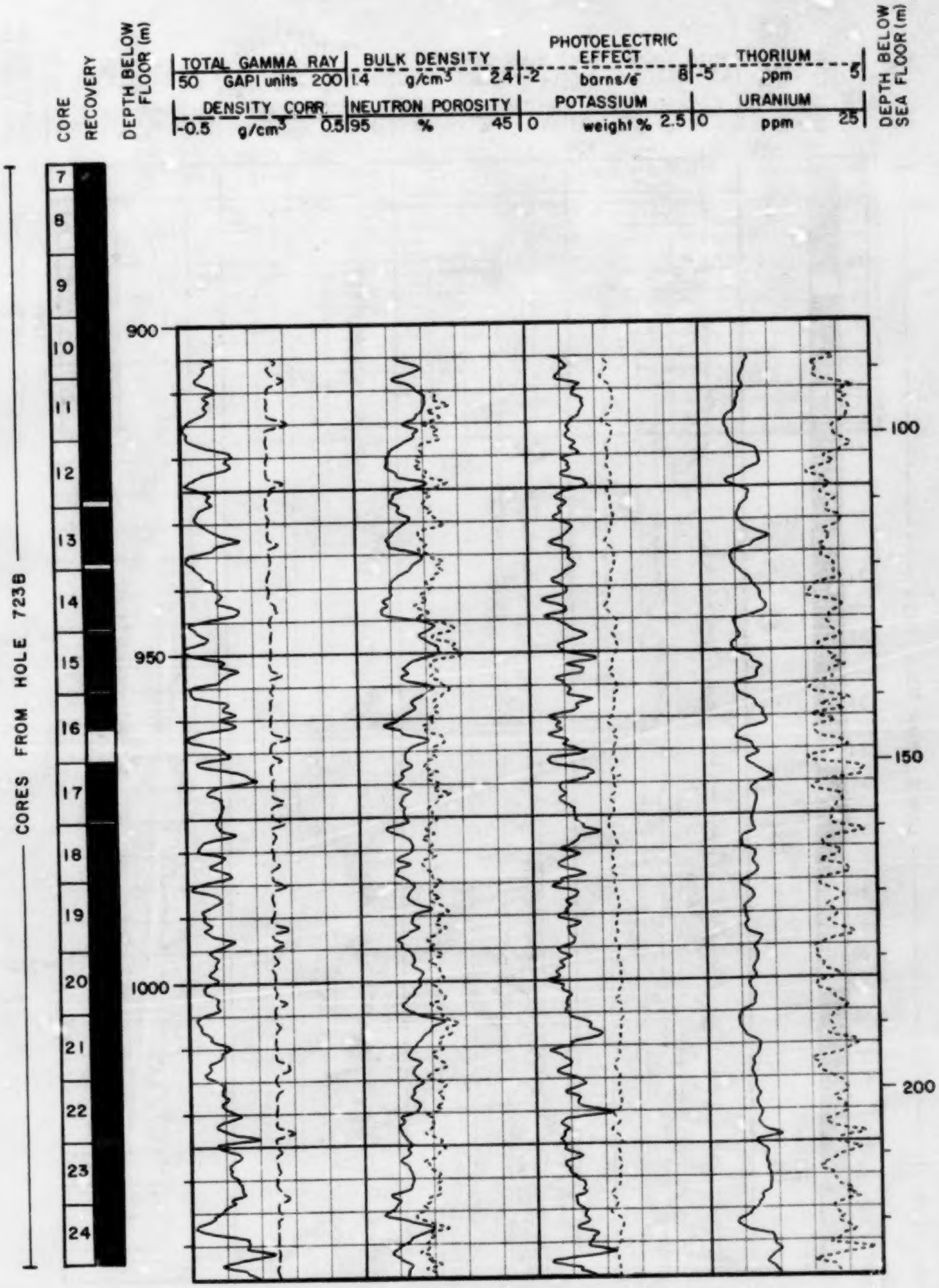

Summary Log for Hole 723B (continued)

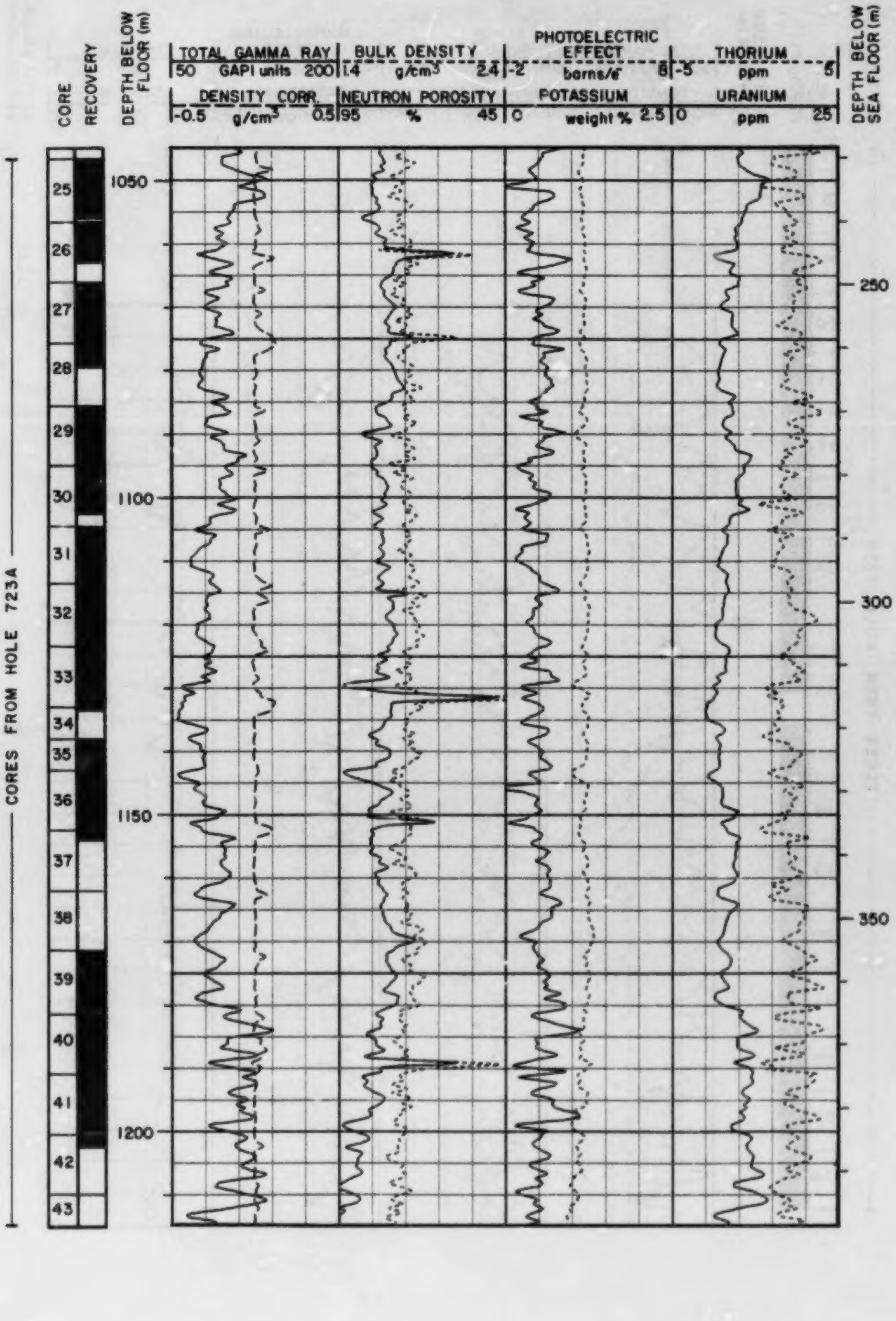

Summary Log for Hole 723B (continued)

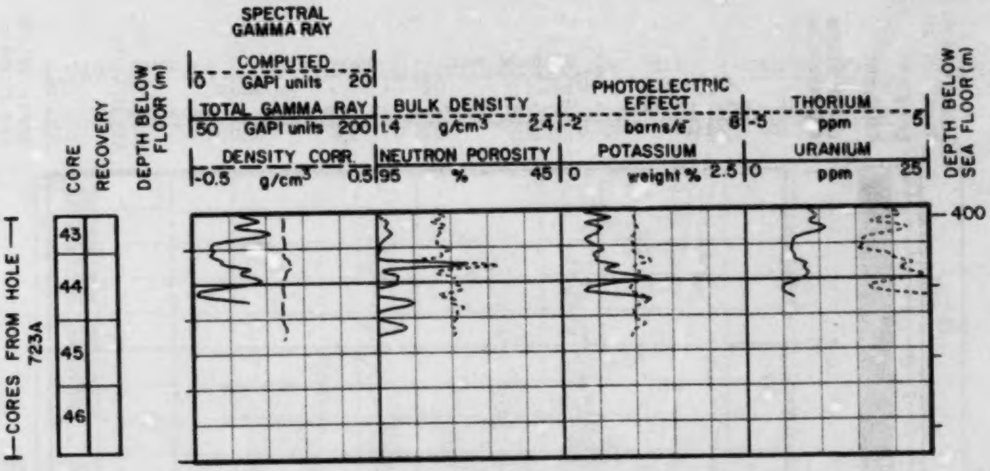

Summary Log for Hole 723B (continued)

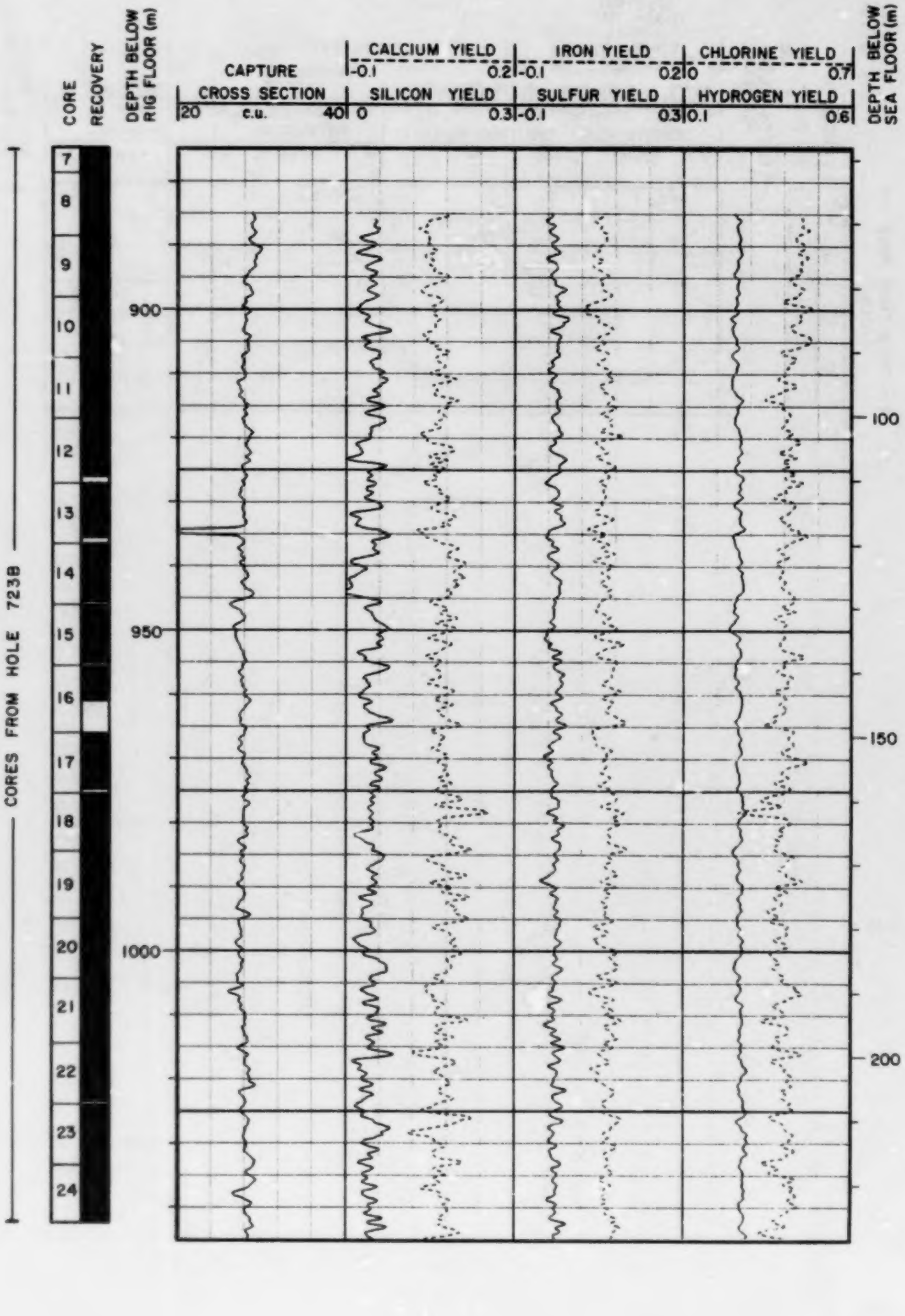

Summary Log for Hole 723B (continued)

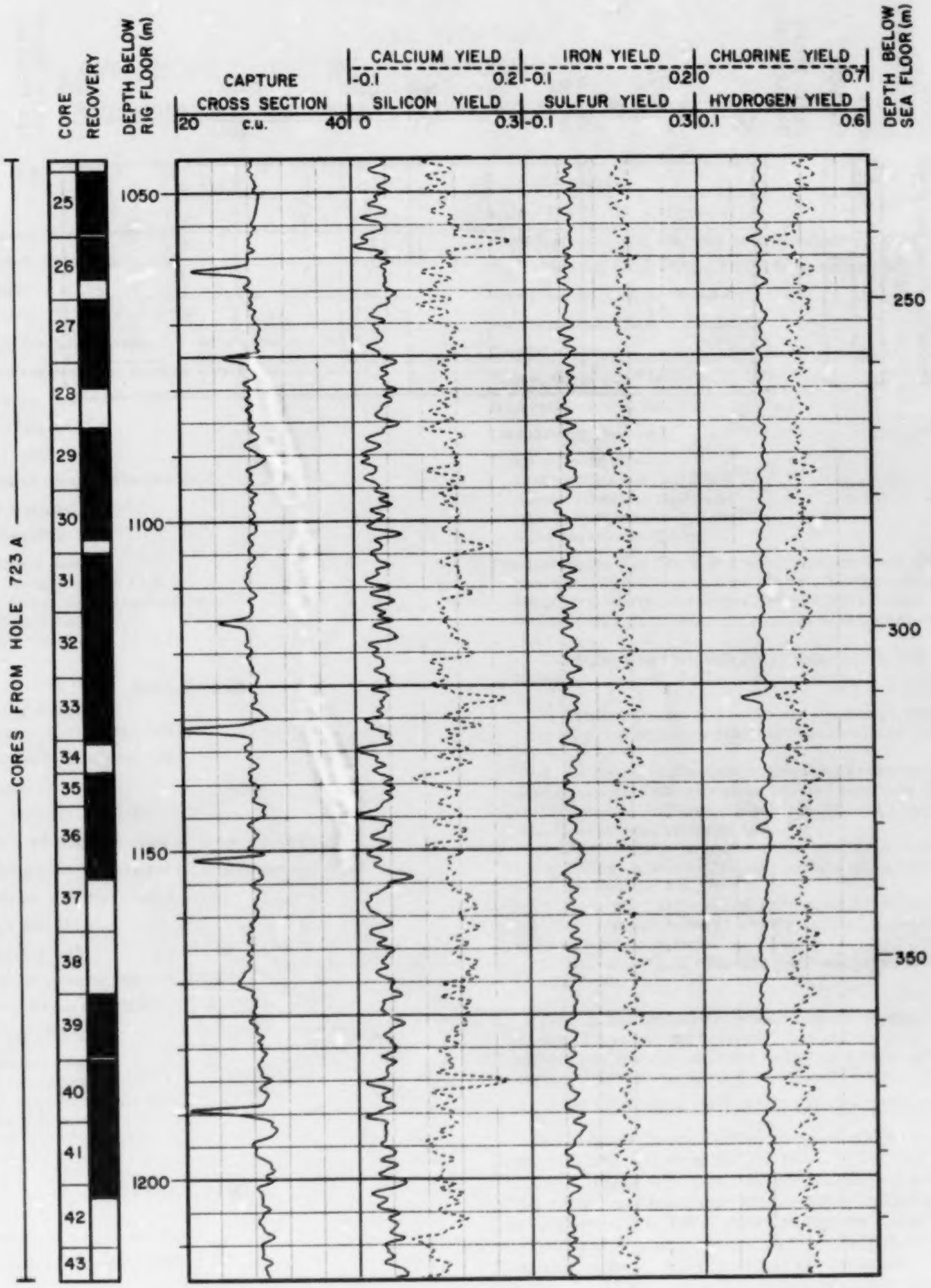

Summary Log for Hole 723B (continued)

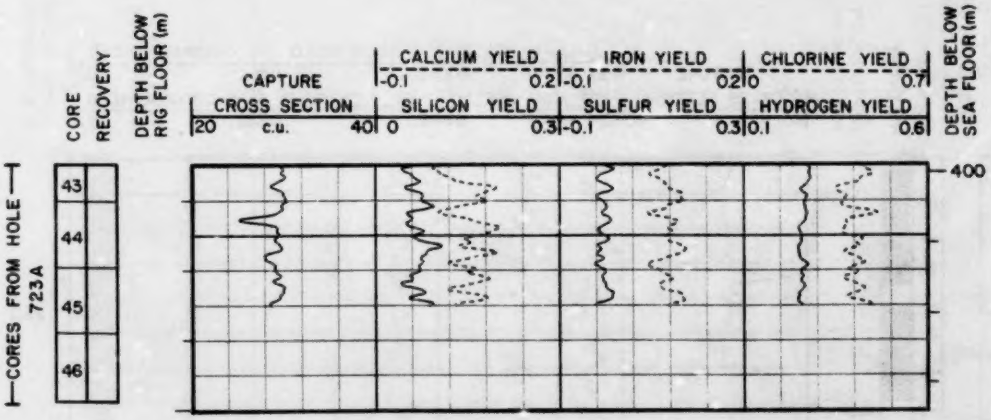

12. SITE 724[1]

Shipboard Scientific Party[2]

HOLE 724A

Date occupied: 20 September 1987

Date departed: 20 September 1987

Time on hole: 16 hr

Position: 18°27.713′N, 57°47.147′E

Water depth (sea level; corrected m, echo-sounding): 592.8

Water depth (rig floor; corrected m, echo-sounding): 603.3

Bottom felt (m, drill pipe): 602.5

Penetration (m): 44.5

Number of cores: 5

Total length of cored section (m): 44.5

Total core recovered (m): 44.8

Core recovery (%): 100.7

Oldest sediment cored:
Depth sub-bottom (m): 44.8
Nature: foraminifer nannofossil ooze
Age: Pleistocene
Measured velocity (km/s): 1.6

HOLE 724B

Date occupied: 20 September 1987

Date departed: 21 September 1987

Time on hole: 15 hr

Position: 18°27.713′N, 57°47.147′E

Water depth (sea level; corrected m, echo-sounding): 592.8

Water depth (rig floor; corrected m, echo-sounding): 603.3

Bottom felt (m, drill pipe): 602.0

Penetration (m): 257.7

Number of cores: 27

Total length of cored section (m): 257.7

Total core recovered (m): 213.7

Core recovery (%): 82.9

Oldest sediment cored:
Depth sub-bottom (m): 257.7
Nature: calcareous clayey silt
Age: early Pliocene
Measured velocity (km/s): —

HOLE 724C

Date occupied: 21 September 1987

Date departed: 21 September 1987

Time on hole: 16 hr

Position: 18°27.713′N, 57°47.147′E

Water depth (sea level; corrected m, echo-sounding): 592.8

Water depth (rig floor; corrected m, echo-sounding): 603.3

Bottom felt (m, drill pipe): 603.2

Penetration (m): 252.4

Number of cores: 27

Total length of cored section (m): 252.4

Total core recovered (m): 242.7

Core recovery (%): 96.2

Oldest sediment cored:
Depth sub-bottom (m): 252.4
Nature: calcareous clayey silt
Age: early Pliocene
Measured velocity (km/s): —

Principal results: Site 724 is at a water depth of about 600 m in the northern part of the upper slope basin on the continental margin of Oman. It is the central drilling target of a depth transect that corresponds to the vertical extent of a pronounced mid-water oxygen-minimum zone.

The major findings at Site 724 include identification of the following:

1. Laminated facies of late Pliocene age that are similar to, but older than, the organic-carbon- and opal-rich facies found at Site 723.
2. An interval of abundant preservation of radiolarians and diatoms and concomitant poor preservation of planktonic foraminifers that occurs near the Pliocene/Pleistocene boundary and is partially coincident with the laminated facies.
3. The occurrence of shallow-water benthic foraminifers in the upper Pliocene section, which may indicate substantial subsidence of the site over the past 3 to 4 m.y.
4. An ongoing reduction of sulfate over the entire section and low Mg^{2+} concentrations. In contrast to Site 723, diagenetic dolomites were not encountered.
5. Trace amounts of ethane, propane, and butane increase steadily with depth.

Overall, Site 724 provides new information about the subsidence of slope basins between basement ridges and on the history of the carbon-rich, opal-rich laminated facies that are associated with the oxygen-minimum zone along the continental margin.

BACKGROUND AND OBJECTIVES

Site 724 of the Ocean Drilling Program (ODP) is in a water depth of about 593 m at 18°27.713′N, 57°47.147′E, on the continental margin of Oman. The site position is near the center of the upper slope basin that was previously drilled at Site 723. The location of Site 724 is shown in Figures 1 and 2, and the structural and depositional setting of the site is shown in Figure 3. At this location, the slope basin is only about 5 km wide, compared to 15 km at Site 723. It is bounded on the west by a faulted block and on the east by a basement ridge. Both basement features are thought to be ophiolite complexes.

Seismic-reflection profiles of the basin sediments show numerous highly reflective layers that both onlap onto and are de-

---

[1] Prell, W. L., Niitsuma, N., et al., 1989. *Proc. ODP, Init. Repts.*, 117: College Station, TX (Ocean Drilling Program).

[2] Shipboard Scientific Party is as given in the list of Participants preceding the contents.

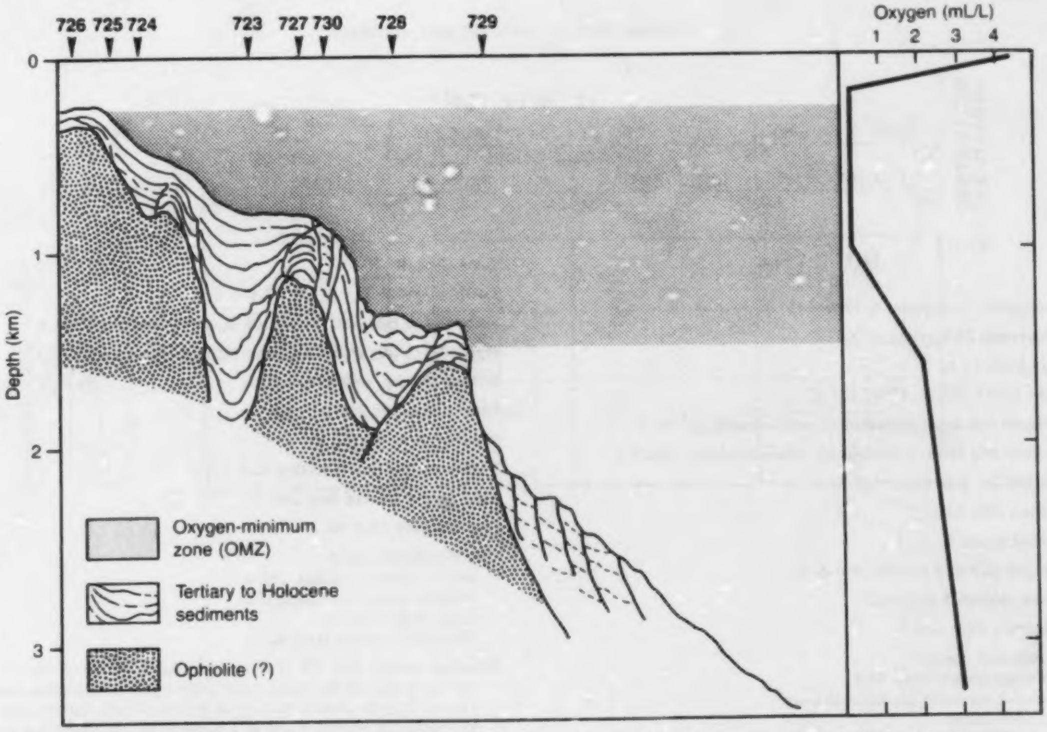

Figure 1. Structure of the Oman margin and the oxygen-minimum zone. The schematic cross section across the margin shows the series of basement ophiolite blocks and the sedimentary basins between them. The concentration of oxygen in the water column (RC2704; unpubl. data, 1986) defines the depth range of the oxygen-minimum zone and where it impinges on the margin.

formed by the adjacent basement structures. The sediments are thickest in the center of the basin and form a syncline-shaped deposit (Fig. 3A) that thickens significantly to the south along the strike of the basin (Fig. 3B). In the shallow sediments near Site 724, some channeling is observed about 5 km to the north, and a large slump scar is noted about 9 km to the south (Fig. 3B). The east-west slope of the sediment surface from the shelf to the seaward edge of the basin is about 2%. The subsurface layers (reflectors) shoal slightly over the basement high, from which they deepen to the south. Comparison of reflector depths at Sites 723 and 724 indicates that the average accumulation rates at Site 724 should be about one-half those at Site 723. Site 724 was located in a water depth of about 600 m to provide samples from the middle of the oxygen-minimum zone in an area with an estimated accumulation rate of about 80 m/m.y. Thus, the site was expected to provide an additional high-resolution sedimentary record of Pliocene-Pleistocene variations of monsoonal upwelling and the oxygen-minimum zone.

The specific objectives for drilling at Site 724 were:

1. To obtain a high-resolution record of the sediments associated with the near-coastal zone of the monsoonal upwelling system, in order to establish the changes in timing and intensity of the monsoon.
2. To provide part of a depth transect that will be used to examine the organic-rich sedimentary facies of the margin and establish their relationship to the oxygen-minimum zone and its spatial variation through time.
3. To document the diagenetic processes associated with the oxygen-minimum zone and the organic-carbon-rich sediments.
4. To search for evidence of changes in the structure of the intermediate water masses of Arabian Sea during the Pliocene-Pleistocene.

OPERATIONS

JOIDES Resolution departed Site 723 at 0030 hr on 20 September 1987. A combined seismic survey of drilling targets OM-3 (Site 724) and OM-4 (Site 725) was begun upon departure. The ship's track during the survey is shown in Figure 4.

After locating the site on the survey line, the beacon was lowered on a taut wireline in 592.8 m water depth at 1045 hr. The position of Site 724 was assessed as 18°27.713′N and 57°47.147′E by the global positioning satellite system.

The mud line of Hole 724A was shot at 1200 hr on 20 September (Table 1). After successfully coring to Core 117-724A-5H with the advanced piston corer (APC) system (0.0 to 44.5 m below seafloor [mbsf] at 100.7% recovery), the core barrel parted during retrieval of Core 117-724A-6H at an overpull of 120,000 lb, and Hole 724A had to be abandoned.

Hole 724B was spudded at 1600 hr on 20 September without offsetting the rig, and five APC cores, averaging 102% recovery, were obtained from the interval 0.0 to 45.0 mbsf before switching to the extended core barrel (XCB) system. Coring of Hole 724B ended at total depth of 257.7 mbsf, the target depth, after cutting Core 117-724B-27X. Average recovery for the 22 XCB cores was 79%. As was the case at Site 723, core expansion caused by gas was severe throughout the cored section. Overall recovery in Hole 724B was 82.9% (Table 1).

After clearing the mudline of Hole 724B at 0800 hr on 21 September, Hole 724C was spudded after offsetting 10 m to the

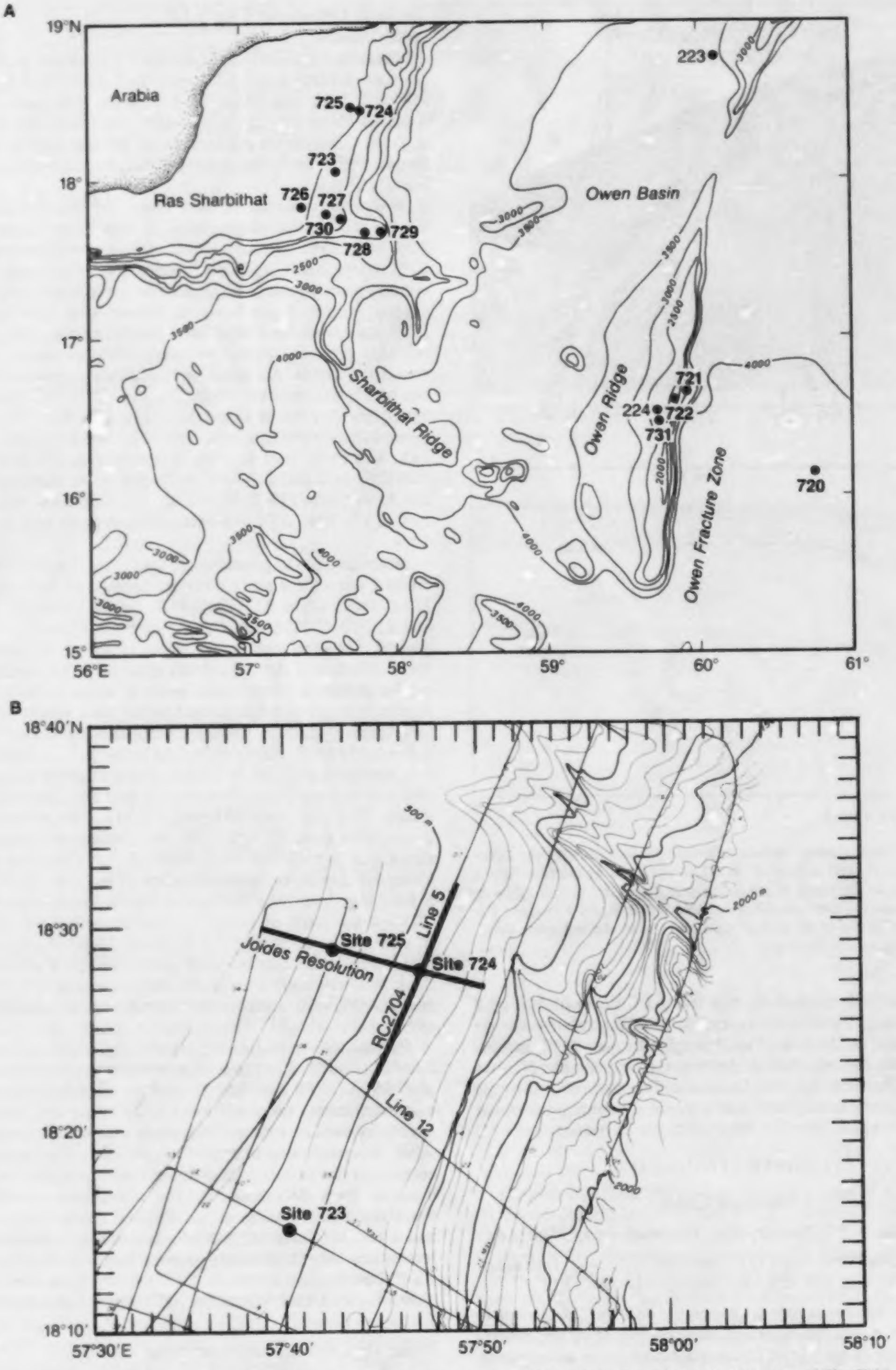
A
19°N
18°
17°
16°
15°
56°E
57°
58°
59°
60°
61°
Arabia
Ras Sharbithat
Owen Basin
Sharbithat Ridge
Owen Ridge
Owen Fracture Zone
223
725
724
723
726
727
730
728
729
721
224
722
731
720
2500
3000
3500
4000
2000
B
18°40′N
18°30′
18°20′
18°10′
57°30′E
57°40′
57°50′
58°00′
58°10′
500 m
2000 m
2000
Site 725
Site 724
Site 723
Joides Resolution
Line 5
RC2704
Line 12

Figure 2. **A.** Bathymetry of the Oman margin (in meters) and the location of Site 724. **B.** Detailed location of Site 724 and the seismic profiles shown in Figure 3. Bathymetry (in meters) and seismic data are from the site survey (RC2704; unpubl. data, 1986).

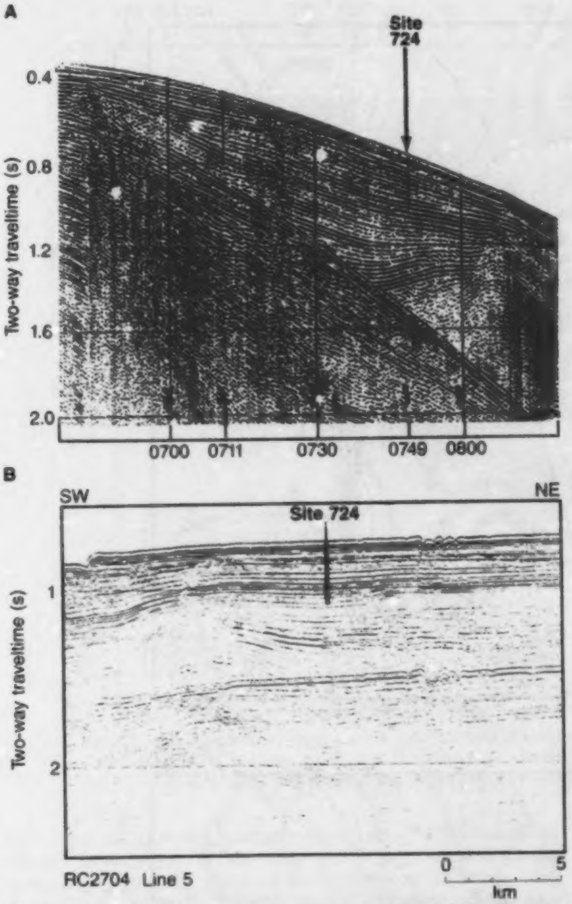

Figure 3. A. Single-channel seismic-reflection profiles showing the structural and depositional setting of Site 724. *JOIDES Resolution* line is perpendicular to the trend of the basin and shows the bounding basement blocks and the syncline-shaped sediment fill. B. RC2704 Line 5 is positioned along the strike of the basin and shows the sediment thickness decreasing to the northeast.

southwest at 0830 hr. Recovery of five APC cores (0.0 to 40.8 mbsf) averaged 105%, whereas coring in XCB mode for the remaining cores to 252.4 mbsf total depth averaged 94%, including voids from core expansion. Average recovery for the 27 cores was 96.2%. The hole was displaced with weighted mud, the pipe was pulled, and the ship was underway in dynamic positioning mode to relocate to Site 725 by 2400 hr on 21 September.

LITHOSTRATIGRAPHY

Lithologic Units

Unit I (Depth, 0–257.7 mbsf; Age, Holocene–early Pliocene)

Cores 117-724A-1H through 117-724A-5H, 117-724B-1H through 117-724B-27X, and 117-724C-1H through 117-724C-27X.

Only one lithologic unit is recognized at Site 724. Unit I is subdivided into two facies, as indicated on Figure 5. The calcareous clayey silt facies (facies I) comprises the entire sedimentary sequence of Hole 724A and the majority of Holes 724B and 724C. A laminated diatomaceous clayey silt facies (facies II) forms beds a few decimeters to meters thick in the lower cores of Holes 724B and 724C (Table 2).

Facies I: Calcareous Clayey Silt

Facies I dominates the sedimentary sequence at Site 724 and consists of black (5Y 2.5/2), very dark gray (5Y 3/1), olive gray (5Y 4/2, 5/2), and olive (5Y 5/3) beds. The beds range from 5 cm to about 250 cm thick, with most beds between 50 and 200 cm. Contacts are predominantly burrow mottled and gradational over a few centimeters, although some contacts are extremely sharp.

Based on smear slide data (areal percentages illustrated in Fig. 6) the average composition of this facies is approximately 30% clay, 25% detrital calcite, 10% quartz (mainly silt size), 20% nannofossils, and 2% foraminifers. The smear slides also contain trace amounts of glauconite, collophane, dolomite, and organic matter. A few horizons contain over 30% nannofossils (55% maximum) and have lower detrital calcite, clay, and quartz contents (Fig. 6). Quartz and clay contents remain fairly constant throughout this facies. Foraminifers increase from an average of 5% in Cores 117-724A-1H, 117-724B-1H, and 117-724C-1H to about 15% in Cores 117-724B-11X and 117-724C-11X. Foraminifers decrease in Cores 117-724B-14X and 117-724C-14X, and from there on, values remain near 2% down to Cores 117-724B-18X and 117-724C-18X. Below the development of facies II in Cores 117-724B-19X to 117-724B-23X and 117-724C-19X to 117-724C-23X, the foraminifer content returns to around 10%.

According to the geochemical data (Figs. 7 and 8 and Table 3), facies I has an average carbonate content of 55% above Cores 117-724B-19X and 117-724C-19X; below Cores 117-724B-23X and 117-724C-23X, the average carbonate content is 47%. In general, the carbonate values from smear slides (nannofossils, foraminifers, and detrital calcite) agree with the geochemical values for particular stratigraphic levels to within 15%, although the former is based on areal percent rather than weight percent. The total organic carbon (TOC) determinations (Table 3) average 1.4% for facies I. Smear slide data show that the light (olive, 5Y 4/3, and olive gray, 5Y 5/2) beds of the calcareous clayey silt facies tend to have more nannofossils and less clay than the dark (black, 5Y 2.5/2, very dark gray, 5Y 3/1, dark olive gray, 5Y 3/2, and olive gray, 5Y 4/2) beds. An unusual development of facies I is a 1- to 1.5-m-thick layer of finely bedded calcareous clayey silt that lacks burrow mottles. (The term "finely bedded" is used here merely to distinguish this layer in facies I from the "laminated" beds of facies II.) The finely bedded layer occurs in all three holes at Site 724 at about 16 mbsf and consists of millimeter- to centimeter-scale beds, averaging about 5 mm in thickness, which are alternately dark olive gray (5Y 3/2) and olive gray (5Y 4/2). Identical sediments were observed at 25 mbsf at Site 723.

Phosphatic or apatite nodules occur at several horizons at Site 724 (Fig. 5). Two types of nodules were observed: a soft yellow brown (10YR 5/6) variety with an elliptical cross section of a mean diameter ranging from 5 to 20 mm and a hard black to dark gray variety with an irregularly shaped cross section of a mean diameter ranging from 2 to 50 mm. The second variety commonly has surface impressions of what may have been woody material (now decomposed). The phosphatic composition of these nodules was demonstrated by X-ray diffraction (XRD) and a test involving crystals of ammonium molybdate and dilute nitric acid, which turn yellow in the presence of phosphorus (G. Shimmield, pers. comm., 1987). One of the hard nodules is illustrated in Figure 9 with its XRD trace shown in Figure 10.

Facies II: Laminated Diatomaceous Clayey Silt

This facies forms beds from 5 to 175 cm thick (average 62 cm) with laminae less than 1 mm thick. The laminae are dark olive gray (5Y 3/2), olive gray (5Y 4/2), and olive (5Y 5/4). Smear slide results from seven laminae yield a mean composi-

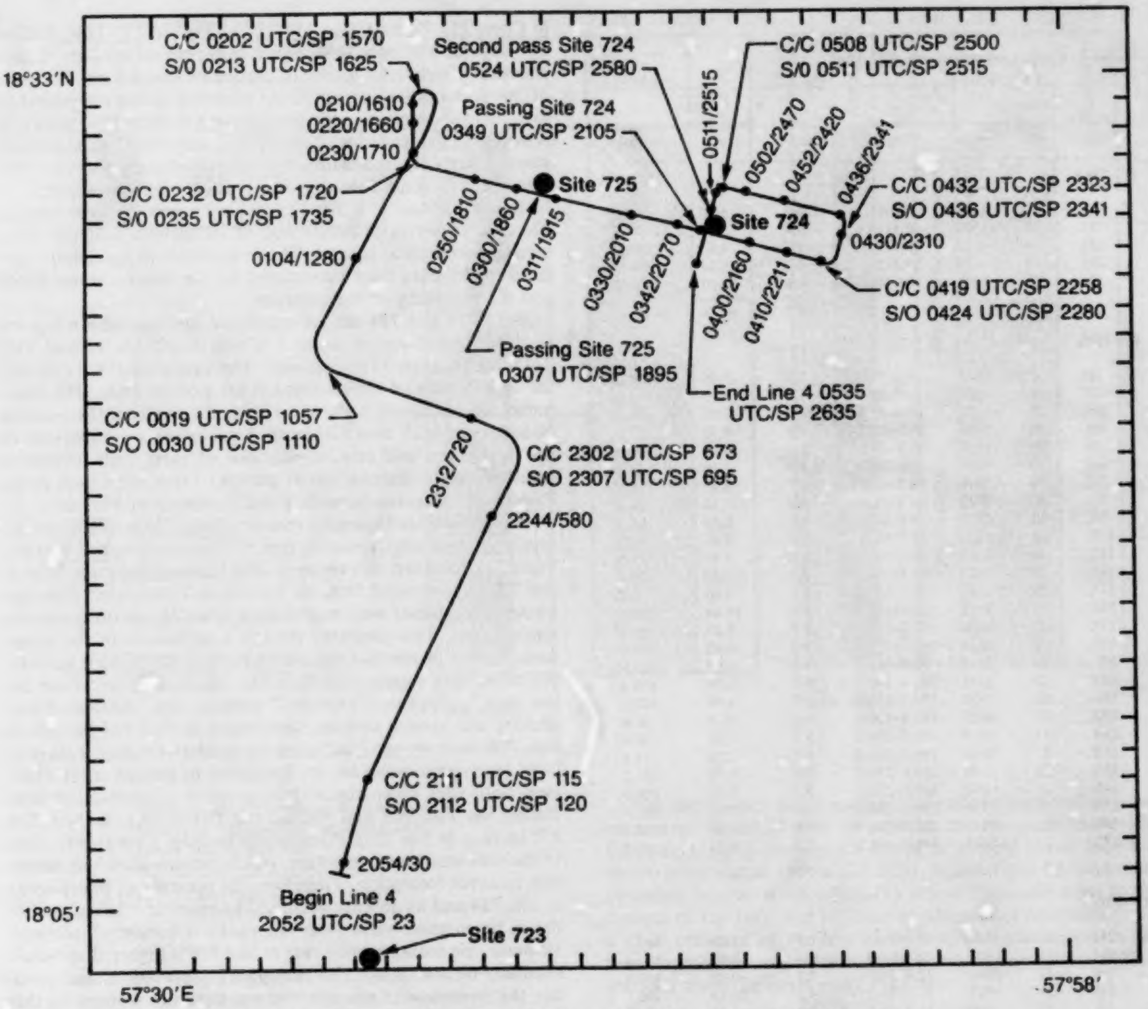
C/C 0202 UTC/SP 1570
S/0 0213 UTC/SP 1625
18°33′N
0210/1610
0220/1660
0230/1710
C/C 0232 UTC/SP 1720
S/0 0235 UTC/SP 1735
0104/1280
Second pass Site 724
0524 UTC/SP 2580
Passing Site 724
0349 UTC/SP 2105
Site 725
0250/1810
0300/1860
0311/1915
0330/2010
0342/2070
Passing Site 725
0307 UTC/SP 1895
C/C 0508 UTC/SP 2500
S/0 0511 UTC/SP 2515
0511/2515
0502/2470
0452/2420
0436/2341
C/C 0432 UTC/SP 2323
S/O 0436 UTC/SP 2341
Site 724
0430/2310
0400/2160
0410/2211
C/C 0419 UTC/SP 2258
S/O 0424 UTC/SP 2280
End Line 4 0535
UTC/SP 2635
C/C 0019 UTC/SP 1057
S/O 0030 UTC/SP 1110
C/C 2302 UTC/SP 673
S/O 2307 UTC/SP 695
2312/720
2244/580
C/C 2111 UTC/SP 115
S/O 2112 UTC/SP 120
2054/30
Begin Line 4
2052 UTC/SP 23
18°05′
Site 723
57°30′E
57°58′

Figure 4. Ship's track during survey of Sites 724 and 725 and positioning at Site 724.

tion of 46% diatoms (60% maximum), 33% clay, 7% detrital calcite, 6% quartz, and 2% nannofossils. Highly similar sediments were found at Sites 723, 725, and 726. Geochemical determinations show that carbonate and organic carbon contents are extremely variable in Cores 117-724B-19X to 117-724B-23X and 117-724C-19X to 117-724C-23X. In these cores both facies I and II are present, which accounts for some of this variability. Average values in this interval are 8% carbonate and 5.5% TOC.

Discussion

The diatomaceous and laminated sediment of facies II appears to indicate a depositional environment that differed intermittently from that represented by the bioturbated calcareous clayey silt of facies I. The preservation of lamination indicates a lack of bioturbation, which implies that the bottom waters were anoxic. The high TOC values in facies II might partly reflect the lack of oxygen in the bottom waters. It is not known if the postulated low oxygen contents were a consequence of high primary productivity in the surface waters and/or the result of a stratified water column through which organic matter fell. The high silica content of facies II might indicate a high production of siliceous organisms. Alternatively, silica might have been largely dissolved in the bioturbated, calcareous sediments, but preserved in the less calcareous, unbioturbated, and laminated sediments. Whatever mechanism is invoked to explain the laminated sediment, late Pliocene conditions were different than in the Pleistocene, because none of the Oman margin sites (723 to 730) recovered laminated sediment in the upper Pleistocene to Holocene section.

Of particular interest at this site is the zone of low foraminifer concentration in Cores 117-724B-15X to 117-724B-23X and 117-724C-15X to 117-724C-23X (Fig. 6). This zone is not restricted to the occurrence of diatomaceous laminated sediment (facies II). The benthic foraminifers apparently remain at nearly constant concentration throughout Cores 117-724B-15X to 117-724B-23X and 117-724C-15X to 117-724C-23X. On the other hand, coccoliths are poorly preserved, planktonic foraminifers are reduced in numbers, and those species that are least resistant to dissolution are missing in this zone (see "Biostratigraphy" section, this chapter). The average carbonate content of facies I in Cores 117-724B-19X to 117-724B-23X and 117-724C-19X to 117-724C-23X is only 36%, which may provide supporting geochemical evidence for a zone of carbonate dissolution. The zone of low foraminifer concentration seems to indicate a period of carbonate dissolution in the late Pliocene to early Pleistocene. It is primarily associated with the occurrence of the laminated sediment (facies II), indicating that the dissolution may be connected to the conditions that led to anoxic bottom waters.

In comparison with Site 723, the sediments deposited at Site 724 contain a greater proportion of terrigenous material (clay, quartz, and detrital calcite). The proportion of terrigenous material might have been determined by the relative water depth and the proximity of the coastline.

Sites 723 and 724 can be correlated lithologically using the finely bedded layer of facies I (Cores 117-724A-2H and 117-724B-2H through 117-723B-4H). The origin of this layer and the significance of the correlation are not yet clear. The laminated diatomaceous beds occur near the Pliocene/Pleistocene boundary at both sites (Table 2). A preliminary comparison of the thicknesses and relative positions of these beds revealed a similarity in the distribution of groups of laminated beds at the Pliocene/Pleistocene boundary and in the upper Pliocene.

A prominent sedimentary feature of Site 723 is a series of dolomitized beds and stringers (see "Lithostratigraphy" section, "Site 723" chapter, this volume). The topmost dolomite layer at Site 723 was recovered from the lowermost Pleistocene. Although Pliocene sediments were recovered at Site 724, no dolomite was encountered. This probably reflects a difference in the diagenetic history of the two sites, because Site 724 lacks a substantial subsurface supply of sulfate and magnesium ions from below (see "Inorganic Chemistry" section, this chapter). Phosphorite and apatite nodules were found at Site 724 but not at Site 723 even though both sites have relatively high values of TOC (one requirement for the formation of phosphorite). However, both sites show major differences in sedimentation rates during the Pliocene and Pleistocene (80 m/m.y. at Site 724, 175 m/m.y. at Site 723). Phosphorite nodules grow slowly, close to the sediment/water interface, which requires slow sedimentation rates for formation. Therefore, the presence of phosphorite at Site 724 and its absence at Site 723 were controlled in part by the sedimentation rates (see "Inorganic Chemistry" section). However, the sedimentation rate at Site 724 is higher than would normally be associated with phosphorite formation, and possibly, the formation of phosphorite was linked to winnowing that left no trace other than the nodules themselves.

BIOSTRATIGRAPHY

Site 724 is on the seaward flank of an upper slope basin. The upper Neogene sediments of this relatively shallow (593 m water depth) site, which is currently within the oxygen-minimum zone, were deposited at a high rate and were expected to record changes in sedimentation resulting from oceanographic and atmospheric circulation.

Planktonic and benthic foraminifers, nannofossils, and radiolarians in the sediments cored at Site 724 were analyzed to obtain biostratigraphic datum levels and to record the faunal changes caused by coastal upwelling. The Pliocene/Pleistocene boundary was recognized at about 130 mbsf (Fig. 11). A plot of faunal datum levels and paleomagnetic reversals vs. depth below seafloor is presented in Figure 12; Table 4 is a detailed listing of these data points.

Throughout the upper part of Hole 724B (0–161.0 mbsf), planktonic and benthic foraminifers and calcareous nannofossils are abundant and moderately to well preserved. Foraminifers exhibit high species diversity, whereas the nannofossils have comparatively low species diversity.

Table 1. Coring summary for Site 724.

Core no.	Date (Sept. 1987)	Time	Depth (mbsf)	Cored (m)	Recovered (m)	Recovery (%)
117-724A-						
1H	20	1240	0.0–6.5	6.5	6.50	100.0
2H	20	1300	6.5–15.9	9.4	9.20	97.9
3H	20	1315	15.9–25.4	9.5	9.65	101.0
4H	20	1330	25.4–34.9	9.5	9.54	100.0
5H	20	1345	34.9–44.5	9.6	9.87	103.0
				44.5	44.76	
117-724B-						
1H	20	1615	0.0–7.0	7.0	7.05	101.0
2H	20	1630	7.0–16.4	9.4	9.75	104.0
3H	20	1650	16.4–25.9	9.5	9.71	102.0
4H	20	1705	25.9–35.4	9.5	9.70	102.0
5H	20	1730	35.4–45.0	9.6	9.97	104.0
6X	20	1810	45.0–54.7	9.7	7.10	73.2
7X	20	1840	54.7–64.4	9.7	5.95	61.3
8X	20	1910	64.4–74.0	9.6	7.18	74.8
9X	20	1935	74.0–83.7	9.7	8.56	88.2
10X	20	2005	83.7–93.4	9.7	3.81	39.3
11X	20	2035	93.4–103.0	9.6	7.59	79.0
12X	20	2055	103.0–112.7	9.7	9.88	102.0
13X	20	2120	112.7–122.4	9.7	0.00	0.0
14X	20	2135	122.4–132.0	9.6	10.04	104.6
15X	20	2200	132.0–141.7	9.7	2.67	27.5
16X	20	2225	141.7–151.4	9.7	10.09	104.0
17X	20	2250	151.4–161.0	9.6	9.97	104.0
18X	20	2315	161.0–170.7	9.7	9.94	102.0
19X	20	2350	170.7–180.4	9.7	9.89	102.0
20X	21	0025	180.4–190.0	9.6	9.45	98.4
21X	21	0110	190.0–199.7	9.7	4.85	50.0
22X	21	0145	199.7–209.4	9.7	1.24	12.8
23X	21	0220	209.4–219.0	9.6	9.74	101.0
24X	21	0250	219.0–228.7	9.7	9.70	100.0
25X	21	0315	228.7–238.4	9.7	9.83	101.0
26X	21	0340	238.4–248.0	9.6	10.06	104.8
27X	21	0425	248.0–257.7	9.7	9.23	95.1
				257.7	212.95	
117-724C-						
1H	21	0830	0.0–2.8	2.8	2.82	101.0
2H	21	0855	2.8–12.2	9.4	9.93	105.0
3H	21	0915	12.2–21.7	9.5	10.05	105.8
4H	21	0935	21.7–31.2	9.5	10.14	106.7
5H	21	1000	31.2–40.8	9.6	9.88	103.0
6X	21	1055	40.8–50.5	9.7	8.94	92.1
7X	21	1120	50.5–60.2	9.7	8.78	90.5
8X	21	1140	60.2–69.8	9.6	8.52	88.8
9X	21	1205	69.8–79.4	9.6	9.57	99.7
10X	21	1225	79.4–89.0	9.6	7.76	80.8
11X	21	1250	89.0–98.6	9.6	9.75	101.0
12X	21	1315	98.6–108.3	9.7	9.82	101.0
13X	21	1345	108.3–117.8	9.5	10.04	105.7
14X	21	1410	117.8–127.4	9.6	8.41	87.6
15X	21	1440	127.4–137.0	9.6	10.12	105.4
16X	21	1505	137.0–146.6	9.6	10.35	107.8
17X	21	1530	146.6–156.3	9.7	9.73	100.0
18X	21	1610	156.3–165.9	9.6	9.33	97.2
19X	21	1655	165.9–175.5	9.6	3.41	35.5
20X	21	1725	175.5–185.2	9.7	9.09	93.7
21X	21	1800	185.2–194.8	9.6	5.86	61.0
22X	21	1840	194.8–204.5	9.7	10.61	109.4
23X	21	1910	204.5–214.1	9.6	10.50	109.4
24X	21	1945	214.1–223.7	9.6	9.69	101.0
25X	21	2015	223.7–233.4	9.7	9.09	93.7
26X	21	2035	233.4–242.9	9.5	10.08	106.1
27X	21	2100	242.9–252.4	9.5	10.43	109.8
				252.4	242.70	

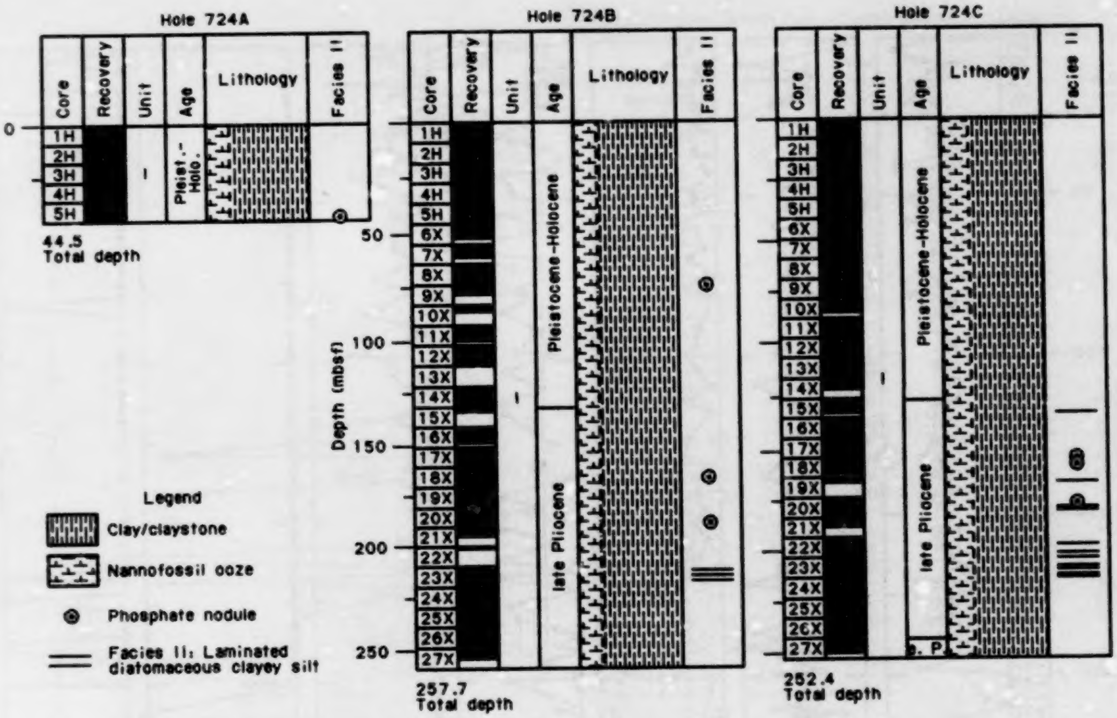

Figure 5. Lithologic summary column for Holes 724A, 724B, and 724C.

Table 2. Stratigraphic occurrence of facies II (laminated diatomaceous clayey silt) at Site 724.

Core, section, interval (cm)	Depth (mbsf)
117-724B-	
23X-5, 62–120	216.02–216.60
23X-6, 118–150	218.08–218.40
23X-7, 0–37	218.40–218.77
23X, CC (0–21)	218.79–219.00
117-724C-	
15X-4, 80–85	132.70–132.75
19X-1, 35–45	166.25–166.35
20X-4, 24–82	180.24–180.82
22X-2, 123–150	197.53–197.80
22X-5, 100–140	201.80–202.20
22X-6, 102–119	203.32–203.49
22X, CC (22–41)	204.31–204.50
23X-1, 106–150	
23X-2, 0–150	205.56–207.58
23X-3, 0–8	
23X-3, 148–150	208.98–210.35
23X-4, 0–135	

Below approximately 161.0 mbsf, the preservation of the calcareous nannofossils becomes poor, and planktonic foraminifers and nannofossils decrease in abundance. At about 225 mbsf this trend reverses: nannofossils and planktonic foraminifers increase in abundance and their preservation improves to a moderate level. These conditions persist to the bottom of the hole. The investigation of calcareous nannofossils in Hole 724C corroborates this general pattern.

The distribution and preservation of siliceous microfossils has an inverse relationship to that of the calcareous nannofossils. Radiolarians and diatoms are absent or present in low amounts to 190 mbsf. From 190 to 229 mbsf, radiolarians become more abundant but the species diversity is low. From 248 mbsf to the bottom of the hole, the radiolarian abundance decreases.

The presence of shallow-water benthic foraminifers in the lower part of the sequence is probably indicative of a subsiding seafloor since the latest early Pliocene.

Planktonic Foraminifers

The distribution of planktonic foraminifers in Hole 724B is similar to that observed in Hole 723A. Highly diverse faunas are found in the upper part of the sequence (Samples 117-724B-1H, CC through 117-724B-16X, CC; 7.0–151 mbsf), where they are abundant and their preservation is good. Pleistocene Zones N23 and N22 are recognized for this part of the section, which consists of foraminifer-bearing nannofossil oozes. The zonal boundary was noted between Samples 117-724B-9X, CC and 117-724B-10X, CC (83.8–93.4 mbsf), as *Globigerinella calida calida* is present in the former but not in the latter sample.

Downhole, foraminifers are rare and moderately well- to poorly preserved (Samples 117-724B-17X, CC through 117-724B-25X, CC; 161.0–238.4 mbsf). Samples 117-724B-26X, CC and 117-724B-27X, CC (248.0–257.7 mbsf) contain common planktonic foraminifers with moderate preservation.

The position of the Pleistocene/Pliocene boundary is difficult to determine because *Globorotalia truncatulinoides* and *Globorotalia tosaensis* are missing at this boundary. An obvious late Pliocene age assemblage is present in Sample 117-724B-19X, CC (180.4 mbsf), because common *Globorotalia acostaensis* and *Globorotalia humerosa* and some *Globorotalia limbata* specimens are found. The absence of the zonal marker of Zone

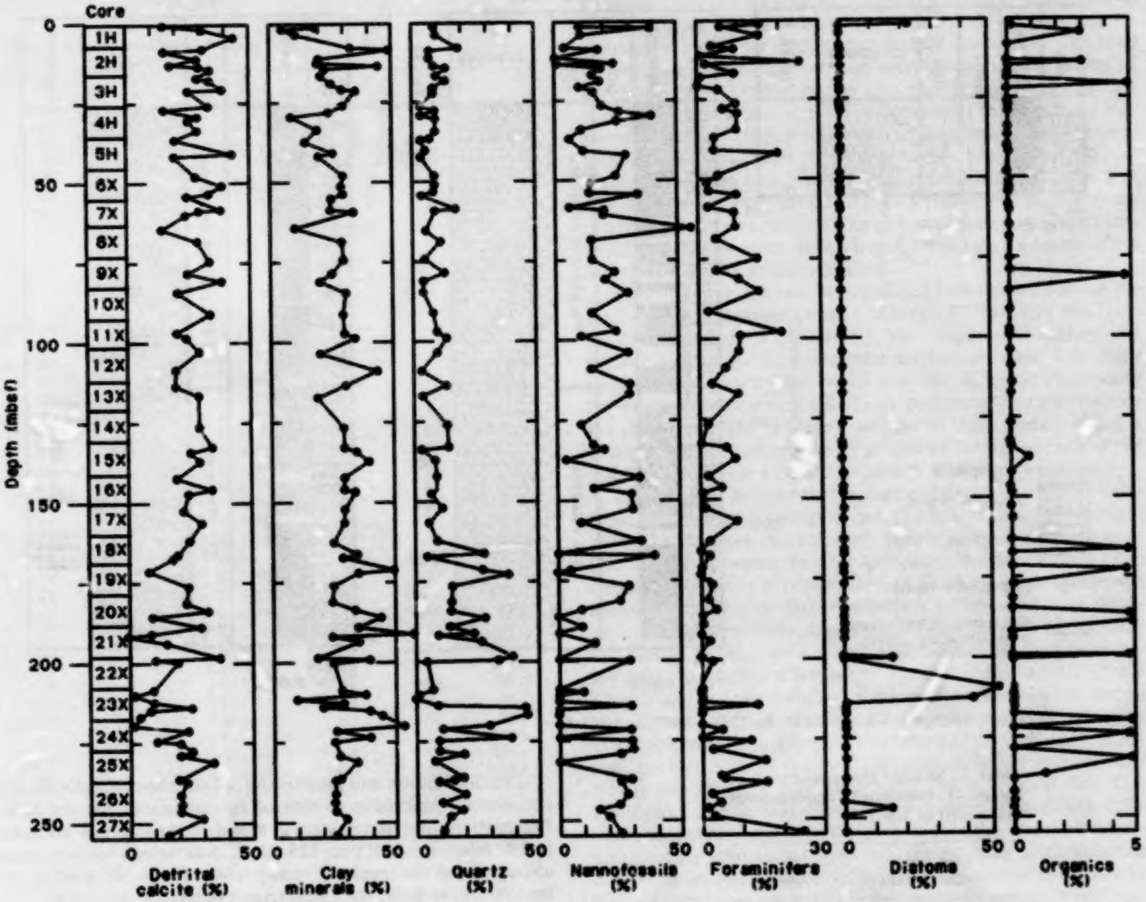

Figure 6. Smear slide data for Holes 724A, 724B, and 724C.

N21 prevented its discrimination from Zone N19–20 in the Pliocene. However, the presence of common *Turborotalia nigriniae* specimens in Samples 117-724B-26X, CC and 117-724B-27X, CC (248.0–257.7 mbsf) shows that the basal part of Hole 724B can be assigned to Zones N19 to N20 and is early to middle Pliocene in age (Fleisher, 1974).

Benthic Foraminifers

The benthic foraminiferal fauna was studied in the core-catcher samples of Hole 724B. The benthic fauna is characterized by its numerous species and high abundance. The state of preservation is moderate to good.

The benthic foraminiferal fauna is dominated by *Bolivina ordinaria*, which comprises between 20% and 70% of the fauna in the samples studied. Other benthic species occurring in high relative abundance throughout the sequence are *Hyalinea baltica* and *Uvigerina peregrina*. Less abundant, but present in most samples, are *Bulimina marginata, Bulimina mexicana, Epistominella* cf. *exigua, Florilus* sp. A, *Stilostomella* spp., and *Uvigerina auberiana*. The foraminiferal fauna is rather uniform in most of the samples, and there are no significant changes in the sequence studied, with the exception of the presence of *Ammonia beccarii* in the lowermost four samples (Samples 117-724B-24X, CC, through 117-724B-27X, CC; 228.7–257.7 mbsf).

According to van Morkhoven et al. (1986), the stratigraphic range for *H. baltica* is upper Pliocene (N21) through Pleistocene (N23). At this site, however, the presence of *H. baltica* throughout the sequence studied places the first occurrence of this species in lower Pliocene (N19) or lower.

Significant in most samples are numerous minor gastropods, pelecypods, and scaphopods. Phosphoritized fish teeth and vertebrae are present throughout the studied sequence.

Calcareous Nannofossils

Three holes were drilled at Site 724 (Fig. 13). Calcareous nannofossils are abundant throughout Hole 724A (6.5–44.5 mbsf), and the preservation is moderate to good. Nannofossils in Hole 724B are abundant with moderate preservation through Sample 117-724B-16X, CC (to 151.4 mbsf). Abundance remains high, but preservation becomes worse and stays poor through Sample 117-724B-18X, CC (151.4–170.7 mbsf). The number of nannofossils decreases to one specimen per 1–10 fields of view whereas preservation remains poor through Sample 117-724B-23X, CC (170.7–219.0 mbsf). At this depth, abundance increases again, and preservation improves to a moderate level. These conditions persist to the bottom of the hole (219.0–257.7 mbsf). Hole 724C has abundant nannofossils with moderate preservation through Sample 117-724C-18X, CC (to 165.9 mbsf). As was the case in

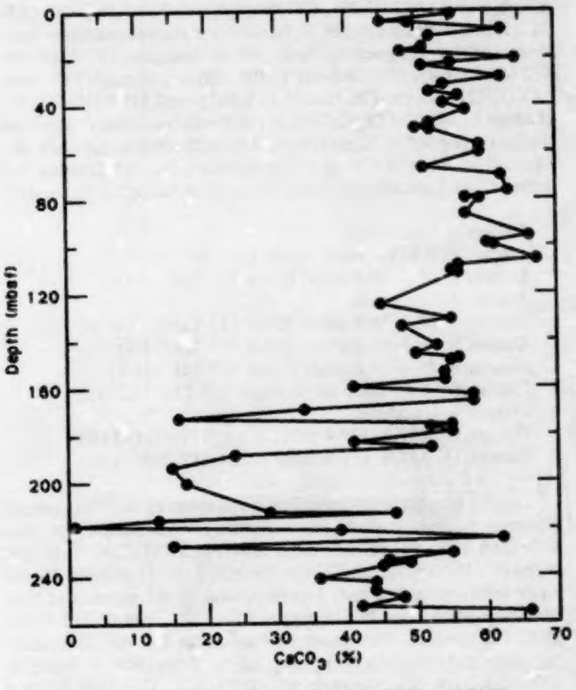

Figure 7. CaCO$_3$ profile (see Table 3) for Holes 724A and 724B.

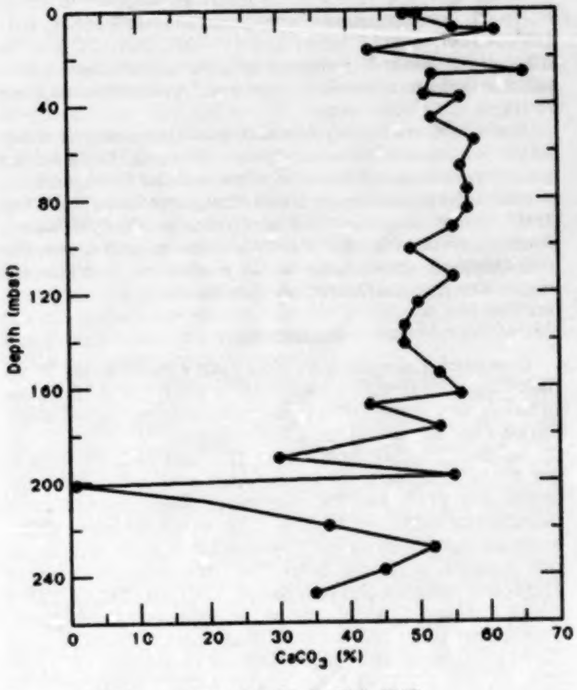

Figure 8. CaCO$_3$ profile (see Table 3) for Hole 724C.

Table 3. Organic carbon and carbonate carbon percentages.

Core, section, interval (cm)	Depth (mbsf)	Total carbon (%)	Inorganic carbon (%)	Organic carbon (%)	CaCO$_3$ (%)
724A-1H-1, 100–102	1.00		6.67		55.6
724C-1H-2, 0–1	1.50	7.16	6.11	1.05	50.9
724C-1H-2, 48–50	1.98		5.85		48.7
724A-1H-3, 100–102	4.00		5.42		45.2
724A-1H-3, 144–145	4.44	6.65	5.91	0.74	49.2
724A-2H-1, 100–102	7.50		7.49		62.4
724C-2H-4, 48–50	7.78		6.63		55.2
724C-2H-5, 0–1	8.80	8.84	7.41	1.43	61.7
724A-2H-3, 100–102	10.50		6.25		52.1
724A-2H-6, 100–102	15.00		6.14		51.2
724A-3H-1, 100–102	16.90		5.80		48.3
724C-3H-4, 48–50	17.18		5.16		43.0
724A-3H-3, 100–102	19.90		7.72		64.3
724A-3H-4, 144–145	21.84	8.01	6.60	1.41	55.0
724A-3H-5, 100–102	22.90		6.18		51.5
724C-4H-4, 48–50	26.68		7.83		65.2
724C-4H-5, 0–1	27.70	8.41	6.31	2.10	52.6
724A-4H-2, 100–102	27.90	8.83	7.50	1.33	62.5
724A-4H-4, 100–102	30.90	7.74	6.57	1.17	54.7
724A-4H-6, 100–102	33.90	6.65	6.33	0.32	52.7
724A-5H-1, 100–102	35.90	7.51	6.82	0.69	56.8
724C-5H-4, 48–50	36.18		6.14		51.2
724C-5H-5, 0–1	37.20	8.31	6.78	1.53	56.5
724A-5H-3, 100–102	38.90	8.01	6.51	1.50	54.2
724A-5H-5, 100–102	41.90	8.25	6.86	1.39	57.1
724C-6X-4, 48–50	45.78		6.28		52.3
724B-6X-2, 70–72	47.20		6.29		52.4
724B-6X-3, 144–145	49.44	6.84	6.09	0.75	50.7
724B-6X-4, 70–73	50.20		6.25		52.1
724C-7X-4, 48–50	55.48		6.97		58.1
724B-7X-2, 70–72	56.90		7.17		59.7
724B-7X-4, 70–72	59.90		7.13		59.4
724C-8X-5, 32–34	66.52		6.75		56.2
724B-8X-2, 80–82	66.70		6.23		51.9
724B-8X-4, 80–82	69.70		7.47		62.2
724C-9X-5, 50–52	76.30		6.91		57.6
724B-9X-2, 90–92	76.40		7.58		63.1
724B-9X-4, 90–92	79.40		6.88		57.3
724B-9X-4, 119–120	79.69	8.77	7.11	1.66	59.2
724C-10X-4, 34–36	84.24		6.93		57.7
724B-10X-2, 90–92	86.10		6.87		57.2
724C-11X-3, 57–59	92.57		6.61		55.1
724B-11X-2, 74–76	95.64		8.01		66.7
724B-11X-4, 74–76	98.64		7.26	60.5	
724B-11X-4, 149–150	99.39	9.30	7.32	1.98	61.0
724C-12X-3, 20–22	101.80		5.99		49.9
724B-12X-2, 98–100	105.48		8.04		67.0
724B-12X-4, 68–70	108.18		6.80		56.6
724B-12X-4, 95–97	108.45		6.72		56.0
724B-12X-5, 119–120	110.19	8.70	6.71	1.99	55.9
724B-12X-6, 88–90	111.38		6.78		56.5
724C-13X-4, 86–88	113.66		6.62		55.1
724C-14X-5, 79–81	124.59		6.00		50.0
724B-14X-2, 80–82	124.70		5.49		45.7
724B-14X-6, 90-92	130.80		6.70		55.8
724B-15X-2, 50–52	134.00		5.79		48.2
724C-15X-5, 90–92	134.30		5.83		48.6
724C-16X-4, 50–52	142.00		5.76		48.0
724B-16X-1, 71–73	142.41		6.47		53.9
724B-16X-3, 91–93	145.61		6.04		50.3
724B-16X-4, 144–145	147.64	8.97	6.78	2.19	56.5
724B-16X-5, 77–79	148.47		6.70		55.8
724B-17X-2, 85–87	153.75		6.52	54.3	
724C-17X-6, 67–69	154.77		6.38		53.2
724B-17X-4, 81–83	156.71		6.49		54.1
724B-17X-6, 105–107	159.95		4.95		41.2
724B-18X-2, 50–52	163.00		7.05		58.7
724C-18X-5, 111–113	163.41		6.75		56.2
724B-18X-4, 57–59	166.07		7.01		58.4
724C-19X-2, 66–68	168.06		5.22		43.5
724B-18X-6, 82–84	169.32		4.18	34.8	
724B-19X-2, 88–90	173.08		1.97		16.4
724B-19X-4, 74–76	175.94		6.66		55.5
724B-19X-5, 0–1	176.70	9.53	6.29	3.24	52.4
724C-20X-2, 76–78	177.76		6.43		53.6
724B-19X-6, 70–72	178.90		6.63	55.2	
724B-20X-2, 125–12	183.15		4.93		41.1

Table 3 (continued).

Core, section, interval (cm)	Depth (mbsf)	Total carbon (%)	Inorganic carbon (%)	Organic carbon (%)	$CaCO_3$ (%)
724B-20X-4, 70–72	185.60		6.25		52.1
724B-20X-6, 75–77	188.65		2.89		24.1
724C-21X-4, 59–61	190.29		3.63		30.2
724B-21X-3, 87–89	193.87		1.87		15.6
724C-22X-3, 76–78	198.56		6.69		55.7
724B-22X, CC (12–14)	200.57		2.08		17.3
724C-22X-5, 74–76	201.54		0.18		1.5
724C-23X-3, 98–100	208.48		2.32		19.3
724B-23X-3, 70–72	213.10		3.50		29.2
724B-23X-4, 0–1	213.90	9.19	5.68	3.51	47.3
724B-23X-5, 70–72	216.10		1.65		13.7
724B-23X-7, 20–22	218.60	5.70	0.21	5.49	1.8
724C-24X-4, 76–78	219.36		4.46		37.2
724B-24X-2, 35–37	220.85		4.72		39.3
724B-24X-4, 93–95	224.43		7.52		62.6
724B-24X-6, 78–80	227.28	9.20	1.88	7.32	15.7
724C-25X-4, 64–66	228.84		6.28		52.3
724B-25X-2, 47–49	230.67		6.64		55.3
724B-25X-4, 30–32	233.50		5.53		46.1
724B-25X-5, 0–1	234.70	7.82	5.88	1.94	49.0
724B-25X-6, 7–9	236.27		5.49		45.7
724C-26X-4, 55–57	238.45		5.51		45.9
724B-26X-2, 132–134	241.22		4.34		36.2
724B-26X-4, 4–6	242.94		5.39		44.9
724B-26X-6, 66–68	246.56		5.38		44.8
724C-27X-4, 58–60	247.98		4.25		35.4
724B-27X-2, 6–8	249.56		5.82		48.5
724B-27X-4, 65–67	253.15		5.08		42.3
724B-27X-6, 7–9	255.57		7.95		66.2

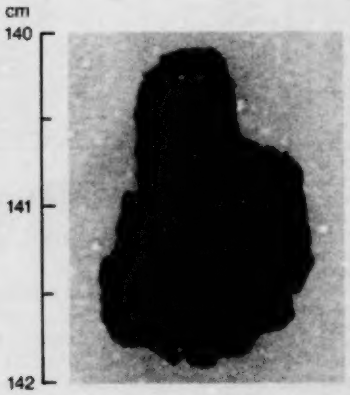

Figure 9. Black (5Y 2.5/1) apatite nodule from Sample 117-724B-5H, 141–142 cm.

Hole 724B, the preservation becomes poor whereas the abundance remains high in Samples 117-724C-19X, CC and 117-724C-20X, CC (165.9–185.2 mbsf). The decrease in nannofossil abundance mimics the pattern in Hole 724B, but abundance increases again in Sample 117-724C-22X, CC (204.5 mbsf) and remains high throughout the remainder of the hole, with moderate preservation (204.5–252.4 mbsf).

As at all of the other Leg 117 sites, the species diversity is comparatively low, and discoasters are not usually found in high concentrations.

Samples down to Samples 117-724A-2H-5, 105–106 cm (13.55 mbsf), 117-724B-1H, CC (7.0 mbsf), and 117-724C-1H, CC (2.8 mbsf) contain *Emiliania huxleyi* and are assigned to Zone NN21. Samples 117-724A-2H, CC to 117-724A-4H, CC (15.90–34.90 mbsf), 117-724B-2H, CC and 117-724B-3H, CC (7.0–25.9 mbsf), and 117-724C-2H, CC through 117-724C-4H, CC (2.8–31.2 mbsf) contain neither *E. huxleyi* nor *Pseudoemiliania lacunosa* and are assigned to Zone NN20. Samples 117-724A-5H, CC (44.5 mbsf), 117-724B-5H-1, 105–106 cm, through 117-724B-18X-3, 121–122 cm (36.45–165.21 mbsf), and 117-724C-5H, CC through 117-724C-17X, CC (31.2–156.3 mbsf) contain *P. lacunosa* and are assigned to Zone NN19. The following datums are recognized in Zone NN19 (see "Explanatory Notes" chapter, this volume), and additional information is tabulated in Table 4.

Datum 1: Uncertain
Datum 2: 2.8–9.4 mbsf (Core 117-724C-2H)
Datum 3: 31.2–40.8 mbsf (Core 117-724C-5H)
Datum 4: Uncertain
Datum 5: 60.2–69.8 mbsf (Core 117-724C-8X)
Datum 6: 60.2–69.8 msbf (Core 117-724C-8X)
Datum 7: 79.4–89.0 mbsf (Core 117-724C-10X)
Datum 8: 98.6–108.3 mbsf (Core 117-724C-12X)
Datum 9: Uncertain
Datum 10: 117.8–127.4 mbsf (Core 117-724C-14X)
Datum 11: 127.4–137.0 mbsf (Core 117-724C-15X)

Datum 11 marks the approximate position of the Pleistocene/Pliocene boundary. Neogene Samples 117-724B-18X, CC and 117-724B-19X, CC (170.7–180.0 mbsf) and 117-724C-18X, CC through 117-724C-22X, CC (165.9–204.5 mbsf) contain *Discoaster brouweri* as the only representative of the genus and thus are assigned to Zone NN18 (upper Pliocene). Sample 117-724B-20X, CC contains *Discoaster pentaradiatus* but not *Discoaster surculus* and, therefore, is assigned to Zone NN17. Samples 117-724B-21X, CC through 117-724B-25X, CC (199.7–238.4 mbsf) contain *D. surculus* but not *Reticulofenestra pseudoumbilica* and are assigned to Zone NN16. Because *D. surculus* was not found in Hole 724C, Samples 117-724C-23X, CC through 117-724C-25X, CC (214.1–233.4 mbsf) are assigned to Zones NN16-17. All sediments below Samples 117-724B-26X-1, 104–105 cm (239.44–257.7 mbsf) and 117-724C-26X, CC (242.9–252.4 mbsf) contain *R. pseudoumbilica* but not *Discoaster asymmetricus* and are assigned to uppermost lower Pliocene Zone NN15.

Traces of Cretaceous species such as *Cribrosphaerella ehrenbergii, Watznaueria barnesae, Micula decussata, Cretarhabdus* spp., *Prediscosphaera intercisa, Cretarhabdus loriei*, and *Microrhabdulus decoratus* are found throughout Holes 724B and 724C. Paleogene species such as *Cyclicargolithus floridanus, Cyclicargolithus abisectus*, and *Cribrocentrum reticulatum*, Eocene-Oligocene species *Sphenolithus predistentus*, and Miocene species *Discoaster deflandrei* are also found.

Radiolarians

Core-catcher samples from Hole 724B were examined for radiolarians. The first 19 cores (to 180.4 mbsf) are either barren or have a very sparse fauna (4 to 5 specimens per strewn slide). Diatoms are also absent from these samples.

Samples 117-724B-20X, CC to 117-724B-24X, CC (190.0–228.7 mbsf) contain a significant number of radiolarians, but species diversity is low. The assemblage closely resembles that found in the lowest part of Hole 723B, except for minor differences associated with an age difference between the radiolarian-rich sequences in the two holes. The last occurrence datum of *Stichocorys peregrina* occurs in Sample 117-724B-22X, CC (209.4 mbsf), marking the upper limit of the *Spongaster pentas* Zone. This species is the only tropical zonal marker found in Hole 724B. Radiolarian abundances decrease in Samples 117-724B-25X, CC and 117-724B-27X, CC (238.4–257.7 mbsf).

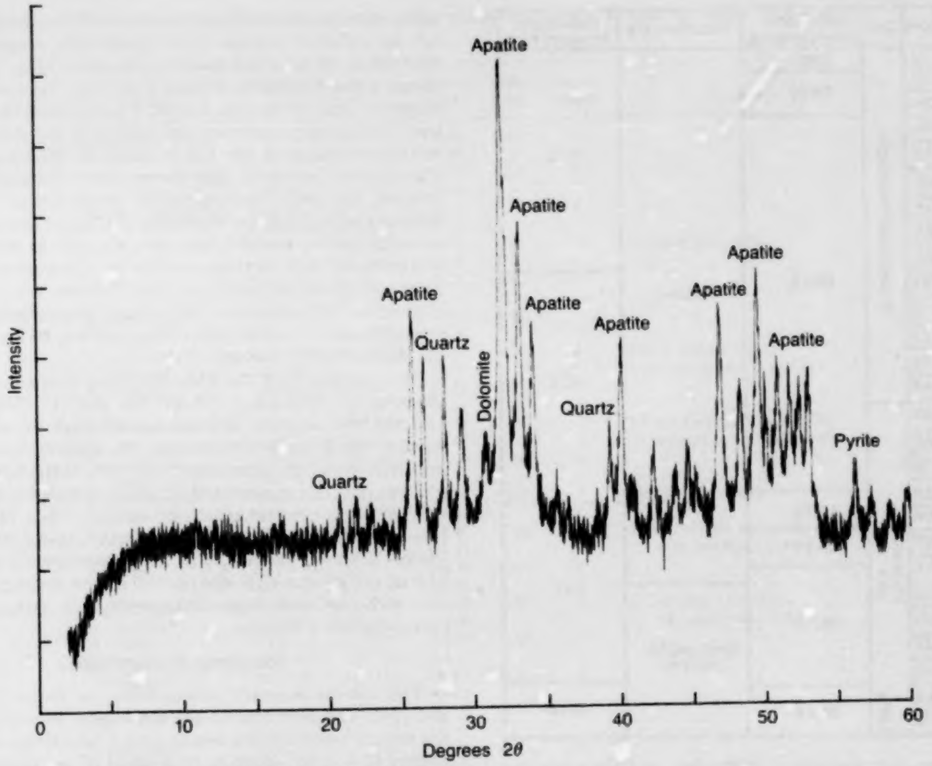

Figure 10. XRD trace of the apatite nodule shown in Figure 9.

Paleoenvironmental Implications

Ammonia beccarii is a well-known neritic benthic foraminiferal species that has a lower depth limit well above 350 m in the modern oceans. Site 724 is today located at a water depth of 593 m, whereas the presence (up to about 10% of the benthic foraminiferal fauna) of *A. beccarii* in the lower part of the sequence studied indicates either a subsiding sea-bottom caused by faulting or downslope transport of material from shallower areas. The uniformity of the color of the phosphorite found throughout the sequence indicates a single source for the material, and thus, we favor the idea of a subsiding sea bottom. Different colors of phosphorite found at one location usually indicate transportation of material from various sources and different ages (redeposition—thanatocoenosis), whereas color uniformity indicates a single source (biocoenosis).

The varying preservation states of the planktonic foraminifers and coccoliths are thought to be related to the reducing conditions in the oxygen-minimum zone, which enhance carbonate dissolution. Reduced planktonic foraminiferal faunas are present in Samples 117-724B-17X, CC through 117-724B-25X, CC (161.0–238.4 mbsf), which are dominated by robust thick-walled species. With the decline of the calcareous fauna is a concomitant increase in abundance of the siliceous fauna.

The nannofossil genus *Helicosphaera* is thought to prefer upwelling areas. This genus is especially numerous in Samples 117-724B-10X, CC (93.4 mbsf), 117-724B-15X, CC (141.7 mbsf), 117-724B-17X, CC (161.0 mbsf), and 117-724C-18X, CC (165.9 mbsf). *Coccolithus pelagicus*, a species known to inhabit cold waters, is found in Samples 117-724B-15X, CC through 117-724B-17X, CC (141.7–161.0 mbsf; lowermost Pleistocene to uppermost Pliocene) and 117-724C-15X, CC through 117-724C-19X, CC (137.0–175.2 mbsf; lowermost Pleistocene to uppermost Pliocene). Interestingly, the large numbers of *Helicosphaera* spp. are always associated with high abundances of *C. pelagicus*, but not all Site 724 samples with high numbers of *C. pelagicus* contain *Helicosphaera* spp. in unusually high concentrations.

PALEOMAGNETISM

Site 724 is at 18°28′N, 57°47′E in a water depth of about 600 m on the Oman margin. Holes 724A, 724B, and 724C were cored to depths of 44.8, 257.7, and 252.4 mbsf, respectively. The lithology consists mainly of calcareous clayey silt.

Magnetic Measurements

The archive halves of five APC cores from Hole 724A (Cores 117-724A-1H through 117-724A-5H) were measured on the pass-through cryogenic magnetometer after alternating field (AF) demagnetization at 5 mT. As for Site 723, the inclinations generally correspond to the expected axial dipole value (33.7°).

Our efforts in measuring discrete samples with the MINISPIN fluxgate spinner magnetometer and the Schonstedt AF demagnetizer proved more fruitful than at Site 723. We selected a peak AF of 5 or 10 mT (depending on the initial intensity) for blanket demagnetization. Stepwise AF demagnetization of samples from Hole 724B suggested that the characteristic magnetization was detectable after AF cleaning at peak fields of 5–10 mT (Figs. 14 through 17). Intensities after AF demagnetization were generally higher than at Site 723: around 1 mA/m down to about 190 mbsf, below which they drop to around 0.1 mA/m. The arithmetic mean intensity is 0.7 mA/m. Figure 18 shows

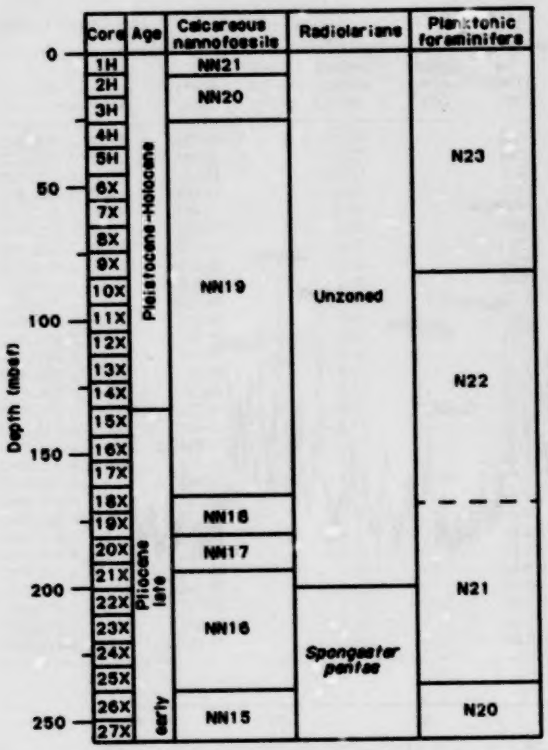

Figure 11. Calcareous nannofossil, radiolarian, and planktonic foraminifer biostratigraphy of Hole 724B.

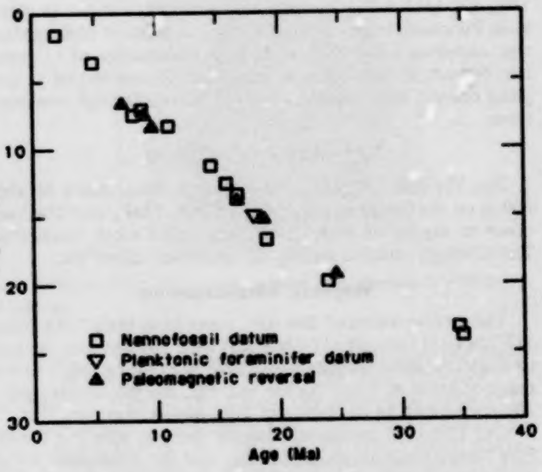

Figure 12. Age-depth plot for Site 724. Events are from Holes 724A and 724B (see Table 4 for a detailed list of events).

that the inclination values of both normally and reversely magnetized specimens are distributed around the expected value for the site.

Downhole plots of declination, inclination, and intensity after AF demagnetization are shown in Figures 19 through 21; points with circular standard deviation (CSD) values greater than 40° are excluded. Samples from Hole 724A, ranging from 0 to 44.5 mbsf, all have downward inclinations (Fig. 19). The two deeper holes, 724B (Fig. 20) and 724C (Fig. 21), show consistent magnetic polarity records for the Pliocene and Pleistocene. At least six polarity transitions are evident in the records, and we tentatively recognize the Chron C1/C1r (Brunhes/Matuyama Chronozone) boundary and Chron C1r–1 (Jaramillo Subchronozone) and more confidently recognize Chron C2 (Olduvai Subchronozone) and the beginning of Chron C2A (Gauss Chronozone). Table 5 lists the core intervals, depths below seafloor, and estimated ages of these transitions. The horizons of the polarity transitions are both consistent between the two holes and concordant with calcareous nannofossil biostratigraphy. Our age estimates give a sedimentation rate of about 80 m/m.y. for this site during the Pleistocene.

Two samples from the 47.6–49.2 mbsf interval of Hole 724B (Samples 117-724B-6X-2, 115–117 cm, and 117-724B-6X-3, 115–117 cm) have negative inclinations, although we assign this interval to the Brunhes Chronozone. No negative inclinations are apparent within the same interval in Hole 724C; however, we did observe reversely magnetized Brunhes specimens in Core 117-723A-9H (see "Paleomagnetism" section, "Site 723" chapter). It is possible that this genuinely reflects geomagnetic field behavior; however, the quality of the paleomagnetic data and the lack of sufficiently tight age control inhibit attempts at correlation with previously suggested geomagnetic events and excursions within the Brunhes.

Magnetic Susceptibility

The volume magnetic susceptibility of Holes 724A, 724B, and 724C was measured on the Bartington Instruments M.S. 1 whole-core susceptibility sensor at 0.1 sensitivity and low-frequency (0.47-kHz) settings. As a result of gas expansion in the deepest cores, the volume magnetic susceptibility of split-core sections was measured from Cores 117-724B-16X to 117-724B-26X and 117-724C-18X to 117-724C-27X. Values obtained during these measurements were multiplied by two during processing. Measurements were made on all cores at 10-cm intervals for a total of 425, 1582, and 1911 measurements for Holes 724A, 724B, and 724C, respectively. Susceptibility values ranged from 50×10^{-6} to 125×10^{-6} and averaged about 100×10^{-6} volume SI units, which is slightly higher than observed at Site 723 and slightly lower than at Sites 722 and 721. To a first-order approximation, the intersite differences in mean susceptibility are inversely related to differences in the relative accumulation rates, which suggests that the variability between sites is due to dilution by nonmagnetic components. At this stage, however, we are unsure as to whether the downhole variability is due to changes in the fluxes of predominantly terrigenous (magnetic) or biogenic (nonmagnetic) components (see "Paleomagnetism" section, "Site 723" chapter).

The susceptibility data for Cores 117-724A-1H to 117-724A-5H, 117-724B-1H to 117-724B-5H, and 117-724C-1H to 117-724C-5H (0–~45 mbsf) are quite similar, and interhole correlations are generally accurate to within ~5 to 10 cm (Fig. 22). Anomalously high values that do not correlate between holes can be attributed to short intervals contaminated by pipe rust and other magnetic contaminants that occur at the core boundaries. Using the Brunhes-Matuyama Chronozone paleomagnetic datums for Holes 724A and 724B (Table 5), the age interval represented by these correlated sequences is approximately 500,000 yr.

Interhole correlations below the limit of APC recovery in Holes 724B and 724C (>45 mbsf) are considerably less detailed. Most of the correlations can be made for gross features only. Although XCB recovery was quite high, the recovered sediments were generally too disturbed for detailed susceptibility

Table 4. Stratigraphic listing of faunal events and paleomagnetic reversals for Holes 724A and 724B.

Event	Core, section, interval (cm)	Depth (mbsf)	Age (Ma)	Source of age	Notes
B *Emiliania huxleyi*	724A-2H-5, 105–106, to 724A-2H, CC	13.55 15.90	0.19	3	
T *Pseudoemiliania lacunosa*	724A-4H, CC 724B-5H-1 105–106	34.90 36.45	0.49	3	
Bruhnes/Matuyama	724B-8X-1, 105–107 724B-8X-2, 105–107	65.45 66.95	0.73	6	
B *Gephyrocapsa parallela*	724B-8X-3, 110–111 724B-8X-5, 100–101	68.50 71.40	0.89	4	North Atlantic data
T Jaramillo	724B-8X-5, 94–96 724B-9X-1, 114–116	71.34 75.14	0.91	6	
T *Reticulofenestra* sp. A	724B-8X, CC, 724B-9X-1, 105–106	74.00 75.05	0.82	3	
T *Gephyrocapsa* "large"	724B-9X-5, 105–106 724B-9X, CC	81.05 83.70	1.10	4	North Atlantic data Long axis greater than 6 μm
B Jaramillo	724B-9X-5, 114–116 724B-10X-1, 105–107	81.18 84.75	0.98	6	
T *Helicosphaera sellii*	724B-12X-1, 135–136 724B-12X-3, 105–106	104.35 107.05			No good published age; event appears to be diachronous
T *Calcidiscus macintyrei*	724B-12X-5, 100–101 724B-12X, CC	110.00 112.70	1.45	6	
B *Gephyrocapsa oceanica*	724B-14X-1, 110–111 724B-14X-3, 104–105	123.50 126.44	1.57	4	North Atlantic data
B *Gephyrocapsa caribbeanica*	724B-14X, CC 724B-15X-1, 103–104	132.00 133.03	1.66	4,8	North Atlantic age consistent with Italian-type section
T Olduvai	724B-15X-2, 68–70 724B-16X-1, 108–110	134.18 142.78	1.66	6	
T *Globigerinoides extremus*	724B-16X-4, 65–67 724B-16X, CC	146.85 151.40	1.80	6	*G. obliquus extremus* in Berggren et al., 1985
B Olduvai	724B-16X-6, 116–118 724B-17X-1, 127–129	150.36 152.67	1.88	6	
T *Discoaster brouweri*	724B-18X-3, 121–122 724B-18X-5, 105–106	165.21 168.05	1.9	6	
Matuyama/Gauss	724B-20X-6, 108–110 724B-21X-2, 141–143	188.98 192.91	2.47	6	
T *Discoaster surculus*	724B-21X-3, 105–106 724B-21X, CC	194.05 199.70	2.4	6	
T *Sphenolithus abies*	724B-25X-1, 135–135 724B-25X-3, 135–136	230.05 233.05	3.47	6	
T *Reticulofenestra pseudoumbilica*	724B-25X, CC 724B-26X-1, 104–105	238.40 239.44	3.5	6	

Note: T = upper limit of event and B = lower limit. Sources of ages are: 3 = oxygen isotope data for Site 723 (N. Niitsuma, unpubl. data); 4 = Takayama and Sato, 1987; 6 = Berggren et al., 1985; and 8 = Sato et al., in press.

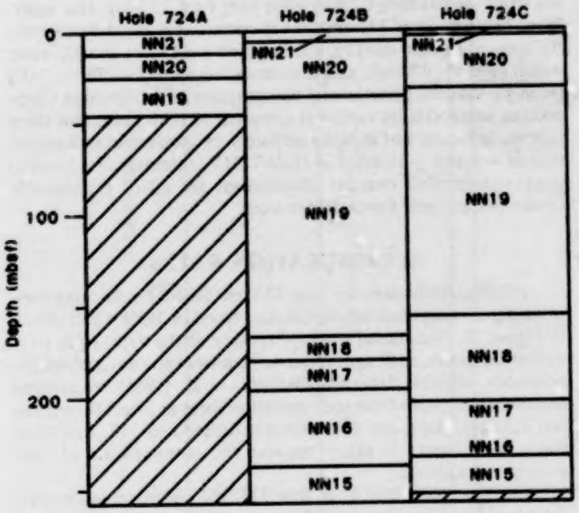

Figure 13. Correlation of calcareous nannofossil zones in Holes 724A, 724B, and 724C.

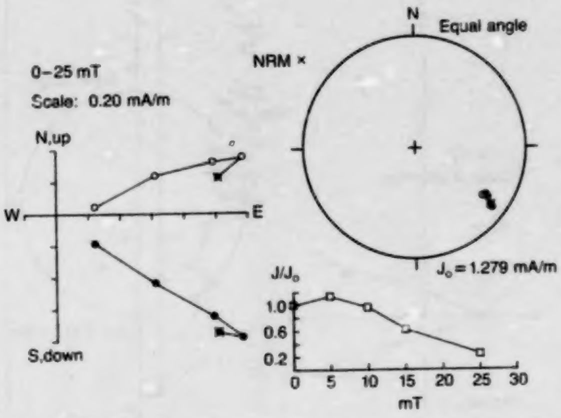

Figure 14. Result of stepwise AF demagnetization for Sample 117-724B-14X-2, 121–123 cm.

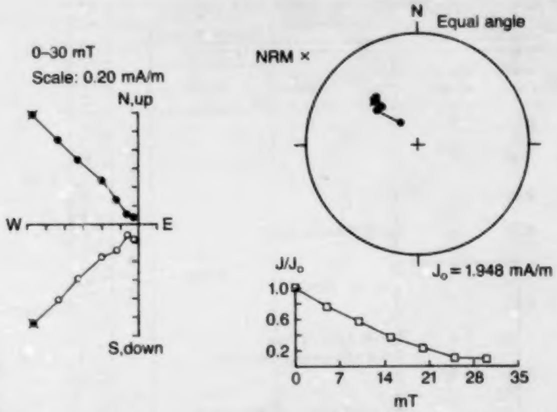

Figure 15. Result of stepwise AF demagnetization for Sample 117-724B-16X-1, 108–110 cm.

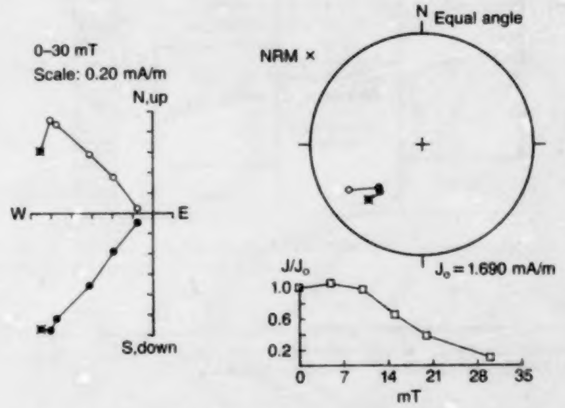

Figure 16. Result of stepwise AF demagnetization for Sample 117-724B-17X-1, 127–129 cm.

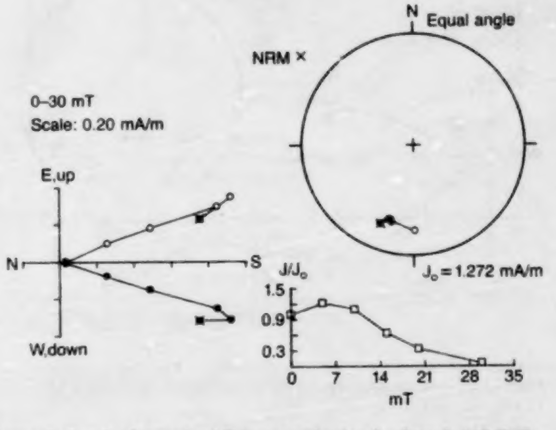

Figure 17. Result of stepwise AF demagnetization for Sample 117-724B-18X-5, 110–112 cm.

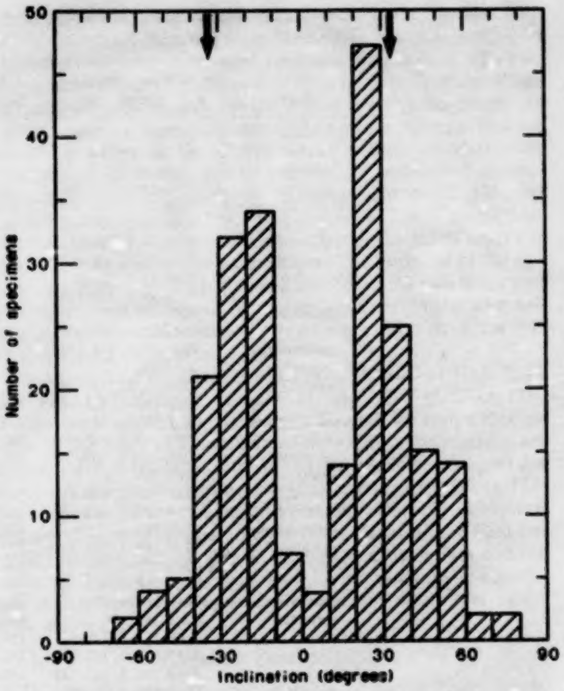

Figure 18. Histogram of magnetic inclination values from Site 724. Arrows show the values expected from the geocentric axial dipole field (33.7°).

correlations. Tentative correlations between Holes 724B and 724C are shown in Figure 23. Detailed interhole correlations based on these data and lithologic marker layers are presented in the "Interhole Correlations" section of this chapter.

Intersite correlations between the two Oman margin sites drilled thus far (723 and 724) are shown in Figure 24. The data are from the Brunhes Chronozone only (<0.73 Ma). The agreement between Sites 723 and 724 is remarkably good despite the differences in core quality, site location (~40 km apart), water depth (800 vs. 570 m), and accumulation rates (~175 vs. ~80 m/m.y). Moderate stretch and compression of the Brunhes Chronozone susceptibility record is apparent at both sites, and there is some indication of missing sediment or condensed sedimentation at ~8 and ~31 mbsf in Hole 724C. Ultimately, we hope to construct detailed intersite correlations for all of the suitable Oman margin and Owen Ridge sites.

ACCUMULATION RATES

Sedimentation rates for Site 724 are based on the magnetostratigraphic and biostratigraphic data listed in Table 4 and shown in Figure 25. Because of the high quality of the data, eight nannofossil datums, with ages from oxygen isotope stratigraphy (N. Niitsuma, unpubl. data) and Berggren et al. (1985) are favored for determination of the sedimentation rates at Site 724 over the last 3.5 m.y. Rates are determined at other Leg 117 sites using these same events to allow between-site comparisons of sediment accumulation.

Over the last 2.4 m.y. at Site 724, the mean sedimentation rate varied between 59 and 142 m/m.y. (Table 6), with an overall mean of 80 m/m.y. This is less by a factor of 2 than the sedimentation rate at nearby Site 723, which is in the center of the

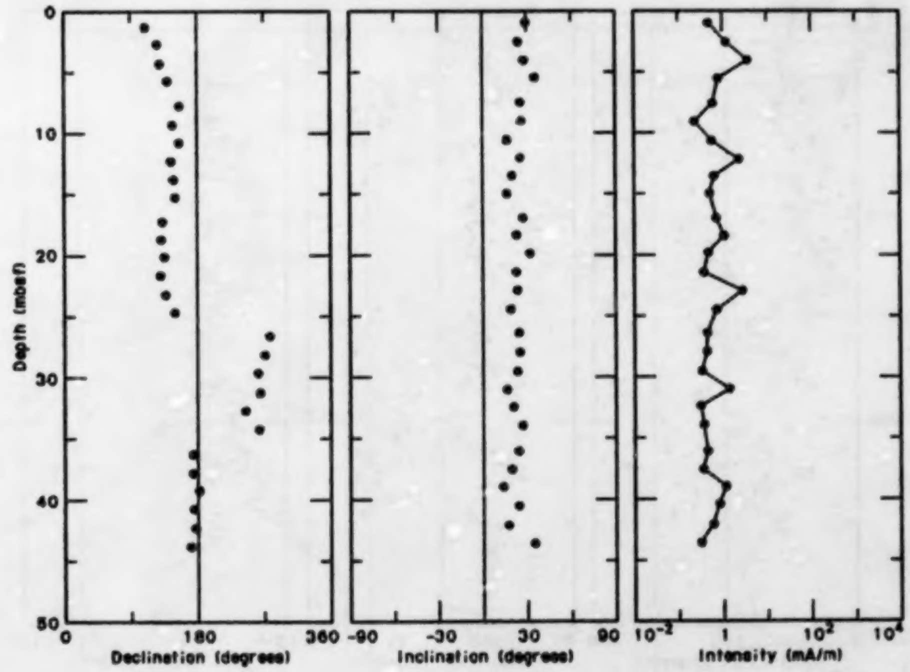

Figure 19. Magnetic declination (relative values), inclination, and intensity profiles for Hole 724A, obtained after AF demagnetization.

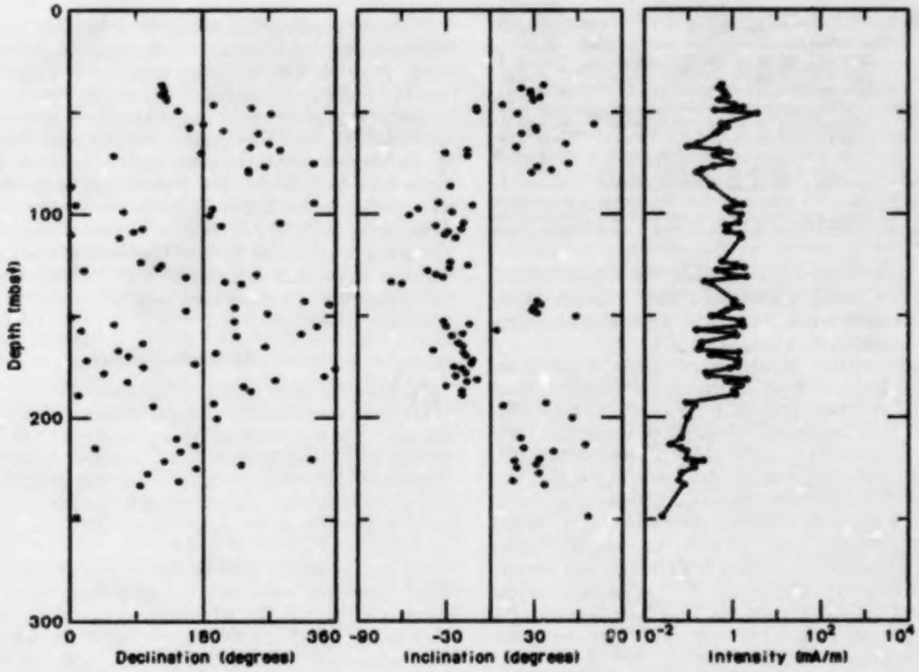

Figure 20. Magnetic declination (relative values), inclination, and intensity profiles for Hole 724B, obtained after AF demagnetization.

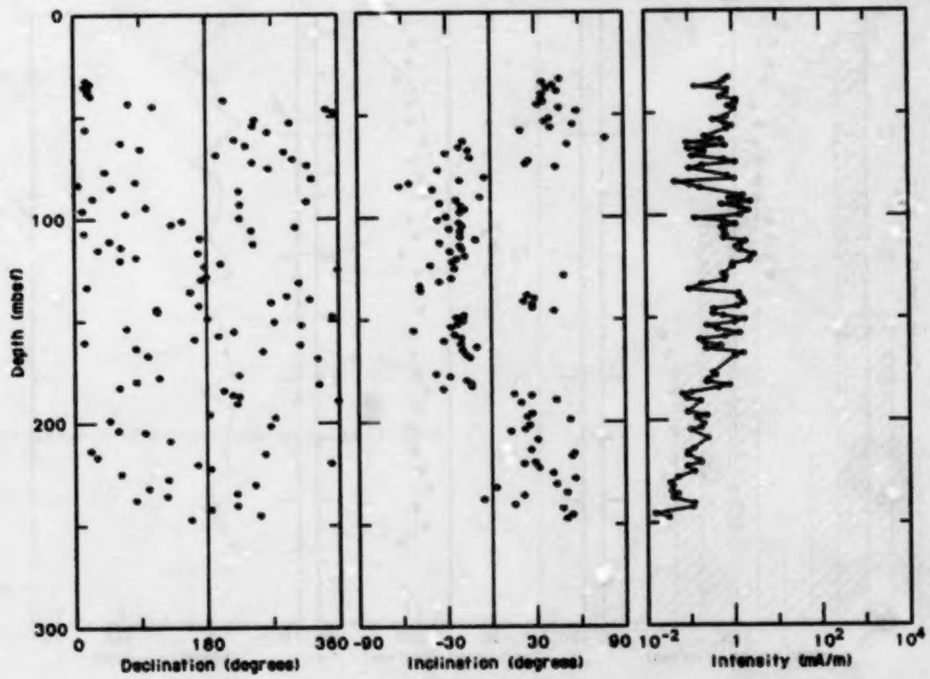

Figure 21. Magnetic declination (relative values), inclination, and intensity profiles for Hole 724C, obtained after AF demagnetization.

Table 5. Polarity transitions in Holes 724B and 724C.

Boundary (Age)	Sample interval	Depth (mbsf)
Brunhes/Matuyama	724B-8X-1, 105 cm, to 724B-8X-2, 105 cm	65.45–66.95
C1/C1r (0.73 Ma)	724C-8X-1, 119 cm, to 724C-8X-2, 119 cm	61.39–62.89
Top of Jaramillo	724B-8X-5, 94 cm, to 724B-9X-1, 114 cm	71.34–75.14
C1r/C1r-1 (0.91 Ma)	724C-9X-1, 119 cm, to 724C-9X-2, 119 cm	70.99–72.49
Bottom of Jaramillo	724B-9X-5, 114 cm, to 724B-10X-1, 105 cm	81.18–84.75
C1r-1/C1r (0.98 Ma)	724C-9X-4, 119 cm, to 724C-9X-5, 119 cm	75.49–76.99
Top of Olduvai	724B-15X-2, 68 cm, to 724B-16X-1, 108 cm	134.18–142.78
C1r/C2 (1.66 Ma)	724C-15X-6, 100 cm, to 724C-16X-1, 110 cm	135.90–138.10
Bottom of Olduvai	724B-16X-6, 116 cm, to 724B-17X-1, 127 cm	150.36–152.67
C2/C2r (1.88 Ma)	724C-16X-6, 118 cm, to 724C-17X-1, 140 cm	145.68–148.00
Matuyama/Gauss	724B-20X-6, 108 cm, to 724B-21X-2, 141 cm	188.98–192.91
C2r/C3 (2.47 Ma)	724C-20X-6, 106 cm, to 724C-21X-1, 117 cm	184.06–186.37

upper slope basin. Prior to 2.4 m.y. at Site 724, a lower rate of accumulation (35 m/m.y.) is associated with a greater abundance of organic-carbon-rich, laminated diatomaceous clayey silts (lithologic facies II).

The mass accumulation of calcium carbonate, organic carbon, and noncarbonate sediment components is calculated from average values between the nannofossil datums (Table 6 and Fig. 26). The rate of bulk sediment accumulation is approximately 12 g/cm^2/1000 yr, lower by a factor of 2 than that at Site 723, and calcium carbonate accounts for more than one-half of the mass accumulated. Preliminary shipboard data suggest that a significant part of the bulk carbonate accumulation is detrital material (see "Lithostratigraphy" section, this chapter). Therefore, carbonate accumulation reflects both pelagic and terrigenous sources. In comparison to nearby Site 723, organic carbon accumulation and concentration at Site 724 (Table 6) are significantly lower. These differences are only partly consistent with the positive correlation of sedimentation rate and organic matter preservation (see Müller and Suess, 1979).

PHYSICAL PROPERTIES

Physical-property measurements at Site 724 were limited by extensive gas-related sediment expansion. Discrete samples were taken from the least disturbed portions of cores for measurement of index properties (wet-bulk density, porosity, and grain density). Vane shear strength was determined only for APC cores of Hole 724A. Wet-bulk density and compressional-wave velocity were measured for the most coherent whole-round core sections with the GRAPE and *P*-wave logging systems. Reliable data acquisition with these systems was limited to the interval between the seafloor and 65 mbsf. Compressional-wave velocity could not be measured with the Hamilton Frame because of the inability to transmit a signal through the expanded sediment. All techniques and equipment used are described in the "Explanatory Notes" chapter.

Index Properties

Variation of index properties in Holes 724A, 724B, and 724C is primarily controlled by changes in sediment texture and composition. The two sediment types identified at Site 724, calcareous clayey silt and laminated diatomaceous clayey silt, are distinguishable on the basis of their physical properties; however, changes between the sediment types are gradational. Index properties measurements for Holes 724A, 724B, and 724C are listed in Table 7.

In the uppermost part of the section at Site 724 (0 to 35 mbsf) grain-size variation is responsible for wide variation in porosity (65% to 41%), water content (46% to 24%), and wet-bulk density (1.63 to 1.96 g/cm^3) (Fig. 27). Sand-rich intervals are characterized by porosities between 50% and 46% and wet-bulk densities between 1.87 to 1.96 g/cm^3. In the finer-grained

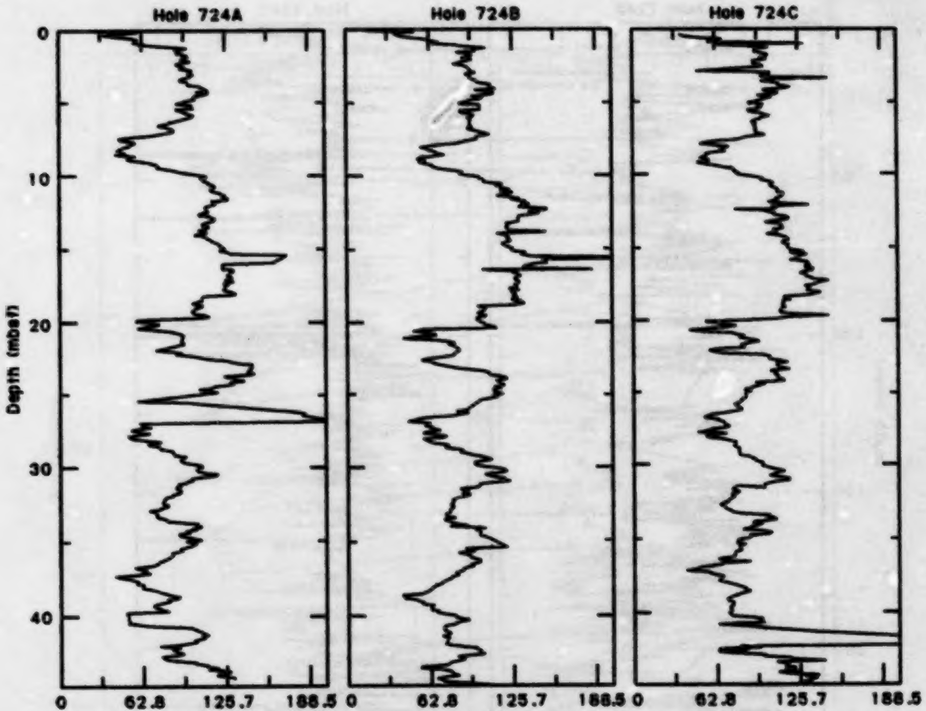

Figure 22. Plots of volume magnetic susceptibility data for 0 to 45 mbsf, Holes 724A, 724B, and 724C. These data were measured on the the first five APC cores of each hole.

sediments, porosity decreases from 62% near the seafloor to 54% at 35 mbsf. The wet-bulk density of these sediments increases from 1.68 to 1.82 g/cm^3 over the same interval.

Between 35 and 185 mbsf, porosity and water content are nearly constant at average values of 55% and 32%, respectively. Below 110 mbsf the variation of these averages is markedly reduced. The change in the degree of porosity variation at 110 mbsf roughly coincides with the disappearance of foraminifers in the sediments. Greater variation of porosity and water content probably reflect textural differences associated with the presence of foraminifers, with foraminifer-bearing sediments typically displaying lower porosity than finer-grained sediments. In the interval between 35 and 185 mbsf, grain density decreases uniformly from 2.73 to 2.55 g/cm^3 and is responsible for a decrease in wet-bulk density from 1.82 g/cm^3 to approximately 1.70 g/cm^3. The decreasing grain density coincides with a general trend of increasing abundance of organic matter and decreasing abundance of calcium carbonate (see "Lithostratigraphy" section).

Low grain density and wet-bulk density and varying porosity and water content characterize the interval between 185 and 230 mbsf. This depth range coincides with the principal occurrence of the diatomaceous clayey silts and dark, organic-rich clayey silts. The highest porosity (73%) and water content (51%) and the lowest wet-bulk density (1.48 g/cm^3) at Site 724 were measured for a sample from a diatom-rich layer at 213.1 mbsf (Sample 117-724B-23X-3, 70–72 cm). The grain density of this sample is low (2.48 g/cm^3) as a consequence of the low density of opal; however, the lowest grain densities (2.32 to 2.47 g/cm^3) are displayed by the dark, organic-rich layers. The high water content and porosity of the diatom-rich sediment are a reflection of the water-retaining attributes of siliceous microfossils. A positive correlation also exists between water content and organic matter abundance, as evidenced by the inverse relationship between water content (and porosity) and grain density in the interval between 185 to 230 mbsf.

Below 230 mbsf there is an insufficient thickness of sediments to document any consistent trends in porosity, water content, and wet-bulk density. Grain density displays a relatively uniform pattern of increase with depth, from 2.56 g/cm^3 at 230 mbsf to 2.74 g/cm^3 near the bottom of Hole 724B (Fig. 27). Foraminifers increase in abundance in this interval, and their reappearance is most likely responsible for the increase in grain density and variation in porosity, water content, and wet-bulk density.

GRAPE and *P*-Wave Logs

Determination of wet-bulk density by the GRAPE and compressional-wave (*P*-wave) velocity with the *P*-wave logger (PWL) was limited by sediment expansion. Continuous GRAPE data were obtained through Cores 117-724B-9X (83.7 mbsf) and 117-724C-9X (79.4 mbsf). In both holes, below approximately 65 mbsf the quality of the data decreases and the density is less than that determined for discrete samples as a consequence of the small fractures associated with sediment expansion. The GRAPE records display a cyclic variation similar to that at Site 723, except that at Site 724 the cycles are roughly half as thick. A tentative correlation of the features of the GRAPE records from Sites 724 and 723 is shown in Figure 28.

Velocity determinations with the PWL represent the only velocity measurements at Site 724. Velocity logs were obtained to depths of 48 mbsf in Hole 724B and 46 mbsf in Hole 724C. The

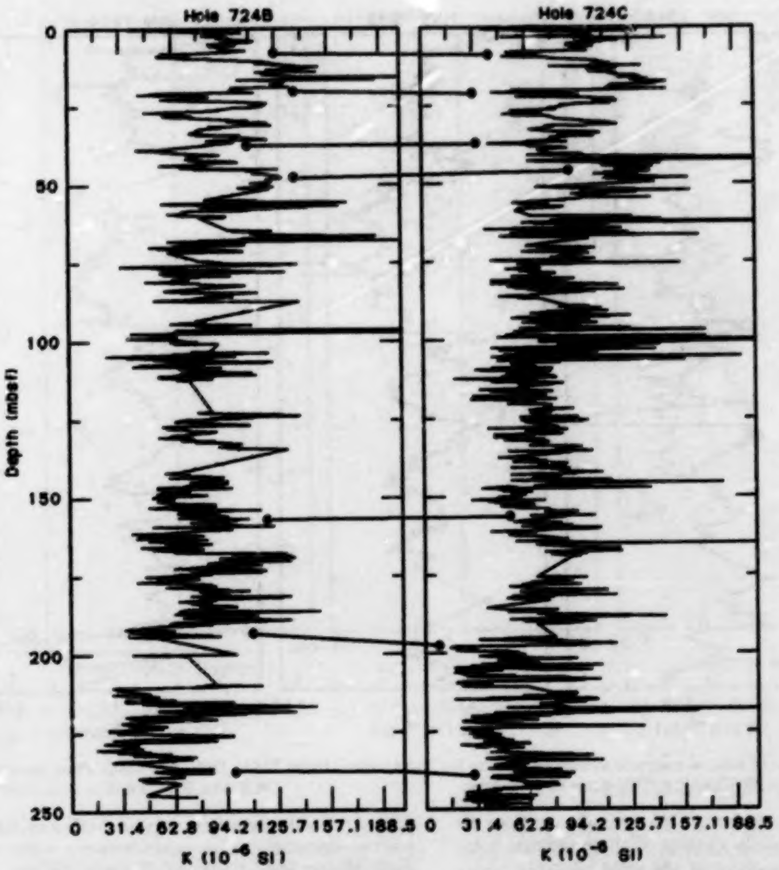

Figure 23. Plots of volume magnetic susceptibility of Holes 724B and 724C with tentative correlation of layers indicated.

measured velocities range from 1540 to 1680 m/s (Fig. 29) and display a pattern of cyclic variation that mimics that of the GRAPE wet-bulk density records.

Vane Shear Strength

Five measurements of vane shear strength were made on cores from Hole 724A (Table 7). The shear strengths varied from 10.29 kPa at 3.9 mbsf to 41.35 kPa at 30.9 mbsf. Below 40 mbsf, expansion-related disturbance made the sediment unsuitable for shear-strength determination.

INORGANIC GEOCHEMISTRY

At Site 724, 14 interstitial-water samples (two from Hole 724A, seven from Hole 724B, and five from Hole 724C) were collected by squeezing. No *in-situ* samples were collected at this site. All analytical results are listed in Tables 8 and 9 and presented in Figure 30. Note that the profiles were compiled by stacking the data sets from all three holes; this procedure may introduce some scatter if the specified depths below seafloor do not strictly correlate.

Salinity, Chloride, and pH

The concentration profiles of salinity, chloride, and pH are shown in Figure 30. As at previous sites, the salinity decrease between 0 and 100 mbsf can be attributed to the loss of sulfate and magnesium from solution (as discussed in the following text).

The chloride profile shows a distinct maximum between the top of the hole and ~80 mbsf, which is similar to the distribution of Cl^- at Site 725. At both sites the maximum is centered in sediments deposited in the mid-Pleistocene, which suggests that bottom water at that time was significantly more saline, at least on this part of the Oman margin. The Cl^- profiles at both sites have been subsequently smoothed by diffusion.

The pH measurements reported in Table 8 and plotted in Figure 30 should be considered to be approximate values only. As at other margin sites, degassing of CO_2 while the pH electrode was immersed in the pore fluid caused a severe upward drift of successive pH measurements; accuracy is therefore poor.

Sulfate and Alkalinity

The sulfate concentration decreases sharply over the upper 50 m of the cored section (Fig. 30), with a gradient (−0.5 mmol/L per m) comparable to that observed at Site 723. However, in contrast to the absence of sulfate at depth at Site 723, SO_4^{2-} is detectable in minor concentrations throughout the deeper part of the cored sequence at Site 724 (Table 8). This may reflect the cessation of sulfate reduction at depth.

Alkalinity increases steadily with depth (Fig. 30). The con-

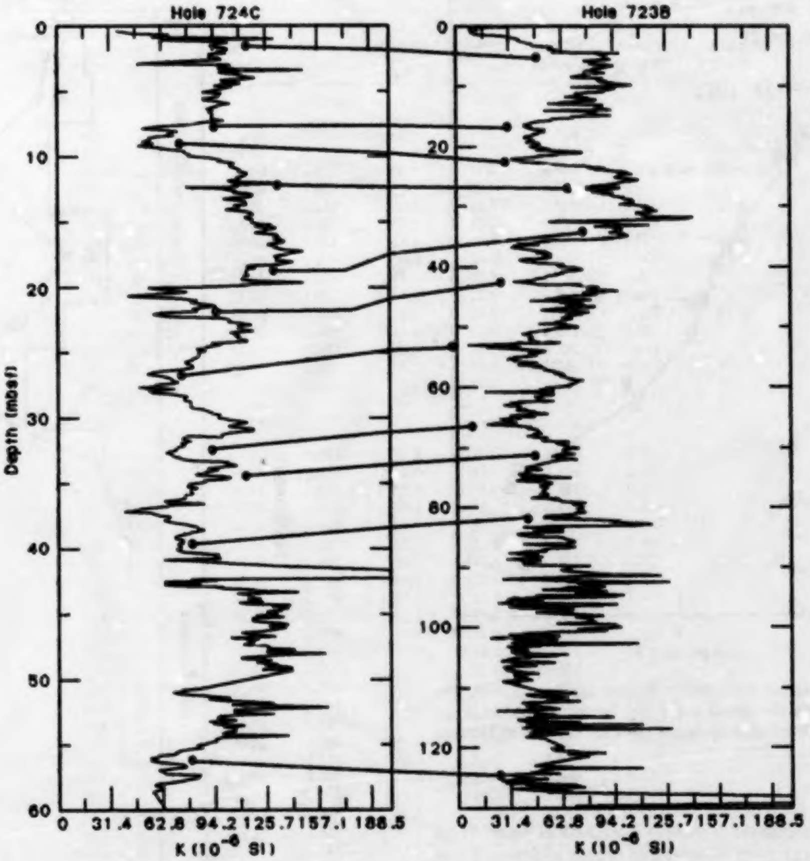

Figure 24. Brunhes Chronozone susceptibility correlations of Holes 723B and 724C from the Oman margin.

centration at 50 mbsf, where sulfate is depleted to < 1 mmol/L, is about 13 mmol/L, ~40 mmol/L less than would be produced by the reduction of 27 mmol/L of SO_4^{2-}. The deficit can be explained by the precipitation of authigenic carbonate minerals, as at previous sites. Below 50 mbsf, the alkalinity increase can be entirely accounted for by the continuing production of ammonia (see the following text) as organic matter is degraded during methanogenesis; methane is abundant at depth at this site (see "Organic Geochemistry" section, this chapter).

Calcium and Magnesium

Calcium and magnesium concentrations both decrease with depth (Fig. 30), with the steepest negative gradients occurring in the top 50 m. The maximum in the Mg/Ca ratio at 9 mbsf can be accounted for by the initial precipitation of calcite followed by the occurrence of dolomitization below ~10 mbsf. The profiles indicate that most of the precipitation of authigenic carbonates occurs in the top 50 m, which is consistent with the alkalinity deficit. Indeed, ~23 mmol/L of Mg^{2+} and 3 mmol/L of Ca^{2+} are consumed from solution in this upper zone to account for 60% of the "missing" alkalinity: presumably the rest of the alkalinity deficit can be attributed to the precipitation as calcite of calcium released to solution during the dolomitization of preexisting biogenic $CaCO_3$.

Ammonia, Phosphate, and Silica

Concentration profiles of these interstitial-water constituents are shown in Figure 30. Ammonia reaches relatively high concentrations, up to ~20 mmol/L, in the lower 200 m of the cored section, which reflects ongoing degradation of organic matter at depth. However, the concentrations in the top 50 m are lower than would be expected given the reduction of ~27 mmol/L of SO_4^{2-}, suggesting that several mmol/L of NH_4^+ have been adsorbed by clay minerals. We cannot determine if such uptake continues at greater depth.

Phosphate concentrations are rather variable at this site, partly as a result of analytical interference from dissolved sulfide (see "Explanatory Notes" chapter). The measured levels are again low, indicating that apatite must be precipitating in the sediments at Site 724; such authigenesis appears to be a universal phenomenon in organic-rich Arabian Sea sediments.

Dissolved silica increases with depth through the upper 50 m to values approaching the solubility of biogenic opal. Highest concentrations occur at ~80 mbsf and below 200 mbsf (Table 8),

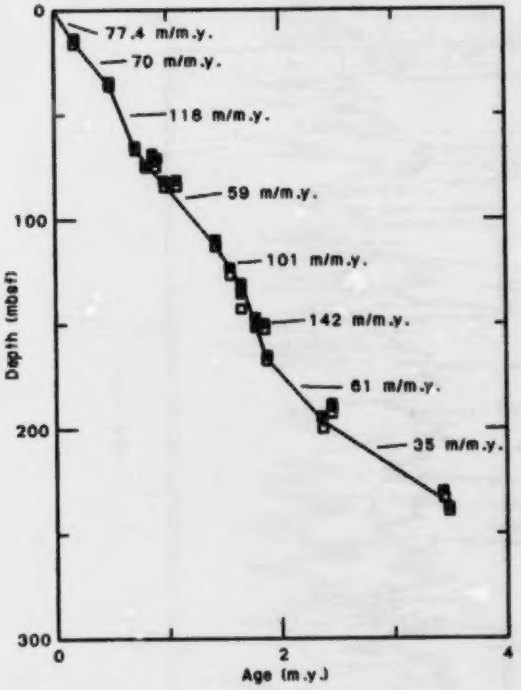

Figure 25. Age-depth plot of stratigraphic datums listed in Table 4. The solid and open boxes are the upper and lower boundaries of each datum, respectively. Indicated sedimentation rates are calculated between reliable nannofossil datum levels.

indicating zones of sediment relatively enriched in opal. High abundances of diatoms were observed in smear slides in Cores 117-724B-22X and 117-724B-23X at ~200–220 mbsf (see "Lithostratigraphy" section), which agrees with the pore-water results.

Dissolved Organic Carbon

The relative abundance of dissolved organic carbon (Table 9; see "Inorganic Geochemistry" section, "Site 723" chapter, for an explanation) in Site 724 pore waters is shown in Figure 30. The profile appears to reflect the general distribution of sedimentary organic carbon in the upper 100 m of the section but is poorly correlated in the lower 150 m. We do not know why this is the case.

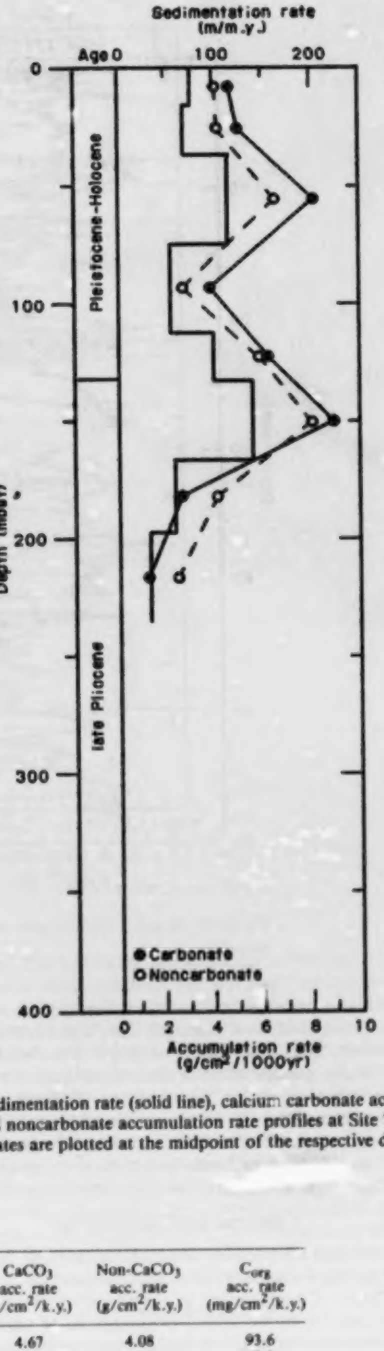

Figure 26. Sedimentation rate (solid line), calcium carbonate accumulation rate, and noncarbonate accumulation rate profiles at Site 724. Accumulation rates are plotted at the midpoint of the respective depth intervals.

Table 6. Sedimentation and accumulation rate data for Site 724.

Depth interval (mbsf)	Age range (Ma)	$CaCO_3$ ($\overline{X}$ %)	C_{org} ($\overline{X}$ %)	Dry-bulk density ($\overline{X}$ g/cm^3)	Sed. rate ($\overline{X}$ m/m.y.)	$CaCO_3$ acc. rate (g/cm^2/k.y.)	Non-$CaCO_3$ acc. rate (g/cm^2/k.y.)	C_{org} acc. rate (mg/cm^2/k.y.)
0.0–14.7	0–0.19	53.4	1.07	1.130	77.4	4.67	4.08	93.6
14.7–35.7	0.19–0.49	54.7	1.27	1.318	70.0	5.05	4.18	117.2
35.7–74.5	0.49–0.82	55.4	1.17	1.251	117.6	8.15	6.56	172.1
74.5–111.4	0.82–1.45	58.6	1.88	1.137	58.6	3.90	2.76	125.3
111.4–132.5	1.45–1.66	51.7	ND	1.214	100.5	6.31	5.89	ND
132.5–166.6	1.66–1.90	52.7	2.19	1.202	142.1	9.00	8.08	374.1
166.6–196.9	1.90–2.40	39.5	3.24	1.136	60.6	2.72	4.16	223.0
196.9–235.0	2.40–3.48	34.0	4.57	1.084	35.3	1.30	2.53	174.9

Note: ND indicates no data from the interval.

Table 7. Physical properties summary for Holes 724A, 724B, and 724C.

Core, section, interval (cm)	Depth (mbsf)	Wet-bulk density (g/cm³)	Porosity (%)	Water content (%)	Grain density (g/cm³)	Dry-bulk density (g/cm³)	Vane shear strength (kPa)
117-724A-							
1H-1, 100–102	1.00	1.770	60.6	35.1	2.726	1.148	
1H-3, 90–92	3.90						10.29
1H-3, 100–102	4.00	1.690	62.3	37.8	2.646	1.051	
2H-1, 100–102	7.50	1.633	65.1	40.9	2.606	0.966	
2H-3, 100–102	10.50	1.866	49.8	27.3	2.609	1.356	12.86
2H-6, 100–102	15.00	1.932	47.5	25.2	2.664	1.446	
3H-1, 100–102	16.90	1.908	48.3	25.9	2.618	1.413	18.65
3H-3, 100–102	19.90	1.679	59.8	36.5	2.541	1.066	
3H-5, 100–102	22.90	1.824	51.1	28.7	2.546	1.300	
4H-2, 100–102	27.90	1.734	56.8	33.6	2.558	1.152	
4H-4, 100–102	30.90	1.894	52.4	28.3	2.740	1.358	41.35
4H-6, 100–102	33.90	1.960	45.8	23.9	2.673	1.491	
5H-1, 100–102	35.90	1.923	49.9	26.6	2.730	1.412	
5H-3, 100–102	38.90	1.825	54.5	30.6	2.683	1.266	30.42
5H-5, 100–102	41.90	1.800	55.4	31.6	2.648	1.232	
117-724B-							
6X-2, 70–72	47.20	1.932	52.8	28.0	2.696	1.391	
6X-4, 70–72	50.20	1.858	50.2	27.7	2.656	1.344	
7X-2, 70–72	56.90	1.741	57.5	33.9	2.587	1.152	
7X-4, 70–72	59.90	1.852	54.4	30.1	2.658	1.295	
8X-2, 80–82	66.70	1.802	53.0	30.1	2.608	1.259	
8X-4, 80–82	69.70	1.711	62.7	37.6	2.665	1.068	
9X-2, 90–92	76.40	1.643	60.7	37.8	2.582	1.022	
9X-4, 90–92	79.40	1.815	54.2	30.6	2.659	1.260	
10X-2, 90–92	86.10	1.774	57.3	33.1	2.623	1.188	
11X-2, 74–76	95.64	1.679	60.6	37.0	2.606	1.058	
11X-4, 74–76	98.64	1.774	54.8	31.6	2.633	1.213	
12X-2, 98–100	105.48	1.671	61.9	38.0	2.532	1.036	
12X-4, 68–70	108.18	1.770	56.2	32.5	2.587	1.194	
12X-6, 88–90	111.38	1.716	57.4	34.3	2.564	1.128	
14X-2, 80–82	124.70	1.773	55.2	31.9	2.561	1.207	
14X-4, 95–97	127.85	1.771	53.8	31.1	2.542	1.220	
14X-6, 90–92	130.80	1.786	55.6	31.9	2.585	1.216	
15X-2, 50–52	134.00	1.810	55.2	31.2	2.651	1.244	
16X-1, 71–73	142.41	1.751	55.9	32.7	2.561	1.178	
16X-3, 91–93	145.61	1.702	55.4	33.3	2.440	1.135	
16X-5, 77–79	148.47	1.746	56.1	32.9	2.508	1.172	
17X-2, 85–87	153.75	1.831	53.6	30.0	2 600	1.281	
17X-4, 81–83	156.71	1.786	53.6	30.7	2.537	1.237	
17X-6, 105–107	159.95	1.769	55.5	32.2	2.565	1.200	
18X-2, 50–52	163.00	1.764	55.7	32.3	2.527	1.193	
18X-4, 57–59	166.07	1.752	56.0	32.8	2.518	1.178	
19X-6, 82–84	179.02	1.725	54.3	32.3	2.471	1.168	
19X-2, 88–90	173.08	1.633	59.8	37.5	2.412	1.020	
19X-4, 74–76	175.94	1.802	52.7	29.9	2.583	1.263	
19X-6, 70–72	178.90	1.804	52.3	29.7	2.514	1.268	
20X-2, 125–127	183.15	1.821	51.4	28.9	2.553	1.295	
20X-4, 70–72	185.60	1.688	55.9	33.9	2.461	1.115	
20X-6, 75–77	188.65	1.643	60.5	37.7	2.439	1.023	
21X-3, 87–89	193.87	1.574	61.9	40.3	2.320	0.939	
22X, CC (12–14)	200.57	1.607	60.2	38.4	2.348	0.991	
23X-3, 70–72	213.10	1.484	73.4	50.7	2.484	0.731	
23X-5, 70–72	216.10	1.766	52.7	30.6	2.467	1.226	
23X-7, 20–22	218.60	1.668	58.0	35.6	2.361	1.073	
24X-2, 35–37	220.85	1.763	57.3	33.3	2.604	1.176	
24X-4, 93–95	224.43	1.702	59.4	35.8	2.504	1.094	
24X-6, 78–80	227.28	1.617	60.0	38.0	2.345	1.003	
25X-2, 47–49	230.67	1.755	56.1	32.7	2.562	1.180	
25X-4, 30–32	233.50	1.830	53.8	30.1	2.609	1.279	
25X-6, 7–9	236.27	1.815	52.6	29.7	2.627	1.276	
26X-2, 132–134	241.22	1.691	60.6	36.7	2.572	1.071	
26X-4, 4–6	242.94	1.808	50.9	28.8	2.580	1.287	
26X-6, 66–68	246.56	1.819	56.6	31.9	2.712	1.239	
27X-2, 6–8	249.56	1.764	58.4	33.9	2.678	1.165	
27X-4, 65–67	253.15	1.721	61.4	36.5	2.741	1.092	
27X-6, 7-9	255.57	1.772	56.3	32.5	2.630	1.195	
117-724C-							
1H-2, 48–50	1.98	1.678	60.3	36.8	2.595	1.060	
2H-4, 48–50	7.78	1.645	61.6	38.4	2.574	1.014	
3H-4, 48–50	17.18	1.786	58.4	33.5	2.702	1.188	

Table 7 (continued).

Core, section, interval (cm)	Depth (mbsf)	Wet-bulk density (g/cm³)	Porosity (%)	Water content (%)	Grain density (g/cm³)	Dry-bulk density (g/cm³)	Vane shear strength (kPa)
117-724C-							
4H-4, 48–50	26.68	1.745	57.0	33.4	2.584	1.162	
5H-4, 48–50	36.18	1.825	53.5	30.0	2.617	1.277	
6X-4, 48–50	45.78	1.804	53.3	30.3	2.634	1.257	
7X-4, 48–50	55.48	1.744	58.7	34.5	2.664	1.143	
8X-5, 32–34	66.52	1.725	57.9	34.4	2.574	1.133	
9X-5, 50–52	76.30	1.819	56.5	31.8	2.746	1.241	
10X-4, 34–36	84.24	1.825	52.5	29.4	2.630	1.288	
11X-3, 57–59	92.57	1.807	55.8	31.7	2.645	1.235	
12X-3, 20–22	101.80	1.904	50.7	27.3	2.701	1.384	
13X-4, 87–89	113.67	1.748	57.1	33.4	2.605	1.163	
14X-5, 79–81	124.59	1.779	54.6	31.5	2.540	1.220	
15X-5, 90–92	134.30	1.848	53.5	29.7	2.672	1.300	
16X-4, 80–82	142.30	1.706	56.8	34.1	2.483	1.124	
17X-6, 67–69	154.77	1.810	55.3	31.3	2.640	1.244	
18X-5, 111–113	163.41	1.797	52.6	30.0	2.591	1.258	
19X-2, 66–68	168.06	1.770	54.3	31.4	2.563	1.214	
20X-2, 76–78	177.76	1.847	53.1	29.5	2.624	1.303	
21X-4, 59–61	190.29	1.613	60.4	38.4	2.384	0.994	
22X-3, 76–78	198.56	1.647	59.0	36.7	2.380	1.042	
22X-5, 74–76	201.54	1.679	57.4	35.0	2.454	1.091	
23X-3, 98–100	208.48	1.651	59.8	37.1	2.466	1.038	
24X-4, 76–78	219.36	1.794	54.7	31.3	2.569	1.233	
25X-4, 64–66	228.84	1.765	57.1	33.1	2.601	1.180	
26X-4, 55–57	238.45	1.799	54.1	30.8	2.618	1.245	
27X-4, 58–60	247.98	1.563	68.4	44.9	2.525	0.862	

ORGANIC GEOCHEMISTRY

Organic Matter Abundance and Character

In Holes 724A, 724B, and 724C, calcium carbonate and total carbon measurements were measured on residues of the headspace samples; the results are given in Table 3. Organic carbon values are, on average, somewhat lower than the values measured in sediments from Site 723, but they show the same trend of a general increase with depth. Several of the samples were subsequently analyzed by Rock-Eval pyrolysis, and the results are given in Table 10. The hydrogen and oxygen indices of Table 10 were recalculated using the total organic carbon (TOC) values from carbon determinations by the coulometric technique because the Rock-Eval TOC values were found to be unreliable. Plotted on a van Krevelen-type diagram (Fig. 31), the samples from Site 724 appear to be slightly shifted to the origin of the axes when compared to the sample plot from the more distal Site 723. Even though such a shift is traditionally considered to be an indication for increasing maturation, the young sediments at Site 724 are unlikely to be in a more advanced stage of thermal maturation. The temperature of maximum pyrolysis (T_{max}), which shifts to higher values during thermal maturation, is still well below the threshold of 435°C for all samples of Site 724. This is indicative for the immature organic matter expected at the site.

Hydrocarbon Gases

The results of interstitial gas analyses by the headspace method are listed in Table 11 and plotted vs. depth in Figure 32. The sharp decrease in interstitial sulfate between 25 and 50 mbsf (see "Inorganic Geochemistry" section) is closely followed by a sharp increase in methane (Fig. 32). The heavier gases, ethane and propane, show a steady increase with depth in both the headspace samples as well as in vacutainer samples from gas pockets (Figs. 32 and 33 and Tables 11 and 12). We believe that the elevated ethane and propane concentrations are of thermogenic origin for lack of a known biogenic source. Methane is dominated by biogenic production, and any elevated thermogenic methane is likely to be masked by the high biogenic contribution. Interstitial sulfate is still present at depth in low concentrations, but apparently does not inhibit methane production. Methane concentrations of 100%, as opposed to CO_2 expected during microbial sulfate reduction, were measured in gas pockets below 150 mbsf. This is in contrast to the results from Site 723, where the methane concentration of the gas pockets never reaches 100% and decreases with depth (see "Organic Geochemistry" section, "Site 723" chapter).

INTERHOLE CORRELATIONS

The upper 45 m at Site 724 has an age range from 0 to about 0.5 Ma and is characterized by cyclic changes in the nature of the sediments that can be identified by visual observation and by variations of magnetic susceptibility and carbonate content. Correlation of the sedimentary sequences and documentation of the correlative horizons between these holes provides valuable information on the relative rate of sedimentation, which is needed for any high-resolution study of Site 724 sediments.

Interhole correlations were made on the basis of visual identification of distinctive layers, as well as on the physical and magnetic properties. The magnetic susceptibility was measured at 10-cm intervals on whole-core sections.

The visual correlation of the cores relied primarily on the core photographs. Twenty-three distinct and traceable layers have been identified in the upper 80 m interval of the correlatable sedimentary sequence at Site 723 and have been labeled OM-a_1, a_2, . . . , through h_4, based on the correlation between Holes 723A and 723B (see "Interhole Correlations" section, "Site 723" chapter). The letter code (e.g., a) refers to the core sequence, and the number code indicates the number of the marker layers in each core. For example, the notation "a_2" corresponds to the second marker layer defined in Core 117-723A-1H, and "b_1" denotes the first marker layer in Core 117-723A-2H. Marker layers a_1 through h_4 were defined from the cored sediments of Hole 723A. The criteria used to define a marker layer is that the layer is dis-

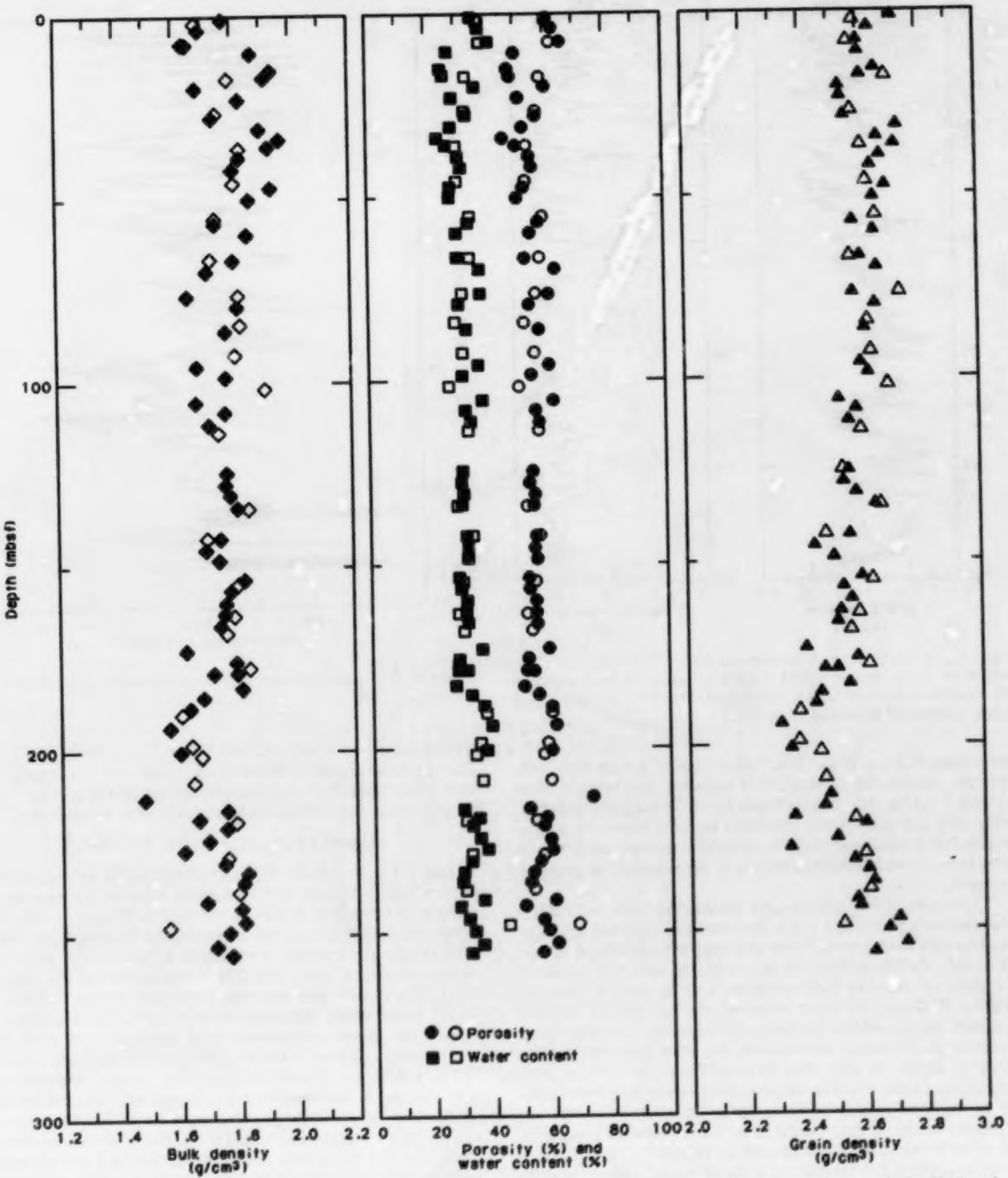

Figure 27. Index properties (wet-bulk density, porosity, water content, and grain density) measured on discrete samples from Holes 724A and 724B (solid symbols) and 724C (open symbols).

tinct enough to be traced in the sedimentary sequence of the other holes and that the character does not change. Useful criteria for recognizing the markers are color boundaries, distinctively colored layers, shape of burrow mottles, and sequence of color change in adjacent sediments. Three new marker layers were defined in the sedimentary sequence at Hole 724A, in addition to those noted at Site 723, and have been labeled c_5, e_3, and h_5, based on the correlation between the sedimentary sequences at Site 724. Table 13 lists the depths of the marker layers in the three holes of Site 724.

Figure 34 shows the magnetic susceptibility curve and positions of individual, visually correlatable layers. The pattern of

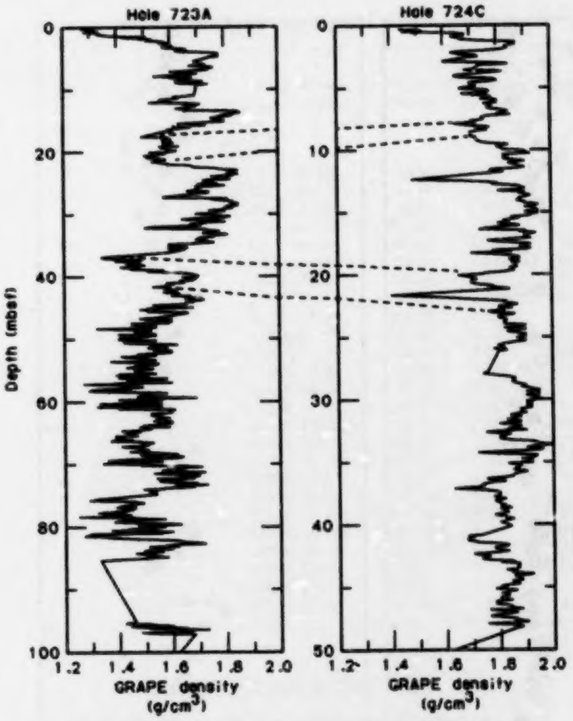

Figure 28. GRAPE wet-bulk density for Holes 723A and 724C. The profiles are based on 10-cm-thick block averages of the data. Note that the depth scale for Hole 723A is half that of Hole 724C. Tentative correlation is indicated by dashed lines.

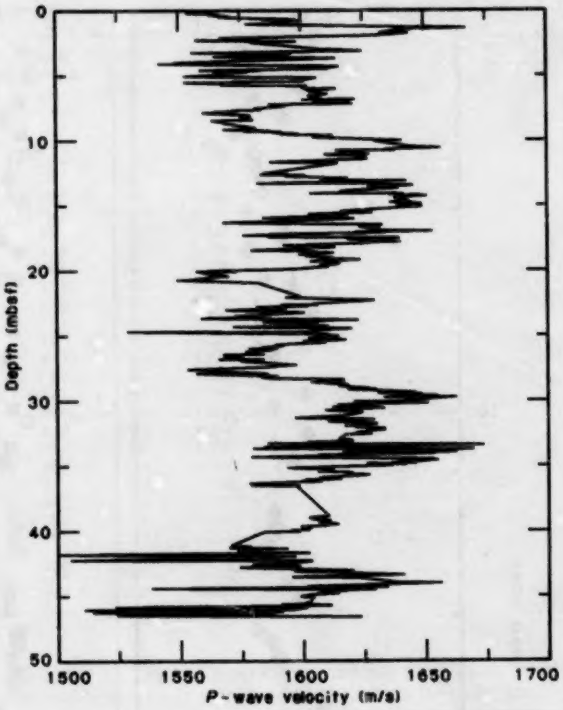

Figure 29. Compressional-wave velocity as measured by the *P*-wave logger in Hole 724C.

the susceptibility and the positions of layers match very well, not only between the three Site 724 holes but also between Sites 723 and 724 (Fig. 35). The stratigraphy of the magnetic susceptibility data and the visually identified layers is extremely consistent in that a particular visually characteristic layer always coincides in depth with a distinct feature in the magnetic susceptibility curve.

The results of the layer-by-layer correlation allow us to calculate true thickness of the layers that coincide with and are separated by core boundaries. Some core tops were expanded by water uptake during drilling. In this case, the observed apparent thickness of the disturbed sediment layer is thicker than the original thickness. In some instances, the top part of the core was missing, for which the apparent thickness is thinner than the original thickness. Fortunately, the three holes were staggered in depth, so that they have different horizons at core boundaries (Table 13). The original thickness of the layers coinciding with core tops or bottoms can be obtained by comparing thickness of the correlative layer in the continuous section of the other holes. The difference can be calculated from the differences in the ODP recorded depths of marker layers between the holes (see "A − B" and "B − C" in Table 13). Table 14 lists the differences between the depth (mbsf) calculated by the ODP Corelog data and the corrected depth (mbsf′) calculated by the layer-by-layer correlation method.

Use of the layer-by-layer method on the double- or triple-cored sedimentary sequences gives us the true stratigraphic thickness after the correction for core-boundary disturbance. Table 15 lists the stratigraphic thickness at Site 723, where most of the marker layers were defined, and Holes 724A, 724B, and 724C. The corrected depths in Holes 724A, 724B, and 724C agree well with each other. The intersite correlation of the marker layers clearly shows the differences in the rate of sedimentation.

SUMMARY AND CONCLUSIONS

Site 724 is in a water depth of about 600 m in the northern part of the ODP Leg 117 operations area on the continental margin of Oman. It is one of the central drilling targets in a depth transect bracketed by water depths ranging from 300 to 1500 m that corresponds vertically to a pronounced mid-water oxygen-minimum zone. Site 724 is positioned on the seaward flank of a slope basin that was previously drilled at Site 723, 45 km to the south. Biogenic material produced by coastal upwelling and eolian components were deposited here at a lower rate (80 m/m.y.) than in the southern part of the basin near Site 723 (175 m/m.y.). The sediments at Site 724 were expected to record changes in sedimentation and oceanographic/atmospheric circulation in considerable detail because of impeded benthic activity in the oxygen-minimum zone. Our intention in investigating Site 724 was to take advantage of the lower sedimentation rates to recover a longer Neogene section than was sampled at Site 723.

Some of the major findings at Site 724 are summarized in Figure 36 and include identification of

1. Laminated facies of late Pliocene age that are similar to, but older than, the facies found at Site 723.
2. A restricted preservation interval of abundant radiolarians and diatoms concomitant with poor preservation of plank-

Table 8. Summary of interstitial water geochemical data, Site 724.

Hole, core, section, interval (cm)	Depth (mbsf)	Vol. (mL)	pH	Alk. (mmol/L)	Sal. (g/kg)	Mg (mmol/L)	Ca (mmol/L)	Cl (mmol/L)	SO_4 (mmol/L)	PO_4 (μmol/L)	NH_4 (mmol/L)	SiO_2 (μmol/L)	Mg/Ca
724C-1H-1, 145-150	1.45	35	7.60	5.00	35.9	55.49	10.29	565	26.3	3.2	0.50	330	5.30
724A-1H-3, 145-150	4.45	35	8.10	5.40	35.0	51.24	8.59	570	19.4	3.8	1.02	512	5.98
724C-2H-4, 145-150	8.75	50	8.00	6.40	36.5	55.32	8.74	564	23.5	4.5	0.65	395	6.33
724A-3H-4, 145-150	21.85	37	7.67	5.74	35.0	45.96	9.03	572	13.9	7.3	1.35	466	5.09
724C-3H-4, 145-150	18.15	45	8.20	6.90	36.3	51.64	9.16	574	22.1	5.3	0.76	404	5.64
724C-4H-4, 145-150	27.65	45	8.20	8.68	36.2	45.38	9.78	575	13.9	3.7	1.02	483	4.64
724C-5H-4, 145-150	37.15	40	8.30	12.70	35.0	39.64	8.84	578	6.6	1.7	1.70	675	4.48
724B-6X-3, 145-150	49.45	31	—	13.02	34.0	32.35	7.47	578	0.9	2.7	2.35	963	4.33
724B-9X-4, 145-150	79.95	39	7.81	13.91	33.0	25.70	6.57	561	0.7	7.1	7.61	1148	3.91
724B-12X-5, 145-150	110.45	33	7.70	19.66	32.5	25.32	6.00	555	1.1	8.5	12.33	998	4.22
724B-16X-4, 145-150	147.65	51	7.70	21.68	32.5	23.31	4.75	557	1.8	3.5	15.04	984	4.91
724B-19X-4, 145-150	176.65	30	7.70	28.45	32.5	20.79	4.72	554	0.7	4.5	18.37	1017	4.40
724B-23X-3, 145-150	213.85	35	7.10	27.18	33.5	18.74	4.55	555	1.5	7.7	19.29	1073	4.12
724B-25X-4, 145-150	234.65	40	7.00	28.75	33.8	17.30	4.80	558	1.8	7.7	19.49	1138	3.60

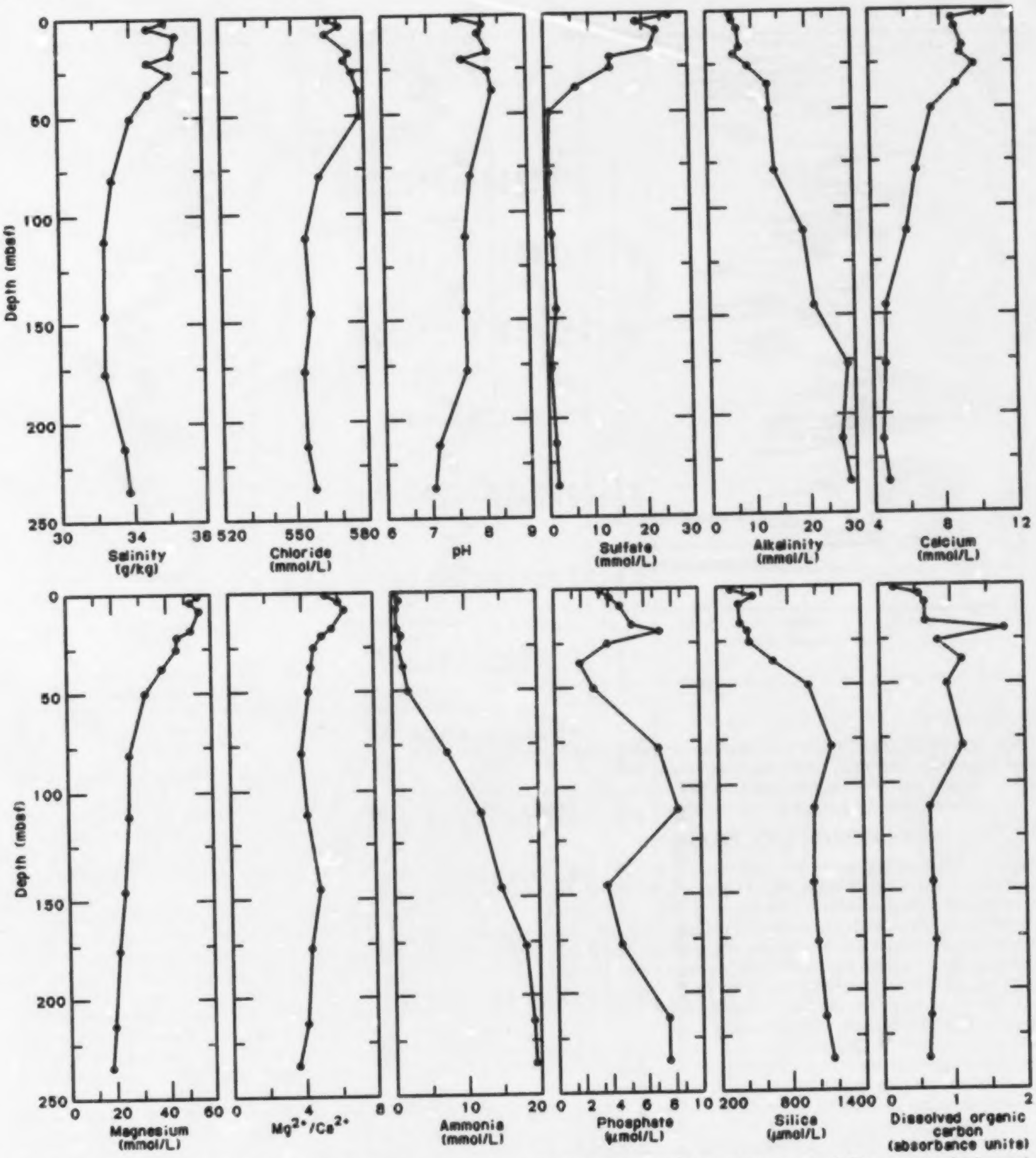

Figure 30. Salinity, chloride, pH, sulfate, alkalinity, calcium, magnesium, Mg/Ca ratio, ammonia, phosphate, dissolved silica, and dissolved organic carbon profiles for Site 724, compiled from data from three holes. Note that the data for dissolved organic carbon are plotted in terms of absorbance units and indicate relative concentration only.

tonic foraminifers. This interval occurs near the Pliocene/Pleistocene boundary and is partially coincident with the laminated facies.

3. The occurrence of shallow-water (less than 300 m) benthic foraminifers in the upper Pliocene section, which may be indicative of substantial subsidence of the site over the past 3 to 4 m.y.

4. Ongoing reduction of sulfate over the entire section and low Mg^{2+} concentrations, but a relative lack of diagenetic dolomite, in comparison to Site 723.

Table 9. Relative dissolved organic carbon concentrations at Site 724.

Core section, interval (cm)	Depth (mbsf)	Dissolved organic carbon (a.u.)
724C-1H-1, 145-150	1.45	0.209
724A-1H-3, 145-150	4.45	0.564
724C-2H-4, 145-150	8.75	0.642
724C-3H-4, 145-150	18.15	0.658
724A-3H-4, 145-150	21.85	1.740
724C-4H-4, 145-150	27.65	0.824
724C-5H-4, 145-150	37.15	1.151
724B-6X-3, 145-150	49.45	0.946
724B-9X-4, 145-150	79.95	1.156
724B-12X-5, 145-150	110.45	0.693
724B-16X-4, 145-150	147.65	0.728
724B-19X-4, 145-150	176.65	0.751
724B-23X-3, 145-150	213.85	0.673
724B-25X-4, 145-150	234.65	0.639

Note: a.u. = absorbance units at 240 nm.

5. Traces of ethane, propane, and butane that increase steadily with depth.

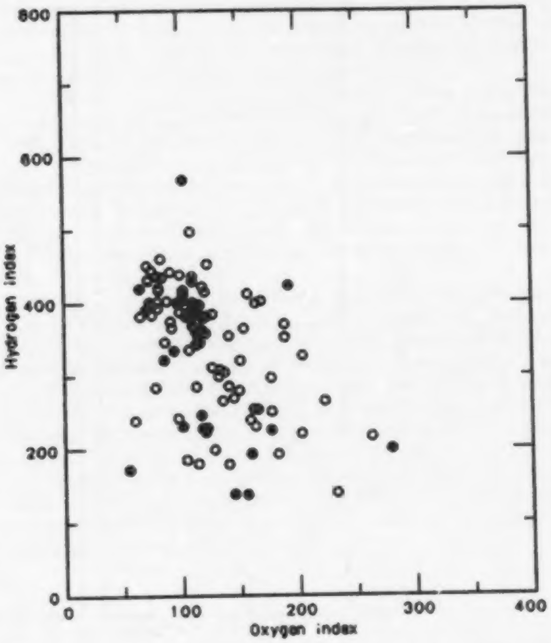

Figure 31. Plot of hydrogen index vs. oxygen index of samples from Holes 724A, 724B, and 724C (dots), compared with samples from Site 723 (circles).

Only one lithologic unit was recognized at Site 724. The section ranges from uppermost lower Pliocene to the Holocene, and the magnetostratigraphy was surprisingly well defined with the Brunhes/Matuyama and Matuyama/Gauss boundaries identified at 60 and 180 mbsf, respectively (Fig. 36). The lithologic unit is comprised of green to olive green calcareous clayey silt high in organic carbon. No dolomite layers were found at this site. Interbedded in the upper Pliocene section are decimeter-scale beds of laminated diatomaceous clayey silt (Fig. 36) that are similar to, but older than, beds previously recognized at Site 723. The upper Pliocene opal-rich facies is clearly identified by the physical-property data, especially by the characteristically low grain density (Fig. 36). This facies is thought to reflect a lack of bioturbation, which led to preservation of the fine-scale laminations of heterogeneous primary input.

The faunal and floral assemblages reveal a complex environmental history at Site 724. Although indicator species generally show that monsoonal upwelling was persistent throughout the Pliocene-Pleistocene, distinct differences exist between the biotic groups (Fig. 36). Radiolarians and diatoms are abundant only in the middle upper Pliocene, an interval where planktonic foraminifers and calcareous nannofossils are rare and poorly preserved. The planktonic foraminifers become abundant and highly diverse and the calcareous nannofossils also become abundant, but with low diversity, in the uppermost Pliocene. Within this same interval, diatoms and radiolarians are sparse or absent. Hence, the production and preservation of opaline and calcareous assemblages seems to be mutually exclusive. The environmental significance of this observed abundance pattern is intriguing but unclear at this time.

Table 10. Results of Rock-Eval pyrolysis of samples from Holes 724A, 724B, and 724C.

Core, section, interval (cm)	Depth (mbsf)	T_{max} (°C)	S_1	S_2	S_3	S_2/S_3	TOC[a]	TOC[b]	HI Index	OI Index
724C-1H-2, 0-1	1.5	421	0.50	1.45	1.64	0.88	0.58	1.05	138	156
724A-1H-3, 144-145	4.44	423	0.27	1.02	1.07	0.95	0.73	0.74	138	145
724C-2H-5, 0-1	8.80	419	0.64	2.76	2.29	1.20	0.74	1.43	193	160
724A-3H-4, 144-145	21.84	423	0.51	3.48	1.65	2.10	1.33	1.41	246	117
724A-4H-2, 100-102	27.90	427	0.34	2.98	1.61	1.85	1.26	1.33	224	121
724A-4H-4, 100-102	30.90	424	0.38	2.65	2.08	1.27	1.86	1.17	226	177
724C-4H-5, 0-1	31.40	417	0.82	4.79	2.48	1.93	1.29	2.10	228	118
724A-4H-6, 100-102	33.90	423	0.10	0.64	0.90	0.71	0.73	0.32	200	280
724A-5H-1, 100-102	35.90	423	0.33	2.92	1.33	2.19	1.34	0.69	423	193
724A-5H-3, 100-102	38.90	422	0.40	3.47	1.52	2.28	1.51	1.50	231	101
724C-5H-5, 0-1	40.90	417	0.69	3.50	1.87	1.87	0.92	1.53	229	122
724A-5H-5, 100-102	41.90	415	1.06	5.97	1.53	3.90	1.85	1.39	429	110
724B-11X-4, 149-150	99.39	415	1.13	6.35	1.69	3.75	2.16	1.98	321	85
724B-12X-5, 119-120	110.19	417	0.99	6.65	1.88	3.53	2.61	1.99	334	94
724B-16X-4, 144-145	147.64	410	2.16	12.41	2.24	5.54	3.63	2.19	567	103
724B-19X-5, 0-1	176.70	407	2.85	12.64	2.27	5.56	3.94	3.24	390	70
724B-23X-4, 0-1	213.90	417	1.18	6.05	1.93	3.13	2.18	3.51	172	55
724B-25X-5, 0-1	234.70	427	0.21	8.12	1.27	6.39	3.76	1.94	419	65

Note: HI = hydrogen index and OI = oxygen index; the hydrogen and oxygen indexes were calculated on the basis of the TOC[b] values. For a detailed description of parameters, see the "Explanatory Notes" chapter (this volume).

[a] TOC values measured by Rock-Eval pyrolysis.

[b] TOC values measured by the difference method.

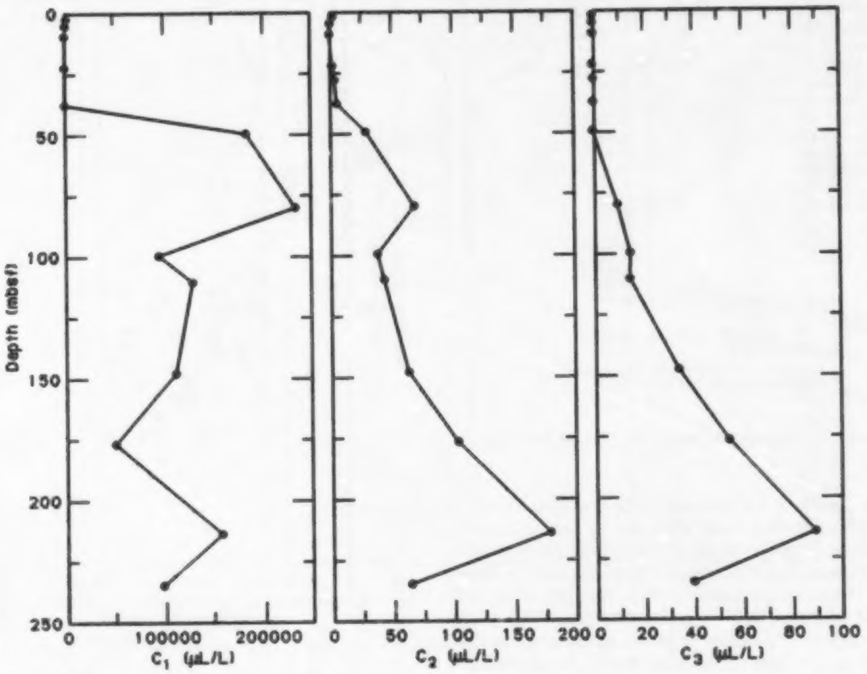

Figure 32. Downhole concentrations of methane (C_1), ethane (C_2), and propane (C_3) in headspace samples from Holes 724A, 724B, and 724C.

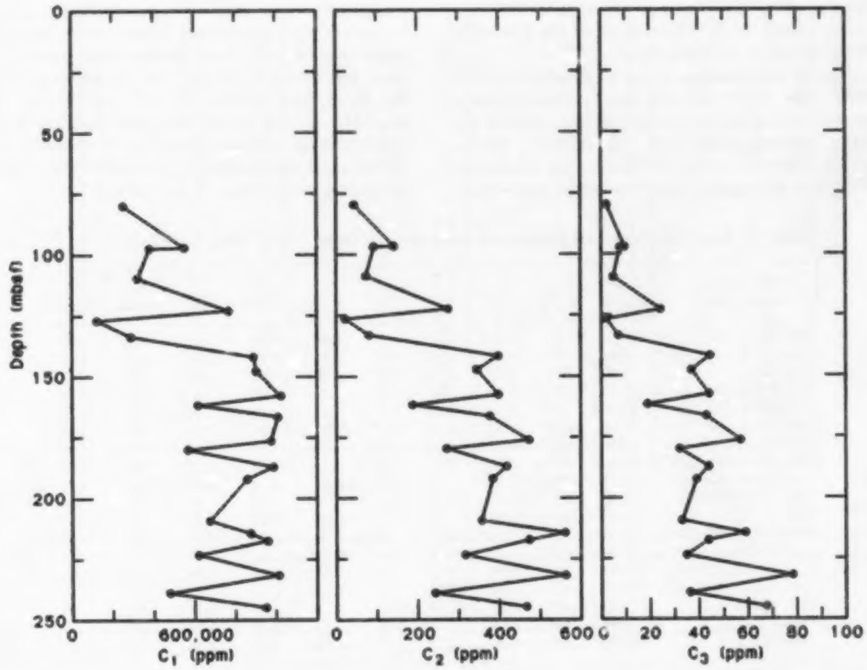

Figure 33. Downhole concentrations of methane (C_1), ethane (C_2), and propane (C_3) in vacutainer samples from gas pockets in Holes 724B and 724C.

Table 11. Concentrations of methane (C_1), ethane (C_2), and propane (C_3) per liter of wet sediment in samples from Holes 724A, 724B, and 724C.

Core, section, interval (cm)	Depth (mbsf)	C_1 (μL/L)	C_2 (μL/L)	C_3 (μL/L)	C_1/C_2
724C-1H-2, 0-1	1.50	659	2		330
724A-1H-3, 144-145	4.44	77			
724C-2H-5, 0-1	8.80	170			
724A-3H-4, 144-145	21.84	427	2		214
724C-4H-5, 0-1	27.70	111	4		28
724C-5H-5, 0-1	37.20	282	6		47
724B-6X-3, 119-120	49.19	184,525	30		6151
724B-9X-4, 119-120	79.69	235,455	70	10	3364
724B-11X-4, 149-150	99.39	95,670	40	15	2392
724B-12X-5, 119-120	110.19	130,940	45	15	2910
724B-16X-4, 144-145	147.64	113,195	65	35	1741
724B-19X-5, 0-1	176.70	51,120	105	55	487
724B-23X-4, 0-1	213.90	160,530	180	90	891
724B-25X-5, 0-1	234.70	99,720	65	40	1534

Note: Values are expressed in μL/L (volume gas/volume wet sediment).

Table 12. Concentrations of methane (C_1), ethane (C_2), and propane (C_3) measured in gas pockets from Holes 724B and 724C.

Core, section, interval (cm)	Depth (mbsf)	C_1 (ppm)	C_2 (ppm)	C_3 (ppm)	C_1/C_2
724B-9X-5, 0	80.00	263,263	50	3	5265
724B-11X-3, 68	97.08	561,013	146	10	3843
724C-11X-6, 75	97.25	392,221	99	9	3962
724B-12X-5, 40	109.40	332,980	78	6	4269
724C-14X-4, 55	122.85	775,644	278	25	2790
724B-14X-3, 145	126.85	130,426	30	3	4348
724B-15X-1, 146	133.46	300,298	89	8	3374
724C-16X-4, 44	141.94	901,650	402	45	2243
724B-16X-4, 135	147.55	915,815	348	38	2632
724B-17X-5, 20	157.60	1,031,869	402	45	2567
724C-18X-4, 95	161.75	635,001	197	20	3223
724B-18X-4, 95	166.45	1,019,407	381	44	2675
724B-19X-4, 120	176.40	985,764	476	58	2071
724C-20X-3, 145	179.95	578,441	279	33	2073
724B-20X-5, 85	187.25	998,695	422	45	2366
724B-21X-2, 78	192.28	868,933	388	40	2240
724C-23X-4, 15	209.15	683,736	361	34	1894
724B-23X-4, 50	214.40	887,847	563	60	1577
724C-24X-3, 35	217.45	967,362	478	45	2024
724B-24X-3, 147	223.47	625,838	325	36	1926
724B-25X-3, 3	231.73	1,015,347	566	79	1794
724C-26X-4, 100	238.90	486,168	251	37	1937
724B-26X-5, 30	244.70	954,141	466	68	2048

A surprising discovery is the occurrence of benthic foraminifers characteristic of shallow water (less than 300 m) in the lower upper Pliocene (Fig. 36). These data indicate that the basin may have subsided several hundred meters (as much as 600 m) during the past 3 to 4 m.y. Although seismic profiles show thickening in the center of the slope basin and thinning against the seaward basement peak, these benthic foraminifer data are the first direct indication of subsidence in the slope basins.

Carbonate and noncarbonate accumulation rates at Site 724 range from 1 to 8 g/cm^2/1000 yr (Fig. 36). Superimposed on these long-term variations in sediment accumulation, both magnetic susceptibility and physical-property data show cyclic variability that may reflect shorter term, climate-related changes in the depositional system dominated by upwelling and eolian input. The production, preservation, and tectonic factors that control these changes are complex and will be the subject of post-cruise research.

Chemical compositions of interstitial waters and gas show that, unlike at Site 723, sulfate is never completely depleted at Site 724. Diagenetic effects associated with organic-matter degradation by sulfate reduction are much less obvious at Site 724. No diagenetic dolomite was encountered, the Ca/Mg ratio is much lower than at Site 723, and gas pockets contain mainly methane. Increased amounts of propane and traces of butane suggest a thermogenic origin for part of the gas.

Overall, Site 724 provides new information about the subsidence of the slope basins and on the history of carbon-rich, opal-rich laminated facies associated with the oxygen-minimum zone along the continental margin.

REFERENCES

Berggren, W. A., Kent, D. V., and Van Couvering, J. A., 1985. The Neogene: Part 2, Neogene geochronology and chronostratigraphy. *In* Snelling, N. J. (Ed.), *The Chronology of the Geological Record*: Geol. Soc. Mem. (London), 10:211–259.

Fleisher, R. L., 1974. Cenozoic planktonic Foraminifera and biostratigraphy, Arabian Sea, Deep Sea Drilling Project, Leg 23A. *In* Whitmarsh, R. B., Weser, O. E., Ross, D. A., et al., *Init. Repts. DSDP*, 23: Washington (U.S. Govt. Printing Office), 1001–1072.

Müller, P. J., and Suess, E., 1979. Productivity, sedimentation rate, and sedimentary organic matter in the oceans—I. Organic carbon preservation. *Deep-Sea Res., Part A*, 26:1347–1362.

Sato, T., Takayama, T., Kato, M., Kudo, T., and Kameo, K., in press. Calcareous microfossil biostratigraphy of the uppermost Cenozoic formations distributed in the coast of the Japan Sea. Part 4: Conclusion. *Sekiyu Gijutsu Kyokaishi*.

Takayama, T., and Sato, T., 1987. Coccolith biostratigraphy of the North Atlantic Ocean, DSDP Leg 94. *In* Ruddiman, W. F., and Kidd, R. B., Thomas, E., et al., *Init. Repts. DSDP*, 94, Pt. 2: Washington (U.S. Govt. Printing Office), 651–702.

van Morkhoven, F. P., Berggren, W. A., and Edwards, A. S., 1986. Cenozoic cosmopolitan deep-water benthic Foraminifera. *Bull. Cent. Rech. Explor.-Prod. Elf-Aquitaine*, Mem. 11.

Ms 117A-111

Table 13. Stratigraphic depths of the marker layers at Site 724.

Layer	Hole 724A		Hole 724B		Hole 724C			
	Core, section, interval (cm)	ODP depth (mbsf)	Core, section, interval (cm)	ODP depth (mbsf)	Core, section, interval (cm)	ODP depth (mbsf)	Holes 724A − 724B	Holes 724B − 724C
OM-a_1	1H-1, 95	0.95	1H-1, 95	0.95	1H-1, 110	1.10	0.00	0.15
a_2	1H-2, 115	2.65	1H-2, 105	2.55			0.10	
b_1	1H-3, 100	4.00	1H-3, 100	4.00	2H-1, 115	3.95	0.00	−0.05
b_3	2H-1, 75	7.25	2H-1, 80	7.80	2H-4, 60	7.90	−0.55	−0.10
c_1	2H-2, 75	8.75	2H-2, 85	9.35			−0.60	
c_2	2H-3, 130	10.80	2H-3, 130	11.30	2H-6, 115	11.45	−0.50	0.15
c_3	2H-4, 70	11.70	2H-4, 75	12.25	2H-7, 50	12.30	−0.55	0.05
c_4	2H-4, 120	12.20	2H-4, 135	12.85			−0.65	
c_5	2H-5, 35	12.85	2H-5, 50	13.50	3H-1, 50	12.70	−0.65	−0.80
d_1	3H-1, 40	16.30	3H-1, 45	16.85	3H-3, 115	16.35	−0.55	−0.50
d_2	3H-1, 150	17.40	3H-2, 5	17.95	3H-4, 65	17.35	−0.55	−0.60
d_3	3H-2, 90	18.30	3H-2, 105	18.95	3H-5, 20	18.40	−0.65	−0.55
d_4	3H-3, 85	19.75	3H-3, 105	20.45	3H-6, 20	19.90	−0.70	−0.55
e_1	3H-4, 15	20.55	3H-4, 35	21.25	3H-6, 105	20.75	−0.70	−0.50
e_2	3H-5, 90	22.80	3H-5, 115	23.55	4H-1, 80	22.50	−0.75	−1.05
e_3	3H-6, 95	24.35	3H-6, 135	25.25	4H-2, 100	24.20	−0.90	−1.05
f_1	4H-1, 85	26.25	4H-1, 60	26.50	4H-4, 20	26.40	−0.25	−0.10
f_2	4H-2, 70	27.60	4H-2, 45	27.85	4H-5, 10	27.80	−0.25	−0.05
g_1	4H-4, 120	31.10	4H-4, 95	31.35	4H-7, 85	31.55	−0.25	−0.20
g_2	4H-6, 25	33.15	4H-6, 5	33.45	5H-1, 150	32.70	−0.30	−0.75
h_1	4H-7, 40	34.80	5H-1, 70	36.10	5H-3, 10	34.30	−1.30	−1.80
h_2	5H-1, 80	35.70	5H-2, 20	37.10	5H-3, 100	35.40	−1.40	−1.70
h_3	5H-2, 60	37.00	5H-2, 150	38.40	5H-4, 85	36.55	−1.40	−1.85
h_4	5H-4, 145	40.85	5H-5, 90	42.30	5H-7, 20	40.40	−1.45	−1.90
h_5	5H-5, 145	42.35	5H-6, 90	43.80	6H-1, 60	41.40	−1.45	−2.40

Note: Depths are based on ODP CORELOG data.

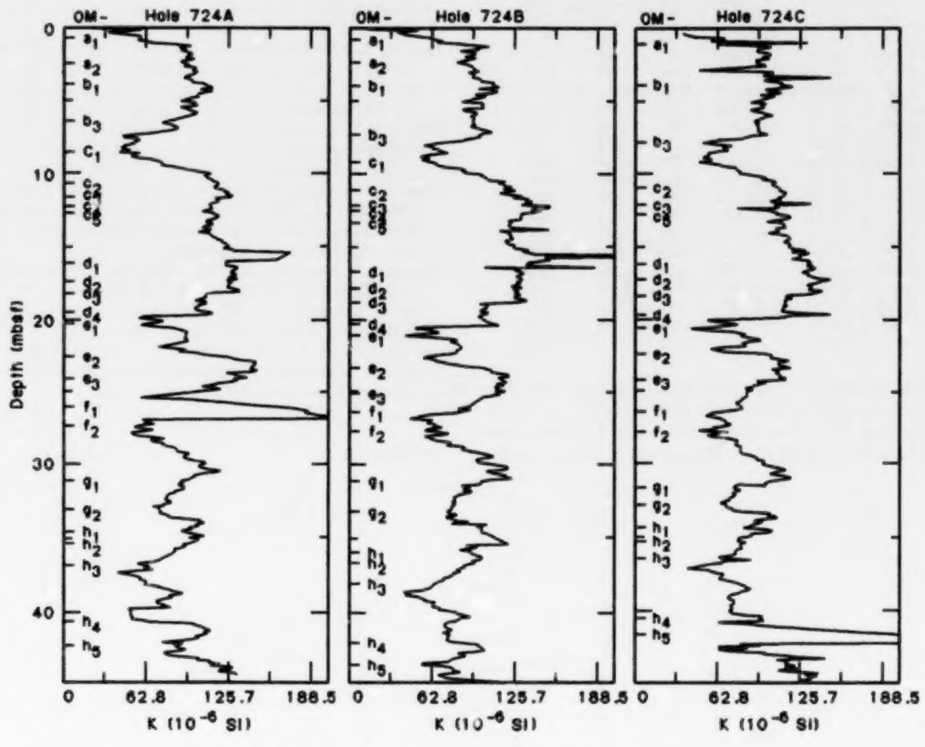

Figure 34. Volume magnetic susceptibility curves and marker layer positions in Holes 724A, 724B, and 724C.

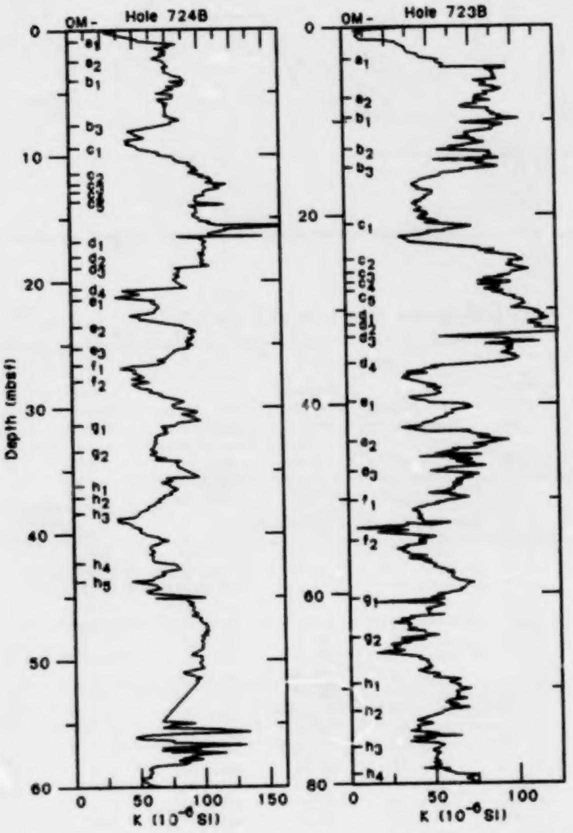

Figure 35. Volume magnetic susceptibility curves and marker layer positions in Holes 723B and 724B.

Table 14. Corrected depth below seafloor of core tops for stratigraphic calculation of depth below seafloor.

	Hole 724A			Hole 724B			Hole 724C		
Core	ODP top depth (mbsf)	Difference	Corrected top depth (mbsf)	ODP top depth (mbsf)	Difference	Corrected top depth (mbsf)	ODP top (mbsf)	Difference	Corrected top depth (mbsf)
1H	0.0	0.0	0.0	0.0	0.0	0.0	0.0	0.0	0.0
2H	6.5	0.7	7.2	7.0	0.1	7.1	2.8	0.0	2.8
3H	15.9	0.2	16.8	16.4	0.2	16.7	12.2	0.8	13.0
4H	25.4	0.6	26.9	25.9	1.0	27.2	21.7	0.5	23.0
5H	34.9	0.1	36.5	35.4	−1.1	35.6	31.2	0.7	33.2
6X							40.8	0.5	43.3

Note: ODP top depth = depth (mbsf) of core top calculated by the ODP CORELOG data; Corrected top depth = depth (mbsf) of core top calculated by the layer-by-layer correlation method. Difference is between the ODP CORELOG data depth and the depth calculated by the layer-by-layer correlation method.

Table 15. Stratigraphic depths of the marker layers at Sites 723 and 724.

	Hole 723B		Hole 724A		Hole 724B		Hole 724C	
Layer	Core, section, interval (cm)	Corrected depth (mbsf)	Core, section, interval (cm)	Corrected depth (mbsf)	Core, section, interval (cm)	Corrected depth (mbsf)	Core, section, interval (cm)	Corrected depth (mbsf)
OM-a_1	1H-3, 35	3.35	1H-1, 95	0.95	1H-1, 95	0.95	1H-1, 110	1.10
a_2	2H-3, 20	7.20	1H-2, 115	2.65	1H-2, 105	2.55		
b_1	2H-4, 65	9.15	1H-3, 100	4.00	1H-3, 100	4.00	2H-1, 115	3.95
b_2	2H-6, 110	12.60						
b_3	3H-1, 95	14.75	2H-1, 75	7.95	2H-1, 80	7.90	2H-4, 60	7.90
c_1	3H-5, 110	20.90	2H-2, 75	9.45	2H-2, 85	9.45		
c_2	4H-1, 85	24.95	2H-3, 130	11.50	2H-3, 130	11.40	2H-6, 115	11.45
c_3	4H-2, 100	26.60	2H-4, 70	12.40	2H-4, 75	12.35	2H-7, 50	12.30
c_4	4H-3, 15	27.25	2H-4, 120	12.90	2H-4, 135	12.95		
c_5	4H-3, 100	28.10	2H-5, 35	13.55	2H-5, 50	13.60	3H-1, 50	13.50
d_1	4H-5, 70	30.80	3H-1, 40	17.20	3H-1, 45	17.15	3H-3, 115	17.15
d_2	4H-6, 10	31.70	3H-1, 150	18.30	3H-2, 5	18.25	3H-4, 65	18.15
d_3	4H-7, 5	33.15	3H-2, 90	19.20	3H-2, 105	19.25	3H-5, 20	19.20
d_4	5H-2, 50	35.30	3H-3, 85	20.65	3H-3, 105	20.75	3H-6, 20	20.70
e_1	5H-5, 20	39.50	3H-4, 15	21.45	3H-4, 35	21.55	3H-6, 105	21.55
e_2	6H-1, 90	43.80	3H-5, 90	23.70	3H-5, 115	23.85	4H-1, 80	23.80
e_3	6H-3, 150	47.40	3H-6, 95	25.25	3H-6, 135	25.55	4H-2, 100	25.50
f_1	6H-5, 120	50.10	4H-1, 85	27.75	4H-1, 60	27.80	4H-4, 20	27.70
f_2	7H-2, 15	54.25	4H-2, 70	29.10	4H-2, 45	29.15	4H-5, 10	29.10
g_1	7H-6, 30	60.40	4H-4, 120	32.60	4H-4, 95	32.65	4H-7, 85	32.85
g_2	8H-2, 60	64.40	4H-6, 25	34.65	4H-6, 5	34.75	5H-1, 150	34.70
h_1	8H-5, 90	69.20	4H-7, 40	36.30	5H-1, 70	36.30	5H-3, 10	36.30
h_2	9H-1, 20	72.10	5H-1, 80	37.30	5H-2, 20	37.30	5H-3, 100	37.20
h_3	9H-3, 135	76.25	5H-2, 60	38.60	5H-2, 150	38.60	5H-4, 85	38.55
h_4	9H-7, 95	81.85	5H-4, 145	42.45	5H-5, 90	42.50	5H-7, 20	42.40
[a]h_5			5H-5, 145	43.95	5H-6, 90	44.00	6X-1, 60	43.90

Note: Depths are based on the correction factor of Table 14. Corrrected depth = corrected depth for stratigraphic thickness.

[a] Top of bioturbated white layer overlain by dark layer.

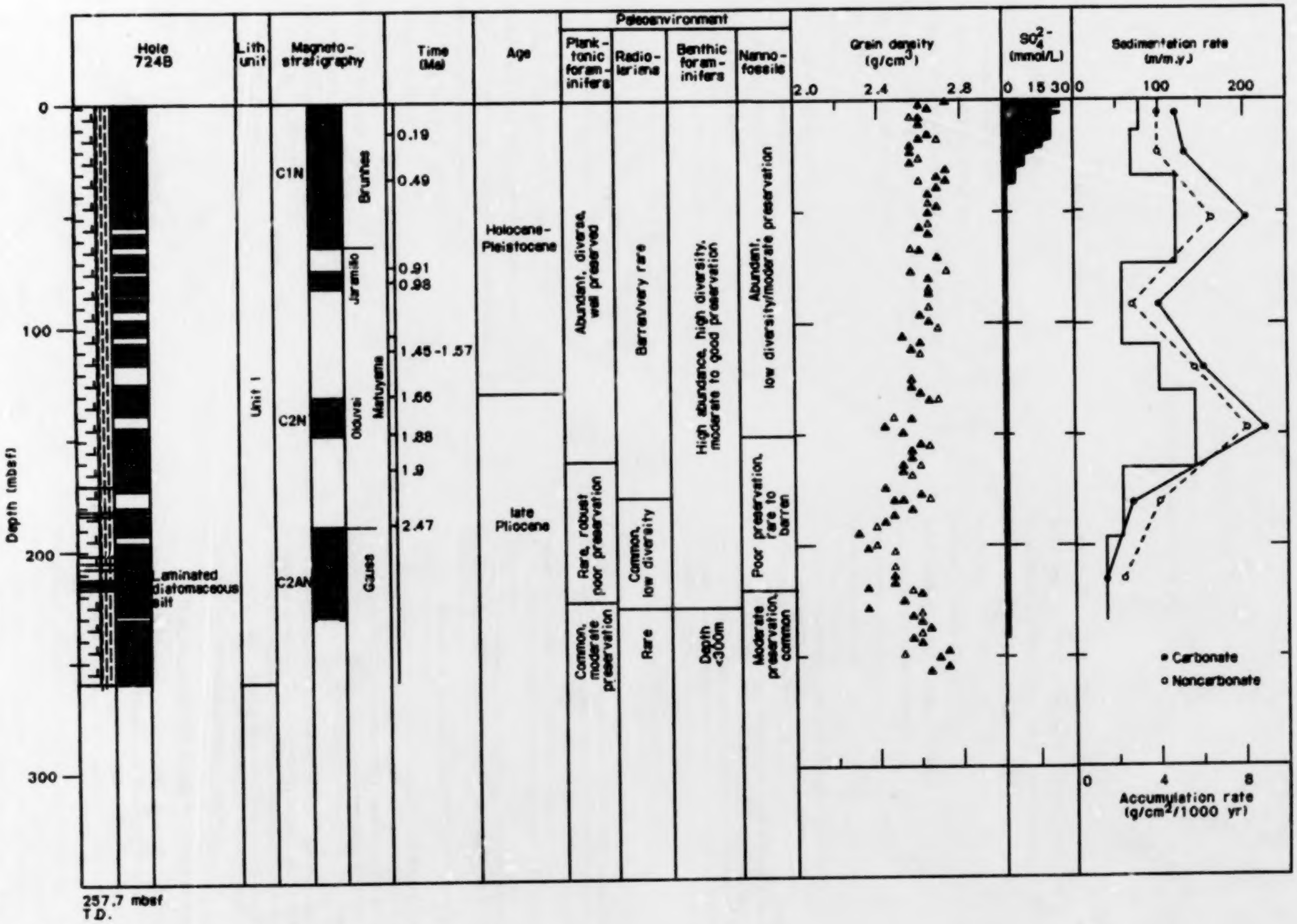

Figure 36. Summary of preliminary shipboard analyses at Site 724.

13. SITE 725[1]

Shipboard Scientific Party[2]

HOLE 725A

Date occupied: 22 September 1987

Date departed: 22 September 1987

Time on hole: 4 hr, 30 min

Position: 18°29.200′N, 57°42.030′E

Water depth (sea level; corrected m, echo-sounding): 311.5

Water depth (rig floor; corrected m, echo-sounding): 322.0

Bottom felt (m, drill pipe): 323.1

Penetration (m): 4.5

Number of cores: 1

Total length of cored section (m): 4.5

Total core recovered (m): 4.5

Core recovery (%): 100%

Oldest sediment cored
Depth sub-bottom (m): 4.5
Nature: nannofossil foraminifer sandy silt

HOLE 725B

Date occupied: 22 September 1987

Date departed: 22 September 1987

Time on hole: 8 hr, 15 min

Position: 18°29.200′N, 57°42.030′E

Water depth (sea level; corrected m, echo-sounding): 311.5

Water depth (rig floor; corrected m, echo-sounding): 322.0

Bottom felt (m, drill pipe): 323.1

Penetration (m): 93.8

Number of cores: 10

Total length of cored section (m): 93.8

Total core recovered (m): 11.2

Core recovery (%): 11.9

Oldest sediment cored
Depth sub-bottom (m): 93.8
Nature: foraminifer-rich calcitic sandy silt
Age: Pleistocene
Measured velocity (km/s): 1.6

HOLE 725C

Date occupied: 22 September 1987

Date departed: 22 September 1987

Time on hole: 9 hr, 45 min

Position: 18°29.200′N, 57°42.030′E

Water depth (sea level; corrected m, echo-sounding): 311.5

Water depth (rig floor; corrected m, echo-sounding): 322.0

Bottom felt (m, drill pipe): 322.7

Penetration (m): 162.8

Number of cores: 17

Total length of cored section (m): 162.8

Total core recovered (m): 98.8

Core recovery (%): 60.6

Oldest sediment cored
Depth sub-bottom (m): 162.8
Nature: nannofossil-rich calcitic sand, silt, and clay
Age: Pleistocene
Measured velocity (km/s): 1.6

Principal results: Site 725 is the shallow landward end point of a depth transect on the Oman continental margin. Our intention at Site 725 was to trace the fluctuations in the upper boundary of the oxygen-minimum zone through time and to evaluate these fluctuations with regard to changes in the monsoon, in tectonic evolution of the margin, and in sea level.

Findings at Site 725 include:

1. Organic- and opal-rich clayey silt alternates with nonlaminated nannofossil ooze and calcitic silty clay. Laminated intervals are confined to the upper part of the lower Pleistocene (lithologic Unit II) and are missing in both the lower (lithologic Unit III) and upper (lithologic Unit I) parts of the section.
2. The sedimentation rate averages about 120 m/m.y. over the top 120 m.
3. Opal occurrences are confined to laminated intervals and sediments having high organic-carbon concentrations of lithologic Units II and III.
4. Cold-water nannoplankton occurrences in the deepest part of the cored section.
5. Persistent occurrence of interstitial sulfate, high alkalinity, and dramatic core expansion suggest replenishment of the interstitial sulfate pool from a deep source comparable to that of Site 723.
6. Elevated ethane and propane gas concentrations with depth imply migration of thermogenic hydrocarbons from deep sources.

Site 725 constitutes a section of Pleistocene age that shows pronounced changes in the depositional environment, which are tentatively attributed to extension and intensification of the mid-water oxygen-minimum zone in the early Pleistocene. These changes were observed at other margin sites and are probably contemporaneous and of a regional rather than local extent.

BACKGROUND AND OBJECTIVES

Site 725 is located at 18°29.200′N and 57°42.030′E on the continental margin of Oman in a water depth of 311 m near the landward edge of the upper slope basin. The location of Site 725 is shown in Figures 1 and 2, and its structural and depositional setting is shown in Figure 3. Site 725 is located in the transitional zone between the continental shelf and the slope basin. The site lies near a faulted block that is thought to be part of an ophiolitic basement and that forms the eastern boundary of the slope basin. Seismic reflection profiles show eastward-dipping layers that both onlap and drape the underlying base-

---

[1] Prell, W. L., Niitsuma, N., et al., 1989. *Proc. ODP, Init. Repts.*, 117: College Station, TX (Ocean Drilling Program).

[2] Shipboard Scientific Party is as given in List of Participants preceding the contents.

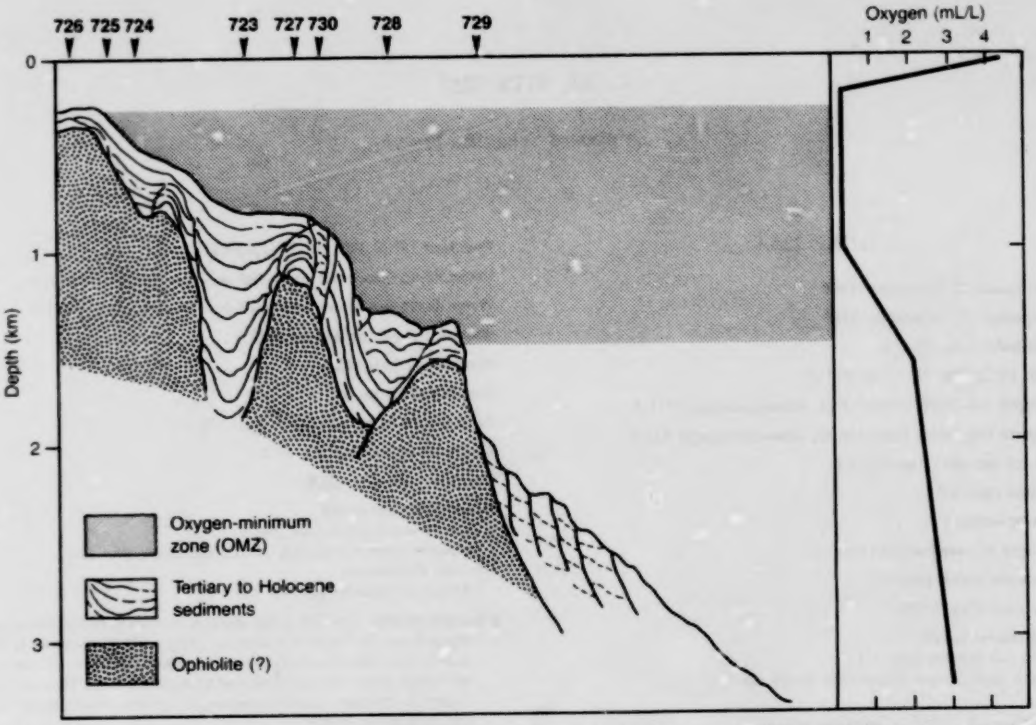

Figure 1. Structure of the Oman margin and the oxygen-minimum zone. The schematic drawing of the Oman margin shows the series of basement ophiolite blocks and the sedimentary basins between them. The concentration of oxygen in the water column (RC2704, unpubl. data) defines the depth range of the oxygen-minimum zone and where it impinges on the margin. The schematic location of Site 725 is indicated.

ment structures. Although the reflectors are generally conformable, some faulting and erosion is indicated by offset and converging reflectors. Site 725 was situated upslope of the original site location to avoid some of the subsurface structure. Preliminary correlation of seismic reflectors within the basin indicated that average accumulation rates should be high at Site 725, although winnowing of shelf-edge sediments might be possible. Site 725 was selected to provide the shallow end-member for a depth transect that spans the depth of the oxygen-minimum zone. The site was expected to provide a high-resolution sedimentary record of the variations of monsoonal upwelling and of the oxygen-minimum zone during the Pliocene-Pleistocene.

Specific objectives for drilling at Site 725 were:

1. To obtain a high-resolution record of the sediments associated with the near-coastal zone of the monsoonal upwelling system so as to establish changes in timing and intensity of the monsoon.
2. To provide the shallow end-member for a depth transect of sediments that will be used to examine the organic-rich sedimentary facies of the margin and to establish their relationship to the oxygen-minimum zone and its spatial variation through time.
3. To document the diagenetic processes associated with the oxygen-minimum zone and organic-rich sediments.
4. To search for evidence of changes in the structure of the intermediate water masses of the Arabian Sea during the Pliocene-Pleistocene.

OPERATIONS

The *JOIDES Resolution* arrived at Site 725 in a dynamic positioning mode by 0230 hr on 22 September 1987. This site, which previously had been surveyed jointly with Site 724, is located in a water depth of 311 m at 18°29.200′N and 57°42.030′E (see Fig. 4, "Operations" section, Site 724 chapter). Upon arrival, a shallow-water beacon was lowered on a taut wire, and by 0430 hr Core 117-725A-1H had been shot. The core barrel parted while shooting Core 117-725A-2H, and Hole 725A had to be abandoned. Recovery of Core 117-725A-1H (0–4.5 meters below seafloor [mbsf]) was 100% (Table 1).

Without offset, Hole 725B was spudded at 0600 hr on September 22 in extended-core-barrel (XCB) coring mode. Ten XCB cores recovered only 11.9% of the cored interval, which was dominated by sand and silt from 0 to 93.8 mbsf. After Core 117-725B-10X had been retrieved, coring in Hole 725B was suspended and the drill string pulled. Hole 725C was spudded at 1415 hr on 22 September, 20 m northeast of Hole 725B, after bit modification.

Three advanced piston corer (APC) cores recovered 100% of the interval from 0 to 28.5 mbsf until an overpull of 80,000 lb made XCB coring necessary. Cores 117-725C-4X through -17X (28.5–162.8 mbsf) showed a much improved recovery, after bit modification, of 52.3% in Hole 725C. Overall recovery in Hole 725C was 60.6%. After reaching total depth, the hole was displaced with weighted mud. After clearing the mud line and retrieving the beacon, the ship was under way to Site 726 by 2400 hr on 22 September 1987.

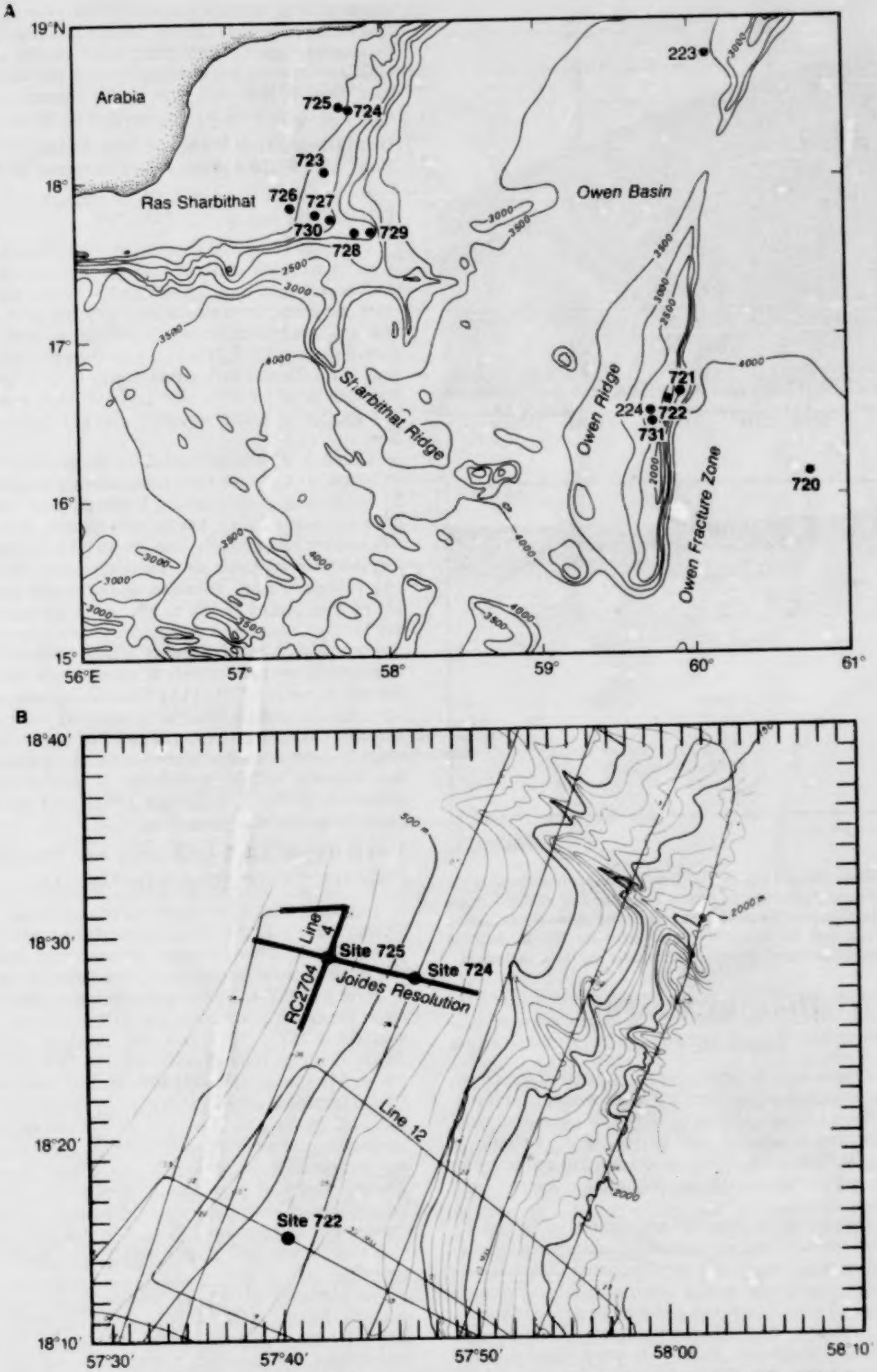
A
19°N
18°
17°
16°
15°
56°E
57°
58°
59°
60°
61°
Arabia
725
724
723
Ras Sharbithat
726
727
730
728
729
Owen Basin
223
3000
3500
2500
4000
Sharbithat Ridge
Owen Ridge
721
224
722
731
2000
720
Owen Fracture Zone
B
18°40′
18°30′
18°20′
18°10′
57°30′
57°40′
57°50′
58°00′
58°10′
500 m
2000 m
Line 4
Site 725
Site 724
RC2704
Joides Resolution
Line 12
Site 722

Figure 2. A. Bathymetry of the Oman margin and the location of Site 725. B. The detailed location of Site 725 and the seismic profiles shown in Figure 3. Bathymetry and seismic data are from the site survey (RC2704, 1986).

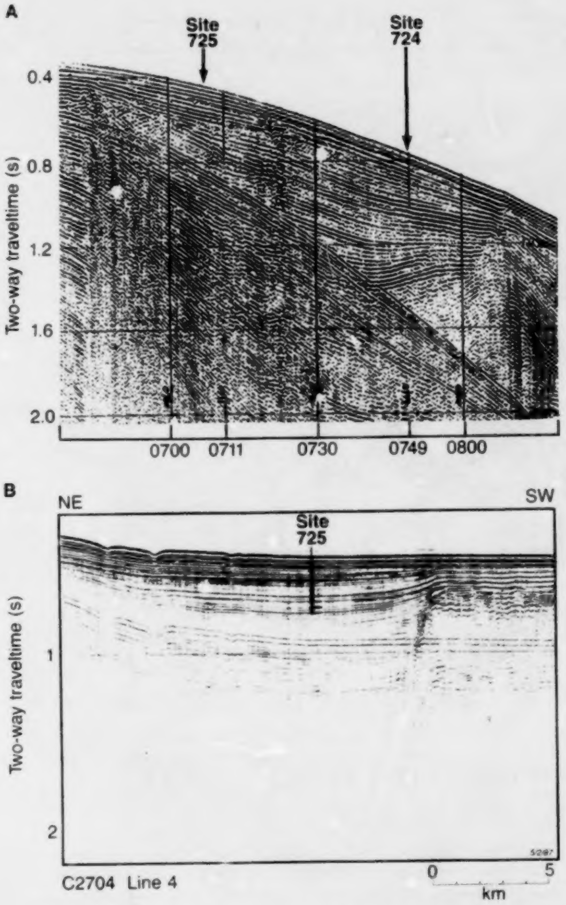

Figure 3. **A.** Single channel seismic (SCS) reflection profiles showing the structural and depositional setting of Site 725. Line 4 of *JOIDES Resolution* is perpendicular to the trend of the basin and shows the bounding basement blocks and the synclinal-shaped sediment fill. **B.** RC2704 Line 4 is along the strike of the basin and shows the thick sediments.

LITHOSTRATIGRAPHY

Lithologic Units

Site 725 is located on the shelf/slope transition of the Oman margin. The recovered sedimentary sequence ranges from Pleistocene to Holocene in age. Coring of Hole 725A was terminated after the first core because of core barrel failure. Because of poor recovery at Hole 725B, lithologic description and interpretation are based predominantly on sediments recovered from Hole 725C.

Sediments recovered at Site 725 are dominated by calcitic marly, nannofossil ooze, but also include calcitic marly calcareous ooze; interbedded clayey silt and laminated diatomaceous mud; and calcitic sand, silt, or clay. Detrital calcite is common to abundant in all these lithologies and may be derived from either an inorganic or a reworked biogenic source. The lithologic section has been divided into three units using visual core descriptions, compositional analyses of smear slides, and carbonate and organic carbon contents as distinguishing parameters. Lithologic Units I and III are compositionally similar; both are dominated by biogenic calcareous components and characterized by bioturbation. Lithologic Unit II contains laminated diatomaceous deposits with interbedded detrital intervals. These sediments contain less inorganic calcite and biogenic carbonate than those in lithologic Unit I. The characteristics and occurrences of these units are summarized in Table 2 and Figure 4.

Unit I (Depth: Hole 725A, 0–4.5 mbsf; Hole 725B, 0–93.8 mbsf; Hole 725C, 0–120.0 mbsf; Age: Pleistocene to Holocene)

Cores 117-725A-1H, 117-725B-1X through 117-725B-10X, and 117-725C-1H through 117-725C-13X.

The composition of lithologic Unit I changes slightly downcore, from calcitic marly calcareous ooze and marly foraminifer nannofossil ooze near the surface to calcitic, marly nannofossil ooze and nannofossil-rich calcitic silty clay at its base. Colors in this unit gradationally darken downcore, from olive (5Y 4/3) and olive gray (5Y 4/2) near the surface, to olive (5Y 4/3), olive gray (5Y 4/2), and dark greenish gray (10Y 5/2) at intermediate levels, to olive (5Y 4/3), olive gray (5Y 4/2), dark olive gray (5Y 4/1 and 5Y 3/2), and very dark gray (5Y 3/1) lower in the section.

Unit I is slightly to moderately bioturbated except in Core 117-725C-11X, where faint laminations are locally developed.

From smear-slide analyses, lithologic Unit I contains 15% to 55% inorganic calcite, 5% to 20% quartz, 10% to 45% clays, 5% to 50% nannofossils, and 2% to 20% foraminifers (including abundant benthics; see "Biostratigraphy" section, this chapter). Feldspars, mica, dolomite, and accessory minerals are present in abundances of 1% to 5%, while phosphate concretions are locally present and glauconite occurs sparsely throughout. Volcanic glass is notably absent in Unit I, and biogenic siliceous components are present only in trace abundances at the base of the unit (Core 117-725C-13X). These compositional ranges indicate that terrigenous material is generally more abundant than biogenic constituents in Unit I and that the terrigenous components become more dominant downcore. In addition, clay content increases and the abundance of silt-size quartz decreases downcore in Unit I, suggesting that Unit I generally becomes more fine-grained downsection.

Unit II (Depth: 120.0–145.4 mbsf; Age: Pleistocene)

Cores 117-725C-13X through 117-725C-16X.

Lithologic Unit II is composed of interbedded calcitic sand-silt-clay, olive gray (5Y 4/2), and laminated diatomaceous beds. These laminated beds contain diatomaceous calcareous clayey silt; diatomaceous calcitic marly nannofossil ooze (olive [5Y 4/3], olive gray [5Y 4/2], and dark olive gray [5Y 3/2]); diatomaceous clayey silt (dark olive gray [5Y 3/2]); and diatomaceous mud (olive [5Y 5/3]). Smear-slide analyses indicate that the darker diatomaceous laminae contain 10% to 30% diatoms, 2% to 5% sponge spicules, 10% to 35% nannofossils, 1% to 5% foraminifers, 25% to 35% clays, 15% to 25% inorganic calcite, and 3% to 20% quartz. The light-colored, diatomaceous laminations have significantly different compositions, however, and average 55% diatoms, 30% clay, 3% inorganic calcite, and 2% to 5% each of quartz, nannofossils, and foraminifers. The calcitic sand-silt-clay intervals are essentially barren of biogenic components and contain 20% to 50% inorganic calcite, 10% to 45% clay, 20% to 30% quartz, and 0% to 5% siliceous biogenic material.

The character of the laminations within the diatomaceous intervals changes in Unit II from more diffuse laminations on a scale of 1 cm in Core 117-725C-14X (129–133 mbsf) to very well-defined, millimeter-scale lamination in Core 117-725C-15X (136–140 mbsf). Often, diatom assemblages within the lighter-colored diatomaceous laminae are nearly monospecific. The contact between the uppermost laminated zone and the overly-

Table 1. Coring summary at Site 725.

Core no.	Date (Sept. 1987)	Time	Depth (mbsf)	Cored (m)	Recovered (m)	Recovery (%)
117-725A-1H	22	0540	0–4.5	4.5	4.53	100.0
117-725B-1X	22	0700	0–7.5	7.5	0.22	2.9
2X	22	0750	7.5–17.1	9.6	0.36	3.8
3X	22	0910	17.1–26.6	9.5	0.62	6.5
4X	22	1015	26.6–36.2	9.6	2.95	30.7
5X	22	1050	36.2–45.7	9.5	2.35	24.7
6X	22	1130	45.7–55.3	9.6	1.03	10.7
7X	22	1205	55.3–64.9	9.6	2.08	21.6
8X	22	1235	64.9–74.5	9.6	0.06	0.6
9X	22	1255	74.5–84.1	9.6	0.78	8.1
10X	22	1320	84.1–93.8	9.7	0.77	7.9
117-725C-1H	22	1445	0–9.0	9.0	9.00	100.0
2H	22	1515	9.0–18.6	9.6	9.66	100.0
3H	22	1540	18.6–28.5	9.9	9.91	100.0
4X	22	1620	28.5–38.0	9.5	4.01	42.2
5X	22	1650	38.0–47.5	9.5	1.00	10.5
6X	22	1715	47.5–57.0	9.5	5.94	62.5
7X	22	1740	57.0–66.5	9.5	0.49	5.2
8X	22	1805	66.5–76.1	9.6	4.18	43.5
9X	22	1825	76.1–85.7	9.6	6.27	65.3
10X	22	1850	85.7–95.3	9.6	0.05	0.5
11X	22	1945	95.3–104.9	9.6	7.06	73.5
12X	22	1935	104.9–114.5	9.6	6.41	66.8
13X	22	1955	114.5–124.1	9.6	3.92	40.8
14X	22	2015	124.1–133.8	9.7	9.66	99.6
15X	22	2030	133.8–143.5	9.7	7.73	79.7
16X	22	2055	143.5–153.2	9.7	3.71	38.2
17X	22	2115	153.2–162.8	9.6	9.76	101.0

Table 2. Lithologic summary at Site 725.

Unit	Description	Facies	Depth (mbsf)	Core	Hole
I	Foraminifer calcitic sandy silts to calcitic marly calcareous ooze and calcitic marly nannofossil ooze to nannofossil-rich sand-silt-clay.	Hemipelagic and calcitic detrital facies	0–4.5 0–93.8 0–120.0	1H 1X to 10X 1H to 13X	A B C
II	Interbedded and laminated diatomaceous clayey silt, diatomaceous mud, and calcitic marly nannofossil ooze, calcitic sand silt clay.	Laminated and detrital facies	120.0–145.4	13H to 16H	C
III	Nannofossil-rich calcitic sand-silt-clay to calcitic marly nannofossil ooze	Hemipelagic and calcitic detrital facies	145.4–162.8	16X to 17X	C

ing unlaminated diatomaceous deposits of Unit II is sharp and lies beneath a basal foraminiferal sand.

Unit III (Depth: 145.4–162.8; Age: Pleistocene)

Cores 117-725C-16X to 117-725C-17X.

Lithologic Unit III is similar to lithologic Unit I in composition and appearance. It is dominated by calcitic marly nannofossil ooze, interbedded with olive (5Y 4/3), olive gray (5Y 4/2), and dark olive gray (5Y 3/2) intervals. Nannofossil-rich calcitic sand-silt-clay is present as a minor lithology, in olive gray (5Y 4/2) and dark olive gray (5Y 3/2) intervals 20 to 75 cm thick. Foraminifers and dispersed shell debris are common in Unit III, and the entire unit is slightly bioturbated.

The marly nannofossil oozes contain 25% to 45% nannofossils, 25% to 35% inorganic calcite, 20% to 25% clay, 5% to 11% quartz, and 2% to 5% each of foraminifers and accessory minerals. The sand-silt-clay intervals contain an average of 25% quartz, 25% clay, 35% inorganic calcite, 10% biogenic carbonate, and 5% accessory minerals.

Discussion

The sedimentary sequence at Site 725 was recovered from a shallow water depth on the Oman margin. For this reason, the depositional record preserved at Site 725 will provide valuable comparisons to correlative deposits from deeper-water environments elsewhere on the margin. The subdivision of the sequence at Site 725 into three lithologic units emphasizes variations in terrigenous and biogenic sediment abundances, as well as differences in depositional and preservational style (i.e., laminated vs. bioturbated intervals). The variations in abundances of sedimentary components are probably related to fluctuating rates of terrigenous sediment supply and marine planktonic productivity, which may have varied in response to climatic fluctuations during the Pleistocene.

At the base of Hole 725C, the bioturbated nannofossil-rich calcitic sand-silt-clays and calcitic marly nannofossil oozes of Unit III contain an important signature of marine planktonic influx (i.e., foraminifers, coccolithophores, and marine organic carbon). Despite the relatively high abundances of terrigenous components (generally greater than 50%), organic carbon con-

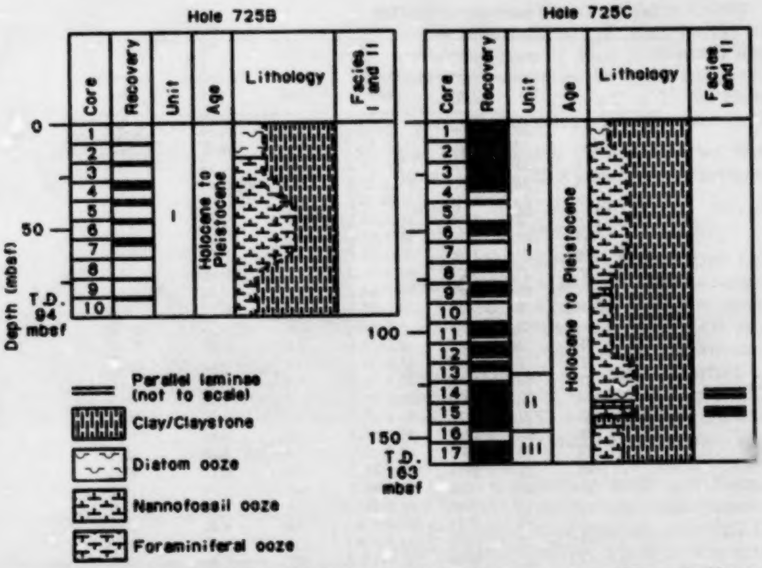

Figure 4. Lithologic summary, Site 725. Lithology is inferred between recovered intervals. Note: No lithologic summary for 725A (recovered only 1 core).

tents near 3% (Table 3 and Fig. 5) are characteristic of lithologic Unit III. The elevated level of organic carbon in lithologic Unit III can be attributed to either an increase in supply, which is related to primary productivity in surface water, or enhanced preservation. Changes in the amount of organic carbon preserved in marine sediments have been attributed to variations in sedimentation rate, bottom-water oxygen contents, and redox potential in the near-surface sediment (see Emerson, 1985, and references therein). Any of these could be factors at Site 725.

A significant contribution of biogenic silica at Site 725 is first evident in lithologic Unit II, which contains diatomaceous laminated intervals. The light layers in these laminated zones contain approximately 60% diatoms, while the dark layers contain lower, but still significant, abundances of biogenic silica or biogenic carbonate. The biogenic content of the darker laminae is lower because they are either diluted by increased detrital supply or because biogenic supply was lower, perhaps from decreased productivity. In the oldest laminated zone, the laminae are thin (millimeter-scale) and well developed. These characteristics, together with the high organic carbon contents (Table 3) and absence of bioturbation in this interval, indicate that conditions at the sediment/water interface were unfavorable for benthic fauna at this time. In addition, laminae reflect repeated short-term variations in sediment supply. Such variations may occur annually or seasonally (Kemper and Zimmerle, 1980).

Repeated short-term (seasonal or annual?) variations in sediment supply are apparent in both the relative importances of biogenic and detrital components and the nature of the detrital constituents. Smear-slide analysis indicates that the lighter laminae contain only fine-grained (predominantly clay-sized) detrital material, in addition to the higher biogenic abundances described earlier. The darker laminae, however, contain a wider range of detrital grain sizes, including minor amounts of sand. Quantitative grain-size and compositional analyses of the terrigenous components in the light and dark laminae will be needed to determine sediment origin and mode of transport.

In lithologic Unit I overlying the laminated deposits of Unit II, the abundance of biogenic calcareous components increases upsection, while widespread bioturbation indicates a return to environmental conditions more favorable for benthic fauna. The transition to a biogenic calcareous sediment assemblage (vs. calcareous and siliceous) is completed by approximately 70 to 80 mbsf, with only marly calcareous nannofossil and foraminifer oozes occurring above that level. This transition is also evident in measurements of sediment density, organic carbon content, and carbonate content (Fig. 5 and Tables 3 and 7).

Although biogenic carbonate abundances increase upsection in Unit I, terrigenous abundances remain high. Inorganic calcite is a major detrital constituent, and its importance is at least partly responsible for the high carbonate abundances throughout lithologic Unit I. The origin of the inorganic calcite is not entirely clear, because it does not always co-vary with other phases that are demonstrably terrigenous (e.g., inorganic calcite increases, while quartz and clays decrease significantly). One explanation for this difference is that the sources and/or the transport processes of these phases are different. However, one possible source is reworking from shelly carbonate sands now forming on the shelf. Reworked foraminifers and aragonitic lenses derived from weathered shells were recognized while describing the Site 725 cores. When crushed, this material closely resembles the "inorganic calcite" observed in smear slides. Shore-based studies will investigate the sources of this calcite further by determining the relationship between calcite and palygorskite. Palygorskite is a known indicator of eolian supply from the Arabian Peninsula (Kolla et al., 1981, Caulet et al., in press), so that co-variation in inorganic calcite and palygorskite will support an eolian interpretation for the inorganic calcite.

In summary, lithologic Units I and III are compositionally similar in biogenic and terrigenous material. A major difference between the two units, however, is the higher organic carbon content of Unit III, which suggests that productivity and/or bottom-water conditions were different during the two periods of deposition. These differences may have developed because of changes in surface or deep-water circulation or they may have resulted from bathymetric changes produced by movement of Site 725.

The presence of upwelling flora in the laminated intervals and the increase in high organic carbon values (2%–3.5%) in

Table 3. Carbonate and organic carbon abundances at Site 725.

Hole, core, section, interval (cm)	Depth (mbsf)	Total carbon (%)	Inorganic carbon (%)	Organic carbon (%)	$CaCO_3$ (%)
117-725C-1H-2, 90-92	2.40	6.95	6.45	0.50	53.7
725A-1H-3, 0-1	3.00	7.15	6.67	0.48	55.6
725C-1H-5, 90-92	6.90	7.17	6.42	0.75	53.5
725C-2H-2, 60-62	11.10	6.86	6.21	0.65	51.7
725C-2H-4, 60-62	14.10	7.08	6.03	1.05	50.2
725C-2H-7, 30-32	18.30	6.76	6.46	0.30	53.8
725C-3H-2, 100-102	21.10	6.32	5.86	0.46	48.8
725C-3H-4, 24-26	23.34	6.26	5.75	0.51	47.9
725C-3H-4, 119-120	24.29	6.83	6.49	0.34	54.1
725C-3H-6, 100-102	27.10	7.39	6.72	0.67	56.0
725C-4H-3, 50-52	32.00	7.00	6.58	0.42	54.8
725B-5X-2, 0-1	37.70	7.04	6.82	0.22	56.8
725C-6X-2, 86-88	49.86	7.46	6.43	1.03	53.6
725C-6X-2, 119-120	50.19	8.68	7.16	1.52	59.6
725C-6X-4, 86-88	52.86	7.11	6.23	0.88	51.9
725C-6X-3, 29-31	69.79	7.16	6.56	0.60	54.6
725C-9X-3. 119-120	80.29	6.93	6.18	0.75	51.5
725C-9X-4, 27-29	80.87	9.19	7.82	1.37	65.1
725C-11X-2, 24-26	97.04	7.84	5.50	2.34	45.8
725C-11X-5, 8-10	101.38	7.18	6.55	0.63	54.6
725C-12X-2, 19-21	106.59	12.32	8.73	3.59	72.7
725C-12X-3, 108-110	108.98	8.98	7.60	1.38	63.3
725C-12X-3, 119-120	109.09	7.79	6.94	0.85	57.8
725C-13X-3, 34-36	117.84	10.72	8.13	2.59	67.7
725C-14X-2, 21-23	125.81	11.68	8.33	3.35	69.4
725C-14X-4, 26-28	128.86	9.47	5.99	3.48	49.9
725C-14X-6, 14-16	131.74	7.91	4.48	3.43	37.3
725C-15X-2, 85-87	136.15	9.34	7.26	2.08	60.5
725C-15X-4, 80-82	139.10	7.41	4.25	3.16	35.4
725C-15X-4, 119-120	139.49	7.41	4.50	2.91	37.5
725C-16X-3, 4-6	146.54	10.54	6.63	3.91	55.2
725C-17X-2, 25-27	154.95	12.12	8.36	3.76	69.6
725C-17X-4, 106-108	158.76	6.87	3.25	3.62	27.1
725C-17X-5, 119-120	160.39	8.58	5.99	2.59	49.9
725C-17X-6, 128-130	161.98	9.12	4.96	4.16	41.3

lithologic Unit II indicate a major depositional change with respect to Units I and III, which supports the hypothesis that upwelling activity was different during the early Pleistocene than today. This may be interpreted in term of fluctuations in the strength of the monsoonal winds (Prell and Streeter, 1982). For that reason, shore-based research will consider both the productivity signal of the biogenic components and the source and transport record of the eolian components to describe sedimentation on the Oman margin in a more comprehensive manner.

BIOSTRATIGRAPHY

Introduction

Both planktonic and benthic foraminiferal fauna as well as nannofossils and radiolarians were studied at Site 725 to establish biostratigraphic zonations. Another objective was to investigate fluctuations in the upper boundary of the oxygen-minimum zone and possible changes in upwelling intensity.

The entire recovered section is referred to the Pleistocene. Planktonic and benthic foraminifers are abundant and well preserved throughout the section; nannofossils are abundant but are poorly preserved. Radiolarians are absent in the upper part of the sequence (Fig. 6). A plot of faunal datum levels vs. depth below the seafloor is presented in Figure 7; for a detailed list of these data points, see Table 4.

Plantonic Foraminifers

Planktonic foraminifers were studied in Hole 725C. The core-catcher samples contain highly diverse, well-preserved faunas throughout the entire sequence, except for Sample 117-725C-15X, CC (143.5 mbsf). This sample yields abundant, robust *Globorotalia tumida tumida* and common *Neogloboquadrina dutertrei* specimens, whereas thin-walled species are present only in low numbers. We believe this distribution of species is related to dissolution processes. The benthic foraminifers also are poorly preserved in this sample.

The presence of *Globigerinella calida calida* in Samples 117-725C-1H, CC through 117-725C-8X, CC (9.0-76.1 mbsf) marks Zone N23. *Globorotalia truncatulinoides* specimens are rare to common in the upper part of the section but disappear below Sample 117-725C-12X, CC (114.5 mbsf). However, some small specimens are again present in the lowermost sample (117-725C-17X, CC; 162.8 mbsf). Thus, the entire sequence is referred to the Pleistocene. The occurrence of *Globigerinoides fistulosus* in the same sample shows that the basal part of the Pleistocene was drilled, as the last appearance of this species has been dated at 1.6 Ma (Berggren et al., 1985).

Benthic Foraminifers

The benthic foraminiferal fauna was studied at Site 725 in the core-catcher samples of Hole 725C. Benthic foraminifers are abundant throughout the sequence, with a maximum abundance of about 140,000 specimens per 10 cm^3 of sediment in Sample 117-725C-1H, CC (9.0 mbsf). Preservation is good to moderate but deteriorates downhole. Diversity is high, which can be expected in water this shallow (311 m).

The benthic foraminiferal fauna of Site 725 is relatively uniform and displays no significant changes during the short time interval recovered by the drilled sequence. However, one can recognize two slightly different assemblages. The first assemblage contains species that are abundant throughout the sequence: *Bolivina ordinaria*, *Cassidulina carinata*, *Cibicidoides wueller-*

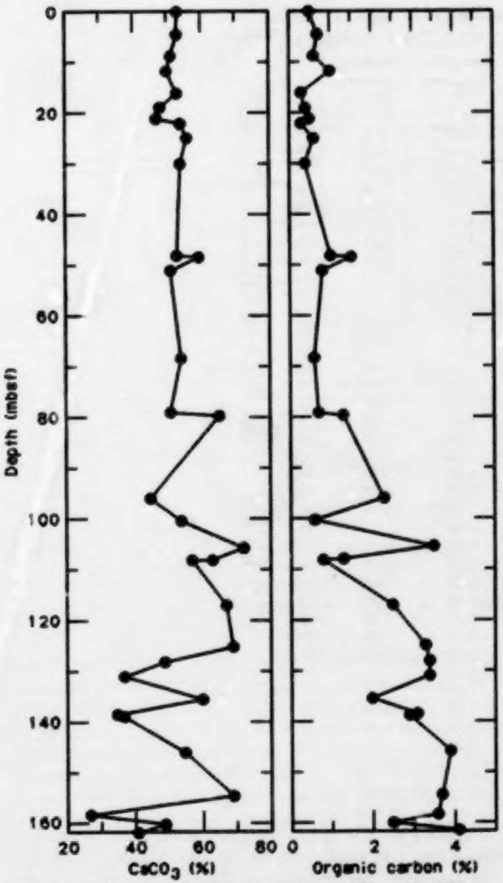

Figure 5. Carbonate and organic carbon profiles, Site 725.

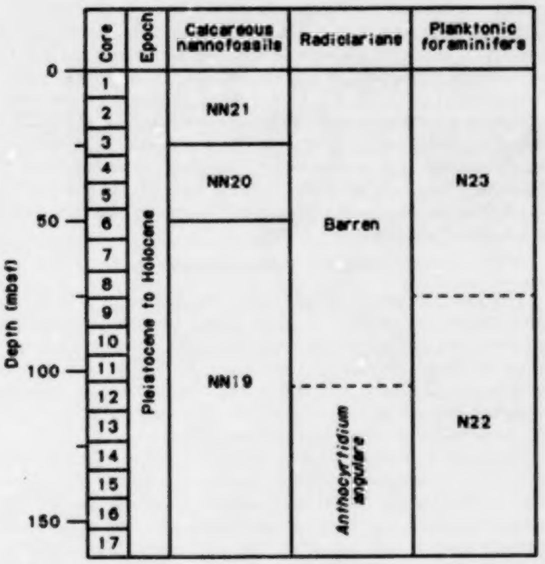

Figure 6. Correlation of planktonic microfossil zones in Hole 725C.

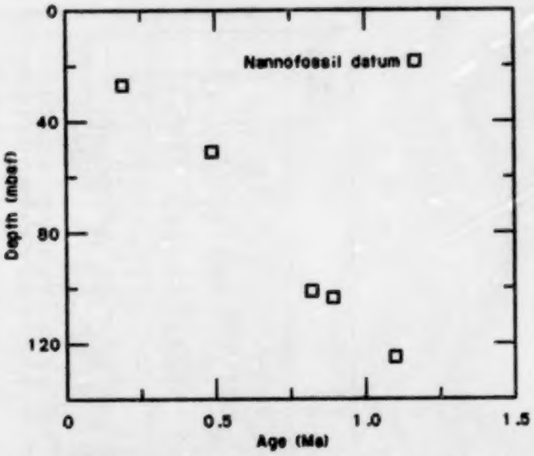

Figure 7. Age-depth plot for Hole 725C. For detailed list of events, see Table 4.

storfi, *Hyalinea balthica*, and *Uvigerina peregrina*. Additional species that occur only in this assemblage are *Ammonia beccarii*, *Lenticulina calcer*, and *Trifarina angulosa*. The other assemblage contains *Florilus* spp., *Globobulimina* spp., *Lenticulina* cf. *falcifer*, and *Uvigerina dirupta*, in addition to those species of the first assemblage. Assemblage 1 occurs in Sections 117-725-1H, CC through -9X, CC (9.0–85.7 mbsf), whereas the second assemblage occurs in Sample 117-725-10X, CC and downhole to the bottom of the recovered sequence (95.3–162.8 mbsf).

The restriction of *Ammonia beccarii* to the upper 85 m may indicate a mid-Pleistocene uplifting at this site. The appearance of assemblage 2 coincides with an increase in the amount of phosphorite found and with a general decrease in the total number of specimens per volume.

Several large lenticuliids and nodosariids were found at Site 725; the diameter of the former often exceeds 5 mm.

Calcareous Nannofossils

Hole 725A

Because of drilling equipment failure, only one core was obtained from Hole 725A. The core-catcher material of this core (Sample 117-725A-1H, CC; 4.5 mbsf) contains *Emiliania huxleyi* and was assigned to Zone NN21 (upper Pleistocene to Holocene).

Holes 725B and 725C

At Hole 725B, penetration was 93.8 m; however, because of bottom-hole conditions, recovery of sediments was poor. The nannofossils recovered from this hole are abundant, but the assemblages are marked by low species diversity, which may be a result of comparatively low temperatures caused by upwelling. Preservation is generally poor. Sediments down to 17.2 mbsf contain *E. huxleyi* and belong to Zone NN21 (Holocene to upper Pleistocene). Below this zone, sediments down to 45.7 mbsf can be placed in Zone NN20 (Pleistocene) based on the absence of *E. huxleyi* and *Pseudoemiliania lacunosa*. The remaining sequence from 45.7 to 93.8 mbsf may belong to Zone NN19 (Pleistocene), although the abundances of *P. lacunosa* range from barren to common.

Nannofossil assemblages in Hole 725C are similar to those in Hole 725B (Fig. 8). Based on the same evidence as the previous hole, sediments down to 18.6 mbsf, underlying sediments down to 47.5 mbsf, and the remaining sediments down to 162.8 mbsf

Table 4. Stratigraphic list of faunal events for Hole 725C.

Event	Core level	Depth (mbsf)	Age (Ma)	Source of age	Notes
B *Emiliania huxleyi*	3H, 118–119	25.78	0.19	3	
	3H, CC	28.50			
T *Pseudoemiliania lacunosa*	6X-2, 118–119	50.18	0.49	3	
	6X-3, 118–119	51.68			
T *Reticulofenestra* sp. A	11X-3, 118–119	99.48	0.82	3	
	11X-5, 93–94	102.23			
B *Gephyrocapsa parallela*	11X-5, 93–94	102.23	[a]0.89	4	
	11X, CC	104.90			
T *Gephyrocapsa* "large"[b]	13X, CC	124.10	[a]1.10	4	
	14X-1, 118–119	125.28			
T *Helicosphaera sellii*	16X, CC	153.20			No good published age; event appears to be diachronous.
	17X-1, 129–130	154.49			

Note: T = upper limit of event and B = lower limit. Sources of ages are: 3 = oxygen isotope data for Site 723 (N. Niitsuma, unpubl. data); 4 = Takayama and Sato, 1987.

[a] North Atlantic data

[b] Long axis greater than 6 μm.

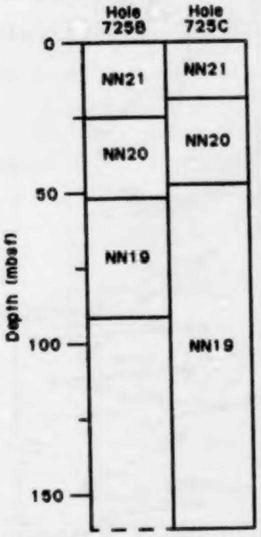

Figure 8. Correlation of calcareous nannofossil zones in Holes 725B and 725C.

were assigned to Zones NN21, NN20, and NN19, respectively. The nannofossil datums recognized in Hole 725C are tabulated in Table 4.

Additional Pleistocene calcareous nannofossil datums (see "Explanatory Notes" section, this volume, for explanation of datums) are recognized in Hole 725B as follows:

Datum 1	Uncertain
Datum 2	17.1–26.6 mbsf in Core 117-725B-3X
Datum 3	45.7–55.3 mbsf in Core 117-725B-6X
Datum 4	Uncertain
Datum 5	84.1–93.8 mbsf in Core 117-725B-10X
Datum 6	84.1–93.8 mbsf in Core 117-725B-10X

Rare reworked specimens were found in a few cores throughout Holes 725B and 725C. These include the Cretaceous species *Microrhabdulus decoratus* and *Discoaster multiradiatus* from the Paleocene or the Eocene.

Radiolarians

Sections 117-725B-1H, CC through 117-725B-10X, CC (7.5–93.8 mbsf) and 117-725C-11X, CC to 117-725C-17X, CC (104.9–162.8 mbsf), which together form a continuous sequence, were examined for radiolarians. The upper 10 cores are barren. However, samples examined below that level have significant radiolarian fauna along with diatoms and sponge spicules. The presence of *Anthocyrtidium angulare* in Samples 117-725C-12X, CC (114.5 mbsf) and 117-725C-14X, CC (133.8 mbsf) places these samples, at least, in the *Anthocyrtidium angulare* Zone. The occurrence of *Lamprocyrtis neoheteroporos* in Samples 117-725C-16X, CC (153.2 mbsf) and 117-725C-17X, CC (162.8 mbsf) suggests that these samples probably lie within the *A. angulare* Zone as well. The fauna at this site is more diverse than at Site 724, although there are still few tropical zonal marker species.

Paleoenvironmental Implications

Many *Helicosphaera* specimens, which seem to prefer upwelling areas (Perch-Nielsen, 1985), as well as *Coccolithus pelagicus*, a cold-water species, were found in the lowermost core-catcher sample in Hole 725C (162.8 mbsf).

The presence of *Ammonia beccarii* in the upper part of the sequence indicates that this site has been at or above its modern water depth since approximately 0.7 Ma. The absence of the same species, together with a significantly different benthic foraminiferal fauna in the lower part of the sequence, might indicate a water depth exceeding 350 m before this date.

PALEOMAGNETISM

Introduction

Site 725 is located at 18°29.20′N, 57°42.03′E in water depth of about 310 m on the Oman margin. Holes 725A, 725B, and 725C were cored to depths of 4.5, 93.8, and 162.8 mbsf, respectively. The lithology consisted mainly of marly nannofossil ooze.

Magnetostratigraphy

As at Sites 723 and 724, natural remanent magnetization (NRM) intensities at Site 725 also were low, generally less than 1 mA/m (arithmetic mean = 0.7 mA/m) after alternating field (AF) demagnetization at 5 to 10 mT. Figure 9 depicts the combined discrete sample declination, inclination, and intensity data for Holes 725A, 725B, and 725C. Points having circular standard deviation values greater than 40° were excluded. Unfortunately, this (rather liberal) filtering procedure did not leave us enough points to permit detailed correlations with the polarity time scale. Reference to the nannofossil stratigraphy (see "Biostratigraphy" section, this chapter) suggests that the shallow and reversed inclination values at 79 mbsf may correspond to the Chron C1/C1r (Brunhes/Matuyama Chronozone) boundary, while the zone of normal inclinations at 100 and 121 mbsf

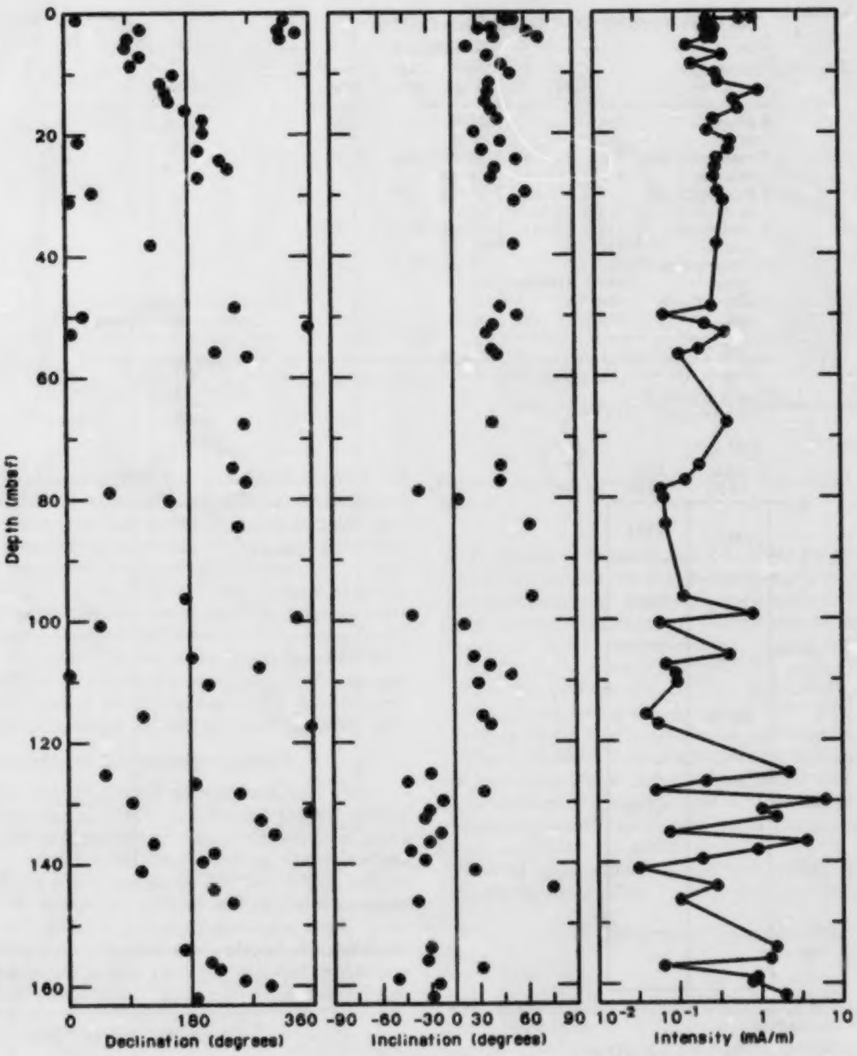

Figure 9. Declination, inclination, and intensity of discrete samples from Holes 725A, 725B, and 725C after AF demagnetization at 5–10 mT.

may be equivalent to Subchron C1r-1 (Jaramillo Subchronozone). Shore-based study of samples collected (but not measured) on board the ship may enable us to make more confident correlations with the polarity time scale.

Figure 10 shows a histogram of inclination values (after filtering) grouped into 10° classes. Inclination values of the normally magnetized specimens agree with the expected geocentric axial dipole value for the site latitude (33.8°). Values for the reversely magnetized specimens appear significantly shallower than expected, which suggests the presence of a normal overprint that was not completely removed by AF demagnetization.

Magnetic Susceptibility

The volume magnetic susceptibility of Site 725 sediments was measured using the Bartington Instruments whole-core susceptibility sensor at the 0.1 sensitivity and low-frequency (0.47 kHz) settings. Intervals of 10 cm were measured at Hole 725C only because of the poor recovery in Holes 725A and 725B. Gas expansion was most severe in Cores 117-725C-16X and -17X; thus, to avoid gaps, archive halves were measured and data were multiplied by two during processing. Susceptibility data for Hole 725C are shown in Figure 11. Poor recovery below Core 117-725C-4H (~32 mbsf) limited the usefulness of the susceptibility data for intersite correlations. Some correlations with Sites 723 and 724 are possible for the first four cores of Hole 725C, however.

While the gaseous nature of Hole 725C sediment precluded measuring susceptibility continuously, the self-extrusion of Hole 725C sediments during core-splitting provided copious amounts of material that could not be curated, which we found suitable for magnetic extractions. Approximately 0.25 kg of wet sediment obtained from the top of Section 117-725C-5H-1 (~38 mbsf) was dispersed in ~1 L of Calgon solution. The slurry was continuously agitated while two bar magnets (sheathed in para-

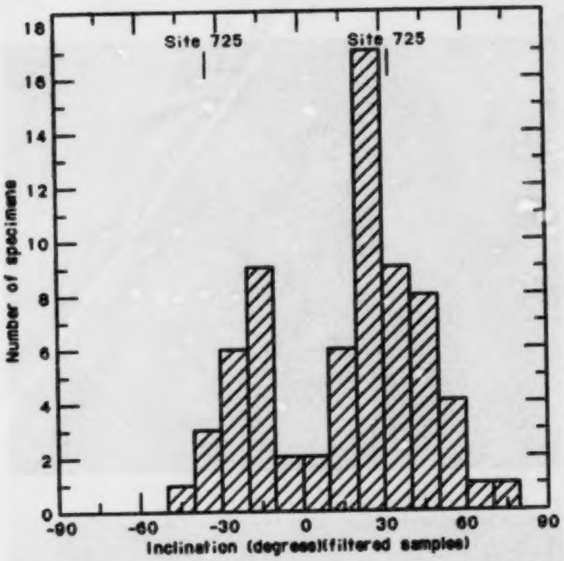

Figure 10. Inclination values grouped into 10° classes. Arrows indicate the expected geocentric axial dipole value for the site latitude.

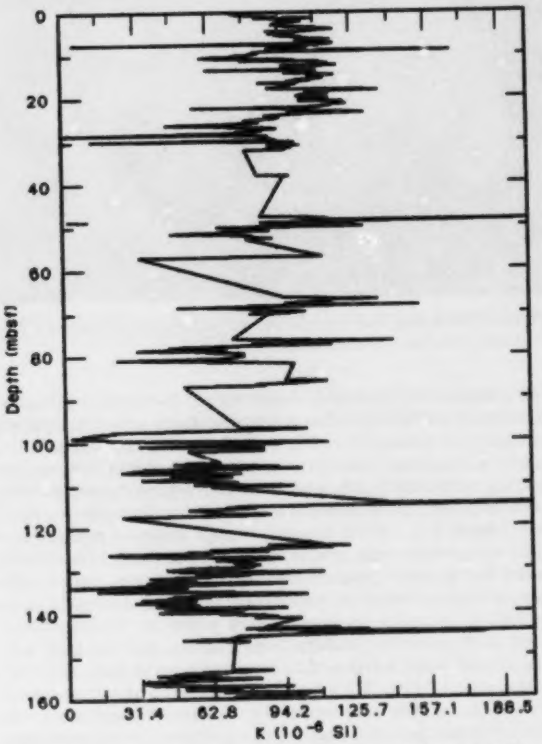

Figure 11. Whole-core magnetic susceptibility record for Hole 725C.

film) were positioned at the top and bottom levels of the beaker. The magnets were removed after several minutes, and the adhering magnetic residue was washed into a separate beaker each time. This process was repeated approximately 15 times for each of two aliquots of sediment. This extraction procedure was then applied to the primary extracts for purification. The efficiency of the extraction is unknown. Visual inspection indicated that the extracted grains were quite coarse (medium silt), which suggests that the finer grains contributing to the NRM either were not abundant or were not extracted.

The initiative for extracting magnetic particles came from our desire to observe the grain sizes, shapes, and textures that contributed to susceptibility and remanence. The slight downhole decrease in NRM intensity from 0 to ~100 mbsf (Fig. 9) suggests that fine-grained ferrimagnetic particles may be dissolving or altering to nonmagnetic phases. The final purified extraction was divided into highly magnetic and less magnetic fractions by passing a bar magnet under the beaker containing the purified extraction and drawing the most magnetic particles to one side. These grains were removed by pipette, dried, and mounted on an SEM sample stub for observation at high magnification. Photographs of the observed grains are shown in Figures 12 through 14.

Observation of the grains indicated that they were remarkably uniform in size (fine to coarse silt) and were generally well rounded and well preserved. Uniformity of size may have been a consequence of the extraction procedure. The degree of grain roundness was surprising in that an extract from margin sediment might be expected to be more angular. However, the roundness is consistent with an eolian mode of deposition, as suggested by the XRD data presented in the "Paleomagnetism" section of the Site 722 chapter.

Some indication of grain pitting and dissolution can be seen in many of the photographs. Striking examples of this can be seen in Figure 13 and in the upper right quadrant of Figure 14. Extensive pitting was apparent for about 10% of the grains, while moderate pitting included perhaps another 10%. Generally, however, the preservation of the grains was very good. To better understand the history of magnetic mineral deposition, we intend to conduct more thorough shore-based magnetic and morphometric analyses of magnetic extracts from Leg 117 sediments.

ACCUMULATION RATES

Sedimentation rates for the top 100 m (lithologic Unit I) of Site 725 are calculated between nannofossil datums with ages based on oxygen isotope stratigraphy (Table 4; Niitsuma, unpublished data). The mean rate for the last million years ranges from 79 to 152 m/m.y. (Table 5, Fig. 15), with an overall average of 124 m/m.y. If we include two additional nannofossil datums recognized at Site 725, with ages based on North Atlantic data (Table 4), the mean rate is 114 m/m.y. for the last 1.1 m.y. (Fig. 15). These values are typical of hemipelagic sedimentation in the upper slope basin. No reliable stratigraphic markers were found below 125 mbsf, therefore, sedimentation rate are unavailable for lithologic Units II and III.

The mass accumulation of calcium carbonate, organic carbon, and noncarbonate sediment components were calculated from average values between nannofossil datums (Table 6, Fig. 16). Based on the homogeneous sediment character in lithologic Unit I, this large variation in accumulation rate is unexpected and may be attributed to uncertainties in the age model. Postcruise studies that obtain a more precise age model for Site 725 will be necessary to verify these rate changes.

PHYSICAL PROPERTIES

Introduction

Physical properties measured on discrete samples of sediment recovered from Site 725 included only index properties (wet-bulk density, porosity, water content, and grain density). The sediments recovered were not sufficiently indurated to allow

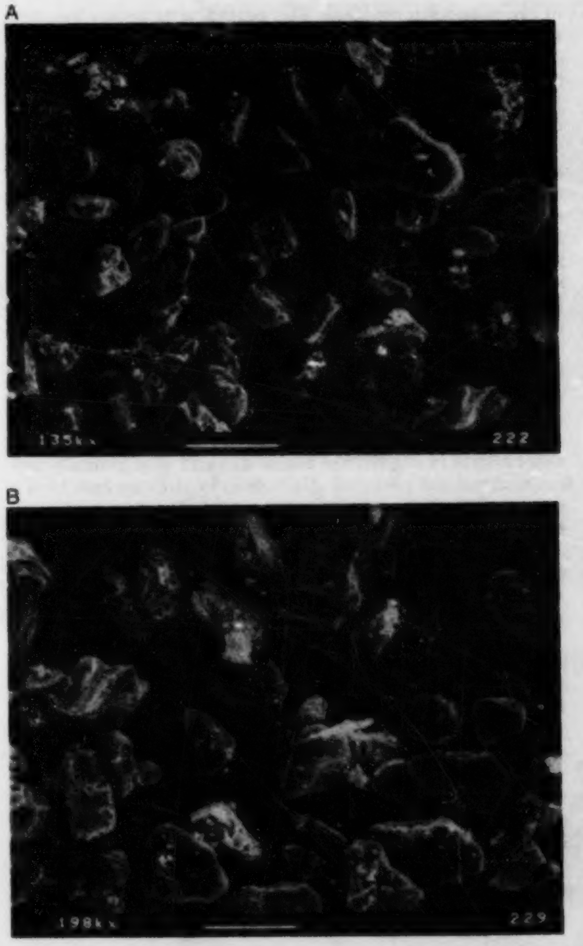

Figure 12. Scanning electron microscope photograph of magnetic concentrates from Site 725 sediments.

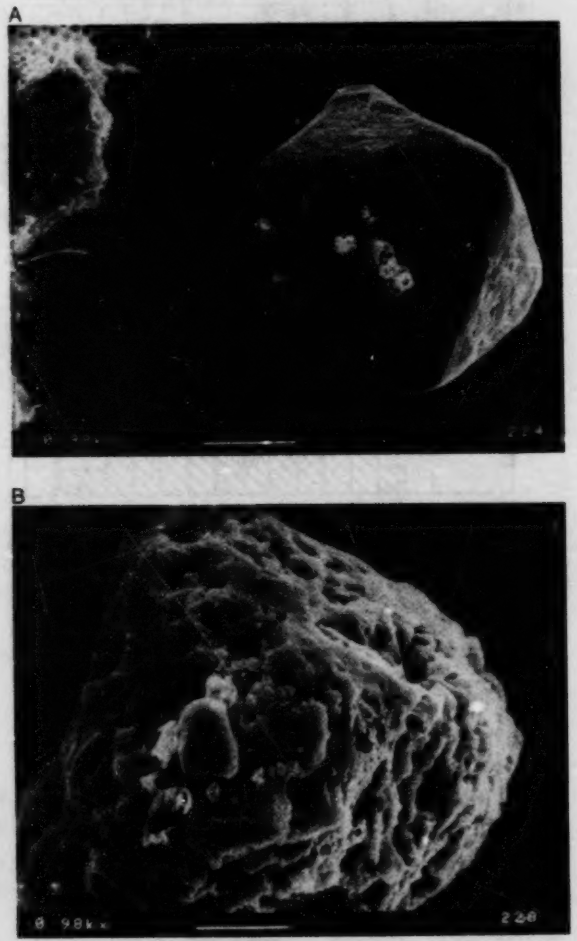

Figure 13. Scanning electron microscope photograph of magnetic concentrates from Site 725 sediments.

compressional-wave velocities to be measured with the Hamilton Frame Velocimeter. The coarse-grained noncohesive sediments common in the upper part of this site were not suitable for measuring shear strengths with the Wykeham-Farrance vane shear device. The properties that were determined for discrete samples from Holes 725A and 725B, and Hole 725C are listed in Tables 6 and 7, respectively. Wet-bulk density was measured on all whole-round core sections that were at least 80 cm long using the GRAPE logging system. Acquisition of compressional-wave velocity data using the *P*-wave logger was successful only on the cores recovered using the APC coring system. All techniques and equipment used are described in the "Explanatory Notes" (this volume).

Index Properties

Lithologic Unit I

Lithologic Unit I (0–121.0 mbsf) is made up of several sediment types that, on the basis of visual description, were not divided into facies or subunits. However, index properties of the sediments in lithologic Unit I do show two distinct trends (Fig. 17) that are related to minor changes in sediment composition and a decrease in grain size downsection. From the seafloor to 70 mbsf, lithologic Unit I is a coarse-grained unit that consists primarily of foraminifer-rich, calcitic, sandy silt and calcitic, marly, nannofossil ooze, throughout which the percentages of calcium carbonate (average of 53%) and organic carbon (<1%) are nearly constant with depth (see "Lithostratigraphy" section, this chapter, Fig. 15). At 70 mbsf, average values of porosity and water content decrease gradually with depth from 51% to 49% and 30% to 28%, respectively. Wet-bulk density reflects the downsection decrease in water content, which increases from 1.87 g/cm^3 near the seafloor to 1.93 g/cm^3 at 70 mbsf. Variations in the values of porosity, water content, and wet-bulk density may be partly attributed to local variation in sediment composition and fabric, but may also be a result of the inevitable disturbance during core recovery of unconsolidated sands and silts. The low porosity and density gradients determined here are typical of coarse-grained sediments, which decrease volume slowly during the early stages of compaction (Meade, 1966). Because of the strong possibility of disturbance, however, the porosities, water contents, and bulk densities reported here should be considered as lower and upper bounds, respectively, on the *in-situ* values.

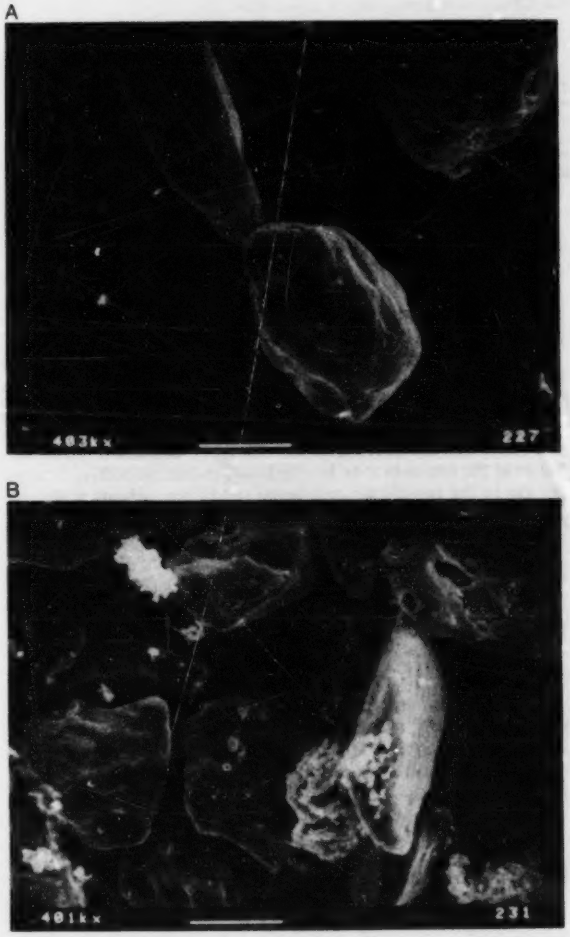

Figure 14. Scanning electron microscope photograph of magnetic concentrates from Site 725 sediments.

In the lower part of lithologic Unit I (75–121 mbsf), the physical property trends change in response to the increasing abundance of terrigenous clay, as well as to gradual increases in both calcium carbonate and organic carbon throughout the section (see "Lithostratigraphy" section, Fig. 15). Although no distinct sedimentologic boundary was identified, physical properties change abruptly near the top of Core 117-725C-9X (76 mbsf), where porosity and water content increase to 66% and 42%, respectively. Between 76 and 121 mbsf, porosity and water content decrease gradually and uniformly to 64% and 40%, respectively. One deviation from this trend occurs in a sample taken from a calcitic silty clay, Sample 117-725C-12X-3, 108–110 cm, which shows inexplicably low porosity and water content coupled with high wet-bulk density. Grain density generally decreases from 2.60 to 2.55 g/cm^3 over this interval in which diatoms become increasingly abundant with depth and nannofossils replace a portion of the terrigenous material (see "Lithostratigraphy" section, this chapter; Fig. 17). Wet-bulk density shows considerable variation over this interval (1.62–1.83 g/cm^3) and averages 1.68 g/cm^3.

Lithologic Unit II

Within the laminated layers of calcitic marly nannofossil ooze and diatomaceous clayey silt and mud of lithologic Unit II (121.0–145.4 mbsf) porosity, water content, and wet-bulk density are relatively constant, with the exception of one sample taken from one of the diatomaceous layers in Sample 117-725C-14X-6, 14–16 cm. The highest porosity (71%) and water content (50%) measured at Site 725 were measured in this diatomaceous interval. Porosity and water content average 63% and 39%, respectively, for the entire unit. Wet-bulk density averages 1.66 g/cm^3 through lithologic Unit II as a whole and decreases to 1.44 g/cm^3 within the diatomaceous mud. Grain densities continue to decrease downsection, with a minimum value of 2.31 g/cm^3 in the diatom-rich layer of Core 117-725C-14X.

Lithologic Unit III

Within lithologic Unit III (145.4–162.8 mbsf), index properties resume the downsection trends established in the base of lithologically similar Unit I. Porosity and water content at the base of this unit average 59% and 37%, respectively. Wet-bulk densities and grain densities measure 1.66 and 2.59 g/cm^3, respectively.

GRAPE and *P*-Wave Logs

Data collected by the GRAPE logging system were of good quality in Hole 725C, in part because of the relatively low gas content of the section (Figs. 18 and 19). The major gaps in the records correspond to intervals of no recovery, rather than areas of low data quality. The general pattern of density variation displayed on the GRAPE records follows that of the wet-bulk densities determined for discrete samples. In the uppermost 70 m of Hole 725C, GRAPE records show relatively high density (1.9 g/cm^3) that varies less than 0.2 g/cm^3. As with the discrete samples, density decreases and variability of the values increases abruptly near 80 mbsf. A close correspondence between the GRAPE logs and discrete samples continues downsection to lithologic Unit III, where the quality of the GRAPE data degrades as the diameter of the core decreases, producing a gap between the sediment and core liner.

Good quality *P*-wave logs were obtained in Cores 117-725C-1H through -4H. The high, near-surface values, 1600 to 1700 m/s, reflect the low densities of the coarse-grained sediment. The *P*-wave record for Cores 117-725C-5X through -11X is of poor quality because of spotty recovery, but does reflect the decrease in density displayed in the GRAPE records. At depths below 100 mbsf, incomplete filling of the core liners resulted in a lack of coupling between sediment and liner that prevented the transmission of *P*-wave signals.

Patterns of cyclic variation on a scale of several meters displayed on the records from Sites 721, 722, 723, and 724 are not well defined at Site 725 because of the low variability in both density and velocity in the surficial sediments.

INORGANIC GEOCHEMISTRY

Introduction

Eight interstitial water samples were collected at Site 725 by squeezing: one each from Holes 724A and 724B and the remainder from Hole 724C. No *in-situ* samples were collected from this site. All analytical results are listed in Tables 8 and 9 and presented in Figures 20 and 21. These profiles are compiled from data from all three holes.

Salinity, Chloride, and pH

The concentration profiles of salinity, chloride, and pH are shown in Figure 20. There is a loss of salinity with depth (~2 g/

Table 5. Sedimentation and accumulation rate data for Site 725.

Depth interval (mbsf)	Age range (m.y.)	$CaCO_3$ ($\bar{x}$ %)	C_{org} ($\bar{x}$ %)	Dry-bulk density ($\bar{x}$ g/cm^3)	Sed. rate ($\bar{x}$ m/m.y.)	$CaCO_3$ acc. rate (g/cm^2/k.y.)	Non-$CaCO_3$ acc. rate (g/cm^2/k.y.)	C_{org} acc. rate (mg/cm^2/k.y.)
0–27.1	0–0.19	52.5	0.57	1.41	142.6	10.56	9.55	114.6
27.1–50.9	0.19–0.49	55.8	0.32	1.54	79.3	6.81	5.40	39.1
50.9–100.9	0.49–0.82	54.6	1.21	1.19	151.5	9.84	8.18	218.1

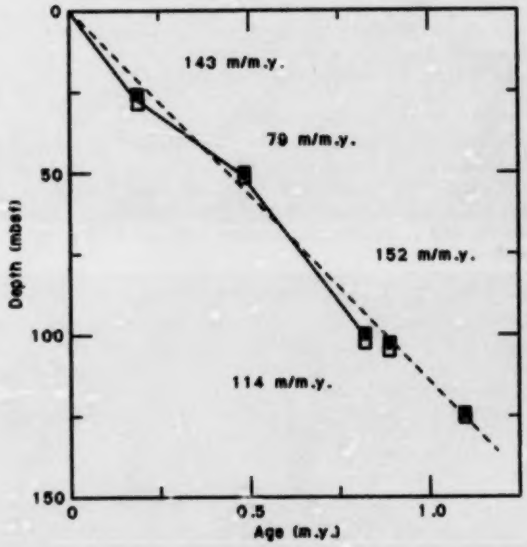

Figure 15. Age-depth plot of stratigraphic datums listed in Table 4. The filled and open boxes are the upper and lower depths of each datum level, respectively. Indicated sedimentation rates (solid lines) are calculated between reliable nannofossil datum levels. The dashed line represents the mean sedimentation rate for the last 1.1 m.y. at Site 725, based on a best fit to all stratigraphic data.

kg over 160 m) of the same magnitude as occurs at Site 724. This decrease may also be attributed to depletion of sulfate and magnesium ions that are involved in microbial degradation and diagenetic reactions, respectively.

The chloride profile at Site 725 displays similar structure to that seen at Site 724, where a broad maximum was observed between 20 and 100 mbsf. However, at Site 725 the chloride maximum extends over a greater depth zone and reaches higher concentrations (+14 mmol/L relative to the topmost sample, compared to a ~10 mmol/L increase at Site 724). We believe that this chloride maximum may represent burial of late Pleistocene seawater that was more saline than modern bottom water. Subsequent diffusion is gradually smoothing this signal. It is not clear why the chloride maximum is seen only at Sites 724 and 725.

pH values measured at this site are biased by sample degassing. However, Site 725 has a slightly higher pH than Site 724, although this may result from the lower depressurization of these samples (Site 725 was one-half as deep as Site 724).

Sulfate and Alkalinity

Sulfate depletion occurs over the upper 110 m of the cored section (Fig. 20), giving a gradient of ~ −0.25 mmol/L/m. This is one-half the gradient of Site 724, despite the higher rate of sedimentation at this site (see "Biostratigraphy" section, this chapter). Below ~110 mbsf, sulfate is constant at ~1 mmol/L, similar to the distribution seen at Site 724.

In contrast to sulfate, the alkalinity increase observed at this site is more than three times that at Site 724. Approximately 30 mmol/L of titration alkalinity was observed at the point where the sulfate concentration approaches zero, compared with ~10 mmol/L at the previous site. Although an alkalinity deficit (about 20 mmol/L) still occurs at this site, the absolute difference between the profiles at the base of the sulfate reduction zones at the two sites may be attributed to less carbonate precipitation in the rapidly accumulating sandy terrigenous sediment of Site 725. Faster sedimentation would cause concentration gradients for alkalinity, magnesium, and calcium to become less steep, which in turn would reduce the downward flux of the alkaline earths, and thus alkalinity, to reaction sites at depth. The increase in alkalinity below 110 mbsf is probably from ammonia production during methanogenesis (see below).

Calcium and Magnesium

Both calcium and magnesium concentrations (Fig. 20) decrease with depth, although calcium displays a subsurface maximum at ~50 mbsf. The profiles indicate that little reaction is occurring in these sediments, while diffusion plays a major role in determining the gradients observed (especially for magnesium). The low magnesium/calcium ratio, low alkalinity deficit, and high accumulation rate of the sediment conspire to limit dolomite diagenesis in the upper 150 m of this site.

Ammonia, Phosphate, Silica, and Dissolved Organic Carbon (DOC)

The distribution of these constituents is shown in Figure 20. Ammonia concentrations increase down the length of the cored section, with a gradient (~0.13 mmol/L/m) similar to that observed at Site 724.

Phosphate concentrations are low and variable (perhaps due to analytical difficulties). The low values are most likely caused by the phosphatization of biogenic skeletal debris and/or apatite precipitation on calcite tests.

Dissolved silica increases rapidly at 40 to 50 mbsf from ~300 μmol/L to ~1200 μmol/L, which is near the saturation limit of opal-CT at this water depth. This rapid increase suggests that biogenic silica should be observed in the sediment in greater amounts from 50 mbsf. In a similar fashion, DOC (Table 9 and Fig. 20) increases over the same depth zone, suggesting that greater amounts of biogenic matter occur within the sediment column below 50 mbsf. Total organic carbon (see "Organic Geochemistry" section, this chapter) and sediment smear-slide descriptions (see "Lithostratigraphy" section, this chapter) indicate relatively constant organic matter concentrations of ~1.0 wt% over the top 80 m of Site 725, but increasing (to 3.5 wt%) and variable concentrations of organic matter and diatoms below. The interstitial water geochemistry presented here broadly confirms these observations.

Table 6. Physical properties summary for Holes 725A and 725B.

Core, section, interval (cm)	Depth (mbsf)	Wet-bulk density (g/cm^3)	Porosity (%)	Water content (%)	Grain density (g/cm^3)	Dry-bulk density (g/cm^3)
117-725A-1H-1, 100-102	1.00	1.883	49.4	26.9	2.615	1.376
725A-1H-3, 100-102	4.00	1.844	51.9	28.8	2.642	1.312
725B-5X-1, 100-102	37.20	1.970	46.9	24.4	2.681	1.490
725B-6X, CC 15-17	46.49	2.039	40.4	20.3	2.608	1.625
725B-7X-1, 130-132	56.60				2.643	

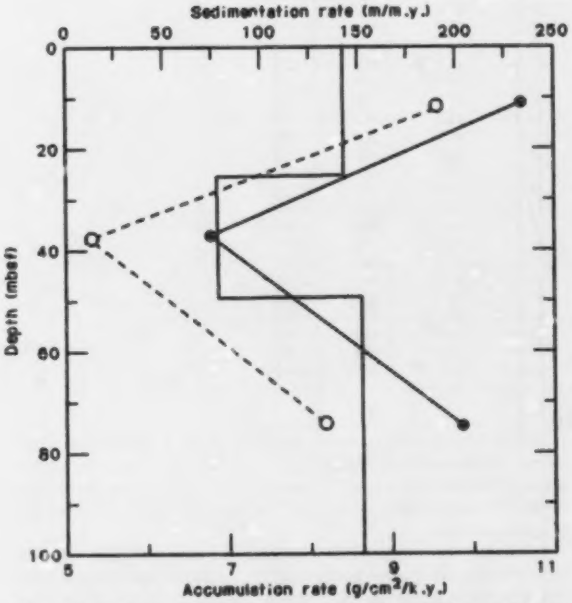

Figure 16. Sedimentation rate (m/m.y.; solid line), calcium carbonate accumulation rate (g/cm^2/k.y.; filled circles), and noncarbonate accumulation rate (g/cm^2/k.y.; open circles) vs. depth (mbsf) at Site 725. Accumulation rates are plotted at the midpoint of the respective depth intervals.

ORGANIC GEOCHEMISTRY

Abundance and Character of Organic Matter

The headspace residues as well as the physical properties residues of 35 samples (mainly from Hole 725C) were analyzed for their calcium carbonate and organic carbon content; the results are given in Table 3 and plotted vs. depth in Figure 5. Organic carbon and calcium carbonate values are fairly constant in the upper 80 mbsf of lithologic Unit I, and organic carbon averages only 0.65%, a low value when compared to previous sites drilled on the Oman margin. The entire lithologic Unit I down to 120 mbsf (see "Lithostratigraphy" section, this chapter), which consists of foraminifer-rich, calcitic, calcareous ooze and sandy silt, has an average value of 1.0%. Organic carbon concentrations vary widely in the lower 40 m of Unit I and reach high values of 3.6%, which are characteristic for the underlying unit of laminated and diatomaceous sediments that comprise lithologic Unit II (120.0–145.4 mbsf). We believe that the facies and composition of Unit II indicate suboxic deposition during some part of the lower Pleistocene. Average organic carbon concentrations are 3.06%. Below Unit II, sediments have the same aspect as those in lithologic Unit I and consist of nannofossil-rich calcitic sand, silt, and clay that averages 3.61% organic carbon. Sparse pyrolysis results (Table 10) indicate that samples from lithologic Unit I with low organic carbon values have low hydrogen index (HI) values, an indication of relatively refractory organic matter. Two samples from Units II and III show high values that appear to be related to the higher organic carbon content. Currently, we are not certain whether influx determines the relative freshness of the organic matter, or whether preservational signals prevail (Fig. 21).

Hydrocarbon Gases

Because of the very shallow water depth (311 m), safety considerations made a stringent hydrocarbon monitoring program necessary at Site 725. Gas pockets occurred only in the last four cores of Hole 725C; results of analyses of the vacutainer samples are given in Table 11. Methane is the most abundant gas, but considerable amounts of thermogenic ethane and propane were detected in gas pockets of Core 117-725C-17X (Table 11). Headspace samples were taken at regular intervals in Hole 725C; results appear in Table 12. Again, a steady increase of the thermogenic gases, ethane and propane, was observed with depth.

SUMMARY AND CONCLUSIONS

Site 725 marks a shallow landward end point of a depth transect designed to recover sediments from a water depth range of 300 to 1500 m on the Oman continental margin. This transect brackets the vertical extent of a pronounced mid-water oxygen-minimum zone. Site 725 is located on the landward flank of the prominent slope basin that had been drilled at Sites 723 and 724. The goal for Site 725 was to trace the fluctuations in the upper boundary of the oxygen-minimum zone through time and to evaluate these fluctuations with regard to changes in the monsoonal upwelling, eolian transport, and eustatic sea level. Continuity of the sedimentary section and the benthic foraminifer assemblages were expected to reveal any differential tectonic movement of the basement blocks and the slope basins.

Some of the major findings at Site 725 are summarized in Figure 22 and include the following:

1. Identification of the alternation of millimeter-scale laminated organic- and opal-rich clayey silt with nonlaminated nannofossil ooze and calcitic silty clay. The laminated intervals are confined to a brief interval in the lower Pleistocene.
2. The average sedimentation rate is about 120 m/m.y.
3. Opal occurrences are confined to sediments with high organic carbon concentrations and overlap the laminated intervals.
4. Cold-water nannoplankton occurrences at the base of the section and abundant but low-diversity assemblages throughout the overlying section.
5. Persistent occurrence of interstitial sulfate, high alkalinities, and dramatic core expansion, which indicate replenishment of the interstitial sulfate pool at depth, comparable to Site 723.
6. A maximum in the chloride concentration at about 80 mbsf (~0.7 Ma), which was also seen at Site 724, suggests that mid-Pleistocene bottom water on the upper margin was significantly more saline than it is today.

Table 7. Physical properties summary for Hole 725C.

Core, section, interval (cm)	Depth (mbsf)	Wet-bulk density (g/cm^3)	Porosity (%)	Water content (%)	Grain density (g/cm^3)	Dry-bulk density (g/cm^3)
117-725C-1H-2, 90-92	2.40	1.915	50.8	27.2	2.724	1.395
1H-6, 90-92	8.40	1.842	53.6	29.8	2.749	1.293
2H-2, 60-62	11.10	1.953	45.7	24.0	2.635	1.484
2H-4, 60-62	14.10	1.815	51.7	29.2	2.647	1.286
2H-7, 30-32	18.30	1.924	46.2	24.6	2.665	1.450
3H-2, 100-102	21.10	1.956	47.5	24.9	2.673	1.469
3H-4, 24-26	23.34	1.956	47.6	24.9	2.639	1.468
3H-6, 100-102	27.10	1.936	46.8	24.8	2.656	1.457
4X-3, 50-52	32.00	1.998	45.0	23.1	2.714	1.537
6X-2, 86-88	49.86	1.810	52.7	29.8	2.677	1.271
6X-4, 86-88	52.86	1.840	51.9	28.9	2.617	1.308
8X-3, 29-31	69.79	1.935	47.2	25.0	2.664	1.452
9X-4, 27-29	80.87	1.622	66.5	42.0	2.592	0.941
11X-2, 24-26	97.04	1.622	64.7	40.9	2.556	0.959
11X-5, 8-10	101.38	1.838	52.5	29.3	2.631	1.300
12X-2, 19-21	106.59	1.586	66.8	43.2	2.513	0.901
12X-3, 108-110	108.98	1.802	66.6	37.8	2.633	1.120
13X-3, 34-36	117.84	1.631	63.0	39.6	2.524	0.985
14X-2, 21-23	125.81	1.623	65.5	41.3	2.621	0.952
14X-4, 26-28	128.86	1.670	61.1	37.5	2.513	1.044
14X-6, 14-16	131.74	1.444	71.0	50.4	2.309	0.716
15X-2, 85-87	136.15	1.737	59.9	35.3	2.662	1.123
15X-4, 80-82	139.10	1.604	64.6	41.3	2.484	0.942
16X-3, 4-6	146.54	1.673	60.2	36.9	2.476	1.056
17X-2, 25-27	154.95	1.653	59.4	36.8	2.436	1.044
17X-4, 106-108	158.76	1.664	58.2	35.9	2.499	1.068
17X-6, 128-130	161.98	1.663	60.8	37.4	2.506	1.040

7. Elevated ethane and propane gas concentrations with depth imply migration of thermogenic hydrocarbons from deep sources.

The section penetrated at Site 725 ranges from the Holocene to the lower Pleistocene and has been subdivided into three lithologic units (Fig. 22).

Lithologic Unit I (0–120 mbsf) comprises foraminifer-rich, calcitic, sandy silt to calcitic, marly, calcareous ooze; calcitic, marly, nannofossil ooze; and nannofossil-rich sand, silt, or clay. This lithology is coarser and has more detrital carbonate than similar sediments at Sites 723 and 724. It is considered to be a hemipelagic facies dominated by influx of detrital calcite, eolian silts and clays, and biogenic components from coastal upwelling and modified by slight winnowing or nondeposition of fine-grained material. Organic carbon content is less than 1% over the upper 80 m and varies between 1% and 2% in the lower part of the unit.

Lithologic Unit II (120–145.4 mbsf) is composed of diatomaceous clayey silt and diatomaceous mud intercalated with calcitic marly nannofossil ooze and calcitic sand, silt, and clay (Fig. 25). Diatom-rich beds form laminae on less than a centimeter scale and are dominated by frustrules of two diatom species. The unit is believed to indicate anoxic depositional conditions. Organic carbon content ranges between 2% and 3% in this laminated unity.

Lithologic Unit III (145–162.8 mbsf) is similar to Unit I and is composed of nannofossil-rich, calcitic sand, silt, and clay and calcitic, marly, nannofossil ooze. All units were found to contain less than 2% authigenic dolomite and traces of apatite and fish scales. Organic carbon content averages 3%.

Like previous sites on the margin, Site 725 contains partially overlapping intervals of cold-water nannoplankton species and a robust, radiolarian fauna dominated by Spumellarians (Fig. 22). In contrast to the other sites, these occurrences are confined to the lower Pleistocene. However, the opal-rich sediments coincide with the laminated facies, as observed at other sites.

Mass accumulation rates obtained with a preliminary age model are depicted in Figure 22. These rates may vary by almost a factor of two downhole. However, some of this variation may be attributed to uncertainties in the age and depth of biostratigraphic datums.

Comparison of Site 725 with Site 723 demonstrates that the ratio of organic matter accumulation to clastic and biogenic accumulation is higher at Site 723 in the center of the basin than at Site 725. This pattern of accumulation may indicate a persistent spatial inhomogeneity of primary production and preservation, or an influx of allochthonous organic-carbon-rich material.

Even though dolomite was encountered in trace amounts throughout the cores, the extent of dolomitization was insignificant when compared to the pronounced dolomitization observed at Site 723. Interstitial water profiles at Site 725 show an increase in chloride concentrations with depth. Sulfate ions are never depleted at depth, even though increasing ammonia and alkalinity concentrations imply ongoing sulfate reduction at depth (Fig. 22). Thus, a replenishment of the interstitial sulfate pool by ascending water may be implied. The persistence of sulfate reduction is in accord with relatively low methane concentrations in gas pockets. Cores more than 100 mbsf show increasing (up to 90 μL/L) ethane and propane concentrations that are believed to indicate thermal hydrocarbon generation at depth.

Site 725 constitutes a complete section of Pleistocene age that shows significant changes in the oceanographic and depositional environment, such as the frequency of upwelling indicators, the accumulation of carbon, and the preservation of laminated facies. Similar associations were observed at Sites 723 and 724, and these associations seem roughly contemporaneous. If these facies prove to be synchronous, they will provide constraints on the regional vs. local origin and possible extent of the oxygen-minimum zone. A preliminary interpretation of the heterogeneity observed in organic matter abundance and preservation of primary sediment structures (i.e., the laminations) is

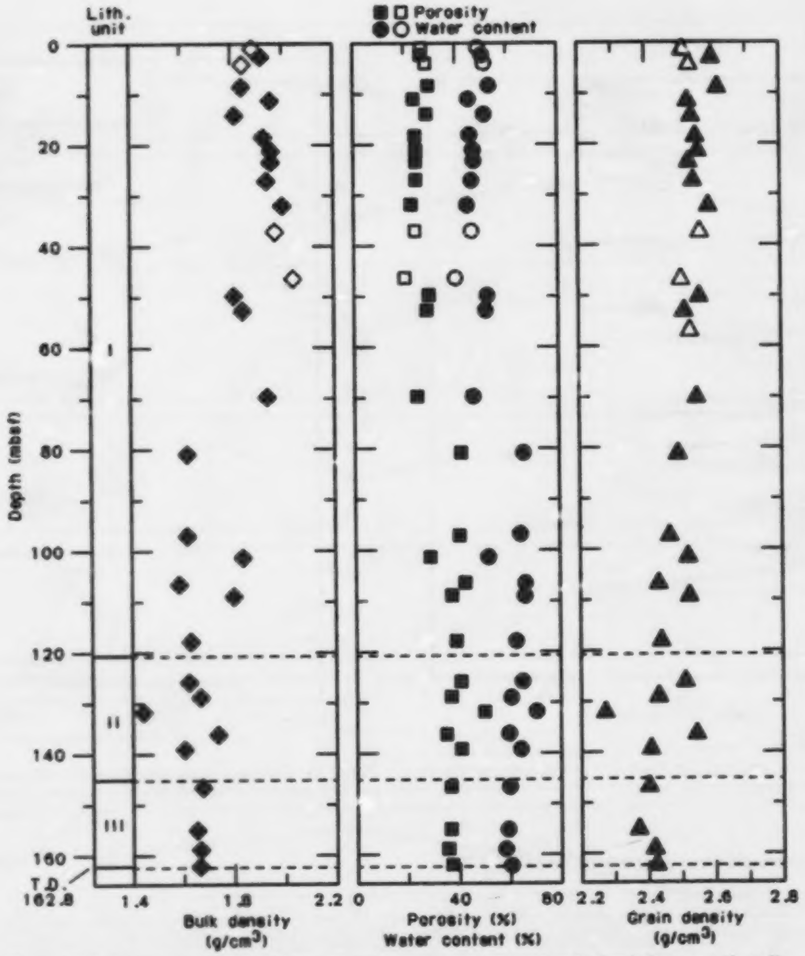

Figure 17. Index properties (bulk density, porosity, water content, and grain density) measured on discrete samples from Holes 725A, 725B, and 725C. Hole 725A and 725B = open symbols; Hole 725C = closed symbols.

that the mid-water oxygen-minimum zone expanded, perphaps in response to enhanced productivity, and was more stable during the early Pleistocene.

REFERENCES

Berggren, W. A., Kent, D. V., and Van Couvering, J. A., 1985. The Neogene: Part 2, Neogene geochronology and chronostratigraphy. *In* Snelling, N. J. (Ed.), *The Chronology of the Geological Record*. Geol. Soc. Mem. (London), 10:211-260.

Caulet, J. P., Debrabant, P., and Fieux, M., in press. Dynamique des masses d'eau océanique et sedimentation quaternaire sur la marge de l'Afrique de l'Est et dans le bassin de Somalie. Resultats préliminaires de la mission MD44 INDUSOM du Marion-Dufresnes. *CRAS.*

Emerson, S., 1985. Organic carbon preservation in marine sediments. *In* Sundquist, E. T., and Broecker, W. S. (Eds.), *The Carbon Cycle and Atmospheric* CO_2*: Natural Variations Archean to Present*. Geophys. Monogr., 3:78-87.

Kemper, E., and Zimmerle, W., 1980. Facies pattern of a Cretaceous/Tertiary subtropical upwelling system (Great Syrian Desert) and an Aptian/Albian boreal upwelling system (NW Germany). *In* Thiede, J., and Suess, E. (Eds.), *Coastal Upwelling* (Pt. B): New York (Plenum Press), 29-72.

Kolla, V., Kostecki, J. A., Robinson, F., and Biscaye, P. E., 1981. Distributions and origins of clay minerals and quartz in surface sediments of the Arabian Sea. *J. Sediment. Petrol.*, 51:563-569.

Meade, R. H., 1966. Factors influencing the early stages of compaction of clays and sands-review. *J. Sediment. Petrol.*, 36:149-165.

Perch-Nielsen, K., 1985. Cenzoic calcareous nannofossils. *In* Bolli, H., Saunders, J., and Perch-Nielsen, K. (Eds.), *Plankton Stratigraphy*: Cambridge (Cambridge Univ. Press), 427-554.

Prell, W. L., and Streeter, H. F., 1982. Temporal and spatial patterns of monsoonal upwelling along Arabia: a modern analogue for the interpretation of Quaternary SST anomalies. *J. Mar. Res.*, 40:143-155.

Takayama, T., and Sato, T., 1987. Coccolith biostratigraphy of the North Atlantic Ocean, Deep Sea Drilling Project Leg 94. *In* Ruddiman, W. F., Kidd, R. B., Thomas, E., et al., *Init. Repts. DSDP*, 94, Pt. 2: Washington (U.S. Govt. Printing Office), 651-702.

Ms 117A-112

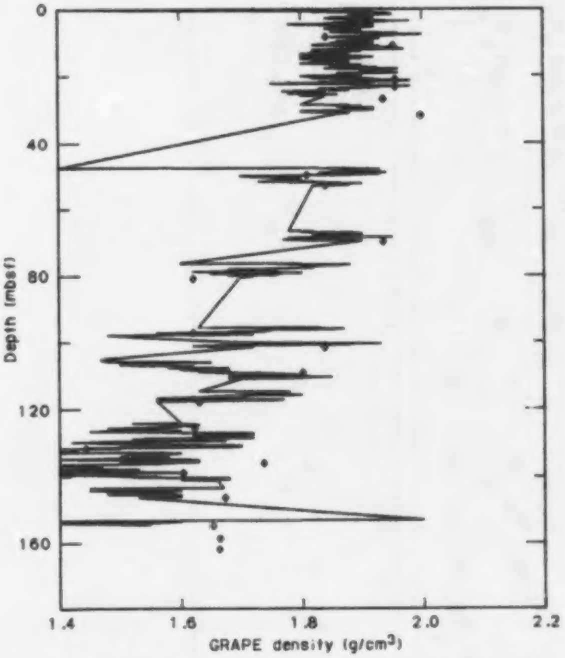

Figure 18. GRAPE wet-bulk density (solid line) and wet-bulk density from discrete samples (diamonds) for Hole 725C. GRAPE profile is based on 10-cm-block averages of the data.

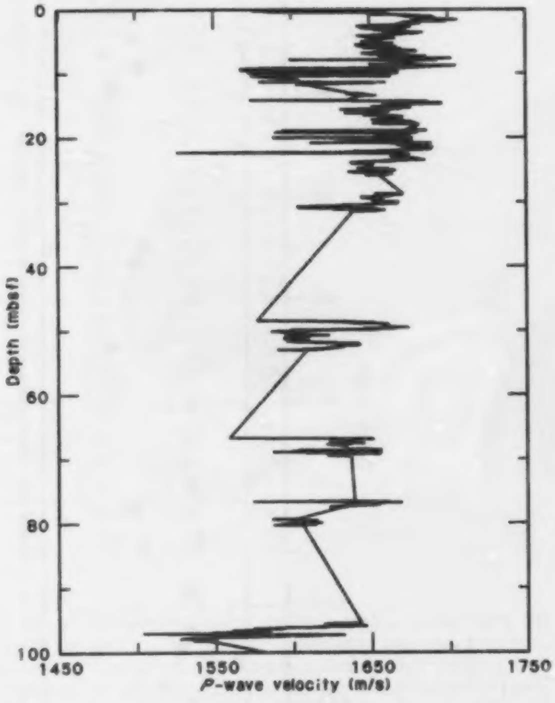

Figure 19. Compressional-wave velocity as measured by the *P*-wave logger in Cores 117-725C-1H through Section 117-725C-11X-2.

Table 8. Summary of interstitial-water geochemical data at Site 725.

Core, section, interval (cm)	Depth (mbsf)	Vol. (mL)	pH	Alk. (mmol/L)	Sal. (g/kg)	Mg (mmol/L)	Ca (mmol/L)	Cl (mmol/L)	SO_4 (mmol/L)	PO_4 (μmol/L)	NH_4 (mmol/L)	SiO_2 (μmol/L)	Mg/Ca (μmol/L)
117-725A-1H-2, 145-150	2.95	30	7.70	3.67	35.6	54.32	10.63	576	27.2	2.8	0.65	183	5.11
725B-5X-1, 145-150	37.65	30	8.15	4.77	35.6	46.[illegible]1	13.03	583	21.3	1.6	1.40	310	3.54
725C-3H-4, 145-150	24.55	42	8.37	4.66	35.5	46.95	11.96	584	21.5	1.2	1.02	248	3.93
725C-6X-2, 145-150	50.45	39	8.29	10.56	35.4	43.60	12.00	587	15.5	6.4	3.10	914	3.63
725C-9X-3, 145-150	80.55	40	8.05	17.31	36.0	41.90	13.49	592	13.5	3.6	4.53	1272	3.11
725C-12X-3, 145-150	109.35	43	7.96	27.16	34.8	31.12	8.75	583	0.8	5.1	9.15	1195	3.56
725C-15X-4, 145-150	139.75	45	8.32	32.20	34.2	27.41	7.34	569	1.1	2.0	16.47	1262	3.73
725C-17X-5, 145-150	160.65	38	7.95	33.93	34.2	22.13	5.39	565	0.8	2.0	21.34	1135	4.11

Table 9. Dissolved organic carbon concentrations at Site 725.

Core, section, interval (cm)	Depth (mbsf)	Dissolved organic carbon (a.u.)
117-725A-1H-2, 145-150	2.95	0.097
725C-3H-4, 145-150	37.65	0.455
725B-5X-1, 145-150	24.55	0.625
725C-6X-2, 145-150	50.45	1.085
725C-9X-3, 145-150	80.55	0.891
725C-12C-3, 145-150	109.35	1.187
725C-15X-4, 145-150	139.75	1.031
725C-17X-5, 145-150	160.65	0.995

Note: a.u. = absorbance units.

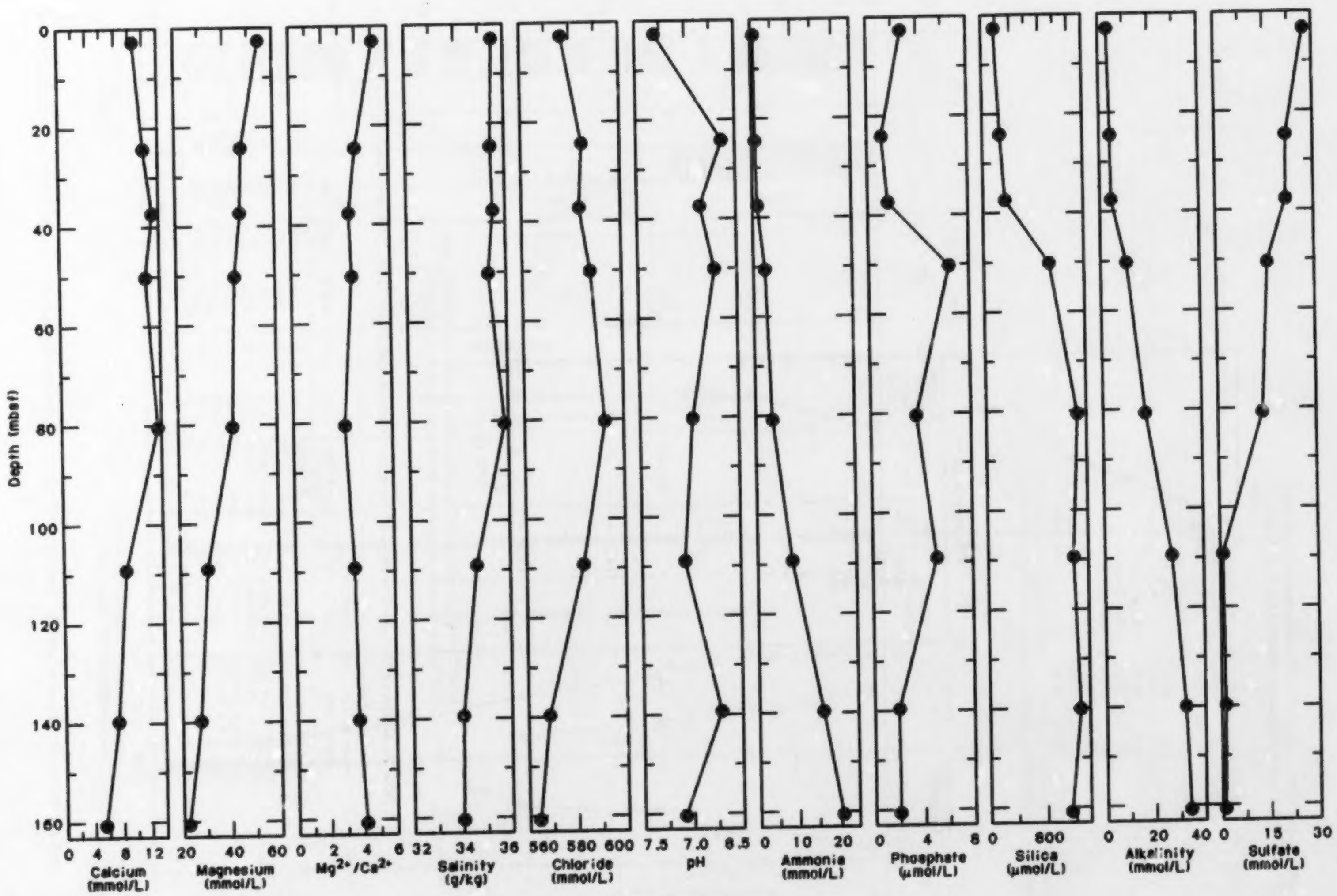

Figure 20. Profiles of interstitial water concentrations for Site 725, compiled from data from three holes.

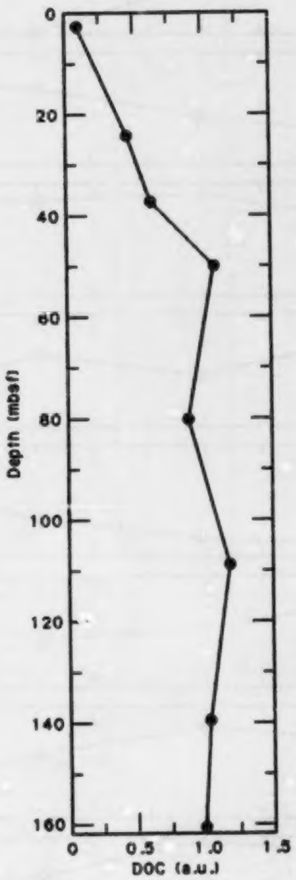

Figure 21. Dissolved organic carbon (DOC) profile for Site 725, compiled from data from three holes (expressed as absorbance units).

Table 10. Results of Rock-Eval pyrolysis of headspace residues from Holes 725A, 725B, and 725C.

Core, section, interval (cm)	Depth (mbsf)	T_{max} (°C)	S_1	S_2	S_3	S_2/S_3	TOC[a]	TOC[b]	HI	OI
117-725A-1H-1, 0-3	3.00	413	0.17	0.70	1.46	0.47	0.45	0.48	146	304
725C-3H-4, 119-120	24.29	412	0.04	0.25	1.04	0.24	0.18	0.34	73	305
725C-6X-2, 119-120	50.19	416	0.31	2.02	1.50	1.34	0.82	1.52	133	99
725C-9X-3, 119-120	80.39	418	0.31	1.49	1.16	1.28	0.45	0.75	199	155
725C-12X-3, 119-120	109.09	415	0.45	1.89	1.25	1.51	0.50	0.85	222	147
725C-15X-4, 119-120	139.49	403	3.61	10.37	2.58	4.01	2.64	2.91	356	89
725C-17X-5, 119-120	160.39	400	2.18	8.64	2.54	3.40	2.21	2.59	333	98

Note: HI = hydrogen index and OI = oxygen index; the hydrogen and oxygen indexes were calculated on the basis of the TOC[b] values. For a detailed description of parameters, see "Explanatory Notes," chapter (this volume).

[a] TOC values are measured by Rock-Eval pyrolysis.

[b] TOC values measured by difference method.

Table 11. Concentrations of methane (C_1), ethane (C_2), and propane (C_3) measured in gas pockets from Hole 725C.

Core, section, interval (cm)	Depth (mbsf)	C_1 (ppm)	C_2 (ppm)	C_3 (ppm)	C_1/C_2
117-725C-14X-6, 28	131.88	412,173	134	19	3,076
15X-3, 14	136.94	255,992	74	11	3,459
16X-1, 145	144.95	142,217	30	5	4,741
17X-6, 30	161.00	799,315	295	52	2,709

Table 12. Concentrations of methane (C_1), ethane (C_2), and propane (C_3) per liter of wet sediment in samples from Holes 725A, 725B, and 725C.

Core, section, interval (cm)	Depth (mbsf)	C_1 (µL/L)	C_2 (µL/L)	C_3 (µL/L)	C_1/C_2
117-725A-1H-3, 0-1	3.00	342			
725B-5X-2, 0-1	37.70	11			
725C-3H-4, 119-120	24.29	38			
725C-6X-2, 119-120	50.19	95	2		48
725C-9X-3, 119-120	80.29	304	6		51
725C-12X-3, 119-120	109.09	52,023	18	3	2,890
725C-15X-4, 119-120	139.49	54.575	29	22	1,882
725C-17X-5, 119-120	160.39	62,010	48	38	1,292

Note: Values are expressed in µm (volume gas/volume wet sediment).

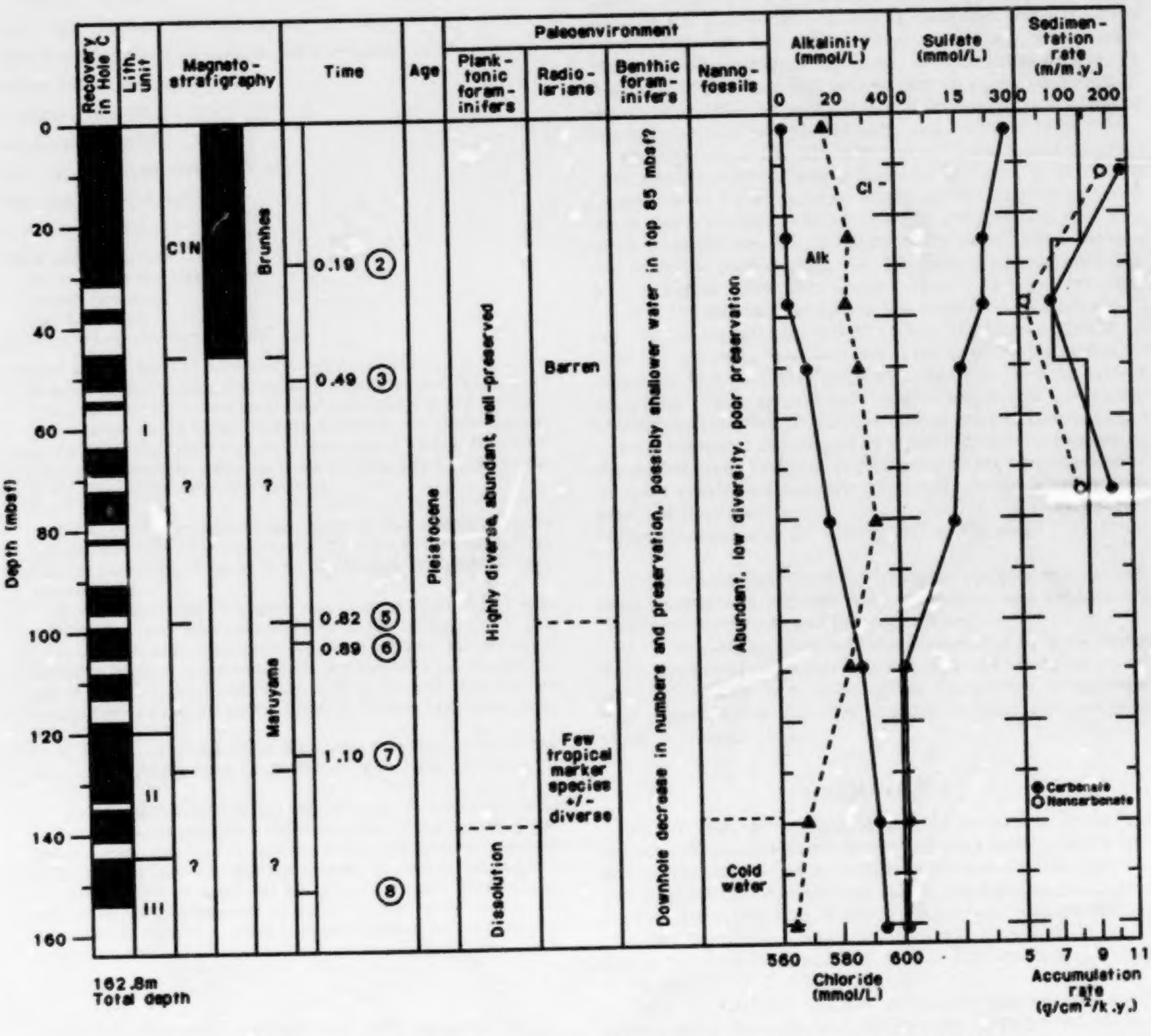

Figure 22. Summary chart outlining preliminary shipboard findings at Site 725. Numbers in circles: nannofossil marker horizons.

14. SITE 726[1]

Shipboard Scientific Party[2]

HOLE 726A

Date occupied: 23 September 1987

Date departed: 24 September 1987

Time on hole: 20 hr, 15 min

Position: 17°48.965′N, 57°22.290′E

Water depth (sea level, corrected m, echo-sounding): 330.8

Water depth (rig floor; corrected m, echo-sounding): 341.3

Bottom felt (m, drill pipe): 340.1

Penetration (m): 186.3

Number of cores: 22

Total length of cored section (m): 186.3

Total core recovered (m): 110.1

Core recovery (%): 59.1

Oldest sediment cored
Depth sub-bottom (m): 186.3
Nature: limestone
Age: Eocene (?)
Measured velocity (km/s): 5.89–6.13

Principal results: Site 726 is located on what was assumed to be a pre-Neogene basement high that coincides with the shelf break. This shelf is landward of a slope basin filled with thick (up to 2 km) Neogene sediment on the Oman continental margin. The main objective at Site 726 was to identify the nature and age of rocks that underlie Neogene hemipelagic sediments in much of the Leg 117 study area.

Of note are the following findings:

1. Repeated alternations from anoxic to oxic conditions in the bottom water resulted in alterations of bioturbated lag deposits with laminated organic-rich layers in the hemipelagic Miocene to Holocene sediment.
2. The preservation of biogenic opal in upper Pliocene sediments parallels opal occurrences at other sites on the margin.
3. Shallow-water nummulitic limestones are dolomitized and are similar to limestones overlying ophiolitic basement on Masirah Island in age and facies. Cementation of the limestone occurred in distinct phases and may be partly related to vadose, fresh-water aquifers.
4. Erosion of shallow-water limestones or nondeposition at the site occurred during much of the Paleogene and lower Miocene.

The recovered section at Site 726 shows the influence that local tectonism and position of the site to the upper boundary of the oxygen-minimum zone have on sediment facies. Hemipelagic sediments of the Neogene reflect repeated oscillations between anoxia and oxia in bottom waters since the late Miocene. Over much of the Oman continental margin, basement appears to be overlain by shallow-water carbonate sediments, which have been uplifted and cemented by vadose cements.

BACKGROUND AND OBJECTIVES

Site 726 is located in a water depth of about 330 m at 17° 48.965′N, 57°22.290′E on the continental margin of Oman. Much of the Oman margin is characterized by a narrow shelf bordered by an extremely steep continental slope, which is thought to be a megashear associated with formation of the margin (Whitmarsh, 1979; Stein and Cochran, 1985). However, the margin between Ras Sharbithat and Ras al Madrakah has a relatively wide continental shelf (about 50 miles) and a series of linear sedimentary basins along the upper continental slope (Fig. 1). This area of the slope and margin may be partly composed of the upthrust ophiolite complex that is observed on the island of Masirah north of Site 726 (Moseley and Abbotts, 1979).

The location of Site 726 is shown in Figure 2, and its structural and depositional setting is shown in Figure 3. Site 726 is located about 5 km landward of the eastern edge of a faulted block that is thought to be an ophiolite complex (Fig. 3B). This block forms the western boundary of the slope basin. The seismic reflection profiles (Figs. 3A, 3B) show gently eastward-dipping reflective layers from about 0.12 to 0.22 s that are truncated to the east and are draped like a conformable pelagic (?) cap. The strong reflector at 0.22 s (Figs. 3A, 3B) is underlain by more diffuse reflections that are thought to be the ophiolitic basement. However, deep structure is observed near the eastern fault (Fig. 3B). In general, this location reveals older, conformable reflectors having an unknown relationship to basement and that are truncated and draped by pelagic sediments. Because of the shallow water depth of Site 726, sediments were expected to be more sandy and possibly winnowed, compared with sediments of slope basins.

Specific objectives for drilling at Site 726 were:

1. To obtain samples of the basement complex and its overlying sediments to help constrain the tectonic and depositional history of the margin and the slope basins.
2. To provide an additional shallow-water end-member for a depth transect of sediments that will be used to examine the organic-rich sedimentary facies of the margin and to establish their relationship to the oxygen-minimum zone and its spatial variation through time.

OPERATIONS

JOIDES Resolution departed Site 725 at 2400 hr on 22 September 1987 and relocated to Site 726 for a seismic survey and drilling operations. We established a seismic dip line and confirmed the RC2704 strike line during good global positioning satellite (GPS) coverage, retrieved seismic gear, and lowered the taut-wire beacon in a water depth of 331 m at 1000 hr on 23 September. The final position of Site 726 was established as 17°48.965′N, 57°22.290′E (Fig. 4).

Core 117-726A-1H was shot at 1200 hr, followed by a rapid succession of five advanced piston corer (APC) cores (0–54.1 meters below seafloor [mbsf]) and a deployment of the *in-situ* pore-water sampler after Core 117-726A-4H. An overpull of

---

[1] Prell, W. D., Niitsuma, N., et al., 1989. *Proc. ODP, Init. Repts.*, 117: College Station, TX (Ocean Drilling Program).

[2] Shipboard Scientific Party is as given in list of Participants preceding the contents.

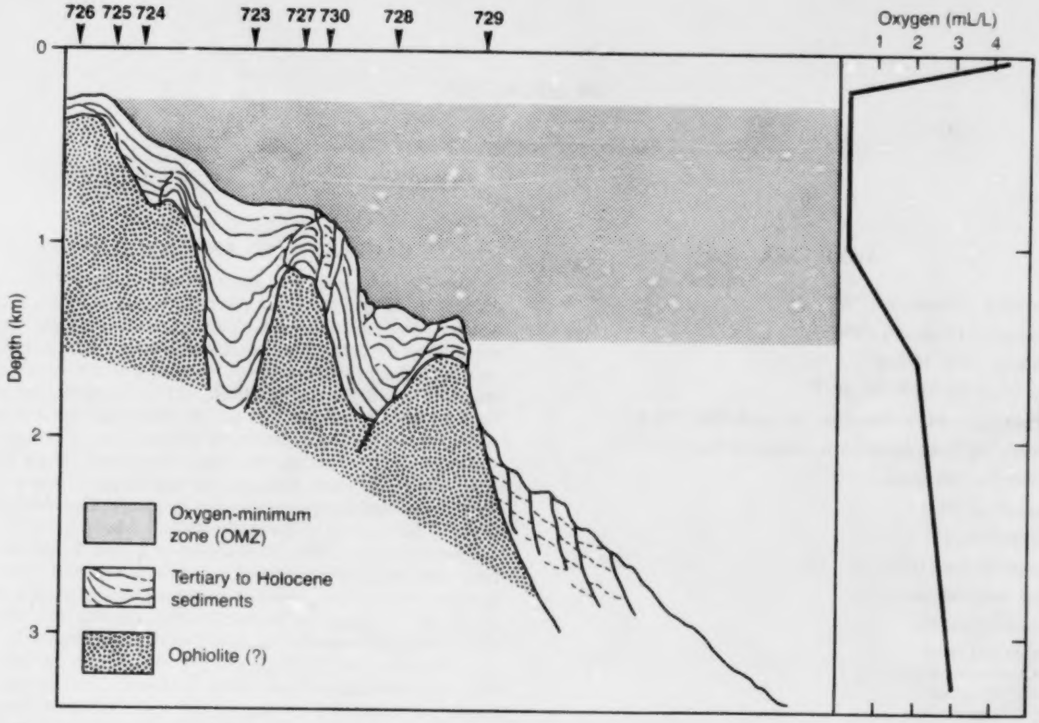

Figure 1. Structure of the Oman margin and the oxygen-minimum zone: the schematic seismic-reflection profile shows a series of basement ophiolite blocks and the sedimentary basins between them. The concentration of oxygen in the water column (RC2704, unpubl. data) defines the depth range of the oxygen-minimum zone and where it impinges on the margin. Schematic location of Site 726 is indicated.

80,000 lb when retrieving Core 117-726A-6H made coring in extended-core-barrel (XCB) mode necessary, starting with Core 117-726A-7X. Recovery in the section cored by the APC was 103%. By 0120 hr, 24 September, Core 117-726A-22X had been retrieved from a total depth of 186.3 mbsf. Core 117-726A-22X was stuck in the bit and the bottom-hole assembly (BHA) had to be pulled out to recover the core barrel on the rig floor. In the cemented dolomite that composed the section below Core 117-726A-16X, penetration and recovery decreased (recovery in the interval cored by the XCB was 40.7% and generally below 10% in the limestone/dolomite), and the hoped-for penetration into ophiolitic basement seemed unattainable within the allocated time (Table 1). Thus, we terminated Hole 726A, displaced it with mud, and pulled the drill string. We were under way to Site 727 by 0830 hr on 24 September.

LITHOSTRATIGRAPHY

Introduction

The sediments and rocks recovered at Site 726 are divided into two lithologic units (Fig. 5). Unit I is composed of two subunits, which are composed of (1) silty clays of Pleistocene and Holocene age and (2) an alternation between organic-carbon-rich silty clays and foraminifer-rich clayey silts of Pleistocene to late Miocene age. Unit II is composed of Eocene (?) shallow-water limestones and dolomites.

Unit I (Depth: 0–131.1 mbsf; Age: Holocene to late Miocene)

Core 117-726-1H to Section 117-726A-14X, CC.

Lithologic Unit I is divided into two subunits that consist of bioturbated calcareous silty clays and alternations of organic-carbon-rich silty clays and foraminifer-rich silts.

Subunit IA (Depth: 0–32.05 mbsf)

Subunit IA consists of calcareous silty clays to marly calcareous ooze with increasing foraminifer content upsection. The color varies from olive (5Y 4/3 to 4/4) to dark olive gray (5Y 3/2). The sediment is composed of 10% to 30% foraminifers, 5% to 40% nannofossils, 10% to 40% detrital calcite, 30% clay, 5% to 15% quartz, and 0% to 2% dolomite (Fig. 6). Small shell fragments are abundant, while soft and hard phosphorite concretions are rare. Bioturbation is not clearly visible in the first two cores due to slight drilling disturbance and lack of differences in lithology. However, mottling occurs in Cores 117-726A-3H and 117-726A-4H. Organic carbon values range from 0.4% to 1.1%, while the carbonate content varies from 53% to 63% (Fig. 7 and Table 2).

Subunit IB (Depth: 32.05–131.1 mbsf)

Subunit IB consists of a suite of laminated, organic-rich, silty clays to marly nannofossil ooze to chalk, interspersed with foraminifer-rich muds. The subunit is Pleistocene to late Miocene in age. The coarse-grained, foraminifer-rich muds are

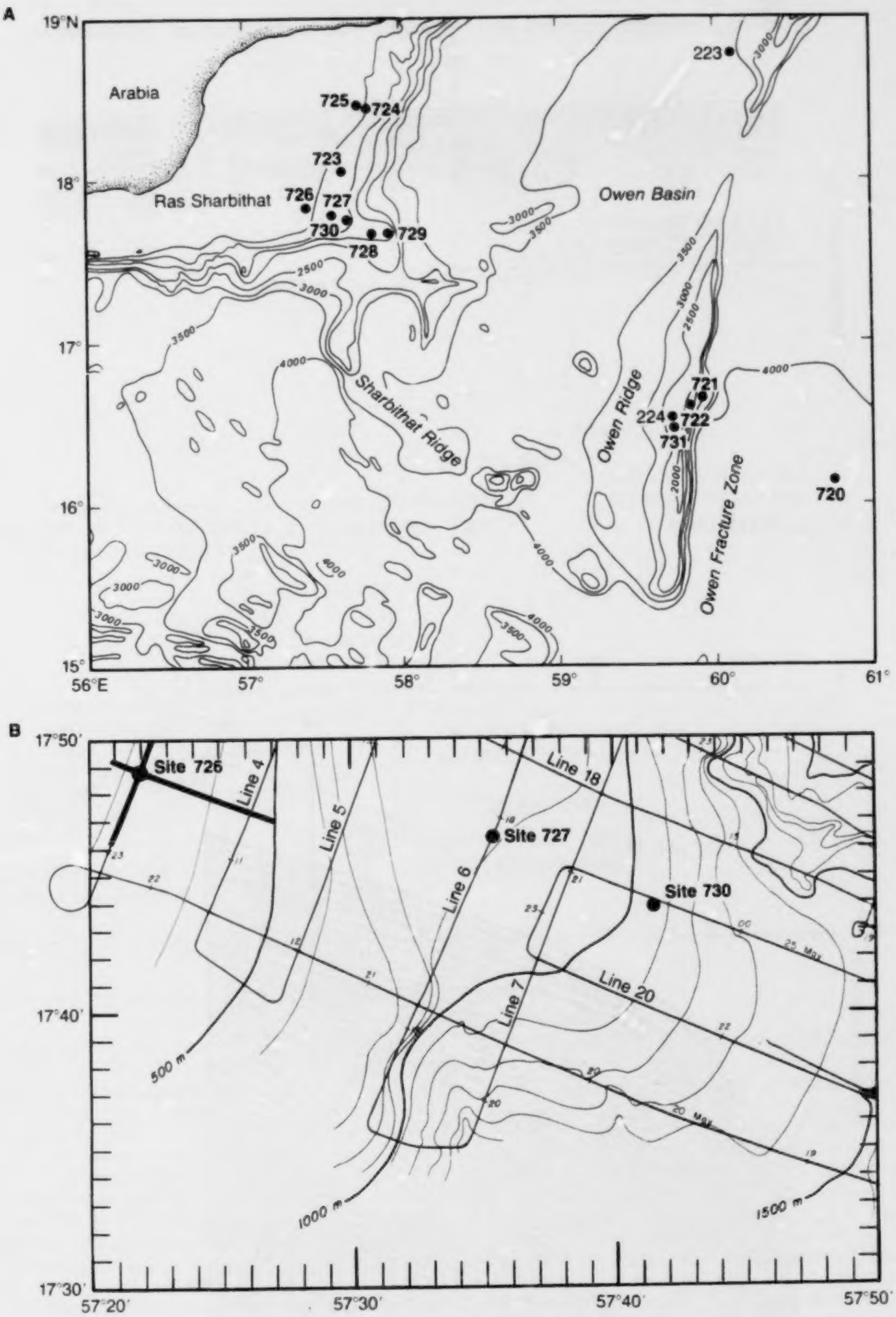
A
19°N
18°
17°
16°
15°
56°E
57°
58°
59°
60°
61°
Arabia
Ras Sharbithat
223
725
724
723
726
727
730
729
728
Owen Basin
Sharbithat Ridge
Owen Ridge
Owen Fracture Zone
721
224
722
731
720
2000
2500
3000
3500
4000
B
17°50′
17°40′
17°30′
57°20′
57°30′
57°40′
57°50′
Site 726
Site 727
Site 730
Line 4
Line 5
Line 6
Line 7
Line 18
Line 20
500 m
1000 m
1500 m
25 May
20 May

Figure 2. **A.** Bathymetry of the Oman margin and the location of Site 726. **B.** Detailed location of Site 726 and seismic profiles shown in Figure 3. Bathymetry data from the site survey (RC2704, 1986).

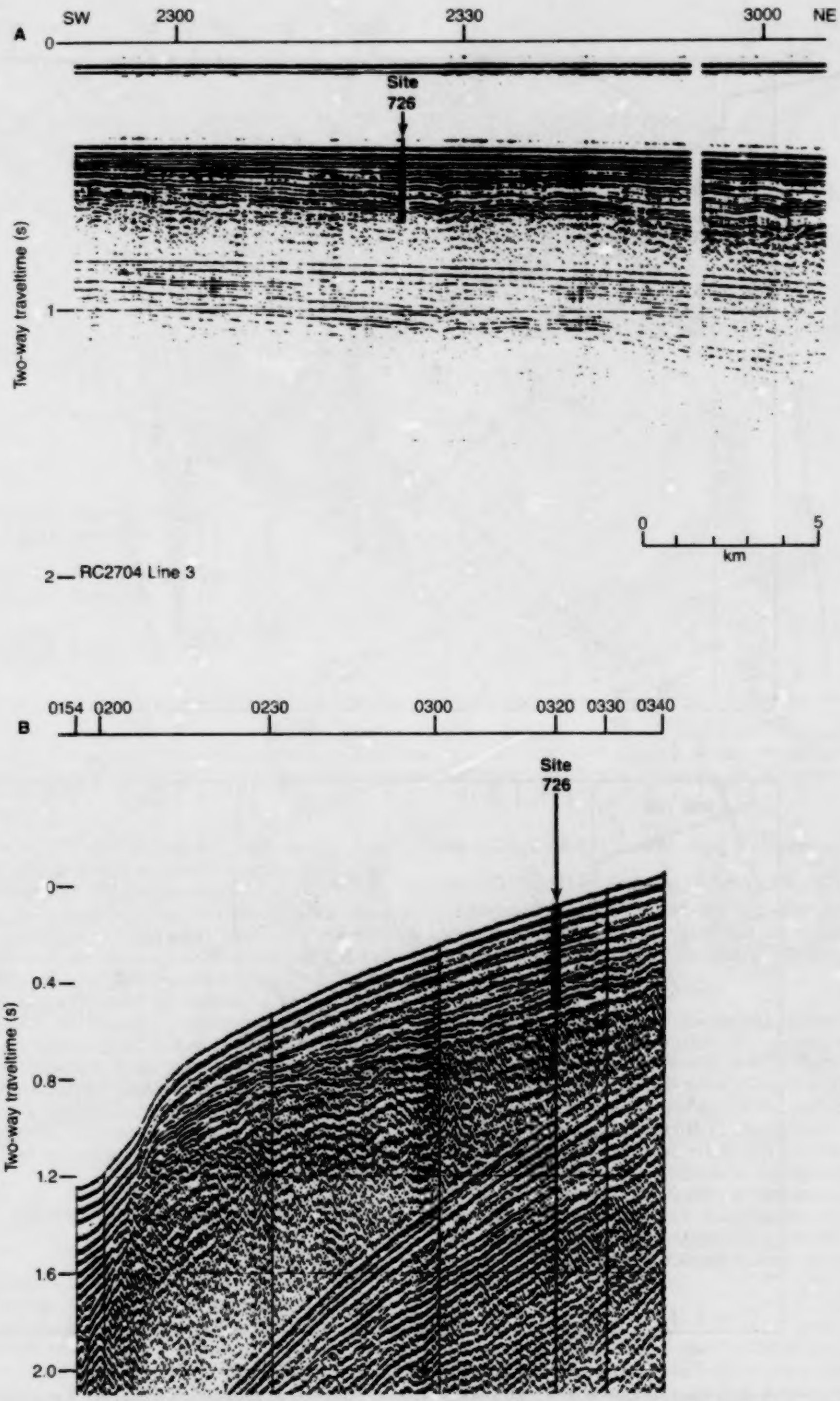

Figure 3. **A.** Single-channel seismic-reflection profiles showing the structural and depositional setting of Site 726. RC2704 Line 3 is along the strike of the basement block and shows the continuity of the basement (?) reflector. **B.** Line 5, *JOIDES Resolution*, is perpendicular to the trend of the faulted basin and shows bounding basement blocks and truncated sediments.

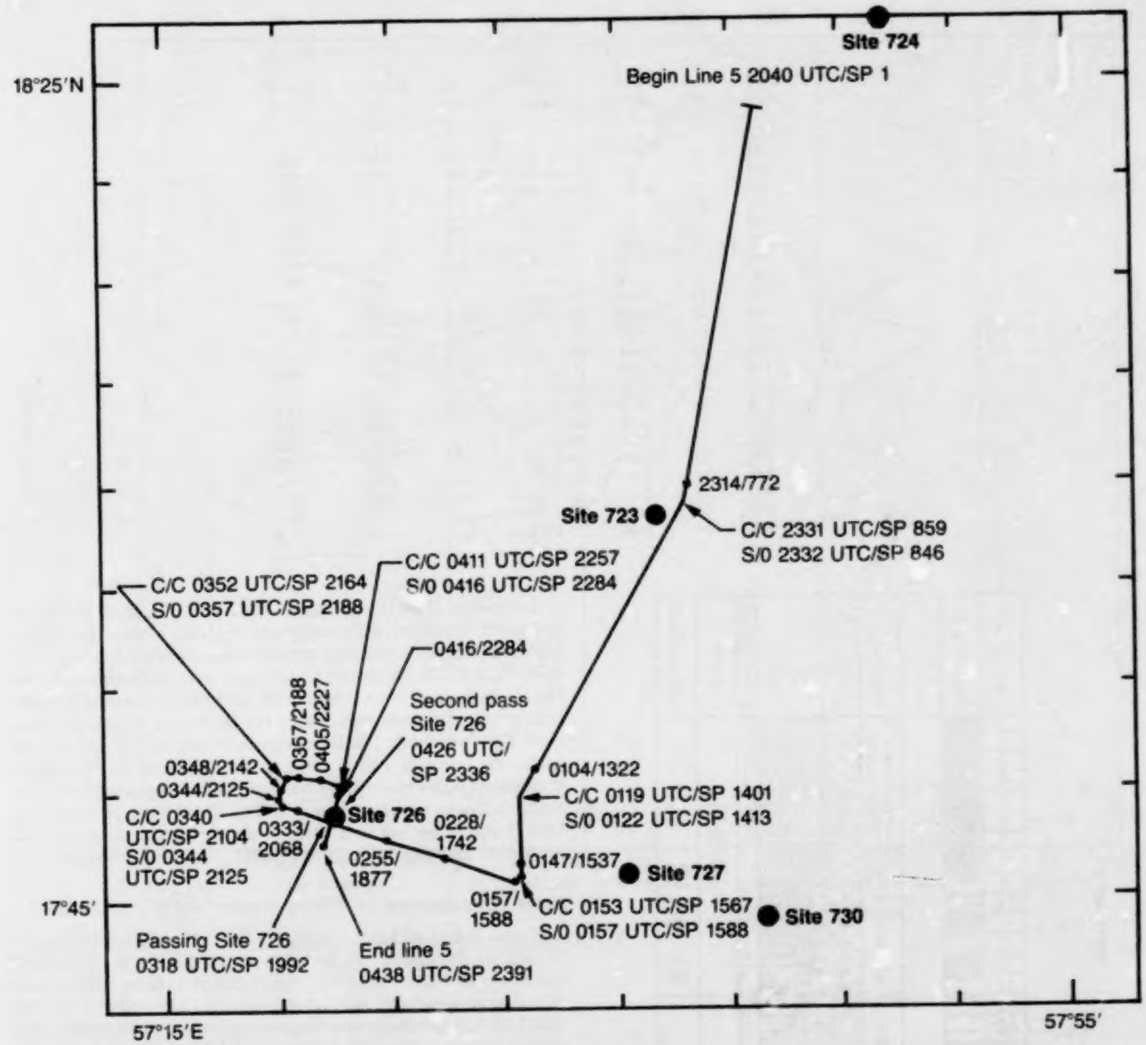
Site 724
Begin Line 5 2040 UTC/SP 1
18°25′N
2314/772
Site 723
C/C 2331 UTC/SP 859
S/0 2332 UTC/SP 846
C/C 0411 UTC/SP 2257
S/0 0416 UTC/SP 2284
C/C 0352 UTC/SP 2164
S/0 0357 UTC/SP 2188
0416/2284
0357/2188
0405/2227
Second pass
Site 726
0426 UTC/
SP 2336
0348/2142
0344/2125
0104/1322
C/C 0119 UTC/SP 1401
S/0 0122 UTC/SP 1413
C/C 0340
UTC/SP 2104
S/0 0344
UTC/SP 2125
0333/
2068
Site 726
0228/
1742
0255/
1877
0147/1537
Site 727
17°45′
0157/
1588
C/C 0153 UTC/SP 1567
S/0 0157 UTC/SP 1588
Site 730
Passing Site 726
0318 UTC/SP 1992
End line 5
0438 UTC/SP 2391
57°15′E
57°55′

Figure 4. Ship's track line during relocation from Site 725 and seismic survey of Site 726.

thought to represent lag deposits, as explained below. Colors range from olive (5Y 4/3 to 4/4) to dark olive gray (5Y3/2) to very dark gray (5Y 3/1) for the silty clays and marly oozes, and from olive (5Y 4/3 to 4/4) to olive gray (5Y 4/2) for the foraminifer-rich layers. Subunit IB displays little to no bioturbation, and laminations are preserved in 1- to 2-m-thick beds in Cores 117-726A-5H to 117-726A-9X (41.3–77.5 mbsf). This interval has a higher clay content (35% to 65%) and a higher content of organic carbon (3% to 4.8%) than the other parts of Subunit IB. The discrete laminated beds are composed of individual laminae 1 to 5 cm thick. Only in Core 117-726A-9X do the laminae contain relatively high amounts of diatoms (up to 25%, 76.2–77.5 mbsf, Fig. 6). Black phosphatic concretions having a diameter of 0.5 to 1.5 cm occur throughout Subunit IB (Fig. 8).

The nonlaminated part of Subunit IB consists of locally dolomitic, foraminifer-bearing marly nannofossil ooze to mud, with an average inorganic calcite content of 15% (Fig. 6). A coarse-grained part of the nonlaminated portion is developed as lag deposits, which are composed of foraminifer-rich muds and nannofossil-foraminifer oozes and which are interbedded with the more organic-rich lithologies of Subunit IB. These are found in two intervals, from Cores 117-726A-4H to 117-726A-6H (32.2–50.9 mbsf) and from Cores 117-726A-8X to 117-726A-14X (65.1–131.1 mbsf). Thus, they overlap with the upper and the lower portions of the laminated zone (Fig. 5). The lag layers are slightly to inversely graded, 3 to 30 cm thick, and have their maximum grain size at the base or in the middle of the beds (Figs. 9 through 11). These layers often show bioturbation mottling with distinctive infill patterns of foraminifer-rich muds into the underlying, nonbioturbated to sparsely bioturbated facies of Subunit IB (Figs. 9 and 10). In the interval from Cores 117-726A-11X to 117-726A-14X (92.4–131.1 mbsf), they form composite lag beds, which become more abundant downhole. Compositionally, lag deposits concentrate phosphorite concretions having a diameter of 1 mm to 0.5 cm, fish bones and fish teeth, and many foraminifer tests with phosphatic incrustations. Be-

Table 1. Coring summary for Site 726.

Core no.	Date (Sept. 1987)	Time (UTC)	Depth (mbsf)	Cored (m)	Recovered (m)	Recovery (%)
117-726A-						
1H	23	1230	0–6.9	6.9	6.90	100.0
2H	23	1250	6.9–16.3	9.4	9.92	105.0
3H	23	1310	16.3–25.8	9.5	9.93	104.0
4H	23	1325	25.8–35.3	9.5	9.61	101.0
5H	23	1430	35.3–44.7	9.4	9.93	105.0
6H	23	1455	44.7–54.1	9.4	0.05	106.0
7X	23	1535	54.1–63.6	9.5	7.91	83.2
8X	23	1550	63.6–73.2	9.6	9.44	98.3
9X	23	1605	73.2–82.8	9.6	5.22	54.4
10X	23	1620	82.8–92.4	9.6	7.23	75.3
11X	23	1635	92.4–102.1	9.7	7.04	72.6
12X	23	1645	102.1–111.8	9.7	0.24	2.5
13X	23	1700	111.8–121.4	9.6	8.67	90.3
14X	23	1730	121.4–131.1	9.7	2.72	28.0
15X	23	1800	131.1–140.7	9.6	1.09	11.3
16X	23	1850	140.7–148.1	7.4	0.59	8.0
17X	23	1950	148.1–154.1	6.0	0.35	5.8
18X	23	2045	154.1–164.1	10.0	0.20	2.0
19X	23	2150	164.1–173.7	9.6	1.79	18.6
20X	23	2330	173.7–183.4	9.7	1.08	11.1
21X	24	0120	183.4–183.8	0.4	0.12	30.0
22X	24	0830	183.8–186.3	2.5	0.18	7.2

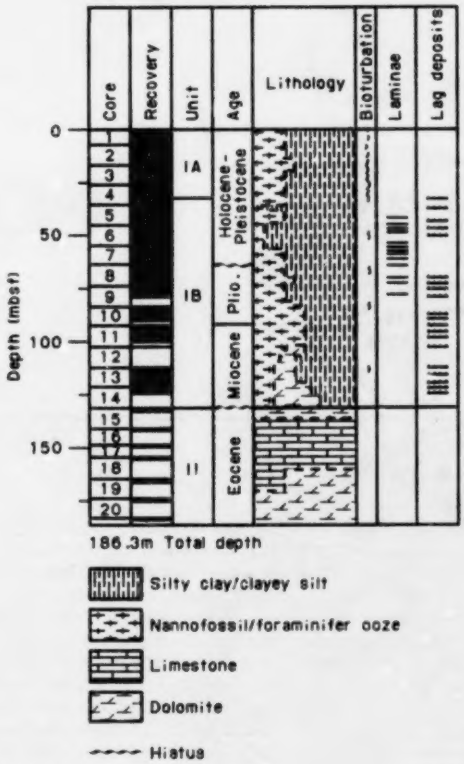

Figure 5. Lithostratigraphy of Site 726.

low Core 117-726A-11X, the lag layers are more and more affected by dolomitization (Fig. 5).

Unit II (Depth: 131.1–186.3 mbsf; Age: Eocene [?])

Core 117-726-15X to Section 117-726A-22X, CC.

Lithologic Unit II is composed of a partly dolomitized shallow-water limestone with carbonate contents higher than 95%. Although recovery was low throughout lithologic Unit II, two primary and one diagenetic facies types were distinguished. The former includes a large foraminifer- and algae-dominated facies with primary components, while the latter is a dolomitized facies. The foraminifer facies is characteristic of the top of the carbonate complex and is progressively replaced by the algae-dominated facies toward the base of the recovered section. The dolomite facies occurs in a zone at the transition from Unit I to Unit II and in the last four cores of the carbonate sequence. Cementation and dolomitization generally increase downhole.

Facies IIA (Foraminifer-Bearing Wackestone to Packstone)

Facies IIA (Fig. 12) is a white, indistinctly bedded, foraminifer-bearing wackestone to packstone containing centimeter-sized specimens of *Nummulites* cf. *planulatus* and *Actinocyclina* (see "Biostratigraphy" section, this chapter). The matrix of this weakly lithified rock is micritic, with cementation concentrated at the grain contacts in the form of a meniscuslike cement, which is a possible indicator of cementation in the vadose zone (e.g., Bathurst, 1975). The interparticle porosity in the foraminifer-bearing wackestone is high (see "Physical Properties" section, this chapter).

Facies IIB (Algae-Dominated Wackestone)

Facies IIB displays 1- to 4-cm-thick, irregularly shaped, calcitic spheres of oncolithic algae (Figs. 13 and 14) and 1-cm-thick branches of coralline algae (Fig. 15). A portion of the coralline algae is concentrated in beds up to 5 cm thick and was observed in nongrowth positions. Both characteristics indicate reworking and transport of the bioclasts by currents.

Facies IIC (Biomoldic Dolomite)

Dolomitized equivalents of Facies IIA and IIB are found at the top and the base of the recovered carbonate sequence. The dolomites are light gray (2.5Y 7/2) to gray (2.5Y 6/0), contain silt-sized rhombs, and show abundant biomoldic casts of the foraminifer and other fossils found in Facies IIA and IIB. Ex-

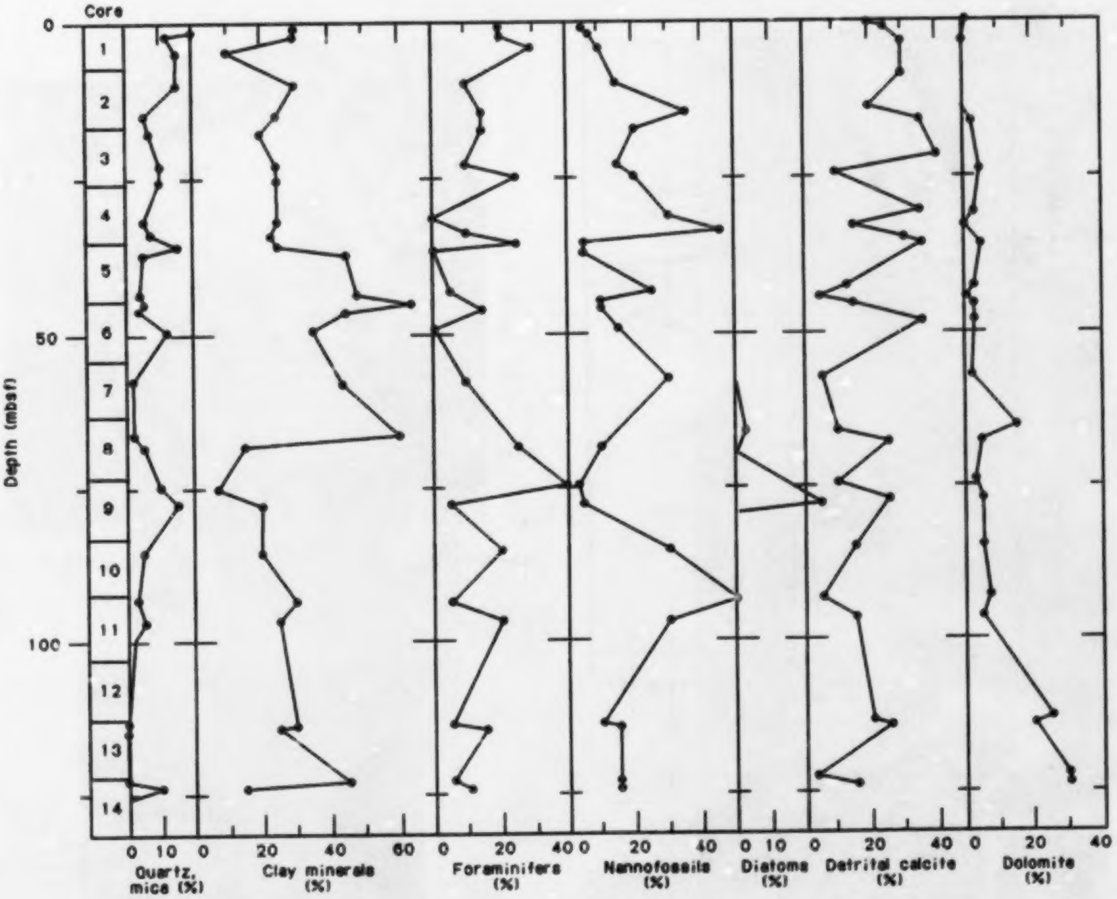

Figure 6. Smear-slide composition (in areal percentage) of lithologic Unit I.

cept for an occurrence at the contact with lithologic Unit I, dolomitization increases downhole. Based on thin sections from rocks in Cores 117-726A-16X to 117-726A-22X, the following preliminary stages of progressive diagenesis can be established:

1. Meniscuslike, micritic calcite cements the contacts of larger grains, while micritic calcite cementation affects the rock matrix (Core 117-726A-16X, 141 mbsf; Figs. 12 and 13).
2. Dolomitization of the rock matrix destroys most of its fabric, while larger fossils are not affected and remain calcitic (e.g., Core 117-726A-19X, 164 mbsf; Fig. 15).
3. Dissolution of calcitic allochems, such as large foraminifers, algae, etc., creates a biomoldic porosity (Fig. 16). On the surface of these molds, drusy dolomite crystals may grow to form a dolomitic spar in a relatively late stage of diagenesis. Locally, a final calcite spar follows the dolomitic spar.

The general downhole increase in diagenesis and lithification within lithologic Unit II results in a decrease in porosity downhole. Porosity decreases from about 40% in the upper part of Unit II to nearly zero in the lower part (see "Physical Properties" section, this chapter).

Discussion

Unit II

The foraminifer and algae facies indicate a warm, shallow-water environment. Diagenetic fabrics in the carbonate and lower dolomite complex document increasing lithification with depth, which begins with a grain-contact cementation in the upper part and proceeds to dolomitization in the lower portion of the sequence at Site 726. This pattern could be interpreted as a "frozen" diagenetic zonation, which still displays the diagenetic pattern achieved during or immediately after deposition of the upper part of Unit II. For instance, a diagenetic zonation similar to that described here is expected from several diagenetic models, including a groundwater-seawater mixing zone established after tectonic uplift. However, the question remains as to why these limestones were not fully cemented later. The unconformity between lithologic Units I and II could indicate a long phase of uplift and erosion, and contact with meteoric pore waters would cement the limestone within a short period of time. Without a better understanding of the local tectonic history, however, we cannot hope to answer this question.

Dolomitic zones found above, and especially below, the unconformity, as well as the relatively early onset of lithification

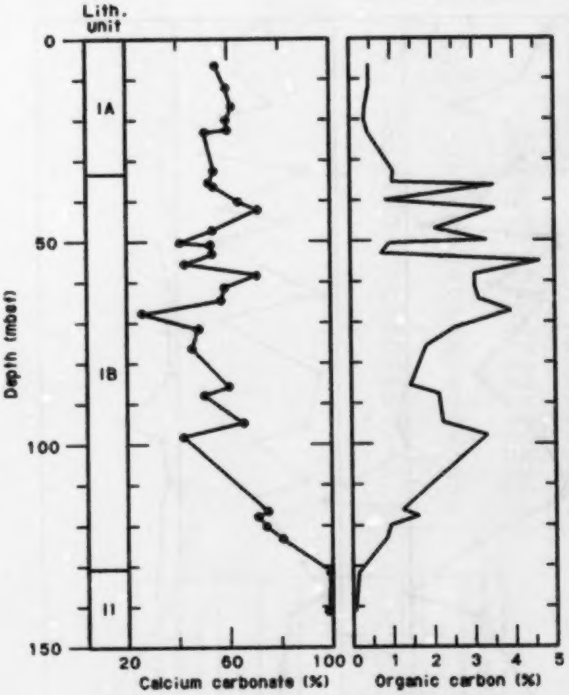

Figure 7. Carbonate and organic carbon contents at Site 726.

Table 2. Carbonate and organic carbon data from Site 726.

Core, section, interval (cm)	Depth (mbsf)	Total carbon (%)	Inorganic carbon (%)	Organic carbon (%)	$CaCO_3$ (%)
117-726A-					
1H-5, 52-54	6.52	7.32	6.78	0.54	56.5
2H-4, 60-62	12.00	7.84	7.30	0.54	60.8
2H-7, 60-62	16.50	7.99	7.56	0.43	63.0
3H-3, 50-52	19.80	7.75	7.29	0.46	60.7
3H-4, 145-150	22.25	7.88	7.32	0.56	61.0
3H-5, 50-52	22.80	6.82	6.30	0.52	52.5
4H-5, 50-52	32.30	7.83	6.73	1.10	56.1
4H-7, 30-32	35.10	7.60	6.46	1.14	53.8
5H-1, 80-82	36.10	10.38	6.72	3.66	56.0
5H-3, 130-132	39.60	8.80	7.88	0.92	65.6
5H-5, 52-54	41.82	12.50	8.81	3.69	73.4
6H-2, 50-52	46.70	8.78	6.68	2.10	55.6
6H-4, 50-52	49.70	8.49	5.09	3.40	42.4
6H-4, 119-120	50.39	7.63	6.59	1.04	54.9
6H-6, 50-52	52.70	7.50	6.65	0.85	55.4
7X-1, 98-100	55.08	10.11	5.32	4.79	44.3
7X-3, 100-102	58.10	11.85	8.72	3.13	72.6
7X-5, 100-102	61.10	10.40	7.21	3.19	60.1
8X-1, 52-54	64.12	10.30	7.03	3.27	58.6
8X-3, 52-54	67.12	7.33	3.25	4.08	27.1
8X-6, 27-29	71.37	8.67	6.05	2.62	50.4
9X-2, 117-119	75.87	7.69	5.75	1.94	47.9
9X-2, 119-120	75.89	7.51	5.60	1.91	46.7
10X-2, 127-129	85.57	9.03	7.45	1.58	62.1
10X-4, 31-33	87.61	8.56	6.27	2.29	52.2
11X-2, 60-62	94.50	10.44	8.09	2.35	67.4
11X-4, 100-102	97.90	8.65	5.20	3.45	43.3
13X-3, 130-132	116.10	10.54	9.24	1.30	77.0
13X-4, 119-120	117.49	10.43	8.73	1.70	72.7
13X-6, 66-68	119.96	10.23	9.18	1.05	76.5
14X-2, 5-7	122.95	10.86	9.93	0.93	82.7
15X-1, 58-60	131.68	12.41	12.17	0.24	101.4
16X, CC 22-24	141.13	12.26	12.07	0.19	100.5

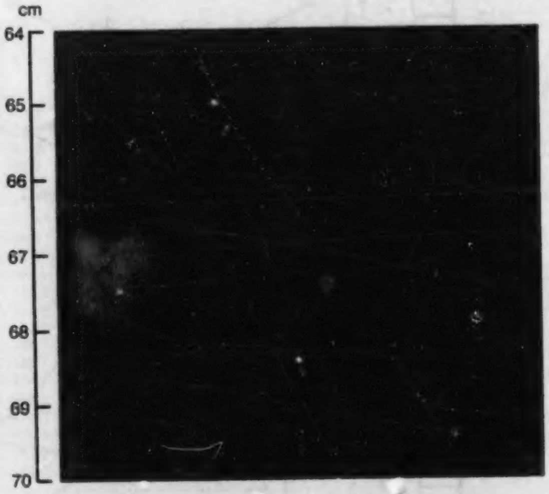

Figure 8. Large phosphorite concretions (1.5 cm), Subunit IB (Section 117-726A-6H-6, 64-70 cm).

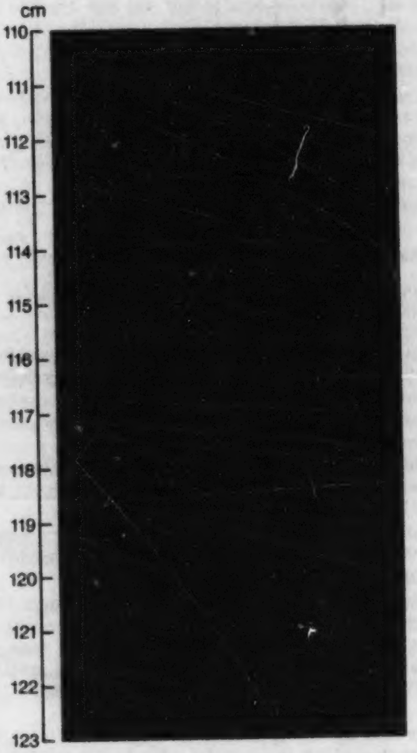

Figure 9. Bioturbated infill of foraminifer mud from an overlying lag deposit into sparsely to unbioturbated silty clay; Subunit B (Section 117-736A-5H-6, 110-123 cm).

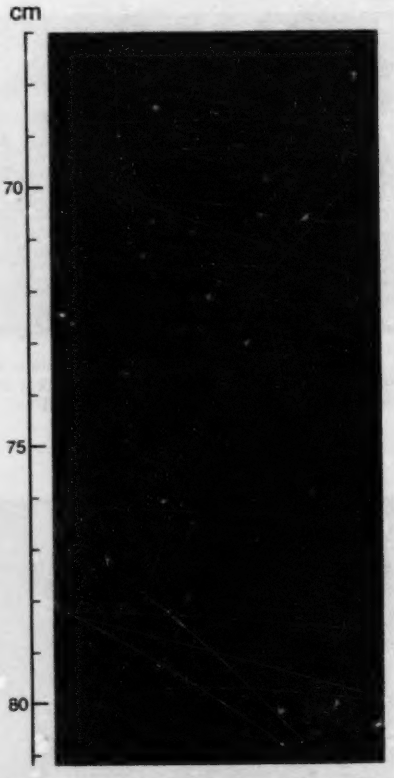

Figure 10. Foraminifer-rich lag deposit that exhibits a relatively coarse-grained, sharp base and that shows bioturbated infill into the underlying, sparsely bioturbated silty clay; Subunit IB (Section 117-726A-5H-1, 67–82 cm).

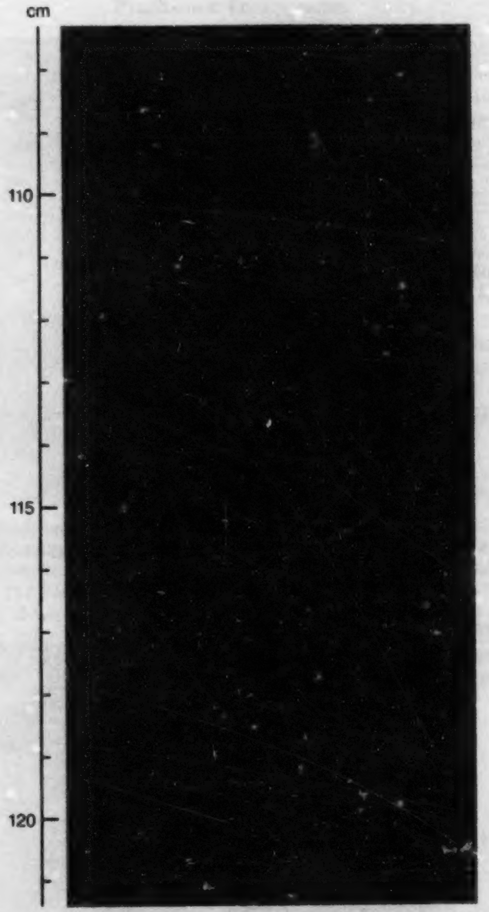

Figure 11. Lag deposit composed of foraminifer-rich mud having an inversely graded base; Subunit IB (Section 117-726A-13X-3, 107–121 cm).

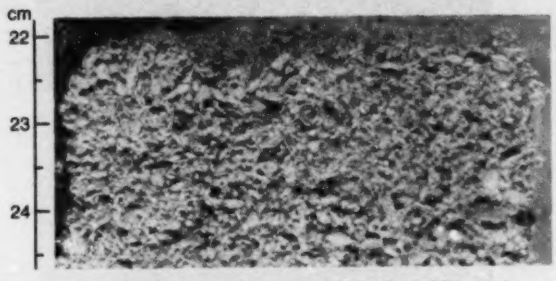

Figure 12. Nummulitic wackestone to packstone that exhibits grain contact cementation and high interparticle porosity; Unit II (Section 117-726A-16X, CC, 2–25 cm, Facies IIA).

(110 m in chalky layers of Unit I), may result from diagenetic effects of both the lateral movements of pore water in the porous carbonates and the high heat-flow values. Pore waters from lithologic Unit I show increasing chlorinity and sulfate values downhole, and a decreasing magnesium/calcium ratio (see "Inorganic Geochemistry" section, this chapter). In addition, heat-flow measurement gives a value that is three times higher than that at the other sites drilled at the Oman margin (see "*In-Situ* Pore-Water Sampling and Downhole Temperature and Heat-Flow Measurements" chapter, this volume).

The recovered Paleogene carbonates may correlate with similar, but more lithified, shallow-water limestones and dolomites found in Oman (Powers et al., 1966) and on the island of Masirah (Moseley and Abbotts, 1979). The uplift of the carbonate sequence at Site 726 occurred sometime between the Eocene and the late Miocene, as documented by the unconformity. It may be related to compressional movements along dextral, northeast-striking, strike-slip faults that took up differential movements between the Indian and the African-Arabian plates (Mosely and Abbotts, 1979; Whitmarsh, 1979).

Unit I

Three observations regarding the sediments of lithologic Unit I at Site 726 are briefly discussed as follows:

1. The increase of lag deposits downhole documents a high degree of reworking in the upper Miocene section. Reworking may indicate that Site 726 had a somewhat shallower water depth in the late Miocene than it does today. This may be explained by a combination of the effects of subsidence, sedimentation, and sea-level variation (Haq et al., 1987).

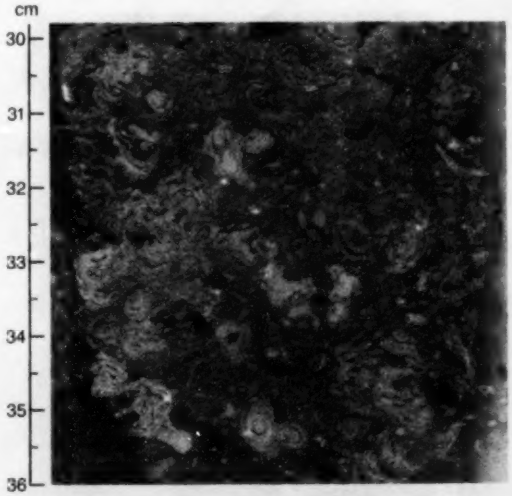

Figure 13. Incompletely cemented, highly porous, oncolithic limestone with cementation occurring at the grain contacts; Unit II (Section 117-726A-16X, CC, 30-36 cm, Facies IIA).

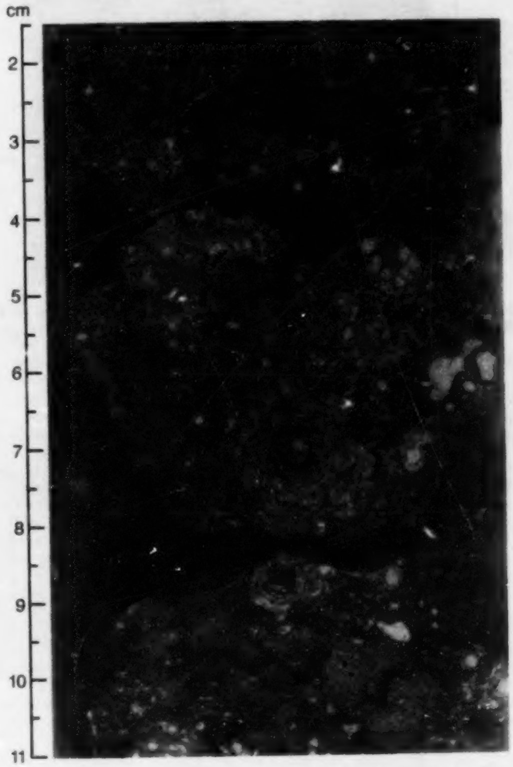

Figure 14. Calcareous dolomite showing calcitic, oncolithic algae embedded in a dolomitic matrix. Upper part shows shell layers; Unit II (Section 117-726A-19X-1, 1-11 cm, Facies IIB).

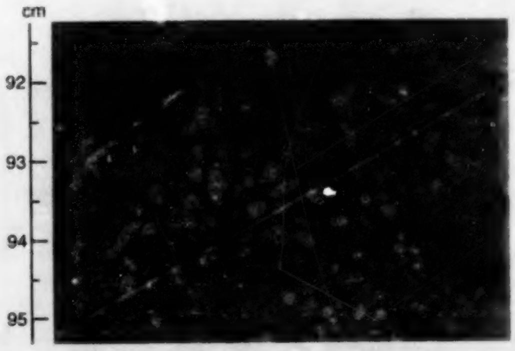

Figure 15. Calcareous, dolomitic wackestone that contains redeposited branches of red algae (calcitic). The matrix of the rock is dolomitized; Unit II (Section 117-726A-19X-1, 91-96 cm, Facies IIB).

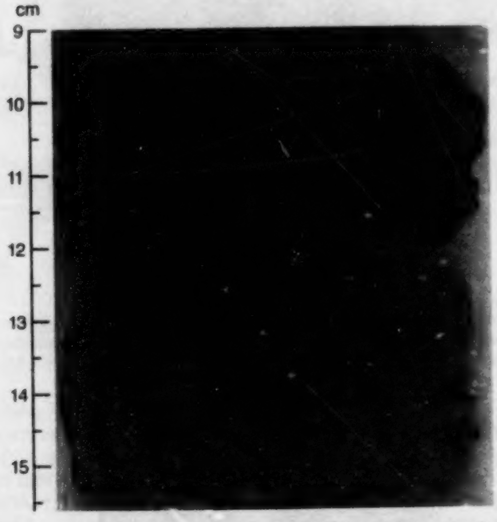

Figure 16. Biomoldic dolomite with molds of foraminifers that locally display a rim of calcite spar; Unit II (Section 117-726A-15X-1, 9-16 cm, Facies IIC).

2. The alternation between bioturbated lag deposits and nonbioturbated to sparsely bioturbated, organic-rich sediments may indicate repeated, drastic changes in the environment at Site 726. Explanations might include oscillations of the top of the oxygen-minimum zone, fluctuations in the intensity of oxygen depletion, sea-level variations, or the development of countercurrents in the upwelling system.

3. Laminated and sparsely bioturbated sediments that lack intercalated lag beds occur between Cores 117-726A-6H and 117-726A-8X (50.9-65.1 mbsf). These sediments, which include the Pleistocene/Pliocene boundary, may indicate a period characterized by a relatively stable and well-developed oxygen-minimum zone (see also Sites 723, 724, and 725 chapters).

BIOSTRATIGRAPHY

The recovered section at Site 726 ranges from Holocene to Eocene (?) in age. A pronounced hiatus separates the upper Miocene from the Eocene (?). The carbonate complex recovered at the bottom of the hole contains probable Eocene (?) species of the benthic foraminiferal genus *Nummulites* and the solely Eocene genus *Actinocyclina*. A plot of faunal datum levels and paleomagnetic reversals vs. depth below the seafloor is presented in Figure 17; for a detailed list of these data points, see Table 3.

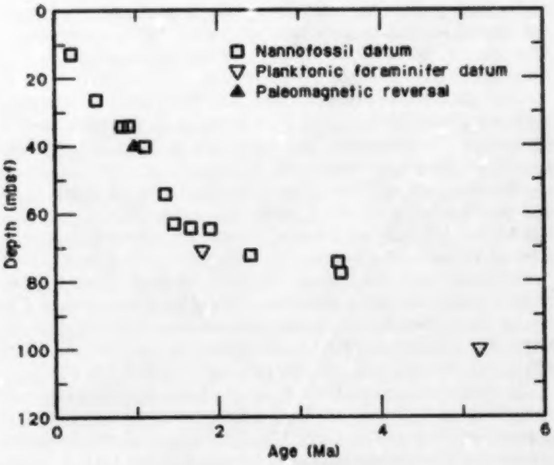

Figure 17. Age-depth plot for Hole 726A. For a detailed list of events, see Table 3.

Planktonic Foraminifers

Planktonic foraminifers were studied in core-catcher samples of Hole 726A. The upper part of the recovered section (Sections 117-726A-1H through 117-726A-7H, CC; 6.9–63.6 mbsf) consists of pelagic, calcitic, clayey silt and contains common to abundant planktonic foraminifers and highly diverse assemblages. The state of preservation is moderate to good. Below this level, foraminifers are sparse, and preservation of the tests is poor. No small foraminifers were found in the basal part of the section (Sections 117-726A-17X, CC through 117-726A-22X, CC; 154.1–186.3 mbsf), which is composed of shallow-water carbonates of Eocene age.

The upper part of the sequence was referred to Zones N22 and N23, which indicate a Pleistocene age. The lower limit of Zone N23 was found in Sample 117-726A-3H, CC (25.8 mbsf) because this sample contains *Globigerinella calida calida* specimens. The lower limit of Zone N22, which corresponds to the Pleistocene/Pliocene boundary, was placed between Samples 117-726A-7X, CC and 117-726A-8X, CC (63.6–73.2 mbsf) because the latter sample contains obvious Pliocene species, such as *Globoquadrina altispira* and *Globorotalia limbata*. Zones N19 and N20 could not be discriminated from Zone N21, as *Globorotalia tosaensis* is not present in the lower Pleistocene and upper Pliocene sediments. The lower boundary of Zones N19 and N20 was tentatively placed between Samples 117-726A-9X, CC and 117-726A-10X, CC (82.8–92.4 mbsf) because *Sphaeroidinella dehiscens immatura* specimens could not be found in the latter sample.

Below this level *Globorotalia tumida tumida* disappears, which justifies the referral to Zone N17. We made no attempt to

Table 3. Stratigraphic list of faunal events and paleomagnetic reversals for Hole 726A.

Event		Core level	Depth (mbsf)	Age (Ma)	Source of age	Notes
B	*Emiliania*	2H-3, 118–119	11.08	0.19	3	
	huxleyi	2H-5, 118–119	14.08			
T	*Pseudoemiliania*	3H, CC	25.08	0.49	3	
	lacunosa	4H-1, 118–119	26.98			
T	*Reticulofenestra*	4H-5, 118–119	32.98	0.82	3	
	sp. *A*	4H, CC	35.30			
B	*Gephyrocapsa*	4H-5, 118–119	32.98	•0.89	4	•North Atlantic data.
	parallela	4H, CC	35.30			
T	*Gephyrocapsa*	4H, CC	35.30	•1.10	4	•North Atlantic data.
	•"large"	5H, CC	44.70			••Long axis greater than 6 μm.
B	Jaramillo	5H-3, 45–47	38.75	0.98	6	
		5H-3, 115–117	39.45			
T	*Helicosphaera*	6H-5, 118–119	51.88			No good published age; event appears to be diachronous.
	sellii	6H, CC	54.10			
B	*Gephyrocapsa*	6H, CC	54.10	•1.36	4	•North Atlantic data.
	••"large"	7X-1, 118–119	55.28			•Long axis greater than 6 μm.
T	*Calcidiscus*	7X-5, 118–119	61.28	1.45	6	
	macintyrei	7X, CC	63.60			
B	*Gephyrocapsa*	7X, CC	63.60	•1.66	4,8	•North Atlantic age consistent with Italian-type section.
	caribbeanica	8X-1, 118–119	64.78			
T	*Discoaster*	7X, CC	63.60	1.9	6	
	brouweri	8X-1, 118–119	64.78			
T	*Globigerinoides*	8X-4, 65–67	68.75	•1.80	6	•*G. obliquus extremus* in Berggren et al., 1985.
	extremus	8X, CC	73.20			
T	*Discoaster*	8X-5, 103–104	70.63	2.4	6	
	pentaradiatus	8X, CC	73.20			
T	*Sphenolithus*	8X, CC	73.20	3.47	6	
	abies	9X-1, 118–119	74.38			
T	*Reticulofenestra*	9X-3, 92–93	77.12	3.5	6	
	pseudoumbilica	9X-4, 15–16	77.85			
B	*Globorotalia*	11X-4, 65–67	97.55	5.20	6	
	tumida tumida	11X, CC	102.10			

Note: T = upper limit and B = lower limit. Sources of age are 3 = oxygen isotope data for Site 723 (N. Niitsuma. unpubl. data); 4 = Takayama and Sato, 1987; 6 = Berggren et al., 1985; 8 = Sato et al., in press.

distinguish Zones N16 and N17 as only sparse specimens of upper Miocene *Globorotalia tumida* subspecies were found.

Benthic Foraminifers

Benthic foraminiferal fauna was studied at Site 726 in the core-catcher samples of Hole 726A. Core-catcher Samples 117-726A-15X, CC (140.7 mbsf) and 117-726A-19X, CC through 117-726A-21X, CC (173.7–183.8 mbsf) contain lithified limestone. Thus, studies of thin sections are required to determine the foraminiferal fauna at the species level.

Benthic foraminiferal fauna at this site varies considerably in its diversity, as well as in its state of preservation. Abundance is high throughout the sequence, except for the sample located just above the limestone (Sample 117-726A-14X, CC; 131.1 mbsf), which contains only a few benthic foraminifers. Preservation is good in the uppermost sample, but becomes moderate by Sample 117-726A-2H, CC (16.3 mbsf). This coincides with the appearance of phosphoritized teeth and vertebrae. The phosphorite becomes nodular in Sample 117-726A-7X, CC (63.6 mbsf). Preservation of benthic foraminiferal tests becomes poor in Sample 117-726A-11X, CC (102.1 mbsf), and the size fraction analyzed through Sample 117-726A-14X, CC (131.1 mbsf) is strongly dominated by crystalline carbonate fluorapatite, [$Ca_5F(PO_4)_3$]. A correlation exists between the state of preservation and the amount of phosphorite present. In samples with many phosphoritized teeth and vertebrae, the preservation deteriorates and the abundance decreases. Only occasionally are phosphoritized foraminifers found.

Three samples from within the limestone (117-726A-16X, CC through 117-726A-18X, CC; 148.1–164.1 mbsf) are semilithified; benthic foraminifers have been affected by calcitic recrystallization.

The planktonic/benthic (P/B) ratio at this site is highly variable; it decreases gradually from about 75% in Sample 117-726A-1H, CC (6.9 mbsf) to about 10% in Sample 117-726A-5H, CC (44.7 mbsf). The ratio increases to more than 75% in Samples 117-726A-6H, CC (54.1 mbsf) and 117-726A-7X, CC (63.6 mbsf); and finally decreases to a value below 10% in the remaining samples (below 63.6 mbsf).

Three different assemblages of benthic foraminifers can be recognized at Site 726. The first assemblage (I) is found in the upper part of the sequence (Samples 117-726A-1H, CC through 117-726A-7X, CC; 6.9–63.6 mbsf). Abundant species are *Bolivina ordinaria*, *Cancris* sp. A, *Cibicidoides wuellerstorfi*, *Hyalinea balthica*, and *Uvigerina peregrina*.

The second assemblage (II) found in Samples 117-726A-8X, CC through 117-726A-14X, CC (54.1–131.1 mbsf) yields high abundances of *Bolivina* sp. A., *Lenticulina calcer*, and *Lenticulina* sp. C, as well as some species found in assemblage I (*B. ordinaria* and *U. peregrina*).

The transition from assemblage I to assemblage II occurs somewhere within Core 117-726A-8X (63.6–73.2 mbsf) and coincides with a significant decrease in the P/B ratio (from about 90% planktonic foraminifers to less than 10%). Phosphoritized bones occur in most parts of the sequence, whereas phosphorite in nodular form occurs only in the basal part of benthic foraminiferal assemblage I. Crystalline carbonate fluorapatite occurs only in the basal part of benthic foraminiferal assemblage II, where the P/B ratio is low.

A third assemblage (III) is found in the limestone samples studied (Samples 117-726A-16X, CC through 117-726A-18X, CC; 148.1–164.1 mbsf). These yielded abundant specimens of *Nummulites* spp. Species recognized are *N.* cf. *planulatus* and *N.* cf. *pratti*, which are both Eocene. The presence of specimens of the genus *Actinocyclina* in a thin section from Sample 117-726A-16X, CC (148.1 mbsf) confirms this age because this genus only occurs during the Eocene.

Calcareous Nannofossils

Calcareous nannofossil floras from Hole 726A, which was the only hole drilled at this site, range from fairly abundant in the upper part to barren in the weakly cemented, partially dolomitized limestone below 140.7 mbsf.

Sediments from the mud line to 11.08 mbsf contain *Emiliania huxleyi* and can be correlated with Zone NN21 (Holocene to Pleistocene). Below Zone NN21, sediments from 11.08 to 25.8 mbsf are placed in Zone NN20 (Pleistocene) because both *E. huxleyi* and *Pseudoemiliania lacunosa* are absent. Underlying sediments from 25.8 to 63.6 mbsf contain *P. lacunosa* and no discoasters, which places these sediments in Zone NN19 (Pleistocene to uppermost Pliocene).

The Pleistocene/Pliocene boundary is located between 63.60 and 64.78 mbsf (between Samples 117-726A-7X, CC and 117-726A-8X-1, 118–119 cm). *Discoaster brouweri* is the only representative of the genus in Samples 117-726A-8X-1, 118–119 cm, down to 117-726A-8X-5, 103–104 cm (64.78–70.63 mbsf). There appears to be a hiatus just below the Pleistocene/Pliocene boundary. The top of *Discoaster pentaradiatus*, which marks the boundary between Zones NN18 and NN17, occurs between Samples 117-726A-8X-5, 103–104 cm, and 117-726A-8X, CC (70.63–73.20 mbsf).

D. surculus is extremely rare in the hole, and the sediments ranging from 73.2 mbsf to 77.12 mbsf were tentatively placed in Zones NN17 to NN16 (Fig. 18). The top of *Reticulofenestra pseudoumbilica* occurs between Samples 117-726A-9X-3, 92–93 cm, and 117-726A-9X-4, 15–16 cm. (77.12–77.85 mbsf). This marks the NN16/NN15 zonal boundary.

The sediments from 77.85 mbsf down to 92.4 mbsf were placed in Zones NN15 to NN12, although age-diagnostic species, such as *Amaurolithus tricorniculatus* and *Ceratolithus rugosus* are absent. Underlying sediments from 92.4 to 102.1 mbsf are characterized by comparatively abundant and well-preserved discoasters, such as *D. Brouweri*, *D. pentaradiatus*, *D. variabilis*, *D. surculus*, *D. quinqueramus*, and *D. berggrenii*, and belong to Zone NN11. Sediments from 102.1 to 131.1 mbsf contain no age-diagnostic species. Based on the absence of *Discoaster quinqueramus*, however, these sediments were tentatively

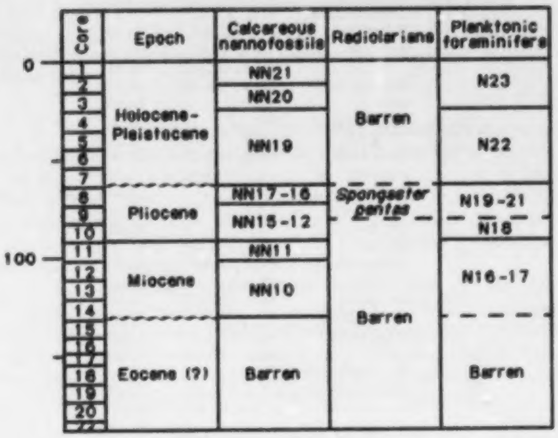

Figure 18. Correlation of planktonic microfossil zones in Hole 736A.

placed in Zone NN10. Calcareous nannofossils are completely absent in the remaining sedimentary sequence.

Radiolarians

Radiolarians are absent from most of the sedimentary sequence recovered at Site 726, except for the interval between Samples 117-726A-8X-2, 85-87 cm, and 117-726A-9X, CC (65.9-82.8 mbsf). In these sediments, there is a good, well-preserved radiolarian fauna belonging to the *Spongaster pentas* Zone, but species diversity is low. Sponge spicules and diatoms are also common in this interval.

Paleoenvironmental Implications

The Miocene and Pliocene sediments at this site are characterized by frequent lag deposits interbedded with hemipelagic sediments. The sedimentation rate is less than 15 m/m.y., and there is abundant phosphorite. We believe this indicates current winnowing. We suggest that during periods of low sea level, the fine-grained fraction of the sediment eroded away, concentrating the phosphorite initially into coarse-grained sediments and ultimately into nodular deposits (Baturin, 1971; Burnett, 1977). The very low P/B ratio is a further indication of shallow water. The sudden increase in the sedimentation rate (to about 45 m/m.y.) in the Pleistocene together with an increasing P/B ratio suggest a significant deepening of this site, either from eustatic sea-level changes, tectonic activity, or a significant change in climatic conditions. The major part of this subsidence took place during the uppermost Pliocene, but may have been initiated much earlier. The Eocene (?) limestone contains nummulitids and indicates that it was deposited in a shallow-water (less than 200 m) environment.

PALEOMAGNETISM

Site 726 is located at 17°49′N, 57°22′E in a water depth of 331 m on the Oman margin. Hole 726A was cored to 186.3 mbsf; the lithology consisted of nannofossil-rich calcitic clay to clayey silt (Unit I) and dolomitic limestone (Unit II).

Magnetic Measurements

Paleomagnetic measurements were conducted on discrete samples using the Minispin magnetometer and the Schonstedt alternating-field (AF) demagnetizer. Detailed research on the stability of the samples during AF demagnetization will be made during post-cruise studies. However, some step-wise AF demagnetizations were performed on specimens from Cores 117-726A-5H and 117-726A-7X and 117-726A-8X. Some of these (Figs. 19 through 21) show quite stable behavior with convex intensity demagnetization curves and median destructive fields up to about 15 mT.

Most of the specimens were AF demagnetized at a blanket AF field of 10 mT. Over the more weakly magnetized intervals of the section, we used a field of 5 mT. Figure 22 shows plots of declination, inclination, and intensity after AF demagnetization. Only specimens with circular standard deviation values of less than 40 are plotted. Over the interval 0 to 40 mbsf, the intensities are relatively uniform and average about 0.2 mA/m. Between about 40 and 70 mbsf, intensities fluctuate from about 0.1 to 5 mA/m, and between about 70 and 100 mbsf, they are more uniform and average about 0.2 mA/m. The sediments below about 100 mbsf were too weakly magnetized to measure. The arithmetic mean intensity is 0.7 mA/m.

Magnetostratigraphy

Although inclination values correspond well to the expected axial dipole values (Fig. 23), correlation of the paleomagnetic record at Site 726 with the polarity time scale is not straightforward. Ignoring isolated points, the section is normally magnetized down to about 39 mbsf, and then reversely magnetized to

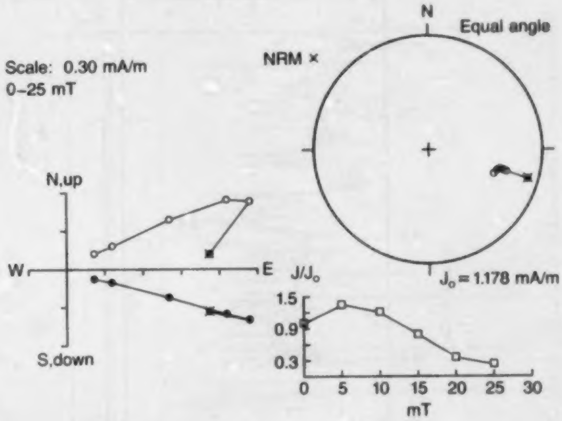

Figure 19. Results of step-wise AF demagnetization of discrete specimen from Hole 726A.

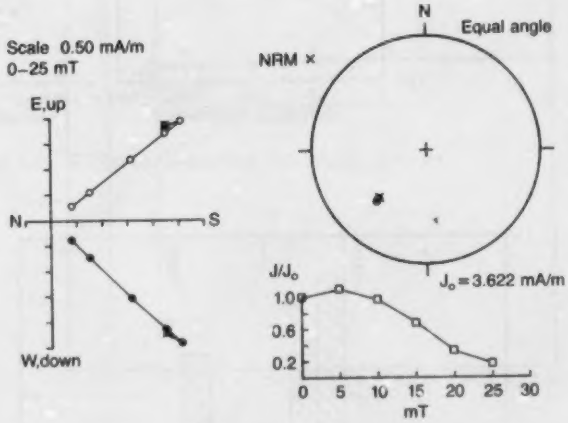

Figure 20. Results of step-wise AF demagnetization of discrete specimen from Hole 726A.

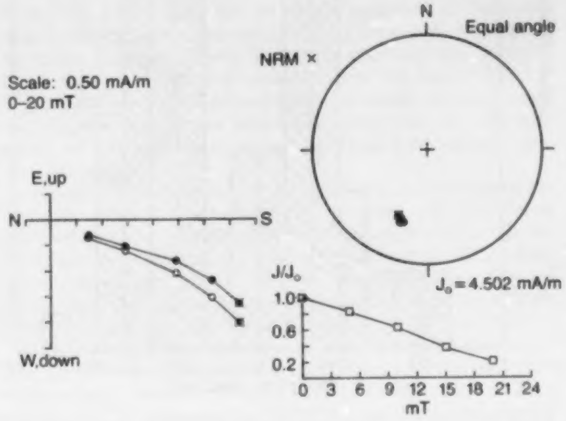

Figure 21. Results of step-wise AF demagnetization of discrete specimen from Hole 726A.

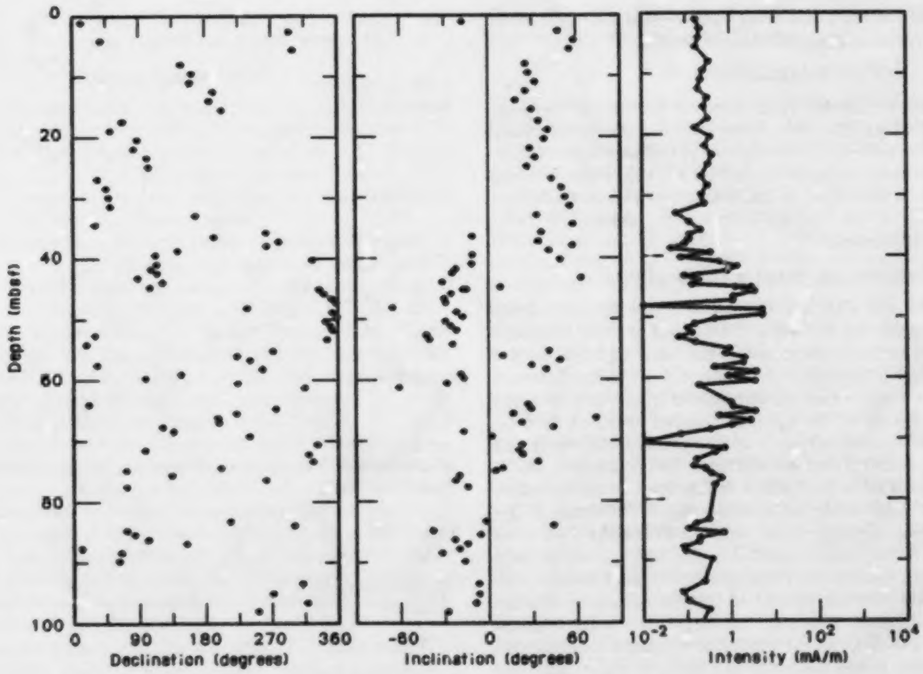

Figure 22. Declination, inclination, and intensity after AF demagnetization of discrete specimens from Hole 726A.

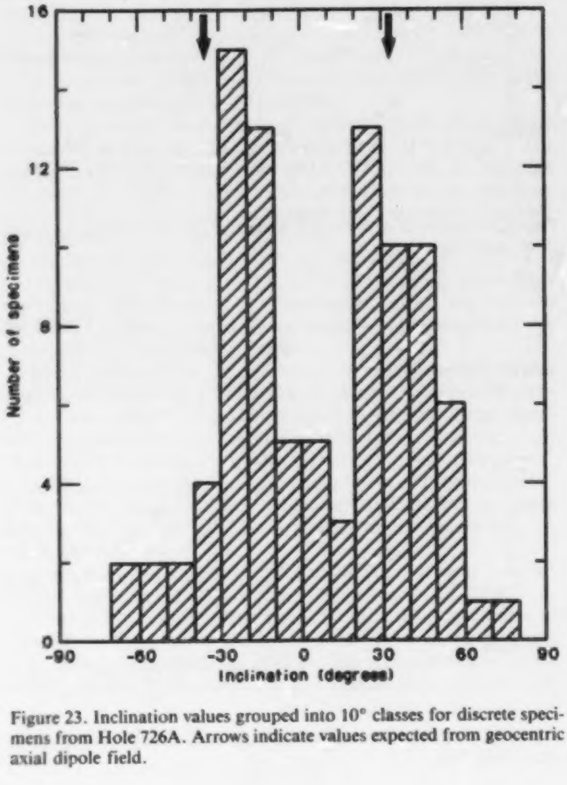

Figure 23. Inclination values grouped into 10° classes for discrete specimens from Hole 726A. Arrows indicate values expected from geocentric axial dipole field.

about 55 mbsf. A series of well-defined polarity transitions occurs between 55 and about 75 mbsf; between 75 and 100 mbsf, the section is reversely magnetized. The nannofossil stratigraphy (see "Biostratigraphy" section, this chapter) shows that the top of acme *Reticulofenestra* sp. A and the first appearance datum (FAD) of *Gephyrocapsa parallela* occur within Core 117-726A-4H (25.8–35.3 mbsf). Although both of these datums significantly predate the Chron C1/C1r (Brunhes/Matuyama Chronozone) boundary (Takayama and Sato, 1987), we find no suggestion of a polarity transition above the base of Core 117-726A-4H. Therefore, we tentatively assigned the transition at 39 mbsf (between intervals 117-726A-5H-3, 45 cm, and 117-726A-5H-3, 115 cm) to the bottom of Subchron C1r-1 (Jaramillo Subchronozone).

The FAD of *Gephyrocapsa oceanica* and the last appearance datum (LAD) of *Discoaster brouweri*, respectively, approximate to the upper and lower boundaries of Chron C2 (Olduvai Subchronozone; Takayama and Sato, 1987). These datums occur within Core 117-726A-8X (63.6–73.2 mbsf) and do coincide roughly with the upper and lower boundaries of a normally magnetized interval. However, interpretation of the normally magnetized interval between about 55 and 60 mbsf then becomes difficult because the only well-documented potential subchron corresponding approximately to this time interval is the Cobb Mountain Subchronozone, which may have lasted for only about 0.02 m.y. (Clement and Robinson, 1987). For this reason, we are reluctant to correlate any of the normally magnetized intervals within this part of the section with the polarity time scale. Nannofossil Zones NN18 to NN11 were placed within Cores 117-726A-8X to 117-726A-11X (63.6–102.1 mbsf). Therefore, the reversely magnetized interval below about 75 mbsf corresponds in time to several normal and reversed chrons, and for this reason we were reluctant to correlate it with the reversal time scale.

The only available evidence that might explain the anomalous paleomagnetic record below about 50 mbsf is the suggestion of increased influence of current-controlled deposition, in the form of several lag deposits, which begin in Core 117-726-4H (see "Lithostratigraphy" section, this chapter). Although we avoided obvious lag deposits during sampling, an overall coarsening of the terrigenous (and magnetic) fraction as a result of winnowing could be one explanation for failure of the sediments to preserve an interpretable paleomagnetic record over this interval. However, this does not agree with the stable behavior of several specimens from this interval during AF demagnetization.

Magnetic Susceptibility

The volume magnetic susceptibility of Hole 726A sediments was measured using Bartington Instruments whole-core sensor at the 0.1 sensitivity and low-frequency (0.47 kHz) settings. Hole 726A was cored in the APC mode to Core 117-726A-6H (54.1 mbsf); drilling then continued in XCB mode to Core 117-726A-22X (186.3 mbsf).

Two lithologic units were encountered. Lithologic Subunit IA, a marly nannofossil ooze, extends from the surface to ~32 mbsf and is characterized by low susceptibility values (40 to 90 × 10^{-6} volume SI units), compared to the other Oman margin sites (Fig. 24). Lithologic Subunit IB (32–131.1 mbsf) contains alternating layers of organic-rich silty clay and foraminiferal sand. The susceptibility values of Unit IB are slightly lower than those of Unit IA. Toward the base of Unit IB, susceptibility values are consistently negative (−15 × 10^{-6} volume SI units) and natural remanent magnetization (NRM) intensities approach the noise level of the instrument, indicating the virtual disappearance of ferrimagnetic particles and the predominance of diamagnetic components. We are uncertain whether this condition is of depositional or diagenetic origin. However, the chemical data for this hole do not reveal any clear gradients at this level. Smear slide and carbonate analyses over the 110 to 120 mbsf interval indicate increasing percentages of biogenic carbonate and euhedral dolomite, which suggests that these components may be the cause of the diamagnetism (see "Lithostratigraphy" and "Inorganic Geochemistry" sections, this chapter). The calculated volume magnetic susceptibility of a sample of pure calcite (or dolomite) is ~13 × 10^{-6} volume SI units. Lithologic Unit II, which consists of dolomitic limestone, was observed from ~130 mbsf to the base of Hole 726A. Carbonate analyses on these sediments often exceeded 100% because of the effect of dolomite. Although recovery of lithologic Unit II was poor, the measured susceptibilities were commonly negative, which presumably also reflects the diamagnetism of calcium carbonate and dolomite.

Detailed correlations between Hole 726A and other Oman margin sites were difficult to establish. The nannofossil biozonations of Hole 726A indicate that the Brunhes/Matuyama Chronozone boundary should be positioned at about 30 mbsf (see "Biostratigraphy" section, this chapter). Using this tentative chronostratigraphic datum, Hole 726A data may be compared with the well-defined Brunhes Chronozone susceptibility data from Hole 723B (Fig. 25). Although gross similarities of the two profiles are apparent, detailed correlations between sites are generally not possible. No obvious correlations of Hole 726A with other Oman margin sites were apparent below the Brunhes Chronozone.

ACCUMULATION RATES

At Site 726, magnetostratigraphic and biostratigraphic data were used to determine sedimentation rates for the top 100 m of sediment (most of lithologic Unit I). Rates over the last 3.5 m.y. were calculated between nannofossil datums where ages were determined from oxygen-isotope stratigraphy (Niitsuma, unpubl. data; Berggren et al., 1985; Table 3). For the last 1.45 m.y., the mean rate varied between 24 and 66 m/m.y., with an average of 45 m/m.y. These rates are the lowest measured in the upper slope basin and are similar to those found in pelagic deposits on the Owen Ridge (see Owen Ridge site chapters, this volume). The higher mean sedimentation rate near the top of Site 726 (Fig. 26) corresponds to the sediments containing abundant small shell fragments and more foraminifer shells than in older sediments of lithologic Subunit IA (see "Lithostratigraphy" section, this chapter).

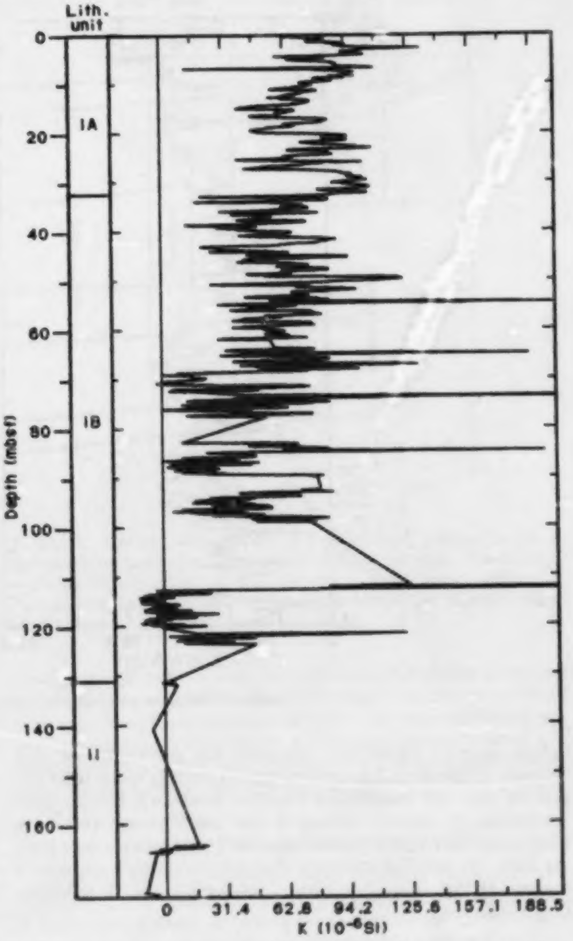

Figure 24. Whole-core, magnetic-susceptibility stratigraphy for Hole 726A.

A hiatus, which represents about 450,000 yr of missing sediment accumulation, is located near 63 mbsf (Fig. 26). Below this level, sediments are characterized by coarse-grained lag deposits interbedded with organic-carbon-rich, nannofossil-foraminifer oozes. In accordance with periods of nondeposition and winnowing, the average sedimentation rate is a factor-of-three lower than rates in more recent deposits (15 vs. 45 m/m.y.).

The mass accumulation of calcium carbonate, organic carbon, and noncarbonate sediment components is calculated from average values between the nannoplankton datum levels (Table 4; Fig. 27). The accumulation of calcium carbonate and noncar-

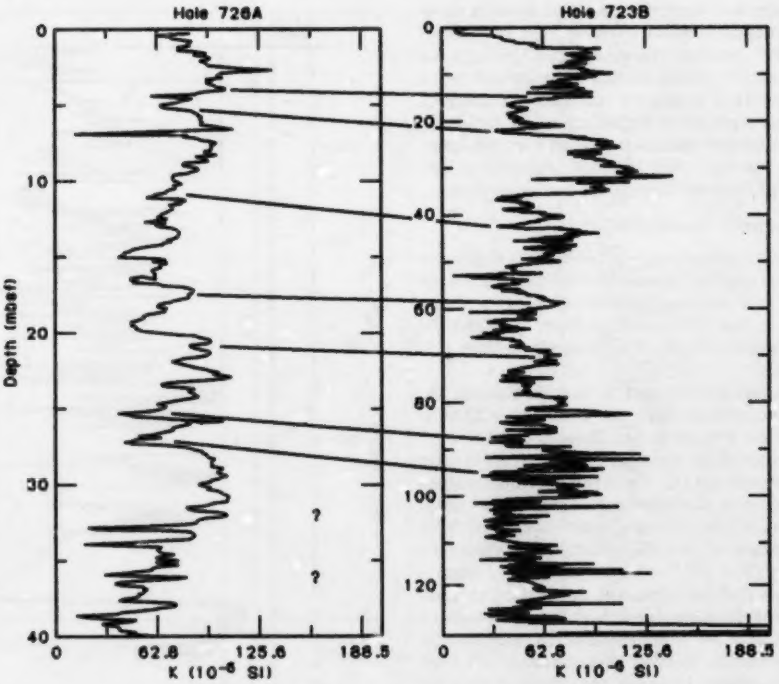

Figure 25. Possible correlation of magnetic susceptibility features between Holes 726A and 723B.

bonate increase upsection, following the sedimentation rate changes. Organic carbon concentrations and accumulations are greatest near the Pleistocene/Pliocene boundary. Similar concentrations of organic carbon in the late Pliocene and early Pleistocene have been observed at other Oman margin sites (i.e., see Sites 723 and 724 chapters, this volume), which suggests a regional change in organic carbon production and/or preservation at this time.

PHYSICAL PROPERTIES

Introduction

Physical-properties measurements at Site 726 included index properties (wet-bulk density, grain density, porosity, and water content), wet-bulk densities determined using the GRAPE, and compressional-wave velocities determined with the *P*-wave logger (PWL). Measurements using the GRAPE and PWL systems were conducted on cores that were sufficiently coherent and at least 80 cm long. In additional, wet-bulk densities measured using GRAPE special 2-min counts were performed on discrete samples taken from the dolomite and limestone recovered from lithologic Unit II. Compressional-wave velocities were measured on discrete samples beginning at Core 117-726A-15X using the Hamilton Frame. Compressional-wave data were not collected in the cores preceding Core 117-726A-15X because the gas-induced expansion of the sediment resulted in a poor signal transmission. Vane shear strengths were not measured because the sediments were coarse-grained and sufficiently indurated to preclude using the Wykeham-Farrance vane shear device. The properties determined at Site 726 are listed in Table 5. All techniques and equipment used are described in the "Explanatory Notes" (this volume).

Index Properties

Lithologic Unit I

Lithologic Unit I (0–131.1 mbsf) is divided into two subunits that differ in bulk density, porosity, water content, and grain density. Subunit IA (0–32.1 mbsf) is a calcareous silty clay to marly calcareous ooze that displays nearly constant index properties (Fig. 28). In Subunit IA, porosity averages 53%, water content averages 30%, wet-bulk density averages 1.84 g/cm^3, and grain density averages 2.67 g/cm^3.

Subunit IB (32.1–131.1 mbsf) is an organic-rich silty clay and marly nannofossil ooze/chalk, with occasional diatomaceous horizons. The boundary between Subunits IA and IB is marked by an increase in porosity and water content and a decrease in bulk and grain densities (Fig. 28). From the boundary to 36 mbsf, porosity increases from 53% to 63%, water content increases from 30% to 41%, wet-bulk density decreases from 1.84 to 1.61 g/cm^3, and grain density decreases from 2.68 to 2.46 g/cm^3. These changes in index properties most likely result from an increase in organic carbon from 1.1% to 3.6% (see "Lithostratigraphy" section, this chapter). The amount of organic carbon remains high to a depth of 70 mbsf. As a result, porosity and water content are high and bulk and grain densities are low to this depth. Abundant diatoms in the interval 60 to 70 mbsf contribute to the high porosity and low densities.

The interval from 70 to 100 mbsf displays trends of decreasing porosity (65%–58%) and water content (41%–34%) and increasing wet-bulk density (1.62 to 1.76 g/cm^3) and grain density (2.56 to 2.70 g/cm^3). From 70 to 85 mbsf, these trends probably result from the decrease in organic carbon (2.62% to 1.5%; see "Lithostratigraphy" section, this chapter). However, the interval from 85 to 100 mbsf shows an increase in organic carbon

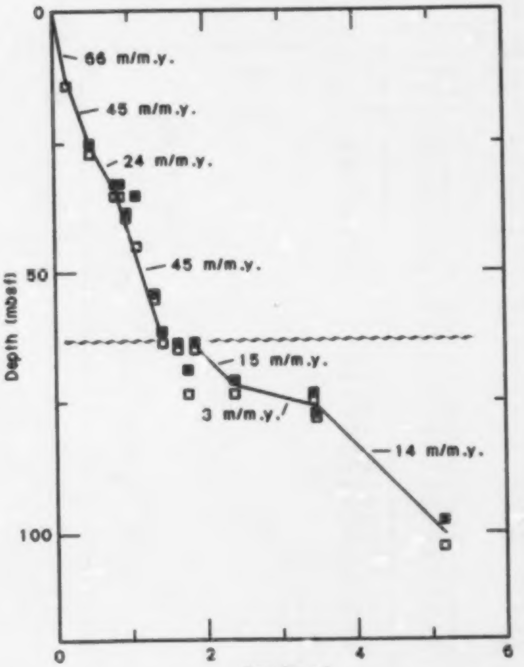

Figure 26. Age-depth plot of stratigraphic datums listed in Table 3. The filled and open boxes represent the upper and lower depths of each datum level, respectively. Indicated sedimentation rates are calculated between reliable nannofossil and foraminifer datum levels.

(1.58% to 3.45%), which suggests that organic carbon content has a diminishing control over physical properties. Porosity and water content decrease and wet-bulk and grain densities increase, between 115 mbsf and the bottom of Unit I (131 mbsf) in response to the increase in dolomite below Core 117-726A-12X.

Lithologic Unit II

Unit II (131.1–186.3 mbsf) consists of dolomite and limestone. Wet-bulk densities, from the GRAPE special 2-min counts, steadily increase from 1.98 to 2.75 g/cm^3 as a result of the downsection increase in cementation and dolomitization (see "Lithostratigraphy" section, this chapter).

Compressional-Wave Velocities

Compressional-wave velocities were determined on the limestone and dolomite samples recovered from lithologic Unit II.

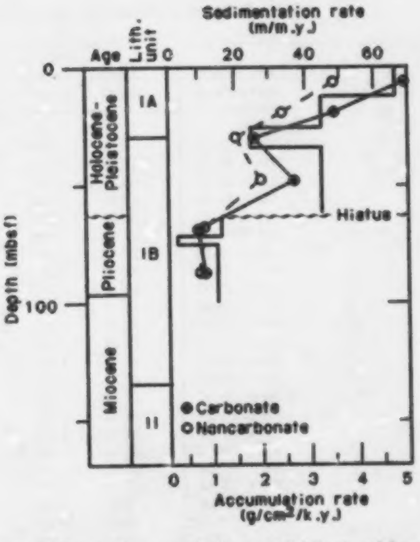

Figure 27. Sedimentation rate (m/m.y.; solid line), calcium carbonate accumulation rate (g/cm^2/k.y.; closed circles), and noncarbonate accumulation rates (g/cm^2/k.y.; open circles) vs. depth (mbsf) at Site 726. Accumulation rates are plotted at the midpoint of the respective depth intervals.

Measurements parallel and perpendicular to bedding show that these samples are anisotropic with respect to the direction of propagation of the compressional wave. Velocities measured parallel to bedding are consistently higher than those measured perpendicular to bedding; 4245 to 6134 m/s and 4194 to 5889 m/s, respectively (Table 5). Velocity anisotropies range from 1.2% to 7.1%.

GRAPE and *P*-Wave Logs

GRAPE wet-bulk densities were obtained for Cores 117-726A-1H to 117-726A-14X, which corresponds to lithologic Unit I. The primary factor affecting the quality of the GRAPE data is the degree of core disturbance that resulted from sediment expansion. Quality of data is good to a depth of 80 mbsf and clearly shows the transition between the two subunits in lithologic Unit I. In the first 50 mbsf interval, the data correlate well with the wet-bulk densities measured on the discrete samples (Fig. 29).

P-wave logs were obtained throughout lithologic Unit I (Cores 117-726A-1H through 117-726A-14X; Fig. 30). Below this interval, there was insufficient contact between the sediment and the core liner to provide adequate signal transmission. Although the

Table 4. Sedimentation and accumulation rate data for Site 726.

Depth interval (mbsf)	Age range (m.y.)	$CaCO_3$ ($\bar{x}$ %)	C_{org} ($\bar{x}$ %)	Dry-bulk density ($\bar{x}$ g/cm$_3$)	Sed. rate ($\bar{x}$ m/m.y.)	$CaCO_3$ acc. rate (g/cm^2/k.y.)	Non-$CaCO_3$ acc. rate (g/cm^2/k.y.)	C_{org} acc. rate (mg/cm^2/k.y.)
0–12.6	0–0.19	58.7	0.54	1.261	66.3	4.91	3.45	45.1
12.6–26.0	0.19–0.49	59.3	0.49	1.305	44.7	3.46	2.37	28.6
26.0–34.1	0.49–0.82	56.1	1.1	1.305	24.5	1.79	1.40	35.2
34.1–62.4	0.82–1.45	57.6	2.54	1.012	44.9	2.62	1.93	115.4
64.2–71.9	1.90–2.40	45.4	3.32	0.889	15.4	0.62	0.75	45.5
71.9–75.0	2.40–3.48	ND	ND	ND	2.9	ND	ND	ND
75.0–99.8	3.48–5.20	53.3	2.25	1.002	14.4	0.77	0.67	32.5

Note: ND = no data from interval.

Table 5. Physical properties summary for Hole 726A.

Core, section, interval (cm)	Depth (mbsf)	Wet-bulk density (g/cm^3)	Porosity (%)	Water content (%)	Grain density (g/cm^3)	Dry-bulk density (g/cm^3)	Velocity (m/s)	
117-726A-								
1H-5, 52-54	6.52	1 849	50.5	28.0	2.639	1.332		
2H-4, 60-62	12.00	1.776	57.1	33.0	2.683	1.190		
2H-7, 60-62	16.50	1.847	52.4	29.0	2.672	1.311		
3H-3, 50-52	19.80	1.760	57.9	33.7	2.625	1.166		
3H-5, 50-52	22.80	1.879	50.7	27.7	2.647	1.359		
3H-7, 50-52	25.80	1.906	51.2	27.5	2.750	1.382		
4H-3, 50-52	29.30	1.841	51.0	28.4	2.624	1.319		
4H-5, 50-52	32.30	1.841	53.0	29.5	2.679	1.297		
4H-7, 30-32	35.10	1.733	58.7	34.7	2.717	1.131		
5H-1, 80-82	36.10	1.606	63.4	40.5	2.456	0.956		
5H-3, 130-132	39.60	1.601	63.9	40.9	2.573	0.946		
5H-5, 52-54	41.82	1.594	67.5	43.4	2.590	0.902		
6H-2, 50-52	46.70	1.681	59.9	36.5	2.555	1.068		
6H-4, 50-52	49.70	1.684	60.8	37.0	2.581	1.062		
6H-6, 50-52	52.70	1.743	58.4	34.3	2.643	1.145		
7X-1, 98-100	55.08	1.572	62.4	40.7	2.409	0.933		
7X-3, 100-102	58.10	1.592	65.5	42.2	2.580	0.921		
7X-5, 100-102	61.10	1.683	61.3	37.3	2.597	1.055		
8X-1, 52-54	64.12	1.469	73.5	51.3	2.485	0.716		
8X-3, 52-54	67.12	1.614	60.6	38.4	2.404	0.993		
8X-6, 27-29	71.37	1.623	65.0	41.0	2.560	0.957		
9X-2, 117-119	75.87	1.517	67.9	45.9	2.641	0.821		
10X-2, 127-129	85.57	1.610	64.2	40.8	2.551	0.953		
10X-4, 31-33	87.61	1.739	59.6	35.1	2.687	1.128		
11X-2, 60-62	94.50	1.609	65.6	41.8	2.619	0.936		
11X-4, 99-101	97.89	1.769	58.4	33.8	2.695	1.171		
13X-3, 130-132	116.10	1.585	69.0	44.6	2.649	0.879		
13X-6, 66-68	119.96	1.913	49.7	26.6	2.709	1.404		
14X-2, 5-7	122.95	1.942	46.5	24.5	2.697	1.466		
15X-1, 41-43	131.51	2.387					^{a}4194	^{b}4245
15X-1, 58-60	131.68	2.326	30.0	13.2	2.760	2.019		
16X, CC 22-24	141.13	1.988	45.5	23.4	2.683	1.522		
17X, CC 30-32	148.40	2.105					^{a}2230	
19X-1, 91-93	165.01	2.614					^{a}5388	^{b}5511
20X, CC 37-39	174.72	2.736					^{a}5597	^{b}6009
21X, CC 3-5	183.43	2.758					^{a}5889	^{b}6134

[a] Velocity measurement perpendicular to bedding.
[b] Velocity measurement parallel to bedding.

velocity profile is discontinuous, it correlates with the GRAPE profile. The velocity values obtained with the PWL vary between 1600 and 1650 m/s in Subunit IA and decrease sharply to 1550 m/s in the lower density sediments of Subunit IB.

INORGANIC GEOCHEMISTRY

Five interstitial-water samples were collected by squeezing at Site 726 and analyzed for alkalinity, pH, salinity, magnesium, calcium, chloride, sulfate, phosphate, ammonia, and silica (Table 6). The Barnes *in-situ* sampler was used once at a depth of 34.8 mbsf, where it collected pristine interstitial water.

Salinity, Chloride, and pH

The concentration profiles of chloride, salinity, and pH are shown in Figure 31. Both salinity and chloride increase with depth, with salinity being uniformly constant at 36.3 g/kg below 5.95 mbsf. Chloride is ~20 mmol/L greater at the base of Hole 726A than at the top. These chloride concentrations were the highest measured during Leg 117. The chloride maximum at a depth of ~80 m probably results from a different phenomenon than that observed at Sites 724 and 725. At both these latter sites, the maximum occurs in sediments deposited in the middle Pleistocene, whereas sediments at 80 mbsf at Site 726 are much older (at least Pliocene age). We are unable to explain the chloride maximum at this site. The pH shows minimal variation downhole and ranges between 7.93 and 7.55.

Sulfate and Alkalinity

Unlike other sites investigated during Leg 117, Site 726 is characterized by high sulfate concentrations over the length of the cored section (down to ~118 mbsf). Over this depth interval, sulfate decreases from 26.5 to 25.5 mmol/L, with a minimum of 22.6 mmol/L at 76 mbsf. Alkalinity produced through the oxidation of organic matter is very low and reaches a maximum of 5.63 mmol/L in Core 117-726A-9X at 76 mbsf. There is some indication that the more pronounced decrease in sulfate between 34 to 50 mbsf is responsible for adding 2.7 mmol/L of alkalinity to the pore water over the same interval. The concentration and distribution of alkalinity and sulfate at Site 726 suggest that the sediment is low in labile organic matter, and that the slow accumulation rate of the sediments allows sulfate to diffuse from overlying seawater to depths of up to 50 mbsf. Further evidence for this hypothesis is outlined below. Table 7 and Figure 32 indicate that levels of dissolved organic carbon (DOC) are much lower at this site than at Sites 723, 724, and 725, which is consistent with the proposed interpretation.

Ammonia, Phosphate, and Silica

Both ammonia and phosphate, products of organic matter degradation, increase with depth, reaching maximum concentrations of 0.69 mmol/L and 8.1 μmol/L at 76 mbsf, respectively. Assuming Redfield stoichiometry for the organic matter, the reduction of ~6 mmol/L of sulfate at Site 726 should produce ~0.9 mmol/L of ammonia and ~45 μmol/L of phosphate. Thus, Figure 31 indicates that little ammonia removal

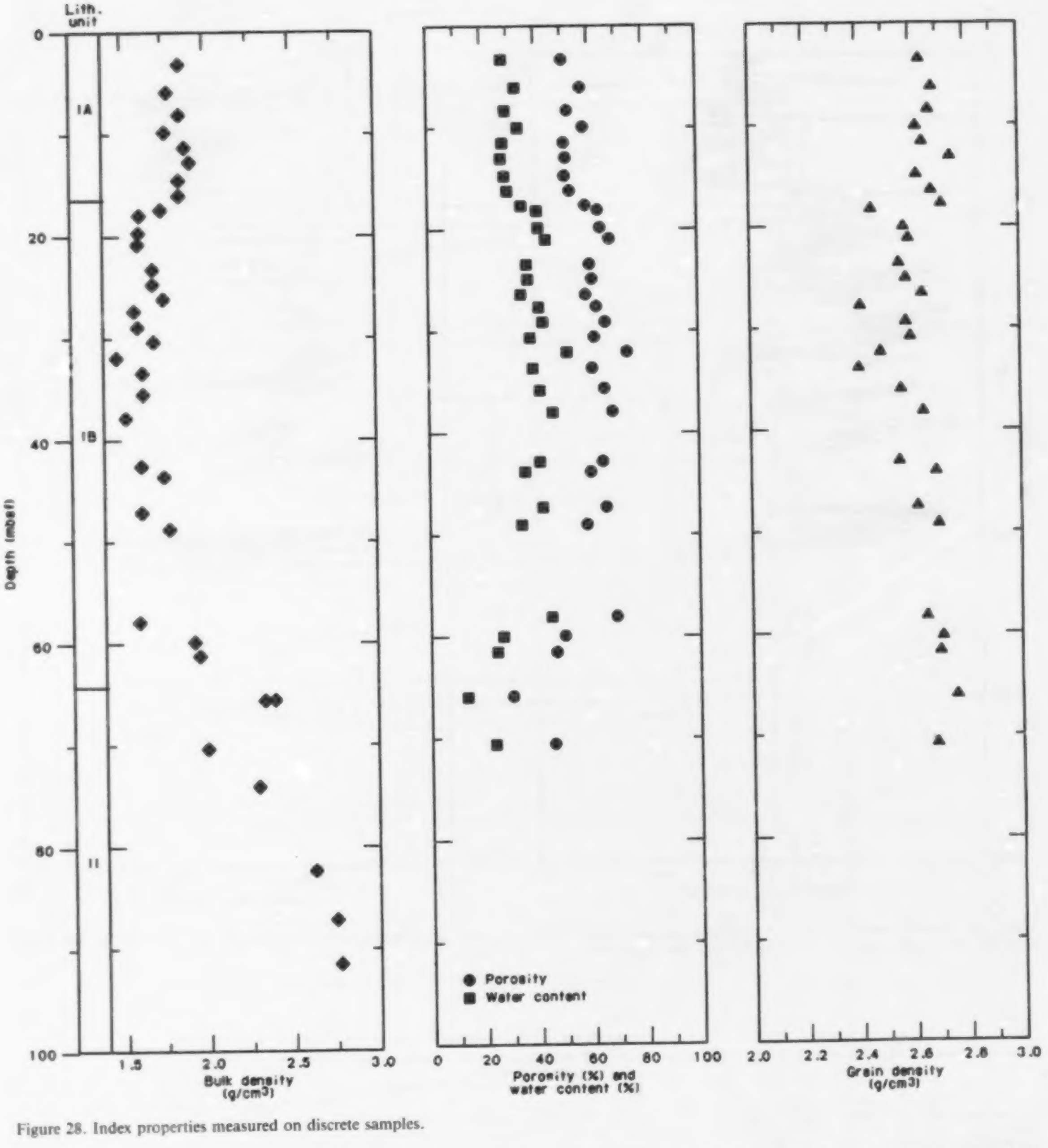

Figure 28. Index properties measured on discrete samples.

onto clays occurs, but phosphate stripping is obvious, in particular over the depth interval from 20 to 40 mbsf. Mineralogical identification (see below) from residues left after sieving for benthic foraminifers reveals large quantities of phosphorite throughout the core. Large nodules and pellets are concentrated at the upper Pliocene unconformity in Section 117-726A-7X, CC. Below 100 mbsf, crystalline carbonate fluorapatite becomes abundant, corresponding to the observed decrease in phosphate below 76 mbsf.

Dissolved silica in the interstitial waters increases from bottom-water values (130–140 μmol/L) to a maximum of 964 μmol/L at 76 mbsf (Fig. 31). The concentration of silica is less here than at previous sites and may reflect control by two limiting mechanisms. First, the slow accumulation rate allows considerable opal-A solution to occur over the upper few meters of the sediment column, thereby reducing the content of opal available for later dissolution. Second, the level of biogenic silica at this site is low (except in the lower Pliocene, 70–90 mbsf) and in-

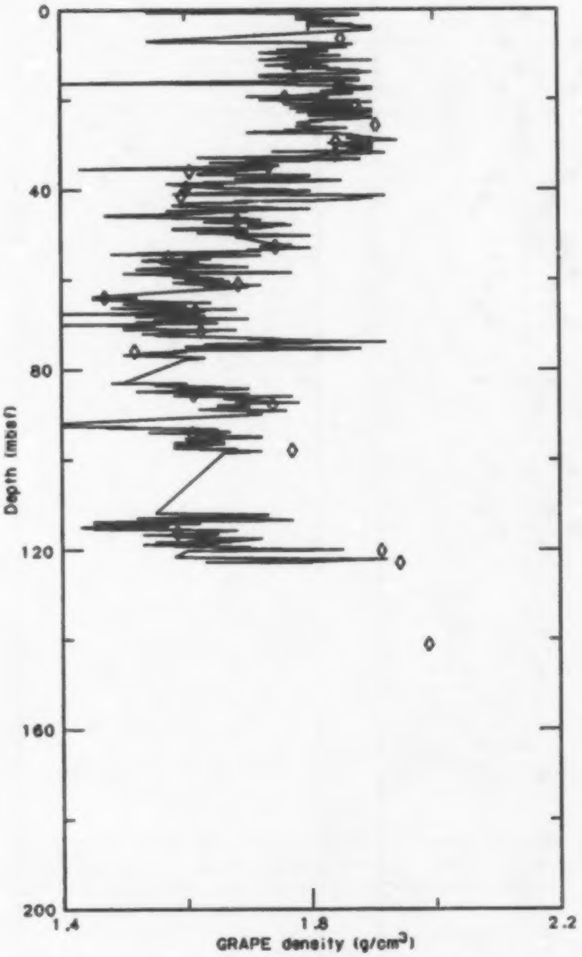

Figure 29. GRAPE wet-bulk density (solid line) and wet-bulk density from discrete samples (diamonds). GRAPE data are 10-cm-block averages.

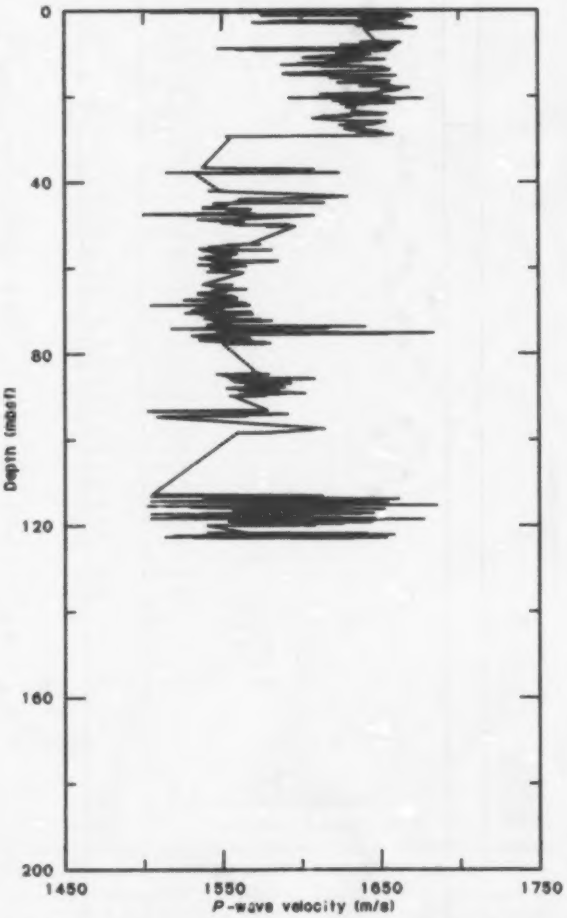

Figure 30. Compressional-wave velocity as measured by the *P*-wave logger.

Table 6. Summary of geochemical data for interstitial water at Hole 726A.

Core, section, interval (cm)	Depth (mbsf)	Vol. (mL)	pH	Alk. (mmol/L)	Sal. (g/kg)	Mg (mmol/L)	Ca (mmol/L)	Cl (mmol/L)	SO_4 (mmol/L)	PO_4 (µmol/L)	NH_4 (mmol/L)	SiO_2 (µmol/L)	Mg/Ca
117-726A-1H-4, 145-150	5.95	41	7.93	4.41	35.8	53.31	11.15	574	26.5	2.1	0.07	147	4.78
117-726A-3H-4, 145-150	22.25	35	7.76	3.04	36.3	50.96	13.42	582	26.4	0.7	0.22	251	3.80
117-726I-4H-7, 0-1	34.80	10	7.80	2.69	36.3	50.71	13.67	588	26.1	1.1	0.27	461	3.71
117-726A-6H-4, 145-150	50.65	41	7.78	5.43	36.3	45.89	15.80	588	22.6	7.0	0.58	885	2.90
117-726A-9X-2, 145-150	76.15	49	7.89	5.63	36.3	45.80	17.00	595	22.59	8.1	0.69	964	2.69
117-726A-13X-4, 145-150	117.75	63	7.55	3.42	36.3	45.90	18.72	593	25.5	2.6	0.21	427	2.45

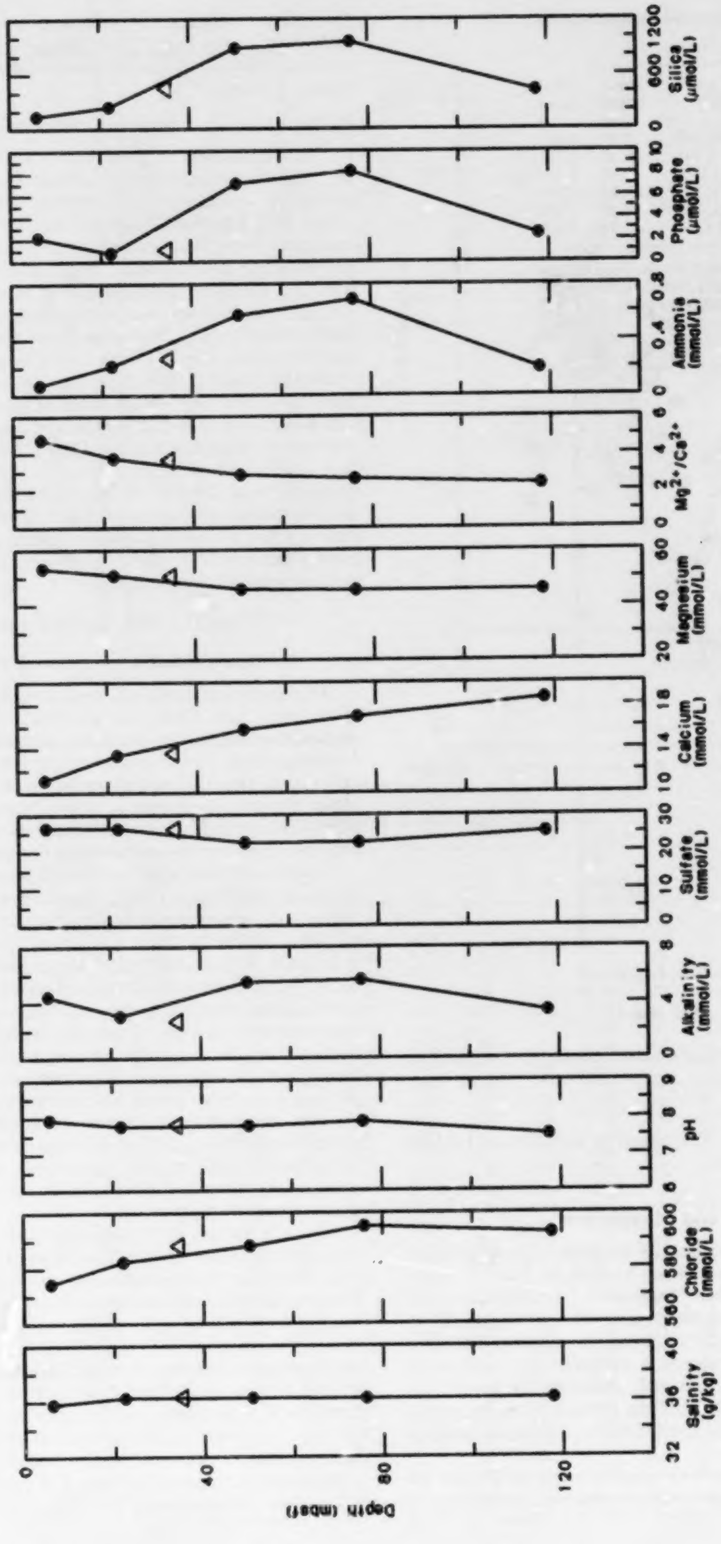

Figure 31. Distribution of concentrations in interstitial waters at Site 726.

Table 7. Dissolved organic carbon at Site 726.

Core, section, interval (cm)	Depth (mbsf)	DOC (a.u.)
117-726A-1H-4, 145	5.95	0.097
3H-4, 145	22.25	0.175
4I-7, 1	34.80	0.168
6H-4, 145	50.65	0.393
9X-2, 145	76.15	0.695
13X-4, 145	117.75	0.169

For explanation of parameters given, see "Explanatory Notes" (this volume); a.u. = absorbance units.

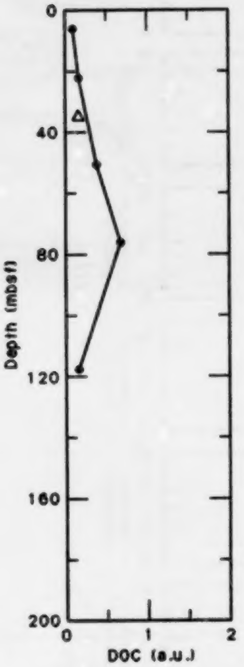

Figure 32. Distribution of dissolved organic carbon (DOC) at Site 726, expressed as absorbance units.

insufficient for dissolution to proceed to equilibrium (~1000 μmol/L) with opal at depth.

Calcium and Magnesium

Profiles of dissolved calcium and magnesium are displayed in Figure 31. Calcium increases from 11.2 mmol/L at ~6 mbsf to 18.7 mmol/L at ~118 mbsf. Magnesium decreases from 53.3 to 45 mmol/L over the same depth interval, and the profile is vertical below 50 mbsf. This distribution indicates that diffusion is absent, which rules out alteration of basalt as a control of magnesium geochemistry at this site. However, the linear calcium gradient between 50 mbsf and the bottom of the hole indicates that calcium is diffusing upward from an unknown source below the cored section.

The curvature evident in both profiles between 10 and 40 mbsf indicates that the greatest degree of reaction, probably dolomitization of preexisting calcite, occurs in this interval. Smear slide descriptions (see "Lithostratigraphy" section, this chapter) indicate abundant dolomite rhombohedra throughout the Pleistocene section.

Sediment Mineralogy

The distribution of phosphorite at this site is of great interest. The first occurrence of noticeable solid-phase phosphatic material is in Sections 117-726A-2H, CC and 117-726A-3H, CC where yellow brown collophane replaces an assemblage of fish teeth and bones that resulted from thanatocaenosis. At the upper Pliocene unconformity (~63 mbsf) in Section 117-726A-7H, CC, we found a lag deposit of large (2 to 3 cm diameter) phosphorite nodules (carbonate fluorapatite) and pellets. These nodules and pellets exist throughout Cores 117-726A-8X, -9X and -10X (down to 92 mbsf). In the upper Miocene (Core 117-726A-11X), highly crystalline, transparent crystal aggregates of pure carbonate fluorapatite (francolite) were found within benthic foraminifer tests and as separate, coherent aggregates. These increase in abundance through Core 117-726A-14X (~130 mbsf). The general morphology, crystal form, and chemistry of the phosphorite at this site will require further study, but it is possible that phosphatization proceeds when sediment accumulation rates are low. However, organic matter diagenesis supplies sufficient phosphorus to the locus of mineralization (often the calcite substrate of foraminifers).

ORGANIC GEOCHEMISTRY

Abundance and Character of Organic Matter

Thirty-one samples of physical properties and headspace residues from Hole 726A were analyzed for organic carbon and carbonate content. The sample suite covers all lithologic units. Lithologic Unit I was subdivided into two subunits on lithological grounds (see "Lithostratigraphy" section, this chapter). Lithologic Subunit IA extends to approximately 32 mbsf and comprises bioturbated, nannofossil-rich, silty clay. Organic carbon concentrations are low and uniform (on average 0.67%; Table 2).

In contrast, lithologic Subunit IB (extending to 131.1 mbsf) shows elevated organic carbon concentrations in which hydrogen-rich organic matter predominates (high hydrogen index [HI] values; Figs. 33 and 34; Table 8). Subunit IB is similar in character to Subunit IA in the major lithology, except that it is less bioturbated and is composed of frequent lag deposits of silt- to sand-sized placers containing apatite, foraminifer tests, and other coarse-grained residues. These lag deposits seem disturbed by bioturbation. As suggested by the saw-tooth patterns in both the organic carbon concentration plot and the highly correlative HI, organic carbon in the bioturbated lag deposits and in the few centimeters of sediments on either side, is low (below 2%) and more refractory. In contrast, organic carbon concentrations in the interbedded, slightly bioturbated, hemipelagic silty clays reach values of up to 4.8% (Table 2), and the organic matter is characterized by high values.

The sole sample (117-726A-15X-1, 58–60 cm) analyzed of the dolomitic shallow-water limestones of Eocene age that comprise lithologic Unit II contained only 0.24% organic carbon. The calculated carbonate content of this sample is over 100%, a result of the fact that we are dealing with dolomite instead of carbonate. Smear slides of Cores 117-726A-13X and 117-726A-14X (see "Lithostratigraphy" section, this chapter) indicate a substantial amount of dolomite at the base of Subunit IA, and, therefore, the calculated carbonate values of these samples are too high. A sample of limestone from 141 mbsf has the lowest organic carbon value measured in Hole 726A.

Both the abundance and degree of preservation of sedimentary organic matter potentially reflect different oceanographic

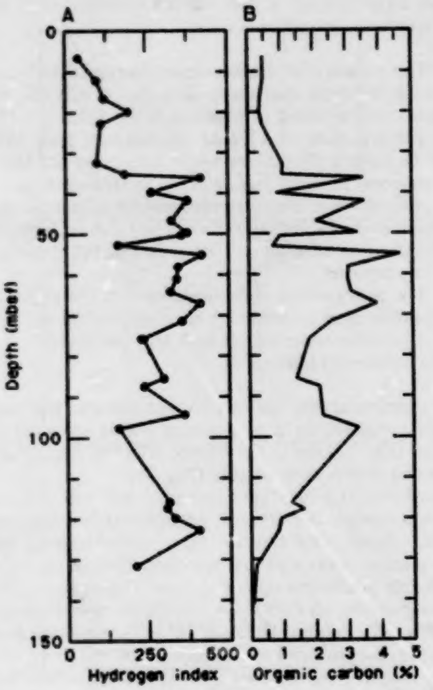

Figure 33. Downhole plot of organic carbon with hydrogen index values.

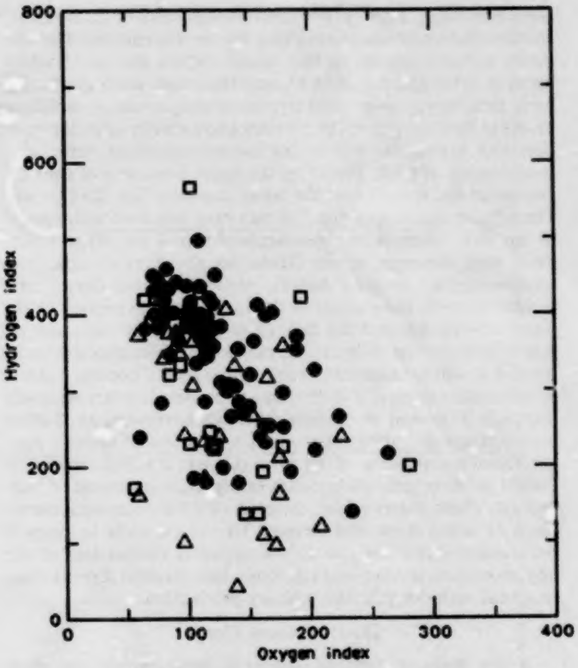

Figure 34. Plot of hydrogen index vs. oxygen index values of samples from sites within the oxygen-minimum zone on the Oman margin. Closed circles indicate samples from Site 723, triangles denote samples from Site 724, and squares depict samples from Site 726.

Table 8. Results of Rock-Eval pyrolysis of samples from Hole 726A.

Core, section, interval (cm)	Depth (mbsf)	T_{max} (°C)	S_1	S_2	S_3	S_2/S_3	TOC	HI	OI
117-726A-									
1H-5, 52-54	6.52	409	0.04	0.23	0.75	0.30	0.54	42	138
2H-4, 60-62	12.00	418	0.10	0.53	0.93	0.56	0.54	98	172
2H-7, 60-62	16.50	414	0.10	0.52	0.90	0.57	0.43	120	209
3H-3, 50-52	19.80	420	0.15	1.10	1.04	1.05	0.56	196	186
3H-5, 50-52	22.80	417	0.11	0.58	0.84	0.69	0.52	111	161
4H-5, 50-52	32.30	414	0.26	1.11	1.07	1.03	1.10	100	97
4H-7, 30-32	35.10	417	0.26	2.12	1.30	1.63	1.14	186	114
5H-1, 80-81	36.10	412	2.56	15.35	2.87	5.34	3.66	419	78
5H-3, 130-132	39.60	416	0.32	2.46	1.41	1.74	0.92	267	153
5H-5, 52-54	41.82	412	2.27	13.90	3.37	4.12	3.69	376	91
6H-2, 50-52	46.70	413	1.18	6.91	2.04	3.38	2.10	329	97
6H-4, 50-52	49.70	413	1.82	12.82	2.88	4.45	3.40	377	84
6H-4, 119-120	50.39	415	0.50	3.73	1.86	2.00	1.04	358	178
6H-6, 50-52	52.70	418	0.30	1.39	1.49	0.93	0.85	163	175
7X-1, 98-100	55.08	411	3.17	20.17	3.25	6.20	4.79	421	67
7X-3, 100-102	58.10	411	1.93	10.93	2.95	3.70	3.13	349	94
7X-5, 100-02	61.10	413	1.50	10.96	2.60	4.21	3.19	343	81
8X-1, 52-54	64.12	410	2.43	10.63	2.81	3.78	3.27	325	86
8X-3, 52-54	67.12	405	3.21	17.00	2.76	6.15	4.08	416	68
8X-6, 27-29	71.37	410	1.27	9.40	2.39	3.93	2.62	358	91
9X-2, 117-119	75.87	410	0.78	4.55	2.21	2.05	1.94	234	113
9X-2, 119-120	75.89	414	0.66	4.59	2.41	1.90	1.91	240	126
10X-2, 127-129	85.57	408	0.63	4.80	2.10	2.28	1.58	303	132
10X-4, 31-33	87.61	415	0.60	5.56	2.23	2.49	2.29	242	97
11X-2, 60-62	94.50	414	0.97	8.58	2.45	3.50	2.35	365	104
11X-4, 100-102	97.90	414	0.57	5.60	2.08	2.69	3.45	162	60
13X-3, 130-132	116.10	417	0.36	4.12	2.15	1.91	1.30	316	165
13X-4, 119-120	117.49	415	1.10	5.22	1.78	2.93	1.70	307	104
13X-6, 66-68	119.96	416	0.38	3.50	1.46	2.39	1.05	333	139
14X-2, 5-7	122.95	418	0.37	3.79	1.23	3.08	0.93	407	132

Note: HI = hydrogen index and OI = oxygen index. TOC values from coulometric determination. For a detailed description of parameters, refer to "Explanatory Notes" chapter (this volume).

conditions (e.g., high vs. low productivity) and/or different environmental conditions prevailing during deposition. The disparity between organic carbon concentrations and preservation between lithologic Subunits IA and IB, which seem quite similar in their inorganic sedimentary components, can be explained by either fluctuations in the primary productivity or in the position and oxygen content of the oxygen-minimum zone, or a combination of both. Presently, the upper boundary of the oxygen-minimum zone is near the water depth of Site 726 (331 m). The relative position of Site 726 may have migrated with respect to the zone, where the oxygen-depleted top of the oxygen-minimum zone impinges on the Oman margin. This scenario also implies that we consider benthic remineralization during oxic conditions to be more effective than when anoxia prevails in the water column because the lack of oxygen in bottom water inhibits bioturbation. Minimal or nonexistent bioturbation limits the rate at which oxidants (principally oxygen if bottom water is oxygenated, sulfate if it is anoxic) are delivered, either passively (through diffusion) or actively (through advection) to shallow buried sediments, thus enhancing preservation of organic matter. Visual examination of the cores suggests that bioturbation is limited in the organic-carbon-rich hemipelagic sequences of Subunit IB. These observations, coupled with the occasional occurrence of laminations and elevated HI values, seem to support the scenario described above. The apparent fluctuations of the oxygen-minimum zone might possibly have resulted directly from temporal variations during primary production.

Hydrocarbon Gases

A few measurements of interstitial hydrocarbon gas show consistently low methane concentrations, and no trace of thermogenic gas noted at other sites on the Oman margin (Table 9). The low values for biogenic methane imply that organic matter degradation during bacterial diagenesis in the entire sedimentary section is dominated by sulfate reduction.

SUMMARY AND CONCLUSIONS

Site 726 marks the end point of a depth transect that brackets the depth range of a pronounced oxygen-minimum zone across the Oman continental margin. The site is located on what was assumed to be a pre-Neogene basement high that coincides with the shelf break, landward of a slope basin filled with thick (up to 2 km) Neogene sediment accumulations. The main objective at Site 726 was to identify the nature and age of rocks that underlie Neogene hemipelagic sediments covering much of the Leg 117 study area. Rapid vertical movements of the basement are evident in seismic images and provided the subsidence necessary for the immense sedimentation rates found in slope basins off Oman. Another reason for drilling at Site 726 was to investigate the facies of sediments at the present upper boundary of this oxygen-minimum zone and to examine the record for changes in the position of the oxygen-minimum zone in the Neogene.

Table 9. Results of headspace analysis for interstitial gas at Site 726.

Core, section, interval (cm)	Depth (mbsf)	C_1 (μL/L)
117-726A-		
3H-4, 119–120	21.99	32
6H-4, 119–120	50.39	35
9X-2, 119–20	75.89	54
13X-4, 119–120	117.49	19

The main findings at Site 726 are summarized in Figure 35 and include the identification of:

1. The recovery of shallow-water limestones of Eocene age (?) similar to those that unconformably overlie the ophiolitic basement on the island of Masirah to the north.
2. The discovery of a hiatus that spans at least 30 m.y. between the Eocene (?) shallow-water limestones and the hemipelagic sediment cover of late Miocene to Holocene age.
3. Indications of repeated alternations of anoxic conditions that result in laminated layers (which are also organic-rich) with conditions of winnowing and oxygenation that result in bioturbated lag deposits.
4. The preservation of biogenic opal in the upper Pliocene that parallels opal preservation at other sites on the margin.
5. A possible water source with high chlorinity in or overlying the Eocene (?) limestones.

The section at Site 726 was divided into two lithologic units that are separated by a pronounced hiatus spanning the time from the late Miocene to the Eocene. The lithologic character of these units differs considerably (Fig. 35).

Unit I (0–131.1 mbsf) is subdivided into two subunits. Subunit IA comprises bioturbated, phosphorite-bearing, nannofossil-rich, calcitic, silty clay to clayey silt—sediments similar to those found at other sites that are typical for the deposits underlying highly productive upwelling cells. The mean sedimentation rate for Subunit IA (NN21 to NN19) is approximately 45 m/m.y. (Fig. 35). Subunit IB is similar in composition to Subunit IA, but is characterized by laminated intervals in its upper half and by frequent lag deposits throughout the subunit (Fig. 35). These lag deposits contain sand-sized foraminifers, phosphoritic grains, fish teeth, and bones that are intercalated in the hemipelagic sequence. These deposits are considered indicators of current winnowing. The frequency of these lag deposits decreases upsection, which indicate progressive deepening of the site. This inference is supported by the increase of the planktonic-benthic ratio upsection. In accordance with recurrent winnowing or nondeposition, the section of Subunit IB is greatly compressed and has an average sedimentation rate of about 15 m/m.y. (Fig. 35).

Lithologic Unit II was only sparsely recovered from 131.1 to 186.3 mbsf and consists of nummulitic and oncolitic limestone of Eocene (?) age, which was variably cemented by dolomite and calcite. These shallow-water sediments appear to correspond to limestone occurrences described from the Arabian peninsula and the ophiolite complex of Masirah, where similar sediments unconformably overlie ophiolitic basement. The base of this recovered section may be slightly silicified.

Paleontological investigation revealed two major hiatuses. The first separates Pleistocene from upper Pliocene hemipelagic sediments, while the second corresponds to the transition from Eocene (?) limestone to upper Miocene transgressive biogenic and eolian upwelling deposits (Fig. 35). The hiatus between upper Pliocene and Pleistocene truncates an interval where radiolarians and diatoms indicate influence of colder water or water of different nutrient composition at the site. This interval seems coeval with similar occurrences at the deeper water Sites 723 and 724, where an opal-rich interval was expanded.

Laminated deposits occur in the upper Pliocene and the lower Pleistocene section (Fig. 35). The upper Pliocene laminations coincide with the opal-rich zone and alternate with lag deposits, while only about one-half of the lower Pleistocene laminations are associated with lag deposits. This interval of laminated deposits spans a large range of accumulation rates and possibly several hiatuses. The association of laminated sequences, lag

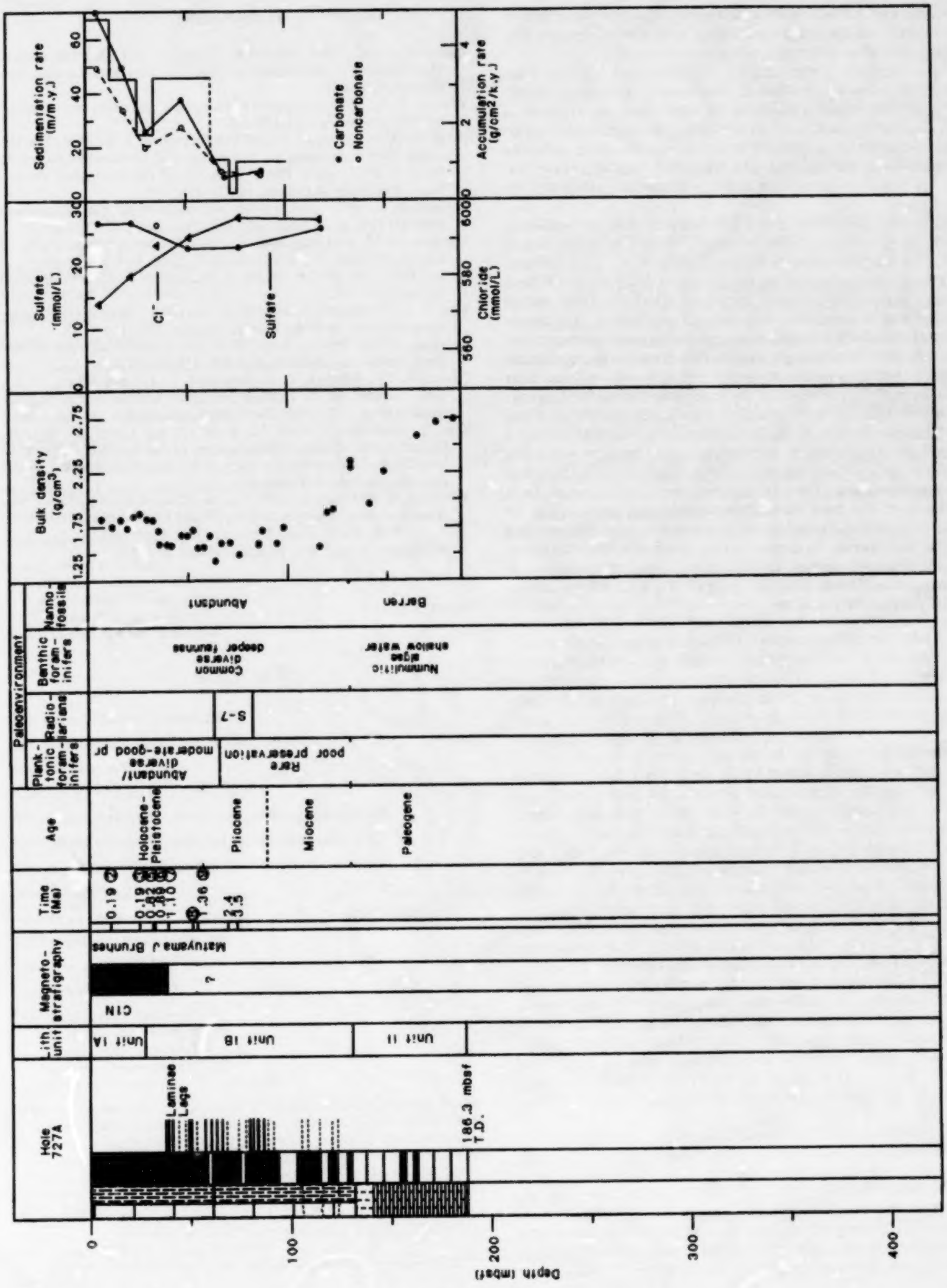

Figure 35. Summary chart outlining preliminary shipboard findings at Site 726.

deposits, and variations in bioturbation indicate variations in the intensity of the oxygen-minimum zone and of current winnowing, possibly by the upwelling countercurrent.

Poor recovery in the variably indurated and lithified limestone and dolostone precluded continuously sampling interstitial water and impeded sampling for interstitial gas. However, a high chloride concentration of 600 mmol/L suggests that hypersaline water either is present in the subsurface or is advected horizontally to the site (Fig. 35). Chemical data also show that Site 726 has more phosphate and less silica than other sites on the margin.

Sediments recovered at Site 726 did not yield the nature or age of the igneous basement complex that underlies this area of the Oman margin. However, by comparison with sediments overlying ophiolitic basement on the island of Masirah, we believe that the shallow-water limestone sequence recovered here and at Site 729 may be associated with ophiolitic basement. The occurrence of the shallow-water, biogenic, carbonate sediments implies that the Oman margin may have been a starved carbonate platform before possible subaerial exposure and erosion near the wave base during much of the Paleogene and early Neogene. We believe that the hemipelagic sediments deposited since the late Miocene on top of the shallow-water carbonates record a progressive deepening of the environment, because placerlike lag deposits are less frequent and the planktonic-benthic ratio increases upsection. The environment alternated between states conducive to the formation of lamination and preservation of labile organic matter and those conducive to bioturbation and current winnowing. Evidence linking the oscillations to either eustatic sea level, vertical tectonic movements, or variations in the oxygen-minimum zone are inconclusive and will be the focus of post-cruise research.

REFERENCES

Bathurst, R.G.C., 1975. *Carbonate Sediments and Their Diagenesis.* Developments in Sedimentology (Vol. 12): New York-London-Amsterdam (Elsevier).

Baturin, G. N., 1971. Formation of phosphate sediments and water dynamics. *Oceanology*, 11:372-376.

Berggren, W. A., Kent, D. V., and Van Couvering, J. A., 1985. The Neogene: Part 2, Neogene geochronology and chronostratigraphy. *In* Snelling, N. J. (Ed.), *The Chronology of the Geological Record.* Geol. Soc. Mem. (London), 10:211-259.

Burnett, W. C., 1977. Geochemistry and origin of phosphorite deposits from off Peru and Chile. *Geol. Soc. Am. Bull.*, 88:813-823.

Clement, B. M., and Robinson, F., 1987. The magnetostratigraphy of Leg 94 sediments. *In* Ruddiman, W. F., Kidd, R. B., Thomas, E., et al., *Init. Repts. DSDP*, 94, Pt. 2: Washington (U.S. Govt. Printing Office), 635-650.

Haq, B. U., Hardenbol, J., and Vail, P. R., 1987. Chronology of fluctuating sea levels since the Triassic. *Science*, 235:1156-1167.

Moseley, F., and Abbotts, I. L., 1979. The ophiolite melange of Masirah, Oman. *J. Geol. Soc. London*, 136:713-724.

Powers, R. W., Ramirez, L. F., Redmond, C. D., and Elberg, E. L., 1966. Geology of the Arabian peninsula: sedimentary geology of Saudi Arabia. *U.S. Geol. Surv. Prof. Pap.*, 560D.

Sato, T., Takayama, T., Kato, M., Kudo, T., and Kamei, K., in press. Calcareous microfossil biostratigraphy of the uppermost Cenozoic formations distributed in the coast of the Japan Sea. Part 4: Conclusion. *Sekiyu Gijutsu Kyokaishi.*

Takayama, T., and Sato, T., 1987. Coccolith biostratigraphy of the North Atlantic Ocean, Deep Sea Drilling Project Leg 94. *In* Ruddiman, W. F., Kidd, R. B., Thomas, E., et al., *Init. Repts. DSDP*, 94, Pt. 2: Washington (U.S. Govt. Printing Office), 651-702.

Ms 117A-113

15. SITE 727[1]

Shipboard Scientific Party[2]

HOLE 727A

Date occupied: 24 September 1987

Date departed: 25 September 1987

Time on hole: 17 hr

Position: 17°46.096′N, 57°35.216′E

Water depth (sea level; corrected m, echo-sounding): 914.50

Water depth (rig floor; corrected m, echo-sounding): 925

Bottom felt (m, drill pipe): 921.50

Penetration (m): 182.40

Number of cores: 19

Total length of cored section (m): 182.20

Total core recovered (m): 188.40

Core recovery (%): 103.4

Oldest sediment cored:
Depth sub-bottom (m): 182.40
Nature: marly nannofossil ooze
Age: late Pliocene (NN18)
Measured velocity (km/s): —

HOLE 727B

Date occupied: 25 September 1987

Date departed: 25 September 1987

Time on hole: 4 hr, 30 min

Position: 17°46.096′N, 57°35.216′E

Water depth (sea level; corrected m, echo-sounding): 914.5

Water depth (rig floor; corrected m, echo-sounding): 925

Bottom felt (m, drill pipe): 918.8

Penetration (m): 27.10

Number of cores: 3

Total length of cored section (m): 27.10

Total core recovered (m): 27.95

Core recovery (%): 103.1

Oldest sediment cored:
Depth sub-bottom (m): 27.10
Nature: marly nannofossil ooze
Age: late Pleistocene (NN18)
Measured velocity (km/s): 1.52–1.61

Principal results: Site 727 is located in the northwestern Arabian Sea on the continental margin off the shore of Oman. The location corresponds to a second drilling target near the center of the pronounced oxygen-minimum zone (OMZ) that impinges on the margin underneath a zone of high biogenic productivity. We drilled Site 727 to complement the continuous and expanded sections of late Neogene to Holocene sediments previously recovered at Site 723, to trace the imprint of the OMZ through time, and to investigate diagenetic sedimentary processes.

Major findings at Site 727 include the identification of

1. a uniform lithology of marly nannofossil oozes ranging in age from latest Pliocene to Holocene;
2. calcareous nannofossils indicative of cold water and upwelling in the lower Pleistocene and only traces of opal in the uppermost Pliocene; and
3. complete sulfate depletion by 50 mbsf, replenished at depth by an unknown source. The sulfate increase is associated with a continuous downsection increase in alkalinity.

Our findings at Site 727 confirm many of the biotic and depositional trends observed at other sites on the Oman margin. However, the lack of laminated facies at Site 727, which lies at the same depth and covers the same time span as Site 723, poses questions about the character and spatial extent of the processes that led to the formation of laminated facies.

BACKGROUND AND OBJECTIVES

Site 727 is located in water depths of about 915 m at 17°46.096′N and 57°35.216′E on the continental margin of Oman. The location of Site 727 is shown in Figures 1 and 2, and its structural and depositional setting is shown in Figure 3. The site is located in the southern part of the slope basin, which is about 15 km wide here, and is bounded on the west by a faulted block and on the east by a basement ridge. Both basement features are thought to be ophiolite complexes.

The seismic reflection profiles of the basin sediments show numerous highly reflective layers in the upper 0.4 s that both onlap and drape the adjacent basement structures. The sediments are thickest in the center of the basin (more that 2000 m, based on sonobuoy data; Mountain and Prell, this volume) and thus form a syncline-shaped deposit (Fig. 3A). Along the strike of the basin (Fig. 3B), the shallow subsurface layers (0–0.4 s) dip gently to both the southwest and the northeast and are relatively conformable. In the deeper layers, some deformational, erosional, and slump-related structures are observed and appear to be associated with the basement peaks.

Site 727 was located within a zone of continuous westward dipping reflectors (Figure 3A) on the seaward margin of the slope basin. The preliminary correlation of seismic reflectors within the basin indicates that the average accumulation rates are highest in the southern part of the basin near the location of Site 723. They were expected to be somewhat lower at Site 727 because it is not in the center of the basin (Fig. 3A).

Specific objectives for drilling at Site 727 were

1. to obtain a high-resolution record of the sediments associated with the near-coastal zone of the monsoonal upwelling system, in order to establish the changes in timing and intensity of the monsoon; and
2. to provide a deep-water section in the depth transect of sites across the Oman margin that can be used to examine the organic-rich sedimentary facies of the margin and establish their relationship to the OMZ and its spatial variation through time.

---

[1] Prell, W. L., Niitsuma, N., et al., 1989. *Proc. ODP, Init. Repts.*, 117: College Station, TX (Ocean Drilling Program).

[2] Shipboard Scientific Party is as given in the list of Participants preceding the contents.

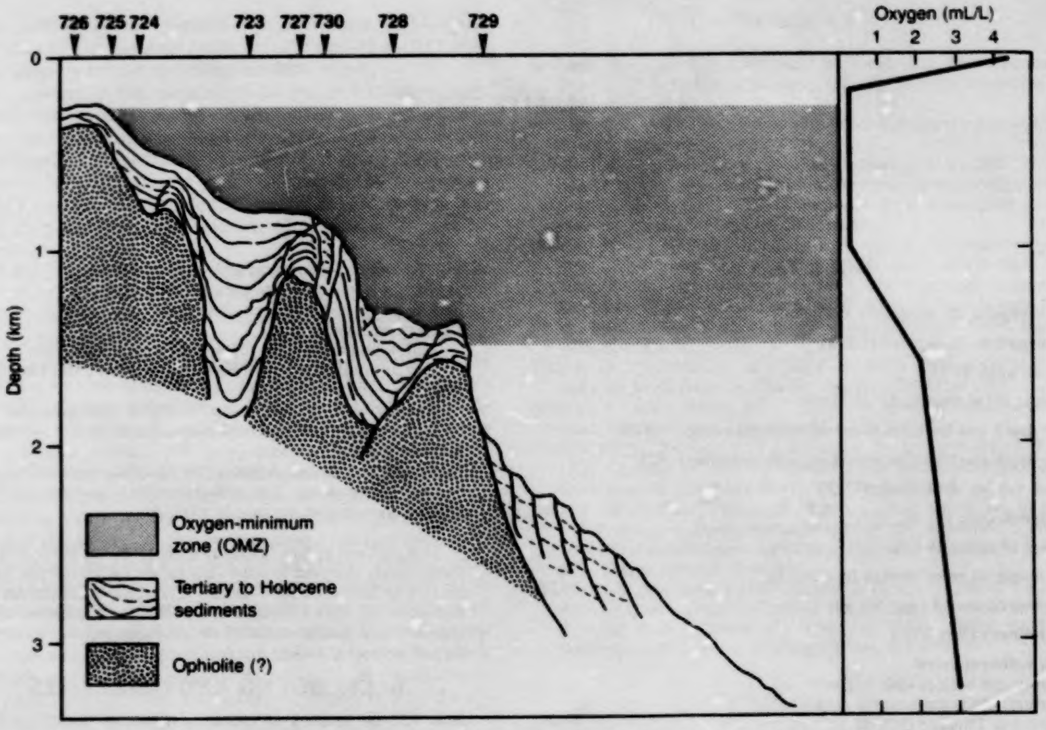

Figure 1. Structure of the Oman margin and the oxygen-minimum zone (OMZ). The schematic profile shows the series of basement ophiolite blocks and the sedimentary basins between them. The concentration of oxygen in the water column (RC2704, unpubl. data) defines the depth range of the OMZ and where it impinges on the margin.

OPERATIONS

The ship departed Site 726 at 0830 hr on 24 September 1987 and surveyed Site 727 with the seismic gear streamed before the site was occupied and drilling operations began. We dropped the beacon in water depths of 914 m upon passing the site for the second time and retrieved the seismic gear. The ship attained dynamic positioning mode by 1230 hr on 24 September. The exact location of Site 727 was obtained from Global Positioning System (GPS) as 17°46.096′N and 57°35.216′E (Fig. 4).

The first of 10 APC cores was shot at 1430 hr, followed by 9 XCB cores to a total depth of 182.2 mbsf in Hole 727A. We switched to the XCB mode after reaching 95.4 mbsf due to a pull-out force of 110,000 lbs upon retrieving Core 117-727A-10H. Recovery in the section cored by the APC was 104%. Recovery with the XCB continued to be excellent down to total depth and averaged 102% in calcareous oozes and clayey silts, even though gas expansion was less severe than at other sites. *In-situ* pore-water samples were collected after Cores 117-727A-9H and -10X (Table 1).

At 0030 hr on 25 September, the hole was displaced with mud and the string was pulled after we reached target depth in Hole 727A. Without offsetting the rig, the bit was positioned to shoot the mud line of Hole 727B, which consists of three APC cores from 0 to 27.1 mbsf, an interval which was cored from 0215 to 0345 hr on 25 September 1987. These cores had 103% recovery. Operations at Site 727 were finished after pulling the string, and the ship set out to survey Sites 728 and 729 by 0600 hr on 25 September 1987.

LITHOSTRATIGRAPHY

Lithologic Units

Sediments recovered from Site 727 range from Holocene to late Pliocene in age. Visual core descriptions, smear slide analyses, and calcium carbonate contents indicate a uniform lithology. A single lithologic unit, consisting of calcitic marly nannofossil ooze to calcitic marly calcareous ooze, has been assigned to the entire sedimentary column (Fig. 5).

Unit I (Depth: Hole 727A, 0–182.4 mbsf; Hole 727B, 0–27.1 mbsf; Age: late Pliocene to Pleistocene)

Cores 117-727B-1H through -19X; Cores 117-727B-1H to -3H.

Lithologic Unit I consists of sediments which grade between calcitic marly nannofossil ooze and calcitic marly calcareous ooze. The sediments range in color from olive (5Y 4/3) to olive gray (5Y 4/2, 5/2), and dark olive gray (5Y 3/2).

Smear slide analyses indicate that the sediment in Unit I is dominated by biogenic carbonate. The carbonate is composed primarily of nannofossils (as much as 55%), but it also contains as much as 20% foraminifers. The nonbiogenic component is dominated by clay (15%–35%) and detrital calcite (15%–40%). Other minerals, usually comprising less than 10% of the sediment, include quartz, trace amounts of dolomite, and opaque minerals (Table 2). Given the resolution of these preliminary data, the mineralogical components show no significant variations within the sedimentary column.

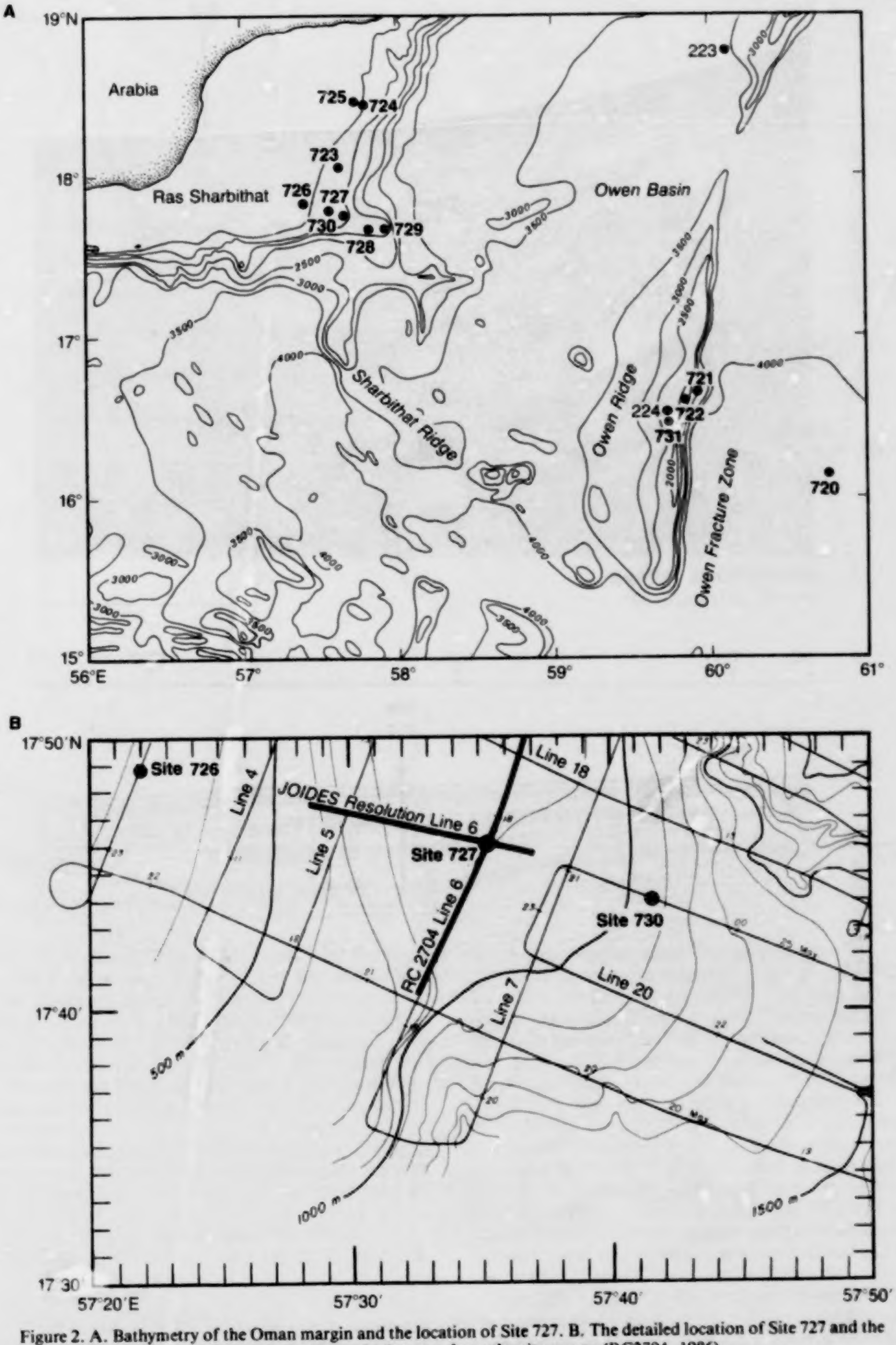
A
19°N
18°
17°
16°
15°
56°E
57°
58°
59°
60°
61°
Arabia
Ras Sharbithat
725
724
723
726
727
730
728
729
223
Owen Basin
Sharbithat Ridge
Owen Ridge
Owen Fracture Zone
721
224
722
731
720
2500
3000
3500
4000
B
17°50′N
17°40′
17°30′
57°20′E
57°30′
57°40′
57°50′
Site 726
Line 4
Line 5
JOIDES Resolution Line 6
Site 727
RC 2704 Line 6
Line 18
Site 730
Line 20
Line 7
500 m
1000 m
1500 m

Figure 2. A. Bathymetry of the Oman margin and the location of Site 727. B. The detailed location of Site 727 and the seismic profiles shown in Figure 3. Bathymetric data are from the site survey (RC2704, 1986).

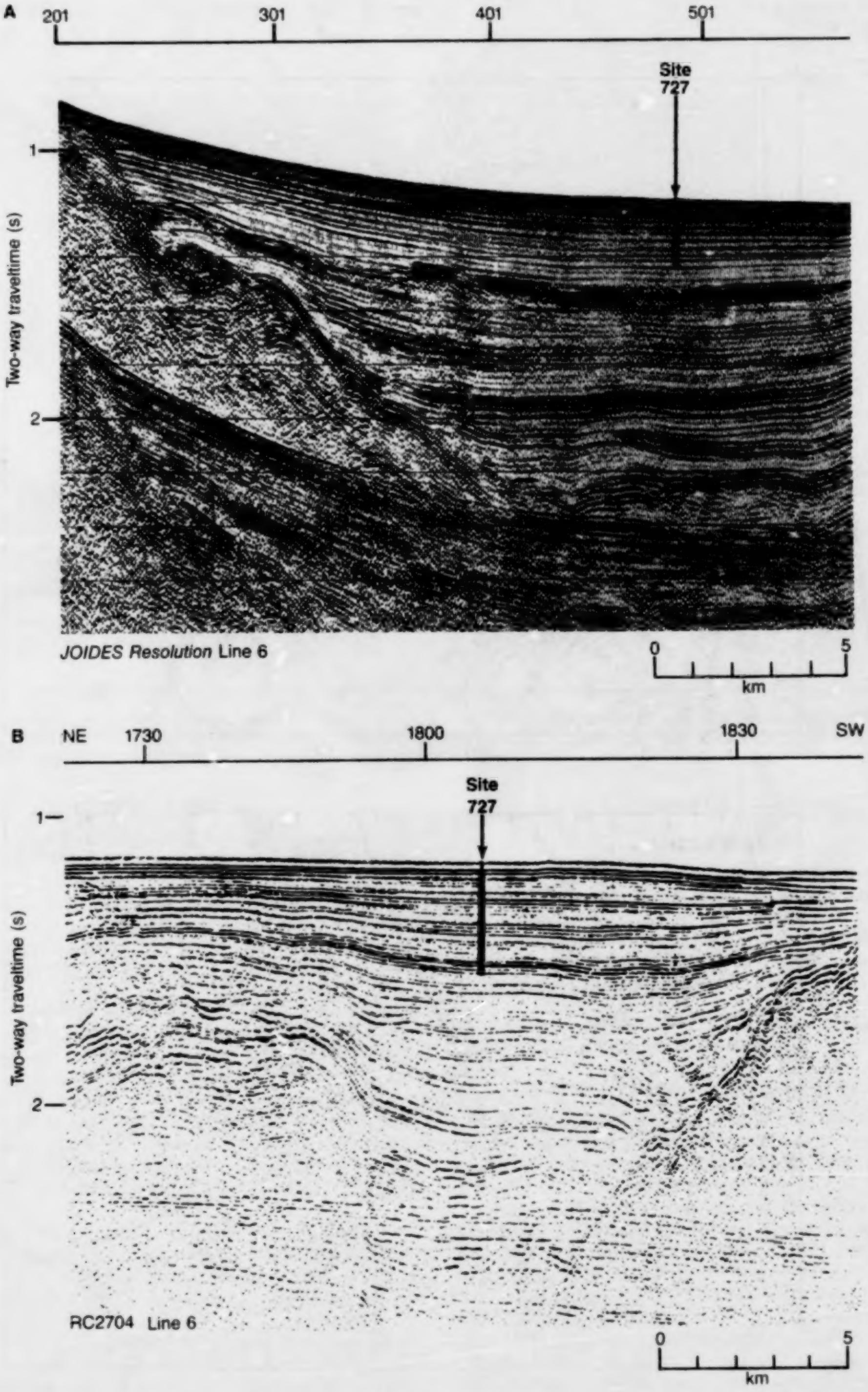

Figure 3. A. Single-channel-seismic (SCS) reflection profiles showing the structural and depositional setting of Site 727. Line 18 is perpendicular to the trend of the basin and shows the bounding basement blocks and the synclinal-shaped sediment fill. The relative position of Site 727 is projected. B. Line 6 is along the strike of the basin and shows the sediment thickness decreasing to the northeast and southwest.

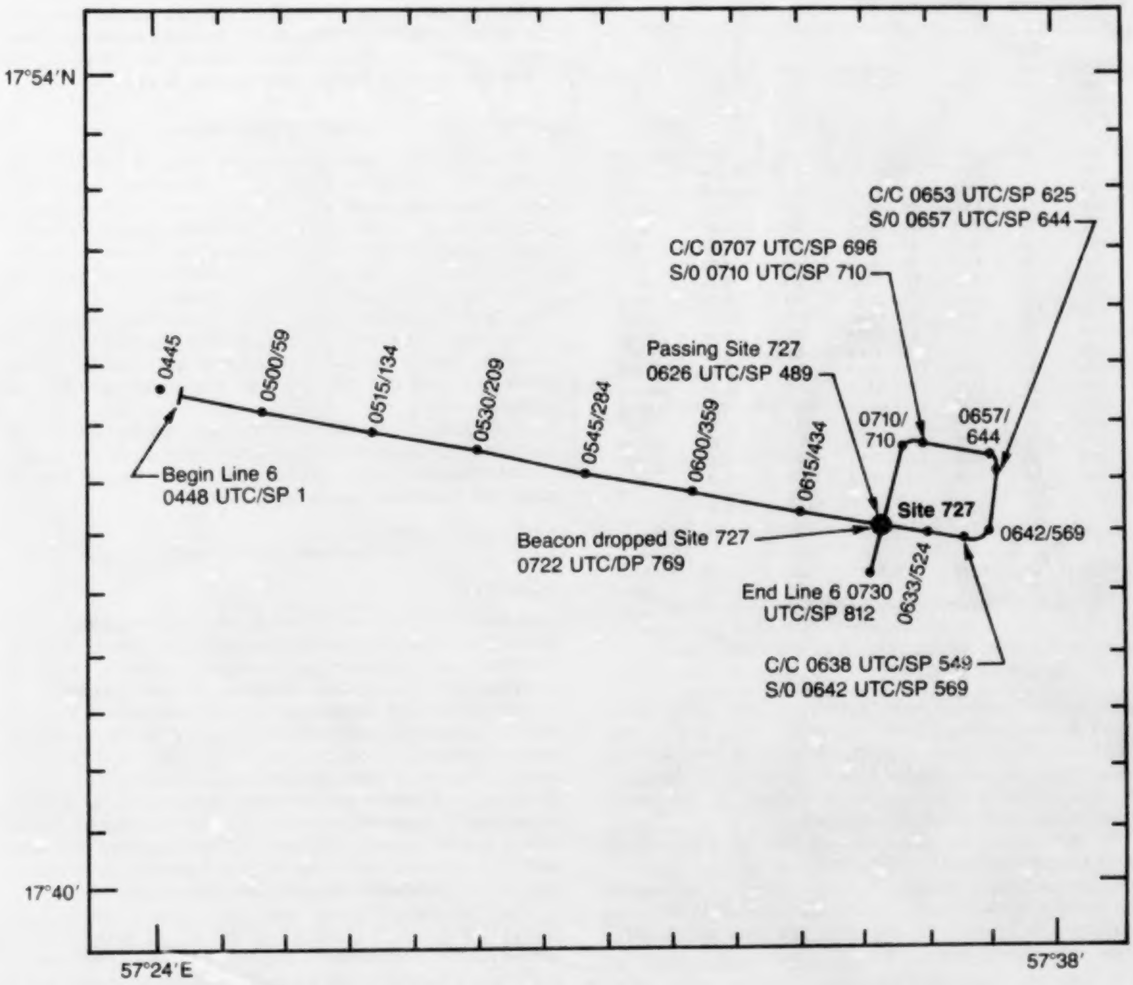
17°54′N
17°40′
57°24′E
57°38′
0445
0500/59
0515/134
0530/209
0545/284
0600/359
0615/434
Begin Line 6
0448 UTC/SP 1
Passing Site 727
0626 UTC/SP 489
C/C 0707 UTC/SP 696
S/0 0710 UTC/SP 710
C/C 0653 UTC/SP 625
S/0 0657 UTC/SP 644
0710/
710
0657/
644
Site 727
0642/569
Beacon dropped Site 727
0722 UTC/DP 769
End Line 6 0730
UTC/SP 812
0633/524
C/C 0638 UTC/SP 549
S/0 0642 UTC/SP 569

Figure 4. Track line of *JOIDES Resolution* during the survey of Site 727.

The calcium carbonate content (Table 3 and Fig. 6) ranges from 46% to 70% and averages 58%. Foraminifer and nannofossil data (see "Biostratigraphy" section, this chapter) indicate that carbonate preservation is good from the top of the section through Core 117-727A-10H (0–94 mbsf) and moderate from Cores 117-727A-10H to -19X (94–182 mbsf). The organic carbon content (Table 3 and Fig. 6) ranges from 0.80% to 4.96%, with the highest values occurring from Cores 117-727A-14X to -16X (126–165 mbsf).

Deviations from the major lithology encompass a total sediment thickness of less than 1 m and are as follows: (1) greenish gray (5GY 5/1) nannofossil-rich calcitic clayey sand (Sample 117-727A-14X-2, 120–121 cm), and (2) dark olive gray (5Y 3/2) nannofossil-rich calcitic silty clay (Samples 117-727B-3H-2, 28–41 cm; 117-727B-3H-2, 93–103 cm; and 117-727B-3H-4, 58–88 cm).

Discussion

The uniform lithology at Site 727 indicates that this site has been under the influence of a relatively constant (dominantly hemipelagic) depositional regime since the late Pliocene. Site 727 occupies the same sedimentary basin as Site 723 (located 28 km north of Site 727). By comparison, Sites 727 and 723 have similar lithologies from the upper Pliocene through the Pleistocene with the exception that no laminated sediments were identified at Site 727. Preliminary estimates, based largely on sediment accumulation rates and benthic foraminifer data, indicate that the two sites were at similar paleodepths from the late Pliocene through the early Pleistocene. During this interval, silica-rich laminated sediments with high organic carbon content were deposited at Site 723; sediments deposited at Site 727, on the other hand, contained only trace amounts of biogenic silica, had high organic carbon contents (up to 5%), and were not laminated. These observations suggest small-scale horizontal heterogeneity in the environmental and depositional conditions within the OMZ.

Site 724, located 70 km north-northwest of Site 727 in the same sedimentary basin, occupied a much shallower paleodepth throughout the Pliocene and Pleistocene. Laminae at Site 724, however, occur only below the Pliocene-Pleistocene boundary,

Table 1. Coring summary, Site 727.

Core no.	Date (Sept. 1987)	Time	Depth (mbsf)	Cored (m)	Recovered (m)	Recovery (%)
117-727A-						
1H	24	1505	0-9.5	9.5	9.57	101.0
2H	24	1520	9.5-18.9	9.4	9.19	97.7
3H	24	1540	18.9-28.4	9.5	9.95	105.0
4H	24	1600	28.4-37.8	9.4	9.88	105.0
5H	24	1715	37.8-47.3	9.5	9.85	103.0
6H	24	1735	47.3-56.8	9.5	9.98	105.0
7H	24	1755	56.8-66.4	9.6	10.03	104.5
8H	24	1815	66.4-76.1	9.7	10.18	104.9
9H	24	1835	76.1-85.8	9.7	10.20	105.1
10H	24	1900	85.8-95.4	9.6	10.45	108.8
11X	24	2045	95.4-105.0	9.6	9.99	104.0
12X	24	2110	105.0-114.6	9.6	9.52	99.1
13X	24	2130	114.6-124.0	9.4	10.14	107.9
14X	24	2150	124.0-133.7	9.7	10.67	110.0
15X	24	2210	133.9-143.6	9.7	9.80	101.0
16X	24	2240	143.6-153.3	9.7	9.73	100.0
17X	24	2300	153.3-163.0	9.7	9.87	102.0
18X	24	2320	163.0-172.7	9.7	9.95	102.0
19X	24	2350	172.7-182.4	9.7	9.45	97.4
				182.2	188.40	
117-727B-						
1H	25	0230	0-8.2	8.2	8.15	99.4
2H	25	0250	8.2-17.6	9.4	9.91	105.0
3H	25	0315	17.6-27.1	9.5	9.89	104.0
				27.1	27.95	

suggesting the possibility of both temporal and vertical heterogeneity in the conditions necessary for the formation of laminated sediments. Detailed stratigraphic, paleontologic, and sedimentologic studies are needed to map the paleodistribution of laminated sediments accurately and to evaluate the environmental conditions under which they formed.

The continuous, uniform nature of Site 727 sediments are ideal for the development of high-resolution faunal, oxygen-isotope, and carbonate records. A comparison of these records with similar records from the Owen Ridge will help to determine the differences between the nearshore and open-marine monsoonal upwelling regimes.

BIOSTRATIGRAPHY

Introduction

Site 727 is located in water depths of 914 m. The Pleistocene-Pliocene boundary was recognized at about 150 mbsf, based on calcareous nannofossil data (Fig. 7). A plot of faunal datum levels and paleomagnetic reversals vs. depth below the seafloor is presented in Figure 8; for a detailed listing of these data points see Table 4.

Siliceous microfossils at this site are absent down to 143.6 mbsf. Below this level only rare fragments are found. Calcareous microfossils (planktonic and benthic foraminifers and nannofossils) are present throughout Hole 727A. Preservation is moderate to good and the abundance of planktonic foraminifers and nannofossils is high. Benthic foraminifers are rare to few in the upper 47.3 m, but they become more abundant below this level.

Planktonic Foraminifers

The drilled sequence of Site 727 contains highly diverse planktonic foraminiferal assemblages. All core-catcher samples studied yielded abundant specimens, except for the lowermost Core 117-727A-19X. Preservation of the tests is moderate to good. The presence of *Globorotalia truncatulinoides* shows that the age of the sediments throughout the entire sequence is Pleistocene, except for the lowermost Sample 117-727A-19X, CC (182.4 mbsf), which may be late Pliocene in age.

Benthic Foraminifers

We studied the benthic foraminifer fauna of Site 727 in the core-catcher samples of Hole 727A. Abundance varied from few to rare in the upper five samples (9.5–47.3 mbsf). Benthic foraminifers are abundant in the next three samples (56.8–76.1 mbsf) and become common further downhole (below 85.8 mbsf). Preservation is good to moderate. The planktonic/benthic (P/B) ratio is high throughout the sequence studied.

Benthic foraminifer fauna at this site are characterized by a high relative abundance of uvigerinoids, especially *Uvigerina peregrina*. Additional species that commonly occur throughout the sequence are *Bolivina ordinaria, Cassidulina carinata,* and *Hyalinea baltica*.

The stability in the faunal composition and the high P/B ratio indicate no major variations in the water depth and suggest that the present location in the upper middle bathyal zone already was established in the late Pliocene.

Calcareous Nannofossils

Hole 727A

A high abundance and moderate to good preservation characterize the calcareous nannofossil assemblages from Hole 727A. However, there is comparatively low species diversity. The cored sediments range in age from Holocene to latest Pliocene.

The nannofossil assemblages in sediments down to 23.08 mbsf are composed predominantly of such placoliths as *Gephyrocapsa oceanica, G. caribbeanica, G. parallela,* and *Emiliania huxleyi*. Therefore, these sediments are assigned to Zone NN21 (Holocene to Pleistocene). Underlying sediments as far down as 41.98 mbsf contain neither *E. huxleyi* nor *Pseudoemiliania lacunosa* and are referred to Zone NN20 (Pleistocene). The presence of *P. lacunosa* and the absence of discoasters in sediments from 42 to 179.90 mbsf place this section in Zone NN19.

The Pleistocene/Pliocene boundary is placed between Samples 117-727A-16X-3, 118–119 cm, and 117-727A-16X-5, 114–115 cm (147.78–150.74 mbsf). The top of *Discoaster brouweri* is between 179.90 and 182.40 mbsf. We assigned sediments below this level down to the bottom of the hole to Zone NN18 (upper Pliocene).

As has been the case at previous sites, nannofossil species such as *Ceratolithus cristatus, Rhabdosphaera clavigera,* and *Oolithotus antillarum* are absent in this hole. *Pseudoemiliania lacunosa* is also rare throughout Zones NN19 and NN18. It is noteworthy that we recognized *Coccolithus pelagicus,* which is a typical cold-water species, in sediments below 163.0 mbsf.

Hole 727B

A total of 27.95 m of sediments was recovered from the second hole at Site 727. Sediments from the mud line to 17.6 mbsf contain *Emiliania huxleyi* and belong to Zone NN21 (Holocene to Pleistocene). We assigned underlying sediments down to the bottom of this hole to Zone NN20 (Pleistocene) because they contain neither *E. huxleyi* nor *P. lacunosa*.

Radiolarians

Most of the recovered material at Site 727 is barren of radiolarians. Rare, non-age-diagnostic fragments only were found in Samples 117-727A-15X, CC (143.6 mbsf), and 117-727A-17X, CC, through -19X, CC (163.0–182.4 mbsf).

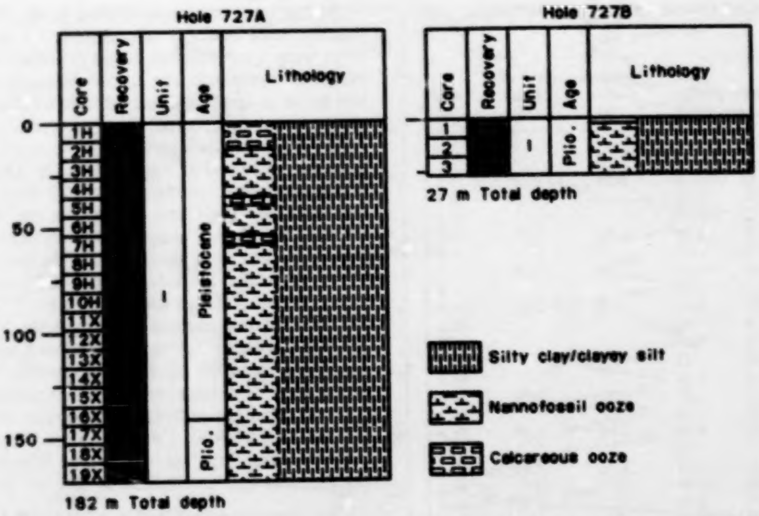

Figure 5. Lithostratigraphic summary columns, Site 727. Black bars represent recovery in Holes 727A and 727B.

Table 2. Smear slide summary, Site 727.

Component	Range	Average
Nannofossils	15%-55%	36%
Clay	15%-35%	26%
Detrital calcite	15%-40%	23%
Foraminifers	00%-20%	7%
Other minerals[a]	03%-12%	8%

[a] Primarily quartz with trace amounts of dolomite and opaque minerals.

Paleoenvironmental Implications

The high P/B ratio suggests that no major changes in the water depth at this site has occurred since the late Pliocene.

PALEOMAGNETISM

Introduction

Sediments recovered at Site 727 were homogeneous and comprised foraminifer-bearing marly nannofossil ooze and calcareous clayey silt. One discrete paleomagnetic sample per section was obtained from Hole 727A, and the magnetic susceptibility of whole-core sections was measured in both holes.

Magnetostratigraphy

We measured the natural remanent magnetization (NRM) of discrete samples with the Molspin Minispin spinner magnetometer. Magnetic cleaning was accomplished with the Schonstedt Alternating Field (AF) Demagnetizer. We selected peak AF demagnetization fields of 5 or 10 mT, depending on the initial intensity. Stepwise demagnetization of a sample from the uppermost part (117-727A-1H-6, 115-117 cm) is shown in Figure 9. As indicated by this example, samples from the upper 70 m interval had relatively high magnetic intensities ranging from 0.5 to 5.9 mA/m and high stability (median destructive field about 20 mT). Below ~100 mbsf, magnetic intensity was generally <0.5 mA/m. The samples from this interval were demagnetized at 5 mT peak AF. The overall logarithmic mean of the magnetic intensity is 0.6 mA/m.

Figure 10 shows downhole plots of magnetic directions and intensities. These plots were obtained after filtering all data with circular standard deviations (CSD) >40°. As also illustrated in the histogram in Figure 11, the inclination values of normal and reversed polarity show a rather asymmetric distribution; while positive inclinations are distributed around the value expected from the geocentric axial dipole field (32.7°), negative inclinations mostly range from −30° to 0°. The smaller absolute inclination values of reversed polarity may be explained by the insufficient removal of secondary magnetic overprints.

The inclination plot in Figure 10 shows that Hole 727A sediment is clearly divided into at least five polarity intervals. We assigned the normal polarity zone between 0 and about 80 mbsf to the Brunhes Chronozone (C1), and the interval below 80 mbsf to the Matuyama Chronozone. The two normal polarity zones, ranging from 96 to 105 mbsf and from about 160 mbsf to the bottom of the hole, can be assigned to the Jaramillo and Olduvai Subchronozones (C1r-1 and C2), respectively (Table 5). These assignments are concordant with the biostratigraphic datums of calcareous nannoplankton (see "Biostratigraphy" section, this chapter).

Magnetic Susceptibility

The magnetic susceptibility of Holes 727A and 727B were measured with the Bartington Susceptibility Meter (Model MS1) and a whole-core, pass-through sensor coil of 80-mm inner diameter (Model MS2C) at the 0.1 sensitivity and low-frequency (0.47 kHz) settings. All measurements were made at 10-cm intervals. The excellent recovery and core quality obtained at Site 727 resulted in one of the highest quality susceptibility records yet produced from Leg 117 drilling on the Oman margin.

The susceptibility values observed at Site 727 were similar in magnitude to those measured at Site 723. The approximate range of values is 30×10^{-6} to 100×10^{-6} volume SI units (Fig. 12). On average, these values are considerably lower than those values obtained from the other Oman margin sites (i.e., 724, 725, and 726). Since Sites 723 and 727 have the two highest accumulation rates of the margin sites (~180 and ~95 m/m.y., respec-

Table 3. Inorganic carbon, organic carbon, and carbonate, Site 727.

Core, section, interval (cm)	Depth (mbsf)	Total carbon (%)	Inorganic carbon (%)	Organic carbon (%)	$CaCO_3$ (%)
117-727A-					
1H-2, 100-102	2.50	10.05	6.64	3.41	55.3
1H-4, 100-102	5.50	6.71			55.9
1H-6, 100-102	8.50	7.79			64.9
2H-2, 50-52	11.50	8.36	6.81	1.55	56.7
2H-4, 50-52	14.50	6.67			55.6
3H-2, 100-102	21.40	10.67	7.39	3.28	61.6
3H-4, 78-80	24.18	6.88			57.3
3H-4, 119-120	24.59	8.84	6.82	2.02	56.8
3H-6, 34-36	26.74	7.30			60.8
4H-2, 6-8	29.96	8.39			69.9
4H-4, 6-8	32.96	7.22			60.1
4H-6, 6-8	35.96	8.24			68.6
5H-2, 71-73	40.01	7.83	7.03	0.80	58.6
5H-4, 32-34	42.62	7.35			61.2
6H-2, 50-52	49.30	8.70	7.13	1.57	59.4
6H-4, 111-113	52.91	8.01			66.7
6H-4, 119-120	52.99	9.21	8.12	1.09	67.6
6H-6, 8-10	54.88	7.98			66.5
6H-6, 50-52	55.30	5.76			48.0
7H-2, 123-125	59.53	8.14	6.54	1.60	54.5
7H-4, 8-10	61.38	6.20			51.7
7H-6, 8-10	64.38	7.25			60.4
8H-2, 24-26	68.14	10.26	8.04	2.22	67.0
8H-4, 40-42	71.30	7.52			62.6
8H-6, 8-10	73.98	7.48			62.3
9H-3, 27-29	79.37	7.57	6.65	0.92	55.4
9H-5, 119-120	83.29	8.19	7.09	1.10	59.1
9H-6, 63-65	84.23	6.90			57.5
10H-3, 80-82	88.32	9.93	6.68	3.25	55.6
10H-5, 90-92	91.42	7.76			64.6
10H-7, 88-90	94.40	7.16			59.6
11X-2, 76-78	97.66	7.97	6.27	1.70	52.2
11X-4, 25-27	100.15	6.73			56.1
11X-6, 85-87	103.75	7.20			60.0
12X-2, 98-100	107.48	9.73	7.59	2.14	63.2
12X-4, 98-100	110.48	7.53			62.7
12X-4, 144-145	110.94	10.43	7.77	2.66	64.7
12X-6, 98-100	113.48	7.24			60.3
13X-2, 0-1	116.10	9.24	7.12	2.12	59.3
13X-2, 93-95	117.03	8.39	6.52	1.87	54.3
13X-4, 102-104	120.12	6.78			56.5
13X-6, 80-82	122.90	7.40			61.6
14X-2, 98-100	126.48	10.63	7.16	3.47	59.6
14X-4, 133-135	129.83	6.31			52.6
14X-4, 149-150	129.99	9.59	5.95	3.64	49.6
14X-7, 18-20	133.18	7.18			59.8
15X-2, 28-30	135.68	11.16	6.93	4.23	57.7
15X-4, 17-19	138.57	6.35			52.9
15X-5, 119-120	141.09	12.23	7.27	4.96	60.6
15X-6, 58-60	141.98	7.24			60.3
16X-2, 80-82	145.90	10.43	6.37	4.06	53.1
16X-4, 60-62	148.70	6.30			52.5
16X-4, 149-150	149.59	8.41	5.76	2.65	48.0
16X-6, 114-116	152.24	5.53			46.1
17X-2, 94-96	155.74	8.74	5.87	2.87	48.9
17X-4, 95-97	158.75	6.39			53.2
17X-5, 0-1	159.30	10.70	6.63	4.07	55.2
17X-6, 120-122	162.00	5.50			45.8
18X-2, 84-86	165.34	10.74	6.92	3.82	57.6
18X-3, 119-120	167.19	9.18	8.13	1.05	67.7
18X-4, 104-106	168.54	7.77			64.7
18X-6, 98-100	171.48	7.68			64.0
19X-1, 135-137	174.05	10.49	7.64	2.85	63.6
19X-3, 0-1	175.70	9.86	7.91	1.95	65.9
19X-3, 128-130	176.98	7.39			61.6
19X-5, 95-97	179.65	6.34			52.8

tively), the lower susceptibility values are most probably attributable to dilution by nonmagnetic components.

The practical utility of susceptibility as a high-resolution stratigraphic tool could be demonstrated at Site 727. The data for the first 10 APC cores of Hole 727A, which were plotted while the hole was being drilled in the XCB mode, indicated that the mud line was missed and that several meters of sediment were not recovered. Since an objective of this site was to obtain a high-resolution upper Neogene sequence, a decision was made to spud-in a second hole so that the uppermost sediments could be recored. The susceptibility data of the three 727B APC cores indicated that ~4 meters of surficial sediment were not recovered at Hole 727A (Fig. 13).

Detailed correlations of Site 727 with other Oman margin sites and with the Owen Ridge sites are clearly apparent when the data are plotted at approximately equivalent time intervals. Figure 14 shows the susceptibility-derived correlations between Holes 723B and 727A from the Oman margin and Hole 722B from the Owen Ridge for the Brunhes Chronozone (0.73 Ma). No detailed correlations were possible between Site 727 and other margin sites below the Brunhes Chronozone since a susceptibility record of equal quality to Site 727 was not available at the time of writing; however, correlations exist between Site 727 and other Owen Ridge sites beyond the Jaramillo Subchronozone (>0.98 Ma). Detailed interhole correlations based on these susceptibility data and distinct lithologic marker layers are presented in the "Interhole Correlation" section of this chapter.

ACCUMULATION RATES

Magneto- and biostratigraphic data are used to determine sedimentation rates at Site 727 for the last 1.9 m.y. (Table 4). Sedimentation rates are calculated between nannofossil datums whose ages are based on oxygen-isotope stratigraphy (Niitsuma, unpublished data) and Berggren et al. (1985a, 1985b); this information is given in Table 4 and Figure 15. Rates vary between 60 and 133 m/m.y., with a mean of 95 m/m.y. for the last 1.9 m.y.

Much of the variation in sedimentation rate at the top of Hole 727A (Fig. 16) is based on the location and age of the LAD of *Pseudoemiliania lacunosa*. We assigned an age of 0.49 m.y. to this datum based on the oxygen-isotope data in nearby Site 723 (Niitsuma, unpublished data). However, if an age close to 0.40 m.y. is used, there is little variation in the mean sedimentation rate of 105 m/m.y. for the top 120 m of Site 727.

Since sediments are relatively homogeneous at Site 727 (see "Lithostratigraphy" section, this chapter), large variations in mean sedimentation rate are unexpected. Post-cruise analysis of the stratigraphic datums is necessary to determine whether the variations in mean sedimentation rate based on the present age model are correct.

In comparison with nearby Site 723, sediments accumulated at Site 727 at almost one half the rate of Site 723. These differences are attributed to the differences in tectonic setting of the two sites: Site 727 is near the edge and Site 723 is in the center of the upper slope basin.

The mass accumulation rates of calcium carbonate, organic carbon, and noncarbonate sediment components are calculated from average values between the nannoplankton datum levels (Table 6). During the Pleistocene to late Pliocene, sediments accumulated at Site 727 at rates between 7 and 13 $\mathrm{g/cm^2/k.y.}$ These values are comparable with those observed at Site 725 to the north. The high rates of organic carbon accumulation near the Pliocene/Pleistocene boundary (Table 6) are associated with sediments containing more biogenic silica (see "Lithostratigraphy" section, this chapter), an association which is observed at other Oman margin sites.

Based on smear slide analyses, sediments at Site 727 and at all other Oman margin sites contain abundant detrital calcite. Therefore, the accumulation of calcium carbonate in Figure 16 contains both detrital and pelagic components. Until the relative contributions of these components are determined, the accumulation of calcite cannot be used to infer changes in biogenic calcium carbonate production in surface waters.

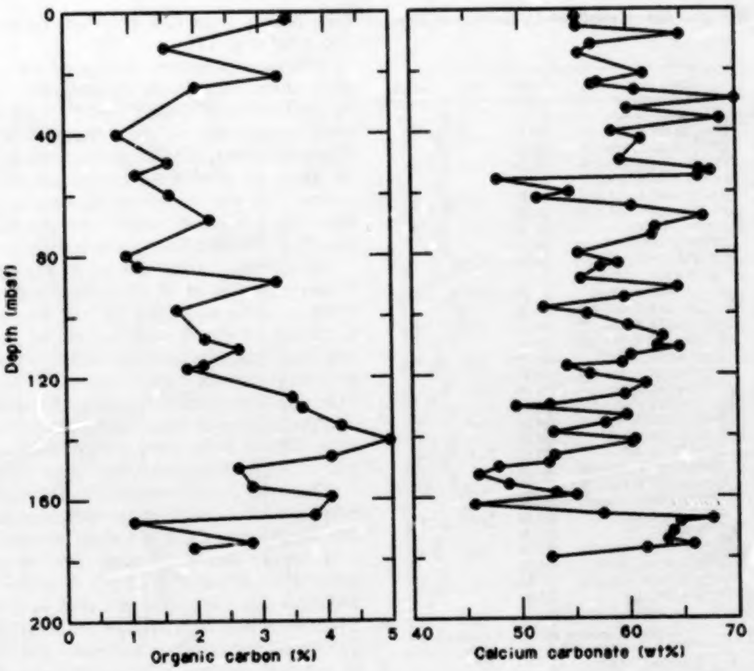

Figure 6. Calcium carbonate and organic carbon content, Site 727. The highest values of organic carbon occur from 126 to 165 mbsf.

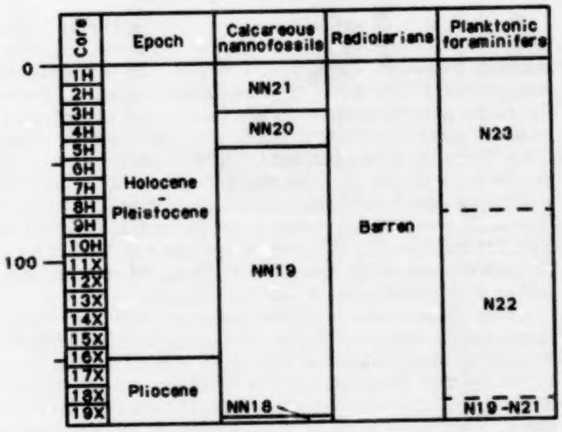
Core
Epoch
Calcareous nannofossils
Radiolarians
Planktonic foraminifers
0
100
1H
2H
3H
4H
5H
6H
7H
8H
9H
10H
11X
12X
13X
14X
15X
16X
17X
18X
19X
Holocene - Pleistocene
Pliocene
NN21
NN20
NN19
NN18
Barren
N23
N22
N19-N21

Figure 7. Correlation of planktonic microfossil zones in Hole 727A.

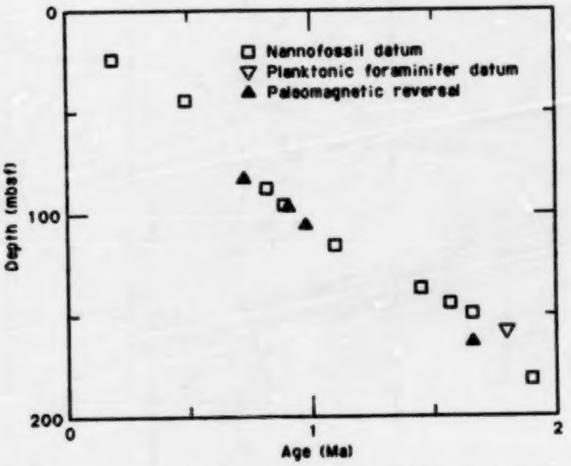

Figure 8. Age-depth plot for Hole 727A. For a detailed listing of events, see Table 4.

PHYSICAL PROPERTIES

Introduction

The problems we experienced at Sites 723, 724, and 725 in measuring the physical properties of sediments disturbed by gas-induced expansion were also encountered at Site 727. Physical properties measured on discrete samples included index properties (wet-bulk density, porosity, water content, and grain density), thermal conductivity, and vane shear strength (Table 7). We could not measure compressional-wave velocities with the Hamilton Frame Velocimeter because the sediments were not sufficiently indurated.

The GRAPE and *P*-wave logger were used to measure continuous wet-bulk density and compressional-wave velocity profiles in core sections longer than 80 cm. Acquisition of reliable data with the GRAPE and *P*-wave logging systems was limited to sediments recovered from depths <65 mbsf.

Table 4. Biostratigraphic listing of faunal events and paleomagnetic reversals for Hole 727A.

Event	Core, section, interval (cm)	Depth (mbsf)	Age (Ma)	Source of age
B *Emiliania huxleyi*	117-727A-3H-3, 118–119	23.08	0.19	3
	117-727A-3H-5, 118–119	26.08		
T *Pseudoemiliania lacunosa*	117-727A-5H-3, 118–119	41.98	0.49	3
	117-727A-5H-5, 118–119	44.98		
Brunhes/Matuyama	117-727A-9H-4, 115–117	81.75	0.73	6
	117-727A-9H-5, 115–117	83.25		
T *Reticulofenestra* sp. A	117-727A-9H, CC	85.80	0.82	3
	117-727A-10H-3, 118–119	88.70		
B *Gephyrocapsa parallela*	117-727A-10H-7, 118–119	94.70	[a]0.89	4
	117-727A-10H, CC			
T Jaramillo	117-727A-10H-8, 85–87	95.87	0.91	6
	117-727A-11X-1, 101–103	96.41		
B Jaramillo	117-727A-11X-6, 124–126	104.14	0.98	6
	117-727A-12X-1, 101–103	106.01		
T *Gephyrocapsa* "large"[b]	117-727A-12X, CC	114.60	[a]1.10	4
	117-727A-13X-1, 118–119	115.78		
T *Helicosphaera sellii*	117-727A-14X-1, 118–119	125.18	[c]	
	117-727A-14X-3, 114–115	128.14		
T *Calcidiscus macintyrei*	117-727A-15X-1, 106–107	134.96	1.45	6
	117-727A-15X-3, 116–117	138.06		
B *Gephyrocapsa oceanica*	117-727A-15X, CC	143.60	[a]1.57	4
	117-727A-16X-1, 118–119	144.78		
B *Gephyrocapsa caribbeanica*	117-727A-16X-3, 118–119	147.78	[d]1.66	4, 8
	117-727A-16X-5, 114–115	150.74		
T *Globigerinoides extremus*	117-727A-16X, CC	153.30	[e]1.8	6
	117-727A-17X, CC	163.00		
T Olduvai	117-727A-17X-6, 126–128	162.06	1.66	6
	117-727A-18X-1, 94–96	163.94		
T *Discoaster brouweri*	117-727A-19X-5, 120–121	179.90	1.9	6
	117-727A-19X, CC	182.40		

Note: T = upper limit of event and B = lower limit. Sources of ages are: 3 = oxygen isotope data for Site 723 (N. Niitsuma, unpubl. data); 4 = Takayama and Sato, 1987; 6 = Berggren et al., 1985b; and 8 = Sato et al., in press.

[a] North Atlantic data.

[b] Long axis greater than 6 μm.

[c] No good published age; event appears to be diachronous.

[d] North Atlantic age consistent with Italian-type section.

[e] *G. obliquus extremus* cited in Berggren et al., 1985b.

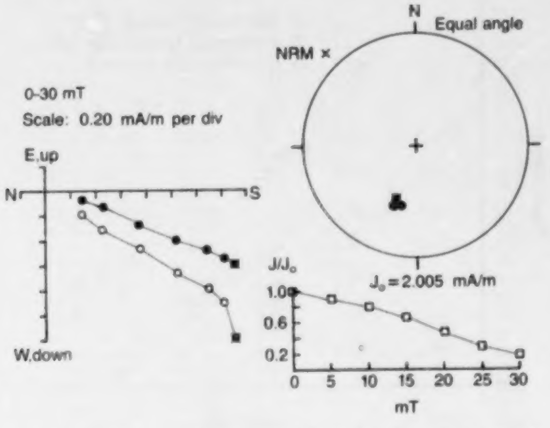

Figure 9. Result of stepwise alternating field (AF) demagnetization for Sample 117-727A-1H-6, 115–117 cm, from 0 to 30 mT.

Index Properties

The uniform lithology of marly nannofossil ooze at Site 727 is characterized by a gradual change in index properties with increasing burial depth. Porosity and water content decrease from 66% and 43%, respectively, at the seafloor to values of 56% and 33% at 180 mbsf (Fig. 17). Grain density shows little variation about an average value of 2.59 g/cm^3; as a consequence, decreasing water content is responsible for an increase in wet-bulk density from 1.58 g/cm^3 at the seafloor to 1.80 g/cm^3 at 180 mbsf (Fig. 17).

The most prominent feature of the index properties profiles is the sharp reduction in the variability of water content, porosity, and wet-bulk density which occurs at 88 mbsf. This depth roughly coincides with the depth at which foraminifer abundance decreases, suggesting that greater water content variability above 88 mbsf is a consequence of textural variation. The coarse grain size of intervals enriched in foraminifers may cause those layers to exhibit lower water content and higher bulk density than adjacent finer-grained sediment.

In addition to the change in the uniformity of the index property profiles at 88 mbsf, there is a 6% increase in porosity (56% to 62%) and a 0.13 g/cm^3 decrease in wet-bulk density (1.80 to 1.67 g/cm^3) over the interval from 84 to 88 mbsf (Fig. 17). These porosity and bulk density changes reflect an increase in average organic carbon content from 1.10% to 3.25% (see "Organic Geochemistry" section, this chapter). Between 88 mbsf and the bottom of Hole 727A (182.4 mbsf), porosity decreases from 62% to 56%, water content decreases from 38% to 33%, and wet-bulk density increases from 1.67 to 1.75 g/cm^3.

These trends are reversed in the interval between 126 and 165 mbsf, coinciding with an increase in organic carbon content. In this depth range there is a slight decrease (0.05 g/cm^3) in wet-bulk density and an increase (3%) in porosity (Fig. 17). The lowest grain densities (2.43 to 2.46 g/cm^3) occur between 138 to 146 mbsf and correspond to a peak in the organic carbon abundance (4.06%–4.96%). Below 165 mbsf a slight increase in grain density, decreases in porosity and water content, and an increase in wet-bulk density reflect decreasing abundance of organic matter and sediment dewatering controlled by increasing overburden pressure.

GRAPE and *P*-Wave Logs

Determination of wet-bulk density by the GRAPE and compressional-wave velocity with the *P*-wave logger was limited by sediment expansion. Continuous GRAPE data were obtained through Core 117-727A-10H (95.4 mbsf); however, below 65 mbsf the quality of the data decreases as a consequence of expansion-related fractures. Between 65 and 95 mbsf the character of the GRAPE records is retained, but GRAPE estimates of wet-bulk density are less than densities determined for discrete samples and there is more high-frequency noise in the data. The GRAPE records display a cyclic variation similar to that observed at Sites 723 and 724. The thickness of the cycles at Site 727 is on the scale of those at Site 724, roughly 2–3 m, and approximately half as thick as the cycles at Site 723 (Fig. 18).

Compressional-wave velocities measured with the *P*-wave logger are the only velocity data obtained at Site 727. Reliable *P*-wave logs were obtained to a depth of 38 mbsf in Hole 727A before sediment disturbance halted signal transmission through the core sections. Velocities range from 1520 to 1610 m/s and display a pattern of cyclic variation similar to that contained in the GRAPE records (Fig. 19).

Thermal Conductivity

Thermal conductivity measurements were made on alternate cores in Hole 727A through Core 117-727A-10X and on Cores 117-727B-1H and 117-727B-3H in Hole 727B (Table 7). The sediment conductivity ranges from 0.97 to 1.54 $W \cdot m^{-1} \cdot K^{-1}$ and averages 1.23 $W \cdot m^{-1} \cdot K^{-1}$. With the exception of a low conductivity at 0.50 mbsf (0.95 $W \cdot m^{-1} \cdot K^{-1}$) and higher values between 12 and 18 mbsf (1.44–1.54 $W \cdot m^{-1} \cdot K^{-1}$) and 33 and 37 mbsf (1.34–1.37 $W \cdot m^{-1} \cdot K^{-1}$), most values are clustered about 1.2 $W \cdot m^{-1} \cdot K^{-1}$ and there is little change in conductivity with depth (Fig. 20). Although the thermal conductivity of sediments

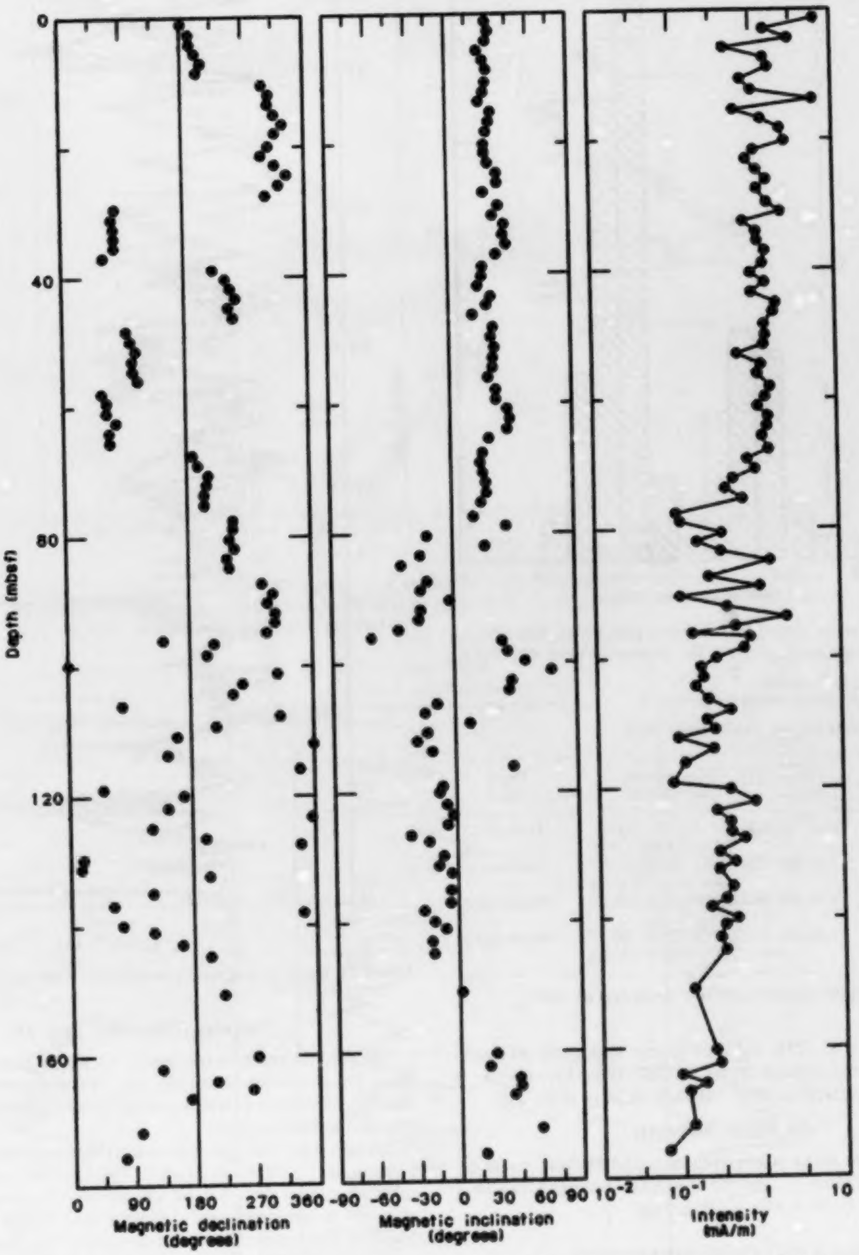

Figure 10. Plots of magnetic declination (relative values), inclination, and intensity against the sub-bottom depth of Hole 727A, obtained by shipboard measurements after AF demagnetization at 5 or 10 mT and filtering circular standard deviation values greater than 40°.

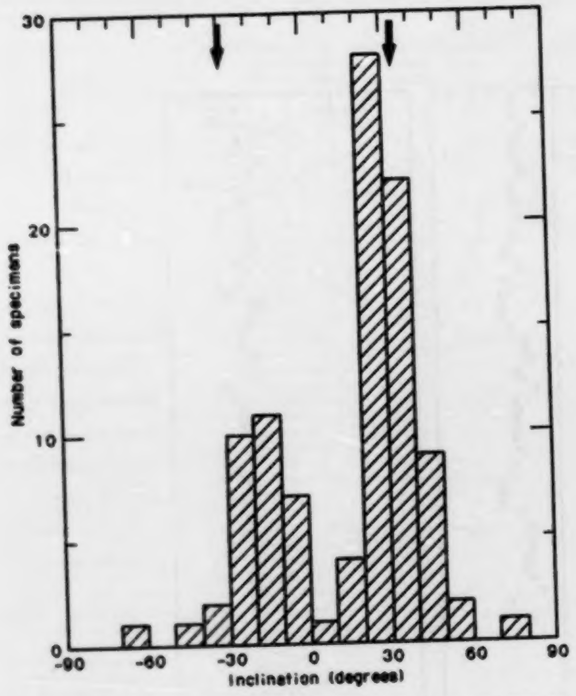

Figure 11. Histogram of magnetic inclination values from Site 727. Arrows show the values expected from the geocentric axial dipole field (32.7°).

Table 5. Magnetozone boundaries in Hole 727A.

Boundary	Age (Ma)	Core, section, interval (cm)	Depth (mbsf)
Brunhes/Matuyama (C1/C1r)	0.73 Ma	117-727A-9H-4, 115 to 117-727A-9H-5, 115	81.75-83.25
Top of Jaramillo (C1r/C1r-1)	0.91 Ma	117-727A-10H-8, 85 to 117-727A-11X-1, 101	95.87-96.41
Bottom of Jaramillo (C1r-1/C1r)	0.98 Ma	117-727A-11X-6, 124 to	104.14-106.01
Top of Olduvai (C1r/C2)	1.66 Ma	117-727A-17X-6, 107 to 117-727A-16X-5, 104	162.06-163.94

Note: Ages of chronozone boundaries are after Berggren et al., 1985b.

from Holes 727A and 727B does not appear to depend on burial depth over the measurement range, conductivity does display a strong positive correlation with wet-bulk density (Fig. 21).

Vane Shear Strength

Only three vane shear strength measurements were made on cores at Site 727 (Table 7). The shear strengths range from 16.2 kPa at 11.7 mbsf to 30.4 kPa at 21.1 mbsf.

INORGANIC GEOCHEMISTRY

Introduction

Nine interstitial water samples were collected at Site 727, seven by squeezing and two using the *in-situ* water sampling tool. All analytical data are listed in Table 8 and presented in Figure 22.

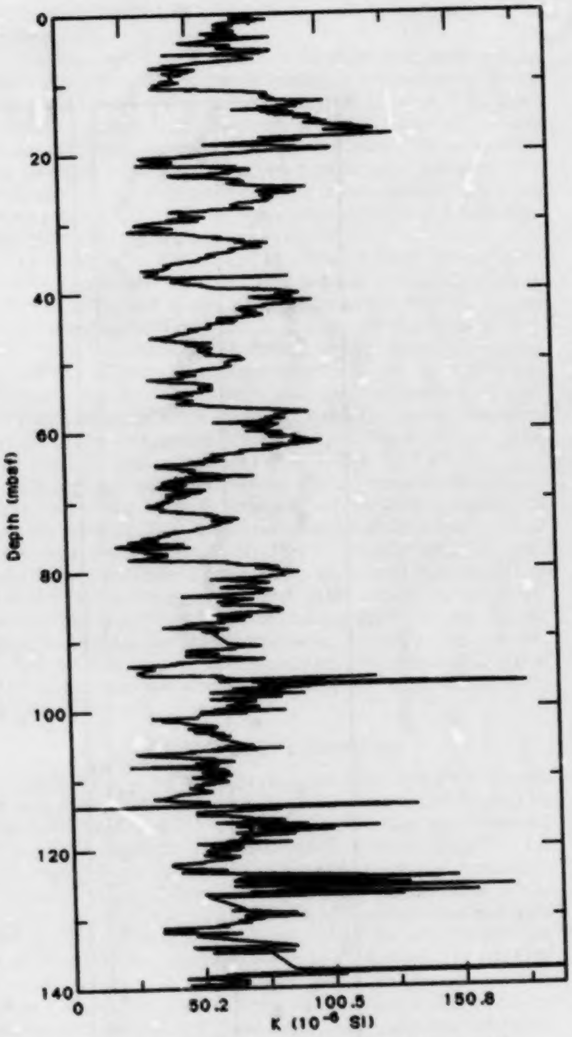

Figure 12. Plots of magnetic susceptibility data for Hole 727A.

Salinity, Chloride, and pH

Salinity decreases with depth, as we have observed at most other Oman margin sites (Fig. 22). This is attributable to the reduction of sulfate as well as a significant downward decrease in the magnesium content.

More important, the chloride concentration decreases from 569 mmol/L at the top of Hole 727A to 554 mmol/L at ~170 mbsf. A similar distribution was observed at Site 723, which we ascribed to the downward diffusion of chloride toward a more brackish fluid at depth, or the upward advection of such a fluid.

The pH appears to decrease with depth, but, as at other margin sites, the data are not considered to be reliable due to steady loss of CO_2 during pH measurement.

Sulfate and Alkalinity

The sulfate gradient over the upper 40 m at this site, ~ −0.5 mmol/L/m, is similar to that at Site 723. The sulfate concentra-

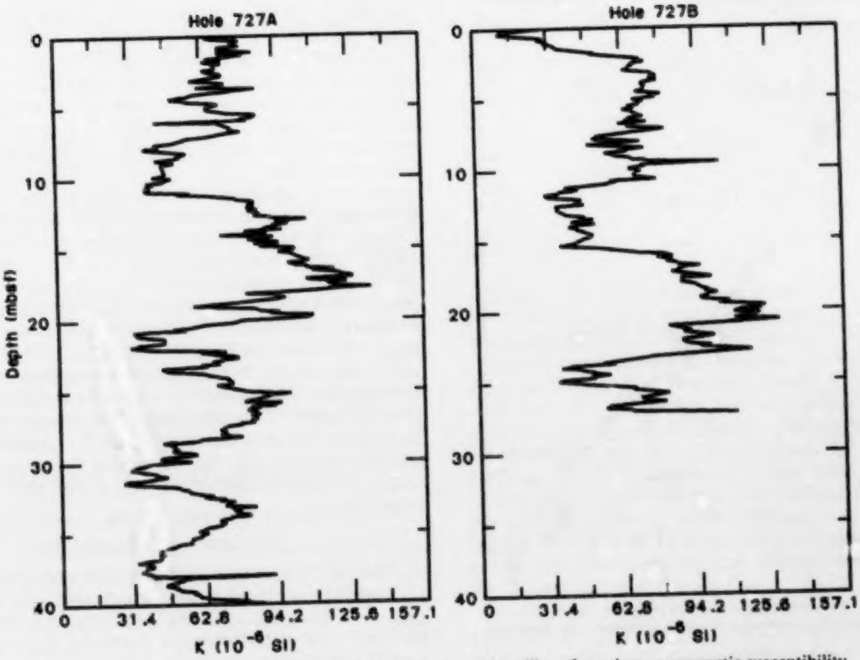

Figure 13. An illustration of the high-resolution stratigraphic utility of continuous magnetic susceptibility measurements. As shown by the susceptibility data of Hole 727B, the first core of Hole 727A missed the mud line and ~4 meters of surficial sediment.

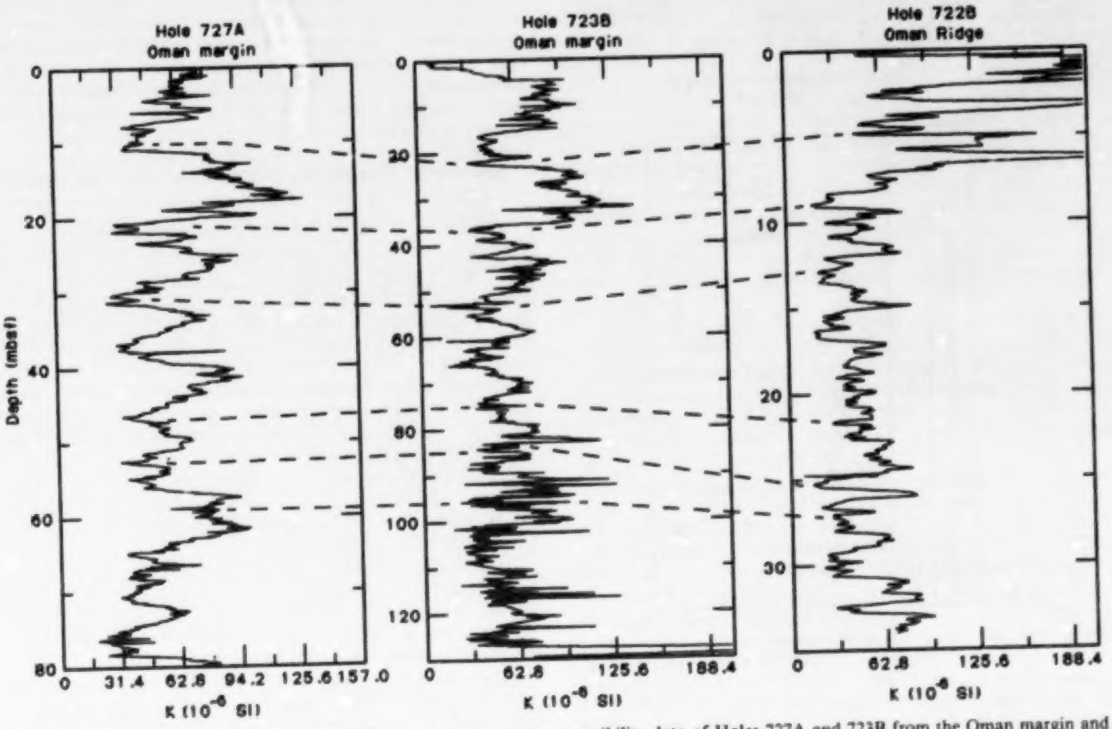

Figure 14. Brunhes Chronozone correlations between the magnetic susceptibility data of Holes 727A and 723B from the Oman margin and Hole 722B from the Owen Ridge.

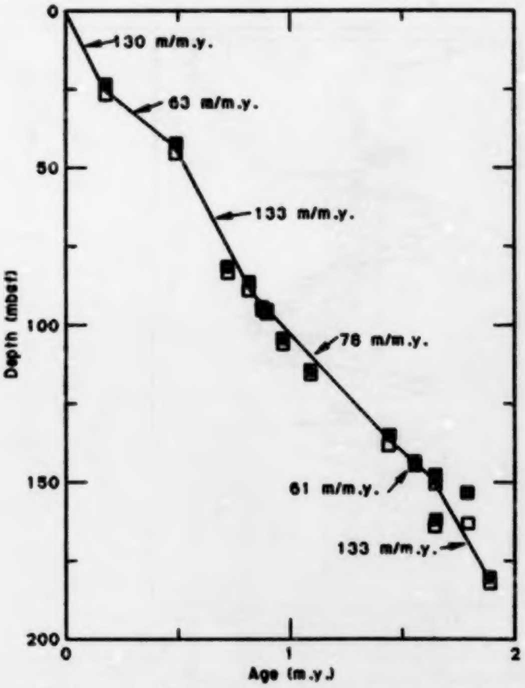

Figure 15. Age-depth plot of stratigraphic datums listed in Table 6. The filled and open dots are the upper and lower depths of each datum level, respectively. Indicated sedimentation rates (solid lines) are calculated between nannofossil datum levels whose ages are based on oxygen-isotope stratigraphy (N. Niitsuma, unpubl. data) or Berggren et al. (1985b).

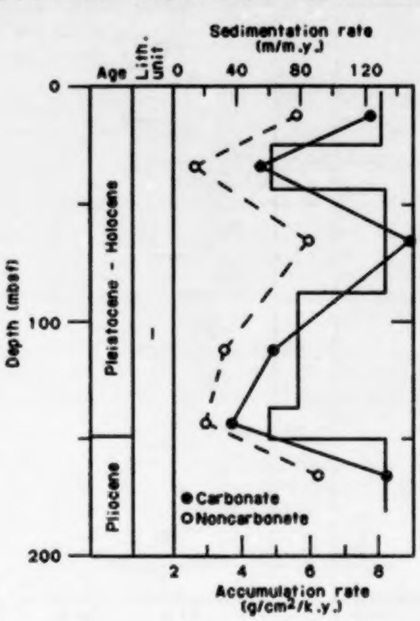

Figure 16. Sedimentation rate (m/m.y.; solid line), calcium carbonate accumulation rate (g/cm^2/k.y.; dots), and noncarbonate accumulation rate (g/cm^2/k.y.; circles) vs. depth at Site 727. Accumulation rates are plotted at the midpoint of the respective depth intervals.

tion falls to zero near 50 mbsf but increases at greater depths to levels >1 mmol/L (Table 8 and Fig. 22). As at Site 723, the presence of SO_4^{2-} in the lower half of the hole suggests that upward diffusion from a sulfate-enriched fluid at depth is responsible for the unusual distribution. Joint consideration of the sulfate and chloride profiles implies that the fluid may have been derived from the leaching of gypsum or anhydrite by relatively fresh water.

Moderate alkalinities are observed at Site 727. As we have discussed in previous reports for margin sites, the alkalinity distribution can be attributed to three processes: (1) production of HCO_3^- (which dominates), NH_4^+, and H_2S during sulfate reduction; (2) consumption of HCO_3^- by precipitating carbonate phases; and (3) production of NH_4^+ during methanogenesis. Process (1) appears to be restricted largely to the upper 50 m, although the reduction of upward-diffusing SO_4^{2-} at greater depths may be important. The calcium and magnesium profiles (see below) indicate that process (2) is important only in the top 50 m. The ~25 mmol/L increase in alkalinity between 50 and 180 mbsf corresponds to an increase of similar magnitude in the ammonia concentration (Fig. 22), suggesting that process (3) may be a major contributor to alkalinity below the upper zone of sulfate reduction.

Calcium and Magnesium

Most of the curvature in the calcium and magnesium profiles occurs in the top 60 m of the section (Fig. 22), suggesting that diagenetic reactions involving these ions are confined to this upper zone. The slight increase in the Mg^{2+}/Ca^{2+} ratio between 6 and 25 mbsf, coupled with a concurrent decrease in the calcium concentration, indicates that calcite may be precipitating in this interval. The decrease of magnesium between 25 and ~60 mbsf is attributed to the formation of dolomite in this zone. We cannot determine whether this occurs via replacement of pre-existing calcite or by direct precipitation. The flat nature of the profiles in the lower half of the section indicates that alteration of basement rocks is not influencing the distribution of dissolved magnesium and calcium over the top 200 m of the sedimentary column at this site.

Ammonia, Phosphate, Silica, and Dissolved Organic Carbon

A comparison of the ammonia and sulfate profiles indicates that ammonia must be being removed from solution over the top ~35 m of the cored section, presumably by the uptake of NH_4^+ by clay minerals (Fig. 22). The magnesium distribution does not indicate that ammonium is exchanging directly for magnesium in clays. The increase in the dissolved ammonia concentration below ~40 mbsf may reflect saturation of the clays by ammonia, although a generally higher organic carbon concentration in this zone could be related to enhanced ammonia production if the more abundant organic matter at depth had a lower C:N ratio (i.e., was less refractory).

Dissolved phosphate levels are much lower than would be predicted on the basis of the observed ammonia concentrations. As at other sites, the phosphate deficiency is probably due to the precipitation of apatite phases.

The rather low gradient of the dissolved silica profile (Fig. 22) over the top 40 m of the section (~20 μmol/L/m) indicates that the sediments at Site 727 are relatively depleted in opal. There is no indication in the profile that zones enriched in opal occur in the cored section.

The dissolved organic carbon (DOC) profile shown in Figure 23 and the data listed in Table 9 suggest that relatively high concentrations of sedimentary organic matter should be encountered at a depth of roughly 40 mbsf. However, the organic car-

Table 6. Sedimentation and accumulation rate data for Site 727.

Depth interval (mbsf)	Age range (m.y.)	$CaCO_3$ ($\bar{x}$ %)	C_{org} ($\bar{x}$ %)	Dry-bulk density ($\bar{x}$ g/cm^3)	Sed. rate ($\bar{x}$ m/m.y.)	$CaCO_3$ acc. rate (g/cm^2/k.y.)	Non-$CaCO_3$ acc. rate (g/cm^2/k.y.)	C_{org} acc. rate (mg/cm^2/k.y.)
0-24.6	0-0.19	58.0	2.57	1.03	129.5	7.74	5.60	342.8
24.6-43.5	0.19-0.49	63.2	0.80	1.14	63.0	4.54	2.64	57.5
43.5-87.3	0.49-0.82	59.9	1.42	1.12	132.7	8.90	5.96	211.0
87.3-136.5	0.82-1.45	58.4	2.79	1.08	78.1	4.93	3.51	235.3
136.5-149.3	1.45-1.66	55.9	4.51	1.10	61.0	3.75	2.96	302.6
149.3-181.2	1.66-1.90	56.8	2.75	1.09	132.9	8.23	6.26	398.4

bon distribution reported in the "Organic Geochemistry" section (this chapter) indicates that DOC and sedimentary organic carbon distributions are poorly correlated at this site. We do not know why the correlation is excellent at some sites (e.g., Site 728) and not at others. The differences may be related to spatial and/or temporal variations of either the type or quality (i.e., extent of degradation) of buried organic matter.

ORGANIC GEOCHEMISTRY

Organic Matter Abundance and Character

We investigated 30 sediment samples from Hole 727A by carbon analysis and Rock-Eval pyrolysis. Organic carbon concentrations average 2.51% and range from 0.80% to 4.96% in the only lithologic unit recognized (Table 3 and Fig. 24).

A slight trend to high organic carbon values as well as high hydrogen index values appears with depth in Figure 24. Assuming a uniform sedimentation rate, the variation in organic carbon concentrations might be the sedimentary expression of variations in the primary productivity.

When the hydrogen and oxygen indices of samples from Site 727 (Table 10) are plotted in a "van Krevelen-type" diagram together with these indices from Site 722 on the Owen Ridge (dots) and from Site 726 on the Oman margin (triangles), samples from Hole 727A (diamonds) plot for the most part in a cluster characterized by a hydrogen index between 200 and 400, and an oxygen index less than 150 (Fig. 25). This may be viewed as a manifestation of the relatively pristine nature of organic matter deposited under oxygen-depleted conditions at the center of the OMZ at Site 727, as compared with organic matter buried under oxygenated water at Site 722 (2034-m water depth). The wide spread of values from Site 726 may be due to sporadically oxic/suboxic/anoxic conditions prevalent at Site 726 (water depth 331 m). Alternatively, the source of the organic matter may be different in the three sectors of the upwelling system and may be related to a spatial zonation of primary producers.

Hydrocarbon Gases

The rapid decrease of interstitial sulfate to negligible amounts below 60 mbsf (see "Inorganic Geochemistry" section, this chapter) is mirrored by a steady increase of biogenic methane measured in headspace samples (Fig. 26 and Table 11). Below the depth of sulfate depletion, we observed the first gas pockets, almost entirely composed out of biogenic methane with small amounts of thermogenic ethane and propane in the hydrocarbon fraction (Table 12). The increase of ethane and propane concentration with depth (Figs. 26 and 27) is in concordance with findings at other sites on the Oman margin.

INTERHOLE CORRELATION

The two holes drilled at Site 727 are located at 915 mbsl in the southern part of the slope basin, previously drilled at Site 723. Holes 727A and 727B were drilled without offset; Hole 727A was drilled to 95.4 mbsf with the APC and to 182.4 mbsf with the XCB, while Hole 727B penetrated 27.1 mbsf with the APC. Recovery from APC coring was almost perfect in these holes, and the top of Hole 727B obtained the mud line.

Detailed correlations in the upper 55 m of the drilled sediments at Site 727 are given here. The upper interval has an age range from 0 to about 0.5 Ma, and is characterized by cyclic changes in the nature of sediments that can be identified by visual observation and by variations of magnetic susceptibility and $CaCO_3$ content. The coherence and similarity of sediments among these holes provides valuable information on the relative rate of sedimentation, which is necessary information for any high-resolution study of depositional environments. The essence of the interhole correlation process is outlined in the "Explanatory Notes" chapter.

Hole-to-hole correlations were made on the basis of visual identification of distinctive layers, as well as physical and magnetic properties. Magnetic susceptibility was measured at 10-cm intervals before splitting the sections. Photographs were taken of the split cores.

Visual correlation of the cores relied primarily on the core photographs. We determined 26 distinct and traceable layers in the upper 55 m of sediment at Sites 723 and 724, which have been denoted as OM-a_1, . . . , h_3, and h_5, based on the correlation between the holes at Sites 723 and 724 (see "Interhole Correlation" sections, "Site 723" and "Site 724" chapters). The letter code (i.e., a, b, c, . . .) refers to the sequence of cores, and the number subscript indicates the marker layer sequence in each core. For example, the notation "a_2" corresponds to the second marker layer defined in Core 117-723A-1H, and "b_1" denotes the first marker layer in Core 117-723A-2H. The marker layers a_1–h_4 were defined on the cored sediments of Hole 723A. Three marker layers (c_5, e_3, and h_5) were defined on the sedimentary sequence at Hole 724A in addition to those noted at Site 723.

The criteria for defining a marker layer are that the layer is distinct enough to trace in the sedimentary sequence of the other holes and that its character does not change. The useful criteria for recognizing the marker are color boundaries, distinctly colored layers, shape of bioturbation, and sequence of color change in surrounding sediments. Table 13 lists the depth of the marker layers in two holes of Site 727.

Figure 28 shows the magnetic susceptibility curve and positions of individual, visually correlatable layers. The pattern of the susceptibility and the positions of layers match very well, not only among the two holes, but also between Sites 723 and 727 (Fig. 28). The stratigraphy of the magnetic susceptibility data and the visually identified layers are extremely consistent in that a particular visually characteristic layer always coincides in depth with a distinct feature in the magnetic susceptibility curve. In this way the lithologic marker layer correlations are confirmed using the susceptibility data, which are quantitative.

The results of the layer-by-layer correlation allow us to calculate the true thickness of these layers that coincide with and are separated by core boundaries. Core tops occasionally were ex-

Table 7. Physical properties summary, Hole 727A.

Core, section, interval (cm)	Depth (mbsf)	Wet-bulk density (g/cm^3)	Porosity (%)	Water content (%)	Grain density (g/cm^3)	Dry-bulk density (g/cm^3)	Thermal conductivity (W·m^{-1}·K^{-1})	Vane shear strength (kPa)
117-727A-								
1H-2, 100–102	2.50	1.589	65.7	42.4	2.614	0.915		
1H-4, 100–102	5.50	1.650	54.3	33.7	2.599	1.094		
1H-6, 100–102	8.50	1.572	67.0	43.7	2.564	0.885		
2H-2, 50–52	11.50	1.761	55.4	32.2	2.599	1.193		
2H-2, 100–101	12.00						1.44	
2H-4, 50–52	14.50	1.759	58.4	34.0	2.700	1.161		
2H-4, 100–101	15.00						1.54	
2H-6, 50–52	17.50	1.734	56.4	33.3	2.560	1.156		29.0
2H-6, 100–101	18.00						1.13	
3H-2, 100–102	21.40	1.551	67.0	44.2	2.548	0.865		
3H-4, 78–80	24.18	1.582	57.3	37.1	2.583	0.995		
3H-6, 36–38	26.76	1.814	61.5	34.7	2.689	1.184		
4H-2, 6–8	29.96	1.624	64.0	40.4	2.589	0.968		
4H-2, 80–81	30.70						1.20	
4H-4, 6–8	32.96	1.803	53.4	30.3	2.534	1.256		
4H-4, 80–81	33.70						1.37	
4H-6, 6–8	35.96	1.691	61.0	36.9	2.650	1.066		
4H-6, 80–81	36.70						1.34	
5H-2, 71–73	40.01	1.848	51.3	28.4	2.642	1.323		
5H-4, 32–34	42.62	1.677	59.4	36.3	2.501	1.068		
6H-2, 50–52	49.30	1.691	56.6	34.3	2.535	1.112		
6H-2, 80–81	49.60						1.27	
6H-4, 80–81	52.60						1.15	
6H-4, 111–113	52.91	1.699	61.6	37.1	2.678	1.068		
6H-6, 8–10	54.88	1.608	62.5	39.8	2.469	0.968		
6H-6, 80–81	55.60						1.17	
7H-2, 123–125	59.53	1.753	56.5	33.0	2.592	1.175		
7H-4, 8–10	61.38	1.786	53.5	30.7	2.563	1.238		
7H-6, 8–10	64.38	1.639	65.0	40.6	2.633	0.973		
8H-2, 24–26	68.14	1.680	61.8	37.7	2.643	1.047		
8H-2, 78–79	68.68						1.20	
8H-4, 40–42	71.30	1.628	61.1	38.4	2.445	1.002		
8H-4, 78–79	71.68						1.20	
8H-6, 8–10	73.98	1.748	58.6	34.4	2.677	1.147		
8H-6, 78–79	74.68						1.16	
9H-3, 27–29	79.37	1.848	50.8	28.2	2.639	1.328		
9H-6, 63–65	84.23	1.797	55.8	31.8	2.662	1.226		
10X-2, 75–76	86.77						1.16	
10X-3, 80–82	88.32	1.670	62.0	38.0	2.590	1.035		
10X-4, 75–76	89.77						1.24	
10X-5, 90–92	91.42	1.717	60.7	36.2	2.694	1.095		
10X-6, 75–76	92.77						1.21	
10X-7, 88–90	94.40	1.697	59.8	36.1	2.570	1.084		
11X-2, 76–78	97.66	1.720	59.0	35.1	2.601	1.116		
11X-4, 25–27	100.15	1.656	61.0	37.7	2.559	1.031		
11X-6, 85–87	103.75	1.755	57.3	33.5	2.629	1.168		
12X-2, 98–100	107.48	1.723	60.4	35.9	2.660	1.104		
12X-4, 98–100	110.48	1.749	56.3	33.0	2.615	1.172		
12X-6, 98–100	113.48	1.712	58.7	35.1	2.562	1.111		
13X-2, 93–95	117.03	1.765	58.0	33.6	2.667	1.171		
13X-4, 102–104	120.12	1.706	60.1	36.1	2.594	1.090		
13X-6, 80–82	122.90	1.671	60.0	36.8	2.515	1.057		
14X-2, 98–100	126.48	1.638	63.2	39.5	2.557	0.990		
14X-4, 133–135	129.83	1.687	59.1	35.9	2.561	1.082		
14X-7, 18–20	133.18	1.654	61.5	38.1	2.536	1.023		
15X-2, 28–30	135.68	1.660	61.6	38.0	2.597	1.028		
15X-4, 17–19	138.57	1.638	60.6	37.9	2.464	1.017		
15X-6, 58–60	141.98	1.685	57.9	35.2	2.433	1.092		
16X-2, 80–82	145.90	1.655	58.4	36.1	2.434	1.058		
16X-4, 60–62	148.70	1.812	54.6	30.9	2.641	1.252		
16X-6, 114–116	152.24	1.701	57.8	34.8	2.518	1.109		
17X-2, 94–96	155.74	1.754	58.8	34.4	2.668	1.151		
17X-4, 95–97	158.75	1.691	59.8	36.2	2.556	1.079		
17X-6, 120–122	162.00	1.700	57.7	34.8	2.521	1.109		
18X-2, 84–86	165.34	1.690	60.4	36.6	2.610	1.071		
18X-4, 104–106	168.54	1.643	62.5	38.9	2.572	1.003		
18X-6, 98–100	171.48	1.663	61.7	38.0	2.568	1.031		
19X-1, 135–137	174.05	1.692	58.8	35.6	2.525	1.090		
19X-3, 128–130	176.98	1.731	60.6	35.8	2.639	1.111		
19X-5, 95–97	179.65	1.751	56.0	32.8	2.576	1.178		
117-727B-								
1H-1, 50–51	0.50					0.970		
1H-3, 50–52	3.50	1.569	66.4	43.3	2.510	0.889	1.19	
1H-5, 50–51	6.50						1.23	
2H-3, 50–52	11.70	1.465	72.8	50.9	2.544	0.719		16.2
3H-1, 50–51	18.10						1.44	
3H-3, 50–52	21.10	1.529	67.3	45.1	2.438	0.839	1.14	30.4
3H-5, 50–51	24.10						1.17	

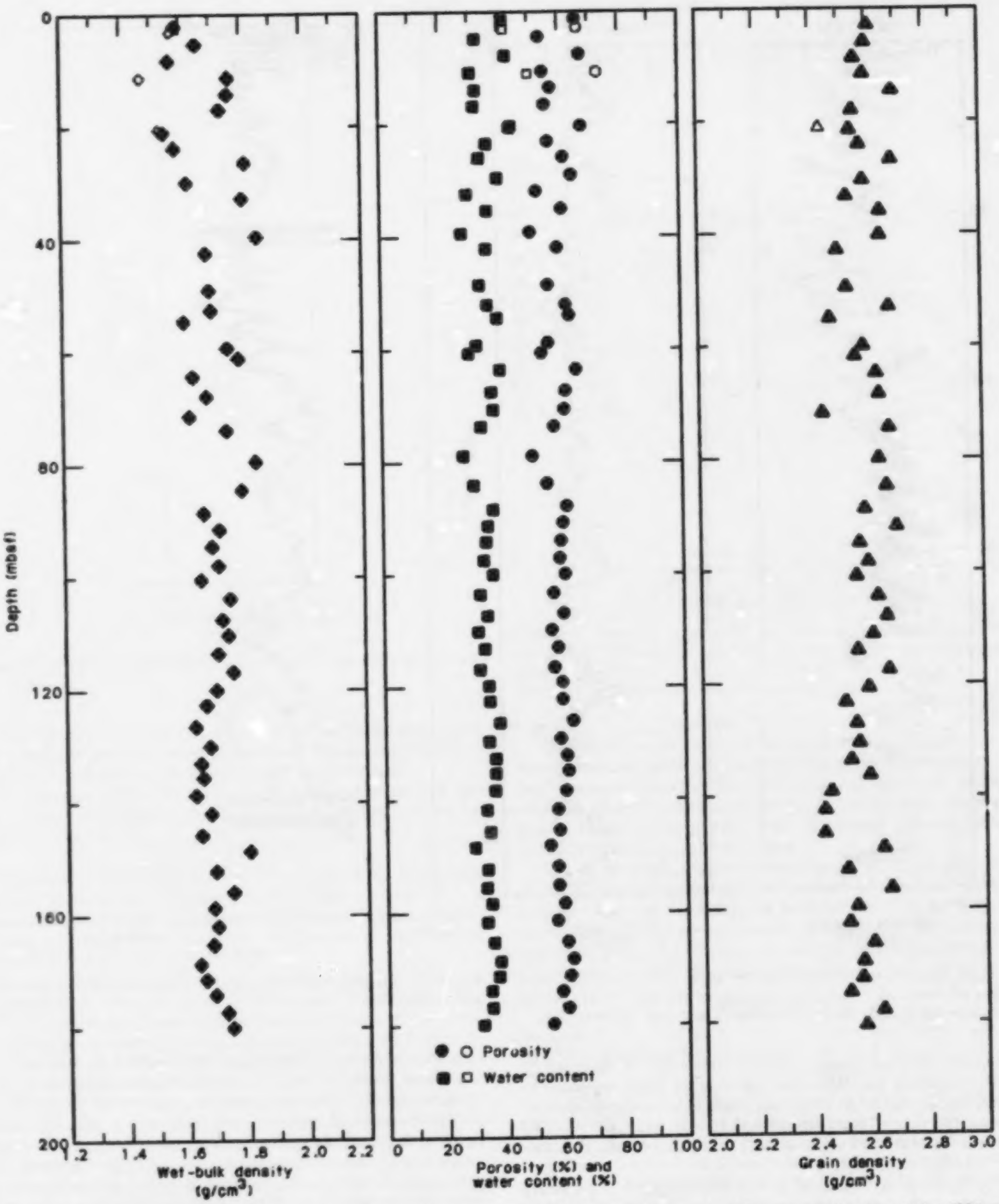

Figure 17. Index properties (wet-bulk density, porosity, water content, and grain density) measured on discrete samples from Holes 727A and 727B. Closed symbols represent values for Hole 727A, and open symbols, Hole 727B.

panded by water uptake during drilling. In this case, the apparent thickness of the disturbed sediment layer is observed to be thicker than the original thickness. In some instances, the top part of the core was missing; in this case, apparent thickness is observed to be thinner than the original thickness. Fortunately, the two holes were staggered in depth so that they have different horizons at core boundaries (Table 13).

The original thickness of layers coinciding with core tops or bottoms can be obtained by comparing the thickness of the correlative layer in the continuous section of the other holes. The

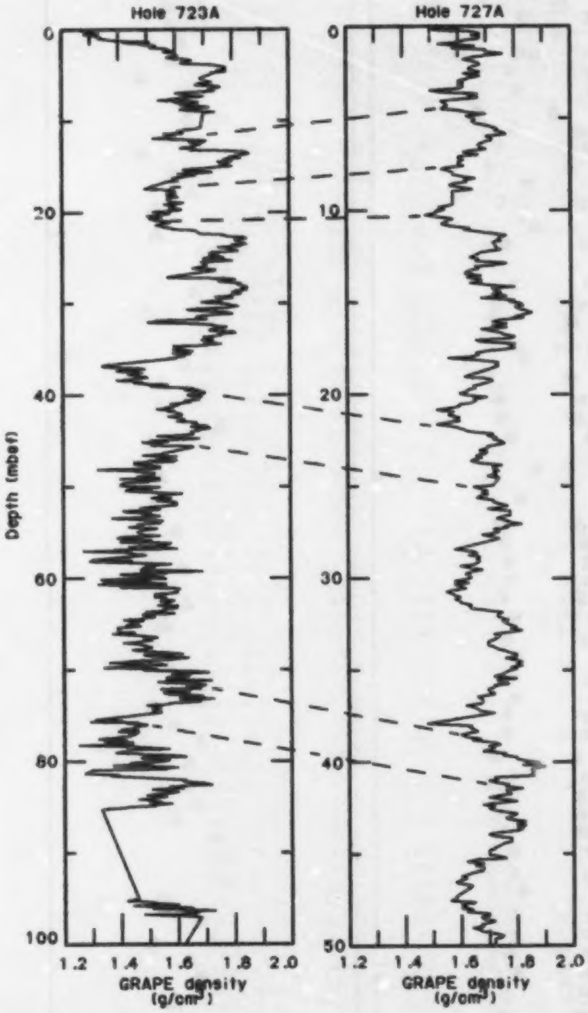

Figure 18. GRAPE wet-bulk density for Holes 723A and 727A. The profiles are based on 10-cm-block averages of the data. Note that the depth scale for Hole 723A is approximately half that of Hole 727A.

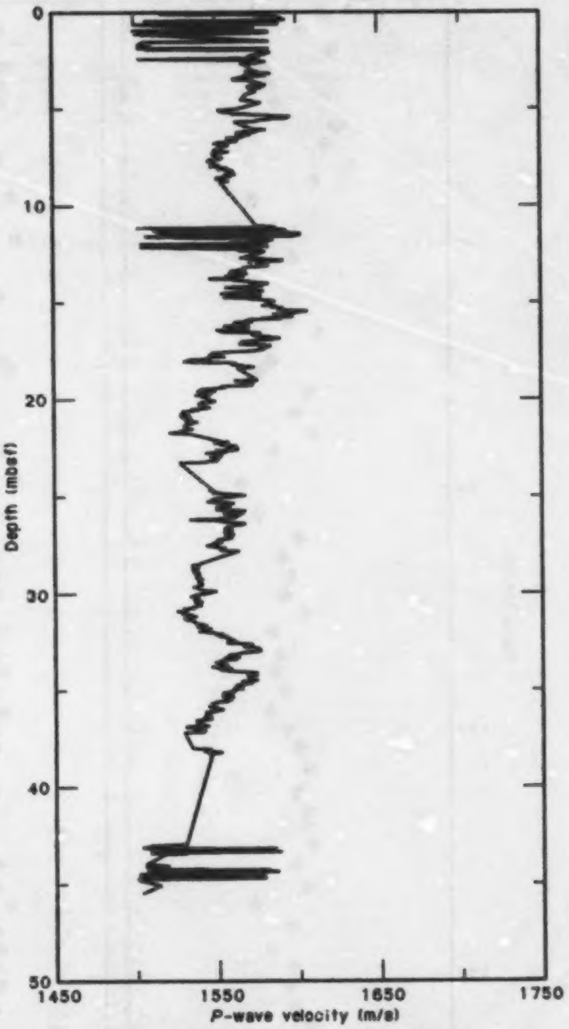

Figure 19. Compressional-wave velocity as measured by the *P*-wave logger in Hole 727A.

calculation of the amount of the difference can be achieved by the differences in the ODP depths of marker layers between the holes ("727B – 727A" in Table 13). Table 14 gives the differences between the depth (mbsf) calculated by the ODP CORELOG data and the corrected depth (mbsf) calculated by the layer-by-layer correlation method.

The layer-by-layer method on the double-cored sedimentary sequences gives us true stratigraphic thickness after the correction for core-boundary disturbance. Table 15 shows the stratigraphic thickness at Sites 723 and 724, where the marker layers were defined, and Holes 727A and 727B. The corrected depths in Hole 727A and 727B agree well with each other. The intersite correlation of the marker layers shows clearly the differences in the rate of sedimentation.

SUMMARY AND CONCLUSIONS

Site 727 is located in the northwestern Arabian Sea on the Oman continental margin and corresponds to a second drilling target (in addition to Site 723) near the center of a slope basin. The water depth of Site 727 (914 m) lies near the bottom of the pronounced OMZ that impinges on the continental margin underneath a zone of high biogenic productivity. Site 727 was located in the southern part of a slope basin formed by a narrow half-graben in what is presumed to be ophiolitic basement. Biogenic material produced by coastal upwelling and eolian components are deposited here at high rates (~95 m/m.y.). Our intentions in drilling Site 727 were (1) to complement the continuous and expanded sections of upper Neogene to Recent sediments previously recovered at Site 723, (2) to trace the imprint of the OMZ through time, and (3) to investigate diagenetic sedimentary processes.

Some of the major findings at Site 727 are summarized in Figure 29 and include the identification of

1. a uniform lithology, lacking laminations and silica, ranging in age from latest Pliocene to Holocene;

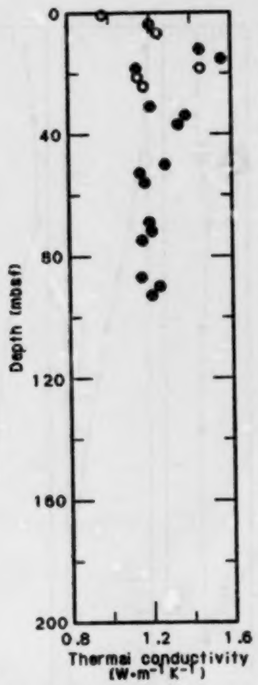

Figure 20. Thermal conductivity vs. depth for Holes 727A (dots) and 727B (circles).

2. calcareous nannofossils that are indicative of cold water and upwelling and that occur in the lower Pleistocene (traces of opal are found only in the uppermost Pliocene); and
3. complete sulfate depletion by 50 mbsf but increasing sulfate downsection associated with a continuous downsection increase in alkalinity.

The section penetrated at Site 727 ranges from uppermost Pliocene to Holocene. The magnetostratigraphy at Site 727 was especially well defined so that the Brunhes-Matuyama boundary, the Jaramillo subchronozone, and the top of the Olduvai were identified.

Only one lithologic unit was recognized at Site 727. The unit comprises homogeneous green to olive green foraminifer-bearing marly nannofossil ooze and calcitic marly nannofossil ooze. The calcium carbonate and organic carbon contents of this facies vary between 40% to 70% and 1% to 7%, respectively. The mean sedimentation rates at Site 727 (60–133 m/m.y.) are consistently lower than those at Site 723 (129–240 m/m.y.), and the section appears to have been deposited continuously. Magnetic susceptibility shows consistent downhole variability that correlates with other margin and ridge sites and reflects climate-related changes in the depositional system, which is dominated by upwelling and eolian input.

The benthic foraminifers are more abundant at Site 727 than at any of the margin sites, but they show few faunal changes, indicating little or no changes due to increasing depth. Faunal and floral assemblages indicate that monsoonal upwelling was persistent throughout the time of deposition. However, some calcareous nannoplankton indicator species only occur in the upper Pliocene and lower Pleistocene. Opal occurs only in traces during this same interval.

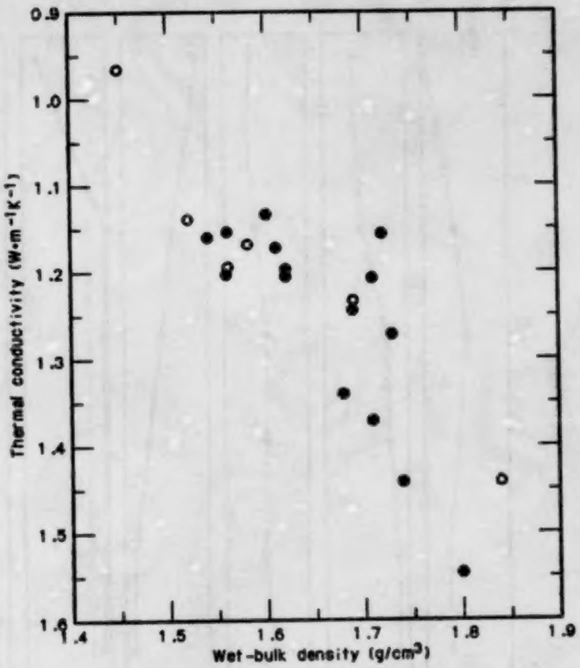

Figure 21. Thermal conductivity vs. wet-bulk density for Holes 727A (dots) and 727B (circles). GRAPE data were used to estimate wet-bulk density for intervals of conductivity measurement which lack a corresponding discrete-sample wet-bulk density determination.

Chemical compositions of interstitial waters show a downsection increase, indicating a possible sub-bottom supply of sulfate. Diagenetic remineralization at Site 727 appears to be dominated by fermentation reactions and methanogenesis. Similar to previous sites on the margin, Site 727 showed a strong increase in ethane and propane with depth.

Site 727 provides confirmation of many of the biotic and depositional trends observed at other sites on the Oman margin. However, the lack of laminated facies at Site 727, which lies at the same depth and covers the same time span as Site 723, poses questions about the heterogeneity of the processes, such as the OMZ, that preserve the laminated facies.

REFERENCES

Berggren, W. A., Kent, D. V., Flynn, J. J., and Van Couvering, J. A., 1985a. Cenozoic geochronology. *Geol. Soc. Am. Bull.*, 96:1407–1418.

Berggren, W. A., Kent, D. V., and Van Couvering, J. A., 1985b. The Neogene: Part 2, Neogene geochronology and chronostratigraphy. *In* Snelling, N. J. (Ed.), *The Chronology of the Geological Record*, Geol. Soc. Mem. (London), 10:211–260.

Sato, T., Takayama, T., Kato, M., Kudo, T., and Kameo, K., in press. Calcareous microfossil biostratigraphy of the uppermost Cenozoic formations distributed in the coast of the Japan Sea. Part 4: Conclusion. *Sekiyu Gijutsu Kyokaishi.*

Takayama, T., and Sato, T., 1987. Coccolith biostratigraphy of the North Atlantic Ocean, Deep Sea Drilling Project Leg 94. *In* Ruddiman, W. F., Kidd, R. B., Thomas, E., et al., *Init. Repts. DSDP,* 94, Pt. 2: Washington (U.S. Govt. Printing Office), 651–702.

Ms 117A-114

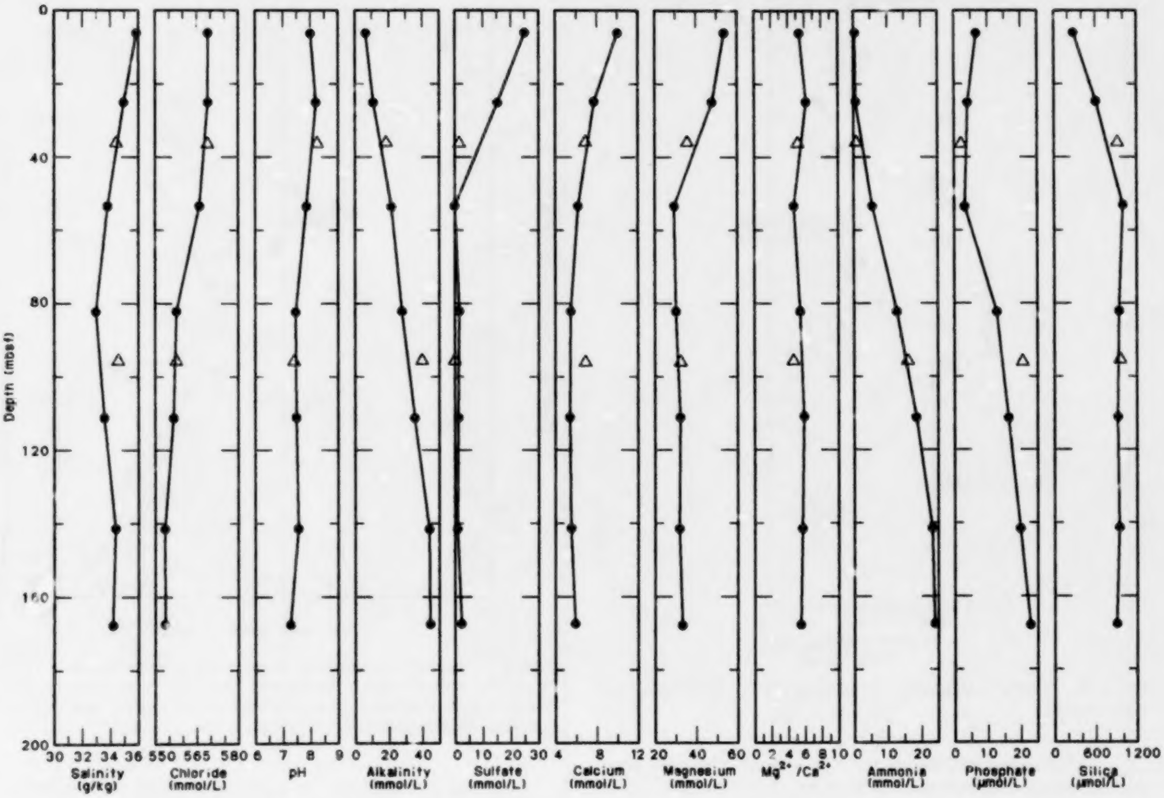

Figure 22. Concentration profiles vs. depth for Site 727.

Table 8. Summary of interstitial water geochemical data, Site 727.

Core, section, interval (cm)	Depth (mbsf)	Vol. (ml)	pH	Alk. (mmol/L)	Sal. (g/kg)	Mg (mmol/L)	Ca (mmol/L)	Cl (mmol/L)	SO_4 (mmol/L)	PO_4 (µmol/L)	NH_4 (mmol/L)	SiO_2 (µmol/L)	Mg/CA
1H-4, 145-150	5.95	47	7.99	6.34	35.8	53.49	9.94	569	24.6	5.5	0.50	285	5.38
3H-4, 145-150	24.85	54	8.19	10.96	34.9	47.81	7.75	569	15.2	3.0	0.64	603	6.17
4I-6, 0-1	35.90	10	8.26	18.26	34.4	36.09	6.91	569	1.6	1.1	0.82	925	5.22
6H-4, 145-150	53.25	47	7.86	21.48	33.8	29.89	6.27	566	0	2.3	5.59	990	4.77
9H-4, 145-150	82.05	36	7.48	27.60	33.0	30.76	5.56	558	1.6	11.6	12.71	940	5.53
11I-1, 0-1	95.40	10	7.42	39.57	34.6	32.94	6.96	558	0	19.1	16.08	953	4.73
12X-4, 145-150	110.95	37	7.51	35.34	33.6	32.68	5.47	557	1.3	15.0	18.57	923	5.97
15X-5, 145-150	141.35	36	7.58	44.07	34.4	32.33	5.58	554	1.0	18.6	23.29	942	5.79
18X-3, 145-150	167.45	50	7.30	44.56	34.2	33.66	6.00	554	2.4	21.6	24.08	904	5.61

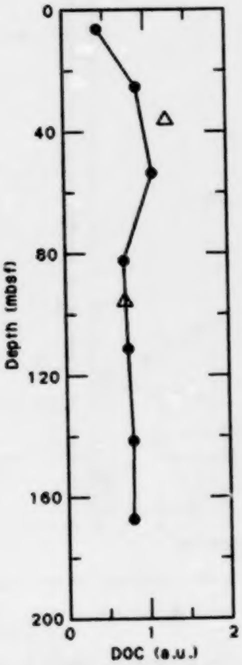

Figure 23. Dissolved organic carbon (DOC) profile for Site 727 in absorbance units (a.u.). Triangles represent the *in-situ* samples.

Table 9. Relative dissolved organic carbon concentrations at Site 727.

Core, section, interval (cm)	Dissolved organic carbon (a.u.)
117-727A-	
1H-4, 145-150	0.437
3H-4, 145-150	0.894
4I-4, 0-1	1.260
6H-4, 145-150	1.087
9H-4, 145-150	0.730
11I-1, 0-1	0.743
12X-4, 145-150	0.769
15X-5, 145-150	0.820
18X-3, 145-150	0.805

Note: a.u. = absorbance units.

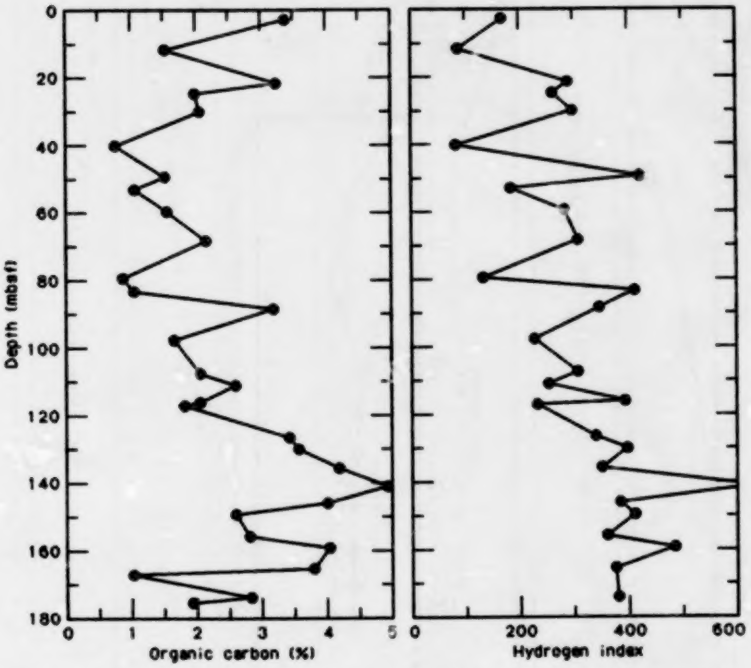

Figure 24. Downhole plot of organic carbon and the hydrogen index values from Rock-Eval pyrolysis.

Table 10. Results of Rock-Eval pyrolysis of samples from Hole 727A.

Core, section, interval (cm)	Depth (mbsf)	T_{max} (°C)	S_1	S_2	S_3	S_2/S_3	TOC	HI	OI
1H-2, 100-102	2.50	418	1.07	5.82	2.97	1.95	3.41	170	87
2H-2, 50-52	11.50	419	0.26	1.40	1.55	0.90	1.55	90	100
3H-2, 100-102	21.40	415	1.77	9.63	3.35	2.87	3.28	293	102
3H-4, 119-120	24.59	415	0.88	5.32	2.44	2.18	2.02	263	120
4H-2, 6-8	29.96	416	0.97	6.34	2.66	2.38	2.11	300	126
5H-2, 71-73	40.01	417	0.08	0.71	1.24	0.57	0.80	88	155
6H-2, 50-52	49.30	417	0.90	6.66	2.51	2.65	1.57	424	159
6H-4, 119-120	52.99	417	0.37	2.07	2.00	1.03	1.09	189	183
7H-2, 123-125	59.53	413	0.56	4.59	2.24	2.04	1.60	286	140
8H-2, 24-26	68.14	418	0.94	6.93	2.43	2.85	2.22	312	109
9H-3, 27-29	79.37	416	0.23	1.27	1.38	0.92	0.92	138	150
9H-5, 119-120	83.29	411	0.80	4.57	1.85	2.47	1.10	415	168
10H-3, 80-82	88.32	414	1.69	11.38	3.34	3.40	3.25	350	102
11H-2, 76-78	97.66	413	0.50	3.91	2.28	1.71	1.70	230	134
12H-2, 98-100	107.48	433	0.80	6.65	2.78	2.39	2.14	310	129
12H-4, 144-145	110.94	415	1.03	6.86	2.34	2.93	2.66	257	87
13H-2, 0-1	116.10	414	1.18	8.39	2.69	3.11	2.12	395	126
13H-2, 93-95	117.03	418	0.59	4.43	2.37	1.86	1.87	237	127
14H-2, 98-100	126.48	411	2.01	11.89	3.64	3.26	3.47	342	104
14H-4, 149-150	129.99	406	3.42	14.58	3.53	4.13	3.64	400	96
15H-2, 28-30	135.68	415	2.08	15.05	4.27	3.52	4.23	355	100
15H-5, 119-120	141.09	402	6.01	31.50	4.57	6.89	4.96	635	92
16H-2, 80-82	145.90	406	3.20	15.71	4.10	3.83	4.06	386	100
16H-4, 149-150	149.59	408	1.90	10.98	2.65	4.14	2.65	414	100
17H-2, 94-96	155.74	408	1.98	10.38	3.76	2.76	2.87	361	131
17H-5, 0-1	159.30	407	4.18	19.81	3.63	5.45	4.07	486	89
18H-2, 84-86	165.34	413	2.32	14.38	4.00	3.59	3.82	376	104
19H-1, 135-137	174.05	415	1.67	10.85	3.42	3.17	2.85	380	120

Note: HI = hydrogen index and OI = organic index. For a detailed description of parameters, see "Explanatory Notes" chapter (this volume).

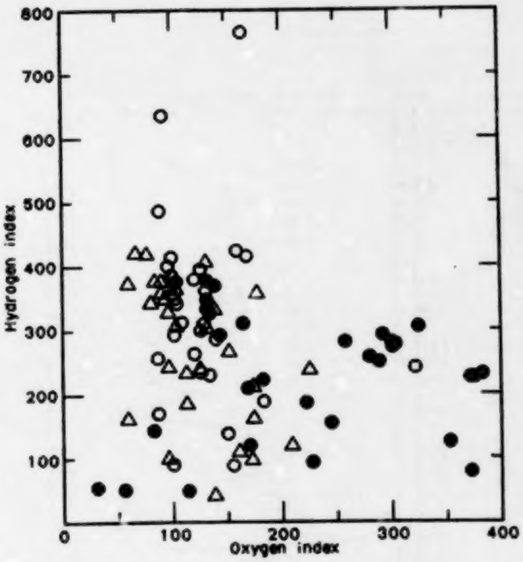

Figure 25. Plot of hydrogen vs. oxygen index of samples from Hole 727A (diamonds), Site 722 (dots), and Site 726 (triangles).

Table 11. Results of headspace analysis of interstitial gas at Hole 727A.

Core, section, interval (cm)	Depth (mbsf)	C_1 (mL/L)	C_2 (μL/L)	C_3 (μL/L)
3H-4, 119–120	24.59	77	2	
9H-5, 119–120	83.29	90813	10	3
12X-4, 144–145	110.94	66321	9	
13X-2, 0–1	116.10	103211	17	4
14X-4, 149–150	129.99	70643	26	10
15X-5, 119–120	141.09	57481	60	26
16X-4, 149–150	149.59	65125	30	10
17X-5, 0–1	159.30	77434	58	22
18X-3, 119–120	167.19	87741	30	13
19X-3, 0–1	175.70	107735	45	20

Note: Values are expressed as μL/L (volume gas/volume wet sediment).

Table 12. Results of gas analysis of vacutainer samples from Hole 727A.

Core, section, interval (cm)	Depth (mbsf)	C_1 (ppm)	C_2 (ppm)	C_3 (ppm)	C_1/C_2
8H-2, 40	68.30	1024211	70	3	14631
9H-6, 140	85.00	972155	74	4	13137
10H-6, 75	92.77	1027567	79	4	13007
11X-6, 27	103.17	1015621	83	4	12236
12X-5, 50	111.50	863423	73	4	11828
13X-6, 70	122.80	945271	93	5	10164
14X-5, 105	131.05	932922	111	6	8405
15X-4, 140	139.80	950363	101	5	9410
16X-5, 145	151.05	1002150	105	6	9544
17X-5, 75	160.05	984137	121	7	8133
18X-5, 105	170.05	946265	139	10	6808

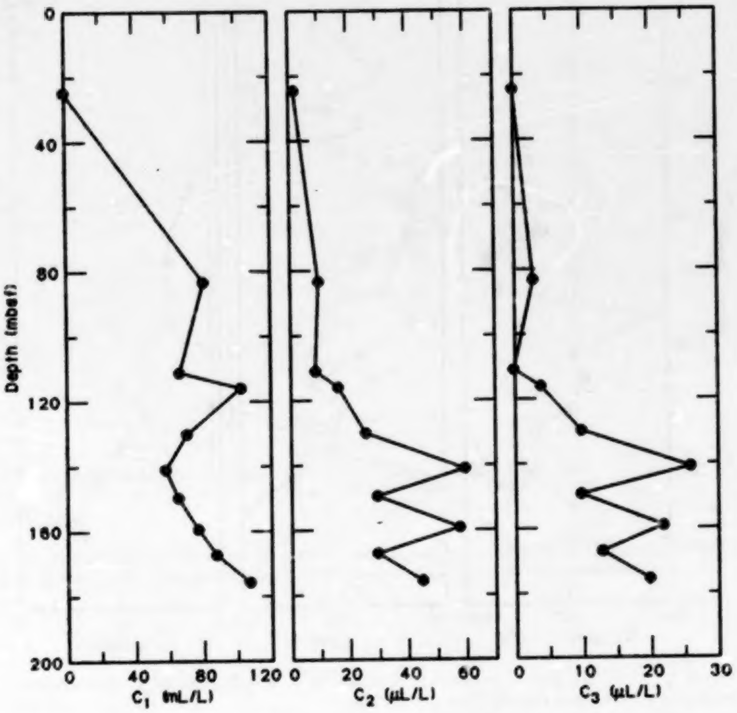

Figure 26. Downhole plot of methane (C_1), ethane (C_2), and propane (C_3) concentrations measured with the headspace technique.

Table 13. Stratigraphic depths of the marker layers at Site 727 for layer-by-layer correlation to the Oman margin.

	Hole 727A		Hole 727B		
Layer	Core, section, interval (cm)	ODP depth (mbsf)	Core, section, interval (cm)	ODP depth (mbsf)	Holes 727B − 727A
OM-a_1			1H-2, 15	1.65	
a_2			1H-3, 55	3.55	
b_1	1H-3, 15	3.15	1H-5, 60	6.60	3.45
b_2	1H-4, 90	5.40	2H-1, 120	9.40	4.00
b_3	1H-5, 80	6.80	2H-2, 110	10.80	4.00
c_1	2H-1, 50	10.00	2H-5, 40	14.60	4.60
c_2	2H-2, 125	12.25	2H-6, 115	16.85	4.60
c_3	2H-3, 95	13.45			
c_4	2H-4, 30	14.30			
c_5	2H-4, 55	14.55			
d_1	2H-5, 100	16.50	3H-2, 35	19.45	2.95
d_2	2H-6, 15	17.15	3H-2, 100	20.10	2.95
d_3	2H-6, 110	18.10	3H-3, 55	21.15	3.05
d_4	3H-1, 90	19.80	3H-4, 75	22.85	3.05
e_1	3H-3, 5	21.95	3H-6, 5	25.15	3.25
e_2	3H-5, 25	25.15			
e_3	3H-5, 130	26.20			
f_1	3H-7, 25	28.15			
f_2	4H-2, 95	30.85			
g_1	4H-4, 100	33.90			
g_2	4H-7, 40	37.80			
h_1	5H-4, 40	42.70			
h_3	5H-6, 135	46.65			
h_4	6H-3, 95	51.25			
h_5	6H-4, 95	52.75			

Note: Depths are based on ODP CORELOG data

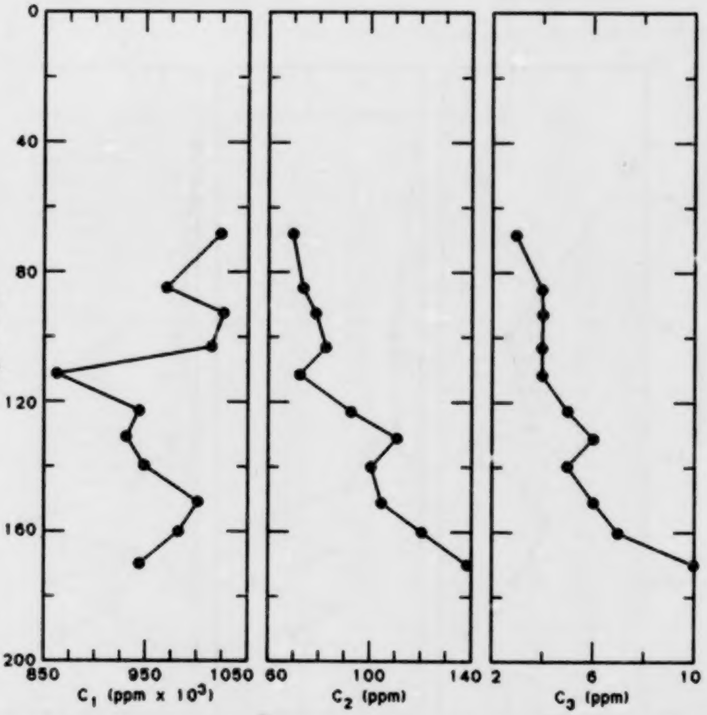

Figure 27. Downhole plot of methane (C_1), ethane (C_2), and propane (C_3) concentrations measured in vacutainer samples from gas pockets.

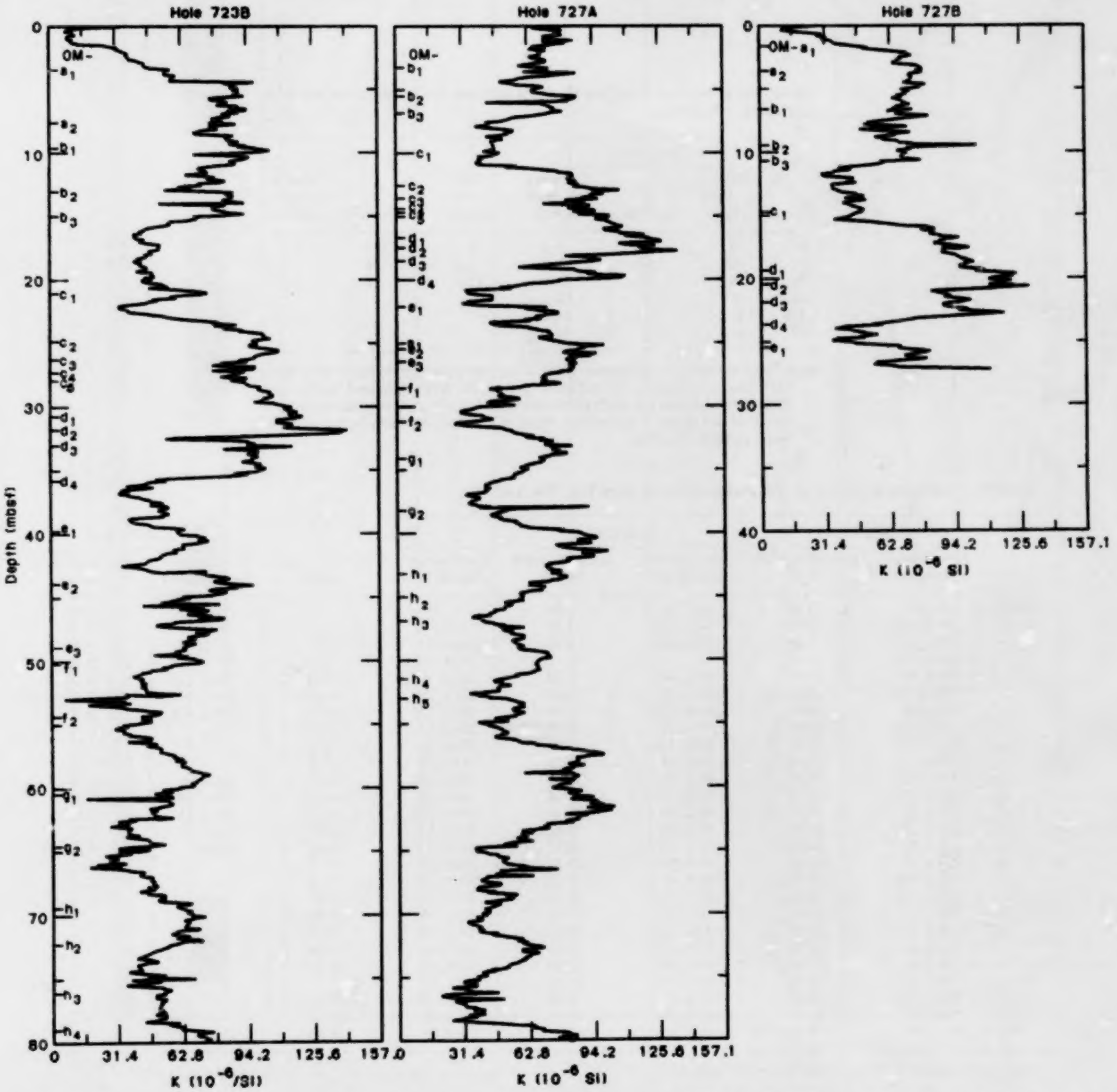

Figure 28. Magnetic susceptibility curve and positions of the marker layers in Holes 727A and 727B. Magnetic susceptibility curve and positions of the marker layers in Holes 723B and 727A. Note the similarity of the curves from these two different sites.

Table 14. Corrected sub-bottom depth of core-top for stratigraphic sub-bottom depth calculation.

	Hole 727A			Hole 727B		
Core	ODP top depth (mbsf)	Difference	Corrected top depth (mbsf)	ODP top depth (mbsf)	Difference	Corrected top depth (mbsf)
1H	0	3.4	3.4	0	0	0
2H	9.5	0.6	13.5	8.2	−0.6	7.6
3H	18.9	0.1	23.0	17.6	1.6	18.6
4H	28.4		32.5			
5H	37.8		41.9			
6H	47.3		51.4			

Note: ODP top depth = sub-bottom depth of core top calculated by the ODP CORELOG data. Difference = the difference between the depth calculated by the ODP CORELOG data and the depth calculated by the layer-by-layer correlation method. Corrected top depth = sub-bottom depth of core top calculated by the layer-by-layer correlation method.

Table 15. Stratigraphic depths of the marker layers at Sites 723, 724, and 727.

	Hole 723B		Hole 724A		Hole 727A		Hole 727B	
Layer	Core, section, interval (cm)	Corrected depth (mbsf)	Core, section, interval (cm)	Corrected depth (mbsf)	Core, section, interval (cm)	Corrected depth (mbsf)	Core, section, interval (cm)	Corrected depth (mbsf)
OM-a_1	1H-3, 35	3.35	1H-1, 95	0.95			1H-2, 15	1.65
a_2	2H-3, 20	7.20	1H-2, 115	2.65			1H-3, 55	3.55
b_1	2H-4, 65	9.15	1H-3, 100	4.00	1H-3, 15	6.55	1H-5, 60	6.60
b_2	2H-6, 110	12.60			1H-4, 90	8.80	2H-1, 120	8.80
b_3	3H-1, 95	14.75	2H-1, 40	7.60	1H-5, 80	10.20	2H-2, 110	10.20
c_1	3H-5, 110	20.90	2H-2, 75	9.45	2H-1, 50	14.00	2H-5, 40	14.00
c_2	4H-1, 85	24.95	2H-3, 130	11.50	2H-2, 125	16.25	2H-6, 115	16.25
c_3	4H-2, 100	26.60	2H-4, 70	12.40	2H-3, 95	17.45		
c_4	4H-3, 15	27.25	2H-4, 120	12.90	2H-4, 30	18.30		
c_5	4H-3, 100	28.10	2H-5, 35	13.55	2H-4, 55	18.55		
d_1	4H-5, 70	30.80	3H-1, 40	17.20	2H-5, 100	20.50	3H-2, 35	20.45
d_2	4H-6, 10	31.70	3H-1, 150	18.30	2H-6, 15	21.15	3H-2, 100	21.10
d_3	4H-7, 5	33.15	3H-2, 90	19.20	2H-6, 110	22.10	3H-3, 55	22.15
d_4	5H-2, 50	35.30	3H-3, 85	20.65	3H-1, 90	23.90	3H-4, 75	23.85
e_1	5H-5, 20	39.50	3H-4, 15	21.45	3H-3, 5	26.05	3H-6, 5	26.15
e_2	6H-1, 90	43.80	3H-5, 90	23.70	3H-5, 25	29.25		
e_3	6H-3, 150	47.40	3H-6, 95	25.25	3H-5, 130	30.30		
f_1	6H-5, 120	50.10	4H-1, 85	27.75	3H-7, 25	32.25		
f_2	7H-2, 15	54.25	4H-2, 70	29.10	4H-2, 95	34.95		
g_1	7H-6, 30	60.40	4H-4, 120	32.60	4H-4, 100	38.00		
g_2	8H-2, 60	64.40	4H-6, 25	34.65	4H-7, 40	41.90		
h_1	8H-5, 90	69.20	4H-7, 40	36.30	5H-4, 40	46.80		
h_2	9H-1, 20	72.10	5H-1, 80	37.30				
h_3	9H-3, 135	76.25	5H-2, 60	38.60	5H-6, 135	50.75		
h_4	9H-7, 95	81.85	5H-4, 145	42.45	6H-3, 95	55.35		
h_5			5H-5, 145	43.95	6H-4, 95	56.85		

Note: Depths based on the correction factors of Table 14.

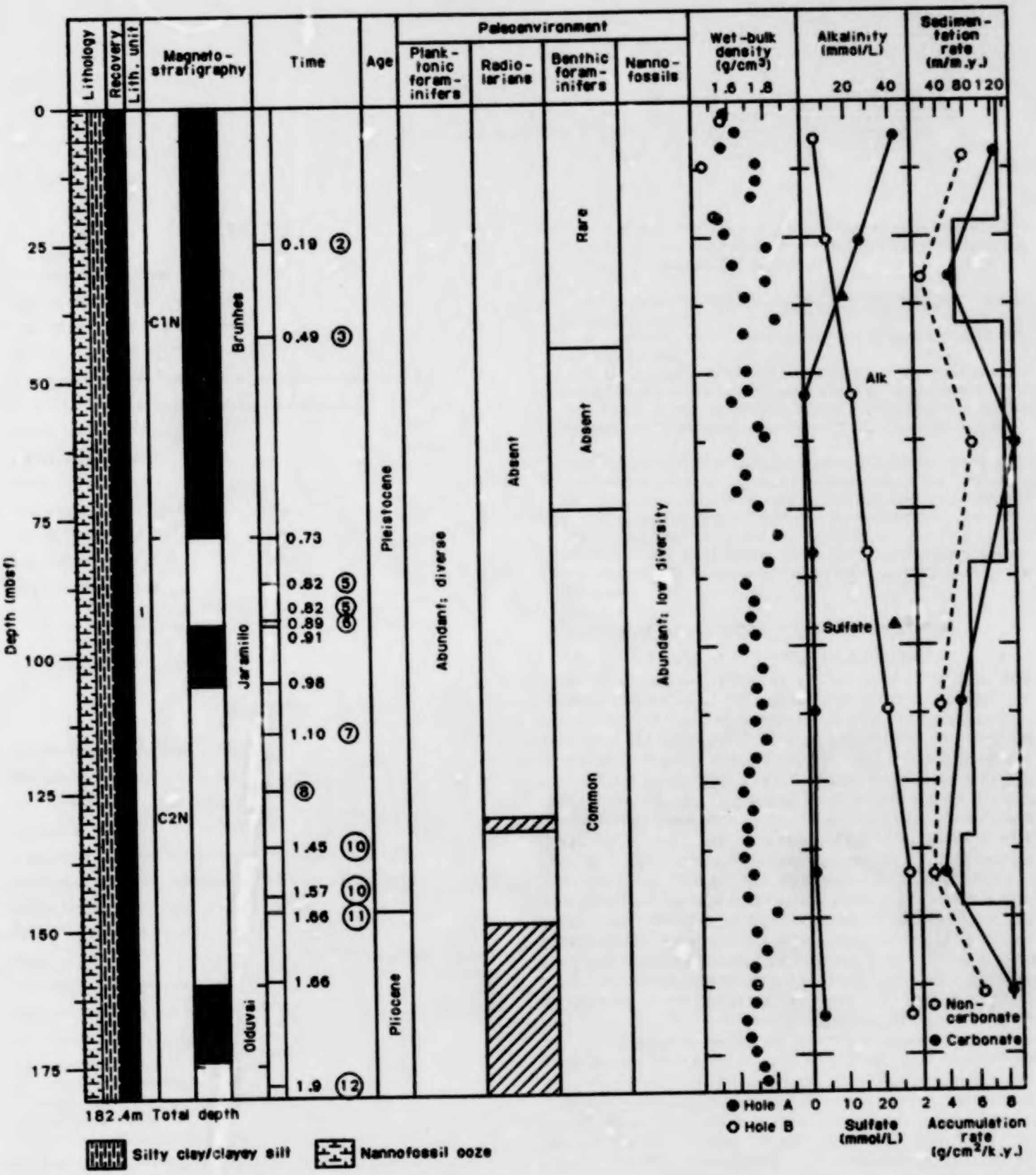

Figure 29. Summary chart of preliminary shipboard findings, Site 727.

16. SITE 728[1]

Shipboard Scientific Party[2]

HOLE 728A

Date occupied: 25 September 1987

Date departed: 26 September 1987

Time on hole: 1 day, 13 hr, 30 min

Position: 17°40.790′N, 57°49.553′E

Water depth (sea level; corrected m, echo-sounding): 1427.8

Water depth (rig floor; corrected m, echo-sounding): 1438.3

Bottom felt (m, drill pipe): 1433.4

Penetration (m): 346.40

Number of cores: 36

Total length of cored section (m): 346.40

Total core recovered (m): 343.72

Core recovery (%): 99.2

Oldest sediment cored
Depth sub-bottom (m): 346.40
Nature: foraminifer nannofossil chalk
Age: late Miocene
Measured velocity (km/s): 1.55–1.66

HOLE 728B

Date occupied: 26 September 1987

Date departed: 28 September 1987

Time on hole: 1 day, 3 hr, 30 min

Position: 17°40.790′N, 57°49.553′E

Water depth (sea level; corrected m, echo-sounding): 1427.8

Water depth (rig floor; corrected m, echo-sounding): 1438.3

Bottom felt (m, drill pipe): 1435.8

Penetration (m): 347.70

Number of cores: 37

Total length of cored section (m): 347.70

Total core recovered (m): 349.50

Core recovery (%): 100.5

Oldest sediment cored
Depth sub-bottom (m): 347.70
Nature: foraminifer nannofossil chalk
Age: late Miocene
Measured velocity (km/s): 1.56

Principal results: Site 728 is located on the Oman margin at a water depth where the lower part of the oxygen-minimum zone intersects the continental slope. The purpose of drilling at Site 728 was to trace the evolution and fluctuation of the oxygen-minimum zone through time. A second intention was to investigate tectonic movements of basement by comparing the sediments in two adjacent slope basins.

Major findings at Site 728 include:

1. An expanded Pliocene section, which is well constrained by paleomagnetic data;
2. Common occurrence of opaline microfossils in the Miocene and Pliocene intervals; and
3. Indication for rapid vertical movement of the site from upper bathyal depths in the late Miocene, rising to neritic depths in the early Pliocene, and subsiding to middle bathyal depths in the late Pliocene and Pleistocene, as indicated by benthic foraminifers.

A zone of high organic-carbon concentrations that was encountered at 80 to 110 mbsf may reflect the movement of Site 728 through the oxygen-minimum zone during the late Pliocene. This zone, high in organic carbon, coincides with maxima in alkalinity of interstitial waters and in uranium concentrations from logs, as well as with the depletion of interstitial sulfate. The elevated organic carbon concentrations (up to 5.5%) appear to foster significant bacterial activity at this depth.

BACKGROUND AND OBJECTIVES

Site 728 is located at 17°40.790′N and 57°49.553′E, on the continental margin of Oman in a water depth of 1428 m, near the center of the deeper of two slope basins (Fig. 1). The location of Site 728 is shown in Figure 2, and its structural and depositional setting is shown in Figure 3. At this location, the deeper slope basin is about 8 km wide and is much smaller in extent than the adjacent basin upslope, where Sites 723, 724, and 727 are located. This deeper basin is bounded on the west by the faulted block that forms the seaward edge of the upper basin. On the east, the basin is bounded by a basement peak that has substantial sediment cover and an eastern scarp that descends to about 2500 m. Both basement features are thought to be ophiolitic. The seismic-reflection profiles of the basin sediments show numerous reflective layers that both onlap onto and are deformed by the adjacent basement structures. The surface layer and shallow reflectors dip seaward from the upper basin toward the lower constraining basement peak. The sediments are thickest in the center of the basin and form a syncline-shaped deposit (Fig. 3); these thin significantly by pinching out and onlapping to both east and west. This deeper basin is not a linear feature like the upper basin, and extends only about 15 km along the trend (northeast-southwest) of the basement ridges. Average accumulation rates at Site 728 were expected to be between 50 and 60 m/m.y. on the basis of preliminary stratigraphy of piston cores taken during the site survey cruise (RC2704). The site was expected to provide a high-resolution sedimentary record that is more pelagic than the other margin sites, but that still reflects the proximal variations of monsoonal upwelling and the oxygen-minimum zone during the Pliocene-Pleistocene.

Specific objectives for drilling at Site 728 were as follows:

1. To obtain a high-resolution record of the sediments associated with the proximal zone of the monsoonal upwelling system to establish changes in timing and intensity of the monsoon.

---

[1] Prell, W. L., Niitsuma, N., et al., 1989. *Proc. ODP, Init. Repts.*, 117: College Station, TX (Ocean Drilling Program).

[2] Shipboard Scientific Party is as given in list of Participants preceding the contents.

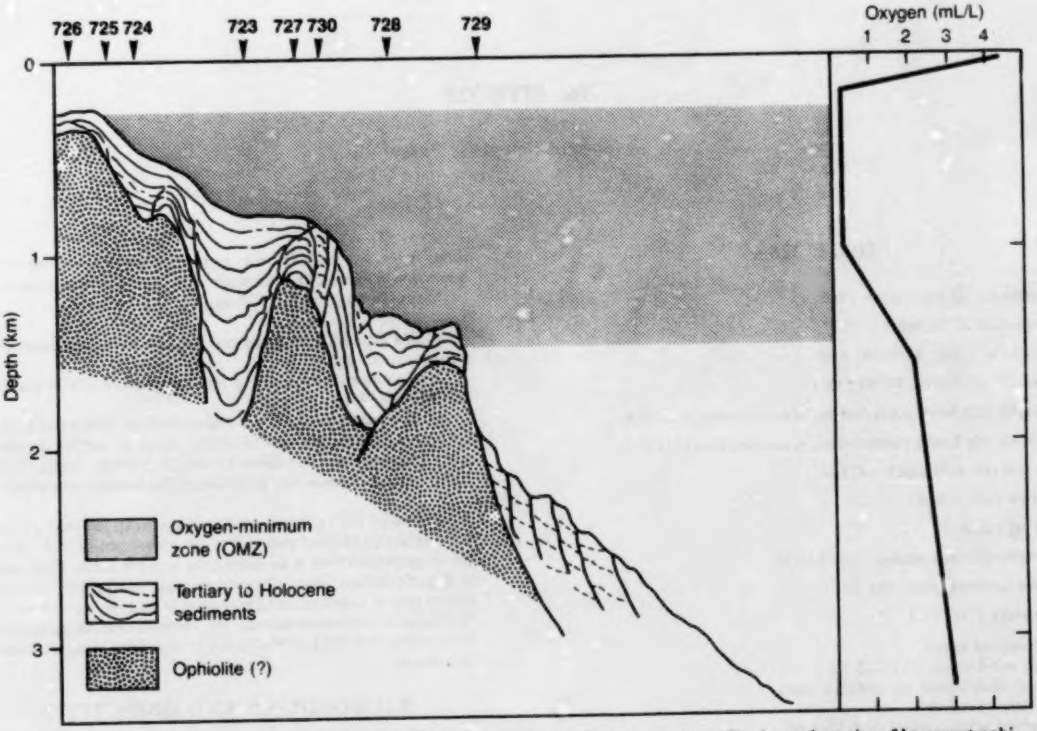

Figure 1. Structure of the Oman margin and the oxygen-minimum zone. The schematic profile shows the series of basement ophiolite blocks and the sedimentary basins between them. The concentration of oxygen in the water column (RC2704, unpubl. data) defines the depth range of the oxygen and where it impinges on the margin.

2. To provide the deepwater end-member of a depth transect that will be used to examine the organic-rich sedimentary facies of the margin to establish their diagenetic history and their relationship to the oxygen-minimum zone and its spatial variation through time.

3. To search for evidence of changes in the structure of the intermediate water masses of the Arabian Sea during the Pliocene-Pleistocene.

OPERATIONS

Site 728 was surveyed jointly with Site 729 on 25 September 1987, after drilling operations at Site 727 had terminated. The ship left Site 727 at 0600 hr with the seismic gear deployed, crossed the future Site 728, and continued to Site 729, where a beacon was dropped at 0900 hr. The *JOIDES Resolution* then returned to Site 728 and dropped a beacon at 1130 hr in a water depth of 1427.8 m. The ship's track line is plotted in Figure 4 according to global positioning system (GPS) navigation fixes. The position of Site 728 was assessed as 17°40.790′N and 59°49.553′E. Seismic gear was retrieved, and the ship positioned by 1230 hr. The mudline of Hole 727A was shot at 1500 hr on 25 September.

Nine APC cores recovered 103% of the sediments from the interval 0 to 85.7 mbsf, after which an overpull of 80,000 lb necessitated a switch to extended-core barrel (XCB) coring mode. Hole 728A was terminated at 0745 hr on 26 September, at a total depth of 346.4 mbsf (Core 117-728A-36X) with an overall recovery as high as 99% owing to cutting shoe modification and favorable sediments (Table 1). The hole was conditioned, swept with mud, displaced with polymer, and prepared for logging. After the lockable flapper valve had been opened and a wiper trip, the bit was positioned at 80 mbsf.

Two logging strings were successfully run in Hole 728A. String 1 consisted of a combination of resistivity (DIT), sonic (BHC), gamma ray (GR), and caliper (CAL) logs, while string 2 ran a combination of gamma spectometry (GST), neutron porosity (CNT), and spectral gamma ray (NGT) logs. At 2315 hr, logging tools were rigged down, the string was pulled out of Hole 728A, the ship moved 10 m northwest, and Hole 728B was spudded at 0100 hr on 26 September. Nine advanced corer (APC) cores were followed by XCB coring to Core 117-728A-37X, a total depth of 347.7 mbsf. The *in-situ* pore-water sampler was deployed after Cores 117-728B-6H, -12X, -17X, and -25X. Overall recovery again averaged 100% for the entire hole, with 104% for the interval from 0 to 77.3 mbsf cored in APC mode. The performance of the XCB system was extraordinary at this site.

Hole 728B was displaced with heavy mud, the string cleared the mudline, and at 2400 hr on 27 September, the ship was under way to Site 729 in dynamic positioning mode.

LITHOSTRATIGRAPHY

Lithologic Units

The two holes drilled at Site 728 are located in a water depth of 1428 m near the center of a lower slope basin. Hole 728B is 10 m northwest of Hole 728A. APC recovery was almost perfect in these holes, and the top of Hole 728B recovered the mudline. The age range of the sedimentary sequence is Pleistocene to late Miocene, the longest continuous section recovered on the Oman margin. The sediments are mostly marly nannofossil ooze and

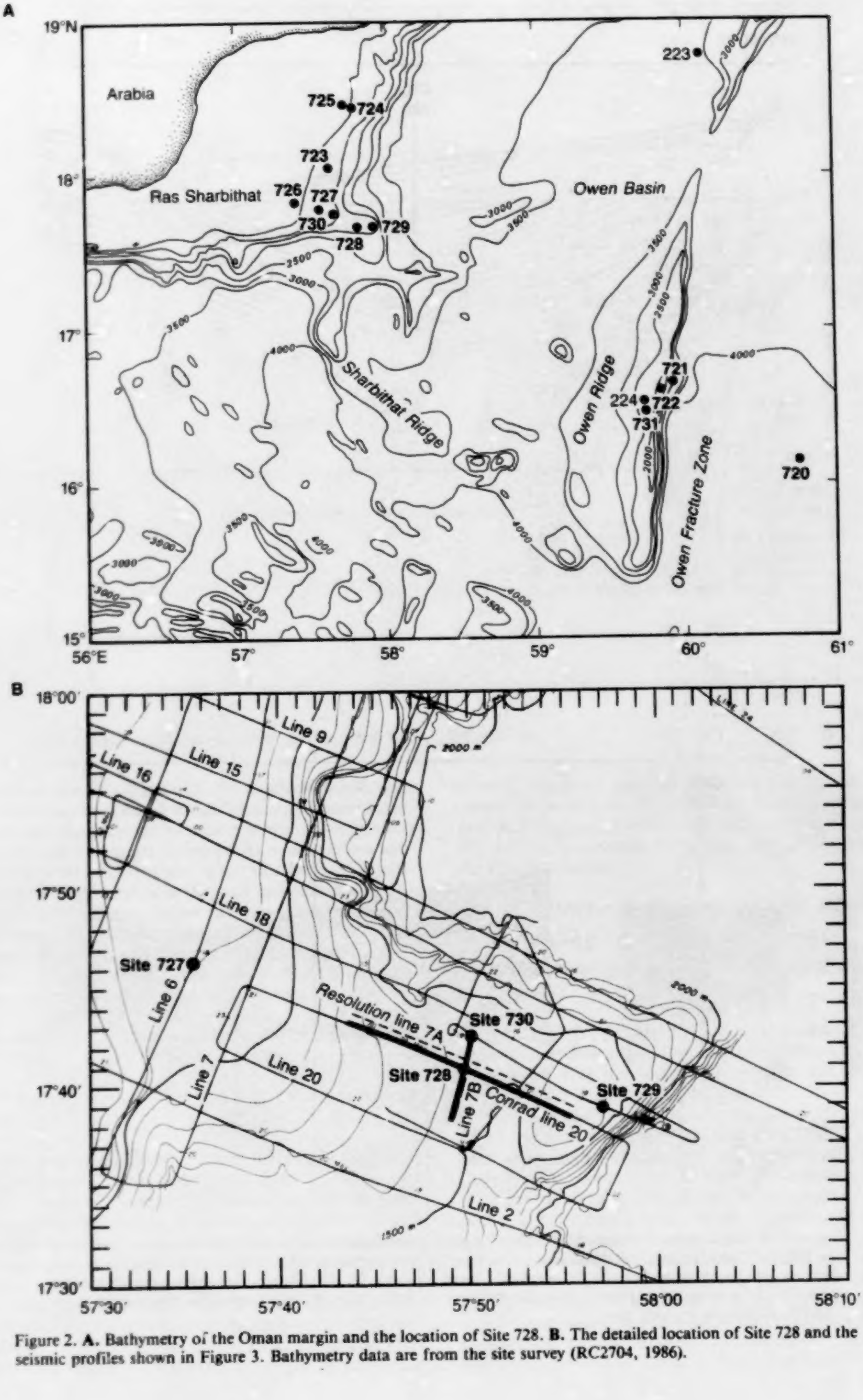
A
19°N
18°
17°
16°
15°
56°E
57°
58°
59°
60°
61°
Arabia
Ras Sharbithat
725
724
723
726
727
730
728
729
223
Owen Basin
Sharbithat Ridge
Owen Ridge
Owen Fracture Zone
721
224
722
731
720
2500
3000
3500
4000
2000
B
18°00′
17°50′
17°40′
17°30′
57°30′
57°40′
57°50′
58°00′
58°10′
Line 9
Line 15
Line 16
Line 18
Line 6
Line 7
Line 20
Line 2
Line 24
Site 727
Site 730
Site 728
Site 729
Resolution line 7A
Line 7B
Conrad line 20
2000 m
1500 m

Figure 2. **A.** Bathymetry of the Oman margin and the location of Site 728. **B.** The detailed location of Site 728 and the seismic profiles shown in Figure 3. Bathymetry data are from the site survey (RC2704, 1986).

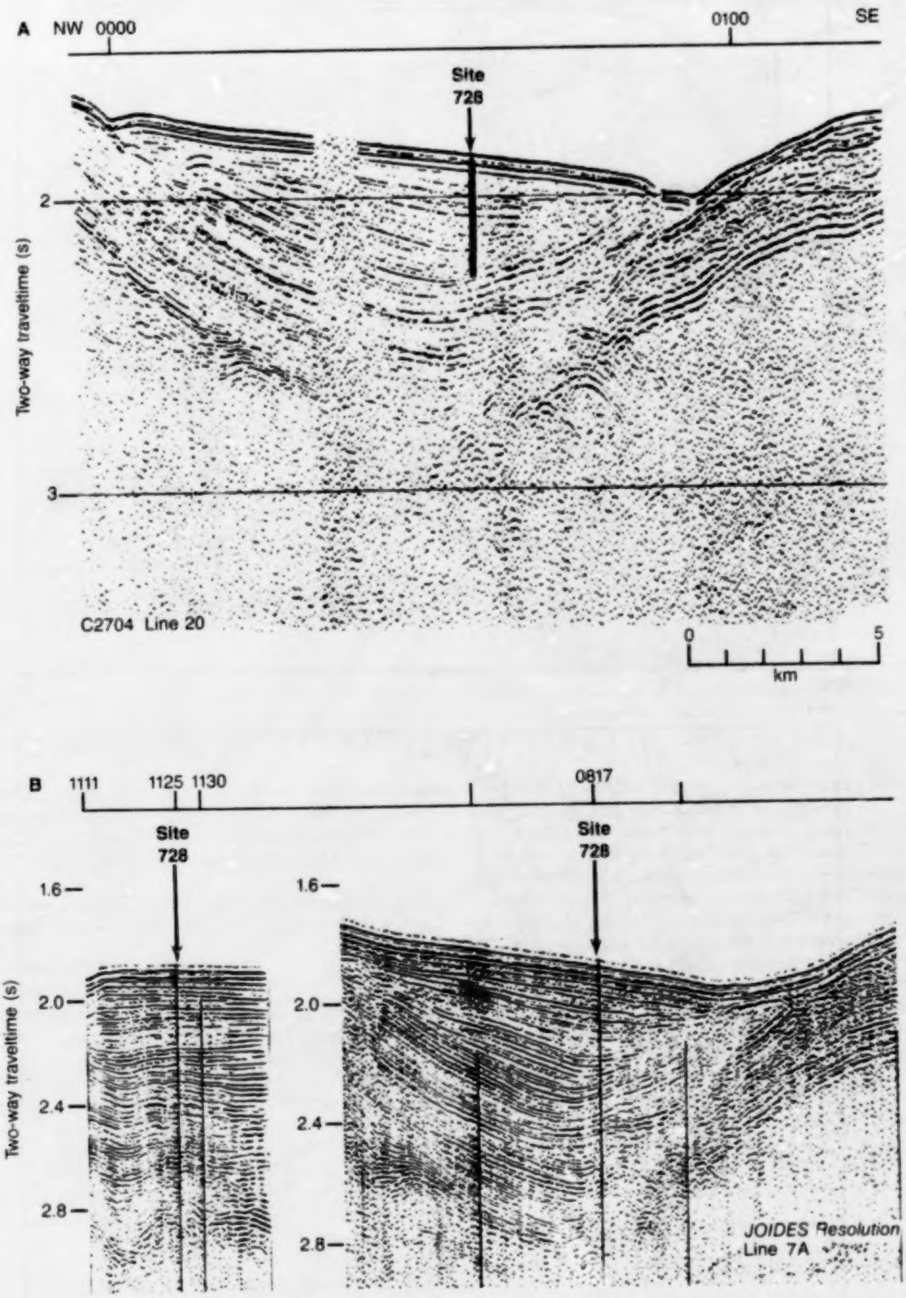

Figure 3. **A.** Single-channel seismic (SCS) reflection profiles showning the structural and depositional setting of Site 728. RC2704 Line 20 and *JOIDES Resolution* Line 7A are perpendicular to the trend of the basin and shows the bounding basement blocks and the synclinal-shaped sediment fill. **B.** *JOIDES Resolution* Line 7B is along the strike of the basement ridges and shows the relatively uniform sediment thickness and horizontal reflectors at Site 728. (All times are local time.)

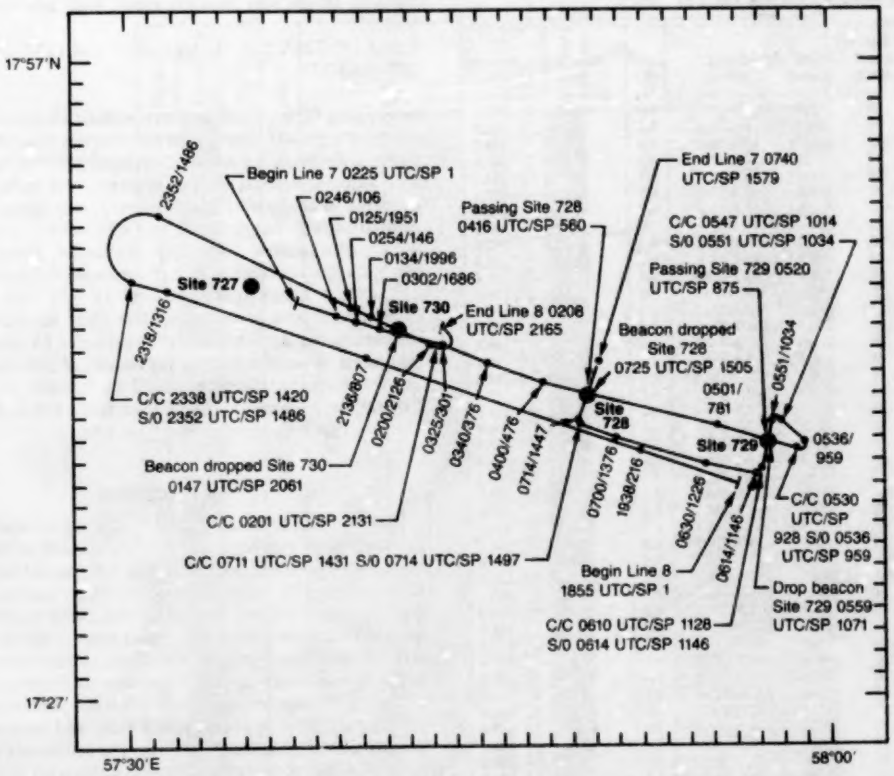
17°57'N
17°27'
57°30'E
58°00'
2352/1486
Begin Line 7 0225 UTC/SP 1
0246/106
0125/1951
0254/146
0134/1996
0302/1686
Site 727
Site 730
Passing Site 728
0416 UTC/SP 560
End Line 8 0208
UTC/SP 2165
End Line 7 0740
UTC/SP 1579
C/C 0547 UTC/SP 1014
S/0 0551 UTC/SP 1034
Passing Site 729 0520
UTC/SP 875
Beacon dropped
Site 728
0725 UTC/SP 1505
0501/
781
0551/1034
2318/1316
C/C 2338 UTC/SP 1420
S/0 2352 UTC/SP 1486
2136/807
0200/2126
0325/301
0340/376
0400/476
0714/1447
Site
728
0700/1376
1938/216
0630/1226
0614/1146
Site 729
0536/
959
Beacon dropped Site 730
0147 UTC/SP 2061
C/C 0201 UTC/SP 2131
C/C 0711 UTC/SP 1431 S/0 0714 UTC/SP 1497
Begin Line 8
1855 UTC/SP 1
C/C 0610 UTC/SP 1128
S/0 0614 UTC/SP 1146
C/C 0530
UTC/SP
928 S/0 0536
UTC/SP 959
Drop beacon
Site 729 0559
UTC/SP 1071

Figure 4. Ship's track during survey and approach to Sites 728 and 729.

are considered as one lithologic unit. We subdivided lithologic Unit I into three subunits, based on carbonate and organic carbon contents and the presence of minor biogenic components (Fig. 5 and Table 2). The upper subunit (IA) is rich in foraminifers. The middle subunit (IB) grades downward from a foraminifer-bearing, marly nannofossil ooze to marly nannofossil and nannofossil oozes. The upper part is dark and more uniform in color, whereas the lower part contains pronounced light and dark cycles that are heavily mottled (bioturbated). Siliceous microfossils are present throughout. Subunit IC is siliceous-bearing, marly nannofossil ooze, often with more than 10% diatoms.

Subunit IA (Depth: 0–58 mbsf; Age: Holocene to early Pleistocene)

Cores 117-728A-1H through -6H and 117-728B-1H through 117-728B-7H.

Subunit IA consists of marly foraminifer-nannofossil ooze and foraminifer-bearing, marly nannofossil ooze. The upper two cores contain abundant foraminifers (more than 10% in smear slides). Foraminifers decrease in abundance within this unit and are only present in minor amounts throughout the hole below 58 mbsf. Smear-slide analysis indicates 20%–50% nannofossils and a variable terrigenous component dominated by clay, and clay and silt-sized detrital calcite (often 20% or more). Calcium carbonate determined coulometrically varies between 50% and 60% (Fig. 6 and Table 2). Subunit IA is similar to the upper sequence observed at other margin sites, although the carbonate content is greater, and the sedimentation rate is significantly slower (34 m/m.y. vs. 80–175 m/m.y.). Variable-thickness, light and dark intervals are olive (5Y 4/2, 4/3) and light olive gray (5Y 5/2, 5/3), mottled throughout, with pyrite flecks visible in the lighter intervals.

Subunit IB (Depth: 58–320 mbsf; Age: early Pleistocene to Miocene)

Cores 117-728A-7H through -33X and 117-728B-8H through 117-728B-34X.

Subunit IB consists mostly of foraminifer-bearing, marly nannofossil ooze with alternating dark beds, olive (5Y 4/4, 4/3), olive gray (5Y 4/2), dark olive gray (5Y 3/2); and lighter beds, olive gray (5Y 5/2) and olive (5Y 5/3). In the lower part, these become lighter in color and more nannofossil rich; light olive gray (5Y 6/2), olive gray (5Y 5/2), and olive (5Y 5/3) nannofossil ooze, containing approximately 70% nannofossils; mottling (bioturbation) is more pronounced. Siliceous microfossils are present throughout this unit. Within the unit, organic carbon gradually decreases in content (Fig. 6), which corresponds to the presence of the lighter, more nannofossil-rich beds.

The abundance of detrital calcite (clay and silt-sized) decreases downward within this unit, from 15% to 25% to less than 10% below 120 mbsf. Thus, in the upper Pleistocene (Subunit IA and upper Subunit IB), detrital calcite is a major component, and in older sediments its abundance is reduced. Quartz is generally present in low abundance (less than 10%) in the up-

Table 1. Coring summary for Site 728.

Core no.	Date (Sept. 1987)	Time (Local)	Depth (mbsf)	Cored (m)	Recovered (m)	Recovery (%)
117-728A-1H	25	1550	0-9.6	9.6	9.63	100.0
2H	25	1615	9.6-19.1	9.5	9.72	102.0
3H	25	1635	19.1-28.5	9.4	9.78	104.0
4H	25	1700	28.5-38.0	9.5	9.83	103.0
5H	25	1740	38.0-47.5	9.5	9.69	102.0
6H	25	1805	47.5-57.0	9.5	10.03	105.6
7H	25	1825	57.0-66.5	9.5	9.86	104.0
8H	25	1845	66.5-76.1	9.6	9.90	103.0
9H	25	1910	76.1-85.7	9.6	9.85	102.0
10X	25	1945	85.7-95.3	9.6	9.18	95.6
11X	25	2010	95.3-104.9	9.6	8.87	92.4
12X	25	2035	104.9-114.5	9.6	5.34	55.6
13X	25	2055	114.5-124.2	9.7	8.52	87.8
14X	25	2115	124.2-133.9	9.7	9.61	99.1
15X	25	2140	133.9-143.5	9.6	9.10	94.8
16X	25	2200	143.5-153.1	9.6	9.05	94.3
17X	25	2225	153.1-162.8	9.7	9.66	99.6
18X	25	2245	162.8-172.5	9.7	8.52	87.8
19X	25	2305	172.5-182.2	9.7	9.81	101.0
20X	25	2325	182.2-191.8	9.6	9.59	99.9
21X	25	2355	191.8-201.5	9.7	9.91	102.0
22X	26	0030	201.5-211.1	9.6	9.93	103.0
23X	26	0100	211.1-220.8	9.7	9.34	96.3
24X	26	0130	220.8-230.5	9.7	9.88	102.0
25X	26	0200	230.5-240.1	9.6	9.91	103.0
26X	26	0235	240.1-249.8	9.7	10.18	104.9
27X	26	0305	249.8-259.5	9.7	9.93	102.0
28X	26	0340	259.5-269.1	9.6	9.96	104.0
29X	26	0405	269.1-278.8	9.7	9.70	100.0
30X	26	0435	278.8-288.5	9.7	10.00	103.1
31X	26	0505	288.5-298.1	9.6	9.99	104.0
32X	26	0530	298.1-307.8	9.7	10.02	103.3
33X	26	0600	307.7-317.5	9.7	9.96	102.0
34X	26	0630	317.5-327.2	9.7	9.83	101.0
35X	26	0655	327.2-336.8	9.6	9.87	103.0
36X	26	0730	336.8-346.4	9.6	9.77	102.0
117-728B-1H	27	0115	0-1.2	1.2	1.24	103.0
2H	27	0220	1.2-10.7	9.5	10.02	105.5
3H	27	0245	10.7-20.1	9.4	10.02	106.6
4H	27	0310	20.1-29.6	9.5	9.98	105.0
5H	27	0345	29.6-29.1	9.5	9.88	104.0
6H	27	0420	39.1-48.6	9.5	9.84	103.0
7H	27	0615	48.6-58.1	9.5	10.09	106.2
8H	27	0650	58.1-67.7	9.6	10.01	104.3
9H	27	0725	67.7-77.3	9.6	10.02	104.4
10X	27	0825	77.3-86.9	9.6	9.68	101.0
11X	27	0855	86.9-96.5	9.6	9.43	98.2
12X	27	0925	96.5-106.1	9.6	9.55	99.5
13X	27	1050	106.1-115.8	9.7	9.65	99.5
14X	27	1125	115.8-125.5	9.7	9.77	101.0
15X	27	1145	125.5-135.1	9.6	9.73	101.0
16X	27	1205	135.1-144.7	9.6	9.13	95.1
17X	27	1235	144.7-154.4	9.7	8.38	86.4
18X	27	1415	154.4-164.1	9.7	9.46	97.5
19X	27	1440	164.1-173.8	9.7	9.75	100.0
20X	27	1505	173.8-183.5	9.7	9.47	97.6
21X	27	1535	183.5-193.2	9.7	9.65	99.5
22X	27	1600	193.2-202.8	9.6	9.82	102.0
23X	27	1625	202.8-212.5	9.7	10.02	103.3
24X	27	1650	212.5-222.2	9.7	9.74	100.0
25X	27	1720	222.2-231.8	9.6	9.96	104.0
26X	27	1900	231.8-241.5	9.7	6.83	70.4
27X	27	1925	241.5-251.2	9.7	9.94	102.0
28X	27	1950	251.2-260.8	9.6	9.76	101.0
29X	27	2015	260.8-270.5	9.7	9.90	102.0
30X	27	2040	270.5-280.2	9.7	10.04	103.5
31X	27	2105	280.2-289.8	9.6	9.68	101.0
32X	27	2125	289.8-299.5	9.7	9.90	102.0
33X	27	2150	299.5-309.2	9.7	9.98	103.0
34X	27	2215	309.2-318.8	9.6	10.06	104.8
35X	27	2240	318.8-328.5	9.7	9.40	96.9
36X	27	2305	328.5-338.1	9.6	9.86	103.0
37X	27	2330	338.1-347.7	9.6	9.86	103.0

per section of Site 728 and at other margin sites (723, 724, and 727). Below 250 mbsf (lower Subunits IB and IC) at Site 728, quartz grains can be found in greater abundance (up to 30% in isolated samples).

Subunit IC (Depth: 320–349 mbsf; Age: late Miocene)

Cores 117-728A-34X through -36X and 117-728B-35X through 117-728B-37X.

Subunit IC is similar to lower Subunit IB described above, but contains a greater abundance of siliceous microfossils. The siliceous assemblage is composed primarily of diatoms (10%–35%), with silicoflagellates, sponge spicules, and radiolarians present in minor abundances. The sediments are diatom-bearing nannofossil, marly nannofossil, and nannofossil oozes and are intensely bioturbated. Generally, the darker layers contain more silica. Color is similar to that in the base of Subunit IB (olive 5Y 4/3, 4/2, 3/2 and light olive gray 5Y 6/2, 5/3, 5/2). Calcium carbonate is 10% lower in the dark intervals within Subunit IC relative to the dark intervals in Subunits IA and IB. Calcium carbonate decreases from a maximum at 250 mbsf to low and variable concentrations observed in Subunit IC (Table 2 and Fig. 6). An increase in quartz abundance below 250 mbsf is obvious in this unit.

Discussion

Subunit IA, foraminifer-rich marly nannofossil ooze, is represented at all margin sites. The proportion of biogenic to terrigenous sediment is highest at Site 728 (more than 50%), which is consistent with its position on the outer margin in a more pelagic setting. Clay and detrital calcite, presumably of eolian origin, dominate the terrigenous component in the modern environment. Foraminifers are an abundant component of the smear-slide assemblage in upper Pleistocene sediments.

Lower Pleistocene and upper Pliocene sediments (upper Subunit IB) are more organic carbon-rich, and trace amounts of siliceous microfossils are preserved. The sediments are marly nannofossil ooze, uniformly olive (5Y 4/3), with few foraminifers. The upper section of Subunit IB correlates with an interval of organic carbon and silica preservation found at margin Sites 723, 724, and 726. At shallower depths and nearer the center of the oxygen-minimum zone (i.e., Site 723), organic carbon values increase to more than 8%; at Site 728, the maximum value is 5% (Table 2 and Fig. 6). During this depositional period, silica preservation is enhanced at shallow sites, and occasionally forms laminated diatomite at Sites 723, 724, and 726; however, no laminae were observed at Site 728. Detrital calcite is abundant within this interval of Subunit IB (often greater than 20%). Thus, Site 728 contains a facies that is correlative with the laminated zone at other margin sites, but the variations in sedimentary facies are not as pronounced.

Lithologic changes in minor components occur within Subunit IB between the upper Miocene and the upper Pliocene. Upper Miocene sediments have more pronounced cycles of light olive nannofossil ooze and darker marly nannofossil ooze and, as a rule, are intensely bioturbated. Mean organic carbon content is about 1%, and detrital calcite is a minor component. Organic carbon increases gradually during the Pliocene to maximum values in the upper Pliocene. The sediment becomes a darker and more uniform marly nannofossil ooze. Detrital calcite, interpreted as an eolian component, increases in Cores 117-728A-14X and 117-728B-15X in the upper Pliocene. These changes suggest that the deposition of the organic carbon-rich interval observed at the other margin sites began in the early Pliocene.

In the upper Miocene (below 320 mbsf) silica is preserved (up to 30%) in marly nannofossil ooze that is intensely bioturbated and shows pronounced light and dark cycles. Preliminary stratigraphy indicates this may be correlated with a Miocene interval of silica preservation that was observed on the Owen Ridge

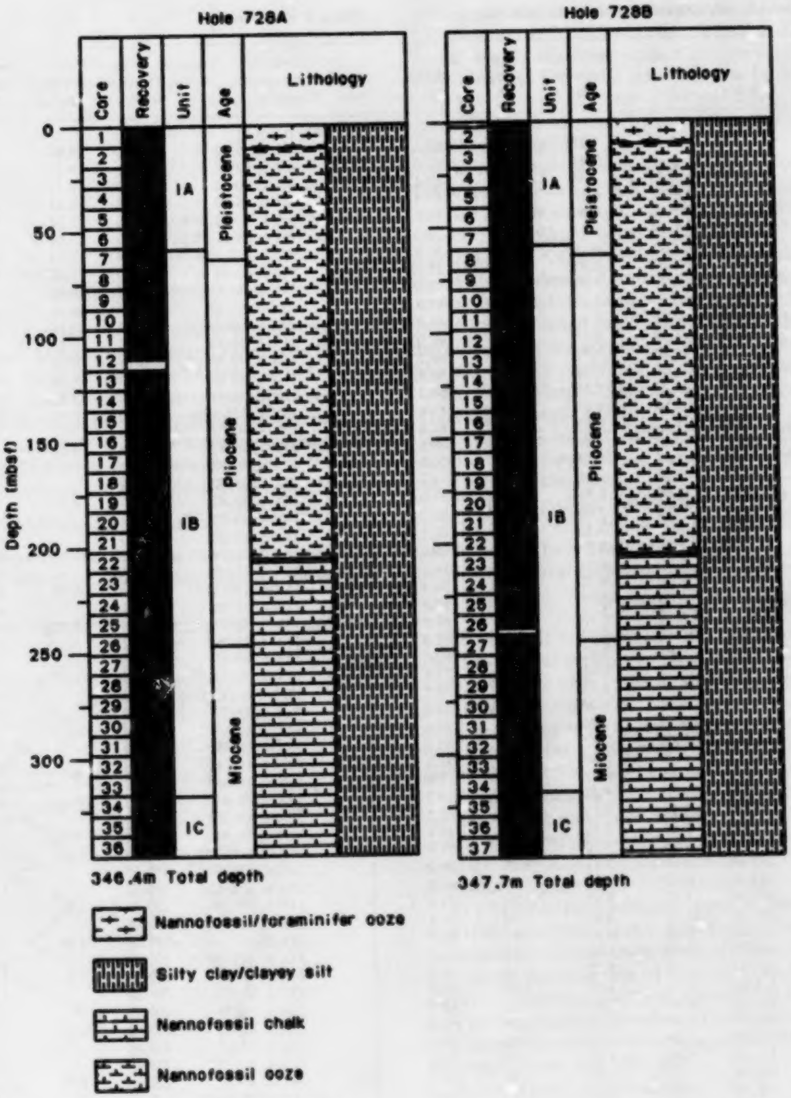
Hole 728A
Hole 728B
Core
Recovery
Unit
Age
Lithology
Depth (mbsf)
0
50
100
150
200
250
300
IA
IB
IC
Pleistocene
Pliocene
Miocene
346.4m Total depth
347.7m Total depth
Nannofossil/foraminifer ooze
Silty clay/clayey silt
Nannofossil chalk
Nannofossil ooze

Figure 5. Lithologic summary for Site 728.

and which occurred at approximately 7 Ma (see "Lithostratigraphy" section, Site 722 chapter, this volume).

Significant amounts of quartz are observed in Miocene sediments below 250 mbsf. The increase may be related to increased supply of terrigenous sediment, or to a change in the depositional environment, which increases the flux of quartz. The shallow sites nearer the continent today have the highest fraction of quartz. Site 728 may have been located in shallower water during the late Miocene (see "Biostratigraphy" section, this chapter), and the abundance of quartz is consistent with this observation. The decrease in quartz in the uppermost Miocene suggests that the site subsided below the shallow-water depositional environment at that time.

BIOSTRATIGRAPHY

Introduction

Site 728 is located in a deep slope basin in 1428 m of water. The age of the sediments ranges from late Miocene to Holocene (Fig. 7). A plot of faunal datum levels and paleomagnetic reversals vs. depth below the seafloor is presented in Figure 8; for a detailed listing of these events, see Table 3. Benthic and planktonic foraminifers are common to abundant, and preservation is good down to approximately 50 mbsf. Below 66.5 mbsf, planktonic foraminifers are few to rare, with moderate to poor preservation. Benthic foraminifers remain common down to 160 mbsf, but preservation is moderate to poor. Below this level, preserva-

Table 2. Calcium carbonate and organic carbon determinations.

Core, section, interval (cm)	Depth (mbsf)	Total carbon (%)	Inorganic carbon (%)	Organic carbon (%)	CaCO$_3$ (%)
117-728A-					
1H-2, 100-102	2.50	8.74	7.21	1.53	60.1
2H-2, 80-82	11.90	8.13	7.44	0.69	62.0
3H-2, 80-82	21.40	9.27	7.49	1.78	62.4
3H-4, 119-120	24.79	7.90	6.86	1.04	57.1
4H-2, 80-82	30.80	7.79	6.60	1.19	55.0
5H-2, 80-82	40.30	8.95	7.77	1.18	64.7
6H-2, 80-82	49.80	7.92	6.11	1.81	50.9
6H-4, 80-82	52.80	8.82	6.45	2.37	53.7
6H-4, 119-120	53.19	8.51	6.24	2.27	52.0
6H-6, 80-82	55.80	6.67	5.99	0.68	49.9
7H-2, 80-82	59.30	7.96	5.91	2.05	49.2
7H-4, 80-82	62.30	7.78	5.52	2.26	46.0
7H-6, 80-82	65.30	10.01	7.98	2.03	66.5
8H-2, 80-82	68.80	9.13	7.18	1.95	59.8
8H-4, 80-82	71.80	9.45	4.11	5.34	34.2
8H-6, 80-82	74.80	8.05	4.97	3.08	41.4
9H-2, 80-82	78.40	11.22	7.54	3.68	62.8
9H-4, 80-82	81.40	10.67	5.86	4.81	48.8
9H-4, 119-120	81.79	11.11	6.14	4.97	51.2
9H-6, 80-82	84.40	9.68	6.45	3.23	53.7
10X-2, 80-82	88.00	10.09	6.84	3.25	57.0
10X-4, 80-82	91.00	10.98	7.95	3.03	66.2
10X-6, 80-82	94.00	10.11	7.26	2.85	60.5
11X-2, 80-82	97.60	8.05	5.57	2.48	46.4
11X-4, 78-80	100.58	9.00	6.51	2.49	54.2
11X-6, 80-82	103.60	8.20	6.77	1.43	56.4
12X-1, 70-72	105.60	8.50	5.75	2.75	47.9
12X-2, 119-120	107.59	8.88	5.93	2.95	49.4
13X-1, 80-82	115.30	10.48	7.27	3.21	60.6
14X-2, 80-82	126.50	9.63	7.22	2.41	60.1
15X-2, 72-74	136.12	10.18	6.41	3.77	53.4
15X-4, 119-120	139.59	10.18	6.78	3.40	56.5
16X-2, 80-82	145.80	8.32	5.29	3.03	44.1
17X-2, 73-75	155.33	9.57	6.46	3.11	53.8
18X-2, 135-137	165.65	10.63	7.87	2.76	65.6
18X-4, 119-120	168.49	11.36	8.60	2.76	71.6
19X-2, 93-95	174.93	11.15	8.12	3.03	67.6
20X-2, 118-120	184.88	9.62	7.11	2.51	59.2
21X-2, 56-58	193.86	8.06	5.17	2.89	43.1
21X-5, 0-1	197.80	9.06	5.95	3.11	49.6
22X-2, 79-81	203.79	7.94	5.02	2.92	41.8
23X-2, 80-82	213.40	9.98	7.11	2.87	59.2
24X-2, 69-71	222.99	9.70	7.43	2.27	61.9
25X-2, 85-87	232.85	8.37	6.43	1.94	53.6
26X-2, 21-23	241.81	10.32	8.63	1.69	71.9
27X-2, 116-118	252.46	8.68	6.81	1.87	56.7
28X-3, 7-9	262.57	10.74	7.41	3.33	61.7
29X-2, 51-53	271.11	8.04	5.78	2.26	48.2
30X-2, 134-136	281.64	7.64	5.94	1.70	49.5
31X-2, 126-128	291.26	6.45	4.74	1.71	39.5
32X-4, 77-79	303.37	5.49	4.47	1.02	37.2
33X-4, 94-96	313.24	8.09	6.81	1.28	56.7
34X-3, 77-79	321.27	6.68	4.78	1.90	39.8
35X-2, 104-106	329.74	4.93	3.45	1.48	28.7
36X-3, 32-35	340.12	7.97	6.41	1.56	53.4
1H-2, 100-102	2.50	8.74	7.21	1.53	60.1
1H-4, 100-102	5.50		7.26		60.5
1H-6, 100-102	8.50		6.12		51.0
2H-2, 80-82	11.90	8.13	7.44	0.69	62.0
2H-4, 80-82	14.90		7.68		64.0
2H-6, 80-82	17.90		7.50		62.5
3H-2, 80-82	21.40	9.27	7.49	1.78	62.4
3H-4, 80-82	24.40		6.95		57.9
3H-4, 119-120	24.79	7.90	6.86	1.04	57.1
3H-6, 28-30	26.88		6.76		56.3
4H-2, 80-82	30.80	7.79	6.60	1.19	55.00
4H-4, 80-82	33.80		6.47		53.9
4H-6, 80-82	36.80		8.48		70.6
5H-2, 80-82	40.30	8.95	7.77	1.18	64.7
5H-4, 80-82	43.30		7.36		61.3
5H-6, 80-82	46.30		6.39		53.2
6H-2, 80-82	49.80	7.92	6.11	1.81	50.9
6H-4, 80-82	52.80	8.82	6.45	2.37	53.7
6H-4, 119-120	53.19	8.51	6.24	2.27	52.0
6H-6, 80-82	55.80	6.67	5.99	0.68	49.9
7H-2, 80-82	59.30	7.96	5.91	2.05	49.2
7H-4, 80-82	62.30	7.78	5.52	2.26	46.0
117-728A- (Cont.)					
7H-6, 80-82	65.30	10.01	7.98	2.03	66.5
8H-2, 80-82	68.80	9.13	7.18	1.95	59.8
8H-4, 80-82	71.80	9.45	4.11	5.34	34.2
8H-6, 80-82	74.80	8.05	4.97	3.08	41.4
9H-2, 80-82	78.40	11.22	7.54	3.68	62.8
9H-4, 80-82	81.40	10.67	5.86	4.81	48.8
9H-4, 119-120	81.79	11.11	6.14	4.97	51.2
9H-6, 80-82	84.40	9.68	6.45	3.23	53.7
10X-2, 80-82	88.00	10.09	6.84	3.25	57.0
10X-4, 80-82	91.00	10.98	7.95	3.03	66.2
10X-6, 80-82	94.00	10.11	7.26	2.85	60.5
11X-2, 80-82	97.60	8.05	5.57	2.48	46.4
11X-4, 78-80	100.58	9.00	6.51	2.49	54.2
11X-6, 80-82	103.60	8.20	6.77	1.43	56.4
12X-1, 70-72	105.60	8.50	5.75	2.75	47.9
12X-2, 119-120	107.59	8.88	5.93	2.95	49.4
12X-3, 70-72	108.60		5.08		42.3
13X-1, 80-82	115.30	10.48	7.27	3.21	60.6
13X-3, 80-82	118.30		6.90		57.5
13X-5, 80-82	121.30		7.01		58.4
14X-2, 80-82	126.50	9.63	7.22	2.41	60.1
14X-4, 80-82	129.50		6.99		58.2
14X-6, 80-82	132.50		7.17		59.7
15X-2, 72-74	136.12	10.18	6.41	3.77	53.4
15X-4, 73-75	139.13		6.51		54.2
15X-4, 119-120	139.59	10.18	6.78	3.40	56.5
15X-6, 94-96	142.34		5.74		47.8
16X-2, 80-82	145.80	8.32	5.29	3.03	44.1
16X-4, 92-94	148.92		6.70		55.8
16X-6, 80-82	151.80		5.23		43.6
17X-2, 73-75	155.33	9.57	6.46	3.11	53.8
17X-4, 69-71	158.29		8.14		67.8
17X-6, 75-77	161.35		6.61		55.1
18X-2, 135-137	165.65	10.63	7.87	2.76	65.6
18X-4, 101-103	168.31		7.11		59.2
18X-4, 119-120	168.49	11.36	8.60	2.76	71.6
18X-6, 61-63	170.91		8.10		67.5
19X-2, 93-95	174.93	11.15	8.12	3.03	67.6
19X-4, 98-100	177.98		6.91		57.6
19X-7, 31-33	181.81		6.97		58.1
20X-2, 118-120	184.88	9.62	7.11	2.51	59.2
20X-4, 106-108	187.76		4.64		38.7
20X-6, 122-124	190.92		6.61		55.1
21X-2, 56-58	193.86	8.06	5.17	2.89	43.1
21X-4, 72-74	197.02		7.15		59.6
21X-5, 0-1	197.80	9.06	5.95	3.11	49.6
21X-6, 103-105	200.33		5.95		49.6
22X-2, 79-81	203.79	7.94	5.02	2.92	41.8
22X-4, 80-82	206.80		6.26		52.2
22X-6, 76-78	209.76		5.21		43.4
23X-2, 80-82	213.40	9.98	7.11	2.87	59.2
23X-4, 80-82	216.40		7.45		62.1
23X-6, 80-82	219.40		6.77		56.4
24X-2, 69-71	222.99	9.79	7.43	2.27	61.9
24X-4, 69-71	225.99		5.83		48.6
24X-4, 138-140	226.68		6.97		58.1
24X-6, 79-81	229.09		8.59		71.6
25X-2, 85-87	232.85	8.37	6.43	1.94	53.6
25X-4, 48-50	235.48		7.50		62.5
25X-6, 147-149	239.47		5.69		47.4
26X-2, 21-23	241.81	8.60	8.63	0.00	71.9
26X-5, 72-74	246.82		7.31		60.9
27X-2, 116-118	252.46	8.68	8.81	1.87	56.7
27X-4, 17-19	254.47		4.26		35.5
27X-6, 107-109	258.37		7.03		58.6
28X-3, 7-9	262.57	10.74	7.41	3.33	61.7
28X-6, 137-139	268.37		6.74		56.1
28X-7, 41-43	268.91		7.07		58.9
29X-2, 51-53	271.11	8.04	5.78	2.26	48.2
29X-5, 67-69	275.77		7.68		64.0
30X-2, 134-136	281.64	7.64	5.94	1.70	49.5
30X-4, 115-117	284.45		5.00		41.7
31X-2, 126-128	291.26	6.45	4.74	1.71	39.5
31X-CC, 30-32	298.23		5.19		43.2
32X-4, 77-79	303.37	5.49	4.47	1.02	37.2
32X-6, 93-95	306.53		5.66		47.2

Table 2 (continued).

Core, section, interval (cm)	Depth (mbsf)	Total carbon (%)	Inorganic carbon (%)	Organic carbon (%)	$CaCO_3$ (%)
117-728A- (Cont.)					
33X-4, 94–96	313.24	8.09	6.81	1.28	56.7
33X-5, 96–98	314.76		5.32		44.3
34X-3, 77–79	321.27	6.68	4.78	1.90	39.8
34X-CC, 33–35	327.28		3.47		28.9
35X-2, 104–106	329.74	4.93	3.45	1.48	28.7
35X-6, 64–66	335.34		8.55		71.2
36X-3, 32–35	340.12	7.97	6.41	1.56	53.4
36X-6, 103–106	345.33		4.34		36.2

tion is good, but benthic foraminifers are rare. Calcareous nannofossils are abundant throughout the cored sequence. Preservation is moderate in Hole 728A down to 269.1 mbsf. From 269.1 to 346.4 mbsf, preservation is moderate to poor. Preservation throughout Hole 728B is moderate. Siliceous microfossils are not present in the upper 38 m. Only a few radiolarians are found between 38 and 76.1 mbsf, but below this level to the bottom of the hole, radiolarians are common and well preserved.

Planktonic Foraminifers

The planktonic foraminiferal fauna in the core-catcher samples of Hole 728A is abundant, and preservation of the tests is good in the upper part of the sequence (Samples 117-728A-1H, CC, through 117-728A-6H, CC; 9.6–57.0 mbsf), which is composed mainly of Pleistocene marly nannofossil oozes. Sample 117-728A-7H, CC (66.5 mbsf) and underlying sediments contain few to rare planktonic foraminifers; preservation ranges from moderate to poor. These sediments are Pliocene and late Miocene in age.

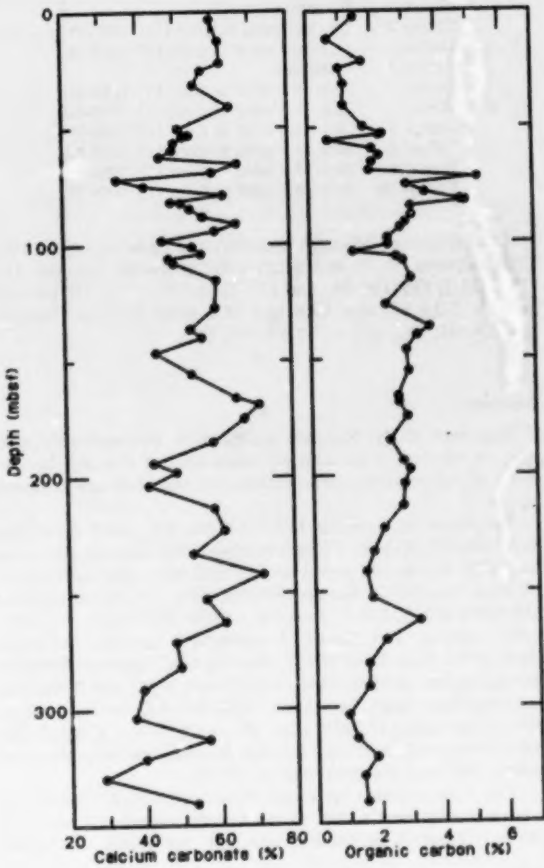

Figure 6. Calcium carbonate and organic carbon content.

The uppermost six core-catcher samples contain *Globigerinella calida calida* and/or *Globorotalia truncatulinoides*. Both species indicate a Pleistocene age. The Pleistocene/Pliocene boundary tentatively was placed between Samples 117-728A-6H, CC and 117-728A-7H, CC (57.0–66.5 mbsf), based on the last appearances of *Globorotalia limbata* and *Globigerinoides obliquus extremus* in the latter sample. The *Globorotalia tosaensis–G. truncatulinoides* lineage could not be used to discern this boundary because only a few specimens could be found. For the same reason, Zone N21 could not be distinguished from Zones N19a and N20. Pliocene sediments were found in Samples 117-728A-7H, CC, through 117-728A-25X, CC (66.5–240.1 mbsf). The fact that thick-walled *Globorotalia tumida tumida* specimens dominate the assemblages indicates that dissolution processes have affected the shells.

The lower part of the section (117-728A-26X, CC, through 117-728A-36X, CC; 249.8–346.4 mbsf) was assigned to the upper Miocene, based on rare specimens of *Globorotalia tumida plesiotumida* and *Globorotalia tumida merotumida*.

Benthic Foraminifers

The benthic foraminiferal fauna was studied at Site 728 in the core-catcher samples of Hole 728A. Abundances range from common in the upper part (above 160 mbsf) to rare in the lower part (below 160 mbsf) of the recovered sequence. Preservation is good in the upper 50 m, but becomes moderate to poor downhole to about 160 mbsf; preservation in the remainder of the sequence (below 160 mbsf) is good.

The planktonic/benthic (P/B) ratio is about 100% in the upper 60 m, but gradually decreases to below 10% at approximately 160 mbsf. This ratio remains below 10% in most of the samples downhole, and increases slightly in the lowermost five samples (approximately 305–345 mbsf).

The benthic foraminiferal fauna at Site 728 can be divided into three assemblages that intergrade. Thus, sharp boundaries between these assemblages are difficult to define. However, one can define the intervals of transition from one assemblage to another. The transition from Assemblage I to Assemblage II occurs between approximately 143 and 163 mbsf, and the transition from Assemblage II to Assemblage III occurs between approximately 230 and 250 mbsf.

Assemblage I is characterized by the presence of abundant *Cassidulina carinata* and *Bulimina aculeata*, which occur solely in this assemblage. Other species that are found exclusively in Assemblage I, but in lower relative abundance, are *Ehrenbergina trigona, Globocassidulina subglobosa, Pullenia subcarinata*, and *Quadrimorphina laevigata*. These species are found together with those also found in Assemblage III: *Cibicidoides wuellerstorfi, Melonis barleeanum, Pullenia bulloides*, and *Uvigerina spinicostata*. However, *M. barleeanum* and *P. bulloides* are found only in the lower part of Assemblage I.

Species characterizing Assemblage II are *Ammonia beccarii* and *Melonis pompiolides*. In Assemblage II, those species common in Assemblage I are absent or occur in low relative abundance.

Assemblage III is characterized by the high abundance of *Melonis barleeanum, Pullenia bulloides*, and *Uvigerina spinicostata*. Other species found in Assemblage III are *Cibicidoides wuellerstorfi* and *Uvigerina peregrina*.

Data from the previous sites drilled during Leg 117 as well as information from other areas (e.g., Ingle et al., 1980; Pflum

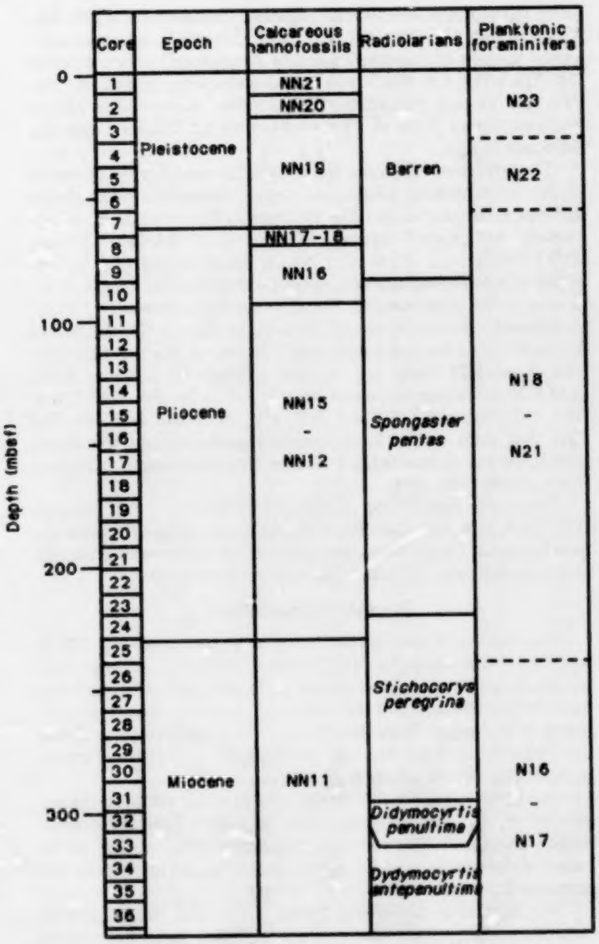

Figure 7. Correlation of planktonic microfossil zones in Hole 728A.

and Frerichs, 1976; van Morkhoven et al., 1986) indicate that these three assemblages include species characteristic of certain water depths. The species in Assemblage I seem to prefer a water depth that exceeds 500 m and can be considered characteristic of the upper middle bathyal zone. Assemblage II contains shallow-water species and accordingly can be regarded as characteristic of the neritic zone (above 150 m), whereas Assemblage III contains species that prefer the depth range between those species occurring in Assemblages I and II. Thus, Assemblage III would indicate an upper bathyal environment. The transition from Assemblage I to the "shallow water" assemblage (II) occurs over the same interval where the P/B ratio reaches less than 10%. These two indicators suggest substantial subsidence of Site 728 through time. The absence of "shallow water" species in Assemblage III indicates a slightly deeper environment during this time.

Calcareous Nannofossils

The holes drilled at Site 728 provide a nearly identical biostratigraphic sequence from the Pleistocene to the upper Miocene (Fig. 9). Calcareous nannofossils are abundant and moderately well preserved in Hole 728A to 269.1 mbsf. From 269.1 to 346.4 mbsf, nannofossils are abundant, but preservation deteriorates and ranges from moderate to poor. Nannofossils are abundant throughout Hole 728B, where preservation ranges from moderate to good.

Quaternary

In Hole 728A, sediments from the mudline to 10.78 mbsf, and in Hole 728B, sediments from the mudline to 1.2 mbsf contain *Emiliania huxleyi* and thus were assigned to Zone NN21 (uppermost Pleistocene to Holocene). Sediments from Samples 117-728A-2H-3, 118–119 cm, down to 177-728A-2H, CC (13.78–19.10 mbsf) and in Sample 117-728B-2H, CC (10.7 mbsf) in Hole 728B contain neither *E. huxleyi* nor *Pseudoemiliania lacunosa* and were assigned to Pleistocene Zone NN20. *P. lacunosa* is present, but *Discoaster brouweri* is absent in Samples 117-728A-3H-1, 118–119 cm, through 117-728A-7H-5, 125–126 cm (20.26–64.25 mbsf), and 117-728B-3H, CC, through 117-728B-7H, CC (20.1–58.1 mbsf); thus, these intervals were assigned to Zone NN19. The following datum levels were recognized in Zone NN19 (see "Explanatory Notes" chapter, this volume, for explanation of datums).

Hole 728B

Datum 1	Uncertain
Datum 2	1.2–10.7 mbsf in Core 117-728B-2H
Datum 3	10.7–20.1 mbsf in Core 117-728B-3H
Datum 4	Uncertain
Datum 5	29.6–39.1 mbsf in Core 117-728B-5H
Datum 6	29.6–39.1 mbsf in Core 117-728B-5H
Datum 7	39.1–48.6 mbsf in Core 117-728B-6H
Datum 8	48.6–58.1 mbsf in Core 117-728B-7H
Datum 9	48.6–58.1 mbsf in Core 117-728B-7H
Datum 10	48.6–58.1 mbsf in Core 117-728B-7H

The Pleistocene/Pliocene boundary can be recognized in Hole 728A between 61.25 and 64.25 mbsf (between Samples 117-728A-7H-3, 125–126 cm, and 117-728A-7H-5, 125–126 cm) and in Hole 728B between 48.6 and 58.1 mbsf (between Samples 117-728-6H, CC, and 117-718B-7H, CC).

Neogene

Zonation of the Neogene sediments is not extremely accurate, as has been true with all other sites of this leg, because some of the tropical zonal markers are absent or are extremely rare.

Sediments in Samples 117-728A-7H, CC (66.5 mbsf) and 117-728B-8H, CC (67.7 mbsf) in Hole 728B contain *Discoaster brouweri*, but not *D. pentaradiatus* and were assigned to upper Pliocene Zone NN18. Samples 117-728A-3H, 118–119 cm, through 117-728A-11X-1, 118–119 cm (76.1–96.48 mbsf), contain *Discoaster surculus*. The top of *D. surculus* is used to distinguish Zone NN16 from Zone NN17. The top of *D. pentaradiatus* was not recognized in Hole 728A, thus Zones NN17 and NN18 cannot be differentiated. Sample 117-728B-9H, CC, belongs to Zone NN17; Samples 117-728B-10X, CC, and -11X, CC (86.9–96.5 mbsf) contain *D. surculus*, but not *Reticulofenestra pseudoumbilica*, and were assigned to Zone NN16.

The zonal markers for Zones NN13 and NN14, *Ceratolithus rugosus* and *Amaurolithus tricorniculatus*, are absent and thus, the only possible alternative, although not a very satisfactory

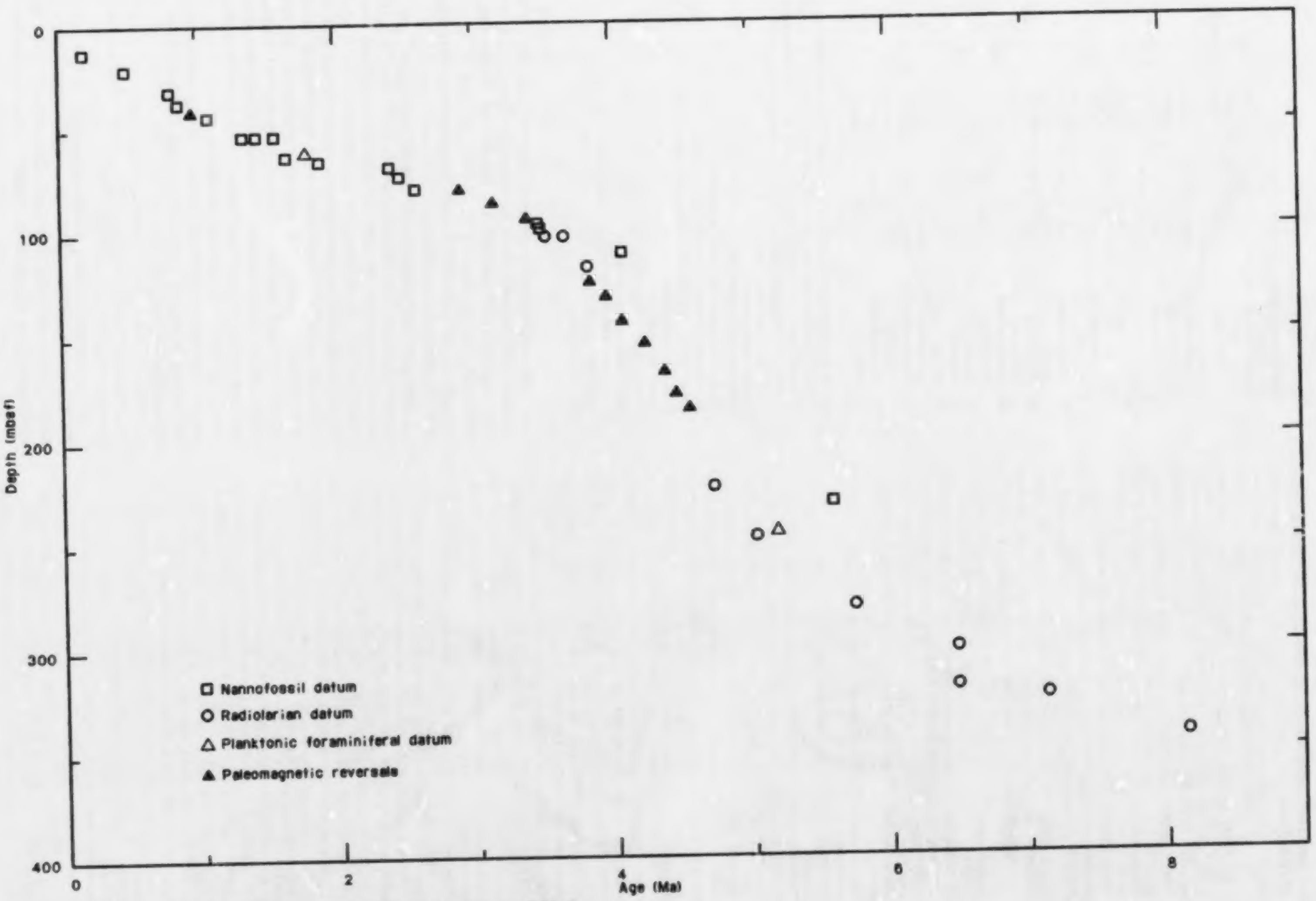

Figure 8. Age-depth plot for Hole 728A. For a detailed listing of events, see Table 3.

Table 3. Stratigraphic list of faunal events and paleomagnetic reversals for Hole 728A.

Event	Core, section, interval (cm)	Depth (mbsf)	Age (Ma)	Source of age
B *Emiliania huxleyi*	2H-1, 118–119 2H-3, 118–119	10.78 13.78	0.19	3
T *Pseudoemiliania lacunosa*	2H, CC 3H-1, 118–119	19.10 20.28	0.49	3
T *Reticulofenestra* sp. A	4H-1, 118–119 4H-3, 118–119	29.68 32.68	0.82	3
B *Gephyrocapsa parallela*	4H-5, 118–119 4H, CC	35.68 38.00	[a]0.89	4
B Jaramillo	5H-2, 120–122 5H-3, 120–122	40.70 42.20	0.98	5
[b]T *Gephyrocapsa* "large"	5H-3, 118–119 5H-5, 118–119	42.18 45.19	[a]1.10	4
[c]T *Helicosphaera sellii*	6H-1, 118–119 6H-2, 118–119	48.68 51.68		
[b]B *Gephyrocapsa* "large"	6H-3, 118–119 6H-5, 118–119	51.68 54.69	[a]1.36	4
T *Calcidiscus macintyrei*	6H-3, 118–119 6H-5, 118–119	51.68 54.68	1.45	5
B *Gephyrocapsa oceanica*	6H-3, 118–119 6H-5, 118–119	51.68 54.68	[a]1.57	4
T *Globigerinoides extremus*	6H, CC 7H, CC	57.00 66.50	[d]1.8	5
B *Gephyrocapsa caribbeanica*	7H-3, 125–126 7H-5, 125–126	61.25 64.25	[e]1.66	6
T *Discoaster brouweri*	7H-5, 125–126 7H, CC	64.25 66.50	1.9	5
T *Discoaster surculus*	8H-1, 118–119 8H-3, 118–119	67.68 70.68	2.4	5
Matuyama/Gauss	8H-4, 120–122 8H-5, 120–122	72.20 73.70	2.47	5
T *Discoaster tamalis*	9H-1, 118–119 9H-3, 118–119	77.28 80.28	[f]2.6	5
T Kaena	9H-2, 120–122 9H-3, 120–122	78.80 80.30	2.92	5
B Mammoth	9H-6, 120–122 10X-1, 120–122	84.80 86.90	3.18	5
Gauss/Gilbert	10X-5, 120–122 10X-6, 120–122	92.90 94.40	3.40	5
T *Sphenelithus abies*	10X, CC 11X-1, 118–119	95.30 96.48	3.47	5
T *Reticulofenestra pseudoumbilica*	11X-1, 118–119 11X-3, 118–119	96.48 99.48	3.5	5
T *Phormostichoartus doliolum*	11X-4, 85–87 11X, CC	100.65 104.90	3.53–3.55	1
B *Amphirhopalum ypsilon*	11X-4, 85–87 11X, CC	100.65 104.90	3.77–3.79	1
B *Discoaster asymmetricus*	12X-3, 118–119 12X, CC	109.08 114.50	[g]4.1	5
B *Spongaster tetras tetras*	12X, CC 13X-4, 85–87	114.40 120.95	3.83–3.85	1
T Cochiti	13X-5, 120–122 14X-1, 115–117	121.70 125.35	3.88	5
B Cochiti	14X-5, 120–122 14X-6, 119–121	131.40 132.89	3.97	5
T Nunivak	15X-6, 120–122 16X-1, 120–122	142.60 144.70	4.10	5
[h]T *Spongodiscus ambus*	15X-4, 85–87 15X, CC	139.25 143.50		
T *Didymocyrtis penultima*	16X-4, 85–87 16X, CC	148.85 153.10		
B Nunivak	16X-6, 108–110 17X-2, 120–122	152.08 155.80	4.24	5
T Sidufjall	18X-3, 129–130 18X-4, 111–113	167.08 168.41	4.40	5
B Sidufjall	19X-3, 125–127 19X-4, 122–124	176.75 178.22	4.47	5
T Thvera	20X-2, 97–99 20X-3, 112–114	184.67 186.32	4.57	5
T *Solenosphaera omnitubus*	23X, CC 24X-4, 85–87	220.80 226.15	4.7–4.8	2
T *Discoaster quinqueramus*	24X, CC 25X-1, 116–119	230.50 231.68	[i]5.6	5
B *Globorotalia tumida tumida*	25X, CC 26X, CC	240.10 249.80	5.2	5
T *Siphostichartus corona*	26X-4, 85–87 26X, CC	245.45 249.80	5.0–5.1	5

Table 3 (continued).

Event	Core, section, interval (cm)	Depth (mbsf)	Age (Ma)	Source of age
T *Stichocorys delmontensis*	26X-4, 85–87 26X, CC	245.45 249.80		
T *Stichocorys johnsoni*	29X, CC 30X-4, 85–87	278.80 284.15	[j]5.7–5.8	2
B *Spongodiscus ambus*	30X, CC 31X-4, 85–87	288.50 293.82		
S. delmontensis →*S. pereorina*	31X, CC 32X, CC	298.10 307.60	6.1–6.7	2
T *Calocycletta caepa*	32X-4, 85–87 32X, CC	303.45 307.80	[k]6.2–6.6	2
B *Stichocorys peregrina*	33X-4, 85–87 33X, CC	313.15 317.50		
B *Solenosphaera omnitubus*	33X, CC 34X-4, 85–87	317.50 322.35	6.3–6.5	2
T *Diartus hughesi*	24X-4, 85–87 34X, CC	322.85 327.20	7.1–7.2	2
T *Dictyocoryne ontongensis*	35X-4, 85–87 35X, CC	332.55 336.80		
T *Botryostrobus miralestensis*	36X-4, 85–87 36X, CC	342.15 346.40	[l]8.1–8.2	2
T *Didymocyrtis laticonus*	36X-4, 85–87 36X, CC	342.15 346.40		

Note: T = upper limit of event and B = lower limit; "an evolutionary transition." Sources of age are: 1 = Johnson et al., in press; 2 = Johnson and Nigrini, 1985; 3 = oxygen-isotope data for Site 723 (Niitsuma, unpubl. data); 4 = Takayama and Sato, 1987; 5 = Berggren et al., 1985; and 6 = Sato et al., in press.

[a] North Atlantic data.

[b] Long axis greater than 6 μm.

[c] No good published age; event appears to be diachronous.

[d] *G. obliquus extremus* in Berggren et al., 1985.

[e] North Atlantic age consistent with Italian-type section.

[f] Equatorial region only.

[g] Should be lower.

[h] ? Reworking or T may be between 11X-4 and 11X, CC.

[i] Age appears to be erroneous.

[j] *E.* cf. *diaphanes* in Johnson and Nigrini, 1985.

[k] Age in western Pacific.

[l] May be reworked.

one, was to combine uppermost Miocene and lower Pliocene Zones NN12 through NN15. Samples 117-728A-11X-3, 118–119 cm, through 117-728A-24X, CC (99.48–230.50 mbsf) and 117-728B-12X, CC, through 117-728B-24X, CC, (106.1–222.2 mbsf) contain *R. pseudoumbilica* and *Discoaster asymmetricus*, but not *Discoaster quinqueramus*.

Discoaster quinqueramus, the marker species for Zone NN11 (upper Miocene), is present from Sample 117-728A-25X-1, 118–119 cm, to the bottom of the hole (231.68–346.4 mbsf) and from 117-728B-25X, CC, to the bottom of the hole (231.8–347.7 mbsf).

Several reworked species include *Chiasmolithus grandis* and *Discoaster barbadiensis* from the Eocene, and *D. exilis, D. deflandrei, D. quinqueramus, Cyclicargolithus floridanus,* and *Sphenolithus moriformis* from the Oligocene-Miocene. *D. variabilis, S. abies,* and *R. pseudoumbilica* from the Miocene-Pliocene were encountered throughout both holes. Reworked Cretaceous species found in Hole 728A include *Watznaveria barnesae, Arkhangelskiella* spp., *Eiffelithus eximius, Microrhabdulus decoratus, Prediscosphaera* spp., *Cribrosphaerella ehrenbergii,* and *Tranolithus phacelosus.*

Radiolarians

The core-catcher samples of Cores 117-728A-1H through 117-728A-4H (9.6–38.0 mbsf) are barren of radiolarians. Between Cores 117-728A-5H and 117-728A-8H (47.5–76.1 mbsf), a few radiolarian fragments were found in the core-catcher sam-

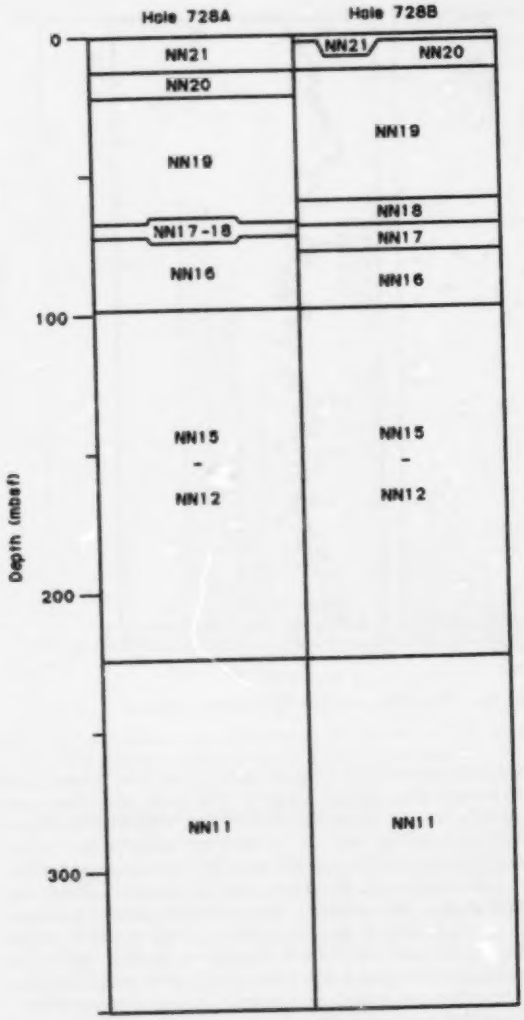

Figure 9. Correlation of calcareous nannofossil zones in Hole 728A and Hole 728B.

ples. However, radiolarians are common and well preserved from Sample 117-728A-9H, CC to Sample 117-728A-36X, CC (85.7–346.4 mbsf). The top of this siliceous sequence coincides with a pronounced spike in clay content, as shown by downhole logging ("Downhole Measurements" section, this chapter), and a change in porosity, as shown by the physical properties measurements (see "Physical Properties" section, this chapter). The radiolarians are generally mixed with varying quantities of mineral fragments, sponge spicules, and diatoms. Samples 117-728A-9H, CC through 117-728A-23X (85.7–220.8 mbsf) are in the *Spongaster pentas* Zone. Since *S. pentas* and *S. berminghami* are virtually absent, the *S. pentas/Stichocorys peregrina* boundary has been approximated to the LAD of *Solenosphaera omnitubus*. The *S. peregrina* Zone extends from Samples 117-728A-24X-4, 85–87 cm, to 117-728A-31X-4, 85–87 cm (226.15–293.82 mbsf). Samples 117-728A-31X, CC, and 117-72-32X-4, 85–87 cm (298.10–303.45 mbsf), lie within the *Didymocyrtis penultima* Zone and Samples 117-728A-32X, CC, to 117-728A-36X, CC (307.80–336.8 mbsf), lie within the *Didymocyrtis antepenultima* Zone.

Environmental Implications

The nannofossil genus, *Helisphaera*, which is thought to prefer areas of upwelling, was found in abundance in Samples 117-7A-4H, CC, through 117-728A-8H, CC (38.0–76.mbsf). *Coccolithus pelagicus*, a cold-water species, was present in unusually high numbers in Samples 117-728A-6H, CC, and 117-728A-7H, CC (48.6–58.1 mbsf).

The three different benthic foraminiferal assemblages found at Site 728 and the variation in the P/B ratio indicate that this site was located in the upper bathyal zone during the late Miocene. The water depth decreased in early Pliocene, and Site 728 was located in the neritic zone. During the late Pliocene, a significant increase occurred in water depth to the modern depth of Site 728 in the upper middle bathyal zone.

The fact that robust, thick-walled *Globorotalia tumida* subspecies dominate the planktonic foraminiferal assemblages in the Pliocene and upper Miocene may be caused by dissolution. These processes may have been enhanced in an extended or intensified oxygen-minimum zone during these time intervals.

PALEOMAGNETISM

Magnetic Measurements

At Site 728, we used the pass-through cryogenic magnetometer for all measurements in Cores 117-728A-1H through 117-728A-13X after pass-through alternating field (AF) demagnetization at 5 mT. Unfortunately, we were again frustrated by a combination of high scatter and incomplete removal of steep overprints, probably induced by coring or retrieval through the drill string.

Therefore, as at previous sites, paleomagnetic information at Site 728 was obtained using the Minispin fluxgate magnetometer and the Schonstedt AF demagnetizer. These efforts were successful; Figure 10 shows one of the better paleomagnetic records obtained during Leg 117. Our record covers sub-bottom depths of 0 to 200 m; below this interval, the sediments were too weakly magnetized to provide reliable data. An arithmetic mean intensity of 0.96 mA/m was obtained after AF demagnetization at 10 mT. Figure 11 indicates that inclination values for this interval correspond well to the expected axial dipole values.

Magnetostratigraphy

Table 4 lists the sub-bottom depths, depths within the cores, and ages (after Berggren et al., 1985) of the inferred polarity transitions. The main points of interest are (1) the absence of a Chron C1/C1r (Brunhes/Matuyama Chronozone) boundary—again after reference to the nannofossil stratigraphy (see "Biostratigraphy" section, this chapter), we interpret the first normal-to-reverse transition as the lower boundary of Subchron C1r-1 (Jaramillo Subchronozone); (2) the absence of Chron C2 (Olduvai Subchronozone), again as inferred from the nannofossil stratigraphy; and (3) the relatively high degree of detail with which Chrons C2Ar and C3 (upper and middle Gilbert Chronozone) are recorded: the Cochiti, Nunivak, and Sidufjall subchronozones appear to be present, together with the upper part of the Thvera Subchronozone. Figure 12 shows an age vs. depth curve based on the correlations with the polarity time scale.

Magnetic Susceptibility

The volume magnetic susceptibility of Site 728 sediments recovered from the Oman margin was measured using Bartington Instruments' whole-core sensor at 0.1 sensitivity and low-frequency (0.47 kHz) settings. Short intervals of pipe rust contamination in the XCB core tops appear as regular ~ 10-m spikes in

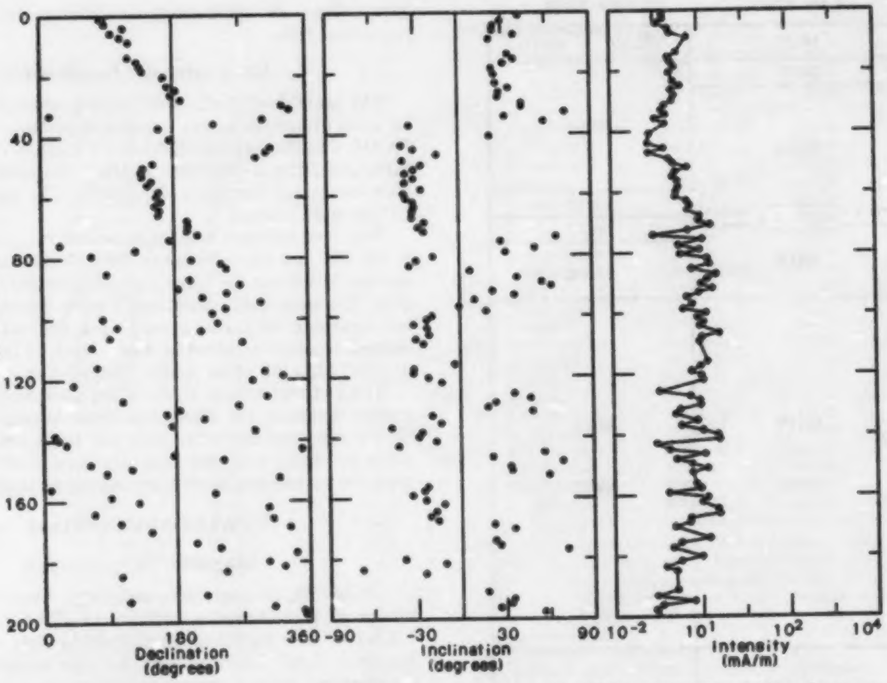

Figure 10. Declination, inclination and intensity for discrete samples from Hole 728A, obtained by shipboard measurements.

the susceptibility data. Susceptibilities were measured at 8 cm intervals, which resulted in approximately 4000 measurements each for Holes 728A and 728B. Recovery and core quality were excellent at both holes.

The susceptibility records of Holes 728A and 728B show well-defined variations that extend to the base of each hole (Fig. 13). The average amplitude of the Site 728 susceptibility variability is 30 to 100 × 10^{-6} volume SI units. These fluctuations can be correlated between holes over most of the recovered sequence with an accuracy of approximately 8 cm. A composite susceptibility record will be constructed for this site (and all others) as part of our shore-based research. Interhole correlations based on these data and lithologic marker layers are presented in the "Interhole Correlation" section of this chapter.

The high-quality susceptibility records obtained for Holes 728A and 728B can be correlated to other Oman margin and Owen Ridge sites. An example of the Brunhes Chronozone correlations possible between Holes 728A and 723B (Oman margin) and Hole 722B (Owen Ridge) is shown in Figure 14. Although the susceptibility record of each hole has a unique character, major and minor correlative features are apparent. Since the susceptibility data of Site 728 show well-defined variations over most of the recovered sequence, detailed correlations between the margin and ridge sites should be possible to at least the Matuyama/Gauss Chronozone boundary (2.47 Ma).

ACCUMULATION RATES

Sedimentation rates for Site 728 are based on magnetostratigraphic and biostratigraphic datum levels identified in Hole 728A (Table 3). Rates for the last 2.4 m.y. were determined between nannofossil datums that were assigned ages based on oxygen-isotope stratigraphy (N. Niitsuma, unpubl. data) or from Berggren et al. (1985). Over the last 1.9 m.y., average sedimentation rates varied from 15 to 65 m/m.y., with an overall mean of 34 m/m.y. (Fig. 15 and Table 5). This mean rate is low compared with those at other margin sites and reflects differences in depositional setting. Site 728, in the lower slope basin, receives mostly a pelagic influx, compared to the dominance of hemipelagic sedimentation in the upper slope basin (see "Lithostratigraphy" section, this chapter). Because of the low rate of sediment accumulation at Site 728 in this interval, errors in the age model may account for some of the high variability., Mean rates of sedimentation from 8.2 to 2.4 m.y. (23–88 m/m.y.) are based on a best fit to the reliable stratigraphic datums listed in Table 3. The mass accumulation of calcium carbonate, organic carbon, and noncarbonate sediment components are calculated from average values within intervals where the mean sedimentation rate is calculated (Table 5, Fig. 16).

At Site 728, sediments in the late Pliocene are characterized by a low mean sedimentation rate, high organic carbon concentrations (3%–4%), and the accumulation of siliceous microfossils. Similar associations were found at other Oman margin sites (see "Site 724" chapter, this volume), where accumulations occurred at more than twice the rate of Site 728. Upper Miocene to lower Pliocene sediments were deposited rapidly (~88 m/m.y.), with accumulation of organic carbon and abundant siliceous microfossils. These associations are thought to reflect sedimentation in environments of high biological productivity. Benthic foraminifer data from Site 728 (see "Biostratigraphy" section, this chapter) indicate that this site was at a depth near 350 m in the late Miocene and early Pliocene, when rapid deposition occurred, and has since subsided to its present depth of 1400 m. These results suggest that changes in the tectonic setting in addition to surface productivity are responsible for the variations in sediment accumulation at Site 728 during the Neogene.

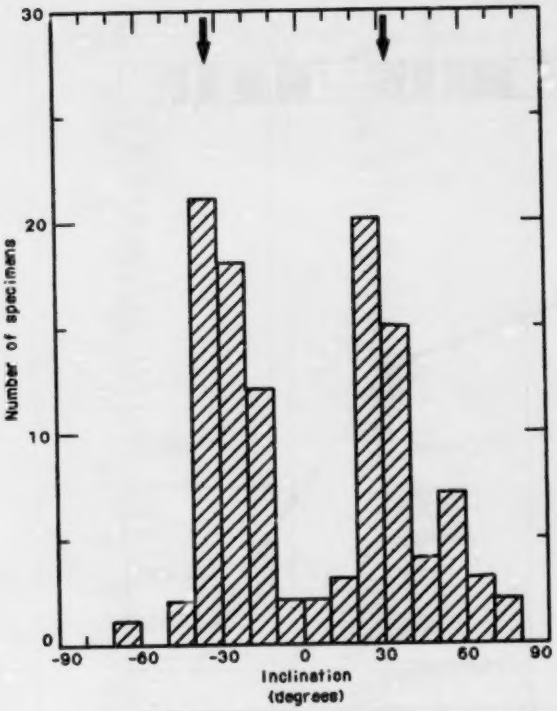

Figure 11. Inclination values grouped into 10° classes. Arrows indicate the expected geocentric axial dipole values for the site latitude.

Table 4. Magnetozone boundaries in Hole 728A.

Boundary	Age (Ma)	Sample interval (cm)	Depth (mbsf)
Bottom of Jaramillo (C1r-1/C1r)	0.98	5H-2, 120/5H-3, 120	40.70/42.20
Matuyama/Gauss (C2r/C2A)	2.47	8H-4, 120/8H-5, 120	72.20/73.70
Top of Kaena (C2A/C2A-1)	2.92	9H-2, 120/9H-3, 120	78.80/80.30
Bottom of Mammoth (C2A-2/C2A)	3.18	9H-6, 120/10X-1, 120	84.80/86.90
Gauss/Gilbert (C2A/C2Ar)	3.40	10X-5, 120/10X-6, 120	92.90/94.40
Top of Cochiti (C2Ar/C3.1)	3.88	13X-5, 120/14X-1, 115	121.70/125.35
Bottom of Cochiti (C3.1/C3.1r)	3.97	14X-5, 120/14X-6, 119	131.40/132.89
Top of Nunivak (C3.1r/C3.2)	4.10	15X-6, 120/16X-1, 120	142.60/144.70
Bottom of Nunivak (C3.2/C3.2r)	4.24	16X-6, 108/17X-2, 120	152.08/155.80
Top of Sidufjall (C3.2r/C3.2r-1)	4.40	18X-3, 128/18X-4, 111	167.08/168.41
Bottom of Sidufjall (C3.2r-1/C3.2r)	4.47	19X-3, 125/19X-4, 122	176.75/178.22
Top of Thvera (C3.2r/C3.3)	4.57	20X-2, 97/20X-3, 112	184.67/186.32

Note: Ages of chronozone boundaries are after Berggren et al. (1985).

PHYSICAL PROPERTIES

Introduction

Physical properties measured on discrete samples of sediments recovered from Site 728 include index properties (wet-bulk density, porosity, water content, and grain density), thermal conductivity, vane shear strength, and compressional-wave velocity (Tables 6 and 7). Wet-bulk density was measured on all whole-round cores that were at least 80 cm in length using the GRAPE logging system. Acquisition of compressional-wave velocity data using the *P*-wave logger was limited to the interval between the seafloor and approximately 100 mbsf. All techniques and equipment used are described in the "Explanatory Notes" (this volume).

Index Properties

As observed at the other sites on the Oman margin, the sequences of marly nannofossil ooze at Site 728 show relatively low wet-bulk and grain densities, as well as high porosities and water contents (Fig. 17). This may be a result of fairly high concentrations of organic material at this site, as well as of the common occurrence of radiolarians and diatoms from Core 117-728A-9H to total depth.

Lithologic Subunit IA

Within the marly foraminifer-nannofossil to foraminifer-bearing marly nannofossil oozes of lithologic Subunit IA (0–58 mbsf), porosity and water contents decrease from 60% to 55% and 36% to 33%, respectively, in response to increasing overburden pressure. Within this subunit, the foraminifers are abundant in some intervals and may account for the variability in index properties. Grain density is variable at all depths (ranging from 2.50 to 2.73 g/cm^3), but decreases downsection as the organic carbon content increases from 1% to 2%. Wet-bulk density varies widely in this interval, but overall values of bulk density increase from 1.70 to 1.75 g/cm^3. An exception to these trends occurs in an interval between 36 and 43 mbsf (Sections 117-728A-4H-6 to 117-728A-5H-4). Here, a maximum porosity of 64% and a minimum wet-bulk density of 1.62 g/cm^3 coincide with a local maximum in calcium carbonate (65%–71%), most likely in the form of foraminifers. The wet-bulk density of this interval is correspondingly low (1.62 g/cm^3).

Lithologic Subunit IB

Several distinct trends in physical properties can be identified within the marly nannofossil ooze and chalk of lithologic Subunit IB (58–320 mbsf) that are related to the presence of siliceous microfossils in the sequences below Section 117-728A-8H, CC (76 mbsf) and to variations in the abundance of organic carbon throughout the section (see "Lithostratigraphy" section, Fig. 6, this chapter). Index properties in Cores 117-728A-7H through 117-728A-9H (58–85 mbsf) display gradients opposite to those expected in a consolidating section because of a rapid increase in organic carbon from 2% at the base of Core 117-728A-6H to maxima of 4.5% and 5.0% at depths of 72 and 82 mbsf. Grain density is markedly lower throughout this interval (2.50 to 2.63 g/cm^3) and decreases gradually with depth to 2.55 g/cm^3 at 85 mbsf. As observed in the overlying sediments, wet-bulk density shows considerable variation. In this interval, however density decreases with depth (1.75 to 1.65 g/cm^3) in response to decreases in grain density. The coincident increases in porosity (55%–62%) and water content (33%–41%) result from the open-fabric framework that is characteristic of organic-rich sediments.

Within the interval of siliceous-bearing, marly nannofossil ooze between 85 mbsf and the base of lithologic Subunit IB, index properties closely track the variation in organic carbon content. Between 85 and 170 mbsf, porosity and water content remain high and increase slightly to maximum values of 65% and 42%, respectively, in an interval between 150 and 170 mbsf. Wet-bulk density is correspondingly low (1.60 g/cm^3) in this interval, which, in addition to being high in organic carbon, is especially rich in calcium carbonate (see Fig. 6, "Lithostratigra-

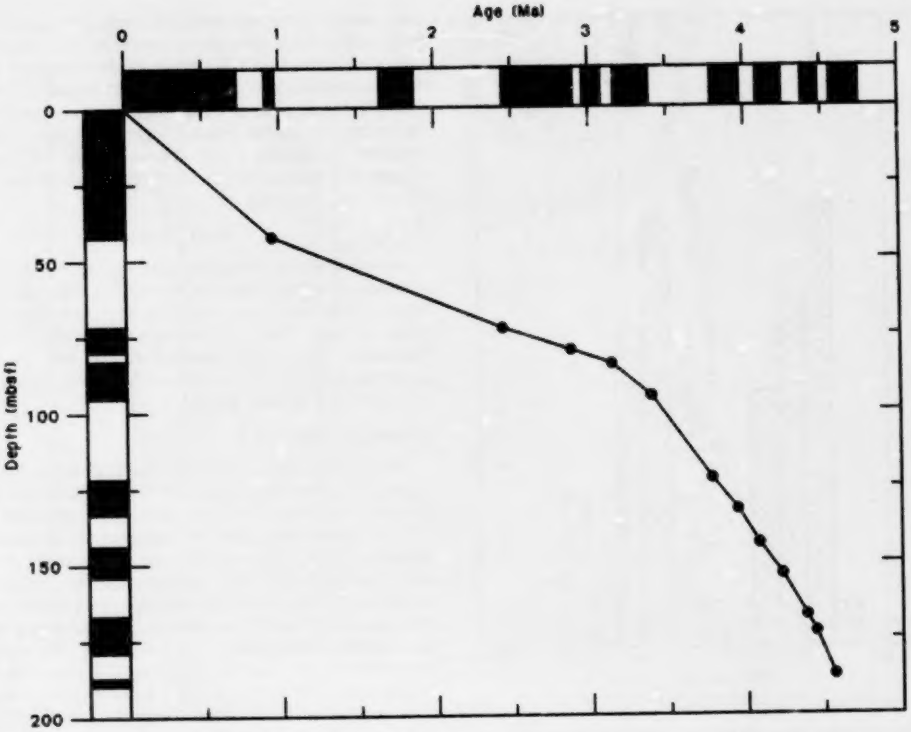

Figure 12. Age-depth curve for the upper 200 mbsf for Hole 728A, using magnetic chronozone boundaries.

phy" section, this chapter). Grain density varies from 2.45 to 2.65 g/cm³ and averages 2.55 g/cm³ between 85 and 170 mbsf.

Below 170 mbsf to the base of lithologic Subunit IB at 320 mbsf, porosity, water content, and wet-bulk density resume normal downsection gradients; porosity decreases from 63% to 59%, water content decreases from 41% to 36%, and wet-bulk density increases from 1.62 to 1.72 g/cm³. Grain density varies throughout this interval at all depths, but generally increases from an average of 2.58 to 2.65 g/cm³ in response to a decrease from 3.0% to 1.3% in organic carbon.

Lithologic Subunit IC

Within lithologic Subunit IC (320–349 mbsf), index properties are found to vary significantly with minor changes in sediment composition. Samples from the layers of marly nannofossil and diatomaceous chalks are distinctly higher in porosity (64%–67%) and water content (41%–43%) and lower in wet-bulk density (1.59 to 1.63 g/cm³) than the more calcareous nannofossil chalks. Grain densities show a less consistent correlation but tend to be lower in the siliceous and clay-rich units (2.50 to 2.60 g/cm³) than in the nannofossil-rich layers (2.51 to 2.65 g/cm³).

Compressional-Wave Velocity

Compressional-wave velocity was measured perpendicular to bedding on discrete samples from all cores in Holes 728A and 728B from which suitable samples could be extracted. Velocities were also measured parallel to bedding on samples that were sufficiently indurated to allow a cubic sample to be cut (Tables 6 and 7; Fig. 18).

Velocities measured in the uppermost 100 m of Hole 728A vary from 1515 to 1594 m/s but correspond well to velocities measured by the *P*-wave logger (Fig. 19) and reflect the slight decrease in bulk density measured in the discrete samples (Fig. 17) and on the continuous GRAPE density logs (Fig. 20). Velocities could not be successfully measured in the friable and brittle sediments recovered from depths greater than 100 and less than 220 mbsf, with the curious exception of one core from each of the two holes at 180 mbsf (Fig. 18). Compressional-wave velocities in the more indurated nannofossil chalks below 220 mbsf are variable but again reflect the slight downhole decrease in density. Anisotropy in compressional-wave velocity shows no consistent correlation with density or sub-bottom depth. Velocities measured parallel to bedding averaged 3.0% greater than those measured perpendicular to bedding.

Thermal Conductivity

Thermal conductivity, measured on even-numbered cores from Cores 117-728A-1H to 117-728A-26X, decreases consistently with depth from approximately 1.45 W/m K near the seafloor to an average of 1.25 W/m K at 250 mbsf. Below this depth, the sediments were too stiff to allow insertion of the needle probes. The observed downsection decrease at first appeared to be attributed to the friable nature of the sediments below 100 mbsf, but a positive correlation between thermal conductivity and wet-bulk density (Fig. 21) suggests that thermal conductivity decreases in response to the gradual downsection decrease in wet-bulk density.

Vane Shear Strength

Vane shear strength increases from 10 kPa near the seafloor to 135.7 kPa at 70 mbsf. The sharp decrease in shear strength below this level coincides with the change in sediment composition to more siliceous and organic-rich sediments.

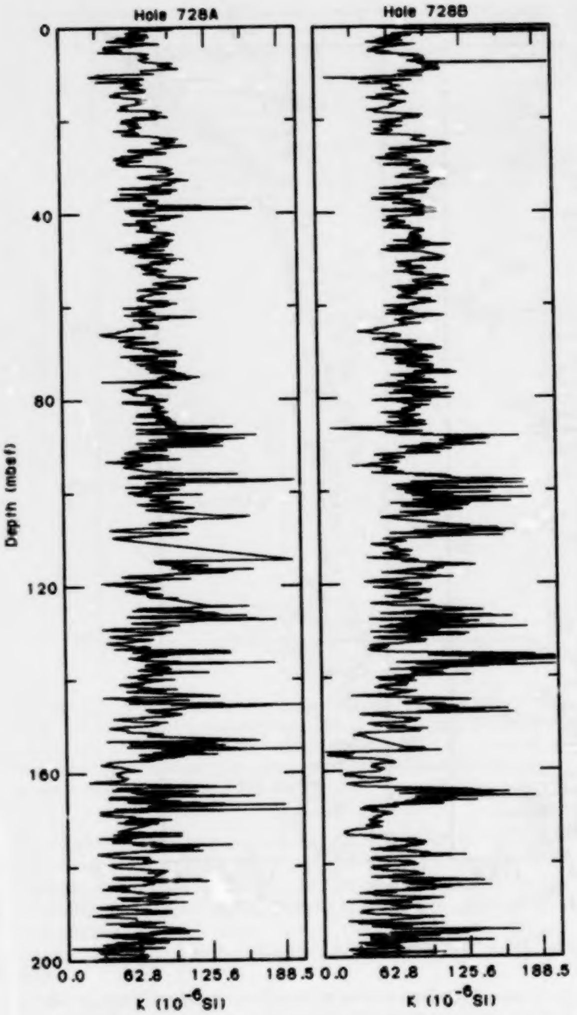

Figure 13. Whole-core magnetic susceptibility data for Holes 728A and 728B. Regular ~ 10-m susceptibility spikes are caused by pipe rust contamination of the XCB core tops.

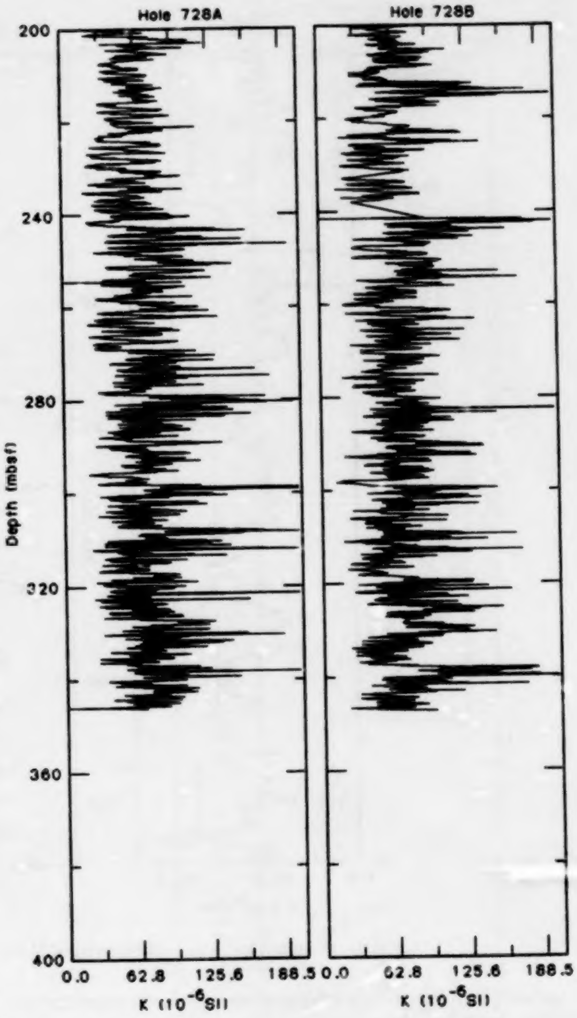

Figure 13 (continued).

GRAPE and *P*-Wave Logs

The quality of data obtained from the GRAPE and *P*-wave logging systems was generally very good at Site 728. Continuous GRAPE data were obtained to total depth in Holes 728A and 728B. The pattern of bulk-density variation determined by the GRAPE records corresponds to that of the discrete samples, although the quality of the match between the two data sets varies with depth. Between 0 and 85 mbsf, the discrete samples display a large variation and are approximately 0.05 to 0.10 g/cm^3 lower than the GRAPE values, perhaps as a result of the addition of water to the sediments during coring, splitting, and/or sampling. A reduction in the disturbance of the discrete samples may contribute to the improved match between the two data sets between 85 and 150 mbsf. Below 150 mbsf, the GRAPE and discrete-measurement records overlap, but the GRAPE system consistently underestimated the wet-bulk density because cores did not completely fill the liners.

P-wave velocity logs were obtained in Cores 117-728A-1H through -10X and Core 117-782B-1H through Section 117-728B-14X-2. These velocities average 1590 m/s to a depth of 30 mbsf. At greater depths, the values decrease gradually to 1550 m/s at 95 mbsf. This negative gradient in part reflects the decrease in wet-bulk density associated with changes in texture and composition of the sediment but may also be accentuated by the increasing thickness of drilling slurry around the sediment cores.

SEISMIC STRATIGRAPHY

Site 728 is located in the distal slope basin of the Oman margin. This basin is separated from an outer basement high by a major normal fault (Fig. 22). The basin is flanked on the northwest by a complexly faulted region that is uplifted in relation to the slope basin. Here, we first examine the relationship between seismic traveltime and core depth to provide a basis for regional extrapolation across a seismic section from the very detailed information available at Site 728. Next, we provide a preliminary seismic interpretation of the seismic section in Figure 22, keyed to the data from Site 728. Implicit in such a discussion of a sin-

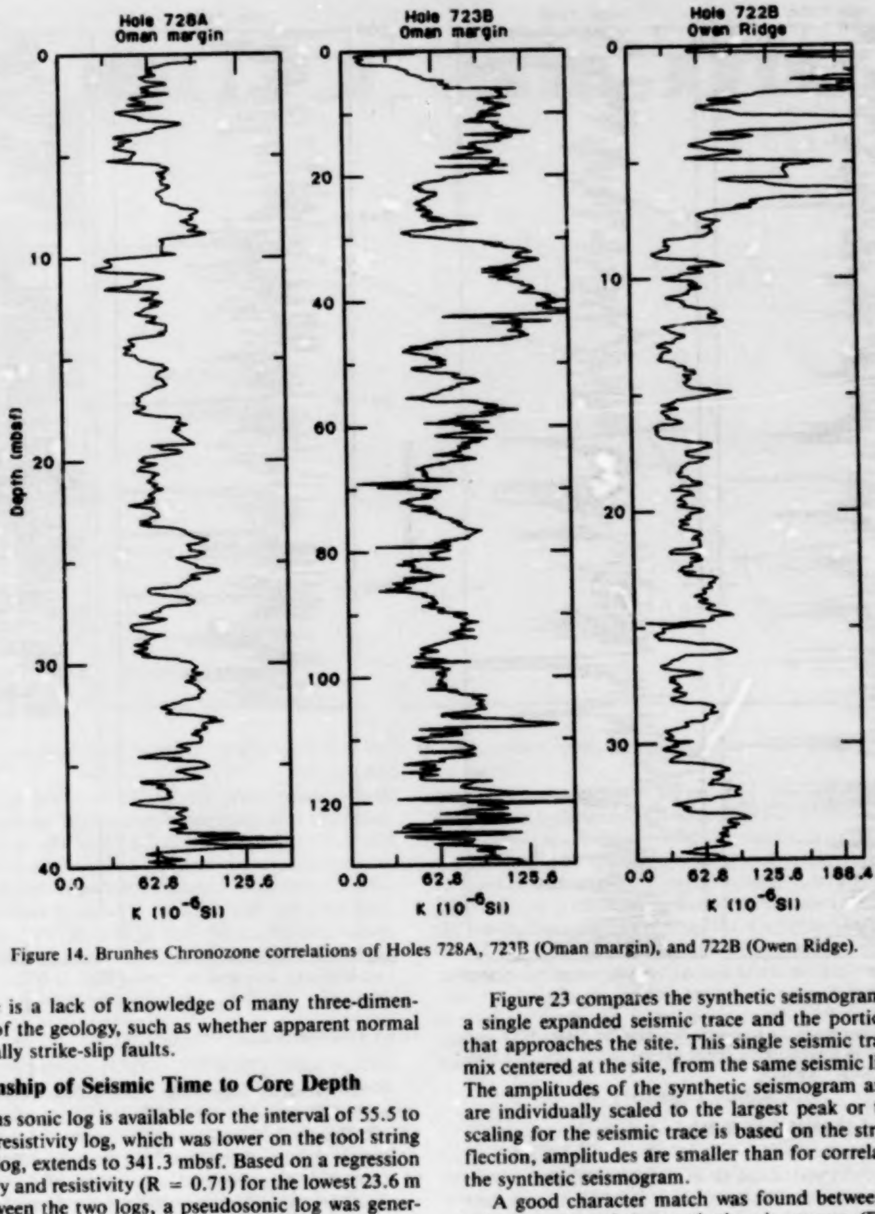

Figure 14. Brunhes Chronozone correlations of Holes 728A, 723B (Oman margin), and 722B (Owen Ridge).

gle seismic line is a lack of knowledge of many three-dimensional aspects of the geology, such as whether apparent normal faults are actually strike-slip faults.

Relationship of Seismic Time to Core Depth

A continuous sonic log is available for the interval of 55.5 to 327.6 mbsf. A resistivity log, which was lower on the tool string than the sonic log, extends to 341.3 mbsf. Based on a regression between velocity and resistivity (R = 0.71) for the lowest 23.6 m of overlap between the two logs, a pseudosonic log was generated for the short interval of 327.6 to 341.3 mbsf (see "Downhole Measurements" section, this chapter). A composite sonic log was used to calculate a synthetic seismogram for Site 728. No density log was available, thus, a constant density was assumed. This assumption probably does not degrade the accuracy of the synthetic seismogram much because a synthetic seismogram calculated for Site 723 using a constant-density assumption was almost identical to that calculated from both sonic and density logs (see "Seismic Stratigraphy" section, Site 723 chapter). The synthetic seismogram was calculated based on a convolutional model with interbed multiples and a wavelet estimate for the *Conrad* (see "Seismic Stratigraphy" section, Site 720 chapter).

Figure 23 compares the synthetic seismogram for Site 728 to a single expanded seismic trace and the portion of Figure 22 that approaches the site. This single seismic trace is a 10-trace mix centered at the site, from the same seismic line as Figure 22. The amplitudes of the synthetic seismogram and seismic trace are individually scaled to the largest peak or trough. Because scaling for the seismic trace is based on the strong seafloor reflection, amplitudes are smaller than for correlative portions of the synthetic seismogram.

A good character match was found between the composite seismic trace and the synthetic seismogram (Fig. 23) down to 2.19 s (267 mbsf), and a tentative match can be extended to 2.23 s (300 mbsf). Below 300 mbsf, the synthetic seismogram indicates much higher amplitudes than the composite seismic trace. Similar high amplitudes were observed on the seismic section adjacent to the site, with the same wavelength between peaks. Furthermore, the strongest seismic reflector intersects the site at 2.28 s, the location of the strongest peak on the synthetic seismogram. The inconsistency of seismic reflector amplitudes between the seismic section and the composite trace from the same section probably results from the substantial dip of these deeper reflectors, which causes averaging of a peak with its adjacent trough across a 10-trace mix. Sonic traveltimes are considered to

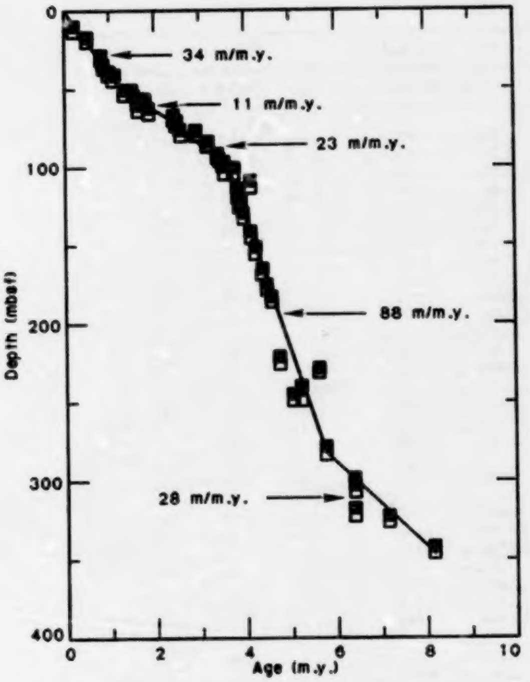

Figure 15. Age-depth plot of stratigraphic datums listed in Table 5. The filled and open boxes are upper and lower depths of each datum level, respectively. Indicated mean sedimentation rates (solid lines) are determined by a best fit to the data. Rates calculated between reliable datums younger than 1.9 m.y. are listed in Table 5.

be reliable in the lower portion of Site 728 down to the lowest sonic log value at 327.6 mbsf (see "Downhole Measurements" section, this chapter), and the deepest seismic reflector on the synthetic seismogram (at 338 mbsf) is caused by velocity contrasts above this level, rather than by the short pseudosonic log. Thus, the match with the seismic peak at 2.28 s is probably correct.

Based on the match of the synthetic seismogram with the seismic section, a continuous match between core depth and seismic reflectors can be made for the depth interval 55.5 to 338 mbsf. We identified three significant seismic reflectors on the seismic section, on the basis of downhole changes in lithostratigraphy and logs.

An impedance rise occurs at 88 mbsf (Fig. 23), immediately below the 63-85 mbsf zone of rapid variations in log responses,

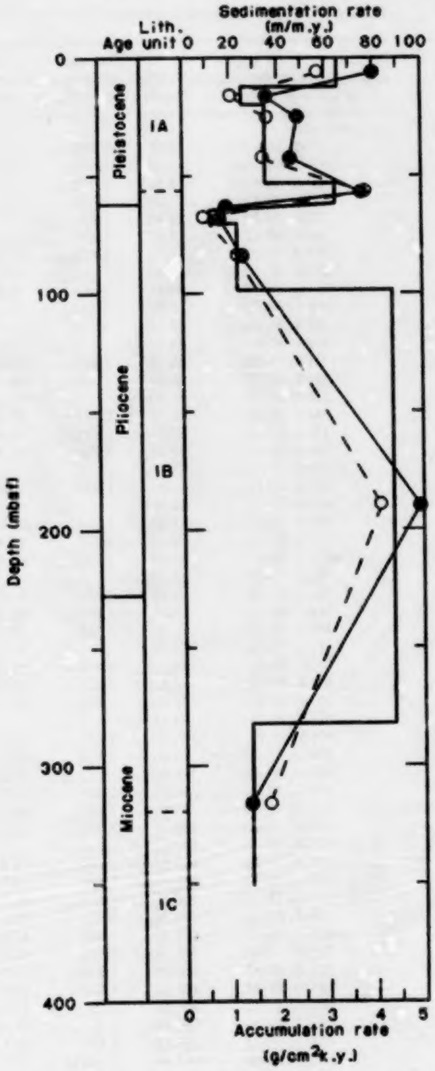

Figure 16. Sedimentation rate (m/m.y.; solid line), calcium carbonate accumulation rate (g/cm^2/k.y.; dots), and noncarbonate accumulation rate (g/cm^2/k.y.; open circles) vs. depth (mbsf) at Site 728. Accumulation rates are plotted at the midpoint of the respective depth intervals.

Table 5. Sedimentation and accumulation rate data for Site 728.

Depth interval (mbsf)	Age range (m.y.)	$CaCO_3$ ($\bar{x}$ %)	C_{org} ($\bar{x}$ %)	Dry-bulk density ($\bar{x}$ g/cm^3)	Sed. rate ($\bar{x}$ m/m.y.)	$CaCO_3$ acc. rate (g/cm^2/k.y.)	Non-$CaCO_3$ acc. rate (g/cm^2/k.y.)	C_{org} acc. rate (mg/cm^2/k.y.)
0.0-12.3	0-0.19	58.4	1.11	1.05	64.7	3.97	2.83	75.4
12.3-19.7	0.19-0.49	63.3	ND	1.11	24.7	1.74	1.01	ND
19.7-31.2	0.49-0.82	57.7	1.34	1.20	34.8	2.41	1.77	56.0
31.2-53.2	0.82-1.45	57.5	1.91	1.13	34.9	2.27	1.68	75.3
53.2-61.5	1.45-1.66	49.6	1.37	1.18	63.8	3.73	3.79	103.1
61.5-64.5	1.66-1.90	46.0	2.26	1.18	15.0	0.81	0.96	40.0
64.5-70.0	1.90-2.40	63.2	1.99	1.09	11.0	0.76	0.44	23.9
70.0-98.0	2.40-3.6	52.2	3.67	1.04	23.3	1.27	1.16	89.0
98.0-282.0	3.6-5.7	54.4	2.59	1.03	87.6	4.91	4.11	233.7
282.0-350.0	5.7-8.15	43.7	1.49	1.12	27.8	1.36	1.75	46.4

Note: ND = no data for the interval.

Table 6. Physical properties summary for Hole 728A.

Core, section, interval (cm)	Depth (mbsf)	Wet-bulk density (g/cm^3)	Porosity (%)	Water content (%)	Gain density (g/cm^3)	Dry-bulk density (g/cm^3)	Velocity (m/s)	Thermal conductivity (W/mK)	Vane shear strength (kPa)
117-728A-									
1H-2, 100-102	2.50	1.581	64.3	41.7	2.686	0.922			
1H-4, 100-102	5.50	1.671	60.9	37.3	2.701	1.047			
1H-6, 100-102	8.50	1.751	57.3	33.5	2.724	1.164			10.0
2H-2, 80-82	11.90	1.646	56.8	35.4	2.640	1.064		1.36	
2H-4, 80-82	14.90	1.676	57.5	35.1	2.738	1.087		1.35	
2H-6, 80-82	17.90	1.699	56.0	33.8	2.735	1.124		1.54	
3H-2, 80-82	21.40	1.651	58.2	36.1	2.678	1.056			
3H-4, 80-82	24.40	1.797	53.4	30.4	2.667	1.251			
3H-6, 28-30	26.88	1.804	52.4	29.8	2.750	1.267			18.1
4H-2, 80-82	30.80	1.781	54.4	31.3	2.639	1.223		1.53	
4H-4, 80-82	33.80	1.738	53.7	31.6	2.637	1.188		1.43	
4H-5, 57-60	35.77						[a]1594		
4H-6, 80-82	36.80	1.623	64.1	40.5	2.581	0.966		1.31	
5H-2, 80-82	40.30	1.628	59.9	37.7	2.630	1.015			
5H-3, 50-53	41.50						[a]1550		
5H-4, 80-82	43.30	1.759	57.3	33.3	2.677	1.173			
5H-6, 80-82	46.30	1.745	55.9	32.8	2.587	1.172			40.8
6H-2, 80-82	49.80	1.789	53.6	30.7	2.641	1.240		1.44	
6H-4, 75-77	52.75								96.1
6H-4, 80-82	52.80	1.716	57.0	34.0	2.502	1.132		1.36	
6H-6, 75-78	55.75						[a]1555		
6H-6, 80-82	55.80	1.764	56.1	32.6	2.609	1.190		1.44	
7H-2, 80-82	59.30	1.745	55.6	32.6	2.554	1.176			
7H-4, 80-82	62.30	1.747	55.3	32.4	2.522	1.181			78.1
7H-6, 75-78	65.25						[a]1515		
7H-6, 80-82	65.30	1.727	57.7	34.2	2.620	1.136			
8H-2, 80-82	68.80	1.669	60.3	37.0	2.575	1.051		1.30	
8H-4, 80-82	71.80	1.669	61.1	37.5	2.584	1.042		1.19	135.7
8H-6, 75-78	74.75						[a]1564		
8H-6, 80-82	74.80	1.790	55.6	31.8	2.626	1.221		1.48	
9H-2, 80-82	78.40	1.628	63.9	40.2	2.566	0.973			61.3
9H-4, 80-82	81.40	1.672	62.6	38.4	2.604	1.031			
9H-6, 75-78	84.35						[a]1594		
9H-6, 80-82	84.40	1.754	58.9	34.4	2.654	1.150			
10X-2, 80-82	88.00	1.636	63.4	39.7	2.556	0.986		1.17	
10X-4, 80-82	91.00	1.562	65.8	43.2	2.460	0.887		1.17	39.6
10X-6, 80-82	94.00	1.666	60.8	37.4	2.526	1.043		1.26	
11X-2, 80-82	97.60	1.697	61.4	37.0	2.656	1.068			
11X-4, 78-80	100.58	1.714	59.8	35.8	2.610	1.101			75.7
11X-6, 75-78	103.55						[a]1578		
11X-6, 80-82	103.60	1.762	56.8	33.0	2.584	1.181			
12X-1, 70-72	105.60	1.662	63.7	39.3	2.622	1.009		1.23	
12X-3, 70-72	108.60	1.669	61.9	38.0	2.557	1.034		1.19	
13X-1, 80-82	115.30	1.613	63.5	40.3	2.486	0.963			
13X-3, 80-82	118.30	1.624	62.2	39.2	2.473	0.987			
13X-5, 80-82	121.30	1.625	65.7	41.5	2.530	0.961			
14X-2, 80-82	126.50	1.639	63.2	39.5	2.564	0.991		1.25	
14X-4, 80-82	129.50	1.625	65.2	41.1	2.626	0.957		1.19	
14X-6, 80-82	132.50	1.605	65.5	41.8	2.543	0.934		1.26	
15X-2, 72-74	136.12	1.651	63.3	39.3	2.597	1.002			
15X-4, 73-75	139.13	1.527	66.7	44.8	2.432	0.843			
15X-6, 94-96	142.34	1.621	65.3	41.3	2.607	0.952			
16X-2, 80-82	145.80	1.605	65.2	41.6	2.539	0.937		1.13	
16X-4, 80-82	148.80							1.21	
16X-4, 92-94	148.92	1.677	62.8	38.4	2.648	1.03[illegible]			
16X-6, 80-82	151.80	1.674	62.9	38.5	2.659	1.029		1.23	
17X-2, 73-75	155.33	1.619	62.7	39.7	2.534	0.977			
17X-4, 69-71	158.29	1.644	64.8	40.4	2.629	0.980			
17X-6, 75-77	161.35	1.631	63.3	39.8	2.546	0.963			
18X-2, 80-82	165.10							1.10	
18X-2, 135-137	165.65	1.617	65.7	41.6	2.607	0.944			
18X-4, 80-82	168.10							1.05	
18X-4, 101-103	168.31	1.586	68.2	44.1	2.488	0.887			
18X-6, 50-52	170.80							1.14	
18X-6, 61-63	170.91	1.624	64.7	40.8	2.667	0.961	[a]1669		
19X-2, 93-95	174.93	1.671	62.7	38.4	2.603	1.029			
19X-4, 98-100	177.98	1.616	64.6	41.0	2.548	0.954			
19X-7, 31-33	181.81	1.660	63.6	39.3	2.644	1.008			
20X-2, 80-82	184.50							1.06	
20X-2, 118-120	184.88	1.629	63.9	40.2	2.533	0.974			
20X-4, 80-82	187.50							1.18	
20X-4, 106-108	187.76	1.673	60.1	36.8	2.484	1.057			
20X-6, 80-82	190.50							1.24	
20X-6, 122-124	190.92	1.658	62.9	38.8	2.564	1.014			
21X-2, 56-58	193.86	1.708	60.6	36.3	2.641	1.087			
21X-4, 72-74	197.02	1.681	63.6	38.8	2.609	1.029			
21X-6, 103-105	200.33	1.670	60.5	37.1	2.517	1.050			

Table 6 (continued).

Core, section, interval (cm)	Depth (mbsf)	Wet-bulk density (g/cm^3)	Porosity (%)	Water content (%)	Gain density (g/cm^3)	Dry-bulk density (g/cm^3)	Velocity (m/s)	Thermal conductivity (W/mK)	Vane shear strength (kPa)
117-728A- (Cont.)									
22X-2, 80-82	203.80	1.690	60.8	36.9	2.587	1.067		1.20	
22X-4, 80-82	206.80	1.630	66.1	41.5	2.662	0.953		1.14	
22X-6, 76-78	209.76	1.691	59.6	36.1	2.527	1.081			
22X-6, 80-82	209.80							1.26	
23X-2, 80-82	213.40	1.621	62.5	39.5	2.455	0.981			
23X-4, 80-82	216.40	1.661	62.0	38.2	2.550	1.026			
23X-6, 80-82	219.40	1.676	61.5	37.6	2.555	1.046			
24X-2, 69-71	222.99	1.659	63.4	39.2	2.616	1.009			
24X-2, 80-82	223.00							1.09	
24X-4, 69-71	225.99	1.696	62.0	37.5	2.633	1.060			
24X-4, 80-82								1.19	
24X-4, 138-140	226.68	1.668	64.1	39.4	2.663	1.012	^{a}1557		
24X-6, 79-81	229.09	1.733	61.2	36.2	2.663	1.105		1.04	
25X-2, 85-87	232.85	1.737	60.1	35.5	2.629	1.121			
25X-4, 48-50	235.48	1.733	58.1	34.4	2.628	1.138	^{a}1616		
25X-6, 147-149	239.47	1.768	57.1	33.1	2.587	1.183			
26X-2, 21-23	241.81	1.664	61.9	38.1	2.528	1.030	^{a}1617		
26X-2, 21-23	241.81						^{b}1603		
26X-2, 80-82	242.40							1.28	
26X-4, 80-82	245.40							1.19	
26X-5, 72-74	246.82	1.721	57.6	34.3	2.565	1.131	^{a}1579		
26X-5, 72-74	246.82						^{b}1638		
26X-6, 80-82	248.80							1.23	
27X-2, 116-118	252.46	1.743	58.8	34.6	2.654	1.140	^{a}1574		
27X-4, 17-19	254.47	1.776	55.9	32.3	2.620	1.203	^{a}1601		
27X-4, 17-19	254.47						^{b}1637		
27X-6, 107-109	258.37	1.737	56.6	33.4	2.546	1.157	^{a}1611		
27X-6, 107-109	258.37						^{b}1648		
28X-3, 7-9	262.57	1.693	62.0	37.5	2.628	1.058			
28X-6, 137-139	268.37	1.679	63.1	38.5	2.659	1.033			
28X-7, 41-43	268.91	1.677	60.5	36.9	2.450	1.057			
29X-2, 51-53	271.11	1.760	59.7	34.7	2.617	1.149			
29X-5, 67-69	275.77	1.718	59.0	35.2	2.511	1.114	^{a}1624		
30X-2, 134-136	281.64	1.741	57.7	34.0	2.604	1.150	^{a}1575		
30X-2, 134-136	281.64						^{b}1614		
30X-4, 114-116	284.44	1.744	56.5	33.2	2.541	1.166	^{a}1557		
30X-4, 114-116	284.44						^{b}1615		
31X-2, 126-128	291.26	1.727	59.4	35.2	2.546	1.119	^{a}1612		
31X, CC, 30-32	298.23	1.834	55.5	31.0	2.659	1.266	^{a}1615		
31X, CC, 30-32	298.23						^{b}1623		
32X-4, 77-79	303.37	1.727	59.3	35.2	2.618	1.120	^{a}1562		
32X-4, 77-79	303.37						^{b}1592		
32X-6, 93-95	306.53	1.649	62.5	38.8	2.545	1.009	^{a}1534		
32X-6, 93-95	306.53						^{b}1585		
33X-4, 94-96	313.24	1.751	59.6	34.9	2.730	1.140	^{a}1567		
33X-4, 94-96	313.24						^{b}1601		
33X-5, 96-98	314.76	1.736	57.5	33.9	2.573	1.147	^{a}1573		
33X-5, 96-98	314.76						^{b}1625		
34X-3, 77-80	321.27	1.591	67.0	43.1	2.564	0.905			
34X, CC, 30-33	327.25	1.778	58.3	33.6	2.646	1.181	^{a}1599		
34X, CC, 30-33	327.25						^{b}1554		
35X-2, 104-107	329.74	1.608	64.0	40.8	2.501	0.952			
35X-6, 63-66	335.33	1.704	60.8	36.6	2.594	1.081	^{a}1573		
36X-3, 32-35	340.12	1.632	65.0	40.8	2.605	0.966			
36X-6, 103-106	345.33	1.654	61.0	37.8	2.506	1.029	^{a}1556		

[a] Velocity measurement perpendicular to bedding.
[b] Velocity measurement parallel to bedding.

associated partly with very organic-rich horizons and perhaps also partly with phosphorite horizons (see "Downhole Measurements" and "Organic Geochemistry" sections, this chapter). Little lithologic change can be found between 88 and 314 mbsf, near the bottom of Site 728. This approximately 88-mbsf base of the highly variable zone corresponds to a trough at 1.97 s on the seismic section, which is traced laterally in Figure 22, based on the fact that the peak at 1.99 s is from a later part of the wavelet that intersects the same horizon. For convenience in subsequent discussions, this seismic horizon is called reflector A and the seismic sequence between this reflector and the seafloor is called sequence SF-A.

An even larger impedance rise at 226 mbsf is caused by a porosity decrease downhole, rather than a mineralogical change (see "Downhole Measurements" section, this chapter). This horizon may be significant for two reasons. First, it occurs within a short depth interval (about 219-229 mbsf) of very slow sedimentation rates or possibly a hiatus, bracketed by long depth intervals of much higher sedimentation rates (see "Accumulation Rates" section, this chapter). Second, it is the approximate lower boundary of an interval thought to represent deposition in a neritic environment; this interval extends from about 143-163 to 230-250 mbsf (see "Biostratigraphy" section, this chapter). The 226-mbsf impedance change is associated with a seismic trough at 2.14 s, which is correlated away from Site 728 with the aid of the immediately underlying peak. This seismic horizon is referred to as reflector B, and the seismic sequence between reflectors B and A is sequence A-B.

Table 7. Physical properties summary for Hole 728B.

Core, section, interval (cm)	Depth (mbsf)	Wet-bulk density (g/cm³)	Porosity (%)	Water content (%)	Gain density (g/cm³)	Dry-bulk density (g/cm³)	Velocity (m/s)
1H-1, 92-94	0.92	1.706	59.8	35.9	2.682	1.094	
2H-2, 89-90	3.58	1.736	58.4	34.5	2.645	1.138	
3H-2, 90-92	13.10	1.708	61.1	36.6	2.718	1.082	
4H-2, 90-92	22.50	1.729	58.4	34.6	2.634	1.131	
5H-2, 90-92	32.00	1.793	56.6	32.3	2.707	1.213	
6H-2, 90-92	41.50	1.727	58.6	34.8	2.603	1.127	
7H-2, 90-92	51.00	1.688	58.1	35.3	2.399	1.093	
8H-2, 90-92	60.50	1.731	57.5	34.0	2.527	1.142	
9H-2, 90-92	70.10	1.689	59.9	36.3	2.619	1.076	
10X-2, 91-93	79.71	1.650	62.4	38.7	2.519	1.011	
11X-2, 90-92	89.30	1.608	66.2	42.2	2.404	0.930	
12X-2, 90-92	98.90	1.624	62.2	39.3	2.570	0.986	
13X-2, 90-92	108.50	1.618	65.3	41.4	2.657	0.949	
14X-2, 90-92	118.20	1.600	64.3	41.1	2.521	0.942	
16X-2, 94-96	137.54	1.620	64.1	40.5	2.516	0.963	
17X-6, 90-92	153.10	1.648	67.3	41.8	2.604	0.959	
18X-2, 99-101	156.89	1.623	63.9	40.3	2.520	0.969	
19X-4, 71-73	169.31	1.690	62.4	37.8	2.624	1.051	[a]1646
20X-6, 95-97	182.25	1.627	61.8	38.9	2.467	0.994	
21X-3, 100-102	187.50	1.651	59.8	37.1	2.476	1.038	
22X-2, 78-80	195.48	1.638	61.8	38.6	2.512	1.005	
23X-3, 70-72	206.50	1.639	62.6	39.1	2.543	0.998	
24X-3, 56-58	216.06	1.673	62.4	38.2	2.569	1.033	
25X-5, 70-72	228.90	1.734	59.1	34.9	2.623	1.128	
26X, CC, 40-42	238.53	1.663	61.1	37.6	2.504	1.037	
27X-6, 131-133	250.31	1.687	58.1	35.3	2.475	1.092	
28X-4, 115-117	256.85	1.716	58.9	35.2	2.653	1.112	[a]1594
28X-4, 115-117	256.85						[b]1593
29X-4, 144-146	266.74	1.801	53.3	30.3	2.632	1.254	[a]1634
29X-4, 144-146	266.74						[b]1700
30X-4, 77-79	275.77	1.624	60.8	38.3	2.480	1.001	[a]1598
30X-4, 77-79	275.77						[b]1638
31X-4, 118-120	285.88	1.717	59.5	35.5	2.651	1.107	[a]1581
31X-4, 118-120	285.88						[b]1627
32X-4, 124-126	295.54	1.788	56.1	32.3	2.667	1.208	[a]1567
32X-4, 124-126	295.54						[b]1619
33X-4, 116-118	305.16	1.687	58.6	35.6	2.527	1.086	
34X-5, 16-18	315.36	1.685	61.5	37.4	2.583	1.055	
35X-4, 106-108	324.36	1.796	59.5	34.0	2.739	1.186	[a]1557
35X-4, 106-108	324.36						[b]1622
36X-4, 109-111	334.09	1.695	59.6	36.0	2.586	1.084	[a]1599
36X-4, 109-111	334.09						[b]1603
37X-5, 80-82	344.90	1.689	61.8	37.5	2.567	1.056	[a]1549
37X-5, 80-82	344.90						[b]1656

[a] Velocity measurement perpendicular to bedding.

[b] Velocity measurement parallel to bedding.

Two beds having very low velocities at 314-319 and 322-327 mbsf (Fig. 22), thought to be highly siliceous (see "Downhole Measurements" section, this chapter), cause the large-amplitude reflectors at the bottom of the synthetic seismogram (Fig. 23). A trough at 2.25 s lies between these two beds (320 mbsf) and is easily correlated across the section with the aid of bracketing high-amplitude peaks. This seismic horizon is referred to as reflector C; sequence B-C immediately overlies it.

Seismic Interpretation

Depositional patterns in the distal slope basin penetrated by Site 728 occur in two seismically distinctive styles, with the boundary between the two styles occurring near reflector C.

Below seismic reflector C, seismic sequences are of relatively uniform thickness throughout the portion of Figure 22 in which they can be identified. No significant onlapping is evident. The sequences are bounded on the southeast by a major normal fault that has dropped the slope basin with respect to the adjacent basement high. Pronounced drag folding is associated with this normal faulting. This folding is responsible for most of the synclinal structure of the sequence between reflector C and a deeper reflector referred to as reflector D; differential sedimentation rates within sequences overlying reflector C also contribute to the synclinal structure. In the section shown in Figure 22, all of sequence C-D southeast of the fault has been eroded away, and channeling in the fault zone has eroded a small part of sequence C-D northwest of the fault. Horizons deeper than reflector C extend at least as far to the northwest as the buried channel near the left margin of Figure 22. Most reflectors cannot be traced with confidence farther to the northwest because of at least two normal faults, but bedding attitudes clearly continue upslope without significant change.

No convincing seismic evidence can be seen of any influence of faulting on the deposition of units older than seismic reflector C. A small normal fault 1.5 km northwest of the main normal fault appears to end at reflector D, but the seismic reflector pattern here is barely coherent enough to identify the fault. This fault may represent a deep accommodation of strain buildup associated with post-C movement of the major fault, rather than a faulting event that ended at reflector D time. Within the uncertainties implicit in seismic interpretation of a single line, we hypothesize that deposition of sequences older than reflector C is a relatively uniform sedimentation upon an originally flat or gently sloping seafloor (e.g., continental shelf). We have seen no evidence on the Oman margin of pelagic drape that resulted in thicknesses as uniform as those below reflector C.

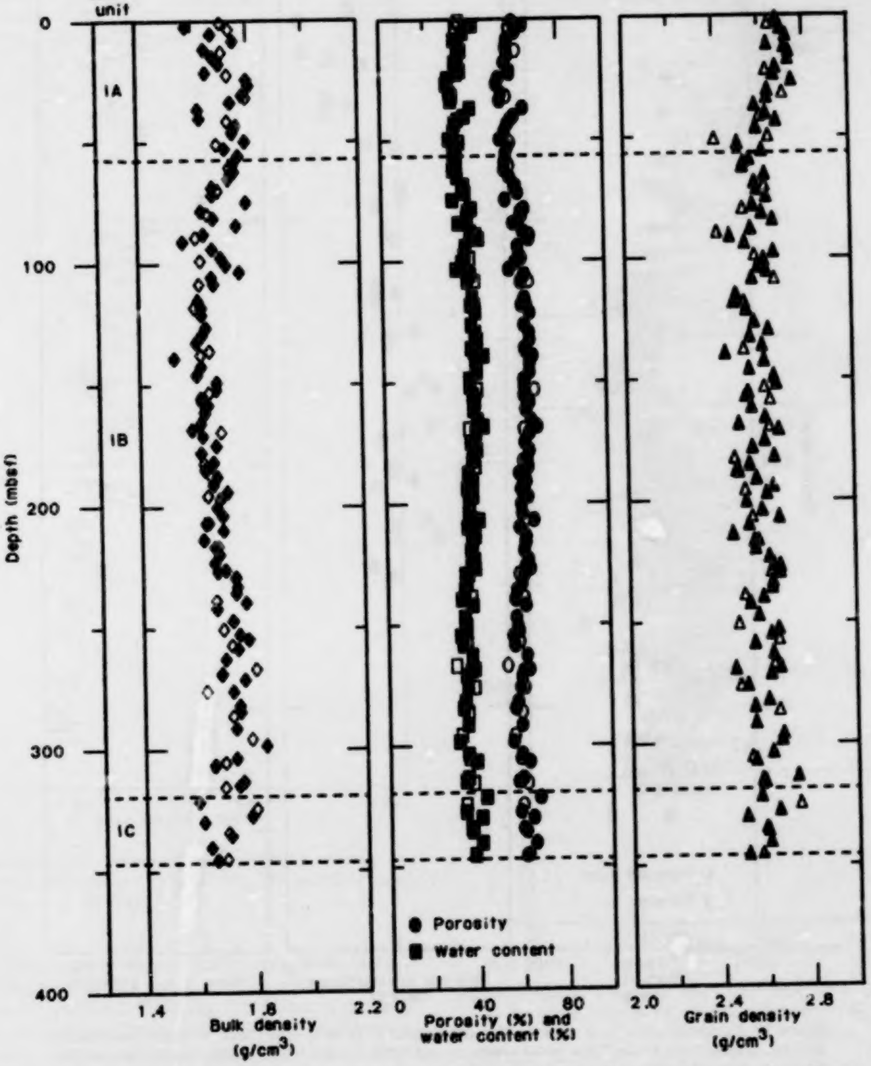

Figure 17. Index properties (wet-bulk density, porosity, water content, and grain density) measured on discrete samples from Holes 728A (solid symbols) and 728B (open symbols).

Above reflector C, seismic sequences exhibit a pronounced thickening in the central portion of the basin, with onlapping obvious toward the northwest topographic high and less certain toward the southeast. This thickening is proportionally greatest for sequence B-C, and least for the youngest sequence SF-A. Channel and levee systems were active during deposition of the three sequences SF-A, A-B, and B-C. The buried channel for sequences B-C and A-B is indicated by dashed lines near the left margin of Figure 22. The modern channel is evident on the seafloor in Figure 22. These two channels probably are primarily erosional. The deeper channel appears to cut down into sequence C-D, and farther to the northeast the erosional relief on the modern channel is more than 180 m. Existence of both modern and buried levees indicates that some spillover of portions of the turbidites occurs. However, no turbidites were identified at Site 728 (see "Lithostratigraphy" and "Downhole Measurements" sections, this chapter), presumably indicating that the turbidite component at Site 728 is minor in comparison to the pelagic component.

Sequences SF-A, A-B, and B-C are bounded on the southeast by seismic reflector C or a horizon very near it. Onlapping onto this reflector is evident only in the lower portion of sequence SF-A and uppermost portion of A-B. The strong seafloor wavelet pattern precludes determination of whether the upper part of sequence SF-A onlaps reflector C. Continuity of seismic reflectors within most of sequence A-B and all of sequence B-C suddenly becomes poor 1.2 km southeast of Site 728 (Fig. 22). The somewhat chaotic reflector pattern within this region (bounded by a dashed line and reflector C in Fig. 22) is suggestive of a slump. However, the lateral movement of this

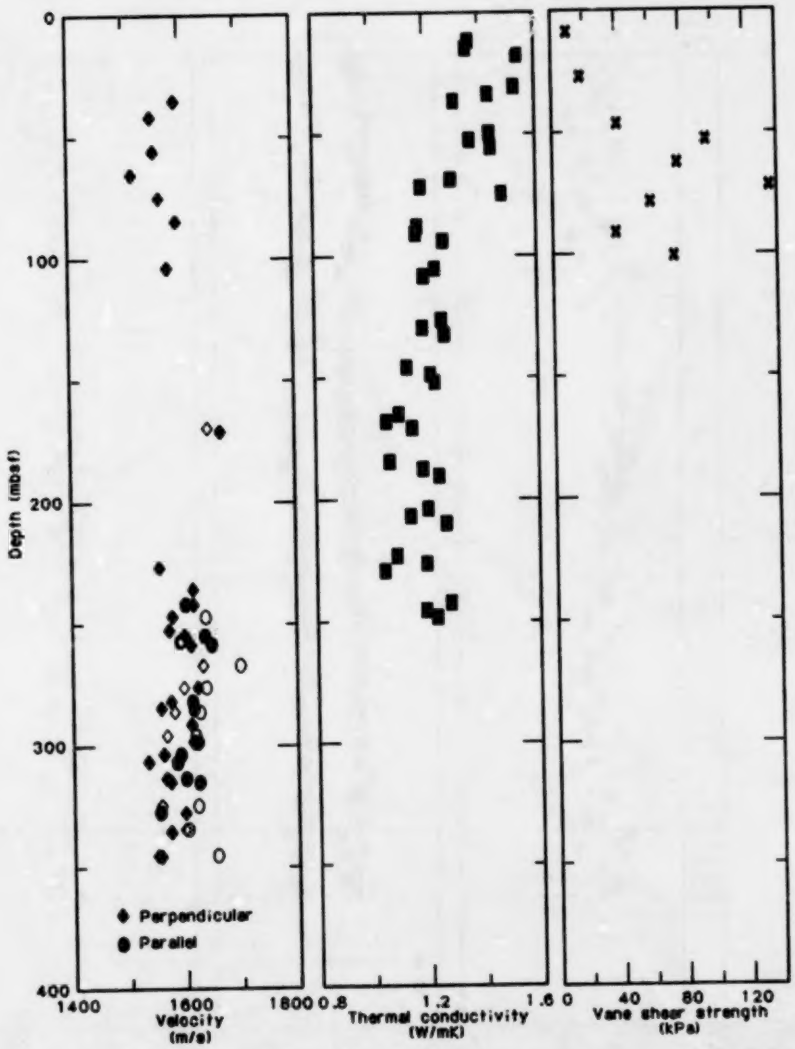

Figure 18. Compressional-wave velocity, thermal conductivity, and vane shear strength measured on discrete samples from Holes 728A (solid symbols) and 728B (open symbols). The designations perpendicular and parallel refer to the orientation of propagation of the compressional wave relative to bedding.

possibly slumped region must have been minor in the plane of Figure 22, because its northwest boundary is too close to vertical for the slump to have preceded deposition of sequences A-B and B-C. This small slump probably has an origin similar to that observed at Site 721 (see "Seismic Stratigraphy" section, Site 721 chapter): gravitational instability of pelagic sediments deposited on an initial slope, with a basal slump plane composed of weak diatomaceous sediments (in this case, the siliceous beds found at 314–319 and 322–327 mbsf at Site 728).

The morphology of sequences SF-A, A-B, and B-C suggests that the depositional environment is somewhat similar to that occurring today in this slope basin and inferred throughout the penetrated section at Site 723 (see "Seismic Stratigraphy" section, Site 723 chapter). Pelagic deposition occurred along a seafloor sloping gently to the southeast, with highest accumulation rates in the most rapidly subsiding central portion of the slope basin. However, unlike Site 723, draping of the sequences over the seaward high (in this case, sequence C-D) is almost completely absent. Therefore, seismic horizon C must have been a topographic high that precluded further downslope southeastward motion of sediments.

This topographic high created by tilting of C-D and deeper sequences was pronounced at the beginning of deposition of sequence B-C, as indicated by sudden thinning of the reflectors immediately overlying reflector C at Site 728. A small hiatus there above reflector C is thus possible, but none was detected. The seaward thinning of sequence A-B is substantially less than that of B-C, and the thinning of sequence SF-A is even smaller. Thus, the topographic relief established at reflector C time (about 7.7 Ma; see "Accumulation Rates" section, this chapter) must

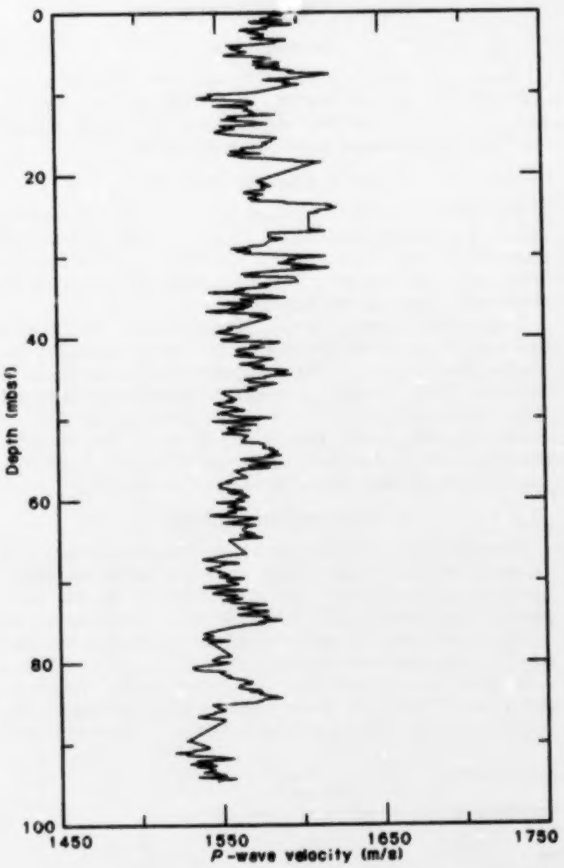

Figure 19. Compressional-wave velocity as measured by the *P*-wave logger in Cores 117-728A-1H through 117-728A-10X. The profile is based on 10-cm-block averages of the data.

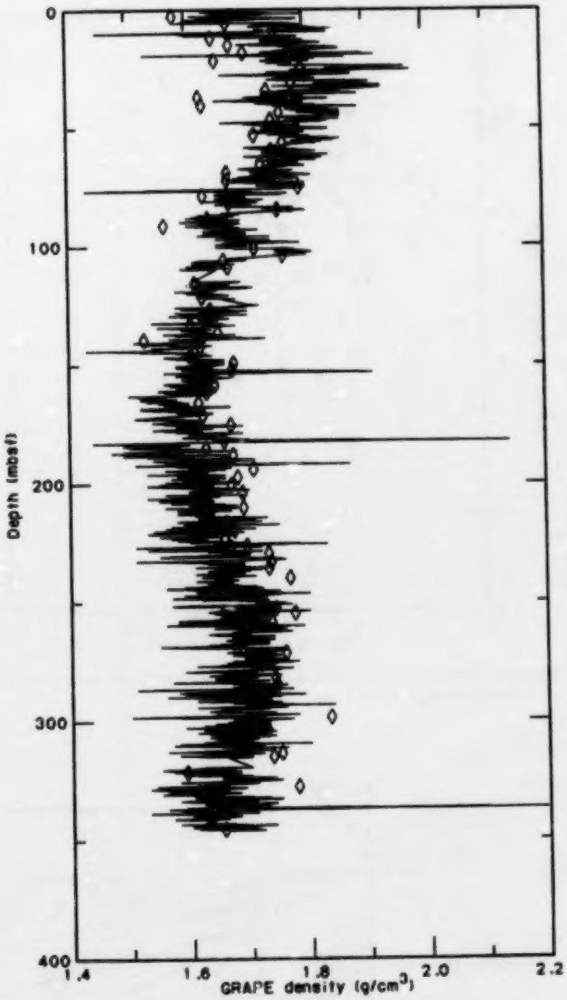

Figure 20. GRAPE wet-bulk density for Hole 728A. The profile is based on 10-cm-block averages of the data. Triangle = discrete sample measurement.

have gradually diminished since then. Finally, within the last 0.5 Ma, sediments have overtopped sequence C-D and spilled into the adjacent channel (dashed lines in Fig. 22). Channel building undoubtedly preceded this spillover, probably fed partially from the topographically higher southwest and from the adjacent basement high. Channel cutting preferentially developed on the updip extension of the major normal fault that bounds the basement high.

In summary, our preferred seismic interpretation of the sequences below and penetrated by Site 728 involves a substantial change in depositional environment, which occurred approximately at the base of Site 728. This distal slope basin may have been part of a rather uniform shelf or slope environment until reflector C time (about 7.7 Ma). At that time, the basin was initiated through normal faulting on the northwest flank of the present basement high, and this basin has been filling almost to the present day.

This seismic interpretation is in conflict with one important observation from Site 728: benthic foraminifers from the interval 143–163 to 230–250 mbsf indicate deposition in the neritic zone, shallower than 150 m below sea level (see "Biostratigraphy" section, this chapter). This interval corresponds to the lower half of sequence A-B, a sequence that shows clear updip onlapping toward a channel that was active during the time that this sequence was deposited. Based on the seismic stratigraphic pattern, a depth of less than 150 m for Site 728 would probably have made the channel subaerial, and would certainly have made the two highs flanking the slope basin subaerial, as faulting preceded deposition of sequence A-B. However, both sedimentological and log evidence indicates a remarkably uniform sediment composition between 85 and 320 mbsf (see "Lithostratigraphy" and "Downhole Measurements" sections, this chapter), a period that encompasses benthic foraminiferal evidence of a transition from upper bathyal to neritic to upper middle bathyal zones (see "Biostratigraphy" section, this chapter). Post-cruise studies will investigate both alternative seismic interpretations and the possibility that the foraminifers were reworked and deposited at the site by channel spillover.

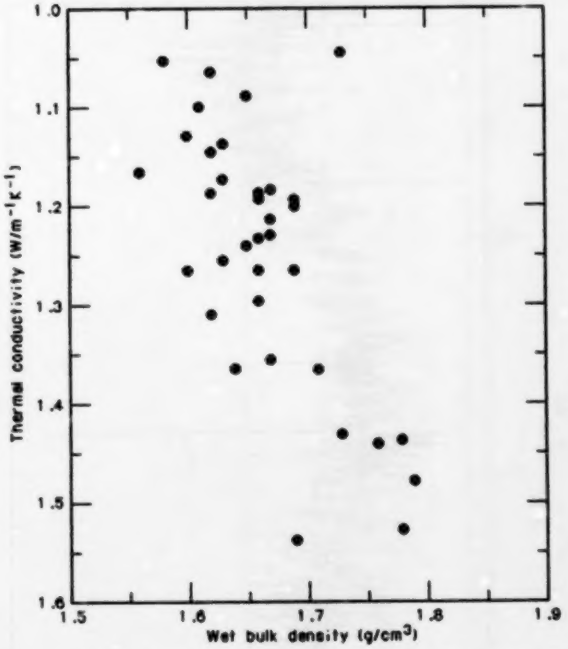

Figure 21. Cross plot of thermal conductivity and wet-bulk density measured on discrete samples from Hole 728A.

INORGANIC CHEMISTRY

Introduction

Twenty-one interstitial water samples were collected at Site 728, 17 by squeezing (Holes 728A and 728B), and the remaining four with the Barnes *in-situ* sampler (Hole 728B only). All data are listed in Table 8 and presented in Figure 24.

Salinity, Chloride, and pH

The distributions of several of the pore-water constituents measured at this site, including salinity, are similar to those seen elsewhere on the Oman margin. The decrease in salinity between ~25 and ~100 mbsf (Fig. 24) is clearly a result of the depletion of sulfate over this interval.

Little variation is seen in the chloride profile. The chloride data give no indication that fresher water is present below the cored section at this site. The pH profile shows a maximum in the upper 100 m. However, a significant difference between pH values measured in Holes 728A and 728B occurs at approximately the same depths (Fig. 24 and Table 8). This variation may be an analytical artifact, rather than being real, and it suggests that the pH data should be viewed with caution.

Alkalinity and Sulfate

Alkalinity increases from the top of the cored section to a maximum of ~15 mmol/L near 100 mbsf, before decreasing linearly to about 5 mmol/L at ~350 mbsf (Fig. 24). The steep positive slope between ~10 and ~100 mbsf reflects sulfate reduction in this zone, but as has often been observed on the margin, the maximum concentration is about 30 to 35 mmol/L, less than would be predicted from the sulfate profile. This deficiency can be explained by the precipitation of authigenic carbonates, possibly both calcite and dolomite, as discussed next.

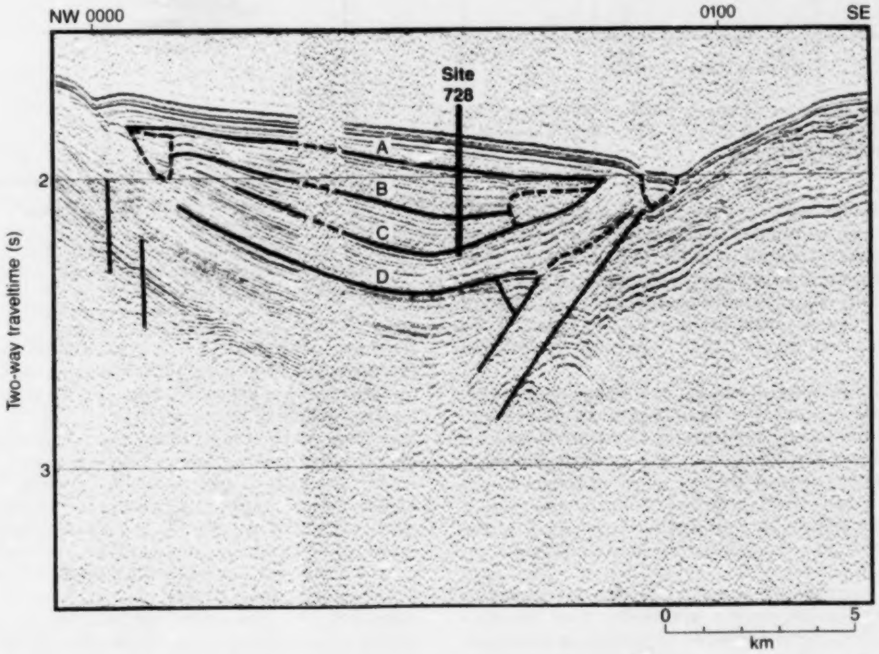

Figure 22. Seismic line 20 of *Robert Conrad* site survey cruise RC2704 across Site 728. Highlights indicate inferred locations of significant seismic reflectors (light lines, dashed where uncertain), faults (heavy lines), and slump and channels (short, dashed lines).

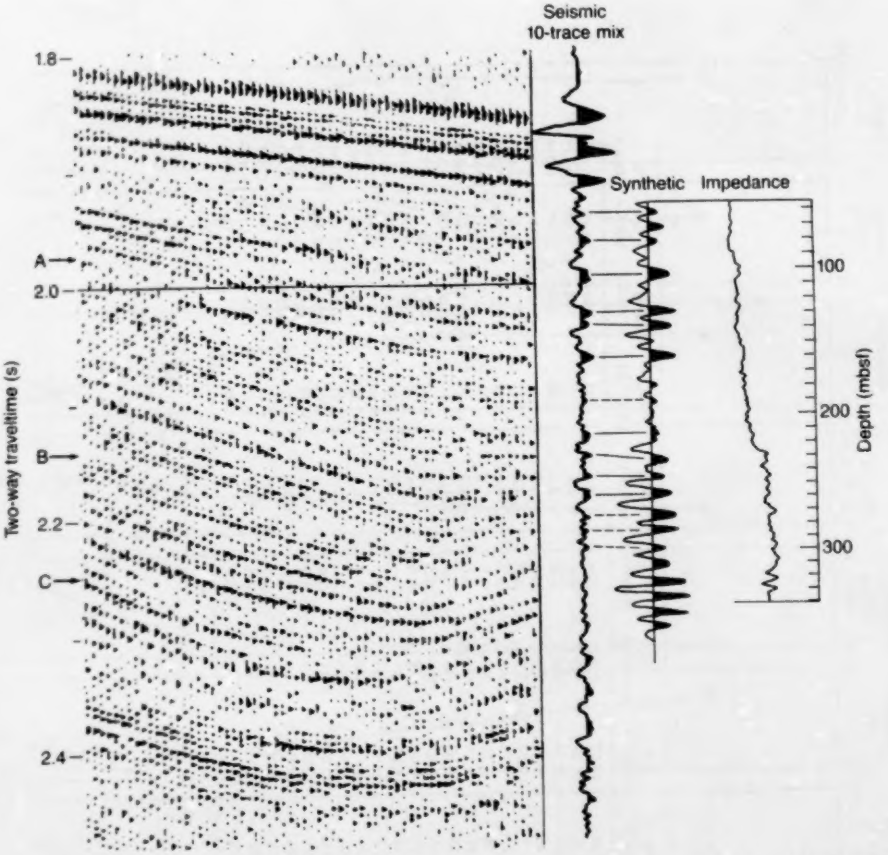

Figure 23. Comparison of a synthetic seismogram for Site 728 with a composite seismic trace (10-trace mix) at the site and with the seismic line of Figure 22. All three are plotted as a function of two-way time; a corresponding depth scale for Site 728 is shown at right.

Sulfate reduction is pronounced between ~25 and ~80 mbsf. The concentration decreases almost linearly in this interval, with a gradient of ~ −0.5 mmol/L/m; dissolved sulfate is absent from interstitial water below about 80 mbsf. There is no indication from the data that a sulfate source exists at depth, as was observed at Sites 723 and 724. This observation is consistent with the chloride distribution.

Calcium and Magnesium

Both calcium and magnesium concentrations decrease over the top 80 m at this site (Fig. 24). Below this zone, calcium increases steadily, while the magnesium concentration continues to decrease. The curvature in the profiles strongly implies that the major zone of precipitation of authigenic carbonates lies between about 70 and 100 mbsf. This interval is marked by a pronounced increase in the organic carbon concentration (see "Organic Geochemistry" section, this chapter), a maximum in the dissolved organic carbon profile (see below), a high uranium content (see "Downhole Measurements" section, this chapter), and an alkalinity maximum. Joint consideration of all these data suggests that the organic carbon-rich zone is supporting very active, bacterially mediated diagenesis. The reaction zone is estimated as 20 to 30 m thick.

Ammonia, Phosphate, Silica, and Dissolved Organic Carbon

The ammonia concentration increases with depth to ~200 mbsf (Fig. 24); below this zone, the concentration does not vary. Maximum curvature in the profile is observed between ~50 and ~150 mbsf, which is consistent with the extensive suite of data (described above) that indicates a maximum in diagenetic reactivity centered on the organic carbon maximum.

Dissolved phosphate concentrations are low at Site 728, as is the case at all other margin sites. Apatite precipitation is believed to be responsible for the lack of phosphate in the pore waters.

The dissolved silica concentration increases with depth to a maximum of ~1200 μmol/L at about 200 mbsf. This profile is similar to those observed previously on both the Owen Ridge (Sites 720 and 721) and the margin, and reflects dissolution of opal. There are two subtle maxima at ~100 and ~225 mbsf in the profile shown in Figure 24, which suggests that the sedimentary opal concentration is higher at these depths. This interpretation agrees with biostratigraphic observations (see "Biostratigraphy" section, this chapter).

The relative concentration of dissolved organic carbon (Fig. 25) shows a distinct broad maximum between ~60 and ~130

Table 8. Summary of interstitial water geochemical data for Site 728.

Core, section, interval (cm)	Depth (mbsf)	Vol. (mL)	pH	Alk. (mmol/L)	Sal. (g/kg)	Mg (mmol/L)	Ca (mmol/L)	Cl (mmol/L)	SO_4 (mmol/L)	PO_4 (μmol/L)	NH_4 (mmol/L)	SiO_2 (μmol/L)	Mg/Ca	DOC (a.u.)
728A-1H-4, 145–150	5.95	33	7.50	3.83	33.0	52.36	10.27	558	25.4	6.1	0.22	293	5.10	0.141
728B-2H-4, 145–150	7.15	50	7.30	3.73	35.5	52.32	10.23	559	24.0	6.2	0.17	305	5.11	0.113
728A-3H-4, 145–150	25.05	38	7.90	4.13	35.4	52.14	9.54	565	24.4	6.2	0.40	394	5.47	0.294
728B-4H-4, 145–150	26.05	50	7.70	4.78	35.8	56.05	9.84	556	26.1	5.3	—	—	5.70	0.260
728B-7I-1, 0–1	48.60	10	8.20	9.19	34.7	48.05	9.02	570	16.3	4.0	2.52	775	5.33	2.059
728A-6H-4, 145–150	53.45	45	8.10	9.35	35.0	46.45	8.15	568	12.7	10.6	1.89	929	5.70	0.987
728B-7H-4, 145–150	54.55	45	7.70	10.15	35.5	43.54	8.20	569	12.7	7.2	1.51	995	5.31	0.898
728A-9H-4, 145–150	82.05	35	8.00	13.63	32.6	33.91	6.65	565	0.0	8.2	3.43	1046	5.10	1.328
728B-10X-4, 145–150	83.25	50	7.20	17.49	33.2	33.30	6.60	565	0.0	11.4	1.19	1038	5.05	1.535
728B-13I-1, 0–1	106.10	10	7.40	18.19	32.8	31.90	8.95	565	0.5	10.2	3.36	1016	3.56	1.225
728A-12X-2, 145–150	107.85	60	8.00	15.56	32.5	32.81	8.04	565	0.0	6.4	4.14	1127	4.08	1.360
728A-15X-4, 145–150	139.85	48	7.70	13.30	32.2	28.10	8.06	565	0.0	12.0	4.89	1098	3.49	1.172
728B-18I-1, 0–1	154.40	10	7.70	16.11	32.4	28.53	9.62	560	0.0	19.7	4.54	1081	2.97	1.168
728A-18X-4, 145–150	168.75	42	7.60	12.57	32.3	28.34	8.54	564	1.3	10.9	5.21	1053	3.32	0.980
728A-21X-4, 145–150	197.75	30	7.20	12.02	32.2	25.14	9.59	564	0.0	12.6	5.75	1225	3.12	0.891
728A-24X-3, 145–150	225.25	35	7.20	10.58	32.1	24.35	9.99	563	0.0	9.8	5.84	1233	2.44	0.795
728B-26I-1, 0–1	231.80	10	7.60	11.91	32.4	23.83	10.98	560	0.0	8.4	6.01	1143	2.17	0.735
728A-27X-4, 145–150	255.75	30	7.20	8.99	32.0	23.09	10.37	563	0.0	12.7	5.90	1235	2.23	0.685
728A-30X-4, 145–150	284.75	30	7.30	7.75	32.0	22.35	11.35	562	0.0	9.9	5.75	1153	1.97	0.557
728A-33X-4, 145–150	313.75	33	7.40	6.18	32.2	22.86	11.40	561	0.3	8.8	5.71	1129	2.01	0.470
728A-36X-4, 145–150	342.75	45	7.40	5.57	32.0	22.35	12.09	560	0.0	9.3	5.69	1227	1.84	0.396

Note: DOC = dissolved organic carbon; a.u. = absorption units.

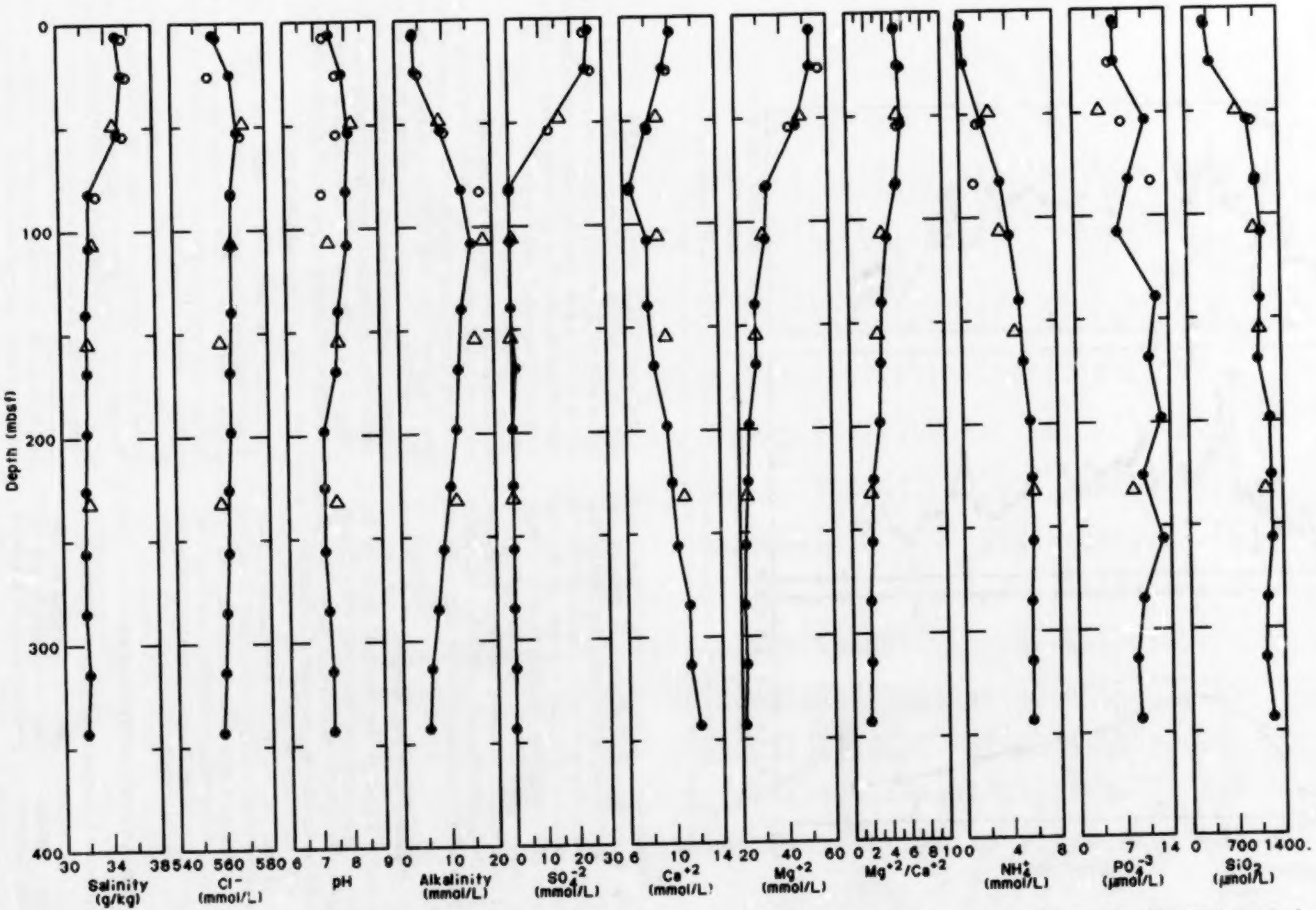

Figure 24. Salinity, chloride, pH profiles, alkalinity, sulfate, calcium, magnesium, Mg/Ca ratio, ammonia, phosphate, and silica profiles for Site 728. Data from Hole 728A are joined by the solid line; open circles represent samples from Hole 728B and triangles represent the *in-situ* samples (all from Hole 728B).

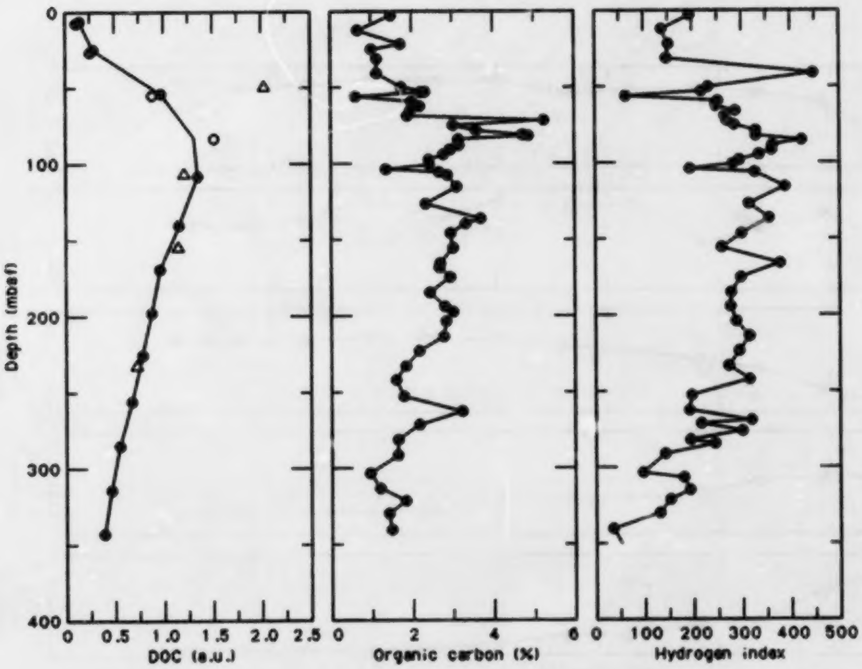

Figure 25. **A.** Dissolved organic carbon distribution at Site 728 symbols as in Figure 24. **B.** Downhole plot of organic carbon. **C.** The ratio of hydrogen-index values from pyrolysis for samples of Hole 728A.

mbsf, which correlates well with the sedimentary organic carbon enrichment in the same depth interval. We presume that this correlation reflects the partial solution of degraded organic matter produced during diagenesis in the organic carbon-rich zone. Because the diffusion coefficient is so low for the high molecular weight humic acids that probably make up most of the dissolved organic carbon (DOC), the DOC profile is less damped by diffusion than the profiles of most other pore-water constituents. For this reason, the DOC profile is a reasonably faithful proxy for the general distribution of reactive organic matter at this site.

In-Situ Pore-Water Samples

As can be seen in Figure 24, the analytical results for the four *in-situ* pore-water samples agree reasonably well with measurements made on the samples extracted by squeezing. Some discrepancy exists between the respective sets of calcium and alkalinity data, with the *in-situ* samples having slightly higher concentrations of both. This may reflect precipitation of calcite induced by decreasing pressure during core recovery. There is no indication that magnesium is affected in a similar way. The high relative DOC concentration measured in the *in-situ* sample collected from Core 117-728B-71 (Table 8) probably signifies contamination by an unknown organic compound.

ORGANIC GEOCHEMISTRY

Character and Abundance of Organic Matter

Fifty-five samples of physical properties and headspace residues from Hole 728A were analyzed for organic carbon and carbonate content (Table 2), and most were analyzed further by Rock-Eval pyrolysis (Table 9).

Organic carbon values are fairly constant in the upper 70 m and average 1.6%, after which a sharp increase occurs (Fig. 25) to an average value of approximately 2.5% (70–225 mbsf interval). The organic carbon values slowly level out with depth and decline at about 225 mbsf to values similar to those measured in the top of the section. Note the sharp organic carbon spikes between 70 and 82 mbsf (Fig. 25), which appear to correlate with uranium, as measured with the geochemical logging tool (see "Downhole Measurements" section, this chapter).

The hydrogen and oxygen indexes, plotted in a "van Krevelen"-type diagram (Fig. 26), exhibit the same scatter as was observed for samples from other sites. When compared to samples from the Owen Ridge (Site 722; dots in Fig. 26), the samples from Site 728 (open circles in Fig. 26) seem to be characterized by slightly lower oxygen indexes. These appear to be more comparable to values obtained from coeval sediments of Site 727 (triangles in Fig. 26), which were deposited in the center of the oxygen-minimum zone at a water depth of approximately 910 m.

Hydrocarbon Gases

Because of the lack of crimp caps, only seven headspace samples were collected from Hole 728A. In addition, several samples from the Hole 728B were collected and sealed in tin cans for shore-based gas analysis. Results of the headspace gas analyses from Hole 728A are given in Table 10. In these data, we observed a trend of increasing gas concentrations with depth in both biogenic methane and thermogenic ethane and propane. The sharp decline in gas concentrations between the headspace samples of Cores 117-728A-18X and 117-728A-21X is not corroborated by the gas analysis of vacutainer samples (Table 11). The results from Sample 117-728A-21X-5, 0–1 cm (Table 10), seem to be unreliable for lack of correlation with the vacutainer samples, possibly because of a sample-handling artifact. Gas analyses of vacutainer samples were severely hampered by gas pockets often filling with water and because moisture entered the vacutainer under high pressure. The results of those analyses,

Table 9. Results of Rock-Eval pyrolysis of samples from Hole 728A.

Core, section, interval (cm)	Depth (mbsf)	T_{max} (°C)	S_1	S_2	S_3	PI	S_2/S_3	PC	TOC	HI	OI
117-728A-											
1H-2, 100-102	2.50	420	0.48	2.99	2.05	0.14	1.45	0.28	1.53	195	133
2H-2, 80-82	11.90	412	0.21	0.96	1.16	0.18	0.82	0.09	0.69	139	168
3H-2, 80-82	21.40	416	0.39	2.79	1.52	0.12	1.83	0.26	1.78	156	85
4H-2, 80-82	30.80	423	0.23	1.79	1.58	0.11	1.13	0.16	1.19	150	132
5H-2, 80-82	40.30	417	0.55	5.30	2.52	0.09	2.10	0.48	1.18	449	213
6H-2, 80-82	49.80	415	0.50	4.27	1.72	0.11	2.48	0.39	1.81	235	95
6H-4, 80-82	52.80	418	0.47	5.26	2.58	0.08	2.03	0.47	2.37	221	108
6H-6, 80-82	55.80	415	0.09	0.46	1.25	0.17	0.36	0.04	0.68	67	183
7H-2, 80-82	59.30	420	0.43	5.23	2.50	0.08	2.09	0.47	2.05	255	121
7H-4, 80-82	62.30	413	0.75	5.65	2.35	0.12	2.40	0.53	2.26	250	103
7H-6, 80-82	65.30	413	0.61	5.90	2.04	0.09	2.89	0.54	2.03	290	100
8H-2, 80-82	68.80	419	0.60	5.24	2.50	0.10	2.09	0.48	1.95	268	128
8H-4, 80-82	71.80	417	1.77	14.56	3.60	0.11	4.04	1.36	5.34	272	67
8H-6, 80-82	74.80	416	1.02	8.90	2.91	0.10	3.05	0.82	3.08	288	94
9H-2, 80-82	78.40	414	1.68	12.15	3.64	0.12	3.33	1.15	3.68	330	98
9H-4, 80-82	81.40	414	2.04	15.94	3.87	0.11	4.11	1.49	4.18	331	80
9H-6, 80-82	84.40	416	1.86	13.76	3.41	0.12	4.03	1.30	3.23	426	105
10X-2, 80-82	88.00	413	1.50	11.94	2.69	0.11	4.43	1.12	3.25	367	82
10X-4, 80-82	91.00	416	1.30	11.05	3.85	0.11	2.87	1.02	3.03	364	127
10X-6, 80-82	94.00	413	1.22	9.66	3.56	0.11	2.71	0.90	2.85	338	124
11X-2, 80-82	97.60	412	0.83	7.40	2.75	0.10	2.69	0.68	2.48	298	110
11X-4, 78-80	100.58	416	1.05	7.08	1.84	0.13	3.84	0.67	2.49	284	73
11X-6, 80-82	103.60	418	0.41	2.81	1.77	0.13	1.58	0.26	1.43	196	123
12X-1, 70-72	105.60	412	0.92	9.05	2.66	0.09	3.40	0.83	2.75	329	96
13X-1, 80-82	115.30	412	1.68	12.62	2.62	0.12	4.81	1.19	3.21	393	81
14X-2, 80-82	126.50	414	0.77	6.88	3.50	0.10	1.96	0.63	2.41	267	145
15X-2, 72-74	136.20	415	1.41	12.11	3.66	0.10	3.30	1.12	3.77	321	97
16X-2, 80-82	145.80	408	1.19	9.17	2.84	0.11	3.22	0.86	3.03	302	93
17X-2, 73-75	155.33	406	1.36	8.21	2.34	0.14	3.50	0.79	3.11	263	75
18X-2, 135-137	165.65	408	1.63	10.57	2.79	0.13	3.78	1.01	2.76	382	101
19X-2, 93-95	174.93	412	1.15	9.14	2.59	0.11	3.52	0.85	3.03	301	85
20X-2, 118-120	184.88	410	0.95	7.05	2.26	0.12	3.11	0.66	2.51	280	90
21X-2, 56-58	193.86	413	0.88	8.12	2.51	0.10	3.23	0.75	2.89	280	85
22X-2, 79-81	203.79	412	0.81	8.50	2.53	0.09	3.35	0.77	2.92	291	86
23X-2, 80-82	213.40	408	1.51	9.15	2.60	0.14	3.51	0.88	2.87	318	90
24X-2, 69-71	222.99	414	0.70	6.76	2.53	0.09	2.67	0.62	2.27	297	111
25X-2, 85-87	232.85	410	0.70	5.34	3.63	0.12	1.47	0.50	1.94	275	187
26X-2, 21-23	241.81	417	0.74	5.35	3.21	0.12	1.66	0.50	1.69	316	189
27X-2, 116-118	252.46	419	0.41	3.77	2.56	0.10	1.47	0.34	1.87	201	136
28X-3, 7-9	262.57	413	0.86	6.52	3.66	0.12	1.78	0.61	3.33	195	109
28X-7, 41-43	268.91	411	0.83	5.13	3.41	0.14	1.50	0.49	1.60	320	213
29X-2, 51-53	271.11	412	0.67	4.96	3.33	0.12	1.48	0.46	2.26	219	147
29X-5, 67-69	275.77	413	0.49	3.53	2.52	0.12	1.40	0.33	1.17	301	[a]215
30X-2, 134-136	281.64	413	0.49	3.36	2.74	0.13	1.22	0.32	1.70	197	161
30X-4, 115-117	284.45	411	0.77	5.17	2.46	0.13	2.10	0.49	2.10	246	[a]117
31X-2, 126-128	291.26	412	0.42	2.53	2.65	0.14	0.95	0.24	1.71	147	154
31X, CC, 30-32	298.31	415	0.41	3.57	2.51	0.12	1.42	0.33	1.69	211	[a]148
32X-4, 77-79	303.37	411	0.25	1.01	1.93	0.20	0.52	0.10	1.02	99	189
32X-6, 93-95	306.53	407	0.42	1.86	2.37	0.18	0.78	0.19	1.02	182	[a]232
33X-5, 96-98	314.76	413	0.39	2.80	2.25	0.12	1.24	0.76	1.43	195	[a]157
34X-3, 77-79	321.27	413	0.45	2.97	2.42	0.13	1.22	0.28	1.90	156	127
34X, CC, 33-35	327.21	414	0.44	2.19	2.05	0.16	1.06	0.21	1.23	178	[a]166
35X-2, 104-106	329.74	412	0.42	1.97	2.31	0.18	0.85	0.19	1.48	133	156
36X-3, 33-35	340.13	410	0.16	0.61	1.58	0.21	0.38	0.06	1.56	39	101

Note: For a detailed description of the parameters, see "Explanatory Notes" chapter (this volume).

[a] Organic carbon values were measured by the Rock-Eval apparatus, and the HI and OI index were calculated with these values.

which were clearly influenced by moisture, are omitted from Table 11. The first gas pockets occurred at a depth of 170 mbsf, well after the depth where interstitial sulfate is depleted (80 mbsf, see "Inorganic Geochemistry" section, this chapter), and biogenic methane is the dominant gas.

DOWNHOLE MEASUREMENTS

Operations

Two logging runs of Schlumberger tool strings were conducted in Hole 728A. We ran a seismic stratigraphic combination (see "Explanatory Notes," this volume) consisting of sonic (BHC), resistivity (DIT), and gamma ray (GR) tools in the open-hole interval. We obtained downgoing logs from the base of pipe (76 mbsf) to 326.2 mbsf. The pipe was raised during upcoming logging, so that we obtained upcoming logs from 342.4 to 55.5 mbsf. After lowering pipe to 85.6 mbsf, we ran a modified geochemical combination. The tool string consisted of spectral gamma ray (NGT), neutron porosity (CNT-G), gamma spectrometry (GST), and accelerometer (GPIT) tools. We selected this tool combination instead of the usual second and third Schlumberger strings (see "Explanatory Notes," this volume) because the density tools run at Sites 722 and 723 had encountered bowspring sticking while entering pipe. We obtained downgoing logs using this tool string from just above the seafloor to 323.6 mbsf. No downgoing NGT logs were attempted because irradiation of the formation by this tool might preclude reliable logging of natural gamma rays. We obtained upcoming logs from the entire tool string for the interval from 340.7 mbsf to just above the seafloor, including a repeat pass for a short through-pipe interval.

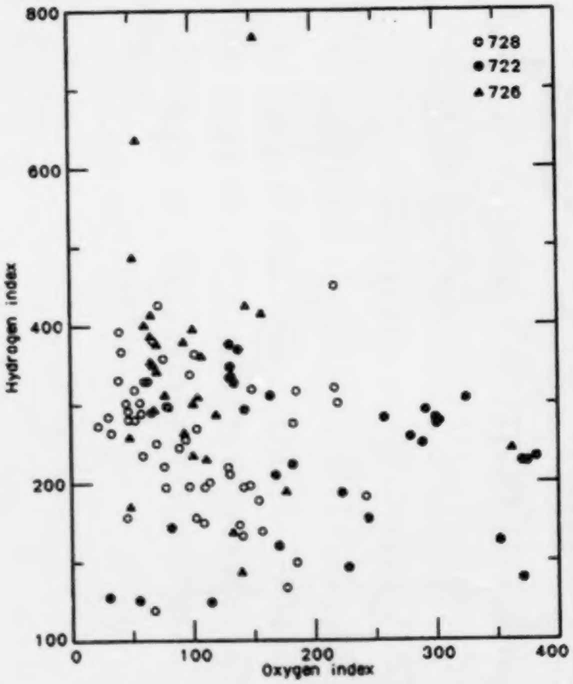

Figure 26. Plot of hydrogen index vs. oxygen index of samples from Site 728 (circles), together with results from Site 722 (dots) and Site 726 (triangles).

Table 10. Results of headspace analysis for interstitial gas at Site 728.

Core, section, interval (cm)	Depth (mbsf)	C_1 (μL/L)	C_2 (μL/L)	C_3 (μL/L)
117-728A-3H-4, 119-120	24.79	51		
6H-4, 119-120	53.19	86	3	
9H-4, 119-120	81.79	49,405	26	6
12X-2, 119-120	107.59	81,635	10	3
15X-4, 119-120	139.59	173,043	38	32
18X-4, 119-120	168.49	227,275	45	40
21X-5, 0-1	197.80	3,500	5	15

Table 11. Results of gas analysis of vacutainer samples from gas pockets at Site 728.

Core, section, interval (cm)	Depth (mbsf)	C_1 (ppm)	C_2 (ppm)	C_3 (ppm)	C_1/C_2
117-728A-18X-6, 10-11	170.40	239,374	30	12	7979
728B-21X-3, 50-51	187.00	899,279	171	82	5259
728B-22X-5, 10-11	199.30	763,225	149	75	5122
728B-23X-3, 145-146	207.25	686,529	122	61	5627
728A-22X-6, 0-1	209.00	262,683	42	20	6254
728B-25X-6, 135-136	231.05	970,184	186	99	5216
728B-27X-1, 30-31	241.80	1,039,019	225	116	4618
728B-29X-6, 140-141	269.70	767,684	188	126	4083
728B-32X-7, 5-6	298.85	459,903	102	65	4508
728A-33X-2, 25-26	309.55	839,872	225	152	3733
728B-34X-7, 10-11	318.30	339,831	76	53	4471
728A-34X-4, 130-131	323.30	813,833	231	164	3523

Very little fill was present in the bottom of the hole, so the bottoms of the two tool strings reached within 2 and 4 m, respectively, of the 346.6 mbsf total drilled depth. The wireline heave compensator was used for only the first run and part of the second run. Seas were extremely flat, and the compensator was observed to be aggravating, rather than reducing, variations in cable tension. We did not encounter bridges during logging of the site. Actual time for logging operations was near the scheduled time: we spent 4.5 hr for hole preparation and 12.5 hr for logging.

Processing and Editing

Log quality was generally good. Based on comparison of downgoing with upcoming logs, reproducibility was excellent. Only upcoming logs are shown here, with the exceptions of the upper GPIT magnetometer data and uppermost NGT data.

GPIT magnetometer data were used for depth shifting of the logs. When expressed as inclination, the magnetometer data show a distinctive pattern of vertical upward and downward magnetizations (Fig. 27), with very sharp transitions at pipe connections that make depth shifting precise and unambiguous. Of relevance to paleomagnetic studies on cores are two observations: (1) cores were exposed to a field of only 0.5 to 1.5 Oe during passage through the pipe (Fig. 27), far less than the magnetization of core barrels; and (2) drill-string magnetization is small at the center of the Monel collar, about 15 m above the base of pipe, where multishot core orientation occurs. Of relevance to downhole magnetometer studies is the observation that drill-string magnetization can be detected to a distance of only about 4 m below the base of pipe. Downhole magnetometer data for the openhole interval were obtained, but are not presented here because the weak sediment magnetization (see "Paleomagnetism" section, this chapter) was dominated by the effect of tool wobbling on the vector sum of tool magnetization and the earth's magnetic field; substantial reprocessing will be needed to eliminate this source of variance.

Data from the NGT tool were reprocessed post-cruise (see "Explanatory Notes" chapter, this volume). The NGT data for the interval from 0 to 85.6 mbsf were obtained through pipe and thus were attenuated (Figs. 28 through 30). To correct for pipe attenuation, we used a gain model (Fig. 31), based on pipe thickness variations, that was nearly identical to the one used at Site 723. The main exception is that the bottom-hole assembly (BHA) was 10 m shorter at Site 728 than at Site 723. To transform from pipe thickness to gain, we used the magnitude of baseline shifts at the top and bottom of the BHA. These shifts imply that pipe attenuation differs for potassium, thorium, and uranium: the maximum gains used were 6 for potassium, 4.5 for thorium, and 3 for uranium (Fig. 31). The gain factor for uranium used at this site is only one-half that estimated for Site 723 (Fig. 31). It is unlikely that both are correct. Even a comparison of downgoing and upcoming logs from Site 728 implies somewhat different gains. Thus, gain-corrected total values for potassium, thorium, and uranium in the interval at 0 to 85.6 mbsf are tentative, but percentage changes in these logs as a function of depth within this interval are not affected.

A total GR log was recomputed from the potassium, thorium, and uranium gain-corrected abundances (Fig. 31). The interval at 54 to 86 mbsf was logged through pipe with the NGT, but through open hole with the GR tool. Comparison of the two runs indicates that gain correction recreated a moderately accurate log. In particular, the peak at 72 mbsf in the GR log is reproduced by the NGT log. The lower flank of this peak is much broader on the GR log than on the NGT log.

Overheating of the data acquisition computer prevented logging of the entire through-pipe interval in a single pass. While the GST was stopped at 45 mbsf, irradiation of the formation

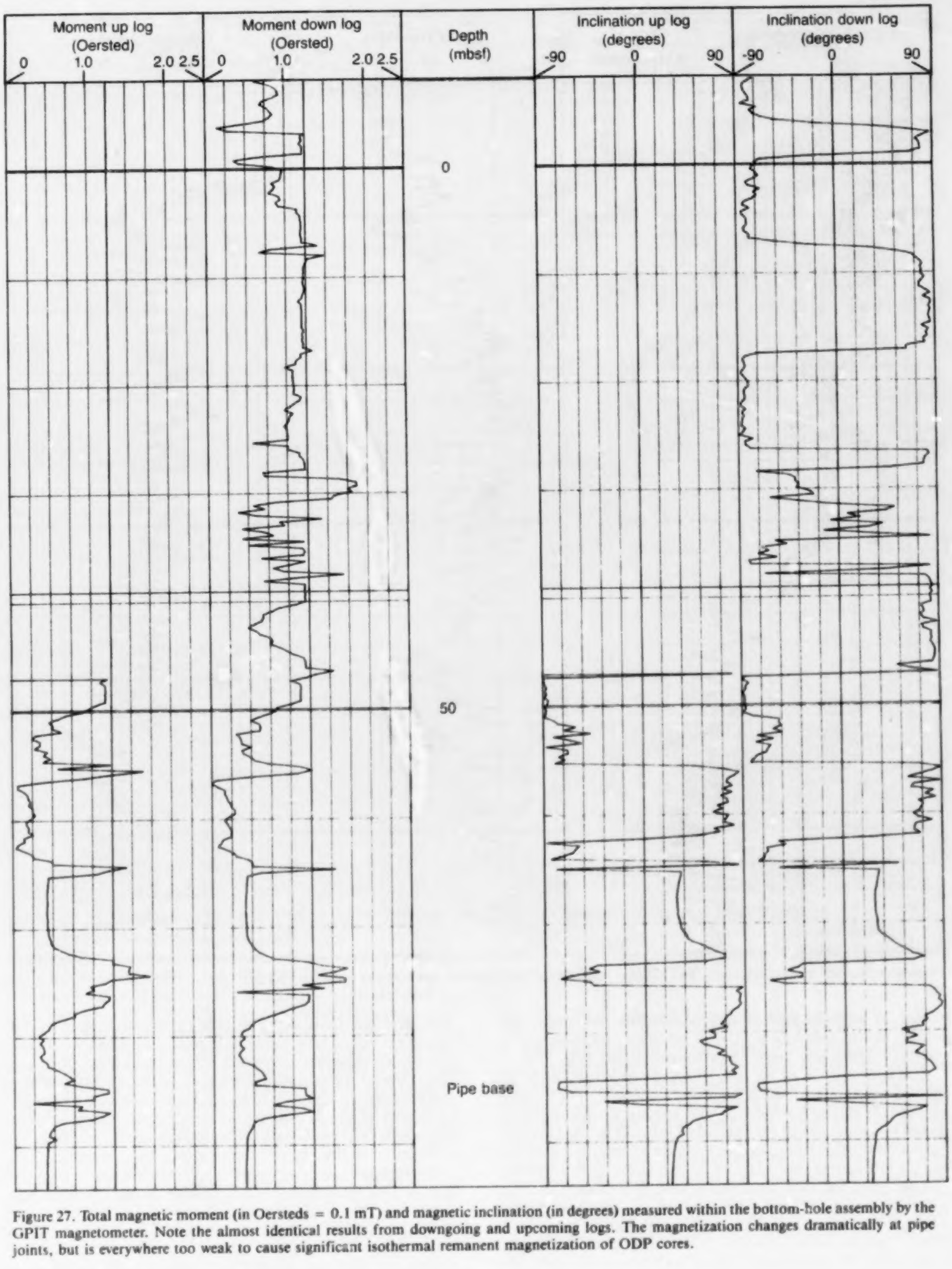

Figure 27. Total magnetic moment (in Oersteds = 0.1 mT) and magnetic inclination (in degrees) measured within the bottom-hole assembly by the GPIT magnetometer. Note the almost identical results from downgoing and upcoming logs. The magnetization changes dramatically at pipe joints, but is everywhere too weak to cause significant isothermal remanent magnetization of ODP cores.

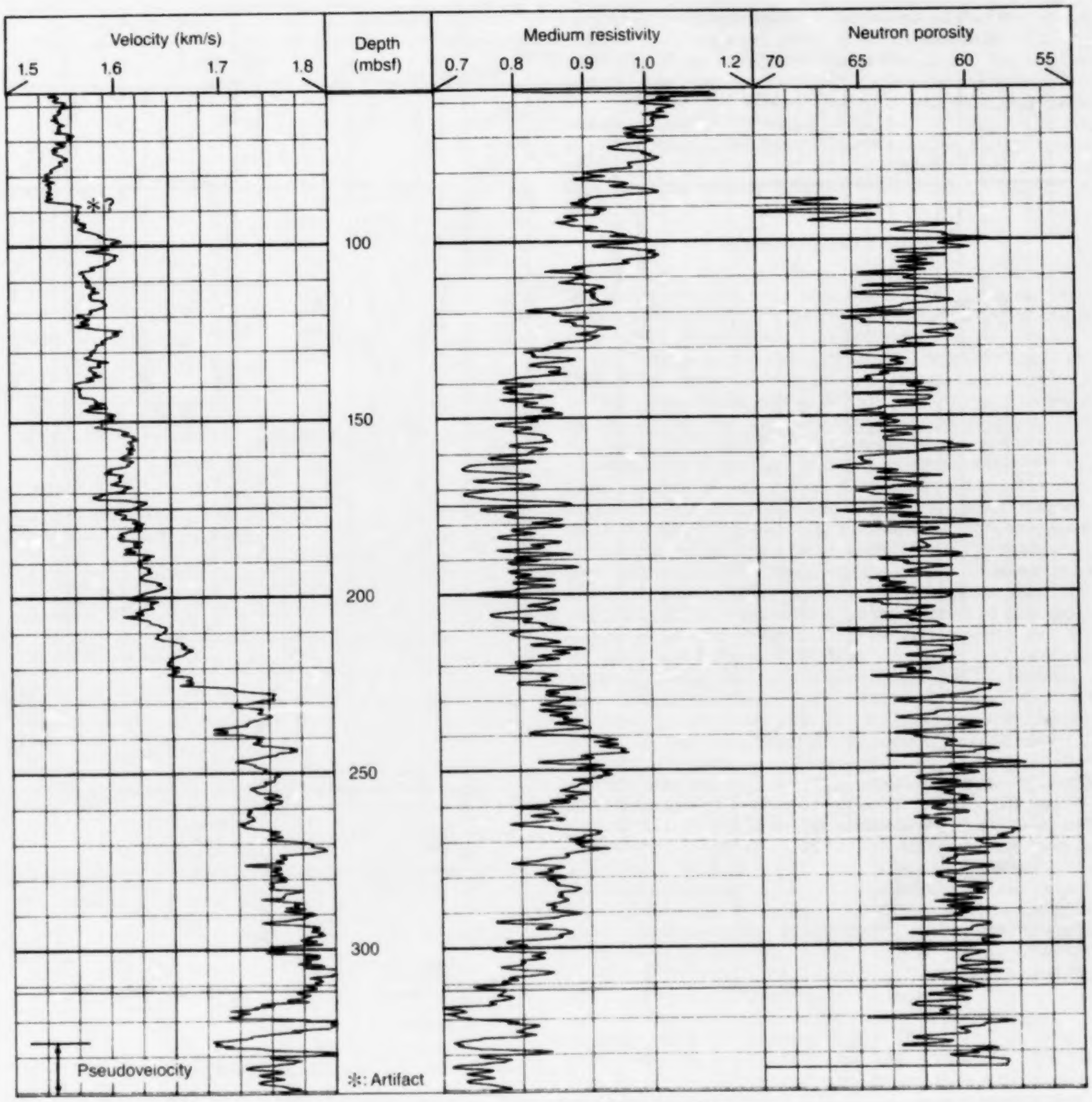

Figure 28. Sound velocity, resistivity, and neutron porosity for the openhole part of Hole 728A.

created an artificial peak in natural GR logs obtained subsequently at this depth (Fig. 31). In addition, subsequent logs above this depth also exhibit an erroneous offset (Fig. 31).

The bottom 30 m of the hole shows gradual increases in potassium and thorium, and a decrease in uranium. These trends are partially artifacts associated with residual gamma radiation caused by irradiation of the bottom of the hole by the GST during the short calibration run. No accurate correction is possible, and the downgoing logs might be more reliable for this interval.

Logs from the GST were reprocessed post-cruise (see "Explanatory Notes" chapter, this volume) to determine relative yields of potassium, titanium, and gadolinium in addition to better yields for silicon, calcium, iron, sulfur, chlorine, and hydrogen (Fig. 32). Significant upward baseline shifts of iron, titanium, and potassium occur as pipe is entered because of high concentrations of these elements in pipe. Based on this offset, a pipe contribution was subtracted from each of these three logs. The shape of the correction model is similar to the model of steel thickness in Figure 35B, except for the low-iron Monel collar evident at 62–72 mbsf on the iron log. Following this pipe correction, GST yields were normalized to 100% total (Fig. 37), as described in the "Explanatory Notes" (this volume).

Sonic logging at Site 728 used a borehole-compensated tool (BHC). This backup tool is less reliable in high-porosity sediments than the normal long-spaced sonic (LSS) tool because of its short source-receiver spacing. At Site 728, the long (1.5 m) source-receiver pairs worked reliably below 87 mbsf, but water arrivals preceded and masked the formation arrival for all of

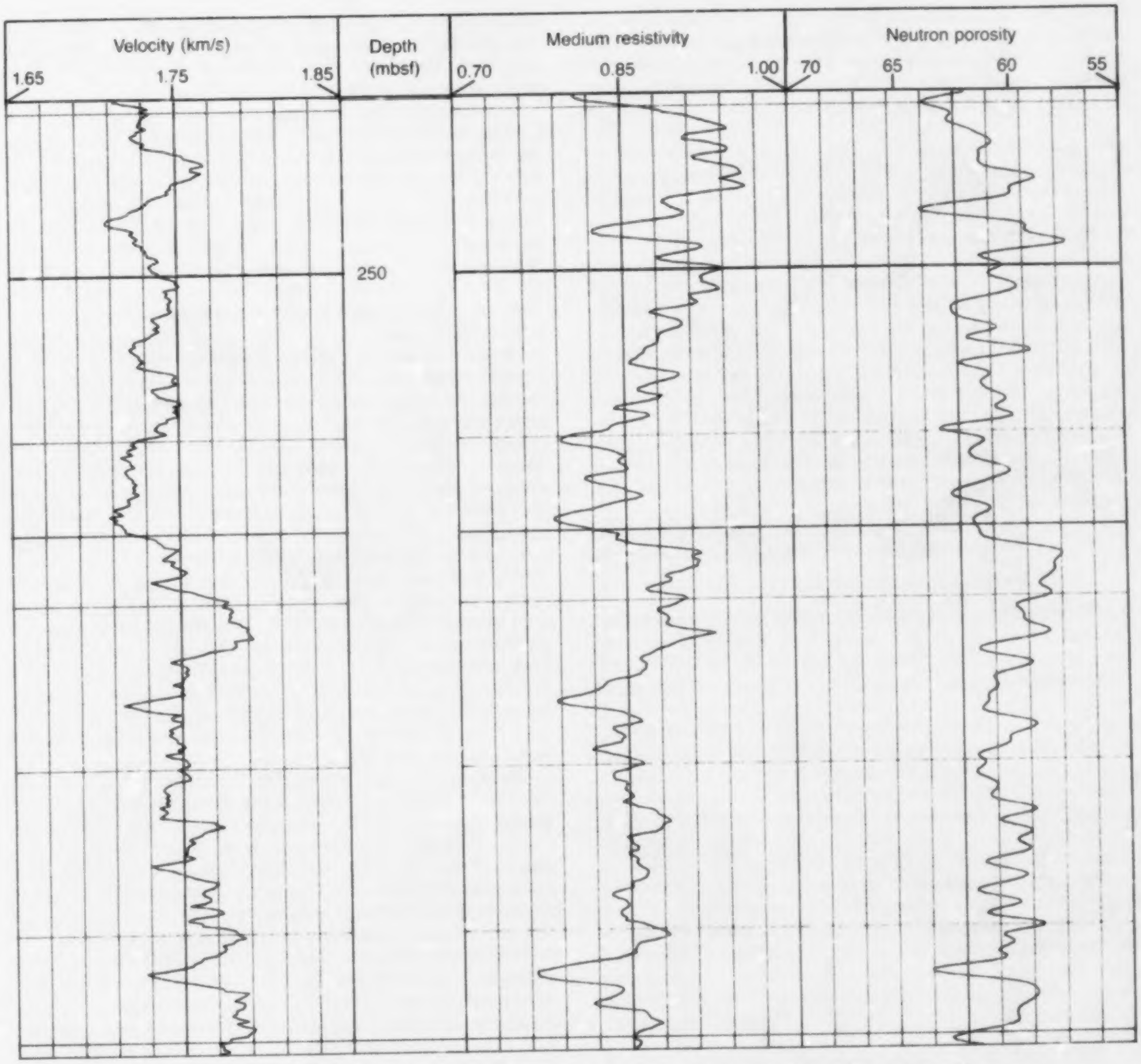

Figure 29. Expanded part of Figure 28, showing the small-scale correlation between velocity, resistivity, and neutron porosity.

one short (0.9 m) source-receiver pair and the upper part (55.5–182.0 mbsf) of the second pair. We replaced the upper part of the second pair with predicted values based on the LSS pair, using a regression (R = 0.99) of short-spaced traveltime on long-spaced traveltime for the reliable interval 182–243 mbsf. The sonic log was then recalculated, using both long-spaced pairs and the single, partially reconstructed, short-spaced pair. This sonic log (Fig. 28) is considered preliminary and will probably be replaced by a sonic log based on waveform analysis. The velocity increase at 87 mbsf in Figure 28 is probably an artifact, caused by water arrivals preceding formation arrivals, even on the long source-receiver pair.

The resistivity tool obtained data down to a depth 13.6 m nearer the bottom of the hole than the sonic tool because of their relative positions on the seismic stratigraphic tool string. For use in a synthetic seismogram, we generated pseudovelocities for this final 13.6-m interval, based on a regression (R = 0.71) of velocity on medium induction resistivity in the overlying 23.6-m interval (Fig. 28).

Mineralogical Variations

The sediments penetrated at Hole 728A were assigned to a single sedimentological unit. These marly nannofossil oozes are dominantly biogenic calcite and clay, with subsidiary opal and organic matter (see "Lithostratigraphy" section, this chapter). Here, we first examine the evidence for variations in clay mineral abundance, then examine that for calcite and organic carbon. Opal abundance is discussed in the next section. The most reliable determination of mineralogic variations is through multi-log inversion. However, clay matrix values for the inversion are unknown at present, so we have postponed log inversion pending availability of results from X-ray diffraction and X-ray fluorescence.

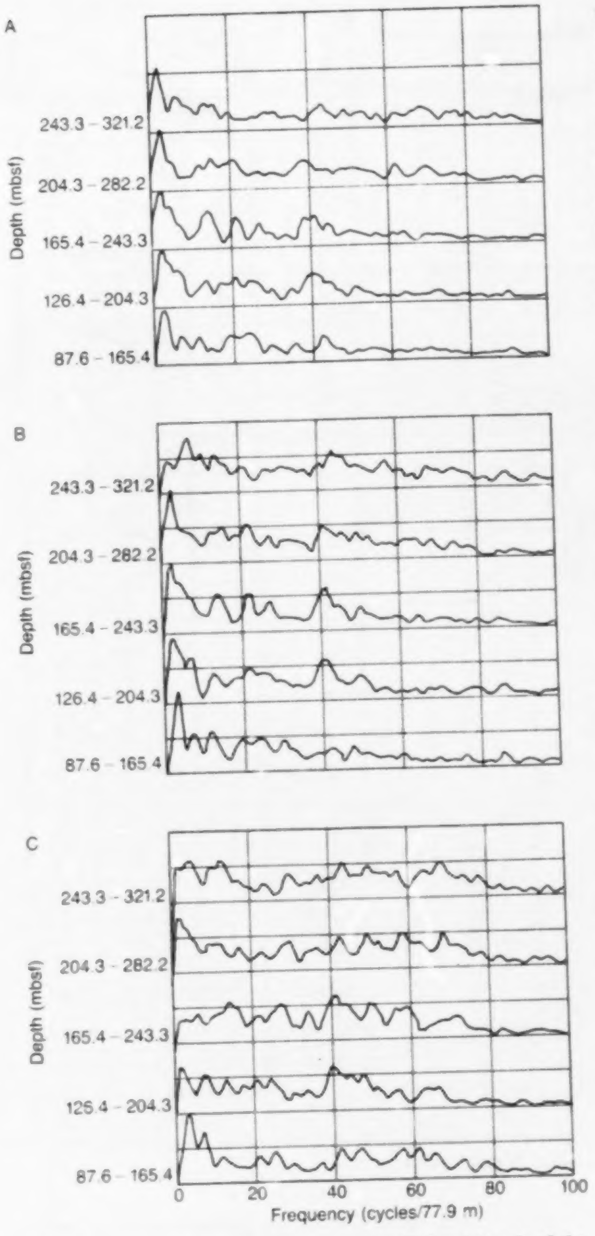

Figure 30. Amplitude spectra for overlapping 77.9-m intervals of the openhole logs for Site 728. **A.** Spectral gamma ray logs. **B.** Gamma ray logs. **C.** Resistivity logs.

The GR log is usually a good indicator of total clay mineral content, because clay minerals contain much higher levels of potassium, thorium, and uranium than do most other minerals. At Site 728, potassium and thorium are strongly correlated (Fig. 31) and thus are present predominantly in the same component. The thorium/potassium ratio is relatively constant at 4 to 6 $\times 10^{-4}$, suggesting that smectite or palygorskite is the volumetrically dominant clay mineral. Potassium concentrations of 0.5% to 1.2% below 85 mbsf and up to 2.6% above 85 mbsf are too high for smectite alone (potassium = 0%–0.6%; Fertl, 1979) and imply significant illite (potassium = 3.5%–8.3%; Fertl, 1979), especially in parts of the top 85 m.

Uranium exhibits only a moderate visual correlation with potassium and thorium and thus is not confined to the clay minerals. A concentration of uranium of 3 to 6 ppm (Fig. 31) is too high for any clay mineral except chlorite. The uranium/thrium ratio is about 1 (Fig. 31), whereas uranium/thorium ratios of kaolinite, illite, and smectite are less than 0.3 (Fertl, 1979). The uranium/potassium ratio below 85 mbsf is about 5, which is consistent with smectite, but inconsistent with other clay minerals. Together, uranium, uranium/thorium, and uranium/potassium cannot be reconciled with any clay mineral or mixture of clay minerals.

Two alternative components for the uranium at Site 728 are organic matter and phosphorite. Uranium tends to be precipitated at the redox fronts associated with organic matter, and a high correlation between uranium and abundance of organic matter was found at nearby Site 723 (see Site 723 chapter, this volume). Both organic carbon (see "Organic Geochemistry" section, this chapter) and uranium are present at Site 728 in only about one-half the concentrations found at Site 723. Accordingly, a correlation between organic carbon and uranium is present at Site 728 (Fig. 31), but this correlation is weaker than at Site 723. Probably the uranium log at Site 728 reflects a dominant uranium contribution from organic matter and slightly smaller contribution from clay minerals. Phosphorite has a very high uranium content and may be responsible for at least some of the high-amplitude uranium fluctuations. Phosphorite is present in rare concentrated horizons, rather than as a dilute component throughout the site (see "Lithostratigraphy" section, this chapter). Thus, phosphorite is unlikely to influence most of the uranium log from Site 728.

Based on core descriptions (see "Lithostratigraphy" section, this chapter), biogenic calcite is the dominant nonclay component throughout Site 728. Variations in calcite abundance downhole may be indicated most readily by the potassium and thorium logs (Fig. 31) because calcite dilutes clays that contain potassium and thorium. Both are much more common than other minerals throughout Site 728, except near the very bottom of the hole. However, variations in percentages of different clay mineral components could substantially degrade the accuracy of potassium and thorium logs as indicators of total clay content and, therefore, as an inverse of carbonate content.

The calcium log (Fig. 33) is relatively insensitive to clay mineral variations and responds largely to calcite variations. This log is probably the best indicator of relative calcite abundance. When compared to core analyses of calcite content (see "Organic Geochemistry" section, this chapter), the calcium log shows general similarity.

Sound Velocity and Porosity

Preliminary *P*-wave velocities logged at Site 728 range from 1.54 km/s at 55–81 mbsf to 1.80 km/s in three thin beds below 300 mbsf (Fig. 28). A gradual compaction profile is present, as well as small-scale (10 m) variability and two velocity baseline shifts, at 87 and 226 mbsf. The measured velocity compaction profile at Site 728 is consistently lower than empirical velocity/depth trends, which range from 1.58 km/s at 55 mbsf to 1.87 km/s at 340 mbsf for terrigenous sediments, and from 1.65 to 2.10 km/s for the same depth range in calcareous sediments (Hamilton, 1979).

The 87-mbsf velocity increase may be associated with the major character change observed on potassium, thorium, and uranium logs, from high-frequency, high-amplitude variations above 85 mbsf to much lower-amplitude variations below. However, as previously discussed, the velocity change may be an artifact.

In contrast, the velocity increase at 226 mbsf is accompanied by a significant neutron porosity decrease and subtle resistivity increase. The porosity change is not evident in pycnometer data (see "Physical Properties" section, this chapter). The qualitatively determined ooze/chalk transition occurs at about 210 mbsf (see "Lithostratigraphy" section, this chapter), and a change in cementation might affect velocity more than it would affect porosity. Geochemical logs (Fig. 33) show a more gradual boundary, with increasing calcium and decreasing titanium over the interval of 215–227 mbsf).

A resistivity log is usually a good indicator of relative porosity, with substantially higher signal-to-noise ratio than neutron porosity logs. Measured formation resistivity depends on both porosity and the resistivity of formation water. The latter decreases at a relatively uniform rate with increasing depth because of increasing temperature, partially masking the overall compaction trend but not affecting the interpretation of porosity fluctuations. A marked long-wavelength variation is present in the resistivity log from Site 728 (Fig. 28). Resistivity decreases from 55 to 163–172 mbsf, then increases down to 245 mbsf, then decreases again below that depth. A similar trend is evident in the potassium and particularly in the thorium logs (Fig. 31). This trend is partially present in the neutron porosity log (Fig. 28), but no trend of increasing neutron porosity below 245 mbsf is evident. Corresponding broad porosity trends are subtle but clearly present in discrete core measurements of porosity and density and are very clear in GRAPE densities (see "Physical Properties" section, this chapter). However, no corresponding broad trends are evident in the velocity log (Fig. 28), for unknown reasons.

The correspondence of long-wavelength trends between thorium, potassium, resistivity, and neutron porosity logs is echoed by a similar correlation of short-wavelength (< 20 m) variations among these logs. Further, although the velocity log lacks the long-wavelength trends of these other logs, it does exhibit a good correlation of short-wavelength variations. For example, Figure 29 focuses on a 58-m interval of Figure 28, illustrating the correlation between velocity, resistivity, and neutron porosity.

Correlation between thorium, potassium, resistivity, porosity, and velocity is very common in deep-sea sediments and arises from the fact that the fibrous, disorganized arrangement of clay minerals at shallow depths causes higher porosity than is associated with most other minerals (e.g., Hamilton and Bachman, 1982). However, this was not the pattern seen at Site 728. Clay content, as indicated by potassium and thorium, is positively correlated with velocity and resistivity and negatively correlated with porosity; this is the opposite of the normal relationship. An additional component must be present that impacts on porosity more than clay. Further, this component must be more common in clay-poor horizons than in clay-rich ones. This component cannot be calcite, as calcite is much faster than clay. It is unlikely to be organic matter (the primary cause of porosity fluctuations at nearby Site 723), because organic matter is more common in clay-rich than clay-poor zones and because uranium is not well-correlated with the porosity logs at this site.

Biogenic opal may be the primary cause of porosity fluctuations at Site 728. Biogenic opal is common below 70 mbsf (see "Biostratigraphy" section, this chapter), reaching levels of greater than 20% in some layers below 320 mbsf (see "Lithostratigraphy" section, this chapter). Two beds with very low velocity and high porosity at 314–319 and 322–327 mbsf (Fig. 28) probably are highly siliceous. A low and variable amount of opal throughout the interval below 70 mbsf may account for the observed interlog correlations and the fact that velocities are lower than empirical models for terrigenous and calcareous sediments. However, high-resolution quantitative determination of opal content will be necessary to test this hypothesis. One observation not obviously accounted for by opal is the absence from the velocity log of the long-wavelength trends seen in resistivity, potassium, and thorium logs.

The correlation between gamma ray and resistivity logs, possibly associated with fluctuations in biogenic opal, can also be examined in the frequency domain. Figure 30 shows normalized amplitude spectra of 77.9 m (512 point) overlapping windows from the gamma ray, spectral gamma ray, and shallow-focused resistivity logs. The frequency spectrum varies somewhat between depth windows, but is very similar for different logs from the same depth window. The similar spectra for the two gamma ray logs indicate that ship heave did not impart spurious frequency to the logs because the logging speed for the GRT was three times as fast as that for the NGT. Similar spectra for the resistivity log, when compared with the two gamma ray logs, indicate that both properties are undergoing similar cyclic variations. This does not identify the cause of these variations, although opal appears likely. A consistent high-frequency component is present in the spectra, at about 38 to 43 cycles per 77.9 m, or a period of 1.8 to 2.0 m. This cyclicity is also obvious in the log plots as a function of depth, although not at the compressed scales of Figures 28 through 33.

INTERHOLE CORRELATIONS

Here, we provide detailed correlations for the upper 30 m of the drilled sediments at Site 728. This upper interval ranges in age from 0 to about 0.5 Ma and is characterized by cyclic changes in the nature of sediments that can be identified by visual observation and by variations of magnetic susceptibility and $CaCO_3$ content. The coherence and similarity of sediments among these holes provide valuable information about the relative rate of sedimentation, which is necessary information for any high-resolution study of depositional environments. The essence of the interhole-correlation process is described in the "Explanatory Notes" chapter (this volume).

Hole-to-hole correlations were based on visual identification of distinctive layers, as well as on physical and magnetic properties. Magnetic susceptibility was measured at 10-cm intervals on whole-core sections. Photographs of the split cores were taken.

Visual correlation of cores relied primarily on these core photographs. Twenty-six distinct, traceable layers were determined in the correlatable sedimentary sequence at Sites 723 and 724 and were notated as OM-a_1, ·····, h_3, and h_5, based on the correlation between the holes at Sites 723 and 724 (see "Lithostratigraphy" sections, Site 723 and Site 724 chapters, this volume). The letter code (i.e., a, b, c, . . .) refers to the sequence of cores, and the number code indicates the number of marker layers in each core. For example, the notation "a_2" corresponds to the second marker layer defined in Core 117-723A-1H, and "b_1" denotes the first marker layer in Core 117-723A-2H. The marker layers a_1 through h_4 were defined on the cored sediments of Hole 723A. Three marker layers, c_5, e_3, and h_5, were defined on the sedimentary sequence at Hole 724A, in addition to those noted at Site 723. The criterion for defining a marker layer was that the layer be distinct enough for tracing in the sedimentary sequence of the other holes and that its character not change. Useful criteria for recognizing the marker are color boundaries, distinctly colored layers, shape of bioturbations, and sequence of color change in surrounding sediments. Table 12 lists the depth of the marker layers in two holes of Site 728.

Figure 34 shows the magnetic susceptibility curve and positions of individual, visually correlatable layers. The pattern of the susceptibility and the positions of layers match very well, not only among the two holes, but also between Sites 723 and

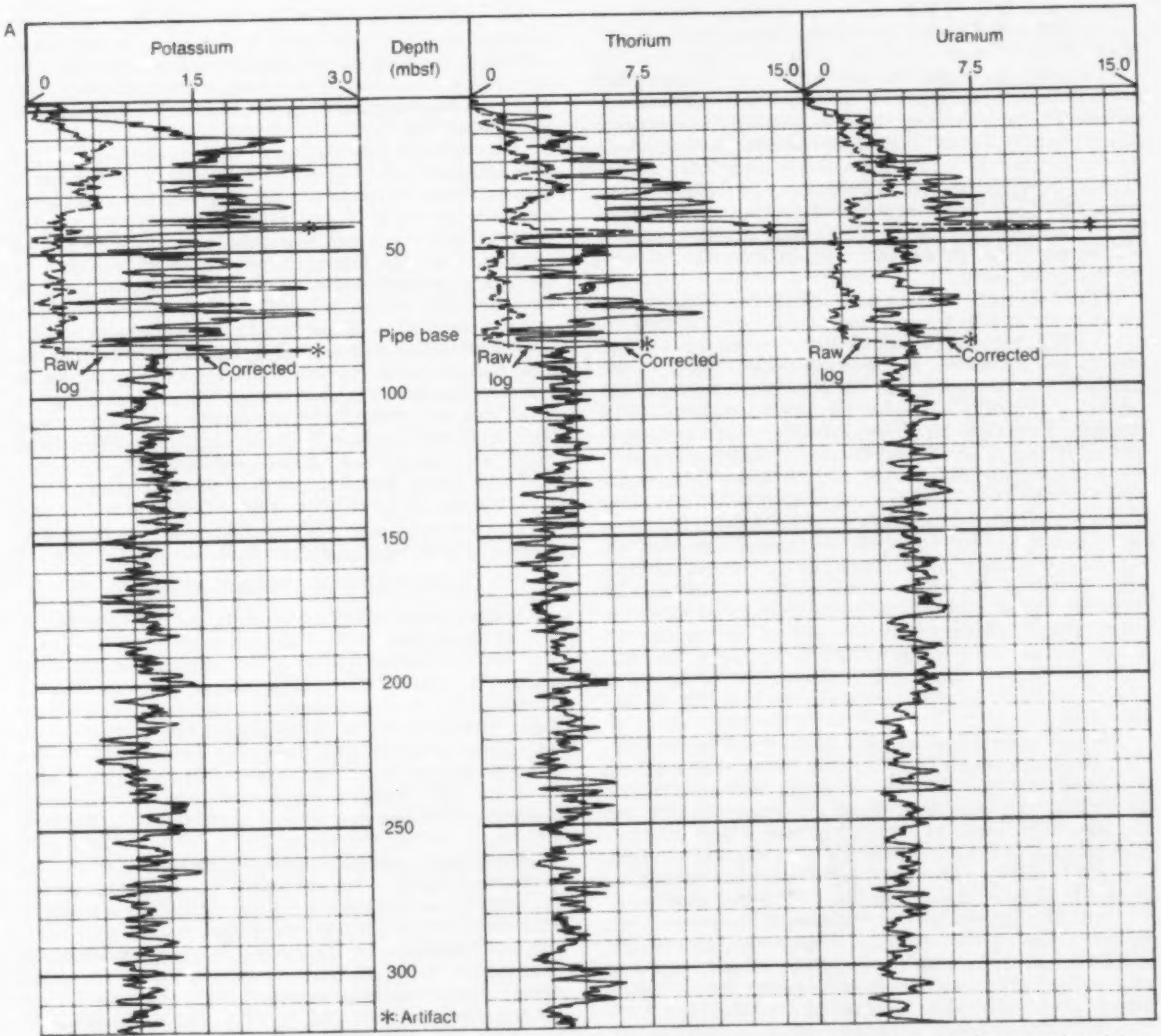

Figure 31. **A.** Potassium, thorium, and uranium logs, both before (dashed) and after (solid) correction of through-pipe logs for attenuation of signal by pipe. Core measurements of organic carbon percentages are shown for comparison with uranium log. **B.** Gain factors used for correction of through-pipe logs, spectral gamma ray logs (both before and after applying gain factors), and openhole gamma ray logs.

728 (Fig. 35). The stratigraphy of the magnetic susceptibility data and the visually identified layers is extremely consistent in that a particular visually characteristic layer always coincides in depth with a distinct feature in the magnetic susceptibility curve. In this way, the lithologic correlations could be verified with the magnetic data, which are quantitative and less ambiguous.

The results of this layer-by-layer correlation allowed us to calculate the true thickness of these layers that coincide with and are separated by core boundaries. Occasionally, core tops were expanded by water uptake during drilling. In this case, the apparent thickness of the disturbed sediment layer was observed to be thicker than the original thickness. In some instances, the top part of the core was missing; in this case, apparent thickness was observed to be thinner than the original thickness. Fortunately, the two holes were staggered in depth, so that they have different horizons at core boundaries (Table 12). The original thickness of layers coinciding with core tops or bottoms can be obtained by comparing thickness of the correlative layer in the continuous section of the other holes. The amount of the difference can be calculated by the differences in the ODP depths of marker layers between the holes ("Holes 728B − 728A" in Table 12). Table 13 gives the differences between the depth (mbsf) calculated by the ODP CORELOG data and the corrected depth (mbsf), calculated by the layer-by-layer correlation method. The mudline was not clearly recognized in Core 117-728A-1H, while according to the layer-by-layer correlation, the top of Core 117-728A-1H obtained the mudline.

The layer-by-layer method on the double-cored sedimentary sequences gives us true stratigraphic thickness after correcting for any core-boundary disturbance. Table 14 shows the stratigraphic thickness at Sites 723 and 724, where the marker layers were defined, and at Holes 728A and 728B. The corrected depths in

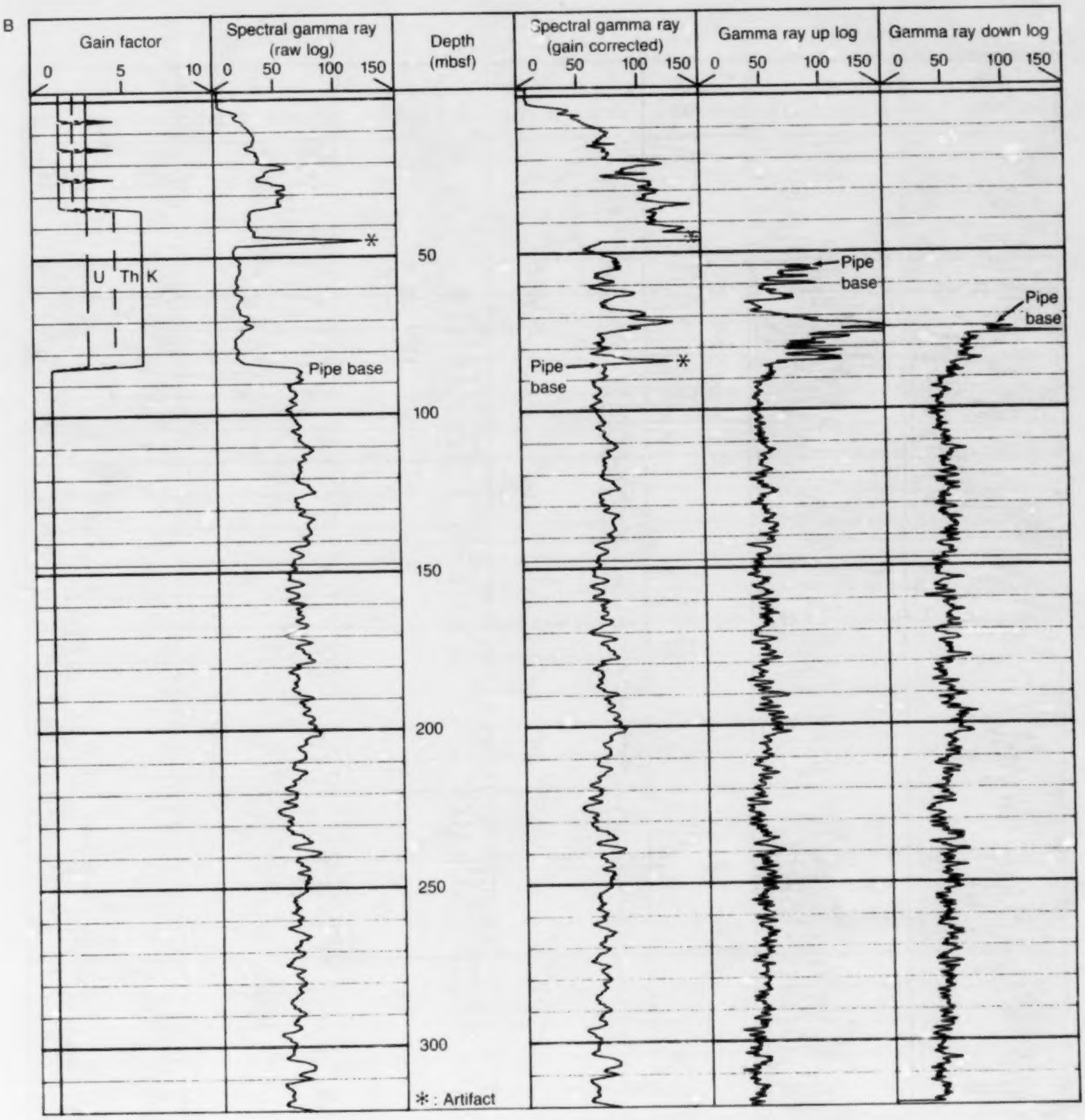

Figure 31 (continued).

Hole 728A and 728B agree well. The intersite correlation of the marker layers clearly shows the differences in sedimentation rate.

SUMMARY AND CONCLUSIONS

Site 728 is located on the Oman margin at a water depth where the lower part of the pronounced mid-water oxygen-minimum zone intersects the continental slope. The location is in a distal slope basin formed by a narrow half-graben in what is presumed to be ophiolitic basement. Biogenic material produced by coastal upwelling and eolian components is deposited here at high rates (11–88 m/m.y.). The purpose of drilling at Site 728 was to provide a margin site that accumulated dominantly pelagic sediments that could be used to trace the evolution and fluctuation of the oxygen-minimum zone through time. A second intention, in conjunction with drilling at Sites 726, 727, 729, and 730, was to investigate the tectonic movements of adjacent ophiolite blocks by coring the sediments in the two adjacent half-graben basins.

Major findings at Site 728 include:

1. An expanded Pliocene section, which is well constrained by paleomagnetic data;

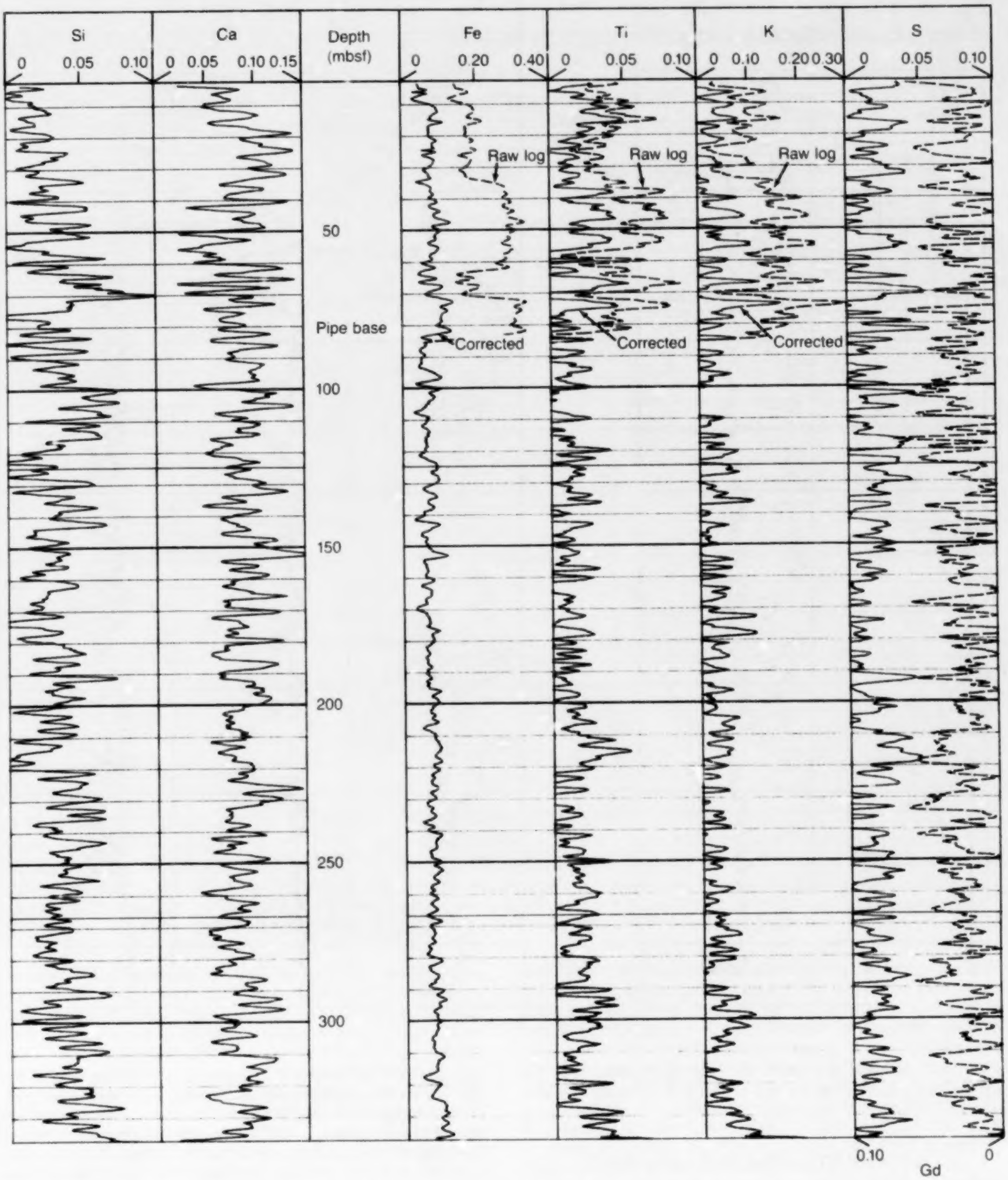

Figure 32. Reprocessed geochemical logs from gamma spectrometry tool. Fe, Ti, and K are shown both before (dashed) and after (solid) correction for pipe contribution.

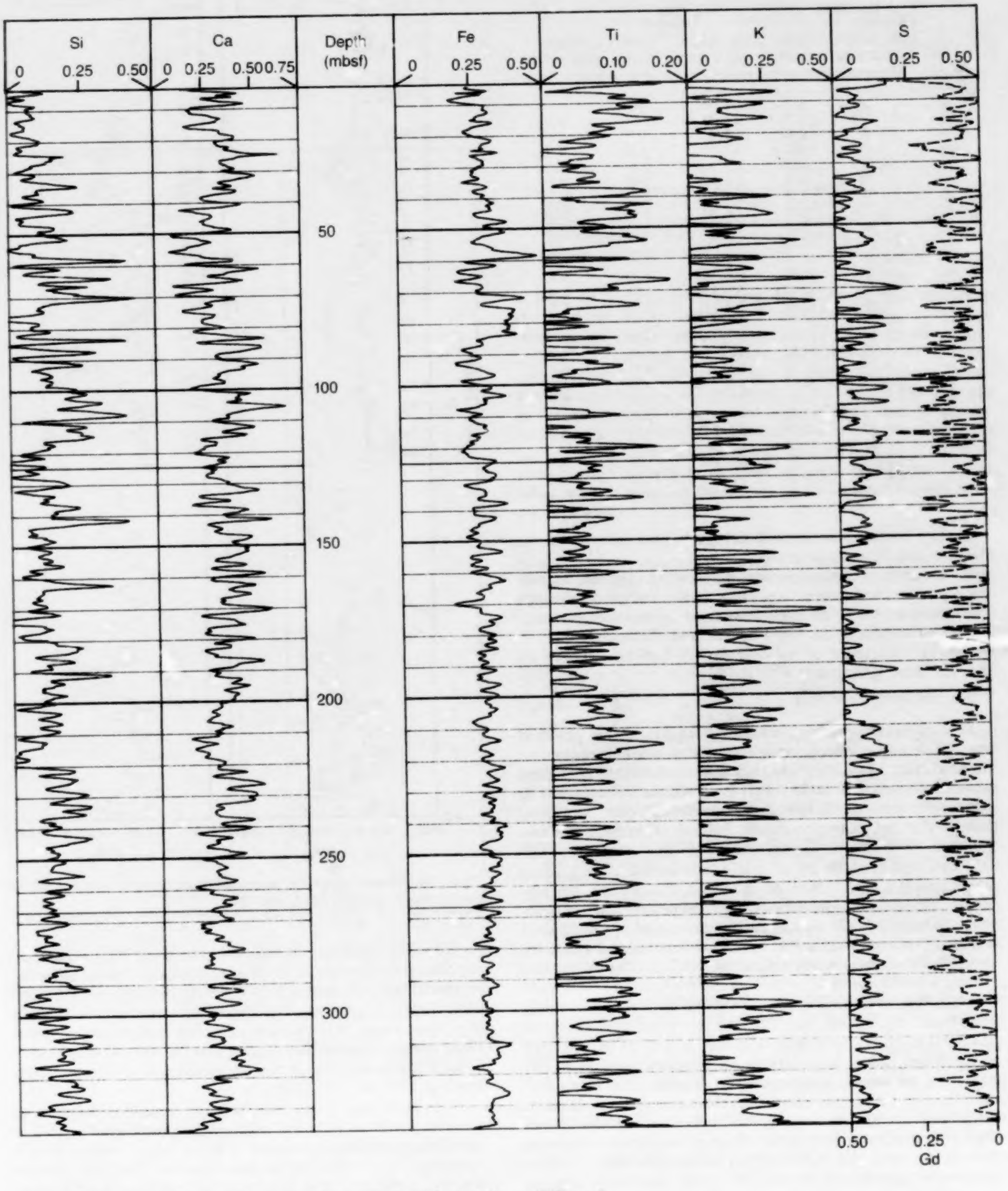

Figure 33. Geochemical logs of Figure 32, after normalization of yields to 100% total.

Table 12. List of marker layers in Site 728.

Layer	Hole 728A Core, section, interval (cm)	Hole 728A ODP depth	Hole 728B Core, section, interval (cm)	Hole 728B ODP depth	Holes 728B − 728A
OM-					
a_1			1-1, 65	0.65	
a_2	1-1, 135	1.35	2-1, 45	1.65	0.35
b_1	1-2, 90	2.40	2-2, 5	2.75	0.35
b_2	1-3, 110	4.10	2-3, 30	4.50	0.40
b_3	1-4, 40	4.90	2-3, 110	5.30	0.40
c_1	1-5, 70	6.70	2-4, 135	7.05	0.35
c_2	1-6, 50	8.00	2-5, 115	8.35	0.35
c_3	1-6, 115	8.65	2-6, 30	9.00	0.35
c_4	1-7, 40	9.40	2-6, 95	9.65	0.25
c_5	2-1, 35	9.95			
d_1	2-2, 5	11.15	3-1, 90	11.60	0.45
d_2	2-2, 25	11.35	3-1, 110	11.80	0.45
d_3	2-2, 50	11.60	3-1, 130	12.00	0.40
e_1	2-2, 95	12.05	3-2, 35	12.55	0.50
e_2	2-2, 140	12.50	3-2, 80	13.00	0.50
e_3	2-3, 60	13.20	3-2, 145	13.65	0.45
f_1	2-4, 20	14.30	3-3, 115	14.85	0.55
f_2	2-4, 55	14.65	3-4, 5	15.25	0.60
g_1	2-5, 35	15.95	3-4, 130	16.50	0.55
g_2	2-5, 105	16.65	3-5, 60	17.30	0.65
h_1	2-6, 70	17.80	3-6, 35	18.55	0.75
h_2	2-7, 35	18.95	3-6, 140	19.60	0.65
h_3	3-1, 90	20.00			
h_4	3-2, 65	21.25	4-1, 120	21.30	0.05
h_5	3-2, 150	22.10	4-2, 40	22.00	−0.10

2. The common occurrence of opaline microfossils in the Miocene and Pliocene intervals;

3. Indications of rapid vertical movement of the site, as indicated by benthic foraminifers, from upper bathyal in the late Miocene to neritic in the early Pliocene, and subsiding to middle bathyal depths in the late Pliocene and Pleistocene;

4. The occurrence of an organic-rich interval between 70 and 225 mbsf (Pliocene), with the highest values at the Pliocene/Pleistocene boundary.

One lithologic unit was recognized in the section cored at Site 728, which encompasses sediment deposited since the late Miocene (Fig. 36). Lithologic Unit I was subdivided into three subunits. Subunit IA (0–58 mbsf) is composed of Holocene to upper Pleistocene marly foraminifer-nannofossil ooze with common bivalve and gastropod debris. Subunit IB includes the section from 58 to 320 mbsf, is of late Pleistocene to late late Miocene age, and is made up of marly nannofossil ooze grading into chalk at about 200 mbsf. Siliceous microfossils are preserved, but make up less than 10% of the sedimentary components. Subunit IC (320–349.5 mbsf) is composed of nannofossil and marly nannofossil chalks, which are interbedded with dark olive, diatomaceous, marly nannofossil chalks. The age of this subunit is late Miocene.

A significant finding at Site 728 is the presence of siliceous microfossils throughout much of the recovered section. Opal-rich Subunit IC is coeval with opal-rich sediments encountered on the Owen Ridge. Radiolarians are common from 85 to 347 mbsf; they are usually accompanied by diatoms. Planktonic foraminifers are poorly preserved over the same interval. Nannofossil floras are low in diversity, but well preserved. An assemblage with presumed cold-water affinities was recognized in the interval spanning the Pliocene/Pleistocene boundary. Benthic foraminifer assemblages at Site 728 exhibit significant changes in paleowater depth. From 0 to 150 mbsf, benthic foraminifers are abundant, and the ratio of planktonic to benthic foraminifers is high in the uppermost 60 m, whereafter it gradually decreases. The uppermost assemblage reflects upper middle bathyal (>500 m water depth) conditions. In the lower Pliocene and upper Miocene, the interval from approximately 150 to 240 mbsf, an assemblage characteristic of a neritic environment (<150 m water depth) is present. The upper Miocene section contains rare foraminifers that indicate an upper bathyal environment. Thus, benthic foraminifers suggest that the site was very shallow in the Pliocene and that it rapidly subsided to its modern water depth of 1423 m.

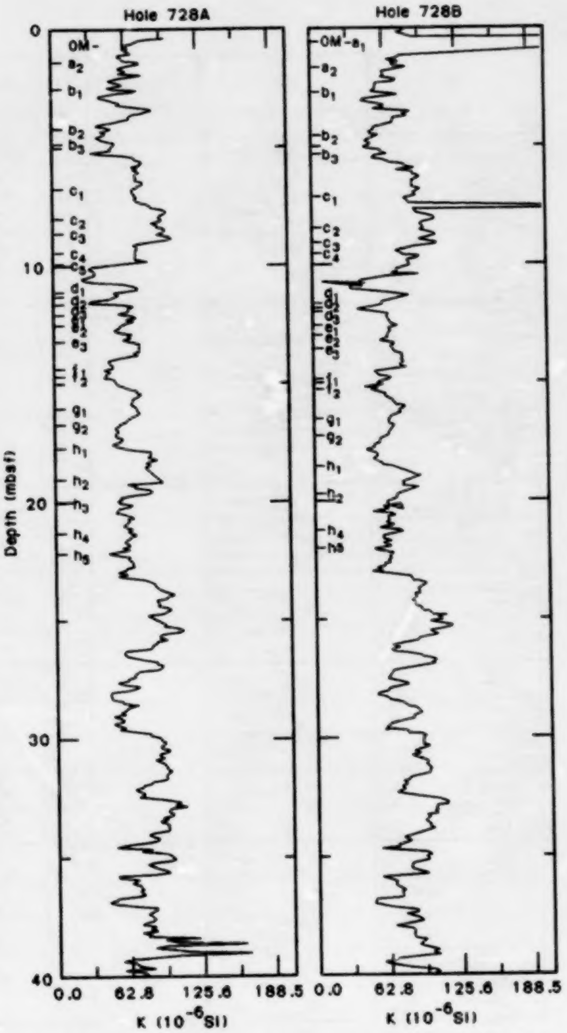

Figure 34. Volume magnetic susceptibility curve and positions of the marker layers in Holes 728A and 728B.

A zone of high organic carbon concentrations that was encountered at 80 to 110 mbsf may reflect a prolonged episode of upwelling or may be associated with the major change in sedimentation rate evident in the late Pliocene (Fig. 36). Detailed logs from this site show maximum concentrations of uranium that correlate well with total organic carbon at this depth, and the zone coincides with maxima in alkalinity in pore waters as well as with the depletion of interstitial sulfate. The elevated organic carbon concentrations (up to 5.3%) appear to foster sig-

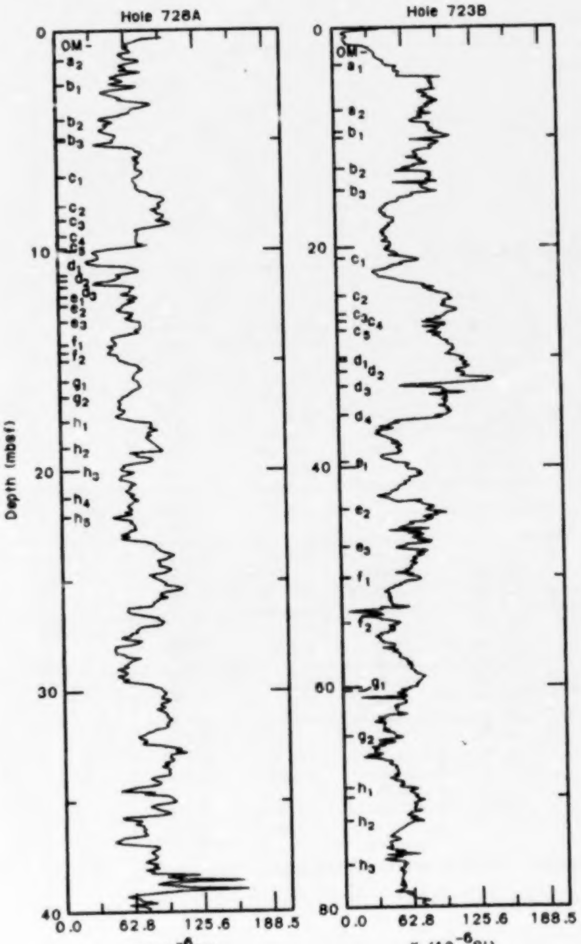

Figure 35. Volume magnetic susceptibility curve and positions of the marker layers in Holes 723B and 728A.

Table 13. Corrected depths below seafloor of core top for stratigraphic depth calculation.

	Hole 728A			Hole 728B		
Core	ODP top depth	Difference	Corrected top depth	ODP top depth	Difference	Corrected top depth
1H	0	0.4	0.4	0	0	0
2H	9.6	0.1	10.1	1.2	0	1.2
3H	19.1	0	19.8	10.7	0	10.7
4H				20.1	0.7	20.8

ODP top depth = depth below seafloor of core top calculated using ODP core data. Difference = difference between depth calculated using ODP core data and depth calculated using layer-to-layer correlation method. Corrected top depth = depth below seafloor of core top calculated using layer-to-layer correlation method.

nificant bacterial activity at this depth, which corresponds to the depth of sulfate depletion in interstitial waters. Both Miocene and Pleistocene sediments are low in total organic carbon.

Site 728 provided several important constraints on the environmental and depositional history of the Oman margin. First, we recovered biosiliceous sediments of Miocene to Pliocene age at this site that can be compared to the Owen Ridge sediments. Second, the site provided additional control on the subsidence history of the slope basins. Combined with findings at other sites on the Oman margin, these findings should permit a detailed reconstruction of the history of the Oman margin in postcruise research.

REFERENCES

Berggren, W. A., Kent, D. V., Flynn, J. J., and Van Couvering, J. A., 1985. Cenozoic geochronology. *Geol. Soc. Am. Bull.*, 96:1407–1418.

Berggren, W. A., Kent, D. V., and Van Couvering, J. A., 1985. The Neogene: Part 2, Neogene geochronology and chronostratigraphy. *In* Snelling N. J. (Ed.), *The Chronology of the Geological Record.* Geol. Soc. Mem. (London), 10:211–259.

Fertl, H. H., 1979. *Gamma Ray Spectral Data Assists in Complex Formation Evaluation*: Houston (Dresser-Atlas).

Hamilton, E. L., 1979. Sound velocity gradients in marine sediments. *J. Acoust. Soc. Am.*, 65:909–922.

Hamilton, E. L., and Bachman, R. T., 1982. Sound velocity and related properties of marine sediments. *J. Acoust. Soc. Am.*, 72:1891–1904.

Ingle, C. J., Jr., Keller, G., and Kolpack, R. L., 1980. Benthic foraminiferal biofacies, sediments and water masses of the southern Peru-Chile Trench area, southeastern Pacific Ocean. *Micropaleontology*, 26:113–150.

Johnson, D. A., in press. Pliocene-Pleistocene radiolarian events and magnetostratigraphic calibrations for the tropical Indian Ocean. *Mar. Micropaleontol.*

Johnson, D. A., and Nigrini, C. A., 1985. Synchronous and time-transgressive Neogene radiolarian datum levels in the equatorial Indian and Pacific oceans. *Mar. Micropaleontol.*, 9:489–523.

Pflum, C. E., and Frerichs, W. E., 1976. Gulf of Mexico deep-water foraminifers. *Cushman Found. Foram. Res., Spec. Publ.* 14.

Sato, T., Takayama, T., Kato, M., Kudo, T., and Kameo, K., in press. Calcareous microfossil biostratigraphy of the uppermost Cenozoic formations distributed in the coast of the Japan Sea. Part 4: Conclusion. *Sekiyu Gijutsu Kyokaishi.*

Takayama, T., and Sato, T., 1987. Coccolith biostratigraphy of the North Atlantic Ocean, Deep Sea Drilling Project Leg 94. *In* Ruddiman, W. T., Kidd, R. B., et al., *Init. Repts. DSDP*, 94, Pt 2: Washington (U.S. Govt. Printing Office), 651–702.

van Morkhoven, F. P., Berggren, W. A., and Edwards, A. S., 1986. Cenozoic cosmopolitan deep-water benthic foraminifera. *Bull. Cent. Rech. Explor.-Prod. Elf-Aquitaine Mem.*, 11.

Ms 117A-115

Table 14. Stratigraphic depths of the marker layers at Sites 723, 724, and 728.

	Hole 723B		Hole 724A		Hole 728A		Hole 728B	
Layer	Core, section, interval (cm)	Corrected depth	Core, section, interval (cm)	Corrected depth	Core, section, interval (cm)	Corrected depth	Core, section, interval (cm)	Corrected depth
OM-a_1	1-3, 35	3.35	1-1, 95	0.95			1-1, 65	0.65
a_2	2-3, 20	7.20	1-2, 115	2.65	1-1, 135	1.75	2-1, 45	1.65
b_1	2-4, 65	9.15	1-3, 100	4.00	1-2, 90	2.80	2-2, 5	2.75
b_2	2-6, 110	12.60			1-3, 110	4.50	2-3, 30	4.50
b_3	3-1, 95	14.75	2-1, 75	7.95	1-4, 40	5.30	2-3, 110	5.30
c_1	3-5, 110	20.90	2-2, 75	9.45	1-5, 70	7.10	2-4, 135	7.05
c_2	4-1, 85	24.95	2-3, 130	11.50	1-6, 50	8.40	2-5, 115	8.35
c_3	4-2, 100	26.60	2-4, 70	12.40	1-6, 115	9.05	2-6, 30	9.00
c_4	4-3, 15	27.25	2-4, 120	12.90	1-7, 40	9.80	2-6, 95	9.65
c_5	4-3, 100	28.10	2-5, 35	13.55	2-1, 35	10.45		
d_1	4-5, 70	30.80	3-1, 40	17.20	2-2, 5	11.65	3-1, 90	11.60
d_2	4-6, 10	31.70	3-1, 150	18.30	2-2, 25	11.85	3-1, 110	11.80
d_3	4-7, 5	33.15	3-2, 90	19.20	2-2, 50	12.10	3-1, 130	12.00
d_4	5-2, 50	35.30	3-3, 85	20.65				
e_1	5-5, 20	39.50	3-4, 15	21.45	2-2, 95	12.55	3-2, 35	12.55
e_2	6-1, 90	43.80	3-5, 90	23.70	2-2, 140	13.00	3-2, 80	13.00
e_3	6-3, 150	47.40	3-6, 95	25.25	2-3, 60	13.70	3-2, 145	13.65
f_1	6-5, 120	50.10	4-1, 85	27.75	2-4, 20	14.80	3-3, 115	14.85
f_2	7-2, 15	54.25	4-2, 70	29.10	2-4, 55	15.15	3-4, 5	15.25
g_1	7-6, 30	60.40	4-4, 120	32.60	2-5, 35	16.45	3-4, 120	16.50
g_2	8-2, 60	64.40	4-6, 25	34.65	2-5, 105	17.15	3-5, 60	17.30
h_1	8-5, 90	69.20	4-7, 40	36.30	2-6, 70	18.30	3-6, 35	18.55
h_2	9-1, 20	72.10	5-1, 80	37.30	2-7, 35	19.45	3-6, 140	19.60
h_3	9-3, 135	76.25	5-2, 60	38.60	3-1, 90	20.70		
h_4	9-7, 95	81.85	5-4, 145	42.45	3-2, 65	21.95	4-1, 120	22.00
h_5			5-5, 145	43.95	3-2, 150	22.80	4-2, 40	22.70

Note: Depths based on the correction factors of Table 13. Corrected depth = corrected depth for stratigraphic thickness.

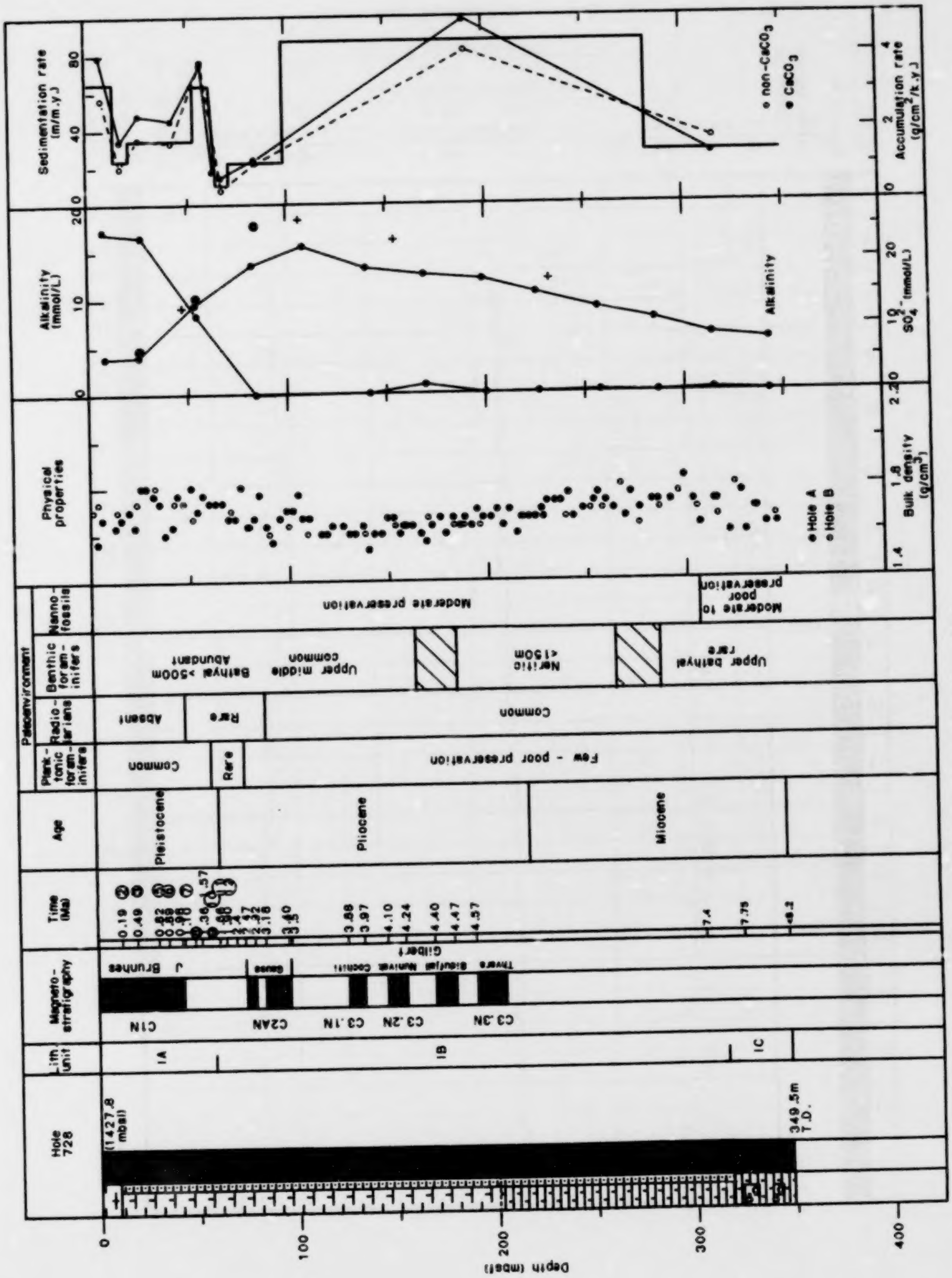

Figure 36. Summary of shipboard results, Site 728. Numbers in circles = nannofossil datum levels.

Summary Log for Hole 728A

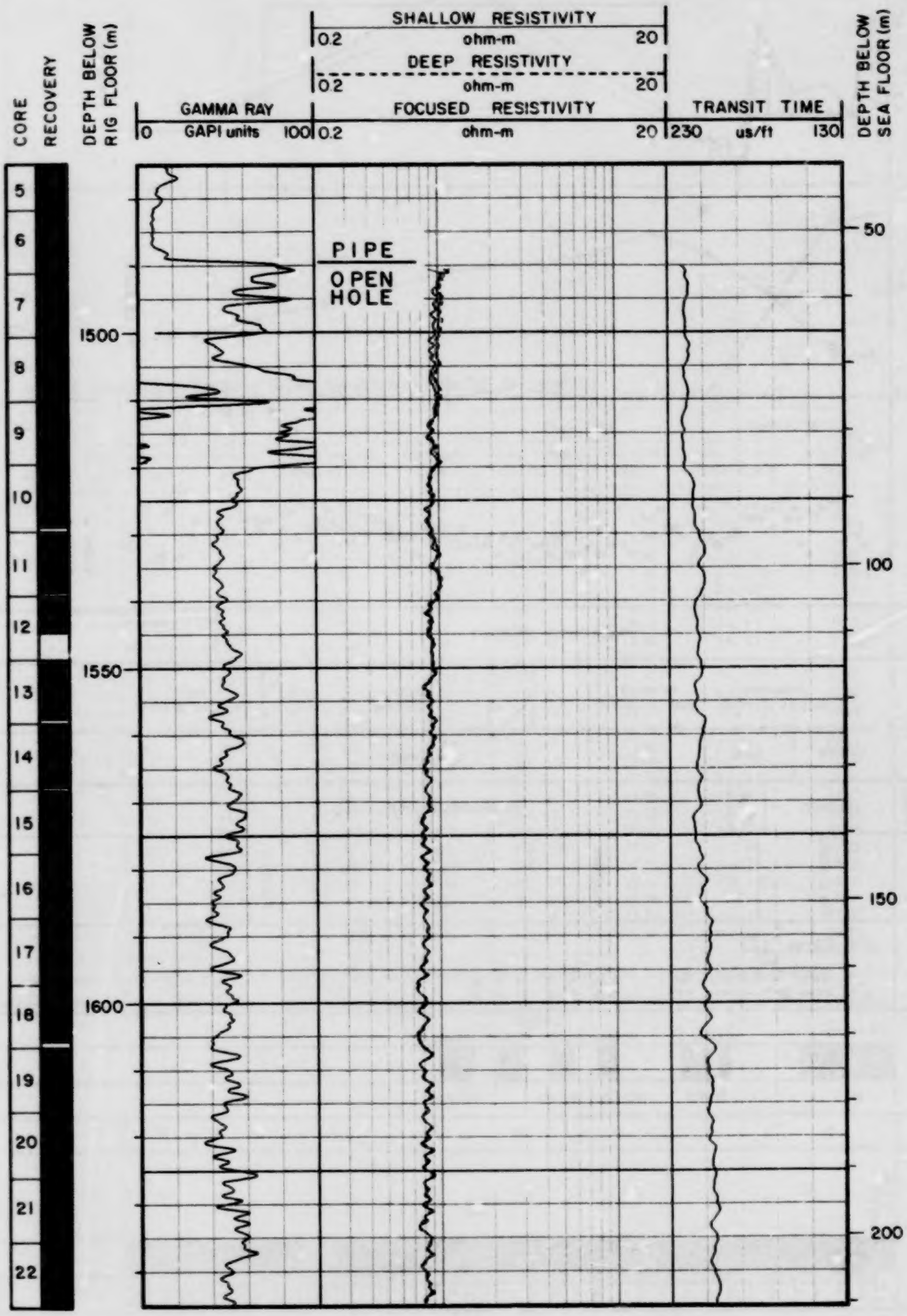

Summary Log for Hole 728A (continued)

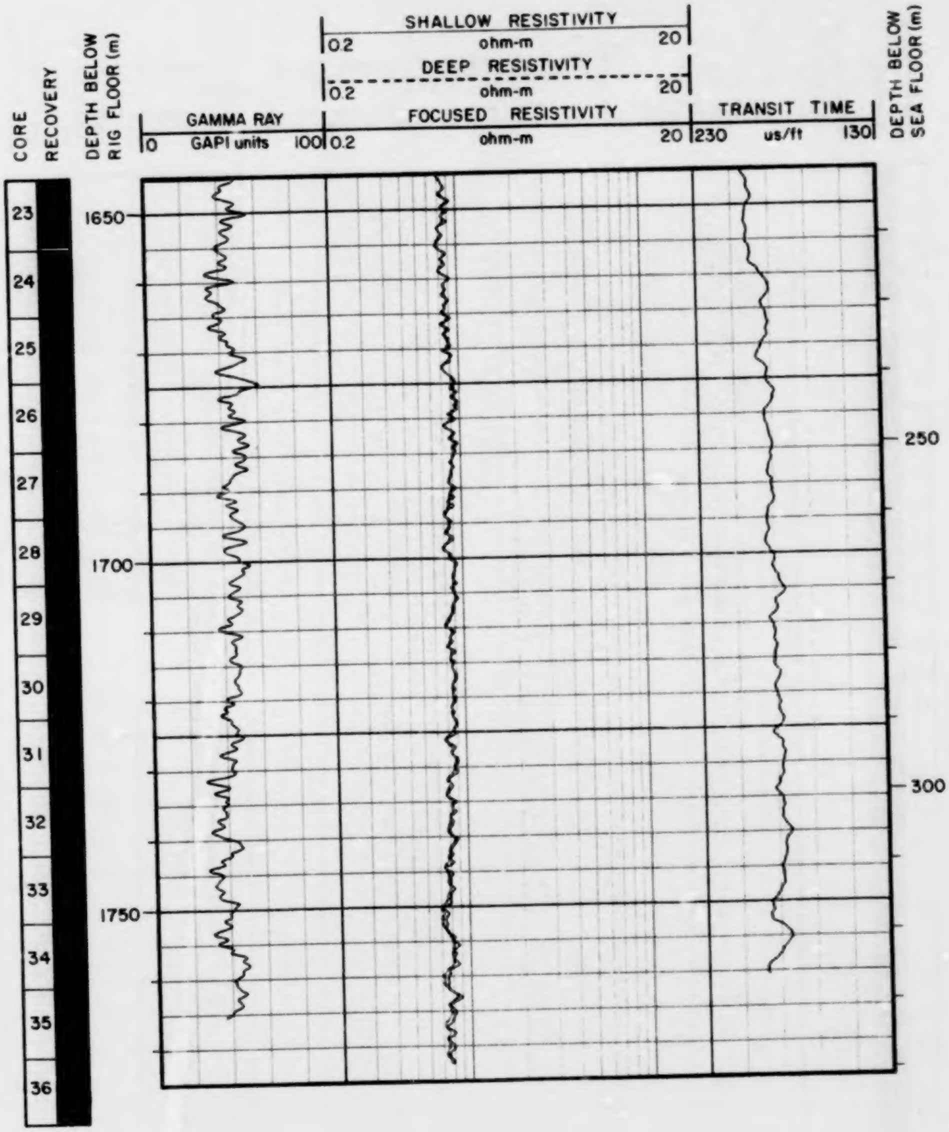

Summary Log for Hole 728A (continued)

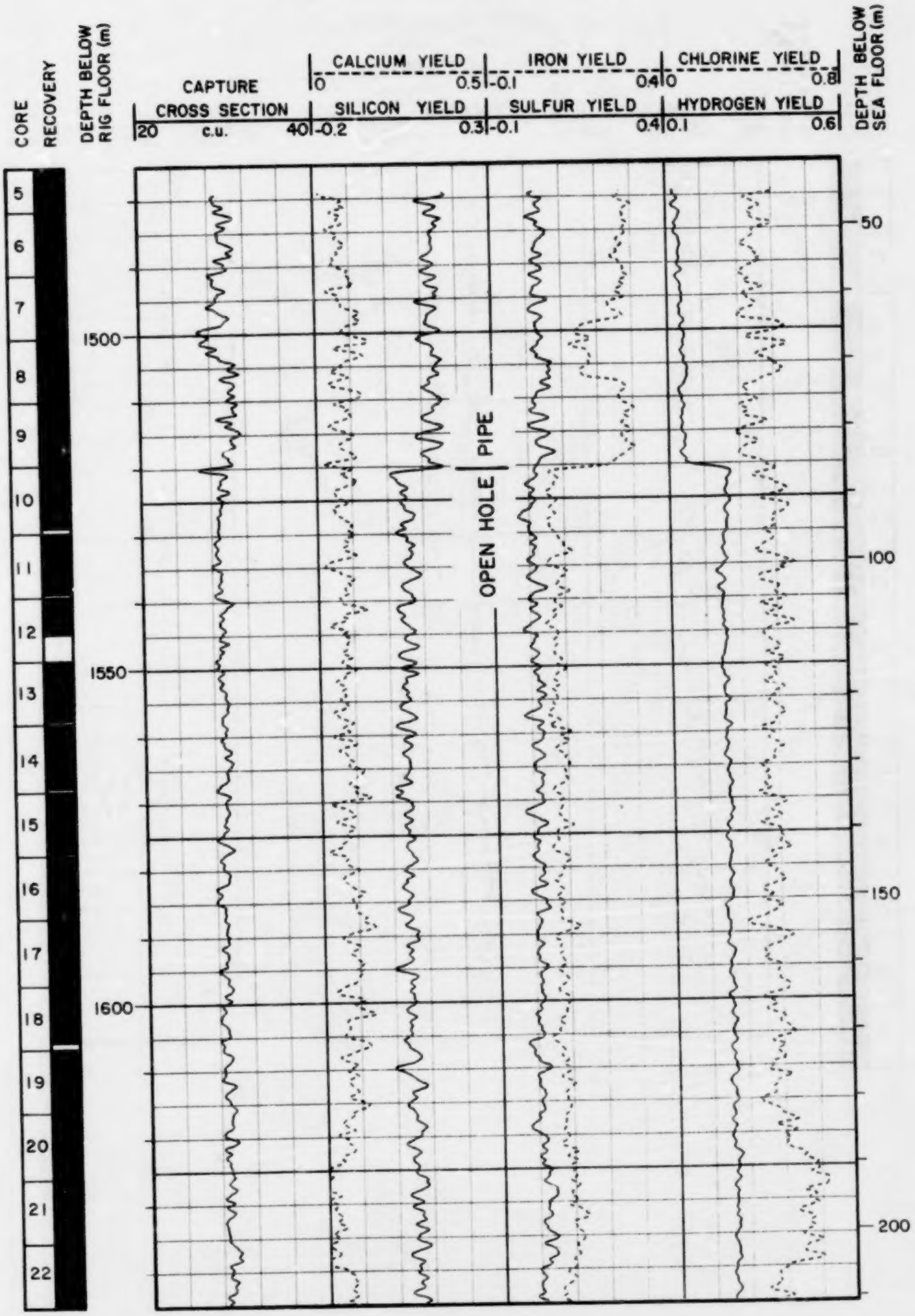

Summary Log for Hole 728A (continued)

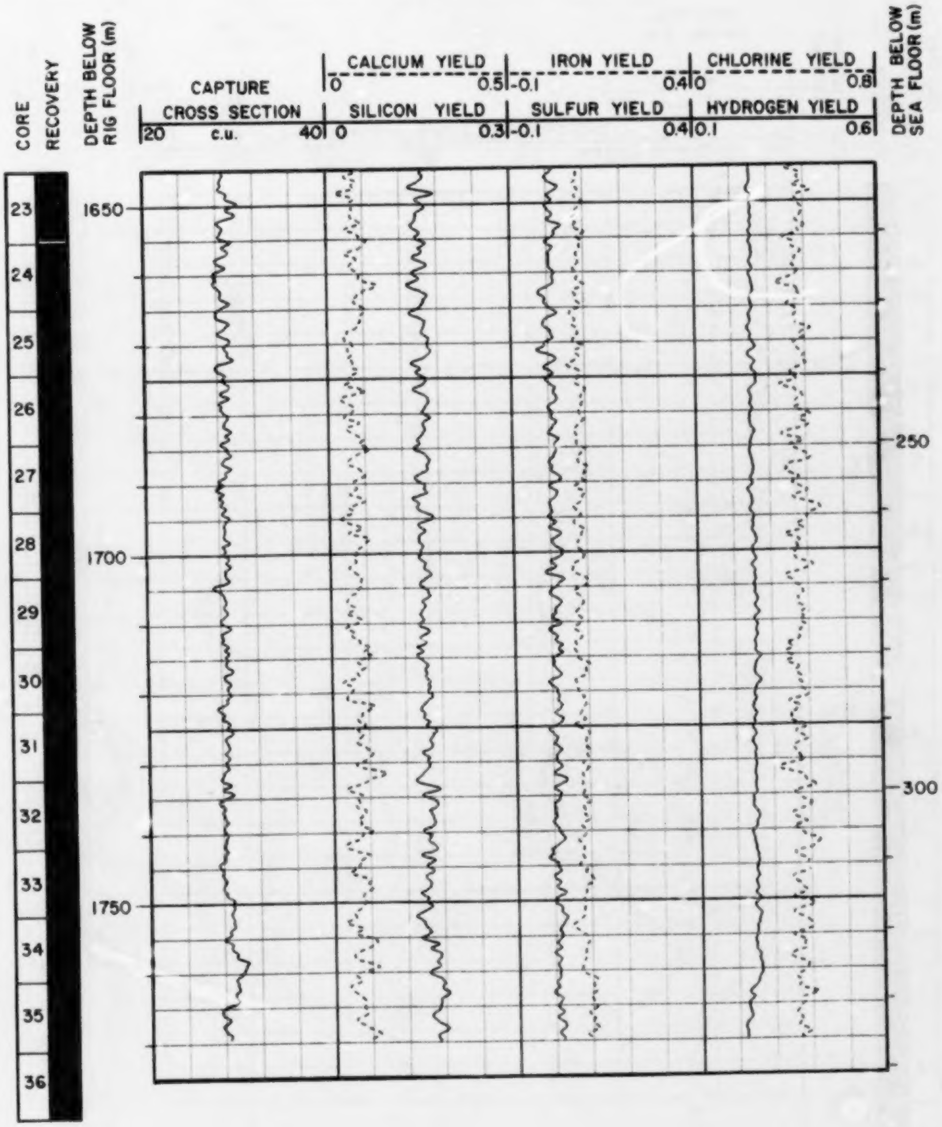

Summary Log for Hole 728A (continued)

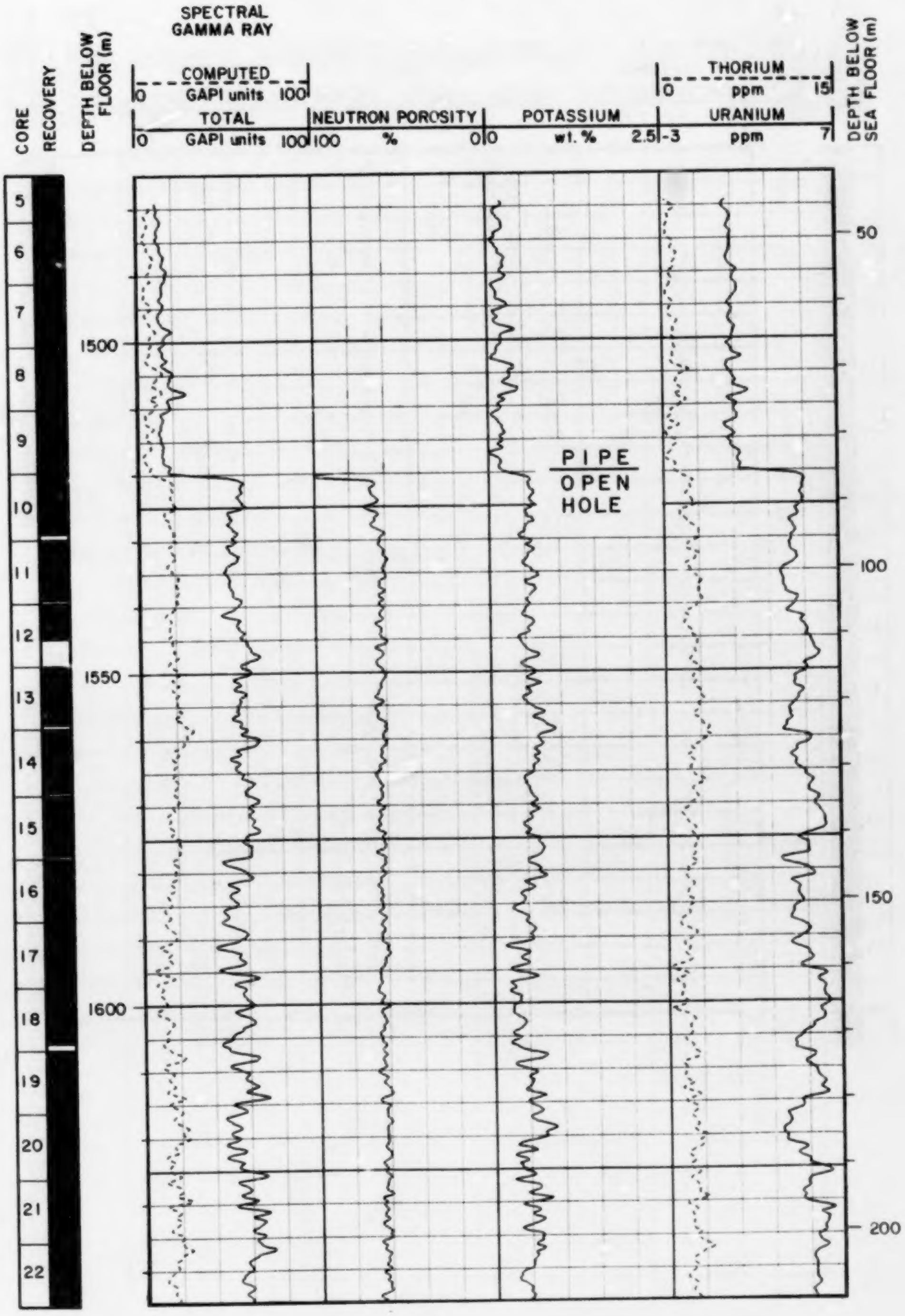

Summary Log for Hole 728A (continued)

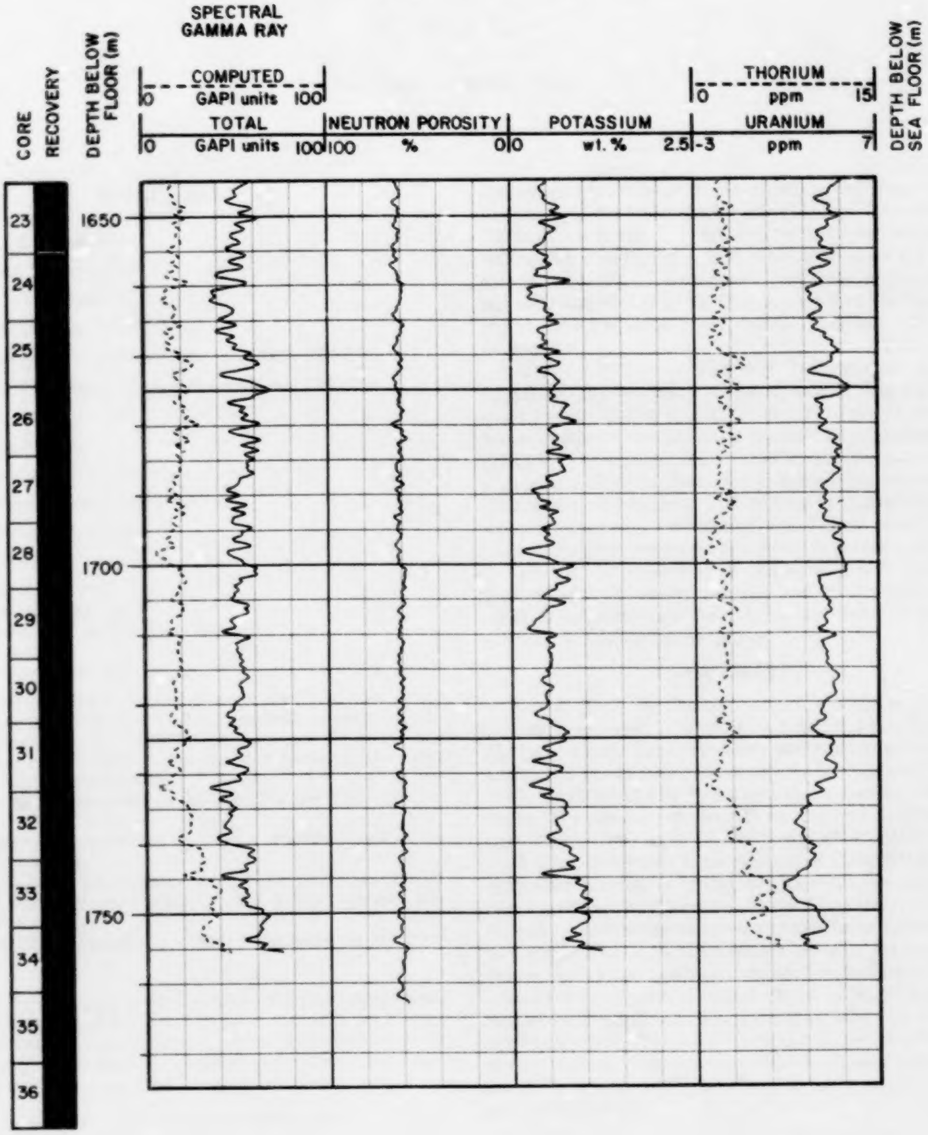

17. SITE 729[1]

Shipboard Scientific Party[2]

HOLE 729A

Date occupied: 28 September 1987

Date departed: 28 September 1987

Time on hole: 16 hr, 30 min

Position: 17°38.715′N, 57°57.221′E

Water depth (sea level; corrected m, echo-sounding): 1398.5

Water depth (rig floor; corrected m, echo-sounding): 1409.0

Bottom felt (m, drill pipe): 1403.8

Penetration (m): 109.1

Number of cores: 13

Total length of cored section (m): 109.1

Total core recovered (m): 31.72

Core recovery (%): 29.1

Oldest sediment cored:
Depth sub-bottom (m): 109.1
Nature: nummulitic, shallow-water limestone
Age: Undetermined
Measured velocity (km/s): –

Principal results: Site 729 is situated in water depths of 1400 m off Oman's shore on a basement block of presumed ophiolitic origin. Our objectives in drilling Site 729 were to recover the oldest sediments on one of the blocks, to penetrate to underlying strata, and possibly to recover igneous rock.

We obtained the following results in drilling Site 729:

1. shallow-water carbonates underlie a condensed Quaternary hemipelagic sequence;
2. shallow-water limestones at Site 729 are similar in character and facies to those recovered at Site 726, 60 km to the west on a second basement ridge; and
3. the limestone sequence apparently is not cemented and dolomitized.

The results of drilling at Site 729 show that pre-Neogene basement, which today is characterized by the mosaic of tectonic structures in the Neogene, may have been a starved carbonate platform in the Paleogene. It may have been uplifted and eroded in the Oligocene and broken into slope basins and ridges in the Neogene.

BACKGROUND AND OBJECTIVES

Site 729 is located in water depths of about 1400 m at 17°38.715′N and 57°57.221′E on the continental margin of Oman (Fig. 1). This area of the slope and margin may be composed, in part, of the upthrust ophiolite complex that is observed on the island of Masirah to the north of Site 726 (Moseley and Abbotts, 1979). Slope basins between ophiolite blocks lie at water depths ranging from 1500 m to 500 m and thus accumulate sediments coincident in water depth with the intermediate-water masses of the Arabian Sea. Site 729 is located on the deepest and most distal basement block that forms the seaward boundary of the lower slope basin (Fig. 1). The location of Site 729 is shown in Figure 2, and its structural and depositional setting is shown in Figure 3. Site 729 is located on the brow of the east-facing scarp of a basement peak that is thought to be an ophiolite complex (Fig. 3). This block forms the eastern boundary of the lower slope basin and is faulted just west (landward) of Site 729.

Seismic reflection profiles (Fig. 3) show a pelagic cap in the uppermost 0.05 s (about 40 mbsf) that is underlain by a relatively transparent zone to 0.2 s (about 170 mbsf). Diffuse reflections, which are thought to be the ophiolitic basement, occur at about 0.35 s or about 310 mbsf (Fig. 3B). In general, this location reveals older conformable reflectors that have an unknown relationship to basement and that are truncated and draped by pelagic sediments. We selected Site 729 to obtain samples of older, truncated sediments and possible underlying basement.

Our specific objective for drilling at Site 729 was to obtain samples of the basement complex and its overlying sediments in order to help constrain the tectonic and depositional history of the margin and the slope basins.

OPERATIONS

The *JOIDES Resolution* reached Site 729 in dynamic positioning mode after a transit of 1.5 hr from Site 728. Since Site 729 had been surveyed previously and marked with a beacon, no additional survey was performed. At 0600 hr on 28 September 1987, the ship was positioned over the beacon in 1398.8 m water depth. The position of Site 729 as obtained by global positioning system (GPS) is 17°38.715′N and 57°57.221′E.

Because the goal of our drilling at Site 729 was to retrieve ophiolitic basement overlain by limestone, we used the rotary core barrel (RCB) system to cut the first core at 1030 hr on 28 September. After first satisfying recoveries in nannofossil oozes to Core 117-729A-4R (26.3 mbsf), recovery dropped sharply in brittle limestones, of which only pebble-sized fragments were recovered from Cores 117-729A-5R to -13R (109.1 mbsf total depth). Hole conditions deteriorated rapidly, and we abandoned drilling in Hole 729A after Core 117-729A-13R. The overall recovery rate for Hole 729A was 29.1% (Table 1). By 2230 hours on 28 September 1987, the ship was underway to Site 730 with no further delays.

LITHOSTRATIGRAPHY

Lithologic Units

We subdivided sediments and rocks recovered at Site 729 into two lithologic units. Lithologic Unit I is composed of foraminifer muds of Quaternary age, while Unit II is a fossiliferous, shallow-water limestone (Fig. 4).

Unit I (Depth: 0–28.35 mbsf; Age: Holocene-Pleistocene)

Core 117-729A-1R through Section 117-729A-4R-5, 5 cm.

Unit I is composed of nannofossil-foraminifer-rich mud to marly nannofossil ooze. The grain sizes include clay- (30%–80%), silt- (15%–40%), and sand-sized particles (5%–30%).

---

[1] Prell, W. L., Niitsuma, N., et al., 1989. *Proc. ODP, Init. Repts.*, 117: College Station, TX (Ocean Drilling Program).

[2] Shipboard Scientific Party is as given in the list of Participants preceding the contents.

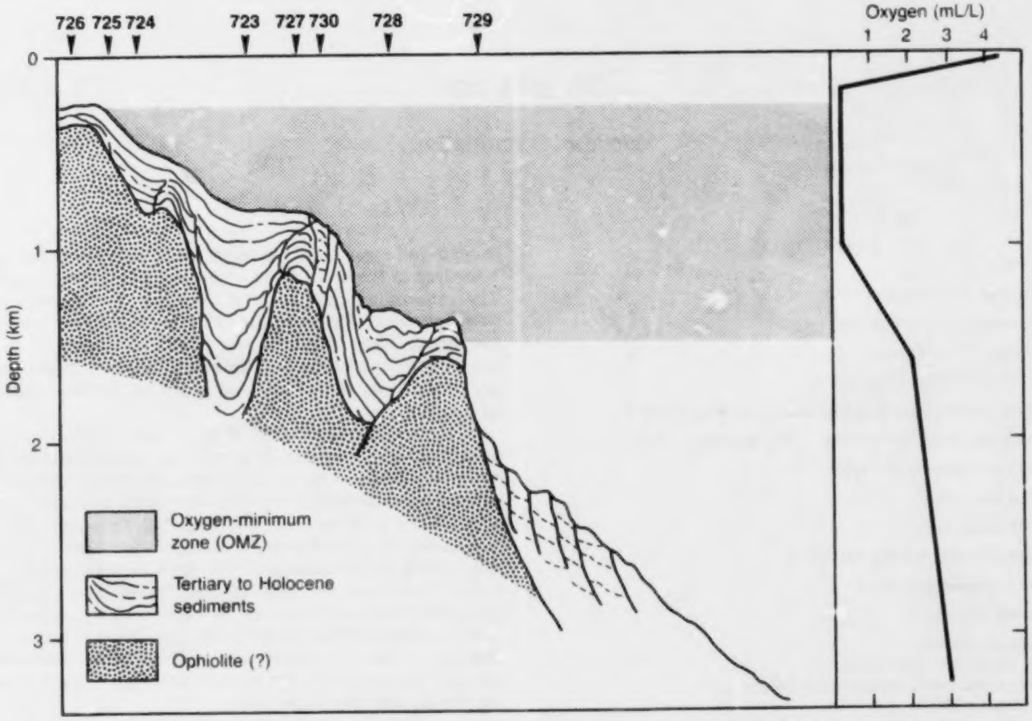

Figure 1. Structure of the Oman margin and the oxygen-minimum zone (OMZ). The schematic profile shows the series of basement ophiolite blocks and the sedimentary basins between them. The concentration of oxygen in the water column (RC-2704, unpubl. date) defines the depth range of the OMZ and where it impinges on the margin. The schematic location of Site 729 is indicated.

The sand fraction is composed mainly of foraminifer tests, which exhibit their highest occurrence toward the top of Unit I. This foraminifer-rich facies is replaced downhole by a nannofossil-dominated facies. The sediments are olive in color (5Y 4/3 to 5/3) and display burrow mottling in Cores 117-729A-3R and -4R. The upper two cores do not show burrow mottling because of drilling disturbance.

Unit I exhibits slight differences in lithology, which are expressed as indistinct alternations of light and dark layers between 0.2 and 1.5 m thick. The light layers are more coarse grained and foraminifer rich, while some of the dark layers seem, from smear slide analyses, to have a higher content of organic carbon. Organic carbon values range from 0.5% to 1.7% (Table 2). Trace amounts of authigenic dolomite rhombs occur in Cores 117-729A-3R and -4R, while phosphorite concretions are found 5 cm above the transition from Unit I to Unit II. That transition appears in Core 117-729A-4R as a relatively sharp boundary.

Unit II (Depth: 28.35–109.1 mbsf; Age: undetermined)

Sections 117-729A-4R-5, 5 cm, through 117-729A-13R.

Unit II is a large foraminifer- to algae-bearing carbonate sequence which is relatively weakly cemented and highly porous. The recovery within Unit II was so low (0%–2.5%) that we could not establish a detailed stratigraphy of the carbonate sequence. The uppermost part of Unit II (Core 117-729A-4R, 28.3–32.0 mbsf) contains a white, highly calcareous, weakly cemented, and friable foraminifer-wackestone with a fine-grained micritic matrix. The facies contains whole and fragmented speciments of large, benthic foraminifers which reach a diameter of 0.5–1 cm. Further downhole, carbonates were only recovered in Core 117-729A-10R (70–80 mbsf) with 24 cm of algae-dominated wackestone. Thin-section examination of this facies reveals an encrusting, oncolithic type of algae and branches of red algae. Foraminifer tests are filled with two generations of cement: early fibrous rim cement and a later blocky spar. The matrix of the rock is dolomitized.

Discussion

The weakly cemented to partly dolomitized rocks of Unit II are shallow-water carbonates. The presence of red algae indicates shallow water (tens of meters deep) with normal salinities (Flügel, 1982). Facies and diagenetic patterns appear to be similar to those observed in the Eocene carbonates recovered at Site 726 approximately 50 km west of Site 729. These similarities include (1) the occurrence of foraminifer-rich and algae-dominated facies in the upper and lower parts of the recovered sequences, respectively; (2) the low degree of cementation in the upper facies, and (3) initiation of matrix dolomitization in the lower facies. However, a dolomitized zone which we found at the transition from Unit I to Unit II at Site 726 was not encountered at Site 729. Implications regarding the time gap between Unit I and II are discussed for Site 726 (see "Lithostratigraphy" section, "Site 726" chapter, this volume) and are not repeated here.

Unit I is composed of a condensed Quaternary sequence. The relatively large grain size of the sediment and the occurrence of clayey to silty sand layers are due mainly to the high foraminifer content (10%–40%). Site 729 is located on a somewhat isolated promontory off the Oman margin in a water depth of 1400 m (see "Background and Objectives" section, this chapter) and the silty sand layers may represent winnowed

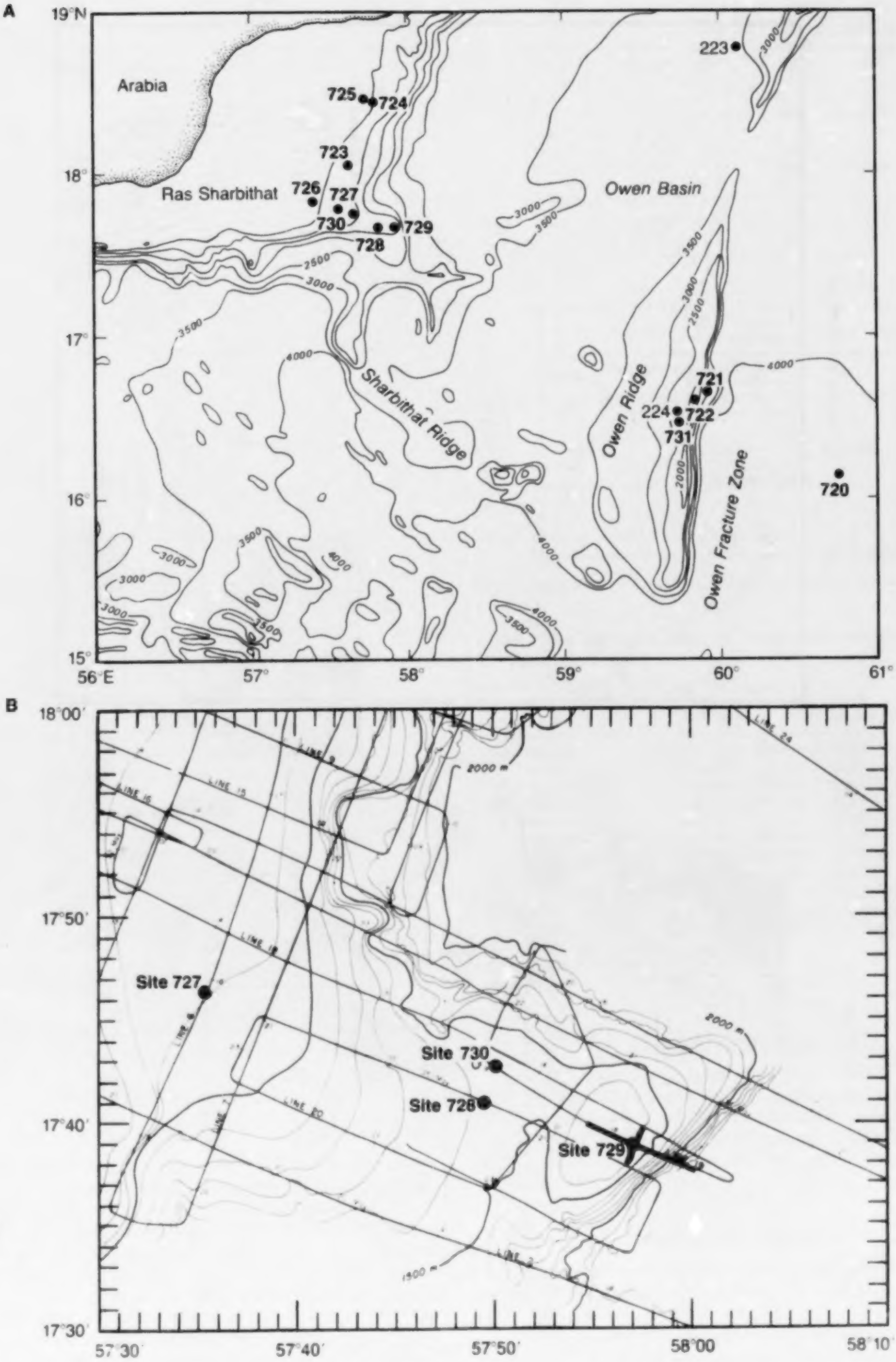
A
19°N
18°
17°
16°
15°
56°E
57°
58°
59°
60°
61°
Arabia
Ras Sharbithat
Owen Basin
Sharbithat Ridge
Owen Ridge
Owen Fracture Zone
223
725
724
723
726
727
730
728
729
721
224
722
731
720
2500
3000
3500
4000
2000
B
18°00′
17°50′
17°40′
17°30′
57°30′
57°40′
57°50′
58°00
58°10′
Site 727
Site 730
Site 728
Site 729
2000 m
1500 m
LINE 15
LINE 16
LINE 19
LINE 20
LINE 24
LINE 2

Figure 2. A. Bathymetry of the Oman margin and the location of Site 729. B. The detailed location of Site 729 and the seismic profiles shown in Figure 3. Bathymetric data are from the site survey (RC2704, 1986).

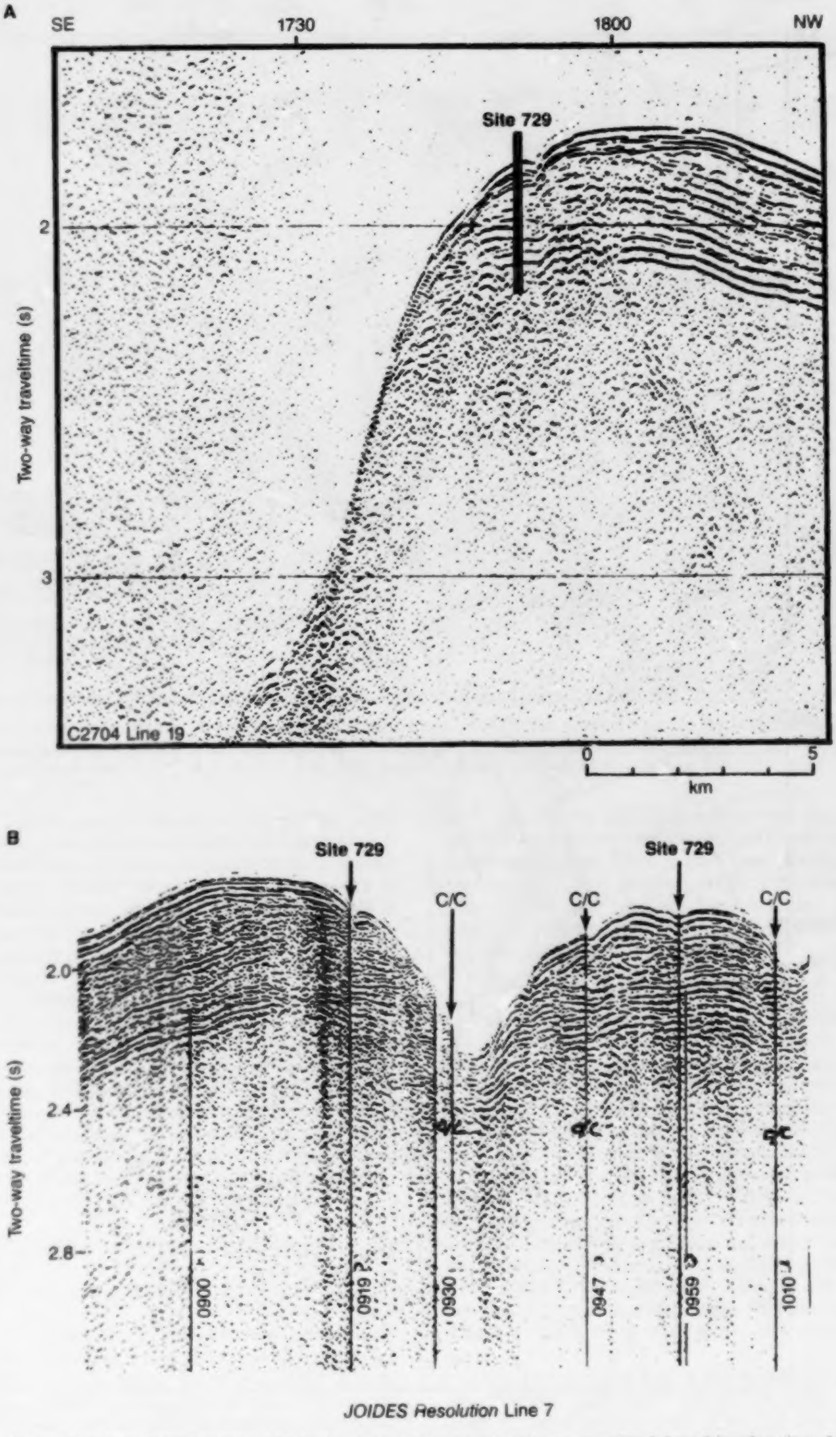

Figure 3. Single-channel seismic (SCS) reflection profiles showing the structural and depositional setting of Site 726. A. RC-2704 Line 19 is perpendicular to the strike of the basement block and shows the faulting near the crest. B. *JOIDES Resolution* Line 7 shows both dip and strike sections of the basement peak. The profile indicates two passes made by the *JOIDES Resolution*. C/C = course change.

Table 1. Coring summary, Site 729.

Core no.	Date (Sept. 1987)	Time (local)	Depth (mbsf)	Cored (m)	Recovered (m)	Recovery (%)
117-729A-						
1R	28	1105	0–3.2	3.2	3.26	102.0
2R	28	1135	3.2–12.7	9.5	8.81	92.7
3R	28	1210	12.7–22.3	9.6	9.68	101.0
4R	28	1300	22.3–26.3	4.0	9.67	242.0
5R	28	1325	26.3–31.9	5.6	0	0
6R	28	1350	31.9–41.4	9.5	0.01	0.1
7R	28	1430	41.4–51.0	9.6	0	0
8R	28	1505	51.0–60.6	9.6	0.01	0.1
9R	28	1530	60.6–70.3	9.7	0.02	0.2
10R	28	1600	70.3–80.0	9.7	0.24	2.5
11R	28	1750	80.0–89.7	9.7	0.02	0.2
12R	28	1715	89.7–99.4	9.7	0	0
13R	28	1745	99.4–109.1	9.7	0	0
				109.1	31.72	

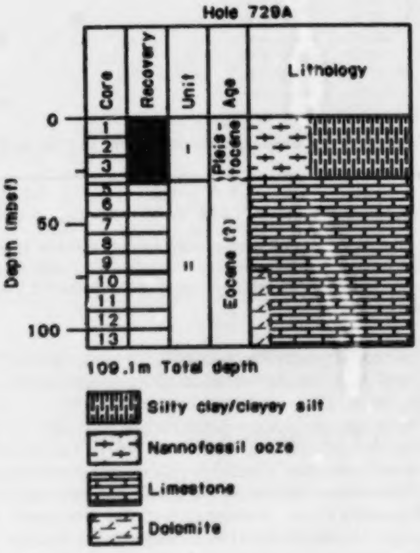
Hole 729A
Core
Recovery
Unit
Age
Lithology
0
50
100
Depth (mbsf)
1
2
3
5
6
7
8
9
10
11
12
13
I
II
Pleis-tocene
Eocene (?)
109.1m Total depth
Silty clay/clayey silt
Nannofossil ooze
Limestone
Dolomite

Figure 4. Lithologic summary, Site 729.

deposits. We have listed in Table 2 a few of the carbonate and organic carbon measurements which characterize this unit.

BIOSTRATIGRAPHY

Introduction

The uppermost sediments recovered at Site 729 are marly foraminifer nannofossil oozes of Pleistocene to Holocene age. However, below 26 m, we recovered a lithified limestone.

Only the uppermost lithologic unit contains planktonic foraminifers and calcareous nannofossils, which are abundant and have moderate to good preservation. Benthic foraminifers are common and have moderate to good preservation in Unit I. Benthic foraminifers are also present in the limestone, but the preservation deteriorated dramatically. No siliceous microfossils were found at this site (Fig. 5). For a detailed listing of faunap events see Table 3.

Table 2. Carbonate and organic carbon data, Site 729.

Core, section, interval (cm)	Depth (mbsf)	Total carbon (%)	Inorganic carbon (%)	Organic carbon (%)	$CaCO_3$ (wt%)
117-729A-					
1R-3, 10–12	3.10	9.30	8.29	1.01	69.1
2R-3, 39–41	6.59	8.73	7.03	1.70	58.6
2R-6, 39–41	11.09	9.32	8.82	0.50	73.5
3R-1, 70–72	13.40	8.92	8.25	0.67	68.7
3R-3, 70–72	16.40	9.43	8.60	0.83	71.6
3R-6, 60–62	20.80	8.44	7.37	1.07	61.4
4R-1, 60–62	22.90	9.08	7.74	1.34	64.5
4R-3, 41–43	25.71	7.27	6.72	0.55	56.0

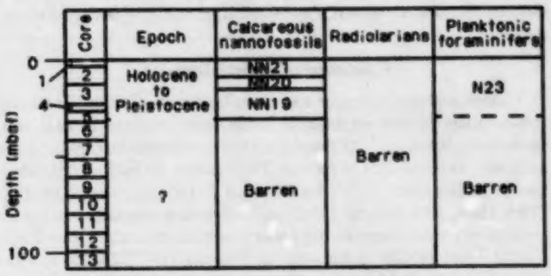
Core
Epoch
Calcareous nannofossils
Radiolarians
Planktonic foraminifers
0
1
4
100
Depth (mbsf)
2
3
5
6
7
8
9
10
11
12
13
Holocene to Pleistocene
?
NN21
NN20
NN19
Barren
Barren
N23
Barren

Figure 5. Correlation of planktonic microfossil zones in Hole 729A.

Table 3. Stratigraphic listing of faunal events for Hole 729A.

Event	Sample or section, interval (cm)	Depth (mbsf)	Age (Ma)	Source of age
B *Emiliania*	117-729A-2R-3, 105–106	7.25	0.19	1
huxley	117-729A-2R-5, 105–106	10.25		
T *Pseudoemiliana*	117-729A-3R-1, 105–106	13.75	0.49	1
lacunosa	117-729A-3R-3, 105–106	16.75		
B *Gephyrocapsa*	117-729A-3R, CC	22.30	[a]0.89	3
parallela	117-729A-4R-1, 105–106	23.35		
T [b]*Geophyrocapsa*	117-729A-4R-1, 105–106	23.35	[a]1.10	3
large	117-729A-4R-3, 105–106	26.35		

Note: T = upper limit and B = lower limit. Sources of ages are: 1 = oxygen isotope data for Site 723 (N. Niitsuma, unpubl. data) and 3 = Takayama and Sato, 1987.

[a] North Atlantic data.

[b] Long axis greater than 6 μm.

Planktonic Foraminifers

The first three core-catcher samples (3.2–22.3 mbsf) in Hole 729A contained abundant and well-preserved planktonic foraminifer assemblages. *Globigerinella calida calida* and *Globorotalia truncatulinoides* indicate a Pleistocene age. The lower part of the section, which is composed of shallow-water carbonates, is barren.

Benthic Foraminifers

The benthic foraminiferal fauna was studied in the core catchers of Hole 729A. Preservation in the upper three samples (117-729A-1R, CC, through -3R, CC; 3.2–22.3 mbsf) is good to moderate, whereas the remainder of the sequence consists of lithified or semilithified limestone with sharply deteriorating states of preservation. In order to investigate the foraminiferal fauna in the limestone, shore-based studies of thin sections will have to be conducted.

The planktonic/benthic (P/B) ratio is about 99% in the upper three samples where benthic foraminifers are rare and have moderate diversity.

Common benthic foraminiferal species in the unconsolidated uppermost Pleistocene interval of Hole 729A are *Bolivina ordinaria, Cibicidoides wuellerstorfi, Hoeglundina elegans, Melonis barleeanum, Osangularia culter, Pullenia subcarinata, Sigmoilinopsis schlumbergeri*, and *Uvigerina hispida*. The faunal composition and the high P/B ratio indicates that Site 729 was located in the upper middle bathyal zone during the Pleistocene.

The benthic foraminiferal fauna in the underlying limestone was not investigated. However, the presence of larger foraminifers of nummulitid and amphistegid types indicates that this part of the sequence was deposited in a shallow-water environment.

Calcareous Nannofossils

Calcareous nannofossils are abundant with moderate to good preservation in the uppermost three core catchers at this site. Sediments down to 7.25 mbsf contain *Emiliania huxleyi* and are assigned to Zone NN21 (upper Pleistocene to Holocene). Sediments in Samples 117-729A-2R-5, 105–106 cm, down to 117-729A-3R-1, 105–106 cm (10.25–13.75 mbsf), contain neither *E. huxleyi* nor *Pseudoemiliania lacunosa* and are assigned to Pleistocene Zone NN20. Sediments in Sample 117-729A-3R-3, 105–106 cm, down to 117-729A-4R-5, 4 cm (16.75–28.3 mbsf), contain *P. lacunosa* and belong to Zone NN19 (lower Pleistocene to uppermost Pliocene). Below this, the lithology changes from a marly nannofossil ooze to a partially lithified limestone which does not contain any calcareous nannofossils (Fig. 5 and Table 3).

Radiolarians

This site is barren of siliceous microfossils.

Paleoenvironmental Implications

The presence of limestone which contains larger foraminifers in the lower part of the sequence indicates a very shallow-water (<200 m) environment during the depositional period.

ACCUMULATION RATES

Sedimentation rates at Site 729 are based on four nannofossil datums identified in the top 26 m (Fig. 6). The mean rate increases upsection from 18 to 46 m/m.y. The higher rate is associated with the foraminifer-rich interval at the top of the site (see "Lithostratigraphy" section, this chapter). The low rate of sedimentation for the hemipelagic deposits at Site 729 may be attributed to postdepositional winnowing, which is thought to be responsible for the silty foraminiferal sand layers found at this site (see "Lithostratigraphy" section, this chapter).

We calculated the mass accumulation rates of calcium carbonate, organic carbon, and noncarbonate sediment components from average values between the datum levels (Table 4). Total accumulation averages 2.6 g/cm^2/k.y. over the past 1.1 m.y., with more than half of this value attributed to calcium carbonate. Organic carbon accumulations are comparable to the calculated rates for the pelagic deposits at Owen Ridge sites (see Owen Ridge site chapters, this volume).

PHYSICAL PROPERTIES

The measurement and analysis of physical properties at Site 729 were restricted by a very low recovery rate in Cores 117-729A-5R through -13R. Physical properties measurements were limited to index properties (wet-bulk density, porosity, water content, and grain density) determined for sediments from Cores 117-729A-1R to -4R.

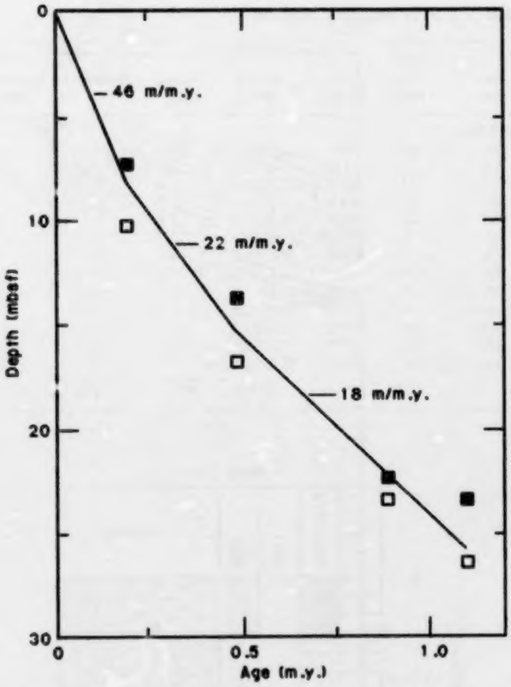

Figure 6. Age-depth plot of stratigraphic datums listed in Table 3. The filled and open dots are the upper and lower depths of each datum level, respectively. Indicated sedimentation rates are calculated between nannofossil datum levels.

Two lithologic units were identified at Site 729. Unit I is a nannofossil-foraminifer-rich mud to a marly nannofossil ooze (see "Lithostratigraphy" section, this chapter) extending from the sea floor to approximately 24 mbsf. The interval from 0 to 13 mbsf shows a slight increase in porosity from 64% to 67% and in water content from 41% to 43%; grain density remains roughly constant at 1.61 g/cm^3. The interval from 13 to 24 mbsf shows an abrupt decrease in porosity from 67% to 56% and in water content from 43% to 32%; wet-bulk density, on the other hand, increases from 1.61 to 1.80 g/cm^3 (Table 5). These data are presented with the cautionary note that drilling disturbances occurred throughout these sediments.

Unit II (24–109 mbsf) is characterized by a very friable and highly disturbed nummulitic limestone. Because of the high degree of drilling disturbance, index properties were not determined for these sediments.

INORGANIC GEOCHEMISTRY

Recovery was poor at Site 729, and only two interstitial water samples were collected, both by squeezing. The standard suite of analytical measurements was performed on the samples; the results are listed in Table 6.

The data indicate that diagenetic activity is not pronounced in the sediments at this site. Little difference from expected bottom-water concentrations of most constituents is seen in the top 30 m. Sulfate reduction over the top ~30 m is hardly evident.

Table 4. Sedimentation and accumulation rate data for Site 724.

Depth interval (mbsf)	Age range (m.y.)	$CaCO_3$ ($\bar{x}$ %)	C_{org} ($\bar{x}$ %)	Dry-bulk density ($\bar{x}$ g/cm^3)	Sed. rate ($\bar{x}$ m/m.y.)	$CaCO_3$ acc. rate (g/cm^2/k.y.)	Non-$CaCO_3$ acc. rate (g/cm^2/k.y.)	C_{org} acc. rate (mg/cm^2/k.y.)
0-8.75	0-0.19	63.9	1.36	0.948	46.0	2.79	1.57	59.3
8.75-15.25	0.19-0.49	71.1	0.59	1.004	21.7	1.55	0.63	12.9
15.25-22.30	0.49-0.89	65.8	1.08	1.122	17.6	1.30	0.68	21.3
22.30-26.00	0.89-1.10	56.0	0.55	1.224	17.6	1.21	0.95	11.8

Table 5. Physical properties summary, Hole 729A.

Core, section, interval (cm)	Depth (mbsf)	Wet-bulk density (g/cm^3)	Porosity (%)	Water content (%)	Grain density (g/cm^3)	Dry-bulk density (g/cm^3)
117-729A-						
1R-3, 10-12	3.10	1.621	64.3	40.7	2.650	0.962
2R-3, 40-42	6.60	1.611	66.1	42.0	2.664	0.934
2R-6, 40-42	11.10	1.605	67.1	42.8	2.705	0.918
3R-1, 70-72	13.40	1.706	60.1	36.1	2.624	1.090
3R-3, 70-72	16.40	1.700	61.1	36.8	2.696	1.074
3R-6, 60-62	20.80	1.770	56.2	32.5	2.636	1.194
4R-1, 60-62	22.90	1.725	61.1	36.3	2.574	1.099
4R-3, 41-43	25.71	1.796	55.8	31.8	2.711	1.224

Table 6. Summary of interstitial water geochemical data, Site 729.

Sample, interval (cm)	Depth (mbsf)	Vol. (mL)	pH	Alk. (mmol/L)	Sal. (g/kg)	Mg (mmol/L)	Ca (mmol/L)	Cl (mmol/L)	SO_4 (mmol/L)	PO_4 (μmol/L)	NH_4 (mmol/L)	SiO_2 (μmol/L)	Mg/Ca
117-729A-													
1R-2, 145-150	2.95	44	7.50	3.74	35.8	52.63	10.02	562	24.6	3.0	0.13	198	5.25
3R-4, 145-150	18.65	36	7.50	2.34	35.9	57.84	10.27	562	24.3	1.5	0.14	350	6.63

The shallow gradient of dissolved silica (~15 μmol/L/m) is among the lowest observed on the margin and indicates that the sediments at Site 729 are opal depleted.

ORGANIC GEOCHEMISTRY

The sediments recovered at Site 729 on the Oman margin were divided into two lithologic units. Eight physical property samples from Unit I, which consists of marly foraminifer-nannofossil oozes of Pleistocene age, were analyzed for their inorganic and organic carbon contents. The results are listed in Table 2. No gas pockets were observed.

SUMMARY AND CONCLUSIONS

Site 729 is situated in water depths of 1400 m on the Oman continental margin in the northwestern Indian Ocean. One of eight sites on the Arabian margin, Site 729 is located on a basement block of presumed ophiolitic origin. Adjacent ridges of ophiolite blocks confine a series of deep slope basins at various depth ranges on the Oman margin. Neogene sections in these basins have been the prime target of drilling on the margin during Leg 117. The objective of Site 729 was to recover the oldest sediments on one of the blocks, to penetrate to underlying strata, and possibly to recover igneous rock. Once the nature and age of the underlying rocks are established, we hoped to use our findings to delineate the tectonic history of the basement ridges and basins.

The main results obtained by drilling at Site 729 are:

1. Shallow-water carbonates underlie a condensed Quaternary hemipelagic sequence.
2. The shallow-water limestones at Site 729 are similar in character and facies to those recovered at Site 726, 60 km to the west on a second basement ridge.
3. The limestone sequence apparently is not cemented and/or dolomitized.

The sediments recovered at Site 729 were sudivided into two lithologic units. Unit I (0-26.3 mbsf) consists of marly, foraminifer-nannofossil oozes of Pleistocene age. Unit II, although very sparsely recovered, is believed to be composed of nummulitic shallow-water limestones with oncoliths, uncemented and very brittle. Our failure to recover any coherent portion of this unit down to a total depth of 109.1 mbsf led to the decision to abandon Site 729 without reaching basement for fear of drilling complications.

This site confirmed that the basement structures are overlain (probably unconformably) by shallow-water limestones of Paleogene(?) age. A similar sequence is observed on the island of Masirah to the north, where shallow-water limestones of Eocene age unconformably overlie the allochthonous ophiolite series.

REFERENCES

Flügel, E., 1982. *Microfacies Analysis of Limestones*: New York (Springer-Verlag).

Moseley, F., and Abbotts, I. L., 1979. The ophiolite melange of Masirah, Oman. *J. Geol. Soc. Lon.*, 136:713-724.

Takayama, T., and Sato, T., 1987. Coccolith biostratigraphy of the North Atlantic Ocean, Deep Sea Drilling Project Leg 94. *In* Ruddiman, W. F., Kidd, R. B., et al., *Init. Repts. DSDP*, 94, Pt. 2: Washington (U.S. Govt. Printing Office), 651-702.

Ms 117A-116

18. SITE 730[1]

Shipboard Scientific Party[2]

HOLE 730A

Date occupied: 29 September 1987

Date departed: 30 September 1987

Time on hole: 1 day, 10 hr, 45 min

Position: 17°43.885′N, 57°41.519′E

Water depth (sea level; corrected m, echo-sounding): 1065.8

Water depth (rig floor; corrected m, echo-sounding): 1076.3

Bottom felt (m, drill pipe): 1071.4

Penetration (m): 403.9

Number of cores: 42

Total length of cored section (m): 403.9

Total core recovered (m): 323.66

Core recovery (%): 80

Oldest sediment cored:
Depth sub-bottom (m): 403.9
Nature: Foraminifer nannofossil chalk
Age: late early Miocene (NN4)
Measured velocity (km/s): 2.03–2.06

Principal results: Site 730 is situated on the Oman continental margin near the bottom of the pronounced oxygen-minimum zone (OMZ) that impinges on the margin. The age of sediments and hiatuses, and the evolution of the sediment facies, were expected to be useful in reconstructing the subsidence as well as the erosional and tectonic history of the slope basins and the prominent basement ridges.

Some major findings at Site 730 include the identification of

1. a significant hiatus ranging in age from Pleistocene to upper Miocene;
2. the occurrence of siliceous sediments in the middle and upper Miocene that appear earlier here but are generally equivalent to the siliceous facies recovered on the Owen Ridge;
3. the appearance of *Globerigina bulloides*, an upwelling indicator, in the lower middle Miocene, which is earlier than its appearance on the Owen Ridge; and
4. the presence of slumps, faults, and turbidites in the middle Miocene that indicate tectonic instability of the marginal slope basins.

The sediments at Site 730 range from the Holocene to the late early Miocene in age and include one prominent hiatus. Opal deposition and upwelling began earlier on the Oman margin than it did on the offshore Owen Ridge. Site 730 also provided information about the tectonic stability and uplift history of the slope basins and their associated basement ridges.

BACKGROUND AND OBJECTIVES

Site 730 is located at 17°43.885′N and 57°41.519′E in a water depth of 1065.8 m and was the last site drilled on the Oman continental margin. It was selected during operations on Leg 117 and added to the operations schedule after Site 729 was abandoned due to hole conditions. Similar to previous Sites 723 and 727, Site 730 is located near the bottom of the pronounced OMZ that impinges on the margin (Fig. 1).

Site 730 is positioned to the east of a ridge that is presumably ophiolitic basement and separates the upper and lower slope sedimentary basins. The location of Site 730 is shown in Figures 2A and 2B, and its structural and depositional setting is shown in Figures 3A and 3B. The seismic reflection profiles (Figs. 3A and 3B) show that the sediments of the upper basin, which were previously drilled only 6 km to the west at Site 727, onlap eastward onto the ridge and are thinned and tilted by tectonic movement of the ridge. East of the basement ridge, the profiles reveal a prominent unconformity (at about 0.05 s) that truncates eastward-dipping reflectors that extend from about 0.5 to 0.20 s. The eastward-dipping reflectors extend downsection through a zone of relatively diffuse reflections (0.2–0.3 sbsf) to a thick zone of discontinuous dipping reflectors with variable amplitude from 0.3 to about 0.8 sbsf.

The eastward-dipping sediments are truncated to the east by a series of high-angle faults that form a series of steps extending down to the basin where Site 728 is located. These sediments are interpreted as the faulted and tilted remnants of a former slope basin. We moved upsection on the eastward-dipping reflectors and cored through the upper unconformity to recover older slope basin sediments. The ages of the sediments and the hiatus and the evolution of the sediment facies were expected to be useful in reconstructing the subsidence as well as the erosional and tectonic history of the slope basins and the prominent basement ridges.

Specific objectives for drilling at Site 730 were

1. to obtain a high-resolution record of older slope basin sediments that are associated with the proximal zone of the monsoonal upwelling system in order to establish long-term changes in monsoonal timing and intensity;
2. to provide another deep-water component of a depth transect that will be used to examine the organic-rich sedimentary facies of the margin and to establish their diagenetic history and relationship to the OMZ and its spatial variation through time; and
3. to provide constraints on the uplift and erosional history of the basement ridges and their intervening slope basins.

OPERATIONS

After the Science Operator gave us permission to drill a new site (Site 730), *JOIDES Resolution* left Site 729 at 2230 on 28 September 1987 and headed west to Site 730 with the seismic gear deployed. After a survey of 22 nmi, we located the site and dropped the beacon at 0545 hr on 22 September. By 0630 the mud line of Hole 730A was shot in water depths of 1065.8 m. According to the global positioning system (GPS), Site 730 is located at 17°43.885′N and 57°41.519′E; furthermore, we drilled only one hole here.

We recovered 104% of the cored interval with the advanced hydraulic piston corer (APC) system in Cores 117-730A-1H to

---

[1] Prell, W. L., Niitsuma, N., et al., 1989. *Proc. ODP, Init. Repts.*, 117: College Station, TX (Ocean Drilling Program).

[2] Shipboard Scientific Party is as given in the list of Participants preceding the contents.

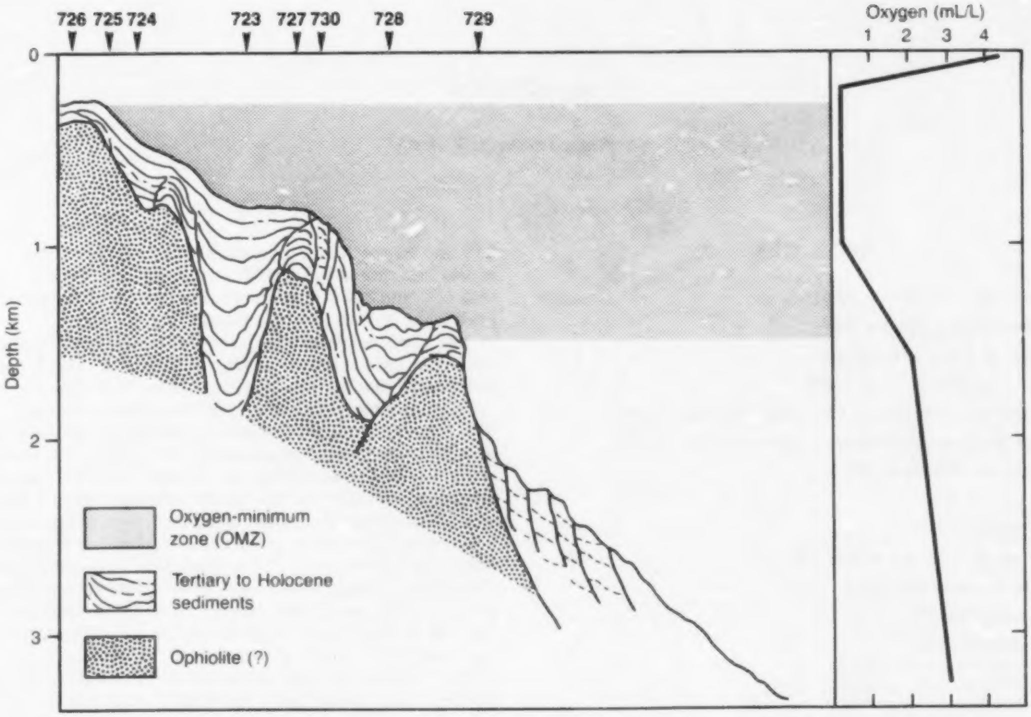

Figure 1. Structure of the Oman margin and the oxygen-minimum zone (OMZ). The schematic profile shows the series of basement ophiolite blocks and the sedimentary basins between them. The concentration of oxygen in the water column (RC2704, unpubl. data) defines the depth range of the OMZ and where it impinges on the margin.

-5H (0–46.3 mbsf). During retrieval of Core 117-730A-5H, a maximum overpull of 60,000 pounds was registered, and we switched the coring mode to the extended core barrel (XCB) system. The total depth of Hole 730A was reached at 403.9 mbsf, when the core barrel parted upon retrieval of Core 117-730A-43X. Recovery with the XCB in the interval from 46.3 to 403.9 mbsf was 75%, which gives an average recovery rate of 80% at Site 730 (Table 1). The long-standing recovery record of 3,841 m, established during Leg 108, was broken with a core recovery of 3,920.2 m during operations on Site 730.

The hole was displaced with heavy mud, and the ship was under way to Site 731 by 1630 hr on 30 September 1987.

LITHOSTRATIGRAPHY

Lithology

The sediments recovered at Site 730 are subdivided into three lithologic units (Fig. 4). Unit I is composed of a relatively thin interval of marly calcareous ooze of Quaternary age, and Unit II is composed of a diatom-bearing sequence of diatomaceous marly nannofossil ooze and diatomaceous silty clays that are late Miocene to middle Miocene age. Unit III, on the other hand, represents calcareous marly chalks and chalks which contain a significant amount of slump horizons and calcareous turbidites. Unit III comprises a lower Miocene to middle Miocene sequence. Table 2 lists the carbonate and organic carbon percentages determined for Site 730; Figure 5 shows the carbonate content of Site 730 sediments.

Unit I (Depth: 0–15.2 mbsf; Age: Holocene to Pleistocene)

Core 117-730A-1H through Section 117A-730A-2H-5, 90 cm.

Unit I is composed of marly to muddy nannofossil-foraminifer ooze and is terminated by an unconformity at 15.2 mbsf. The sediment is olive (5Y 4/3) to olive gray (5Y 5/2) in color and contains 20%–45% foraminifers and 15%–30% nannofossils. Fragments of bivalves and a solitary coral (Fig. 6) were found in this sequence. Authigenic dolomite rhombs occur in proportions of 1%–3%. The lower boundary of this sequence appears as a relatively dark-colored, 50-cm-thick, muddy and bioturbated layer. Sediment from this layer was found within burrows in a 60-cm-thick zone below this horizon (Fig. 7). Also, a single vertical burrow filled with the sediment of Unit I that was 2.25 m long and had a diameter of 2 cm appeared on the split face. Between 2 and 7 m above this major boundary, three horizons approximately 15 cm thick of predominantly vertical burrows were noted. These zones may represent minor hiatuses.

Unit II (Depth: 15.2–201.0 mbsf; Age: middle to late Miocene)

Sections 117-730A-2H-5, 90 cm, through 117-730A-21X, CC.

Unit II is composed of alternating relatively carbonate-rich and carbonate-poor layers which display 0.5–2-m-thick pairs of light and dark layers. Unit II is subdivided into three subunits, based on the presence of diatoms, the differences in carbonate

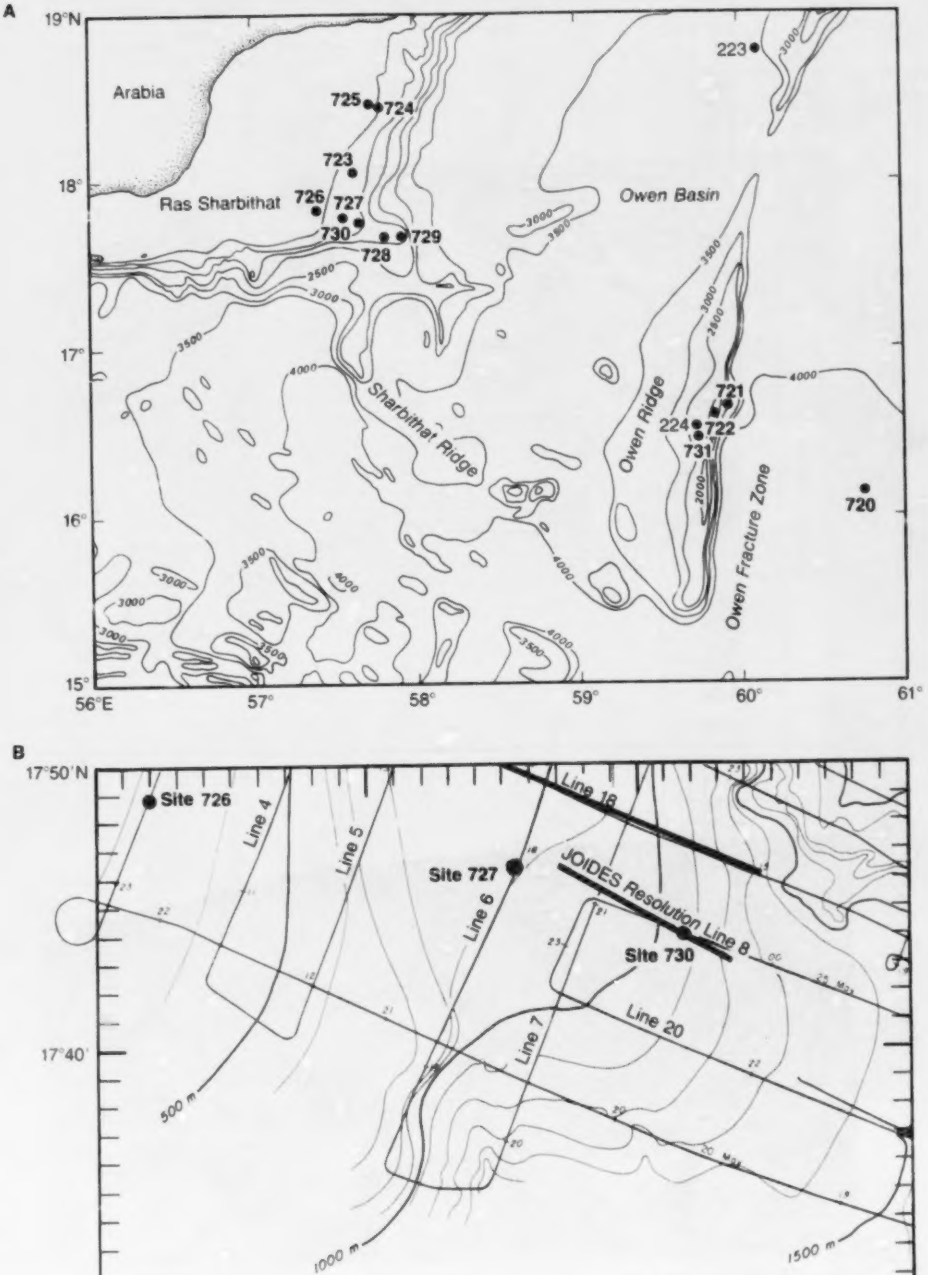
A
19°N
18°
17°
16°
15°
56°E
57°
58°
59°
60°
61°
Arabia
Ras Sharbithat
725
724
723
726
727
730
728
729
223
Owen Basin
Sharbithat Ridge
Owen Ridge
Owen Fracture Zone
721
224
722
731
720
2500
3000
3500
4000
2800
2000
B
17°50'N
17°40'
17°30'
57°20'E
58°30'
57°40'
57°50'
Site 726
Line 4
Line 5
Site 727
Line 6
Line 18
JOIDES Resolution Line 8
Site 730
Line 20
Line 7
500 m
1000 m
1500 m

Figure 2. **A.** Bathymetry of the Oman margin and the location of Site 730. **B.** Detailed location of Site 730 and the seismic profiles shown in Figure 3. Bathymetry data are from the site survey (RC2704, 1986).

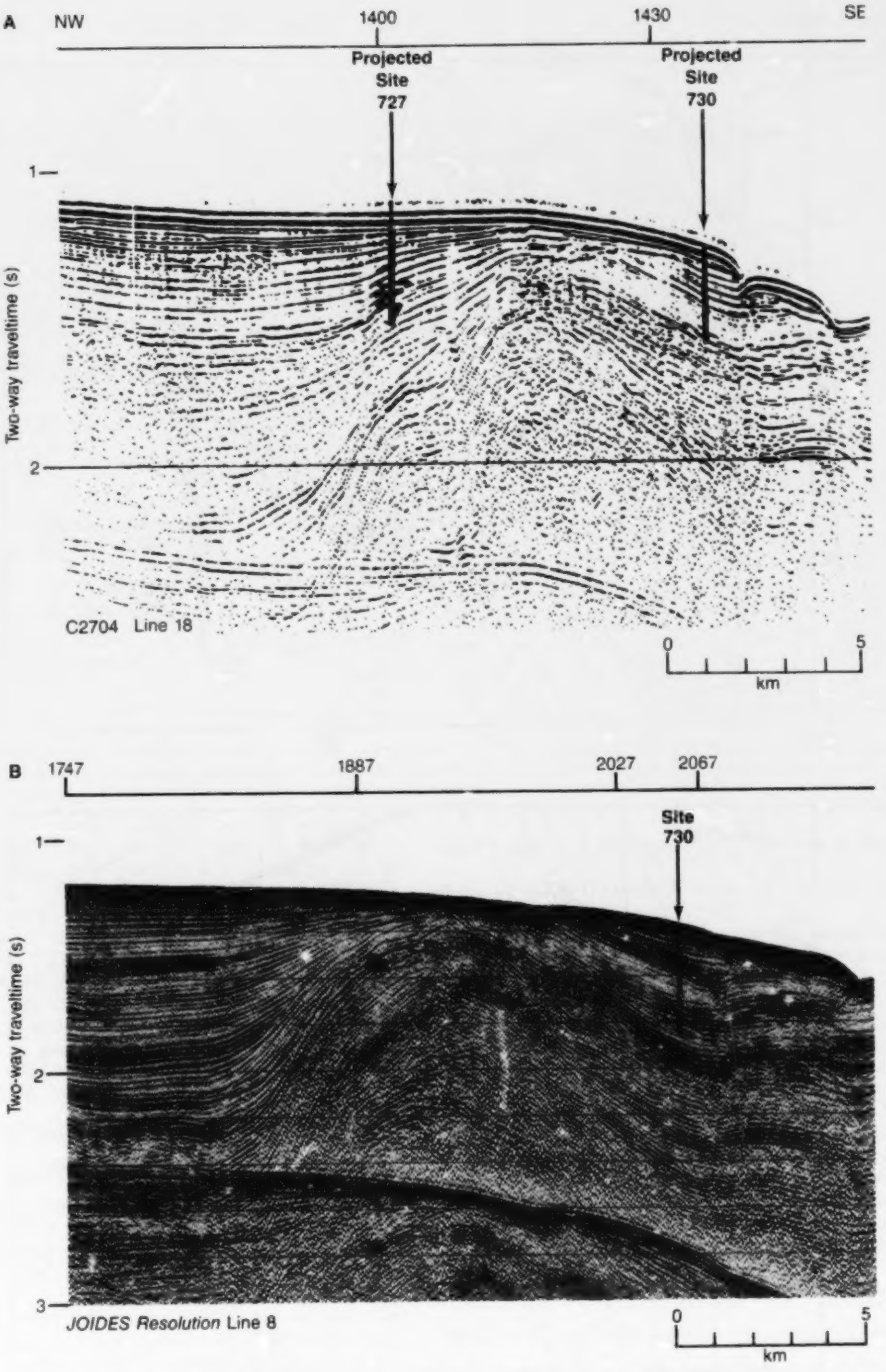

Figure 3. Single channel seismic (SCS) reflection profiles showing the structural and depositional setting of Site 730. A. RC2704 Line 8. B. *JOIDES Resolution* Line 18. Both profiles are perpendicular to the trend of the basin and show the bounding basement blocks and the dipping and truncated slope basin sediments.

Table 1. Coring summary, Site 730.

Core no.	Date (Sept. 1987)	Time (local)	Depth (mbsf)	Cored (m)	Recovered (m)	Recovery (%)
1H	29	1045	0-8.3	8.3	8.32	100.0
2H	29	1100	8.3-17.8	9.5	9.94	104.0
3H	29	1130	17.8-27.3	9.5	9.99	105.0
4H	29	1200	27.3-36.8	9.5	9.97	105.0
5H	29	1230	36.8-46.3	9.5	10.07	106.0
6X	29	1300	46.3-55.8	9.5	9.52	100.0
7X	29	1325	55.8-65.5	9.7	9.53	98.2
8X	29	1344	65.5-75.2	9.7	9.41	97.0
9X	29	1405	75.2-84.9	9.7	9.87	102.0
10X	29	1425	84.9-94.6	9.7	9.44	97.3
11X	29	1445	94.6-104.2	9.6	9.34	97.3
12X	29	1505	104.2-113.9	9.7	9.34	96.3
13X	29	1520	113.9-123.5	9.6	8.03	83.6
14X	29	1540	123.5-133.2	9.7	9.79	101.0
15X	29	1600	133.2-142.9	9.7	9.58	98.7
16X	29	1620	142.9-152.6	9.7	9.62	99.2
17X	29	1640	152.6-162.2	9.6	9.16	95.4
18X	29	1705	162.2-171.9	9.7	9.40	96.9
19X	29	1740	171.9-181.6	9.7	9.47	97.6
20X	29	1805	181.6-191.2	9.6	9.01	93.8
21X	29	1835	191.2-200.9	9.7	9.86	101.0
22X	29	1905	200.9-210.6	9.7	9.81	101.0
23X	29	1930	210.6-220.2	9.6	9.96	104.0
24X	29	1950	220.2-229.9	9.7	9.85	101.0
25X	29	2015	229.9-239.6	9.7	9.49	97.8
26X	29	2040	239.6-249.2	9.6	7.25	75.5
27X	29	2105	249.2-258.9	9.7	6.24	64.3
28X	29	2150	258.9-268.6	9.7	5.71	58.8
29X	29	2220	268.6-278.2	9.6	7.03	73.2
30X	29	2245	278.2-287.9	9.7	8.78	90.5
31X	29	2305	287.9-297.6	9.7	9.54	98.3
32X	29	2330	297.6-307.2	9.6	1.14	11.9
33X	30	0005	307.2-316.9	9.7	6.70	69.1
34X	30	0045	316.9-326.6	9.7	2.34	24.1
35X	30	0130	326.6-336.2	9.6	1.99	20.7
36X	30	0215	336.2-345.9	9.7	1.02	10.5
37X	30	0335	345.9-355.6	9.7	4.72	48.6
38X	30	0430	355.6-365.2	9.6	2.63	27.4
39X	30	0540	365.2-374.9	9.7	3.49	36.0
40X	30	0720	374.9-384.6	9.7	9.79	101.0
41X	30	0915	384.6-394.2	9.6	1.93	20.1
42X	30	1040	394.2-403.9	9.7	5.59	57.6
				403.9	323.66	

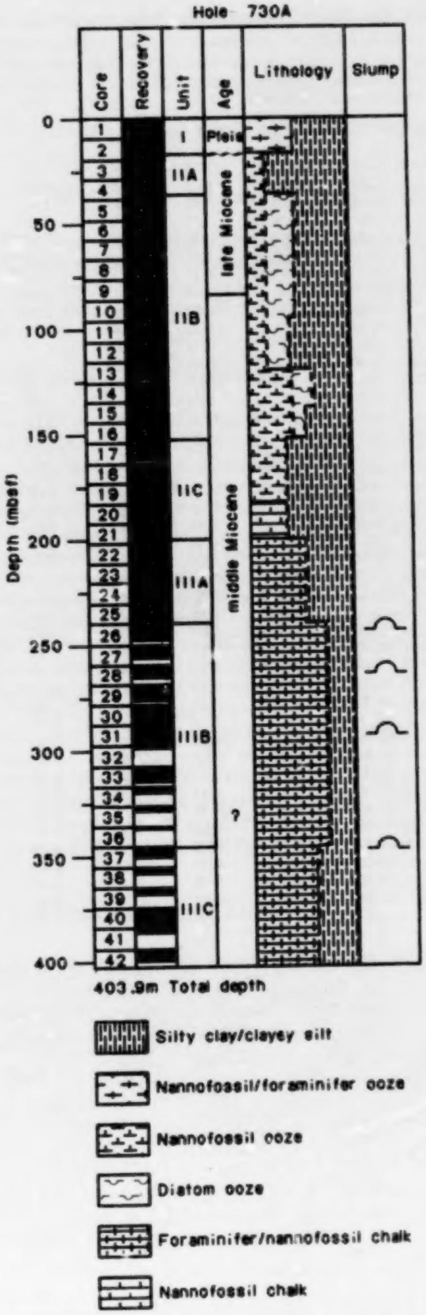
Hole 730A
Core
Recovery
Unit
Age
Lithology
Slump
Depth (mbsf)
0
50
100
150
200
250
300
350
400
1
2
3
4
5
6
7
8
9
10
11
12
13
14
15
16
17
18
19
20
21
22
23
24
25
26
27
28
29
30
31
32
33
34
35
36
37
38
39
40
41
42
I
IIA
IIB
IIC
IIIA
IIIB
IIIC
Pleis
late Miocene
middle Miocene
?
403.9m Total depth
Silty clay/clayey silt
Nannofossil/foraminifer ooze
Nannofossil ooze
Diatom ooze
Foraminifer/nannofossil chalk
Nannofossil chalk

Figure 4. Lithologic summary of Site 730. ⌒ = slump horizons.

and organic carbon content, and distinctions in trace fossil assemblages.

Subunit IIA (Depth: 15.2-33.2 mbsf)

Subunit IIA is composed of distinct alternations between carbonate-rich and carbonate-poor layers with pairs of light and dark layers about 60 cm thick. These sediments are olive (5Y 4/3) to dark olive (5Y 3/3) in color. Bioturbation mottling is abundant throughout this subunit and includes traces of *Zoophycus*. The carbonate content ranges from 30% to 40%, and organic carbon displays values from 1% to 1.5%.

Subunit IIB (Depth: 33.2-150.45 mbsf)

Subunit IIB is a dominantly carbonate-poor (Fig. 5), diatomaceous marly nannofossil ooze with alternating carbonate-rich and carbonate-poor layers that have an organic carbon content from 2% to 4% (Table 2). Colors range from olive gray (5Y 5/2) to olive (5Y 4/3) in the light layers and dark olive gray (5Y 3/2) in the dark layers.

Evidence of bioturbation is seen throughout Subunit IIB. Bioturbation displays the typical infill pattern of dark-colored sediment into the top of the light layers and of light-colored sediment into the top of the dark layers. Some of the dark-colored layers seem to have a slightly lesser degree of bioturbation when compared with the light-colored ones. Among the trace fossils observed are *Planolites*, *Teichichnus*, and *Chondrites*, whereas *Zoophycus* is relatively rare. The diatom content ranges between 10% and 40% (Fig. 8) and shows two major patterns in its distribution. On a large scale, the highest diatom content and the

Table 2. Calcium carbonate and organic carbon contents, Site 730.

Core, section, interval (cm)	Depth (mbsf)	Total carbon (%)	Inorganic carbon (%)	Organic carbon (%)	$CaCO_3$ (%)
117-730A-					
1H-3, 78-80	3.78	8.75	7.47	1.28	62.2
2H-2, 78-80	10.58	9.73	8.81	0.92	73.4
3H-2, 130-132	20.60	5.88	4.27	1.61	35.6
4H-2, 78-80	29.58	7.07	5.56	1.51	46.3
5H-2, 80-82	39.10	4.88	2.89	1.99	24.1
6X-2, 105-107	48.85	5.47	2.08	3.39	17.3
7X-1, 130-132	57.10	5.21	2.33	2.88	19.4
8X-2, 109-111	68.09	4.27	2.18	2.09	18.2
9X-2, 78-80	77.48	4.98	2.35	2.63	19.6
10X-2, 78-80	87.18	8.28	6.40	1.88	53.3
11X-2, 110-112	97.20	6.78	3.68	3.10	30.7
12X-2, 78-80	106.48	8.83	4.79	4.04	39.9
13X-2, 128-130	116.68	7.69	5.93	1.76	49.4
14X-2, 78-80	125.78	8.42	8.04	0.38	67.0
15X-2, 30-32	135.00	9.24	8.42	0.82	70.1
16X-2, 14-16	144.54	7.69	6.78	0.91	56.5
17X-2, 73-75	154.83	6.14	4.99	1.15	41.6
18X-2, 36-38	164.06	7.07	6.14	0.93	51.2
19X-2, 60-62	174.00	9.39	9.35	0.04	77.9
20X-2, 93-95	184.03	8.31	7.54	0.77	62.8
21X-2, 78-80	193.48	6.87	6.01	0.86	50.1
22X-2, 123-125	203.63	6.46	5.48	0.98	45.7
23X-2, 88-90	212.98	6.64	6.00	0.64	50.0
24X-2, 71-73	222.41	7.62	7.27	0.35	60.6
25X-2, 87-89	232.27	7.55	6.94	0.61	57.8
26X-4, 72-74	244.82	10.50	10.36	0.14	86.3
27X-4, 91-93	254.61	9.89	9.79	0.10	81.6
28X-4, 80-82	264.20	9.32	9.00	0.32	75.0
29X-3, 65-67	272.25	11.25	11.19	0.06	93.2
29X-5, 70-72	275.30	6.58	6.21	0.37	51.7
30X-6, 59-61	286.29	8.64	8.46	0.18	70.5
31X-1, 87-90	288.77	6.79	6.38	0.41	53.2
32X-1, 48-50	298.08	11.26	11.21	0.05	93.4
33X-1, 29-31	307.49	10.91	10.86	0.05	90.5
34X-1, 50-52	317.40	11.67	11.30	0.37	94.1
35X-1, 17-19	326.77	11.43	11.30	0.13	94.1
37X-1, 81-83	346.71	10.55	10.36	0.19	86.3
38X-2, 21-23	357.31	7.63	7.36	0.27	61.3
39X-1, 75-77	365.95	10.75	10.70	0.05	89.1
40X-2, 20-22	376.60	9.07	9.02	0.05	75.1
41X-1, 54-56	385.14	5.58	5.48	0.10	45.7
42X-1, 97-99	395.17	10.55	10.53	0.02	87.7

lowest carbonate content (Fig. 5) are observed in the upper part of Subunit IIB. On a scale of beds, dark layers are richer in diatoms and poorer in nannofossils compared with the lighter, carbonate-rich layers (Fig. 8). The difference in carbonate content between most light and dark layers is 10%–15%.

The lower interval of Subunit IIB (Sections 117-730A-13X-5, 20 cm, to 117-730A-16X-6; 120.1–150.5 mbsf) has a relatively high carbonate content (55%–75%; Fig. 5) with 5%–15% diatoms (Fig. 8). Sediment colors range from light gray (5Y 7/2) to light olive gray (5Y 6/2) to olive gray (5Y 5/2) to olive (5Y 4/3). The sediments display well-developed light and dark alterations which have an average thickness of 1.5 m. Mottling by bioturbation is well developed, and organic carbon values are relatively low (~ 1%).

Subunit IIC (Depth: 150.45–201.0 mbsf)

Subunit IIC shows a well-developed to indistinctly developed light-dark alternation on the scale of 1–1.5 m. Sediment colors range from light olive gray (5Y 6/2) to olive gray (5Y 5/2) to olive (5Y 5/3). Subunit IIC is composed of 35%–80% carbonate (with a mean of roughly 50%) and less than 5% foraminifers. Less than 2% of the components are diatoms, which distinguishes this subunit from the diatomaceous Subunit IIB. Bio-

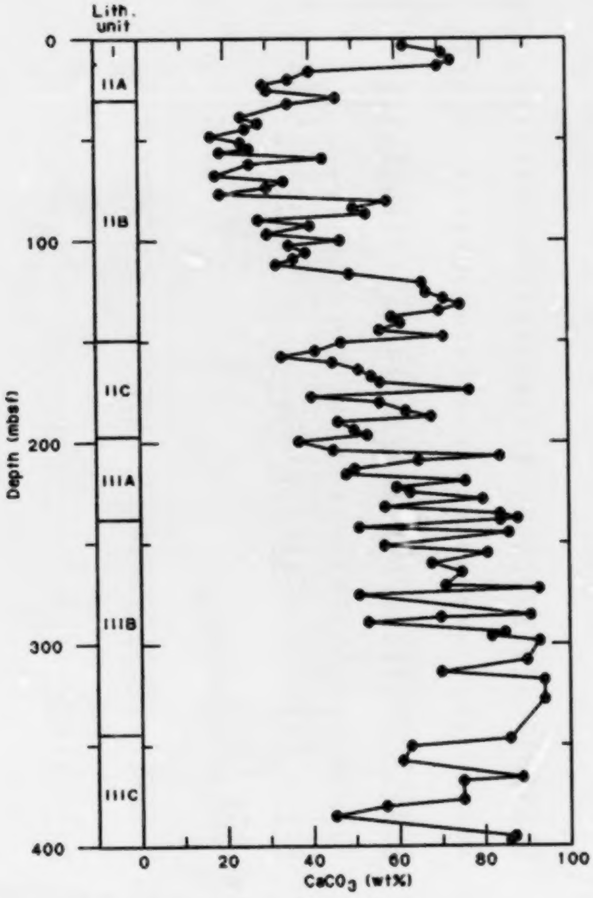

Figure 5. Carbonate contents of Hole 730A.

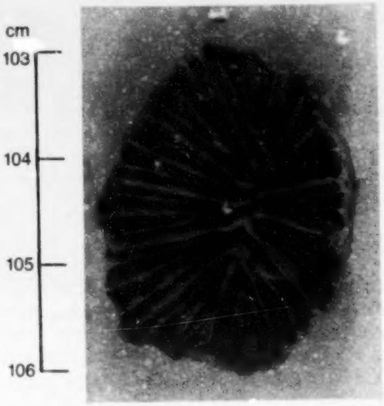

Figure 6. Solitary coral in Unit I (Section 117-730A-2H-1, 103–106 cm).

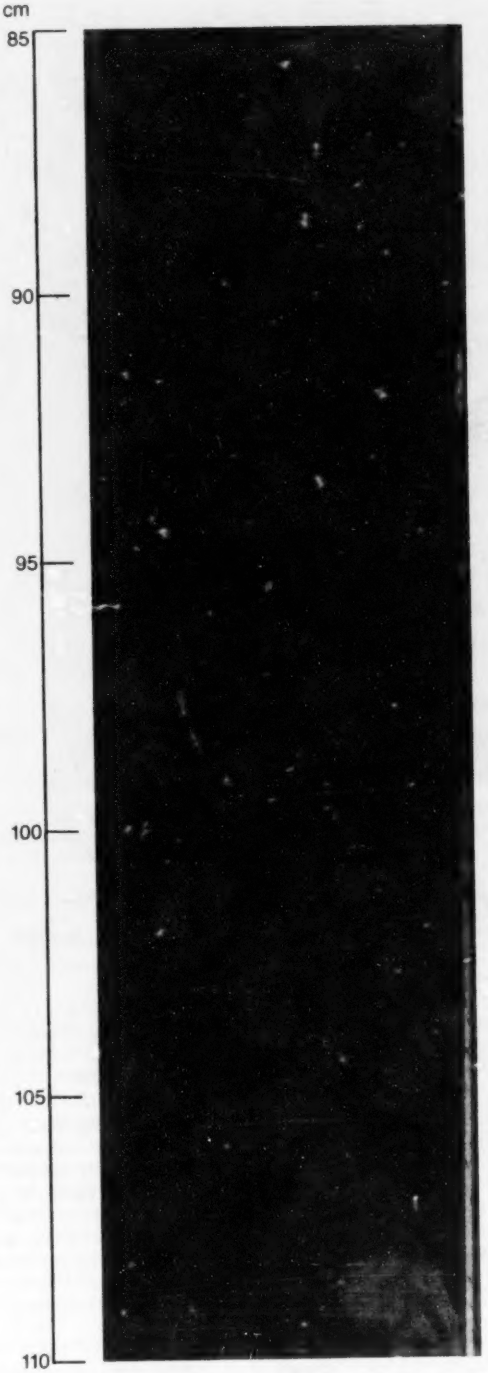

Figure 7. Bioturbated contact defining the unconformity between Units I and II (Section 117-730A-2H-5, 85–110 cm).

turbation and trace fossils are the same as described in Subunit IIB. The ooze-chalk transition occurs at roughly 180 mbsf. The first set of subvertical joints and features of other small offsets are found in Core 117-730A-20X (184.5 mbsf).

Unit III (Depth: 201.0–403.9 mbsf; Age: middle Miocene to early Miocene)

Sections 117-730A-21X, CC, through 117-730A-42X, CC

Unit III is composed of chalk with relatively high carbonate and foraminifer contents. It is subdivided into three subunits that are composed of two pelagic chalk sequences separated by a chalk layer that contains slump deposits and calcareous turbidites.

Subunit IIIA (Depth: 201.0–239.6 mbsf)

Subunit IIIA is comprised of foraminifer-rich marly chalk to chalk. Carbonate contents range from 50% to 90% (Fig. 5). The sequence displays a well-developed light-dark alternation spaced 0.9–1.5 m apart. Colors vary from light gray (5Y 7/2) to light olive gray (5Y 6/2) to olive gray (5Y 5/2) and are related to fluctuations in the carbonate content. Light-colored layers have a higher foraminifer (30%) and nannofossil (~70%) content and a lower amount of detrital calcite (roughly 5%) compared with the dark layers which possess foraminifer, nannofossil, and detrital calcite contents of about 5%, 50%, and 20%, respectively (Fig. 8). A trace fossil assemblage that is rich in *Zoophycus* is found throughout this subunit. Only one 5-cm-thick turbidite layer was encountered in Subunit IIIA (Core 117-730A-24X, 227.7 mbsf). It is composed mainly of tests of planktonic foraminifers and contains some pyrite grains at its base.

A number of subvertical joints several centimeters long that display small-scale offsets were found throughout this sequence. The most spectacular feature is a steeply dipping fault zone in Sample 117-730A-24X-4, 70 cm (225.4 mbsf). It displays several smeared faults, one of which may show reverse faulting (Figs. 9 and 10).

Subunit IIIB (Depth: 239.6–347.1 m)

Subunit IIIB is a pelagic foraminifer-bearing nannofossil chalk and marly chalk that is interrupted by slump horizons and calcareous turbidites; the latter are composed of foraminifer silts and sands. Four larger slump horizons, each roughly 1.5–2 m thick, are recognized in Cores 117-730A-26X (239.5–242.2 mbsf), -28X (262.4–263.8 mbsf), -31X (294–296.2 mbsf), and -37X (345.9–347.1 mbsf). The turbidites are interbedded with the pelagic chalks and the slump horizons and have an abundance of one to four turbidites per core. Turbidites are more common and have a larger grain size in the lower part of this section (Cores 117-730A-32X to -36X, 297.6–347.1 mbsf).

The colors of the chalks range from white (5Y 8/1) to light gray (5Y 7/2) to olive gray (5Y 5/2). Carbonate contents vary between 50% and 95% (Fig. 5), and organic carbon contents are below 1%. Foraminifers occur with an abundance of roughly 10% (Fig. 8).

The composition of the slump horizons is similar to the underlying and overlying chalks. The slumps are 1.5–2 m thick and often display laminated shear zones 20–50 cm thick at the base. This is followed by a zone composed of overturned folds separated by minor shear surfaces (Figs. 11, 12, and 13).

The frequency of the foraminifer-bearing turbidites as well as their content of large shallow-water foraminifers increases downsection. Turbidites in Cores 117-730A-25X to -28X (223–

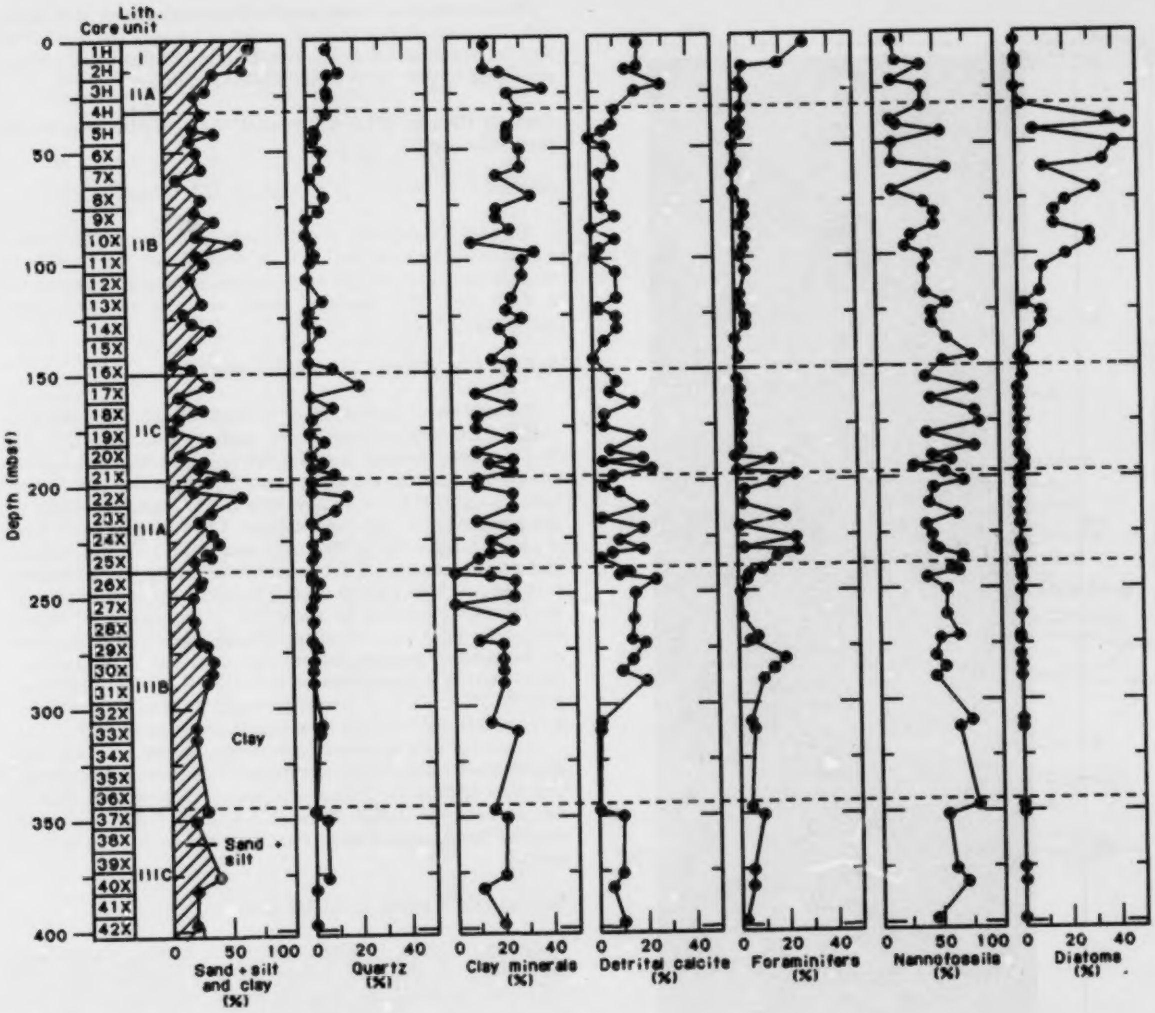

Figure 8. Smear slide data for Site 730, in area percent.

269 mbsf) are composed mainly of planktonic and minor amounts of benthic foraminifers and range from a few centimeters thick up to 20 cm thick. However, turbidites from Core 117-730A-29X to -36X (269–346 mbsf) are thicker and display a higher amount of large nummulitic foraminifers with a diameter of 0.5 cm. Those layers have a sharp base and show grading and imbrication.

In Core 117-730A-36X the nummulitic turbidites contain a small percentage of black, rounded clay intraclasts (0.5 cm diameter) with a few percentage of nannofossils that are the same age as the pelagic intervals. Thin sections show an isopachous rim cement in the chambers of planktonic foraminifers in Cores 117-730A-22X through -35X (259–326 mbsf). However, *Nummulitidae* of the turbidites, which are originally composed of high-magnesium calcite (Bathurst, 1975), display a much higher degree of dissolution and syntaxial calcite overgrowth.

Subunit IIIC (Depth: 347.1–403.9 m)

Subunit IIIC is composed of foraminifer-bearing marly nannofossil chalk to chalk and contains only a few turbidites in comparison to Subunit IIIB. The chalk exhibits a light-dark layering that ranges in color from white (5Y 8/1) to light gray (5Y 7/1) to olive gray (5Y 4/2). Some of the dark layers are thin and have a nodular appearance due to the presence of compacted, partly cemented burrows (Figs. 14 and 15). In the carbonate-rich layers, cross sections of less-compacted burrows show diffuse haloes, possibly of pyrite, which give the rock a spotty appearance (Fig. 14).

Only a few turbidites were encountered (Cores 117-730A-40X and -42X). They are between 10 and 35 cm thick and are composed entirely of benthic foraminifer sands.

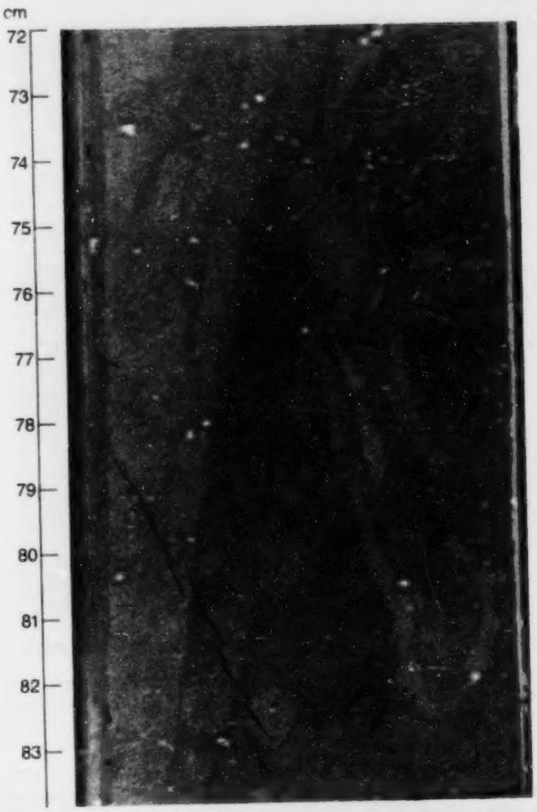

Figure 9. Steeply dipping faults with smeared fault planes. Offset of burrow in lower right corner seems to indicate reverse faulting in Subunit IIIA (Section 117-730A-24X-4, 72-84 cm).

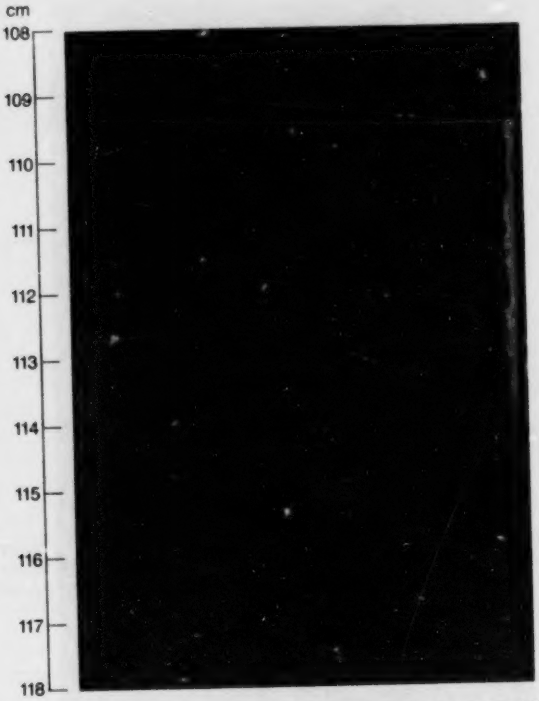

Figure 10. Set of subvertical joints that show a small offset in the bioturbation pattern of Subunit IIIA (Section 117-730A-24X-6, 108-118 cm).

Discussion

The following observations are worth mentioning regarding the environment and tectonic development of Site 730.

1. The turbidites found in Unit III indicate decreasing turbidite activity upsection. They document a trend from relatively proximal, thick, sandy turbidites with large shallow-water foraminifers toward thin, distal turbidites that contain dominantly planktonic and benthic foraminifers. This may indicate the gradual drowning of an isolated source area with abundant large-foraminifer sands and shallow-water environments. Other explanations may include the gradual uplifting of Site 730 to a more isolated position in the basin or other changes in paleogeography.
2. Slump horizons document tectonic activity during the lower part of the middle Miocene, which may indicate a syndepositional phase of steepening seafloor at Site 730. However, faulting may have continued from the middle Miocene into the Holocene.
3. The hiatus encountered between Unit I and Unit II indicates a considerable period of nondeposition and supposed erosion that ended in the Pleistocene. The hiatus may document the generation of relief combined with tectonic uplift.
4. The carbonate curve at Site 730 displays a generally decreasing trend through the early to late Miocene. The curve shows the change from relatively high values (85%) at the end of the early Miocene to relatively low values (30%-50%) at the beginning of the late Miocene. This trend was also noticed for the Owen Ridge sites (Sites 721, 722, and 731). It documents the transition from an environment that is dominated by the production of calcareous nannofossils to a system that is dominated by terrigenous input.

BIOSTRATIGRAPHY

Introduction

Site 730 is located in water depths of 1065 m on the Oman margin to the east of a ridge that separates two of the sedimentary basins on the upper slope. Abundant calcareous nannofossils and benthic foraminifers with good preservation are found in the uppermost three samples (0-27.3 mbsf). Below this level down to 258.9 mbsf, benthic foraminifers are few to rare, but with good to moderate preservation. Nannofossils are abundant, usually with moderate preservation. Below 258.9 mbsf benthic foraminifers are few to rare, but the preservation has been affected by calcitic recrystallization and lithification. Nannofossils in this interval are heavily overgrown, especially the asteroliths. Planktonic foraminifers are abundant with good preservation in the uppermost sample (8.3 mbsf). In Cores 117-730A-2H through -16X (17.8-152.6 mbsf), planktonic foraminifers are few and poorly preserved. Below 152.6 mbsf their abundance increases and preservation improves to moderate and good.

Siliceous microfossils are absent in the uppermost three core-catcher samples (0-27.3 mbsf). From 36.8 to 191.2 mbsf radiolarians are common and well preserved. From 200.9 to 278.2

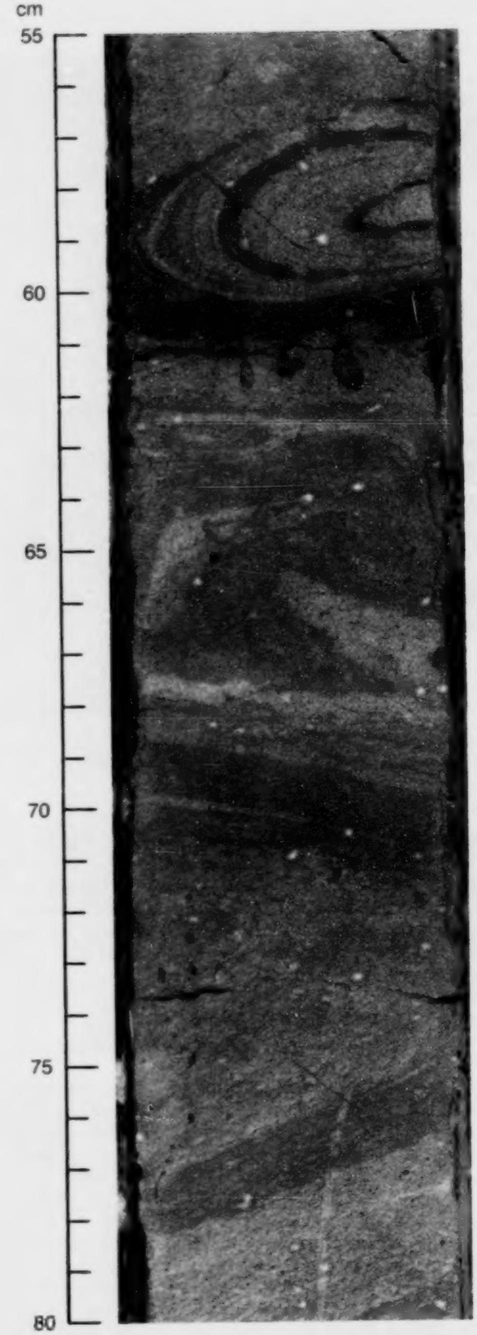

Figure 11. Upper portion of a slump horizon displaying overturned folds in Subunit IIIB (Section 117-730A-26X-1, 55–80 cm).

mbsf their abundance decreases and preservation is moderate. Diatoms and sponge spicules are present in the interval of radiolarian occurrences; below 278.2 mbsf no siliceous microfossils were found. A synopsis of microfossil zonations is presented in Figure 16.

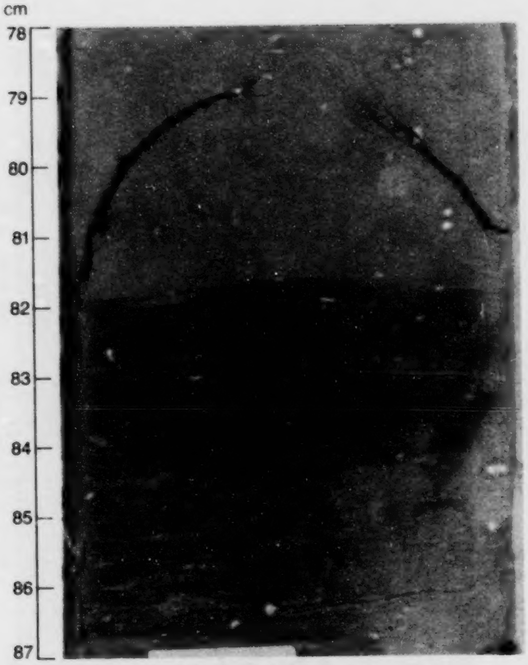

Figure 12. Shear horizons in the lower portion of the slump depicted in Figure 11. The horizon shows an offset in the bioturbation pattern of Subunit IIIB (Section 117-730A-26X-2, 78–87 cm).

A pronounced hiatus was recognized between 15.35 and 17.8 mbsf. Most of the Pleistocene, all of the Pliocene, and part of the upper Miocene are missing. A plot of faunal datum levels vs. depth below sea floor is presented in Figure 17; for a detailed listing of these data points see Table 3.

Planktonic Foraminifers

We studied planktonic foraminifers in core-catcher samples from Hole 730A. The first sample (117-730A-1H, CC; 8.3 mbsf) contains a highly diverse Pleistocene fauna (N23), and the preservation of tests is good.

A few moderately well-preserved specimens were found in Samples 117-730A-2H, CC, through 117-730A-16X, CC (17.8–152.6 mbsf). This part of the recovered sequence is assigned to the upper and middle Miocene and points to a hiatus somewhere in Core 117-730A-2H. Sample 117-730A-2H, CC, yields rare occurrences of *Globorotalia tumida plesiotumida* or *Globorotalia tumida merotumida*, which are zonal markers for N16–N17 (upper Miocene). Samples 117-730A-3X, CC, through 117-730A-9X, CC (27.3–86.4), are barren. Zones N13–N14 (middle Miocene), exemplified by the presence of *Globorotalia siakensis*, were recognized in Samples 117-730A-13X, CC, through 117-730A-16X, CC (123.5–154.0 mbsf). No attempts were made to discern the zonal boundary between N13 and N14, which is defined by the first appearance of *Globigerinoides nepenthes*, because this species was only found in highly scattered occurrences.

Below Sample 117-730A-16X, CC (152.6 mbsf), planktonic foraminifers are common to abundant and moderately well preserved. The *Globorotalia fohsi* evolutionary lineage (Zones N10–N12) was found in Samples 117-730A-17X, CC, through 117-730A-31X, CC (162.2–297.6 mbsf). The zonal boundaries are tentative because they are based on first appearances of the

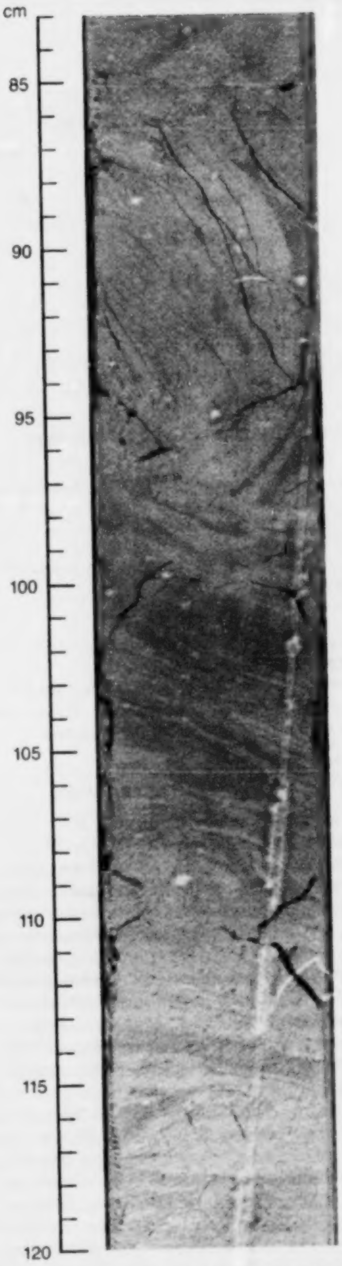

Figure 13. Upper portion of slump horizon displaying shear surfaces and overturned folds in Subunit IIIB (Section 117-730A-31X-5, 83–120 cm).

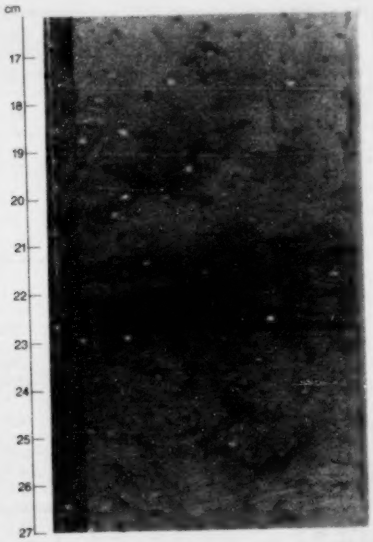

Figure 14. Diagenetic alternations of bedding chalk. Haloed, little compacted burrows in the chalk layers are contrasted by compacted nodular burrows in the clay-rich layers of Subunit IIIC (Section 117-730A-40X-1, 16–27 cm).

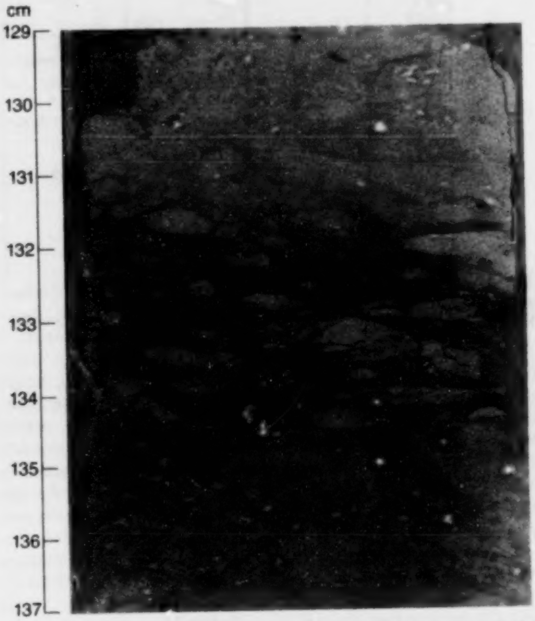

Figure 15. Nodular character of a relatively clay-rich layer that exhibits flattened burrow cross sections with high carbonate content in Subunit IIIC (Section 117-730A-40X-6, 129–137 cm).

morphologic transitional series from *Globorotalia peripheronda* to fully developed *Globorotalia fohsi*. The first appearance of *Orbulina universa*, which marks the lower limit of Zone N9, was found in Sample 117-730A-31X, CC (297.6 mbsf).

The basal part of the recovered section, Samples 117-730A-32X, CC, through 117-730A-42X, CC (307.2–403.9 mbsf), is referred to lower Miocene Zone N8. *Globigerinoides sicanus* is present and *Orbulina universa* is absent in these sediments.

Benthic Foraminifers

The abundance of benthic foraminifers in core-catcher samples from Hole 730A is high only in the upper three samples

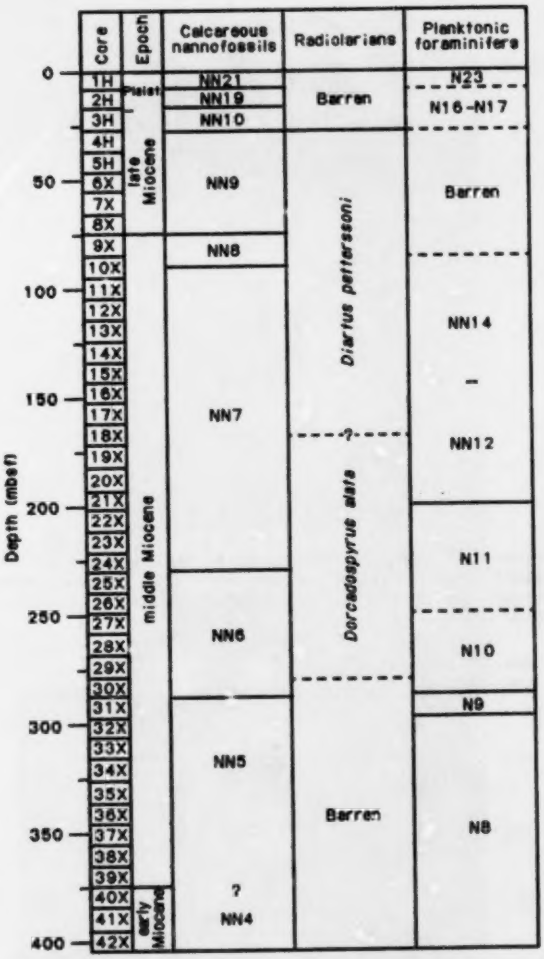

Figure 16. Correlation of planktonic microfossil zones in Hole 730A.

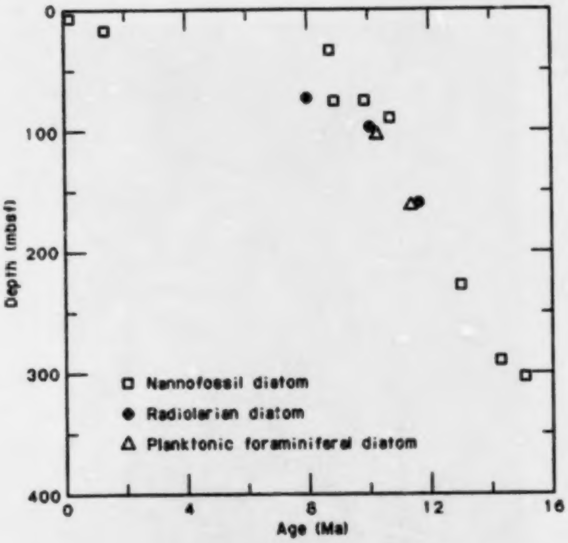

Figure 17. Age-depth plot for Hole 730A. For a detailed listing of the events, see Table 3.

(117-730A-1H, CC, through -3H, CC; 8.3-27.3 mbsf), which corresponds approximately to the interval of marly nannofossil ooze (Unit I). Below Sample 117-730A-3H, CC (27.3 mbsf), abundance ranges from few to rare, and preservation is good to moderate for most of the sequence. Calcitic recrystallization in combination with lithification of the sediments below Sample 117-730A-27X, CC (258.9 mbsf), affects preservation in the part of the sequence studied.

The planktonic/benthic (P/B) ratio is variable. It decreases gradually from more than 99 in the uppermost sample (117-730A-1H, CC; 8.3 mbsf) to 0 in Sample 117-730A-6X, CC (55.8 mbsf); it remains low down to Sample 117-730A-19X, CC (181.6 mbsf). An exception for an excursion exists up to about 90 around 100 mbsf. Below Sample 117-730A-19X, CC (181.6 mbsf), the P/B ratio is consistently higher than 90.

The benthic foraminiferal fauna of Site 730 is quite uniform. An upper middle bathyal faunal assemblage is found throughout the sequence. It is characterized by the presence of *Bulimina truncana, Cibicidoides wuellerstorfi, Hoeglundina elegans, Melonis barleeanum,* and *Pullenia bulloides* in most samples. Species which are present in lower relative abundance are *Bulimina mexicana, Sigmoilinopsis schlumbergeri, Sphaeroidina bulloides,* and *Uvigerina auberiana.*

Below Sample 117-730A-24X, CC (229.9 mbsf), thick turbidite sequences occur which contain such shallow-water species as *Amphistegina* spp. and *Elphidium macellum*; nummulitids are common as well.

Calcareous Nannofossils

Nannofossils are abundant throughout Hole 730A. Sediments down to Sample 117-730A-1H, CC (8.3 mbsf), contain abundant specimens of *Emiliania huxleyi* and are assigned to Zone NN21 (uppermost Pleistocene to Holocene). The presence of *Pseudoemiliania lacunosa* and *Gephyrocapsa caribbeanica* in Sample 117-730A-2H-5, 105-106 cm, assigns these sediments to the Pleistocene part of Zone NN19. The presence of *Sphenolithus abies, Reticulofenestra pseudoumbilica,* and such discoasters as *D. brouweri, D. pentaradiatus, D. neohamatus,* and *D. pansus* places Sample 117-730A-2H, CC, in Zone NN10 (upper Miocene). Therefore, the lower part of Zone NN19 and Zones NN18 through NN11 are missing somewhere between 15.35 mbsf and 17.8 mbsf.

Samples down to 117-730A-4H-3, 105-106 cm (31.35 mbsf), contain the same species as in 117-730A-2H, CC, together with *Discoaster calcaris* and *D. bollii* and may also be assigned to Zone NN10. Nannofossils exhibit good preservation in the three uppermost samples. The top of *Discoaster hamatus* occurs between Samples 117-730A-4H-3, 105-106 cm, and 117-730A-4H-5, 105-106 cm, and marks the top of Zone NN9. The total range of *D. hamatus* defines Zone NN9. The bottom of this fossil occurs between Samples 117-730A-8X, CC, and 117-730A-9X-1, 105-106 cm (75.20-76.25 mbsf). In this zone, sporadic occurrences of *Catinaster calyculus* and *C. coalitus* are recognized.

Sediments below 76.25 mbsf down to the bottom of *Catinaster coalitus* are assigned to middle Miocene Zone NN8. Samples 117-730A-10X-5, 105-106 cm, down to 117-730A-24X-5, 105-106 cm (91.95-227.25 mbsf), belong to Zone NN7 (middle Miocene) based on the absence of *C. coalitus* and the presence of *Discoaster kugleri.* The age of the boundary between Zones NN8

Table 3. Stratigraphic listing of faunal events for Hole 730A.

Event	Core, section, interval (cm)	Depth (mbsf)	Age (Ma)	Source of age
B *Emiliania huxleyi*	117-730A-1H, CC	8.30	0.19	3
	117-730A-2H-1, 117–118	8.82		
B *Geophyrocapsa* "large"[a]	117-730A-2H-5, 105–106	15.35	[b]1.36	4
	117-730A-2H, CC	17.80		
T *Discoaster hamatus*	117-730A-4H-3, 105–106	31.35	8.85	6
	117-730A-4H-5, 105–106	34.35		
T *Stichocorys wolffii*	117-730A-8X-4, 85–87	70.85	[c]8.0–8.2	2
	117-730A-8X, CC	75.20		
T *Catinaster coalitus*	117-730A-8X, CC	75.20	9.0	6
	117-730A-9X-1, 105–106	76.25		
B *Discoaster hamatus*	117-730A-8X, CC	75.20	10.0	6
	117-730A-9X-1, 105–106	76.25		
B *Catinaster coalitus*[d]	117-730A-10X-3, 105–106	88.95	10.8	6
	117-730A-10X-5, 105–106	91.95		
T *Cyrtocapsella japonica*	117-730A-10X, CC	94.60	10.0–10.3	2
	117-730A-11X-4, 85–87	99.95		
T *Globorotalia mayeri*	117-730A-11X-4, 65–67	99.75	10.4	6
	117-730A-11X, CC	104.25		
T *Lithopera thornburgi*	117-730A-16X, CC	152.60		
	117-730A-17X-4, 85–87	157.65		
T *Cyrtocapsella cornuta*	117-730A-17X-4, 85–87	157.95	11.6–11.9	2
	117-730A-17X, CC	162.20		
T *Globorotalia fohsi*	117-730A-17X, CC	162.20	11.5	6
	117-730A-18X-2, 65–67	164.35		
B *Diartus petterssoni*	117-730A-18X-4, 85–87	167.55		
	117-730A-18X, CC	171.90		
T *Lithopera renzae*	117-730A-19X-4, 85–87	177.25		
	117-730A-19X, CC	181.60		
B *Discoaster kugleri*	117-730A-24X-5, 105–106	227.25	13.1	6
	117-730A-24X, CC	229.90		
T *Sphenolithus heteromorphus*	117-730A-30X, CC	287.90	14.4	6
	117-730A-31X-1, 105–106	288.95		
B *Orbulina universa*	117-730A-31X-3, 65–67	291.55	15.2	6
	117-730A-31X, CC	297.60		

Note: T = upper limit of event and B = lower limit. Sources of ages are: 2 = Johnson and Nigrini, 1985; 3 = oxygen isotope data for Site 723 (N. Niitsuma, unpubl. data); 4 = Takayama and Sato, 1987; and 6 = Berggren et al., 1985.

[a] Long axis greater than 6 μm.

[b] North Atlantic data.

[c] Pacific Ocean data.

[d] Should be lower.

and NN7 was estimated by Berggren et al. (1985) as 10.8 Ma. In Hole 730A, this datum coincides with the highest occurrence of *Coccolithus miopelagicus*. Samples 117-730A-24X, CC, through 117-730A-30X, CC (229.9–287.9 mbsf), belong to Zone NN6 (middle Miocene) based on the absence of *Discoaster kugleri* and *Sphenolithus heteromorphus*.

Bukry's (1973) zonation shows the last appearance datum (LAD) of *Cyclicargolithus floridanus* coinciding with the first appearance datum (FAD) of *Discoaster kugleri* (NN7/NN6 boundary). According to Bukry (1975), however, the LAD of *C. floridanus*, which is often used as a surrogate criterion for the NN7/NN6 boundary, is within Zone NN7 as defined by the FAD of *D. kugleri* in some areas, including Site 563 (North Atlantic). In the present hole, however, the LAD of *C. floridanus* is clearly recognizable and coincides with the FAD of *D. kugleri*. Nannofossil preservation ranges from good to poor, with moderate preservation between 36.8 and 249.2 mbsf in most samples.

Below 249.2 mbsf the preservation of the coccoliths becomes abruptly poorer and almost all specimens, especially asteroliths, are heavily overgrown. Below 287.9 mbsf, sediments down to the bottom of the hole (Samples 117-730A-31X, CC, through -42X, CC) contain *Sphenolithus heteromorphus*, together with *C. floridanus* and *Discoaster deflandrei*. *Discoaster druggii* and sporadic occurrences of *Hayaster perplexus* are also recognized. Because *Helicosphaera ampliaperta* is not recognized in this hole, these sediments are assigned to Zones NN5 and NN4 (middle to lower Miocene).

Radiolarians

Radiolarians are common and well preserved in the samples from Cores 117-730A-4H through -20X (36.8–191.2 mbsf). They decrease in abundance, and preservation is only moderate between Samples 117-730A-21X, CC, and 117-730A-25X-4, 85–87 cm (200.9–235.25 mbsf). From Sample 117-730A-25X, CC, to Sample 117-730A-29X, CC (239.6–278.2 mbsf), there is a further decrease in abundance and even more deterioration in the preservation state. Both above and below these intervals, the recovered sediments are barren of siliceous microfossils. Diatoms and sponge spicules are common to abundant thoughout the silica-rich interval. Sponge spicules are particularly robust, but they do show pitting due to dissolution in the sections where radiolarians are less abundant.

From Samples 117-730A-4H-4, 85–87 cm, to 117-730A-18X-4, 85–87 cm (32.65–167.55 mbsf), the radiolarians belong to the *Diartus petterssoni* Zone. The FAD of *D. petterssoni* is in Sample 117-730A-18X-4, 85–87 cm, and this event normally marks the *D. petterssoni*/*Dorcadospyris alata* zonal boundary. Thus, the sediments from Samples 117-730A-18X, CC, to 117-730A-29X, CC (171.9–278.2 mbsf), appear to belong to the *D. alata* Zone. However, the LAD of *Liriospyris parkeri* and *D. alata* should also coincide approximately with this boundary, but we observed neither of these species. In addition, placement of the *D. petterssoni*/*D. alata* boundary between Samples 117-730A-18X-4, 85–87 cm, and 117-730A-18X, CC (168.35–171.9 mbsf), is inconsistent with the nannofossil zonal data.

Paleoenvironmental Implications

The occurrence of rare *Globigerina bulloides* specimens and the first appearance of biogenic silica during the middle Miocene indicates that upwelling conditions were present in this area at that time. These conditions may be related to the onset of the monsoon system. However, a full analysis of the planktonic foraminiferal and radiolarian faunas found at Oman margin Site 730 is necessary to establish the onset and variations in the monsoon system during the Miocene.

PALEOMAGNETISM

Magnetic Measurements

We measured the archive halves of Cores 117-730A-1H through -5H on the pass-through cryogenic magnetometer after alternating-field (AF) demagnetization at 5 mT. The records were again dominated by high scatter and incompletely removed coring overprints, and no useful information was obtaine[illegible]igure 18 shows the results of MINISPIN measurements of [illegible] samples (after AF demagnetization at 5 or 10 mT) for the [illegible]val from 0 to 150 mbsf. Only samples with circular standard [illegible]viations (CSDs) of <40° are plotted.

A major hiatus occurs within Core 117-730A-2H (8.3–17.8 mbsf) separating sediments of Pleistocene and late Miocene age. Intensities average around 0.5 mA/m over the interval from 40 to 110 mbsf and are slightly lower both above and below. The most striking aspect of the records is the long normally magnetized interval between about 50 and 110 mbsf, spanning nannofossil Zones NN9 through NN7; the upper part may be correlative with Chron C5 (Chronozone 11).

Magnetic Susceptibility

The volume magnetic susceptibility of Hole 730A sediments was measured on the Bartington Susceptibility Meter (Model MS1) and a whole-core, pass-through sensor coil at the 0.1 sen-

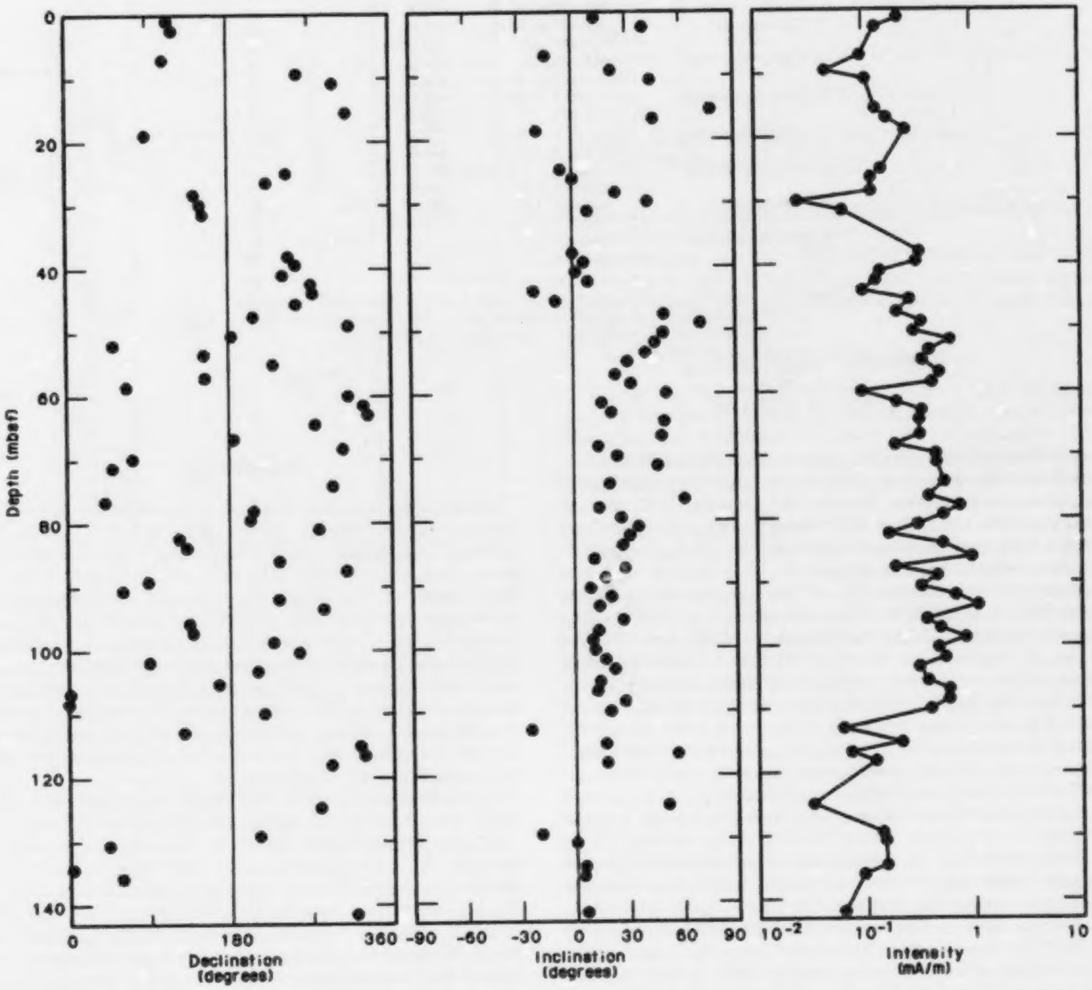

Figure 18. Declination, inclination, and intensity for discrete samples from Hole 730A, after 5–10 mT demagnetization. Only samples with circular standard deviations (CSDs) of <40° are plotted.

sitivity and 0.47 kHz low-frequency settings. Hole 730A was cored with the APC to Core 117-730A-5H (46.3 mbsf) and cored in the XCB mode from Cores 117-730A-6X to -42X (403.9 mbsf). Measurements were performed at 8-cm intervals. Susceptibility data vary from ~25 to 140 × 10^{-6} SI units (Fig. 19).

Sedimentological investigations have indicated three lithologic units (see "Lithostratigraphy" section, this chapter). Unit I consists of a marly nannofossil ooze that extends from the top to 15.2 mbsf. A disconformable hiatus spanning nannofossil Zones NN21–NN10 was found in Core 117-730A-2H at the base of Unit I (see "Biostratigraphy" section, this chapter). Although the hiatus is not conspicuous sedimentologically, the susceptibility data are very high (~200 × 10^{-6} SI units) over the interval containing the hiatus horizon. The susceptibility peak is centered at Sample 117-730A-2H-5, 70 cm, or 15.00 mbsf.

Although core-top pipe rust contamination is apparent in most XCB cores, this interval of high susceptibility is within Core 117-730A-2H; therefore, the data most probably reflect real changes in the concentration and grain size of ferrimagnetic grains. A tentative conclusion, which is consistent with the visual descriptions of Core 117-730A-2H, is that this horizon is a coarse lag-type deposit from a previous erosional or failure event.

Unit II extends from 15.2 to 201.0 mbsf and comprises marly nannofossil oozes and diatomaceous silty clays of late to middle Miocene age. Most of the sediments in Unit II were recovered by XCB coring, and rust contamination is common, as evidenced by the regular ~10-m spikes. Structure within the susceptibility data of Unit II is apparent, but sedimentological interpretations are wanting in the absence of detailed data. Preliminary comparisons of the susceptibility data and the visual core descriptions did not indicate any simple associations.

Unit III extends from 201.0 to 403.9 mbsf and is dominated by foraminifer-bearing nannofossil chalks. The susceptibility data of Unit III are somewhat lower in value than those of Unit II. However, as with Unit II, we could establish no simple relationships between susceptibility data and core descriptions.

ACCUMULATION RATES

Sedimentation rates for Site 730 are based on the biostratigraphic datum levels listed in Table 3. We recognized a pronounced hiatus between 15 and 18 mbsf, which represents almost 8 m.y. of missing section (see "Biostratigraphy" section, this chapter). Because of poor stratigraphic control above the hiatus, only the FAD of *Emiliania huxleyi* was used to estimate the mean rate of sedimentation in the late Pleistocene (44 m/m.y.; Fig. 20). Based on a best fit to the biostratigraphic datums, the mean sedimentation rate was 49 m/m.y. in the interval from 8 to 15 Ma (Fig. 20). Therefore, the late Pleistocene and Miocene rates of sediment accumulation at Site 730 are similar. These values are also similar to rates determined in pelagic sediments of comparable age on the Owen Ridge (see Owen Ridge site chapters, this volume).

PHYSICAL PROPERTIES

Introduction

Physical properties measured on discrete samples of sediments recovered from Site 730 include index properties (wet-bulk density, porosity, water content, and grain density), compressional-wave velocity, and vane shear strength. The properties that were determined for discrete samples are listed in Table 4. Wet-bulk density and compressional-wave velocity were measured on all whole-round core sections longer than 80 cm using the GRAPE and *P*-wave logging systems. All techniques and equipment used are described in the "Explanatory Notes" (this volume).

The relatively high recovery rate at Site 730 provided a high sampling frequency. With this large data set, we could distinguish the boundaries between the three lithologic units identified at Site 730 by the transitions in the physical properties profiles.

Index Properties

Unit I

Relatively little change in index properties is displayed in the thin interval of marly nannofossil foraminifer ooze that makes up Unit I (0–15.2 mbsf; Fig. 21). Average values for porosity, water content, wet-bulk density, and grain density in Unit I are 63%, 39%, 1.67 g/cm^3, and 2.66 g/cm^3, respectively.

Unit II

Unit II (15.2–201.0 mbsf) is characterized by the occurrence of high porosity and water content and low grain and wet-bulk density in association with an increased abundance of siliceous microfossils and organic matter. Transitions in the index property profiles mark the boundaries between nannofossil silty clay to marly nannofossil ooze (Subunit IIA), diatomaceous marly nannofossil ooze (Subunit IIB), and marly nannofossil ooze (Subunit IIC).

Index-property profiles for Subunit IIA (15.2–33.2 mbsf) show increases in porosity from 57% to 72% and in water content from 33% to 49%; wet-bulk density, on the other hand, decreases from 1.76 to 1.50 g/cm^3 with increasing depth (Fig. 21). These changes reflect the downsection decrease in grain size in this interval. Grain density is 2.60 g/cm^3 at the top and bottom of Subunit IIA; however, it decreases from the top of Subunit IIA to a minimum value of 2.48 g/cm^3 at 26.1 mbsf (Fig. 21). The low grain density at this depth coincides with a minimum in the calcium carbonate percentage (Fig. 5).

Subunit IIB (33.2–150.45 mbsf) contains sediment with the highest porosity and water content and lowest wet-bulk density and grain density at Site 730. Between 33.2 and 62.6 mbsf, porosity and water content are essentially constant, with average values of 78% and 58%, respectively. Grain density varies from 2.45 and 2.22 g/cm^3 in this interval and is accompanied by variations in wet-bulk density from 1.41 to 1.33 g/cm^3 (Fig. 21). The interval from 33.2 to 62.6 mbsf contains the highest abundance of diatoms and radiolarians at Site 730 (see "Biostratigraphy" section, this chapter) and organic carbon percentages as high as 3.39% (see "Organic Geochemistry" section, this chapter).

Because of their low grain densities and high water retentiveness, the abundant siliceous microfossils and organic material are responsible for the high porosity and water content and low densities. From 62.6 mbsf to the base of Subunit IIB, there is a progressive decrease in diatom and radiolarian abundance which is accompanied by decreases in porosity (from 78% to 71%) and water content (from 60% to 47%) as well as by increases in grain density (from 2.22 to 2.66 g/cm^3) and wet-bulk density (from 1.33 to 1.55 g/cm^3). The pattern of increasing grain and wet-bulk density is reversed between 92.9 and 109.5 mbsf (Fig. 21). Minimum values of grain density (2.36 g/cm^3) and wet-bulk density (1.40 g/cm^3) in this interval correspond to a peak in organic carbon concentration (4.04%) at 106.5 mbsf.

The downsection trends of decreasing porosity and water content and increasing grain and wet-bulk density that characterize the lower portion of Subunit IIB are reversed in Subunit IIC (120.1–150.5 mbsf). The top of Subunit IIC is marked by slight decreases in porosity and water content; wet-bulk density increases from 1.55 to 1.66 g/cm^3. Grain density changes only slightly across the boundary between Subunit IIB and IIC, decreasing from 2.66 to 2.64 g/cm^3. Normal compaction trends resume between 137.9 mbsf and the base of Subunit IIC, and porosity decreases to 66%, water content decreases to 41%, and

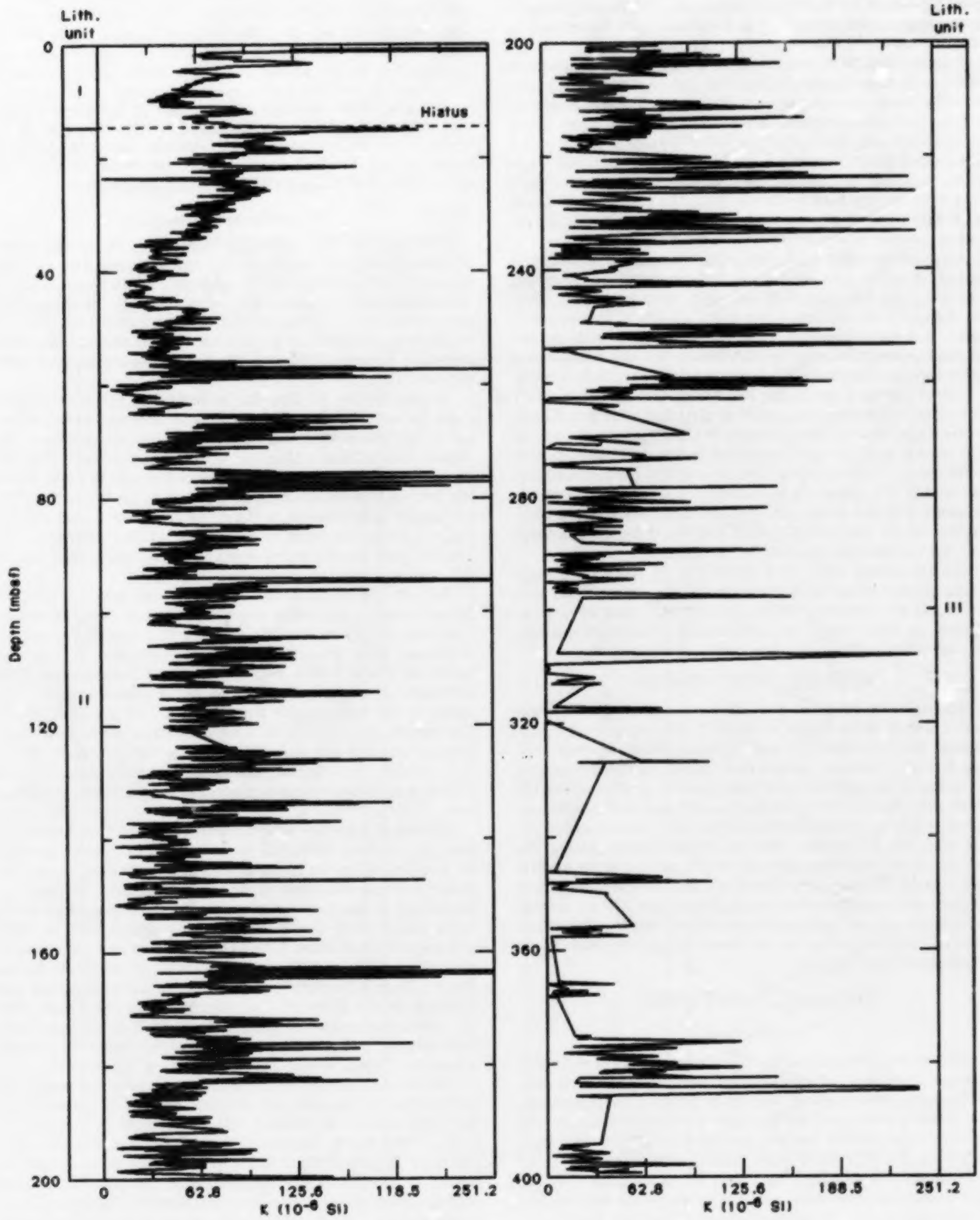

Figure 19. Magnetic susceptibility (K) data for Hole 730A.

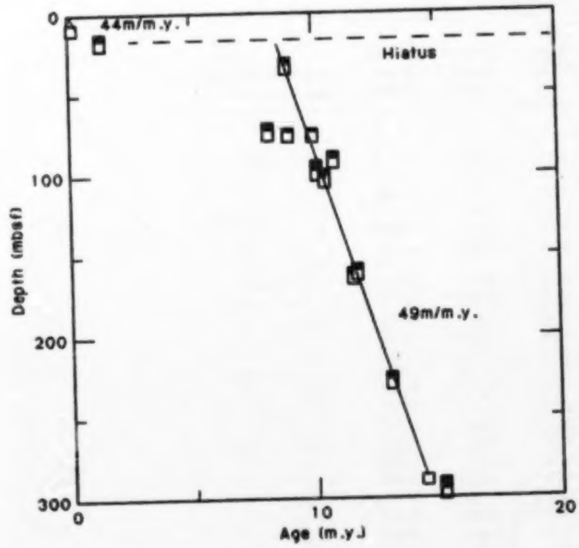

Figure 20. Age-depth plot of stratigraphic datums listed in Table 3. The filled and open boxes are the upper and lower depths of each datum level, respectively. The sedimentation rates indicated are calculated from a best fit of the reliable datums.

grain and wet-bulk density increase to 2.71 and 1.64 g/cm^3, respectively (Fig. 21).

Unit III

The marly nannofossil ooze/chalk and foraminiferal nannofossil chalk of Unit III (201.0–403.9 mbsf) are characterized by a uniform decrease in porosity and water content and increase in wet-bulk density with increasing depth. Boundaries between the five subunits of Unit III cannot be distinguished on the basis of index properties. Index-property profiles for Unit III are divided into two segments by gradient changes that occur at approximately 294 mbsf (Fig. 21). In the interval between 201.0 and 293.6 mbsf, there is a gradual decrease in porosity from 62% to 53% and in water content from 38% to 29%. There is a concomitant rise in wet-bulk density from 1.67 to 1.86 g/cm^3.

Concentrations of siliceous microfossils and organic carbon decrease over this interval, but because of their low initial value there is only a slight increase in grain density from 2.59 to 2.64 g/cm^3. From 293.6 mbsf to the bottom of Hole 730A (403.9 mbsf), gradients are reduced as porosity and water content decrease to 44% and 23%, respectively, and wet-bulk density increases to 1.96 g/cm^3. Grain density is essentially constant below 293.6 mbsf with an average value of 2.65 g/cm^3. Siliceous microfossils are absent below 289.7 mbsf; and, as a consequence of the lack of significant compositional variation, changes in porosity, water content, and wet-bulk density primarily reflect sediment compaction in response to increasing overburden pressure.

Two well-lithified chalks were sampled in Unit III at 272.3 mbsf (Sample 117-730A-29X-3, 65–67 cm) and 285.5 mbsf (Sample 117-730A-30X-6, 58–60 cm). These rocks are characterized by anomalously low porosity and water content and low wet-bulk density (Fig. 21 and Table 4).

Compressional-Wave Velocity

Compressional-wave velocity was measured on discrete samples from all three lithologic units at Site 730, including not only the indurated chalks but also the lower density nannofossil oozes and diatomaceous silty clays (Table 4 and Fig. 21). Within Units I and II compressional-wave velocity shows relatively little variation and a consistent trend of increasing velocity with depth from approximately 1500 m/s near the seafloor to 1575 m/s at the base of Unit II. This increase in compressional-wave velocity reflects a relatively rapid increase in wet-bulk density with depth from <1.4 to 1.6 g/cm^3 (Figs. 21 and 23).

Within the nannofossil oozes and chalks of Unit III, the variation in compressional-wave velocity increases significantly. This variation is most likely the result of differences in relative abundances of clay minerals, foraminifers, and nannofossils as well as sharp changes in the degree of induration encountered in this sequence of interbedded ooze and chalk. The affect of induration on compressional-wave velocity is illustrated by two samples of exceptionally well-indurated chalk (Samples 117-730A-29X-3, 65–67 cm, and 117-730A-30X-5, 125–127 cm), where the velocities measured perpendicular to bedding are 2078 and 2450 m/s, respectively. These values deviate significantly from the general velocity-depth profile (Fig. 22).

The relationship between velocity and density for the sequences at Site 730 shows a well-defined trend that closely matches the empirical correlation of Hamilton (1978) for calcareous sediments and chalks (Fig. 23). Variation of the data on the velocity-density crossplot is similar to that shown on the velocity-depth profile. The diatomaceous silty clays and diatomaceous marly nannofossil oozes of Unit II, all with densities of 1.6 g/cm^3 or less, show a well-defined velocity-density relationship. In contrast, the relationship between the marly nannofossil oozes/chalks and the foraminiferal nannofossil chalks of Unit III is characterized by a markedly higher variation, with no consistent relationship between velocity and calcium carbonate content.

Anisotropy of the compressional-wave velocity for 36 samples of chalk from Unit III shows no consistent relationship to either density or sub-bottom depth. Eight percent of the samples displayed small negative anisotropies (velocity parallel to bedding less than that perpendicular to bedding) that probably resulted from errors in measurement if the surfaces of the samples were not exactly parallel. Anisotropy of the remaining 33 samples ranged from 0.1% to 5.5%, with a mean of 1.7%.

GRAPE and *P*-Wave Logs

Continuous GRAPE wet-bulk density data were determined to a depth of approximately 290 mbsf at Site 730. Reliable data were obtained for Cores 117-730A-1H to -16X (0–152 mbsf). From the seafloor to 152 mbsf, the GRAPE wet-bulk densities correlate well with the wet-bulk density measurements obtained from discrete samples (Fig. 24). The transition from Unit I to Unit II (15.2 mbsf) is clearly shown as a drop in the wet-bulk density from 1.70 to 1.65 g/cm^3. The boundary from Subunit IIA to Subunit IIB (33.2 mbsf) is shown by a decrease from 1.50 to 1.40 g/cm^3. The transition from Unit II to Unit III (201.0 mbsf) is evidenced by an increase in the density/depth gradient, as also noted in the discrete samples.

The quality of the GRAPE data diminishes from Core 117-730A-17X to Core 117-730A-42X as the result of a decrease in the recovered core diameter giving smaller density values. Therefore, at depths greater than 152 mbsf the discrete sample data are consistently higher than the GRAPE wet-bulk density data by 0.5 to 1.5 g/cm^3. However, both sets of data continue to track along the same gradients.

The cyclic variations in the GRAPE data are not very well defined since the cycle intervals vary considerably with depth. The thickness of the intervals are on the order of 1–2 m. This trend corresponds to the smaller-scale cyclic variations evident at Sites 721 and 722.

Reliable compressional-wave velocity measurements with the *P*-wave logger were obtained from Cores 117-730A-1H to -10X

Table 4. Physical properties summary for Hole 730A.

Core, section, interval (cm)	Depth (mbsf)	Wet-bulk density (g/cm³)	Porosity (%)	Water content (%)	Grain density (g/cm³)	Dry-bulk density (g/cm³)	Velocity (m/s)	Vane shear strength (kPa)
117-730A-								
1H-3, 78-80	3.78	1.643	64.9	40.5	2.656	0.978		
1H-5, 78-80	6.78	1.706	59.0	35.4	2.634	1.102		
2H-2, 78-80	10.58	1.612	66.1	42.0	2.697	0.935		
2H-4, 30-32	13.10							10.5
2H-4, 78-80	13.58	1.721	61.0	36.3	2.647	1.096		
2H-6, 78-80	16.58	1.761	56.7	33.0	2.601	1.179		
2H-7, 30-33	17.60						[a]1517	
3H-2, 130-132	20.60	1.639	65.5	40.9	2.709	0.968		
3H-4, 80-82	23.10	1.570	65.9	43.0	2.529	0.895		46.1
3H-6, 80-82	26.10	1.600	64.1	41.1	2.478	0.943	[a]1446	
4H-2, 78-80	29.58	1.597	64.8	41.6	2.537	0.932		
4H-4, 78-80	32.58	1.503	72.2	49.2	2.602	0.764		
4H-7, 8-10	36.38							106.9
4H-7, 17-19	36.47	1.382	79.6	59.0	2.653	0.567	[a]1467	
5H-2, 80-82	39.10	1.369	79.3	59.3	2.449	0.557		
5H-4, 80-82	42.10	1.342	78.3	59.8	2.282	0.540		
5H-6, 78-80	45.08	1.414	73.9	53.5	2.329	0.657	[a]1537	182.6
6X-2, 105-107	48.85	1.342	79.6	60.8	2.427	0.526		
6X-4, 80-82	51.60	1.370	76.1	56.9	2.367	0.591		
6X-6, 92-94	54.72	1.343	77.5	59.1	2.250	0.549	[a]1502	
7X-1, 130-132	57.10	1.338	80.3	61.5	2.409	0.515		
7X-3, 69-71	59.49	1.407	75.7	55.1	2.446	0.632	[a]1525	
7X-5, 80-82	62.60	1.333	77.7	59.7	2.217	0.537	[a]1533	
8X-2, 109-111	68.09	1.492	73.8	50.7	2.553	0.736	[a]1543	
8X-4, 103-105	71.03	1.511	68.6	46.5	2.468	0.808		
8X-6, 73-75	73.73	1.465	72.7	50.8	2.433	0.721		
9X-2, 78-80	77.48	1.490	72.7	50.0	2.552	0.745		
9X-4, 90-92	80.60	1.553	66.3	43.7	2.546	0.874	[a]1542	
9X-6, 140-142	84.10	1.487	70.6	48.7	2.463	0.763		
10X-2, 78-80	87.18	1.519	68.3	46.0	2.449	0.820		
10X-4, 78	80	90.18	1.447	75.2	53.3	2.519	0.676	
10X-6, 47-49	92.87	1.463	71.2	49.9	2.360	0.733	[a]1570	
11X-2, 110-112	97.20	1.397	74.2	54.4	2.368	0.637		
11X-4, 71-73	99.81	1.636	63.0	39.5	2.570	0.991		
11X-6, 69-71	102.79	1.597	66.2	42.5	2.618	0.919	[a]1540	
12X-2, 78-80	106.48	1.526	69.4	46.6	2.497	0.815		
12X-4, 78-80	109.48	1.618	62.9	39.8	2.505	0.974		
12X-6, 76-78	112.46	1.521	70.4	47.4	2.600	0.800		
13X-2, 127-129	116.67	1.548	70.7	46.8	2.662	0.824		
13X-5, 85-87	120.75	1.662	62.0	38.2	2.644	1.027	[a]1563	
14X-2, 78-80	125.78	1.686	59.7	36.3	2.593	1.074		
14X-4, 61-63	128.61	1.629	63.2	39.8	2.559	0.981		
14X-6, 64-67	131.64	1.593	64.7	41.6	2.534	0.930	[a]1577	
15X-2, 31-33	135.01	1.539	67.4	44.9	2.570	0.848		
15X-4, 23-25	137.93	1.501	73.8	50.4	2.622	0.745		
15X-6, 30-32	141.00	1.572	66.2	43.1	2.543	0.894		
16X-2, 14-16	144.54	1.640	65.3	40.8	2.695	0.970		
16X-4, 26-28	147.66	1.642	66.1	41.2	2.709	0.965		
16X-6, 24-26	150.64	1.476	69.8	48.5	2.378	0.760		
16X-6, 104-107	151.44						[a]1538	
17X-2, 73-75	154.83	1.668	62.2	38.2	2.587	1.030		
17X-4, 70-72	157.80	1.636	63.1	39.5	2.539	0.990		
17X-6, 58-61							[a]1650	
17X-6, 63-65	160.73	1.651	63.0	39.1	2.557	1.005		
18X-2, 36-38	164.06	1.665	62.9	38.7	2.656	1.021		
18X-4, 30-32	167.00	1.810	56.7	32.1	2.726	1.230		
18X-6, 32-34	170.02	1.635	62.7	39.3	2.520	0.993		
19X-2, 60-62	174.00	1.733	57.8	34.2	2.589	1.140		
19X-4, 80-82	177.20	1.728	61.3	36.3	2.714	1.100		
19X-6, 60-62	180.00	1.733	61.0	36.1	2.732	1.108		
19X-6, 62-64	180.02						[a]1632	
19X-6, 62-64	180.02						[b]1655	
20X-2, 93-95	184.03	1.681	61.5	37.5	2.658	1.051	[a]1586	
20X-2, 93-95	184.03						[b]1619	
20X-4, 96-98	187.06	1.690	61.7	37.4	2.655	1.058	[a]1557	
20X-4, 96-98	187.06						[b]1570	
20X-6, 50-52	189.60	1.717	59.0	35.2	2.630	1.113		
21X-2, 78-80	193.48	1.747	59.5	34.9	2.712	1.137		
21X-4, 44-46	196.14	1.645	62.2	38.7	2.598	1.008	[a]1562	
21X-4, 44-46	196.14						[b]1597	
21X-6, 69-71	199.39	1.747	55.5	32.6	2.618	1.178	[a]1661	
21X-6, 69-71	199.39						[b]1705	
22X-2, 123-125	203.63	1.747	56.7	33.2	2.591	1.167	[a]1655	

Table 4 (continued).

Core, section, interval (cm)	Depth (mbsf)	Wet-bulk density (g/cm^3)	Porosity (%)	Water content (%)	Grain density (g/cm^3)	Dry-bulk density (g/cm^3)	Velocity (m/s)	Vane shear strength (kPa)
117-730A- (Cont.)								
22X-2, 123–125	203.63						[b]1690	
22X-4, 120–122	206.60	1.717	60.5	36.1	2.691	1.097	[a]1614	
22X-4, 120–122	206.60						[b]1606	
22X-6, 57–59	208.97	1.800	56.8	32.3	2.730	1.218	[a]1699	
22X-6, 57–59	208.97						[a]1701	
23X-2, 88–90	212.98	1.783	57.4	33.0	2.789	1.195	[a]1696	
23X-2, 88–90	212.98						[b]1719	
23X-4, 94–96	216.04	1.754	56.2	32.8	2.629	1.178		
23X-6, 120–122	219.30	1.662	62.7	38.6	2.634	1.020	[a]1576	
23X-6, 120–122	219.30						[b]1608	
24X-2, 71–73	222.41	1.725	59.0	35.1	2.675	1.120	[a]1665	
24X-2, 71–73	222.41						[b]1703	
24X-4, 21–23	224.91	1.752	60.5	35.4	2.736	1.132	[a]1677	
24X-4, 21–23	224.91						[b]1688	
24X-6, 47–49	228.17	1.773	56.2	32.5	2.653	1.198	[a]1724	
24X-6, 47–49	228.17						[b]1762	
25X-2, 87–89	232.27	1.705	58.9	35.4	2.630	1.101	[a]1651	
25X-2, 87–89	232.27						[b]1664	
25X-4, 107–109	235.47	1.768	59.0	34.2	2.736	1.164	[a]1632	
25X-4, 107–109	235.47						[b]1659	
25X-6, 84–86	238.24	1.832	54.4	30.5	2.708	1.274	[a]1739	
25X-6, 84–86	238.24						[b]1794	
26X-2, 102–104	242.12	1.819	56.0	31.5	2.783	1.245	[a]1632	
26X-2, 102–104	242.12						[b]1643	
26X-4, 72–74	244.82	1.862	52.6	29.0	2.706	1.322	[a]1787	
26X-4, 72–74	244.82						[b]1799	
27X-2, 27–29	250.97	1.768	56.5	32.7	2.758	1.189	[a]1616	
27X-2, 27–29	250.97						[b]1620	
27X-4, 91–93	254.61	1.820	57.4	32.3	2.724	1.232		
28X-1, 137–139	260.27	1.799	56.2	32.0	2.724	1.223	[a]1609	
28X-1, 137–139	260.27						[b]1643	
28X-4, 80–82	264.20	1.813	55.2	31.2	2.677	1.247	[a]1655	
28X-4, 80–82	264.20						[b]1665	
29X-2, 31–33	270.41	1.844	55.1	30.6	2.785	1.280	[a]1668	
29X-2, 31–33	270.41						[b]1714	
29X-3, 65–67	272.25	2.001	45.0	23.0	2.741	1.541	[a]2078	
29X-3, 65–67	272.25						[b]2197	
29X-5, 70–72	275.30	1.778	56.0	32.3	2.600	1.204	[a]1657	
29X-5, 70–72	275.30						[b]1683	
30X-5, 125–127	285.45	2.070	38.5	19.0	2.634	1.676	[a]2450	
30X-5, 125–127	285.45						[b]2434	
30X-6, 58–60	286.28	1.763	57.9	33.6	2.652	1.171	[a]1609	
30X-6, 58–60	286.28						[b]1633	
31X-1, 87–89	288.77	1.716	60.0	35.8	2.696	1.101		
31X-4, 124–126	293.64	1.855	52.8	29.1	2.639	1.315	[a]1684	
31X-4, 124–126	293.64						[b]1661	
31X-6, 53–55	295.93	1.855	53.8	29.7	2.699	1.304	[a]1699	
31X-6, 53–55	295.93						[b]1700	
32X-1, 48–50	298.08	1.932	48.4	25.7	2.658	1.436		
33X-1, 29–31	307.49	1.833	53.4	29.8	2.618	1.287	[a]1674	
33X-1, 29–31	307.49						[b]1702	
33X-5, 2–4	313.22	1.888	50.0	27.1	2.688	1.376	[a]1691	
33X-5, 2–4	313.22						[b]1709	
34X-1, 50–52	317.40	1.834	54.0	30.2	2.640	1.280	[a]1697	
35X-1, 17–19	326.37	1.922	50.2	26.7	2.585	1.408		
37X-1, 81–83	346.71	1.846	52.1	28.9	2.641	1.313	[a]1683	
37X-1, 81–83	346.71						[b]1706	
37X, CC, 30–32	350.45	1.903	52.1	28.0	2.626	1.370		
38X-2, 21–23	357.31	1.875	52.7	28.8	2.704	1.335		
39X-1, 75–77	365.95	1.860	53.2	29.3	2.679	1.315	[a]1631	
39X-1, 75–77	365.95						[b]1646	
39X-2, 92–94	367.62	1.883	52.1	28.4	2.684	1.349	[a]1683	
39X-2, 92–94	367.62						[b]1731	
40X-2, 20–22	376.60	1.845	52.9	29.4	2.639	1.303		
40X-4, 53–55	379.93	1.940	49.9	26.3	2.781	1.429	[a]1803	
40X-4, 53–55	379.93						[b]1871	
41X-1, 54–56	385.14	1.688	47.3	28.7	2.698	1.204	[a]1653	
41X-1, 54–56	385.14						[b]1641	
42X-1, 98–100	395.18	1.875	46.3	25.3	2.574	1.400	[a]1887	
42X-1, 98–100	395.18						[b]1918	
42X-3, 16–18	397.36	1.963	44.1	23.0	2.543	1.512	[a]2031	
42X-3, 16–18	397.36						[b]2057	

[a] Velocity measurement perpendicular to bedding.

[b] Velocity measurement parallel to bedding.

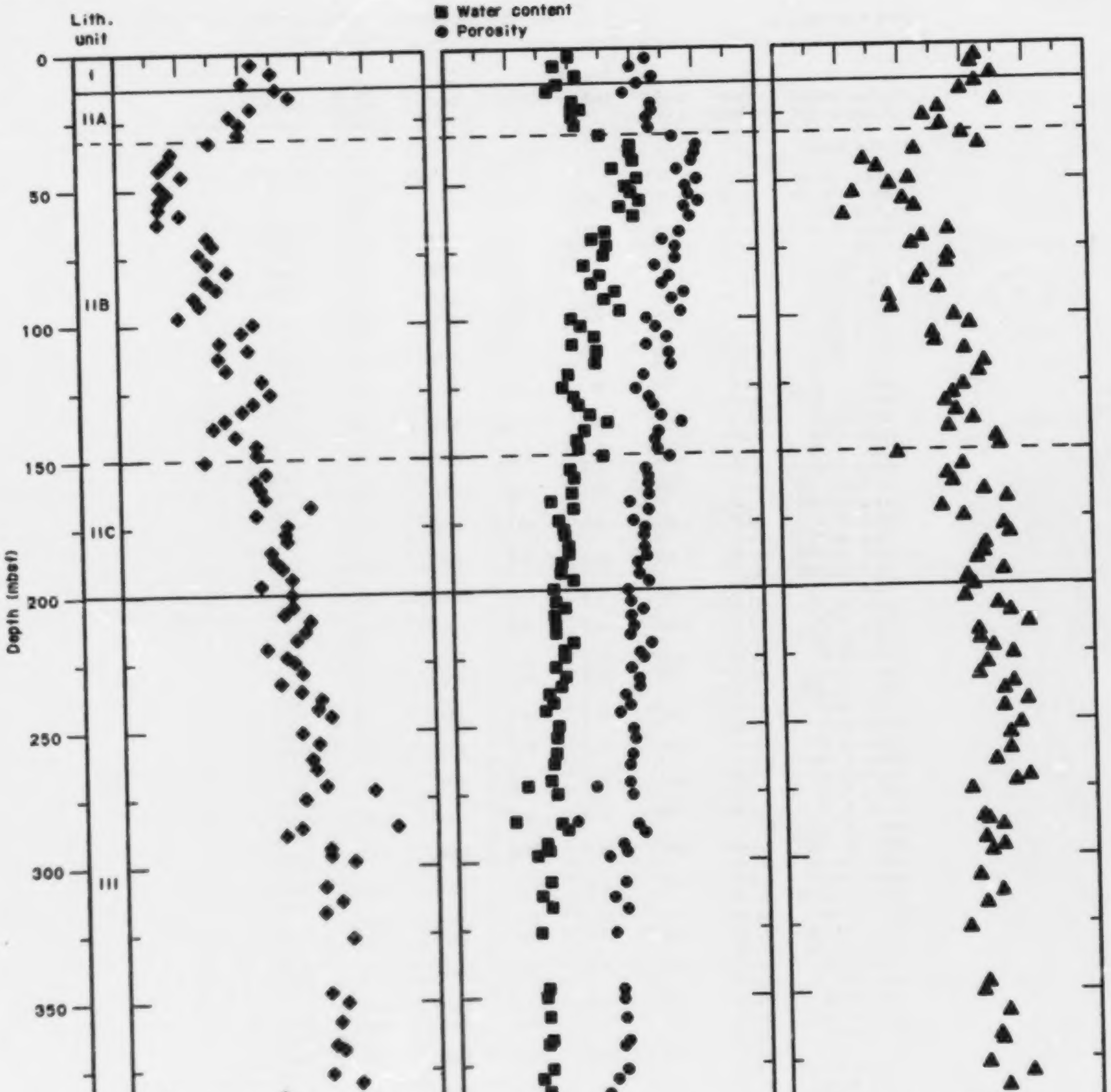

Figure 21. Index properties (wet-bulk density, porosity, water content, and grain density) measured on discrete samples for Hole 730A.

(0–95 mbsf; Fig. 25). We were unable to determine *P*-wave data for the interval from 95 to 135 mbsf since the sediments were not making sufficient contact with the core liner. The *P*-wave logger data display a trend similar to that contained in the GRAPE records. However, the density minimum zone seen in the GRAPE data between 25 and 75 mbsf is not reflected in the *P*-wave data.

The interval from 0 to 25 mbsf shows a decrease in compressional-wave velocity from 1575 m/s to 1550 m/s; from 25 to 95 mbsf the velocities average 1535 m/s. An increase in velocity from 1525 to 1675 m/s was measured in the interval from 135 to 250 mbsf. The *P*-wave logger data values are consistently less than the compressional-wave velocity measurements determined from discrete samples. The discrepancy between the discrete and

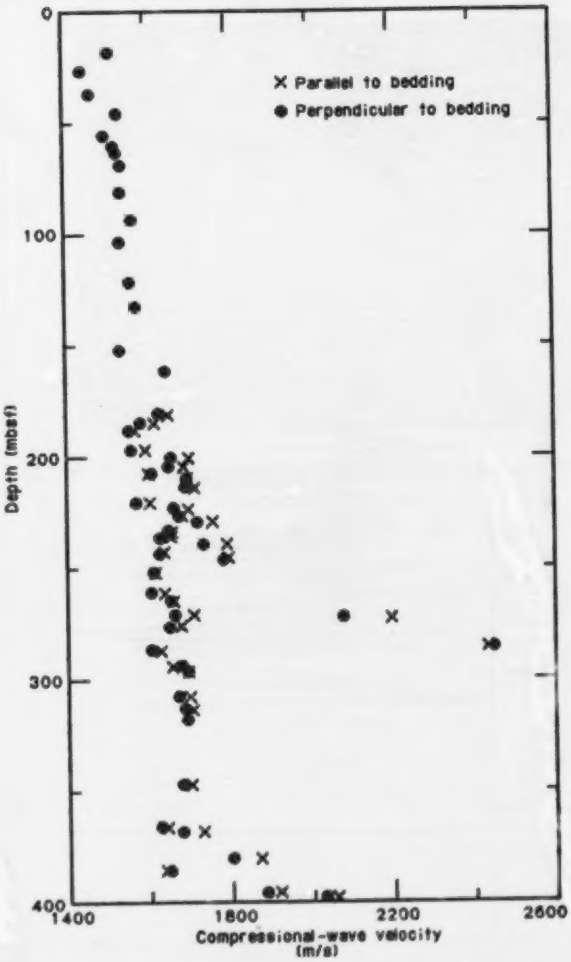

Figure 22. Compressional-wave velocity as measured on discrete samples in the Hamilton Frame Velocimeter for Hole 730A.

P-wave velocities results from the decrease in core diameter and an increase in drilling-induced sediment slurry surrounding intact sediment blocks.

Vane Shear Strength

Four vane shear strength measurements made on cores from the upper 45 m of the section at Site 730 (Table 4) define a consistent trend of rapidly increasing shear strength as well as a markedly higher rate of increase in shear strength below the hiatus in Cores 117-730-H-5. In the Pleistocene section (0–15.2 mbsf), vane shear strength increases at a rate of 0.80 kPa/m, as compared with an average rate of 6.3 kPa/m in the section underlying the Pleistocene/upper Miocene hiatus.

The consistently high shear strengths obtained from this section of Site 730 cores could be the result of previous burial to depths greater than present sub-bottom positions. However, because of the limited number of measurements at this site and the lack of comparable data from other sites on the Oman margin, any detailed interpretation of these results would be highly speculative.

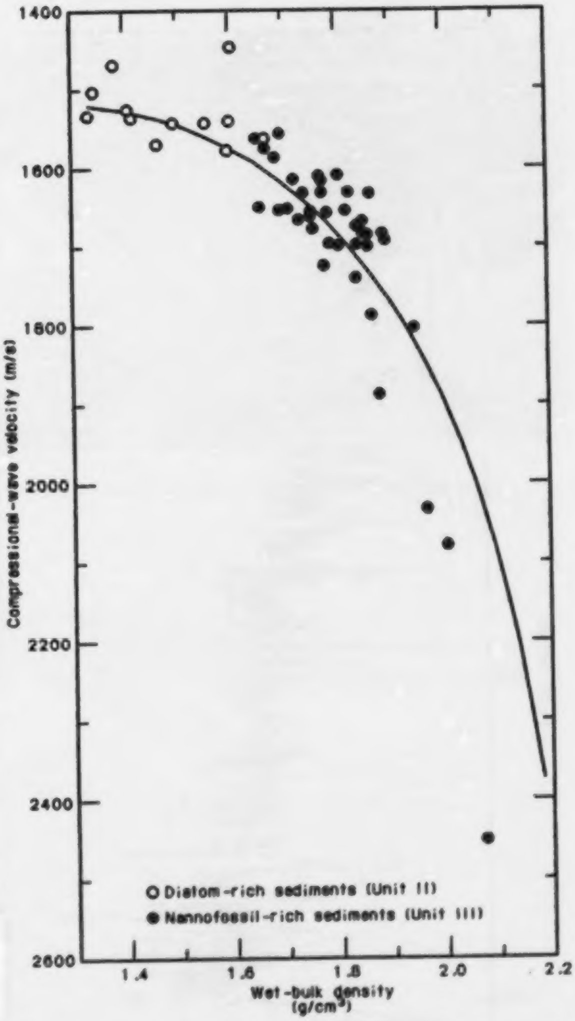

Figure 23. Wet-bulk density vs. compressional-wave velocity measured perpendicular to bedding on discrete samples. The solid line is an empirical correlation for velocity vs. density in calcareous marine sediments (30% calcium carbonate) from Hamilton (1978).

SEISMIC STRATIGRAPHY

Site 730 is located on the slope of a submarine terrace which separates two slope basins that form the southeast corner of the Oman margin. Seismic features display patterns that might be critical for interpreting the evolution of the Oman margin.

The area between the two slope basins is displayed on the shipboard seismic line (Fig. 26) as an anticlinal structure with east- and westward-dipping reflectors. The western basin has a different pattern of reflectors than the slope-adjacent terrace, indicating different lithologies or ages for the western slope ba-

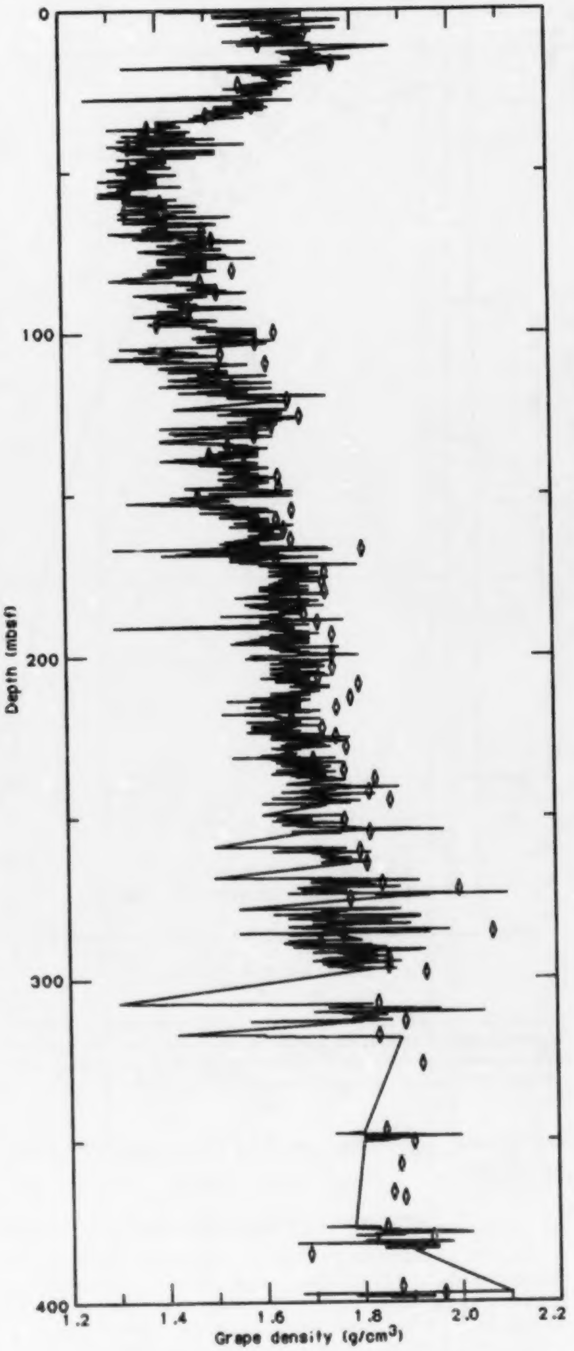

Figure 24. GRAPE wet-bulk density for Hole 730A. The profile is based on 10-cm-block averages of the data. Diamond-shaped symbols represent wet-bulk densities determined for discrete samples.

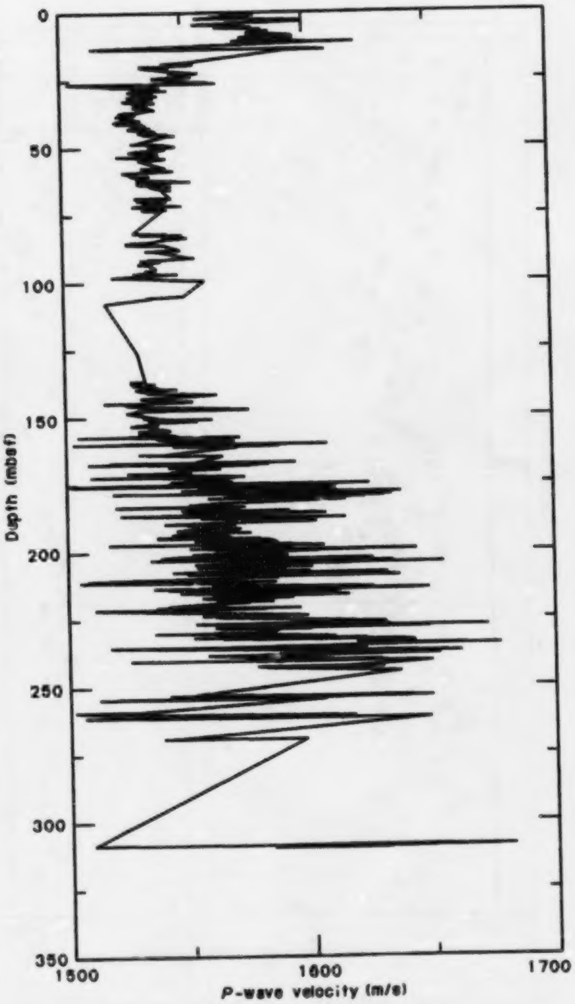

Figure 25. Compressional-wave velocity as measured by the P-wave logger for Hole 730A. The profile is based on 10-cm-block averages of the data.

sin and the slope terrace (Figs. 26 and 27). The detailed seismic connection between the two areas is unclear.

Seismic Unit A (Fig. 27) is a Quaternary sequence that forms a thin veneer over underlying sequences. This unit has parallel reflectors that are locally concordant as well as discordant to the underlying sequences. The thickness of this unit remains constant along the seismic section shown (Fig. 26).

Seismic Units B, C, and D (Fig. 27) belong to the Miocene section recovered at Site 730. Unit B has well-developed clinoforms with eastward-prograding reflectors. Older reflectors of Unit B are truncated by younger reflectors that produce onlap toward the east and toplap toward the center of the anticline.

Seismic Unit C has a uniform thickness and is a relatively homogeneous layer seismically, which seems to correlate with the upper portion of the chalk encountered at Site 730 (see "Lithostratigraphy" section, this chapter). At the top of the anticline,

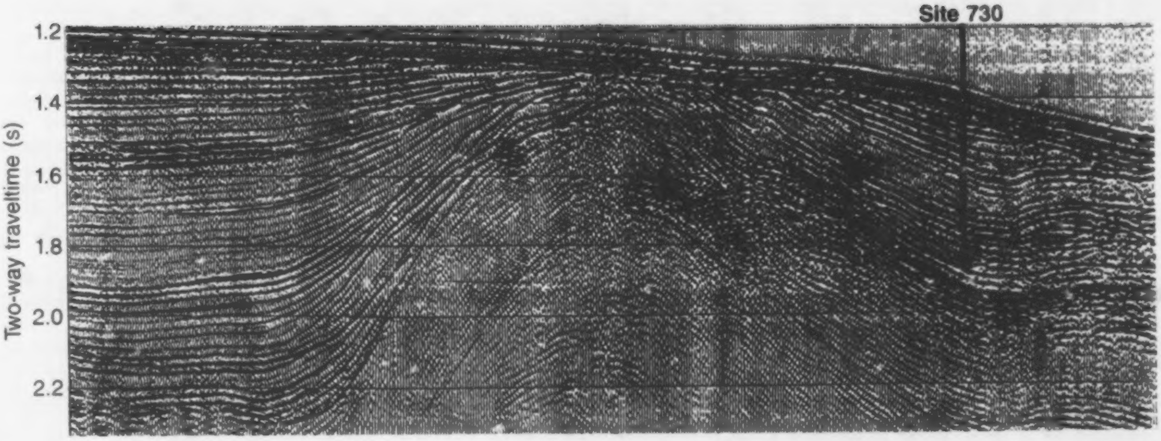

Figure 26. Seismic line on the submarine terrace showing location of Site 730. See Figure 2 for location of *JOIDES Resolution* Line 8.

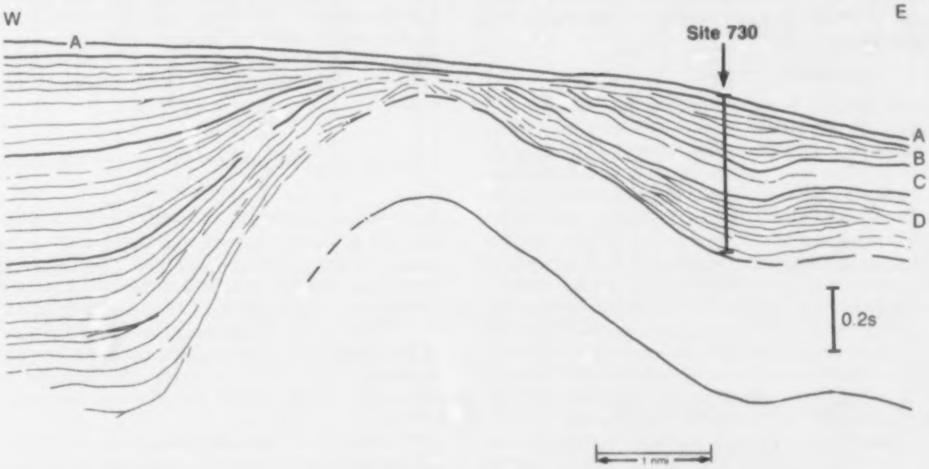

Figure 27. Schematic interpretation of Figure 26 showing seismic reflectors A–D.

some reflectors of seismic Unit C truncate older reflectors of this sequence and are in turn truncated by seismic Unit A.

Seismic Unit D, an eastward-thickening sequence, corresponds to middle and early Miocene chalks recovered at Site 730. Reflectors are discontinuous throughout this section and show numerous downlap and toplap patterns. At the top of the anticline, the reflectors appear to be irregular, wavy-shaped, and locally moundlike.

Discussion

The following observations seem to be critical for the interpretation of the basin development of the Oman margin.

Seismic Unit D is equivalent to middle to early Miocene chalks recovered at Site 730 which contains turbidites and slump horizons. This observation is consistent with the irregular patterns of truncating reflectors found in this unit. The lower portion of the turbidite-chalk sequence recovered at Site 730 contains redeposited, large benthic foraminifers, which could be derived from shallow-water carbonates developed at the top of the anticline, where wavy reflectors may indicate progradational lobes of carbonate sands. Unit D thickens eastward, suggesting that the depositional slope faced in this direction. If this conclusion is correct, seismic Unit D was a shallow-water facies (50–100 m water depth) only in the area of the top of the anticline.

Seismic Units B and C exhibit large-scale clinoforms, indicating progradation of sediment wedges to the east and leading to a contemporaneous overlapping of thin layers at the top of the anticline. It is not clear whether this overlap is related to erosional truncation followed by short phases of sedimentation or whether overlapping layers represent condensed equivalents of the thick Miocene sediments encountered at Site 730. The offlap pattern and overlap of thin layers on the anticline show that the shallow-water carbonates in seismic Unit D became somewhat submerged to allow a smooth veneer of sediment to occur on the anticline. This interpretation is supported by the waning occurrence of turbidite beds upsection in Site 730. On the other hand, submergence was not strong enough to develop a general draping pattern. Instead, the offlap pattern observed may indicate outer shelf conditions with roughly 200–400 m of water depth.

While the western slope basin has well-developed sediments of Pliocene and Quaternary age, we did not find any equivalent sediments on the anticline near Site 730 except for the thin veneer of Quaternary sediments in Unit A. This phenomenon might be interpreted as being the result of a recent uplift with accompanying erosion or nondeposition.

INORGANIC GEOCHEMISTRY

Introduction

We collected 15 interstitial water samples by squeezing from Hole 730A. Analytical results are listed in Table 5 and are presented in Figures 28 and 29.

Salinity, Chloride, and pH

Salinity decreases with depth at this site (Fig. 28) as a direct consequence of the reduction of sulfate and loss of magnesium from solution between ~25 and ~200 mbsf. In contrast, no significant variation is seen in the chloride content (Fig. 28), and the pH varies only slightly between maximum and minimum values of ~7.7 and ~7.1 (Fig. 28). The pH is lower than that of seawater, probably as a consequence of the production of H_2S during sulfate reduction.

Alkalinity and Sulfate

The highest alkalinity measured at this location (~6.8 mmol/L at 110 mbsf) is significantly lower than is observed at most other Oman margin sites (Fig. 28). The greatest rate of addition of alkalinity to pore solution (i.e., greatest positive slope) coincides well with the maximum negative slope in the sulfate profile (Fig. 28). However, the absolute alkalinity concentration is much lower than should be present considering that sulfate is fully reduced at depth. This presumably reflects a high degree of removal of dissolved inorganic carbon from pore waters by precipitation of authigenic carbonates. The observed magnesium distribution supports this interpretation (see below). A second reason for the low alkalinity at depth is the relatively low ammonia content.

The depth at which the sulfate concentration goes to zero (~250 mbsf) is substantially greater at this site than that observed at nearby Site 727 (~55 mbsf). This contrast is most probably a function of the difference in sedimentation rate between the two locations. Sedimentation at Site 727 has apparently been continuous throughout the Pleistocene, whereas much of the Pleistocene and Pliocene are missing at Site 730. The high organic carbon concentrations present in the upper Miocene chalks clearly provide a metabolizable substrate for sulfate-reducing bacteria in Hole 730A, suggesting that, despite its age, the organic matter is still viable as an energy source for bacteria: it must have been preserved to some extent when it was initially buried during the late Miocene. However, the presence of dissolved sulfate at considerable depths in the hole, coupled with the associated relatively low ammonia concentrations, suggests that such preservation has been moderate at best. The shallower depth at which sulfate is fully depleted in Hole 727A is consistent with the implication that a higher oxidant demand is associated with the more rapidly buried (thus somewhat "fresher") organic matter at this site.

It is interesting to note that we found no indication in either the sulfate or chloride data for the presence of a relatively fresh, sulfate-enriched fluid at depth at this site, as there was at nearby Site 727. This contrast may arise because Site 730 is located on the outer shoulder of an elevation (possibly a horst?), which would preclude significant lateral advection of fluids from the west.

Calcium and Magnesium

Concentrations of calcium generally increase linearly with depth at this site (Fig. 28), suggesting that distribution is controlled mainly by the upward diffusion of calcium from an unknown source below the base of the cored section. In contrast, the curvature in the magnesium profile between ~50 and ~250 mbsf (Fig. 28) indicates that dolomitization is occurring in this zone.

Ammonia, Phosphate, Silica, and Dissolved Organic Carbon

Ammonia concentrations are relatively low in Hole 730A, but they generally increase with depth even in the absence of sulfate reduction below ~225 mbsf (Fig. 28). Although methane content was not measured at this site, it is apparent that the increase in ammonia below ~200 m depth reflects production of NH_3 during methanogenesis. We suggest that because the organic matter in the upper ~110 m at Site 730 is old (and at best moderately preserved), it is likely to be nitrogen depleted. Such a depletion would explain the relatively low ammonia concentrations at depth.

As observed previously, phosphate concentrations are low throughout the hole, which is again attributed to the precipitation of small quantities of apatite (Fig. 28).

Maxima in the dissolved silica profile record two intervals, near 170 and 275 mbsf, where the sediments appear to be rela-

Table 5. Summary of interstitial water data, Site 730.

Core, sample interval (cm)	Depth (mbsf)	Vol. (mL)	pH	Alk. (mmol/L)	Sal. (g/kg)	Mg (mmol/L)	Ca (mmol/L)	Cl (mmol/L)	SO_4 (mmol/L)	PO_4 (μmol/L)	NH_4 (mmol/L)	SiO_2 (μmol/L)	Mg/Ca	DOC (a.u.)
117-730A-														
1H-4, 145–150	5.95		7.64	3.48	35.2	52.94	10.65	563	26.1	2.5	0.13	170	4.97	0.075
3H-4, 145–150	23.75	65	7.11	2.84	35.2	51.33	10.98	564	26.1	2.3	0.16	576	4.67	0.110
6X-4, 145–150	52.25	62	7.23	3.71	35.0	49.72	12.04	568	23.1	2.4	0.22	917	4.13	0.223
9X-4, 145–150	81.15	53	7.47	5.29	34.3	41.66	12.39	565	14.9	3.5	0.35	1065	3.36	0.532
12X-4, 145–150	110.15	41	7.40	6.33	33.6	35.89	12.28	566	7.6	2.5	0.74	1129	2.92	0.726
15X-4, 145–150	139.15	51	7.68	6.75	32.6	32.72	12.98	562	3.7	1.7	1.01	1097	2.52	0.793
18X-4, 145–150	168.15	46	7.45	5.34	32.6	30.29	13.11	564	2.2	1.6	1.22	1252	2.31	0.731
21X-4, 145–150	197.15	31	7.59	5.17	32.4	28.41	14.19	564	0.4	3.5	1.48	1103	2.00	0.680
24X-4, 145–150	226.15	25	7.61	4.34	32.4	28.26	14.58	564	0.4	3.2	1.60	1008	1.94	0.467
27X-2, 140–150	252.10	58	7.39	4.10	32.3	27.58	15.02	564	0	4.6	1.84	998	1.84	0.406
29X-4, 140–150	274.50	44	7.42	3.73	32.3	27.84	15.08	557	0	3.0	2.03	1141	1.85	0.340
33X-3, 140–150	331.60	30	7.42	3.27	32.2	28.07	15.41	564	0	2.0	2.29	850	1.82	0.305
37X-2, 140–150	348.80	30	7.16	3.12	32.2	26.99	16.81	567	0	1.0	2.64	800	1.61	0.292
39X-1, 140–150	366.60	25	7.15	2.76	32.2	26.93	16.79	569	0	1.0	2.88	733	1.60	0.223
42X-2, 140–150	397.10	35	7.48	1.92	32.2	26.68	17.04	566	0	0.7	2.49	669	1.57	0.236

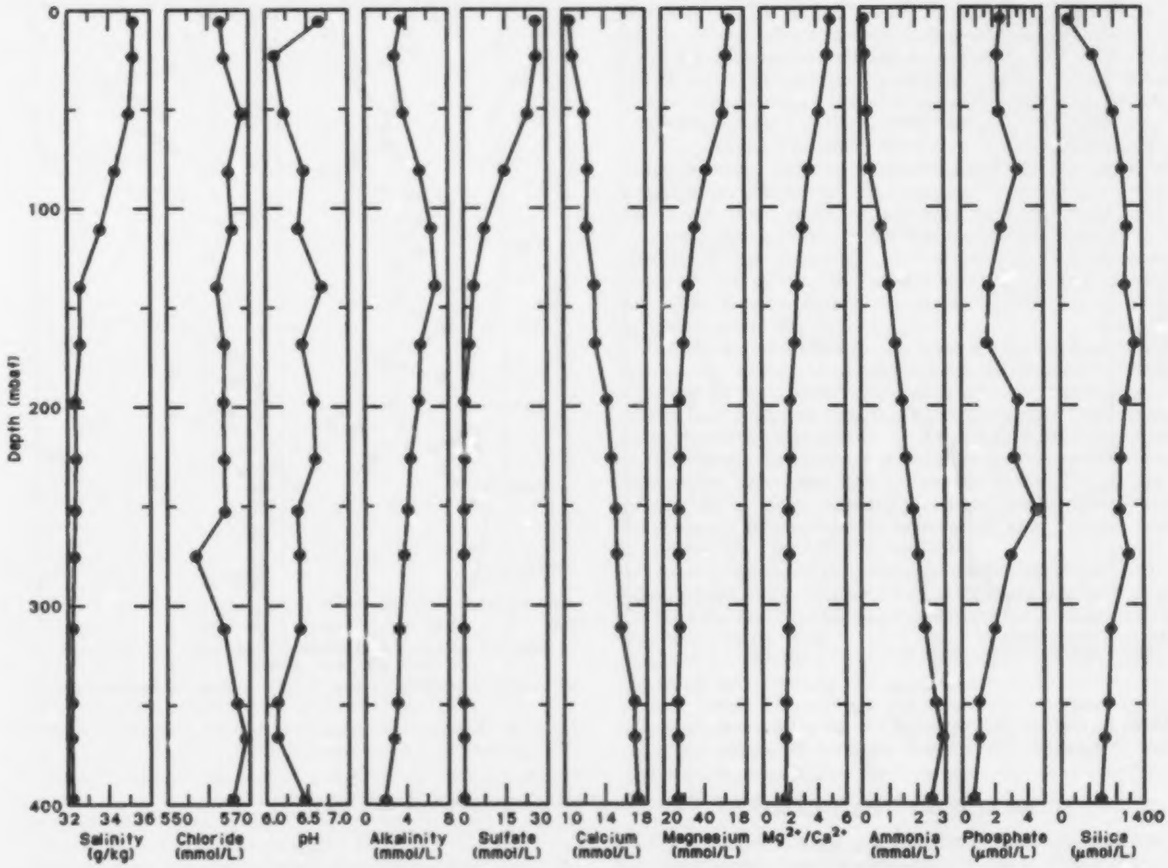

Figure 28. Concentration profiles vs. depth for Site 730.

tively enriched in opal (Fig. 28). The upper zone of enrichment is consistent with the observed abundance of siliceous microfossils in the hole (see "Biostratigraphy" section, this chapter). Radiolarian skeletons and diatom frustules are relatively rare in Core 117-730A-29X (~275 mbsf), but sponge spicules are common. This may account for the high dissolved silica concentration measured in the pore-water sample from that core. Biogenic silica is practically absent from the sediments below Core 117-730A-29X, which is reflected by the decreasing dissolved SiO_2 concentration below ~275 mbsf (Fig. 28).

Dissolved organic carbon (DOC) concentrations (Fig. 29) are lower at Site 730 than at the majority of Oman margin sites, which is consistent with the reduced level of diagenetic activity characteristic at this location. The DOC profile agrees only approximately with the organic carbon distribution (see "Organic Geochemistry" section, this chapter). Organic carbon concentrations range between 2% and 4% from ~40 to 110 mbsf. However, the absence of pronounced sulfate reduction, alkalinity, and metabolite production, and the rather low DOC in the pore waters of this zone suggests that the organic matter, even though abundant in places, may be relatively refractory when compared with other sites on the margin. This tentative conclusion is in agreement with the unusual history of sedimentation at this site, which has resulted in the presence of "old" organic matter in the near-surface strata.

ORGANIC GEOCHEMISTRY

Organic Matter Abundance and Character

We analyzed 44 samples, taken from all three lithologic units, for organic carbon and carbonate content (Table 2) and performed Rock-Eval pyrolysis on most of the above samples (Table 6).

Unit I consists of marly nannofossil ooze to a depth of 36.6 mbsf, and organic carbon values vary from 0.92% to 1.61%. The first 80 m of Unit II consist of marly nannofossil ooze and diatomaceous silty clays to a depth of 191 mbsf and are characterized by high organic carbon values that average 2.6%. The lower part of Unit II has distinctly lower values averaging 0.7% (Fig. 30 and Table 2). Unit III consists of foraminifer nannofossil chalks, and organic carbon values rarely exceed 0.5%.

The hydrogen (HI) and oxygen (OI) indices, plotted in a "van Krevelen-type" diagram (Fig. 31), cluster in an area which is characterized by somewhat lower HI when compared with samples from other margin sites. This might indicate that the organic matter is slightly more degraded at Site 730 than in comparison with Site 726.

Hydrocarbon Gases

Several unconformities, which could be effective seals for hydrocarbons, were visible on the seismic lines (see "Seismic Stra-

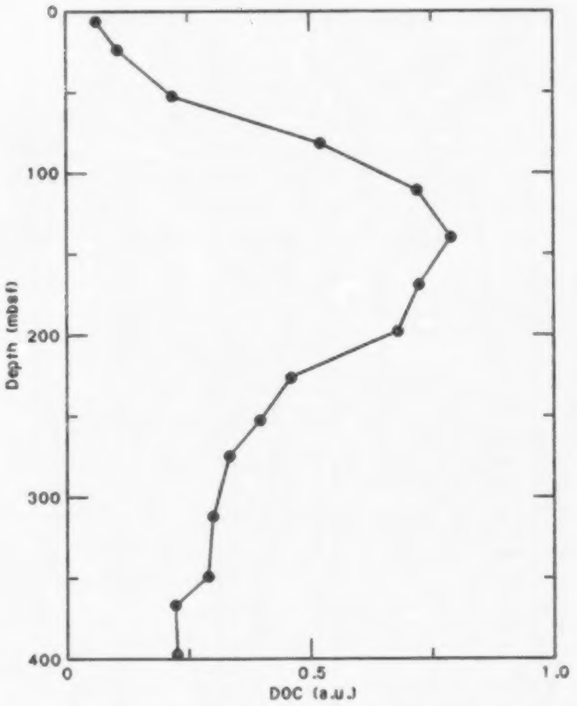

Figure 29. Profile of the relative concentration of dissolved organic carbon (DOC) at Site 730, plotted in absorbance units (a.u.).

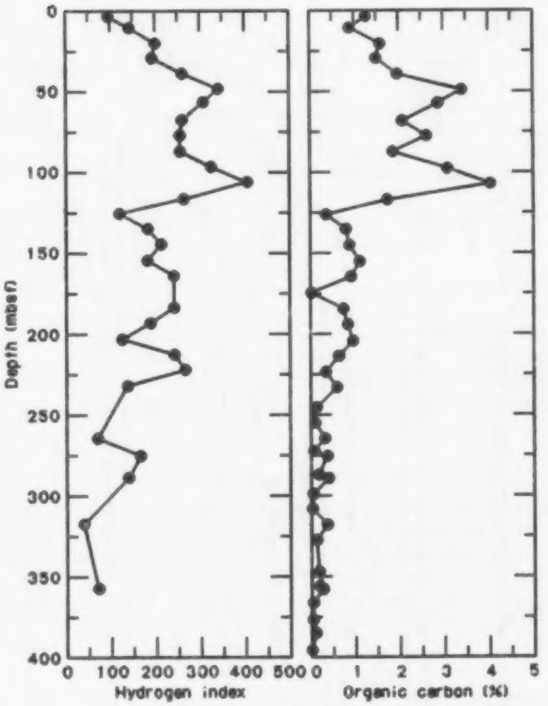

Figure 30. Downhole plot of organic carbon and hydrogen index values from pyrolysis for samples from Hole 730A.

Table 6. Results of Rock-Eval pyrolysis of sediment samples from Hole 730A.

Core, section interval (cm)	Depth (mbsf)	T_{max} (°C)	S_1	S_2	S_3	S_2/S_3	TOC	HI	OI
117-730A-									
1H-3, 78-80	3.78	424	0.21	1.24	1.77	0.70	1.28	96	138
2H-2, 78-80	10.58	426	0.18	1.33	1.35	0.98	0.92	144	146
3H-2, 130-132	20.60	424	0.37	3.23	1.80	1.79	1.61	200	111
4H-2, 78-80	29.58	420	0.33	2.95	3.63	0.81	1.51	195	240
5H-2, 80-82	39.10	416	0.74	5.22	4.22	1.23	1.99	262	212
6H-2, 105-107	48.90	415	1.57	11.63	2.78	4.18	3.39	343	82
7X-1, 130-132	57.00	411	2.03	8.92	2.19	4.07	2.88	309	76
8X-2, 109-111	68.09	418	0.85	5.46	2.28	2.39	2.09	261	109
9X-2, 78-80	77.48	417	0.91	6.74	2.05	3.28	2.63	256	77
10X-2, 78-80	87.18	419	0.69	4.85	2.32	2.09	1.88	257	123
11X-2, 110-112	97.20	413	1.88	10.14	3.92	2.58	3.10	327	126
12X-2, 78-80	106.48	418	2.27	16.39	3.58	4.57	4.04	405	88
13X-2, 128-130	116.68	416	0.70	4.68	4.53	1.03	1.76	265	257
14X-2, 78-80	125.78	417	0.12	0.46	1.69	0.27	0.38	121	444
15X-2, 30-32	135.00	417	0.29	1.51	1.93	0.78	0.82	184	235
16X-2, 14-16	144.54	416	0.36	1.93	1.48	1.30	0.91	212	162
17X-2, 73-75	154.83	421	0.30	2.12	1.78	1.19	1.15	184	154
18X-2, 36-38	164.06	419	0.27	2.25	1.91	1.17	0.93	241	205
20X-2, 93-95	184.03	417	0.28	1.86	1.60	1.16	0.77	241	207
21X-2, 78-80	193.48	414	0.31	1.63	1.40	1.16	0.86	189	162
22X-2, 123-125	203.63	414	0.25	1.24	1.40	0.88	0.98	126	142
23X-2, 88-90	212.98	417	0.27	1.56	1.68	0.92	0.64	243	262
24X-2, 71-73	222.41	417	0.17	0.93	1.47	0.63	0.35	265	420
25X-2, 87-89	232.27	412	0.20	0.84	1.58	0.53	0.61	137	259
28X-4, 80-82	264.20	408	0.05	0.23	1.04	0.22	0.32	71	325
29X-5, 70-72	275.30	410	0.13	0.61	1.50	0.40	0.37	164	405
31X-1, 87-89	288.77	409	0.15	0.57	1.88	0.30	0.41	139	458
34X-1, 50-52	317.40	422	0	0.15	0.47	0.31	0.37	40	127
38X-2, 21-23	357.31	410	0.03	0.19	1.24	0.15	0.27	70	459

Note: HI = hydrogen index and OI = oxygen index. For a detailed description of parameters, see "Explanatory Notes" chapter (this volume).

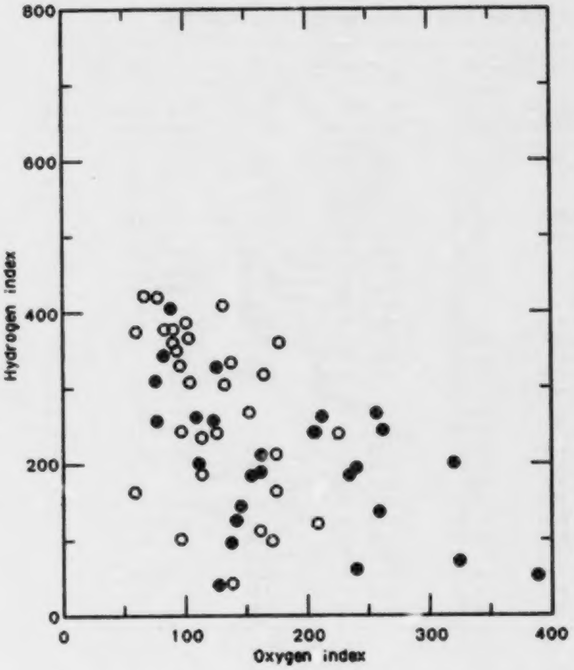

Figure 31. Plot of hydrogen index vs. oxygen index of samples from Hole 730A (dots), together with results from Hole 726A (circles).

tigraphy" section, this chapter), thereby warranting a careful monitoring of hydrocarbon gases during drilling. Gas pockets were virtually absent, however, and the only vacutainer sample collected from a suspected gas pocket (117-730A-17X-5, 145 cm) had a relatively low concentration of methane (28,481 ppm). Interstitial sulfate is depleted at a depth of 200 mbsf (see "Inorganic Geochemistry" section, this chapter), and the very low background values of organic carbon below this depth (average 0.25%) almost preclude the formation of biogenic methane.

INTERHOLE CORRELATIONS

Layer-by-Layer Correlation at Site 730

The one hole drilled at Site 730 is located in a water depth of 1066 m on the eastern flank of a midslope basement high that separates the slope basin into a shallow part and a deeper part. Hole 730A was drilled to 46.3 mbsf with the APC system and to 403.9 mbsf with the XCB. Recovery of APC-drilled cores was almost perfect in the hole, and the top of Hole 730A obtained the mud line. The age sedimentary sequence is mainly from middle to late Miocene age and is covered unconformably by late Pleistocene sediments.

We obtained detailed correlations in the upper 13 m of the covered sediments at Site 730. The upper interval has an age range from 0 to 0.3 Ma and is characterized by cyclic changes in the nature of sediments that can be identified by visual observation and by variations of magnetic susceptibility and $CaCO_3$ content.

Site-to-site correlations were made on the basis of visual identification of distinctive layers, as well as on physical and magnetic properties. Magnetic susceptibility was measured continuously and at 10-cm intervals before splitting the sections. Photographs were taken of the split cores.

Visual core correlations relied primarily on the core photographs. We were able to determine 26 distinct and traceable layers in the correlatable sedimentary sequence at Sites 723 and 724. These layers have been notated as OM-$a_1, \ldots h_4$, and h_5, based on correlations between holes at Sites 723 and 724 (see "Lithostratigraphy" sections, "Site 723" and "Site 724" chapters, this volume). The letter code (i.e., a, b, c, etc.) refers to the sequence of cores, and the number code indicates the number of marker layers in each core. For example, the notation "a_2" corresponds to the second marker layer defined in Core 117-723A-1H, and "b_1" denotes the first marker layer in Core 117-723A-2H. Marker layers a_1–h_4 were defined on the cored sediments of Hole 723A. Three marker layers (c_5, e_3, and h_5) were defined on the sedimentary sequence at Hole 724A in addition to those noted at Site 723.

Criteria for defining a marker layer are (1) the layer is distinct enough to trace in the sedimentary sequence of the other holes and (2) the character of the layer does not change. Useful criteria for recognizing a marker layer include color boundaries, distinctly colored layers, shape of bioturbations, and sequences of color change in surrounding sediments. We have traced the same marker layers from Sites 723 and 724 to Sites 727 and 728. At Site 730, the upper 16 marker layers are traced. Table 7 lists the depth of the traced marker layers in the Oman margin sites (i.e., Sites 723, 724, 727, 728, and 730).

Figure 32 shows the magnetic susceptibility curve and the positions of individual, visually correlatable layers. The pattern of the magnetic susceptibility and the positions of the layers match very well between Sites 728 and 730. The stratigraphy of the magnetic susceptibility data and the visually identified layers are extremely consistent in that a particular visually characteristic layer always coincides in depth with a distinct feature in the magnetic susceptibility curve. Since stratigraphic control in the top of Site 730 is poor, these site-to-site correlations should prove useful in future studies on the Pleistocene section of Site 730.

SUMMARY AND CONCLUSIONS

Site 730 is the last site drilled on the Oman continental margin and was added to the operations schedule after Site 729 was abandoned due to poor hole conditions. Similar to Sites 723 and 727, the site is located near the bottom of the pronounced OMZ that impinges on the margin. Site 730 is positioned to the east of a ridge that is presumably ophiolitic basement and that separates the upper and lower sedimentary basins. Sediments of the upper basin, which were previously drilled only 6 km to the west at Site 727, onlap eastward onto the ridge and are thinned and tilted by tectonic movement of the ridge. East of the basement ridge, seismic reflection profiles reveal a prominent unconformity that truncates eastward-dipping beds.

We moved upsection on the eastward-dipping reflectors and cored through the unconformity to recover older strata at Site 730 than those previously cored at Site 727. The age of sediments and hiatuses, and the evolution of the sediment facies, were expected to be useful in reconstructing the subsidence, as well as the erosional and tectonic history, of the slope basins and the prominent basement ridges.

Some of the major findings at Site 730 are summarized in Figure 33 and include the identification of

1. a significant hiatus ranging in age from Pleistocene to upper Miocene;
2. the occurrence of siliceous sediments in the middle and late Miocene that appear earlier here but are generally equivalent to the siliceous facies recovered on the Owen Ridge;
3. the appearance of *Globerigina bulloides*, an upwelling indicator, in the lower middle Miocene, which is earlier than its appearance on the Owen Ridge; and

Table 7. List of stratigraphic depth marker layers at Sites 723, 724, 727, 728, and ODP depth of marker layers at Site 730.

	Hole 723B		Hole 724A		Holes 727A and B		Holes 728A and B		Hole 730A	
Layer	Core, section, interval (cm)	Corrected depth (mbsf)	Core, section, interval (cm)	Corrected depth (mbsf)	Core, section, interval (cm)	Corrected depth (mbsf)	Core, section, interval (cm)	Corrected depth (mbsf)	Core, section, interval (cm)	ODP depth (mbsf)
OM-a_1	1H-3, 35	3.35	1H-1, 95	0.95	1H-2, 15	1.65	1H-1, 65	0.65		
a_2	2H-3, 20	7.20	1H-2, 115	2.65	1H-3, 55	3.55	1H-1, 135	1.75	1H-1, 120	1.20
b_1	2H-4, 65	9.15	1H-3, 100	4.00	1H-3, 15	6.55	1H-2, 90	2.80	1H-2, 85	2.35
b_2	2H-6, 110	12.60			1H-4, 90	8.80	1H-3, 110	4.50	1H-3, 115	4.15
b_3	3H-1, 95	14.75	2H-1, 75	7.95	1H-5, 80	10.20	1H-4, 40	5.30	1H-4, 55	5.05
c_1	3H-5, 110	20.90	2H-2, 75	9.45	2H-1, 50	14.00	1H-5, 70	7.10	1H-5, 25	6.25
c_2	4H-1, 85	24.95	2H-3, 130	11.50	2H-2, 125	16.25	1H-6, 50	8.40	1H-5, 110	7.10
c_3	4H-2, 100	26.60	2H-4, 70	12.40	2H-3, 95	17.45	1H-6, 115	9.05	1H-6, 10	7.60
c_4	4H-3, 15	27.25	2H-4, 120	12.90	2H-4, 30	18.30	1H-7, 40	9.80	2H-1, 35	8.65
c_5	4H-3, 100	28.10	2H-5, 35	13.55	2H-4, 55	18.55	2H-1, 35	10.45		
d_1	4H-5, 70	30.80	3H-1, 40	17.20	2H-5, 100	20.50	2H-2, 5	11.65	2H-2, 45	10.25
d_2	4H-6, 10	31.70	3H-1, 150	18.30	2H-6, 15	21.15	2H-2, 25	11.85	2H-2, 65	10.45
d_3	4H-7, 5	33.15	3H-2, 90	19.20	2H-6, 110	22.10	2H-2, 50	12.10	2H-2, 95	10.75
d_4	5H-2, 50	35.30	3H-3, 85	20.65	3H-1, 90	23.90			2H-2, 130	11.10
e_1	5H-5, 20	39.50	3H-4, 15	21.45	3H-3, 5	26.05	2H-2, 95	12.55	2H-3, 55	11.85
e_2	6H-1, 90	43.80	3H-5, 90	23.70	3H-5, 25	29.25	2H-2, 140	13.00	2H-3, 115	12.45
e_3	6H-3, 150	47.40	3H-6, 95	25.25	3H-5, 130	30.30	2H-3, 60	13.70	2H-4, 40	13.20
f_1	6H-5, 120	50.10	4H-1, 85	27.75	3H-7, 25	32.25	2H-4, 20	14.80		
f_2	7H-2, 15	54.25	4H-2, 70	29.10	4H-2, 95	34.95	2H-4, 55	15.15		
g_1	7H-6, 30	60.40	4H-4, 120	32.60	4H-4, 100	38.00	2H-5, 35	16.45		
g_2	8H-2, 60	64.40	4H-6, 25	34.65	4H-7, 40	41.90	2H-5, 105	17.15		
h_1	8H-5, 90	69.20	4H-7, 40	36.30	5H-4, 40	46.80	2H-6, 70	18.30		
h_2	9H-1, 20	72.10	5H-1, 80	37.30			2H-7, 35	19.45		
h_3	9H-3, 135	76.25	5H-2, 60	38.60	5H-6, 135	50.75	3H-1, 90	20.70		
h_4	9H-7, 95	81.85	5H-4, 145	42.45	6H-3, 95	55.35	3H-2, 65	21.95		
h_5			5H-5, 145	43.95	6H-4, 95	56.85	3H-2, 150	22.80		

Note: Corrected depth = corrected depth for stratigraphic thickness.

4. the presence of slumps, faults, and turbidites in the middle Miocene that indicate tectonic instability of the marginal slope basins.

The sediments at Site 730 range from Holocene to late early Miocene age and have been divided into three lithologic units. Unit I consists of marly nannofossil ooze to a sub-bottom depth of 15.2 mbsf. No siliceous fossils occur in this unit. A major hiatus spanning nannofossil Zones NN21–NN10 was found in Core 117-730A-2H; it separates lithologically similar sediments of Pleistocene and late Miocene age (Fig. 33). The rate of sedimentation in the interval above the hiatus was established as 44 m/m.y.

Unit II comprises marly nannofossil oozes and diatomaceous silty clays, which are late and middle Miocene age, and extends downsection to 201 mbsf. Diatom frustules and radiolaria are abundant from 33 to 150 mbsf, where they begin to decrease in abundance and completely disappear by the early middle Miocene (about 280 mbsf).

Foraminifer nannofossil chalks dominate Unit III, which extends downsection to about 404 mbsf. Unit III is late early Miocene (NN4) age (Fig. 33). Such structural features as slump beds 10–200 cm thick, recumbent folds, and high-angle faults that offset bioturbation traces and color laminations characterize this unit. Turbidites that contain shallow-water material are commonly associated with the slump structures in the middle of Unit III, but they are rare at the base of Unit III. Throughout the recovered section, the occurrence of siliceous microfossils coincides with poor preservation of planktonic and benthic foraminifers, which are progressively recrystallized with depth.

The chemical compositions of interstitial waters show no indication of a sub-bottom supply of sulfate, and diagenetic reactions appear to be dominated by carbonate cementation and methanogenesis (Fig. 33). High values of organic carbon (2%–3%) occur only in the upper part of Unit II (upper Miocene) and are distinctly lower (<1%) throughout the remaining section (Fig. 33).

Site 730 provided several types of new information about the Oman margin. First, it showed that opal deposition and upwelling began earlier on the Oman margin than it did on the offshore Owen Ridge. Second, it provided information about the tectonic stability and uplift history of the slope basins and their associated basement ridges.

REFERENCES

Bathurst, R.G.C., 1975. *Carbonate sediments and their diagenesis.* Developments in Sedimentary (Vol. 12): New York-London-Amsterdam (Elsevier).

Berggren, W. A., Kent, D. V., and Van Couvering, J. A., 1985. The Neogene: Part 2, Neogene chronology and chronostratigraphy. *In* Snelling, N. J. (Ed.), *The Chronology of the Geological Record*: Geol. Soc. Mem. (London), 10:211–260.

Bukry, D., 1973. Low-latitude coccolith biostratigraphic zonation. *In* Edgar, N. T., Saunders, J. B., et al., *Init. Repts. DSDP*, 15: Washington (U.S. Govt. Printing Office), 685–703.

________, 1975. Coccolith and silicoflagellate stratigraphy, northwestern Pacific Ocean, Deep Sea Drilling Project Leg 32. *In* Larson, R. L., Moberly, R., et al., *Init. Repts. DSDP*, 32: Washington (U.S. Govt. Printing Office), 677–701.

Hamilton, E. L., 1978. Sound velocity-density relations in sea-floor sediments and rocks. *J. Acoustic. Soc. Am.*, 63:366–377.

Johnson, D. A., and Nigrini, C. A., 1985. Synchronous and time-transgressive Neogene radiolarian datum levels in the equatorial Indian and Pacific Oceans. *Mar. Micropaleontol.*, 9:489–523.

Takayama, T., and Sato, T., 1987. Coccolith biostratigraphy of the North Atlantic Ocean, Deep Sea Drilling Project Leg 94. *In* Ruddiman, W. F., Kidd, R. B., et al., *Init. Repts. DSDP*, 94, Pt. 2: Washington (U.S. Govt. Printing Office), 651–702.

Ms 117A-117

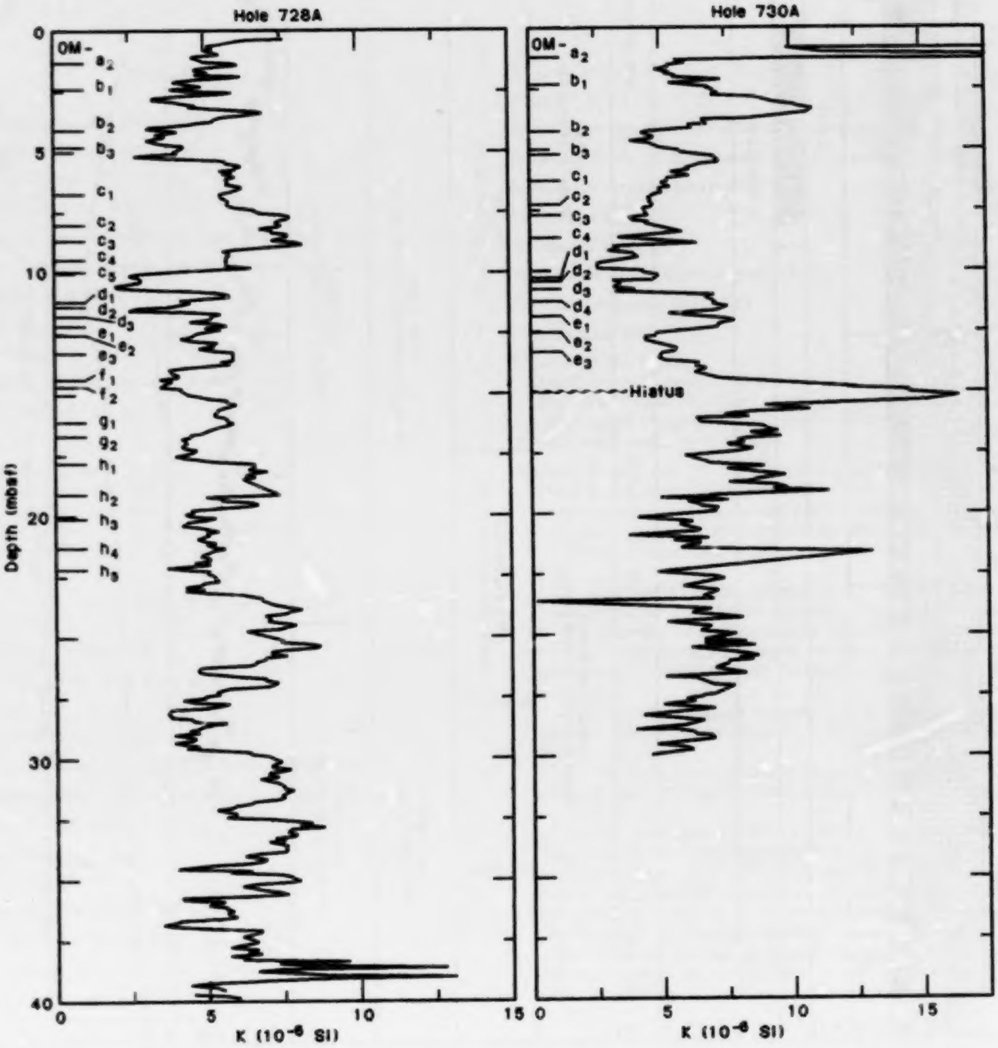

Figure 32. Volume magnetic susceptibility curve and positions of the marker layers in Holes 728A and 730A.

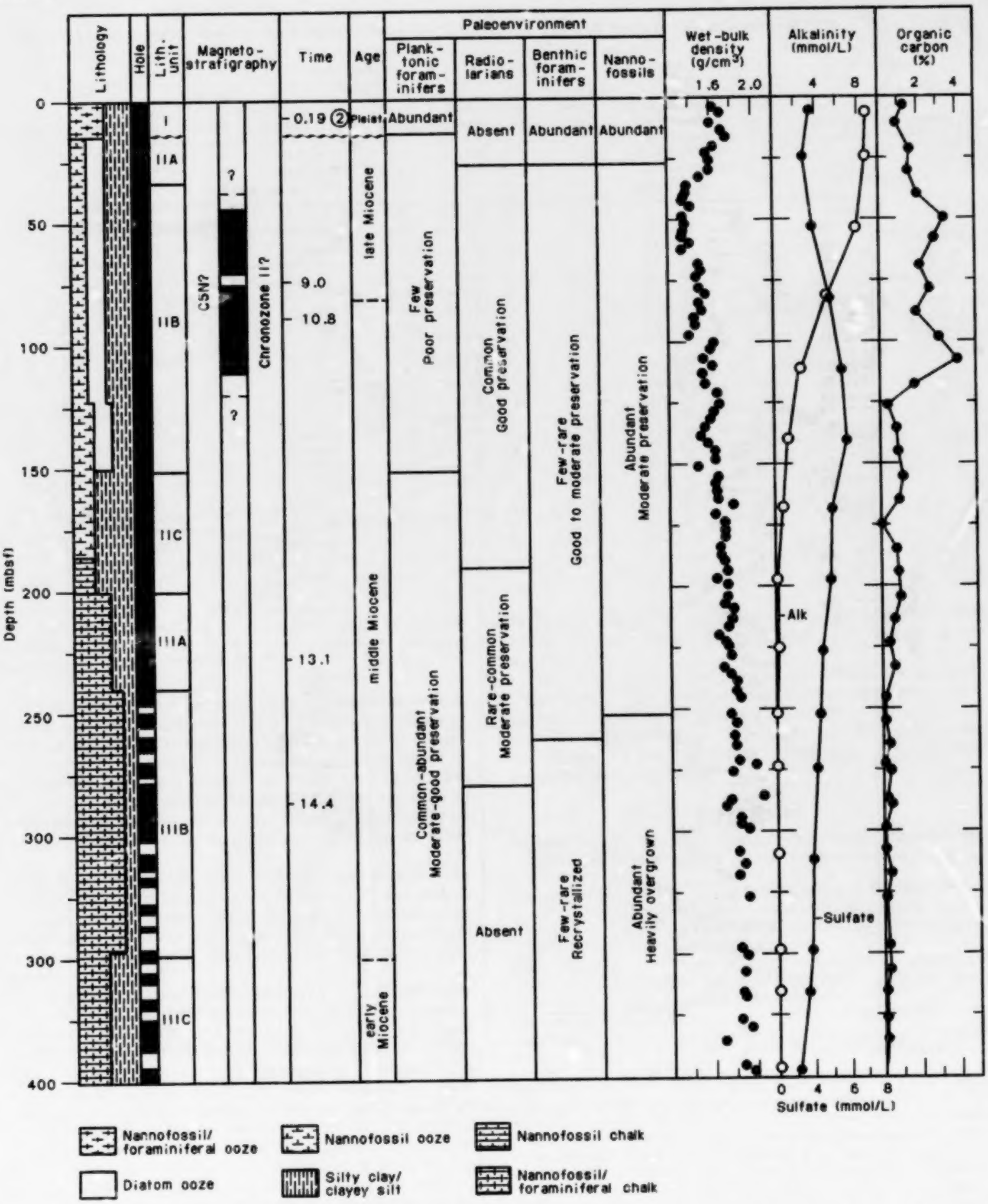

Figure 33. Summary chart outlining preliminary shipboard findings at Site 730.

19. SITE 731[1]

Shipboard Scientific Party[2]

HOLE 731A

Date occupied: 1 October 1987

Date departed: 4 October 1987

Time on hole: 2 days, 17 hr, 30 min

Position: 16°28.229′N, 59°42.149′E

Water depth (sea level; corrected m, echo-sounding): 2365.8

Water depth (rig floor; corrected m, echo-sounding): 2376.3

Bottom felt (m, drill pipe): 2370.9

Penetration (m): 409.0

Number of cores: 43

Total length of cored section (m): 409.0

Total core recovered (m): 359.28

Core recovery (%): 87.8

Oldest sediment cored:
Depth sub-bottom (m): 409.0
Nature: turbiditic silty clay
Age: early Miocene to late Oligocene (NP25?)
Measured velocity (km/s): 1.67–1.75

HOLE 731B

Date occupied: 4 October 1987

Date departed: 5 October 1987

Time on hole: 1 day, 12 hr, 45 min

Position: 16°28.229′N, 59°42.149′E

Water depth (sea level; corrected m, echo-sounding): 2365.8

Water depth (rig floor; corrected m, echo-sounding): 2376.3

Bottom felt (m, drill pipe): 2370.9

Penetration (m): 457.1

Number of cores: 5

Total length of cored section (m): 48.4

Total core recovered (m): 14.97

Core recovery (%): 31

Oldest sediment cored:
Depth sub-bottom (m): 457.1
Nature: turbiditic silty clay
Age: early Miocene to late Oligocene (NP25?)
Measured velocity (km/s): 1.58

HOLE 731C

Date occupied: 5 October 1987

Date departed: 9 October 1987

Time on hole: 4 days, 3 hr, 15 min

Position: 16°28.229′N, 59°42.149′E

Water depth (sea level; corrected m, echo-sounding): 2365.8

Water depth (rig floor; corrected m, echo-sounding): 2376.3

Bottom felt (m, drill pipe): 2370.9

Penetration (m): 994.2

Number of cores: 24

Total length of cored section (m): 154.7

Total core recovered (m): 59.81

Core recovery (%): 39

Oldest sediment cored:
Depth sub-bottom (m): 994.2
Nature: turbiditic silty clay
Age: early Miocene to late Oligocene (NP25?)
Measured velocity (km/s): 2.24

Principal Results: Site 731 is located in the western Arabian Sea on the Owen Ridge. Scientific objectives for drilling at Site 731 were to recover a continuous Neogene and possibly Paleogene sequence of pelagic and turbiditic sediments from the crest of the Owen Ridge.

The most significant findings at Site 731 are:

1. The thick turbidite sequence from 320 to 994 mbsf, which is characteristic of deep-sea fan deposition from the Indus Fan;
2. The gradual transition from clastic turbiditic depositional mode to pelagic sedimentation in the upper lower Miocene, which marks the uplift of Owen Ridge over the reach of turbidites and above the lysocline;
3. The onset of opaline sedimentation in the upper Miocene concomitant with the onset of cyclic variations in sedimentary properties;
4. The excellent correlation of magnetic susceptibility records between all three sites on the Owen Ridge (721, 722, and 731).

Site 731 penetrated to 994.2 mbsf and recovered sediments that range from possibly Oligocene (NP25) to late Pleistocene in age. The section here and at nearby Sites 721 and 722 provide an excellent record of the onset and evolution of monsoonal upwelling from the late middle Miocene to the Pliocene-Pleistocene. They provide insights into the relationship of orbital changes and the uplift of the Himalaya to the history of monsoon-related upwelling and eolian sedimentation on the Owen Ridge, as well as on tectonic uplift of Owen Ridge and the evolution of Owen Basin.

BACKGROUND AND OBJECTIVES

Site 731 is located at 16°28.229′N and 59°42.149′E in 2366 m water depth, just below the crest of the Owen Ridge. The location of Site 731 is shown in Figure 1, and its depositional and structural setting is shown in Figure 2. The site was selected near the intersection of seismic Lines 35 and 45 collected on the site survey (RC2704). The site is located about 6 km south of DSDP Site 224, which penetrated 792 mbsf to basement. Total sediment thickness at Site 731 is about 1.5 s (about 1800 m) and the target depth was to recover as much of the section as time permitted. The upper 0.42 s of the section (~400 mbsf) is characterized by relatively smooth, low-amplitude parallel reflectors that lie above a prominent but smooth reflector, which was denoted seismic reflector C at Sites 721 and 722. This reflector

---

[1] Prell, W. L., Niitsuma, N., et al., 1989. *Proc. ODP, Init. Repts.*, 117: College Station, TX (Ocean Drilling Program).

[2] Shipboard Scientific Party is as given in the list of Participants preceding the contents.

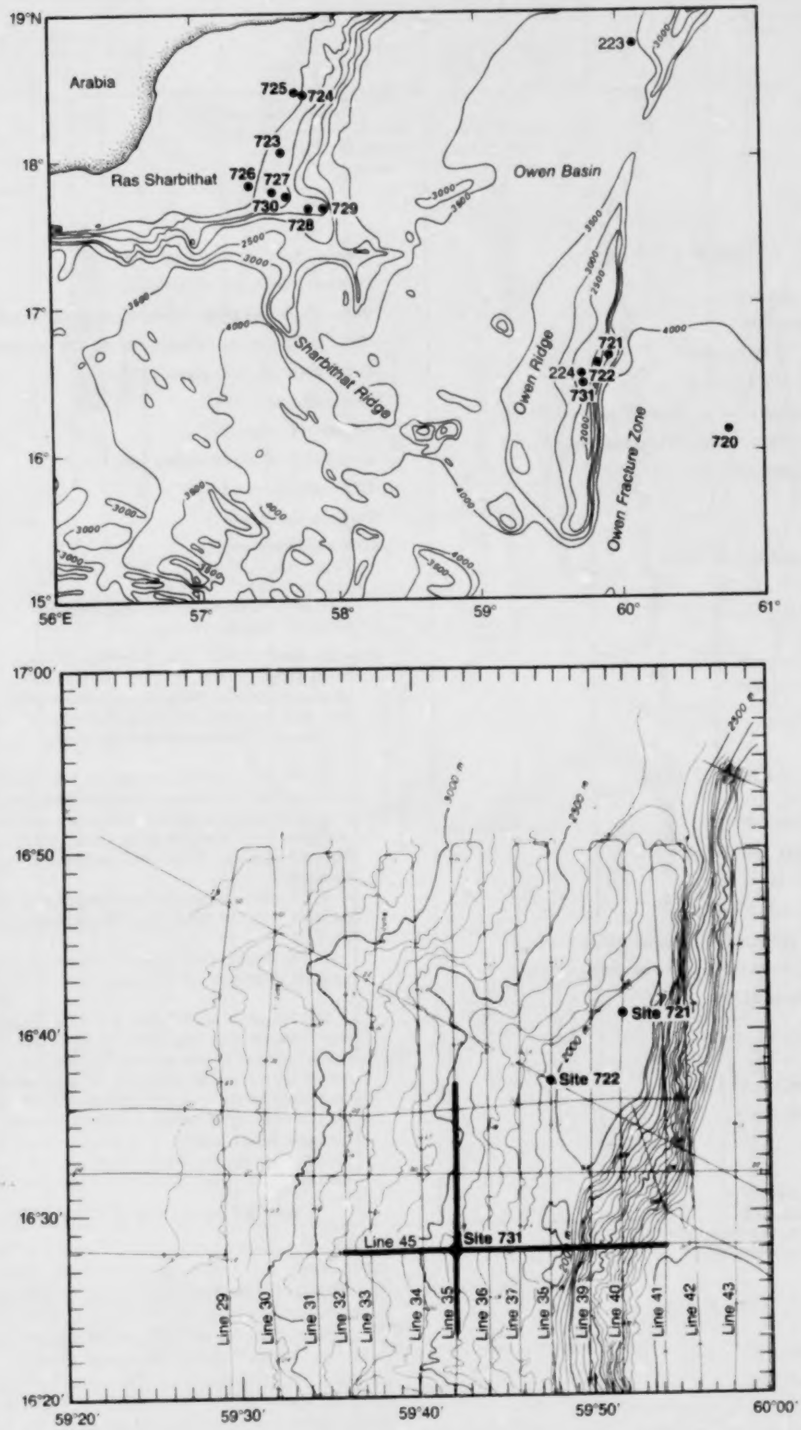
19°N
18°
17°
16°
15°
56°E
57°
58°
59°
60°
61°
Arabia
Ras Sharbithat
725
724
723
726
727
730
728
729
223
Owen Basin
Sharbithat Ridge
Owen Ridge
Owen Fracture Zone
721
224
722
731
720
2500
3000
3500
4000
2000
17°00′
16°50′
16°40′
16°30′
16°20′
59°20′
59°30′
59°40′
59°50′
60°00′
3000 m
2500 m
2000 m
Site 721
Site 722
Site 731
Line 45
Line 29
Line 30
Line 31
Line 32
Line 33
Line 34
Line 35
Line 36
Line 37
Line 35
Line 39
Line 40
Line 41
Line 42
Line 43

Figure 1. The location of Site 731 on the Owen Ridge. Bathymetry is from the Sea Beam site survey data (Prell, unpubl. data). The portions of RC2704 seismic lines Lines 35 and 45 (shown in Fig. 2) crossing Site 731 are indicated by the heavy lines.

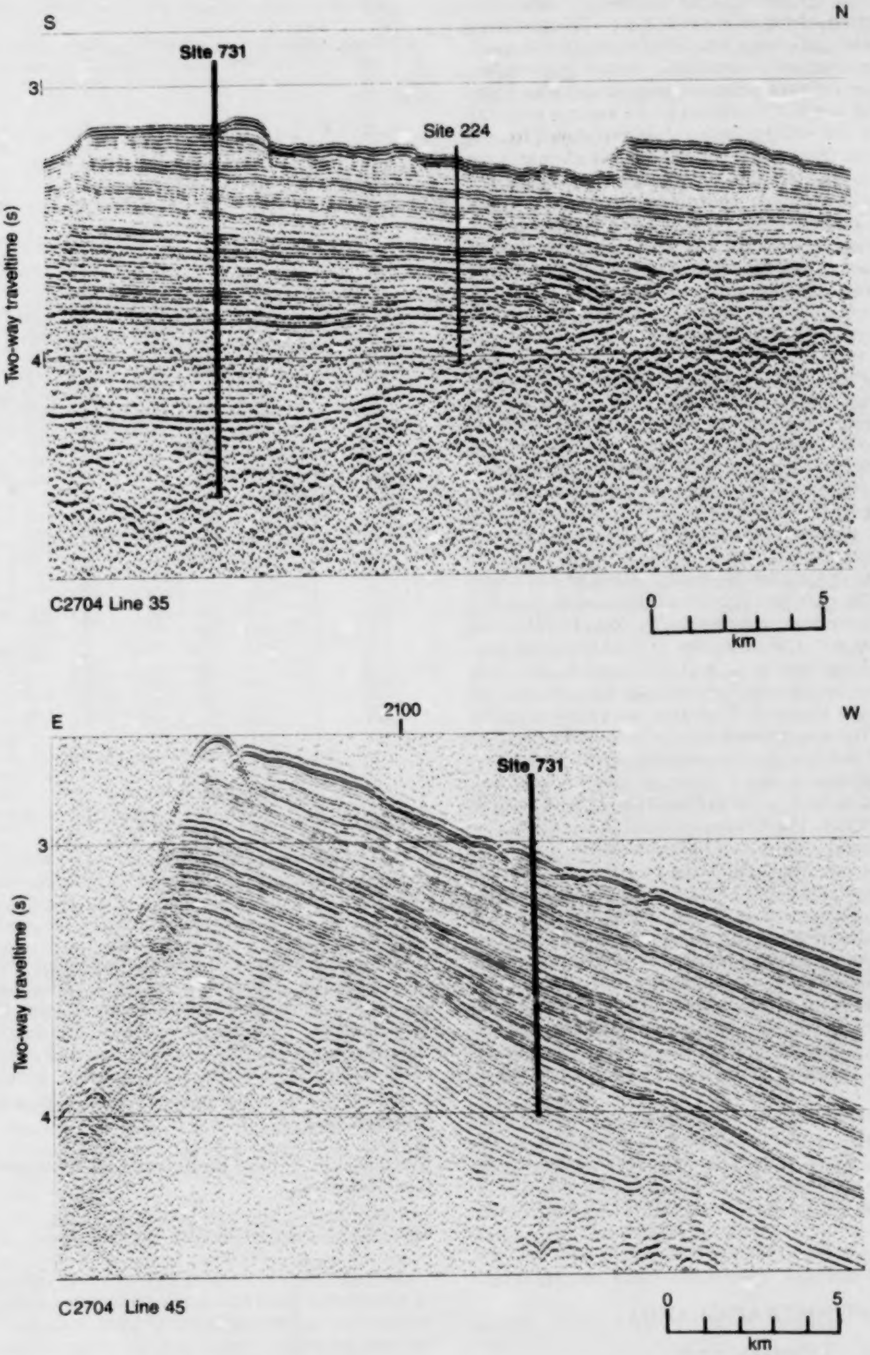
S
N
Site 731
Site 224
3
4
Two-way traveltime (s)
C2704 Line 35
0
5
km
E
2100
W
Site 731
3
4
Two-way traveltime (s)
C2704 Line 45
0
5
km

Figure 2. The seismic reflection profiles, Lines 35 and 45 of RC2704, that intersect Site 731. Track lines are shown in Figure 1.

marks the top of the turbiditic sequence that formed the lithologic Unit IV at Sites 721 and 722. The sequence of high-amplitude reflectors extends down to about 0.75 s (~750 mbsf) and onlap onto the basement peak where DSDP Site 224 was cored. This high-amplitude sequence is underlain from 0.75 s to 1.10 s by lower-amplitude reflectors that are parallel and also onlap northward onto basement. Correlation of the sections at DSDP Site 224 and Sites 721 and 722 with the seismic data from the site survey indicates that seismic reflector C, which marks the upper boundary of the turbidites, is of late early Miocene age and that the boundary between the high-amplitude and low-amplitude reflection sequences may be about late Oligocene in age. The age of the lower sequences is unknown, but is expected to postdate the lower Eocene sediments recovered at DSDP Site 224.

OPERATIONS

The seismic survey of Site 731 began at 0600 hr on 1 October after a 13-hr transit from Site 730. By 0730 Site 731 had been located, the beacon was deployed, the seismic gear was retrieved, and the rig was positioned in 2366 m water depth. The position was assessed as 16°28.229′N and 59°42.149′E by Global Positioning Satellite (GPS). After 76 stands of pipe had been tripped, the ship was inclined 5° to perform a bending stress test with bending joint and stress sub incorporated in the string. The test was finished successfully and the mud line of Hole 731A was shot by 2030 hr on 1 October. Hydraulic piston (APC) Cores 117-731A-1H to -7H recovered 102.5% of the interval from 0.0 to 67.0 mbsf, and extended core barrel (XCB) Cores 117-731A-8X through -43X (67.0–409.0 mbsf) yielded 88% of the cored sediments (Table 1). Upon cutting Core 117-731A-43X, the XCB cutting shoe broke, and attempts to dislodge the remnants of the shoe with a center bit failed. The string was pulled to the rig floor, and Hole 731B was spudded after offsetting the rig 10 m north at 0600 on 4 October. The hole was drilled with a polycrystalline diamond drilling bit and a center bit to 408.7 mbsf and coring commenced in XCB mode to Core 117-731B-5X (408.7–457.1 mbsf total depth). The core barrel flared at this depth and after attempts to grind it down had failed, coring in Hole 731B was terminated. Recovery in Hole 731B averaged 31% (Table 1).

Again the rig was offset 10 m to the north, and Hole 731C was spudded with a rotary coring (RCB) assembly at 1815 on 5 October. We drilled and spot-cored through the very thick turbidite sequence previously encountered on Owen Ridge, hoping to reach underlying sediments in the remaining time allocated for Leg 117. At a total depth of 994.2 mbsf, still in lower Miocene to upper Oligocene(?) turbidites, coring was suspended and the hole was prepared for logging. Hole 731C had 111.5 m core recovered, and total recovery during Leg 117 was established at 4367.2 m.

The hole was conditioned for logging, and two logging runs were performed with the bit positioned at 85 mbsf; 14 m of fill was encountered at the bottom of the hole. Two logging strings were run: the first consisted of DIT, BHC, GR, and CAL, while the second combined GST, CNT, NGT, and GPIT. Logging conditions were good, and log quality was excellent.

The ship was underway to Mauritius at 1700 hr on 9 October, 1987.

Table 1. Coring summary, Site 731.

Core no.	Date (Oct. 1987)	Time	Depth (mbsf)	Cored (m)	Recovered (m)	Recovery (m)
117-731A-						
1H	1	2125	0–9.8	9.8	9.87	101.0
2H	1	2155	9.8–19.3	9.5	9.84	103.0
3H	1	2225	19.3–28.8	9.5	9.94	104.0
4H	1	2300	28.8–38.3	9.5	9.77	103.0
5H	1	2340	38.3–47.8	9.5	9.22	97.0
6H	2	0015	47.8–57.3	9.5	9.94	104.0
7H	2	0050	57.3–67.0	9.7	10.10	104.1
8X	2	0235	67.0–76.7	9.7	6.01	61.9
9X	2	0320	76.7–86.4	9.7	8.60	88.6
10X	2	0400	86.4–96.0	9.6	9.65	100.0
11X	2	0440	96.0–105.7	9.7	9.32	96.1
12X	2	0515	105.7–115.4	9.7	9.74	100.0
13X	2	0555	115.4–125.0	9.6	9.17	95.5
14X	2	0635	125.0–134.7	9.7	7.37	76.0
15X	2	0725	134.7–144.4	9.7	9.61	99.1
16X	2	0800	144.4–154.0	9.6	9.68	101.0
17X	2	0835	154.0–163.7	9.7	9.76	100.0
18X	2	0925	163.7–173.4	9.7	9.83	101.0
19X	2	1105	173.4–183.1	9.7	9.77	101.0
20X	2	1145	183.1–192.8	9.7	9.69	99.9
21X	2	1215	192.8–202.5	9.7	8.81	90.8
22X	2	1245	202.5–212.2	9.7	9.60	98.9
23X	2	1315	212.2–221.9	9.7	9.49	97.8
24X	2	1350	221.9–231.6	9.7	8.69	89.6
25X	2	1430	231.6–241.3	9.7	9.78	101.0
26X	2	1610	241.3–250.9	9.6	7.12	74.1
27X	2	1645	250.9–260.6	9.7	9.45	97.4
28X	2	1720	260.6–270.2	9.6	9.70	101.0
29X	2	1810	270.2–279.9	9.7	9.79	101.0
30X	2	1930	279.9–289.6	9.7	9.86	101.0
31X	2	2135	289.6–299.2	9.6	5.22	54.4
32X	2	2210	299.2–308.9	9.7	9.31	96.0
33X	3	0015	308.9–315.5	6.6	4.49	68.0
34X	3	0210	315.5–322.1	6.6	4.12	62.4
35X	3	0355	322.1–331.7	9.6	9.31	97.0
36X	3	0535	331.7–341.3	9.6	0.13	1.4
37X	3	0720	341.3–351.0	9.7	9.63	99.3
38X	3	0850	351.0–360.7	9.7	9.87	102.0
39X	3	1010	360.7–370.4	9.7	5.40	55.7
40X	3	1305	370.4–380.0	9.6	6.69	69.7
41X	3	1505	380.0–389.7	9.7	4.59	47.3
42X	3	1430	389.7–399.4	9.7	1.70	17.5
43X	3	1730	399.4–409.0	9.6	9.65	100.0
				409.0	359.28	

LITHOSTRATIGRAPHY

Lithologic Units

Sediments recovered at Site 731 range from late Oligocene(?) or early Miocene to late Pleistocene or Holocene in age. Lithologies consist predominantly of nannofossil and marly nannofossil ooze and chalk, fine-grained turbidites, and coarse-grained turbidites; occurrences of foraminifer-nannofossil chalk and siliceous-bearing to diatomaceous marly nannofossil ooze/chalk are locally important. The sedimentary sequence is divided into four lithologic units based on visual core descriptions, smear slide analysis of sediment composition, and calcium carbonate contents (Figs. 3, 4, and 5; Tables 2 and 3). Lithologic Unit I is divided into two subunits. Three lithofacies are identified in lithologic Unit IV.

Unit I (Depth: 0–146.5 mbsf; Age: late Miocene to late Pleistocene/Holocene)

Core 117-731A-1H to Section 117-731A-16X-2, 60 cm.

Lithologic Unit I consists of alternating light and dark beds of nannofossil ooze and marly nannofossil ooze, with limited occurrences of foraminifer-nannofossil ooze, diatomaceous foraminifer-nannofossil ooze, and diatomaceous marly nannofossil ooze. Nannofossil-rich calcitic silty clay is present in very minor amounts. These lithologies are interbedded on a scale of 0.05–1.50 m. The relative abundance of diatoms in the upper 66 m of Unit I is used to define lithologic Subunit IA, while Subunit IB contains only trace amounts of diatoms (Fig. 4).

Table 1 (continued).

Core no.	Date (Oct. 1987)	Time	Depth (mbsf)	Cored (m)	Recovered (m)	Recovery (m)
Hole 731B-						
1X	4	2145	408.7-418.3	9.6	0.83	8.6
2X	4	2300	418.3-428.1	9.8	0.95	9.7
3X	5	0030	428.1-437.7	9.6	2.31	24.0
4X	5	0220	437.7-447.4	9.7	6.47	66.7
5X	5	1330	447.4-457.1	9.7	4.41	45.4
				48.4	14.97	
Hole 731C-						
1W	6	0810	351.7-502.4	150.7	2.55	1.7
2R	6	1015	502.4-512.1	9.7	6.35	65.4
3W	6	1300	512.1-560.2	48.1	3.02	6.3
4R	6	1415	560.2-569.9	9.7	1.38	14.2
5W	6	1615	569.9-618.1	48.2	7.22	15.0
6R	6	1730	618.1-627.8	9.7	1.22	12.6
7W	6	2045	627.8-675.9	48.1	4.68	9.7
8R	6	2155	675.9-685.6	9.7	5.77	59.5
9W	7	0025	685.6-733.6	48.0	8.25	17.2
10R	7	0140	733.6-743.3	9.7	2.17	22.4
11W	7	0430	743.3-791.5	48.2	9.65	20.0
12R	7	0555	791.5-801.1	9.6	4.05	42.2
13W	7	0900	801.1-849.4	48.3	9.64	20.0
14R	7	1020	849.4-859.1	9.7	2.18	22.5
15W	7	1315	859.1-907.3	48.2	6.72	13.9
16R	7	1445	907.3-916.7	9.4	3.36	35.7
17R	7	1615	916.7-926.4	9.7	4.98	51.3
18R	7	1755	926.4-936.1	9.7	0.60	6.2
19R	7	1910	936.1-945.7	9.6	4.64	48.3
20R	7	2050	945.7-955.4	9.7	4.97	51.2
21R	7	2220	955.4-965.1	9.7	3.16	32.6
22R	7	2350	965.1-974.8	9.7	4.86	50.1
23R	8	0205	974.8-984.5	9.7	4.77	49.2
24R	8	0415	984.5-994.2	9.7	5.35	55.1
				642.5	111.54	

Subunit IA (Depth: 0–66.3 mbsf)

Subunit IA consists of gradationally interbedded nannofossil ooze, foraminifer-nannofossil ooze, and marly nannofossil ooze. The marly nannofossil oozes commonly grade to foraminifer-bearing or diatomaceous marly nannofossil oozes. Beds range in thickness from 0.05 to 1.50 m, generally with gradational and burrow-mottled contacts. Bioturbation is minor to moderate throughout Subunit IA, although identifiable trace fossils are absent. Light beds range in color from light gray (5Y 7/1, 5Y 7/2) and light greenish gray (10Y 7/2, 10Y 6/2, 5GY 7/1) to light olive gray (5Y 6/2) and pale olive (5Y 6/3). Dark beds range from pale olive (5Y 6/3) to olive (5Y 5/4, 5Y 5/3, 5Y 4/3). Dark beds contain 5%–20% more silty clay and 5%–20% more diatoms than the light beds. The average calcium carbonate content in Subunit IA is 66%, with a range from 48% to 78% (Table 3; Fig. 5). The higher calcium carbonate contents occur in the lighter beds.

Smear slide analysis (Fig. 4) indicates that nannofossils are the dominant sedimentary component in Subunit IA, although clay and detrital calcite abundances equal or exceed nannofossil contents in some of the marly nannofossil ooze beds. Foraminifer abundances exceed 10% in the first two cores at Hole 731A (approximately 0–20 mbsf), but fall below 10% for the remainder of the subunit. Nannofossil abundances range from 25% to 70%, with highest values in the lighter beds. Diatom abundances vary from 0% to 20%, with highest values in a diatomaceous foraminifer-nannofossil ooze in Core 117-731A-2H, a diatomaceous marly nannofossil ooze in Core 117-731A-4H, and a diatomaceous nannofossil-rich silty clay in Core 117-731A-7H.

Clays and detrital calcite are the dominant terrigenous components, with abundances ranging from 5% to 30% for each; highest values are found in the darker beds of marly nannofossil ooze and calcitic silty clay. Other minerals present include quartz, mica, volcanic ash, dolomite, and opaque minerals, with abundances generally less than 5%.

Subunit IB (Depth: 66.3–146.5 mbsf)

Subunit IB also consists of alternating light and dark beds of nannofossil ooze and marly nannofossil ooze, but is distinguished from Subunit IA by the decreased abundance or absence of diatoms and foraminifers in smear slides (Fig. 4). Characteristics of the light and dark beds (colors, bedding thickness, and degree of bioturbation) are generally similar to those of Subunit IA, although white (5Y 8/1) nannofossil oozes and olive gray (5Y 4/2) to dark olive gray (5Y 3/2) nannofossil-rich calcitic silty clays are also observed in Subunit IB. Identifiable trace fossils, including *Planolites* and *Zoophycus*, are first identified in Subunit IB. Carbonate contents in Subunit IB average 67% and range from 46% to 85%, similar to the values in Subunit IA (Fig. 5; Table 3).

Smear slide analysis (Fig. 4) indicates that nannofossils remain the dominant sediment component in Subunit IB, with abundances ranging from 35% to 85%. As in Subunit IA, highest nannofossil contents occur in the lightest-colored beds. Foraminifer contents range from 0% to 8%, and average approximately 5%. Diatoms are present at abundances less than 5%, and are absent in much of Subunit IB. Clay contents range from 8% to 30%, averaging approximately 20%. Detrital calcite contents range from 0% to 30%, and average approximately 15%. Quartz abundances range from 0% to 10%, while mica, opaque minerals, and dolomite are present at abundances less than 5%.

Two unconformities are located within Subunit IB, and are tentatively located in Section 117-731A-10X, CC, to Core 117-731A-12X on the basis of nannofossil and radiolarian biostratigraphy (see "Biostratigraphy" section, this chapter). Although these unconformities presently are identified only from paleontological analysis, several lithostratigraphic features within these cores can be proposed as possible locations of the unconformities. The first hiatus superposes upper Pliocene sediments on lower Pliocene deposits, and lies between Sections 117-731A-10X, CC, and -11X-4. In contrast to the overlying beds, sharp contacts were observed at Section 117-731A-11X-1, 70 and 138 cm, while sharp and irregular contacts occurred at Section 117-731A-11X-2, 13, 45, 90, and 105 cm. The superjacent beds in Section 117-731A-11X-2 are distinctive in both color and degree of bioturbation, suggesting that the unconformity (or several smaller unconformities) occurs in that interval. The older unconformity superposes lower Pliocene sediments on upper Miocene deposits, and is located in Core 117-731A-12X. Sharp and irregular contacts occur at Section 117-731A-12X-6, 84-113 cm, while sharp bedding contacts occur at Section 117-731A-12X-7, 6-7 cm. These relationships suggest that the second hiatus at Site 731 is located within one of these intervals. More detailed biostratigraphic study will be required to locate these unconformities more precisely.

Unit II (Depth: 146.5–240.9 mbsf; Age: late Miocene)

Section 117-731A-16X-2, 60 cm, through Section 117-731A-25X-7.

Lithologic Unit II consists of alternating light and dark beds of nannofossil ooze/chalk, marly nannofossil ooze/chalk, diatomaceous marly nannofossil ooze/chalk, diatomaceous nannofossil-rich silty clay/claystone, and nannofossil-rich diatoma-

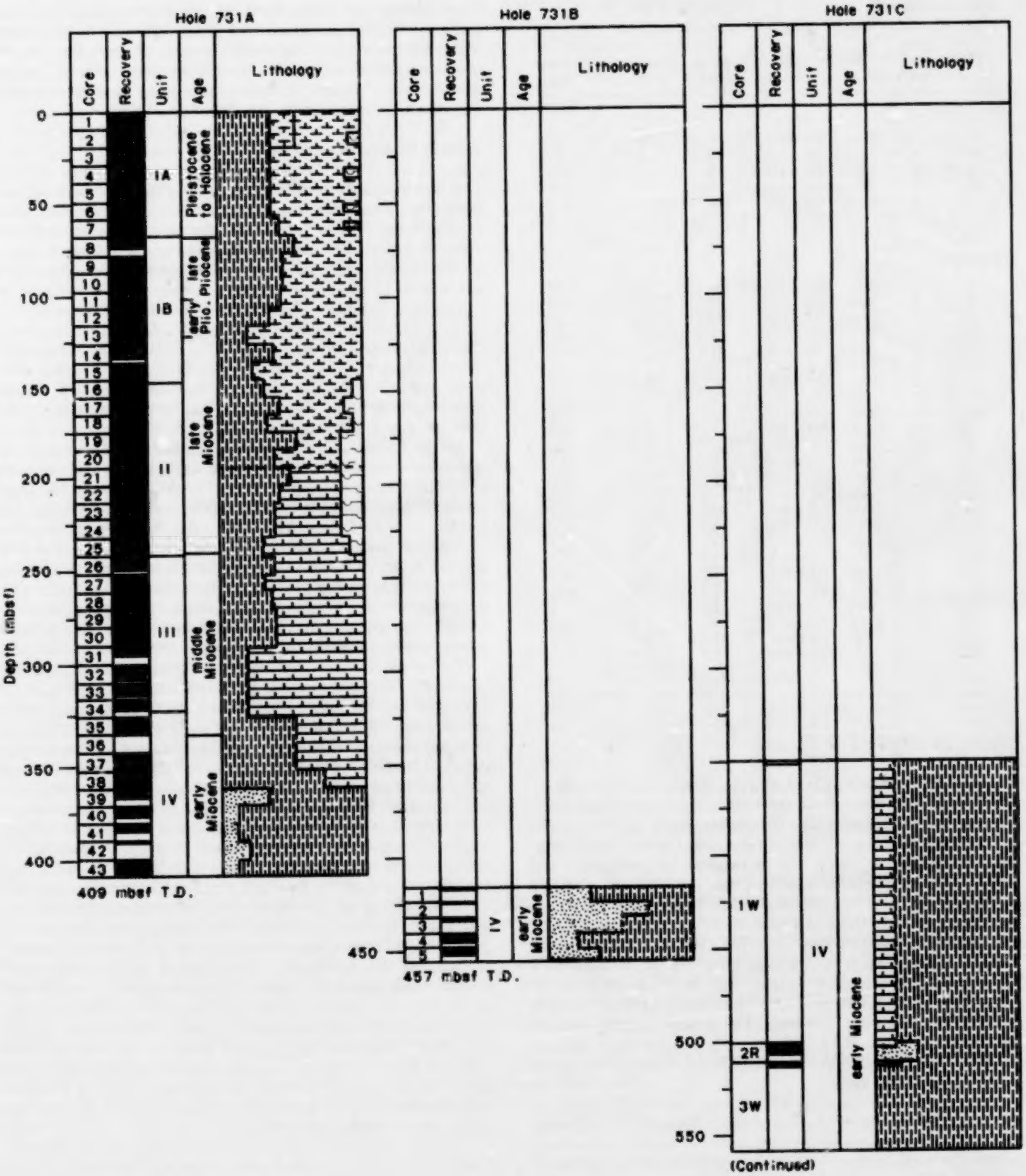

Figure 3. Lithostratigraphic summary, Site 731.

ceous mud/mudstone. Contacts between the light and dark beds are gradational. The transition from soft sediment (ooze/clay/mud) to lithified sediment (chalk/claystone/mudstone) is placed at the top of Core 117-731A-21X (192.8 mbsf). Colors of the light layers include light gray (5Y 7/1, 5Y 7/2, 5Y 6/1), light olive gray (5Y 6/2), light greenish gray (5GY 7/1, 10Y 7/2), and pale olive (5Y 6/3). The darker layers, which contain 20%–40% more terrigenous material and 5%–20% more diatoms than the light layers, are light olive gray (5Y 6/2), olive gray (5Y 5/2, 5Y 4/2), gray (5Y 6/1), olive (5Y 5/3, 5Y 4/3), and dark olive gray

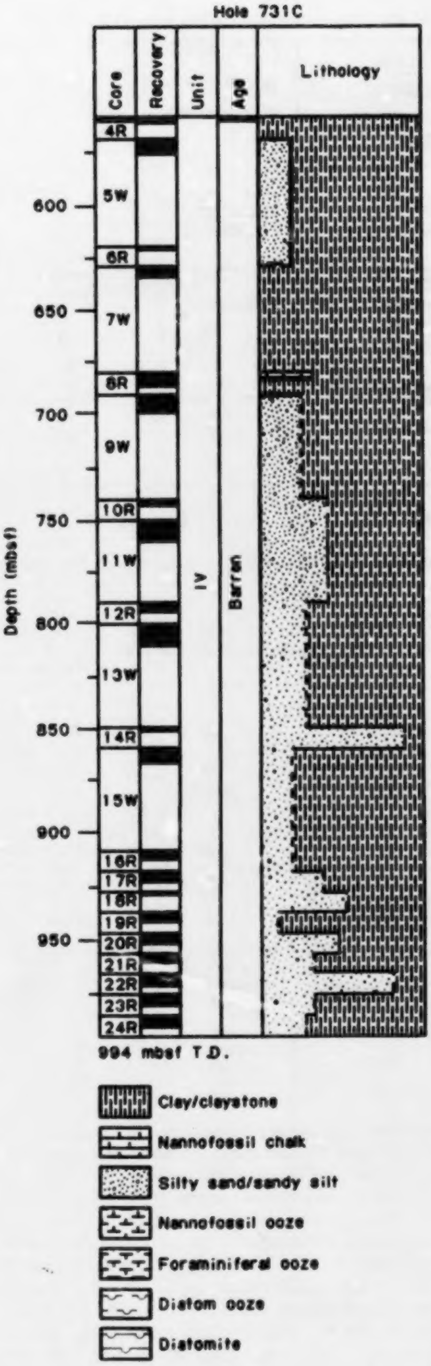

Figure 3 (continued).

(5Y 3/2). The calcium carbonate content (Table 3; Fig. 5) in lithologic Unit II averages 40%, and ranges from 9% to 77%, reflecting the increased, but variable, importance of biogenic silica and detrital components in that unit. Bed thicknesses generally range between 10 cm and 50 cm, with minor to common bioturbation, including *Zoophycus*, *Chondrites*, and *Planolites*. Purple concentric laminations around large burrows are first observed in Core 117-731A-25X, and are interpreted as redox halos, perhaps formed by the precipitation of dissolved Mn^{2+} or Fe^{2+} at a redox front surrounding the burrow. The concentric halos are best developed in the lighter layers, and become more common in Unit III.

Results of smear slide analyses (Fig. 4) reflect the compositional variability within lithologic Unit II and illustrate the compositional differences between lithologic Units I and II. Nannofossil abundances remain high in the light layers; values range from 50% to 75%. The light layers also contain 3%-7% diatoms, 0%-5% foraminifers, 0%-12% detrital calcite, and 16%-25% clay, so that their compositions are essentially unchanged from those of lithologic Unit I. The dark layers, however, have significantly different compositions, containing only 7%-35% nannofossils, but 10%-35% diatoms, 0%-5% radiolarians, 0%-2% foraminifers, 5%-22% detrital calcite, and 15%-40% clay. Sponge spicules, silicoflagellates, quartz, mica, and opaque minerals are all present in low abundances (0%-5%) throughout lithologic Unit II.

Lithologic Unit II is the youngest/shallowest interval at Site 731 that contains vertical to subvertical sets of parallel, millimeter-width, filled fractures. In some instances, millimeter-scale offsets are visible across these fractures, indicating microfaulting. These structures are well developed in the diatomaceous marly nannofossil chalks and nannofossil-rich diatomaceous mudstones of Cores 117-731A-21X and -24X. Similar features were previously observed at Sites 722 and 730 (see "Lithostratigraphy" sections, "Site 722" and "Site 730" chapters, this volume), also with best development in opal-rich horizons. The fracture sets often are closely associated with slumped intervals. These associations suggest that the fractures may result from volume changes during opal diagenesis, pressure or extension associated with slumping, or other causes. A better understanding of the implications of these structures for diagenetic, tectonic, and sediment loading histories will require more detailed shore-based study.

Although available biostratigraphic data do not indicate that unconformities are present in Core 117-731A-25X, the presence of angular fragments within that interval suggests that slumping probably has influenced that interval to some extent. The fragments are composed of olive (5Y 5/3) diatomaceous marly nannofossil chalk, reach dimensions of approximately 2 cm by 1 cm, and have well-defined edges with angular corners. The fragments are found in beds of light gray (5Y 7/1) nannofossil chalk, generally 5-20 cm above the underlying gradational contact. Burrows within the adjacent nannofossil chalk do not continue through the marly nannofossil chalk fragments. The composition, position, and unburrowed nature of the fragments suggests that they are transported rip-up clasts, while their shape and compositional similarity to underlying beds suggests that the distance of transport was small. Interpretations of the effect of mass movements on this portion of Unit II require further biostratigraphic, sedimentologic, and physical properties data.

Unit III (Depth: 240.9-320.1 mbsf; Age: middle to late Miocene)

Section 117-731A-25X-7, 31 cm, through Section 117-731A-34X-3, 60 cm.

Lithologic Unit III consists of interbedded nannofossil chalk, calcitic marly nannofossil chalk, and limited occurrences of nannofossil-rich calcitic silty claystone. Contacts between these lithologies are gradational. Color variations in the unit are less marked than in Unit II, with light layers ranging from white (5Y

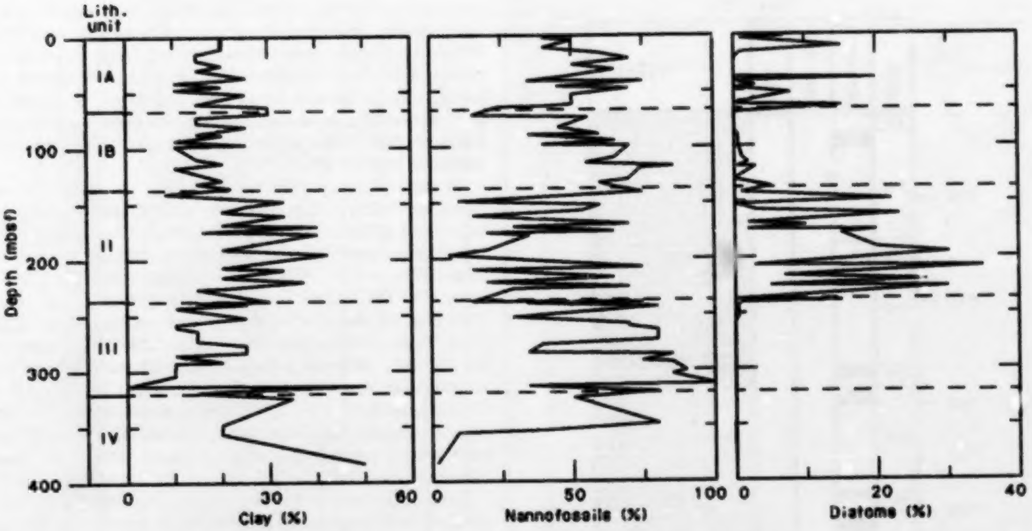

Figure 4. Abundances of clay, nannofossils, and diatoms in smear slides from Hole 731A, illustrating characteristic compositions of lithologic units. Roman numerals indicate lithologic units.

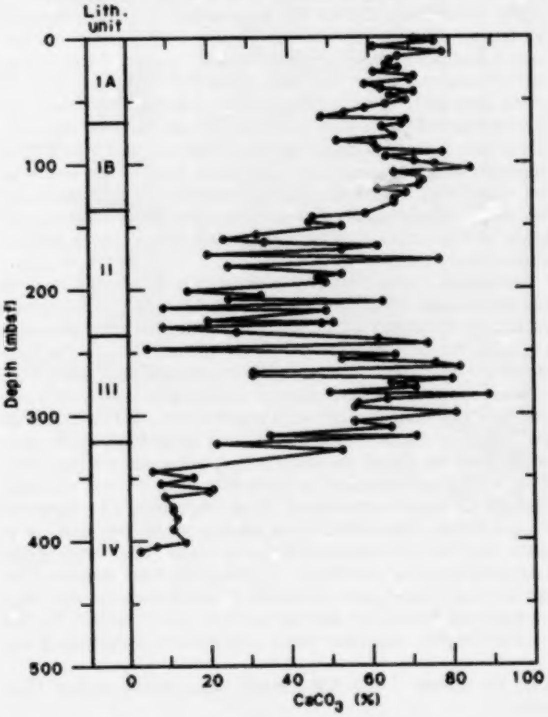

Figure 5. Calcium carbonate abundances, Site 731.

Table 2. Lithostratigraphic summary, Site 731.

Lithologic unit	Cores	Depth (mbsf)	Age
IA Nannofossil ooze, marly nannofossil ooze, nannofossil-foraminifer ooze, diatomaceous marly nannofossil ooze	731A-1H to -7H-6	0.0–66.3	Pleistocene/Holocene
IB Nannofossil ooze, marly nannofossil ooze	731A-7H-6 to -16X-2	66.3–146.5	late Miocene to early Pleistocene
II Nannofossil and marly nannofossil ooze/chalk to nannofossil-rich diatomaceous mud/mudstone	731A-16X-2 to -25X-7	146.5–240.9	late Miocene to middle Miocene
III Nannofossil chalk, marly nannofossil chalk	731A-25X-7 to -34X-3	240.9–320.1	middle Miocene
IV Interbedded siltstones to nannofossil chalk, mud turbidites, sand turbidites	731A-34X-3 to -43X; 731B-1X to -5X; 731C-1W to -24R	320.1–409.0 408.6–457.1 351.7–994.2	late Oligocene(?) to early Miocene

8/1) to light gray (5Y 7/1, 5Y 7/2, N7/), light greenish gray (5GY 7/1, 10Y 7/1, 5G 7/1), pale olive (5Y 6/3), and gray (5Y 6/1). Dark layers range from greenish gray (10Y 6/2, 10Y 5/2, 10Y 4/2, 5G 6/1, 5G 5/1, 5GY 6/1, 5GY 5/1) and gray (5Y 5/1) to olive (5Y 5/3, 5Y 5/4), olive gray (5Y 5/2), and brown (10YR 5/3). Bed thicknesses range from 0.01 m to greater than 1 m, and bioturbation is minor to abundant throughout Unit III. Purple redox(?) halos around large burrows (described for Unit II) are common in Unit III. Average calcium carbonate content in Unit III is 63%, with values ranging from 31% to 89% (Fig. 5; Table 3). The increased carbonate content reflects the absence of biogenic silica, which diluted the carbonate content of Unit II.

Smear slide analyses confirm the carbonate-rich nature of Unit III, with compositional ranges of 30%–90% nannofossils, 0%–30% detrital calcite, 10%–25% clay, 0%–2% foraminifers, and 0%–2% diatoms (Fig. 4). Other minerals are present in only trace amounts. Light layers generally contain 30%–40% more nannofossils than the dark layers, with correspondingly lower abundances of terrigenous material (clays and inorganic calcite).

Vertical to subvertical parallel sets of filled, millimeter-scale fractures and microfaults, described previously for Unit II, are also observed in Cores 117-731A-28X and -29X of Unit III. Unlike most other occurrences, these fracture sets are developed in

Table 3. Calcium carbonate and organic carbon contents, Site 731.

Core, section, interval (cm)	Depth (mbsf)	Total carbon (%)	Inorganic carbon (%)	Organic carbon (%)	$CaCO_3$ (%)
117-731A-					
1H-1, 96-98	0.96	9.95	8.58	1.37	71.5
1H-3, 80-82	3.80		9.12		76.0
1H-5, 80-82	6.80		7.38		61.5
2H-2, 80-82	12.10	9.62	9.36	0.26	78.0
2H-4, 80-82	15.10		8.15		67.9
2H-6, 80-82	18.10		7.83		65.2
3H-2, 80-82	21.60	8.56	7.77	0.79	64.7
3H-4, 80-82	24.60		8.07		67.2
3H-6, 80-82	27.60		7.43		61.9
4H-2, 80-82	31.10	9.03	8.52	0.51	71.0
4H-4, 80-82	34.10		8.40		70.0
4H-6, 80-82	37.10		7.16		59.6
5H-2, 80-82	40.60	7.79	7.58	0.21	63.1
5H-4, 80-82	43.60		8.56		71.3
5H-6, 80-82	46.60		7.84		65.3
6H-2, 80-82	50.10	8.89	8.29	0.60	69.1
6H-4, 80-82	53.10		7.68		64.0
6H-6, 80-82	56.10		7.09		59.1
7H-2, 80-82	59.60	6.73	6.50	0.23	54.2
7H-4, 80-82	62.60		5.81		48.4
7H-6, 80-82	65.60		8.28		69.0
8X-2, 64-66	69.14	8.72	8.22	0.50	68.5
8X-3, 81-83	70.81		7.56		63.0
9X-2, 80-82	79.00	9.50	7.98	1.52	66.5
9X-4, 80-82	82.00		6.32		52.7
9X-6, 39-41	84.59		7.43		61.9
10X-2, 80-82	88.70	8.00	7.50	0.50	62.5
10X-4, 80-82	91.70		9.46		78.8
10X-6, 80-82	94.70		7.68		64.0
11X-2, 92-94	98.42	9.48	8.60	0.88	71.6
11X-4, 92-94	101.42		9.13		76.1
11X-6, 92-94	104.42		10.27		85.6
12X-2, 80-82	108.00	8.39	8.01	0.38	66.7
12X-4, 77-79	110.97		8.73		72.7
12X-6, 77-79	113.97		8.80		73.3
13X-2, 84-86	117.74	8.98	8.70	0.28	72.5
13X-4, 82-84	120.72		7.49		62.4
13X-6, 99-101	123.89		8.30		69.1
14X-3, 77-79	128.77	8.34	8.01	0.33	66.7
14X-5, 75-77	131.75		7.94		66.1
15X-4, 100-101	140.20	7.59	7.16	0.43	59.6
15X-6, 62-64	142.82		5.58		46.5
16X-2, 103-105	146.93	6.15	5.50	0.65	45.8
16X-4, 121-123	150.11		6.36		53.0
17X-2, 125-127	156.75	5.02	3.87	1.15	32.2
17X-4, 123-125	159.73		2.91		24.2
17X-6, 113-115	162.63		4.19		34.9
18X-2, 101-103	166.21	8.15	7.53	0.62	62.7
18X-4, 61-63	168.81		6.41		53.4
18X-6, 100-102	172.20		2.44		20.3
19X-3, 86-88	177.26	9.46	9.27	0.19	77.2
19X-6, 92-94	181.82		3.03		25.2
20X-4, 67-69	188.27	7.13	6.36	0.77	53.0
20X-6, 30-32	190.90		5.73		47.7
21X-2, 56-58	194.86	6.50	5.99	0.51	49.9
21X-6, 48-50	200.78		1.87		15.6
22X-2, 99-101	204.99	4.68	4.01	0.67	33.4
22X-4, 98-100	207.98		3.06		25.5
22X-6, 20-22	210.20		7.60		63.3
23X-2, 70-72	214.40	2.79	1.18	1.61	9.8
23X-4, 70-72	217.40		5.97		49.7
24X-2, 108-110	224.48	3.76	2.47	1.29	20.6
24X-4, 69-71	227.09		6.21		51.7
24X-6, 18-20	229.58		1.14		9.5
25X-2, 90-92	234.00	4.77	3.33	1.44	27.7
25X-4, 94-96	237.02	5.80			48.3
25X-6, 90-92	240.00		7.49		62.4
26X-2, 100-102	243.80	9.00	8.97	0.03	74.7
26X-4, 100-102	246.80		0.68		5.7
27X-2, 79-81	253.19	8.21	8.01	0.20	66.7
27X-4, 52-54	255.92		6.46		53.8
27X-6, 120-122	259.60		9.14		76.1
28X-2, 59-61	262.69	10.07	9.84	0.23	82.0
28X-4, 63-65	265.73		3.77		31.4
28X-6, 58-60	268.68		3.77		31.4
29X-2, 80-82	272.50	9.91	9.70	0.21	80.8
29X-4, 91-93	275.61		7.81		65.1
29X-6, 92-94	278.62		8.54		71.1
30X-2, 71-73	282.11	6.28	6.08	0.20	50.7
30X-4, 76-78	285.16		10.71		89.2
30X-6, 116-118	288.56		7.74		64.5
31X-2, 51-53	291.61	7.06	6.95	0.11	57.9
31X-CC, 18-20	294.53		6.74		56.1
32X-1, 28-30	299.48	9.83	9.78	0.05	81.5
32X-5, 46-48	305.66		6.77		56.4
33X-2, 25-27	310.65	7.93	7.88	0.05	65.6
34X-1, 73-75	316.23	4.26	4.22	0.04	35.2
34X-2, 69-71	317.69		8.62		71.8
35X-1, 78-80	322.88	2.73	2.68	0.05	22.3
35X-5, 37-39	328.47		6.42		53.5
37X-3, 25-27	344.55	0.87	0.80	0.07	6.7
37X-6, 84-86	349.64		1.93		16.1
38X-3, 31-33	354.31	1.10	1.00	0.10	8.3
38X-6, 67-69	359.17		2.61		21.7
39X-1, 48-50	361.18	2.55	2.46	0.09	20.5
39X-3, 111-113	364.81		1.18		9.8
40X-2, 137-139	373.27	1.64	1.43	0.21	11.9
40X-4, 91-93	375.81		1.43		11.9
41X-2, 90-92	382.40	1.73	1.53	0.20	12.7
42X-1, 68-70	390.38	1.61	1.42	0.19	11.8
43X-2, 52-54	401.42	1.84	1.76	0.08	14.7
43X-4, 79-81	404.69		0.93		7.8
43X-6, 92-94	407.82		0.38		3.2
117-731B-					
1X-1, 17-19	408.77		1.43		11.9
2X-1, 34-36	418.64		1.11		9.3
3X-1, 80-82	428.90		1.60		13.3
4X-1, 80-82	438.50		1.63		13.6
4X-3, 47-49	441.17		1.22		10.2
5X-1, 40-43	447.80		1.36		11.3
117-731C-					
2R-2, 76-78	504.66		1.37		11.4
2R-3, 121-123	506.61		0.72		6.0
4R-1, 36-38	560.56		1.36		11.3
5W-4, 74-76	575.14		1.19		9.9
6R-1, 94-96	619.04		1.05		8.8
7W-1, 53-55	628.33		1.20		10.0
8R-1, 62-64	676.52		1.20		10.0
8R-4, 26-28	680.66		1.20		10.0
10R-1, 22-24	733.82		0.02		0.2
10R-2, 3-5	735.13		1.33		11.1
10R-2, 43-45	735.53		1.79		14.9
11W-5, 137-139	750.67		1.68		14.0
12R-1, 94-96	792.44		1.10		9.2
12R-2, 137-139	794.37		1.34		11.2
12R-3, 95-97	795.45		1.64		13.7
14R-1, 39-41	849.79		1.61		13.4
14R-2, 53-55	851.43		1.19		9.9
16R-1, 137-139	908.67		1.18		9.8
16R-2, 60-62	909.40		1.32		11.0
16R-3, 6-8	910.36		1.45		12.1
17R-2, 142-145	919.62		1.20		10.0
17R-4, 2-4	921.22		1.53		12.7
19R-1, 141-143	937.51		1.65		13.7
19R-3, 8-10	939.18		1.64		13.7
20R-1, 34-36	946.04		1.29		10.8
20R-3, 1-63	949.31		1.34		11.2
20R-4, 20-22	950.40		1.44		12.0
21R-1, 17-19	955.57		1.43		11.9
21R-2, 121-123	958.11		1.54		12.8
22R-2, 82-84	967.42		1.49		12.4
23R-2, 83-85	977.13		1.40		11.7
24R-2, 136-138	987.36		1.51		12.6

sediments that lack biogenic silica, suggesting that processes other than diagenetic volume changes of opal (see "Lithostratigraphy" section, "Site 722" chapter, this volume) can produce these structures. Angular clasts of marly nannofossil chalk, similar to those described at the base of Unit II, also occur in Section 117-731A-25X-5. This suggests that episodic slumping occurred throughout deposition of the sediments at the Unit III/Unit II transition. However, neither the clast occurrences nor the fracture development in Unit III provide further insight to the depositional, diagenetic, or deformational implications of these two types of features.

Unit IV (Depths: Hole 731A, 320.1–409.0 mbsf; Hole 731B, 408.6–457.1 mbsf; Hole 731C, 351.7–994.2 mbsf; Age: late Oligocene(?) to early Miocene)

Section 117-731A-34X-3, 60 cm, through Core 117-731A-43X; Core 117-731B-1X through 117-731B-5X; Cores 117-731C-1W through 117-731C-24R.

The top of lithologic Unit IV is defined by the top of the uppermost (youngest) clastic-based turbidite, based on criteria used at Site 721 and 722 (see "Lithostratigraphy" sections, "Site 721" and "Site 722" chapters, this volume). Although Unit IV is dominated by turbidites, the relative abundances of biogenic carbonate, coarse detrital components, and fine-grained detrital components can be used to distinguish three separate lithofacies. These are characterized as follows:

1. Mixed turbidite-carbonate lithofacies: The mixed turbidite-carbonate lithofacies is best-developed at the top of Unit IV, where it forms a transitional zone between the carbonate chalks of Unit III and the terrigenous turbidites that occur below 360 mbsf (Section 117-731A-38X-6, 95 cm). This lithofacies also occurs in Cores 117-731C-1W to -3W, -7W, -8R, and -13W as thin (< 20 cm thick) intervals; upper and lower contacts of these occurrences are generally obscured or destroyed by drilling disturbance. This lithofacies is characterized by clayey siltstones/silty claystones interbedded with nannofossil chalk, forming beds that grade from basal terrigenous sediments to biogenic carbonate caps. The silty claystones to clayey siltstones are generally sharp-based and thin (< 10 cm), with colors of greenish gray (5GY 5/1, 5G 6/1, 5BG 5/1), gray (5Y 5/1), olive gray (5Y 4/2), dark gray (N4/) and dark greenish gray (5GY 4/1). The carbonate caps are bioturbated nannofossil chalks to marly nannofossil chalks, with colors of olive gray (5Y 5/2) and gray (5Y 6/1) to light gray (10YR 7/1), or brown (10YR 5/3) and grayish brown (10YR 5/2) to light grayish brown (10YR 6/2). Complete gradational sequences range from 10 cm to approximately 60 cm in thickness. Calcium carbonate contents in the lithofacies average 21%, but vary from 6% in a basal turbidite to 53% in a carbonate cap (Table 3; Fig. 5). Smear slide analyses also reflect this compositional variability, with one basal turbidite containing 10% nannofossils, 40% quartz, 20% clay, and 30% detrital calcite (Fig. 4). One carbonate cap, however, contains 80% nannofossils and 20% clay.

2. Mud turbidite lithofacies: The second lithofacies in Unit IV occurs below 360 mbsf, and consists of gradationally interbedded clayey siltstones or siltstones and silty claystones. The interbedded lithologies form fining-upward beds 3–30 cm thick; they generally begin with a sharp-based or scoured contact and parallel-laminated siltstone or clayey siltstone, and grade upward to uniform silty claystone (Fig. 6). The upper 1–5 cm of the beds is commonly bioturbated. Ripple cross-lamination and low angle cross-stratification are observed in a few of the basal siltstones, and slumping and dewatering structures are rarely present in the silty claystones. The fining-upward beds are commonly stacked, forming intervals of repeated mud turbidites as thick as 3 m. Colors are relatively uniform through this lithofacies, including dark gray (N4/, 5Y 4/1, 10YR 4/1), dark greenish gray (5BG 4/1, 5GY 4/1, 5B 4/1, 5G 4/1), dark brown (10YR 4/3, 10YR 3/3), dark grayish brown 10YR 4/2, 10YR3/2), and very dark gray (5Y 3/1). Calcium carbonate contents are low below 360 mbsf, and average approximately 10% (Fig. 5; Table 3), with detrital calcite providing most of the carbonate seen in Unit IV. Smear slide analyses indicate that quartz, clay, and detrital calcite are the dominant constituents of the mud turbidite lithofacies. Abundances range from 15% to 50% quartz, 10%–70% clay, and 10%–30% detrital calcite. Quartz and detrital calcite are generally enriched in the siltstone and clayey siltstone intervals, while clays dominate in the silty claystones. Feldspar, mica, volcanic ash, heavy minerals, and opaque minerals are present at abundances of 0%–5% each.

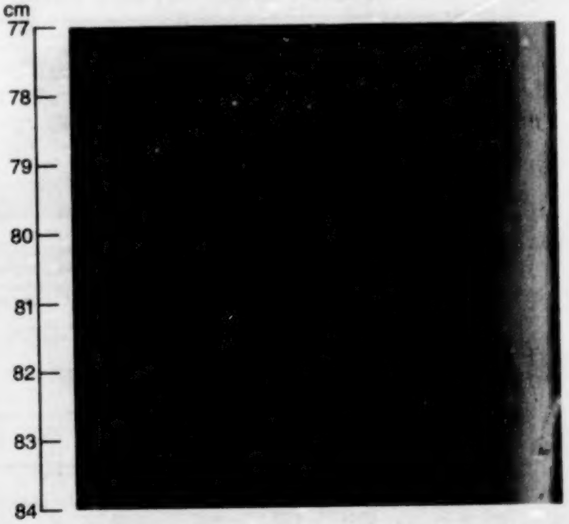

Figure 6. Photograph of the mud turbidite lithofacies in Unit IV, showing a stacked sequence of fining-upward, siltstone to claystone beds (Section 117-731C-12R-2, 77–84 cm).

3. Coarse-grained turbidite lithofacies: The third lithofacies in Unit IV is characterized by significant amounts of coarse-grained clastics, including silty sandstones/sandy siltstones and sandstones. These coarser clastics occur in two modes: either as the coarse-grained base of a fining-upward sequence, which can extend into a siltstone or a thin silty claystone cap, or as a discrete, ungraded to slightly fining-upward, coarse-grained bed, generally with sharp upper and lower contacts. Bed thicknesses range from approximately 10 cm to as much as 150 cm in both modes of occurrence. Primary sedimentary structures are rare to absent in the coarse-grained turbidites, with a diffuse parallel lamination as the most common structure. The sandstones and siltstones are dominated by quartz and detrital calcite, with feldspars, amphiboles, pyroxenes, mica, and opaque minerals also present. Rock fragments, including chert and chlorite-rich schist, are present in trace amounts. The sandstones in the coarse-grained turbidite lithofacies are commonly poorly cemented and friable; locally, however, the sandstones are heavily cemented with calcite. The cemented intervals show no significant difference in grain composition from the weakly cemented sandstones.

Within Unit IV, the mixed turbidite-carbonate lithofacies is generally restricted to depths shallower than 360 mbsf. The mud turbidite lithofacies and the coarse-grained turbidite lithofacies, however, are not depth-restricted in the interval from 360 to 994 mbsf. The relative abundances of these two lithofacies are generally represented by the proportions of coarse clastics and fine clastics shown in Figure 3. The data from Hole 731C suggest a general downhole increase in the importance of coarse clastics, which is supported by the results of downhole logging (see "Downhole Measurements" section, this chapter). The lithologic summary from Hole 731B, however, indicates that coarse clastics are also important within the upper portions of Unit IV.

Discussion

Site 731

The sequence of lithostratigraphic units at Site 731 records the tectonic evolution of the Owen Ridge and variations in marine planktonic productivity, dissolution, and terrigenous sediment supply from the Oligocene to the Holocene. Deposition at Site 731 during the late Oligocene(?) to early middle Miocene was dominated by terrigenous turbidites, and coarse-grained and fine-grained sediments apparently were supplied by distinct depositional processes. The intervals of stacked mud turbidites represent deposition by repeated low-velocity events (predominantly from suspended load), perhaps either downfan from distributary channels or in overbank regions away from leveed distributaries. The interbedded coarse-grained turbidite lithofacies, however, indicates that coarse clastic input to Site 731 was sustained episodically, perhaps by distributary channel migration or by sand transport to distal lobe depocenters during early stages of Indus Fan construction (predominantly by bed-load transport).

The coarse-grained turbidite and the mud turbidite lithofacies are interbedded throughout the interval from 360 to 994 mbsf, so that no large-scale fining-upward trend is evident in sediments recovered from that portion of Unit IV. The absence of such a trend indicates that both bed-load and suspended load depositional processes were active into the middle Miocene at Site 731; this suggests that relatively stable depositional conditions were maintained until that time. Turbidite influence decreased and pelagic carbonate deposition was periodically important at Site 731 during the late early to middle Miocene, producing the mixed turbidite-carbonate lithofacies at the top of Unit IV. This transition in depositional style reflects the tectonic uplift of the Owen Ridge, which moved Site 731 above the level of turbidite deposition during the middle Miocene. Owen Ridge uplift, however, began in the early Miocene (Whitmarsh, 1974), indicating that Site 731 was not affected by the first stages of uplift. The relatively rapid change from interbedded coarse-grained and mud turbidites to the mixed carbonate-turbidite lithofacies suggests that uplift at Site 731, once initiated, quickly influenced deposition at that site. The relatively thin transitional zone (the mixed turbidite-carbonate lithofacies) may record relatively rapid uplift of Site 731 through the zone of episodic turbidite suspended-load deposition.

During the middle Miocene, Site 731 was uplifted above the zone of turbidite influence, and pelagic deposition became dominant. The decrease in turbidite supply is recorded by a decrease in sedimentation rate above 305 mbsf (see "Accumulation Rates" section, this chapter). Because of the loss of turbidite input, the major controls on sedimentation became the rates of supply and preservation of biogenic calcium carbonate and biogenic silica, and the rate of terrigenous supply, which was probably dominated by eolian processes (Kolla et al., 1981).

During the middle Miocene, carbonate was the dominant biogenic constituent, producing the nannofossil chalks and marly nannofossil chalks of Unit III. Abundant bioturbation in Unit III records the presence of oxygenated bottom waters throughout this time. Relatively low organic carbon contents in Unit III (see "Organic Geochemistry" section, this chapter) indicate conditions of low productivity and/or significant organic matter recycling in the water column and surface sediments.

The planktonic productivity/preservation signal changed at approximately the beginning of the late Miocene, however, with the onset of significant biosiliceous sedimentation in Unit II. Smear slide data show that diatom abundances reach their maximum within 20 m of the base of Unit II, and gradually decrease above that level. Diatom-poor nannofossil oozes/chalks and marly nannofossil oozes/chalks are interbedded throughout Unit II, recording repeated fluctuations in the biogenic carbonate vs. biogenic silica production/preservation balance through the late Miocene. Organic carbon contents are generally high but variable in Unit II, perhaps recording both increased productivity and enhanced preservation at this time. Bioturbation in Unit II again records the presence of oxygenated bottom waters, but an increased sedimentation rate (observed above 205 mbsf; see "Accumulation Rates" section, this chapter) may have enhanced both organic carbon and opal preservation at that time.

Biogenic carbonate also dominates pelagic input from the upper Miocene to the Holocene, producing the nannofossil oozes and marly nannofossil oozes of Unit I. More variable conditions of production and preservation are indicated by Subunit IA, with its variable biosiliceous and organic carbon contents (see "Organic Geochemistry" section, this chapter).

Reduced sedimentation rates and/or the presence of unconformities through the Pliocene section at Site 731 may limit its usefulness for high resolution studies. The enhanced record of biogenic silica production and preservation in Units IA and II at Site 731, however, will provide data for valuable comparisons with the correlative records at Sites 721 and 722.

BIOSTRATIGRAPHY

Introduction

Site 731 was the third site drilled on the crest of the Owen Ridge after Sites 721 and 722. Planktonic microfossil biostratigraphy has been established for this site and is depicted in Figures 7, 9, and 10. Planktonic foraminifers are abundant to common with good preservation in the five uppermost core-catcher samples (down to 47.8 mbsf) in Hole 731A. Below this interval down to 308.9 mbsf, the planktonic foraminifers are rare and the preservation is poor; sediments below 308.9 mbsf are barren of planktonic foraminifers. Benthic foraminifers are abundant down to 86.4 mbsf, common from this level down to 154.0 mbsf, and rare to few from this level down to 299.2 mbsf. Below 299.2 mbsf, benthic foraminifers are few with poor preservation.

Throughout the length of Hole 731A, preservation states of the calcareous nannofossils show many changes, but they remain abundant down to 289.6 mbsf. From this level down to the bottom of the hole abundance varies from barren to abundant. Preservation of the nannofossils is poor below 370.1 mbsf. All five samples in Hole 731B were barren of nannofossils. Nannofossils range from abundant to barren throughout Hole 731C, but the preservation is poor, with all of the specimens being heavily overgrown.

Radiolarians are present in Hole 731A down to 279.9 mbsf but below this level the sediments are barren of radiolarians. Few specimens are present in the two uppermost core catcher samples, and the preservation is moderate to good. From 28.8 to 192.8 mbsf there is an increase in the abundance and the state of preservation of the radiolarians, while from 202.5 mbsf to 221.9 mbsf we noted a slight decrease in the abundance and

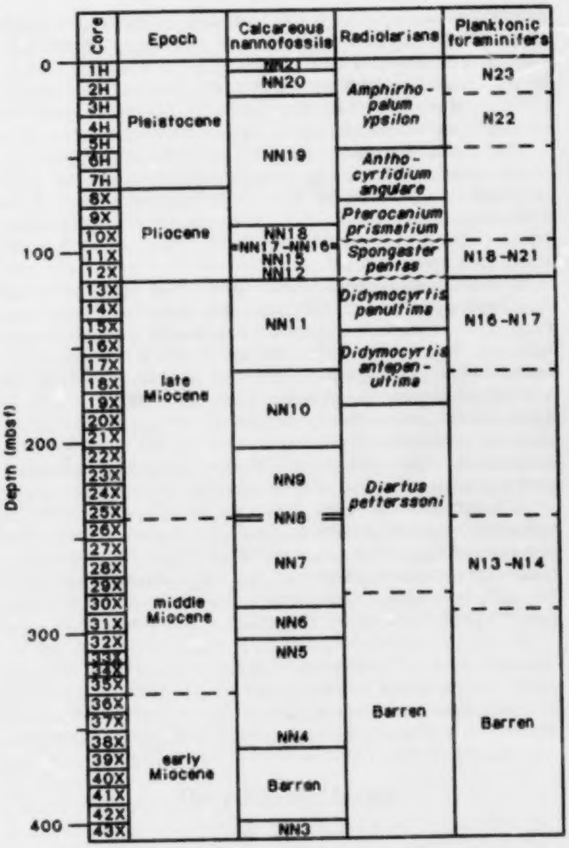

Figure 7. Correlation of planktonic microfossil groups in Hole 731A.

state of preservation of radiolarians. In 117-731A-28X, CC, and -29X, CC (270.2–279.9 mbsf), radiolarians are rare and many have been pyritized. Diatoms are common from 154.0 mbsf to 260.6 mbsf. Holes 731B and 731C are barren of siliceous microfossils.

Two hiatuses have been recognized based on the radiolarian data. Some of the middle Pliocene (2.4 Ma to less than 3.4 Ma) and lowermost Pliocene to uppermost Miocene (around 4.3 Ma to 6.1 Ma) sediments appear to be missing at this site. The calcareous nannofossil zonal markers are missing in this part of the sequence so it is nearly impossible to recognize a hiatus in Hole 731A. A plot of faunal datum levels and paleomagnetic reversals vs. depth below sea level is presented in Figure 8; for a detailed listing see Table 4.

Planktonic Foraminifers

The drilled sequence in Hole 731A contains abundant to common and well-preserved planktonic foraminifers in the interval from 9.8 to 47.8 mbsf (Samples 117-731A-1H, CC, through 117-731A-5H, CC), which is composed of Pleistocene marly-nannofossil oozes. Rare and poorly preserved specimens were found in Samples 117-731A-6H, CC, through 117-731A-32X, CC (57.3–308.9 mbsf). This part of the sequence ranges from the Pliocene to the middle Miocene. The underlying sediments, which are comprised of sandy turbidites, did not yield planktonic foraminifers.

The first appearance of *Globigerinella calida calida* was noted in Sample 117-731A-2H, CC (19.3 mbsf), which marks the lower limit of Zone N23. The lower boundary of Zone N22, which is based on the first appearance (FA) of *Globorotalia truncatulinoides*, was found in Sample 117-731A-5H, CC (47.8 mbsf). However, the boundary is not reliable because this species is very rare in this area. Other foraminifers are also rare, and thus the Pleistocene/Pliocene boundary could not be approximated.

A Pliocene foraminiferal assemblage was noted in Sample 117-731A-11X, CC (105.7 mbsf), which was assigned to Zones N19 to N21. A substantial hiatus occurs somewhere in this interval because the Pliocene is too condensed (see "Calcareous Nannofossils" and "Radiolarians" discussions below).

Upper Miocene sediments range from Sample 117-731A-13X, CC, through 117-731A-17X, CC (125.0–163.7 mbsf), pointed out by *Globorotalia tumida merotumida* and *Globorotalia tumida plesiotumida* (Zones N16–N17). The lower limit of this zone is not its true boundary as the underlying sediments are barren of planktonic foraminifers.

The presence of *Globorotalia mayeri* and the lack of *Globorotalia fohsi* in Samples 117-731A-26X, CC, through 117-731A-30X, CC (250.9–289.6 mbsf), indicate middle Miocene sediments (Zones N13–N14). The remainder of the section does not contain planktonic foraminifers.

Benthic Foraminifers

The benthic foraminiferal fauna of Site 731 was studied in the core catchers of Hole 731A. Benthic foraminifers are abundant and well-preserved in the upper part of the sequence (Samples 117-731A-1H, CC, through -9X, CC; 9.8–86.4 mbsf). Below 86.4 mbsf, benthic foraminifers are common and moderately well preserved. Below Sample 117-731A-16, CC (154.0 mbsf), the benthic foraminifers are few to rare and poorly preserved. Samples below Sample 117-731A-31X, CC (299.2 mbsf), are essentially barren with only a few poorly preserved specimens in some of the samples. The core catchers of Hole 731B and 731C were all within the turbiditic sequence and were barren. The preservation is good in the upper 115 m below which it becomes moderate to poor. Pyritized benthic and planktonic foraminiferal tests are abundant throughout the sequence studied.

The P/B (planktonic/benthic) ratio is above 90% in the uppermost seven samples (down to 67.0 mbsf); it decreases and remains low (0%–25%), with the exception of a few excursions at around 105 and 145 mbsf, down to Sample 117-731A-25X, CC (241.3 mbsf). Below 241.3 mbsf, the P/B ratio increases to more than 75% and is continuously high down to the level where both benthic and planktonic foraminifers disappear (299.2 mbsf).

The benthic foraminiferal fauna can be divided into three slightly different assemblages. Assemblage I is present in the uppermost seven samples (9.8–67.0 mbsf) and is characterized by high relative abundances of *Cassidulina carinata, Chilostomella oolina, Epistominella exigua, Globocassidulina subglobosa*, and *Pullenia subcarinata*. Additional species are *Ehrenbergina trigona, Melonis barleeanum, Pullenia bulloides, Sigmoilinopsis schlumbergeri*, and *Uvigerina peregrina*.

Assemblage II dominates the fauna in the interval 76.7–115.4 mbsf and is characterized by high relative abundances of *Melonis pompilioides*. Additional species are *Eggerella bradyi, Pullenia bulloides, Quadrimorphina laevigata* A, *Sigmoilopsis schlumbergeri*, and *Uvigerina spinicostata*.

Assemblage III is present below 125.0 mbsf and is characterized by high relative abundances of *Cibicidoides wuellerstorfi, Melonis pompilioides*, and *Pullenia bulloides*. Species present in lower relative abundances are *Eggerella bradyi, Globocassidulina subglobosa, Laticarinina halophora*, and *Melonis barleeanum*.

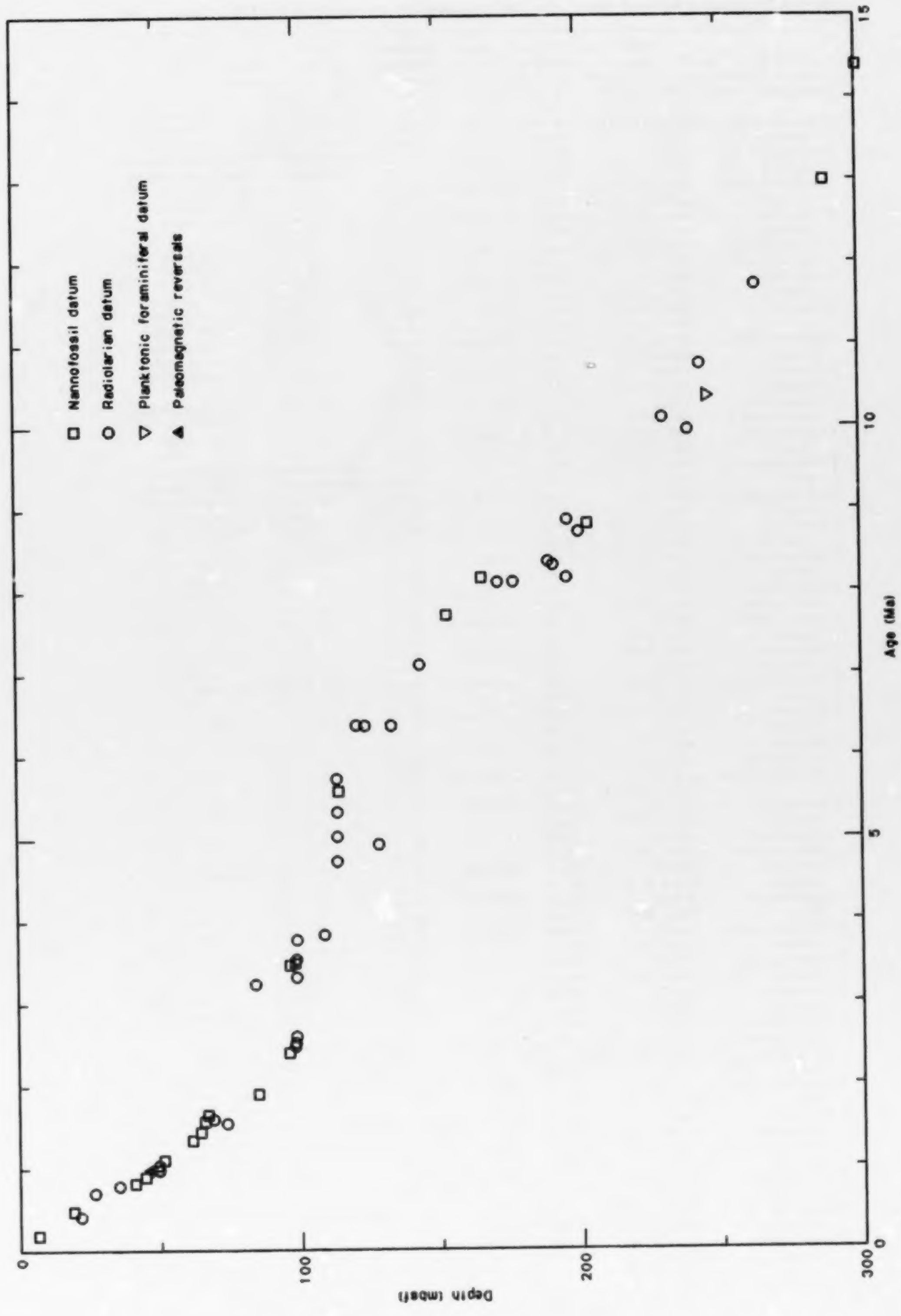

Figure 8. Age-depth plot for Hole 731A. For a detailed listing of events see Table 4.

Table 4. Stratigraphic listing of faunal events and paleomagnetic reversals for Hole 731A.

Event	Core level	Depth (mbsf)	Age (Ma)	Source of age	Notes
B *Emiliania huxleyi*	1H-4, 115–117 1H-5, 115–117	5.62 7.15	0.19	3	
T *Pseudoemiliania lacunosa*	2H-6, 115–117 2H-CC	18.45 19.30	0.49	3	
T *Stylatractus universus*	2H-CC 3H-4, 85–87	19.30 24.65	0.37–0.46	1	Cores MD81-369, RC14-22 and VM34-35; DSDP 214 data probably less accurate.
T *Anthocyrtidium nosicoae*	3H-4, 85–87 3H-CC	24.65 28.80	0.66–0.76	1	
B *Pterocorys hertwigii*	4H-4, 85–87 4H-CC	34.15 38.30	0.76–0.84	1	
T *Reticulofenestra* sp. A (acme)	5H-2, 115–117 5H-3, 115–117	40.95 42.45	0.82	3	
B *Gephyrocapsa parallela*	5H-4, 115–117 5H-5, 115–117	43.95 45.45	[a]0.89	4	
B Jaramillo	5H-5, 115–117 5H-6, 45–47	45.45 46.25	0.98	6	
T *Anthocyrtidium angulare*	5H-CC 6H-4, 85–87	47.80 53.15	0.94–1.04	1	
B *Lamprocyrtis nigriniae*	5H-CC 6H-4, 85–87	47.80 53.15	1.02–1.07	1	
T *Lamprocyrtis neoheteroporos*	5H-CC 6H-4, 85–87	47.80 53.15	0.94–1.04	1	
T *Gephyrocapsa* "large"[b]	6H-3, 115–117 6H-4, 115–117	51.95 53.45	[a]1.10	4	
T *Helicosphaera sellii*	6H-6, 115–117 6H-CC	56.45 57.30			No good published ages; event may be diachronous.
B *Gephyrocapsa* "large"[b]	7H-3, 115–117 7H-4, 115–117	61.45 62.95	[a]1.36	4	
T *Calcidiscus macintyrei*	7H-5, 115–117 7H-6, 115–117	64.45 65.95	1.45	6	
B *Gephyrocapsa oceanica*	7H-6, 115–117 7H-CC	65.95 67.00	[a]1.57	4	
B *Gephyrocapsa caribbeanica*	7H-CC 8X-1, 115–117	67.00 68.15	[c]1.66	4,8	
B *Anthocyrtidium angulare*	7H-CC 8X-4, 85–87	67.00 72.35	1.52–1.64	1	
T *Pterocanium prismatium*	8X-4, 85–87 8X-CC	72.35 76.70	1.52–1.56	1	
T *Phormostichoartus fistula*	9X-4, 85–87 9X-CC	82.05 86.40	3.26–3.28	1	? Too high; possible reworking.
T *Discoaster brouweri*	9X-5, 115–117 9X-CC	83.85 86.40	1.9	6	
T *Discoaster pentaradiatus*	10X-CC 11X-1, 115–117	96.00 97.15	2.4	6	
T *Sphenolithus abies*	10X-CC 11X-1, 115–117	96.00 97.15	3.47	6	
B *Theocalyptra davisiana*	10X-CC 11X-4, 85–87	96.00 101.35	2.42–2.44	1	
B *Lamprocyrtis neoheteroporos*	10X-CC 11X-4, 85–87	96.00 101.35	2.51–2.53	1	
T *Stichocorys peregrina*	10X-CC 11X-4, 85–87	96.00 101.35	2.62–2.64	1	
T *Lychnodictyum audax*	10X-CC 11X-4, 85–87	96.00 101.35	3.33–3.35	1	
T *Phormostichoartus doliolum*	10X-CC 11X-4, 85–87	96.00 101.35	3.53–3.55	1	
B *Amphirhopalum ypsilon*	10X-CC 11X-4, 85–87	96.00 101.35	3.77–3.79	1	
T *Didymocyrtis penultima*	10X-CC 11X-4, 85–87	96.00 101.35			
T *Reticulofenestra pseudoumbilica*	11X-1, 115–117 11X-2, 116–118	97.15 98.66	3.5	6	
T *Spongodiscus ambus*	11X-4, 85–87 11X-CC	101.35 105.70			
B *Spongaster tetras tetras*	11X-CC 12X-4, 85–87	105.70 111.05	3.83–3.85	1	
T *Spongaster berminghami*	11X-CC 12X-4, 85–87	105.70 111.70			
T *Stichocorys johnsoni*	12X-4, 85–87 12X-CC	111.05 115.40	5.7–5.8	[d]2	
T *Solenosphaera omnitubus*	12X-4, 85–87 12X-CC	111.05 115.40	4.7–4.8	2	
T *Acrobotrys tritubus*	12X-4, 85–87 12X-CC	111.05 115.40	5.3–5.4	2	Rare in Site 731.
T *Siphostichartus corona*	12X-4, 85–87 12X-CC	111.05 115.40	5.0–5.1	2	

Table 4 (continued).

Event	Core level	Depth (mbsf)	Age (Ma)	Source of age	Notes
T *Stichocorys delmontensis*	12X-4, 85–87	111.05			
	12X-CC	115.40			
T *Discoaster quinqueramus*	12X-5, 115–117	112.85	5.6	6	Age appears to be erroneous.
	12X-6, 115–177	114.35			
B *Spongodiscus ambus*	12X-CC	115.40			
	13X-4, 85–87	120.70			
S. delmontensis → *S. peregrina*	12X-CC	115.40	6.1–6.7	2	
	13X-CC	125.00			
T *Calocycletta caepa*	13X-4, 85–87	120.70	[e]6.2–6.6	2	
	13X-CC	125.00			
T *Botryostrobus bramlettei*	13X-CC	125.00	4.9–5.0	2	Should be higher.
	14X-4, 85–87	130.35			
B *Stichocorys peregrina*	13X-CC	125.00			
	14X-4, 85–87	130.35			
T *Didymocyrtis antepenultima*	14X-4, 85–87	130.35			
	14X-CC	134.70			
B *Solemosphaera omnitubus*	14X-4, 85–87	130.35	6.3–6.5	2	
	14X-CC	134.70			
T *Diartus hughesi*	15X-4, 85–87	140.95	7.1–7.2	2	
	15X-CC	144.40			
T *Dictyocoryne ontongensis*	16X-4, 85–87	149.75			
	16X-CC	154.00			
B *Acrobotrys tritubus*	16X-4, 85–87	149.75	7.7–7.8	2	Rare in Site 731.
	16X-CC	154.00			
B *Discoaster quinqueramus*	17X-CC	163.70	8.2	6	
	18X-1, 135–137	165.05			
T *Botryostrobus miralestensis*	18X-4, 85–87	169.05	8.1–8.2	2	
	18X-CC	173.40			
T *Diartus petterssoni*	18X-CC	173.40	8.1–8.2	2	
	19X-4, 85–87	178.75			
T *Didymocyrtis laticonus*	19X-4, 85–87	178.75			
	19X-CC	183.10			
D. petterssoni → *D. hughesi*	19X-4, 85–87	178.75	8.3–8.5	2	
	21X-4, 85–87	198.15			
T *Stichocorys wolffii*	20X-4, 85–87	188.45	[e]8.1–8.2	2	
	20X-CC	192.80			
B *Spongaster berminghami*	20X-CC	192.80	7.9–8.0	2	
	21X-4, 85–87	198.15			
B *Botryostrobus bramlettei*	20X-CC	192.80	8.8–9.0	2	
	21X-4, 85–87	198.15			
B *Diartus hughesi*	21X-4, 85–87	198.15	8.7–8.8	2	
	21X-CC	202.50			
T *Discoaster hamatus*	21X-CC	202.50	8.85	6	
	22X-1, 129–131	203.79			
T *Cyrtocapsella japonica*	24X-4, 85–87	227.25	10.0–10.3	2	
	24X-CC	231.60			
B *Discoaster hamatus*	25X-5, 115–116	238.75	10.0	6	
	25X-6, 115–116	240.25			
T *Globorotalia mayeri*	25X-CC	241.30	10.4	[f]6	
	26X-CC	250.90			
B *Catinaster coalitus*	25X-CC	241.30	10.8	6	
	26X-3, 117–119	245.47			
T *Lithopera thornburgi*	27X-4, 85–97	256.27			
	27X-CC	260.60			
T *Cyrtocapsella cornuta*	27X-CC	260.60	11.6–11.9	2	
	28X-4, 85–87	265.96			
B *Discoaster kugleri*	30X-5, 115–116	287.05	13.1	6	
	30X-CC	289.60			
T *Sphenolithus heteromorphus*	31X-CC	299.20	14.4	6	
	32X-1, 115–116	300.35			

Note: T = upper limit, B indicates lower limit, and → = an evolutionary transition. Sources of ages are: 1 = Johnson et al., in press; 2 = Johnson and Nigrini, 1985; 3 = oxygen isotope data for Site 723 (N. Niitsuma, unpubl. data); 4 = Takayama and Sato, 1987; 6 = Berggren et al, 1985; and 8 = Sato et al., in press.

[a] North Atlantic data.

[b] Long axis greater than 6 μm.

[c] North Atlantic age consistent with Italian-type section.

[d] *E.* cf. *diaphanes* cited in this source.

[e] Age in western Pacific.

[f] *G. siakensis* cited in this source.

Calcareous Nannofossils

Hole 731A

Sample 117-731A-1H-5, 115–117 cm (5.62 mbsf), contains *Emiliania huxleyi* and is assigned to Pleistocene-Holocene Zone NN21. Samples 117-731A-1H-5, 115–117 cm (7.15–18.45 mbsf) contain neither *Emiliania huxleyi* nor *Pseudoemiliania lacunosa*, and are therefore assigned to Pleistocene Zone NN20 (Fig. 9).

Sediments from 19.3 mbsf down to 83.85 mbsf (Samples 117-731A-2H, CC through 117-713A-9X-5, 115–117 cm) contain *P. lacunosa*, but no discoasters and are assigned to Zone NN19 (uppermost Pliocene to Pleistocene). In Samples 117-731A-7H, CC (67.0 mbsf), and -8X, CC (76.6 mbsf), we recognized some reworked Miocene and Pliocene species such as *Cyclicargolithus floridanus, Discoaster brouweri, D. quinqueramus, Reticulofenestra pseudoumbilica*, and *Sphenolithus moriformis*.

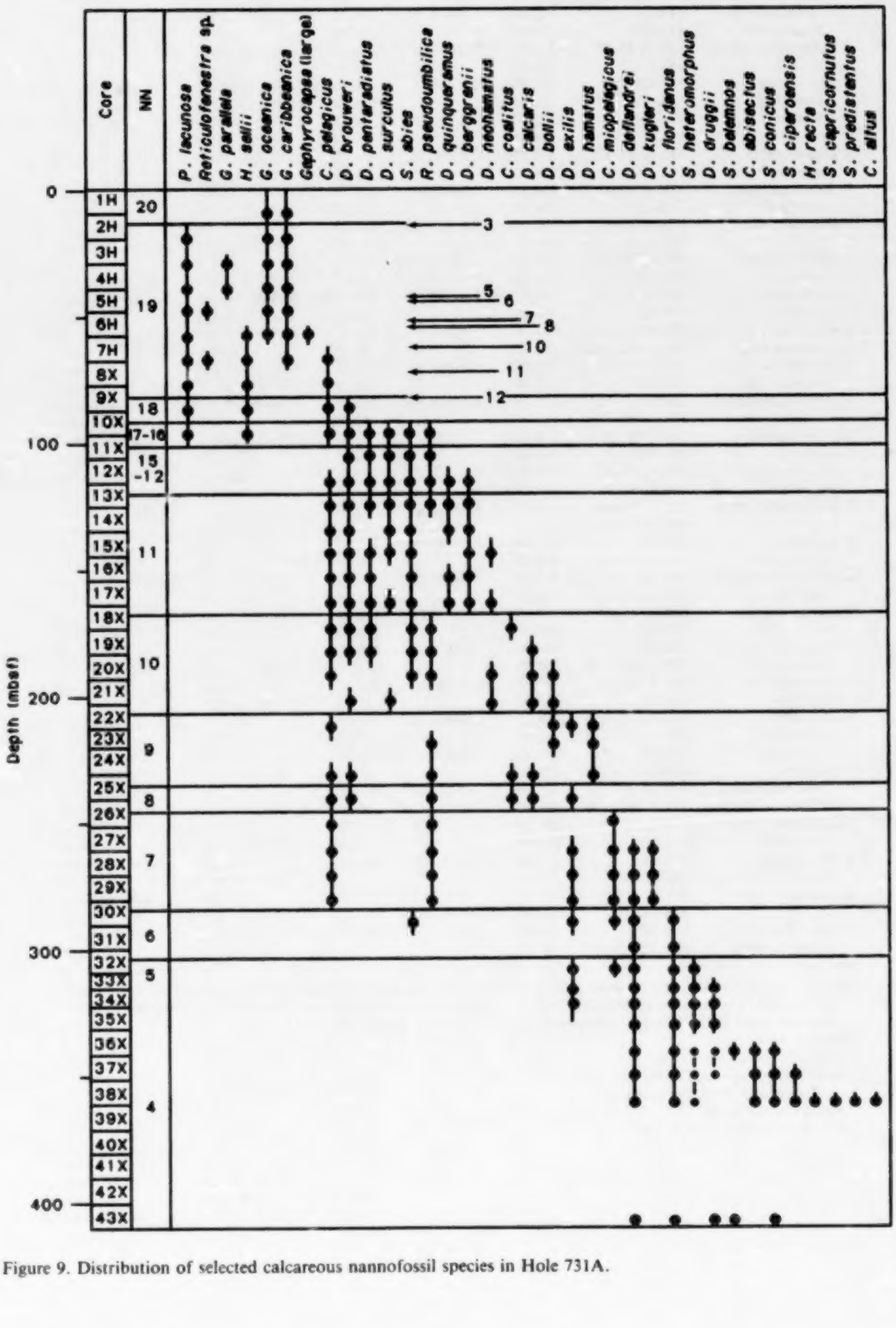

Figure 9. Distribution of selected calcareous nannofossil species in Hole 731A.

Nannofossils are abundant throughout this sequence with moderate to good preservation down to 38.3 mbsf. The preservation is poor throughout the remainder of Zone NN19.

The approximate position of the Pliocene/Pleistocene boundary is between Samples 117-731A-7H, CC, and 117-731A-8X-1, 115–117 cm (67.0–68.15 mbsf). Samples 117-731A-9X, CC (86.4 mbsf) and 117-731A-10X, CC (96.0 mbsf) contain rare specimens of *Discoaster brouweri*, but no specimens of *D. pentaradiatus* and is assigned to upper Pliocene Zone NN18. Nannofossils are abundant but poorly preserved.

Samples 117-731A-10X, CC (96.0 mbsf), through 117-731A-11X-1, 115–117 cm (97.15 mbsf), contain abundant nannofossils having moderate preservation. The assemblage contains *Discoaster brouweri, D. pentaradiatus*, and a few *D. surculus* and is assigned to Zone NN17.

As has been the case at the other sites of this leg, the zonal markers *Amaurolithus tricorniculatus* and *Ceratolithus rugosus* are missing and we must combine Zones NN15 through NN12. Samples 117-731A-11X-2, 116–118 cm, and -12X-5, 115–117 cm (98.66–112.85 mbsf), are given such a zonal assignment. Nannofossils having moderate to good preservation are abundant within these zones. The length of these zones is somewhat abbreviated, but without the ability to recognize these as four distinct zones, it is impossible to determine if a hiatus is present or a slow rate of sedimentation is responsible for this thin sedimentary section.

Samples 117-731A-12X-6, 115–117 cm, through -17X, CC (114.35–163.7 mbsf), contain *D. quinqueramus* and are assigned to Zone NN11 (upper Miocene). A diverse assemblage of discoasters is found in this zone, which in addition to *D. quinqueramus*, include: *D. berggrenii, D. brouweri, D. challengeri, D. neohamatus, D. neorectus, D. pentaradiatus, D. surculus, D. triradiatus*, and *D. variabilis*. Nannofossils are abundant with moderate preservation throughout this zone.

Neither *Discoaster hamatus* nor *D. quinqueramus* was found in Samples 117-731A-18X-1, 135–137 cm, through -21X, CC (165.05–202.5 mbsf), and so this interval can be assigned to upper Miocene Zone NN10. Nannofossils are abundant, and the preservation ranges from moderate to poor. The lowermost sample in this zone contains a few reworked specimens of *D. hamatus*.

D. hamatus is present in Samples 117-731A-22X-1, 129–131 cm, through 117-731A-25X-5, 115–116 cm (203.79–238.75 mbsf). These sediments are assigned to Zone NN9. Sample 117-731A-25X, CC (241.3 mbsf), lacks *D. hamatus* but contains *Catinaster coalitus* and is, therefore, assigned to Zone NN8 (middle to upper Miocene). Zone NN7 is characterized by the presence of *Discoaster kugleri* and the absence of *C. coalitus*. Samples 117-731A-26X-3, 117–119 cm, through 117-731A-30X5, 115–116 cm (245.47–287.05 mbsf) are assigned to this zone. Abundant, moderately well-preserved nannofossils are found in Zones NN9 through NN7.

Preservation becomes poor, specifically the nannofossils are heavily overgrown, and hinders a confident identification of the nannofossils in Samples 117-731-30X, CC, and -31X, CC (289.6–299.2 mbsf). Specimens tentatively identified as *Cyclicargolithus floridanus* were noted. The last appearance datum (LAD) of this species is used as one of the criteria for recognizing the top of Zone NN6. No *Sphenolithus heteromorphus* specimens were recognized which is consistent with the NN6 zonal assignment.

Sediments below Sample 117-731A-32X-1, 115-116 cm (300.35 mbsf) contain *S. heteromorphus*. *Helicosphaera ampliaperta*, whose LAD is used to define the top of Zone NN4, is not present in this region and so it is necessary to combine Zones NN5 and NN4. Nannofossils are abundant, but poorly preserved in Cores 117-731A-32X, CC, through -34X, CC; rare in 117-731A-35X, CC, and -36X, CC, and the preservation is moderate; abundant in 117-731A-37X, CC, and common in -38X, CC, and the preservation is moderate. Reworked Paleogene species are common. These include: *Chiasmolithus altus, Cyclicargolithus abisectus, Discoaster barbadiensis, Helicospheara recta, S. capricornutus, S. ciperoensis, S. conicus*, and *S. predistentus*.

Sample 117-731A-40X-1, 69 cm (371.1 mbsf), contains *S. belemnos* and *Discoaster druggii* and is assigned to lower Miocene Zones NN3 to NN2. Nannofossils are abundant, but the spheroliths and asteroliths are strongly overgrown. Sample 117-731A-39X, CC (370.4 mbsf), was barren of nannofossils. Sample 117-731A-40X-1, 81 cm, contains rare, poorly preserved nannofossils, but it can be placed somewhere in the early Miocene. Samples 117-731-40X, CC, through -42X, CC (380.0–399.4 mbsf), are barren of nannofossils. Sample 117-731A-43X, CC (409.0 mbsf), contains abundant, poorly preserved nannofossils including *S. belemnos* and *D. druggii* and can be placed in lower Miocene Zone NN3. Drilling in Hole 731A stopped at a depth of 409.0 mbsf due to mechanical problems.

Hole 731B

Coring at Hole 731B commenced at 408.7 mbsf after the overlying section had been drilled and washed. Only five XCB cores were recovered from this hole before it, too, was abandoned because of mechanical problems. All five core-catcher samples (418.3–457.1 mbsf) are barren of nannofossils.

Hole 731C

Hole 731C was drilled down to a depth of 351.7 mbsf. At this point, washing commenced and continued to 502.4 mbsf. Sample 117-731C-1W-2, 39 cm, contains *S. heteromorphus* and *D. druggii* in an abundant, moderately preserved assemblage. A zonal assignment of NN5–NN4 (lower to middle Miocene) is given to this sample (Fig. 10). Sample 117-731C-1W, CC (502.4 mbsf), is barren of nannofossils. A rotary core was taken immediately below the washed core. Sample 117-731C-2R, CC (512.1 mbsf), contains abundant, well-preserved nannofossils. *Sphenolithus belemnos, S. dissimilis*, and *Cyclicargolithus abisectus* are present. This sample is assigned to Zone NN2. Washing of the hole continued from 512.1 to 560.1 mbsf. Within this interval, Sample 117-731C-3W-2, 80 cm, was found to contain *D. druggii, C. abisectus, Triquetrorhabdulus carinatus*, and *S. belemnos*, in an abundant but poorly preserved assemblage, and can be assigned to lower Miocene Zone NN2. Sample 117-731C-3W, CC (560.2 mbsf), contains rare nannofossils with moderate to poor preservation. Age-diagnostic taxa are not recognizable, but a presumably reworked specimen of the Eocene genus *Chiasmolithus* was noted. Core 117-731C-4R was taken immediately below the washed interval, but the core catcher was barren of nannofossils. Hole 731C was washed from 569.9 mbsf to 618.1 mbsf. The core catcher of -5W contains rare, poorly preserved nannofossils which are not age-diagnostic. Core 117-731C-6R, was taken immediately below the washed interval. Sample 117-731C-6R, CC, contains rare, poorly preserved, non-age-diagnostic forms. Core 117-731C-7W is from the washed interval between 627.8 mbsf and 675.9 mbsf. An abundant, but poorly preserved, nannofossil flora is contained in Sample 117-731C-7W-2, 83–84 cm. This assemblage is composed of *C. abisectus, Dictyococcites bisectus*, and *Coccolithus eopelagicus* together with long-ranging species such as *Cyclicargolithus floridanus* and *S. moriformis*. Therefore, this sample is referred tentatively to upper Oligocene Zone NP25. Below this, sediments down to the bottom of the hole are all barren or have so few nannofossils that they should be considered barren. The one and only brief flicker of hope was in Sample 117-731C-13W-5, 75 cm (Core 13W spanned from 801.1 to 849.4 mbsf). An abundant, yet poorly preserved nannofossil assemblage which includes *Cycli-*

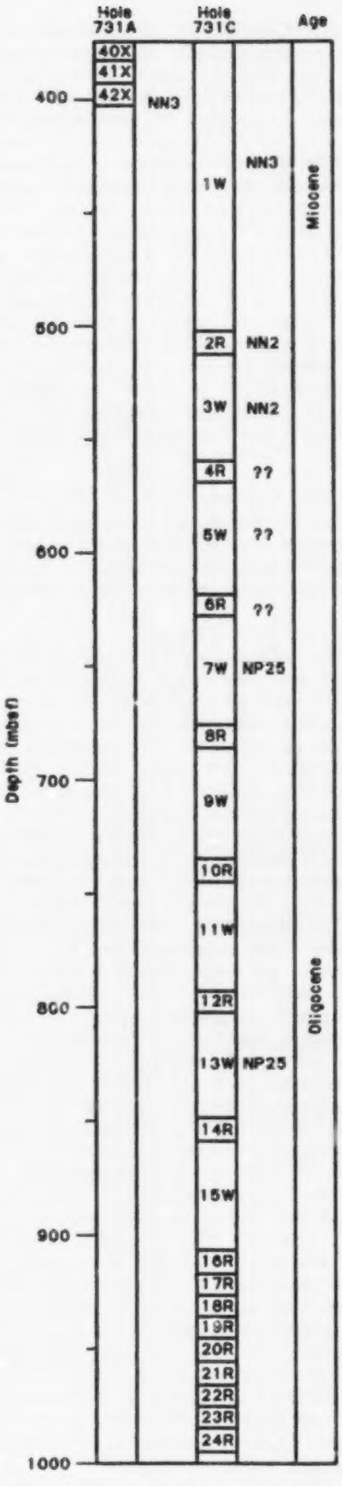

Figure 10. Distribution of selected calcareous nannofossil zones in Hole 731C.

cargolithus abisectus, C. floridanus, Discoaster deflandrei, Helicosphaera euphratis, H. recta, Sphenolithus ciperoensis, and *S. dissimilis*. A zonal assignment of NP25 (upper Oligocene) has been given to this sample.

Radiolarians

In Hole 731A all samples from Cores 117-731A-1H, CC, through 117-731A-29X (9.8–279.9 mbsf) contain radiolarians. Below this level all samples are barren. Diatoms are a common component of the siliceous fauna between Samples 117-731A-16X, CC (154.0 mbsf), and 117-731A-27X, CC (260.6 mbsf). No siliceous microfossils occur in any of the material recovered at Holes 731B or 731C.

Samples 117-731A-1H, CC (9.8 mbsf) and 117-731A-2H, CC (19.3 mbsf) contain a few, moderately well-preserved radiolarians which appear to belong to the *Amphirhopalum ypsilon* Zone. Both preservation and abundance improve below Sample 117-731A-3H-4, 85–87 cm (24.65 mbsf), and remain relatively good through Sample 117-731A-20X, CC (192.8 mbsf). The *A. ypsilon/Anthocyrtidium angulare* zonal boundary lies between Samples 117-731A-5H, CC (47.8 mbsf), and 117-731A-6H-4, 85–87 cm (53.15 mbsf). Based on a single fragment of *Pterocanium prismatium*, Sample 117-731A-8X, CC (76.7 mbsf), has been placed in the *P. prismatium* Zone. *P. prismatium* is also very rare in samples from Cores 117-731A-9X and 117-731A-10X, but they are, nevertheless, placed in the *P. prismatium* Zone because *Stichocorys peregrina* is also absent. A hiatus probably occurs in the upper part of Core 117-731A-11X, because Sample 117-731A-11X-4, 85–87 cm (101.35 mbsf), belongs to the lower part of the *Spongaster pentas* Zone; *Lychnodictyum audax, Phormostichoartus fistula*, and *Phormostichoartus doliolum* are all present. Another hiatus lies within Core 117-731-12X, as the *Stichocorys peregrina* Zone is entirely missing. Sample 117-731A-12X, CC (115.4 mbsf), lies within the *Didymocyrtis penultima* Zone which continues through Sample 117-731A-15X-4, 85–87 cm (140.5 mbsf). The LAD of *Diartus hughesi* in Sample 117-731A-15X, CC (144.4 mbsf), denotes the top of the *Didymocyrtis antepenultima* Zone and its transition from *Diartus petterssoni* between Samples 117-731A-19X-4, 85–87 cm (178.75 mbsf), and 117-731A-19X, CC (183.1 mbsf), marks the boundary with the *D. petterssoni* Zone. The remainder of the radiolarian bearing sediment apparently belongs to this zone. Samples from Cores 117-731A-21X through 117-731A-23X show a slight decrease in radiolarian abundance and preservation; Samples 117-731A-28X, CC (270.2 mbsf), and 117-731A-29X, CC (279.9 mbsf), contain only rare radiolarians and many of those in 117-731A-29X, CC, have been pyritized.

Paleoenvironmental Implications

As with planktonic foraminifers, calcareous nannofossils attain their maximum diversity in tropical areas. According to McIntyre and Bé (1967), tropical and subtropical assemblages contain over three times more species than subarctic and subantarctic assemblages and thus, conform to present ideas on latitudinal changes in diversity. Many species such as *Coccolithus pelagicus* are obviously controlled by temperature; this species seems to be extremely rare or absent in tropical waters. In contrast with this, most species of *Sphenolithus*, some species of *Helicosphaera*, and probably all species of *Scyphosphaera* are absent in boreal waters (Martini, 1970).

Roth (1974) superimposed the paleotemperature curve based on planktonic foraminiferal assemblages on the stratigraphic changes of the nannofossil diversity values from DSDP Site 167 (Magellan Rise, central Pacific Ocean) and suggested that the species diversity of nannofossils was highest during times of warm temperatures and lowest during times of low temperatures.

Figure 11 shows the calcareous nannofossil species diversity in the operations area of Leg 117 (northwest Indian Ocean) compared to the typical tropical region (for example the tropical Pacific) in each calcareous nannofossil one. For example, in the the sediments referred to Zone NN5 (lower middle Miocene) in the tropical region, about 17 species commonly occur. These are: *Coccolithus miopelagicus*, *C. pelagicus*, *Cyclicargolithus floridanus*, *Calcidiscus leptoporus*, *C. macintyrei*, *Discoaster aulakos*, *D. deflandrei*, *D. exilis*, *D. variabilis*, *Helicosphaera granulata*, *H. carteri*, *Reticulofenestra pseudoumbilica*, *Sphenolithus abies*, *S. heteromorphus*, *S. moriformis*, *Triquetrorhabdulus rugosus*, and *Coronocyclus* sp. During Leg 117, we recognized common occurrences of all but the last two species mentioned above in Zone NN5 in both the Owen Ridge sites and the Oman margin sites. This means that about 88% of the total tropical flora was recognized in the area studied on this leg. This assemblage is considered to be similar to the tropical flora. The species diversity, however, gradually decreases upward and in Zone NN8 the nannofossil assemblage is about 64% of the tropical one. In Zone NN9 the flora is again "subtropical" (about 85%) and then rapidly becomes less diversified until Zone NN12 (about 36%). After that the diversity is around 50%, although it increases slightly upward. Based on this rough estimation, we can conclude that the calcareous nannofossils in this area were first affected by upwelling in the early late Miocene (about 9.5 Ma).

PALEOMAGNETISM

Magnetic Measurements

Paleomagnetic measurements were made on discrete specimens using the MINISPIN spinner magnetometer after alternating field (AF) demagnetization using the Schonstedt demagnetizer. Figure 12 shows the combined data from Holes 731A and 731C after AF demagnetization at 5 or 10 mT (depending on the initial intensity) and removal of points with circular standard deviations greater than 40°. Figure 13 shows the distributions of intensities (plotted on a logarithmic scale) for the pelagic sediments (above around 300 mbsf) and the turbiditic sediments (below around 300 mbsf), respectively. Intensities in the pelagic oozes average around 0.2 mA/m; significantly higher values (around 6.3 mA/m) occur in the turbidites. The inclination data for the relatively weakly magnetized pelagic oozes and chalks are significantly more scattered in comparison with the correlative intervals at the other Owen Ridge sites (Sites 721 and 722); this is partly a result of weaker intensities at Site 731, but may also reflect instrumental problems (increased noise level of the MINISPIN because of irregular spinning) during occupation of the site.

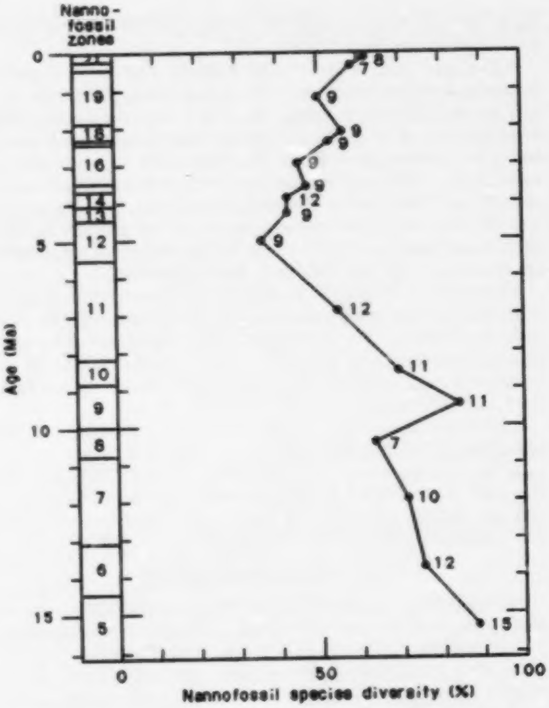

Figure 11. Calcareous nannofossil species diversity for Zones NN5 through NN21. Number is number of species occurring.

Because the AF demagnetization behavior of the Pleistocene and Pleistocene oozes on the Owen Ridge was relatively well-documented from efforts at previous Leg 117 sites, we confined such studies to specimens from the turbidite sequence. They showed variable behavior during demagnetization. The Zijderveldt plot for specimen from Core 117-731A-37X (Fig. 14) shows an example of a specimen which shows no sign of univectorial decay of the magnetization toward the origin, together with evidence of possible acquisition of anhysteretic remanent magnetization (ARM) above 25 mT. The Zijderveldt plots in Figures 15–16 of specimens from Cores 117-731A-40X and -43X show removal of a low coercivity overprint, followed by apparently univectorial decay toward the origin; however, they then exhibit increasing intensity (probably ARM acquisition) at fields greater than 30 mT. We are uncertain whether this behavior reflects intrinsic properties of the sediments or inadequacies of the shipboard AF demagnetizer. More careful AF and thermal demagnetization experiments will be performed on turbidite samples during post-cruise studies.

Magnetostratigraphy

Biostratigraphic datums of calcareous nannoplankton (see "Biostratigraphy" section, this chapter) were used in assignment of the polarity intervals above 100 mbsf. The top of acme *Reticulofenestra* sp. A and the first appearance datum of *Gephyrocapsa parallela* occur within Core 117-731A-5H. These datums occur between the Chron C1/C1r (Brunhes/Matuyama Chronozone) boundary and Subchron C1r-1 (Jaramillo Subchronozone). The last appearance datum of *Helicosphaera sellii* occurs in Core 117-731A-6H, and this datum predates Subchron C1r-1. In the shipboard results (Fig. 12), the uppermost reverse-to-normal transition was found at around 50 mbsf. Shore-based remeasurements with 15 mT AF demagnetization indicate that the boundary occurs between Samples 117-731-5H-5, 115 cm, and -5H-6, 45 cm. This suggests that, as at almost all of the other Oman margin and Owen Ridge sites, the Brunhes/Matuyama boundary has not been recorded clearly and that this first transition is the older Jaramillo boundary. Between this transition and the top of the turbidite sequence, a significant number of points were eliminated from the data set because of high circular standard deviations. Moreover, many of the remaining points do not accord with the expected axial dipole inclination for the site latitude (30.6°), as is reflected in Figure 13C. Therefore, we are reluctant to make any further correlations with the polarity time-scale on the basis of the shipboard data. Shore-based study of additional samples may significantly improve the paleomagnetic record over this interval.

Within the turbidite sequence the inclinations are consistently shallower (generally less than 10°) than in the pelagic sediments (Figs. 13C and -D). This implies that Site 731 was located significantly closer to the equator during the period of turbidite de-

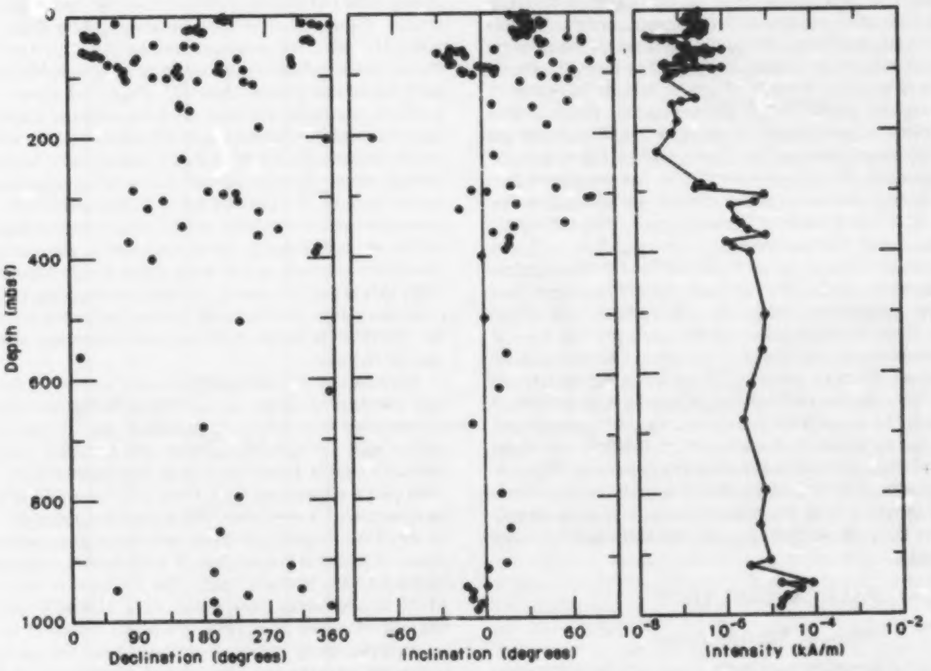

Figure 12. Plots of magnetic declination (relative values), inclination, and intensity vs. depth of Holes 731A and 731C, obtained after AF demagnetization at 5 or 10 mT and filtering circular standard deviation values greater than 40°.

position than at the present day. The mean of the absolute inclinations, excluding anomalously high values from Cores 117-731A-32X and -37X, is 11.0°, giving a paleolatitude of 5.6°. Some caution is required in using these data for quantitative estimation of paleolatitude because of the possibility of inclination error in what may be possibly rapidly deposited and nonbioturbated sediments; also no precise age control is available at present for the turbidites.

Magnetic Susceptibility

The volume magnetic susceptibility of Hole 731A sediments was measured using the Bartington Instruments' whole-core sensor at the 0.1 sensitivity and low-frequency (0.47 kHz) settings. Measurements were made at 5-cm intervals for a total of about 6800 measurements.

Four lithologic units were recognized at Hole 731A (see "Lithostratigraphy" section, this chapter). Lithologic Subunit IA (0-66.3 mbsf) is comprised of a marly nannofossil ooze with minor biosiliceous components. Unit I exhibits regular susceptibility fluctuations of ~1 m wavelength and about 30-100 × 10^{-6} volume SI units amplitude. The Hole 731A susceptibility record of Subunit IA can be correlated on a virtual point-for-point basis with Sites 721 and 722 which are also from the Owen Ridge (Fig. 17). Susceptibility fluctuations of ~2-3 m and ~4-5 m wavelengths are also apparent. If ~40 m/m.y. is used for the sedimentation rate of Site 731, these wavelengths correspond roughly to the ~19-23 k.y, ~41 k.y., and ~100 k.y. Milankovitch orbital isolation periodicities.

Lithologic Subunit IB (66.3-146.5 mbsf) is also a marly nannofossil ooze, but with no significant biosiliceous material. The susceptibility data representative of Unit IB are not significantly different in character from the data of Subunit IA (Fig. 18). However, pipe rust contamination of the upper ~1 m of the XCB cores did obscure many of the correlatable features which were apparent at Sites 721 and 722.

Lithologic Unit II (146.5-240.9 mbsf) consists of a marly diatom-rich nannofossil ooze. The susceptibility data from this unit are slightly lower in value than Unit I but a regular cyclicity of about ~1 m is apparent, despite XCB-coring disturbance and pipe rust contamination. The depression of susceptibility values near ~220 mbsf is coincident with increases in sediment porosity and biosiliceous (diatom) components, which suggests that this interval of low values may be due to dilution by biogenic sediment (Fig. 18). Flux data for the different components are required to say this with confidence, however.

Lithologic Unit III (240.9-320.1 mbsf) consists of nannofossil chalks without biosiliceous components. Susceptibility data in the lower part of this unit are generally higher and more variable than the overlying units (Fig. 19). The higher values reflect an increase in terrigenous component supply which was noted in the visual core descriptions of Unit III sediments.

Lithologic Unit IV (320.1-409.0 mbsf in Hole 731A) consists of numerous turbidite layers which are intercalated with higher carbonate pelagic layers. As with Sites 721 and 722, the turbidite layers are indicated by high susceptibility values, which presumably reflects the increased grain size and concentration of ferrimagnetic particles.

ACCUMULATION RATES

Sedimentation rates for the top 300 m of Site 731 are based on the mean depth and age of magneto- and biostratigraphic datum levels identified in Holes 731A (Table 5 and Fig. 20). Because of uncertainties in the shipboard paleomagnetic data (see "Explanatory Notes" chapter, this volume), we favor the nannofossil biostratigraphic datums for the determination of the sedimentation rates at Leg 117 sites. For the interval from 0 to 2.4

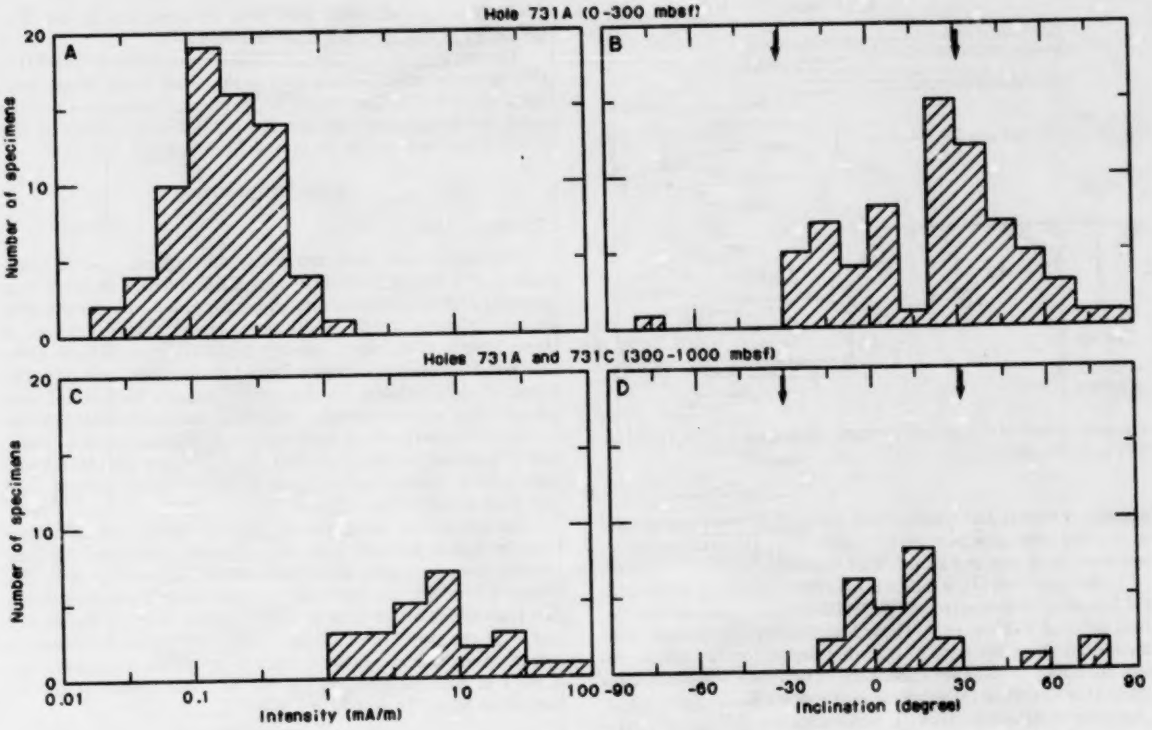

Figure 13. Histograms of magnetic inclination and intensity values from the interval above 300 mbsf of Hole 731A (A and B) and below 300 mbsf of Holes 731A and 731C (C and D). Arrows show the inclination values expected from the geocentric axial dipole field (30.6°).

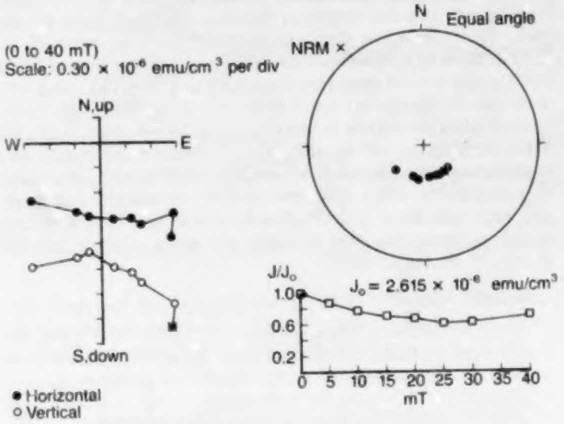

Figure 14. Result of stepwise AF demagnetization for Sample 117-731A-37X-3, 137–139 cm.

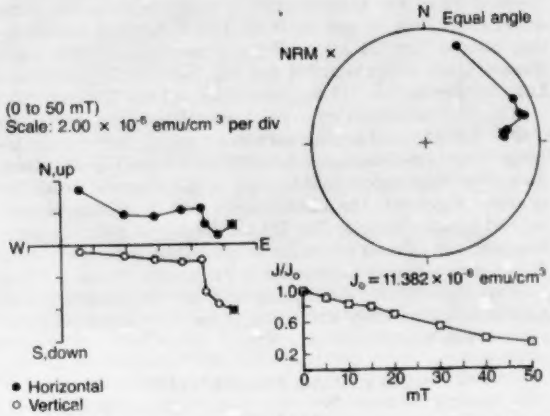

Figure 15. Result of stepwise AF demagnetization for Sample 117-731A-40X-1, 32–34 cm.

m.y., we used six nannofossil datums with ages based on oxygen isotope stratigraphy (N. Niitsuma, unpubl. data) and from Berggren et al. (1985) to determine variations in the mean sedimentation (Tables 4 and 5). These same biohorizons are used to determine the mean sedimentation rate at other Leg 117 sites to permit the comparison of sediment accumulation of hemipelagic deposits on the Oman margin and the pelagic sediments on the Owen Ridge.

Site 731 encountered the same sedimentary sequence as in nearby Sites 721 and 722, and the same four lithologic units are identified at all three sites. These lithologic units reflect the changing depositional environment of the site due to the uplift of the Owen Ridge, and variations in surface plankton activity. At Site 731, one or more gaps in sediment accumulation are evident between 97 and 115 mbsf. These gaps represent a hiatus that spans more than 3 m.y. The comparable section at Site 722

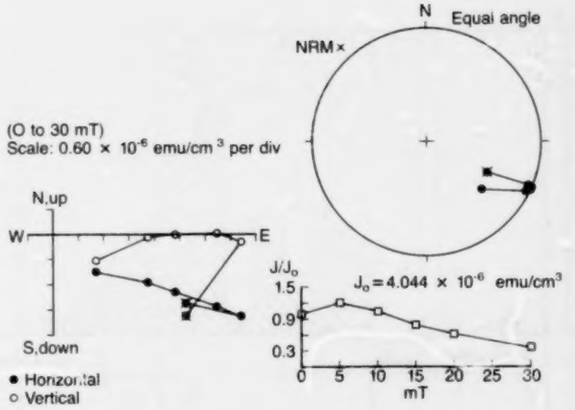

Figure 16. Result of stepwise AF demagnetization for Sample 117-731A-43X-1, 22-24 cm.

appears complete and undisturbed. Because of poor age control in the turbidite sequence of lithologic Unit IV, no estimate of sedimentation rate can be made at this time.

Lithologic Unit III, a nannofossil chalk deposited in the middle Miocene, is characterized by relatively low mean sedimentation rates of 9-30 m/m.y. These low rates reflect pelagic sedimentation above the zone of turbidite deposition but still in waters corrosive to calcium carbonate. The transition from Unit III to II is identified by an increase in opal-rich sediments which characterize lithologic Unit II. Sedimentation rates which average 30-35 m/m.y. are associated with the upper Miocene opal-rich sediments of lithologic Unit II (Fig. 20 and Table 5).

The nannofossil oozes/chalks of lithologic Unit I ranging from late Miocene to Holocene were deposited at mean rates of 20-69 m/m.y., but sedimentation is interrupted by the hiatus noted above (Fig. 20 and Table 5). The Pleistocene sedimentation rates at Site 731 are similar to, but slightly higher than, those at Owen Ridge Sites 721 and 722. However, further downhole the rates at Site 731 are lower than at Sites 721 and 722.

The mass accumulation of calcium carbonate, noncarbonate (100 − $CaCO_3$), and organic carbon are calculated from the average values between selected datums (Table 5 and Fig. 21). These data allow independent examination of the temporal variability in each component. The accumulation rates of calcium carbonate and noncarbonate at Site 731 mostly mirror the sedimentation rate, and calcium carbonate accumulation is generally twice that of noncarbonate in Pliocene to Pleistocene deposits. These rates are characteristic of areas having a high production of calcium carbonate shells of coccolithophores and foraminifers with minimal postdepositional dissolution.

PHYSICAL PROPERTIES

Introduction

Physical properties measured on discrete samples of sediment from Site 731 include index properties (wet-bulk density, porosity, water content, and grain density), compressional-wave velocity, thermal conductivity, and vane shear strength. The properties determined for Holes 731A, 731B, and 731C are listed in Tables 6, 7, and 8, respectively. The GRAPE and *P*-wave logging systems were used to measure the wet-bulk density and compressional-wave velocity of all whole-round sections that substantially filled the core liner and were longer than 80 cm. All techniques and equipment used are described in the "Explanatory Notes" chapter (this volume).

The pattern of variation of physical properties at Site 731 is similar to the patterns displayed at the other Owen Ridge sites, Sites 721 and 722. Transitions in the physical properties profiles mark the boundaries between the four lithologic units at Site 731 in a manner similar to that at Sites 721 and 722.

Index Properties

Lithologic Unit I

The nannofossil ooze and marly nannofossil ooze of lithologic Unit I (0-146.5 mbsf) display normal trends of decreasing porosity and water content and increasing wet-bulk density with increasing burial depth. In lithologic Unit I, porosity decreases from 75% to 61%, water content decreases from 52% to 37%, and wet-bulk density increases from 1.49 to 1.67 g/cm^3 (Fig. 22). Grain density exhibits no consistent change downsection and varies about an average value of 2.57 g/cm^3. Lithologic Subunit IA (0-66.3 mbsf), which is characterized by intermittent biosiliceous intervals, is distinguished from Subunit IB (66.3-146.5 mbsf) by a greater variability in porosity, water content, and wet-bulk density (Fig. 22).

The uppermost sediments of lithologic Unit I are characterized by higher porosity and water content and lower wet-bulk density than sediments near the seafloor at Sites 721 and 722. These differences are attributed to the siliceous-microfossil-rich intervals which are present in Subunit IA at Site 731 but do not occur at the other Owen Ridge sites. The values for porosity, water content, and wet-bulk density at the base of lithologic Unit I at Site 731 are comparable to those values at similar depths at Sites 721 and 722.

Lithologic Unit II

Downsection trends of index properties present in lithologic Unit I are reversed in lithologic Unit II (146.5-240.9 mbsf) reflecting the greater abundance of biogenic silica in the nannofossil oozes and diatomaceous marly nannofossil oozes of this unit. With increasing depth in lithologic Unit II, porosity increases from 63% to 66%, water content increases from 39% to 43%, grain density decreases from 2.68 to 2.52 g/cm^3, and wet-bulk density decreases from 1.67 to 1.57 g/cm^3 (Fig. 22). Variation of index properties in lithologic Unit II correlates well with the concentrations of organic carbon, calcium carbonate, and siliceous microfossils (see "Lithostratigraphy" section, this chapter). Sediments with a low concentration of calcium carbonate and high concentrations of organic carbon and biogenic silica are characterized by high porosity and water content and low grain and wet-bulk density.

Lithologic Unit III

Index properties in lithologic Unit III (240.9-320.1 mbsf) display a rapid and uniform change from the properties that characterize the nannofossil and marly nannofossil chalks at the base of lithologic Unit II and the terrigenous turbidites of lithologic Unit IV. A pronounced break in slope in the profiles of porosity, water content, and wet-bulk density occurs at 295 mbsf. This depth coincides with reductions in the concentrations of both calcium carbonate and organic carbon (see "Lithostratigraphy" section, this chapter). Between 240.9 and 294.5 mbsf porosity decreases from 66% to 49%, water content decreases from 43% to 27%, and wet-bulk density increases from 1.57 to 1.88 g/cm^3 (Fig. 22). Below 295 mbsf, gradients in the porosity, water content, and wet-bulk density profiles are sharply reduced as porosity and water content decrease to 46% and 24%, respectively, and wet-bulk density increases to 1.97 g/cm^3. The grain density

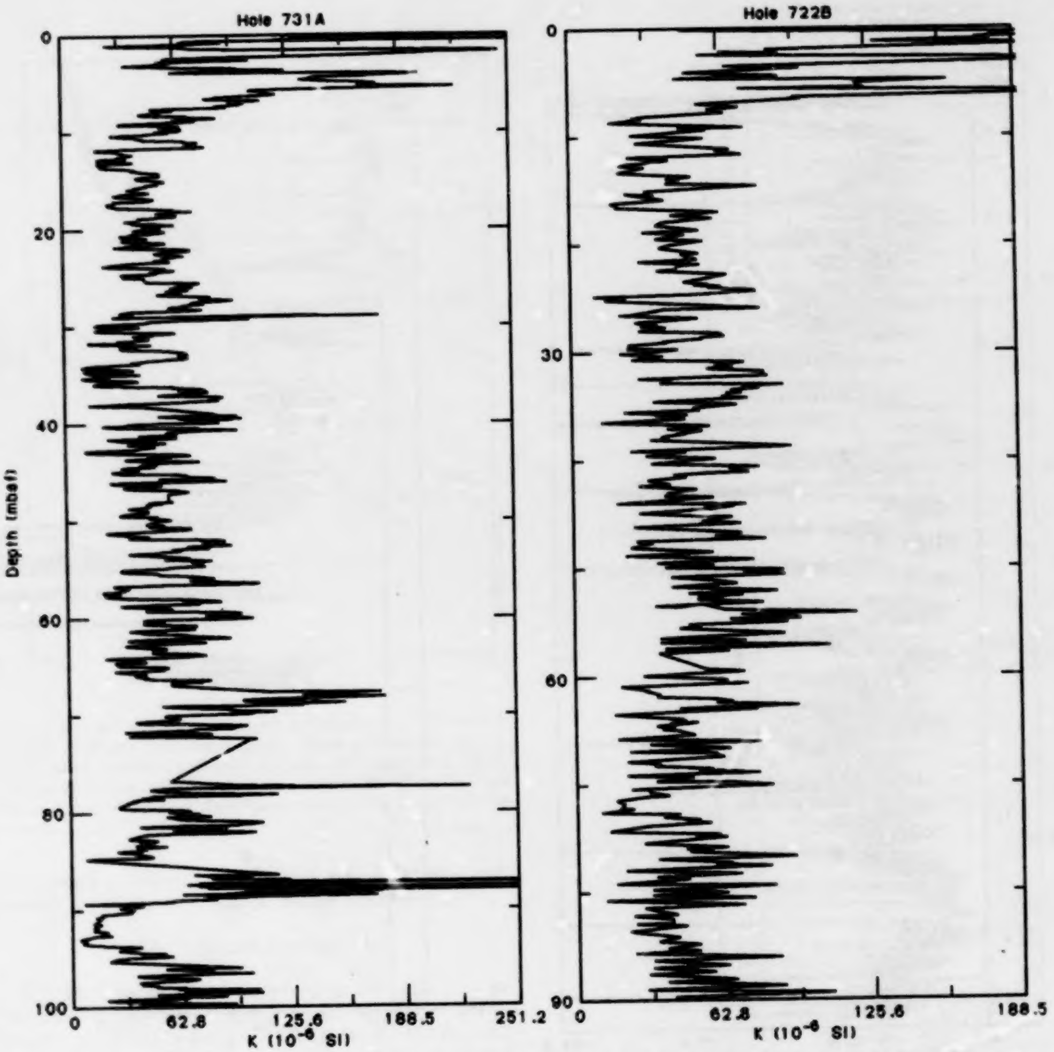

Figure 17. Volume magnetic susceptibility of Hole 731A (0–100 mbsf) compared to Hole 722B (0–90 mbsf), also from the Owen Ridge.

profile does not display a distinct gradient change in lithologic Unit III. Overall there is an increase in grain density from 2.52 g/cm^3 at 240.9 mbsf to 2.63 g/cm^3 at 320.1 mbsf (Fig. 22).

Lithologic Unit IV

Sediments of lithologic Unit IV (320.1–994.2 mbsf) exhibit volume reduction with depth that accompanies increasing overburden pressure. Within lithologic Unit IV properties of the coarse-grained turbidites (silty sandstones) and the fine-grained turbidites (claycy siltstones to claystones) differ. Downsection changes for fine-grained turbidites include decreases in porosity (48% to 31%) and water content (25% to 14%) and an increase in wet-bulk density (1.96 to 2.23 g/cm^3) (Fig. 22). Grain density of these sediments shows little change with increasing depth and averages 2.70 g/cm^3. The porosity profile of the fine-grained turbidites in lithologic Unit IV parallels the porosity profile at the nearby DSDP Site 222 (Arabian Basin), which has been used by Hamilton (1976) as a reference section for terrigenous deep-sea sediments. However, the porosity values at Site 731 are approximately 5%–8% less than the porosities at Site 222.

Index properties of the coarse-grained turbidites vary with the degree of cementation. Seven poorly cemented sandstones and four well-cemented sandstones were sampled between 428 mbsf and the base of lithologic Unit IV. Between 735.1 and 988.6 mbsf, the poorly cemented silty sandstones display downsection decreases in porosity (31% to 26%) and water content (14% to 11%) and increase in wet-bulk density (2.27 to 2.34 g/cm^3) (Tables 7 and 8). Grain density averages 2.69 g/cm^3 for these sandstones. Wet-bulk density, as determined by the 2-minute gamma ray attenuation porosity evaluator (GRAPE) technique, was the only index property measured for the well-cemented calcitic silty sandstones (Tables 7 and 8). The wet-bulk density of these sandstones averages 2.64 g/cm^3. The grain density of these sediments was not determined, but using the aver-

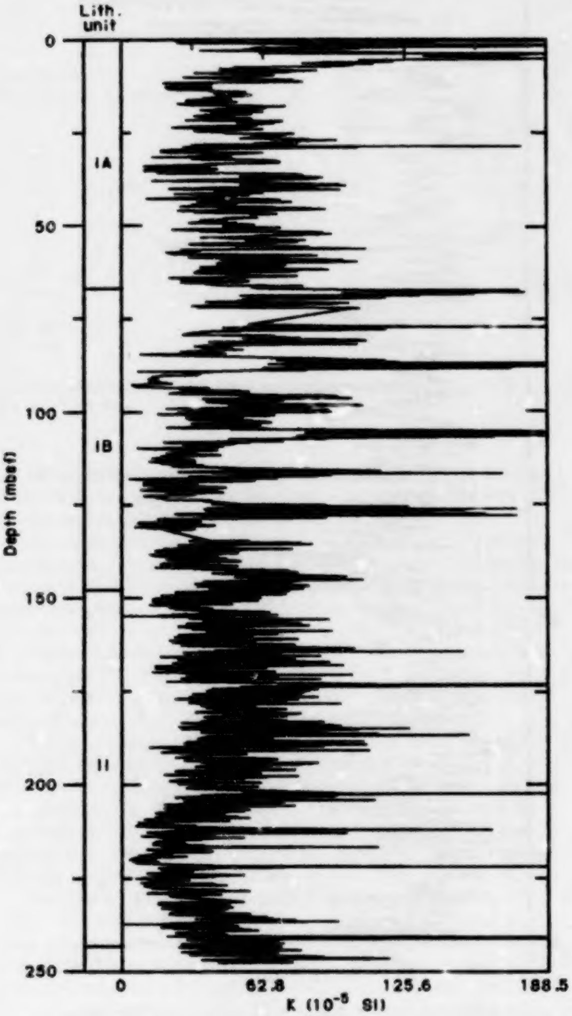

Figure 18. Volume magnetic susceptibility of Hole 731A. Measurements were made at 5-cm intervals.

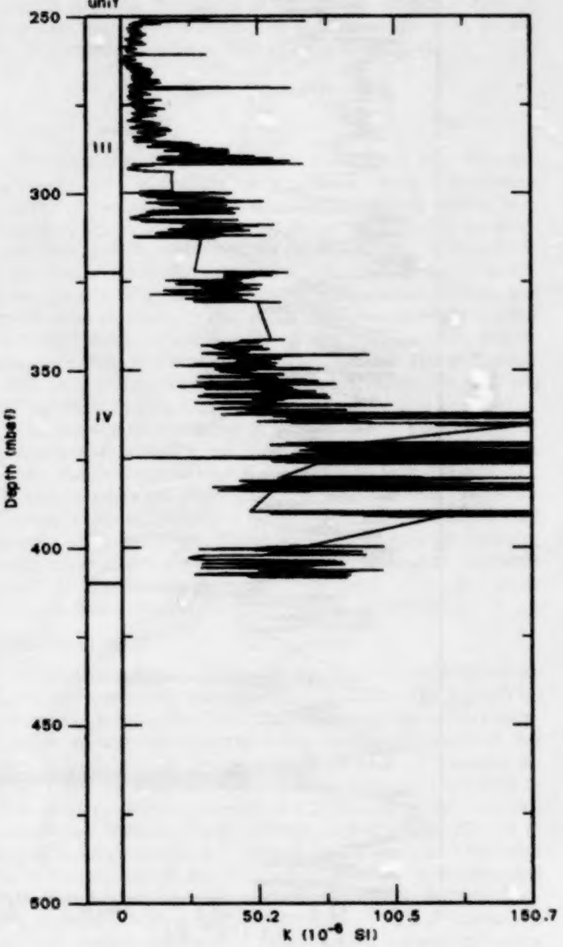

Figure 19. Volume magnetic susceptibility of Hole 731A, 250 mbsf to total depth.

Table 5. Sedimentation and accumulation rate data for Site 731.

Depth interval (mbsf)	Age range (m.y.)	$CaCO_3$ ($\bar{x}$ %)	C_{org} ($\bar{x}$ %)	Dry-bulk density ($\bar{x}$ g/cm^3)	Sed. rate ($\bar{x}$ m/m.y.)	$CaCO_3$ acc. rate (g/cm^2/k.y.)	Non-$CaCO_3$ acc. rate (g/cm^2/k.y.)	C_{org} acc. rate (mg/cm^2/k.y.)
0-6.4	0-0.19	73.7	1.37	0.741	33.7	1.84	0.657	34.2
6.4-18.9	0.19-0.49	68.2	0.26	0.984	41.7	2.80	1.30	10.7
18.9-41.7	0.49-0.82	65.4	0.50	0.934	69.1	4.22	2.23	32.3
41.7-65.2	0.82-1.45	61.6	0.42	0.982	37.3	2.26	1.41	15.4
65.2-85.1	1.45-1.9	63.6	1.01	0.996	44.2	2.80	1.60	44.5
85.1-97	1.9-2.4	68.4	0.50	1.010	23.8	1.64	0.760	24.3
115-142.5	5.75-7.15	66.1	0.35	1.029	19.6	0.683	1.33	7.06
142.5-203.1	7.15-8.85	42.8	0.65	0.882	35.6	1.80	1.34	20.4
203.1-288.3	8.85-13.1	49.3	0.65	0.937	20.0	0.950	0.924	12.2
288.3-299.8	13.1-14.4	65.0	0.08	1.474	8.85	0.457	0.848	1.04

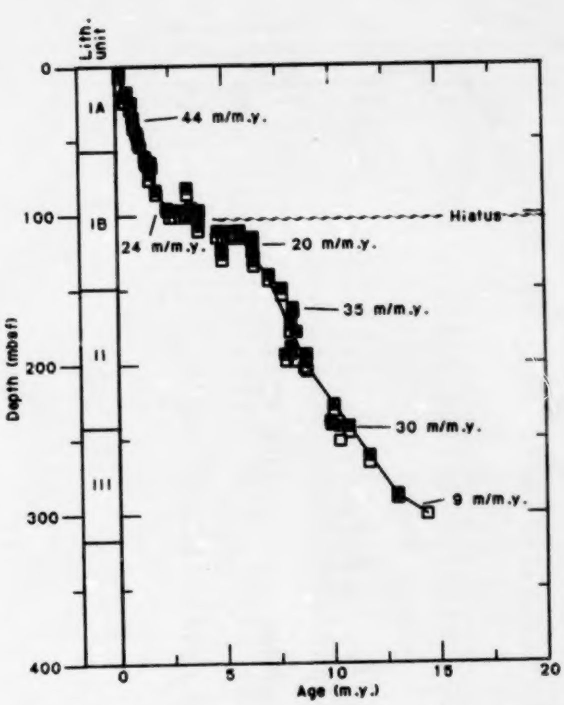

Figure 20. Age-depth plot of stratigraphic datums for Site 731 listed in Table 4. The solid and open boxes are the upper and lower depths of each datum level. Indicated sedimentation rates are based on a best fit to all stratigraphic data. Sedimentation rates calculated between reliable nannofossil datum levels in the top 85 m are listed in Table 5 and shown in Figure 21.

age grain density of the poorly cemented sandstones (2.69 g/cm^3) the porosity (ϕ) can be estimated using the equation:

$$(\phi) = [(\delta_s - \delta_{bw})/(\delta_{bw} - \delta_f)] \cdot 100$$

where δ_s = grain density, δ_{bw} = wet-bulk density, and δ_f = interstitial fluid density (assumed to be 1.025 g/cm^3). The estimated porosities range from 2% to 8% (Table 8). The porosity of Sample 117-731B-3X-1, 10–12 cm, could not be determined because its wet-bulk density (2.71 g/cm^3) is greater than the assumed grain density.

Compressional-Wave Velocity

At Site 731 compressional-wave velocities were measured perpendicular to bedding on discrete samples from cores recovered throughout Holes 731A, 731B, and 731C (Fig. 23). At depths greater than 200 mbsf, velocities were also measured parallel to bedding. The instrument-induced variation in the velocities is comparable in magnitude to that found at Sites 721 and 722. The velocity data from the nannofossil oozes/chalks and the uppermost clay-rich turbidites correlate well with wet-bulk density and display trends and gradients that are identical to those found at the other Owen Ridge sites. At this site, however, the extension of drilling to nearly 1000 mbsf has provided the opportunity to: (1) measure the velocity of the coarse-grained turbidites (silty-sandstones) recovered between 428 mbsf and total depth; (2) extend the velocity-density relationships of the turbidites to densities in excess of 2.6 g/cm^3; and (3) examine the development of velocity anisotropy in the more consolidated portions of the turbidite sequences.

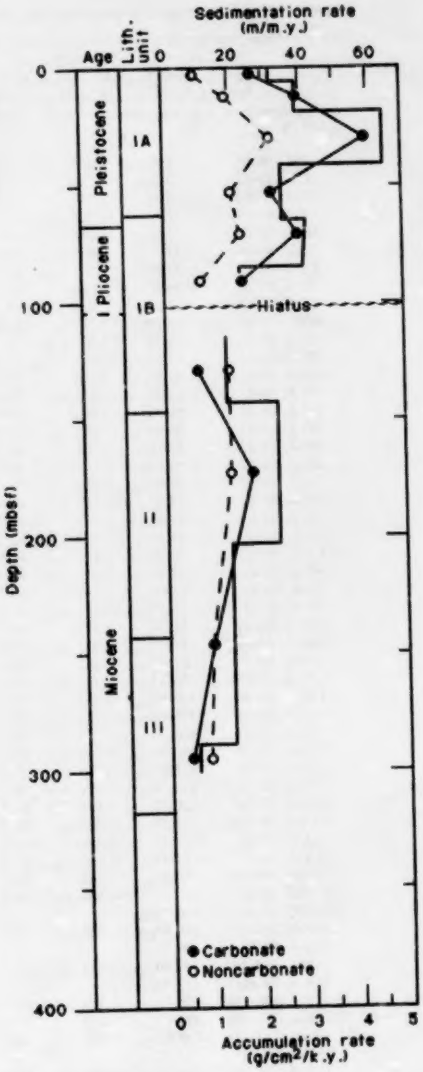

Figure 21. Sedimentation rate (m/m.y., solid line), calcium carbonate accumulation rate (g/cm^2/k.y., dots), and noncarbonate accumulation rate (g/cm^2/k.y., circles) vs. depth (mbsf) at Site 731. Accumulation rates are plotted at the midpoint of the respective depth intervals.

Within lithologic Unit I, compressional-wave velocity increases from 1510 m/s at depths just below the seafloor to 1570 m/s at 146.5 mbsf (Fig. 23). In the diatomaceous sequences of lithologic Unit II, velocity decreases slightly to a minimum value of 1540 m/s at 220 mbsf. As the biosiliceous sediment component decreases through lithologic Unit III, compressional-wave velocities increases rapidly to about 1650 m/s at 320 mbsf.

The relationships between wet-bulk density and compressional-wave velocity are well defined for both the nannofossil oozes/chalks and clay-rich turbidites for densities less than 2.0 g/cm^3 and 2.4 g/cm^3, respectively (Fig. 24). Given the limited

Table 6. Physical properties summary for Hole 731A.

Core, section, interval (cm)	Depth (mbsf)	Wet-bulk density (g/cm³)	Porosity (%)	Water content (%)	Grain density (g/cm³)	Dry-bulk density (g/cm³)	Velocity (m/s)	Thermal conductivity (w/m/ – k)	Vane shear strength (kPa)
117-731A-									
1H-1, 96-98	0.96	1.486	74.9	51.7	2.563	0.718			
1H-3, 80-82	3.80	1.510	72.8	49.4	2.593	0.764			7.1
1H-5, 80-82	6.80	1.590	61.9	39.9	2.609	0.956			
2H-2, 80-82	12.10	1.608	63.0	40.1	2.546	0.963		1.28	
2H-4, 80-82	15.10	1.658	66.4	41.0	2.681	0.977		1.25	12.9
2H-6, 80-82	18.10	1.692	63.9	38.7	2.625	1.038	[a]1511	1.29	
3H-2, 80-82	21.60	1.536	67.0	44.7	2.493	0.850			
3H-4, 80-82	24.60	1.480	69.2	47.9	2.550	0.770			18.5
3H-6, 80-82	27.60	1.658	63.7	39.4	2.682	1.005	[a]1507		
4H-2, 80-82	31.10	1.707	67.0	40.2	2.588	1.021		1.36	
4H-4, 80-82	34.10	1.497	72.7	49.8	2.505	0.751		1.13	36.1
4H-6, 80-82	37.10	1.667	62.1	38.2	2.574	1.030	[a]1572	1.34	
5H-2, 80-82	40.60	1.724	59.7	35.5	2.635	1.112			
5H-4, 80-82	43.60	1.655	63.3	39.2	2.621	1.007			22.3
5H-6, 80-82	46.60	1.563	68.1	44.7	2.490	0.865	[a]1529		
6H-2, 80-82	50.10	1.658	63.5	39.2	2.637	1.007		1.30	
6H-4, 80-82	53.10	1.655	60.5	37.5	2.562	1.035		1.27	
6H-6, 80-82	56.10	1.670	61.8	37.9	2.526	1.037	[a]1551	1.35	
7H-2, 80-82	59.60	1.658	55.6	34.3	2.519	1.089			
7H-4, 80-82	62.60	1.532	68.4	45.7	2.380	0.832			68.4
7H-6, 80-82	65.60	1.629	64.2	40.4	2.625	0.971	[a]1547		
8X-2, 64-66	69.14	1.694	62.1	37.6	2.664	1.057		1.35	27.6
8X-3, 80-82	70.80	1.616	64.8	41.1	2.586	0.952	[a]1545	1.33	
9X-2, 80-82	79.00	1.581	66.4	43.0	2.576	0.901			
9X-4, 80-82	82.00	1.712	60.1	36.0	2.675	1.095			37.2
9X-6, 39-41	84.59	1.635	61.7	38.7	2.498	1.002	[a]1545		
10X-2, 80-82	88.70	1.723	60.7	36.1	2.676	1.101		1.36	
10X-4, 80-82	91.70	1.623	62.6	39.5	2.505	0.982		1.10	42.0
10X-6, 82-84	94.72	1.601	63.9	40.9	2.558	0.947	[a]1534	1.15	
11X-2, 92-94	98.42	1.731	59.3	35.1	2.705	1.123			
11X-4, 92-94	101.42	1.683	59.5	36.2	2.533	1.074			49.3
11X-6, 92-94	104.42	1.684	59.5	36.2	2.539	1.075	[a]1550		
12X-2, 80-82	108.00	1.667	61.9	38.1	2.518	1.033		1.39	
12X-4, 77-79	110.97	1.659	60.7	37.5	2.532	1.038		1.14	
12X-6, 77-79	113.97	1.700	59.9	36.1	2.591	1.086	[a]1541	1.31	
13X-2, 84-86	117.74	1.657	59.7	36.9	2.489	1.046	[a]1559		
13X-4, 82-84	120.72	1.643	61.1	38.1	2.500	1.017			
13X-6, 99-101	123.89	1.665	63.4	39.0	2.499	1.015	[a]1560		
14X-3, 77-79	128.77	1.696	61.7	37.3	2.630	1.064		1.36	
14X-5, 75-77	131.75	1.650	62.3	38.7	2.556	1.012	[a]1578	1.36	
15X-4, 100-102	140.20	1.654	62.0	38.4	2.621	1.019	[a]1639		
15X-6, 62-64	142.82	1.665	60.5	37.2	2.578	1.045			
16X-2, 80-82	146.70							1.13	
16X-2, 103-105	146.93	1.669	62.9	38.6	2.679	1.025			
16X-4, 80-82	149.70							1.33	
16X-4, 100-102	149.90	1.682	63.1	38.4	2.639	1.036			
16X-6, 80-82	152.70							1.24	
17X-2, 125-127	156.75	1.489	68.7	47.3	2.367	0.785	[a]1551		
17X-4, 122-124	159.72	1.513	70.3	47.6	2.524	0.793	[a]1551		
17X-6, 113-115	162.63	1.553	66.4	43.8	2.464	0.873			
18X-2, 80-82	166.00							1.40	
18X-2, 102-104	166.22	1.584	64.4	41.7	2.482	0.924	[a]1565		
18X-4, 61-63	168.81	1.677	62.9	38.4	2.542	1.033	[a]1600		
18X-6, 80-82	172.00							0.99	
18X-6, 100-102	172.20	1.392	74.2	54.6	2.244	0.632			
19X-3, 86-88	177.26	1.624	62.5	39.4	2.529	0.984	[a]1550		
19X-6, 92-94	181.82	1.519	67.3	45.4	2.443	0.830	[a]1582		
20X-2, 80-82	185.40							1.39	
20X-4, 68-70	188.28	1.569	67.6	44.2	2.536	0.876	[a]1532		
20X-4, 80-82	188.40							1.09	
20X-6, 30-32	190.90	1.487	68.0	46.8	2.376	0.791	[a]1554		
20X-6, 80-82	191.40							1.29	
21X-2, 56-58	194.86	1.606	65.9	42.0	2.605	0.931	[a]1554		
21X-6, 48-50	200.78	1.418	72.3	52.3	2.364	0.677	[a]1571		
21X-6, 48-50	200.78						1572		
22X-2, 80-82	204.80							1.09	
22X-2, 99-101	204.99	1.409	73.2	53.2	2.332	0.659	[a]1551		
22X-2, 99-101	204.99						1555		
22X-4, 80-82	207.80							1.04	
22X-4, 98-100	207.98	1.385	76.1	56.3	2.404	0.606	[a]1558		
22X-6, 21-23	210.21	1.570	68.1	44.4	2.604	0.872	[a]1537		
22X-6, 21-23	210.21						1573		
22X-6, 80-82	210.80							0.94	
23X-2, 70-72	214.40	1.368	77.0	57.6	2.360	0.580	[a]1541		
23X-4, 70-72	217.40	1.524	69.2	46.5	2.521	0.815	[a]1538		

Table 6 (continued).

Core, section, interval (cm)	Depth (mbsf)	Wet-bulk density (g/cm³)	Porosity (%)	Water content (%)	Grain density (g/cm³)	Dry-bulk density (g/cm³)	Velocity (m/s)	Thermal conductivity (w/m/−k)	Vane shear strength (kPa)
117-731A-									
23X-4, 70-72	217.40						1560		
24X-2, 108-110	224.48	1.400	72.3	52.9	2.310	0.660	^{a}1549		
24X-2, 108-110	224.48						1591		
24X-4, 69-71	227.09	1.539	66.7	44.4	2.489	0.856	^{a}1555		
24X-4, 69-71	227.09						1575		
24X-6, 18-20	229.58	1.389	75.9	56.0	2.339	0.611			
25X-2, 90-92	234.00	1.427	74.4	53.4	2.433	0.665	^{a}1554		
25X-2, 90-92	234.00						1586		
25X-4, 94-96	237.04	1.550	66.9	44.2	2.512	0.865	^{a}1558		
25X-4, 94-96	237.04						1584		
25X-6, 90-92	240.00	1.574	65.8	42.8	2.520	0.900			
26X-2, 100-102	243.80	1.625	62.7	39.5	2.551	0.983	^{a}1556		
26X-2, 100-102	243.80						1562		
26X-4, 100-102	246.80	1.587	67.4	43.5	2.676	0.896	^{a}1603		
26X-4, 100-102	246.80						1605		
27X-2, 79-81	253.19	1.661	60.6	37.4	2.581	1.041	^{a}1591		
27X-2, 79-81	253.19						1614		
27X-4, 52-54	255.92	1.677	62.3	38.0	2.678	1.039	^{a}1579		
27X-4, 52-54	255.92						1598		
27X-6, 120-122	259.60	1.687	59.3	36.0	2.604	1.080	^{a}1591		
27X-6, 120-122	259.60						1610		
28X-2, 59-61	262.69	1.705	61.0	36.6	2.712	1.081	^{a}1582		
28X-2, 59-61	262.69						1596		
28X-4, 63-65	265.73	1.638	64.1	40.1	2.692	0.982	^{a}1602		
28X-4, 63-65	265.73						1639		
28X-6, 58-60	268.68	1.727	57.7	34.2	2.596	1.137	^{a}1608		
28X-6, 58-60	268.68						1651		
29X-2, 80-82	272.50	1.753	58.0	33.9	2.662	1.159	^{a}1616		
29X-2, 80-82	272.50						1629		
29X-4, 91-93	275.61	1.761	57.8	33.7	2.673	1.168	^{a}1597		
29X-4, 91-93	275.61						1632		
29X-6, 92-94	278.62	1.805	54.2	30.7	2.630	1.250	^{a}1616		
29X-6, 92-94	278.62						1631		
30X-2, 71-73	282.11	1.833	53.1	29.7	2.682	1.289	^{a}1655		
30X-2, 71-73	282.11						1708		
30X-4, 76-78	285.16	1.821	51.1	28.8	2.664	1.297	^{a}1585		
30X-4, 76-78	285.16						1614		
30X-6, 116-118	288.56	1.890	51.7	28.0	2.757	1.360	^{a}1614		
30X-6, 116-118	288.56						1618		
31X-2, 51-53	291.61	1.876	48.5	26.5	2.632	1.380	^{a}1640		
31X-2, 51-53	291.61						1630		
31X-CC, 18-20	294.53	2.014	42.9	21.8	2.677	1.574	^{a}1704		
31X-CC, 18-20	294.53						1698		
32X-1, 28-30	299.48	2.017	42.5	21.6	2.689	1.582	^{a}1835		
32X-1, 28-30	299.48						1904		
32X-5, 46-48	305.66	1.808	49.0	27.7	2.754	1.306	^{a}1608		
32X-5, 46-48	305.66						1614		
33X-2, 25-27	310.65	1.965	46.9	24.5	2.705	1.485	^{a}1663		
33X-2, 25-27	310.65	1691							
34X-1, 73-75	316.23	1.848	52.8	29.3	2.632	1.307	^{a}1609		
34X-1, 73-75	316.23						1648		
34X-2, 69-71	317.69	1.972	45.6	23.7	2.651	1.505	^{a}1606		
34X-2, 69-71	317.69						1702		
35X-1, 77-79	322.87	1.961	47.8	25.0	2.698	1.471	^{a}1637		
35X-1, 77-79	322.87						1655		
35X-5, 37-39	328.47	1.951	48.8	25.6	2.704	1.451	^{a}1669		
35X-5, 37-39	328.47						1675		
37X-3, 25-27	344.55	2.022	46.5	23.6	2.783	1.545	^{a}1657		
37X-6, 84-86	349.64	2.075	39.5	19.5	2.589	1.671			
38X-3, 31-33	354.31	2.001	43.1	22.1	2.665	1.560	^{a}1659		
38X-3, 31-33	354.31						1681		
38X-6, 66-68	359.16	1.978	47.9	24.8	2.768	1.487	^{a}1619		
38X-6, 66-68	359.16						1628		
39X-1, 48-50	361.18	1.873	53.3	29.1	2.683	1.327	^{a}1582		
39X-1, 48-50	361.18						1624		
39X-3, 110-112	364.80	1.847	48.8	27.1	2.733	1.348	^{a}1595		
39X-3, 110-112	364.80						1587		
40X-2, 137-139	373.27	2.006	45.3	23.1	2.708	1.542	^{a}1649		
40X-2, 137-139	373.27						1654		
40X-4, 91-93	375.81	2.010	44.9	22.9	2.727	1.551	^{a}1665		
40X-4, 91-93	375.81						1670		
41X-2, 91-93	382.41	1.918	48.0	25.7	2.622	1.426	^{a}1596		
41X-2, 91-93	382.41						1594		
42X-1, 68-70	390.38	1.916	49.0	26.2	2.728	1.414	^{a}1592		
42X-1, 68-70	390.38						1629		
43X-2, 52-54	401.42	1.979	45.9	23.8	2.714	1.508	^{a}1643		

Table 6 (continued).

Core, section, interval (cm)	Depth (mbsf)	Wet-bulk density (g/cm^3)	Porosity (%)	Water content (%)	Grain density (g/cm^3)	Dry-bulk density (g/cm^3)	Velocity (m/s)	Thermal conductivity (w/m/ – k)	Vane shear strength (kPa)
117-731A-									
43X-2, 52–54	401.42						1707		
43X-4, 79–81	404.69	1.992	44.5	22.9	2.661	1.535	[a]1685		
43X-4, 79–81	404.69						1715		
43X-6, 92–94	407.82	1.976	46.1	23.9	2.692	1.503	[a]1668		
43X-6, 92–94	407.82						1748		

[a] Velocity measurement perpendicular to bedding; others measured parallel to bedding.

Table 7. Physical properties summary for Hole 731B.

Core, section, interval (cm)	Depth (mbsf)	Wet-bulk density (g/cm^3)	Porosity (%)	Water content (%)	Grain density (g/cm^3)	Dry-bulk density (g/cm^3)	Velocity (m/s)	Coarse-grained turbidites
117-731B-								
1X-1, 17–19	408.77	2.034	44.0	22.1	2.731	1.583	[a]1642	
1X-1, 17–19	408.77						1659	
2X-1, 34–36	418.64				2.637			ss
3X-1, 10–12	428.20	2.705					[a]4429	css
3X-1, 10–12	428.20						4638	css
3X-1, 80–82	428.90	2.021	41.3	20.9	2.658	1.599		
4X-1, 80–82	438.50				2.683			ss
4X-3, 47–49	441.17	2.176	46.1	21.7	2.752	1.704	[a]1627	
4X-3, 47–49	441.17						1653	
5X-1, 40–42	447.80	1.916	51.0	27.3	2.755	1.394	[a]1582	
5X-1, 40–42	447.80						1572	

Note: css = calcitic silty sandstone (well indurated) and ss = silty sandstone.

[a] Velocity measurement perpendicular to bedding; others measured parallel to bedding.

number of sandstone samples, the density-velocity relationship for the coarse-grained turbidites is less well-defined.

At Site 731, as at Sites 721 and 722, the variation of the velocities measured both parallel and perpendicular to bedding increases in the fine-grained turbidites of lithologic Unit IV. Four samples of poorly cemented silty sandstone recovered from depths between 900 and 1000 mbsf transmit compressional waves slightly faster than the adjacent clay-rich layers (Table 7), but are more readily distinguished by their low anisotropy (Fig. 25). In contrast, compressional-wave velocities measured perpendicular to bedding for well-indurated calcitic silty sandstone are markedly higher, ranging from 3801 to 4429 m/s.

The different lithologies recovered at Site 731 show distinctly different patterns of velocity anisotropy (Fig. 25). Within the nannofossil-rich sequences of lithologic Units I, II, and III, anisotropy varies considerably from 0.1% to 5.8% with an average value of 1.7% and little if any correlation to wet-bulk density. Anisotropy of the turbidites ranged from 0.3% to 15.1%, with considerable variation at all sub-bottom depths. On average, anisotropy of the turbidites increases with density, as a result of increased compaction and the resultant increases in preferred orientation of the platy-clay minerals. The poorly cemented silty sandstones displayed weak anisotropy. Two of the four poorly cemented sandstone samples display small negative anisotropies (velocity parallel to bedding less than that perpendicular to bedding), whereas anisotropy of the two remaining samples ranges from 1.2% to 3.3%. Velocity anisotropy of the calcitic silty sandstones is high, averaging 8.9%, but also highly variable, with values ranging from 4.6% to 18.4%.

Vane Shear Strength

Vane shear strengths were measured in Cores 117-731A-1H through -11X (0–102 mbsf). Throughout the seven APC cores, which sampled lithologic Subunit IA, shear strength increased at an average rate of 1.10 kPa/m to a maximum value of 68.4 kPa at 62.6 mbsf. In lithologic Subunit IB, beginning in Core 117-731A-8X, the shear strength dropped to 27.6 kPa and increased downsection at a rate of only 0.65 kPa/m. The low shear strengths in this unit probably reflect an increase in drilling-induced disturbance caused by the XCB coring system rather than a true decreases in shear strength associated with the change in lithology. These findings are identical to those found at Site 721 and 722 where shear strength gradients of 1.10 to 1.20 kPa/m were recorded in the intervals recovered by the APC and where markedly lower shear strengths and gradients were encountered in the XCB cores.

Thermal Conductivity

Thermal conductivity was measured on alternate cores from Hole 731A through Core 117-731A-22X (212 mbsf). Sediments recovered from greater depths were too stiff for insertion of the needle probes or too friable and brittle for accurate measurement. Through Subunits IA and IB, thermal conductivity varies from about 1.10 to 1.40 W/m·K, with a mean value for the unit of 1.30 W/m·K (Fig. 26). At depths greater than about 70 mbsf, the lowest values may result from insertion of the probe into slurry between the drilling biscuits rather than into the "undisturbed" sediment.

Within lithologic Unit II, thermal conductivity decreases downsection in tandem with the decrease in wet-bulk density. The markedly higher variability of thermal conductivity in this layer is most likely related to changes in sediment constituents, particularly the abundance of diatoms and organic matter which is responsible for the high variability of bulk density within this unit. However, given the relatively well-defined relationship between thermal conductivity and density (Fig. 27), it is likely that

Table 8. Physical properties summary for Hole 731C.

Core, section, interval (cm)	Depth (mbsf)	Wet-bulk density (g/cm^3)	Porosity (%)	Water content (%)	Grain density (g/cm^3)	Dry-bulk density (g/cm^3)	Velocity (m/s)	Coarse-grained turbidites
117-731C-								
2R-2, 76-78	504.66	2.092	38.2	18.7	2.646	1.700	[a]1724	
2R-2, 76-78	504.66						1776	
2R-3, 121-123	506.61	2.029	41.2	20.8	2.627	1.607	[a]1700	
2R-3, 121-123	506.61						1745	
4R-1, 36-38	560.56	2.120	39.9	19.3	2.755	1.711	[a]1709	
4R-1, 36-38	560.56						1803	
5W-4, 74-76	575.14	2.120	38.6	18.7	2.757	1.724	[a]1770	
5W-4, 74-76	575.14						1902	
6R-1, 94-96	619.04	2.084	39.7	19.5	2.709	1.678	[a]1748	
6R-1, 94-96	619.04						1831	
7W-1, 53-55	628.33	2.088	39.4	19.3	2.714	1.684	[a]1705	
7W-1, 53-55	628.33						1762	
8R-1, 62-64	676.52	2.082	44.4	21.9	2.779	1.627		
8R-4, 26-28	680.66	2.118	39.4	19.1	2.751	1.714	[a]1718	
8R-4, 26-28	680.66						1847	
10R-1, 22-24	733.82	2.208	36.7	17.0	2.766	1.832	[a]1815	
10R-1, 22-24	733.82						1966	
10R-2, 3-5	735.13	2.270	31.3	14.1	2.714	1.949	[a]1902	ss
10R-2, 43-45	735.53	2.216	34.3	15.9	2.760	1.865	[a]1830	
10R-2, 43-45	735.53						1899	
11W-1, 47-49	743.77	2.657	2.0				[a]3878	css
11W-1, 47-49	743.77						4691	css
11W-5, 137-139	750.67	2.204	34.8	16.2	2.761	1.847	[a]1779	
11W-5, 137-139	750.67						1854	
12R-1, 94-96	792.44	2.270	26.8	12.1	2.646	1.995	[a]2028	ss
12R-2, 137-139	794.37	2.201	33.9	15.8	2.715	1.854	[a]1832	
12R-2, 137-139	794.37						1912	
12R-3, 95-97	795.45	2.185	33.1	15.5	2.712	1.845	[a]1837	
12R-3, 95-97	795.45						1952	
14R-1, 27-29	849.67	2.566	8.0				[a]3801	css
14R-1, 27-29	849.67						4004	css
14R-1, 39-41	849.79	2.205	30.8	14.3	2.676	1.889	[a]2076	
14R-1, 39-41	849.79						2157	
16R-1, 137-139	908.67	2.222	31.0	14.3	2.636	1.904	[a]1910	
16R-1, 137-139	908.67						2143	
16R-2, 60-62	909.40	2.245	29.4	13.4	2.655	1.944	[a]1969	ss
16R-2, 60-62	909.40						1942	ss
16R-3, 6-8	910.36	2.232	30.3	13.9	2.594	1.922	[a]1938	
16R-3, 6-8	910.36						2124	
17R-2, 143-145	919.63	2.302	24.5	10.9	2.678	2.051	[a]2220	ss
17R-2, 143-145	919.63						2246	ss
17R-4, 2-4	921.22	2.227	31.0	14.2	2.699	1.910	[a]1925	
17R-4, 2-4	921.22						2085	
19R-1, 141-143	937.51	2.279	29.4	13.2	2.665	1.977	[a]1949	
19R-1, 141-143	937.51						2141	
19R-3, 8-10	939.18	2.330	29.1	12.8	2.711	2.031	[a]1980	
19R-3, 8-10	939.18						2094	
20R-1, 33-35	946.03	2.252	32.0	14.5	2.707	1.924	[a]1885	
20R-1, 33-35	946.03						2153	
20R-3, 61-63	949.31	2.260	32.2	14.6	2.710	1.930	[a]1862	
20R-3, 61-63	949.31						2166	
20R-4, 20-22	950.40	2.331	28.3	12.5	2.740	2.040	[a]1967	
20R-4, 20-22	950.40						2158	
21R-1, 17-19	955.57	2.272	33.7	15.2	2.721	1.927	[a]1853	
21R-1, 17-19	955.57						2107	
21R-2, 121-123	958.11	2.245	31.0	14.1	2.678	1.927	[a]1838	
21R-2, 121-123	958.11						2054	
21R-3, 0-2	958.40	2.629	3.7				[a]4331	css
21R-3, 0-2	958.40						4667	css
22R-1, 90-92	966.00	2.286	28.2	12.6	2.670	1.997	[a]2001	ss
22R-2, 82-84	967.42	2.265	29.6	13.4	2.689	1.962	[a]1975	
22R-2, 82-84	967.42						2243	
22R-4, 15-17	969.75	2.250	28.3	12.9	2.665	1.960	[a]1983	
22R-4, 15-17	969.75						2207	
23R-1, 68-70	975.48	2.320	30.2	13.4	2.711	2.010	[a]1951	
23R-1, 68-70	975.48						2196	
23R-2, 83-85	977.13	2.434	27.2	11.4	2.737	2.156	[a]2346	ss
23R-2, 83-85	977.13						2426	ss
23R-4, 13-15	979.43	2.237	29.2	13.4	2.759	1.938	[a]1959	
23R-4, 13-15	979.43						2289	
24R-1, 54-56	985.04	2.249	29.9	13.6	2.639	1.943	[a]1942	
24R-1, 54-56	985.04						2175	
24R-2, 136-138	987.36	2.226	30.5	14.1	2.675	1.913	[a]1875	
24R-2, 136-138	987.36						2067	
24R-3, 110-112	988.60	2.336	26.3	11.5	2.722	2.066	[a]2247	ss
24R-3, 110-112	988.60						2241	ss

Note: css = calcitic silty sandstone (well indurated) and ss = silty sandstone.

[a] Velocity measurement perpendicular to bedding; others measured parallel to bedding.

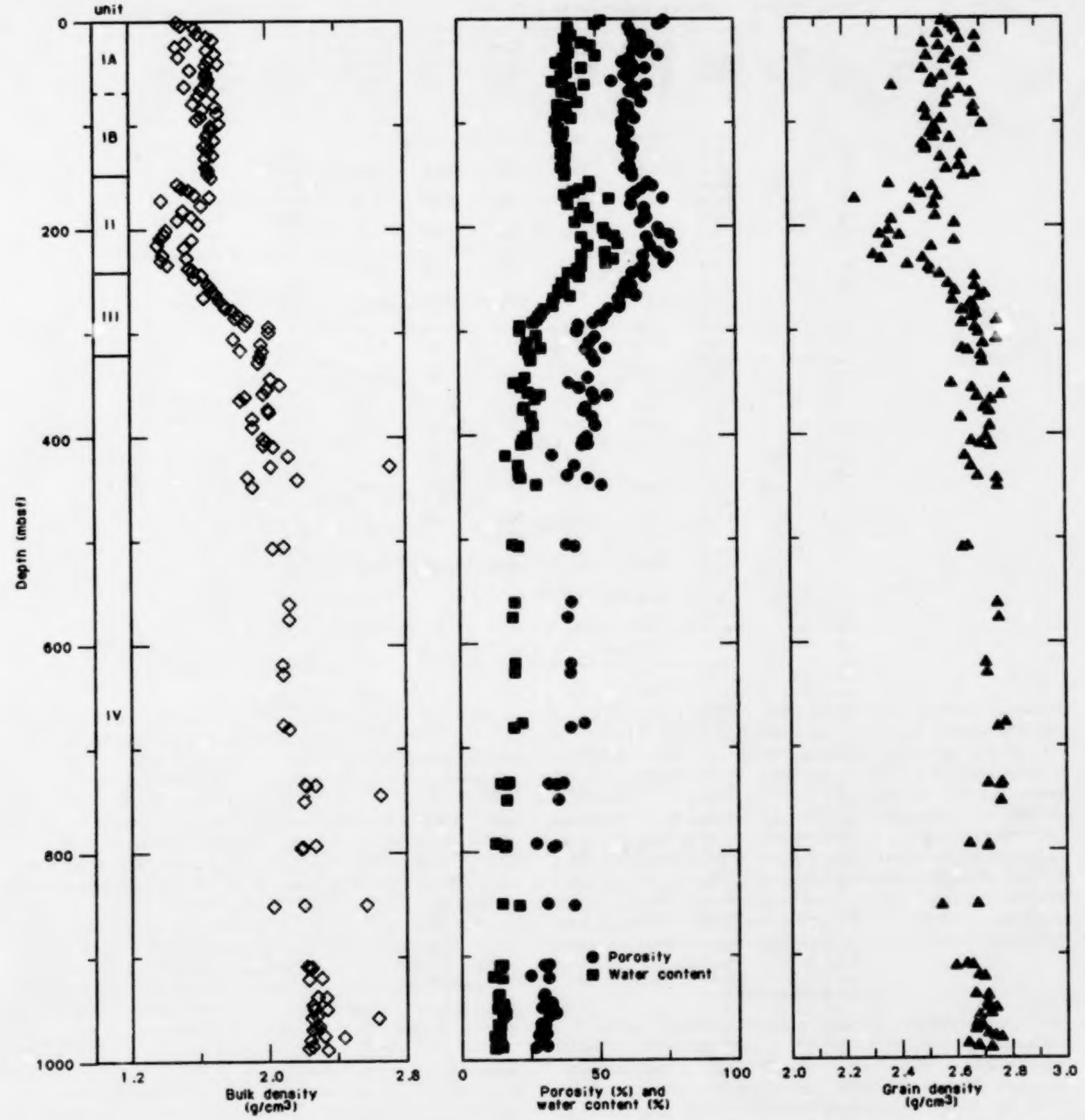

Figure 22. Index properties (wet-bulk density, porosity, water content, and grain density) measured on discrete samples for Holes 731A, 731B, and 731C.

some of the scatter also results from the increased drilling disturbance of this low density layer and inherent difficulties in positioning the probes into undisturbed sediment in the whole-round core sections.

GRAPE and P-Wave Logs

GRAPE and *P*-wave logger records of very good quality were obtained for the entire interval cored in Hole 731A (Figs. 28 and 29). The measurements of both logging systems correspond well to measurements made on discrete samples. The cyclic variation on the scale of 1-2 m in lithologic Unit I, which is present in the GRAPE and *P*-wave logs from Sites 721 and 722, is also present in the records from Site 731. Although the character of the logs from all of the Owen Ridge sites is similar, the correlation of features of the logs from Site 731 with features of the logs from Sites 721 and 722 is not readily apparent.

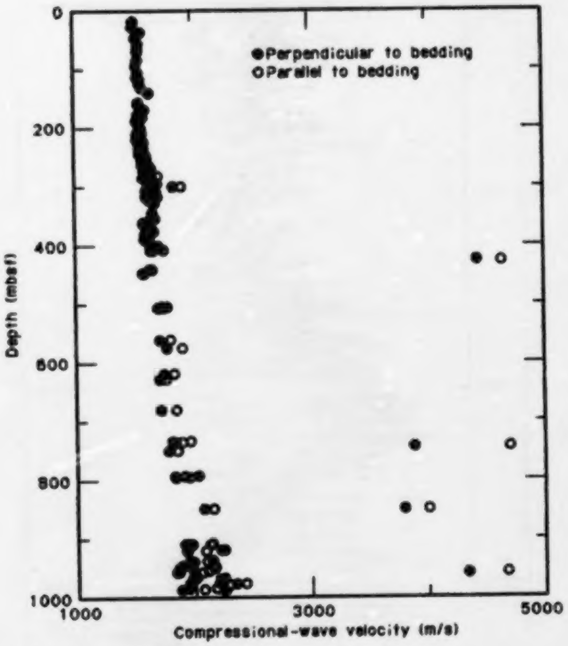

Figure 23. Compressional-wave velocity as measured on discrete samples in the Hamilton Frame Velocimeter for Holes 731A, 731B, and 731C.

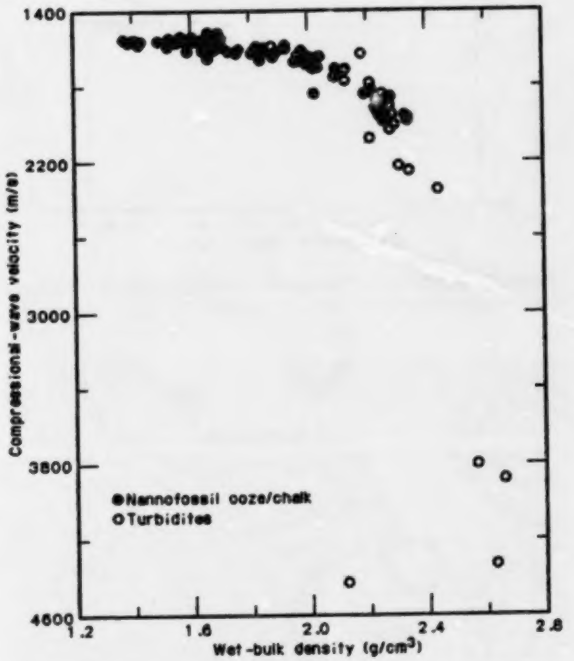

Figure 24. Wet-bulk density vs. compressional-wave velocity measured on discrete samples for Holes 731A, 731B, and 731C.

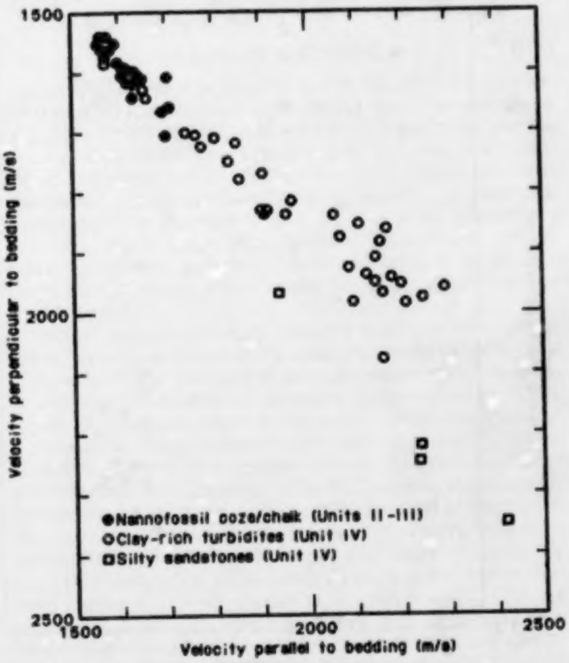

Figure 25. Crossplot of compressional-wave velocity measured perpendicular and parallel to bedding on discrete samples for Holes 731A, 731B, and 731C.

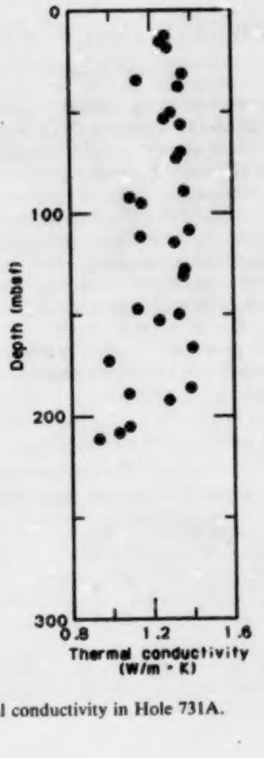

Figure 26. Thermal conductivity in Hole 731A.

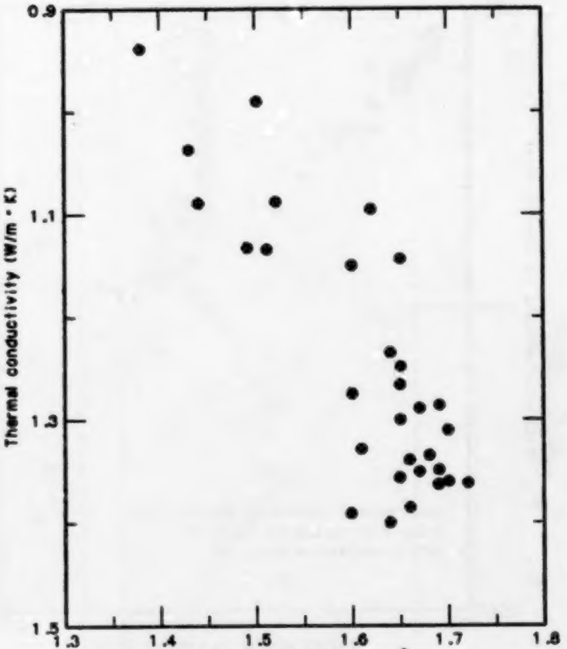

Figure 27. Thermal conductivity vs. wet-bulk density for Hole 731A. GRAPE densities were used to estimate wet-bulk density for intervals of conductivity which lack corresponding discrete-sample wet-bulk density determinations.

INORGANIC GEOCHEMISTRY

Introduction

Twenty-five interstitial water samples were collected by squeezing from Holes 731A (16 samples), 731B (1 sample), and 731C (8 samples). A single *in-situ* sample was collected from Hole 731A with the *in-situ* water sampler. All analytical data are listed in Table 9 and displayed as composite plots in Figure 30. The deepest sample, collected at 989 mbsf, appears to contain a significant proportion of seawater as indicated by calcium and chloride concentrations which are lower than expected and salinity, sulfate, and magnesium levels which are apparently too high. The *in-situ* sample also appears to have been contaminated by the addition of some seawater.

In general, the pore-water profiles at this site are very similar to the results from the two previous Owen Ridge sites (721 and 722). The one significant difference is that Site 731 was drilled to a much greater depth; the interstitial water data span nearly 1 km of section, which permits a better definition of the diagenetic reaction paths on the ridge.

Salinity, Chloride, and pH

The decrease in salinity over the top ~150 m (Fig. 30) reflects sulfate reduction and magnesium depletion in the pore waters, a phenomenon which was almost universally encountered during Leg 117. In contrast, the chloride content increases with depth, from about 560 mmol/L near the top of Hole 731A (equivalent to a bottom water salinity of ~35‰) to ~580 mmol/L near the bottom of Hole 731C (Table 9). The higher concentrations occur in the turbidite unit (lithologic Unit IV) only, and it appears that Cl^- is currently diffusing upward from the turbidites into the overlying nannofossil chalks (Fig. 30). A similar increase in the chloride concentration with depth was noted at both sites drilled previously on the Owen Ridge. This distribution can potentially be explained by either or both of two processes. First, the high chloride levels at depth could simply represent burial of more saline bottom water during the late Oligocene to early Miocene. Rapid accumulation of the turbidites would obviate the subsequent loss of salt via diffusion from the deeper part of the sequence. The second possibility is that the formation of authigenic clay minerals during the alteration of both volcanic ash and detrital silicates in the turbidites could increase the salinity by incorporating water into interlayer sites in the clays. However, given the limited volume of smectites observed in the turbidites (see "Inorganic Geochemistry" section, "Site 721" chapter, this volume), we believe that this mechanism is unlikely to account for the observed increase in the chloride content. Bottom water would have had to have been about

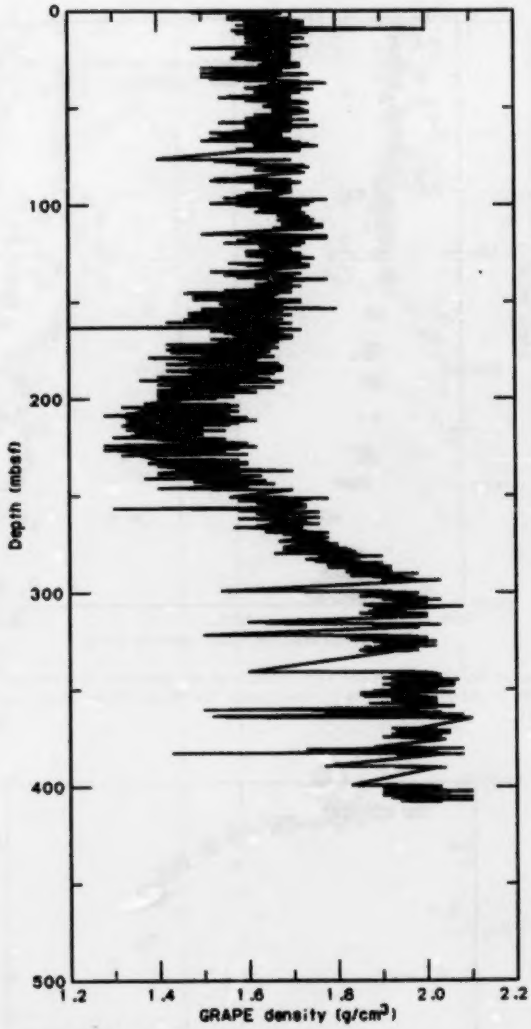

Figure 28. GRAPE wet-bulk density for Hole 731A. The profile is based on 10-cm-block averages of the data.

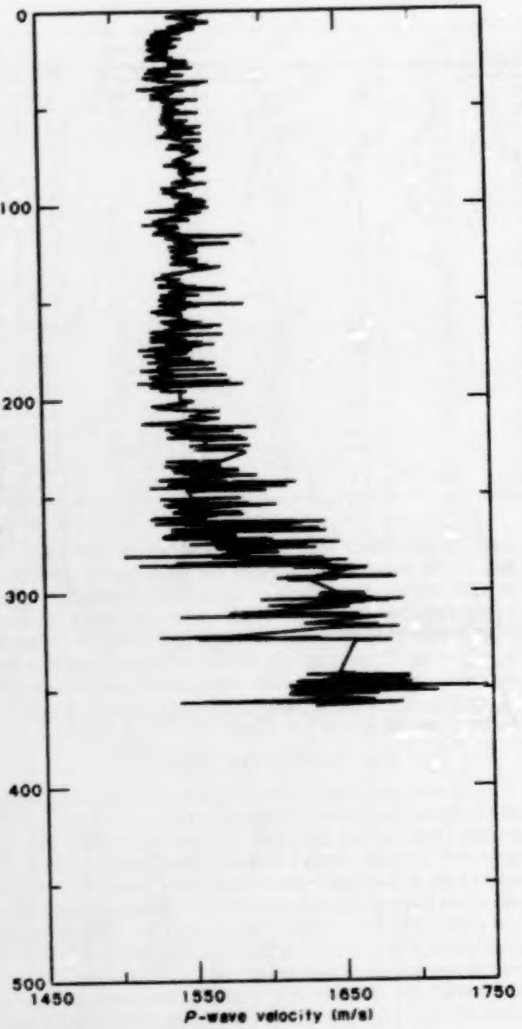

Figure 29. Compressional-wave velocity as measured by the *P*-wave logger for Hole 731A. The profile is based on 10-cm-block averages of the data.

1 g/kg saltier during the early Miocene in order to produce a 20 mmol/L increase in the chloride concentration; we consider this to be a reasonable possibility and prefer it to the alteration hypothesis.

It is interesting to note that the topmost pore-water sample at Site 731 contained 559 mmol/L Cl^-, similar to that at Site 721 (556 mmol/L). The chloride content measured in the shallowest sample at Site 722 (549 mmol/L) is somewhat lower which may be the result of an analytical error. Several sites on the Oman margin had significantly higher concentrations of chloride, ranging up to 570 mmol/L, in near-surface interstitial waters. Such high levels probably indicate the influence of inflow at intermediate depths of high-salinity water from the Red Sea and the Persian Gulf.

The pH profile (Fig. 30) shows little variation with depth. Measured values are ~0.5 pH units less than "normal" seawater pH, which can probably be explained by the production of H_2S during sulfate reduction.

Alkalinity and Sulfate

The alkalinity profile (Fig. 30) is very similar to the distributions seen at Sites 721 and 722 on the northern Owen Ridge. A maximum of ~9 mmol/L at 90 mbsf results from a balance between production and consumption of HCO_3^-. Above 90 mbsf, the rate of production of HCO_3^- ion during sulfate reduction exceeds the rate of consumption as authigenic carbonates are precipitated. The opposite is probably true in the nannofossil oozes and chalks below the maximum. As noted by Gieskes (1981, and references therein), chemical alteration of volcanic ash in the turbidites (see below) may be consuming alkalinity at greater depths.

Sulfate depletion is nearly complete at depths below about 250 m but minor concentrations appear to persist to the bottom of the hole. The greatest rate of reduction occurs in the top 60 m, as evidenced by the slope of the upper portion of the profile in Figure 30. The persistence of sulfate to considerable depths at this site differs from the distribution observed at Site 721, where no sulfate was detectable between 100 and 380 mbsf (see "Inorganic Geochemistry" section, "Site 721" chapter, this volume), but bears some similarity to the profile measured at Site 722. It was thought (see "Inorganic Geochemistry" section, "Site 722" chapter, this volume) that the trapping of seawater during the rapid emplacement of the turbidite facies, coupled with a relatively low input of labile organic matter, might account for the presence of the residual interstitial sulfate at depth at Site 722; a similar phenomenon might account for the distribution seen at Site 731. Presumably, the absence of sulfate in the 100–380 mbsf interval in Hole 721A resulted from a slightly higher oxidant demand compared to Sites 722 and 731. This may in part reflect the shallower water column at the former site, which would encourage the deposition of slightly less oxidized organic matter at the sediment-water interface.

Note that sulfate is depleted at many of the Oman margin sites at depths very similar to that seen at Site 731. We find this to be very surprising given that the sediments at the margin sites are deposited within the oxygen minimum, contain generally higher organic carbon contents, and accumulate at a faster rate. All three of these factors should result in complete depletion of sulfate at considerably shallower depths on the margin than on Owen Ridge, but no such contrast is observed. We are unable to explain this seeming enigma at present, but it has important implications for any hypothesis which attempts to account for the accumulation of organic matter under the oxygen minimum on the Oman margin. The major question which such a hypothesis will need to embrace is: why isn't there a profound difference in the distribution of dissolved sulfate between the ridge and the margin?

Calcium and Magnesium

Calcium and magnesium distributions at Site 731 (Fig. 30) are very similar to those observed at Sites 721 and 722. The depletion of magnesium with depth is attributed to precipitation of dolomite or dolomitization of pre-existing calcite, and to the alteration of volcanic ash in the turbidites (to magnesian smectite or sepiolite?). Smear slide observations indicate that ash is a common constituent, ranging up to 10% by volume (see "Lithostratigraphy" section, this chapter). The calcium minimum appears to reflect two controls: first, precipitation of calcite at relatively shallow depths (which leads to an increase in the Mg/Ca ratio; see Fig. 30); and second, release of Ca^{2+} during alteration of feldspars (and ash?) in the turbidites. Smear slide observations indicate that alteration of feldspars is a common phenomenon in the turbidite facies (S. Clemens, pers. comm.). Calcium

Table 9. Summary of interstitial water geochemical data, Site 731.

Hole, core, section, interval (cm)	Depth (mbsf)	Vol. (mL)	pH	Alk. (mmol/L)	Sal. (g/kg)	Mg (mmol/L)	Ca (mmol/L)	Cl (mmol/L)	SO_4 (mmol/L)	PO_4 (μmol/L)	NH_4 (mmol/L)	SiO_2 (μmol/L)	Mg/Ca	DOC (a.u.)
731A-1H-4, 145-150	5.95	52	7.65	5.60	34.2	51.15	8.06	559	22.2	9.8	0.16	722	6.34	0.243
731A-3H-4, 145-150	25.25	45	7.41	7.83	34.2	49.55	6.96	562	16.1	11.9	0.96	815	7.12	0.623
731A-6H-4, 145-150	53.75	50	7.60	8.77	33.2	41.50	6.51	563	9.3	12.0	1.61	982	6.37	0.885
731A-7I-6, 145-150	64.80	13	7.65	6.80	33.9	44.37	7.21	565	12.1	1.4	1.28	788	6.15	0.429
731A-9X-4, 145-150	82.65	35	7.64	9.06	32.5	37.99	6.68	560	6.0	8.7	1.79	918	5.69	0.908
731A-12X-4, 145-150	111.65	33	7.58	7.68	32.3	34.92	7.84	559	4.2	5.8	1.84	957	4.45	0.605
731A-15X-4, 145-150	140.65	34	7.44	6.33	32.2	33.23	8.66	561	3.9	4.7	1.66	963	3.84	0.453
731A-18X-4, 145-150	169.65	42	7.45	5.33	32.2	31.45	9.09	562	3.5	4.2	1.63	1114	3.46	0.378
731A-21X-4, 145-150	198.75	51	7.56	3.41	32.2	30.27	9.71	559	3.2	3.2	1.46	1223	3.12	0.300
731A-24X-4, 145-150	227.85	41	7.30	4.52	32.1	29.19	10.47	559	2.0	1.9	1.38	1126	2.79	0.256
731A-27X-4, 145-150	256.85	48	7.45	3.44	32.0	28.26	10.69	557	2.0	0.7	1.25	1219	2.64	0.172
731A-30X-4, 145-150	285.85	28	7.58	2.39	32.1	27.71	10.84	555	1.7	0.2	1.18	698	2.56	0.120
731A-33X-2, 145-150	311.85	18	7.63	1.67	32.1	27.31	12.11	560	0.5	0.1	1.01	417	2.25	0.186
731A-37X-1, 140-150	347.20	25	7.67	2.24	32.0	27.22	12.28	561	0.0	0.2	0.50	310	2.22	0.121
731A-40X-2, 140-150	374.80	14	7.84	2.25	32.3	28.66	13.86	564	2.0	0.1	0.17	317	2.07	0.179
731A-43X-4, 140-150	405.30	27	7.87	2.16	32.1	27.22	14.03	565	0.2	0.1	0.35	230	1.94	0.143
731B-3X-1, 140-150	429.50	35	7.84	2.10	33.0	27.65	14.24	577	4.4	0.5	0.68	168	1.94	0.106
731C-2R-2, 140-150	505.30	26	7.79	1.79	31.3	25.58	16.22	560	1.1	0.4	0.41	174	1.58	0.133
731C-10R-1, 140-150	735.00	15	8.27	0.83	32.2	19.89	20.07	580	1.1	0.6	0.79	90	0.99	0.183
731C-12R-1, 140-150	792.90	12	8.10	1.14	32.2	20.04	21.84	579	2.1	0.1	0.61	100	0.92	0.166
731C-14R-1, 140-150	850.80	16	8.18	1.28	32.1	19.08	24.44	580	0.7	1.0	0.82	110	0.78	0.140
731C-16R-2, 140-150	910.20	10	7.73	0.71	32.3	22.05	24.55	580	2.4	0.3	0.56	96	0.90	0.193
731C-19R-2, 140-150	939.00	5	—	—	32.8	21.36	25.64	579	2.4	0.5	0.59	110	0.83	0.224
731C-22R-3, 140-150	969.50	14	8.26	1.20	32.5	20.89	25.47	582	1.1	0.5	0.82	78	0.82	0.160
731C-24R-3, 140-150	968.90	7	—	1.04	33.6	24.93	24.55	575	5.1	0.1	0.69	86	1.02	0.160

may also diffuse upward into the drilled section from an unknown source at greater depths. The approximately vertical form of the profile between 900 and 1000 mbsf suggests, however, that such a contribution is at best minor.

Ammonia, Phosphate, Silica, and Dissolved Organic Carbon

Ammonia, phosphate and dissolved silica distributions at Site 731 (Fig. 30) are almost identical in form to those observed at Sites 721 and 722. Ammonia concentrations are relatively low compared to levels which would be expected if organic matter with a composition equivalent to Redfield stoichiometry was being degraded. The deficiency implies that the buried organic material at the site has a higher C:N ratio than does the organic substrate in buried sediments on the Oman margin, where the concentration of ammonia produced per mole of sulfate reduced is significantly higher. It is possible that the uptake of NH_4^+ by clay minerals may also contribute to the relative ammonia deficiency in pore waters at Site 731, but we are unable to assess this.

Phosphate concentrations generally decrease with depth to values below ~250 mbsf which are near the analytical detection limit (Table 9). The profile is attributed to the precipitation of authigenic apatite in lithologic Units I–IV (nannofossil oozes and chalks) and to very limited diagenetic activity in the turbidites at depth.

The dissolved silica distribution clearly outlines the change from opal-bearing nannofossil ooze and chalk to opal-poor terrigenous turbidites at the boundary between lithologic Units III and IV (at about 320 mbsf; see "Lithostratigraphy" section, this chapter). Silica must be diffusing downward into lithologic Unit IV where it is presumably precipitated as quartz overgrowths. Indeed, the dissolved silica concentrations measured in the lower 200 m of lithologic Unit IV are very near the solubility limit for quartz, which is ~100 μmol/L at 20°C (Blatt et al., 1980).

The dissolved organic carbon (DOC) profile measured at Site 731 (Fig. 30) broadly reflects the distribution of organic carbon in the drilled section. The highest DOC levels occur between 50 and 90 mbsf, approximately coincident with a local maximum of the organic carbon concentration at about 75 mbsf (see "Organic Geochemistry" section, this chapter). Other pronounced sedimentary organic carbon maxima at ~150 and ~225 mbsf do not reflect such a direct association with DOC. This may be the result of smearing of the DOC profile by diffusion or a lower level of reactivity of the organic matter buried in the deeper horizons. The DOC maximum occurs within the zone of rapid sulfate reduction and coincides with the peak in the alkalinity profile. These three sets of data indicate clearly that diagenetic activity at this site is most pronounced in the upper 100 m. Organic matter in the carbon-rich bands at greater depths is apparently not subject to significant continuing degradation.

ORGANIC GEOCHEMISTRY

Forty-two physical property samples of Hole 731A, covering all four lithologic units, were analyzed for their organic carbon content (Fig. 31) and pyrolysis characteristics (Table 10). Sediments of lithologic Units I (0–146.5 mbsf) and II (146.5–240.9 mbsf) have an average organic carbon content of 0.71%. These values are more or less comparable with those measured in samples from other sites on the Owen Ridge (721, 722), although in these latter sites organic carbon values as high as 3.68% have been measured (see "Organic Geochemistry" sections, "Site 721" and "Site 722" chapters, this volume). Sediments of lithologic Units III and IV are characterized by very low organic carbon concentrations (average 0.12%). As the organic carbon values of lithologic Unit IV are within the limit of detection, no further organic carbon measurements were made on sediments of this lithologic unit recovered in Holes 731B and 731C. The results of the Rock-Eval pyrolysis are given in Table 10. The hydrogen indices are comparable with the results from the other Owen Ridge sites, but are generally lower than values measured in samples from the Oman margin sites.

DOWNHOLE MEASUREMENTS

Logging

Operations

Logging operations at Hole 731C began at 0415 hr on 8 October, with a hole conditioning program similar to that used at Site 720. The seismic stratigraphic combination was rigged up at 1610 hr. At this site the seismic stratigraphic combination consisted of borehole compensated sonic (BHC), dual induction resistivity (DIT), and gamma ray (GR) tools. This tool string was run from 1655 to 2155. Downgoing logs were obtained from the

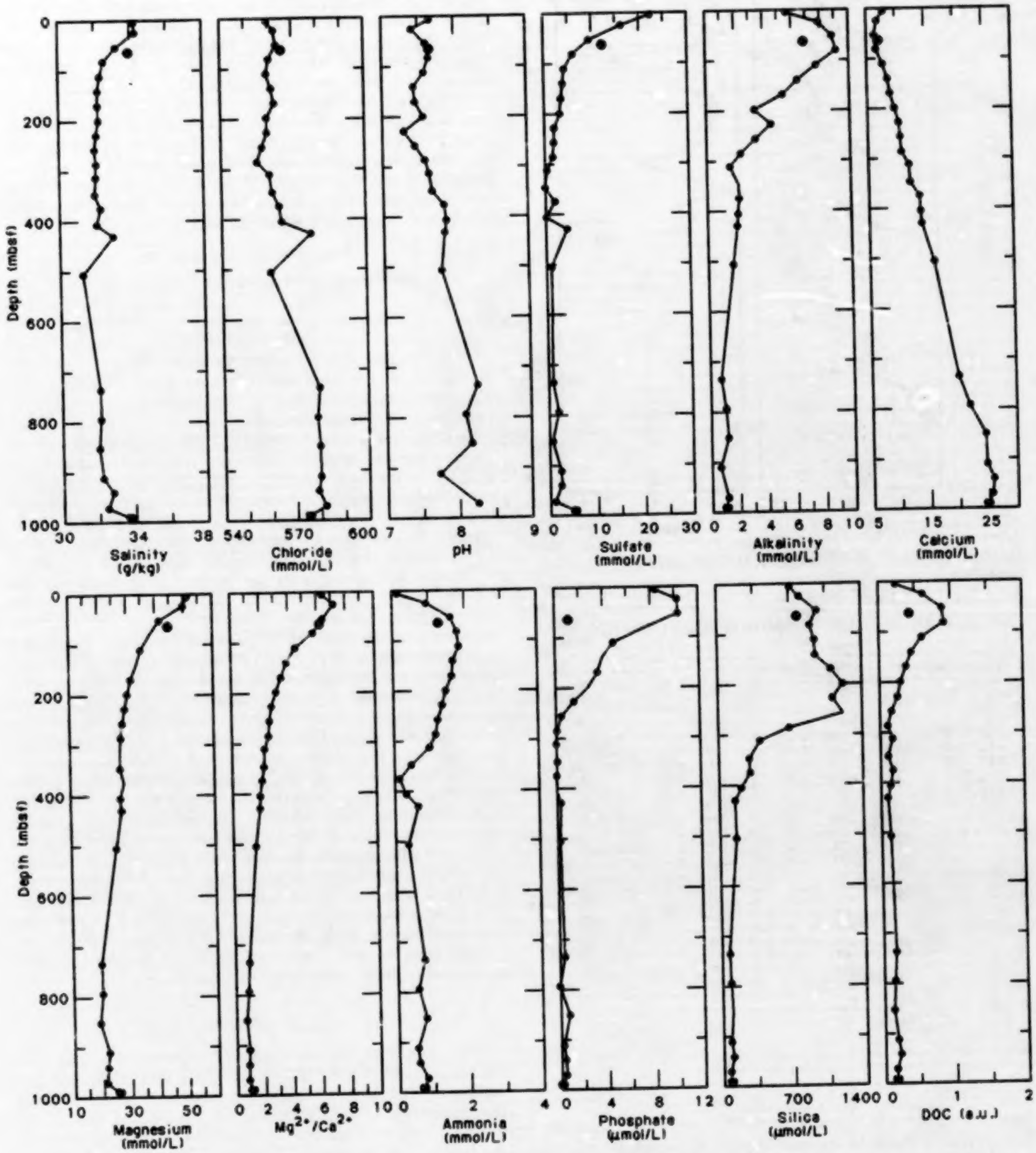

Figure 30. Concentrations vs. depth for Site 731. Compiled by stacking data from Holes 731A, 731B, and 731C. The large dot represents the *in-situ* sample. Parentheses enclose the lowermost point, which is believed to be partly contaminated with seawater. It is not clear why anomalously high sulfate concentrations were measured at 375 and 430 mbsf. The data shown in other profiles indicate that the presence of sulfate in these two samples cannot simply be attributed to contamination with drilling fluid. Dissolved organic carbon measured in absorbance units.

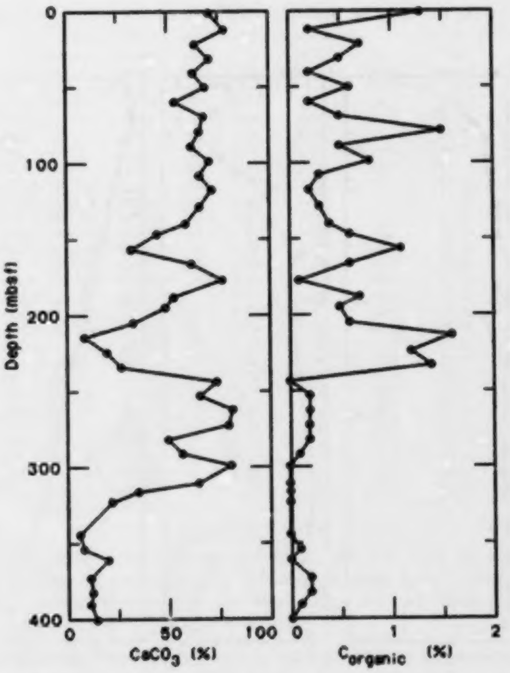

Figure 31. Downhole plot of $CaCO_3$ and organic carbon for samples of Hole 731A.

Table 10. Results of Rock-Eval pyrolysis of samples from Hole 731A.

Core, section, interval (cm)	Depth	T_{max} (°C)	S_1	S_2	S_3	S_2/S_3	TOC	HI	OI
117-731A-									
1H-1, 96-98	0.96	429	0.44	2.52	2.67	0.94	1.37	184	195
2H-2, 80-82	12.10	424	0.10	0.33	1.57	0.21	0.26	127	604
3H-2, 80-82	21.60	430	0.24	1.63	2.00	0.81	0.79	206	253
4H-2, 80-82	31.10	421	0.15	0.55	1.72	0.31	0.51	108	337
6H-2, 80-82	50.10	428	0.12	0.48	1.80	0.26	0.60	80	300
8X-2, 64-66	69.14	427	0.08	0.47	1.50	0.31	0.50	94	300
9X-2, 80-82	79.00	429	0.46	4.17	2.39	1.74	1.52	274	157
10X-2, 80-82	88.70	422	0.15	0.78	1.74	0.44	0.50	156	348
11X-2, 92-94	98.42	429	0.09	0.71	1.39	0.51	0.88	81	158
12X-2, 80-82	108.00	422	0.14	0.66	1.62	0.40	0.38	174	426
13X-2, 84-86	117.74	421	0.07	0.40	1.33	0.30	0.28	143	475
14X-3, 77-79	128.77	420	0.08	0.44	1.31	0.33	0.33	133	397
15X-4, 100-101	140.20	414	0.11	0.34	1.42	0.23	0.43	79	330
16X-2, 103-105	146.93	417	0.16	0.70	1.62	0.43	0.65	108	249
17X-2, 125-127	156.75	425	0.38	2.22	2.15	1.03	1.15	193	187
18X-2, 101-103	166.21	426	0.21	1.19	1.49	0.79	0.62	192	240
20X-4, 67-69	188.27	421	0.21	1.38	1.65	0.83	0.87	159	190
21X-2, 56-58	194.86	414	0.19	0.61	1.53	0.39	0.51	120	300
22X-2, 99-101	204.99	424	0.20	1.56	1.68	0.92	0.67	233	251
23X-2, 70-72	214.40	423	0.57	3.76	1.68	2.23	1.61	233	104
24X-2, 108-110	224.48	424	0.42	2.92	1.69	1.72	1.29	226	131
25X-2, 90-92	234.00	427	0.36	3.34	1.90	1.75	1.44	232	132

Note: HI = hydrogen index and OI = oxygen index. Results of samples from Units III and IV have been omitted because of the very low organic carbon values.

base of pipe (85 mbsf) to 973 mbsf. Upcoming logs were obtained from 979 mbsf to the base of pipe (65 mbsf after raising pipe during logging).

The geochemical combination was run between 2319 hr on 8 October and 1100 hr on 9 October. At this site the geochemical combination consisted of spectral gamma ray (NGT), neutron porosity (CNT-G), gamma spectroscopy (GST), and accelerometer (GPIT) tools. Downgoing logs were obtained from the seafloor to 966 mbsf. The gamma spectroscopy tool was not activated during this run, because the downgoing logging speed is too fast for this tool and because its irradiation effect on the formation degrades the quality of the spectral gamma ray tool. With the gamma spectroscopy tool activated, upcoming logs were obtained from 968 mbsf to the seafloor. A short repeat section (129–78 mbsf) was also logged.

Rigdown from logging was completed at 1140 hr on 9 October. In all, 12 hr was used for hole conditioning and 19.5 hr was used for logging. No significant problems or delays were encountered, and the total time for logging operations was almost identical to the 32 hr scheduled. No bridges were encountered, so the sidewall entry sub was not needed. The wireline heave compensator was not used either, because seas were flat.

Log Quality and Editing

Most logs were of good quality and required no editing. Replicability of results was generally very good, as indicated by agreement of downgoing and upcoming logs. Subsequently, only upcoming logs are discussed. Geochemical logs obtained through pipe will require gain correction for pipe attenuation, but this correction has not been undertaken yet. Logs from four tools warranted some reprocessing: sonic, gamma spectroscopy, resistivity, and spectral gamma ray.

The upcoming sonic log was generally of high quality. No cycle skipping was detected. However, of the two source-receiver spacings in the BHC sonic tool, the short (0.9 m) spacing records the direct water waves before formation refracted waves in sediments with very slow velocities (high porosities). Consequently, no formation traveltimes were obtained from the short source-receiver spacing in the intervals 68.4–245.8 mbsf, 319.3–378.4 mbsf, and several other shorter low-velocity intervals. This problem rarely occurs even with the longer (1.5 m) source-receiver spacing. Revised short-spaced traveltimes were estimated for these intervals from the long-spaced traveltimes, based on a regression equation (R = 0.921) between short- and long-spaced traveltimes for the interval 585.7–616.1 mbsf, in which both spacings were reliable. Sonic velocities were then recalculated, using an algorithm described in Arthur et al. (in press). This reprocessed velocity log (Fig. 32) is likely to be quite accurate in general, but it may slightly overestimate the lowest velocities.

The resistivity logs at Site 731 exhibited the same low quality of calibration in the chalks that occurred in this unit at Site 722 (see "Downhole Measurements" section, "Site 722" chapter, this volume). Unlike at Site 722, the spherically focused log was consistent with medium and deep resistivity logs in the chalks, but all three logs have rare spurious spikes in the chalks (e.g., Fig. 32). No editing of these spikes has been undertaken yet. The gamma spectroscopy and spectral gamma log data were reprocessed post-cruise as described in the "Explanatory Notes" chapter (this volume). Data from both tools appeared to be of good quality, based on internal calibration tests.

Hole Deviation

Deviation from vertical of the borehole was measured with the GPIT accelerometer tool during both downgoing and upcoming runs of the geochemical combination (Fig. 33). Because this tool string is neither centralized nor padded against the borehole wall, tool wobble causes local deviation errors of as much as 0.5° in the top half of the hole and as much as 1.5° in the deepest part of the hole. Nevertheless, the pattern of hole deviation is easily seen.

From 80 to 320 mbsf, the hole is deviated by about 0.5° to the southeast. In the upper turbidites (320–460 mbsf), the hole deviation changes to near-vertical, with associated loss of accuracy of measurements of deviation azimuth. With continued

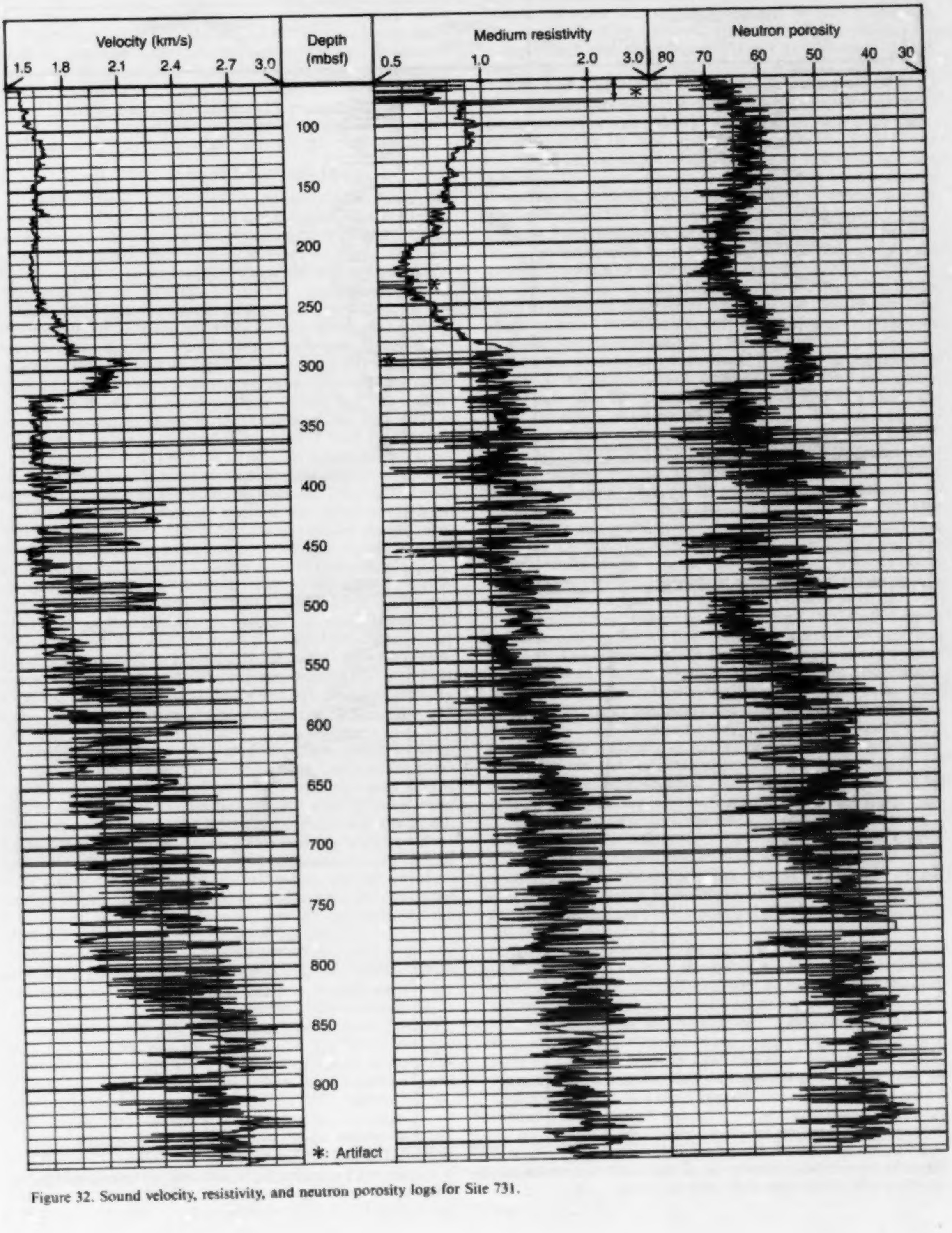

Figure 32. Sound velocity, resistivity, and neutron porosity logs for Site 731.

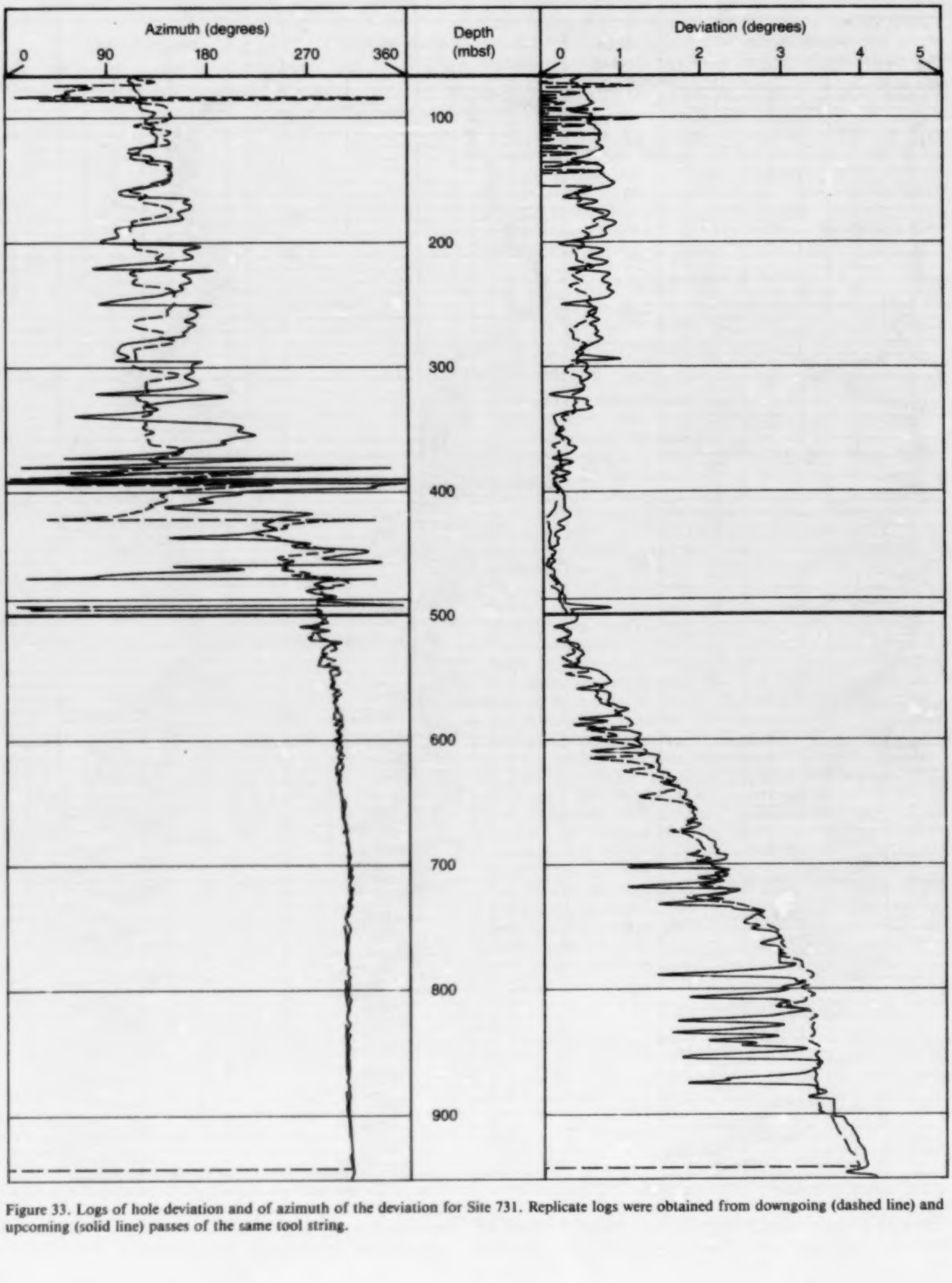

Figure 33. Logs of hole deviation and of azimuth of the deviation for Site 731. Replicate logs were obtained from downgoing (dashed line) and upcoming (solid line) passes of the same tool string.

penetration of the turbidites, this deviation increases gradually to a maximum of 4° toward the northwest.

This magnitude of hole deviation is sufficient to have a slight effect on magnetic inclinations in cores and to be detectable as inclined bedding in cores. Core orientation using the inclined bedding is possible. Such orientation would have an accuracy of 30°-45° in azimuth, sufficient to assist in polarity determination for the low-inclination paleomagnetic results from the lower turbidites (see "Paleomagnetism" section, this chapter).

Log Responses of Lithologic Units

Lithologic Unit I (0-146.5 mbsf) consists of nannofossil ooze and marly nannofossil ooze, with rare biogenic silica in the upper 66 m (see "Lithostratigraphy" section, this chapter). Open-hole logging of this unit began at 65 mbsf. Calcium values are high throughout the interval 65-146.5 mbsf, and potassium and thorium values are low (Figs. 34 and 35), consistent with smear slide identification of this unit as a nannofossil ooze with low clay content. Velocity and resistivity increase downhole and neutron porosities decrease. These changes partially reflect some increase of compaction with depth but also result from a gradual decrease in clay content and increase in calcite, as indicated by the potassium and calcium logs (Figs. 34 and 35). The unconformity at about 115 mbsf is not obvious on any log though a significant increase in titanium occurs at 117 mbsf (Fig. 35).

Lithologic Unit II (146.5-240.9 mbsf) is similar to Unit I, except that clay content is higher and diatoms sometimes constitute 20% or more of the sediment volume. This high diatom content affects both porosity-sensitive and geochemical logs. Even minor diatom content substantially increases porosity; resistivity and velocity are decreased accordingly. Porosity fluctuations at Site 731 are similar in character to those for comparable ages at Site 722 (see "Site 722" chapter, this volume): a slow cyclic increase in porosity downhole from 118 to 192 mbsf, rapid porosity increase between 192 and 200 mbsf, highest porosities between 200 and 246 mbsf, then rapid porosity decrease down to 286 mbsf (Fig. 32). Of these porosity changes only the increase between 118 and 170 mbsf may arise partly or entirely from clay mineral increase (Figs. 34 and 35). Based on porosity alone, maximum diatom abundance occurs between 200 and 246 mbsf.

A silicon abundance log shows maximum silicon between 145 and 242 mbsf (Fig. 34), a depth range that closely corresponds to the boundaries of Unit II. Within this interval, the highest silicon log yields are between 202 and 242 mbsf, very similar to the 200-246 mbsf interval of maximum porosity. Silica in either diatoms or clay minerals could account for these two correlations. However, the very high porosities, the lack of a correlation between potassium and silicon, and the actual reduction of potassium in the highest silicon zone 202-242 mbsf (Fig. 34) all indicate that diatoms, not clay minerals, are the dominant silicon component in lithologic Unit II.

Organic carbon is highest at about 200-240 mbsf (see "Organic Geochemistry" section, this chapter), corresponding with the interval of highest porosities. However, organic carbon levels are too low to dominate the character of the uranium log, as occurred at Site 728 (see "Downhole Measurements" section, "Site 728" chapter, this volume). Instead, the broad trends in the uranium log in the upper few hundred meters of both Site 731 and 722 parallel those of potassium (Figs. 34 and 35) and "Downhole Measurements" section, "Site 722" chapter, this volume), and suggest that much of the uranium is in clays.

Smear slides indicate that clay mineral abundance is somewhat higher in lithologic Unit II than in Unit I (see "Lithostratigraphy" section, this chapter). Increased iron, potassium, and thorium beneath 140-142 mbsf (Figs. 34 and 35) are consistent with this observation. Calcium abundance is significantly lower in Unit II than in Units I and III (Fig. 34), but with gradational boundaries rather than sudden changes at the unit boundaries. The calcium lowering is caused primarily by diatom dilution but is augmented near the lithologic Unit I/Unit II boundary by clay dilution.

Lithologic Unit III (240.9-320.1 mbsf) is composed of about 75% nannofossils and 15%-20% clay, with no diatoms. Accordingly, relative calcium abundance reaches some of the highest values at Site 731, and porosities are rather low (Figs. 32 and 34). Based on log responses alone, the unit is divided into two subunits. The upper subunit is a continuation of the gradual downward decrease in porosity and increase in velocity that began in lithologic Unit II. These changes probably reflect a gradual downward increase in the ratio of biogenic calcite to opal. The lithostratigraphic basis for the Unit II/III boundary is the lowest occurrence of biogenic opal in smear slides (see "Lithostratigraphy" section, this chapter). However, the lowest occurrence indicated by biostratigraphic studies of core-catcher samples is in Core 117-731C-29X, only 6 m shallower than the base of the log-determined subunit at 286 mbsf.

The second subunit of lithologic Unit III, as indicated by logs, is in the interval 286-315 mbsf. The subunit has a gradational base from 315 to 322 mbsf, characterized by a major decrease in calcium and increases in potassium, thorium, and iron. The base is close to the sedimentologically determined base of lithologic Unit III at 320.1 mbsf. Calcium is very high in this subunit, and silicon, iron, potassium, thorium, and uranium are quite low (Figs. 34 and 35). Porosities are low, as indicated by the velocity, resistivity, and neutron porosity logs (Fig. 32). This unit is more distinctive on the velocity and neutron porosity logs than on the resistivity log, because the latter reveals only the lower porosity of this subunit, while the former respond to both its lower porosity and its lower clay content. All of the log responses suggest a relatively pure chalk with low porosity.

In contrast to lithologic Units I-III, Unit IV (320-994 mbsf) is almost entirely detrital (see "Lithostratigraphy" section, this chapter). The interval 320-360 mbsf is thought to represent a transition zone from strong dominance of biogenic calcite above to even stronger dominance of terrigenous turbidites below. Biogenic calcite is very rare below the transition zone (see "Lithostratigraphy" and "Biostratigraphy" sections, this chapter), but detrital calcite is present to varying degrees and averages about 10%. The low but variable response of the calcium log in the turbidites (Fig. 34) probably reflects variations in detrital calcite content, though some contribution from plagioclase is possible.

Based on log responses, the majority of the transition is accomplished in the rather short interval 315-322 mbsf. Calcite (Ca log) decreases markedly, and clay abundance increases substantially (K, Th, and Fe logs; Figs. 34 and 35). The more gradual transition deduced from cores is also evident in nearly all of the geochemical logs, with a poorly defined base at about 355-380 mbsf.

The turbidites of lithologic Unit IV have a complex mineralogy, as indicated by both smear slides and log responses. The dominant minerals are clay (probably mainly illite and chlorite) and quartz, but mica and detrital calcite are abundant and feldspar and hornblende are common (see "Lithostratigraphy" section, this chapter). Changes in the relative abundances of these minerals cause few consistent patterns to be obvious in the logs. For example, potassium and thorium are positively correlated with porosity logs over some intervals (indicating that the potassium and thorium are dominantly in the clay minerals), but negatively correlated with porosity over other intervals (indicating that mica and/or potassium feldspar in the silts contribute more potassium and thorium than do the clays). These complexities can be handled by post-cruise mineralogical inversion of the logs.

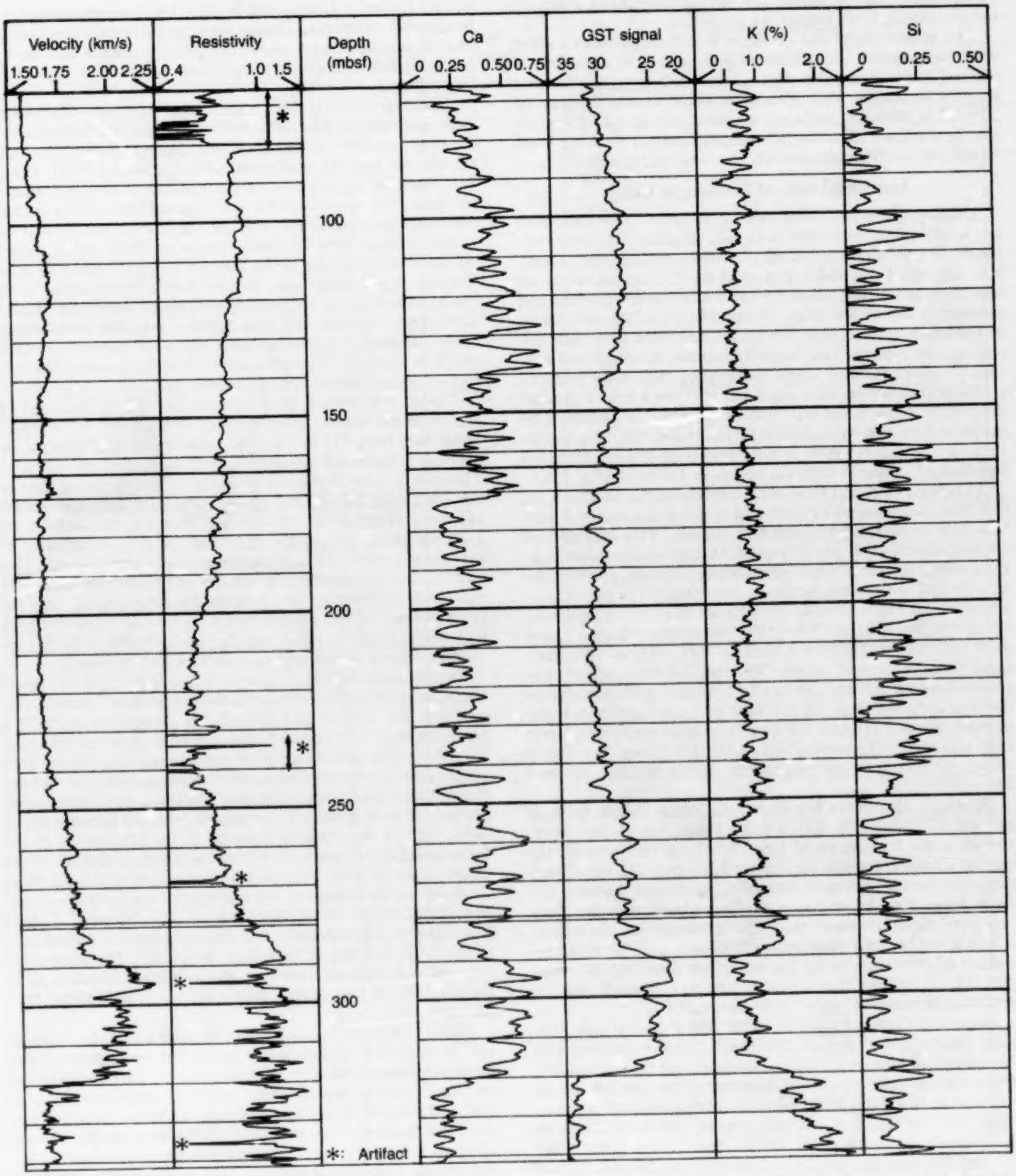

Figure 34. Comparison of velocity and resistivity logs with geochemical logs of potassium volume percent, calcium and silicon relative yields, and total formation signal from the GST tool.

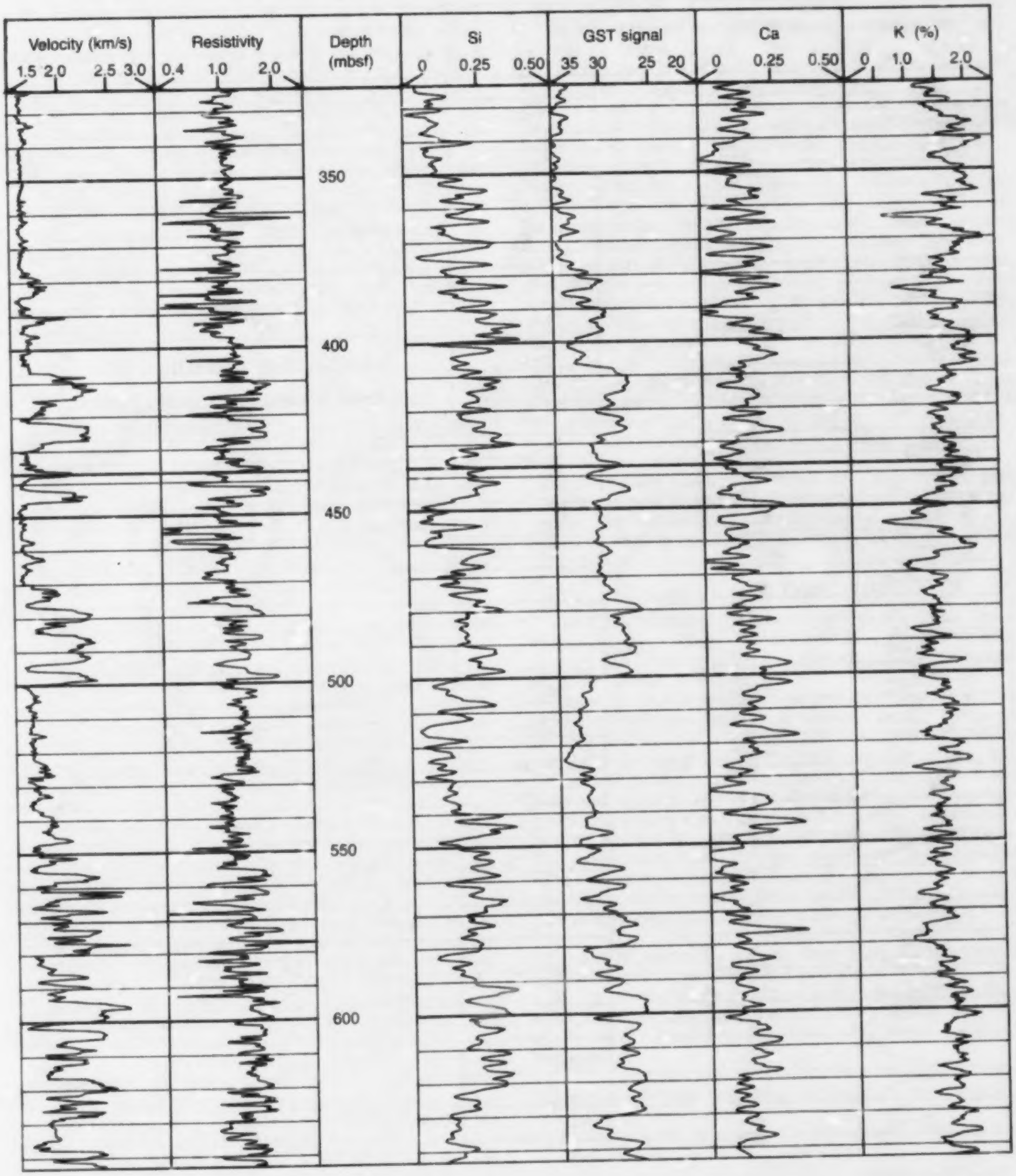

Figure 34 (continued).

Clay-rich and silt-rich units are best defined on the velocity log (Fig. 32). Superimposed on the overall compaction trend of the velocity log is a bimodal character, alternating between low-velocity clays and higher-velocity silts and sands. Neither is a complete end point in the clay/quartz continuum, but the two relative end points are well developed. In the interval 317–530 mbsf, clay-rich beds dominate, with most of the sands occurring in clusters in the two short intervals 404–443 and 470–500 mbsf. From 530 to 840 mbsf, clay-rich and sand-rich beds are present in about equal proportions. Below 840 mbsf, sand-rich

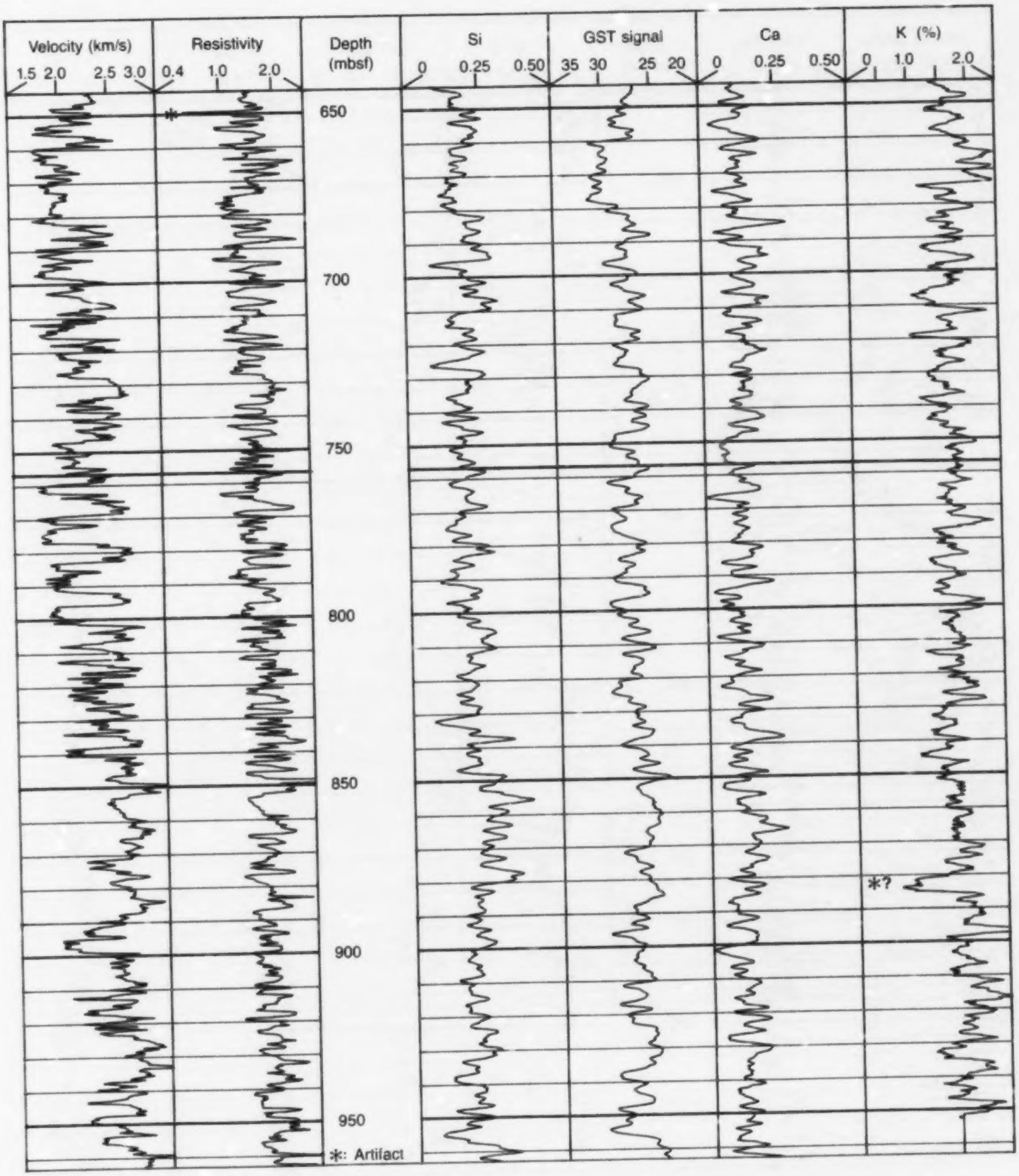

Figure 34 (continued).

beds slightly predominate. Throughout the turbidites, there is very little evidence of fining-upward or coarsening-upward sequences, as indicated by either porosity or clay indicator logs. Most individual turbidites have thicknesses of less than a meter (see "Lithostratigraphy" section, this chapter). The vertical resolution of the logs is not sufficient for detection of fining-upward patterns on this scale.

The velocity increase as a function of depth is greater in the turbidites of Site 731 than in most other regions. The empirical curve of velocity vs. depth of Hamilton (1979), based on 20 areas of terrigenous sediments, predicts a velocity of 1.9 km/s at the top of the turbidites and 2.3 km/s at the bottom of Site 731. In contrast, average velocities at Site 731 increase from about 1.65 km/s in the upper 50 m of the turbidites to about 2.6 km/s in the lowest 100 m of sediments penetrated (Fig. 32). Similarly low velocities were found in the upper turbidites at Site 722 (see "Downhole Measurements" section, "Site 722" chapter, this volume). Nearly all of this difference between turbidite velocities of Owen Ridge and other regions can be attributed to the downhole change from clay dominance to silt dominance. The clay base line compaction trend increases from 1.6 to 2.0 km/s downhole, and the silt and sand base line increases from 2.1 to 2.8 km/s. The 1.9 km/s prediction is less than 0.1 km/s higher than the average of clay and silt baselines near the top of the turbidites. Near the bottom of the hole, the 2.3 km/s predicted average is only about 0.1 km/s higher than the average of clay and silt base lines.

INTERHOLE CORRELATIONS

Layer-by-layer Correlation at Site 731

The three holes drilled at Site 731 are located in 2366 m water depth on the west of the Owen Ridge flank, 23 km west-southwest of Site 721 and 14 km west-southwest of Site 722. Hole 731A was drilled to 67.0 mbsf with the APC and to 409.0 mbsf with the XCB. Recovery with the APC was almost perfect, but the top of Hole 731A did not obtain the mud line. Holes 731B and 731B were drilled from 408.7 and 502.4 mbsf to 457.1 and 994.2 mbsf with the XCB and RCB, respectively. The age of the sedimentary sequence ranges from the late Oligocene(?) to Pleistocene.

We attempt detailed correlations in the upper 300 m of the covered sediments in Hole 731A. The upper interval has an age range from 0 to 14 Ma, and is characterized by cyclic changes in the nature of sediments that can be identified by visual observation and by variations of magnetic susceptibility and $CaCO_3$ content. Correlation of the sedimentary coherence and similarity among the sites of the Owen Ridge provides valuable information on the relative rate of sedimentation, which is necessary information for study of depositional environments and sedimentation.

Site-to-site correlations were made on the basis of visual identification of distinctive layers, as well as on physical and magnetic properties. The magnetic susceptibility was measured continuously and at 10-cm intervals before splitting the sections. Photographs were taken of the split cores.

The visual correlation of the cores relied primarily on the core photographs. Twenty-six distinct and traceable marker horizons have been determined in the correlatable sedimentary sequence at Sites 721 and 722, and have been notated as OR-a_0, . . . , y_1, and y_2, based on the correlation between the holes at Sites 721 and 722 (see "Interhole Correlations" sections, "Site 721" and "Site 722" chapters, this volume). The letter code (i.e., a, b, c, . . .) refers to the sequence of cores, and the number code indicates the number of marker horizons in each core. For example, the notation "a_2" corresponds to the second marker horizon defined in Core 117-721A-1H, and "b_1" denotes the first marker layer in Core 117-721A-2H. The criterion to define a marker horizon is that the horizon is distinct enough to trace it in the sedimentary sequence of the other holes and that the character does not change. The useful criteria for recognizing the marker are color boundaries, distinctly colored layers, shape of bioturbations, and sequence of color change in surrounding sediments. These marker horizons have been traced between Sites 721 and 722. At Site 731, forty-two marker horizons are traced. Below y_2 horizon, six marker horizons, z_1 to z_6, were newly identified and traced between Sites 731 and 722. Table 11 (OR = Owen Ridge; notation is omitted in table) lists the depth of the traced marker horizons in the Owen Ridge Sites 721, 722,and 731.

The pattern of the magnetic susceptibility and the positions of marker layers match very well between Sites 722 and 731 (Fig. 17). The stratigraphy of the magnetic susceptibility data and the visually identified layers are extremely consistent in that a particular visually characteristic layer always coincides in depth with a distinct feature in the magnetic susceptibility curve.

Because Site 731 has not double-cored the sedimentary sequences, we can not calculate true stratigraphic thickness after the correction for core-boundary disturbance. The intersite correlation of the marker horizons, a_0 to a_4, indicates that the top 2 m of the surface sediments was missing in Core 117-731A-1H (Fig. 36). The layer-by-layer correlation allows us to determine the existence and time interval of hiatuses. The disconformable contact was observed at the horizon 75 cm below the marker horizon h_1, and the marker horizon n_1 was identified at 480 cm below the contact. The thickness between h_1 and n_1 is 49.75 m at Site 721, while the thickness at Site 731 is 5.55 m. The hiatus above the marker n_1 was also found at Site 722. The coincidence of the horizon of hiatus at Site 731 and 722 indicates that the horizon above the marker n_1 may have a character similar to a basal plane of a submarine slide.

Another sharp contact is observed 19.75 m below the previous hiatus, and marker x_1 was identified 2.10 m below the contact. The thickness for the missing interval at Site 731 is calculated as 80.80 m based on occurrence of the markers at Site 721 and 74.90 m at Site 722.

SUMMARY AND CONCLUSIONS

Site 731 is located in the western Arabian Sea on the Owen Ridge. The Owen Ridge is an asymmetric, northeast-trending ridge 300 km offshore Oman that dips steeply to the east and gently to the west.

The main scientific objectives for drilling at Site 731 were to recover a continuous Neogene sequence of pelagic sediments from the crest of the Owen Ridge. The second objective was to penetrate and possibly recover a thick sequence of turbiditic sediments in order to reconstruct the tectonic history of Owen Ridge and adjacent Owen Basin. The sedimentary sequence recovered here, along with those at Site 721 and 722, was expected to yield records of long-term and short-term variations in the biotic, sedimentologic, and chemical response of the depositional system to initiation of and changes in the monsoonal circulation system, and of tectonic control on facies evolution.

The most significant findings at Site 731 are (Fig. 37):

1. The thick turbidite sequence from 320 to 994 mbsf, which is characteristic of deep-sea fan deposition;
2. The gradual transition from clastic turbiditic depositional mode to pelagic sedimentation in the lower middle Miocene, which marks the uplift over the reach of turbidites and above the lysocline;
3. The onset of opaline sedimentation in the upper Miocene concomitant with the onset of cyclic variations in sedimentary properties;
4. The excellent correlation of magnetic susceptibility records between all three sites on the Owen Ridge (721, 722, and 723).

Site 731 penetrated to 994.2 mbsf and recovered sediments that range from possibly Oligocene (NP25) to late Pleistocene in age. The section has been divided into four major lithologic units:

Unit I (0–146.5 mbsf) consists of alternating light and dark layers of foraminifer-nannofossil ooze, marly nannofossil ooze, and nannofossil ooze with biosiliceous intervals of late Pleisto-

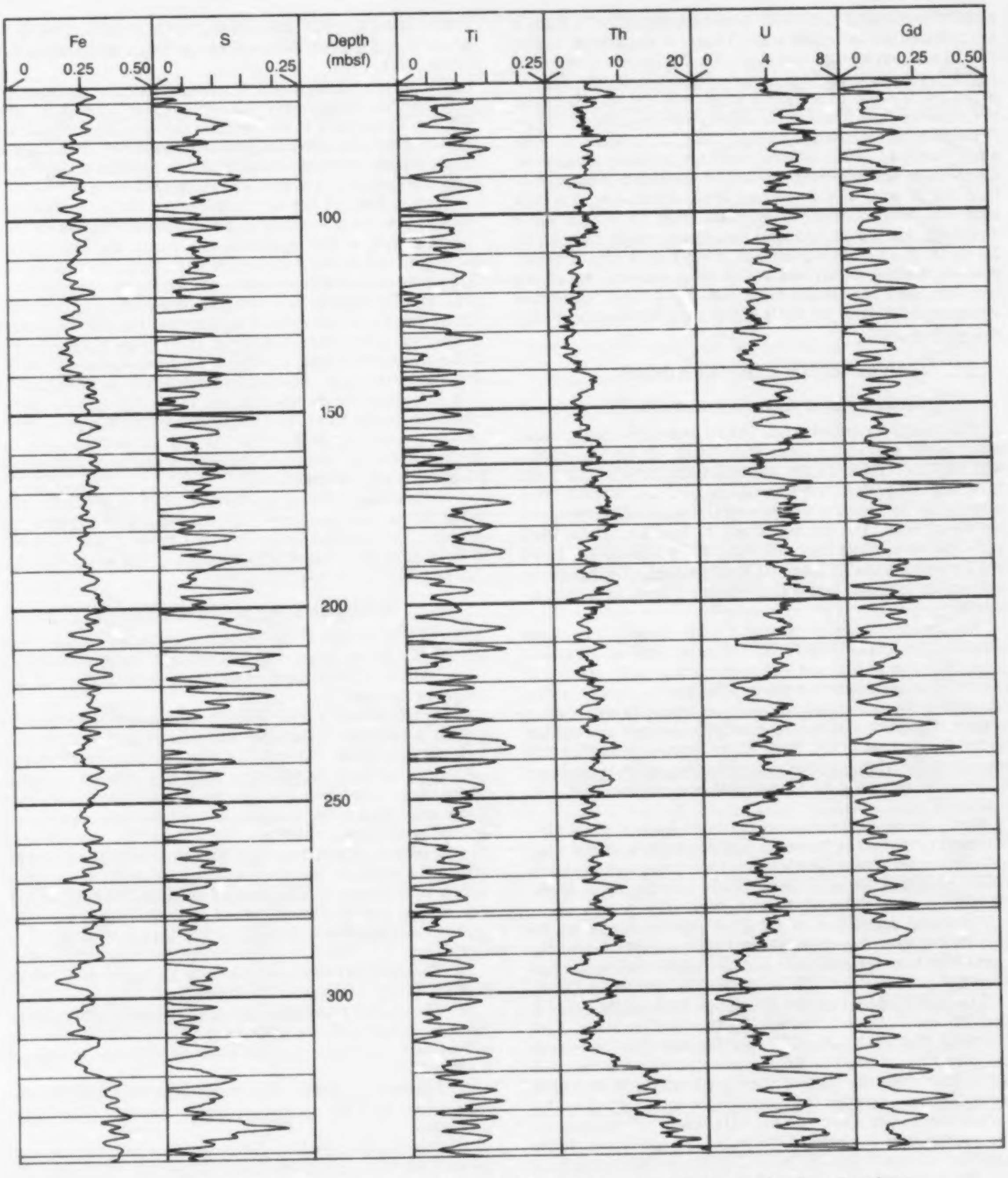

Figure 35. Geochemical logs of iron, sulfur, titanium, and gadolinium yields, and of thorium and uranium abundance by volume.

cene to late Miocene age. The uppper part of Unit I (0–66.3 mbsf) contains variable amounts (as much as 20%) of opaline material, which decreases in the remainder of lithologic Unit I. The amount of opal found in Unit I at Site 731 appears to exceed the opal content found in coeval sediments of Sites 721 and 722 on the Owen Ridge. As at Sites 721 and 722, the sediments here reveal strong cyclicity indicated by changes in colors, bulk densities, carbonate content, and particularly well by magnetic susceptibility on whole-round cores. Two hiatus horizons were recognized at 97 mbsf and 117 mbsf, which correspond to the late Pliocene and early Pliocene to middle late Miocene ages, respectively.

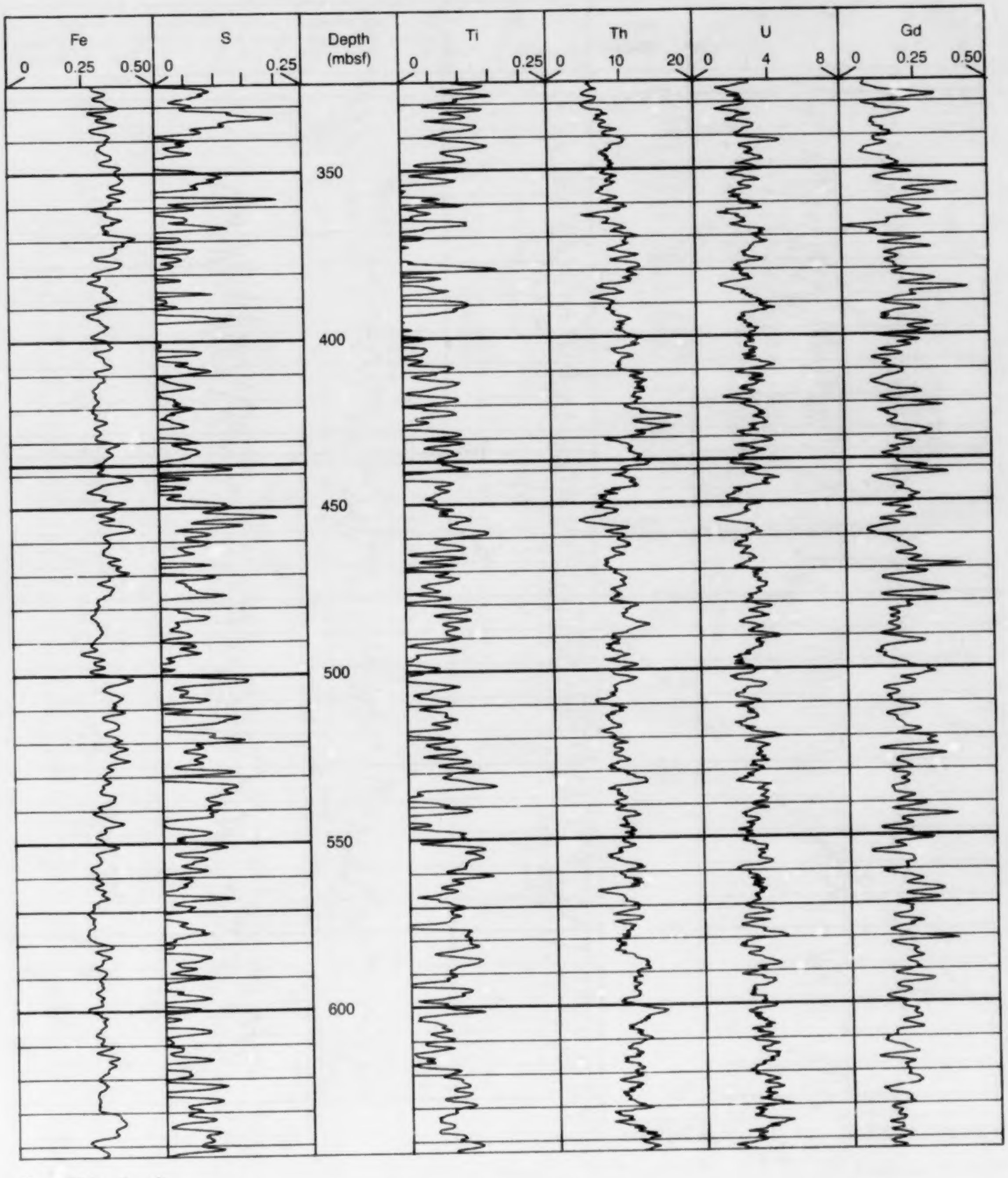

Figure 35 (continued).

Lithologic Unit II (146.5–240.9 mbsf) is composed of nannofossil oozes, diatomaceous marly nannofossil oozes, minor nannofossil-rich siliceous muds, and alternations of nannofossil chalks and diatomaceous muds of late Miocene age. Biogenic opal is an abundant component and its influence on the physical properties of the sediment is clearly observed in the density, porosity, and velocity measured onbord ship and by downhole logging. The abundance of opal (as much as 35% from smear slides) is the major difference between lithologic Units I and II.

Lithologic Unit III (240.9–320.1 mbsf) consists of cyclic bedding of nannofossil chalks and marly nannofossil chalks. This lithology is observed in the physical properties by a steady in-

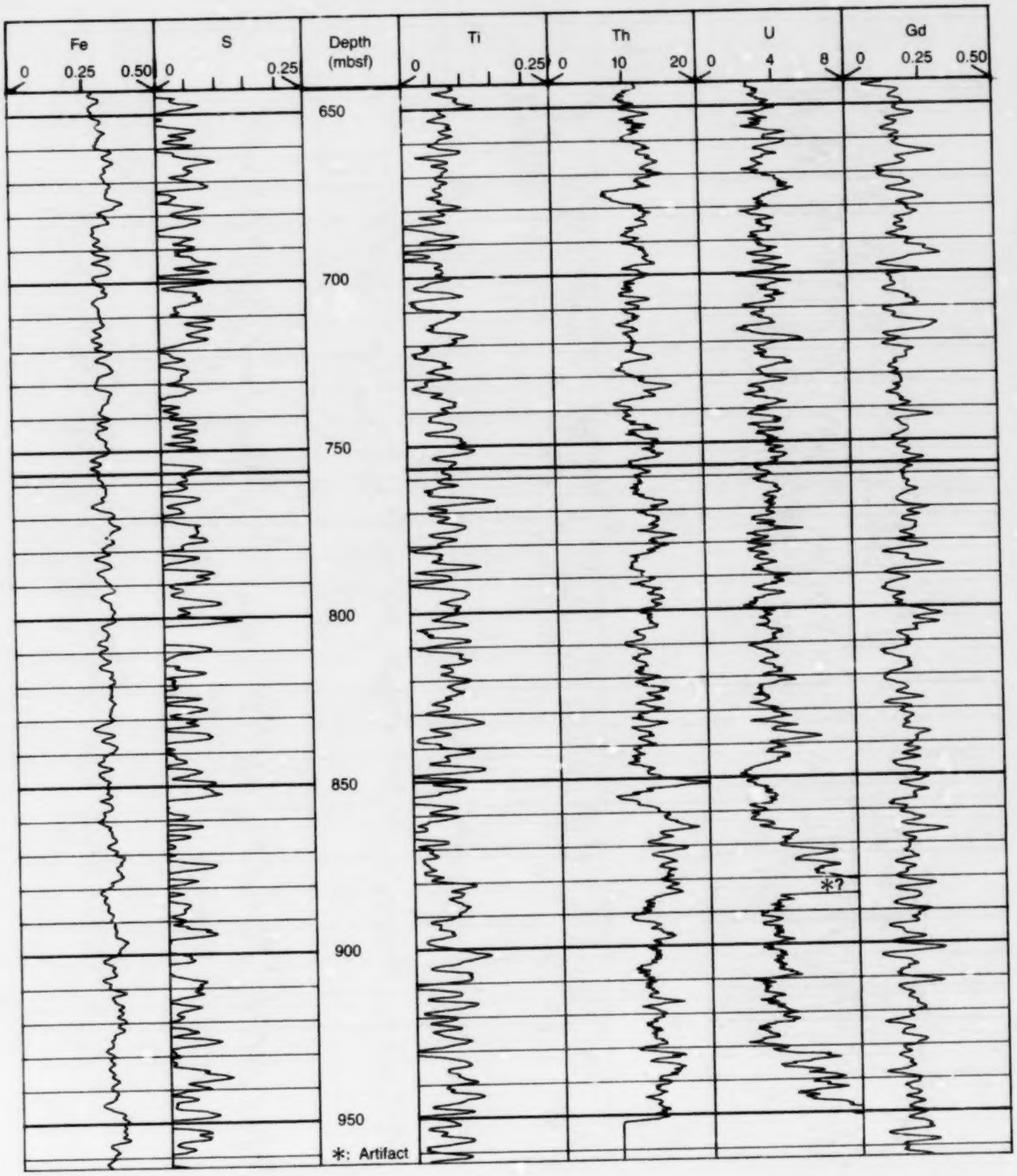

Figure 35 (continued).

crease in bulk density (Fig. 37) and velocity values, and low porosity.

Lithologic Unit IV (320.1–994.2 mbsf) is primarily composed of turbidites of silty clays grading upward to nannofossil chalks on the scale of beds and coarsening downsection to almost barren silty clays with coarse bases of early Miocene to Oligocene(?) age. Mud turbidites of 5–10 cm thickness are frequent and are stacked into beds of 2–3 m thickness. A transition zone between Units IV and III is found between 320.1 and 359.5 mbsf, which may designate the time when the ridge was uplifted above the influence of turbidites and above the lysocline. This latter boundary is indicated by improved preservation of planktonic calcare-

Table 11. List of the stratigraphic depth of the marker horizons at Sites 721 and 722, and ODP depth (based on core logs) of the marker horizons in Site 731.

	Hole 721B		Hole 722B		Hole 731A	
	Core, section, interval (cm)	Corrected depth (mbsf)	Core, section, interval (cm)	Corrected depth (mbsf)	Core, section, interval (cm)	ODP depth (mbsf)
a_0	1H-2, 105	2.95	1H-2, 85	2.35	1H-1, 75	0.75
a_1	1H-3, 90	3.90	1H-3, 50	3.50	1H-2, 75	2.25
a_2	1H-5, 45	6.45	2H-1, 25	6.05	1H-4, 15	4.65
a_3	1H-6, 32	7.82	2H-2, 20	7.50	1H-5, 45	6.45
a_4	2H-2, 85	11.25	2H-4, 65	10.95	2H-1, 60	10.40
b_1	2H-4, 85	14.25	2A-3, 20	14.20	2H-4, 55	14.85
b_2	2H-6, 115	17.55	3H-2, 105	17.95	2H-6, 120	18.50
b_3	2H-7, 40	18.30	3H-3, 45	18.85	2H-7, 45	19.25
b_4	3H-1, 140	20.50	3H-5, 10	21.50	3H-2, 85	21.65
c_1	3H-3, 130	23.40	3H-7, 15	24.55	3H-6, 35	27.15
c_2	3H-4, 130	24.90	4H-1, 85	26.35		
c_3	3H-5, 105	26.15	4H-2, 60	27.60	4H-2, 150	31.80
c_4	3H-6, 110	27.70	4H-3, 85	29.35	4H-4, 120	34.50
c_5	3H-7, 50	28.60	4H-4, 40	30.40	4H-5, 80	35.60
c_6	4H-1, 75	29.75	4H-5, 5	31.55	4H-6, 80	37.10
c_7	4H-2, 20	30.70	4H-5, 100	32.50		
$d_{1'}$	4H-3, 70	32.70	4H-6, 140	34.40	5H-1, 45	38.75
d_1	4H-4, 0	33.50	4A-4, 5	35.45	5H-2, 5	39.85
$d_{2'}$	4H-4, 70	34.20	5H-1, 70	36.00	5H-2, 100	40.80
d_2	4H-4, 145	34.95	5H-2, 10	36.90	5H-3, 75	42.05
$d_{3'}$	4H-6, 85	37.35	5H-3, 100	39.30	5H-5, 75	45.05
d_3	4H-7, 30	38.30	5H-4, 30	40.10	5H-6, 70	46.50
d_4	5H-1, 125	41.05	5H-5, 20	41.50	6H-2, 30	49.60
e_1	5H-6, 75	48.05	6H-3, 130	49.30		
e_2	6H-1, 35	50.25	6H-5, 60	51.60	7H-2, 30	59.10
e_3	6H-2, 95	52.35	6H-6, 130	53.80	7H-4, 135	63.15
f_1	6H-4, 115	55.55	7H-1, 45	56.05	8X-1, 95	67.95
f_2	6H-5, 60	56.50	7H-1, 140	57.00	8X-2, 120	69.70
f_3	6H-7, 15	59.05	7H-3, 85	59.45	8X-4, 100	72.50
f_4	7H-3, 45	62.95	7H-5, 100	62.60	9X-2, 80	79.00
f_5	7H-4, 65	64.65	7H-6, 120	64.40	9X-3, 90	80.60
g_1	7H-5, 45	65.95	7A-4, 40	65.70	9X-4, 85	82.05
g_2	8H-1, 85	70.35	8H-3, 75	69.25	10X-1, 5	86.45
g_3	8H-2, 50	71.50	8H-4, 120	71.20	10X-2, 20	88.10
g_4	8H-3, 70	73.20	8H-5, 140	72.90	10X-3, 15	89 55
h_1	8H-7, 50	79.00	9H-3, 50	79.00	11X-1, 5	96.05
h_2	9H-1, 35	79.45	9H-3, 110	79.60		
h_3	9H-2, 60	81.20	9H-4, 110	81.10		
h_4	9H-4, 40	84.00	9H-6, 60	83.60		
i_1	9H-5, 45	85.35	9H-7, 50	85.00		
i_2	9H-7, 40	88.50	10X-2, 60	86.40		
i_*	10X-2, 50	90.40	10X-3, 75	88.05		
i_3	10X-4, 25	93.15	10X-5, 40	90.70		
i_4	10X-4, 120	94.10	10X-5, 135	91.65		
i_5	10X-6, 75	96.65	10A-3, 25	93.95		
j_1	11X-1, 120	98.90	11X-2, 5	95.65		
j_2	11X-2, 130	100.50	11X-3, 35	97.45		
j_3	11X-3, 70	101.40	11X-3, 80	97.90		
j_4	11X-4, 65	102.85	11X-4, 50	99.10		
j_5	11X-5, 90	104.60	11A-2, 95	101.05		
k_1	12X-1, 55	108.65	11A-3, 100	102.60		
k_2			12X-3, 45	107.05		
l_1	13X-1, 60	115.40	12A-1, 45	108.75		
l_2	13X-2, 60	116.90	12A-2, 45	110.25		
l_3	13X-4, 40	119.70	13X-1, 65	112.95		
l_4	13X-6, 30	122.30	13X-3, 45	115.75		
m_1	14X-2, 115	127.05	13A-1, 50	119.00		
m_2	14X-3, 120	128.60	13A-2, 90	120.90		
m_3	14X-4, 70	129.60	13A-3, 35	121.85		
n_1	15X-1, 75	134.85	14X-3, 90	126.90	11X-4, 110	101.60
n_2	15X-2, 135	136.95	14X-4, 65	128.15	11X-5, 130	103.30
n_3	15X-3, 130	138.40	14X-5, 20	129.20	11X-6, 90	104.40
n_4	15X-6, 15	141.75	15X-1, 95	133.55	12X-2, 55	107.75
o_1	16X-2, 70	146.00	14A-4, 100	134.60	12X-4, 70	110.90
o_2	16X-3, 30	147.10	14A-5, 15	135.75	12X-5, 10	111.80
p_1	17X-1, 95	154.40	15A-2, 120	140.50		
p_2	17X-2, 45	155.45	15A-3, 65	141.45		
p_3	17X-3, 90	157.40	15A-4, 45	142.75		
p_4	17X-4, 70	158.70	16X-2, 35	144.15		
p_5	17X-5, 100	160.50	16X-3, 75	146.05		
p_6	17X-6, 90	161.90	16X-4, 15	146.95		
q_1	18X-1, 120	164.40	16X-5, 35	148.65		
q_2	18X-2, 90	165.60	16X-5, 130	149.60		
q_3	18X-3, 45	166.65	16X-6, 60	150.40		
q_4	18X-4, 100	168.70	16A-3, 100	151.90		
q_5	18X-5, 70	169.90	16A-4, 30	152.70		
q_6	18X-6, 90	171.60	17X-2, 5	154.05		
r_1	19X-1, 110	174.00	17X-4, 145	158.45		
r_2	19X-2, 55	174.95	17X-5, 75	159.25		
r_3	19X-4, 70	178.10	17X-C, 20	161.90		
r_4	19X-5, 100	179.90	18X-1, 125	163.45		

Table 11 (continued).

	Hole 721B		Hole 722B		Hole 731A	
	Core, section, interval (cm)	Corrected depth (mbsf)	Core, section, interval (cm)	Corrected depth (mbsf)	Core, section, interval (cm)	ODP depth (mbsf)
s_1	20X-2, 105	185.15	18X-4, 130	168.00		
s_2	20X-3, 100	186.60	18X-6, 50	170.20		
s_3	20X-4, 65	187.75	18X-7, 5	171.25		
s_4	20X-4, 140	188.5	19X-1, 90	176.80		
t_1	21X-1, 20	192.50	19X-5, 90	182.80		
t_2	21X-2, 110	194.90	20X-1, 110	184.80		
u_1	22X-3, 30	205.30	20A-2, 90	188.15		
u_2	22X-4, 65	207.15	20A-3, 75	189.75		
v_1	23X-2, 45	213.65	21X-2, 40	195.20		
v_2	23X-3, 120	215.90	21X-3, 90	197.20		
w_1	24X-2, 60	223.40	22X-6, 50	211.00		
w_2	24X-3, 100	225.30	22A-4, 120	213.40		
x_1	25X-3, 125	234.75	23X-3, 130	217.00	13X-3, 25	118.65
x_2	25X-5, 65	237.15	23X-5, 45	219.15	13X-4, 110	121.00
y_1	26X-3, 50	243.60	24X-3, 45	224.45	14X-3, 80	128.80
y_2	26X-4, 90	245.50	24X-4, 75	226.25	14X-4, 120	130.70
z_1			27X-2, 120	249.2	15X-5, 90	141.60
z_2			29X-1, 110	267.00	18X-6, 75	171.95
z_3			31X-2, 120	288.00	19X-6, 120	182.10
z_4			35X-4, 55	329.05	25X-4, 80	236.90
z_5			37X-3, 40	346.80	27X-4, 60	256.00
z_6			38X-4, 65	358.25	28X-4, 75	265.85

Note: Corrected depth = corrected depth for stratigraphic thickness. Depths are based on ODP CORELOG data. Core number + A = the marker layer was not identified in Hole B, but was identified in Hole A, and the core number listed is from Hole 731A.

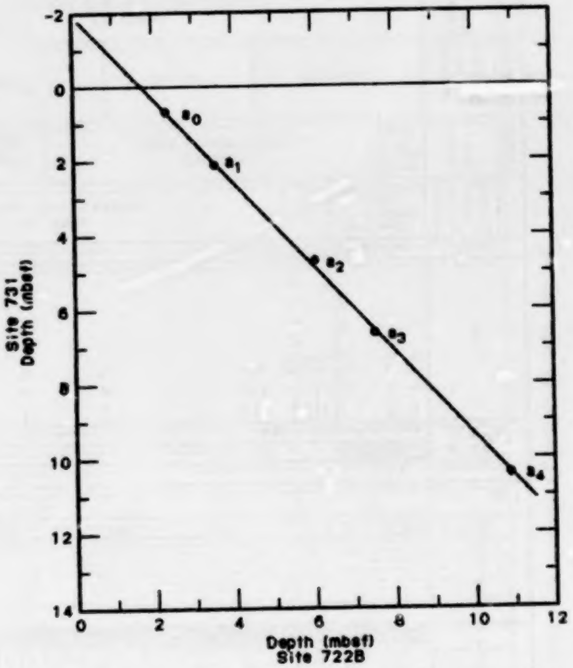

Figure 36. Correlation of the corrected sub-bottom depths at Hole 722B and depth at Site 731 for the marker horizons a_0–a_4. This graph shows that the top 2 m of surface sediments are missing in the cored sedimentary sequence at Site 731.

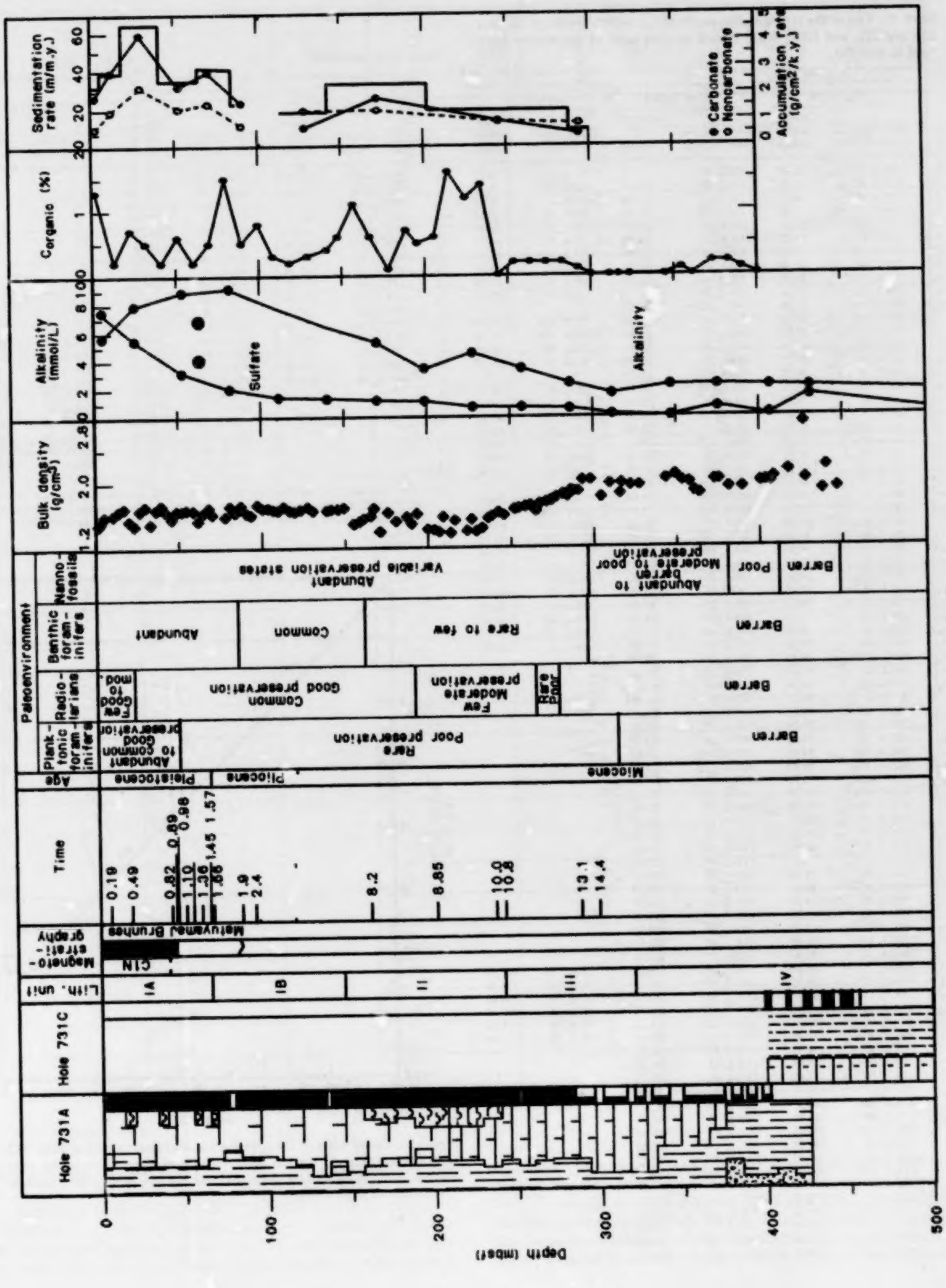
Depth (mbsf)
0
100
200
300
400
500
Hole 731A
Hole 731C
Lith. unit
IA
IB
II
III
IV
Magnetostratigraphy
C1N
Brunhes
Matuyama
Time
0.19
0.49
0.82
0.89
0.98
1.10
1.36
1.45
1.57
1.66
1.9
2.4
8.2
8.85
10.0
10.8
13.1
14.4
Age
Pleistocene
Pliocene
Miocene
Paleoenvironment
Planktonic foraminifers
Abundant to common Good preservation
Rare Poor preservation
Barren
Radiolarians
Few Good to mod.
Common Good preservation
Few Moderate preservation
Rare Poor
Barren
Benthic foraminifers
Abundant
Common
Rare to few
Barren
Nannofossils
Abundant Variable preservation states
Abundant to barren Moderate to poor preservation
Poor
Barren
Bulk density (g/cm3)
1.2
2.0
2.8
Alkalinity (mmol/L)
0
2
4
6
8
10
Sulfate
Alkalinity
Corganic (%)
1
2
Sedimentation rate (m/m.y.)
20
40
60
Carbonate
Noncarbonate
Accumulation rate (g/cm2/k.y.)
0
1
2
3
4
5

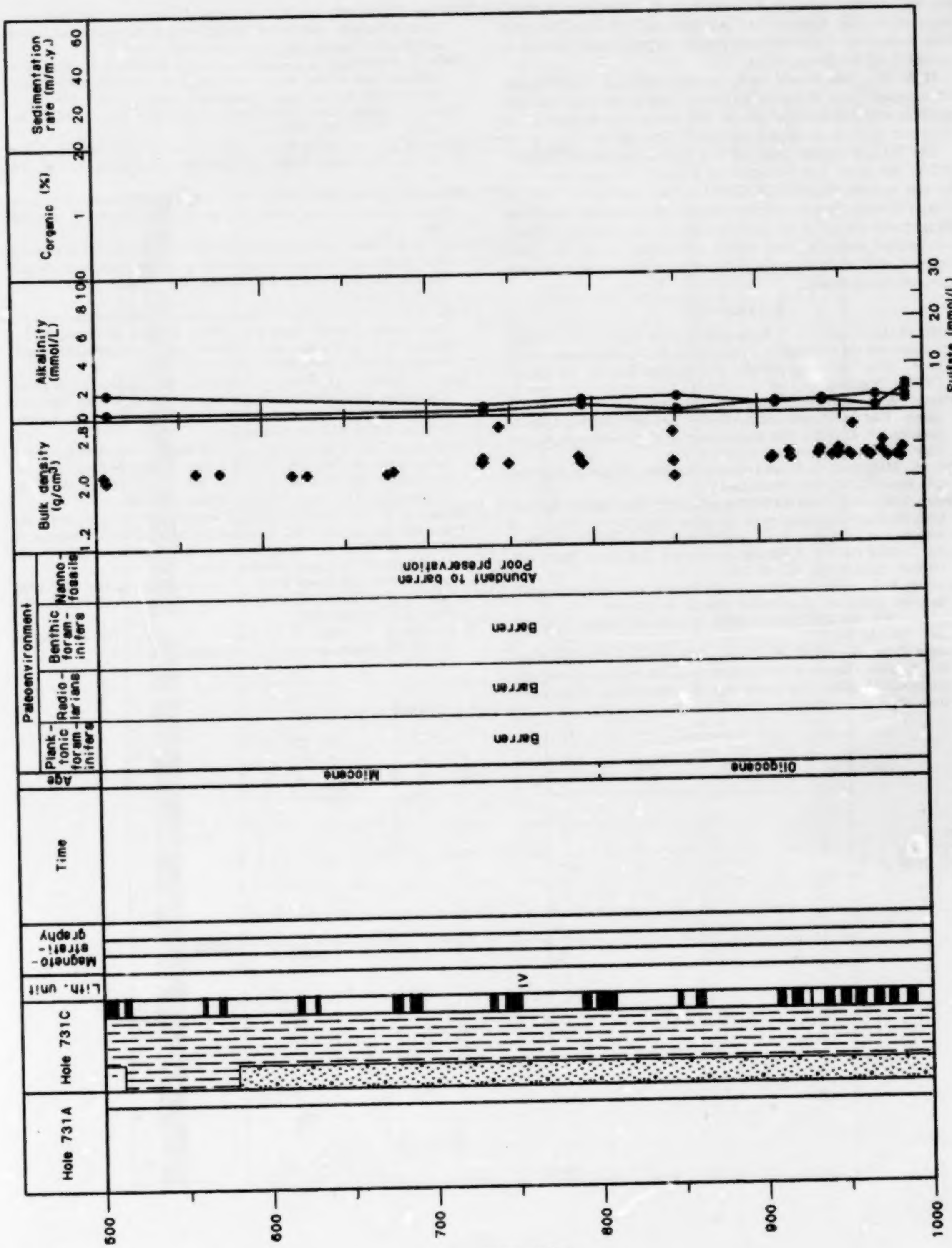

Figure 37. Summary chart of the preliminary shipboard findings, Site 731.

ous tests toward younger sediments, and the increased abundance of benthic foraminifers in lithologic Unit III. The trend from turbiditic to increasingly pelagic deposition is related to the uplift of the Owen Ridge.

Hole 731C was logged under good conditions with two tool combinations over 968 m of the 994-m-deep hole. Log quality is excellent and will provide insight into lithologic changes in the thick and sparsely recovered turbiditic Unit IV.

Site 731 and nearby Sites 721 and 722 provide an excellent record of the onset and evolution of monsoonal upwelling from the late middle Miocene to the Pliocene-Pleistocene. This sequence should provide insights into the relationship of orbital changes and the uplift of the Himalaya to the history of monsoon-related upwelling and eolian sedimentation on the Owen Ridge, as well as on tectonic uplift of Owen Ridge and the evolution of Owen Basin.

REFERENCES

Arthur, M. A., Srivastrava, S. P., Jarrard, R., and Aksu, A. E., in press. Seismic and log correlation ... *In* Arthur, M. A., Srirastrava, S. P., et al., *Proc. ODP, Sci. Results*, 105: College Station, TX (Ocean Drilling Program).

Berggren, W. A., Kent, D. V., and Van Couvering, J. A., 1985. The Neogene: Part 2, Neogene geochronology and chronostratigraphy. *In* Snelling, N. J. (Ed.), *The Chronology of the Geological Record*: Geol. Soc. Mem. (London), 10:211-259.

Blatt, H., Middleton, G. V., and Murray, R., 1980. *Origin of Sedimentary Rocks*: New Jersey (Prentice-Hall).

Gieskes, J. M., 1981. Deep sea drilling interstitial water studies: implications for chemical alteration of the ocean crust, Layers I and II. *In* Warme, J. E., Douglas, R. C., and Winterer, E. L. (Eds.), *The Deep Sea Drilling Project: A Decade of Progress*, Soc. Econ. Paleontol. Mineral. Spec. Publ., 32:149-168.

Hamilton, E. L., 1976. Variations of density and porosity with depth in deep-sea sediments. *J. Sediment. Petrol.*, 46:280-300.

________, 1979. Sound velocity gradients in marine sediments. *J. Acoust. Soc. Am.*, 65:909-922.

Johnson, D. A., Nigrini, C. A., Caulet, J. P., Schneider, D., and Kent, D., in press. Pliocene-Pleistocene radiolarian events and magnetostratigraphic calibrations for the tropical Indian Ocean. *Mar. Micropaleontol.*

Johnson, D. A., and Nigrini, C. A., 1985. Synchronous and time-transgressive Neogene radiolarian datum levels in the equatorial Indian and Pacific Oceans. *Mar. Micropaleontol.*, 9:489-523.

Kolla, V., Kostecki, J. A., Robinson, F., and Biscaye, P. E., 1981. Distribution and origins of clay minerals and quartz in surface sediments of the Arabian Sea. *J. Sediment. Petrol.*, 51:563-569.

Martini, E., 1970. Standard Palaeogene calcareous nannoplankton zonation. *Nature*, 226:560-561.

McIntyre, A., and Bé, A.W.H., 1967. Modern Coccolithophoridae of the Atlantic Ocean—I: placoliths and cyrtoliths. *Deep-Sea Res.*, 14:561-597.

Mountain, G., and Prell, W. L., 1987. Leg 117 ODP site survey: a revised history of Owen Basin. *Eos, Trans. Am. Geophys. Union*, 68:424.

Prell, W. L., 1984. Monsoonal climate of the Arabian Sea during the late Quaternary: a response to changing solar radiation. *In* Berger, A., and Imbrie, J. (Eds.), *Milankovitch and Climate*: Dordrecht (D. Reidel), 349-366.

Roth, P. H., 1974. Calcareous nannofossils from the northwestern Indian Ocean, Leg 24, Deep Sea Drilling Project. *In* Fisher, R. L., Bunce, E. T., et al., *Init. Repts. DSDP*, 24: Washington (U.S. Govt. Printing Office), 969-994.

Sato, T., Takayama, T., Kato, M., Kudo, T., and Kameo, K., in press. Calcareous microfossil biostratigraphy of the uppermost Cenozoic formations distributed in the coast of the Japan Sea. Part. 4: Conclusion. *Sekiyu Gijutsu Kyokaishi.*

Takayama, T., and Sato, T., 1987. Coccolith biostratigraphy of the North Atlantic Ocean, Deep Sea Drilling Project Leg 94. *In* Ruddiman, W. F., Kidd, R. B., Thomas, E., et al., *Init. Repts. DSDP*, 94, Pt. 2: Washington (U.S. Govt Printing Office), 651-702.

Whitmarsh, R. B., 1974. Summary of general features of Arabian Sea and Red Sea Cenozoic history based on Leg 23 cores. *In* Whitmarsh, R. B., Weser, O. E., Ross, D. A., et al., *Init. Repts. DSDP*, 23: Washington (U.S. Govt. Printing Office), 1115-1123.

________, 1979. The Owen Basin off the southeast margin of Arabia and the evolution of the Owen Fracture Zone. *Geophys. J. R. Astron. Soc.*, 58:441-470.

Whitmarsh, R. B., Weser, O. E., Ross, D. A., et al., 1974. *Init. Repts. DSDP*, 23: Washington (U.S. Govt. Printing Office).

Ms 117A-108

Summary Log for Hole 731C (continued)

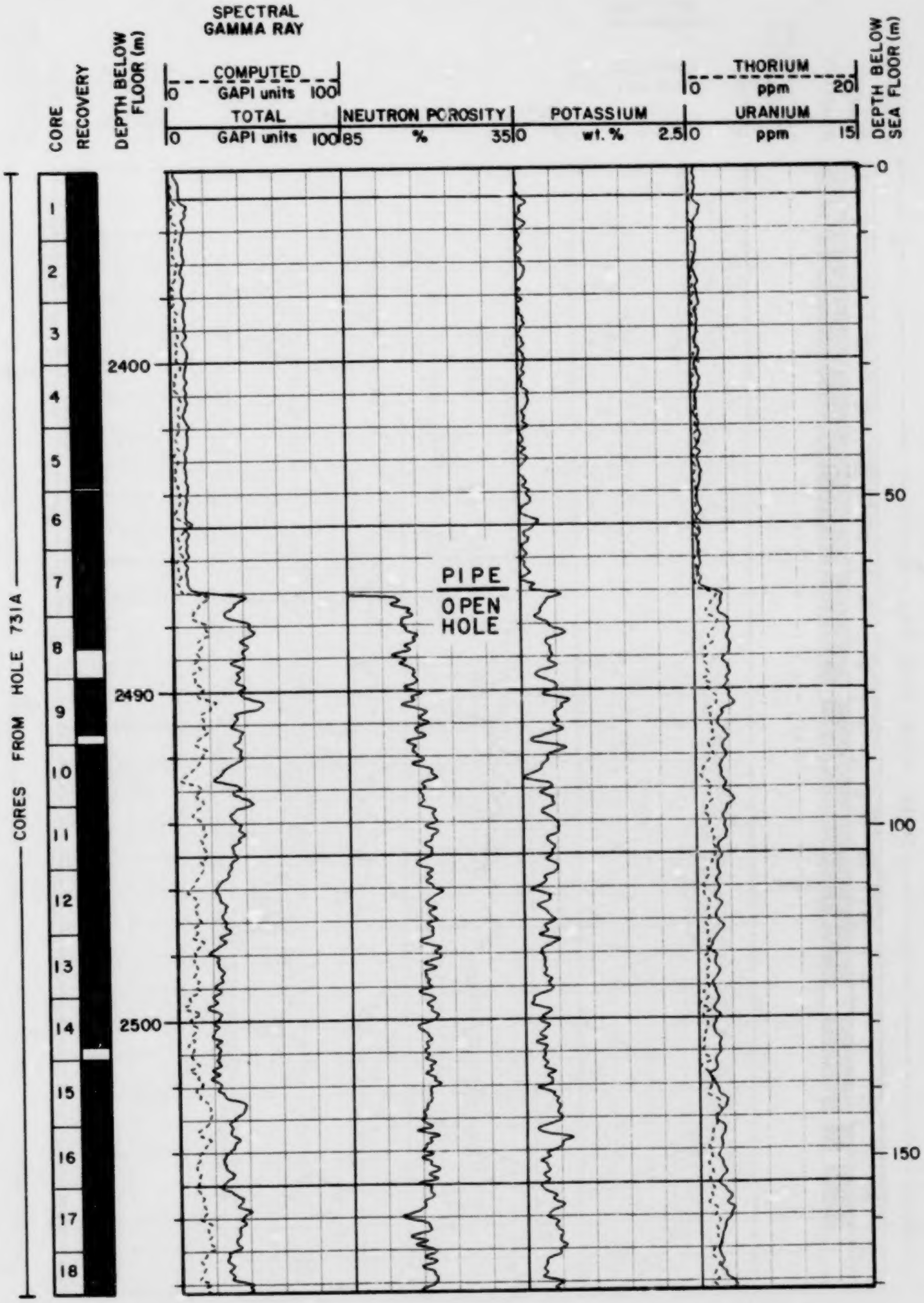

Summary Log for Hole 731C (continued)

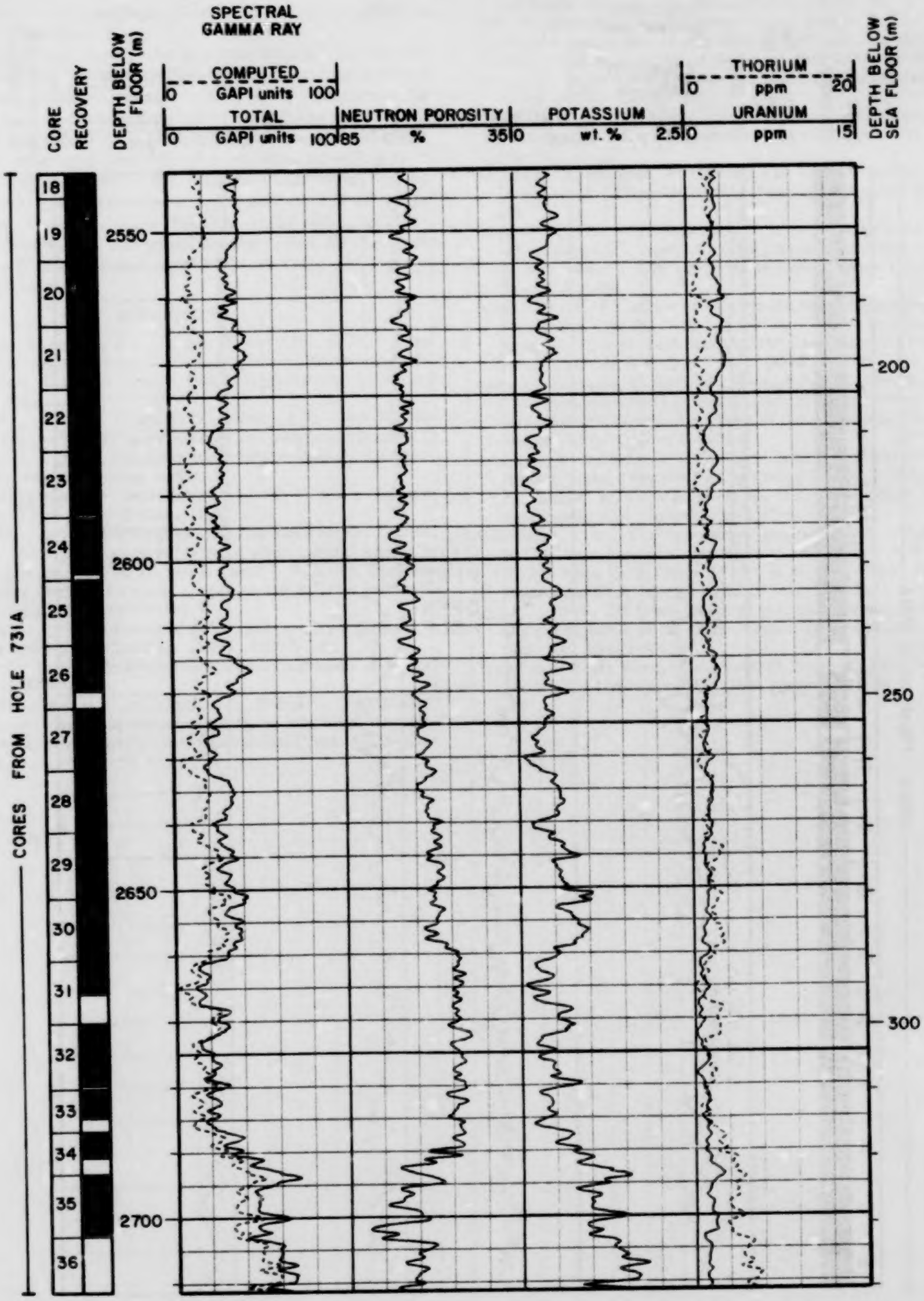

Summary Log for Hole 731C (continued)

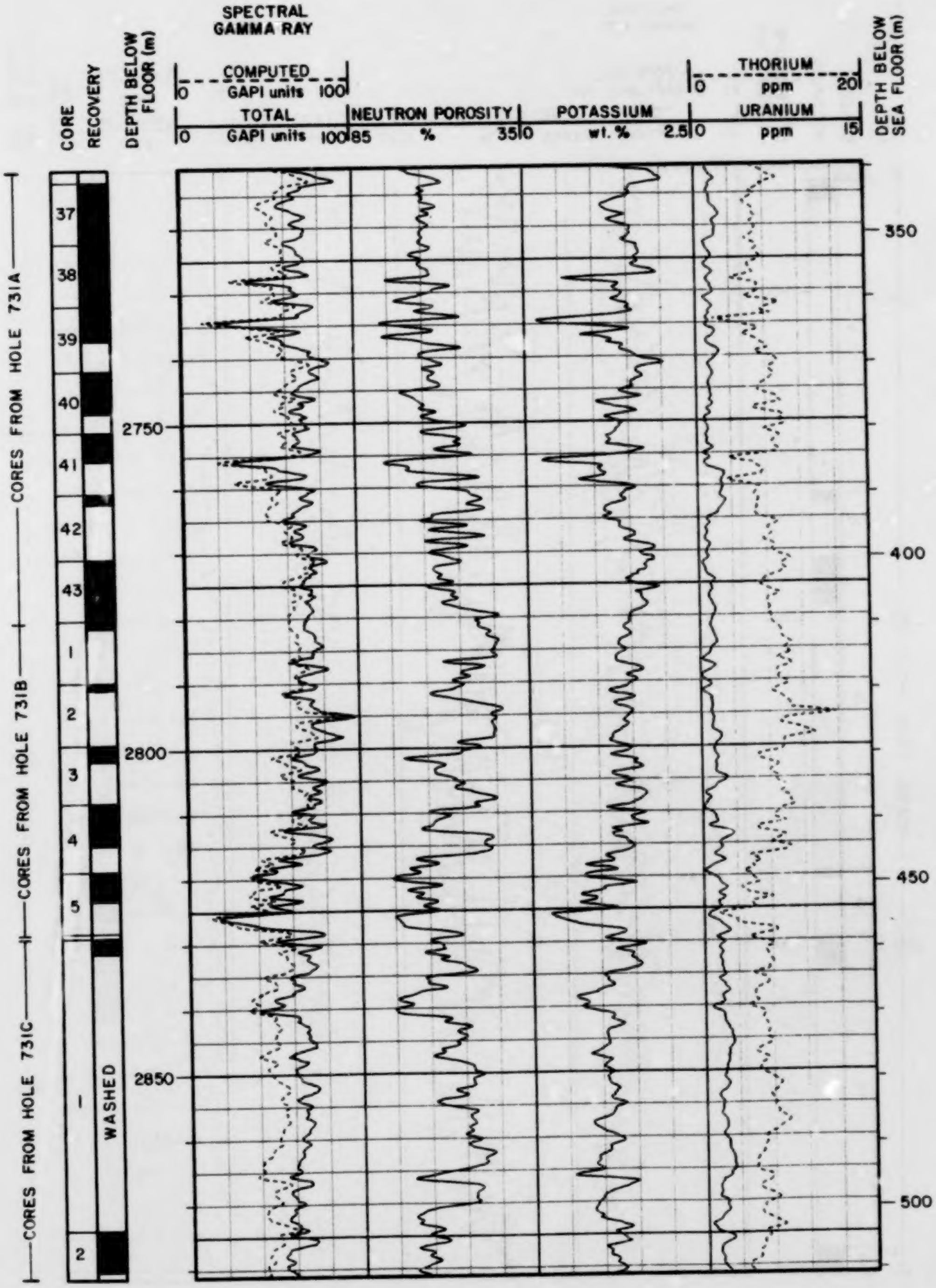

Summary Log for Hole 731C (continued)

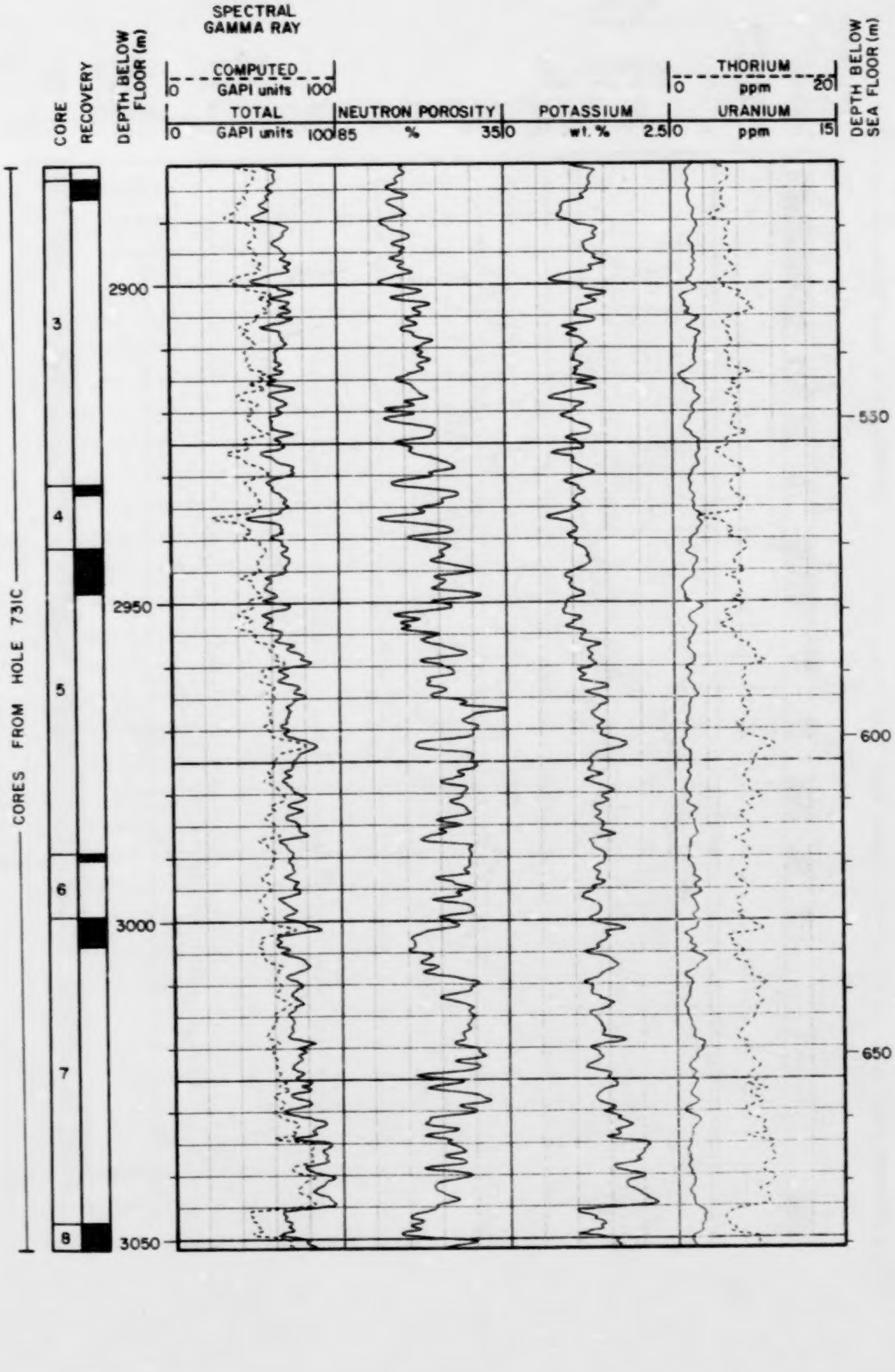

Summary Log for Hole 731C (continued)

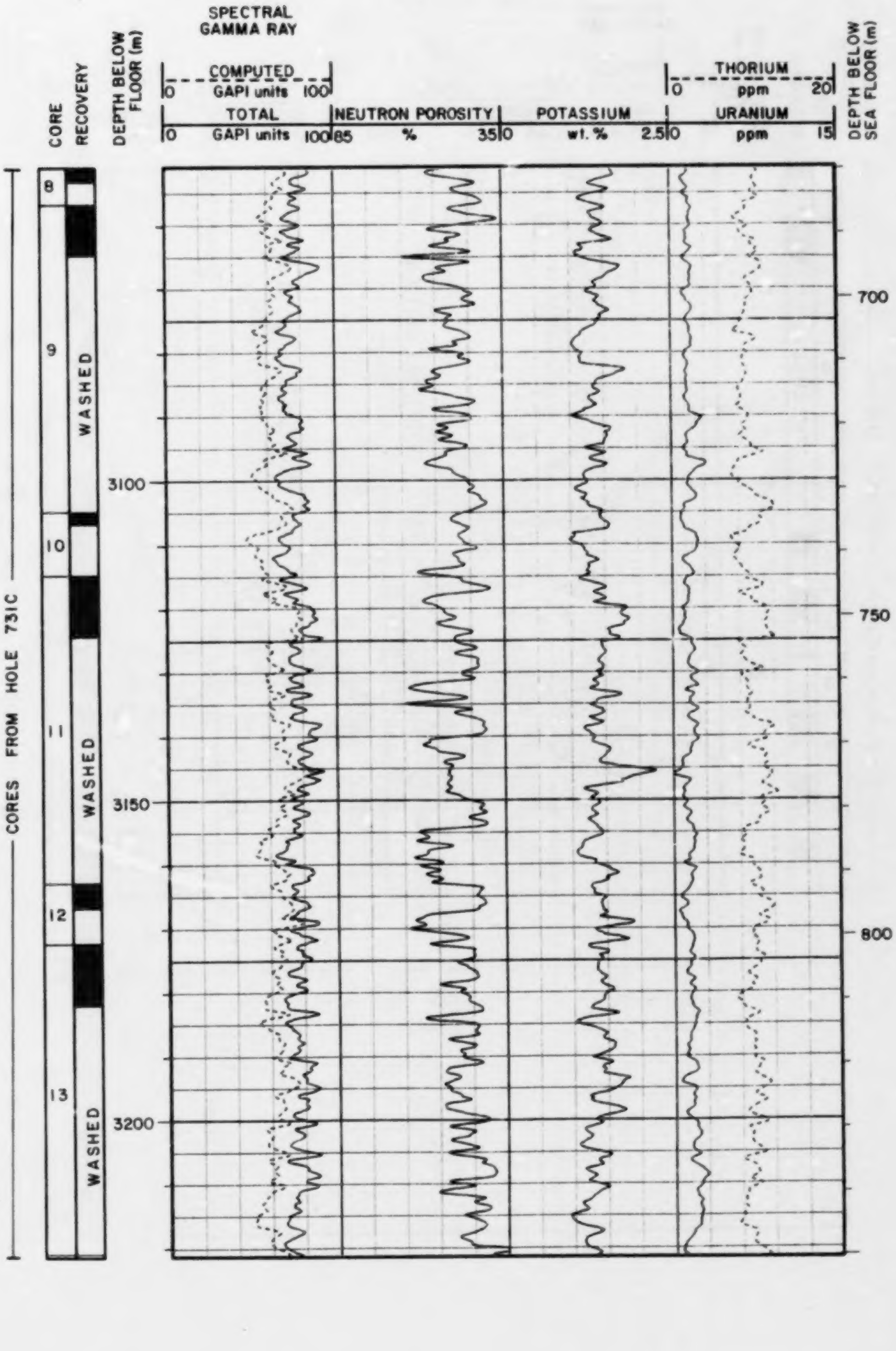

Summary Log for Hole 731C (continued)

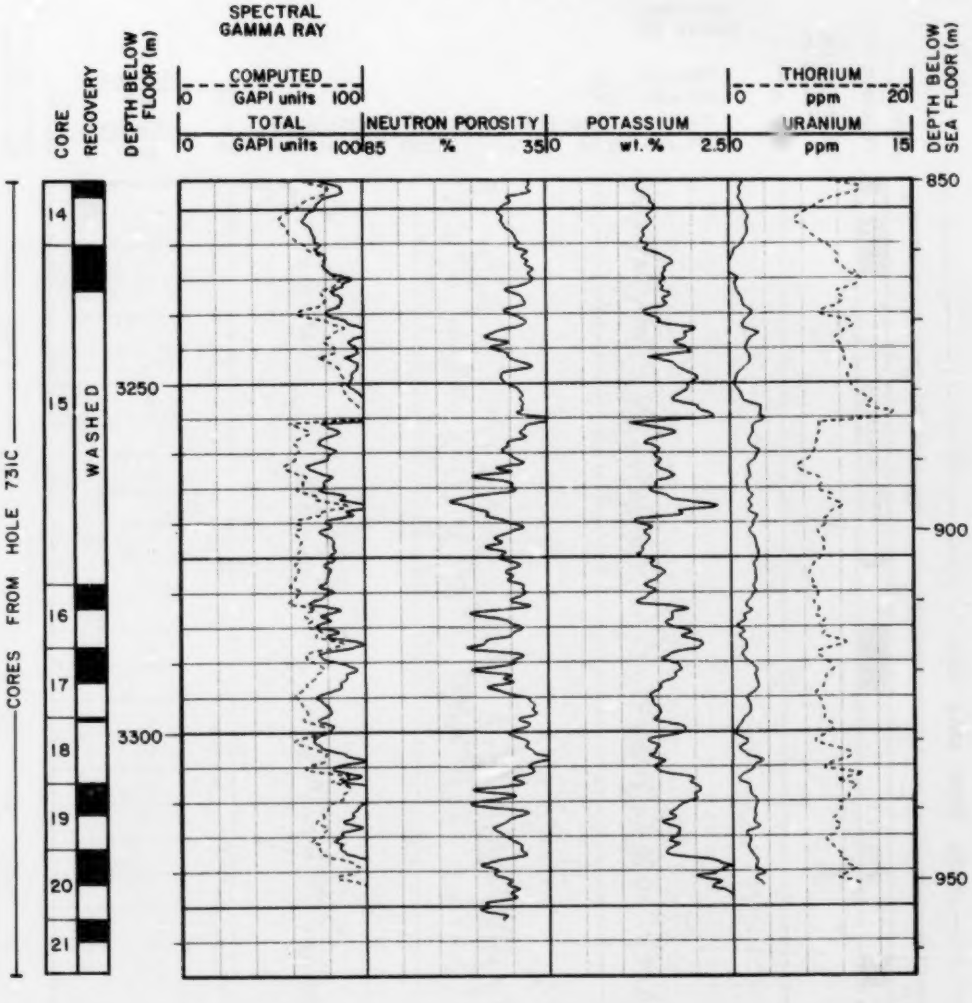

Summary Log for Hole 731C (continued)

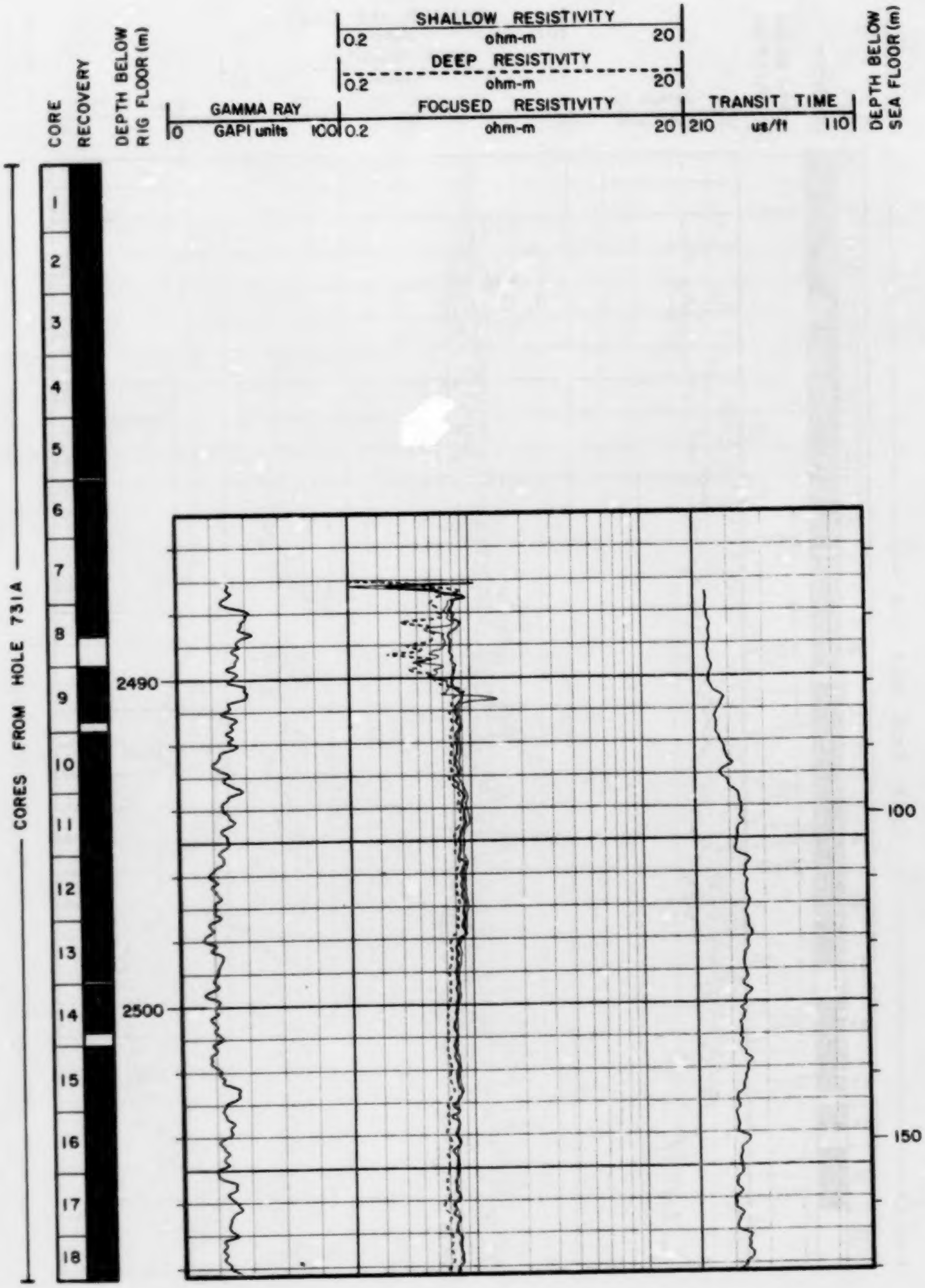

Summary Log for Hole 731C (continued)

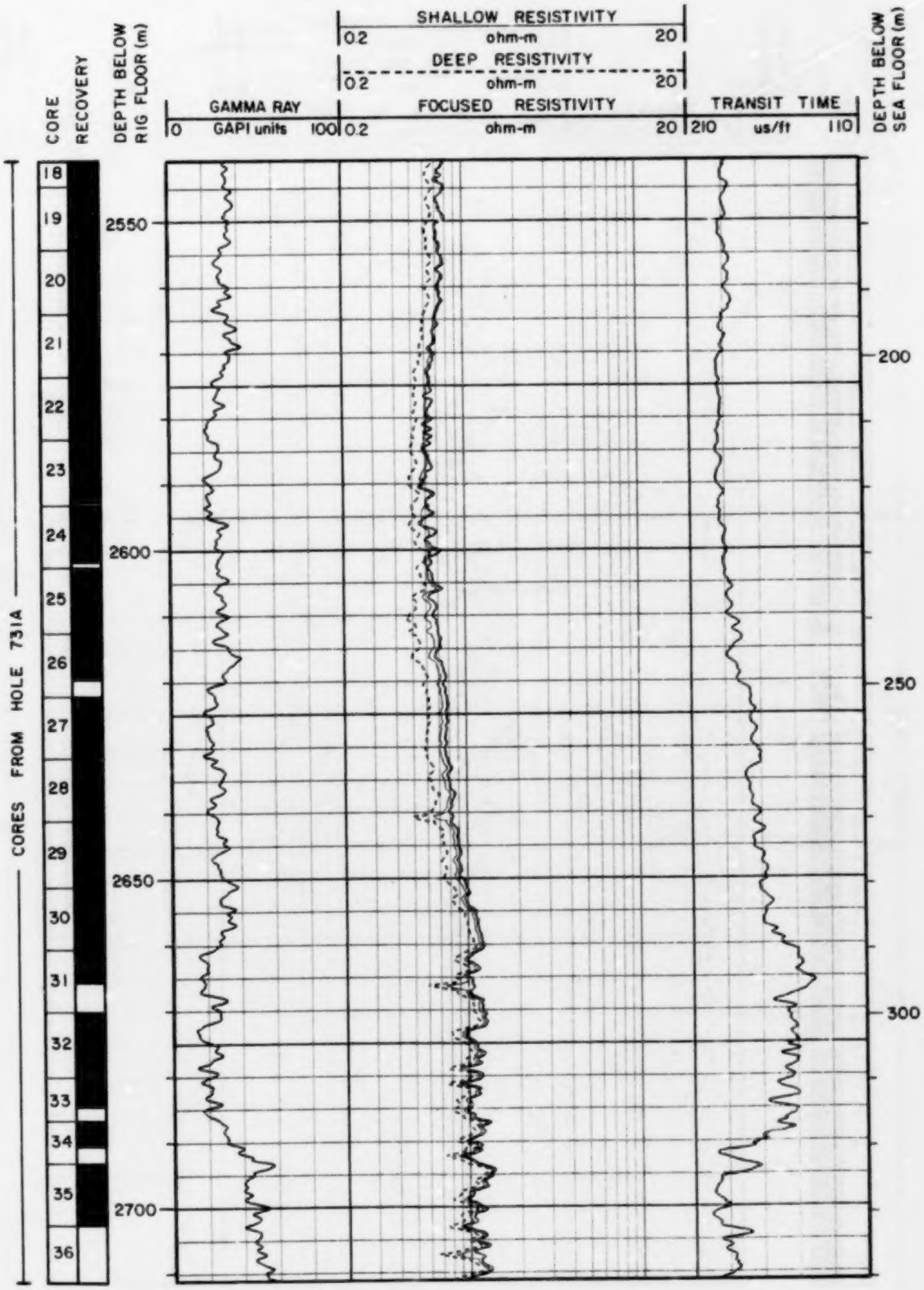

Summary Log for Hole 731C (continued)

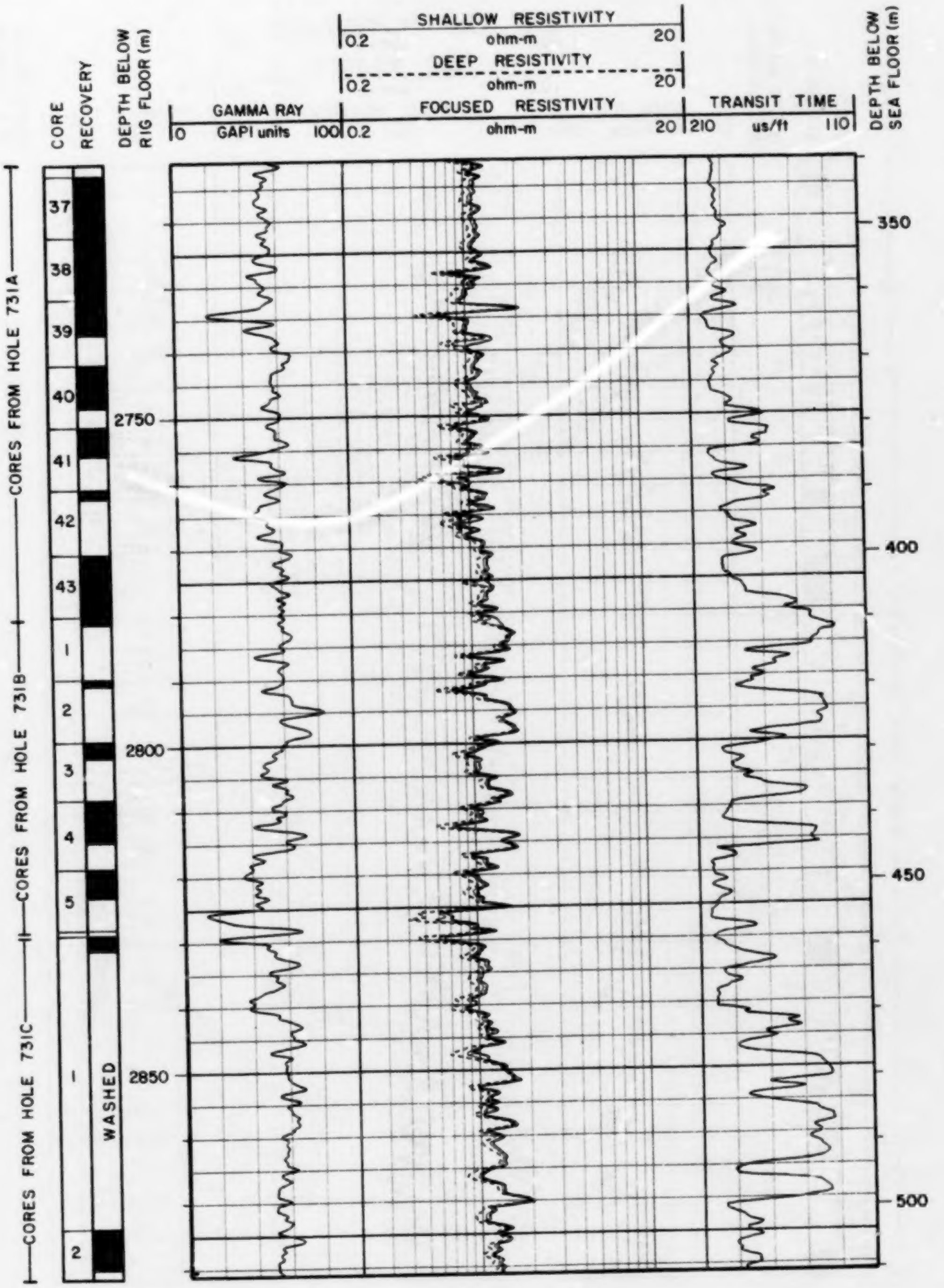

Summary Log for Hole 731C (continued)

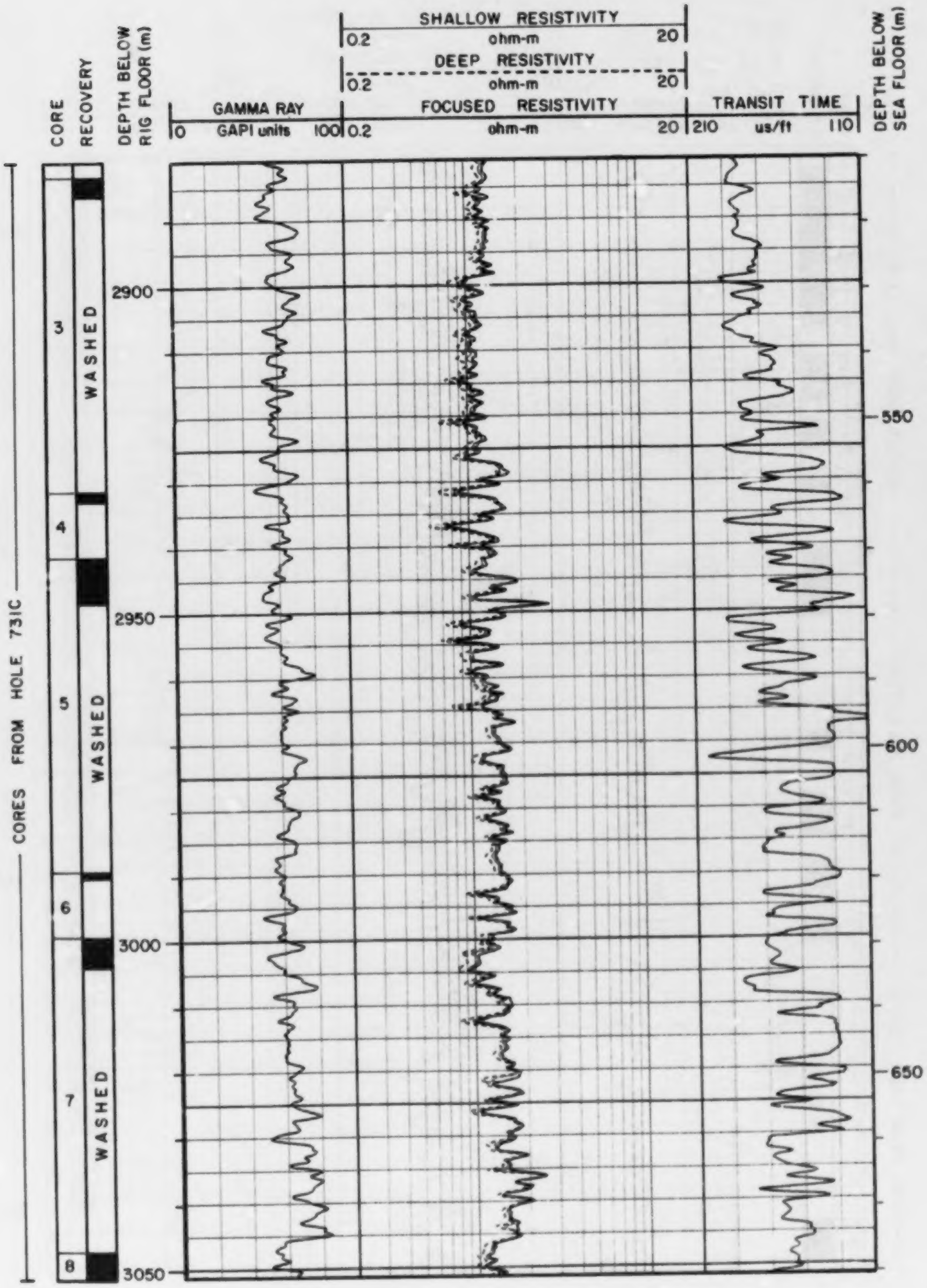

Summary Log for Hole 731C (continued)

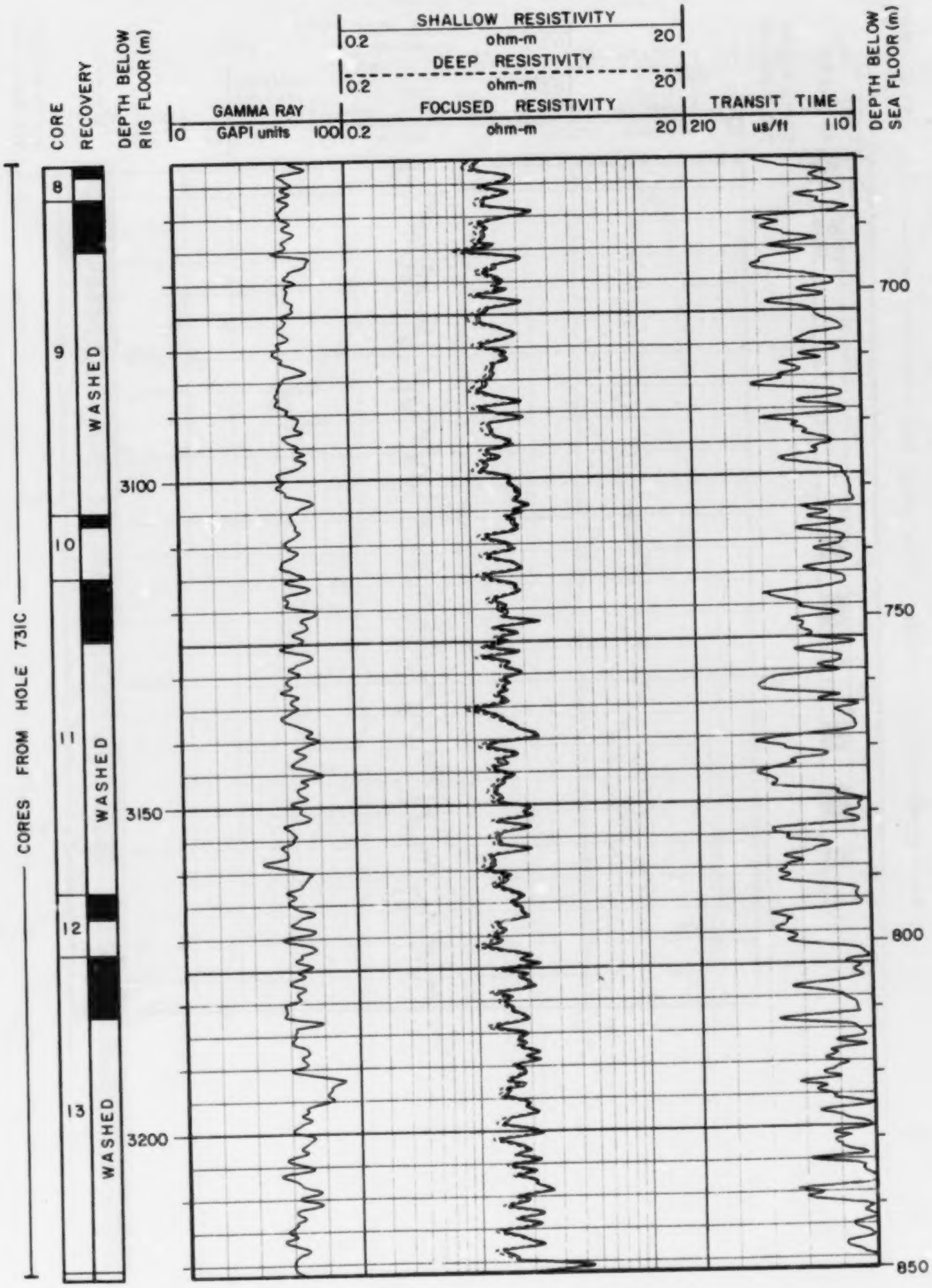

Summary Log for Hole 731C (continued)

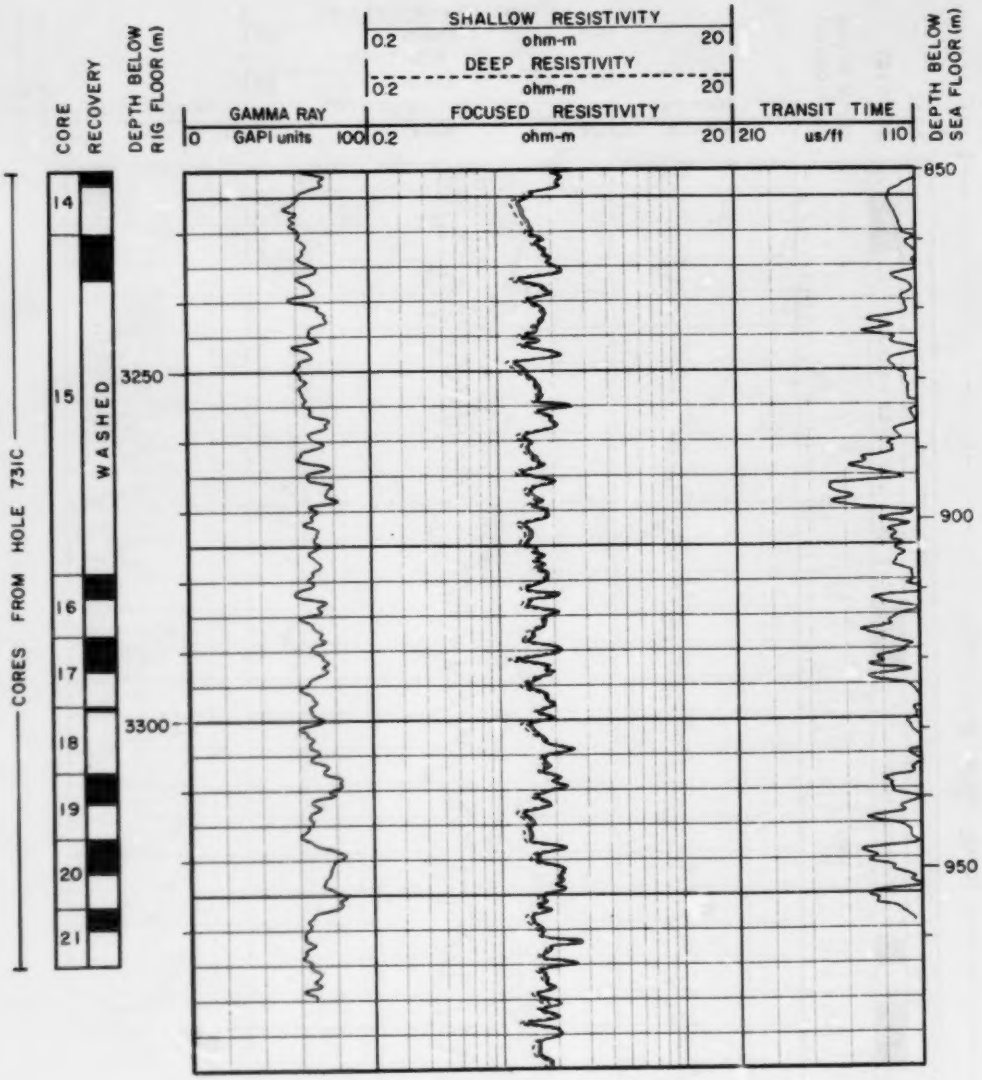

Summary Log for Hole 731C (continued)

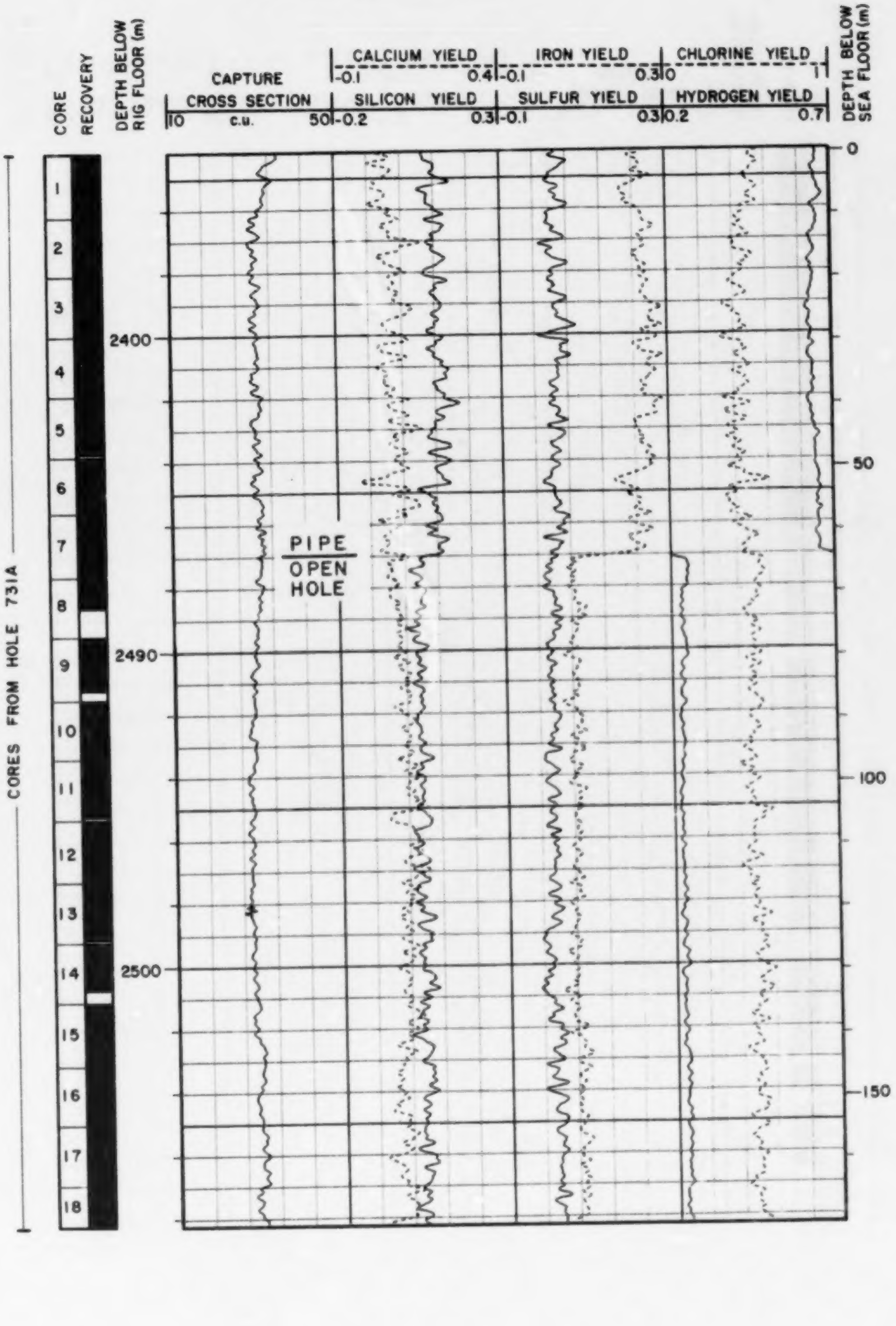

Summary Log for Hole 731C (continued)

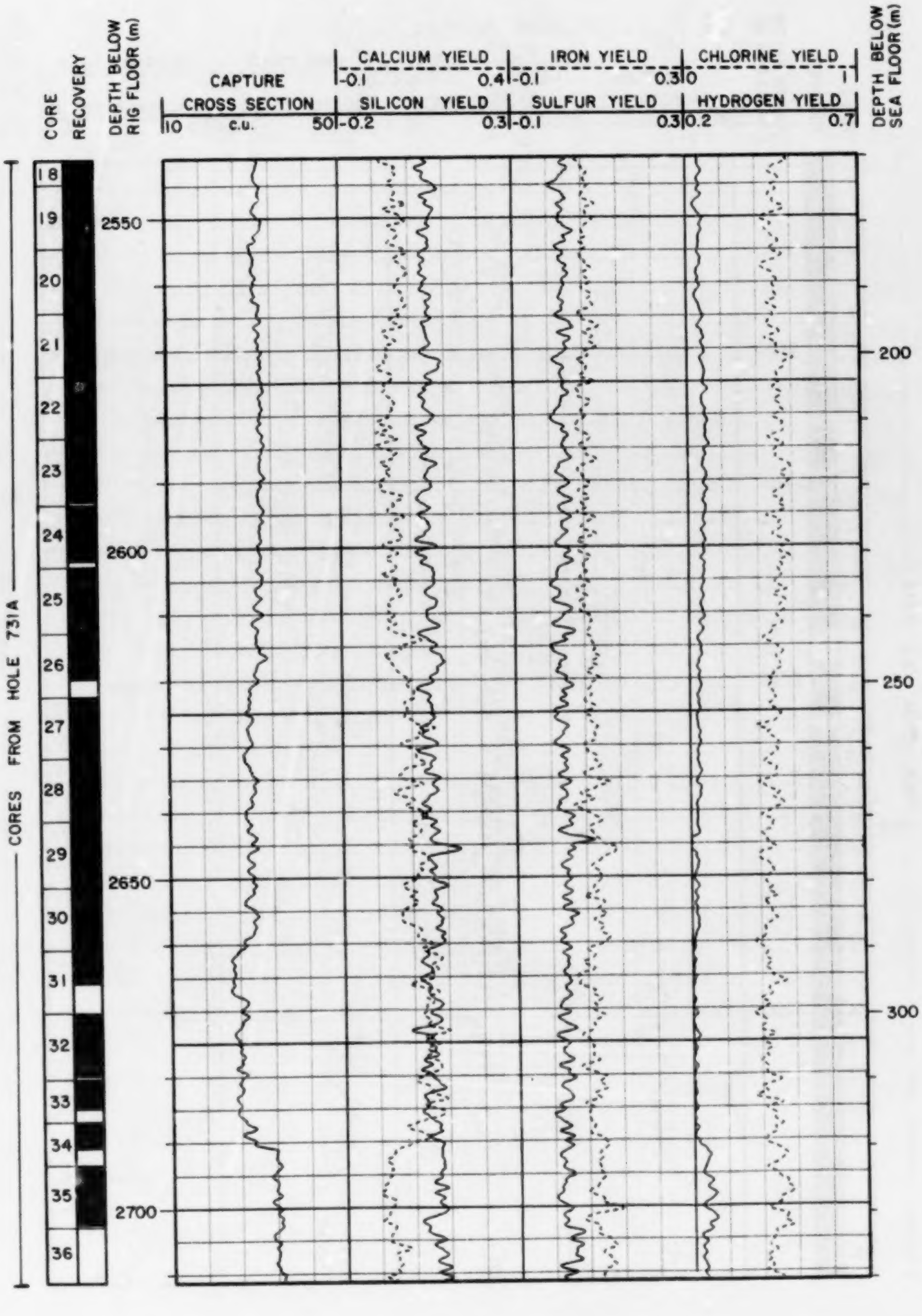

Summary Log for Hole 731C (continued)

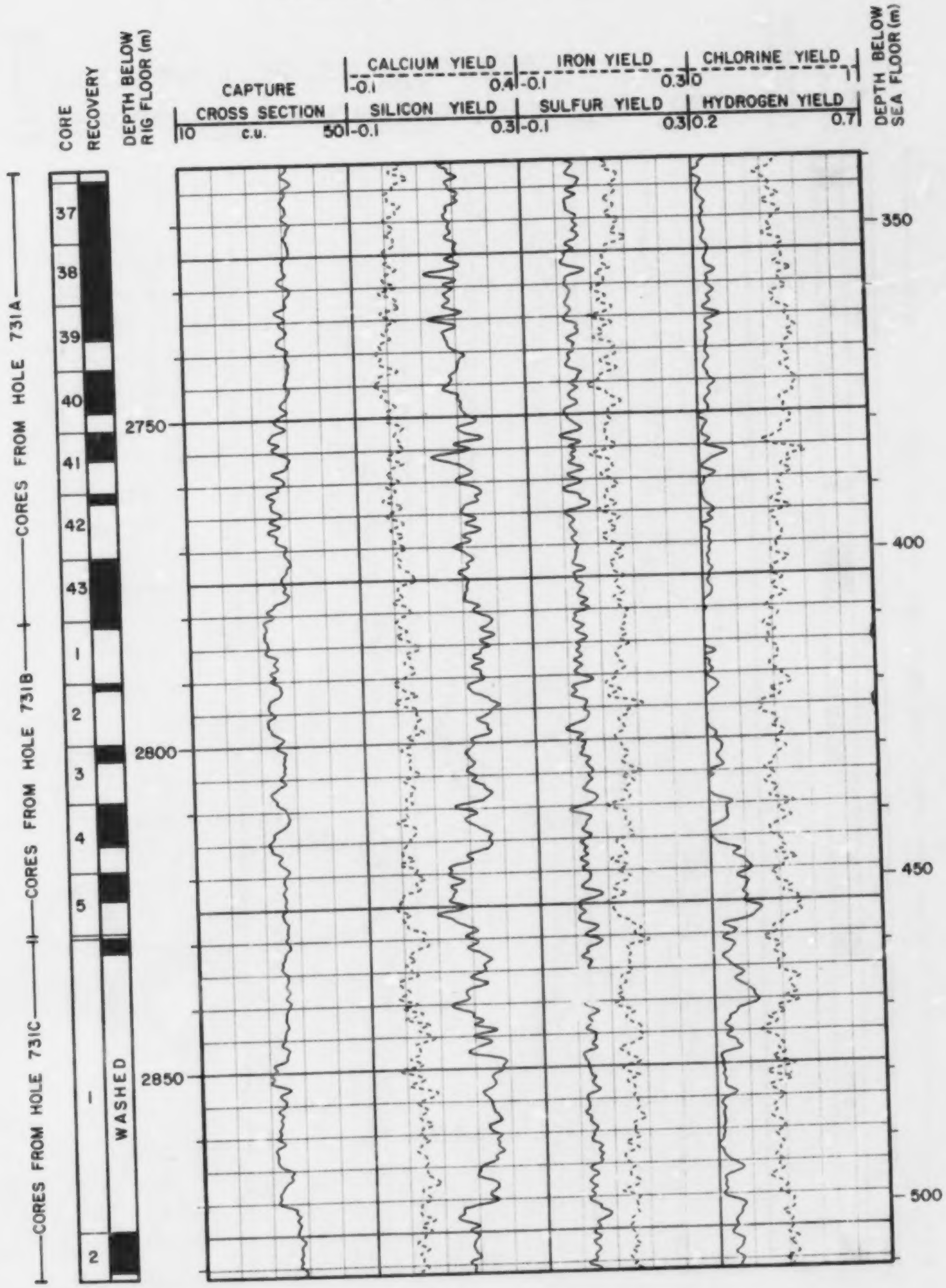

Summary Log for Hole 731C (continued)

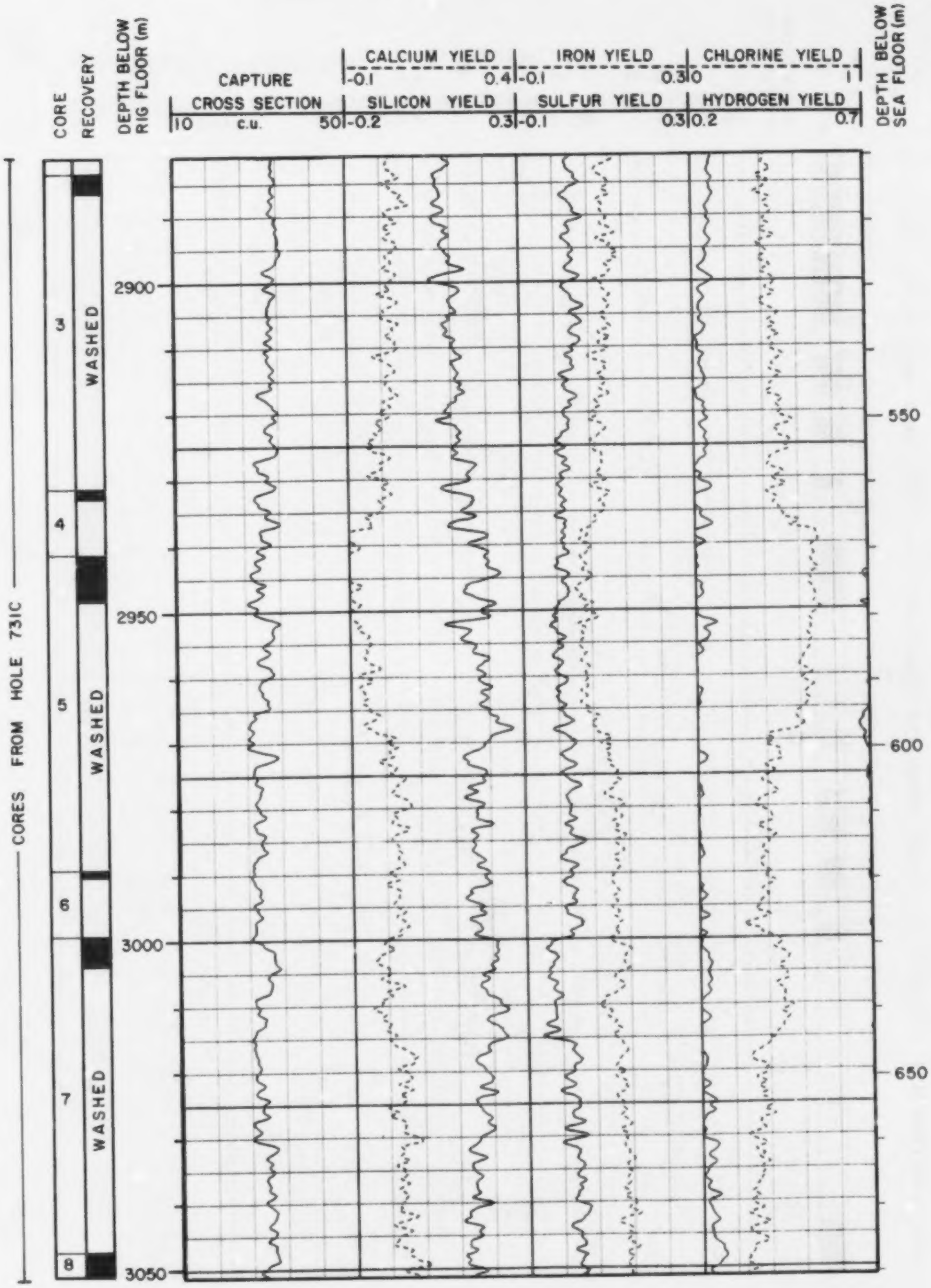

Summary Log for Hole 731C (continued)

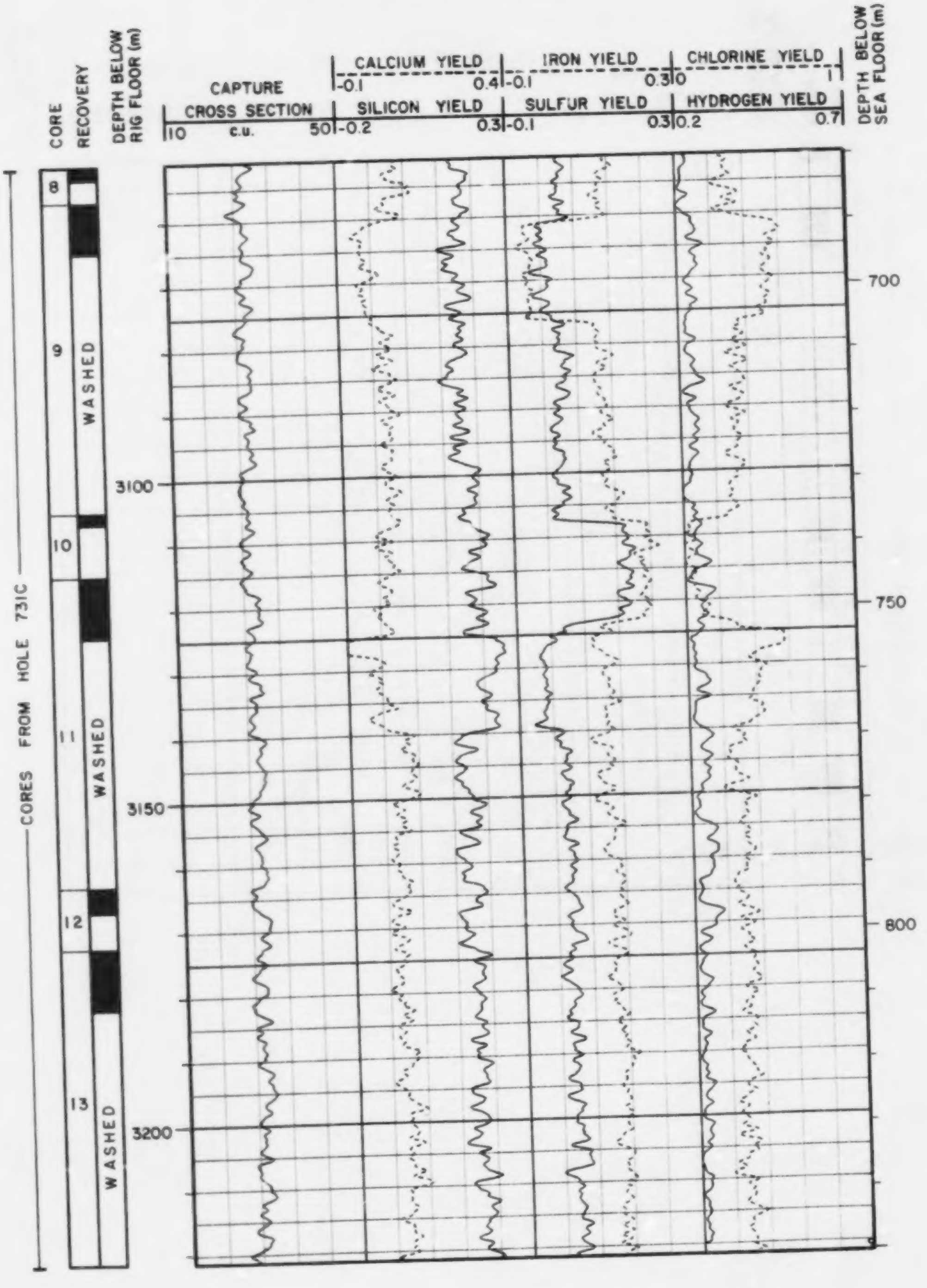

Summary Log for Hole 731C (continued)

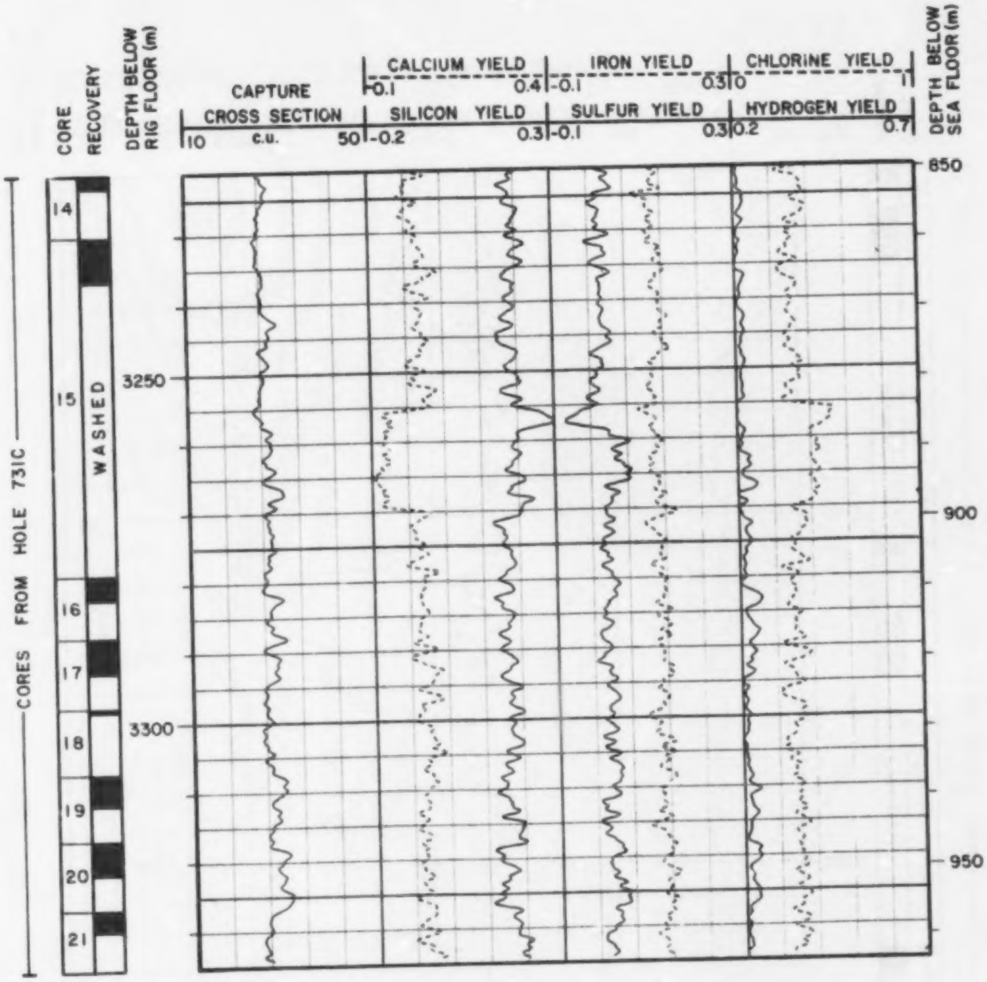

SECTION 3: CORES

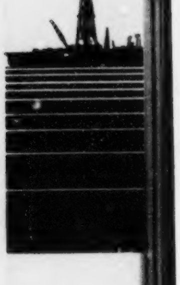

SITE 720 HOLE A CORE 1H CORED INTERVAL 4048.3-4057.7 mbsl; 0.0-9.4 mbsf

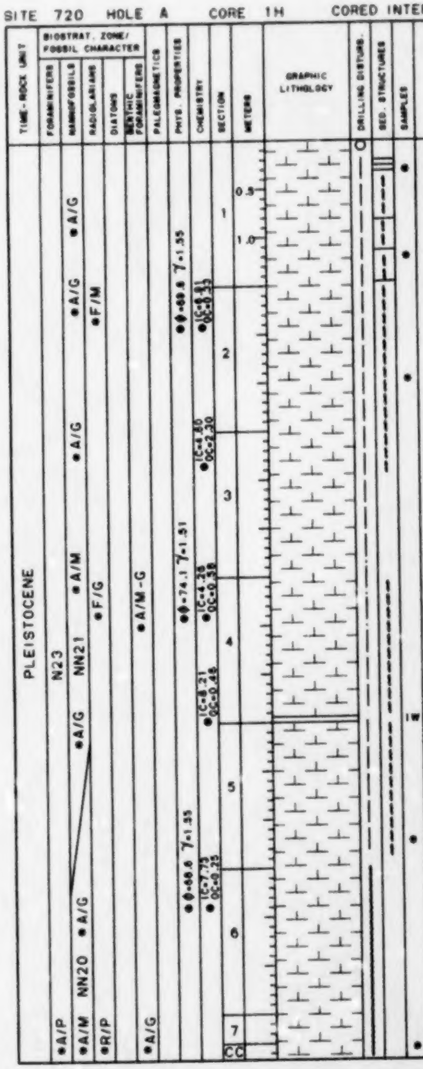
TIME-ROCK UNIT
BIOSTRAT. ZONE/ FOSSIL CHARACTER
FORAMINIFERS
NANNOFOSSILS
RADIOLARIANS
DIATOMS
BENTHIC FORAMINIFERS
PALEOMAGNETICS
PHYS. PROPERTIES
CHEMISTRY
SECTION
METERS
GRAPHIC LITHOLOGY
DRILLING DISTURB.
SED. STRUCTURES
SAMPLES
PLEISTOCENE
N23
●A/P
NN20
NN21
●A/M
●A/G
●A/G
●A/M
●A/G
●A/G
●A/G
●R/P
●F/G
●F/M
●A/G
●A/M-G
●φ=68.6 γ=1.55
●φ=74.1 γ=1.51
●φ=69.8 γ=1.55
●IC=7.73 OC=0.25
●IC=8.21 OC=0.46
●IC=4.28 OC=0.38
●IC=4.80 OC=2.30
●IC=8.81 OC=0.33
1
2
3
4
5
6
7
CC
0.5
1.0
IW

LITHOLOGIC DESCRIPTION

NANNOFOSSIL OOZE and FORAMINIFER-BEARING NANNOFOSSIL OOZE

Section 3, 116-138 cm, and Section 5, 142 cm, to CC, are moderately to highly disturbed. Remainder of core is slightly disturbed to undisturbed.

Major lithology: NANNOFOSSIL OOZE and FORAMINIFER-BEARING NANNOFOSSIL OOZE, gray (5Y 6/1) to light olive gray (5Y 6/2) and grayish green (5G 5/2). Slightly bioturbated throughout, with faint color banding at cm scale common.

SMEAR SLIDE SUMMARY (%):

	1, 29 D	1, 119 D	5, 130 D	CC D	2, 98 M
TEXTURE:					
Sand	10	1	10	10	15
Silt	10	7	15	45	15
Clay	80	92	75	45	70
COMPOSITION:					
Access. minerals	2	—	1	Tr	2
Bioclasts	—	—	5	—	—
Clay	5	—	8	3	3
Diatoms	Tr	Tr	—	—	—
2 Dolomite	—	Tr	—	—	—
Feldspar	—	Tr	1	—	—
Foraminifers	5	7	5	20	5
Volcanic glass	—	2	2	2	5
Glauconite	—	—	—	Tr	—
Mica	—	—	1	Tr	—
Nannofossils	80	84	75	70	80
Opaques	—	2	—	—	—
Quartz	3	5	2	5	5
Radiolarians	5	—	Tr	Tr	—
Sponge spicules	—	—	Tr	Tr	—

Information on Core Description Forms, for ALL sites, represents field notes taken aboard ship. Some of this information has been refined in accord with post-cruise findings, but production schedules prohibit definitive correlation of these forms with subsequent findings. Thus the reader should be alerted to the occasional ambiguity or discrepancy.

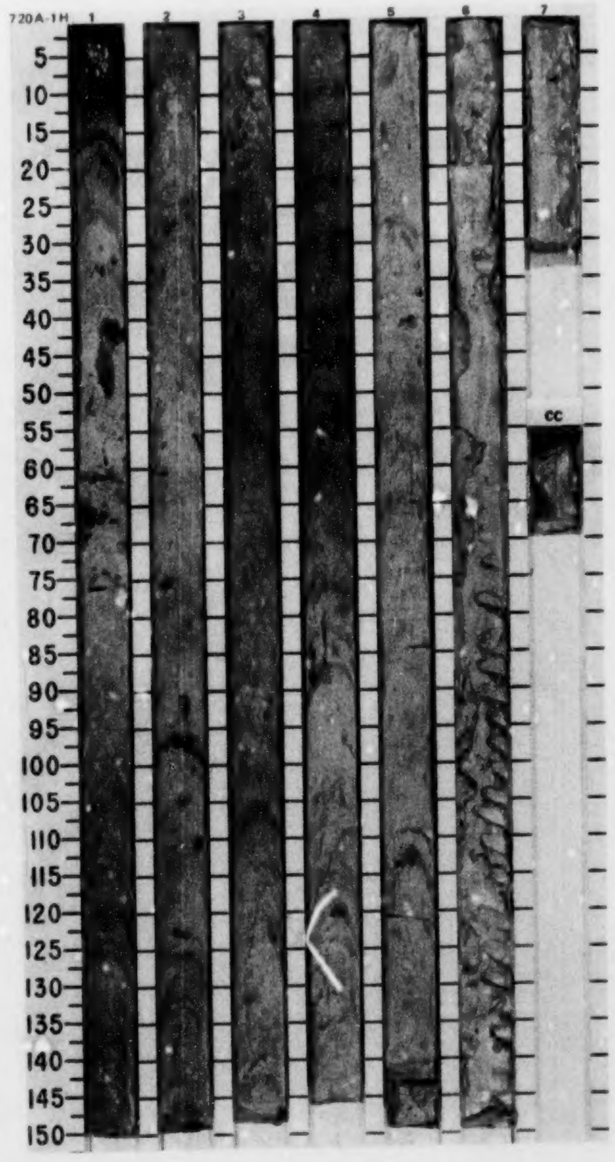
720A-1H
1
2
3
4
5
6
7
CC
5
10
15
20
25
30
35
40
45
50
55
60
65
70
75
80
85
90
95
100
105
110
115
120
125
130
135
140
145
150

SITE 720 HOLE A CORE 2H CORED INTERVAL 4057.7-4067.3 mbsl; 9.4-19.0 mbsf

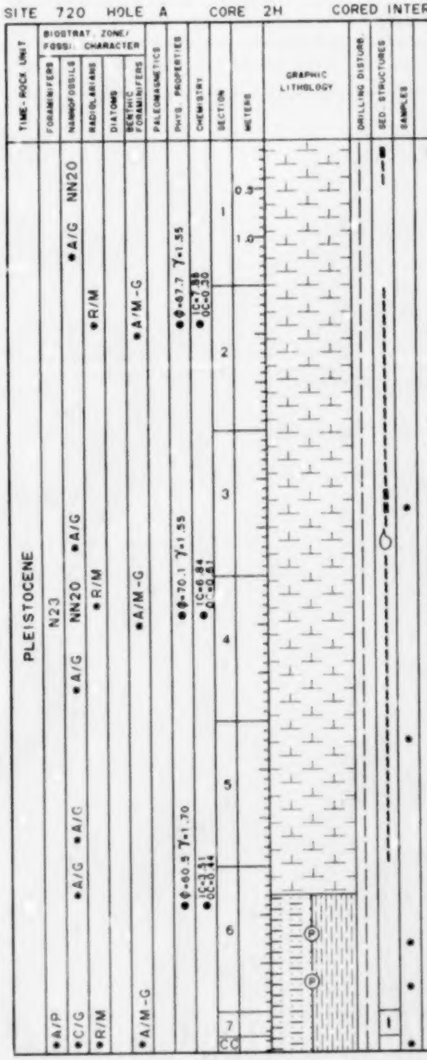
TIME-ROCK UNIT
BIOSTRAT. ZONE/ FOSSIL CHARACTER
FORAMINIFERS
NANNOFOSSILS
RADIOLARIANS
DIATOMS
BENTHIC FORAMINIFERS
PALEOMAGNETICS
PHYS. PROPERTIES
CHEMISTRY
SECTION
METERS
GRAPHIC LITHOLOGY
DRILLING DISTURB.
SED. STRUCTURES
SAMPLES
PLEISTOCENE
N23
●A/P
●A/G NN20
●A/G
NN20
●A/G
●A/G
●C/G
●R/M
●R/M
●R/M
●A/M-G
●A/M-G
●A/M-G
●Φ=67.7 γ=1.55
●Φ=70.1 γ=1.55
●Φ=60.5 γ=1.70
●IC=7.88 OC=0.30
●IC=6.84 OC=0.61
●IC=3.31 OC=0.44
1
2
3
4
5
6
7
CC
0.5
1.0
P
P

LITHOLOGIC DESCRIPTION

NANNOFOSSIL OOZE, MUD, and CLAYEY SILT

CC is moderately disturbed. Remainder of core is undisturbed.

Major lithologies:
- a. NANNOFOSSIL OOZE, greenish gray (5GY 5/1) to light greenish gray (5GY 7/1), light gray (5Y 7/1), and olive gray (5Y 5/2). Slight to moderate bioturbation throughout, with minor faint color banding. Section 1 to Section 6, 32 cm.
- b. Interbedded MUD and CLAYEY SILT, dark gray (5Y 4/1) and very dark grayish brown (10YR 3/2) to black (5Y 2.5/1). Silty intervals average 2 cm in thickness, mud layers average 2-5 cm in thickness. Silty intervals generally have sharp bases and gradational tops. Section 6, 32 cm, to CC.

SMEAR SLIDE SUMMARY (%):

	3, 81 M	5, 27 D	6, 80 D	6, 125 D	CC D
TEXTURE:					
Sand	—	10	—	—	2
Silt	20	10	70	75	60
Clay	80	80	30	25	38
COMPOSITION:					
Access. minerals	3	2	4	4	Tr
Bioclasts	—	—	Tr	—	—
Clay	5	5	23	23	5
Diatoms	Tr	—	—	—	—
Feldspar	—	—	4	4	5
Foraminifers	5	10	4	—	—
Volcanic glass	3	2	4	4	15
Mica	2	3	4	4	—
Inorganic calcite	—	—	9	9	—
Nannofossils	75	75	—	—	35
Plant debris	—	Tr	—	—	—
Quartz	5	3	45	50	40
Radiolarians	—	Tr	—	—	—
Sponge spicules	2	—	—	—	—

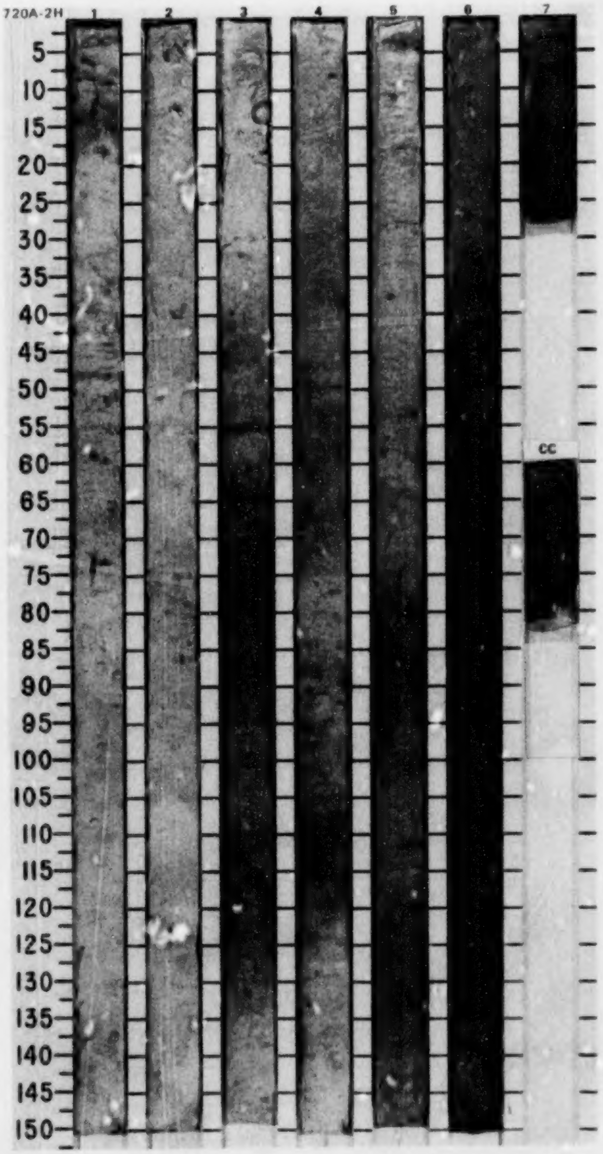
720A-2H
1
2
3
4
5
6
7
CC
5
10
15
20
25
30
35
40
45
50
55
60
65
70
75
80
85
90
95
100
105
110
115
120
125
130
135
140
145
150

SITE 720 HOLE A CORE 3H CORED INTERVAL 4067.3-4076.9 mbsl; 19.0-28.6 mbsf

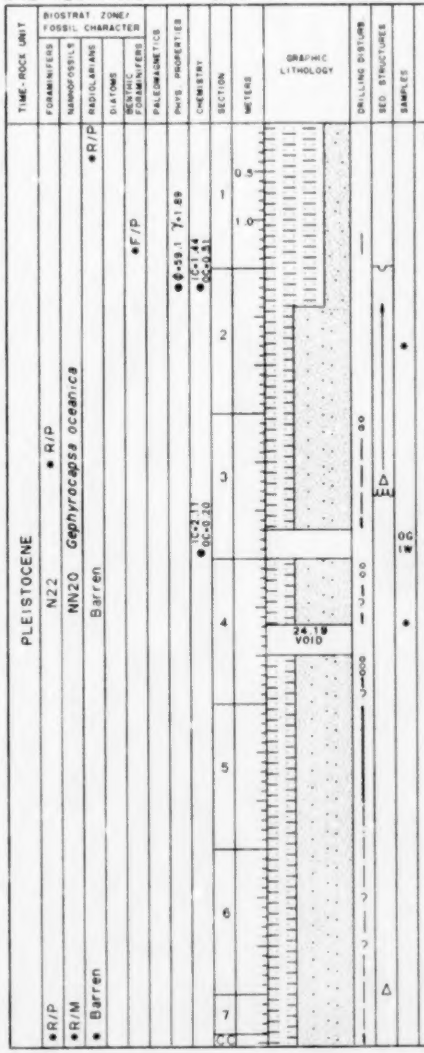
TIME-ROCK UNIT
BIOSTRAT. ZONE/ FOSSIL CHARACTER
FORAMINIFERS
NANNOFOSSILS
RADIOLARIANS
DIATOMS
BENTHIC FORAMINIFERS
PALEOMAGNETICS
PHYS. PROPERTIES
CHEMISTRY
SECTION
METERS
GRAPHIC LITHOLOGY
DRILLING DISTURB.
SED. STRUCTURES
SAMPLES
PLEISTOCENE
N22
• R/P
NN20 Gephyrocapsa oceanica
Barren
•R/P
•F/P
•φ=59.1 γ=1.89
•IC=1.44 OC=0.51
•IC=2.11 OC=0.20
•R/P
•R/M
• Barren
0.5
1.0
1
2
3
4
5
6
7
CC
24.19 VOID
OG
IW

LITHOLOGIC DESCRIPTION

MUD, SILTY SAND, and SAND

Section 3, 100-120 cm, and Section 5 to CC, are highly disturbed. Remainder of core is slightly disturbed to undisturbed.

Major lithologies:

a. Thinly interbedded MUD and SILTY SAND, dark grayish brown (10YR 4/2) to very dark gray (5Y 3/1). SILTY SAND layers are 1-5 cm thick, generally with sharp bases and gradational tops; some bases show scour and small-scale load structures. MUD layers are 1-10 cm thick with no obvious structures. Section 1 to Section 2, 42 cm.

b. SAND to SILTY SAND and MUD, very dark gray (5Y 3/1) and dark grayish brown (10YR 4/2), respectively. SAND layers have sharp bases, several of which are scoured. SANDS fine upward; layers are 40-200 cm thick. MUD layers overlay sand layers gradationally, and are homogeneous. Section 2, 42 cm to CC.

SMEAR SLIDE SUMMARY (%):

	2, 91 D	4, 63 D
TEXTURE:		
Sand	40	2
Silt	40	70
Clay	20	28
COMPOSITION:		
Access. minerals	8	2
Clay	—	25
Dolomite	2	—
Feldspar	20	10
Foraminifers	—	3
Volcanic glass	20	5
Mica	—	5
Inorganic calcite	—	10
Nannofossils	—	5
Quartz	45	40

CORE 117–720A–4X NO RECOVERY

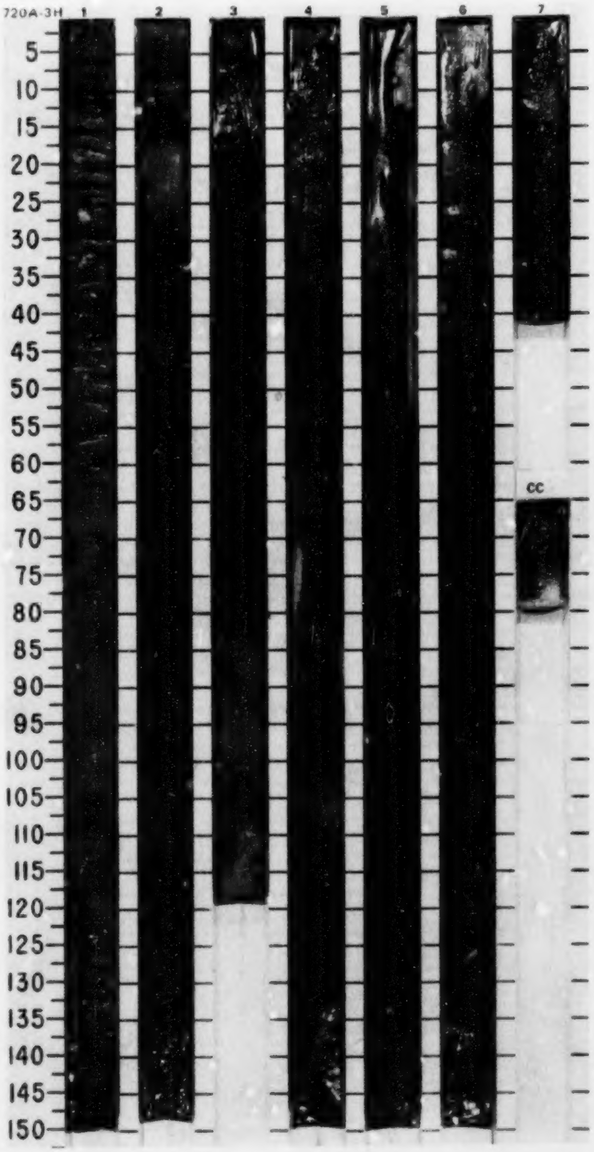
720A-3H
1
2
3
4
5
6
7
CC
5
10
15
20
25
30
35
40
45
50
55
60
65
70
75
80
85
90
95
100
105
110
115
120
125
130
135
140
145
150

SITE 720 HOLE A CORE 5X CORED INTERVAL 4086.5-4096.2 mbsl; 38.2-47.9 mbsf

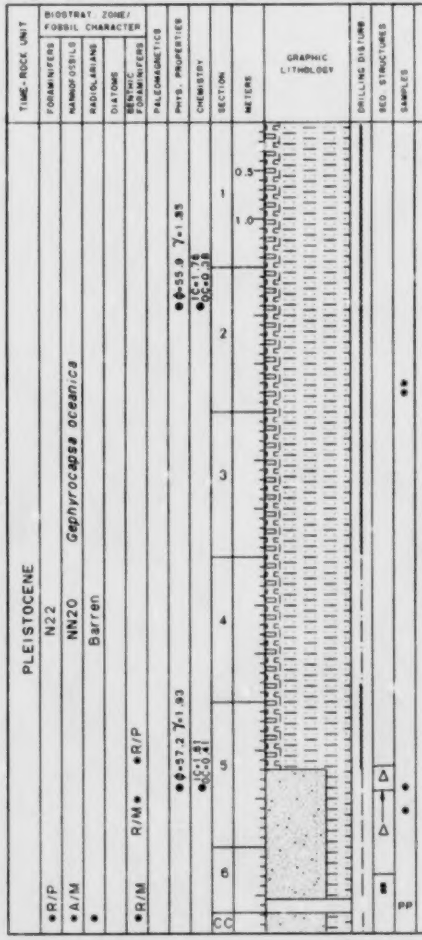
TIME-ROCK UNIT
BIOSTRAT. ZONE/ FOSSIL CHARACTER
FORAMINIFERS
NANNOFOSSILS
RADIOLARIANS
DIATOMS
BENTHIC FORAMINIFERS
PALEOMAGNETICS
PHYS. PROPERTIES
CHEMISTRY
SECTION
METERS
GRAPHIC LITHOLOGY
DRILLING DISTURB.
SED. STRUCTURES
SAMPLES
PLEISTOCENE
N22
NN20
Gephyrocapsa oceanica
Barren
●R/P
●A/M
●
●R/M
R/M●
●R/P
●Φ=55.9 γ=1.85
●Φ=57.2 γ=1.93
●IC=1.76 OC=0.38
●IC=1.81 OC=0.41
1
2
3
4
5
6
CC
0.5
1.0
PP

LITHOLOGIC DESCRIPTION

NANNOFOSSIL OOZE to CALCAREOUS MUD, and interbedded MUD and SANDY SILT/SILTY SAND

Section 1 to Section 5, 70 cm, is highly disturbed. Remainder of core is undisturbed to slightly disturbed.

Major lithologies:
- a. NANNOFOSSIL OOZE to CALCAREOUS MUD, dark gray (5Y 4/1) to greenish gray (5GY 6/1), highly disturbed to soupy. Section 1 to Section 5, 70 cm.
- b. Interbedded MUD and SANDY SILT/SILTY SAND, dark gray (5Y 4/1) and very dark gray (5Y 3/1), respectively. Sand layers are 2-40 cm thick, have sharp bases, and fine upward to gradational tops. Overlain by homogeneous mud layers, 1-10 cm thick. Section 5, 70 cm, to CC.

Minor lithology: Nannofossil ooze, yellowish brown (10YR 5/4). Section 2, 129-133 cm.

SMEAR SLIDE SUMMARY (%):

	2, 121 D	2, 130 M	5, 88 D	5,112 D
TEXTURE:				
Sand	5	5	40	
Silt	50	20	15	55
Clay	45	75	80	5
COMPOSITION:				
Access. minerals	5	3	10	
Clay	30	10	30	—
Dolomite	Tr	—	—	—
Feldspar	5	—	5	20
Foraminifers	10	—	—	—
Volcanic glass	10	—	—	—
Mica	5	2	10	5
Inorganic calcite	10	10	—	—
Nannofossils	—	70	5	—
Quartz	25	5	50	65
Radiolarians	—	Tr	—	—

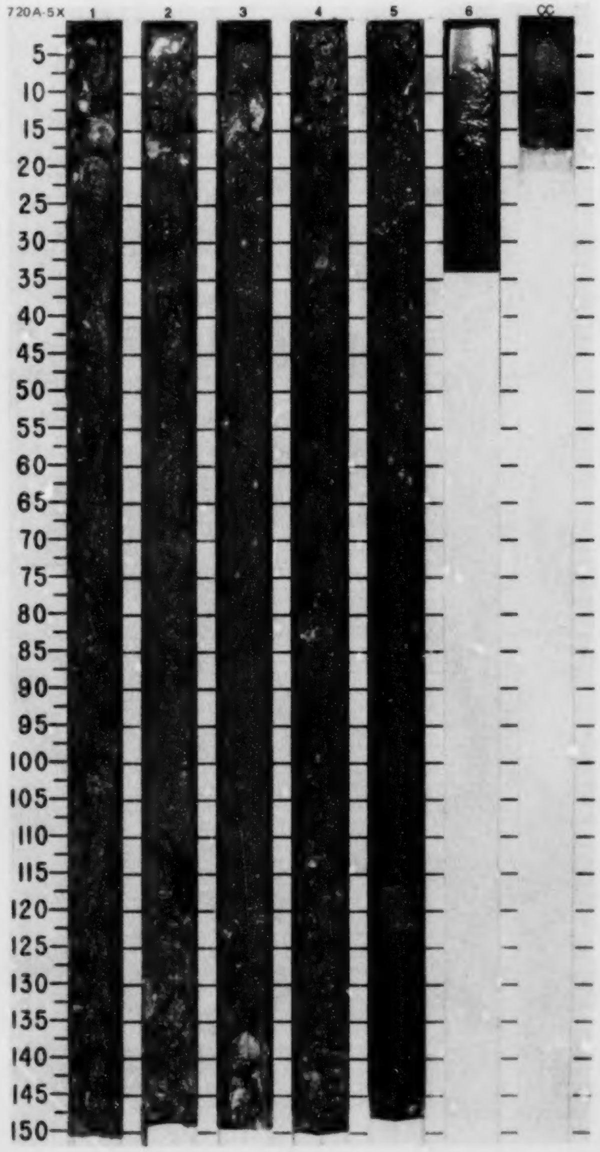
720A-5X
1
2
3
4
5
6
CC
5
10
15
20
25
30
35
40
45
50
55
60
65
70
75
80
85
90
95
100
105
110
115
120
125
130
135
140
145
150

SITE 720 HOLE A CORE 6X CORED INTERVAL 4096.2-4105.9 mbsl; 47.9-57.6 mbsf

TIME-ROCK UNIT	BIOSTRAT. ZONE/ FOSSIL CHARACTER					PALEOMAGNETICS	PHYS. PROPERTIES	CHEMISTRY	SECTION	METERS	GRAPHIC LITHOLOGY	DRILLING DISTURB.	SED. STRUCTURES	SAMPLES
	FORAMINIFERS	NANNOFOSSILS	RADIOLARIANS	DIATOMS	BENTHIC FORAMINIFERS									
PLEISTOCENE	N22 C/P ●	*Pseudoemiliania lacunosa* NN19 A/G ● A/G ●	Barren ●		A/M ● ● F/M		γ=1.67 ϕ=69.5 ●	● [illegible] OC=0.33	1 CC	0.5				●●

LITHOLOGIC DESCRIPTION

NANNOFOSSIL-RICH MUD and NANNOFOSSIL OOZE

Entire core is undisturbed to slightly disturbed.

Major lithology: NANNOFOSSIL-RICH MUD and NANNOFOSSIL OOZE, gray (5Y 5/1), with minor bioturbation.

Minor lithology: Nannofossil-rich sand-silt-clay, black (10Y 3/1), with sharp bases, sharp-to-gradational tops. Section 1, 10-13, 30-31, 38-39, and 47-53 cm.

SMEAR SLIDE SUMMARY (%):

	1, 21 D	1, 30 M
TEXTURE:		
Sand	—	40
Silt	—	30
Clay	95	30
COMPOSITION:		
Access. minerals	—	15
Clay	2	—
Feldspar	—	30
Foraminifers	—	Tr
Nannofossils	95	25
Quartz	3	30

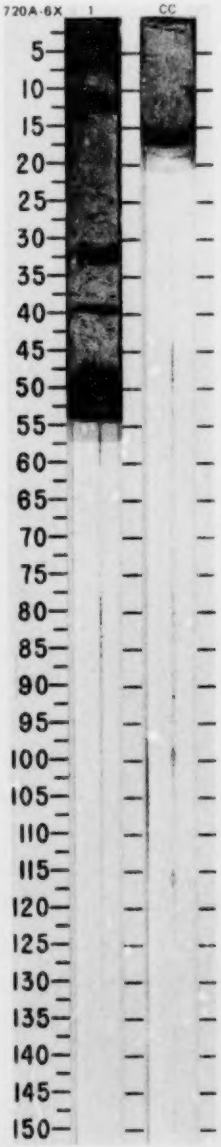

SITE 720 HOLE A CORE 7X CORED INTERVAL 4105.9-4115.6 mbsl; 57.6-67.3 mbsf

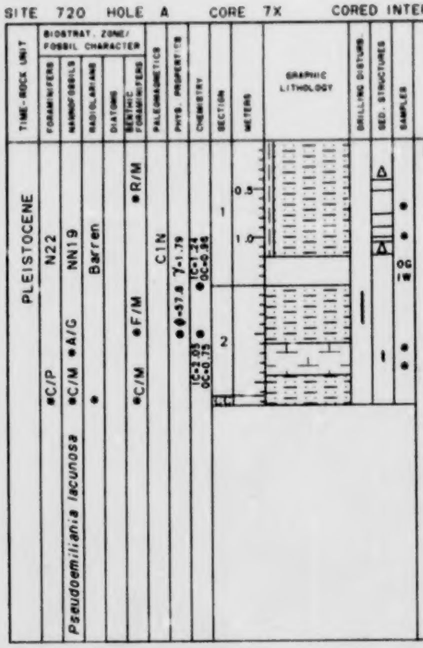
TIME-ROCK UNIT
BIOSTRAT. ZONE/ FOSSIL CHARACTER
FORAMINIFERS
NANNOFOSSILS
RADIOLARIANS
DIATOMS
BENTHIC FORAMINIFERS
PALEOMAGNETICS
PHYS. PROPERTIES
CHEMISTRY
SECTION
METERS
GRAPHIC LITHOLOGY
DRILLING DISTURB.
SED. STRUCTURES
SAMPLES
PLEISTOCENE
N22
●C/P
Pseudoemiliania lacunosa
NN19
●C/M ●A/G
Barren
●
●R/M
●F/M
●C/M
C1N
●φ=57.8 γ=1.79
●IC=1.24 OC=0.96
●IC=2.05 OC=0.75
1
2
CC
0.5
1.0
OG
IW

LITHOLOGIC DESCRIPTION

MUD

Major lithology: MUD, very dark gray (5Y 3/1, 5YR 3/1) to gray (5Y 5/1), slightly bioturbated.

Minor lithologies:
a. Clayey-silt (mud), very dark gray (5Y 3/1), forms interbeds approximately 1 cm thick, with sharp bases and gradational tops. Section 1, 45-46, 57-58, 78-79, 82-83, 89-90, 93-94, 98-99, 102-103, 109-110, and 114-115 cm.
b. Nannofossil ooze, gray (5Y 5/1), slightly bioturbated. Section 2, 81-92 cm.

SMEAR SLIDE SUMMARY (%):

	1, 70 D	1, 98 M	2, 66 M	2, 84 M
TEXTURE:				
Sand	—	5	—	—
Silt	10	65	5	15
Clay	90	30	95	85
COMPOSITION:				
Access. minerals	—	—	1	3
Clay	5	5	—	—
Dolomite	—	—	—	Tr
Feldspar	5	10	1	5
Foraminifers	—	—	2	2
Volcanic glass	—	Tr	—	—
Inorganic calcite	—	—	—	—
Mica	5	5	—	—
Nannofossils	Tr	—	94	80
Quartz	85	80	2	10

CORE 117–720A–8X NO RECOVERY

CORE 117–720A–9X NO RECOVERY

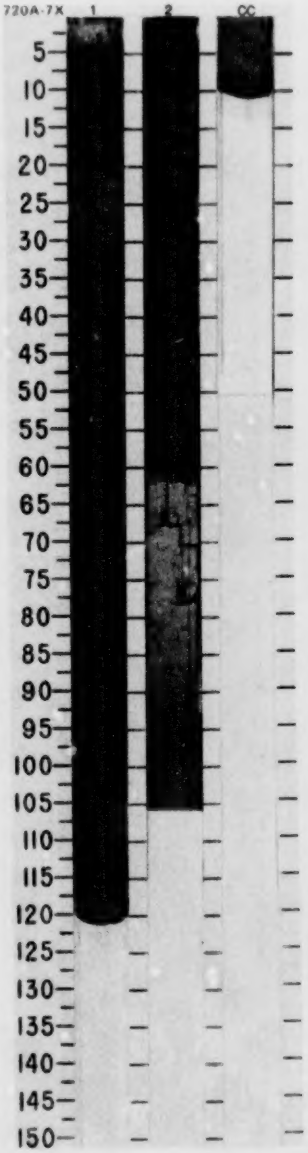
720A-7X
1
2
CC
5
10
15
20
25
30
35
40
45
50
55
60
65
70
75
80
85
90
95
100
105
110
115
120
125
130
135
140
145
150

SITE 720 HOLE A CORE 10X CORED INTERVAL 4135.0-4144.7 mbsl; 86.7-96.4 mbsf

TIME-ROCK UNIT	BIOSTRAT. ZONE/ FOSSIL CHARACTER					PALEOMAGNETICS	PHYS. PROPERTIES	CHEMISTRY	SECTION	METERS	GRAPHIC LITHOLOGY	DRILLING DISTURB.	SED. STRUCTURES	SAMPLES	LITHOLOGIC DESCRIPTION
	FORAMINIFERS	NANNOFOSSILS	RADIOLARIANS	DIATOMS	BENTHIC FORAMINIFERS										
PLEISTOCENE	Barren ● N22	F/M ● NN19	● Barren	R/P ●					CC					●	SANDY SILT

SANDY SILT

Entire core is undisturbed.

Major lithology: SANDY SILT, very dark gray (5Y 3/1).

SMEAR SLIDE SUMMARY (%):

	CC, 8 D
TEXTURE:	
Sand	30
Silt	50
Clay	20
COMPOSITION:	
Clay	5
Feldspar	5
Volcanic glass	Tr
Mica	5
Quartz	80
Rock fragments	5

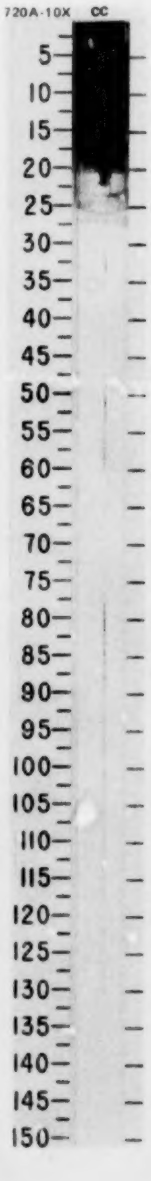
720A-10X
CC
5
10
15
20
25
30
35
40
45
50
55
60
65
70
75
80
85
90
95
100
105
110
115
120
125
130
135
140
145
150

SITE 720 HOLE A CORE 11X CORED INTERVAL 4144.7-4154.3 mbsl; 96.4-106.0 mbsf

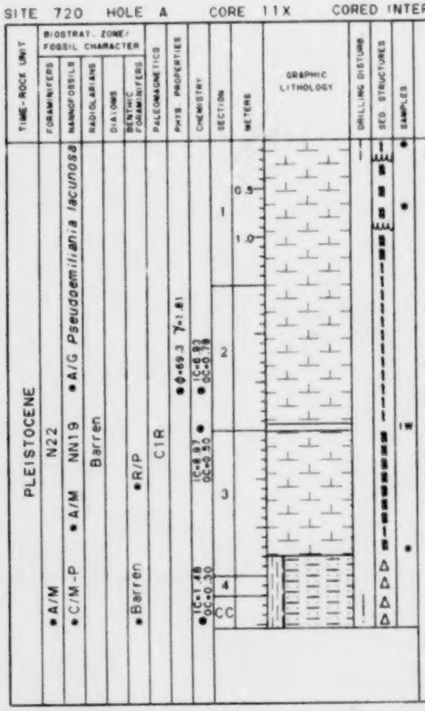
TIME-ROCK UNIT
BIOSTRAT. ZONE/ FOSSIL CHARACTER
FORAMINIFERS
NANNOFOSSILS
RADIOLARIANS
DIATOMS
BENTHIC FORAMINIFERS
PALEOMAGNETICS
PHYS. PROPERTIES
CHEMISTRY
SECTION
METERS
GRAPHIC LITHOLOGY
DRILLING DISTURB.
SED. STRUCTURES
SAMPLES
PLEISTOCENE
N22
●A/M
●C/M-P
●A/M
NN19
●A/G Pseudoemiliania lacunosa
Barren
●R/P
●Barren
C1R
●Φ=69.3 γ=1.81
●IC=6.92 OC=0.78
IC=6.87 OC=0.50●
●IC=1.48 OC=0.30
1
2
3
4
CC
0.5
1.0
IW

LITHOLOGIC DESCRIPTION

NANNOFOSSIL OOZE, and interbedded MUD and SILTY MUD

Entire core is undisturbed to slightly disturbed.

Major lithologies:
- a. NANNOFOSSIL OOZE, very dark gray (2.5Y 3/0), olive gray (5Y 4/2), and light olive gray (5Y 6/2), slightly to moderately bioturbated throughout, with faint color banding in Section 2. Section 1 to Section 3, 130 cm.
- b. Interbedded MUD and SILTY MUD, very dark gray (5Y 3/1) to dark gray (5Y 4/1), form upward-fining intervals 5-20 cm thick with sharp, silty mud bases. Section 3, 130 cm, to CC.

SMEAR SLIDE SUMMARY (%):

	1, 7 D	1, 70 D	3, 123 D
TEXTURE:			
Silt	5	5	10
Clay	95	95	90
COMPOSITION:			
Clay	10	—	—
Foraminifers	2	Tr	
Nannofossils	70	95	80
Quartz	20	3	20

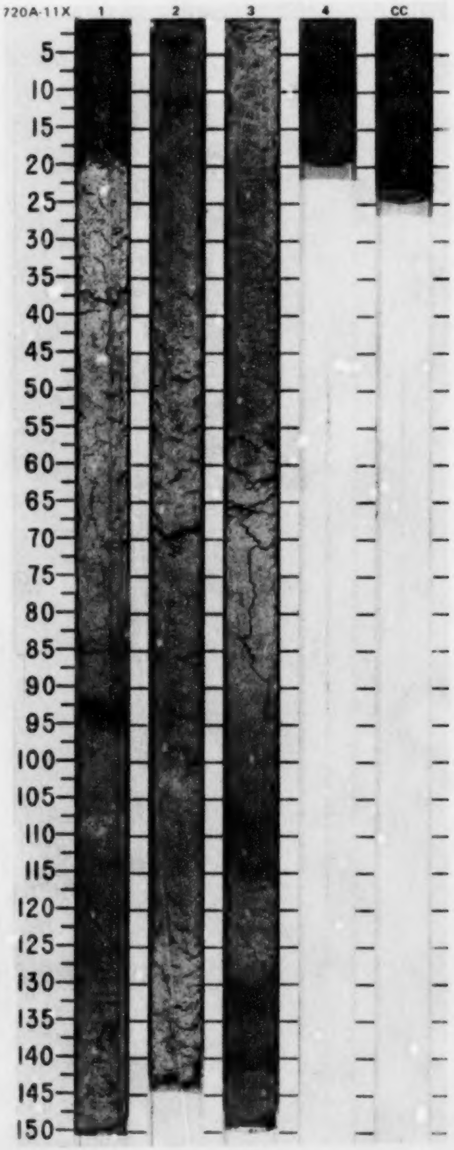
720A-11X
1
2
3
4
CC
5
10
15
20
25
30
35
40
45
50
55
60
65
70
75
80
85
90
95
100
105
110
115
120
125
130
135
140
145
150

SITE 720 HOLE A CORE 12X CORED INTERVAL 4154.3-4164.0 mbsl; 106.0-115.7 mbsf

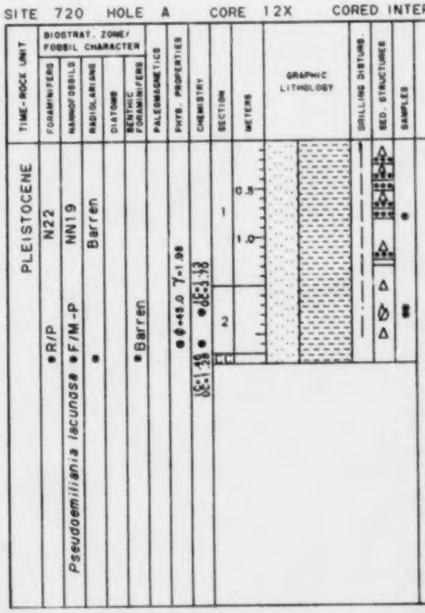
TIME-ROCK UNIT
BIOSTRAT. ZONE/ FOSSIL CHARACTER
FORAMINIFERS
NANNOFOSSILS
RADIOLARIANS
DIATOMS
BENTHIC FORAMINIFERS
PALEOMAGNETICS
PHYS. PROPERTIES
CHEMISTRY
SECTION
METERS
GRAPHIC LITHOLOGY
DRILLING DISTURB.
SED. STRUCTURES
SAMPLES
PLEISTOCENE
N22
●R/P
NN19
Pseudoemiliania lacunosa ●F/M-P
Barren
●
●Barren
●ϕ-45.0 γ-1.98
0.5
1.0
1
2
CC

LITHOLOGIC DESCRIPTION

SILT and CLAY

Entire core is undisturbed to slightly disturbed.

Major lithology: SILT and CLAY, dark olive gray (5Y 3/2) to very dark gray (5Y 3/1), fining slightly upward from sharp base over intervals of 3-15 cm. SILT zones are micaceous; zone at Section 2, 21-25 cm, contains abundant charcoal.

SMEAR SLIDE SUMMARY (%):

	1, 60 D	2, 25 M	2, 29 M
TEXTURE:			
Sand	30	20	
Silt	5	30	70
Clay	5	40	10
COMPOSITION:			
Access. minerals	1	—	3
Calcareous frag.	—	—	Tr
Clay	65	10	—
Feldspar	—	20	20
Fish remains	—	Tr	—
Volcanic glass	—	5	—
Inorganic calcite	—	15	—
Mica	1	15	7
Nannofossils	Tr	—	—
Opaques	—	Tr	—
Plant debris	—	5	—
Quartz	33	30	60
Rock fragments	—	—	10

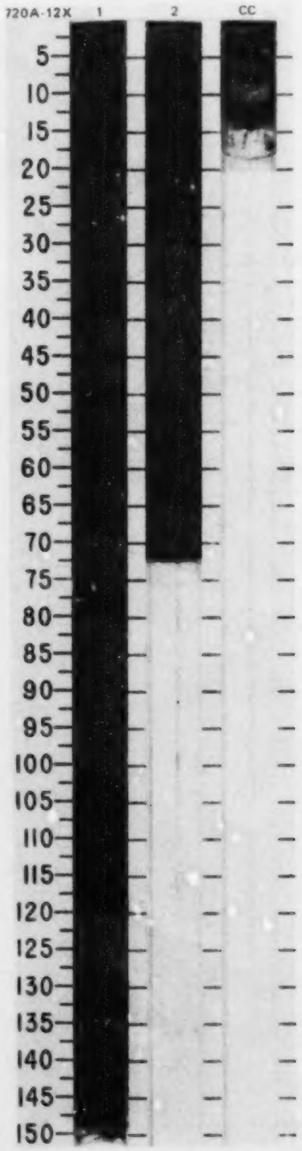
720A-12X
1
2
CC
5
10
15
20
25
30
35
40
45
50
55
60
65
70
75
80
85
90
95
100
105
110
115
120
125
130
135
140
145
150

SITE 720 HOLE A CORE 13X CORED INTERVAL 4164.0-4173.7 mbsl; 115.7-125.4 mbsf

TIME-ROCK UNIT	BIOSTRAT. ZONE/ FOSSIL CHARACTER					PALEOMAGNETICS	PHYS. PROPERTIES	CHEMISTRY	SECTION	METERS	GRAPHIC LITHOLOGY	DRILLING DISTURB.	SED. STRUCTURES	SAMPLES	LITHOLOGIC DESCRIPTION
	FORAMINIFERS	NANNOFOSSILS	RADIOLARIANS	DIATOMS	BENTHIC FORAMINIFERS										
PLEISTOCENE	N22 R/P●	*Pseudoemiliania lacunosa* NN19 F/M-P●	Barren ●		R/M●				1 CC						CLAY and SILTY CLAY Section 1 is highly disturbed. CC is slightly disturbed. Major lithology: CLAY and SILTY CLAY, dark gray (5Y 4/1).

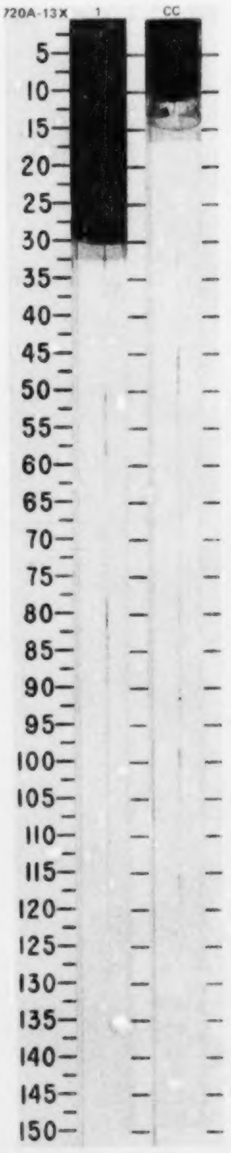
720A-13X
1
CC
5
10
15
20
25
30
35
40
45
50
55
60
65
70
75
80
85
90
95
100
105
110
115
120
125
130
135
140
145
150

SITE 720 HOLE A CORE 14X CORED INTERVAL 4173.7-4183.3 mbsl; 125.4-135.0 mbsf

TIME-ROCK UNIT	BIOSTRAT. ZONE/ FOSSIL CHARACTER FORAMINIFERS	NANNOFOSSILS	RADIOLARIANS	DIATOMS		PALEOMAGNETICS	PHYS. PROPERTIES	CHEMISTRY	SECTION	METERS	GRAPHIC LITHOLOGY	DRILLING DISTURB.	SED. STRUCTURES	SAMPLES
PLEISTOCENE	●R/P N22	●C/M-P NN19 *Pseudoemiliania lacunosa*	● Barren		●R/M		●γ=1.84 ●φ=54.4	● IC=1.87 OC=0.32	1 CC	0.5	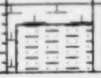			● ●

LITHOLOGIC DESCRIPTION

CALCAREOUS MUD and NANNOFOSSIL OOZE

Entire core is highly disturbed.

Major lithology: CALCAREOUS MUD and NANNOFOSSIL OOZE, light gray (5Y 7/1) to very dark gray (5Y 3/1).

SMEAR SLIDE SUMMARY

	1, 18 D	1, 34 D
TEXTURE:		
Silt	10	20
Clay	90	80
COMPOSITION:		
Clay	10	45
Feldspar	5	10
Hornblende	—	Tr
Inorganic calcite	10	20
Mica	—	10
Nannofossils	70	5
Opaques	—	Tr
Quartz	5	10

CORE 117-720A-15X NO RECOVERY

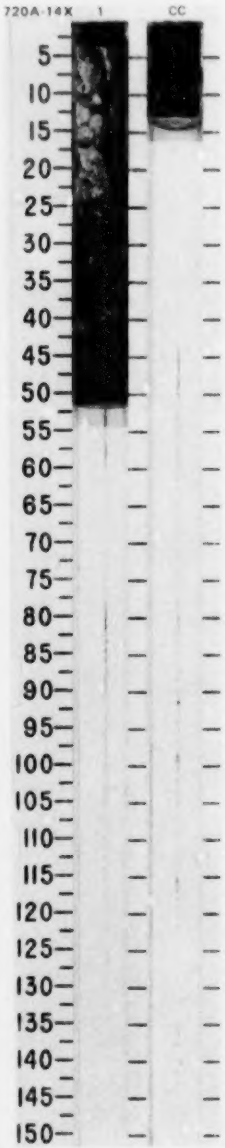
720A-14X
1
CC
5
10
15
20
25
30
35
40
45
50
55
60
65
70
75
80
85
90
95
100
105
110
115
120
125
130
135
140
145
150

SITE 720 HOLE A CORE 16X CORED INTERVAL 4193.0-4202.7 mbsl; 144.7-154.4 mbsf

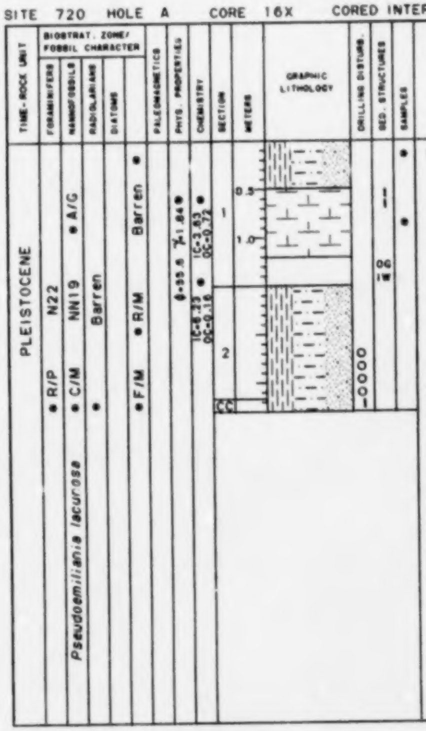
TIME-ROCK UNIT
BIOSTRAT. ZONE/ FOSSIL CHARACTER
FORAMINIFERS
NANNOFOSSILS
RADIOLARIANS
DIATOMS
PALEOMAGNETICS
PHYS. PROPERTIES
CHEMISTRY
SECTION
METERS
GRAPHIC LITHOLOGY
DRILLING DISTURB.
SED. STRUCTURES
SAMPLES
PLEISTOCENE
● R/P N22
● C/M NN19 ● A/G
Pseudoemiliania lacunosa
● Barren
● F/M ● R/M Barren ●
ϕ=55.6 γ=1.84 ●
IC=6.23 OC=0.16 ● IC=3.63 OC=0.72 ●
1
2
CC
0.5
1.0
OG
IW

LITHOLOGIC DESCRIPTION

MUD, MUDDY SILT, SANDY SILT, and NANNOFOSSIL OOZE

Section 2, 75 cm, to CC is highly disturbed. Remainder of the core is undisturbed.

Major lithologies:
- a. MUD, MUDDY SILT, and SANDY SILT, gray (5Y 5/1) to very dark gray (5Y 3/1), uniform. Section 1, 0-47 cm, and Section 2 to CC.
- b. NANNOFOSSIL OOZE, greenish gray (5G 6/1) to dark greenish gray (5GY 4/1), with minor bioturbation. Section 1, 47-120 cm.

SMEAR SLIDE SUMMARY (%):

	1, 17 D	1, 88 D
TEXTURE:		
Sand	20	—
Silt	60	7
Clay	20	93
COMPOSITION:		
Access. minerals	5	—
Diatoms	—	Tr
Dolomite	Tr	—
Feldspar	5	—
Foraminifers	Tr	3
Volcanic glass	15	Tr
Inorganic calcite	10	5
Mica	5	—
Nannofossils	—	90
Opaques	—	Tr
Quartz	60	2

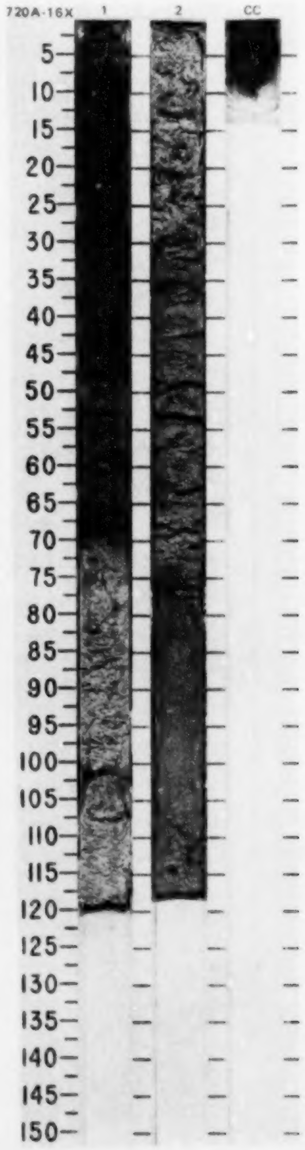
720A-16X
1
2
CC
5
10
15
20
25
30
35
40
45
50
55
60
65
70
75
80
85
90
95
100
105
110
115
120
125
130
135
140
145
150

CORE 117-720A-17X NO RECOVERY

CORE 117-720A-18X NO RECOVERY

SITE 720 HOLE A CORE 19X CORED INTERVAL 4222.0-4231.7 mbsl; 173.7-183.4 mbsf

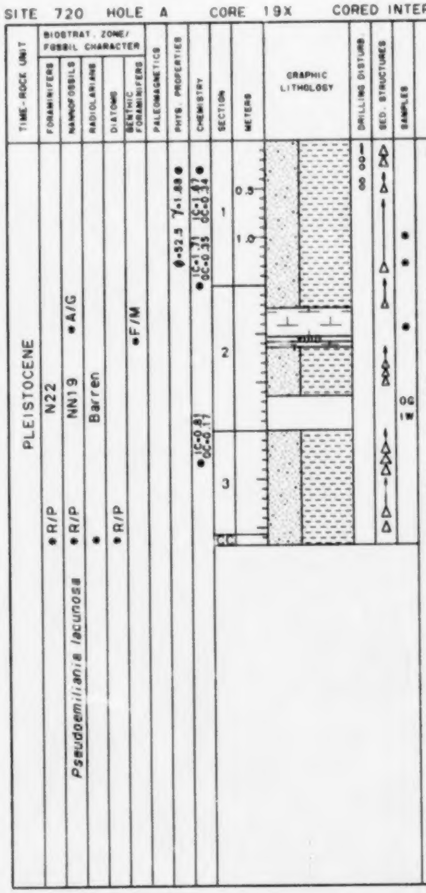
TIME-ROCK UNIT
BIOSTRAT. ZONE/ FOSSIL CHARACTER
FORAMINIFERS
NANNOFOSSILS
RADIOLARIANS
DIATOMS
BENTHIC FORAMINIFERS
PALEOMAGNETICS
PHYS. PROPERTIES
CHEMISTRY
SECTION
METERS
GRAPHIC LITHOLOGY
DRILLING DISTURB.
SED. STRUCTURES
SAMPLES
PLEISTOCENE
N22
•R/P
NN19
•A/G
•R/P
Pseudoemiliania lacunosa
Barren
•
•R/P
•F/M
φ=52.5 γ=1.88
IC=1.71 OC=0.35
IC=1.67 OC=0.34
IC=0.81 OC=0.17
1
2
3
CC
0.5
1.0
OG
IW

LITHOLOGIC DESCRIPTION

CLAY to SILTY SAND

Entire core is undisturbed to slightly disturbed.

Major lithology: CLAY to SILTY SAND, grading from very dark gray (5Y 3/1) silty sand at base to olive gray (5Y 4/2) mud over 10-80 cm intervals. Sequence repeated throughout core.

Minor lithology: Nannofossil ooze, greenish gray (5GY 6/1), bioturbated. Section 2, 26-67 cm.

SMEAR SLIDE SUMMARY (%):

	1, 100 D	1, 126 D	2, 43 D
TEXTURE:			
Sand	—	80	—
Silt	8	20	10
Clay	92	90	
COMPOSITION:			
Access. minerals	2	20	
Clay	90	—	5
Feldspar	2	20	—
Foraminifers	—	—	2
Volcanic glass	—	15	—
Inorganic calcite	—	—	10
Mica	2	5	1
Nannofossils	2	—	80
Quartz	2	40	2

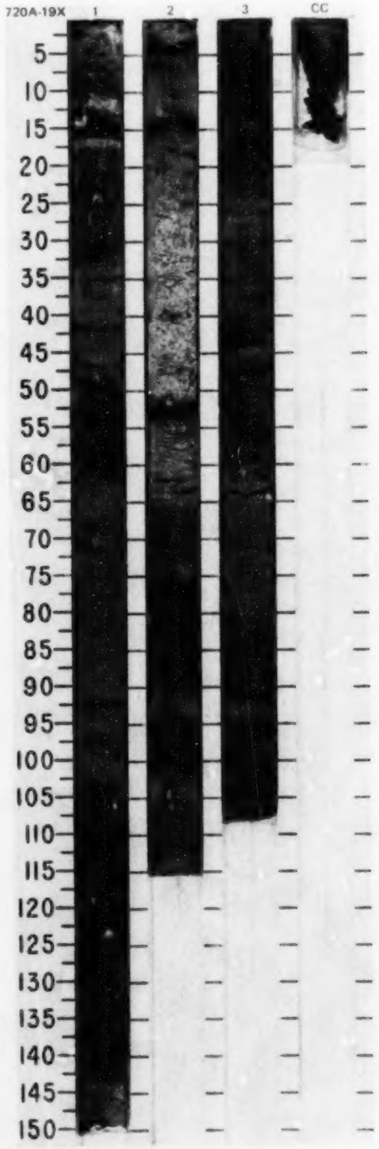
720A-19X
1
2
3
CC
5
10
15
20
25
30
35
40
45
50
55
60
65
70
75
80
85
90
95
100
105
110
115
120
125
130
135
140
145
150

SITE 720 HOLE A CORE 20X CORED INTERVAL 4231.7-4241.3 mbsl; 183.4-193.0 mbsf

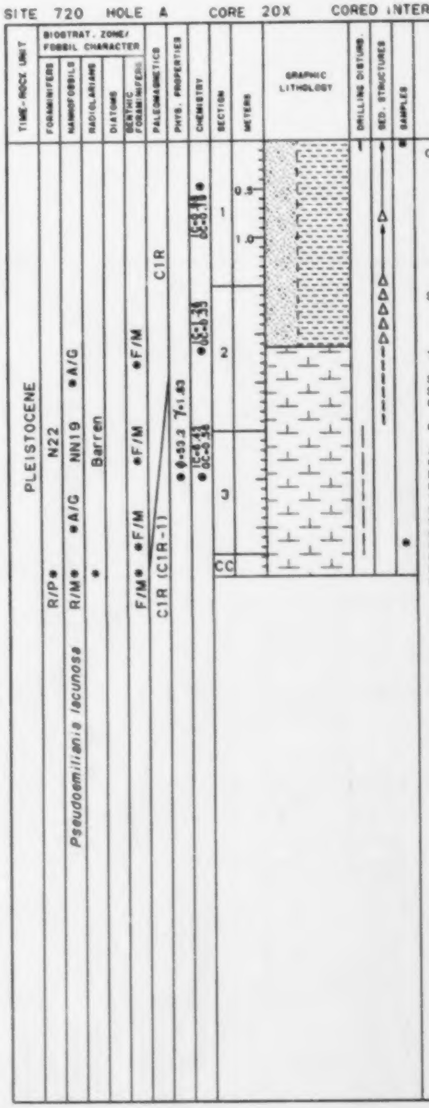
TIME-ROCK UNIT
BIOSTRAT. ZONE/ FOSSIL CHARACTER
FORAMINIFERS
NANNOFOSSILS
RADIOLARIANS
DIATOMS
BENTHIC FORAMINIFERS
PALEOMAGNETICS
PHYS. PROPERTIES
CHEMISTRY
SECTION
METERS
GRAPHIC LITHOLOGY
DRILLING DISTURB.
SED. STRUCTURES
SAMPLES
PLEISTOCENE
N22
R/P●
NN19
●A/G
●A/G
R/M●
Pseudoemiliania lacunosa
Barren
●
●F/M
●F/M
●F/M
F/M●
C1R
C1R (C1R-1)
● φ-53.2 γ-1.83
IC-3.11 OC-0.18 ●
● IC-1.36 OC-0.35
● IC-4.43 OC-0.38
1
2
3
CC
0.5
1.0

LITHOLOGIC DESCRIPTION

CLAY to SILTY SAND and NANNOFOSSIL OOZE

Entire core is undisturbed to slightly disturbed.

Major lithologies:
- a. CLAY to SILTY SAND, grading from very dark gray (5Y 3/1) silty sand at base to olive gray (5Y 4/2) mud over 10-80 cm intervals. Sequence repeated from Section 1 to Section 2, 64 cm.
- b. NANNOFOSSIL OOZE, greenish gray (5GY 5/1) to dark greenish gray (5GY 4/1), bioturbated, with foraminifers common. Section 2, 64 cm, to CC.

SMEAR SLIDE SUMMARY (%):

	1, 2 M	3, 118 D
TEXTURE:		
Sand	5	5
Silt	25	25
Clay	70	70
COMPOSITION:		
Access. minerals	—	2
Clay	10	—
Diatoms	5	—
Foraminifers	—	2
Volcanic glass	5	—
Inorganic calcite	10	20
Mica	—	2
Nannofossils	60	70
Quartz	5	4
Radiolarians	Tr	—
Silicoflagellates	Tr	—
Sponge spicules	5	—

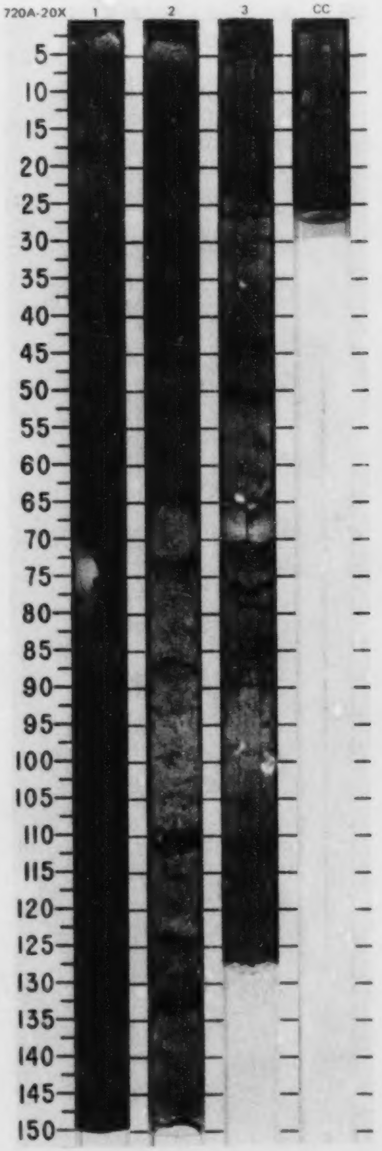
720A-20X
1
2
3
CC
5
10
15
20
25
30
35
40
45
50
55
60
65
70
75
80
85
90
95
100
105
110
115
120
125
130
135
140
145
150

SITE 720 HOLE A CORE 21X CORED INTERVAL 4241.3-4251.0 mbsl; 193.0-202.7 mbsf

TIME-ROCK UNIT	BIOSTRAT. ZONE/ FOSSIL CHARACTER					PALEOMAGNETICS	PHYS. PROPERTIES	CHEMISTRY	SECTION	METERS	GRAPHIC LITHOLOGY	DRILLING DISTURB.	SED. STRUCTURES	SAMPLES	LITHOLOGIC DESCRIPTION
	FORAMINIFERS	NANNOFOSSILS	RADIOLARIANS	DIATOMS	BENTHIC FORAMINIFERS										
PLEISTOCENE	N22	*P. lacunosa* NN19 ●R/M	Barren ●		●R/M	C1R (C1R-1)	$\phi=53.3$ $\gamma=2.11$ ●	IC=1.35 OC=0.25 ●	1 CC	0.5	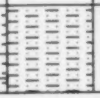	ǀ			MUD Section 1, 0-16 cm, is highly disturbed. Remainder of the core is undisturbed. Major lithology: MUD, very dark gray (5Y 3/1).

SITE 720 HOLE A CORE 22X CORED INTERVAL 4251.0-4260.7 mbsl; 202.7-212.4 mbsf

TIME-ROCK UNIT	BIOSTRAT. ZONE/ FOSSIL CHARACTER					PALEOMAGNETICS	PHYS. PROPERTIES	CHEMISTRY	SECTION	METERS	GRAPHIC LITHOLOGY	DRILLING DISTURB.	SED. STRUCTURES	SAMPLES	LITHOLOGIC DESCRIPTION
	FORAMINIFERS	NANNOFOSSILS	RADIOLARIANS	DIATOMS	BENTHIC FORAMINIFERS										
PLEISTOCENE	●Barren	*Pseudoemiliania lacunosa* NN19 ●R/P	Barren ●		Barren ● ●Barren	C1R (C1R-1)		IC=1.14 OC=0.21 ●	1 CC	0.5	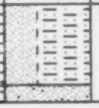	ǀ	△ △		SAND and MUD Section 1, 0-26 cm, highly disturbed. Remainder of the core is undisturbed. Major lithology: Interbedded SAND and MUD, very dark gray (5Y 3/1), form upward-fining sequences with sharp bases and gradational tops.

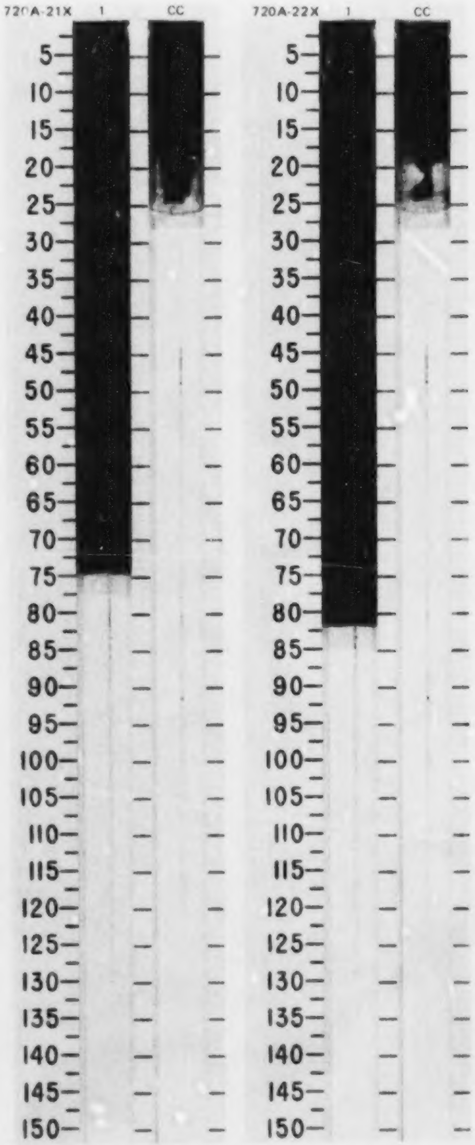

SITE 720 HOLE A CORE 23X CORED INTERVAL 4260.7-4270.3 mbsl; 212.4-222.0 mbsf

TIME-ROCK UNIT	BIOSTRAT. ZONE/ FOSSIL CHARACTER					PALEOMAGNETICS	PHYS. PROPERTIES	CHEMISTRY	SECTION	METERS	GRAPHIC LITHOLOGY	DRILLING DISTURB.	SED. STRUCTURES	SAMPLES	LITHOLOGIC DESCRIPTION
	FORAMINIFERS	NANNOFOSSILS	RADIOLARIANS	DIATOMS	BENTHIC FORAMINIFERS										
PLEISTOCENE	Barren ●	*Pseudoemiliania lacunosa* NN19 R/P ●	Barren ●		R/P ●				CC	–	▨				SILTY SAND Entire core is moderately disturbed. Major lithology: SILTY SAND, very dark gray (5Y 3/1).

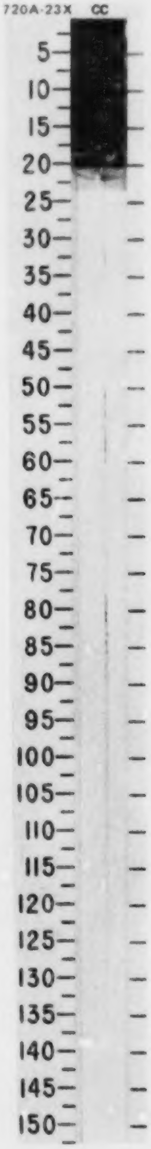
720A-23X
CC
5
10
15
20
25
30
35
40
45
50
55
60
65
70
75
80
85
90
95
100
105
110
115
120
125
130
135
140
145
150

SITE 720 HOLE A CORE 24X CORED INTERVAL 4270.3-4280.0 mbsl; 222.0-231.7 mbsf

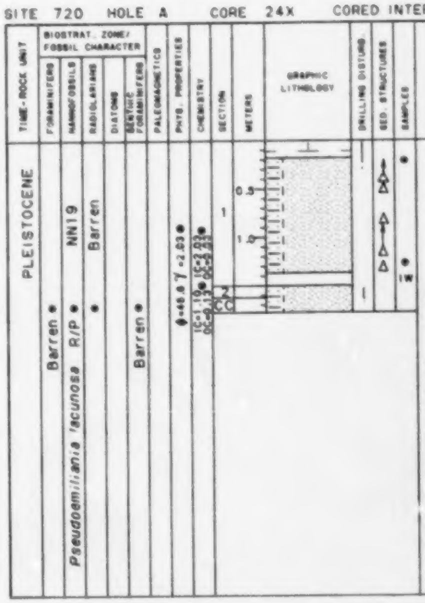
TIME-ROCK UNIT
BIOSTRAT. ZONE/ FOSSIL CHARACTER
FORAMINIFERS
NANNOFOSSILS
RADIOLARIANS
DIATOMS
BENTHIC FORAMINIFERS
PALEOMAGNETICS
PHYS. PROPERTIES
CHEMISTRY
SECTION
METERS
GRAPHIC LITHOLOGY
DRILLING DISTURB.
SED. STRUCTURES
SAMPLES
PLEISTOCENE
Barren
Pseudoemiliania lacunosa R/P
NN19
Barren
Barren
ϕ=48.0 γ=2.03
IC=1.10 OC=0.13
IC=2.93
1
2
CC
0.5
1.0
IW

LITHOLOGIC DESCRIPTION

SAND and MUD

Section 1, 0-18 cm, and Section 2 are highly disturbed. Remainder of the core is undisturbed.

Major lithology: Interbedded SAND and MUD, very dark gray (5Y 3/1), form upward-fining sequences with sharp bases and gradational tops. SAND layers are 10-30 cm thick and MUD layers are 1-10 cm thick. SAND is micaceous.

Minor lithology: Nannofossil ooze, dark gray (5Y 3/1) to dark greenish gray (5GY 4/1), highly disturbed. Section 1, 0-18 cm.

SMEAR SLIDE SUMMARY (%):

	20 D	134 D
TEXTURE:		
Silt	40	60
Clay	60	40
COMPOSITION:		
Access. minerals	2	2
Clay	60	40
Feldspar	2	3
Foraminifers	Tr	—
Volcanic glass	4	5
Inorganic calcite	5	10
Mica	2	5
Nannofossils	Tr	—
Quartz	25	35

CORE 117–720A–25X NO RECOVERY

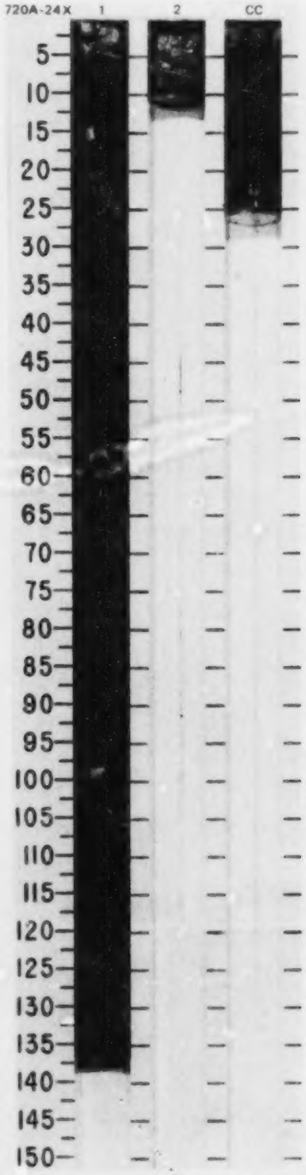
720A-24X
1
2
CC
5
10
15
20
25
30
35
40
45
50
55
60
65
70
75
80
85
90
95
100
105
110
115
120
125
130
135
140
145
150

SITE 720 HOLE A CORE 26X CORED INTERVAL 4289.7-4299.3 mbsl; 241.4-251.0 mbsf

TIME-ROCK UNIT	BIOSTRAT. ZONE/ FOSSIL CHARACTER					PALEOMAGNETICS	PHYS. PROPERTIES	CHEMISTRY	SECTION	METERS	GRAPHIC LITHOLOGY	DRILLING DISTURB.	SED. STRUCTURES	SAMPLES
	FORAMINIFERS	NANNOFOSSILS	RADIOLARIANS	DIATOMS	BENTHIC FORAMINIFERS									
PLEISTOCENE	●Barren	●Barren *Pseudoemiliania lacunosa* NN19	Barren		●Barren	C1R	ϕ=50.3 γ=1.97 ●	IC=1.87 OC=0.21 ●	1 CC	0.5	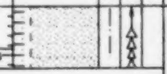			

LITHOLOGIC DESCRIPTION

SAND and MUD

Section 1, 0-12 cm, is highly disturbed. Remainder of the core is undisturbed.

Major lithology: Interbedded SAND and MUD, very dark gray (5Y 3/1), form upward-fining sequences with sharp bases and gradational tops. SAND layers are 10-20 cm thick and MUD layers are 1-10 cm thick. SAND is micaceous.

SITE 720 HOLE A CORE 27X CORED INTERVAL 4299.3-4308.8 mbsl; 251.0-260.5 mbsf

TIME-ROCK UNIT	BIOSTRAT. ZONE/ FOSSIL CHARACTER					PALEOMAGNETICS	PHYS. PROPERTIES	CHEMISTRY	SECTION	METERS	GRAPHIC LITHOLOGY	DRILLING DISTURB.	SED. STRUCTURES	SAMPLES
	FORAMINIFERS	NANNOFOSSILS	RADIOLARIANS	DIATOMS	BENTHIC FORAMINIFERS									
PLEISTOCENE	●Barren	●R/P *Pseudoemiliania lacunosa* NN19	● Barren		●Barren			IC=0.84 OC=0.29 ●	1 CC	0.5	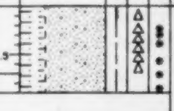			

LITHOLOGIC DESCRIPTION

SILTY SAND, SILT, and MUD

Entire core is slightly to moderately disturbed.

Major lithology: SILTY SAND, SILT, and MUD, very dark gray (5Y 3/1) to dark gray (5Y 4/2), form upward-fining sequences with sharp, sandy bases and gradational tops. SAND layers are 5-20 cm thick and MUD layers are 2-20 cm thick.

SMEAR SLIDE SUMMARY (%):

	1, 24 D	1, 29 D	1, 39 D	1, 57 D	CC, 1 D	CC, 19 D
TEXTURE:						
Sand	—	40	20	15	15	30
Silt	5	50	65	70	75	60
Clay	95	10	15	15	10	10
COMPOSITION:						
Access. minerals	—	5	—	—	—	5
Clay	30	—	—	—	—	—
Feldspar	10	10	15	10	15	10
Hornblende	—	—	—	Tr	Tr	—
Inorganic calcite	Tr	Tr	5	Tr	Tr	—
Mica	15	20	20	15	10	5
Quartz	45	65	60	75	75	80

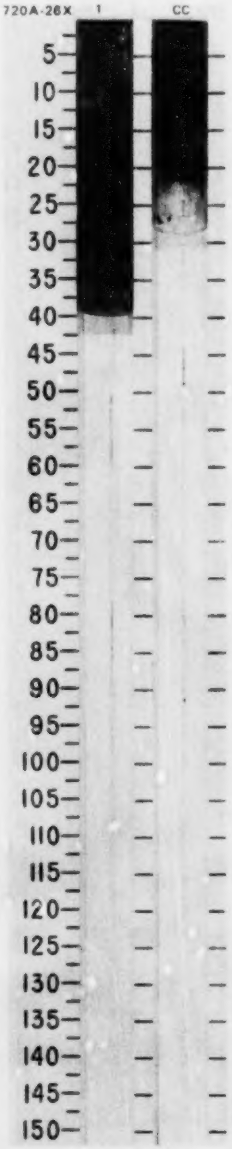
720A-26X
1
CC
5
10
15
20
25
30
35
40
45
50
55
60
65
70
75
80
85
90
95
100
105
110
115
120
125
130
135
140
145
150

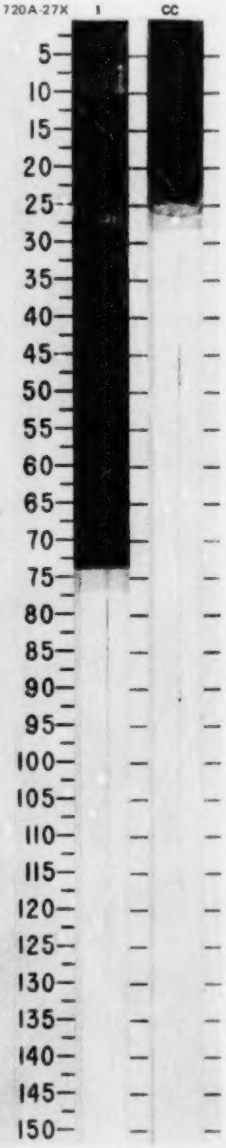
720A-27X
1
CC
5
10
15
20
25
30
35
40
45
50
55
60
65
70
75
80
85
90
95
100
105
110
115
120
125
130
135
140
145
150

SITE 720 HOLE A CORE 28X CORED INTERVAL 4308.8-4318.4 mbsl; 260.5-270.1 mbsf

TIME-ROCK UNIT	BIOSTRAT. ZONE/ FOSSIL CHARACTER					PALEOMAGNETICS	PHYS. PROPERTIES	CHEMISTRY	SECTION	METERS	GRAPHIC LITHOLOGY	DRILLING DISTURB.	SED. STRUCTURES	SAMPLES	LITHOLOGIC DESCRIPTION
	FORAMINIFERS	NANNOFOSSILS	RADIOLARIANS	DIATOMS	BENTHIC FORAMINIFERS										
PLEISTOCENE	Barren ●	*Pseudoemiliania lacunosa* NN19 R/P ●	Barren ●		R/P ●			IC=2.07 ● OC=1.44	1	0.5 1.0				●	SAND and MUD Section 1, 0-23 cm, is highly disturbed. Remainder of the core is moderately disturbed. Major lithology: Interbedded SAND and MUD, dark gray (5Y 4/1). SAND layers are 2-30 cm thick and MUD layers are 3-35 cm thick.

SMEAR SLIDE SUMMARY (%):

	1, 87 D
TEXTURE:	
Sand	40
Silt	50
Clay	10
COMPOSITION:	
Clay	5
Inorganic calcite	2
Mica	15
Nannofossils	1
Quartz	76
Rock fragments	1

SITE 720 HOLE A CORE 29X CORED INTERVAL 4318.4-4328.1 mbsl; 270.1-279.8 mbsf

TIME-ROCK UNIT	BIOSTRAT. ZONE/ FOSSIL CHARACTER					PALEOMAGNETICS	PHYS. PROPERTIES	CHEMISTRY	SECTION	METERS	GRAPHIC LITHOLOGY	DRILLING DISTURB.	SED. STRUCTURES	SAMPLES	LITHOLOGIC DESCRIPTION
	FORAMINIFERS	NANNOFOSSILS	RADIOLARIANS	DIATOMS	BENTHIC FORAMINIFERS										
PLEISTOCENE	N22 R/P ●	*Pseudoemiliania lacunosa* NN19 F/P ●	Barren ●		R/P ●				1 CC						MUD Entire core is moderately disturbed. Major lithology: MUD, dark olive gray (5Y 3/2), silty, with minor sand lenses.

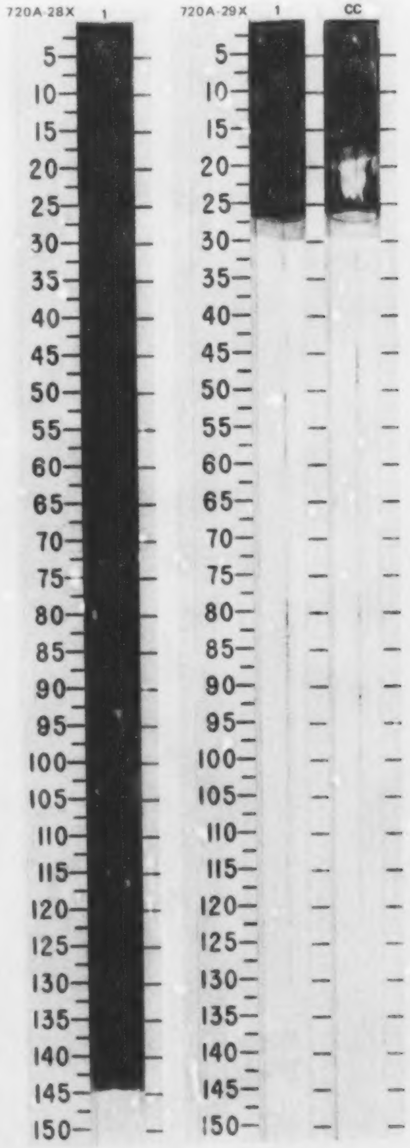

SITE 720 HOLE A CORE 30X CORED INTERVAL 4328.1-4337.7 mbsl; 279.8-289.4 mbsf

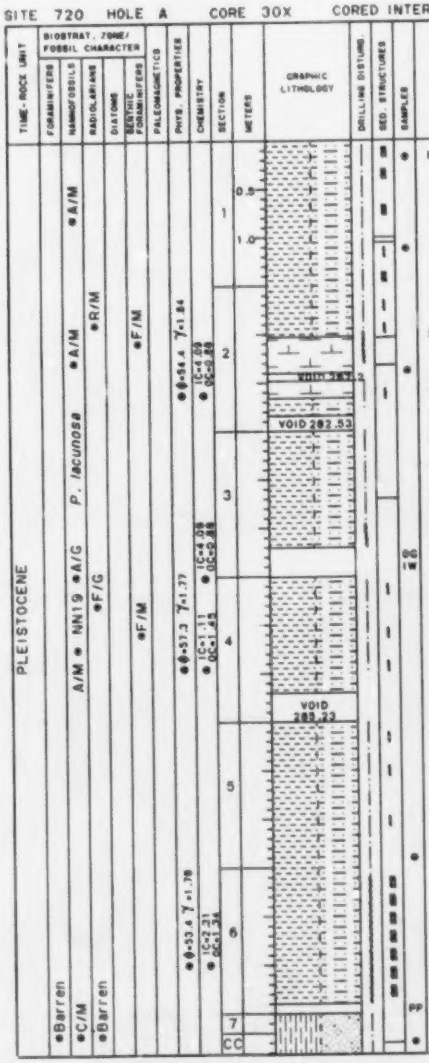
TIME-ROCK UNIT
BIOSTRAT. ZONE/ FOSSIL CHARACTER
FORAMINIFERS
NANNOFOSSILS
RADIOLARIANS
DIATOMS
BENTHIC FORAMINIFERS
PALEOMAGNETICS
PHYS. PROPERTIES
CHEMISTRY
SECTION
METERS
GRAPHIC LITHOLOGY
DRILLING DISTURB.
SED. STRUCTURES
SAMPLES
PLEISTOCENE
●Barren
●C/M
A/M ● NN19 ●A/G
P. lacunosa
●A/M
●A/M
●Barren
●F/G
●R/M
●F/M
●F/M
●ϕ=54.4 γ=1.84
●ϕ=57.3 γ=1.77
●ϕ=53.4 γ=1.78
● IC=4.69 OC=0.89
● IC=4.08 OC=0.88
● IC=1.11 OC=1.45
● IC=2.31 OC=1.34
1
2
3
4
5
6
7
CC
0.5
1.0
VOID 282.2
VOID 282.53
VOID 285.23
OG
IW
PP

LITHOLOGIC DESCRIPTION

MUD and CLAY

Entire core is moderately to highly disturbed.

Major lithology: MUD and CLAY, olive gray (10Y 4/2), dark olive gray (5Y 3/2), dark greenish gray (5GY 4/1), and greenish gray (5GY 5/1), in alternating color bands 20-30 cm thick. Bioturbated and mottled throughout.

Minor lithologies:
a. Nannofossil ooze, gray (10Y 6/1) and bioturbated. Section 2, 56-115 cm.
b. Silty clay and sandy silt, dark gray (5Y 4/1) and gray (5Y 5/1), respectively, interbedded on a scale of 5-10 cm. Sandy silt is micaceous. Section 7 to CC.

SMEAR SLIDE SUMMARY (%):

	1, 18 D	1, 113 M	2, 90 D	3, 75 M	5, 140 D	CC, 10 M
TEXTURE:						
Sand	—	5	—	—	—	5
Silt	40	40	10	5	20	75
Clay	60	55	90	90	80	20
COMPOSITION:						
Access. minerals	5	—	—	—	—	—
Clay	55	30	5	50	85	10
Feldspar	—	5	—	—	—	10
Foraminifers	—	Tr	—	—	—	—
Inorganic calcite	30	35	30	20	—	30
Mica	—	5	5	—	—	10
Nannofossils	5	5	50	10	5	—
Quartz	—	20	10	15	10	40
Radiolarians	5	—	—	5	—	—

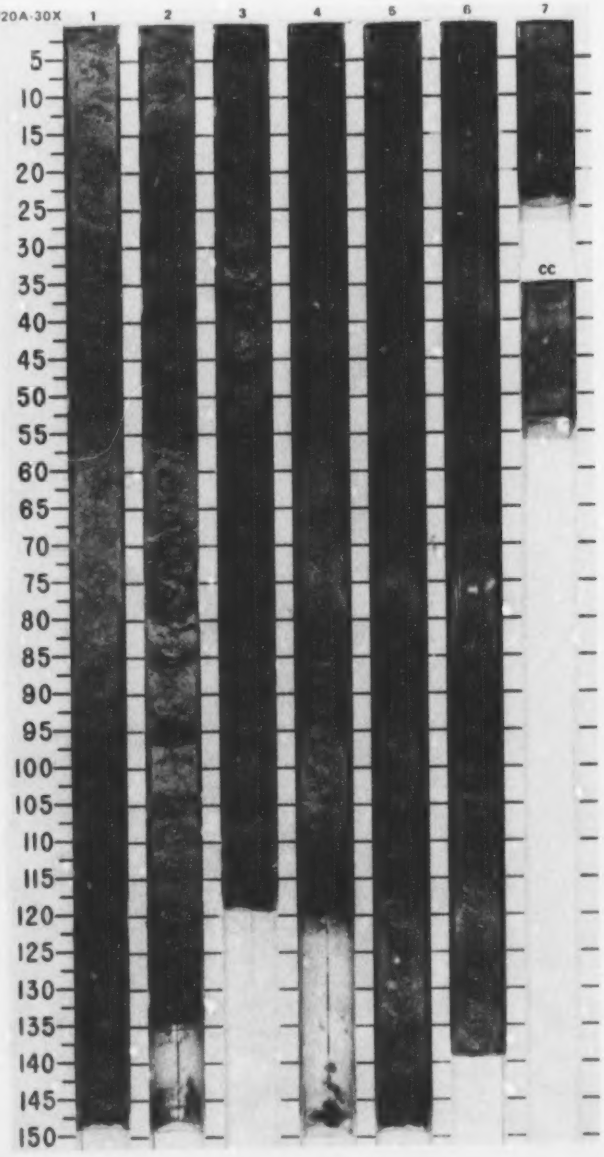
720A-30X
1
2
3
4
5
6
7
CC
5
10
15
20
25
30
35
40
45
50
55
60
65
70
75
80
85
90
95
100
105
110
115
120
125
130
135
140
145
150

SITE 720 HOLE A CORE 31X CORED INTERVAL 4337.7-4347.3 mbsl; 289.4-299.0 mbsf

TIME-ROCK UNIT	BIOSTRAT. ZONE/ FOSSIL CHARACTER					PALEOMAGNETICS	PHYS. PROPERTIES	CHEMISTRY	SECTION	METERS	GRAPHIC LITHOLOGY	DRILLING DISTURB.	SED. STRUCTURES	SAMPLES
	FORAMINIFERS	NANNOFOSSILS	RADIOLARIANS	DIATOMS	BENTHIC FORAMINIFERS									
PLEISTOCENE	*Pseudoemiliania lacunosa* ●Barren	NN19 ●R/M-P	Barren ●		●R/P				1 CC	0.5	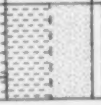		Δ	● ●●

LITHOLOGIC DESCRIPTION

SAND and CLAY

Entire core is slightly disturbed.

Major lithology: SAND and CLAY, very dark gray (5Y 3/1) and dark gray (5Y 4/1), respectively. Interbedded to form upward-fining intervals of 10-20 cm, with sharp-based sand layers and gradational transition to clay layers.

SMEAR SLIDE SUMMARY (%):

	4 D	26 D	13 M
TEXTURE:			
Sand	5	—	25
Silt	85	5	55
Clay	10	95	20
COMPOSITION:			
Clay	5	9	5
20			
Feldspar	10	—	15
Inorganic calcite	20	—	
Quartz	60	5	40

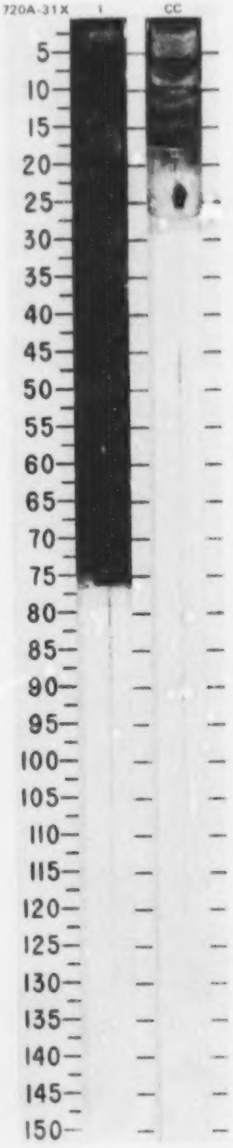
720A-31X
1
CC
5
10
15
20
25
30
35
40
45
50
55
60
65
70
75
80
85
90
95
100
105
110
115
120
125
130
135
140
145
150

SITE 720 HOLE A CORE 32X CORED INTERVAL 4347.3-4356.9 mbsl; 299.0-308.6 mbsf

TIME-ROCK UNIT	BIOSTRAT. ZONE/ FOSSIL CHARACTER: FORAMINIFERS	NANNOFOSSILS	RADIOLARIANS	DIATOMS	BENTHIC FORAMINIFERS	PALEOMAGNETICS	PHYS. PROPERTIES	CHEMISTRY	SECTION	METERS
PLEISTOCENE	●Barren	*P. lacunosa* NN19 ●R/M-P	Barren ●		●R/M		ϕ=50.4 γ=1.89 ●	IC=1.34 OC=0.38 ●	1 2 CC	0.5 1.0

LITHOLOGIC DESCRIPTION

SILT and MUD

Section 1, 0-21 cm, and Section 2, 108-128 cm, highly disturbed. Remainder of core is slightly to moderately disturbed.

Major lithology: SILT and MUD, dark gray (5Y 4/1) to gray (5Y 5/1), with locally abundant bioturbation and mottling. Also contains five zones, each 1-3 cm thick, of black (5Y 2.5/1) detrital carbonate-bearing silt.

SMEAR SLIDE SUMMARY (%):

	1, 77 M	1, 111 D	2, 37 D
TEXTURE:			
Sand	5	—	20
Silt	60	15	70
Clay	35	85	10
COMPOSITION:			
Clay	20	85	—
Feldspar	5	3	20
Inorganic calcite	25	Tr	20
Mica	10	2	5
Organic debris	—	—	Tr
Plant debris	10	—	—
Quartz	30	10	55
Siliceous frag.	—	Tr	—

SITE 720 HOLE A CORE 33X CORED INTERVAL 4356.9-4366.5 mbsl; 308.6-318.2 mbsf

TIME-ROCK UNIT	BIOSTRAT. ZONE/ FOSSIL CHARACTER: FORAMINIFERS	NANNOFOSSILS	RADIOLARIANS	DIATOMS	BENTHIC FORAMINIFERS	PALEOMAGNETICS	PHYS. PROPERTIES	CHEMISTRY	SECTION	METERS
PLEISTOCENE	Barren●	*P. lacunosa* NN19 R/M-P●	Barren ●		Barren●			IC=1.60 OC=0.15 ●	1	

LITHOLOGIC DESCRIPTION

MUD and SILT

Entire core is moderately to highly disturbed.

Major lithology: Interbedded MUD and SILT, very dark gray (5Y 3/1), with micaceous silt layers at 10-12, 16-18, and 26-34 cm.

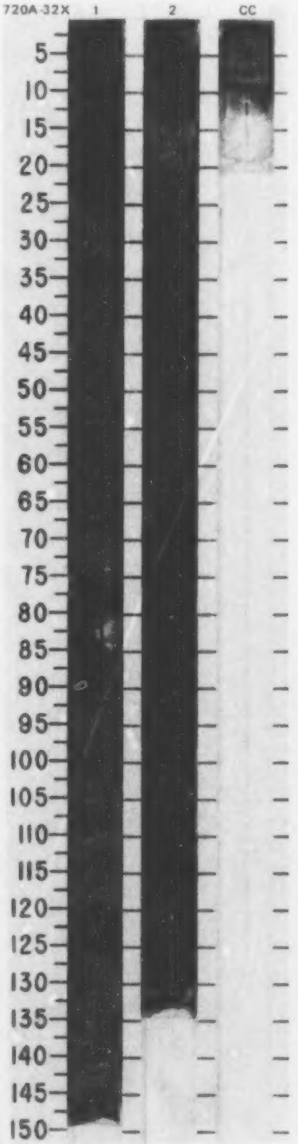
720A-32X
1
2
CC
5
10
15
20
25
30
35
40
45
50
55
60
65
70
75
80
85
90
95
100
105
110
115
120
125
130
135
140
145
150

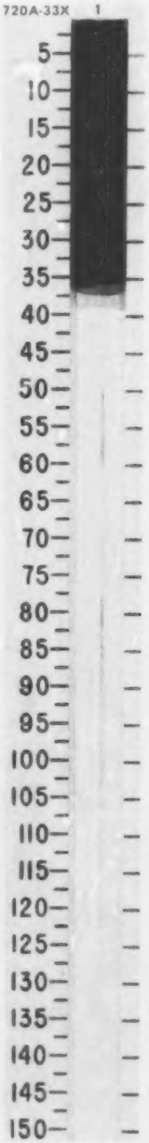
720A-33X
1
5
10
15
20
25
30
35
40
45
50
55
60
65
70
75
80
85
90
95
100
105
110
115
120
125
130
135
140
145
150

CORE 117–720A–34X NO RECOVERY

CORE 117–720A–35X NO RECOVERY

SITE 720 HOLE A CORE 36X CORED INTERVAL 4385.7-4395.3 mbsl; 337.4-347.0 mbsf

TIME-ROCK UNIT	BIOSTRAT. ZONE/ FOSSIL CHARACTER					PALEOMAGNETICS	PHYS. PROPERTIES	CHEMISTRY	SECTION	METERS	GRAPHIC LITHOLOGY	DRILLING DISTURB.	SED. STRUCTURES	SAMPLES
	FORAMINIFERS	NANNOFOSSILS	RADIOLARIANS	DIATOMS	BENTHIC FORAMINIFERS									
PLEISTOCENE	N22 ●R/P	*Pseudoemiliania lacunosa* NN19 ●R/G	Barren ●		●R/M		ϕ=52.1 γ=1.88 ●	IC=1.62 OC=0.27 ●	1 CC	0.5	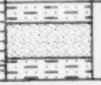			● ●

LITHOLOGIC DESCRIPTION

MUD and SAND

Section 1, 0-9 cm, is highly disturbed. Remainder of the core is slightly disturbed to undisturbed.

Major lithology: Interbedded MUD and SILT, very dark gray (5Y 3/1), with sharp-based sand at 22-59 cm, grading up to overlying mud.

SMEAR SLIDE SUMMARY (%):

	1, 17 D	54 D
TEXTURE:		
Sand	—	80
Silt	40	20
Clay	60	—
COMPOSITION:		
Access. minerals	Tr	3
Clay	60	—
Dolomite	Tr	—
Feldspar	3	10
Volcanic glass	2	5
Inorganic calcite	10	5
Mica	—	2
Nannofossils	Tr	—
Quartz	25	75

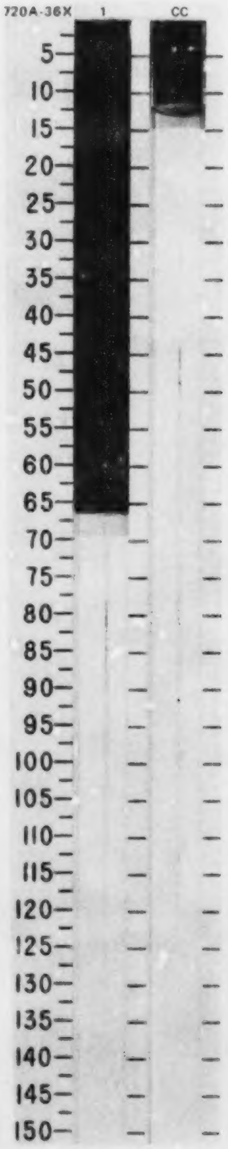

SITE 720 HOLE A CORE 37X CORED INTERVAL 4395.3-4404.9 mbsl; 347.0-356.6 mbsf

TIME-ROCK UNIT	BIOSTRAT. ZONE/ FOSSIL CHARACTER					PALEOMAGNETICS	PHYS. PROPERTIES	CHEMISTRY	SECTION	METERS	GRAPHIC LITHOLOGY	DRILLING DISTURB.	SED. STRUCTURES	SAMPLES
	FORAMINIFERS	NANNOFOSSILS	RADIOLARIANS	DIATOMS	BENTHIC FORAMINIFERS									
PLEISTOCENE	Barren ●	*P. lacunosa* NN19 R/M ●	Barren ●		Barren ●		ϕ=48.3 γ=1.94 ●	IC=1.62 OC=0.28 ●	1 CC	0.5				

LITHOLOGIC DESCRIPTION

MUD and SAND

Entire core slightly to moderately disturbed.

Major lithology: Interbedded MUD and SAND, very dark gray (5Y 3/1), form upward-fining sequences on a scale of 10-20 cm. Sharp-based micaceous sand grades into overlying uniform mud.

SITE 720 HOLE A CORE 38X CORED INTERVAL 4404.9-4414.5 mbsl; 356.6-366.2 mbsf

TIME-ROCK UNIT	BIOSTRAT. ZONE/ FOSSIL CHARACTER					PALEOMAGNETICS	PHYS. PROPERTIES	CHEMISTRY	SECTION	METERS	GRAPHIC LITHOLOGY	DRILLING DISTURB.	SED. STRUCTURES	SAMPLES
	FORAMINIFERS	NANNOFOSSILS	RADIOLARIANS	DIATOMS	BENTHIC FORAMINIFERS									
PLEISTOCENE	Barren ●	*P. lacunosa* NN19 R/M ●	Barren ●		Barren ●				CC				Δ	

LITHOLOGIC DESCRIPTION

MUD and SAND

Entire core is moderately disturbed.

Major lithology: Interbedded MUD and SAND, very dark gray (5Y 3/1), forms one upward-fining sequence, with sharp-based micaceous sand grading into overlying uniform mud.

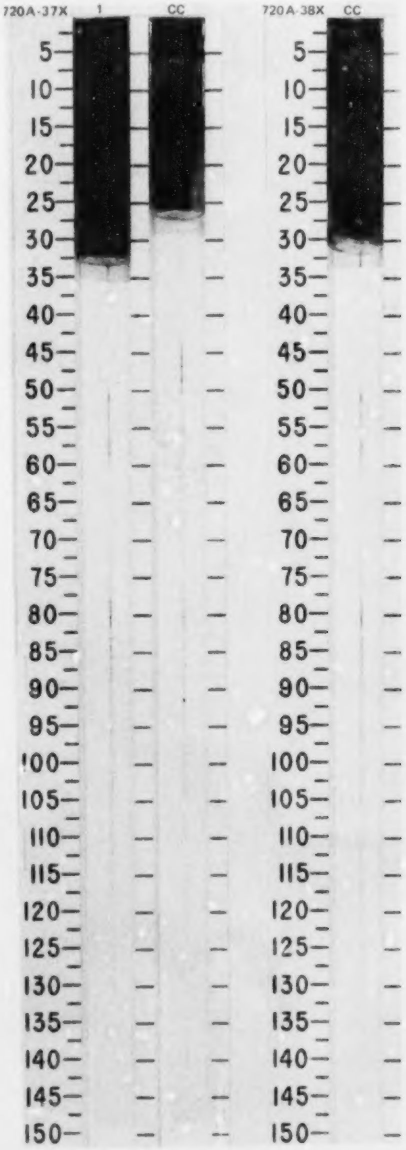

SITE 720 HOLE A CORE 39X CORED INTERVAL 4414.5-4424.2 mbsl; 366.2-375.9 mbsf

TIME-ROCK UNIT	BIOSTRAT. ZONE/ FOSSIL CHARACTER FORAMINIFERS	NANNOFOSSILS	RADIOLARIANS	DIATOMS	BENTHIC FORAMINIFERS	PALEOMAGNETICS	PHYS. PROPERTIES	CHEMISTRY	SECTION	METERS	GRAPHIC LITHOLOGY	DRILLING DISTURB.	SED. STRUCTURES	SAMPLES
PLEISTOCENE	N22 R/P●	*Pseudoemiliania lacunosa* NN19 A/M●	Barren ●		R/P●		ϕ=48.4 γ=1.89 ●	IC=8.06 OC=0.54 ●	1 CC	0.5	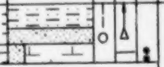			●●

LITHOLOGIC DESCRIPTION

MUD and SAND

Section 1 is slightly deformed. CC is undeformed.

Major lithology: Interbedded MUD and SAND, very dark gray (5Y 3/1). Forms one upward-fining sequence, with sharp-based micaceous sand grading into overlying uniform mud.

Minor lithology: Calcareous silty clay to clayey foraminiferal ooze, very dark gray (5Y 3/1) to olive gray (5Y 5/2). Overconsolidated zone. CC, 8-18 cm.

SMEAR SLIDE SUMMARY (%):

	CC, 9 M	CC, 15 D
TEXTURE:		
Sand	5	5
Silt	25	10
Clay	70	85
COMPOSITION:		
Access. minerals	3	1
Clay	60	20
Feldspar	2	—
Foraminifers	Tr	3
Volcanic glass	3	2
Inorganic calcite	10	10
Mica	2	2
Nannofossils	10	60
Quartz	10	2

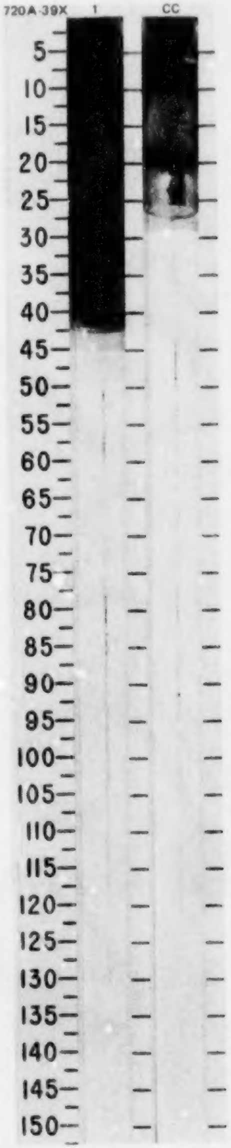

SITE 720 HOLE A CORE 40X CORED INTERVAL 4424.2-4433.5 mbsl; 375.9-385.2 mbsf

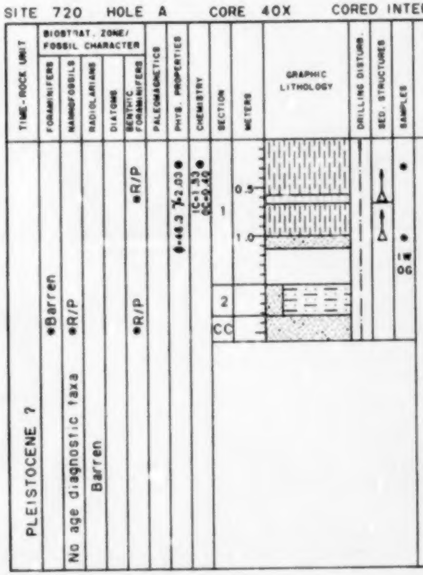
TIME-ROCK UNIT
BIOSTRAT. ZONE/ FOSSIL CHARACTER
FORAMINIFERS
NANNOFOSSILS
RADIOLARIANS
DIATOMS
BENTHIC FORAMINIFERS
PALEOMAGNETICS
PHYS. PROPERTIES
CHEMISTRY
SECTION
METERS
GRAPHIC LITHOLOGY
DRILLING DISTURB.
SED. STRUCTURES
SAMPLES
PLEISTOCENE ?
●Barren
No age diagnostic taxa ●R/P
Barren
●R/P
●R/P
ϕ=48.3 γ=2.03 ●
IC=1.53 OC=0.40 ●
1
2
CC
0.5
1.0
IW
OG

LITHOLOGIC DESCRIPTION

MUD and SAND

Section 1, 0-10 cm, is highly disturbed. Remainder of core is undisturbed.

Major lithology: Interbedded MUD and SAND, very dark gray (5Y 3/1), form upward-fining sequences with sharp-based micaceous sand grading into overlying uniform mud.

Minor lithology: Sandy mud to muddy sand, black (10YR 2/1). Section 1, 58-64 cm.

SMEAR SLIDE SUMMARY (%):

	1, 29 D	1, 102 D
TEXTURE:		
Sand	—	25
Silt	20	50
Clay	80	25
COMPOSITION:		
Access. minerals	3	5
Clay	80	25
Feldspar	2	5
Volcanic glass	Tr	10
Inorganic calcite	10	10
Mica	Tr	Tr
Nannofossils	—	Tr
Quartz	5	45

SITE 720 HOLE A CORE 41X CORED INTERVAL 4433.5-4443.2 mbsl; 385.2-394.9 mbsf

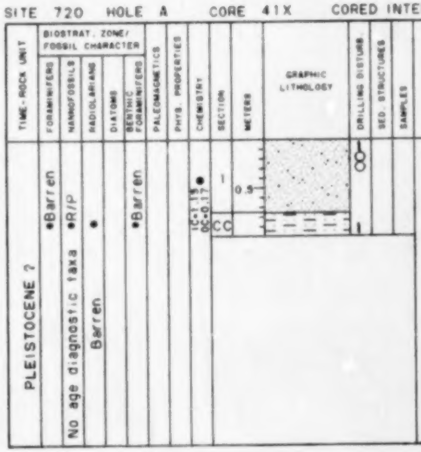
TIME-ROCK UNIT
BIOSTRAT. ZONE/ FOSSIL CHARACTER
FORAMINIFERS
NANNOFOSSILS
RADIOLARIANS
DIATOMS
BENTHIC FORAMINIFERS
PALEOMAGNETICS
PHYS. PROPERTIES
CHEMISTRY
SECTION
METERS
GRAPHIC LITHOLOGY
DRILLING DISTURB.
SED. STRUCTURES
SAMPLES
PLEISTOCENE ?
●Barren
No age diagnostic taxa ●R/P
Barren ●
●Barren
IC=1.15 OC=0.17 ●
1
CC
0.5

LITHOLOGIC DESCRIPTION

SILTY SAND and MUD

Section 1, 0-34 cm, is highly disturbed. Remainder of the core is undisturbed.

Major lithologies:
a. SILTY SAND, dark olive gray (5Y 3/2), structureless. Section 1.
b. MUD, very dark gray (5Y 3/1), uniform. CC.

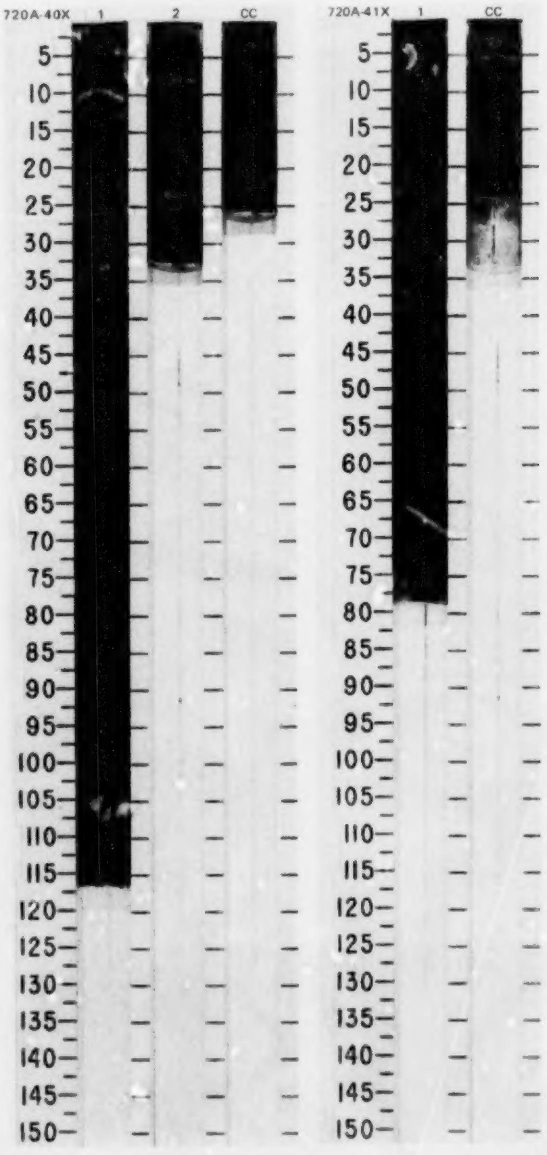
720A-40X
1
2
CC
720A-41X
1
CC
5
10
15
20
25
30
35
40
45
50
55
60
65
70
75
80
85
90
95
100
105
110
115
120
125
130
135
140
145
150

SITE 720 HOLE A CORE 42X CORED INTERVAL 4443.2-4452.9 mbsl; 394.9-404.6 mbsf

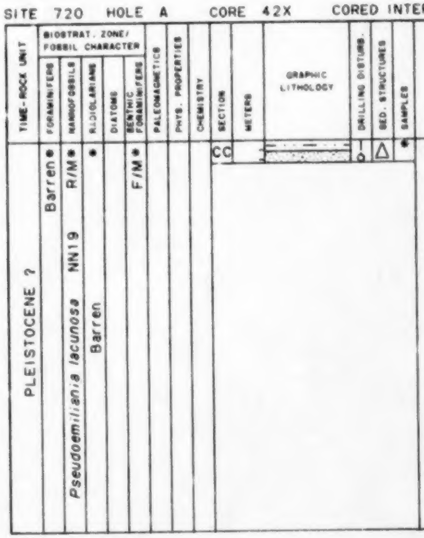
TIME-ROCK UNIT
BIOSTRAT. ZONE/ FOSSIL CHARACTER
FORAMINIFERS
NANNOFOSSILS
RADIOLARIANS
DIATOMS
BENTHIC FORAMINIFERS
PALEOMAGNETICS
PHYS. PROPERTIES
CHEMISTRY
SECTION
METERS
GRAPHIC LITHOLOGY
DRILLING DISTURB.
SED. STRUCTURES
SAMPLES
PLEISTOCENE ?
Barren ●
Pseudoemiliania lacunosa NN19 R/M ●
● Barren
F/M ●
CC

LITHOLOGIC DESCRIPTION

MUD and SANDY SILT

Entire core is moderately to highly disturbed.

Major lithology: Interbedded MUD and SANDY SILT, very dark gray (5Y 3/1), form one upward-fining sequence 24 cm thick, with sharp-based micaceous sandy silt grading into overlying uniform mud.

SMEAR SLIDE SUMMARY (%):

	CC, 4 D
TEXTURE:	
Silt	40
Clay	60
COMPOSITION:	
Access. minerals	3
Clay	60
Feldspar	2
Inorganic calcite	15
Mica	Tr
Quartz	20

SITE 720 HOLE A CORE 43X CORED INTERVAL 4452.9-4462.6 mbsl; 404.6-414.3 mbsf

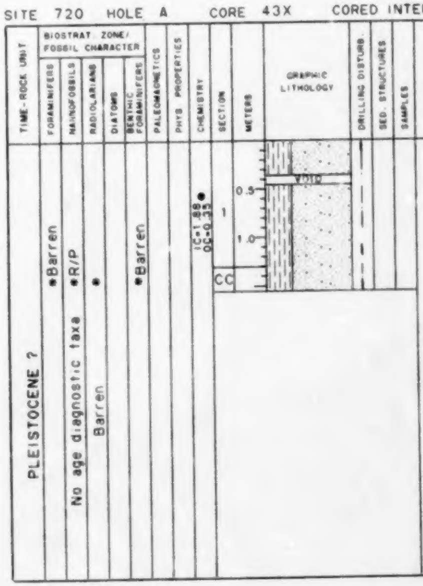
TIME-ROCK UNIT
BIOSTRAT. ZONE/ FOSSIL CHARACTER
FORAMINIFERS
NANNOFOSSILS
RADIOLARIANS
DIATOMS
BENTHIC FORAMINIFERS
PALEOMAGNETICS
PHYS. PROPERTIES
CHEMISTRY
SECTION
METERS
GRAPHIC LITHOLOGY
DRILLING DISTURB.
SED. STRUCTURES
SAMPLES
PLEISTOCENE ?
●Barren
No age diagnostic taxa ●R/P
● Barren
●Barren
IC=1.88 ●
OC=0.35
1
CC
0.5
1.0
VOID

LITHOLOGIC DESCRIPTION

MUD and SANDY SILT

Entire core is moderately to highly disturbed.

Major lithology: Interbedded MUD, dark gray (5Y 4/1) and homogeneous, and sandy silt, olive gray (5Y 4/2).

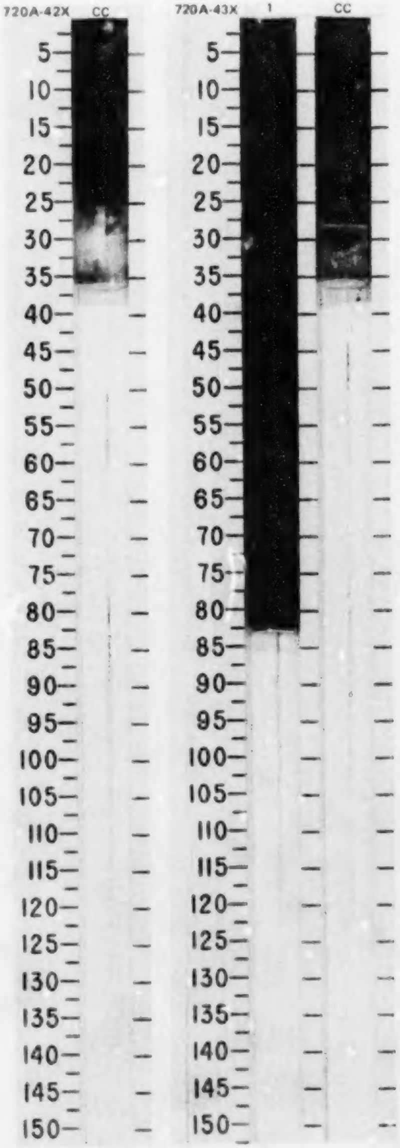
720A-42X
CC
720A-43X
1
CC
5
10
15
20
25
30
35
40
45
50
55
60
65
70
75
80
85
90
95
100
105
110
115
120
125
130
135
140
145
150

SITE 721 HOLE A CORE 1H CORED INTERVAL 1944.8-1954.6 mbsl; 0.0-9.8 mbsf

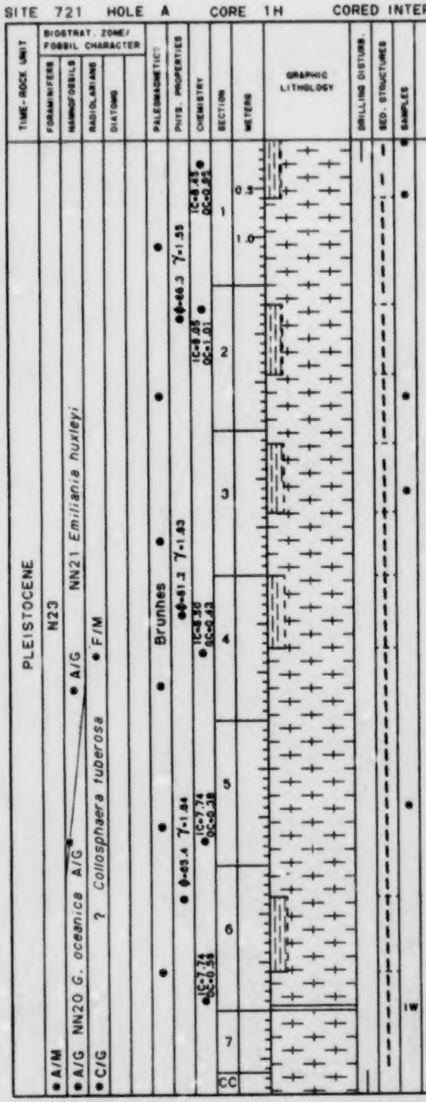
TIME-ROCK UNIT
BIOSTRAT. ZONE/ FOSSIL CHARACTER
FORAMINIFERS
NANNOFOSSILS
RADIOLARIANS
DIATOMS
PALEOMAGNETICS
PHYS. PROPERTIES
CHEMISTRY
SECTION
METERS
GRAPHIC LITHOLOGY
DRILLING DISTURB.
SED. STRUCTURES
SAMPLES
PLEISTOCENE
N23
• A/M
NN20 G. oceanica A/G
• A/G
NN21 Emiliania huxleyi
• A/G
? Collosphaera tuberosa
• C/G
• F/M
Brunhes
•Φ=66.3 γ=1.55
•Φ=61.2 γ=1.83
• Φ=65.4 γ=1.84
IC=8.45 OC=0.85
IC=8.05 OC=1.01
IC=8.30 OC=0.43
IC=7.74 OC=0.38
IC=7.74 OC=0.58
1
2
3
4
5
6
7
CC
0.5
1.0
IW

LITHOLOGIC DESCRIPTION

FORAMINIFER-NANNOFOSSIL OOZE

Section 1, 0-8 cm, is slightly disturbed. Remainder of core is undisturbed.

Major lithology: FORAMINIFER-NANNOFOSSIL OOZE. Alternating light and dark bands, light greenish gray (10Y 5/2, 6/2) to olive (5Y 4/3, 4/4). Slight to moderate burrow-mottling throughout. Dark layers contain 10-20% more terrigenous clay than do light layers.

SMEAR SLIDE SUMMARY (%):

	1, 1 D	1, 58 M	2, 115 D	3, 62 M	5, 98 D
TEXTURE:					
Sand	—	10	—	—	—
Silt	25	20	10	25	10
Clay	75	70	90	75	90
COMPOSITION:					
Access. minerals	Tr	5	—	—	Tr
Clay	15	—	25	20	10
Dolomite	Tr	—	—	Tr	Tr
Foraminifers	15	10	5	20	5
Volcanic glass	—	Tr	—	—	—
Inorganic calcite	5	10	—	5	5
Mica	Tr	—	—	—	—
Nannofossils	65	70	65	50	80
Quartz	Tr	5	5	5	Tr
Radiolarians	—	—	Tr	—	—
Sponge spicules	Tr	—	—	—	—

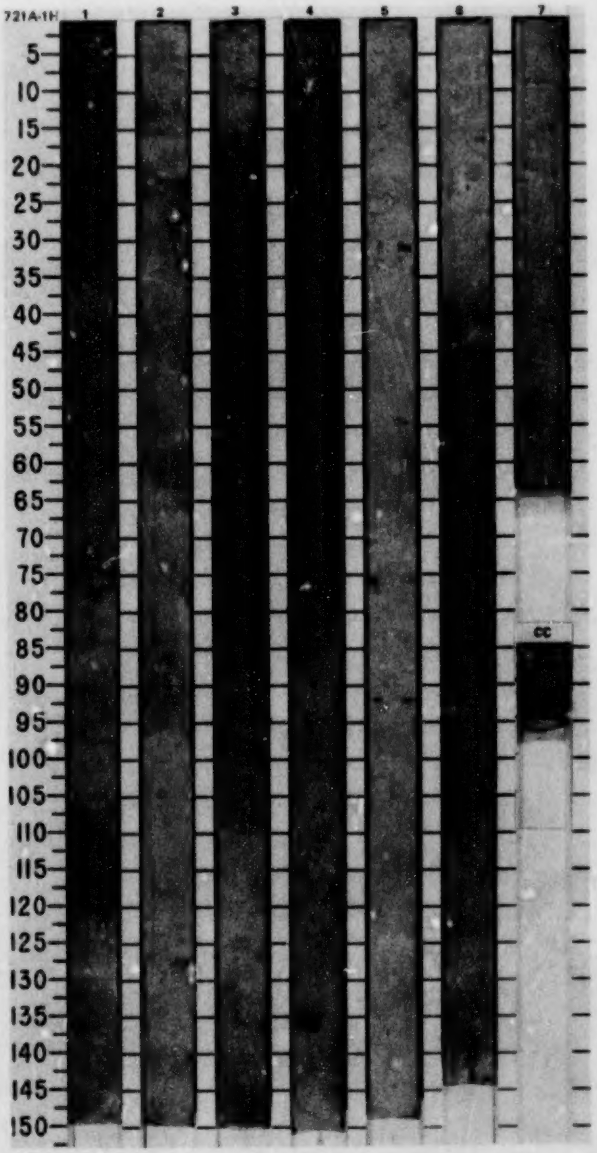
721A-1H
1
2
3
4
5
6
7
CC
5
10
15
20
25
30
35
40
45
50
55
60
65
70
75
80
85
90
95
100
105
110
115
120
125
130
135
140
145
150

SITE 721 HOLE A CORE 2H CORED INTERVAL 1954.6-1964.3 mbsl; 9.8-19.5 mbsf

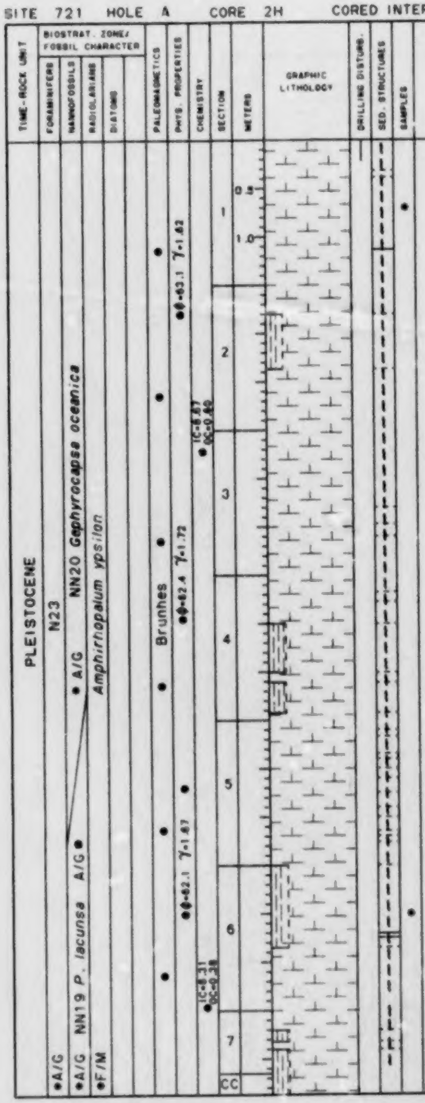
TIME-ROCK UNIT
BIOSTRAT. ZONE/ FOSSIL CHARACTER
FORAMINIFERS
NANNOFOSSILS
RADIOLARIANS
DIATOMS
PALEOMAGNETICS
PHYS. PROPERTIES
CHEMISTRY
SECTION
METERS
GRAPHIC LITHOLOGY
DRILLING DISTURB.
SED. STRUCTURES
SAMPLES
PLEISTOCENE
N23
●A/G
NN20 Gephyrocapsa oceanica
● A/G
NN19 P. lacunsa A/G●
●A/G
Amphirhopalum ypsilon
●F/M
Brunhes
●Φ=63.1 γ=1.82
●Φ=62.4 γ=1.72
●Φ=62.1 γ=1.87
IC=8.87 OC=0.80
IC=8.31 OC=0.38
1
2
3
4
5
6
7
CC
0.5
1.0

LITHOLOGIC DESCRIPTION

NANNOFOSSIL OOZE

Section 1, 5-15 cm, is slightly disturbed. Remainder of core is undisturbed.

Major lithology: NANNOFOSSIL OOZE. Alternating light and dark bands of light greenish gray (10Y 7/2, 6/2) to dark greenish gray (10Y 5/4, 5/2, 4/2) and olive (5Y 4/4). Slight to moderate burrow-mottling throughout. Dark layers contain 10-20% more terrigenous silty clay than do light layers.

SMEAR SLIDE SUMMARY (%):

	1, 70 D	6, 50 D
TEXTURE:		
Sand	—	5
Silt	20	15
Clay	80	80
COMPOSITION:		
Clay	10	5
Dolomite	—	Tr
Foraminifers	Tr	10
Inorganic calcite	5	10
Nannofossils	80	75
Quartz	5	Tr
Radiolarians	—	Tr

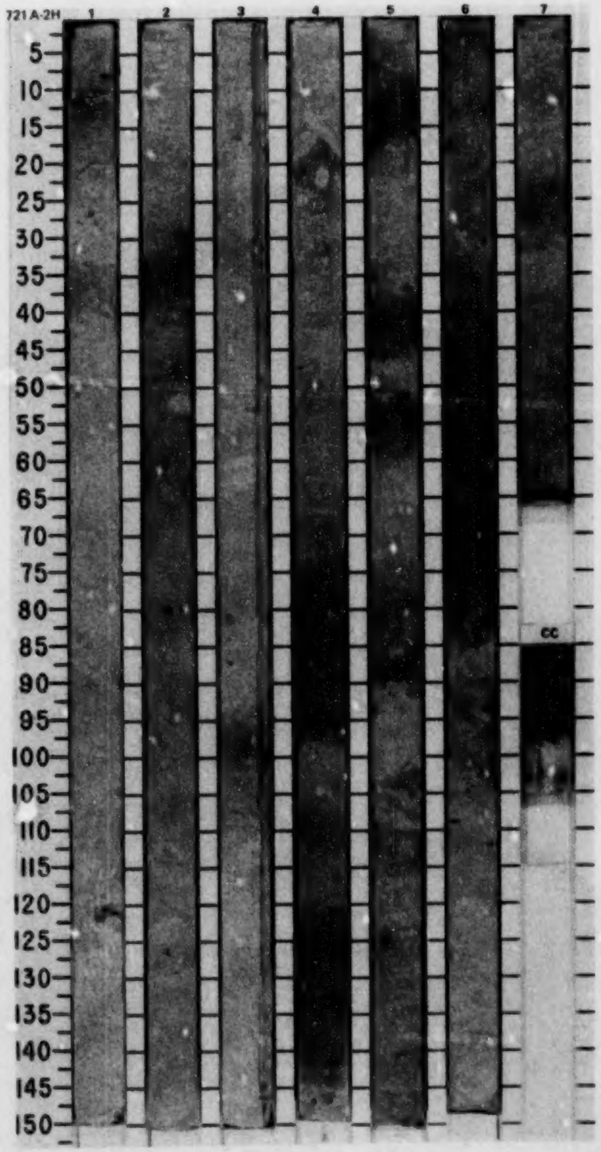
721A-2H
1
2
3
4
5
6
7
CC
5
10
15
20
25
30
35
40
45
50
55
60
65
70
75
80
85
90
95
100
105
110
115
120
125
130
135
140
145
150

SITE 721 HOLE A CORE 3H CORED INTERVAL 1964.3-1974.0 mbsl; 19.5-29.2 mbsf

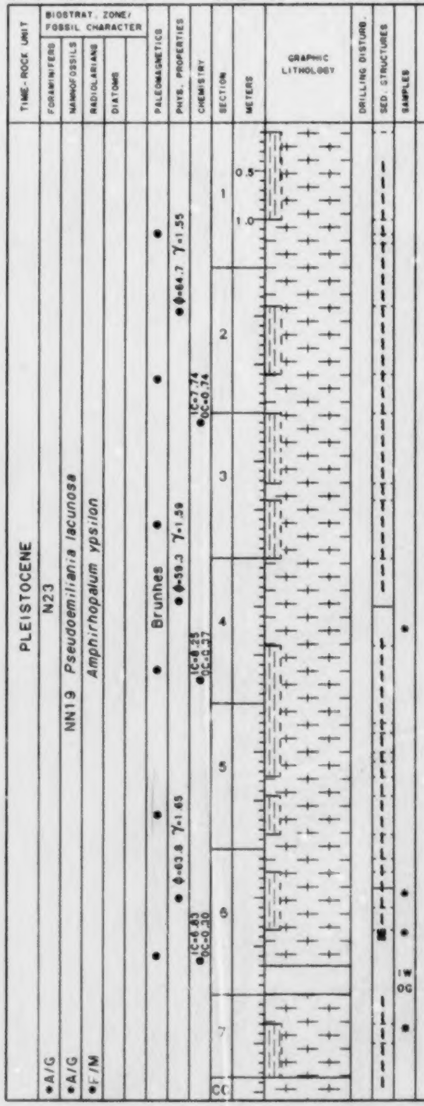
TIME-ROCK UNIT
BIOSTRAT. ZONE/ FOSSIL CHARACTER
FORAMINIFERS
NANNOFOSSILS
RADIOLARIANS
DIATOMS
PALEOMAGNETICS
PHYS. PROPERTIES
CHEMISTRY
SECTION
METERS
GRAPHIC LITHOLOGY
DRILLING DISTURB.
SED. STRUCTURES
SAMPLES
PLEISTOCENE
N23
NN19 Pseudoemiliania lacunosa
Amphirhopalum ypsilon
•A/G
•A/G
•F/M
Brunhes
•φ=64.7 γ=1.55
•φ=59.3 γ=1.59
•φ=63.8 γ=1.65
•IC=7.74 OC=0.74
•IC=8.25 OC=0.37
•IC=6.83 OC=0.30
0.5
1.0
1
2
3
4
5
6
7
CC
IW
OG

LITHOLOGIC DESCRIPTION

FORAMINIFER-NANNOFOSSIL OOZE

No drilling disturbance.

Major lithology: FORAMINIFER-NANNOFOSSIL OOZE. Alternating light and dark bands of light greenish gray (10Y 5/2, 6/2, 7/2) to olive gray (5Y 5/2) and olive (5Y 5/3). Slight to moderate burrow-mottling throughout. Dark layers contain 10-20% more terrigenous clay than do light layers.

SMEAR SLIDE SUMMARY (%):

	4, 72	6, 46	6, 88	7, 32
	72	46	88	32
	D	M	M	M
TEXTURE:				
Sand	—	—	—	5
Silt	25	5	40	30
Clay	75	95	60	65
COMPOSITION:				
Access. minerals	Tr	—	—	
Clay	10	20	10	10
Diatoms	—	—	Tr	—
Dolomite	Tr	—	—	Tr
Inorganic calcite	5	5	25	5
Mica	—	—	5	—
Nannofossils	70	80	50	50
Quartz	Tr	—	—	5
Radiolarians	—	—	—	Tr
Silicoflagellates	—	—	—	Tr
Sponge spicules	—	—	—	Tr

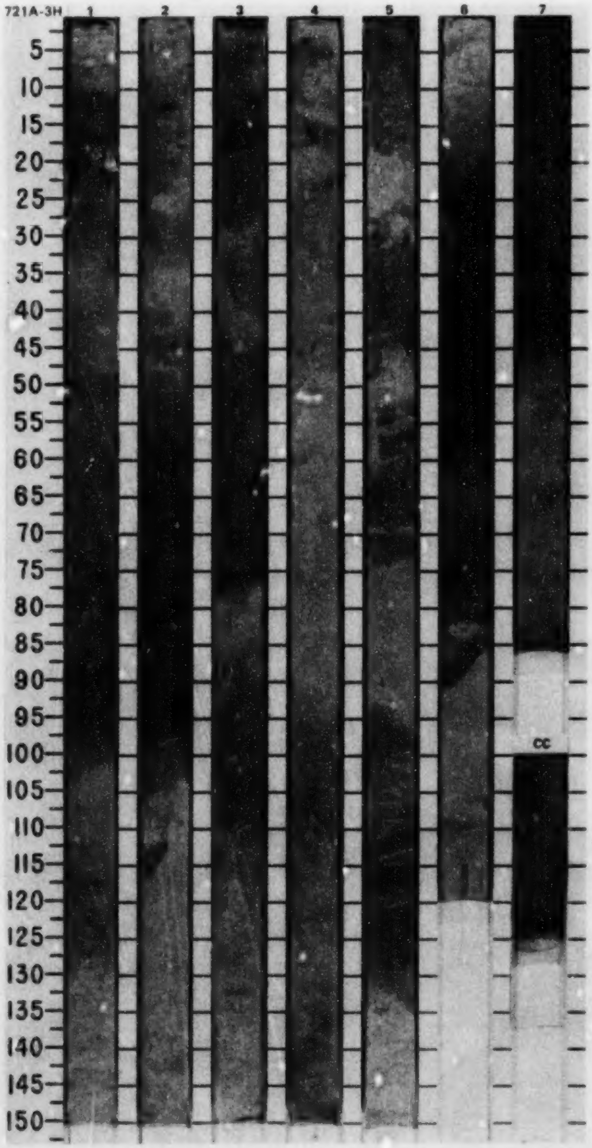
721A-3H
1
2
3
4
5
6
7
5
10
15
20
25
30
35
40
45
50
55
60
65
70
75
80
85
90
95
100
105
110
115
120
125
130
135
140
145
150
CC

SITE 721 HOLE A CORE 4H CORED INTERVAL 1974.0-1983.7 mbsl; 29.2-38.9 mbsf

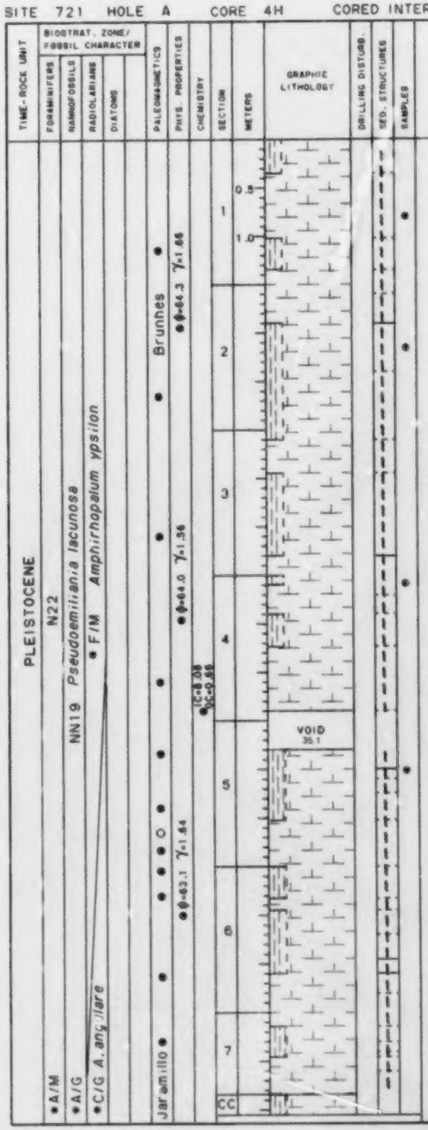
TIME-ROCK UNIT
BIOSTRAT. ZONE/ FOSSIL CHARACTER
FORAMINIFERS
NANNOFOSSILS
RADIOLARIANS
DIATOMS
PALEOMAGNETICS
PHYS. PROPERTIES
CHEMISTRY
SECTION
METERS
GRAPHIC LITHOLOGY
DRILLING DISTURB.
SED. STRUCTURES
SAMPLES
PLEISTOCENE
•A/M N22
•A/G NN19 Pseudoemiliania lacunosa
•C/G A. angulare
• F/M Amphirhopalum ypsilon
Brunhes
Jaramillo
• φ=64.3 γ=1.66
• φ=64.0 γ=1.56
• φ=63.1 γ=1.64
IC=8.08
OC=0.89
1
2
3
4
5
6
7
CC
0.5
1.0
VOID
35.1

LITHOLOGIC DESCRIPTION

NANNOFOSSIL OOZE

No drilling disturbance. Voids in Section 4, 143-150 cm, and Section 5, 0-30 cm.

Major lithology: NANNOFOSSIL OOZE. Alternating light and dark bands of light olive gray (5Y 6/2) to light greenish gray (10Y 5/2, 6/1) to pale olive (5Y 6/4) and olive (5Y 5/3, 5/4). Slight to moderate burrow-mottling throughout. Dark layers contain 10-20% more terrigenous clay than do light layers.

SMEAR SLIDE SUMMARY (%):

	1, 80 D	2, 66 D	4, 9 D	5, 52 D	5, 53 D
TEXTURE:					
Sand	—	—	—	—	5
Silt	5	20	10	20	20
Clay	95	80	90	75	80
COMPOSITION:					
Access. minerals	—	Tr	Tr	Tr	
Clay	20	5	12	35	27
Dolomite	3	5	—	5	3
Feldspar	—	—	1	—	—
Foraminifers	5	3	1	10	10
Inorganic calcite	10	10	5	15	10
Mica	—	—	—	Tr	Tr
Nannofossils	60	75	80	30	45
Pteropod	—	—	—	—	Tr
Quartz	2	2	1	5	5
Radiolarians	—	—	Tr	Tr	—
Sponge spicules	—	Tr	Tr	—	—

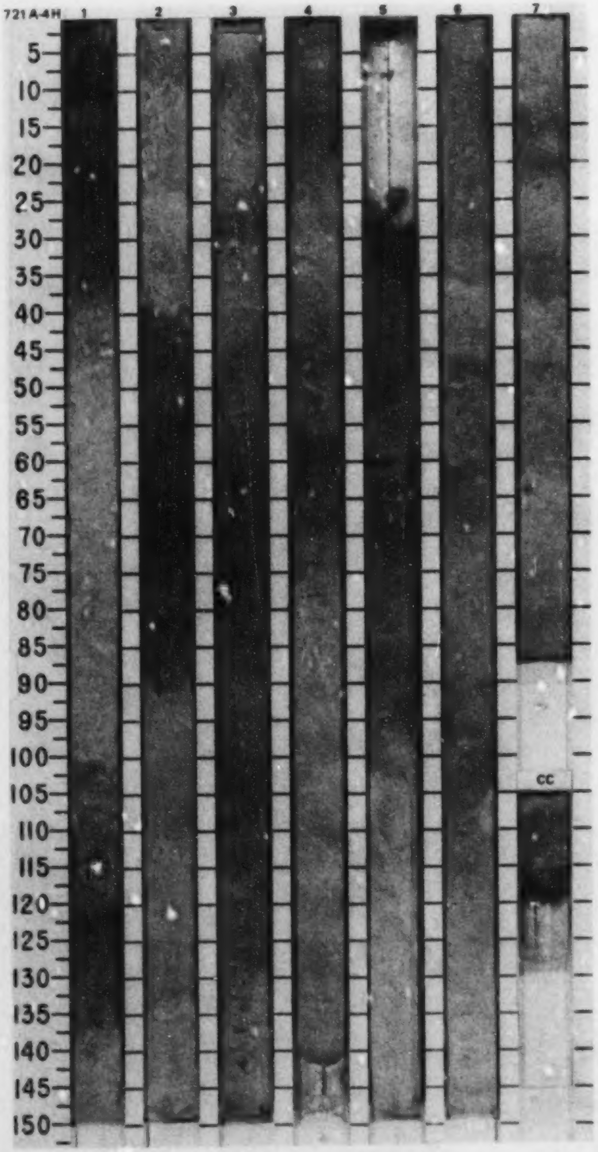
721A-4H
1
2
3
4
5
6
7
CC
5
10
15
20
25
30
35
40
45
50
55
60
65
70
75
80
85
90
95
100
105
110
115
120
125
130
135
140
145
150

SITE 721 HOLE A CORE 5H CORED INTERVAL 1983.7-1993.3 mbsl; 38.9-48.5 mbsf

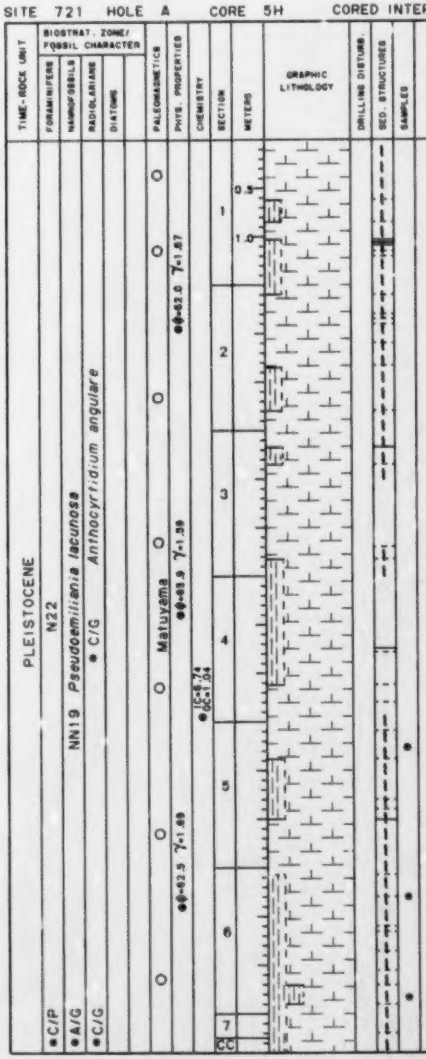

LITHOLOGIC DESCRIPTION

NANNOFOSSIL OOZE

No drilling disturbance.

Major lithology: NANNOFOSSIL OOZE. Alternating light and dark bands of light olive gray (5Y 6/2) to light greenish gray (10Y 5/2, 6/2) and olive (5Y 4/3, 5/3). Slight to moderate burrow-mottling throughout. Dark layers enriched in terrigenous components relative to light layers.

Minor lithology: Marly nannofossil ooze, dark olive gray (5Y 3/2), Section 6, 120-135 cm.

SMEAR SLIDE SUMMARY (%):

	5, 27 D	6, 15 D	6, 131 D
TEXTURE:			
Sand	1	1	10
Silt	7	15	35
Clay	92	84	55
COMPOSITION:			
Access. minerals	Tr	Tr	2
Clay	—	13	20
Diatoms	Tr	21	
Dolomite	Tr	—	Tr
Feldspar	—	—	2
Foraminifers	Tr	1	1
Volcanic glass	1	—	Tr
Inorganic calcite	5	10	30
Mica	Tr	1	—
Nannofossils	92	70	35
Quartz	1	Tr	8
Radiolarians	Tr	2	Tr
Silicoflagellates	—	1	—
Sponge spicules	Tr	1	—

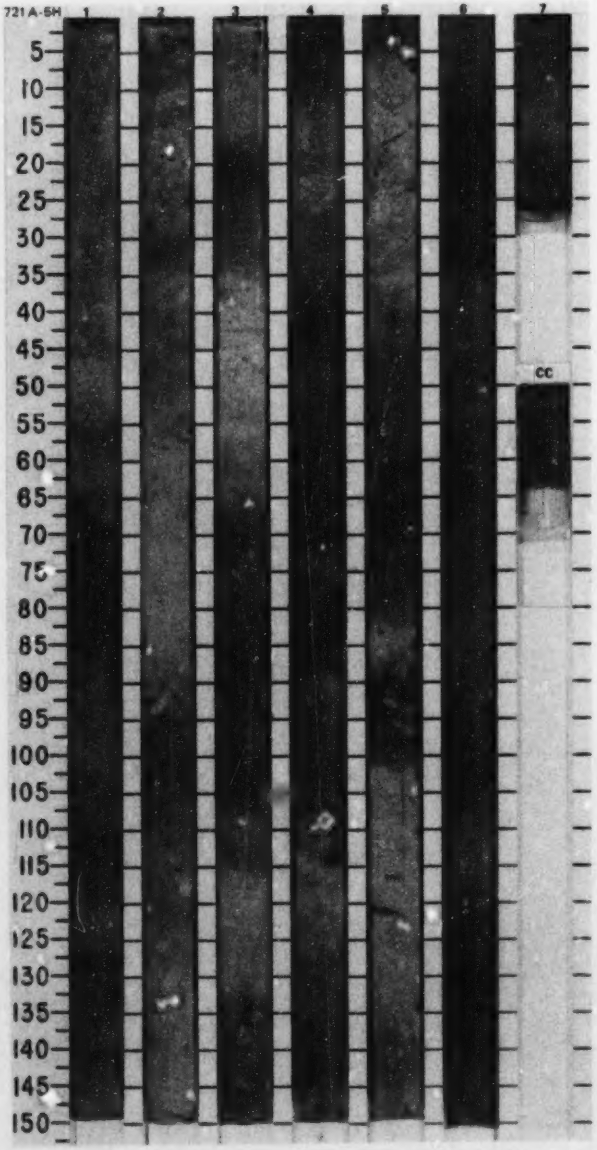
721A-5H
1
2
3
4
5
6
7
CC
5
10
15
20
25
30
35
40
45
50
55
60
65
70
75
80
85
90
95
100
105
110
115
120
125
130
135
140
145
150

SITE 721 HOLE A CORE 6H CORED INTERVAL 1993.3-2002.6 mbsl; 48.5-57.8 mbsf

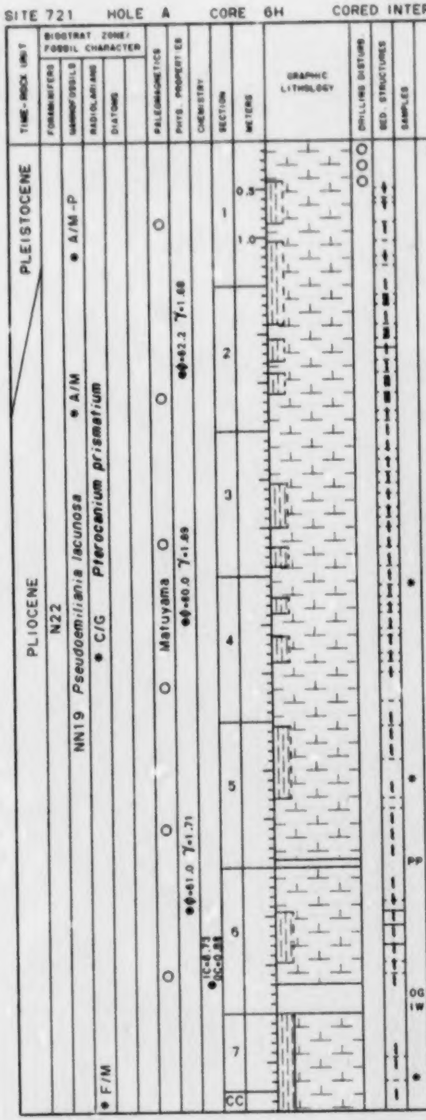
TIME-ROCK UNIT
BIOSTRAT. ZONE/ FOSSIL CHARACTER
FORAMINIFERS
NANNOFOSSILS
RADIOLARIANS
DIATOMS
PALEOMAGNETICS
PHYS. PROPERTIES
CHEMISTRY
SECTION
METERS
GRAPHIC LITHOLOGY
DRILLING DISTURB.
SED. STRUCTURES
SAMPLES
PLEISTOCENE
PLIOCENE
N22
● A/M-P
● A/M
NN19 Pseudoemiliania lacunosa
● C/G Pterocanium prismatium
● F/M
Matuyama
●φ=62.2 γ=1.68
●φ=60.0 γ=1.69
●φ=61.0 γ=1.71
●IC=8.73 OC=0.88
1
2
3
4
5
6
7
CC
0.5
1.0
PP
OG
IW

LITHOLOGIC DESCRIPTION

NANNOFOSSIL OOZE

Section 1, 10-40 cm, soupy. Remainder of core undisturbed.

Major lithology: NANNOFOSSIL OOZE. Alternating light and dark bands of light olive gray (5Y 6/2) to pale olive (5Y 6/3) to olive gray (5Y 5/2, 6/2) and olive (5Y 4/3, 4/4). Slight to moderate burrow-mottling throughout. Dark layers contain 10-20% more terrigenous clay than do light layers.

Minor lithology: Foraminifer sand. Concentrated in a layer in Section 1, 69 cm, and in burrows in Section 2, 17, 63, and 66 cm.

SMEAR SLIDE SUMMARY (%):

	4, 9 D	5, 61 D	7, 65 D
TEXTURE:			
Sand	—	—	15
Silt	20	10	35
Clay	80	90	50
COMPOSITION:			
Clay	—	—	8
Diatoms	—	2	Tr
Dolomite	Tr	Tr	Tr
Feldspar	—	Tr	—
Foraminifers	5	7	15
Inorganic calcite	5	5	25
Mica	10	—	—
Nannofossils	75	80	50
Quartz	5	1	1
Radiolarians	—	2	1
Silicoflagellates	—	1	—
Sponge spicules	—	2	Tr

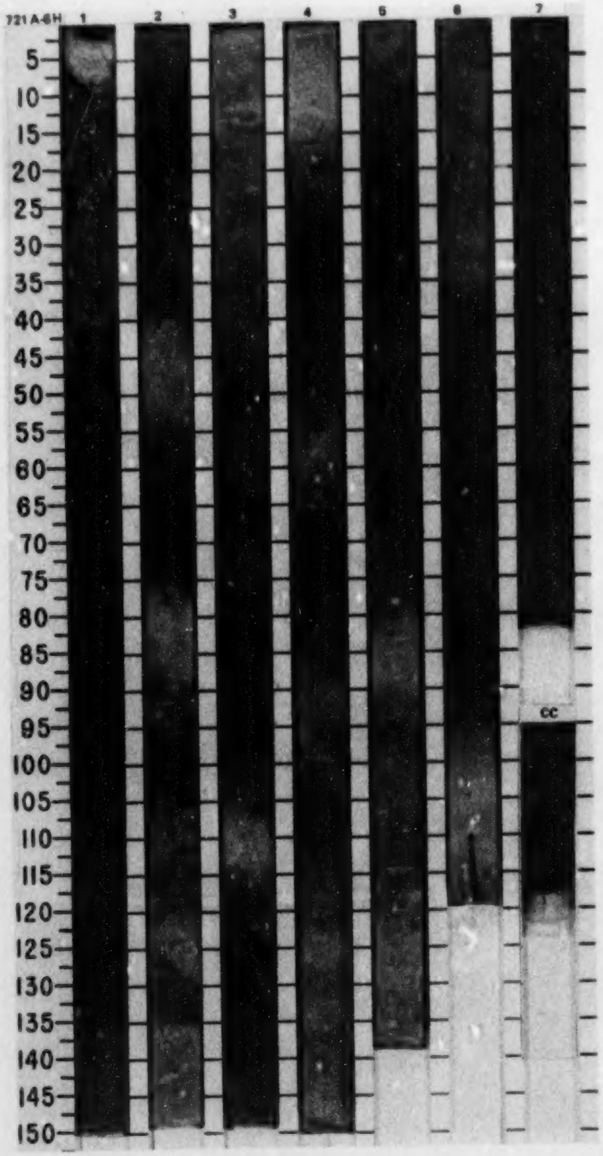
721A-6H
1
2
3
4
5
6
7
CC
5
10
15
20
25
30
35
40
45
50
55
60
65
70
75
80
85
90
95
100
105
110
115
120
125
130
135
140
145
150

SITE 721 HOLE A CORE 7H CORED INTERVAL 2002.6-2012.1 mbsl; 57.8-67.3 mbsf

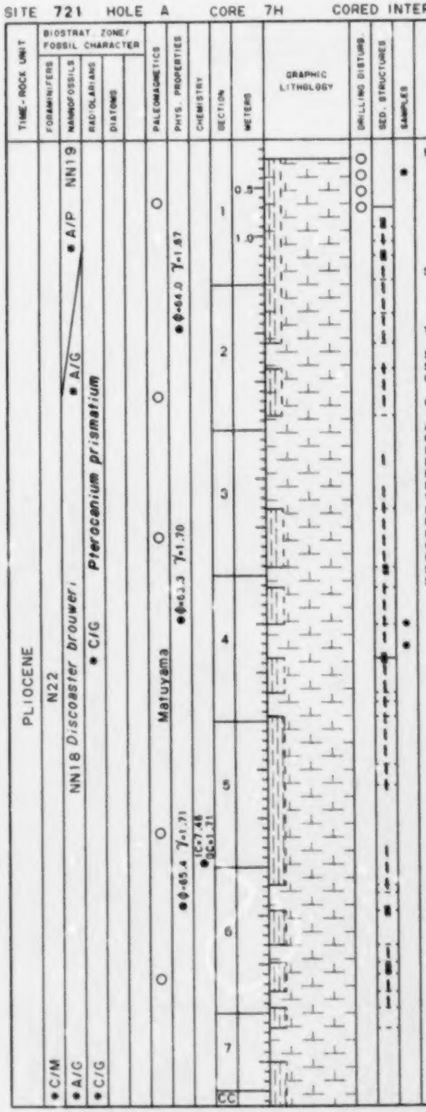
TIME-ROCK UNIT
BIOSTRAT. ZONE/ FOSSIL CHARACTER
FORAMINIFERS
NANNOFOSSILS
RADIOLARIANS
DIATOMS
PALEOMAGNETICS
PHYS. PROPERTIES
CHEMISTRY
SECTION
METERS
GRAPHIC LITHOLOGY
DRILLING DISTURB.
SED. STRUCTURES
SAMPLES
PLIOCENE
N22
NN18 Discoaster brouweri
NN19
● A/P
● A/G
● C/G
Pterocenium prismatium
● C/M
● A/G
● C/G
Matuyama
●Φ=64.0 γ=1.87
●Φ=63.3 γ=1.70
●Φ=65.4 γ=1.71
IC=7.48
OC=1.71
1
2
3
4
5
6
7
CC
0.5
1.0

LITHOLOGIC DESCRIPTION

NANNOFOSSIL OOZE

Void Section 1, 0-18 cm, soupy, in Section 1, 10-70 cm. Remainder of core is undisturbed.

Major lithology: NANNOFOSSIL OOZE. Alternating light and dark bands of pale olive (5Y 6/3) to olive (5Y 4/3, 5/3). Slight to moderate burrow-mottling throughout. Dark layers enriched in terrigenous clay relative to light layers.

SMEAR SLIDE SUMMARY (%):

	1, 35 D	4, 50 D	4, 72 D
TEXTURE:			
Sand	5	5	10
Silt	15	20	15
Clay	80	75	75
COMPOSITION:			
Access. minerals	1	1	1
Clay	10	11	5
Diatoms	—	Tr	—
Dolomite	—	Tr	—
Feldspar	Tr	—	—
Foraminifers	2	3	8
Volcanic glass	—	15	Tr
Inorganic calcite	15	—	15
Mica	—	—	Tr
Nannofossils	70	65	75
Quartz	2	5	1
Radiolarians	Tr	—	Tr
Silicoflagellates	—	Tr	Tr
Sponge spicules	Tr	Tr	Tr

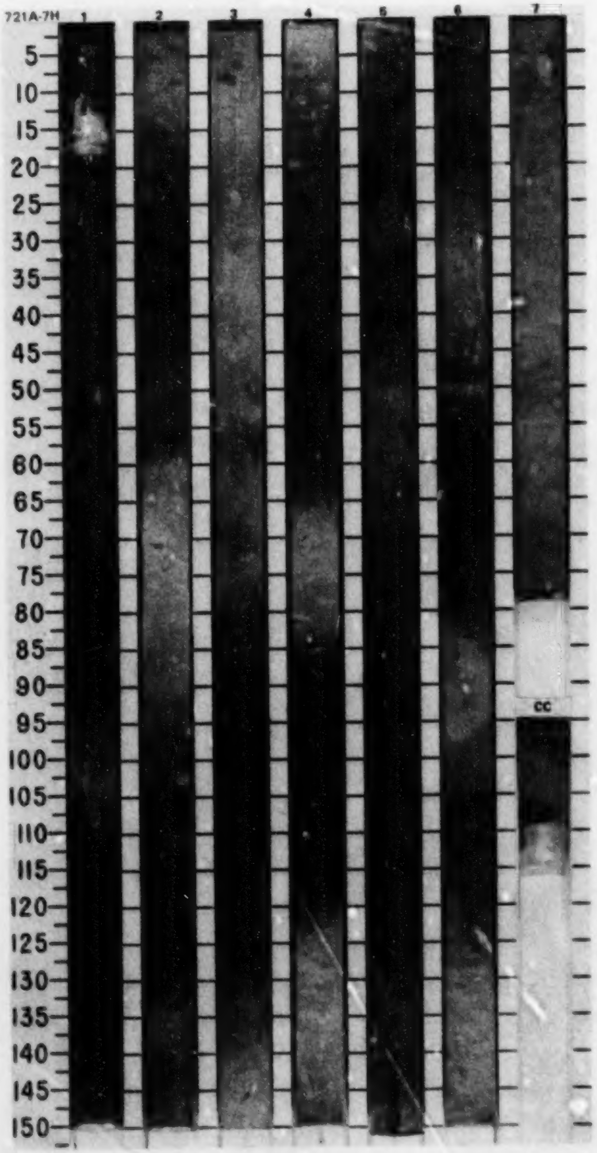
721A-7H
1
2
3
4
5
6
7
CC
5
10
15
20
25
30
35
40
45
50
55
60
65
70
75
80
85
90
95
100
105
110
115
120
125
130
135
140
145
150

SITE 721 HOLE A CORE 8H CORED INTERVAL 2012.1-2021.6 mbsl; 67.3-76.8 mbsf

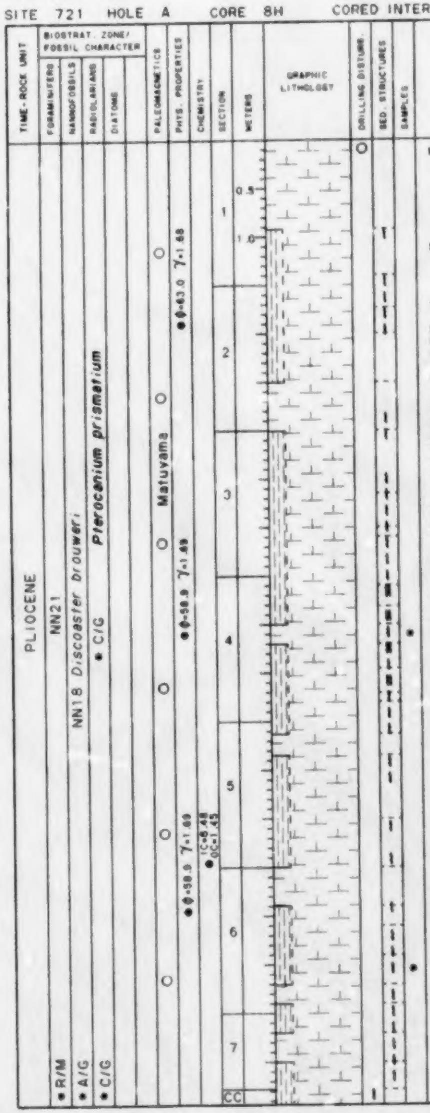
TIME-ROCK UNIT
BIOSTRAT. ZONE/ FOSSIL CHARACTER
FORAMINIFERS
NANNOFOSSILS
RADIOLARIANS
DIATOMS
PALEOMAGNETICS
PHYS. PROPERTIES
CHEMISTRY
SECTION
METERS
GRAPHIC LITHOLOGY
DRILLING DISTURB.
SED. STRUCTURES
SAMPLES
PLIOCENE
NN21
NN18 Discoaster brouweri
• C/G Pterocanium prismatium
• R/M
• A/G
• C/G
Matuyama
●ϕ=63.0 γ=1.68
●ϕ=58.9 γ=1.89
●ϕ=58.0 γ=1.89
●IC=8.48 OC=1.45
1
2
3
4
5
6
7
CC
0.5
1.0

LITHOLOGIC DESCRIPTION

NANNOFOSSIL OOZE

Section 1, 0-2 cm, soupy. Remainder of core is undisturbed. Major lithology: NANNOFOSSIL OOZE. Alternating light and dark bands of light gray (5Y 7/2) to light olive gray (5Y 6/2) and olive (5Y 4/3, 5/3, 4/4). Slight to moderate burrow-mottling throughout. Dark layers enriched in terrigenous clay relative to light layers.

SMEAR SLIDE SUMMARY (%):

	4, 80 D	6, 106 D
TEXTURE:		
Sand	—	5
Silt	15	15
Clay	80	85
COMPOSITION:		
Access. minerals	1	Tr
Diatoms	—	1
Feldspar	1	—
Foraminifers	5	—
Volcanic glass	Tr	Tr
Inorganic calcite	10	10
Mica	2	—
Nannofossils	80	84
Quartz	1	2
Radiolarians	Tr	1
Silicoflagellates	Tr	2
Sponge spicules	Tr	—

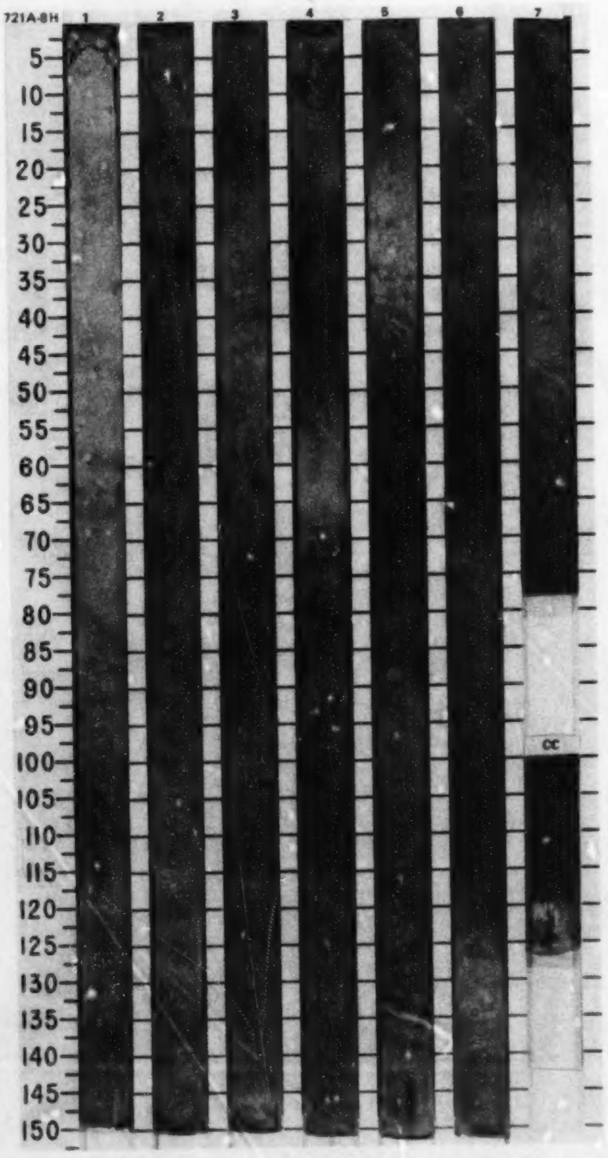
721A-8H
1
2
3
4
5
6
7
CC
5
10
15
20
25
30
35
40
45
50
55
60
65
70
75
80
85
90
95
100
105
110
115
120
125
130
135
140
145
150

SITE 721 HOLE A CORE 9H CORED INTERVAL 2021.6-2031.2 mbsl; 76.8-86.4 mbsf

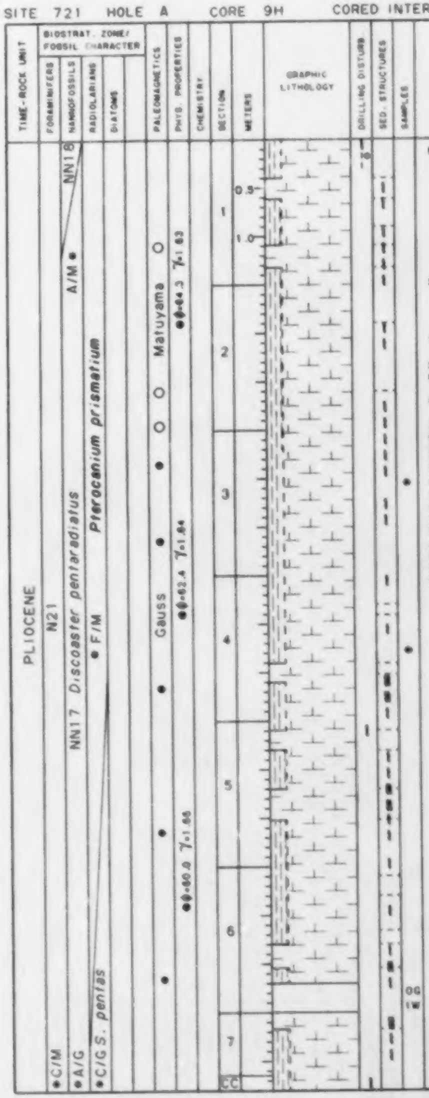
TIME-ROCK UNIT
BIOSTRAT. ZONE/ FOSSIL CHARACTER
FORAMINIFERS
NANNOFOSSILS
RADIOLARIANS
DIATOMS
PALEOMAGNETICS
PHYS. PROPERTIES
CHEMISTRY
SECTION
METERS
GRAPHIC LITHOLOGY
DRILLING DISTURB.
SED. STRUCTURES
SAMPLES
PLIOCENE
N21
NN18
NN17 Discoaster pentaradiatus
A/M
Pterocanium prismatium
F/M
C/G S. pentas
C/M
A/G
C/G
Matuyama
Gauss
φ=64.3 γ=1.83
φ=62.4 γ=1.84
φ=60.0 γ=1.86
0.5
1.0
1
2
3
4
5
6
7
CC
OG
IW

LITHOLOGIC DESCRIPTION

NANNOFOSSIL OOZE

Section 1, 0-7 cm, slightly disturbed, 7-10 cm, soupy. Remainder of core is undisturbed.

Major lithology: NANNOFOSSIL OOZE. Alternating light and dark bands of light olive gray (5Y 6/2) to olive (5Y 4/3, 5/3, 4/4) and olive gray (5Y 4/2). Slight to moderate burrow-mottling throughout. Dark layers enriched in terrigenous clay relative to light layers.

SMEAR SLIDE SUMMARY (%):

	3, 55 D	4, 78 D	5, 91 D
TEXTURE:			
Silt	15	3	5
Clay	85	97	95
COMPOSITION:			
Access. minerals	—	Tr	—
Clay	5	—	3
Diatoms	—	—	Tr
Dolomite	—	Tr	—
Foraminifers	3	3	1
Volcanic glass	—	Tr	Tr
Inorganic calcite	10	2	5
Mica	1	Tr	—
Nannofossils	80	93	90
Pore space	1	—	—
Quart	Tr	1	Tr
Radiolarians	Tr	Tr	Tr
Silicoflagellates	Tr	1	1
Sponge spicules	—	Tr	—

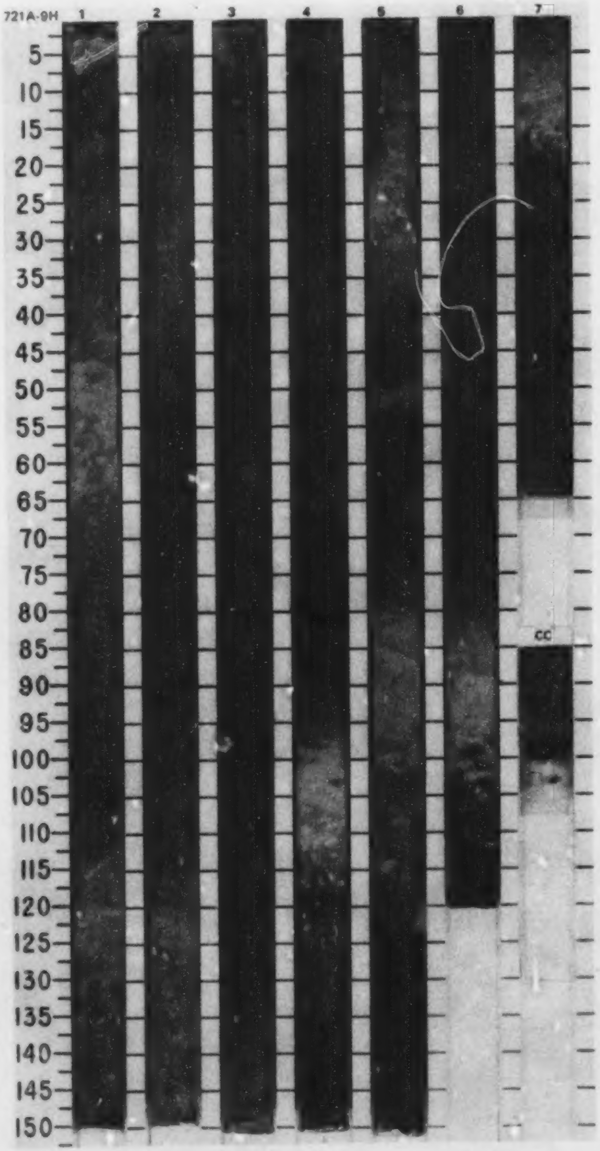
721A-9H
1
2
3
4
5
6
7
CC
5
10
15
20
25
30
35
40
45
50
55
60
65
70
75
80
85
90
95
100
105
110
115
120
125
130
135
140
145
150

SITE 721 HOLE B CORE 1H CORED INTERVAL 1944.8-1954.2 mbsl; 0.0-9.4 mbsf

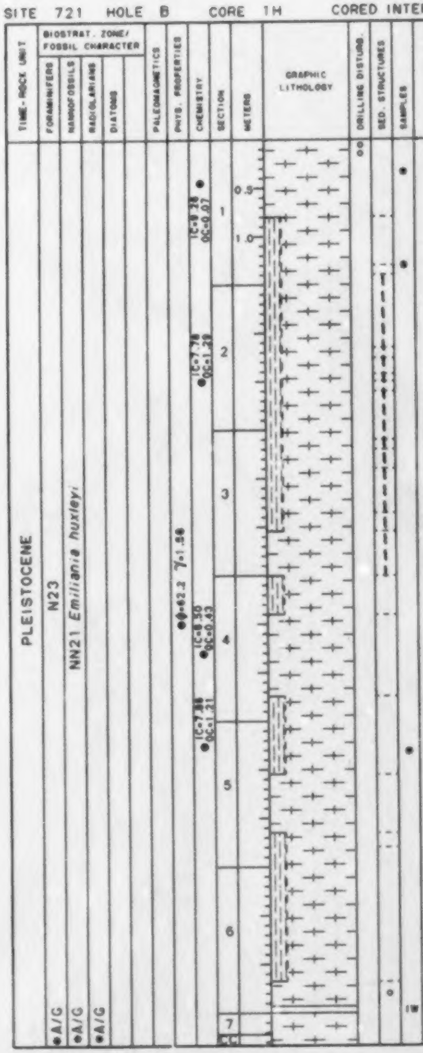
TIME-ROCK UNIT
BIOSTRAT. ZONE/ FOSSIL CHARACTER
FORAMINIFERS
NANNOFOSSILS
RADIOLARIANS
DIATOMS
PALEOMAGNETICS
PHYS. PROPERTIES
CHEMISTRY
SECTION
METERS
GRAPHIC LITHOLOGY
DRILLING DISTURB.
SED. STRUCTURES
SAMPLES
PLEISTOCENE
N23
NN21 *Emiliania huxleyi*
●A/G
●A/G
●A/G
●φ=62.2 γ=1.56
●IC=8.28 OC=0.07
●IC=7.78 OC=1.29
●IC=8.50 OC=0.43
●IC=7.88 OC=1.21
1
2
3
4
5
6
7
CC
0.5
1.0
IW

LITHOLOGIC DESCRIPTION

FORAMINIFER-NANNOFOSSIL OOZE

Section 1, 0-5 cm, soupy. Remainder of core is undisturbed.

Major lithology: FORAMINIFER-NANNOFOSSIL OOZE. Alternating light and dark bands of light gray (5Y 7/1) to gray (5Y 6/1) to olive (5Y 5/3, 4/4) to olive gray (5Y 4/2). Slight to moderate burrow-mottling throughout. Dark layers contain 10-20% more terrigenous clay than do light layers.

Minor lithology: Foraminifer sand. Concentration in burrows in Section 1, 90-91 cm, and Section 6, 58-61 cm.

SMEAR SLIDE SUMMARY (%):

	1, 34 D	1, 130 D	6, 31 D
TEXTURE:			
Sand	20	20	10
Silt	20	15	12
Clay	60	65	78
COMPOSITION:			
Access. minerals	Tr	—	Tr
Clay	—	5	8
Diatoms	Tr	—	—
Feldspar	—	—	Tr
Fish remains	—	Tr	—
Foraminifers	35	20	10
Volcanic glass	Tr	—	Tr
Inorganic calcite	5	10	10
Mica	—	Tr	1
Nannofossils	60	65	70
Quartz	—	Tr	1
Silicoflagellates	Tr	—	—
Sponge spicules	Tr	Tr	Tr

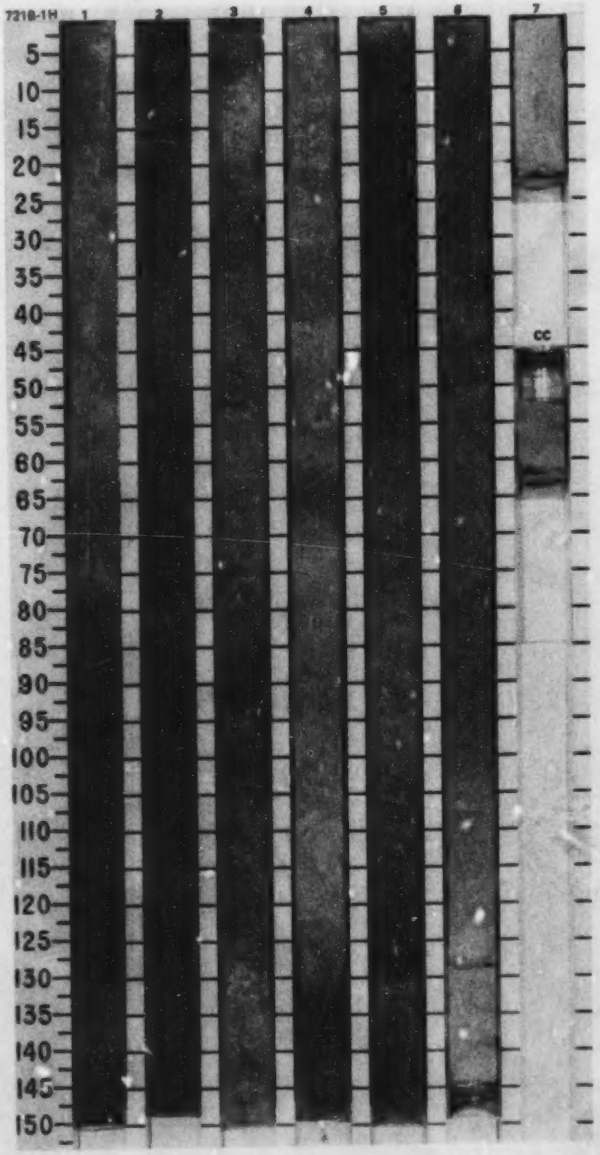
721B-1H
1
2
3
4
5
6
7
CC
5
10
15
20
25
30
35
40
45
50
55
60
65
70
75
80
85
90
95
100
105
110
115
120
125
130
135
140
145
150

SITE 721 HOLE B CORE 2H CORED INTERVAL 1954.2-1963.9 mbsl; 9.4-19.1 mbsf

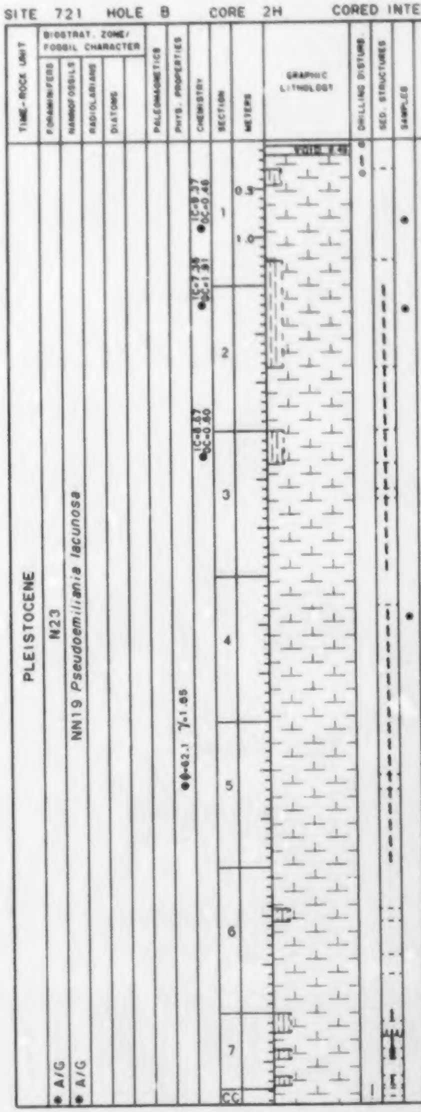
TIME-ROCK UNIT
BIOSTRAT. ZONE/ FOSSIL CHARACTER
FORAMINIFERS
NANNOFOSSILS
RADIOLARIANS
DIATOMS
PALEOMAGNETICS
PHYS. PROPERTIES
CHEMISTRY
SECTION
METERS
GRAPHIC LITHOLOGY
DRILLING DISTURB.
SED. STRUCTURES
SAMPLES
PLEISTOCENE
N23
NN19 Pseudoemiliania lacunosa
A/G
A/G
IC=8.37 OC=0.46
IC=7.38 OC=1.91
IC=8.57 OC=0.60
φ=62.1 γ=1.65
0.5
1.0
VOID
1
2
3
4
5
6
7
CC

LITHOLOGIC DESCRIPTION

NANNOFOSSIL OOZE

Section 1, 0-7 cm, soupy; 7-12 cm, void; 12-30 cm, very disturbed; and 47-52 cm, soupy. Remainder of core is undisturbed.

Major lithology: NANNOFOSSIL OOZE. Alternating light and dark bands of light gray (5Y 7/1, 7/2), light greenish gray (10Y 6/1, 6/2), light olive gray (5Y 6/2), and pale olive (5Y 6/3) to olive (5Y 5/3, 4/4). Slight to moderate burrow-mottling throughout. Dark layers contain 10-20% more terrigenous silty clay than do light layers.

SMEAR SLIDE SUMMARY (%):

	1, 84 D	4, 43 D
TEXTURE:		
Sand	10	5
Silt	17	15
Clay	73	80
COMPOSITION:		
Access. minerals	Tr	
Clay	3	
Dolomite	Tr	
Foraminifers	7	5
Volcanic glass	Tr	Tr
Inorganic calcite	20	13
Mica	Tr	1
Nannofossils	70	80
Quartz	Tr	1
Radiolarians	Tr	
Sponge spicules	Tr	

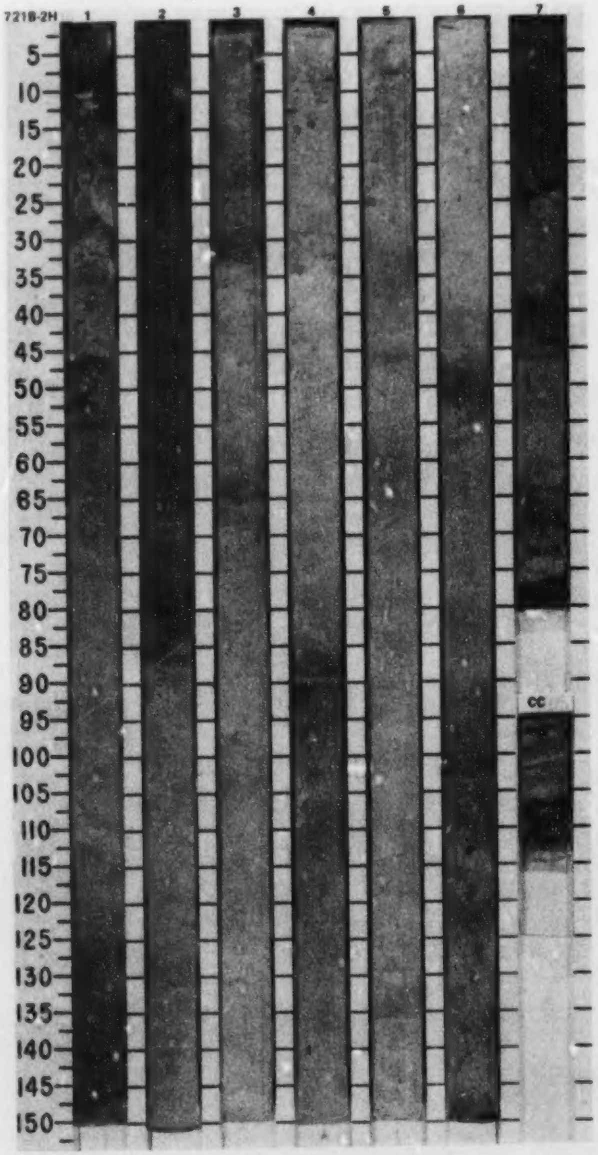
721B-2H
1
2
3
4
5
6
7
CC
5
10
15
20
25
30
35
40
45
50
55
60
65
70
75
80
85
90
95
100
105
110
115
120
125
130
135
140
145
150

SITE 721 HOLE B CORE 3H CORED INTERVAL 1963.9-1973.6 mbsl; 19.1-28.8 mbsf

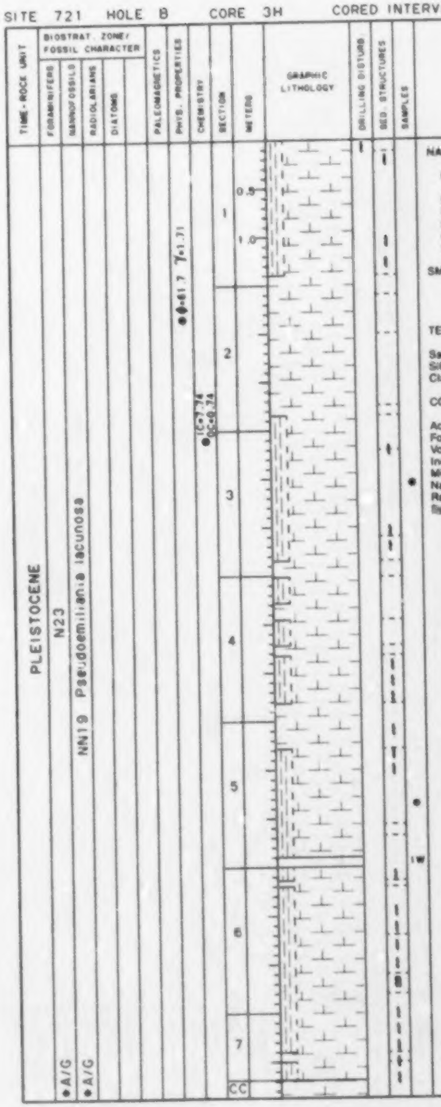
TIME-ROCK UNIT
BIOSTRAT. ZONE/ FOSSIL CHARACTER
FORAMINIFERS
NANNOFOSSILS
RADIOLARIANS
DIATOMS
PALEOMAGNETICS
PHYS. PROPERTIES
CHEMISTRY
SECTION
METERS
GRAPHIC LITHOLOGY
DRILLING DISTURB.
SED. STRUCTURES
SAMPLES
PLEISTOCENE
N23
NN19 Pseudoemiliania lacunosa
●A/G
●A/G
●ϕ=61.7 γ=1.71
●IC=7.74 OC=0.74
0.5
1.0
1
2
3
4
5
6
7
CC
IW

LITHOLOGIC DESCRIPTION

NANNOFOSSIL OOZE

No drilling disturbance.

Major lithology: NANNOFOSSIL OOZE. Alternating light and dark bands of light olive gray (5Y 6/2) to pale olive (5Y 6/3) and olive (5Y 5/3). Slight to moderate burrow-mottling throughout. Dark layers are enriched in terrigenous clay compared to light layers. Minor lithology: Foraminifer sand. Concentrated as lags in Section 4, 15-20, 38-42, and 135-145 cm.

SMEAR SLIDE SUMMARY (%):

	3, 57 D	5, 85 D
TEXTURE:		
Sand	5	5
Silt	10	10
Clay	85	85
COMPOSITION:		
Access. minerals	Tr	
Foraminifers	5	5
Volcanic glass	Tr	
Inorganic glass	10	10
Mica	Tr	
Nannofossils	85	85
Radiolarians		Tr
Sponge spicules		Tr

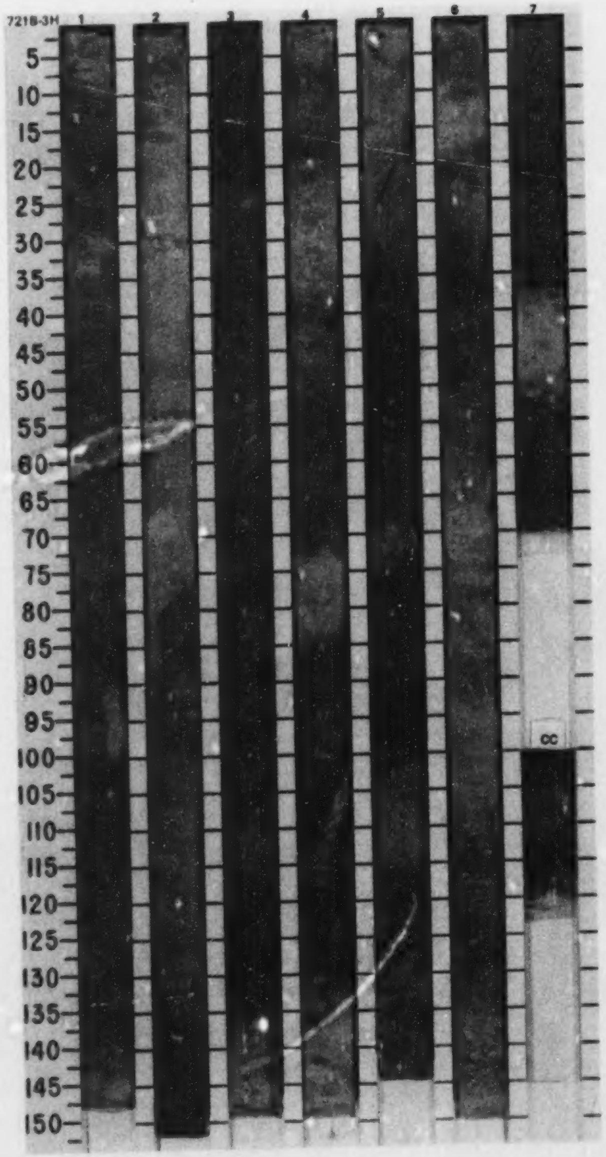
721B-3H
1
2
3
4
5
6
7
CC
5
10
15
20
25
30
35
40
45
50
55
60
65
70
75
80
85
90
95
100
105
110
115
120
125
130
135
140
145
150

SITE 721 HOLE B CORE 4H CORED INTERVAL 1973.6-1983.3 mbsl; 28.8-38.5 mbsf

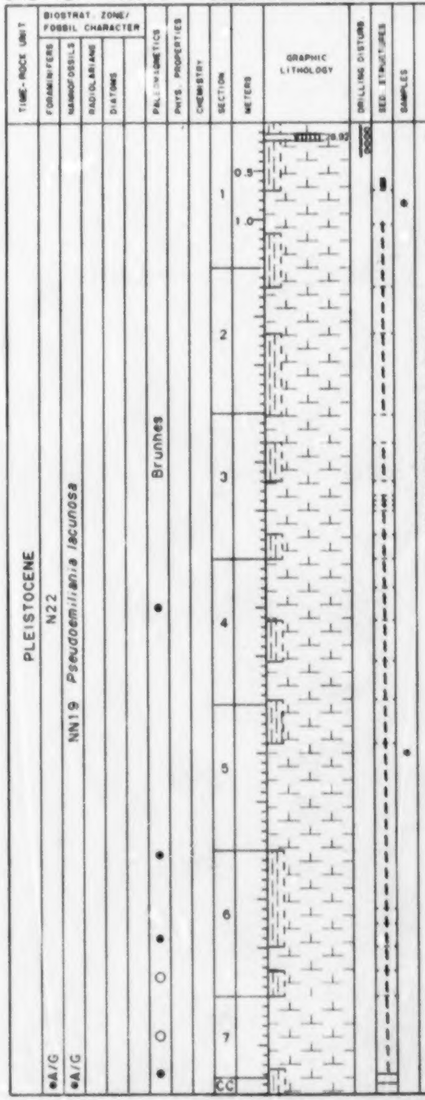
TIME-ROCK UNIT
BIOSTRAT. ZONE/ FOSSIL CHARACTER
FORAMINIFERS
NANNOFOSSILS
RADIOLARIANS
DIATOMS
PALEOMAGNETICS
PHYS. PROPERTIES
CHEMISTRY
SECTION
METERS
GRAPHIC LITHOLOGY
DRILLING DISTURB.
SED. STRUCTURES
SAMPLES
PLEISTOCENE
N22
NN19 Pseudoemiliania lacunosa
Brunhes
●A/G
●A/G
0.5
1.0
28.92
1
2
3
4
5
6
7
CC

LITHOLOGIC DESCRIPTION

NANNOFOSSIL OOZE

Section 1, 0-30 cm, very disturbed; void in Section 1, 13-20 cm.

Major lithology: NANNOFOSSIL OOZE. Alternating light and dark bands of light gray (5Y 6/1) to light olive gray (5Y 6/2) and olive (5Y 4/3, 5/3, 5/4). Slight to moderate burrow-mottling throughout. Dark layers contain 10-20% more terrigenous clay than do light layers.

SMEAR SLIDE SUMMARY (%):

	1, 83 D	5, 50 D
TEXTURE:		
Sand	5	3
Silt	10	7
Clay	85	90
COMPOSITION:		
Access. minerals	Tr	Tr
Dolomite	Tr	
Foraminifers	5	3
Volcanic glass	Tr	
Inorganic calcite	10	7
Mica	Tr	Tr
Nannofossils	85	90
Quartz	Tr	
Radiolarians		Tr
Silicoflagellates	Tr	
Sponge spicules	Tr	Tr

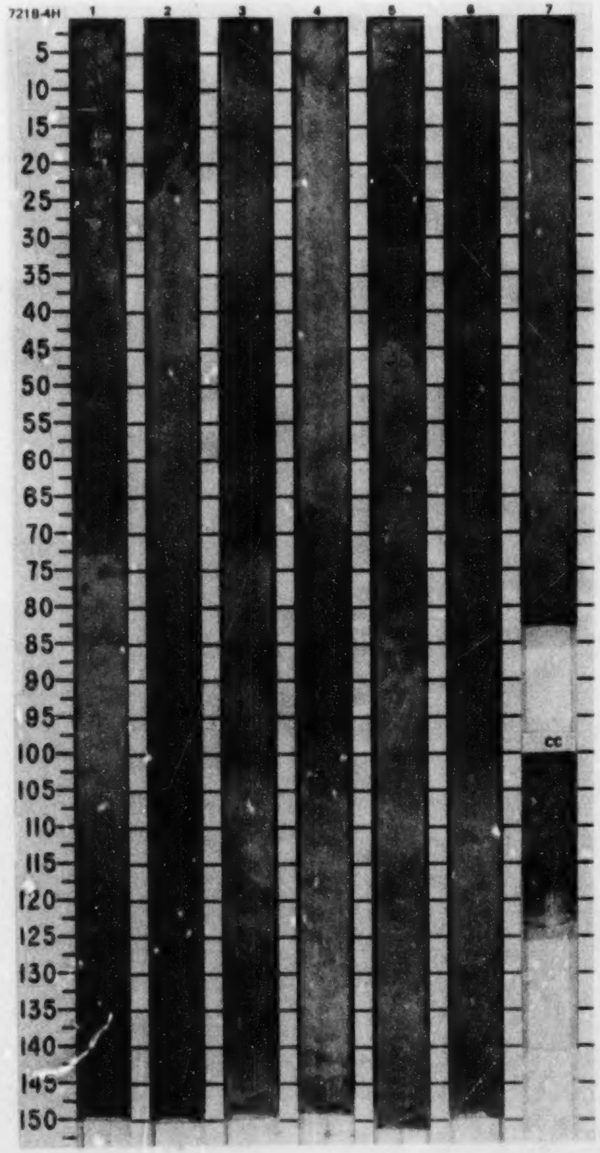
721B-4H
1
2
3
4
5
6
7
CC
5
10
15
20
25
30
35
40
45
50
55
60
65
70
75
80
85
90
95
100
105
110
115
120
125
130
135
140
145
150

SITE 721 HOLE B CORE 5H CORED INTERVAL 1983.3-1992.9 mbsl; 38.5-48.1 mbsf

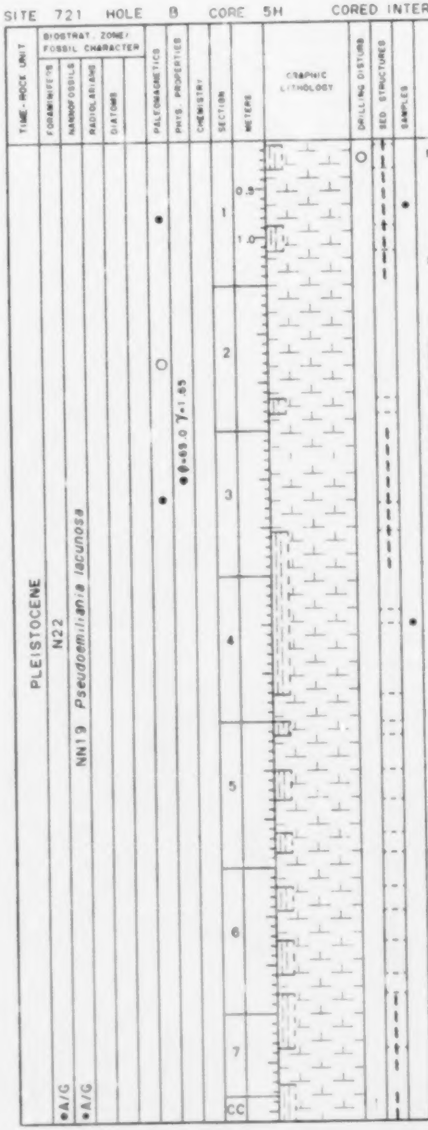
TIME-ROCK UNIT
BIOSTRAT. ZONE/ FOSSIL CHARACTER
FORAMINIFERS
NANNOFOSSILS
RADIOLARIANS
DIATOMS
PALEOMAGNETICS
PHYS. PROPERTIES
CHEMISTRY
SECTION
METERS
GRAPHIC LITHOLOGY
DRILLING DISTURB.
SED. STRUCTURES
SAMPLES
PLEISTOCENE
N22
NN19 Pseudoemiliania lacunosa
•A/G
•A/G
•φ=69.0 γ=1.65
0.5
1.0
1
2
3
4
5
6
7
CC

LITHOLOGIC DESCRIPTION

NANNOFOSSIL OOZE

No drilling disturbance.

Major lithology: NANNOFOSSIL OOZE. Alternating light and dark bands of light gray (5Y 7/1, 7/2) and light olive gray (5Y 6/2) to light greenish gray (10Y 6/1) and olive (5Y 5/3). Slight to moderate burrow-mottling throughout. Dark layers enriched in terrigenous components relative to light layers.

SMEAR SLIDE SUMMARY (%):

	1, 67 D	4, 51 D
TEXTURE:		
Sand	1	5
Silt	25	25
Clay	74	70
COMPOSITION:		
Access. minerals	Tr	
Diatoms		Tr
Foraminifers	3	7
Volcanic glass	Tr	
Inorganic calcite	10	6
Nannofossils	85	82
Quartz	2	2
Radiolarians		1
Silicoflagellates		Tr
Sponge spicules		Tr

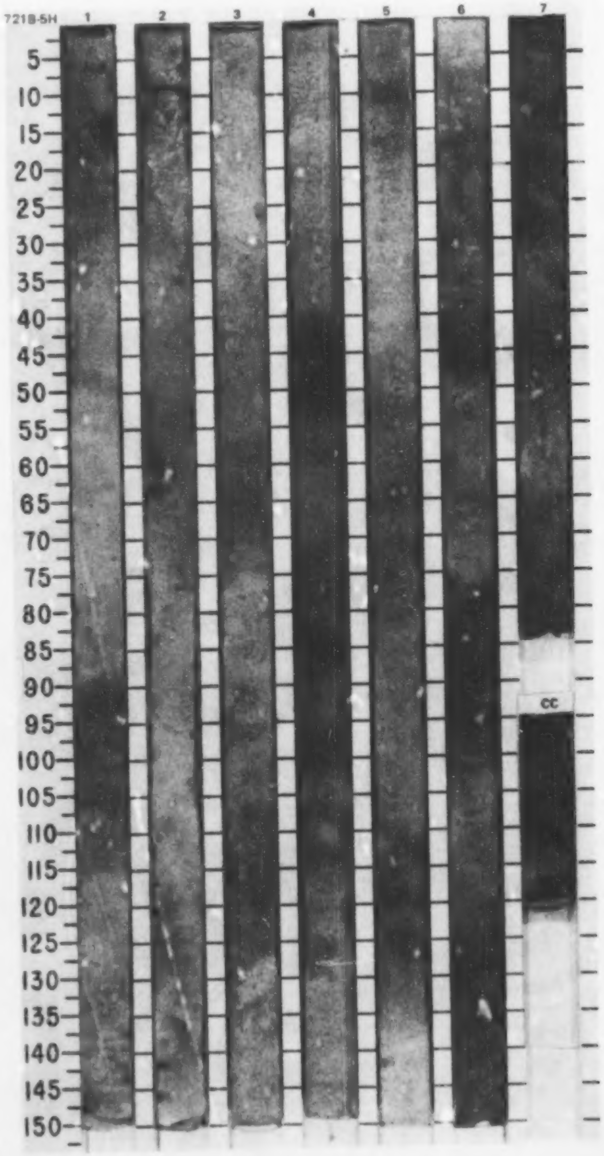
721B-5H
1
2
3
4
5
6
7
CC
5
10
15
20
25
30
35
40
45
50
55
60
65
70
75
80
85
90
95
100
105
110
115
120
125
130
135
140
145
150

SITE 721 HOLE B CORE 6H CORED INTERVAL 1992.9-2002.2 mbsl; 48.1-57.4 mbsf

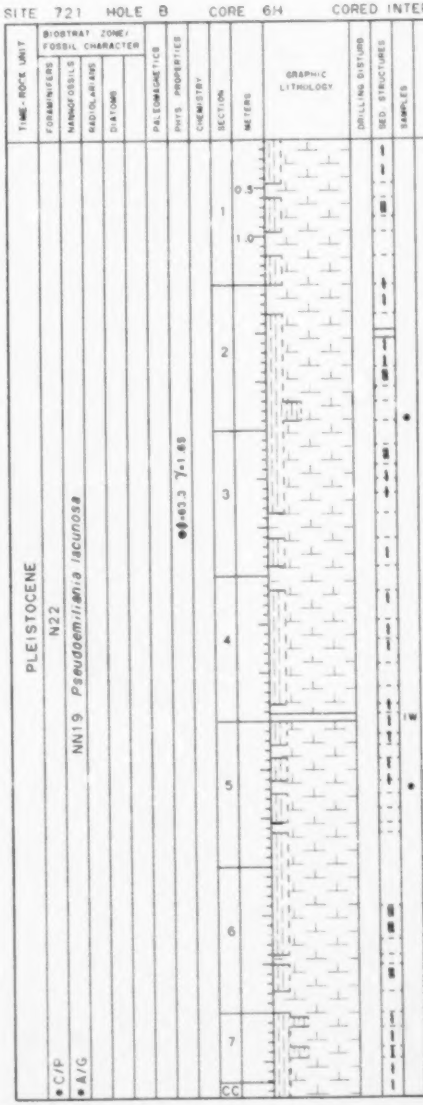
TIME-ROCK UNIT
BIOSTRAT. ZONE/ FOSSIL CHARACTER
FORAMINIFERS
NANNOFOSSILS
RADIOLARIANS
DIATOMS
PALEOMAGNETICS
PHYS. PROPERTIES
CHEMISTRY
SECTION
METERS
GRAPHIC LITHOLOGY
DRILLING DISTURB.
SED. STRUCTURES
SAMPLES
PLEISTOCENE
N22
NN19 Pseudoemiliania lacunosa
● C/P
● A/G
●ϕ=63.3 γ=1.65
0.5
1.0
1
2
3
4
5
6
7
CC
IW

LITHOLOGIC DESCRIPTION

FORAMINIFER-BEARING NANNOFOSSIL OOZE

No drilling disturbance

Major lithology: FORAMINIFER-BEARING NANNOFOSSIL OOZE. Alternating light and dark bands of light olive gray (5Y 6/2) and pale olive (5Y 6/3) to olive gray (5Y 5/2, 4/2) and olive (5Y 4/3, 5/3). Slight to moderate burrow-mottling throughout. Dark layers contain 10-20% more terrigenous clay than do light layers.

Minor lithology: Foraminifer-bearing marly nannofossil ooze, dark olive gray (5Y 3/2), Section 2, 122-132 cm, and Section 7, 6-20 and 35-48 cm.

SMEAR SLIDE SUMMARY (%):

	2, 138 D	5, 69 D
TEXTURE:		
Sand	7	5
Silt	8	14
Clay	85	81
COMPOSITION:		
Access. minerals	1	
Dolomite	Tr	Tr
Foraminifers	7	7
Volcanic glass	1	Tr
Inorganic calcite	3	3
Mica	1	Tr
Nannofossils	80	87
Quartz	2	
Siliceous frag.	5	3

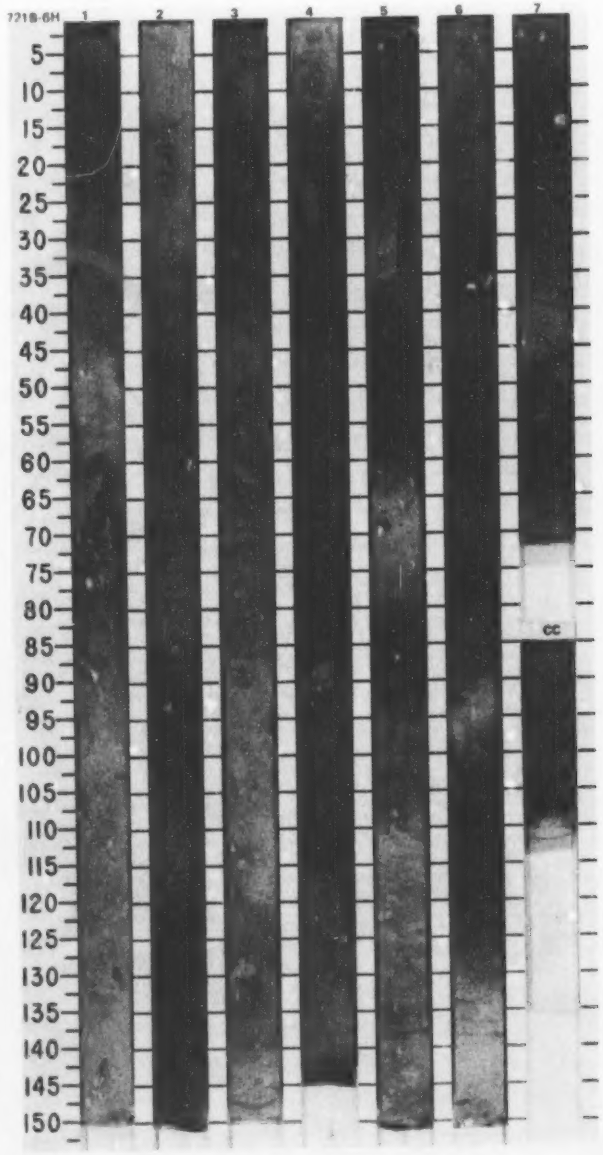
721B-6H
1
2
3
4
5
6
7
CC
5
10
15
20
25
30
35
40
45
50
55
60
65
70
75
80
85
90
95
100
105
110
115
120
125
130
135
140
145
150

SITE 721 HOLE B CORE 7H CORED INTERVAL 2002.2-2011.7 mbsl; 57.4-66.9 mbsf

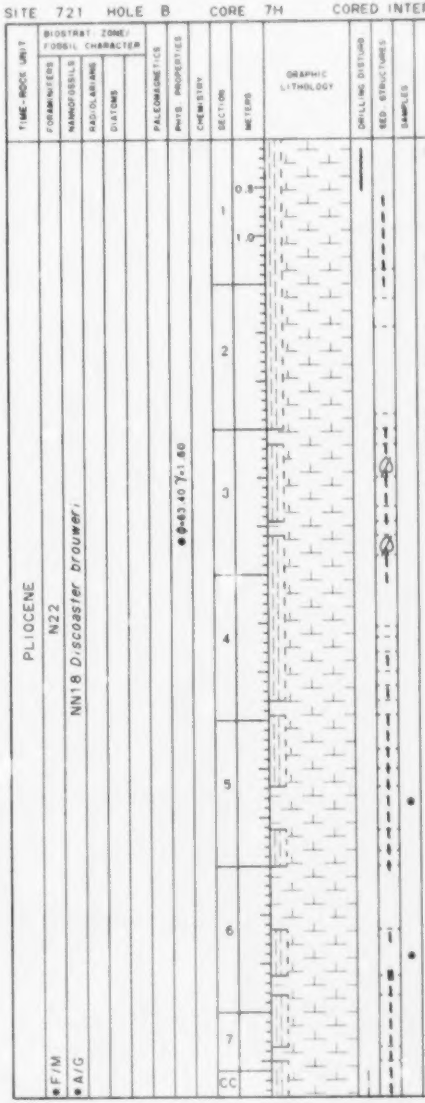
TIME-ROCK UNIT
BIOSTRAT. ZONE/ FOSSIL CHARACTER
FORAMINIFERS
NANNOFOSSILS
RADIOLARIANS
DIATOMS
PALEOMAGNETICS
PHYS. PROPERTIES
CHEMISTRY
SECTION
METERS
GRAPHIC LITHOLOGY
DRILLING DISTURB.
SED. STRUCTURES
SAMPLES
PLIOCENE
N22
●F/M
NN18 Discoaster brouweri
●A/G
●φ=63.40 γ=1.80
1
2
3
4
5
6
7
CC
0.5
1.0

LITHOLOGIC DESCRIPTION

FORAMINIFER-BEARING NANNOFOSSIL OOZE

No drilling disturbance.

Major lithology: FORAMINIFER-BEARING NANNOFOSSIL OOZE. Alternating light and dark bands of light olive gray (5Y 6/2) to olive (5Y 4/3, 5/3, 4/4). Slight to moderate burrow-mottling throughout. Dark layers enriched in terrigenous clay relative to light layers.

SMEAR SLIDE SUMMARY (%):

	5, 88 D	6, 96 D
TEXTURE:		
Silt	20	20
Clay	80	80
COMPOSITION:		
Clay	10	
Diatoms		Tr
Foraminifers	10	10
Inorganic calcite	Tr	5
Nannofossils	80	75
Quartz	Tr	5
Radiolarians		

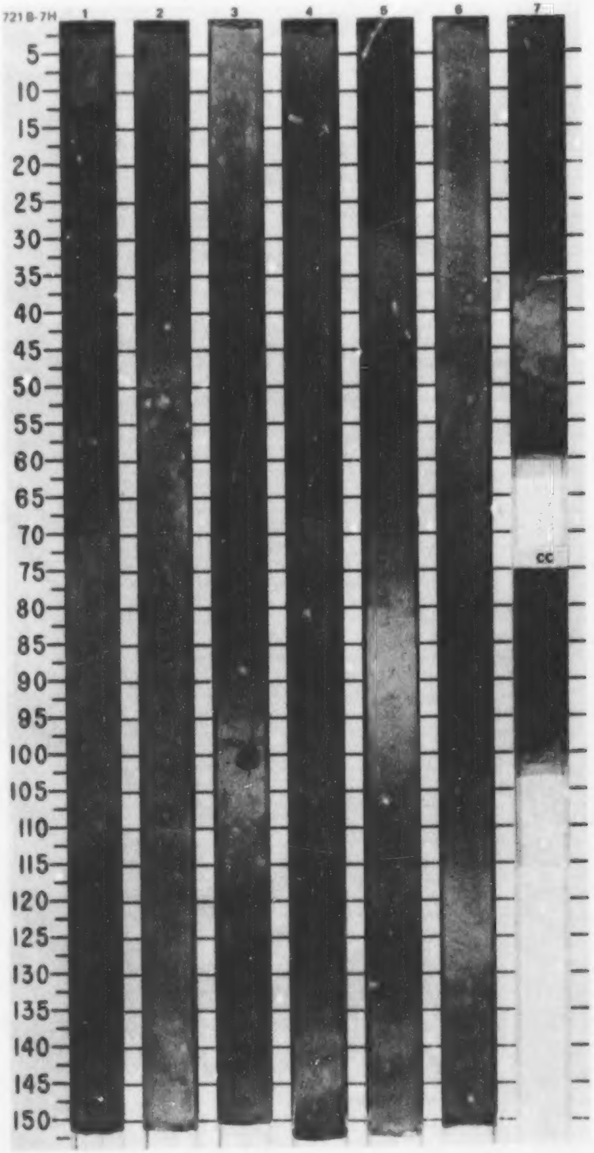
721B-7H
1
2
3
4
5
6
7
CC
5
10
15
20
25
30
35
40
45
50
55
60
65
70
75
80
85
90
95
100
105
110
115
120
125
130
135
140
145
150

SITE 721 HOLE B CORE 8H CORED INTERVAL 2011.7-2021.2 mbsl; 66.9-76.4 mbsf

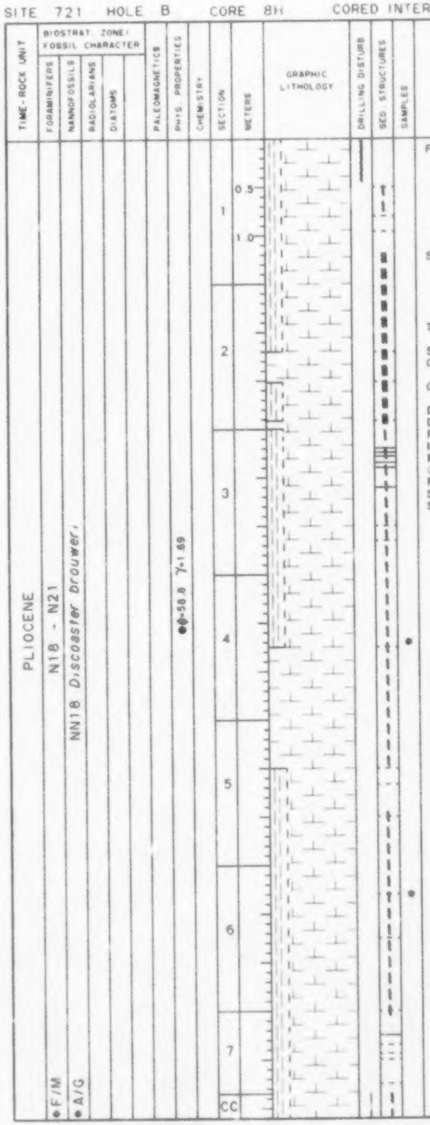
TIME-ROCK UNIT
BIOSTRAT. ZONE/ FOSSIL CHARACTER
FORAMINIFERS
NANNOFOSSILS
RADIOLARIANS
DIATOMS
PALEOMAGNETICS
PHYS. PROPERTIES
CHEMISTRY
SECTION
METERS
GRAPHIC LITHOLOGY
DRILLING DISTURB.
SED. STRUCTURES
SAMPLES
PLIOCENE
N18 - N21
NN18 Discoaster brouweri
• F/M
• A/G
●ϕ=58.8 γ=1.69
0.5
1.0
1
2
3
4
5
6
7
CC

LITHOLOGIC DESCRIPTION

FORAMINIFER-BEARING NANNOFOSSIL OOZE

Section 1, 0-53 cm, very disturbed. Remainder of core is undisturbed.

Major lithology: FORAMINIFER-BEARING NANNOFOSSIL OOZE. Alternating light and dark bands of light gray (5Y 7/1) to light olive gray (5Y 6/2) and olive (5Y 5/4, 5/3, 4/4). Slight to moderate burrow-mottling throughout. Dark layers enriched in terrigenous clay relative to light layers.

SMEAR SLIDE SUMMARY (%):

	4, 70 D	6, 30 D
TEXTURE:		
Silt	20	20
Clay	80	80
COMPOSITION:		
Diatoms	3	5
Dolomite		Tr
Foraminifers	9	10
Inorganic calcite	9	Tr
Nannofossils	73	80
Quartz		Tr
Radiolarians	4	5
Silicoflagellates		Tr
Sponge spicules	1	

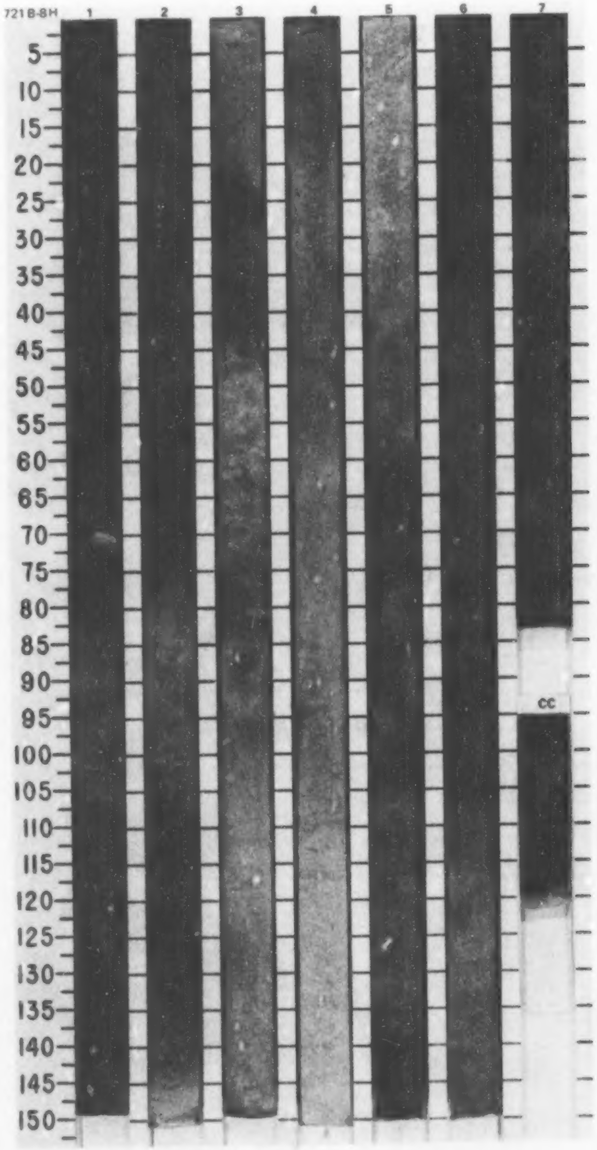
721B-8H
1
2
3
4
5
6
7
CC
5
10
15
20
25
30
35
40
45
50
55
60
65
70
75
80
85
90
95
100
105
110
115
120
125
130
135
140
145
150

SITE 721 HOLE B CORE 9H CORED INTERVAL 2021.2-2030.8 mbsl; 76.4-86.0 mbsf

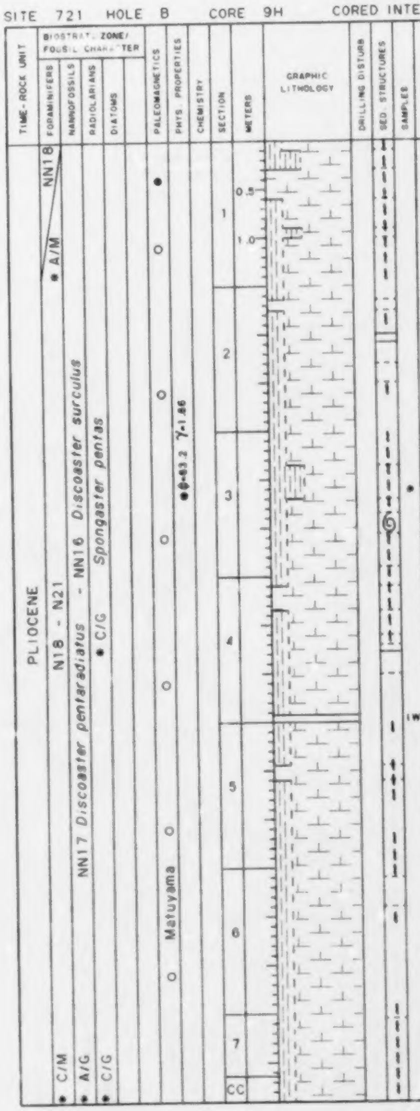
TIME-ROCK UNIT
BIOSTRAT. ZONE/ FOSSIL CHARACTER
FORAMINIFERS
NANNOFOSSILS
RADIOLARIANS
DIATOMS
PALEOMAGNETICS
PHYS. PROPERTIES
CHEMISTRY
SECTION
METERS
GRAPHIC LITHOLOGY
DRILLING DISTURB.
SED. STRUCTURES
SAMPLES
PLIOCENE
NN18
A/M
N18 - N21
NN17 Discoaster pentaradiatus - NN16 Discoaster surculus
C/G Spongaster pentas
C/M
A/G
C/G
Matuyama
ϕ-63.2 γ-1.86
0.5
1.0
1
2
3
4
5
6
7
CC
IW

LITHOLOGIC DESCRIPTION

FORAMINIFER-BEARING NANNOFOSSIL OOZE

Section 1, 0-7 cm, slightly disturbed, 7-10 cm, soupy. Remainder of core is undisturbed.

Major lithology: FORAMINIFER-BEARING NANNOFOSSIL OOZE. Alternating light and dark bands of light olive gray (5Y 6/2) to olive (5Y 4/3, 5/3, 4/4) and olive gray (5Y 4/2). Slight to moderate burrow-mottling throughout. Dark layers enriched in terrigenous clay relative to light layers.

Minor lithology: Marly nannofossil ooze, dark olive gray (5Y 3/2). Section 1, 10-28 and 90-100 cm, and Section 3, 35-60 cm. Moderate burrow-mottling.

SMEAR SLIDE SUMMARY (%):

	3, 61 D
TEXTURE:	
Silt	15
Clay	85
COMPOSITION:	
Clay	35
Foraminifers	10
Inorganic calcite	5
Mica	Tr
Nannofossils	40
Radiolarians	Tr
Unspec. minerals	10

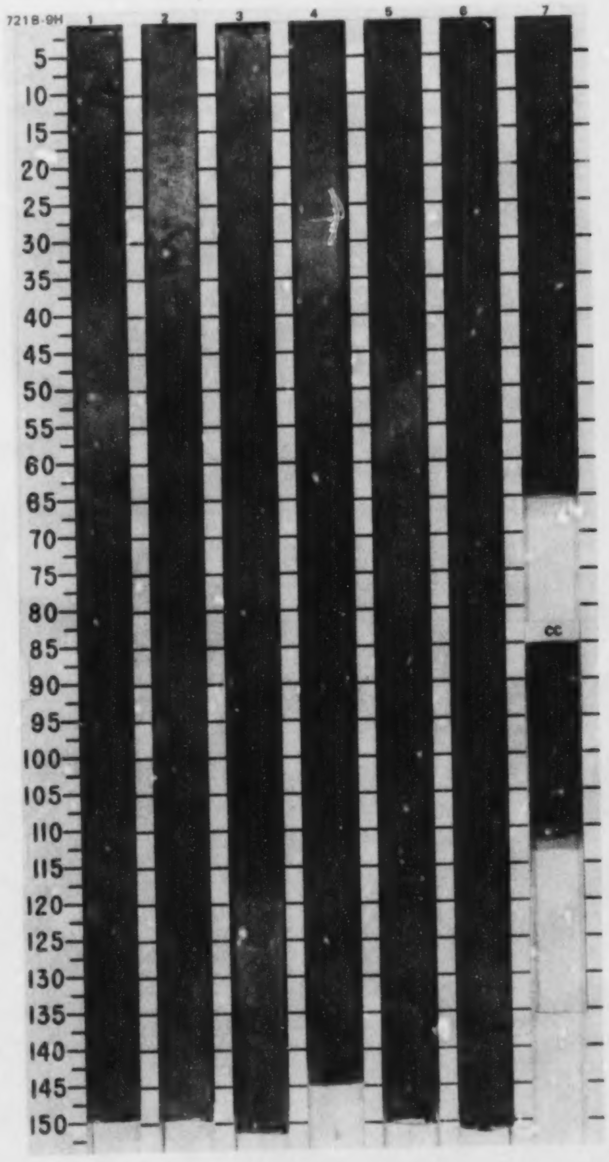
721B-9H
1
2
3
4
5
6
7
CC
5
10
15
20
25
30
35
40
45
50
55
60
65
70
75
80
85
90
95
100
105
110
115
120
125
130
135
140
145
150

SITE 721 HOLE B CORE 10X CORED INTERVAL 2030.8-2040.4 mbsl; 86.0-95.6 mbsf

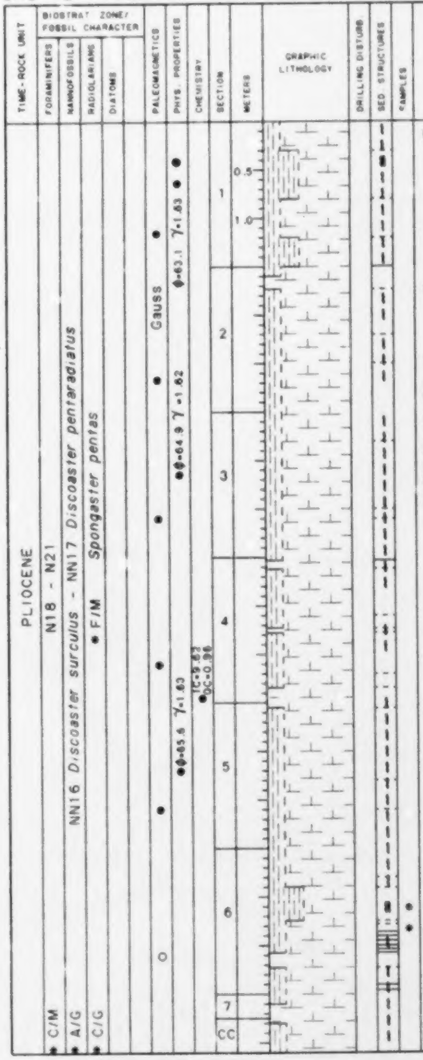
TIME-ROCK UNIT
BIOSTRAT. ZONE/ FOSSIL CHARACTER
FORAMINIFERS
NANNOFOSSILS
RADIOLARIANS
DIATOMS
PALEOMAGNETICS
PHYS. PROPERTIES
CHEMISTRY
SECTION
METERS
GRAPHIC LITHOLOGY
DRILLING DISTURB.
SED. STRUCTURES
SAMPLES
PLIOCENE
N18 - N21
C/M
NN16 Discoaster surculus - NN17 Discoaster pentaradiatus
A/G
F/M Spongaster pentas
C/G
Gauss
γ=1.63
ϕ=63.1
ϕ=64.9 γ=1.62
ϕ=65.6 γ=1.63
TC=9.62
OC=0.96
1
2
3
4
5
6
7
CC
0.5
1.0

LITHOLOGIC DESCRIPTION

NANNOFOSSIL OOZE to FORAMINIFER-BEARING NANNOFOSSIL OOZE

Section 5, 70-105 cm, slightly disturbed. Remainder of core is undisturbed

Major lithology: NANNOFOSSIL OOZE to FORAMINIFER-BEARING NANNOFOSSIL OOZE. Alternating light and dark bands of light olive gray (5Y 6/2) to olive (5Y 4/3, 5/3, 4/4) and olive gray (5Y 4/2). Slight to moderate burrow-mottling throughout. Dark layers enriched in terrigenous clay relative to light layers.

Minor lithology: Marly nannofossil ooze, dark olive gray (5Y 3/2). Section 1, 35-72 and 120-150 cm, and Section 6, 43-74 cm. Moderate burrow-mottling.

SMEAR SLIDE SUMMARY (%):

	6, 81 D	6, 81 D
TEXTURE:		
Silt	10	5
Clay	90	95
COMPOSITION:		
Access. minerals	3	
Clay	59	20
Foraminifers	5	10
Inorganic calcite	6	5
Nannofossils	27	65
Quartz		Tr

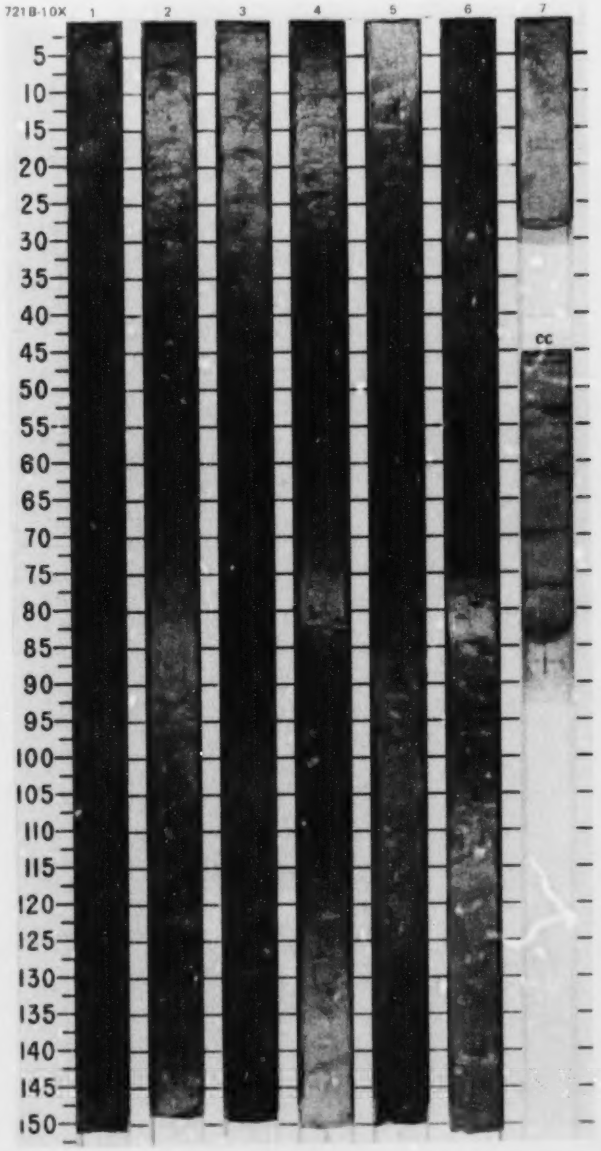
721B-10X
1
2
3
4
5
6
7
CC
5
10
15
20
25
30
35
40
45
50
55
60
65
70
75
80
85
90
95
100
105
110
115
120
125
130
135
140
145
150

SITE 721 HOLE B CORE 11X CORED INTERVAL 2040.4-2050.0 mbsl; 95.6-105.2 mbsf

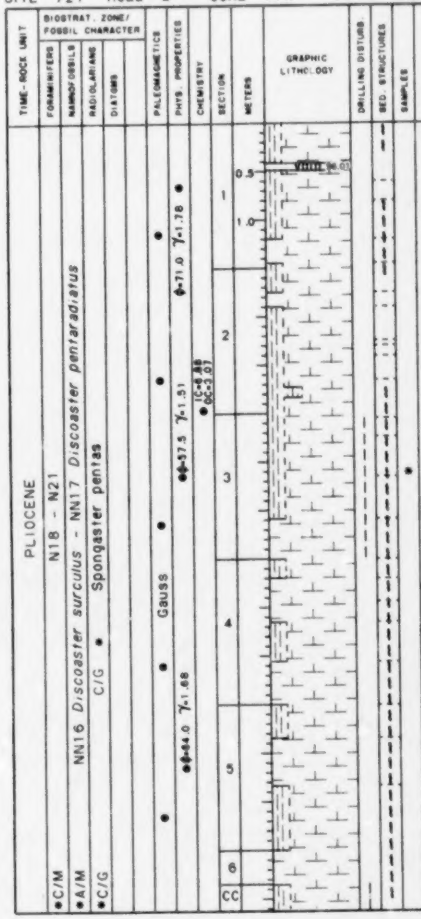
TIME-ROCK UNIT
BIOSTRAT. ZONE/ FOSSIL CHARACTER
FORAMINIFERS
NANNOFOSSILS
RADIOLARIANS
DIATOMS
PALEOMAGNETICS
PHYS. PROPERTIES
CHEMISTRY
SECTION
METERS
GRAPHIC LITHOLOGY
DRILLING DISTURB.
SED. STRUCTURES
SAMPLES
PLIOCENE
N18 - N21
NN16 Discoaster surculus - NN17 Discoaster pentaradiatus
C/G ● Spongaster pentas
●C/M
●A/M
●C/G
Gauss
φ=71.0 γ=1.78
●φ=57.5 γ=1.51
●φ=64.0 γ=1.68
IC=8.88
OC=3.07
1
2
3
4
5
6
CC
0.5
1.0
VOID

LITHOLOGIC DESCRIPTION

NANNOFOSSIL OOZE to FORAMINIFER-BEARING NANNOFOSSIL OOZE

Void in Section 1, 40-43 cm. Remainder of core is undisturbed.

Major lithology: NANNOFOSSIL OOZE to FORAMINIFER-BEARING NANNOFOSSIL OOZE. Alternating light and dark bands of light olive gray (5Y 6/2) to olive (5Y 4/3, 5/3, 4/4) and olive gray (5Y 4/2). Slight to moderate burrow-mottling throughout. Dark layers enriched in terrigenous clay relative to light layers.

Minor lithology: Marly nannofossil ooze, dark olive gray (5Y 3/2). Section 2, 122-132 cm.

SMEAR SLIDE SUMMARY (%)

	3, 61 D
TEXTURE:	
Silt	10
Clay	90
COMPOSITION:	
Access. minerals	Tr
Clay	20
Foraminifers	Tr
Inorganic calcite	5
Nannofossils	70
Radiolarians	5

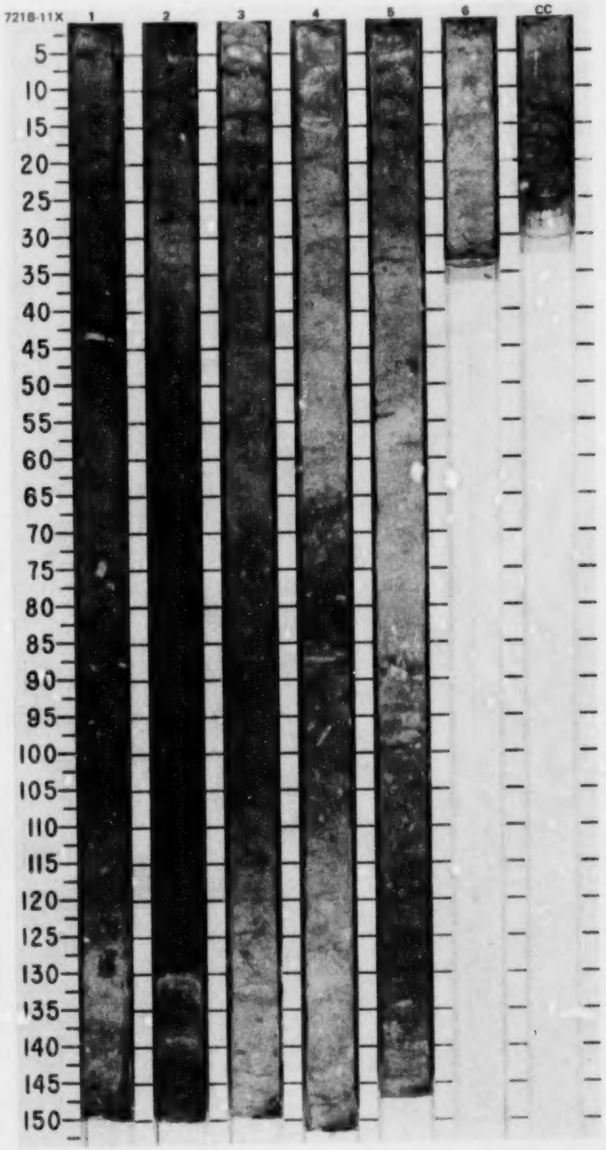
721B-11X
1
2
3
4
5
6
CC
5
10
15
20
25
30
35
40
45
50
55
60
65
70
75
80
85
90
95
100
105
110
115
120
125
130
135
140
145
150

SITE 721 HOLE B CORE 12X CORED INTERVAL 2050.0-2059.6 mbsl; 105.2-114.8 mbsf

TIME-ROCK UNIT	BIOSTRAT. ZONE/ FOSSIL CHARACTER					PALEOMAGNETICS	PHYS. PROPERTIES	CHEMISTRY	SECTION	METERS	GRAPHIC LITHOLOGY	DRILLING DISTURB.	SED. STRUCTURES	SAMPLES	LITHOLOGIC DESCRIPTION
	FORAMINIFERS	NANNOFOSSILS	RADIOLARIANS	DIATOMS											
PLIOCENE	●C/M N18 - N21	●A/M	●C/G *Spongaster pentas*		NN16 *Discoaster surculus* - NN17 *Discoaster pentaradiatus*	● ●	●ϕ=62.4 γ=1.65	●IC=8.38 OC=1.36	1 2 3 CC	0.5 1.0				● ● IW OG	**FORAMINIFER-BEARING NANNOFOSSIL OOZE** Section 1, 23-34 and 47-48 cm, soupy; 0-120 cm, slightly disturbed; and 28-31 cm, void. Remainder of core is undisturbed. Major lithology: FORAMINIFER-BEARING NANNOFOSSIL OOZE. Alternating light and dark bands of light olive gray (5Y 6/2) to olive (5Y 4/3, 5/3, 4/4) and olive gray (5Y 4/2). Slight to moderate burrow-mottling throughout. Dark layers enriched in terrigenous clay relative to light layers. Minor lithology: Marly nannofossil ooze, dark olive gray (5Y 3/2). Section 1, 60-120 cm. Moderate burrow-mottling.

SMEAR SLIDE SUMMARY (%):

	1, 42 D	1, 88 D
TEXTURE:		
Silt	15	35
Clay	85	65
COMPOSITION:		
Clay	15	55
Foraminifers	10	15
Inorganic calcite	5	10
Mica		Tr
Nannofossils	70	15
Quartz	Tr	5
Siliceous frag.	Tr	

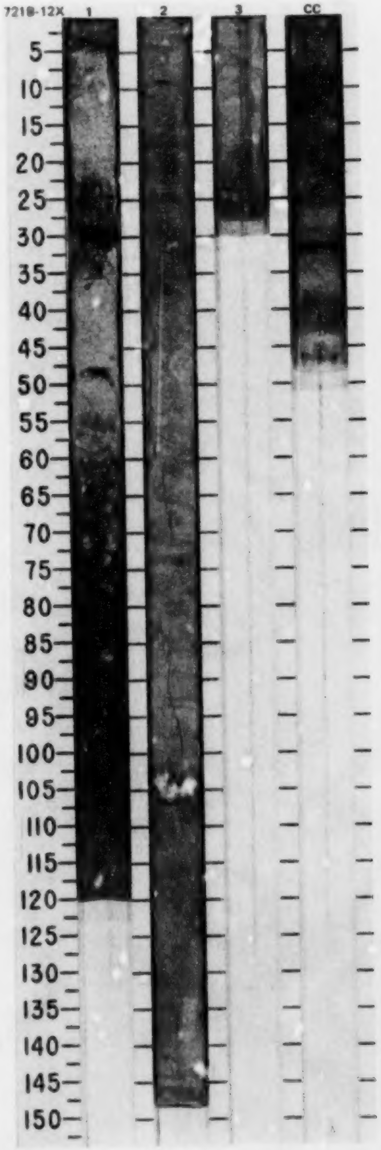

SITE 721 HOLE B CORE 13X CORED INTERVAL 2059.6-2069.2 mbsl; 114.8-124.4 mbsf

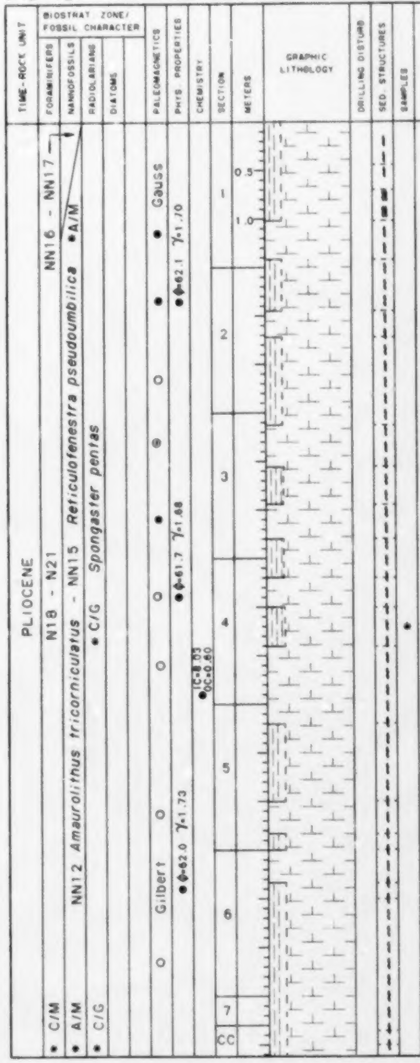
TIME-ROCK UNIT
BIOSTRAT. ZONE/FOSSIL CHARACTER
FORAMINIFERS
NANNOFOSSILS
RADIOLARIANS
DIATOMS
PALEOMAGNETICS
PHYS. PROPERTIES
CHEMISTRY
SECTION
METERS
GRAPHIC LITHOLOGY
DRILLING DISTURB.
SED. STRUCTURES
SAMPLES
PLIOCENE
N18 - N21
NN16 - NN17
• C/M
NN12 Amaurolithus tricorniculatus - NN15 Reticulofenestra pseudoumbilica
•A/M
• A/M
• C/G Spongaster pentas
• C/G
Gauss
Gilbert
●Φ=62.1 γ=1.70
●Φ=61.7 γ=1.88
●Φ=62.0 γ=1.73
IC=8.03
OC=0.60
0.5
1.0
1
2
3
4
5
6
7
CC

LITHOLOGIC DESCRIPTION

FORAMINIFER-BEARING NANNOFOSSIL OOZE

No drilling disturbance.

Major lithology: FORAMINIFER-BEARING NANNOFOSSIL OOZE. Alternating light and dark bands of light olive gray (5Y 6/2) to olive (5Y 4/3, 5/3, 4/4) and olive gray (5Y 4/2). Slight to moderate burrow-mottling throughout. Dark layers enriched in terrigenous clay relative to light layers.

SMEAR SLIDE SUMMARY (%):

	4, 70 D
TEXTURE:	
Silt	10
Clay	90
COMPOSITION:	
Access. minerals	2
Clay	20
Foraminifers	10
Inorganic calcite	3
Mica	Tr
Nannofossils	65
Quartz	Tr

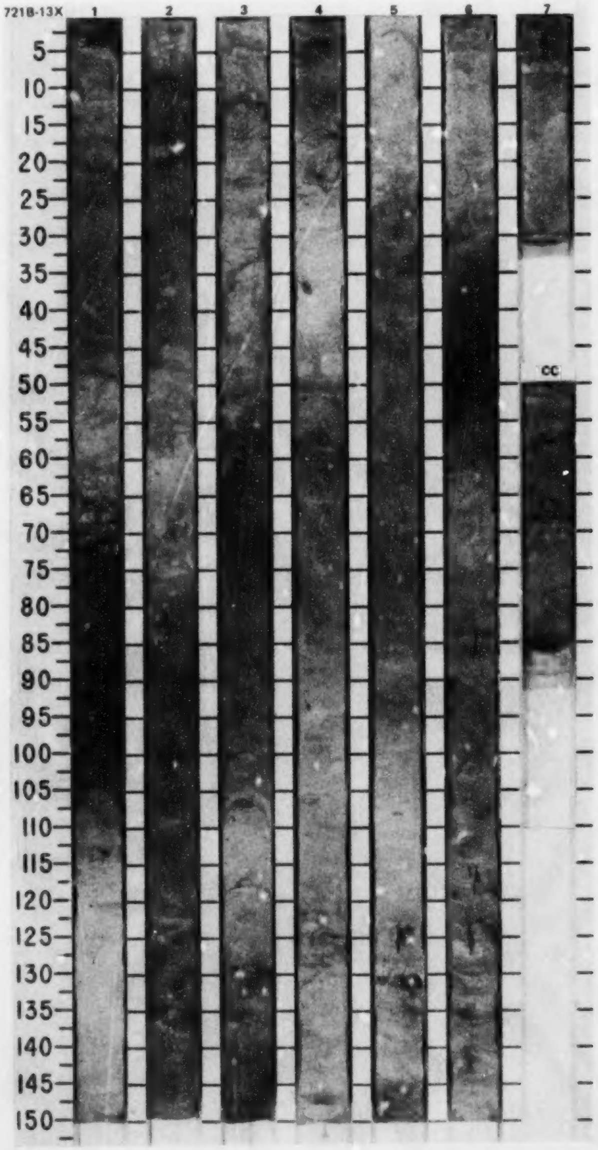
721B-13X
1
2
3
4
5
6
7
CC
5
10
15
20
25
30
35
40
45
50
55
60
65
70
75
80
85
90
95
100
105
110
115
120
125
130
135
140
145
150

SITE 721 HOLE B CORE 14X CORED INTERVAL 2069.2-2078.9 mbsl; 124.4-134.1 mbsf

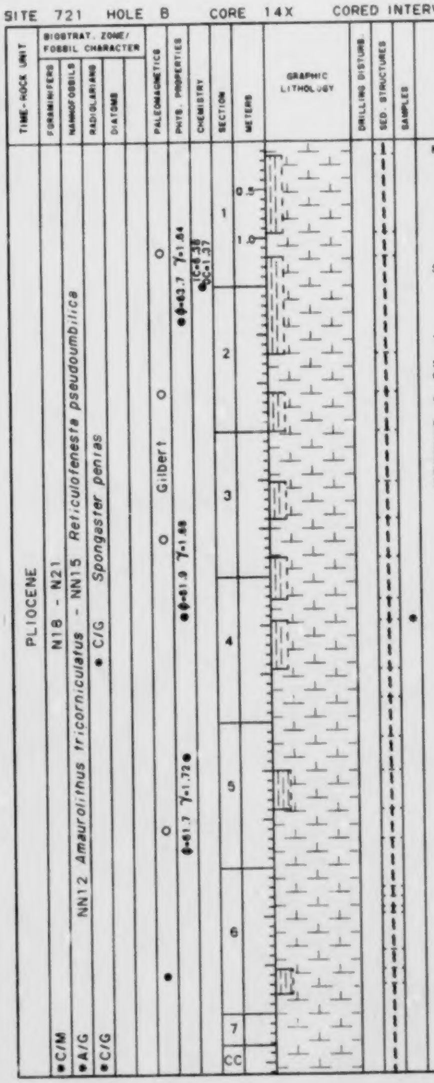
TIME-ROCK UNIT
BIOSTRAT. ZONE/ FOSSIL CHARACTER
FORAMINIFERS
NANNOFOSSILS
RADIOLARIANS
DIATOMS
PALEOMAGNETICS
PHYS. PROPERTIES
CHEMISTRY
SECTION
METERS
GRAPHIC LITHOLOGY
DRILLING DISTURB.
SED. STRUCTURES
SAMPLES
PLIOCENE
N18 - N21
NN12 Amaurolithus tricorniculatus - NN15 Reticulofenestra pseudoumbilica
● C/G Spongaster pentas
●C/M
●A/G
●C/G
Gilbert
●ϕ=63.7 γ=1.84
●ϕ=61.9 γ=1.88
ϕ=61.7 γ=1.72●
IC=8.38
OC=1.37
0.5
1.0
1
2
3
4
5
6
7
CC

LITHOLOGIC DESCRIPTION

NANNOFOSSIL OOZE to FORAMINIFER-BEARING NANNOFOSSIL OOZE

Minor drilling disturbance Section 1, 10-20 cm.

Major lithology: NANNOFOSSIL OOZE to FORAMINIFER-BEARING NANNOFOSSIL OOZE. Altern::ting lighter and darker sediments of light greenish gray (10Y 6/2, 6/4) to dark greenish gray (10Y 5/4, 5/2) and olive (5Y 4/3). Banding on a 5-130 cm scale. Minor bioturbation throughout. Dark layers generally have 10-20% more terrigenous silty clay than ligh' layers.

SMEAR SLIDE SUMMARY (%):

	4, 48 D
TEXTURE:	
Silt	20
Clay	80
COMPOSITION:	
Clay	10
Foraminifers	5
Inorganic calcite	Tr
Nannofossils	80
Quartz	Tr
Radiolarians	5

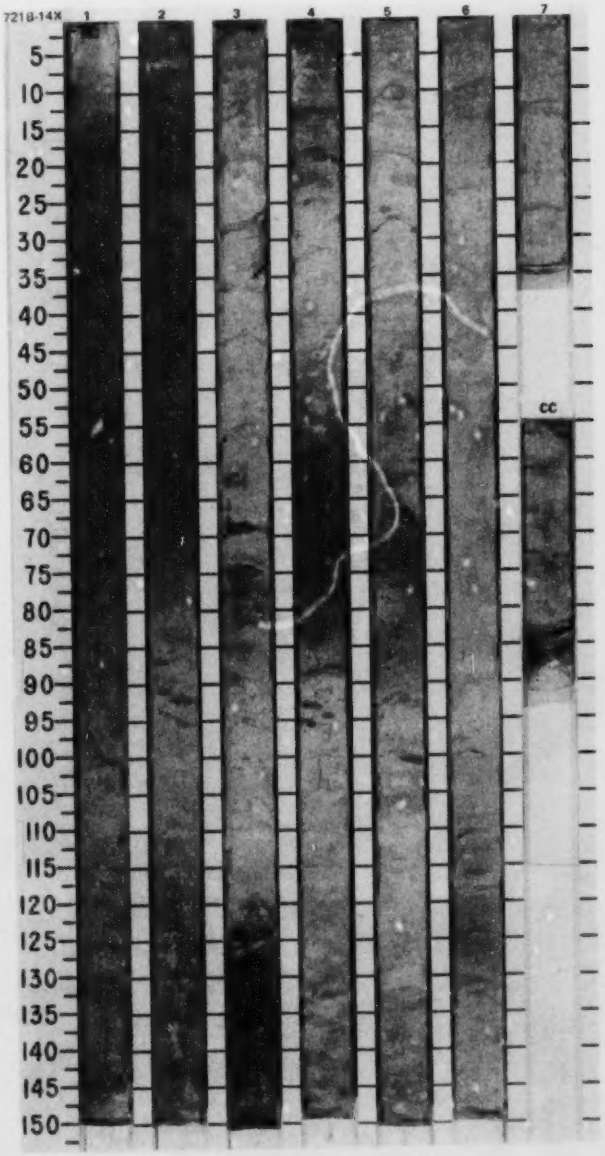
721B-14X
1
2
3
4
5
6
7
CC
5
10
15
20
25
30
35
40
45
50
55
60
65
70
75
80
85
90
95
100
105
110
115
120
125
130
135
140
145
150

SITE 721 HOLE B CORE 15X CORED INTERVAL

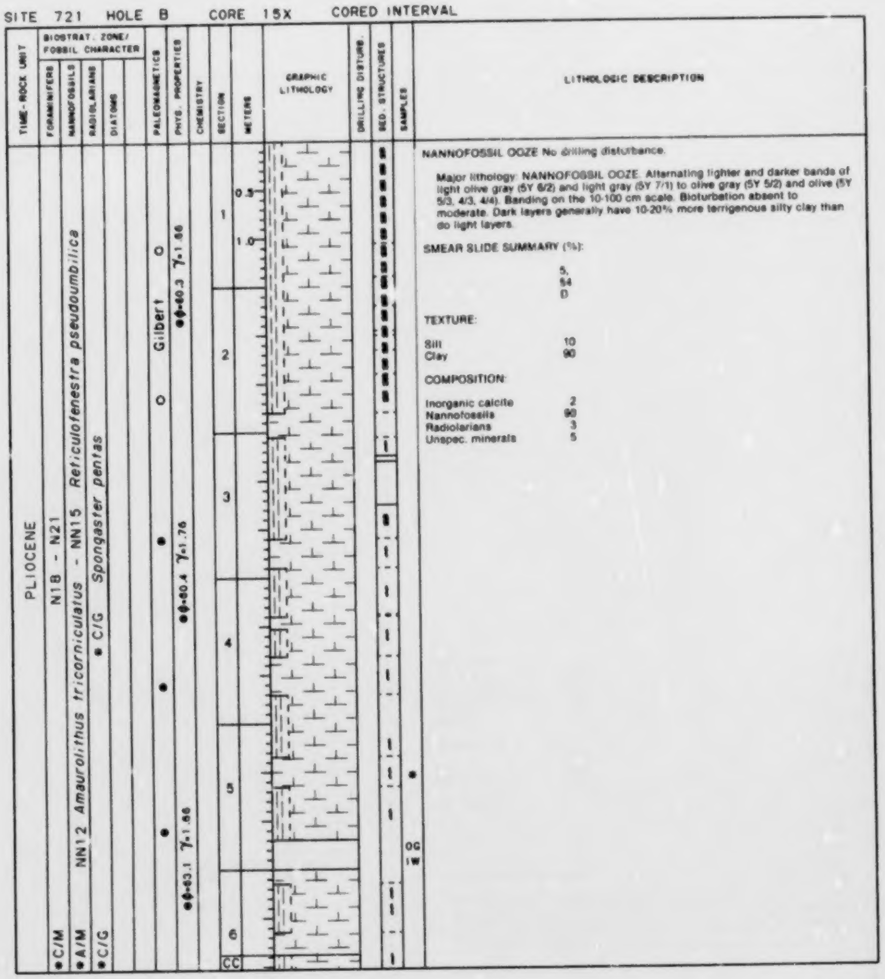
TIME-ROCK UNIT
BIOSTRAT. ZONE/FOSSIL CHARACTER
FORAMINIFERS
NANNOFOSSILS
RADIOLARIANS
DIATOMS
PALEOMAGNETICS
PHYS. PROPERTIES
CHEMISTRY
SECTION
METERS
GRAPHIC LITHOLOGY
DRILLING DISTURB.
SED. STRUCTURES
SAMPLES
PLIOCENE
●C/M N18 - N21
●A/M NN12 Amaurolithus tricorniculatus - NN15 Reticulofenestra pseudoumbilica
●C/G ● C/G Spongaster pentas
Gilbert
●ϕ=60.3 γ=1.66
●ϕ=60.4 γ=1.76
●ϕ=63.1 γ=1.66
0.5
1.0
1
2
3
4
5
6
CC
OG
IW

LITHOLOGIC DESCRIPTION

NANNOFOSSIL OOZE No drilling disturbance.

Major lithology: NANNOFOSSIL OOZE. Alternating lighter and darker bands of light olive gray (5Y 6/2) and light gray (5Y 7/1) to olive gray (5Y 5/2) and olive (5Y 5/3, 4/3, 4/4). Banding on the 10-100 cm scale. Bioturbation absent to moderate. Dark layers generally have 10-20% more terrigenous silty clay than do light layers.

SMEAR SLIDE SUMMARY (%):

	5, 54 D
TEXTURE:	
Silt	10
Clay	90
COMPOSITION:	
Inorganic calcite	2
Nannofossils	90
Radiolarians	3
Unspec. minerals	5

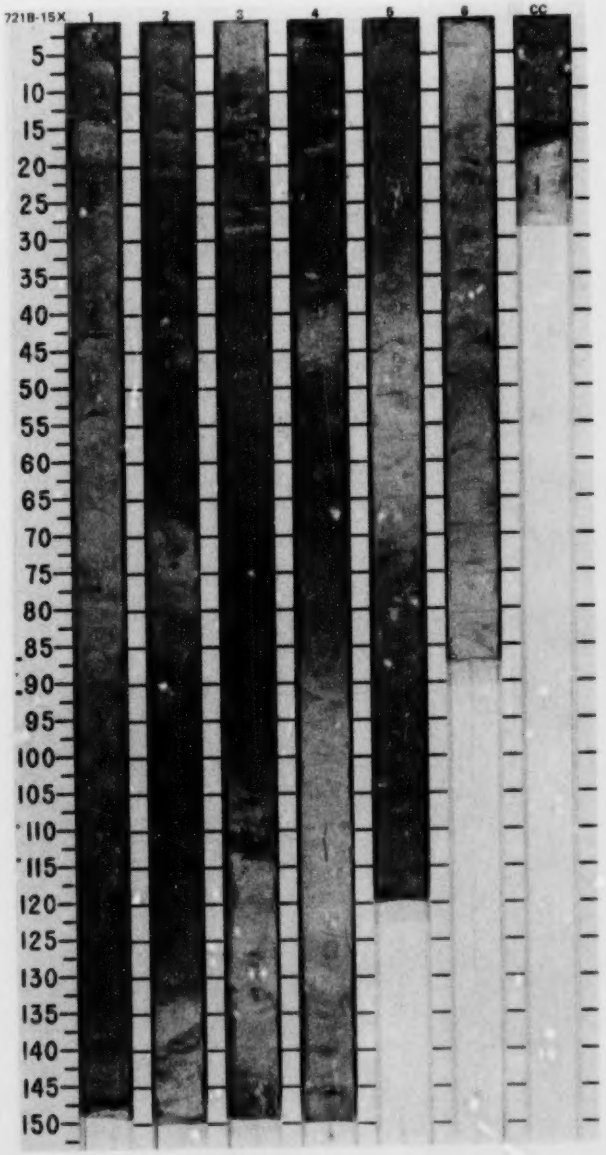
721B-15X
1
2
3
4
5
6
CC
5
10
15
20
25
30
35
40
45
50
55
60
65
70
75
80
85
90
95
100
105
110
115
120
125
130
135
140
145
150

SITE 721 HOLE B CORE 16X CORED INTERVAL 2088.6-2098.3 mbsl; 143.8-153.5 mbsf

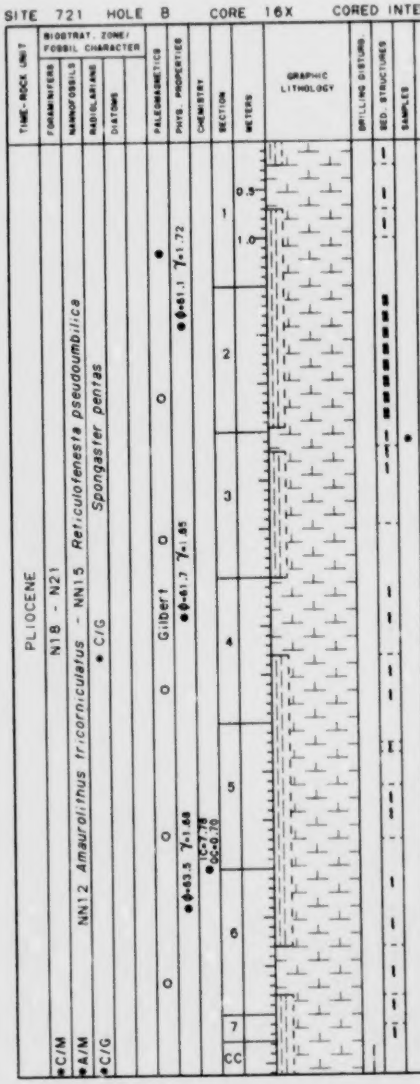
TIME-ROCK UNIT
BIOSTRAT. ZONE/ FOSSIL CHARACTER
FORAMINIFERS
NANNOFOSSILS
RADIOLARIANS
DIATOMS
PALEOMAGNETICS
PHYS. PROPERTIES
CHEMISTRY
SECTION
METERS
GRAPHIC LITHOLOGY
DRILLING DISTURB.
SED. STRUCTURES
SAMPLES
PLIOCENE
N18 - N21
NN12 Amaurolithus tricorniculatus - NN15 Reticulofenesta pseudoumbilica
● C/G Spongaster pentas
●C/M
●A/M
●C/G
Gilbert
●ϕ=61.1 γ=1.72
●ϕ=61.7 γ=1.85
●ϕ=63.5 γ=1.88
●IC=7.78 OC=0.70
0.5
1.0
1
2
3
4
5
6
7
CC

LITHOLOGIC DESCRIPTION

NANNOFOSSIL OOZE to FORAMINIFER-BEARING NANNOFOSSIL OOZE

Moderate drilling disturbance, CC.

Major lithology: NANNOFOSSIL OOZE to FORAMINIFER-BEARING NANNOFOSSIL OOZE. Alternating lighter and darker bands of light gray (5Y 7/1, 7/2) to pale olive (5Y 6/3) and olive (5Y 5/3, 5/4, 4/3, 4/4). Banding on a 20-150 cm scale. Bioturbation absent to moderate. Dark layers generally have 10-20% more terrigenous silty clay than do light layers.

SMEAR SLIDE SUMMARY (%):

	3, 8 D
TEXTURE:	
Silt	10
Clay	90
COMPOSITION:	
Access. minerals	5
Clay	10
Diatoms	Tr
Foraminifers	10
Inorganic calcite	Tr
Mica	Tr
Nannofossils	75
Radiolarians	Tr

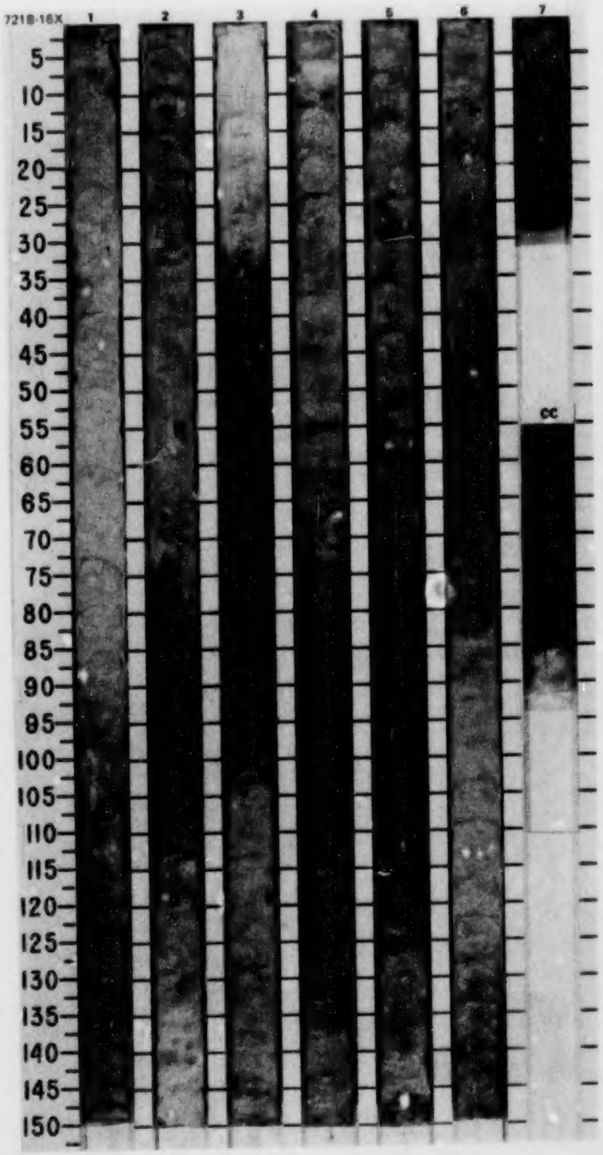
721B-16X
1
2
3
4
5
6
7
CC
5
10
15
20
25
30
35
40
45
50
55
60
65
70
75
80
85
90
95
100
105
110
115
120
125
130
135
140
145
150

SITE 721 HOLE B CORE 17X CORED INTERVAL 2098.3-2108.0 mbsl; 153.5-163.2 mbsf

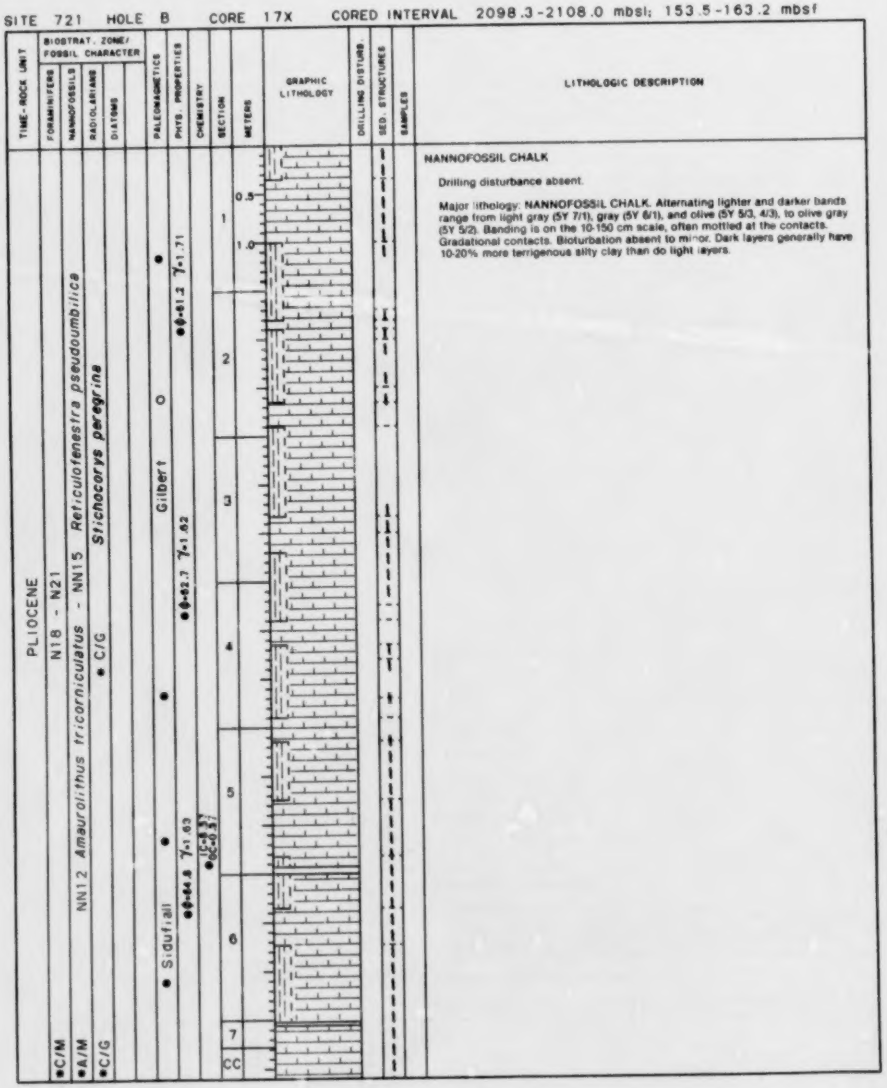
TIME-ROCK UNIT
BIOSTRAT. ZONE/ FOSSIL CHARACTER
FORAMINIFERS
NANNOFOSSILS
RADIOLARIANS
DIATOMS
PALEOMAGNETICS
PHYS. PROPERTIES
CHEMISTRY
SECTION
METERS
GRAPHIC LITHOLOGY
DRILLING DISTURB.
SED. STRUCTURES
SAMPLES
PLIOCENE
N18 - N21
NN12 Amaurolithus tricorniculatus - NN15 Reticulofenestra pseudoumbilica
Stichocorys peregrina
● C/G
●C/M
●A/M
●C/G
Gilbert
Sidufjall
●φ=61.2 γ=1.71
●φ=62.7 γ=1.62
●φ=64.8 γ=1.63
●IC=8.37 OC=0.37
1
2
3
4
5
6
7
CC
0.5
1.0

LITHOLOGIC DESCRIPTION

NANNOFOSSIL CHALK

Drilling disturbance absent.

Major lithology: NANNOFOSSIL CHALK. Alternating lighter and darker bands range from light gray (5Y 7/1), gray (5Y 6/1), and olive (5Y 5/3, 4/3), to olive gray (5Y 5/2). Banding is on the 10-150 cm scale, often mottled at the contacts. Gradational contacts. Bioturbation absent to minor. Dark layers generally have 10-20% more terrigenous silty clay than do light layers.

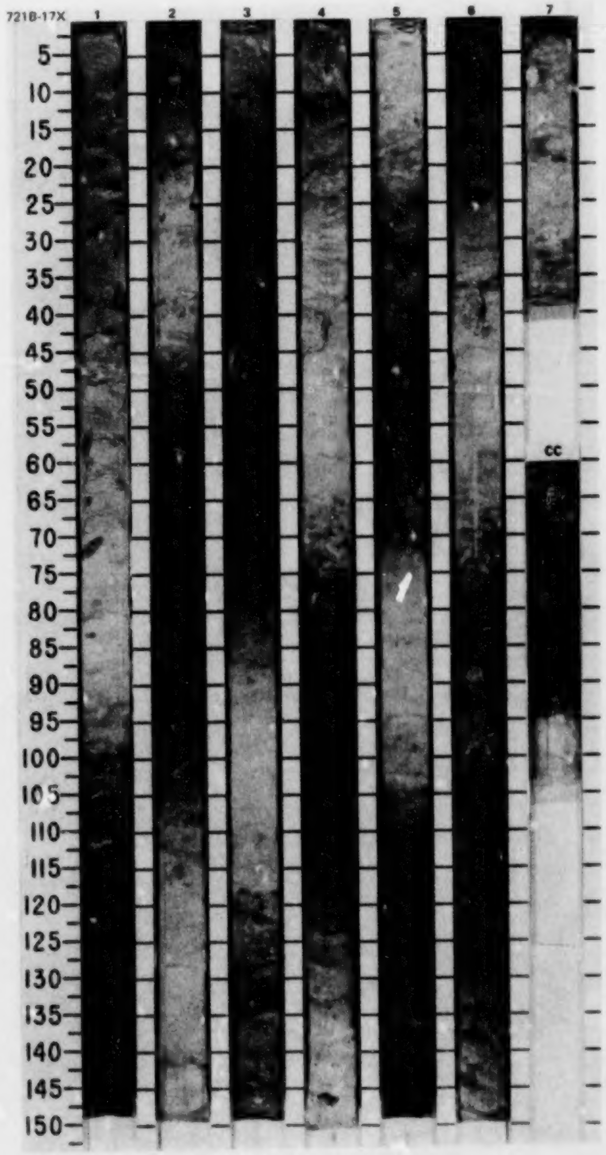
721B-17X
1
2
3
4
5
6
7
CC
5
10
15
20
25
30
35
40
45
50
55
60
65
70
75
80
85
90
95
100
105
110
115
120
125
130
135
140
145
150

SITE 721 HOLE B CORE 18X CORED INTERVAL 2108.0-2117.7 mbsl: 163.2-172.9 mbsf

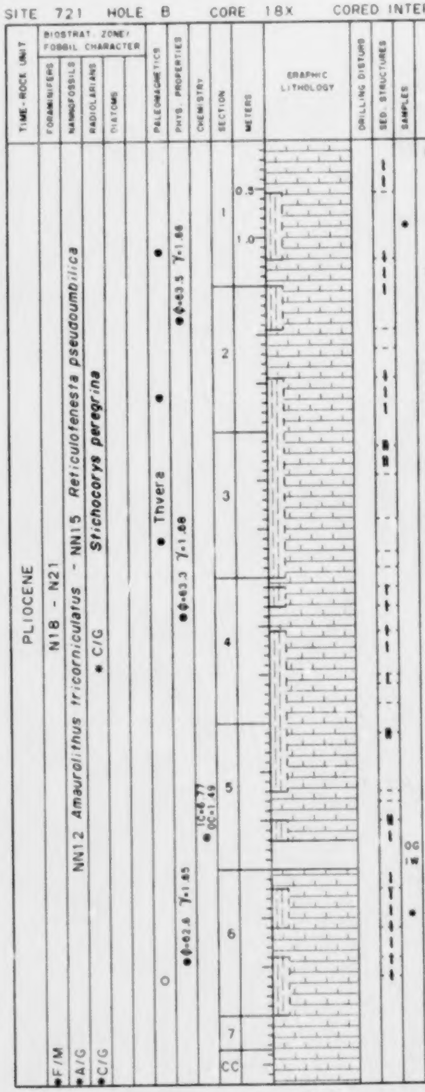
TIME-ROCK UNIT
BIOSTRAT. ZONE/ FOSSIL CHARACTER
FORAMINIFERS
NANNOFOSSILS
RADIOLARIANS
DIATOMS
PALEOMAGNETICS
PHYS. PROPERTIES
CHEMISTRY
SECTION
METERS
GRAPHIC LITHOLOGY
DRILLING DISTURB.
SED. STRUCTURES
SAMPLES
PLIOCENE
N18 - N21
NN12 Amaurolithus tricorniculatus - NN15 Reticulofenesta pseudoumbilica
Stichocorys peregrina
• C/G
• Thvera
○
•φ=63.5 γ=1.86
•φ=63.3 γ=1.88
•φ=62.6 γ=1.85
• TC=6.77 OC=1.49
0.5
1.0
1
2
3
4
5
6
7
CC
OG
IW
•F/M
•A/G
•C/G

LITHOLOGIC DESCRIPTION

NANNOFOSSIL CHALK to FORAMINIFER-BEARING NANNOFOSSIL CHALK

Early stages of drilling biscuits; some splitting disturbance.

Major lithology: NANNOFOSSIL CHALK to FORAMINIFER-BEARING NANNOFOSSIL CHALK. Alternating lighter and darker bands on a 10-70 cm scale, light gray (5Y 7/1), gray (5Y 6/1), light olive gray (5Y 6/2), and pale olive (5Y 6/3) to olive (5Y 5/3, 4/3). Bioturbation absent to moderate. Dark layers generally have 10-20% more terrigenous silty clay than do light layers.

SMEAR SLIDE SUMMARY (%):

	1, 84 D	6, 45 D
TEXTURE:		
Sand	5	5
Silt	10	10
Clay	85	85
COMPOSITION:		
Access. minerals		1
Diatoms	Tr	Tr
Foraminifers	5	3
Volcanic glass		Tr
Inorganic calcite	10	10
Mica	Tr	Tr
Nannofossils	85	85
Quartz	Tr	1
Radiolarians	Tr	Tr
Silicoflagellates	Tr	Tr
Sponge spicules	Tr	Tr

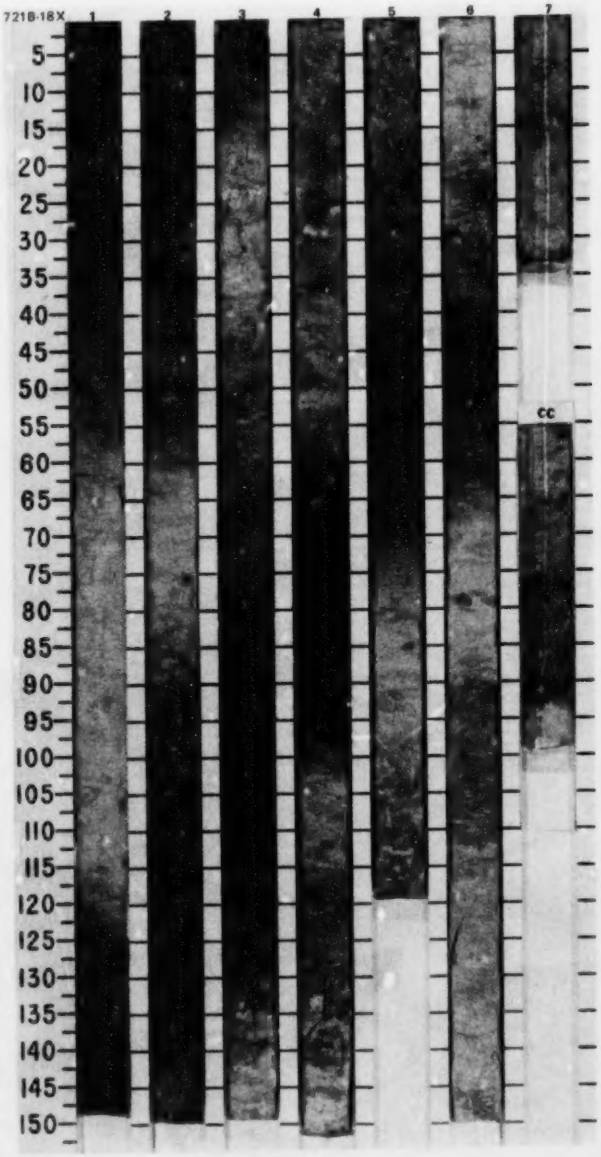
721B-18X
1
2
3
4
5
6
7
CC
5
10
15
20
25
30
35
40
45
50
55
60
65
70
75
80
85
90
95
100
105
110
115
120
125
130
135
140
145
150

SITE 721 HOLE B CORE 19X CORED INTERVAL 2117.7-2127.4 mbsl; 172.9-182.6 mbsf

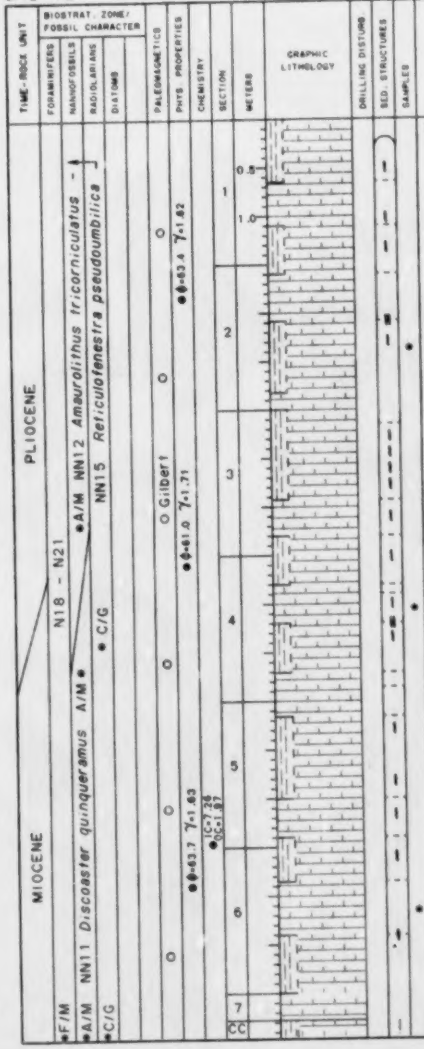
TIME-ROCK UNIT
BIOSTRAT. ZONE/ FOSSIL CHARACTER
FORAMINIFERS
NANNOFOSSILS
RADIOLARIANS
DIATOMS
PALEOMAGNETICS
PHYS. PROPERTIES
CHEMISTRY
SECTION
METERS
GRAPHIC LITHOLOGY
DRILLING DISTURB.
SED. STRUCTURES
SAMPLES
PLIOCENE
MIOCENE
N18 - N21
●F/M
●A/M NN12 Amaurolithus tricorniculatus
NN11 Discoaster quinqueramus A/M ●
●A/M
NN15 Reticulofenestra pseudoumbilica
● C/G
●C/G
O Gilbert
●ϕ=63.4 γ=1.82
●ϕ=61.0 γ=1.71
●ϕ=63.7 γ=1.83
●IC=7.26 OC=1.87
0.5
1.0
1
2
3
4
5
6
7
CC

LITHOLOGIC DESCRIPTION

NANNOFOSSIL CHALK

Undisturbed core.

Major lithology: NANNOFOSSIL CHALK. Alternating lighter and darker bands range from light gray (5Y 7/1), light olive gray (5Y 6/2), and pale olive (5Y 6/3) to olive (5Y 5/4, 7/3, 5/3). Bioturbation absent to moderate. Light layers generally have 10-20% less terrigenous silty clay than do dark layers.

SMEAR SLIDE SUMMARY (%):

	2, 85 D	4, 55 D	6, 65 D
TEXTURE:			
Sand		2	2
Silt	10	8	8
Clay	90	90	90
COMPOSITION:			
Access. minerals	1	Tr	Tr
Foraminifers	Tr	2	2
Volcanic glass			Tr
Inorganic calcite	8	7	7
Mica		Tr	Tr
Nannofossils	90	90	90
Quartz	Tr		Tr
Radiolarians	Tr	Tr	Tr
Silicoflagellates	1	1	1
Sponge spicules	Tr		

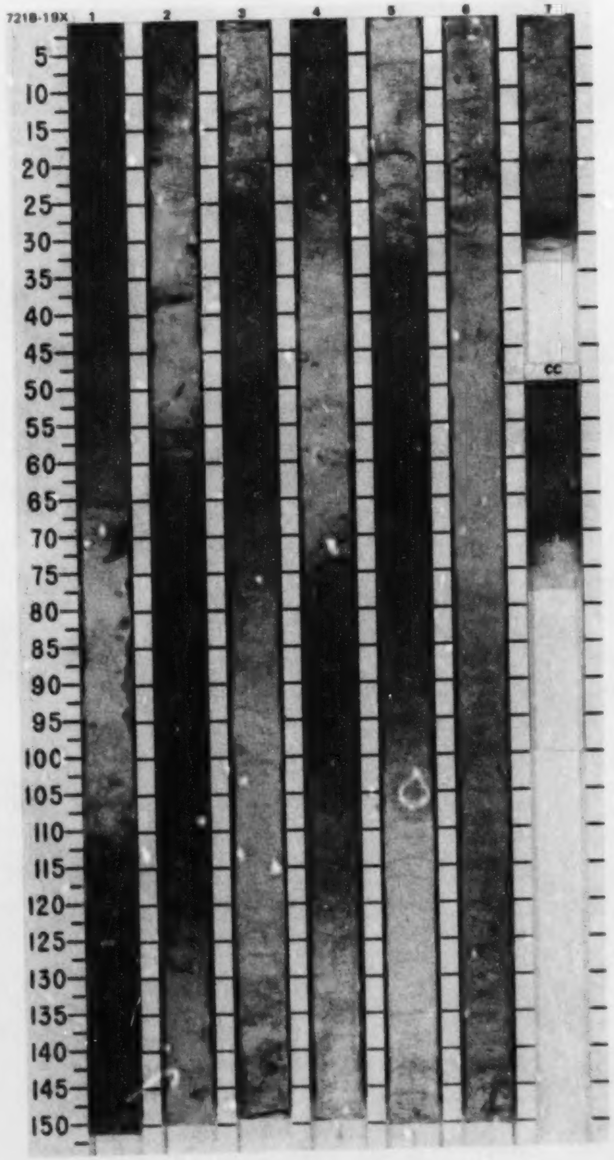
721B-19X
1
2
3
4
5
6
7
CC
5
10
15
20
25
30
35
40
45
50
55
60
65
70
75
80
85
90
95
100
105
110
115
120
125
130
135
140
145
150

SITE 721 HOLE B CORE 20X CORED INTERVAL 2127.4-2137.1 mbsl; 182.6-192.3 mbsf

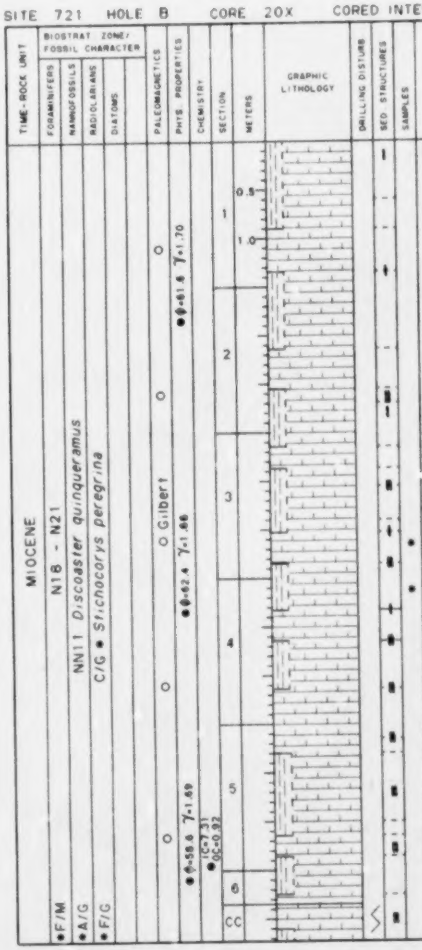
TIME-ROCK UNIT
BIOSTRAT. ZONE/ FOSSIL CHARACTER
FORAMINIFERS
NANNOFOSSILS
RADIOLARIANS
DIATOMS
PALEOMAGNETICS
PHYS. PROPERTIES
CHEMISTRY
SECTION
METERS
GRAPHIC LITHOLOGY
DRILLING DISTURB.
SED. STRUCTURES
SAMPLES
MIOCENE
N18 - N21
NN11 Discoaster quinqueramus
C/G ● Stichocorys peregrina
●F/M
●A/G
●F/G
O
O
O Gilbert
O
O
●ϕ=61.8 γ=1.70
●ϕ=62.4 γ=1.66
●ϕ=58.6 γ=1.69
●IC=7.31
OC=0.92
1
2
3
4
5
6
CC
0.5
1.0

LITHOLOGIC DESCRIPTION

NANNOFOSSIL CHALK to FORAMINIFER-BEARING NANNOFOSSIL CHALK

Slightly disturbed, Section 6, 0-30 cm; very disturbed CC, 20-30 cm.

Major lithology: NANNOFOSSIL CHALK to FORAMINIFER-BEARING NANNOFOSSIL CHALK. Alternating lighter and darker layers. Colors range from light gray (5Y 7/1), light olive gray (5Y 6/2), and pale olive (5Y 6/3), to olive (5Y 5/4, 4/4). Banding on a scale of 10-70 cm. Bioturbation, absent to moderate, shows up as mottling over gradational contacts. Light layers generally have 10-20% less terrigenous silty clay than do dark layers.

SMEAR SLIDE SUMMARY (%):

	3, 115 D	4, 12 D
TEXTURE:		
Sand	5	
Silt	5	20
Clay	90	80
COMPOSITION:		
Access. minerals	Tr	1
Diatoms	Tr	
Dolomite		Tr
Foraminifers	5	
Volcanic glass	Tr	
Inorganic calcite	5	15
Mica	Tr	Tr
Nannofossils	90	80
Quartz	Tr	Tr
Radiolarians	Tr	Tr
Silicoflagellates	Tr	4
Sponge spicules	Tr	Tr

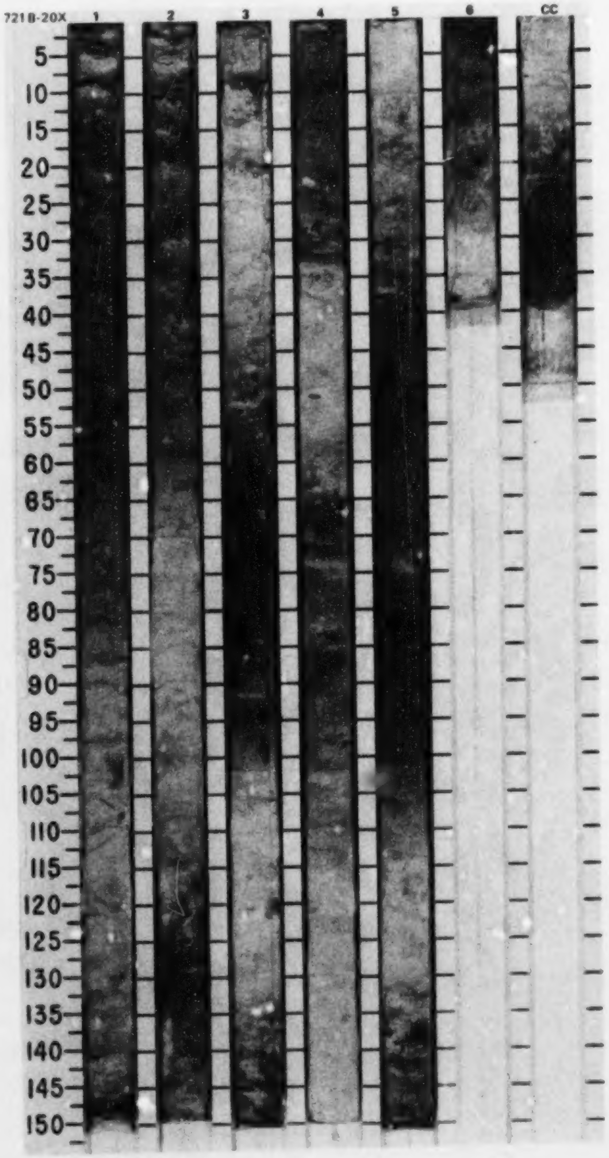
721B-20X
1
2
3
4
5
6
CC
5
10
15
20
25
30
35
40
45
50
55
60
65
70
75
80
85
90
95
100
105
110
115
120
125
130
135
140
145
150

SITE 721 HOLE B CORE 21X CORED INTERVAL 2137.1-2146.8 mbsl; 192.3-202.0 mbsf

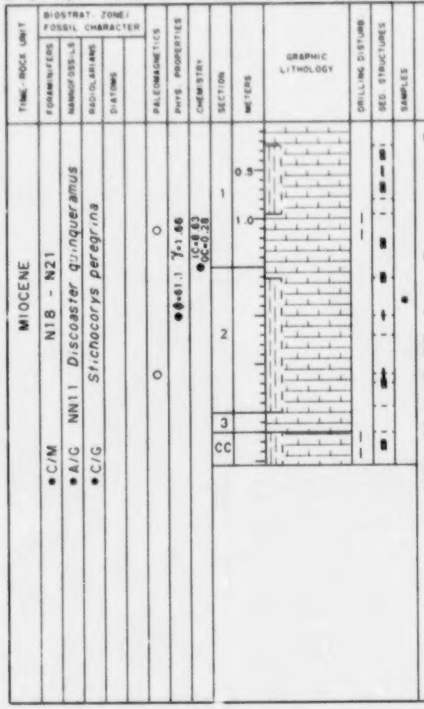
TIME-ROCK UNIT
BIOSTRAT. ZONE/FOSSIL CHARACTER
FORAMINIFERS
NANNOFOSSILS
RADIOLARIANS
DIATOMS
PALEOMAGNETICS
PHYS. PROPERTIES
CHEMISTRY
SECTION
METERS
GRAPHIC LITHOLOGY
DRILLING DISTURB.
SED. STRUCTURES
SAMPLES
MIOCENE
●C/M N18 - N21
●A/G NN11 Discoaster quinqueramus
●C/G Stichocorys peregrina
φ=61.1 γ=1.86
IC=8.63
OC=0.28
1
2
3
CC
0.5
1.0

LITHOLOGIC DESCRIPTION

NANNOFOSSIL CHALK

Slightly disturbed, Section 1, 95-105 cm; Section 3, CC, 10-25 cm.

Major lithology: NANNOFOSSIL CHALK. Alternating lighter and darker layers. Colors range from light gray (5Y 7/1) and olive gray (5Y 5/2) to olive gray (5Y 5/3, 4/3, 5/4). Layering is on a scale of 15-50 cm. Bioturbation absent to strong. Contacts mottled by bioturbation. Light layers generally have 10-20% less terrigenous silty clay than do dark layers.

SMEAR SLIDE SUMMARY (%):

	2, 36 D
TEXTURE:	
Silt	10
Clay	90
COMPOSITION:	
Access. minerals	Tr
Volcanic glass	Tr
Inorganic calcite	9
Mica	1
Nannofossils	90
Quartz	Tr
Radiolarians	Tr
Silicoflagellates	Tr

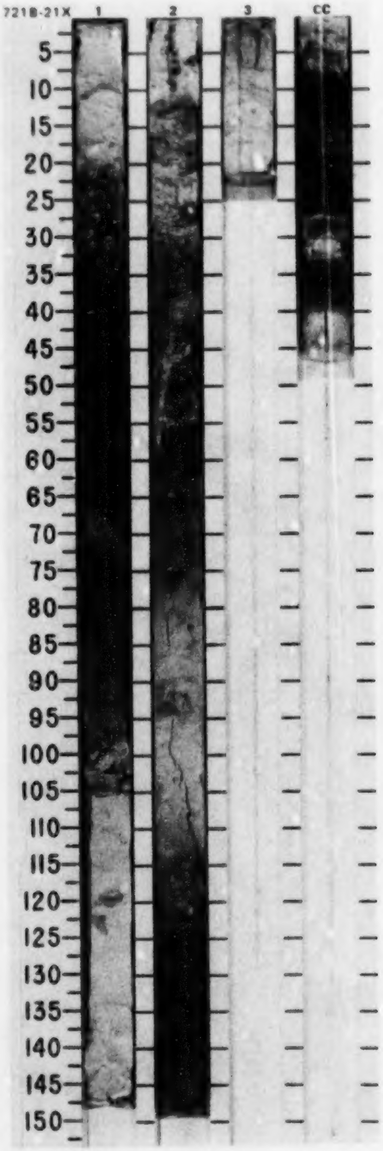
721B-21X
1
2
3
CC
5
10
15
20
25
30
35
40
45
50
55
60
65
70
75
80
85
90
95
100
105
110
115
120
125
130
135
140
145
150

SITE 721 HOLE B CORE 22X CORED INTERVAL 2146.8-2156.5 mbsl; 202.0-211.7 mbsf

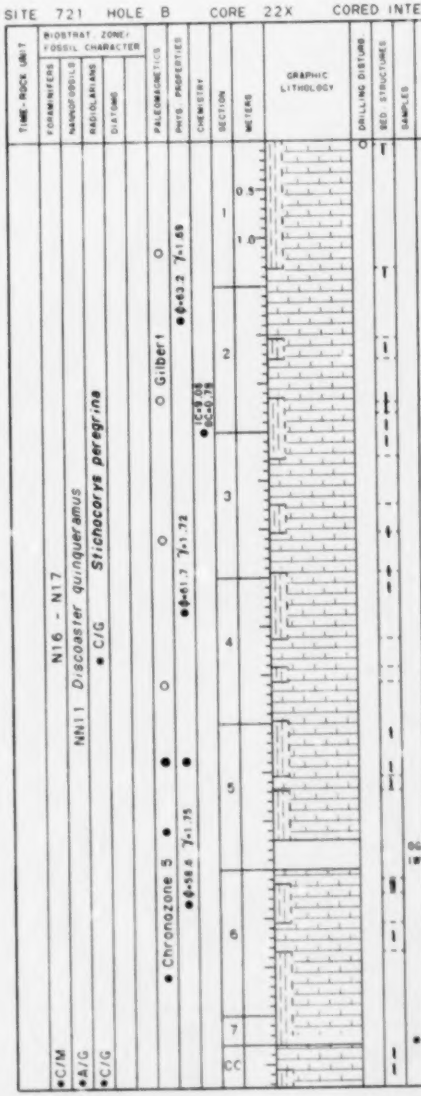
TIME-ROCK UNIT
BIOSTRAT. ZONE/ FOSSIL CHARACTER
FORAMINIFERS
NANNOFOSSILS
RADIOLARIANS
DIATOMS
PALEOMAGNETICS
PHYS. PROPERTIES
CHEMISTRY
SECTION
METERS
GRAPHIC LITHOLOGY
DRILLING DISTURB.
SED. STRUCTURES
SAMPLES
N16 - N17
NN11 Discoaster quinqueramus
• C/G Stichocorys peregrina
•C/M
•A/G
•C/G
○ Gilbert
• Chronozone 5
•φ=63.2 γ=1.69
•φ=61.7 γ=1.72
•φ=58.8 γ=1.75
•IC=9.08 OC=0.79
0.5
1.0
1
2
3
4
5
6
7
CC
OG
IW

LITHOLOGIC DESCRIPTION

NANNOFOSSIL CHALK

Undisturbed core.

Major lithology: NANNOFOSSIL CHALK. Alternating lighter and darker layers. Colors range from light gray (5Y 7/1) and light olive gray (5Y 5/4, 4/4, 4/3) to live gray (5Y 4/2). Layers range from 20-130 cm. Bioturbation absent to moderate, causing mottled gradational contacts. Light layers generally have 10-20% less terrigenous silty clay than the dark layers.

SMEAR SLIDE SUMMARY (%):

	7, 28 D
TEXTURE:	
Sand	2
Silt	8
Clay	90
COMPOSITION:	
Diatoms	Tr
Foraminifers	2
Inorganic calcite	3
Nannofossils	85
Silicoflagellates	10
Sponge spicules	Tr

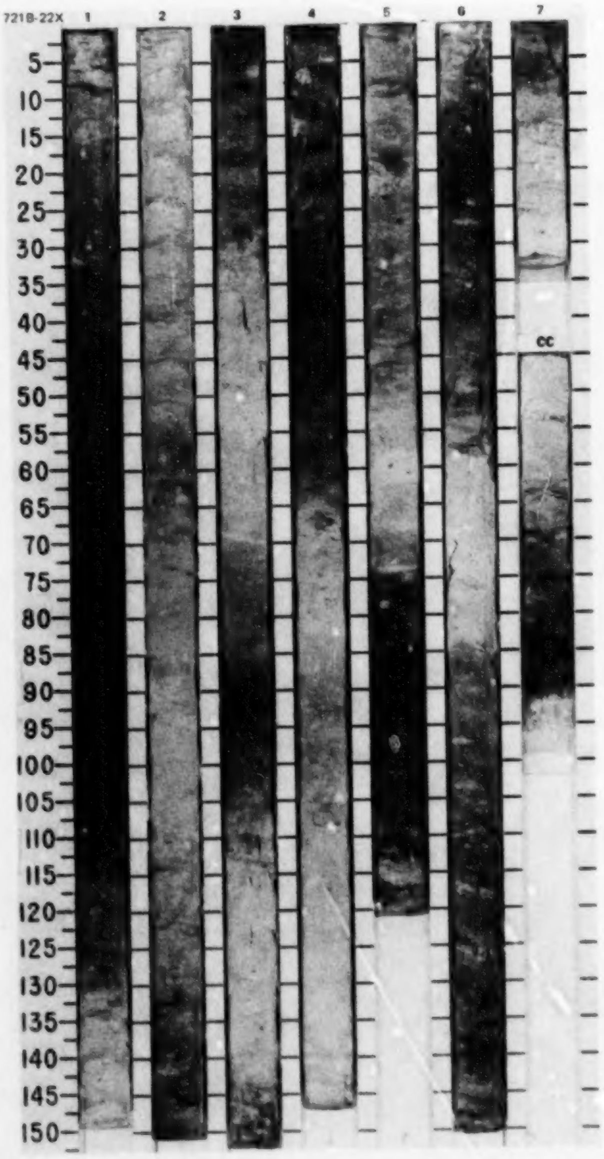
721B-22X
1
2
3
4
5
6
7
CC
5
10
15
20
25
30
35
40
45
50
55
60
65
70
75
80
85
90
95
100
105
110
115
120
125
130
135
140
145
150

SITE 721 HOLE B CORE 23X CORED INTERVAL 2156.5-2166.1 mbsl; 211.7-221.3 mbsf

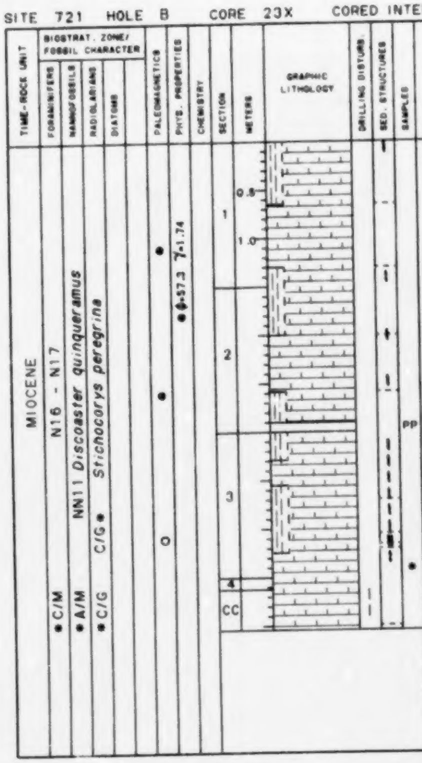
TIME-ROCK UNIT
BIOSTRAT. ZONE/ FOSSIL CHARACTER
FORAMINIFERS
NANNOFOSSILS
RADIOLARIANS
DIATOMS
PALEOMAGNETICS
PHYS. PROPERTIES
CHEMISTRY
SECTION
METERS
GRAPHIC LITHOLOGY
DRILLING DISTURB.
SED. STRUCTURES
SAMPLES
MIOCENE
N16 - N17
NN11 Discoaster quinqueramus
Stichocorys peregrina
C/G
● C/M
● A/M
● C/G
● φ=57.3 γ=1.74
1
2
3
4
CC
0.5
1.0
PP

LITHOLOGIC DESCRIPTION

NANNOFOSSIL CHALK

CC disturbed, 0-20 cm.

Major lithology: NANNOFOSSIL CHALK. Alternating light and dark layers. Color ranges from light gray (5Y 7/1, 7/2), pale olive (5Y 6/3), and olive (5Y 5/3, 4/3) to very dark gray (5Y 3/1). Layers range from 10-70 cm thick. Bioturbation ranges from absent to moderate; mottling over gradational contacts. Light layers generally have 10-20% less terrigenous silty clay than do dark layers.

SMEAR SLIDE SUMMARY (%):

	3, 136 D
TEXTURE:	
Sand	1
Silt	5
Clay	94
COMPOSITION:	
Access. minerals	Tr
Dolomite	Tr
Foraminifers	Tr
Inorganic calcite	5
Mica	Tr
Nannofossils	85
Silicoflagellates	10
Sponge spicules	Tr

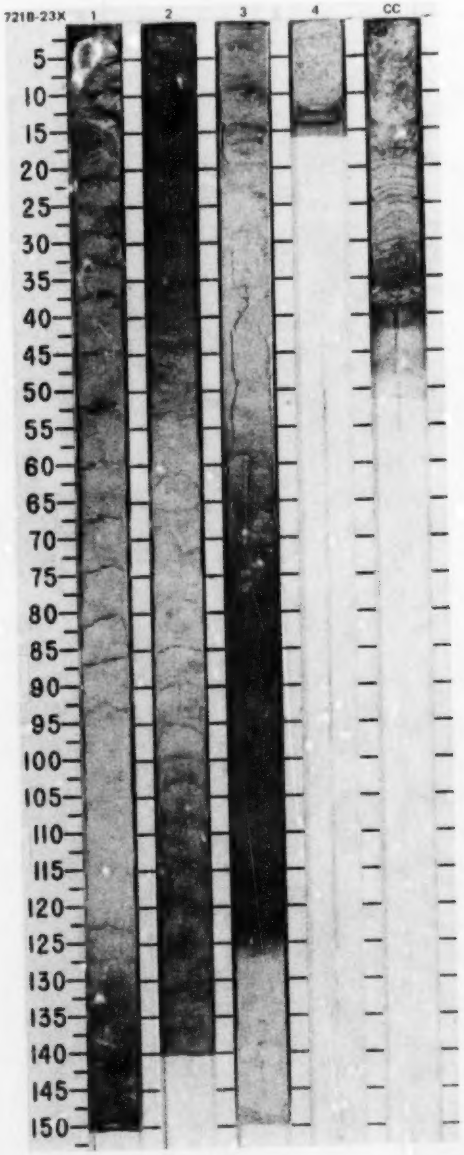
721B-23X
1
2
3
4
CC
5
10
15
20
25
30
35
40
45
50
55
60
65
70
75
80
85
90
95
100
105
110
115
120
125
130
135
140
145
150

SITE 721 HOLE B CORE 24X CORED INTERVAL 2166.1-2175.3 mbsl; 221.3-230.5 mbsf

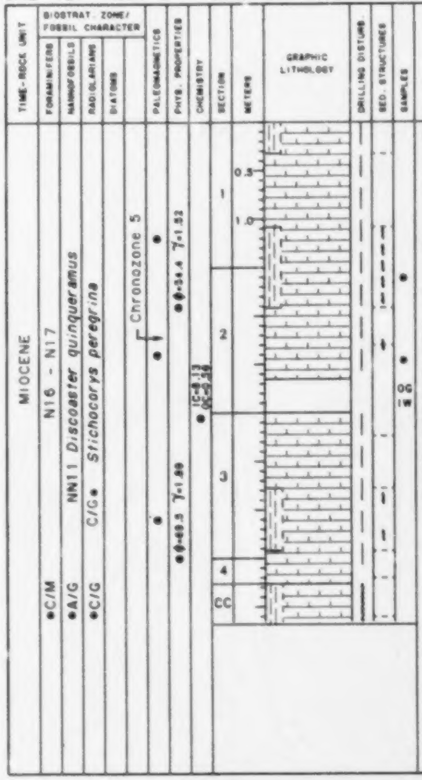
TIME-ROCK UNIT
BIOSTRAT. ZONE/ FOSSIL CHARACTER
FORAMINIFERS
NANNOFOSSILS
RADIOLARIANS
DIATOMS
PALEOMAGNETICS
PHYS. PROPERTIES
CHEMISTRY
SECTION
METERS
GRAPHIC LITHOLOGY
DRILLING DISTURB.
SED. STRUCTURES
SAMPLES
MIOCENE
●C/M N16 - N17
●A/G NN11 Discoaster quinqueramus
●C/G C/G● Stichocorys peregrina
Chronozone 5
●φ=54.4 γ=1.82
●φ=69.5 γ=1.60
●IC=8.13 OC=0.38
1
2
3
4
CC
0.5
1.0
OG
IW

LITHOLOGIC DESCRIPTION

NANNOFOSSIL CHALK

Drilling biscuits forming; slightly disturbed throughout. CC very disturbed.

Major lithology: NANNOFOSSIL CHALK. Alternating light and dark layers. Color ranges from light gray (5Y 7/1), light olive gray (5Y 6/2), and pale olive (5Y 6/3) to olive (5Y 4/3, 5/3). Bioturbation absent to minor. Dark layers generally have 10-20% more terrigenous silty clay than do light layers.

SMEAR SLIDE SUMMARY (%):

	2, 11 D	2, 96 D
TEXTURE:		
Sand	Tr	
Silt	5	10
Clay	95	90
COMPOSITION:		
Access. minerals		Tr
Diatoms	Tr	
Foraminifers	5	Tr
Inorganic calcite	3	2
Nannofossils	92	88
Quartz	Tr	Tr
Radiolarians	Tr	Tr
Silicoflagellates	Tr	10
Sponge spicules		Tr

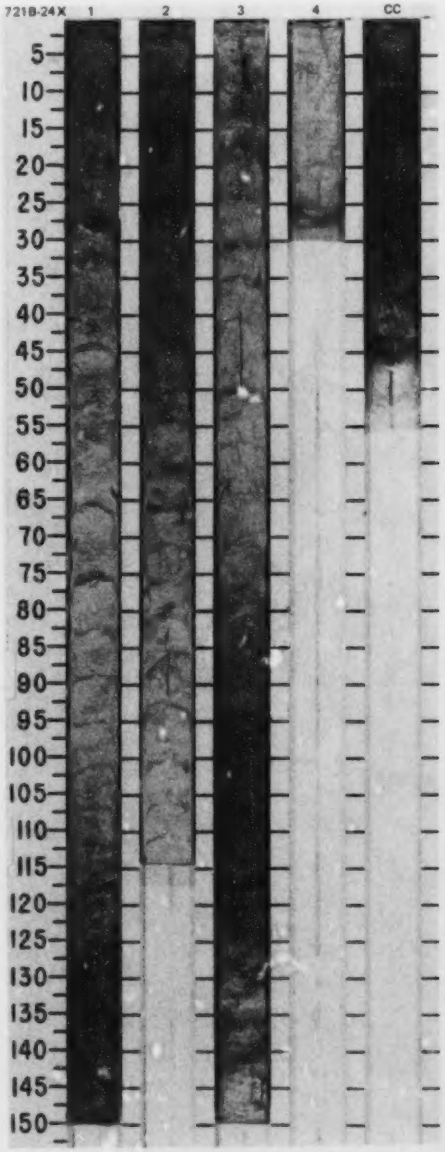
721B-24X
1
2
3
4
CC
5
10
15
20
25
30
35
40
45
50
55
60
65
70
75
80
85
90
95
100
105
110
115
120
125
130
135
140
145
150

SITE 721 HOLE B CORE 25X CORED INTERVAL 2175.3-2184.9 mbsl; 230.5-240.1 mbsf

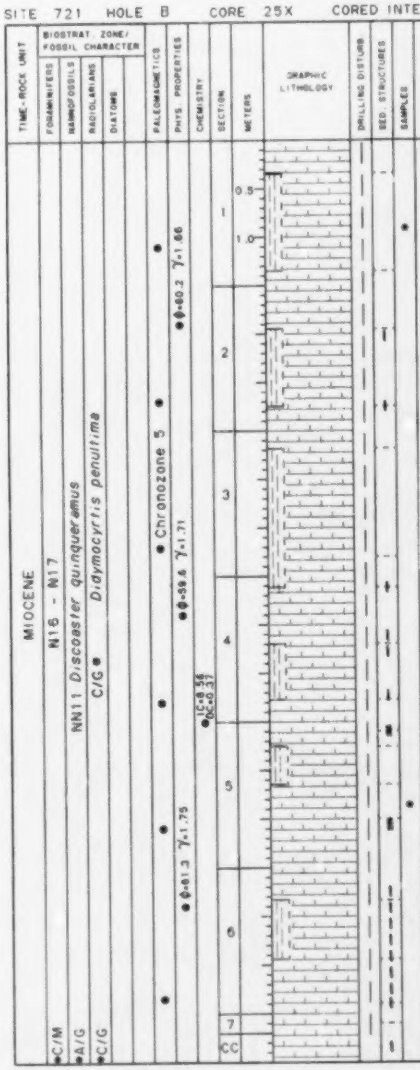

LITHOLOGIC DESCRIPTION

NANNOFOSSIL CHALK to FORAMINIFER-BEARING NANNOFOSSIL CHALK

Drilling biscuits throughout; slightly disturbed.

Major lithology: NANNOFOSSIL CHALK to FORAMINIFER-BEARING NANNOFOSSIL CHALK. Alternating light and dark layers. Colors range from light gray (5Y 7/1), gray (5Y 6/1), light olive gray (5Y 6/2), and pale olive (5Y 6/3), to olive (5Y 5/3). Light layers generally have less terrigenous silty clay than do dark layers.

SMEAR SLIDE SUMMARY (%):

	1, 91 D	5, 85 D
TEXTURE:		
Sand		1
Silt	15	20
Clay	85	79
COMPOSITION:		
Diatoms	Tr	
Dolomite	Tr	
Foraminifers		5
Volcanic glass	Tr	Tr
Inorganic calcite	10	5
Mica	Tr	
Nannofossils	85	85
Quartz	Tr	2
Radiolarians	Tr	1
Silicoflagellates	5	2
Sponge spicules	Tr	Tr

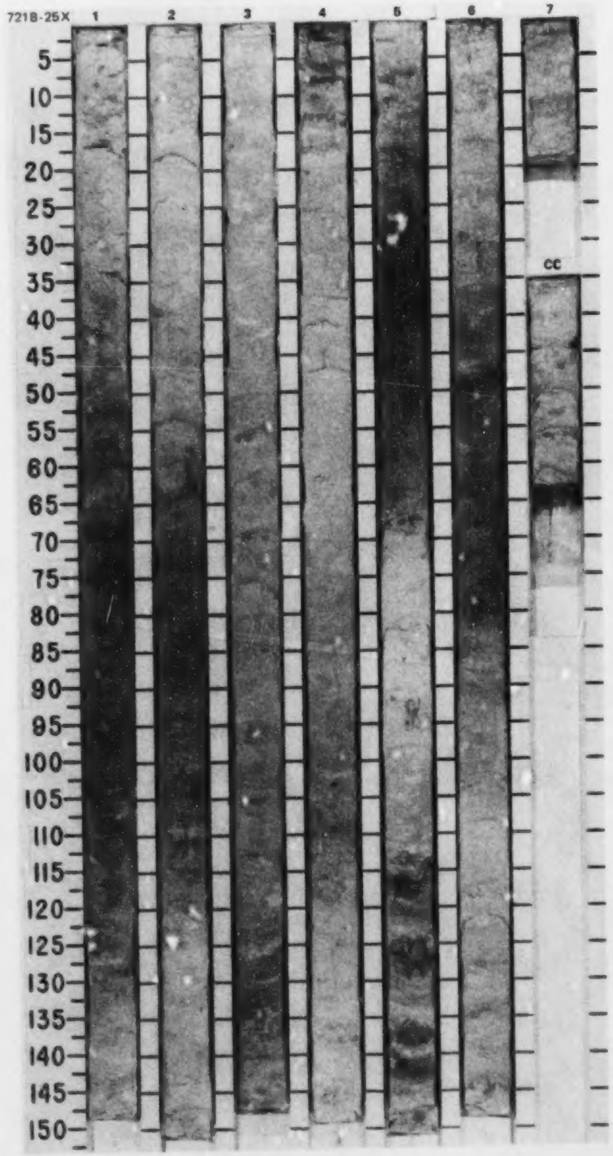
721B-25X
1
2
3
4
5
6
7
CC
5
10
15
20
25
30
35
40
45
50
55
60
65
70
75
80
85
90
95
100
105
110
115
120
125
130
135
140
145
150

SITE 721 HOLE B CORE 26X CORED INTERVAL 2184.9-2194.6 mbsl; 240.1-249.8 mbsf

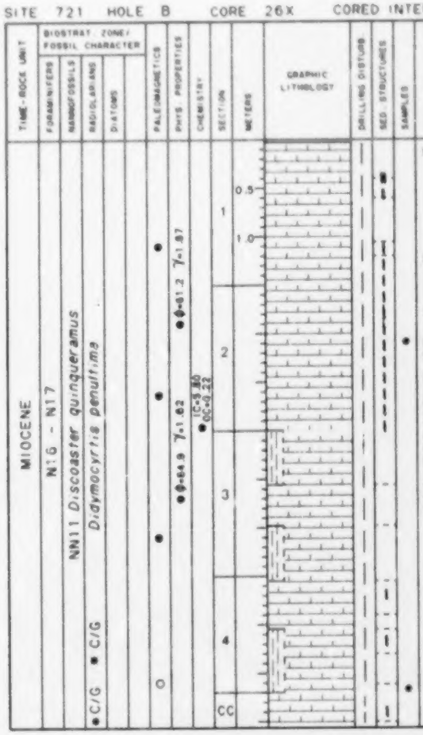
TIME-ROCK UNIT
BIOSTRAT. ZONE/ FOSSIL CHARACTER
FORAMINIFERS
NANNOFOSSILS
RADIOLARIANS
DIATOMS
PALEOMAGNETICS
PHYS. PROPERTIES
CHEMISTRY
SECTION
METERS
GRAPHIC LITHOLOGY
DRILLING DISTURB.
SED. STRUCTURES
SAMPLES
MIOCENE
N16 - N17
NN11 Discoaster quinqueramus
Didymocyrtis penultima
●C/G
● C/G
● C/G
ϕ=61.2 γ=1.87
ϕ=64.9 γ=1.82
IC=5.80
OC=0.22
1
2
3
4
CC
0.5
1.0

LITHOLOGIC DESCRIPTION

NANNOFOSSIL CHALK

Drilling biscuits throughout; slightly disturbed.

Major lithology: NANNOFOSSIL CHALK. Alternating light and dark layers, ranging from light olive gray (5Y 6/2) to light gray (5Y 7/1) for light layers, and olive (5Y 5/3) to pale olive (5Y 6/3) for dark layers. Light layers generally have less terrigenous silty clay than do dark layers.

SMEAR SLIDE SUMMARY (%):

	2, 58 D	4, 11 D
TEXTURE:		
Silt	5	5
Clay	95	95
COMPOSITION:		
Diatoms	Tr	Tr
Foraminifers	Tr	5
Volcanic glass		Tr
Inorganic calcite	3	2
Mica	Tr	Tr
Nannofossils	95	93
Quartz		Tr
Radiolarians		Tr
Silicoflagellates	2	Tr
Sponge spicules	Tr	

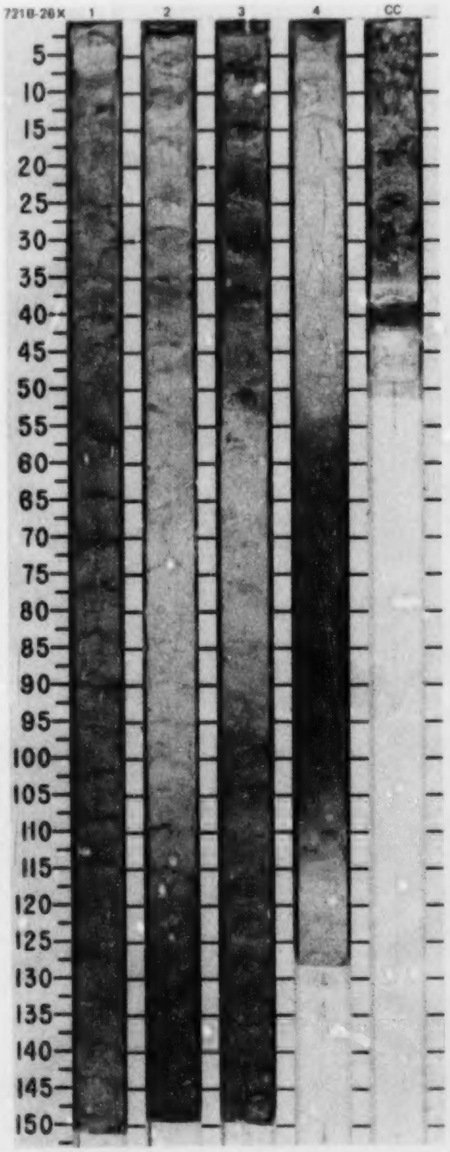
721B-26X
1
2
3
4
CC
5
10
15
20
25
30
35
40
45
50
55
60
65
70
75
80
85
90
95
100
105
110
115
120
125
130
135
140
145
150

SITE 721 HOLE B CORE 27X CORED INTERVAL 2194.6-2204.4mbsl; 249.8-259.6 mbsf

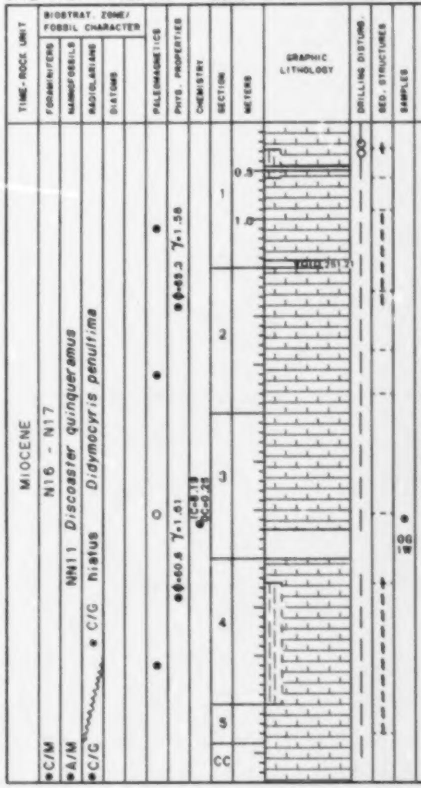
TIME-ROCK UNIT
BIOSTRAT. ZONE/ FOSSIL CHARACTER
FORAMINIFERS
NANNOFOSSILS
RADIOLARIANS
DIATOMS
PALEOMAGNETICS
PHYS. PROPERTIES
CHEMISTRY
SECTION
METERS
GRAPHIC LITHOLOGY
DRILLING DISTURB.
SED. STRUCTURES
SAMPLES
MIOCENE
N16 - N17
NN11 Discoaster quinqueramus
C/G hiatus Didymocyris penultima
●C/M
●A/M
●C/G
●ϕ=65.3 γ=1.58
●ϕ=60.6 γ=1.61
IC=8.13
OC=0.25
1
2
3
4
5
CC
0.5
1.0
VOID
OG
IW

LITHOLOGIC DESCRIPTION

NANNOFOSSIL CHALK

Section 1, 0-2 and 15-21 cm, soupy; void in Section 1, 48-50 cm; drilling biscuits throughout; slightly disturbed.

Major lithology: NANNOFOSSIL CHALK. Alternating light and dark layers, ranging from light olive gray (5Y 6/2) to light gray (5Y 7/1) for light layers, and olive (5Y 5/3) to olive gray (5Y 5/2) for dark layers. Light layers generally have less terrigenous silty clay than do dark layers.

SMEAR SLIDE SUMMARY (%):

	3, 113 D	4, 104 D
TEXTURE:		
Silt	3	10
Clay	97	90
COMPOSITION:		
Access. minerals		Tr
Diatoms	Tr	Tr
Foraminifers	3	
Inorganic calcite	3	4
Nannofossils	94	90
Quartz	Tr	Tr
Radiolarians	Tr	Tr
Silicoflagellates	Tr	1
Sponge spicules	Tr	5

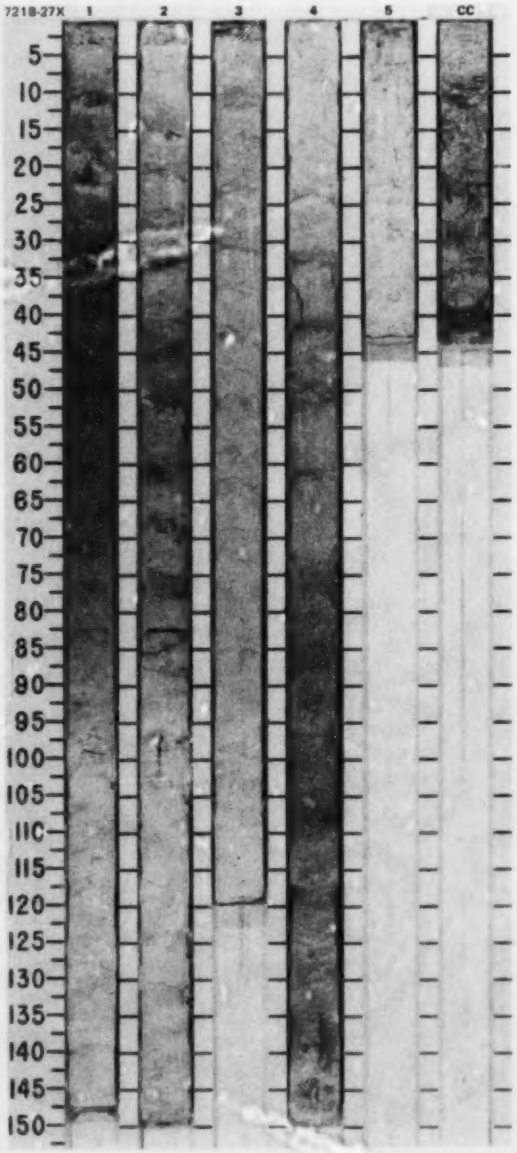
721B-27X
1
2
3
4
5
CC
5
10
15
20
25
30
35
40
45
50
55
60
65
70
75
80
85
90
95
100
105
110
115
120
125
130
135
140
145
150

SITE 721 HOLE B CORE 28X CORED INTERVAL 2204.4-2214.2 mbsl; 259.6-269.4 mbsf

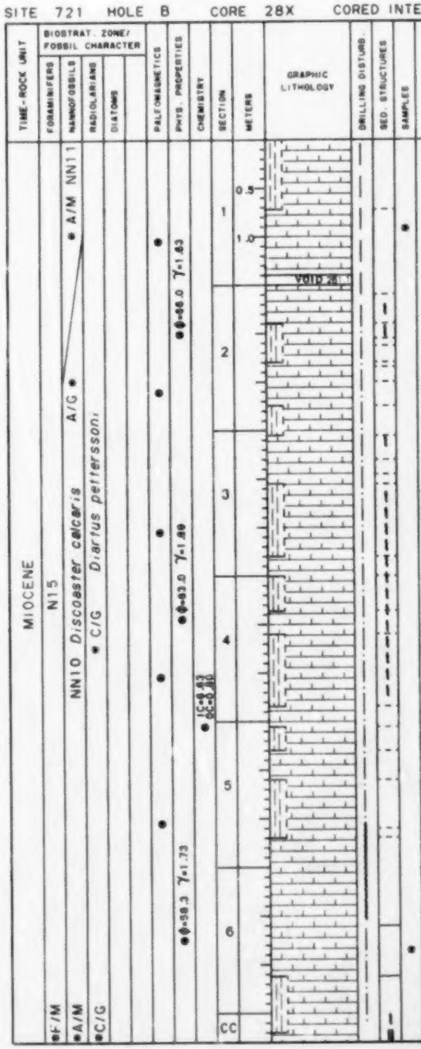
TIME-ROCK UNIT
BIOSTRAT. ZONE/ FOSSIL CHARACTER
FORAMINIFERS
NANNOFOSSILS
RADIOLARIANS
DIATOMS
PALEOMAGNETICS
PHYS. PROPERTIES
CHEMISTRY
SECTION
METERS
GRAPHIC LITHOLOGY
DRILLING DISTURB.
SED. STRUCTURES
SAMPLES
MIOCENE
N15
NN10 Discoaster calcaris
• A/M NN11
A/G •
• C/G Diartus petterssoni
•F/M
•A/M
•C/G
•ϕ=66.0 γ=1.63
•ϕ=63.0 γ=1.69
•ϕ=58.3 γ=1.73
• IC=8.63 OC=0.90
1
2
3
4
5
6
CC
0.5
1.0
VOID

LITHOLOGIC DESCRIPTION

NANNOFOSSIL CHALK

Void in Section 1, 140-150 cm; drilling biscuits throughout; slightly disturbed.

Major lithology: NANNOFOSSIL CHALK. Alternating light and dark layers, ranging from light olive gray (5Y 6/2) and light gray (5Y 7/1) to white (5Y 8/1) for light layers, and olive (5Y 5/3, 4/3) and pale olive (5Y 5/3) to olive gray (5Y 4/2, 5/2) for dark layers. Light layers generally have 10-20% less terrigenous silty clay than do dark layers.

SMEAR SLIDE SUMMARY (%):

	1, 91 D	6, 85 D
TEXTURE:		
Sand	5	
Silt	5	
Clay	90	100
COMPOSITION:		
Access. minerals	Tr	
Diatoms	Tr	Tr
Foraminifers	Tr	
Inorganic calcite	7	
Mica	Tr	
Nannofossils	90	100
Radiolarians	1	
Silicoflagellates	2	Tr
Sponge spicules	Tr	Tr

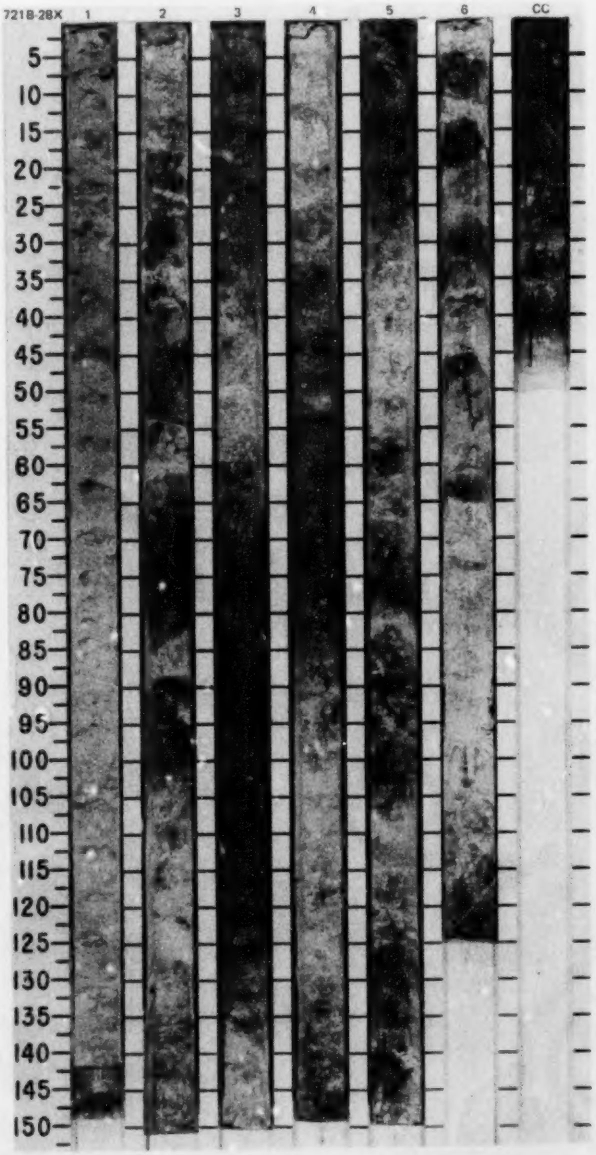
721B-28X
1
2
3
4
5
6
CC
5
10
15
20
25
30
35
40
45
50
55
60
65
70
75
80
85
90
95
100
105
110
115
120
125
130
135
140
145
150

SITE 721 HOLE B CORE 29X CORED INTERVAL 2214.2-2224.0 mbsl: 269.4-279.2 mbsf

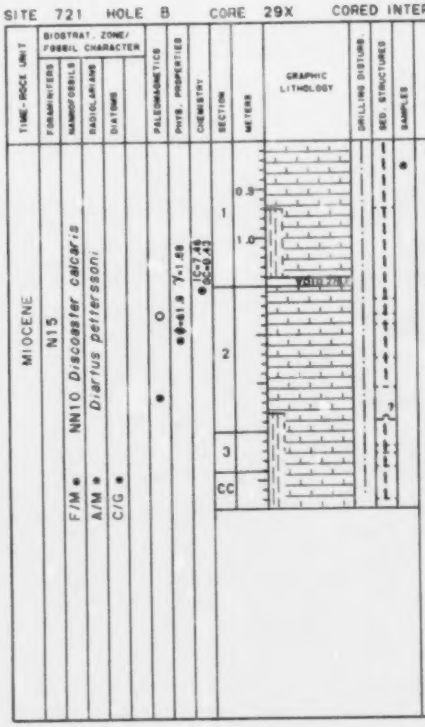
TIME-ROCK UNIT
BIOSTRAT. ZONE/ FOSSIL CHARACTER
FORAMINIFERS
NANNOFOSSILS
RADIOLARIANS
DIATOMS
PALEOMAGNETICS
PHYS. PROPERTIES
CHEMISTRY
SECTION
METERS
GRAPHIC LITHOLOGY
DRILLING DISTURB.
SED. STRUCTURES
SAMPLES
MIOCENE
N15
F/M ● NN10 Discoaster calcaris
A/M ● Diartus petterssoni
C/G ●
○
●
●ϕ=61.9 γ=1.88
●IC=7.46 OC=0.43
1
2
3
CC
0.5
1.0
VOID

LITHOLOGIC DESCRIPTION

NANNOFOSSIL CHALK

Void in Section 1, 143-150 cm; possible wash in Section 1, 0-4 cm; drilling biscuits throughout; slightly disturbed.

Major lithology: NANNOFOSSIL CHALK. Alternating light and dark layers, ranging from light olive gray (5Y 6/2) and light gray (5Y 7/1) to white (5Y 8/1) for light layers, and olive (5Y 5/3, 4/3) and pale olive (5Y 6/3) to olive gray (5Y 5/2, 4/2) for dark layers. Light layers generally have 10-20% less terrigenous silty clay than do dark layers.

SMEAR SLIDE SUMMARY (%):

	1, 28 D
TEXTURE:	
Sand	2
Silt	8
Clay	90
COMPOSITION:	
Diatoms	Tr
Foraminifers	Tr
Inorganic calcite	10
Nannofossils	90
Radiolarians	Tr
Silicoflagellates	Tr
Sponge spicules	Tr

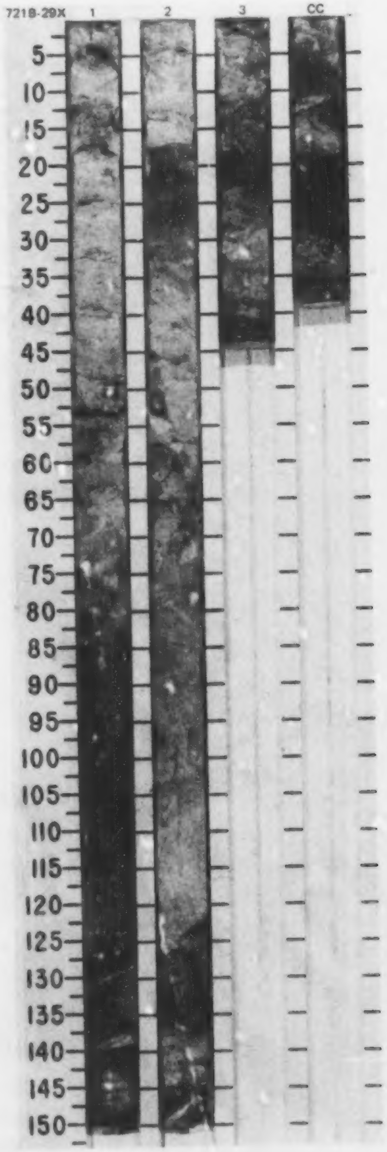
721B-29X
1
2
3
CC
5
10
15
20
25
30
35
40
45
50
55
60
65
70
75
80
85
90
95
100
105
110
115
120
125
130
135
140
145
150

SITE 721 HOLE B CORE 30X CORED INTERVAL 2224.0-2233.8 mbsl; 279.2-289.0 mbsf

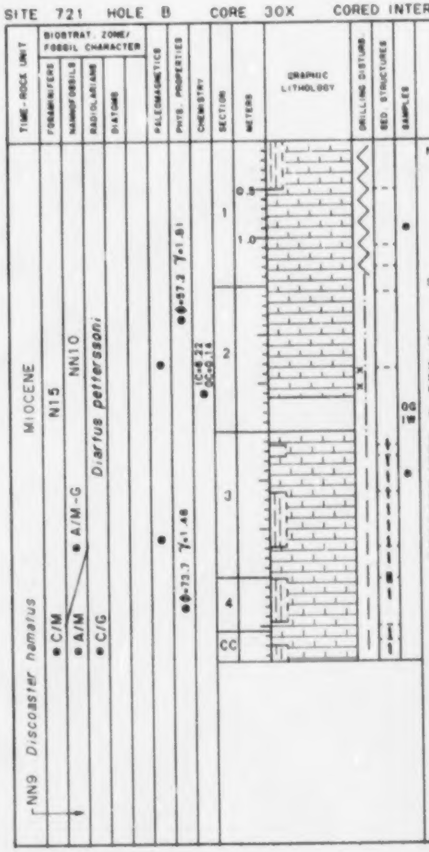
TIME-ROCK UNIT
BIOSTRAT. ZONE/ FOSSIL CHARACTER
FORAMINIFERS
NANNOFOSSILS
RADIOLARIANS
DIATOMS
PALEOMAGNETICS
PHYS. PROPERTIES
CHEMISTRY
SECTION
METERS
GRAPHIC LITHOLOGY
DRILLING DISTURB.
SED. STRUCTURES
SAMPLES
MIOCENE
NN9 Discoaster hamatus
N15
● C/M
NN10
● A/M-G
● A/M
Diartus petterssoni
● C/G
●Φ=57.2 γ=1.81
●Φ=73.7 γ=1.48
● IC=8.22
OC=0.14
1
2
3
4
CC
0.5
1.0
OG
IW

LITHOLOGIC DESCRIPTION

NANNOFOSSIL CHALK to FORAMINIFER-BEARING NANNOFOSSIL CHALK

Drilling biscuits throughout; slightly disturbed.

Major lithology: NANNOFOSSIL CHALK to FORAMINIFER-BEARING NANNOFOSSIL CHALK. Alternating light and dark layers, ranging from light olive gray (5Y 6/2) to light gray (5Y 7/1, 6/1) and light greenish gray (5G 7/1) to light bluish gray (5B 7/1) for light layers, and olive (5Y 4/3) to olive gray (5Y 5/2) for dark layers. Light layers generally have less terrigenous silty clay than do dark layers. Some layers seem brecciated, especially in Section 2, 107-115 cm.

SMEAR SLIDE SUMMARY (%):

	1, 90 M	3, 45 D
TEXTURE:		
Sand	5	5
Silt	10	5
Clay	85	90
COMPOSITION:		
Access. minerals	Tr	
Diatoms		Tr
Foraminifers	5	5
Volcanic glass		Tr
Inorganic calcite		5
Nannofossils	85	90
Plant debris	3	
Quartz		Tr
Radiolarians	Tr	Tr
Silicoflagellates	7	Tr
Sponge spicules	Tr	Tr

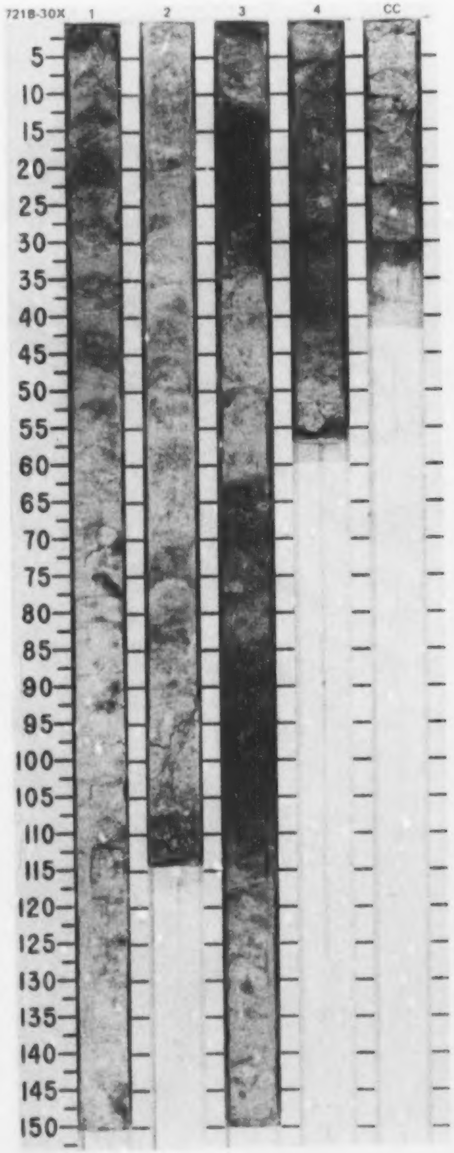
721B-30X
1
2
3
4
CC
5
10
15
20
25
30
35
40
45
50
55
60
65
70
75
80
85
90
95
100
105
110
115
120
125
130
135
140
145
150

SITE 721 HOLE B CORE 31X CORED INTERVAL 2233.8-2243.6 mbsl; 289.0-298.8 mbsf

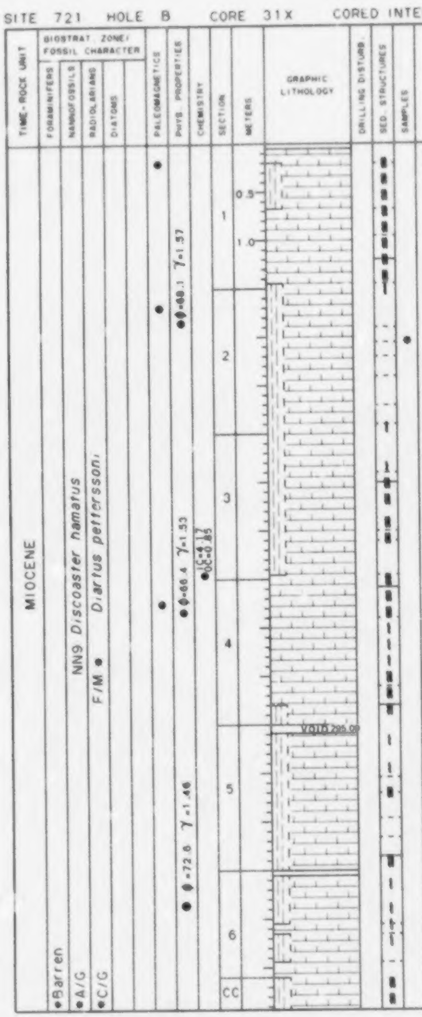
TIME-ROCK UNIT
BIOSTRAT. ZONE/ FOSSIL CHARACTER
FORAMINIFERS
NANNOFOSSILS
RADIOLARIANS
DIATOMS
PALEOMAGNETICS
PHYS. PROPERTIES
CHEMISTRY
SECTION
METERS
GRAPHIC LITHOLOGY
DRILLING DISTURB.
SED. STRUCTURES
SAMPLES
MIOCENE
●Barren
NN9 Discoaster hamatus
●A/G
F/M ● Diartus petterssoni
●C/G
●φ=68.1 γ=1.57
●φ=66.4 γ=1.53
● φ=72.6 γ=1.46
●IC=4.17 OC=0.85
1
2
3
4
5
6
CC
0.5
1.0
VOID 295.09

LITHOLOGIC DESCRIPTION

SILICEOUS-BEARING FORAMINIFER-NANNOFOSSIL CHALK to NANNOFOSSIL CHALK

Voids in Section 1, 0-2 cm, Section 5, 0-6 cm, and Section 6, 0-6 cm. Drilling biscuits throughout; slightly disturbed.

Major lithology: SILICEOUS-BEARING FORAMINIFER-NANNOFOSSIL CHALK to NANNOFOSSIL CHALK. Alternating light and dark layers ranging from light olive gray (5Y 6/2) and light gray (5Y 7/1) to light greenish gray (5GY 7/1) for light layers, and olive (5Y 5/3, 4/3, 5/4) to pale olive (5Y 6/3, 6/4) and olive gray (5Y 5/2) for dark layers. Dark layers generally have more terrigenous silty clay and siliceous microfossils than do light layers.

SMEAR SLIDE SUMMARY (%):

	2, 60 D
TEXTURE:	
Silt	5
Clay	95
COMPOSITION:	
Cement	15
Clay	10
Diatoms	3
Foraminifers	Tr
Nannofossils	70
Quartz	Tr
Radiolarians	2

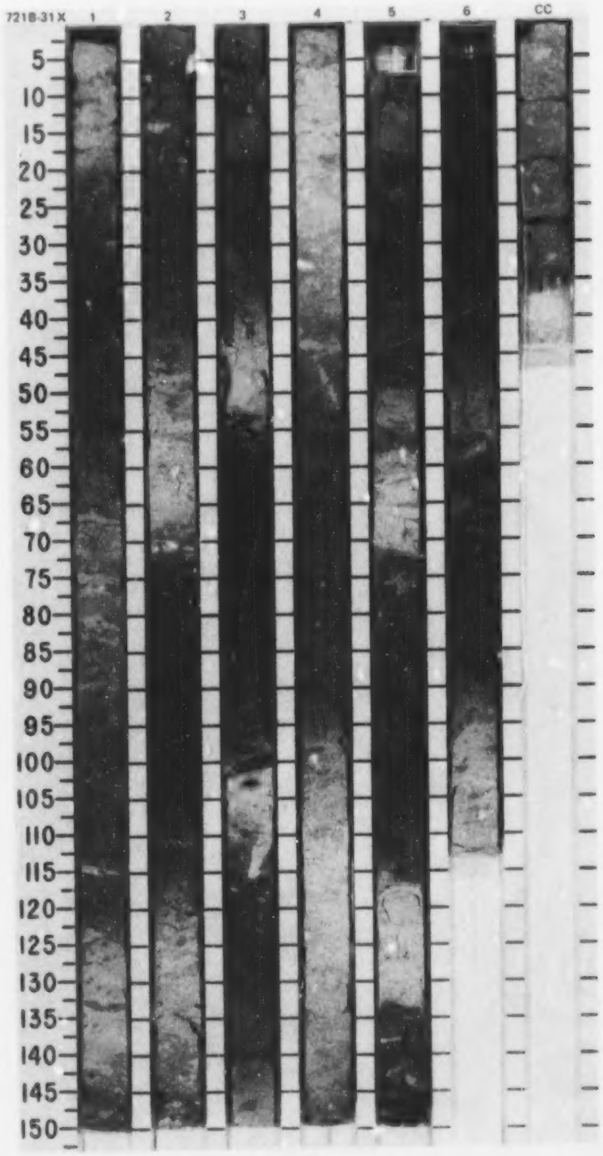
721B-31X
1
2
3
4
5
6
CC
5
10
15
20
25
30
35
40
45
50
55
60
65
70
75
80
85
90
95
100
105
110
115
120
125
130
135
140
145
150

SITE 721 HOLE B CORE 32X CORED INTERVAL 2243.6-2253.2 mbsl; 298.8-308.4 mbsf

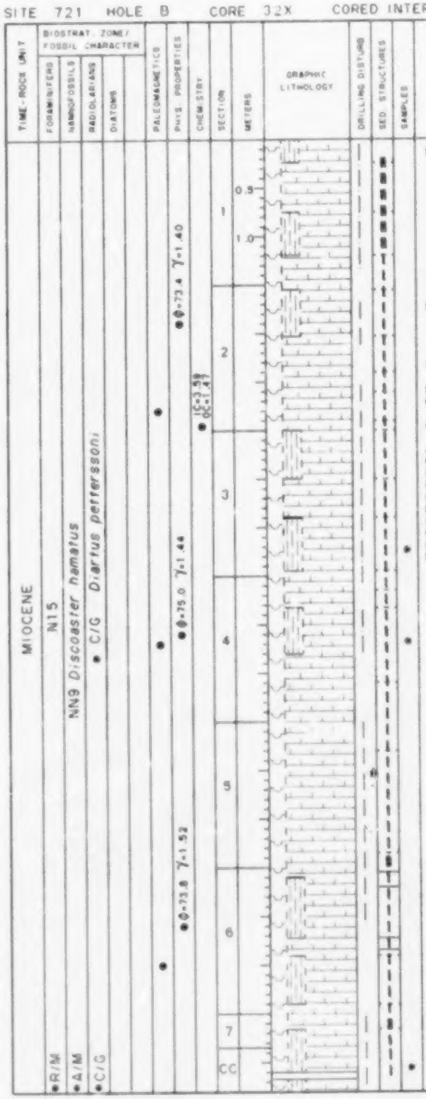
TIME-ROCK UNIT
BIOSTRAT. ZONE/ FOSSIL CHARACTER
FORAMINIFERS
NANNOFOSSILS
RADIOLARIANS
DIATOMS
PALEOMAGNETICS
PHYS. PROPERTIES
CHEMISTRY
SECTION
METERS
GRAPHIC LITHOLOGY
DRILLING DISTURB.
SED. STRUCTURES
SAMPLES
MIOCENE
N15
NN9 Discoaster hamatus
● C/G Diartus petterssoni
●R/M
●A/M
●C/G
●Φ=73.4 γ=1.40
●Φ=75.0 γ=1.44
●Φ=73.8 γ=1.52
IC=3.59
OC=1.47
1
2
3
4
5
6
7
CC
0.5
1.0

LITHOLOGIC DESCRIPTION

SILICEOUS-BEARING NANNOFOSSIL CHALK

Drilling biscuits throughout; slightly disturbed.

Major lithology: SILICEOUS-BEARING NANNOFOSSIL CHALK. Alternating light and dark layers ranging from light gray (5Y 7/1) for light layers to olive (5Y 5/3) for dark layers. Dark layers enriched in terrigenous silty clay and siliceous microfossil compared to light layers. Zoophycos and Chondrites burrows present.

Minor lithology: Diatomaceous nannofossil chalk associated with olive (5Y 4/3, 4/4) layers.

SMEAR SLIDE SUMMARY (%):

	3, 124 D	4, 68 D	CC, 21 D
TEXTURE:			
Silt	20	20	30
Clay	80	80	70
COMPOSITION:			
Access. minerals			1
Clay	Tr		30
Diatoms	20	20	20
Dolomite			Tr
Foraminifers		Tr	Tr
Inorganic calcite	Tr		5
Nannofossils	80	80	40
Quartz	Tr	Tr	Tr
Silicoflagellates		Tr	3
Sponge spicules			1

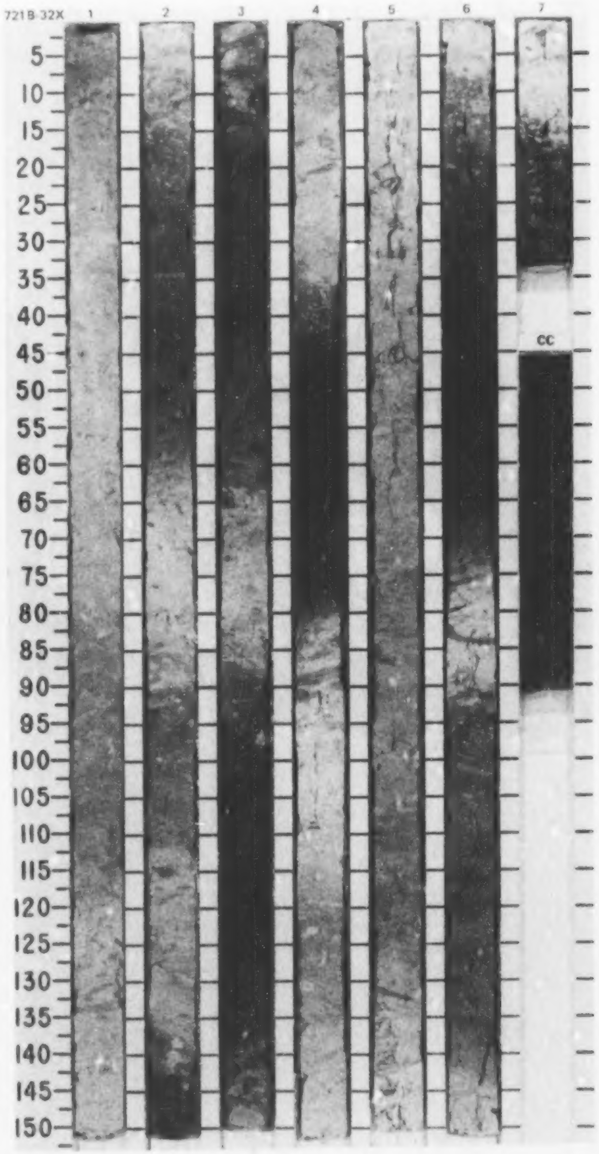
721B-32X
1
2
3
4
5
6
7
CC
5
10
15
20
25
30
35
40
45
50
55
60
65
70
75
80
85
90
95
100
105
110
115
120
125
130
135
140
145
150

SITE 721 HOLE B CORE 33X CORED INTERVAL 2253.2-2262.8 mbsl; 308.4-318.0 mbsf

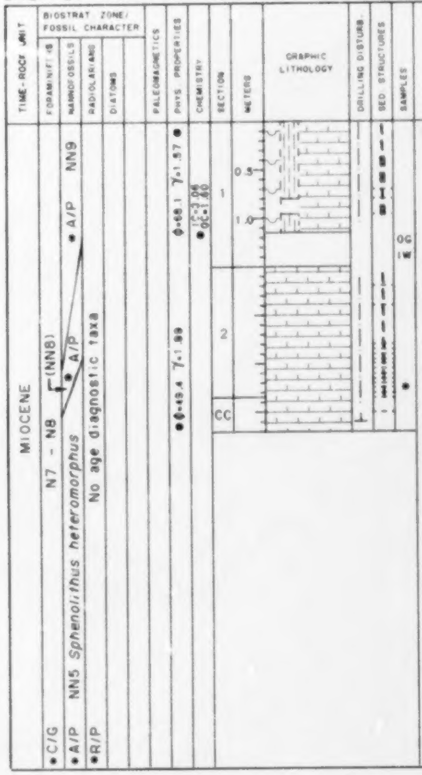
TIME-ROCK UNIT
BIOSTRAT. ZONE/ FOSSIL CHARACTER
FORAMINIFERS
NANNOFOSSILS
RADIOLARIANS
DIATOMS
PALEOMAGNETICS
PHYS. PROPERTIES
CHEMISTRY
SECTION
METERS
GRAPHIC LITHOLOGY
DRILLING DISTURB.
SED. STRUCTURES
SAMPLES
MIOCENE
●C/G N7 - N8 (NN8)
●A/P NN5 Sphenolithus heteromorphus
● A/P
● A/P NN9
●R/P No age diagnostic taxa
φ=68.1 γ=1.57 ●
●φ=49.4 γ=1.99
●IC=3.06 OC=1.80
1
2
CC
0.5
1.0
OG
IW
●

LITHOLOGIC DESCRIPTION

DIATOMACEOUS NANNOFOSSIL CHALK to NANNOFOSSIL CHALK

Drilling biscuits throughout; moderately disturbed.

Major lithology:
a. Diatomaceous nannofossil chalk, in Section 1. Alternating light and dark layers, ranging from light gray (5Y 7/1) for light layers to olive (5Y 5/3) for dark layers. Dark layers are enriched in terrigenous silty clay and siliceous microfossils compared to light layers.
b. Nannofossil chalk, light greenish gray (5BG 7/1) to greenish gray (5G 6/1), in Section 2 and CC. Slight to moderate burrow-mottling. Transition from lithologic Units II to III is located at the base of Section 1.

SMEAR SLIDE SUMMARY (%):

	2, 126 M
TEXTURE:	
Clay	100
COMPOSITION:	
Diatoms	Tr
Dolomite	Tr
Foraminifers	Tr
Inorganic calcite	Tr
Nannofossils	100
Quartz	Tr
Radiolarians	Tr
Silicoflagellates	Tr
Sponge spicules	Tr

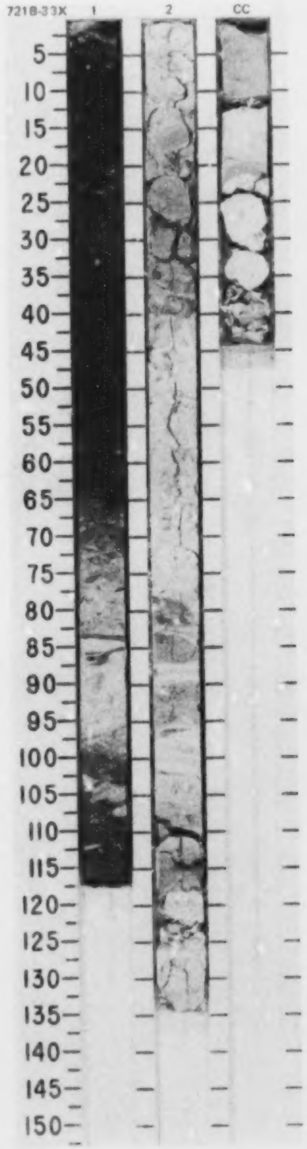
721B-33X
1
2
CC
5
10
15
20
25
30
35
40
45
50
55
60
65
70
75
80
85
90
95
100
105
110
115
120
125
130
135
140
145
150

SITE 721 HOLE B CORE 34X CORED INTERVAL 2262.8-2272.5 mbsl; 318.0-327.7 mbsf

TIME-ROCK UNIT: MIOCENE

BIOSTRAT. ZONE/FOSSIL CHARACTER

- FORAMINIFERS: ● R/M N7 - N8
- NANNOFOSSILS: ● A/P NN4 *Helicosphaera ampliaperta* - NN5 *Sphenolithus heteromorphus*
- RADIOLARIANS: ● R/P No age diagnostic taxa
- DIATOMS:

PALEOMAGNETICS:

PHYS. PROPERTIES: ●ϕ=50.7 γ=1.93 ●ϕ=52.0 γ=1.98

CHEMISTRY: ●IC=10.81 OC=0.00

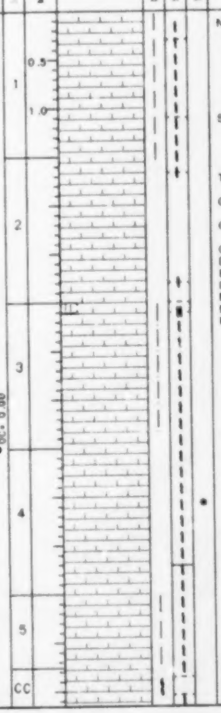
SECTION
METERS
GRAPHIC LITHOLOGY
DRILLING DISTURB.
SED. STRUCTURES
SAMPLES
0.5
1
1.0
2
3
4
5
CC

LITHOLOGIC DESCRIPTION

NANNOFOSSIL CHALK

Drilling biscuits present throughout. Slight to moderate disturbance.

Major lithology: NANNOFOSSIL CHALK. White (2.5Y 8/0) and light greenish gray (5BG 7/1) to greenish gray (5G 6/1, 5/1). Slight to moderate burrow-mottling.

SMEAR SLIDE SUMMARY (%):

	4, 56 D
TEXTURE:	
Clay	100
COMPOSITION:	
Clay	20
Dolomite	Tr
Foraminifers	3
Inorganic calcite	Tr
Mica	Tr
Nannofossils	77
Radiolarians	Tr

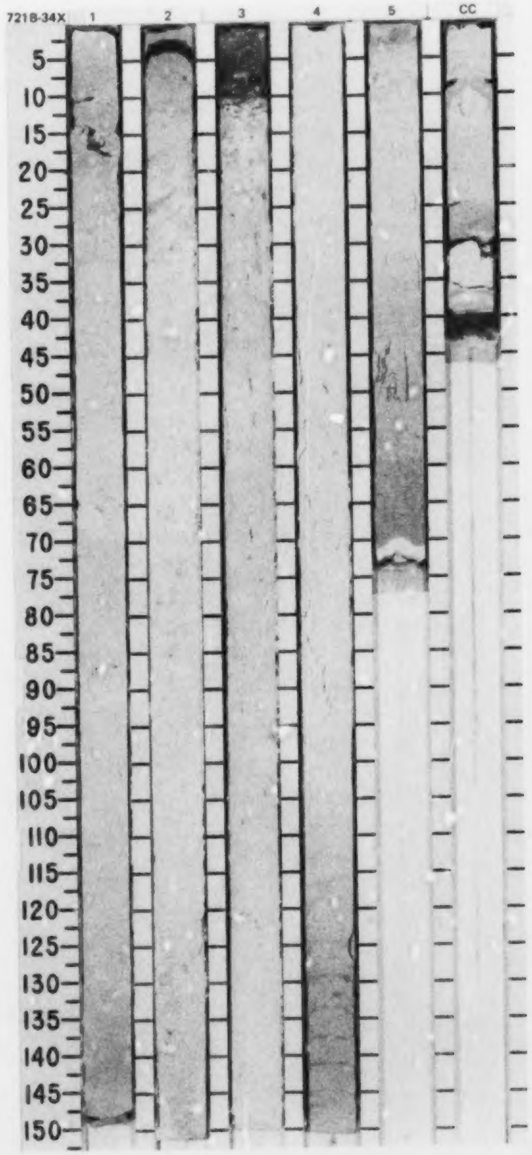
721B-34X
1
2
3
4
5
CC
5
10
15
20
25
30
35
40
45
50
55
60
65
70
75
80
85
90
95
100
105
110
115
120
125
130
135
140
145
150

SITE 721 HOLE B CORE 35X CORED INTERVAL 2272.5-2282.2 mbsl; 327.7-337.4 mbsf

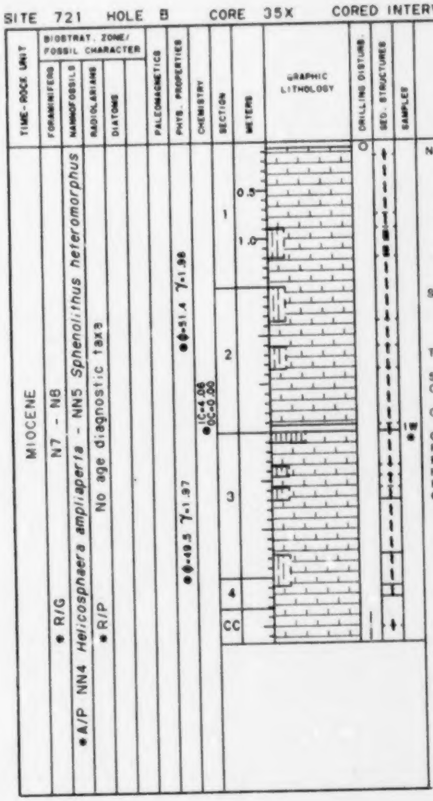
TIME-ROCK UNIT
BIOSTRAT. ZONE/ FOSSIL CHARACTER
FORAMINIFERS
NANNOFOSSILS
RADIOLARIANS
DIATOMS
PALEOMAGNETICS
PHYS. PROPERTIES
CHEMISTRY
SECTION
METERS
GRAPHIC LITHOLOGY
DRILLING DISTURB.
SED. STRUCTURES
SAMPLES
MIOCENE
● R/G N7 - N8
●A/P NN4 Helicosphaera ampliaperta - NN5 Sphenolithus heteromorphus
● R/P No age diagnostic taxa
●Φ-51.4 γ-1.98
●Φ-49.5 γ-1.97
●IC=4.06 OC=0.00
1
2
3
4
CC
0.5
1.0
1W
●

LITHOLOGIC DESCRIPTION

NANNOFOSSIL CHALK

Void in Section 1, 0-8 cm. Drilling biscuits present throughout. Slight to moderate disturbance.

Major lithology: NANNOFOSSIL CHALK. Alternating light and dark layers of white (2.5Y 8/0), light greenish gray (5BG 7/1), and light bluish gray (5B 7/1) to greenish gray (5G 6/1, 5/1). Slight to moderate burrow-mottling.

Minor lithology: Calcareous silty claystone. Greenish gray (5BG 5/1) layers in Section 3.

SMEAR SLIDE SUMMARY (%):

	3, 1 D
TEXTURE:	
Silt	30
Clay	70
COMPOSITION:	
Clay	10
Feldspar	10
Foraminifers	Tr
Inorganic calcite	30
Nannofossils	10
Quartz	40

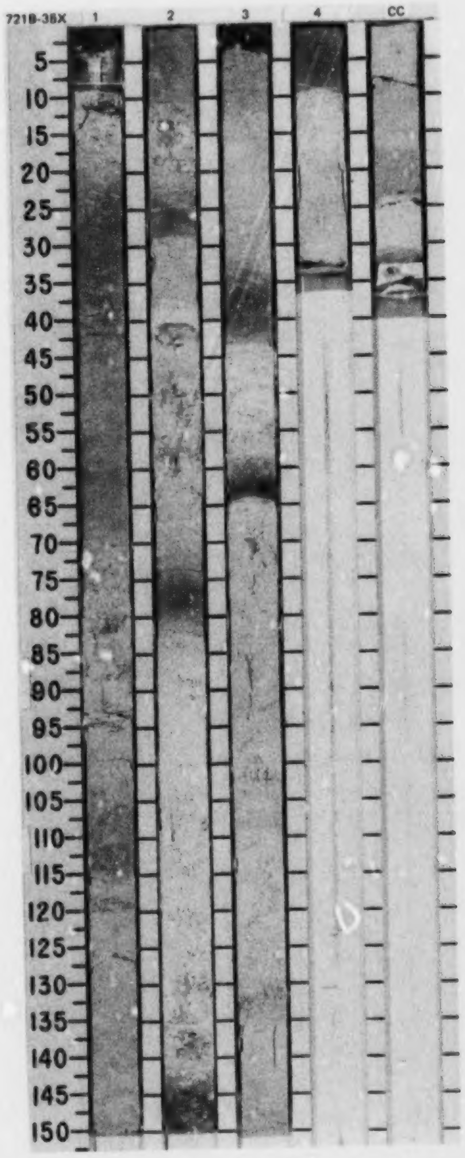
721B-35X
1
2
3
4
CC
5
10
15
20
25
30
35
40
45
50
55
60
65
70
75
80
85
90
95
100
105
110
115
120
125
130
135
140
145
150

SITE 721 HOLE B CORE 36X CORED INTERVAL 2282.2-2291.8 mbsl; 337.4-347.0 mbsf

TIME-ROCK UNIT	BIOSTRAT. ZONE/ FOSSIL CHARACTER: FORAMINIFERS	NANNOFOSSILS	RADIOLARIANS	DIATOMS		PALEOMAGNETICS	PHYS. PROPERTIES	CHEMISTRY	SECTION	METERS	GRAPHIC LITHOLOGY	DRILLING DISTURB.	SED. STRUCTURES	SAMPLES
MIOCENE	●R/M N7 - N8	●A/P NN4 *Helicosphaera ampliaperta* - NN5 *Sphenolithus heteromorphus*	● Barren				●ϕ=47.6 γ=2.10	●IC=10.55 OC= 0.37	1 2 3 CC	0.5 1.0	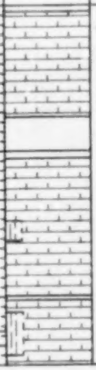			IW OG ● ●

LITHOLOGIC DESCRIPTION

NANNOFOSSIL CHALK

Voids in Section 1, 0-6 cm; Section 2, 0-5 cm, and Section 3, 0-2 cm. Section 1, 6-11 cm, very disturbed. Drilling biscuits present throughout. Remainder of core has slight to moderate disturbance.

Major lithology: NANNOFOSSIL CHALK, white (2.5Y 8/0) and light greenish gray (5B 7/1, 5BG 7/1) to greenish gray (5G 6/1, 5BG 6/1). Slight to moderate burrow-mottling. Pyrite grains on core face at Section 1, 35 cm, and Section 3, 20-21 cm.

Minor lithology: Marly nannofossil chalk, light brownish gray (2.5Y 6/2), found in CC from 33 to 38 cm. This indicates the transition from lithologic Units III to IV.

SMEAR SLIDE SUMMARY (%):

	CC, 15 D	CC, 36 M
TEXTURE:		
Silt	5	10
Clay	95	90
COMPOSITION:		
Clay	10	10
Inorganic calcite	10	10
Nannofossils	80	70
Quartz	Tr	10

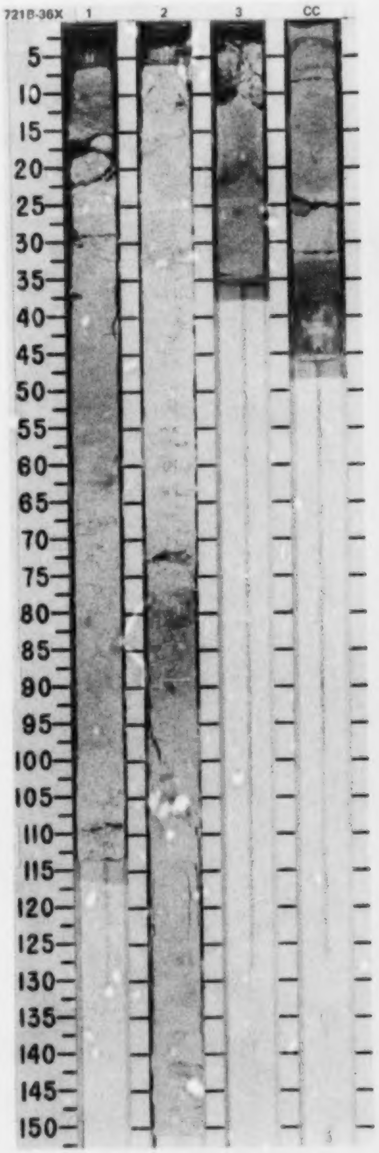

SITE 721 HOLE B CORE 37X CORED INTERVAL 2291.8-2301.4 mbsl; 347.0-356.6 mbsf

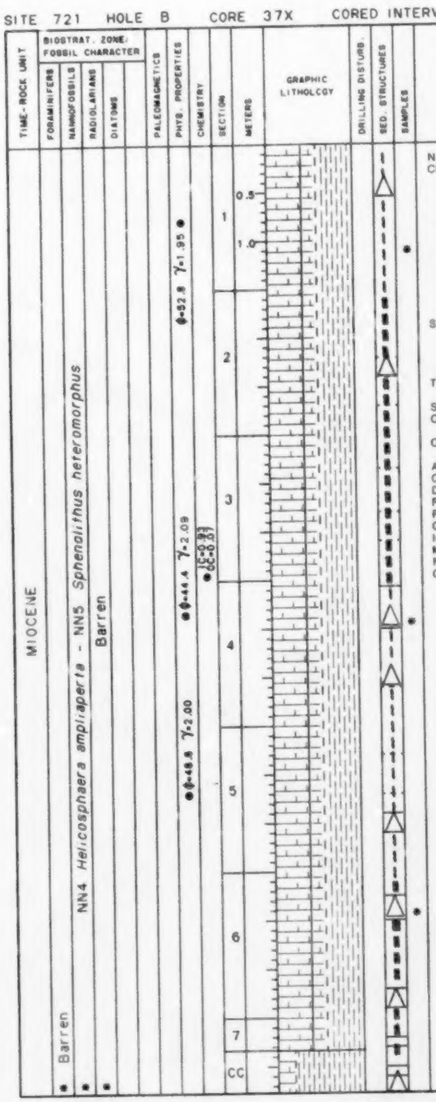
TIME-ROCK UNIT
BIOSTRAT. ZONE/ FOSSIL CHARACTER
FORAMINIFERS
NANNOFOSSILS
RADIOLARIANS
DIATOMS
PALEOMAGNETICS
PHYS. PROPERTIES
CHEMISTRY
SECTION
METERS
GRAPHIC LITHOLOGY
DRILLING DISTURB.
SED. STRUCTURES
SAMPLES
MIOCENE
Barren
NN4 Helicosphaera ampliaperta - NN5 Sphenolithus heteromorphus
Barren
ϕ=52.8 γ=1.95
ϕ=44.4 γ=2.09
IC=0.93 OC=0.07
ϕ=48.8 γ=2.00
1
2
3
4
5
6
7
CC
0.5
1.0

LITHOLOGIC DESCRIPTION

NANNOFOSSIL CHALK, MARLY NANNOFOSSIL CHALK, CALCAREOUS SILTY CLAYSTONE, and SILTY CLAYSTONE

Moderate drilling disturbance. Drilling biscuits common.

Major lithology: Interbedded NANNOFOSSIL CHALK, MARLY NANNOFOSSIL CHALK, CALCAREOUS SILTY CLAYSTONE, and SILTY CLAYSTONE. Sequences grade from greenish gray (5GY 5/1 5G 5/1) SILTY CLAYSTONE with sharp contacts at the base to yellowish brown (10YR 5/4), dark yellowish brown (10YR 4/4), olive (5Y 4/3), and olive gray (5Y 5/2) SILTY CLAYSTONE and CALCAREOUS SILTY CLAYSTONE to light gray (10YR 7/1) MARLY NANNOFOSSIL CHALK and NANNOFOSSIL CHALK. Slight mottling in the CHALK and CALCAREOUS SILTY CLAYSTONE.

SMEAR SLIDE SUMMARY (%):

	1, 110 D	4, 44 D	6, 44 D
TEXTURE:			
Silt	5	20	20
Clay	95	80	80
COMPOSITION:			
Access. minerals		5	
Clay	15	15	15
Dolomite		Tr	
Feldspar		10	
Foraminifers		Tr	
Gypsum	5	5	
Inorganic calcite	10	35	30
Mica		Tr	
Nannofossils	70	5	35
Quartz		25	20

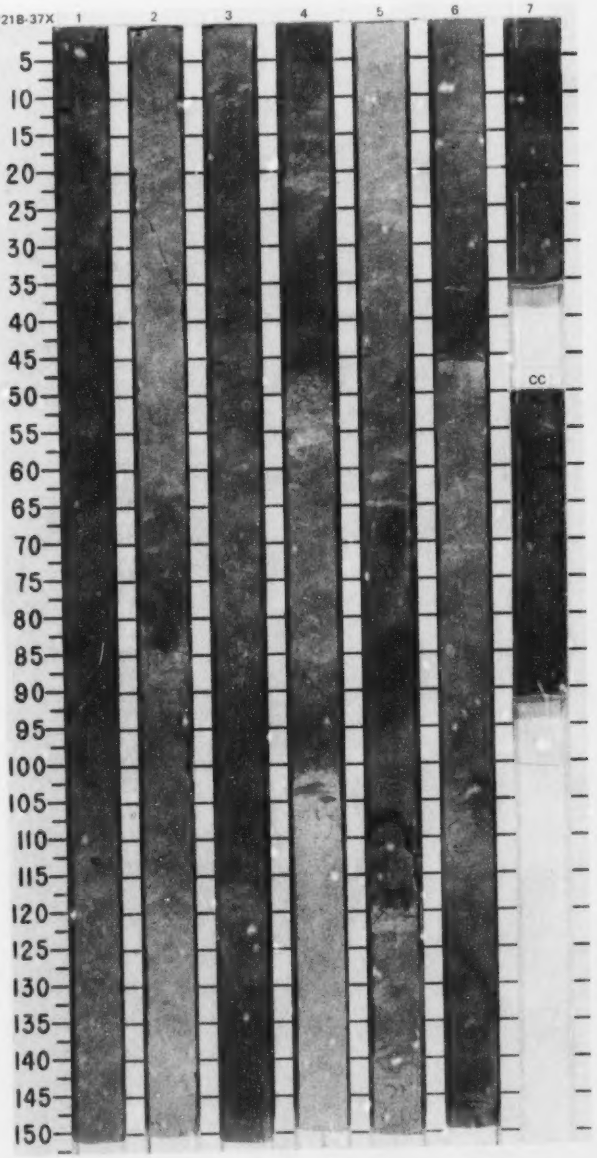
721B-37X
1
2
3
4
5
6
7
CC
5
10
15
20
25
30
35
40
45
50
55
60
65
70
75
80
85
90
95
100
105
110
115
120
125
130
135
140
145
150

SITE 721 HOLE B CORE 38X CORED INTERVAL 2301.4-2311.1 mbsl; 356.6-366.3 mbsf

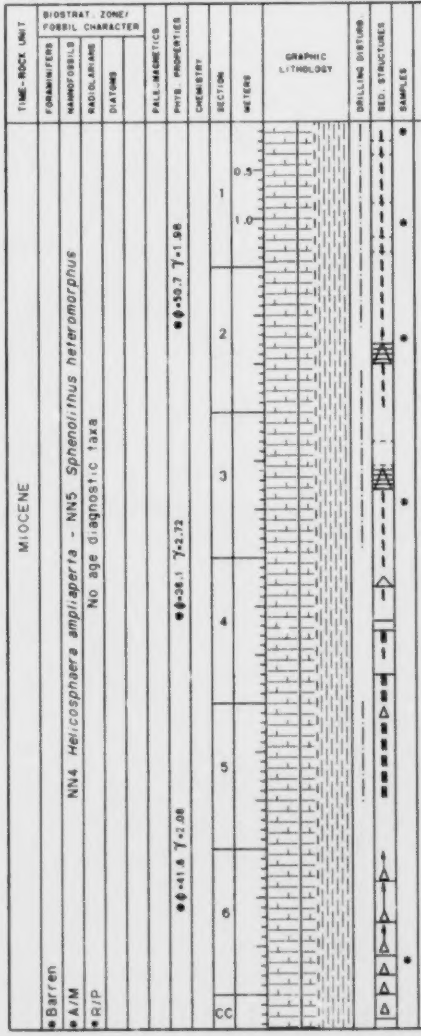
TIME-ROCK UNIT
BIOSTRAT. ZONE/ FOSSIL CHARACTER
FORAMINIFERS
NANNOFOSSILS
RADIOLARIANS
DIATOMS
PALEOMAGNETICS
PHYS. PROPERTIES
CHEMISTRY
SECTION
METERS
GRAPHIC LITHOLOGY
DRILLING DISTURB.
SED. STRUCTURES
SAMPLES
MIOCENE
●Barren
●A/M
NN4 Helicosphaera ampliaperta - NN5 Sphenolithus heteromorphus
●R/P
No age diagnostic taxa
●φ=50.7 γ=1.98
●φ=38.1 γ=2.72
●φ=41.6 γ=2.08
1
2
3
4
5
6
CC
0.5
1.0

LITHOLOGIC DESCRIPTION

NANNOFOSSIL CHALK, MARLY NANNOFOSSIL CHALK, CALCAREOUS SILTY CLAYSTONE, and SILTY CLAYSTONE

Moderate drilling disturbance. Drilling biscuits common.

Major lithology: Interbedded NANNOFOSSIL CHALK, MARLY NANNOFOSSIL CHALK, CALCAREOUS SILTY CLAYSTONE, and SILTY CLAYSTONE. Sequences grade from greenish gray (5GY 5/1, 5G 5/1) SILTY CLAYSTONE with sharp contacts at the base to grayish brown (10YR 5/2), brown (10YR 5/3), dark brown (10YR 3/3), and olive (5Y 4/3, 5/3) SILTY CLAYSTONE and CALCAREOUS SILTY CLAYSTONE to light gray (10YR 7/1) marly NANNOFOSSIL CHALK and NANNOFOSSIL CHALK. Slight mottling in the CHALK and CALCAREOUS SILTY CLAYSTONE. Millimeter-sized layers of pyrite grains common between 83 and 150 cm in Section 5.

SMEAR SLIDE SUMMARY (%):

	1, 11 D	1, 104 D	2, 73 M	3, 93 D	6, 113 M
TEXTURE:					
Silt	20	1	20	5	50
Clay	80	99	80	95	50
COMPOSITION:					
Access. minerals			5	Tr	5
Clay	70	10	50	25	35
Dolomite	Tr			Tr	Tr
Foraminifers				Tr	
Volcanic glass	Tr				
Inorganic calcite	10	3	10	5	10
Nannofossils	10	80	25	65	Tr
Pyrite	Tr	Tr			
Quartz	10	2	10	5	50

CORE 117–721B–39X NO RECOVERY

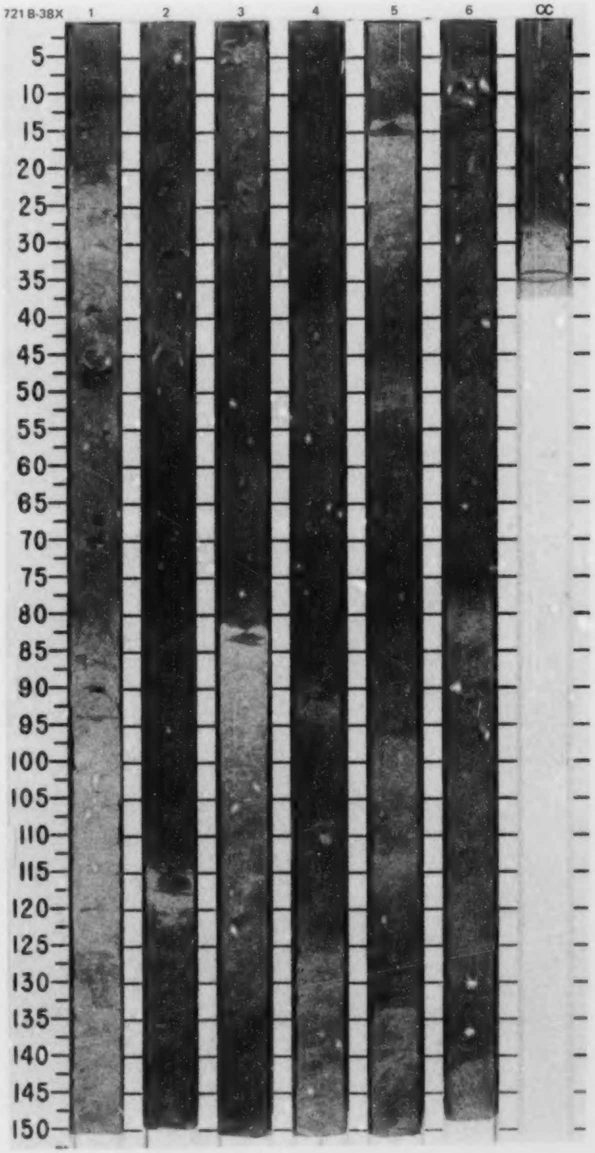
721B-38X
1
2
3
4
5
6
CC
5
10
15
20
25
30
35
40
45
50
55
60
65
70
75
80
85
90
95
100
105
110
115
120
125
130
135
140
145
150

SITE 721 HOLE B CORE 40X CORED INTERVAL 2320.7-2330.4 mbsl; 375.9-385.6 mbsf

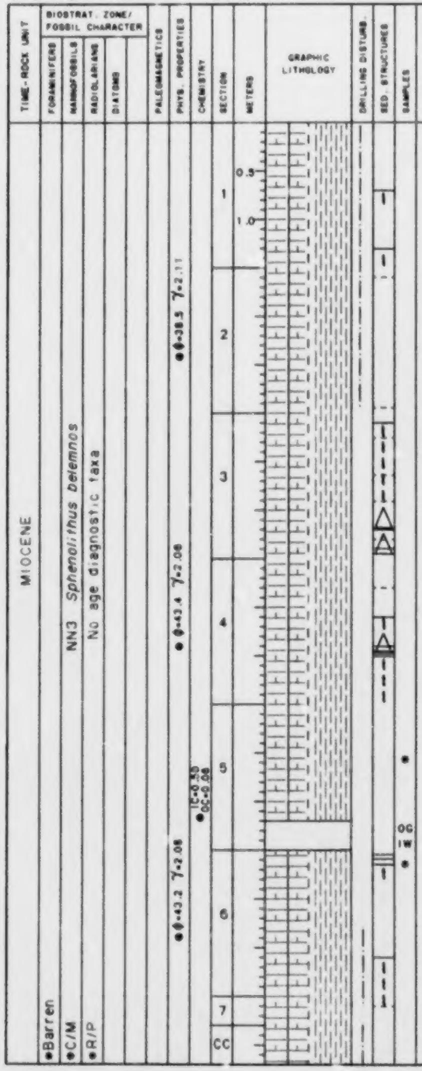
TIME-ROCK UNIT
BIOSTRAT. ZONE/ FOSSIL CHARACTER
FORAMINIFERS
NANNOFOSSILS
RADIOLARIANS
DIATOMS
PALEOMAGNETICS
PHYS. PROPERTIES
CHEMISTRY
SECTION
METERS
GRAPHIC LITHOLOGY
DRILLING DISTURB.
SED. STRUCTURES
SAMPLES
MIOCENE
●Barren
●C/M
NN3 Sphenolithus belemnos
●R/P
No age diagnostic taxa
●Φ=38.5 γ=2.11
●Φ=43.4 γ=2.08
●Φ=43.2 γ=2.08
●IC=0.50 OC=0.06
0.5
1.0
1
2
3
4
5
6
7
CC
OG
IW

LITHOLOGIC DESCRIPTION

CALCAREOUS SILTY CLAYSTONE, SILTY CLAYSTONE, and CLAYEY SILTSTONE

Moderate drilling disturbance. Drilling biscuits common.

Major lithology: Interbedded CALCAREOUS SILTY CLAYSTONE, SILTY CLAYSTONE, and CLAYEY SILTSTONE. Sequences grade from black (10YR 2.5/1), dark bluish gray (5B 4/1), dark gray (N 4/0), and dark brown (10YR 3/3) SILTY CLAYSTONE and some coarser CLAYEY SILTSTONE with sharp contacts at the base to grayish brown (10YR 5/2), dark brown (10YR 4/3), and olive (5Y 4/3) SILTY CLAYSTONE and CALCAREOUS SILTY CLAYSTONE. Slight mottling in the SILTY CLAYSTONE.

SMEAR SLIDE SUMMARY (%):

	5, 57 M	6, 15 M
TEXTURE:		
Silt	30	40
Clay	70	60
COMPOSITION:		
Access. minerals	Tr	5
Clay	65	52
Dolomite	Tr	3
Inorganic calcite	15	10
Nannofossils	5	5
Quartz	15	25

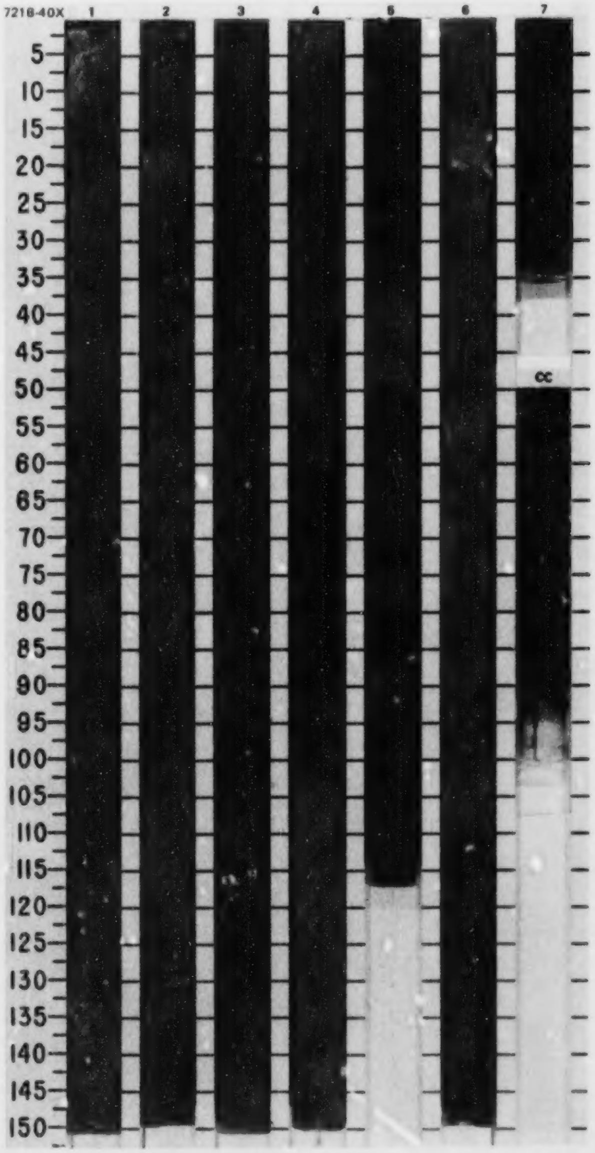
721B-40X
1
2
3
4
5
6
7
CC
5
10
15
20
25
30
35
40
45
50
55
60
65
70
75
80
85
90
95
100
105
110
115
120
125
130
135
140
145
150

SITE 721 HOLE B CORE 41X CORED INTERVAL 2330.4-2340.0 mbsl; 385.6-395.2 mbsf

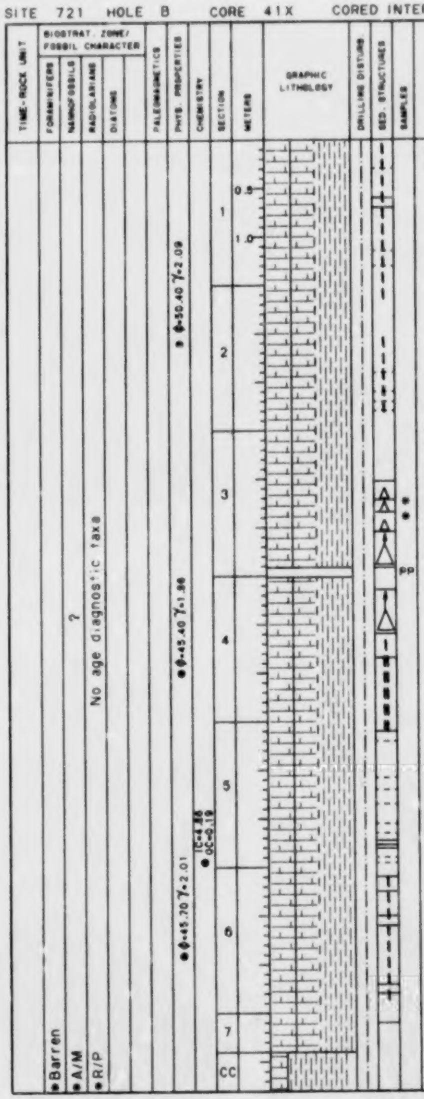
TIME-ROCK UNIT
BIOSTRAT. ZONE/ FOSSIL CHARACTER
FORAMINIFERS
NANNOFOSSILS
RADIOLARIANS
DIATOMS
PALEOMAGNETICS
PHYS. PROPERTIES
CHEMISTRY
SECTION
METERS
GRAPHIC LITHOLOGY
DRILLING DISTURB.
SED. STRUCTURES
SAMPLES
?
No age diagnostic taxa
• Barren
• A/M
• R/P
• ϕ=50.40 γ=2.09
• ϕ=45.40 γ=1.96
• ϕ=45.70 γ=2.01
• IC=4.86 OC=0.19
1
2
3
4
5
6
7
CC
0.5
1.0
*
*
PP

LITHOLOGIC DESCRIPTION

NANNOFOSSIL CHALK, CALCAREOUS SILTY CLAYSTONE, SILTY CLAYSTONE, and CLAYEY SILTSTONE

Moderate drilling disturbance. Drilling biscuits common.

Major lithology: Interbedded NANNOFOSSIL CHALK, CALCAREOUS SILTY CLAYSTONE, SILTY CLAYSTONE, and CLAYEY SILTSTONE. Sequences grade from dark greenish gray (5G 4/1), greenish gray (5GY 5/1, 5G 5/1), and dark gray (N 4/0) SILTY CLAYSTONE and CLAYEY SILTSTONE with sharp contacts at the base, to grayish brown (10YR 5/2), brown (10YR 5/3), dark grayish brown (10YR 4/2), and olive gray (5Y 4/2) SILTY CLAYSTONE and CALCAREOUS SILTY CLAYSTONE to light gray (10YR 7/0) NANNOFOSSIL CHALK. Slight mottling in the CHALK and CALCAREOUS SILTY CLAYSTONE. Millimeter-sized layers of pyrite grains found in Section 6 and in the CC. FORAMINIFER SAND at 87-88 cm in Section 3.

SMEAR SLIDE SUMMARY (%):

	3, 74 M	3, 89 D
TEXTURE:		
Sand	10	
Silt	50	
Clay	40	100
COMPOSITION:		
Cement		10
Clay		10
Foraminifers	60	10
Inorganic calcite	Tr	Tr
Nannofossils	10	70
Quartz		Tr

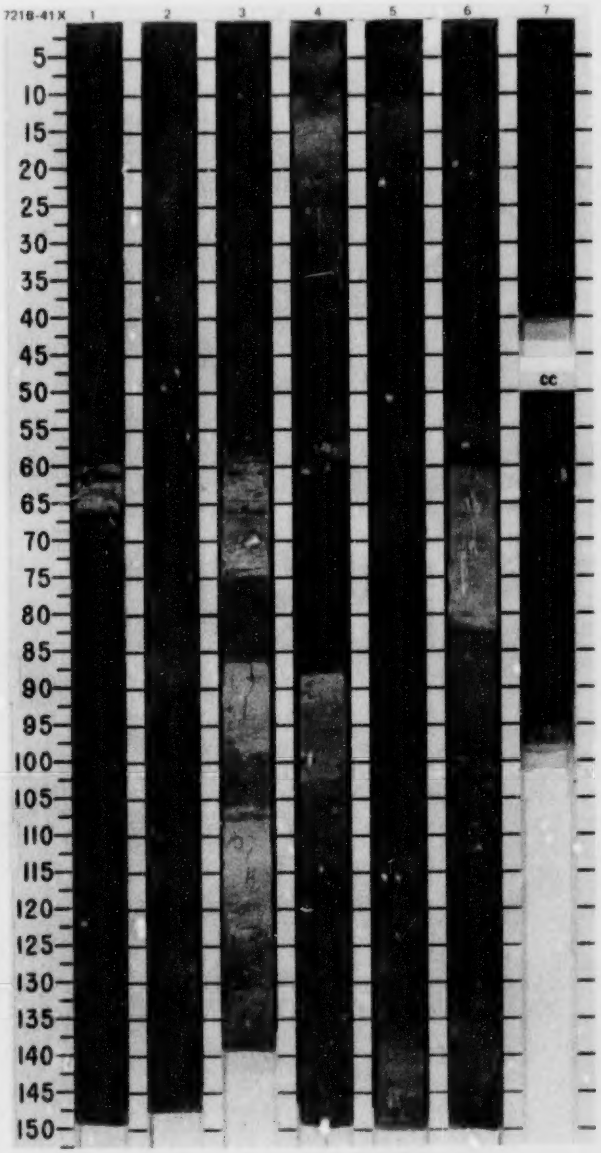
721B-41X
1
2
3
4
5
6
7
CC
5
10
15
20
25
30
35
40
45
50
55
60
65
70
75
80
85
90
95
100
105
110
115
120
125
130
135
140
145
150

SITE 721 HOLE B CORE 42X CORED INTERVAL 2340.0-2349.7 mbsl; 395.2-404.9 mbsf

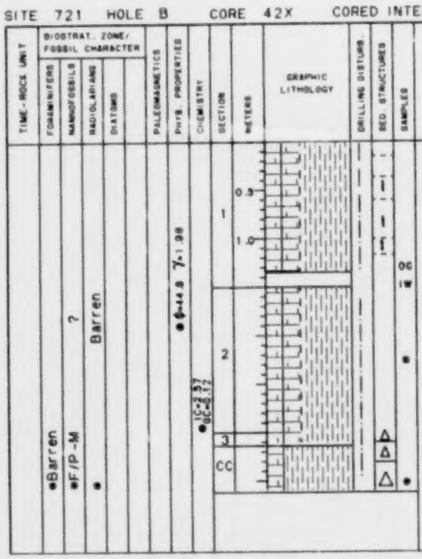
TIME-ROCK UNIT
BIOSTRAT. ZONE/ FOSSIL CHARACTER
FORAMINIFERS
NANNOFOSSILS
RADIOLARIANS
DIATOMS
PALEOMAGNETICS
PHYS. PROPERTIES
CHEMISTRY
SECTION
METERS
GRAPHIC LITHOLOGY
DRILLING DISTURB.
SED. STRUCTURES
SAMPLES
●Barren
●F/P-M
?
●
Barren
●φ=44.8 γ=1.98
●IC=2.57 OC=0.12
1
2
3
CC
0.5
1.0
OG
IW
●
●

LITHOLOGIC DESCRIPTION

SILTY CLAYSTONE and CLAYEY SILTSTONE

Moderate drilling disturbance. Drilling biscuits common.

Major lithology: SILTY CLAYSTONE and CLAYEY SILTSTONE. Sequences contain 30-200 cm layers of dark greenish gray (5GY 4/1, 5G 4/1) SILTY CLAYSTONE with sharp contacts at the base, thin (<50 cm thick) layers of dark grayish brown (10YR 4/2) SILTY CLAYSTONE and rare marly nannofossil chalk. Millimeter-sized layers of pyrite grains found at the base of some of the clayey siltstone.

SMEAR SLIDE SUMMARY (%):

	2, 77 D	CC, 43 M
TEXTURE:		
Sand		50
Silt	10	40
Clay	90	10
COMPOSITION:		
Access. minerals		5
Clay	15	
Feldspar		5
Inorganic calcite	20	25
Mica		20
Nannofossils	45	
Quartz	20	45

SITE 721 HOLE B CORE 43X CORED INTERVAL 2349.7-2359.3 mbsl; 404.9-414.5 mbsf

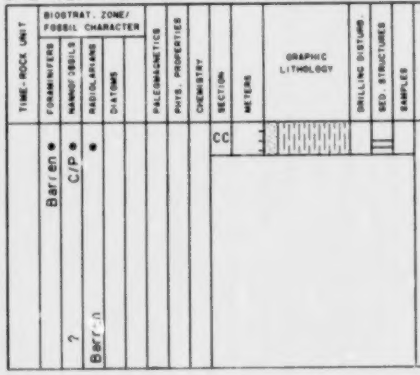
TIME-ROCK UNIT
BIOSTRAT. ZONE/ FOSSIL CHARACTER
FORAMINIFERS
NANNOFOSSILS
RADIOLARIANS
DIATOMS
PALEOMAGNETICS
PHYS. PROPERTIES
CHEMISTRY
SECTION
METERS
GRAPHIC LITHOLOGY
DRILLING DISTURB.
SED. STRUCTURES
SAMPLES
Barren ●
C/P ●
?
●
Barren
CC

LITHOLOGIC DESCRIPTION

CLAYEY SILTSTONE

Moderate drilling disturbance.

Major lithology: CLAYEY SILTSTONE, dark gray (5Y 4/1). SANDY SILT layer 1 cm thick, located at 19 cm, contains detrital calcite and mica.

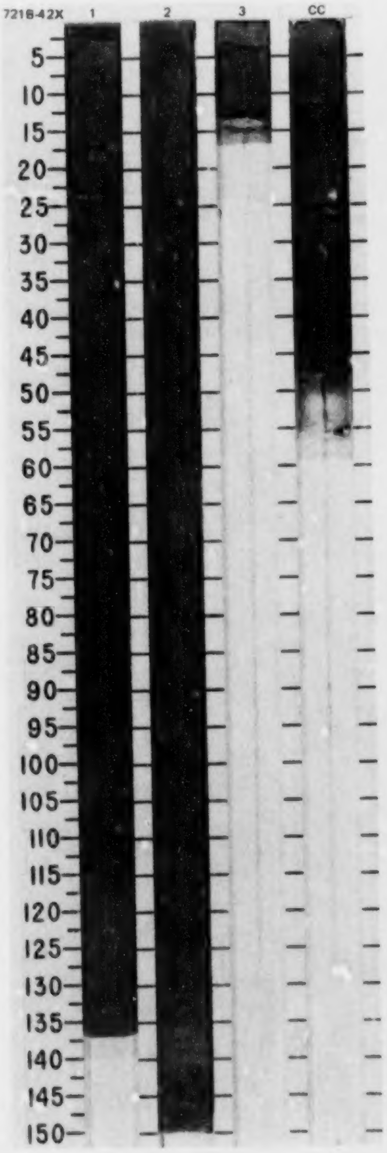
721B-42X
1
2
3
CC
5
10
15
20
25
30
35
40
45
50
55
60
65
70
75
80
85
90
95
100
105
110
115
120
125
130
135
140
145
150

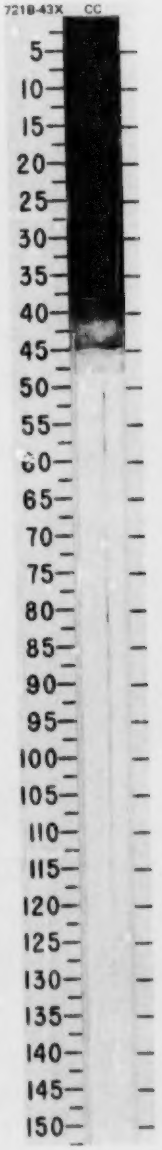
721B-43X
CC
5
10
15
20
25
30
35
40
45
50
55
60
65
70
75
80
85
90
95
100
105
110
115
120
125
130
135
140
145
150

SITE 721 HOLE B CORE 44X CORED INTERVAL 2359.3-2369.0 mbsl; 414.5-424.2 mbsf

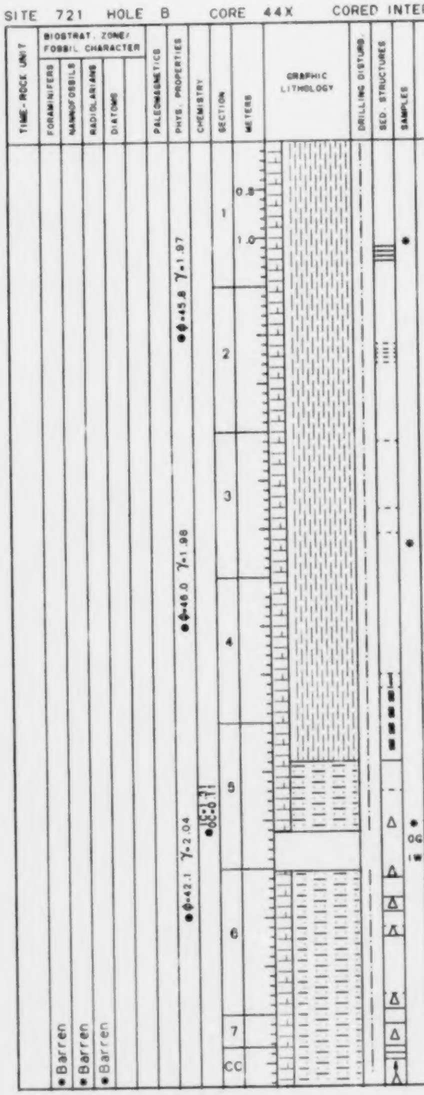
TIME-ROCK UNIT
BIOSTRAT. ZONE/FOSSIL CHARACTER
FORAMINIFERS
NANNOFOSSILS
RADIOLARIANS
DIATOMS
PALEOMAGNETICS
PHYS. PROPERTIES
CHEMISTRY
SECTION
METERS
GRAPHIC LITHOLOGY
DRILLING DISTURB.
SED. STRUCTURES
SAMPLES
● Barren
● Barren
● Barren
●ϕ=45.8 γ=1.97
●ϕ=46.0 γ=1.98
●ϕ=42.1 γ=2.04
1
2
3
4
5
6
7
CC
0.5
1.0
OG
IW

LITHOLOGIC DESCRIPTION

CLAYSTONE, SILTY CLAYSTONE, CLAYEY SILTSTONE, and SILTY SANDSTONE

Moderate drilling disturbance. Drilling biscuits common.

Major lithology: Interbedded CLAYSTONE, SILTY CLAYSTONE, CLAYEY SILTSTONE, and SILTY SANDSTONE, dark reddish gray (5YR 4/2). Sequences appear to fine upward. Foraminifer sand concentrated at 0-11 cm in Section 6.

Minor lithology: CALCAREOUS CLAYSTONE, light greenish gray (5G 7/1) to light gray (5Y 6/1). Slight to moderate mottling.

SMEAR SLIDE SUMMARY (%):

	1, 108 D	4, 127 D	5, 103 D
TEXTURE:			
Sand			50
Silt	30	15	30
Clay	70	85	20
COMPOSITION:			
Access. minerals	2	1	5
Clay	70	75	20
Dolomite	Tr		
Feldspar	2		10
Volcanic glass	1		10
Inorganic calcite	10	10	12
Mica		Tr	3
Nannofossils	Tr	10	
Quartz	15	1	40
Silicoflagellates	Tr	3	

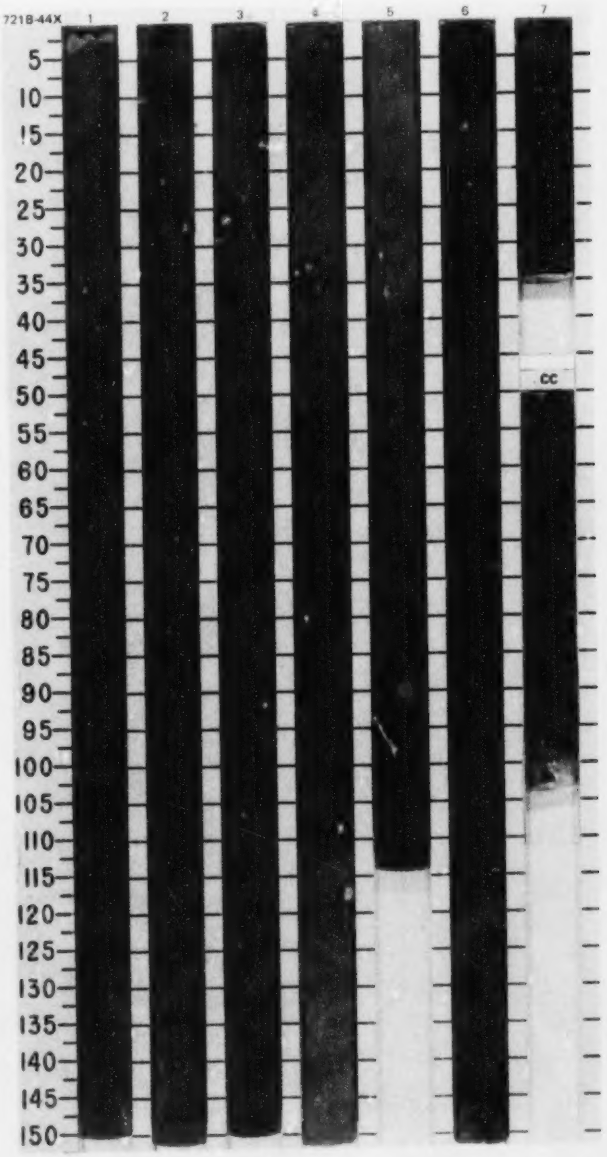
721B-44X
1
2
3
4
5
6
7
CC
5
10
15
20
25
30
35
40
45
50
55
60
65
70
75
80
85
90
95
100
105
110
115
120
125
130
135
140
145
150

SITE 721 HOLE C CORE 1H CORED INTERVAL 1944.8-1948.4 mbsl; 0.0-3.6 mbsf

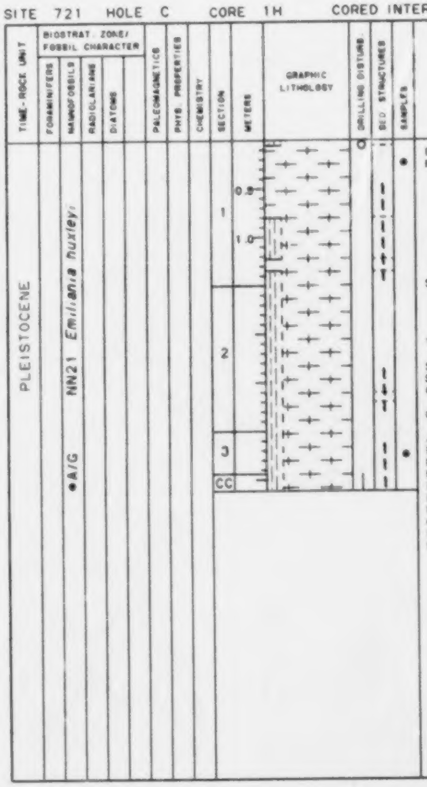
TIME-ROCK UNIT
BIOSTRAT. ZONE/ FOSSIL CHARACTER
FORAMINIFERS
NANNOFOSSILS
RADIOLARIANS
DIATOMS
PALEOMAGNETICS
PHYS. PROPERTIES
CHEMISTRY
SECTION
METERS
GRAPHIC LITHOLOGY
DRILLING DISTURB.
SED. STRUCTURES
SAMPLES
PLEISTOCENE
●A/G NN21 Emiliania huxleyi
1
2
3
CC
0.5
1.0

LITHOLOGIC DESCRIPTION

FORAMINIFER-NANNOFOSSIL OOZE to FORAMINIFER-BEARING NANNOFOSSIL OOZE

Section 1, 0-5 cm, and the CC are highly disturbed. Remainder of core is undisturbed.

Major lithology: FORAMINIFER-NANNOFOSSIL OOZE to FORAMINIFER-BEARING NANNOFOSSIL OOZE. Alternating light and dark bands of light gray (5Y 6/1) to olive (5Y 4/3, 5/3). Slight to moderate burrow-mottling throughout. Dark layers contain more terrigenous clay than do light layers.

SMEAR SLIDE SUMMARY (%):

	1, 24 D	3, 24 D
TEXTURE:		
Sand	35	10
Silt	15	20
Clay	50	70
COMPOSITION:		
Access. minerals		1
Diatoms	Tr	Tr
Dolomite	Tr	
Feldspar		1
Foraminifers	35	15
Inorganic calcite	15	11
Nannofossils	50	70
Quartz	Tr	2
Radiolarians	Tr	Tr
Sponge spicules	Tr	Tr

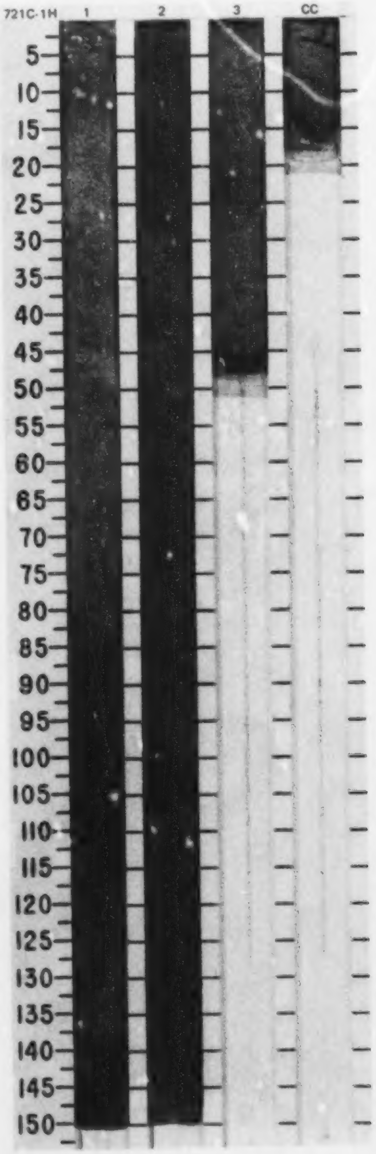
721C-1H
1
2
3
CC
5
10
15
20
25
30
35
40
45
50
55
60
65
70
75
80
85
90
95
100
105
110
115
120
125
130
135
140
145
150

SITE 721 HOLE C CORE 2H CORED INTERVAL 1948.4-1958.1 mbsl; 3.6-13.3 mbsf

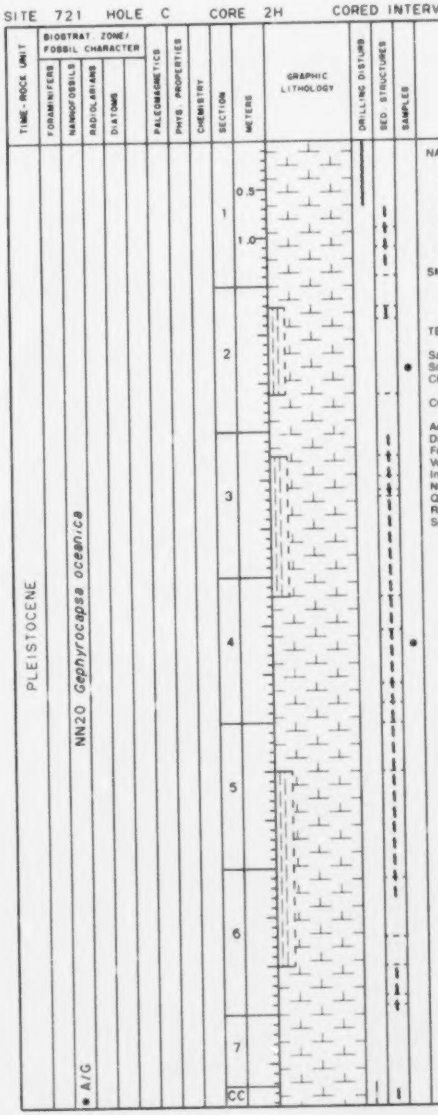
TIME-ROCK UNIT
BIOSTRAT. ZONE/ FOSSIL CHARACTER
FORAMINIFERS
NANNOFOSSILS
RADIOLARIANS
DIATOMS
PALEOMAGNETICS
PHYS. PROPERTIES
CHEMISTRY
SECTION
METERS
GRAPHIC LITHOLOGY
DRILLING DISTURB.
SED. STRUCTURES
SAMPLES
PLEISTOCENE
NN20 Gephyrocapsa oceanica
● A/G
0.5
1.0
1
2
3
4
5
6
7
CC

LITHOLOGIC DESCRIPTION

NANNOFOSSIL OOZE

Section 1, 0-61 cm, is very disturbed. Remainder of core is undisturbed.

Major lithology: NANNOFOSSIL OOZE. Alternating light and dark bands, light gray (5Y 7/1, 6/1), light olive gray (5Y 6/2), and pale olive (5Y 6/3), to olive (5Y 4/3, 5/3). Slight to moderate burrow-mottling throughout. Dark layers contain more terrigenous silty clay than do light layers. Black pyrite spots seen throughout, especially as burrow linings.

SMEAR SLIDE SUMMARY (%):

	2, 88 D	4, 67 D
TEXTURE:		
Sand	10	10
Silt	20	15
Clay	70	75
COMPOSITION:		
Access. minerals	Tr	Tr
Diatoms		1
Foraminifers	10	7
Volcanic glass	Tr	Tr
Inorganic calcite	20	17
Nannofossils	70	75
Quartz	Tr	Tr
Radiolarians	Tr	Tr
Sponge spicules	Tr	

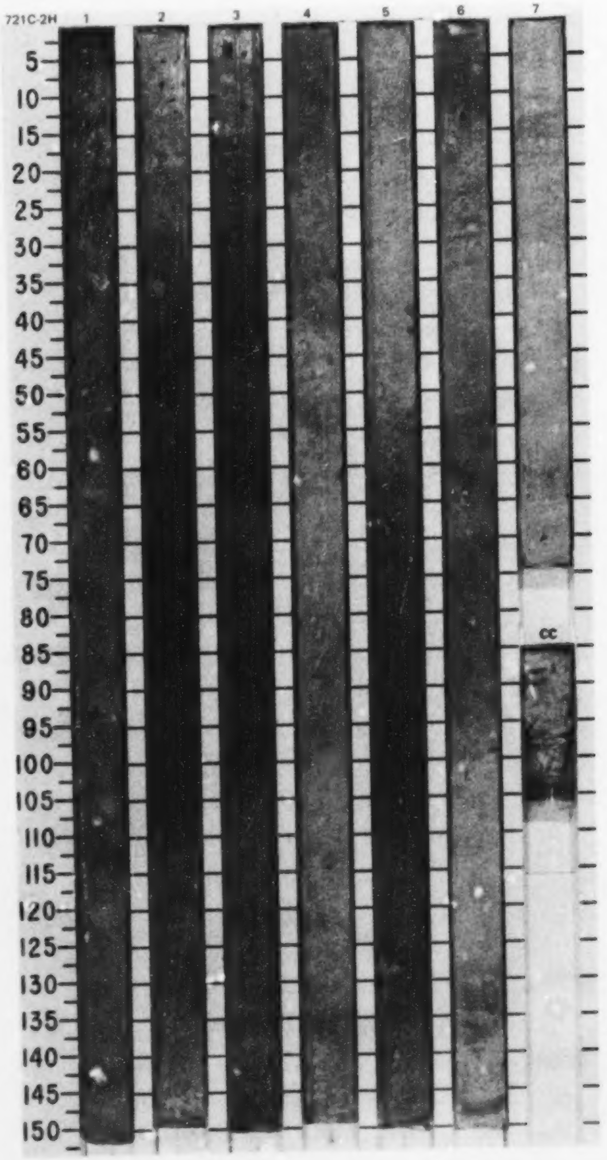
721C-2H
1
2
3
4
5
6
7
CC
5
10
15
20
25
30
35
40
45
50
55
60
65
70
75
80
85
90
95
100
105
110
115
120
125
130
135
140
145
150

SITE 721 HOLE C CORE 3H CORED INTERVAL 1958.1-1967.8 mbsl; 13.3-23.0 mbsf

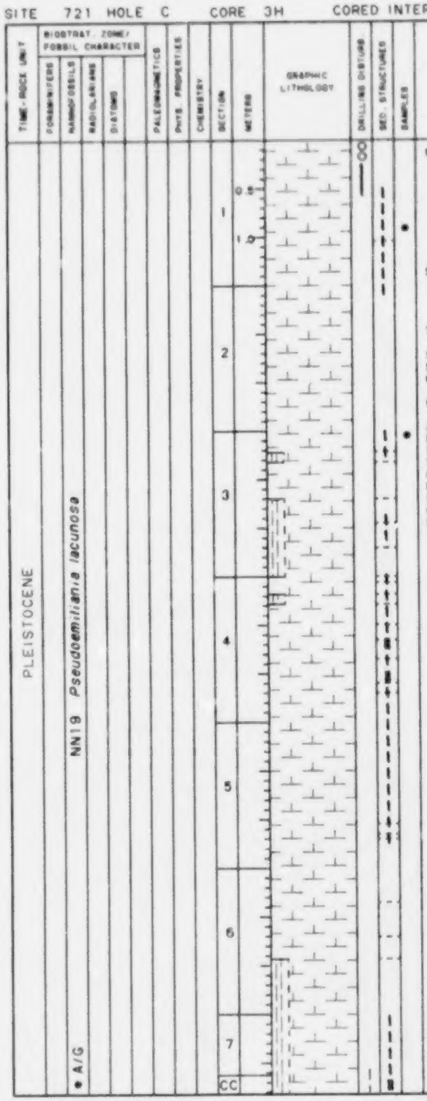
TIME-ROCK UNIT
BIOSTRAT. ZONE/ FOSSIL CHARACTER
FORAMINIFERS
NANNOFOSSILS
RADIOLARIANS
DIATOMS
PALEOMAGNETICS
PHYS. PROPERTIES
CHEMISTRY
SECTION
METERS
GRAPHIC LITHOLOGY
DRILLING DISTURB.
SED. STRUCTURES
SAMPLES
PLEISTOCENE
NN19 Pseudoemiliania lacunosa
• A/G
0.5
1.0
1
2
3
4
5
6
7
CC

LITHOLOGIC DESCRIPTION

NANNOFOSSIL OOZE

Section 1, 0-15 cm, soupy; 15-57 cm, stretched and moderately disturbed. Remainder of core undisturbed.

Major lithology: NANNOFOSSIL OOZE. Alternating light and dark bands of light gray (5Y 7/1) and light olive gray (5Y 6/2) to olive (5Y 5/3, 4/3, 5/4, 4/4). Slight to moderate burrow-mottling throughout. Dark layers contain more terrigenous silty clay than do light layers. Foraminifers visible on core face.

SMEAR SLIDE SUMMARY (%):

	1, 90 D	3, 4 D
TEXTURE:		
Sand	1	1
Silt	9	9
Clay	90	90
COMPOSITION:		
Access. minerals	Tr	Tr
Dolomite	Tr	
Foraminifers	1	1
Volcanic glass	Tr	
Inorganic calcite	9	9
Mica		Tr
Nannofossils	90	90
Quartz	Tr	Tr
Sponge spicules	Tr	

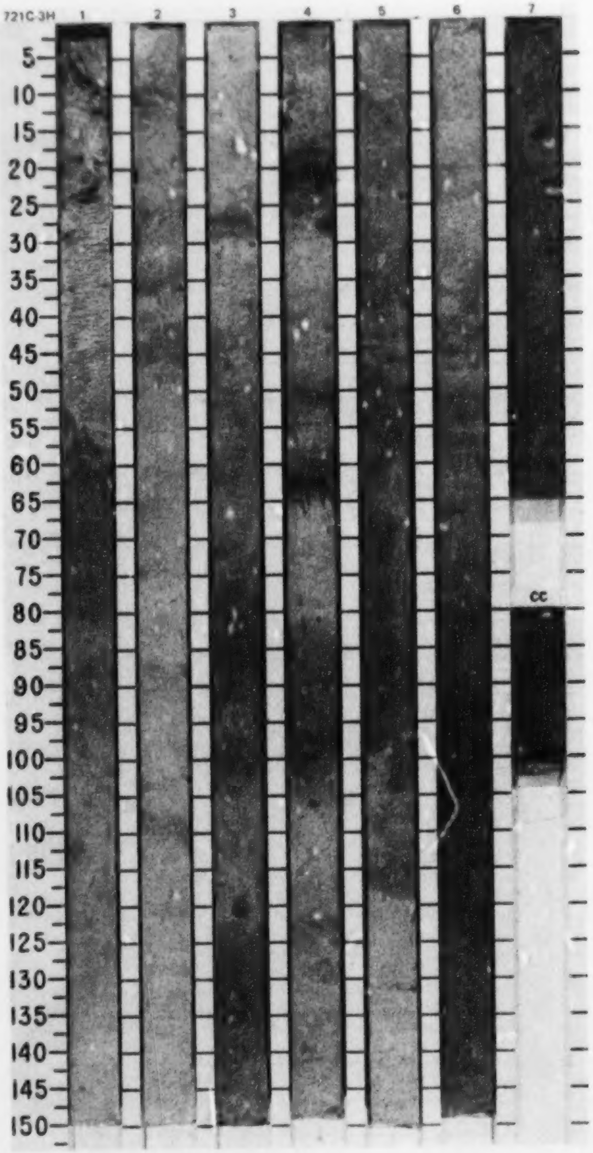
721C-3H
1
2
3
4
5
6
7
CC
5
10
15
20
25
30
35
40
45
50
55
60
65
70
75
80
85
90
95
100
105
110
115
120
125
130
135
140
145
150

SITE 721 HOLE C CORE 4H CORED INTERVAL 1967.8-1977.5 mbsl; 23.0-32.7 mbsf

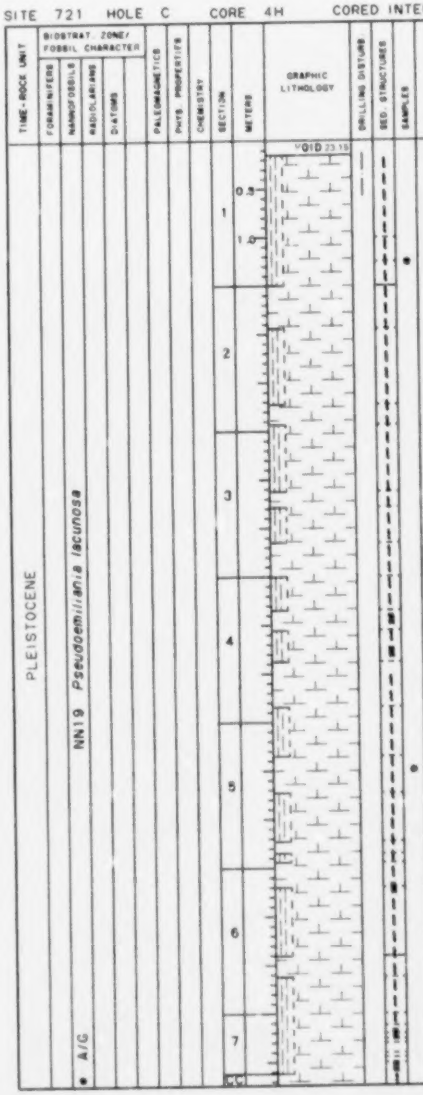
TIME-ROCK UNIT
BIOSTRAT. ZONE/ FOSSIL CHARACTER
FORAMINIFERS
NANNOFOSSILS
RADIOLARIANS
DIATOMS
PALEOMAGNETICS
PHYS. PROPERTIES
CHEMISTRY
SECTION
METERS
GRAPHIC LITHOLOGY
DRILLING DISTURB.
SED. STRUCTURES
SAMPLES
PLEISTOCENE
NN19 Pseudoemiliania lacunosa
A/G
VOID 23.15
0.5
1.0
1
2
3
4
5
6
7
CC

LITHOLOGIC DESCRIPTION

NANNOFOSSIL OOZE

Void 0-13 cm, in Section 1. Section 1, 13-30 cm, soupy and moderately disturbed. Remainder of core is undisturbed.

Major lithology: NANNOFOSSIL OOZE. Alternating light and dark bands of light olive gray (5Y 6/2), light greenish gray (5GY 7/1, 10Y 6/2), light gray (5Y 6/1), pale olive (5Y 6/3), and olive (5Y 5/3, 5/4, 4/3), to olive gray (5Y 5/2, 4/2). Slight to moderate burrow-mottling throughout. Dark layers contain 10-20% more terrigenous silty clay than do light layers. Some burrows lined with black pyrite grains.

SMEAR SLIDE SUMMARY (%):

	1, 127 D	5, 49 D
TEXTURE:		
Sand	20	
Silt	15	15
Clay	65	85
COMPOSITION:		
Access. minerals	1	Tr
Diatoms	10	
Feldspar		Tr
Foraminifers	10	Tr
Volcanic glass		Tr
Inorganic calcite	10	14
Mica		Tr
Nannofossils	65	85
Quartz	Tr	1
Radiolarians	Tr	
Silicoflagellates	1	
Sponge spicules	3	Tr

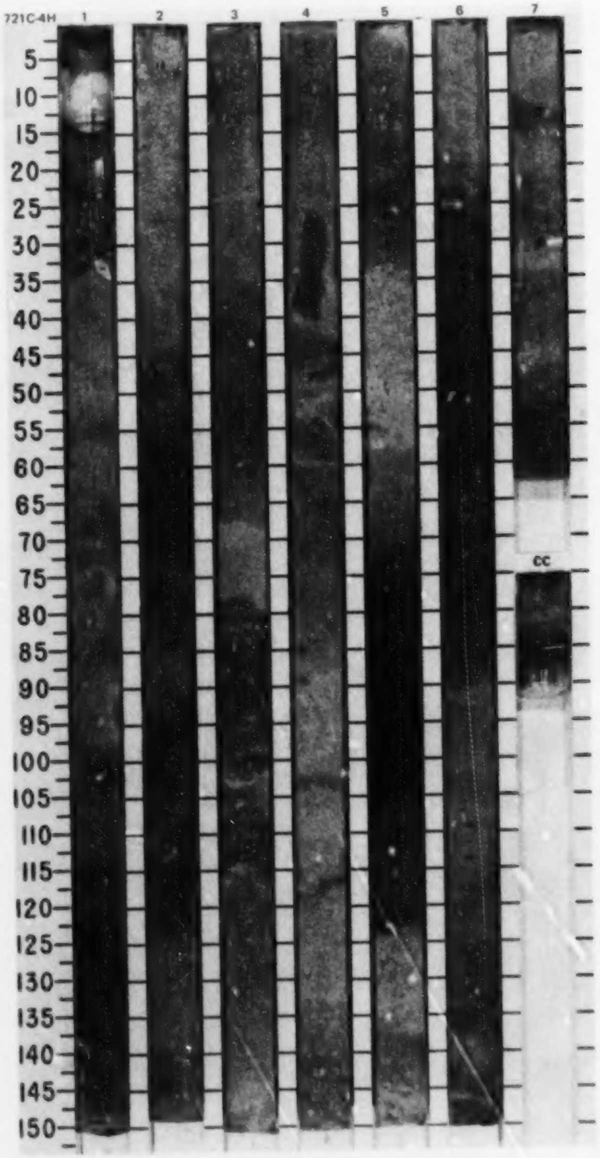
721C-4H
1
2
3
4
5
6
7
CC
5
10
15
20
25
30
35
40
45
50
55
60
65
70
75
80
85
90
95
100
105
110
115
120
125
130
135
140
145
150

SITE 721 HOLE C CORE 5H CORED INTERVAL 1977.5-1987.2 mbsl; 32.7-42.4 mbsf

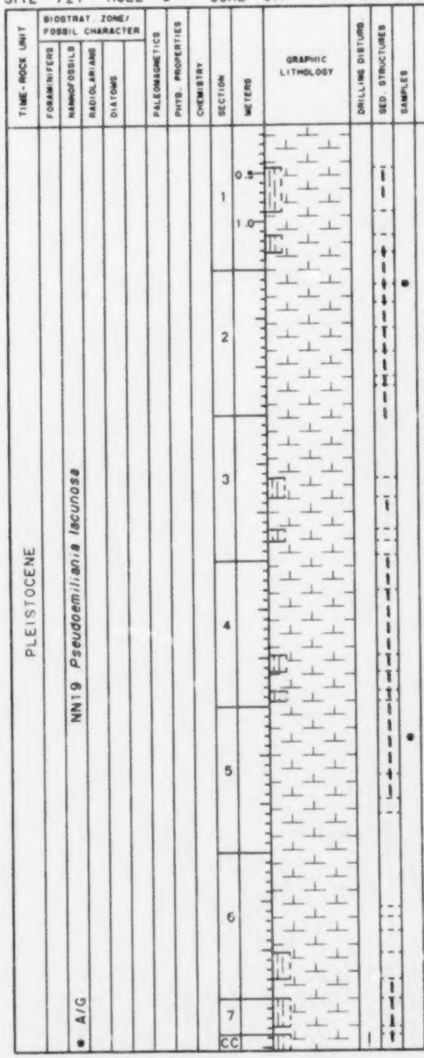
TIME-ROCK UNIT
BIOSTRAT. ZONE/FOSSIL CHARACTER
FORAMINIFERS
NANNOFOSSILS
RADIOLARIANS
DIATOMS
PALEOMAGNETICS
PHYS. PROPERTIES
CHEMISTRY
SECTION
METERS
GRAPHIC LITHOLOGY
DRILLING DISTURB.
SED. STRUCTURES
SAMPLES
PLEISTOCENE
NN19 Pseudoemiliania lacunosa
A/G
0.5
1.0
1
2
3
4
5
6
7
CC

LITHOLOGIC DESCRIPTION

NANNOFOSSIL OOZE

No drilling disturbance.

Major lithology: NANNOFOSSIL OOZE. Alternating light and dark bands, light greenish gray (5GY 7/1, 10Y 6/2), light gray (5Y 7/2), and light olive gray (5Y 6/2) to olive gray (5Y 5/2), pale olive (5Y 6/3), and olive (5Y 4/3, 5/3). Slight to moderate burrow-mottling throughout. Dark layers enriched in terrigenous components relative to light layers. Foraminifers visible on core face.

SMEAR SLIDE SUMMARY (%):

	2, 16 D	5, 32 D
TEXTURE:		
Sand	1	
Silt	14	15
Clay	85	85
COMPOSITION:		
Access. minerals	Tr	Tr
Diatoms	Tr	
Dolomite	Tr	
Foraminifers	1	Tr
Volcanic glass		Tr
Inorganic calcite	13	15
Mica	1	Tr
Nannofossils	85	85
Radiolarians	Tr	
Sponge spicules		Tr

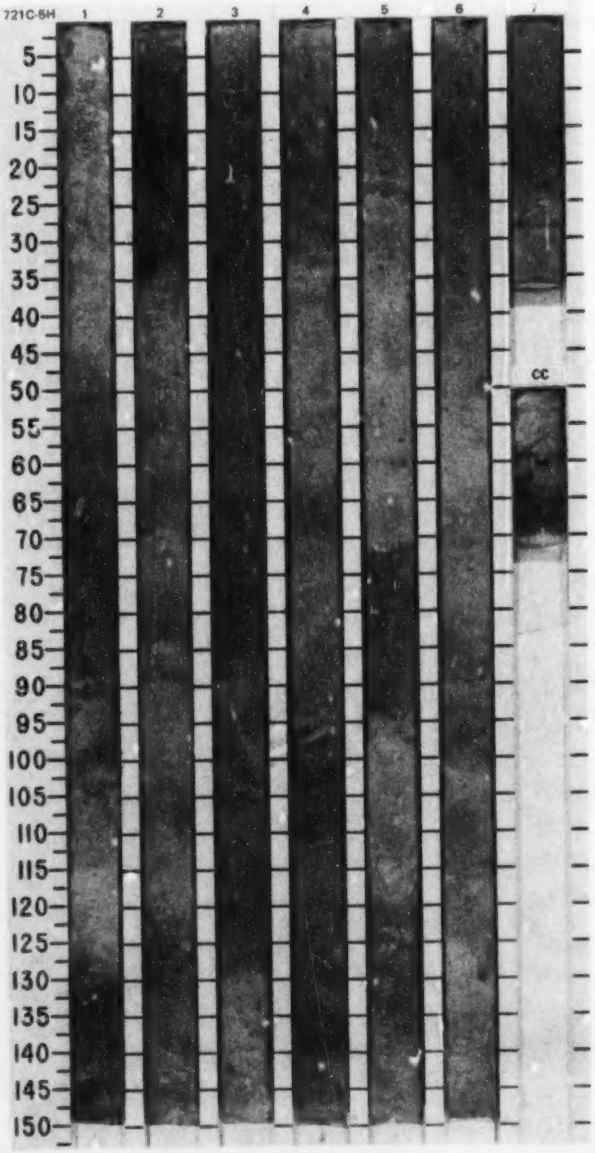
721C-5H
1
2
3
4
5
6
7
CC
5
10
15
20
25
30
35
40
45
50
55
60
65
70
75
80
85
90
95
100
105
110
115
120
125
130
135
140
145
150

SITE 721 HOLE C CORE 6H CORED INTERVAL

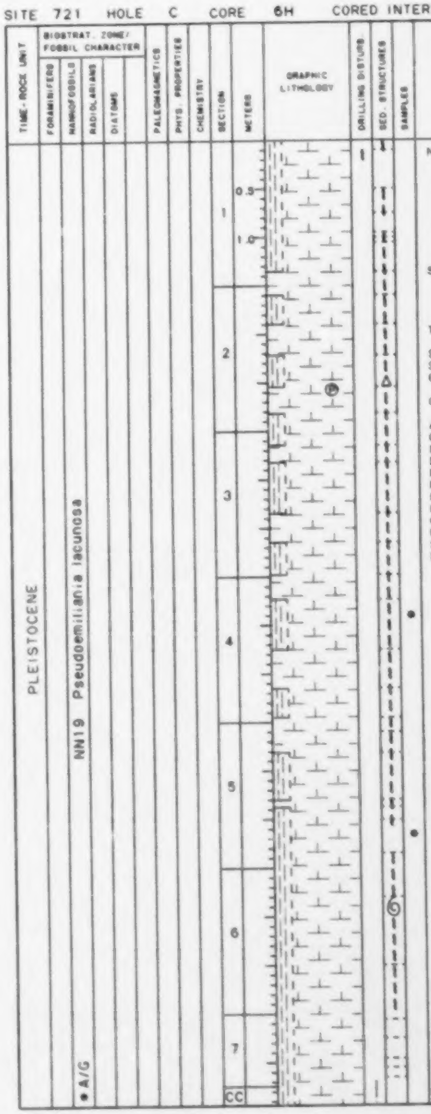
TIME-ROCK UNIT
BIOSTRAT. ZONE/ FOSSIL CHARACTER
FORAMINIFERS
NANNOFOSSILS
RADIOLARIANS
DIATOMS
PALEOMAGNETICS
PHYS. PROPERTIES
CHEMISTRY
SECTION
METERS
GRAPHIC LITHOLOGY
DRILLING DISTURB.
SED. STRUCTURES
SAMPLES
PLEISTOCENE
NN19 Pseudoemiliania lacunosa
• A/G
0.5
1.0
1
2
3
4
5
6
7
CC

LITHOLOGIC DESCRIPTION

NANNOFOSSIL OOZE

Section 1, 0-20 cm, highly disturbed. Remainder of core undisturbed.

Major lithology: NANNOFOSSIL OOZE. Alternating light and dark bands, light gray (5Y 6/1) and olive gray (5Y 6/2) to olive gray (5Y 5/2) and olive (5Y 4/3, 4/4, 5/4, 5/3). Slight to moderate burrow-mottling throughout. Dark layers contain 10-20% more terrigenous silty clay than do light layers. Foraminifers visible on core face.

SMEAR SLIDE SUMMARY (%):

	4, 40 D	5, 115 D
TEXTURE:		
Sand	5	
Silt	15	15
Clay	80	85
COMPOSITION:		
Access. minerals		Tr
Clay	5	10
Diatoms	Tr	
Dolomite		Tr
Feldspar	Tr	
Foraminifers	5	5
Inorganic calcite	Tr	10
Nannofossils	80	74
Quartz	5	1
Radiolarians	5	Tr
Silicoflagellates	Tr	
Sponge spicules		Tr

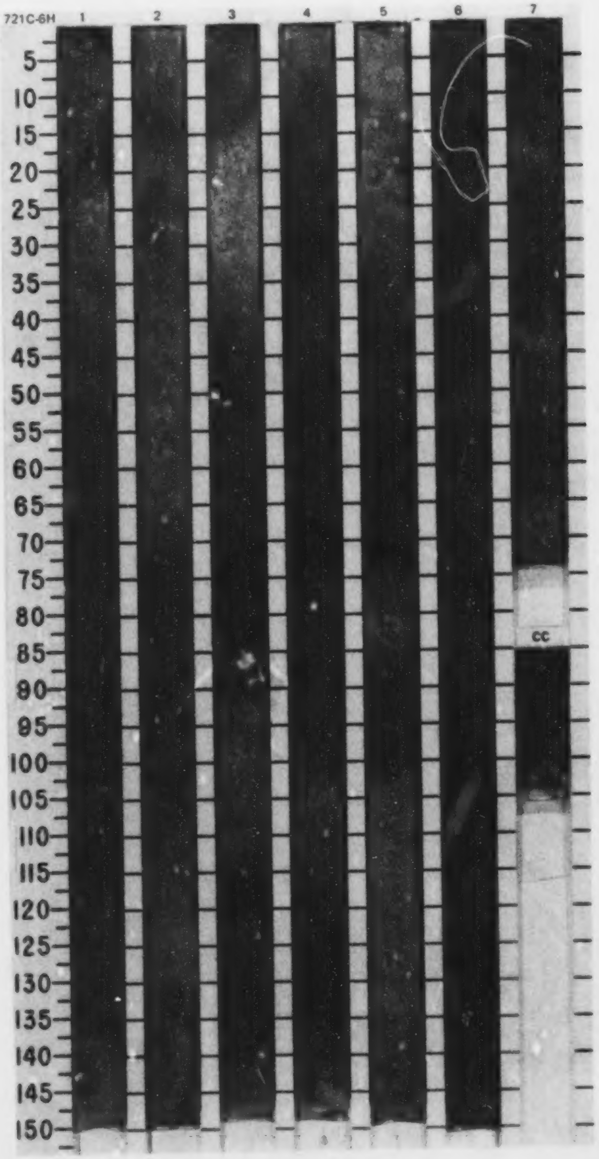
721C-6H
1
2
3
4
5
6
7
CC
5
10
15
20
25
30
35
40
45
50
55
60
65
70
75
80
85
90
95
100
105
110
115
120
125
130
135
140
145
150

SITE 721 HOLE C CORE 7H CORED INTERVAL 1996.8-2006.1 mbsl; 52.0-61.3 mbsf

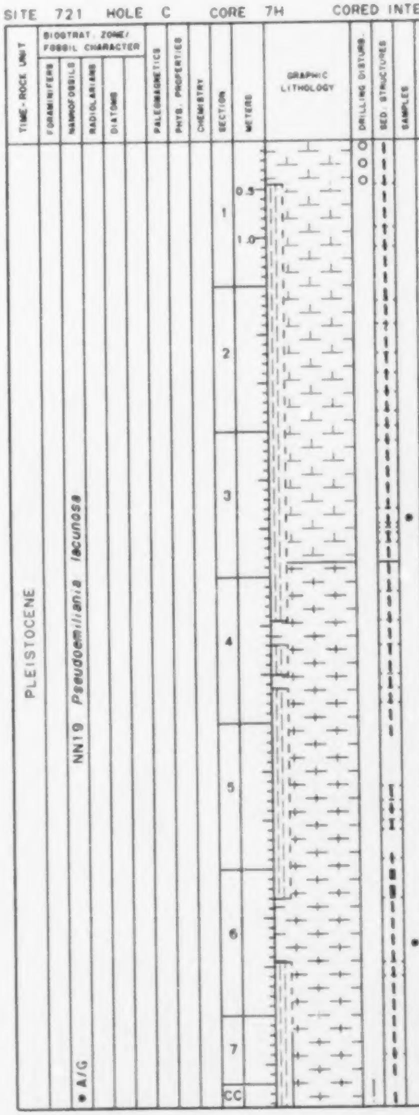
TIME-ROCK UNIT
BIOSTRAT. ZONE/ FOSSIL CHARACTER
FORAMINIFERS
NANNOFOSSILS
RADIOLARIANS
DIATOMS
PALEOMAGNETICS
PHYS. PROPERTIES
CHEMISTRY
SECTION
METERS
GRAPHIC LITHOLOGY
DRILLING DISTURB.
SED. STRUCTURES
SAMPLES
PLEISTOCENE
NN19 Pseudoemiliania lacunosa
* A/G
0.5
1.0
1
2
3
4
5
6
7
CC

LITHOLOGIC DESCRIPTION

FORAMINIFER-NANNOFOSSIL OOZE to NANNOFOSSIL OOZE

Section 1, 10-45 cm, soupy. Remainder of core is undisturbed.

Major lithology: FORAMINIFER-NANNOFOSSIL OOZE to NANNOFOSSIL OOZE. Alternating light and dark bands, light greenish gray (10Y 6/2) and light gray (5Y 7/1) to olive gray (5Y 5/2, 4/2) and olive (5Y 4/3, 5/3, 5/4). Slight to moderate burrow-mottling throughout. Dark layers enriched in terrigenous silty clay relative to light layers.

SMEAR SLIDE SUMMARY (%):

	3, 90 D	6, 77 D
TEXTURE:		
Sand	10	15
Silt	20	30
Clay	70	55
COMPOSITION:		
Access. minerals		2
Clay	10	15
Feldspar	Tr	
Foraminifers	10	15
Gypsum		Tr
Inorganic calcite	Tr	3
Mica	Tr	
Nannofossils	70	65
Quartz	10	
Radiolarians	Tr	
Silicoflagellates	Tr	

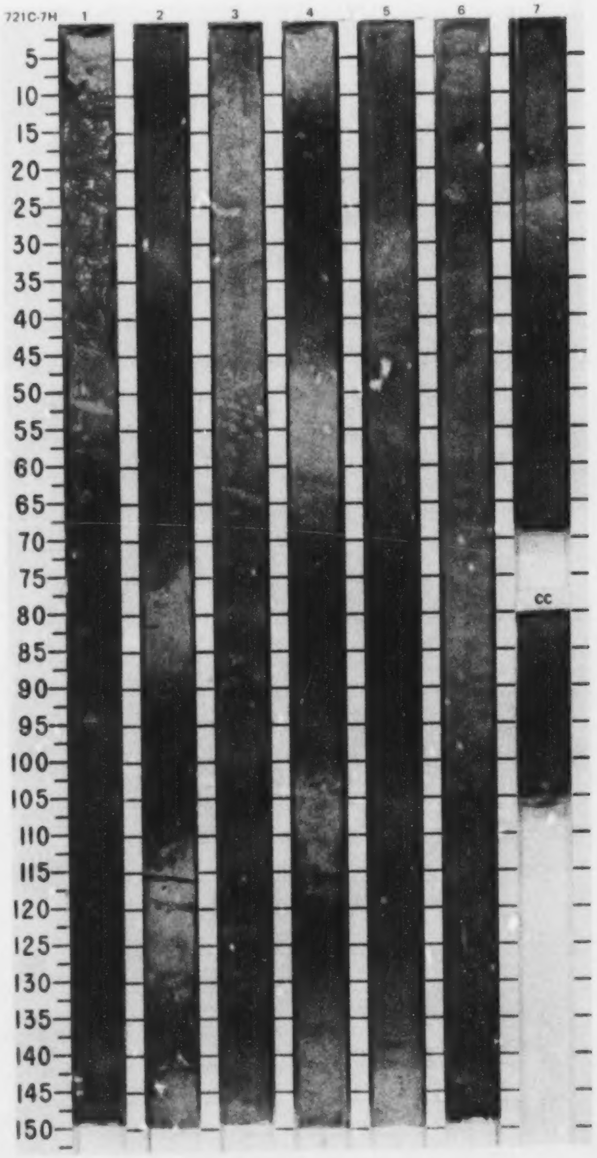
721C-7H
1
2
3
4
5
6
7
CC
5
10
15
20
25
30
35
40
45
50
55
60
65
70
75
80
85
90
95
100
105
110
115
120
125
130
135
140
145
150

SITE 721 HOLE C CORE 8H CORED INTERVAL 2006.1-2015.6 mbsl; 61.3-70.8 mbsf

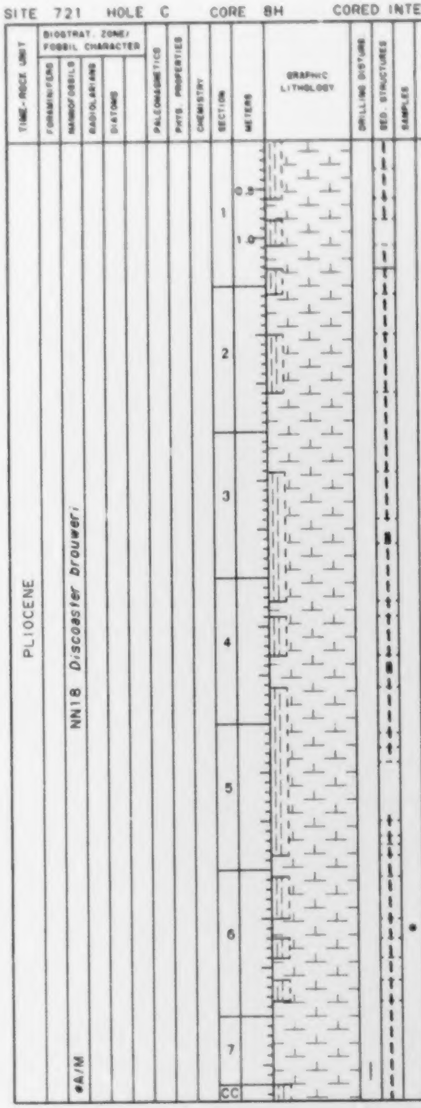
TIME-ROCK UNIT
BIOSTRAT. ZONE/ FOSSIL CHARACTER
FORAMINIFERS
NANNOFOSSILS
RADIOLARIANS
DIATOMS
PALEOMAGNETICS
PHYS. PROPERTIES
CHEMISTRY
SECTION
METERS
GRAPHIC LITHOLOGY
DRILLING DISTURB.
SED. STRUCTURES
SAMPLES
PLIOCENE
NN18 Discoaster brouweri
#A/M
0.5
1.0
1
2
3
4
5
6
7
CC

LITHOLOGIC DESCRIPTION

NANNOFOSSIL OOZE

No drilling disturbance.

Major lithology: NANNOFOSSIL OOZE. Alternating light and dark bands, light olive gray (5Y 6/2) and pale olive (5Y 6/3) to olive gray (5Y 5/2, 4/2) and olive (5Y 4/3, 5/3, 4/4). Slight to moderate burrow-mottling throughout. Dark layers enriched in terrigenous silty clay relative to light layers.

SMEAR SLIDE SUMMARY (%):

	6, 60 D
TEXTURE:	
Sand	5
Silt	30
Clay	65
COMPOSITION:	
Access. minerals	Tr
Clay	20
Foraminifers	15
Gypsum	Tr
Inorganic calcite	5
Nannofossils	60
Radiolarians	Tr

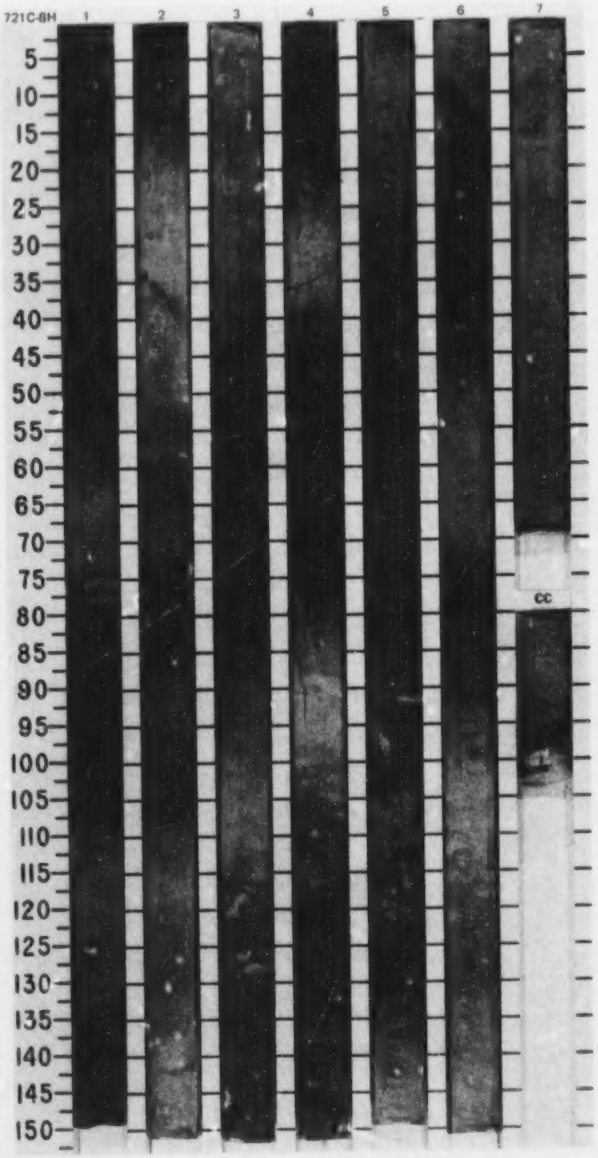
721C-8H
1
2
3
4
5
6
7
CC
5
10
15
20
25
30
35
40
45
50
55
60
65
70
75
80
85
90
95
100
105
110
115
120
125
130
135
140
145
150

SITE 721 HOLE C CORE 9H CORED INTERVAL 2015.6-2025.1 mbsl; 70.8-80.3 mbsf

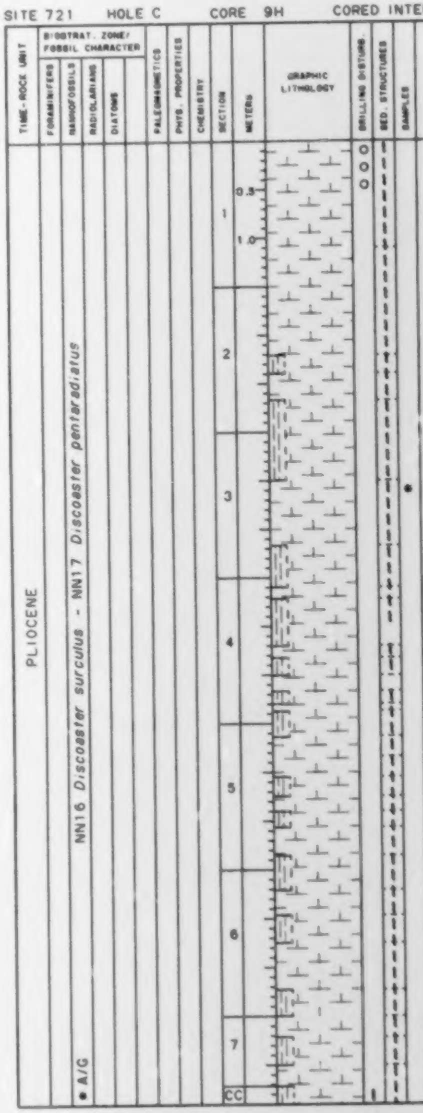
TIME-ROCK UNIT
BIOSTRAT. ZONE/ FOSSIL CHARACTER
FORAMINIFERS
NANNOFOSSILS
RADIOLARIANS
DIATOMS
PALEOMAGNETICS
PHYS. PROPERTIES
CHEMISTRY
SECTION
METERS
GRAPHIC LITHOLOGY
DRILLING DISTURB.
SED. STRUCTURES
SAMPLES
PLIOCENE
NN16 Discoaster surculus - NN17 Discoaster pentaradiatus
• A/G
0.5
1.0
1
2
3
4
5
6
7
CC

LITHOLOGIC DESCRIPTION

NANNOFOSSIL OOZE

Section 1, 0-38 cm, soupy. Remainder of core is undisturbed.

Major lithology: NANNOFOSSIL OOZE. Alternating light and dark bands, light gray (5Y 7/1), pale yellow (5Y 7/3), and light olive gray (5Y 6/2) to olive (5Y 4/3, 5/3, 4/4) and olive gray (5Y 4/2). Slight to moderate burrow-mottling throughout. Dark layers enriched in terrigenous clay relative to light layers.

SMEAR SLIDE SUMMARY (%):

	3, 60 D
TEXTURE:	
Silt	20
Clay	80
COMPOSITION:	
Clay	10
Diatoms	5
Foraminifers	Tr
Inorganic calcite	Tr
Nannofossils	85
Quartz	Tr

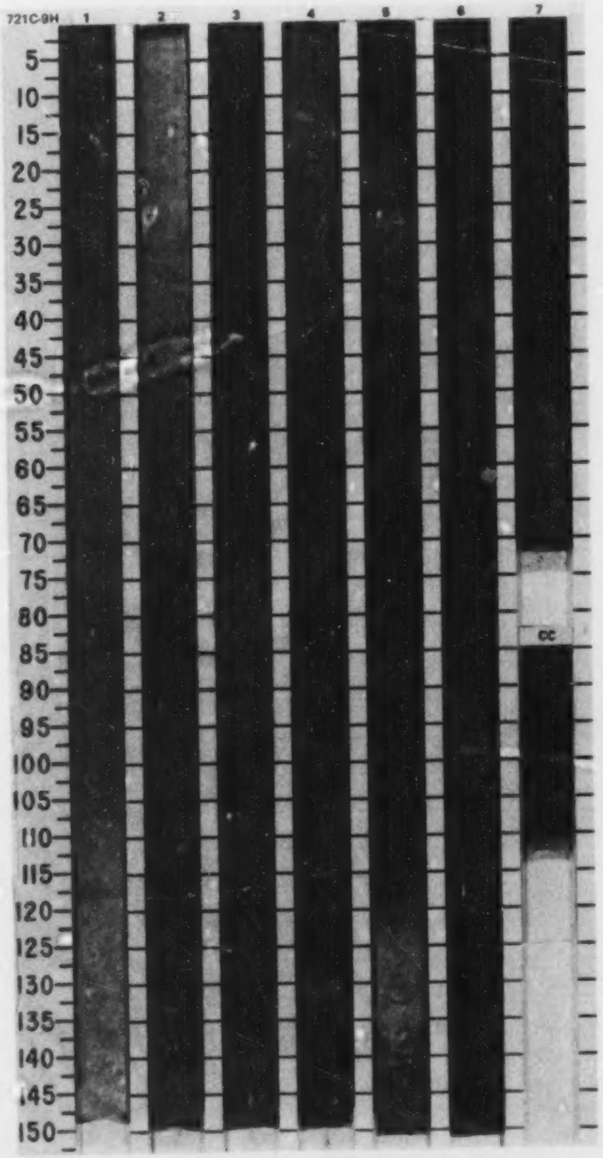
721C-9H
1
2
3
4
5
6
7
CC
5
10
15
20
25
30
35
40
45
50
55
60
65
70
75
80
85
90
95
100
105
110
115
120
125
130
135
140
145
150

SITE 721 HOLE C CORE 10H CORED INTERVAL 2025.1-2034.7 mbsl; 80.3-89.9 mbsf

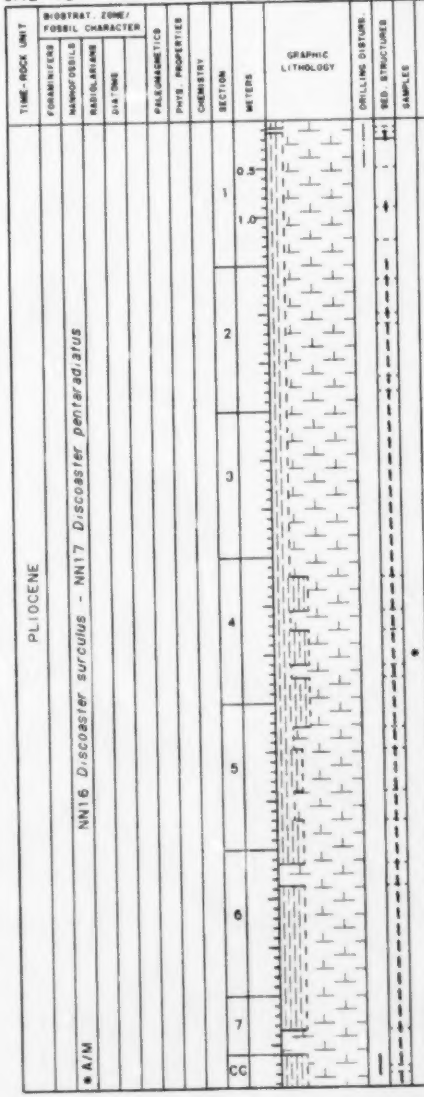
TIME-ROCK UNIT
BIOSTRAT. ZONE/ FOSSIL CHARACTER
FORAMINIFERS
NANNOFOSSILS
RADIOLARIANS
DIATOMS
PALEOMAGNETICS
PHYS. PROPERTIES
CHEMISTRY
SECTION
METERS
GRAPHIC LITHOLOGY
DRILLING DISTURB.
SED. STRUCTURES
SAMPLES
PLIOCENE
NN16 Discoaster surculus - NN17 Discoaster pentaradiatus
A/M
0.5
1.0
1
2
3
4
5
6
7
CC

LITHOLOGIC DESCRIPTION

NANNOFOSSIL OOZE

Section 1, 0-20 cm, moderately disturbed. Remainder of core is undisturbed.

Major lithology: NANNOFOSSIL OOZE. Alternating light and dark bands, pale olive (5Y 6/3) to olive (5Y 4/3, 5/3, 5/4) and olive gray (5Y 4/2). Slight to moderate burrow-mottling throughout. Dark layers enriched in terrigenous clay relative to light layers.

Minor lithology: Marly nannofossil ooze, dark olive gray (5Y 3/2), in Section 4, 148-150 cm; Section 5, 0-25 cm; Section 7, 10-35 cm; and CC.

SMEAR SLIDE SUMMARY (%):

	4, 100 D
TEXTURE:	
Silt	90
Clay	90
COMPOSITION:	
Clay	30
Inorganic calcite	20
Nannofossils	40
Quartz	10

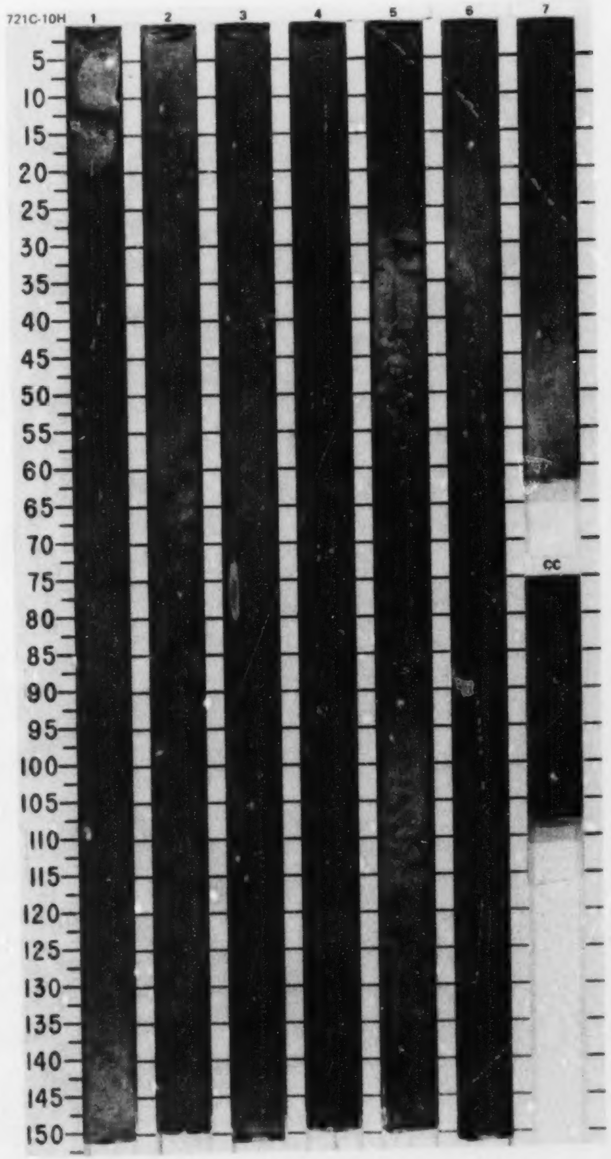
721C-10H
1
2
3
4
5
6
7
CC
5
10
15
20
25
30
35
40
45
50
55
60
65
70
75
80
85
90
95
100
105
110
115
120
125
130
135
140
145
150

SITE 721 HOLE C CORE 11X CORED INTERVAL 2034.7-2044.3 mbsl; 89.9-99.5 mbsf

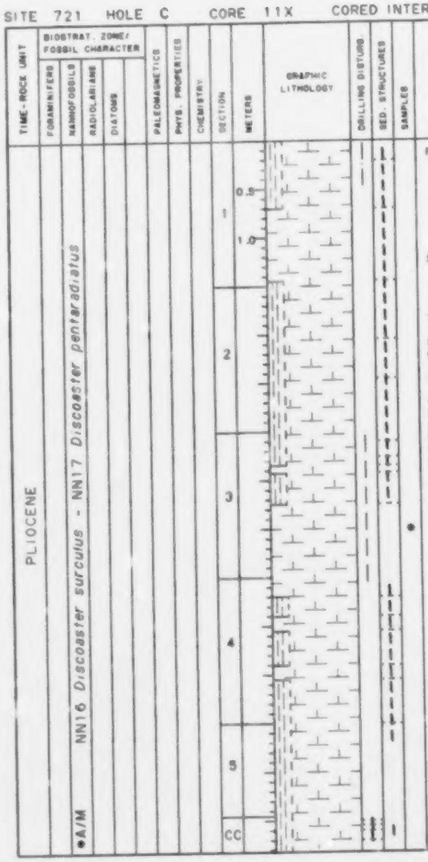
TIME-ROCK UNIT
BIOSTRAT. ZONE/ FOSSIL CHARACTER
FORAMINIFERS
NANNOFOSSILS
RADIOLARIANS
DIATOMS
PALEOMAGNETICS
PHYS. PROPERTIES
CHEMISTRY
SECTION
METERS
GRAPHIC LITHOLOGY
DRILLING DISTURB.
SED. STRUCTURES
SAMPLES
PLIOCENE
•A/M
NN16 *Discoaster surculus* - NN17 *Discoaster pentaradiatus*
1
2
3
4
5
CC
0.5
1.0

LITHOLOGIC DESCRIPTION

NANNOFOSSIL OOZE

Section 1, 0-23 cm, moderately disturbed. Remainder of core is undisturbed.

Major lithology: NANNOFOSSIL OOZE. Alternating light and dark bands, light olive gray (5Y 6/2) and pale olive (5Y 6/3) to olive (5Y 4/3, 5/3, 5/4, 4/4). Slight to moderate burrow-mottling throughout. Dark layers enriched in terrigenous silty clay relative to light layers.

SMEAR SLIDE SUMMARY (%):

	3, 100 D
TEXTURE:	
Silt	20
Clay	80
COMPOSITION:	
Clay	10
Diatoms	5
Inorganic calcite	5
Mica	Tr
Nannofossils	80
Quartz	Tr

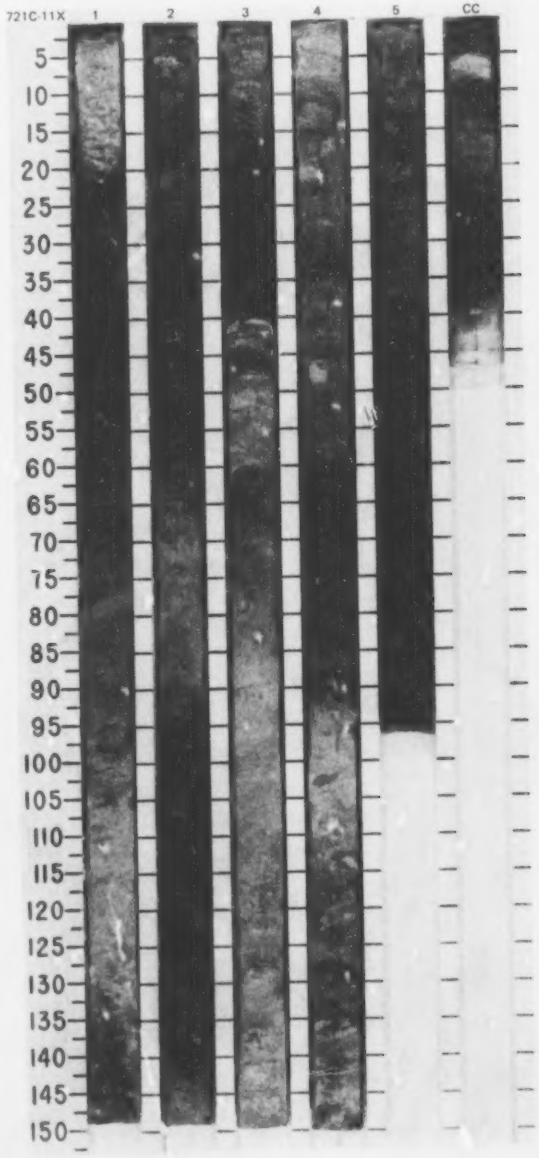
721C-11X
1
2
3
4
5
CC
5
10
15
20
25
30
35
40
45
50
55
60
65
70
75
80
85
90
95
100
105
110
115
120
125
130
135
140
145
150

SITE 721 HOLE C CORE 12X CORED INTERVAL 2044.3-2053.9 mbsl; 99.5-109.1 mbsf

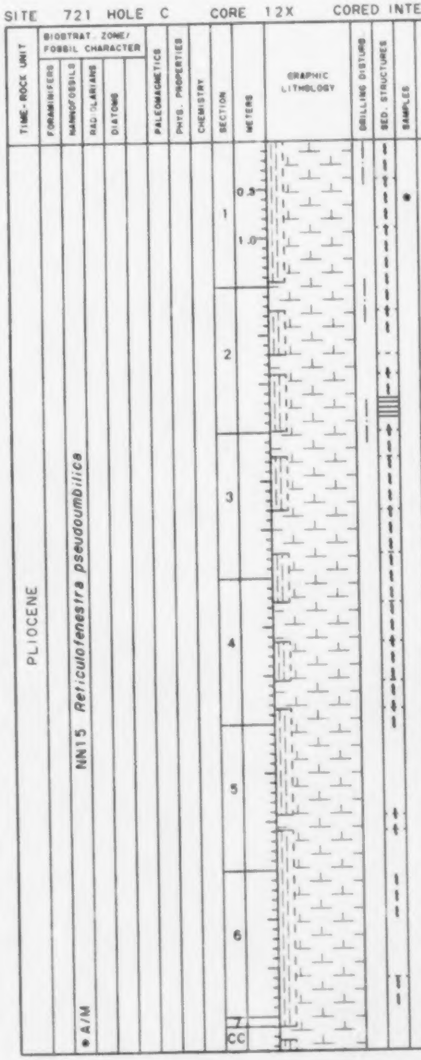
TIME-ROCK UNIT
BIOSTRAT. ZONE/ FOSSIL CHARACTER
FORAMINIFERS
NANNOFOSSILS
RADIOLARIANS
DIATOMS
PALEOMAGNETICS
PHYS. PROPERTIES
CHEMISTRY
SECTION
METERS
GRAPHIC LITHOLOGY
DRILLING DISTURB.
SED. STRUCTURES
SAMPLES
PLIOCENE
NN15 Reticulofenestra pseudoumbilica
• A/M
0.5
1.0
1
2
3
4
5
6
7
CC

LITHOLOGIC DESCRIPTION

NANNOFOSSIL OOZE

Section 1, 0-10 cm, very disturbed. Remainder of core is undisturbed.

Major lithology: NANNOFOSSIL OOZE. Alternating light and dark bands, light olive gray (5Y 6/2) and pale olive (5Y 6/3) to olive (5Y 4/3, 5/3, 4/4). Slight to moderate burrow-mottling throughout. Dark layers enriched in terrigenous silty clay relative to light layers.

SMEAR SLIDE SUMMARY (%):

	1, 60 D
TEXTURE:	
Sand	5
Silt	15
Clay	80
COMPOSITION:	
Clay	10
Foraminifers	5
Inorganic calcite	Tr
Mica	Tr
Nannofossils	85
Quartz	Tr

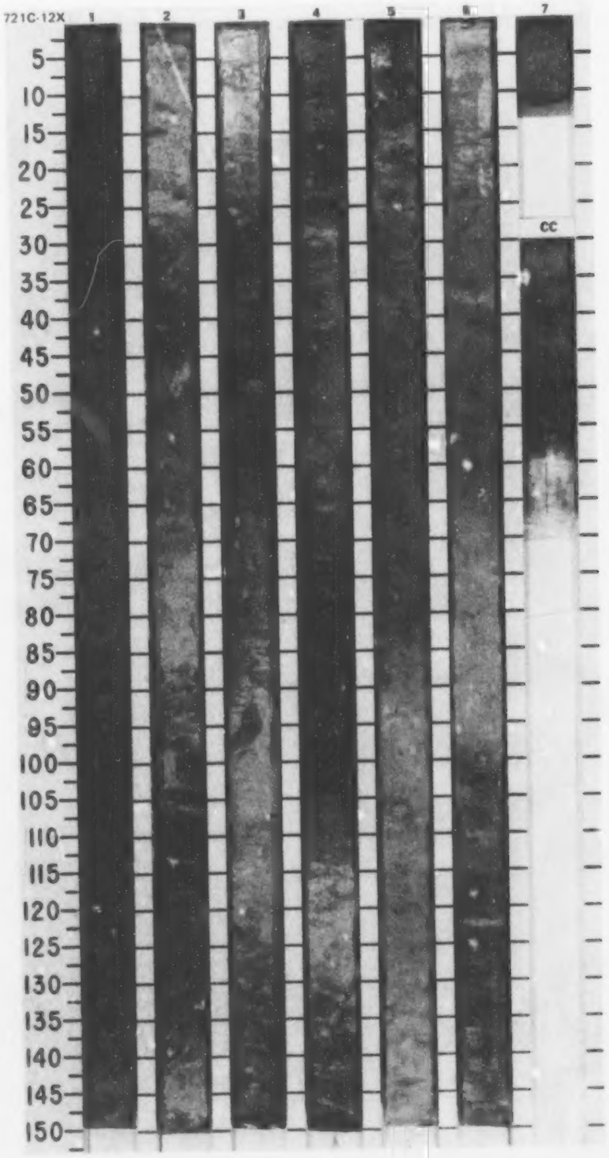
721C-12X
1
2
3
4
5
6
7
CC
5
10
15
20
25
30
35
40
45
50
55
60
65
70
75
80
85
90
95
100
105
110
115
120
125
130
135
140
145
150

SITE 721 HOLE C CORE 13X CORED INTERVAL 2053.9-2063 mbsl; 109.1-118.7 mbsf

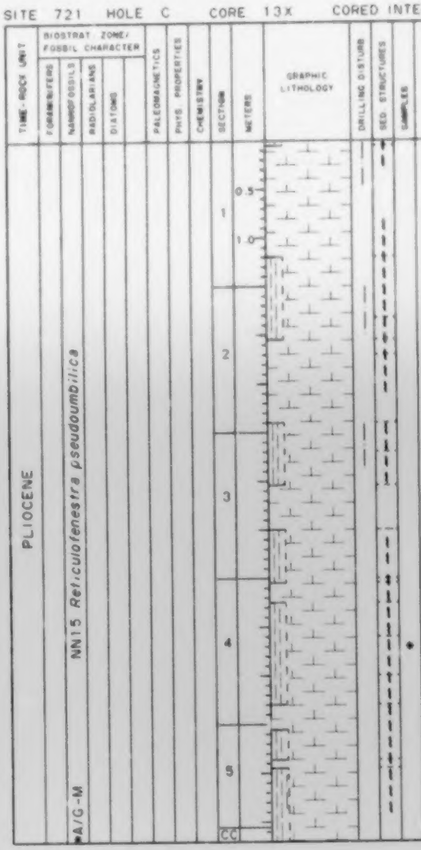
TIME-ROCK UNIT
BIOSTRAT. ZONE/ FOSSIL CHARACTER
FORAMINIFERS
NANNOFOSSILS
RADIOLARIANS
DIATOMS
PALEOMAGNETICS
PHYS. PROPERTIES
CHEMISTRY
SECTION
METERS
GRAPHIC LITHOLOGY
DRILLING DISTURB.
SED. STRUCTURES
SAMPLES
PLIOCENE
NN15 Reticulofenestra pseudoumbilica
A/G-M
0.5
1.0
1
2
3
4
5
CC

LITHOLOGIC DESCRIPTION

NANNOFOSSIL OOZE

Section 1, 0-5 cm, and Section 2, 0-80 cm, moderately disturbed. Remainder of core is undisturbed.

Major lithology: NANNOFOSSIL OOZE. Alternating light and dark bands, light gray (5Y 6/1) and light olive gray (5Y 6/2) to olive (5Y 4/3, 5/3) and olive gray (5Y 5/2). Slight to moderate burrow-mottling throughout. Dark layers enriched in terrigenous silty clay relative to light layers.

SMEAR SLIDE SUMMARY (%):

	4, 70 D
TEXTURE:	
Silt	20
Clay	80
COMPOSITION:	
Clay	10
Foraminifers	Tr
Inorganic calcite	5
Mica	Tr
Nannofossils	85
Quartz	Tr

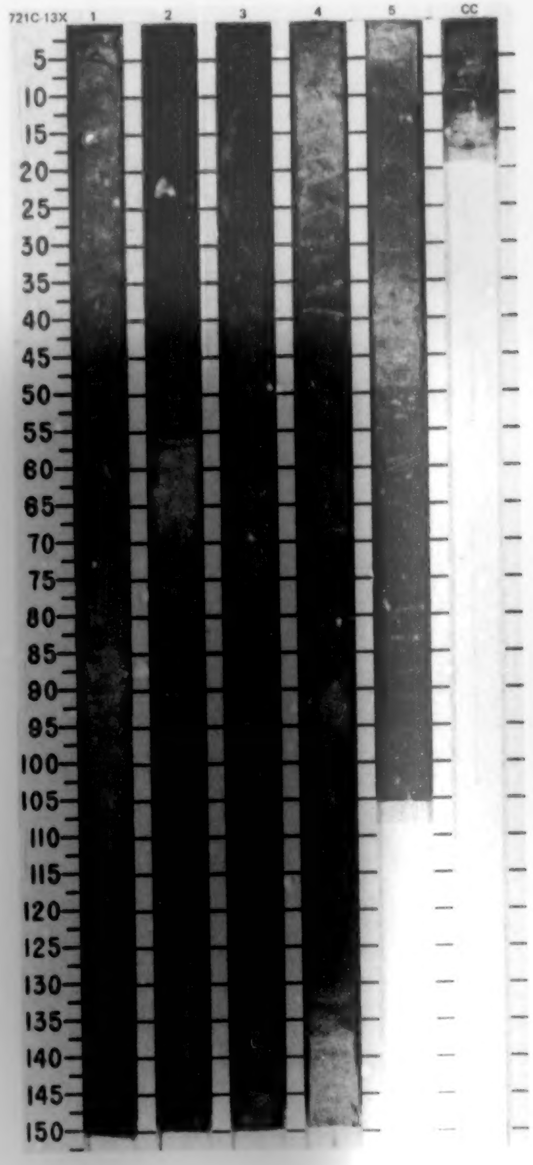
721C-13X
1
2
3
4
5
CC
5
10
15
20
25
30
35
40
45
50
55
60
65
70
75
80
85
90
95
100
105
110
115
120
125
130
135
140
145
150

SITE 721 HOLE C CORE 14X CORED INTERVAL 2063.5-2073.1 mbsl; 118.7-128.3 mbsf

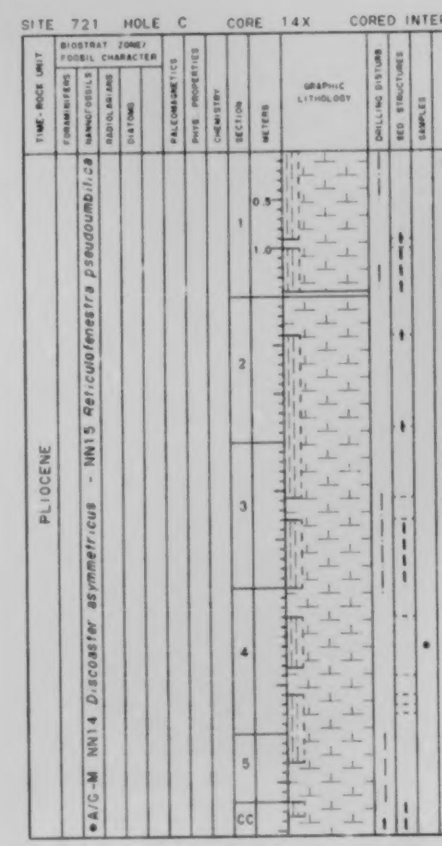
TIME-ROCK UNIT
BIOSTRAT. ZONE/ FOSSIL CHARACTER
FORAMINIFERS
NANNOFOSSILS
RADIOLARIANS
DIATOMS
PALEOMAGNETICS
PHYS. PROPERTIES
CHEMISTRY
SECTION
METERS
GRAPHIC LITHOLOGY
DRILLING DISTURB.
SED. STRUCTURES
SAMPLES
PLIOCENE
●A/G-M NN14 Discoaster asymmetricus - NN15 Reticulofenestra pseudoumbilica
0.5
1.0
1
2
3
4
5
CC

LITHOLOGIC DESCRIPTION

NANNOFOSSIL OOZE

Voids in Section 1, 146-150 cm, and Section 2, 149-150 cm. Most of core slightly to moderately disturbed.

Major lithology: NANNOFOSSIL OOZE. Alternating light and dark bands, light gray (5Y 7/1), light olive gray (5Y 6/2), and pale olive (5Y 6/3) to olive (5Y 4/3, 5/3) and olive gray (5Y 5/2). Slight to moderate burrow-mottling throughout. Dark layers enriched in terrigenous silty clay relative to light layers.

SMEAR SLIDE SUMMARY (%):

	4, 60 D
TEXTURE	
Silt	10
Clay	90
COMPOSITION	
Clay	10
Diatoms	10
Dolomite	Tr
Foraminifers	Tr
Inorganic calcite	5
Mica	Tr
Nannofossils	75
Quartz	Tr
Radiolarians	Tr

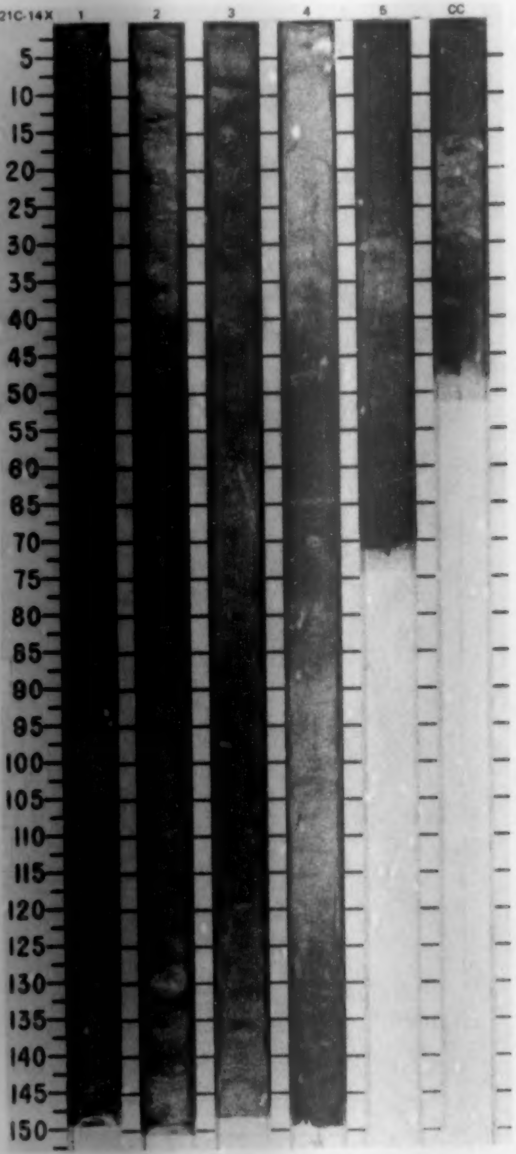
721C-14X
1
2
3
4
5
CC
5
10
15
20
25
30
35
40
45
50
55
60
65
70
75
80
85
90
95
100
105
110
115
120
125
130
135
140
145
150

SITE 721 HOLE C CORE 15X CORED INTERVAL 2073.1-2082.8 mbsl; 128.3-138.0 mbsf

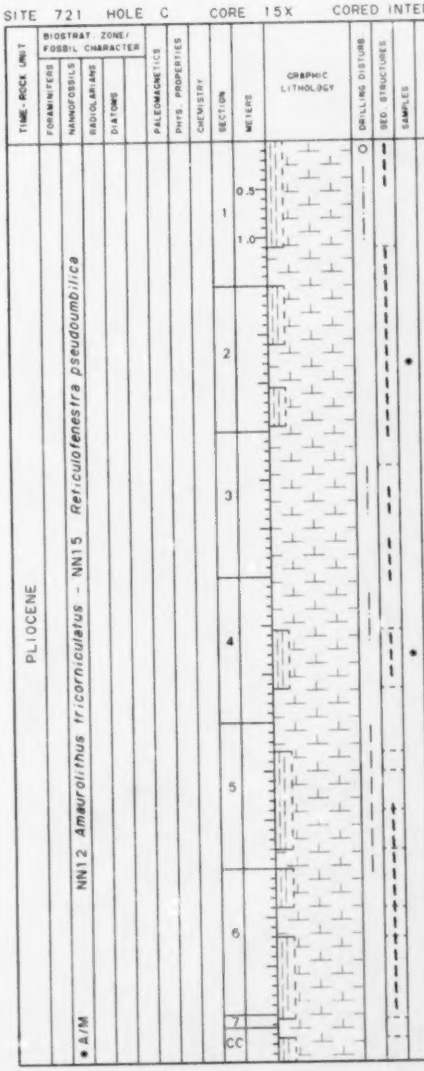
TIME-ROCK UNIT
BIOSTRAT. ZONE/ FOSSIL CHARACTER
FORAMINIFERS
NANNOFOSSILS
RADIOLARIANS
DIATOMS
PALEOMAGNETICS
PHYS. PROPERTIES
CHEMISTRY
SECTION
METERS
GRAPHIC LITHOLOGY
DRILLING DISTURB.
SED. STRUCTURES
SAMPLES
PLIOCENE
NN12 Amaurolithus tricorniculatus - NN15 Reticulofenestra pseudoumbilica
A/M
0.5
1.0
1
2
3
4
5
6
7
CC

LITHOLOGIC DESCRIPTION

NANNOFOSSIL OOZE

Core is slightly to moderately disturbed throughout.

Major lithology: NANNOFOSSIL OOZE. Alternating light and dark bands of light gray (5Y 7/1, 6/1) and light olive gray (5Y 6/2) to olive (5Y 4/3, 5/3) and olive gray (5Y 5/2). Slight to moderate burrow-mottling throughout. Dark layers enriched in terrigenous silty clay relative to light layers.

SMEAR SLIDE SUMMARY (%):

	2, 80 D	4, 80 D
TEXTURE:		
Silt	15	20
Clay	85	80
COMPOSITION:		
Clay	10	10
Diatoms	10	Tr
Foraminifers	Tr	5
Inorganic calcite	Tr	5
Mica	Tr	Tr
Nannofossils	80	75
Quartz	Tr	5
Radiolarians	Tr	Tr

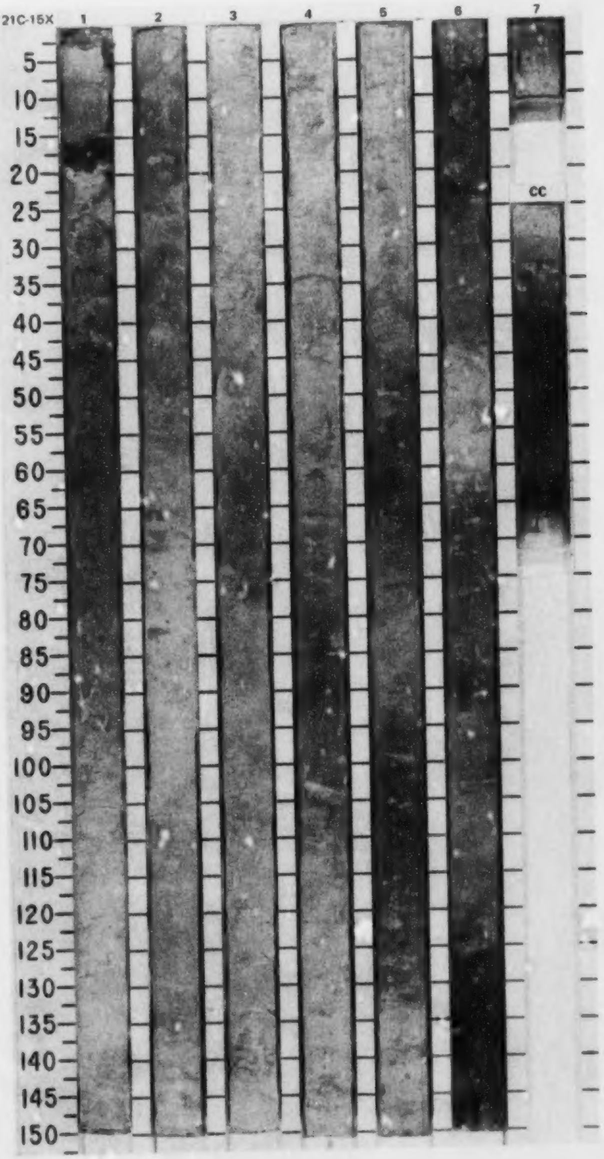
721C-15X
1
2
3
4
5
6
7
CC
5
10
15
20
25
30
35
40
45
50
55
60
65
70
75
80
85
90
95
100
105
110
115
120
125
130
135
140
145
150

SITE 722 HOLE A CORE 1H CORED INTERVAL 2027.8-2037.6 mbsl; 0-9.8 mbsf

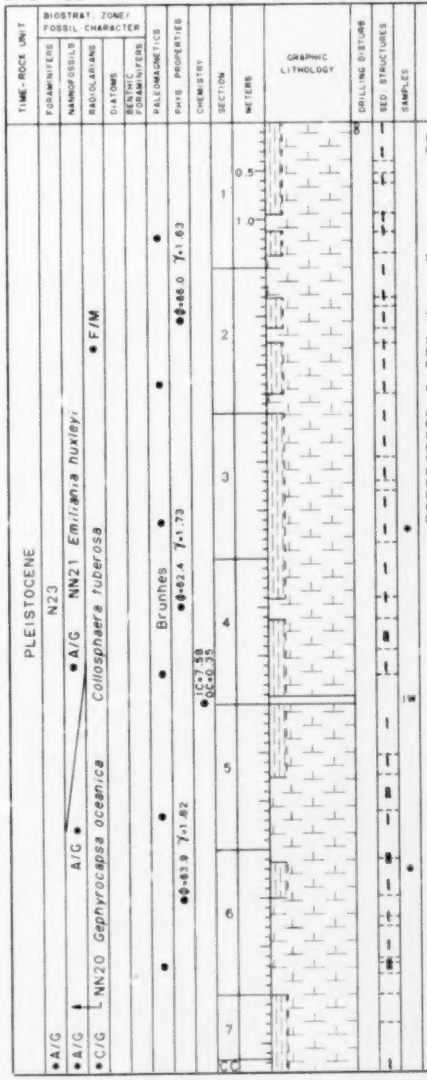
TIME-ROCK UNIT
BIOSTRAT. ZONE/ FOSSIL CHARACTER
FORAMINIFERS
NANNOFOSSILS
RADIOLARIANS
DIATOMS
BENTHIC FORAMINIFERS
PALEOMAGNETICS
PHYS. PROPERTIES
CHEMISTRY
SECTION
METERS
GRAPHIC LITHOLOGY
DRILLING DISTURB.
SED. STRUCTURES
SAMPLES
PLEISTOCENE
N23
•A/G
•A/G NN21 Emiliania huxleyi
A/G •
•A/G
NN20 Gephyrocapsa oceanica
•C/G
Collosphaera tuberosa
• F/M
Brunhes
•φ=66.0 γ=1.63
•φ=62.4 γ=1.73
•φ=63.9 γ=1.82
•IC=7.58 OC=0.35
1
2
3
4
5
6
7
CC
0.5
1.0
IW

LITHOLOGIC DESCRIPTION

Interbedded NANNOFOSSIL OOZE and FORAMINIFER-BEARING NANNOFOSSIL OOZE

Section 1, 0-5 cm, is highly disturbed.

Major lithology: Interbedded nannofossil ooze and foraminifer-bearing nannofossil ooze. Contacts are gradational. Beds range from light greenish gray (5GY 7/1, 10Y 6/2) to olive gray (5Y 5/2) and olive (5Y 4/3, 5/3). Bioturbation is minor to moderate throughout, with some pyrite(?)-impregnated burrows.

SMEAR SLIDE SUMMARY (%):

	3, 121 D	6, 20 D
TEXTURE:		
Sand	10	3
Silt	20	17
Clay	70	80
COMPOSITION:		
Access. minerals	1	Tr
Clay	10	5
Feldspar		1
Foraminifers	10	2
Volcanic glass	Tr	Tr
Inorganic calcite	18	10
Mica		1
Nannofossils	60	80
Quartz	1	1
Sponge spicules	Tr	

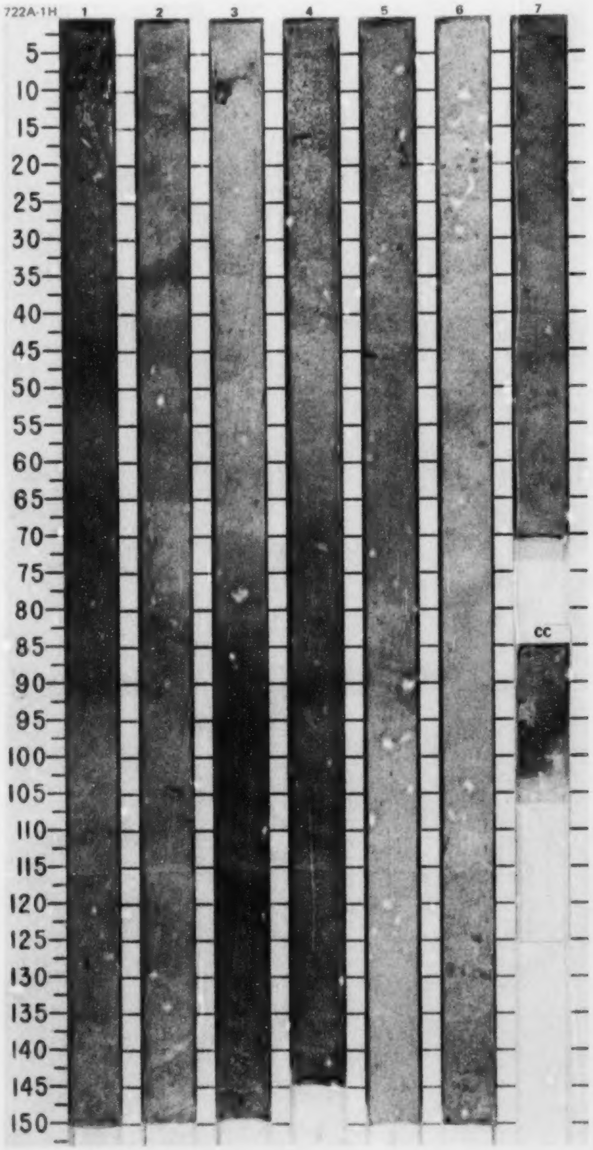
722A-1H
1
2
3
4
5
6
7
CC
5
10
15
20
25
30
35
40
45
50
55
60
65
70
75
80
85
90
95
100
105
110
115
120
125
130
135
140
145
150

SITE 722 HOLE A CORE 2H CORED INTERVAL 2037.6-2047.2 mbsl; 9.8-19.4 mbsf

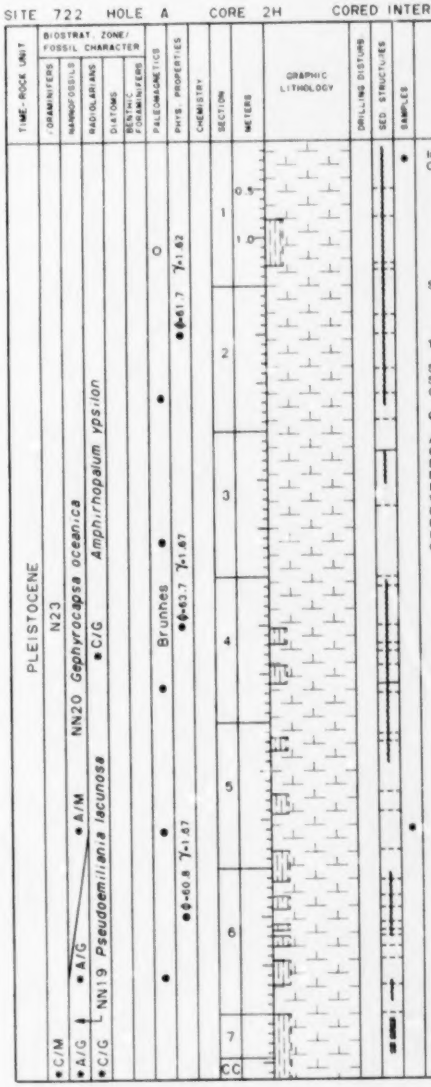
TIME-ROCK UNIT
BIOSTRAT. ZONE/FOSSIL CHARACTER
FORAMINIFERS
NANNOFOSSILS
RADIOLARIANS
DIATOMS
BENTHIC FORAMINIFERS
PALEOMAGNETICS
PHYS. PROPERTIES
CHEMISTRY
SECTION
METERS
GRAPHIC LITHOLOGY
DRILLING DISTURB.
SED. STRUCTURES
SAMPLES
PLEISTOCENE
N23
NN20 Gephyrocapsa oceanica
NN19 Pseudoemiliania lacunosa
Amphirhopalum ypsilon
●C/M
●A/G
●A/G
●A/M
●C/G
●C/G
Brunhes
●ϕ=61.7 γ=1.62
●ϕ=63.7 γ=1.67
●ϕ=60.8 γ=1.67
0.5
1.0
1
2
3
4
5
6
7
CC

LITHOLOGIC DESCRIPTION

Interbedded NANNOFOSSIL OOZE and FORAMINIFER-BEARING NANNOFOSSIL OOZE

Entire core is undisturbed.

Major litholog; Interbedded NANNOFOSSIL OOZE and FORAMINIFER-BEARING NANNOFOSSIL OOZE. Contacts are gradational. Beds range from light gray (5Y 7/1) to light olive gray (5Y 7/2, 6/2) and light olive (5Y 6/3, 5/3). Bioturbation is minor to moderate throughout, with some pyrite(?)-impregnated burrows.

SMEAR SLIDE SUMMARY (%):

	1, 20 D	5, 107 D
TEXTURE:		
Sand	2	10
Silt	8	20
Clay	90	70
COMPOSITION:		
Access. minerals	Tr	1
Clay	5	10
Dolomite		Tr
Feldspar		1
Foraminifers	2	5
Volcanic glass		1
Inorganic calcite	8	20
Mica	Tr	
Nannofossils	85	60
Quartz	Tr	2

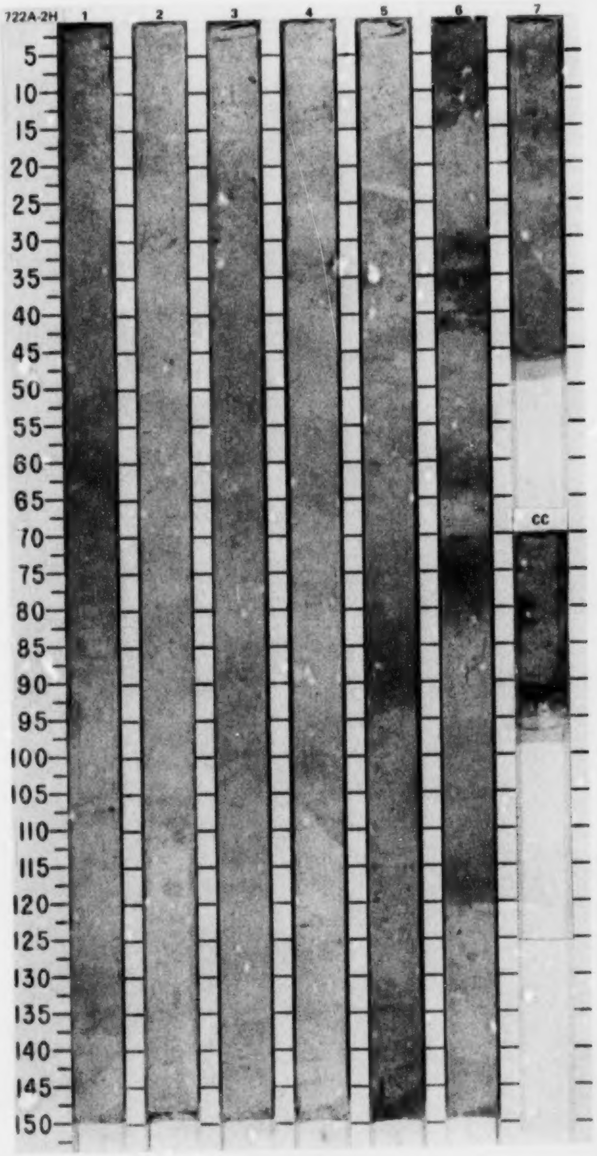
722A-2H
1
2
3
4
5
6
7
CC
5
10
15
20
25
30
35
40
45
50
55
60
65
70
75
80
85
90
95
100
105
110
115
120
125
130
135
140
145
150

SITE 722 HOLE A CORE 3H CORED INTERVAL 2047.2-2056.8 mbsl; 19.4-29.0 mbsf

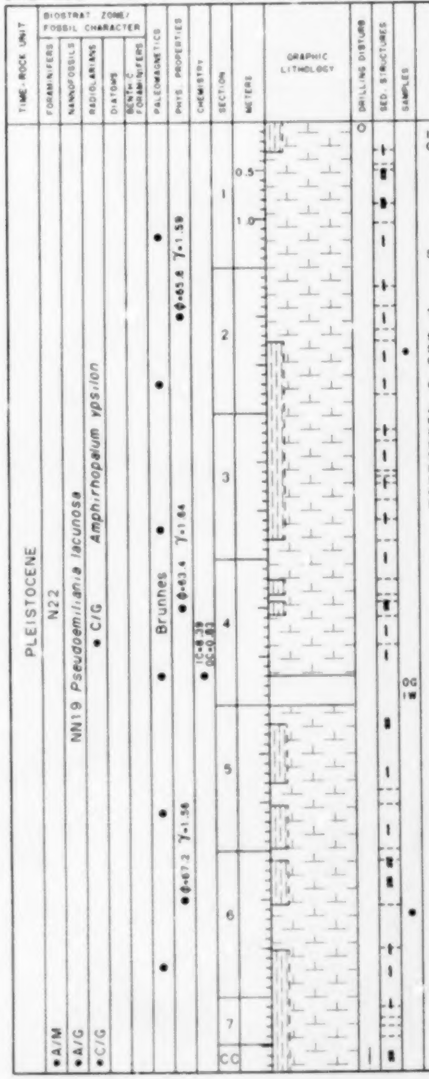
TIME-ROCK UNIT
BIOSTRAT. ZONE/ FOSSIL CHARACTER
FORAMINIFERS
NANNOFOSSILS
RADIOLARIANS
DIATOMS
BENTHIC FORAMINIFERS
PALEOMAGNETICS
PHYS. PROPERTIES
CHEMISTRY
SECTION
METERS
GRAPHIC LITHOLOGY
DRILLING DISTURB.
SED. STRUCTURES
SAMPLES
PLEISTOCENE
N22
NN19 Pseudoemiliania lacunosa
● C/G Amphirhopalum ypsilon
● A/M
● A/G
● C/G
Brunnes
● ϕ=65.8 γ=1.59
● ϕ=63.4 γ=1.64
● ϕ=67.2 γ=1.56
IC=8.39 OC=0.83
0.5
1.0
1
2
3
4
5
6
7
CC
OG
IW

LITHOLOGIC DESCRIPTION

Interbedded NANNOFOSSIL OOZE and FORAMINIFER-BEARING NANNOFOSSIL OOZE

Section 1, 1-10 cm, soupy; CC, 10-20 cm, moderately disturbed.

Major lithology: Interbedded NANNOFOSSIL OOZE and FORAMINIFER-BEARING NANNOFOSSIL OOZE. Beds range from light olive gray (5Y 6/2) to light gray (5Y 7/1), olive (5Y 4/3, 5/3), and pale olive (5Y 6/3). Contacts are gradational. Bioturbation is minor to moderate throughout.

SMEAR SLIDE SUMMARY (%):

	2, 86 D	6, 65 D
TEXTURE:		
Sand	15	
Silt	10	15
Clay	75	85
COMPOSITION:		
Access. minerals	1	
Clay	10	5
Dolomite		Tr
Foraminifers	10	5
Volcanic glass	Tr	
Inorganic calcite	18	15
Nannofossils	60	75
Quartz	1	Tr
Radiolarians	Tr	

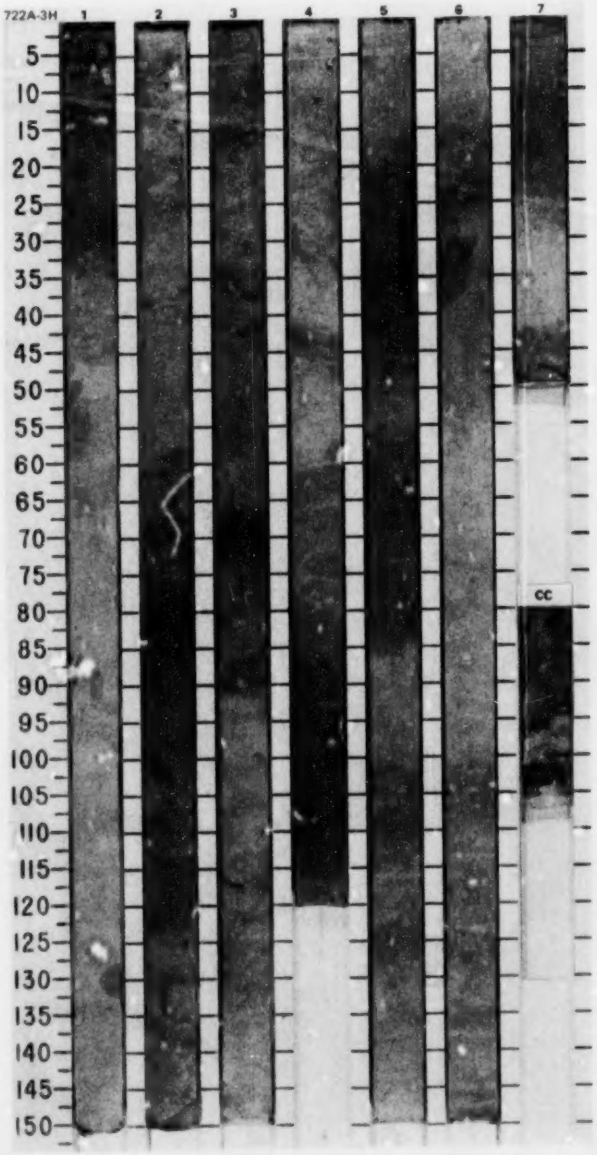
722A-3H
1
2
3
4
5
6
7
CC
5
10
15
20
25
30
35
40
45
50
55
60
65
70
75
80
85
90
95
100
105
110
115
120
125
130
135
140
145
150

SITE 722 HOLE A CORE 4H CORED INTERVAL 2056.8-2066.4 mbsl; 29.0-38.6 mbsf

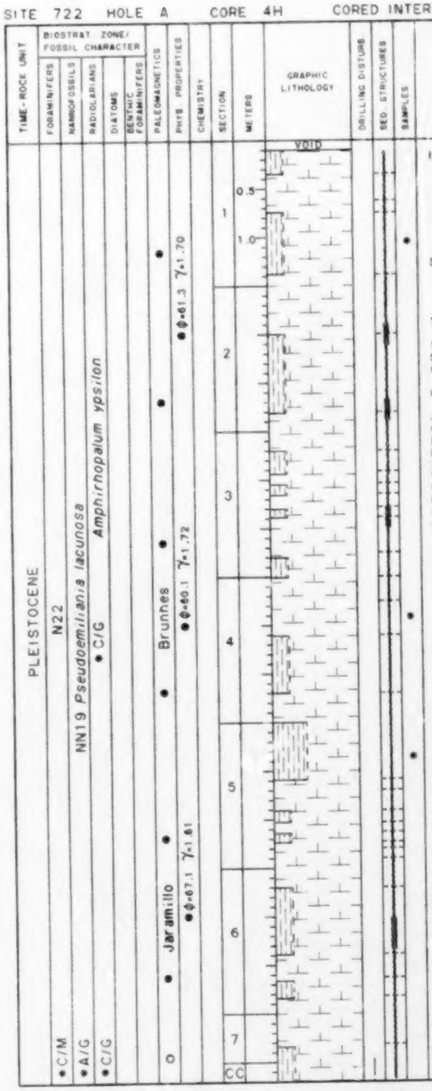
TIME-ROCK UNIT
BIOSTRAT. ZONE/ FOSSIL CHARACTER
FORAMINIFERS
NANNOFOSSILS
RADIOLARIANS
DIATOMS
BENTHIC FORAMINIFERS
PALEOMAGNETICS
PHYS. PROPERTIES
CHEMISTRY
SECTION
METERS
GRAPHIC LITHOLOGY
DRILLING DISTURB.
SED. STRUCTURES
SAMPLES
PLEISTOCENE
N22
NN19 Pseudoemiliania lacunosa
Amphirhopalum ypsilon
● C/G
● C/M
● A/G
● C/G
Brunhes
Jaramillo
● φ=61.3 γ=1.70
● φ=60.1 γ=1.72
● φ=67.1 γ=1.61
0.5
1.0
1
2
3
4
5
6
7
CC
VOID

LITHOLOGIC DESCRIPTION

Interbedded NANNOFOSSIL OOZE and MARLY NANNOFOSSIL OOZE

Entire core is undisturbed to slightly disturbed.

Major lithology: Interbedded NANNOFOSSIL OOZE and MARLY NANNOFOSSIL OOZE. Contacts are gradational. Beds range from light olive gray (5Y 6/2) to light gray (5Y 7/2) and light olive (5Y 6/3, 5/3). Bioturbation is minor to moderate throughout.

SMEAR SLIDE SUMMARY (%):

	1, 105 M	4, 43 D	5, 35 D
TEXTURE:			
Sand	35	5	5
Silt	25	10	15
Clay	40	85	80
COMPOSITION:			
Access. minerals	1	1	1
Clay			20
Diatoms		80	
Dolomite	1		
Foraminifers	40	2	5
Volcanic glass	Tr		Tr
Inorganic calcite	16	12	13
Mica			Tr
Nannofossils	40	5	60
Quartz	2	Tr	1

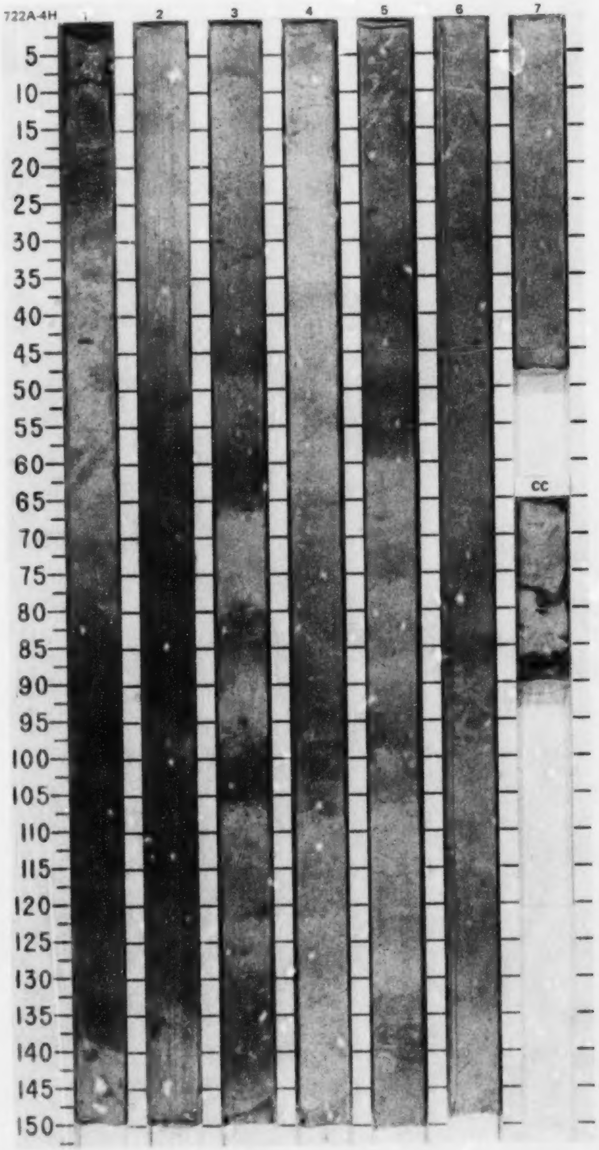
722A-4H
1
2
3
4
5
6
7
CC
5
10
15
20
25
30
35
40
45
50
55
60
65
70
75
80
85
90
95
100
105
110
115
120
125
130
135
140
145
150

SITE 722 HOLE A CORE 5H CORED INTERVAL 2066.4-2076.0 mbsl; 38.6-48.2 mbsf

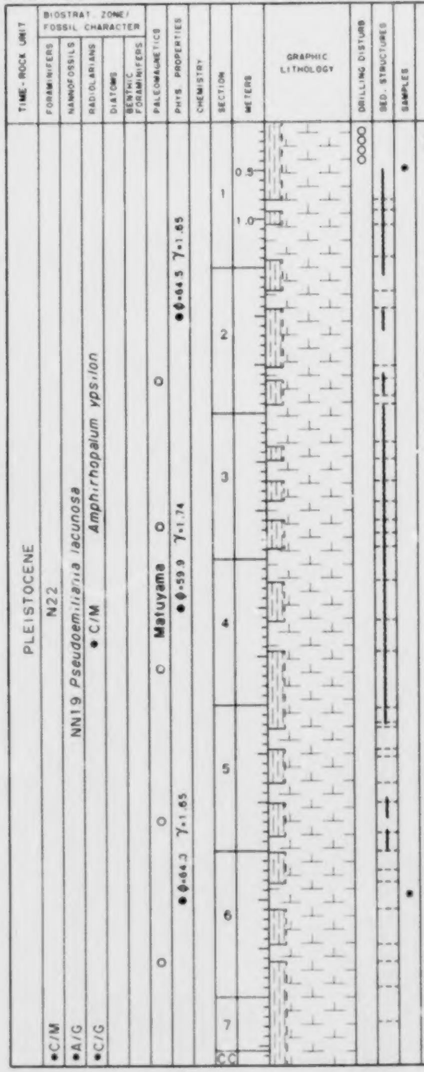
TIME-ROCK UNIT
BIOSTRAT. ZONE/ FOSSIL CHARACTER
FORAMINIFERS
NANNOFOSSILS
RADIOLARIANS
DIATOMS
BENTHIC FORAMINIFERS
PALEOMAGNETICS
PHYS. PROPERTIES
CHEMISTRY
SECTION
METERS
GRAPHIC LITHOLOGY
DRILLING DISTURB.
SED. STRUCTURES
SAMPLES
PLEISTOCENE
N22
NN19 Pseudoemiliania lacunosa
• C/M Amphirhopalum ypsilon
Matuyama
•ϕ=64.5 γ=1.65
•ϕ=59.9 γ=1.74
•ϕ=64.3 γ=1.65
•C/M
•A/G
•C/G
0.5
1.0
1
2
3
4
5
6
7
CC

LITHOLOGIC DESCRIPTION

Interbedded NANNOFOSSIL OOZE and FORAMINIFER-BEARING NANNOFOSSIL OOZE

Section 1, 0-47 cm, is soupy.

Major lithology: Interbedded NANNOFOSSIL OOZE and FORAMINIFER-BEARING NANNOFOSSIL OOZE. Contacts are gradational. Beds range from light olive gray (5Y 7/2, 6/2) to light gray (5Y 7/2). Bioturbation is minor throughout.

SMEAR SLIDE SUMMARY (%):

	1, 59 D	6, 44 D
TEXTURE:		
Silt	20	20
Clay	80	80
COMPOSITION:		
Clay	10	10
Foraminifers	5	5
Inorganic calcite	5	5
Mica		Tr
Nannofossils	80	75
Quartz		5

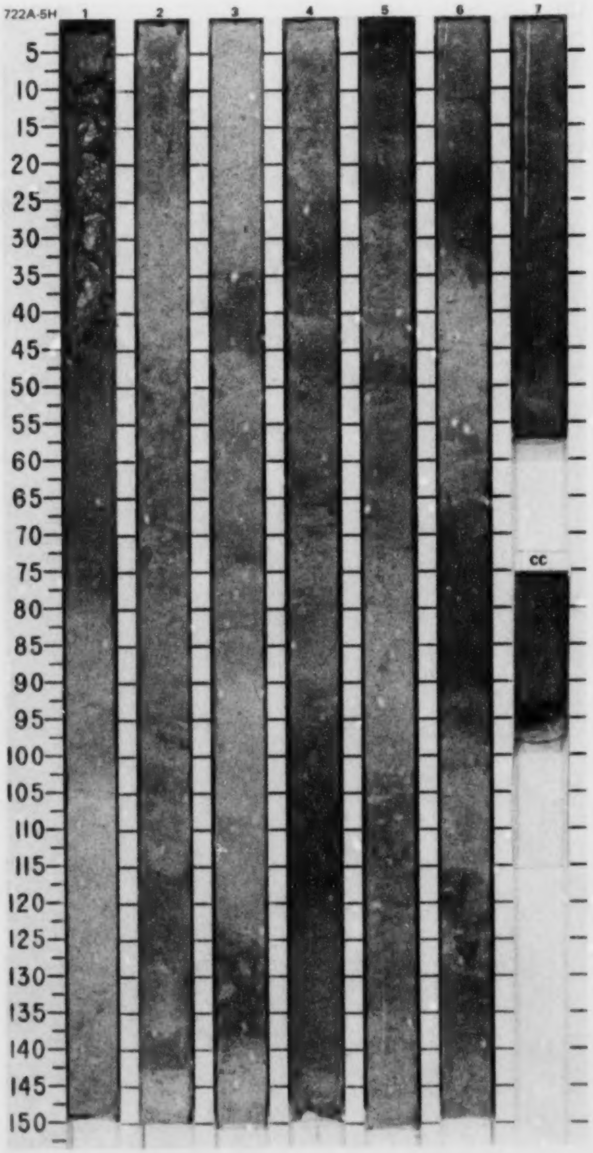
722A-5H
1
2
3
4
5
6
7
CC
5
10
15
20
25
30
35
40
45
50
55
60
65
70
75
80
85
90
95
100
105
110
115
120
125
130
135
140
145
150

SITE 722 HOLE A CORE 6H CORED INTERVAL 2076.0-2085.3 mbsl; 48.2-57.5 mbsf

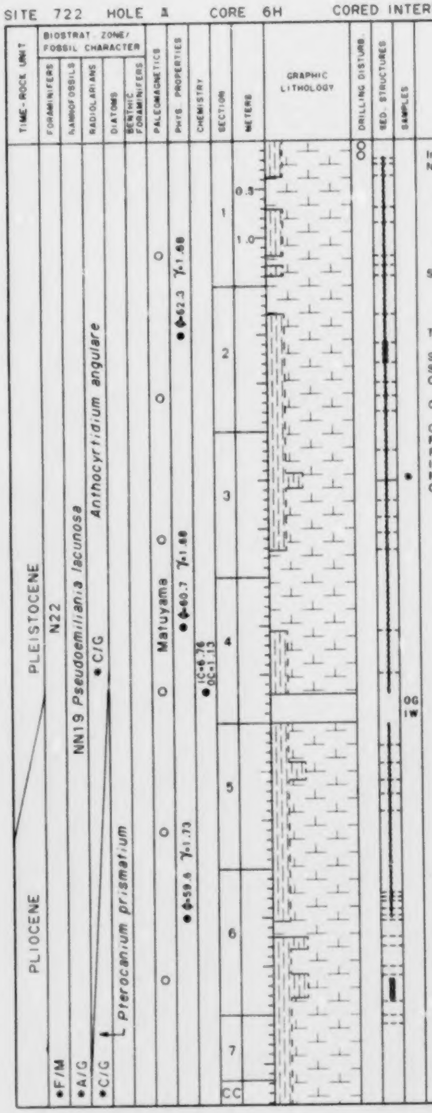

LITHOLOGIC DESCRIPTION

Interbedded FORAMINIFER BEARING NANNOFOSSIL OOZE and MARLY NANNOFOSSIL OOZE

Section 1, 0-15 cm, is soupy.

Major lithology: Interbedded FORAMINIFER-BEARING NANNOFOSSIL OOZE and MARLY NANNOFOSSIL OOZE. Contacts are gradational. Beds range from light gray (5Y 7/2) to olive gray (5Y 6/1, 6/2), pale olive (5Y 6/3), and olive (5Y 5/3, 4/3). Bioturbation is minor to moderate throughout.

SMEAR SLIDE SUMMARY (%):

	3, 49 D
TEXTURE:	
Sand	5
Silt	40
Clay	55
COMPOSITION:	
Clay	30
Feldspar	Tr
Foraminifers	5
Inorganic calcite	30
Nannofossils	30
Quartz	5

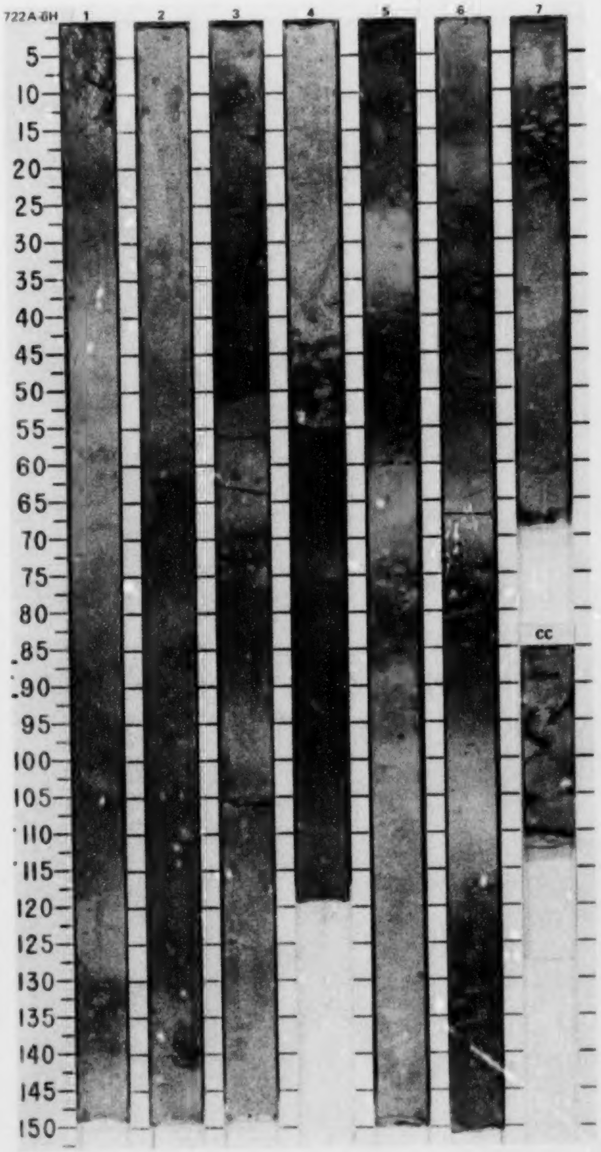
722A-6H
1
2
3
4
5
6
7
CC
5
10
15
20
25
30
35
40
45
50
55
60
65
70
75
80
85
90
95
100
105
110
115
120
125
130
135
140
145
150

SITE 722 HOLE A CORE 7H CORED INTERVAL 2085.3-2095.0 mbsl; 57.5-67.2 mbsf

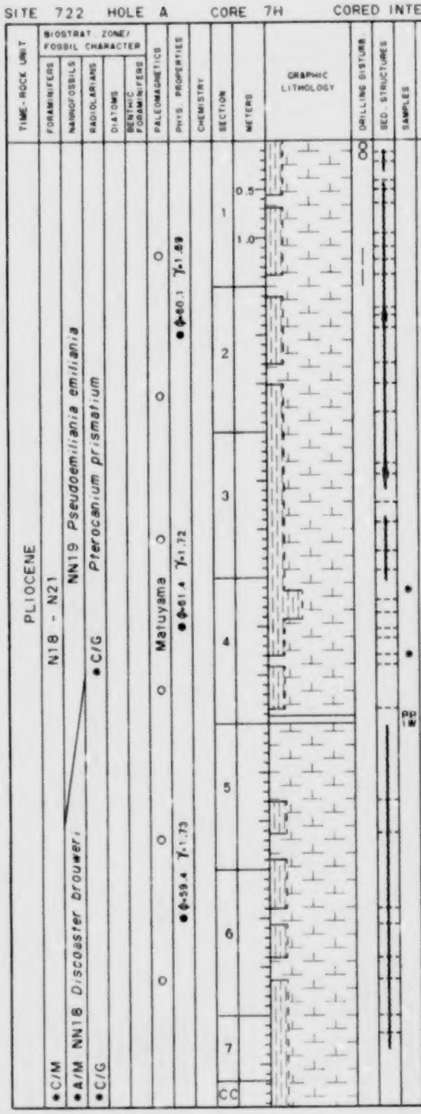
TIME-ROCK UNIT
BIOSTRAT. ZONE/ FOSSIL CHARACTER
FORAMINIFERS
NANNOFOSSILS
RADIOLARIANS
DIATOMS
BENTHIC FORAMINIFERS
PALEOMAGNETICS
PHYS. PROPERTIES
CHEMISTRY
SECTION
METERS
GRAPHIC LITHOLOGY
DRILLING DISTURB.
SED. STRUCTURES
SAMPLES
PLIOCENE
N18 - N21
●C/M
NN19 Pseudoemiliania emiliania
●A/M NN18 Discoaster brouweri
●C/G Pterocanium prismatium
●C/G
Matuyama
●Φ-60.1 γ-1.69
●Φ-61.4 γ-1.72
●Φ-59.4 γ-1.73
1
2
3
4
5
6
7
CC
0.5
1.0
PP
IW

LITHOLOGIC DESCRIPTION

Interbedded NANNOFOSSIL OOZE and MARLY NANNOFOSSIL OOZE

Section 1, 0-10 cm, soupy; Section 1, 140-150 cm, slightly disturbed.

Major lithology: interbedded NANNOFOSSIL OOZE and MARLY NANNOFOSSIL OOZE. Contacts are gradational. Beds range from light olive gray (5Y 6/2) to light gray (5Y 7/2), olive (5Y 4/4, 5/4, 5/3, 4/3), pale olive (5Y 6/3), and dark olive gray (5Y 3/2). Bioturbation is minor to moderate throughout.

SMEAR SLIDE SUMMARY (%):

	4, 13 D	4, 86 D
TEXTURE:		
Sand	5	5
Silt	20	10
Clay	75	
COMPOSITION:		
Access. minerals	2	2
Clay	25	20
Diatoms	Tr	
Foraminifers	5	5
Inorganic calcite	15	3
Mica	3	
Nannofossils	40	70
Quartz	10	
Radiolarians	Tr	
Sponge spicules	Tr	

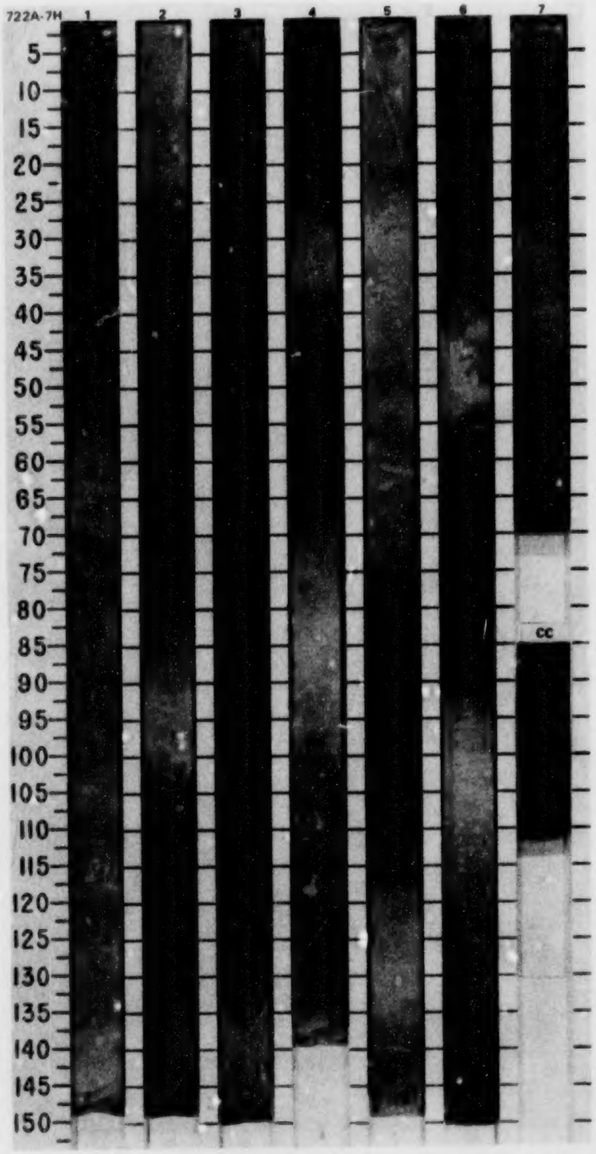
722A-7H
1
2
3
4
5
6
7
CC
5
10
15
20
25
30
35
40
45
50
55
60
65
70
75
80
85
90
95
100
105
110
115
120
125
130
135
140
145
150

SITE 722 HOLE A CORE 8H CORED INTERVAL 2095.0-2104.6 mbsl; 67.20-76.80 mbsf

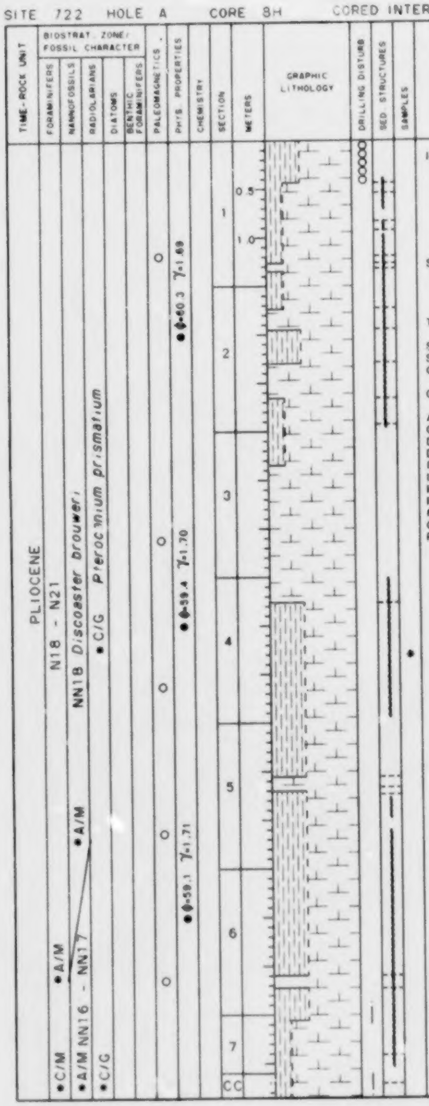
TIME-ROCK UNIT
BIOSTRAT. ZONE/ FOSSIL CHARACTER
FORAMINIFERS
NANNOFOSSILS
RADIOLARIANS
DIATOMS
BENTHIC FORAMINIFERS
PALEOMAGNETICS
PHYS. PROPERTIES
CHEMISTRY
SECTION
METERS
GRAPHIC LITHOLOGY
DRILLING DISTURB.
SED. STRUCTURES
SAMPLES
PLIOCENE
N18 - N21
NN18 Discoaster brouweri
C/G Pterocnium prismatium
C/M
A/M
A/M NN16 - NN17
A/M
C/G
ϕ=60.3 γ=1.69
ϕ=59.4 γ=1.70
ϕ=59.1 γ=1.71
1
2
3
4
5
6
7
CC
0.5
1.0

LITHOLOGIC DESCRIPTION

Interbedded **NANNOFOSSIL OOZE** and **MARLY NANNOFOSSIL OOZE**

Section 1, 0-35 cm, soupy; CC moderately disturbed.

Major lithology: Interbedded **NANNOFOSSIL OOZE** and **MARLY NANNOFOSSIL OOZE**. Contacts are gradational. Beds range from light olive gray (5Y 6/2) to olive gray (5Y 5/2), olive (5Y 5/3, 5/4), and pale olive (5Y 6/3). Bioturbation is minor to moderate throughout.

SMEAR SLIDE SUMMARY (%):

	4, 80 D
TEXTURE:	
Sand	5
Silt	30
Clay	65
COMPOSITION:	
Access. minerals	Tr
Clay	25
Diatoms	Tr
Dolomite	Tr
Foraminifers	5
Inorganic calcite	5
Mica	Tr
Nannofossils	65
Pyrite	Tr
Quartz	Tr
Radiolarians	Tr

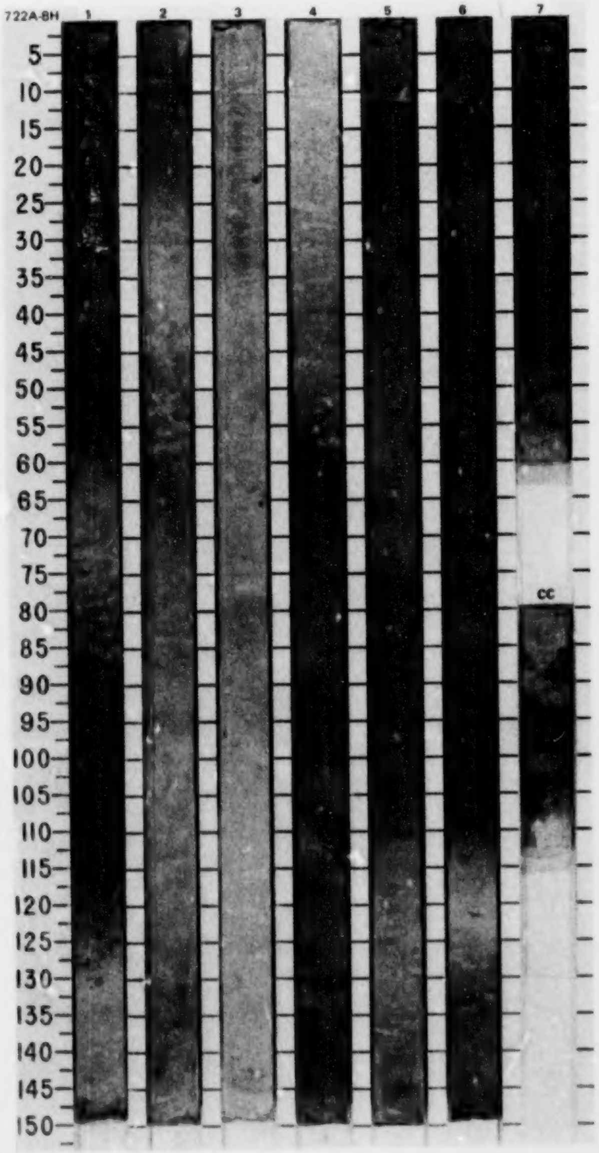
722A-8H
1
2
3
4
5
6
7
CC
5
10
15
20
25
30
35
40
45
50
55
60
65
70
75
80
85
90
95
100
105
110
115
120
125
130
135
140
145
150

SITE 722 HOLE A CORE 9H CORED INTERVAL 2104.6-2114.3 mbsl; 76.8-86.5 mbsf

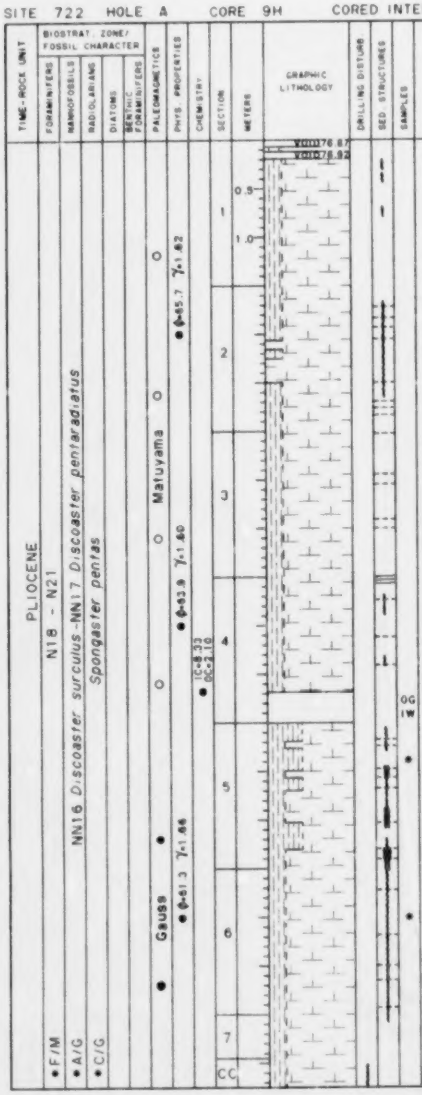

LITHOLOGIC DESCRIPTION

Interbedded NANNOFOSSIL OOZE and MARLY NANNOFOSSIL OOZE

Section 1, 5-10 cm, and CC are very disturbed.

Major lithology: NANNOFOSSIL OOZE and MARLY NANNOFOSSIL OOZE. Contacts are gradational. Beds range from light olive gray (5Y 6/2) to light gray (5Y 4/2), olive (5Y 4/4, 4/3, 5/4, 5/3), and dark olive gray (5Y 3/2). Section 5, 125-135 cm, is strongly bioturbated. Bioturbation is minor to moderate throughout the remainder of the core.

SMEAR SLIDE SUMMARY (%):

	5, 39 D	6, 52 M
TEXTURE:		
Silt	20	10
Clay	80	90
COMPOSITION:		
Access. minerals	2	
Clay	29	10
Diatoms	Tr	
Foraminifers	3	5
Gypsum		Tr
Inorganic calcite	4	5
Nannofossils	57	80
Quartz	4	
Radiolarians		Tr
Sponge spicules	Tr	

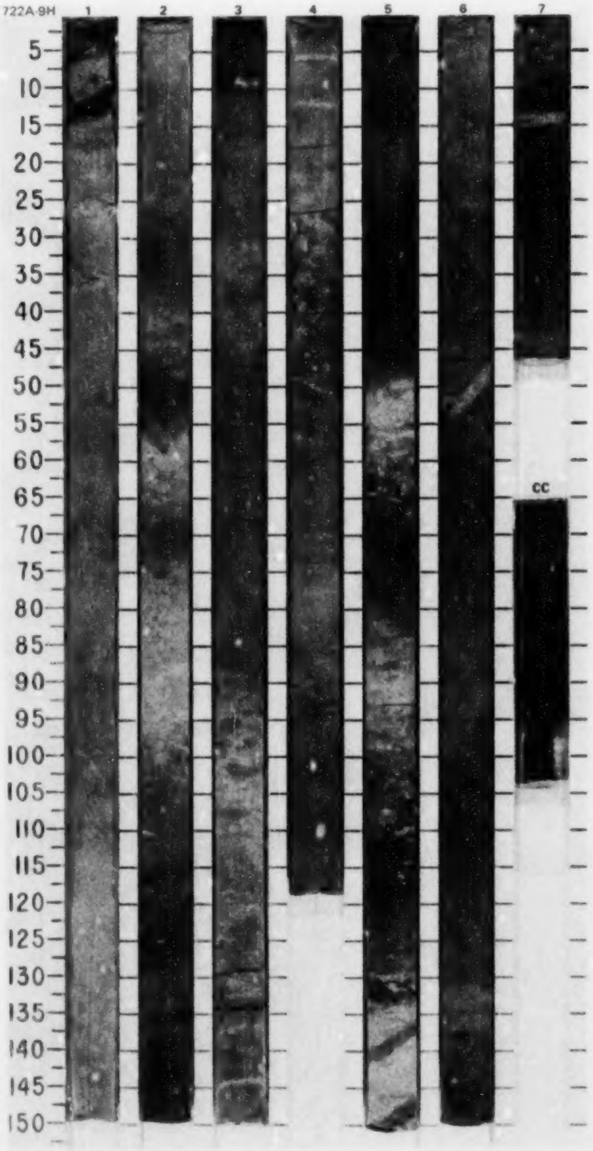
722A-9H
1
2
3
4
5
6
7
CC
5
10
15
20
25
30
35
40
45
50
55
60
65
70
75
80
85
90
95
100
105
110
115
120
125
130
135
140
145
150

SITE 722 HOLE A CORE 10X CORED INTERVAL 2114.3-2124.0 mbsl; 86.5-96.2 mbsf

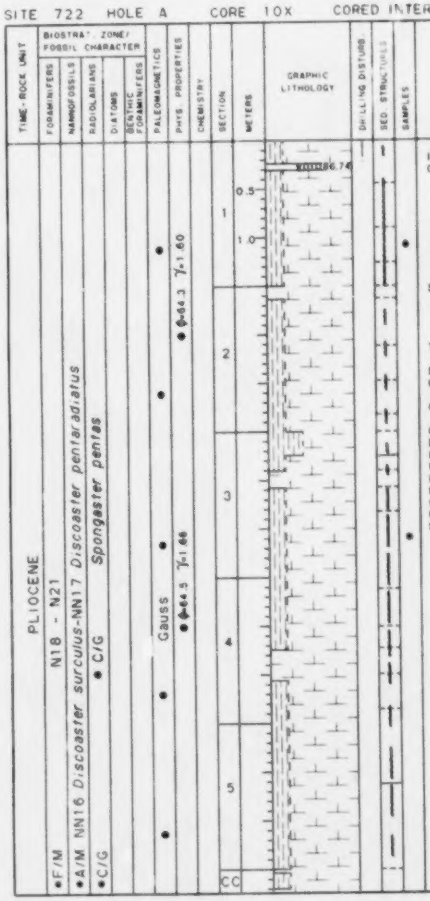
TIME-ROCK UNIT
BIOSTRAT. ZONE/ FOSSIL CHARACTER
FORAMINIFERS
NANNOFOSSILS
RADIOLARIANS
DIATOMS
BENTHIC FORAMINIFERS
PALEOMAGNETICS
PHYS. PROPERTIES
CHEMISTRY
SECTION
METERS
GRAPHIC LITHOLOGY
DRILLING DISTURB.
SED. STRUCTURES
SAMPLES
PLIOCENE
●F/M N18 - N21
●A/M NN16 Discoaster surculus-NN17 Discoaster pentaradiatus
●C/G ● C/G Spongaster pentas
Gauss
●φ=64.3 γ=1.60
●φ=64.5 γ=1.66
1
2
3
4
5
CC
0.5
1.0
86.74

LITHOLOGIC DESCRIPTION

Interbedded NANNOFOSSIL OOZE, FORAMINIFER-BEARING NANNOFOSSIL OOZE, and MARLY NANNOFOSSIL OOZE

Section 1, 1-18 cm, is moderately disturbed.

Major lithology: Interbedded NANNOFOSSIL OOZE, FORAMINIFER-BEARING NANNOFOSSIL OOZE, and MARLY NANNOFOSSIL OOZE. Contacts are gradational. Beds range from light olive gray (5Y 6/2) to olive gray (5Y 5/2), olive (5Y 4/3, 5/3, 5/4), and dark olive gray (5Y 3/2). Bioturbation is minor to moderate throughout.

SMEAR SLIDE SUMMARY (%):

	1, 108 D	3, 108 D
TEXTURE:		
Silt	20	25
Clay	80	75
COMPOSITION:		
Clay	10	10
Diatoms	Tr	Tr
Dolomite		Tr
Foraminifers	Tr	10
Inorganic calcite	10	15
Nannofossils	80	64
Quartz	Tr	Tr
Radiolarians	Tr	1
Silicoflagellates		Tr

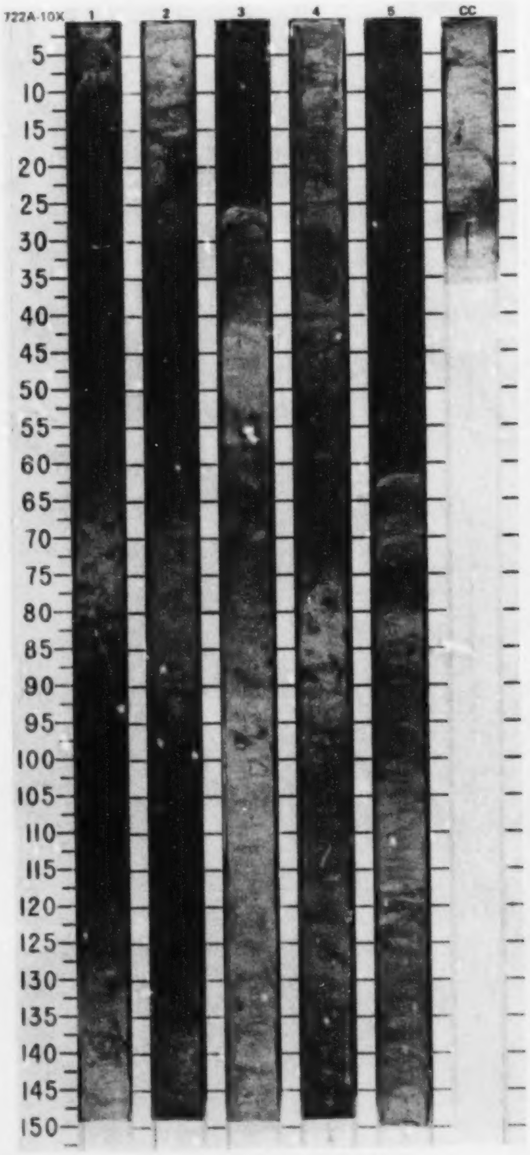
722A-10X
1
2
3
4
5
CC
5
10
15
20
25
30
35
40
45
50
55
60
65
70
75
80
85
90
95
100
105
110
115
120
125
130
135
140
145
150

SITE 722 HOLE A CORE 11X CORED INTERVAL 2124.0-2133.7 mbsl; 96.2-105.9 mbsf

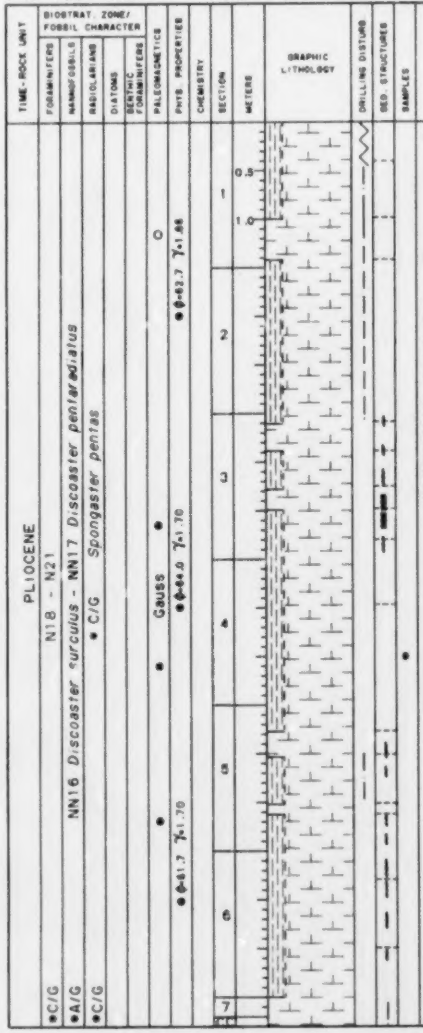
TIME-ROCK UNIT
BIOSTRAT. ZONE/ FOSSIL CHARACTER
FORAMINIFERS
NANNOFOSSILS
RADIOLARIANS
DIATOMS
BENTHIC FORAMINIFERS
PALEOMAGNETICS
PHYS. PROPERTIES
CHEMISTRY
SECTION
METERS
GRAPHIC LITHOLOGY
DRILLING DISTURB.
SED. STRUCTURES
SAMPLES
PLIOCENE
N18 - N21
NN16 Discoaster surculus - NN17 Discoaster pentaradiatus
• C/G Spongaster pentas
•C/G
•A/G
•C/G
Gauss
●φ=62.7 γ=1.86
●φ=64.0 γ=1.70
●φ=61.7 γ=1.70
1
2
3
4
5
6
7
CC
0.5
1.0

LITHOLOGIC DESCRIPTION

NANNOFOSSIL OOZE

Section 1, 0-50 cm, is very disturbed. Section 1, 50-150 cm, Section 3, 0-60 cm, Section 5, 15-25 cm, and CC are moderately disturbed. Section 2, 0-150 cm, is slightly disturbed.

Major lithology: NANNOFOSSIL OOZE. Beds range from gray (5Y 6/1) to light olive gray (5Y 6/2), light greenish gray (10Y 6/1), and olive (5Y 5/3, 4/3, 4/4). Contacts are gradational. Bioturbation is minor to moderate throughout.

SMEAR SLIDE SUMMARY (%):

	4, 100 D
TEXTURE:	
Silt	20
Clay	80
COMPOSITION:	
Clay	10
Diatoms	Tr
Dolomite	Tr
Foraminifers	5
Inorganic calcite	5
Nannofossils	75
Quartz	Tr
Radiolarians	5
Silicoflagellates	Tr

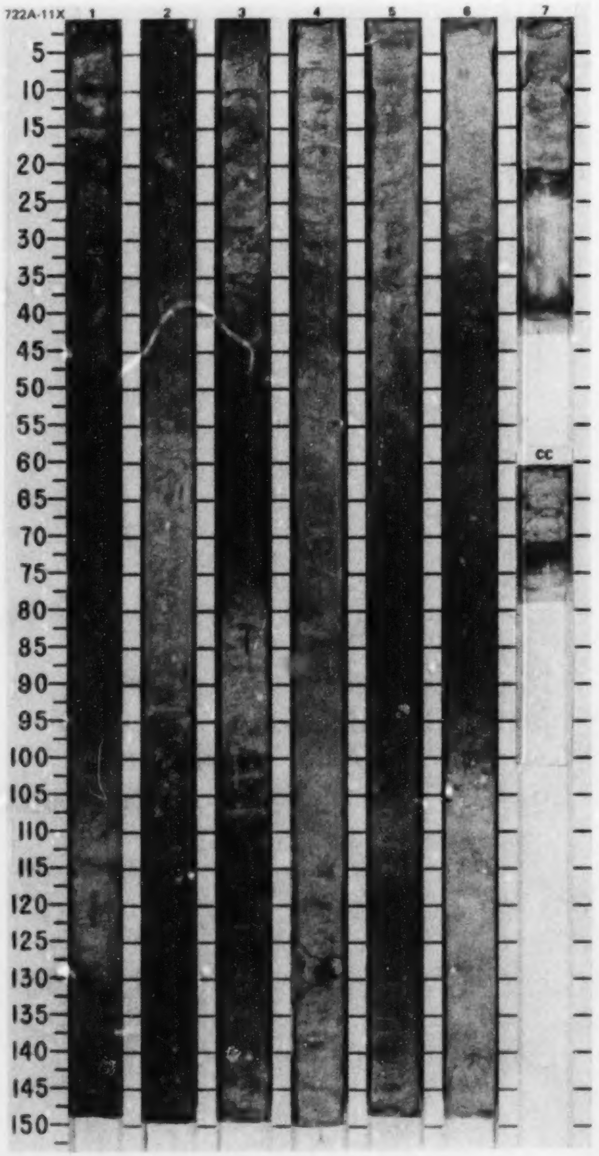
722A-11X
1
2
3
4
5
6
7
CC
5
10
15
20
25
30
35
40
45
50
55
60
65
70
75
80
85
90
95
100
105
110
115
120
125
130
135
140
145
150

SITE 722 HOLE A CORE 12X CORED INTERVAL 2133.7-2143.4 mbsl; 105.9-115.6 mbsf

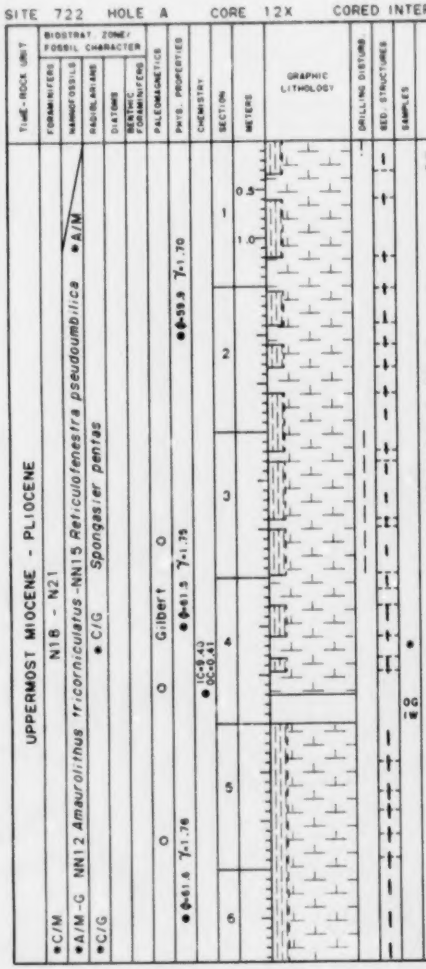
TIME-ROCK UNIT
BIOSTRAT. ZONE/ FOSSIL CHARACTER
FORAMINIFERS
NANNOFOSSILS
RADIOLARIANS
DIATOMS
BENTHIC FORAMINIFERS
PALEOMAGNETICS
PHYS. PROPERTIES
CHEMISTRY
SECTION
METERS
GRAPHIC LITHOLOGY
DRILLING DISTURB.
SED. STRUCTURES
SAMPLES
UPPERMOST MIOCENE - PLIOCENE
●C/M N18 - N21
●A/M-G NN12 Amaurolithus tricorniculatus-NN15 Reticulofenestra pseudoumbilica ●A/M
●C/G ●C/G Spongaster pentas
O Gilbert O O O
●Φ=59.9 γ=1.70
●Φ=61.5 γ=1.75
●Φ=61.6 γ=1.76
●IC=9.40 OC=0.41
1
2
3
4
5
6
0.5
1.0
●
OG
IW

LITHOLOGIC DESCRIPTION

Interbedded NANNOFOSSIL OOZE and FORAMINIFER-BEARING NANNOFOSSIL OOZE

Section 1, 0-10 cm, is moderately disturbed. Section 3, 0-150 cm, is slightly disturbed.

Major lithology: Interbedded NANNOFOSSIL OOZE and FORAMINIFER-BEARING NANNOFOSSIL OOZE. Contacts are gradational. Beds range from light olive gray (5Y 6/2) to light gray (5Y 7/1), olive gray (5Y 5/2), and olive (5Y 5/3, 5/4, 4/4). Bioturbation is minor throughout.

SMEAR SLIDE SUMMARY (%):

	4, 70 D
TEXTURE:	
Silt	20
Clay	80
COMPOSITION:	
Clay	10
Diatoms	Tr
Foraminifers	10
Inorganic calcite	5
Nannofossils	75
Quartz	Tr
Radiolarians	Tr

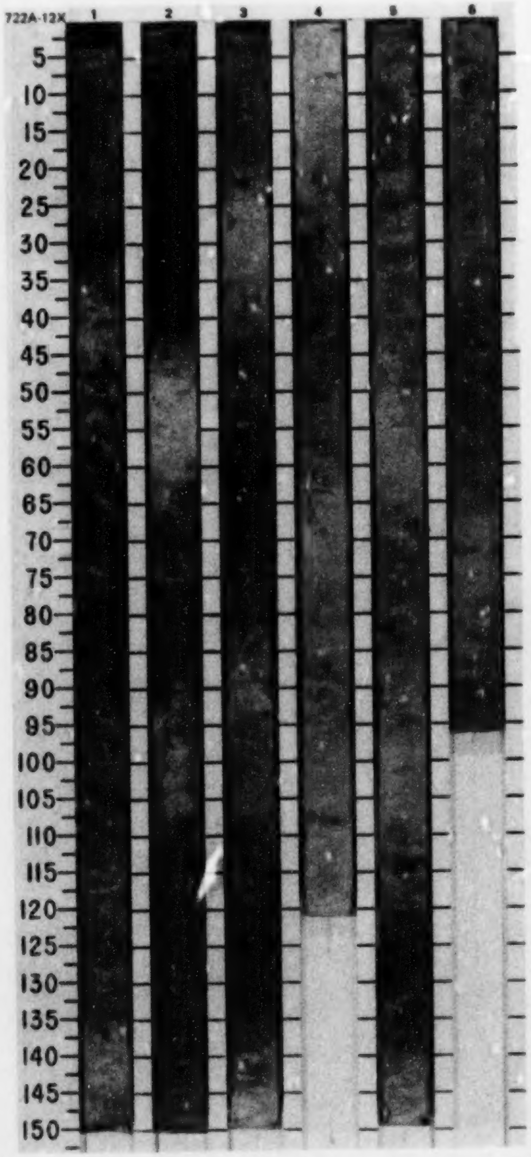
722A-12X
1
2
3
4
5
6
5
10
15
20
25
30
35
40
45
50
55
60
65
70
75
80
85
90
95
100
105
110
115
120
125
130
135
140
145
150

SITE 722 HOLE A CORE 13X CORED INTERVAL 2143.4-2153.1 mbsl; 115.6-125.3 mbsf

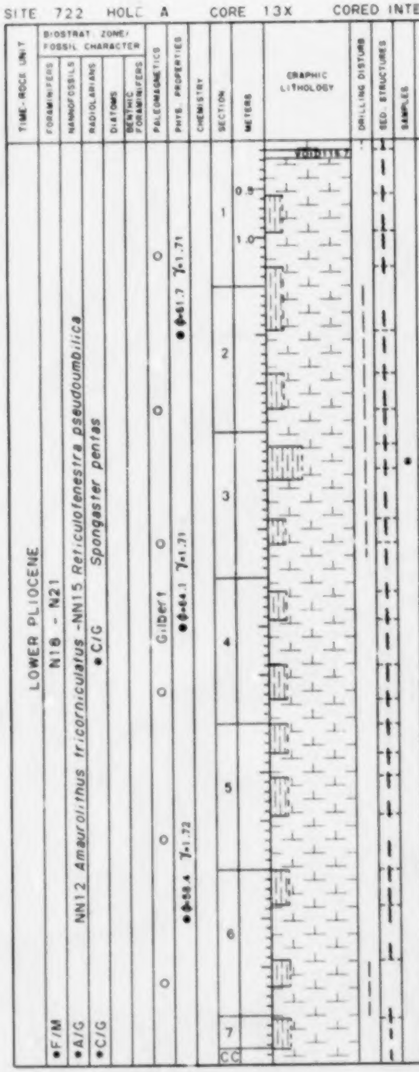
TIME-ROCK UNIT
BIOSTRAT. ZONE/ FOSSIL CHARACTER
FORAMINIFERS
NANNOFOSSILS
RADIOLARIANS
DIATOMS
BENTHIC FORAMINIFERS
PALEOMAGNETICS
PHYS. PROPERTIES
CHEMISTRY
SECTION
METERS
GRAPHIC LITHOLOGY
DRILLING DISTURB.
SED. STRUCTURES
SAMPLES
LOWER PLIOCENE
●F/M
N18 - N21
●A/G
NN12 Amaurolithus tricorniculatus -NN15 Reticulofenestra pseudoumbilica
●C/G
●C/G
Spongaster pentas
Gilbert
●φ=61.7 γ=1.71
●φ=64.1 γ=1.71
●φ=58.4 γ=1.72
1
2
3
4
5
6
7
CC
0.5
1.0

LITHOLOGIC DESCRIPTION

NANNOFOSSIL OOZE

Section 1, 0-10 cm, and Section 6, 110-150 cm, are moderately disturbed. Section 2, 0 cm, to Section 3, 150 cm, is slightly disturbed.

Major lithology: NANNOFOSSIL OOZE. Beds range from gray (5Y 6/1) to light olive gray (5Y 6/2), light gray (5Y 7/1), olive gray (5Y 5/2), olive (5Y 5/3, 4/3), and pale olive (5Y 6/3). Contacts are gradational. Bioturbation is minor throughout.

SMEAR SLIDE SUMMARY (%):

	3, 31 D
TEXTURE:	
Sand	5
Silt	30
Clay	65
COMPOSITION:	
Access. minerals	2
Clay	25
Foraminifers	5
Inorganic calcite	15
Mica	3
Nannofossils	45
Quartz	5

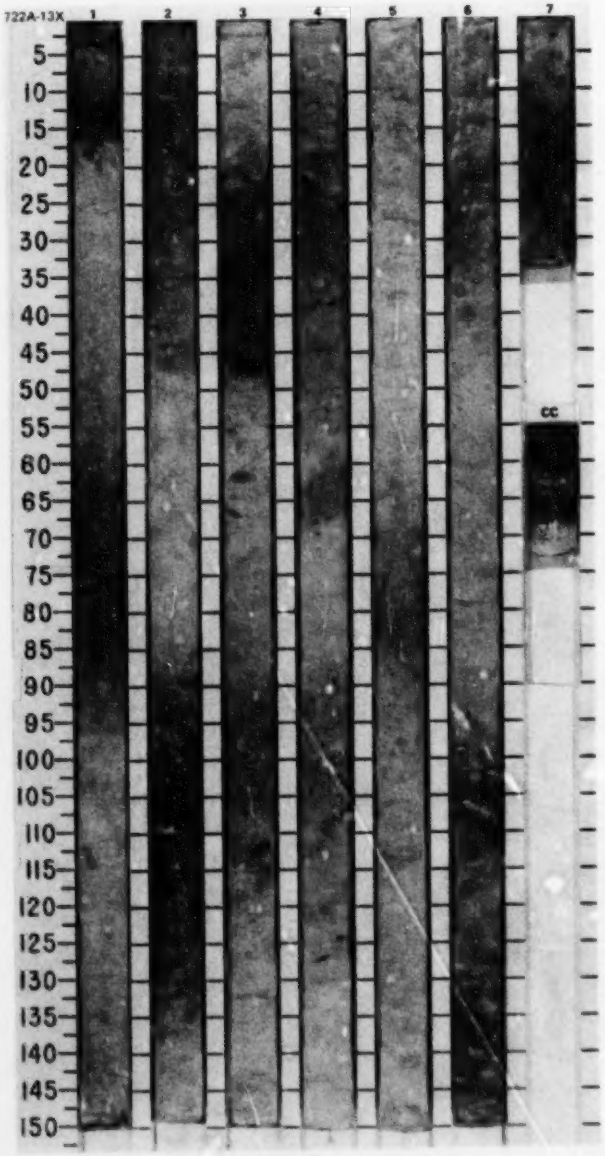
722A-13X
1
2
3
4
5
6
7
CC
5
10
15
20
25
30
35
40
45
50
55
60
65
70
75
80
85
90
95
100
105
110
115
120
125
130
135
140
145
150

SITE 722 HOLE A CORE 14X CORED INTERVAL 2153.1-2162.7 mbsl; 125.3-134.9 mbsf

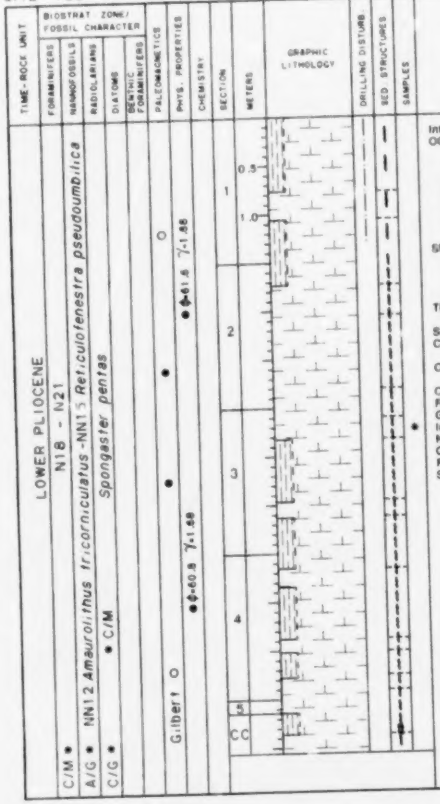
TIME-ROCK UNIT
BIOSTRAT. ZONE/ FOSSIL CHARACTER
FORAMINIFERS
NANNOFOSSILS
RADIOLARIANS
DIATOMS
BENTHIC FORAMINIFERS
PALEOMAGNETICS
PHYS. PROPERTIES
CHEMISTRY
SECTION
METERS
GRAPHIC LITHOLOGY
DRILLING DISTURB.
SED. STRUCTURES
SAMPLES
LOWER PLIOCENE
N18 - N21
C/M ●
NN12 Amaurolithus tricorniculatus -NN15 Reticulofenestra pseudoumbilica
A/G ●
Spongaster pentas
C/G ●
● C/M
Gilbert
○
●
●
○
●ϕ=61.6 γ=1.88
●ϕ=60.8 γ=1.88
1
2
3
4
5
CC
0.5
1.0

LITHOLOGIC DESCRIPTION

Interbedded NANNOFOSSIL OOZE and FORAMINIFER-BEARING NANNOFOSSIL OOZE

Section 1, 0-30 cm, is moderately disturbed.

Major lithology: Interbedded NANNOFOSSIL OOZE and FORAMINIFER-BEARING NANNOFOSSIL OOZE. Contacts are gradational. Beds range from gray (5Y 6/1) to light olive gray (5Y 6/2), light gray (5Y 7/1, olive (5Y 5/3, 5/4), and pale olive (5Y 6/3). Bioturbation is minor throughout.

SMEAR SLIDE SUMMARY (%):

	3, 23 D
TEXTURE:	
Silt	10
Clay	90
COMPOSITION:	
Clay	15
Foraminifers	5
Gypsum	Tr
Inorganic calcite	5
Nannofossils	74
Quartz	Tr
Radiolarians	1
Sponge spicules	

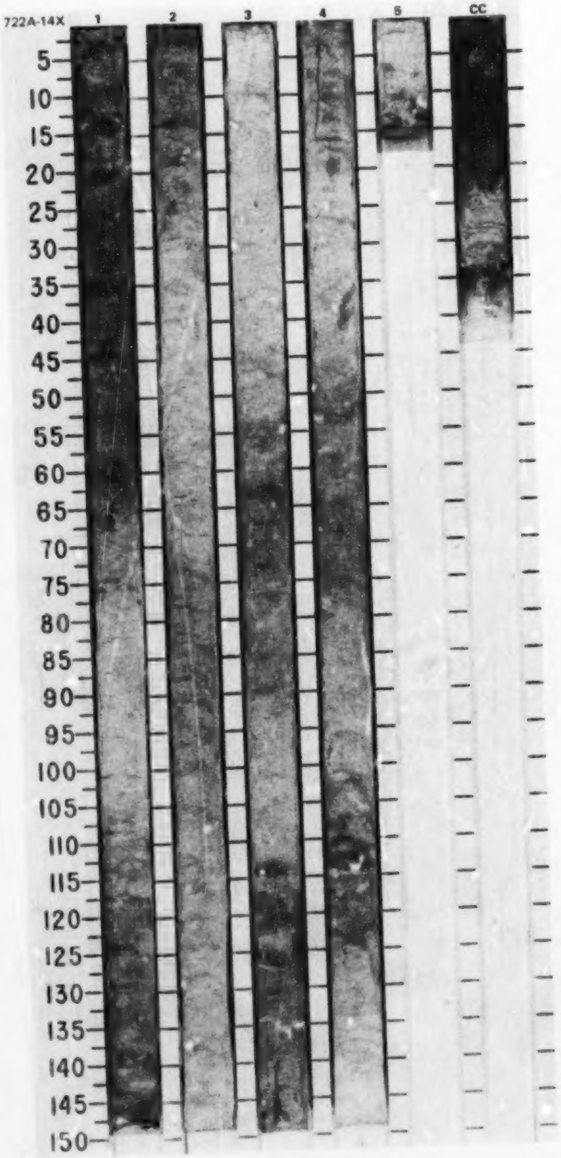
722A-14X
1
2
3
4
5
CC
5
10
15
20
25
30
35
40
45
50
55
60
65
70
75
80
85
90
95
100
105
110
115
120
125
130
135
140
145
150

SITE 722 HOLE A CORE 15X CORED INTERVAL 2162.7-2172.4 mbsl; 134.9-144.6 mbsf

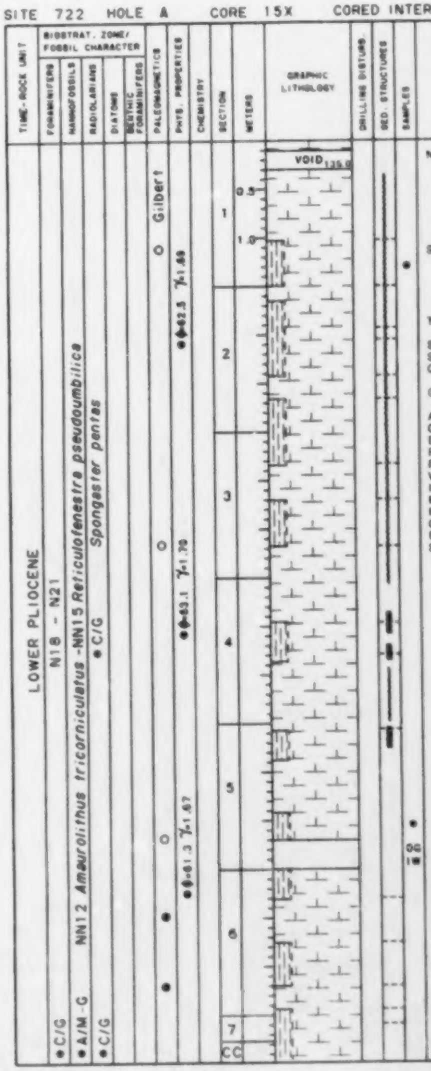
TIME-ROCK UNIT
BIOSTRAT. ZONE/ FOSSIL CHARACTER
FORAMINIFERS
NANNOFOSSILS
RADIOLARIANS
DIATOMS
BENTHIC FORAMINIFERS
PALEOMAGNETICS
PHYS. PROPERTIES
CHEMISTRY
SECTION
METERS
GRAPHIC LITHOLOGY
DRILLING DISTURB.
SED. STRUCTURES
SAMPLES
LOWER PLIOCENE
● C/G N18 - N21
● A/M-G NN12 Amaurolithus tricorniculatus -NN15 Reticulofenestra pseudoumbilica
● C/G ● C/G Spongaster pentas
○ Gilbert
●ϕ=62.5 γ=1.69
●ϕ=63.1 γ=1.70
●ϕ=61.3 γ=1.67
1
2
3
4
5
6
7
CC
0.5
1.0
VOID
135.0
OG
IW

LITHOLOGIC DESCRIPTION

NANNOFOSSIL OOZE

Entire core is undisturbed.

Major lithology: NANNOFOSSIL OOZE. Beds range from light gray (5Y 7/1) to light olive gray (5Y 6/2) and olive (5Y 5/3, 4/4). Contacts are gradational. Bioturbation is minor to moderate throughout.

SMEAR SLIDE SUMMARY (%):

	1, 136 D	5, 108 D
TEXTURE:		
Sand	3	
Silt	12	5
Clay	85	95
COMPOSITION:		
Access. minerals	1	
Clay	15	4
Diatoms	Tr	1
Feldspar	Tr	
Foraminifers	2	Tr
Volcanic glass	Tr	
Inorganic calcite	10	5
Mica	1	Tr
Nannofossils	70	90
Quartz	1	
Radiolarians	Tr	Tr
Sponge spicules		Tr

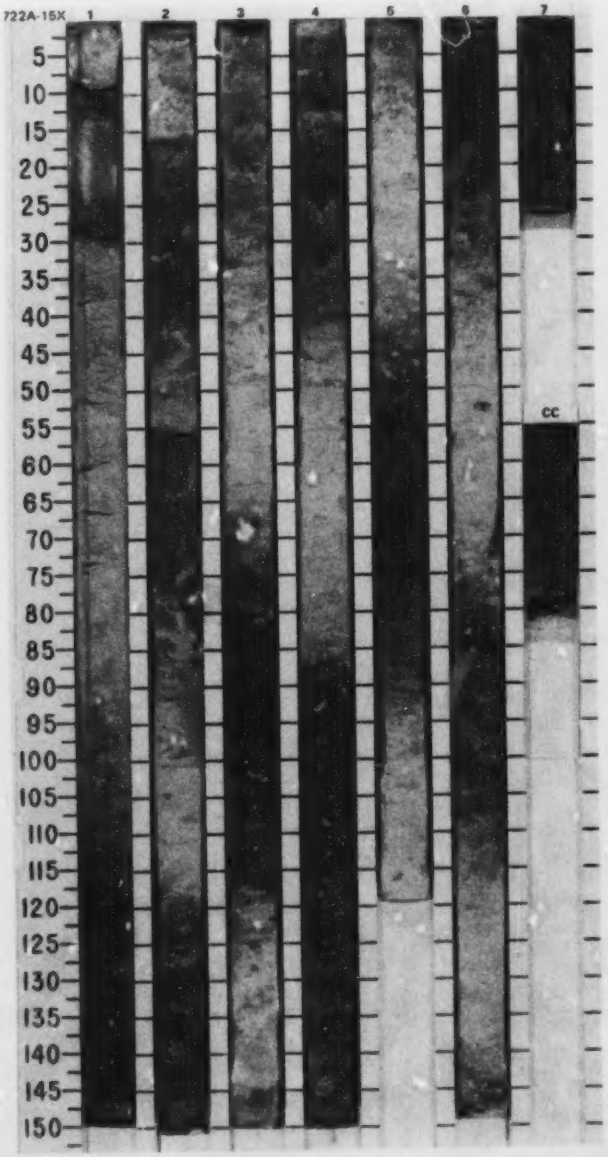
722A-15X
1
2
3
4
5
6
7
CC
5
10
15
20
25
30
35
40
45
50
55
60
65
70
75
80
85
90
95
100
105
110
115
120
125
130
135
140
145
150

SITE 722 HOLE A CORE 16X CORED INTERVAL 2172.4-2182.1 mbsl; 144.6-154.3 mbsf

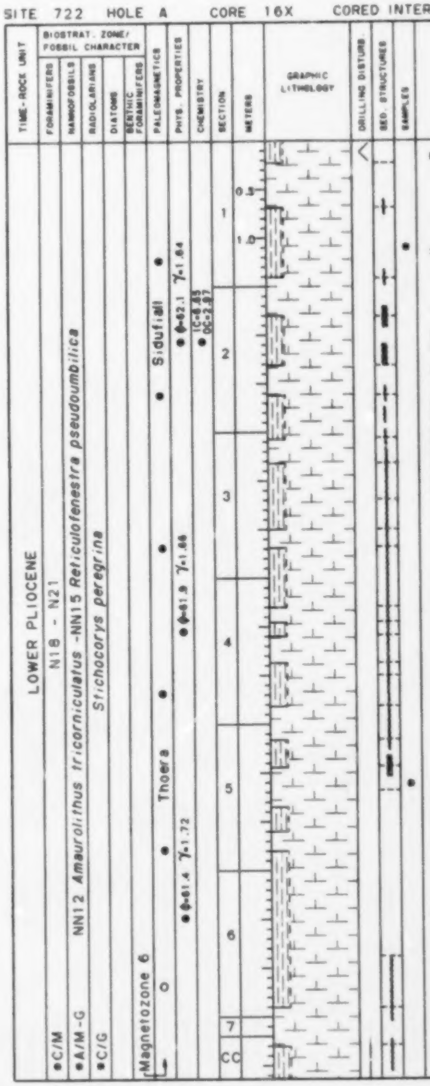
TIME-ROCK UNIT
BIOSTRAT. ZONE/ FOSSIL CHARACTER
FORAMINIFERS
NANNOFOSSILS
RADIOLARIANS
DIATOMS
BENTHIC FORAMINIFERS
PALEOMAGNETICS
PHYS. PROPERTIES
CHEMISTRY
SECTION
METERS
GRAPHIC LITHOLOGY
DRILLING DISTURB.
SED. STRUCTURES
SAMPLES
LOWER PLIOCENE
●C/M N18 - N21
●A/M-G NN12 Amaurolithus tricorniculatus -NN15 Reticulofenestra pseudoumbilica
●C/G Stichocorys peregrina
Sidufjall
Thvera
Magnetozone 6
●φ=62.1 γ=1.64
●φ=61.9 γ=1.86
●φ=61.4 γ=1.72
●IC=8.85 OC=2.87
1
2
3
4
5
6
7
CC
0.5
1.0

LITHOLOGIC DESCRIPTION

NANNOFOSSIL OOZE

Section 1, 0-10 cm, and CC are slightly disturbed.

Major lithology: NANNOFOSSIL OOZE. Beds range from light gray (5Y 7/1) to light olive gray (5Y 6/2) and olive (5Y 5/3, 4/4). Contacts are gradational. Bioturbation is minor to moderate throughout.

SMEAR SLIDE SUMMARY (%):

	1, 110 D	5, 61 D
TEXTURE:		
Silt	10	7
Clay	90	93
COMPOSITION:		
Access. minerals	1	1
Clay	20	3
Diatoms	Tr	
Foraminifers	Tr	Tr
Volcanic glass	Tr	Tr
Inorganic calcite	9	6
Nannofossils	70	90
Quartz	Tr	Tr
Sponge spicules	Tr	

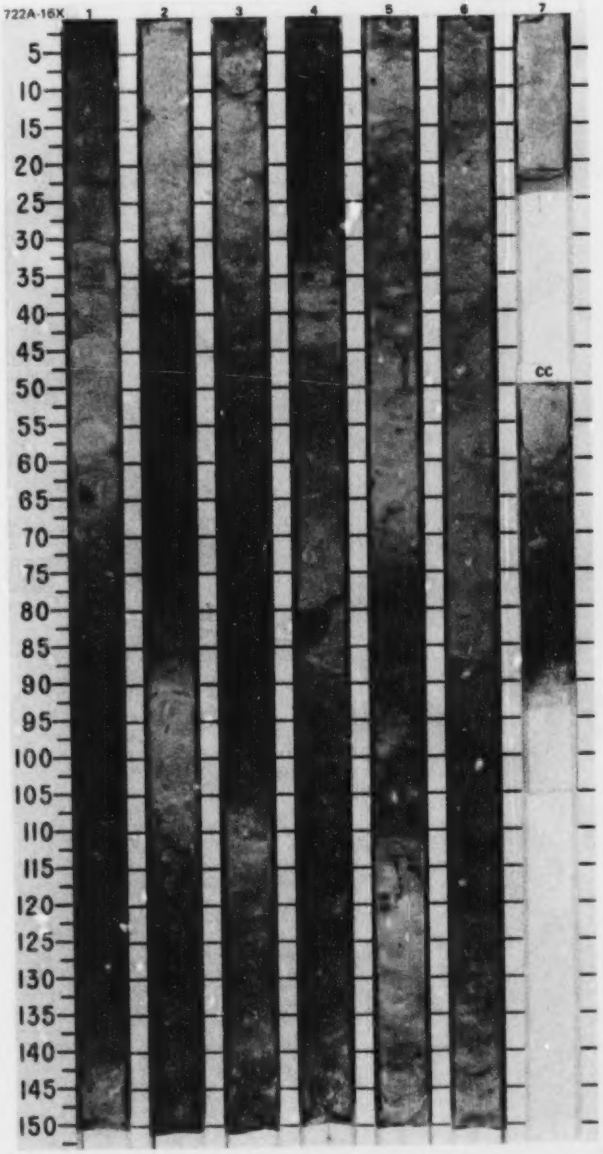
722A-16X
1
2
3
4
5
6
7
CC
5
10
15
20
25
30
35
40
45
50
55
60
65
70
75
80
85
90
95
100
105
110
115
120
125
130
135
140
145
150

SITE 722 HOLE A CORE 17X CORED INTERVAL 2182.1-2191.7 mbsl; 154.3-163.9 mbsf

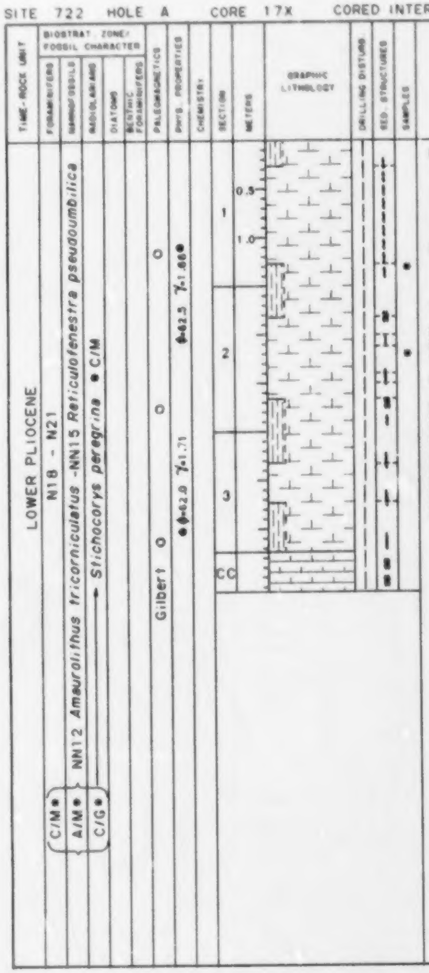
TIME-ROCK UNIT
BIOSTRAT. ZONE/ FOSSIL CHARACTER
FORAMINIFERS
NANNOFOSSILS
RADIOLARIANS
DIATOMS
BENTHIC FORAMINIFERS
PALEOMAGNETICS
PHYS. PROPERTIES
CHEMISTRY
SECTION
METERS
GRAPHIC LITHOLOGY
DRILLING DISTURB.
SED. STRUCTURES
SAMPLES
LOWER PLIOCENE
C/M
N18 - N21
A/M
NN12 Amaurolithus tricorniculatus -NN15 Reticulofenestra pseudoumbilica
C/G
Stichocorys peregrina ● C/M
Gilbert
φ=62.5 γ=1.88
γ=1.71
φ=62.0
1
2
3
CC
0.5
1.0

LITHOLOGIC DESCRIPTION

NANNOFOSSIL CHALK

Entire core is slightly disturbed by drilling biscuit formation.

Major lithology: NANNOFOSSIL CHALK. Beds range from light olive gray (5Y 6/2) to light gray (5Y 7/1) and olive (5Y 5/3, 5/4, 4/3). Contacts are gradational. Bioturbation is minor to moderate throughout.

SMEAR SLIDE SUMMARY (%):

	1, 139 D	2, 76 D
TEXTURE:		
Sand		3
Silt	5	7
Clay	95	90
COMPOSITION:		
Access. minerals	Tr	
Clay	10	
Diatoms		Tr
Foraminifers	Tr	3
Volcanic glass	Tr	
Inorganic calcite	5	7
Mica		Tr
Nannofossils	85	90
Radiolarians		Tr
Sponge spicules	Tr	

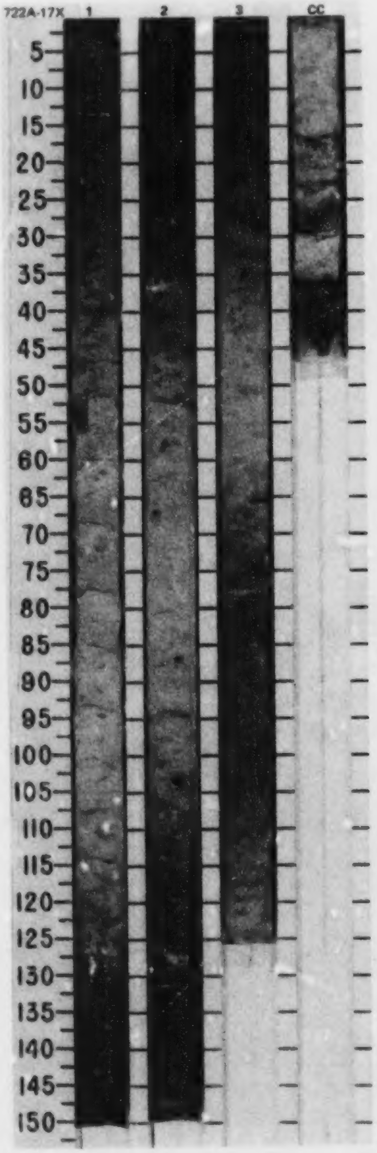
722A-17X
1
2
3
CC
5
10
15
20
25
30
35
40
45
50
55
60
65
70
75
80
85
90
95
100
105
110
115
120
125
130
135
140
145
150

SITE 722 HOLE A CORE 18X CORED INTERVAL 2191.7-2201.4 mbsl; 163.9-173.6 mbsf

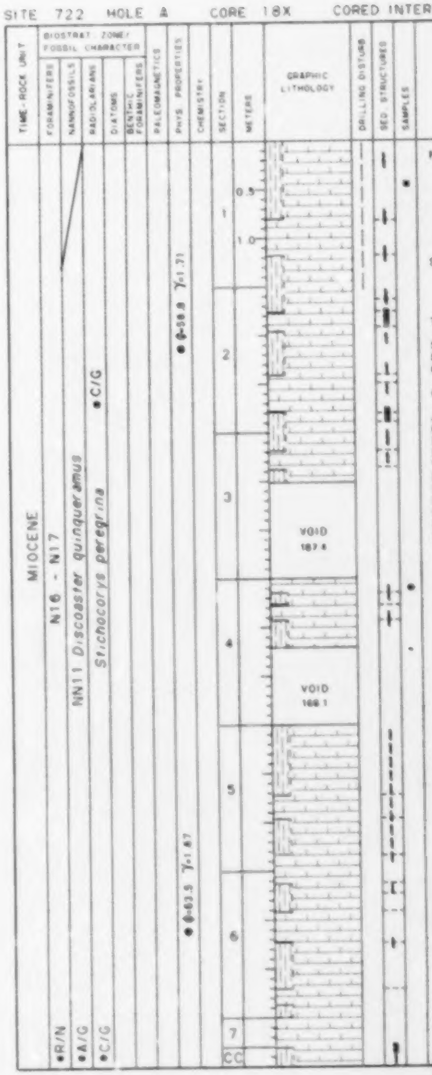
TIME-ROCK UNIT
BIOSTRAT. ZONE/ FOSSIL CHARACTER
FORAMINIFERS
NANNOFOSSILS
RADIOLARIANS
DIATOMS
BENTHIC FORAMINIFERS
PALEOMAGNETICS
PHYS. PROPERTIES
CHEMISTRY
SECTION
METERS
GRAPHIC LITHOLOGY
DRILLING DISTURB.
SED. STRUCTURES
SAMPLES
MIOCENE
N16 - N17
NN11 Discoaster quinqueramus
Stichocorys peregrina
●C/G
●R/N
●A/G
●C/G
● ϕ-58.9 γ-1.71
● ϕ-63.5 γ-1.87
0.5
1.0
1
2
3
4
5
6
7
CC
VOID 187.4
VOID 168.1

LITHOLOGIC DESCRIPTION

NANNOFOSSIL CHALK

Core extruded on drilling deck, reconstructed on catwalk. Section 1, 0-150 cm, is slightly disturbed.

Major lithology: NANNOFOSSIL CHALK. Beds range from gray (5Y 6/1) to light gray (5Y 7/1, 7/2), olive (5Y 5/3, 4/3, 5/4), and pale olive (5Y 6/3). Contacts are gradational. Bioturbation is minor to moderate throughout.

SMEAR SLIDE SUMMARY (%):

	1, 52 D	4, 10 D
TEXTURE:		
Sand	2	2
Silt	5	10
Clay	93	88
COMPOSITION:		
Access. minerals	Tr	
Clay	13	4
Diatoms		Tr
Foraminifers	1	1
Volcanic glass	Tr	Tr
Inorganic calcite	5	10
Nannofossils	80	85
Quartz	1	Tr
Radiolarians	Tr	
Silicoflagellates		Tr
Sponge spicules	Tr	

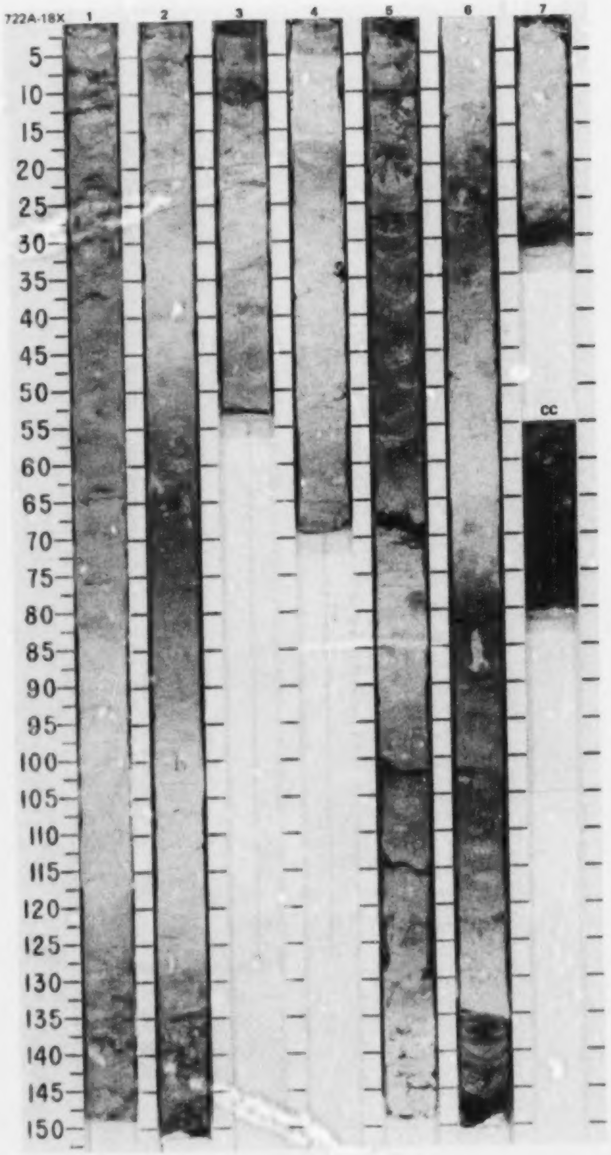
722A-18X
1
2
3
4
5
6
7
CC
5
10
15
20
25
30
35
40
45
50
55
60
65
70
75
80
85
90
95
100
105
110
115
120
125
130
135
140
145
150

SITE 722 HOLE A CORE 19X CORED INTERVAL 2201.4-2211.1 mbsl; 173.6-183.3 mbsf

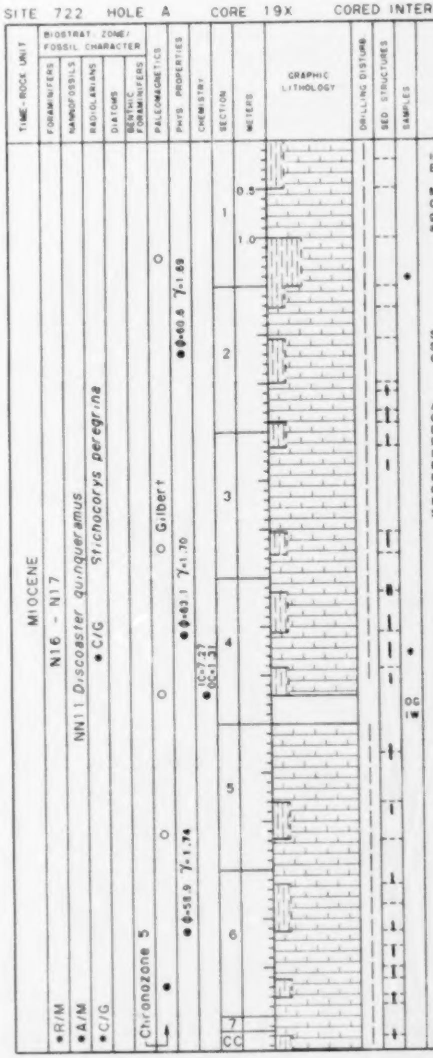
TIME-ROCK UNIT
BIOSTRAT. ZONE/ FOSSIL CHARACTER
FORAMINIFERS
NANNOFOSSILS
RADIOLARIANS
DIATOMS
BENTHIC FORAMINIFERS
PALEOMAGNETICS
PHYS. PROPERTIES
CHEMISTRY
SECTION
METERS
GRAPHIC LITHOLOGY
DRILLING DISTURB.
SED. STRUCTURES
SAMPLES
MIOCENE
N16 - N17
NN11 Discoaster quinqueramus
• C/G Stichocorys peregrina
• R/M
• A/M
• C/G
Chronozone 5
O Gilbert
● φ=60.8 γ=1.89
● φ=63.1 γ=1.70
● φ=58.9 γ=1.74
● IC=7.27 OC=1.31
1
2
3
4
5
6
7
CC
0.5
1.0
OG
IW

LITHOLOGIC DESCRIPTION

Interbedded NANNOFOSSIL CHALK and MARLY NANNOFOSSIL CHALK
Entire core is slightly disturbed.

Major lithology: Interbedded NANNOFOSSIL CHALK and MARLY NANNOFOSSIL CHALK. Contacts are gradational. Beds range from gray (5Y 6/1) to light olive gray (5Y 6/2), light gray (5Y 7/1, 7/2), olive gray (5Y 5/2), olive (5Y 4/3, 5/3, 4/4, 5/4), and pale olive (5Y 6/3). Bioturbation is minor to moderate throughout.

SMEAR SLIDE SUMMARY (%):

	1, 142 D	4, 77 D
TEXTURE:		
Sand	4	5
Silt	8	10
Clay	90	85
COMPOSITION:		
Access. minerals	2	Tr
Clay	20	7
Diatoms	Tr	
Foraminifers		5
Inorganic calcite	7	8
Mica		Tr
Nannofossils	70	80
Quartz	1	
Radiolarians	Tr	Tr
Sponge spicules		Tr

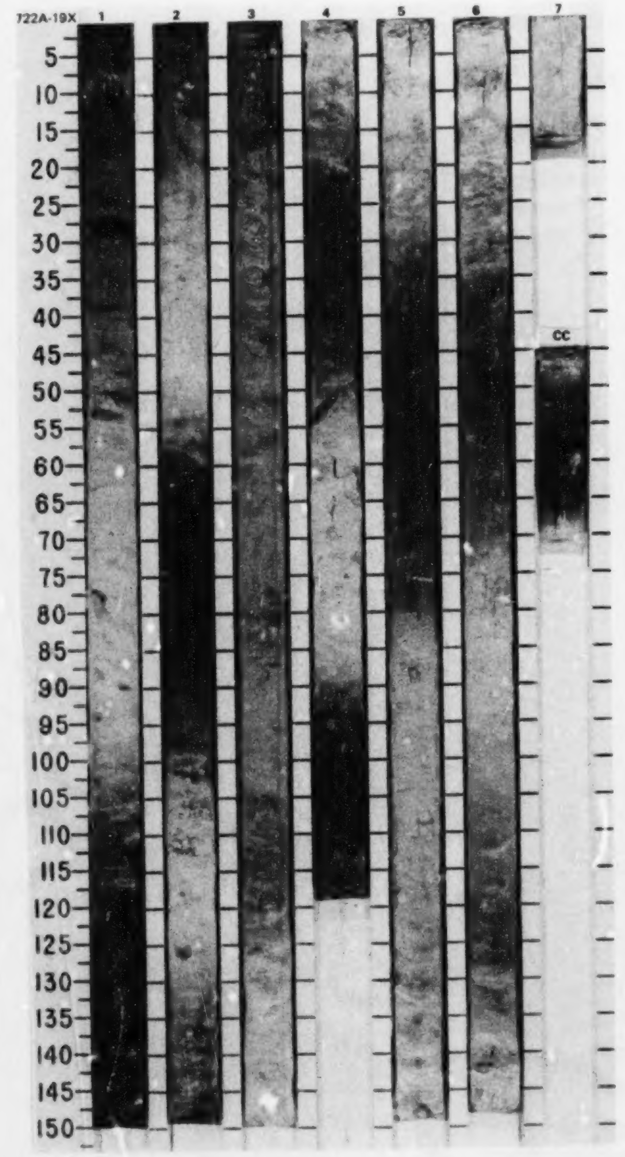
722A-19X
1
2
3
4
5
6
7
CC
5
10
15
20
25
30
35
40
45
50
55
60
65
70
75
80
85
90
95
100
105
110
115
120
125
130
135
140
145
150

SITE 722 HOLE A CORE 20X CORED INTERVAL 2211.1-2220.8 mbsl; 183.3-193.0 mbsf

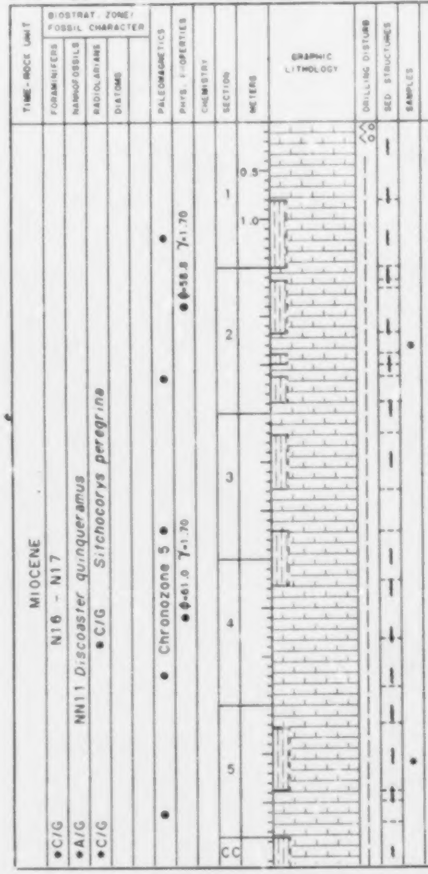
TIME-ROCK UNIT
BIOSTRAT. ZONE/ FOSSIL CHARACTER
FORAMINIFERS
NANNOFOSSILS
RADIOLARIANS
DIATOMS
PALEOMAGNETICS
PHYS. PROPERTIES
CHEMISTRY
SECTION
METERS
GRAPHIC LITHOLOGY
DRILLING DISTURB.
SED. STRUCTURES
SAMPLES
MIOCENE
N16 - N17
NN11 Discoaster quinqueramus
Sitchocorys peregrina
●C/G
●A/G
●C/G
●C/G
Chronozone 5
●φ=58.8 γ=1.70
●φ=61.0 γ=1.70
1
2
3
4
5
CC
0.5
1.0

LITHOLOGIC DESCRIPTION

NANNOFOSSIL CHALK

Section 1, 0-10 cm, is very disturbed/soupy. Remainder of core is slightly disturbed.

Major lithology: NANNOFOSSIL CHALK. Beds range from light olive gray (5Y 6/2) to light gray (5Y 7/1), olive (5Y 5/3), and pale olive (5Y 6/3). Contacts are gradational. Bioturbation is minor throughout.

SMEAR SLIDE SUMMARY (%):

	2, 81 D	57 D
TEXTURE:		
Silt	5	15
Clay	95	85
COMPOSITION:		
Access. minerals		1
Clay	4	20
Diatoms		1
Feldspar		Tr
Foraminifers	Tr	Tr
Volcanic glass		1
Inorganic calcite	5	10
Nannofossils	90	65
Quartz	1	2
Radiolarians	Tr	Tr
Sponge spicules	Tr	

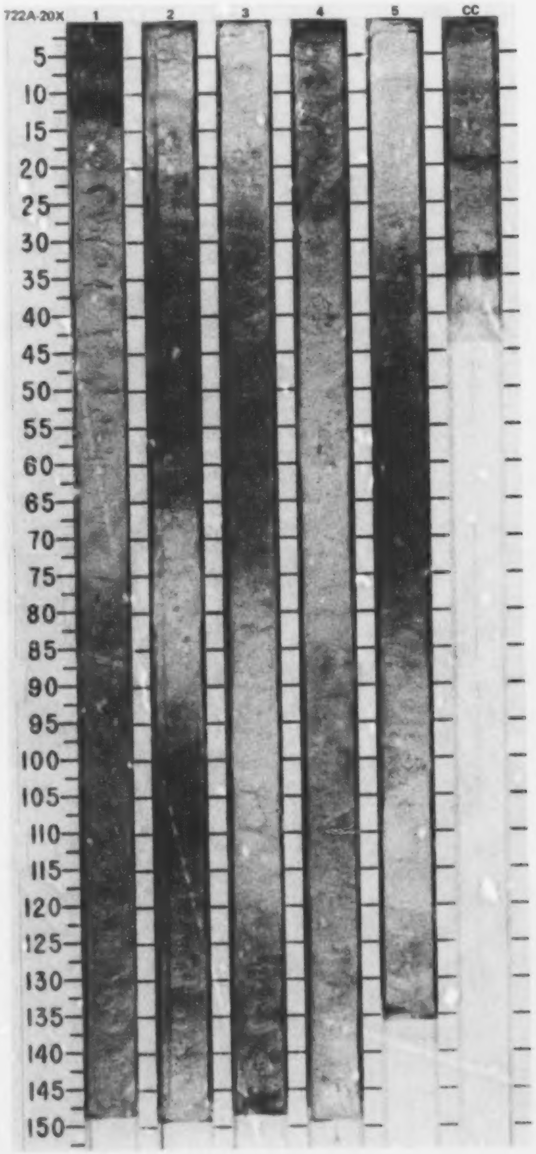
722A-20X
1
2
3
4
5
CC
5
10
15
20
25
30
35
40
45
50
55
60
65
70
75
80
85
90
95
100
105
110
115
120
125
130
135
140
145
150

SITE 722 HOLE A CORE 21X CORED INTERVAL 2220.8-2230.5 mbsl; 193.0-202.7 mbsf

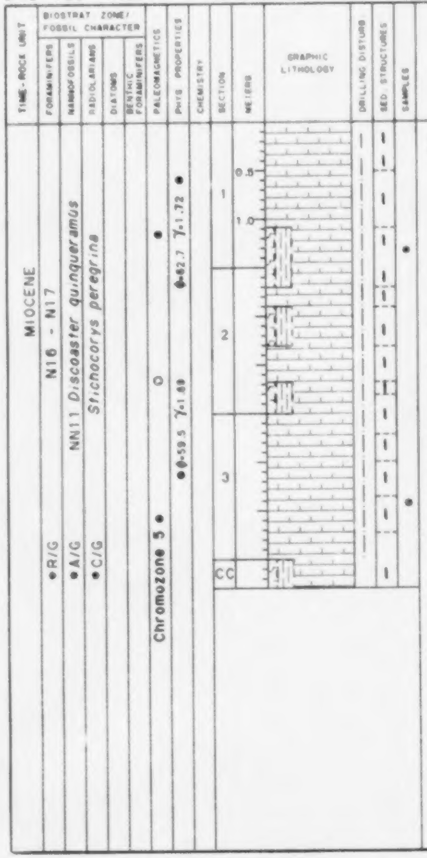
TIME-ROCK UNIT
BIOSTRAT. ZONE/ FOSSIL CHARACTER
FORAMINIFERS
NANNOFOSSILS
RADIOLARIANS
DIATOMS
BENTHIC FORAMINIFERS
PALEOMAGNETICS
PHYS. PROPERTIES
CHEMISTRY
SECTION
METERS
GRAPHIC LITHOLOGY
DRILLING DISTURB.
SED. STRUCTURES
SAMPLES
MIOCENE
N16 - N17
●R/G
NN11 Discoaster quinqueramus
●A/G
Stichocorys peregrina
●C/G
Chromozone 5
Φ=62.7 γ=1.72
Φ=59.5 γ=1.89
1
2
3
CC
0.5
1.0

LITHOLOGIC DESCRIPTION

Interbedded NANNOFOSSIL CHALK and DIATOM-BEARING NANNOFOSSIL CHALK

Entire core is moderately disturbed.

Major lithology: Interbedded NANNOFOSSIL CHALK and DIATOM- BEARING NANNOFOSSIL CHALK. Contacts are gradational. Beds range from light gray (5Y 7/1) to gray (5Y 6/1), pale olive (5Y 6/3), and olive (5Y 4/3). Bioturbation is minor throughout. Diatom content is higher in the darker pale olive and olive beds.

SMEAR SLIDE SUMMARY (%):

	1, 133 D	3, 100 D
TEXTURE:		
Sand	5	2
Silt	15	8
Clay	80	90
COMPOSITION:		
Access. minerals	1	Tr
Clay	20	
Diatoms	10	
Dolomite	Tr	
Feldspar	1	
Foraminifers	Tr	2
Volcanic glass		Tr
Inorganic calcite	5	8
Nannofossils	60	90
Quartz	3	
Radiolarians	Tr	Tr
Sponge spicules	Tr	Tr

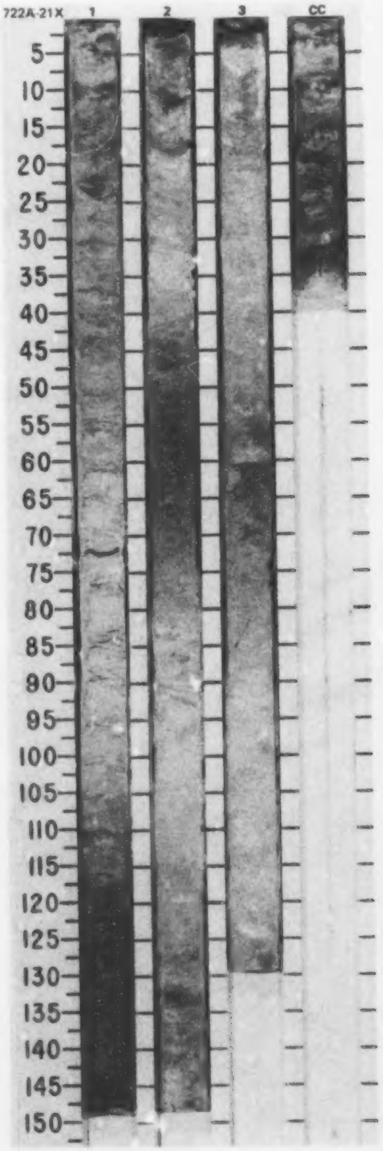
722A-21X
1
2
3
CC
5
10
15
20
25
30
35
40
45
50
55
60
65
70
75
80
85
90
95
100
105
110
115
120
125
130
135
140
145
150

SITE 722 HOLE A CORE 22X CORED INTERVAL 2230.5-2240.2 mbsl; 202.7-212.4 mbsf

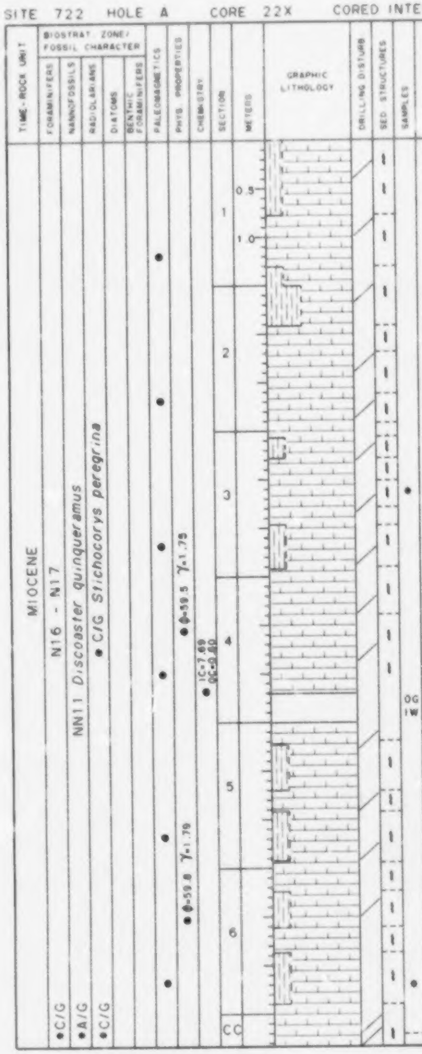
TIME-ROCK UNIT
BIOSTRAT. ZONE/ FOSSIL CHARACTER
FORAMINIFERS
NANNOFOSSILS
RADIOLARIANS
DIATOMS
BENTHIC FORAMINIFERS
PALEOMAGNETICS
PHYS. PROPERTIES
CHEMISTRY
SECTION
METERS
GRAPHIC LITHOLOGY
DRILLING DISTURB.
SED. STRUCTURES
SAMPLES
MIOCENE
N16 - N17
NN11 Discoaster quinqueramus
● C/G Stichocorys peregrina
●C/G
●A/G
●C/G
●ϕ=59.5 γ=1.75
●ϕ=59.8 γ=1.79
● IC=7.69 OC=0.80
1
2
3
4
5
6
CC
0.5
1.0
OG
IW

LITHOLOGIC DESCRIPTION

Interbedded NANNOFOSSIL CHALK and MARLY NANNOFOSSIL CHALK

Entire core is moderately disturbed.

Major lithology: Interbedded NANNOFOSSIL CHALK and MARLY NANNOFOSSIL CHALK. Contacts are gradational. Beds range from light gray (5Y 7/1, 7/2) to light olive gray (5Y 6/2), gray (5Y 6/1), olive gray (5Y 5/2), and olive (5Y 5/3, 4/2). Bioturbation is minor to moderate throughout.

SMEAR SLIDE SUMMARY (%):

	3, 65 D	6, 119 D
TEXTURE:		
Sand	1	10
Silt	5	10
Clay	94	80
COMPOSITION:		
Access. minerals	Tr	1
Clay	9	20
Diatoms	Tr	
Feldspar		1
Foraminifers	1	5
Volcanic glass	Tr	Tr
Inorganic calcite	5	10
Mica		1
Nannofossils	85	60
Quartz		2
Radiolarians	Tr	
Sponge spicules	Tr	

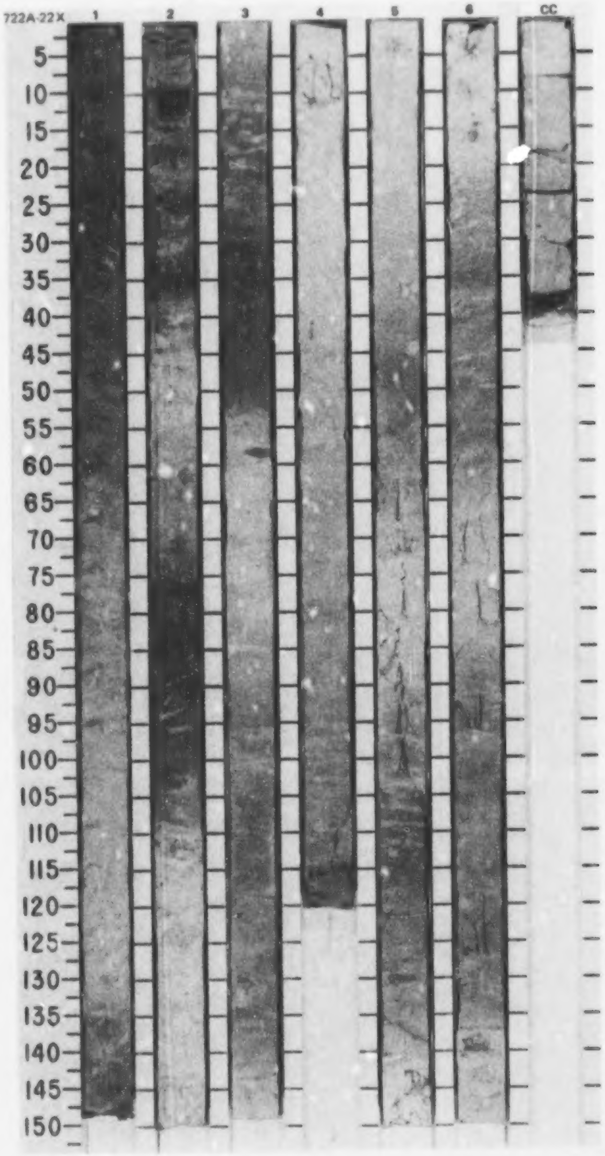
722A-22X
1
2
3
4
5
6
CC
5
10
15
20
25
30
35
40
45
50
55
60
65
70
75
80
85
90
95
100
105
110
115
120
125
130
135
140
145
150

SITE 722 HOLE A CORE 23X CORED INTERVAL 2240.2-2249.8 mbsl; 212.4-22.0 mbsf

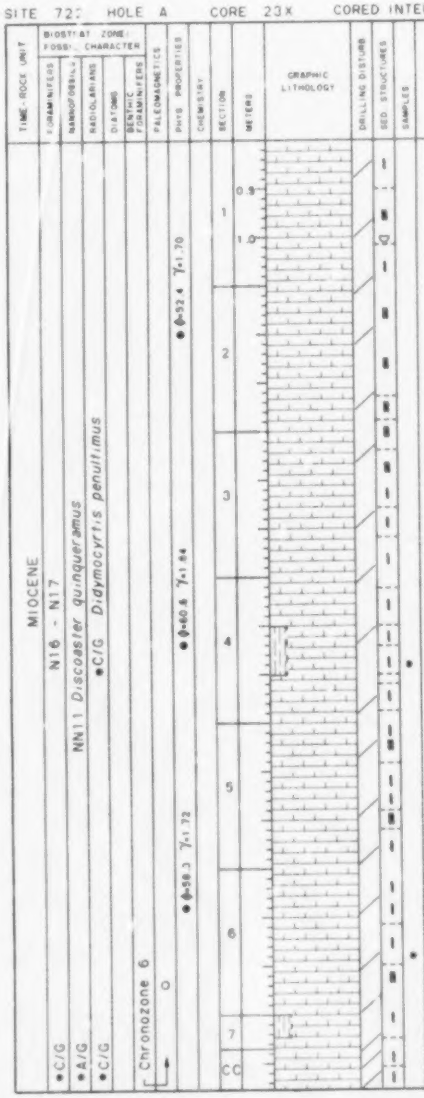
TIME-ROCK UNIT
BIOSTRAT. ZONE/ FOSSIL CHARACTER
FORAMINIFERS
NANNOFOSSILS
RADIOLARIANS
DIATOMS
BENTHIC FORAMINIFERS
PALEOMAGNETICS
PHYS. PROPERTIES
CHEMISTRY
SECTION
METERS
GRAPHIC LITHOLOGY
DRILLING DISTURB.
SED. STRUCTURES
SAMPLES
MIOCENE
N16 - N17
NN11 Discoaster quinqueramus
●C/G Didymocyrtis penultimus
●C/G
●A/G
●C/G
Chronozone 6
●ϕ=52.4 γ=1.70
●ϕ=60.6 γ=1.84
●ϕ=58.3 γ=1.72
1
2
3
4
5
6
7
CC
0.5
1.0

LITHOLOGIC DESCRIPTION

Interbedded NANNOFOSSIL CHALK and DIATOM-BEARING NANNOFOSSIL CHALK

Entire core is slightly disturbed.

Major lithology: Interbedded NANNOFOSSIL CHALK and DIATOM-BEARING NANNOFOSSIL CHALK. Contacts are gradational. Beds range from white (10Y 8/1) to light gray (5Y 7/1, 7/2), light greenish gray (10Y 7/1), light olive gray (5Y 6/2), pale olive (5Y 6/3), and olive (5Y 5/3). Bioturbation is minor to moderate throughout. Diatom-bearing chalk is generally pale olive to olive.

SMEAR SLIDE SUMMARY (%):

	4, 90 D	6, 90 D
TEXTURE:		
Sand	5	3
Silt	15	7
Clay	80	90
COMPOSITION:		
Access. minerals	1	
Clay	14	4
Diatoms	5	Tr
Dolomite	Tr	
Feldspar	1	
Foraminifers	2	3
Volcanic glass	Tr	
Inorganic calcite	10	6
Mica		Tr
Nannofossils	65	86
Quartz	2	Tr
Radiolarians	Tr	Tr
Silicoflagellates	Tr	Tr
Sponge spicules		Tr

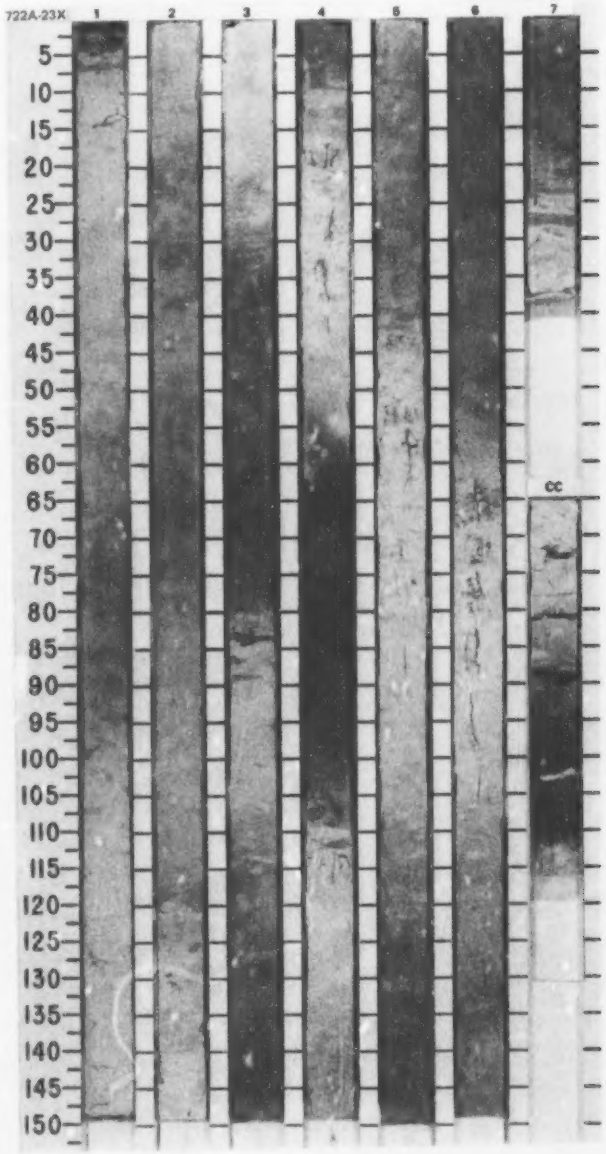
722A-23X
1
2
3
4
5
6
7
CC
5
10
15
20
25
30
35
40
45
50
55
60
65
70
75
80
85
90
95
100
105
110
115
120
125
130
135
140
145
150

SITE 722 HOLE A CORE 24X CORED INTERVAL 2249.8-2259.5 mbsl; 222.0-231 .7 mbsf

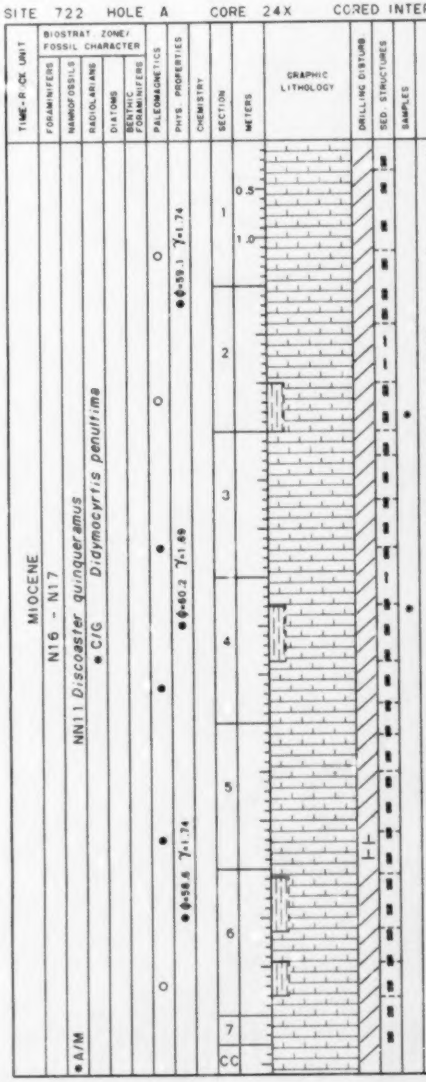
TIME-ROCK UNIT
BIOSTRAT. ZONE/ FOSSIL CHARACTER
FORAMINIFERS
NANNOFOSSILS
RADIOLARIANS
DIATOMS
BENTHIC FORAMINIFERS
PALEOMAGNETICS
PHYS. PROPERTIES
CHEMISTRY
SECTION
METERS
GRAPHIC LITHOLOGY
DRILLING DISTURB.
SED. STRUCTURES
SAMPLES
MIOCENE
N16 - N17
NN11 Discoaster quinqueramus
● A/M
● C/G Didymocyrtis penultima
● φ=59.1 γ=1.74
● φ=60.2 γ=1.69
● φ=58.8 γ=1.74
0.5
1.0
1
2
3
4
5
6
7
CC

LITHOLOGIC DESCRIPTION

NANNOFOSSIL CHALK

Entire core is slightly to moderately fractured.

Major lithology: NANNOFOSSIL CHALK. Beds range from white (5Y 8/1) to light olive gray (5Y 7/1), light gray (5Y 7/1), olive gray (5Y 5/2), and pale olive (5Y 6/3). Entire core is moderately bioturbated.

SMEAR SLIDE SUMMARY (%):

	2, 133 D	4, 34 D
TEXTURE:		
Sand	5	
Silt	10	10
Clay	85	90
COMPOSITION:		
Access. minerals	1	
Clay	15	5
Diatoms	2	
Foraminifers	Tr	Tr
Inorganic calcite	10	5
Mica	Tr	Tr
Nannofossils	70	90
Quartz	2	
Radiolarians	Tr	Tr
Silicoflagellates		Tr
Sponge spicules	Tr	

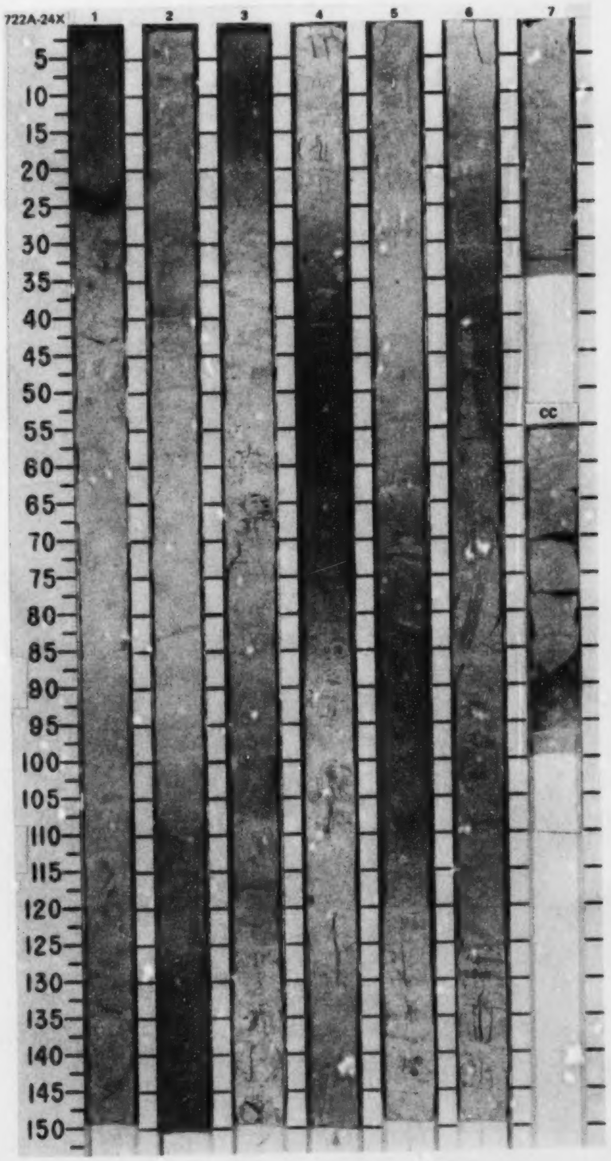
722A-24X
1
2
3
4
5
6
7
CC
5
10
15
20
25
30
35
40
45
50
55
60
65
70
75
80
85
90
95
100
105
110
115
120
125
130
135
140
145
150

SITE 722 HOLE A CORE 25X CORED INTERVAL 2259.5-2269.5 mbsl; 231.7-241.7 mbsf

TIME-ROCK UNIT	BIOSTRAT. ZONE/ FOSSIL CHARACTER					PALEOMAGNETICS	PHYS. PROPERTIES	CHEMISTRY	SECTION	METERS	GRAPHIC LITHOLOGY	DRILLING DISTURB.	SED. STRUCTURES	SAMPLES	LITHOLOGIC DESCRIPTION
	FORAMINIFERS	NANNOFOSSILS	RADIOLARIANS	DIATOMS	BENTHIC FORAMINIFERS										
MIOCENE	N16 - N17 ●R/G	NN11 *Discoaster quinqueramus* ●A/M	*Didymocyrtis penultima* ●C/G				●ϕ=38.6 γ=1.76●		1 CC	0.5 1.0				● ●	Interbedded NANNOFOSSIL CHALK and DIATOM-BEARING NANNOFOSSIL CHALK

Entire core is slightly fractured throughout.

Major lithology: Interbedded NANNOFOSSIL CHALK and DIATOM- BEARING NANNOFOSSIL CHALK. Contacts are gradational. Beds range from white (5Y 8/1) to light olive gray (5Y 6/2) and light gray (5Y 7/1). Bioturbation is minor throughout.

SMEAR SLIDE SUMMARY (%):

	1, 33 D	1, 91 D
TEXTURE:		
Silt	5	15
Clay	95	85
COMPOSITION:		
Access. minerals		Tr
Clay	7	9
Diatoms	Tr	5
Dolomite		Tr
Foraminifers	Tr	
Inorganic calcite	3	5
Nannofossils	90	80
Radiolarians	Tr	1
Silicoflagellates	Tr	Tr
Sponge spicules	Tr	Tr

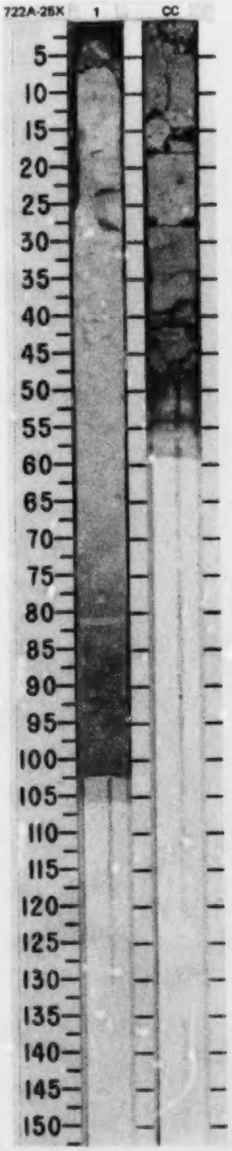

SITE 722 HOLE A CORE 26X CORED INTERVAL 2269.5-2278.8 mbsl; 241.7-251.0 mbsf

TIME-ROCK UNIT	BIOSTRAT. ZONE/ FOSSIL CHARACTER: FORAMINIFERS	NANNOFOSSILS	RADIOLARIANS	DIATOMS	BENTHIC FORAMINIFERS	PALEOMAGNETICS	PHYS. PROPERTIES	CHEMISTRY	SECTION	METERS	GRAPHIC LITHOLOGY	DRILLING DISTURB.	SED. STRUCTURES	SAMPLES	LITHOLOGIC DESCRIPTION
MIOCENE	N16 - N17 ●R/G	N11 *Discoaster quinqueramus* ●A/M	*Didymocyrtis antepenultimus* ●C/G				ϕ=63.1 γ=1.63 ●		1 CC	0.5 1.0	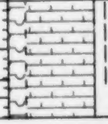	| | |	| ⊥ |	●	FORAMINIFER-BEARING DIATOM-NANNOFOSSIL CHALK

FORAMINIFER-BEARING DIATOM-NANNOFOSSIL CHALK

Entire core is slightly disturbed.

Major lithology: FORAMINIFER-BEARING DIATOM-NANNOFOSSIL CHALK. Beds range from light olive gray (5Y 6/2) to light gray (5Y 7/1). Contacts are gradational. Bioturbation is minor throughout.

SMEAR SLIDE SUMMARY (%):

	1, 60 D
TEXTURE:	
Silt	30
Clay	70
COMPOSITION:	
Clay	15
Diatoms	15
Foraminifers	5
Inorganic calcite	5
Nannofossils	59
Radiolarians	Tr
Silicoflagellates	1
Sponge spicules	Tr

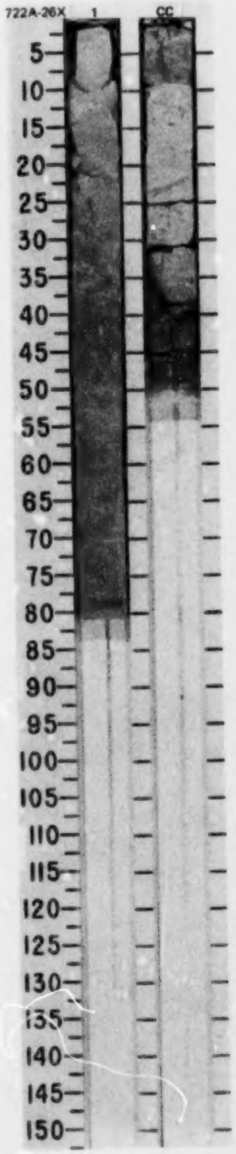

SITE 722 HOLE A CORE 27X CORED INTERVAL 2278.8-2288.5 mbsl; 251.0-260.7 mbsf

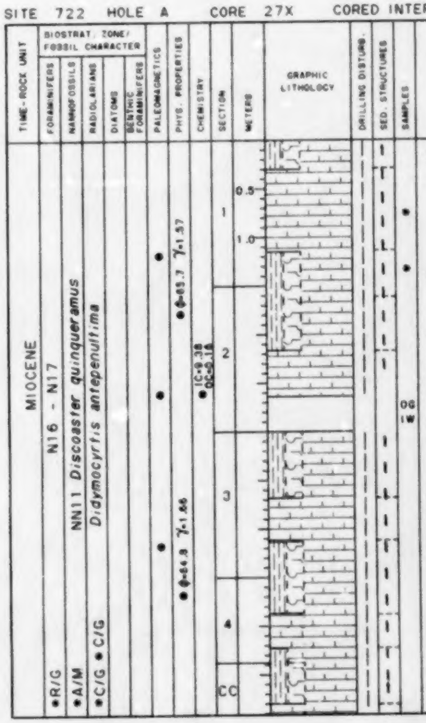
TIME-ROCK UNIT
BIOSTRAT. ZONE/ FOSSIL CHARACTER
FORAMINIFERS
NANNOFOSSILS
RADIOLARIANS
DIATOMS
BENTHIC FORAMINIFERS
PALEOMAGNETICS
PHYS. PROPERTIES
CHEMISTRY
SECTION
METERS
GRAPHIC LITHOLOGY
DRILLING DISTURB.
SED. STRUCTURES
SAMPLES
MIOCENE
N16 - N17
NN11 Discoaster quinqueramus
Didymocyrtis antepenultima
●R/G
●A/M
●C/G ● C/G
●φ=65.7 γ=1.57
●φ=64.8 γ=1.66
●IC=9.38 OC=0.18
1
2
3
4
CC
0.5
1.0
OG
IW

LITHOLOGIC DESCRIPTION

RADIOLARIAN-BEARING DIATOM-NANNOFOSSIL CHALK

Section 1 to Section 4 is slightly disturbed.

Major lithology: RADIOLARIAN-BEARING DIATOM-NANNOFOSSIL CHALK. Beds range from light olive gray (5Y 6/2) to light gray (5Y 7/2), olive (5Y 5/3, 4/3), and pale olive (5Y 6/3). Contacts are gradational. Bioturbation is minor throughout. Siliceous components are more abundant in the pale olive and olive beds.

SMEAR SLIDE SUMMARY (%):

	1, 75 D	1, 143 D
TEXTURE:		
Silt	15	40
Clay	85	60
COMPOSITION:		
Access. minerals	Tr	
Clay	4	10
Diatoms	1	25
Dolomite	Tr	
Foraminifers	7	3
Inorganic calcite	5	5
Nannofossils	80	50
Quartz	Tr	
Radiolarians	3	5
Silicoflagellates	Tr	2
Sponge spicules		Tr

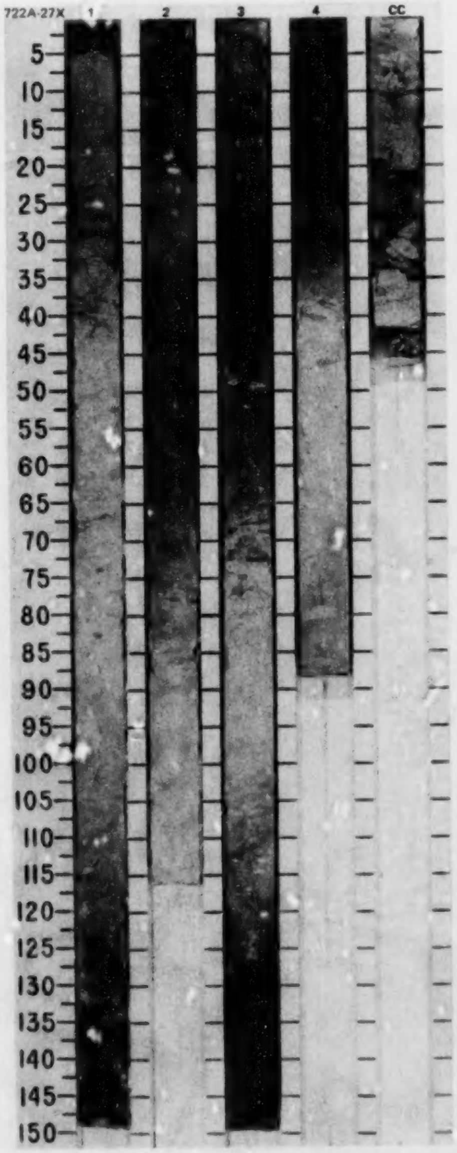
722A-27X
1
2
3
4
CC
5
10
15
20
25
30
35
40
45
50
55
60
65
70
75
80
85
90
95
100
105
110
115
120
125
130
135
140
145
150

SITE 722 HOLE A CORE 28X CORED INTERVAL 2288.5-2298.2 mbsl; 260.7-270.4 mbsf

TIME-ROCK UNIT	BIOSTRAT. ZONE/ FOSSIL CHARACTER					PALEOMAGNETICS	PHYS. PROPERTIES	CHEMISTRY	SECTION	METERS	GRAPHIC LITHOLOGY	DRILLING DISTURB.	SED. STRUCTURES	SAMPLES	LITHOLOGIC DESCRIPTION
	FORAMINIFERS	NANNOFOSSILS	RADIOLARIANS	DIATOMS	BENTHIC FORAMINIFERS										
MIOCENE	N16 - N17 R/M*	NN11 *Discoaster quinqueramus* A/M*	*Didymocyrtis antepenultima* C/G*						CC						DIATOM-NANNOFOSSIL CHALK CC is very disturbed. Major lithology: DIATOM-NANNOFOSSIL CHALK.

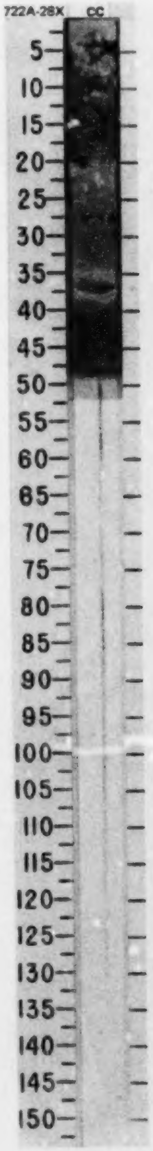
722A-28X
CC
5
10
15
20
25
30
35
40
45
50
55
60
65
70
75
80
85
90
95
100
105
110
115
120
125
130
135
140
145
150

SITE 722 HOLE A CORE 29X CORED INTERVAL 2298.2-2307.8 mbsl; 270.4-280.0 mbsf

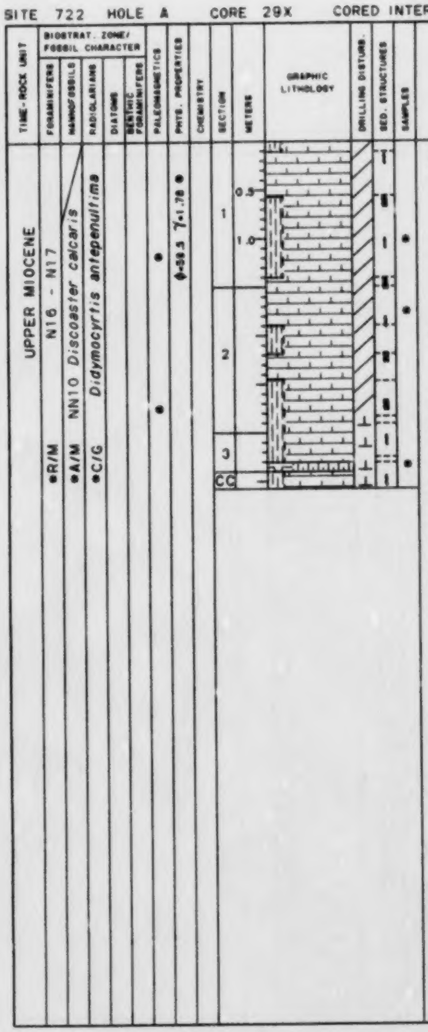
TIME-ROCK UNIT
BIOSTRAT. ZONE/ FOSSIL CHARACTER
FORAMINIFERS
NANNOFOSSILS
RADIOLARIANS
DIATOMS
BENTHIC FORAMINIFERS
PALEOMAGNETICS
PHYS. PROPERTIES
CHEMISTRY
SECTION
METERS
GRAPHIC LITHOLOGY
DRILLING DISTURB.
SED. STRUCTURES
SAMPLES
UPPER MIOCENE
●R/M N16 - N17
●A/M NN10 Discoaster calcaris
●C/G Didymocyrtis antepenultima
ϕ=58.5 γ=1.78 ●
1
2
3
CC
0.5
1.0

LITHOLOGIC DESCRIPTION

Interbedded NANNOFOSSIL CHALK and DIATOM-BEARING NANNOFOSSIL CHALK

Section 1 to Section 2 is slightly fractured. Section 3 and CC are moderately fractured.

Major lithology: INTERBEDDED NANNOFOSSIL CHALK and DIATOM-BEARING NANNOFOSSIL CHALK. Contacts are gradational. Beds range from light olive gray (5Y 6/2) to light greenish gray (10Y 7/1, 7/2), olive gray (5Y 5/2), olive (5Y 5/3, 4/3, 4/4), pale olive (5Y 5/4), and dark greenish gray (10Y 5/2). Bioturbation is minor to moderate throughout.

Minor lithology: Diatomaceous silty claystone, dark olive gray (5Y 3/2). Section 3, 30-40 cm.

SMEAR SLIDE SUMMARY (%):

	1, 101 D	2, 25 D	3, 39 M
TEXTURE:			
Silt	25	5	50
Clay	75	95	50
COMPOSITION:			
Access. minerals	Tr	Tr	Tr
Clay	10	8	33
Diatoms	10	Tr	33
Dolomite	Tr	Tr	Tr
Foraminifers	5	2	Tr
Inorganic calcite	10	Tr	11
Nannofossils	65	90	5
Quartz	Tr	Tr	11
Radiolarians	Tr	Tr	5
Silicoflagellates	Tr		2
Sponge spicules	Tr	Tr	Tr

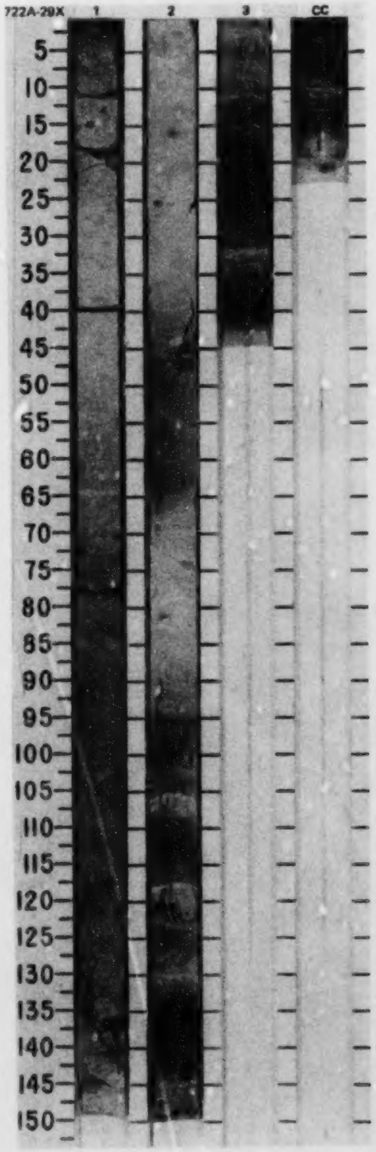
722A-29X
1
2
3
CC
5
10
15
20
25
30
35
40
45
50
55
60
65
70
75
80
85
90
95
100
105
110
115
120
125
130
135
140
145
150

SITE 722 HOLE B CORE 1H CORED INTERVAL 2027.8-2033.3 mbsl; 0.0-5.5 mbsf

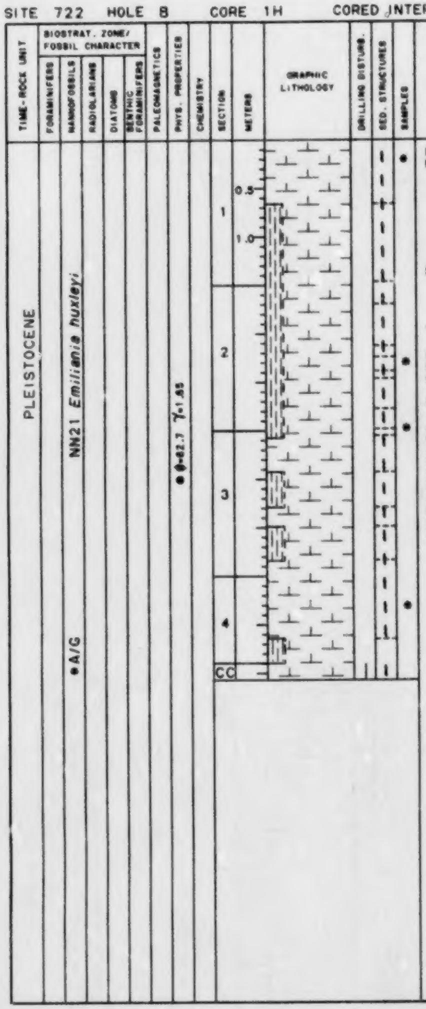
TIME-ROCK UNIT
BIOSTRAT. ZONE/ FOSSIL CHARACTER
FORAMINIFERS
NANNOFOSSILS
RADIOLARIANS
DIATOMS
BENTHIC FORAMINIFERS
PALEOMAGNETICS
PHYS. PROPERTIES
CHEMISTRY
SECTION
METERS
GRAPHIC LITHOLOGY
DRILLING DISTURB.
SED. STRUCTURES
SAMPLES
PLEISTOCENE
NN21 Emiliania huxleyi
● A/G
● φ=62.7 γ=1.85
1
2
3
4
CC
0.5
1.0

LITHOLOGIC DESCRIPTION

Interbedded FORAMINIFER-BEARING NANNOFOSSIL OOZE and FORAMINIFER-NANNOFOSSIL OOZE

CC is slightly disturbed.

Major lithology: Interbedded FORAMINIFER-BEARING NANNOFOSSIL OOZE and FORAMINIFER-NANNOFOSSIL OOZE. Contacts are gradational. Beds range from light olive gray (5Y 6/2) to light greenish gray (10Y 5/2, 6/2), olive (5Y 4/3, 5/3, 5/4), and pale olive (5Y 6/3). Bioturbation is minor throughout.

SMEAR SLIDE SUMMARY (%):

	1, 20 D	2, 78 D	2, 149 M	4, 30 D
TEXTURE:				
Sand	15	5	20	
Silt	20	10	30	20
Clay	65	85	50	80
COMPOSITION:				
Access. minerals	2		3	
Clay	15	10	15	10
Diatoms		10		Tr
Foraminifers	15	5	5	5
Inorganic calcite	5	5	5	10
Mica		Tr	Tr	
Nannofossils	60	65	55	75
Pyrite			15	
Quartz	Tr	5	2	Tr
Radiolarians	3			Tr

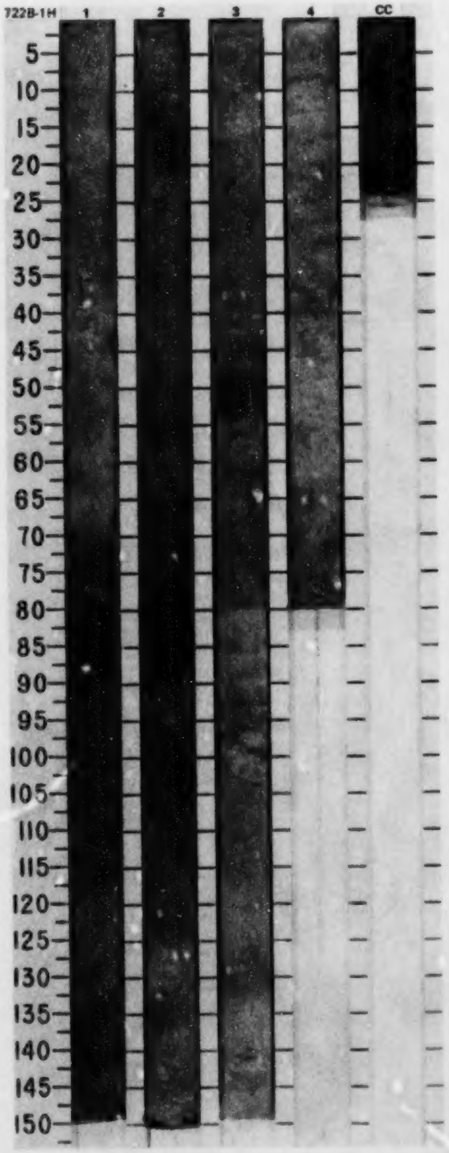
722B-1H
1
2
3
4
CC
5
10
15
20
25
30
35
40
45
50
55
60
65
70
75
80
85
90
95
100
105
110
115
120
125
130
135
140
145
150

SITE 722 HOLE B CORE 2H CORED INTERVAL 2033.3-2042.9 mbsl; 5.5-15.1 mbsf

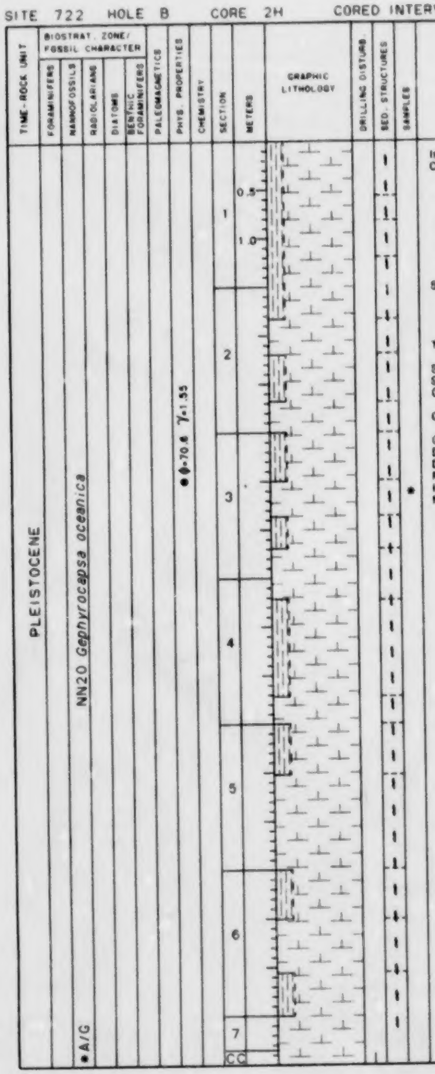
TIME-ROCK UNIT
BIOSTRAT. ZONE/ FOSSIL CHARACTER
FORAMINIFERS
NANNOFOSSILS
RADIOLARIANS
DIATOMS
BENTHIC FORAMINIFERS
PALEOMAGNETICS
PHYS. PROPERTIES
CHEMISTRY
SECTION
METERS
GRAPHIC LITHOLOGY
DRILLING DISTURB.
SED. STRUCTURES
SAMPLES
PLEISTOCENE
NN20 Gephyrocapsa oceanica
● A/G
● ϕ-70.6 γ-1.55
0.5
1.0
1
2
3
4
5
6
7
CC
*

LITHOLOGIC DESCRIPTION

Interbedded NANNOFOSSIL OOZE and FORAMINIFER-BEARING NANNOFOSSIL OOZE

CC is slightly disturbed.

Major lithology: Interbedded NANNOFOSSIL OOZE and FORAMINIFER-BEARING NANNOFOSSIL OOZE. Contacts are gradational. Beds range from gray (5Y 6/1) to light olive gray (5Y 6/2), light gray (5Y 7/1), olive gray (5Y 5/2), olive (5Y 5/4, 5/3), and pale olive (5Y 6/3). Bioturbation is minor throughout, with some pyrite(?)-lined burrows.

SMEAR SLIDE SUMMARY (%):

	3, 60 D
TEXTURE:	
Sand	5
Silt	10
Clay	80
COMPOSITION:	
Clay	10
Diatoms	Tr
Dolomite	Tr
Foraminifers	5
Inorganic calcite	5
Nannofossils	80

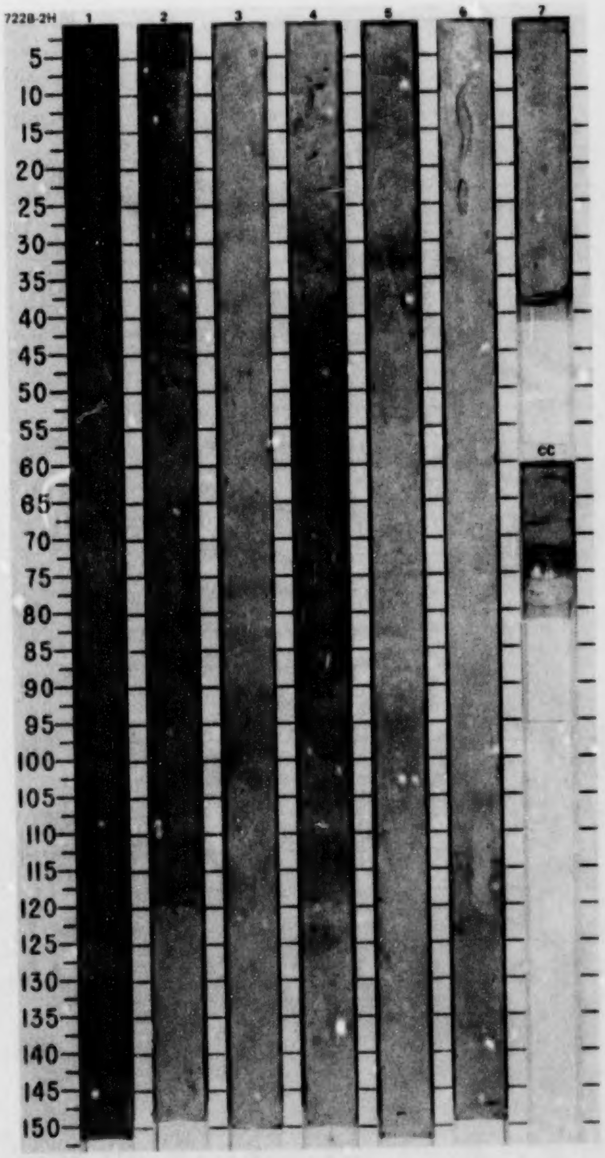
722B-2H
1
2
3
4
5
6
7
CC
5
10
15
20
25
30
35
40
45
50
55
60
65
70
75
80
85
90
95
100
105
110
115
120
125
130
135
140
145
150

SITE 722 HOLE B CORE 3H CORED INTERVAL 2042.9-2052.5 mbsl; 15.1-24.7 mbsf

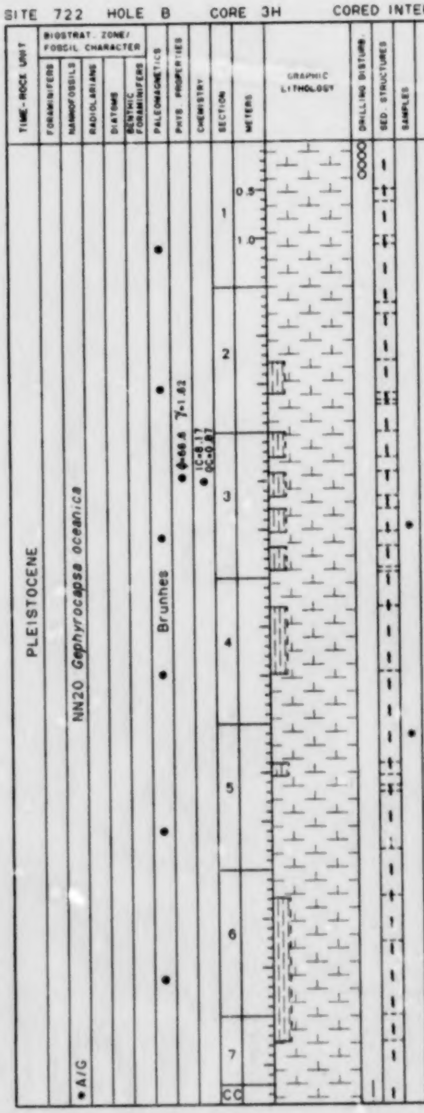

LITHOLOGIC DESCRIPTION

Interbedded NANNOFOSSIL OOZE and FORAMINIFER-BEARING NANNOFOSSIL OOZE

Section 1, 0-40 cm, is soupy. CC is moderately disturbed.

Major lithology: Interbedded NANNOFOSSIL OOZE and FORAMINIFER-BEARING NANNOFOSSIL OOZE. Contacts are gradational. Beds range from light olive gray (5Y 6/2) to light gray (5Y 7/1, 7/2), olive gray (5Y 5/2), olive (5Y 5/3, 5/4, 4/3), pale olive (5Y 6/3), and dark greenish gray (10Y 5/2). Bioturbation is minor throughout.

SMEAR SLIDE SUMMARY (%):

	3, 96 D	5, 11 D
TEXTURE:		
Silt	20	15
Clay	80	85
COMPOSITION:		
Access. minerals	Tr	Tr
Clay	7	5
Dolomite	Tr	Tr
Foraminifers	8	10
Volcanic glass	Tr	
Inorganic calcite	5	5
Nannofossils	80	80
Quartz	Tr	Tr

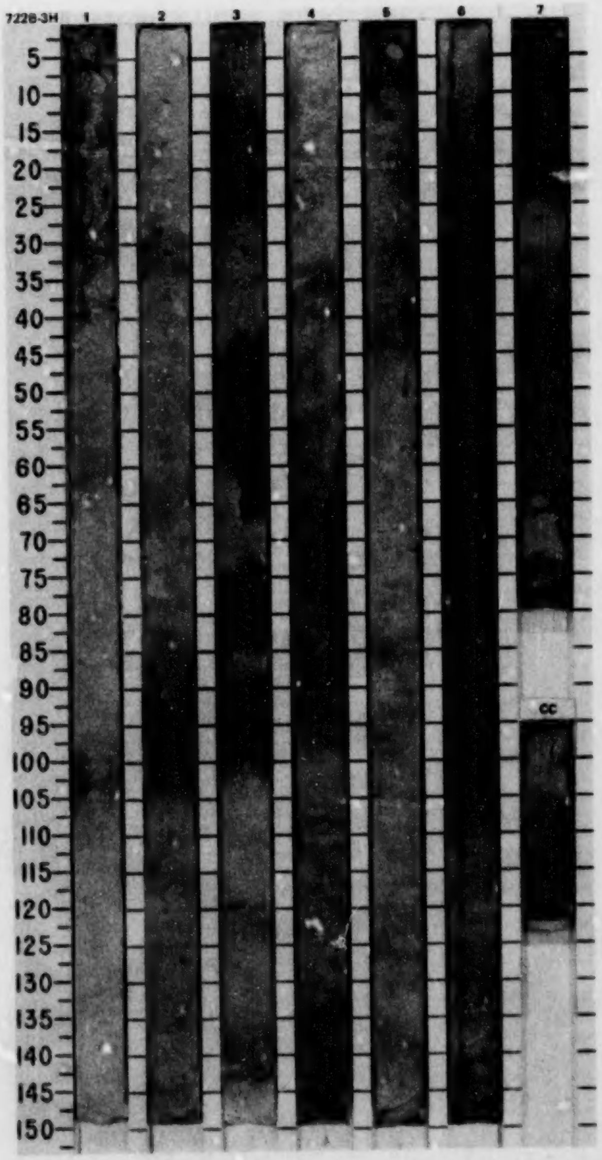
722B-3H
1
2
3
4
5
6
7
CC
5
10
15
20
25
30
35
40
45
50
55
60
65
70
75
80
85
90
95
100
105
110
115
120
125
130
135
140
145
150

SITE 722 HOLE B CORE 4H CORED INTERVAL 2052.5-2062.1 mbsl; 24.7-34.3 mbsf

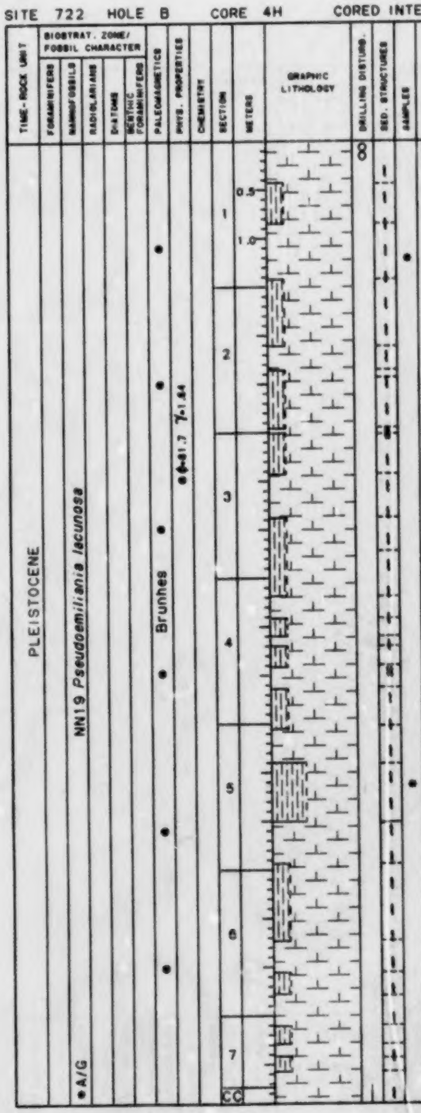
TIME-ROCK UNIT
BIOSTRAT. ZONE/ FOSSIL CHARACTER
FORAMINIFERS
NANNOFOSSILS
RADIOLARIANS
DIATOMS
BENTHIC FORAMINIFERS
PALEOMAGNETICS
PHYS. PROPERTIES
CHEMISTRY
SECTION
METERS
GRAPHIC LITHOLOGY
DRILLING DISTURB.
SED. STRUCTURES
SAMPLES
PLEISTOCENE
NN19 Pseudoemiliania lacunosa
●A/G
Brunhes
●ϕ=61.7 γ=1.84
0.5
1.0
1
2
3
4
5
6
7
CC

LITHOLOGIC DESCRIPTION

Interbedded FORAMINIFER-BEARING NANNOFOSSIL OOZE and FORAMINIFER-BEARING MARLY NANNOFOSSIL OOZE

Section 1, 0-20 cm, is soupy. CC is slightly disturbed.

Major lithology: Interbedded FORAMINIFER-BEARING NANNOFOSSIL OOZE and FORAMINIFER-BEARING MARLY NANNOFOSSIL OOZE. Contacts are gradational except for sharp contact at Section 5, 100 cm. Beds range from gray (5Y 6/1) to light olive gray (5Y 6/2), light gray (5Y 7/1, 7/2), light greenish gray (10Y 6/2), olive gray (5Y 5/2), olive (5Y 5/4, 5/3, 4/4, 4/3), and pale olive (5Y 6/3). Bioturbation is minor to moderate throughout.

SMEAR SLIDE SUMMARY (%):

	1, 121 D	5, 62 D
TEXTURE:		
Sand	10	10
Silt	15	10
Clay		
COMPOSITION:		
Access. minerals	Tr	1
Clay	10	25
Dolomite	Tr	
Foraminifers	12	7
Volcanic glass	Tr	Tr
Inorganic calcite	10	9
Mica	1	Tr
Nannofossils	65	55
Quartz	2	3

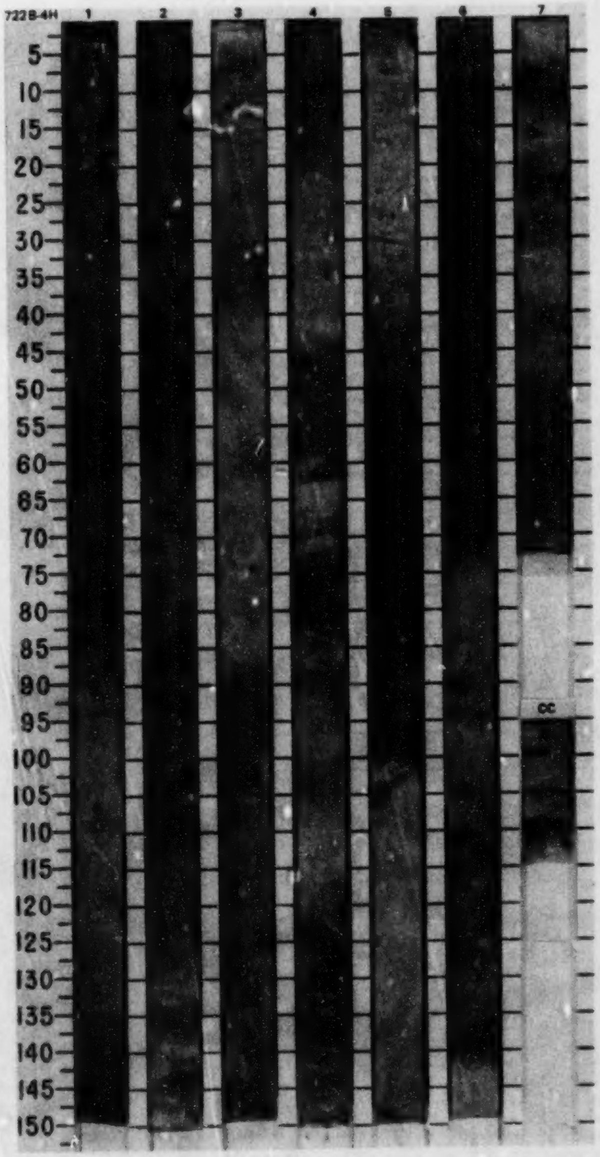
722B-4H
1
2
3
4
5
6
7
CC
5
10
15
20
25
30
35
40
45
50
55
60
65
70
75
80
85
90
95
100
105
110
115
120
125
130
135
140
145
150

SITE 722 HOLE B CORE 5H CORED INTERVAL 2062.1-2071.7 mbsl; 34.3-43.9 mbsf

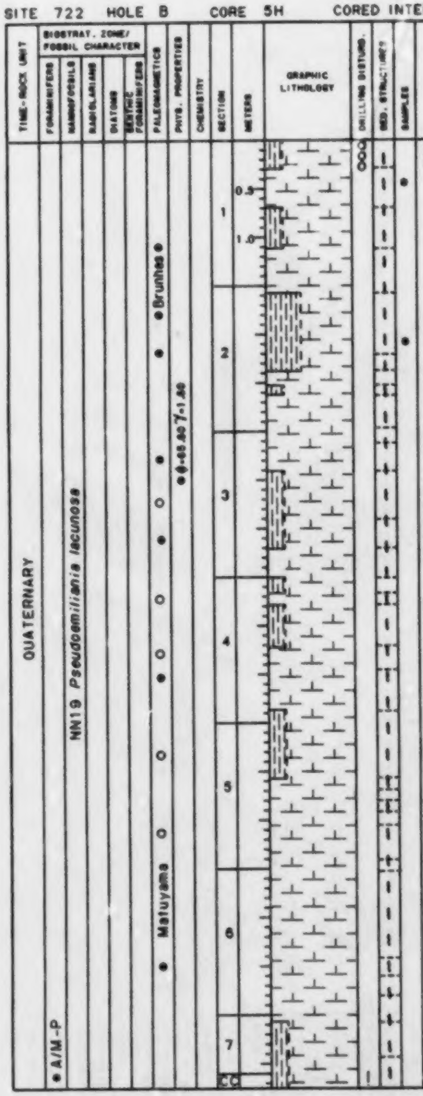
TIME-ROCK UNIT
BIOSTRAT. ZONE/ FOSSIL CHARACTER
FORAMINIFERS
NANNOFOSSILS
RADIOLARIANS
DIATOMS
BENTHIC FORAMINIFERS
PALEOMAGNETICS
PHYS. PROPERTIES
CHEMISTRY
SECTION
METERS
GRAPHIC LITHOLOGY
DRILLING DISTURB.
SED. STRUCTURES
SAMPLES
QUATERNARY
● A/M-P
NN19 Pseudoemiliania lacunosa
● Brunhes ●
Matuyama
●ϕ-65.80 γ-1.80
1
2
3
4
5
6
7
CC
0.5
1.0

LITHOLOGIC DESCRIPTION

Interbedded NANNOFOSSIL OOZE and FORAMINIFER-BEARING NANNOFOSSIL OOZE

Section 1, 0-30 cm, is soupy. CC is moderately disturbed.

Major lithology: Interbedded NANNOFOSSIL OOZE and FORAMINIFER-BEARING NANNOFOSSIL OOZE. Contacts are gradational. Beds range from light olive gray (5Y 6/2) to light gray (5Y 7/1, 7/2), light greenish gray (10Y 6/2), olive gray (5Y 5/2), olive (5Y 5/3, 5/4), and pale olive (5Y 6/4). Bioturbation is minor throughout.

SMEAR SLIDE SUMMARY (%):

	1, 43 D	2, 59 D
TEXTURE:		
Sand		10
Silt	10	10
Clay	90	80
COMPOSITION:		
Access. minerals	Tr	2
Clay	3	20
Diatoms		1
Foraminifers	1	6
Volcanic glass	Tr	Tr
Inorganic calcite	10	6
Mica		Tr
Nannofossils	85	60
Quartz	1	1
Radiolarians		Tr
Silicoflagellates		2

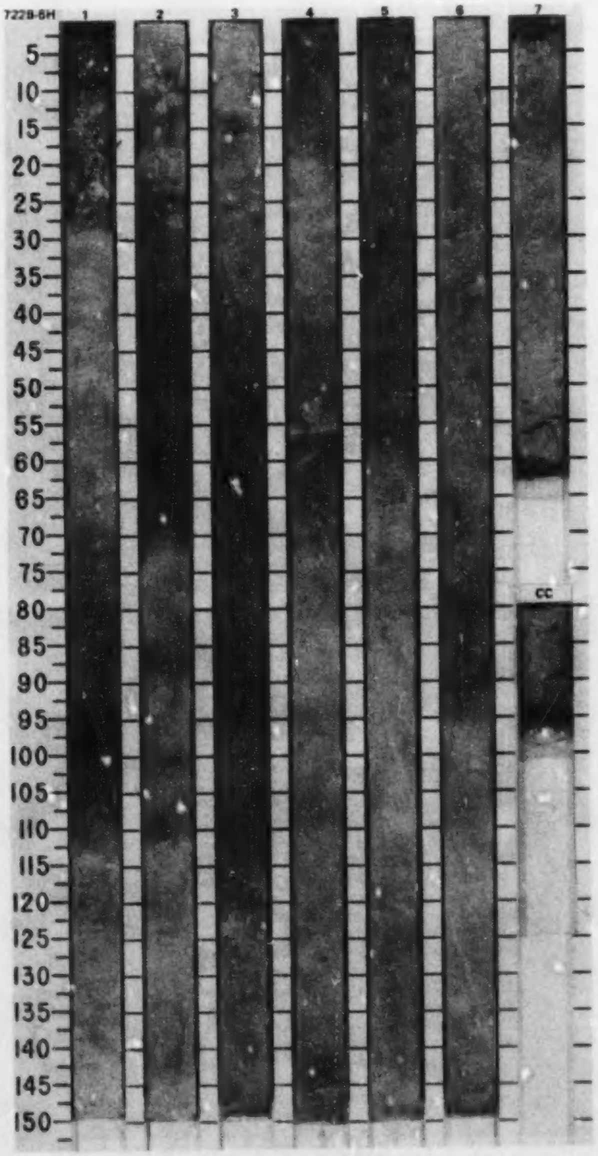
722B-5H
1
2
3
4
5
6
7
CC
5
10
15
20
25
30
35
40
45
50
55
60
65
70
75
80
85
90
95
100
105
110
115
120
125
130
135
140
145
150

SITE 722 HOLE B CORE 6H CORED INTERVAL 2071.7-2081.0 mbsl; 43.9-53.2 mbsf

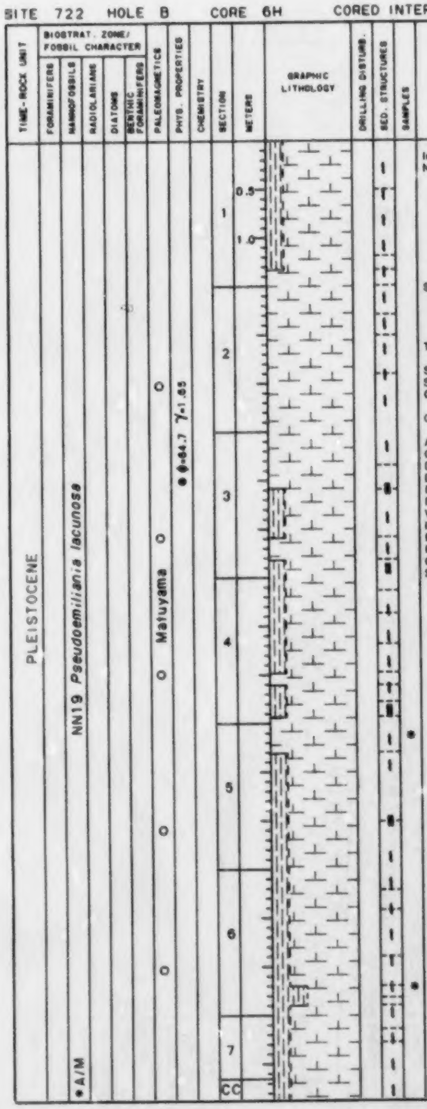
TIME-ROCK UNIT
BIOSTRAT. ZONE/ FOSSIL CHARACTER
FORAMINIFERS
NANNOFOSSILS
RADIOLARIANS
DIATOMS
BENTHIC FORAMINIFERS
PALEOMAGNETICS
PHYS. PROPERTIES
CHEMISTRY
SECTION
METERS
GRAPHIC LITHOLOGY
DRILLING DISTURB.
SED. STRUCTURES
SAMPLES
PLEISTOCENE
NN19 Pseudoemiliania lacunosa
• A/M
Matuyama
● ϕ=64.7 γ=1.65
0.5
1.0
1
2
3
4
5
6
7
CC

LITHOLOGIC DESCRIPTION

Interbedded NANNOFOSSIL OOZE and FORAMINIFER-BEARING MARLY NANNOFOSSIL OOZE

Entire core is undisturbed.

Major lithology: Interbedded NANNOFOSSIL OOZE and FORAMINIFER-BEARING MARLY NANNOFOSSIL OOZE. Contacts are gradational. Beds range from light olive gray (5Y 6/2) to light gray (5Y 7/2), light greenish gray (10Y 6/2), olive gray (5Y 5/2), olive (5Y 5/3, 4/3), pale olive (5Y 6/3), and dark olive gray (5Y 3/2). Bioturbation is minor to moderate throughout.

SMEAR SLIDE SUMMARY (%):

	5, 11 D	6, 129 D
TEXTURE:		
Sand	2	10
Silt	18	15
Clay	80	75
COMPOSITION:		
Access. minerals		2
Clay	5	25
Diatoms		Tr
Dolomite	Tr	
Feldspar		2
Foraminifers	2	12
Volcanic glass	Tr	Tr
Inorganic calcite	18	9
Mica	Tr	Tr
Nannofossils	75	45
Quartz	Tr	5
Silicoflagellates		Tr

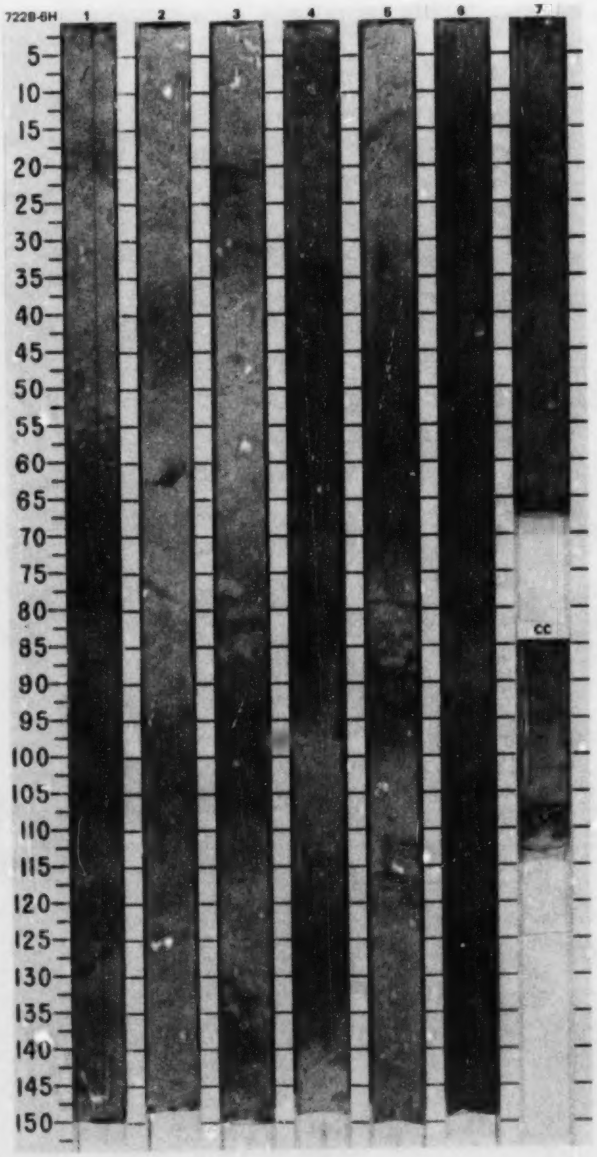
722B-6H
1
2
3
4
5
6
7
CC
5
10
15
20
25
30
35
40
45
50
55
60
65
70
75
80
85
90
95
100
105
110
115
120
125
130
135
140
145
150

SITE 722 HOLE B CORE 7H CORED INTERVAL 2081.0-2090.7 mbsl; 53.2-62.9 mbsf

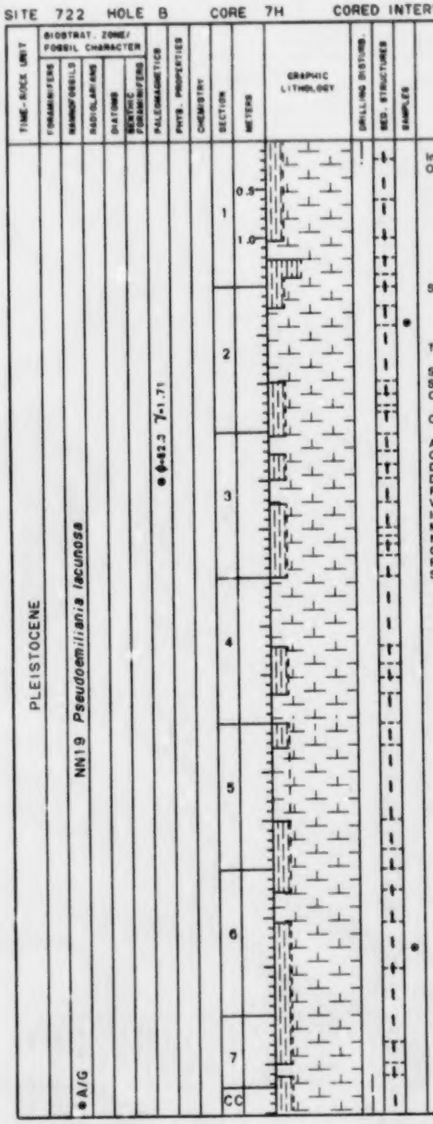
TIME-ROCK UNIT
BIOSTRAT. ZONE/ FOSSIL CHARACTER
FORAMINIFERS
NANNOFOSSILS
RADIOLARIANS
DIATOMS
BENTHIC FORAMINIFERS
PALEOMAGNETICS
PHYS. PROPERTIES
CHEMISTRY
SECTION
METERS
GRAPHIC LITHOLOGY
DRILLING DISTURB.
SED. STRUCTURES
SAMPLES
PLEISTOCENE
NN19 Pseudoemiliania lacunosa
● A/G
● φ-82.3 γ-1.71
1
2
3
4
5
6
7
CC
0.5
1.0

LITHOLOGIC DESCRIPTION

Interbedded NANNOFOSSIL OOZE and FORAMINIFER-BEARING NANNOFOSSIL OOZE

Section 1, 0-10 cm, is moderately disturbed. CC is slightly disturbed.

Major lithology: INTERBEDDED NANNOFOSSIL OOZE and FORAMINIFER-BEARING NANNOFOSSIL OOZE. Contacts are gradational. Beds range from light olive gray (5Y 7/1) to olive gray (5Y 5/2, 4/2), olive (5Y 4/3, 5/3), dark greenish gray (10Y 5/2), and dark olive gray (5Y 3/2) Bioturbation is minor throughout.

SMEAR SLIDE SUMMARY (%):

	2, 39 D	6, 81 D
TEXTURE:		
Sand	3	15
Silt	7	10
Clay	90	75
COMPOSITION:		
Access. minerals		1
Clay	10	20
Diatoms		Tr
Dolomite		Tr
Foraminifers	5	15
Volcanic glass	Tr	Tr
Inorganic calcite	5	7
Mica	Tr	
Nannofossils	80	55
Quartz		2
Radiolarians	Tr	Tr
Sponge spicules		Tr

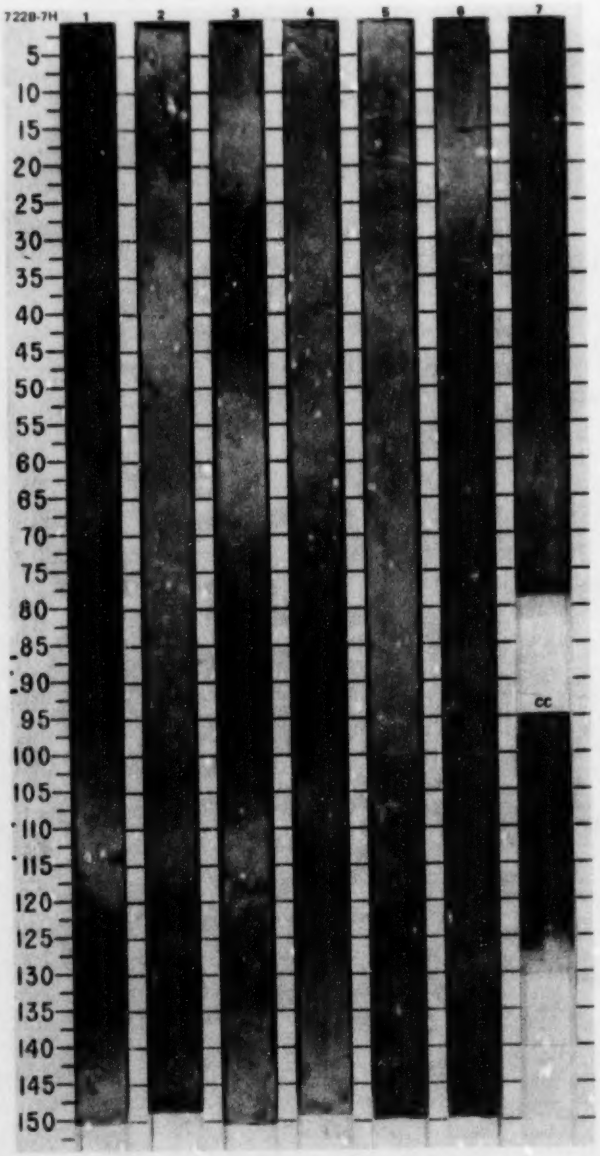
722B-7H
1
2
3
4
5
6
7
CC
5
10
15
20
25
30
35
40
45
50
55
60
65
70
75
80
85
90
95
100
105
110
115
120
125
130
135
140
145
150

SITE 722 HOLE B CORE 8H CORED INTERVAL 2090.7-2100.3 mbsl; 62.9-72.5 mbsf

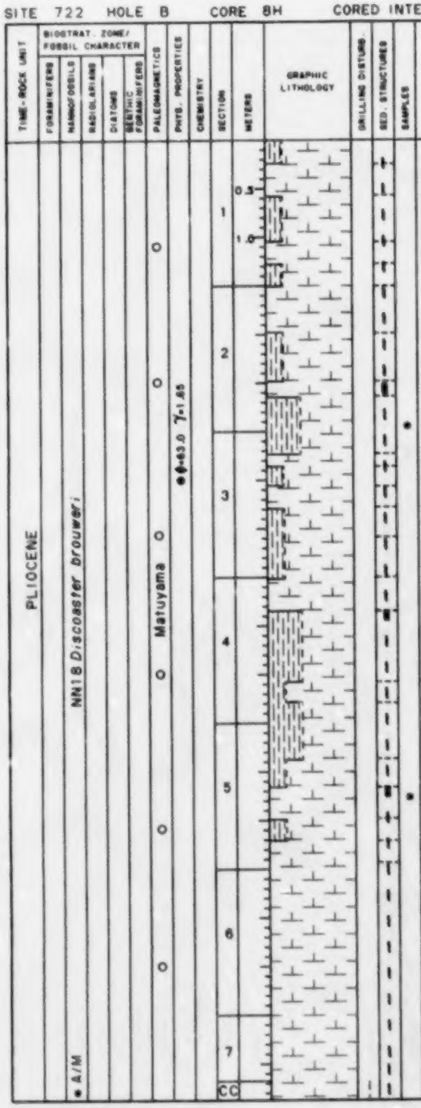
TIME-ROCK UNIT
BIOSTRAT. ZONE/ FOSSIL CHARACTER
FORAMINIFERS
NANNOFOSSILS
RADIOLARIANS
DIATOMS
BENTHIC FORAMINIFERS
PALEOMAGNETICS
PHYS. PROPERTIES
CHEMISTRY
SECTION
METERS
GRAPHIC LITHOLOGY
DRILLING DISTURB.
SED. STRUCTURES
SAMPLES
PLIOCENE
NN18 Discoaster brouweri
● A/M
Matuyama
●ϕ=63.0 γ=1.65
0.5
1.0
1
2
3
4
5
6
7
CC

LITHOLOGIC DESCRIPTION

Interbedded NANNOFOSSIL OOZE and FORAMINIFER-BEARING MARLY NANNOFOSSIL OOZE CC is slightly disturbed.

Major lithology: Interbedded NANNOFOSSIL OOZE and FORAMINIFER-BEARING MARLY NANNOFOSSIL OOZE. Contacts are gradational. Beds range from light olive gray (5Y 6/2) to light gray (5Y 7/2, 7/1), light greenish gray (10Y 6/2), olive gray (5Y 5/2, 4/2), olive (5Y 4/3, 5/3, 5/4), pale olive (5Y 6/3), and dark greenish gray (10Y 5/2). Bioturbation is minor to moderate throughout.

SMEAR SLIDE SUMMARY (%):

	2, 145 D	5, 77 D
TEXTURE:		
Sand	7	1
Silt	10	4
Clay	83	95
COMPOSITION:		
Accress. minerals	2	Tr
Clay	23	10
Diatoms	Tr	
Dolomite	Tr	Tr
Feldspar	1	
Foraminifers	6	1
Volcanic glass	Tr	
Inorganic calcite	5	4
Mica	Tr	
Nannofossils	60	85
Quartz	3	Tr
Radiolarians	Tr	
Sponge spicules		Tr

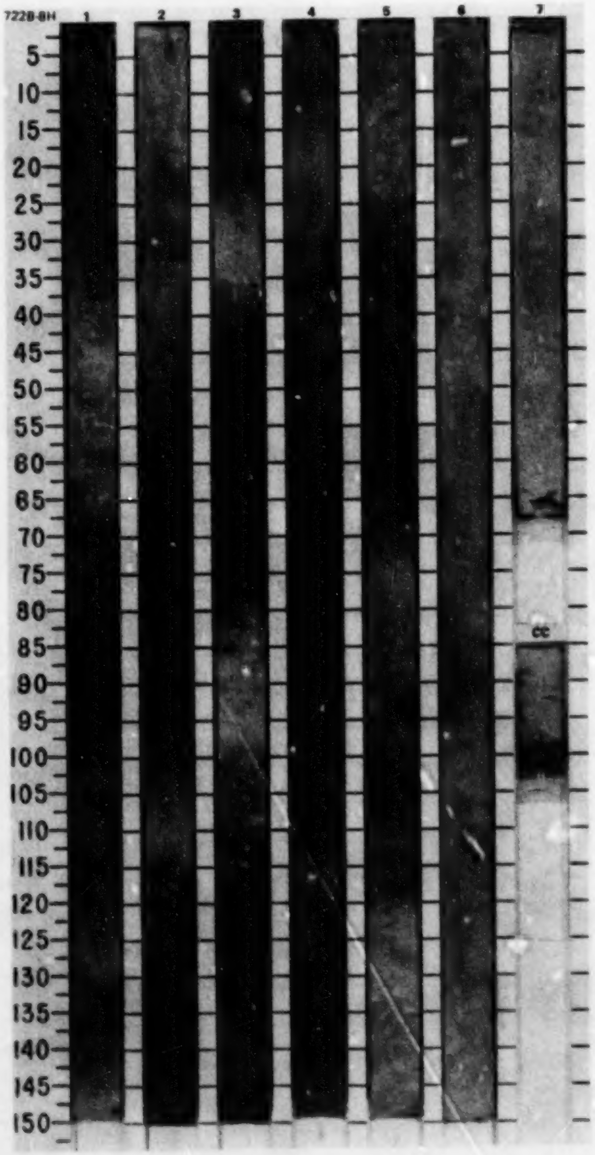
722B-8H
1
2
3
4
5
6
7
CC
5
10
15
20
25
30
35
40
45
50
55
60
65
70
75
80
85
90
95
100
105
110
115
120
125
130
135
140
145
150

SITE 722 HOLE B CORE 9H CORED INTERVAL 2100.3-2110.0 mbsl; 72.5-82.2 mbsf

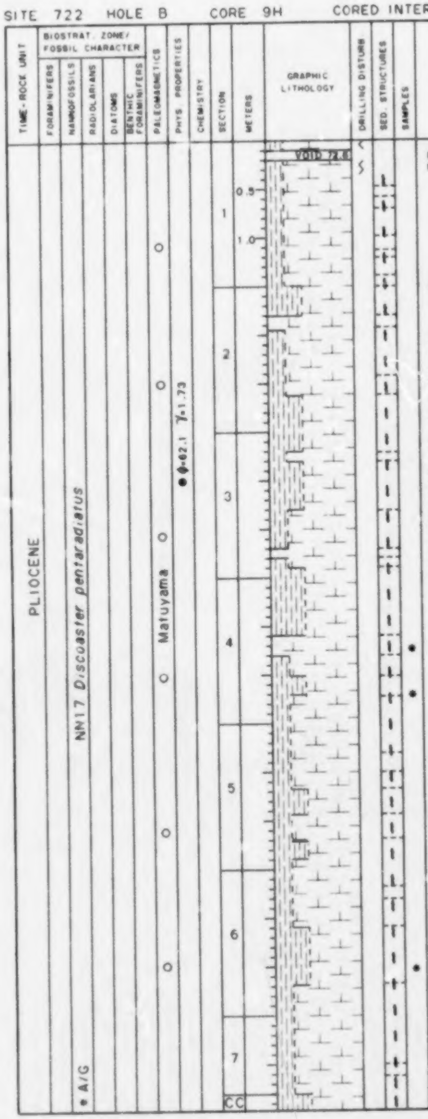
TIME-ROCK UNIT
BIOSTRAT. ZONE/ FOSSIL CHARACTER
FORAMINIFERS
NANNOFOSSILS
RADIOLARIANS
DIATOMS
BENTHIC FORAMINIFERS
PALEOMAGNETICS
PHYS. PROPERTIES
CHEMISTRY
SECTION
METERS
GRAPHIC LITHOLOGY
DRILLING DISTURB.
SED. STRUCTURES
SAMPLES
PLIOCENE
NN17 Discoaster pentaradiatus
● A/G
Matuyama
●Φ=62.1 γ=1.73
0.5
1.0
1
2
3
4
5
6
7
CC
VOID 72.6

LITHOLOGIC DESCRIPTION

Interbedded MARLY NANNOFOSSIL OOZE and FORAMINIFER-BEARING MARLY NANNOFOSSIL OOZE

Section 1, 0-30 cm, is disturbed.

Major lithology: Interbedded MARLY NANNOFOSSIL OOZE and FORAMINIFER-BEARING MARLY NANNOFOSSIL OOZE. Contacts are gradational. Beds range from light gray (5Y 7/1, 7/2) to light greenish gray (10Y 6/2), olive (5Y 5/4, 4/3), and pale olive (5Y 6/3, 6/4). Bioturbation is minor throughout.

SMEAR SLIDE SUMMARY (%):

	4, 73 D	4, 121 D	6, 102 D
TEXTURE:			
Sand	5	10	5
Silt	15	15	10
Clay	80	75	85
COMPOSITION:			
Access. minerals	Tr	1	2
Clay	9	20	35
Diatoms	Tr		Tr
Feldspar			Tr
Foraminifers	5	7	2
Volcanic glass	Tr		1
Inorganic calcite	15	14	5
Mica	Tr		
Nannofossils	70	55	50
Quartz	Tr	3	5
Radiolarians	1	Tr	Tr
Sponge spicules	Tr	Tr	

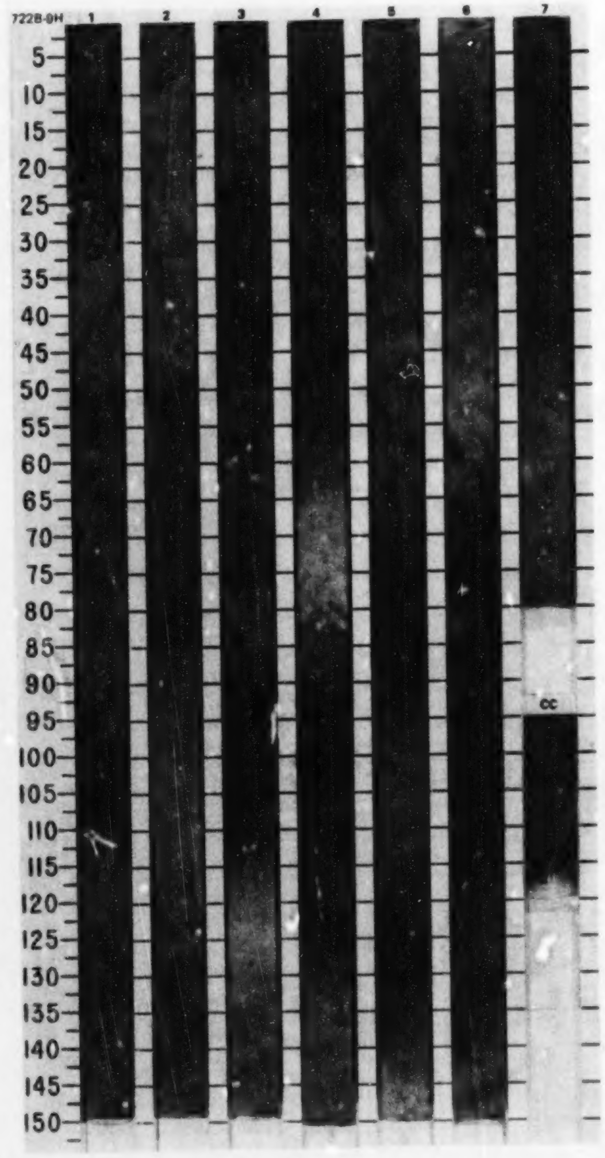
722B-9H
1
2
3
4
5
6
7
CC
5
10
15
20
25
30
35
40
45
50
55
60
65
70
75
80
85
90
95
100
105
110
115
120
125
130
135
140
145
150

SITE 722 HOLE B CORE 10H CORED INTERVAL 2110.0-2119.7 mbsl; 82.2-91.9 mbsf

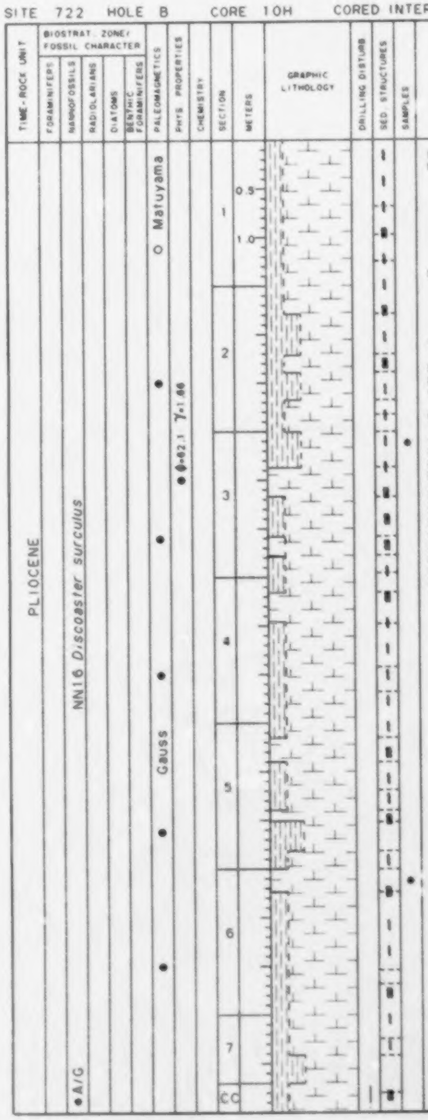
TIME-ROCK UNIT
BIOSTRAT. ZONE/ FOSSIL CHARACTER
FORAMINIFERS
NANNOFOSSILS
RADIOLARIANS
DIATOMS
BENTHIC FORAMINIFERS
PALEOMAGNETICS
PHYS. PROPERTIES
CHEMISTRY
SECTION
METERS
GRAPHIC LITHOLOGY
DRILLING DISTURB.
SED. STRUCTURES
SAMPLES
PLIOCENE
NN16 Discoaster surculus
A/G
Matuyama
Gauss
φ=62.1 γ=1.86
0.5
1.0
1
2
3
4
5
6
7
CC

LITHOLOGIC DESCRIPTION

Interbedded FORAMINIFER-BEARING NANNOFOSSIL OOZE and MARLY NANNOFOSSIL OOZE

CC is moderately disturbed.

Major lithology: Interbedded FORAMINIFER-BEARING NANNOFOSSIL OOZE and MARLY NANNOFOSSIL OOZE. Contacts are gradational. Beds range from light olive gray (5Y 6/2) to olive (5Y 5/3, 4/4, 4/3, 5/4), pale olive (5Y 6/3), and dark olive gray (5Y 6/3). Bioturbation is minor to moderate throughout.

SMEAR SLIDE SUMMARY (%):

	3, 12 D	6, 12 D
TEXTURE:		
Sand	10	5
Silt	20	15
Clay	70	80
COMPOSITION:		
Access. minerals	3	Tr
Clay	30	5
Diatoms		Tr
Dolomite	Tr	
Feldspar	3	
Foraminifers	Tr	5
Volcanic glass	1	Tr
Inorganic calcite	10	14
Mica	1	
Nannofossils	40	75
Quartz	12	1
Radiolarians	Tr	Tr
Sponge spicules		Tr

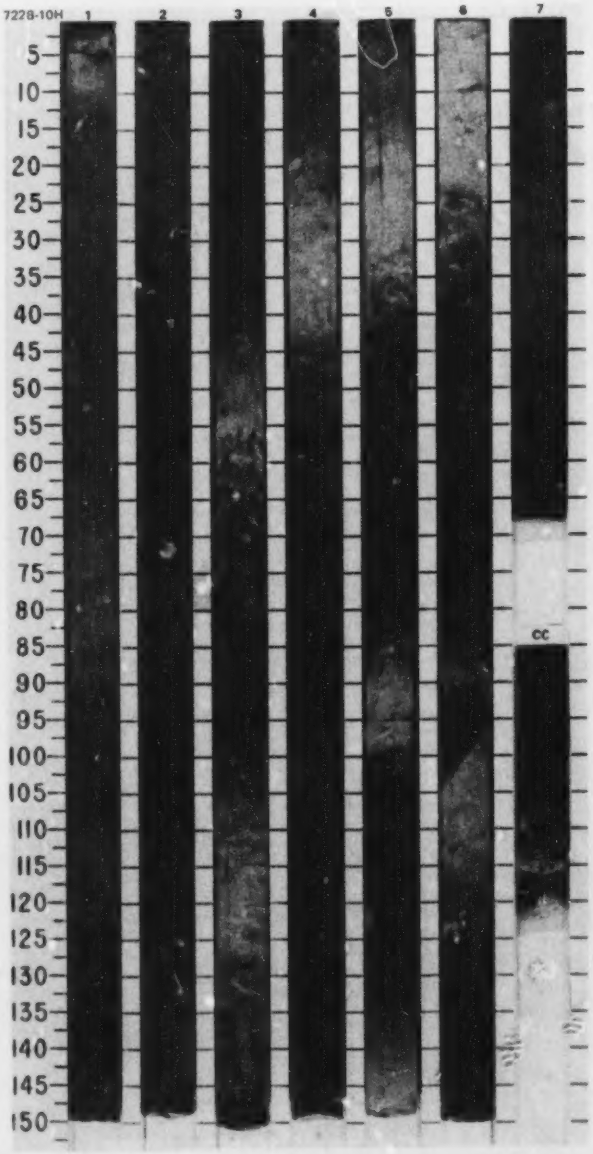
722B-10H
1
2
3
4
5
6
7
CC
5
10
15
20
25
30
35
40
45
50
55
60
65
70
75
80
85
90
95
100
105
110
115
120
125
130
135
140
145
150

SITE 722 HOLE B CORE 11X CORED INTERVAL 2119.7-2129.3 mbsl; 91.9-101.5 mbsf

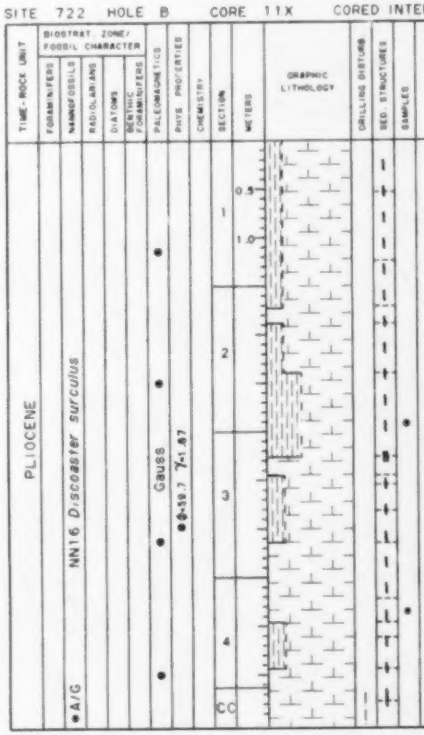
TIME-ROCK UNIT
BIOSTRAT. ZONE/ FOSSIL CHARACTER
FORAMINIFERS
NANNOFOSSILS
RADIOLARIANS
DIATOMS
BENTHIC FORAMINIFERS
PALEOMAGNETICS
PHYS. PROPERTIES
CHEMISTRY
SECTION
METERS
GRAPHIC LITHOLOGY
DRILLING DISTURB.
SED. STRUCTURES
SAMPLES
PLIOCENE
NN16 Discoaster surculus
●A/G
Gauss
●φ=59.7 γ=1.87
1
2
3
4
CC
0.5
1.0

LITHOLOGIC DESCRIPTION

Interbedded NANNOFOSSIL OOZE and MARLY NANNOFOSSIL OOZE

CC is moderately disturbed.

Major lithology: Interbedded NANNOFOSSIL OOZE and MARLY NANNOFOSSIL OOZE. Contacts are gradational. Beds range from light olive gray (5Y 6/2) to light gray (5Y 7/1), olive (5Y 5/4, 4/4, 4/3), and pale olive (5Y 6/3). Bioturbation is minor to moderate throughout.

SMEAR SLIDE SUMMARY (%):

	2, 146 D	4, 36 D
TEXTURE:		
Sand	15	5
Silt	10	10
Clay	75	85
COMPOSITION:		
Access. minerals	2	Tr
Clay	30	10
Diatoms		Tr
Feldspar	2	
Foraminifers	2	10
Inorganic calcite	8	10
Mica	1	
Nannofossils	45	70
Quartz	10	Tr
Radiolarians		Tr

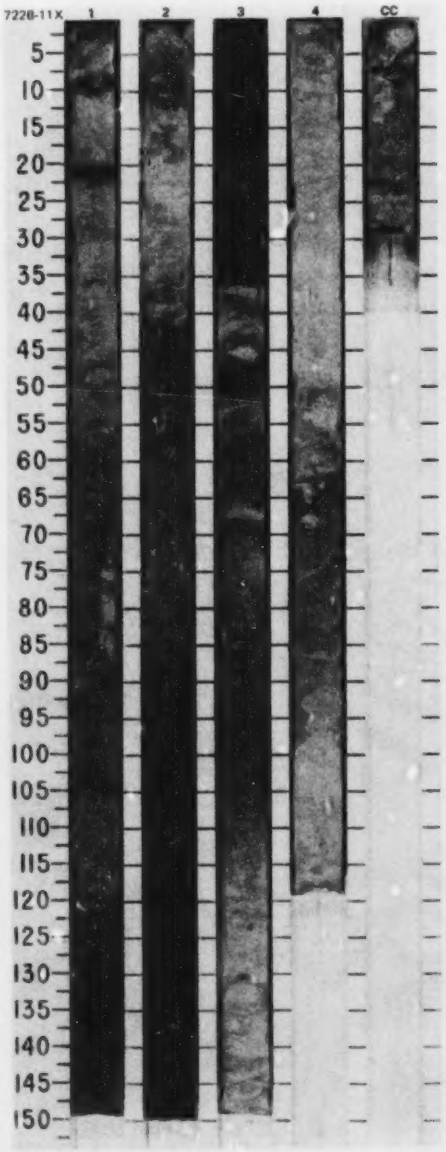
722B-11X
1
2
3
4
CC
5
10
15
20
25
30
35
40
45
50
55
60
65
70
75
80
85
90
95
100
105
110
115
120
125
130
135
140
145
150

SITE 722 HOLE B CORE 12X CORED INTERVAL 2129.3-2139.0 mbsl; 101.5-111.2 mbsf

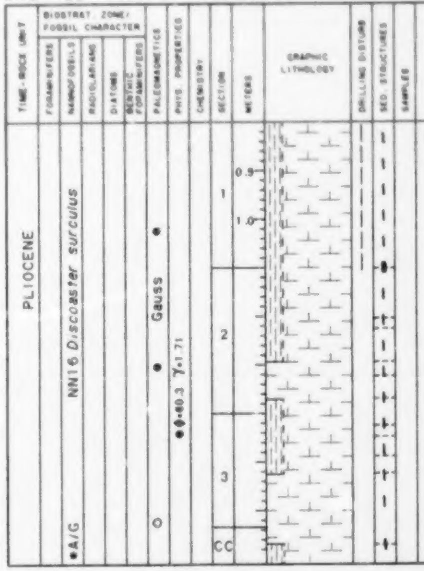
TIME-ROCK UNIT
BIOSTRAT. ZONE/ FOSSIL CHARACTER
FORAMINIFERS
NANNOFOSSILS
RADIOLARIANS
DIATOMS
BENTHIC FORAMINIFERS
PALEOMAGNETICS
PHYS. PROPERTIES
CHEMISTRY
SECTION
METERS
GRAPHIC LITHOLOGY
DRILLING DISTURB.
SED. STRUCTURES
SAMPLES
PLIOCENE
NN16 Discoaster surculus
●A/G
Gauss
●ϕ=60.3 γ=1.71
1
2
3
CC
0.5
1.0

LITHOLOGIC DESCRIPTION

NANNOFOSSIL OOZE

Section 1 is slightly disturbed; initial stages of biscuit formation due to drilling.

Major lithology: NANNOFOSSIL OOZE. Beds range from white (5Y 8/1) to light olive gray (5Y 6/2), light gray (5Y 7/1, 7/2), olive (5Y 5/3, 5/4), and pale olive (5Y 6/3). Bioturbation is minor to moderate throughout.

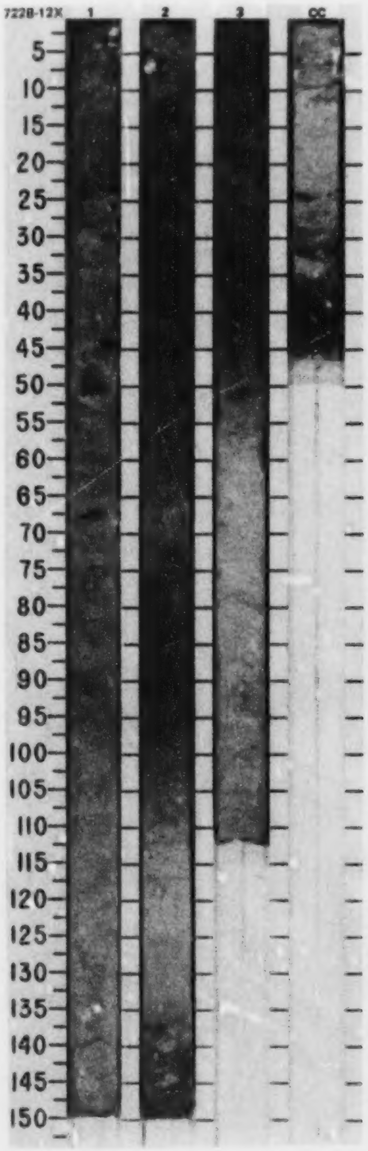
722B-12X
1
2
3
CC
5
10
15
20
25
30
35
40
45
50
55
60
65
70
75
80
85
90
95
100
105
110
115
120
125
130
135
140
145
150

SITE 722 HOLE B CORE 13X CORED INTERVAL 2148.7-2158.3 mbsl; 120.9-130.5 mbsf

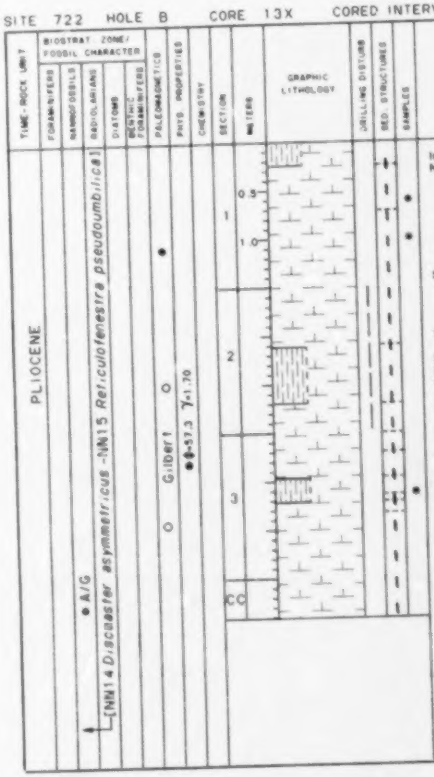
TIME-ROCK UNIT
BIOSTRAT. ZONE/ FOSSIL CHARACTER
FORAMINIFERS
NANNOFOSSILS
RADIOLARIANS
DIATOMS
BENTHIC FORAMINIFERS
PALEOMAGNETICS
PHYS. PROPERTIES
CHEMISTRY
SECTION
METERS
GRAPHIC LITHOLOGY
DRILLING DISTURB.
SED. STRUCTURES
SAMPLES
PLIOCENE
● A/G
[NN14 Discoaster asymmetricus -NN15 Reticulofenestra pseudoumbilica]
Gilbert
●Φ-57.3 γ-1.70
0.5
1.0
1
2
3
CC

LITHOLOGIC DESCRIPTION

Interbedded FORAMINIFER-BEARING NANNOFOSSIL OOZE and MARLY NANNOFOSSIL OOZE

Section 2 is slightly disturbed.

Major lithology: Interbedded FORAMINIFER-BEARING NANNOFOSSIL OOZE and MARLY NANNOFOSSIL OOZE. Contacts are gradational. Beds range from light olive gray (5Y 6/2) to olive gray (5Y 7/1), light greenish gray (10Y 7/1, 7/2), olive (5Y 5/3), and pale olive (5Y 6/3). Bioturbation is minor throughout.

SMEAR SLIDE SUMMARY (%):

	1, 61 D	1, 100 D	3, 61 D
TEXTURE:			
Sand	10	5	10
Silt	10	15	15
Clay	80	80	75
COMPOSITION:			
Access. minerals		Tr	3
Clay	5	10	
Feldspar			2
Foraminifers	10	5	2
Volcanic glass		Tr	Tr
Inorganic calcite	10	8	10
Mica	Tr	1	25
Nannofossils	75	75	50
Quartz	Tr		8
Radiolarians	Tr	1	

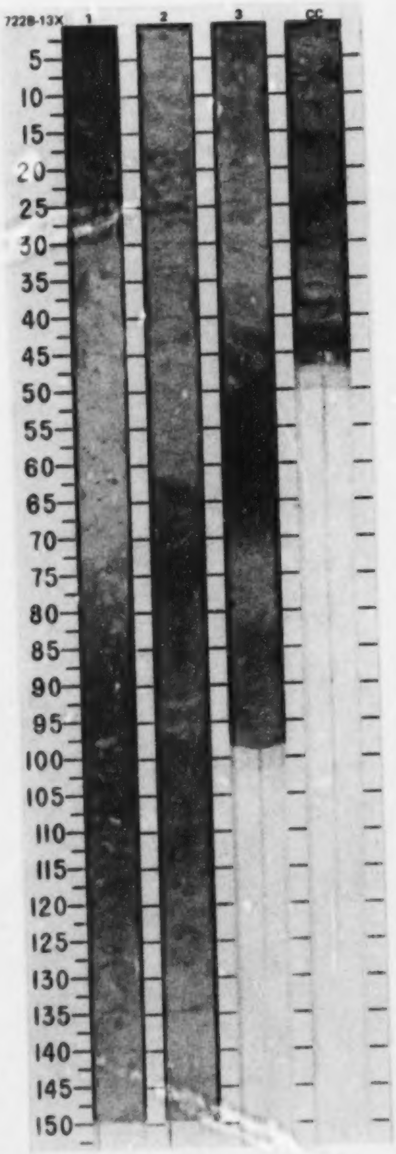
722B-13X
1
2
3
CC
5
10
15
20
25
30
35
40
45
50
55
60
65
70
75
80
85
90
95
100
105
110
115
120
125
130
135
140
145
150

SITE 722 HOLE B CORE 14X CORED INTERVAL 2148.7-2158.3 mbsl; 120.9-130.5 mbsf

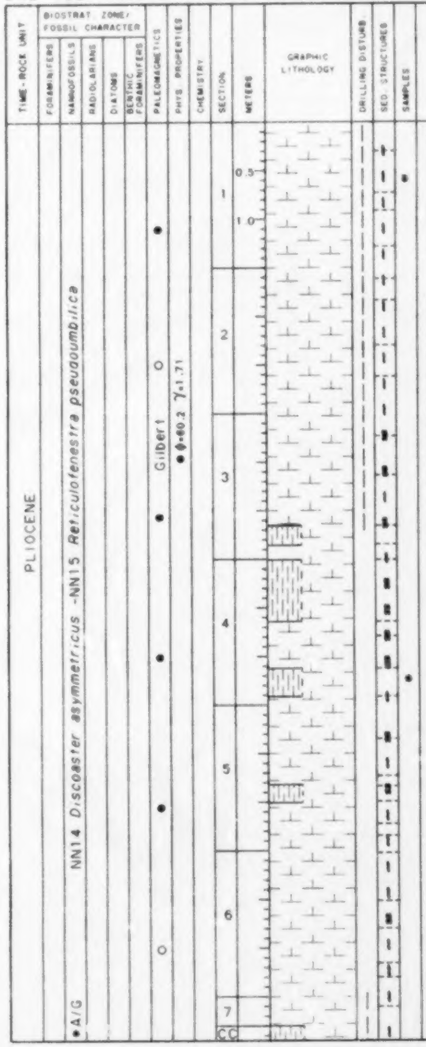

LITHOLOGIC DESCRIPTION

Interbedded NANNOFOSSIL OOZE and MARLY NANNOFOSSIL OOZE

Sections 1-3 and Section 7 are slightly disturbed. CC is moderately disturbed

Major lithology: Interbedded NANNOFOSSIL OOZE and MARLY NANNOFOSSIL OOZE. Contacts are gradational. Beds range from light olive gray (5Y 6/2) to light gray (5Y 7/1), light greenish gray (10Y 7/1, 7/2, 6/2), and olive (5Y 5/3). Bioturbation is minor to moderate throughout.

SMEAR SLIDE SUMMARY (%):

	1, 59 D	4, 124 D
TEXTURE:		
Sand	2	10
Silt	8	15
Clay	90	75
COMPOSITION:		
Access. minerals	Tr	3
Clay		30
Diatoms	Tr	Tr
Foraminifers	3	Tr
Volcanic glass		Tr
Inorganic calcite	7	9
Mica		1
Nannofossils	90	45
Quartz		10
Radiolarians	Tr	2
Silicoflagellates		Tr
Sponge spicules		Tr

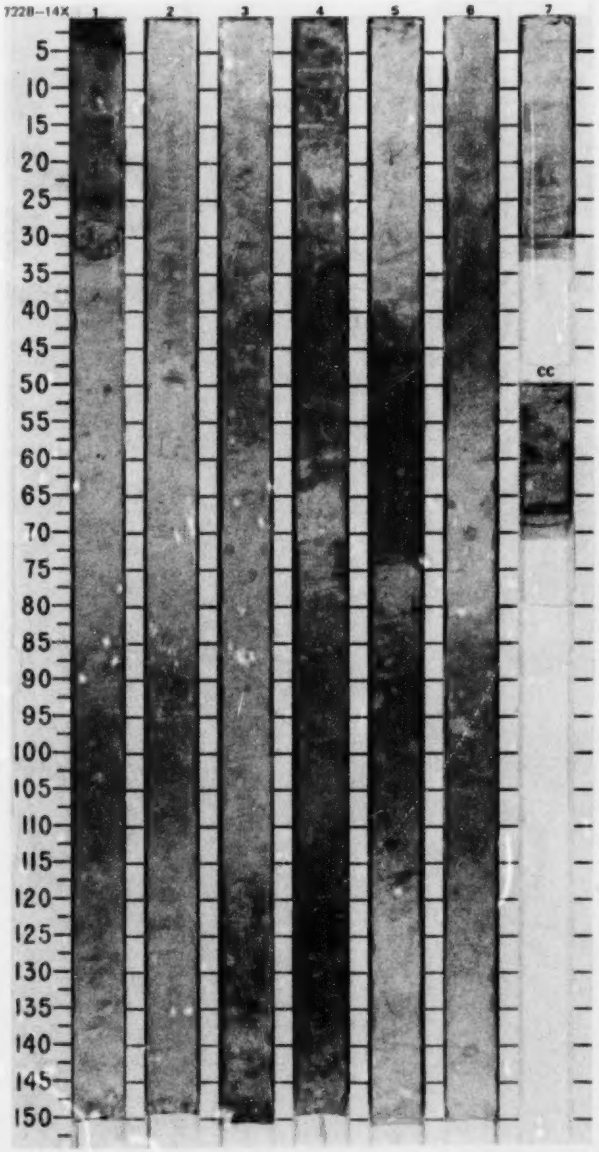
722B-14X
1
2
3
4
5
6
7
CC
5
10
15
20
25
30
35
40
45
50
55
60
65
70
75
80
85
90
95
100
105
110
115
120
125
130
135
140
145
150

SITE 722 HOLE B CORE 15X CORED INTERVAL 2158.3-2168.0 mbsl; 130.5-140.2 mbsf

TIME-ROCK UNIT	BIOSTRAT. ZONE/ FOSSIL CHARACTER: FORAMINIFERS	NANNOFOSSILS	RADIOLARIANS	DIATOMS	BENTHIC FORAMINIFERS	PALEOMAGNETICS	PHYS. PROPERTIES	CHEMISTRY	SECTION	METERS	GRAPHIC LITHOLOGY	DRILLING DISTURB.	SED. STRUCTURES	SAMPLES
PLIOCENE		NN14 *Discoaster asymmetricus* -NN15 *Reticulofenestra pseudoumbilica* * A/G				O			1 CC	0.5 1.0				*

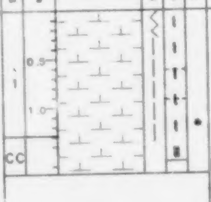

LITHOLOGIC DESCRIPTION

NANNOFOSSIL OOZE

Section 1, 0-15 cm, is very disturbed. Section 1, 15-129 cm, is slightly disturbed.

Major lithology: NANNOFOSSIL OOZE. Beds range from light olive gray (5Y 6/2) to light greenish gray (10Y 7/1). Contacts are gradational. Bioturbation is minor to moderate throughout.

SMEAR SLIDE SUMMARY (%):

	1, 117 D
TEXTURE:	
Sand	3
Silt	7
Clay	90
COMPOSITION:	
Access. minerals	Tr
Diatoms	Tr
Foraminifers	3
Volcanic glass	Tr
Inorganic calcite	7
Nannofossils	90
Quartz	Tr
Radiolarians	Tr

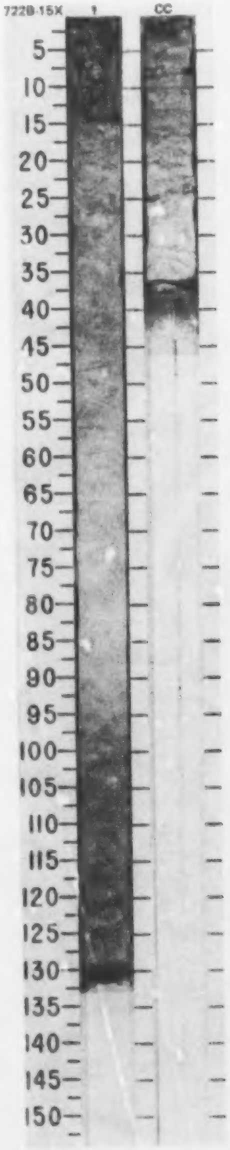

SITE 722 HOLE B CORE 16X CORED INTERVAL 2168.0-2177.7 mbsl; 140.2-149.9 mbsf

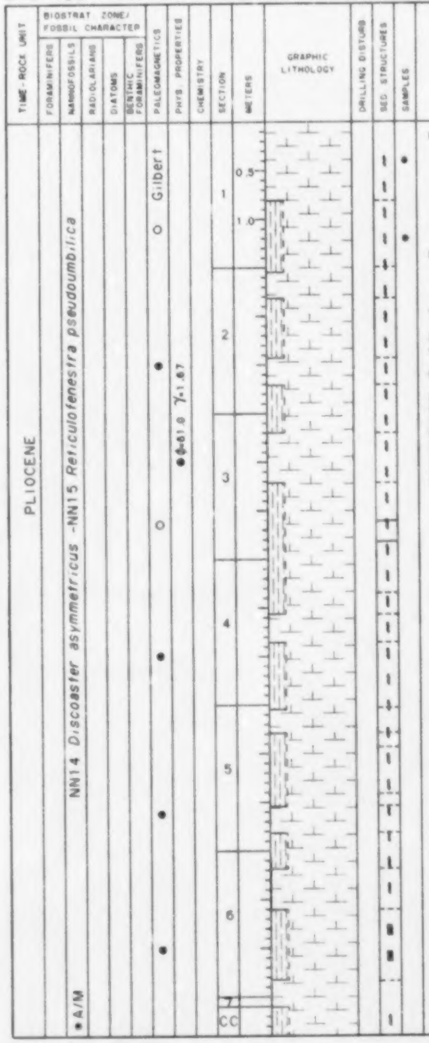
TIME-ROCK UNIT
BIOSTRAT. ZONE/ FOSSIL CHARACTER
FORAMINIFERS
NANNOFOSSILS
RADIOLARIANS
DIATOMS
BENTHIC FORAMINIFERS
PALEOMAGNETICS
PHYS. PROPERTIES
CHEMISTRY
SECTION
METERS
GRAPHIC LITHOLOGY
DRILLING DISTURB.
SED. STRUCTURES
SAMPLES
PLIOCENE
NN14 Discoaster asymmetricus -NN15 Reticulofenestra pseudoumbilica
A/M
Gilbert
φ=61.0 γ=1.67
0.5
1.0
1
2
3
4
5
6
7
CC

LITHOLOGIC DESCRIPTION

Interbedded NANNOFOSSIL OOZE and DIATOM-BEARING NANNOFOSSIL OOZE

CC is moderately disturbed.

Major lithology: INTERBEDDED NANNOFOSSIL OOZE and DIATOM- BEARING NANNOFOSSIL OOZE. Contacts are gradational. Beds range from light olive gray (5Y 6/2) to light gray (5Y 7/1), light greenish gray (5Y 6/3), olive gray (5Y 4/2), and olive (5Y 4/3, 4/4, 5/3). Bioturbation is minor to moderate throughout. Diatom-bearing beds occur as darker, more clayey beds.

SMEAR SLIDE SUMMARY (%):

	1, 40 D	1, 120 D
TEXTURE:		
Silt	10	20
Clay	90	80
COMPOSITION:		
Clay	10	10
Diatoms	Tr	10
Dolomite	Tr	Tr
Foraminifers	Tr	5
Inorganic calcite	5	5
Nannofossils	85	70
Quartz	Tr	Tr
Silicoflagellates		Tr

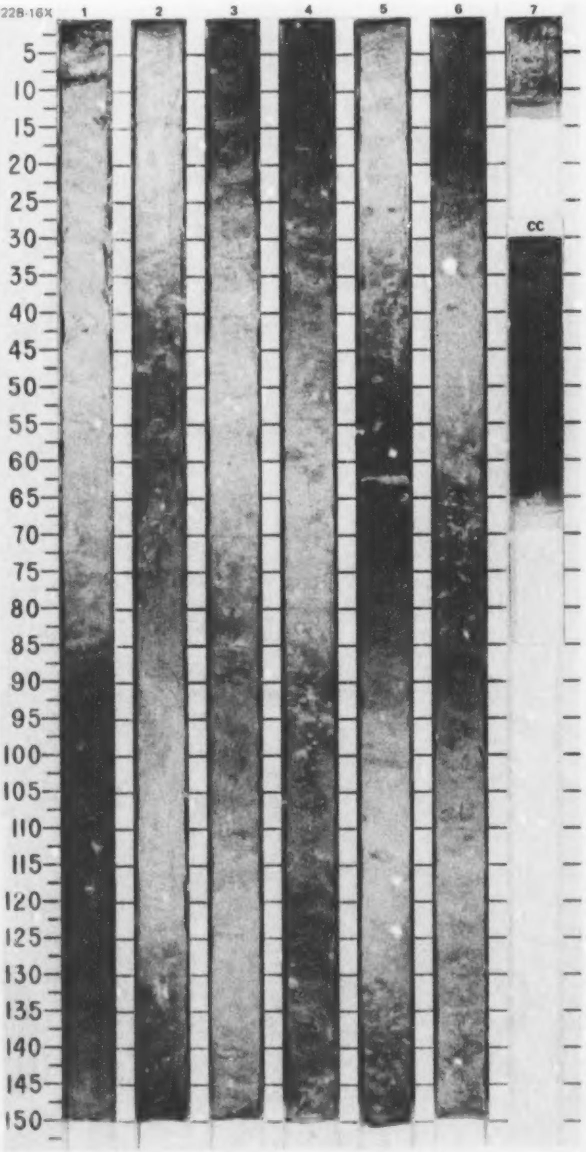
722B-16X
1
2
3
4
5
6
7
CC
5
10
15
20
25
30
35
40
45
50
55
60
65
70
75
80
85
90
95
100
105
110
115
120
125
130
135
140
145
150

SITE 722 HOLE B CORE 17X CORED INTERVAL 2177.7-2187.3 mbsl; 149.9-159.5 mbsf

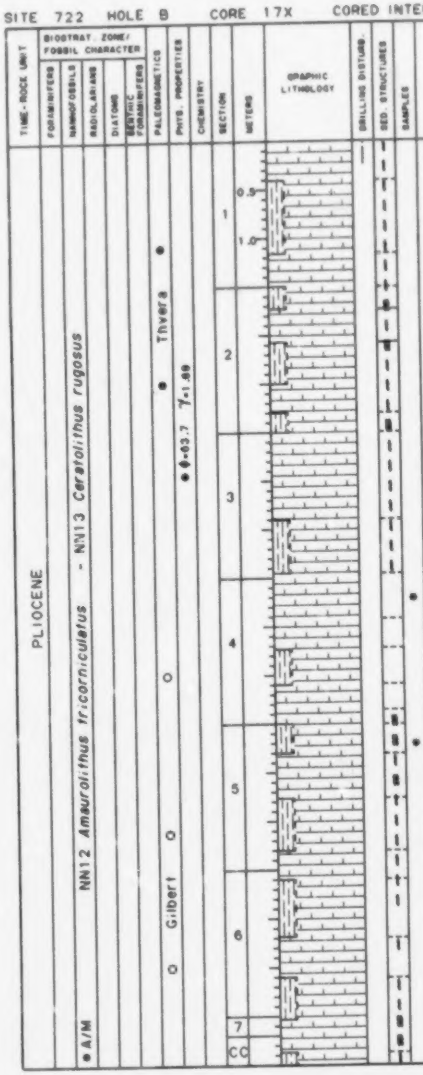
TIME-ROCK UNIT
BIOSTRAT. ZONE/ FOSSIL CHARACTER
FORAMINIFERS
NANNOFOSSILS
RADIOLARIANS
DIATOMS
BENTHIC FORAMINIFERS
PALEOMAGNETICS
PHYS. PROPERTIES
CHEMISTRY
SECTION
METERS
GRAPHIC LITHOLOGY
DRILLING DISTURB.
SED. STRUCTURES
SAMPLES
PLIOCENE
NN12 Amaurolithus tricorniculatus - NN13 Ceratolithus rugosus
● A/M
Thvera
Gilbert
● φ=63.7 γ=1.89
1
2
3
4
5
6
7
CC
0.5
1.0

LITHOLOGIC DESCRIPTION

NANNOFOSSIL CHALK

Section 1, 0-10 cm, is moderately disturbed.

Major lithology: NANNOFOSSIL CHALK. Beds range from light gray (5Y 7/1) to light greenish gray (10Y 7/1, 6/2), olive gray (5Y 5/2), olive (5Y 5/3, 4/2, 4/3), and dark greenish gray (10Y 5/2). Contacts are gradational except for a sharp contacts in Section 2, 20-110 cm. Bioturbation is minor to moderate throughout.

SMEAR SLIDE SUMMARY (%):

	4, 21 D	5, 21 D
TEXTURE:		
Silt	10	10
Clay	90	90
COMPOSITION:		
Clay	10	10
Diatoms	5	Tr
Foraminifers	5	
Inorganic calcite	Tr	5
Nannofossils	80	85
Quartz	Tr	Tr

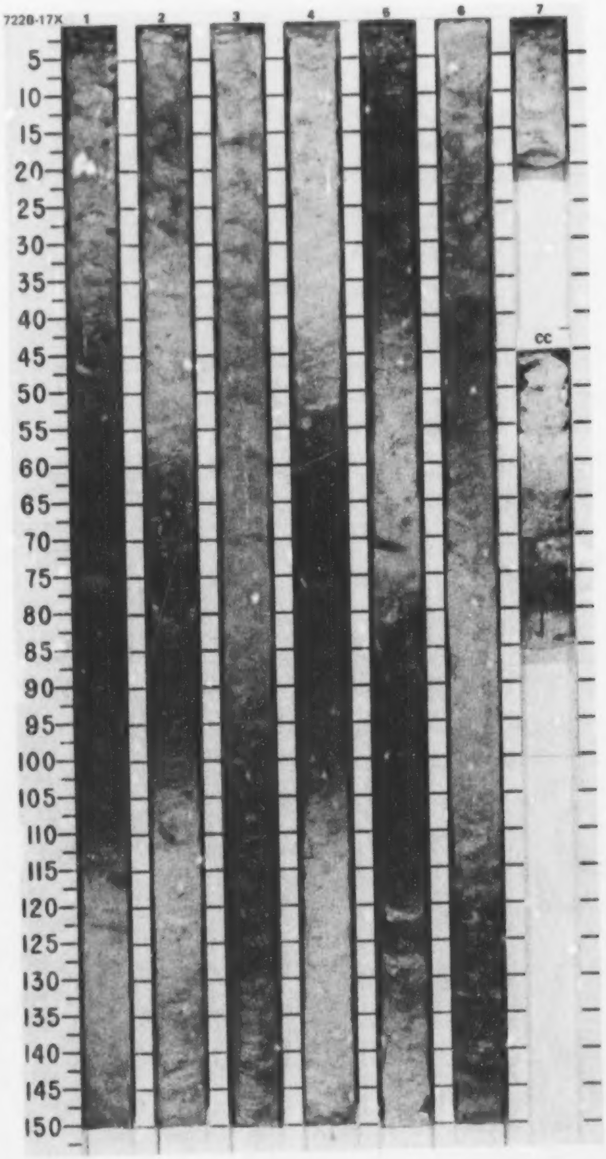
722B-17X
1
2
3
4
5
6
7
CC
5
10
15
20
25
30
35
40
45
50
55
60
65
70
75
80
85
90
95
100
105
110
115
120
125
130
135
140
145
150

SITE 722 HOLE B CORE 18X CORED INTERVAL 2187.3-2197.0 mbsl; 159.5-169.2 mbsf

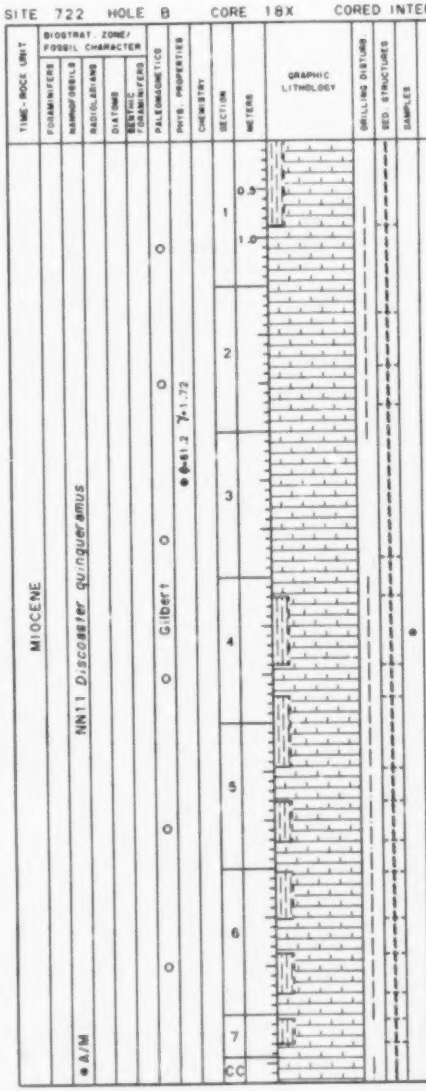
TIME-ROCK UNIT
BIOSTRAT. ZONE/ FOSSIL CHARACTER
FORAMINIFERS
NANNOFOSSILS
RADIOLARIANS
DIATOMS
BENTHIC FORAMINIFERS
PALEOMAGNETICS
PHYS. PROPERTIES
CHEMISTRY
SECTION
METERS
GRAPHIC LITHOLOGY
DRILLING DISTURB.
SED. STRUCTURES
SAMPLES
MIOCENE
NN11 Discoaster quinqueramus
● A/M
Gilbert
● ϕ-61.2 γ-1.72
0.5
1.0
1
2
3
4
5
6
7
CC

LITHOLOGIC DESCRIPTION

NANNOFOSSIL CHALK

Section 1, 70 cm, to Section 2, 150 cm, is slightly disturbed. Section 4 to Section 6 is slightly to moderately disturbed. CC is moderately disturbed.

Major lithology: NANNOFOSSIL CHALK. Beds range from gray (5Y 6/1) to light olive gray (5Y 6/2), light gray (5Y 7/1), olive gray (5Y 5/2), and olive (5Y 5/3). Contacts are gradational. Bioturbation is minor throughout.

SMEAR SLIDE SUMMARY (%):

	4, 60 D
TEXTURE:	
Silt	10
Clay	90
COMPOSITION:	
Clay	10
Diatoms	Tr
Foraminifers	Tr
Inorganic calcite	5
Nannofossils	85
Quartz	Tr

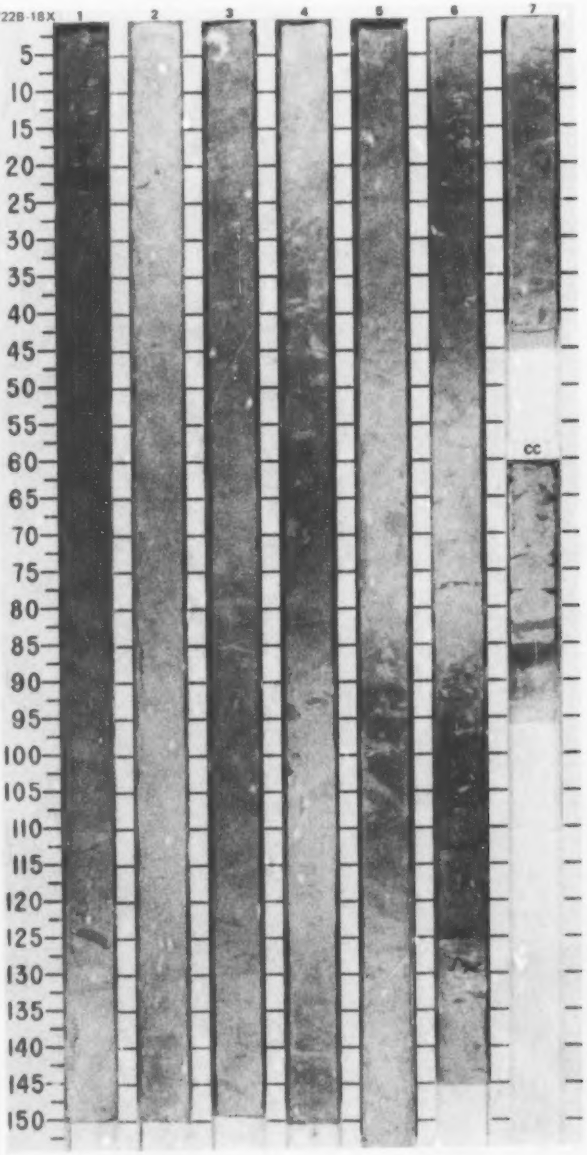
722B-18X
1
2
3
4
5
6
7
CC
5
10
15
20
25
30
35
40
45
50
55
60
65
70
75
80
85
90
95
100
105
110
115
120
125
130
135
140
145
150

SITE 722 HOLE B CORE 19X CORED INTERVAL 2197.0-2206.7 mbsl; 169.2-178.9 mbsf

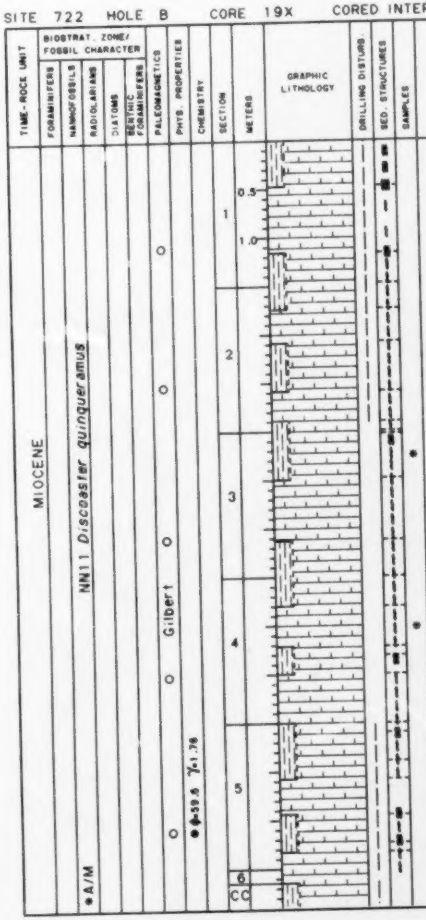
TIME-ROCK UNIT
BIOSTRAT. ZONE/ FOSSIL CHARACTER
FORAMINIFERS
NANNOFOSSILS
RADIOLARIANS
DIATOMS
BENTHIC FORAMINIFERS
PALEOMAGNETICS
PHYS. PROPERTIES
CHEMISTRY
SECTION
METERS
GRAPHIC LITHOLOGY
DRILLING DISTURB.
SED. STRUCTURES
SAMPLES
MIOCENE
NN11 Discoaster quinqueramus
* A/M
Gilbert
● ϕ=59.6 γ=1.76
1
2
3
4
5
6
CC
0.5
1.0

LITHOLOGIC DESCRIPTION

NANNOFOSSIL CHALK

Section 1 to Section 2 is slightly disturbed. CC is moderately disturbed.

Major lithology: NANNOFOSSIL CHALK. Beds range from light olive gray (5Y 6/2) to light gray (5Y 7/1), light greenish gray (10Y 7/1), olive gray (5Y 5/2, 4/2), olive (5Y 5/3, 4/3), pale olive (5Y 6/3), dark greenish gray (5Y 6/3), and dark olive gray (5Y 3/2). Contacts are gradational. Bioturbation is minor to strong.

SMEAR SLIDE SUMMARY (%):

	3, 25 D	4, 51 D
TEXTURE:		
Silt	10	10
Clay	90	90
COMPOSITION:		
Clay	10	20
Diatoms	Tr	1
Foraminifers	Tr	5
Inorganic calcite	5	5
Nannofossils	85	69
Organic debris	Tr	
Quartz	Tr	Tr
Radiolarians		Tr
Sponge spicules	Tr	Tr

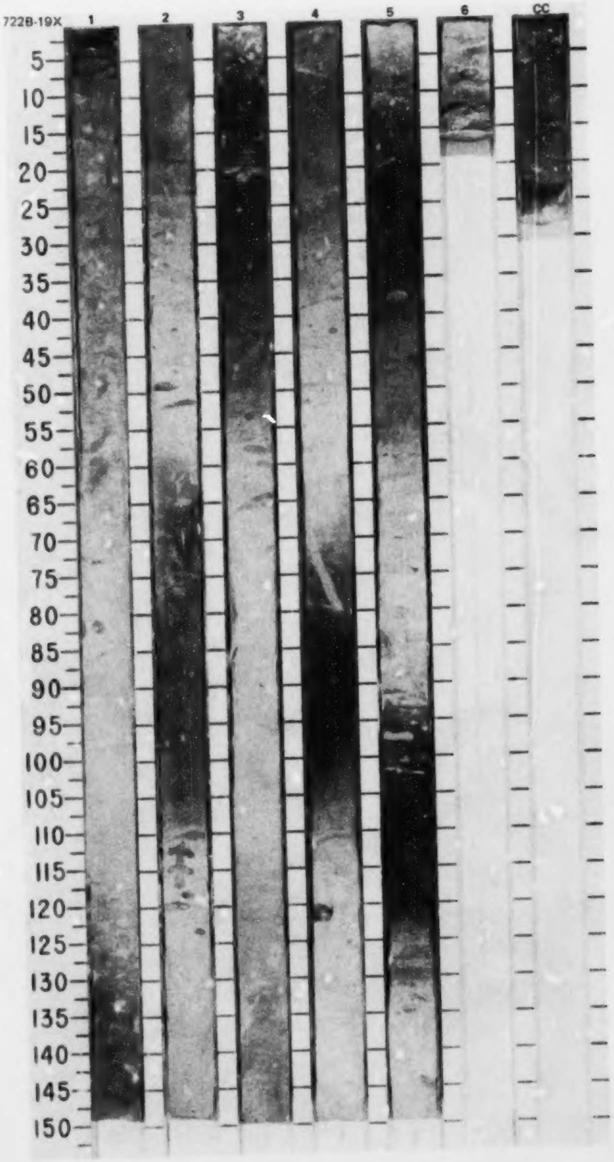
722B-19X
1
2
3
4
5
6
CC
5
10
15
20
25
30
35
40
45
50
55
60
65
70
75
80
85
90
95
100
105
110
115
120
125
130
135
140
145
150

SITE 722 HOLE B CORE 20X CORED INTERVAL 2206.7-2216.3 mbsl; 178.9-188.5 mbsf

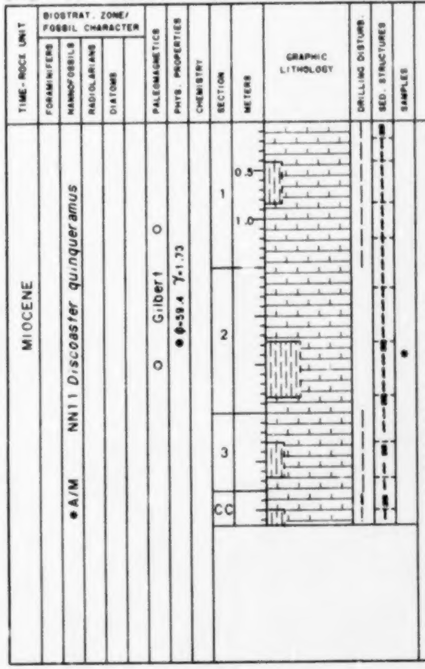
TIME-ROCK UNIT
BIOSTRAT. ZONE/ FOSSIL CHARACTER
FORAMINIFERS
NANNOFOSSILS
RADIOLARIANS
DIATOMS
PALEOMAGNETICS
PHYS. PROPERTIES
CHEMISTRY
SECTION
METERS
GRAPHIC LITHOLOGY
DRILLING DISTURB.
SED. STRUCTURES
SAMPLES
MIOCENE
● A/M NN11 Discoaster quinqueramus
○ Gilbert ○
● ϕ-59.4 γ-1.73
1
2
3
CC
0.5
1.0

LITHOLOGIC DESCRIPTION

Interbedded NANNOFOSSIL CHALK and MARLY NANNOFOSSIL CHALK

Section 1 is slightly disturbed. CC is moderately disturbed.

Major lithology: Interbedded NANNOFOSSIL CHALK and MARLY NANNOFOSSIL CHALK. Contacts are gradational. Beds range from light olive gray (5Y 6/2) to light gray (5Y 7/1), olive gray (5Y 5/2), olive (5Y 5/3), pale olive (5Y 6/3), and dark greenish gray (10Y 4/3). Bioturbation is minor to moderate throughout.

SMEAR SLIDE SUMMARY (%):

	2, 93 D
TEXTURE:	
Silt	10
Clay	90
COMPOSITION:	
Clay	25
Diatoms	1
Foraminifers	5
Inorganic calcite	7
Mica	3
Nannofossils	55
Quartz	3
Radiolarians	1
Rock fragments	Tr

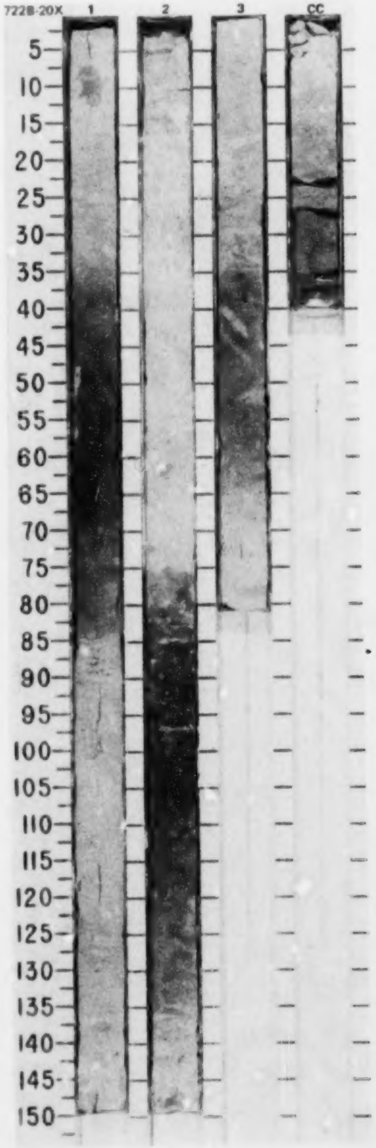
722B-20X
1
2
3
CC
5
10
15
20
25
30
35
40
45
50
55
60
65
70
75
80
85
90
95
100
105
110
115
120
125
130
135
140
145
150

SITE 722 HOLE B CORE 21X CORED INTERVAL 2216.3-2226.0 mbsl; 188.5-198.2 mbsf

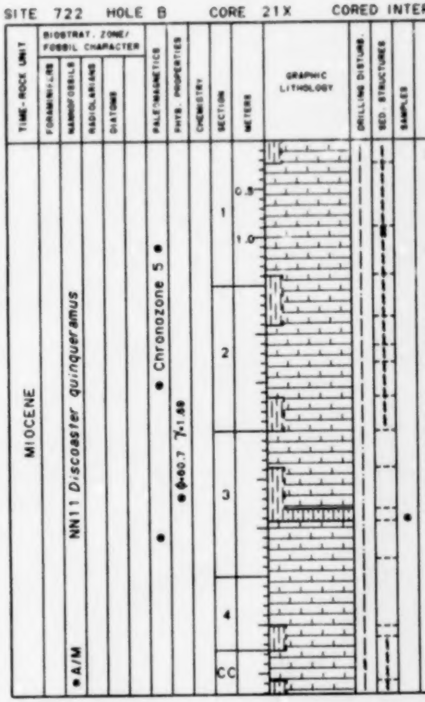
TIME-ROCK UNIT
BIOSTRAT. ZONE/ FOSSIL CHARACTER
FORAMINIFERS
NANNOFOSSILS
RADIOLARIANS
DIATOMS
PALEOMAGNETICS
PHYS. PROPERTIES
CHEMISTRY
SECTION
METERS
GRAPHIC LITHOLOGY
DRILLING DISTURB.
SED. STRUCTURES
SAMPLES
MIOCENE
NN11 Discoaster quinqueramus
● A/M
● Chronozone 5 ●
●
● ϕ=60.7 γ=1.88
1
2
3
4
CC
0.5
1.0

LITHOLOGIC DESCRIPTION

NANNOFOSSIL CHALK

Major lithology: NANNOFOSSIL CHALK. Beds range from light olive gray (5Y 6/2) to light gray (5Y 7/1), light greenish gray (10Y 6/1), olive gray (5Y 5/2), and olive (5Y 5/3, 4/3). Contacts are gradational. Bioturbation is minor to moderate throughout. Minor lithology: Silica-bearing calcitic silty claystone, dark olive gray (5Y 3/2). Section 3, 86-92 cm.

SMEAR SLIDE SUMMARY (%):

	3, 90 M
TEXTURE:	
Sand	5
Silt	40
Clay	55
COMPOSITION:	
Clay	48
Diatoms	5
Dolomite	1
Gypsum	Tr
Inorganic calcite	10
Mica	3
Nannofossils	5
Organic debris	4
Quartz	20
Radiolarians	2
Sponge spicules	2

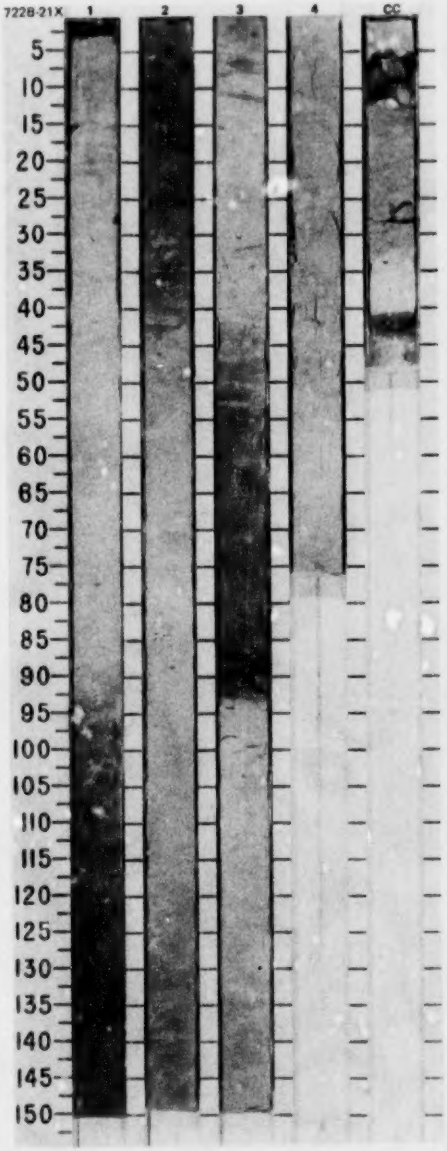
722B-21X
1
2
3
4
CC
5
10
15
20
25
30
35
40
45
50
55
60
65
70
75
80
85
90
95
100
105
110
115
120
125
130
135
140
145
150

SITE 722 HOLE B CORE 22X CORED INTERVAL 2226.0-2235.7 mbsl; 198.2-207.9 mbsf

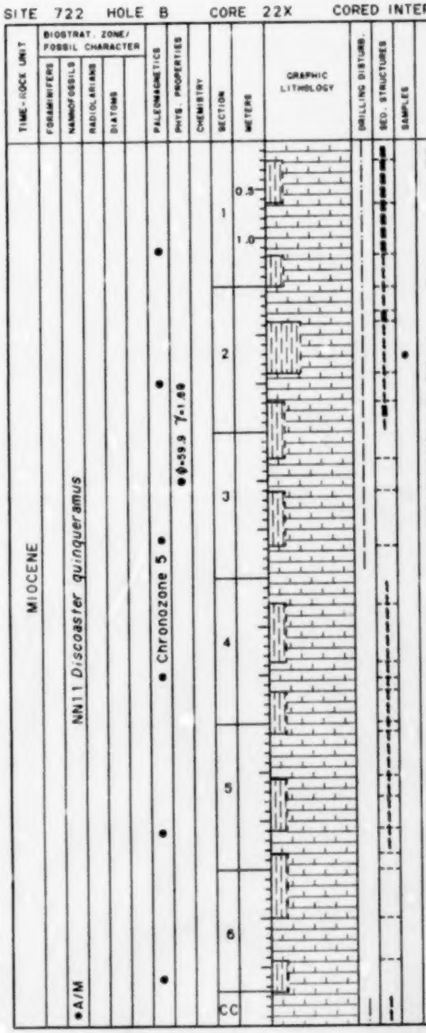
TIME-ROCK UNIT
BIOSTRAT. ZONE/ FOSSIL CHARACTER
FORAMINIFERS
NANNOFOSSILS
RADIOLARIANS
DIATOMS
PALEOMAGNETICS
PHYS. PROPERTIES
CHEMISTRY
SECTION
METERS
GRAPHIC LITHOLOGY
DRILLING DISTURB.
SED. STRUCTURES
SAMPLES
MIOCENE
NN11 Discoaster quinqueramus
●A/M
Chronozone 5
●Φ=59.9 γ=1.89
1
2
3
4
5
6
CC
0.5
1.0

LITHOLOGIC DESCRIPTION

Interbedded DIATOM-BEARING NANNOFOSSIL CHALK and MARLY NANNOFOSSIL CHALK

Section 1 and CC are moderately disturbed. Sections 2 and 3 are slightly disturbed.

Major lithology: Interbedded DIATOM-BEARING NANNOFOSSIL CHALK and MARLY NANNOFOSSIL CHALK. Contacts are gradational. Beds range from white (5Y 8/1) to gray (5Y 6/1), light gray (5Y 7/1, 7/2), and olive (5Y 5/3, 5/4, 4/3). Bioturbation is minor to moderate throughout.

SMEAR SLIDE SUMMARY (%):

	2, 71 D
TEXTURE:	
Silt	20
Clay	80
COMPOSITION:	
Access. minerals	2
Clay	30
Diatoms	5
Foraminifers	3
Inorganic calcite	3
Nannofossils	55
Organic debris	2
Quartz	Tr
Radiolarians	Tr

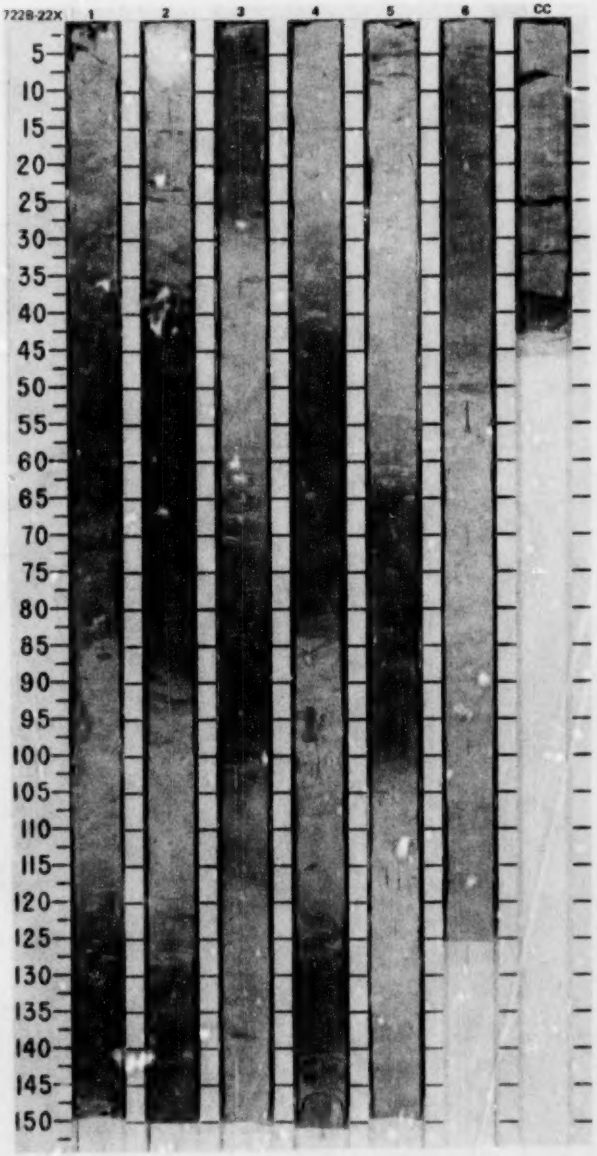
722B-22X
1
2
3
4
5
6
CC
5
10
15
20
25
30
35
40
45
50
55
60
65
70
75
80
85
90
95
100
105
110
115
120
125
130
135
140
145
150

SITE 722 HOLE B CORE 23X CORED INTERVAL 2235.7-2245.3 mbsl; 207.9-217.5 mbsf

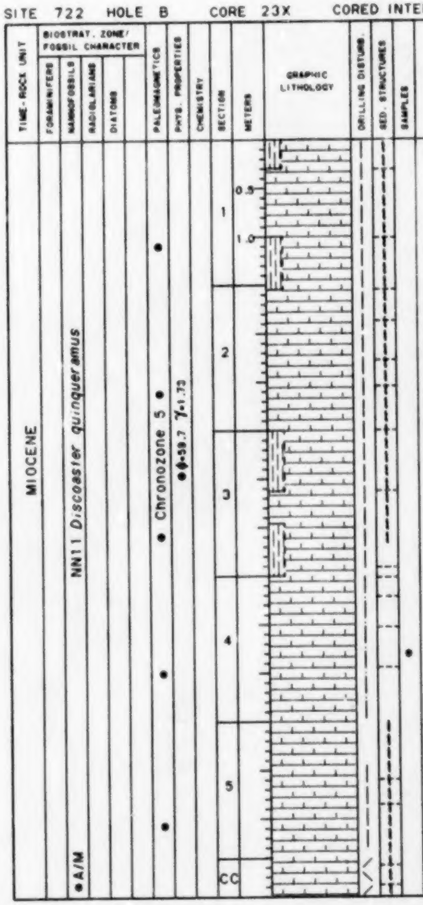
TIME-ROCK UNIT
BIOSTRAT. ZONE/FOSSIL CHARACTER
FORAMINIFERS
NANNOFOSSILS
RADIOLARIANS
DIATOMS
PALEOMAGNETICS
PHYS. PROPERTIES
CHEMISTRY
SECTION
METERS
GRAPHIC LITHOLOGY
DRILLING DISTURB.
SED. STRUCTURES
SAMPLES
MIOCENE
NN11 Discoaster quinqueramus
• A/M
Chronozone 5
•ϕ=59.7 γ=1.73
0.5
1.0
1
2
3
4
5
CC

LITHOLOGIC DESCRIPTION

NANNOFOSSIL CHALK

Sections 1-3 are slightly disturbed. CC is highly fragmented.

Major lithology: NANNOFOSSIL CHALK. Beds range from light olive gray (5Y 7/1, 7/2) to olive gray (5Y 5/2) and pale olive (5Y 6/3). Contacts are gradational. Bioturbation is minor throughout.

SMEAR SLIDE SUMMARY (%):

	4, 80 D
TEXTURE:	
Silt	5
Clay	95
COMPOSITION:	
Clay	10
Foraminifers	5
Inorganic calcite	Tr
Nannofossils	85
Quartz	Tr

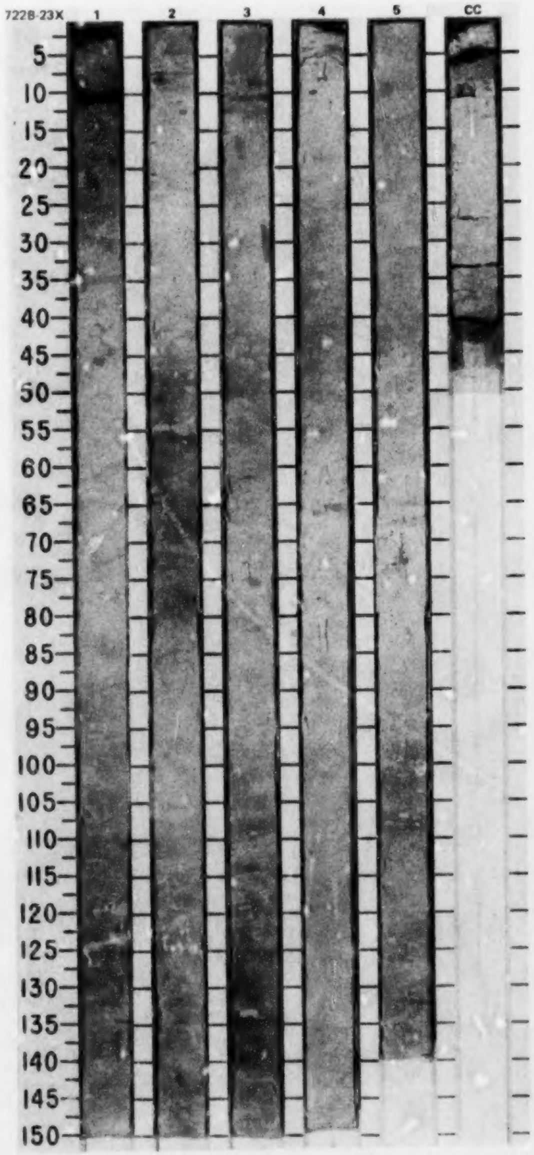
722B-23X
1
2
3
4
5
CC
5
10
15
20
25
30
35
40
45
50
55
60
65
70
75
80
85
90
95
100
105
110
115
120
125
130
135
140
145
150

SITE 722 HOLE B CORE 24X CORED INTERVAL 2245.3-2255.0 mbsl; 217.5-227.2 mbsf

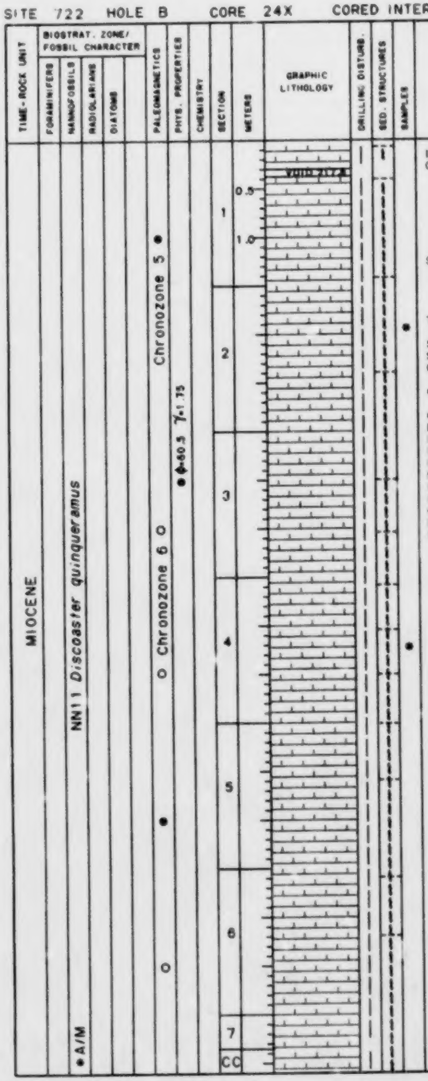
TIME-ROCK UNIT
BIOSTRAT. ZONE/ FOSSIL CHARACTER
FORAMINIFERS
NANNOFOSSILS
RADIOLARIANS
DIATOMS
PALEOMAGNETICS
PHYS. PROPERTIES
CHEMISTRY
SECTION
METERS
GRAPHIC LITHOLOGY
DRILLING DISTURB.
SED. STRUCTURES
SAMPLES
MIOCENE
NN11 Discoaster quinqueramus
• A/M
Chronozone 5 •
○ Chronozone 6 ○
•
○
• ϕ-60.5 γ-1.75
1
2
3
4
5
6
7
CC
0.5
1.0
VOID 217.8

LITHOLOGIC DESCRIPTION

Interbedded NANNOFOSSIL CHALK and DIATOM-BEARING NANNOFOSSIL CHALK

Entire core is slightly disturbed.

Major lithology: Interbedded NANNOFOSSIL CHALK and DIATOM- BEARING NANNOFOSSIL CHALK. Contacts are gradational. Beds range from light olive gray (5Y 6/2) to light gray (5Y 7/1). Bioturbation is minor throughout.

SMEAR SLIDE SUMMARY (%):

	2, 44 D	4, 72 D
TEXTURE:		
Sand		5
Silt	10	30
Clay	90	65
COMPOSITION:		
Clay	20	15
Diatoms	1	5
Dolomite		Tr
Foraminifers	5	3
Inorganic calcite		15
Mica		2
Nannofossils	74	50
Pyrite		3
Quartz		5
Radiolarians	Tr	1
Sponge spicules	Tr	1

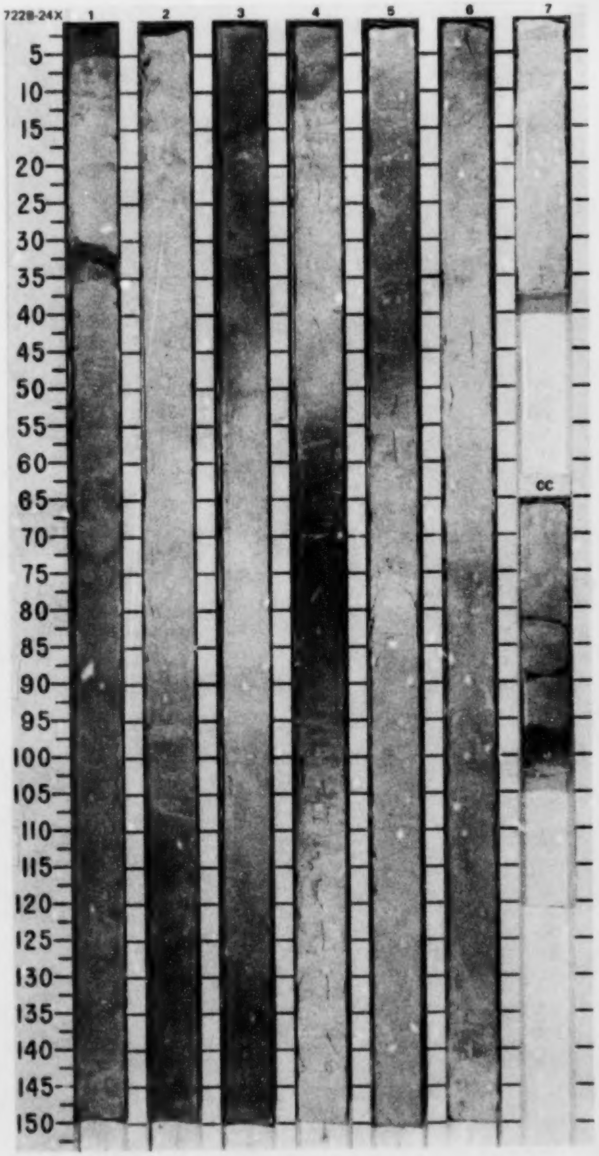
722B-24X
1
2
3
4
5
6
7
CC
5
10
15
20
25
30
35
40
45
50
55
60
65
70
75
80
85
90
95
100
105
110
115
120
125
130
135
140
145
150

SITE 722 HOLE B CORE 25X CORED INTERVAL 2255.0-2264.7 mbsl; 227.2-236.9 mbsf

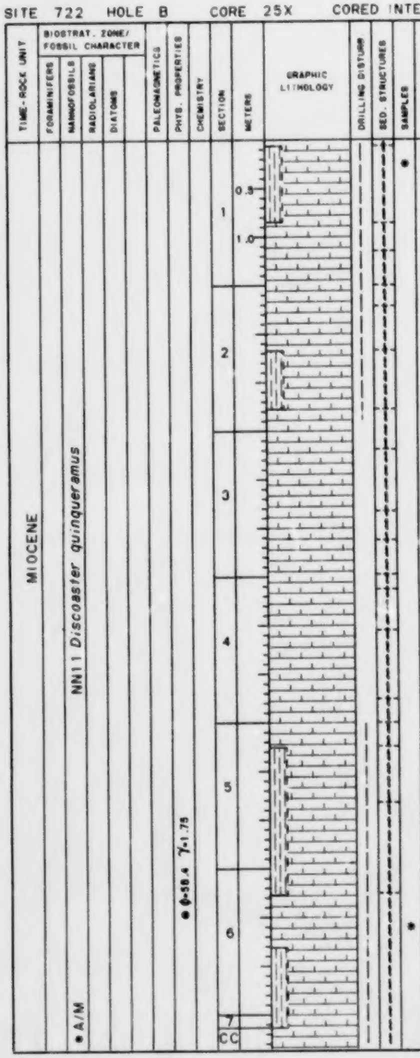
TIME-ROCK UNIT
BIOSTRAT. ZONE/ FOSSIL CHARACTER
FORAMINIFERS
NANNOFOSSILS
RADIOLARIANS
DIATOMS
PALEOMAGNETICS
PHYS. PROPERTIES
CHEMISTRY
SECTION
METERS
GRAPHIC LITHOLOGY
DRILLING DISTURB.
SED. STRUCTURES
SAMPLES
MIOCENE
NN11 Discoaster quinqueramus
● A/M
● φ=58.4 γ=1.75
1
2
3
4
5
6
7
CC
0.5
1.0

LITHOLOGIC DESCRIPTION

Interbedded NANNOFOSSIL CHALK and DIATOM-BEARING NANNOFOSSIL CHALK

Sections 1-2, 5-7, and CC are slightly disturbed.

Major lithology: Interbedded NANNOFOSSIL CHALK and DIATOM- BEARING NANNOFOSSIL CHALK. Contacts are gradational. Beds range from white (5Y 8/1) to light olive gray (5Y 7/1, 7/2), olive gray (5Y 5/2), and olive (5Y 5/3). Bioturbation is minor throughout.

SMEAR SLIDE SUMMARY (%):

	1, 25 D	6, 60 D
TEXTURE:		
Silt	15	20
Clay	85	80
COMPOSITION:		
Clay	10	10
Diatoms	5	1
Dolomite	Tr	
Foraminifers	5	5
Inorganic calcite	5	3
Nannofossils	75	78
Quartz	Tr	
Radiolarians		3
Rock fragments		Tr

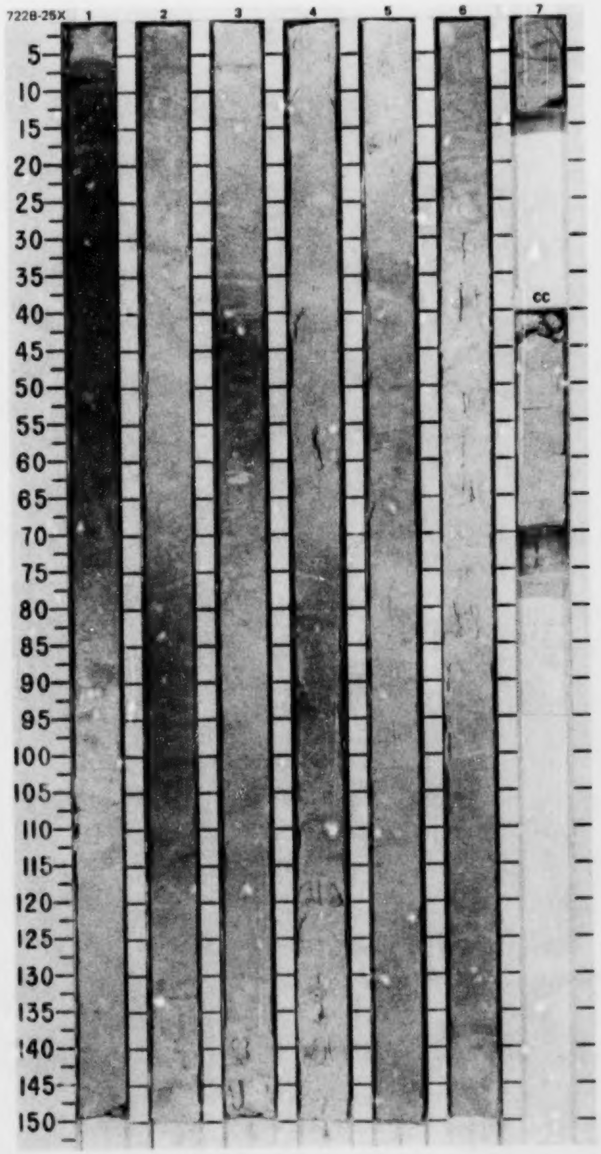
722B-25X
1
2
3
4
5
6
7
CC
5
10
15
20
25
30
35
40
45
50
55
60
65
70
75
80
85
90
95
100
105
110
115
120
125
130
135
140
145
150

SITE 722 HOLE B CORE 26X CORED INTERVAL 2264.7-2274.3 mbsl; 236.9-246.5 mbsf

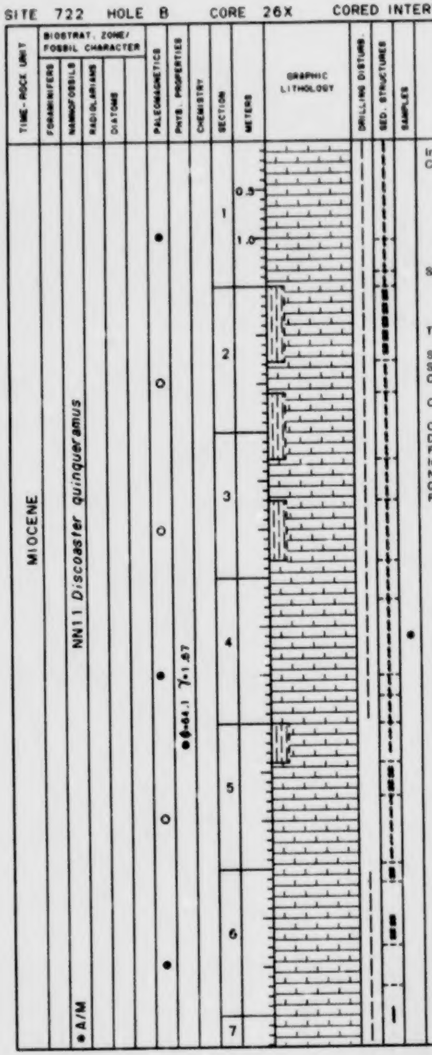
TIME-ROCK UNIT
BIOSTRAT. ZONE/ FOSSIL CHARACTER
FORAMINIFERS
NANNOFOSSILS
RADIOLARIANS
DIATOMS
PALEOMAGNETICS
PHYS. PROPERTIES
CHEMISTRY
SECTION
METERS
GRAPHIC LITHOLOGY
DRILLING DISTURB.
SED. STRUCTURES
SAMPLES
MIOCENE
NN11 Discoaster quinqueramus
● A/M
●ϕ=64.1 γ=1.67
0.5
1.0
1
2
3
4
5
6
7

LITHOLOGIC DESCRIPTION

Interbedded NANNOFOSSIL CHALK and DIATOM-BEARING NANNOFOSSIL CHALK

Sections 1-4 and Section 6 are slightly disturbed.

Major lithology: Interbedded NANNOFOSSIL CHALK and DIATOM- BEARING NANNOFOSSIL OOZE. Contacts are gradational. Beds range from light olive gray (5Y 6/2) to light gray (5Y 7/2, 7/1), olive gray (5Y 5/2), and olive (5Y 5/3). Bioturbation is minor to moderate throughout.

SMEAR SLIDE SUMMARY (%):

	4, 60 D
TEXTURE:	
Sand	5
Silt	10
Clay	85
COMPOSITION:	
Clay	10
Diatoms	5
Foraminifers	5
Inorganic calcite	Tr
Nannofossils	80
Quartz	Tr
Radiolarians	Tr

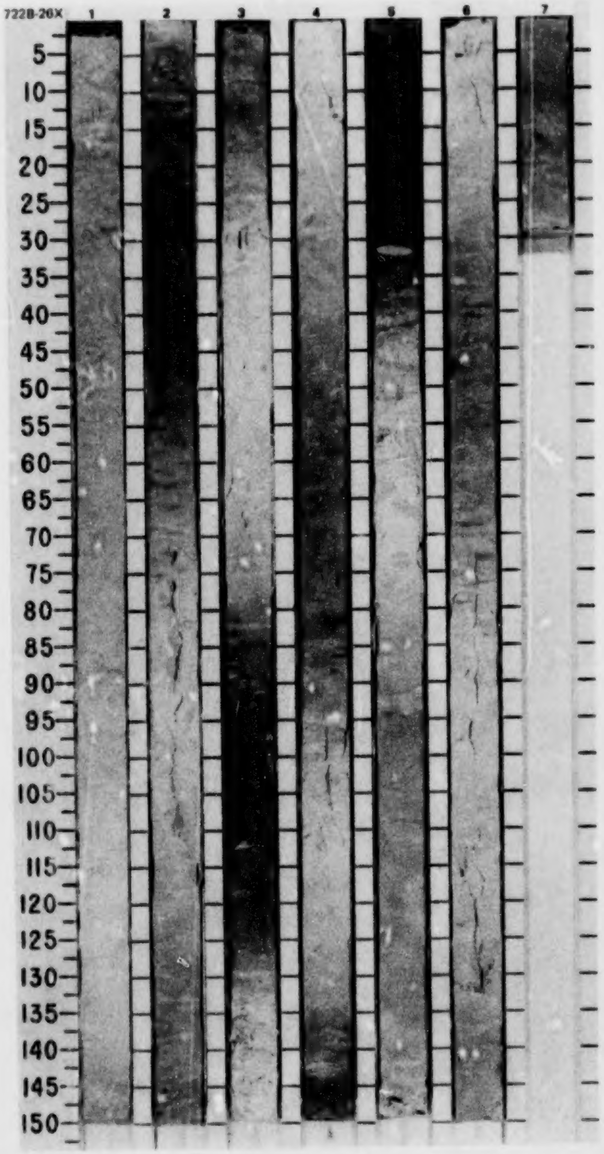
722B-26X
1
2
3
4
5
6
7
5
10
15
20
25
30
35
40
45
50
55
60
65
70
75
80
85
90
95
100
105
110
115
120
125
130
135
140
145
150

SITE 722 HOLE B CORE 27X CORED INTERVAL 2274.3-2284.0 mbsl; 246.5-256.2 mbsf

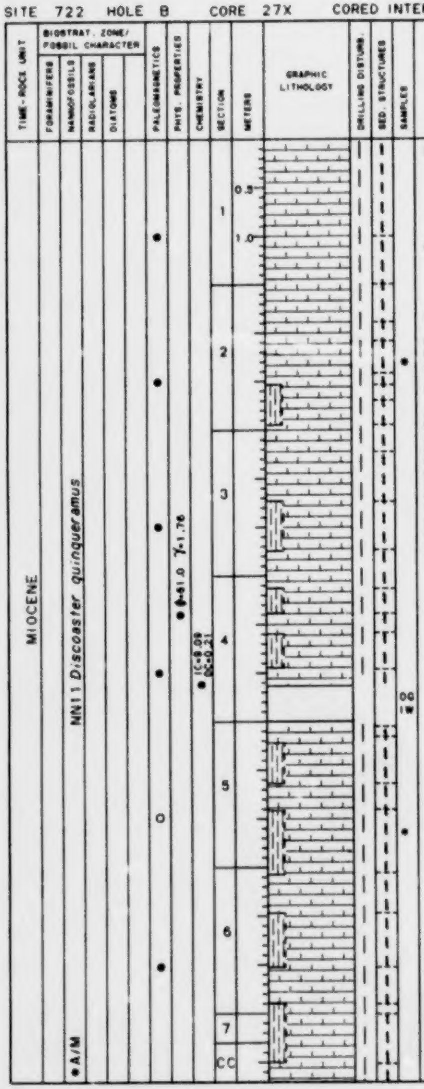
TIME-ROCK UNIT
BIOSTRAT. ZONE/ FOSSIL CHARACTER
FORAMINIFERS
NANNOFOSSILS
RADIOLARIANS
DIATOMS
PALEOMAGNETICS
PHYS. PROPERTIES
CHEMISTRY
SECTION
METERS
GRAPHIC LITHOLOGY
DRILLING DISTURB.
SED. STRUCTURES
SAMPLES
MIOCENE
NN11 Discoaster quinqueramus
• A/M
• φ=61.0 γ=1.76
• IC=8.09 OC=0.21
0.5
1.0
1
2
3
4
5
6
7
CC
OG
IW

LITHOLOGIC DESCRIPTION

Interbedded NANNOFOSSIL CHALK and DIATOM-NANNOFOSSIL CHALK

Major lithology: Interbedded NANNOFOSSIL CHALK and DIATOM-NANNOFOSSIL CHALK. Contacts are gradational. Beds range from white (5Y 8/1) to gray (5Y 6/1), light gray (5Y 7/1, 6/1), light greenish gray (10Y 7/1, 6/2), olive gray (5Y 5/2), olive (5Y 5/3, 4/3, 5/4), and pale olive (5Y 6/3). Bioturbation is minor throughout. The diatom-nannofossil chalk occurs mainly as darker beds.

SMEAR SLIDE SUMMARY (%):

	2, 80 D	5, 114 D
TEXTURE:		
Sand	5	
Silt	20	15
Clay	75	85
COMPOSITION:		
Access. minerals		Tr
Clay	10	
Diatoms	20	2
Dolomite	Tr	
Foraminifers		5
Inorganic calcite	Tr	10
Nannofossils	70	80
Quartz	Tr	Tr
Radiolarians	Tr	3
Silicoflagellates	Tr	Tr
Sponge spicules	Tr	Tr

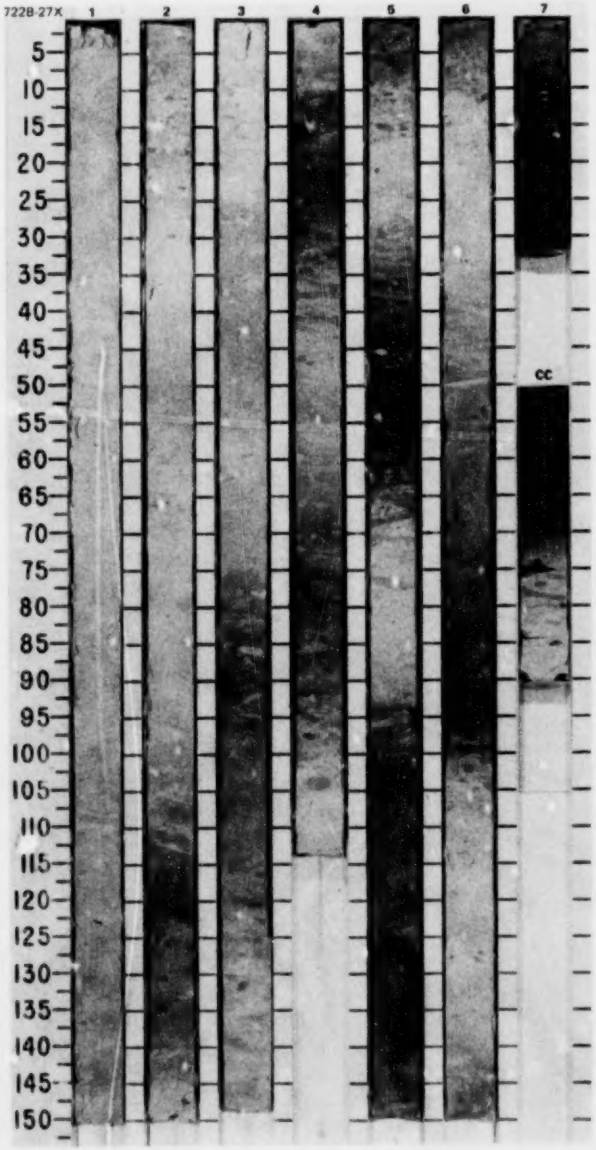
722B-27X
1
2
3
4
5
6
7
CC
5
10
15
20
25
30
35
40
45
50
55
60
65
70
75
80
85
90
95
100
105
110
115
120
125
130
135
140
145
150

SITE 722 HOLE B CORE 28X CORED INTERVAL 2284.0-2293.7 mbsl; 256.2-265.9 mbsf

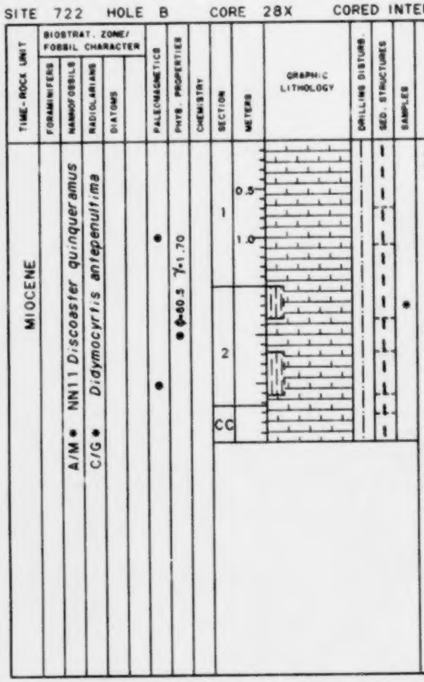
TIME-ROCK UNIT
BIOSTRAT. ZONE/ FOSSIL CHARACTER
FORAMINIFERS
NANNOFOSSILS
RADIOLARIANS
DIATOMS
PALEOMAGNETICS
PHYS. PROPERTIES
CHEMISTRY
SECTION
METERS
GRAPHIC LITHOLOGY
DRILLING DISTURB.
SED. STRUCTURES
SAMPLES
MIOCENE
A/M ● NN11 Discoaster quinqueramus
C/G ● Didymocyrtis antepenultima
● ϕ=60.5 γ=1.70
1
2
CC
0.5
1.0

LITHOLOGIC DESCRIPTION

Interbedded NANNOFOSSIL CHALK and DIATOM-BEARING NANNOFOSSIL CHALK

Entire core is moderately disturbed.

Major lithology: Interbedded NANNOFOSSIL CHALK and DIATOM-NANNOFOSSIL CHALK. Contacts are gradational. Beds range from light olive gray (5Y 6/2) to light gray (5Y 7/1) and olive gray (5Y 5/2). Bioturbation is minor throughout.

SMEAR SLIDE SUMMARY (%):

	2, 20 D
TEXTURE:	
Sand	5
Silt	15
Clay	80
COMPOSITION:	
Clay	10
Diatoms	5
Dolomite	Tr
Foraminifers	5
Nannofossils	80
Quartz	Tr
Radiolarians	Tr
Silicoflagellates	Tr

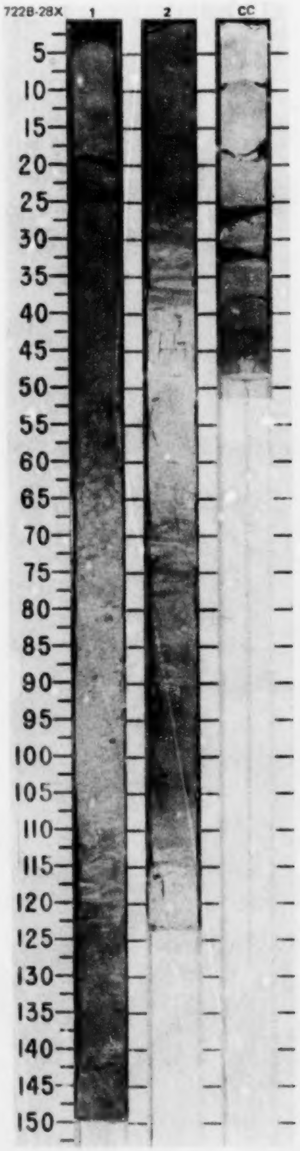
722B-28X
1
2
CC
5
10
15
20
25
30
35
40
45
50
55
60
65
70
75
80
85
90
95
100
105
110
115
120
125
130
135
140
145
150

SITE 722 HOLE B CORE 29X CORED INTERVAL 2293.7-2303.4 mbsl; 265.9-275.6 mbsf

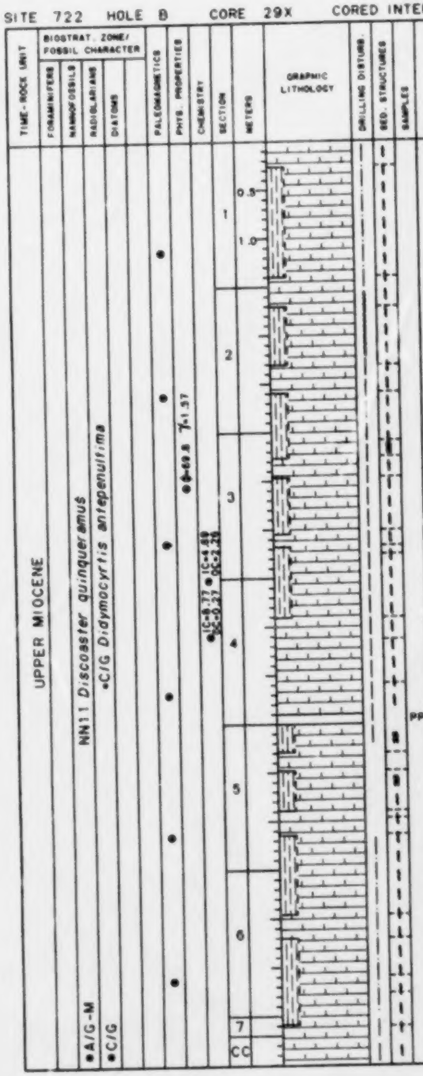
TIME-ROCK UNIT
BIOSTRAT. ZONE/ FOSSIL CHARACTER
FORAMINIFERS
NANNOFOSSILS
RADIOLARIANS
DIATOMS
PALEOMAGNETICS
PHYS. PROPERTIES
CHEMISTRY
SECTION
METERS
GRAPHIC LITHOLOGY
DRILLING DISTURB.
SED. STRUCTURES
SAMPLES
UPPER MIOCENE
NN11 Discoaster quinqueramus
•C/G Didymocyrtis antepenultima
•A/G-M
•C/G
•φ=69.8 γ=1.57
•IC=6.77 OC=0.27
•IC=4.89 OC=2.25
1
2
3
4
5
6
7
CC
0.5
1.0
PP

LITHOLOGIC DESCRIPTION

Interbedded NANNOFOSSIL CHALK and DIATOM-BEARING NANNOFOSSIL CHALK

Section 2, 0-70 cm, is very disturbed. Section 1 and Section 5, 50 cm, to Section 7, 20 cm, are moderately disturbed. Remainder of the core is slightly disturbed.

Major lithology: Interbedded NANNOFOSSIL CHALK and DIATOM- BEARING NANNOFOSSIL CHALK. Contacts are gradational. Beds range from gray (5Y 6/1) to light olive gray (5Y 6/2), light gray (5Y 7/2, 7/1), olive gray (5Y 5/2, 4/3, 4/2), and olive (5Y 5/3). Bioturbation is minor to moderate throughout.

SMEAR SLIDE SUMMARY (%):

	1, 4 D
TEXTURE:	
Sand	40
Silt	30
Clay	30
COMPOSITION:	
Access. minerals	1
Cement	30
Clay	20
Feldspar	1
Hornblende	1
Mica	3
Opaques	4
Quartz	40

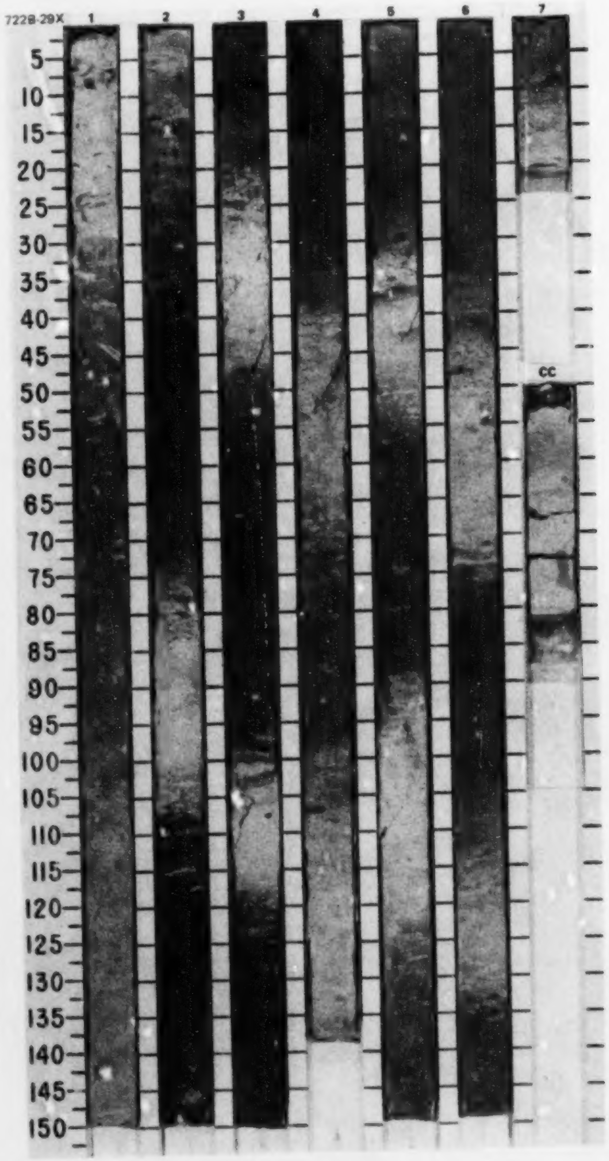
722B-29X
1
2
3
4
5
6
7
CC
5
10
15
20
25
30
35
40
45
50
55
60
65
70
75
80
85
90
95
100
105
110
115
120
125
130
135
140
145
150

SITE 722 HOLE B CORE 30X CORED INTERVAL 2303.4-2313.1 mbsl; 275.6-285.3 mbsf

TIME-ROCK UNIT	BIOSTRAT. ZONE/ FOSSIL CHARACTER					PALEOMAGNETICS	PHYS. PROPERTIES	CHEMISTRY	SECTION	METERS	GRAPHIC LITHOLOGY	DRILLING DISTURB.	SED. STRUCTURES	SAMPLES	LITHOLOGIC DESCRIPTION
	FORAMINIFERS	NANNOFOSSILS	RADIOLARIANS	DIATOMS											
MIOCENE	N15 ●R/M	NN10 *Discoaster calcaris* ●A/M	*Didymocyrtis antepenultima* ●C/G			O			1 2 CC	0.5 1.0	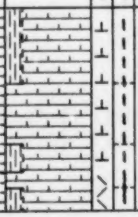				Interbedded NANNOFOSSIL CHALK and DIATOM-BEARING NANNOFOSSIL CHALK CC is highly fragmented. Remainder of the core is moderately fractured. Major lithology: Interbedded NANNOFOSSIL CHALK and DIATOM- BEARING NANNOFOSSIL CHALK. Contacts are gradational. Beds range from gray (5Y 6/1) to light gray (5Y 7/1) and olive gray (5Y 5/2). Bioturbation is minor throughout.

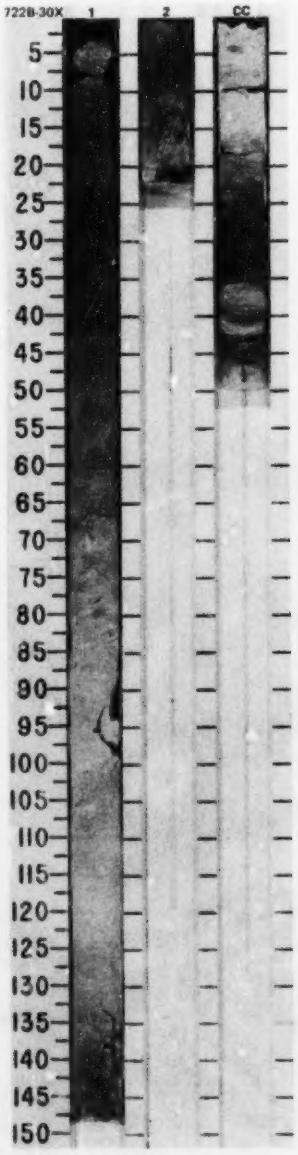
722B-30X
1
2
CC
5
10
15
20
25
30
35
40
45
50
55
60
65
70
75
80
85
90
95
100
105
110
115
120
125
130
135
140
145
150

SITE 722 HOLE B CORE 31X CORED INTERVAL 2313.1-2322.8 mbsl; 285.3-295.0 mbsf

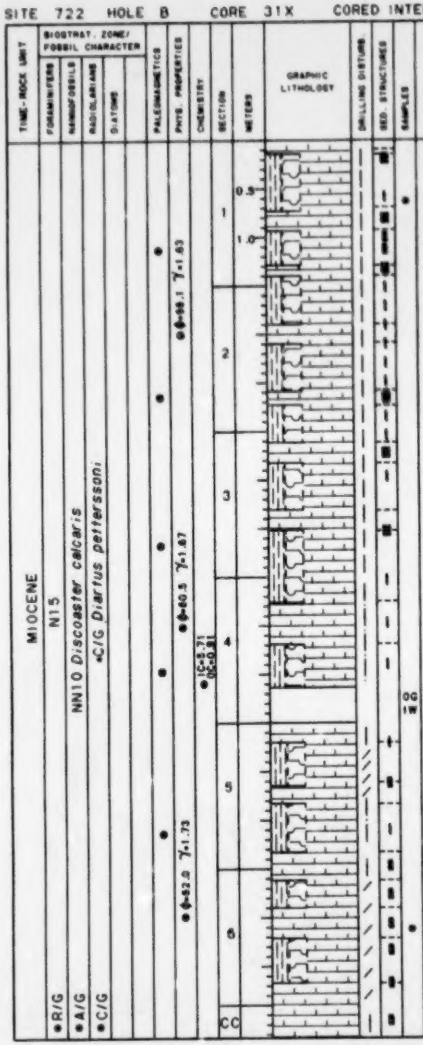
TIME-ROCK UNIT
BIOSTRAT. ZONE/ FOSSIL CHARACTER
FORAMINIFERS
NANNOFOSSILS
RADIOLARIANS
DIATOMS
PALEOMAGNETICS
PHYS. PROPERTIES
CHEMISTRY
SECTION
METERS
GRAPHIC LITHOLOGY
DRILLING DISTURB.
SED. STRUCTURES
SAMPLES
MIOCENE
N15
NN10 Discoaster calcaris
•C/G Diartus petterssoni
•R/G
•A/G
•C/G
•φ=68.1 γ=1.63
•φ=60.5 γ=1.87
•φ=62.0 γ=1.73
•IC=5.71 OC=0.81
1
2
3
4
5
6
CC
0.5
1.0
OG
IW

LITHOLOGIC DESCRIPTION

Interbedded NANNOFOSSIL CHALK and DIATOM-BEARING NANNOFOSSIL CHALK

Section 5, 20-85 cm, and Section 6, 25-140 cm, are slightly fractured. Section 1, Section 3, and CC are slightly disturbed. Remainder of the core is moderately disturbed.

Major lithology: Interbedded NANNOFOSSIL CHALK and DIATOM-BEARING NANNOFOSSIL CHALK. Contacts are gradational. Beds range from gray (5Y 6/1) to light olive gray (5Y 6/2), light gray (5Y 7/1), olive gray (5Y 5/2), and olive (5Y 5/3, 4/3). Bioturbation is minor to strong throughout and most evidant across contacts.

SMEAR SLIDE SUMMARY (%):

	1, 63 D	6, 57 D
TEXTURE:		
Sand	10	
Silt	10	10
Clay	80	90
COMPOSITION:		
Clay	10	10
Diatoms	10	5
Foraminifers	Tr	
Inorganic calcite	5	Tr
Mica		Tr
Nannofossils	65	85
Quartz	5	Tr
Radiolarians	5	Tr
Silicoflagellates	Tr	Tr
Sponge spicules	Tr	Tr

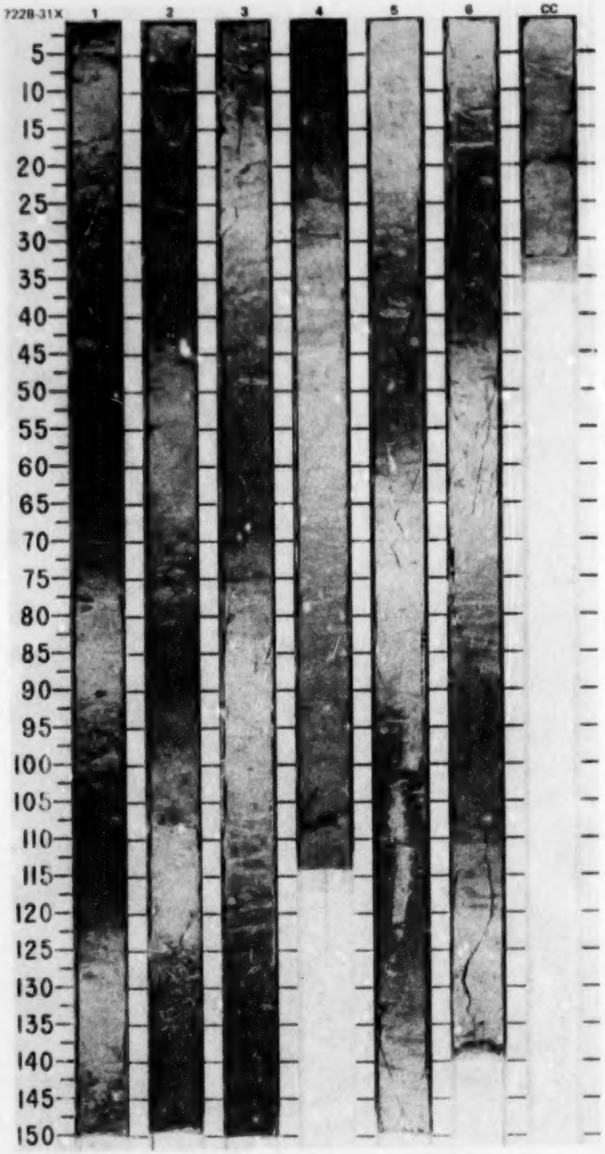
722B-31X
1
2
3
4
5
6
CC
5
10
15
20
25
30
35
40
45
50
55
60
65
70
75
80
85
90
95
100
105
110
115
120
125
130
135
140
145
150

SITE 722 HOLE B CORE 32X CORED INTERVAL 2322.8-2332.5 mbsl; 295.0-304.7 mbsf

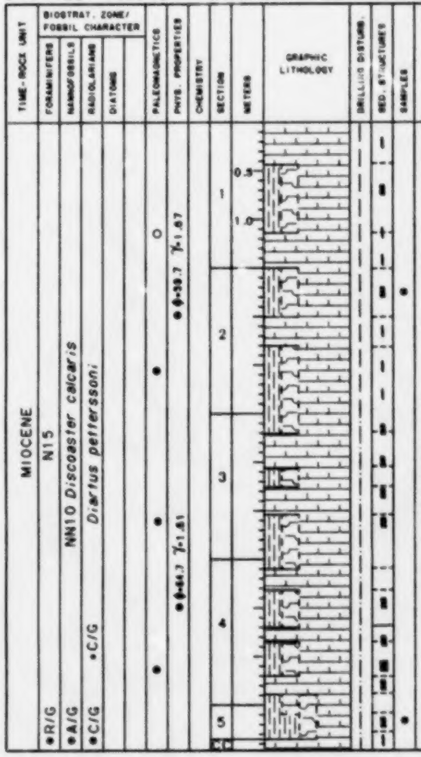
TIME-ROCK UNIT
BIOSTRAT. ZONE/ FOSSIL CHARACTER
FORAMINIFERS
NANNOFOSSILS
RADIOLARIANS
DIATOMS
PALEOMAGNETICS
PHYS. PROPERTIES
CHEMISTRY
SECTION
METERS
GRAPHIC LITHOLOGY
DRILLING DISTURB.
SED. STRUCTURES
SAMPLES
MIOCENE
N15
NN10 Discoaster calcaris
Diartus petterssoni
•R/G
•A/G
•C/G
•C/G
● ϕ=59.7 γ=1.87
● ϕ=64.7 γ=1.81
0.5
1.0
1
2
3
4
5
CC

LITHOLOGIC DESCRIPTION

Interbedded NANNOFOSSIL CHALK and DIATOMACEOUS MARLY NANNOFOSSIL CHALK

Sections 1-2 are slightly disturbed. Sections 3-CC are moderately disturbed.

Major lithology: Interbedded NANNOFOSSIL CHALK and DIATOMACEOUS MARLY NANNOFOSSIL CHALK. Contacts are gradational except for sharp contact in Section 4, 73 cm. Beds range from light olive gray (5Y 6/2) to light gray (5Y 7/1, 7/2), olive (5Y 4/3, 4/2), pale olive (5Y 6/3), and dark olive gray (5Y 3/2). Bioturbation is minor to moderate throughout.

SMEAR SLIDE SUMMARY (%):

	2, 25 D	5, 16 M
TEXTURE:		
Sand		10
Silt	10	10
Clay	90	80
COMPOSITION:		
Clay	10	30
Diatoms	10	15
Inorganic calcite	Tr	
Mica		Tr
Nannofossils	80	45
Quartz		5
Radiolarians	Tr	5
Silicoflagellates	Tr	Tr
Sponge spicules		Tr

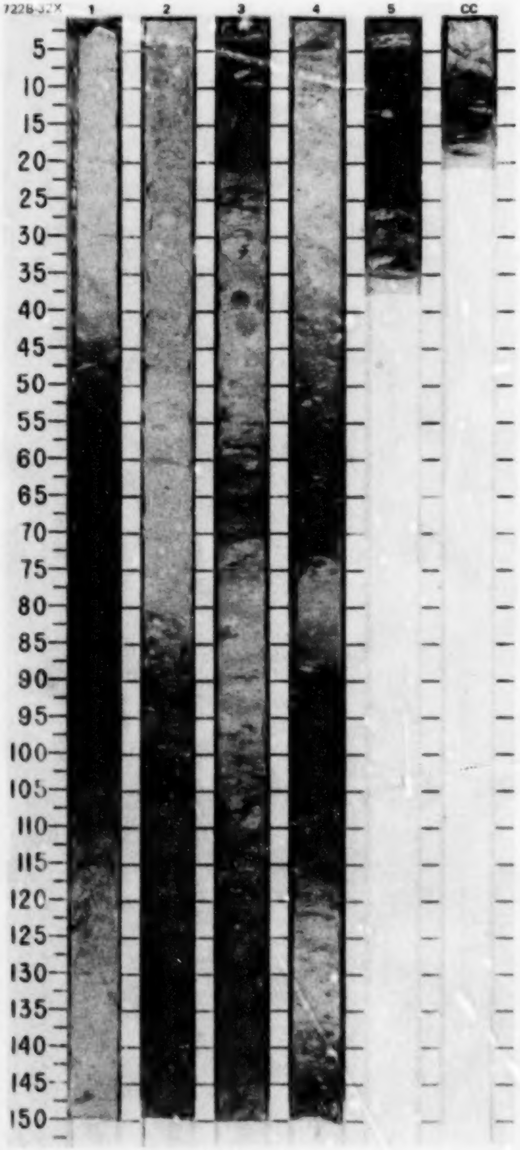
722B-32X
1
2
3
4
5
CC
5
10
15
20
25
30
35
40
45
50
55
60
65
70
75
80
85
90
95
100
105
110
115
120
125
130
135
140
145
150

SITE 722 HOLE B CORE 33X CORED INTERVAL 2332.5-2342.1 mbsl; 304.7-314.3 mbsf

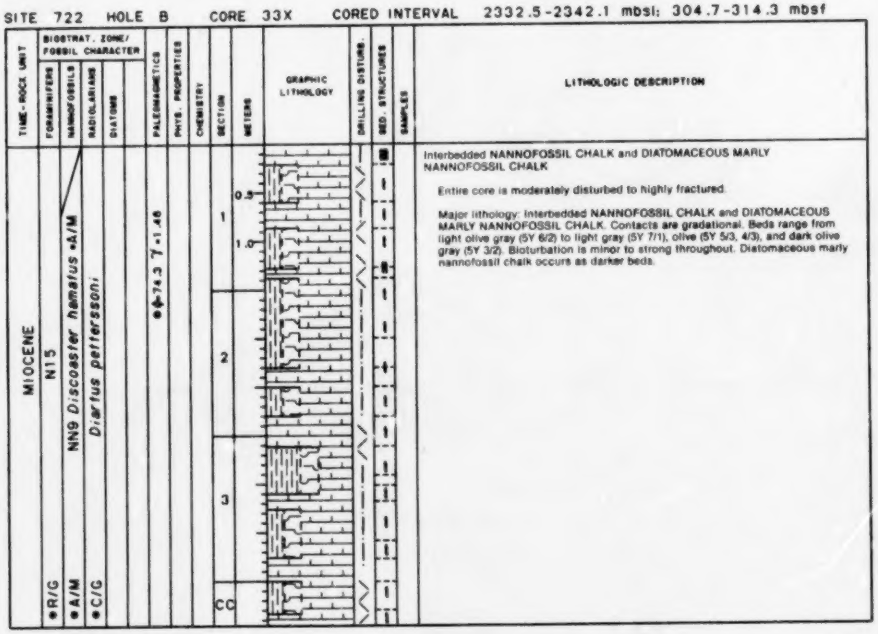
TIME-ROCK UNIT
BIOSTRAT. ZONE/ FOSSIL CHARACTER
FORAMINIFERS
NANNOFOSSILS
RADIOLARIANS
DIATOMS
PALEOMAGNETICS
PHYS. PROPERTIES
CHEMISTRY
SECTION
METERS
GRAPHIC LITHOLOGY
DRILLING DISTURB.
SED. STRUCTURES
SAMPLES
LITHOLOGIC DESCRIPTION
MIOCENE
N15
NN9 Discoaster hamatus •A/M
Diartus petterssoni
•R/G
•A/M
•C/G
•ɸ-74.3 γ-1.48
1
2
3
CC
0.5
1.0

Interbedded NANNOFOSSIL CHALK and DIATOMACEOUS MARLY NANNOFOSSIL CHALK

Entire core is moderately disturbed to highly fractured.

Major lithology: Interbedded NANNOFOSSIL CHALK and DIATOMACEOUS MARLY NANNOFOSSIL CHALK. Contacts are gradational. Beds range from light olive gray (5Y 6/2) to light gray (5Y 7/1), olive (5Y 5/3, 4/3), and dark olive gray (5Y 3/2). Bioturbation is minor to strong throughout. Diatomaceous marly nannofossil chalk occurs as darker beds.

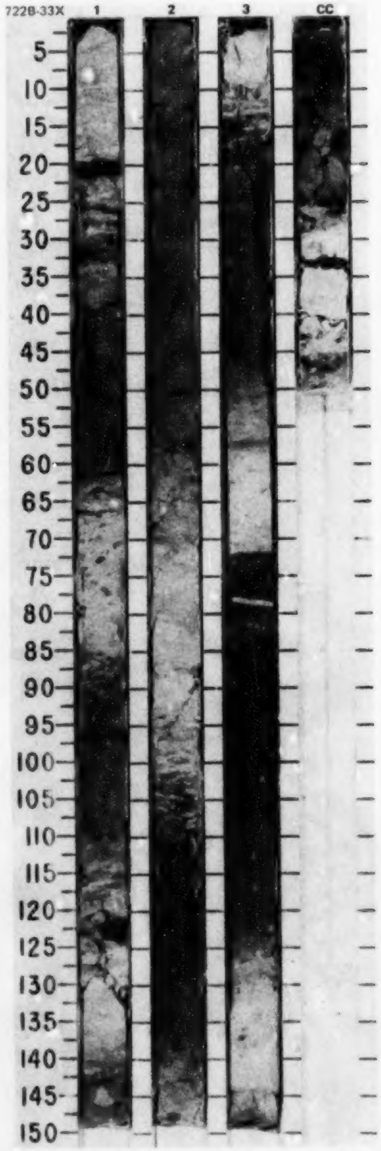
722B-33X
1
2
3
CC
5
10
15
20
25
30
35
40
45
50
55
60
65
70
75
80
85
90
95
100
105
110
115
120
125
130
135
140
145
150

SITE 722 HOLE B CORE 34X CORED INTERVAL 2342.1-2351.8 mbsl; 314.3-324.0 mbsf

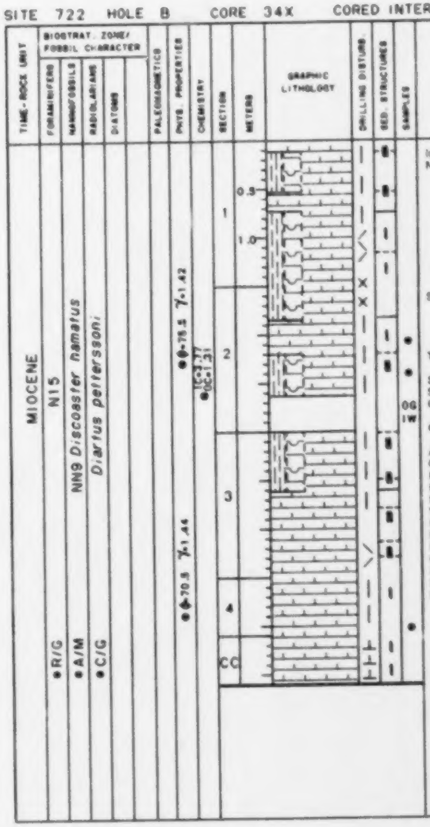
TIME-ROCK UNIT
BIOSTRAT. ZONE/ FOSSIL CHARACTER
FORAMINIFERS
NANNOFOSSILS
RADIOLARIANS
DIATOMS
PALEOMAGNETICS
PHYS. PROPERTIES
CHEMISTRY
SECTION
METERS
GRAPHIC LITHOLOGY
DRILLING DISTURB.
SED. STRUCTURES
SAMPLES
MIOCENE
N15
NN9 Discoaster hamatus
Diartus petterssoni
●R/G
●A/M
●C/G
●Φ-75.5 γ-1.42
●Φ-70.5 γ-1.44
IC-2.77
●OC-1.31
0.5
1.0
1
2
3
4
CC
OG
IW

LITHOLOGIC DESCRIPTION

Interbedded NANNOFOSSIL CHALK and DIATOMACEOUS MARLY NANNOFOSSIL CHALK

Entire core is slightly disturbed to brecciated.

Major lithology: Interbedded NANNOFOSSIL CHALK and DIATOMACEOUS MARLY NANNOFOSSIL CHALK. Contacts are gradational except for sharp contact in Section 2, 35 cm. Beds range from light olive gray (5Y 6/2) to light gray (5Y 7/1), olive gray (5Y 5/2), and olive (5Y 4/3, 5/3). Bioturbation is minor to strong throughout. Subvertical, en echelon dewatering (?) structures are present in darker, diatomaceous beds.

SMEAR SLIDE SUMMARY (%):

	2, 57 D	2, 90 D	4, 52 D
TEXTURE:			
Sand		5	
Silt	14	20	10
Clay	86	75	90
COMPOSITION:			
Access. minerals	Tr	2	Tr
Clay	6	40	5
Diatoms	12	15	7
Feldspar		1	
Foraminifers			Tr
Volcanic glass		Tr	
Inorganic calcite	1	2	2
Mica	Tr	1	Tr
Nannofossils	80	35	85
Quartz	Tr	3	1
Radiolarians	1	1	
Silicoflagellates	Tr		
Sponge spicules			Tr

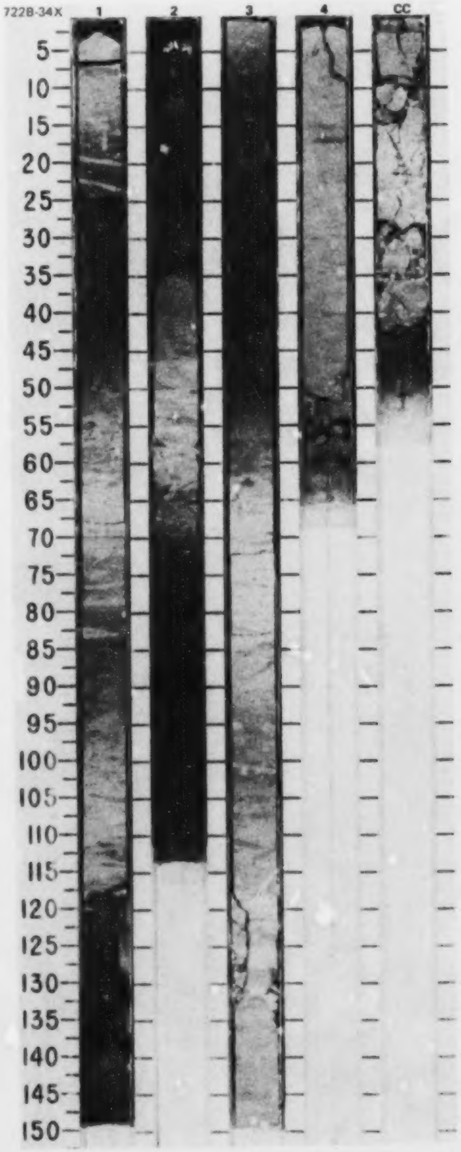
722B-34X
1
2
3
4
CC
5
10
15
20
25
30
35
40
45
50
55
60
65
70
75
80
85
90
95
100
105
110
115
120
125
130
135
140
145
150

SITE 722 HOLE B CORE 35X CORED INTERVAL 2351.8-2361.5 mbsl; 324.0-337.7 mbsf

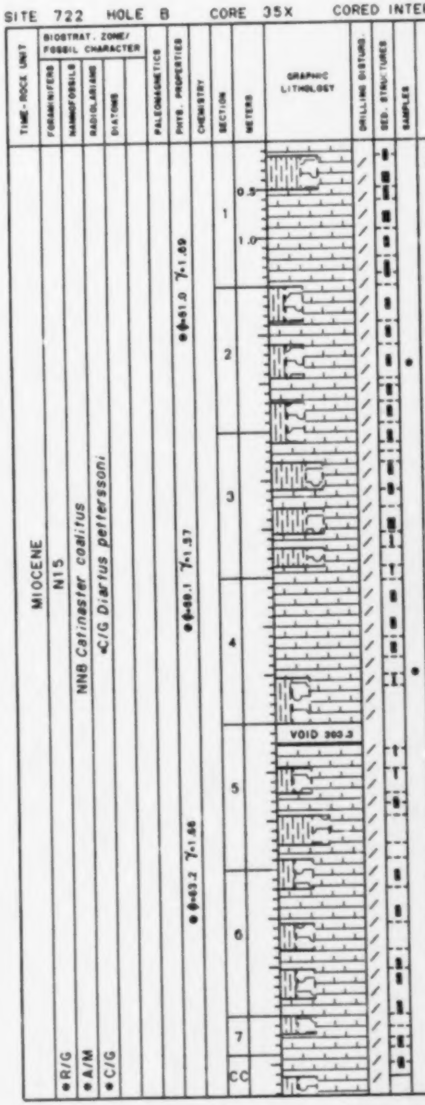
TIME-ROCK UNIT
BIOSTRAT. ZONE/ FOSSIL CHARACTER
FORAMINIFERS
NANNOFOSSILS
RADIOLARIANS
DIATOMS
PALEOMAGNETICS
PHYS. PROPERTIES
CHEMISTRY
SECTION
METERS
GRAPHIC LITHOLOGY
DRILLING DISTURB.
SED. STRUCTURES
SAMPLES
MIOCENE
N15
NNB Catinaster coalitus
•C/G Diartus petterssoni
•R/G
•A/M
•C/G
•φ=51.0 γ=1.69
•φ=60.1 γ=1.57
•φ=63.2 γ=1.56
1
2
3
4
5
6
7
CC
0.5
1.0
VOID 303.3

LITHOLOGIC DESCRIPTION

Interbedded NANNOFOSSIL CHALK and DIATOMACEOUS MARLY NANNOFOSSIL CHALK

Entire core is slightly fractured.

Major lithology: Interbedded NANNOFOSSIL CHALK and DIATOMACEOUS MARLY NANNOFOSSIL CHALK. Contacts are gradational except for sharp contacts in Section 6, 137 cm, and CC, 24 cm. Beds range from white (5Y 8/1) to gray (5Y 6/1), light olive gray (5Y 6/2), light gray (5Y 7/2, 7/1), light greenish gray (5GY 7/1, 10Y 6/2), olive (5Y 5/4, 5/3, 4/3), pale olive (5Y 6/3), and dark greenish gray (5GY 6/1). Bioturbation is minor to strong throughout. Subvertical, en echelon dewatering (?) structures are present in light and dark beds, but are larger and more prevalent in darker beds. Concentric purple alteration rings around burrows occur within the lighter beds.

SMEAR SLIDE SUMMARY (%):

	2, 80 D	4, 98 D
TEXTURE:		
Sand	10	
Silt	20	3
Clay	70	97
COMPOSITION:		
Access. minerals	2	
Clay	35	7
Diatoms	20	1
Feldspar	Tr	
Foraminifers		1
Inorganic calcite	3	1
Mica		Tr
Nannofossils	35	90
Quartz	5	
Radiolarians		Tr
Silicoflagellates	Tr	
Sponge spicules	Tr	

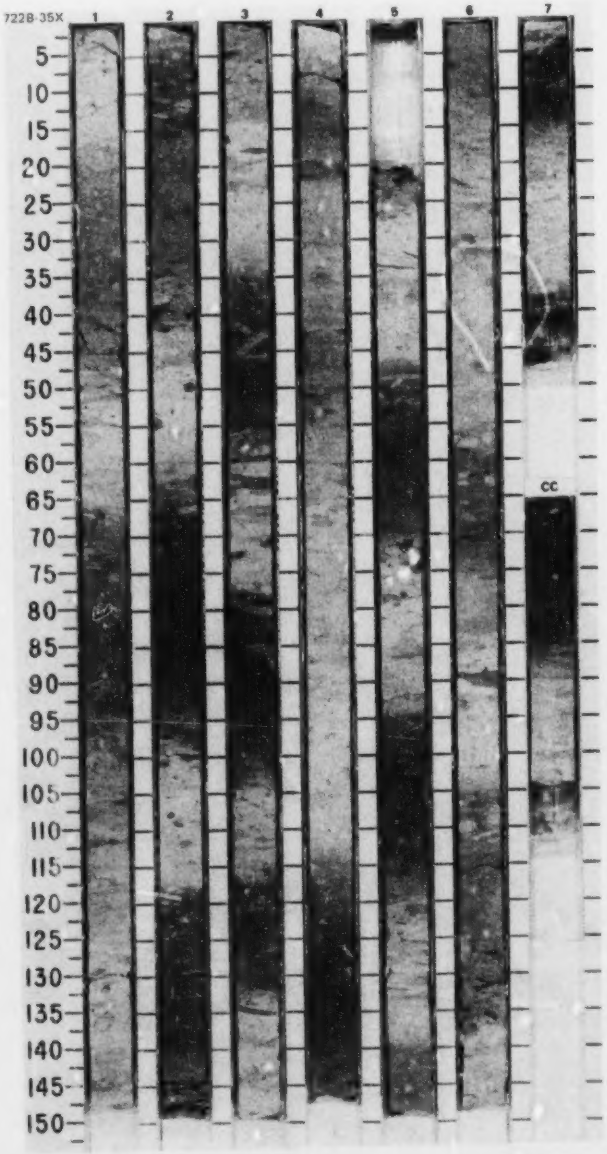
722B-35X
1
2
3
4
5
6
7
CC
5
10
15
20
25
30
35
40
45
50
55
60
65
70
75
80
85
90
95
100
105
110
115
120
125
130
135
140
145
150

SITE 722 HOLE B CORE 36X CORED INTERVAL 2361.5-2371.2 mbsl; 333.7-343.4 mbsf

TIME-ROCK UNIT	BIOSTRAT. ZONE/ FOSSIL CHARACTER: FORAMINIFERS	BIOSTRAT. ZONE/ FOSSIL CHARACTER: NANNOFOSSILS	BIOSTRAT. ZONE/ FOSSIL CHARACTER: RADIOLARIANS	BIOSTRAT. ZONE/ FOSSIL CHARACTER: DIATOMS	PALEOMAGNETICS	PHYS. PROPERTIES	CHEMISTRY	SECTION	METERS
MIOCENE	N14 ● R/B	NN8 *Catinaster coalitus* ● A/G-M	*Diartus petterssoni* ● C/M ● C/M			●ϕ=52.9 γ=1.72		1	0.5 1.0
								2	
						●ϕ=63.7 γ=1.84		3	
								4	
								CC	

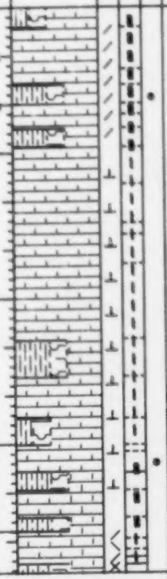
GRAPHIC LITHOLOGY
DRILLING DISTURB.
SED. STRUCTURES
SAMPLES

LITHOLOGIC DESCRIPTION

Interbedded NANNOFOSSIL CHALK and DIATOMACEOUS MARLY NANNOFOSSIL CHALK

Section 1 is slightly fractured. Section 2 to Section 4, 90 cm, is moderately fractured. CC is highly fragmented.

Major lithology: Interbedded NANNOFOSSIL CHALK and DIATOMACEOUS MARLY NANNOFOSSIL CHALK. Contacts are gradational except for sharp contact at Section 4, 28 cm. Beds range from light gray (5Y 7/2, 7/1) to light greenish gray (10Y 7/1, 6/2), olive (5Y 5/4, 4/3), pale olive (5Y 6/3), and dark greenish gray (5GY 7/1, 6/1). Bioturbation is minor to moderate throughout the core. Concentric purple calcite alteration rings around burrows occur within the lighter beds.

SMEAR SLIDE SUMMARY (%):

	1, 93 D	4, 22 D
TEXTURE:		
Sand	5	5
Silt	20	5
Clay	75	90
COMPOSITION:		
Access. minerals	1	Tr
Clay	35	5
Diatoms	15	1
Dolomite	Tr	
Feldspar	1	
Foraminifers		1
Volcanic glass	Tr	
Inorganic calcite	1	3
Mica	1	
Nannofossils	40	85
Quartz	5	
Radiolarians	Tr	4
Silicoflagellates	Tr	
Sponge spicules	1	1

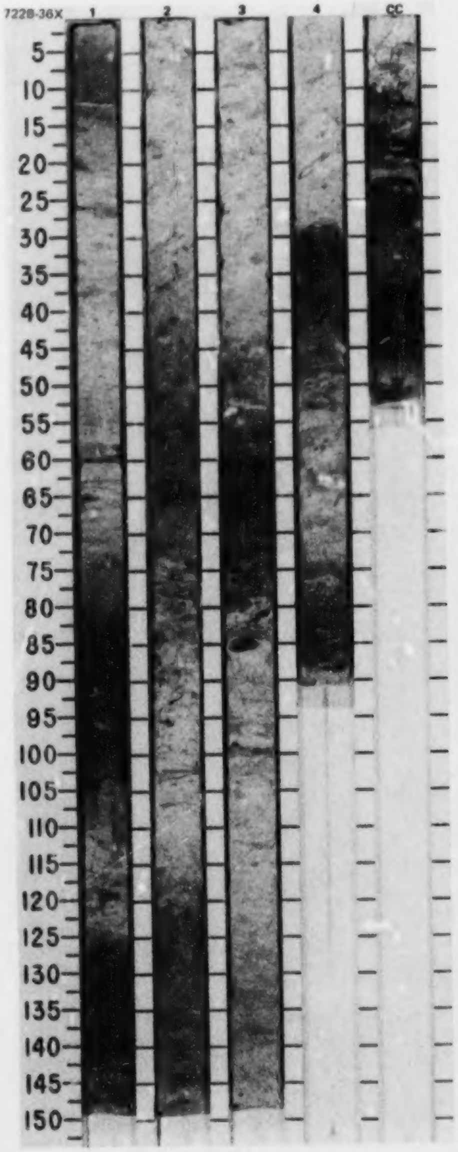
722B-36X
1
2
3
4
CC
5
10
15
20
25
30
35
40
45
50
55
60
65
70
75
80
85
90
95
100
105
110
115
120
125
130
135
140
145
150

SITE 722 HOLE B CORE 37X CORED INTERVAL 2371.2-2380.9 mbsl; 343.4-353.1 mbsf

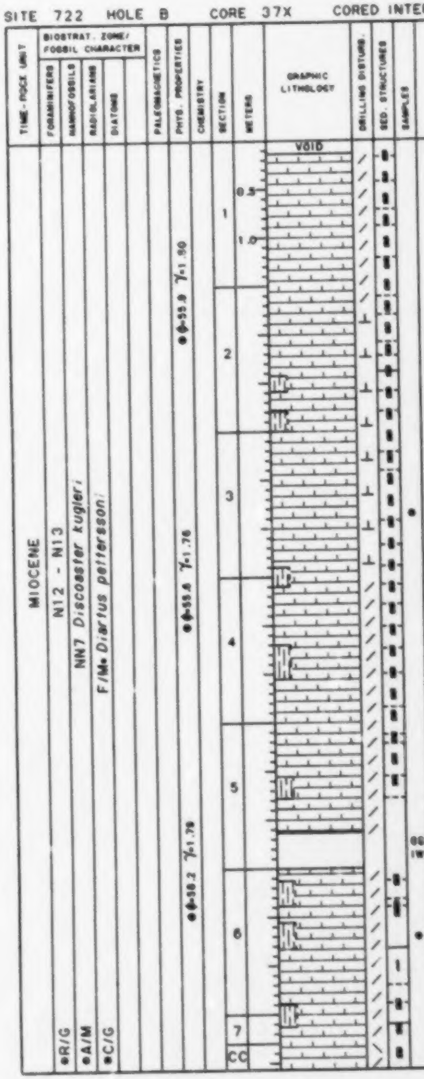
TIME-ROCK UNIT
BIOSTRAT. ZONE/ FOSSIL CHARACTER
FORAMINIFERS
NANNOFOSSILS
RADIOLARIANS
DIATOMS
PALEOMAGNETICS
PHYS. PROPERTIES
CHEMISTRY
SECTION
METERS
GRAPHIC LITHOLOGY
DRILLING DISTURB.
SED. STRUCTURES
SAMPLES
MIOCENE
N12 - N13
NN7 Discoaster kugleri
F/M• Diartus petterssoni
●R/G
●A/M
●C/G
●ϕ=55.9 γ=1.90
●ϕ=55.6 γ=1.76
●ϕ=58.2 γ=1.78
1
2
3
4
5
6
7
CC
0.5
1.0
VOID
OG
IW

LITHOLOGIC DESCRIPTION

NANNOFOSSIL CHALK

Section 1, 0 cm, to Section 2, 20 cm, and Section 3, 10 cm, to Section 7, 30 cm, are slightly fractured. Section 2, 20 cm, to Section 3, 0 cm, is moderately fractured. CC is highly fragmented.

Major lithology: NANNOFOSSIL CHALK. Beds range from white (5Y 8/1) to gray (5Y 5/1), light olive gray (5Y 6/2), light gray (5Y 7/1), light greenish gray (5G 7/1, 5GY 7/1, 10Y 6/2), greenish gray (5GY 6/1), olive (5Y 5/3), and dark greenish gray (10Y 5/2). Contacts are gradational except for Section 2, 93 cm, and Section 6, 84 cm. Bioturbation is minor to moderate throughout. Lighter beds contain burrows encircled by concentric purple alteration rings.

SMEAR SLIDE SUMMARY (%):

	3, 85 D	6, 71 D
TEXTURE:		
Silt	5	10
Clay	95	90
COMPOSITION:		
Access. minerals	Tr	1
Clay	5	20
Diatoms	1	1
Dolomite		1
Feldspar		1
Foraminifers	1	Tr
Inorganic calcite	2	
Mica		1
Nannofossils	90	70
Quartz		5
Radiolarians	1	
Silicoflagellates		Tr

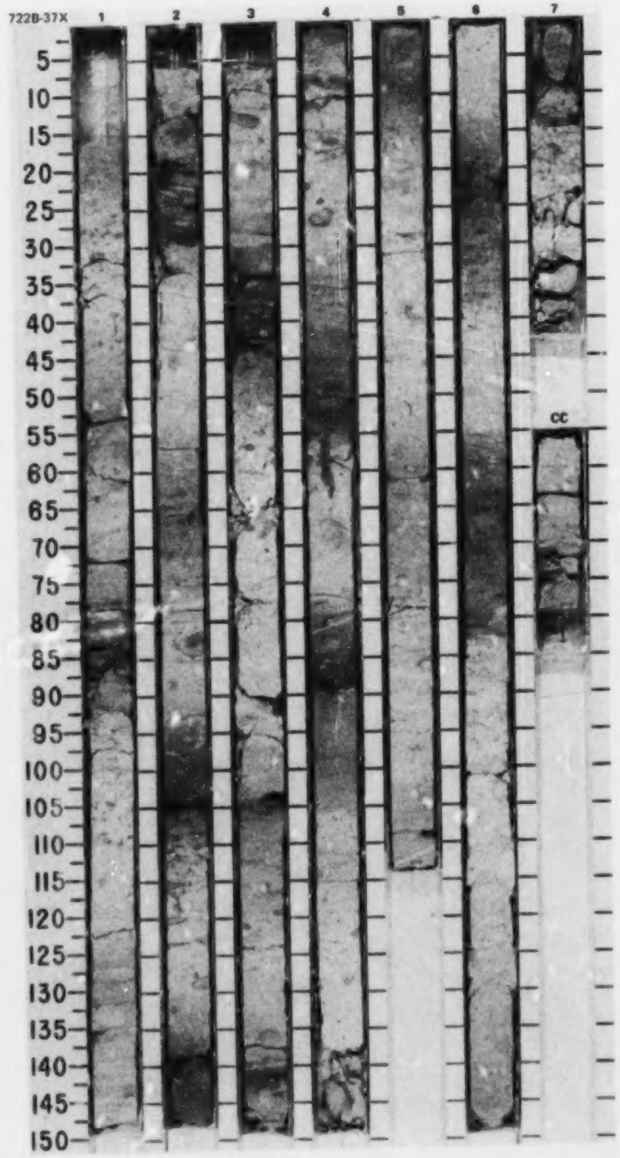
722B-37X
1
2
3
4
5
6
7
CC
5
10
15
20
25
30
35
40
45
50
55
60
65
70
75
80
85
90
95
100
105
110
115
120
125
130
135
140
145
150

SITE 722 HOLE B CORE 38X CORED INTERVAL 2380.9-2390.6 mbsl; 353.1-362.8 mbsf

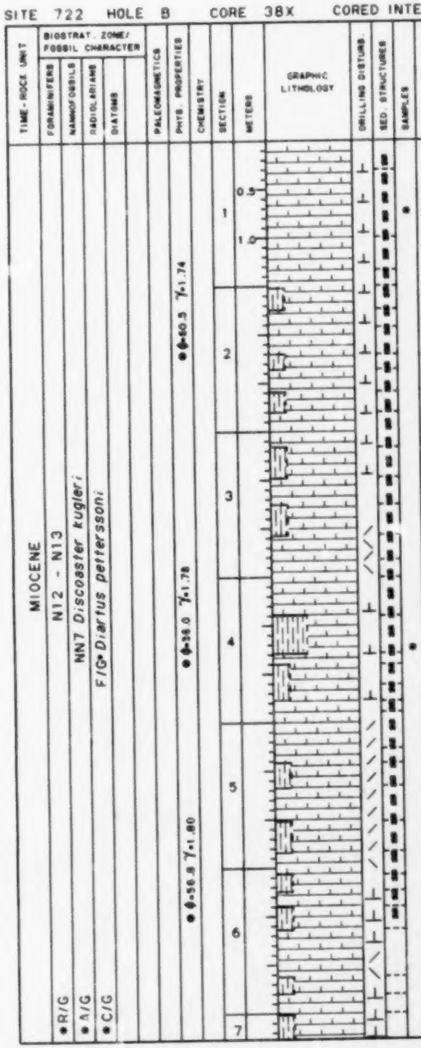
TIME-ROCK UNIT
BIOSTRAT. ZONE/ FOSSIL CHARACTER
FORAMINIFERS
NANNOFOSSILS
RADIOLARIANS
DIATOMS
PALEOMAGNETICS
PHYS. PROPERTIES
CHEMISTRY
SECTION
METERS
GRAPHIC LITHOLOGY
DRILLING DISTURB.
SED. STRUCTURES
SAMPLES
MIOCENE
N12 - N13
NN7 Discoaster kugleri
F/G• Diartus petterssoni
●R/G
●A/G
●C/G
●ϕ=60.5 γ=1.74
●ϕ=56.0 γ=1.78
●ϕ=56.8 γ=1.80
1
2
3
4
5
6
7
0.5
1.0

LITHOLOGIC DESCRIPTION

Interbedded NANNOFOSSIL CHALK and MARLY NANNOFOSSIL CHALK

Entire core is slightly fractured to highly fragmented.

Major lithology: Interbedded NANNOFOSSIL CHALK and MARLY NANNOFOSSIL CHALK. Contacts are gradational. Beds range from white (5Y 8/1) to light gray (5Y 7/1), light greenish gray (5GY 7/1, 10Y 7/1), greenish gray (5G 5/1, 5G 6/1, 5GY 6/1), and dark greenish gray (10Y 4/2, 5/2). Bioturbation is moderate throughout. Lighter beds contain burrows encircled by concentric purple alteration rings.

SMEAR SLIDE SUMMARY (%):

	1, 72 D	4, 72 D
TEXTURE:		
Sand		5
Silt	5	10
Clay	95	85
COMPOSITION:		
Access. minerals	Tr	2
Clay	5	30
Diatoms	Tr	
Dolomite		Tr
Feldspar		2
Foraminifers	Tr	2
Volcanic glass	Tr	Tr
Inorganic calcite	5	5
Nannofossils	90	55
Quartz		4
Radiolarians	Tr	Tr
Sponge spicules	Tr	Tr

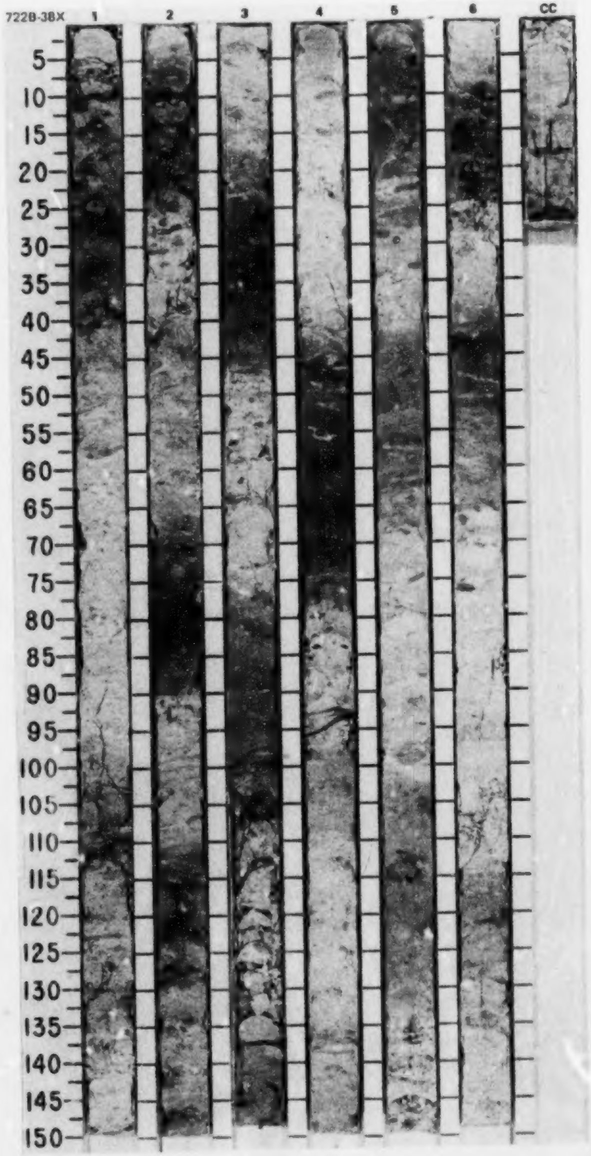
722B-38X
1
2
3
4
5
6
CC
5
10
15
20
25
30
35
40
45
50
55
60
65
70
75
80
85
90
95
100
105
110
115
120
125
130
135
140
145
150

SITE 722 HOLE B CORE 39X CORED INTERVAL 2390.6-2400.3 mbsl; 362.372.5 mbsf

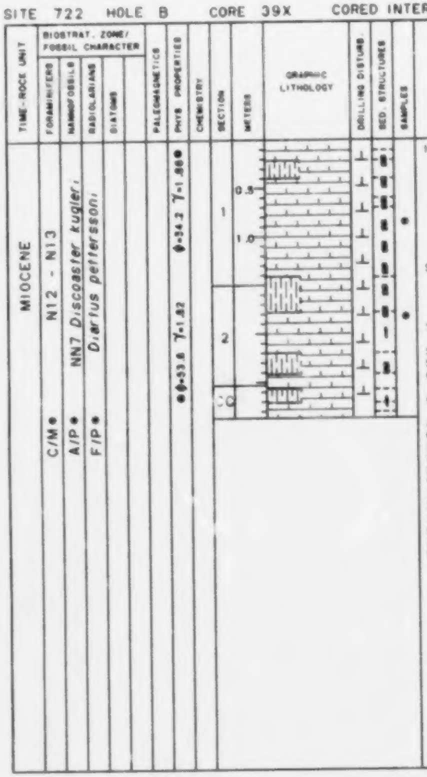
TIME-ROCK UNIT
BIOSTRAT. ZONE/ FOSSIL CHARACTER
FORAMINIFERS
NANNOFOSSILS
RADIOLARIANS
DIATOMS
PALEOMAGNETICS
PHYS. PROPERTIES
CHEMISTRY
SECTION
METERS
GRAPHIC LITHOLOGY
DRILLING DISTURB.
SED. STRUCTURES
SAMPLES
MIOCENE
N12 - N13
NN7 Discoaster kugleri
Diartus petterssoni
C/M●
A/P●
F/P●
●ϕ=53.6 γ=1.82
ϕ=34.2 γ=1.86●
1
2
CC
0.5
1.0

LITHOLOGIC DESCRIPTION

Interbedded NANNOFOSSIL CHALK and MARLY NANNOFOSSIL CHALK

Entire core is moderately fractured.

Major lithology: Interbedded NANNOFOSSIL CHALK and MARLY NANNOFOSSIL CHALK. Contacts are gradational. Beds range from white (5Y 8/1) to light gray (N7), light greenish gray (5BG 7/1, 5G 7/1, 5GY 7/1), and greenish gray (5GY 6/1). Bioturbation is minor to moderate throughout. Lighter beds contain burrows encircled by concentric purple alteration rings.

SMEAR SLIDE SUMMARY (%)

	1, 85 D	2, 32 D
TEXTURE:		
Sand		5
Silt	5	10
Clay	95	85
COMPOSITION:		
Access. minerals	Tr	2
Clay	5	25
Dolomite	Tr	Tr
Feldspar		Tr
Foraminifers	Tr	Tr
Volcanic glass	Tr	Tr
Inorganic calcite	5	8
Mica		Tr
Nannofossils	90	60
Quartz		1
Radiolarians	Tr	Tr
Sponge spicules	Tr	Tr

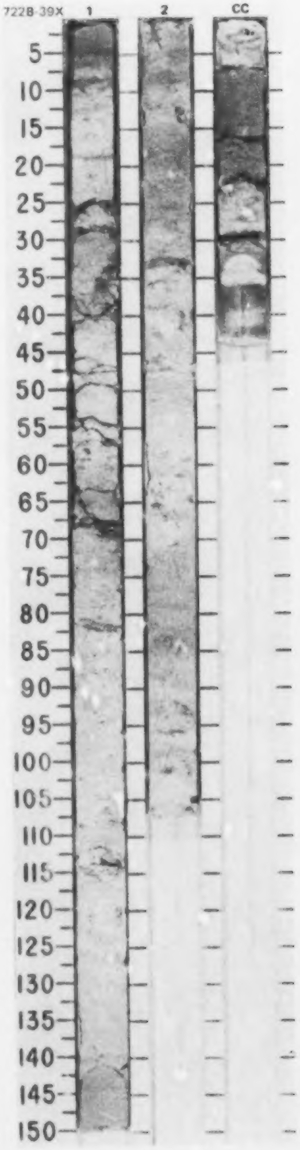
722B-39X
1
2
CC
5
10
15
20
25
30
35
40
45
50
55
60
65
70
75
80
85
90
95
100
105
110
115
120
125
130
135
140
145
150

SITE 722 HOLE B CORE 40X CORED INTERVAL 2400.3-2410.0 mbsl; 372.5-382.2 mbsf

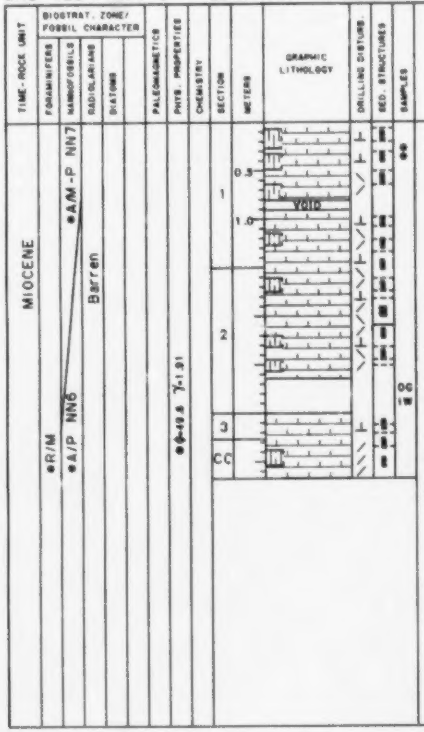
TIME-ROCK UNIT
BIOSTRAT. ZONE/ FOSSIL CHARACTER
FORAMINIFERS
NANNOFOSSILS
RADIOLARIANS
DIATOMS
PALEOMAGNETICS
PHYS. PROPERTIES
CHEMISTRY
SECTION
METERS
GRAPHIC LITHOLOGY
DRILLING DISTURB.
SED. STRUCTURES
SAMPLES
MIOCENE
●R/M
●AM-P NN7
●A/P NN6
Barren
●ϕ-49.6 γ-1.91
1
2
3
CC
0.5
1.0
VOID
OG
IW

LITHOLOGIC DESCRIPTION

Interbedded NANNOFOSSIL CHALK and FORAMINIFER-BEARING NANNOFOSSIL CHALK

Entire core is slightly fractured to highly fragmented.

Major lithology: Interbedded NANNOFOSSIL CHALK and FORAMINIFER-BEARING NANNOFOSSIL CHALK. Contacts are gradational except for sharp contact at Section 2, 70 cm. Beds range from white (5Y 8/1) to gray (5Y 5/1), light gray (N7, 5Y 7/1), light greenish gray (5GY 7/1), greenish gray (5G 5/1, 6/1, 5GY 6/1), and olive gray (5Y 5/2). Bioturbation is moderate to strong throughout. Lighter beds contain concentric purple alteration rings around burrows.

SMEAR SLIDE SUMMARY (%):

	1, 27 D	1, 30 M
TEXTURE:		
Sand	1	10
Silt	4	5
Clay	95	85
COMPOSITION:		
Access. minerals	Tr	Tr
Clay	10	10
Dolomite	Tr	
Foraminifers	2	10
Inorganic calcite	3	5
Nannofossils	85	75

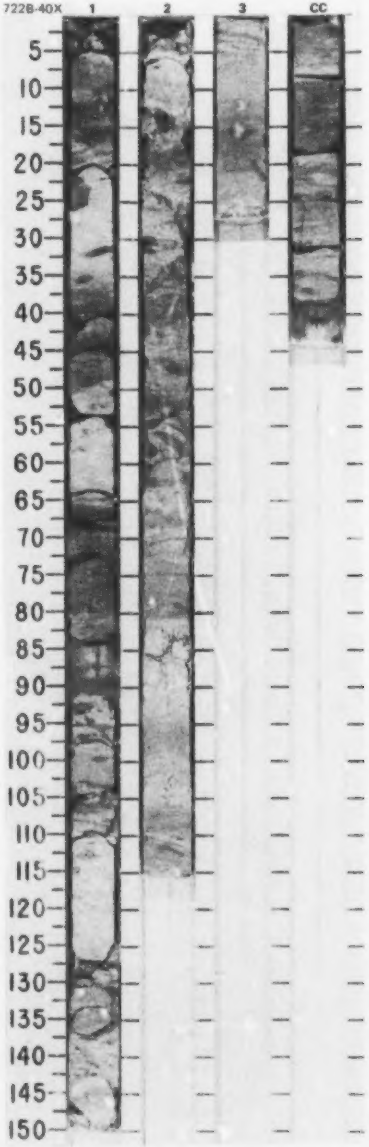
722B-40X
1
2
3
CC
5
10
15
20
25
30
35
40
45
50
55
60
65
70
75
80
85
90
95
100
105
110
115
120
125
130
135
140
145
150

SITE 722 HOLE B CORE 41X CORED INTERVAL 2410.0-2419.6 mbsl; 382.2-391.8 mbsf

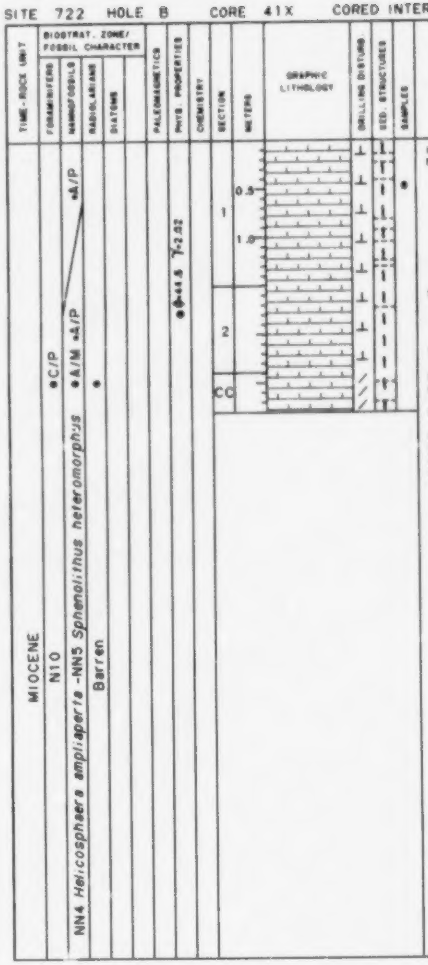
TIME-ROCK UNIT
BIOSTRAT. ZONE/ FOSSIL CHARACTER
FORAMINIFERS
NANNOFOSSILS
RADIOLARIANS
DIATOMS
PALEOMAGNETICS
PHYS. PROPERTIES
CHEMISTRY
SECTION
METERS
GRAPHIC LITHOLOGY
DRILLING DISTURB.
SED. STRUCTURES
SAMPLES
MIOCENE
N10
NN4 Helicosphaera ampliaperta -NN5 Sphenolithus heteromorphus
Barren
●C/P
●A/M ●A/P
●A/P
●φ=44.5 γ=2.02
1
2
CC
0.5
1.0

LITHOLOGIC DESCRIPTION

Interbedded NANNOFOSSIL CHALK and FORAMINIFER-BEARING NANNOFOSSIL CHALK

Core liner shattered, stratigraphy may be disturbed. Entire core is slightly to moderately fractured.

Major lithology: Interbedded NANNOFOSSIL CHALK and FORAMINIFER-BEARING NANNOFOSSIL CHALK. Contacts are gradational. Beds range from white (2.5Y 8/1) to light gray (N7), light greenish gray (5GY 7/1, 5G 7/1), and greenish gray (5GY 6/1). Bioturbation is minor throughout. Lighter beds contain burrows encircled by concentric purple alteration rings.

SMEAR SLIDE SUMMARY (%):

	1, 48 D
TEXTURE:	
Silt	5
Clay	95
COMPOSITION:	
Clay	5
Dolomite	Tr
Inorganic calcite	5
Nannofossils	90

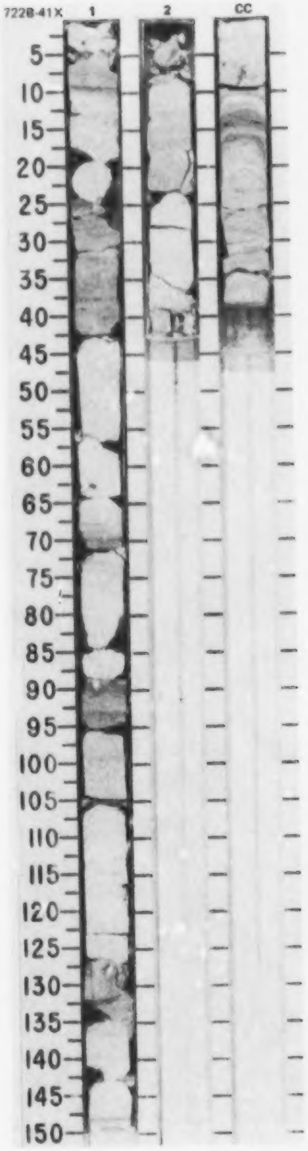
722B-41X
1
2
CC
5
10
15
20
25
30
35
40
45
50
55
60
65
70
75
80
85
90
95
100
105
110
115
120
125
130
135
140
145
150

SITE 722 HOLE B CORE 42X CORED INTERVAL 2419.6-2429.2 mbsl; 391.8-401.4 mbsf

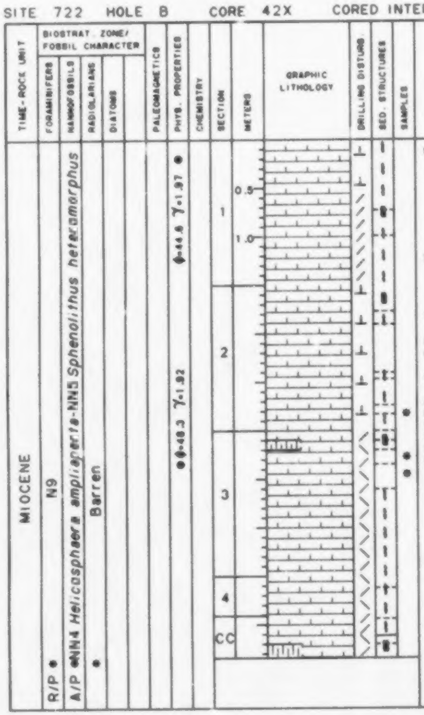
TIME-ROCK UNIT
BIOSTRAT. ZONE/ FOSSIL CHARACTER
FORAMINIFERS
NANNOFOSSILS
RADIOLARIANS
DIATOMS
PALEOMAGNETICS
PHYS. PROPERTIES
CHEMISTRY
SECTION
METERS
GRAPHIC LITHOLOGY
DRILLING DISTURB.
SED. STRUCTURES
SAMPLES
MIOCENE
R/P ● N9
A/P ●NN4 Helicosphaera ampliaperta-NN5 Sphenolithus heteromorphus
● Barren
ϕ=44.6 γ=1.97 ●
●ϕ=48.3 γ=1.92
1
2
3
4
CC
0.5
1.0

LITHOLOGIC DESCRIPTION

Interbedded NANNOFOSSIL CHALK and MARLY NANNOFOSSIL CHALK

Entire core is slightly fractured to highly fragmented.

Major lithology: Interbedded NANNOFOSSIL CHALK and MARLY NANNOFOSSIL CHALK. Contacts are gradational. Beds range from white (N8) to gray (5Y 5/1, 6/1) and light gray (5Y 7/1). Bioturbation is minor to moderate throughout. Diagenetic fronts (stylolites?) occur within the lighter beds.

SMEAR SLIDE SUMMARY (%):

	2, 131 D	3, 17 D	3, 45 D
TEXTURE:			
Silt	20	15	10
Clay	80	85	90
COMPOSITION:			
Access. minerals		5	Tr
Clay	10	35	10
Dolomite	Tr	Tr	1
Inorganic calcite	10	5	8
Nannofossils	80	50	80
Quartz	Tr	5	1

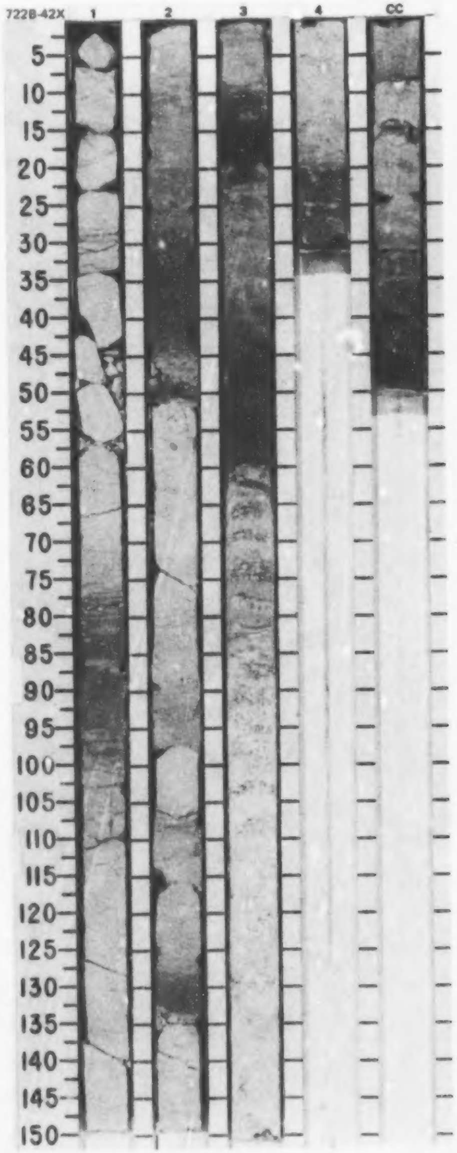
722B-42X
1
2
3
4
CC
5
10
15
20
25
30
35
40
45
50
55
60
65
70
75
80
85
90
95
100
105
110
115
120
125
130
135
140
145
150

SITE 722 HOLE B CORE 43X CORED INTERVAL 2429.2-2438.9 mbsl; 401.4-411.1 mbsf

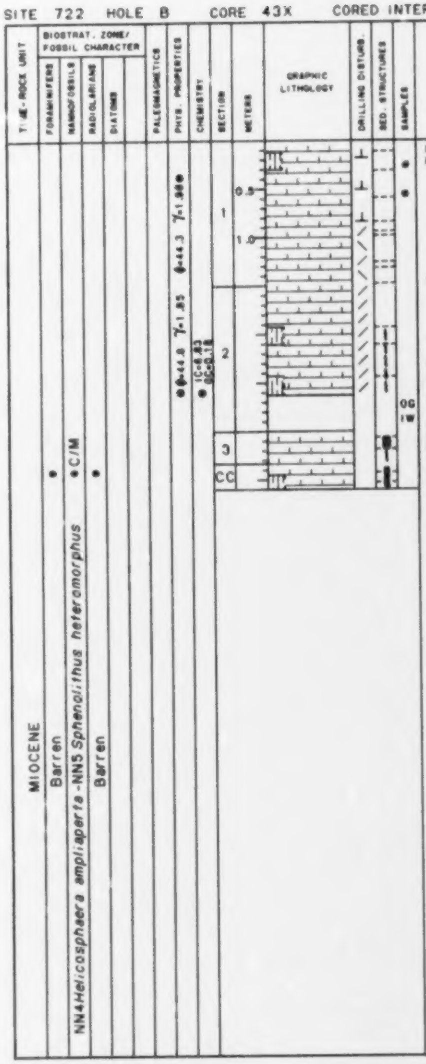
TIME-ROCK UNIT
BIOSTRAT. ZONE/ FOSSIL CHARACTER
FORAMINIFERS
NANNOFOSSILS
RADIOLARIANS
DIATOMS
PALEOMAGNETICS
PHYS. PROPERTIES
CHEMISTRY
SECTION
METERS
GRAPHIC LITHOLOGY
DRILLING DISTURB.
SED. STRUCTURES
SAMPLES
MIOCENE
Barren
NN4Helicosphaera ampliaperta-NN5 Sphenolithus heteromorphus
●C/M
Barren
●ϕ=44.8 γ=1.85 ϕ=44.3 γ=1.98●
● IC=8.83 OC=0.18
1
2
3
CC
0.5
1.0
OG
IW

LITHOLOGIC DESCRIPTION

Interbedded NANNOFOSSIL CHALK and FORAMINIFER-BEARING NANNOFOSSIL CHALK

Entire core is slightly fractured to highly fragmented.

Major lithology: Interbedded NANNOFOSSIL CHALK and FORAMINIFER-BEARING NANNOFOSSIL CHALK. Contacts are gradational. Beds range from white (5Y 8/0, 2.5Y 8/0, 5Y 8/1) to light gray (2.5Y 7/2, 5Y 7/1), light brownish gray (2.5Y 6/2), gray (5Y 6/1), light olive gray (5Y 6/2), olive gray (5Y 5/2, 4/3), and light greenish gray (10Y 7/1, 6/1). Bioturbation is minor to strong throughout.

SMEAR SLIDE SUMMARY (%):

	1, 25 D	1, 56 D
TEXTURE:		
Silt	20	20
Clay	80	80
COMPOSITION:		
Access. minerals	Tr	Tr
Clay		10
Dolomite	5	
Foraminifers	5	10
Inorganic calcite	10	Tr
Nannofossils	80	80
Quartz	Tr	Tr

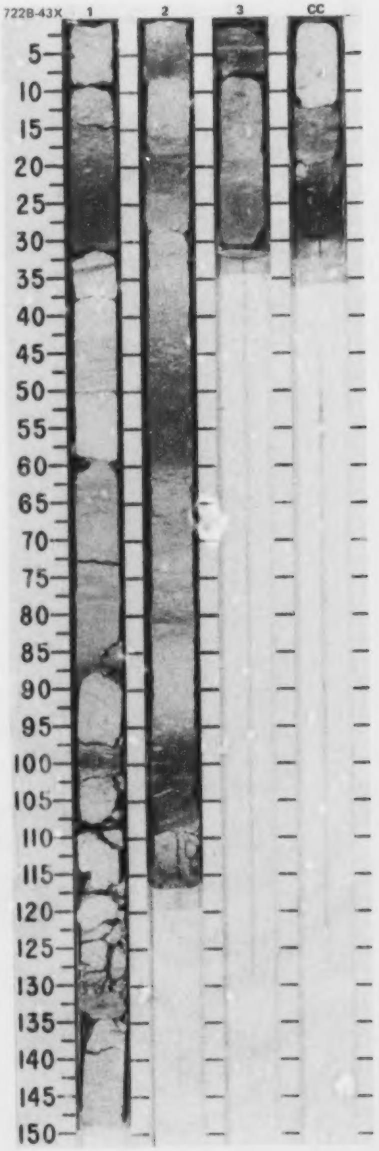
722B-43X
1
2
3
CC
5
10
15
20
25
30
35
40
45
50
55
60
65
70
75
80
85
90
95
100
105
110
115
120
125
130
135
140
145
150

SITE 722 HOLE B CORE 44X CORED INTERVAL 2438.9-2448.6 mbsl; 411.1-420.8 mbsf

TIME-ROCK UNIT	BIOSTRAT. ZONE/ FOSSIL CHARACTER: FORAMINIFERS	NANNOFOSSILS	RADIOLARIANS	DIATOMS	PALEOMAGNETICS	PHYS. PROPERTIES	CHEMISTRY	SECTION
MIOCENE	Barren	NN4 *Helicosphaera ampliaperta* -NN5 *Sphenolithus heteromorphus*	Barren			●ϕ-38.8 γ-2.14		1
								2
						●ϕ-38.2 γ-1.86		3
								4
								5
	●	● C/P	●					CC

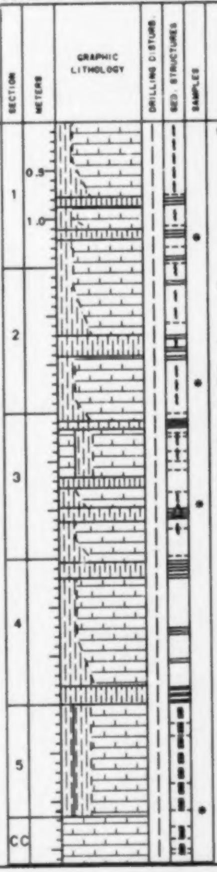
METERS
0.5
1.0
GRAPHIC LITHOLOGY
DRILLING DISTURB.
SED. STRUCTURES
SAMPLES

LITHOLOGIC DESCRIPTION

Interbedded NANNOFOSSIL CHALK and MARLY NANNOFOSSIL CHALK

Entire core is slightly disturbed.

Major lithology: Interbedded NANNOFOSSIL CHALK and MARLY NANNOFOSSIL CHALK. Contacts are gradational. Beds range from gray (5Y 6/1) to olive gray (5Y 5/2, 4/3, 4/2), pale brown (10YR 6/3), brown (10YR 5/3), and yellowish brown (10YR 5/4). Bioturbation is minor throughout.

Minor lithology: Silty claystone, greenish gray (5G 5/1, 6/1), with parallel laminae. Basal contact usually sharp, upper contact gradational with major lithology.

SMEAR SLIDE SUMMARY (%):

	1, 120 M	2, 120 D	3, 95 D	5, 111 D
TEXTURE:				
Silt	40	20	30	20
Clay	60	80	70	80
COMPOSITION:				
Access. minerals	1		3	Tr
Clay	60	15	60	10
Dolomite	2	Tr	Tr	
Volcanic glass	2		Tr	
Inorganic calcite	10	10	7	5
Nannofossils	Tr	70	20	85
Quartz	25	5	10	Tr

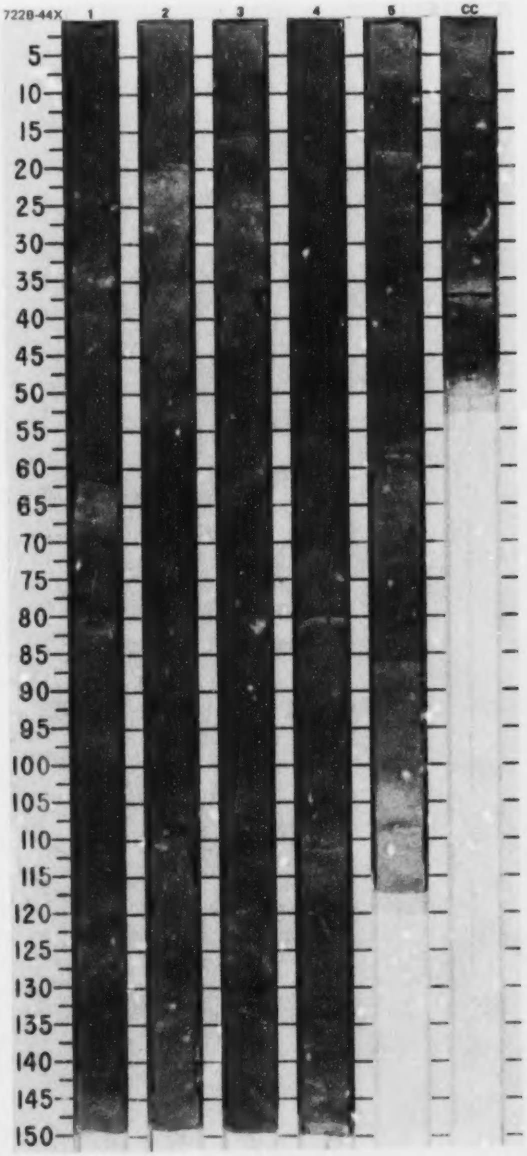
722B-44X
1
2
3
4
5
CC
5
10
15
20
25
30
35
40
45
50
55
60
65
70
75
80
85
90
95
100
105
110
115
120
125
130
135
140
145
150

SITE 722 HOLE B CORE 45X CORED INTERVAL 2448.6-2458.3 mbsl; 420.8-430.5 mbsf

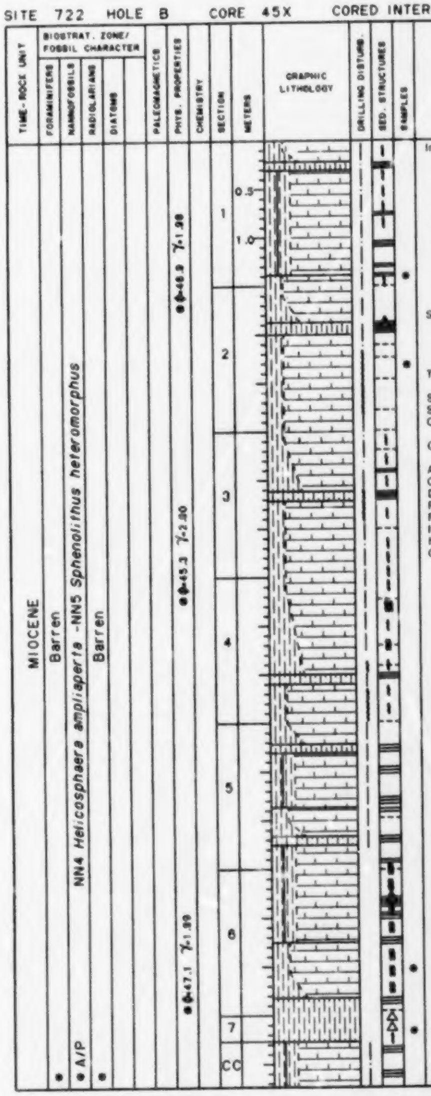
TIME-ROCK UNIT
BIOSTRAT. ZONE/ FOSSIL CHARACTER
FORAMINIFERS
NANNOFOSSILS
RADIOLARIANS
DIATOMS
PALEOMAGNETICS
PHYS. PROPERTIES
CHEMISTRY
SECTION
METERS
GRAPHIC LITHOLOGY
DRILLING DISTURB.
SED. STRUCTURES
SAMPLES
MIOCENE
Barren
NN4 *Helicosphaera ampliaperta* -NN5 *Sphenolithus heteromorphus*
Barren
●
● A/P
●
●Φ=48.9 γ=1.98
●Φ=45.3 γ=2.00
●Φ=47.1 γ=1.99
1
2
3
4
5
6
7
CC
0.5
1.0

LITHOLOGIC DESCRIPTION

Interbedded NANNOFOSSIL CHALK and MARLY NANNOFOSSIL CHALK

Entire core is slightly to very disturbed.

Major lithology: Interbedded NANNOFOSSIL CHALK and MARLY NANNOFOSSIL CHALK. Contacts are gradational. Beds range from olive gray (5Y 5/2) to olive (5Y 4/2), greenish gray (5Y 5/1), light brownish gray (10YR 6/2), pale brown (10YR 6/3), and brown (10YR 5/3). Bioturbation is minor to strong throughout.

Minor lithology: Silty claystone, greenish gray (5G 5/1, 6/1). Parallel laminae present. Basal contacts sharp, upper contacts gradational with major lithology.

SMEAR SLIDE SUMMARY (%):

	1, 140 M	2, 82 D	6, 103 M	7, 16 M
TEXTURE:				
Sand				20
Silt	35	30	30	70
Clay	65	70	70	10
COMPOSITION:				
Access. minerals	Tr	5	10	10
Clay	60	20	65	5
Dolomite	Tr		Tr	5
Feldspar				10
Foraminifers				Tr
Inorganic calcite	20	10	10	10
Nannofossils	5	50	5	
Quartz	15	15	10	60

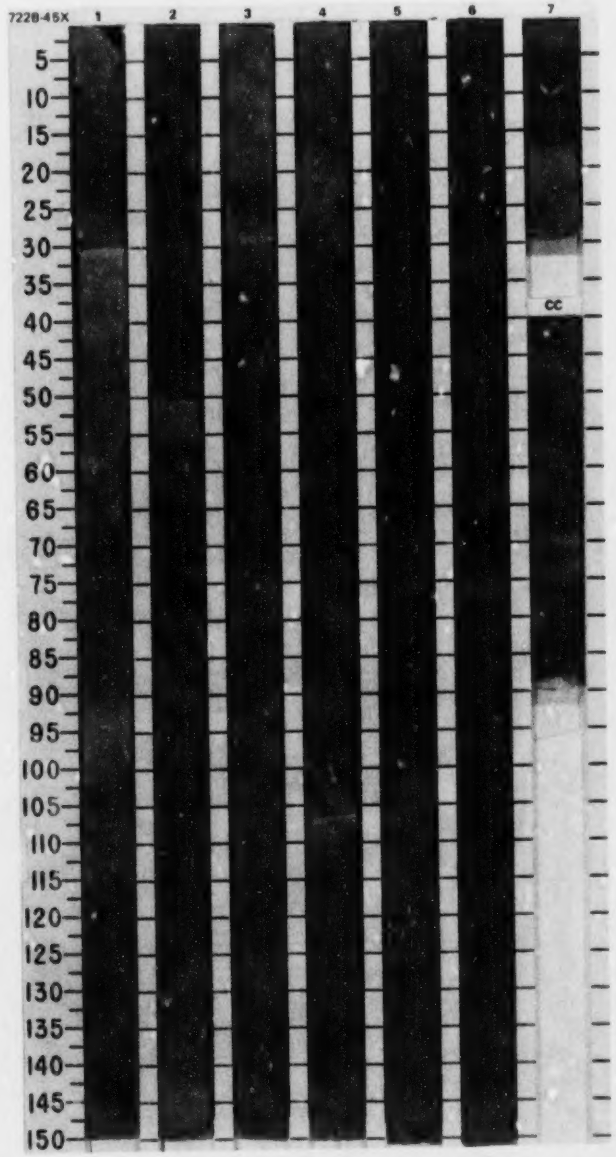
722B-45X
1
2
3
4
5
6
7
CC
5
10
15
20
25
30
35
40
45
50
55
60
65
70
75
80
85
90
95
100
105
110
115
120
125
130
135
140
145
150

SITE 722 HOLE B CORE 46X CORED INTERVAL 2458.3-2468.0 mbsl; 430.5-440.2 mbsf

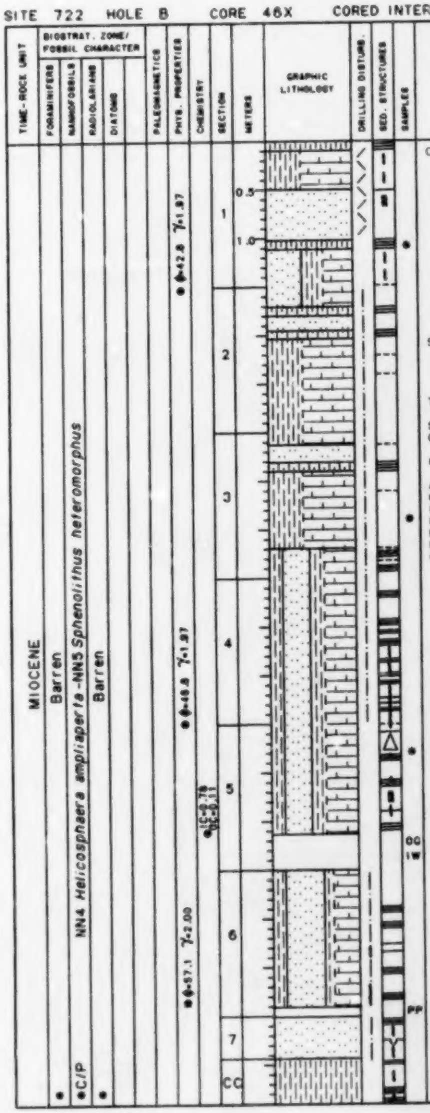
TIME-ROCK UNIT
BIOSTRAT. ZONE/ FOSSIL CHARACTER
FORAMINIFERS
NANNOFOSSILS
RADIOLARIANS
DIATOMS
PALEOMAGNETICS
PHYS. PROPERTIES
CHEMISTRY
SECTION
METERS
GRAPHIC LITHOLOGY
DRILLING DISTURB.
SED. STRUCTURES
SAMPLES
MIOCENE
Barren
NN4 Helicosphaera ampliaperta-NN5 Sphenolithus heteromorphus
Barren
●
●C/P
●
●ϕ=42.8 γ=1.97
●ϕ=48.8 γ=1.97
●ϕ=57.1 γ=2.00
●IC=8.78 OC=0.11
1
2
3
4
5
6
7
CC
0.5
1.0
OG
IW
PP

LITHOLOGIC DESCRIPTION

CLAYEY SILTSTONE and MARLY NANNOFOSSIL CHALK

Section 1 is highly fragmented; remainder of the core is moderately disturbed.

Major lithologies:

a. CLAYEY SILTSTONE, olive (5Y 4/3), gradationally interbedded with nannofossil chalk and minor siltstone.

b. MARLY NANNOFOSSIL CHALK. Gradationally interbedded with and usually overlying clayey siltstone. Beds range from dark brown (10YR 4/3) to dark grayish brown (10YR 4/2) and light brownish gray (10YR 6/2). Contacts are gradational. Bioturbation is moderate throughout.

Minor lithology: Siltstone, greenish gray (5G 5/1, 6/1). Contains parallel laminae. Gradationally interbedded with and usually underlying siltstone. Basal contact with underlying nannofossil chalk is usually sharp.

SMEAR SLIDE SUMMARY (%):

	1, 109 M	3, 89 D	5, 35 D
TEXTURE:			
Silt	85	40	15
Clay	15	60	85
COMPOSITION:			
Access. minerals	15	2	5
Clay	15	10	80
Feldspar	5		
Inorganic calcite	35	10	10
Mica	5		
Nannofossils	Tr	75	Tr
Quartz	25	3	5

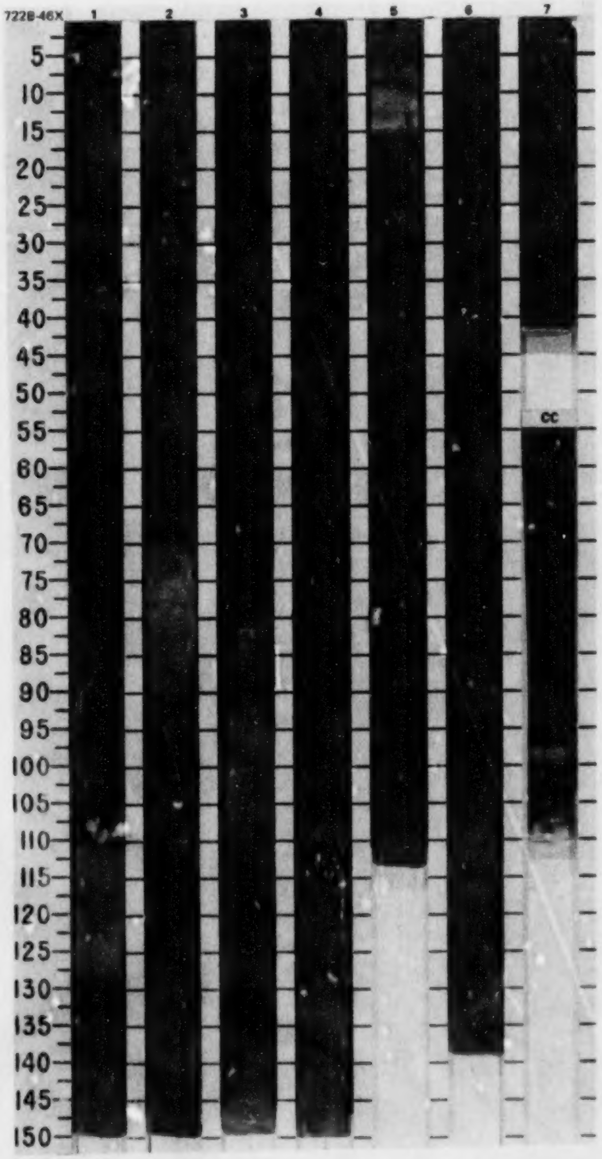
722B-46X
1
2
3
4
5
6
7
CC
5
10
15
20
25
30
35
40
45
50
55
60
65
70
75
80
85
90
95
100
105
110
115
120
125
130
135
140
145
150

CORE 117–722B–47X NO RECOVERY

SITE 722 HOLE B CORE 48X CORED INTERVAL 2477.6-2487.2 mbsl; 449.8-459.4 mbsf

TIME-ROCK UNIT	BIOSTRAT. ZONE/ FOSSIL CHARACTER: FORAMINIFERS	NANNOFOSSILS	RADIOLARIANS	DIATOMS	PALEOMAGNETICS	PHYS. PROPERTIES	CHEMISTRY	SECTION	METERS	GRAPHIC LITHOLOGY	DRILLING DISTURB.	SED. STRUCTURES	SAMPLES	LITHOLOGIC DESCRIPTION
MIOCENE	Barren ●	NN4 *Helicosphaera ampliaperta*-NN5 *Sphenolithus heteromorphus* ●F/P	Barren ●			ϕ=47.7 γ=2.01 ●		1 CC	0.5	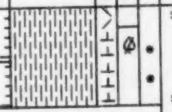			● ●	SILTY CLAYSTONE

Moderately fractured to very fragmented throughout.

Major lithology: SILTY CLAYSTONE, dark grayish brown (10YR 4/2). Layer of plant debris (1 cm thick) at Section 1, 45 cm.

SMEAR SLIDE SUMMARY (%):

	1, 45 M	2, 19 D
TEXTURE:		
Sand	20	
Silt	50	5
Clay	30	95
COMPOSITION:		
Clay	15	80
Feldspar	5	
Inorganic calcite	30	10
Mica	15	Tr
Plant debris	10	
Quartz	25	10
Rock fragments		Tr

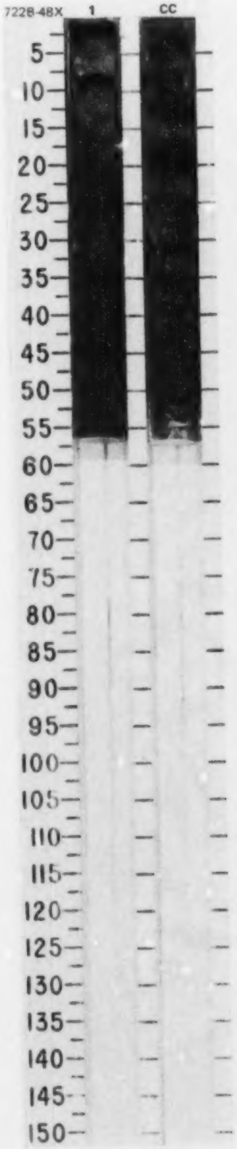
722B-48X
1
CC
5
10
15
20
25
30
35
40
45
50
55
60
65
70
75
80
85
90
95
100
105
110
115
120
125
130
135
140
145
150

SITE 722 HOLE B CORE 49X CORED INTERVAL 2487.2-2496.8 mbsl; 459.8-469.0 mbsf

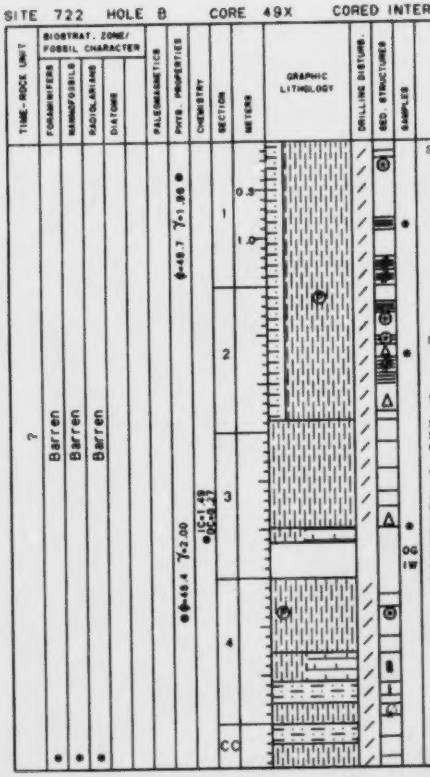
TIME-ROCK UNIT
BIOSTRAT. ZONE/ FOSSIL CHARACTER
FORAMINIFERS
NANNOFOSSILS
RADIOLARIANS
DIATOMS
PALEOMAGNETICS
PHYS. PROPERTIES
CHEMISTRY
SECTION
METERS
GRAPHIC LITHOLOGY
DRILLING DISTURB.
SED. STRUCTURES
SAMPLES
?
Barren
Barren
Barren
φ=48.7 γ=1.96
φ=48.4 γ=2.00
IC=1.49
OC=0.27
1
2
3
4
CC
0.5
1.0
OG
IW

LITHOLOGIC DESCRIPTION

SILTY CLAYSTONE

Entire core slightly fractured.

Major lithology: SILTY CLAYSTONE, very dark grayish brown (10YR 3/2). Interbedded with marly nannofossil chalk and mudstone. Contacts are sharp. Charcoal-rich bands (1-2 cm thick) and sandy beds (1 cm thick) are common. Pyrite concretions(?) occur in Sections 1, 2, and 4.

Minor lithologies:
- a. Marly nannofossil chalk, olive gray (5Y 5/2). Moderately bioturbated and interbedded with silty claystone and and mudstone. Contacts are sharp.
- b. Mudstone, gray (5Y 5/1). Interbedded with marly nannofossil chalk and silty claystone. Contacts are sharp. Bioturbation is minor; mica flakes are common.

SMEAR SLIDE SUMMARY (%):

	1, 88 D	2, 70 D	3, 103 M
TEXTURE:			
Sand	50		
Silt	35	25	50
Clay	15	75	50
COMPOSITION:			
Access. minerals	2	Tr	5
Clay	15	60	30
Feldspar	3		
Inorganic calcite	5	20	5
Mica	15	Tr	
Nannofossils		Tr	50
Quartz	60	20	10
Rock fragments	Tr		

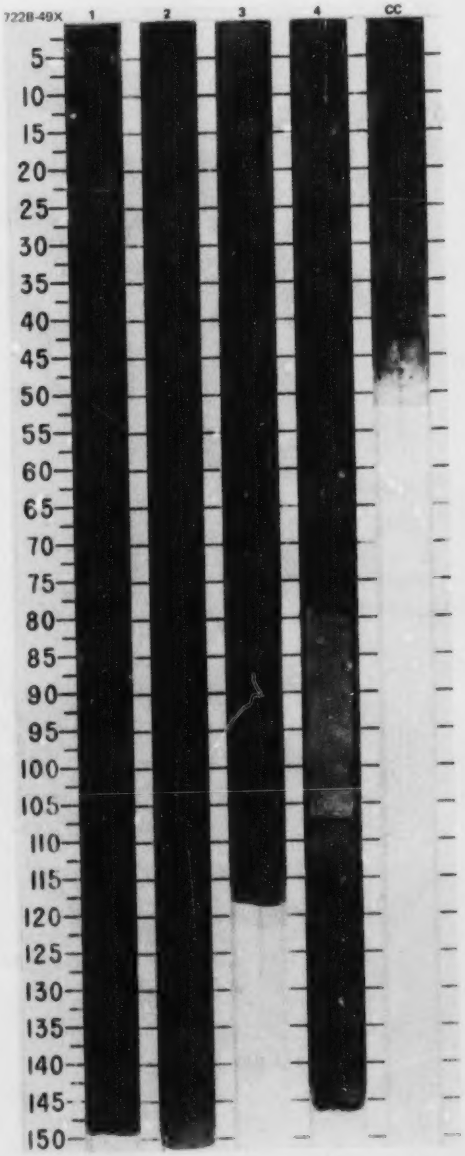
722B-49X
1
2
3
4
CC
5
10
15
20
25
30
35
40
45
50
55
60
65
70
75
80
85
90
95
100
105
110
115
120
125
130
135
140
145
150

SITE 722 HOLE B CORE 50X CORED INTERVAL 2496.8-2506.4 mbsl; 469.0-478.6 mbsf

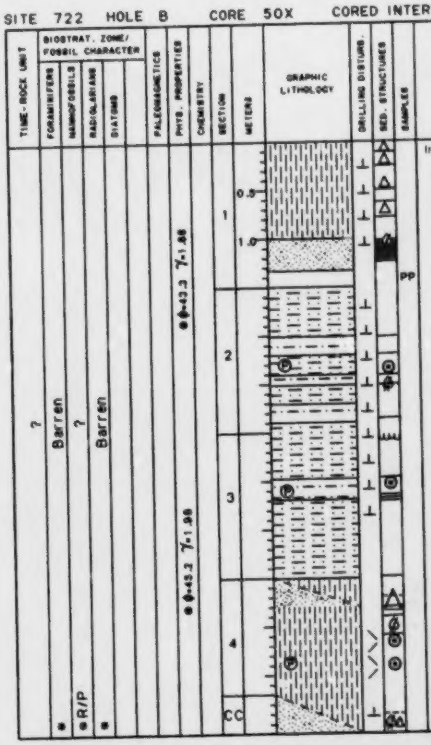
TIME-ROCK UNIT
BIOSTRAT. ZONE/ FOSSIL CHARACTER
FORAMINIFERS
NANNOFOSSILS
RADIOLARIANS
DIATOMS
PALEOMAGNETICS
PHYS. PROPERTIES
CHEMISTRY
SECTION
METERS
GRAPHIC LITHOLOGY
DRILLING DISTURB.
SED. STRUCTURES
SAMPLES
?
Barren
?
Barren
●
●R/P
●
●ϕ=43.3 γ=1.88
●ϕ=43.2 γ=1.98
1
2
3
4
CC
0.5
1.0
PP

LITHOLOGIC DESCRIPTION

Interbedded SANDY MUDSTONE and MUDSTONE

Entire core is moderately fractured.

Major lithology: Interbedded, massive SANDY MUDSTONE and MUDSTONE, gray (5YR 3/1). Contacts sharp. Contain disseminated pyrite- and charcoal-rich bands (1-2 cm thick), in Sections 2-3.

Minor lithologies:
a. Silty claystone, very dark gray (5YR 3/1). Sections 1, 4, and CC.
b. Sandy siltstone, very dark grayish brown (10YR 3/2). Fines upward into silty claystone. Sections 1, 4, and CC.

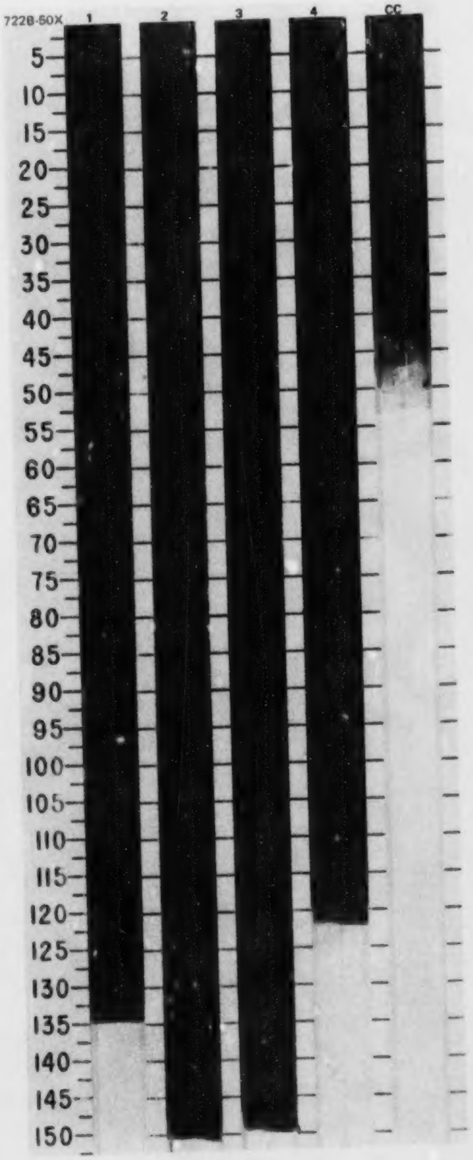
722B-50X
1
2
3
4
CC
5
10
15
20
25
30
35
40
45
50
55
60
65
70
75
80
85
90
95
100
105
110
115
120
125
130
135
140
145
150

SITE 722 HOLE B CORE 51X CORED INTERVAL 2506.4-2516.0 mbsl; 478.6-488.2 mbsf

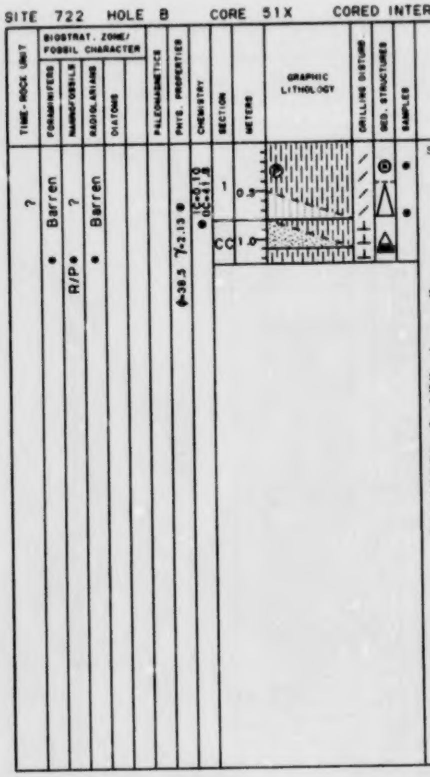
TIME-ROCK UNIT
BIOSTRAT. ZONE/ FOSSIL CHARACTER
FORAMINIFERS
NANNOFOSSILS
RADIOLARIANS
DIATOMS
PALEOMAGNETICS
PHYS. PROPERTIES
CHEMISTRY
SECTION
METERS
GRAPHIC LITHOLOGY
DRILLING DISTURB.
SED. STRUCTURES
SAMPLES
?
Barren
R/P
?
Barren
φ=38.5 γ=2.13
IC=0.10
OC=11.8
1
CC
0.5
1.0

LITHOLOGIC DESCRIPTION

SILTY CLAYSTONE

Section 1 is slightly fractured. CC is moderately fractured.

Major lithology: SILTY CLAYSTONE, massive, very dark grayish brown (2.5Y 4/2). Gradationally interbedded with and overlying clayey sand and sandstone.

Minor lithologies:
- a. Clayey sand, grades upward into silty claystone. Contains charcoal-rich bands (1-2 cm thick) and parallel laminae.
- b. Sandstone, grades upward into clayey siltstone.

SMEAR SLIDE SUMMARY (%):

	1, 28 D	1, 75 D
TEXTURE:		
Sand		50
Silt	20	15
Clay	80	35
COMPOSITION:		
Access. minerals		3
Clay	80	35
Feldspar	Tr	2
Volcanic glass		10
Inorganic calcite	10	10
Mica	Tr	
Nannofossils	Tr	
Quartz	10	40

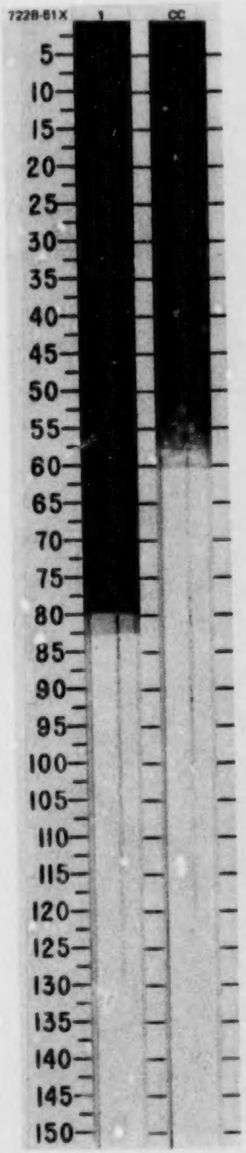
722B-51X
1
CC
5
10
15
20
25
30
35
40
45
50
55
60
65
70
75
80
85
90
95
100
105
110
115
120
125
130
135
140
145
150

SITE 722 HOLE B CORE 52X CORED INTERVAL 2516.0-2525.7 mbsl; 488.2-497.9 mbsf

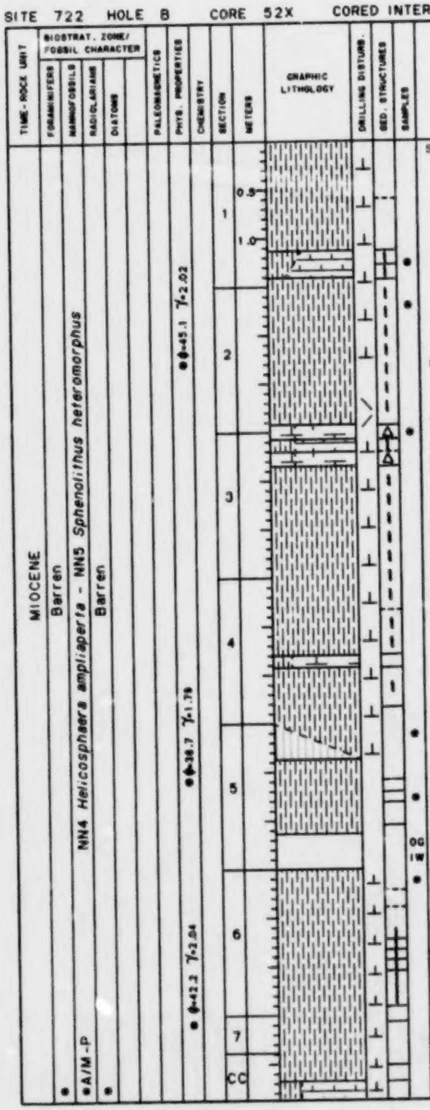
TIME-ROCK UNIT
BIOSTRAT. ZONE/ FOSSIL CHARACTER
FORAMINIFERS
NANNOFOSSILS
RADIOLARIANS
DIATOMS
PALEOMAGNETICS
PHYS. PROPERTIES
CHEMISTRY
SECTION
METERS
GRAPHIC LITHOLOGY
DRILLING DISTURB.
SED. STRUCTURES
SAMPLES
MIOCENE
● Barren
●A/M-P NN4 Helicosphaera ampliaperta - NN5 Sphenolithus heteromorphus
● Barren
●φ=45.1 γ=2.02
●φ=36.7 γ=1.76
●φ=42.2 γ=2.04
1
2
3
4
5
6
7
CC
0.5
1.0
OG
IW

LITHOLOGIC DESCRIPTION

SILTY CLAYSTONE

Entire core is moderately disturbed.

Major lithology: **SILTY CLAYSTONE**, massive. Beds range from dark gray (5Y 4/1) to dark olive (5Y 3/2, 3/1), very dark greenish gray (10Y 4/2), olive gray (5Y 4/2), dark reddish brown (5YR 3/2), dark grayish brown (10YR 4/2), and dark grayish green (10Y 5/2). Contains upward-fining carbonate turbidites (5 cm thick). Interbedded with nannofossil chalk and foraminifer-bearing nannofossil chalk. Contacts are sharp.

Minor lithologies:
a. Nannofossil chalk and foraminifer-bearing nannofossil chalk, massive, light gray (5Y 7/1, 10YR 7/2) to gray (5Y 6/1). Interbedded with silty claystone. Contacts are sharp. Minor bioturbation throughout.
b. Clayey sand, dark gray (5Y 4/1). Grades upward into silty claystone, Section 5, 0-40 cm.

SMEAR SLIDE SUMMARY (%):

	1, 126 D	2, 20 D	3, 1 D	5, 12 D	5, 78 D	6, 13 D
TEXTURE:						
Sand	2		5	59	60	
Silt	8	32	5	15	40	10
Clay	90	68	90	25	60	90
COMPOSITION:						
Access. minerals	2		5	5		
Clay	20	65	10	25	60	90
Dolomite					Tr	
Feldspar				2		
Foraminifers	2		5			
Volcanic glass				10	Tr	
Inorganic calcite	8	10	5	10	15	7
Mica	Tr		Tr			
Nannofossils	70	3	80			Tr
Quartz	Tr	20		45	20	3

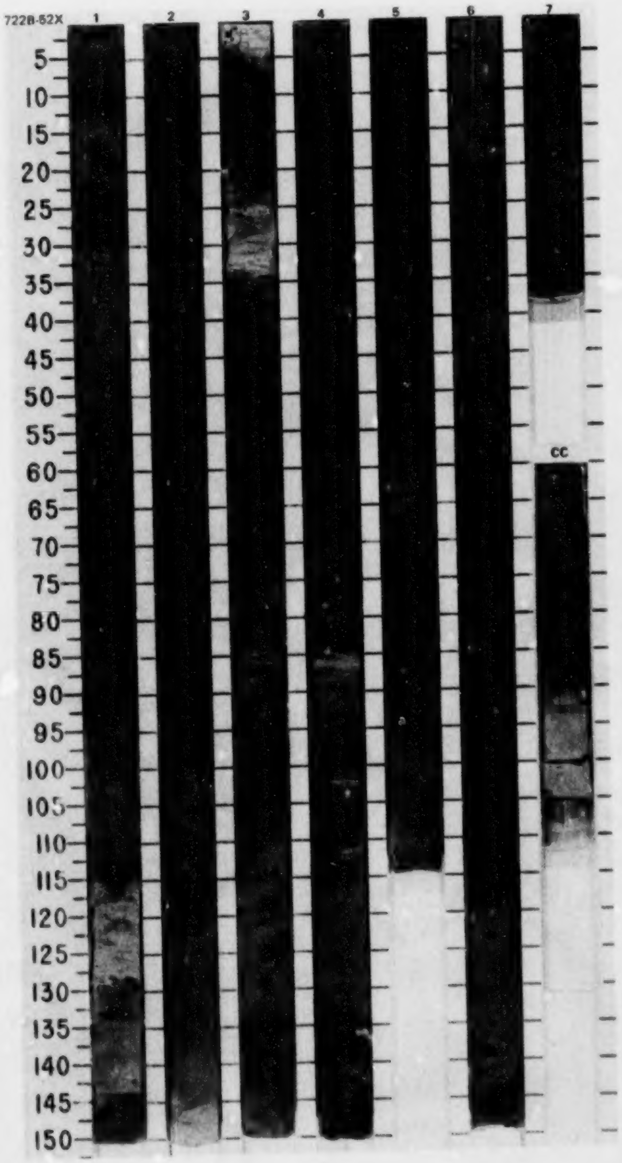
722B-52X
1
2
3
4
5
6
7
CC
5
10
15
20
25
30
35
40
45
50
55
60
65
70
75
80
85
90
95
100
105
110
115
120
125
130
135
140
145
150

SITE 722 HOLE B CORE 53X CORED INTERVAL 2525.7-2535.4 mbsl; 497.9-507.6 mbsf

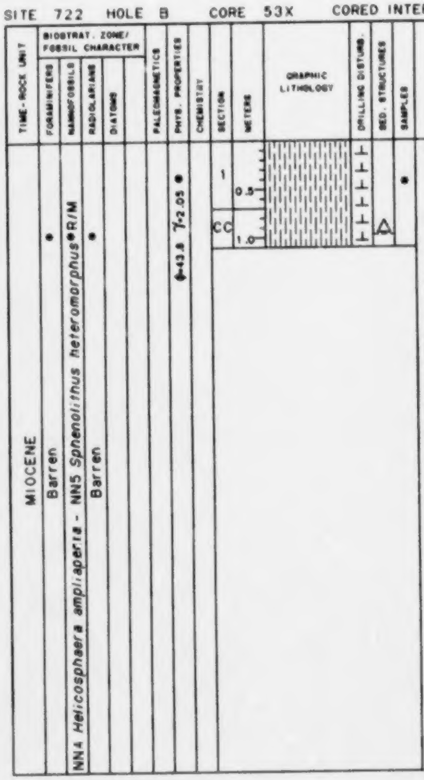
TIME-ROCK UNIT
BIOSTRAT. ZONE/ FOSSIL CHARACTER
FORAMINIFERS
NANNOFOSSILS
RADIOLARIANS
DIATOMS
PALEOMAGNETICS
PHYS. PROPERTIES
CHEMISTRY
SECTION
METERS
GRAPHIC LITHOLOGY
DRILLING DISTURB.
SED. STRUCTURES
SAMPLES
MIOCENE
Barren
NN4 Helicosphaera ampliaperta - NN5 Sphenolithus heteromorphus R/M
Barren
φ=43.8 γ=2.05
1
CC
0.5
1.0

LITHOLOGIC DESCRIPTION

SILTY CLAYSTONE

Entire core moderately fractured.

Major lithology: SILTY CLAYSTONE, massive, dark gray (5YR 4/1).

SMEAR SLIDE SUMMARY (%):

	1, 41 D
TEXTURE:	
Silt	40
Clay	60
COMPOSITION:	
Access. minerals	2
Clay	60
Dolomite	Tr
Feldspar	1
Volcanic glass	1
Inorganic calcite	15
Mica	1
Quartz	20

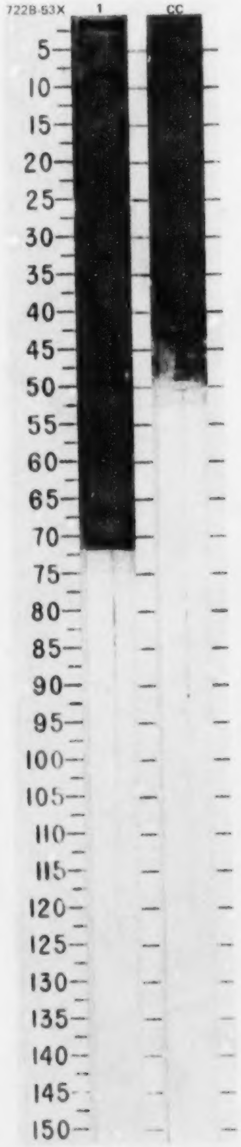
722B-53X
1
CC
5
10
15
20
25
30
35
40
45
50
55
60
65
70
75
80
85
90
95
100
105
110
115
120
125
130
135
140
145
150

SITE 722 HOLE B CORE 54X CORED INTERVAL 2535.4-2545.0 mbsl; 507.6-517.2 mbsf

TIME-ROCK UNIT	BIOSTRAT. ZONE/ FOSSIL CHARACTER				PALEOMAGNETICS	PHYS. PROPERTIES	CHEMISTRY	SECTION	METERS	GRAPHIC LITHOLOGY	DRILLING DISTURB.	SED. STRUCTURES	SAMPLES
	FORAMINIFERS	NANNOFOSSILS	RADIOLARIANS	DIATOMS									
MIOCENE	● Barren	● Barren	● Barren					1 CC	0.5	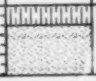			

LITHOLOGIC DESCRIPTION

SILTY CLAYSTONE and MICACEOUS SAND

Entire core is highly fragmented.

Major lithologies:
a. SILTY CLAYSTONE, massive, light gray (10YR 7/2) to yellowish brown (10YR 5/4).
b. MICACEOUS SAND, dark gray (10YR 4/1).

SMEAR SLIDE SUMMARY (%):

	1, 17 D	1, 23 D
TEXTURE:		
Sand	80	
Silt	10	60
Clay	10	40
COMPOSITION:		
Access. minerals	5	Tr
Clay	10	40
Feldspar	5	
Volcanic glass	Tr	Tr
Inorganic calcite	10	30
Mica	10	
Quartz	60	30

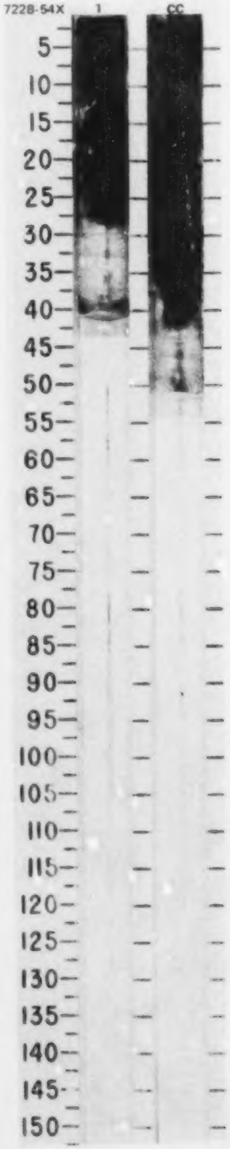
722B-54X
1
CC
5
10
15
20
25
30
35
40
45
50
55
60
65
70
75
80
85
90
95
100
105
110
115
120
125
130
135
140
145
150

SITE 722 HOLE B CORE 55X CORED INTERVAL 2545.0-2554.7 mbsl; 517.2-526.9 mbsf

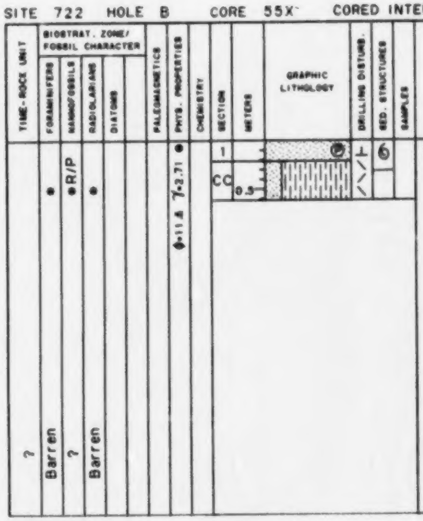
TIME-ROCK UNIT
BIOSTRAT. ZONE/ FOSSIL CHARACTER
FORAMINIFERS
NANNOFOSSILS
RADIOLARIANS
DIATOMS
PALEOMAGNETICS
PHYS. PROPERTIES
CHEMISTRY
SECTION
METERS
GRAPHIC LITHOLOGY
DRILLING DISTURB.
SED. STRUCTURES
SAMPLES
?
Barren
R/P
?
Barren
ϕ=11.4 γ=2.71
1
CC
0.5

LITHOLOGIC DESCRIPTION

SILTY CLAYSTONE and MICACEOUS SAND

Major lithologies:
a. SILTY CLAYSTONE, massive, dark gray (5YR 4/1).
b. MICACEOUS SAND, dark gray (10YR 4/1), pyrite present.

SMEAR SLIDE SUMMARY (%):

	2, 135 D
TEXTURE:	
Silt	30
Clay	70
COMPOSITION:	
Clay	40
Diatoms	10
Foraminifers	Tr
Inorganic calcite	15
Nannofossils	20
Opaques	2
Quartz	5
Radiolarians	Tr
Silicoflagellates	2
Sponge spicules	3
Zeolites	3

SITE 722 HOLE B CORE 56X CORED INTERVAL 2554.7-2564.4 mbsl; 526.9-536.6 mbsf

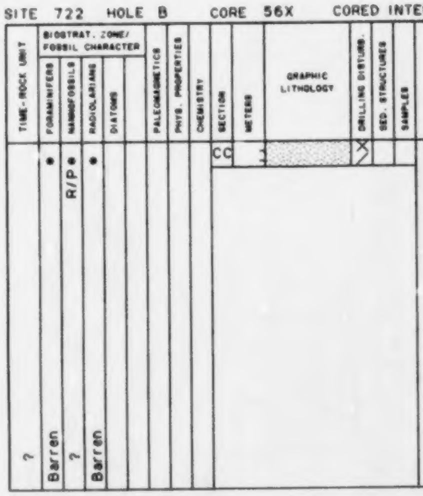
TIME-ROCK UNIT
BIOSTRAT. ZONE/ FOSSIL CHARACTER
FORAMINIFERS
NANNOFOSSILS
RADIOLARIANS
DIATOMS
PALEOMAGNETICS
PHYS. PROPERTIES
CHEMISTRY
SECTION
METERS
GRAPHIC LITHOLOGY
DRILLING DISTURB.
SED. STRUCTURES
SAMPLES
?
Barren
R/P
?
Barren
CC

LITHOLOGIC DESCRIPTION

SANDSTONE

Entire core is slightly fractured to brecciated.

Major lithology: SANDSTONE, dark gray (5Y 4/1), with minor parallel laminae. Fine-grained, moderately sorted. Quartz, feldspar, chlorite, mica, and pyrite visible in hand-sample.

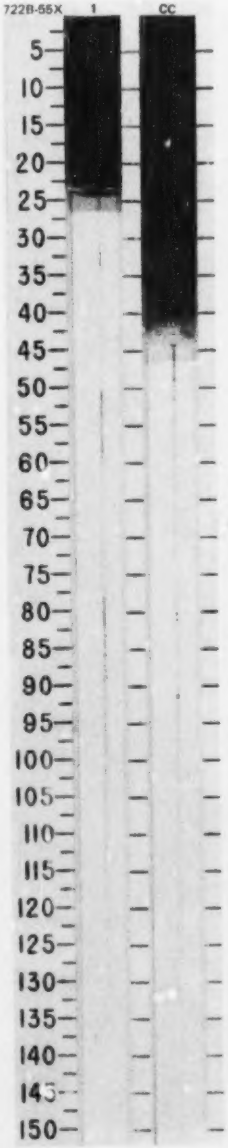
722B-55X
1
CC
5
10
15
20
25
30
35
40
45
50
55
60
65
70
75
80
85
90
95
100
105
110
115
120
125
130
135
140
145
150

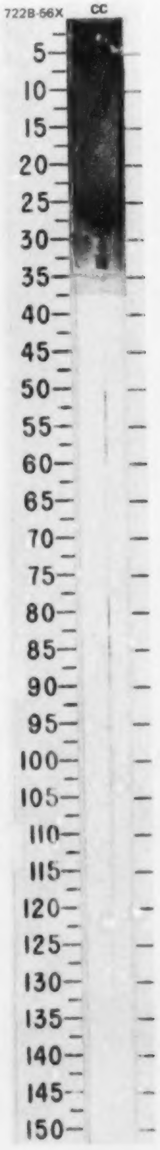
722B-56X
CC
5
10
15
20
25
30
35
40
45
50
55
60
65
70
75
80
85
90
95
100
105
110
115
120
125
130
135
140
145
150

SITE 722 HOLE B CORE 57X CORED INTERVAL 2564.4-2574.0 mbsl; 536.6-546.2 mbsf

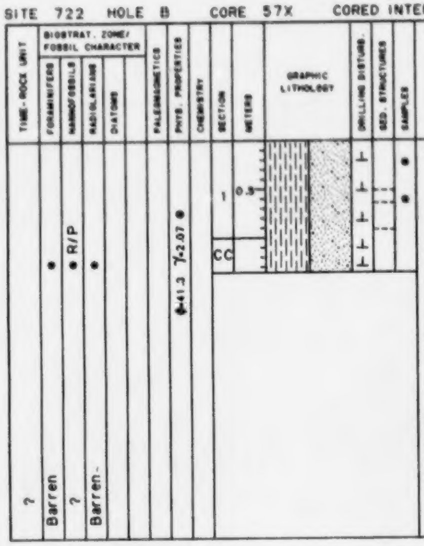
TIME-ROCK UNIT
BIOSTRAT. ZONE/ FOSSIL CHARACTER
FORAMINIFERS
NANNOFOSSILS
RADIOLARIANS
DIATOMS
PALEOMAGNETICS
PHYS. PROPERTIES
CHEMISTRY
SECTION
METERS
GRAPHIC LITHOLOGY
DRILLING DISTURB.
SED. STRUCTURES
SAMPLES
?
Barren
? ● R/P
Barren-
φ-41.3 γ-2.07 ●
1
0.5
CC

LITHOLOGIC DESCRIPTION

CLAYEY SILTSTONE and SILTY SAND

Entire core moderately fractured.

Major lithologies:
a. CLAYEY SILTSTONE, dark gray (10YR 4/1), interbedded with silty sand. Contacts obscured by drilling deformation.
b. Silty sand, gray (10YR 4/1).

SMEAR SLIDE SUMMARY (%):

	1, 23 D	1, 61 D
TEXTURE:		
Sand		40
Silt	55	40
Clay	45	20
COMPOSITION:		
Access. minerals	3	5
Clay	45	20
Dolomite	Tr	
Feldspar	2	5
Volcanic glass	3	10
Inorganic calcite	10	20
Mica	2	Tr
Quartz	35	40

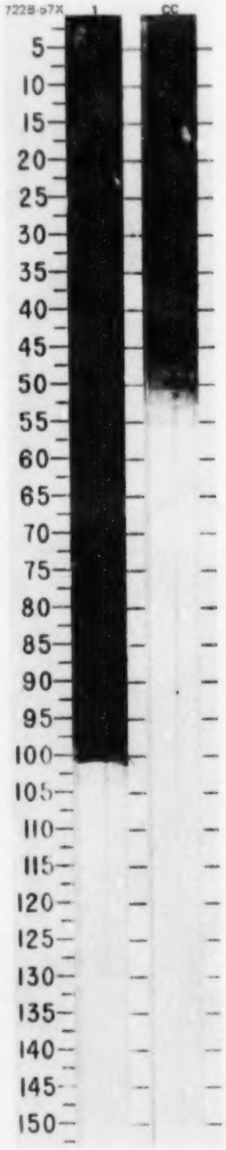
722B-57X
1
CC
5
10
15
20
25
30
35
40
45
50
55
60
65
70
75
80
85
90
95
100
105
110
115
120
125
130
135
140
145
150

SITE 722 HOLE B CORE 58X CORED INTERVAL 2574.0-2583.7 mbsl; 546.2-555.9 mbsf

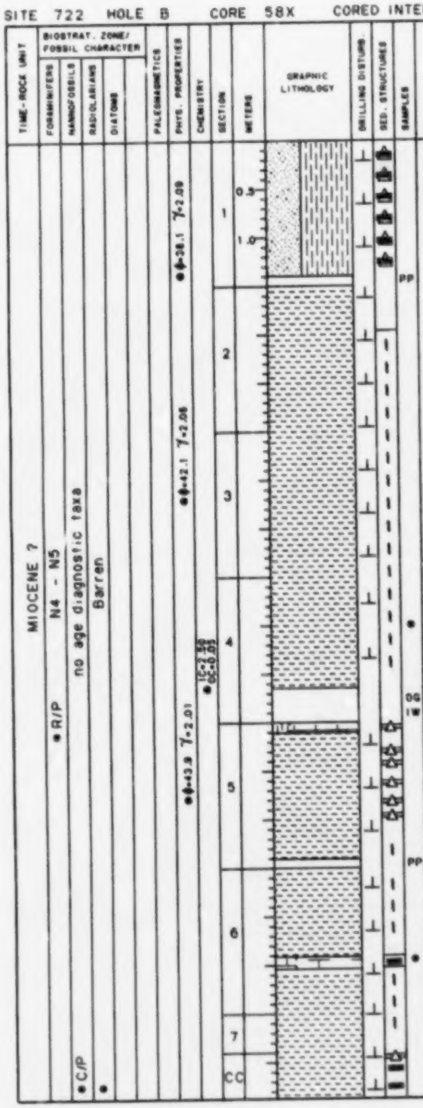
TIME-ROCK UNIT
BIOSTRAT. ZONE/ FOSSIL CHARACTER
FORAMINIFERS
NANNOFOSSILS
RADIOLARIANS
DIATOMS
PALEOMAGNETICS
PHYS. PROPERTIES
CHEMISTRY
SECTION
METERS
GRAPHIC LITHOLOGY
DRILLING DISTURB.
SED. STRUCTURES
SAMPLES
MIOCENE ?
● R/P N4 - N5
● C/P no age diagnostic taxa
● Barren
●φ=38.1 γ=2.09
●φ=42.1 γ=2.06
●φ=43.9 γ=2.01
●IC=2.50 OC=0.05
1
2
3
4
5
6
7
CC
0.5
1.0
PP
OG
IW
PP

LITHOLOGIC DESCRIPTION

CLAYSTONE and NANNOFOSSIL CHALK

Moderately disturbed throughout.

Major lithology: CLAYSTONE, dark gray (5YR 4/1) to olive (5Y 4/3), olive gray (5Y 4/2), reddish brown (5YR 4/3), greenish gray (5G 5/1), and reddish gray (5YR 4/2). Interbedded with NANNOFOSSIL CHALK. Minor bioturbation throughout.

Minor lithology: Interbedded clayey silt and silty sand, dark gray (5YR 4/1). Silty sand has sharp basal contacts and fines upward into clayey silt. Silty sand/clayey silt units are 10-20 cm thick.

SMEAR SLIDE SUMMARY (%):

	4, 50 D	6, 93 M
TEXTURE:		
Silt	10	10
Clay	90	90
COMPOSITION:		
Access. minerals	Tr	
Cement		5
Clay	70	20
Dolomite	Tr	Tr
Foraminifers		3
Inorganic calcite	10	5
Mica	Tr	
Nannofossils	10	67
Quartz	10	Tr
Rock fragments		Tr

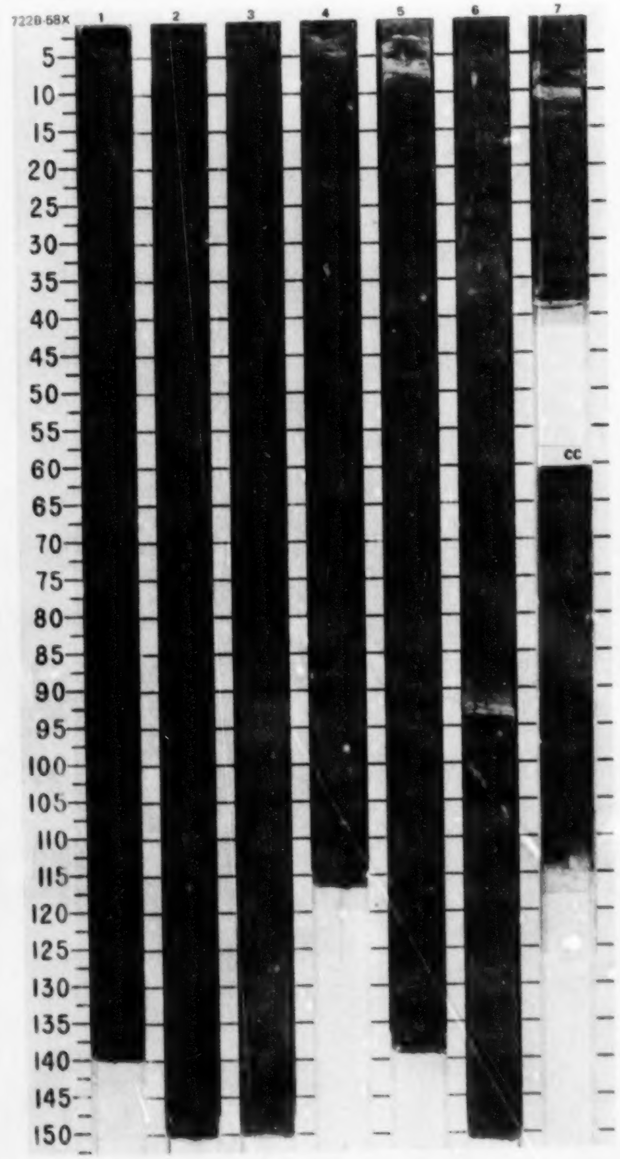
722B-58X
1
2
3
4
5
6
7
CC
5
10
15
20
25
30
35
40
45
50
55
60
65
70
75
80
85
90
95
100
105
110
115
120
125
130
135
140
145
150

SITE 722 HOLE B CORE 59X CORED INTERVAL 2583.7-2593.4 mbsl; 555.9-565.6 mbsf

TIME-ROCK UNIT	BIOSTRAT. ZONE/ FOSSIL CHARACTER					PALEOMAGNETICS	PHYS. PROPERTIES	CHEMISTRY	SECTION	METERS
	FORAMINIFERS	NANNOFOSSILS	RADIOLARIANS	DIATOMS						
MIOCENE	Barren ●	NN3 *Sphenolithus belemnos* ●C/P	Barren ●				ϕ=42.4 γ=2.04 ●		1 CC	0.5 1.0

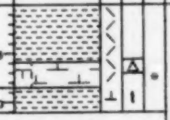
GRAPHIC LITHOLOGY
DRILLING DISTURB.
SED. STRUCTURES
SAMPLES

LITHOLOGIC DESCRIPTION

CLAYSTONE

Moderately fractured to highly fragmented throughout.

Major lithology: CLAYSTONE, olive (5Y 4/2) to dark gray (5YR 4/1) and greenish gray (5GY 5/1). Carbonate turbidite(?) in Section 1, 64-75 cm.

SMEAR SLIDE SUMMARY (%):

	1, 73 M
TEXTURE:	
Sand	20
Silt	20
Clay	60
COMPOSITION:	
Foraminifers	20
Inorganic calcite	30
Nannofossils	50

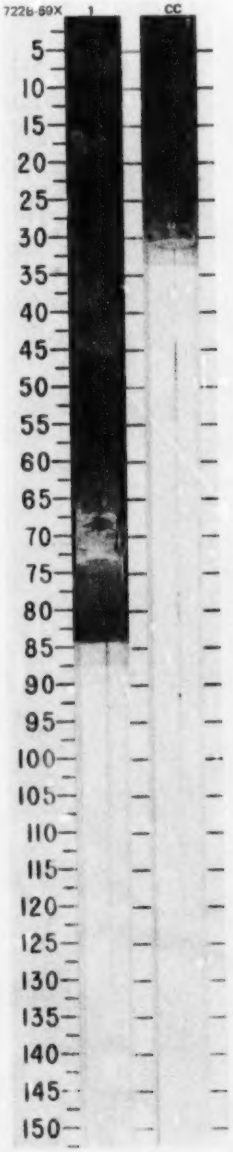
722B-59X
1
CC
5
10
15
20
25
30
35
40
45
50
55
60
65
70
75
80
85
90
95
100
105
110
115
120
125
130
135
140
145
150

SITE 723 HOLE A CORE 1H CORED INTERVAL 807.8-815.6 mbsl; 0.0-7.8 mbsf

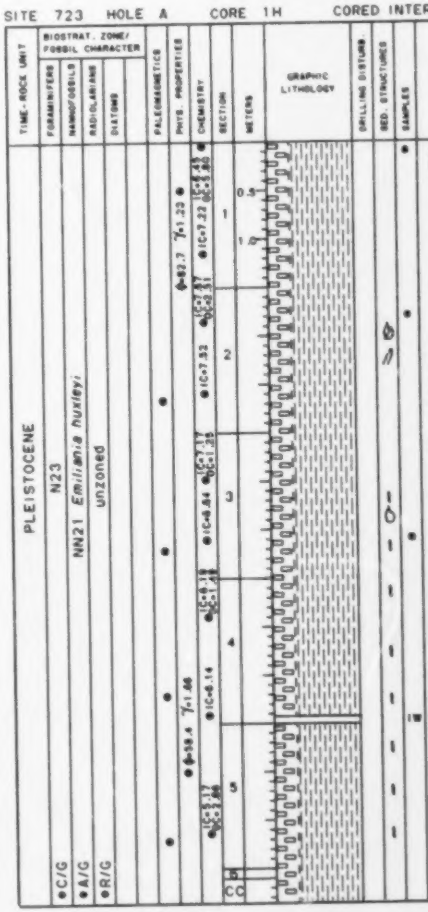
TIME-ROCK UNIT
BIOSTRAT. ZONE/ FOSSIL CHARACTER
FORAMINIFERS
NANNOFOSSILS
RADIOLARIANS
DIATOMS
PALEOMAGNETICS
PHYS. PROPERTIES
CHEMISTRY
SECTION
METERS
GRAPHIC LITHOLOGY
DRILLING DISTURB.
SED. STRUCTURES
SAMPLES
PLEISTOCENE
N23
NN21 Emiliania huxleyi
unzoned
●C/G
●A/G
●R/G
φ=62.7 γ=1.23
φ=58.4 γ=1.66
IC=7.22
IC=7.32
IC=6.84
IC=6.14
1
2
3
4
5
6
CC
0.5
1.0
IW

LITHOLOGIC DESCRIPTION

FORAMINIFER-BEARING MARLY NANNOFOSSIL OOZE and CALCAREOUS CLAYEY SILT

Entire core undisturbed.

Major lithologies: FORAMINIFER-BEARING MARLY NANNOFOSSIL OOZE and CALCAREOUS CLAYEY SILT, olive gray (5Y 4/2, 3/1, 3/2), faintly mottled. Foraminifers and shell fragments (pteropods) common on core face. Variable terrigenous component dominated by clay and silt-sized detrital calcite. Diatoms present (15%) in surface sediment.

SMEAR SLIDE SUMMARY (%):

	1, 10 D	2, 30 D	3, 109 D
TEXTURE:			
Sand	10	5	5
Silt	20	35	25
Clay	70	60	70
COMPOSITION:			
Access. minerals		1	
Clay	40	12	29
Diatoms	15	1	
Dolomite		3	5
Foraminifers	5	15	5
Inorganic calcite	10	30	20
Mica	2	5	3
Nannofossils	20	35	30
Opal		Tr	
Organic debris	5		
Organic debris		5	3
Pteropod			Tr
Quartz	3	3	5
Radiolarians	Tr		

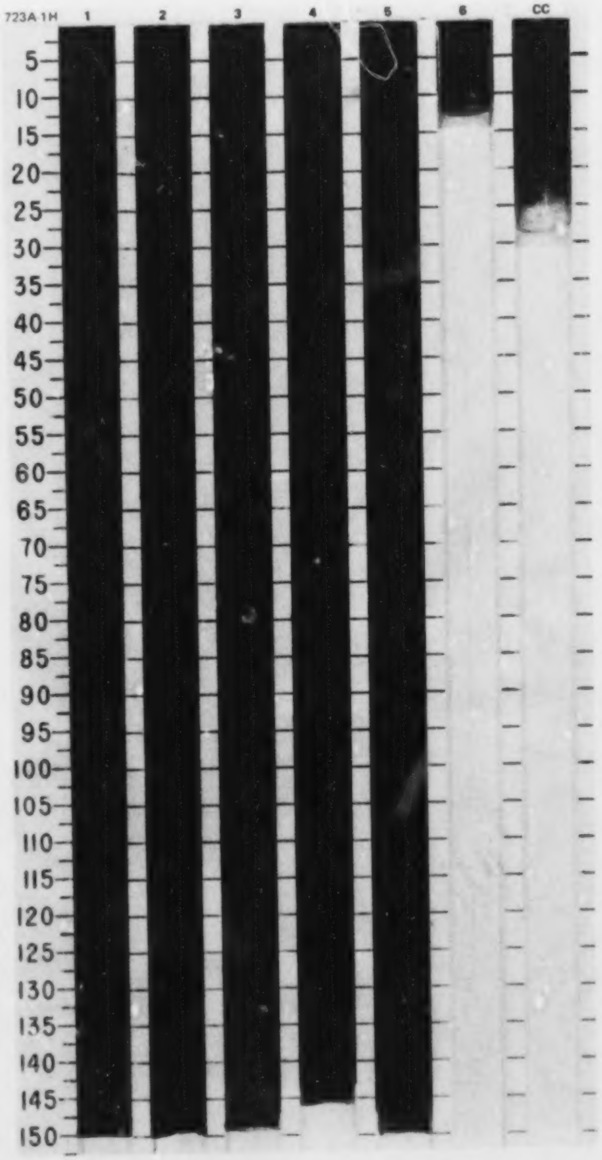
723A-1H
1
2
3
4
5
6
CC
5
10
15
20
25
30
35
40
45
50
55
60
65
70
75
80
85
90
95
100
105
110
115
120
125
130
135
140
145
150

SITE 723 HOLE A CORE 2H CORED INTERVAL 815.6-825.3 mbsl; 7.8-17.5 mbsf

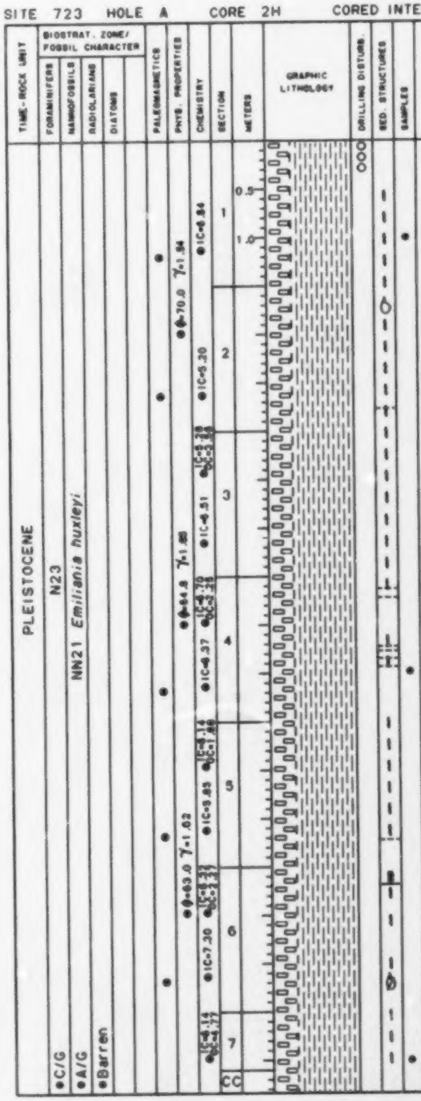
TIME-ROCK UNIT
BIOSTRAT. ZONE/ FOSSIL CHARACTER
FORAMINIFERS
NANNOFOSSILS
RADIOLARIANS
DIATOMS
PALEOMAGNETICS
PHYS. PROPERTIES
CHEMISTRY
SECTION
METERS
GRAPHIC LITHOLOGY
DRILLING DISTURB.
SED. STRUCTURES
SAMPLES
PLEISTOCENE
N23
NN21 Emiliania huxleyi
●C/G
●A/G
●Barren
●φ=70.0 γ=1.94
●φ=64.8 γ=1.80
●φ=63.0 γ=1.02
●IC=8.84
●IC=5.20
●IC=6.51
●IC=8.37
●IC=5.85
●IC=7.30
1
2
3
4
5
6
7
CC
0.5
1.0

LITHOLOGIC DESCRIPTION

FORAMINIFER-BEARING MARLY NANNOFOSSIL OOZE and CALCAREOUS CLAYEY SILT

Entire core undisturbed.

Major lithologies: FORAMINIFER-BEARING MARLY NANNOFOSSIL OOZE and CALCAREOUS CLAYEY SILT, olive gray (5Y 4/2, 4/3) and dark olive gray (5Y 3/2, 3/1, 2.5/1). Increased color contrast and mottling. Section 6 contains centimeter-scale light and dark layers. Foraminifers and shell fragments (pteropods) common on core face. Shell debris concentrated in burrows. Variable terrigenous component dominated by clay and silt-sized detrital calcite.

SMEAR SLIDE SUMMARY (%):

	2, 145 M	4, 99 D
TEXTURE:		
Sand	5	15
Silt	50	30
Clay	45	55
COMPOSITION:		
Clay	40	25
Dolomite	Tr	Tr
Feldspar		Tr
Foraminifers	5	15
Hornblende		Tr
Inorganic calcite	25	30
Mica	5	5
Nannofossils	Tr	10
Other	20	
Pellets		10
Quartz	5	5
Rock fragments		Tr
Sponge spicules	Tr	

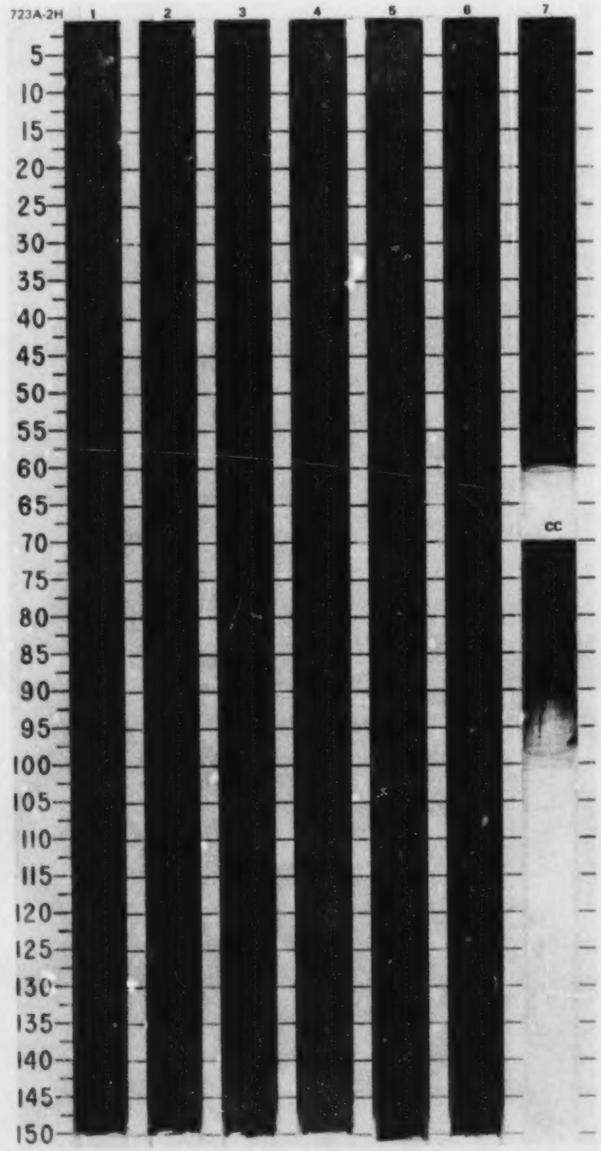
723A-2H
1
2
3
4
5
6
7
CC
5
10
15
20
25
30
35
40
45
50
55
60
65
70
75
80
85
90
95
100
105
110
115
120
125
130
135
140
145
150

SITE 723 HOLE A CORE 3H CORED INTERVAL 825.3-834.9 mbsl; 17.5-27.1 mbsf

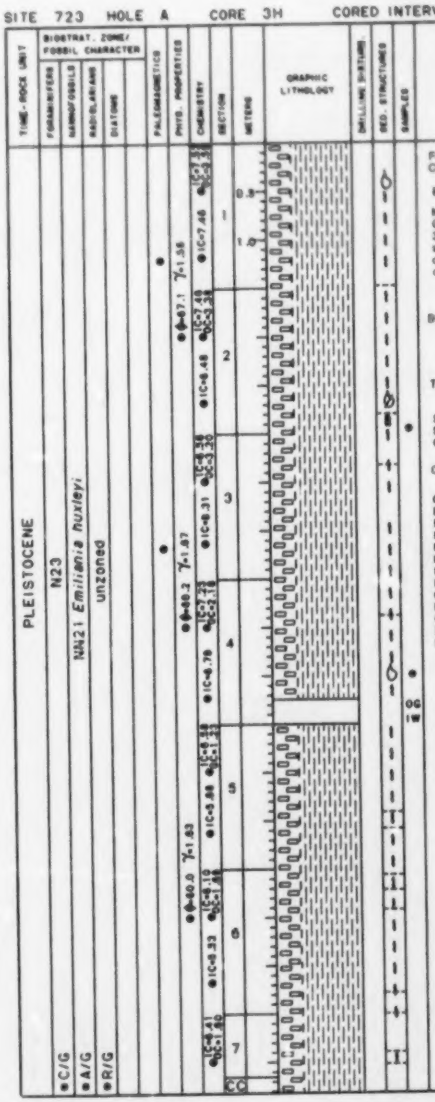

LITHOLOGIC DESCRIPTION

FORAMINIFER-BEARING MARLY NANNOFOSSIL OOZE and CALCAREOUS CLAYEY SILT

Entire core undisturbed.

Major lithologies: FORAMINIFER-BEARING MARLY NANNOFOSSIL OOZE and CALCAREOUS CLAYEY SILT, olive gray (5Y 4/2, 4/3) and dark olive gray (5Y 3/2, 3/1, 2.5/1). Increased color contrast and mottling. Section 6 contains centimeter-scale light and dark layers. Foraminifers and shell fragments (pteropods) common on core face. Shell debris concentrated in burrows. Variable terrigenous component dominated by clay and silt-sized detrital calcite.

SMEAR SLIDE SUMMARY (%):

	2, 145 M	4, 90 D
TEXTURE:		
Sand	5	15
Silt	50	30
Clay	45	55
COMPOSITION:		
Clay	40	25
Dolomite	Tr	Tr
Feldspar		Tr
Foraminifers	5	15
Hornblende		Tr
Inorganic calcite	25	30
Mica	5	5
Nannofossils	Tr	10
Other	20	
Pellets		10
Quartz	5	5
Rock fragments		Tr
Sponge spicules	Tr	

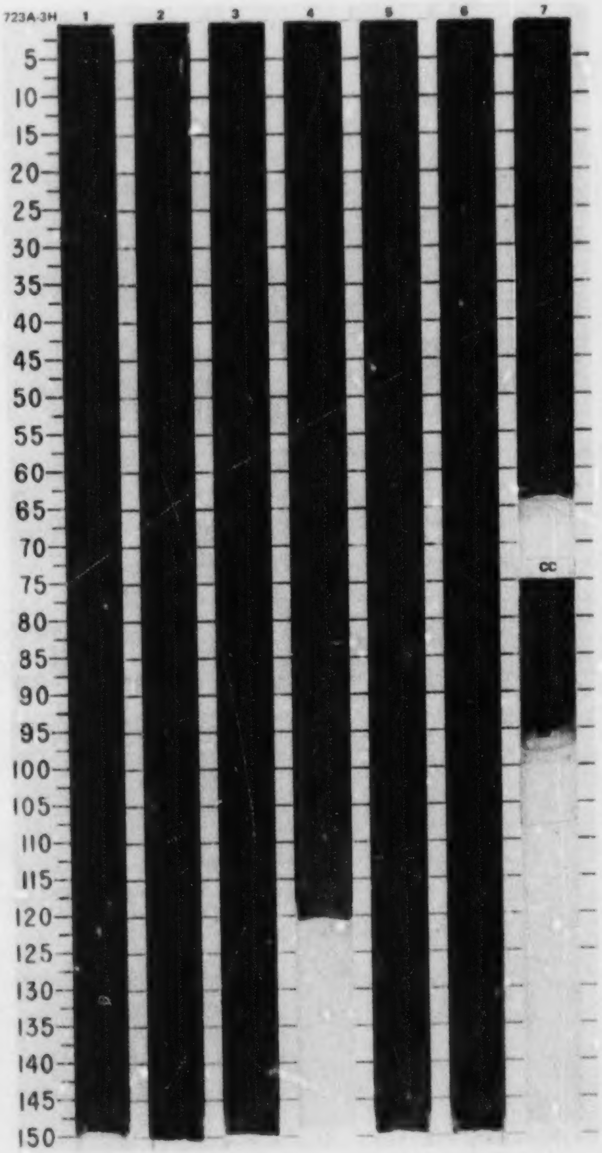
723A-3H
1
2
3
4
5
6
7
CC
5
10
15
20
25
30
35
40
45
50
55
60
65
70
75
80
85
90
95
100
105
110
115
120
125
130
135
140
145
150

SITE 723 HOLE A CORE 4H CORED INTERVAL 834.9-844.6 mbsl; 27.1-36.8 mbsf

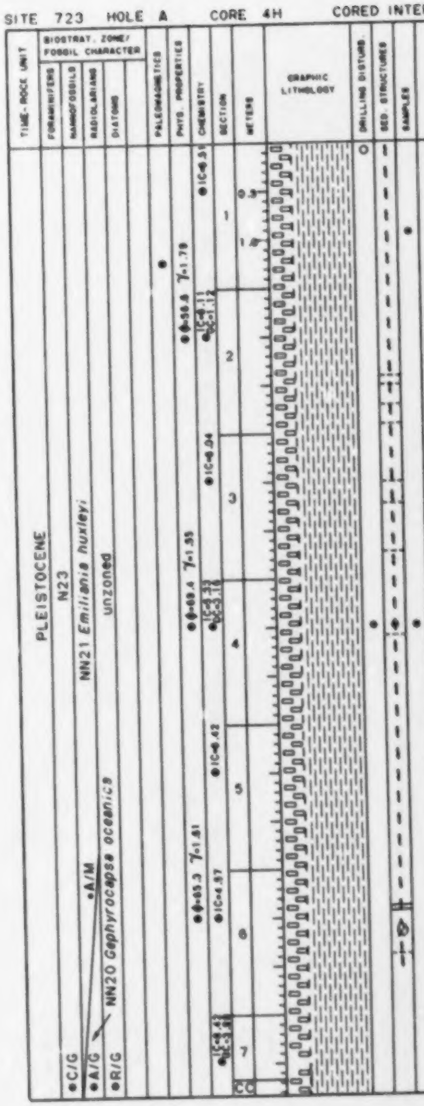
TIME-ROCK UNIT
BIOSTRAT. ZONE/ FOSSIL CHARACTER
FORAMINIFERS
NANNOFOSSILS
RADIOLARIANS
DIATOMS
PALEOMAGNETICS
PHYS. PROPERTIES
CHEMISTRY
SECTION
METERS
GRAPHIC LITHOLOGY
DRILLING DISTURB.
SED. STRUCTURES
SAMPLES
PLEISTOCENE
N23
NN21 Emiliania huxleyi
unzoned
●A/M
NN20 Gephyrocapsa oceanica
●C/G
●A/G
●R/G
●ϕ=56.6 γ=1.79
●ϕ=60.4 γ=1.55
●ϕ=65.3 γ=1.81
●IC=6.51
●IC=6.04
●IC=6.42
●IC=4.97
0.5
1.0
1
2
3
4
5
6
7
CC

LITHOLOGIC DESCRIPTION

FORAMINIFER-BEARING MARLY NANNOFOSSIL OOZE and CALCAREOUS CLAYEY SILT

Section 1, 0-15 cm, soupy; remainder undisturbed.

Major lithologies: FORAMINIFER-BEARING MARLY NANNOFOSSIL OOZE and CALCAREOUS CLAYEY SILT, olive gray (5Y 4/2, 4/3) and dark olive gray (5Y 3/2, 3/1, 2.5/1). Increased color contrast and mottling. Foraminifers and shell fragments (pteropods) common on core face. Variable terrigenous component dominated by clay and silt-sized detrital calcite.

Minor lithology: Section 4, 0-60 cm, diatomaceous silty clay, olive gray (5Y 4/2).

SMEAR SLIDE SUMMARY (%):

	1, 93 D	4, 44 D
TEXTURE:		
Sand		5
Silt	60	30
Clay	40	65
COMPOSITION:		
Access. minerals	2	5
Clay	30	24
Diatoms	Tr	20
Dolomite	2	
Foraminifers	3	10
Inorganic calcite	40	10
Mica	5	3
Nannofossils	10	10
Organic debris	3	5
Pellets		5
Pteropod		Tr
Quartz	5	3

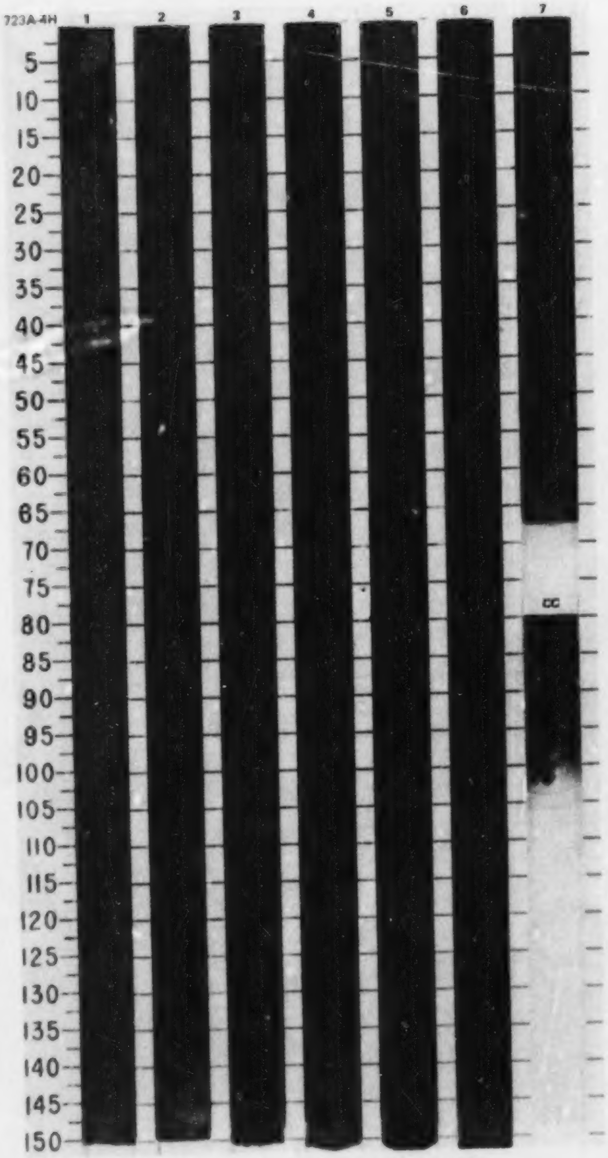
723A-4H
1
2
3
4
5
6
7
CC
5
10
15
20
25
30
35
40
45
50
55
60
65
70
75
80
85
90
95
100
105
110
115
120
125
130
135
140
145
150

SITE 723 HOLE A CORE 5H CORED INTERVAL 844.6-854.2 mbsl; 36.8-46.4 mbsf

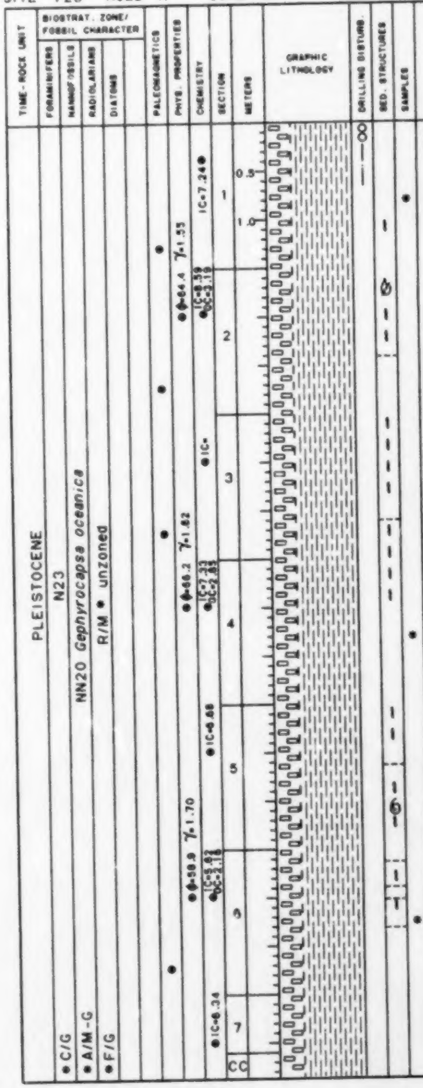
TIME-ROCK UNIT
BIOSTRAT. ZONE/ FOSSIL CHARACTER
FORAMINIFERS
NANNOFOSSILS
RADIOLARIANS
DIATOMS
PALEOMAGNETICS
PHYS. PROPERTIES
CHEMISTRY
SECTION
METERS
GRAPHIC LITHOLOGY
DRILLING DISTURB.
SED. STRUCTURES
SAMPLES
PLEISTOCENE
N23
NN20 Gephyrocapsa oceanica
R/M • unzoned
• C/G
• A/M-G
• F/G
●ϕ=64.4 γ=1.55
●ϕ=66.2 γ=1.82
●ϕ=58.9 γ=1.70
IC=7.24●
●IC=8.59 OC=3.19
●IC=
●IC=7.33 OC=2.85
●IC=6.66
●IC=5.82 OC=2.18
●IC=6.34
1
2
3
4
5
6
7
CC
0.5
1.0

LITHOLOGIC DESCRIPTION

FORAMINIFER-BEARING MARLY NANNOFOSSIL OOZE and CALCAREOUS CLAYEY SILT

Section 1, 0-50 cm, moderately disturbed; remainder slightly disturbed by gas expansion cracks and separation.

Major lithologies: FORAMINIFER-BEARING MARLY NANNOFOSSIL OOZE and CALCAREOUS CLAYEY SILT, olive gray (5Y 4/2, 4/3) and dark olive gray (5Y 3/2). Foraminifers common on core face. Shell debris concentrated in burrows. Variable terrigenous component dominated by clay and silt-sized detrital calcite.

SMEAR SLIDE SUMMARY (%):

	1, 80 D	4, 80 D	6, 74 D
TEXTURE:			
Sand	10	30	20
Silt	30	40	40
Clay	60	30	40
COMPOSITION:			
Clay	15	25	10
Diatoms	Tr	Tr	Tr
Dolomite	Tr	2	Tr
Foraminifers	10	20	5
Inorganic calcite	15	5	50
Mica			5
Nannofossils	55	25	10
Organic debris		5	
Quartz	5	8	20
Silicoflagellates			Tr

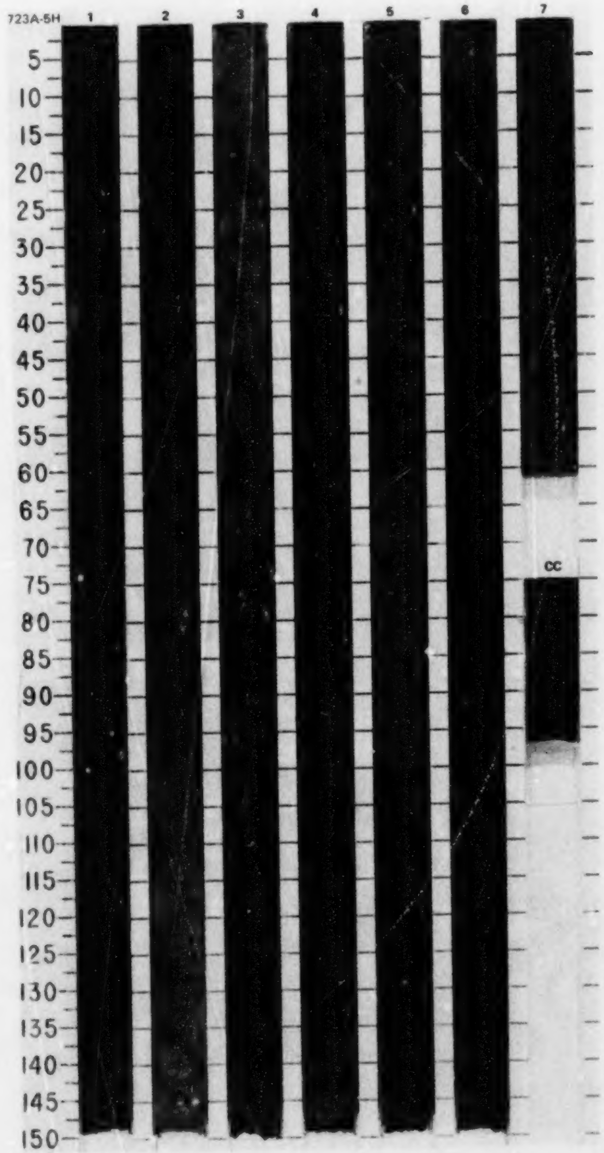
723A-5H
1
2
3
4
5
6
7
CC
5
10
15
20
25
30
35
40
45
50
55
60
65
70
75
80
85
90
95
100
105
110
115
120
125
130
135
140
145
150

SITE 723 HOLE A CORE 6H CORED INTERVAL 854.2-863.9 mbsl: 46.4-56.1 mbsf

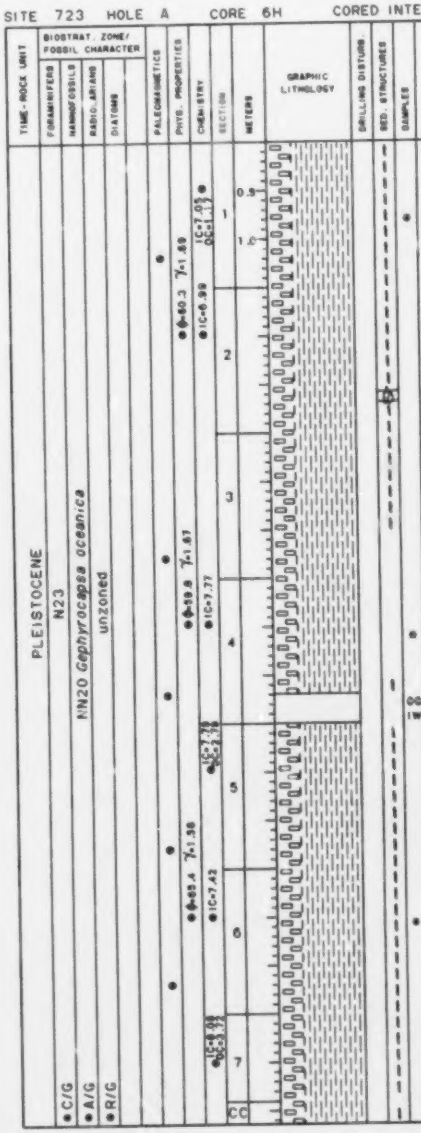
TIME-ROCK UNIT
BIOSTRAT. ZONE/ FOSSIL CHARACTER
FORAMINIFERS
NANNOFOSSILS
RADIOLARIANS
DIATOMS
PALEOMAGNETICS
PHYS. PROPERTIES
CHEMISTRY
SECTION
METERS
GRAPHIC LITHOLOGY
DRILLING DISTURB.
SED. STRUCTURES
SAMPLES
PLEISTOCENE
N23
NN20 Gephyrocapsa oceanica
unzoned
● C/G
● A/G
● R/G
●φ=60.3 γ=1.89
●φ=59.8 γ=1.87
●φ=65.4 γ=1.98
IC=7.05 OC=1.17 ●
●IC=6.99
●IC=7.77
●IC=7.42
0.5
1.0
1
2
3
4
5
6
7
CC
OG
IW

LITHOLOGIC DESCRIPTION

FORAMINIFER-BEARING MARLY NANNOFOSSIL OOZE and CALCAREOUS CLAYEY SILT

Entire core slightly disturbed by gas expansion (numerous small voids). Sediment appears continuous across voids within core.

Major lithologies: FORAMINIFER-BEARING MARLY NANNOFOSSIL OOZE and CALCAREOUS CLAYEY SILT, olive gray (5Y 5/2, 4/2, 4/3) and dark olive gray (5Y 3/2, 2.5/1). Increased color contrast and mottling. Foraminifers common on core face. Variable terrigenous component dominated by clay and silt-sized detrital calcite.

SMEAR SLIDE SUMMARY (%):

	1, 80 D	4, 60 D	6, 55 M
TEXTURE:			
Silt	35	45	50
Clay	65	55	50
COMPOSITION:			
Access. minerals	10	10	10
Clay	20	15	30
Diatoms			Tr
Dolomite	Tr	Tr	Tr
Foraminifers	7	7	10
Volcanic glass		Tr	
Inorganic calcite	13	18	20
Mica	Tr		
Nannofossils	40	40	10
Organic debris			5
Quartz	10	10	15
Sponge spicules			Tr

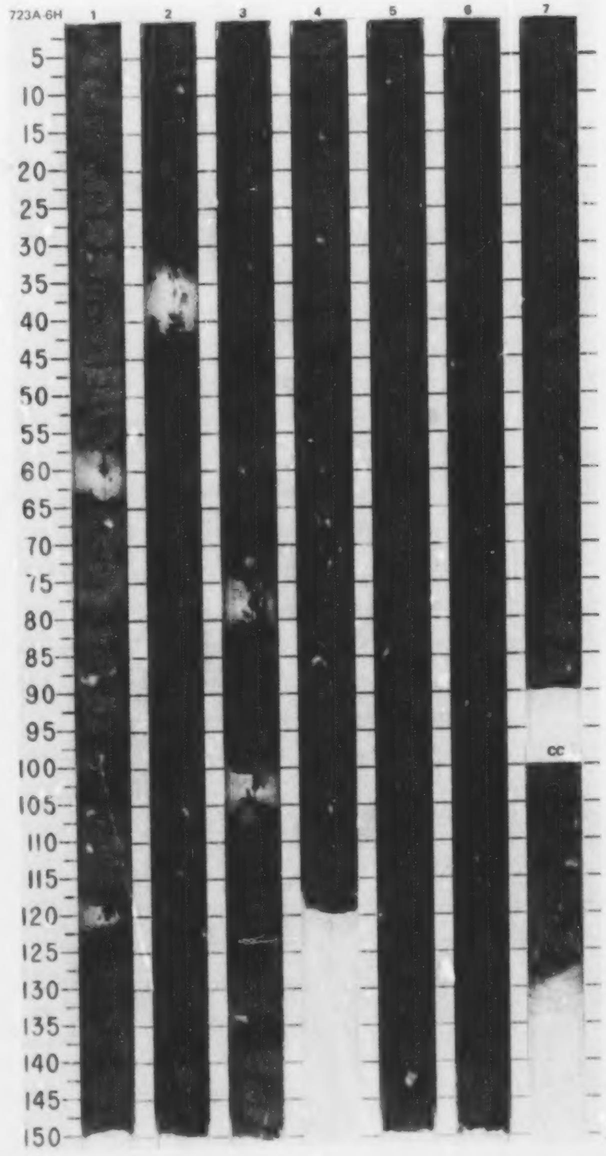
723A-6H
1
2
3
4
5
6
7
CC
5
10
15
20
25
30
35
40
45
50
55
60
65
70
75
80
85
90
95
100
105
110
115
120
125
130
135
140
145
150

SITE 723 HOLE A CORE 7H CORED INTERVAL 863.9-873.6 mbsl; 56.1-65.8 mbsf

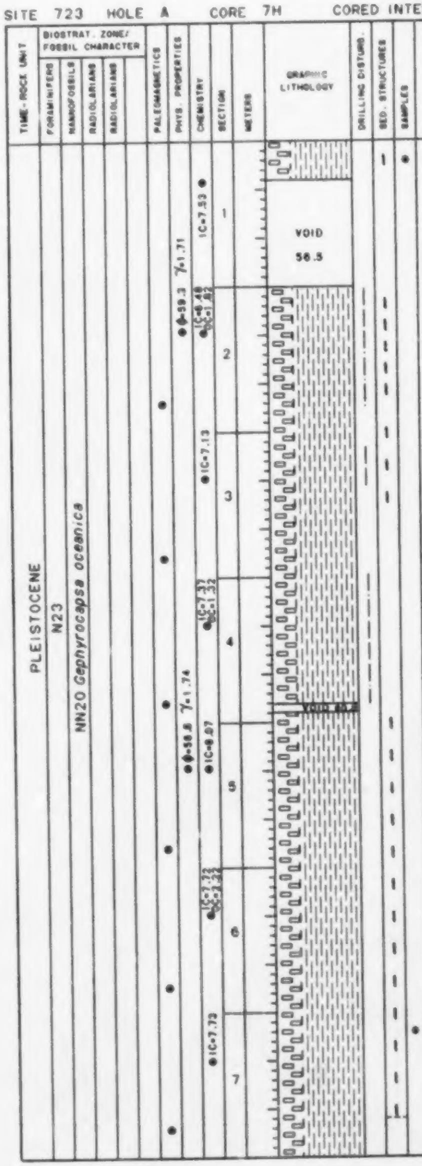
TIME-ROCK UNIT
BIOSTRAT. ZONE/ FOSSIL CHARACTER
FORAMINIFERS
NANNOFOSSILS
RADIOLARIANS
RADIOLARIANS
PALEOMAGNETICS
PHYS. PROPERTIES
CHEMISTRY
SECTION
METERS
GRAPHIC LITHOLOGY
DRILLING DISTURB.
SED. STRUCTURES
SAMPLES
PLEISTOCENE
N23
NN20 Gephyrocapsa oceanica
●Φ=59.3 γ=1.71
●Φ=58.8 γ=1.74
IC=7.53
IC=6.48
OC=1.82
IC=7.13
IC=7.37
OC=1.32
IC=8.07
IC=7.32
OC=2.32
IC=7.73
1
2
3
4
5
6
7
VOID
56.5
VOID

LITHOLOGIC DESCRIPTION

FORAMINIFER-BEARING MARLY NANNOFOSSIL OOZE and CALCAREOUS CLAYEY SILT

Entire core slightly to moderately disturbed by gas expansion (numerous small voids). Expanded beyond length cored. Sediment appears continuous across voids within core.

Major lithologies: FORAMINIFER-BEARING MARLY NANNOFOSSIL OOZE and CALCAREOUS CLAYEY SILT, olive gray (5Y 4/2, 4/3) and dark olive gray (5Y 3/1). Foraminifers common on core face. Variable terrigenous component dominated by clay and silt-sized detrital calcite.

SMEAR SLIDE SUMMARY (%):

	1, 20 D	7, 20 D
TEXTURE:		
Sand	5	10
Silt	25	35
Clay	70	55
COMPOSITION:		
Access. minerals	2	2
Clay	20	30
Dolomite		Tr
Feldspar		1
Foraminifers	6	6
Volcanic glass	Tr	1
Inorganic calcite	15	20
Nannofossils	50	35
Pteropod		Tr
Quartz	2	5
Sponge spicules	Tr	

(CON'T.)

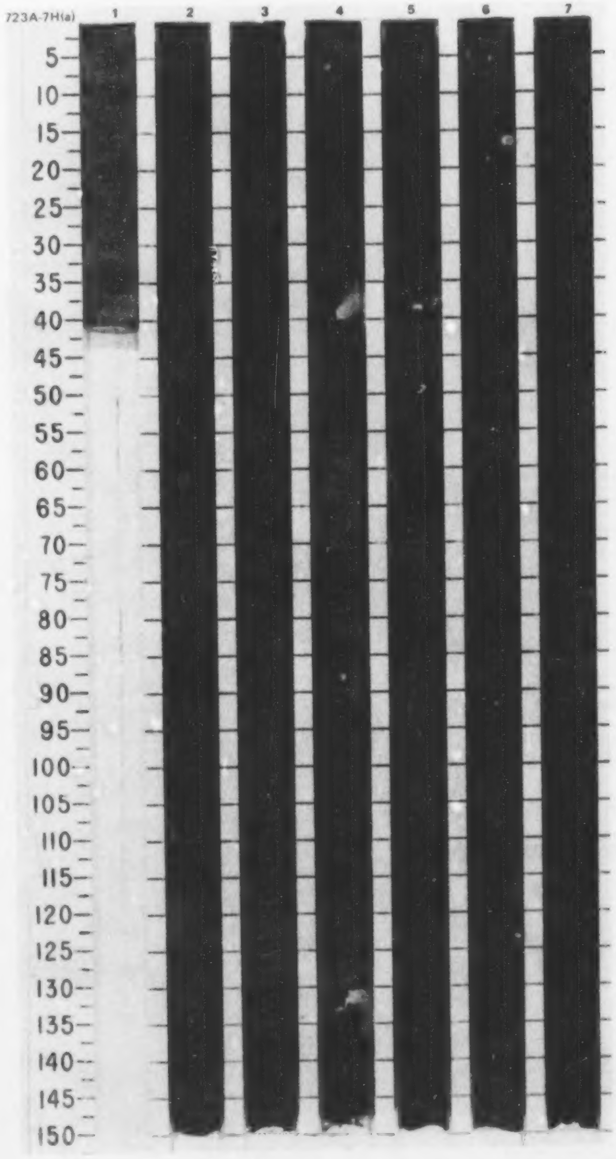
723A-7H(a)
1
2
3
4
5
6
7
5
10
15
20
25
30
35
40
45
50
55
60
65
70
75
80
85
90
95
100
105
110
115
120
125
130
135
140
145
150

SITE 723 HOLE A CORE 7H CORED INTERVAL 863.9-873.6 mbsl; 56.1-65.8 mbsf

TIME-ROCK UNIT	BIOSTRAT. ZONE/ FOSSIL CHARACTER: FORAMINIFERS	NANNOFOSSILS	RADIOLARIANS	DIATOMS		PALEOMAGNETICS	PHYS. PROPERTIES	CHEMISTRY	SECTION	METERS	GRAPHIC LITHOLOGY	DRILLING DISTURB.	SED. STRUCTURES	SAMPLES	LITHOLOGIC DESCRIPTION
	●C/G	●A/G	●Barren				ϕ=65.3 γ=1.56 ●	●IC=4.95 OC=5.51 IC=8.07●	8 CC	0.5 1.0			!		(CON'T.)

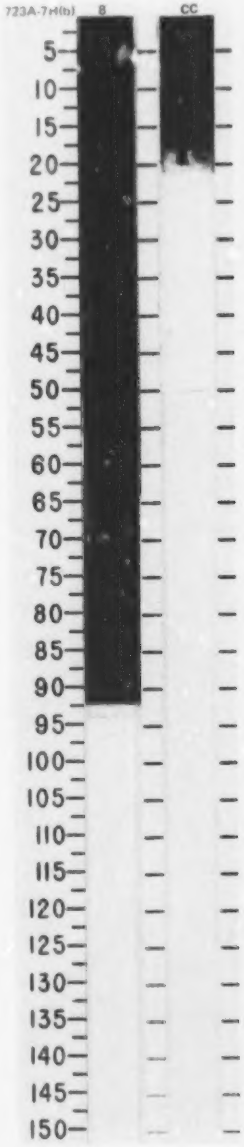
723A-7H(b)
8
CC
5
10
15
20
25
30
35
40
45
50
55
60
65
70
75
80
85
90
95
100
105
110
115
120
125
130
135
140
145
150

SITE 723 HOLE A CORE 8H CORED INTERVAL 873.6-883.2 mbsl; 65.8-75.4 mbsf

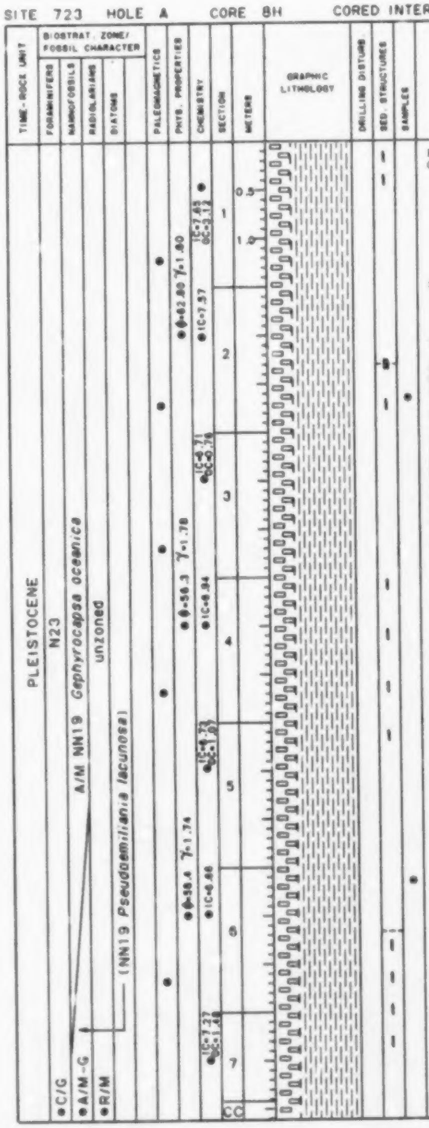
TIME-ROCK UNIT
BIOSTRAT. ZONE/ FOSSIL CHARACTER
FORAMINIFERS
NANNOFOSSILS
RADIOLARIANS
DIATOMS
PALEOMAGNETICS
PHYS. PROPERTIES
CHEMISTRY
SECTION
METERS
GRAPHIC LITHOLOGY
DRILLING DISTURB.
SED. STRUCTURES
SAMPLES
PLEISTOCENE
N23
A/M NN19 Gephyrocapsa oceanica
unzoned
(NN19 Pseudoemiliania lacunosa)
●C/G
●A/M-G
●R/M
●φ=62.80 γ=1.80
●φ=56.3 γ=1.78
●φ=58.4 γ=1.74
IC=7.45 OC=3.12
●IC=7.57
IC=6.71 OC=0.76
●IC=6.94
IC=6.73 OC=1.07
●IC=6.86
IC=7.27 OC=1.48
0.5
1.0
1
2
3
4
5
6
7
CC

LITHOLOGIC DESCRIPTION

FORAMINIFER-BEARING MARLY NANNOFOSSIL OOZE and CALCAREOUS CLAYEY SILT

Entire core slightly disturbed by gas expansion (numerous small voids). Sediment appears continuous across voids within core.

Major lithologies: FORAMINIFER-BEARING MARLY NANNOFOSSIL OOZE and CALCAREOUS CLAYEY SILT, olive gray (5Y 5/3, 4/2, 4/3, 4/4) and dark olive gray (5Y 3/2). Mottling less obvious. Foraminifers common on core face. Variable terrigenous component dominated by clay and silt-sized detrital calcite.

SMEAR SLIDE SUMMARY (%):

	2, 114 D	6, 14 D
TEXTURE:		
Sand	15	5
Silt	20	30
Clay	65	65
COMPOSITION:		
Access. minerals	2	2
Clay	25	20
Dolomite	1	1
Foraminifers	2	1
Volcanic glass	Tr	Tr
Inorganic calcite	25	25
Mica		1
Nannofossils	40	45
Pteropod		Tr
Quartz	5	3
Sponge spicules		Tr

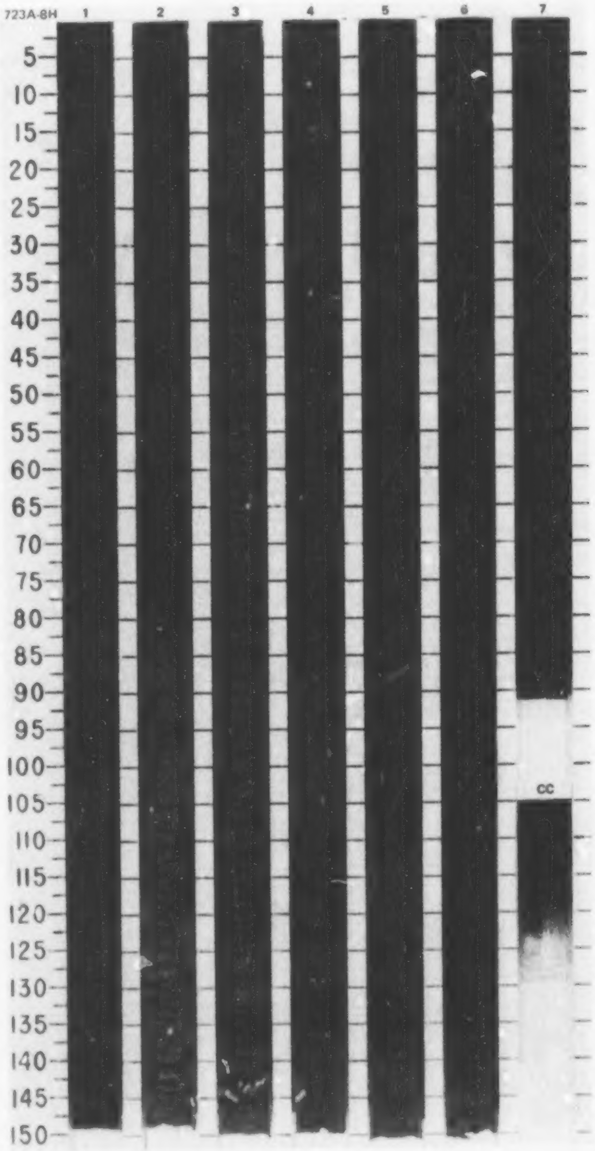
723A-8H
1
2
3
4
5
6
7
CC
5
10
15
20
25
30
35
40
45
50
55
60
65
70
75
80
85
90
95
100
105
110
115
120
125
130
135
140
145
150

SITE 723 HOLE A CORE 9H CORED INTERVAL 883.2-892.9 mbsl; 75.4-85.1 mbsf

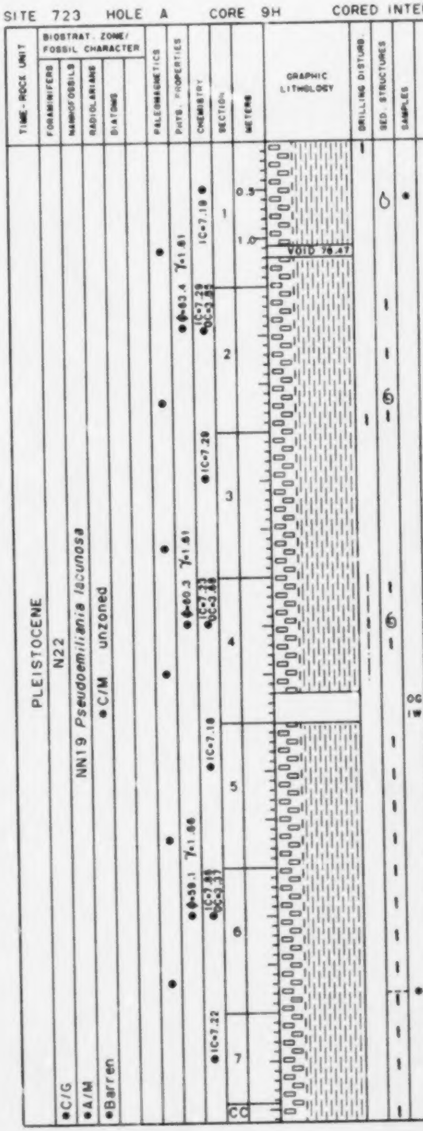
TIME-ROCK UNIT
BIOSTRAT. ZONE/ FOSSIL CHARACTER
FORAMINIFERS
NANNOFOSSILS
RADIOLARIANS
DIATOMS
PALEOMAGNETICS
PHYS. PROPERTIES
CHEMISTRY
SECTION
METERS
GRAPHIC LITHOLOGY
DRILLING DISTURB.
SED. STRUCTURES
SAMPLES
PLEISTOCENE
N22
NN19 Pseudoemiliania lacunosa
●C/M unzoned
●C/G
●A/M
●Barren
IC=7.18 ●
●φ=63.4 γ=1.81
IC=7.29 OC=3.85
●IC=7.28
●φ=60.3 γ=1.81
IC=7.23 OC=3.88
●IC=7.18
●φ=59.1 γ=1.86
IC=7.86 OC=3.37
●IC=7.22
0.5
1.0
VOID 76.47
1
2
3
4
5
6
7
CC
OG
IW

LITHOLOGIC DESCRIPTION

FORAMINIFER-BEARING MARLY NANNOFOSSIL OOZE and CALCAREOUS CLAYEY SILT

Section 4, 59-69 cm, heavily disturbed; Section 4, 95-115 cm, moderately disturbed; remainder of core slightly disturbed by gas expansion (numerous small voids). Sediment appears continuous across voids within core.

Major lithologies: FORAMINIFER-BEARING MARLY NANNOFOSSIL OOZE and CALCAREOUS CLAYEY SILT, olive gray (5Y 4/2, 4/3) and dark olive gray (5Y 3/2), mottled. Foraminifers common on core face. Variable terrigenous component dominated by clay and silt-sized detrital calcite.

SMEAR SLIDE SUMMARY (%):

	1, 57 D	6, 136 D
TEXTURE:		
Sand	15	20
Silt	25	20
Clay	60	60
COMPOSITION:		
Access. minerals	1	2
Clay	25	30
Dolomite	Tr	Tr
Feldspar	1	1
Foraminifers	15	7
Inorganic calcite	16	25
Nannofossils	40	30
Quartz	2	5

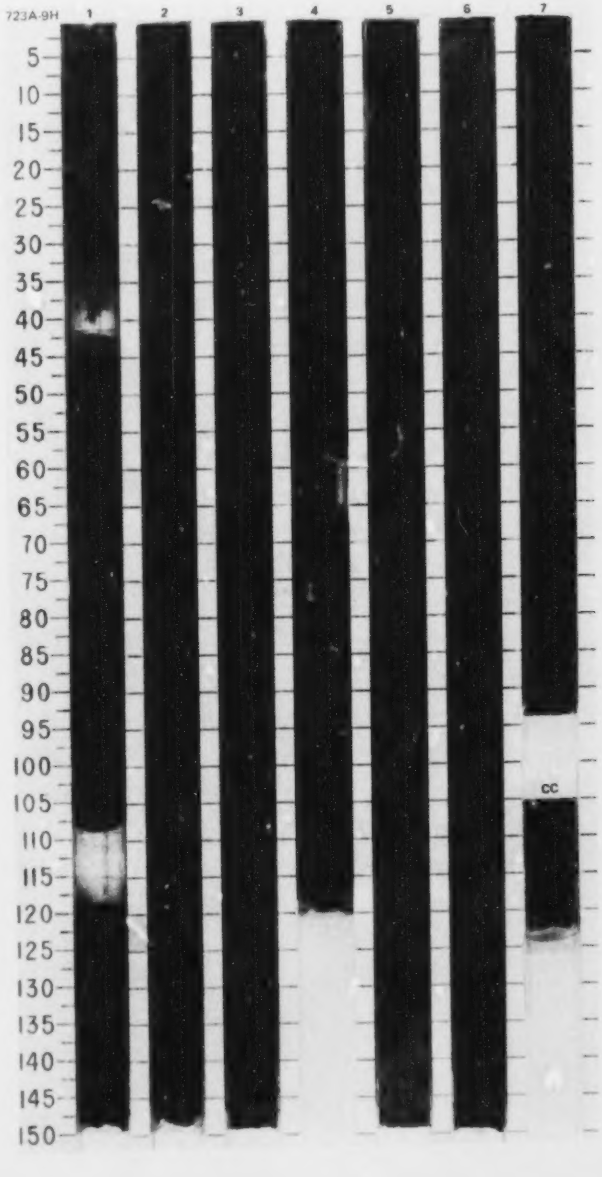
723A-9H
1
2
3
4
5
6
7
CC
5
10
15
20
25
30
35
40
45
50
55
60
65
70
75
80
85
90
95
100
105
110
115
120
125
130
135
140
145
150

CORE 117–723A–10X NO RECOVERY

SITE 723 HOLE A CORE 11X CORED INTERVAL 902.6-912.2 mbsl; 94.8-104.4 mbsf

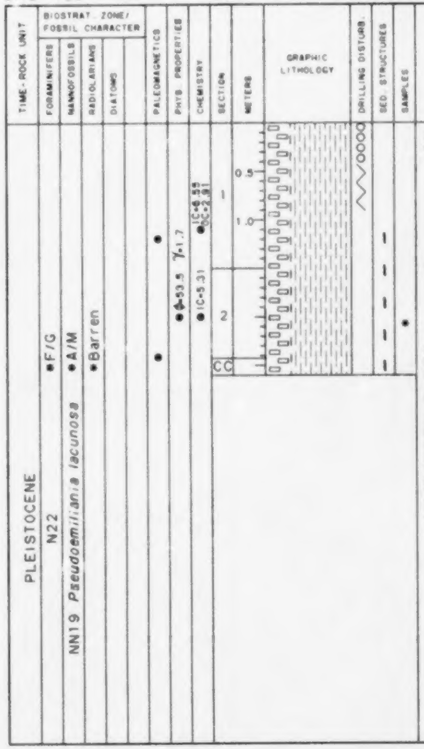
TIME-ROCK UNIT
BIOSTRAT. ZONE/ FOSSIL CHARACTER
FORAMINIFERS
NANNOFOSSILS
RADIOLARIANS
DIATOMS
PALEOMAGNETICS
PHYS. PROPERTIES
CHEMISTRY
SECTION
METERS
GRAPHIC LITHOLOGY
DRILLING DISTURB.
SED. STRUCTURES
SAMPLES
PLEISTOCENE
N22
●F/G
NN19 Pseudoemiliania lacunosa
●A/M
●Barren
●Φ-53.5 γ-1.7
●IC-6.59 OC-2.91
●IC-5.31
1
2
CC
0.5
1.0

LITHOLOGIC DESCRIPTION

FORAMINIFER-BEARING MARLY NANNOFOSSIL OOZE and CALCAREOUS CLAYEY SILT

Section 1, 0-100 cm, soupy and very disturbed; remainder slightly disturbed by gas expansion.

Major lithologies: FORAMINIFER-BEARING MARLY NANNOFOSSIL OOZE and CALCAREOUS CLAYEY SILT, olive gray (5Y 4/2) and dark olive gray (5Y 3/2), mottled. Variable terrigenous component dominated by clay and silt-sized detrital calcite.

SMEAR SLIDE SUMMARY (%):

	2, 58 D
TEXTURE:	
Sand	15
Silt	35
Clay	50
COMPOSITION:	
Access. minerals	2
Clay	30
Feldspar	1
Foraminifers	2
Volcanic glass	Tr
Inorganic calcite	30
Mica	Tr
Nannofossils	28
Quartz	7

CORE 117–723A–12X NO RECOVERY

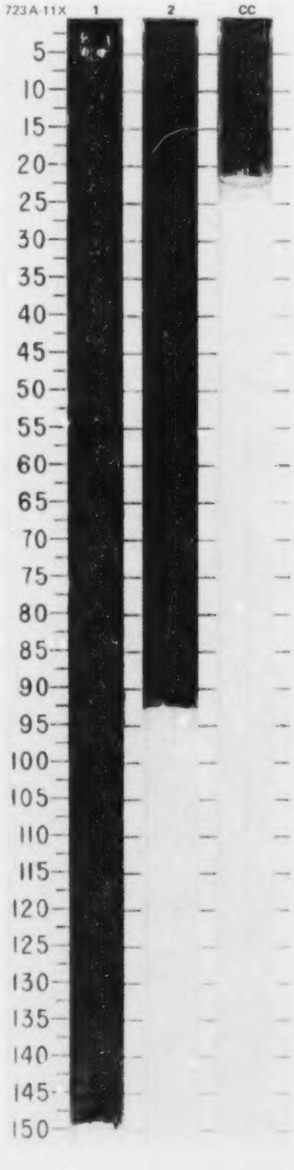
723A-11X
1
2
CC
5
10
15
20
25
30
35
40
45
50
55
60
65
70
75
80
85
90
95
100
105
110
115
120
125
130
135
140
145
150

SITE 723 HOLE A CORE 13X CORED INTERVAL 921.9-931.6 mbsl; 114.1-123.8 mbsf

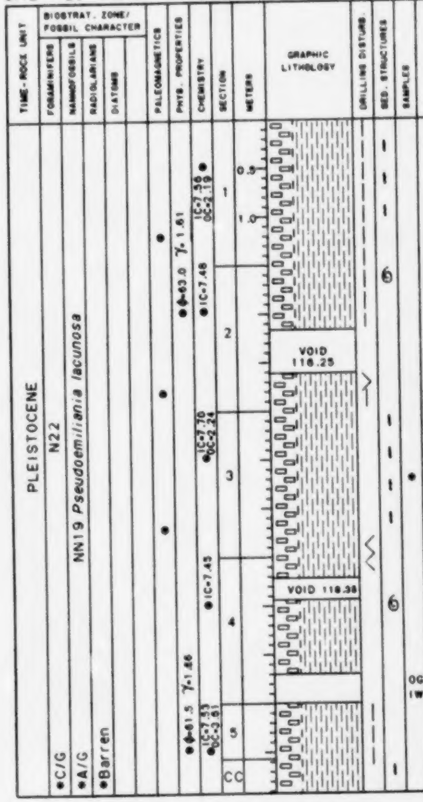
TIME-ROCK UNIT
BIOSTRAT. ZONE/ FOSSIL CHARACTER
FORAMINIFERS
NANNOFOSSILS
RADIOLARIANS
DIATOMS
PALEOMAGNETICS
PHYS. PROPERTIES
CHEMISTRY
SECTION
METERS
GRAPHIC LITHOLOGY
DRILLING DISTURB.
SED. STRUCTURES
SAMPLES
PLEISTOCENE
N22
NN19 Pseudoemiliania lacunosa
●C/G
●A/G
●Barren
●Φ=63.0 γ=1.61
●Φ=61.5 γ=1.86
IC=7.56 OC=2.19
●IC=7.48
IC=7.70 OC=2.24
●IC=7.45
IC=7.53 OC=3.61
1
2
3
4
5
CC
0.5
1.0
VOID 116.25
VOID 118.38
OG
IW

LITHOLOGIC DESCRIPTION

FORAMINIFER-BEARING MARLY NANNOFOSSIL OOZE and CALCAREOUS CLAYEY SILT

Entire core slightly to moderately disturbed by gas expansion (voids increasing in size, sediment below space often disturbed by splitting wire). Sediment appears continuous across voids within core.

Major lithologies: FORAMINIFER-BEARING MARLY NANNOFOSSIL OOZE and CALCAREOUS CLAYEY SILT, olive gray (5Y 4/2), mottled. Foraminifers and shell fragments common on core face. Variable terrigenous component dominated by clay and silt-sized detrital calcite.

SMEAR SLIDE SUMMARY (%):

	3, 65 D
TEXTURE:	
Sand	10
Silt	34
Clay	56
COMPOSITION:	
Access. minerals	2
Clay	30
Feldspar	1
Foraminifers	8
Volcanic glass	Tr
Inorganic calcite	20
Mica	Tr
Nannofossils	36
Pteropod	Tr
Quartz	3
Rock fragments	Tr

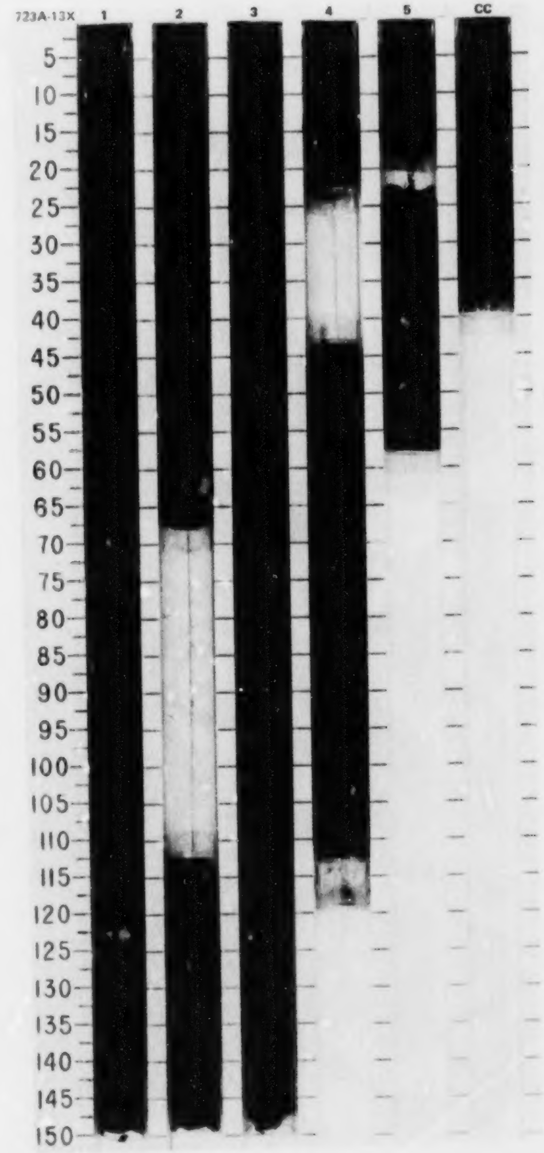
723A-13X
1
2
3
4
5
CC
5
10
15
20
25
30
35
40
45
50
55
60
65
70
75
80
85
90
95
100
105
110
115
120
125
130
135
140
145
150

SITE 723 HOLE A CORE 14X CORED INTERVAL 931.6-941.2 mbsl; 123.8-133.4 mbsf

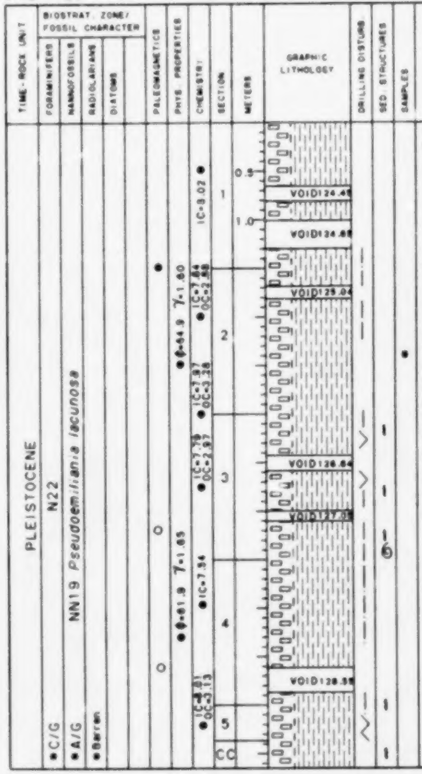
TIME-ROCK UNIT
BIOSTRAT. ZONE/ FOSSIL CHARACTER
FORAMINIFERS
NANNOFOSSILS
RADIOLARIANS
DIATOMS
PALEOMAGNETICS
PHYS. PROPERTIES
CHEMISTRY
SECTION
METERS
GRAPHIC LITHOLOGY
DRILLING DISTURB.
SED. STRUCTURES
SAMPLES
PLEISTOCENE
N22
NN19 Pseudoemiliania lacunosa
●C/G
●A/G
●Barren
IC=8.02
φ=64.9 γ=1.60
IC=7.64 OC=2.88
IC=7.97 OC=3.26
IC=7.78 OC=2.97
φ=61.9 γ=1.65
IC=7.34
IC=8.81 OC=3.13
1
2
3
4
5
CC
0.5
1.0
VOID 124.45
VOID 124.85
VOID 125.04
VOID 126.84
VOID 127.05
VOID 128.35

LITHOLOGIC DESCRIPTION

FORAMINIFER-BEARING MARLY NANNOFOSSIL OOZE and CALCAREOUS CLAYEY SILT

Entire core slightly to moderately disturbed by gas expansion (numerous voids). Sediment appears continuous across voids within core.

Major lithologies: FORAMINIFER-BEARING MARLY NANNOFOSSIL OOZE and CALCAREOUS CLAYEY SILT, olive gray (5Y 4/2) and dark olive gray (5Y 3/2), faintly mottled. Foraminifers present on core face. Variable terrigenous component dominated by clay and silt-sized detrital calcite.

SMEAR SLIDE SUMMARY (%):

	2, 89 D
TEXTURE:	
Sand	10
Silt	30
Clay	60
COMPOSITION:	
Access. minerals	Tr
Clay	25
Dolomite	Tr
Foraminifers	5
Inorganic calcite	20
Nannofossils	45
Quartz	5

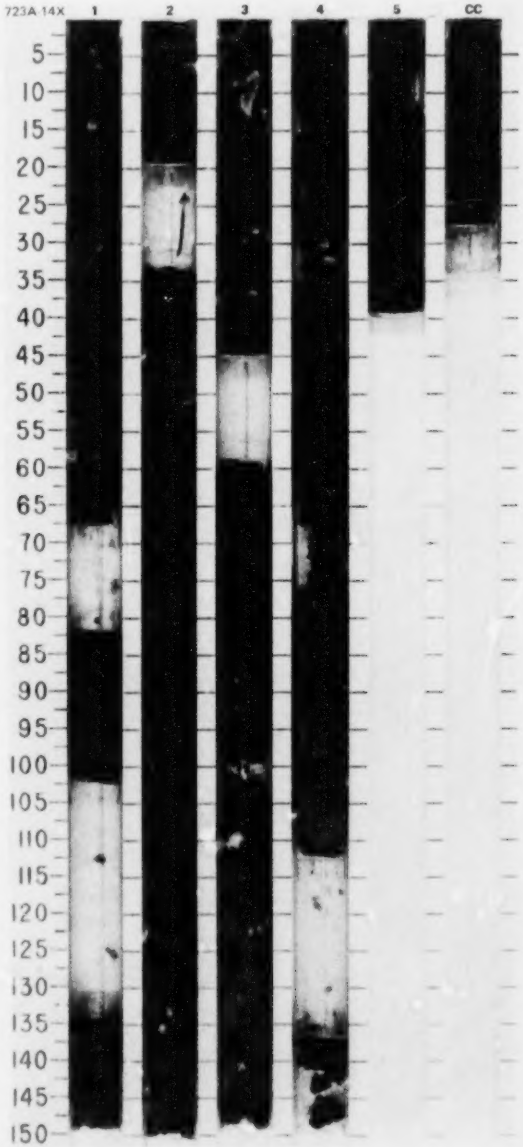
723A 14X
1
2
3
4
5
CC
5
10
15
20
25
30
35
40
45
50
55
60
65
70
75
80
85
90
95
100
105
110
115
120
125
130
135
140
145
150

SITE 723 HOLE A CORE 15X CORED INTERVAL 941.2-950.9 mbsl; 133.4-143.1 mbsf

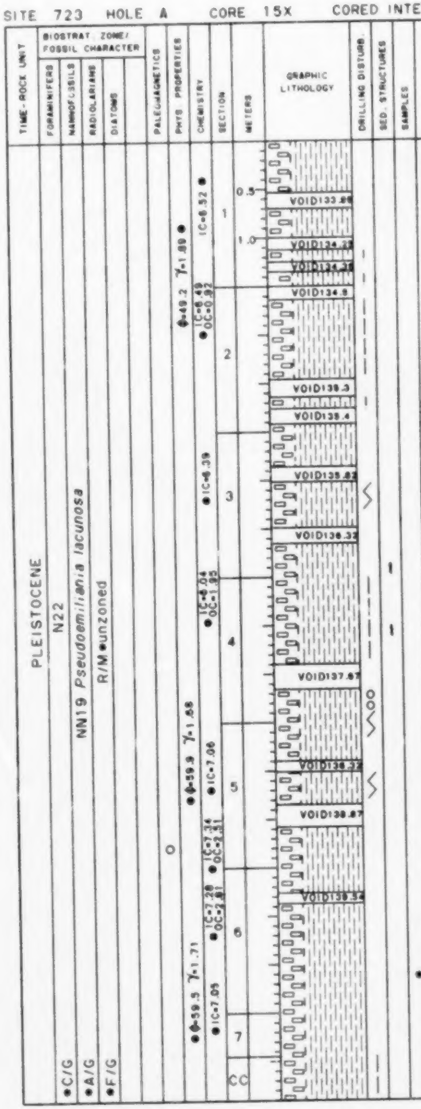
TIME-ROCK UNIT
BIOSTRAT. ZONE/ FOSSIL CHARACTER
FORAMINIFERS
NANNOFOSSILS
RADIOLARIANS
DIATOMS
PALEOMAGNETICS
PHYS. PROPERTIES
CHEMISTRY
SECTION
METERS
GRAPHIC LITHOLOGY
DRILLING DISTURB.
SED. STRUCTURES
SAMPLES
PLEISTOCENE
N22
NN19 Pseudoemiliania lacunosa
R/M●unzoned
●C/G
●A/G
●F/G
●Φ=49.2 γ=1.89 ●
●Φ=59.9 γ=1.88
●Φ=59.5 γ=1.71
IC=6.52 ●
● IC=6.49 OC=0.92
●IC=6.39
● IC=6.04 OC=1.95
●IC=7.06
● IC=7.34 OC=2.31
● IC=7.28 OC=2.81
●IC=7.05
1
2
3
4
5
6
7
CC
0.5
1.0
VOID133.86
VOID134.23
VOID134.38
VOID134.8
VOID135.3
VOID135.4
VOID135.82
VOID136.32
VOID137.67
VOID138.32
VOID138.87
VOID139.34

LITHOLOGIC DESCRIPTION

FORAMINIFER-BEARING MARLY NANNOFOSSIL OOZE and CALCAREOUS CLAYEY SILT

Entire core slightly to moderately disturbed by gas expansion. (numerous voids). Sediment appears continuous across voids within core except for Section 4, 130-150 cm, (soupy) sediment missing(?).

Major lithologies: FORAMINIFER-BEARING MARLY NANNOFOSSIL OOZE and CALCAREOUS CLAYEY SILT, olive gray (5Y 4/2, 4/3) and dark olive gray, faintly mottled. Foraminifers rare on core face. Variable terrigenous component dominated by clay and silt-sized detrital calcite.

SMEAR SLIDE SUMMARY (%):

	6, 111 D
TEXTURE:	
Sand	20
Silt	35
Clay	45
COMPOSITION:	
Access. minerals	Tr
Clay	20
Feldspar	1
Foraminifers	4
Inorganic calcite	30
Mica	Tr
Nannofossils	25
Quartz	20
Sponge spicules	Tr

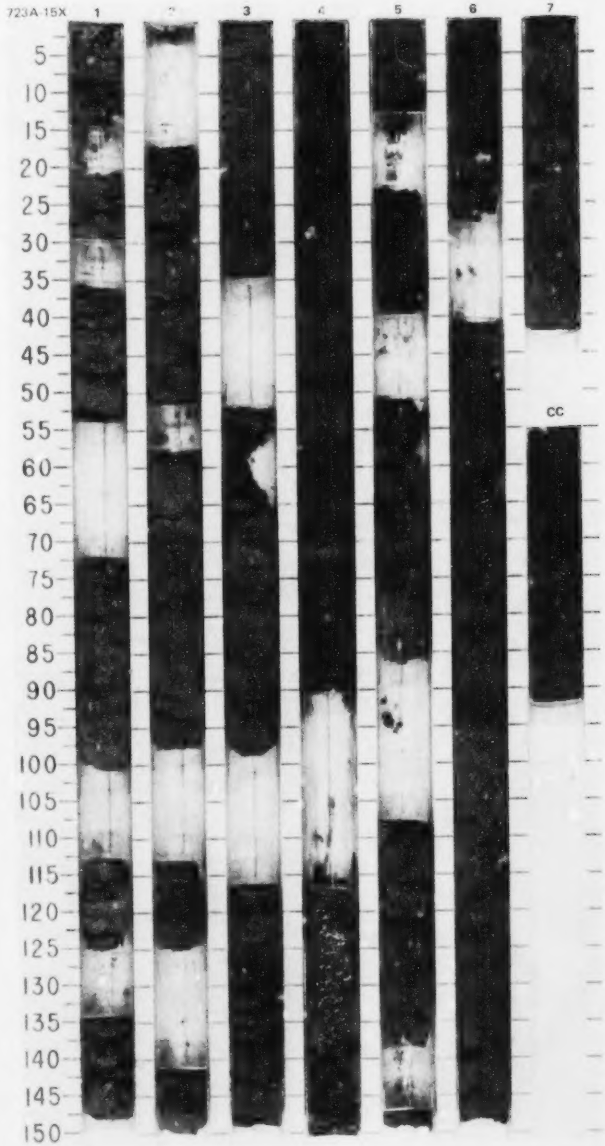
723A-15X
1
2
3
4
5
6
7
CC
5
10
15
20
25
30
35
40
45
50
55
60
65
70
75
80
85
90
95
100
105
110
115
120
125
130
135
140
145
150

CORE 117–723A–16X NO RECOVERY

SITE 723 HOLE A CORE 17X CORED INTERVAL 960.6-970.2 mbsl; 152.8-162.4 mbsf

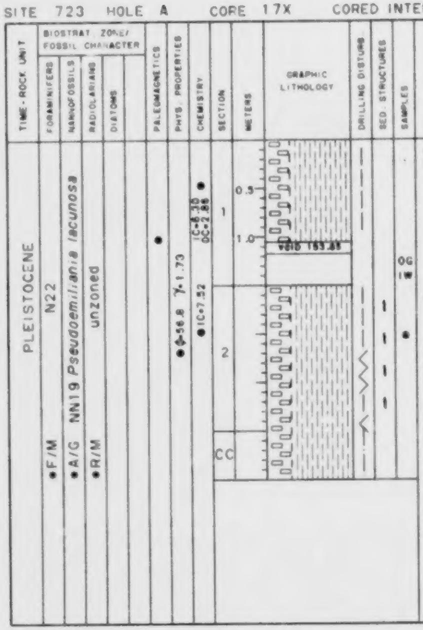
TIME-ROCK UNIT
BIOSTRAT. ZONE/ FOSSIL CHARACTER
FORAMINIFERS
NANNOFOSSILS
RADIOLARIANS
DIATOMS
PALEOMAGNETICS
PHYS. PROPERTIES
CHEMISTRY
SECTION
METERS
GRAPHIC LITHOLOGY
DRILLING DISTURB.
SED. STRUCTURES
SAMPLES
PLEISTOCENE
●F/M N22
●A/G NN19 Pseudoemiliania lacunosa
●R/M unzoned
●Φ=56.8 γ=1.73
IC=6.30 OC=2.88
●IC=7.52
1
2
CC
0.5
1.0
VOID 153.85
OG
IW

LITHOLOGIC DESCRIPTION

FORAMINIFER-BEARING MARLY NANNOFOSSIL OOZE and CALCAREOUS CLAYEY SILT

Entire core slightly to moderately disturbed by gas expansion (numercus voids). Section 1, soupy top(?). Sediment appears continuous across voids within core.

Major lithologies: FORAMINIFER-BEARING MARLY NANNOFOSSIL OOZE and CALCAREOUS CLAYEY SILT, olive gray (5Y 4/3) and dark olive gray (5Y 3/2), faintly mottled. Foraminifers rare on core face. Variable terrigenous component dominated by clay and silt-sized detrital calcite.

SMEAR SLIDE SUMMARY (%):

	2, 51 D
TEXTURE:	
Sand	5
Silt	15
Clay	80
COMPOSITION:	
Access. minerals	1
Clay	30
Foraminifers	2
Volcanic glass	Tr
Inorganic calcite	10
Nannofossils	50
Quartz	2
Sponge spicules	Tr

CORE 117–723A–18X NO RECOVERY

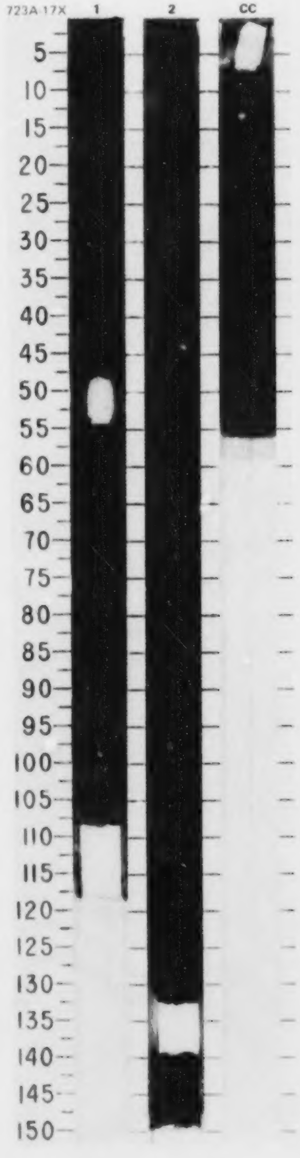
723A-17X
1
2
CC
5
10
15
20
25
30
35
40
45
50
55
60
65
70
75
80
85
90
95
100
105
110
115
120
125
130
135
140
145
150

SITE 723 HOLE A CORE 19X CORED INTERVAL 979.9-989.6 mbsl; 172.1-181.8 mbsf

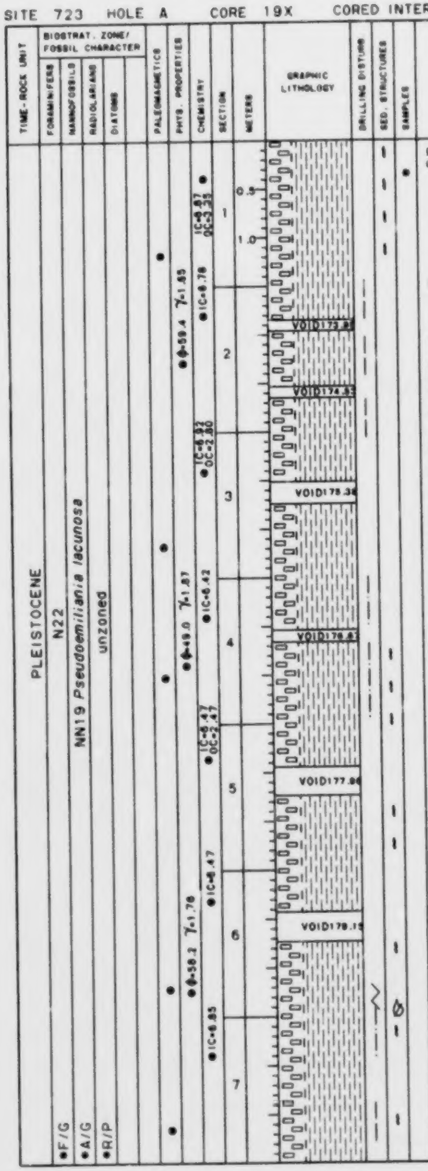
TIME-ROCK UNIT
BIOSTRAT. ZONE/FOSSIL CHARACTER
FORAMINIFERS
NANNOFOSSILS
RADIOLARIANS
DIATOMS
PALEOMAGNETICS
PHYS. PROPERTIES
CHEMISTRY
SECTION
METERS
GRAPHIC LITHOLOGY
DRILLING DISTURB.
SED. STRUCTURES
SAMPLES
PLEISTOCENE
N22
NN19 Pseudoemiliania lacunosa
unzoned
●F/G
●A/G
●R/P
●Φ=59.4 γ=1.85
●Φ=49.0 γ=1.87
●Φ=58.2 γ=1.76
IC=8.87 OC=3.35
●IC=8.78
●IC=6.82 OC=2.80
●IC=6.42
●IC=6.47 OC=2.47
●IC=6.47
●IC=6.85
1
2
3
4
5
6
7
0.5
1.0
VOID173.8
VOID174.5
VOID175.3
VOID176.8
VOID177.8
VOID179.1

LITHOLOGIC DESCRIPTION

FORAMINIFER-BEARING MARLY NANNOFOSSIL OOZE and CALCAREOUS CLAYEY SILT

Entire core slightly to moderately disturbed by gas expansion (numerous voids). Sediment appears continuous across voids within core.

Major lithologies: FORAMINIFER-BEARING MARLY NANNOFOSSIL OOZE and CALCAREOUS CLAYEY SILT, olive gray (5Y 4/2, 5/3) and dark olive gray (5Y 3/2), faintly mottled. Foraminifers present on core face. Variable terrigenous component dominated by clay and silt-sized detrital calcite.

SMEAR SLIDE SUMMARY (%):

	1, 35 D
TEXTURE:	
Sand	10
Silt	24
Clay	66
COMPOSITION:	
Access. minerals	2
Clay	20
Dolomite	Tr
Feldspar	1
Foraminifers	6
Volcanic glass	Tr
Inorganic calcite	20
Nannofossils	46
Quartz	5
Sponge spicules	Tr

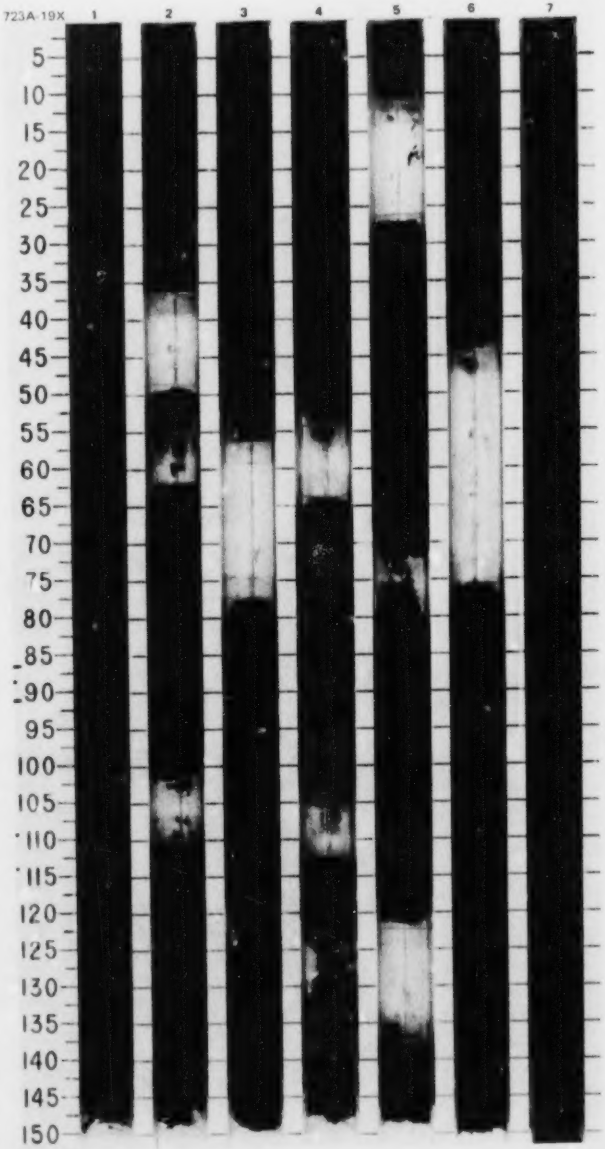
723A-19X
1
2
3
4
5
6
7
5
10
15
20
25
30
35
40
45
50
55
60
65
70
75
80
85
90
95
100
105
110
115
120
125
130
135
140
145
150

SITE 723 HOLE A CORE 20X CORED INTERVAL 989.6-999.2 mbsl; 181.8-191.4 mbsf

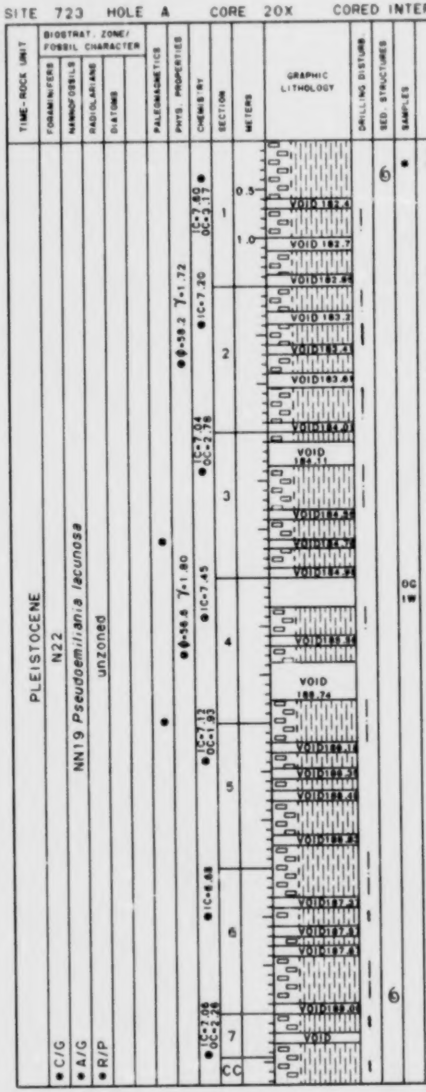
TIME-ROCK UNIT
BIOSTRAT. ZONE/ FOSSIL CHARACTER
FORAMINIFERS
NANNOFOSSILS
RADIOLARIANS
DIATOMS
PALEOMAGNETICS
PHYS. PROPERTIES
CHEMISTRY
SECTION
METERS
GRAPHIC LITHOLOGY
DRILLING DISTURB.
SED. STRUCTURES
SAMPLES
PLEISTOCENE
N22
NN19 Pseudoemiliania lacunosa
unzoned
● C/G
● A/G
● R/P
●φ=58.2 γ=1.72
●φ=56.6 γ=1.80
IC=7.60 OC=3.17 ●
●IC=7.20
●IC=7.04 OC=2.78
●IC=7.45
●IC=7.12 OC=1.93
●IC=6.68
●IC=7.06 OC=2.26
1
2
3
4
5
6
7
CC
0.5
1.0
VOID 182.4
VOID 182.7
VOID 183.2
VOID 184.11
VOID 186.74
VOID
OG
IW

LITHOLOGIC DESCRIPTION

FORAMINIFER-BEARING MARLY NANNOFOSSIL OOZE and CALCAREOUS CLAYEY SILT

Entire core moderately disturbed by gas expansion (numerous voids).

Major lithologies: FORAMINIFER-BEARING MARLY NANNOFOSSIL OOZE and CALCAREOUS CLAYEY SILT, olive gray (5Y 4/2, 4/3) and dark olive gray (5Y 3/2), faintly mottled. Foraminifers present on core face. Variable terrigenous component dominated by clay and silt-sized detrital calcite.

SMEAR SLIDE SUMMARY (%):

	1, 25 D
TEXTURE:	
Sand	15
Silt	20
Clay	65
COMPOSITION:	
Access. minerals	Tr
Clay	25
Dolomite	Tr
Foraminifers	7
Volcanic glass	Tr
Inorganic calcite	20
Nannofossils	40
Quartz	8

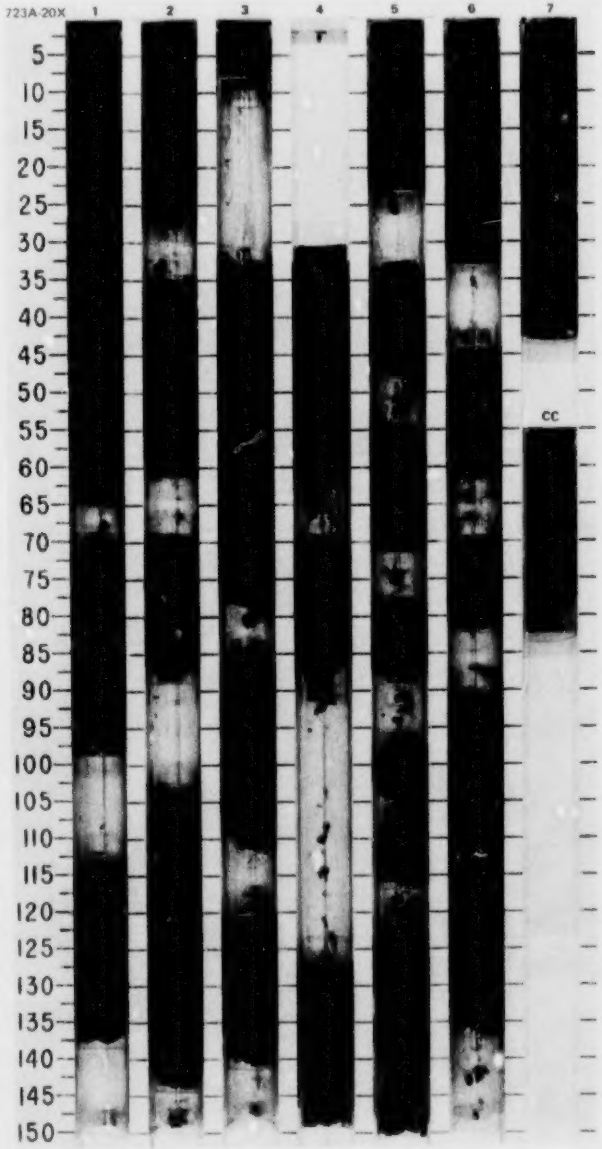
723A-20X
1
2
3
4
5
6
7
CC
5
10
15
20
25
30
35
40
45
50
55
60
65
70
75
80
85
90
95
100
105
110
115
120
125
130
135
140
145
150

SITE 723 HOLE A CORE 21X CORED INTERVAL 999.2-1008.9 mbsl; 191.4-201.1 mbsf

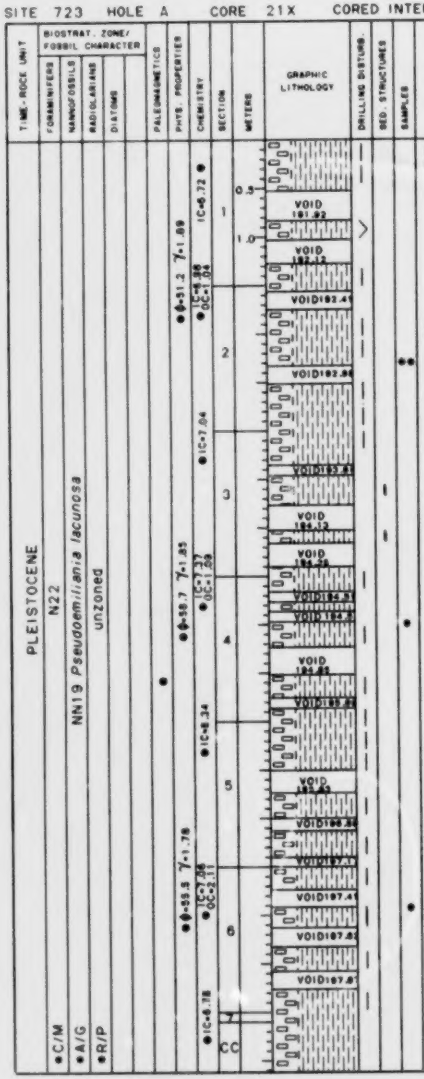
TIME-ROCK UNIT
BIOSTRAT. ZONE/ FOSSIL CHARACTER
FORAMINIFERS
NANNOFOSSILS
RADIOLARIANS
DIATOMS
PALEOMAGNETICS
PHYS. PROPERTIES
CHEMISTRY
SECTION
METERS
GRAPHIC LITHOLOGY
DRILLING DISTURB.
SED. STRUCTURES
SAMPLES
PLEISTOCENE
N22
NN19 Pseudoemiliania lacunosa
unzoned
●C/M
●A/G
●R/P
●ϕ=51.2 γ=1.89
●ϕ=58.7 γ=1.85
●ϕ=55.5 γ=1.78
IC=6.72 ●
●IC=6.86 OC=1.04
●IC=7.04
●IC=7.37 OC=1.09
●IC=8.34
●IC=7.06 OC=2.11
●IC=6.78
1
2
3
4
5
6
7
CC
0.5
1.0
VOID 191.92
VOID 192.12
VOID192.41
VOID192.86
VOID193.61
VOID 194.13
VOID 194.28
VOID194.51
VOID 194.83
VOID 195.63
VOID196.86
VOID197.41
VOID197.62
VOID197.81

LITHOLOGIC DESCRIPTION

FORAMINIFER-BEARING MARLY NANNOFOSSIL OOZE and CALCAREOUS CLAYEY SILT

Entire core slightly disturbed by gas expansion (numerous voids). Sediment appears continuous across voids within core (except for Section 1, 90 cm, missing sediment?). Firm cohesive units (10 cm) appear.

Major lithologies: FORAMINIFER-BEARING MARLY NANNOFOSSIL OOZE and CALCAREOUS CLAYEY SILT, olive gray (5Y 4/2) and dark olive gray, faintly mottled. Foraminifers on core face, more apparent in dark layers. Variable terrigenous component dominated by silt-sized detrital calcite.

Minor lithology: Clayey siltstone composed of 80% poorly sorted inorganic calcite (Section 2, 79 cm, a lithified interval).

SMEAR SLIDE SUMMARY (%):

	2, 79 D	2, 79 D	4, 58 D	6, 41 D
TEXTURE:				
Sand	10	2	15	10
Silt	46	80	30	40
Clay	44	18	55	50
COMPOSITION:				
Access. minerals	Tr		1	Tr
Clay	34	18	25	20
Diatoms				Tr
Dolomite			Tr	
Foraminifers		1	5	10
Volcanic glass	Tr	Tr	Tr	
Inorganic calcite	50	80	38	40
Mica	1	Tr		
Nannofossils	10	Tr	30	20
Organic debris				5
Quartz	5	1	1	5

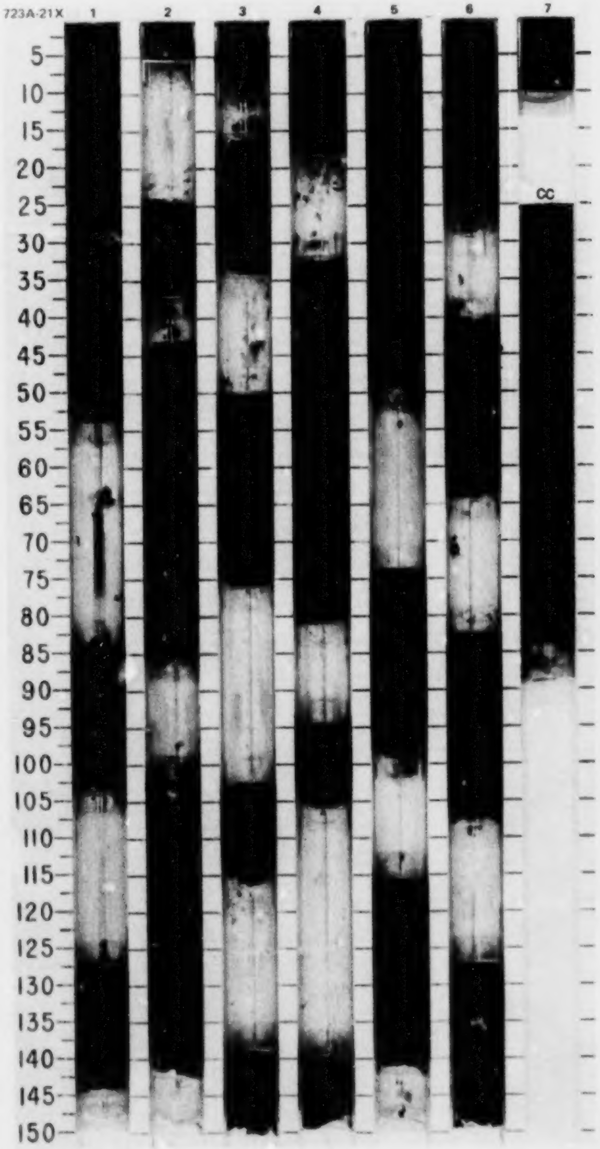
723A-21X
1
2
3
4
5
6
7
CC
5
10
15
20
25
30
35
40
45
50
55
60
65
70
75
80
85
90
95
100
105
110
115
120
125
130
135
140
145
150

SITE 723 HOLE A CORE 22X CORED INTERVAL 1008.9-1018.6 mbsl; 201.1-210.8 mbsf

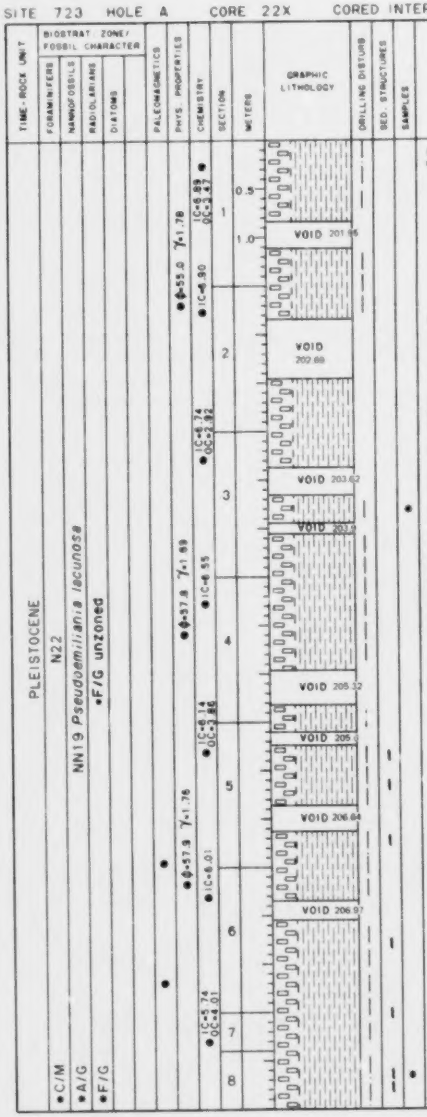
TIME-ROCK UNIT
BIOSTRAT. ZONE/ FOSSIL CHARACTER
FORAMINIFERS
NANNOFOSSILS
RADIOLARIANS
DIATOMS
PALEOMAGNETICS
PHYS. PROPERTIES
CHEMISTRY
SECTION
METERS
GRAPHIC LITHOLOGY
DRILLING DISTURB.
SED. STRUCTURES
SAMPLES
PLEISTOCENE
N22
NN19 Pseudoemiliania lacunosa
•F/G unzoned
•C/M
•A/G
•F/G
•ϕ=55.0 γ=1.78
•ϕ=57.8 γ=1.89
•ϕ=57.9 γ=1.76
IC=6.89 OC=3.47
•IC=6.90
•IC=6.74 OC=2.92
•IC=6.55
•IC=6.14 OC=3.86
•IC=6.01
•IC=5.74 OC=4.01
0.5
1.0
1
2
3
4
5
6
7
8
VOID 201.95
VOID 202.69
VOID 203.62
VOID 203.9
VOID 205.32
VOID 205.6
VOID 206.64
VOID 206.97

LITHOLOGIC DESCRIPTION

FORAMINIFER-BEARING MARLY NANNOFOSSIL OOZE and CALCAREOUS CLAYEY SILT

Entire core moderately disturbed by gas expansion (numerous voids). Sediment appears continuous across voids within core.

Major lithologies: FORAMINIFER-BEARING MARLY NANNOFOSSIL OOZE and CALCAREOUS CLAYEY SILT, olive gray (5Y 4/2) and dark olive gray, faintly mottled. Foraminifers common on core face. Variable terrigenous component dominated by clay and silt-sized detrital calcite.

Minor lithology: Diatom-bearing(?) calcareous clayey silt, dark olive gray (5Y 3/2). Occurs in bottom of Section 7, and in Section 8.

SMEAR SLIDE SUMMARY (%):

	3, 80 D	8, 25 M
TEXTURE:		
Sand	15	15
Silt	55	25
Clay	30	60
COMPOSITION:		
Access. minerals		3
Clay	20	35
Diatoms		3
Dolomite		Tr
Foraminifers	5	2
Volcanic glass		Tr
Inorganic calcite	55	25
Mica		1
Nannofossils	10	25
Quartz	10	6
Radiolarians		Tr
Silicoflagellates		Tr
Sponge spicules	Tr	Tr

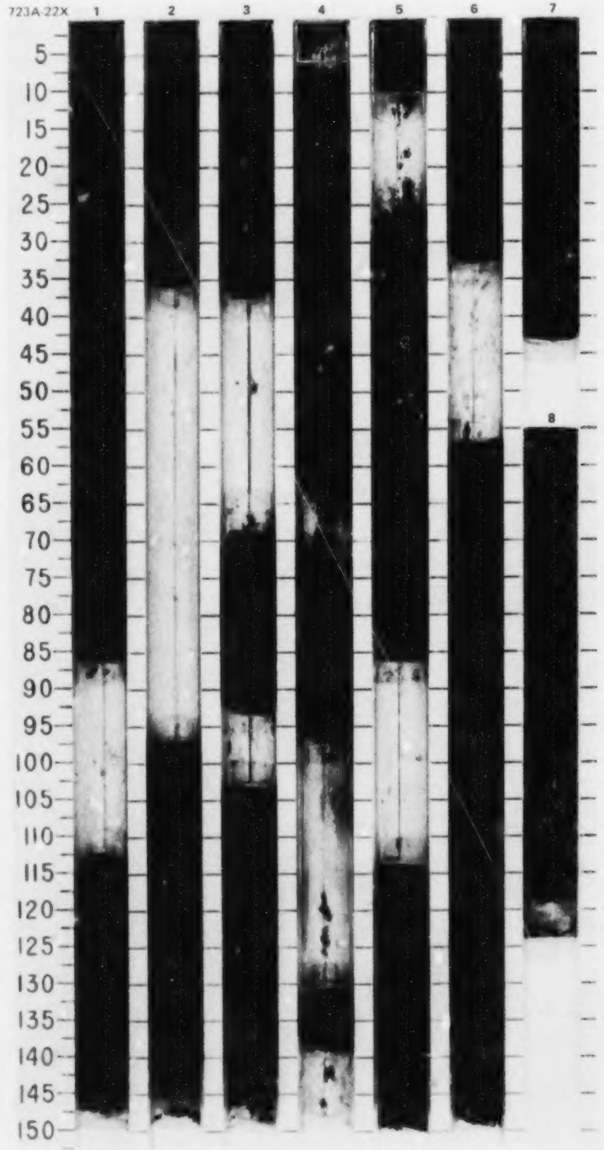
723A-22X
1
2
3
4
5
6
7
8
5
10
15
20
25
30
35
40
45
50
55
60
65
70
75
80
85
90
95
100
105
110
115
120
125
130
135
140
145
150

SITE 723 HOLE A CORE 23X CORED INTERVAL 1018.6-1028.2 mbsl; 210.8-220.4 mbsf

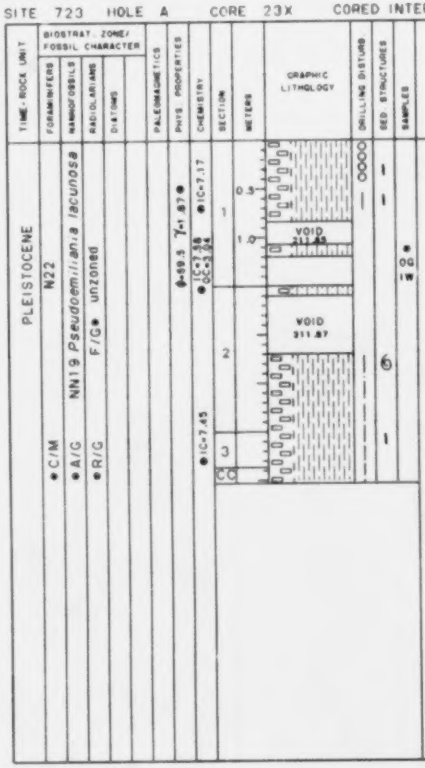
TIME-ROCK UNIT
BIOSTRAT. ZONE/ FOSSIL CHARACTER
FORAMINIFERS
NANNOFOSSILS
RADIOLARIANS
DIATOMS
PALEOMAGNETICS
PHYS. PROPERTIES
CHEMISTRY
SECTION
METERS
GRAPHIC LITHOLOGY
DRILLING DISTURB.
SED. STRUCTURES
SAMPLES
PLEISTOCENE
N22
NN19 Pseudoemiliania lacunosa
F/G● unzoned
●C/M
●A/G
●R/G
ϕ=59.5 γ=1.87●
●IC=7.17
●IC=7.58 OC=1.04
●IC=7.45
1
2
3
CC
0.5
1.0
VOID 211.45
VOID 211.87
●
OG
IW

LITHOLOGIC DESCRIPTION

FORAMINIFER-BEARING MARLY NANNOFOSSIL OOZE and CALCAREOUS CLAYEY SILT

Section 1, 0-50 cm, soupy, remainder of core slightly disturbed by gas expansion (two large voids). Sediment appears continuous across voids within core.

Major lithologies: FORAMINIFER-BEARING MARLY NANNOFOSSIL OOZE and CALCAREOUS CLAYEY SILT, olive gray (5Y 4/2) and dark olive gray, faintly mottled. Variable terrigenous component dominated by clay and silt-sized detrital calcite.

SMEAR SLIDE SUMMARY (%):

	1, 122 D
TEXTURE:	
Sand	15
Silt	15
Clay	70
COMPOSITION:	
Access. minerals	1
Clay	30
Dolomite	Tr
Foraminifers	5
Inorganic calcite	22
Mica	1
Nannofossils	40
Quartz	1
Sponge spicules	Tr

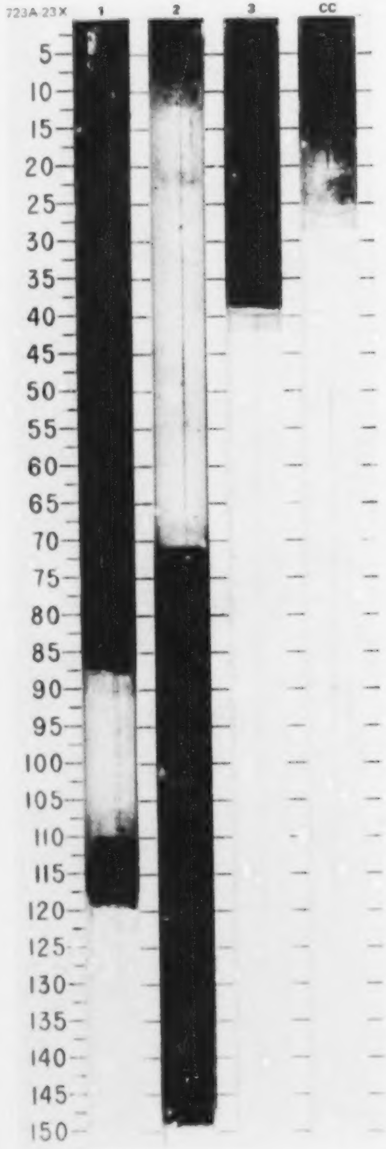
723A-23X
1
2
3
CC
5
10
15
20
25
30
35
40
45
50
55
60
65
70
75
80
85
90
95
100
105
110
115
120
125
130
135
140
145
150

SITE 723 HOLE A CORE 24X CORED INTERVAL 1028.2-1037.9 mbsl; 220.4-230.1 mbsf

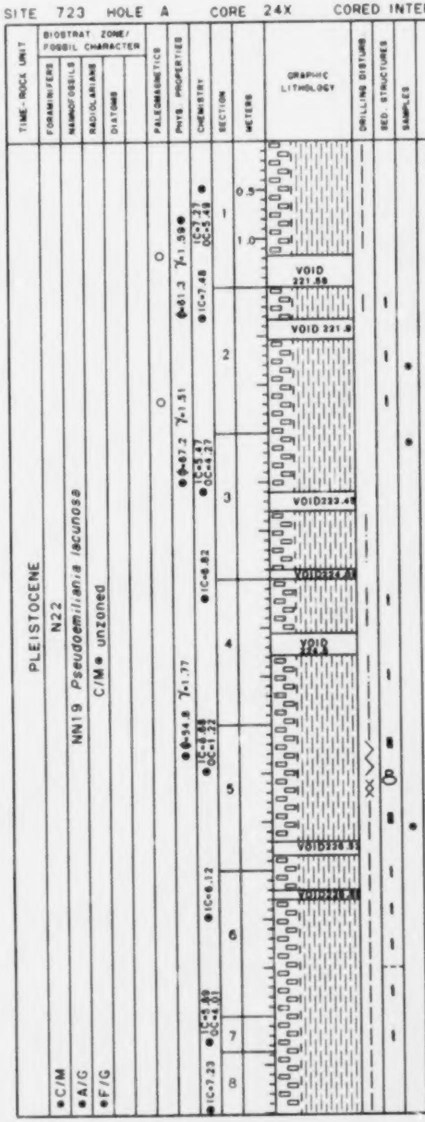
TIME-ROCK UNIT
BIOSTRAT. ZONE/ FOSSIL CHARACTER
FORAMINIFERS
NANNOFOSSILS
RADIOLARIANS
DIATOMS
PALEOMAGNETICS
PHYS. PROPERTIES
CHEMISTRY
SECTION
METERS
GRAPHIC LITHOLOGY
DRILLING DISTURB.
SED. STRUCTURES
SAMPLES
PLEISTOCENE
N22
NN19 Pseudoemiliania lacunosa
C/M● unzoned
●C/M
●A/G
●F/G
●Φ-61.3 γ-1.59●
●Φ-67.2 γ-1.51
●Φ-54.8 γ-1.77
IC=7.27 OC=5.49 ●
●IC=7.48
●IC=5.47 OC=4.27
●IC=6.82
●IC=6.68 OC=1.22
●IC=6.12
IC=5.89 OC=4.01 ●
●IC=7.23
1
2
3
4
5
6
7
8
0.5
1.0
VOID 221.59
VOID 221.9
VOID223.45
VOID224.
VOID 224.9
VOID226.3
VOID226.

LITHOLOGIC DESCRIPTION

FORAMINIFER-BEARING MARLY NANNOFOSSIL OOZE and CALCAREOUS CLAYEY SILT

Section 5, 50-95 cm, heavily disturbed, remainder slightly disturbed by gas expansion (numerous voids). Sediment appears continuous across voids within core.

Major lithologies: FORAMINIFER-BEARING MARLY NANNOFOSSIL OOZE and CALCAREOUS CLAYEY SILT, olive gray (5Y 4/2, 4/3) and dark olive gray (5Y 3/2, 3/1), faintly mottled. Variable terrigenous component dominated by clay and silt-sized detrital calcite.

Minor lithologies:

a. Thin sand layer (quartz and inorganic calcite), Section 3, 10 cm.
b. Lithified section (same composition as core?) with bioturbation structures, Section 5, 64-67 cm.

SMEAR SLIDE SUMMARY (%):

	2, 82 D	3, 10 M	5, 108 D
TEXTURE:			
Sand	10	60	10
Silt	20	20	55
Clay	70	20	35
COMPOSITION:			
Access. minerals	Tr	5	2
Clay	35		20
Diatoms	Tr	Tr	
Dolomite	Tr		
Feldspar		10	
Foraminifers	2		2
Inorganic calcite	25	40	55
Nannofossils	35		15
Quartz	3	45	6
Radiolarians	Tr		
Sponge spicules	Tr		

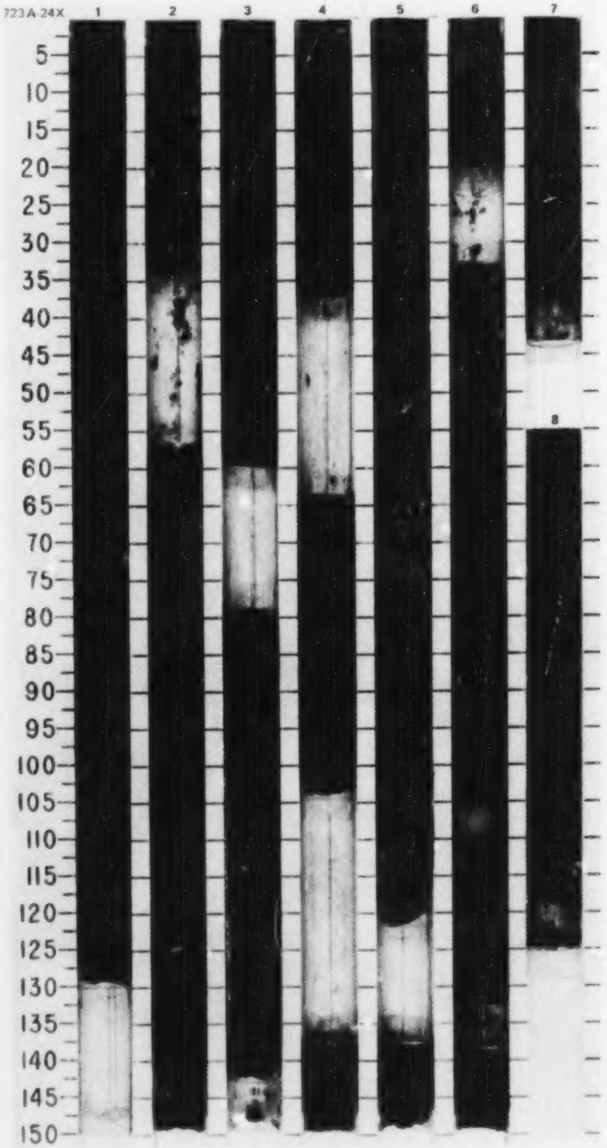
723A-24X
1
2
3
4
5
6
7
8
5
10
15
20
25
30
35
40
45
50
55
60
65
70
75
80
85
90
95
100
105
110
115
120
125
130
135
140
145
150

SITE 723 HOLE A CORE 25X CORED INTERVAL 1037.9-1047.6 mbsl; 230.1-239.8 mbsf

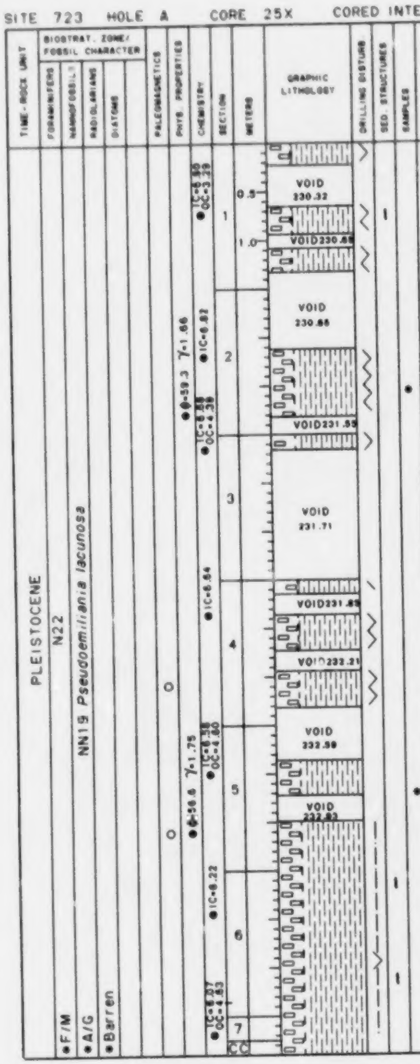

LITHOLOGIC DESCRIPTION

FORAMINIFER-BEARING MARLY NANNOFOSSIL OOZE and CALCAREOUS CLAYEY SILT

Sections 1-5 heavily disturbed, remainder slightly disturbed by gas expansion (numerous voids). Sediment appears continuous across voids within core. Sediment crumbles readily.

Major lithologies: FORAMINIFER-BEARING MARLY NANNOFOSSIL OOZE and CALCAREOUS CLAYEY SILT, dark olive gray (5Y 3/2). Foraminifers common lower in core on less disturbed core face. Variable terrigenous component dominated by clay and silt-sized detrital calcite.

SMEAR SLIDE SUMMARY (%)

	2, 105 D	5, 63 D
TEXTURE:		
Silt	40	40
Clay	60	60
COMPOSITION:		
Access. minerals	10	10
Bioclasts		Tr
Clay	20	25
Dolomite	Tr	Tr
Foraminifers	5	
Inorganic calcite	15	25
Mica	Tr	
Nannofossils	40	30
Organic debris	Tr	Tr
Quartz	10	10
Sponge spicules		Tr

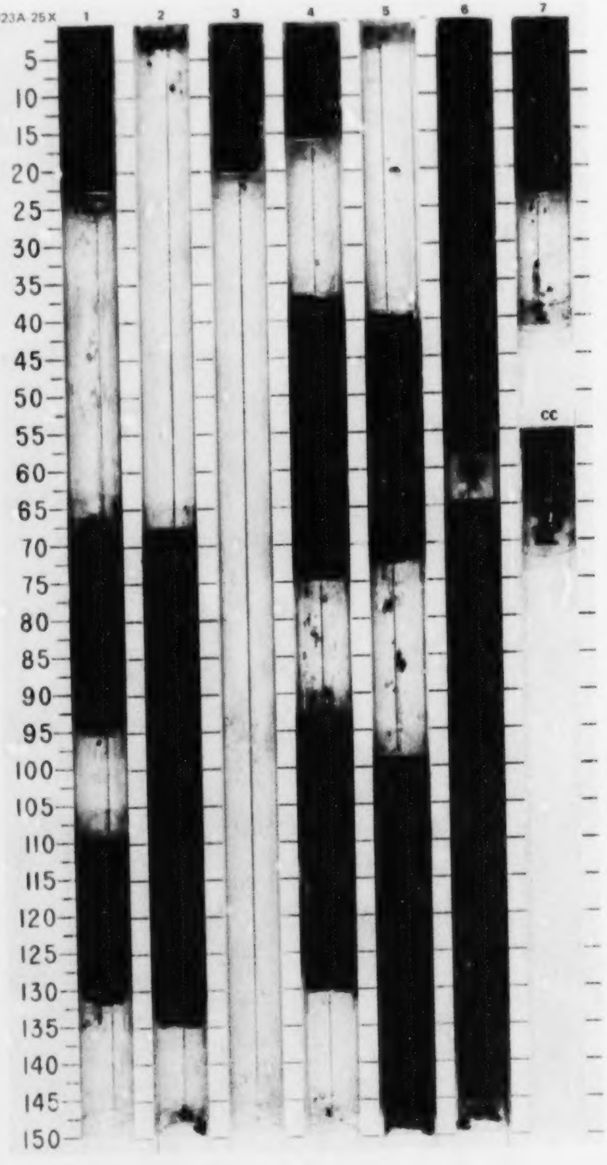
723A-25X
1
2
3
4
5
6
7
CC
5
10
15
20
25
30
35
40
45
50
55
60
65
70
75
80
85
90
95
100
105
110
115
120
125
130
135
140
145
150

SITE 723 HOLE A CORE 26X CORED INTERVAL 1047.6-1057.2 mbsl; 239.8-249.4 mbsf

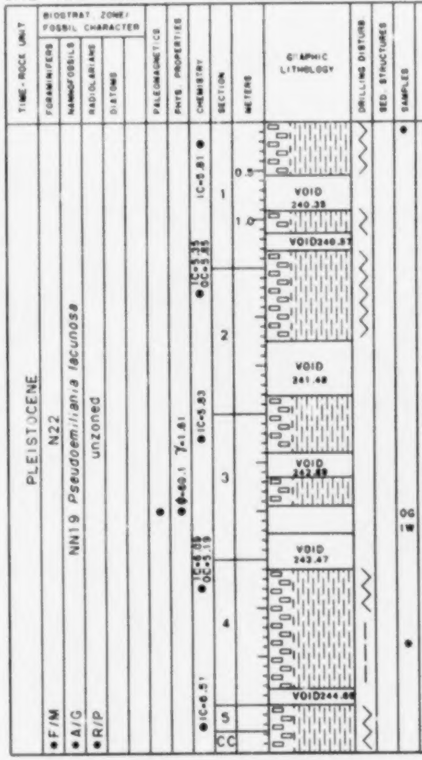
TIME-ROCK UNIT
BIOSTRAT. ZONE/ FOSSIL CHARACTER
FORAMINIFERS
NANNOFOSSILS
RADIOLARIANS
DIATOMS
PALEOMAGNETICS
PHYS. PROPERTIES
CHEMISTRY
SECTION
METERS
GRAPHIC LITHOLOGY
DRILLING DISTURB.
SED. STRUCTURES
SAMPLES
PLEISTOCENE
N22
NN19 Pseudoemiliania lacunosa
unzoned
●F/M
●A/G
●R/P
●φ-60.1 γ-1.81
IC-5.81
IC-5.35 OC-5.85
IC-5.83
IC-6.08 OC-5.19
IC-6.51
1
2
3
4
5
CC
0.5
1.0
VOID 240.35
VOID240.57
VOID 241.48
VOID 242.49
VOID 243.47
VOID244.88
OG
IW

LITHOLOGIC DESCRIPTION

FORAMINIFER-BEARING MARLY NANNOFOSSIL OOZE and CALCAREOUS CLAYEY SILT

Entire core (except lower Section 4) heavily disturbed by gas expansion (numerous voids). Sediment appears continuous across voids within core. Crumbles readily, and firm intervals separate into clasts. Section 5 and CC partly full.

Major lithologies: FORAMINIFER-BEARING MARLY NANNOFOSSIL OOZE and CALCAREOUS CLAYEY SILT, dark olive gray (5Y 3/2). Foraminifers visible on surface lower in core. Variable terrigenous component dominated by clay and silt-sized detrital calcite.

SMEAR SLIDE SUMMARY (%):

	1, 9 D	4, 88 D
TEXTURE:		
Silt	45	40
Clay	55	60
COMPOSITION:		
Access. minerals	10	2
Bioclasts		5
Clay	25	30
Dolomite	Tr	Tr
Foraminifers	5	5
Inorganic calcite	25	15
Nannofossils	20	25
Organic debris	5	5
Pellets	Tr	2
Quartz	10	10
Radiolarians		Tr
Sponge spicules	Tr	1

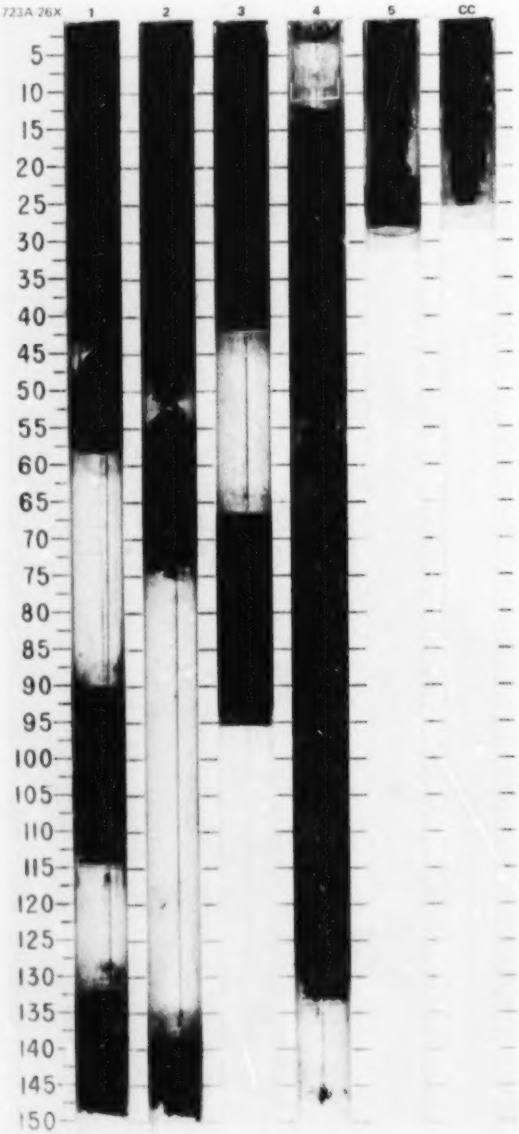
723A 26X
1
2
3
4
5
CC
5
10
15
20
25
30
35
40
45
50
55
60
65
70
75
80
85
90
95
100
105
110
115
120
125
130
135
140
145
150

SITE 723 HOLE A CORE 27X CORED INTERVAL 1057.2-1066.9 mbsl; 249.4-259.1 mbsf

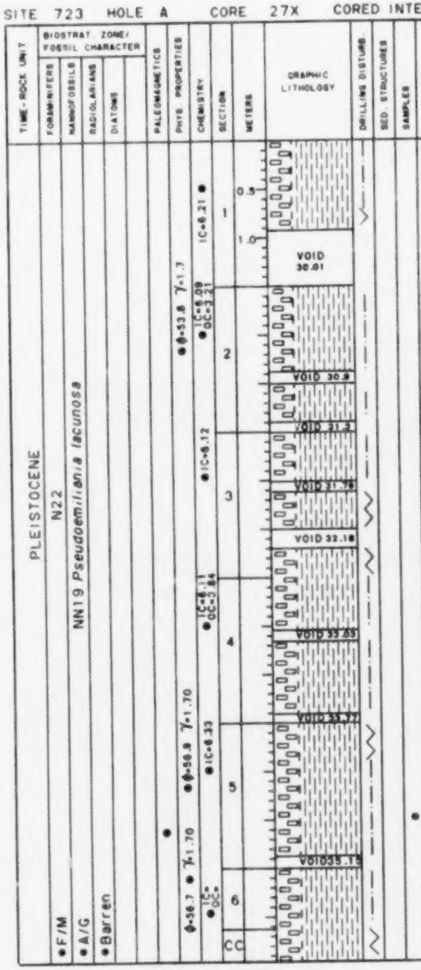
TIME-ROCK UNIT
BIOSTRAT. ZONE/ FOSSIL CHARACTER
FORAMINIFERS
NANNOFOSSILS
RADIOLARIANS
DIATOMS
PALEOMAGNETICS
PHYS. PROPERTIES
CHEMISTRY
SECTION
METERS
GRAPHIC LITHOLOGY
DRILLING DISTURB.
SED. STRUCTURES
SAMPLES
PLEISTOCENE
N22
NN19 Pseudoemiliania lacunosa
●F/M
●A/G
●Barren
●ϕ=53.8 γ=1.7
●ϕ=56.9 γ=1.70
ϕ=56.7 ● γ=1.70
IC=6.21 ●
●IC=6.09 OC=3.21
●IC=6.12
●IC=6.11 OC=3.84
●IC=6.33
●IC= OC=
1
2
3
4
5
6
CC
0.5
1.0
VOID 30.01
VOID 30.9
VOID 31.3
VOID 31.76
VOID 32.18
VOID 33.03
VOID 33.77
VOID35.15

LITHOLOGIC DESCRIPTION

FORAMINIFER-BEARING MARLY NANNOFOSSIL OOZE and CALCAREOUS CLAYEY SILT

Entire core moderately to heavily disturbed by gas expansion (numerous voids). Sediment appears continuous across voids within core. Crumbles readily, and firm intervals separate into clasts.

Major lithologies: FORAMINIFER-BEARING MARLY NANNOFOSSIL OOZE and CALCAREOUS CLAYEY SILT, dark olive gray (5Y 3/2). Foraminifers visible on core face, also mica flakes(?) on Section 6 face. Variable terrigenous component dominated by clay and silt-sized detrital calcite.

SMEAR SLIDE SUMMARY (%):

	5, 98 D
TEXTURE:	
Silt	55
Clay	45
COMPOSITION:	
Access. minerals	10
Bioclasts	5
Clay	20
Dolomite	Tr
Foraminifers	Tr
Inorganic calcite	30
Mica	Tr
Nannofossils	20
Quartz	15
Radiolarians	Tr
Sponge spicules	Tr

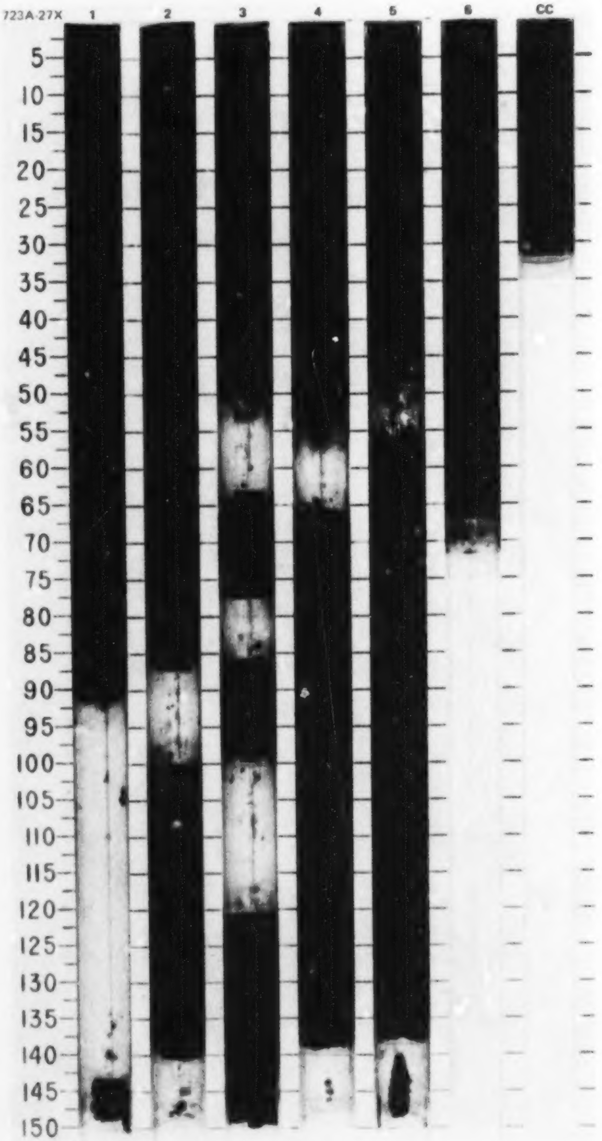
723A-27X
1
2
3
4
5
6
CC
5
10
15
20
25
30
35
40
45
50
55
60
65
70
75
80
85
90
95
100
105
110
115
120
125
130
135
140
145
150

SITE 723 HOLE A CORE 28X CORED INTERVAL 1066.9-1076.5 mbsl; 259.1-268.7 mbsf

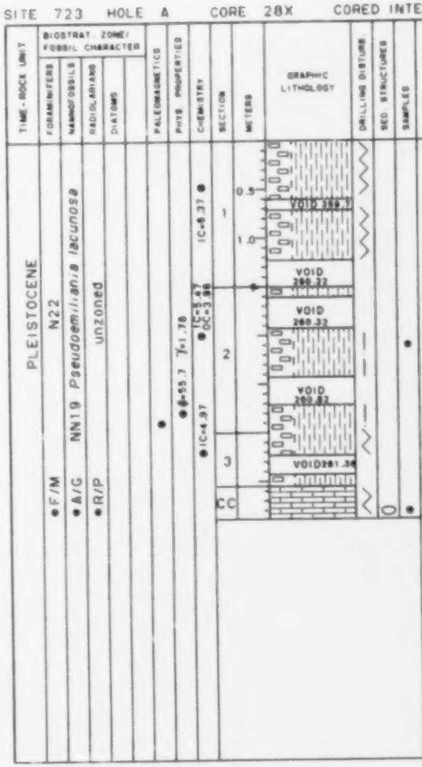
TIME-ROCK UNIT
BIOSTRAT. ZONE/ FOSSIL CHARACTER
FORAMINIFERS
NANNOFOSSILS
RADIOLARIANS
DIATOMS
PALEOMAGNETICS
PHYS. PROPERTIES
CHEMISTRY
SECTION
METERS
GRAPHIC LITHOLOGY
DRILLING DISTURB.
SED. STRUCTURES
SAMPLES
PLEISTOCENE
N22
NN19 Pseudoemiliania lacunosa
unzoned
F/M
A/G
R/P
φ=55.7 γ=1.78
IC=8.37
IC=5.47 OC=3.96
IC=4.97
1
2
3
CC
0.5
1.0
VOID 259.7
VOID 260.22
VOID 260.32
VOID 260.82
VOID 261.34

LITHOLOGIC DESCRIPTION

FORAMINIFER-BEARING MARLY NANNOFOSSIL OOZE and CALCAREOUS CLAYEY SILT

Section 1, 0-10 cm, soupy, remainder moderately disturbed by gas expansion (numerous voids). Sediment appears continuous across voids within core. Crumbles readily, and firm intervals separate into clasts.

Major lithologies: FORAMINIFER-BEARING MARLY NANNOFOSSIL OOZE and CALCAREOUS CLAYEY SILT, dark olive gray (5Y 3/2). Foraminifers present on core face. Variable terrigenous component dominated by clay and silt-sized detrital calcite.

Minor lithology: Limestone, dark olive gray (5Y 3/2) with well preserved foraminifers, found in bottom of CC.

SMEAR SLIDE SUMMARY (%):

	2, 60 D	CC, 25 D	CC, 25 D
TEXTURE:			
Sand		20	15
Silt	35	20	55
Clay	65	60	30
COMPOSITION:			
Access. minerals	10		
Cement			15
Clay	15	40	30
Dolomite	Tr		35
Foraminifers	5	20	20
Inorganic calcite	25		
Nannofossils	20		
Organic debris	5	Tr	
Quartz	20		
Spar cement		40	

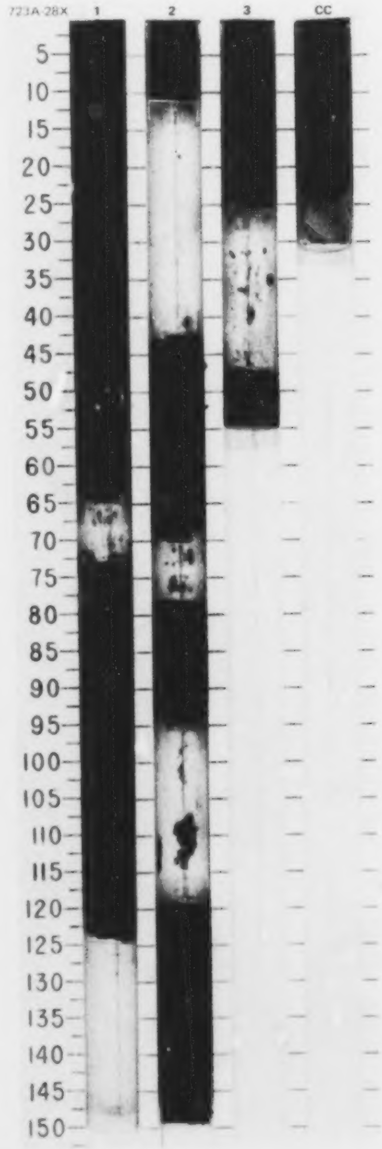
723A-28X
1
2
3
CC
5
10
15
20
25
30
35
40
45
50
55
60
65
70
75
80
85
90
95
100
105
110
115
120
125
130
135
140
145
150

SITE 723 HOLE A CORE 29X CORED INTERVAL 1076.5-1086.1 mbsl: 268.7-278.3 mbsf

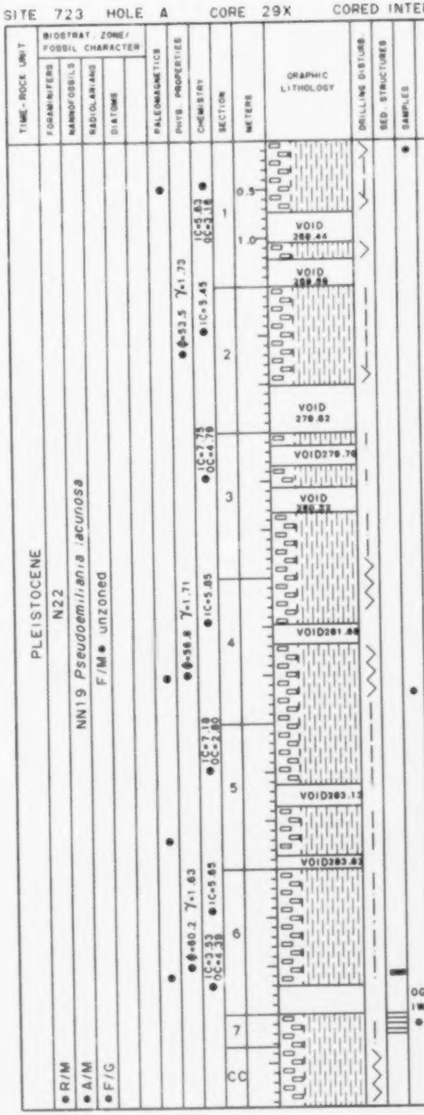
TIME-ROCK UNIT
BIOSTRAT. ZONE/ FOSSIL CHARACTER
FORAMINIFERS
NANNOFOSSILS
RADIOLARIANS
DIATOMS
PALEOMAGNETICS
PHYS. PROPERTIES
CHEMISTRY
SECTION
METERS
GRAPHIC LITHOLOGY
DRILLING DISTURB.
SED. STRUCTURES
SAMPLES
PLEISTOCENE
N22
NN19 Pseudoemiliania lacunosa
F/M● unzoned
●R/M
●A/M
●F/G
●φ=53.5 γ=1.73
●φ=56.8 γ=1.71
●φ=60.2 γ=1.63
IC=5.83 OC=3.18
●IC=5.45
●IC=7.75 OC=4.70
●IC=5.85
●IC=7.18 OC=2.80
●IC=5.65
●IC=3.53 OC=4.38
1
2
3
4
5
6
7
CC
0.5
1.0
VOID 268.44
VOID
VOID 270.02
VOID270.7
VOID
VOID281.6
VOID283.1
VOID283.6
OG
IW

LITHOLOGIC DESCRIPTION

FORAMINIFER-BEARING MARLY NANNOFOSSIL OOZE and CALCAREOUS CLAYEY SILT

Entire core moderately disturbed by gas expansion (numerous voids). Sediment appears continuous across voids within core. Crumbles readily, and firm intervals separate into clasts.

Major lithologies: FORAMINIFER-BEARING MARLY NANNOFOSSIL OOZE and CALCAREOUS CLAYEY SILT, olive gray (5Y 4/2) and dark olive gray (5Y 3/2, 3/1). Foraminifers visible on core face. Variable terrigenous component dominated by clay and silt-sized detrital calcite.

Minor lithology: Parallel laminae preserved in firmer intervals, lower Section 6 and Section 7. Individual light and dark layers are 0.1-1.0 mm thick. Smear slide from one light layer is muddy diatomaceous ooze.

SMEAR SLIDE SUMMARY (%):

	1, 11 D	4, 118 D	7, 13 M
TEXTURE:			
Silt	60	55	75
Clay	40	45	25
COMPOSITION:			
Access. minerals	10	9	2
Clay	28	25	20
Diatoms			60
Dolomite	Tr	Tr	Tr
Foraminifers	Tr	5	Tr
Volcanic glass		Tr	
Inorganic calcite	25	25	8
Nannofossils	10	20	5
Organic debris	4	5	Tr
Pellets	3		
Quartz	20	10	5
Radiolarians		Tr	
Silicoflagellates			Tr
Sponge spicules	Tr	1	Tr

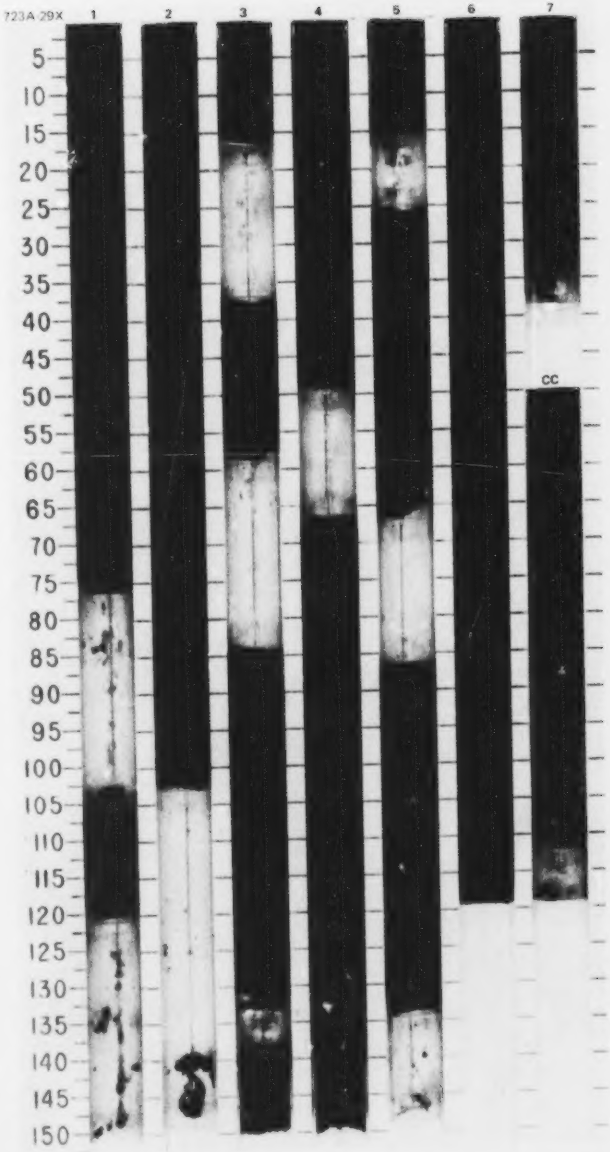
723A-29X
1
2
3
4
5
6
7
CC
5
10
15
20
25
30
35
40
45
50
55
60
65
70
75
80
85
90
95
100
105
110
115
120
125
130
135
140
145
150

SITE 723 HOLE A CORE 30X CORED INTERVAL 1088.1-1095.7 mbsl; 278.3-287.9 mbsf

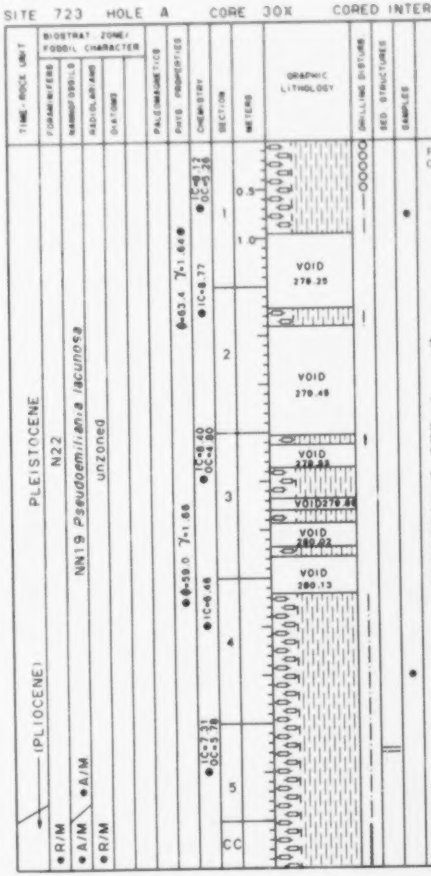
TIME-ROCK UNIT
BIOSTRAT. ZONE/ FOSSIL CHARACTER
FORAMINIFERS
NANNOFOSSILS
RADIOLARIANS
DIATOMS
PALEOMAGNETICS
PHYS. PROPERTIES
CHEMISTRY
SECTION
METERS
GRAPHIC LITHOLOGY
DRILLING DISTURB.
SED. STRUCTURES
SAMPLES
PLEISTOCENE
(PLIOCENE)
N22
NN19 Pseudoemiliania lacunosa
unzoned
●R/M
●A/M
●A/M
●R/M
φ=63.4 γ=1.64
φ=59.0 γ=1.66
IC=8.12 OC=5.26
IC=8.77
IC=8.40 OC=4.80
IC=8.46
IC=7.31 OC=5.78
1
2
3
4
5
CC
0.5
1.0
VOID 278.25
VOID 279.45
VOID 279.83
VOID 279.86
VOID 280.02
VOID 280.13

LITHOLOGIC DESCRIPTION

FORAMINIFER-BEARING MARLY NANNOFOSSIL CHALK and CALCAREOUS CLAYEY SILTSTONE

Section 1, 0-50 cm, soupy, remainder moderately disturbed by gas expansion (numerous voids). Firm intervals separate into clasts. Flow across between firm sections occurred when cut with saw.

Major lithologies: FORAMINIFER-BEARING MARLY NANNOFOSSIL CHALK and CALCAREOUS CLAYEY SILTSTONE, dark olive gray (5Y 3/2). Foraminifers visible on core face. Variable terrigenous component dominated by clay and silt-sized detrital calcite.

Minor lithologies:
a. Limestone fragments (0.5 cm) in soupy upper Section 1.
b. Faint laminae preserved in upper Section 5.

SMEAR SLIDE SUMMARY (%):

	1, 77 D	4, 100 M
TEXTURE:		
Sand		10
Silt	35	50
Clay	65	40
COMPOSITION:		
Access. minerals	5	
Clay	15	20
Dolomite	Tr	
Foraminifers	15	5
Inorganic calcite	15	50
Nannofossils	40	10
Quartz	9	10
Sponge spicules	1	5

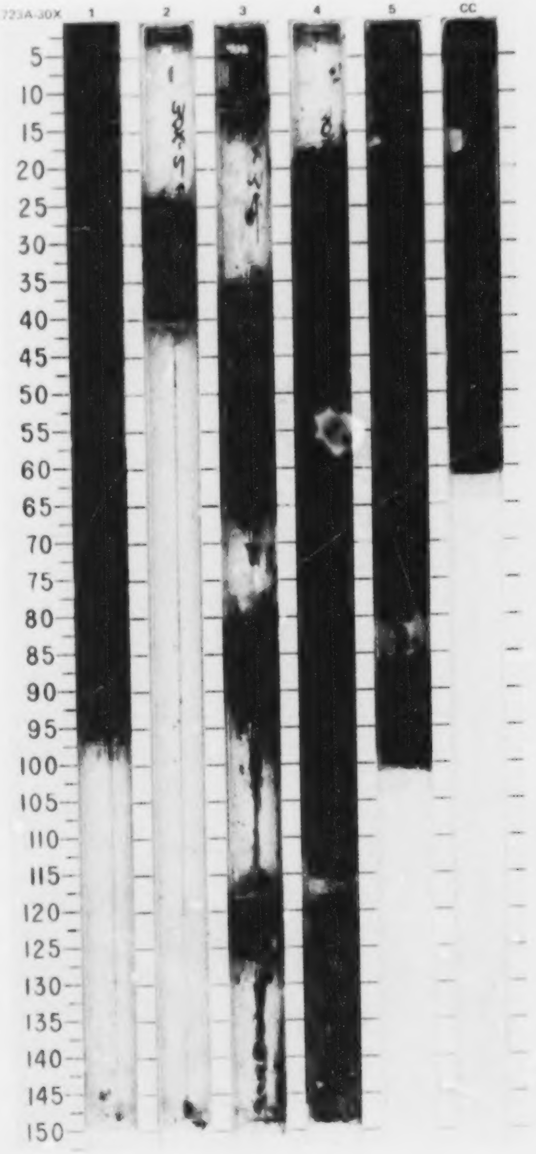
723A-30X
1
2
3
4
5
CC
5
10
15
20
25
30
35
40
45
50
55
60
65
70
75
80
85
90
95
100
105
110
115
120
125
130
135
140
145
150

SITE 723 HOLE A CORE 31X CORED INTERVAL 1095.7-1105.3 mbsl; 287.9-297.5 mbsf

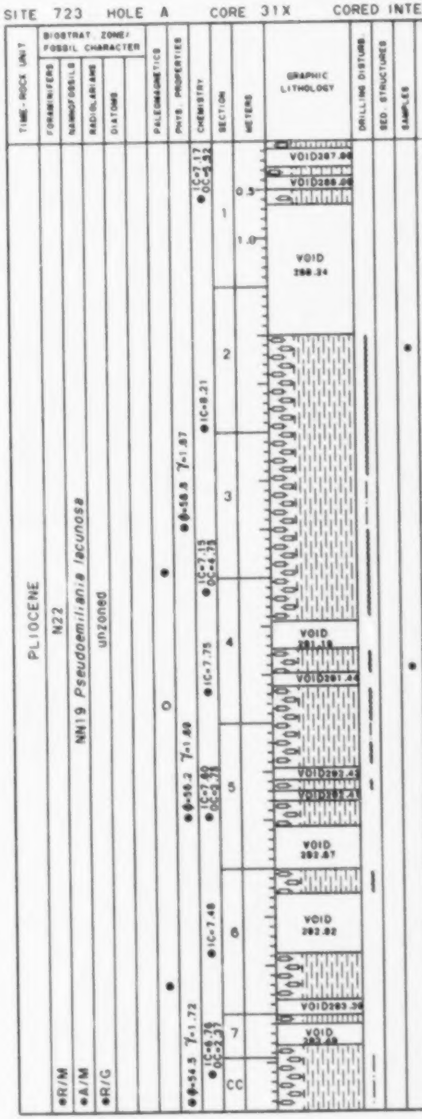
TIME-ROCK UNIT
BIOSTRAT. ZONE/ FOSSIL CHARACTER
FORAMINIFERS
NANNOFOSSILS
RADIOLARIANS
DIATOMS
PALEOMAGNETICS
PHYS. PROPERTIES
CHEMISTRY
SECTION
METERS
GRAPHIC LITHOLOGY
DRILLING DISTURB.
SED. STRUCTURES
SAMPLES
PLIOCENE
N22
NN19 Pseudoemiliania lacunosa
unzoned
●R/M
●A/M
●R/G
●φ=58.8 γ=1.97
●φ=50.2 γ=1.80
●φ=54.3 γ=1.72
●IC=7.17 OC=1.92
●IC=8.21
●IC=7.15 OC=4.75
●IC=7.75
●IC=7.80 OC=3.75
●IC=7.48
●IC=6.78 OC=2.37
1
2
3
4
5
6
7
CC
0.5
1.0
VOID287.06
VOID288.06
VOID 288.34
VOID 291.18
VOID291.44
VOID292.43
VOID 292.87
VOID 292.82
VOID293.36

LITHOLOGIC DESCRIPTION

FORAMINIFER-BEARING MARLY NANNOFOSSIL CHALK and CALCAREOUS CLAYEY SILTSTONE

Entire core heavily disturbed by gas expansion (numerous voids). Crumbles readily, and firm intervals separate into clasts. Cut with wire in order to preserve laminae. Section 2 soupy, missing sediment(?).

Major lithologies: FORAMINIFER-BEARING MARLY NANNOFOSSIL CHALK and CALCAREOUS CLAYEY SILTSTONE, dark olive gray (5Y 3/2). Foraminifers present on core face. Variable terrigenous component dominated by clay and silt-sized detrital calcite.

SMEAR SLIDE SUMMARY (%):

	2, 65 D	4, 93 D
TEXTURE		
Silt	40	30
Clay	60	70
COMPOSITION:		
Clay	29	30
Foraminifers	5	3
Inorganic calcite	29	14
Mica	3	
Nannofossils	14	50
Organic debris	3	
Pellets	5	
Quartz	9	3
Sponge spicules	3	Tr

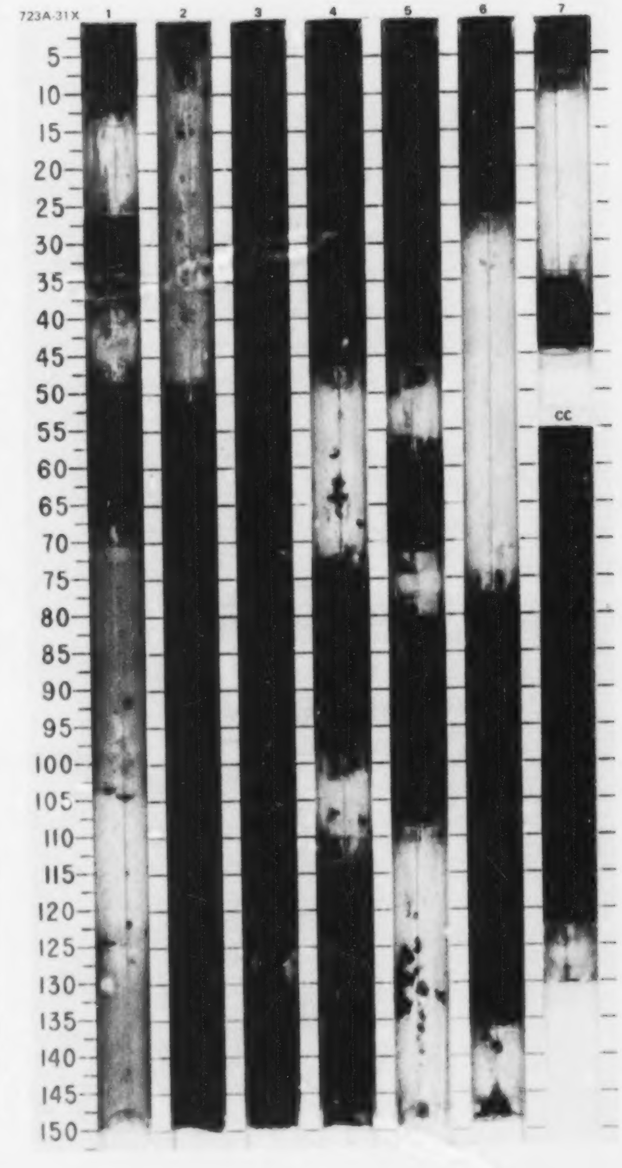
723A-31X
1
2
3
4
5
6
7
CC
5
10
15
20
25
30
35
40
45
50
55
60
65
70
75
80
85
90
95
100
105
110
115
120
125
130
135
140
145
150

SITE 723 HOLE A CORE 32X CORED INTERVAL 1105.3-1114.9 mbsl; 297.5-307.1 mbsf

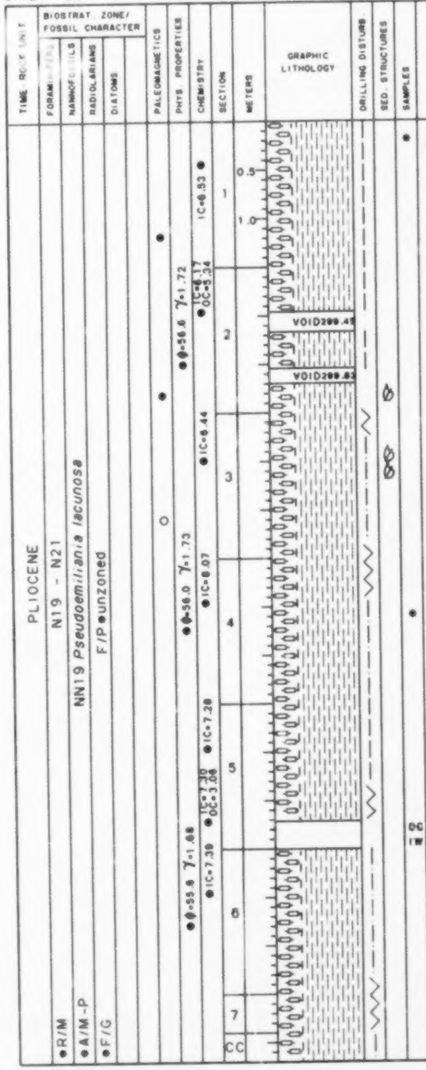
TIME-ROCK UNIT
BIOSTRAT. ZONE/ FOSSIL CHARACTER
FORAMINIFERS
NANNOFOSSILS
RADIOLARIANS
DIATOMS
PALEOMAGNETICS
PHYS. PROPERTIES
CHEMISTRY
SECTION
METERS
GRAPHIC LITHOLOGY
DRILLING DISTURB.
SED. STRUCTURES
SAMPLES
PLIOCENE
N19 - N21
NN19 Pseudoemiliania lacunosa
F/P●unzoned
●R/M
●A/M-P
●F/G
●φ=56.6 γ=1.72
●φ=56.0 γ=1.73
●φ=55.8 γ=1.88
IC=6.53 ●
●IC=6.17 OC=5.34
●IC=6.44
●IC=8.07
●IC=7.28
●IC=7.30 OC=3.06
●IC=7.30
1
2
3
4
5
6
7
CC
0.5
1.0
VOID299.45
VOID299.83
OG
IW

LITHOLOGIC DESCRIPTION

FORAMINIFER-BEARING MARLY NANNOFOSSIL CHALK and CALCAREOUS CLAYEY SILTSTONE

Sections 3, top, Section 4, 10-15 cm, and Section 5, 86-120 cm, very disturbed, remainder moderately disturbed by gas expansion and drilling. Numerous voids. Sediment appears continuous across voids within core, but it becomes more difficult to identify drilling disturbance. Crumbles readily, and firm intervals separate into clasts. Cut with wire in order to preserve laminae.

Major lithologies: FORAMINIFER-BEARING MARLY NANNOFOSSIL CHALK and CALCAREOUS CLAYEY SILTSTONE, olive gray (5Y 4/2, 4/3) and dark olive gray (5Y 3/2, 3/1). Foraminifers present on core face, some shell fragments. Variable terrigenous component dominated by clay and silt-sized detrital calcite.

SMEAR SLIDE SUMMARY (%):

	1, 19 M	4, 58 D
TEXTURE:		
Silt	70	30
Clay	30	70
COMPOSITION:		
Access. minerals	10	
Clay	16	35
Diatoms	2	
Dolomite	5	
Foraminifers	5	8
Inorganic calcite	15	25
Mica	Tr	
Nannofossils	15	25
Organic debris	5	
Pellets	5	
Quartz	20	7
Sponge spicules	2	

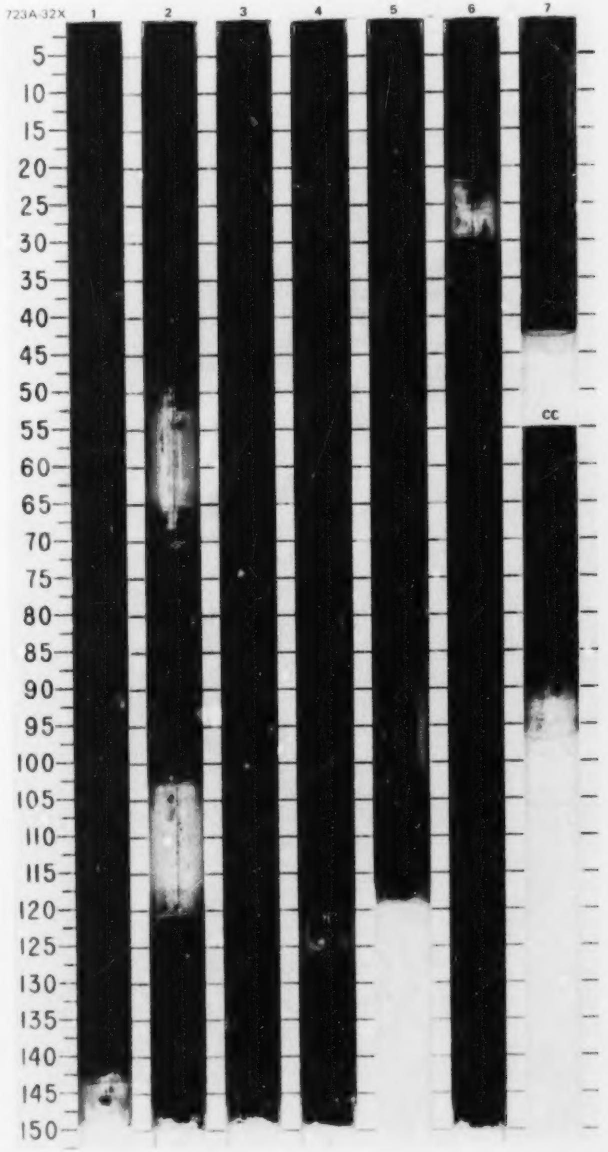
723A-32X
1
2
3
4
5
6
7
CC
5
10
15
20
25
30
35
40
45
50
55
60
65
70
75
80
85
90
95
100
105
110
115
120
125
130
135
140
145
150

SITE 723 HOLE A CORE 33X CORED INTERVAL 1114.9-1124.5 mbsl; 307.1-316.7 mbsf

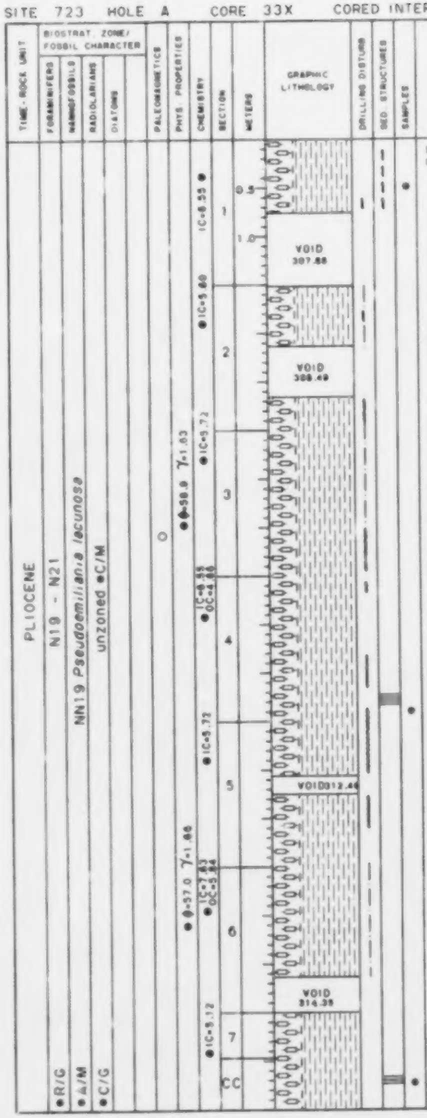
TIME-ROCK UNIT
BIOSTRAT. ZONE/ FOSSIL CHARACTER
FORAMINIFERS
NANNOFOSSILS
RADIOLARIANS
DIATOMS
PALEOMAGNETICS
PHYS. PROPERTIES
CHEMISTRY
SECTION
METERS
GRAPHIC LITHOLOGY
DRILLING DISTURB.
SED. STRUCTURES
SAMPLES
PLIOCENE
N19 - N21
NN19 Pseudoemiliania lacunosa
unzoned ●C/M
●R/G
●A/M
●C/G
●φ=58.9 γ=1.83
●φ=57.0 γ=1.86
IC=8.55 ●
●IC=5.80
●IC=5.72
●IC=8.55 OC=4.88
●IC=5.72
●IC=7.83 OC=5.84
●IC=5.12
1
2
3
4
5
6
7
CC
0.5
1.0
VOID 307.88
VOID 308.49
VOID312.46
VOID 314.35

LITHOLOGIC DESCRIPTION

FORAMINIFER-BEARING MARLY NANNOFOSSIL CHALK and CALCAREOUS CLAYEY SILTSTONE

Entire core moderately disturbed by gas expansion (numerous voids). Sediment appears continuous across voids within core. Crumbles readily, and firm intervals separate into clasts. Cut with wire in order to preserve laminae.

Major lithologies: FORAMINIFER-BEARING MARLY NANNOFOSSIL CHALK and CALCAREOUS CLAYEY SILTSTONE, dark olive gray (5Y 3/2, 3/1). Foraminifers present on core face. Variable terrigenous component dominated by clay and silt-sized detrital calcite.

Minor lithology: Parallel laminae, individual light and dark layers 0.1-1.0 mm thick. Light layers are composed of nannofossils or diatoms, usually dominated by a single species. Section 4, 134-143 cm.

SMEAR SLIDE SUMMARY (%):

	1, 50 D	4, 140 M	CC, 27 M
TEXTURE			
Silt	40	60	40
Clay	60	40	60
COMPOSITION			
Access. minerals	5	Tr	2
Clay	15	10	8
Diatoms	Tr	10	30
Dolomite		3	Tr
Foraminifers	5	10	Tr
Inorganic calcite	20	17	5
Nannofossils	45	40	50
Organic debris	Tr	Tr	
Quartz	10	10	5
Silicoflagellates			Tr
Sponge spicules	Tr	Tr	Tr

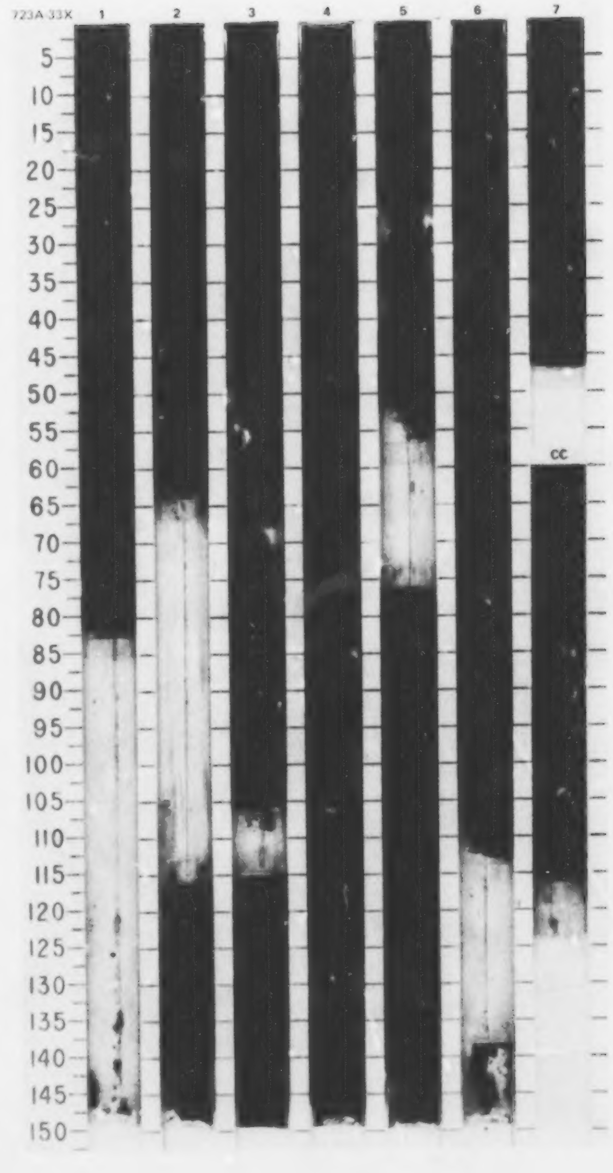
723A 33X
1
2
3
4
5
6
7
CC
5
10
15
20
25
30
35
40
45
50
55
60
65
70
75
80
85
90
95
100
105
110
115
120
125
130
135
140
145
150

SITE 723 HOLE A CORE 34X CORED INTERVAL 1124.5-1129.3 mbsl; 316.7-321.5 mbsf

TIME-ROCK UNIT	BIOSTRAT. ZONE/ FOSSIL CHARACTER: FORAMINIFERS	BIOSTRAT. ZONE/ FOSSIL CHARACTER: NANNOFOSSILS	BIOSTRAT. ZONE/ FOSSIL CHARACTER: RADIOLARIANS	BIOSTRAT. ZONE/ FOSSIL CHARACTER: DIATOMS		PALEOMAGNETICS	PHYS. PROPERTIES	CHEMISTRY	SECTION	METERS	GRAPHIC LITHOLOGY	DRILLING DISTURB.	SED. STRUCTURES	SAMPLES	LITHOLOGIC DESCRIPTION
PLIOCENE	N19 - N21 R/M●	NN19 *Pseudoemiliania lacunosa* A/M●	unzoned C/M●					● IC=6.56 OC=4.13	1			○○○			**FORAMINIFER-BEARING MARLY NANNOFOSSIL CHALK and CALCAREOUS CLAYEY SILTSTONE** Section 1 is soupy and completely disturbed; CC contains two clasts. Major lithologies: FORAMINIFER-BEARING MARLY NANNOFOSSIL CHALK and CALCAREOUS CLAYEY SILTSTONE, dark olive gray (5Y 3/2). Variable terrigenous component dominated by clay and silt-sized detrital calcite. Minor lithology: Limestone, dark olive gray (5Y 3/2), with abundant foraminifers, found in CC.
									CC				∞		

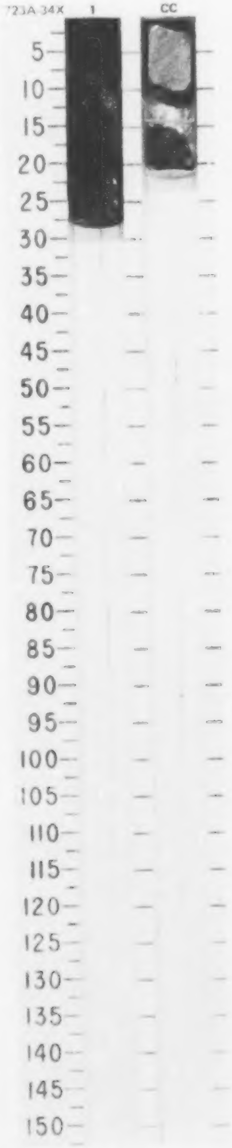

SITE 723 HOLE A CORE 35X CORED INTERVAL 1129.3-1134.1 mbsl; 321.5-326.3 mbsf

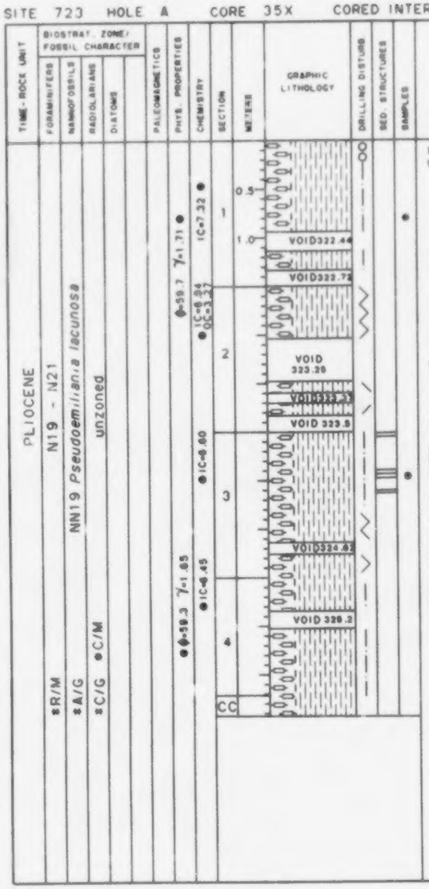
TIME-ROCK UNIT
BIOSTRAT. ZONE/ FOSSIL CHARACTER
FORAMINIFERS
NANNOFOSSILS
RADIOLARIANS
DIATOMS
PALEOMAGNETICS
PHYS. PROPERTIES
CHEMISTRY
SECTION
METERS
GRAPHIC LITHOLOGY
DRILLING DISTURB.
SED. STRUCTURES
SAMPLES
PLIOCENE
N19 - N21
NN19 Pseudoemiliania lacunosa
unzoned
*R/M
*A/G
*C/G ●C/M
φ=59.7 γ=1.71
φ=59.3 γ=1.65
IC=7.32
IC=6.94 OC=3.27
IC=6.60
IC=6.45
1
2
3
4
CC
0.5
1.0
VOID322.44
VOID322.72
VOID 323.20
VOID323.37
VOID 323.5
VOID324.62
VOID 326.2

LITHOLOGIC DESCRIPTION

FORAMINIFER-BEARING MARLY NANNOFOSSIL CHALK and CALCAREOUS CLAYEY SILTSTONE

Section 1, 0-15 cm, soupy; remainder moderately disturbed by gas expansion (numerous voids). Sediment appears continuous across voids within core. Crumbles readily, and firm intervals separate into clasts. Cut with wire in order to preserve laminae.

Major lithologies: FORAMINIFER-BEARING MARLY NANNOFOSSIL CHALK and CALCAREOUS CLAYEY SILTSTONE, dark olive gray (5Y 3/2). Foraminifers present on core face. Variable terrigenous component dominated by clay and silt-sized detrital calcite.

Minor lithology: Parallel laminae, individual light and dark layers 0.1-1.0 mm thick. Light layers are composed of nannofossils or diatoms, usually dominated by a single species. Observed in firm biscuits in Section 3, 5-6, 42-44, and 62-64 cm.

SMEAR SLIDE SUMMARY (%):

	1, 80 D	3, 46 M
TEXTURE:		
Sand	10	
Silt	50	10
Clay	40	90
COMPOSITION:		
Clay	20	10
Diatoms		3
Foraminifers	5	
Inorganic calcite	20	5
Mica	Tr	
Nannofossils	40	82
Pellets	5	
Quartz	10	
Silicoflagellates	Tr	
Sponge spicules	Tr	

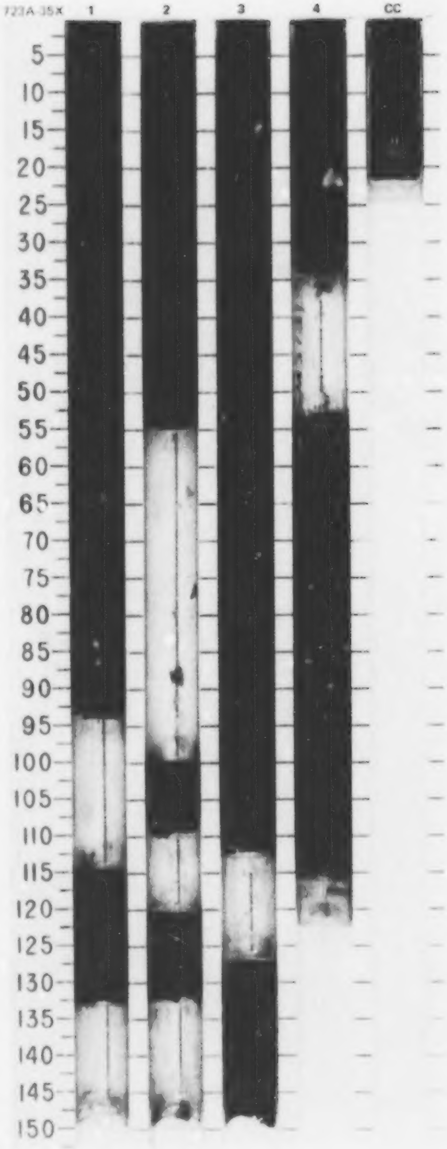
723A-35X
1
2
3
4
CC
5
10
15
20
25
30
35
40
45
50
55
60
65
70
75
80
85
90
95
100
105
110
115
120
125
130
135
140
145
150

SITE 723 HOLE A CORE 36X CORED INTERVAL 1134.1-1143.6 mbsl; 326.3-335.8 mbsf

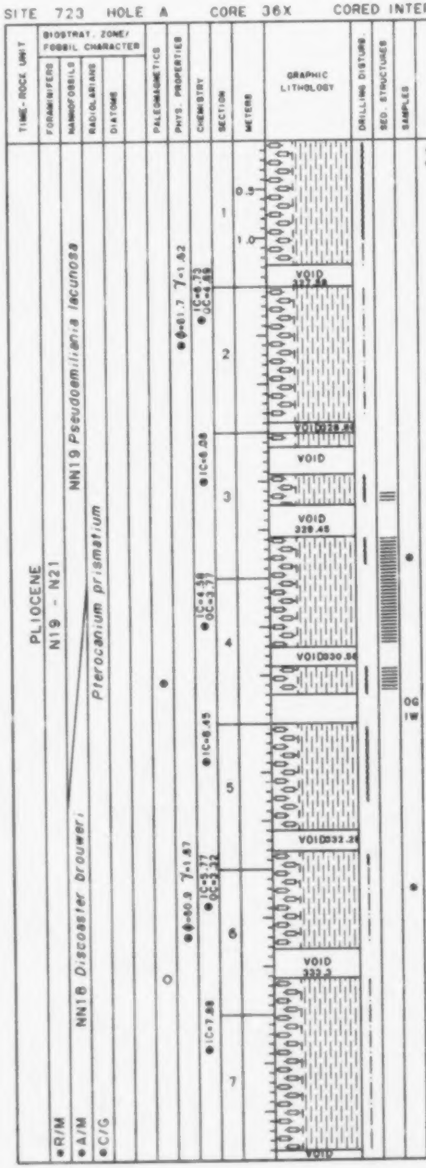
TIME-ROCK UNIT
BIOSTRAT. ZONE/ FOSSIL CHARACTER
FORAMINIFERS
NANNOFOSSILS
RADIOLARIANS
DIATOMS
PALEOMAGNETICS
PHYS. PROPERTIES
CHEMISTRY
SECTION
METERS
GRAPHIC LITHOLOGY
DRILLING DISTURB.
SED. STRUCTURES
SAMPLES
PLIOCENE
N19 - N21
NN19 Pseudoemiliania lacunosa
NN18 Discoaster brouweri
Pterocanium prismatium
●R/M
●A/M
●C/G
●ϕ=61.7 γ=1.82
●ϕ=50.9 γ=1.87
●IC=6.73 OC=4.89
●IC=6.08
●IC=4.58 OC=3.77
●IC=6.45
●IC=3.77 OC=3.32
●IC=7.88
1
2
3
4
5
6
7
0.5
1.0
VOID
VOID 329.45
VOID 332.3
OG
IW

LITHOLOGIC DESCRIPTION

FORAMINIFER-BEARING MARLY NANNOFOSSIL CHALK and CALCAREOUS CLAYEY SILTSTONE

Section 1, 0-115 cm, is soupy and half full. Remainder of core is moderately disturbed by gas expansion (numerous voids). Sediment appears continuous across voids within core. Crumbles readily, and firm intervals separate into clasts. Cut with wire in order to preserve laminae.

Major lithologies: FORAMINIFER-BEARING MARLY NANNOFOSSIL CHALK and CALCAREOUS CLAYEY SILTSTONE, dark olive gray (5Y 3/2, 3/1). Foraminifers present on core face. Variable terrigenous component dominated by clay and silt-sized detrital calcite.

Minor lithology: Parallel laminae, individual light and dark layers 0.1-1.0 mm thick. Light layers are composed of nannofossils or diatoms, usually dominated by a single species. Observed in Section 3, 72-150 cm, throughout Section 4, and Section 6, 24-31 cm. Some white layers are cohesive, cemented(?), and stick out as horizontal white flakes.

SMEAR SLIDE SUMMARY (%):

	3, 139 M	6, 25 D
TEXTURE:		
Silt	5	20
Clay	95	80
COMPOSITION:		
Clay	10	33
Diatoms	79	10
Foraminifers	3	5
Inorganic calcite	3	6
Mica		Tr
Nannofossils	5	40
Pellets		3
Quartz		3

(Con't.)

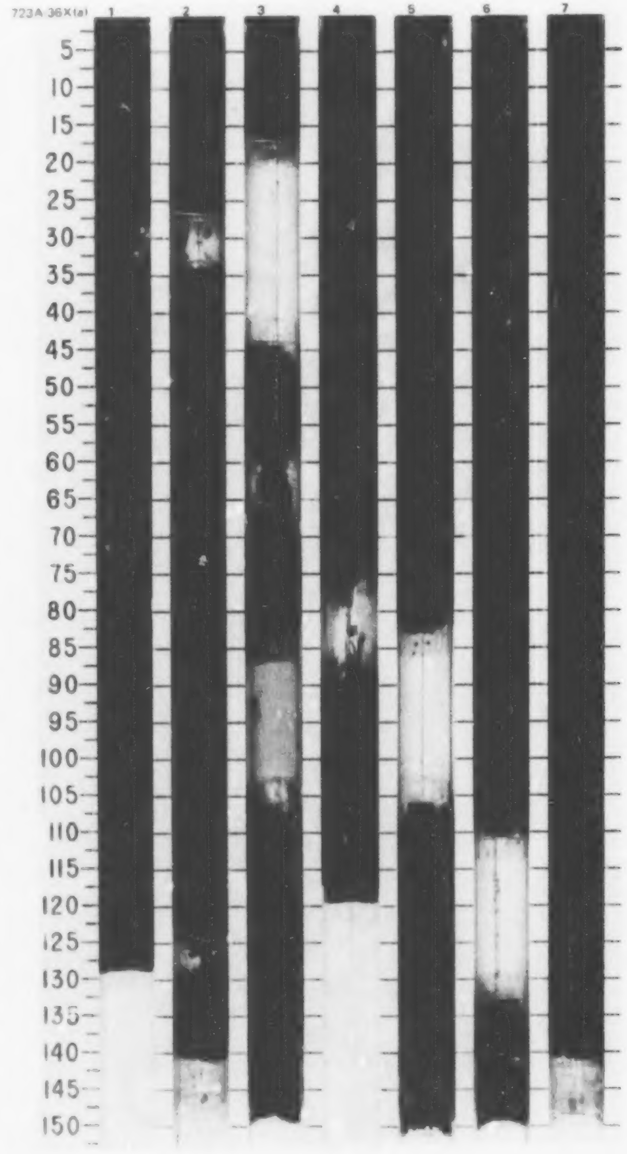
723A-36X(a)
1
2
3
4
5
6
7
5
10
15
20
25
30
35
40
45
50
55
60
65
70
75
80
85
90
95
100
105
110
115
120
125
130
135
140
145
150

SITE 723 HOLE A CORE 36X CORED INTERVAL 1134.1-1143.6 mbsl; 326.3-335.8 mbsf

TIME-ROCK UNIT	FORAMINIFERS	NANNOFOSSILS	RADIOLARIANS	DIATOMS	PALEOMAGNETICS	PHYS. PROPERTIES	CHEMISTRY	SECTION	METERS	GRAPHIC LITHOLOGY	DRILLING DISTURB.	SED. STRUCTURES	SAMPLES	LITHOLOGIC DESCRIPTION
								8 CC	0.5	VOID				(Con't.)

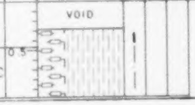

SITE 723 HOLE A CORE 37X CORED INTERVAL 1143.6-1153.2 mbsl; 335.8-345.4 mbsf

TIME-ROCK UNIT	FORAMINIFERS	NANNOFOSSILS	RADIOLARIANS	DIATOMS	PALEOMAGNETICS	PHYS. PROPERTIES	CHEMISTRY	SECTION	METERS
PLIOCENE	N19 - N21 R/M●	NN18 *Discoaster brouweri* A/M●	*Pterocanium prismatium* C/G●		●	φ=65.5 γ=1.34●	IC=5.89 OC=5.99 ●	1 CC	0.5 1.0

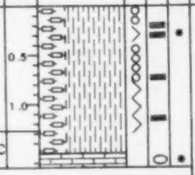

LITHOLOGIC DESCRIPTION

FORAMINIFER-BEARING MARLY NANNOFOSSIL CHALK and CALCAREOUS CLAYEY SILTSTONE

Section 1 is soupy and heavily disturbed. CC contains clast.

Major lithologies: FORAMINIFER-BEARING MARLY NANNOFOSSIL CHALK and CALCAREOUS CLAYEY SILTSTONE, olive gray (5Y 4/2, 4/3) and dark olive gray (5Y 3/2, 3/1), black (5Y 2.5/1) in CC, at 0-2, 4, 6, and 12 cm. Foraminifers present on core face. Variable terrigenous component dominated by clay and silt-sized detrital calcite.

Minor lithology:
a. Parallel laminae, individual light and dark layers 0.1-1.0 mm thick. Light colored layers are composed of nannofossils or diatoms, usually dominated by a single species. Laminae are intermittent and indistinct.
b. Fine-grained limestone, dolomite concretions (?), olive gray (5Y 4/2, 5/2). Contains foraminifers. Found in end of CC.

SMEAR SLIDE SUMMARY (%):

	1, 30 D	CC, 25 M	CC, 25 M
TEXTURE:			
Sand	5	40	10
Silt	45	10	70
Clay	50	50	20
COMPOSITION:			
Cement	20		20
Clay	35	25	30
Diatoms	5	8	
Dolomite	30		30
Foraminifers	Tr	10	20
Inorganic calcite	20		
Nannofossils	15		
Pellets	15		
Quartz	10	5	
Radiolarians	Tr		
Spar cement		50	
Sponge spicules		2	

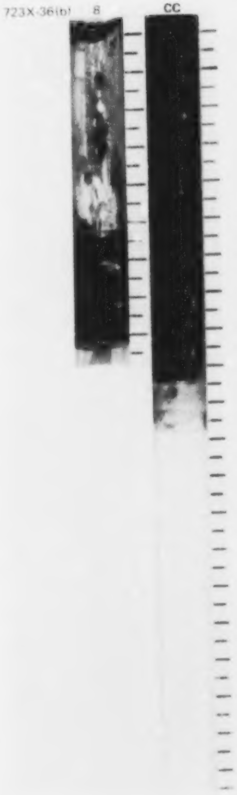

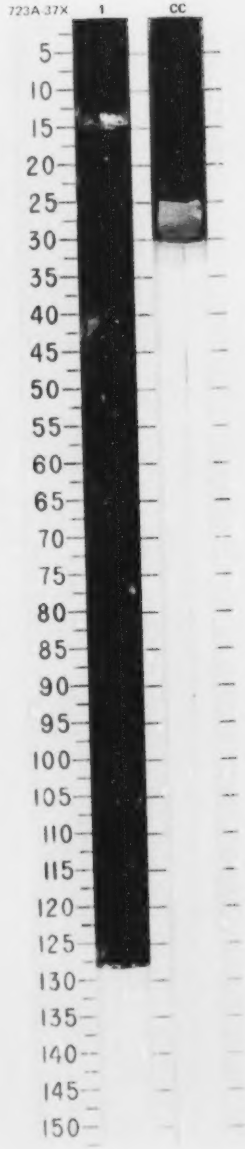

CORE 117–723A–38X NO RECOVERY

SITE 723 HOLE A CORE 39X CORED INTERVAL 1162.8-1172.5 mbsl; 355.0-364.7 mbsf

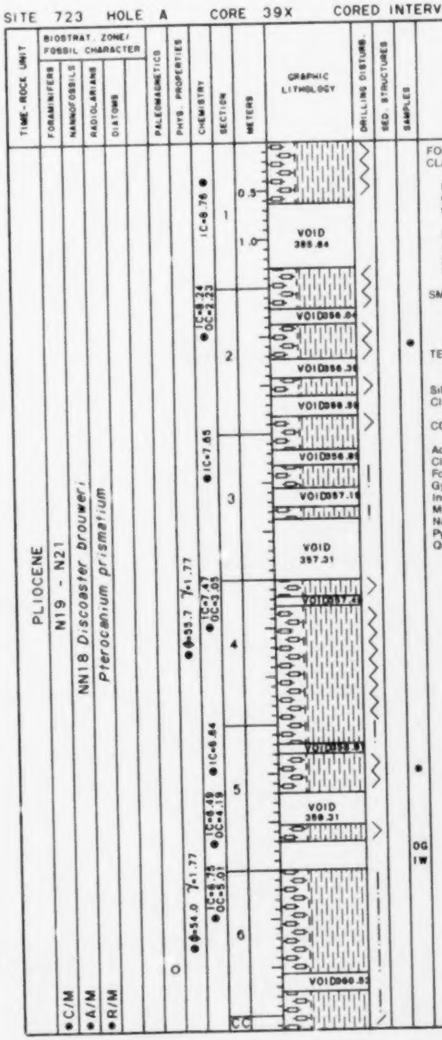
TIME-ROCK UNIT
BIOSTRAT. ZONE/ FOSSIL CHARACTER
FORAMINIFERS
NANNOFOSSILS
RADIOLARIANS
DIATOMS
PALEOMAGNETICS
PHYS. PROPERTIES
CHEMISTRY
SECTION
METERS
GRAPHIC LITHOLOGY
DRILLING DISTURB.
SED. STRUCTURES
SAMPLES
PLIOCENE
N19 - N21
NN18 Discoaster brouweri
Pterocanium prismatium
●C/M
●A/M
●R/M
IC=8.76 ●
●IC=8.24 OC=2.23
●IC=7.65
●IC=7.47 OC=3.05
●IC=8.84
●IC=8.40 OC=4.19
●IC=8.75 OC=5.01
●ϕ=55.7 γ=1.77
●ϕ=54.0 γ=1.77
○
1
2
3
4
5
6
CC
0.5
1.0
VOID 355.84
VOID 356.04
VOID 356.36
VOID 356.86
VOID 356.86
VOID 357.19
VOID 357.31
VOID 357.48
VOID 359.81
VOID 359.31
VOID 360.53
OG
IW

LITHOLOGIC DESCRIPTION

FORAMINIFER-BEARING MARLY NANNOFOSSIL CHALK and CALCAREOUS CLAYEY SILTSTONE

Entire core moderately to heavily disturbed by gas expansion (numerous voids) Crumbles readily, and firm intervals separate into clasts. Cut with wire in order to preserve laminae.

Major lithologies: FORAMINIFER-BEARING MARLY NANNOFOSSIL CHALK and CALCAREOUS CLAYEY SILTSTONE, dark olive gray (5Y 3/2). Foraminifers present on core face. Variable terrigenous component dominated by clay and silt-sized detrital calcite.

SMEAR SLIDE SUMMARY (%):

	2, 58 D	5, 47 D
TEXTURE:		
Silt	40	50
Clay	60	50
COMPOSITION:		
Access. minerals		4
Clay	20	35
Foraminifers	3	5
Gypsum		Tr
Inorganic calcite	45	25
Mica	3	3
Nannofossils	24	25
Pyrite		Tr
Quartz	5	3

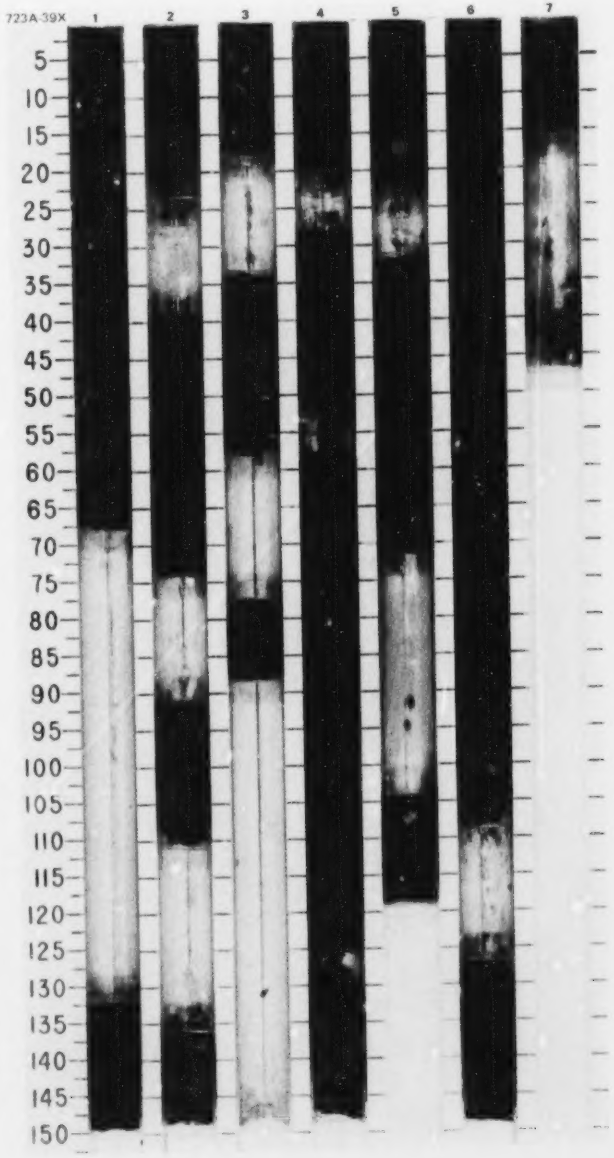
723A-39X
1
2
3
4
5
6
7
5
10
15
20
25
30
35
40
45
50
55
60
65
70
75
80
85
90
95
100
105
110
115
120
125
130
135
140
145
150

SITE 723 HOLE A CORE 40X CORED INTERVAL 1172.5-1182.1 mbsl; 364.7-374.3 mbsf

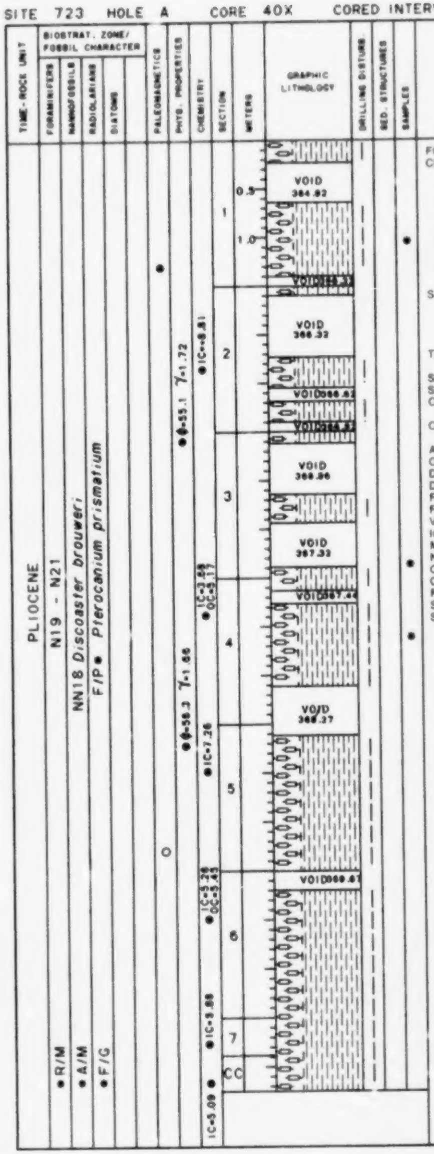
TIME-ROCK UNIT
BIOSTRAT. ZONE/ FOSSIL CHARACTER
FORAMINIFERS
NANNOFOSSILS
RADIOLARIANS
DIATOMS
PALEOMAGNETICS
PHYS. PROPERTIES
CHEMISTRY
SECTION
METERS
GRAPHIC LITHOLOGY
DRILLING DISTURB.
SED. STRUCTURES
SAMPLES
PLIOCENE
N19 - N21
NN18 Discoaster brouweri
F/P● Pterocanium prismatium
●R/M
●A/M
●F/G
●ϕ=55.1 γ=1.72
●ϕ=58.3 γ=1.86
●IC=8.81
●IC=3.88 OC=5.17
●IC=7.26
●IC=5.26 OC=5.43
●IC=5.88
IC=5.09 ●
1
2
3
4
5
6
7
CC
0.5
1.0
VOID 364.92
VOID 366.32
VOID 366.62
VOID 366.86
VOID 367.32
VOID 367.44
VOID 368.27
VOID 369.67

LITHOLOGIC DESCRIPTION

FORAMINIFER-BEARING MARLY NANNOFOSSIL CHALK and CALCAREOUS CLAYEY SILTSTONE

Entire core moderately disturbed by gas expansion (numerous voids). Crumbles readily, and firm intervals separate into clasts. Cut with wire in order to preserve laminas.

Major lithologies: FORAMINIFER-BEARING MARLY NANNOFOSSIL CHALK and CALCAREOUS CLAYEY SILTSTONE, dark olive gray (5Y 3/2, 2.5/2). Color becoming darker in deeper cores. Foraminifers present on core face. Variable terrigenous component dominated by clay and silt-sized detrital calcite.

SMEAR SLIDE SUMMARY (%):

	1, 105 D	3, 146 D	4, 61 D
TEXTURE:			
Sand	5	15	25
Silt	25	45	35
Clay	70	40	40
COMPOSITION:			
Access. minerals	Tr	3	10
Clay	30	35	35
Diatoms			
Dolomite	Tr	Tr	
Feldspar		5	5
Foraminifers	8	2	1
Volcanic glass			Tr
Inorganic calcite	15	25	20
Mica	Tr		2
Nannofossils	40	5	2
Organic debris			
Quartz	7	25	25
Radiolarians			Tr
Spar cement			
Sponge spicules		Tr	Tr

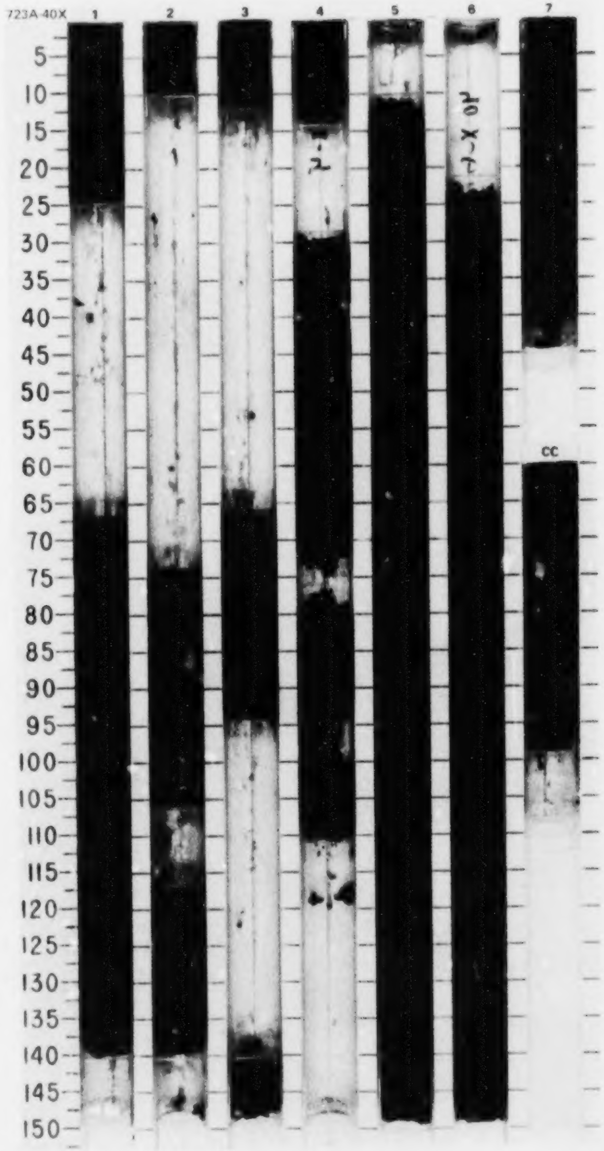
723A-40X
1
2
3
4
5
6
7
CC
5
10
15
20
25
30
35
40
45
50
55
60
65
70
75
80
85
90
95
100
105
110
115
120
125
130
135
140
145
150

SITE 723 HOLE A CORE 41X CORED INTERVAL 1182.1-1191.8 mbsl; 374.3-384.0 mbsf

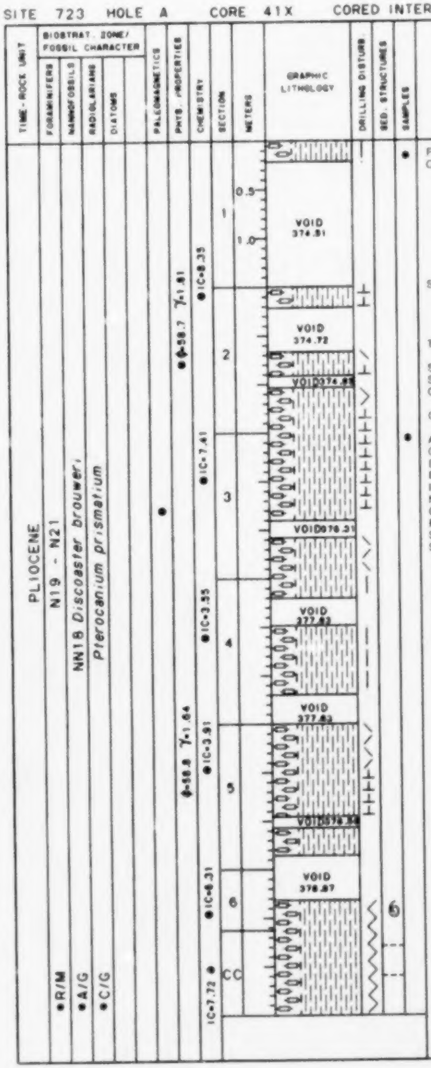
TIME-ROCK UNIT
BIOSTRAT. ZONE/ FOSSIL CHARACTER
FORAMINIFERS
NANNOFOSSILS
RADIOLARIANS
DIATOMS
PALEOMAGNETICS
PHYS. PROPERTIES
CHEMISTRY
SECTION
METERS
GRAPHIC LITHOLOGY
DRILLING DISTURB.
SED. STRUCTURES
SAMPLES
PLIOCENE
N19 - N21
NN18 Discoaster brouweri
Pterocanium prismatium
●R/M
●A/G
●C/G
●φ=58.7 γ=1.81
φ=58.8 γ=1.64
●IC=8.35
●IC=7.41
●IC=3.55
●IC=3.91
●IC=8.31
IC=7.72 ●
1
2
3
4
5
6
CC
0.5
1.0
VOID 374.81
VOID 374.72
VOID 374.85
VOID 376.31
VOID 377.82
VOID 377.83
VOID 378.38
VOID 378.87

LITHOLOGIC DESCRIPTION

FORAMINIFER-BEARING MARLY NANNOFOSSIL CHALK and CALCAREOUS CLAYEY SILTSTONE

CC is soupy and heavily disturbed. Entire core moderately to heavily disturbed by gas expansion (numerous voids). Crumbles readily, and firm intervals separate into clasts. Cut with wire in order to preserve laminae.

Major lithologies: FORAMINIFER-BEARING MARLY NANNOFOSSIL CHALK and CALCAREOUS CLAYEY SILTSTONE, dark olive gray (5Y 3/2, 2.5/2). Variable terrigenous component dominated by clay and silt-sized detrital calcite.

SMEAR SLIDE SUMMARY (%):

	1, 19 D	3, 4 D
TEXTURE:		
Sand	5	20
Silt	55	20
Clay	40	60
COMPOSITION:		
Access. minerals	1	5
Clay	20	25
Diatoms	3	Tr
Foraminifers	Tr	15
Inorganic calcite	45	17
Nannofossils	20	35
Quartz	10	3
Radiolarians	Tr	Tr
Silicoflagellates	Tr	
Sponge spicules	1	Tr

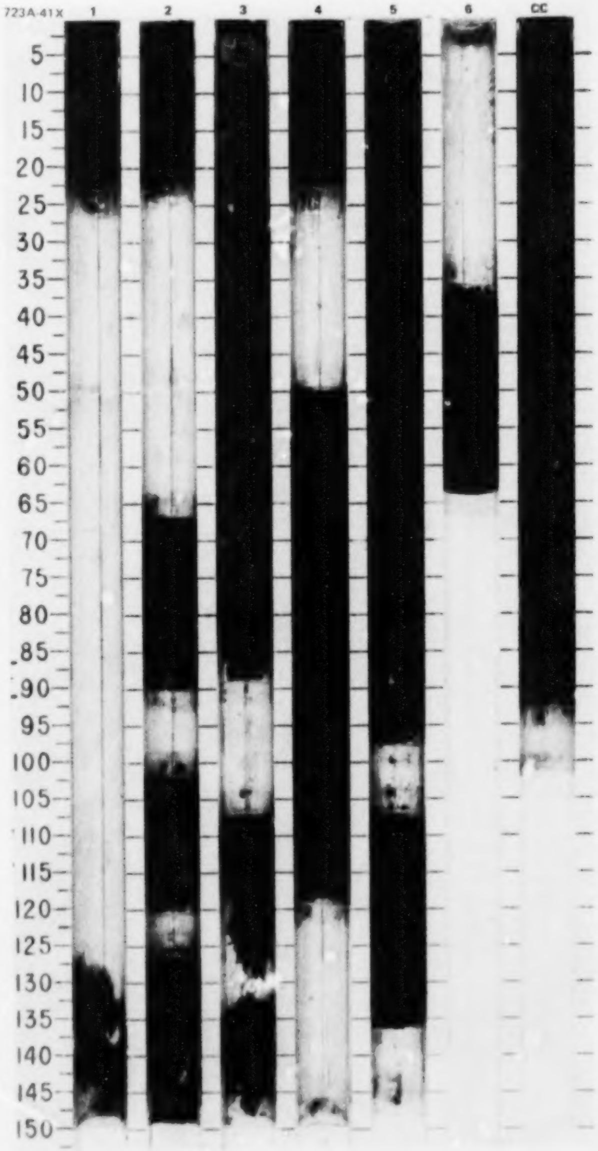
723A-41X
1
2
3
4
5
6
CC
5
10
15
20
25
30
35
40
45
50
55
60
65
70
75
80
85
90
95
100
105
110
115
120
125
130
135
140
145
150

SITE 723 HOLE A CORE 42X CORED INTERVAL 1191.8-1201.4 mbsl; 384.0-393.6 mbsf

TIME-ROCK UNIT	BIOSTRAT. ZONE/ FOSSIL CHARACTER					PALEOMAGNETICS	PHYS. PROPERTIES	CHEMISTRY	SECTION	METERS	GRAPHIC LITHOLOGY	DRILLING DISTURB.	SED. STRUCTURES	SAMPLES
	FORAMINIFERS	NANNOFOSSILS	RADIOLARIANS	DIATOMS										
UPPER PLIOCENE	N19 - N21 ●R/M	NN18 *Discoaster brouweri* ●A/M-G	*Pterocanium prismatium* ●C/G			O	●ϕ-68.9 γ-1.45	IC-3.61 ●	1 2	0.5 1.0	VOID 384.22			● ▬ ▬ ●

LITHOLOGIC DESCRIPTION

FORAMINIFER-BEARING MARLY NANNOFOSSIL CHALK and CALCAREOUS CLAYEY SILTSTONE

Entire core moderately disturbed by gas expansion (numerous voids). Crumbles readily, and firm intervals separate into clasts. Cut with wire in order to preserve laminae.

Major lithologies: FORAMINIFER-BEARING MARLY NANNOFOSSIL CHALK and CALCAREOUS CLAYEY SILTSTONE, dark olive gray (5Y 2.5/2). Variable terrigenous component dominated by clay and silt-sized detrital calcite. Smear slide from dark drill-flow material indicates diatomaceous marly nannofossil chalk.

Minor lithology: Parallel laminae, individual light and dark layers 0.1-1.0 mm thick. Light layers are composed of nannofossils or diatoms; usually dominated by a single species. Laminae are faint and indistinct, occurring in hard biscuits in Section 1.

SMEAR SLIDE SUMMARY (%):

	1, 27 D	2, 21 D
TEXTURE:		
Sand	10	5
Silt	30	30
Clay	60	65
COMPOSITION:		
Access. minerals	5	2
Clay	60	35
Diatoms	1	5
Volcanic glass		15
Inorganic calcite	3	
Nannofossils		30
Quartz	30	12
Radiolarians	Tr	1
Silicoflagellates	Tr	
Sponge spicules	1	Tr

CORE 117–723A–43X NO RECOVERY

SITE 723 HOLE A CORE 44X CORED INTERVAL 1211.1-1220.8 mbsl; 403.3-413.0 mbsf

TIME-ROCK UNIT	BIOSTRAT. ZONE/ FOSSIL CHARACTER				PALEOMAGNETICS	PHYS. PROPERTIES	CHEMISTRY	SECTION	METERS	GRAPHIC LITHOLOGY	DRILLING DISTURB.	SED. STRUCTURES	SAMPLES
	FORAMINIFERS	NANNOFOSSILS	RADIOLARIANS	DIATOMS									
								CC					

LITHOLOGIC DESCRIPTION

FORAMINIFER-BEARING MARLY NANNOFOSSIL LIMESTONE and CALCAREOUS CLAYEY SILTSTONE

Single clast recovered in CC.

Major lithologies: FORAMINIFER-BEARING MARLY NANNOFOSSIL LIMESTONE and CALCAREOUS CLAYEY SILTSTONE with indistinct 1-mm-thick parallel laminated light and dark layers. Wavy bedding in diagenetic(?) and burrow structures.

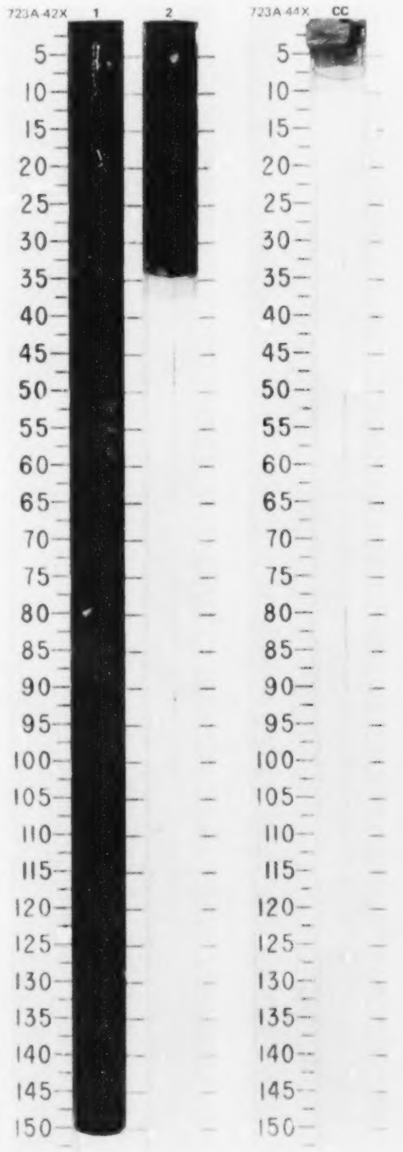

SITE 723 HOLE A CORE 45X CORED INTERVAL 1220.8-1230.4 mbsl; 413.0-422.6 mbsf

TIME-ROCK UNIT	BIOSTRAT. ZONE/ FOSSIL CHARACTER: FORAMINIFERS	NANNOFOSSILS	RADIOLARIANS	DIATOMS	PALEOMAGNETICS	PHYS. PROPERTIES	CHEMISTRY	SECTION	METERS	GRAPHIC LITHOLOGY	DRILLING DISTURB.	SED. STRUCTURES	SAMPLES
		B ● Barren						CC					TS ●

LITHOLOGIC DESCRIPTION

FORAMINIFER-BEARING MARLY NANNOFOSSIL LIMESTONE and CALCAREOUS CLAYEY SILTSTONE

CC contains broken pieces.

Major lithologies: FORAMINIFER-BEARING MARLY NANNOFOSSIL LIMESTONE and CALCAREOUS CLAYEY SILTSTONE contains light and dark layers 0.1-1.0 mm thick, parallel and lenticular lamination.

SMEAR SLIDE SUMMARY (%):

	CC, 26 D	CC, 26 M
TEXTURE:		
Sand		40
Silt	30	10
Clay	70	50
COMPOSITION:		
Clay	27	20
Diatoms		50
Dolomite	59	
Foraminifers	9	5
Spar cement		20
Sponge spicules	5	5

SITE 723 HOLE B CORE 1H CORED INTERVAL 806.2-810.5 mbsl; 0.0-4.3 mbsf

TIME-ROCK UNIT	BIOSTRAT. ZONE/ FOSSIL CHARACTER: FORAMINIFERS	NANNOFOSSILS	RADIOLARIANS	DIATOMS	PALEOMAGNETICS	PHYS. PROPERTIES	CHEMISTRY	SECTION	METERS	GRAPHIC LITHOLOGY	DRILLING DISTURB.	SED. STRUCTURES	SAMPLES
PLEISTOCENE		NN21 *Emiliania huxleyi* ● A/G					●IC=8.17 OC=3.86	1	0.5 1.0				●
							●IC=7.84 OC=2.83	2					
						●Φ=64.9 γ=1.62	●IC=6.41 OC=2.28	3					●
								CC					

LITHOLOGIC DESCRIPTION

FORAMINIFER-BEARING MARLY NANNOFOSSIL OOZE and CALCAREOUS CLAYEY SILT

Entire core undisturbed. Section 1, 0-60 cm, is almost soupy.

Major lithologies: FORAMINIFER-BEARING MARLY NANNOFOSSIL OOZE and CALCAREOUS CLAYEY SILT, olive gray (5Y 4/2) and dark olive gray (5Y 3/2), faintly mottled. Foraminifers and shell fragments (pteropods) common on core face, open burrows in Section 1. Variable terrigenous component dominated by clay and silt-sized detrital calcite.

SMEAR SLIDE SUMMARY (%):

	1, 113 D	3, 98 D
TEXTURE:		
Sand	15	10
Silt	25	35
Clay	60	55
COMPOSITION:		
Access. minerals	3	1
Clay	30	20
Diatoms	3	
Dolomite		1
Feldspar		1
Foraminifers	15	15
Inorganic calcite	10	20
Mica	1	
Nannofossils	35	35
Pteropod	Tr	
Quartz	3	7
Radiolarians	Tr	
Sponge spicules	Tr	

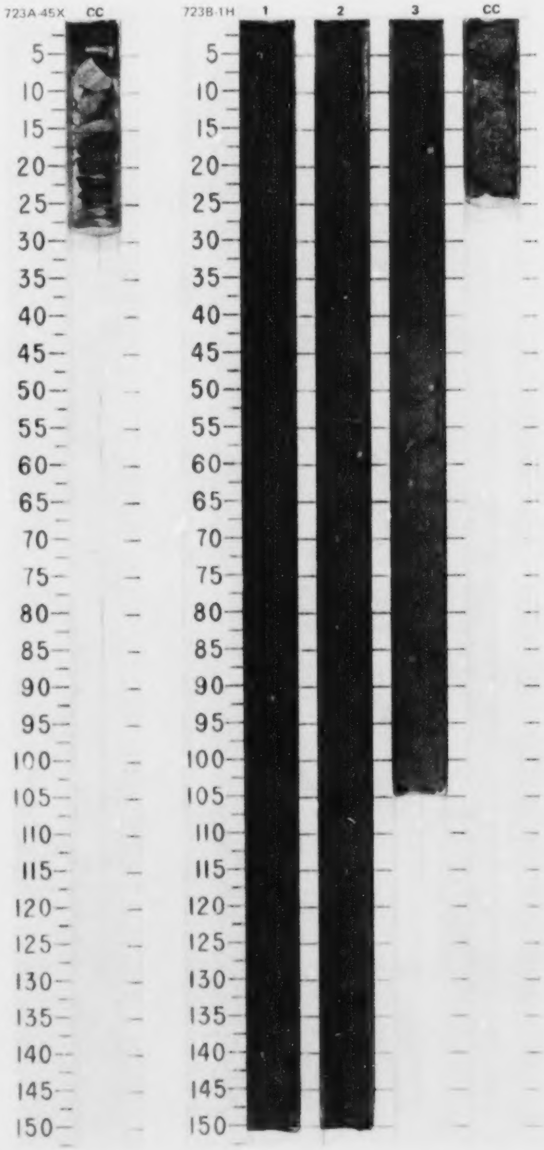

SITE 723 HOLE B CORE 2H CORED INTERVAL 810.5-820.2 mbsl; 4.3-14.0 mbsf

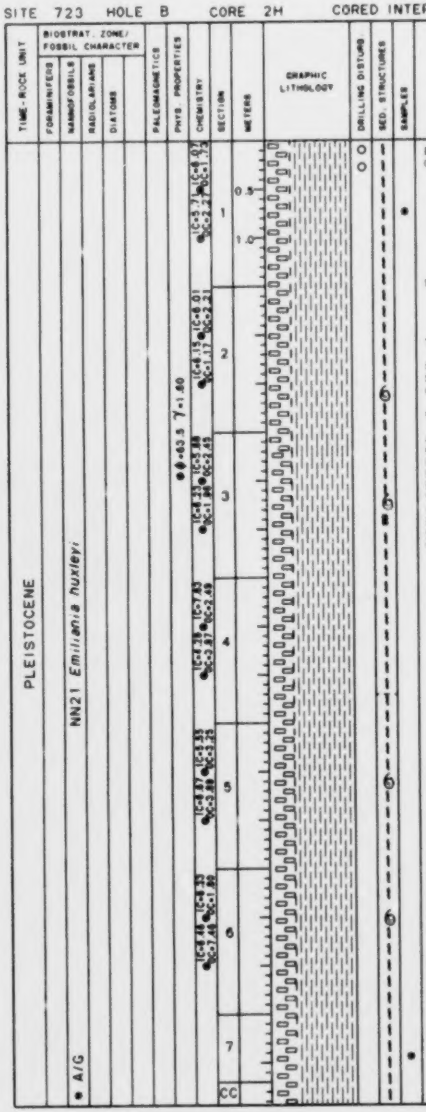
TIME-ROCK UNIT
BIOSTRAT. ZONE/ FOSSIL CHARACTER
FORAMINIFERS
NANNOFOSSILS
RADIOLARIANS
DIATOMS
PALEOMAGNETICS
PHYS. PROPERTIES
CHEMISTRY
SECTION
METERS
GRAPHIC LITHOLOGY
DRILLING DISTURB.
SED. STRUCTURES
SAMPLES
PLEISTOCENE
NN21 Emiliania huxleyi
● A/G
● φ=63.5 γ=1.80
IC=5.71 OC=2.27
IC=6.07 OC=1.73
IC=6.15 OC=1.17
IC=6.01 OC=2.21
IC=6.23 OC=1.89
IC=5.88 OC=2.45
IC=6.28 OC=3.87
IC=7.83 OC=2.49
IC=6.87 OC=3.88
IC=5.55 OC=3.25
IC=6.46 OC=7.46
IC=6.33 OC=1.80
1
2
3
4
5
6
7
CC
0.5
1.0

LITHOLOGIC DESCRIPTION

FORAMINIFER-BEARING MARLY NANNOFOSSIL OOZE and CALCAREOUS CLAYEY SILT

Section 1, 0-15 cm, soupy; remainder of core undisturbed.

Major lithologies: FORAMINIFER-BEARING MARLY NANNOFOSSIL OOZE and CALCAREOUS CLAYEY SILT, olive gray (5Y 4/2) and dark olive gray (5Y 3/2), faintly mottled. Foraminifers and shell fragments (pteropods) common on core face. Variable terrigenous component dominated by clay and silt-sized detrital calcite.

SMEAR SLIDE SUMMARY (%):

	1, 73 D	7, 44 D
TEXTURE		
Sand	15	10
Silt	40	45
Clay	45	45
COMPOSITION		
Access. minerals	2	2
Clay	30	20
Dolomite	Tr	1
Feldspar	5	
Foraminifers	2	1
Volcanic glass	Tr	1
Inorganic calcite	25	30
Mica	1	
Nannofossils	15	25
Quartz	20	20

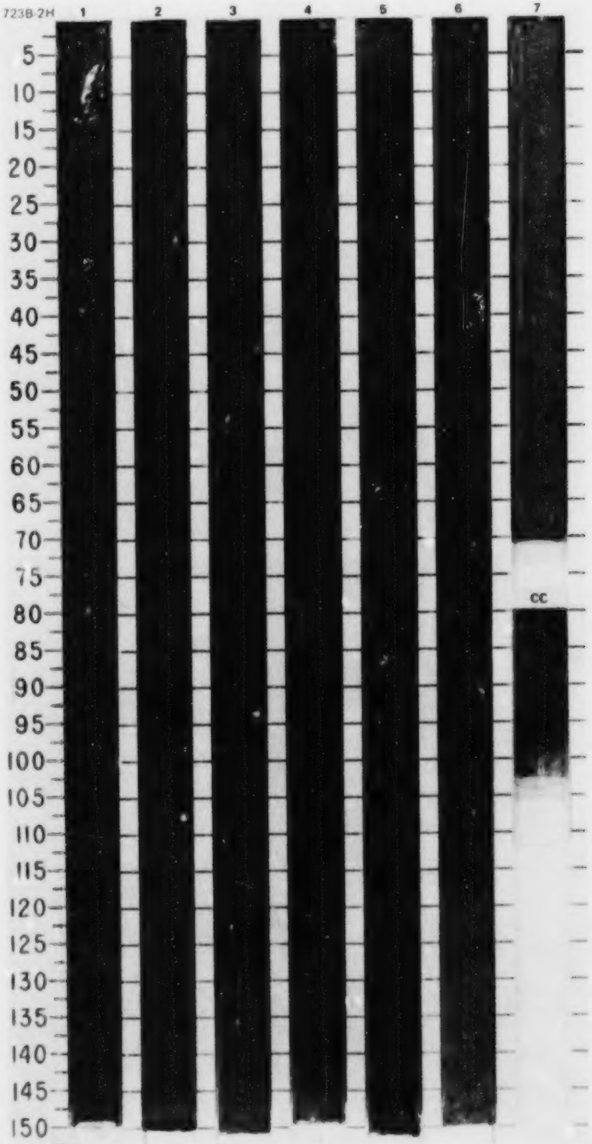
723B-2H
1
2
3
4
5
6
7
CC
5
10
15
20
25
30
35
40
45
50
55
60
65
70
75
80
85
90
95
100
105
110
115
120
125
130
135
140
145
150

SITE 723 HOLE B CORE 3H CORED INTERVAL 820.2-829.6 mbsl; 14.0-23.6 mbsf

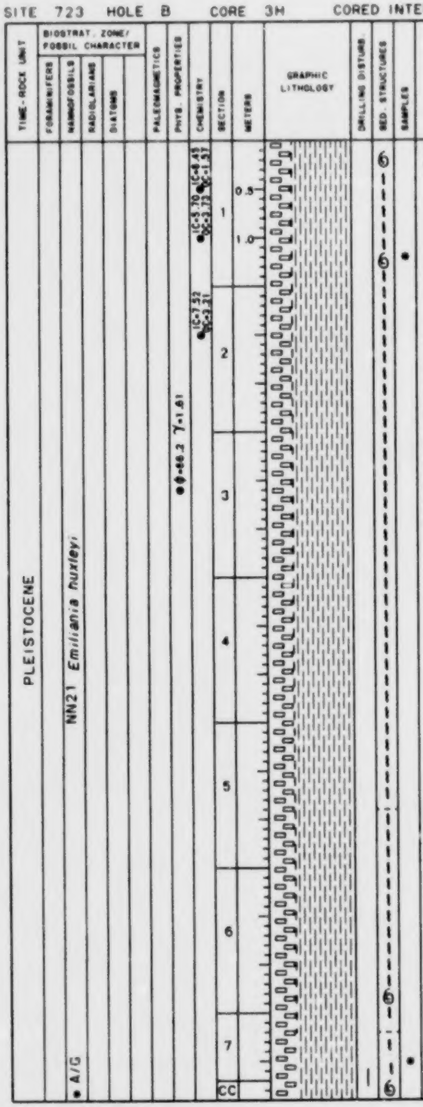

LITHOLOGIC DESCRIPTION

FORAMINIFER-BEARING MARLY NANNOFOSSIL OOZE and CALCAREOUS CLAYEY SILT

Section 1, 0-10 cm, soupy; remainder of core undisturbed.

Major lithologies: FORAMINIFER BEARING MARLY NANNOFOSSIL OOZE and CALCAREOUS CLAYEY SILT, olive gray (5Y 4/2) and dark olive gray (5Y 3/2), mottled. Foraminifers and shell fragments common on core face, with some fragments concentrated in burrows. Variable terrigenous component dominated by clay and silt-sized detrital calcite.

SMEAR SLIDE SUMMARY (%):

	1, 120 D	7, 50 D
TEXTURE:		
Sand	15	25
Silt	25	35
Clay	60	40
COMPOSITION:		
Access. minerals	2	3
Clay	25	20
Dolomite	Tr	
Feldspar		3
Foraminifers	8	4
Inorganic calcite	25	25
Nannofossils	35	20
Quartz	5	25

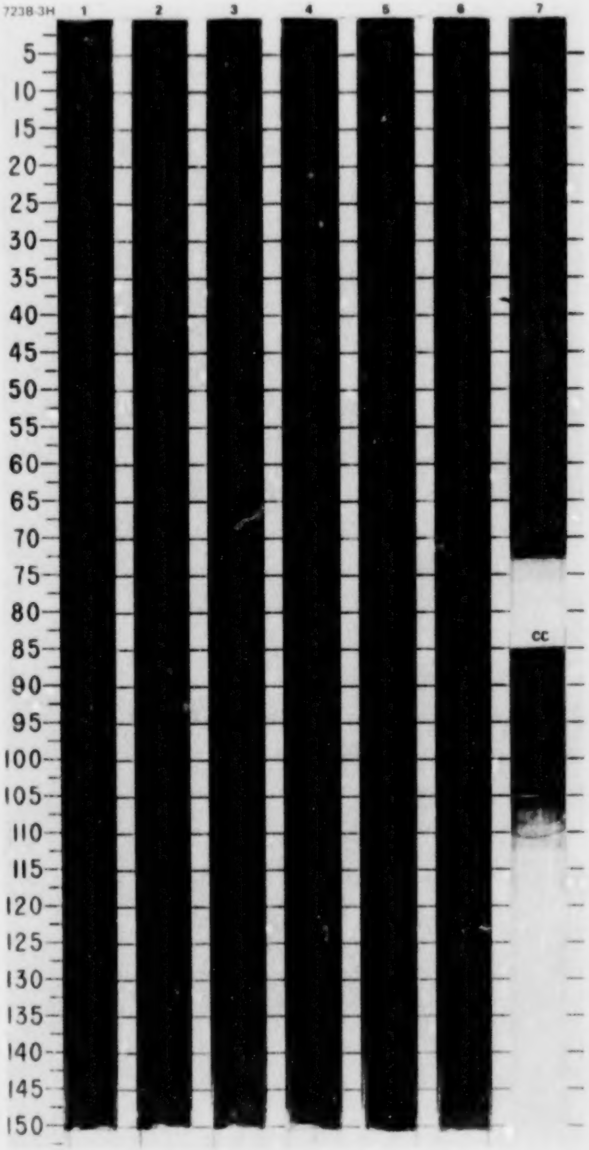
723B-3H
1
2
3
4
5
6
7
CC
5
10
15
20
25
30
35
40
45
50
55
60
65
70
75
80
85
90
95
100
105
110
115
120
125
130
135
140
145
150

SITE 723 HOLE B CORE 4H CORED INTERVAL 829.8-839.5 mbsl; 23.6-33.3 mbsf

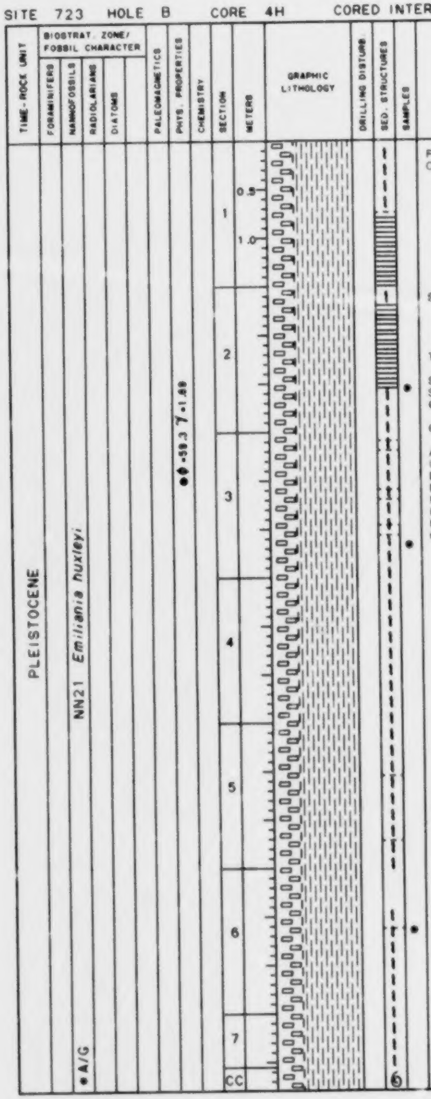
TIME-ROCK UNIT
BIOSTRAT. ZONE/ FOSSIL CHARACTER
FORAMINIFERS
NANNOFOSSILS
RADIOLARIANS
DIATOMS
PALEOMAGNETICS
PHYS. PROPERTIES
CHEMISTRY
SECTION
METERS
GRAPHIC LITHOLOGY
DRILLING DISTURB.
SED. STRUCTURES
SAMPLES
PLEISTOCENE
NN21 Emiliania huxleyi
● A/G
●φ =59.3 γ =1.89
0.5
1.0
1
2
3
4
5
6
7
CC

LITHOLOGIC DESCRIPTION

FORAMINIFER-BEARING MARLY NANNOFOSSIL OOZE and CALCAREOUS CLAYEY SILT

Entire core undisturbed.

Major lithologies: FORAMINIFER-BEARING MARLY NANNOFOSSIL OOZE and CALCAREOUS CLAYEY SILT, irregular intervals of olive gray (5Y 4/2, 4/3) and dark olive gray (5Y 3/2), mottled. Centimeter-scale light and dark layers in bottom of Section 1 and in Section 2. Foraminifers are common on core face. Variable terrigenous component is dominated by clay and silt-sized detrital calcite.

SMEAR SLIDE SUMMARY (%):

	2, 103 D	3, 118 D	6, 67 D
TEXTURE:			
Sand	20	20	15
Silt	35	25	35
Clay	45	55	50
COMPOSITION:			
Access. minerals	3		3
Clay	20	20	30
Dolomite	1	1	
Feldspar	2		2
Foraminifers	4	10	
Inorganic calcite	25	25	35
Nannofossils	25	35	15
Quartz	20	9	15

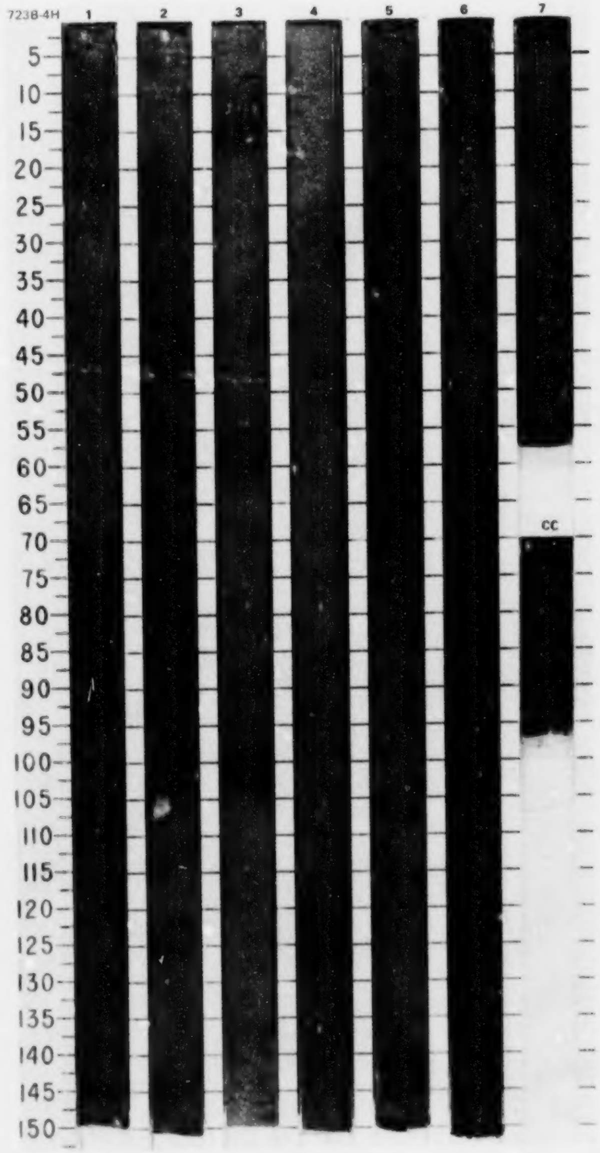
723B-4H
1
2
3
4
5
6
7
CC
5
10
15
20
25
30
35
40
45
50
55
60
65
70
75
80
85
90
95
100
105
110
115
120
125
130
135
140
145
150

SITE 723 HOLE B CORE 5H CORED INTERVAL 839.5-849.1 mbsl; 33.3-42.9 mbsf

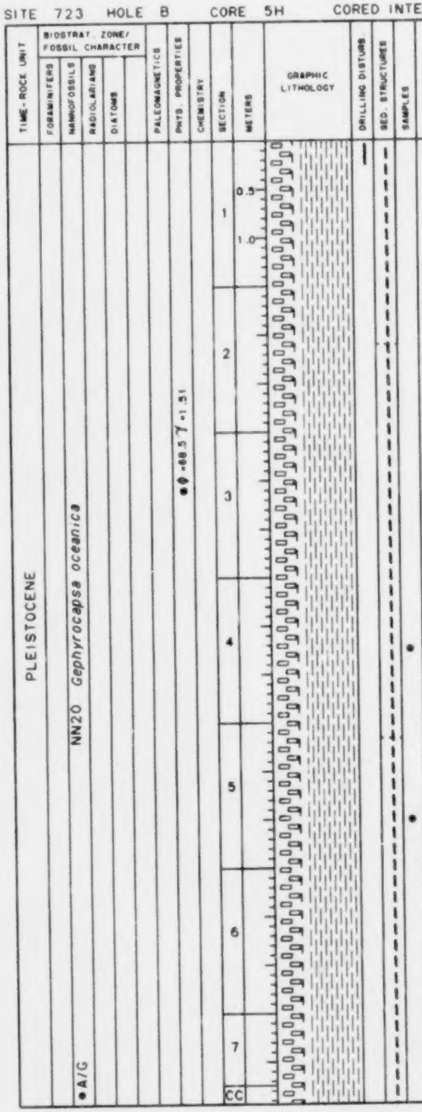
TIME-ROCK UNIT
BIOSTRAT. ZONE/ FOSSIL CHARACTER
FORAMINIFERS
NANNOFOSSILS
RADIOLARIANS
DIATOMS
PALEOMAGNETICS
PHYS. PROPERTIES
CHEMISTRY
SECTION
METERS
GRAPHIC LITHOLOGY
DRILLING DISTURB.
SED. STRUCTURES
SAMPLES
PLEISTOCENE
NN20 Gephyrocapsa oceanica
● A/G
● φ =68.5 γ =1.51
0.5
1.0
1
2
3
4
5
6
7
CC

LITHOLOGIC DESCRIPTION

FORAMINIFER-BEARING MARLY NANNOFOSSIL OOZE and CALCAREOUS CLAYEY SILT

Section 1, 0-15 cm, slightly disturbed; remainder of core undisturbed.

Major lithologies: FORAMINIFER-BEARING MARLY NANNOFOSSIL OOZE and CALCAREOUS CLAYEY SILT, olive gray (5Y 4/2, 5/2) and dark olive gray (5Y 3/2) intervals, mottled. Foraminifers common on core face. Variable terrigenous component dominated by clay and silt-sized detrital calcite.

SMEAR SLIDE SUMMARY (%):

	4, 74 D	5, 100 D
TEXTURE:		
Sand	10	10
Silt	20	20
Clay	70	70
COMPOSITION:		
Access. minerals	2	1
Clay	25	20
Dolomite		Tr
Feldspar	1	
Foraminifers	10	4
Volcanic glass		20
Inorganic calcite	10	
Nannofossils	45	50
Quartz	7	5
Radiolarians	Tr	
Sponge spicules	Tr	

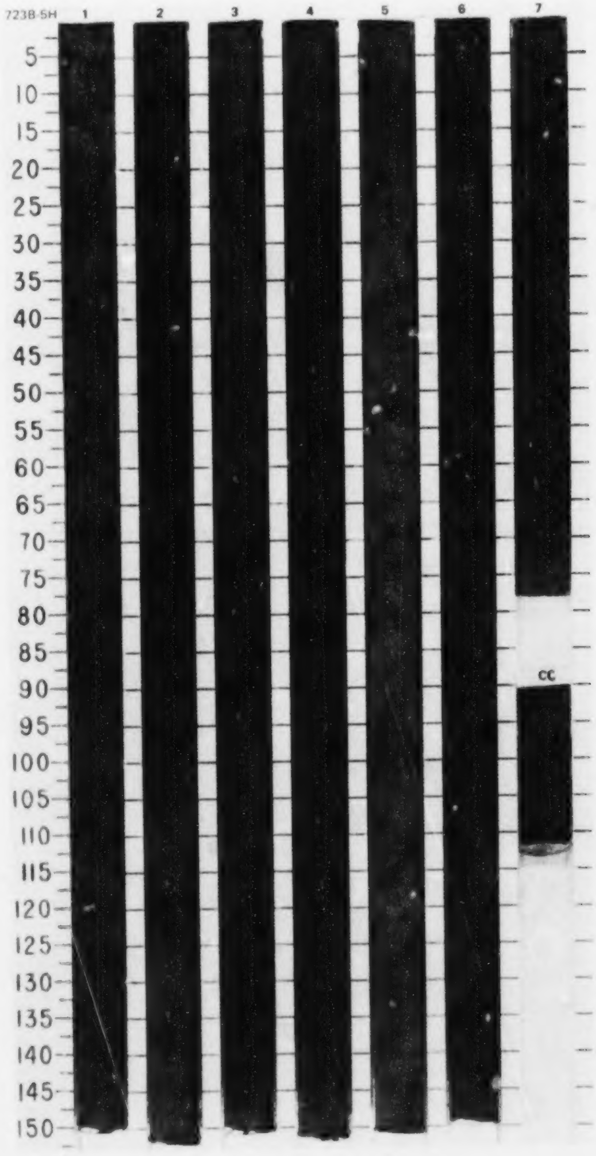
723B-5H
1
2
3
4
5
6
7
CC
5
10
15
20
25
30
35
40
45
50
55
60
65
70
75
80
85
90
95
100
105
110
115
120
125
130
135
140
145
150

SITE 723 HOLE B CORE 6H CORED INTERVAL 849.1-858.8 mbsl; 42.9-52.6 mbsf

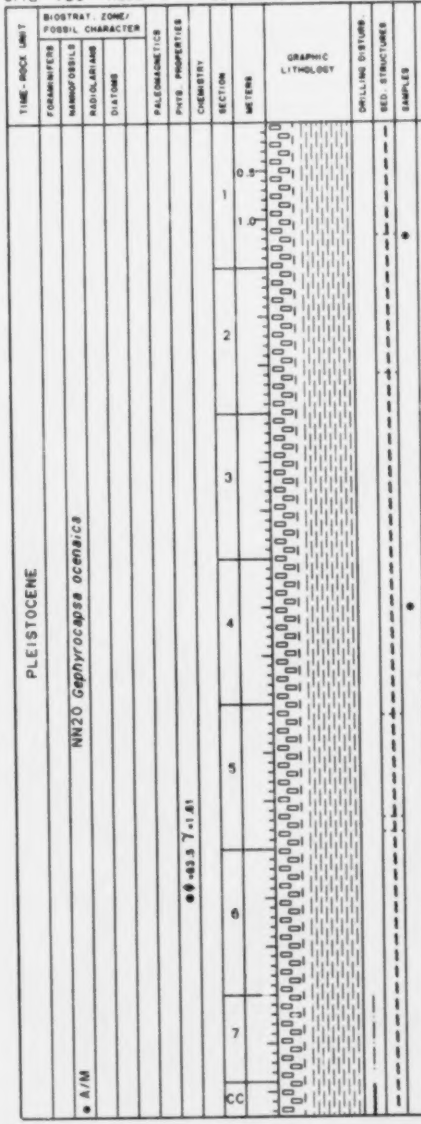
TIME-ROCK UNIT
BIOSTRAT. ZONE/ FOSSIL CHARACTER
FORAMINIFERS
NANNOFOSSILS
RADIOLARIANS
DIATOMS
PALEOMAGNETICS
PHYS. PROPERTIES
CHEMISTRY
SECTION
METERS
GRAPHIC LITHOLOGY
DRILLING DISTURB.
SED. STRUCTURES
SAMPLES
PLEISTOCENE
NN20 Gephyrocapsa oceanica
● A/M
●φ=63.5 γ=1.81
0.5
1.0
1
2
3
4
5
6
7
CC

LITHOLOGIC DESCRIPTION

FORAMINIFER-BEARING MARLY NANNOFOSSIL OOZE and CALCAREOUS CLAYEY SILT

Undisturbed except for minor gas expansion.

Major lithologies: FORAMINIFER-BEARING MARLY NANNOFOSSIL OOZE and CALCAREOUS CLAYEY SILT, olive gray (5Y 4/2, 4/3, 5/3, 5/2) and dark olive gray (5Y 3/2), mottled. Foraminifers common on core face. Variable terrigenous component dominated by clay and silt-sized detrital calcite.

SMEAR SLIDE SUMMARY (%):

	1, 118 D	4, 49 D
TEXTURE:		
Sand	15	
Silt	40	40
Clay	45	60
COMPOSITION:		
Access. minerals	2	2
Clay	30	20
Diatoms	2	
Dolomite		Tr
Feldspar	Tr	1
Foraminifers	1	2
Inorganic calcite	25	20
Nannofossils	15	40
Quartz	25	15
Silicoflagellates	Tr	
Sponge spicules	Tr	

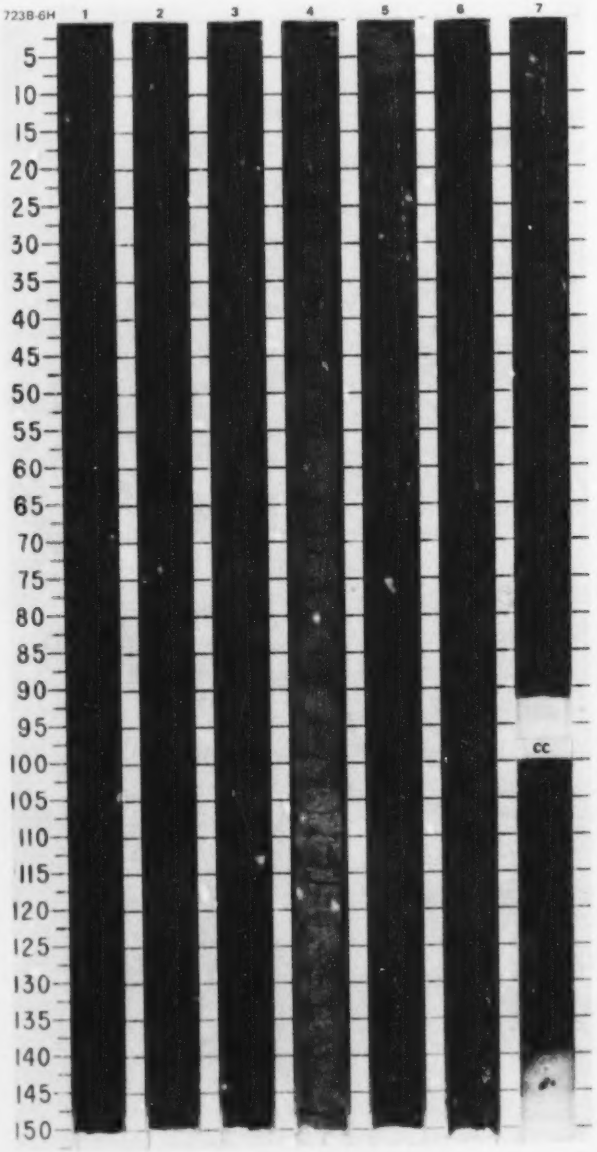
723B-6H
1
2
3
4
5
6
7
CC
5
10
15
20
25
30
35
40
45
50
55
60
65
70
75
80
85
90
95
100
105
110
115
120
125
130
135
140
145
150

SITE 723 HOLE B CORE 7H CORED INTERVAL 858.8-868.5 mbsl; 52.6-62.3 mbsf

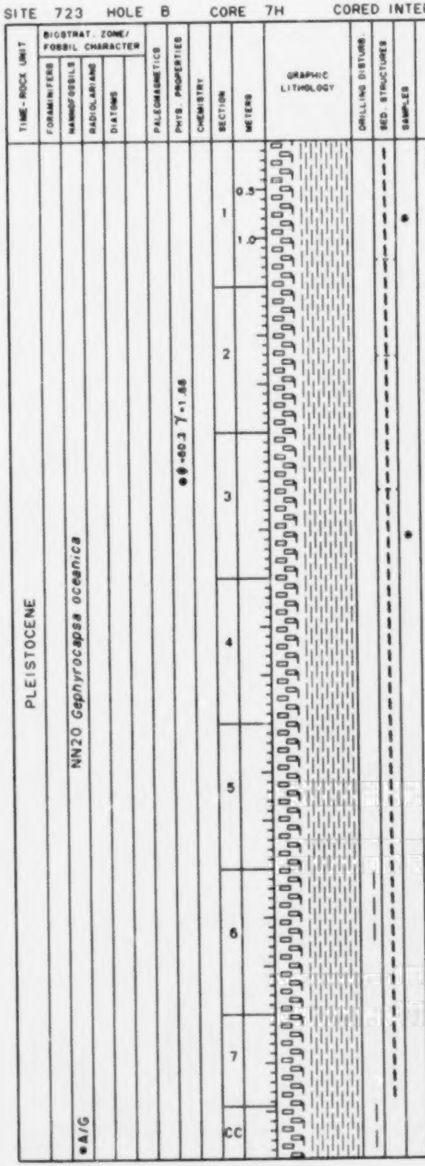
TIME-ROCK UNIT
BIOSTRAT. ZONE/ FOSSIL CHARACTER
FORAMINIFERS
NANNOFOSSILS
RADIOLARIANS
DIATOMS
PALEOMAGNETICS
PHYS. PROPERTIES
CHEMISTRY
SECTION
METERS
GRAPHIC LITHOLOGY
DRILLING DISTURB.
SED. STRUCTURES
SAMPLES
PLEISTOCENE
NN20 Gephyrocapsa oceanica
●A/G
●Φ=60.3 γ=1.88
0.5
1.0
1
2
3
4
5
6
7
CC

LITHOLOGIC DESCRIPTION

FORAMINIFER-BEARING MARLY NANNOFOSSIL OOZE and CALCAREOUS CLAYEY SILT

Entire core slightly disturbed by gas expansion. Numerous small voids. Sediment appears continuous across voids.

Major lithologies: FORAMINIFER-BEARING MARLY NANNOFOSSIL OOZE and CALCAREOUS CLAYEY SILT, olive gray (5Y 4/2, 4/3, 5/3) and dark olive gray (5Y 3/2), mottled. Foraminifers common on core face. Variable terrigenous component dominated by clay and silt-sized detrital calcite.

SMEAR SLIDE SUMMARY (%):

	1, 80 D	3, 108 D
TEXTURE:		
Sand	10	
Silt	30	25
Clay	60	75
COMPOSITION:		
Access. minerals	5	5
Clay	17	7
Dolomite	Tr	Tr
Foraminifers	10	3
Inorganic calcite	10	15
Mica	Tr	
Nannofossils	50	65
Organic debris	3	
Quartz	5	5

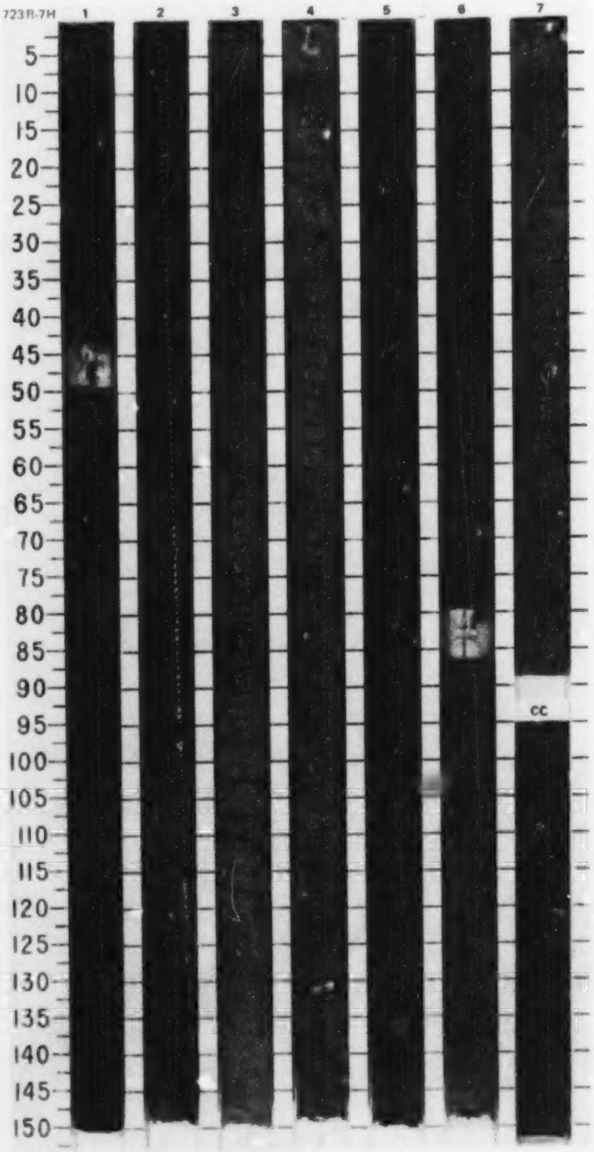
723B-7H
1
2
3
4
5
6
7
CC
5
10
15
20
25
30
35
40
45
50
55
60
65
70
75
80
85
90
95
100
105
110
115
120
125
130
135
140
145
150

SITE 723 HOLE B CORE 8H CORED INTERVAL 868.5-878.1 mbsl; 62.3-71.9 mbsf

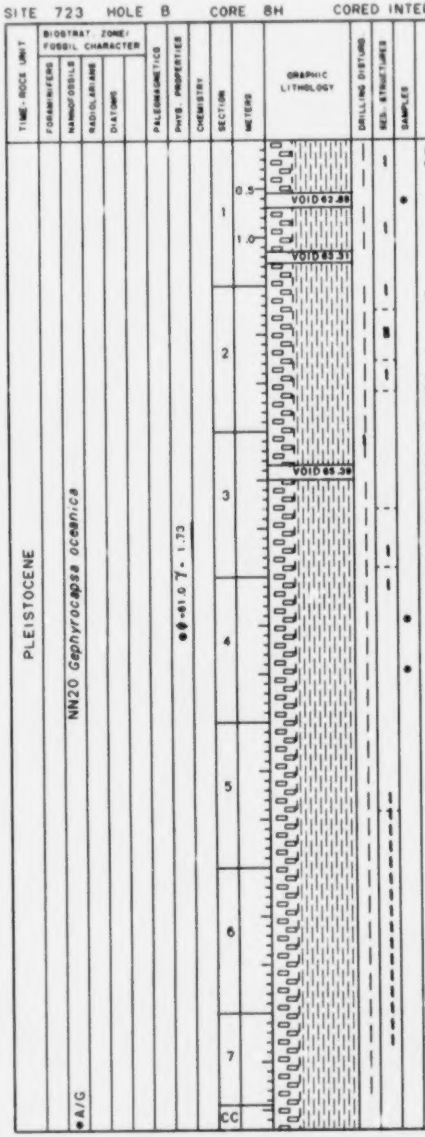
TIME-ROCK UNIT
BIOSTRAT. ZONE/ FOSSIL CHARACTER
FORAMINIFERS
NANNOFOSSILS
RADIOLARIANS
DIATOMS
PALEOMAGNETICS
PHYS. PROPERTIES
CHEMISTRY
SECTION
METERS
GRAPHIC LITHOLOGY
DRILLING DISTURB.
SED. STRUCTURES
SAMPLES
PLEISTOCENE
NN20 Gephyrocapsa oceanica
●A/G
●ϕ=61.0 γ=1.73
1
2
3
4
5
6
7
CC
0.5
1.0
VOID 62.88
VOID 63.31
VOID 65.39

LITHOLOGIC DESCRIPTION

FORAMINIFER-BEARING MARLY NANNOFOSSIL OOZE and CALCAREOUS CLAYEY SILT

Section 3, 0-17 cm, heavily disturbed, remainder slightly disturbed by gas expansion. Numerous small voids. Large (10 cm) voids appear. Sediment appears continuous across voids.

Major lithologies: FORAMINIFER-BEARING MARLY NANNOFOSSIL OOZE and CALCAREOUS CLAYEY SILT, olive gray (5Y 4/2, 4/3) and dark olive gray (5Y 3/2, 3/1), mottled. Foraminifers present on core face. Variable terrigenous component dominated by clay and silt-sized detrital calcite.

SMEAR SLIDE SUMMARY (%):

	2, 62 D	4, 42 M	4, 98 D
TEXTURE:			
Sand		5	
Silt	40	75	55
Clay	60	20	45
COMPOSITION:			
Access. minerals	10	15	10
Clay	48	5	10
Dolomite	Tr	Tr	Tr
Foraminifers	2	5	10
Inorganic calcite	20	30	25
Mica		5	
Nannofossils	10	15	35
Organic debris	Tr		
Quartz	10	20	10
Rock fragments		5	
Sponge spicules			Tr

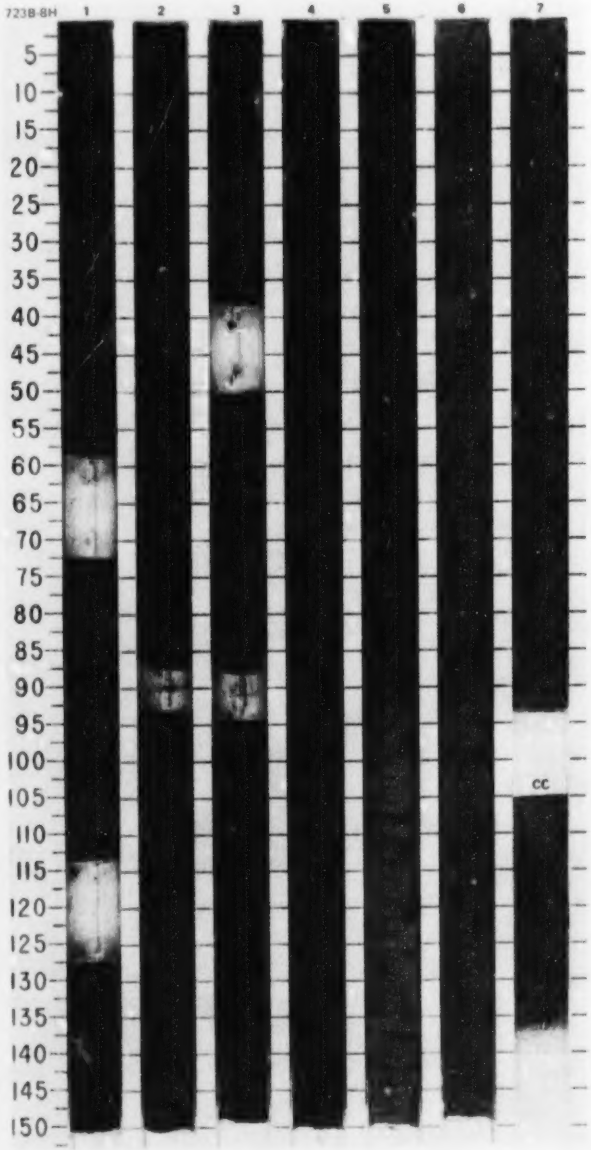
723B-8H
1
2
3
4
5
6
7
CC
5
10
15
20
25
30
35
40
45
50
55
60
65
70
75
80
85
90
95
100
105
110
115
120
125
130
135
140
145
150

SITE 723 HOLE B CORE 9H CORED INTERVAL 878.1-887.8 mbsl; 71.9-81.6 mbsf

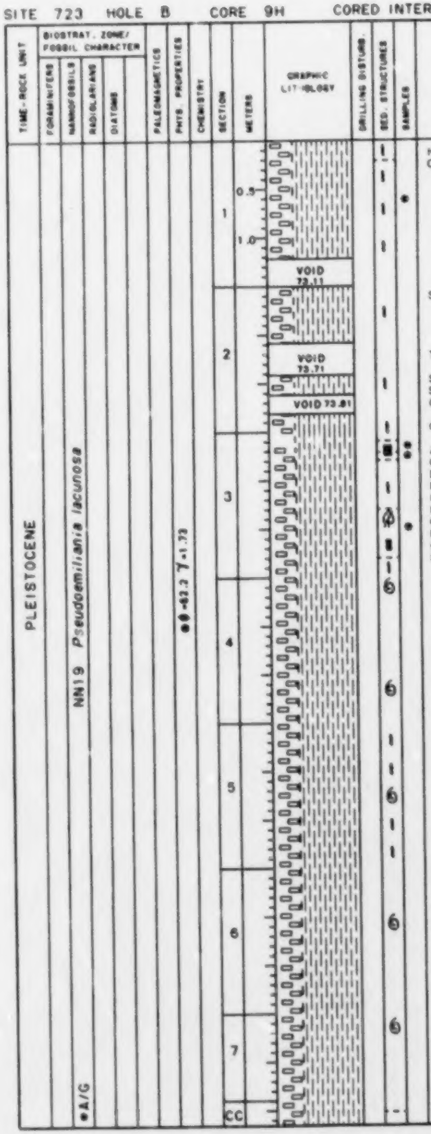
TIME-ROCK UNIT
BIOSTRAT. ZONE/ FOSSIL CHARACTER
FORAMINIFERS
NANNOFOSSILS
RADIOLARIANS
DIATOMS
PALEOMAGNETICS
PHYS. PROPERTIES
CHEMISTRY
SECTION
METERS
GRAPHIC LITHOLOGY
DRILLING DISTURB.
SED. STRUCTURES
SAMPLES
PLEISTOCENE
NN19 Pseudoemiliania lacunosa
●A/G
●Φ-62.2 γ-1.73
1
2
3
4
5
6
7
CC
0.5
1.0
VOID 73.11
VOID 73.71
VOID 73.81

LITHOLOGIC DESCRIPTION

FORAMINIFER-BEARING MARLY NANNOFOSSIL OOZE and CALCAREOUS CLAYEY SILT

Entire core slightly disturbed by gas expansion. Numerous small voids. Sediment appears continuous across voids.

Major lithologies: FORAMINIFER-BEARING MARLY NANNOFOSSIL OOZE and CALCAREOUS CLAYEY SILT, olive gray (5Y 4/2, 4/3) and dark olive gray (5Y 3/2), mottled. Foraminifers common on core face, also abundant shell fragments. Variable terrigenous component dominated by clay and silt-sized detrital calcite. Winnowed or turbidite(?) layer, top of Section 3.

SMEAR SLIDE SUMMARY (%):

	1, 60 D	3, 14 M	3, 23 M	3, 90 D
TEXTURE:				
Sand		5	15	
Silt	45	70	45	60
Clay	55	25	40	40
COMPOSITION:				
Access. minerals	5	10	5	9
Clay	5	10	10	22
Dolomite		2		2
Foraminifers	10	5	20	9
Inorganic calcite	25	38	20	28
Nannofossils	40	15	30	9
Organic debris	Tr			5
Pyrite	5			
Quartz	10	20	15	14
Sponge spicules	Tr	Tr		

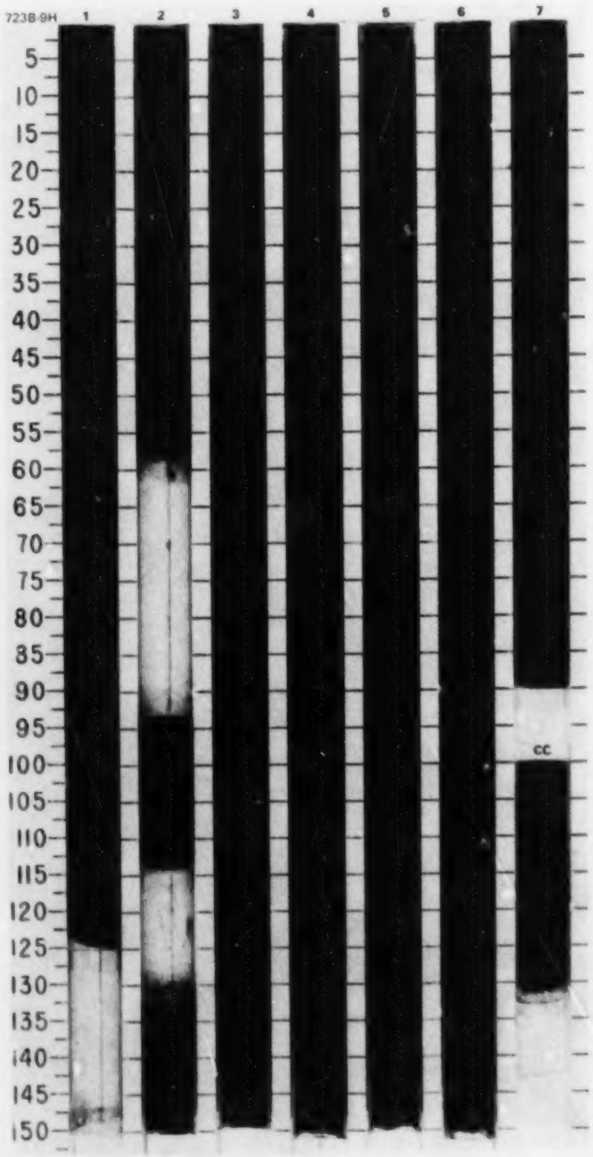
723B-9H
1
2
3
4
5
6
7
CC
5
10
15
20
25
30
35
40
45
50
55
60
65
70
75
80
85
90
95
100
105
110
115
120
125
130
135
140
145
150

SITE 723 HOLE B CORE 10X CORED INTERVAL 887.8-897.4 mbsl; 81.6-91.2 mbsf

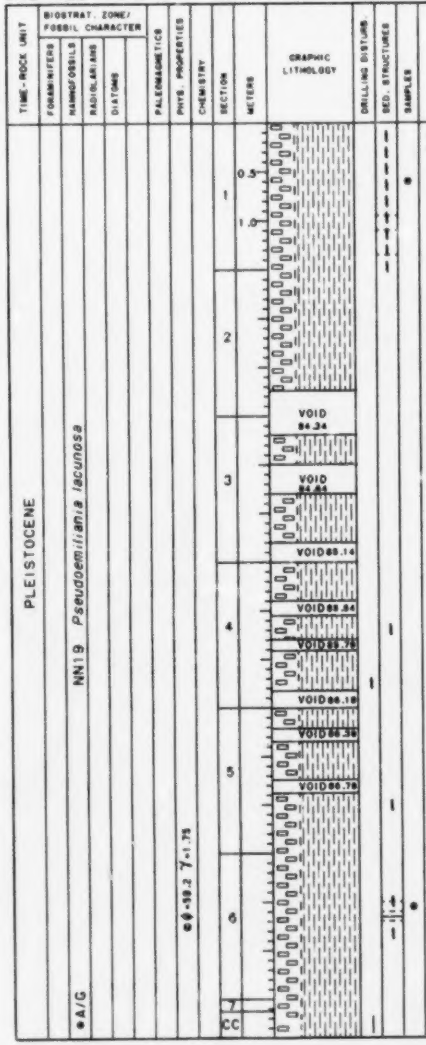
TIME-ROCK UNIT
BIOSTRAT. ZONE/ FOSSIL CHARACTER
FORAMINIFERS
NANNOFOSSILS
RADIOLARIANS
DIATOMS
PALEOMAGNETICS
PHYS. PROPERTIES
CHEMISTRY
SECTION
METERS
GRAPHIC LITHOLOGY
DRILLING DISTURB.
SED. STRUCTURES
SAMPLES
PLEISTOCENE
NN19 Pseudoemiliania lacunosa
●A/G
●ϕ-59.2 γ-1.75
1
2
3
4
5
6
7
CC
0.5
1.0
VOID 84.34
VOID 84.84
VOID 85.14
VOID 85.84
VOID 85.76
VOID 86.18
VOID 86.36
VOID 86.78

LITHOLOGIC DESCRIPTION

FORAMINIFER-BEARING MARLY NANNOFOSSIL OOZE and CALCAREOUS CLAYEY SILT

Entire core slightly disturbed by gas expansion. Numerous small voids. Sediment appears continuous across voids.

Major lithologies: FORAMINIFER-BEARING MARLY NANNOFOSSIL OOZE and CALCAREOUS CLAYEY SILT, olive gray (5Y 4/2, 4/3) and dark olive gray (5Y 3/2, 3/1), mottled. Foraminifers common on core face. Variable terrigenous component dominated by clay and silt-sized detrital calcite.

SMEAR SLIDE SUMMARY (%):

	2, 60 D	6, 55 M
TEXTURE:		
Sand	0	5
Silt	25	45
Clay	75	50
COMPOSITION:		
Access. minerals	2	10
Clay	20	14
Dolomite		1
Foraminifers	3	15
Inorganic calcite	20	15
Nannofossils	50	35
Quartz	5	10
Sponge spicules		Tr

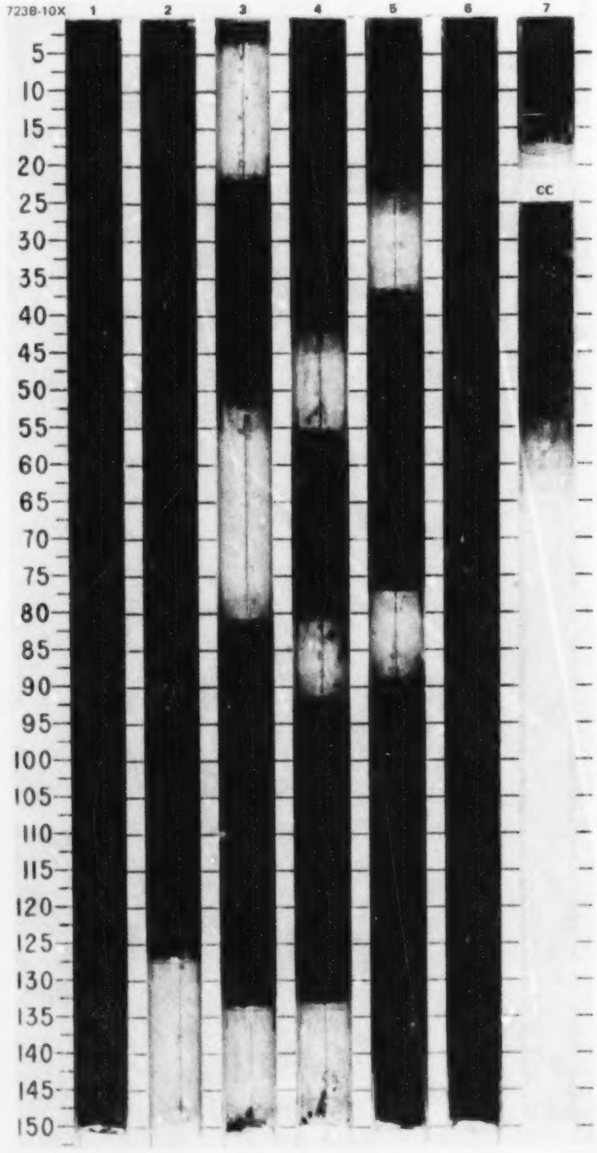
723B-10X
1
2
3
4
5
6
7
CC
5
10
15
20
25
30
35
40
45
50
55
60
65
70
75
80
85
90
95
100
105
110
115
120
125
130
135
140
145
150

SITE 723 HOLE B CORE 11X CORED INTERVAL 897.4-906.9 mbsl; 91.2-100.7 mbsf

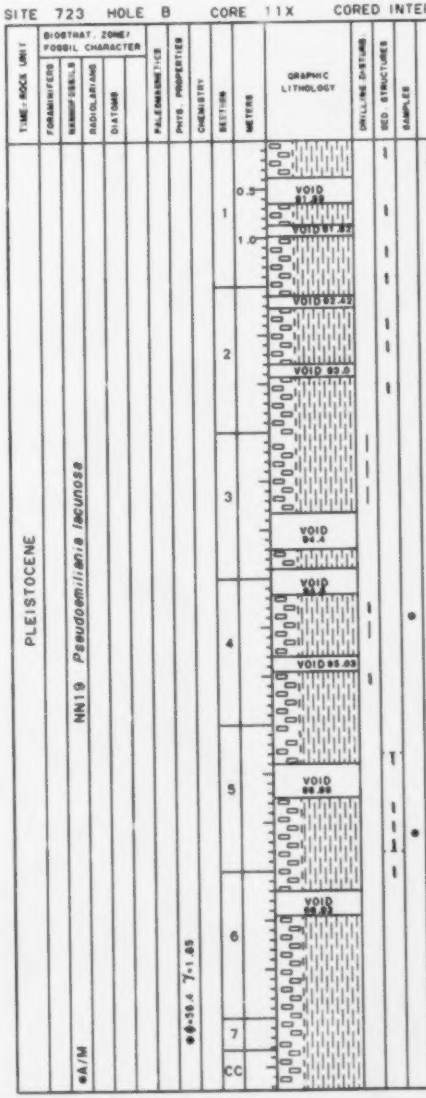
TIME-ROCK UNIT
BIOSTRAT. ZONE/ FOSSIL CHARACTER
FORAMINIFERS
NANNOFOSSILS
RADIOLARIANS
DIATOMS
PALEOMAGNETICS
PHYS. PROPERTIES
CHEMISTRY
SECTION
METERS
GRAPHIC LITHOLOGY
DRILLING DISTURB.
SED. STRUCTURES
SAMPLES
PLEISTOCENE
NN19 Pseudoemiliania lacunosa
●A/M
●Φ=58.4 γ=1.85
1
2
3
4
5
6
7
CC
0.5
1.0
VOID
VOID
VOID 92.42
VOID 93.0
VOID 94.4
VOID
VOID 95.03
VOID
VOID

LITHOLOGIC DESCRIPTION

FORAMINIFER-BEARING MARLY NANNOFOSSIL OOZE and CALCAREOUS CLAYEY SILT

Entire core slightly disturbed by gas expansion, moderate disturbance adjacent to voids. Numerous voids. Sediment appears continuous across voids.

Major lithologies: FORAMINIFER-BEARING MARLY NANNOFOSSIL OOZE and CALCAREOUS CLAYEY SILT, olive gray (5Y 4/2) and dark olive gray (5Y 3/2), mottled. Foraminifers common on core face. Variable terrigenous component dominated by clay and silt-sized detrital calcite.

SMEAR SLIDE SUMMARY (%):

	4, 40 D	5, 112 D
TEXTURE:		
Silt	40	60
Clay	60	40
COMPOSITION:		
Clay	40	30
Dolomite	Tr	
Foraminifers	10	15
Inorganic calcite	30	33
Mica		Tr
Nannofossils	15	12
Organic debris	Tr	3
Quartz	5	7

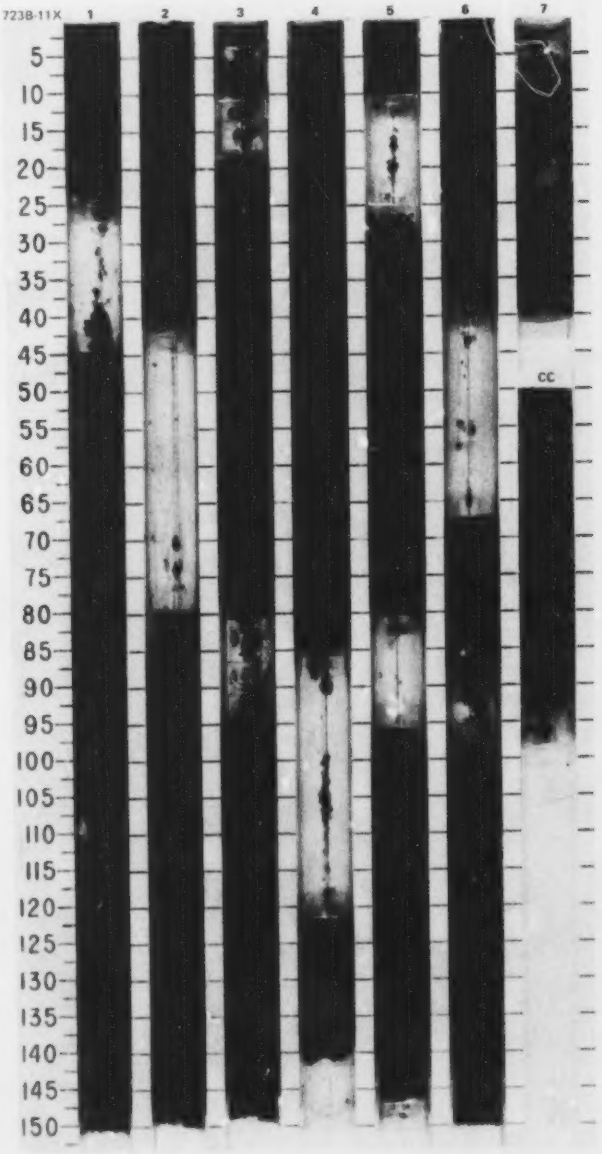
723B-11X
1
2
3
4
5
6
7
CC
5
10
15
20
25
30
35
40
45
50
55
60
65
70
75
80
85
90
95
100
105
110
115
120
125
130
135
140
145
150

SITE 723 HOLE B CORE 12X CORED INTERVAL 906.9-916.5 mbsl; 100.7-110.3 mbsf

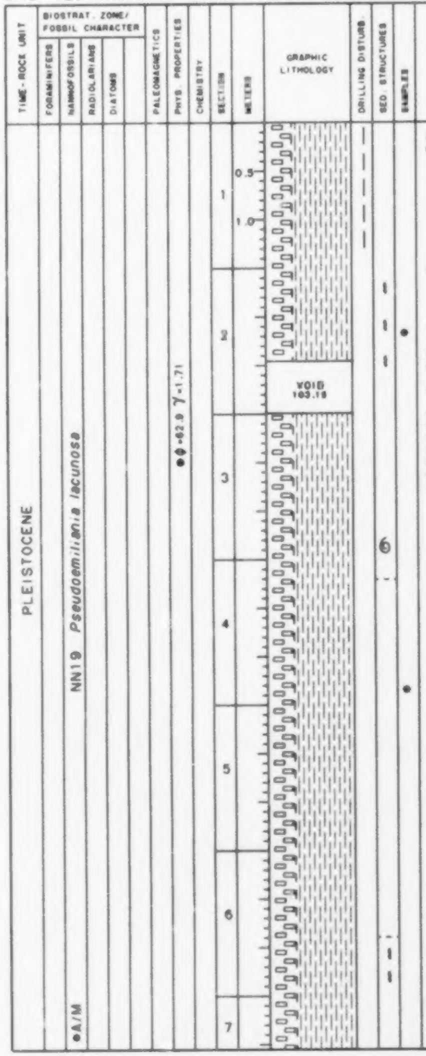
TIME-ROCK UNIT
BIOSTRAT. ZONE/ FOSSIL CHARACTER
FORAMINIFERS
NANNOFOSSILS
RADIOLARIANS
DIATOMS
PALEOMAGNETICS
PHYS. PROPERTIES
CHEMISTRY
SECTION
METERS
GRAPHIC LITHOLOGY
DRILLING DISTURB.
SED. STRUCTURES
SAMPLES
PLEISTOCENE
NN19 Pseudoemiliania lacunosa
•A/M
●Φ=62.9 γ=1.71
0.5
1.0
1
2
3
4
5
6
7
VOID 103.19

LITHOLOGIC DESCRIPTION

FORAMINIFER-BEARING MARLY NANNOFOSSIL OOZE and CALCAREOUS CLAYEY SILT

Entire core slightly disturbed by gas expansion. Numerous voids. Sediment appears continuous across voids.

Major lithologies: FORAMINIFER-BEARING MARLY NANNOFOSSIL OOZE and CALCAREOUS CLAYEY SILT, olive gray (5Y 4/2) and dark olive gray (5Y 3/2, 3/1), mottled. Foraminifers common on core face. Variable terrigenous component dominated by clay and silt sized detrital calcite.

SMEAR SLIDE SUMMARY (%):

	2, 68 D	4, 132 D
TEXTURE:		
Silt	30	40
Clay	70	60
COMPOSITION:		
Clay	20	30
Foraminifers	5	10
Gypsum	Tr	
Inorganic calcite	25	25
Nannofossils	45	30
Quartz	5	5
Sponge spicules		Tr

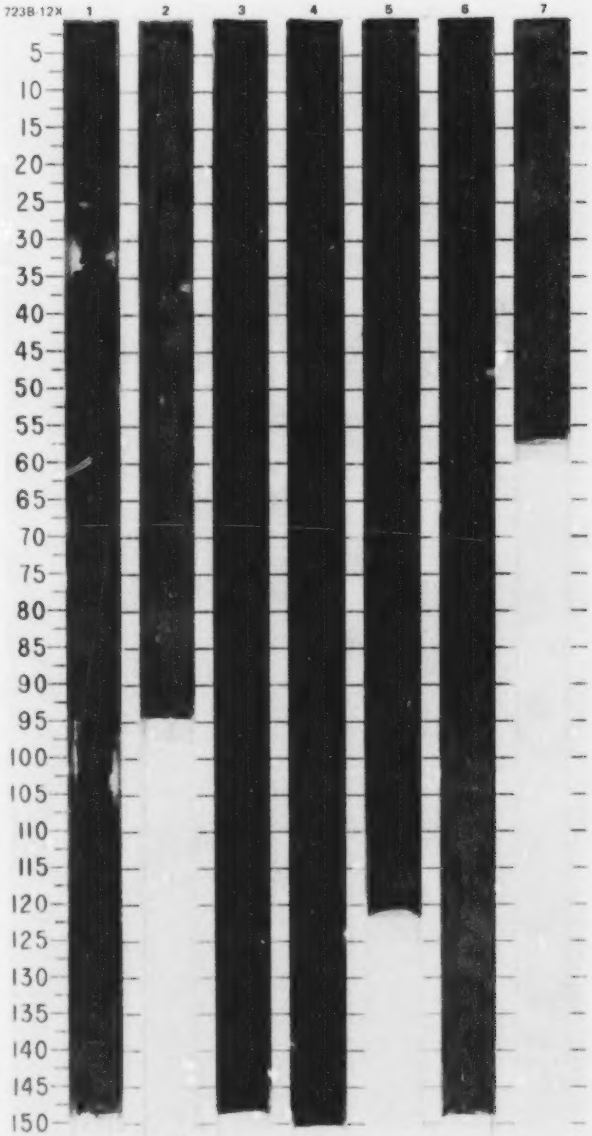
723B-12X
1
2
3
4
5
6
7
5
10
15
20
25
30
35
40
45
50
55
60
65
70
75
80
85
90
95
100
105
110
115
120
125
130
135
140
145
150

SITE 723 HOLE B CORE 13X CORED INTERVAL 916.5-926.5 mbsl; 110.3-119.9 mbsf

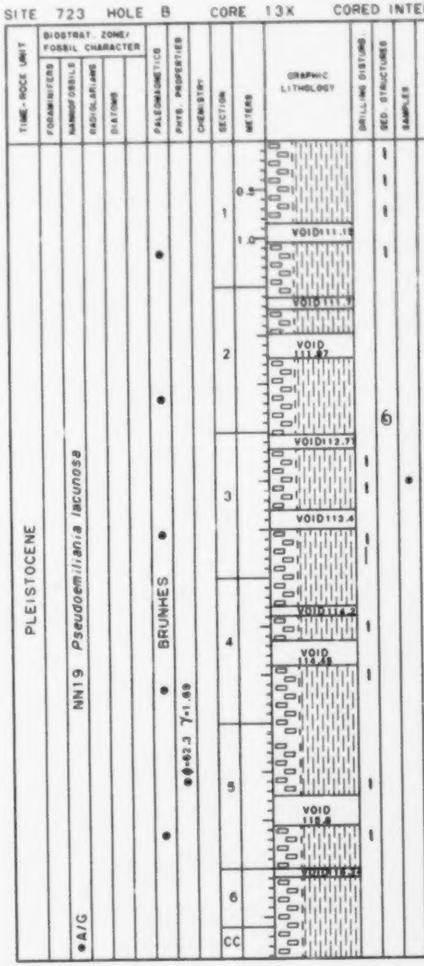

TIME-ROCK UNIT
BIOSTRAT. ZONE/ FOSSIL CHARACTER
FORAMINIFERS
NANNOFOSSILS
RADIOLARIANS
DIATOMS
PALEOMAGNETICS
PHYS. PROPERTIES
CHEMISTRY
SECTION
METERS
GRAPHIC LITHOLOGY
DRILLING DISTURB.
SED. STRUCTURES
SAMPLES
PLEISTOCENE
NN19 *Pseudoemiliania lacunosa*
●A/G
BRUNHES
●φ=62.3 γ=1.69
1
2
3
4
5
6
CC
0.5
1.0
VOID 111.1
VOID 111.7
VOID 111.87
VOID 112.7
VOID 113.4
VOID 114.2
VOID 114.45
VOID 115.8

LITHOLOGIC DESCRIPTION

FORAMINIFER-BEARING MARLY NANNOFOSSIL OOZE and CALCAREOUS CLAYEY SILT

Section 3 is moderately disturbed; remainder is slightly disturbed by gas expansion. Numerous voids. Sediment appears continuous across voids.

Major lithologies: FORAMINIFER-BEARING MARLY NANNOFOSSIL OOZE and CALCAREOUS CLAYEY SILT, olive gray (5Y 4/2), faintly mottled, with only minor variations in color; foraminifers abundant, also shell fragments on core face. Variable terrigenous component dominated by clay and silt-sized detrital calcite.

SMEAR SLIDE SUMMARY (%):

	3, 51 D
TEXTURE:	
Silt	30
Clay	70
COMPOSITION:	
Clay	15
Foraminifers	5
Inorganic calcite	25
Nannofossils	50
Quartz	5

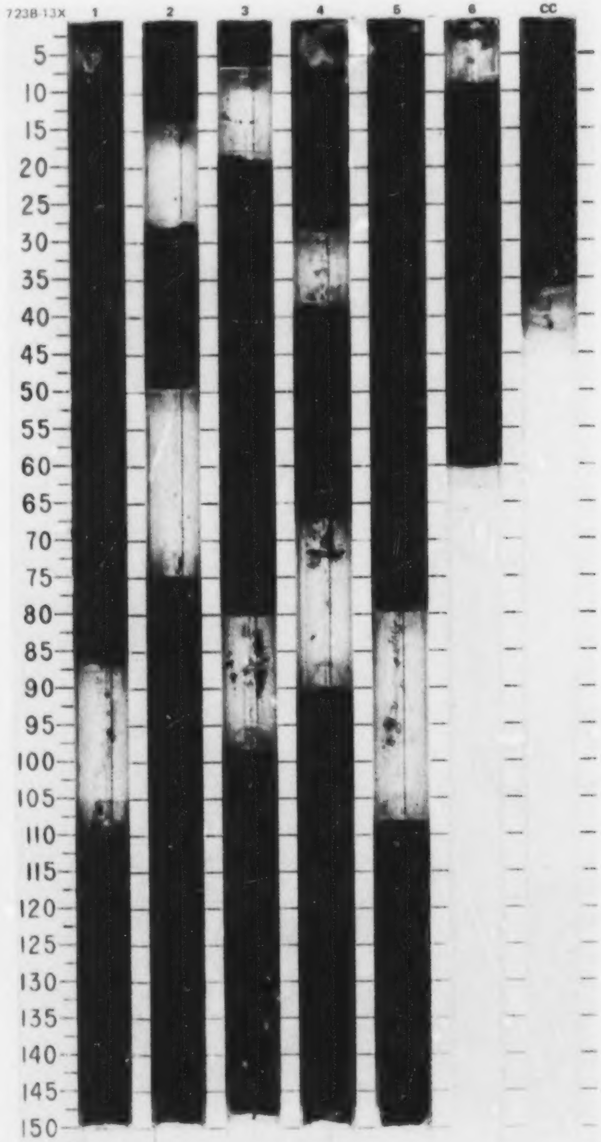

723B-13X
1
2
3
4
5
6
CC
5
10
15
20
25
30
35
40
45
50
55
60
65
70
75
80
85
90
95
100
105
110
115
120
125
130
135
140
145
150

SITE 723 HOLE B CORE 14X CORED INTERVAL 926.1-935.8 mbsl; 119.9-129.6 mbsf

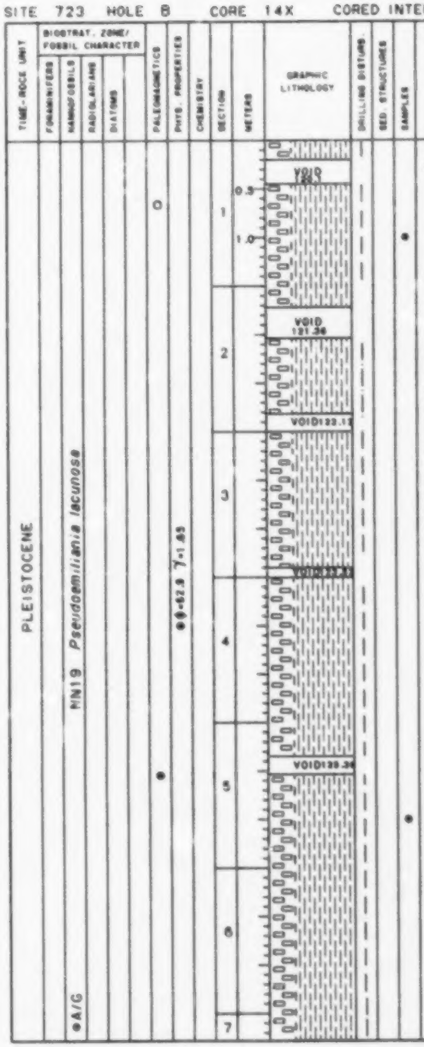
TIME-ROCK UNIT
BIOSTRAT. ZONE/ FOSSIL CHARACTER
FORAMINIFERS
NANNOFOSSILS
RADIOLARIANS
DIATOMS
PALEOMAGNETICS
PHYS. PROPERTIES
CHEMISTRY
SECTION
METERS
GRAPHIC LITHOLOGY
DRILLING DISTURB.
SED. STRUCTURES
SAMPLES
PLEISTOCENE
NN19 Pseudoemiliania lacunosa
●A/G
●φ=62.9 γ=1.93
0.5
1.0
1
2
3
4
5
6
7
VOID
VOID 121.36

LITHOLOGIC DESCRIPTION

FORAMINIFER-BEARING MARLY NANNOFOSSIL OOZE AND CALCAREOUS CLAYEY SILT

Section 2 is moderately disturbed; remainder is slightly disturbed by gas expansion. Numerous voids. Sediment appears continuous across voids. Core surface often separates into 1-mm-thick flakes raised up by splitting wire.

Major lithologies: FORAMINIFER-BEARING MARLY NANNOFOSSIL OOZE and CALCAREOUS CLAYEY SILT, olive gray (5Y 4/3), mottled. Foraminifers present on core face. Variable terrigenous component dominated by clay and silt-sized detrital calcite.

SMEAR SLIDE SUMMARY (%):

	1, 100 D	5, 100 D
TEXTURE:		
Silt	60	50
Clay	40	50
COMPOSITION:		
Access. minerals	5	3
Clay	15	15
Dolomite	Tr	3
Feldspar		Tr
Foraminifers	5	15
Inorganic calcite	30	15
Mica	Tr	
Nannofossils	30	35
Organic debris		9
Quartz	15	7

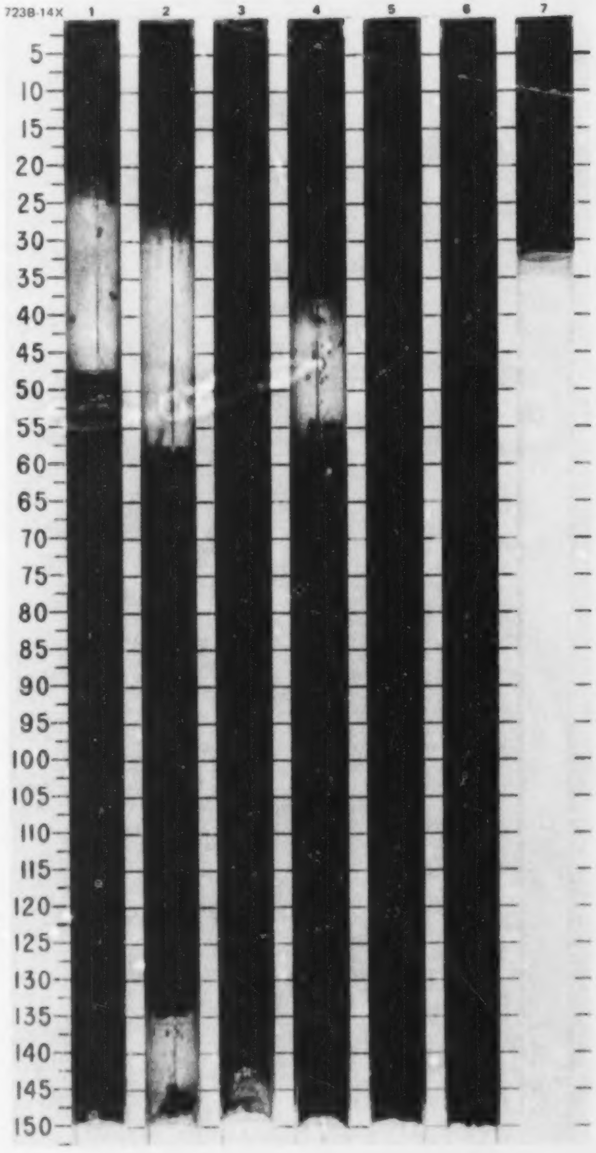
723B-14X
1
2
3
4
5
6
7
5
10
15
20
25
30
35
40
45
50
55
60
65
70
75
80
85
90
95
100
105
110
115
120
125
130
135
140
145
150

SITE 723 HOLE B CORE 15X CORED INTERVAL 935.8-945.4 mbsl; 129.6-139.2 mbsf

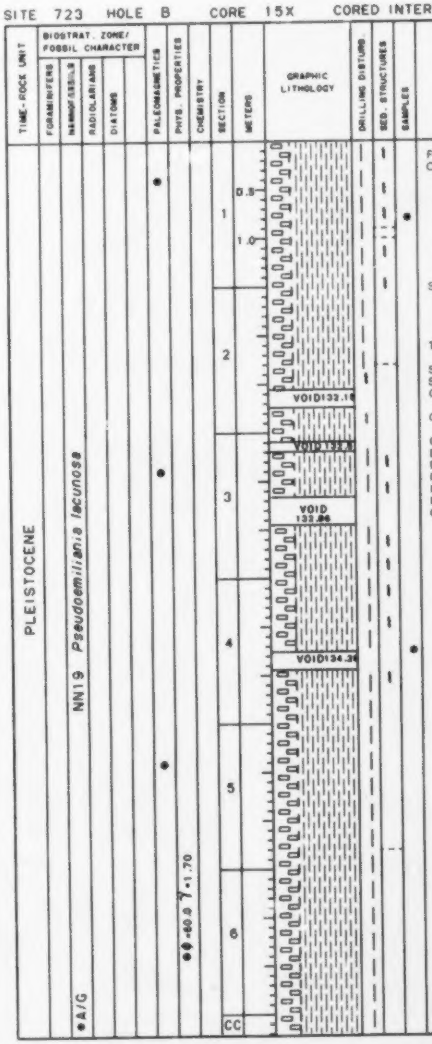
TIME-ROCK UNIT
BIOSTRAT. ZONE/ FOSSIL CHARACTER
FORAMINIFERS
NANNOFOSSILS
RADIOLARIANS
DIATOMS
PALEOMAGNETICS
PHYS. PROPERTIES
CHEMISTRY
SECTION
METERS
GRAPHIC LITHOLOGY
DRILLING DISTURB.
SED. STRUCTURES
SAMPLES
PLEISTOCENE
NN19 Pseudoemiliania lacunosa
●A/G
●ϕ=60.0 γ=1.70
1
2
3
4
5
6
CC
0.5
1.0
VOID132.1
VOID 132.86
VOID134.3

LITHOLOGIC DESCRIPTION

FORAMINIFER-BEARING MARLY NANNOFOSSIL OOZE AND CALCAREOUS CLAYEY SILT

Entire core slightly disturbed by gas expansion. Numerous voids. Sediment appears continuous across voids.

Major lithologies: FORAMINIFER-BEARING MARLY NANNOFOSSIL OOZE and CALCAREOUS CLAYEY SILT, olive gray (5Y 4/2, 4/3) and dark olive gray (5Y 3/2), faintly mottled. Foraminifers less common on core face. Variable terrigenous component dominated by clay and silt-sized detrital calcite.

SMEAR SLIDE SUMMARY (%):

	1, 78 D	4, 78 D
TEXTURE:		
Sand	10	20
Silt	30	20
Clay	60	60
COMPOSITION:		
Clay	10	20
Diatoms	Tr	Tr
Dolomite	Tr	
Foraminifers	10	10
Inorganic calcite	10	20
Nannofossils	65	45
Quartz	5	5

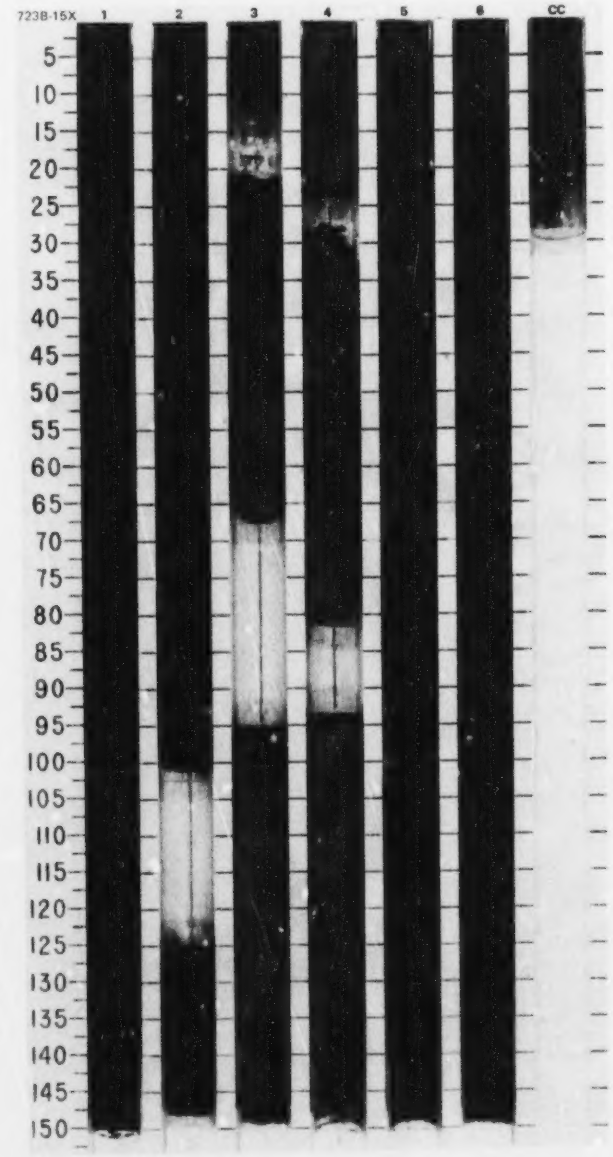
723B-15X
1
2
3
4
5
6
CC
5
10
15
20
25
30
35
40
45
50
55
60
65
70
75
80
85
90
95
100
105
110
115
120
125
130
135
140
145
150

SITE 723 HOLE B CORE 16X CORED INTERVAL 945.4-955.1 mbsl; 139.2-148.9 mbsf

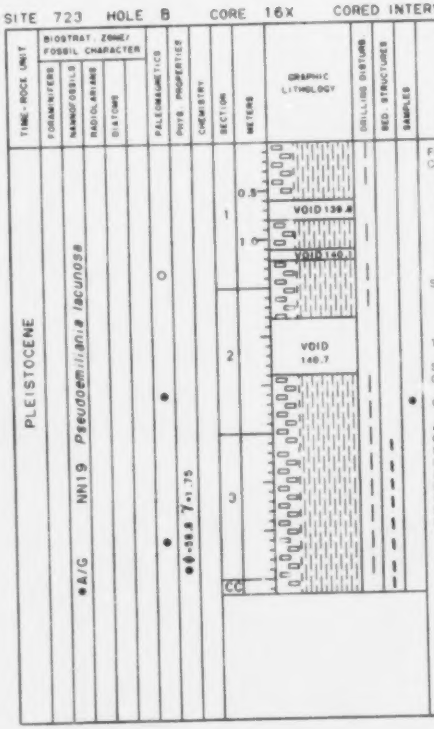
TIME-ROCK UNIT
BIOSTRAT. ZONE/ FOSSIL CHARACTER
FORAMINIFERS
NANNOFOSSILS
RADIOLARIANS
DIATOMS
PALEOMAGNETICS
PHYS. PROPERTIES
CHEMISTRY
SECTION
METERS
GRAPHIC LITHOLOGY
DRILLING DISTURB.
SED. STRUCTURES
SAMPLES
PLEISTOCENE
●A/G NN19 Pseudoemiliania lacunosa
○
●
●
●φ-58.8 γ-1.75
1
2
3
CC
0.5
1.0
VOID 139.8
VOID 140.1
VOID 140.7

LITHOLOGIC DESCRIPTION

FORAMINIFER BEARING MARLY NANNOFOSSIL OOZE and CALCAREOUS CLAYEY SILT

Entire core slightly disturbed by gas expansion. Numerous voids. Sediment appears continuous across voids.

Major lithologies: FORAMINIFER BEARING MARLY NANNOFOSSIL OOZE and CALCAREOUS CLAYEY SILT, olive gray (5Y 4/2), faintly mottled. Foraminifers less common on core face. Variable terrigenous component dominated by clay and silt sized detrital calcite.

SMEAR SLIDE SUMMARY (%):

	2, 80 D	2, 120 D
TEXTURE:		
Silt	25	60
Clay	75	40
COMPOSITION:		
Access. minerals	2	5
Clay	20	25
Dolomite		2
Feldspar		1
Foraminifers	3	7
Inorganic calcite	20	30
Nannofossils	50	15
Pyrite		5
Quartz	5	10

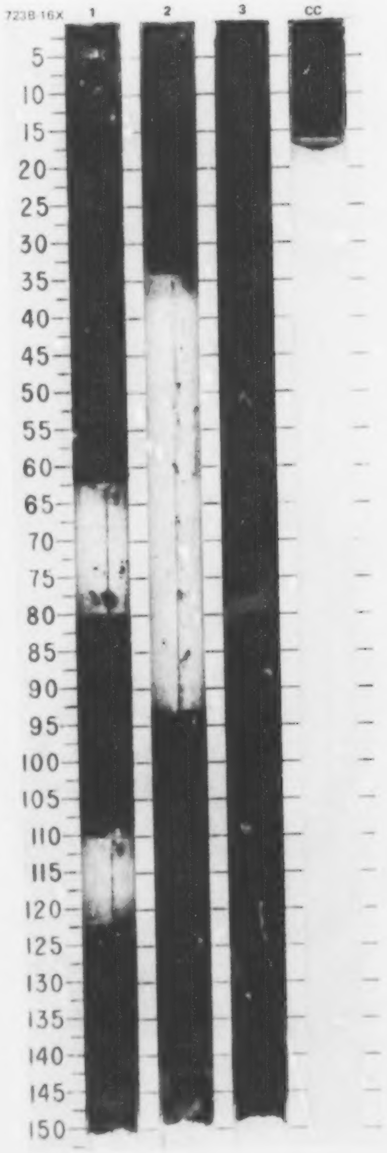
723B-16X
1
2
3
CC
5
10
15
20
25
30
35
40
45
50
55
60
65
70
75
80
85
90
95
100
105
110
115
120
125
130
135
140
145
150

SITE 723 HOLE B CORE 17X CORED INTERVAL 955.1-964.8 mbsl; 148.9-158.6 mbsf

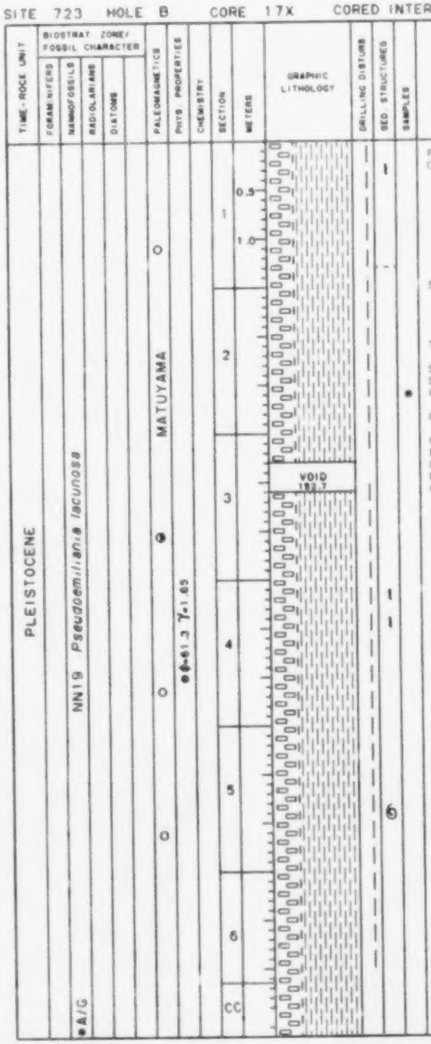
TIME-ROCK UNIT
BIOSTRAT. ZONE/ FOSSIL CHARACTER
FORAMINIFERS
NANNOFOSSILS
RADIOLARIANS
DIATOMS
PALEOMAGNETICS
PHYS. PROPERTIES
CHEMISTRY
SECTION
METERS
GRAPHIC LITHOLOGY
DRILLING DISTURB.
SED. STRUCTURES
SAMPLES
PLEISTOCENE
NN19 Pseudoemiliania lacunosa
●A/G
MATUYAMA
●φ=61.3 γ=1.65
0.5
1.0
1
2
3
4
5
6
CC
VOID 152.7

LITHOLOGIC DESCRIPTION

FORAMINIFER BEARING MARLY NANNOFOSSIL OOZE and CALCAREOUS CLAYEY SILT

Section 6, 84-116 cm, very disturbed. Entire core slightly disturbed by gas expansion. Numerous voids. Sediment appears continuous across voids.

Major lithologies: FORAMINIFER BEARING MARLY NANNOFOSSIL OOZE and CALCAREOUS CLAYEY SILT, olive gray (5Y 4/2) and dark olive gray (5Y 3/2), faintly mottled. Foraminifers less common on core face. Variable terrigenous component dominated by clay and silt-sized detrital calcite.

SMEAR SLIDE SUMMARY (%):

	2, 109 D
TEXTURE:	
Sand	15
Silt	40
Clay	45
COMPOSITION:	
Clay	20
Foraminifers	10
Inorganic calcite	10
Nannofossils	55
Quartz	5

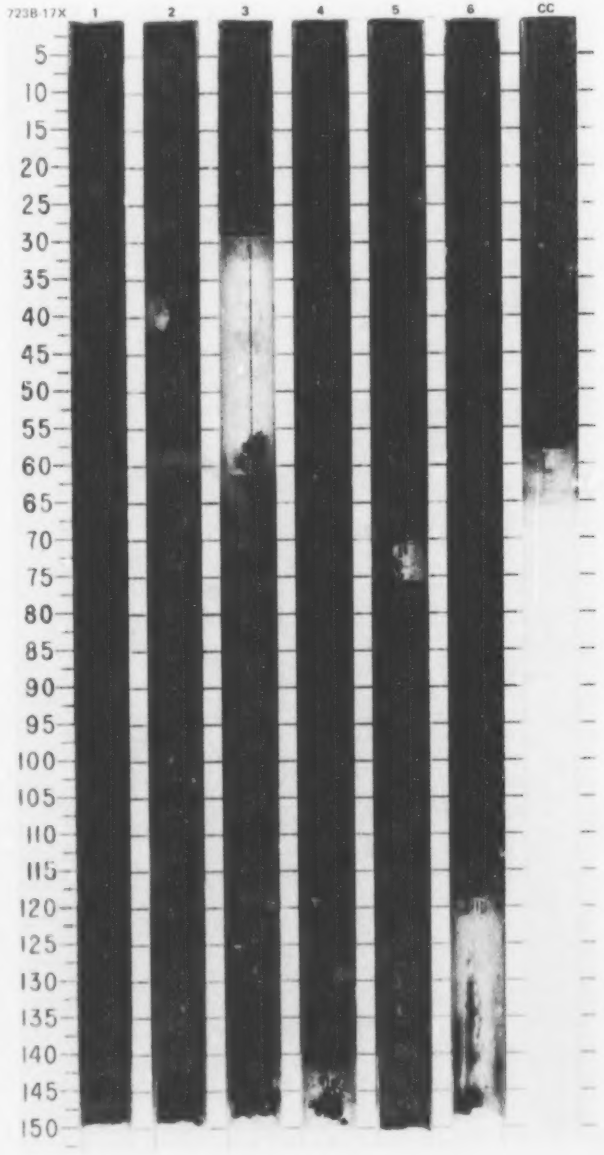
723B-17X
1
2
3
4
5
6
CC
5
10
15
20
25
30
35
40
45
50
55
60
65
70
75
80
85
90
95
100
105
110
115
120
125
130
135
140
145
150

SITE 723 HOLE B CORE 18X CORED INTERVAL 964.8-974.4 mbsl; 158.6-168.2 mbsf

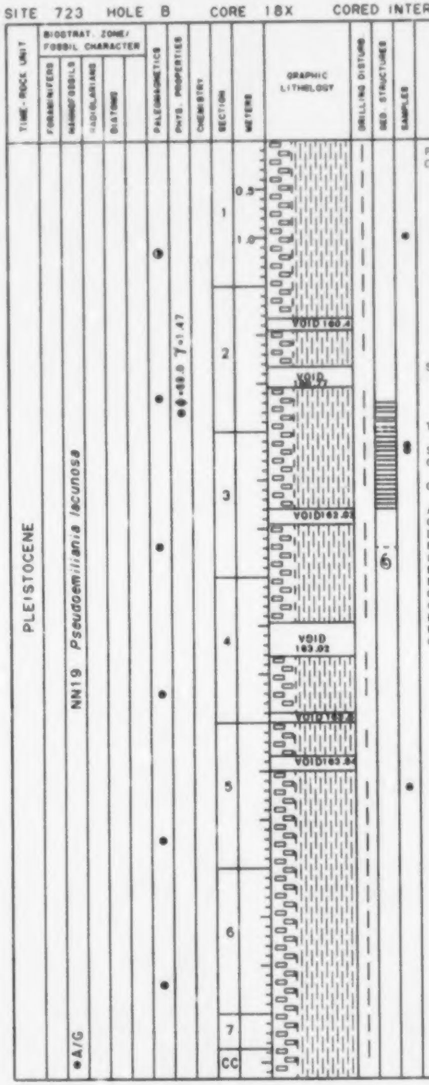
TIME-ROCK UNIT
BIOSTRAT. ZONE/ FOSSIL CHARACTER
FORAMINIFERS
NANNOFOSSILS
RADIOLARIANS
DIATOMS
PALEOMAGNETICS
PHYS. PROPERTIES
CHEMISTRY
SECTION
METERS
GRAPHIC LITHOLOGY
DRILLING DISTURB.
SED. STRUCTURES
SAMPLES
PLEISTOCENE
NN19 *Pseudoemiliania lacunosa*
●A/G
●ϕ=58.0 γ=1.47
0.5
1.0
1
2
3
4
5
6
7
CC
VOID 160.4
VOID
VOID162.02
VOID 163.02
VOID163.84

LITHOLOGIC DESCRIPTION

FORAMINIFER-BEARING MARLY NANNOFOSSIL OOZE and CALCAREOUS CLAYEY SILT

Entire core slightly disturbed by gas expansion. Numerous voids. Sediment appears continuous across voids.

Major lithologies: FORAMINIFER-BEARING MARLY NANNOFOSSIL OOZE and CALCAREOUS CLAYEY SILT, olive gray (5Y 4/2) and dark olive gray (5Y 3/2); no evidence of bioturbation. Foraminifers less common on core face. Variable terrigenous component dominated by clay and silt-sized detrital calcite.

Minor lithologies:
a. Parallel laminae, individual light and dark layers (varves?). Light layers are composed of diatom ooze, in Section 2, 120-150 cm, and Section 3, 0-70 cm. Foraminifers rare in laminated layer.
b. Dark grayish brown (2.5Y 3/2) clay layer 0.5 cm thick, altered ash layer(?), at Section 5, 70 cm.

SMEAR SLIDE SUMMARY (%):

	1, 100 D	3, 15 M	3, 16 D	5, 70 M
TEXTURE:				
Silt	30	10	10	10
Clay	70	90	90	90
COMPOSITION:				
Access. minerals			2	
Clay	25	25	20	54
Diatoms	Tr	65	60	
Foraminifers	7			3
Inorganic calcite	20	5	5	3
Mica		Tr		
Nannofossils	40		10	
Organic debris		Tr		
Other				40
Pellets	3			
Pyrite		2		
Quartz	5	3	3	

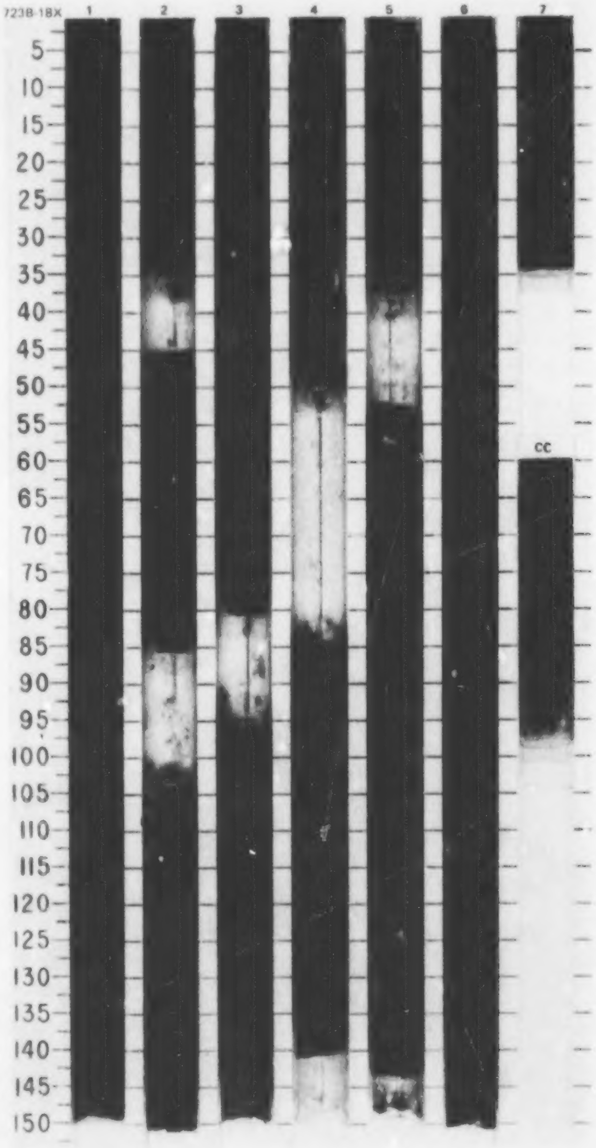
723B-18X
1
2
3
4
5
6
7
CC
5
10
15
20
25
30
35
40
45
50
55
60
65
70
75
80
85
90
95
100
105
110
115
120
125
130
135
140
145
150

SITE 723 HOLE B CORE 19X CORED INTERVAL 974.4-984.1 mbsl; 168.2-177.9 mbsf

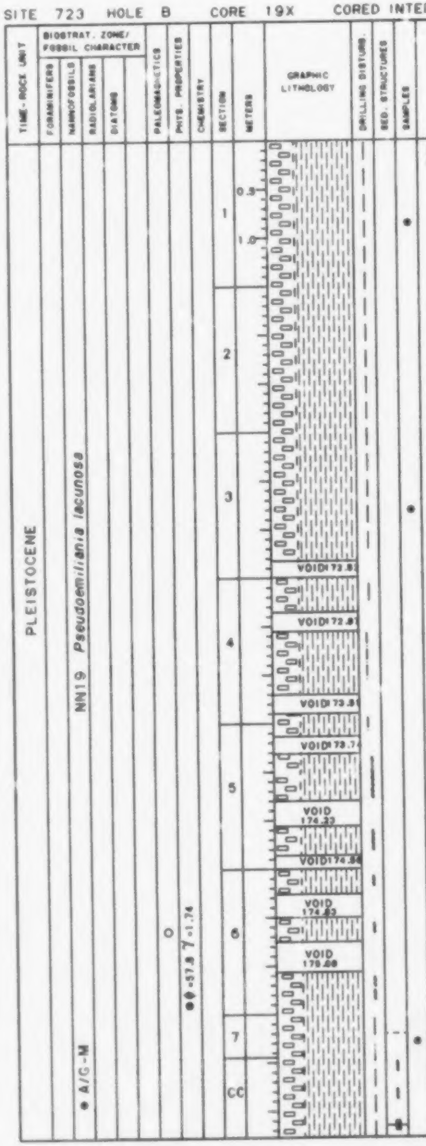
TIME-ROCK UNIT
BIOSTRAT. ZONE/ FOSSIL CHARACTER
FORAMINIFERS
NANNOFOSSILS
RADIOLARIANS
DIATOMS
PALEOMAGNETICS
PHYS. PROPERTIES
CHEMISTRY
SECTION
METERS
GRAPHIC LITHOLOGY
DRILLING DISTURB.
SED. STRUCTURES
SAMPLES
PLEISTOCENE
NN19 Pseudoemiliania lacunosa
A/G-M
○
●◆-57.8 γ-1.74
0.5
1.0
1
2
3
4
5
6
7
CC
VOID 172.8
VOID 172.8
VOID 173.8
VOID 173.7
VOID 174.23
VOID 174.5
VOID 174.83
VOID 175.08

LITHOLOGIC DESCRIPTION

FORAMINIFER-BEARING MARLY NANNOFOSSIL OOZE and CALCAREOUS CLAYEY SILT

Section 1, 0-15 cm, and Sections 5-6 are heavily disturbed, remainder slightly disturbed by gas expansion. Numerous voids, sediment begins to separate into firm clasts and crumbs. Sediment appears continuous across voids.

Major lithologies: FORAMINIFER-BEARING MARLY NANNOFOSSIL OOZE and CALCAREOUS CLAYEY SILT, olive gray (5Y 4/3, 4/2) and dark olive gray (5Y 3/2, 3/3); no evidence of bioturbation. Foraminifers less common on core face. Variable terrigenous component dominated by clay and silt-sized detrital calcite.

SMEAR SLIDE SUMMARY (%):

	1, 86 D	3, 80 D	7, 30 D
TEXTURE:			
Sand		15	20
Silt	40	25	25
Clay	60	60	55
COMPOSITION:			
Access. minerals		Tr	2
Clay	40	25	25
Diatoms	10		
Dolomite		Tr	1
Feldspar		2	1
Foraminifers		5	1
Volcanic glass		Tr	
Gypsum	Tr		
Inorganic calcite	40	20	30
Mica	3	Tr	Tr
Nannofossils		35	20
Organic debris	2		
Quartz	5	13	20
Radiolarians	Tr		
Sponge spicules	Tr	Tr	

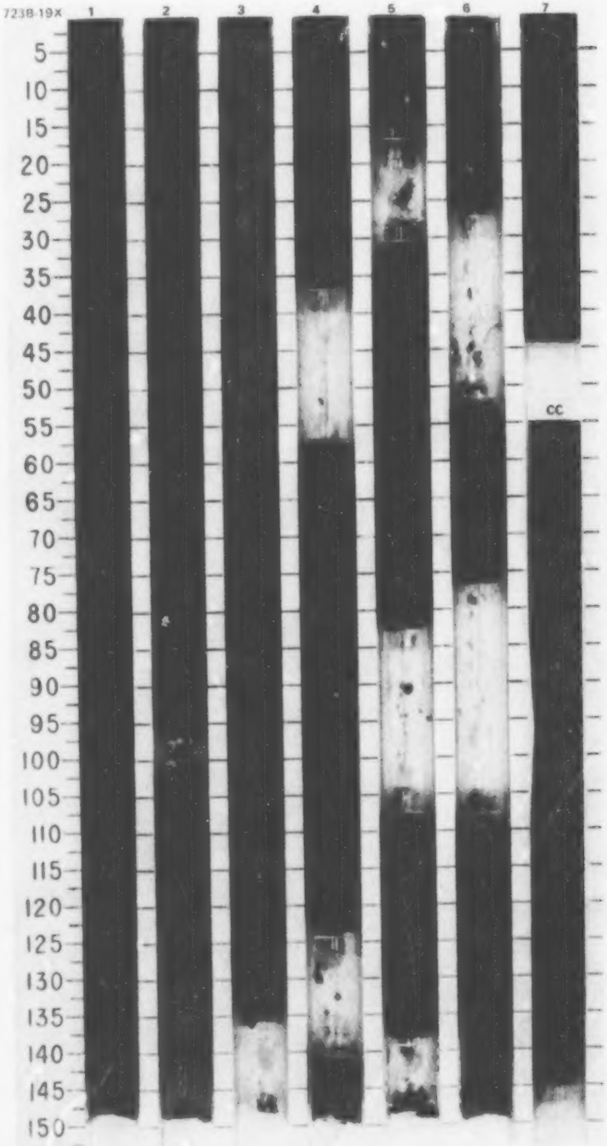
723B-19X
1
2
3
4
5
6
7
CC
5
10
15
20
25
30
35
40
45
50
55
60
65
70
75
80
85
90
95
100
105
110
115
120
125
130
135
140
145
150

SITE 723 HOLE B CORE 20X CORED INTERVAL 984.1-993.8 mbsl; 177.9-187.6 mbsf

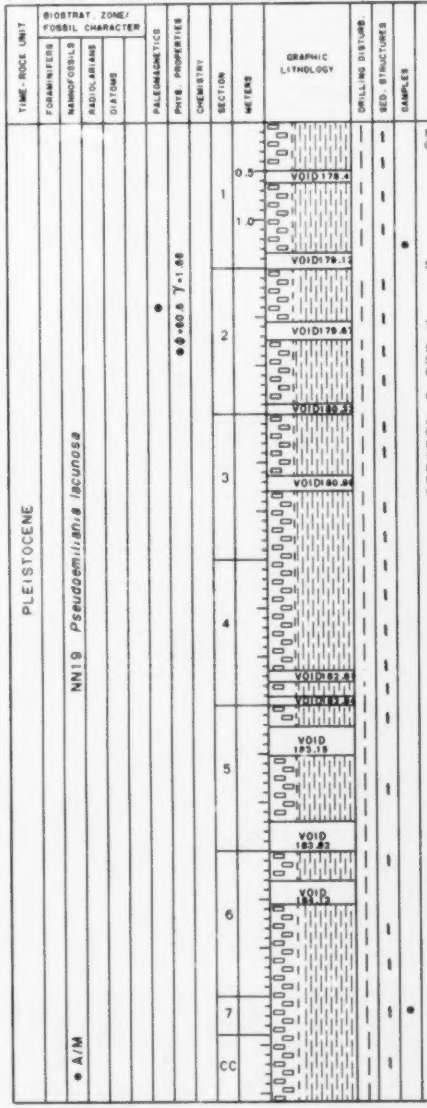
TIME-ROCK UNIT
BIOSTRAT. ZONE/ FOSSIL CHARACTER
FORAMINIFERS
NANNOFOSSILS
RADIOLARIANS
DIATOMS
PALEOMAGNETICS
PHYS. PROPERTIES
CHEMISTRY
SECTION
METERS
GRAPHIC LITHOLOGY
DRILLING DISTURB.
SED. STRUCTURES
SAMPLES
PLEISTOCENE
NN19 Pseudoemiliania lacunosa
• A/M
•ϕ-60.6 γ-1.88
1
2
3
4
5
6
7
CC
0.5
1.0
VOID 178.4
VOID 179.12
VOID 179.67
VOID 180.23
VOID 180.86
VOID 182.61
VOID 182.84
VOID 183.15
VOID 183.82
VOID 184.13

LITHOLOGIC DESCRIPTION

FORAMINIFER-BEARING MARLY NANNOFOSSIL OOZE and CALCAREOUS CLAYEY SILT

Entire core slightly disturbed by gas expansion. Numerous voids. Sediment appears continuous across voids.

Major lithologies: **FORAMINIFER-BEARING MARLY NANNOFOSSIL OOZE** and **CALCAREOUS CLAYEY SILT**, olive gray (5Y 4/2), faintly mottled. Foraminifers present on core face. Variable terrigenous component dominated by clay and silt-sized detrital calcite.

SMEAR SLIDE SUMMARY (%):

	1, 127 D	7, 15 D
TEXTURE:		
Sand	10	15
Silt	20	30
Clay	70	55
COMPOSITION:		
Access. minerals	4	Tr
Clay	20	25
Dolomite	—	Tr
Foraminifers	6	2
Inorganic calcite	10	25
Nannofossils	50	30
Quartz	10	18

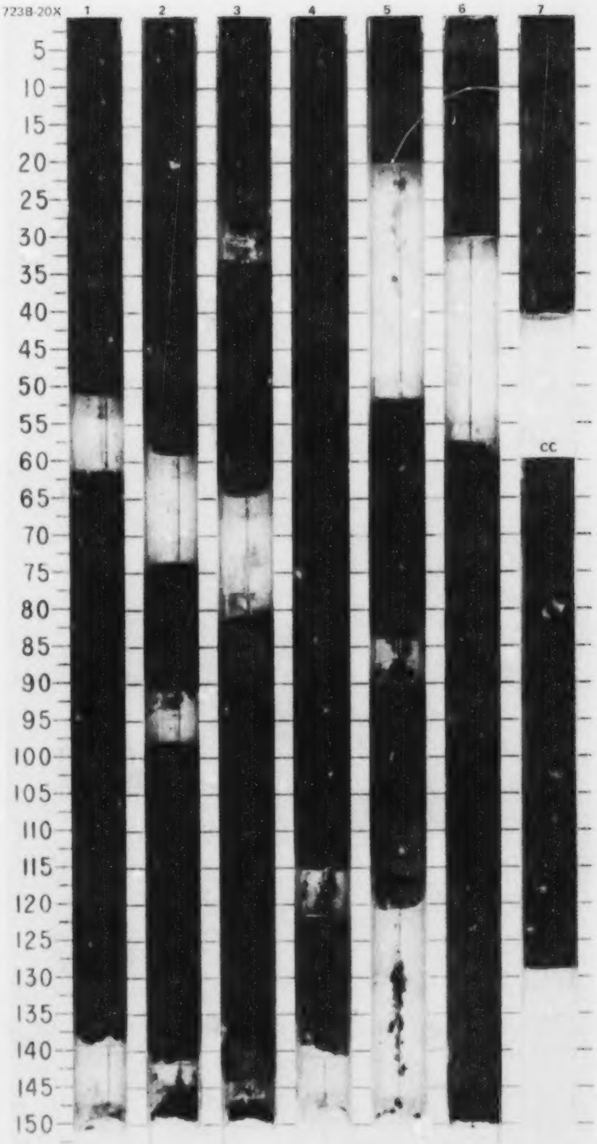
723B-20X
1
2
3
4
5
6
7
CC
5
10
15
20
25
30
35
40
45
50
55
60
65
70
75
80
85
90
95
100
105
110
115
120
125
130
135
140
145
150

SITE 723 HOLE B CORE 21X CORED INTERVAL 993.8-1003.5 mbsl; 187.6-197.3 mbsf

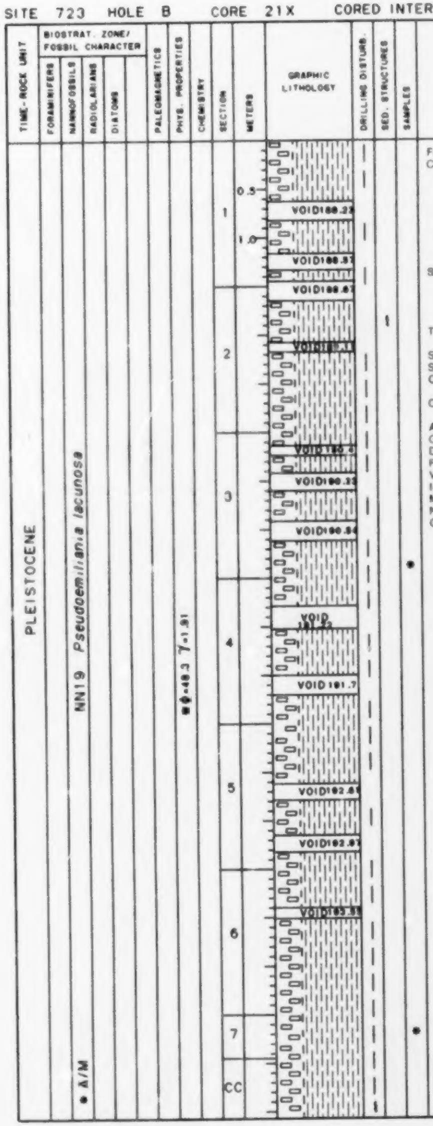
TIME-ROCK UNIT
BIOSTRAT. ZONE/ FOSSIL CHARACTER
FORAMINIFERS
NANNOFOSSILS
RADIOLARIANS
DIATOMS
PALEOMAGNETICS
PHYS. PROPERTIES
CHEMISTRY
SECTION
METERS
GRAPHIC LITHOLOGY
DRILLING DISTURB.
SED. STRUCTURES
SAMPLES
PLEISTOCENE
NN19 Pseudoemiliania lacunosa
• A/M
Φ=48.3 γ=1.91
1
2
3
4
5
6
7
CC
0.5
1.0
VOID188.23
VOID188.57
VOID188.67
VOID189.1
VOID190.0
VOID190.23
VOID190.54
VOID 191.2
VOID 191.7
VOID192.61
VOID192.97
VOID193.55

LITHOLOGIC DESCRIPTION

FORAMINIFER-BEARING MARLY NANNOFOSSIL OOZE and CALCAREOUS CLAYEY SILT

Core moderately disturbed by gas expansion. Numerous voids.

Major lithologies: FORAMINIFER-BEARING MARLY NANNOFOSSIL OOZE and CALCAREOUS CLAYEY SILT, olive gray (5Y 4/2, 4/3). Foraminifers visible on core face. Variable terrigenous component dominated by clay and silt-sized detrital calcite.

SMEAR SLIDE SUMMARY (%):

	3, 38 D	7, 19 D
TEXTURE:		
Sand	15	10
Silt	40	40
Clay	45	50
COMPOSITION:		
Access. minerals	2	3
Clay	25	25
Dolomite	1	Tr
Foraminifers	1	1
Volcanic glass		Tr
Inorganic calcite	35	30
Mica		1
Nannofossils	20	25
Quartz	15	15

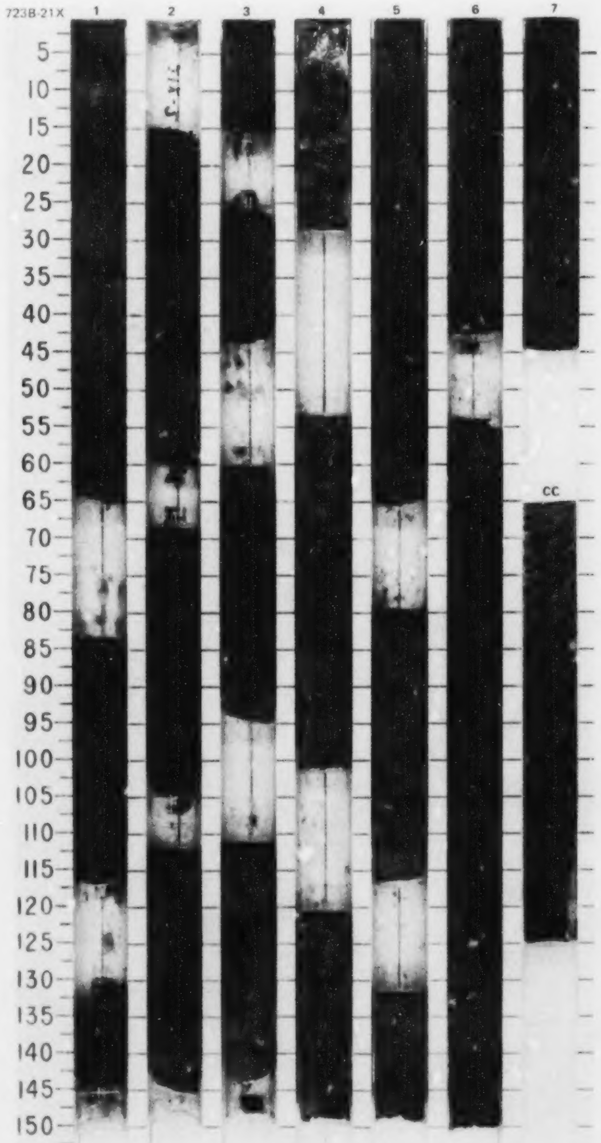
723B-21X
1
2
3
4
5
6
7
CC
5
10
15
20
25
30
35
40
45
50
55
60
65
70
75
80
85
90
95
100
105
110
115
120
125
130
135
140
145
150

SITE 723 HOLE B CORE 22X CORED INTERVAL 1003.5-1013.1 mbsl; 197.3-206.9 mbsf

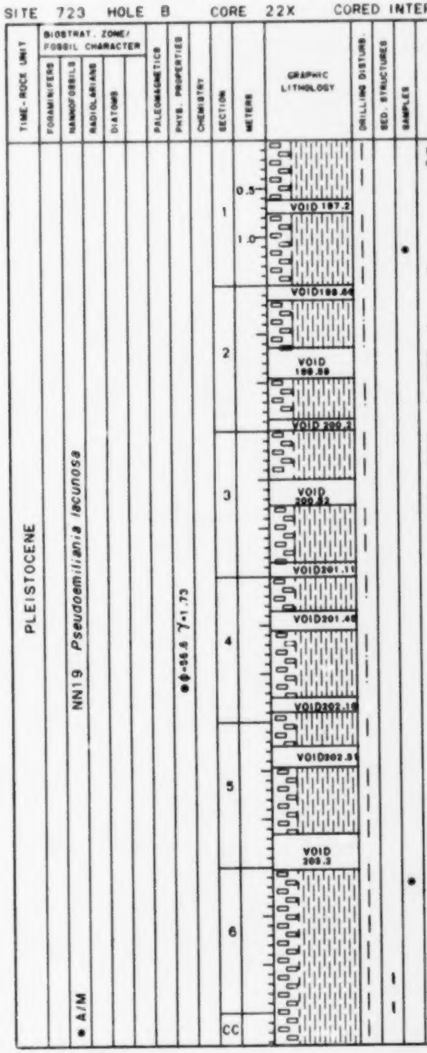
TIME-ROCK UNIT
BIOSTRAT. ZONE/ FOSSIL CHARACTER
FORAMINIFERS
NANNOFOSSILS
RADIOLARIANS
DIATOMS
PALEOMAGNETICS
PHYS. PROPERTIES
CHEMISTRY
SECTION
METERS
GRAPHIC LITHOLOGY
DRILLING DISTURB.
SED. STRUCTURES
SAMPLES
PLEISTOCENE
NN19 Pseudoemiliania lacunosa
• A/M
●ϕ-56.6 γ-1.73
1
2
3
4
5
6
CC
0.5
1.0
VOID 197.2
VOID198.64
VOID 198.89
VOID 200.2
VOID 200.82
VOID201.11
VOID201.46
VOID202.19
VOID202.51
VOID 203.3

LITHOLOGIC DESCRIPTION

FORAMINIFER-BEARING MARLY NANNOFOSSIL OOZE and CALCAREOUS CLAYEY SILT

Core moderately disturbed by gas expansion. Numerous voids.

Major lithologies: FORAMINIFER-BEARING MARLY NANNOFOSSIL OOZE and CALCAREOUS CLAYEY SILT, olive gray (5Y 4/2). Foraminifers visible on core face in Section 1. Variable terrigenous component dominated by clay and silt-sized detrital calcite.

SMEAR SLIDE SUMMARY (%):

	1, 115 D	6, 17 D
TEXTURE:		
Sand	15	15
Silt	35	25
Clay	50	60
COMPOSITION:		
Access. minerals	2	3
Clay	25	25
Dolomite	Tr	Tr
Foraminifers	8	2
Inorganic calcite	25	20
Nannofossils	25	35
Quartz	15	15
Sponge spicules	Tr	Tr

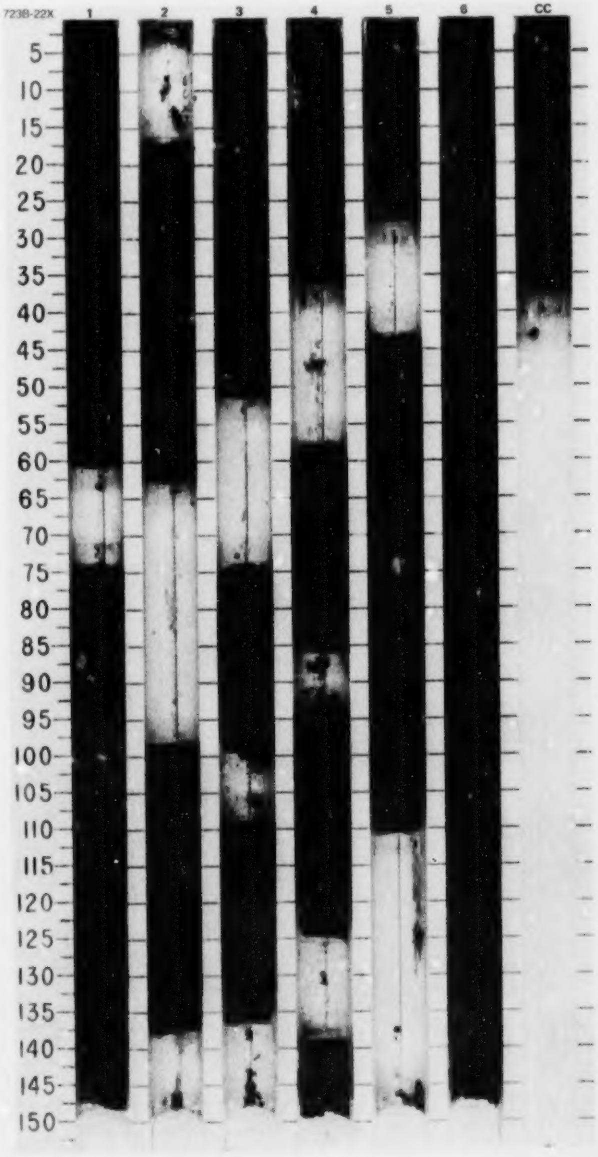
723B-22X
1
2
3
4
5
6
CC
5
10
15
20
25
30
35
40
45
50
55
60
65
70
75
80
85
90
95
100
105
110
115
120
125
130
135
140
145
150

SITE 723 HOLE B CORE 23X CORED INTERVAL 1013.1-1022.7 mbsl; 206.9-216.5 mbsf

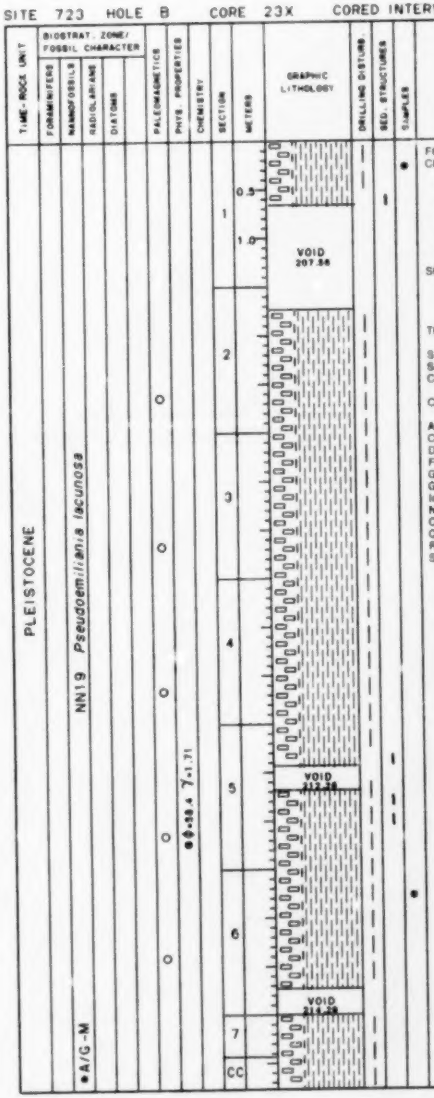
TIME-ROCK UNIT
BIOSTRAT. ZONE/ FOSSIL CHARACTER
FORAMINIFERS
NANNOFOSSILS
RADIOLARIANS
DIATOMS
PALEOMAGNETICS
PHYS. PROPERTIES
CHEMISTRY
SECTION
METERS
GRAPHIC LITHOLOGY
DRILLING DISTURB.
SED. STRUCTURES
SAMPLES
PLEISTOCENE
NN19 Pseudoemiliania lacunosa
•A/G-M
ɸ=58.4 γ=1.71
0.5
1.0
1
2
3
4
5
6
7
CC
VOID 207.98
VOID 212.28
VOID 214.28

LITHOLOGIC DESCRIPTION

FORAMINIFER-BEARING MARLY NANNOFOSSIL OOZE and CALCAREOUS CLAYEY SILT

Core moderately disturbed by gas expansion. Numerous voids.

Major lithologies: FORAMINIFER-BEARING MARLY NANNOFOSSIL OOZE and CALCAREOUS CLAYEY SILT, olive gray (5Y 4/2), faintly mottled in Section 5. Foraminifers less common on core face. Variable terrigenous component dominated by clay and silt-sized detrital calcite.

SMEAR SLIDE SUMMARY (%):

	1, 28 D	6, 28 D
TEXTURE:		
Sand	10	20
Silt	25	25
Clay	65	55
COMPOSITION:		
Access. minerals	5	3
Clay	25	20
Dolomite	Tr	
Foraminifers	5	5
Glauconite	Tr	
Gypsum		Tr
Inorganic calcite	20	30
Nannofossils	40	35
Organic debris		2
Quartz	5	5
Radiolarians	Tr	Tr
Sponge spicules	Tr	Tr

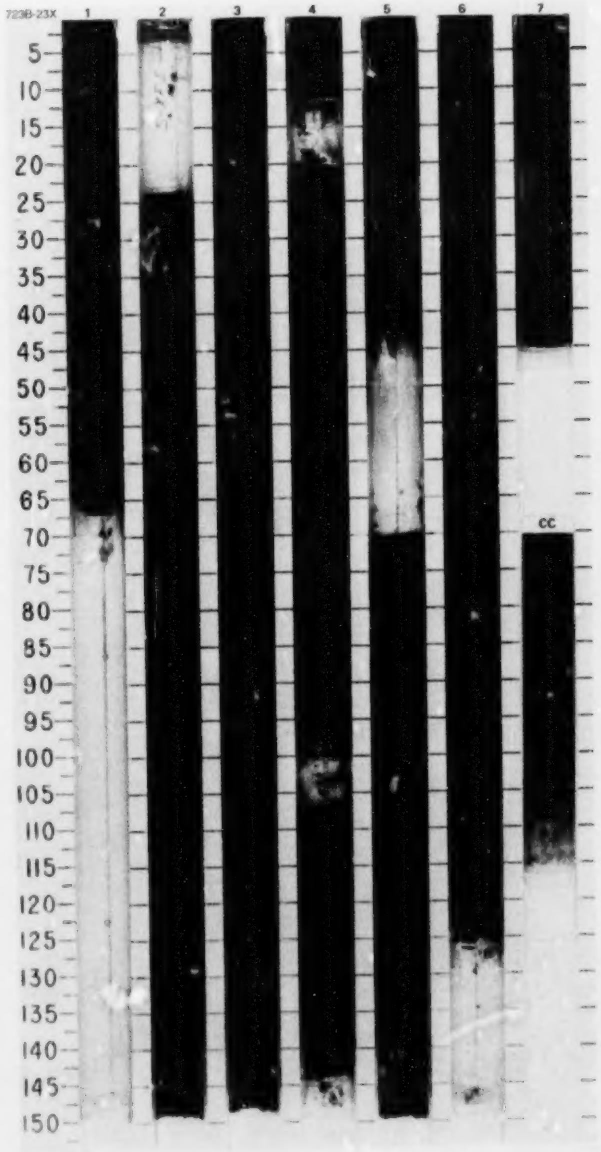
723B-23X
1
2
3
4
5
6
7
CC
5
10
15
20
25
30
35
40
45
50
55
60
65
70
75
80
85
90
95
100
105
110
115
120
125
130
135
140
145
150

SITE 723 HOLE B CORE 24X CORED INTERVAL 1022.7-1032.4 mbsl; 216.5-226.2 mbsf

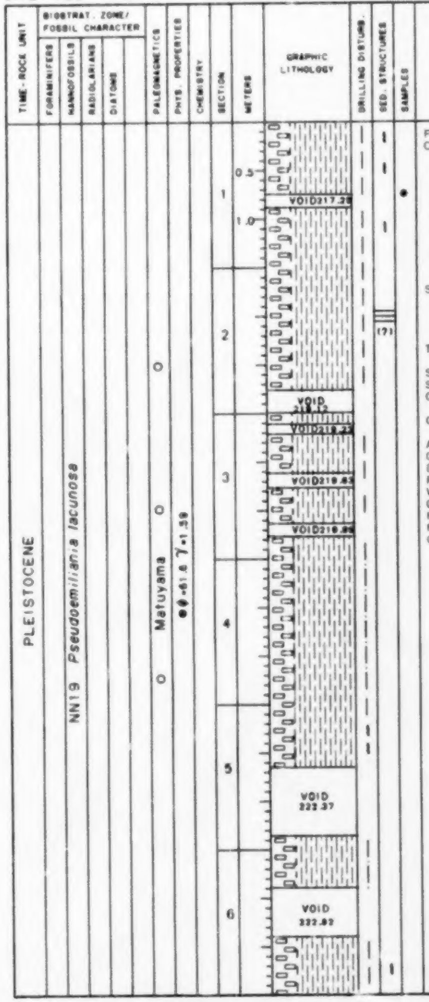
TIME-ROCK UNIT
BIOSTRAT. ZONE/ FOSSIL CHARACTER
FORAMINIFERS
NANNOFOSSILS
RADIOLARIANS
DIATOMS
PALEOMAGNETICS
PHYS. PROPERTIES
CHEMISTRY
SECTION
METERS
GRAPHIC LITHOLOGY
DRILLING DISTURB.
SED. STRUCTURES
SAMPLES
PLEISTOCENE
NN19 Pseudoemiliania lacunosa
Matuyama
●ϕ=61.6 γ=1.59
0.5
1.0
1
2
3
4
5
6
VOID217.28
VOID 218.12
VOID218.22
VOID219.43
VOID219.86
VOID 222.37
VOID 222.92
(?)

LITHOLOGIC DESCRIPTION

FORAMINIFER-BEARING MARLY NANNOFOSSIL OOZE and CALCAREOUS CLAYEY SILT

Core moderately disturbed by gas expansion. Numerous voids.

Major lithologies: FORAMINIFER-BEARING MARLY NANNOFOSSIL OOZE and CALCAREOUS CLAYEY SILT, olive gray (5Y 4/2, 4/3) and dark olive gray (5Y 3/2). Section 1 faintly mottled. Foraminifers less common on core face. Variable terrigenous component dominated by clay and silt-sized detrital calcite.

Minor lithology: Faint parallel-laminated light and dark layers (0.5 cm thick) preserved in drilling biscuits, Section 2, 57-77 cm.

SMEAR SLIDE SUMMARY (%):

	1, 73 D	7, 17 D
TEXTURE:		
Sand	15	25
Silt	25	45
Clay	60	30
COMPOSITION:		
Access. minerals	3	5
Clay	25	15
Dolomite		Tr
Foraminifers	2	Tr
Volcanic glass	Tr	
Glauconite	Tr	
Inorganic calcite	30	35
Nannofossils	35	15
Quartz	5	30

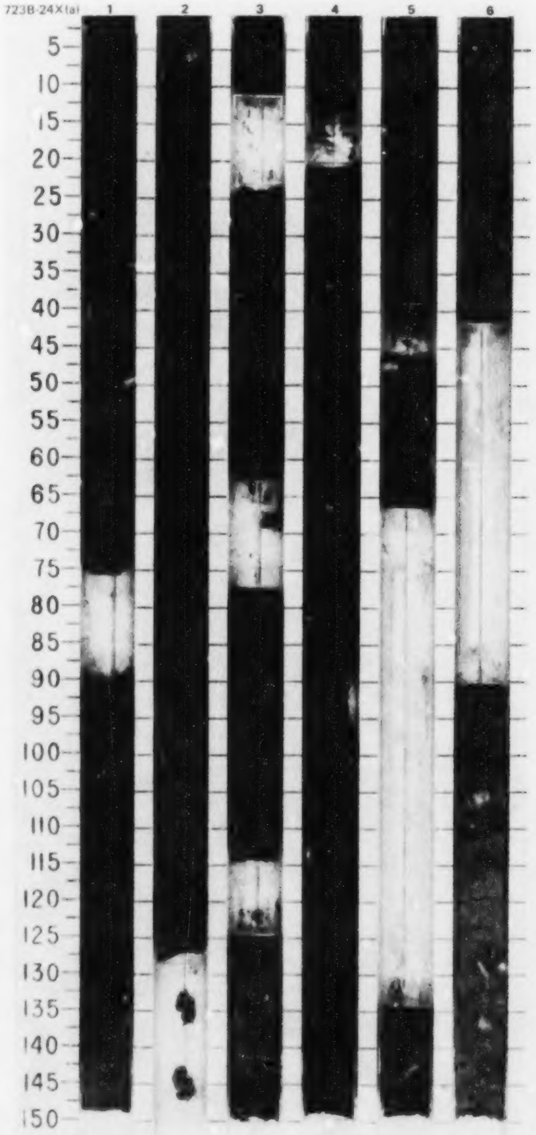
723B-24X(a)
1
2
3
4
5
6
5
10
15
20
25
30
35
40
45
50
55
60
65
70
75
80
85
90
95
100
105
110
115
120
125
130
135
140
145
150

SITE 723 HOLE B CORE 24X CORED INTERVAL 1022.7-1032.4 mbsl; 216.5-226.2 mbsf

TIME-ROCK UNIT	BIOSTRAT. ZONE/ FOSSIL CHARACTER				PALEOMAGNETICS	PHYS. PROPERTIES	CHEMISTRY	SECTION	METERS	GRAPHIC LITHOLOGY	DRILLING DISTURB.	SED. STRUCTURES	SAMPLES	LITHOLOGIC DESCRIPTION
	FORAMINIFERS	NANNOFOSSILS	RADIOLARIANS	DIATOMS										
		•A/M						7				●		
								CC	0.5 1.0					

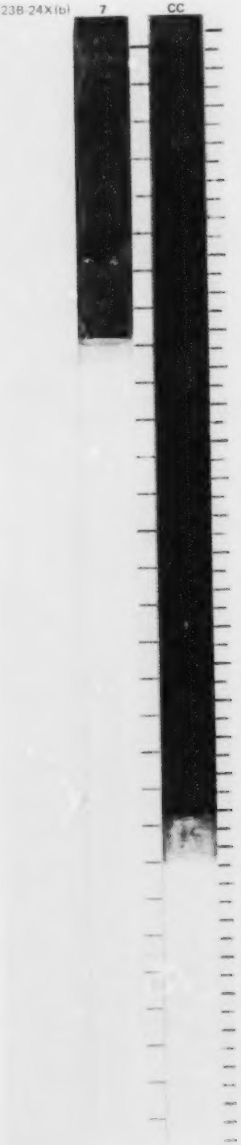

SITE 723 HOLE B CORE 25X CORED INTERVAL 1032.4-1042.1 mbsl; 226.2-235.9 mbsf

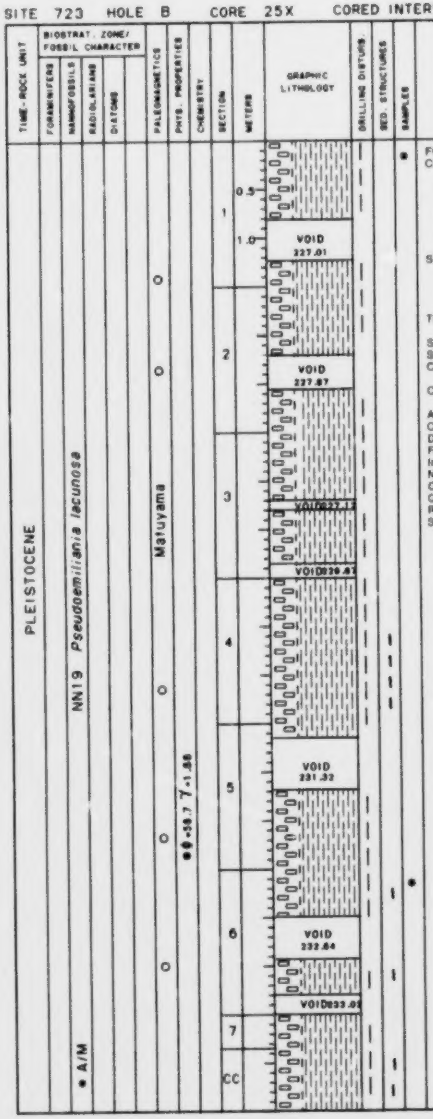
TIME-ROCK UNIT
BIOSTRAT. ZONE/ FOSSIL CHARACTER
FORAMINIFERS
NANNOFOSSILS
RADIOLARIANS
DIATOMS
PALEOMAGNETICS
PHYS. PROPERTIES
CHEMISTRY
SECTION
METERS
GRAPHIC LITHOLOGY
DRILLING DISTURB.
SED. STRUCTURES
SAMPLES
PLEISTOCENE
NN19 Pseudoemiliania lacunosa
• A/M
Matuyama
●Φ=58.7 γ=1.88
1
2
3
4
5
6
7
CC
0.5
1.0
VOID 227.01
VOID 227.87
VOID227.17
VOID229.47
VOID 231.32
VOID 232.64
VOID233.02

LITHOLOGIC DESCRIPTION

FORAMINIFER-BEARING MARLY NANNOFOSSIL OOZE and CALCAREOUS CLAYEY SILT

Core moderately disturbed by gas expansion. Numerous voids.

Major lithologies: FORAMINIFER-BEARING MARLY NANNOFOSSIL OOZE and CALCAREOUS CLAYEY SILT, olive gray (5Y 4/2) and dark olive gray (5Y 3/2), faintly mottled in Section 4 and CC.

SMEAR SLIDE SUMMARY (%):

	1, 18 D	6, 13 D
TEXTURE:		
Sand	20	15
Silt	25	35
Clay	55	50
COMPOSITION:		
Access. minerals	3	2
Clay	35	30
Dolomite		Tr
Foraminifers	5	3
Inorganic calcite	22	25
Nannofossils	20	20
Organic debris	5	5
Quartz	10	15
Radiolarians	Tr	
Sponge spicules	Tr	Tr

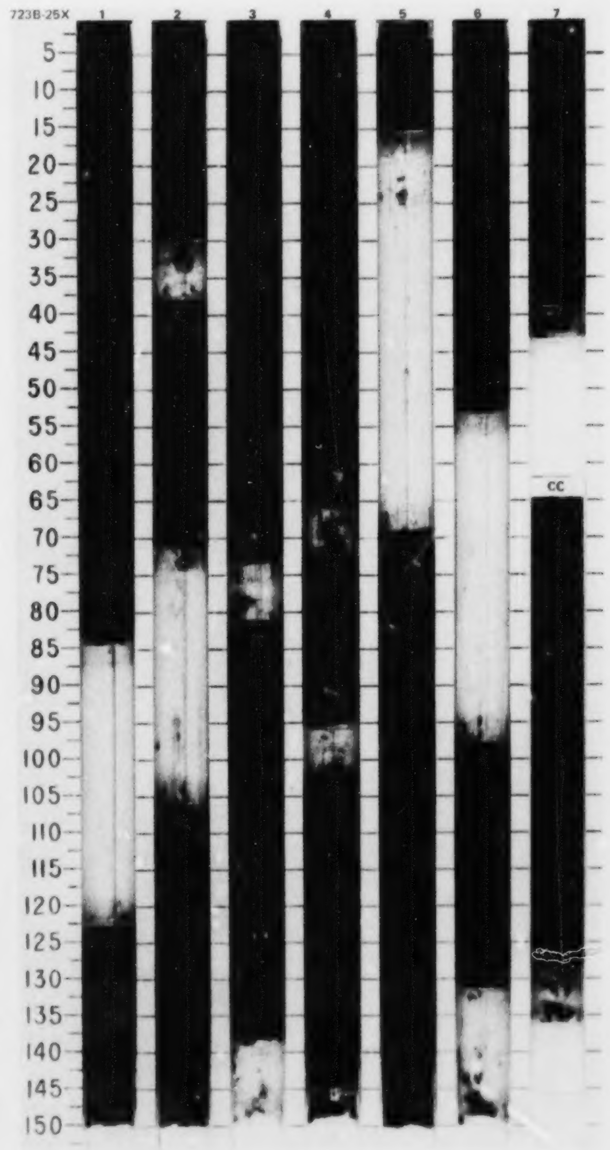
723B-25X
1
2
3
4
5
6
7
CC
5
10
15
20
25
30
35
40
45
50
55
60
65
70
75
80
85
90
95
100
105
110
115
120
125
130
135
140
145
150

SITE 723 HOLE B CORE 26X CORED INTERVAL 1042.1-1051.8 mbsl; 235.9-245.6 mbsf

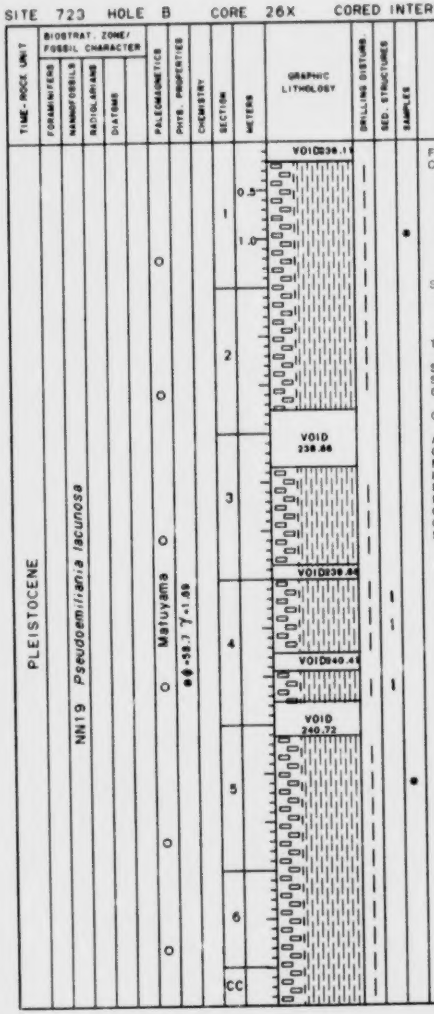
TIME-ROCK UNIT
BIOSTRAT. ZONE/ FOSSIL CHARACTER
FORAMINIFERS
NANNOFOSSILS
RADIOLARIANS
DIATOMS
PALEOMAGNETICS
PHYS. PROPERTIES
CHEMISTRY
SECTION
METERS
GRAPHIC LITHOLOGY
DRILLING DISTURB.
SED. STRUCTURES
SAMPLES
PLEISTOCENE
NN19 Pseudoemiliania lacunosa
Matuyama
φ=58.7 γ=1.89
1
2
3
4
5
6
CC
0.5
1.0
VOID236.1
VOID 238.66
VOID239.86
VOID240.4
VOID 240.72

LITHOLOGIC DESCRIPTION

FORAMINIFER-BEARING MARLY NANNOFOSSIL OOZE and CALCAREOUS CLAYEY SILT

Section 1 cut with saw, heavily broken up. Remainder moderately disturbed by gas expansion. Numerous voids.

Major lithologies: FORAMINIFER-BEARING MARLY NANNOFOSSIL OOZE and CALCAREOUS CLAYEY SILT, dark olive gray (5Y 3/2), faintly mottled in Section 4. Foraminifers less common on core face. Variable terrigenous component dominated by clay and silt-sized detrital calcite.

SMEAR SLIDE SUMMARY (%):

	1, 97 D	5, 59 D
TEXTURE:		
Sand	15	20
Silt	35	20
Clay	50	60
COMPOSITION:		
Access. minerals	3	2
Clay	25	25
Foraminifers	2	1
Inorganic calcite	30	27
Mica	Tr	
Nannofossils	25	35
Organic debris	5	
Quartz	10	10
Sponge spicules	Tr	Tr

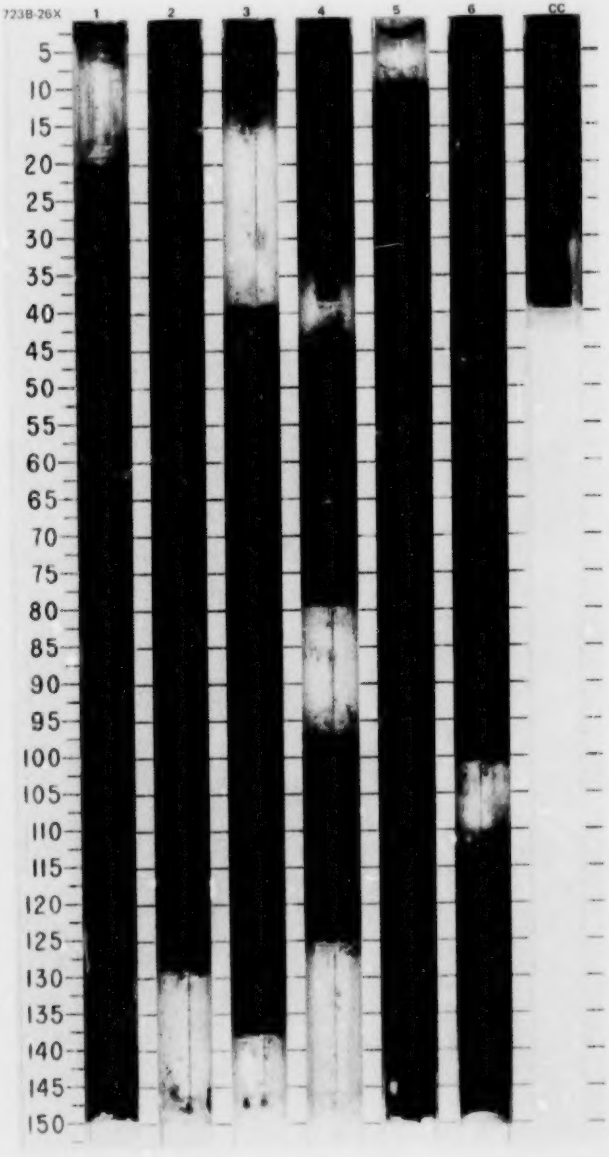
723B-26X
1
2
3
4
5
6
CC
5
10
15
20
25
30
35
40
45
50
55
60
65
70
75
80
85
90
95
100
105
110
115
120
125
130
135
140
145
150

SITE 723 HOLE B CORE 27X CORED INTERVAL 1051.8-1053.45 mbsl; 245.6 mbsf

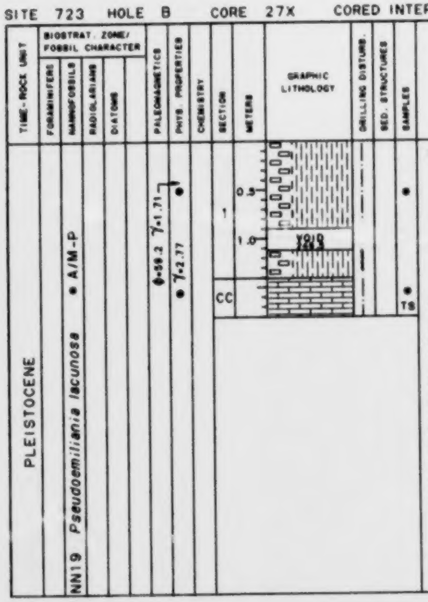
TIME-ROCK UNIT
BIOSTRAT. ZONE/ FOSSIL CHARACTER
FORAMINIFERS
NANNOFOSSILS
RADIOLARIANS
DIATOMS
PALEOMAGNETICS
PHYS. PROPERTIES
CHEMISTRY
SECTION
METERS
GRAPHIC LITHOLOGY
DRILLING DISTURB.
SED. STRUCTURES
SAMPLES
PLEISTOCENE
NN19 Pseudoemiliania lacunosa
● A/M-P
φ=59.2 γ=1.71
● γ=2.77
1
CC
0.5
1.0
VOID
TS

LITHOLOGIC DESCRIPTION

CALCAREOUS CLAYEY SILT and DOLOMITIC LIMESTONE

Section 1 is moderately to heavily disturbed. Two voids.

Major lithologies: CALCAREOUS CLAYEY SILT, olive gray (5Y 4/2). Foraminifers rare on core face. Dolomitic limestone, 40 cm (broken into three clasts), recovered in CC.

SMEAR SLIDE SUMMARY (%)

	1, 53 D	CC, 16 D(TS)
TEXTURE:		
Sand	10	30
Silt	30	45
Clay	60	25
COMPOSITION:		
Access. minerals	2	
Cement		25
Clay	33	25
Dolomite	Tr	25
Foraminifers	Tr	25
Volcanic glass	Tr	
Inorganic calcite	30	
Nannofossils	25	
Quartz	10	

CORE 117–723B–28X NO RECOVERY

CORE 117–723B–29X NO RECOVERY

CORE 117–723B–30X NO RECOVERY

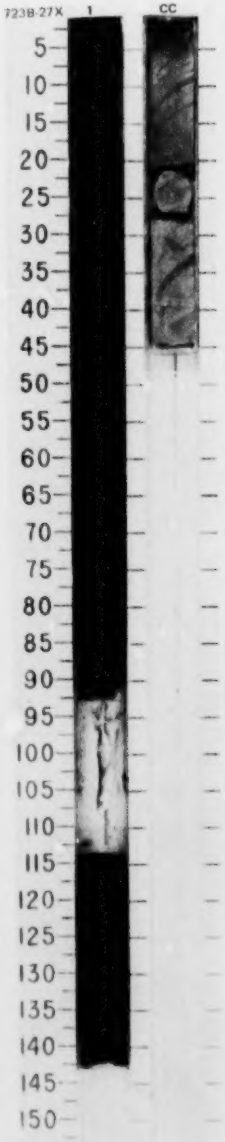
723B-27X
1
CC
5
10
15
20
25
30
35
40
45
50
55
60
65
70
75
80
85
90
95
100
105
110
115
120
125
130
135
140
145
150

SITE 723 HOLE B CORE 31X CORED INTERVAL 1099.9-1109.5 mbsl; 293.7-303.3 mbsf

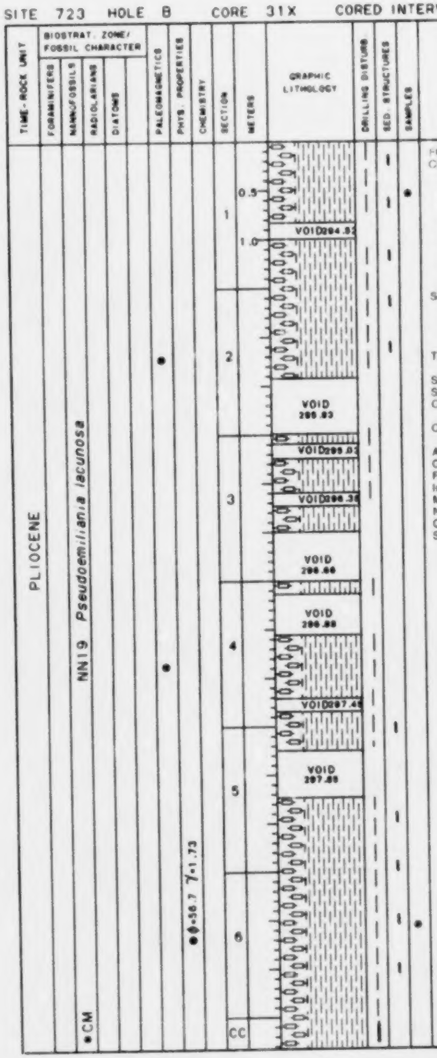
TIME-ROCK UNIT
BIOSTRAT. ZONE/ FOSSIL CHARACTER
FORAMINIFERS
NANNOFOSSILS
RADIOLARIANS
DIATOMS
PALEOMAGNETICS
PHYS. PROPERTIES
CHEMISTRY
SECTION
METERS
GRAPHIC LITHOLOGY
DRILLING DISTURB.
SED. STRUCTURES
SAMPLES
PLIOCENE
NN19 Pseudoemiliania lacunosa
CM
φ=56.7 γ=1.73
1
2
3
4
5
6
CC
0.5
1.0
VOID294.82
VOID 295.83
VOID296.03
VOID296.36
VOID 296.66
VOID 296.88
VOID297.45
VOID 297.85

LITHOLOGIC DESCRIPTION

FORAMINIFER-BEARING MARLY NANNOFOSSIL CHALK and CALCAREOUS CLAYEY SILTSTONE

Section 1, 0-25 cm, heavily disturbed, remainder moderately disturbed by gas expansion. Firm intervals separate into clasts. Numerous voids.

Major lithologies: FORAMINIFER-BEARING MARLY NANNOFOSSIL CHALK and CALCAREOUS CLAYEY SILTSTONE, olive gray (5Y 4/2) and dark olive gray (5Y 3/2), faintly mottled in Sections 1, 2, 5, and 6. Foraminifers present on core face. Variable terrigenous component dominated by clay and silt-sized detrital calcite.

SMEAR SLIDE SUMMARY (%):

	1, 53 D	6, 54 D
TEXTURE:		
Sand	5	20
Silt	20	30
Clay	75	50
COMPOSITION:		
Access. minerals	2	2
Clay	30	25
Foraminifers	2	3
Inorganic calcite	10	25
Mica	1	
Nannofossils	45	25
Quartz	10	20
Sponge spicules	Tr	

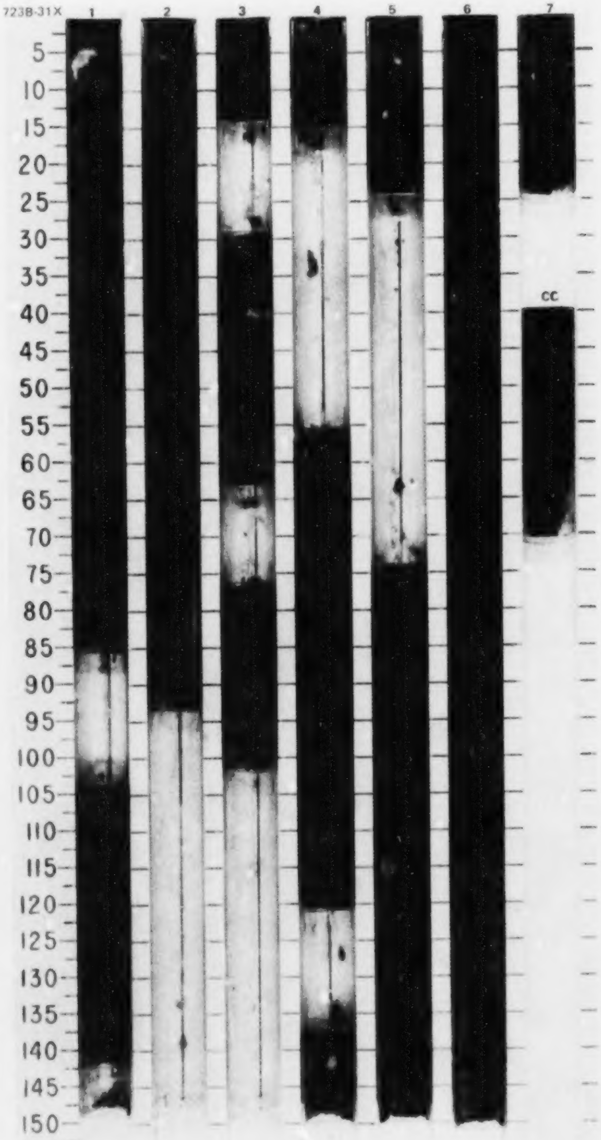
723B-31X
1
2
3
4
5
6
7
CC
5
10
15
20
25
30
35
40
45
50
55
60
65
70
75
80
85
90
95
100
105
110
115
120
125
130
135
140
145
150

CORE 117–723B–32X NO RECOVERY

SITE 723 HOLE B CORE 33X CORED INTERVAL 1119.2-1123.6 mbsl; 313.0-317.4 mbsf

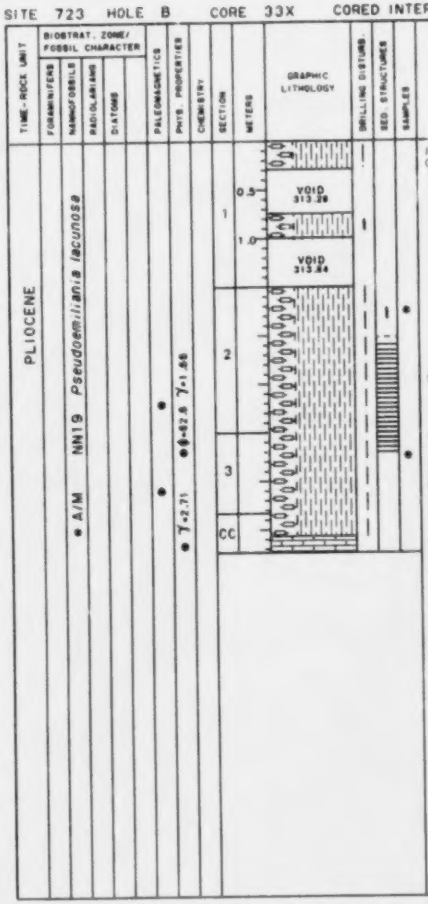
TIME-ROCK UNIT
BIOSTRAT. ZONE/ FOSSIL CHARACTER
FORAMINIFERS
NANNOFOSSILS
RADIOLARIANS
DIATOMS
PALEOMAGNETICS
PHYS. PROPERTIES
CHEMISTRY
SECTION
METERS
GRAPHIC LITHOLOGY
DRILLING DISTURB.
SED. STRUCTURES
SAMPLES
PLIOCENE
● A/M NN19 Pseudoemiliania lacunosa
● γ=2.71
●ϕ=62.6 γ=1.88
1
2
3
CC
0.5
1.0
VOID 313.29
VOID 313.84

LITHOLOGIC DESCRIPTION

FORAMINIFER-BEARING MARLY NANNOFOSSIL CHALK and CALCAREOUS CLAYEY SILTSTONE

Core moderately disturbed by gas expansion. Firm intervals separate into clasts which crumble readily. Cut with wire to preserve laminae. Numerous voids.

Major lithologies: FORAMINIFER-BEARING MARLY NANNOFOSSIL CHALK and CALCAREOUS CLAYEY SILTSTONE, olive gray (5Y 4/2) and dark olive gray (5Y 3/2, 2.5/2). Foraminifers present on core face. Variable terrigenous component dominated by clay and silt-sized detrital calcite.

Minor lithologies:
a. Parallel laminae, individual light and dark layers, 0.1-1.0 mm thick. Light layers are composed of diatomaceous mud, in Section 1, 85-83 cm, Section 2, 52-150 cm, and Section 3, 0-12 cm.
b. Dolomitic limestone with faint burrow structures. Dark gray (5Y 4/1), in CC, 18-34 cm.

SMEAR SLIDE SUMMARY (%):

	2, 22 D	3, 25 D
TEXTURE:		
Sand	20	20
Silt	40	20
Clay	40	60
COMPOSITION:		
Access. minerals	1	1
Clay	25	20
Diatoms	Tr	Tr
Dolomite	Tr	
Feldspar	2	
Foraminifers	Tr	4
Inorganic calcite	30	20
Nannofossils	15	40
Organic debris	2	
Quartz	25	15
Radiolarians	Tr	Tr
Sponge spicules	Tr	

CORE 117–723B–34X NO RECOVERY

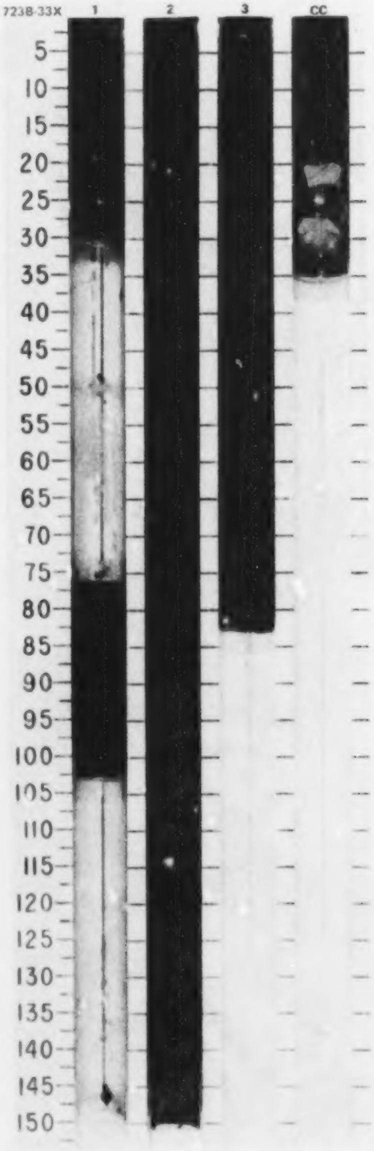
723B-33X
1
2
3
CC
5
10
15
20
25
30
35
40
45
50
55
60
65
70
75
80
85
90
95
100
105
110
115
120
125
130
135
140
145
150

SITE 723 HOLE B CORE 35X CORED INTERVAL 1128.9-1138.7 mbsl; 322.7-332.5 mbsf

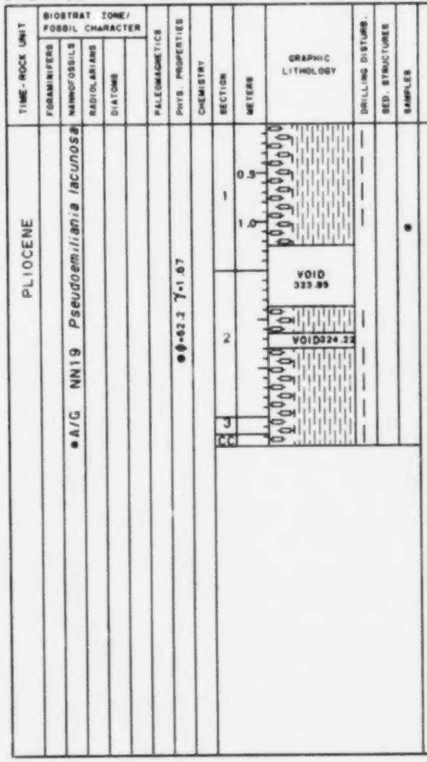
TIME-ROCK UNIT
BIOSTRAT. ZONE/ FOSSIL CHARACTER
FORAMINIFERS
NANNOFOSSILS
RADIOLARIANS
DIATOMS
PALEOMAGNETICS
PHYS. PROPERTIES
CHEMISTRY
SECTION
METERS
GRAPHIC LITHOLOGY
DRILLING DISTURB.
SED. STRUCTURES
SAMPLES
PLIOCENE
●A/G NN19 Pseudoemiliania lacunosa
●ϕ-62.2 γ-1.67
1
2
3
CC
0.5
1.0
VOID 323.89
VOID324.22

LITHOLOGIC DESCRIPTION

FORAMINIFER-BEARING MARLY NANNOFOSSIL CHALK and CALCAREOUS CLAYEY SILTSTONE

Core moderately disturbed by gas expansion. Firm intervals separate into clasts. Numerous voids.

Major lithologies: FORAMINIFER-BEARING MARLY NANNOFOSSIL CHALK and CALCAREOUS CLAYEY SILTSTONE, olive gray (5Y 4/2). No mottling or burrow structures observed. Variable terrigenous component dominated by clay and silt-sized detrital calcite.

SMEAR SLIDE SUMMARY (%):

	1, 108 D
TEXTURE:	
Sand	10
Silt	15
Clay	75
COMPOSITION:	
Access. minerals	2
Clay	30
Diatoms	1
Foraminifers	2
Inorganic calcite	15
Nannofossils	45
Quartz	5
Sponge spicules	Tr

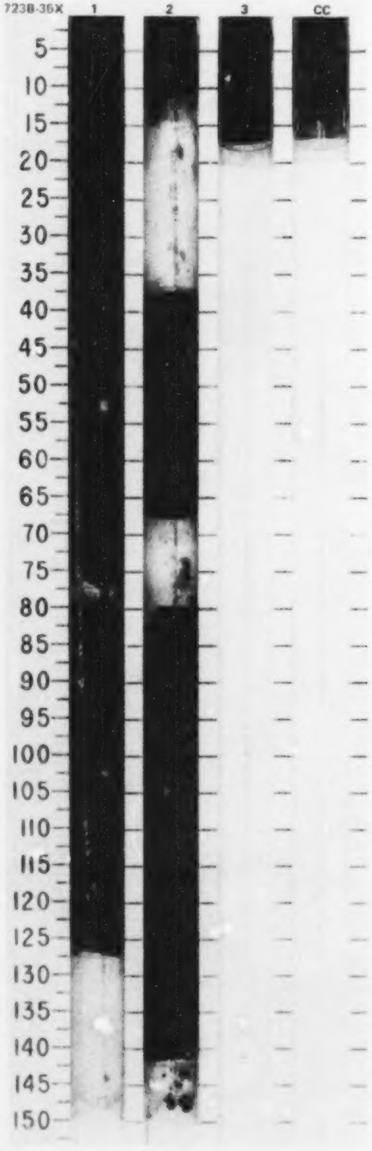
723B-35X
1
2
3
CC
5
10
15
20
25
30
35
40
45
50
55
60
65
70
75
80
85
90
95
100
105
110
115
120
125
130
135
140
145
150

SITE 723 HOLE B CORE 36X CORED INTERVAL 1138.7-1148.4 mbsl; 332.5-342.2 mbsf

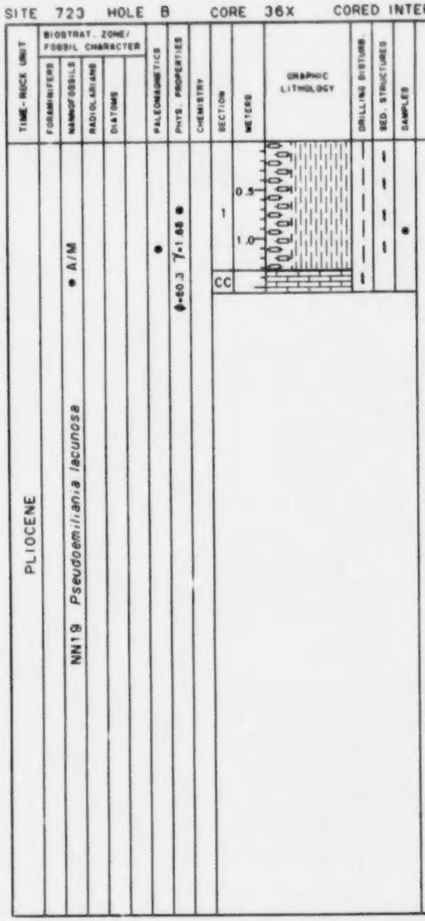
TIME-ROCK UNIT
BIOSTRAT. ZONE/ FOSSIL CHARACTER
FORAMINIFERS
NANNOFOSSILS
RADIOLARIANS
DIATOMS
PALEOMAGNETICS
PHYS. PROPERTIES
CHEMISTRY
SECTION
METERS
GRAPHIC LITHOLOGY
DRILLING DISTURB.
SED. STRUCTURES
SAMPLES
PLIOCENE
NN19 Pseudoemiliania lacunosa
• A/M
φ=60.3 γ=1.68
1
0.5
1.0
CC

LITHOLOGIC DESCRIPTION

FORAMINIFER-BEARING MARLY NANNOFOSSIL CHALK and CALCAREOUS CLAYEY SILTSTONE

Section 1, 0-9 cm, heavily disturbed; remainder moderately disturbed by gas expansion. Firm intervals separate into clasts.

Major lithologies: FORAMINIFER-BEARING MARLY NANNOFOSSIL CHALK and CALCAREOUS CLAYEY SILTSTONE, dark olive gray (5Y 3/2), Section 1 faintly mottled. Variable terrigenous component dominated by clay and silt-sized detrital calcite.

Minor lithology: Dolomitic limestone, with minor parallel laminations. Recrystallized diatoms and broken foraminifers present. Clastic component is predominantly clay, in bottom of CC, 18-22 cm.

SMEAR SLIDE SUMMARY (%):

	1, 94 D
TEXTURE:	
Sand	10
Silt	20
Clay	70
COMPOSITION:	
Access. minerals	2
Clay	20
Diatoms	Tr
Dolomite	Tr
Foraminifers	1
Volcanic glass	Tr
Inorganic calcite	22
Nannofossils	50
Quartz	5
Radiolarians	Tr
Sponge spicules	Tr

CORE 117-723B-37X NO RECOVERY

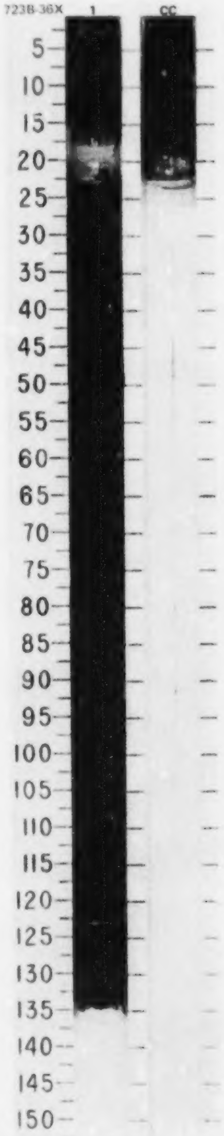
723B-36X
1
CC
5
10
15
20
25
30
35
40
45
50
55
60
65
70
75
80
85
90
95
100
105
110
115
120
125
130
135
140
145
150

SITE 723 HOLE B CORE 38X CORED INTERVAL 1158.1-1167.8 mbsl; 351.9-361.6 mbsf

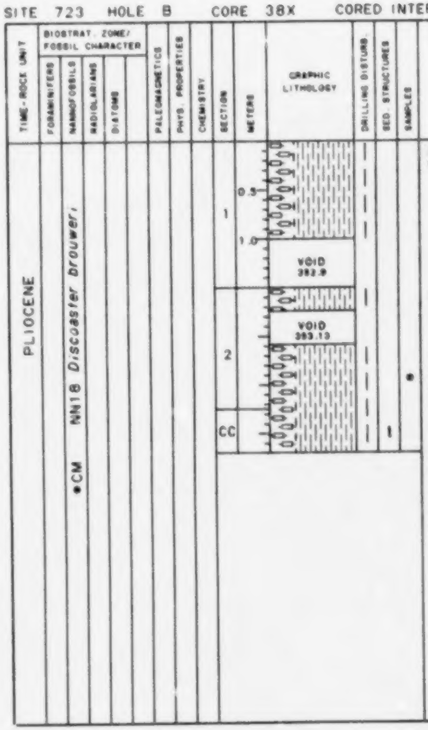
TIME-ROCK UNIT
BIOSTRAT. ZONE/ FOSSIL CHARACTER
FORAMINIFERS
NANNOFOSSILS
RADIOLARIANS
DIATOMS
PALEOMAGNETICS
PHYS. PROPERTIES
CHEMISTRY
SECTION
METERS
GRAPHIC LITHOLOGY
DRILLING DISTURB.
SED. STRUCTURES
SAMPLES
PLIOCENE
•CM NN18 Discoaster brouweri
1
2
CC
0.5
1.0
VOID 352.9
VOID 353.13

LITHOLOGIC DESCRIPTION

FORAMINIFER-BEARING MARLY NANNOFOSSIL CHALK and CALCAREOUS CLAYEY SILTSTONE

Section 1, 0-20 cm, soupy and heavily disturbed; remainder moderately disturbed by gas expansion. Firm intervals seperate into clasts. Numerous voids.

Major lithologies: FORAMINIFER BEARING MARLY NANNOFOSSIL CHALK and CALCAREOUS CLAYEY SILTSTONE, olive gray (5Y 4/2) and dark olive gray (5Y 3/2). CC faintly mottled. Variable terrigenous component dominated by clay and silt-sized detrital calcite.

SMEAR SLIDE SUMMARY (%):

	2, 94 D
TEXTURE:	
Sand	20
Silt	25
Clay	55
COMPOSITION:	
Access. minerals	2
Clay	25
Feldspar	1
Foraminifers	2
Inorganic calcite	20
Nannofossils	30
Quartz	20
Sponge spicules	Tr

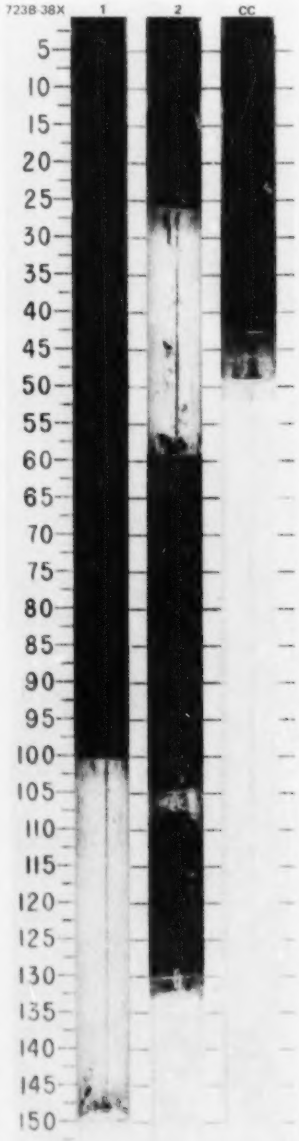
723B-38X
1
2
CC
5
10
15
20
25
30
35
40
45
50
55
60
65
70
75
80
85
90
95
100
105
110
115
120
125
130
135
140
145
150

SITE 723 HOLE B CORE 39X CORED INTERVAL 1167.8-1177.5 mbsl; 361.6-371.3 mbsf

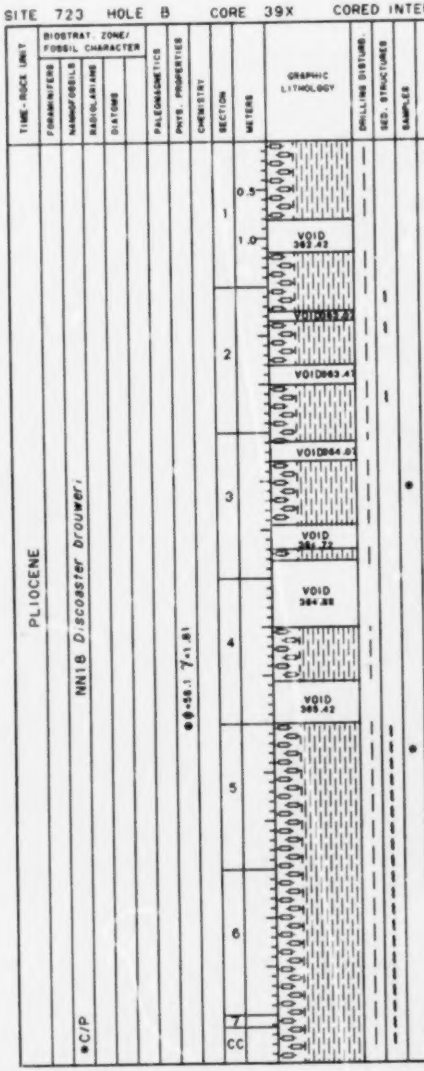
TIME-ROCK UNIT
BIOSTRAT. ZONE/ FOSSIL CHARACTER
FORAMINIFERS
NANNOFOSSILS
RADIOLARIANS
DIATOMS
PALEOMAGNETICS
PHYS. PROPERTIES
CHEMISTRY
SECTION
METERS
GRAPHIC LITHOLOGY
DRILLING DISTURB.
SED. STRUCTURES
SAMPLES
PLIOCENE
NN18 Discoaster brouweri
●C/P
●Φ=58.1 γ=1.81
1
2
3
4
5
6
7
CC
0.5
1.0
VOID 362.42
VOID 363.41
VOID 364.07
VOID 364.88
VOID 365.42

LITHOLOGIC DESCRIPTION

FORAMINIFER-BEARING MARLY NANNOFOSSIL CHALK and CALCAREOUS CLAYEY SILTSTONE

Section 1, 0-10 cm, heavily disturbed, remainder moderately disturbed by gas expansion. Firm intervals separate into clasts. Sediment crumbles adjacent to voids.

Major lithologies: FORAMINIFER-BEARING MARLY NANNOFOSSIL CHALK and CALCAREOUS CLAYEY SILTSTONE, olive gray (5Y 4/2, 4/3) and dark olive gray (5Y 3/2, 2.5/2). Variable terrigenous component dominated by clay and silt-sized detrital calcite.

SMEAR SLIDE SUMMARY (%):

	3, 54 D	5, 26 D
TEXTURE:		
Sand	20	10
Silt	35	50
Clay	45	40
COMPOSITION:		
Access. minerals	1	2
Clay	25	30
Dolomite	Tr	Tr
Foraminifers	4	
Volcanic glass		Tr
Glauconite		Tr
Inorganic calcite	35	28
Nannofossils	20	10
Organic debris		5
Quartz	15	25
Radiolarians		Tr

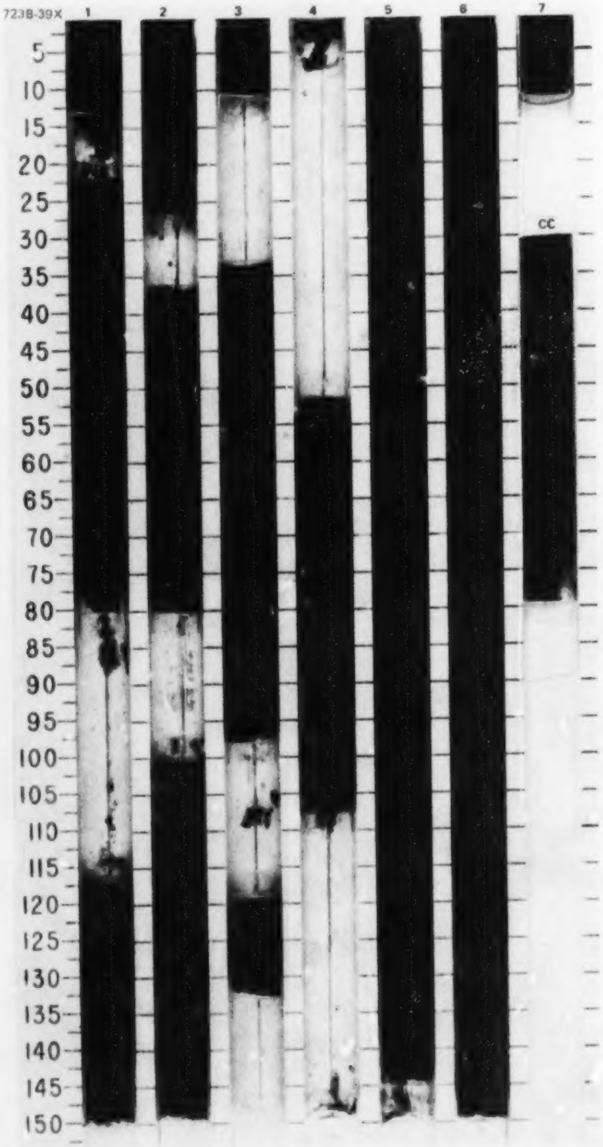
723B-39X
1
2
3
4
5
6
7
CC
5
10
15
20
25
30
35
40
45
50
55
60
65
70
75
80
85
90
95
100
105
110
115
120
125
130
135
140
145
150

SITE 723 HOLE B CORE 40X CORED INTERVAL 1177.5-1187.2 mbsl; 371.3-381.0 mbsf

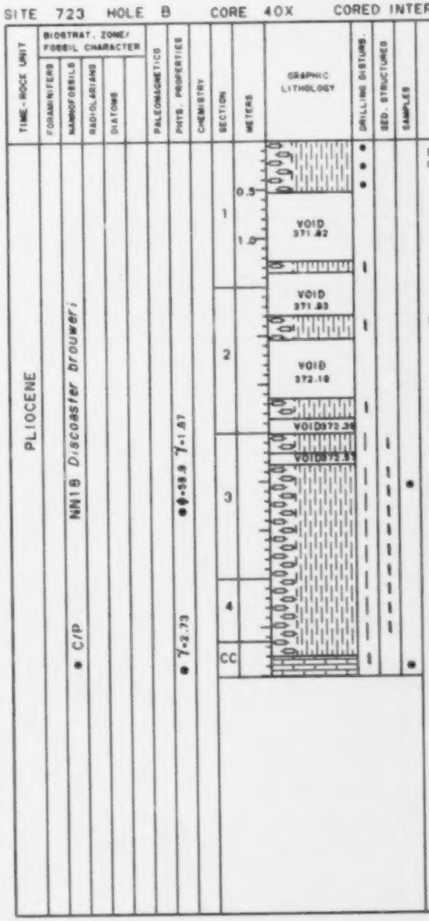
TIME-ROCK UNIT
BIOSTRAT. ZONE/ FOSSIL CHARACTER
FORAMINIFERS
NANNOFOSSILS
RADIOLARIANS
DIATOMS
PALEOMAGNETICS
PHYS. PROPERTIES
CHEMISTRY
SECTION
METERS
GRAPHIC LITHOLOGY
DRILLING DISTURB.
SED. STRUCTURES
SAMPLES
PLIOCENE
NN18 Discoaster brouweri
● C/P
●φ=58.9 γ=1.87
● γ=2.73
1
2
3
4
CC
0.5
1.0
VOID 371.82
VOID 371.93
VOID 372.18
VOID372.29
VOID372.37

LITHOLOGIC DESCRIPTION

FORAMINIFER-BEARING MARLY NANNOFOSSIL CHALK and CALCAREOUS CLAYEY SILTSTONE

Section 1, heavily disturbed; remainder moderately to heavily disturbed by gas expansion. Firm intervals separate into clasts. Numerous voids.

Major lithologies: FORAMINIFER-BEARING MARLY NANNOFOSSIL CHALK and CALCAREOUS CLAYEY SILTSTONE, olive gray (5Y 4/2) and dark olive gray (5Y 3/2), faint burrow mottles. Variable terrigenous component dominated by clay and silt-sized detrital calcite.

Minor lithology: Dolomitic limestone. Fine grained, minor stylolite development, containing foraminifers, in bottom of CC, 15-38 cm.

SMEAR SLIDE SUMMARY (%):

	3, 54 D	CC D
TEXTURE:		
Sand	10	15
Silt	30	5
Clay	60	80
COMPOSITION:		
Access. minerals	2	
Cement		20
Clay	30	35
Diatoms	Tr	
Dolomite		25
Foraminifers	3	20
Inorganic calcite	25	
Nannofossils	30	
Phosphate	Tr	
Quartz	10	

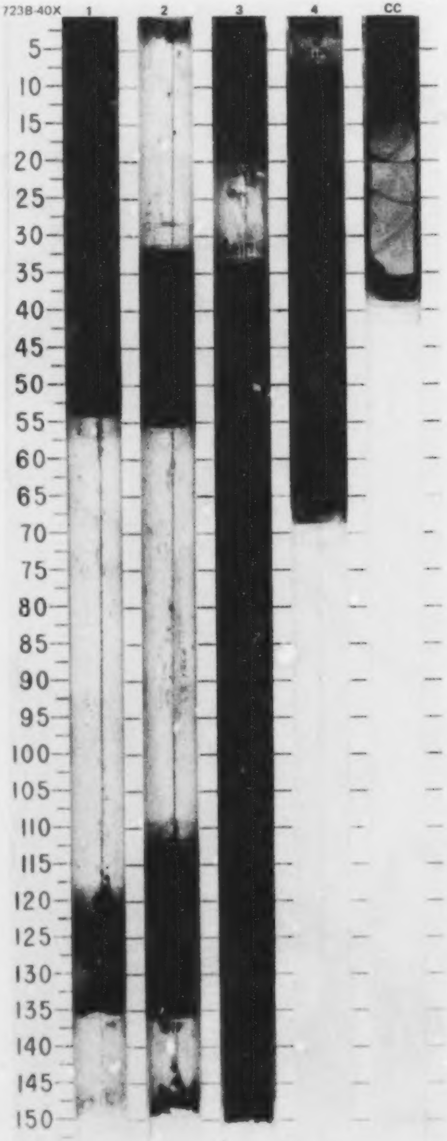
723B-40X
1
2
3
4
CC
5
10
15
20
25
30
35
40
45
50
55
60
65
70
75
80
85
90
95
100
105
110
115
120
125
130
135
140
145
150

SITE 723 HOLE B CORE 41X CORED INTERVAL 1187.2-1196.9 mbsl; 381.0-390.7 mbsf

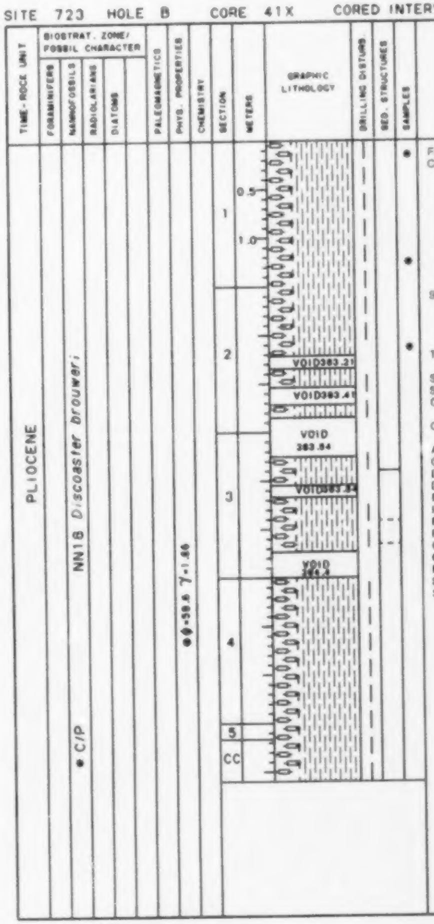
TIME-ROCK UNIT
BIOSTRAT. ZONE/ FOSSIL CHARACTER
FORAMINIFERS
NANNOFOSSILS
RADIOLARIANS
DIATOMS
PALEOMAGNETICS
PHYS. PROPERTIES
CHEMISTRY
SECTION
METERS
GRAPHIC LITHOLOGY
DRILLING DISTURB.
SED. STRUCTURES
SAMPLES
PLIOCENE
NN18 Discoaster brouweri
● C/P
●ϕ=58.6 γ=1.86
1
2
3
4
5
CC
0.5
1.0
VOID383.21
VOID383.41
VOID 383.84
VOID383.84
VOID 384.4

LITHOLOGIC DESCRIPTION

FOHAMINIFER-BEARING MARLY NANNOFOSSIL CHALK and CALCAREC'JS CLAYEY SILTSTONE

Core moderately disturbed by gas expansion. Firm intervals separate into clasts. Numerous voids.

Major lithologies: FORAMINIFER-BEARING MARLY NANNOFOSSIL CHALK and CALCAREOUS CLAYEY SILTSTONE, olive gray (5Y 4/2) and dark olive gray (5Y 3/2, 3/1), irregular light and dark layers. Foraminifers present on core face. Variable terrigenous component dominated by clay- and silt-sized detrital calcite.

SMEAR SLIDE SUMMARY (%):

	1, 15 D	1, 125 D	2, 64 D
TEXTURE:			
Sand	2	5	
Silt	60	40	40
Clay	38	55	60
COMPOSITION:			
Access. minerals	10	5	8
Clay	14	35	45
Diatoms	Tr		20
Dolomite	2	Tr	2
Foraminifers	8	10	
Inorganic calcite	30	18	10
Mica	Tr	Tr	Tr
Nannofossils	20	20	Tr
Organic debris	3	5	5
Quartz	12	5	5
Radiolarians	Tr	Tr	2
Silicoflagellates			1
Sponge spicules	1	1	2

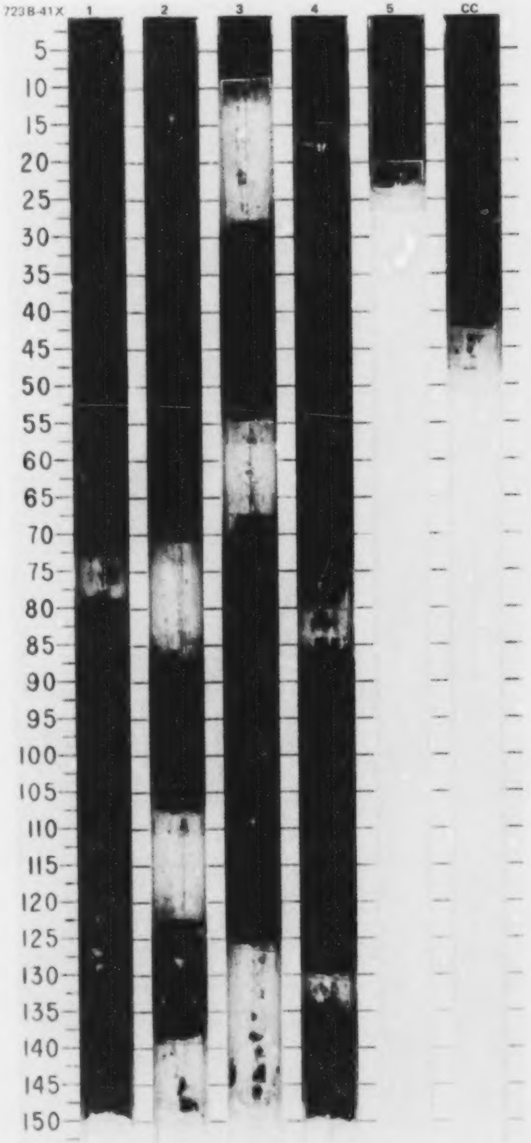
723B-41X
1
2
3
4
5
CC
5
10
15
20
25
30
35
40
45
50
55
60
65
70
75
80
85
90
95
100
105
110
115
120
125
130
135
140
145
150

SITE 723 HOLE B CORE 42X CORED INTERVAL 2012.7-2022.2 mbsl; 400.3-409.8 mbsf

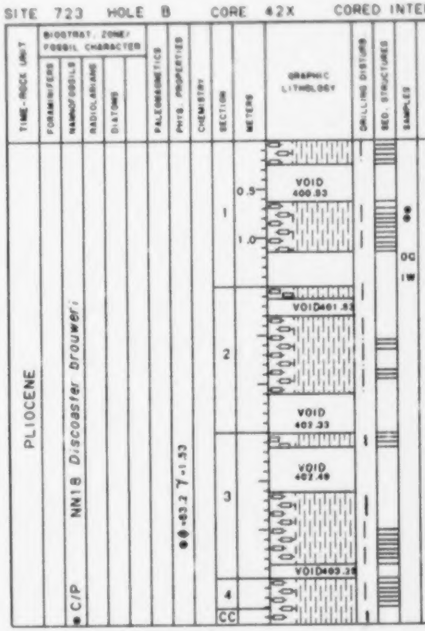
TIME-ROCK UNIT
BIOSTRAT. ZONE/ FOSSIL CHARACTER
FORAMINIFERS
NANNOFOSSILS
RADIOLARIANS
DIATOMS
PALEOMAGNETICS
PHYS. PROPERTIES
CHEMISTRY
SECTION
METERS
GRAPHIC LITHOLOGY
DRILLING DISTURB.
SED. STRUCTURES
SAMPLES
PLIOCENE
NN18 Discoaster brouweri
● C/P
●φ-63.2 γ-1.53
1
2
3
4
CC
0.5
1.0
VOID 400.83
VOID 401.83
VOID 402.33
VOID 402.49
VOID 403.28
OG
IW

LITHOLOGIC DESCRIPTION

CALCAREOUS CLAYEY SILTSTONE and DIATOMACEOUS SHALE

Core moderately disturbed by gas expansion. Firm intervals separate into clasts. Numerous voids.

Major lithologies: CALCAREOUS CLAYEY SILTSTONE, dark olive gray (5Y 3/1), and diatomaceous shale, forming 0.1-1.0-mm-thick laminae. Laminae are faint and indistinct in Section 2. Variable terrigenous component dominated by clay and silt-sized detrital calcite.

SMEAR SLIDE SUMMARY (%):

	1, 72 D	1, 73 D
TEXTURE:		
Silt	45	40
Clay	55	60
COMPOSITION:		
Access. minerals	3	5
Clay	30	49
Cristobalite		2
Diatoms	20	15
Dolomite	Tr	1
Foraminifers	5	Tr
Inorganic calcite	10	10
Mica	Tr	
Nannofossils	20	2
Organic debris	2	5
Quartz	5	7
Radiolarians	1	Tr
Silicoflagellates	1	1
Sponge spicules	2	3

CORE 117-723B-43X NO RECOVERY

SITE 723 HOLE B CORE 44X CORED INTERVAL 2031.8-2041.4 mbsl; 419.4-429.0 mbsf

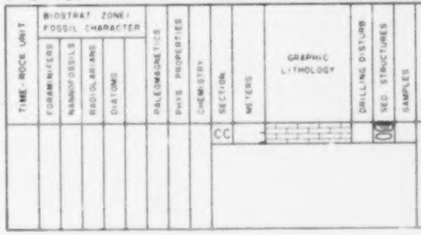
TIME-ROCK UNIT
BIOSTRAT. ZONE/ FOSSIL CHARACTER
FORAMINIFERS
NANNOFOSSILS
RADIOLARIANS
DIATOMS
PALEOMAGNETICS
PHYS. PROPERTIES
CHEMISTRY
SECTION
METERS
GRAPHIC LITHOLOGY
DRILLING DISTURB.
SED. STRUCTURES
SAMPLES
CC

LITHOLOGIC DESCRIPTION

DOLOMITIC LIMESTONE

Dolomitic limestone clast recovered from bottom of CC, 0-22 cm. Contains faint horizontal bedding, laminated facies(?) consisting of diatomaceous shale and calcareous clayey siltstone(?).

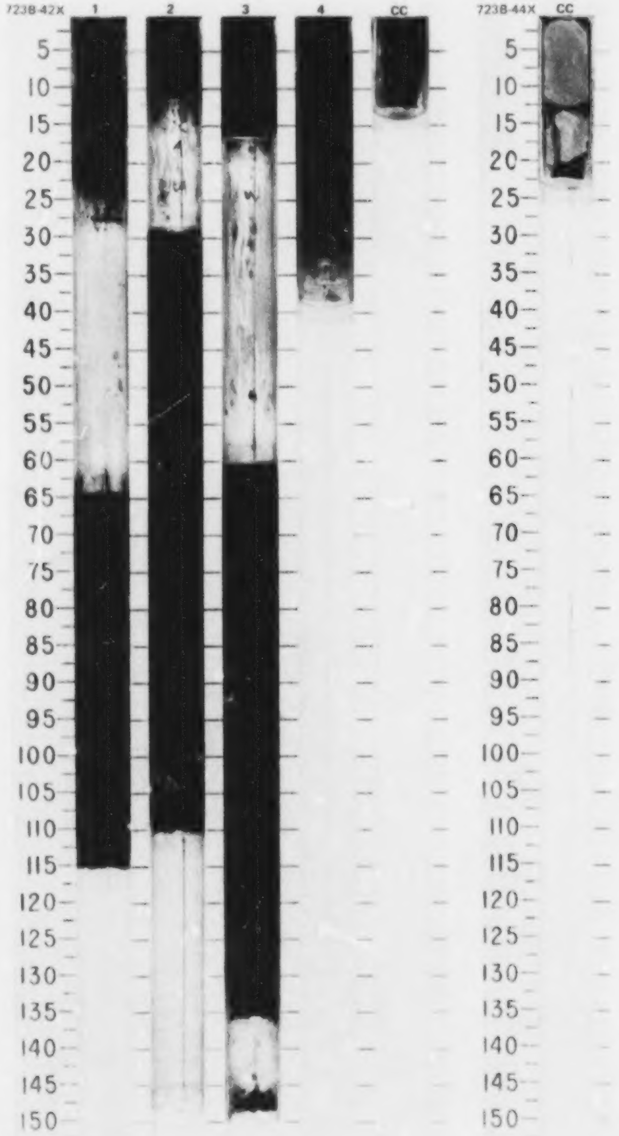
723B-42X
1
2
3
4
CC
723B-44X
CC
5
10
15
20
25
30
35
40
45
50
55
60
65
70
75
80
85
90
95
100
105
110
115
120
125
130
135
140
145
150

SITE 724 HOLE A CORE 1H CORED INTERVAL 592.8-599.3 mbsl; 0.0-6.5 mbsf

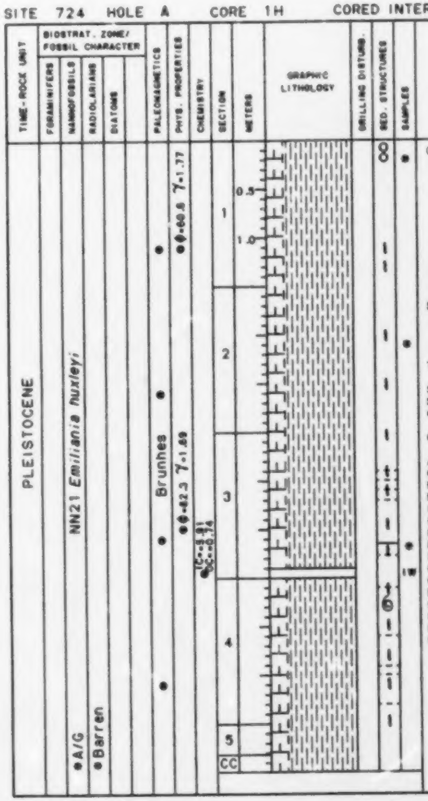
TIME-ROCK UNIT
BIOSTRAT. ZONE/ FOSSIL CHARACTER
FORAMINIFERS
NANNOFOSSILS
RADIOLARIANS
DIATOMS
PALEOMAGNETICS
PHYS. PROPERTIES
CHEMISTRY
SECTION
METERS
GRAPHIC LITHOLOGY
DRILLING DISTURB.
SED. STRUCTURES
SAMPLES
PLEISTOCENE
NN21 Emiliania huxleyi
●A/G
●Barren
Brunhes
●ϕ-60.6 γ-1.77
●ϕ-62.3 γ-1.89
IC-5.91
OC-0.74
0.5
1.0
1
2
3
4
5
CC
IW

LITHOLOGIC DESCRIPTION

CALCAREOUS CLAYEY SILT

Section 1, 0-18 cm, soupy; remainder undisturbed.

Major lithology: CALCAREOUS CLAYEY SILT, olive (5Y 5/3, 4/3), olive gray (5Y 4/2), dark olive gray (5Y 3/2), and very dark olive gray (5Y 3/1). Minor burrow mottling throughout. Contacts gradational and mottled. Millimeter-sized indeterminate shell fragments common. Foraminifers, pteropods, and gastropods visible.

Minor lithology: Section 1, 0-100 cm, diatomaceous clayey silt, dark olive gray (5Y 3/2).

SMEAR SLIDE SUMMARY (%):

	1, 20 D	2, 60 D	3, 118 M
TEXTURE:			
Sand	5	5	
Silt	65	75	75
Clay	30	20	25
COMPOSITION:			
Access. minerals	10	5	15
Clay	18	10	31
Diatoms	20		
Dolomite	1	Tr	2
Feldspar		2	Tr
Foraminifers	15	15	5
Inorganic calcite	15	45	20
Mica	Tr	Tr	Tr
Nannofossils	10	10	Tr
Opaques			5
Organic debris	Tr	3	5
Pellets			2
Quartz	10	10	15
Radiolarians			Tr
Rock fragments	Tr	Tr	
Sponge spicules	Tr		Tr

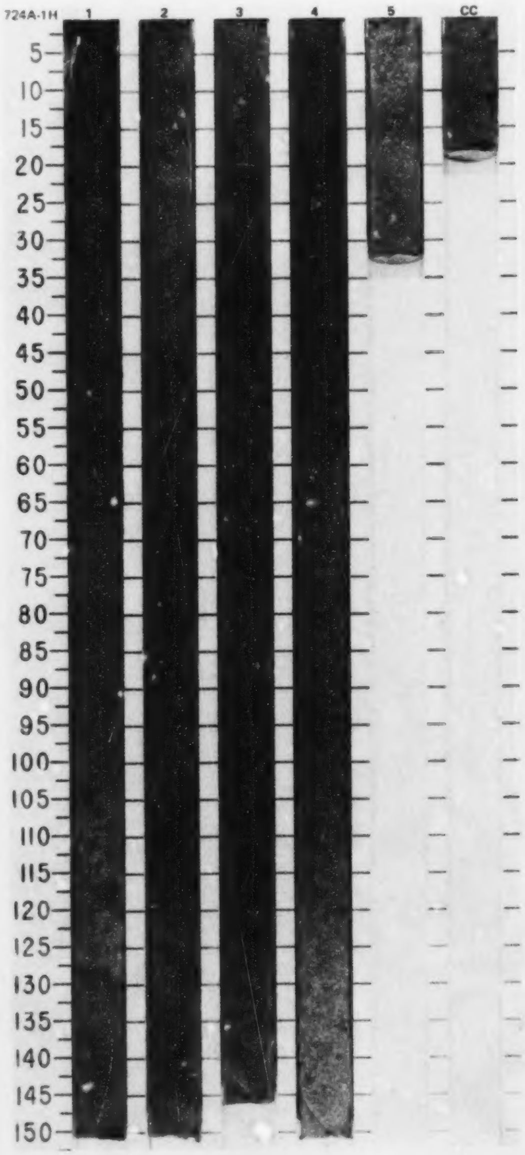
724A-1H
1
2
3
4
5
CC
5
10
15
20
25
30
35
40
45
50
55
60
65
70
75
80
85
90
95
100
105
110
115
120
125
130
135
140
145
150

SITE 724 HOLE A CORE 2H CORED INTERVAL 599.3-608.7 mbsl; 6.5-15.9 mbsf

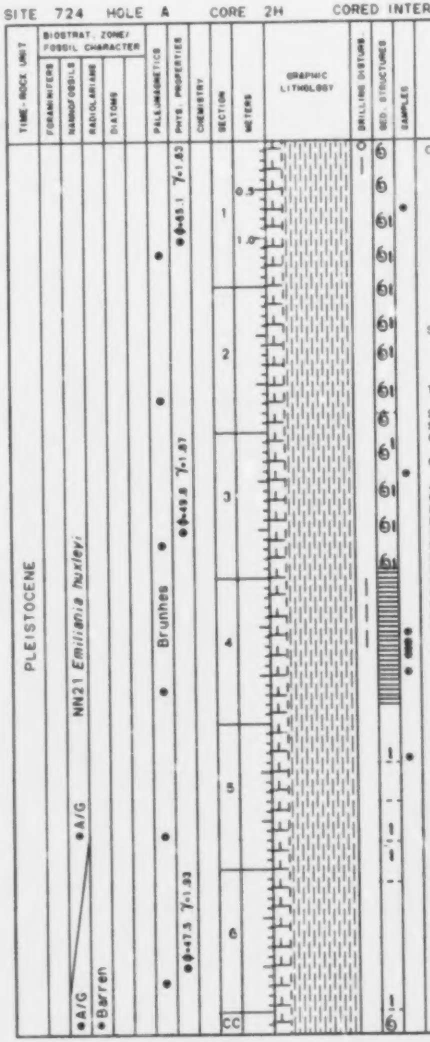
TIME-ROCK UNIT
BIOSTRAT. ZONE/ FOSSIL CHARACTER
FORAMINIFERS
NANNOFOSSILS
RADIOLARIANS
DIATOMS
PALEOMAGNETICS
PHYS. PROPERTIES
CHEMISTRY
SECTION
METERS
GRAPHIC LITHOLOGY
DRILLING DISTURB.
SED. STRUCTURES
SAMPLES
PLEISTOCENE
NN21 Emiliania huxleyi
●A/G
●A/G
●Barren
Brunhes
●Φ=65.1 γ=1.63
●Φ=49.8 γ=1.87
●Φ=47.5 γ=1.93
1
2
3
4
5
6
CC
0.5
1.0

LITHOLOGIC DESCRIPTION

CALCAREOUS CLAYEY SILT

Section 1, 0-5 cm, soupy, Section 1, 5-35 cm, and Section 4, 0-80 cm, slightly disturbed; remainder undisturbed.

Major lithology: CALCAREOUS CLAYEY SILT, olive (5Y 4/3), olive gray (5Y 5/2, 4/2), and dark olive gray (5Y 3/2). Minor burrow mottling throughout. Contacts gradational and mottled. Millimeter-sized indeterminate shell fragments common. Foraminifers, bivalves, scaphopods, pteropods, and gastropods visible.

Minor lithology: Section 3, 140-150 cm, Section 4, 0-120 cm, finely bedded layer. Alternating beds about 5 mm thick of nannofossil silty clay, olive gray (5Y 4/2), and calcitic silty clay, d[illegible] olive gray (5Y 3/2).

SMEAR SLIDE SUMMARY (%):

	1, 70 D	3, 44 D	4, 58 M	4, 66 M	4, 67 M	4, 80 M	4, 96 M
TEXTURE:							
Sand	5	10	15		2	10	
Silt	30	55	85	40	68	75	40
Clay	65	35		60	30	15	60
COMPOSITION:							
Access. minerals	3	6	10	5	5	10	5
Clay	48	20		30	20	10	45
Dolomite	Tr	2	2	Tr	2	6	1
Feldspar	1	1	5	Tr	1	5	
Foraminifers	8	10	10	Tr	5	5	8
Inorganic calcite	15	30	38	30	35	35	20
Mica	Tr	3	5	Tr	2	5	1
Nannofossils	17	15	Tr	25	10	2	15
Opaques		5					
Organic debris	Tr				5		
Pellets					5	5	
Quartz	8	8	25	10	10	15	5
Rock fragments			5			2	

SMEAR SLIDE SUMMARY (%):

	5, 35 M
TEXTURE:	
Sand	2
Silt	53
Clay	45
COMPOSITION:	
Access. minerals	10
Clay	45
Dolomite	6
Feldspar	1
Foraminifers	2
Inorganic calcite	20
Mica	3
Nannofossils	Tr
Opaques	2
Organic debris	3
Quartz	8

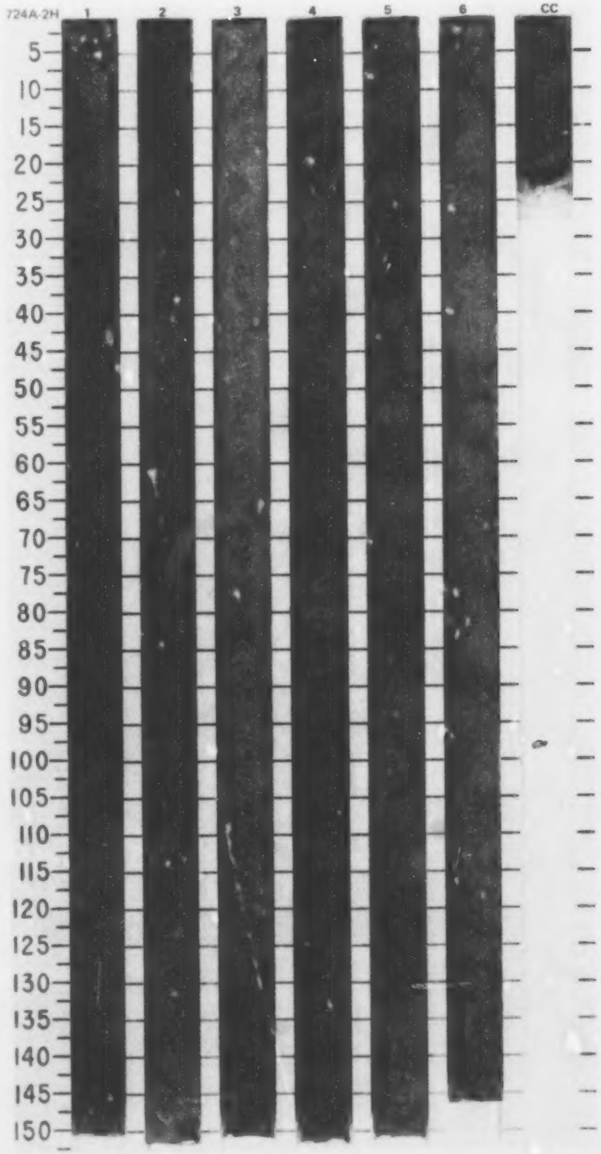
724A-2H
1
2
3
4
5
6
CC
5
10
15
20
25
30
35
40
45
50
55
60
65
70
75
80
85
90
95
100
105
110
115
120
125
130
135
140
145
150

SITE 724 HOLE A CORE 3H CORED INTERVAL 608.7-618.2 mbsl; 15.9-25.4 mbsf

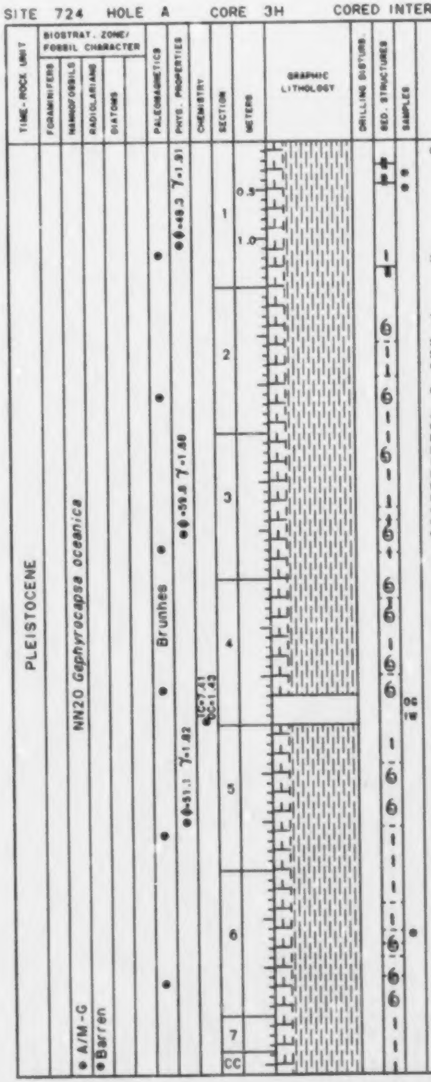
TIME-ROCK UNIT
BIOSTRAT. ZONE/ FOSSIL CHARACTER
FORAMINIFERS
NANNOFOSSILS
RADIOLARIANS
DIATOMS
PALEOMAGNETICS
PHYS. PROPERTIES
CHEMISTRY
SECTION
METERS
GRAPHIC LITHOLOGY
DRILLING DISTURB.
SED. STRUCTURES
SAMPLES
PLEISTOCENE
NN20 Gephyrocapsa oceanica
● A/M-G
● Barren
Brunhes
●ϕ=48.3 γ=1.91
●ϕ=59.8 γ=1.80
●ϕ=51.1 γ=1.82
IC=7.41
OC=1.43
0.5
1.0
1
2
3
4
5
6
7
CC
OG
IW

LITHOLOGIC DESCRIPTION

CALCAREOUS CLAYEY SILT

Entire core undisturbed.

Major lithology: Calcareous clayey silt, olive (5Y 4/3), olive gray (5Y 5/2, 4/2), and dark olive gray (5Y 3/2). Minor to moderate burrow mottling. Contacts gradational and mottled. Millimeter-sized indeterminate shell fragments common. Foraminifers, scaphopods, and gastropods visible.

SMEAR SLIDE SUMMARY (%):

	1, 34 M	1, 50 D	5, 68 D
TEXTURE:			
Sand	2	10	5
Silt	40	55	45
Clay	58	35	50
COMPOSITION:			
Access. minerals	10	8	8
Clay	38	20	35
Dolomite	2	2	2
Feldspar		2	
Foraminifers	2	8	5
Inorganic calcite	25	30	25
Mica	5	5	2
Nannofossils	5	15	15
Opaques	3		
Organic debris	5		Tr
Quartz	7	10	8

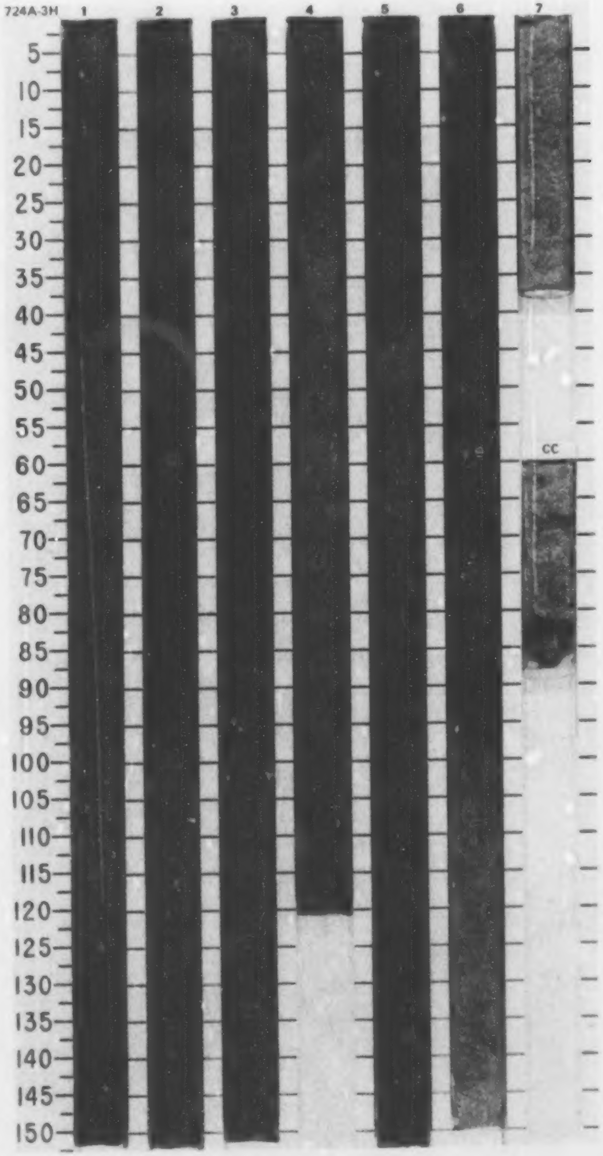
724A-3H
1
2
3
4
5
6
7
CC
5
10
15
20
25
30
35
40
45
50
55
60
65
70
75
80
85
90
95
100
105
110
115
120
125
130
135
140
145
150

SITE 724 HOLE A CORE 4H CORED INTERVAL 618.2-627.7 mbsl; 25.4-34.9 mbsf

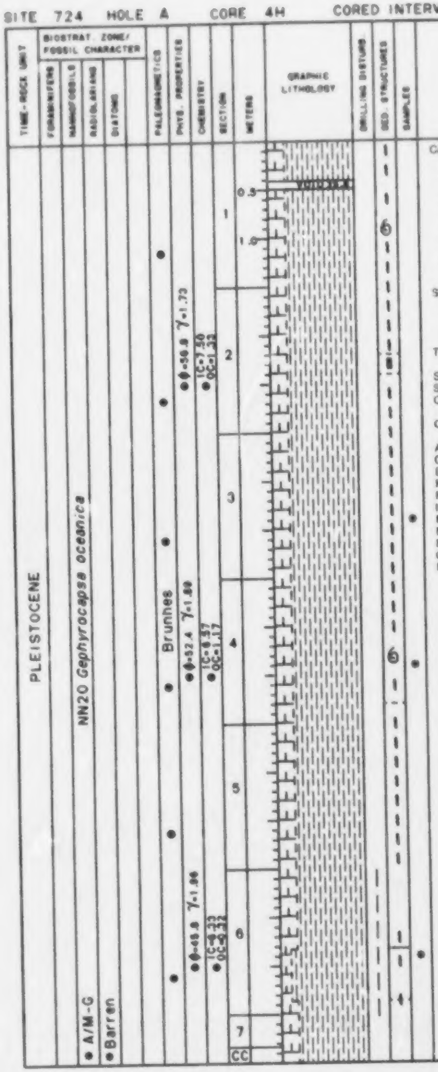
TIME-ROCK UNIT
BIOSTRAT. ZONE/ FOSSIL CHARACTER
FORAMINIFERS
NANNOFOSSILS
RADIOLARIANS
DIATOMS
PALEOMAGNETICS
PHYS. PROPERTIES
CHEMISTRY
SECTION
METERS
GRAPHIC LITHOLOGY
DRILLING DISTURB.
SED. STRUCTURES
SAMPLES
PLEISTOCENE
NN20 Gephyrocapsa oceanica
● A/M-G
● Barren
Brunhes
● φ=56.8 γ=1.73
● φ=52.4 γ=1.80
● φ=48.8 γ=1.96
● IC=7.50 OC=1.33
● IC=6.57 OC=1.17
● IC=6.33 OC=0.32
1
2
3
4
5
6
7
CC
0.5
1.0

LITHOLOGIC DESCRIPTION

CALCAREOUS CLAYEY SILT

Section 6, 0-150 cm, slightly disturbed; remainder undisturbed.

Major lithology: CALCAREOUS CLAYEY SILT, olive (5Y 4/3), olive gray (5Y 5/2, 4/2), and dark olive gray (5Y 3/2). Minor to moderate burrow mottling. Contacts gradational and mottled. Millimeter-sized indeterminate shell fragments common. Foraminifers visible.

Minor lithology: Section 6, 75-135 cm, calcitic clayey silt, olive gray (5Y 5/2). Sharp top contact, burrow-mottled lower contact.

SMEAR SLIDE SUMMARY (%):

	3, 90 D	4, 90 D	6, 90 D
TEXTURE:			
Sand	5	5	10
Silt	45	55	60
Clay	50	40	30
COMPOSITION:			
Access. minerals	10	8	10
Clay	24	13	19
Dolomite	5	5	2
Feldspar	Tr	1	2
Foraminifers	5	8	10
Inorganic calcite	15	25	30
Mica	1	Tr	2
Nannofossils	25	25	10
Pellets	5		
Quartz	10	10	10
Rock fragments		5	5

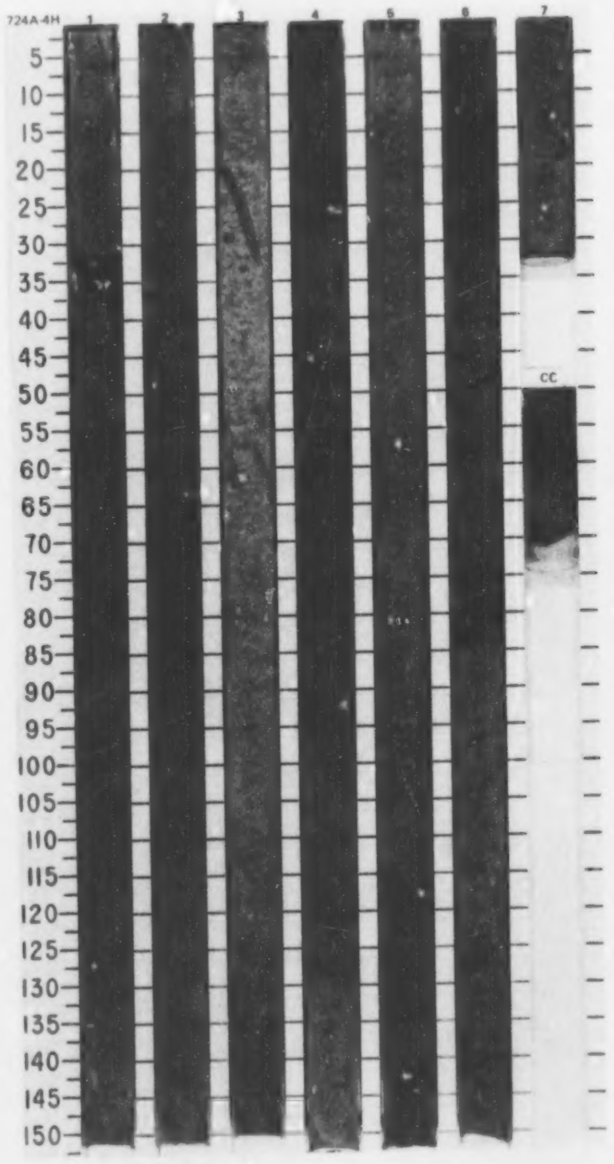
724A-4H
1
2
3
4
5
6
7
CC
5
10
15
20
25
30
35
40
45
50
55
60
65
70
75
80
85
90
95
100
105
110
115
120
125
130
135
140
145
150

SITE 724 HOLE A CORE 5H CORED INTERVAL 627.7-637.3 mbsl; 34.9-44.5 mbsf

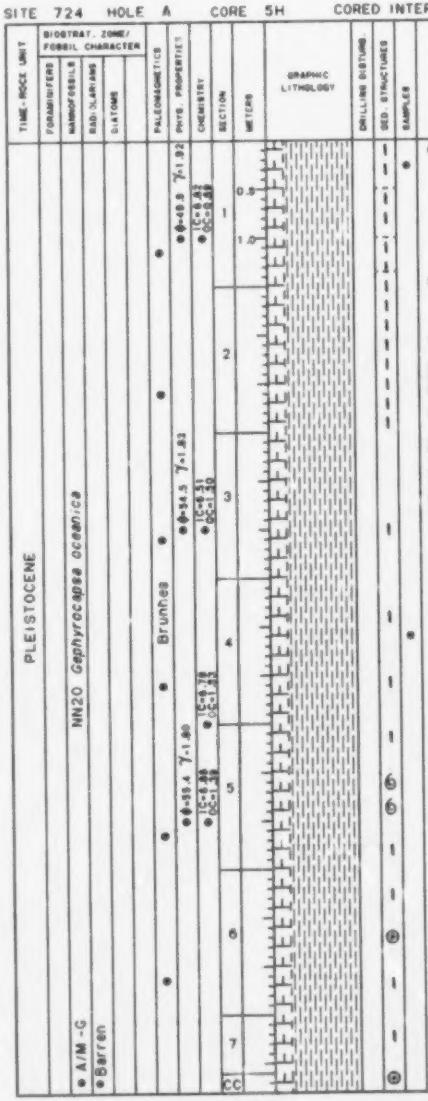
TIME-ROCK UNIT
BIOSTRAT. ZONE/ FOSSIL CHARACTER
FORAMINIFERS
NANNOFOSSILS
RADIOLARIANS
DIATOMS
PALEOMAGNETICS
PHYS. PROPERTIES
CHEMISTRY
SECTION
METERS
GRAPHIC LITHOLOGY
DRILLING DISTURB.
SED. STRUCTURES
SAMPLES
PLEISTOCENE
NN20 Gephyrocapsa oceanica
● A/M -G
● Barren
Brunhes
●Φ=49.8 γ=1.92
●Φ=54.5 γ=1.83
●Φ=55.4 γ=1.80
● IC=8.82 OC=0.50
● IC=8.51 OC=1.30
● IC=8.78 OC=1.33
● IC=8.88 OC=1.39
0.5
1.0
1
2
3
4
5
6
7
CC

LITHOLOGIC DESCRIPTION

CALCAREOUS CLAYEY SILT

Entire core undisturbed.

Major lithology: CALCAREOUS CLAYEY SILT, olive (5Y 4/3), olive gray (5Y 4/2), and dark olive gray (5Y 3/2). Most of the core is dark olive gray (5Y 3/2). Minor burrow mottling generally faint. Contacts gradational and mottled. Millimeter-sized indeterminate shell fragments common. Foraminifers visible. Section 6, 70 cm, and CC, 4 cm, phosphatic nodules, black (5Y 2.5/1) contain foraminifers.

SMEAR SLIDE SUMMARY (%):

	1, 26 D	4, 60 D
TEXTURE:		
Sand	5	10
Silt	80	75
Clay	15	15
COMPOSITION:		
Access. minerals		2
Clay	15	20
Foraminifers	5	3
Inorganic calcite	68	65
Nannofossils	5	5
Quartz	7	5
Rock fragments		?

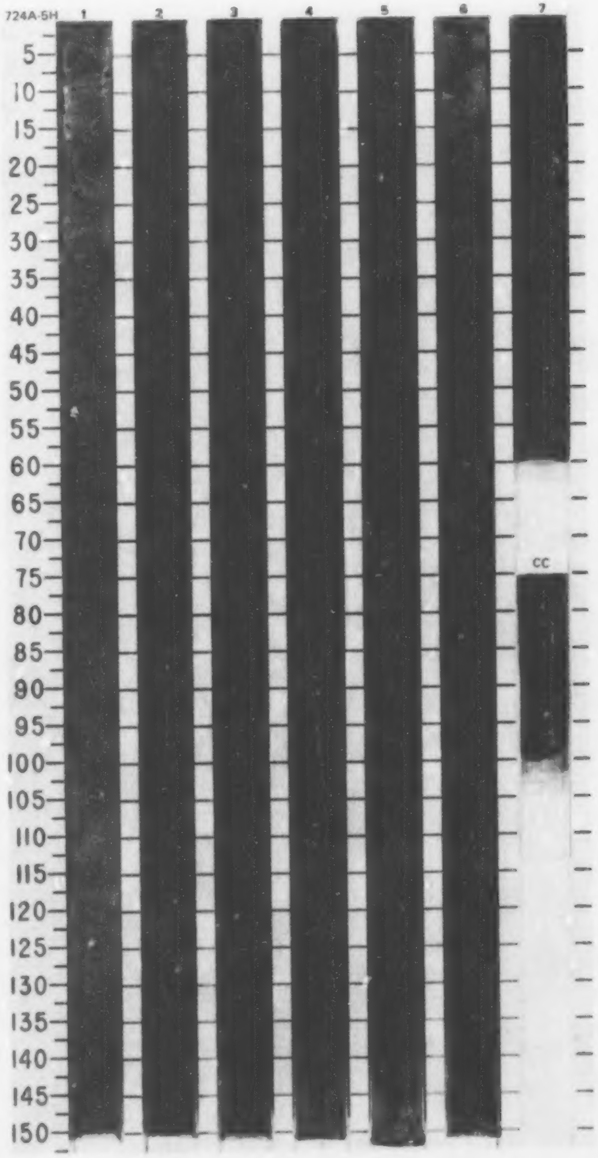
724A-5H
1
2
3
4
5
6
7
CC
5
10
15
20
25
30
35
40
45
50
55
60
65
70
75
80
85
90
95
100
105
110
115
120
125
130
135
140
145
150

SITE 724 HOLE B CORE 1H CORED INTERVAL 592.8-599.8 mbsl; 0.0-7.0 mbsf

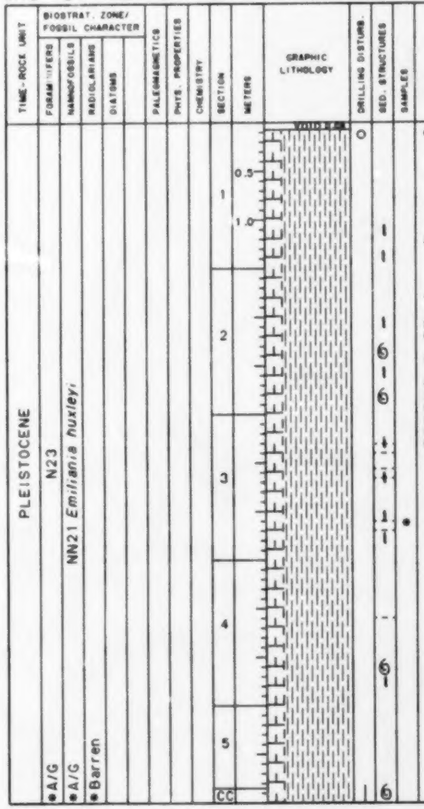
TIME-ROCK UNIT
BIOSTRAT. ZONE/ FOSSIL CHARACTER
FORAMINIFERS
NANNOFOSSILS
RADIOLARIANS
DIATOMS
PALEOMAGNETICS
PHYS. PROPERTIES
CHEMISTRY
SECTION
METERS
GRAPHIC LITHOLOGY
DRILLING DISTURB.
SED. STRUCTURES
SAMPLES
PLEISTOCENE
N23
NN21 Emiliania huxleyi
●A/G
●A/G
●Barren
1
2
3
4
5
CC
0.5
1.0

LITHOLOGIC DESCRIPTION

CALCAREOUS CLAYEY SILT

CC, slightly disturbed; remainder undisturbed.

Major lithology: CALCAREOUS CLAYEY SILT, olive gray (5Y 4/2) and dark olive gray (5Y 3/2). Minor burrow mottling common. Contacts gradational and mottled. Millimeter-sized indeterminate shell fragments common. Foraminifers, bivalves, and scaphopods visible.

SMEAR SLIDE SUMMARY (%):

	3, 112 M
TEXTURE:	
Silt	60
Clay	40
COMPOSITION:	
Clay	40
Inorganic calcite	40
Mica	Tr
Nannofossils	5
Organic debris	5
Quartz	10

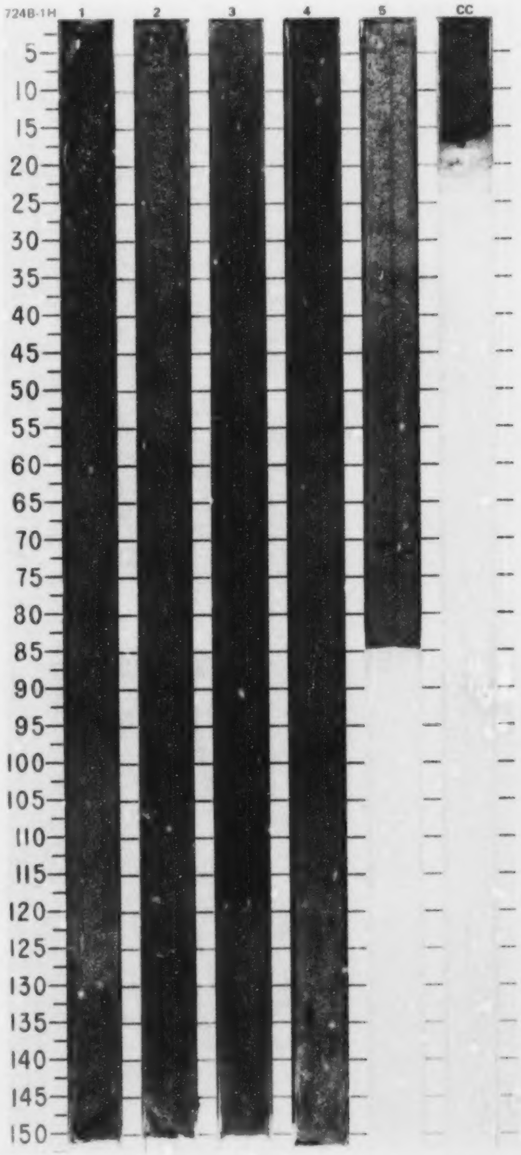
724B-1H
1
2
3
4
5
CC
5
10
15
20
25
30
35
40
45
50
55
60
65
70
75
80
85
90
95
100
105
110
115
120
125
130
135
140
145
150

SITE 724 HOLE B CORE 2H CORED INTERVAL 599.8-609.2 mbsl; 7.0-16.4 mbsf

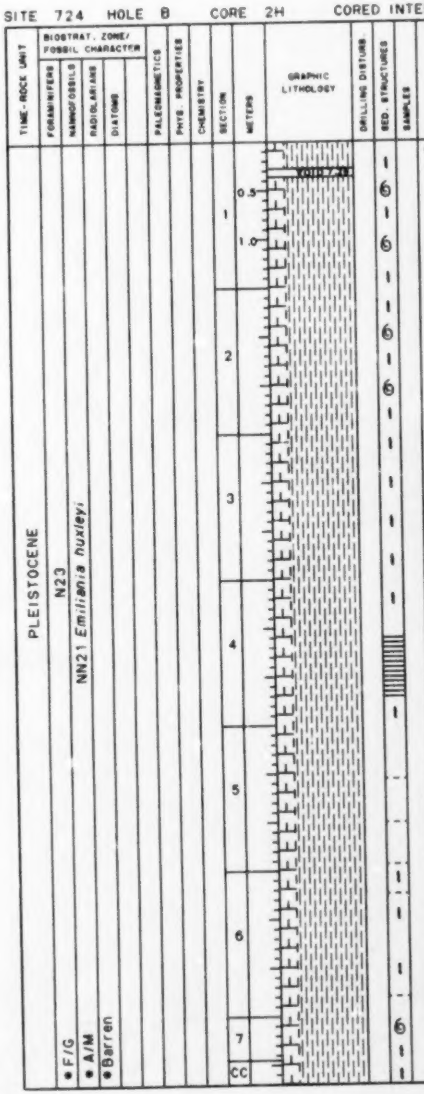
TIME-ROCK UNIT
BIOSTRAT. ZONE/ FOSSIL CHARACTER
FORAMINIFERS
NANNOFOSSILS
RADIOLARIANS
DIATOMS
PALEOMAGNETICS
PHYS. PROPERTIES
CHEMISTRY
SECTION
METERS
GRAPHIC LITHOLOGY
DRILLING DISTURB.
SED. STRUCTURES
SAMPLES
PLEISTOCENE
N23
NN21 Emiliania huxleyi
● F/G
● A/M
● Barren
0.5
1.0
1
2
3
4
5
6
7
CC
VOID

LITHOLOGIC DESCRIPTION

CALCAREOUS CLAYEY SILT

Entire core undisturbed.

Major lithology: CALCAREOUS CLAYEY SILT, olive (5Y 4/3), olive gray (5Y 5/2, 4/2), and dark olive gray (5Y 3/2). Minor burrow mottling common. Contacts gradational and mottled. Millimeter-sized indeterminate shell fragments common.

Minor lithology: Section 4, 60-120 cm, finely bedded layer. Beds 5-10 mm thick of alternating nannofossil silty clay, olive gray (5Y 4/2), and calcitic silty clay, dark olive gray (5Y 3/2).

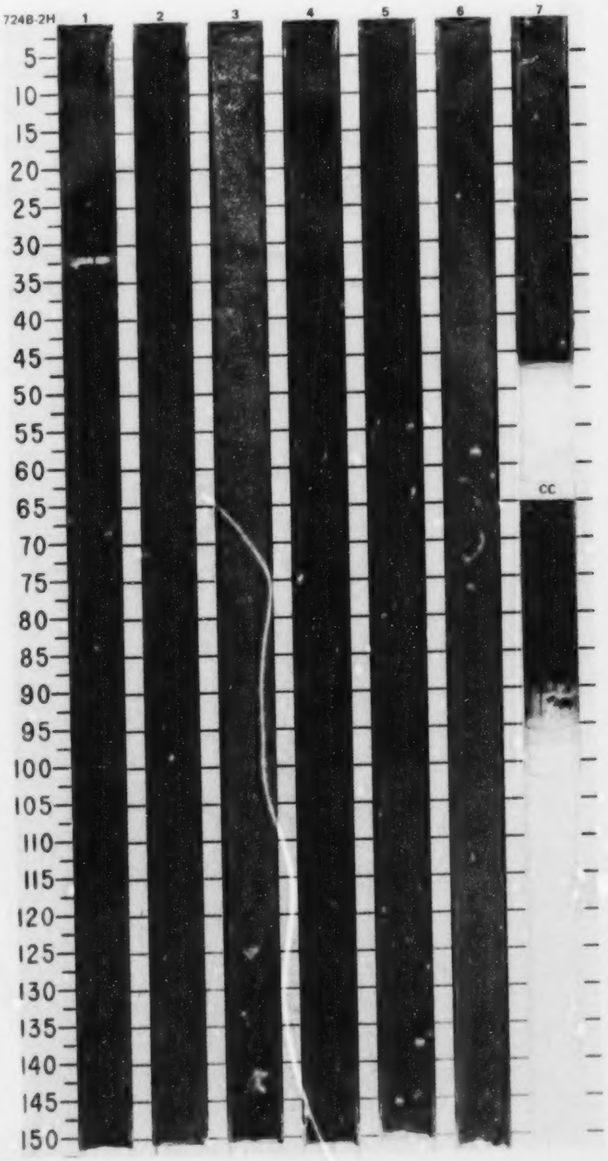
724B-2H
1
2
3
4
5
6
7
CC
5
10
15
20
25
30
35
40
45
50
55
60
65
70
75
80
85
90
95
100
105
110
115
120
125
130
135
140
145
150

SITE 724 HOLE B CORE 3H CORED INTERVAL 609.2-618.7 mbsl; 16.4-25.9 mbsf

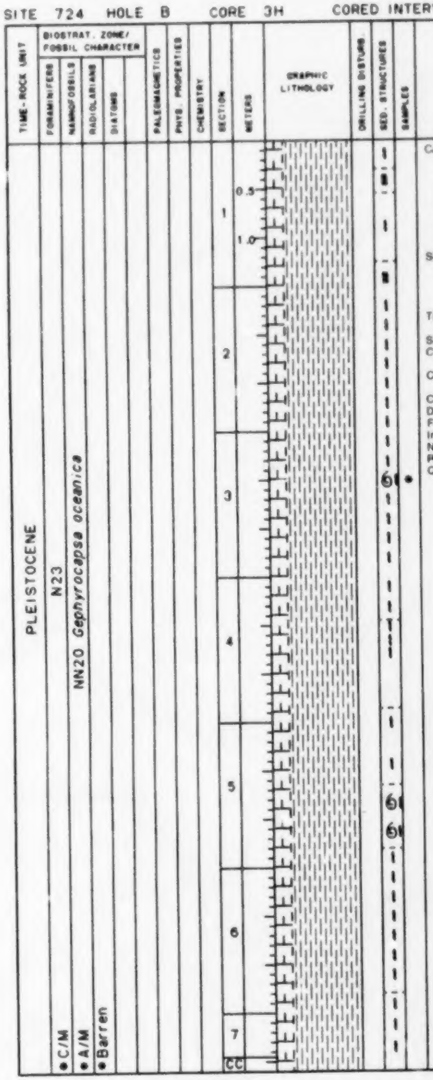
TIME-ROCK UNIT
BIOSTRAT. ZONE/ FOSSIL CHARACTER
FORAMINIFERS
NANNOFOSSILS
RADIOLARIANS
DIATOMS
PALEOMAGNETICS
PHYS. PROPERTIES
CHEMISTRY
SECTION
METERS
GRAPHIC LITHOLOGY
DRILLING DISTURB.
SED. STRUCTURES
SAMPLES
PLEISTOCENE
N23
NN20 Gephyrocapsa oceanica
● C/M
● A/M
● Barren
0.5
1.0
1
2
3
4
5
6
7
CC

LITHOLOGIC DESCRIPTION

CALCAREOUS CLAYEY SILT

Entire core undisturbed.

Major lithology: CALCAREOUS CLAYEY SILT, olive (5Y 4/3), and olive gray (5Y 4/2). Minor to moderate burrow mottling common. Contacts gradational and mottled. Millimeter-sized indeterminate shell fragments common. Foraminifers visible.

SMEAR SLIDE SUMMARY (%):

	3, 51 D
TEXTURE:	
Silt	60
Clay	40
COMPOSITION:	
Clay	31
Dolomite	Tr
Foraminifers	5
Inorganic calcite	45
Nannofossils	7
Pellets	2
Quartz	10

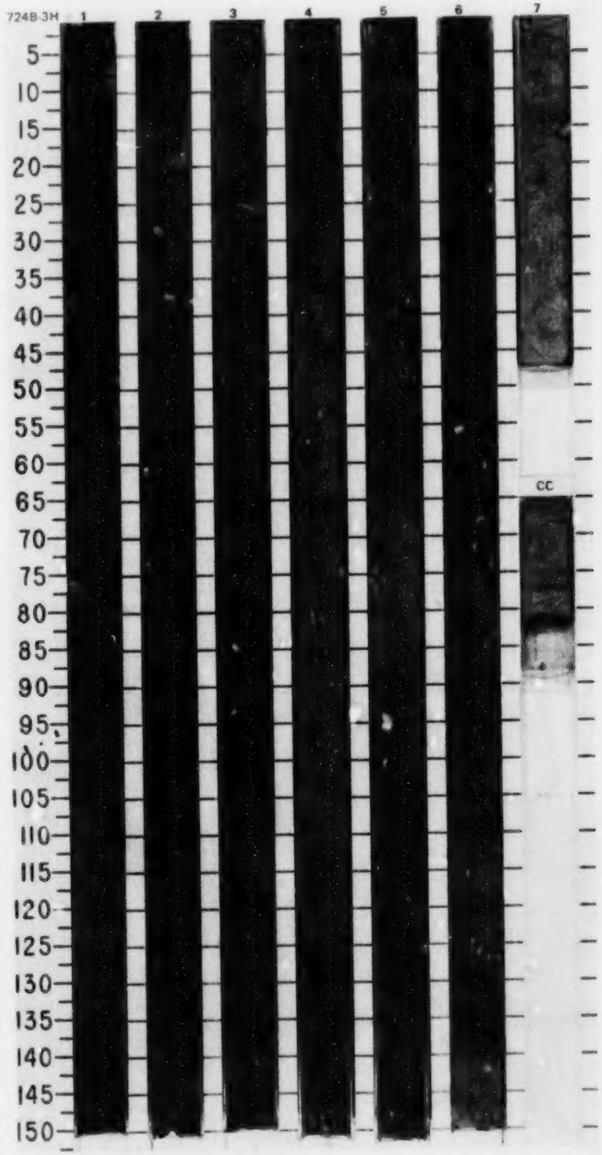
724B-3H
1
2
3
4
5
6
7
CC
5
10
15
20
25
30
35
40
45
50
55
60
65
70
75
80
85
90
95
100
105
110
115
120
125
130
135
140
145
150

SITE 724 HOLE B CORE 4H CORED INTERVAL 618.7-628.2 mbsl; 25.9-35.4 mbsf

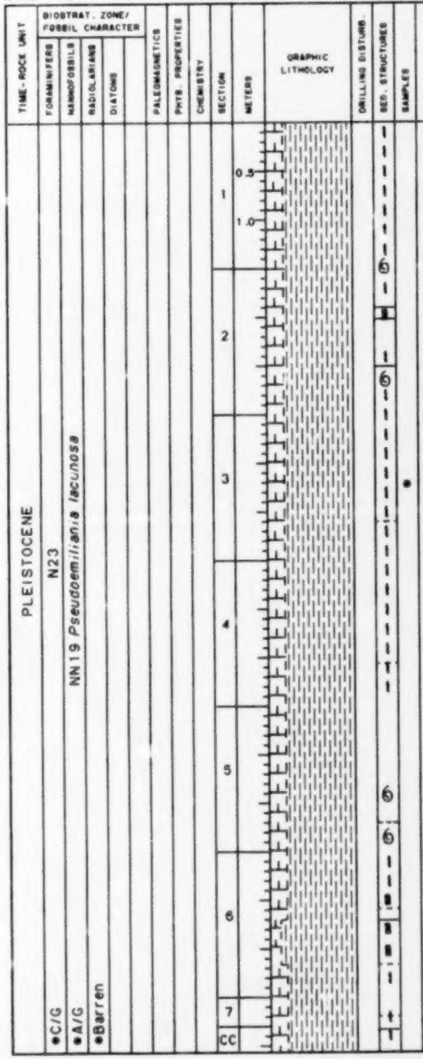
TIME-ROCK UNIT
BIOSTRAT. ZONE/ FOSSIL CHARACTER
FORAMINIFERS
NANNOFOSSILS
RADIOLARIANS
DIATOMS
PALEOMAGNETICS
PHYS. PROPERTIES
CHEMISTRY
SECTION
METERS
GRAPHIC LITHOLOGY
DRILLING DISTURB.
SED. STRUCTURES
SAMPLES
PLEISTOCENE
N23
NN19 Pseudoemiliania lacunosa
●C/G
●A/G
●Barren
1
2
3
4
5
6
7
CC
0.5
1.0

LITHOLOGIC DESCRIPTION

CALCAREOUS CLAYEY SILT

Entire core undisturbed.

Major lithology: CALCAREOUS CLAYEY SILT, olive (5Y 4/3), olive gray (5Y 5/2, 4/2), and dark olive gray (5Y 3/2). Minor to moderate burrow mottling common. Contacts gradational and mottled. Foraminifers and bivalves visible.

Minor lithology: Section 6, 70-120 cm, calcitic clayey silt, olive gray (5Y 5/2). Sharp top and mottled lower contact.

SMEAR SLIDE SUMMARY (%):

	3, 72 D
TEXTURE:	
Silt	30
Clay	70
COMPOSITION:	
Clay	25
Feldspar	2
Foraminifers	2
Gypsum	Tr
Inorganic calcite	25
Nannofossils	33
Pellets	3
Quartz	10

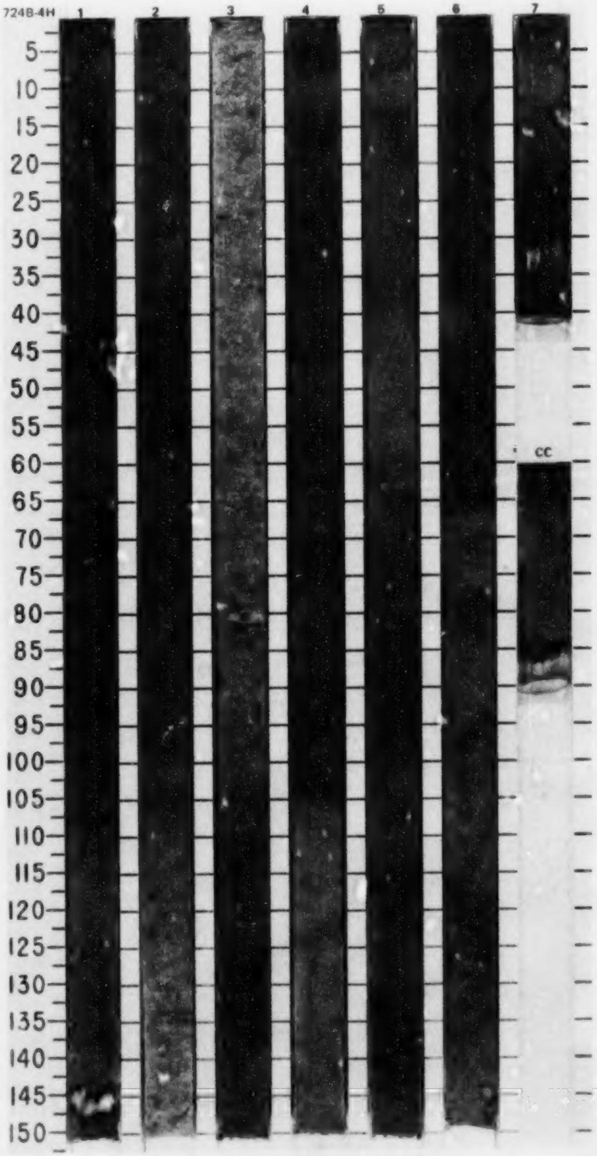
724B-4H
1
2
3
4
5
6
7
CC
5
10
15
20
25
30
35
40
45
50
55
60
65
70
75
80
85
90
95
100
105
110
115
120
125
130
135
140
145
150

SITE 724 HOLE B CORE 5H CORED INTERVAL 628.2-637.8 mbsl; 35.4-45.0 mbsf

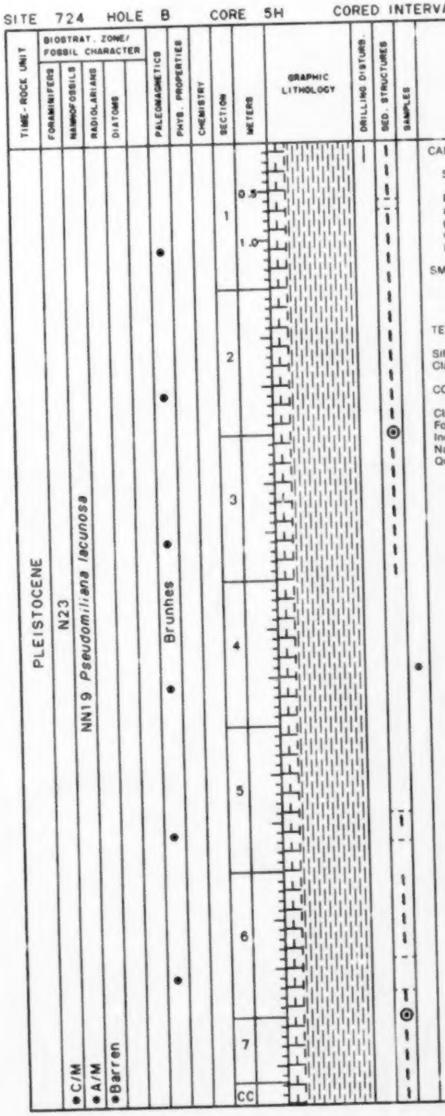
TIME-ROCK UNIT
BIOSTRAT. ZONE/ FOSSIL CHARACTER
FORAMINIFERS
NANNOFOSSILS
RADIOLARIANS
DIATOMS
PALEOMAGNETICS
PHYS. PROPERTIES
CHEMISTRY
SECTION
METERS
GRAPHIC LITHOLOGY
DRILLING DISTURB.
SED. STRUCTURES
SAMPLES
PLEISTOCENE
N23
NN19 Pseudomiliana lacunosa
Brunhes
●C/M
●A/M
●Barren
0.5
1.0
1
2
3
4
5
6
7
CC

LITHOLOGIC DESCRIPTION

CALCAREOUS CLAYEY SILT

Section 1, 0-15 cm, slightly disturbed; remainder undisturbed.

Major lithology: CALCAREOUS CLAYEY SILT, olive (5Y 4/3), olive gray (5Y 4/2), and dark olive gray (5Y 3/2). Minor burrow mottling common. Contacts gradational and mottled. Millimeter-sized indeterminate shell fragments common. Foraminifers visible. Section 2, 142 cm, and Section 6, 140 cm, phosphatic nodules, black (5Y 2.5/1) with irregular outlines.

SMEAR SLIDE SUMMARY (%):

	4, 93 D
TEXTURE:	
Silt	40
Clay	60
COMPOSITION:	
Clay	30
Foraminifers	7
Inorganic calcite	35
Nannofossils	20
Quartz	8

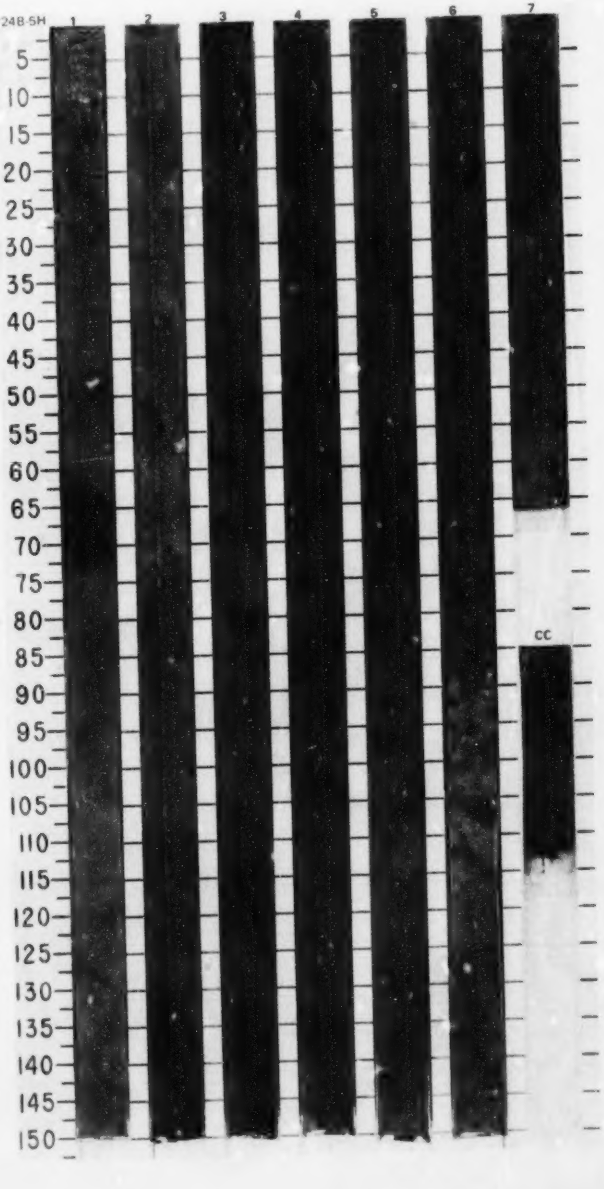
724B-5H
1
2
3
4
5
6
7
CC
5
10
15
20
25
30
35
40
45
50
55
60
65
70
75
80
85
90
95
100
105
110
115
120
125
130
135
140
145
150

SITE 724 HOLE B CORE 6X CORED INTERVAL 637.8-647.5 mbsl; 45.0-54.7 mbsf

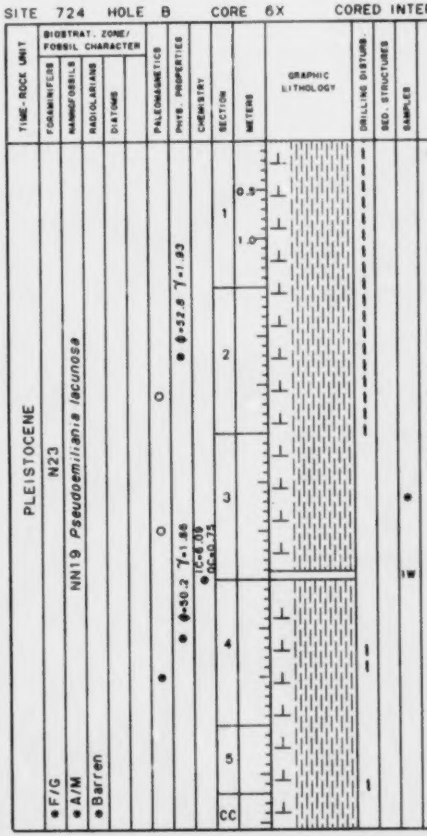
TIME-ROCK UNIT
BIOSTRAT. ZONE/ FOSSIL CHARACTER
FORAMINIFERS
NANNOFOSSILS
RADIOLARIANS
DIATOMS
PALEOMAGNETICS
PHYS. PROPERTIES
CHEMISTRY
SECTION
METERS
GRAPHIC LITHOLOGY
DRILLING DISTURB.
SED. STRUCTURES
SAMPLES
PLEISTOCENE
N23
NN19 Pseudoemiliania lacunosa
● F/G
● A/M
● Barren
● Φ=52.8 γ=1.93
● Φ=50.2 γ=1.86
● IC=6.08 OC=0.75
1
2
3
4
5
CC
0.5
1.0
IW

LITHOLOGIC DESCRIPTION

CALCAREOUS CLAYEY SILT

Entire core undisturbed.

Major lithology: CALCAREOUS CLAYEY SILT, olive gray (5Y 4/2). Minor burrow mottling in Sections 1 and 2, rest of core unmottled. Some mottles filled with olive gray (5Y 5/2) calcitic silt.

SMEAR SLIDE SUMMARY (%):

	3, 68 D
TEXTURE:	
Silt	40
Clay	60
COMPOSITION:	
Clay	30
Dolomite	2
Foraminifers	5
Inorganic calcite	28
Mica	Tr
Nannofossils	25
Quartz	10

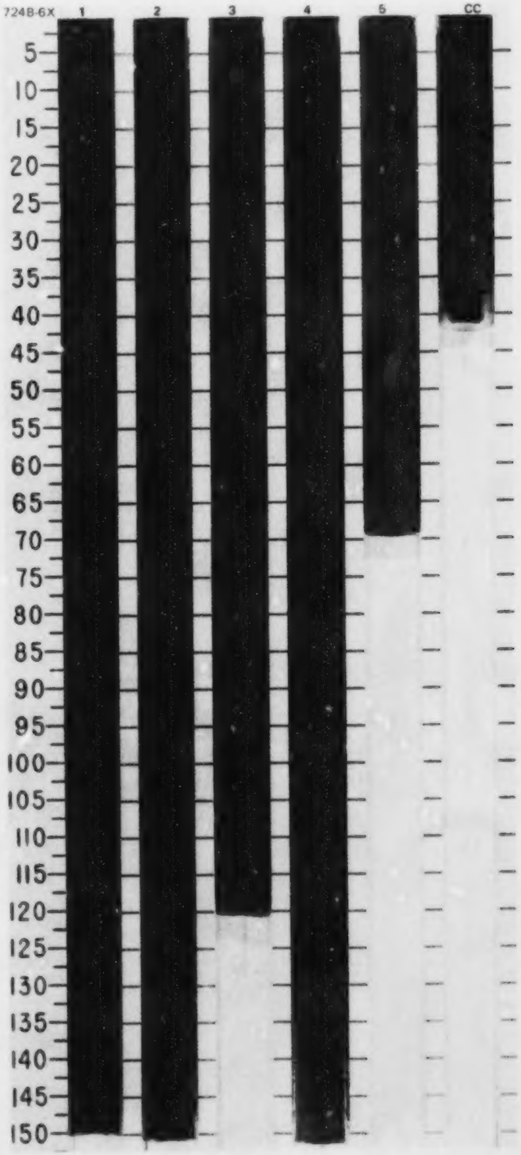
724B-6X
1
2
3
4
5
CC
5
10
15
20
25
30
35
40
45
50
55
60
65
70
75
80
85
90
95
100
105
110
115
120
125
130
135
140
145
150

SITE 724 HOLE B CORE 7X CORED INTERVAL 647.5-657.2 mbsl; 54.7-64.4 mbsf

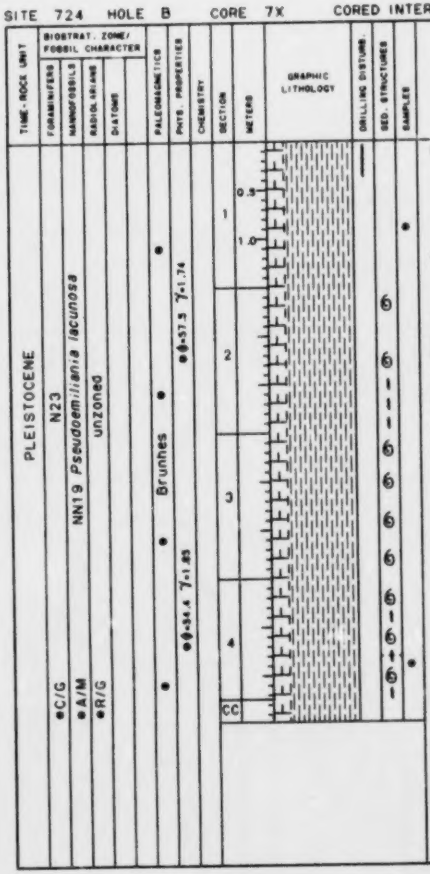
TIME-ROCK UNIT
BIOSTRAT. ZONE/ FOSSIL CHARACTER
FORAMINIFERS
NANNOFOSSILS
RADIOLARIANS
DIATOMS
PALEOMAGNETICS
PHYS. PROPERTIES
CHEMISTRY
SECTION
METERS
GRAPHIC LITHOLOGY
DRILLING DISTURB.
SED. STRUCTURES
SAMPLES
PLEISTOCENE
N23
NN19 Pseudoemiliania lacunosa
unzoned
●C/G
●A/M
●R/G
Brunhes
●Φ=57.5 γ=1.74
●Φ=54.4 γ=1.85
1
2
3
4
CC
0.5
1.0

LITHOLOGIC DESCRIPTION

CALCAREOUS CLAYEY SILT

Section 1, 0-25 cm, very disturbed; remainder undisturbed.

Major lithology: CALCAREOUS CLAYEY SILT, olive (5Y 4/3) and olive gray (5Y 4/2). Occasional faint burrow mottling. Bedding contact is gradational and mottled. Millimeter-sized, indeterminate shell fragments in Sections 2, 3, and 4.

SMEAR SLIDE SUMMARY (%):

	1, 90 D	4, 90 D
TEXTURE:		
Silt	40	45
Clay	60	55
COMPOSITION:		
Clay	25	35
Dolomite	Tr	Tr
Feldspar	Tr	
Foraminifers	10	5
Inorganic calcite	25	30
Nannofossils	35	20
Quartz	5	10

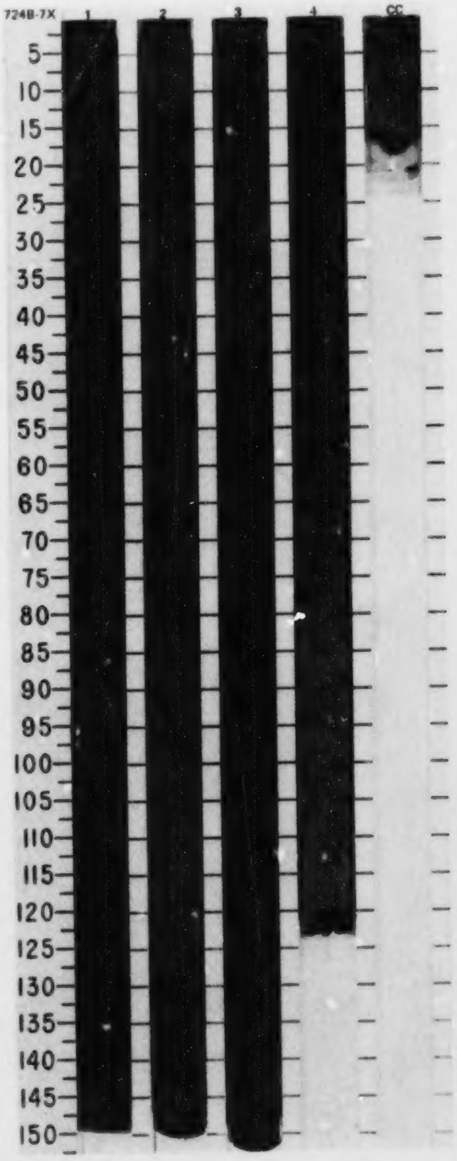
724B-7X
1
2
3
4
CC
5
10
15
20
25
30
35
40
45
50
55
60
65
70
75
80
85
90
95
100
105
110
115
120
125
130
135
140
145
150

SITE 724 HOLE B CORE 8X CORED INTERVAL 657.2-666.8 mbsl; 64.4-74.0 mbsf

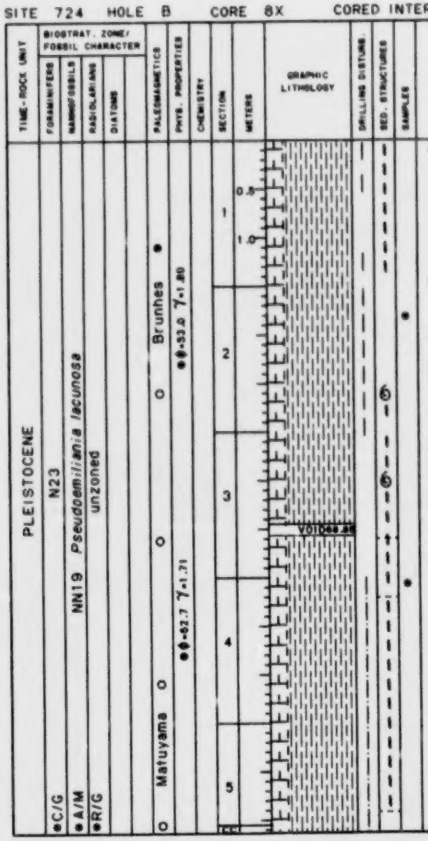
TIME-ROCK UNIT
BIOSTRAT. ZONE/ FOSSIL CHARACTER
FORAMINIFERS
NANNOFOSSILS
RADIOLARIANS
DIATOMS
PALEOMAGNETICS
PHYS. PROPERTIES
CHEMISTRY
SECTION
METERS
GRAPHIC LITHOLOGY
DRILLING DISTURB.
SED. STRUCTURES
SAMPLES
PLEISTOCENE
N23
NN19 Pseudoemiliania lacunosa
unzoned
●C/G
●A/M
●R/G
Brunhes
Matuyama
●Φ=53.0 γ=1.80
●Φ=62.7 γ=1.71
0.5
1.0
1
2
3
4
5
CC
VOID

LITHOLOGIC DESCRIPTION

MARLY NANNOFOSSIL OOZE

Section 4, 0-150 cm, and Section 5, 0-150 cm, moderately disturbed; Section 1, 0-15, 45-55, and 115-125 cm, and Section 2, 0-150 cm, slightly disturbed; remainder undisturbed.

Major lithology: MARLY NANNOFOSSIL OOZE, olive (5Y 4/3), olive gray (5Y 5/2, 4/2), dark olive gray (5Y 3/2), very dark gray (5Y 3/1), and black (5Y 2.5/2). Minor burrow mottling throughout. Bedding contacts are gradational and mottled. Millimeter-sized, indeterminate shell fragments common. Foraminifers visible.

SMEAR SLIDE SUMMARY (%):

	2, 30 D	4, 7 M
TEXTURE:		
Sand	5	
Silt	45	30
Clay	50	70
COMPOSITION:		
Access. minerals	5	
Clay	10	35
Diatoms		Tr
Dolomite		Tr
Foraminifers	10	10
Inorganic calcite	15	20
Nannofossils	55	30
Organic debris		5
Pyrite	Tr	
Quartz	5	Tr
Silicoflagellates		Tr
Sponge spicules		Tr

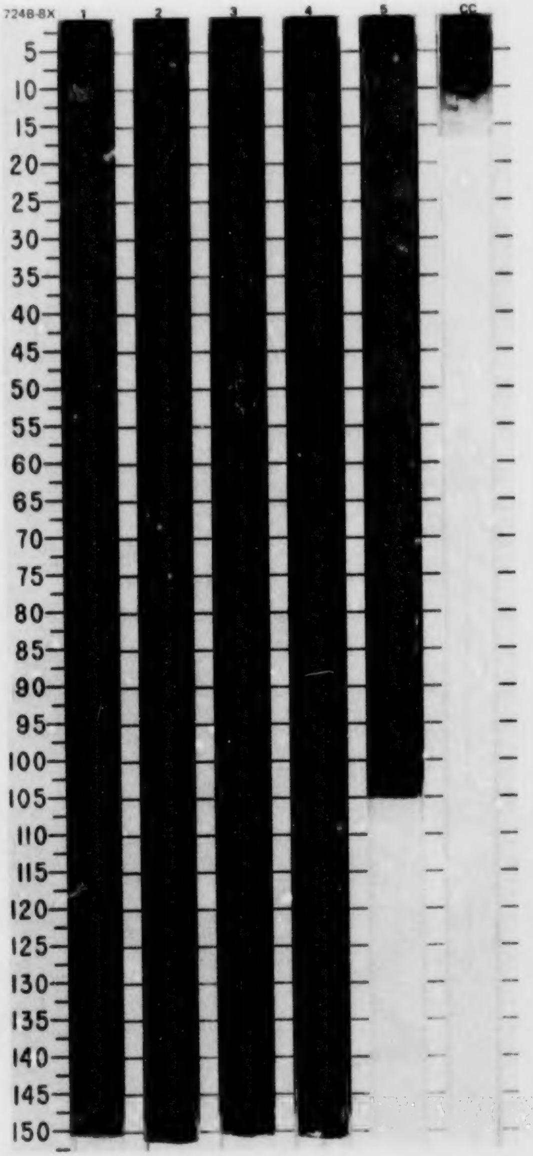
724B-8X
1
2
3
4
5
CC
5
10
15
20
25
30
35
40
45
50
55
60
65
70
75
80
85
90
95
100
105
110
115
120
125
130
135
140
145
150

SITE 724 HOLE B CORE 9X CORED INTERVAL 666.8-676.5 mbsl: 74.0-83.7 mbsf

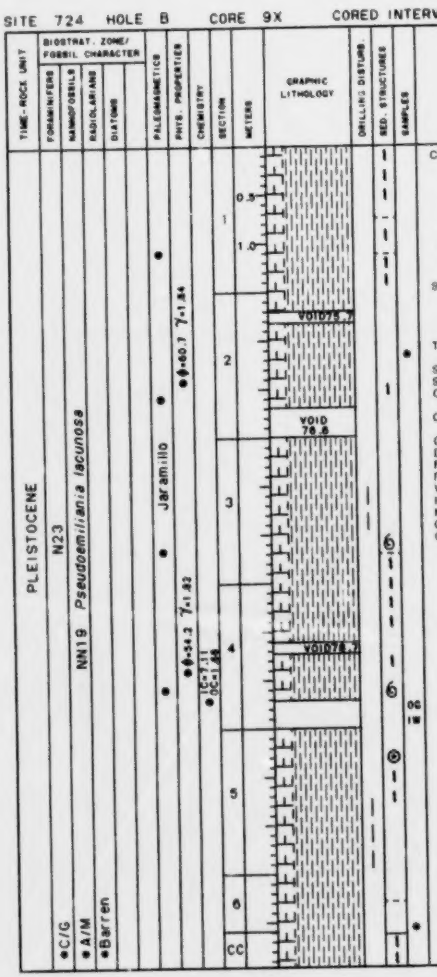

TIME-ROCK UNIT
BIOSTRAT. ZONE/ FOSSIL CHARACTER
FORAMINIFERS
NANNOFOSSILS
RADIOLARIANS
DIATOMS
PALEOMAGNETICS
PHYS. PROPERTIES
CHEMISTRY
SECTION
METERS
GRAPHIC LITHOLOGY
DRILLING DISTURB.
SED. STRUCTURES
SAMPLES
PLEISTOCENE
N23
NN19 Pseudoemiliania lacunosa
•C/G
•A/M
•Barren
Jaramillo
•φ=60.7 γ=1.84
•φ=54.2 γ=1.82
•IC=7.11 OC=1.88
1
2
3
4
5
6
CC
0.5
1.0
VOID 75.7
VOID 76.6
VOID 78.7
OG
IW

LITHOLOGIC DESCRIPTION

CALCAREOUS CLAYEY SILT

Section 3, 60-110 cm, and Section 5, 80-125 cm, slightly disturbed; remainder undisturbed. Voids caused during gas expansion.

Major lithology: CALCAREOUS CLAYEY SILT, olive (5Y 4/3), olive gray (5Y 5/2, 4/2), and dark olive gray (5Y 3/2). Minor burrow mottling throughout. Bedding contacts are gradational and mottled. Millimeter-sized, indeterminate shell fragments common. Foraminifers visible. Section 5, 27 cm, black (5Y 2.5/1) phosphatic nodule.

SMEAR SLIDE SUMMARY (%):

	2, 65 D	6, 52 D
TEXTURE:		
Sand	10	10
Silt	50	50
Clay	40	40
COMPOSITION:		
Clay	30	20
Dolomite	Tr	Tr
Feldspar		Tr
Foraminifers	15	10
Volcanic glass		Tr
Inorganic calcite	35	40
Nannofossils	15	20
Organic debris		5
Quartz	5	5

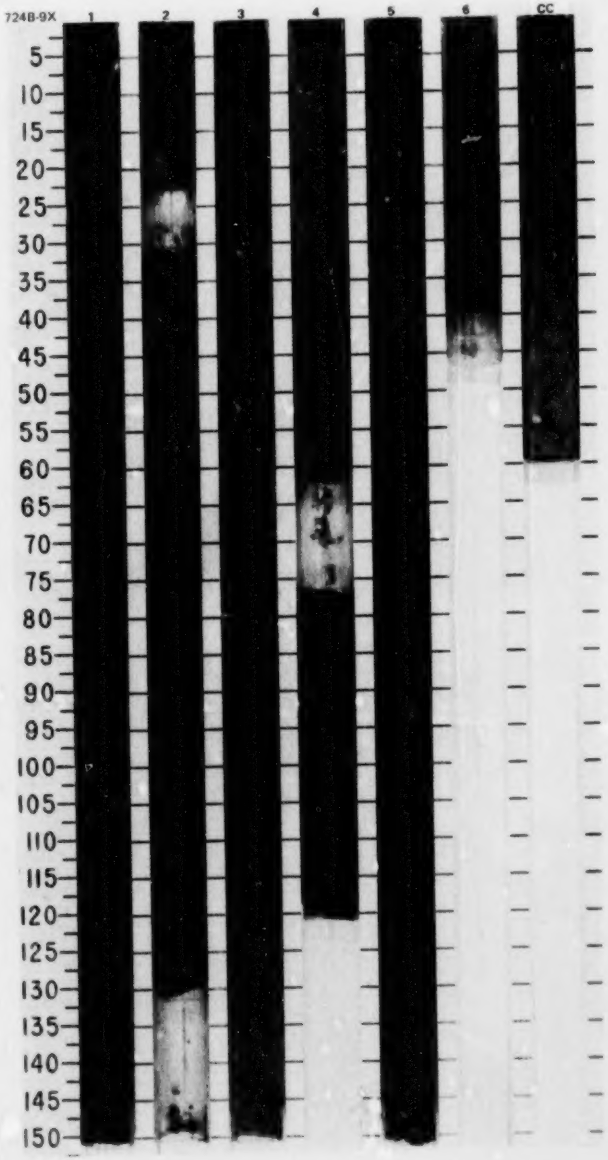

724B-9X
1
2
3
4
5
6
CC
5
10
15
20
25
30
35
40
45
50
55
60
65
70
75
80
85
90
95
100
105
110
115
120
125
130
135
140
145
150

SITE 724 HOLE B CORE 10X CORED INTERVAL 676.5-686.2 mbsl; 83.7-93.4 mbsf

TIME-ROCK UNIT	BIOSTRAT. ZONE/ FOSSIL CHARACTER					PALEOMAGNETICS	PHYS. PROPERTIES	CHEMISTRY
	FORAMINIFERS	NANNOFOSSILS	RADIOLARIANS	DIATOMS				
PLEISTOCENE	N22 ●C/G	NN19 *Pseudoemiliania lacunosa* ●A/M	●Barren			Matuyama O	●ϕ=57.3 γ=1.77	

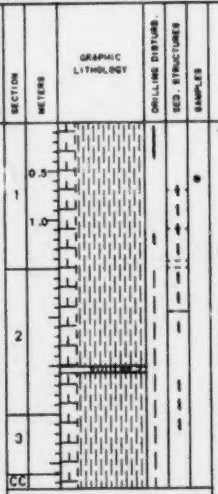
SECTION
METERS
GRAPHIC LITHOLOGY
DRILLING DISTURB.
SED. STRUCTURES
SAMPLES
1
2
3
CC
0.5
1.0

LITHOLOGIC DESCRIPTION

CALCAREOUS CLAYEY SILT

Section 1, 0-30 and 110-130 cm, very disturbed; Section 2, 0-150 cm, and Section 3, 0-60 cm, slightly disturbed; remainder undisturbed. Voids caused during gas expansion.

Major lithology: CALCAREOUS CLAYEY SILT, olive (5Y 4/3), olive gray (5Y 4/2), dark olive gray (5Y 3/2), and black (5Y 2.5/2). Minor burrow mottling common. Bedding contacts are gradational and mottled. Foraminifers visible.

SMEAR SLIDE SUMMARY (%):

	1, 60 D
TEXTURE:	
Sand	5
Silt	35
Clay	60
COMPOSITION:	
Clay	30
Dolomite	Tr
Foraminifers	15
Volcanic glass	Tr
Inorganic calcite	20
Nannofossils	30
Quartz	5

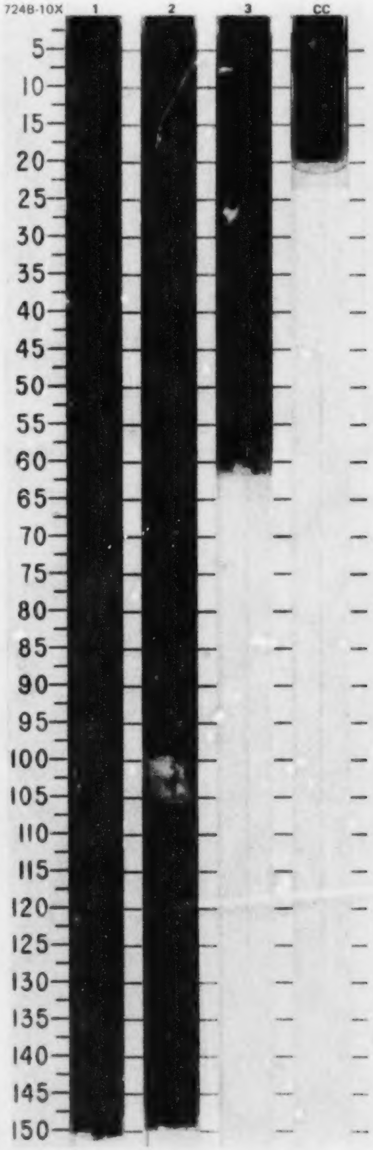
724B-10X
1
2
3
CC
5
10
15
20
25
30
35
40
45
50
55
60
65
70
75
80
85
90
95
100
105
110
115
120
125
130
135
140
145
150

SITE 724 HOLE B CORE 11X CORED INTERVAL 686.2-695.8 mbsl; 93.4-103.0 mbsf

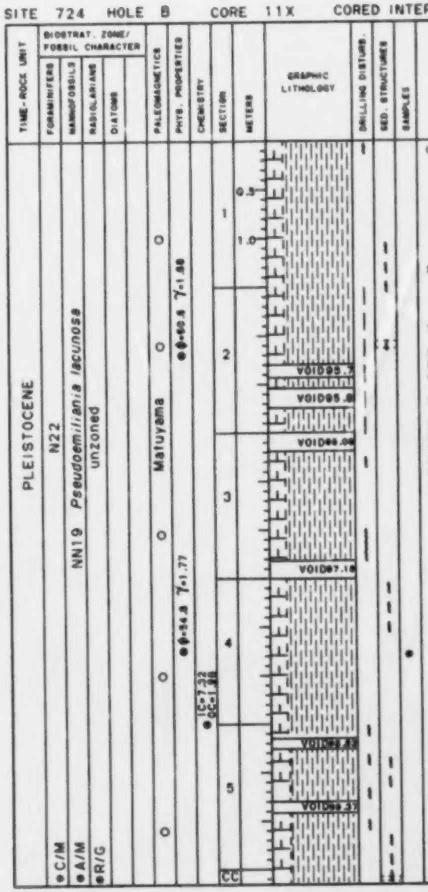
TIME-ROCK UNIT
BIOSTRAT. ZONE/ FOSSIL CHARACTER
FORAMINIFERS
NANNOFOSSILS
RADIOLARIANS
DIATOMS
PALEOMAGNETICS
PHYS. PROPERTIES
CHEMISTRY
SECTION
METERS
GRAPHIC LITHOLOGY
DRILLING DISTURB.
SED. STRUCTURES
SAMPLES
PLEISTOCENE
N22
NN19 Pseudoemiliania lacunosa
unzoned
●C/M
●A/M
●R/G
Matuyama
●ϕ=60.6 γ=1.86
●ϕ=54.8 γ=1.77
●IC=7.32 OC=1.88
1
2
3
4
5
CC
0.5
1.0
VOID95.7
VOID95.8
VOID96.06
VOID97.16
VOID98.83
VOID99.37

LITHOLOGIC DESCRIPTION

CALCAREOUS CLAYEY SILT

Section 1, 0-15 cm, Section 3, 20-25 and 100-130 cm, and Section 5, 10-30 and 75-86 cm, very disturbed; and Section 2, 0-150 cm, slightly disturbed; remainder undisturbed. Voids caused during gas expansion.

Major lithology: CALCAREOUS CLAYEY SILT, dark olive gray (5Y 3/2) and black (5Y 2.5/2). Some minor burrow mottling. Bedding contacts are gradational and mottled. Foraminifers visible.

SMEAR SLIDE SUMMARY (%):

	4, 77 D
TEXTURE:	
Sand	5
Silt	50
Clay	45
COMPOSITION:	
Clay	30
Dolomite	Tr
Foraminifers	20
Inorganic calcite	20
Nannofossils	25
Quartz	5

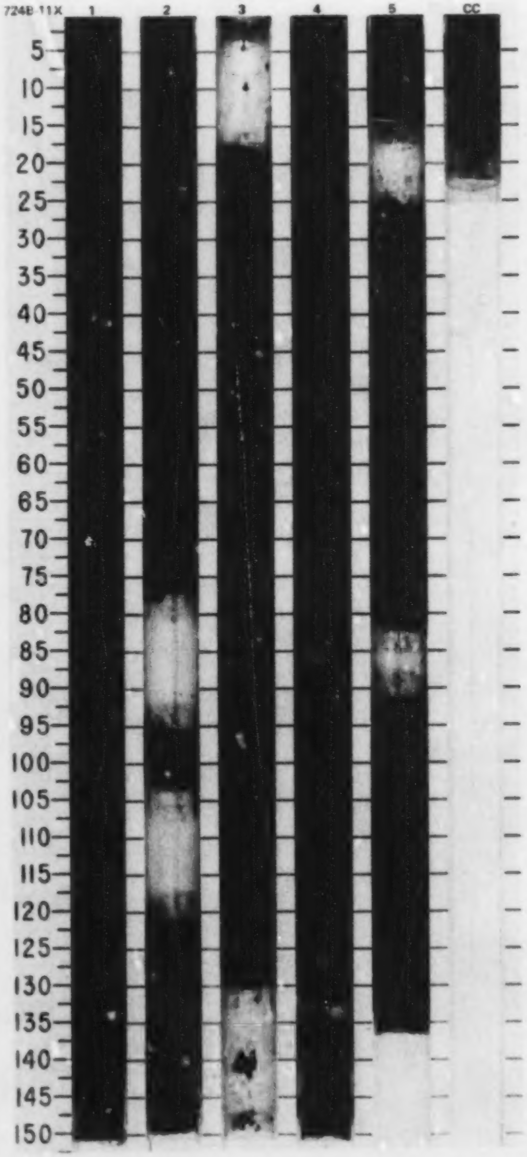
724B-11X
1
2
3
4
5
CC
5
10
15
20
25
30
35
40
45
50
55
60
65
70
75
80
85
90
95
100
105
110
115
120
125
130
135
140
145
150

SITE 724 HOLE B CORE 12X CORED INTERVAL 695.8-705.5 mbsl; 103.0-112.7 mbsf

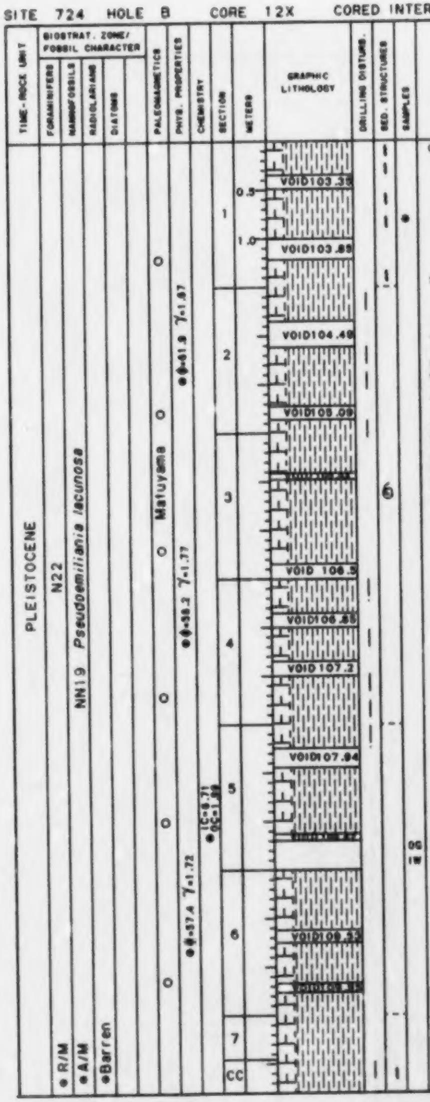
TIME-ROCK UNIT
BIOSTRAT. ZONE/ FOSSIL CHARACTER
FORAMINIFERS
NANNOFOSSILS
RADIOLARIANS
DIATOMS
PALEOMAGNETICS
PHYS. PROPERTIES
CHEMISTRY
SECTION
METERS
GRAPHIC LITHOLOGY
DRILLING DISTURB.
SED. STRUCTURES
SAMPLES
PLEISTOCENE
N22
NN19 Pseudoemiliania lacunosa
● R/M
● A/M
●Barren
Matuyama
●φ=61.9 γ=1.67
●φ=58.2 γ=1.77
●φ=57.4 γ=1.72
●IC=8.71 OC=1.89
0.5
1.0
1
2
3
4
5
6
7
CC
VOID103.35
VOID103.85
VOID104.49
VOID105.09
VOID 106.5
VOID106.85
VOID 107.2
VOID107.94
VOID108.33
OG
IW

LITHOLOGIC DESCRIPTION

CALCAREOUS CLAYEY SILT

Section 2, 69-90 cm, and Section 4, 15-38 and 110-150 cm, moderately disturbed; Section 2, 0-38 and 90-150 cm, and Section 4, 0-15 and 50-110 cm, slightly disturbed; remainder undisturbed. Voids caused during gas expansion.

Major lithology: CALCAREOUS CLAYEY SILT, olive (5Y 4/3), olive gray (5Y 4/2), and dark olive gray (5Y 3/2). Minor burrow mottling in Section 1 only. Bedding contacts are gradational and mottled. Foraminifers visible. Section 3, 75 cm, phosphatized bone.

SMEAR SLIDE SUMMARY (%):

	1, 80 D
TEXTURE:	
Silt	40
Clay	60
COMPOSITION:	
Access. minerals	Tr
Clay	20
Foraminifers	10
Inorganic calcite	30
Mica	Tr
Nannofossils	30
Quartz	10

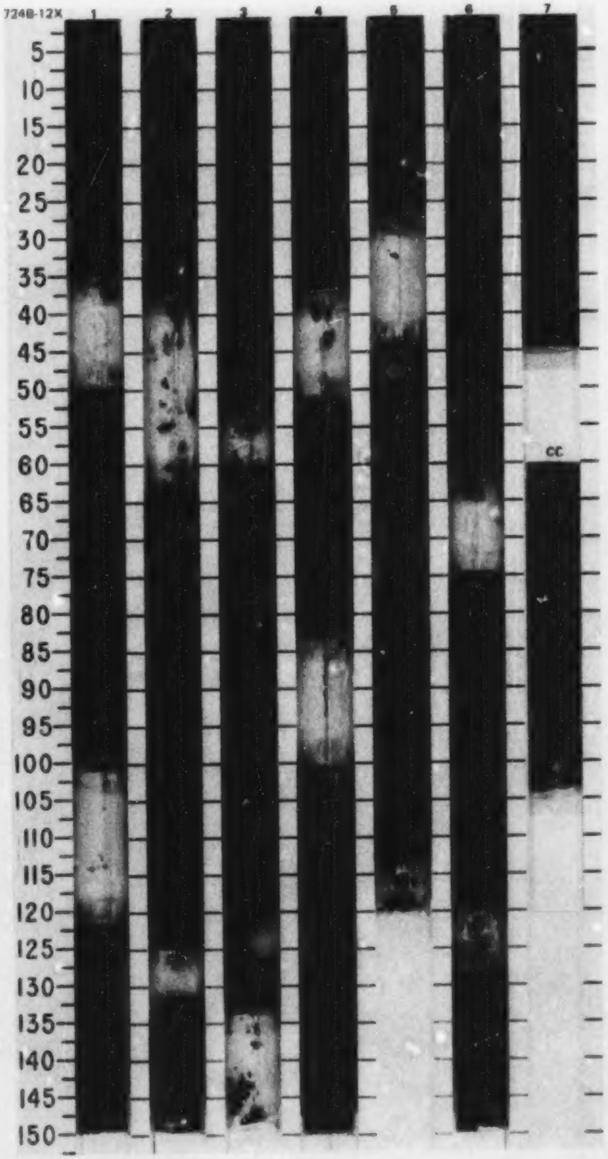
724B-12X
1
2
3
4
5
6
7
CC
5
10
15
20
25
30
35
40
45
50
55
60
65
70
75
80
85
90
95
100
105
110
115
120
125
130
135
140
145
150

CORE 117–724B–13X NO RECOVERY

SITE 724 HOLE B CORE 14X CORED INTERVAL 715.2-724.8 mbsl; 122.4-132.0 mbsf

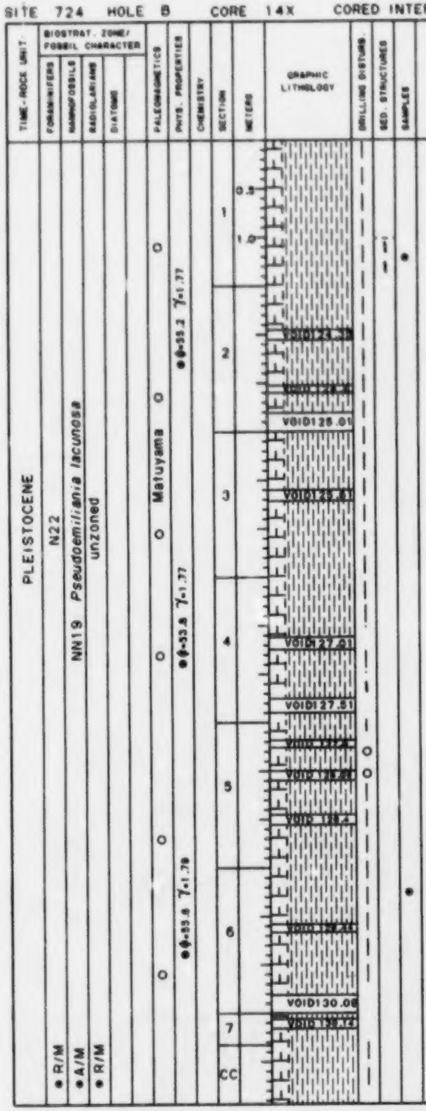

TIME-ROCK UNIT
BIOSTRAT. ZONE/ FOSSIL CHARACTER
FORAMINIFERS
NANNOFOSSILS
RADIOLARIANS
DIATOMS
PALEOMAGNETICS
PHYS. PROPERTIES
CHEMISTRY
SECTION
METERS
GRAPHIC LITHOLOGY
DRILLING DISTURB.
SED. STRUCTURES
SAMPLES
PLEISTOCENE
N22
NN19 Pseudoemiliania lacunosa
unzoned
• R/M
• A/M
• R/M
Matuyama
●φ=55.2 γ=1.77
●φ=53.8 γ=1.77
●φ=53.6 γ=1.79
1
2
3
4
5
6
7
CC
0.5
1.0
VOID125.01
VOID125.61
VOID127.01
VOID127.51
VOID130.08

LITHOLOGIC DESCRIPTION

CALCAREOUS CLAYEY SILT

Section 5, 24-51 cm, soupy; Section 4, 100-125 cm, very disturbed; Section 4, 30-100 cm, moderately disturbed; remainder slightly disturbed. Voids caused during gas expansion.

Major lithology: CALCAREOUS CLAYEY SILT, olive gray (5Y 4/2) and dark olive gray (5Y 3/2). Minor burrow mottling in Section 1 only. Bedding contacts are gradational and mottled. Foraminifers visible.

SMEAR SLIDE SUMMARY (%):

	1, 120 D	6, 29 D
TEXTURE:		
Sand	15	10
Silt	40	30
Clay	45	60
COMPOSITION:		
Access. minerals	2	2
Clay	30	30
Dolomite	Tr	
Feldspar	2	
Foraminifers	Tr	3
Volcanic glass	Tr	Tr
Inorganic calcite	30	20
Mica	1	
Nannofossils	15	30
Quartz	20	15
Sponge spicules		Tr

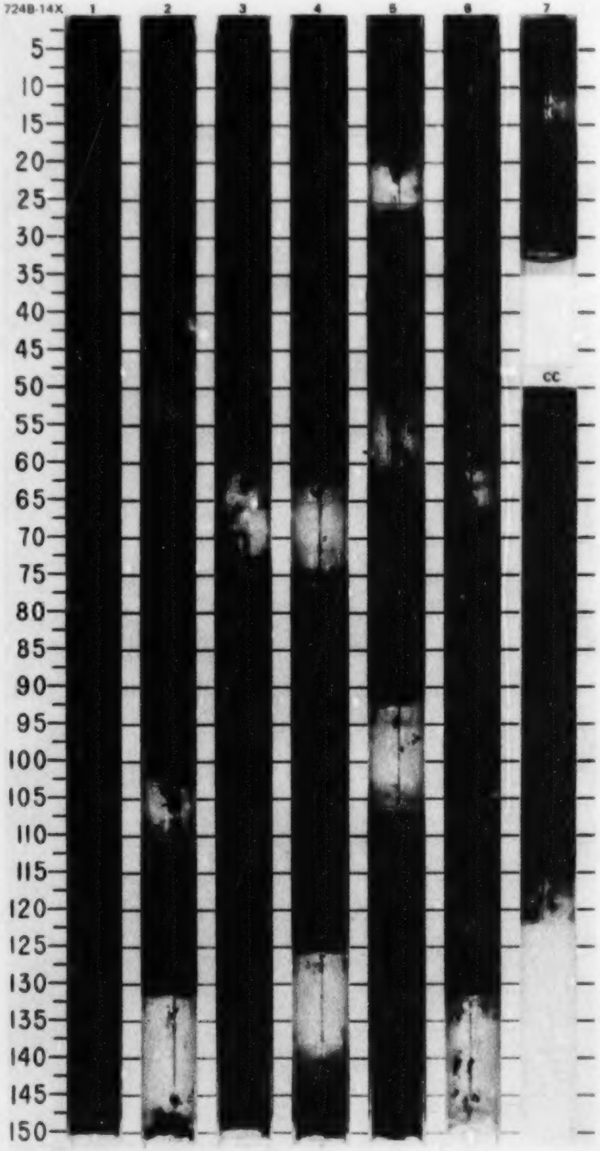

724B-14X
1
2
3
4
5
6
7
CC
5
10
15
20
25
30
35
40
45
50
55
60
65
70
75
80
85
90
95
100
105
110
115
120
125
130
135
140
145
150

SITE 724 HOLE B CORE 15X CORED INTERVAL 724.8-734.5 mbsl; 132.0-141.7 mbsf

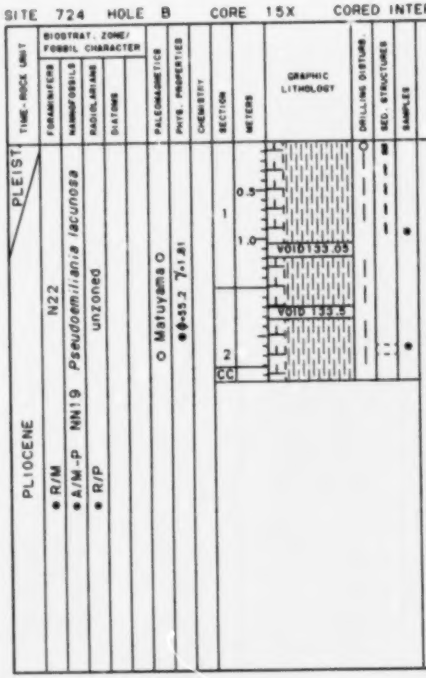
TIME-ROCK UNIT
BIOSTRAT. ZONE/ FOSSIL CHARACTER
FORAMINIFERS
NANNOFOSSILS
RADIOLARIANS
DIATOMS
PALEOMAGNETICS
PHYS. PROPERTIES
CHEMISTRY
SECTION
METERS
GRAPHIC LITHOLOGY
DRILLING DISTURB.
SED. STRUCTURES
SAMPLES
PLEIST.
PLIOCENE
● R/M N22
● A/M-P NN19 Pseudoemiliania lacunosa
● R/P unzoned
O Matuyama O
●ϕ=55.2 γ=1.81
1
2
CC
0.5
1.0
VOID133.05
VOID 133.5

LITHOLOGIC DESCRIPTION

CALCAREOUS CLAYEY SILT

Section 1, 0-10 cm, soupy; Section 1, 10-25 cm, moderately disturbed; remainder slightly disturbed. Voids caused during gas expansion.

Major lithology: CALCAREOUS CLAYEY SILT, olive gray (5Y 4/2) and dark olive gray (5Y 3/2). Minor to moderate burrow mottling. Bedding contacts are gradational and mottled. Foraminifers visible.

SMEAR SLIDE SUMMARY (%):

	1, 94 D	2, 62 D
TEXTURE:		
Sand	20	15
Silt	30	45
Clay	50	40
COMPOSITION:		
Access. minerals	3	2
Clay	30	35
Dolomite	Tr	
Feldspar	1	2
Foraminifers	1	1
Inorganic calcite	35	30
Nannofossils	15	5
Organic debris		5
Quartz	15	20

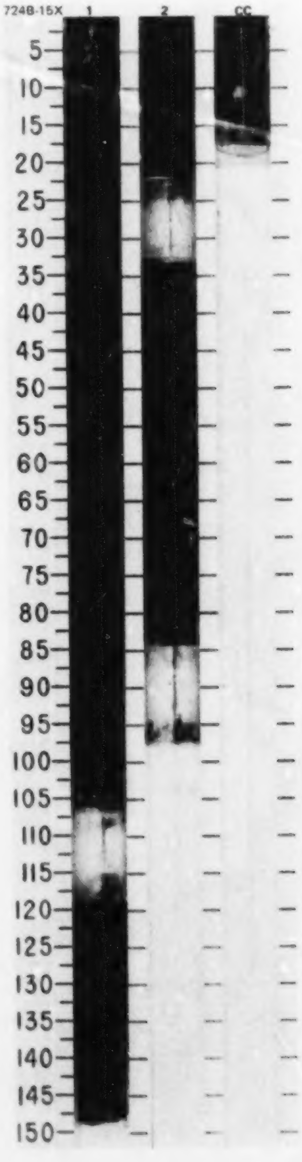
724B-15X
1
2
CC
5
10
15
20
25
30
35
40
45
50
55
60
65
70
75
80
85
90
95
100
105
110
115
120
125
130
135
140
145
150

SITE 724 HOLE B CORE 16X CORED INTERVAL 734.5-744.2 mbsl; 141.7-151.4 mbsf

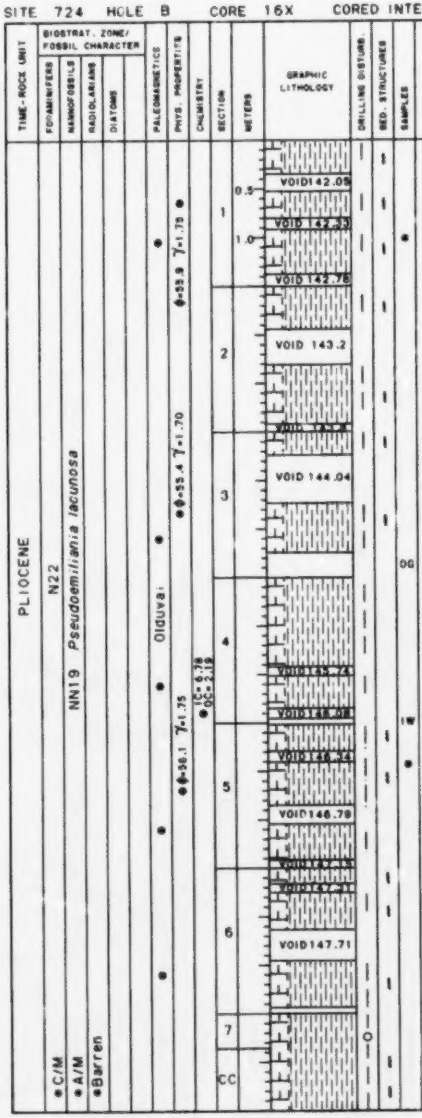
TIME-ROCK UNIT
BIOSTRAT. ZONE/ FOSSIL CHARACTER
FORAMINIFERS
NANNOFOSSILS
RADIOLARIANS
DIATOMS
PALEOMAGNETICS
PHYS. PROPERTIES
CHEMISTRY
SECTION
METERS
GRAPHIC LITHOLOGY
DRILLING DISTURB.
SED. STRUCTURES
SAMPLES
PLIOCENE
N22
NN19 Pseudoemiliania lacunosa
●C/M
●A/M
●Barren
Olduvai
ϕ=55.9 γ=1.75
ϕ=55.4 γ=1.70
ϕ=56.1 γ=1.75
IC=6.78
OC=2.19
1
2
3
4
5
6
7
CC
0.5
1.0
VOID142.05
VOID 142.33
VOID 142.78
VOID 143.2
VOID 144.04
VOID145.74
VOID146.08
VOID146.34
VOID146.70
VOID147.15
VOID147.21
VOID147.71
OG
IW

LITHOLOGIC DESCRIPTION

CALCAREOUS CLAYEY SILT

Section 7, 0-10 cm, soupy; Section 4, 20-30 cm, and Section 5, 0-29 and 40-85 cm, moderately disturbed; remainder slightly disturbed. Voids caused during gas expansion.

Major lithology: CALCAREOUS CLAYEY SILT, olive gray (5Y 4/2) and dark olive gray (5Y 3/2). Minor burrow mottling throughout. Bedding contacts are gradational and mottled. Foraminifers visible.

SMEAR SLIDE SUMMARY (%):

	1, 102 D	5, 43 D
TEXTURE:		
Sand	10	15
Silt	25	20
Clay	65	65
COMPOSITION:		
Access. minerals	2	2
Clay	30	35
Dolomite		Tr
Feldspar	1	
Foraminifers	2	1
Inorganic calcite	20	25
Mica	Tr	
Nannofossils	35	30
Quartz	10	7
Sponge spicules	Tr	Tr

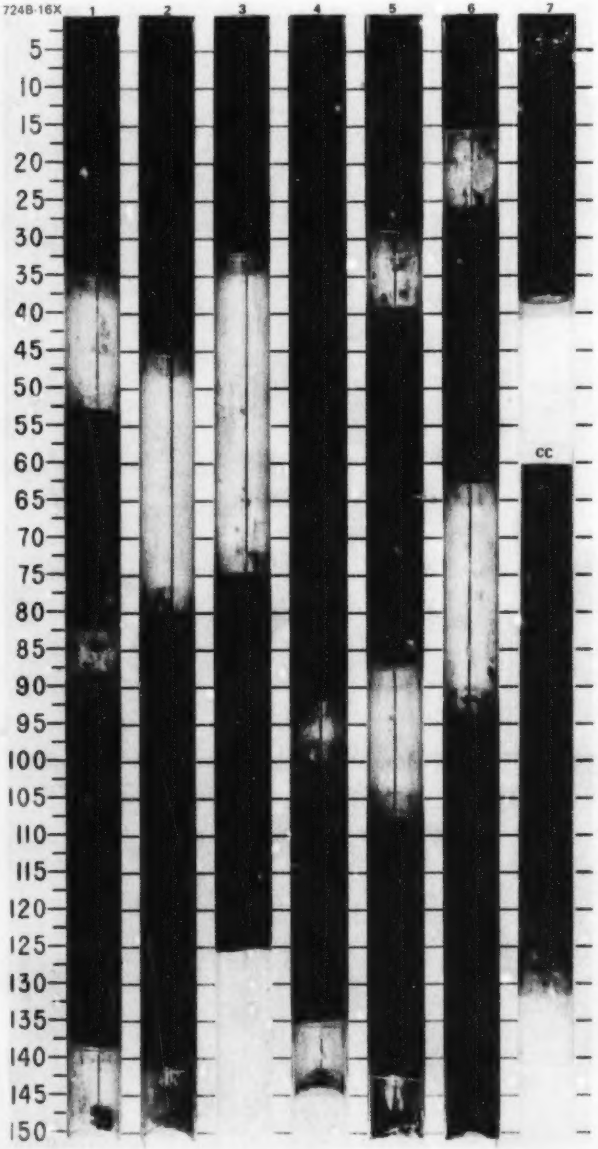
724B-16X
1
2
3
4
5
6
7
CC
5
10
15
20
25
30
35
40
45
50
55
60
65
70
75
80
85
90
95
100
105
110
115
120
125
130
135
140
145
150

SITE 724 HOLE B CORE 17X CORED INTERVAL 744.2-753.8 mbsl; 151.4-161.0 mbsf

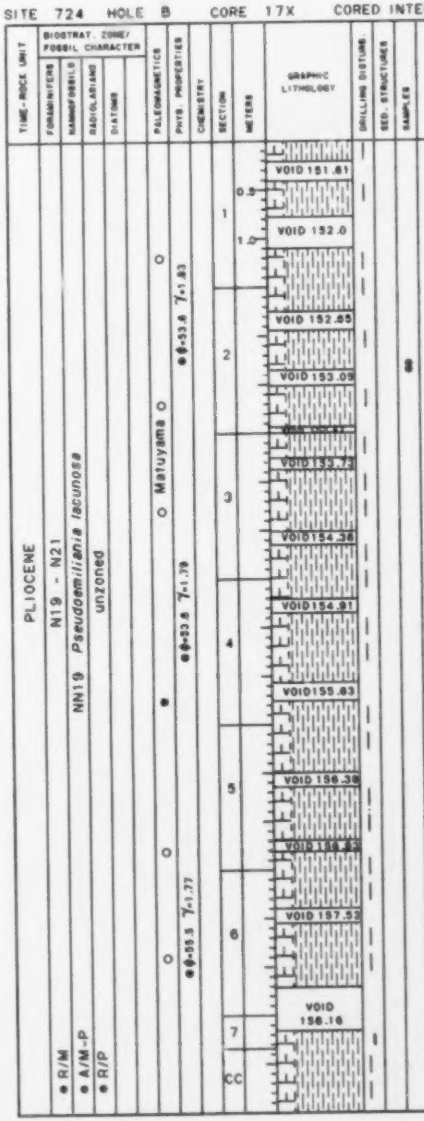
TIME-ROCK UNIT
BIOSTRAT. ZONE/ FOSSIL CHARACTER
FORAMINIFERS
NANNOFOSSILS
RADIOLARIANS
DIATOMS
PALEOMAGNETICS
PHYS. PROPERTIES
CHEMISTRY
SECTION
METERS
GRAPHIC LITHOLOGY
DRILLING DISTURB.
SED. STRUCTURES
SAMPLES
PLIOCENE
N19 - N21
NN19 Pseudoemiliania lacunosa
unzoned
• R/M
• A/M-P
• R/P
Matuyama
•φ=53.6 γ=1.83
•φ=53.6 γ=1.79
•φ=55.5 γ=1.77
1
2
3
4
5
6
7
CC
0.5
1.0
VOID 151.81
VOID 152.0
VOID 152.65
VOID 153.09
VOID 154.38
VOID 154.91
VOID155.83
VOID 156.38
VOID 157.52
VOID 158.16

LITHOLOGIC DESCRIPTION

CALCAREOUS CLAYEY SILT

Section 7, 18-32 cm, very disturbed; Section 1, 40-50 and 110-150 cm, and Section 5, 65-120 cm, moderately disturbed; remainder slightly disturbed. Voids caused during gas expansion.

Major lithology: CALCAREOUS CLAYEY SILT, olive gray (5Y 4/2). Bedding contacts are gradational and mottled. Foraminifers visible.

SMEAR SLIDE SUMMARY (%):

	2, 79 D	2, 83 D
TEXTURE:		
Sand	20	20
Silt	20	20
Clay	60	60
COMPOSITION:		
Access. minerals	2	2
Clay	30	30
Feldspar	1	
Foraminifers	2	3
Inorganic calcite	20	25
Mica		Tr
Nannofossils	30	30
Quartz	15	10
Sponge spicules	Tr	

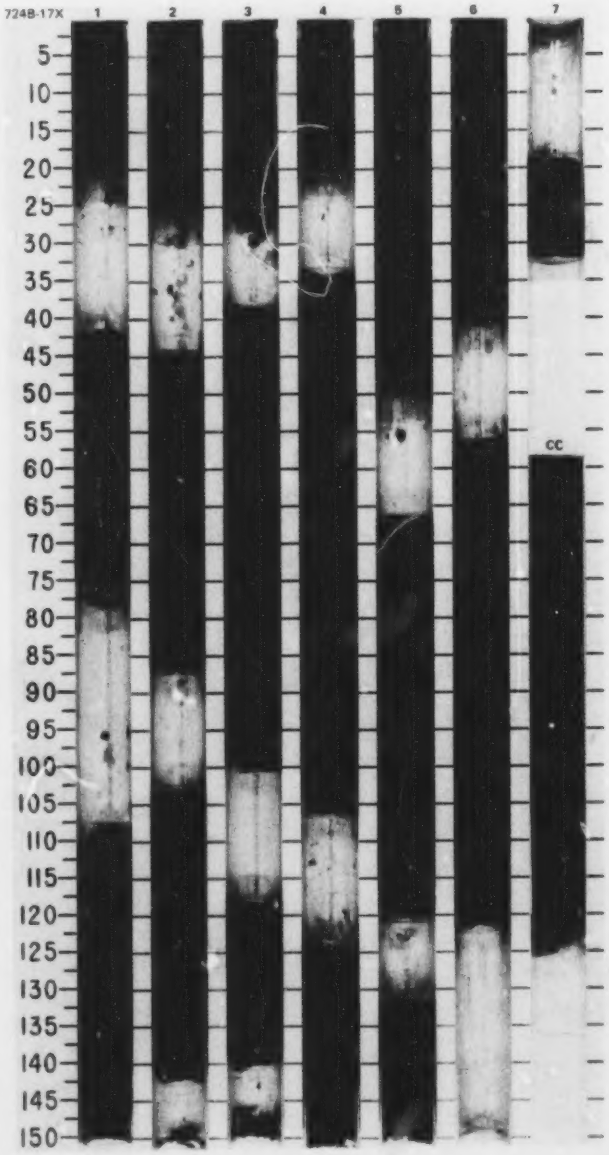
724B-17X
1
2
3
4
5
6
7
CC
5
10
15
20
25
30
35
40
45
50
55
60
65
70
75
80
85
90
95
100
105
110
115
120
125
130
135
140
145
150

SITE 724 HOLE B CORE 18X CORED INTERVAL 753.8-763.5 mbsl; 161.0-170.7 mbsf

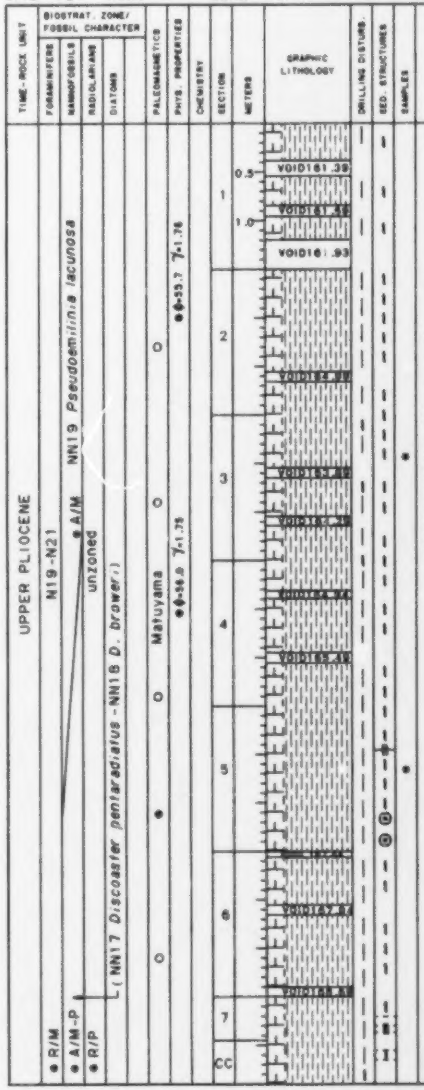
TIME-ROCK UNIT
BIOSTRAT. ZONE/ FOSSIL CHARACTER
FORAMINIFERS
NANNOFOSSILS
RADIOLARIANS
DIATOMS
PALEOMAGNETICS
PHYS. PROPERTIES
CHEMISTRY
SECTION
METERS
GRAPHIC LITHOLOGY
DRILLING DISTURB.
SED. STRUCTURES
SAMPLES
UPPER PLIOCENE
N19-N21
NN19 Pseudoemiliania lacunosa
● A/M
unzoned
(NN17 Discoaster pentaradiatus - NN18 D. brouweri)
● R/M
● A/M-P
● R/P
Matuyama
●φ=55.7 γ=1.76
●φ=56.0 γ=1.75
0.5
1.0
1
2
3
4
5
6
7
CC
VOID161.39
VOID161.58
VOID161.93
VOID

LITHOLOGIC DESCRIPTION

CALCAREOUS CLAYEY SILT

Section 3, 10-20, 64-75, and 135-150 cm, and CC, 35-44 cm, very disturbed; Section 1, 25-38 and 110-120 cm, moderately disturbed; remainder slightly disturbed. Voids caused during gas expansion.

Major lithology: CALCAREOUS CLAYEY SILT, olive gray (5Y 4/2) and dark olive gray (5Y 3/2). Abrupt change from olive gray to dark olive gray in Section 5. Minor burrow mottling throughout. Bedding contacts are gradational and mottled. Foraminifers visible. Section 5, 125 and 116 cm, soft, yellowish brown (10YR 5/8) phosphatic nodules.

SMEAR SLIDE SUMMARY (%):

	3, 44 D	5, 66 D
TEXTURE:		
Sand	10	15
Silt	30	50
Clay	60	35
COMPOSITION:		
Access. minerals	2	3
Clay	25	35
Dolomite		1
Feldspar		5
Foraminifers	3	
Inorganic calcite	25	20
Mica	Tr	1
Nannofossils	35	Tr
Organic debris		5
Quartz	10	30
Sponge spicules		Tr

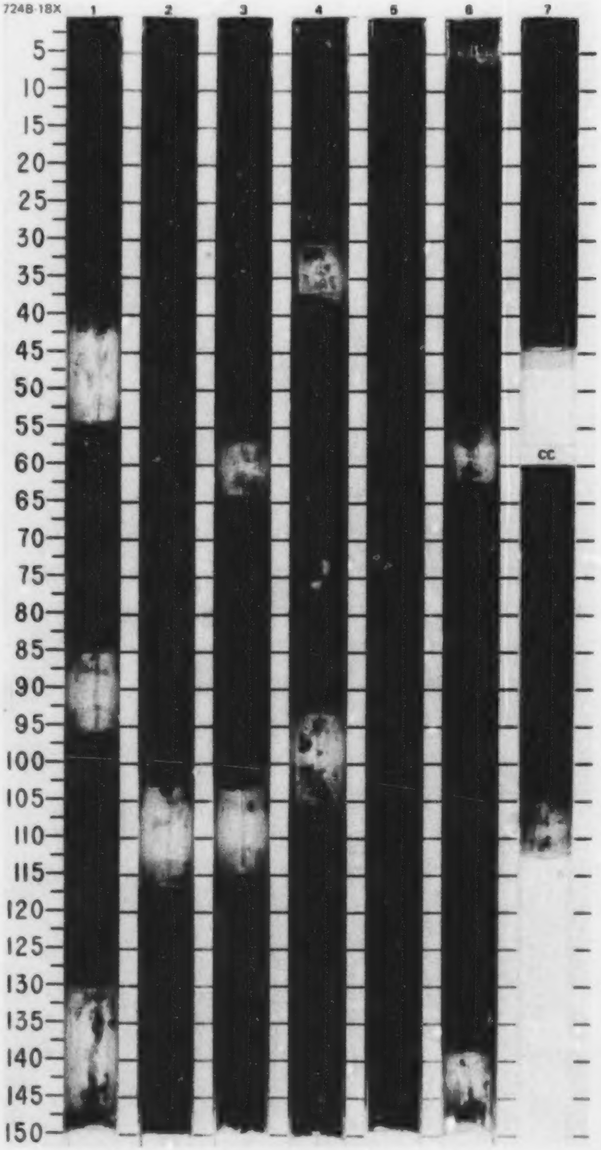
724B-18X
1
2
3
4
5
6
7
CC
5
10
15
20
25
30
35
40
45
50
55
60
65
70
75
80
85
90
95
100
105
110
115
120
125
130
135
140
145
150

SITE 724 HOLE B CORE 19X CORED INTERVAL 763.5-773.2 mbsl; 170.7-180.4 mbsf

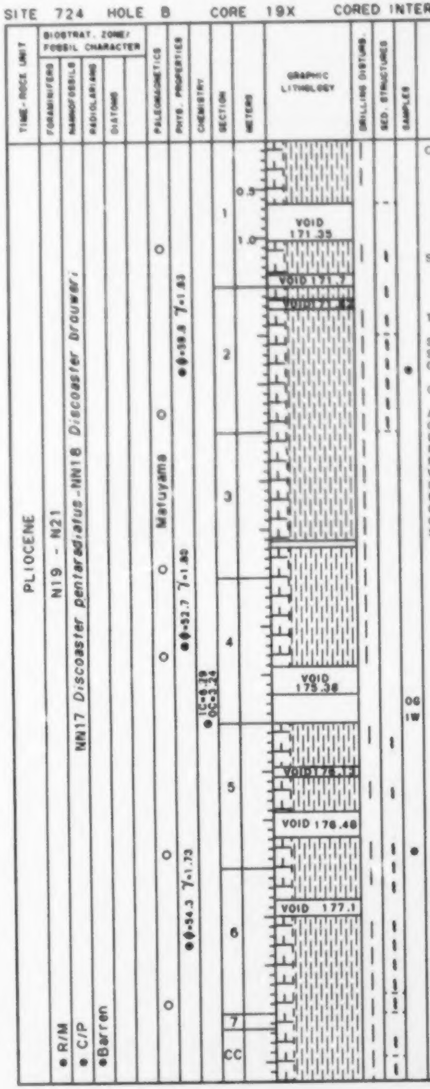
TIME-ROCK UNIT
BIOSTRAT. ZONE/FOSSIL CHARACTER
FORAMINIFERS
NANNOFOSSILS
RADIOLARIANS
DIATOMS
PALEOMAGNETICS
PHYS. PROPERTIES
CHEMISTRY
SECTION
METERS
GRAPHIC LITHOLOGY
DRILLING DISTURB.
SED. STRUCTURES
SAMPLES
PLIOCENE
N19 - N21
NN17 Discoaster pentaradiatus-NN18 Discoaster brouweri
● R/M
● C/P
●Barren
Matuyama
●φ=58.8 γ=1.83
●φ=52.7 γ=1.80
●φ=54.3 γ=1.73
●IC=6.29 OC=3.24
1
2
3
4
5
6
7
CC
0.5
1.0
VOID 171.35
VOID 171.7
VOID 171.82
VOID 175.38
VOID 176.13
VOID 176.48
VOID 177.1
OG
IW

LITHOLOGIC DESCRIPTION

CALCAREOUS CLAYEY SILT

Section 1, 45-60 cm, and Section 7, 0-28 cm, moderately disturbed; remainder slightly disturbed. Voids caused during gas expansion.

Major lithology: CALCAREOUS CLAYEY SILT, olive gray (5Y 4/2) and dark olive gray (5Y 3/2). Minor to moderate burrow mottling. Bedding contacts are gradational and mottled. Foraminifers visible.

SMEAR SLIDE SUMMARY (%):

	2, 98 D	5, 133 D
TEXTURE:		
Sand	20	15
Silt	45	30
Clay	35	55
COMPOSITION:		
Access. minerals	3	2
Clay	25	25
Dolomite	Tr	Tr
Feldspar	5	
Foraminifers		3
Volcanic glass	Tr	
Inorganic calcite	12	25
Nannofossils		30
Organic debris	5	
Quartz	40	15
Sponge spicules	Tr	Tr

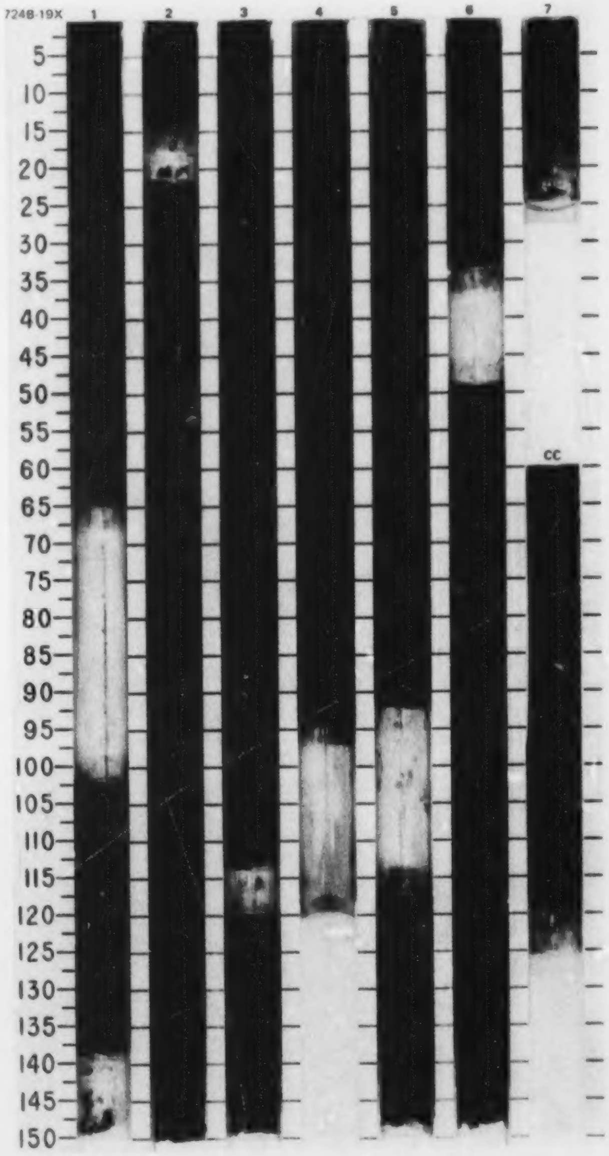
724B-19X
1
2
3
4
5
6
7
CC
5
10
15
20
25
30
35
40
45
50
55
60
65
70
75
80
85
90
95
100
105
110
115
120
125
130
135
140
145
150

SITE 724 HOLE B CORE 20X CORED INTERVAL 773.2-782.8 mbsl; 180.4-190.0 mbsf

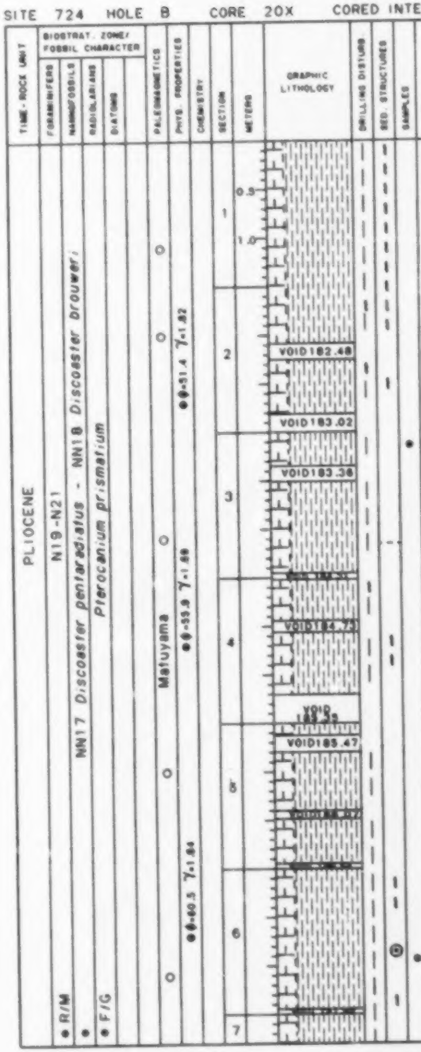
TIME-ROCK UNIT
BIOSTRAT. ZONE/ FOSSIL CHARACTER
FORAMINIFERS
NANNOFOSSILS
RADIOLARIANS
DIATOMS
PALEOMAGNETICS
PHYS. PROPERTIES
CHEMISTRY
SECTION
METERS
GRAPHIC LITHOLOGY
DRILLING DISTURB.
SED. STRUCTURES
SAMPLES
PLIOCENE
N19-N21
NN17 Discoaster pentaradiatus - NN18 Discoaster brouweri
Pterocanium prismatium
• R/M
•
• F/G
Matuyama
●Φ=51.4 γ=1.82
●Φ=55.9 γ=1.88
●Φ=60.5 γ=1.84
1
2
3
4
5
6
7
0.5
1.0
VOID 182.48
VOID 183.02
VOID 183.36
VOID 184.73
VOID 185.33
VOID 185.47

LITHOLOGIC DESCRIPTION

CALCAREOUS CLAYEY SILT

Section 2, 20-30, 76-90, and 120-131 cm, and Section 4, 0-20 cm, very disturbed; remainder slightly disturbed. Voids caused during gas expansion.

Major lithology: CALCAREOUS CLAYEY SILT, olive gray (5Y 4/2) and dark olive gray (5Y 3/2). Minor burrow mottling throughout. Bedding contacts are gradational and mottled. Foraminifers visible. Section 6, 86 cm: phosphatic nodule present.

SMEAR SLIDE SUMMARY (%):

	3, 13 D	6, 92 D
TEXTURE:		
Sand	20	25
Silt	30	30
Clay	50	45
COMPOSITION:		
Access. minerals	3	3
Clay	25	45
Diatoms		Tr
Feldspar	2	6
Foraminifers	2	
Inorganic calcite	28	10
Mica		1
Nannofossils	25	Tr
Organic debris		5
Quartz	15	30
Radiolarians		Tr
Sponge spicules		Tr

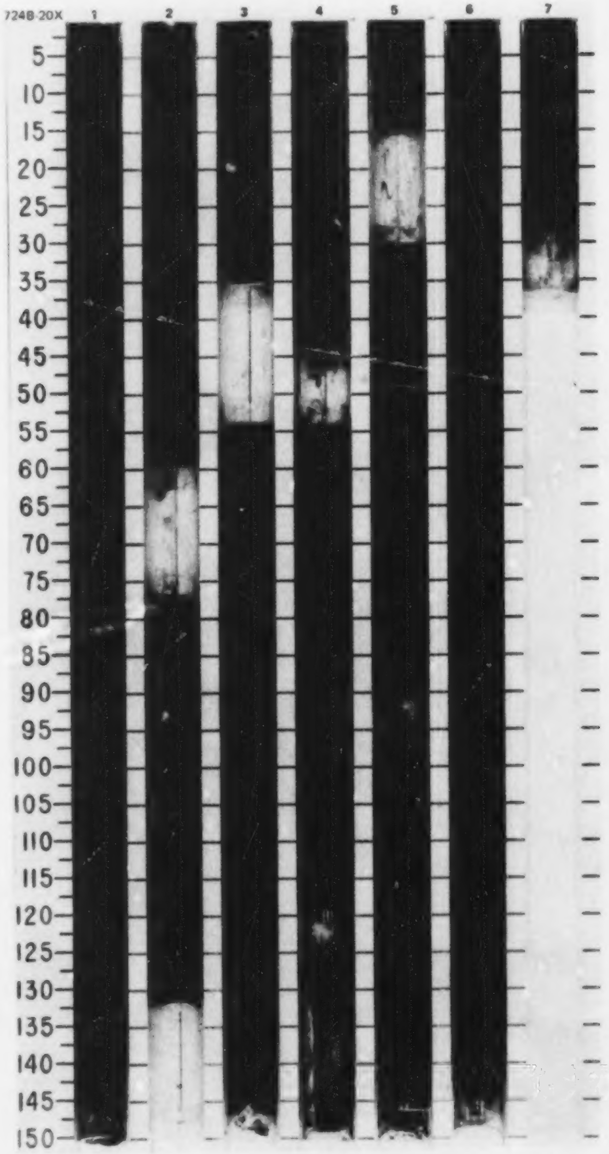
724B-20X
1
2
3
4
5
6
7
5
10
15
20
25
30
35
40
45
50
55
60
65
70
75
80
85
90
95
100
105
110
115
120
125
130
135
140
145
150

SITE 724 HOLE B CORE 21X CORED INTERVAL 782.8-792.5 mbsl; 190.0-199.7 mbsf

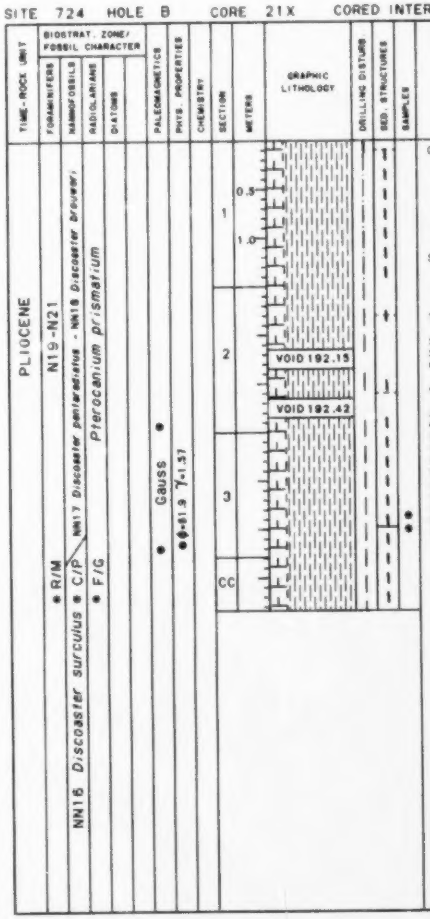
TIME-ROCK UNIT
BIOSTRAT. ZONE/ FOSSIL CHARACTER
FORAMINIFERS
NANNOFOSSILS
RADIOLARIANS
DIATOMS
PALEOMAGNETICS
PHYS. PROPERTIES
CHEMISTRY
SECTION
METERS
GRAPHIC LITHOLOGY
DRILLING DISTURB.
SED. STRUCTURES
SAMPLES
PLIOCENE
N19-N21
• R/M
NN16 Discoaster surculus • C/P
NN17 Discoaster pentaradiatus - NN18 Discoaster brouweri
Pterocanium prismatium
• F/G
Gauss
•ϕ-61.9 γ-1.57
1
2
3
CC
0.5
1.0
VOID 192.15
VOID 192.42

LITHOLOGIC DESCRIPTION

CALCAREOUS CLAYEY SILT

Section 1, 0-20 cm, very disturbed; Section 1, 20-150 cm, moderately disturbed; remainder slightly disturbed. Voids caused during gas expansion.

Major lithology: CALCAREOUS CLAYEY SILT, olive gray (5Y 4/2) and dark olive gray (5Y 3/2). Minor burrow mottling throughout. Bedding contacts are gradational and mottled. Foraminifers visible.

SMEAR SLIDE SUMMARY (%):

	3, 86 D	3, 99 D
TEXTURE:		
Sand	13	20
Silt	32	20
Clay	55	60
COMPOSITION:		
Access. minerals	2	2
Clay	60	25
Dolomite		Tr
Feldspar	3	
Foraminifers	Tr	5
Volcanic glass		12
Inorganic calcite	10	
Mica		1
Nannofossils		45
Quartz	25	10
Sponge spicules		Tr

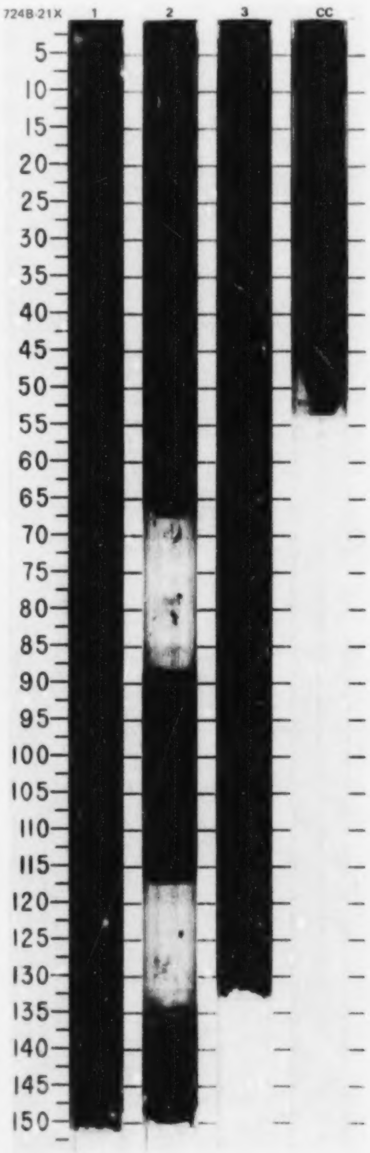
724B-21X
1
2
3
CC
5
10
15
20
25
30
35
40
45
50
55
60
65
70
75
80
85
90
95
100
105
110
115
120
125
130
135
140
145
150

SITE 724 HOLE B CORE 22X CORED INTERVAL 792.5-802.2 mbsl; 199.7-209.4 mbsf

TIME-ROCK UNIT	BIOSTRAT. ZONE/ FOSSIL CHARACTER					PALEOMAGNETICS	PHYS. PROPERTIES	CHEMISTRY	SECTION	METERS	GRAPHIC LITHOLOGY	DRILLING DISTURB.	SED. STRUCTURES	SAMPLES	LITHOLOGIC DESCRIPTION
	FORAMINIFERS	NANNOFOSSILS	RADIOLARIANS	DIATOMS											
PLIOCENE ?	●Barren	●Barren	●F/G *Spongaster pentas*				● ϕ=60.2 γ=1.81 ●		1 CC	0.5 1.0		O		●	

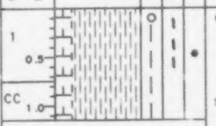

CALCAREOUS CLAYEY SILT

Section 1, 0-10 cm, soupy; remainder slightly disturbed.

Major lithology: CALCAREOUS CLAYEY SILT, dark olive gray (5Y 3/2). Minor burrow mottling throughout.

SMEAR SLIDE SUMMARY (%):

	1, 47 D
TEXTURE:	
Sand	3
Silt	80
Clay	17
COMPOSITION:	
Access. minerals	3
Clay	17
Diatoms	2
Dolomite	Tr
Inorganic calcite	38
Quartz	40
Sponge spicules	Tr

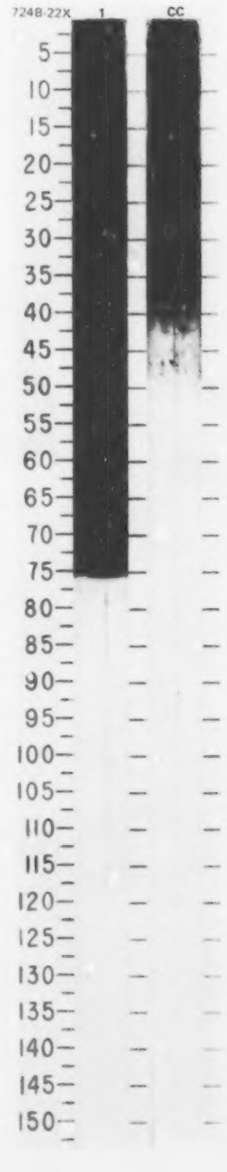
724B-22X
1
CC
5
10
15
20
25
30
35
40
45
50
55
60
65
70
75
80
85
90
95
100
105
110
115
120
125
130
135
140
145
150

SITE 724 HOLE B CORE 23X CORED INTERVAL 802.2-811.8 mbsl; 209.4-219.0 mbsf

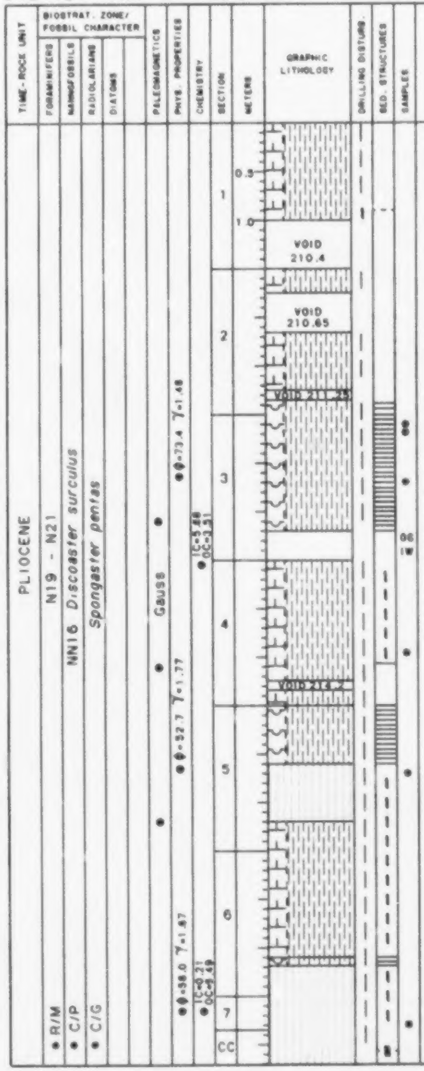
TIME-ROCK UNIT
BIOSTRAT. ZONE/FOSSIL CHARACTER
FORAMINIFERS
NANNOFOSSILS
RADIOLARIANS
DIATOMS
PALEOMAGNETICS
PHYS. PROPERTIES
CHEMISTRY
SECTION
METERS
GRAPHIC LITHOLOGY
DRILLING DISTURB.
SED. STRUCTURES
SAMPLES
PLIOCENE
N19 - N21
NN16 Discoaster surculus
Spongaster pentas
• R/M
• C/P
• C/G
Gauss
●φ=73.4 γ=1.48
●φ=52.7 γ=1.77
●φ=58.0 γ=1.87
●IC=5.88 OC=3.31
●IC=0.21 OC=0.49
1
2
3
4
5
6
7
CC
0.5
1.0
VOID 210.4
VOID 210.65
VOID 211.25
VOID 214.2
OG
IW

LITHOLOGIC DESCRIPTION

CALCAREOUS CLAYEY SILT

Section 1, 85-100 cm, very disturbed; remainder slightly disturbed. Voids caused during gas expansion.

Major lithology: CALCAREOUS CLAYEY SILT, olive gray (5Y 4/2), dark olive gray (5Y 3/2), and black (2.5/2). Minor burrow mottling common. Bedding contacts are gradational and mottled. Foraminifers visible.

Minor lithologies:

a. Section 2, 133-150 cm, Section 3, 0-120 cm, Section 5, 5-45 cm, and Section 6, 115-120 cm: sub-millimeter laminated beds with laminae composed of diatomaceous silty clay, diatomaceous muc, and diatom ooze, olive (5Y 5/4), olive gray (5Y 4/2), and dark olive gray (5Y 3/2).

b. Section 5, 62-120 cm, Section 6, 118-150 cm, Section 7, 0-37 cm, and CC, 0-21 cm, black (5Y 2.5/2) clayey sand (about 45% quartz and 40% clay).

SMEAR SLIDE SUMMARY (%):

	3, 11 D	3, 19 D	3, 70 D	4, 96 D	5, 70 D	7, 30 D
TEXTURE:						
Sand			2	15	35	25
Silt	50	90	38	45	25	30
Clay	50	10	60	40	40	45
COMPOSITION:						
Access. minerals			2		4	
Clay	37	10	60	20	40	45
Diatoms	47	87	10		Tr	
Dolomite				Tr	Tr	
Feldspar			2			5
Fish remains			Tr			
Foraminifers			Tr	15		
Volcanic glass					1	
Inorganic calcite	3	3	10	25	6	5
Mica			1			Tr
Nannofossils	10			30		
Quartz	2		15	10	45	45
Radiolarians	Tr		Tr			
Sponge spicules	1				2	Tr

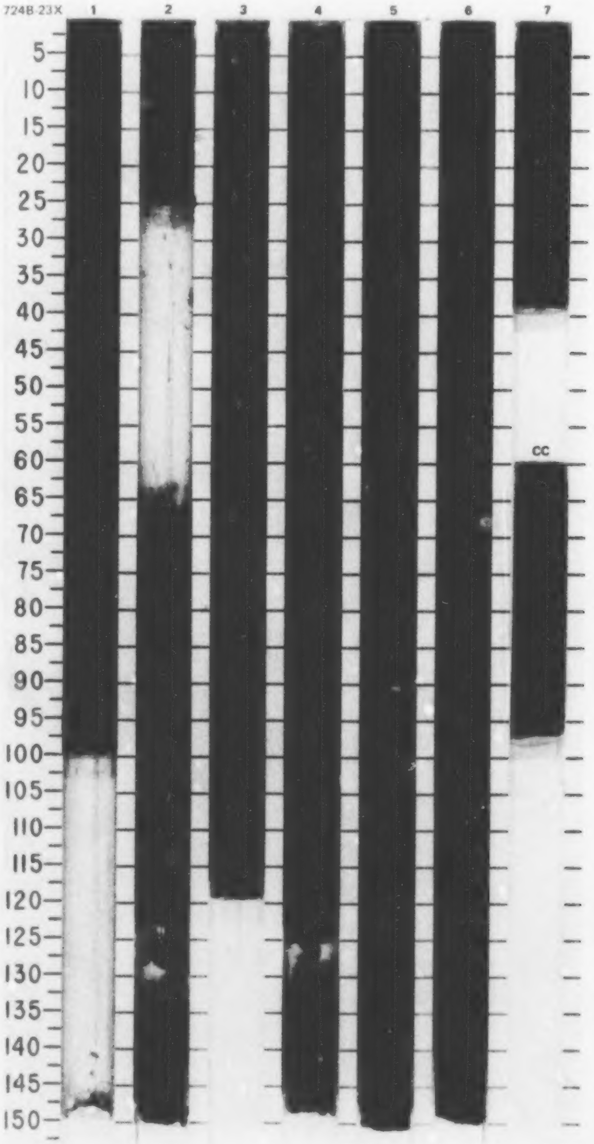
724B-23X
1
2
3
4
5
6
7
CC
5
10
15
20
25
30
35
40
45
50
55
60
65
70
75
80
85
90
95
100
105
110
115
120
125
130
135
140
145
150

SITE 724 HOLE B CORE 24X CORED INTERVAL 811.8-821.5 mbsl; 219.0-228.7 mbsf

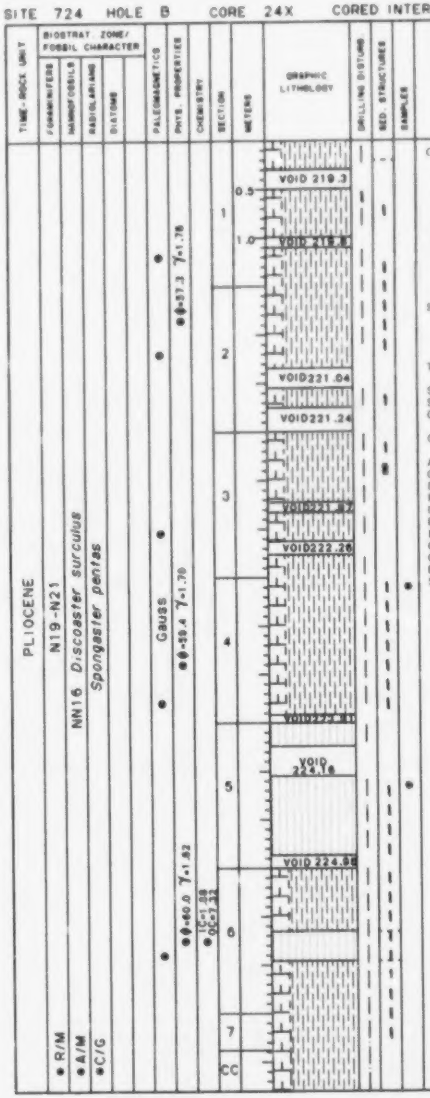
TIME-ROCK UNIT
BIOSTRAT. ZONE/ FOSSIL CHARACTER
FORAMINIFERS
NANNOFOSSILS
RADIOLARIANS
DIATOMS
PALEOMAGNETICS
PHYS. PROPERTIES
CHEMISTRY
SECTION
METERS
GRAPHIC LITHOLOGY
DRILLING DISTURB.
SED. STRUCTURES
SAMPLES
PLIOCENE
N19-N21
NN16 Discoaster surculus
Spongaster pentas
● R/M
● A/M
● C/G
Gauss
●Φ=57.3 γ=1.76
●Φ=59.4 γ=1.70
●Φ=60.0 γ=1.82
● IC=1.08 OC=7.32
1
2
3
4
5
6
7
CC
0.5
1.0
VOID 219.3
VOID 219.8
VOID221.04
VOID221.24
VOID221.87
VOID222.26
VOID 224.16
VOID 224.98

LITHOLOGIC DESCRIPTION

CALCAREOUS CLAYEY SILT

Section 1, 51-65 cm, very disturbed; Section 2, 104-125 cm, Section 3, 126-150 cm, Section 7, 0-37 cm, and CC, 0-40 cm, moderately disturbed; remainder slightly disturbed. Voids caused during gas expansion.

Major lithology: CALCAREOUS CLAYEY SILT, olive gray (5Y 4/2) and dark olive gray (5Y 3/2). Minor burrow mottling throughout. Bedding contacts are gradational and mottled. Foraminifers visible.

Minor lithology: Section 5, 0-150 cm, and Section 6, 63-98 cm, black (5Y 2.5/2) clayey sand.

SMEAR SLIDE SUMMARY (%):

	4, 17 D	5, 65 D
TEXTURE:		
Sand	20	40
Silt	25	20
Clay	55	40
COMPOSITION:		
Access. minerals	3	3
Clay	25	40
Feldspar	2	
Foraminifers	5	
Inorganic calcite	25	10
Mica	Tr	Tr
Nannofossils	30	
Organic debris		5
Quartz	10	40
Radiolarians		Tr
Sponge spicules		2

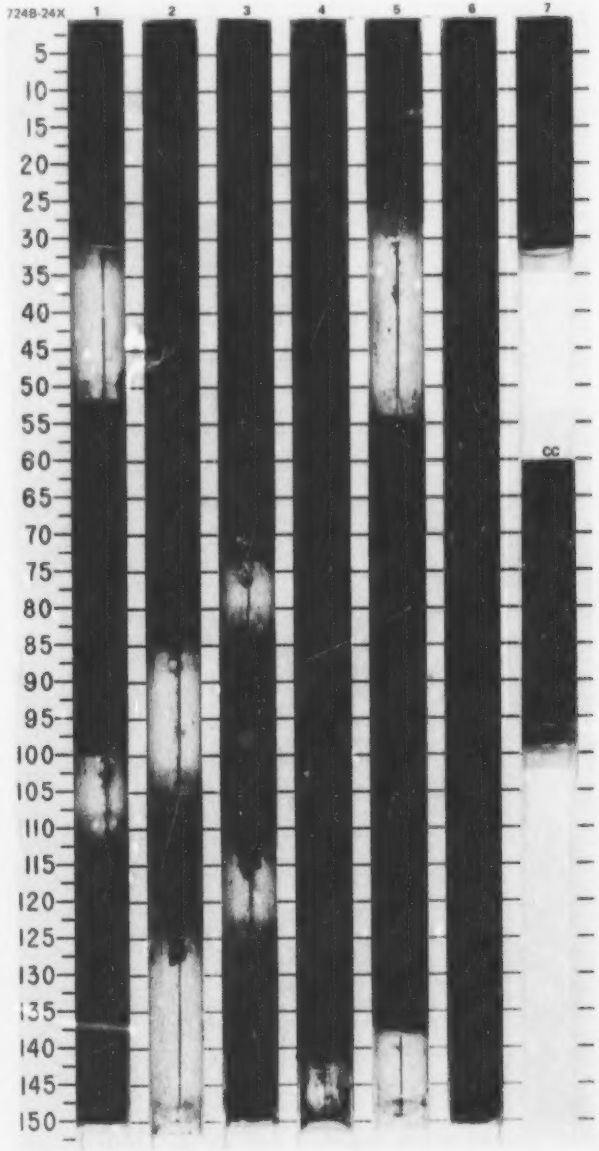
724B-24X
1
2
3
4
5
6
7
CC
5
10
15
20
25
30
35
40
45
50
55
60
65
70
75
80
85
90
95
100
105
110
115
120
125
130
135
140
145
150

SITE 724 HOLE B CORE 25X CORED INTERVAL 821.5-831.2 mbsl; 228.7-238.4 mbsf

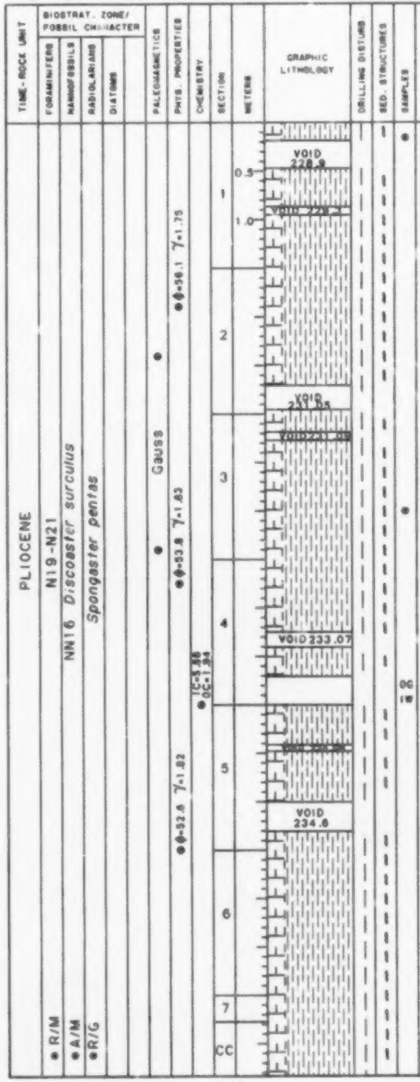
TIME-ROCK UNIT
BIOSTRAT. ZONE/ FOSSIL CHARACTER
FORAMINIFERS
NANNOFOSSILS
RADIOLARIANS
DIATOMS
PALEOMAGNETICS
PHYS. PROPERTIES
CHEMISTRY
SECTION
METERS
GRAPHIC LITHOLOGY
DRILLING DISTURB.
SED. STRUCTURES
SAMPLES
PLIOCENE
N19-N21
NN16 Discoaster surculus
Spongaster pentas
● R/M
● A/M
● R/G
Gauss
●ϕ=56.1 γ=1.75
●ϕ=53.8 γ=1.83
●ϕ=52.6 γ=1.82
●IC=5.88 OC=1.34
1
2
3
4
5
6
7
CC
0.5
1.0
VOID 228.9
VOID 229.3
VOID 231.05
VOID 231.3
VOID 233.07
VOID 234.6
OG
IW

LITHOLOGIC DESCRIPTION

CALCAREOUS CLAYEY SILT

Entire core slightly disturbed. Voids caused during gas expansion.

Major lithology: CALCAREOUS CLAYEY SILT, olive gray (5Y 4/2). Minor burrow mottling throughout. Foraminifers visible.

SMEAR SLIDE SUMMARY (%):

	1, 17 D	3, 101 D
TEXTURE:		
Sand	15	10
Silt	35	30
Clay	50	60
COMPOSITION:		
Access. minerals	3	2
Clay	35	27
Dolomite		Tr
Feldspar		2
Foraminifers		3
Volcanic glass	Tr	
Inorganic calcite	35	25
Mica		1
Nannofossils	15	30
Organic debris	5	
Quartz	7	10
Sponge spicules	Tr	

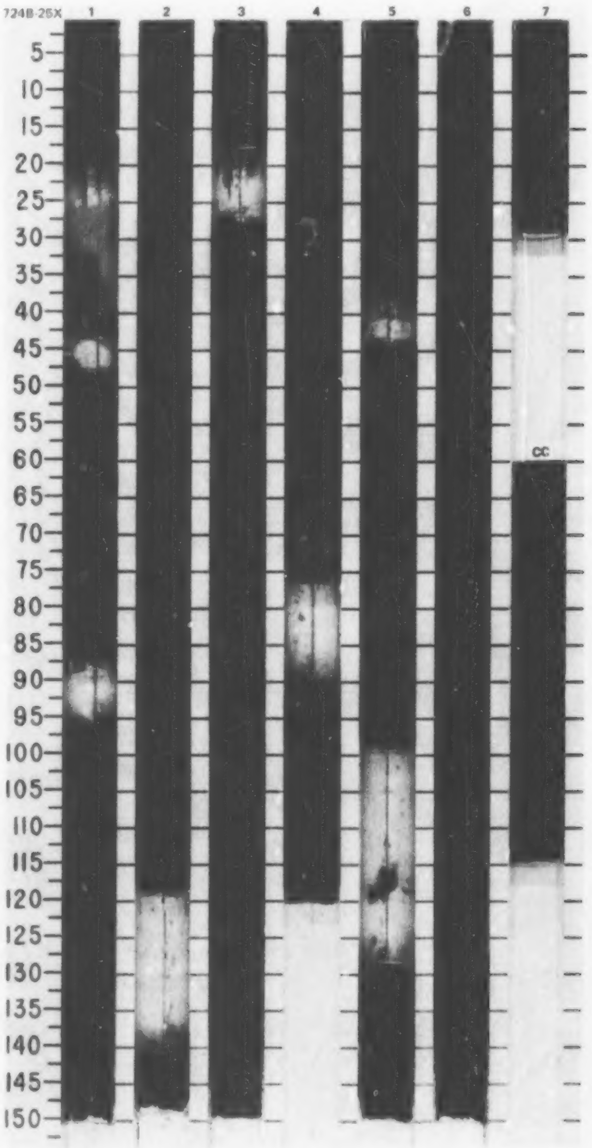
724B-25X
1
2
3
4
5
6
7
CC
5
10
15
20
25
30
35
40
45
50
55
60
65
70
75
80
85
90
95
100
105
110
115
120
125
130
135
140
145
150

SITE 724 HOLE B CORE 26X CORED INTERVAL 831.2-840.8 mbsl; 238.4-248.0 mbsf

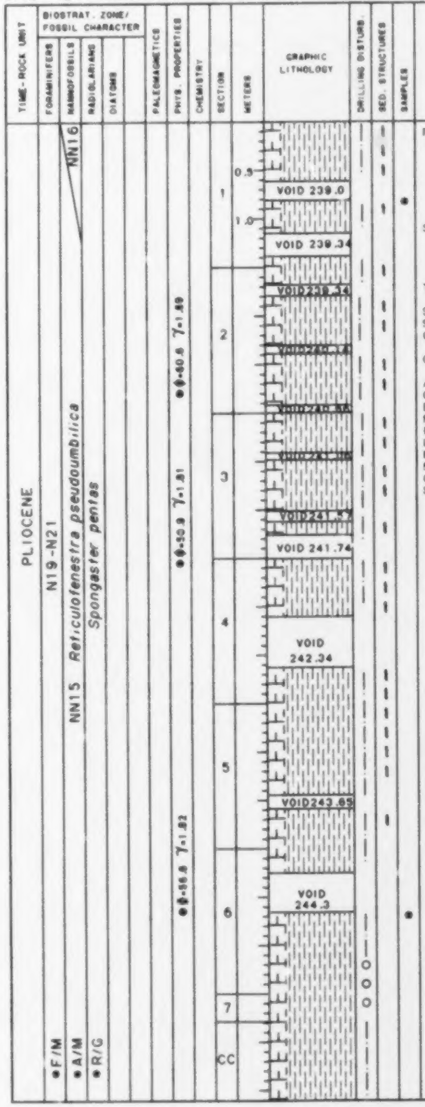
TIME-ROCK UNIT
BIOSTRAT. ZONE/ FOSSIL CHARACTER
FORAMINIFERS
NANNOFOSSILS
RADIOLARIANS
DIATOMS
PALEOMAGNETICS
PHYS. PROPERTIES
CHEMISTRY
SECTION
METERS
GRAPHIC LITHOLOGY
DRILLING DISTURB.
SED. STRUCTURES
SAMPLES
PLIOCENE
N19-N21
NN16
NN15 Reticulofenestra pseudoumbilica
Spongaster pentas
●F/M
●A/M
●R/G
●ϕ=60.6 γ=1.89
●ϕ=50.9 γ=1.81
●ϕ=56.8 γ=1.82
1
2
3
4
5
6
7
CC
0.5
1.0
VOID 239.0
VOID 239.34
VOID 242.34
VOID 241.74
VOID243.65
VOID 244.3

LITHOLOGIC DESCRIPTION

MARLY FORAMINIFER-BEARING NANNOFOSSIL OOZE

Section 6, 90-150 cm, and Section 7, 0-27 cm, soupy; remainder moderately disturbed. Voids caused during gas expansion.

Major lithology: **MARLY FORAMINIFER-BEARING NANNOFOSSIL OOZE**, olive gray (5Y 4/2). Minor burrow mottling throughout. Foraminifers visible.

SMEAR SLIDE SUMMARY (%):

	1, 83 D	6, 69 D
TEXTURE:		
Sand	20	15
Silt	30	25
Clay	50	60
COMPOSITION:		
Access. minerals	2	2
Clay	25	25
Dolomite	1	1
Feldspar	2	
Foraminifers	15	5
Inorganic calcite	15	22
Mica	Tr	
Nannofossils	25	35
Quartz	15	10
Sponge spicules		Tr

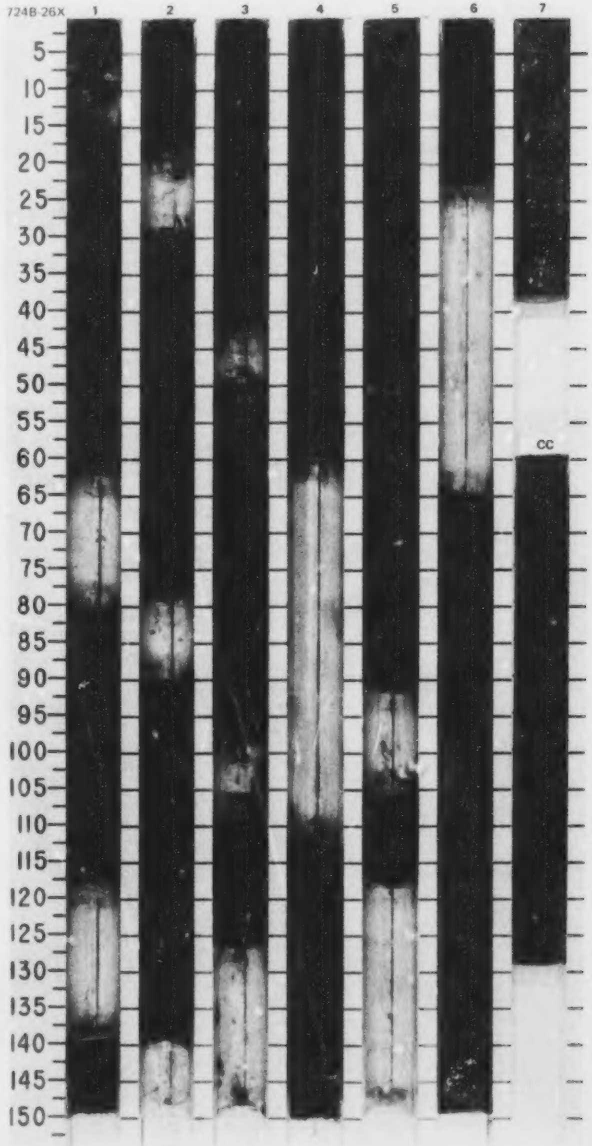
724B-26X
1
2
3
4
5
6
7
CC
5
10
15
20
25
30
35
40
45
50
55
60
65
70
75
80
85
90
95
100
105
110
115
120
125
130
135
140
145
150

SITE 724 HOLE B CORE 27X CORED INTERVAL 840.8-850.5 mbsl; 248.0-257.7 mbsf

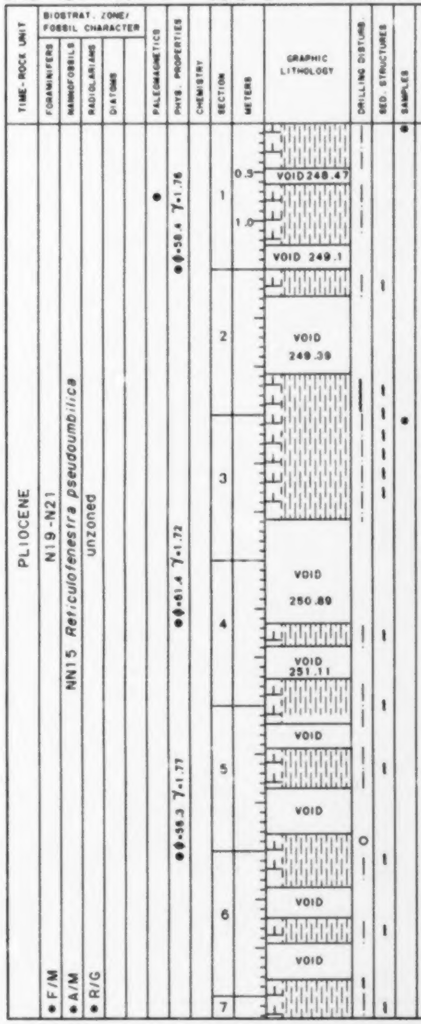
TIME-ROCK UNIT
BIOSTRAT. ZONE/ FOSSIL CHARACTER
FORAMINIFERS
NANNOFOSSILS
RADIOLARIANS
DIATOMS
PALEOMAGNETICS
PHYS. PROPERTIES
CHEMISTRY
SECTION
METERS
GRAPHIC LITHOLOGY
DRILLING DISTURB.
SED. STRUCTURES
SAMPLES
PLIOCENE
N19-N21
NN15 Reticulofenestra pseudoumbilica
unzoned
• F/M
• A/M
• R/G
●φ=58.4 γ=1.76
●φ=61.4 γ=1.72
●φ=58.3 γ=1.77
1
2
3
4
5
6
7
0.5
1.0
VOID 248.47
VOID 249.1
VOID 249.39
VOID 250.89
VOID 251.11
VOID
VOID
VOID
VOID

LITHOLOGIC DESCRIPTION

CALCAREOUS CLAYEY SILT

Section 5, 132-150 cm, soupy; Section 2, 109-150 cm, and Section 6, 132-150 cm, very disturbed; remainder moderately disturbed. Voids caused during gas expansion.

Major lithology: CALCAREOUS CLAYEY SILT, olive (5Y 4/3) and olive gray (5Y 4/2). Minor burrow mottling throughout. Foraminifers visible.

Minor lithology: Section 1, 7 cm (smear slide), diatomaceous calcareous clayey silt grading into calcareous clayey silt.

SMEAR SLIDE SUMMARY (%):

	1, 7 D	3, 6 D
TEXTURE:		
Sand	20	10
Silt	40	40
Clay	40	50
COMPOSITION:		
Access. minerals	2	2
Clay	25	30
Diatoms	15	
Dolomite		Tr
Feldspar	2	2
Foraminifers	1	3
Volcanic glass	Tr	
Inorganic calcite	20	30
Nannofossils	15	20
Quartz	20	13
Radiolarians	Tr	Tr
Sponge spicules		Tr

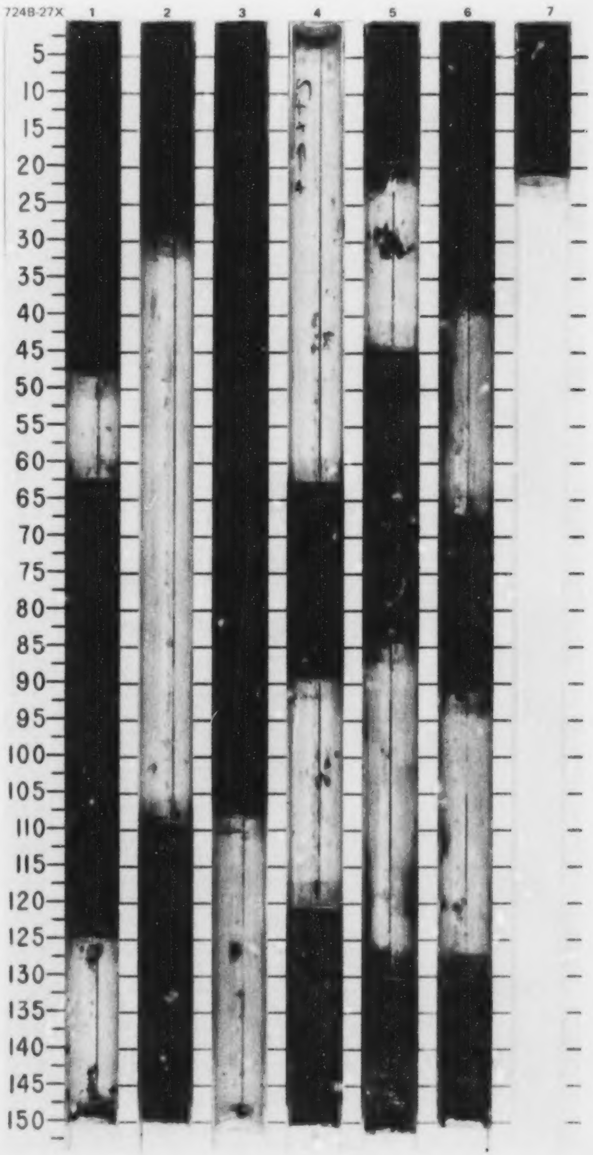
724B-27X
1
2
3
4
5
6
7
5
10
15
20
25
30
35
40
45
50
55
60
65
70
75
80
85
90
95
100
105
110
115
120
125
130
135
140
145
150

SITE 724 HOLE C CORE 1H CORED INTERVAL 592.8-595.6 mbsl; 0.0-2.8 mbsf

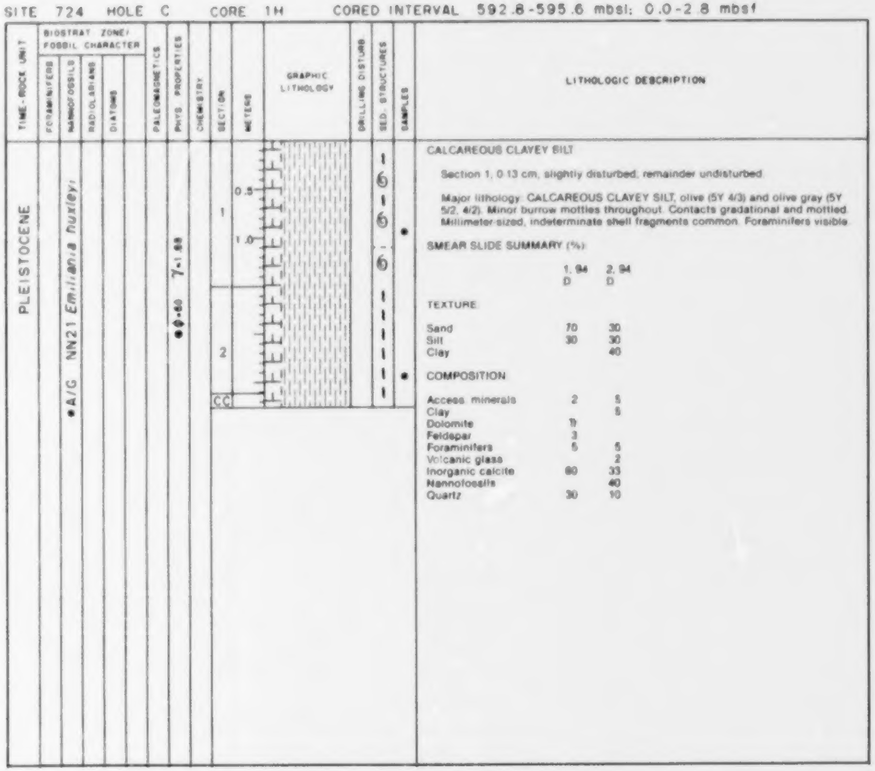
TIME-ROCK UNIT
BIOSTRAT. ZONE/ FOSSIL CHARACTER
FORAMINIFERS
NANNOFOSSILS
RADIOLARIANS
DIATOMS
PALEOMAGNETICS
PHYS. PROPERTIES
CHEMISTRY
SECTION
METERS
GRAPHIC LITHOLOGY
DRILLING DISTURB.
SED. STRUCTURES
SAMPLES
LITHOLOGIC DESCRIPTION
PLEISTOCENE
●A/G NN21 Emiliania huxleyi
●ϕ=60 γ=1.88
1
2
CC
0.5
1.0

CALCAREOUS CLAYEY SILT

Section 1, 0-13 cm, slightly disturbed; remainder undisturbed.

Major lithology: CALCAREOUS CLAYEY SILT, olive (5Y 4/3) and olive gray (5Y 5/2, 4/2). Minor burrow mottles throughout. Contacts gradational and mottled. Millimeter-sized, indeterminate shell fragments common. Foraminifers visible.

SMEAR SLIDE SUMMARY (%):

	1, 94 D	2, 94 D
TEXTURE:		
Sand	70	30
Silt	30	30
Clay		40
COMPOSITION:		
Access. minerals	2	5
Clay		5
Dolomite	Tr	
Feldspar	3	
Foraminifers	5	5
Volcanic glass		2
Inorganic calcite	60	33
Nannofossils		40
Quartz	30	10

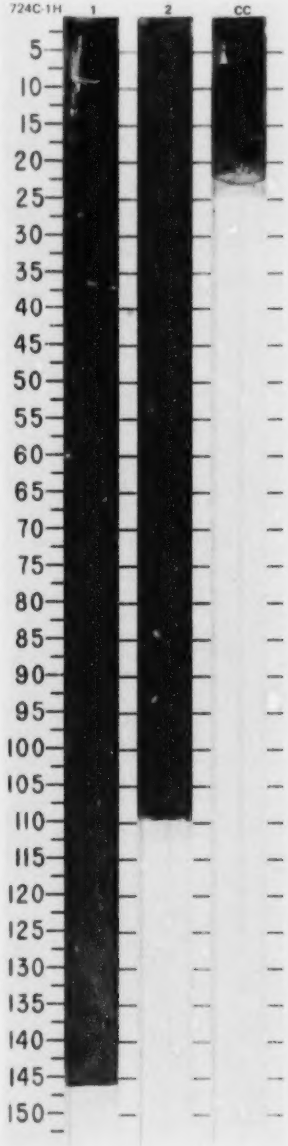
724C-1H
1
2
CC
5
10
15
20
25
30
35
40
45
50
55
60
65
70
75
80
85
90
95
100
105
110
115
120
125
130
135
140
145
150

SITE 724 HOLE C CORE 2H CORED INTERVAL 595.6-605.0 mbsl; 2.8-12.2 mbsf

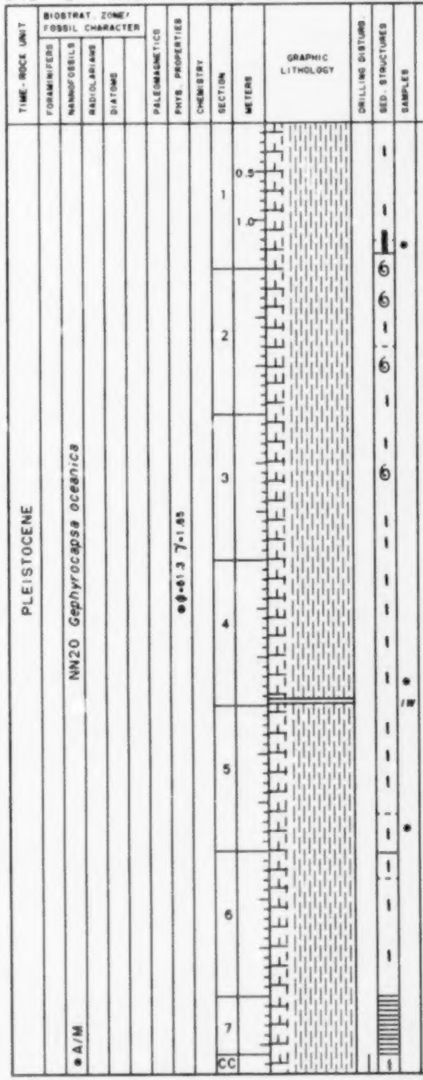
TIME-ROCK UNIT
BIOSTRAT. ZONE/ FOSSIL CHARACTER
FORAMINIFERS
NANNOFOSSILS
RADIOLARIANS
DIATOMS
PALEOMAGNETICS
PHYS. PROPERTIES
CHEMISTRY
SECTION
METERS
GRAPHIC LITHOLOGY
DRILLING DISTURB.
SED. STRUCTURES
SAMPLES
PLEISTOCENE
NN20 Gephyrocapsa oceanica
●A/M
●φ=61.3 γ=1.85
1
2
3
4
5
6
7
CC
0.5
1.0
IW

LITHOLOGIC DESCRIPTION

CALCAREOUS CLAYEY SILT

Section 1, 0-35 cm, and CC, 0-22 cm, moderately disturbed; remainder undisturbed.

Major lithology: CALCAREOUS CLAYEY SILT, olive (5Y 4/3) and olive gray (5Y 5/2, 4/2). Minor burrow mottles throughout. Contacts gradational and mottled. Millimeter-sized, indeterminate shell fragments common. Foraminifers, bivalves and scaphopods visible.

Minor lithology: Section 7, 0-63 cm, finely bedded layer consisting of beds 5-20 mm thick made of gray (5Y 4/1) calcitic silty clay and olive gray (5Y 4/2) nannofossil silty clay.

SMEAR SLIDE SUMMARY (%):

	1, 125 D	4, 127 D	5, 127 D
TEXTURE:			
Sand	30	30	30
Silt	30	25	25
Clay	40	45	45
COMPOSITION:			
Access. minerals	2	2	3
Clay	35	20	23
Dolomite	1		Tr
Foraminifers	4	25	4
Volcanic glass			Tr
Glauconite		Tr	
Inorganic calcite	33	18	35
Mica	1		
Nannofossils	4	25	20
Quartz	20	10	15
Shell debris		Tr	Tr
Sponge spicules	Tr		

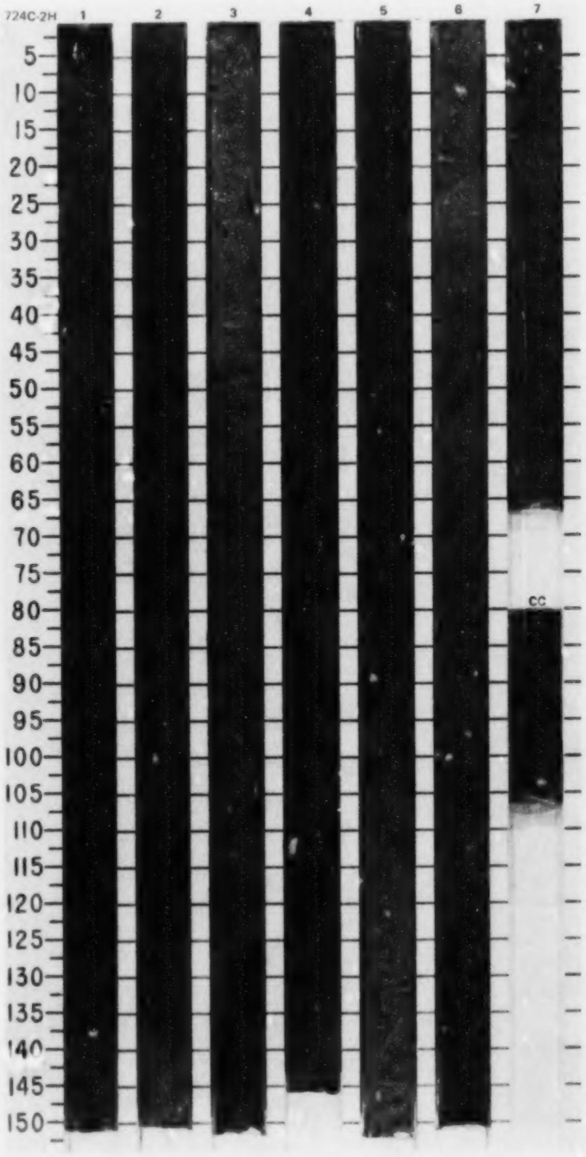
724C-2H
1
2
3
4
5
6
7
CC
5
10
15
20
25
30
35
40
45
50
55
60
65
70
75
80
85
90
95
100
105
110
115
120
125
130
135
140
145
150

SITE 724 HOLE C CORE 3H CORED INTERVAL 605.0-614.5 mbsl; 12.2-21.7 mbsf

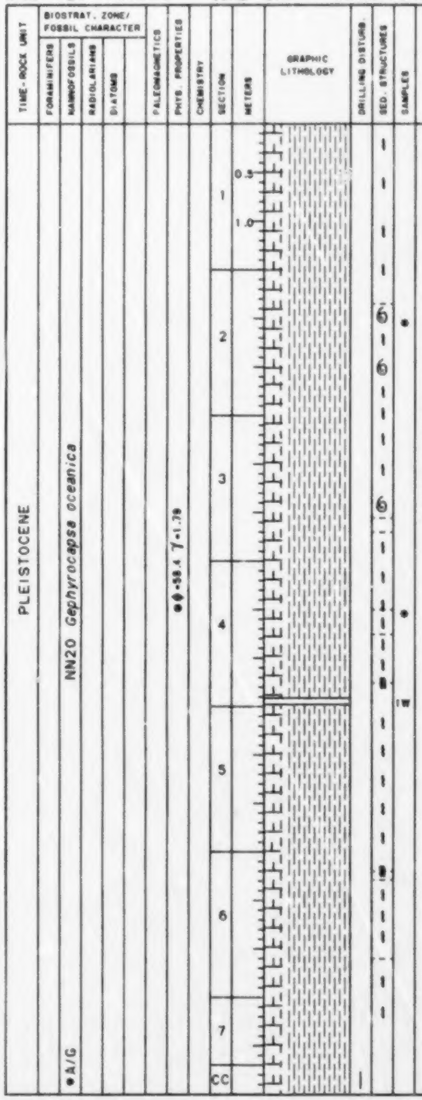
TIME-ROCK UNIT
BIOSTRAT. ZONE/ FOSSIL CHARACTER
FORAMINIFERS
NANNOFOSSILS
RADIOLARIANS
DIATOMS
PALEOMAGNETICS
PHYS. PROPERTIES
CHEMISTRY
SECTION
METERS
GRAPHIC LITHOLOGY
DRILLING DISTURB.
SED. STRUCTURES
SAMPLES
PLEISTOCENE
NN20 Gephyrocapsa oceanica
●A/G
● φ=58.4 γ=1.79
1
2
3
4
5
6
7
CC
0.5
1.0
IW

LITHOLOGIC DESCRIPTION

CALCAREOUS CLAYEY SILT

CC, 0-33 cm, slightly disturbed; remainder undisturbed.

Major lithology: CALCAREOUS CLAYEY SILT, olive (5Y 4/3), olive gray (5Y 5/2, 4/2), and dark olive gray (5Y 3/2). Minor to moderate burrow mottles. Contacts gradational and mottled. Millimeter-sized, indeterminate shell fragments common, locally concentrated in burrows.

SMEAR SLIDE SUMMARY (%):

	2, 55 D	4, 57 D
TEXTURE:		
Sand	25	20
Silt	25	45
Clay	50	35
COMPOSITION:		
Access. minerals	2	3
Clay	25	30
Dolomite	1	1
Foraminifers	1	1
Volcanic glass		Tr
Glauconite		Tr
Inorganic calcite	35	40
Mica	1	
Nannofossils	20	10
Organic debris		5
Quartz	15	10

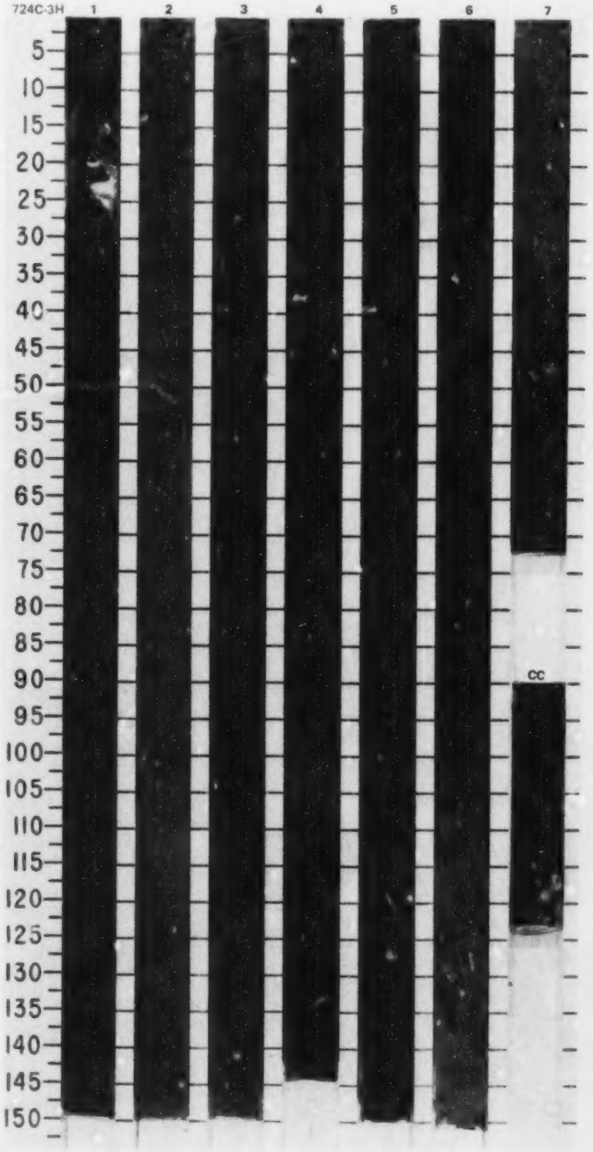
724C-3H
1
2
3
4
5
6
7
CC
5
10
15
20
25
30
35
40
45
50
55
60
65
70
75
80
85
90
95
100
105
110
115
120
125
130
135
140
145
150

SITE 724 HOLE C CORE 4H CORED INTERVAL 614.5-624.0 mbsl; 21.7-31.2 mbsf

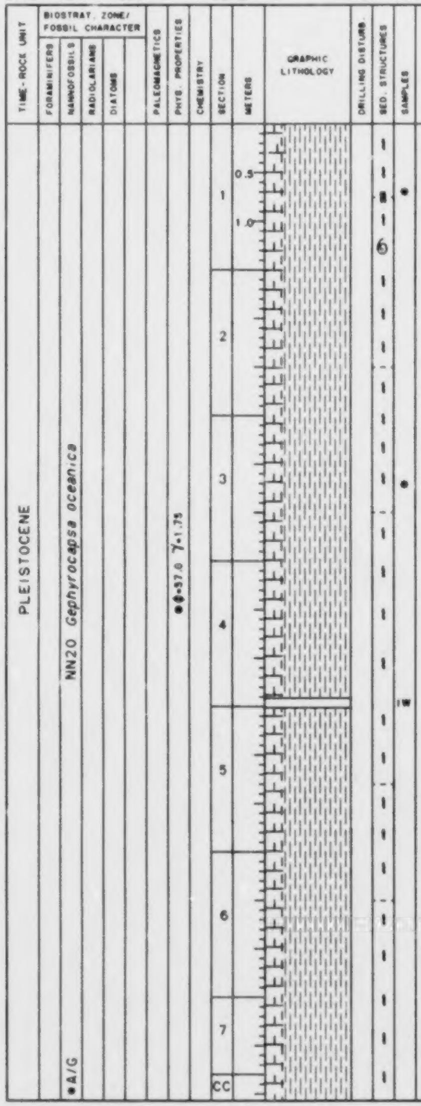
TIME-ROCK UNIT
BIOSTRAT. ZONE/ FOSSIL CHARACTER
FORAMINIFERS
NANNOFOSSILS
RADIOLARIANS
DIATOMS
PALEOMAGNETICS
PHYS. PROPERTIES
CHEMISTRY
SECTION
METERS
GRAPHIC LITHOLOGY
DRILLING DISTURB.
SED. STRUCTURES
SAMPLES
PLEISTOCENE
NN20 Gephyrocapsa oceanica
●A/G
●ϕ=37.0 γ=1.75
0.5
1.0
1
2
3
4
5
6
7
CC
IW

LITHOLOGIC DESCRIPTION

CALCAREOUS CLAYEY SILT

Entire core undisturbed.

Major lithology: CALCAREOUS CLAYEY SILT, olive (5Y 4/3), olive gray (5Y 5/2, 4/2), and dark olive gray (5Y 3/2). Minor to moderate burrow mottles. Contacts gradational and mottled. Millimeter-sized, indeterminate shell fragments scattered throughout. Foraminifers visible.

SMEAR SLIDE SUMMARY (%):

	1, 70 D	3, 70 D
TEXTURE:		
Sand	5	5
Silt	50	35
Clay	45	60
COMPOSITION:		
Clay	30	10
Dolomite	Tr	Tr
Foraminifers	10	10
Inorganic calcite	35	30
Nannofossils	20	40
Pellets		5
Quartz	5	5
Sponge spicules		Tr

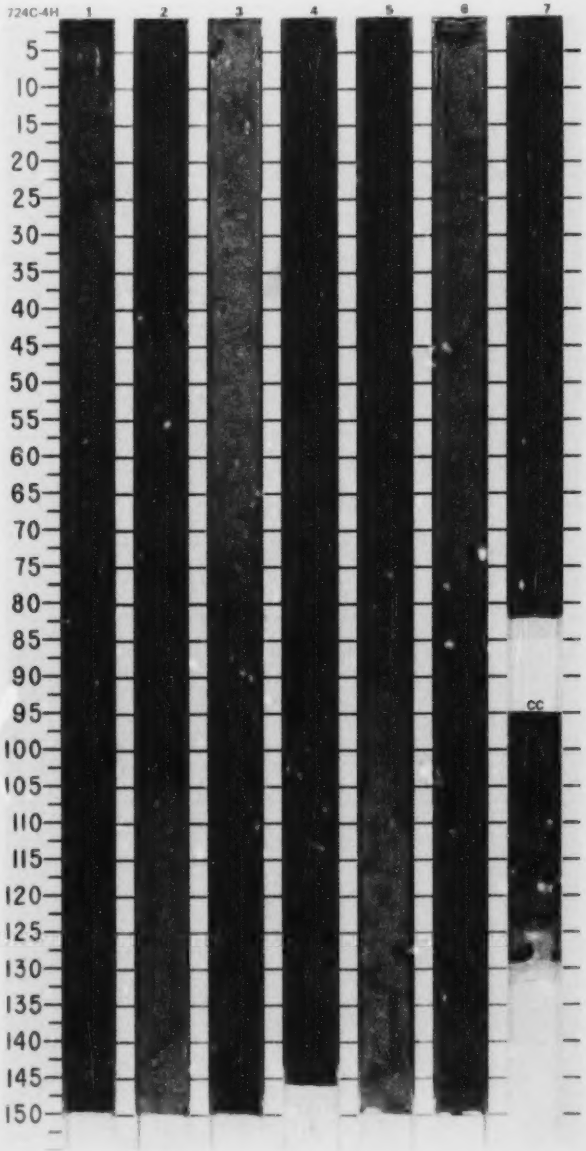
724C-4H
1
2
3
4
5
6
7
CC
5
10
15
20
25
30
35
40
45
50
55
60
65
70
75
80
85
90
95
100
105
110
115
120
125
130
135
140
145
150

SITE 724 HOLE C CORE 5H CORED INTERVAL 624.0-633.6 mbsl; 31.2-40.8 mbsf

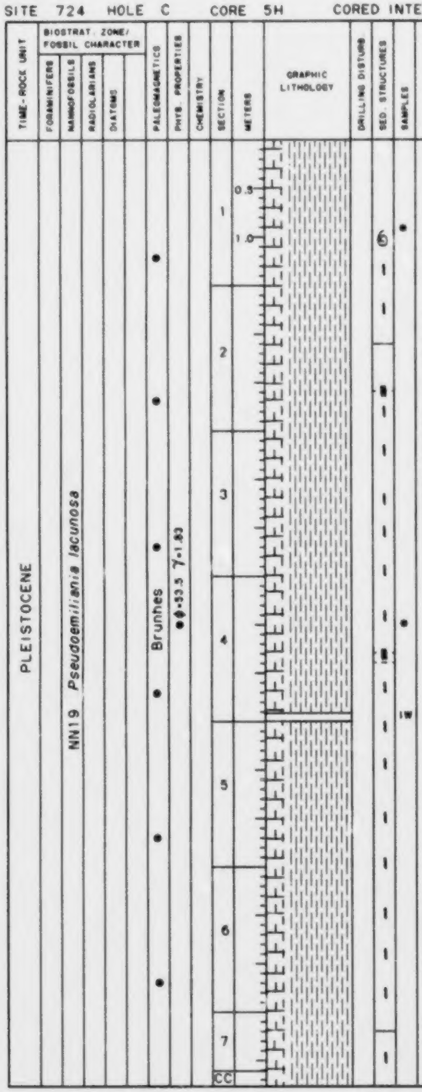
TIME-ROCK UNIT
BIOSTRAT. ZONE/ FOSSIL CHARACTER
FORAMINIFERS
NANNOFOSSILS
RADIOLARIANS
DIATOMS
PALEOMAGNETICS
PHYS. PROPERTIES
CHEMISTRY
SECTION
METERS
GRAPHIC LITHOLOGY
DRILLING DISTURB.
SED. STRUCTURES
SAMPLES
PLEISTOCENE
NN19 Pseudoemiliania lacunosa
Brunhes
●φ=53.5 γ=1.83
1
2
3
4
5
6
7
CC
0.5
1.0
IW

LITHOLOGIC DESCRIPTION

CALCAREOUS CLAYEY SILT

Entire core undisturbed.

Major lithology: CALCAREOUS CLAYEY SILT, olive (5Y 4/3), olive gray (5Y 5/2, 4/2), and dark olive gray (5Y 3/2). Minor to moderate burrow mottles. Contacts gradational and mottled. Millimeter-sized, indeterminate shell fragments scattered throughout. Foraminifers visible.

SMEAR SLIDE SUMMARY (%):

	1, 82 D	4, 49 D
TEXTURE:		
Sand	5	10
Silt	33	40
Clay	62	50
COMPOSITION:		
Access. minerals	Tr	Tr
Clay	15	20
Dolomite	Tr	
Foraminifers	20	20
Volcanic glass	Tr	
Inorganic calcite	20	20
Mica	Tr	Tr
Nannofossils	40	30
Pellets		5
Quartz	5	5

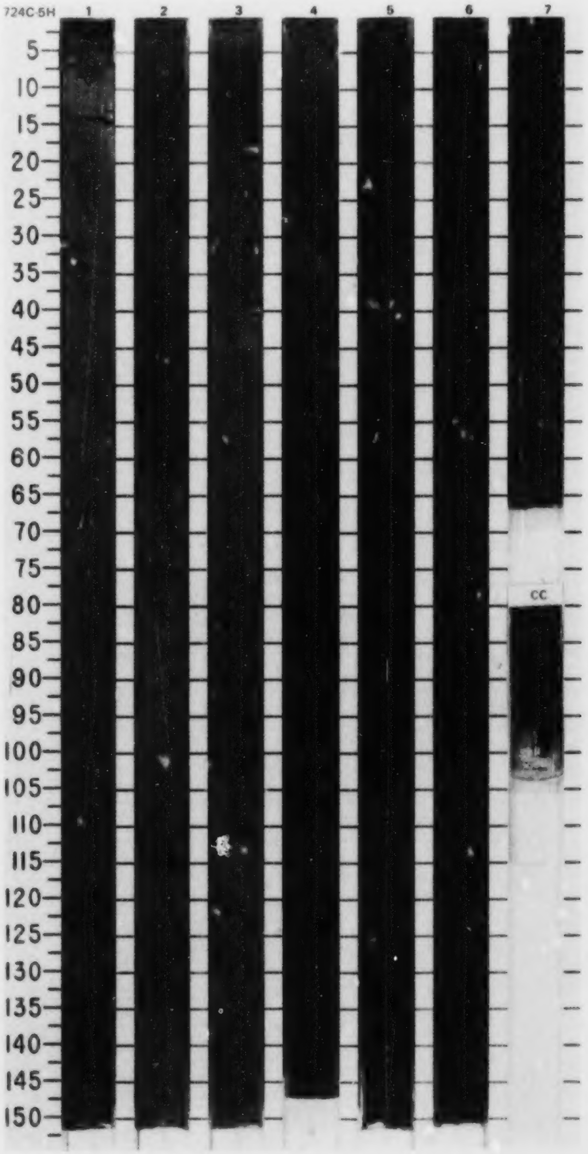
724C-5H
1
2
3
4
5
6
7
CC
5
10
15
20
25
30
35
40
45
50
55
60
65
70
75
80
85
90
95
100
105
110
115
120
125
130
135
140
145
150

SITE 724 HOLE C CORE 6X CORED INTERVAL 633.6-643.3 mbsl; 40.8-50.5 mbsf

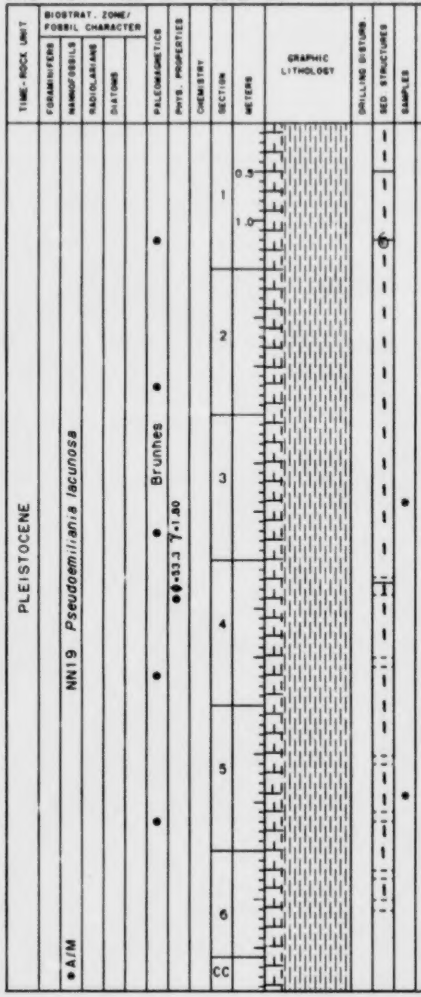
TIME-ROCK UNIT
BIOSTRAT. ZONE/ FOSSIL CHARACTER
FORAMINIFERS
NANNOFOSSILS
RADIOLARIANS
DIATOMS
PALEOMAGNETICS
PHYS. PROPERTIES
CHEMISTRY
SECTION
METERS
GRAPHIC LITHOLOGY
DRILLING DISTURB.
SED. STRUCTURES
SAMPLES
PLEISTOCENE
NN19 Pseudoemiliania lacunosa
A/M
Brunhes
φ=53.3 γ=1.80
0.5
1.0
1
2
3
4
5
6
CC

LITHOLOGIC DESCRIPTION

CALCAREOUS CLAYEY SILT

Entire core undisturbed.

Major lithology: CALCAREOUS CLAYEY SILT, olive (5Y 4/3), olive gray (5Y 5/2, 4/2), and dark olive gray (5Y 3/2). Minor burrow mottles throughout. Contacts gradational and mottled. Millimeter-sized, indeterminate shell fragments common. Foraminifers and pteropods visible.

SMEAR SLIDE SUMMARY (%):

	3, 92 D	5, 92 D
TEXTURE:		
Sand		10
Silt	55	45
Clay	45	45
COMPOSITION:		
Access. minerals	2	2
Clay	30	30
Foraminifers	3	3
Inorganic calcite	40	35
Nannofossil:	15	15
Pellets		5
Quartz	10	10

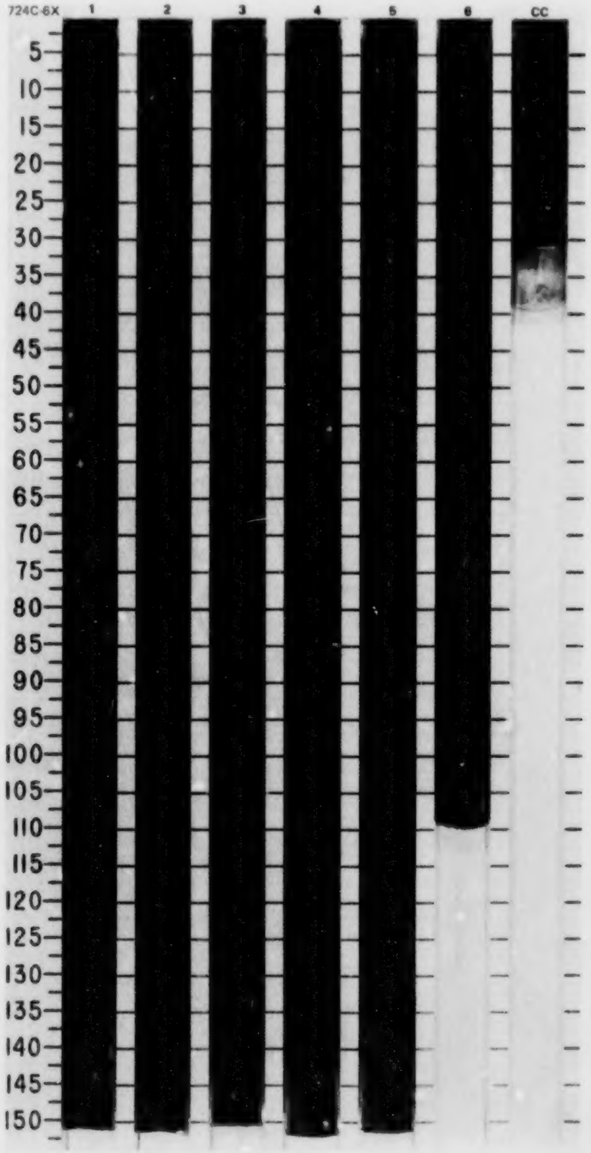
724C-6X
1
2
3
4
5
6
CC
5
10
15
20
25
30
35
40
45
50
55
60
65
70
75
80
85
90
95
100
105
110
115
120
125
130
135
140
145
150

SITE 724 HOLE C CORE 7X CORED INTERVAL 643.3-653.0 mbsl; 50.5-60.2 mbsf

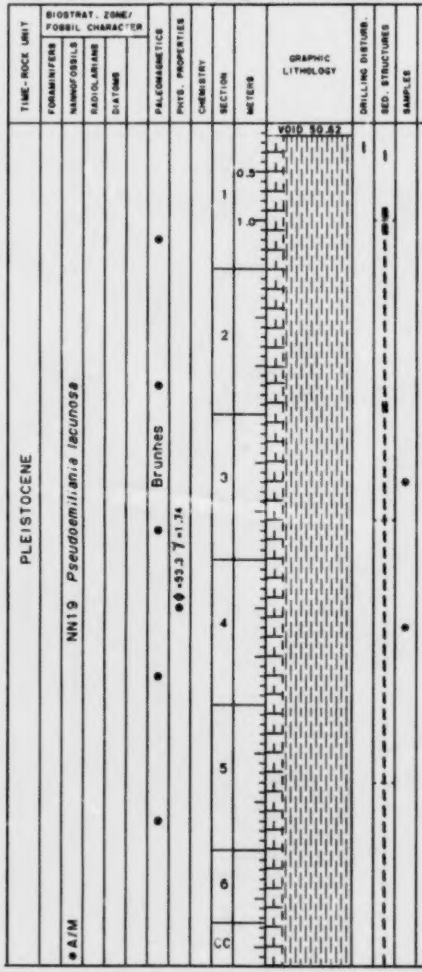
TIME-ROCK UNIT
BIOSTRAT. ZONE/ FOSSIL CHARACTER
FORAMINIFERS
NANNOFOSSILS
RADIOLARIANS
DIATOMS
PALEOMAGNETICS
PHYS. PROPERTIES
CHEMISTRY
SECTION
METERS
GRAPHIC LITHOLOGY
DRILLING DISTURB.
SED. STRUCTURES
SAMPLES
PLEISTOCENE
●A/M
NN19 Pseudoemiliania lacunosa
Brunhes
●ϕ=53.3 γ=1.74
1
2
3
4
5
6
CC
0.5
1.0
VOID 50.62

LITHOLOGIC DESCRIPTION

CALCAREOUS CLAYEY SILT

Entire core undisturbed.

Major lithology: CALCAREOUS CLAYEY SILT, olive (5Y 4/3, 4/4), olive gray (5Y 5/2, 4/2), and dark olive gray (5Y 3/2). Minor to moderate burrow mottling. Contacts gradational and mottled. Millimeter-sized, indeterminate shell fragments common. Foraminifers visible.

SMEAR SLIDE SUMMARY (%):

	3, 70 D	4, 70 D
TEXTURE:		
Silt	55	45
Clay	45	55
COMPOSITION:		
Access. minerals	2	3
Clay	25	30
Foraminifers	3	8
Inorganic calcite	40	25
Nannofossils	7	20
Pellets	5	4
Quartz	18	10

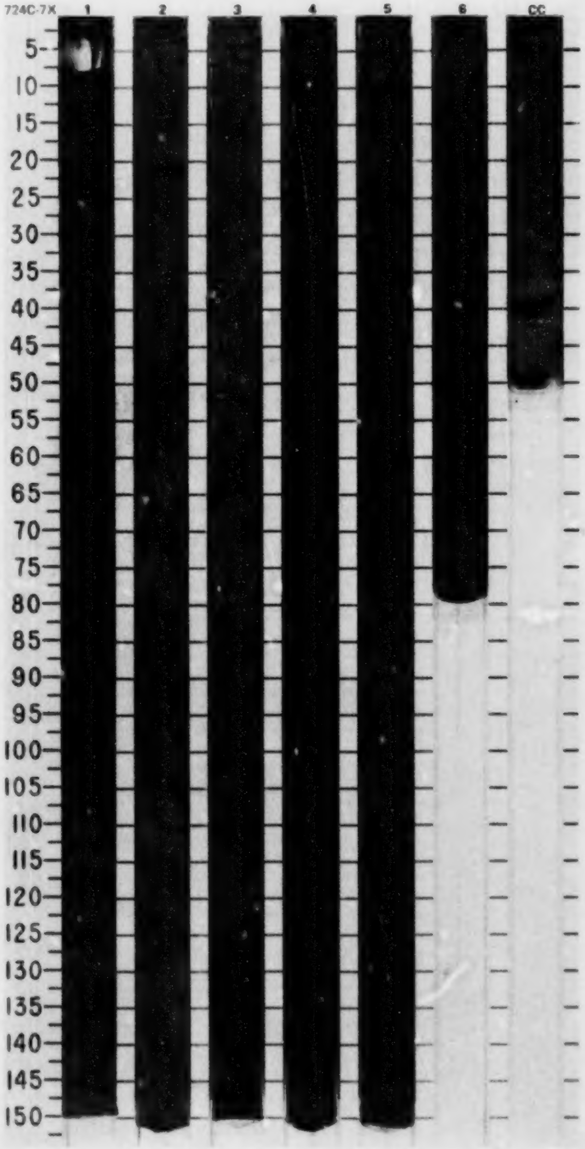
724C-7X
1
2
3
4
5
6
CC
5
10
15
20
25
30
35
40
45
50
55
60
65
70
75
80
85
90
95
100
105
110
115
120
125
130
135
140
145
150

SITE 724 HOLE C CORE 8X CORED INTERVAL 653.0-662.6 mbsl; 60.2-69.8 mbsf

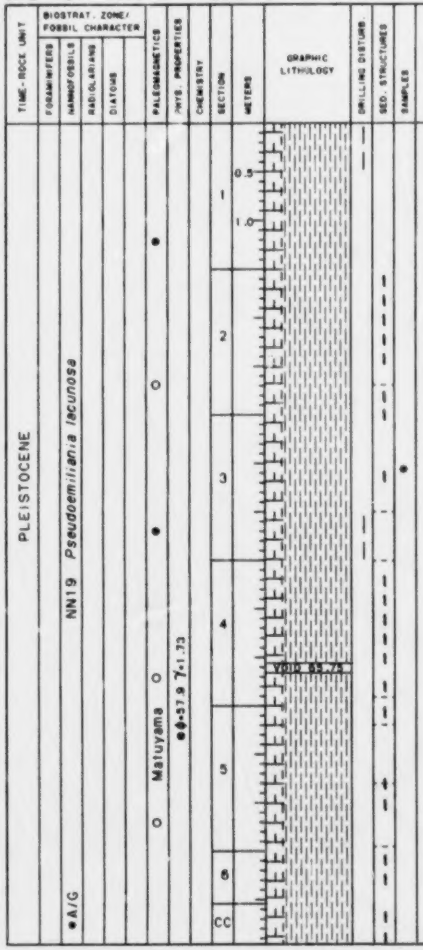
TIME-ROCK UNIT
BIOSTRAT. ZONE/ FOSSIL CHARACTER
FORAMINIFERS
NANNOFOSSILS
RADIOLARIANS
DIATOMS
PALEOMAGNETICS
PHYS. PROPERTIES
CHEMISTRY
SECTION
METERS
GRAPHIC LITHOLOGY
DRILLING DISTURB.
SED. STRUCTURES
SAMPLES
PLEISTOCENE
NN19 Pseudoemiliania lacunosa
●A/G
Matuyama
●Φ=57.9 γ=1.73
0.5
1.0
1
2
3
4
5
6
CC
VOID 85.75

LITHOLOGIC DESCRIPTION

CALCAREOUS CLAYEY SILT

Section 1, 0-50 cm, and Section 3, 110-140 cm, slightly disturbed; remainder undisturbed.

Major lithology: CALCAREOUS CLAYEY SILT, olive (5Y 4/3, 4/4), olive gray (5Y 5/2, 4/2), and dark olive gray (5Y 3/2). Minor burrow mottling common. Contacts gradational and mottled. Millimeter-sized, indeterminate shell fragments common. Foraminifers visible.

SMEAR SLIDE SUMMARY (%):

	3, 56 D
TEXTURE:	
Silt	60
Clay	40
COMPOSITION:	
Clay	30
Foraminifers	5
Inorganic calcite	30
Nannofossils	15
Pellets	7
Quartz	13

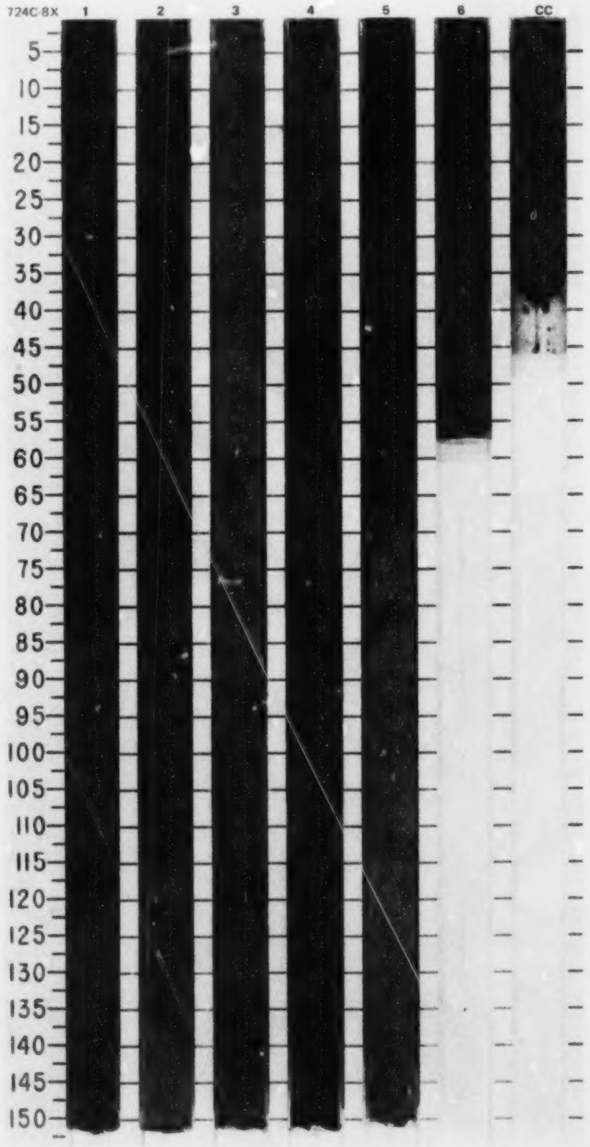
724C-8X
1
2
3
4
5
6
CC
5
10
15
20
25
30
35
40
45
50
55
60
65
70
75
80
85
90
95
100
105
110
115
120
125
130
135
140
145
150

SITE 724 HOLE C CORE 9X CORED INTERVAL 662.6-672.2 mbsl; 69.8-79.4 mbsf

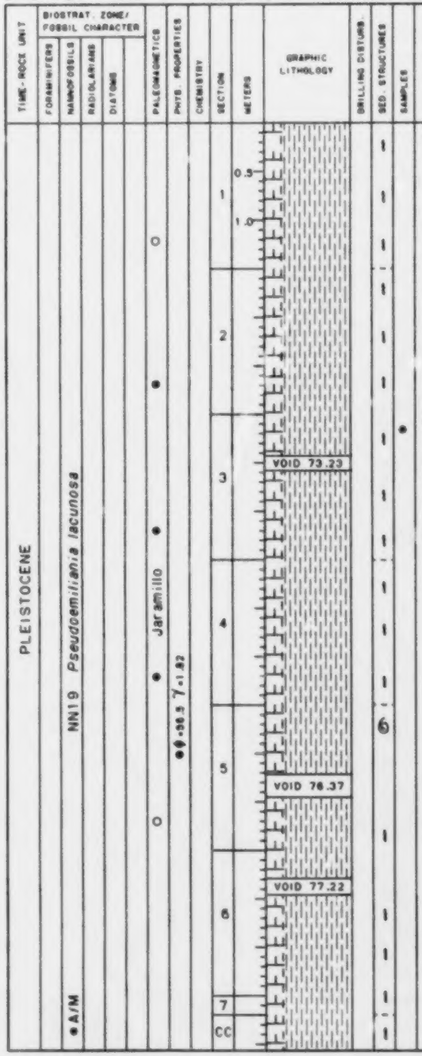
TIME-ROCK UNIT
BIOSTRAT. ZONE/ FOSSIL CHARACTER
FORAMINIFERS
NANNOFOSSILS
RADIOLARIANS
DIATOMS
PALEOMAGNETICS
PHYS. PROPERTIES
CHEMISTRY
SECTION
METERS
GRAPHIC LITHOLOGY
DRILLING DISTURB.
SED. STRUCTURES
SAMPLES
PLEISTOCENE
NN19 Pseudoemiliania lacunosa
●A/M
Jaramillo
●ϕ=56.5 γ=1.82
0.5
1.0
1
2
3
4
5
6
7
CC
VOID 73.23
VOID 76.37
VOID 77.22

LITHOLOGIC DESCRIPTION

CALCAREOUS CLAYEY SILT

Entire core undisturbed. Voids caused by gas expansion.

Major lithology: CALCAREOUS CLAYEY SILT, olive (5Y 4/3), olive gray (5Y 5/2, 4/2), and dark olive gray (5Y 3/2). Minor burrow mottling throughout. Contacts gradational and mottled. Millimeter-sized, indeterminate shell fragments common. Foraminifers visible.

SMEAR SLIDE SUMMARY (%):

	3, 18 D
TEXTURE:	
Silt	50
Clay	50
COMPOSITION:	
Access. minerals	Tr
Clay	25
Foraminifers	5
Inorganic calcite	25
Mica	Tr
Nannofossils	25
Pellets	5
Quartz	15

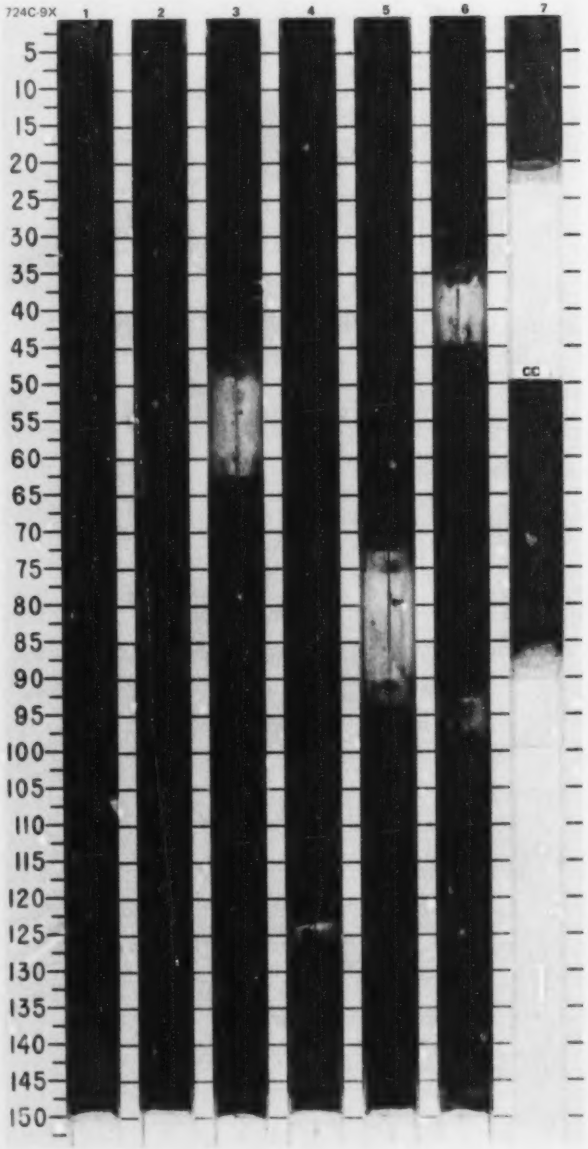
724C-9X
1
2
3
4
5
6
7
CC
5
10
15
20
25
30
35
40
45
50
55
60
65
70
75
80
85
90
95
100
105
110
115
120
125
130
135
140
145
150

SITE 724 HOLE C CORE 10X CORED INTERVAL 672.2-681.8 mbsl; 79.4-89.0 mbsf

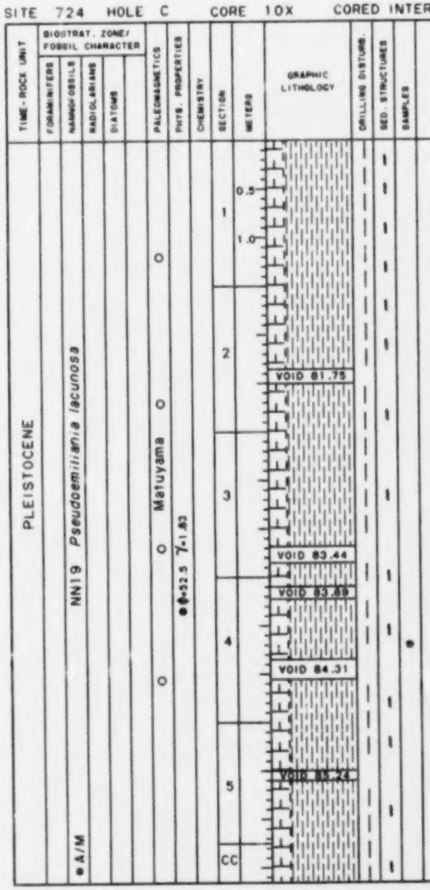
TIME-ROCK UNIT
BIOSTRAT. ZONE/ FOSSIL CHARACTER
FORAMINIFERS
NANNOFOSSILS
RADIOLARIANS
DIATOMS
PALEOMAGNETICS
PHYS. PROPERTIES
CHEMISTRY
SECTION
METERS
GRAPHIC LITHOLOGY
DRILLING DISTURB.
SED. STRUCTURES
SAMPLES
PLEISTOCENE
NN19 Pseudoemiliania lacunosa
● A/M
Matuyama
●ϕ=52.5 γ=1.83
1
2
3
4
5
CC
0.5
1.0
VOID 81.75
VOID 83.44
VOID 83.89
VOID 84.31
VOID 85.24

LITHOLOGIC DESCRIPTION

CALCAREOUS CLAYEY SILT

Entire core lightly disturbed. Voids caused by gas expansion.

Major lithology: CALCAREOUS CLAYEY SILT, olive (5Y 4/3). Minor burrow mottling throughout. Foraminifers visible.

SMEAR SLIDE SUMMARY (%):

	4, 70 D
TEXTURE:	
Silt	50
Clay	50
COMPOSITION:	
Access. minerals	Tr
Clay	30
Dolomite	2
Foraminifers	3
Inorganic calcite	36
Nannofossils	15
Pellets	5
Quartz	10

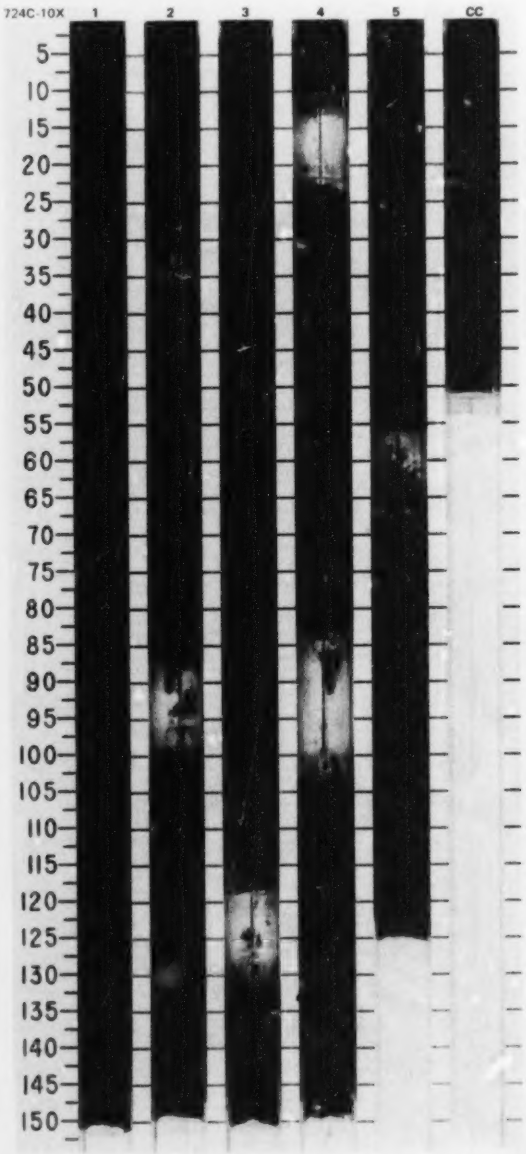
724C-10X
1
2
3
4
5
CC
5
10
15
20
25
30
35
40
45
50
55
60
65
70
75
80
85
90
95
100
105
110
115
120
125
130
135
140
145
150

SITE 724 HOLE C CORE 11X CORED INTERVAL 681.8-691.4 mbsl; 89.0-98.6 mbsf

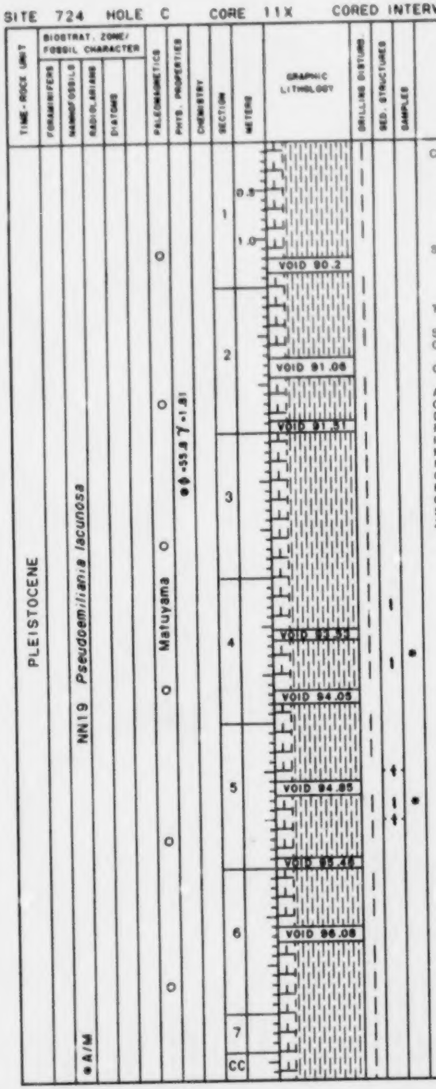
TIME-ROCK UNIT
BIOSTRAT. ZONE/ FOSSIL CHARACTER
FORAMINIFERS
NANNOFOSSILS
RADIOLARIANS
DIATOMS
PALEOMAGNETICS
PHYS. PROPERTIES
CHEMISTRY
SECTION
METERS
GRAPHIC LITHOLOGY
DRILLING DISTURB.
SED. STRUCTURES
SAMPLES
PLEISTOCENE
NN19 Pseudoemiliania lacunosa
● A/M
Matuyama
●φ=55.8 γ=1.81
1
2
3
4
5
6
7
CC
0.5
1.0
VOID 90.2
VOID 91.06
VOID 91.31
VOID 93.32
VOID 94.05
VOID 94.85
VOID 95.46
VOID 96.08

LITHOLOGIC DESCRIPTION

CALCAREOUS CLAYEY SILT

Entire core slightly disturbed. Voids caused by gas expansion.

Major lithology: CALCAREOUS CLAYEY SILT, olive (5Y 4/3) and very dark gray (5Y 3/1). Minor burrow mottling rare. Contacts gradational and mottled. Foraminifers visible.

SMEAR SLIDE SUMMARY (%):

	4, 80 D	5, 82 M
TEXTURE:		
Silt	55	60
Clay	45	40
COMPOSITION:		
Access. minerals	1	2
Clay	35	35
Dolomite	1	3
Foraminifers	10	3
Inorganic calcite	25	30
Mica	Tr	Tr
Nannofossils	10	3
Organic debris		7
Pellets	3	5
Quartz	15	10
Sponge spicules		1
Zircon		Tr

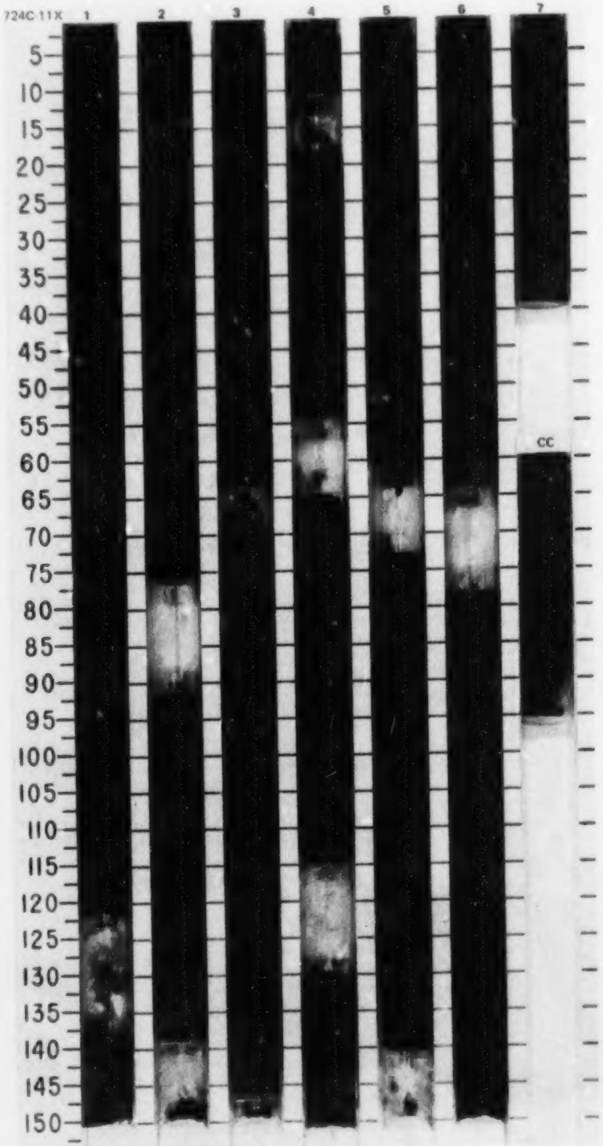
724C-11X
1
2
3
4
5
6
7
CC
5
10
15
20
25
30
35
40
45
50
55
60
65
70
75
80
85
90
95
100
105
110
115
120
125
130
135
140
145
150

SITE 724 HOLE C CORE 12X CORED INTERVAL 691.4-701.1 mbsl; 98.6-108.3 mbsf

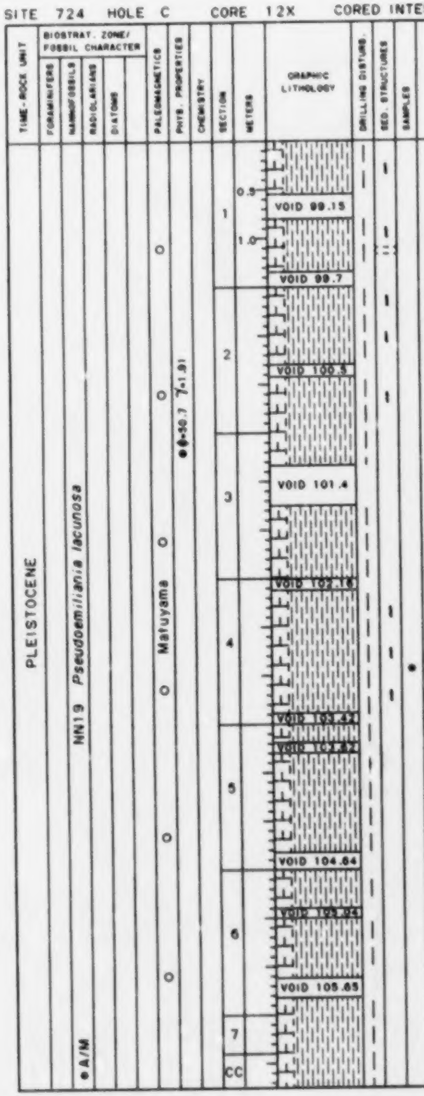
TIME-ROCK UNIT
BIOSTRAT. ZONE/ FOSSIL CHARACTER
FORAMINIFERS
NANNOFOSSILS
RADIOLARIANS
DIATOMS
PALEOMAGNETICS
PHYS. PROPERTIES
CHEMISTRY
SECTION
METERS
GRAPHIC LITHOLOGY
DRILLING DISTURB.
SED. STRUCTURES
SAMPLES
PLEISTOCENE
NN19 *Pseudoemiliania lacunosa*
● A/M
Matuyama
●ϕ=50.7 γ=1.91
1
2
3
4
5
6
7
CC
0.5
1.0
VOID 99.15
VOID 99.7
VOID 100.5
VOID 101.4
VOID 102.16
VOID 104.64
VOID 105.65

LITHOLOGIC DESCRIPTION

CALCAREOUS CLAYEY SILT

Entire core slightly disturbed. Voids caused by gas expansion.

Major lithology: CALCAREOUS CLAYEY SILT, olive (5Y 4/3), olive gray (5Y 4/2), dark olive gray (5Y 3/2), and very dark gray (5Y 3/1). Minor burrow mottling common. Foraminifers visible.

SMEAR SLIDE SUMMARY (%):

	4, 94 D
TEXTURE:	
Silt	30
Clay	70
COMPOSITION:	
Access. minerals	1
Clay	45
Dolomite	2
Foraminifers	7
Inorganic calcite	20
Nannofossils	15
Pellets	5
Quartz	5

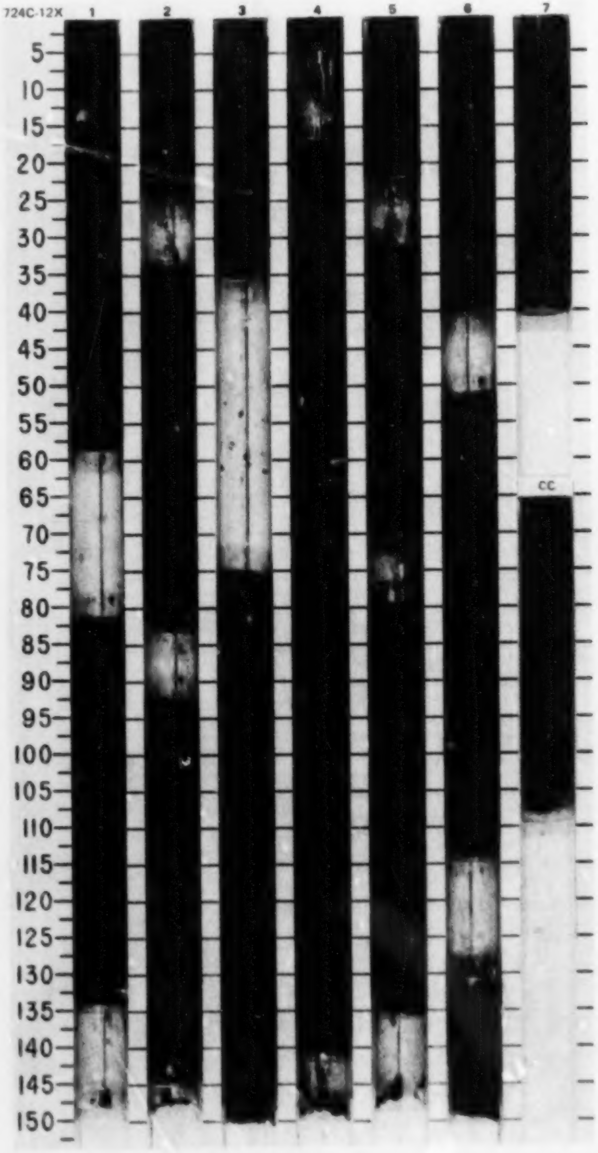
724C-12X
1
2
3
4
5
6
7
CC
5
10
15
20
25
30
35
40
45
50
55
60
65
70
75
80
85
90
95
100
105
110
115
120
125
130
135
140
145
150

SITE 724 HOLE C CORE 13X CORED INTERVAL 701.1-710.6 mbsl; 108.3-117.8 mbsf

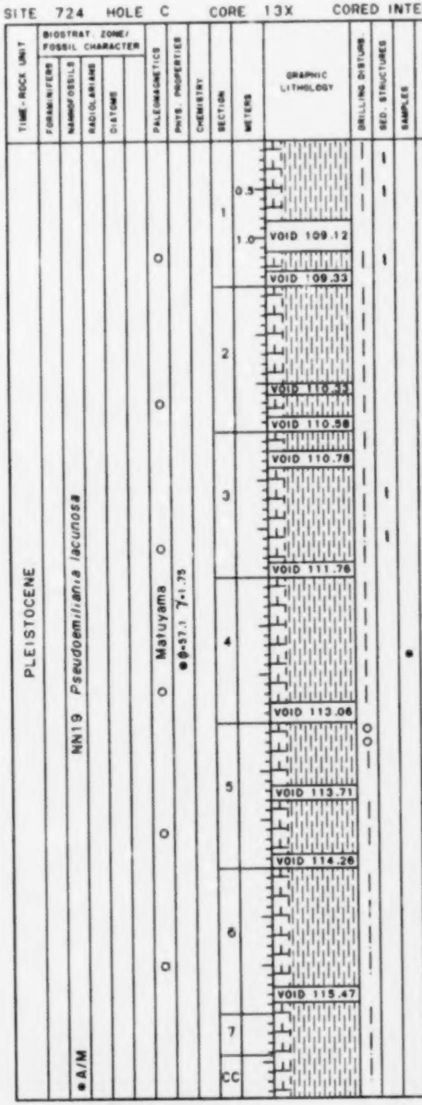
TIME-ROCK UNIT
BIOSTRAT. ZONE/ FOSSIL CHARACTER
FORAMINIFERS
NANNOFOSSILS
RADIOLARIANS
DIATOMS
PALEOMAGNETICS
PHYS. PROPERTIES
CHEMISTRY
SECTION
METERS
GRAPHIC LITHOLOGY
DRILLING DISTURB.
SED. STRUCTURES
SAMPLES
PLEISTOCENE
NN19 Pseudoemiliania lacunosa
• A/M
Matuyama
●Φ=57.1 γ=1.75
1
2
3
4
5
6
7
CC
0.5
1.0
VOID 109.12
VOID 109.33
VOID 110.33
VOID 110.58
VOID 110.78
VOID 111.76
VOID 113.06
VOID 113.71
VOID 114.26
VOID 115.47

LITHOLOGIC DESCRIPTION

CALCAREOUS CLAYEY SILT

Section 5, 0-20 cm, soupy; Section 3, 80-135 cm, and Section 6, 50-130 cm, moderately disturbed; remainder slightly disturbed. Voids caused by gas expansion.

Major lithology: CALCAREOUS CLAYEY SILT, olive (5Y 4/3) and dark olive gray (5Y 3/2). Minor burrow mottling rare. Contacts gradational and mottled. Foraminifers visible.

SMEAR SLIDE SUMMARY (%):

	4, 80 D
TEXTURE:	
Silt	60
Clay	40
COMPOSITION:	
Clay	19
Dolomite	5
Foraminifers	9
Volcanic glass	Tr
Inorganic calcite	28
Nannofossils	28
Organic debris	5
Quartz	5

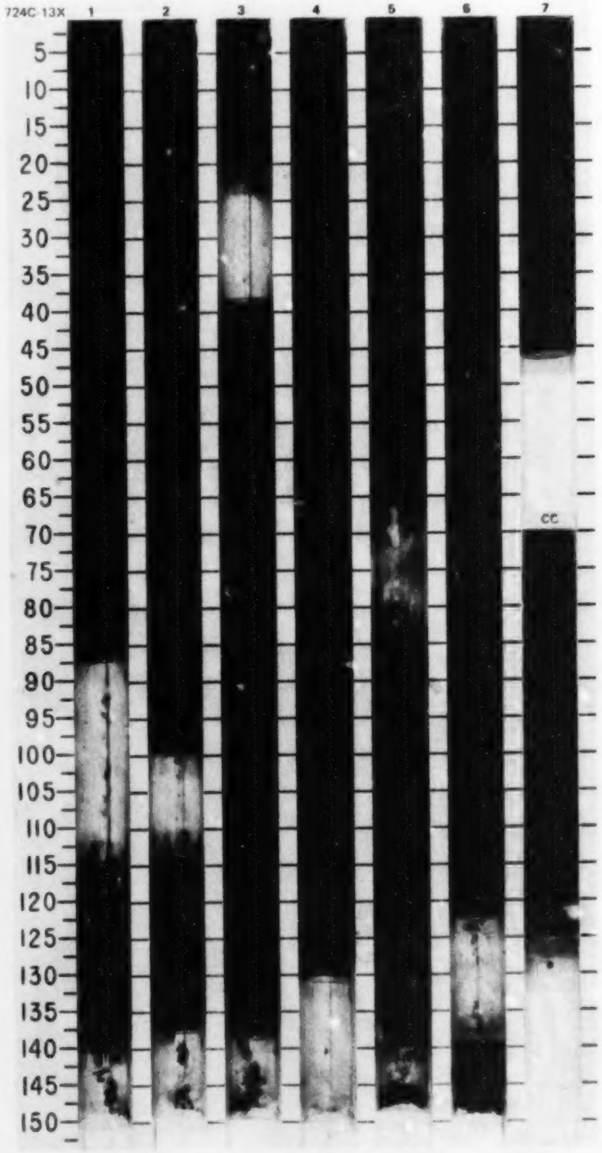
724C-13X
1
2
3
4
5
6
7
CC
5
10
15
20
25
30
35
40
45
50
55
60
65
70
75
80
85
90
95
100
105
110
115
120
125
130
135
140
145
150

SITE 724 HOLE C CORE 14X CORED INTERVAL 710.6-720.2 mbsl; 117.8-127.4 mbsf

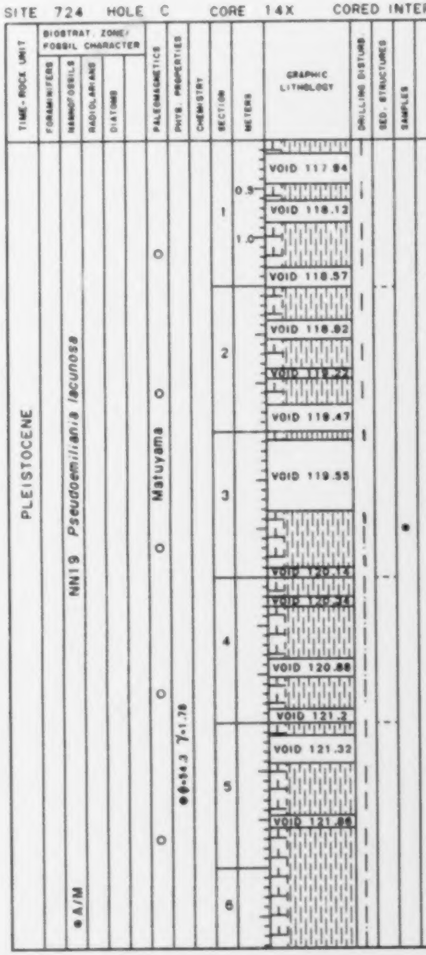
TIME-ROCK UNIT
BIOSTRAT. ZONE/ FOSSIL CHARACTER
FORAMINIFERS
NANNOFOSSILS
RADIOLARIANS
DIATOMS
PALEOMAGNETICS
PHYS. PROPERTIES
CHEMISTRY
SECTION
METERS
GRAPHIC LITHOLOGY
DRILLING DISTURB.
SED. STRUCTURES
SAMPLES
PLEISTOCENE
NN19 Pseudoemiliania lacunosa
●A/M
Matuyama
●φ=54.3 γ=1.78
1
2
3
4
5
6
0.5
1.0
VOID 117.94
VOID 118.12
VOID 118.57
VOID 118.92
VOID 119.22
VOID 119.47
VOID 119.55
VOID 120.14
VOID 120.24
VOID 120.88
VOID 121.2
VOID 121.32
VOID 121.86

LITHOLOGIC DESCRIPTION

CALCAREOUS CLAYEY SILT

Section 3, 0-9, 81-90, and 135-140 cm, very disturbed; Section 3, 90-135 cm, Section 4, 0-150 cm, and Section 6, 0-83 cm, moderately disturbed; remainder slightly disturbed. Voids caused by gas expansion.

Major lithology: CALCAREOUS CLAYEY SILT, olive (5Y 4/3), olive gray (5Y 4/2), and dark olive gray (5Y 3/2). Contacts gradational and mottled. Foraminifers visible.

SMEAR SLIDE SUMMARY (%):

	3, 100 D
TEXTURE:	
Silt	60
Clay	40
COMPOSITION:	
Access. minerals	2
Clay	30
Dolomite	2
Foraminifers	3
Inorganic calcite	30
Nannofossils	10
Pellets	3
Quartz	15
Sponge spicules	3

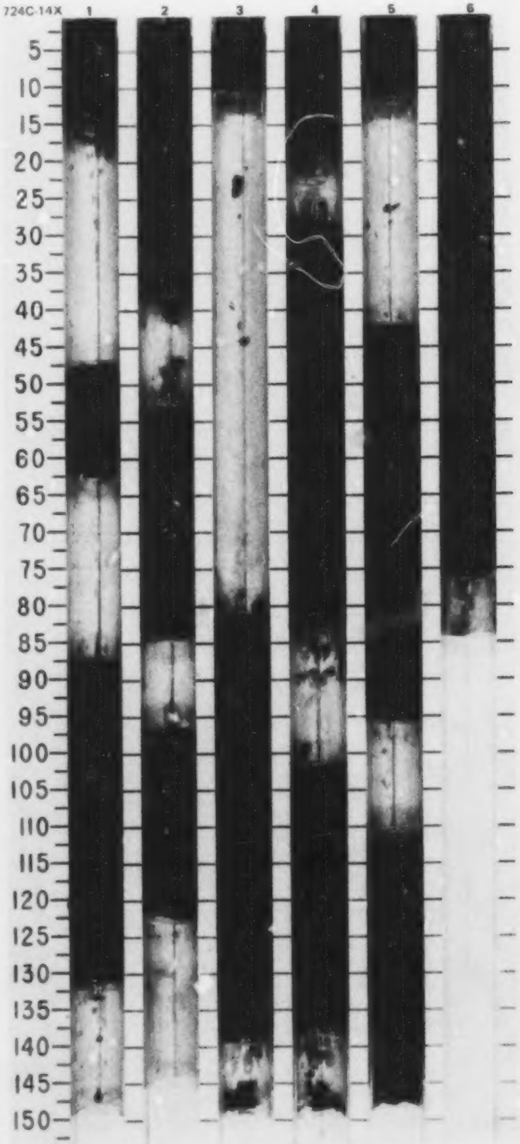
724C-14X
1
2
3
4
5
6
5
10
15
20
25
30
35
40
45
50
55
60
65
70
75
80
85
90
95
100
105
110
115
120
125
130
135
140
145
150

SITE 724 HOLE C CORE 15X CORED INTERVAL 720.2-729.8 mbsl; 127.4-137.0 mbsf

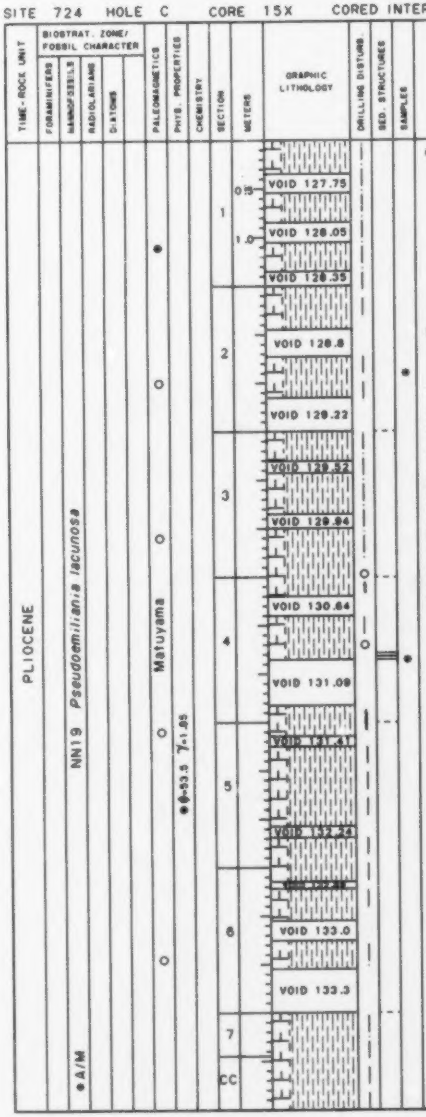
TIME-ROCK UNIT
BIOSTRAT. ZONE/ FOSSIL CHARACTER
FORAMINIFERS
NANNOFOSSILS
RADIOLARIANS
DIATOMS
PALEOMAGNETICS
PHYS. PROPERTIES
CHEMISTRY
SECTION
METERS
GRAPHIC LITHOLOGY
DRILLING DISTURB.
SED. STRUCTURES
SAMPLES
PLIOCENE
NN19 Pseudoemiliania lacunosa
A/M
Matuyama
ϕ=53.5 γ=1.85
1
2
3
4
5
6
7
CC
0.5
1.0
VOID 127.75
VOID 128.05
VOID 128.35
VOID 128.8
VOID 129.22
VOID 129.52
VOID 129.84
VOID 130.64
VOID 131.09
VOID 131.41
VOID 132.24
VOID 133.0
VOID 133.3

LITHOLOGIC DESCRIPTION

CALCAREOUS CLAYEY SILT

Section 3, 135-150 cm, and Section 4, 75-80 cm, soupy; Section 4, 0-5 cm, Section 5, 0-14 cm, Section 6, 0-55 cm, and CC, 30-60 cm, very disturbed; Section 1, 0-150 cm, Section 3, 0-135 cm, Section 6, 77-113 cm, and Section 7, 10-43 cm, moderately disturbed; remainder slightly disturbed. Voids caused by gas expansion.

Major lithology: CALCAREOUS CLAYEY SILT, olive (5Y 4/3), dark olive gray (5Y 3/2), and very dark gray (5Y 3/1). Minor burrow mottling very rare. Contacts gradational and mottled. Foraminifers visible.

Minor lithology: Section 4, 80-85 cm, submillimeter laminated calcitic silty clay, very dark gray (5Y 3/1).

SMEAR SLIDE SUMMARY (%):

	2, 90 D	4, 86 M
TEXTURE:		
Silt	40	35
Clay	60	65
COMPOSITION:		
Clay	35	40
Diatoms		Tr
Dolomite	3	2
Foraminifers	7	10
Gypsum		Tr
Inorganic calcite	25	30
Mica	Tr	
Nannofossils	20	5
Organic debris		3
Pellets	3	
Quartz	5	10
Sponge spicules	2	

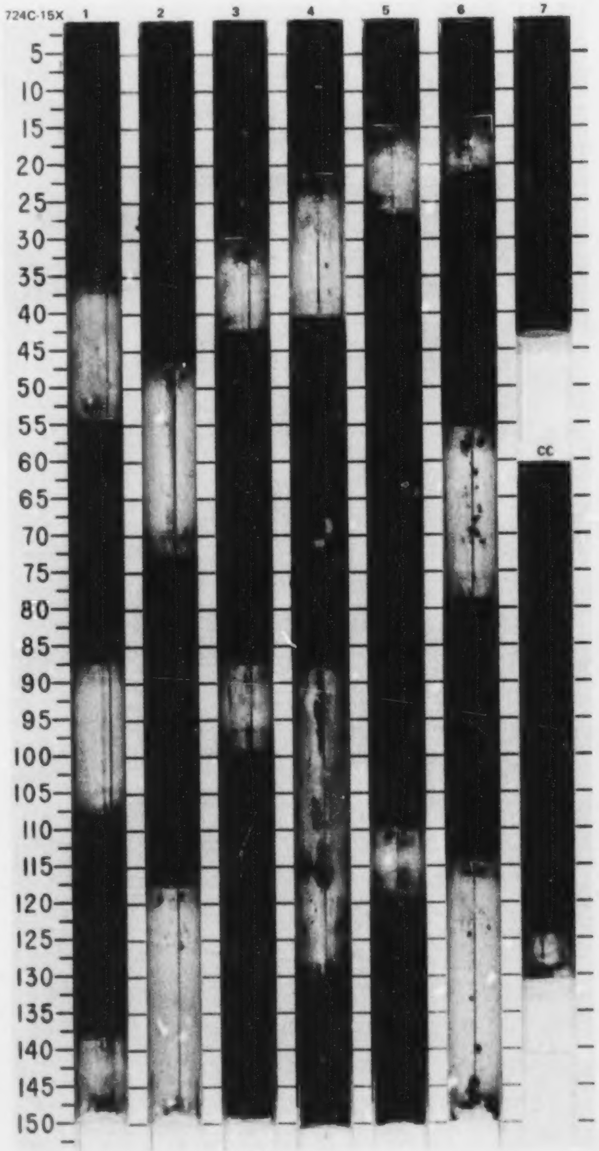
724C-15X
1
2
3
4
5
6
7
CC
5
10
15
20
25
30
35
40
45
50
55
60
65
70
75
80
85
90
95
100
105
110
115
120
125
130
135
140
145
150

SITE 724 HOLE C CORE 16X CORED INTERVAL 729.8-739.4 mbsl; 137.0-146.6 mbsf

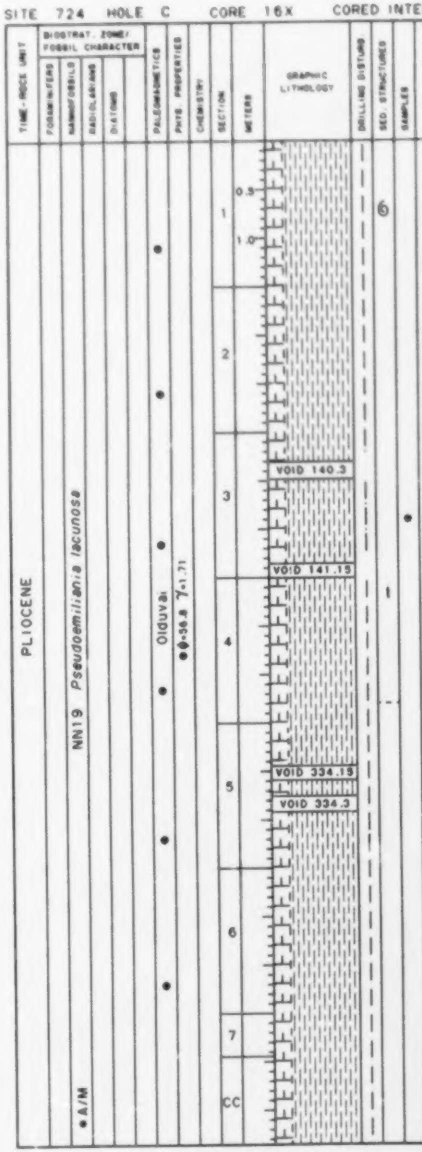
TIME-ROCK UNIT
BIOSTRAT. ZONE/ FOSSIL CHARACTER
FORAMINIFERS
NANNOFOSSILS
RADIOLARIANS
DIATOMS
PALEOMAGNETICS
PHYS. PROPERTIES
CHEMISTRY
SECTION
METERS
GRAPHIC LITHOLOGY
DRILLING DISTURB.
SED. STRUCTURES
SAMPLES
PLIOCENE
NN19 Pseudoemiliania lacunosa
● A/M
Olduvai
●ϕ=56.8 γ=1.71
1
2
3
4
5
6
7
CC
0.5
1.0
VOID 140.3
VOID 141.15
VOID 334.15
VOID 334.3

LITHOLOGIC DESCRIPTION

CALCAREOUS CLAYEY SILT

Section 3, 0-150 cm, moderately disturbed; remainder slightly disturbed. Voids caused by gas expansion.

Major lithology: CALCAREOUS CLAYEY SILT, olive (5Y 4/3), olive gray (5Y 4/2), and dark olive gray (5Y 3/2). Minor burrow mottling very rare. Contacts gradational and mottled. Foraminifers visible.

SMEAR SLIDE SUMMARY (%):

	3, 90 D
TEXTURE:	
Silt	40
Clay	60
COMPOSITION:	
Clay	30
Dolomite	2
Foraminifers	7
Gypsum	Tr
Hornblende	Tr
Inorganic calcite	35
Mica	Tr
Nannofossils	15
Pyrite	1
Quartz	10
Sponge spicules	Tr

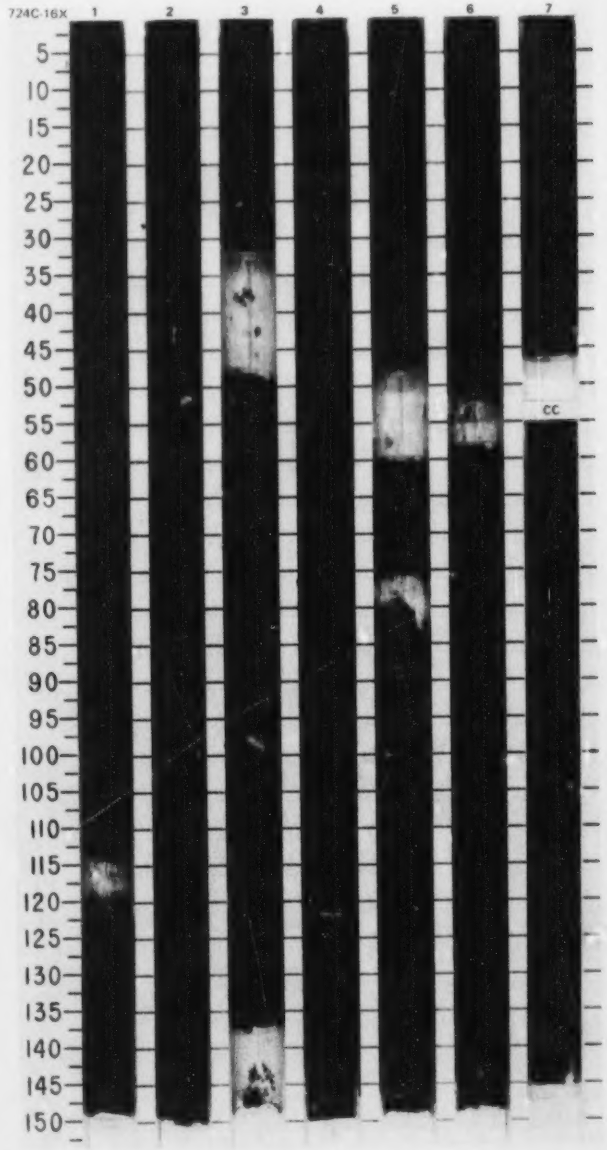
724C-16X
1
2
3
4
5
6
7
CC
5
10
15
20
25
30
35
40
45
50
55
60
65
70
75
80
85
90
95
100
105
110
115
120
125
130
135
140
145
150

SITE 724 HOLE C CORE 17X CORED INTERVAL 739.4-749.1 mbsl; 146.6-156.3 mbsf

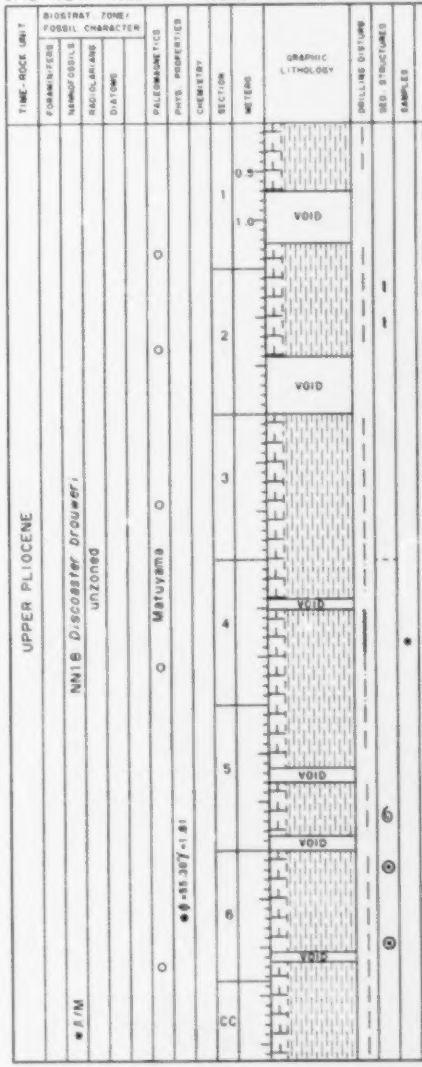
TIME-ROCK UNIT
BIOSTRAT. ZONE/ FOSSIL CHARACTER
FORAMINIFERS
NANNOFOSSILS
RADIOLARIANS
DIATOMS
PALEOMAGNETICS
PHYS. PROPERTIES
CHEMISTRY
SECTION
METERS
GRAPHIC LITHOLOGY
DRILLING DISTURB.
SED. STRUCTURES
SAMPLES
UPPER PLIOCENE
NN18 Discoaster brouweri
unzoned
● A/M
Matuyama
●ϕ=55.30 γ=1.81
1
2
3
4
5
6
CC
0.5
1.0
VOID
VOID
VOID
VOID
VOID
VOID

LITHOLOGIC DESCRIPTION

CALCAREOUS CLAYEY SILT

Section 4, 56-90 cm, very disturbed. Section 4, 0-43 and 96-150 cm, moderately disturbed; remainder slightly disturbed. Voids caused by gas expansion.

Major lithology: CALCAREOUS CLAYEY SILT, olive gray (5Y 4/2) and dark olive gray (5Y 3/2). Minor burrow mottling very rare. Contacts gradational and mottled. Foraminifers visible. Section 6, 8 and 97 cm, black (5Y 2.5/1) phosphatic nodules present. Section 5, 109 cm, fish vertebra present.

SMEAR SLIDE SUMMARY (%):

	4, 86 D
TEXTURE:	
Silt	40
Clay	60
COMPOSITION:	
Clay	30
Dolomite	4
Foraminifers	10
Hornblende	Tr
Inorganic calcite	30
Mica	2
Nannofossils	10
Pellets	5
Quartz	7
Silicoflagellates	2

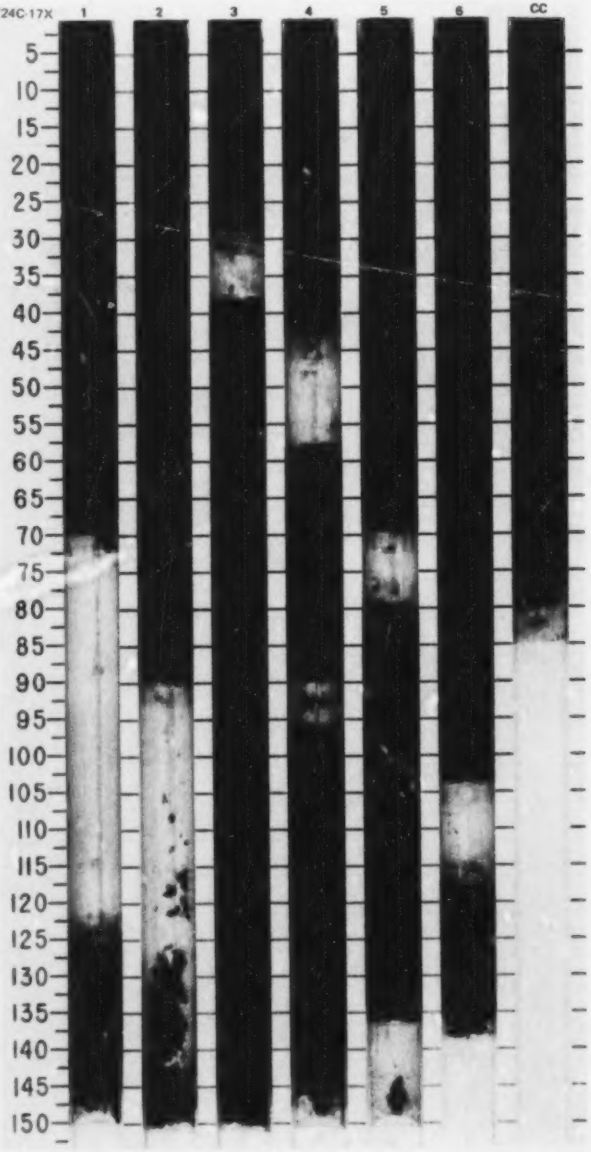
724C-17X
1
2
3
4
5
6
CC
5
10
15
20
25
30
35
40
45
50
55
60
65
70
75
80
85
90
95
100
105
110
115
120
125
130
135
140
145
150

SITE 724 HOLE C CORE 18X CORED INTERVAL 749.1-758.7 mbsl; 156.3-165.9 mbsf

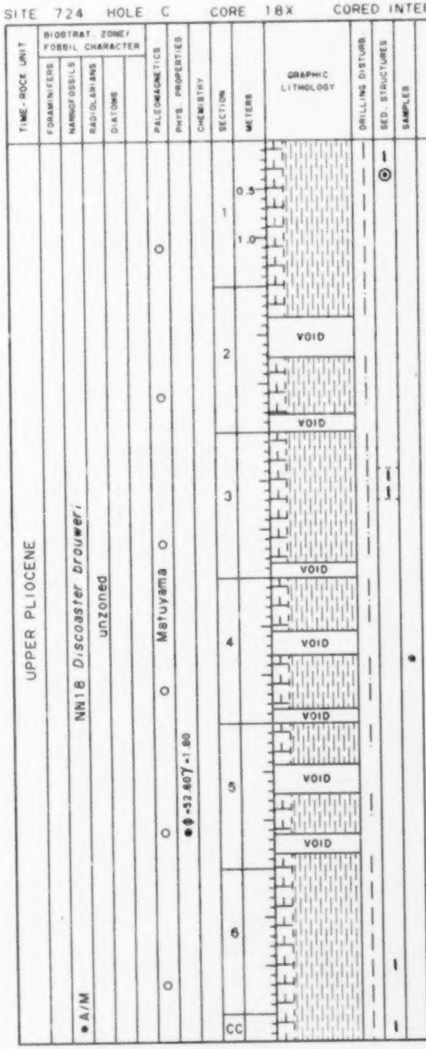
TIME-ROCK UNIT
BIOSTRAT. ZONE/ FOSSIL CHARACTER
FORAMINIFERS
NANNOFOSSILS
RADIOLARIANS
DIATOMS
PALEOMAGNETICS
PHYS. PROPERTIES
CHEMISTRY
SECTION
METERS
GRAPHIC LITHOLOGY
DRILLING DISTURB.
SED. STRUCTURES
SAMPLES
UPPER PLIOCENE
NN18 Discoaster brouweri
unzoned
• A/M
Matuyama
●ϕ=52.60γ=1.80
0.5
1.0
1
2
3
4
5
6
CC
VOID
VOID
VOID
VOID
VOID
VOID
VOID

LITHOLOGIC DESCRIPTION

CALCAREOUS CLAYEY SILT

Sections 2-5 moderately disturbed, remainder slightly disturbed. Voids caused by gas expansion.

Major lithology: CALCAREOUS CLAYEY SILT, light gray (5Y 7/1), olive (5Y 4/3), olive gray (5Y 4/2), and dark olive gray (5Y 3/2). Minor burrow mottling very rare. Contacts gradational and mottled. Foraminifers visible. Section 1, 52 cm, black (5Y 2.5/1) phosphatic nodule present.

SMEAR SLIDE SUMMARY (%):

	4, 85 D
TEXTURE:	
Silt	30
Clay	70
COMPOSITION:	
Clay	28
Dolomite	4
Foraminifers	3
Inorganic calcite	20
Mica	Tr
Nannofossils	40
Quartz	5

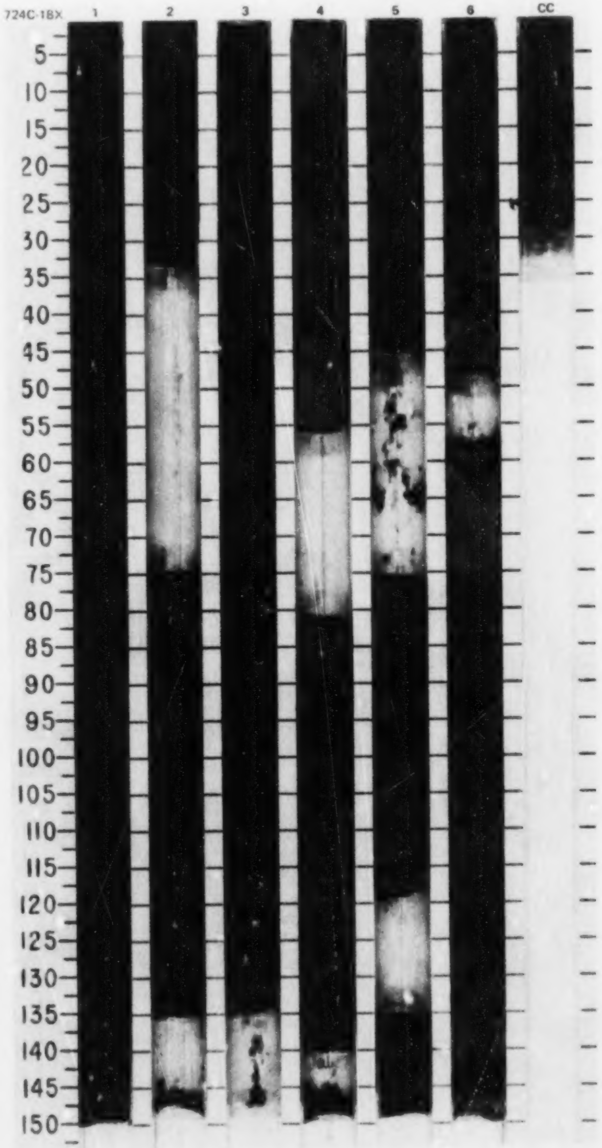
724C-18X
1
2
3
4
5
6
CC
5
10
15
20
25
30
35
40
45
50
55
60
65
70
75
80
85
90
95
100
105
110
115
120
125
130
135
140
145
150

SITE 724 HOLE C CORE 19X CORED INTERVAL 758.7-768.3 mbsl; 165.9-175.5 mbsf

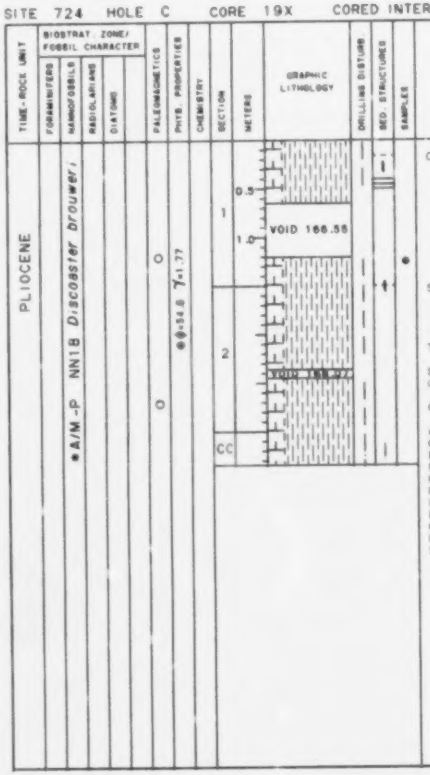
TIME-ROCK UNIT
BIOSTRAT. ZONE/ FOSSIL CHARACTER
FORAMINIFERS
NANNOFOSSILS
RADIOLARIANS
DIATOMS
PALEOMAGNETICS
PHYS. PROPERTIES
CHEMISTRY
SECTION
METERS
GRAPHIC LITHOLOGY
DRILLING DISTURB.
SED. STRUCTURES
SAMPLES
PLIOCENE
●A/M-P NN18 Discoaster brouweri
●Φ=54.8 γ=1.77
1
2
CC
0.5
1.0
VOID 166.55

LITHOLOGIC DESCRIPTION

CALCAREOUS CLAYEY SILT

CC, 0-35 cm, moderately disturbed; remainder slightly disturbed. Voids caused by gas expansion.

Major lithology: CALCAREOUS CLAYEY SILT, olive (5Y 4/3), dark olive gray (5Y 3/2), and black (5Y 2.5/2). Minor burrow mottling rare. Contacts gradational and mottled. Foraminifers visible.

Minor lithology: Section 1, 35-4 cm, black (5Y 2.5/2) diatomaceous mud.

SMEAR SLIDE SUMMARY (%):

	1, 125 D
TEXTURE:	
Silt	30
Clay	70
COMPOSITION:	
Access. minerals	Tr
Clay	50
Dolomite	1
Foraminifers	2
Gypsum	Tr
Inorganic calcite	8
Nannofossils	5
Pellets	2
Quartz	30
Radiolarians	1
Sponge spicules	1

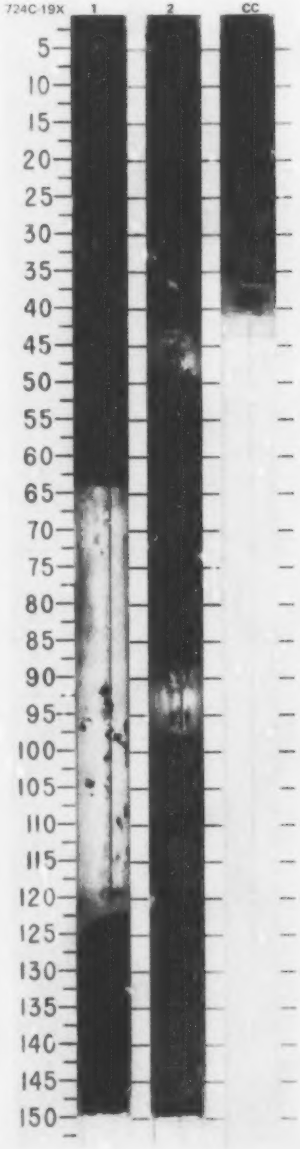
724C-19X
1
2
CC
5
10
15
20
25
30
35
40
45
50
55
60
65
70
75
80
85
90
95
100
105
110
115
120
125
130
135
140
145
150

SITE 724 HOLE C CORE 20X CORED INTERVAL 768.3-778.0 mbsl; 175.5-185.2 mbsf

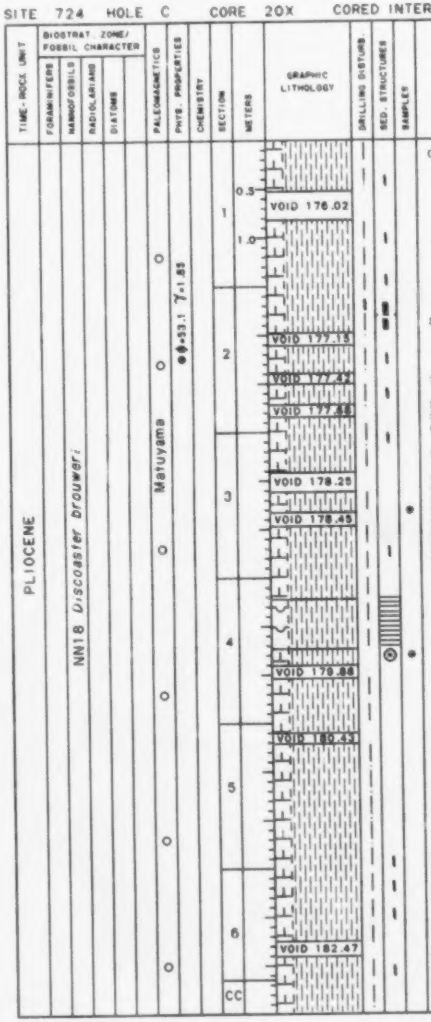
TIME-ROCK UNIT
BIOSTRAT. ZONE/ FOSSIL CHARACTER
FORAMINIFERS
NANNOFOSSILS
RADIOLARIANS
DIATOMS
PALEOMAGNETICS
PHYS. PROPERTIES
CHEMISTRY
SECTION
METERS
GRAPHIC LITHOLOGY
DRILLING DISTURB.
SED. STRUCTURES
SAMPLES
PLIOCENE
NN18 Discoaster brouweri
Matuyama
ϕ=53.1 γ=1.85
1
2
3
4
5
6
CC
0.5
1.0
VOID 176.02
VOID 177.15
VOID 177.42
VOID 177.66
VOID 178.25
VOID 178.45
VOID 179.86
VOID 180.43
VOID 182.47

LITHOLOGIC DESCRIPTION

CALCAREOUS CLAYEY SILT

Section 2, 0-25 cm, very disturbed; Section 2, 25-150 cm., and Section 5, 0-150 cm, moderately disturbed; remainder slightly disturbed. Voids caused by gas expansion.

Major lithology: CALCAREOUS CLAYEY SILT, olive (5Y 4/3), and dark olive gray (5Y 3/2). Minor to moderate burrow mottling common. Contacts gradational and mottled. Foraminifers visible. Section 4, 82 cm, phosphatic nodule present.

Minor lithology: Section 4, 24-82 cm, submillimeter laminated olive (5Y 4/3) diatomaceous mud.

SMEAR SLIDE SUMMARY (%):

	3, 81 D	4, 80 D
TEXTURE:		
Sand		10
Silt	40	40
Clay	60	50
COMPOSITION:		
Access. minerals	1	2
Clay	35	35
Dolomite	1	
Foraminifers	5	3
Inorganic calcite	33	30
Nannofossils	10	15
Phosphate		Tr
Quartz	15	15

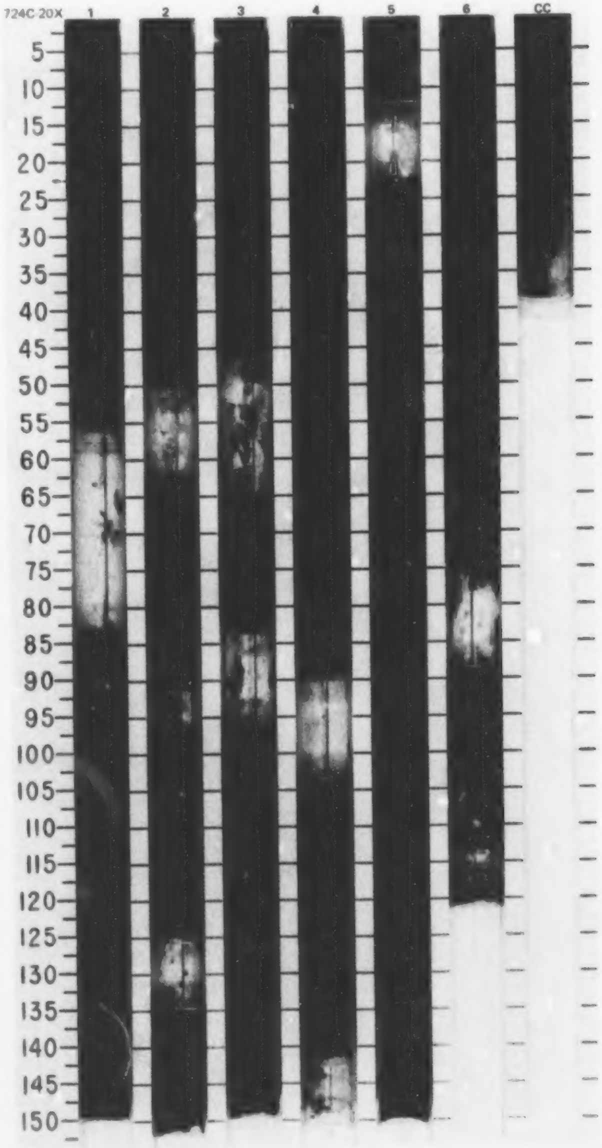
724C-20X
1
2
3
4
5
6
CC
5
10
15
20
25
30
35
40
45
50
55
60
65
70
75
80
85
90
95
100
105
110
115
120
125
130
135
140
145
150

SITE 724 HOLE C CORE 21X CORED INTERVAL 778.0-787..6 mbsl; 185.2-194.8 mbsf

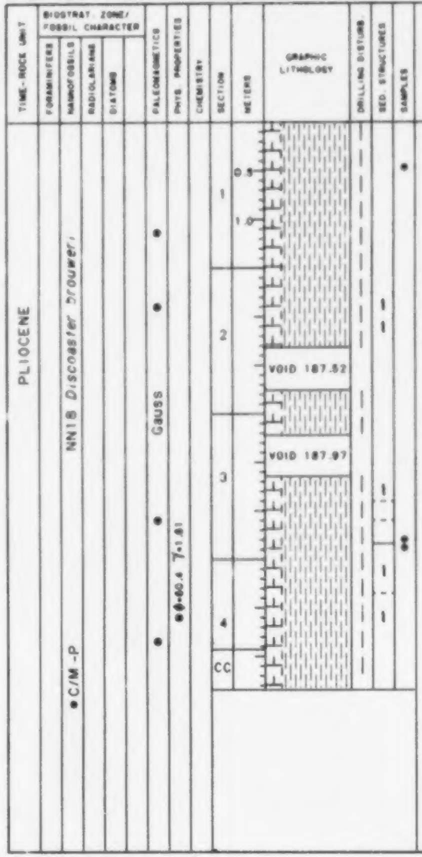
TIME-ROCK UNIT
BIOSTRAT. ZONE/ FOSSIL CHARACTER
FORAMINIFERS
NANNOFOSSILS
RADIOLARIANS
DIATOMS
PALEOMAGNETICS
PHYS. PROPERTIES
CHEMISTRY
SECTION
METERS
GRAPHIC LITHOLOGY
DRILLING DISTURB.
SED. STRUCTURES
SAMPLES
PLIOCENE
NN18 Discoaster brouweri
●C/M -P
Gauss
●ϕ=60.4 γ=1.81
1
2
3
4
CC
0.5
1.0
VOID 187.52
VOID 187.97

LITHOLOGIC DESCRIPTION

CALCAREOUS CLAYEY SILT

Entire core slightly disturbed. Voids caused by gas expansion.

Major lithology: CALCAREOUS CLAYEY SILT, olive gray (5Y 4/2) and dark olive gray (5Y 3/2). Minor burrow mottling common. Contacts gradational and mottled. Foraminifers visible.

SMEAR SLIDE SUMMARY (%):

	1, 48 D	3, 130 D	3, 136 D
TEXTURE:			
Sand	5	5	15
Silt	50	45	30
Clay	45	50	55
COMPOSITION:			
Access. minerals	2	2	2
Clay	35	45	25
Dolomite			Tr
Feldspar		5	
Foraminifers	2		5
Glauconite	Tr	Tr	
Inorganic calcite	30	8	23
Mica	1	Tr	
Nannofossils	10		30
Organic debris	5		
Phosphate		Tr	
Quartz	15	40	15
Sponge spicules		Tr	Tr

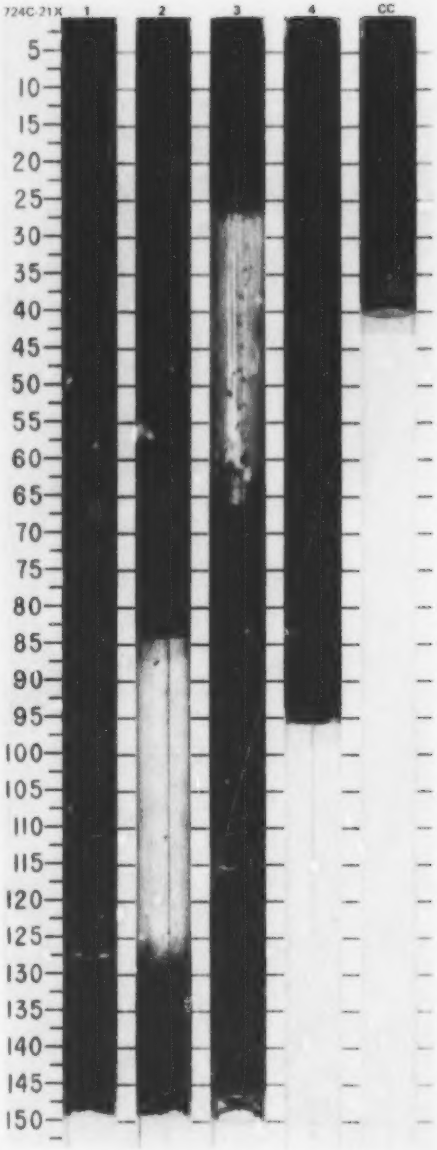
724C-21X
1
2
3
4
CC
5
10
15
20
25
30
35
40
45
50
55
60
65
70
75
80
85
90
95
100
105
110
115
120
125
130
135
140
145
150

SITE 724 HOLE C CORE 22X CORED INTERVAL 787.6-797.3 mbsl; 194.8-204.5 mbsf

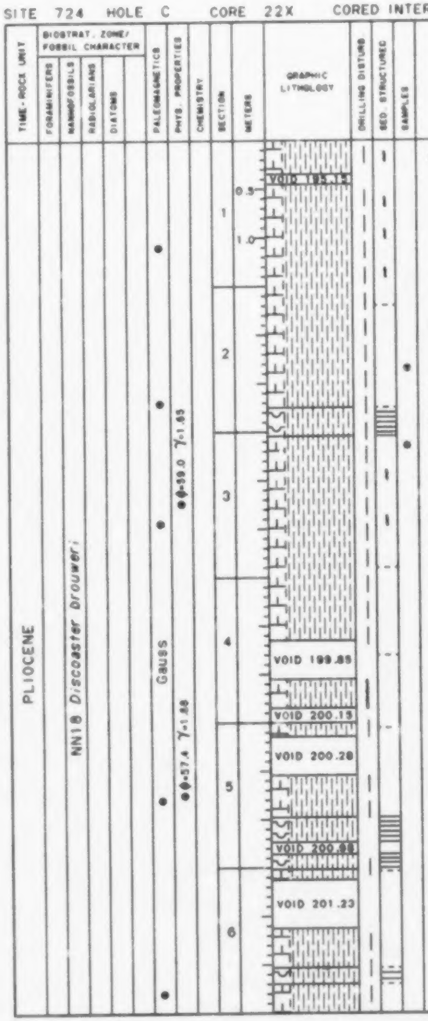

LITHOLOGIC DESCRIPTION

CALCAREOUS CLAYEY SILT

Section 4, 100-140 cm, very disturbed; remainder slightly disturbed. Voids caused by gas expansion.

Major lithology: CALCAREOUS CLAYEY SILT, olive gray (5Y 4/2), dark olive gray (5Y 3/2), and black (5Y 2.5/2). Minor burrow mottling rare. Contacts gradational and mottled.

Minor lithology: Section 2, 123-150 cm, Section 5, 100-140 cm, Section 6, 102-119 cm, and CC, 22-41 cm, centimeter-to millimeter-scale laminated diatomaceous mud, diatomaceous marly nannofossil ooze and diatom ooze, olive (5Y 4/3), olive gray (5Y 4/2), and dark olive gray (5Y 3/2).

SMEAR SLIDE SUMMARY (%):

	2, 85 D	3, 15 D
TEXTURE:		
Sand	10	5
Silt	50	40
Clay	40	55
COMPOSITION:		
Access. minerals	3	2
Clay	40	25
Diatoms	Tr	15
Feldspar	5	
Foraminifers		3
Glauconite	Tr	
Inorganic calcite	12	20
Nannofossils	Tr	30
Organic debris	5	
Phosphate	Tr	
Quartz	35	5
Radiolarians	Tr	Tr
Sponge spicules	Tr	Tr

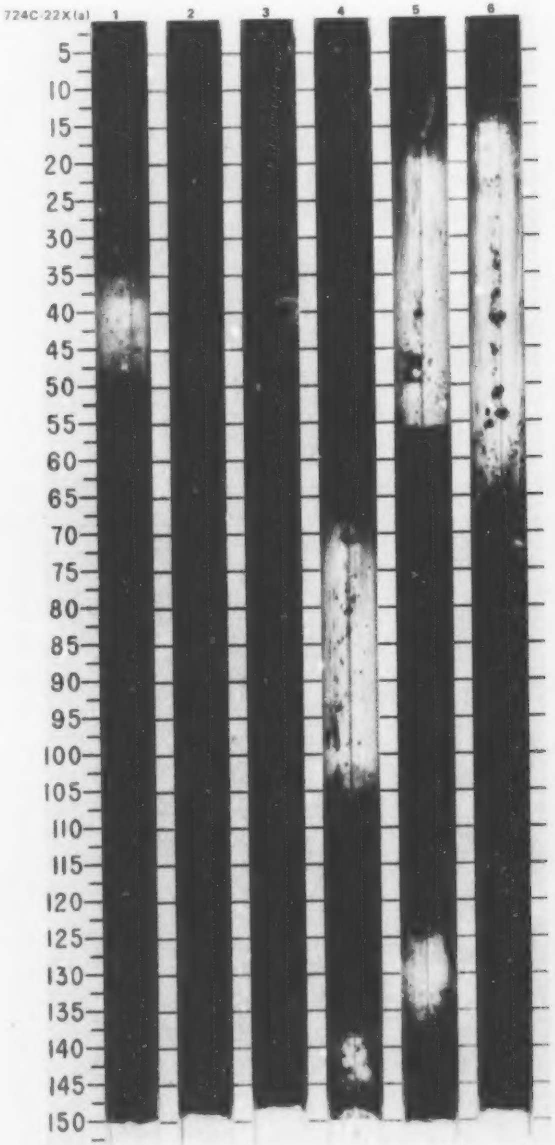

SITE 724 HOLE C CORE 22X CORED INTERVAL 787.6-797.3 mbsl; 194.8-204.5 mbsf

TIME-ROCK UNIT	BIOSTRAT. ZONE/ FOSSIL CHARACTER				PALEOMAGNETICS	PHYS. PROPERTIES	CHEMISTRY	SECTION	METERS	GRAPHIC LITHOLOGY	DRILLING DISTURB.	SED. STRUCTURES	SAMPLES	LITHOLOGIC DESCRIPTION
	FORAMINIFERS	NANNOFOSSILS	RADIOLARIANS	DIATOMS										
								7		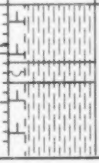				(cont.)
								CC						

724C-22X(b)
7
CC

SITE 724 HOLE C CORE 23X CORED INTERVAL 797.3-806.9 mbsl: 204.5-214.1 mbsf

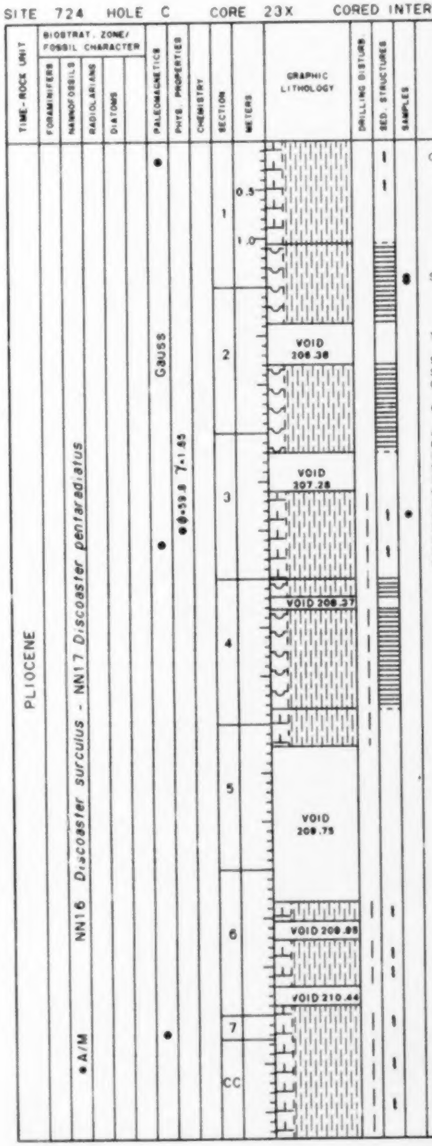
TIME-ROCK UNIT
BIOSTRAT. ZONE/ FOSSIL CHARACTER
FORAMINIFERS
NANNOFOSSILS
RADIOLARIANS
DIATOMS
PALEOMAGNETICS
PHYS. PROPERTIES
CHEMISTRY
SECTION
METERS
GRAPHIC LITHOLOGY
DRILLING DISTURB.
SED. STRUCTURES
SAMPLES
PLIOCENE
NN16 Discoaster surculus - NN17 Discoaster pentaradiatus
●A/M
Gauss
●ϕ=59.8 γ=1.85
1
2
3
4
5
6
7
CC
0.5
1.0
VOID 206.38
VOID 207.28
VOID 208.37
VOID 209.75
VOID 209.95
VOID 210.44

LITHOLOGIC DESCRIPTION

CALCAREOUS CLAYEY SILT

Entire core slightly disturbed. Voids caused by gas expansion.

Major lithologies:
a. Calcareous clayey silt, olive gray (5Y 4/2). Minor burrow mottling.
b. Section 1, 106-150 cm, Section 2, 0-150 cm, Section 3, 0-8 and 148-150 cm, and Section 4, 0-135 cm; sub-millimeter laminated diatomaceous mud and diatom ooze, olive (5Y 4/3), olive gray (5Y 4/2), and dark olive gray (5Y 3/2).

SMEAR SLIDE SUMMARY (%):

	1, 143 M	1, 146 M	3, 85 D
TEXTURE:			
Sand		10	15
Silt	70	65	40
Clay	30	25	45
COMPOSITION:			
Access. minerals	1	1	2
Clay	33	25	45
Diatoms	60	45	Tr
Dolomite		Tr	
Fish remains			Tr
Inorganic calcite	5	15	20
Mica		1	1
Organic debris			5
Phosphate		Tr	
Quartz	1	13	25
Radiolarians			1
Sponge spicules		Tr	1

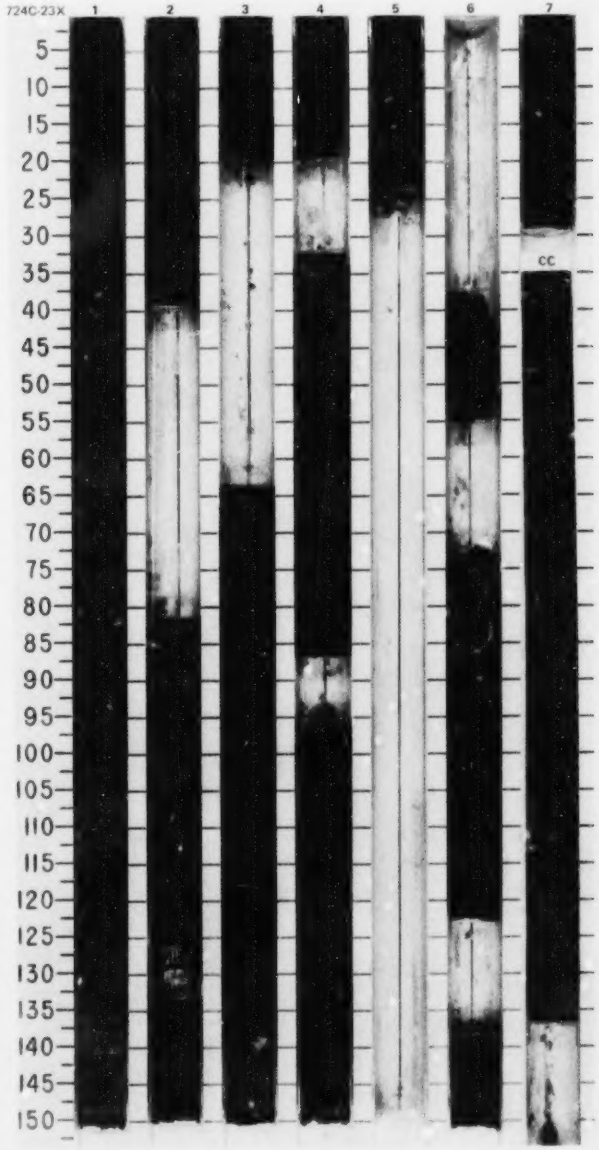
724C-23X
1
2
3
4
5
6
7
CC
5
10
15
20
25
30
35
40
45
50
55
60
65
70
75
80
85
90
95
100
105
110
115
120
125
130
135
140
145
150

SITE 724 HOLE C CORE 24X CORED INTERVAL 806.9-816.5 mbsl; 214.1-223.7 mbsf

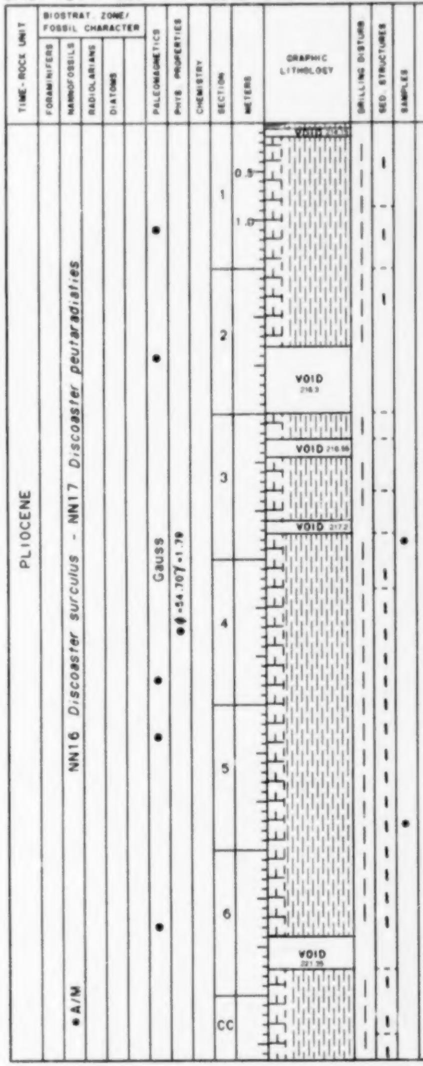
TIME-ROCK UNIT
BIOSTRAT. ZONE/ FOSSIL CHARACTER
FORAMINIFERS
NANNOFOSSILS
RADIOLARIANS
DIATOMS
PALEOMAGNETICS
PHYS. PROPERTIES
CHEMISTRY
SECTION
METERS
GRAPHIC LITHOLOGY
DRILLING DISTURB.
SED. STRUCTURES
SAMPLES
PLIOCENE
NN16 Discoaster surculus - NN17 Discoaster peutaradiaties
• A/M
Gauss
●ϕ=54.70γ=1.79
1
2
3
4
5
6
CC
0.5
1.0
VOID
VOID 216.3
VOID 216.96
VOID 217.2
VOID 221.35

LITHOLOGIC DESCRIPTION

CALCAREOUS CLAYEY SILT

Entire core slightly disturbed. Voids caused by gas expansion.

Major lithology: CALCAREOUS CLAYEY SILT, olive gray (5Y 4/2), dark olive gray (5Y 3/2), and black (5Y 2.5/2). Minor burrow mottling common. Contacts gradational and mottled.

SMEAR SLIDE SUMMARY (%)

	3, 132 D	5, 132 D
TEXTURE		
Sand		20
Silt	45	25
Clay	55	55
COMPOSITION		
Access. minerals	3	2
Clay	55	25
Dolomite		Tr
Feldspar	5	
Foraminifers		13
Glauconite	Tr	
Inorganic calcite	[illegible]	20
Mica	Tr	
Nannofossils		30
Organic debris	5	
Phosphate	Tr	
Quartz	30	10
Sponge spicules	Tr	Tr

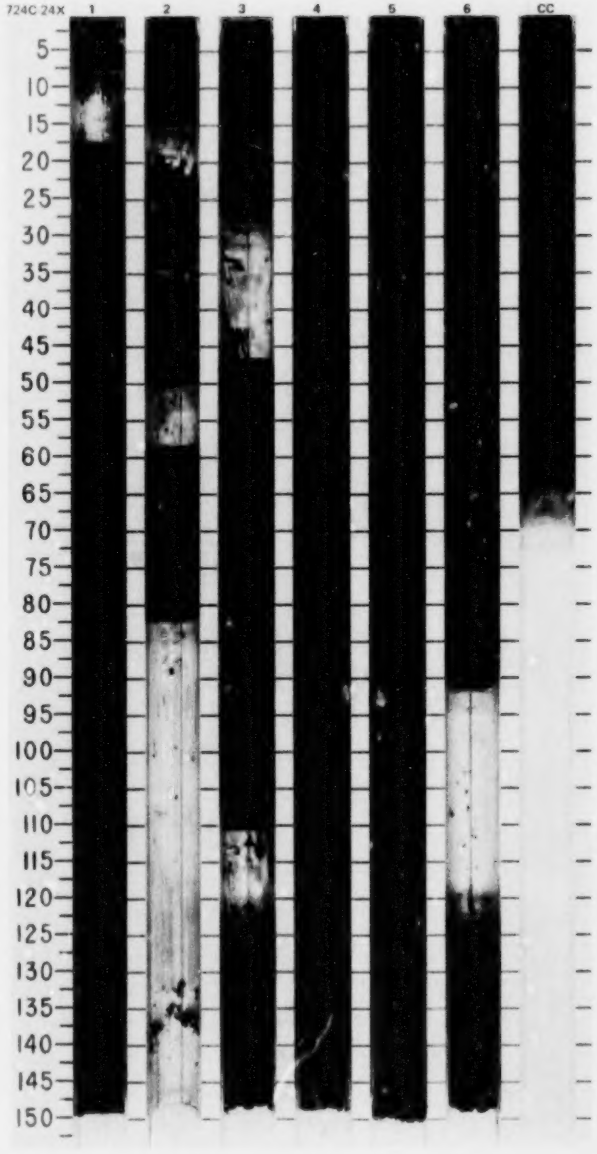
724C 24X
1
2
3
4
5
6
CC
5
10
15
20
25
30
35
40
45
50
55
60
65
70
75
80
85
90
95
100
105
110
115
120
125
130
135
140
145
150

SITE 724 HOLE C CORE 25X CORED INTERVAL 816.5-826.2 mbsl; 223.7-233.4 mbsf

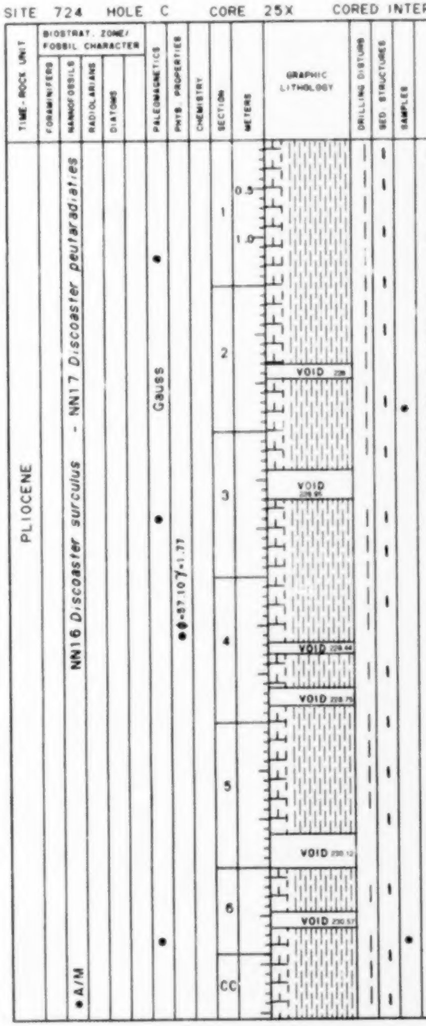
TIME-ROCK UNIT
BIOSTRAT. ZONE/ FOSSIL CHARACTER
FORAMINIFERS
NANNOFOSSILS
RADIOLARIANS
DIATOMS
PALEOMAGNETICS
PHYS. PROPERTIES
CHEMISTRY
SECTION
METERS
GRAPHIC LITHOLOGY
DRILLING DISTURB.
SED. STRUCTURES
SAMPLES
PLIOCENE
NN16 Discoaster surculus - NN17 Discoaster peutaradiaties
• A/M
Gauss
•Φ=57.1 0 γ=1.77
1
2
3
4
5
6
CC
0.5
1.0
VOID
VOID 226.95
VOID 228.44
VOID 228.75
VOID 230.12
VOID 230.57

LITHOLOGIC DESCRIPTION

CALCAREOUS CLAYEY SILT

Entire core slightly disturbed. Voids caused by gas expansion.

Major lithology: CALCAREOUS CLAYEY SILT, olive gray (5Y 4/2). Minor burrow mottling throughout. Foraminifers visible.

SMEAR SLIDE SUMMARY (%):

	2, 129 D	6, 77 D
TEXTURE:		
Sand	20	25
Silt	25	25
Clay	55	50
COMPOSITION:		
Access. minerals	3	3
Clay	30	27
Dolomite	Tr	
Foraminifers	7	5
Glauconite	Tr	
Inorganic calcite	20	20
Nannofossils	25	25
Quartz	15	20
Sponge spicules	Tr	

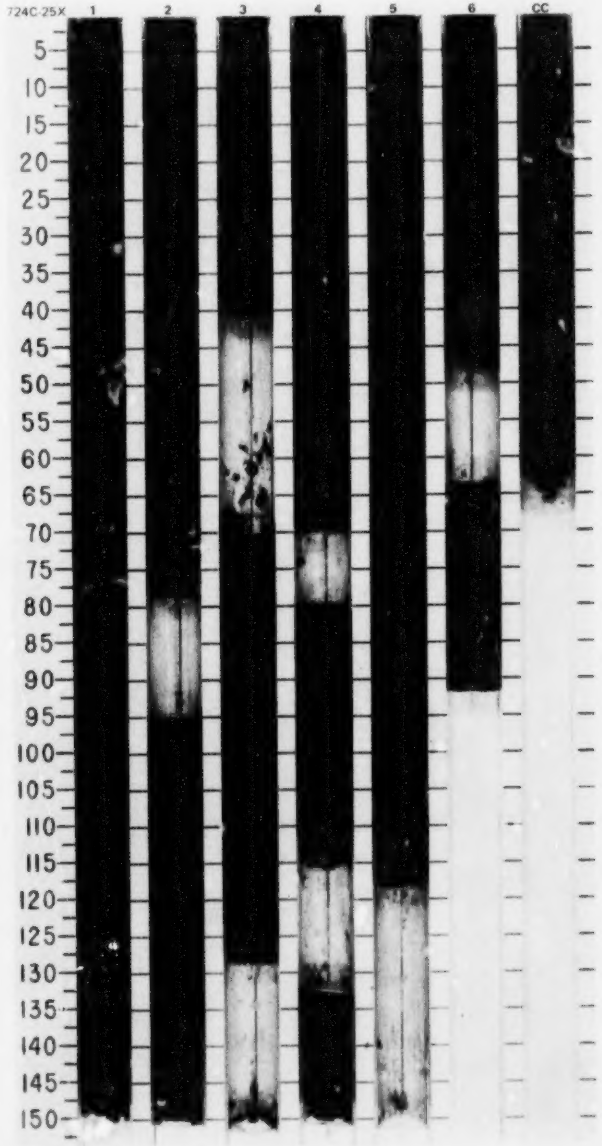
724C-25X
1
2
3
4
5
6
CC
5
10
15
20
25
30
35
40
45
50
55
60
65
70
75
80
85
90
95
100
105
110
115
120
125
130
135
140
145
150

SITE 724 HOLE C CORE 26X CORED INTERVAL 826.2-835.7 mbsl; 233.4-242.9 mbsf

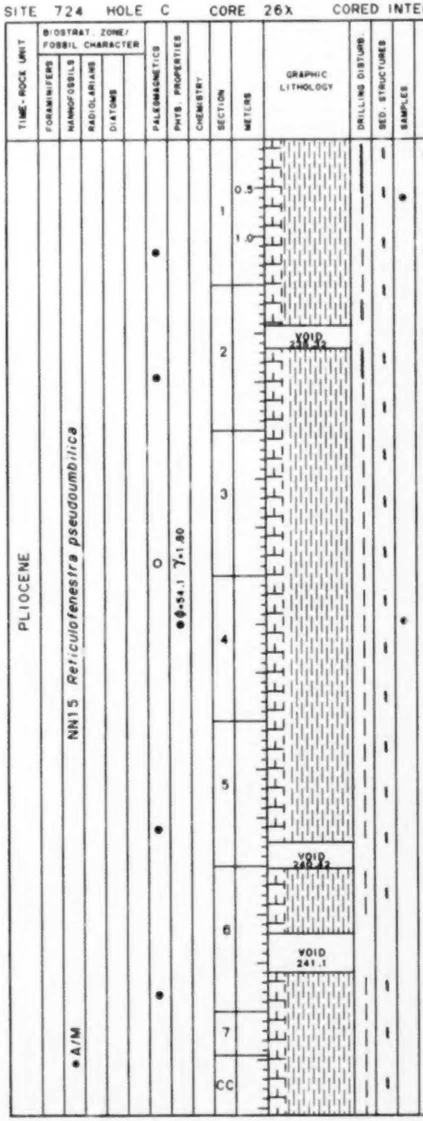
TIME-ROCK UNIT
BIOSTRAT. ZONE/ FOSSIL CHARACTER
FORAMINIFERS
NANNOFOSSILS
RADIOLARIANS
DIATOMS
PALEOMAGNETICS
PHYS. PROPERTIES
CHEMISTRY
SECTION
METERS
GRAPHIC LITHOLOGY
DRILLING DISTURB.
SED. STRUCTURES
SAMPLES
PLIOCENE
NN15 Reticulofenestra pseudoumbilica
● A/M
● φ=54.1 γ=1.80
0.5
1.0
1
2
3
4
5
6
7
CC
VOID 235.42
VOID 240.42
VOID 241.1

LITHOLOGIC DESCRIPTION

CALCAREOUS CLAYEY SILT

Section 1, 0-40 cm, and Section 2, 20-40 and 65-80 cm, remainder slightly disturbed. Voids caused by gas expansion.

Major lithology: CALCAREOUS CLAYEY SILT, olive (5Y 4/3). Minor burrow mottling throughout. Foraminifers visible.

SMEAR SLIDE SUMMARY (%):

	1, 60 D	4, 49 D
TEXTURE:		
Sand	20	20
Silt	25	25
Clay	55	55
COMPOSITION:		
Access. minerals	2	2
Clay	25	25
Dolomite	Tr	1
Feldspar		1
Foraminifers	6	3
Glauconite		Tr
Inorganic calcite	22	20
Nannofossils	30	28
Quartz	15	20
Radiolarians	Tr	

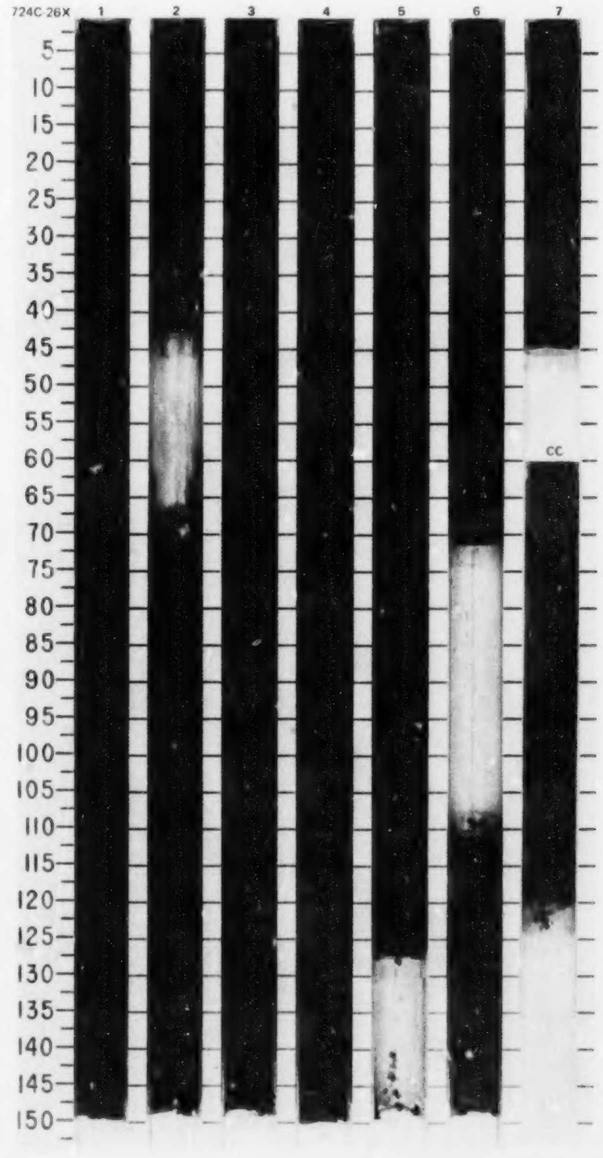
724C-26X
1
2
3
4
5
6
7
CC
5
10
15
20
25
30
35
40
45
50
55
60
65
70
75
80
85
90
95
100
105
110
115
120
125
130
135
140
145
150

SITE 724 HOLE C CORE 27X CORED INTERVAL 835.7-845.2 mbsl; 242.9-252.4 mbsf

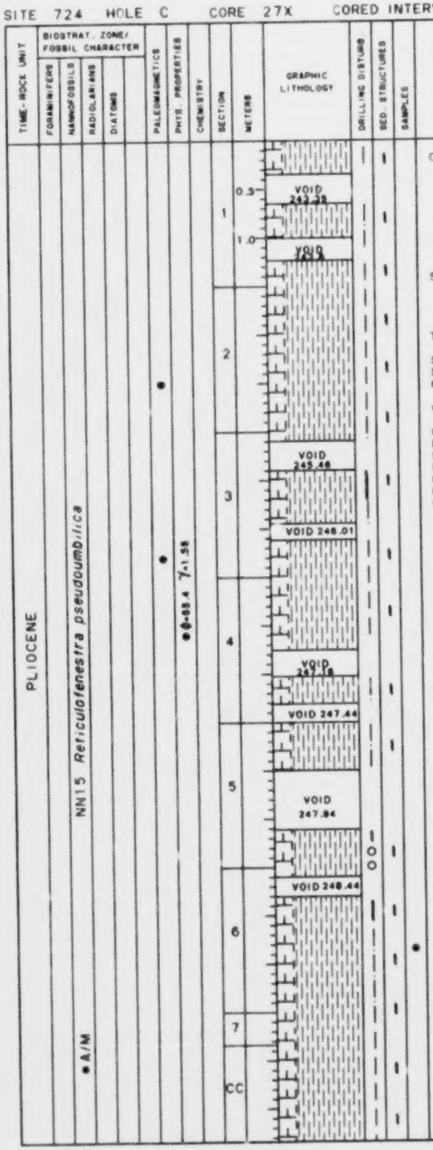
TIME-ROCK UNIT
BIOSTRAT. ZONE/ FOSSIL CHARACTER
FORAMINIFERS
NANNOFOSSILS
RADIOLARIANS
DIATOMS
PALEOMAGNETICS
PHYS. PROPERTIES
CHEMISTRY
SECTION
METERS
GRAPHIC LITHOLOGY
DRILLING DISTURB.
SED. STRUCTURES
SAMPLES
PLIOCENE
NN15 Reticulofenestra pseudoumbilica
●A/M
●φ=69.4 γ=1.98
0.5
1.0
1
2
3
4
5
6
7
CC
VOID 242.33
VOID
VOID 245.48
VOID 246.01
VOID 247.18
VOID 247.44
VOID 247.84
VOID 248.44

LITHOLOGIC DESCRIPTION

CALCAREOUS CLAYEY SILT

Section 3, 40-60 cm, Section 5, 110-150 cm, and Section 6, 30-60 cm, very disturbed; Section 1, 65-100 cm, Section 3, 0-10 and 40-100 cm, Section 4, 100-130 cm, Section 5, 0-50 cm, and Section 6, 60-140 cm, moderately disturbed; remainder slightly disturbed. Voids caused by gas expansion.

Major lithology: CALCAREOUS CLAYEY SILT, olive (5Y 4/3) and olive gray (5Y 4/2). Minor burrow mottling throughout. Foraminifers visible.

SMEAR SLIDE SUMMARY (%):

	6, 83 D
TEXTURE	
Sand	30
Silt	20
Clay	50
COMPOSITION	
Clay	25
Dolomite	Tr
Feldspar	1
Foraminifers	24
Inorganic calcite	15
Nannofossils	25
Quartz	10

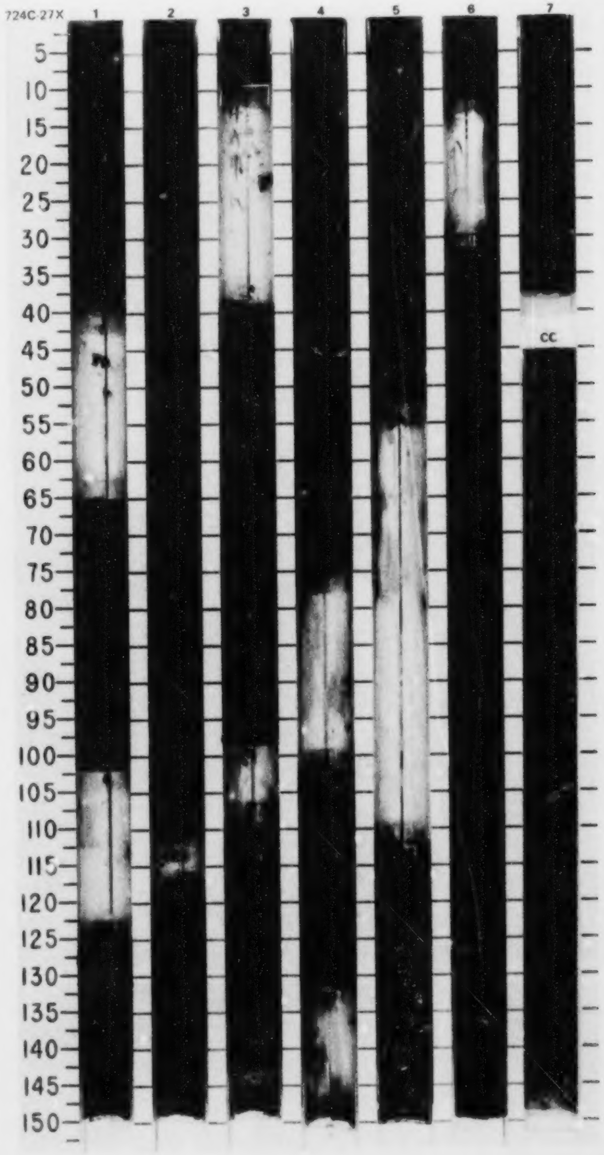
724C-27X
1
2
3
4
5
6
7
CC
5
10
15
20
25
30
35
40
45
50
55
60
65
70
75
80
85
90
95
100
105
110
115
120
125
130
135
140
145
150

SITE 725 HOLE A CORE 1H CORED INTERVAL 311.5-316.0 mbsl; 0.0-4.5 mbsf

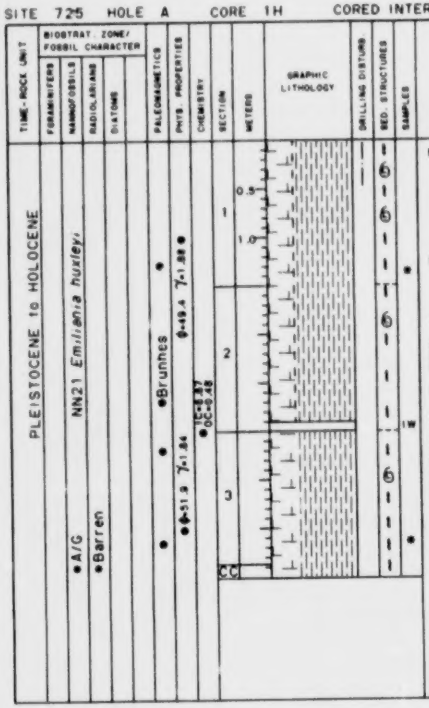
TIME-ROCK UNIT
BIOSTRAT. ZONE/ FOSSIL CHARACTER
FORAMINIFERS
NANNOFOSSILS
RADIOLARIANS
DIATOMS
PALEOMAGNETICS
PHYS. PROPERTIES
CHEMISTRY
SECTION
METERS
GRAPHIC LITHOLOGY
DRILLING DISTURB.
SED. STRUCTURES
SAMPLES
PLEISTOCENE to HOLOCENE
NN21 Emiliania huxleyi
●A/G
●Barren
●Brunnes
ϕ=49.4 γ=1.88
ϕ=51.9 γ=1.84
TC=8.87
OC=0.48
1
2
3
CC
0.5
1.0
IW

LITHOLOGIC DESCRIPTION

NANNOFOSSIL-RICH CALCITIC CLAYEY SAND

Section 1, 0-40 cm, is moderately disturbed. Remainder of core is undisturbed.

Major lithology: NANNOFOSSIL-RICH CALCITIC CLAYEY SAND, olive gray (5Y 5/2). Slightly bioturbated throughout. Shell fragments scattered throughout, especially Section 1, 30-40 cm, Section 2, 50-60 cm, and Section 3, 45-50 cm. Hexagonal, orangish-colored tubes in lower half of Section 1.

SMEAR SLIDE SUMMARY (%):

	1, 135 D	3, 114 D
TEXTURE:		
Sand	50	45
Silt	15	20
Clay	35	35
COMPOSITION:		
Access. minerals	3	3
Clay	10	15
Feldspar	2	2
Foraminifers	4	5
Inorganic calcite	40	40
Nannofossils	25	20
Quartz	16	15
Radiolarians	Tr	
Shell debris		Tr
Sponge spicules	Tr	

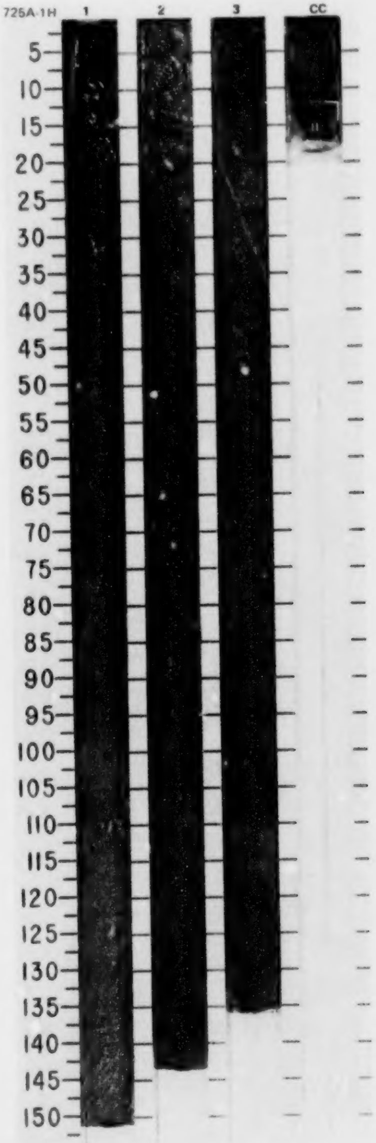
725A-1H
1
2
3
CC
5
10
15
20
25
30
35
40
45
50
55
60
65
70
75
80
85
90
95
100
105
110
115
120
125
130
135
140
145
150

SITE 725 HOLE B CORE 1X CORED INTERVAL 310.5-318.0 mbsl; 0.0-7.5 mbsf

TIME-ROCK UNIT	BIOSTRAT. ZONE/ FOSSIL CHARACTER				PALEOMAGNETICS	PHYS. PROPERTIES	CHEMISTRY	SECTION	METERS	GRAPHIC LITHOLOGY	DRILLING DISTURB.	SED. STRUCTURES	SAMPLES	LITHOLOGIC DESCRIPTION
	FORAMINIFERS	NANNOFOSSILS	RADIOLARIANS	DIATOMS										
PLEISTOCENE to HOLOCENE		NN21 *Emiliania huxleyi* A/G●	unzoned R/M●					CC					●	CALCITIC MARLY CALCAREOUS OOZE

CALCITIC MARLY CALCAREOUS OOZE

CC very disturbed to soupy.

Major lithology: CALCITIC MARLY CALCAREOUS OOZE, olive (5Y 4/3). Fine-grained shell debris dispersed throughout.

SMEAR SLIDE SUMMARY (%):

	CC, 18 D
TEXTURE:	
Sand	45
Silt	25
Clay	30
COMPOSITION:	
Access. minerals	2
Clay	15
Feldspar	2
Foraminifers	20
Volcanic glass	1
Inorganic calcite	30
Nannofossils	15
Quartz	15

SITE 725 HOLE B CORE 2X CORED INTERVAL 318.0-327.6 mbsl; 7.5-17.1 mbsf

TIME-ROCK UNIT	BIOSTRAT. ZONE/ FOSSIL CHARACTER				PALEOMAGNETICS	PHYS. PROPERTIES	CHEMISTRY	SECTION	METERS	GRAPHIC LITHOLOGY	DRILLING DISTURB.	SED. STRUCTURES	SAMPLES	LITHOLOGIC DESCRIPTION
	FORAMINIFERS	NANNOFOSSILS	RADIOLARIANS	DIATOMS										
PLEISTOCENE		NN21 *Emiliania huxleyi* A/M●	Barren●					CC					●	CALCITIC MARLY CALCAREOUS OOZE

CALCITIC MARLY CALCAREOUS OOZE

CC slightly disturbed to undisturbed.

Major lithology: CALCITIC MARLY CALCAREOUS OOZE, olive gray (5Y 4/2). Slightly bioturbated throughout.

SMEAR SLIDE SUMMARY (%):

	CC, 22 D
TEXTURE:	
Sand	35
Silt	25
Clay	40
COMPOSITION:	
Access. minerals	3
Clay	15
Dolomite	Tr
Feldspar	2
Foraminifers	10
Glauconite	Tr
Inorganic calcite	30
Nannofossils	25
Phosphate	Tr
Quartz	15

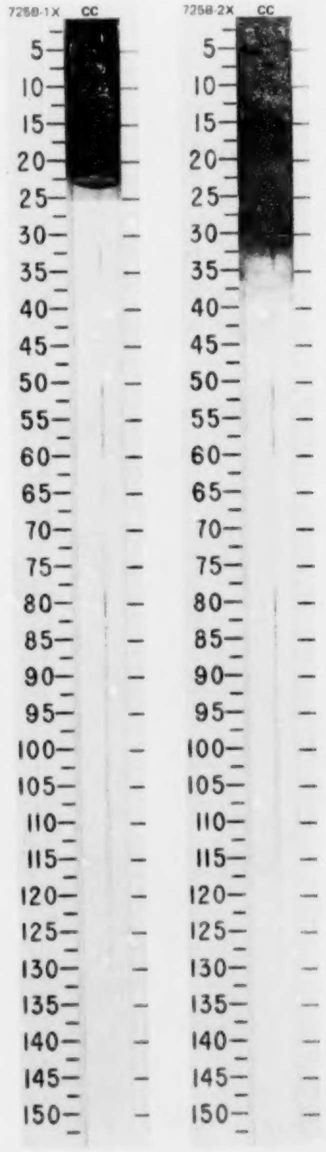

SITE 725 HOLE B CORE 3X CORED INTERVAL 327.6-337.1 mbsl; 17.1-26.6 mbsf

TIME-ROCK UNIT	BIOSTRAT. ZONE/ FOSSIL CHARACTER: FORAMINIFERS	NANNOFOSSILS	RADIOLARIANS	DIATOMS	PALEOMAGNETICS	PHYS. PROPERTIES	CHEMISTRY	SECTION	METERS	GRAPHIC LITHOLOGY	DRILLING DISTURB.	SED. STRUCTURES	SAMPLES
PLEISTOCENE		NN20 *Gephyrocapsa oceanica* C/P ●	Barren ●					1 CC	0.5				● ●

LITHOLOGIC DESCRIPTION

CALCITIC MARLY NANNOFOSSIL OOZE

Section 1 and CC slightly disturbed to undisturbed.

Major lithology: CALCITIC MARLY NANNOFOSSIL OOZE, dark greenish gray (10Y 4/2). Slightly bioturbated.

SMEAR SLIDE SUMMARY (%):

	1, 20 D	CC, 20 D
TEXTURE:		
Sand	40	35
Silt	20	20
Clay	40	45
COMPOSITION:		
Access. minerals	2	2
Clay	15	15
Dolomite	Tr	1
Feldspar	2	3
Foraminifers	6	2
Inorganic calcite	35	32
Nannofossils	25	30
Quartz	15	15

SITE 725 HOLE B CORE 4X CORED INTERVAL 337.1-346.7 mbsl; 26.6-36.2 mbsf

TIME-ROCK UNIT	BIOSTRAT. ZONE/ FOSSIL CHARACTER: FORAMINIFERS	NANNOFOSSILS	RADIOLARIANS	DIATOMS	PALEOMAGNETICS	PHYS. PROPERTIES	CHEMISTRY	SECTION	METERS	GRAPHIC LITHOLOGY	DRILLING DISTURB.	SED. STRUCTURES	SAMPLES
PLEISTOCENE		●A/P NN20 *Gephyrocapsa oceanica*	●Barren					1 2 CC	0.5 1.0				● ●

LITHOLOGIC DESCRIPTION

MARLY NANNOFOSSIL OOZE to MARLY FORAMINIFERAL NANNOFOSSIL OOZE

Section 1, 20-30 and 50-80 cm, and Section 2, 0-77 cm, are soupy. Remainder is very disturbed.

Major lithology: MARLY NANNOFOSSIL OOZE to MARLY FORAMINIFERAL NANNOFOSSIL OOZE, dark greenish gray (10Y 4/2).

SMEAR SLIDE SUMMARY (%):

	1, 140 D	2, 101 D
TEXTURE:		
Sand	20	20
Silt	30	30
Clay	50	50
COMPOSITION:		
Access. minerals	2	2
Clay	15	15
Dolomite	1	
Foraminifers	2	16
Inorganic calcite	30	20
Nannofossils	35	35
Quartz	15	12

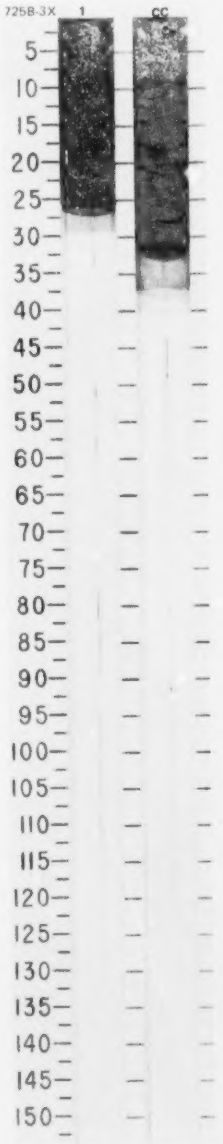
725B-3X
1
CC
5
10
15
20
25
30
35
40
45
50
55
60
65
70
75
80
85
90
95
100
105
110
115
120
125
130
135
140
145
150

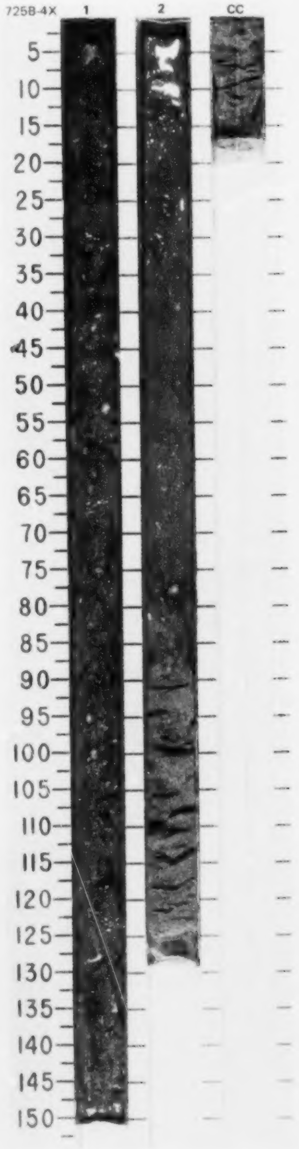
725B-4X
1
2
CC
5
10
15
20
25
30
35
40
45
50
55
60
65
70
75
80
85
90
95
100
105
110
115
120
125
130
135
140
145
150

SITE 725 HOLE B CORE 5X CORED INTERVAL 346.7-356.2 mbsl; 36.2-45.7 mbsf

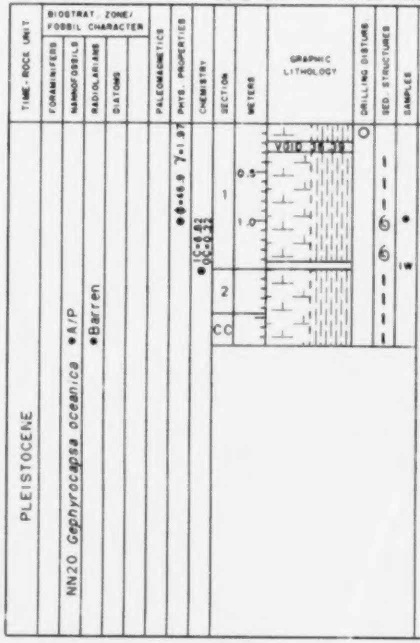
TIME-ROCK UNIT
BIOSTRAT. ZONE/ FOSSIL CHARACTER
FORAMINIFERS
NANNOFOSSILS
RADIOLARIANS
DIATOMS
PALEOMAGNETICS
PHYS. PROPERTIES
CHEMISTRY
SECTION
METERS
GRAPHIC LITHOLOGY
DRILLING DISTURB.
SED. STRUCTURES
SAMPLES
PLEISTOCENE
NN20 Gephyrocapsa oceanica ●A/P
●Barren
●Φ=46.9 γ=1.97
●IC=6.82 OC=0.32
1
2
CC
0.5
1.0
VOID 36-39
IW

LITHOLOGIC DESCRIPTION

MARLY NANNOFOSSIL OOZE

Section 1, 0-19 cm, is very disturbed. Remainder is undisturbed.

Major lithology: MARLY NANNOFOSSIL OOZE, dark greenish gray (10Y 5/2). Slightly bioturbated throughout. Shell fragments abundant at Section 1, 114-116 and 134-136 cm.

SMEAR SLIDE SUMMARY (%):

	1, 98 D
TEXTURE	
Sand	15
Silt	20
Clay	65
COMPOSITION	
Access. minerals	2
Clay	15
Dolomite	Tr
Foraminifers	3
Glauconite	Tr
Inorganic calcite	20
Mica	Tr
Nannofossils	50
Quartz	10

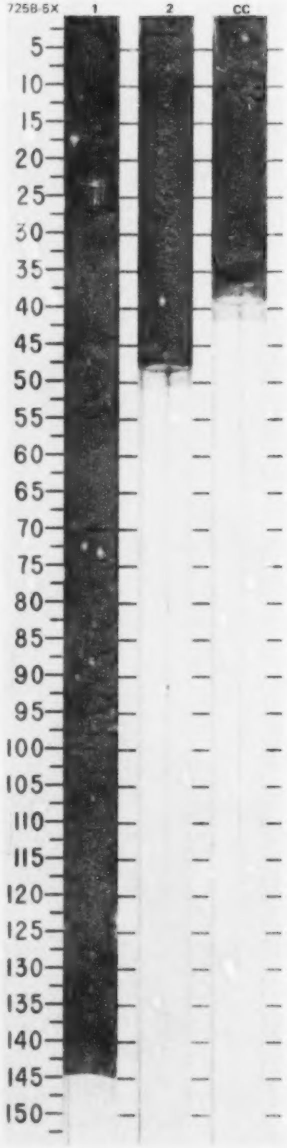
725B-5X
1
2
CC
5
10
15
20
25
30
35
40
45
50
55
60
65
70
75
80
85
90
95
100
105
110
115
120
125
130
135
140
145
150

SITE 725 HOLE B CORE 6X CORED INTERVAL 356.2-365.8 mbsl; 45.7-55.3 mbsf

TIME-ROCK UNIT	BIOSTRAT. ZONE/ FOSSIL CHARACTER: FORAMINIFERS	NANNOFOSSILS	RADIOLARIANS	DIATOMS	PALEOMAGNETICS	PHYS. PROPERTIES	CHEMISTRY	SECTION	METERS	GRAPHIC LITHOLOGY	DRILLING DISTURB.	SED. STRUCTURES	SAMPLES
PLEISTOCENE		NN19 *Pseudoemiliania lacunosa* A/P ●	Barren ●			φ=40.4 γ=2.04 ●		1 CC	0.5				●

LITHOLOGIC DESCRIPTION

MARLY NANNOFOSSIL OOZE

Section 1, 0-20 cm, is soupy. CC is undisturbed. Remainder is moderately disturbed.

Major lithology: MARLY NANNOFOSSIL OOZE, dark greenish gray (10Y 5/2), with minor bioturbation throughout.

SMEAR SLIDE SUMMARY (%):

	1, 51 D
TEXTURE:	
Sand	30
Silt	25
Clay	45
COMPOSITION:	
Access. minerals	2
Clay	15
Dolomite	Tr
Foraminifers	3
Inorganic calcite	30
Nannofossils	30
Quartz	20

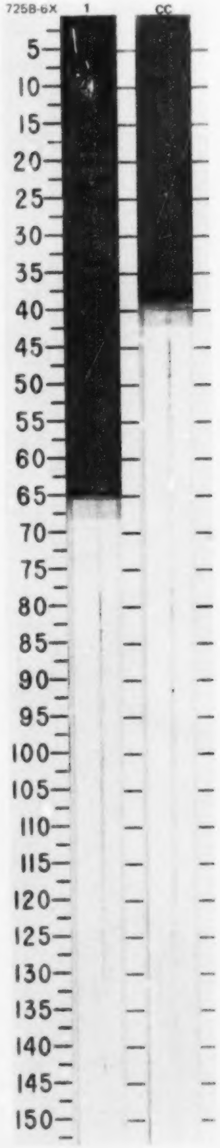
725B-6X
1
CC
5
10
15
20
25
30
35
40
45
50
55
60
65
70
75
80
85
90
95
100
105
110
115
120
125
130
135
140
145
150

SITE 725 HOLE B CORE 7X CORED INTERVAL 365.8-375.4 mbsl; 55.3-64.9 mbsf

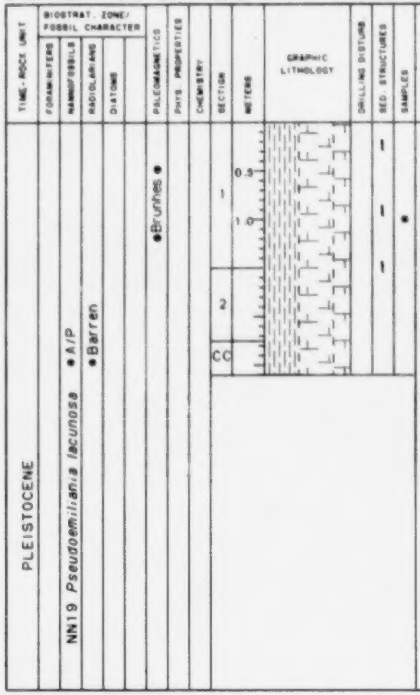

TIME-ROCK UNIT
BIOSTRAT. ZONE/ FOSSIL CHARACTER
FORAMINIFERS
NANNOFOSSILS
RADIOLARIANS
DIATOMS
PALEOMAGNETICS
PHYS. PROPERTIES
CHEMISTRY
SECTION
METERS
GRAPHIC LITHOLOGY
DRILLING DISTURB.
SED. STRUCTURES
SAMPLES
PLEISTOCENE
NN19 Pseudoemiliania lacunosa
● A/P
● Barren
● Brunhes ●
1
2
CC
0.5
1.0

LITHOLOGIC DESCRIPTION

MARLY FORAMINIFERAL NANNOFOSSIL OOZE

Entire core is undisturbed.

Major lithology: MARLY FORAMINIFERAL NANNOFOSSIL OOZE, olive (5Y 4/3), faintly mottled. Slight bioturbation in Section 1. Shell debris at Section 1, 80-90 and 125-130 cm. Abundant benthic foraminifers at Section 1, 75-150 cm.

SMEAR SLIDE SUMMARY (%):

	1, 100 D
TEXTURE:	
Sand	30
Silt	35
Clay	35
COMPOSITION:	
Access. minerals	5
Clay	10
Dolomite	5
Foraminifers	20
Inorganic calcite	10
Nannofossils	40
Quartz	10

CORE 117-725B-8X NO RECOVERY

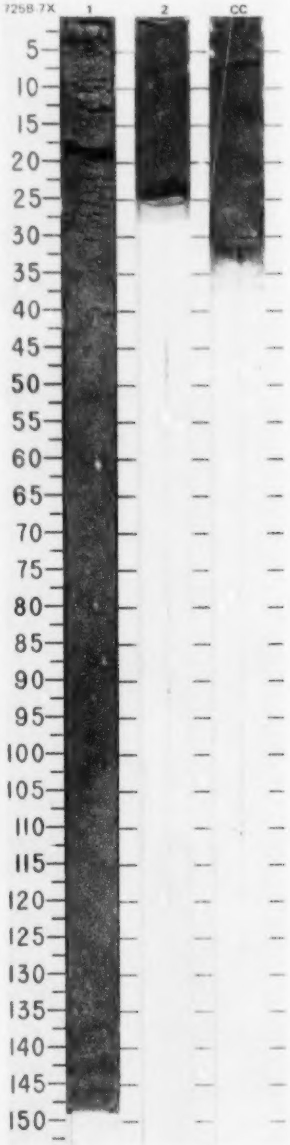

725B-7X
1
2
CC
5
10
15
20
25
30
35
40
45
50
55
60
65
70
75
80
85
90
95
100
105
110
115
120
125
130
135
140
145
150

SITE 725 HOLE B CORE 9X CORED INTERVAL 385.0-394.6 mbsl; 74.5-84.1 mbsf

TIME-ROCK UNIT	BIOSTRAT. ZONE/ FOSSIL CHARACTER				PALEOMAGNETICS	PHYS. PROPERTIES	CHEMISTRY	SECTION	METERS	GRAPHIC LITHOLOGY	DRILLING DISTURB.	SED. STRUCTURES	SAMPLES	LITHOLOGIC DESCRIPTION
	FORAMINIFERS	NANNOFOSSILS	RADIOLARIANS	DIATOMS										
PLEISTOCENE		NN19 *Pseudoemiliania lacunosa* ● A/M	● Barren		●			1 CC	0.5				●	NANNOFOSSIL-RICH CALCITIC CLAYEY SILT Entire core is undisturbed. Major lithology: NANNOFOSSIL-RICH CALCITIC CLAYEY SILT, olive gray (5Y 4/2). Slightly bioturbated.

SMEAR SLIDE SUMMARY (%):

	1
	20
	D
TEXTURE:	
Silt	50
Clay	50
COMPOSITION:	
Access. minerals	2
Clay	30
Dolomite	1
Foraminifers	2
Inorganic calcite	35
Nannofossils	20
Quartz	10

SITE 725 HOLE B CORE 10X CORED INTERVAL 394.6-404.3 mbsl; 84.1-93.8 mbsf

TIME-ROCK UNIT	BIOSTRAT. ZONE/ FOSSIL CHARACTER				PALEOMAGNETICS	PHYS. PROPERTIES	CHEMISTRY	SECTION	METERS	GRAPHIC LITHOLOGY	DRILLING DISTURB.	SED. STRUCTURES	SAMPLES	LITHOLOGIC DESCRIPTION
	FORAMINIFERS	NANNOFOSSILS	RADIOLARIANS	DIATOMS										
PLEISTOCENE		NN19 *Pseudoemiliania lacunosa* ● A/M-G	● Barren		Brunhes ●			1 CC	0.5					NANNOFOSSIL-RICH CALCITIC CLAYEY SILT Entire core is undisturbed. Major lithology: NANNOFOSSIL-RICH CALCITIC CLAYEY SILT, olive gray (5Y 4/2). Slightly bioturbated throughout.

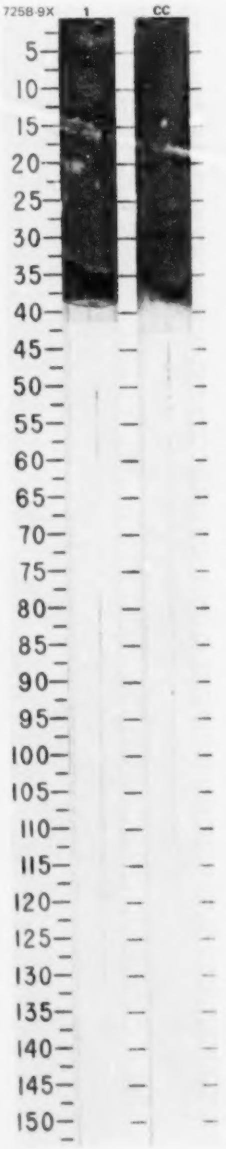
725B-9X
1
CC
5
10
15
20
25
30
35
40
45
50
55
60
65
70
75
80
85
90
95
100
105
110
115
120
125
130
135
140
145
150

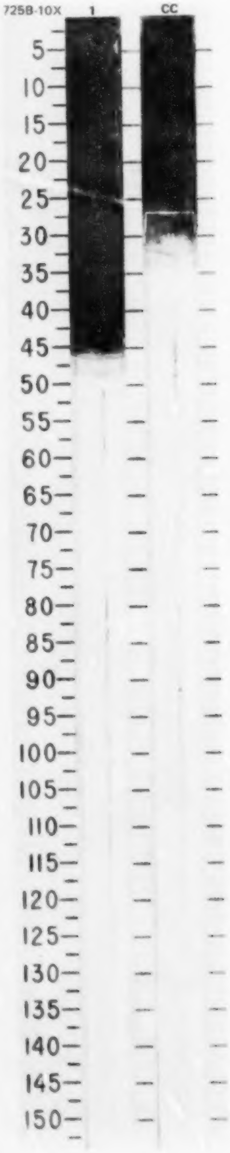
725B-10X
1
CC
5
10
15
20
25
30
35
40
45
50
55
60
65
70
75
80
85
90
95
100
105
110
115
120
125
130
135
140
145
150

SITE 725 HOLE C CORE 1H CORED INTERVAL 310.5-319.5 mbsl; 0.0-9.0 mbsf

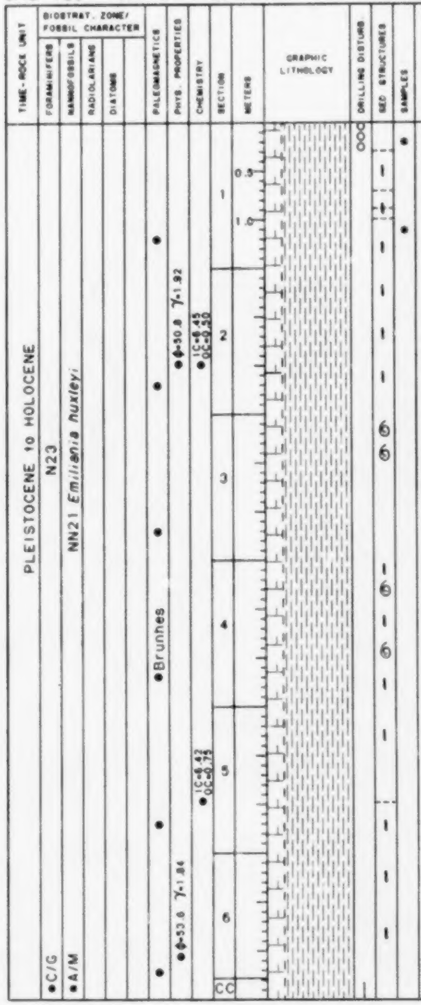
TIME-ROCK UNIT
BIOSTRAT. ZONE/ FOSSIL CHARACTER
FORAMINIFERS
NANNOFOSSILS
RADIOLARIANS
DIATOMS
PALEOMAGNETICS
PHYS. PROPERTIES
CHEMISTRY
SECTION
METERS
GRAPHIC LITHOLOGY
DRILLING DISTURB.
SED. STRUCTURES
SAMPLES
PLEISTOCENE to HOLOCENE
N23
NN21 Emiliania huxleyi
●C/G
●A/M
●Brunhes
●Φ=50.8 γ=1.92
●Φ=53.6 γ=1.84
●IC=8.45 OC=0.50
●IC=8.42 OC=0.75
1
2
3
4
5
6
CC
0.5
1.0

LITHOLOGIC DESCRIPTION

CALCAREOUS CALCITIC CLAYEY SILT to NANNOFOSSIL-RICH CLAYEY SILT

Section 1, 0-25 cm, is soupy. CC is slightly disturbed. Remainder is undisturbed.

Major lithology: CALCAREOUS CALCITIC CLAYEY SILT to NANNOFOSSIL-RICH CLAYEY SILT, olive (5Y 4/3) to olive gray (5Y 4/2). Slightly bioturbated throughout. Shell fragments dispersed throughout, abundant at Section 3, 22 and 43 cm, and Section 4, 45 and 95 cm.

SMEAR SLIDE SUMMARY (%):

	1, 20 D	1, 111 D
TEXTURE:		
Sand	10	20
Silt	50	45
Clay	40	35
COMPOSITION:		
Access. minerals		Tr
Clay	20	20
Dolomite		Tr
Foraminifers	15	
Inorganic calcite	40	55
Nannofossils	10	15
Pellets	10	
Quartz	5	10

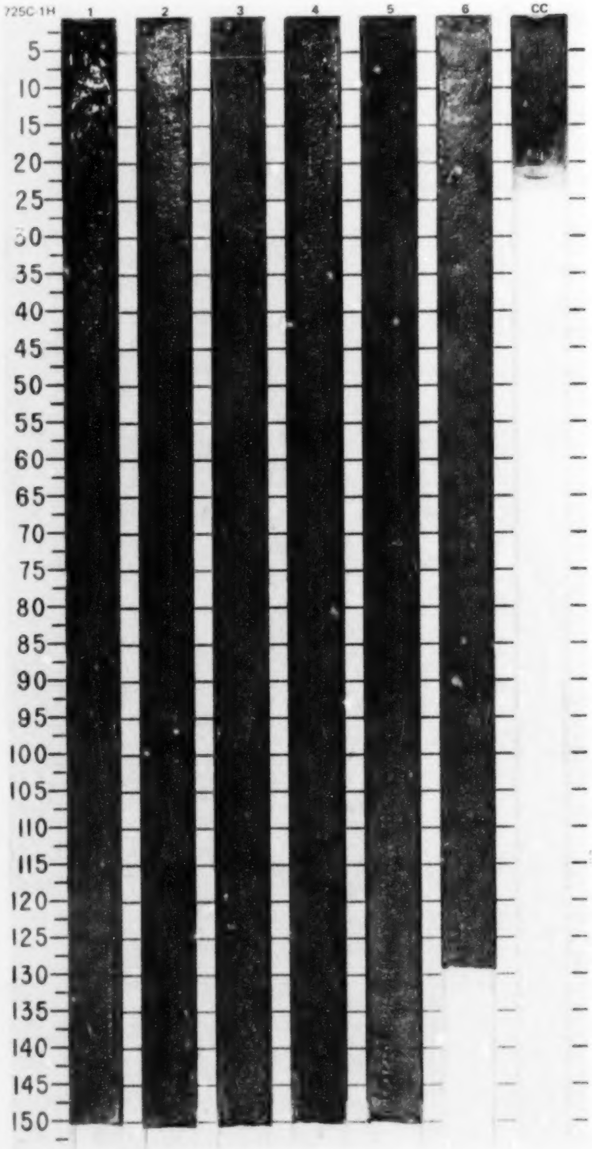
725C-1H
1
2
3
4
5
6
CC
5
10
15
20
25
30
35
40
45
50
55
60
65
70
75
80
85
90
95
100
105
110
115
120
125
130
135
140
145
150

SITE 725 HOLE C CORE 2H CORED INTERVAL 319.5-329.1 mbsl; 9.0-18.6 mbsf

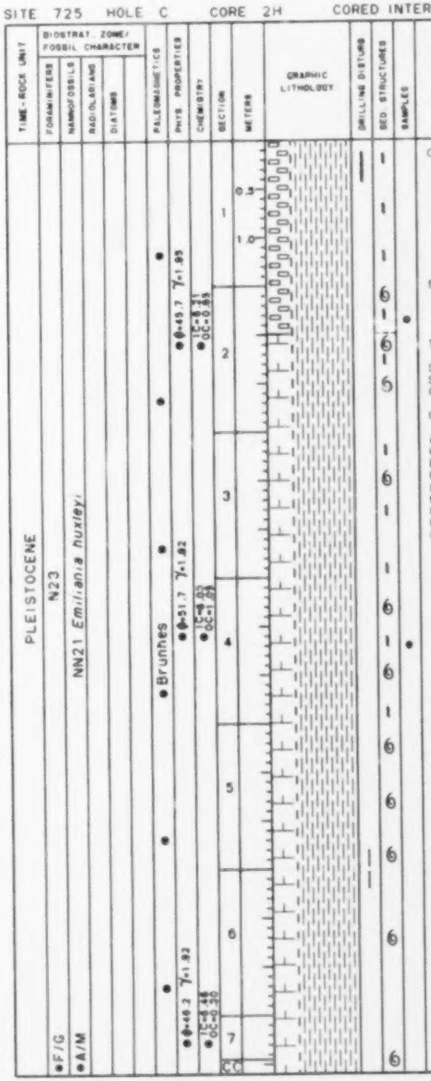
TIME-ROCK UNIT
BIOSTRAT. ZONE/ FOSSIL CHARACTER
FORAMINIFERS
NANNOFOSSILS
RADIOLARIANS
DIATOMS
PALEOMAGNETICS
PHYS. PROPERTIES
CHEMISTRY
SECTION
METERS
GRAPHIC LITHOLOGY
DRILLING DISTURB.
SED. STRUCTURES
SAMPLES
PLEISTOCENE
N23
NN21 Emiliania huxleyi
●F/G
●A/M
●Brunhes
●φ=45.7 γ=1.95
●φ=51.7 γ=1.82
●φ=46.2 γ=1.82
●IC=8.21 OC=0.85
●IC=6.83 OC=1.29
●IC=4.46 OC=0.30
1
2
3
4
5
6
7
CC
0.5
1.0

LITHOLOGIC DESCRIPTION

CALCAREOUS CALCITIC CLAYEY SILT and NANNOFOSSIL-RICH CLAYEY SILT

Section 1, 25-36 cm, is soupy. Section 6, 0-12 cm, is slightly disturbed. Remainder is undisturbed.

Major lithologies:

a. Calcareous calcitic clayey silt, olive (5Y 4/3), slightly bioturbated. Section 1 to Section 2, 40 cm.

b. Nannofossil-rich clayey silt, olive (5Y 4/3), slightly bioturbated. Contains abundant shell fragments. Section 2, 40 cm, to CC.

SMEAR SLIDE SUMMARY (%):

	2, 35 D	4, 70 D
TEXTURE:		
Sand	20	10
Silt	50	50
Clay	30	40
COMPOSITION:		
Access. minerals		2
Clay	20	20
Dolomite		Tr
Foraminifers	15	7
Inorganic calcite	40	38
Mica		3
Nannofossils	15	20
Pellets	5	
Quartz	5	10

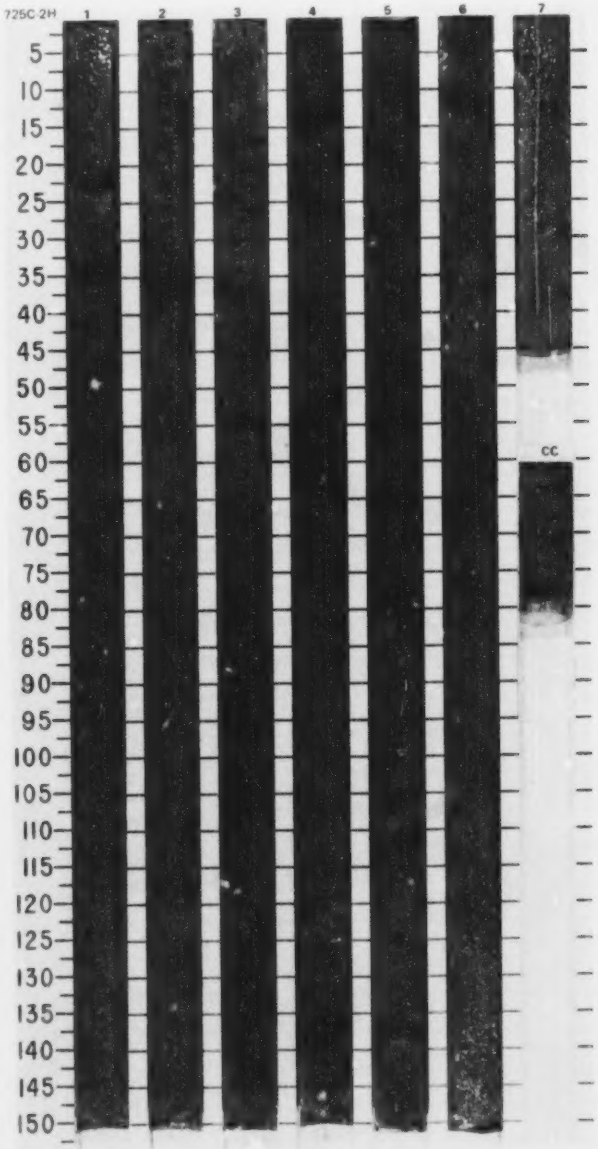
725C 2H
1
2
3
4
5
6
7
CC
5
10
15
20
25
30
35
40
45
50
55
60
65
70
75
80
85
90
95
100
105
110
115
120
125
130
135
140
145
150

SITE 725 HOLE C CORE 3H CORED INTERVAL 329.1-339.0 mbsl; 18.6-28.5 mbsf

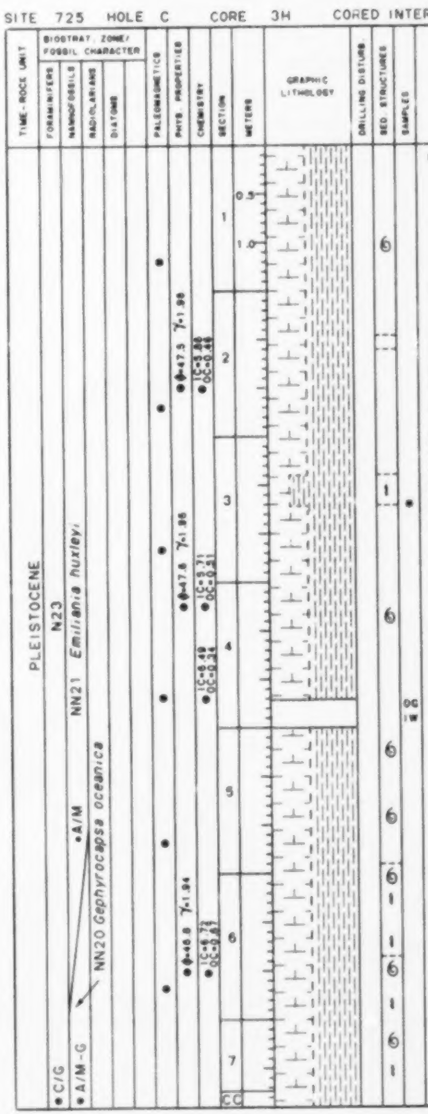
TIME-ROCK UNIT
BIOSTRAT. ZONE/ FOSSIL CHARACTER
FORAMINIFERS
NANNOFOSSILS
RADIOLARIANS
DIATOMS
PALEOMAGNETICS
PHYS. PROPERTIES
CHEMISTRY
SECTION
METERS
GRAPHIC LITHOLOGY
DRILLING DISTURB.
SED. STRUCTURES
SAMPLES
PLEISTOCENE
N23
NN21 Emiliania huxleyi
NN20 Gephyrocapsa oceanica
• C/G
• A/M-G
•A/M
●φ=47.5 γ=1.98
●IC=5.86 OC=0.46
●φ=47.6 γ=1.98
●IC=5.71 OC=0.51
●IC=6.49 OC=0.34
●φ=46.8 γ=1.94
●IC=6.72 OC=0.47
1
2
3
4
5
6
7
CC
0.5
1.0
OG
IW

LITHOLOGIC DESCRIPTION

MARLY CALCITIC NANNOFOSSIL OOZE

Entire core is undisturbed.

Major lithology: MARLY CALCITIC NANNOFOSSIL OOZE, olive (5Y 4/3) to dark greenish gray (10Y 4/2, 4/3). Slightly bioturbated in Sections 6 and 7. Shell fragments scattered throughout interval, abundant in Section 2 and 5.

Minor lithology: Nannofossil-rich calcific clayey silt, dark olive gray (5Y 3/2), with sharp contacts and minor bioturbation. Section 3, 45-75 cm.

SMEAR SLIDE SUMMARY (%):

	3, 70 D	6, 70 D
TEXTURE:		
Silt	50	40
Clay	50	60
COMPOSITION:		
Access. minerals	Tr	
Clay	30	25
Dolomite		Tr
Foraminifers	5	5
Inorganic calcite	30	20
Nannofossils	20	40
Pellets		5
Quartz	15	5

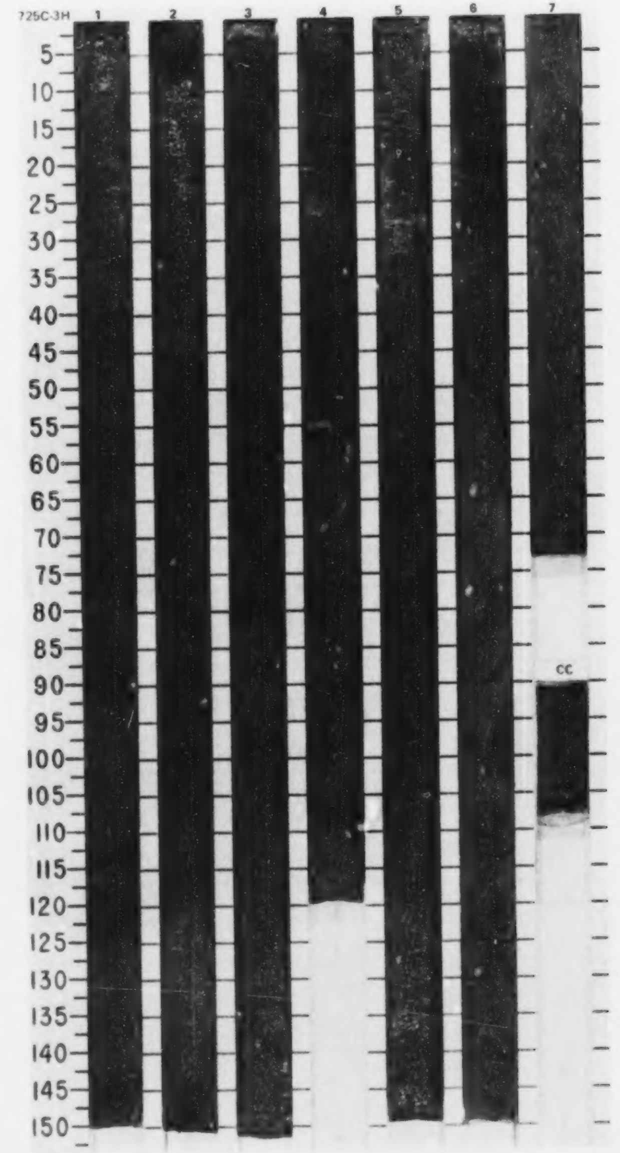
725C-3H
1
2
3
4
5
6
7
CC
5
10
15
20
25
30
35
40
45
50
55
60
65
70
75
80
85
90
95
100
105
110
115
120
125
130
135
140
145
150

SITE 725 HOLE C CORE 4X CORED INTERVAL 339.0-348.5 mbsl; 28.5-38.0 mbsf

TIME-ROCK UNIT	FORAMINIFERS	NANNOFOSSILS	RADIOLARIANS	DIATOMS	PALEOMAGNETICS	PHYS. PROPERTIES	CHEMISTRY	SECTION	METERS	GRAPHIC LITHOLOGY	DRILLING DISTURB.	SED. STRUCTURES	SAMPLES
PLEISTOCENE	N23 ●C/G	NN20 *Gephyrocapsa oceanica* ●A/P-M			● ●	●φ=45.0 γ=2.00	●IC=8.38 OC=0.42	1 2 3 CC	0.5 1.0			⑥ I I ⑥ I I	●

LITHOLOGIC DESCRIPTION

MARLY CALCITIC NANNOFOSSIL OOZE and NANNOFOSSIL-RICH CALCITIC SILTY CLAY

Entire core is undisturbed.

Major lithologies:

a. MARLY CALCITIC NANNOFOSSIL OOZE, dark greenish gray (10Y 4/2). Scaphopod shell at Section 1, 15 cm. Section 1 to Section 2, 36 cm, and Section 3, 33 cm, to CC.

b. NANNOFOSSIL-RICH CALCITIC SILTY CLAY, olive (5Y 4/3), with faint bioturbation and dispersed shell fragments. Section 2, 36 cm, to Section 3, 34 cm.

SMEAR SLIDE SUMMARY (%):

	2, 86 D
TEXTURE:	
Sand	5
Silt	30
Clay	65
COMPOSITION:	
Access. minerals	2
Clay	45
Feldspar	Tr
Foraminifers	3
Inorganic calcite	15
Nannofossils	20
Pellets	5
Quartz	10
Rock fragments	Tr

SITE 725 HOLE C CORE 5X CORED INTERVAL 348.5-358.0 mbsl; 38.0-47.5 mbsf

TIME-ROCK UNIT	FORAMINIFERS	NANNOFOSSILS	RADIOLARIANS	DIATOMS	PALEOMAGNETICS	PHYS. PROPERTIES	CHEMISTRY	SECTION	METERS	GRAPHIC LITHOLOGY	DRILLING DISTURB.	SED. STRUCTURES	SAMPLES
PLEISTOCENE	N23 F/G●	NN20 *Gephyrocapsa oceanica* A/M●			●			1 CC				△ I	●

LITHOLOGIC DESCRIPTION

MARLY CALCITIC NANNOFOSSIL OOZE

Entire core is undisturbed.

Major lithology: MARLY CALCITIC NANNOFOSSIL OOZE, olive gray (5Y 4/2) to dark greenish gray (10Y 5/2), and slightly bioturbated. Section 1, 16 cm, to CC.

Minor lithology: Foraminifer-bearing calcitic clayey silt, dark greenish gray (10Y 4/2). Sharp base and slightly graded. Section 1, 0-16 cm.

SMEAR SLIDE SUMMARY (%):

	1, 8 D
TEXTURE:	
Sand	30
Silt	60
Clay	10
COMPOSITION:	
Access. minerals	3
Clay	10
Dolomite	1
Feldspar	2
Foraminifers	10
Inorganic calcite	50
Mica	1
Nannofossils	3
Pyrite	Tr
Quartz	20

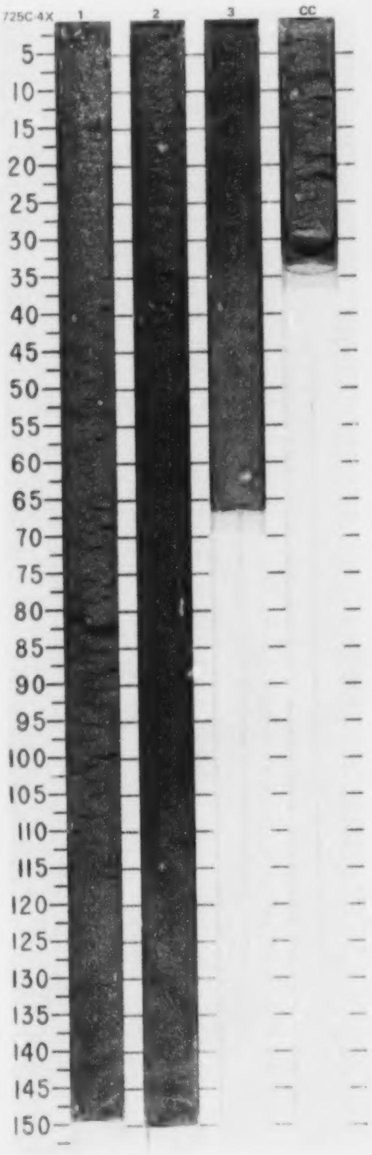

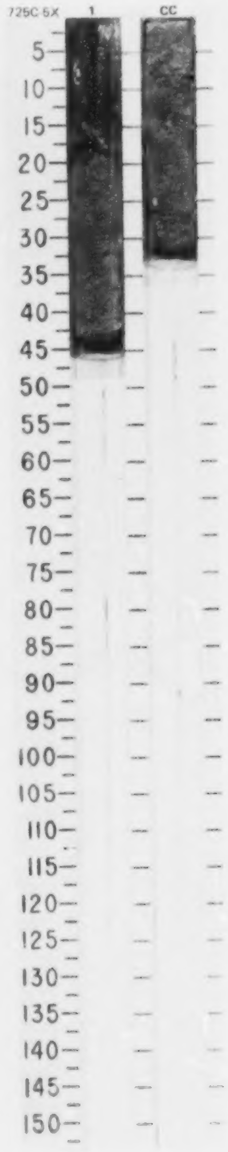

SITE 725 HOLE C CORE 6X CORED INTERVAL 358.0-367.5 mbsl; 47.5-57.0 mbsf

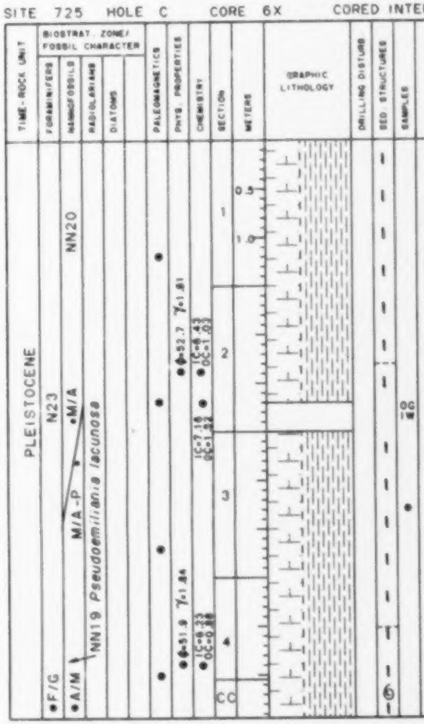
TIME-ROCK UNIT
BIOSTRAT. ZONE/ FOSSIL CHARACTER
FORAMINIFERS
NANNOFOSSILS
RADIOLARIANS
DIATOMS
PALEOMAGNETICS
PHYS. PROPERTIES
CHEMISTRY
SECTION
METERS
GRAPHIC LITHOLOGY
DRILLING DISTURB.
SED. STRUCTURES
SAMPLES
PLEISTOCENE
N23
●F/G
NN20
●M/A
M/A-P
●A/M
NN19 Pseudoemiliania lacunosa
●φ=52.7 γ=1.81
●φ=51.9 γ=1.84
●IC=8.43 OC=1.03
●IC=7.16 OC=1.32
●IC=8.22 OC=0.88
1
2
3
4
CC
0.5
1.0
OG
IW

LITHOLOGIC DESCRIPTION

MARLY CALCITIC NANNOFOSSIL OOZE

Entire core is undisturbed.

Major lithology: MARLY CALCITIC NANNOFOSSIL OOZE, dark greenish gray (10Y 5/2), olive gray (5Y 4/2), and olive (5Y 4/3). Minor bioturbation throughout. Shell fragments rare throughout the core, more common at CC, 10-15 cm.

SMEAR SLIDE SUMMARY (%):

	3, 78 D
TEXTURE:	
Silt	40
Clay	60
COMPOSITION:	
Access. minerals	2
Clay	20
Dolomite	3
Foraminifers	5
Inorganic calcite	30
Nannofossils	30
Quartz	10

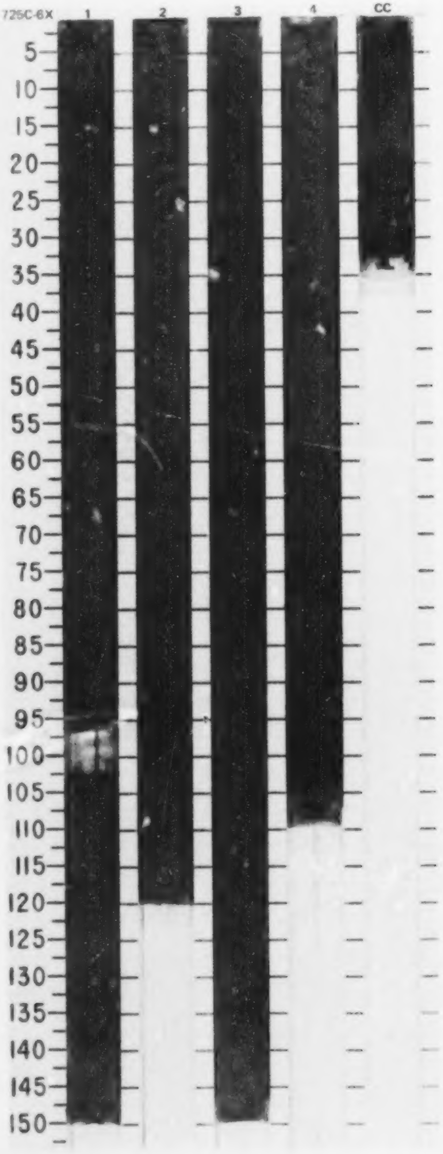
725C-6X
1
2
3
4
CC
5
10
15
20
25
30
35
40
45
50
55
60
65
70
75
80
85
90
95
100
105
110
115
120
125
130
135
140
145
150

SITE 725 HOLE C CORE 7X CORED INTERVAL 367.5-377.0 mbsl; 57.0-66.5 mbsf

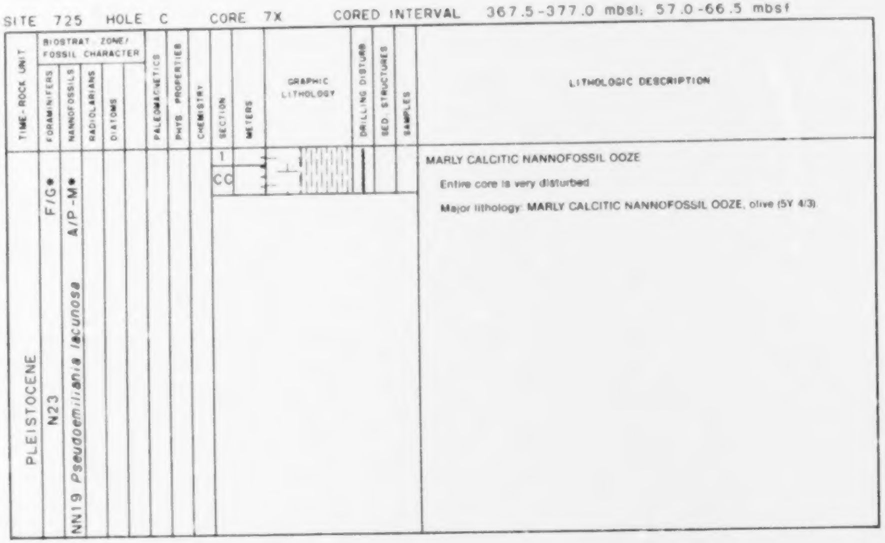
TIME-ROCK UNIT
BIOSTRAT. ZONE/ FOSSIL CHARACTER
FORAMINIFERS
NANNOFOSSILS
RADIOLARIANS
DIATOMS
PALEOMAGNETICS
PHYS. PROPERTIES
CHEMISTRY
SECTION
METERS
GRAPHIC LITHOLOGY
DRILLING DISTURB.
SED. STRUCTURES
SAMPLES
LITHOLOGIC DESCRIPTION
PLEISTOCENE
N23
NN19 *Pseudoemiliania lacunosa*
F/G●
A/P-M●
1
CC

MARLY CALCITIC NANNOFOSSIL OOZE

Entire core is very disturbed.

Major lithology: MARLY CALCITIC NANNOFOSSIL OOZE, olive (5Y 4/3).

SITE 725 HOLE C CORE 8X CORED INTERVAL 377.0-386.6 mbsl; 66.5-76.1 mbsf

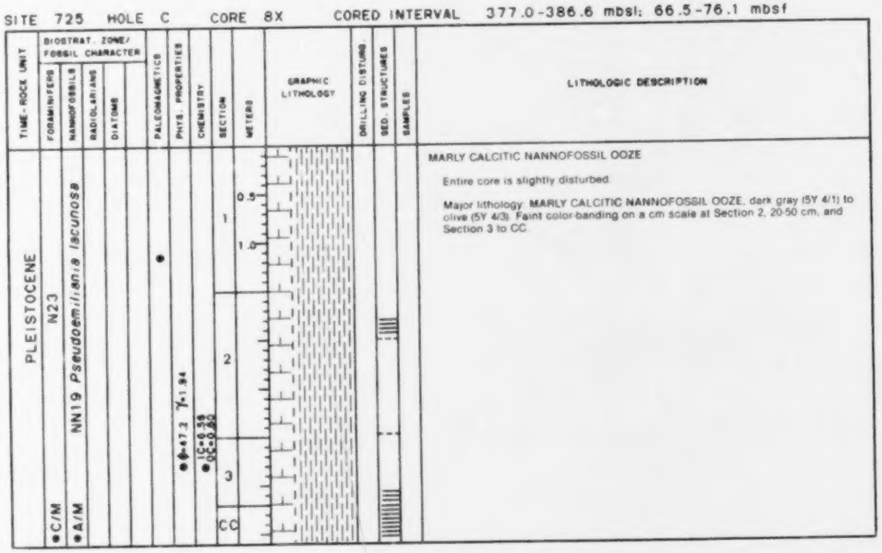
TIME-ROCK UNIT
BIOSTRAT. ZONE/ FOSSIL CHARACTER
FORAMINIFERS
NANNOFOSSILS
RADIOLARIANS
DIATOMS
PALEOMAGNETICS
PHYS. PROPERTIES
CHEMISTRY
SECTION
METERS
GRAPHIC LITHOLOGY
DRILLING DISTURB.
SED. STRUCTURES
SAMPLES
LITHOLOGIC DESCRIPTION
PLEISTOCENE
N23
NN19 *Pseudoemiliania lacunosa*
●C/M
●A/M
●
●Φ=47.2 γ=1.94
●IC=6.59 OC=0.60
0.5
1.0
1
2
3
CC

MARLY CALCITIC NANNOFOSSIL OOZE

Entire core is slightly disturbed.

Major lithology: MARLY CALCITIC NANNOFOSSIL OOZE, dark gray (5Y 4/1) to olive (5Y 4/3). Faint color-banding on a cm scale at Section 2, 20-50 cm, and Section 3 to CC.

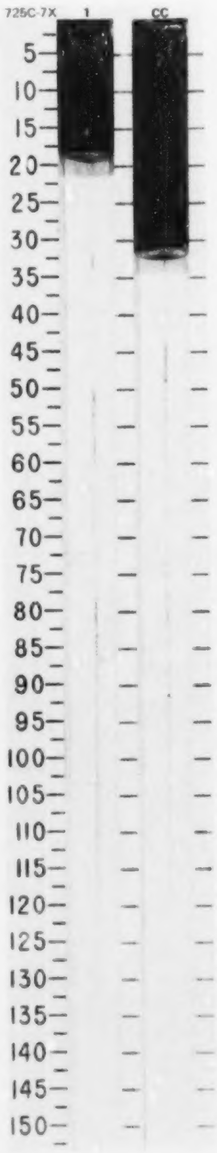
725C-7X
1
CC
5
10
15
20
25
30
35
40
45
50
55
60
65
70
75
80
85
90
95
100
105
110
115
120
125
130
135
140
145
150

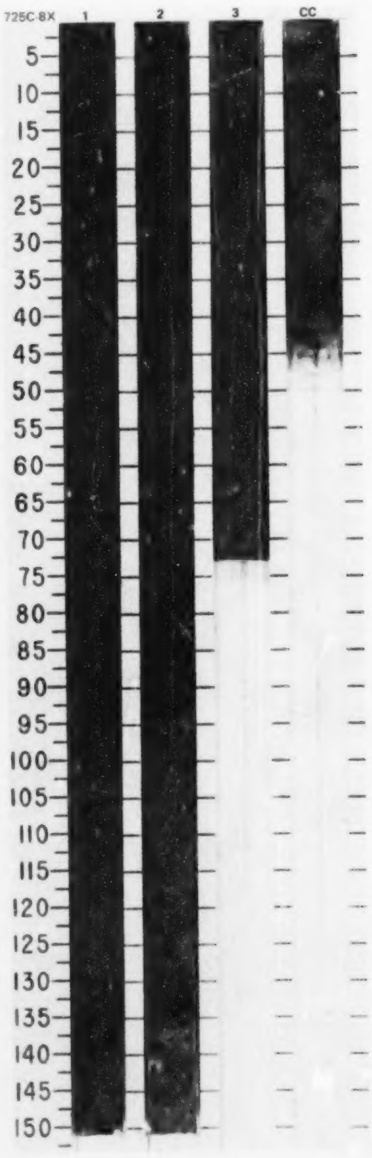
725C-8X
1
2
3
CC
5
10
15
20
25
30
35
40
45
50
55
60
65
70
75
80
85
90
95
100
105
110
115
120
125
130
135
140
145
150

SITE 725 HOLE C CORE 9X CORED INTERVAL 386.6-396.2 mbsl; 76.1-85.7 mbsf

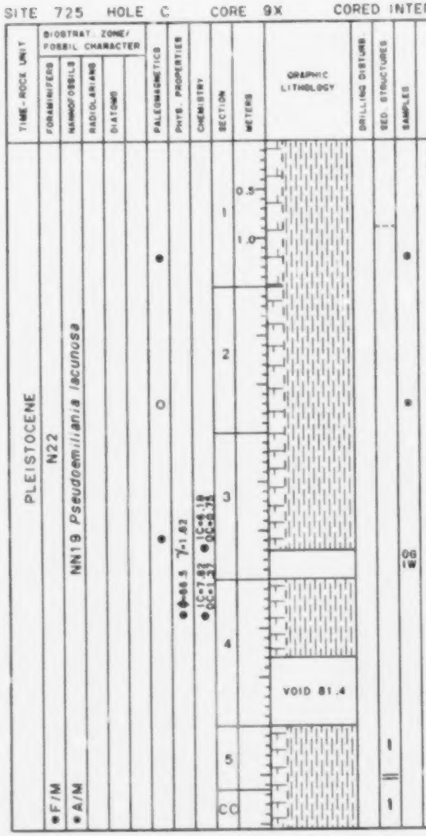
TIME-ROCK UNIT
BIOSTRAT. ZONE/ FOSSIL CHARACTER
FORAMINIFERS
NANNOFOSSILS
RADIOLARIANS
DIATOMS
PALEOMAGNETICS
PHYS. PROPERTIES
CHEMISTRY
SECTION
METERS
GRAPHIC LITHOLOGY
DRILLING DISTURB.
SED. STRUCTURES
SAMPLES
PLEISTOCENE
N22
NN19 *Pseudoemiliania lacunosa*
●F/M
●A/M
●ϕ-66.5 γ-1.82
●IC=7.82 OC=1.37
●IC=8.18 OC=0.75
1
2
3
4
5
CC
0.5
1.0
VOID 81.4
OG
IW

LITHOLOGIC DESCRIPTION

NANNOFOSSIL-RICH CALCITIC SILTY CLAY and FORAMINIFER-RICH CALCITIC SANDY SILT

Entire core is undisturbed.

Major lithologies:
a. NANNOFOSSIL-RICH CALCITIC SILTY CLAY, dark gray (5Y 4/1) to olive (5Y 4/3). Slightly bioturbated in CC. Section 1 and CC.
b. FORAMINIFER-RICH CALCITIC SANDY SILT, olive (5Y 4/3) to olive gray (5Y 4/2). Slightly bioturbated in Section 5. Faint cm-scale laminations in Section 5, 57-64 cm. Section 2 to Section 5.

SMEAR SLIDE SUMMARY (%):

	1, 120 D	2, 120 D
TEXTURE:		
Sand		40
Silt	50	40
Clay	50	20
COMPOSITION:		
Access. minerals	3	
Clay	30	10
Dolomite	2	1
Foraminifers	5	15
Hornblende		2
Inorganic calcite	30	55
Nannofossils	20	5
Pellets		8
Quartz	10	8

CORE 117-725C-10X NO RECOVERY

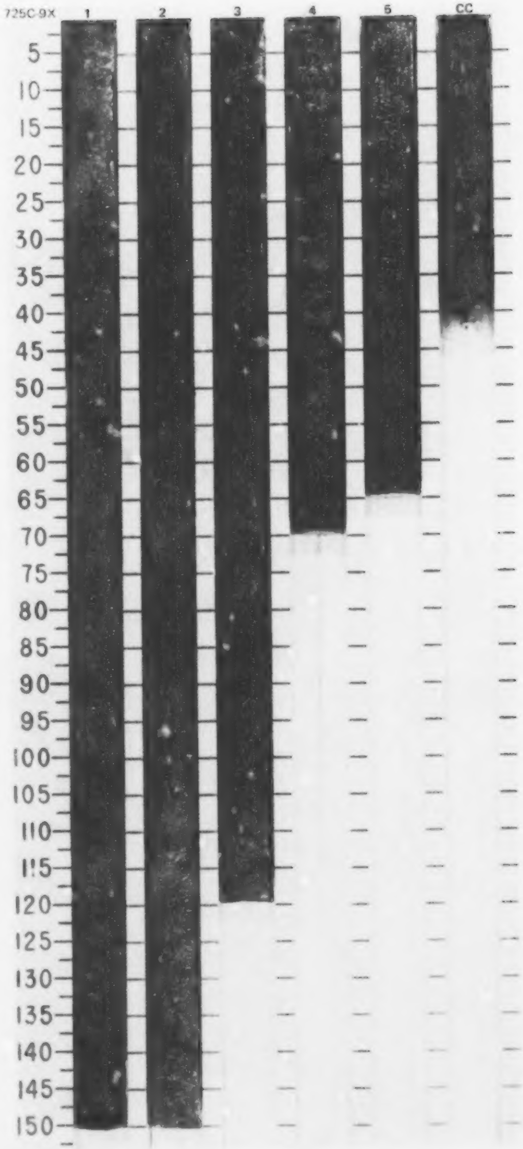
725C-9X
1
2
3
4
5
CC
5
10
15
20
25
30
35
40
45
50
55
60
65
70
75
80
85
90
95
100
105
110
115
120
125
130
135
140
145
150

SITE 725 HOLE C CORE 11X CORED INTERVAL 405.8-415.4 mbsl; 95.3-104.9 mbsf

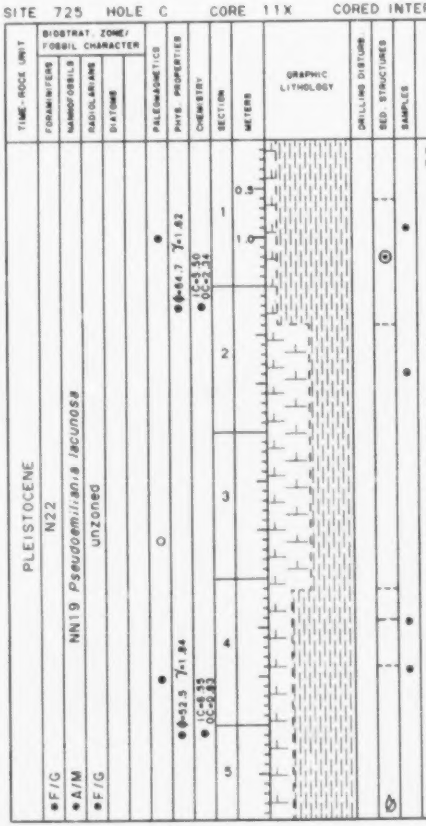
TIME-ROCK UNIT
BIOSTRAT. ZONE/ FOSSIL CHARACTER
FORAMINIFERS
NANNOFOSSILS
RADIOLARIANS
DIATOMS
PALEOMAGNETICS
PHYS. PROPERTIES
CHEMISTRY
SECTION
METERS
GRAPHIC LITHOLOGY
DRILLING DISTURB.
SED. STRUCTURES
SAMPLES
PLEISTOCENE
N22
NN19 Pseudoemiliania lacunosa
unzoned
●F/G
●A/M
●F/G
●Φ=64.7 γ=1.82
●Φ=52.5 γ=1.84
● IC=3.50 OC=2.34
● IC=8.55 OC=0.83
0.5
1.0
1
2
3
4
5

LITHOLOGIC DESCRIPTION

NANNOFOSSIL-RICH CALCITIC SILTY CLAY and MARLY CALCITIC NANNOFOSSIL OOZE

Entire core is undisturbed.

Major lithologies:
a. NANNOFOSSIL-RICH CALCITIC SILTY CLAY, olive (5Y 4/3) to dark olive gray (5Y 3/2). Contains phosphorite concretion at Section 1, 133 cm, and shell debris at Section 5, 95 cm. Section 1 to Section 2, 43 cm, and Section 4, 45 cm, to Section 5.
b. MARLY CALCITIC NANNOFOSSIL OOZE, olive (5Y 4/3). Section 2, 43 cm, to Section 4, 18 cm.

Minor lithology: nannofossil-rich calcitic clayey silt, dark greenish gray (10Y 3/2), with sharp basal contact. Section 4, 18-45 cm.

SMEAR SLIDE SUMMARY (%):

	1, 92 D	2, 90 D	4, 45 D	4, 94 D
TEXTURE:				
Silt	40	25	55	45
Clay	60	75	45	55
COMPOSITION:				
Access. minerals	1		1	2
Clay	35	30	25	35
Dolomite	3		4	3
Foraminifers	3	5	3	5
Gypsum		Tr		
Inorganic calcite	35	15	37	30
Mica	1			
Nannofossils	10	45	20	20
Quartz	10	5	10	5
Radiolarians	Tr			
Sponge spicules	2			

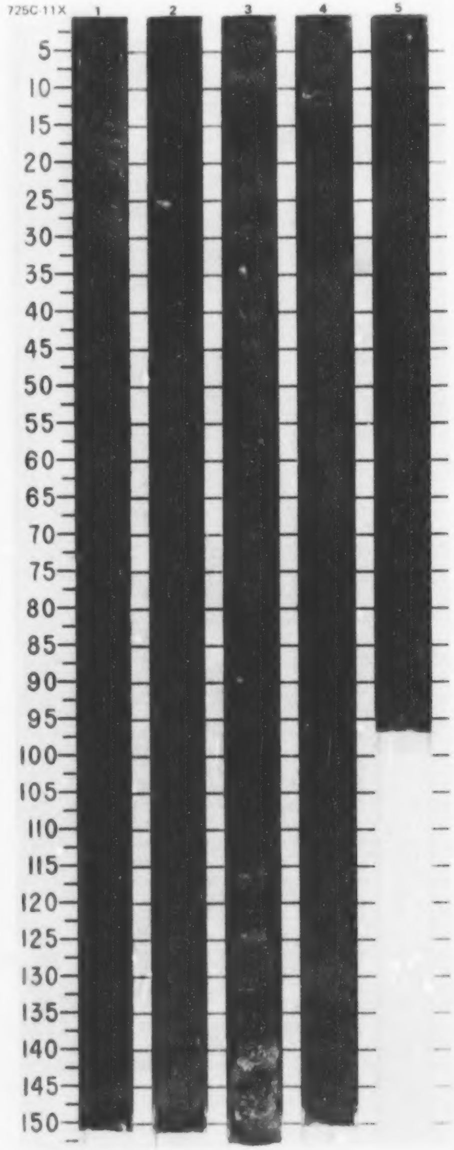
725C-11X
1
2
3
4
5
5
10
15
20
25
30
35
40
45
50
55
60
65
70
75
80
85
90
95
100
105
110
115
120
125
130
135
140
145
150

SITE 725 HOLE C CORE 12X CORED INTERVAL 415.4-425.0 mbsl; 104.9-114.5 mbsf

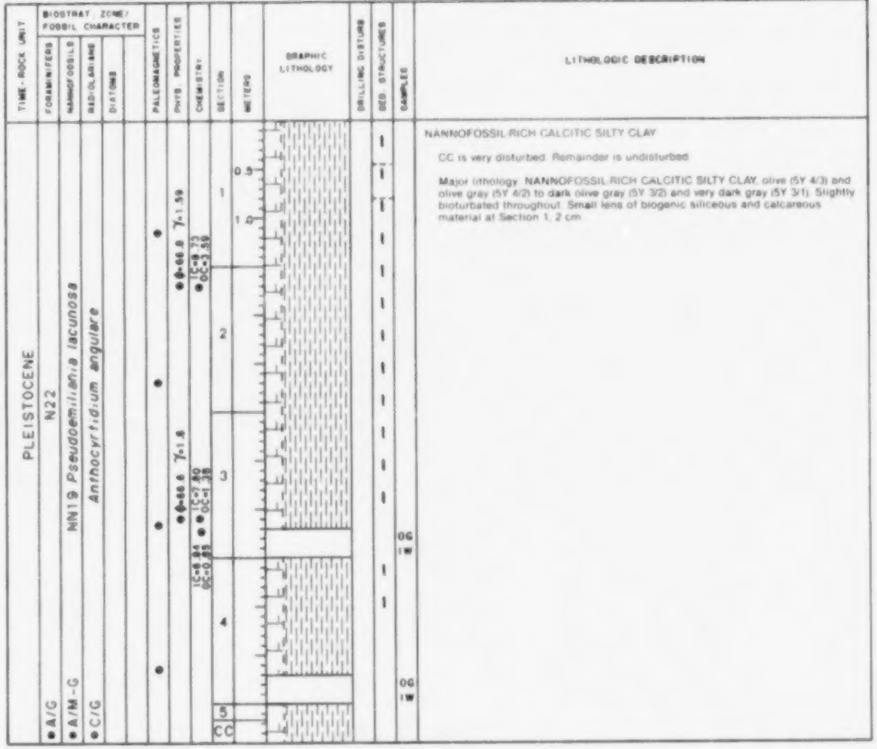
TIME-ROCK UNIT
BIOSTRAT. ZONE/ FOSSIL CHARACTER
FORAMINIFERS
NANNOFOSSILS
RADIOLARIANS
DIATOMS
PALEOMAGNETICS
PHYS. PROPERTIES
CHEMISTRY
SECTION
METERS
GRAPHIC LITHOLOGY
DRILLING DISTURB.
SED. STRUCTURES
SAMPLES
PLEISTOCENE
N22
NN19 Pseudoemiliania lacunosa
Anthocyrtidium angulare
● A/G
● A/M-G
● C/G
● φ=66.0 γ=1.59
● IC=8.73 OC=1.59
● φ=66.6 γ=1.8
● IC=7.90 OC=1.38
● IC=6.84 OC=0.85
0.5
1.0
1
2
3
4
5
CC
OG
IW
OG
IW

LITHOLOGIC DESCRIPTION

NANNOFOSSIL-RICH CALCITIC SILTY CLAY

CC is very disturbed. Remainder is undisturbed.

Major lithology: NANNOFOSSIL-RICH CALCITIC SILTY CLAY, olive (5Y 4/3) and olive gray (5Y 4/2) to dark olive gray (5Y 3/2) and very dark gray (5Y 3/1). Slightly bioturbated throughout. Small lens of biogenic siliceous and calcareous material at Section 1, 2 cm.

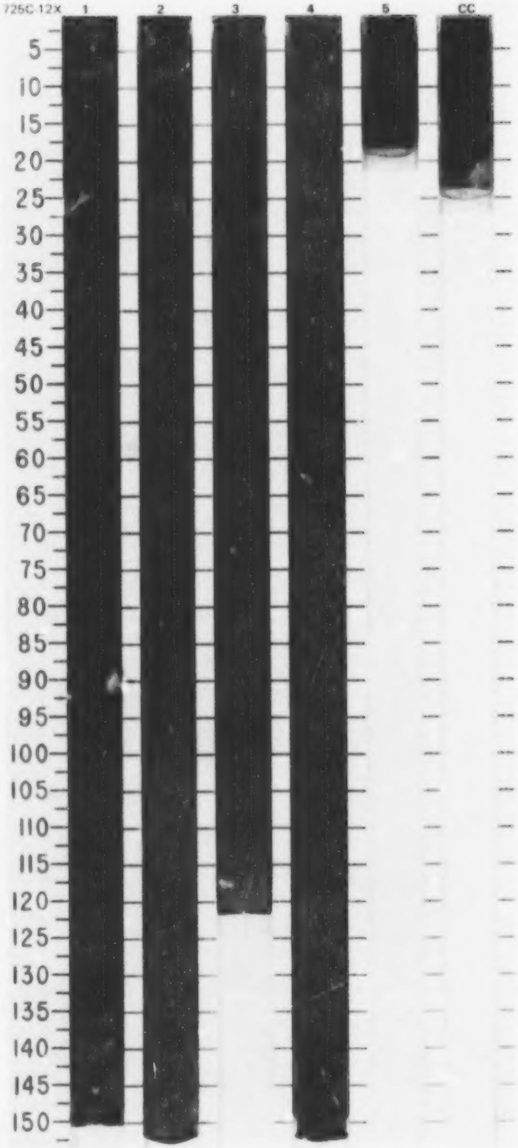
725C-12X
1
2
3
4
5
CC
5
10
15
20
25
30
35
40
45
50
55
60
65
70
75
80
85
90
95
100
105
110
115
120
125
130
135
140
145
150

SITE 725 HOLE C CORE 13X CORED INTERVAL 425.0-434.6 mbsl; 114.5-124.1 mbsf

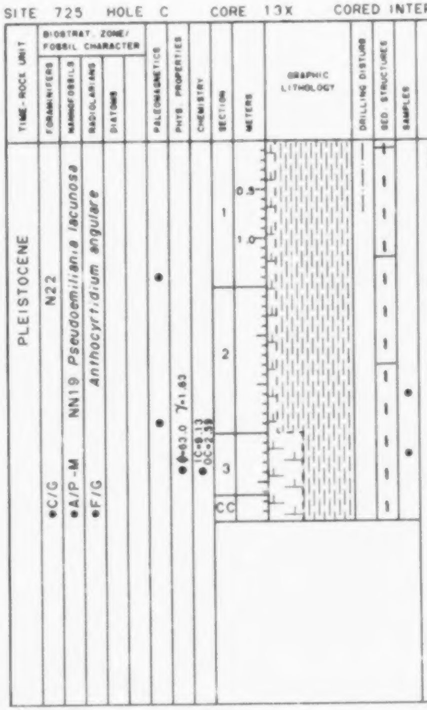
TIME-ROCK UNIT
BIOSTRAT. ZONE/ FOSSIL CHARACTER
FORAMINIFERS
NANNOFOSSILS
RADIOLARIANS
DIATOMS
PALEOMAGNETICS
PHYS. PROPERTIES
CHEMISTRY
SECTION
METERS
GRAPHIC LITHOLOGY
DRILLING DISTURB.
SED. STRUCTURES
SAMPLES
PLEISTOCENE
N22
NN19 Pseudoemiliania lacunosa
Anthocyrtidium angulare
●C/G
●A/P-M
●F/G
●ϕ=63.0 γ=1.83
●IC=0.13 OC=2.38
0.5
1.0
1
2
3
CC

LITHOLOGIC DESCRIPTION

NANNOFOSSIL-RICH CALCITIC SILTY CLAY and CALCITIC MARLY FORAMINIFERAL-NANNOFOSSIL OOZE

Section 1, 0-90 cm, moderately disturbed. Remainder is undisturbed.

Major lithologies:
- a. NANNOFOSSIL-RICH CALCITIC SILTY CLAY, olive gray (5Y 4/2, 5/2) to dark olive gray (5Y 3/2). Minor bioturbation throughout. Sections 1 and 2.
- b. CALCITIC MARLY FORAMINIFERAL-NANNOFOSSIL ooze, olive (5Y 4/3). Section 3 and CC.

SMEAR SLIDE SUMMARY (%):

	2, 110 D	3, 21 D
TEXTURE:		
Silt	45	40
Clay	55	60
COMPOSITION:		
Access. minerals	2	2
Clay	44	28
Diatoms		Tr
Dolomite	4	3
Foraminifers	3	10
Inorganic calcite	30	20
Nannofossils	7	30
Quartz	10	5
Sponge spicules		2

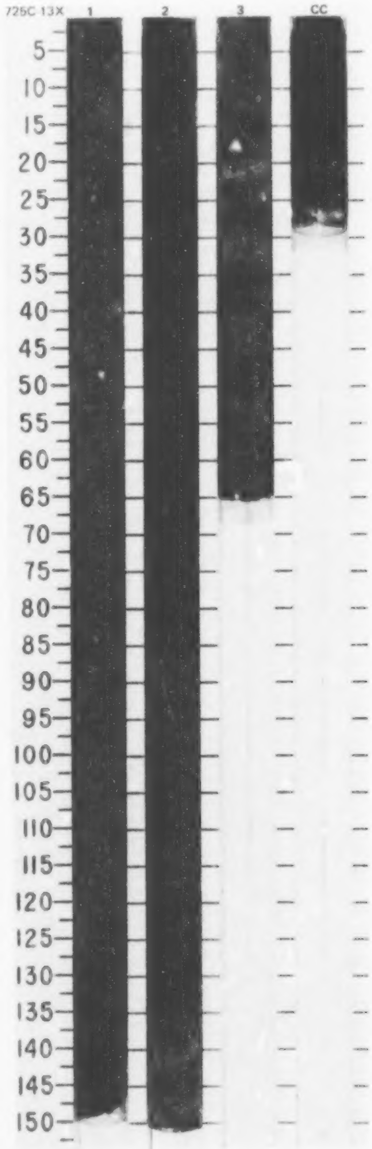
725C 13X
1
2
3
CC
5
10
15
20
25
30
35
40
45
50
55
60
65
70
75
80
85
90
95
100
105
110
115
120
125
130
135
140
145
150

SITE 725 HOLE C CORE 14X CORED INTERVAL 434.6-444.3 mbsl; 124.1-133.8 mbsf

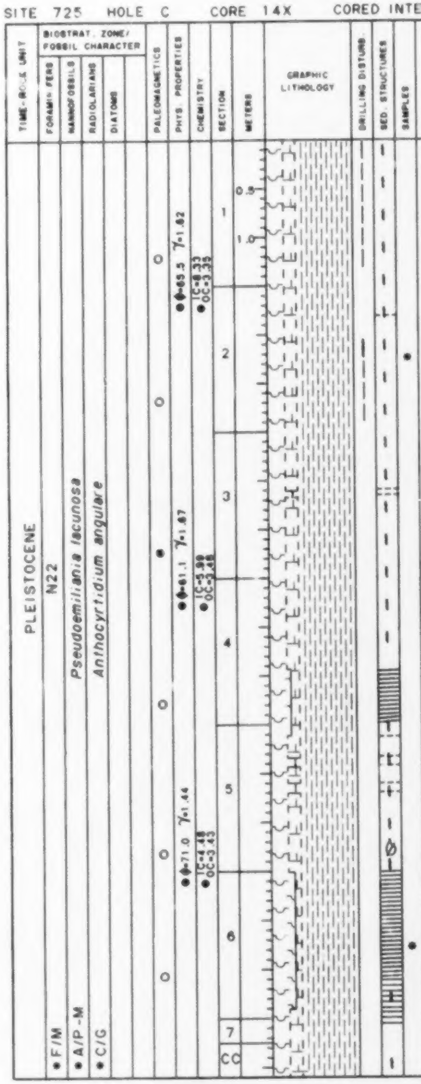
TIME-ROCK UNIT
BIOSTRAT. ZONE/FOSSIL CHARACTER
FORAMINIFERS
NANNOFOSSILS
RADIOLARIANS
DIATOMS
PALEOMAGNETICS
PHYS. PROPERTIES
CHEMISTRY
SECTION
METERS
GRAPHIC LITHOLOGY
DRILLING DISTURB.
SED. STRUCTURES
SAMPLES
PLEISTOCENE
N22
Pseudoemiliania lacunosa
Anthocyrtidium angulare
• F/M
• A/P-M
• C/G
●Φ=65.5 γ=1.82
●Φ=61.1 γ=1.87
●Φ=71.0 γ=1.44
● IC=8.33 OC=3.35
● IC=5.99 OC=3.48
● IC=4.48 OC=3.43
1
2
3
4
5
6
7
CC
0.5
1.0

LITHOLOGIC DESCRIPTION

DIATOMACEOUS CALCAREOUS CLAYEY SILT, and interbedded DIATOMACEOUS CALCAREOUS SILT and DIATOMACEOUS CLAYEY SILT

Section 1 is slightly disturbed. Section 2 is locally slightly to very disturbed. Remainder is undisturbed.

Major lithologies:

a. DIATOMACEOUS CALCAREOUS CLAYEY SILT, dark olive gray (5Y 3/2), olive gray (5Y 4/2), and olive (5Y 4/3). Minor bioturbation throughout. Section 1 to Section 4, 93 cm, and CC.

b. INTERBEDDED and laminated DIATOMACEOUS CALCAREOUS SILT, olive gray (5Y 4/2), and DIATOMACEOUS CLAYEY SILT, dark olive gray (5Y 3/2). Laminations are on scale of 1 cm thick. Calcareous silt beds are 18-80 cm thick, clayey silt beds are 6-13 cm thick. Section 4, 93 cm, through Section 7.

SMEAR SLIDE SUMMARY (%):

	2, 124 D	6, 92 D
TEXTURE:		
Silt	55	65
Clay	45	35
COMPOSITION:		
Access. minerals		1
Clay	35	35
Diatoms	20	30
Dolomite	4	2
Foraminifers	5	
Inorganic calcite	15	15
Nannofossils	10	
Pellets	3	
Quartz	3	15
Sponge spicules	5	2

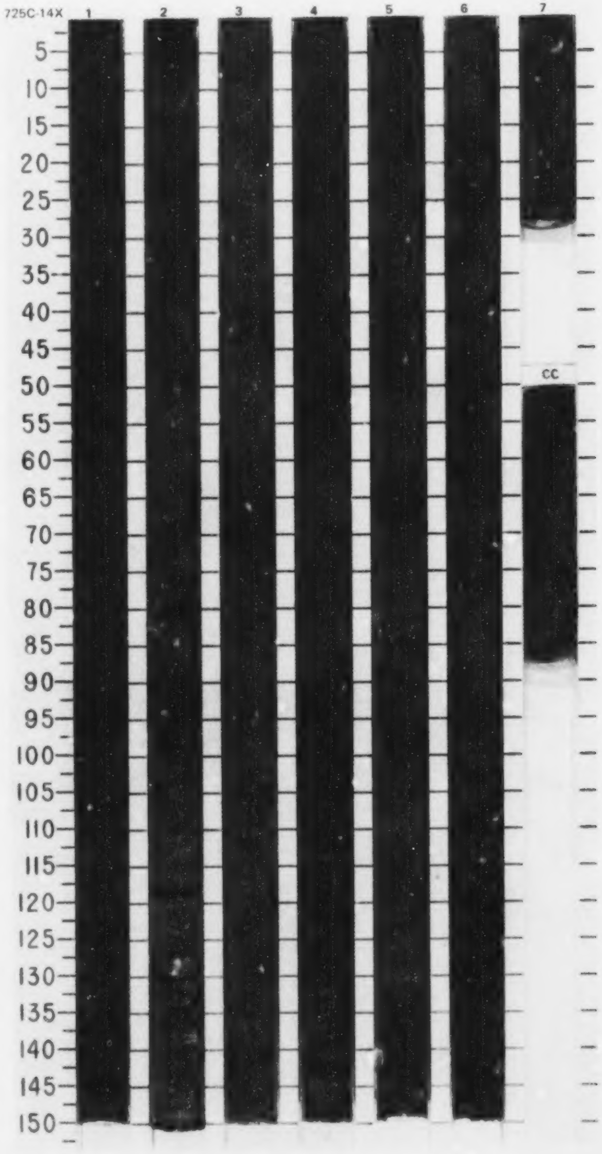
725C-14X
1
2
3
4
5
6
7
CC
5
10
15
20
25
30
35
40
45
50
55
60
65
70
75
80
85
90
95
100
105
110
115
120
125
130
135
140
145
150

SITE 725 HOLE C CORE 15X CORED INTERVAL 444.3-454.0 mbsl; 133.8-143.5 mbsf

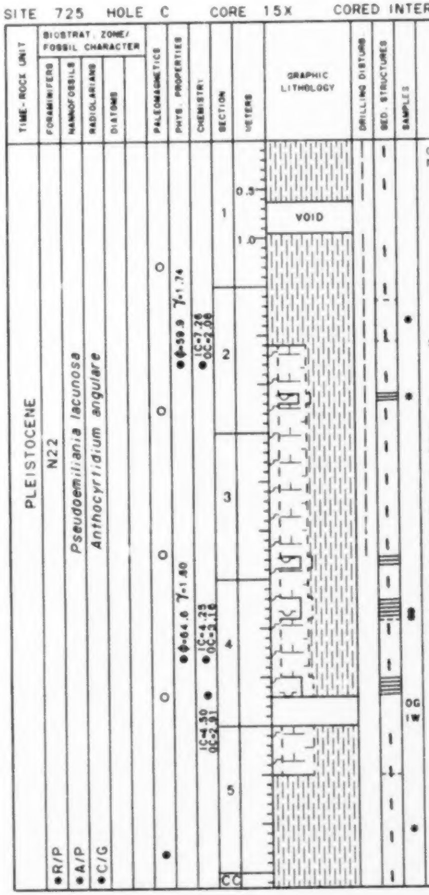
TIME-ROCK UNIT
BIOSTRAT. ZONE/ FOSSIL CHARACTER
FORAMINIFERS
NANNOFOSSILS
RADIOLARIANS
DIATOMS
PALEOMAGNETICS
PHYS. PROPERTIES
CHEMISTRY
SECTION
METERS
GRAPHIC LITHOLOGY
DRILLING DISTURB.
SED. STRUCTURES
SAMPLES
PLEISTOCENE
N22
Pseudoemiliania lacunosa
Anthocyrtidium angulare
●R/P
●A/P
●C/G
●ϕ=59.9 γ=1.74
●ϕ=64.6 γ=1.80
●IC=7.26 OC=2.08
●IC=4.25 OC=3.16
●IC=4.50 OC=2.81
1
2
3
4
5
CC
0.5
1.0
VOID
OG
IW

LITHOLOGIC DESCRIPTION

CALCITIC CLAYEY TO SANDY SILT, and interbedded CALCITIC MARLY NANNOFOSSIL OOZE and DIATOMACEOUS MUD

Section 1 to Section 3 slightly disturbed. Remainder is undisturbed.

Major lithologies:
a. CALCITIC CLAYEY TO SANDY SILT, olive (5Y 4/3) and olive gray (5Y 4/2) to dark greenish gray (10Y 4/2) and very dark gray (5Y 3/2). Minor bioturbation throughout. Section 1 to Section 2, 110 cm.
b. CALCITIC MARLY NANNOFOSSIL OOZE, olive (5Y 4/3), olive gray (5Y 4/2), and dark olive gray (5Y 3/2), and slightly bioturbated. Interbedded with zones of LAMINATED DIATOMACEOUS MUD, olive (5Y 5/3), and DIATOMACEOUS CALCAREOUS CLAYEY SILT, olive gray (5Y 4/2) to dark olive gray (5Y 3/2). Intervals of marly nannofossil ooze are 22-160 cm thick. Section 2, 110 cm, to CC.

SMEAR SLIDE SUMMARY (%):

	2, 35 D	2, 114 D	4, 34 M	4, 40 M	5, 100 D
TEXTURE:					
Sand	30	10	20	5	25
Silt	25	30	40	60	60
Clay	45	60	40	35	15
COMPOSITION:					
Access. minerals		1	2		5
Clay	40	25	25	30	10
Diatoms		10	15	55	
Dolomite					2
Feldspar	3				
Fish remains	Tr				
Foraminifers		1	3	2	
Inorganic calcite	25	25	25	3	48
Mica	Tr				
Nannofossils		35	10	5	5
Organic debris	5				
Phosphate	Tr				
Quartz	25	3	20	5	30
Radiolarians	Tr	Tr	Tr		
Sponge spicules	2		Tr		

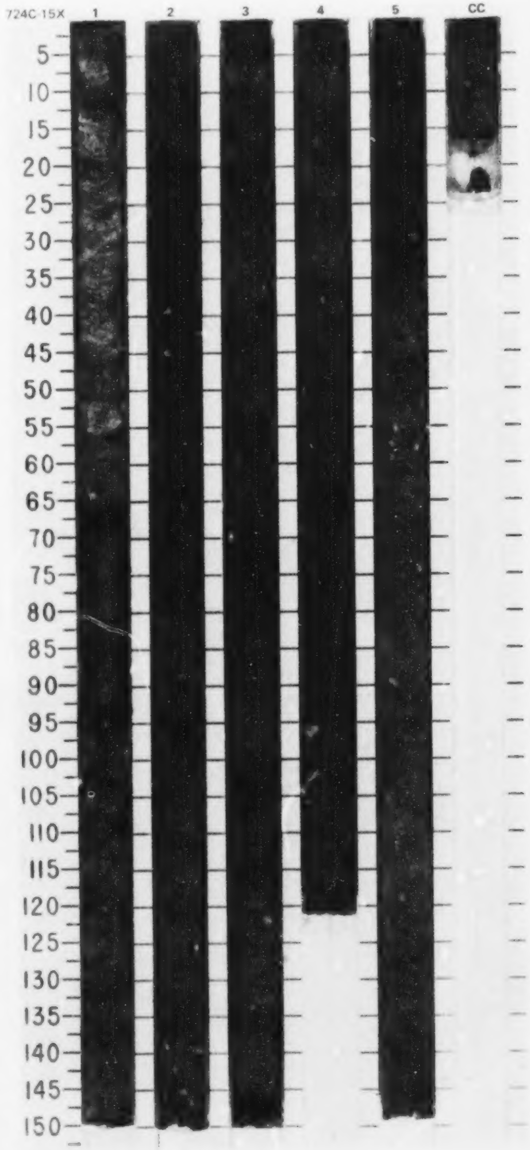
724C 15X
1
2
3
4
5
CC
5
10
15
20
25
30
35
40
45
50
55
60
65
70
75
80
85
90
95
100
105
110
115
120
125
130
135
140
145
150

SITE 725 HOLE C CORE 16X CORED INTERVAL 454.0-463.7 mbsl; 143.5-153.2 mbsf

TIME-ROCK UNIT	FORAMINIFERS	NANNOFOSSILS	RADIOLARIANS	DIATOMS	PALEOMAGNETICS	PHYS. PROPERTIES	CHEMISTRY	SECTION	METERS	DRILLING DISTURB.	SED. STRUCTURES	SAMPLES
PLEISTOCENE	N22 ●C/G	NN19 *Pseudoemiliania lacunosa* ●A	*Anthocyrtidium angulare* ●C/G		● ○	●ϕ-60.2 γ-1.87	●IC-6.63 OC-3.91	1 2 3 CC	0.5 1.0	○		● ● ●

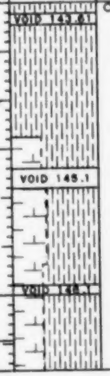
VOID 143.61
VOID 145.1
VOID 148.1

LITHOLOGIC DESCRIPTION

CALCITIC SAND-SILT-CLAY and CALCITIC MARLY NANNOFOSSIL OOZE

CC is slightly disturbed. Remainder is undisturbed.

Major lithologies:
a. CALCITIC SAND-SILT-CLAY, olive gray (5Y 4/2). Slightly bioturbated throughout. Section 1, 0-133 cm.
b. CALCITIC MARLY NANNOFOSSIL OOZE, olive (5Y 4/3), olive gray (5Y 4/2), and dark olive gray (5Y 3/2). Slightly bioturbated throughout, with common burrow mottling at Section 2, 122-144 cm.

SMEAR SLIDE SUMMARY (%):

	1, 132 D	2, 8 D	2, 50 D
TEXTURE:			
Sand	30	10	2
Silt	30	25	30
Clay	40	65	68
COMPOSITION:			
Access. minerals	1	1	
Clay	40	25	25
Diatoms	1	5	
Dolomite		Tr	Tr
Feldspar	2		
Foraminifers		4	2
Volcanic glass			Tr
Inorganic calcite	30	30	25
Nannofossils	Tr	30	43
Organic debris	5		
Quartz	20	5	5
Radiolarians		Tr	
Silicoflagellates		Tr	
Sponge spicules	1		

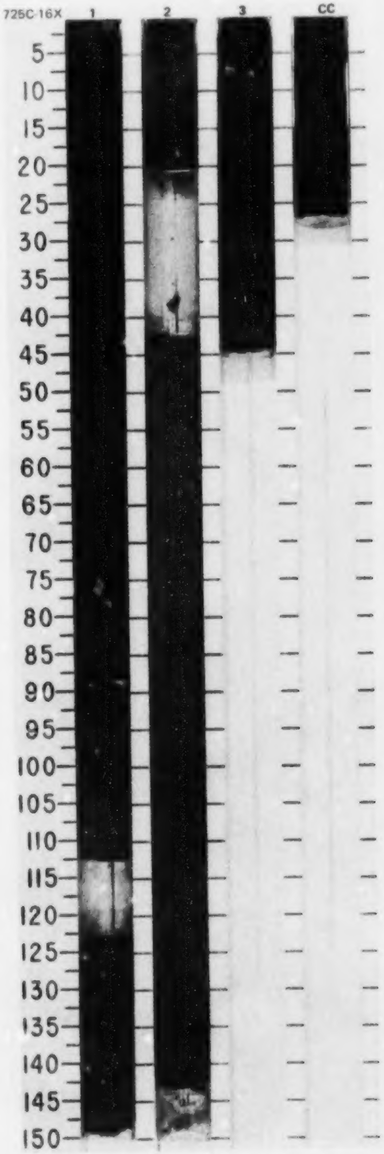
725C-16X
1
2
3
CC
5
10
15
20
25
30
35
40
45
50
55
60
65
70
75
80
85
90
95
100
105
110
115
120
125
130
135
140
145
150

SITE 725 HOLE C CORE 17X CORED INTERVAL 463.7-473.3 mbsl; 153.2-162.8 mbsf

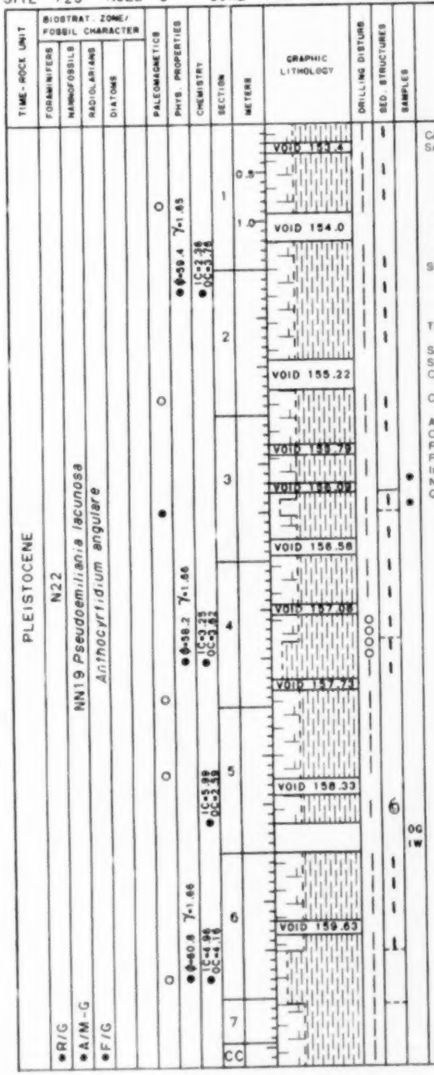
TIME-ROCK UNIT
BIOSTRAT. ZONE/FOSSIL CHARACTER
FORAMINIFERS
NANNOFOSSILS
RADIOLARIANS
DIATOMS
PALEOMAGNETICS
PHYS. PROPERTIES
CHEMISTRY
SECTION
METERS
GRAPHIC LITHOLOGY
DRILLING DISTURB.
SED. STRUCTURES
SAMPLES
PLEISTOCENE
N22
NN19 Pseudoemiliania lacunosa
Anthocyrtidium angulare
●R/G
●A/M-G
●F/G
●Φ=59.4 γ=1.85
●Φ=58.2 γ=1.86
●Φ=60.8 γ=1.86
●IC=2.38 OC=3.76
●IC=3.25 OC=3.62
●IC=5.88 OC=2.59
●IC=4.96 OC=4.16
1
2
3
4
5
6
7
CC
0.5
1.0
VOID 153.4
VOID 154.0
VOID 155.22
VOID 155.79
VOID 156.09
VOID 156.58
VOID 157.08
VOID 157.73
VOID 158.33
VOID 159.63
OG
IW

LITHOLOGIC DESCRIPTION

CALCITIC MARLY NANNOFOSSIL OOZE and NANNOFOSSIL-RICH CALCITIC SAND-SILT-CLAY

Section 4, 56-90 cm, is soupy. Remainder is slightly disturbed.

Major lithology: Interbedded CALCITIC MARLY NANNOFOSSIL OOZE, olive (5Y 4/3) to olive gray (5Y 4/2), and NANNOFOSSIL-RICH CALCITIC SAND-SILT-CLAY, olive gray (5Y 4/2) to dark olive gray (5Y 3/2). Sand-silt-clay intervals are 20-75 cm thick. Minor bioturbation throughout. Shell fragments and foraminifers are common on split surface of core.

SMEAR SLIDE SUMMARY (%):

	3, 65 D	3, 91 D
TEXTURE:		
Sand	15	35
Silt	40	30
Clay	45	35
COMPOSITION:		
Access. minerals	2	2
Clay	20	25
Feldspar	2	3
Foraminifers	5	2
Inorganic calcite	35	35
Nannofossils	25	8
Quartz	11	25

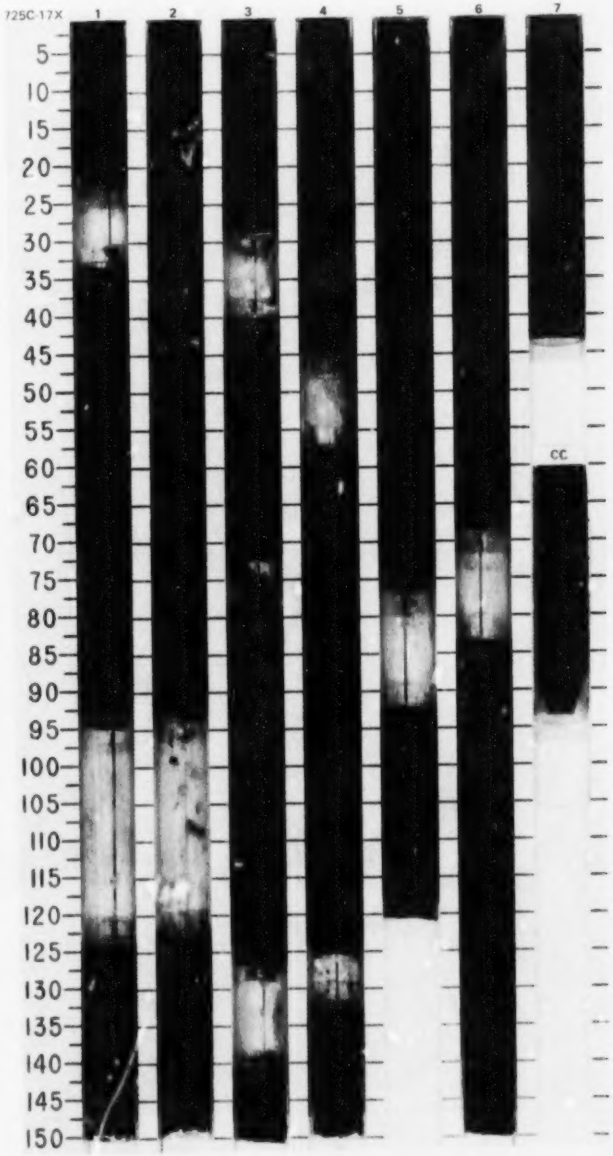
725C-17X
1
2
3
4
5
6
7
CC
5
10
15
20
25
30
35
40
45
50
55
60
65
70
75
80
85
90
95
100
105
110
115
120
125
130
135
140
145
150

SITE 726 HOLE A CORE 1H CORED INTERVAL 330.8-337.7 mbsl; 0.0-6.9 mbsf

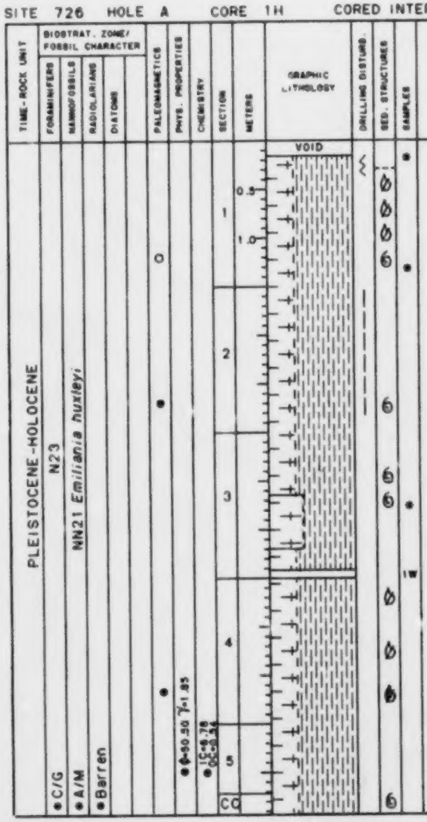
TIME-ROCK UNIT
BIOSTRAT. ZONE/ FOSSIL CHARACTER
FORAMINIFERS
NANNOFOSSILS
RADIOLARIANS
DIATOMS
PALEOMAGNETICS
PHYS. PROPERTIES
CHEMISTRY
SECTION
METERS
GRAPHIC LITHOLOGY
DRILLING DISTURB.
SED. STRUCTURES
SAMPLES
PLEISTOCENE-HOLOCENE
N23
NN21 Emiliania huxleyi
● C/G
● A/M
● Barren
● ϕ=50.50 γ=1.85
● IC=6.78 OC=0.54
1
2
3
4
5
CC
0.5
1.0
VOID
IW

LITHOLOGIC DESCRIPTION

FORAMINIFER CALCITIC CLAYEY SILT and MARLY FORAMINIFER

Major lithology: FORAMINIFER CALCITIC CLAYEY SILT with inorganic calcite and sand-sized foraminifers, olive grey (5Y 4/2) and olive (5Y 4/3) to dark olive grey (5Y 3/2) (surface layer), no clear bedding or bioturbation visible, scattered abundant shell fragments of bivalves, occasionally complete bivalve shells and scaphopods.

Minor lithology: Marly foraminifer nannofossil ooze with detrital calcite, olive gray (5Y 4/3), slightly higher content of foraminifers and nannofossils than the major lithology.

SMEAR SLIDE SUMMARY (%):

	1, 17 D	1, 141 D	3,75 D
TEXTURE:			
Sand		20	10
Silt	60	50	70
Clay	40	30	20
COMPOSITION:			
Access. minerals	1	2	5
Clay	30	30	10
Diatoms	5		
Dolomite		1	Tr
Foraminifers	20	20	30
Inorganic calcite	25	20	30
Mica	2	4	5
Nannofossils	7	5	10
Pellets		3	
Quartz	10	15	10
Radiolarians	Tr		

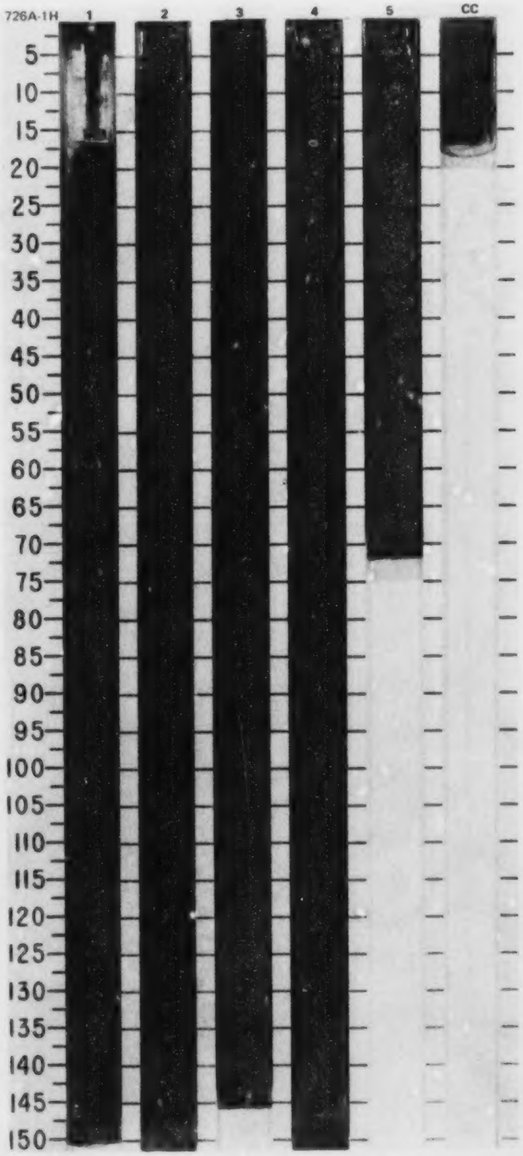
726A-1H
1
2
3
4
5
CC
5
10
15
20
25
30
35
40
45
50
55
60
65
70
75
80
85
90
95
100
105
110
115
120
125
130
135
140
145
150

SITE 726 HOLE A CORE 2H CORED INTERVAL 337.7-347.1 mbsl; 6.9-16.3 mbsf

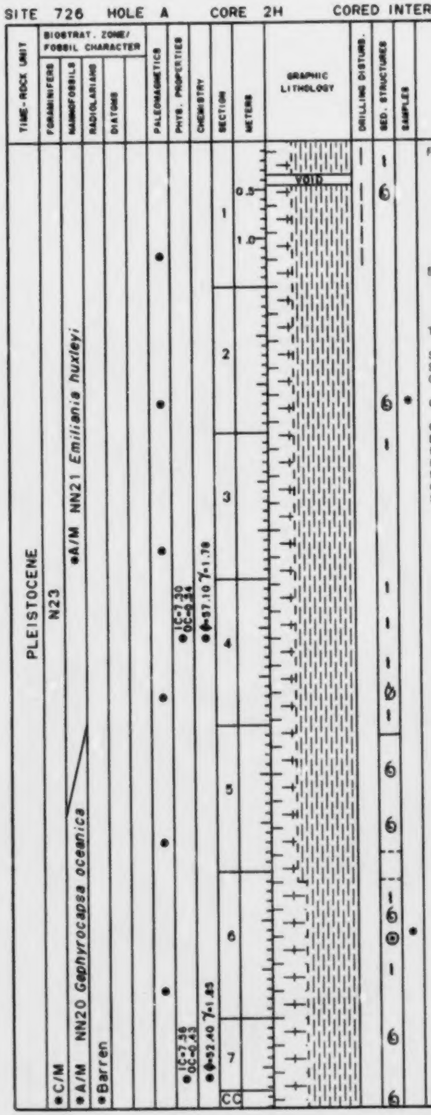
TIME-ROCK UNIT
BIOSTRAT. ZONE/ FOSSIL CHARACTER
FORAMINIFERS
NANNOFOSSILS
RADIOLARIANS
DIATOMS
PALEOMAGNETICS
PHYS. PROPERTIES
CHEMISTRY
SECTION
METERS
GRAPHIC LITHOLOGY
DRILLING DISTURB.
SED. STRUCTURES
SAMPLES
PLEISTOCENE
N23
●C/M
●A/M NN21 Emiliania huxleyi
●A/M NN20 Gephyrocapsa oceanica
●Barren
●IC=7.30 OC=0.34
●IC=7.58 OC=0.43
●Φ=57.10 γ=1.78
●Φ=52.40 γ=1.85
1
2
3
4
5
6
7
CC
0.5
1.0
VOID

LITHOLOGIC DESCRIPTION

FORAMINIFER NANNOFOSSIL CALCITIC CLAYEY SILT

Major lithology: FORAMINIFER NANNOFOSSIL CLAYEY SILT with 30% detrital calcite, olive gray (5Y 4/2) to olive (5Y 4/3), bioturbation visible locally, small-sized shell fragments scattered throughout core.

Minor lithology: Foraminifer marly nannofossil ooze with inorganic calcite, light olive (5Y 5/3), bioturbation clearly visible, 1-2 mm shell fragments, black crusty phosphorite concretions in Section 6.

SMEAR SLIDE SUMMARY (%):

	2, 118 D	6, 62 D
TEXTURE:		
Sand		10
Silt	55	40
Clay	45	50
COMPOSITION:		
Clay	30	25
Dolomite	Tr	Tr
Foraminifers	10	15
Inorganic calcite	30	20
Nannofossils	15	35
Quartz	15	5
Sponge spicules		Tr

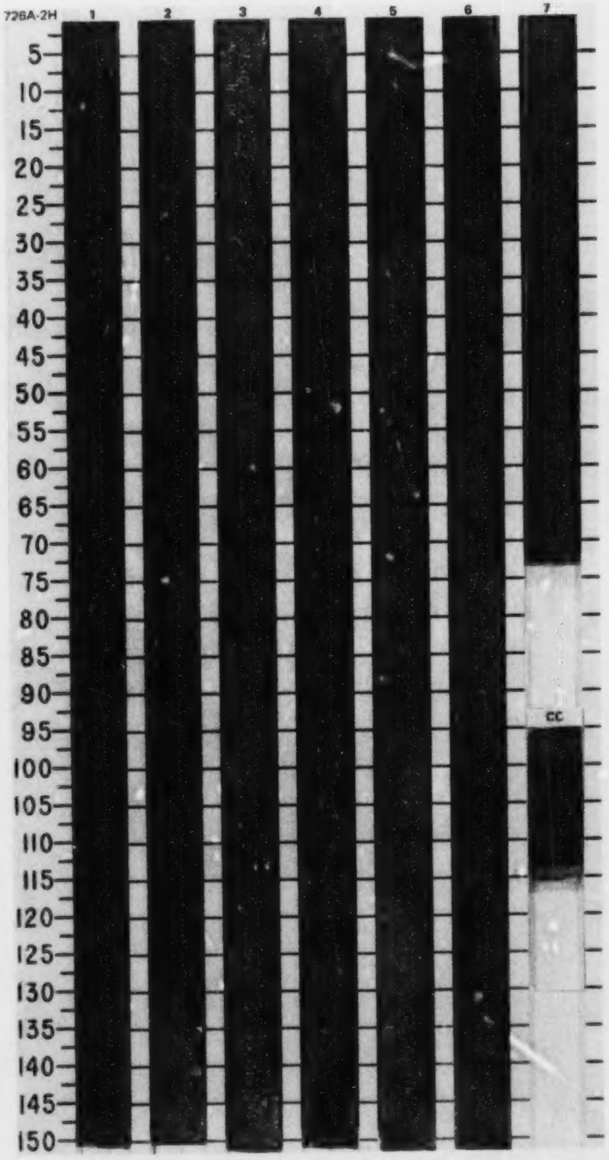
726A-2H
1
2
3
4
5
6
7
CC
5
10
15
20
25
30
35
40
45
50
55
60
65
70
75
80
85
90
95
100
105
110
115
120
125
130
135
140
145
150

SITE 726 HOLE A CORE 3H CORED INTERVAL 347.1-356.6 mbsl; 16.3-25.8 mbsf

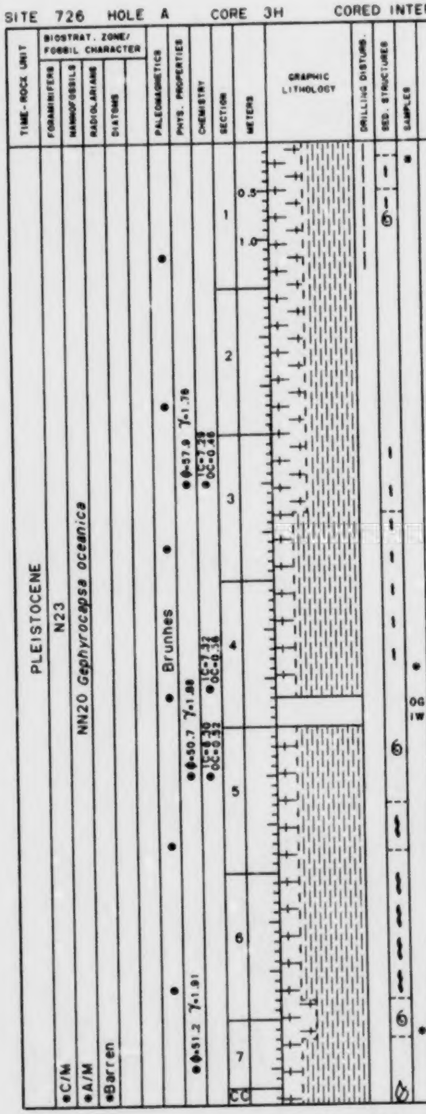
TIME-ROCK UNIT
BIOSTRAT. ZONE/ FOSSIL CHARACTER
FORAMINIFERS
NANNOFOSSILS
RADIOLARIANS
DIATOMS
PALEOMAGNETICS
PHYS. PROPERTIES
CHEMISTRY
SECTION
METERS
GRAPHIC LITHOLOGY
DRILLING DISTURB.
SED. STRUCTURES
SAMPLES
PLEISTOCENE
N23
NN20 Gephyrocapsa oceanica
●C/M
●A/M
●Barren
Brunhes
●φ=57.9 γ=1.76
●φ=50.7 γ=1.88
●φ=51.2 γ=1.91
●IC=7.28 OC=0.46
●IC=7.32 OC=0.36
●IC=8.30 OC=0.32
1
2
3
4
5
6
7
CC
0.5
1.0
OG
IW

LITHOLOGIC DESCRIPTION

FORAMINIFER MARLY NANNOFOSSIL OOZE to NANNOFOSSIL CALCITIC CLAYEY SILT

Major lithology: FORAMINIFER MARLY NANNOFOSSIL OOZE to NANNOFOSSIL CALCITIC CLAYEY SILT, both with 10-40% inorganic calcite, olive gray (5Y 4/2) to olive (5Y 4/3, 4/4), bioturbation ranges from indistinct to clearly visible, shell fragments are scattered throughout the core, occurrence of bivalves and 0.5 cm thick black phosphorite nodules.

SMEAR SLIDE SUMMARY (%):

	1, 20 D	4, 90 D	7, 13 D
TEXTURE:			
Sand	20	10	10
Silt	40	60	40
Clay	40	30	50
COMPOSITION:			
Access. minerals	1	Tr	2
Clay	20	25	25
Dolomite	2	Tr	5
Feldspar		Tr	
Foraminifers	15	10	25
Inorganic calcite	35	40	10
Nannofossils	20	15	20
Quartz	7	10	10
Sponge spicules			3

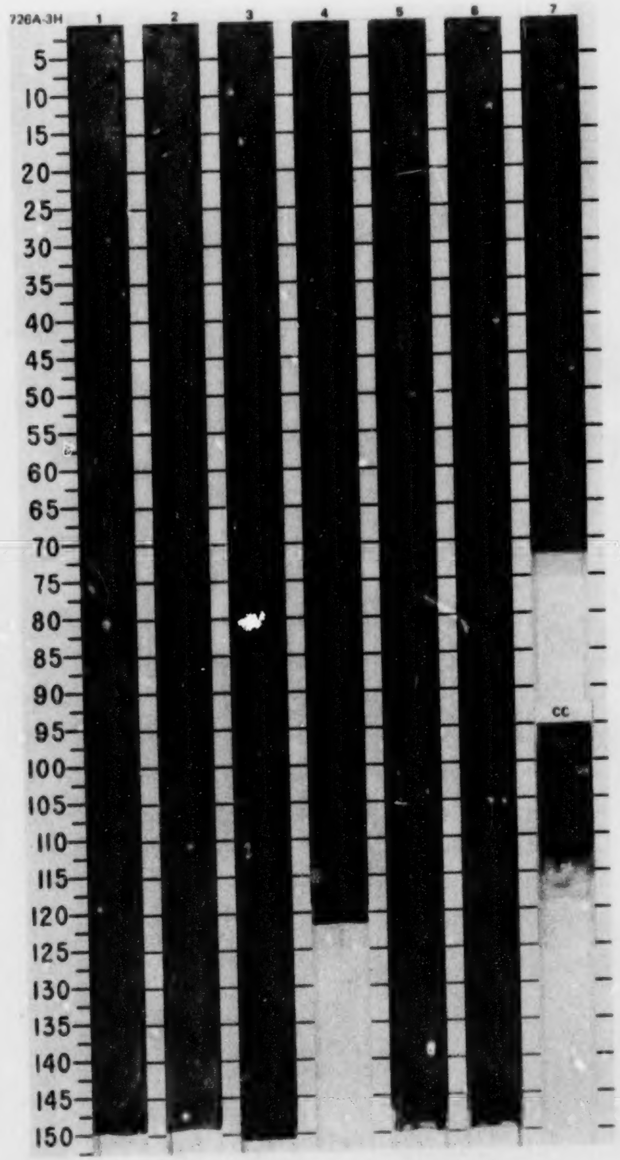
726A-3H
1
2
3
4
5
6
7
CC
5
10
15
20
25
30
35
40
45
50
55
60
65
70
75
80
85
90
95
100
105
110
115
120
125
130
135
140
145
150

SITE 726 HOLE A CORE 4H CORED INTERVAL 356.6-366.1 mbsl; 25.8-35.3 mbsf

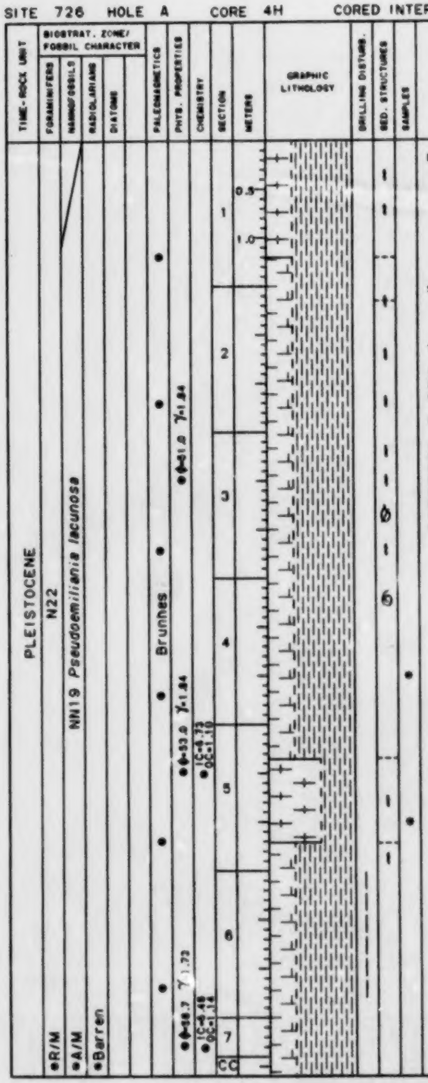
TIME-ROCK UNIT
BIOSTRAT. ZONE/ FOSSIL CHARACTER
FORAMINIFERS
NANNOFOSSILS
RADIOLARIANS
DIATOMS
PALEOMAGNETICS
PHYS. PROPERTIES
CHEMISTRY
SECTION
METERS
GRAPHIC LITHOLOGY
DRILLING DISTURB.
SED. STRUCTURES
SAMPLES
PLEISTOCENE
N22
NN19 Pseudoemiliania lacunosa
●R/M
●A/M
●Barren
Brunhes
●φ-51.0 γ-1.84
●φ-53.0 γ-1.84
●φ-58.7 γ-1.73
●IC-6.73 OC-1.10
●IC-6.48 OC-1.14
1
2
3
4
5
6
7
CC
0.5
1.0

LITHOLOGIC DESCRIPTION

FORAMINIFER-BEARING MARLY CALCITIC NANNOFOSSIL OOZE

Major lithology: FORAMINIFER-BEARING MARLY CALCITIC NANNOFOSSIL OOZE, with 15-35% inorganic calcite and 0-10% foraminifers, olive gray (5Y 4/2) to olive (5Y 4/3), bioturbation mottling is visible in two-thirds of the core, shell fragments occur in localized regions, 0.5 cm thick black phosphorite concretions occur at the top of Section 5.

Minor lithology: Foraminifer-bearing nannofossil calcitic clayey silt, olive gray (5Y 4/2) to olive (5Y 4/2, 4/3), bioturbated, foraminifers visible on core surface.

SMEAR SLIDE SUMMARY (%):

	4, 100 D	5, 100 D
TEXTURE:		
Sand		10
Silt	50	30
Clay	50	60
COMPOSITION:		
Access. minerals	2	
Clay	25	23
Dolomite	3	Tr
Foraminifers		10
Inorganic calcite	35	15
Mica		2
Nannofossils	30	45
Quartz	5	5

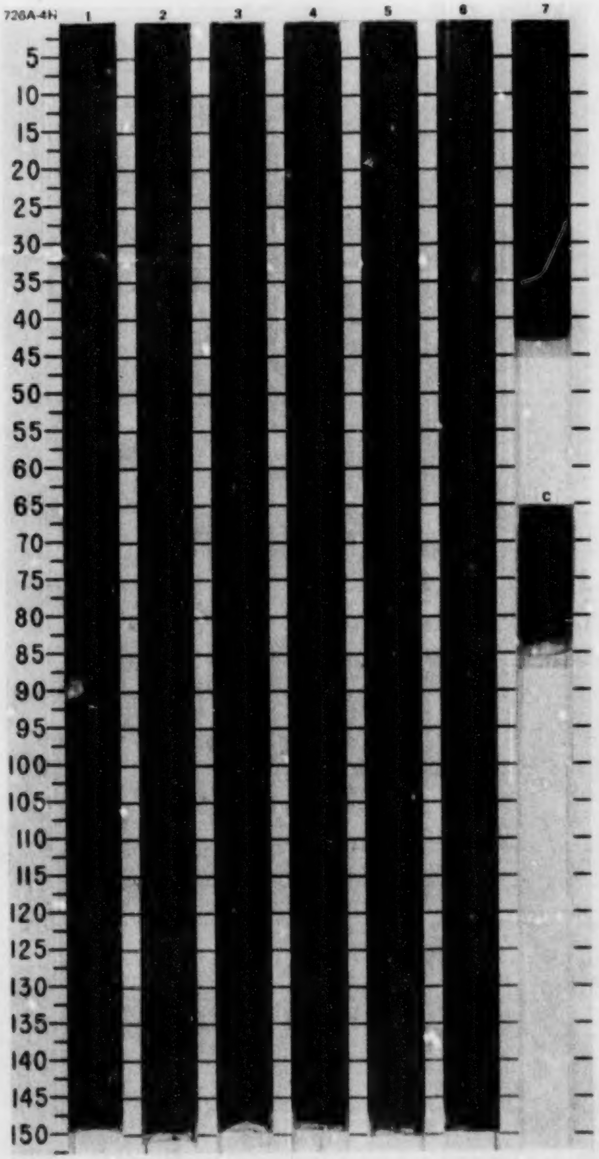
726A-4H
1
2
3
4
5
6
7
C
5
10
15
20
25
30
35
40
45
50
55
60
65
70
75
80
85
90
95
100
105
110
115
120
125
130
135
140
145
150

SITE 726 HOLE A CORE 5H CORED INTERVAL 366.1-375.5 mbsl; 35.3-44.7 mbsf

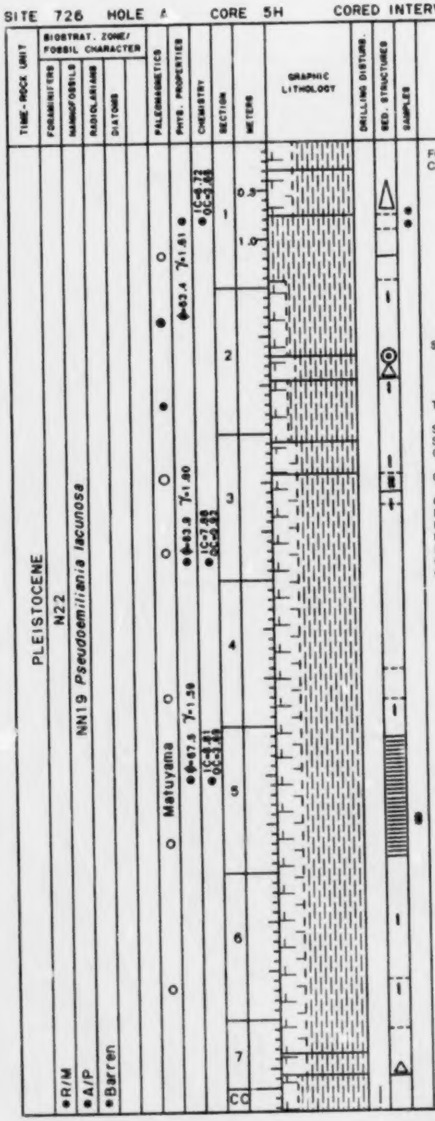
TIME-ROCK UNIT
BIOSTRAT. ZONE/ FOSSIL CHARACTER
FORAMINIFERS
NANNOFOSSILS
RADIOLARIANS
DIATOMS
PALEOMAGNETICS
PHYS. PROPERTIES
CHEMISTRY
SECTION
METERS
GRAPHIC LITHOLOGY
DRILLING DISTURB.
SED. STRUCTURES
SAMPLES
PLEISTOCENE
N22
NN19 Pseudoemiliania lacunosa
●R/M
●A/P
●Barren
Matuyama
● γ=1.81 ● φ=63.4
● φ=63.9 γ=1.90
● φ=67.5 γ=1.59
● IC=6.72 OC=3.65
● IC=7.88 OC=0.53
● IC=8.81 OC=1.69
1
2
3
4
5
6
7
CC
0.5
1.0

LITHOLOGIC DESCRIPTION

FORAMINIFER-BEARING CALCITIC MARLY NANNOFOSSIL OOZE to SILTY CALCAREOUS CLAY

Major lithology:
- a. FORAMINIFER-BEARING CALCITIC MARLY NANNOFOSSIL OOZE, with 35% inorganic calcite, olive (5Y 4/3, 4/4) to dark olive (5Y 4/2), bioturbation in Sections 2-7; two cm-scale laminations of dark olive gray (5Y 3/2) and olive gray (5Y 4/2) layers with 3.7% organic carbon.
- b. SILTY CALCAREOUS CLAY with 35% inorganic calcite, very dark gray (5Y 3/1) to dark olive gray (5Y 3/2), no bioturbation, organic carbon reaches 3.5%.

Minor lithology: Muddy foraminifer ooze with 30% detrital calcite, olive gray (5Y 4/3, 4/4), sand-sized foraminifers, layers show slight upward fining of grain size and bioturbation, phosphorite concretion in Section 2.

SMEAR SLIDE SUMMARY (%):

	1, 73 D	1, 88 D	5, 34 M	5, 95 M
TEXTURE:				
Sand	20			
Silt	50	40	30	20
Clay	30	60	70	80
COMPOSITION:				
Clay	25	45	47	50
Dolomite		5		4
Foraminifers	25		5	5
Inorganic calcite	30	35	15	10
Nannofossils	5	5	25	25
Organic debris		5	3	3
Quartz	15	5	5	3

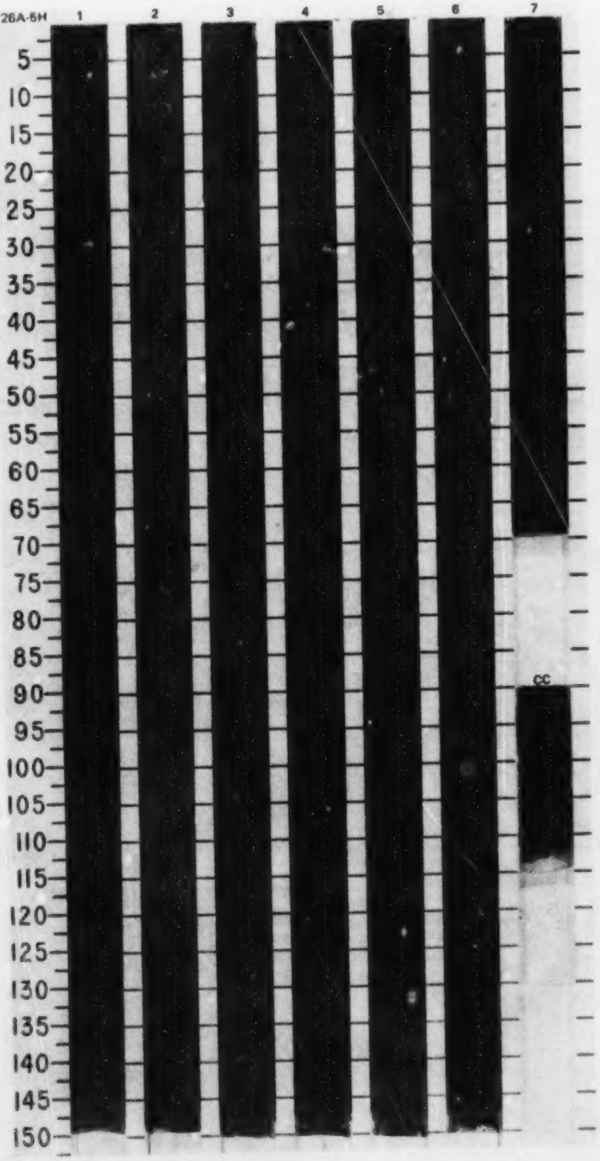
726A-5H
1
2
3
4
5
6
7
CC
5
10
15
20
25
30
35
40
45
50
55
60
65
70
75
80
85
90
95
100
105
110
115
120
125
130
135
140
145
150

SITE 726 HOLE A CORE 6H CORED INTERVAL 375.5-384.9 mbsl; 44.7-54.1 mbsf

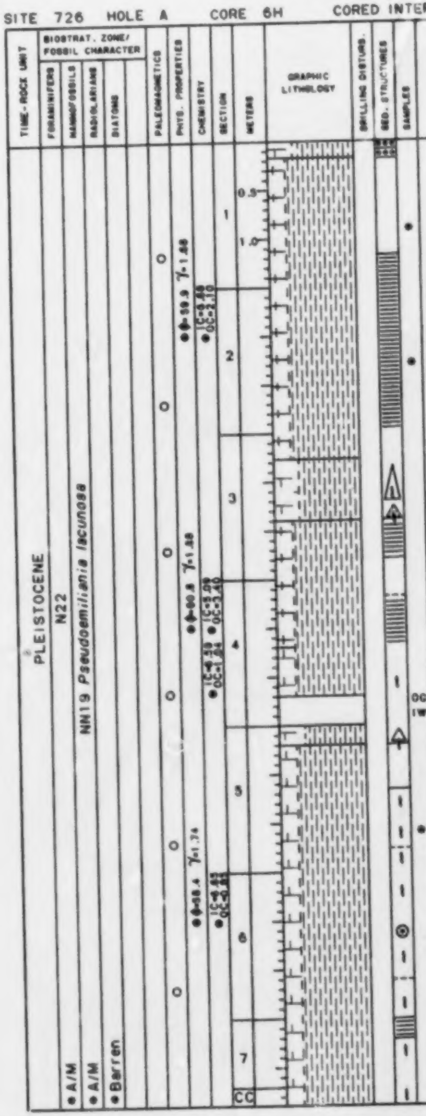
TIME-ROCK UNIT
BIOSTRAT. ZONE/ FOSSIL CHARACTER
FORAMINIFERS
NANNOFOSSILS
RADIOLARIANS
DIATOMS
PALEOMAGNETICS
PHYS. PROPERTIES
CHEMISTRY
SECTION
METERS
GRAPHIC LITHOLOGY
DRILLING DISTURB.
SED. STRUCTURES
SAMPLES
PLEISTOCENE
N22
NN19 Pseudoemiliania lacunosa
● A/M
● A/M
● Barren
● φ=59.9 γ=1.88
● IC=6.68 OC=2.10
● φ=60.8 γ=1.88
● IC=3.09 OC=3.40
● IC=4.59 OC=1.84
● φ=58.4 γ=1.74
● IC=4.85 OC=0.88
0.5
1.0
1
2
3
4
5
6
7
CC
OG
IW

LITHOLOGIC DESCRIPTION

CALCITIC SILTY CLAY with NANNOFOSSILS and FORAMINIFERS

Major lithology: CALCITIC SILTY CLAY with various amounts of NANNOFOSSILS and FORAMINIFERS, olive (5Y 4/3, 4/4) to dark olive gray (5Y 3/1). Sections 1-4 dominantly display cm-scale light-dark laminations with 2-3.5% organic carbon; Sections 4-6 are bioturbated and have organic carbon contents of 1%; and Section 6 has black lithified phosphorite concretions.

Minor lithology: Muddy foraminifer ooze with inorganic calcite, olive (5Y 4/3) to dark greenish gray (10Y 4/2), in 1 to 30 cm thick layers, slightly graded, thicker layers display bioturbation.

SMEAR SLIDE SUMMARY (%):

	1, 88 D	2, 77 D	5, 109 D
TEXTURE:			
Sand	2	2	
Silt	20	38	40
Clay	78	60	60
COMPOSITION:			
Access. minerals	Tr	2	
Clay	64	45	35
Dolomite	1	2	3
Foraminifers	10	15	
Inorganic calcite	5	15	35
Mica	Tr	1	2
Nannofossils	10	10	15
Organic debris	5	5	
Quartz	5	3	10
Sponge spicules	Tr	2	

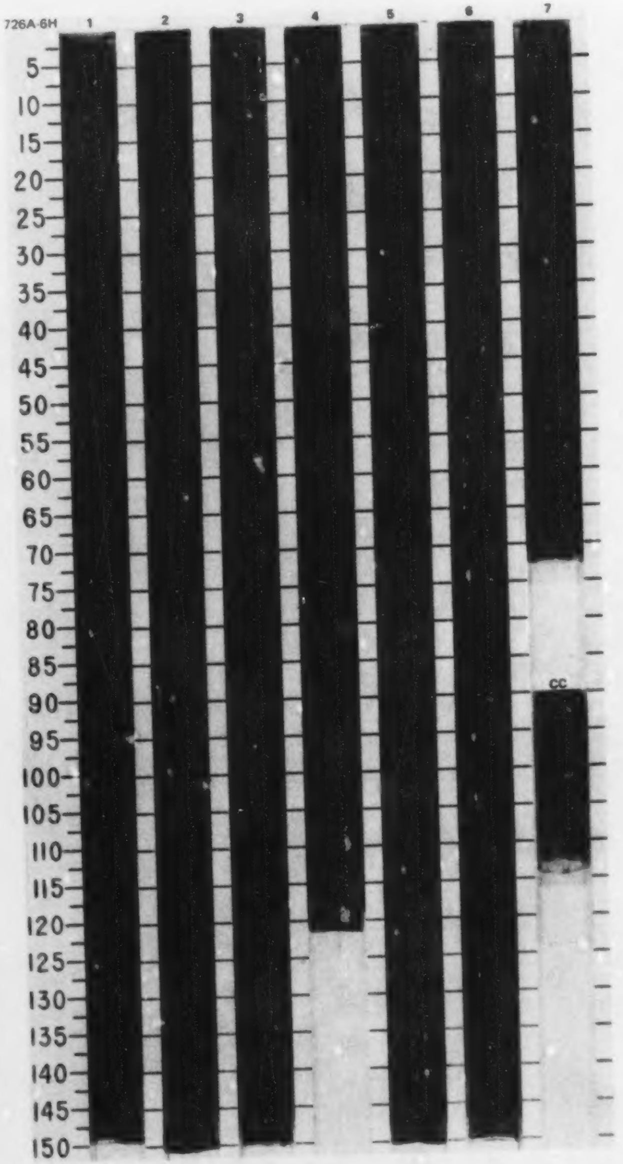
726A-6H
1
2
3
4
5
6
7
CC
5
10
15
20
25
30
35
40
45
50
55
60
65
70
75
80
85
90
95
100
105
110
115
120
125
130
135
140
145
150

SITE 726 HOLE A CORE 7X CORED INTERVAL 384.9-394.4 mbsl; 54.1-63.6 mbsf

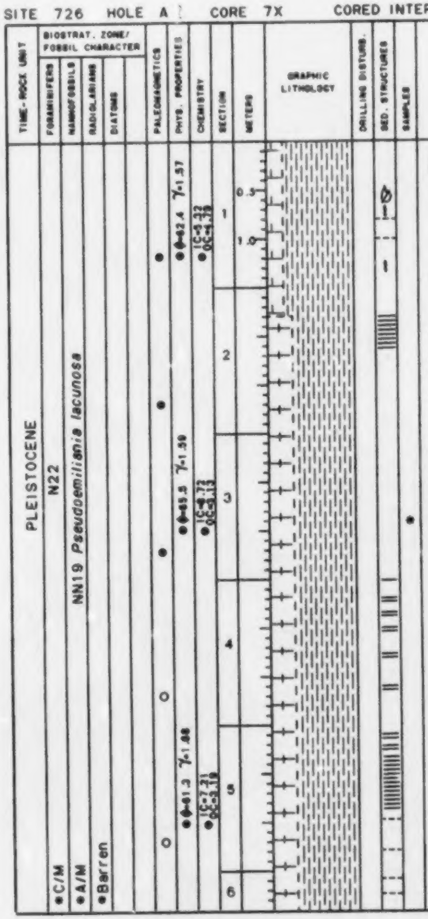
TIME-ROCK UNIT
BIOSTRAT. ZONE/ FOSSIL CHARACTER
FORAMINIFERS
NANNOFOSSILS
RADIOLARIANS
DIATOMS
PALEOMAGNETICS
PHYS. PROPERTIES
CHEMISTRY
SECTION
METERS
GRAPHIC LITHOLOGY
DRILLING DISTURB.
SED. STRUCTURES
SAMPLES
PLEISTOCENE
N22
NN19 Pseudoemiliania lacunosa
●C/M
●A/M
●Barren
●φ=62.4 γ=1.57
●φ=65.5 γ=1.59
●φ=61.3 γ=1.88
●IC=3.32 OC=4.39
●IC=4.72 OC=3.13
●IC=7.21 OC=3.19
1
2
3
4
5
6
0.5
1.0

LITHOLOGIC DESCRIPTION

FORAMINIFER MARLY NANNOFOSSIL OOZE and NANNOFOSSIL CALCITIC SILTY CLAY

Major lithology: FORAMINIFER MARLY NANNOFOSSIL OOZE, and NANNOFOSSIL CALCITIC SILTY CLAY, with variable amounts of inorganic calcite, both dark olive gray (5Y 3/2) to very dark gray (5Y 3/1). Section 1 is predominantly bioturbated, and Sections 2-6 have no macrobioturbation and display sets of 1-5 cm thick light-dark laminations. Organic carbon content varies from 3-4.8%.

SMEAR SLIDE SUMMARY (%):

	3, 90 D
TEXTURE:	
Silt	25
Clay	75
COMPOSITION:	
Access. minerals	Tr
Clay	44
Dolomite	2
Foraminifers	10
Inorganic calcite	5
Mica	Tr
Nannofossils	30
Organic debris	5
Quartz	2
Sponge spicules	2

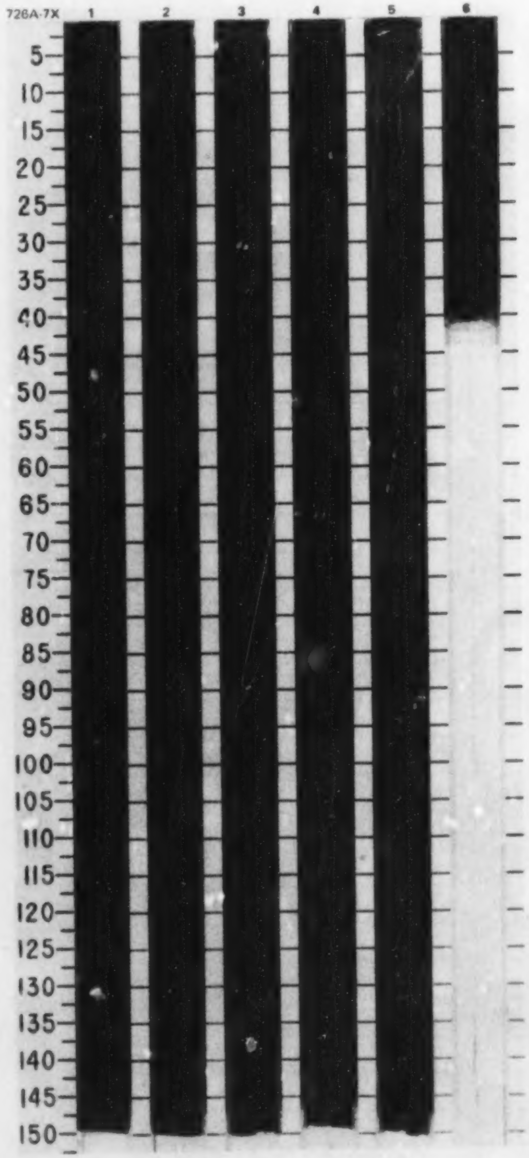
726A-7X
1
2
3
4
5
6
5
10
15
20
25
30
35
40
45
50
55
60
65
70
75
80
85
90
95
100
105
110
115
120
125
130
135
140
145
150

SITE 726 HOLE A CORE 8X CORED INTERVAL 394.4-404.0 mbsl; 63.6-73.2 mbsf

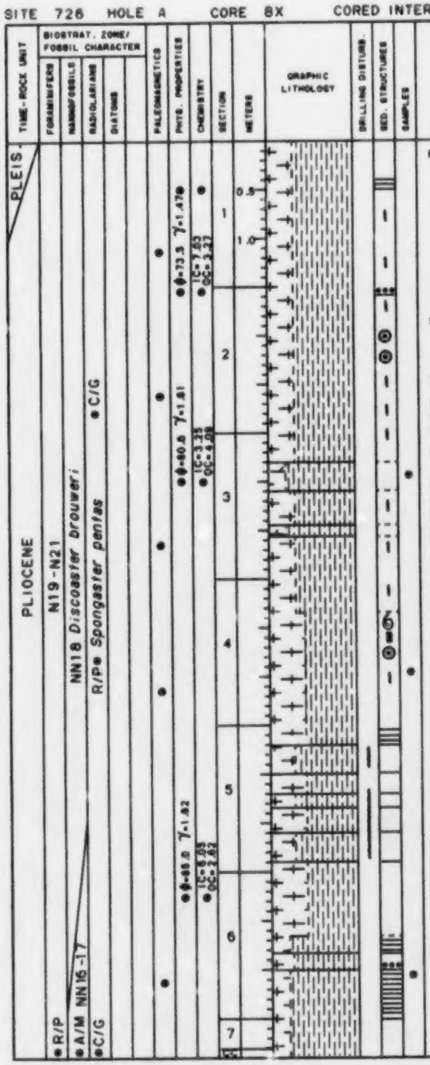
TIME-ROCK UNIT
BIOSTRAT. ZONE/FOSSIL CHARACTER
FORAMINIFERS
NANNOFOSSILS
RADIOLARIANS
DIATOMS
PALEOMAGNETICS
PHYS. PROPERTIES
CHEMISTRY
SECTION
METERS
GRAPHIC LITHOLOGY
DRILLING DISTURB.
SED. STRUCTURES
SAMPLES
PLEIS.
PLIOCENE
N19-N21
NN18 Discoaster brouweri
●C/G
R/P● Spongaster pentas
●R/P
●A/M NN16-17
●C/G
●φ=73.5 γ=1.47●
●φ=60.6 γ=1.81
●φ=65.8 γ=1.82
●
●IC=7.63 OC=3.27
●IC=3.35 OC=4.09
●IC=6.05 OC=2.62
0.5
1.0
1
2
3
4
5
6
7

LITHOLOGIC DESCRIPTION

MARLY FORAMINIFER NANNOFOSSIL OOZE and CALCITIC SILTY CLAY

Major lithologies:
- a. MARLY FORAMINIFER NANNOFOSSIL OOZE with 15-25% inorganic calcite, olive (5Y 4/3), bioturbated. Phosphorite concretions in Sections 2 and 4, and fish bones in Section 4.
- b. CALCITIC SILTY CLAY, olive (5Y 4/3, 4/4), cm-scale laminations, slightly diatomaceous.

Minor lithology:
- a. Muddy foraminiferal nannofossil ooze, with sand-sized foraminifers, olive (5Y 4/3).
- b. Dolomitic silty clay, very dark gray (5Y 3/1); organic carbon content is 4%.

SMEAR SLIDE SUMMARY (%):

	3, 45 D	4, 97 M	6, 106 M
TEXTURE:			
Sand		10	
Silt	30	60	37
Clay	70	30	63
COMPOSITION:			
Access. minerals	3	2	Tr
Clay	61	15	48
Diatoms	2		5
Dolomite	15	5	2
Foraminifers		35	10
Inorganic calcite	10	25	15
Mica	Tr		
Nannofossils		10	10
Organic debris	5	3	5
Quartz	2	5	3
Radiolarians	Tr		Tr
Silicoflagellates	Tr		Tr
Sponge spicules	2		2

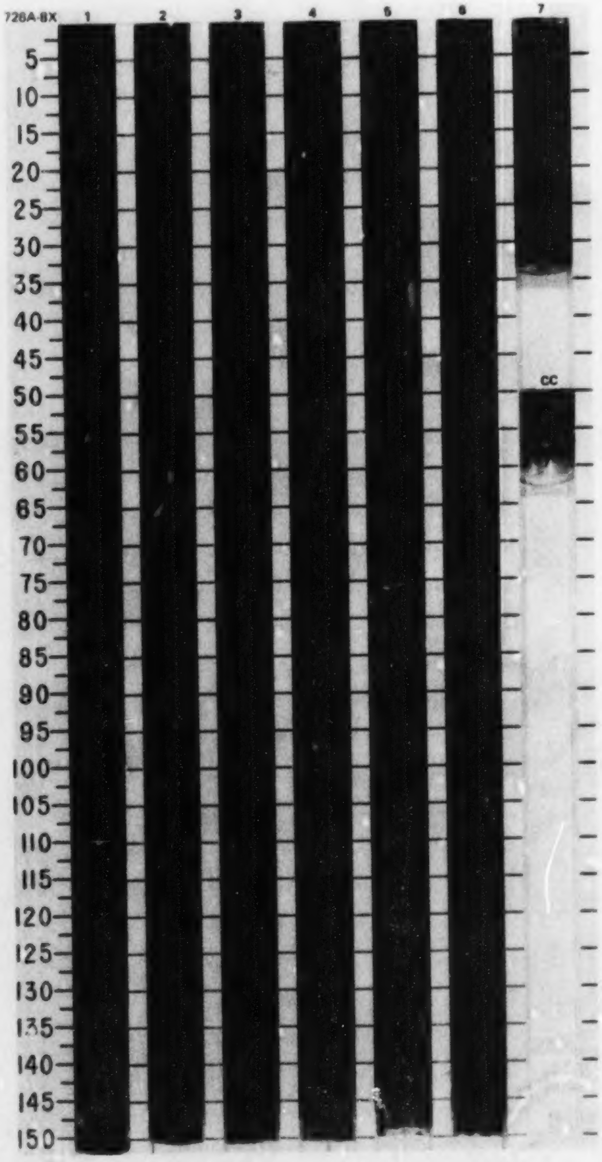
726A-8X
1
2
3
4
5
6
7
CC
5
10
15
20
25
30
35
40
45
50
55
60
65
70
75
80
85
90
95
100
105
110
115
120
125
130
135
140
145
150

SITE 726 HOLE A CORE 9X CORED INTERVAL 404.0-413.6 mbsl; 73.2-82.8 mbsf

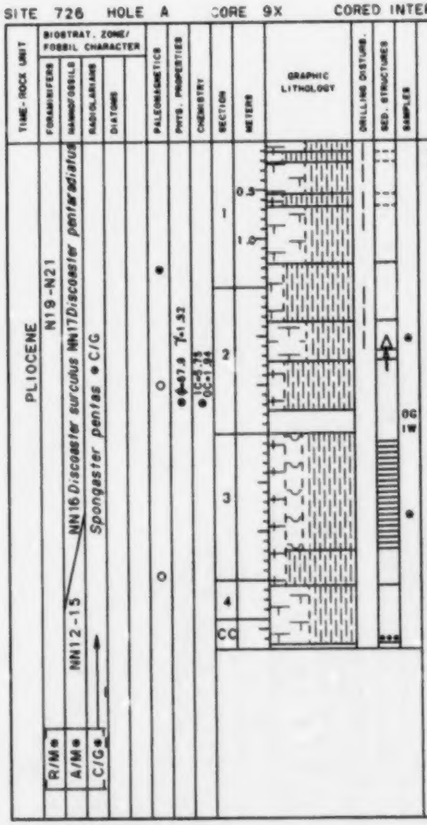
TIME-ROCK UNIT
BIOSTRAT. ZONE/ FOSSIL CHARACTER
FORAMINIFERS
NANNOFOSSILS
RADIOLARIANS
DIATOMS
PALEOMAGNETICS
PHYS. PROPERTIES
CHEMISTRY
SECTION
METERS
GRAPHIC LITHOLOGY
DRILLING DISTURB.
SED. STRUCTURES
SAMPLES
PLIOCENE
N19-N21
NN16 Discoaster surculus NN17 Discoaster pentaradiatus
NN12-15
Spongaster pentas ● C/G
R/M●
A/M●
C/G●
Φ-67.8
γ-1.92
IC-5.75
OC-1.84
1
2
3
4
CC
0.5
1.0
OG
IW

LITHOLOGIC DESCRIPTION

CALCITIC SILTY CLAY, DIATOMACEOUS CALCITIC SILTY CLAY, and FORAMINIFERAL SILTY SAND to SANDY SILT

Major lithologies:

a. CALCITIC SILTY CLAY, olive (5Y 4/3) to dark olive gray (5Y 4/2), slightly mottled.

b. DIATOMACEOUS CALCITIC SILTY CLAY, olive (5Y 4/3) to olive gray (5Y 4/2), faint laminations approximately 2.5 cm thick.

c. FORAMINIFERAL SILTY SAND to SANDY SILT, dark olive gray (5Y 3/2) to very dark gray (5Y 3/1). Ungraded to slightly graded layers, bioturbation recognizable in some parts, benthic foraminifers are coated by black phosphorite, organic carbon content is 2%.

SMEAR SLIDE SUMMARY (%):

	2, 52 M	3, 83 D
TEXTURE:		
Sand	50	
Silt	40	40
Clay	10	60
COMPOSITION:		
Phosphorite	20	
Clay	7	20
Diatoms		25
Dolomite	3	5
Foraminifers	40	5
Inorganic calcite	10	25
Mica	5	
Nannofossils	3	5
Pellets	7	
Quartz	5	15
Radiolarians		Tr

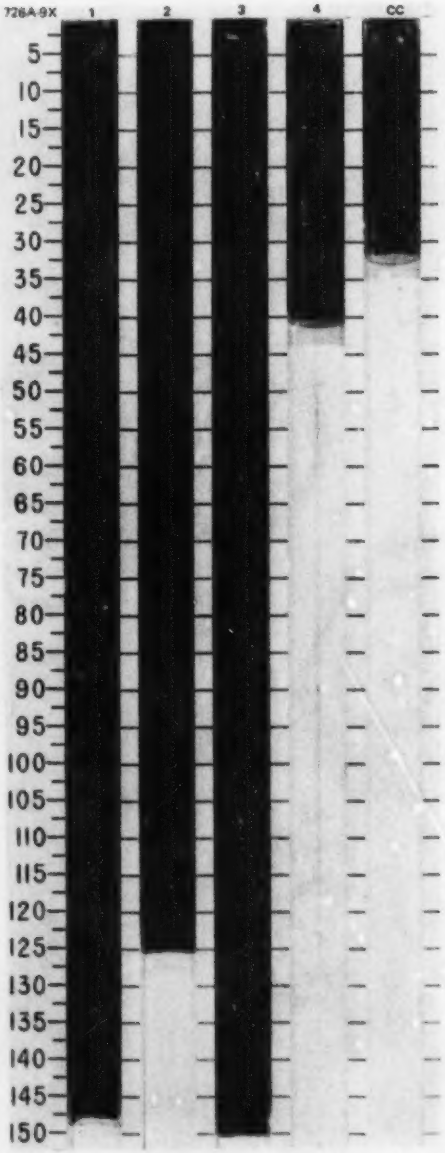
726A-9X
1
2
3
4
CC
5
10
15
20
25
30
35
40
45
50
55
60
65
70
75
80
85
90
95
100
105
110
115
120
125
130
135
140
145
150

SITE 726 HOLE A CORE 10X CORED INTERVAL 413.6-423.2 mbsl; 82.8-92.4 mbsf

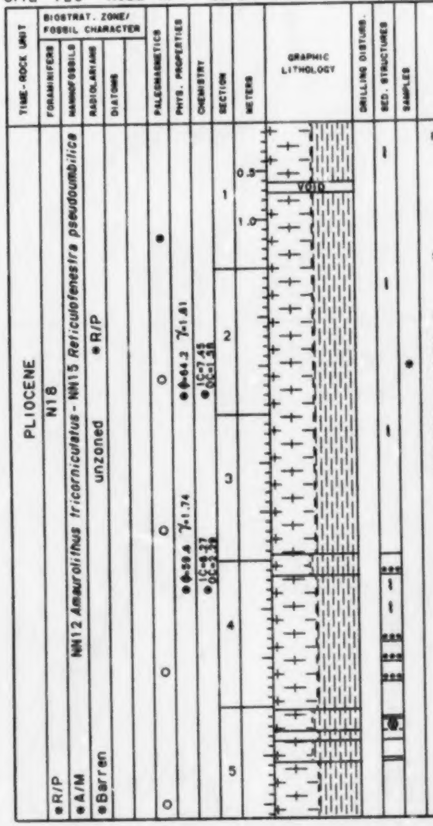
TIME-ROCK UNIT
BIOSTRAT. ZONE/ FOSSIL CHARACTER
FORAMINIFERS
NANNOFOSSILS
RADIOLARIANS
DIATOMS
PALEOMAGNETICS
PHYS. PROPERTIES
CHEMISTRY
SECTION
METERS
GRAPHIC LITHOLOGY
DRILLING DISTURB.
SED. STRUCTURES
SAMPLES
PLIOCENE
N18
NN12 Amaurolithus tricorniculatus - NN15 Reticulofenestra pseudoumbilica
unzoned
● R/P
● R/P
● A/M
● Barren
● Φ=64.2 γ=1.81
● Φ=59.4 γ=1.74
● IC=7.45 OC=1.58
● IC=8.27 OC=2.32
0.5
1.0
1
2
3
4
5
VOID

LITHOLOGIC DESCRIPTION

FORAMINIFERAL MARLY NANNOFOSSIL OOZE

Major lithology: FORAMINIFERAL MARLY NANNOFOSSIL OOZE with 15% inorganic calcite, olive (5Y 4/3), faint bioturbation and laminations visible, organic carbon content is 1.6-2.3%.

Minor lithology: Sandy to silty foraminiferal marly nannofossil ooze in layers of variable thickness, gradational base, layers contain 0.5 cm thick black phosphorite concretions and phosphorite coatings on foraminiferal tests.

SMEAR SLIDE SUMMARY (%):

	2, 100 D
TEXTURE:	
Sand	10
Silt	30
Clay	60
COMPOSITION:	
Access. minerals	Tr
Clay	20
Dolomite	5
Foraminifers	20
Inorganic calcite	15
Nannofossils	30
Organic debris	5
Quartz	5

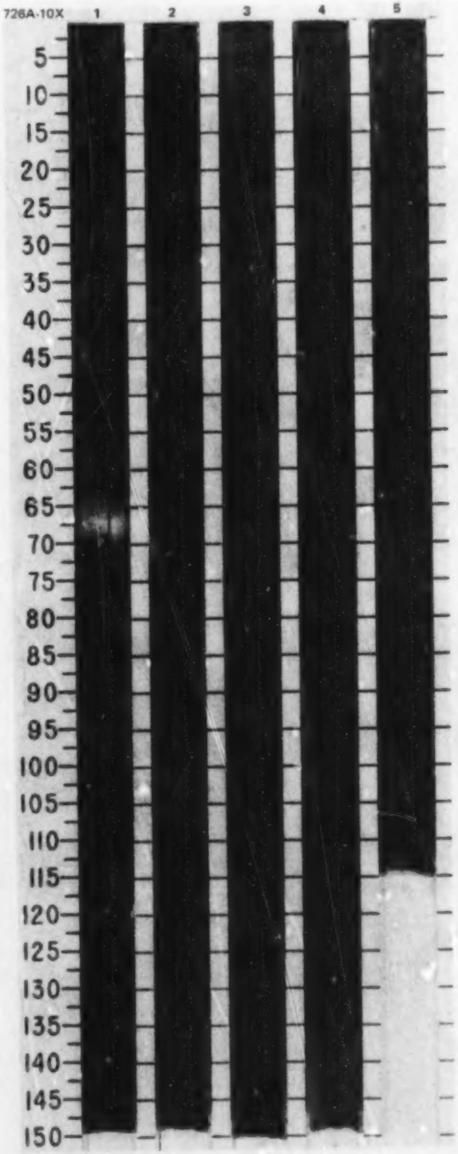
726A-10X
1
2
3
4
5
5
10
15
20
25
30
35
40
45
50
55
60
65
70
75
80
85
90
95
100
105
110
115
120
125
130
135
140
145
150

SITE 726 HOLE A CORE 11X CORED INTERVAL 423.2-432.9 mbsl; 92.4-102.1 mbsf

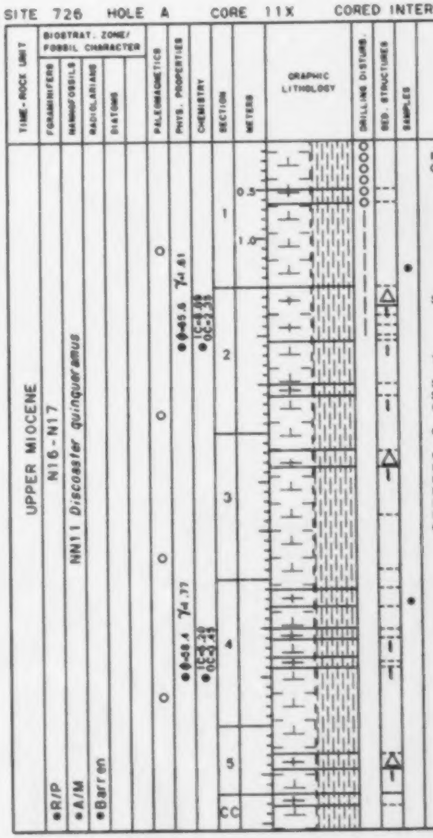
TIME-ROCK UNIT
BIOSTRAT. ZONE/ FOSSIL CHARACTER
FORAMINIFERS
NANNOFOSSILS
RADIOLARIANS
DIATOMS
PALEOMAGNETICS
PHYS. PROPERTIES
CHEMISTRY
SECTION
METERS
GRAPHIC LITHOLOGY
DRILLING DISTURB.
SED. STRUCTURES
SAMPLES
UPPER MIOCENE
N16-N17
NN11 Discoaster quinqueramus
●R/P
●A/M
●Barren
●ϕ=45.6 γ=1.81
●ϕ=58.4 γ=1.77
1
2
3
4
5
CC
0.5
1.0

LITHOLOGIC DESCRIPTION

MARLY NANNOFOSSIL OOZE and FORAMINIFERAL MUDDY NANNOFOSSIL OOZE

Major lithologies:

a. MARLY NANNOFOSSIL OOZE, olive (5Y 4/2) to dark olive gray (5Y 3/2), no clear macrobioturbation except below interbedded layers of lithology B, organic carbon content 2.5-3.5%.

b. FORAMINIFERAL MUDDY NANNOFOSSIL OOZE, coarse grained, with silt- to sand-sized foraminifers, olive (5Y 4/3) to olive gray (5Y 4/2), interbedded with lithology A. Bioturbated, gradational and sharp basal contacts, with bones and fish teeth.

SMEAR SLIDE SUMMARY (%):

	1, 131 D	4, 23 M
TEXTURE:		
Sand		20
Silt	20	30
Clay	80	50
COMPOSITION:		
Clay	30	25
Dolomite	7	5
Fish remains		Tr
Foraminifers	5	20
Inorganic calcite	5	15
Nannofossils	50	30
Quartz	3	5

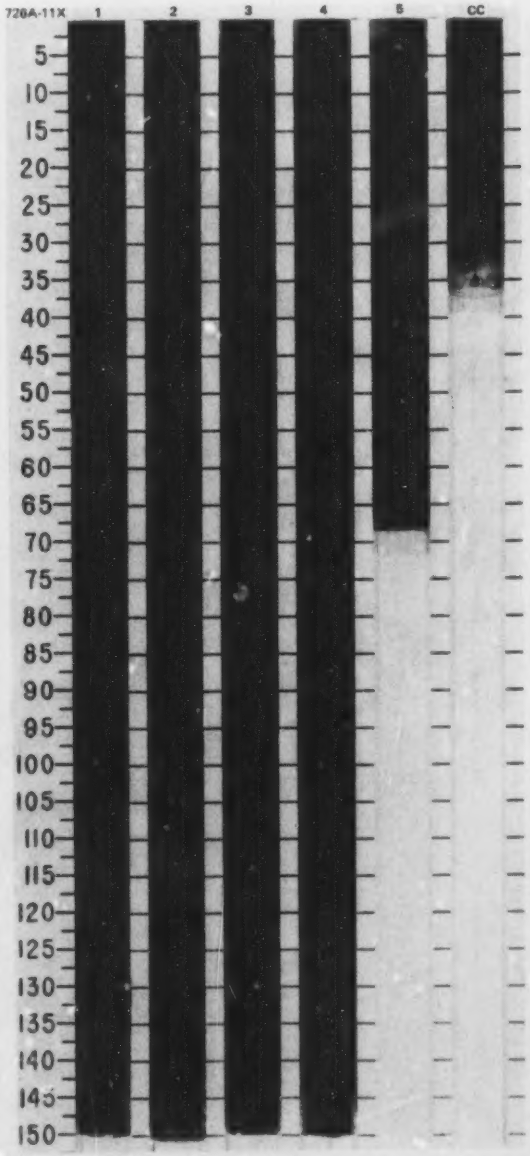
726A-11X
1
2
3
4
5
CC
5
10
15
20
25
30
35
40
45
50
55
60
65
70
75
80
85
90
95
100
105
110
115
120
125
130
135
140
145
150

SITE 726 HOLE A CORE 12X CORED INTERVAL 432.9-442.6 mbsl; 102.1-111.8 mbsf

TIME-ROCK UNIT	BIOSTRAT. ZONE/ FOSSIL CHARACTER				PALEOMAGNETICS	PHYS. PROPERTIES	CHEMISTRY	SECTION	METERS	GRAPHIC LITHOLOGY	DRILLING DISTURB.	SED. STRUCTURES	SAMPLES	LITHOLOGIC DESCRIPTION
	FORAMINIFERS	NANNOFOSSILS	RADIOLARIANS	DIATOMS										
MIOCENE	N16-N17 R/P●	NN10 *Discoaster calcaris* A/M-G●	Barren●					CC						MARLY NANNOFOSSIL OOZE with FORAMINIFERAL MUDDY NANNOFOSSIL OOZE Major lithology: MARLY NANNOFOSSIL OOZE with coarse-grained layers of FORAMINIFERAL MUDDY NANNOFOSSIL OOZE, olive (5Y 4/2). Weak recovery is due to lithified dolostone as found at the base of the CC.

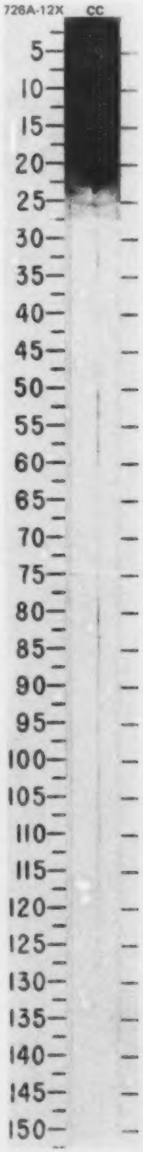
726A-12X
CC
5
10
15
20
25
30
35
40
45
50
55
60
65
70
75
80
85
90
95
100
105
110
115
120
125
130
135
140
145
150

SITE 726 HOLE A CORE 13X CORED INTERVAL 442.6-452.2 mbsl; 111.8-121.4 mbsf

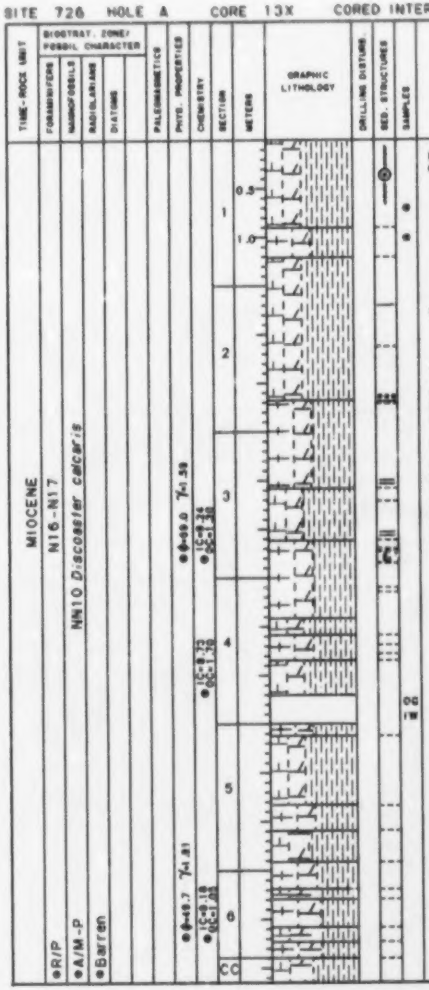
TIME-ROCK UNIT
BIOSTRAT. ZONE/ FOSSIL CHARACTER
FORAMINIFERS
NANNOFOSSILS
RADIOLARIANS
DIATOMS
PALEOMAGNETICS
PHYS. PROPERTIES
CHEMISTRY
SECTION
METERS
GRAPHIC LITHOLOGY
DRILLING DISTURB.
SED. STRUCTURES
SAMPLES
MIOCENE
N16-N17
NN10 Discoaster calcaris
●R/P
●A/M-P
●Barren
●φ=69.0 γ=1.59
●φ=49.7 γ=1.81
●IC=9.24 OC=1.30
●IC=8.72 OC=1.28
●IC=9.18 OC=1.05
1
2
3
4
5
6
CC
0.5
1.0
OG
IW

LITHOLOGIC DESCRIPTION

DOLOMITIC SILTY CLAY, and DOLOMITIC MUDDY FORAMINIFER NANNOFOSSIL OOZE to CHALK

Major lithology:

a. DOLOMITIC SILTY CLAY with 10% nannofossil ooze, dark olive gray (5Y 3/2) to olive (5Y 4/4), bioturbation not clearly visible, brownish, soft, 0.5 cm thick phosphorite concretion in Section 1, organic carbon content is 1.7%.

b. DOLOMITIC MUDDY FORAMINIFER NANNOFOSSIL OOZE to CHALK, olive (5Y 4/4) to light olive (5Y 5/4), 10 cm thick layers and composite layers 5 cm thick, bioturbation not clearly visible. Layers display gradational contacts at base and top, phosphorite coatings on foraminifers, and occasionally shell debris (e.g. gastropods); organic carbon reaches 1-1.3%.

SMEAR SLIDE SUMMARY (%):

	1, 70 D	1, 100 M
TEXTURE:		
Sand		20
Silt	40	40
Clay	60	40
COMPOSITION:		
Clay	30	25
Dolomite	30	20
Foraminifers	5	15
Inorganic calcite	20	25
Nannofossils	10	15
Organic debris	5	
Quartz	Tr	

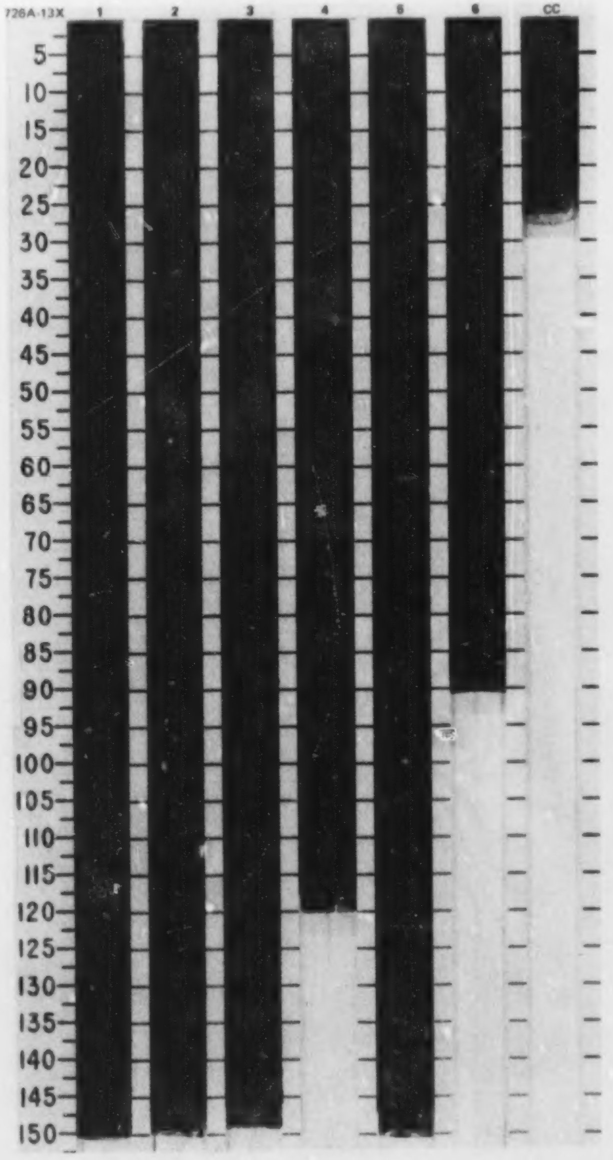
726A-13X
1
2
3
4
5
6
CC
5
10
15
20
25
30
35
40
45
50
55
60
65
70
75
80
85
90
95
100
105
110
115
120
125
130
135
140
145
150

SITE 726 HOLE A CORE 14X CORED INTERVAL 452.2-462.9 mbsl; 121.4-131.1 mbsf

TIME-ROCK UNIT	FORAMINIFERS	NANNOFOSSILS	RADIOLARIANS	DIATOMS	PALEOMAGNETICS	PHYS. PROPERTIES	CHEMISTRY	SECTION	METERS	GRAPHIC LITHOLOGY	DRILLING DISTURB.	SED. STRUCTURES	SAMPLES
MIOCENE	N16-N17 R/P●	NN10 *Discoaster quinqueramus* C/M-P●	Barren●			●ϕ=46.5 γ=1.94	●IC=8.33 OC=2.33	1 2 CC	0.5 1.0				● ●

LITHOLOGIC DESCRIPTION

DOLOMITIC SILTY CLAY, and DOLOMITIC MUDDY FORAMINIFERAL NANNOFOSSIL OOZE to CHALK

Major lithology:
- a. DOLOMITIC SILTY CLAY with 20% nannofossil ooze, olive (5Y 4/3) to dark olive gray (5y 3/2); bioturbation not clearly visible.
- b. DOLOMITIC MUDDY FORAMINIFERAL NANNOFOSSIL OOZE to CHALK, slightly lithified, olive (5Y 4/3) and dark olive (5Y 3/2) to very dark gray (5Y 3/1). Sets of composite 5 cm thick layers contain small phosphorite concretions, bone fragments, and phosphorite-coated foraminifers; organic carbon content is 1%.

SMEAR SLIDE SUMMARY (%):

	1, 90 D	2, 12 M
TEXTURE:		
Sand		10
Silt	40	60
Clay	60	30
COMPOSITION:		
Access. minerals	2	5
Clay	45	15
Dolomite	30	30
Foraminifers	5	10
Inorganic calcite	3	15
Mica	Tr	5
Nannofossils	15	15
Quartz	Tr	5

SITE 726 HOLE A CORE 15X CORED INTERVAL 461.9-471.5 mbsl; 131.1-140.7 mbsf

TIME-ROCK UNIT	FORAMINIFERS	NANNOFOSSILS	RADIOLARIANS	DIATOMS	PALEOMAGNETICS	PHYS. PROPERTIES	CHEMISTRY	SECTION	METERS	GRAPHIC LITHOLOGY	DRILLING DISTURB.	SED. STRUCTURES	SAMPLES
?	●Barren	●Barren	●Barren			ϕ=30.8 γ=2.33 ● ϕγ=2.38	IC=12.17● OC=0.28●	1 CC	0.5 1.0			6 6 6 6	● ●

LITHOLOGIC DESCRIPTION

DOLOMITE

Major lithology: DOLOMITE, massive, biomoldic porosity, olive (5Y 4/3), with 0.5 cm long elliptical molds of Nummulites sp.. No clear bedding features; wispy stylolites at Section 1, 20 cm.

SMEAR SLIDE SUMMARY (%):

	1, 24 D	1, 51 D
TEXTURE:		
Sand	3	
Silt	90	80
Clay	7	20
COMPOSITION:		
Clay	10	10
Dolomite	87	90
Inorganic calcite	3	

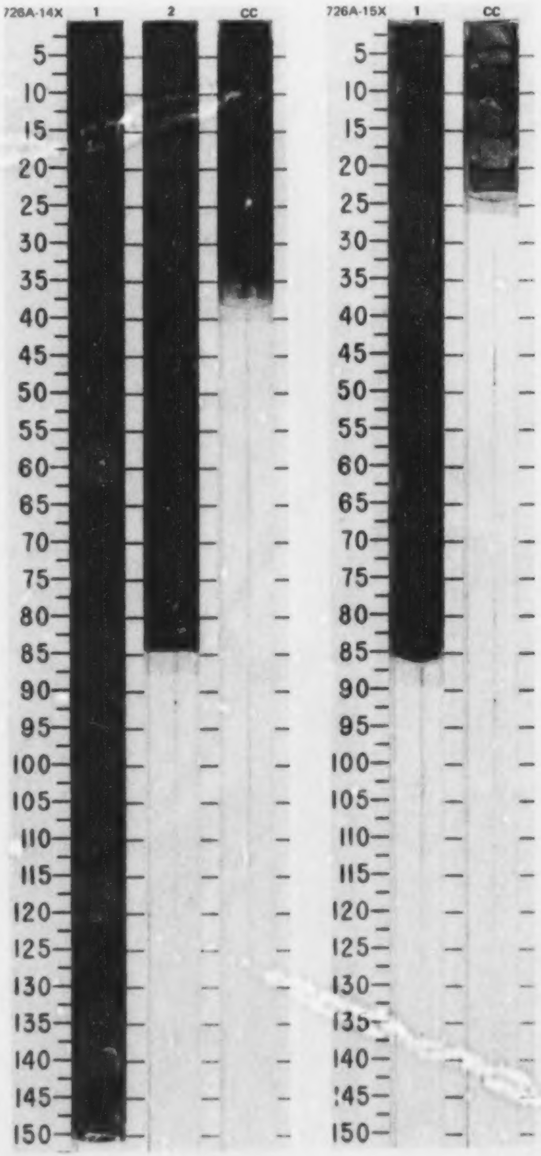

SITE 726 HOLE A CORE 16X CORED INTERVAL 471.5-478.9 mbsl; 140.7-148.1 mbsf

TIME-ROCK UNIT	BIOSTRAT. ZONE/ FOSSIL CHARACTER FORAMINIFERS	NANNOFOSSILS	RADIOLARIANS	DIATOMS	PALEOMAGNETICS	PHYS. PROPERTIES	CHEMISTRY	SECTION	METERS	GRAPHIC LITHOLOGY	DRILLING DISTURB.	SED. STRUCTURES	SAMPLES
?	●Barren	●Barren	●Barren			φ=45.5 γ=1.99 ●	IC=12.07 OC=00.18 ●	1 CC				6 6	● ● ●

LITHOLOGIC DESCRIPTION

NUMMULITIC LIMESTONE

Major lithology: NUMMULITIC LIMESTONE, friable, incompletely cemented, white (5Y 8/2), contains different species of large benthic foraminifers, . packstone to wackestone. Micritic grain contact cementation shows emplacement by dolomite rhombs with high interparticle porosity; organic carbon content is 0.2%.

Minor lithology: Oncolitic limestone, white (5Y 8/2), and wackestone with as large as 2 cm algal oncoliths of round to irregular shape. Grain contact cementation, and high intergrain and interparticle porosity.

SMEAR SLIDE SUMMARY (%):

	1, 5 D	CC, 17 D	CC, 30 D
TEXTURE:			
Sand	50	100	70
Silt	20		10
Clay	30		20
COMPOSITION:			
Algae	20		60
Foraminifers	50	100	5
Micrite	30		35

SITE 726 HOLE A CORE 17X CORED INTERVAL 478.9-484.9 mbsl; 148.1-154.1 mbsf

TIME-ROCK UNIT	BIOSTRAT. ZONE/ FOSSIL CHARACTER FORAMINIFERS	NANNOFOSSILS	RADIOLARIANS	DIATOMS	PALEOMAGNETICS	PHYS. PROPERTIES	CHEMISTRY	SECTION	METERS	GRAPHIC LITHOLOGY	DRILLING DISTURB.	SED. STRUCTURES	SAMPLES
?	Barren●	Barren●	Barren●			γ=2.11 ●		CC			<	6	

LITHOLOGIC DESCRIPTION

NUMMULITIC LIMESTONE to ONCOLITIC LIMESTONE

Major lithology: NUMMULITIC LIMESTONE to ONCOLITIC LIMESTONE, highly fractured due to drilling, white (5Y 8/2).

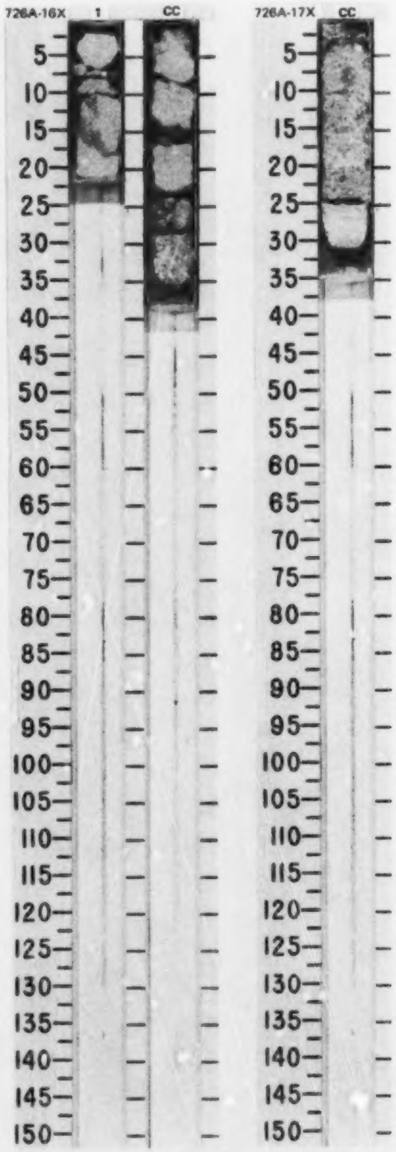

SITE 726 HOLE A CORE 18X CORED INTERVAL 484.9-494.9 mbsl; 154.1-164.1 mbsf

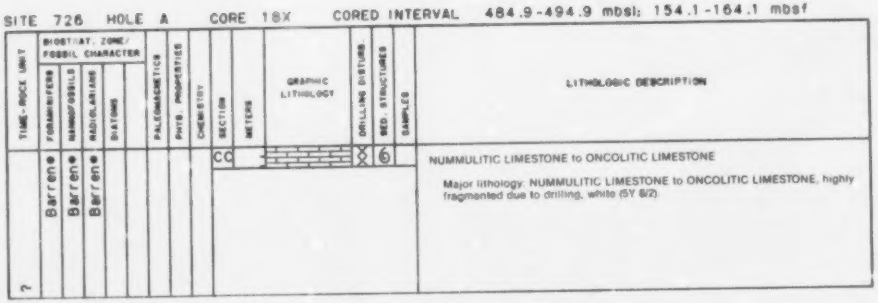
TIME-ROCK UNIT
BIOSTRAT. ZONE/ FOSSIL CHARACTER
FORAMINIFERS
NANNOFOSSILS
RADIOLARIANS
DIATOMS
PALEOMAGNETICS
PHYS. PROPERTIES
CHEMISTRY
SECTION
METERS
GRAPHIC LITHOLOGY
DRILLING DISTURB.
SED. STRUCTURES
SAMPLES
LITHOLOGIC DESCRIPTION
?
Barren
Barren
Barren
CC

NUMMULITIC LIMESTONE to ONCOLITIC LIMESTONE

Major lithology: NUMMULITIC LIMESTONE to ONCOLITIC LIMESTONE, highly fragmented due to drilling, white (5Y 8/2)

SITE 726 HOLE A CORE 19X CORED INTERVAL 494.9-504.5 mbsl; 164.1-173.7 mbsf

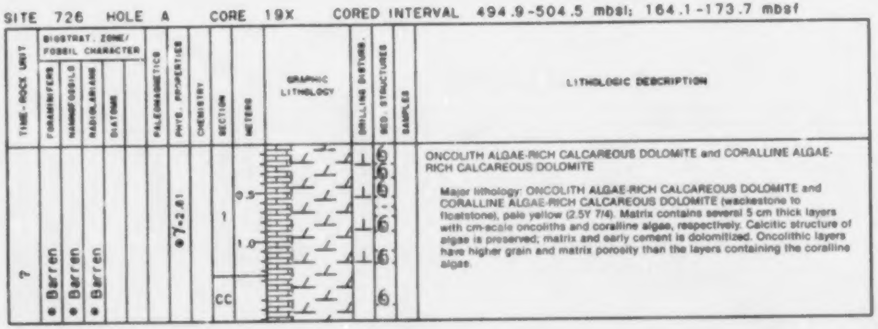
TIME-ROCK UNIT
BIOSTRAT. ZONE/ FOSSIL CHARACTER
FORAMINIFERS
NANNOFOSSILS
RADIOLARIANS
DIATOMS
PALEOMAGNETICS
PHYS. PROPERTIES
CHEMISTRY
SECTION
METERS
GRAPHIC LITHOLOGY
DRILLING DISTURB.
SED. STRUCTURES
SAMPLES
LITHOLOGIC DESCRIPTION
?
● Barren
● Barren
● Barren
●γ=2.81
1
CC
0.5
1.0

ONCOLITH ALGAE-RICH CALCAREOUS DOLOMITE and CORALLINE ALGAE-RICH CALCAREOUS DOLOMITE

Major lithology: ONCOLITH ALGAE-RICH CALCAREOUS DOLOMITE and CORALLINE ALGAE-RICH CALCAREOUS DOLOMITE (wackestone to floatstone), pale yellow (2.5Y 7/4). Matrix contains several 5 cm thick layers with cm-scale oncoliths and coralline algae, respectively. Calcitic structure of algae is preserved; matrix and early cement is dolomitized. Oncolithic layers have higher grain and matrix porosity then the layers containing the coralline algae.

SITE 726 HOLE A CORE 20X CORED INTERVAL 504.5-514.2 mbsl; 173.7-183.4 mbsf

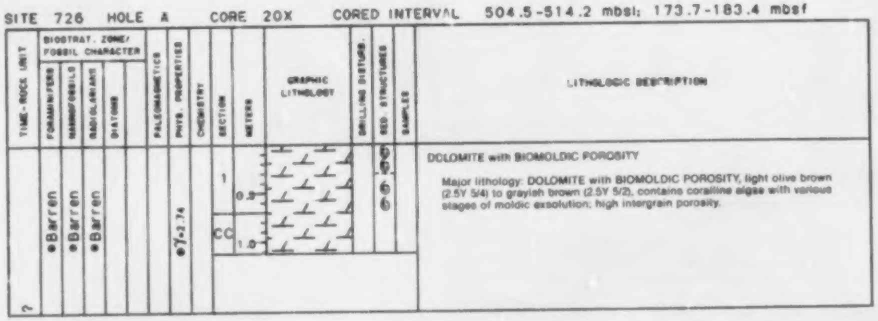
TIME-ROCK UNIT
BIOSTRAT. ZONE/ FOSSIL CHARACTER
FORAMINIFERS
NANNOFOSSILS
RADIOLARIANS
DIATOMS
PALEOMAGNETICS
PHYS. PROPERTIES
CHEMISTRY
SECTION
METERS
GRAPHIC LITHOLOGY
DRILLING DISTURB.
SED. STRUCTURES
SAMPLES
LITHOLOGIC DESCRIPTION
?
●Barren
●Barren
●Barren
●γ=2.74
1
CC
0.5
1.0

DOLOMITE with BIOMOLDIC POROSITY

Major lithology: DOLOMITE with BIOMOLDIC POROSITY, light olive brown (2.5Y 5/4) to grayish brown (2.5Y 5/2), contains coralline algae with various stages of moldic exsolution; high intergrain porosity.

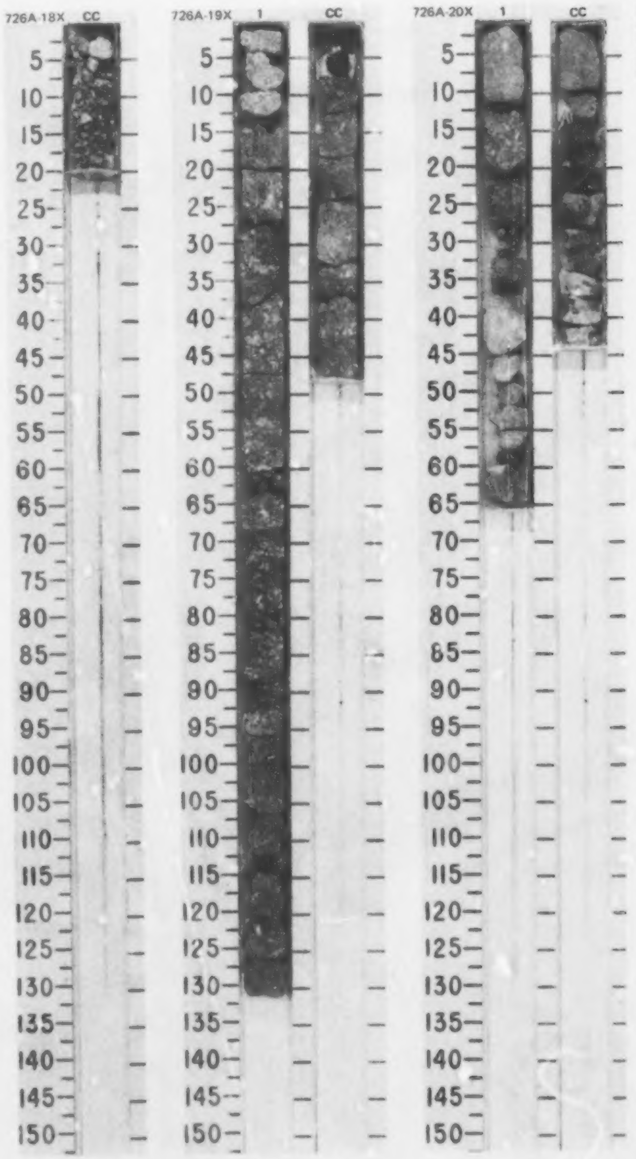
726A-18X
CC
726A-19X
1
CC
726A-20X
1
CC
5
10
15
20
25
30
35
40
45
50
55
60
65
70
75
80
85
90
95
100
105
110
115
120
125
130
135
140
145
150

SITE 726 HOLE A CORE 21X CORED INTERVAL 514.2-514.6 mbsl; 183.4-183.8 mbsf

TIME-ROCK UNIT	BIOSTRAT. ZONE/ FOSSIL CHARACTER					PALEOMAGNETICS	PHYS. PROPERTIES	CHEMISTRY	SECTION	METERS	GRAPHIC LITHOLOGY	DRILLING DISTURB.	SED. STRUCTURES	SAMPLES	LITHOLOGIC DESCRIPTION
	FORAMINIFERS	NANNOFOSSILS	RADIOLARIANS	DIATOMS											
?	Barren●	Barren●	Barren●			γ=2.78●			CC						DOLOMITE Major lithology: DOLOMITE, massive, light gray (2.5 Y 7/2) to gray (2.5Y 6/0), fine grained, porous, no fossils visible.

SITE 726 HOLE A CORE 22X CORED INTERVAL 514.6-517.1 mbsl; 183.8-186.3 mbsf

TIME-ROCK UNIT	BIOSTRAT. ZONE/ FOSSIL CHARACTER					PALEOMAGNETICS	PHYS. PROPERTIES	CHEMISTRY	SECTION	METERS	GRAPHIC LITHOLOGY	DRILLING DISTURB.	SED. STRUCTURES	SAMPLES	LITHOLOGIC DESCRIPTION
	FORAMINIFERS	NANNOFOSSILS	RADIOLARIANS	DIATOMS											
?	Barren●	Barren●	Barren●						CC				6		DOLOMITE Major lithology: DOLOMITE, light gray (2.5Y 7/1, 7/2), fine grained, with molds of brachiopods, gastropods, and coralline algae; traces of calcite are present on drusy surface of molds.

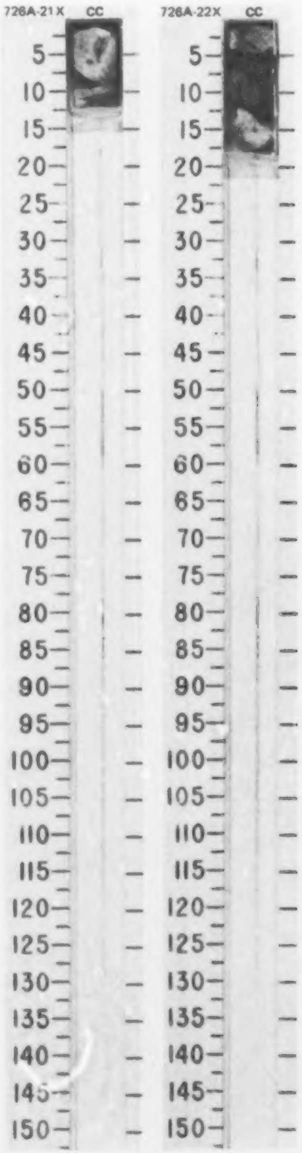

SITE 727 HOLE A CORE 1H CORED INTERVAL 914.8-924.3 mbsl; 0.0-9.5 mbsf

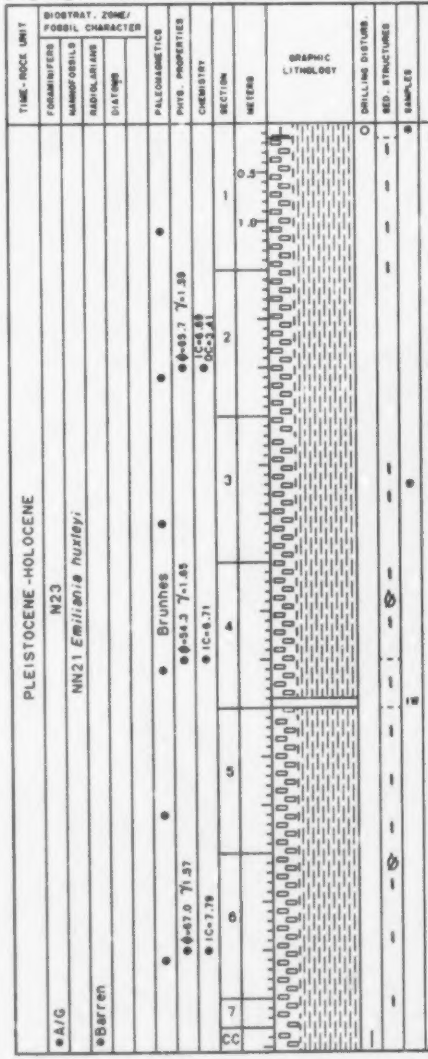
TIME-ROCK UNIT
BIOSTRAT. ZONE/ FOSSIL CHARACTER
FORAMINIFERS
NANNOFOSSILS
RADIOLARIANS
DIATOMS
PALEOMAGNETICS
PHYS. PROPERTIES
CHEMISTRY
SECTION
METERS
GRAPHIC LITHOLOGY
DRILLING DISTURB.
SED. STRUCTURES
SAMPLES
PLEISTOCENE-HOLOCENE
•A/G
N23
NN21 Emiliania huxleyi
•Barren
Brunhes
•ϕ=65.7 γ=1.59
•ϕ=54.3 γ=1.85
•ϕ=67.0 γ=1.57
•IC=6.89 OC=2.41
• IC=6.71
• IC=7.79
0.5
1.0
1
2
3
4
5
6
7
CC
IW

LITHOLOGIC DESCRIPTION

CALCITIC MARLY CALCAREOUS OOZE

Section 1, 0-16 cm, is highly disturbed. Remainder is undisturbed.

Major lithology: CALCITIC MARLY CALCAREOUS OOZE, olive (5Y 4/3), olive gray (5Y 4/2), and dark olive gray (5Y 3/2). Bioturbated throughout, with shell debris dispersed throughout core.

Minor lithology: Nannofossil ooze, olive (5Y 4/3), in Section 1, 0-16 cm.

SMEAR SLIDE SUMMARY (%):

	1, 1 D	3, 70 D
TEXTURE:		
Sand	5	5
Silt	25	45
Clay	70	50
COMPOSITION:		
Access. minerals		Tr
Clay	35	35
Dolomite	1	1
Foraminifers	5	15
Inorganic calcite	20	25
Mica	2	2
Nannofossils	30	15
Quartz	7	7
Sponge spicules	Tr	

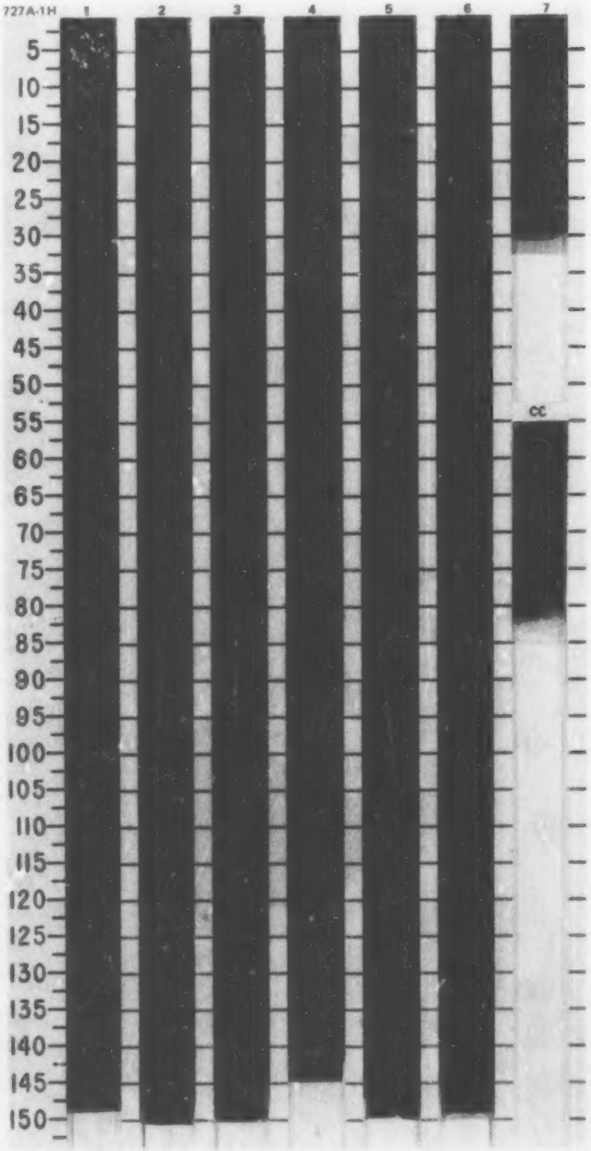
727A-1H
1
2
3
4
5
6
7
CC
5
10
15
20
25
30
35
40
45
50
55
60
65
70
75
80
85
90
95
100
105
110
115
120
125
130
135
140
145
150

SITE 727 HOLE A CORE 2H CORED INTERVAL 924.3-933.7 mbsl; 9.5-18.9 mbsf

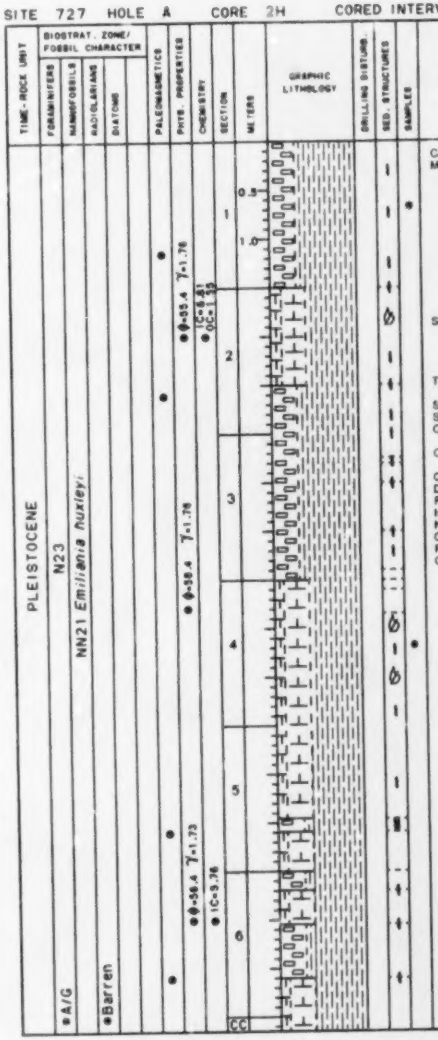
TIME-ROCK UNIT
BIOSTRAT. ZONE/ FOSSIL CHARACTER
FORAMINIFERS
NANNOFOSSILS
RADIOLARIANS
DIATOMS
PALEOMAGNETICS
PHYS. PROPERTIES
CHEMISTRY
SECTION
METERS
GRAPHIC LITHOLOGY
DRILLING DISTURB.
SED. STRUCTURES
SAMPLES
PLEISTOCENE
N23
NN21 Emiliania huxleyi
●A/G
●Barren
●ϕ=55.4 γ=1.76
●ϕ=58.4 γ=1.76
●ϕ=56.4 γ=1.73
●IC=6.81 OC=1.55
●IC=9.76
0.5
1.0
1
2
3
4
5
6
CC

LITHOLOGIC DESCRIPTION

CALCITIC MARLY CALCAREOUS OOZE and FORAMINIFER-BEARING CALCITIC MARLY NANNOFOSSIL OOZE

Entire core is undisturbed.

Major lithologies:
a. CALCITIC MARLY CALCAREOUS OOZE, dark olive gray (5Y 3/2) and bioturbated, in Section 1; Section 2, 100 cm, to Section 3; Section 5, 97-107 cm; and Section 6, 0-20 and 55-110 cm.
b. FORAMINIFER-BEARING CALCITIC MARLY NANNOFOSSIL OOZE, olive (5Y 4/3) and olive gray (5Y 4/2), bioturbated. Section 2, 0-100 cm; Section 4 to Section 5, 97 cm; Section 5, 107-150 cm; Section 6, 20-55 cm; and Section 6, 110 cm to CC.

SMEAR SLIDE SUMMARY (%):

	1, 67 D	4, 67 D
TEXTURE:		
Sand	5	5
Silt	35	40
Clay	60	55
COMPOSITION:		
Clay	35	30
Dolomite	Tr	1
Foraminifers	10	10
Inorganic calcite	20	25
Nannofossils	20	29
Organic debris	5	
Pellets	5	
Quartz	5	5

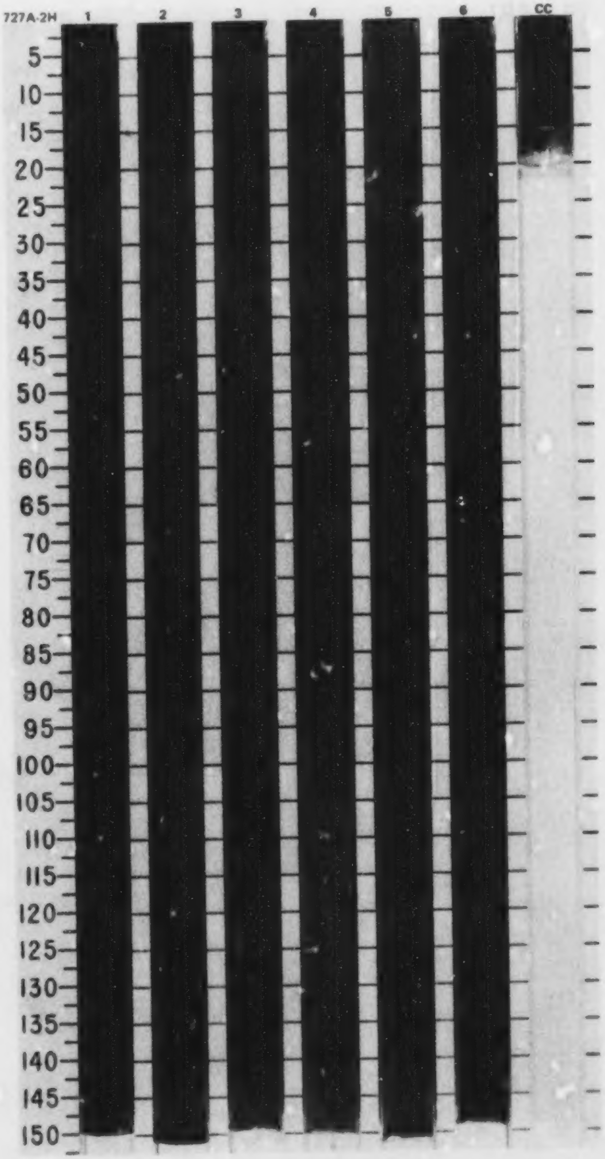
727A-2H
1
2
3
4
5
6
CC
5
10
15
20
25
30
35
40
45
50
55
60
65
70
75
80
85
90
95
100
105
110
115
120
125
130
135
140
145
150

SITE 727 HOLE A CORE 3H CORED INTERVAL 933.7-943.2 mbsl; 18.9-28.4 mbsf

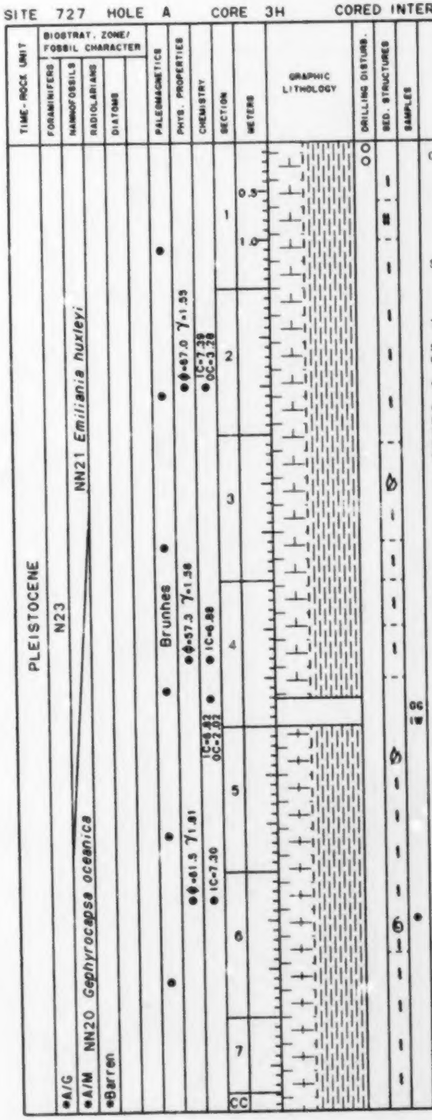
TIME-ROCK UNIT
BIOSTRAT. ZONE/ FOSSIL CHARACTER
FORAMINIFERS
NANNOFOSSILS
RADIOLARIANS
DIATOMS
PALEOMAGNETICS
PHYS. PROPERTIES
CHEMISTRY
SECTION
METERS
GRAPHIC LITHOLOGY
DRILLING DISTURB.
SED. STRUCTURES
SAMPLES
PLEISTOCENE
N23
NN21 *Emiliania huxleyi*
NN20 *Gephyrocapsa oceanica*
●A/G
●A/M
●Barren
Brunhes
●φ=67.0 γ=1.53
●φ=57.3 γ=1.98
●φ=61.5 γ=1.91
IC=7.39
OC=3.28
● IC=6.88
IC=6.82
OC=2.02
● IC=7.30
1
2
3
4
5
6
7
CC
0.5
1.0
OG
IW

LITHOLOGIC DESCRIPTION

CALCITIC MARLY NANNOFOSSIL OOZE

Section 1, 0-10 cm, is highly disturbed. Remainder is undisturbed.

Major lithology: CALCITIC MARLY NANNOFOSSIL OOZE, olive (5Y 4/3) and olive gray (5Y 4/2) to dark olive gray (5Y 3/2). Bioturbated throughout. Small shell fragments dispersed throughout core; intact bryozoan at Section 6, 50-54 cm.

SMEAR SLIDE SUMMARY (%):

	6, 50 D
TEXTURE:	
Silt	30
Clay	70
COMPOSITION:	
Clay	25
Foraminifers	7
Inorganic calcite	20
Nannofossils	45
Quartz	3

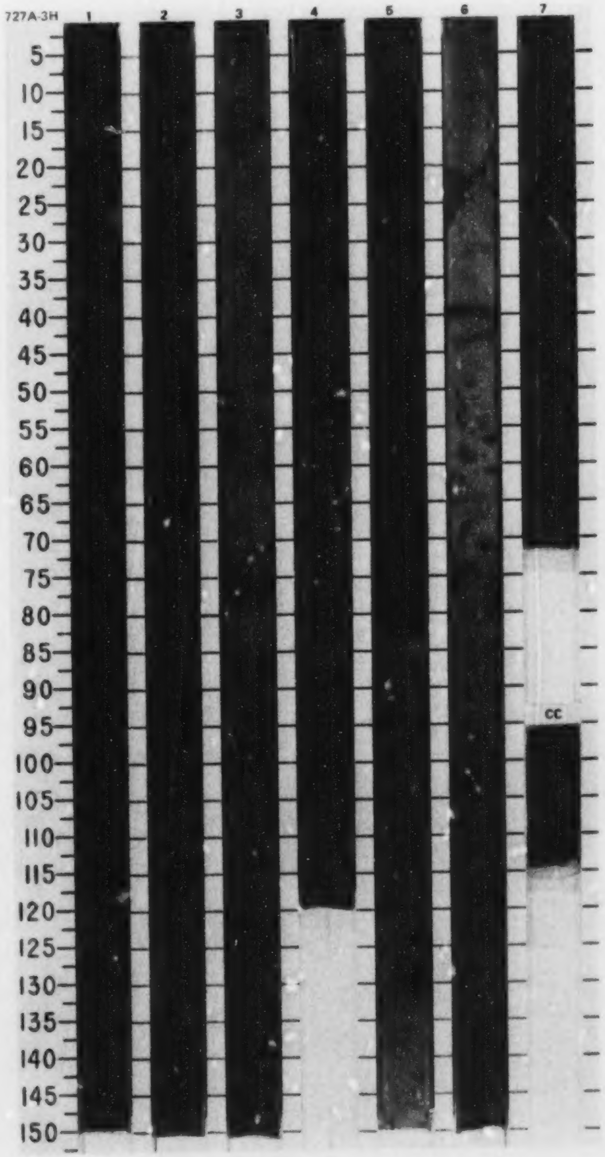
727A-3H
1
2
3
4
5
6
7
CC
5
10
15
20
25
30
35
40
45
50
55
60
65
70
75
80
85
90
95
100
105
110
115
120
125
130
135
140
145
150

SITE 727 HOLE A CORE 4H CORED INTERVAL 943.2-952.6 mbsl; 28.4-37.8 mbsf

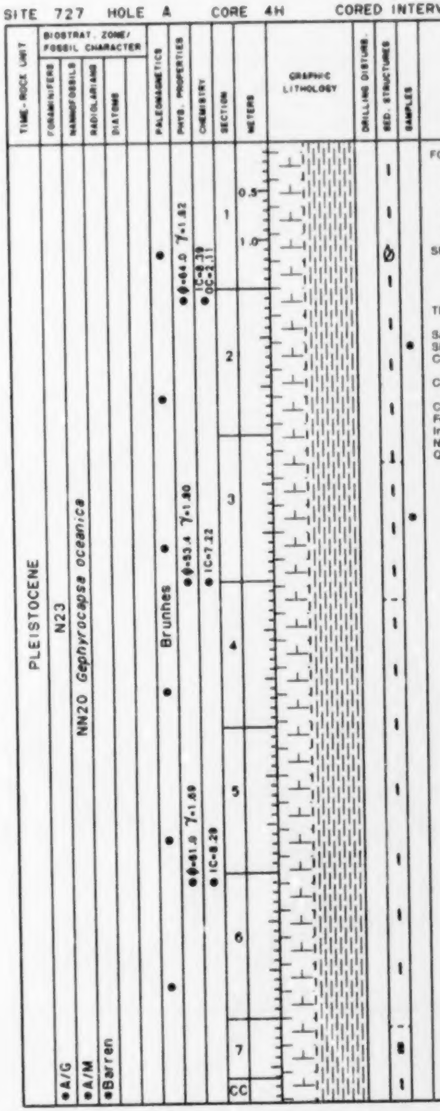
TIME-ROCK UNIT
BIOSTRAT. ZONE/ FOSSIL CHARACTER
FORAMINIFERS
NANNOFOSSILS
RADIOLARIANS
DIATOMS
PALEOMAGNETICS
PHYS. PROPERTIES
CHEMISTRY
SECTION
METERS
GRAPHIC LITHOLOGY
DRILLING DISTURB.
SED. STRUCTURES
SAMPLES
PLEISTOCENE
N23
NN20 Gephyrocapsa oceanica
●A/G
●A/M
●Barren
Brunhes
●φ=64.0 γ=1.82
●φ=53.4 γ=1.80
●φ=61.0 γ=1.69
IC=8.39
OC=2.11
●IC=7.22
●IC=8.29
1
2
3
4
5
6
7
CC
0.5
1.0

LITHOLOGIC DESCRIPTION

FORAMINIFER-BEARING CALCITIC MARLY NANNOFOSSIL OOZE

CC is highly disturbed. Remainder of core is undisturbed.

Major lithology: FORAMINIFER-BEARING CALCITIC MARLY NANNOFOSSIL OOZE, olive (5Y 4/3) and olive gray (5Y 4/2, 5/2). Minor to moderate bioturbation throughout, with small shell fragments sparsely dispersed throughout core.

SMEAR SLIDE SUMMARY (%):

	2, 60 D	3, 87 D
TEXTURE:		
Sand	10	
Silt	45	40
Clay	45	60
COMPOSITION:		
Clay	30	25
Foraminifers	15	10
Inorganic calcite	17	20
Nannofossils	35	35
Quartz	3	10

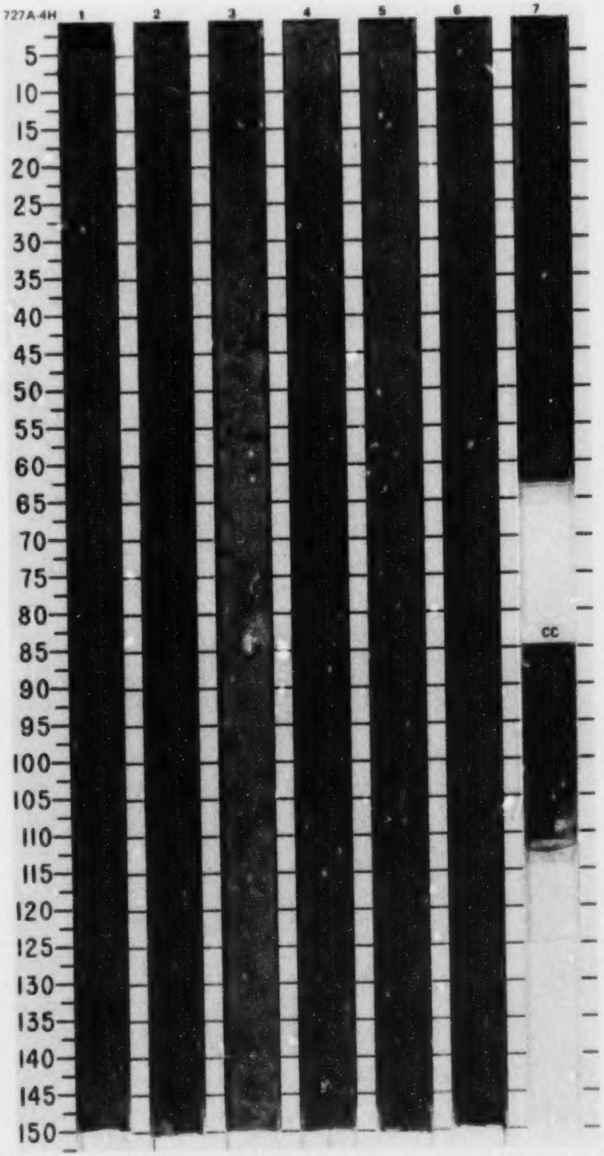
727A-4H
1
2
3
4
5
6
7
CC
5
10
15
20
25
30
35
40
45
50
55
60
65
70
75
80
85
90
95
100
105
110
115
120
125
130
135
140
145
150

SITE 727 HOLE A CORE 5H CORED INTERVAL 952.6-962.1 mbsl; 37.8-47.3 mbsf

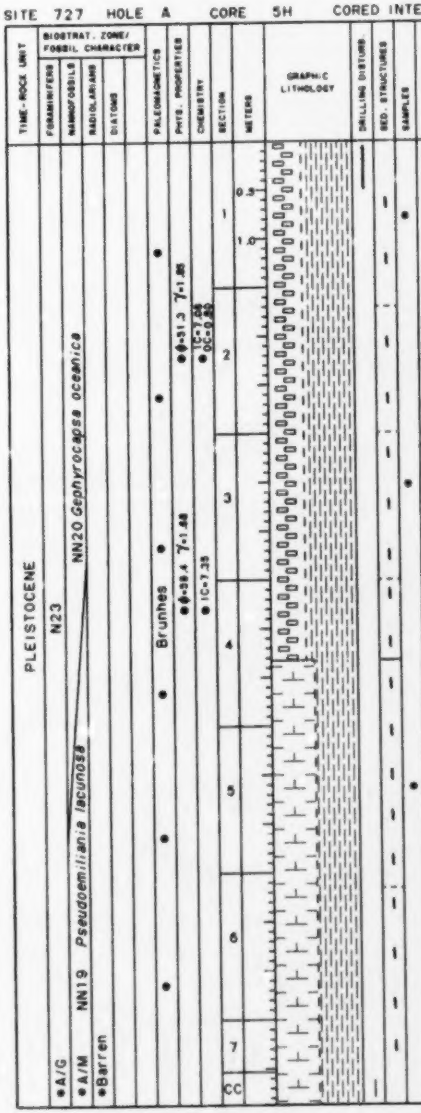

LITHOLOGIC DESCRIPTION

CALCITIC MARLY CALCAREOUS OOZE and FORAMINIFER-BEARING CALCITIC MARLY NANNOFOSSIL OOZE

Section 1, 0-25 cm, is highly disturbed. Remainder of core is undisturbed.

Major lithologies:

a. CALCITIC MARLY CALCAREOUS OOZE, olive (5Y 4/3) to olive gray (5Y 4/2), bioturbated throughout Section 1 through Section 4, 84 cm.

b. FORAMINIFER-BEARING CALCITIC MARLY NANNOFOSSIL OOZE, olive (5Y 4/3) to olive gray (5Y 4/2), bioturbated throughout. Section 4, 84 cm, to CC.

SMEAR SLIDE SUMMARY (%):

	1, 78 D	5, 53 D
TEXTURE:		
Silt	45	45
Clay	55	55
COMPOSITION:		
Access. minerals	2	
Clay	35	25
Dolomite	1	
Foraminifers	15	12
Inorganic calcite	20	20
Nannofossils	20	38
Quartz	7	5

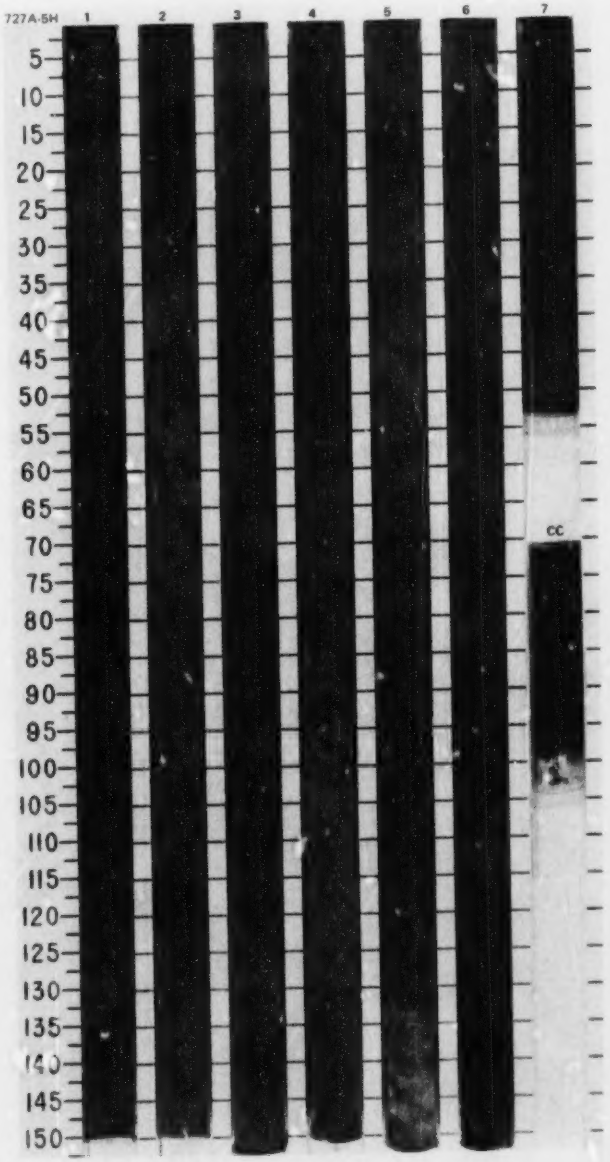
727A-5H
1
2
3
4
5
6
7
CC
5
10
15
20
25
30
35
40
45
50
55
60
65
70
75
80
85
90
95
100
105
110
115
120
125
130
135
140
145
150

SITE 727 HOLE A CORE 6H CORED INTERVAL 962.1-971.6 mbsl; 47.3-56.8 mbsf

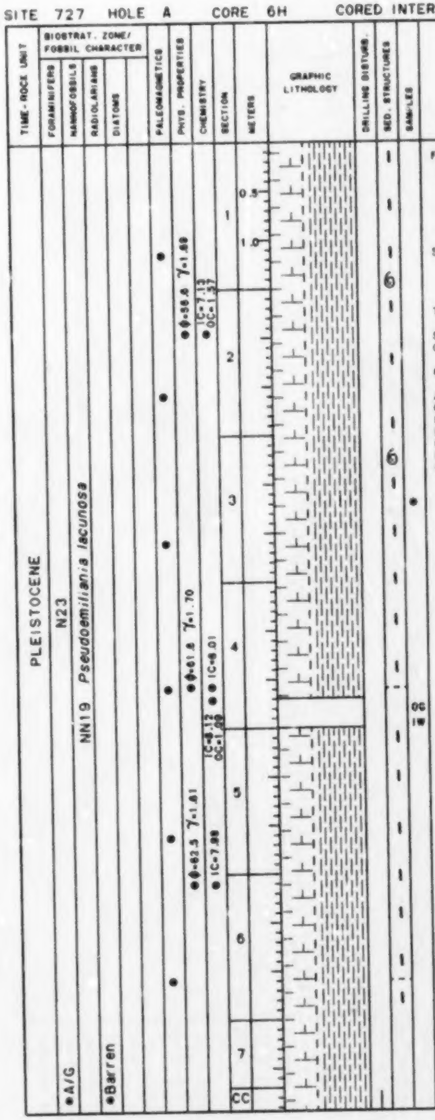
TIME-ROCK UNIT
BIOSTRAT. ZONE/ FOSSIL CHARACTER
FORAMINIFERS
NANNOFOSSILS
RADIOLARIANS
DIATOMS
PALEOMAGNETICS
PHYS. PROPERTIES
CHEMISTRY
SECTION
METERS
GRAPHIC LITHOLOGY
DRILLING DISTURB.
SED. STRUCTURES
SAMPLES
PLEISTOCENE
N23
NN19 Pseudoemiliania lacunosa
●A/G
●Barren
●ϕ=58.6 γ=1.88
●ϕ=61.8 γ=1.70
●ϕ=62.5 γ=1.81
●IC=7.13 OC=1.57
●IC=8.01
IC=8.12 OC=1.09
●IC=7.88
0.5
1.0
1
2
3
4
5
6
7
CC
OG
IW

LITHOLOGIC DESCRIPTION

FORAMINIFER-BEARING CALCITIC MARLY NANNOFOSSIL OOZE

CC is slightly disturbed. Remainder of the core is undisturbed.

Major lithology: FORAMINIFER-BEARING CALCITIC MARLY NANNOFOSSIL OOZE, olive (5Y 4/3) to dark olive gray (5Y 3/2). Bioturbated throughout, with minor dispersed amounts of small shell debris in Sections 1-3.

SMEAR SLIDE SUMMARY (%):

	3, 70 D
TEXTURE:	
Silt	45
Clay	55
COMPOSITION:	
Access. minerals	2
Clay	28
Dolomite	2
Foraminifers	10
Inorganic calcite	20
Nannofossils	35
Quartz	3

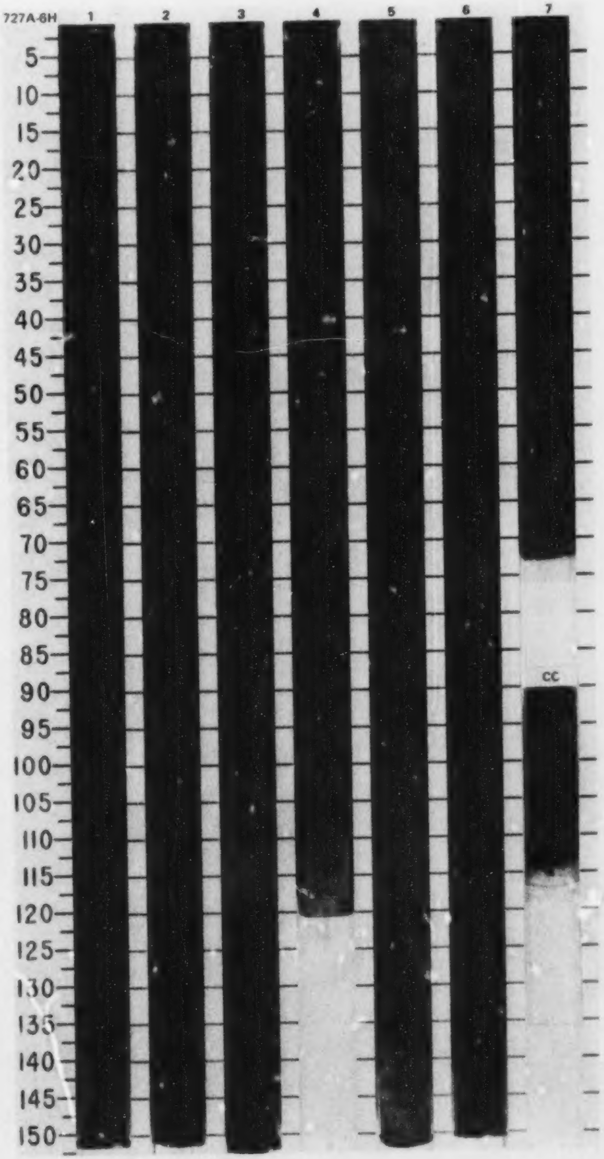
727A-6H
1
2
3
4
5
6
7
CC
5
10
15
20
25
30
35
40
45
50
55
60
65
70
75
80
85
90
95
100
105
110
115
120
125
130
135
140
145
150

SITE 727 HOLE A CORE 7H CORED INTERVAL 971.6-981.2 mbsl; 56.8-66.4 mbsf

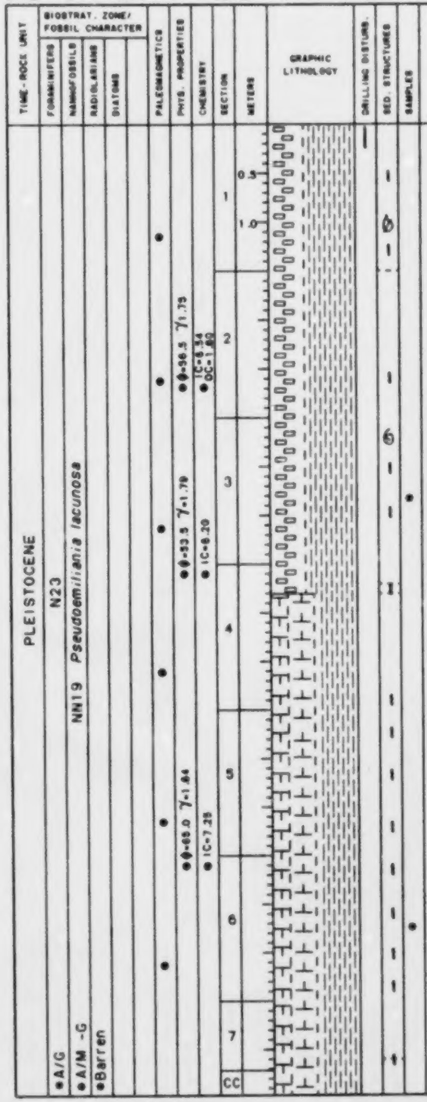
TIME-ROCK UNIT
BIOSTRAT. ZONE/ FOSSIL CHARACTER
FORAMINIFERS
NANNOFOSSILS
RADIOLARIANS
DIATOMS
PALEOMAGNETICS
PHYS. PROPERTIES
CHEMISTRY
SECTION
METERS
GRAPHIC LITHOLOGY
DRILLING DISTURB.
SED. STRUCTURES
SAMPLES
PLEISTOCENE
N23
NN19 Pseudoemiliania lacunosa
●A/G
●A/M -G
●Barren
●ϕ=56.5 γ1.75
●ϕ=53.5 γ=1.79
●ϕ=65.0 γ=1.84
IC=6.54
●OC=1.60
● IC=6.20
● IC=7.25
0.5
1.0
1
2
3
4
5
6
7
CC

LITHOLOGIC DESCRIPTION

CALCITIC MARLY CALCAREOUS OOZE and FORAMINIFER-BEARING CALCITIC MARLY NANNOFOSSIL OOZE

Section 1, 0-30 cm, is highly disturbed. Remainder of core is undisturbed.

Major lithologies:
a. CALCITIC MARLY CALCAREOUS OOZE, olive (5Y 4/3) to dark olive gray (5Y 3/2), bioturbated, in Section 1 to Section 4, 30 cm. Small zones of shell hash, Section 3, 0-50 cm.
b. FORAMINIFER-BEARING CALCITIC MARLY NANNOFOSSIL OOZE, olive (5Y 4/3) and olive gray (5Y 4/2). Section 4, 30 cm, to CC. Bioturbated throughout.

SMEAR SLIDE SUMMARY (%):

	3, 86 D	6, 75 D
TEXTURE:		
Sand		5
Silt	45	45
Clay	55	50
COMPOSITION:		
Access. minerals	2	
Clay	30	25
Dolomite	1	Tr
Foraminifers	15	20
Inorganic calcite	25	20
Nannofossils	20	30
Quartz	7	5

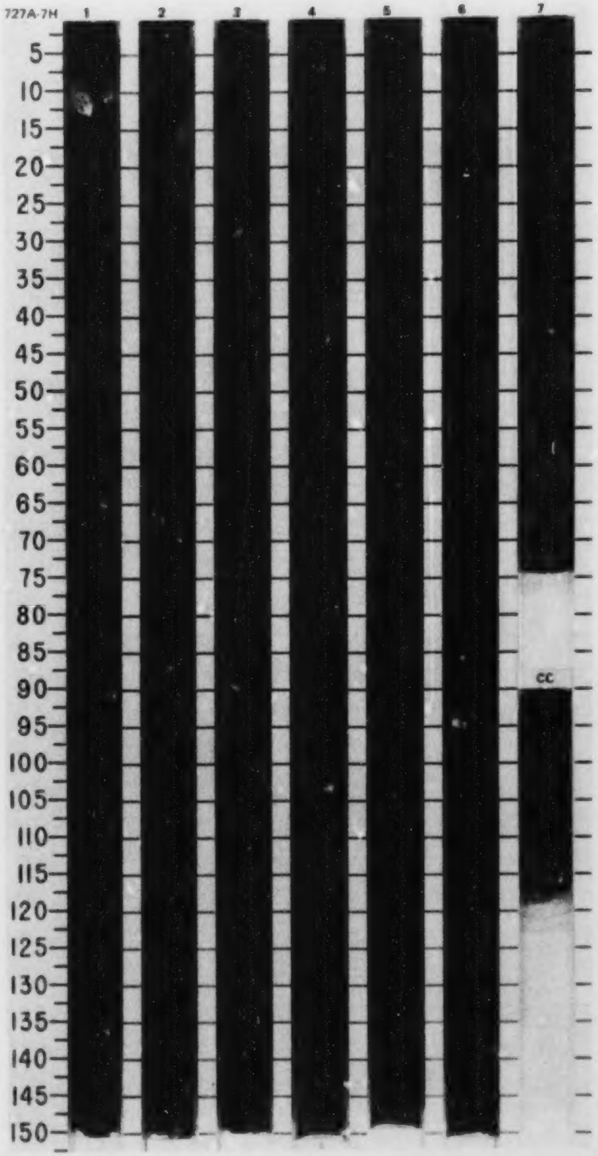
727A-7H
1
2
3
4
5
6
7
CC
5
10
15
20
25
30
35
40
45
50
55
60
65
70
75
80
85
90
95
100
105
110
115
120
125
130
135
140
145
150

SITE 727 HOLE A CORE 8H CORED INTERVAL 981.2-990.0 mbsl; 66.4-76.1 mbsf

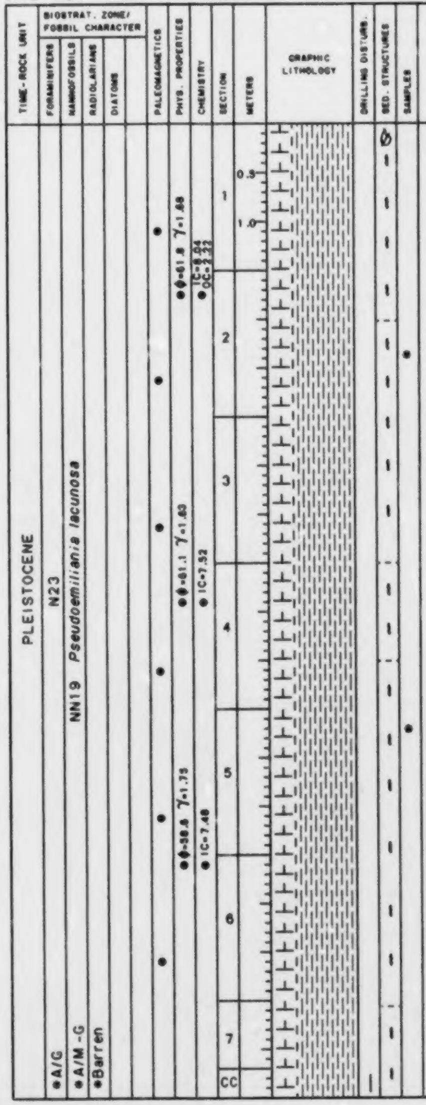
TIME-ROCK UNIT
BIOSTRAT. ZONE/ FOSSIL CHARACTER
FORAMINIFERS
NANNOFOSSILS
RADIOLARIANS
DIATOMS
PALEOMAGNETICS
PHYS. PROPERTIES
CHEMISTRY
SECTION
METERS
GRAPHIC LITHOLOGY
DRILLING DISTURB.
SED. STRUCTURES
SAMPLES
PLEISTOCENE
N23
NN19 Pseudoemiliania lacunosa
●A/G
●A/M-G
●Barren
●Φ=61.8 γ=1.88
●IC=8.04 OC=2.22
●Φ=61.1 γ=1.83
●IC=7.52
●Φ=58.6 γ=1.75
●IC=7.48
1
2
3
4
5
6
7
CC
0.5
1.0

LITHOLOGIC DESCRIPTION

CALCITIC MARLY NANNOFOSSIL OOZE to NANNOFOSSIL-RICH CALCITIC CLAYEY SILT

Entire core is undisturbed.

Major lithology: CALCITIC MARLY NANNOFOSSIL OOZE to NANNOFOSSIL-RICH CALCITIC CLAYEY SILT, olive (5Y 4/3) and olive gray (5Y 4/2) to dark olive gray (5Y 3/2). Minor bioturbation throughout.

SMEAR SLIDE SUMMARY (%):

	2, 86 D	5, 21 D
TEXTURE:		
Silt	30	65
Clay	70	35
COMPOSITION:		
Access. minerals	2	1
Clay	30	25
Dolomite	Tr	1
Foraminifers	10	5
Inorganic calcite	15	40
Nannofossils	40	18
Quartz	3	10

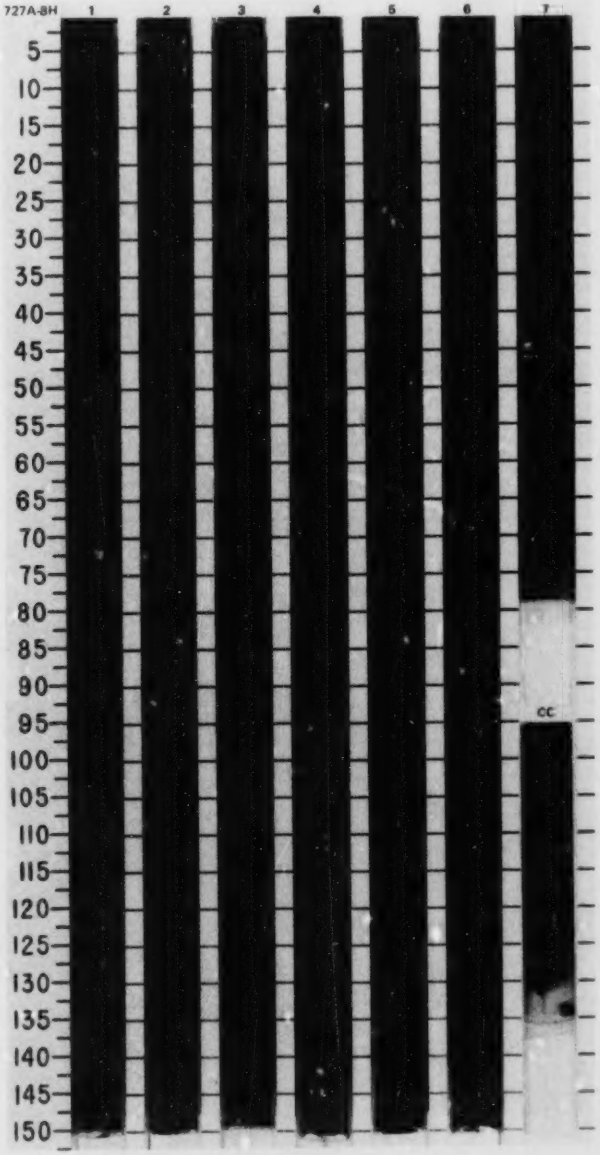
727A-8H
1
2
3
4
5
6
7
CC
5
10
15
20
25
30
35
40
45
50
55
60
65
70
75
80
85
90
95
100
105
110
115
120
125
130
135
140
145
150

SITE 727 HOLE A CORE 9H CORED INTERVAL 990.9-1000.6 mbsl; 76.1-85.8 mbsf

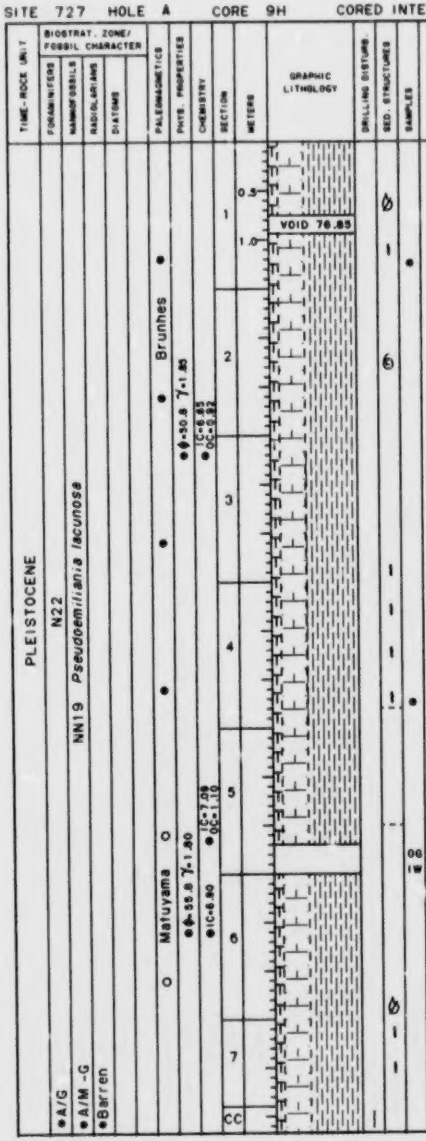
TIME-ROCK UNIT
BIOSTRAT. ZONE/ FOSSIL CHARACTER
FORAMINIFERS
NANNOFOSSILS
RADIOLARIANS
DIATOMS
PALEOMAGNETICS
PHYS. PROPERTIES
CHEMISTRY
SECTION
METERS
GRAPHIC LITHOLOGY
DRILLING DISTURB.
SED. STRUCTURES
SAMPLES
PLEISTOCENE
N22
NN19 Pseudoemiliania lacunosa
●A/G
●A/M -G
●Barren
Brunhes
Matuyama
●φ=50.8 γ=1.85
●φ=55.8 γ=1.80
●IC=6.85 OC=0.82
●IC=7.09 OC=1.10
●IC=6.90
0.5
1.0
1
2
3
4
5
6
7
CC
VOID 76.85
OG
IW

LITHOLOGIC DESCRIPTION

FORAMINIFER-BEARING CALCITIC MARLY NANNOFOSSIL OOZE to CALCITIC MARLY CALCAREOUS OOZE

CC is slightly disturbed. Remainder of core is undisturbed.

Major lithology: FORAMINIFER-BEARING CALCITIC MARLY NANNOFOSSIL OOZE to CALCITIC MARLY CALCAREOUS OOZE, olive (5Y 4/3) and olive gray (5Y 4/2). Minor bioturbation in Sections 1, 3, 4, and 7.

SMEAR SLIDE SUMMARY (%):

	1, 125 D	4, 123 D
TEXTURE:		
Silt	35	50
Clay	65	50
COMPOSITION:		
Clay	30	20
Dolomite	Tr	1
Foraminifers	10	10
Inorganic calcite	20	35
Mica		1
Nannofossils	30	24
Quartz	10	Tr

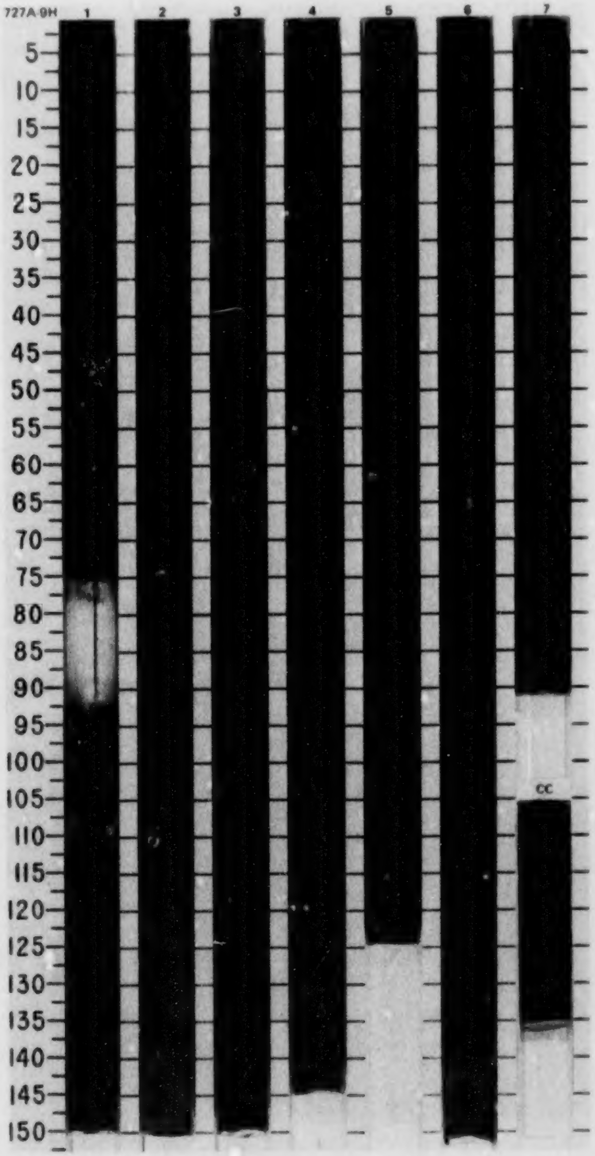
727A-9H
1
2
3
4
5
6
7
CC
5
10
15
20
25
30
35
40
45
50
55
60
65
70
75
80
85
90
95
100
105
110
115
120
125
130
135
140
145
150

SITE 727 HOLE A CORE 10H CORED INTERVAL 1000.6-1010.2 mbsl; 85.8-95.4 mbsf

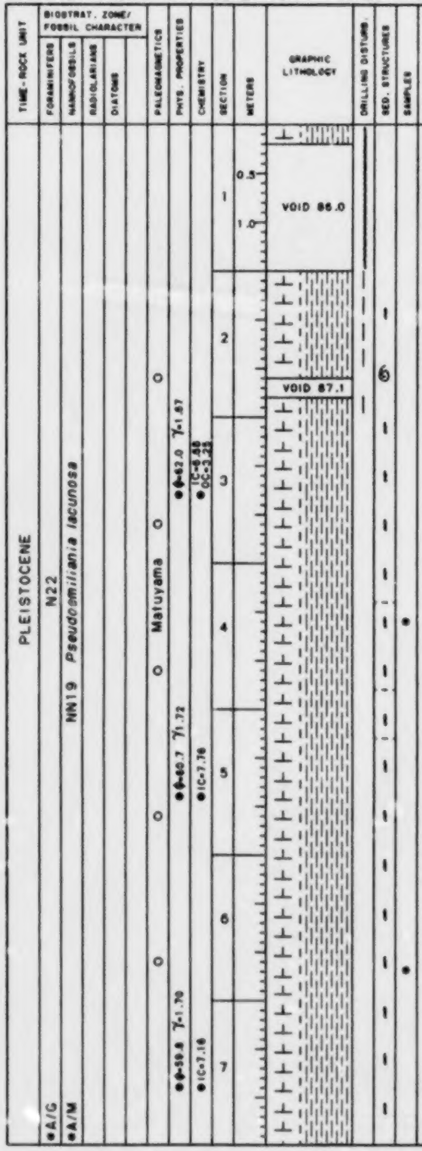
TIME-ROCK UNIT
BIOSTRAT. ZONE/ FOSSIL CHARACTER
FORAMINIFERS
NANNOFOSSILS
RADIOLARIANS
DIATOMS
PALEOMAGNETICS
PHYS. PROPERTIES
CHEMISTRY
SECTION
METERS
GRAPHIC LITHOLOGY
DRILLING DISTURB.
SED. STRUCTURES
SAMPLES
PLEISTOCENE
•A/G
N22
•A/M
NN19 *Pseudoemiliania lacunosa*
Matuyama
•Φ=62.0 γ=1.87
•Φ=60.7 γ1.72
•Φ=59.8 γ=1.70
IC=6.58
•OC=3.23
•IC=7.76
•IC=7.16
1
2
3
4
5
6
7
0.5
1.0
VOID 86.0
VOID 87.1

LITHOLOGIC DESCRIPTION

FORAMINIFER-BEARING CALCITIC MARLY NANNOFOSSIL OOZE

Section 1 is highly disturbed. Remainder of core is undisturbed.

Major lithology: FORAMINIFER-BEARING CALCITIC MARLY NANNOFOSSIL OOZE, olive (5Y 4/3) and olive gray (5Y 5/2, 4/2). Bioturbated throughout core.

SMEAR SLIDE SUMMARY (%):

	4, 83 D	6, 118 D
TEXTURE:		
Silt	50	40
Clay	50	60
COMPOSITION:		
Clay	15	20
Foraminifers	10	10
Inorganic calcite	35	20
Nannofossils	30	45
Quartz	10	5

Cont.

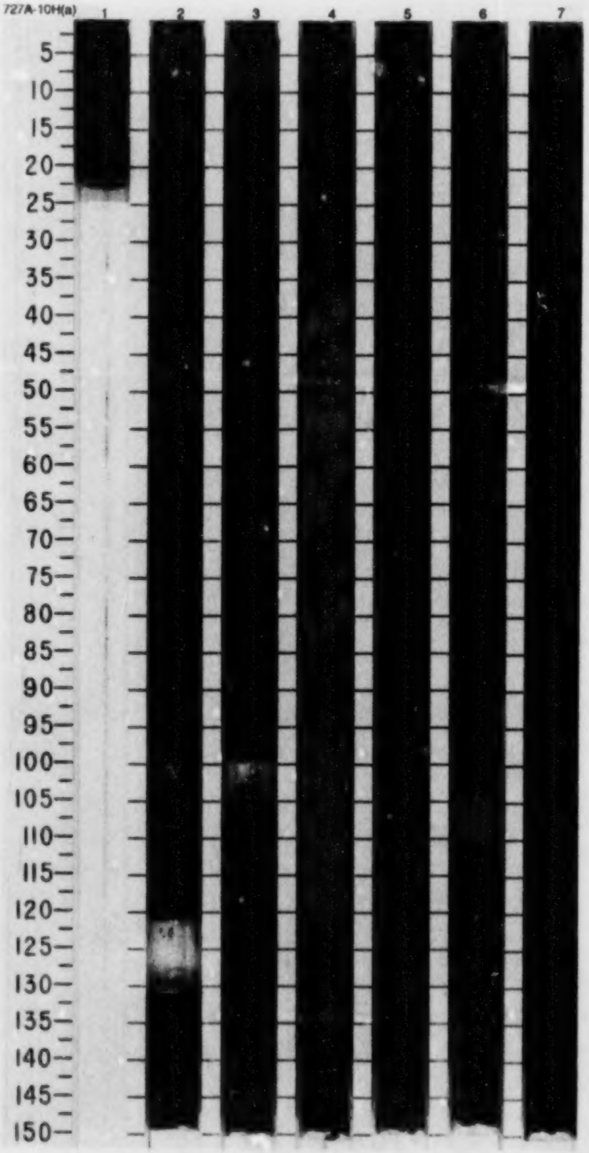
727A-10H(a)
1
2
3
4
5
6
7
5
10
15
20
25
30
35
40
45
50
55
60
65
70
75
80
85
90
95
100
105
110
115
120
125
130
135
140
145
150

SITE 727 HOLE A CORE 10H CORED INTERVAL 1000.6-1010.2 mbsl; 85.8-95.4 mbsf

TIME-ROCK UNIT	BIOSTRAT. ZONE/ FOSSIL CHARACTER				PALEOMAGNETICS	PHYS. PROPERTIES	CHEMISTRY	SECTION	METERS	GRAPHIC LITHOLOGY	DRILLING DISTURB.	SED. STRUCTURES	SAMPLES	LITHOLOGIC DESCRIPTION
	FORAMINIFERS	NANNOFOSSILS	RADIOLARIANS	DIATOMS										
PLEISTOCENE	●A/G N22	●A/M NN19	●Barren					8	0.5					Cont.
								CC	1.0					

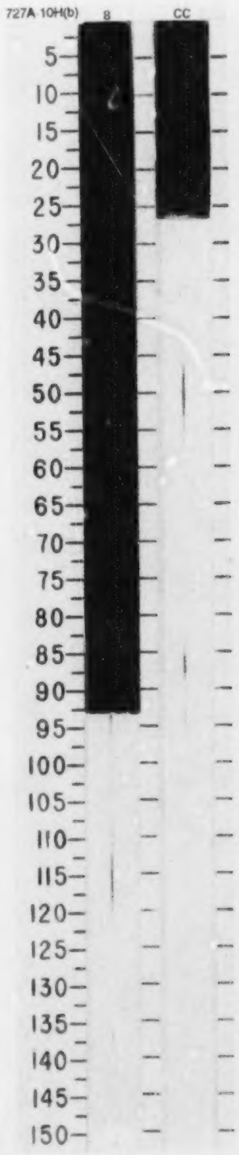
727A 10H(b)
8
CC
5
10
15
20
25
30
35
40
45
50
55
60
65
70
75
80
85
90
95
100
105
110
115
120
125
130
135
140
145
150

SITE 727 HOLE A CORE 11X CORED INTERVAL 1010.2-1019.8 mbsl; 95.4-105.0 mbsf

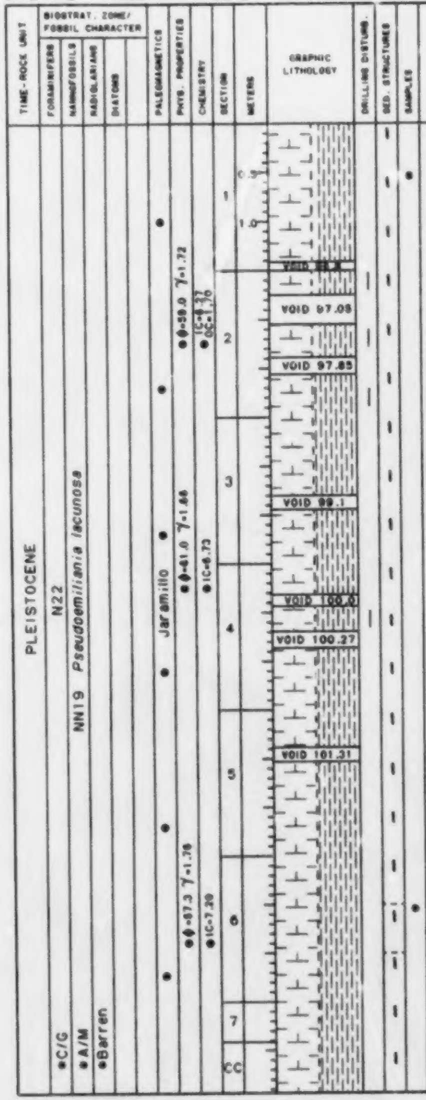
TIME-ROCK UNIT
BIOSTRAT. ZONE/ FOSSIL CHARACTER
FORAMINIFERS
NANNOFOSSILS
RADIOLARIANS
DIATOMS
PALEOMAGNETICS
PHYS. PROPERTIES
CHEMISTRY
SECTION
METERS
GRAPHIC LITHOLOGY
DRILLING DISTURB.
SED. STRUCTURES
SAMPLES
PLEISTOCENE
N22
NN19 Pseudoemiliania lacunosa
●C/G
●A/M
●Barren
Jaramillo
●ϕ=59.0 γ=1.72
●IC=8.37 OC=1.70
●ϕ=61.0 γ=1.86
●IC=6.73
●ϕ=67.3 γ=1.76
●IC=7.20
1
2
3
4
5
6
7
CC
0.5
1.0
VOID 97.05
VOID 97.85
VOID 99.1
VOID 100.0
VOID 100.27
VOID 101.31

LITHOLOGIC DESCRIPTION

CALCITIC MARLY NANNOFOSSIL OOZE

Section 2 and Section 4, 50-70 cm, are slightly disturbed. Remainder of core is undisturbed.

Major lithology: CALCITIC MARLY NANNOFOSSIL OOZE, olive (5Y 4/3) and olive gray (5Y 4/2). Bioturbation minor to common throughout.

SMEAR SLIDE SUMMARY (%):

	1, 54 D	6, 54 D
TEXTURE:		
Sand	5	10
Silt	25	25
Clay	70	65
COMPOSITION:		
Access. minerals	2	2
Clay	20	15
Dolomite	Tr	1
Fish remains	Tr	
Foraminifers	3	4
Inorganic calcite	15	25
Nannofossils	55	50
Quartz	5	3

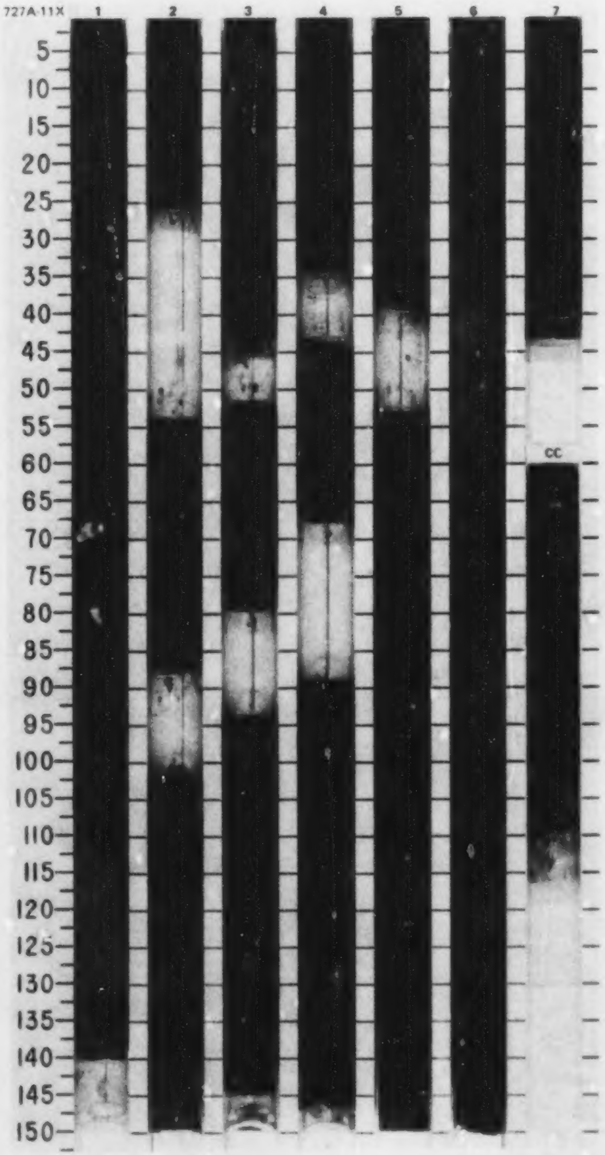
727A-11X
1
2
3
4
5
6
7
CC
5
10
15
20
25
30
35
40
45
50
55
60
65
70
75
80
85
90
95
100
105
110
115
120
125
130
135
140
145
150

SITE 727 HOLE A CORE 12X CORED INTERVAL 1019.8-1029.4 mbsl; 105.0-114.6 mbsf

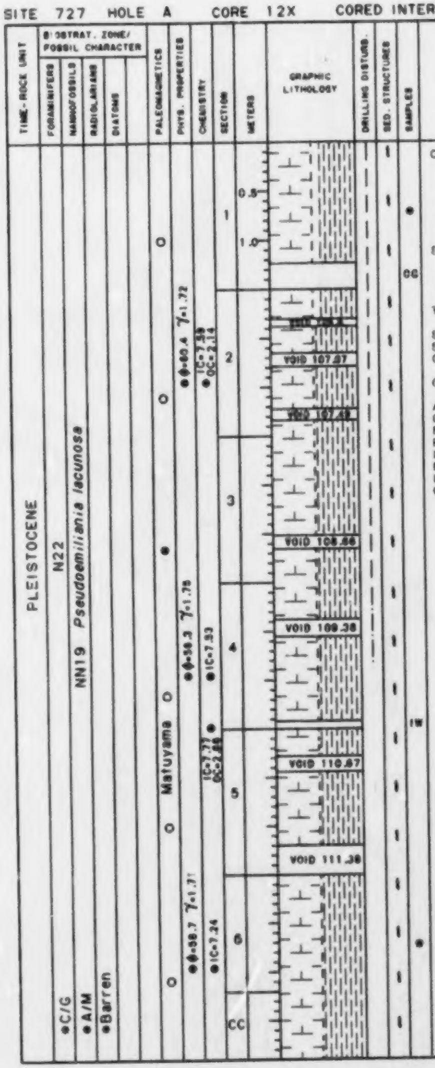
TIME-ROCK UNIT
BIOSTRAT. ZONE/ FOSSIL CHARACTER
FORAMINIFERS
NANNOFOSSILS
RADIOLARIANS
DIATOMS
PALEOMAGNETICS
PHYS. PROPERTIES
CHEMISTRY
SECTION
METERS
GRAPHIC LITHOLOGY
DRILLING DISTURB.
SED. STRUCTURES
SAMPLES
PLEISTOCENE
N22
NN19 Pseudoemiliania lacunosa
●C/G
●A/M
●Barren
Matuyama
●ϕ=60.4 γ=1.72
●ϕ=56.3 γ=1.75
●ϕ=58.7 γ=1.71
●IC=7.59 OC=2.14
●IC=7.53
IC=7.77 OC=2.85 ●
●IC=7.24
1
2
3
4
5
6
CC
0.5
1.0
VOID 107.07
VOID 107.49
VOID 108.66
VOID 109.38
VOID 110.67
VOID 111.38
OG
IW

LITHOLOGIC DESCRIPTION

CALCITIC MARLY NANNOFOSSIL OOZE

Sections 1-3 are slightly disturbed. Section 4, 0-90 cm is moderately disturbed. Remainder of core is undisturbed.

Major lithology: CALCITIC MARLY NANNOFOSSIL OOZE, olive (5Y 4/3), bioturbated.

SMEAR SLIDE SUMMARY (%):

	1, 72 D	6, 72 D
TEXTURE:		
Sand	5	5
Silt	25	30
Clay	70	65
COMPOSITION:		
Access. minerals	3	1
Clay	25	25
Feldspar	1	
Foraminifers	4	3
Inorganic calcite	15	25
Mica	Tr	1
Nannofossils	45	40
Quartz	7	5

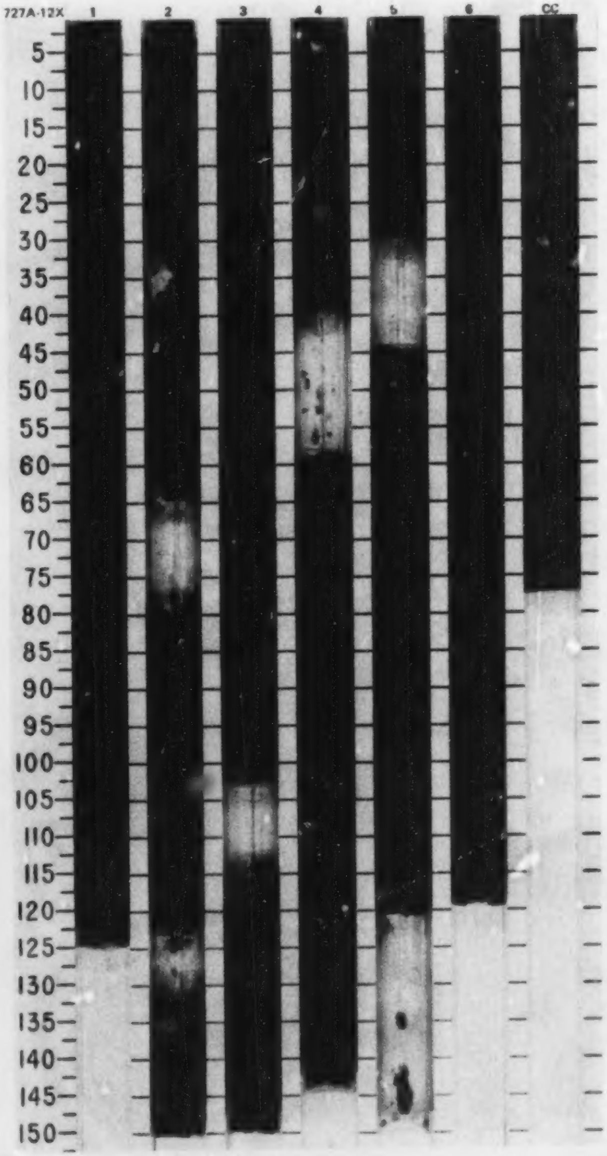
727A-12X
1
2
3
4
5
6
CC
5
10
15
20
25
30
35
40
45
50
55
60
65
70
75
80
85
90
95
100
105
110
115
120
125
130
135
140
145
150

SITE 727 HOLE A CORE 13X CORED INTERVAL 1029.4-1039.0 mbsl; 114.6-124.2 mbsf

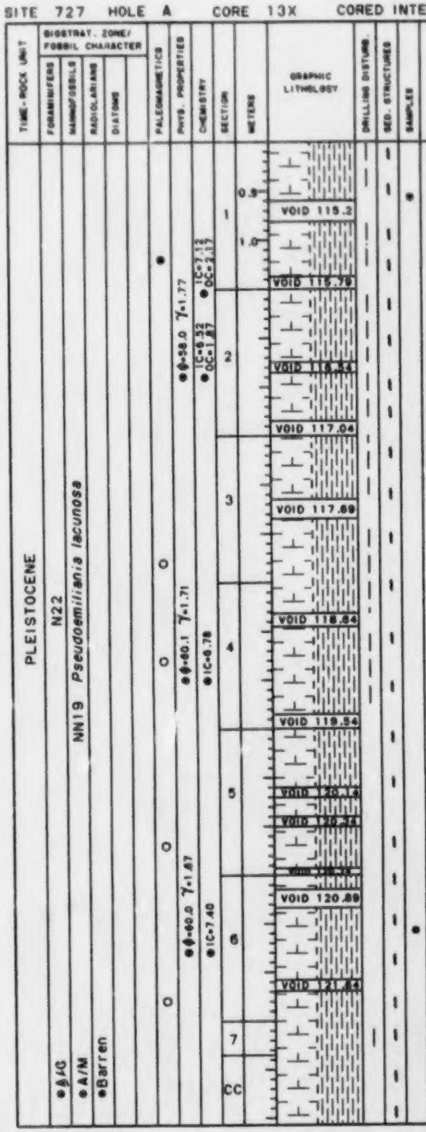
TIME-ROCK UNIT
BIOSTRAT. ZONE/ FOSSIL CHARACTER
FORAMINIFERS
NANNOFOSSILS
RADIOLARIANS
DIATOMS
PALEOMAGNETICS
PHYS. PROPERTIES
CHEMISTRY
SECTION
METERS
GRAPHIC LITHOLOGY
DRILLING DISTURB.
SED. STRUCTURES
SAMPLES
PLEISTOCENE
N22
NN19 Pseudoemiliania lacunosa
●A/G
●A/M
●Barren
●ϕ=58.0 γ=1.77
●ϕ=60.1 γ=1.71
●ϕ=60.0 γ=1.87
●IC=7.12 OC=2.17
●IC=6.52 OC=1.87
●IC=6.78
●IC=7.40
1
2
3
4
5
6
7
CC
0.5
1.0
VOID 115.2
VOID 115.79
VOID 116.54
VOID 117.04
VOID 117.89
VOID 118.64
VOID 119.54
VOID 120.89
VOID 121.64

LITHOLOGIC DESCRIPTION

CALCITIC MARLY NANNOFOSSIL OOZE

Sections 1-4 and Section 7 are slightly to moderately disturbed. Remainder of core is undisturbed.

Major lithology: CALCITIC MARLY NANNOFOSSIL OOZE, olive (5Y 4/3), bioturbated.

SMEAR SLIDE SUMMARY (%):

	1, 58 D	6, 58 D
TEXTURE:		
Sand	10	10
Silt	25	25
Clay	65	65
COMPOSITION:		
Access. minerals	1	1
Clay	25	25
Dolomite	Tr	1
Feldspar	2	1
Foraminifers	4	5
Inorganic calcite	20	20
Nannofossils	40	40
Quartz	8	7

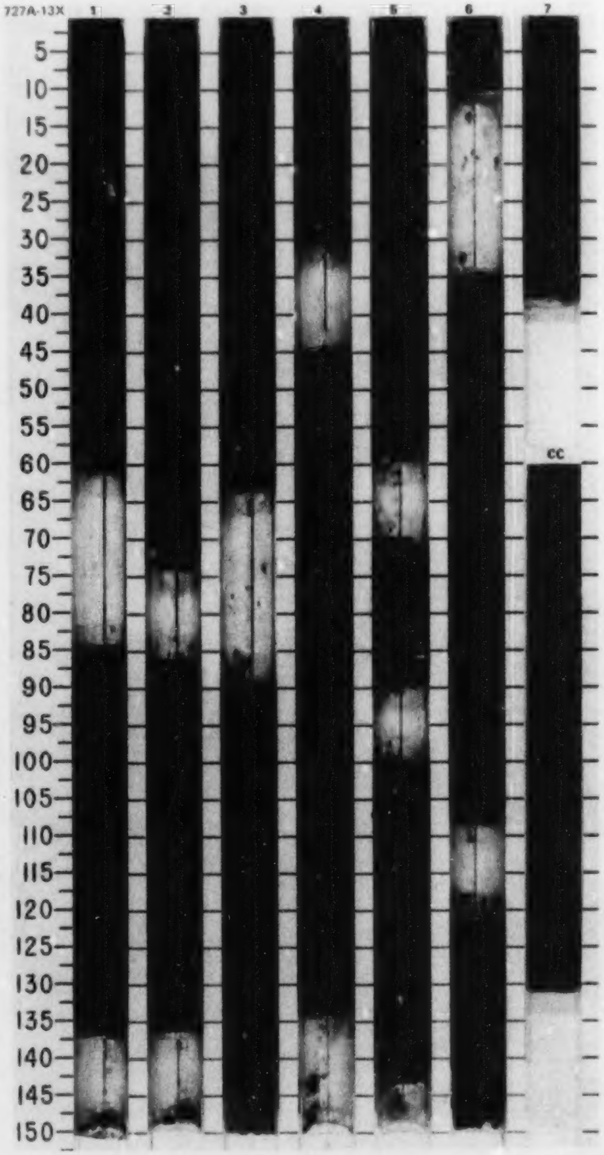
727A-13X
1
2
3
4
5
6
7
CC
5
10
15
20
25
30
35
40
45
50
55
60
65
70
75
80
85
90
95
100
105
110
115
120
125
130
135
140
145
150

SITE 727 HOLE A CORE 14X CORED INTERVAL 1039.0-1048.7 mbsl; 124.0-133.9 mbsf

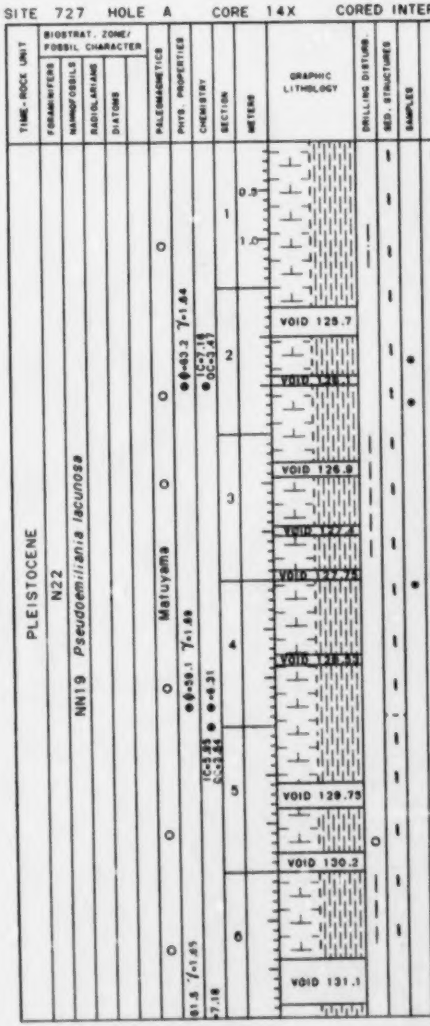
TIME-ROCK UNIT
BIOSTRAT. ZONE/ FOSSIL CHARACTER
FORAMINIFERS
NANNOFOSSILS
RADIOLARIANS
DIATOMS
PALEOMAGNETICS
PHYS. PROPERTIES
CHEMISTRY
SECTION
METERS
GRAPHIC LITHOLOGY
DRILLING DISTURB.
SED. STRUCTURES
SAMPLES
PLEISTOCENE
N22
NN19 Pseudoemiliania lacunosa
Matuyama
φ=63.2 γ=1.64
φ=58.1 γ=1.69
61.5 γ=1.65
IC=7.18 OC=3.47
IC=5.85 OC=3.84
=6.31
=7.18
0.5
1.0
1
2
3
4
5
6
VOID 125.7
VOID 126.1
VOID 126.9
VOID 127.4
VOID 127.75
VOID 128.53
VOID 129.75
VOID 130.2
VOID 131.1

LITHOLOGIC DESCRIPTION

CALCITIC MARLY NANNOFOSSIL OOZE

Section 1, 100-150 cm, Section 5, 120-130 cm, and Section 6, 135-150 cm, are moderately to highly disturbed. Section 3, Section 5, 0-60 cm, and Section 7 are slightly disturbed. Remainder of core is undisturbed.

Major lithology: CALCITIC MARLY NANNOFOSSIL OOZE, olive (5Y 4/3) and olive gray (5Y 5/2). Minor to common bioturbation throughout.

Minor lithology: Nannofossil-rich calcitic clayey sand, greenish gray (5GY 5/1), in Section 2, 120-121 cm.

SMEAR SLIDE SUMMARY (%):

	2, 74 D	2, 120 M	4, 3 D
TEXTURE:			
Sand	5	45	20
Silt	30	15	20
Clay	65	40	60
COMPOSITION:			
Access. minerals	2	2	1
Clay	25	20	15
Dolomite	1		
Feldspar		2	1
Foraminifers	5	1	Tr
Inorganic calcite	20	40	33
Nannofossils	40	20	45
Phosphate	Tr		
Quartz	7	15	5
Radiolarians	Tr		
Sponge spicules	Tr		

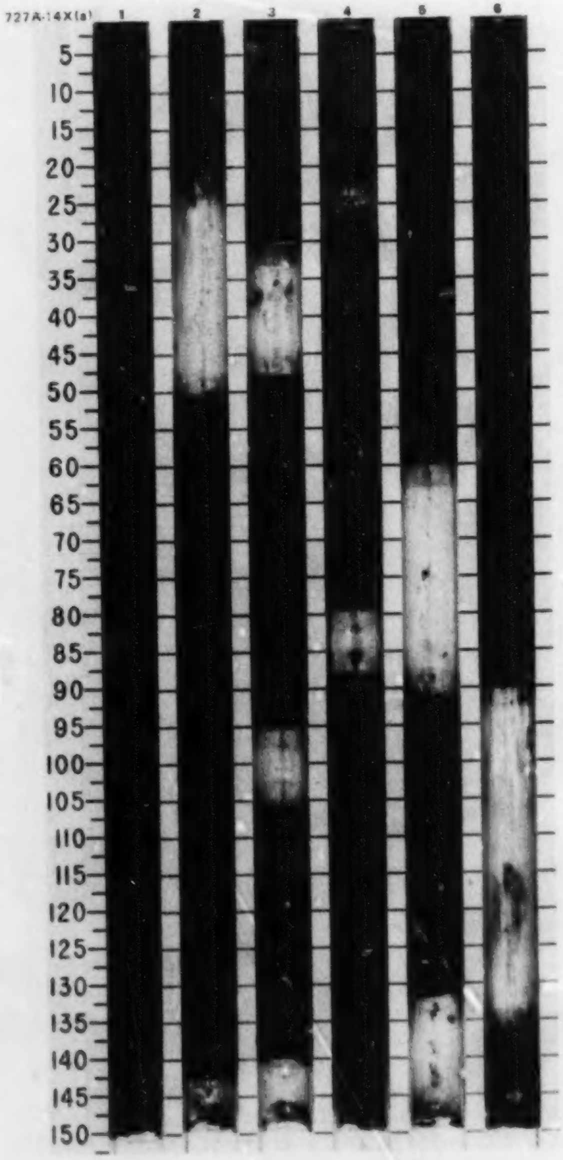
727A-14X(a)
1
2
3
4
5
6
5
10
15
20
25
30
35
40
45
50
55
60
65
70
75
80
85
90
95
100
105
110
115
120
125
130
135
140
145
150

SITE 727 HOLE A CORE 14X CORED INTERVAL 1039.0-1048.7 mbsl; 124.0-133.9 mbsf

TIME-ROCK UNIT	BIOSTRAT. ZONE/ FOSSIL CHARACTER FORAMINIFERS	NANNOFOSSILS	RADIOLARIANS	DIATOMS		PALEOMAGNETICS	PHYS. PROPERTIES	CHEMISTRY	SECTION	METERS	GRAPHIC LITHOLOGY	DRILLING DISTURB.	SED. STRUCTURES	SAMPLES	LITHOLOGIC DESCRIPTION
	● A/G	● A/M	● BARREN				φ=61.5 ● γ=1.65	IC=7.1 ●	7						(cont.)
									CC						

727A-14X(b)
7
CC

SITE 727 HOLE A CORE 15X CORED INTERVAL 1048.7-1058.4 mbsl; 133.9-143.6 mbsf

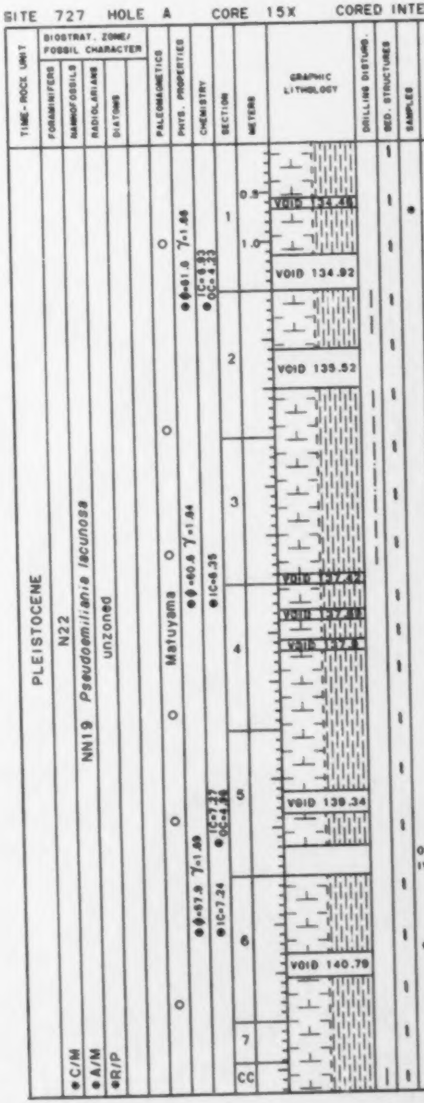
TIME-ROCK UNIT
BIOSTRAT. ZONE/ FOSSIL CHARACTER
FORAMINIFERS
NANNOFOSSILS
RADIOLARIANS
DIATOMS
PALEOMAGNETICS
PHYS. PROPERTIES
CHEMISTRY
SECTION
METERS
GRAPHIC LITHOLOGY
DRILLING DISTURB.
SED. STRUCTURES
SAMPLES
PLEISTOCENE
N22
NN19 Pseudoemiliania lacunosa
unzoned
●C/M
●A/M
●R/P
Matuyama
●Φ=61.0 γ=1.88
●Φ=60.6 γ=1.84
●Φ=57.9 γ=1.89
●IC=8.93 OC=4.33
●IC=8.35
●IC=7.27 OC=4.98
●IC=7.24
1
2
3
4
5
6
7
CC
0.5
1.0
VOID 134.92
VOID 135.52
VOID 139.34
VOID 140.79
OG
IW

LITHOLOGIC DESCRIPTION

CALCITIC MARLY NANNOFOSSIL OOZE

Sections 2 through 3 and CC are slightly to moderately disturbed. Remainder of core is undisturbed.

Major lithology: CALCITIC MARLY NANNOFOSSIL OOZE, OLIVE (5Y 4/3), with minor to moderate bioturbation in Section 1 to Section 6, 80 cm, and CC.

SMEAR SLIDE SUMMARY (%):

	1, 71 D	6, 75 D
TEXTURE:		
Sand	5	10
Silt	20	30
Clay	75	60
COMPOSITION:		
Quartz	5	100
Feldspar		1
Mica		1
Clay	25	25
Accessory Minerals	2	Tr
Foraminifers	3	1
Nannofossils	50	35
Sponge spicules	Tr	

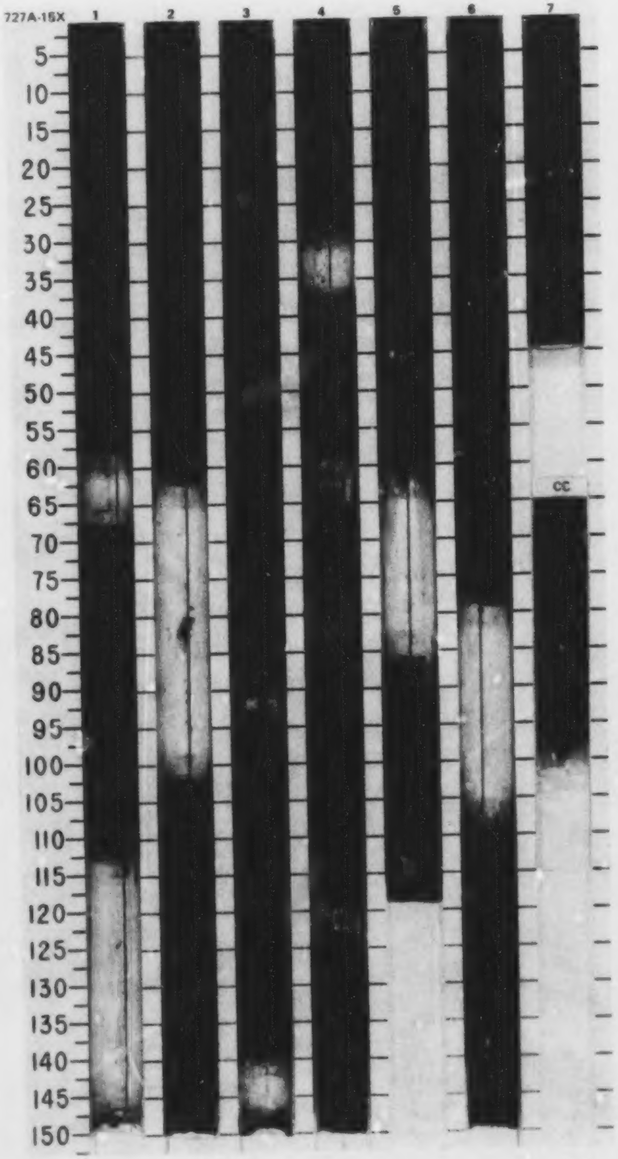
727A-15X
1
2
3
4
5
6
7
CC
5
10
15
20
25
30
35
40
45
50
55
60
65
70
75
80
85
90
95
100
105
110
115
120
125
130
135
140
145
150

SITE 727 HOLE A CORE 16X CORED INTERVAL 1058.4-1068.1 mbsl; 143.6-153.3 mbsf

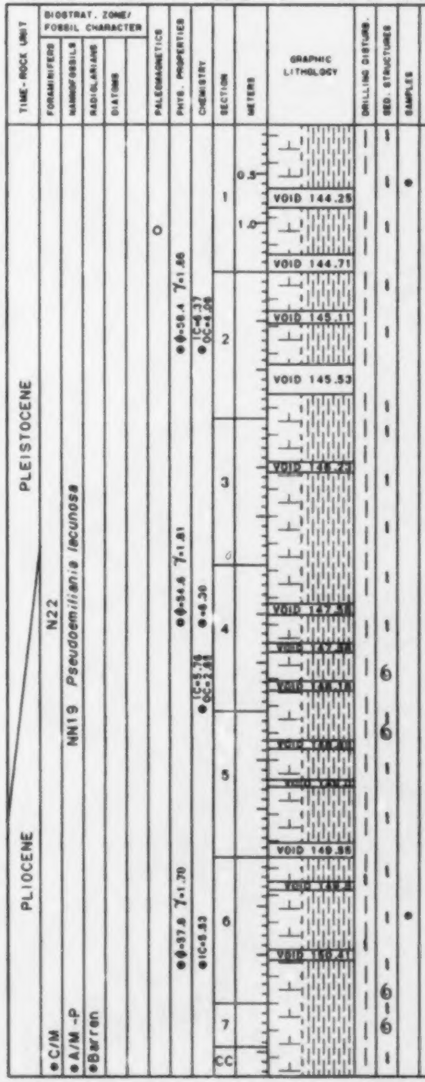
TIME-ROCK UNIT
BIOSTRAT. ZONE/ FOSSIL CHARACTER
FORAMINIFERS
NANNOFOSSILS
RADIOLARIANS
DIATOMS
PALEOMAGNETICS
PHYS. PROPERTIES
CHEMISTRY
SECTION
METERS
GRAPHIC LITHOLOGY
DRILLING DISTURB.
SED. STRUCTURES
SAMPLES
PLEISTOCENE
PLIOCENE
N22
NN19 Pseudoemiliania lacunosa
●C/M
●A/M -P
●Barren
φ=58.4 γ=1.86
φ=54.6 γ=1.81
φ=37.6 γ=1.70
IC=5.53
1
2
3
4
5
6
7
CC
0.5
1.0
VOID 144.25
VOID 144.71
VOID 145.11
VOID 145.53
VOID 149.55

LITHOLOGIC DESCRIPTION

CALCITIC MARLY NANNOFOSSIL OOZE TO FORAMINIFER-BEARING CALCITIC MARLY NANNOFOSSIL OOZE

Entire core is slightly to highly disturbed.

Major lithology: CALCITIC MARLY NANNOFOSSIL OOZE to FORAMINIFER-BEARING CALCITIC MARLY NANNOFOSSIL OOZE, olive (5Y 4/3) and olive gray (5Y 5/2, 4/2). Slightly bioturbated throughout. Dispersed shell debris at Section 4, 98-107 cm, Section 5, 15-25 cm, Section 6, 130-135 cm, and CC, 6-8 cm.

SMEAR SLIDE SUMMARY (%):

	1, 59 D	6, 60 D
TEXTURE:		
Sand	10	20
Silt	30	25
Clay	60	55
COMPOSITION:		
Access. minerals	1	2
Clay	25	25
Dolomite	Tr	1
Feldspar	1	
Foraminifers	5	7
Glauconite		Tr
Inorganic calcite	25	25
Nannofossils	35	30
Quartz	8	10
Shell debris		Tr
Sponge spicules	Tr	

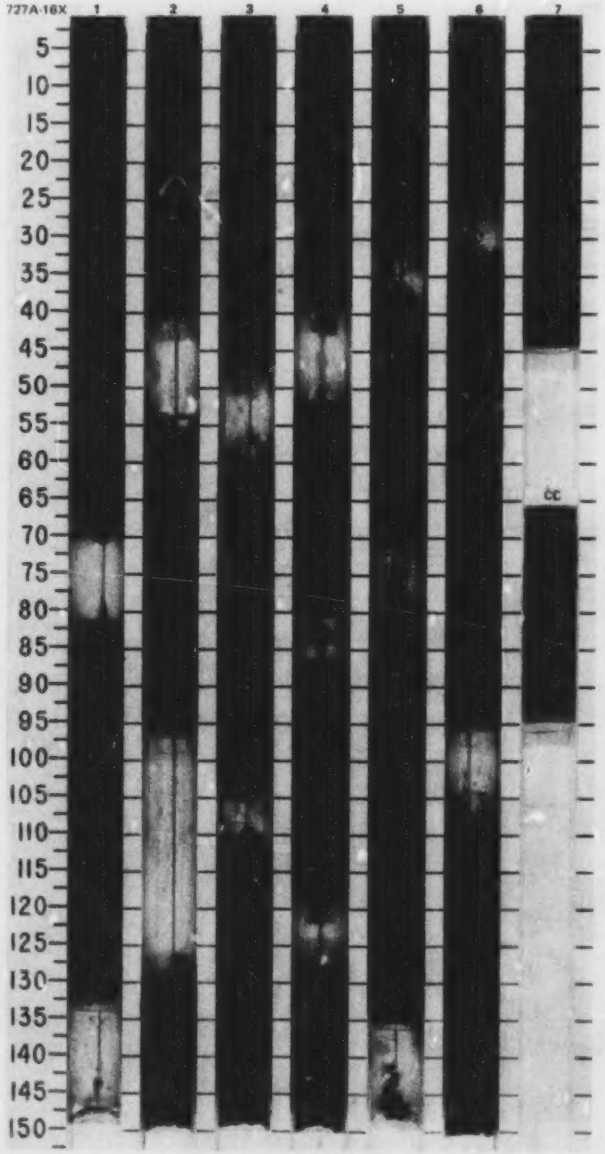
727A-16X
1
2
3
4
5
6
7
CC
5
10
15
20
25
30
35
40
45
50
55
60
65
70
75
80
85
90
95
100
105
110
115
120
125
130
135
140
145
150

SITE 727 HOLE A CORE 17X CORED INTERVAL 1068.1-1077.8 mbsl; 153.3-163.0 mbsf

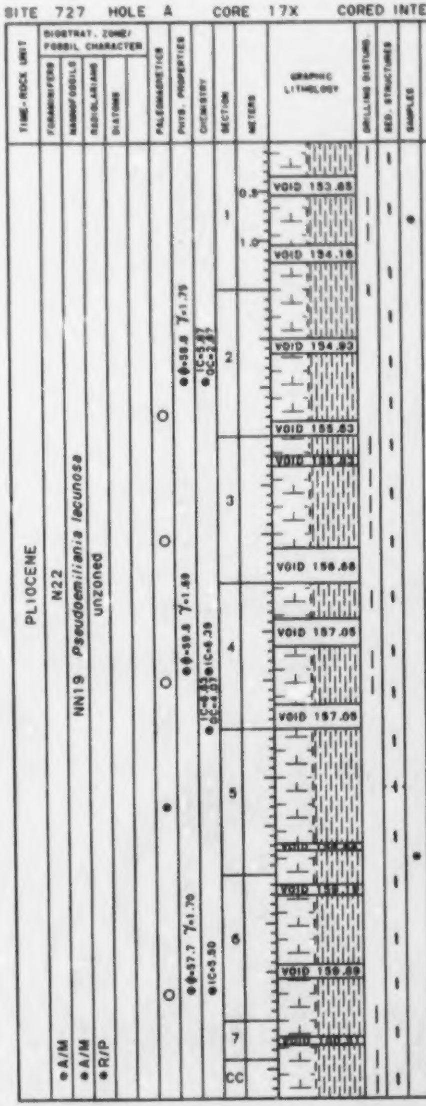
TIME-ROCK UNIT
BIOSTRAT. ZONE/ FOSSIL CHARACTER
FORAMINIFERS
NANNOFOSSILS
RADIOLARIANS
DIATOMS
PALEOMAGNETICS
PHYS. PROPERTIES
CHEMISTRY
SECTION
METERS
GRAPHIC LITHOLOGY
DRILLING DISTURB.
SED. STRUCTURES
SAMPLES
PLIOCENE
N22
NN19 Pseudoemiliania lacunosa
unzoned
● A/M
● A/M
● R/P
●φ=58.8 γ=1.75
●φ=59.8 γ=1.69
●φ=57.7 γ=1.70
IC=5.87 OC=2.87
IC=6.83 OC=4.07
●IC=6.39
●IC=5.50
0.5
1.0
1
2
3
4
5
6
7
CC
VOID 153.65
VOID 154.16
VOID 154.93
VOID 155.63
VOID 156.88
VOID 157.05
VOID 157.08
VOID 159.89

LITHOLOGIC DESCRIPTION

CALCITIC MARLY NANNOFOSSIL OOZE

Sections 1, 3 and 4, 7, and CC are slightly disturbed. Remainder of core is undisturbed.

Major lithology: CALCITIC MARLY NANNOFOSSIL OOZE, olive (5Y 4/3), with minor bioturbation throughout.

SMEAR SLIDE SUMMARY (%):

	1, 80 D	5, 133 D
TEXTURE:		
Sand	15	
Silt	25	30
Clay	60	70
COMPOSITION:		
Access. minerals	1	1
Clay	25	25
Dolomite	1	Tr
Foraminifers	5	Tr
Glauconite	Tr	
Inorganic calcite	25	24
Mica	1	
Nannofossils	35	45
Quartz	7	5

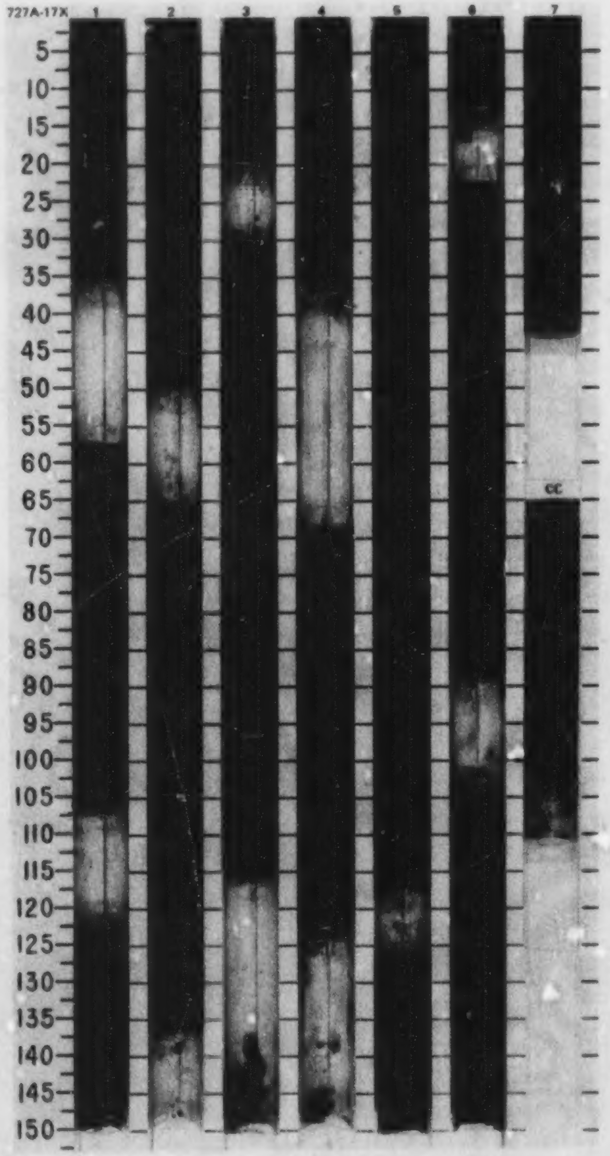
727A-17X
1
2
3
4
5
6
7
CC
5
10
15
20
25
30
35
40
45
50
55
60
65
70
75
80
85
90
95
100
105
110
115
120
125
130
135
140
145
150

SITE 727 HOLE A CORE 18X CORED INTERVAL 1077.8-1087.5 mbsl; 163.0-172.7 mbsf

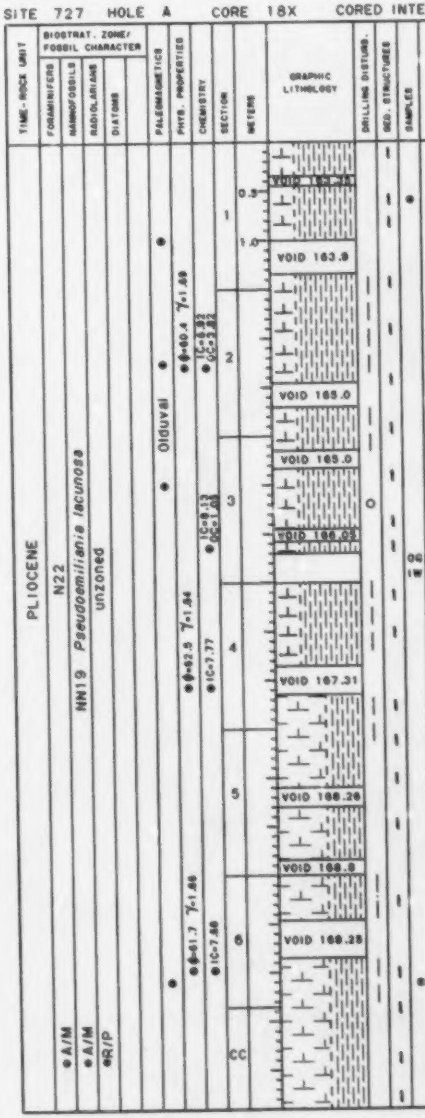
TIME-ROCK UNIT
BIOSTRAT. ZONE/ FOSSIL CHARACTER
FORAMINIFERS
NANNOFOSSILS
RADIOLARIANS
DIATOMS
PALEOMAGNETICS
PHYS. PROPERTIES
CHEMISTRY
SECTION
METERS
GRAPHIC LITHOLOGY
DRILLING DISTURB.
SED. STRUCTURES
SAMPLES
PLIOCENE
N22
NN19 Pseudoemiliania lacunosa
unzoned
●A/M
●A/M
●R/P
Olduvai
●φ=60.4 γ=1.89
●φ=62.5 γ=1.84
●φ=61.7 γ=1.86
●IC=8.92 OC=1.82
●IC=9.13 OC=1.03
●IC=7.77
●IC=7.86
1
2
3
4
5
6
CC
0.5
1.0
VOID 163.8
VOID 165.0
VOID 165.0
VOID 166.05
VOID 167.31
VOID 168.26
VOID 168.8
VOID 169.25
OG
IW

LITHOLOGIC DESCRIPTION

CALCITIC MARLY NANNOFOSSIL OOZE

Section 1, 135 cm, to Section 2, and Sections 4 and 6, are slightly to moderately disturbed. Remainder of core is undisturbed.

Major lithology: CALCITIC MARLY NANNOFOSSIL OOZE, olive (5Y 4/3) and olive gray (5Y 4/2). Minor bioturbation throughout.

SMEAR SLIDE SUMMARY (%):

	1, 60 D	6, 112 D
TEXTURE:		
Sand	20	5
Silt	25	25
Clay	55	70
COMPOSITION:		
Access. minerals	1	1
Clay	25	20
Feldspar	1	
Foraminifers	3	2
Inorganic calcite	30	15
Nannofossils	30	55
Quartz	10	7
Sponge spicules		Tr

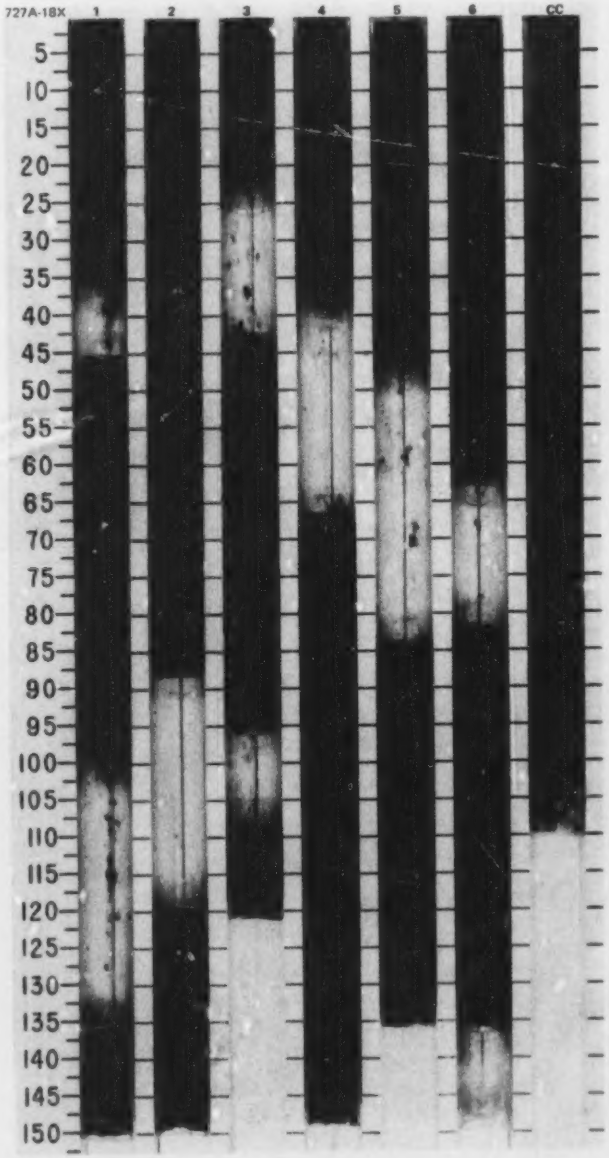
727A-18X
1
2
3
4
5
6
CC
5
10
15
20
25
30
35
40
45
50
55
60
65
70
75
80
85
90
95
100
105
110
115
120
125
130
135
140
145
150

SITE 727 HOLE A CORE 19X CORED INTERVAL 1087.5-1097.2 mbsl; 172.7-182.4 mbsf

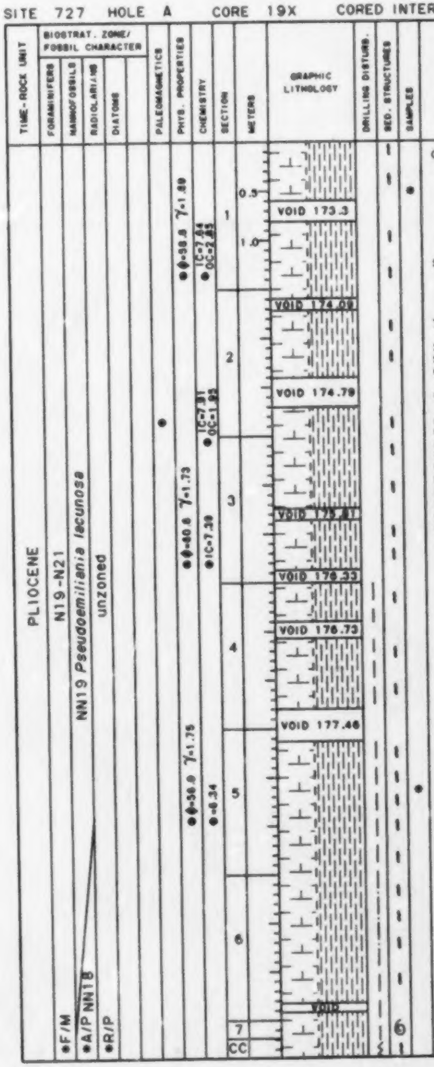
TIME-ROCK UNIT
BIOSTRAT. ZONE/ FOSSIL CHARACTER
FORAMINIFERS
NANNOFOSSILS
RADIOLARIANS
DIATOMS
PALEOMAGNETICS
PHYS. PROPERTIES
CHEMISTRY
SECTION
METERS
GRAPHIC LITHOLOGY
DRILLING DISTURB.
SED. STRUCTURES
SAMPLES
PLIOCENE
N19-N21
NN19 Pseudoemiliania lacunosa
unzoned
●F/M
●A/P NN18
●R/P
●Φ=58.8 γ=1.89
●Φ=60.6 γ=1.73
●Φ=56.9 γ=1.75
●IC=7.64 OC=2.85
●IC=7.31 OC=1.95
●IC=7.39
●=6.34
1
2
3
4
5
6
7
CC
0.5
1.0
VOID 173.3
VOID 174.09
VOID 174.79
VOID 175.81
VOID 176.33
VOID 176.73
VOID 177.46
VOID
6

LITHOLOGIC DESCRIPTION

CALCITIC MARLY NANNOFOSSIL OOZE

Sections 4-7 are slightly disturbed. CC is highly disturbed. Sections 1-3 are undisturbed.

Major lithology: CALCITIC MARLY NANNOFOSSIL OOZE, olive (5Y 4/3) and olive gray (5Y 4/2). Minor bioturbation throughout. Dispersed shell debris at Section 6, 143-146 cm.

SMEAR SLIDE SUMMARY (%):

	1, 51 D	5, 63 D
TEXTURE:		
Sand	10	15
Silt	20	25
Clay	70	60
COMPOSITION:		
Access. minerals	1	2
Clay	30	20
Dolomite	Tr	
Feldspar	1	
Foraminifers	2	3
Inorganic calcite	20	25
Mica	Tr	Tr
Nannofossils	40	40
Quartz	6	10
Sponge spicules	Tr	

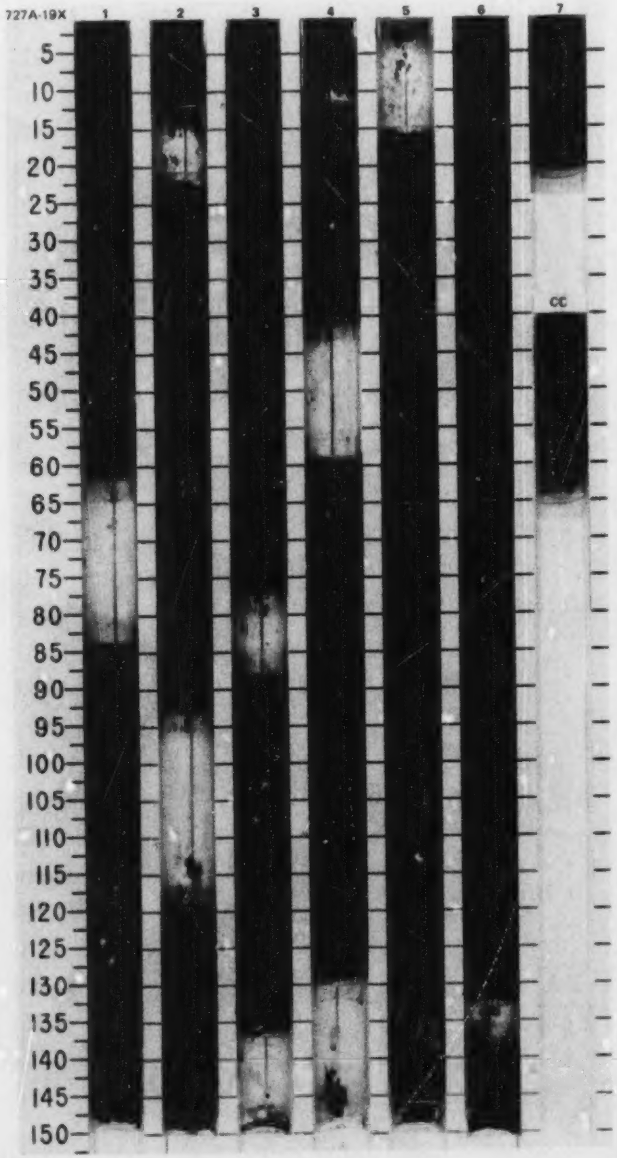
727A-19X
1
2
3
4
5
6
7
CC
5
10
15
20
25
30
35
40
45
50
55
60
65
70
75
80
85
90
95
100
105
110
115
120
125
130
135
140
145
150

SITE 727 HOLE B CORE 1H CORED INTERVAL 914.8-923.0 mbsl; 0.0-8.2 mbsf

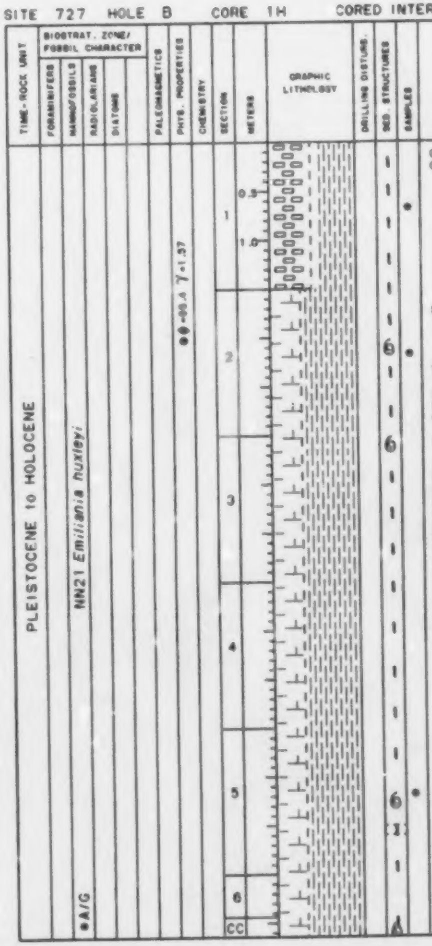
TIME-ROCK UNIT
BIOSTRAT. ZONE/ FOSSIL CHARACTER
FORAMINIFERS
NANNOFOSSILS
RADIOLARIANS
DIATOMS
PALEOMAGNETICS
PHYS. PROPERTIES
CHEMISTRY
SECTION
METERS
GRAPHIC LITHOLOGY
DRILLING DISTURB.
SED. STRUCTURES
SAMPLES
PLEISTOCENE to HOLOCENE
NN21 *Emiliania huxleyi*
●A/G
●Φ=68.4 γ=1.37
0.5
1.0
1
2
3
4
5
6
CC

LITHOLOGIC DESCRIPTION

CALCITIC MARLY CALCAREOUS OOZE and CALCITIC MARLY NANNOFOSSIL OOZE

Section 1, 0-5 cm, is moderately disturbed. Remainder of core is undisturbed.

Major lithologies:

a. CALCITIC MARLY CALCAREOUS OOZE, olive gray (5Y 4/2). Section 1. Bioturbated.

b. CALCITIC MARLY NANNOFOSSIL OOZE, olive (5Y 4/3), in Section 2 to CC; bioturbated. Dispersed shell debris at Section 2, 55-60 cm, Section 3, 7 cm, and CC, 4-5 cm. Whole pelecypod shell at Section 5, 72-78 cm. Section 2 to CC.

SMEAR SLIDE SUMMARY (%):

	1, 60 D	2, 60 D	5, 60 D
TEXTURE:			
Sand	25	15	15
Silt	30	30	30
Clay	45	55	55
COMPOSITION:			
Access. minerals	2	3	2
Clay	20	20	20
Diatoms	4		
Dolomite	1		
Feldspar	2		1
Foraminifers	15	5	2
Volcanic glass		Tr	
Glauconite	Tr		
Inorganic calcite	20	25	25
Nannofossils	25	35	35
Phosphate		Tr	
Quartz	10	12	15
Radiolarians	Tr		
Silicoflagellates	Tr		
Sponge spicules	1		

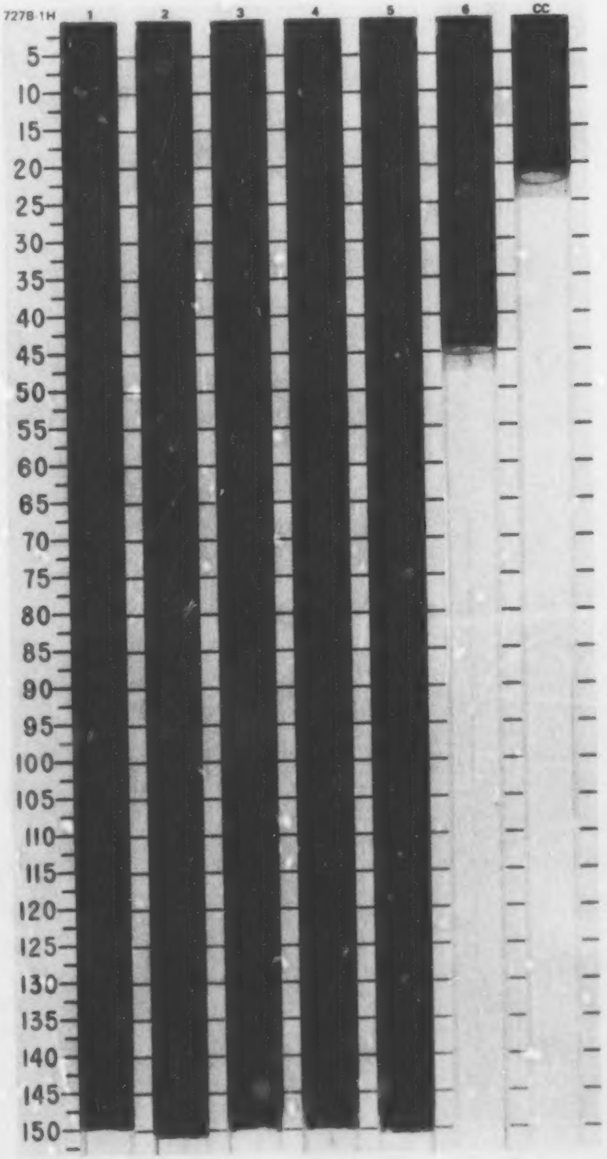
727B-1H
1
2
3
4
5
6
CC
5
10
15
20
25
30
35
40
45
50
55
60
65
70
75
80
85
90
95
100
105
110
115
120
125
130
135
140
145
150

SITE 727 HOLE B CORE 2H CORED INTERVAL 923.0-932.4 mbsl; 8.2-17.6 mbsf

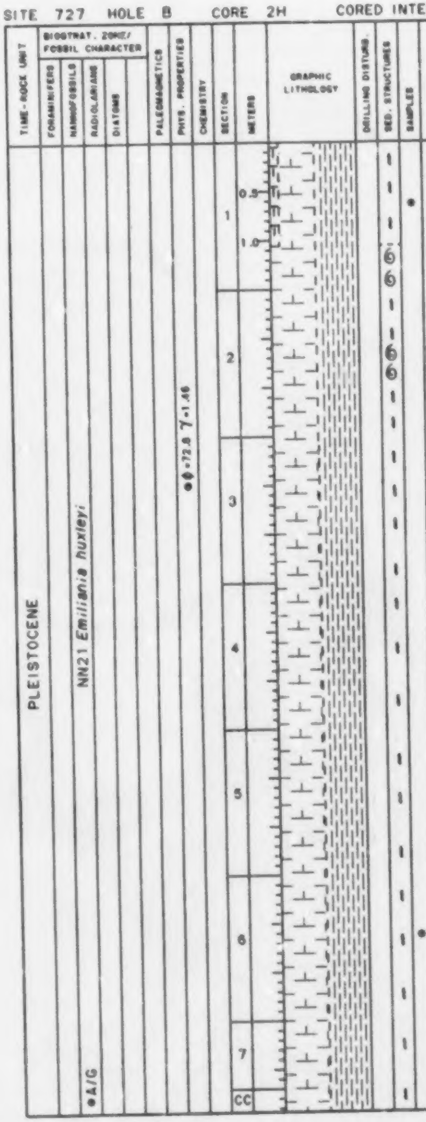
TIME-ROCK UNIT
BIOSTRAT. ZONE/ FOSSIL CHARACTER
FORAMINIFERS
NANNOFOSSILS
RADIOLARIANS
DIATOMS
PALEOMAGNETICS
PHYS. PROPERTIES
CHEMISTRY
SECTION
METERS
GRAPHIC LITHOLOGY
DRILLING DISTURB.
SED. STRUCTURES
SAMPLES
PLEISTOCENE
NN21 Emiliania huxleyi
●A/G
●φ=72.8 γ=1.46
1
2
3
4
5
6
7
CC
0.5
1.0

LITHOLOGIC DESCRIPTION

FORAMINIFER-RICH CALCITIC MARLY NANNOFOSSIL OOZE and CALCITIC MARLY NANNOFOSSIL OOZE

Entire core is undisturbed.

Major lithologies:
a. FORAMINIFER-RICH CALCITIC MARLY NANNOFOSSIL OOZE, olive (5Y 4/3), in Section 1, 0-107 cm; bioturbated. Sparse shell debris.
b. CALCITIC MARLY NANNOFOSSIL OOZE, olive (5Y 4/3) and olive gray (5Y 5/2, 4/2), in Section 1, 107 cm, to CC. Bioturbation common to abundant throughout. Dispersed shell debris throughout. Single small brachiopod(?) valve at Section 1, 129-130 cm.

SMEAR SLIDE SUMMARY (%):

	1, 64 D	6, 64 D
TEXTURE:		
Sand	15	10
Silt	25	20
Clay	60	70
COMPOSITION:		
Access. minerals	2	1
Clay	20	20
Feldspar		Tr
Foraminifers	10	1
Inorganic calcite	20	23
Nannofossils	40	50
Organic debris	2	
Quartz	6	5
Sponge spicules		Tr

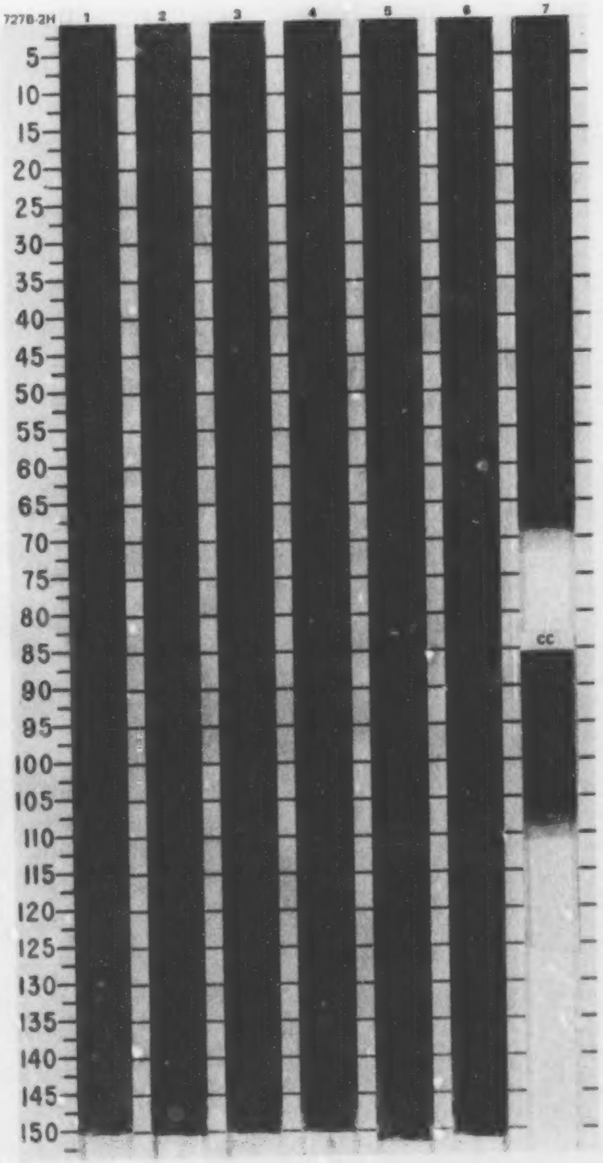
727B-2H
1
2
3
4
5
6
7
CC
5
10
15
20
25
30
35
40
45
50
55
60
65
70
75
80
85
90
95
100
105
110
115
120
125
130
135
140
145
150

SITE 727 HOLE B CORE 3H CORED INTERVAL 932.4-941.9 mbsl; 17.6-27.1 mbsf

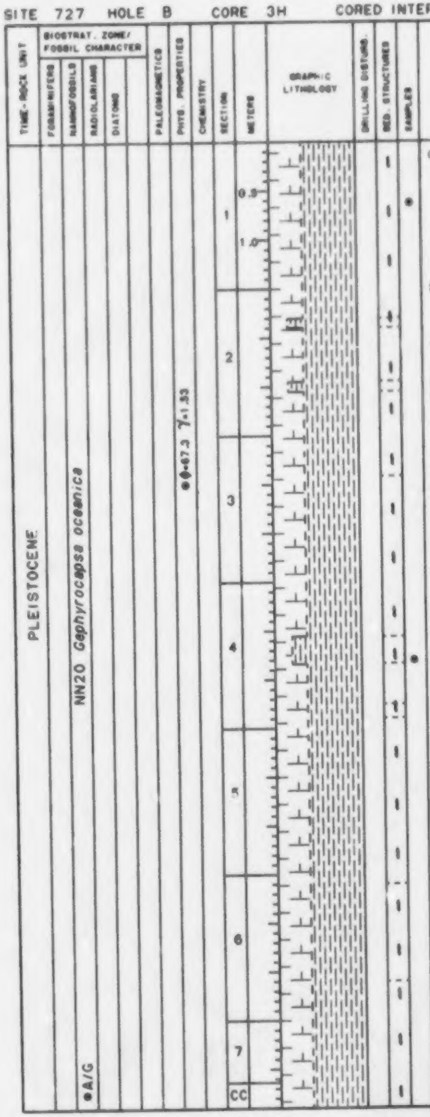
TIME-ROCK UNIT
BIOSTRAT. ZONE/ FOSSIL CHARACTER
FORAMINIFERS
NANNOFOSSILS
RADIOLARIANS
DIATOMS
PALEOMAGNETICS
PHYS. PROPERTIES
CHEMISTRY
SECTION
METERS
GRAPHIC LITHOLOGY
DRILLING DISTURB.
SED. STRUCTURES
SAMPLES
PLEISTOCENE
NN20 Gephyrocapsa oceanica
●A/G
●ϕ=67.3 γ=1.53
1
2
3
4
5
6
7
CC
0.5
1.0

LITHOLOGIC DESCRIPTION

CALCITIC MARLY NANNOFOSSIL OOZE

Entire core is undisturbed.

Major lithology: CALCITIC MARLY NANNOFOSSIL OOZE, olive (5Y 4/3) to olive gray (5Y 4/2); bioturbated.

Minor lithology: Nannofossil-rich calcitic silty clay, dark olive gray (5Y 3/2), in Section 2, 28-41 and 92-103 cm, and Section 4, 58-88 cm. Moderate to abundant bioturbation.

SMEAR SLIDE SUMMARY (%):

	1, 63 D	4, 80 D
TEXTURE:		
Sand	15	20
Silt	30	35
Clay	55	45
COMPOSITION:		
Access. minerals	1	2
Clay	20	25
Feldspar	1	
Foraminifers	3	Tr
Volcanic glass		Tr
Inorganic calcite	30	30
Nannofossils	35	20
Organic debris		5
Quartz	10	18

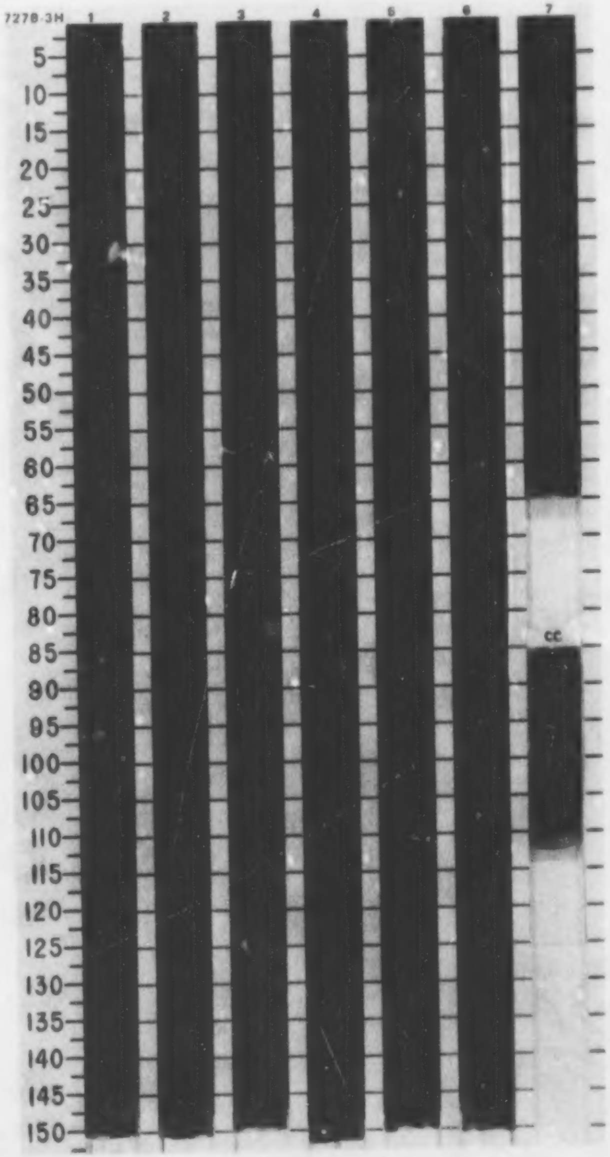
727B-3H
1
2
3
4
5
6
7
CC
5
10
15
20
25
30
35
40
45
50
55
60
65
70
75
80
85
90
95
100
105
110
115
120
125
130
135
140
145
150

SITE 728 HOLE A CORE 1H CORED INTERVAL 1427.8-1437.4 mbsl; 0.0-9.6 mbsf

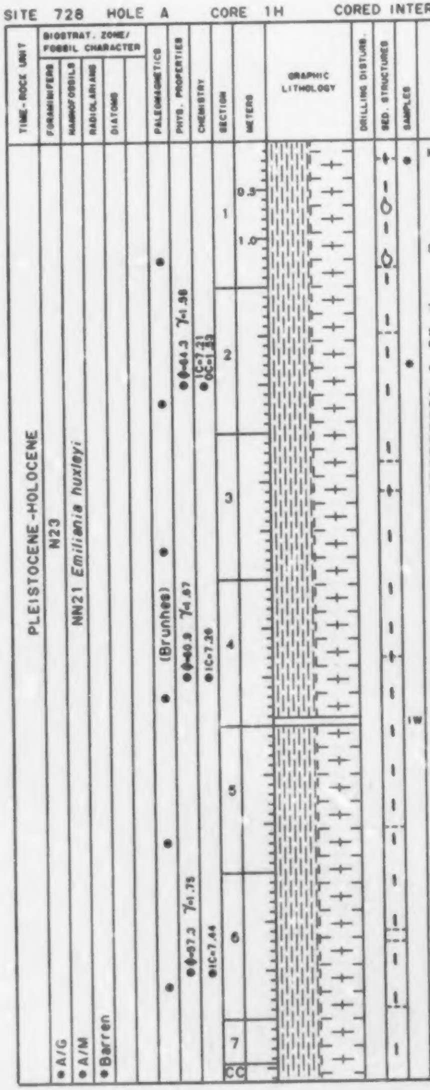
TIME-ROCK UNIT
BIOSTRAT. ZONE/ FOSSIL CHARACTER
FORAMINIFERS
NANNOFOSSILS
RADIOLARIANS
DIATOMS
PALEOMAGNETICS
PHYS. PROPERTIES
CHEMISTRY
SECTION
METERS
GRAPHIC LITHOLOGY
DRILLING DISTURB.
SED. STRUCTURES
SAMPLES
PLEISTOCENE-HOLOCENE
N23
NN21 Emiliania huxleyi
● A/G
● A/M
● Barren
(Brunhes)
●ϕ=64.3 γ=1.98
●IC=7.21 OC=1.53
●ϕ=60.9 γ=1.87
●IC=7.36
●ϕ=57.3 γ=1.75
●IC=7.44
0.5
1.0
1
2
3
4
5
6
7
CC
IW

LITHOLOGIC DESCRIPTION

MARLY FORAMINIFER-NANNOFOSSIL OOZE

Section 1, 0-25 cm, soupy; remainder of core is undisturbed.

Major lithologies: MARLY FORAMINIFER-NANNOFOSSIL OOZE, mottled olive (5Y 4/3, 4/2) and light olive gray (5Y 5/2, 5/3) intervals 20-100 cm thick. Foraminifers and shell fragments abundant on core face.

SMEAR SLIDE SUMMARY (%):

	1, 22 D	2, 80 D
TEXTURE:		
Silt	40	45
Clay	60	55
COMPOSITION:		
Access. Minerals	1	Tr
Clay	20	28
Diatoms	Tr	
Dolomite	Tr	1
Foraminifers	13	10
Inorganic Calcite	20	16
Mica	1	
Nannofossils	40	30
Quartz	5	15

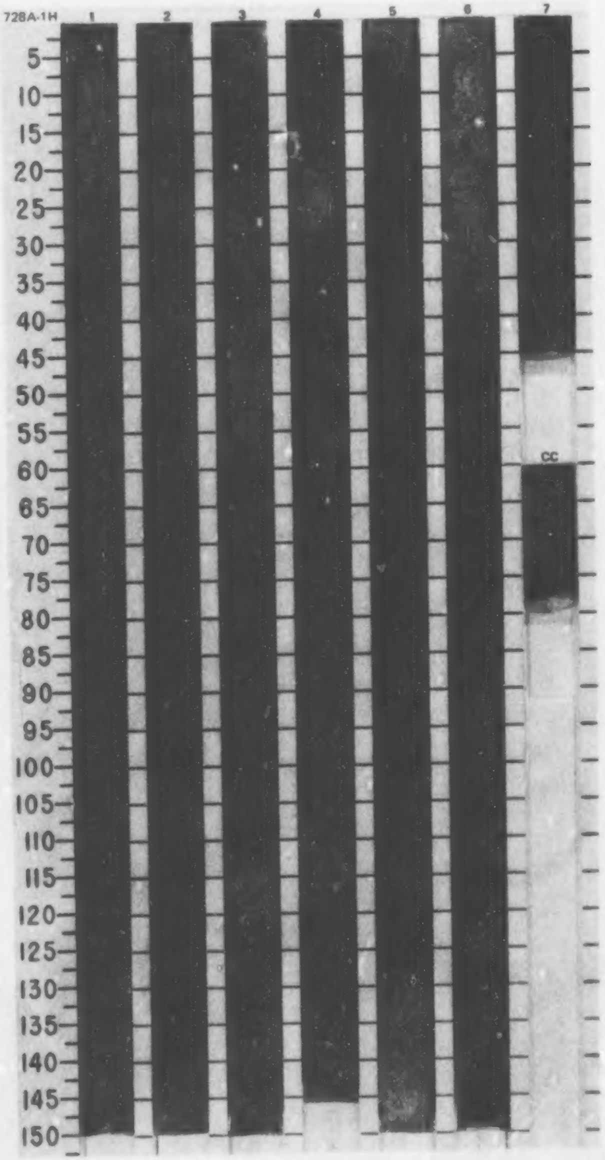
728A-1H
1
2
3
4
5
6
7
CC
5
10
15
20
25
30
35
40
45
50
55
60
65
70
75
80
85
90
95
100
105
110
115
120
125
130
135
140
145
150

SITE 728 HOLE A CORE 2H CORED INTERVAL 1437.4-1446.9 mbsl; 9.6-19.1 mbsf

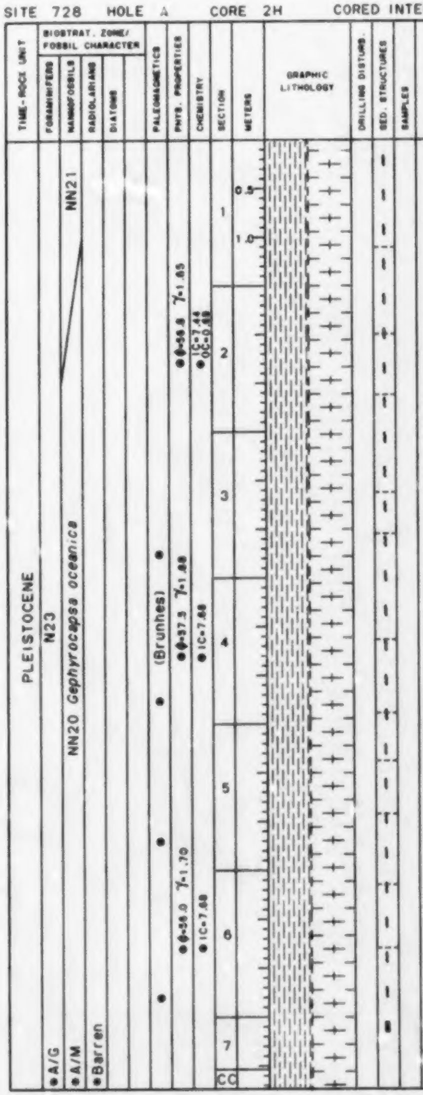
TIME-ROCK UNIT
BIOSTRAT. ZONE/ FOSSIL CHARACTER
FORAMINIFERS
NANNOFOSSILS
RADIOLARIANS
DIATOMS
PALEOMAGNETICS
PHYS. PROPERTIES
CHEMISTRY
SECTION
METERS
GRAPHIC LITHOLOGY
DRILLING DISTURB.
SED. STRUCTURES
SAMPLES
PLEISTOCENE
N23
NN21
NN20 Gephyrocapsa oceanica
(Brunhes)
●φ=56.8 γ=1.85
●IC=7.44 OC=0.68
●φ=57.5 γ=1.88
●IC=7.68
●φ=56.0 γ=1.70
●IC=7.68
1
2
3
4
5
6
7
CC
0.5
1.0
●A/G
●A/M
●Barren

LITHOLOGIC DESCRIPTION

MARLY FORAMINIFER-NANNOFOSSIL OOZE

Section 1, 0-5 cm, soupy; remainder of core is undisturbed.

Major lithologies: MARLY FORAMINIFER-NANNOFOSSIL OOZE, mottled olive (5Y 4/3) and light olive gray (5Y 5/2, 5/3) intervals 20-100 cm thick. Foraminifers common on core face. Pyrite flecks visible in lighter layers.

SMEAR SLIDE SUMMARY (%):

	4, 87 D
TEXTURE:	
Silt	30
Clay	70
COMPOSITION:	
Clay	20
Dolomite	Tr
Foraminifers	12
Inorganic Calcite	15
Nannofossils	50
Quartz	3

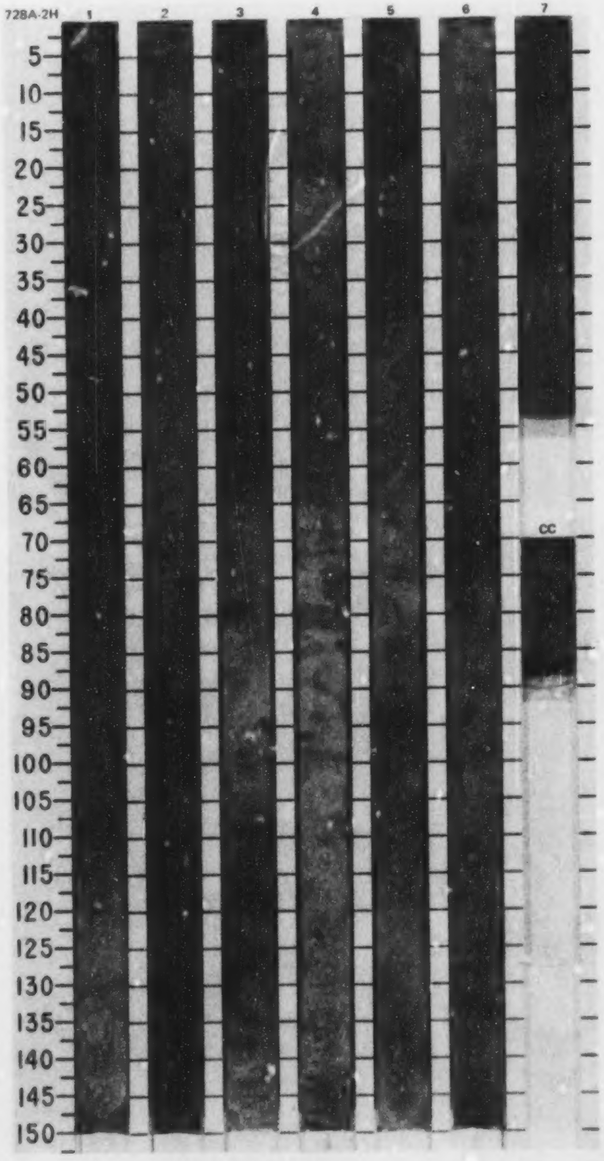
728A-2H
1
2
3
4
5
6
7
CC
5
10
15
20
25
30
35
40
45
50
55
60
65
70
75
80
85
90
95
100
105
110
115
120
125
130
135
140
145
150

SITE 728 HOLE A CORE 3H CORED INTERVAL 1446.9-1456.3 mbsl; 19.1-28.5 mbsf

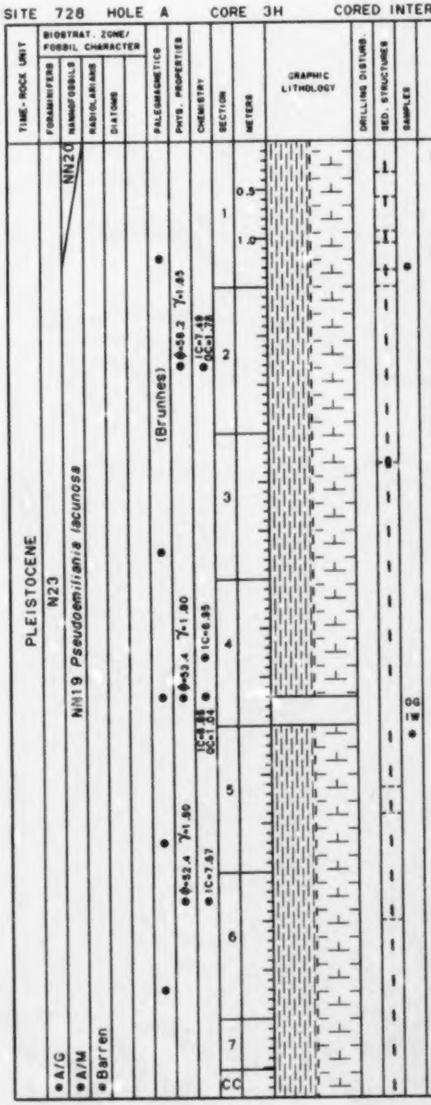
TIME-ROCK UNIT
BIOSTRAT. ZONE/ FOSSIL CHARACTER
FORAMINIFERS
NANNOFOSSILS
RADIOLARIANS
DIATOMS
PALEOMAGNETICS
PHYS. PROPERTIES
CHEMISTRY
SECTION
METERS
GRAPHIC LITHOLOGY
DRILLING DISTURB.
SED. STRUCTURES
SAMPLES
PLEISTOCENE
N23
NN20
NN19 Pseudoemiliania lacunosa
●A/G
●A/M
●Barren
(Brunhes)
●Φ=58.2 γ=1.85
●Φ=53.4 γ=1.80
●Φ=52.4 γ=1.90
●IC=7.49 OC=1.78
●IC=6.95
IC=6.88 OC=1.04
●IC=7.67
0.5
1.0
1
2
3
4
5
6
7
CC
OG
IW

LITHOLOGIC DESCRIPTION

MARLY FORAMINIFER-NANNOFOSSIL OOZE and MARLY NANNOFOSSIL OOZE

Entire core is undisturbed.

Major lithologies: MARLY FORAMINIFER-NANNOFOSSIL OOZE and MARLY NANNOFOSSIL OOZE, mottled olive (5Y 4/3, 4/2) and light olive gray (5Y 5/2, 5/.) intervals 20-100 cm thick. Foraminifers common on core face.

SMEAR SLIDE SUMMARY (%):

	1, 137 D	5, 10 D
TEXTURE:		
Sand	—	—
Silt	20	40
Clay	80	60
COMPOSITION:		
Clay	17	30
Dolomite	Tr	Tr
Foraminifers	5	10
Inorganic Calcite	10	20
Mica	—	Tr
Nannofossils	65	30
Quartz	3	10

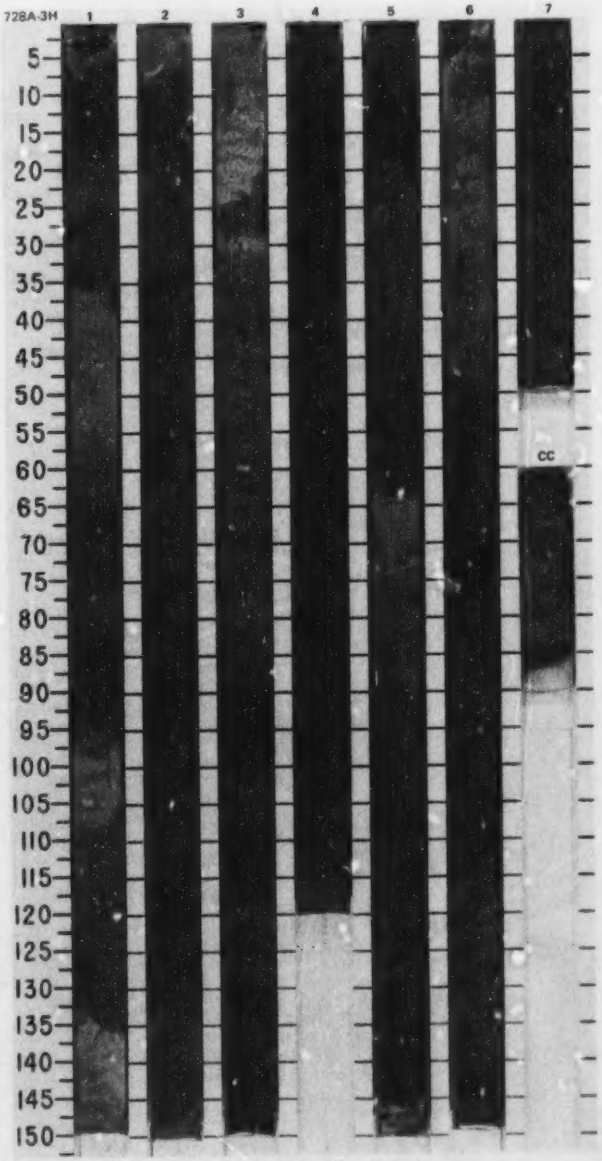
728A-3H
1
2
3
4
5
6
7
CC
5
10
15
20
25
30
35
40
45
50
55
60
65
70
75
80
85
90
95
100
105
110
115
120
125
130
135
140
145
150

SITE 728 HOLE A CORE 4H CORED INTERVAL 1456.3-1465.8 mbsl; 28.5-38.0 mbsf

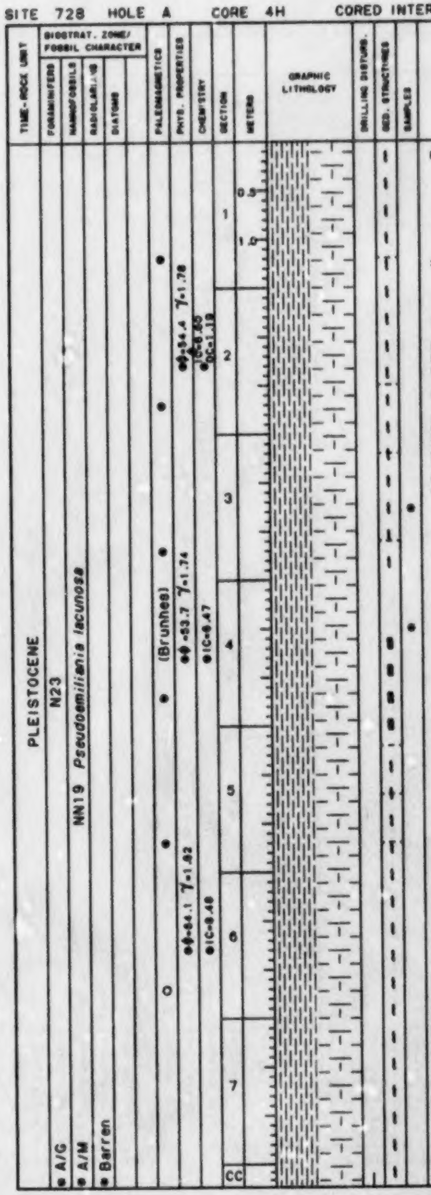
TIME-ROCK UNIT
BIOSTRAT. ZONE/ FOSSIL CHARACTER
FORAMINIFERS
NANNOFOSSILS
RADIOLARIANS
DIATOMS
PALEOMAGNETICS
PHYS. PROPERTIES
CHEMISTRY
SECTION
METERS
GRAPHIC LITHOLOGY
DRILLING DISTURB.
SED. STRUCTURES
SAMPLES
PLEISTOCENE
N23
NN19 Pseudoemiliania lacunosa
● A/G
● A/M
● Barren
(Brunhes)
●ϕ=54.4 γ=1.78
●ϕ=53.7 γ=1.74
●ϕ=54.1 γ=1.82
●IC=6.65
OC=1.19
●IC=6.47
●IC=6.40
1
2
3
4
5
6
7
CC
0.5
1.0

LITHOLOGIC DESCRIPTION

MARLY FORAMINIFER-NANNOFOSSIL OOZE and MARLY NANNOFOSSIL OOZE

Entire core is undisturbed.

Major lithologies: MARLY FORAMINIFER-NANNOFOSSIL OOZE and MARLY NANNOFOSSIL OOZE, mottled olive (5Y 4/3, 4/2, 3/2) and light olive gray (5Y 5/2, 5/3) intervals 20-100 cm thick. Foraminifers common on core face. Color contrast and mottling (bioturbation) increase relative to cores above.

SMEAR SLIDE SUMMARY (%):

	3, 78 D	4, 50 D
TEXTURE:		
Sand	5	5
Silt	15	35
Clay	80	60
COMPOSITION:		
Clay	10	10
Dolomite	—	Tr
Foraminifers	10	20
Inorganic Calcite	20	20
Nannofossils	50	40
Organic Matter	5	—
Quartz	5	10

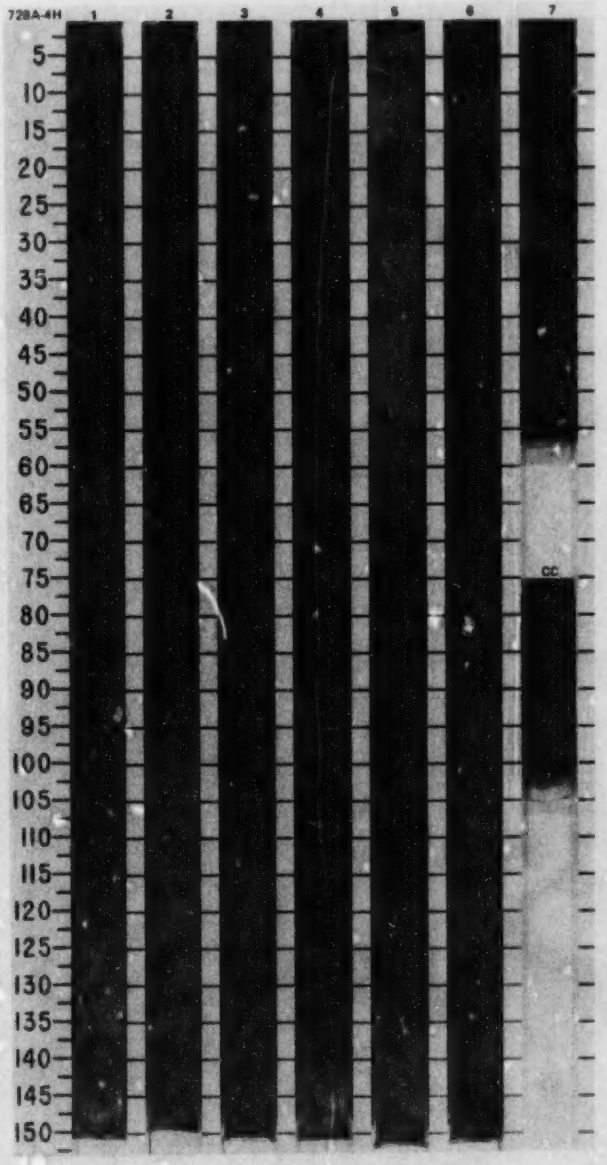
728A-4H
1
2
3
4
5
6
7
CC
5
10
15
20
25
30
35
40
45
50
55
60
65
70
75
80
85
90
95
100
105
110
115
120
125
130
135
140
145
150

SITE 728 HOLE A CORE 5H CORED INTERVAL 1465.8-1475.3 mbsl; 38.0-47.5 mbsf

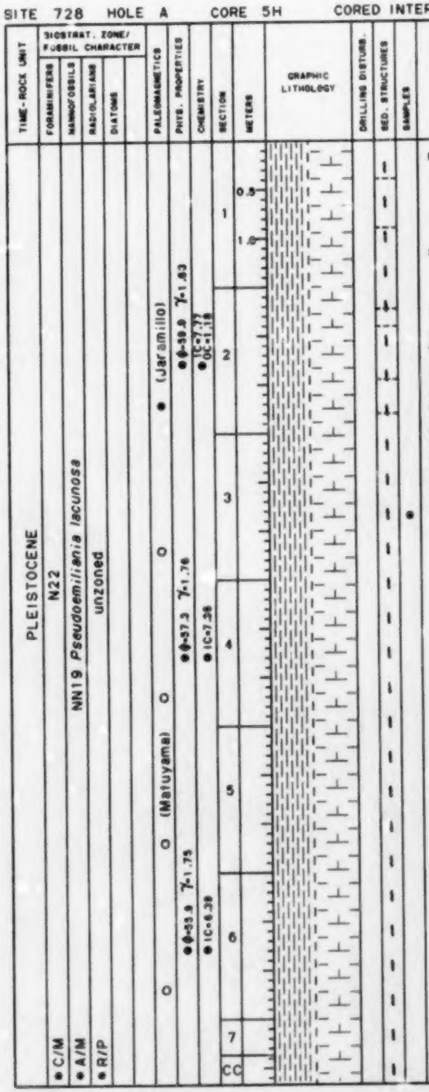
TIME-ROCK UNIT
BIOSTRAT. ZONE/ FOSSIL CHARACTER
FORAMINIFERS
NANNOFOSSILS
RADIOLARIANS
DIATOMS
PALEOMAGNETICS
PHYS. PROPERTIES
CHEMISTRY
SECTION
METERS
GRAPHIC LITHOLOGY
DRILLING DISTURB.
SED. STRUCTURES
SAMPLES
PLEISTOCENE
N22
NN19 Pseudoemiliania lacunosa
unzoned
• C/M
• A/M
• R/P
(Jaramillo)
(Matuyama)
ϕ=59.0 γ=1.83
ϕ=57.3 γ=1.76
ϕ=55.9 γ=1.75
IC=7.77
OC=1.18
IC=7.36
IC=6.39
1
2
3
4
5
6
7
CC
0.5
1.0

LITHOLOGIC DESCRIPTION

MARLY FORAMINIFER-NANNOFOSSIL OOZE and MARLY NANNOFOSSIL OOZE

Entire core is undisturbed.

Major lithology: MARLY FORAMINIFER-NANNOFOSSIL OOZE and MARLY NANNOFOSSIL OOZE, mottled olive (5Y 4/3, 4/2, 3/2) and light olive gray (5Y 5/2, 5/3) intervals 20-100 cm thick. Foraminifers common on core face.

SMEAR SLIDE SUMMARY (%):

	3, 60 D	3, 86 D	5, 82 D
TEXTURE:			
Silt	50	45	55
Clay	50	55	45
COMPOSITION:			
Access. minerals	Tr	—	—
Clay	23	35	30
Diatoms	1	1	—
Dolomite	Tr	2	—
Foraminifers	15	10	10
Inorganic calcite	28	25	30
Nannofossils	25	20	10
Quartz	7	5	20
Radiolarians	—	Tr	—
Sponge Spicules	1	2	—

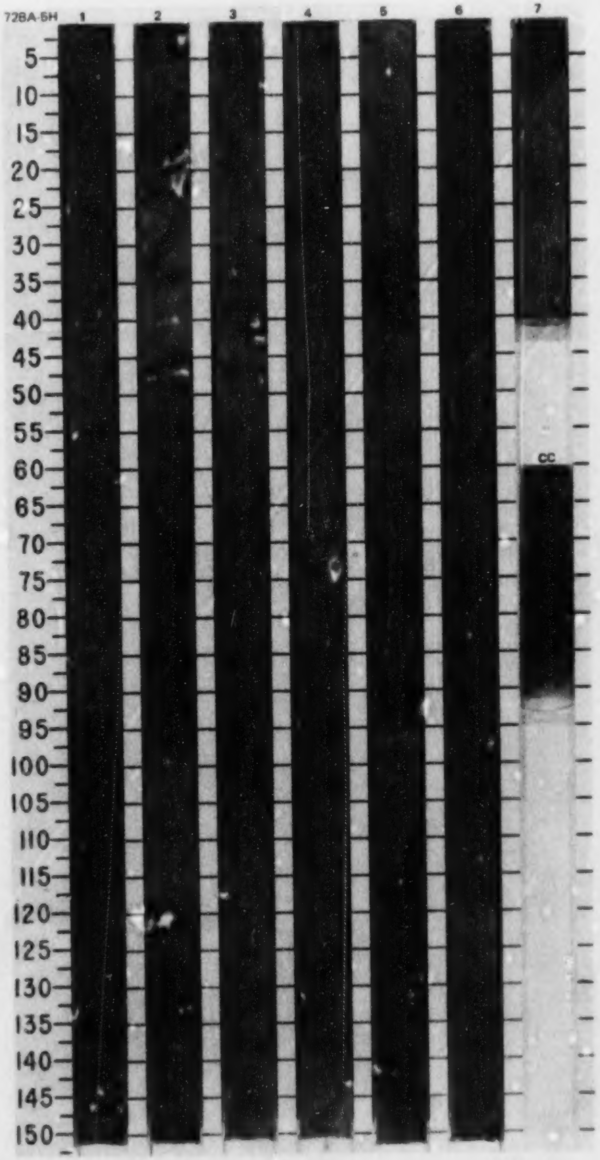
728A-5H
1
2
3
4
5
6
7
CC
5
10
15
20
25
30
35
40
45
50
55
60
65
70
75
80
85
90
95
100
105
110
115
120
125
130
135
140
145
150

SITE 728 HOLE A CORE 6H CORED INTERVAL 1475.3-1484.8 mbsl; 47.5-57.0 mbsf

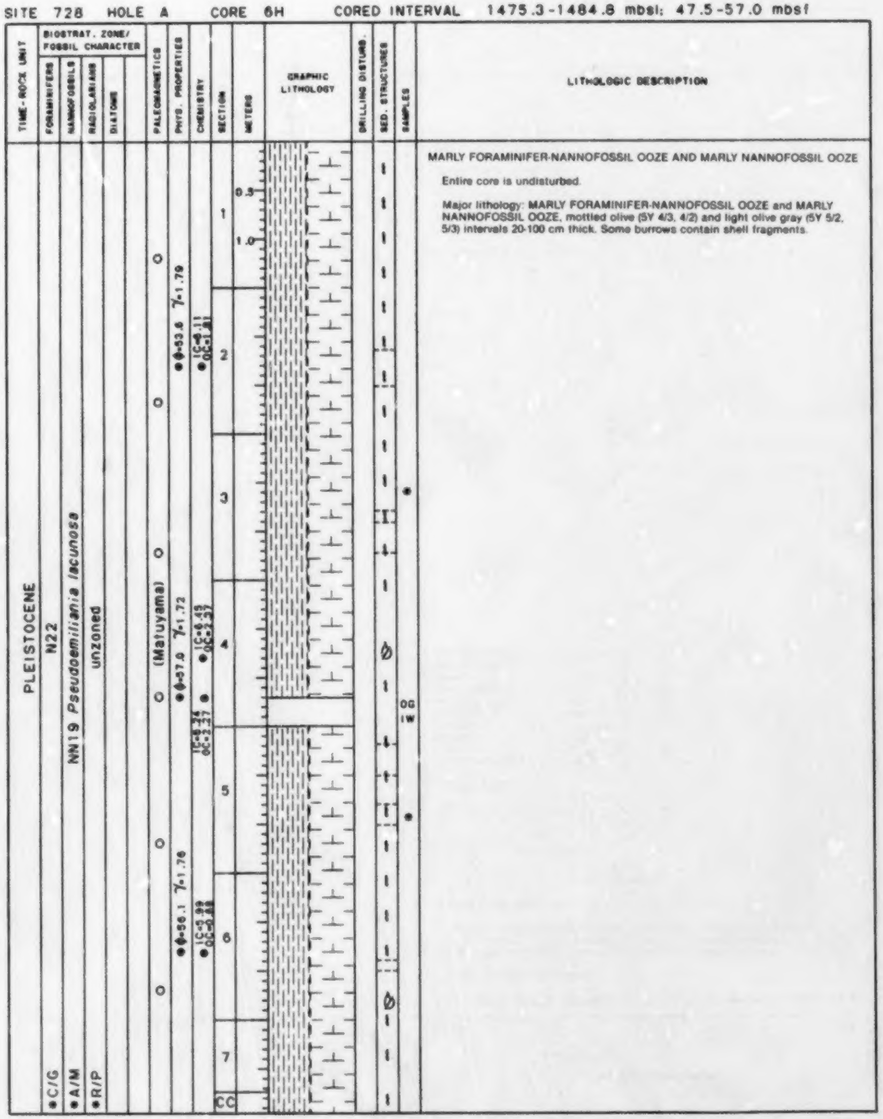
TIME-ROCK UNIT
BIOSTRAT. ZONE/ FOSSIL CHARACTER
FORAMINIFERS
NANNOFOSSILS
RADIOLARIANS
DIATOMS
PALEOMAGNETICS
PHYS. PROPERTIES
CHEMISTRY
SECTION
METERS
GRAPHIC LITHOLOGY
DRILLING DISTURB.
SED. STRUCTURES
SAMPLES
LITHOLOGIC DESCRIPTION
PLEISTOCENE
N22
NN19 Pseudoemiliania lacunosa
unzoned
●C/G
●A/M
●R/P
(Matuyama)
●ϕ=53.6 γ=1.79
●ϕ=57.0 γ=1.72
●ϕ=56.1 γ=1.76
●IC=8.11 OC=1.81
●IC=6.45 OC=2.57
●IC=8.24 OC=2.27
●IC=5.99 OC=0.88
1
2
3
4
5
6
7
CC
0.5
1.0
OG
IW

MARLY FORAMINIFER-NANNOFOSSIL OOZE AND MARLY NANNOFOSSIL OOZE

Entire core is undisturbed.

Major lithology: MARLY FORAMINIFER-NANNOFOSSIL OOZE and MARLY NANNOFOSSIL OOZE, mottled olive (5Y 4/3, 4/2) and light olive gray (5Y 5/2, 5/3) intervals 20-100 cm thick. Some burrows contain shell fragments.

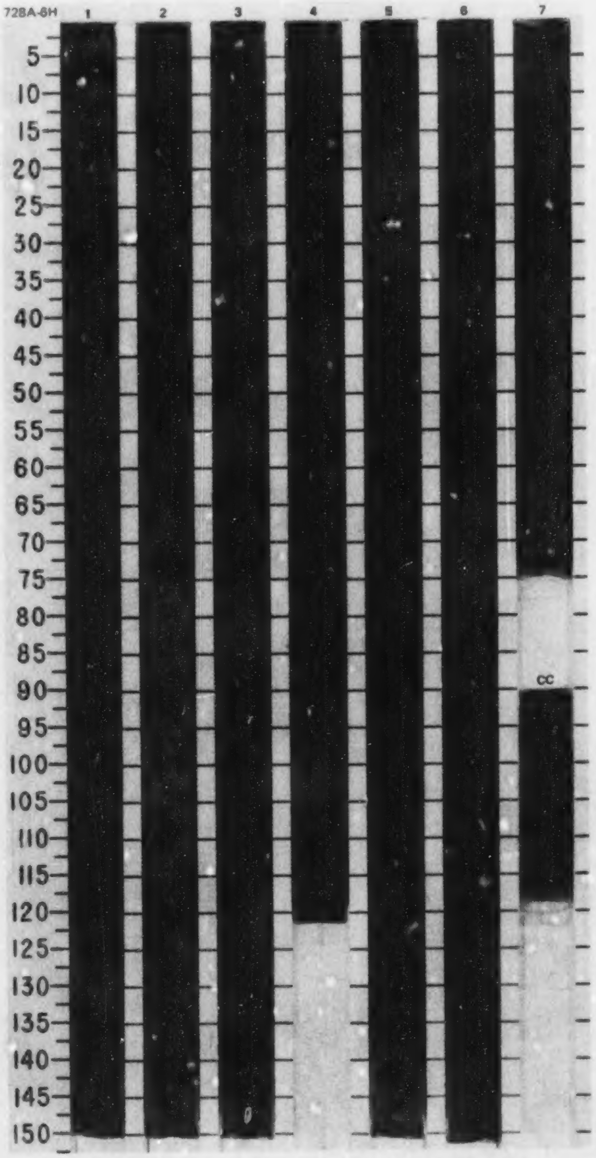
728A-6H
1
2
3
4
5
6
7
CC
5
10
15
20
25
30
35
40
45
50
55
60
65
70
75
80
85
90
95
100
105
110
115
120
125
130
135
140
145
150

SITE 728 HOLE A CORE 7H CORED INTERVAL 1484.8-1494.3 mbsl; 57.0-66.5 mbsf

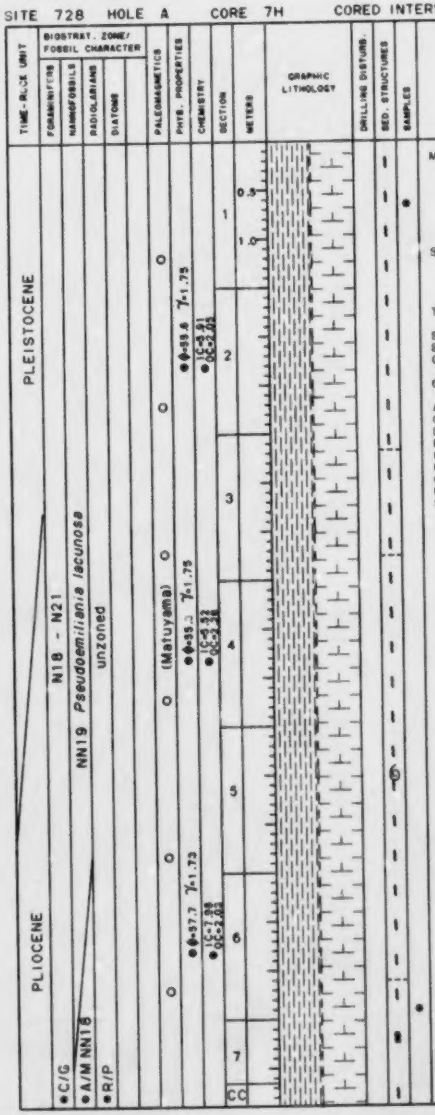
TIME-ROCK UNIT
BIOSTRAT. ZONE/ FOSSIL CHARACTER
FORAMINIFERS
NANNOFOSSILS
RADIOLARIANS
DIATOMS
PALEOMAGNETICS
PHYS. PROPERTIES
CHEMISTRY
SECTION
METERS
GRAPHIC LITHOLOGY
DRILLING DISTURB.
SED. STRUCTURES
SAMPLES
PLEISTOCENE
PLIOCENE
N18 - N21
NN19 Pseudoemiliania lacunosa
unzoned
●C/G
●A/M NN18
●R/P
(Matuyama)
●φ=55.6 γ=1.75
●IC=5.91 OC=2.05
●φ=55.3 γ=1.75
●IC=5.52 OC=2.26
●φ=57.7 γ=1.73
●IC=7.88 OC=2.03
0.5
1.0
1
2
3
4
5
6
7
CC

LITHOLOGIC DESCRIPTION

MARLY NANNOFOSSIL OOZE

Entire core is undisturbed.

Major lithology: MARLY NANNOFOSSIL OOZE, mottled olive (5Y 4/3) and light olive gray (5Y 5/2, 5/3) intervals 20-100 cm thick. Fewer foraminifers observed in smear slides.

SMEAR SLIDE SUMMARY (%):

	1, 65 D	6, 140 D
TEXTURE:		
Sand	10	5
Silt	25	10
Clay	65	85
COMPOSITION:		
Access. minerals	2	—
Clay	20	10
Dolomite	—	1
Foraminifers	2	3
Inorganic calcite	28	5
Nannofossils	45	75
Quartz	3	6
Radiolarians	Tr	—
Sponge Spicules	Tr	—

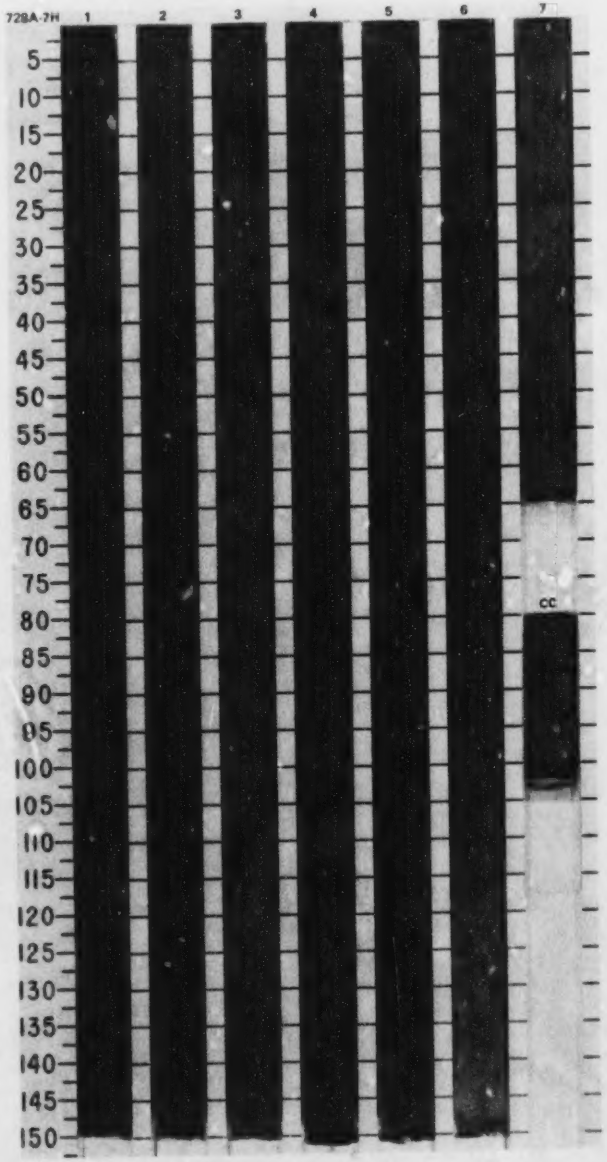
728A-7H
1
2
3
4
5
6
7
CC
5
10
15
20
25
30
35
40
45
50
55
60
65
70
75
80
85
90
95
100
105
110
115
120
125
130
135
140
145
150

SITE 728 HOLE A CORE 8H CORED INTERVAL 1494.3-1503.9 mbsl; 66.5-76.1 mbsf

TIME-ROCK UNIT	BIOSTRAT. ZONE/FOSSIL CHARACTER: FORAMINIFERS	NANNOFOSSILS	RADIOLARIANS	DIATOMS
PLIOCENE	●R/M N18 - N21	●A/M NN16 *Discoaster surculus*; NN17 - NN18	●R/P unzoned	

SECTION	METERS	PALEOMAGNETICS	PHYS. PROPERTIES	CHEMISTRY	SAMPLES
1	0.5 1.0	O			●
2		O	●φ=60.3 γ=1.87	●IC=7.18 OC=1.98	
3		(Matuyama) O			
4		O	●φ=61.1 γ=1.87	●IC=4.11 OC=0.34	
5		●			●
6		(Gauss) ●	●φ=55.6 γ=1.79	●IC=4.87 OC=0.08	
7					
CC					

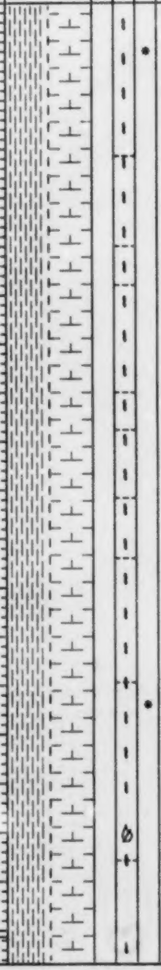
GRAPHIC LITHOLOGY
DRILLING DISTURB.
SED. STRUCTURES

LITHOLOGIC DESCRIPTION

MARLY NANNOFOSSIL OOZE

Entire core is undisturbed.

Major lithology: MARLY NANNOFOSSIL OOZE, mottled olive (5Y 4/3, 4/2, 3/2) and light olive gray (5Y 5/3) intervals 20-100 cm thick. Foraminifers and shell debris present in mm-scale lenses.

SMEAR SLIDE SUMMARY (%):

	1, 58 D	5, 138 D
TEXTURE:		
Sand	10	—
Silt	15	20
Clay	75	80
COMPOSITION:		
Access. minerals	1	2
Clay	25	20
Dolomite	—	Tr
Feldspar	—	1
Foraminifers	5	1
Inorganic calcite	15	10
Nannofossils	49	60
Quartz	5	6

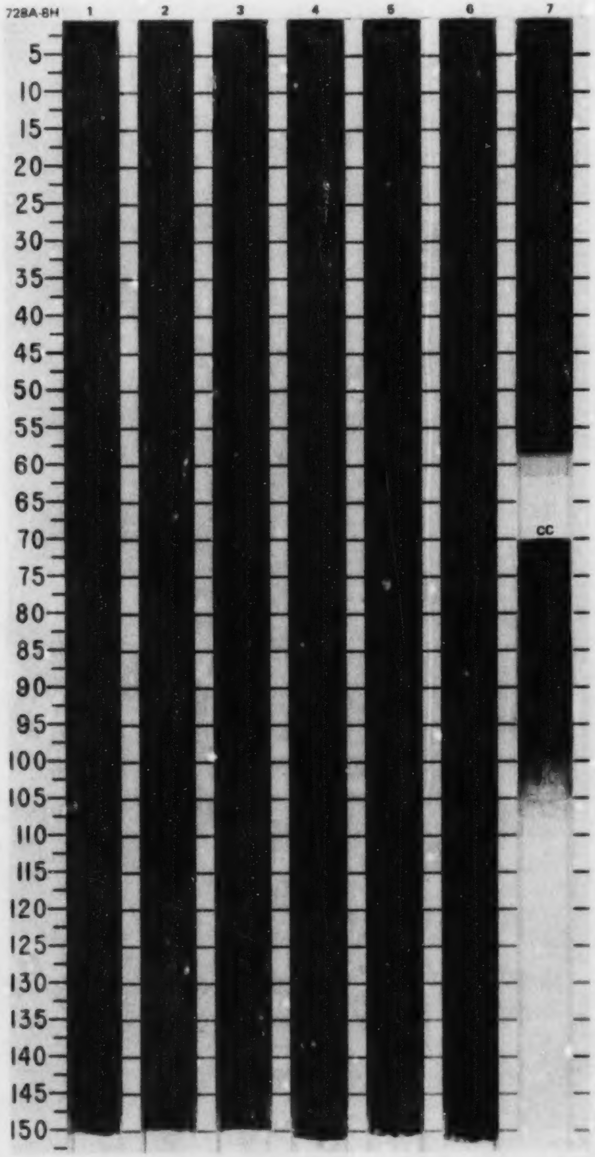
728A-8H
1
2
3
4
5
6
7
CC
5
10
15
20
25
30
35
40
45
50
55
60
65
70
75
80
85
90
95
100
105
110
115
120
125
130
135
140
145
150

SITE 728 HOLE A CORE 9H CORED INTERVAL 1503.9-1513.5 mbsl; 76.1-85.7 mbsf

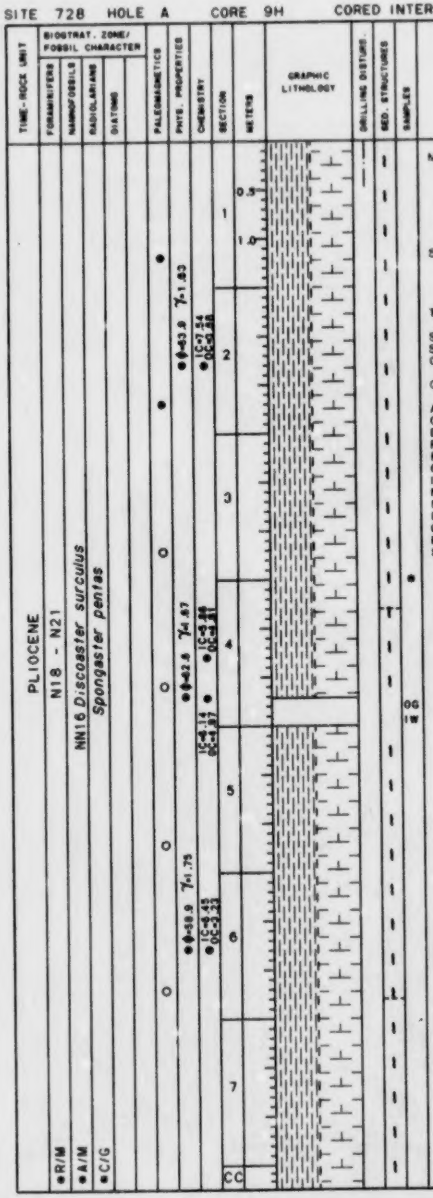
TIME-ROCK UNIT
BIOSTRAT. ZONE/ FOSSIL CHARACTER
FORAMINIFERS
NANNOFOSSILS
RADIOLARIANS
DIATOMS
PALEOMAGNETICS
PHYS. PROPERTIES
CHEMISTRY
SECTION
METERS
GRAPHIC LITHOLOGY
DRILLING DISTURB.
SED. STRUCTURES
SAMPLES
PLIOCENE
N18 - N21
NN16 Discoaster surculus
Spongaster pentas
●R/M
●A/M
●C/G
φ=63.9 γ=1.83
IC=7.54 OC=0.88
φ=42.8 γ=1.87
IC=8.88 OC=1.31
IC=8.14 OC=1.87
φ=58.9 γ=1.75
IC=6.45 OC=3.23
0.5
1.0
1
2
3
4
5
6
7
CC
OG
IW

LITHOLOGIC DESCRIPTION

MARLY NANNOFOSSIL OOZE

Section 1, 0-25 cm, disturbed; remainder of core is undisturbed.

Major lithology: MARLY NANNOFOSSIL OOZE, mottled olive (5Y 4/2, 4/3). Pteropod fragments common on core face. Pyrite flecks common. Smear slides contain trace amounts of siliceous microfossils.

SMEAR SLIDE SUMMARY (%):

	1, 59 D	4, 6 D
TEXTURE:		
Sand	10	—
Silt	20	10
Clay	70	90
COMPOSITION:		
Access. minerals	2	1
Clay	20	20
Diatoms	—	Tr
Feldspar	2	—
Foraminifers	1	1
Glauconite	Tr	—
Inorganic calcite	15	8
Mica	Tr	—
Nannofossils	50	70
Phosphate	Tr	—
Quartz	10	Tr
Radiolarians	—	Tr
Sponge spicules	—	Tr

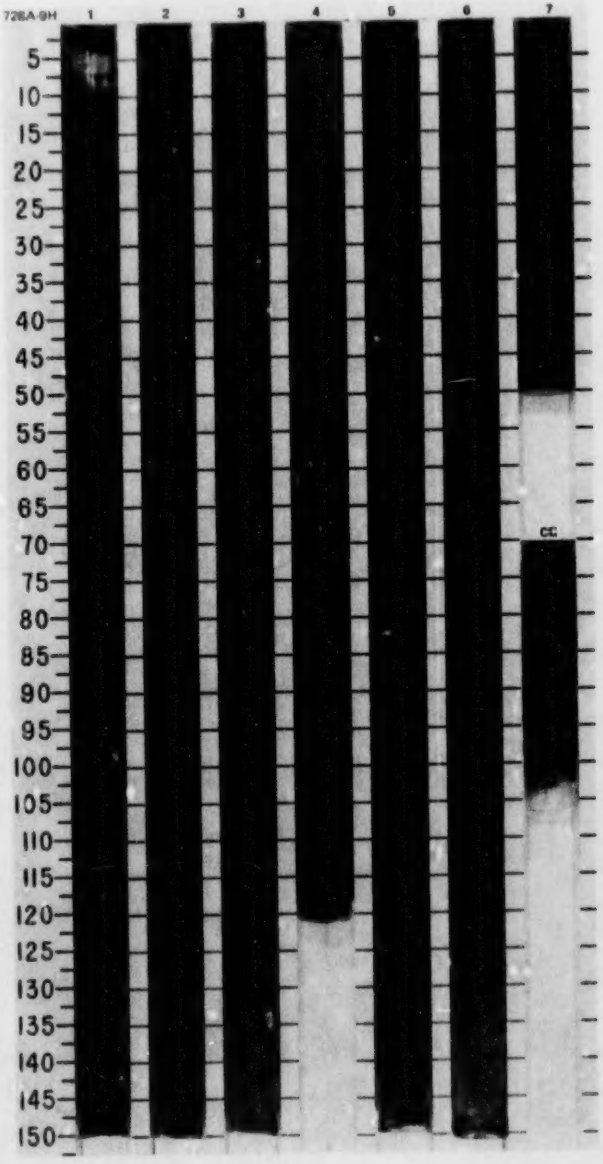
728A-9H
1
2
3
4
5
6
7
CC
5
10
15
20
25
30
35
40
45
50
55
60
65
70
75
80
85
90
95
100
105
110
115
120
125
130
135
140
145
150

SITE 728 HOLE A CORE 10X CORED INTERVAL 1513.5-1523.1 mbsl; 85.7-95.3 mbsf

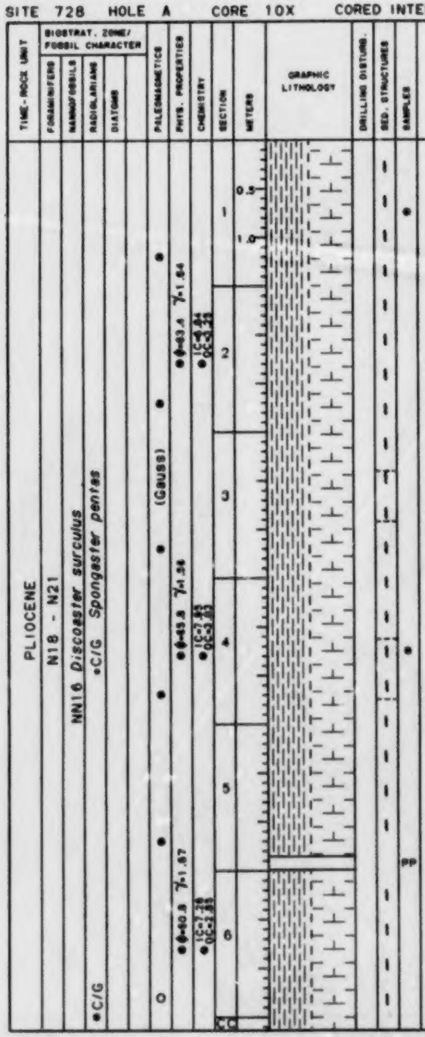
TIME-ROCK UNIT
BIOSTRAT. ZONE/FOSSIL CHARACTER
FORAMINIFERS
NANNOFOSSILS
RADIOLARIANS
DIATOMS
PALEOMAGNETICS
PHYS. PROPERTIES
CHEMISTRY
SECTION
METERS
GRAPHIC LITHOLOGY
DRILLING DISTURB.
SED. STRUCTURES
SAMPLES
PLIOCENE
N18 - N21
NN16 Discoaster surculus
•C/G Spongaster pentas
•C/G
(Gauss)
●φ=63.4 γ=1.64
●IC=6.84 OC=0.35
●φ=45.5 γ=1.56
●IC=7.83 OC=0.83
●φ=60.5 γ=1.67
●IC=7.26 OC=2.85
1
2
3
4
5
6
CC
0.5
1.0
PP

LITHOLOGIC DESCRIPTION

MARLY NANNOFOSSIL OOZE and SILICEOUS-BEARING MARLY NANNOFOSSIL OOZE

Entire core is undisturbed.

Major lithologies: MARLY NANNOFOSSIL OOZE and SILICEOUS- BEARING MARLY NANNOFOSSIL OOZE, mottled olive (5Y 4/3, 4/2) and light olive gray (5Y 5/2, 5/3) intervals of irregular thickness.

SMEAR SLIDE SUMMARY (%):

	1, 73 D	4, 79 D
TEXTURE:		
Sand	10	
Silt	15	20
Clay	80	70
COMPOSITION:		
Access. minerals	2	1
Clay	20	20
Diatoms	1	2
Feldspar	1	—
Foraminifers	1	5
Volcanic glass	6	—
Inorganic calcite	—	20
Mica	1	—
Nannofossils	60	50
Quartz	3	Tr
Radiolarians	1	1
Silicoflagellates	1	1
Sponge spicules	2	1

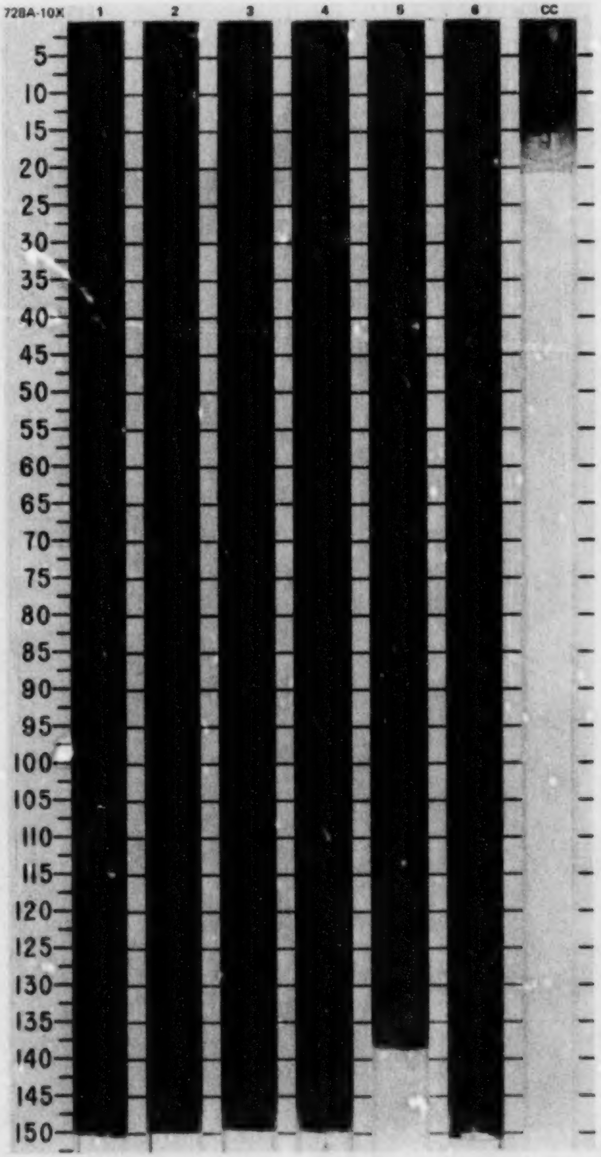
728A-10X
1
2
3
4
5
6
CC
5
10
15
20
25
30
35
40
45
50
55
60
65
70
75
80
85
90
95
100
105
110
115
120
125
130
135
140
145
150

SITE 728 HOLE A CORE 11X CORED INTERVAL 1523.1-1532.7 mbsl; 95.3-104.9 mbsf

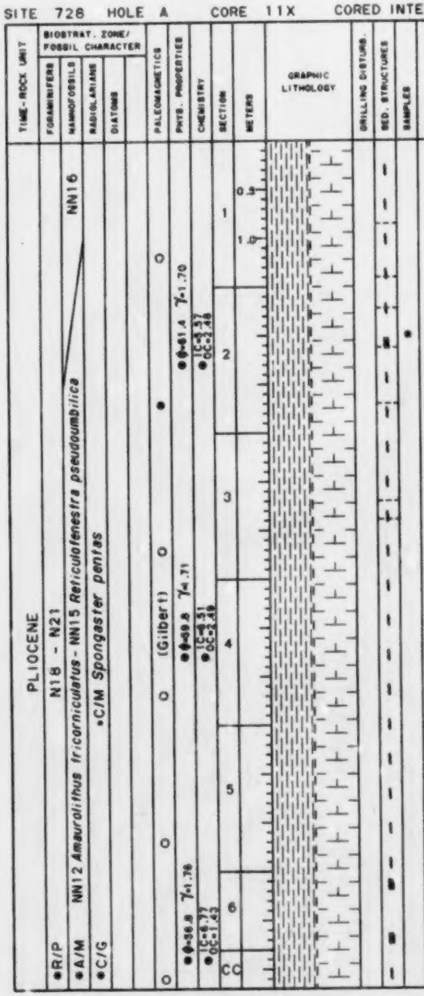
TIME-ROCK UNIT
BIOSTRAT. ZONE/ FOSSIL CHARACTER
FORAMINIFERS
NANNOFOSSILS
RADIOLARIANS
DIATOMS
PALEOMAGNETICS
PHYS. PROPERTIES
CHEMISTRY
SECTION
METERS
GRAPHIC LITHOLOGY
DRILLING DISTURB.
SED. STRUCTURES
SAMPLES
PLIOCENE
●R/P N18 - N21
●A/M NN12 Amaurolithus tricorniculatus - NN15 Reticulofenestra pseudoumbilica
NN16
●C/G ●C/M Spongaster pentas
(Gilbert)
●φ=61.4 γ=1.70
●IC=6.57 OC=2.48
●φ=59.8 γ=1.71
●IC=4.51 OC=2.49
●φ=56.8 γ=1.76
●IC=6.77 OC=1.43
1
2
3
4
5
6
CC
0.5
1.0

LITHOLOGIC DESCRIPTION

MARLY NANNOFOSSIL OOZE

Entire core is undisturbed.

Major lithology: MARLY NANNOFOSSIL OOZE, mottled olive (5Y 4/3, 4/2, 3/2) and light olive gray (5Y 5/3) intervals of irregular thickness. Siliceous microfossils present in trace amounts. Mottling (bioturbation) light to moderate.

SMEAR SLIDE SUMMARY (%):

	2, 50 D	5, 20 D
TEXTURE:		
Sand	10	5
Silt	25	15
Clay	65	80
COMPOSITION:		
Access. minerals	2	2
Clay	25	30
Diatoms	—	Tr
Dolomite	Tr	—
Volcanic glass	—	1
Inorganic calcite	23	15
Nannofossils	40	50
Quartz	10	1
Radiolarians	Tr	Tr
Sponge spicules	Tr	1

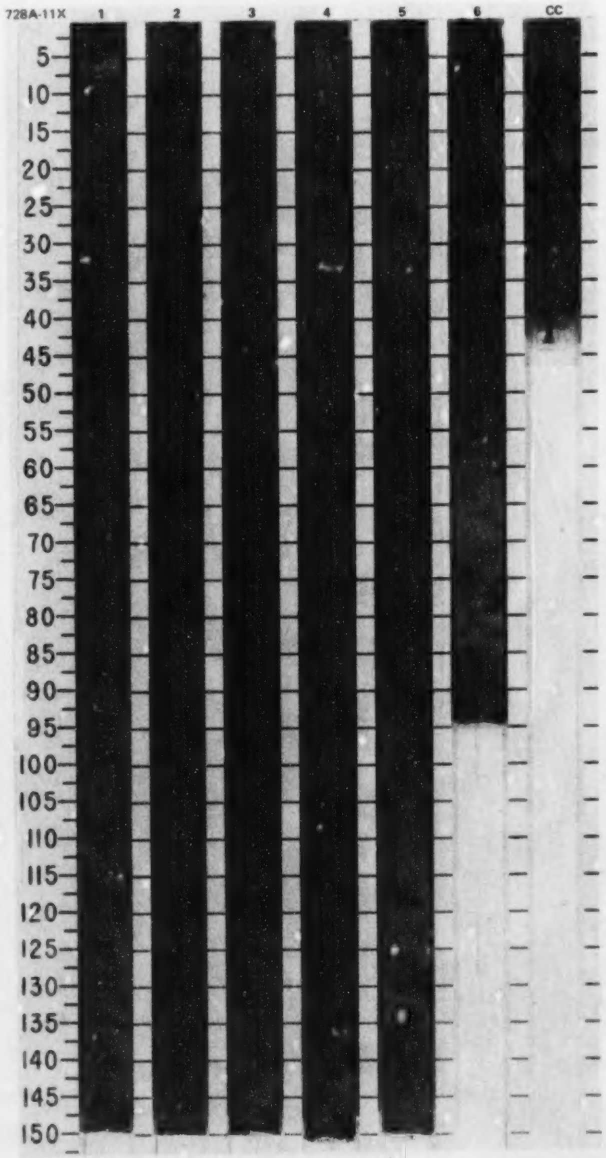
728A-11X
1
2
3
4
5
6
CC
5
10
15
20
25
30
35
40
45
50
55
60
65
70
75
80
85
90
95
100
105
110
115
120
125
130
135
140
145
150

SITE 728 HOLE A CORE 12X CORED INTERVAL 1532.7-1542.3 mbsl; 104.9-114.5 mbsf

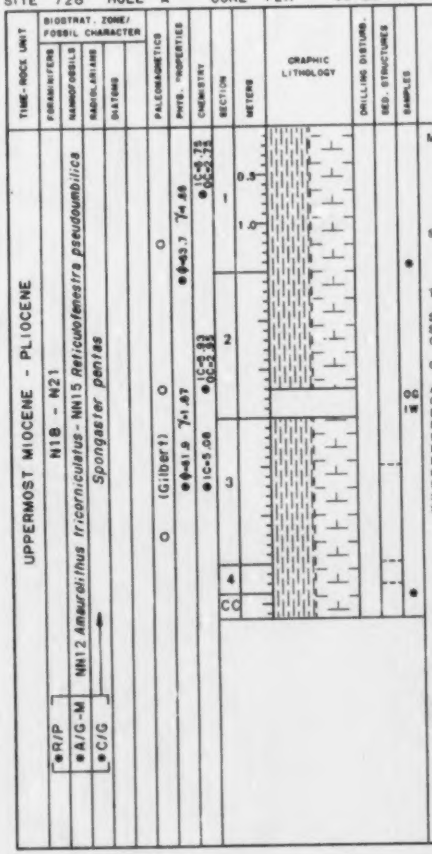
TIME-ROCK UNIT
BIOSTRAT. ZONE/ FOSSIL CHARACTER
FORAMINIFERS
NANNOFOSSILS
RADIOLARIANS
DIATOMS
PALEOMAGNETICS
PHYS. PROPERTIES
CHEMISTRY
SECTION
METERS
GRAPHIC LITHOLOGY
DRILLING DISTURB.
SED. STRUCTURES
SAMPLES
UPPERMOST MIOCENE - PLIOCENE
●R/P N18 - N21
●A/G-M NN12 Amaurolithus tricorniculatus - NN15 Reticulofenestra pseudoumbilica
●C/G Spongaster pentas
O
O
(Gilbert?)
O
●φ=63.7 γ=1.88
●φ=61.9 γ=1.87
●IC=6.78 OC=2.75
●IC=6.93 OC=2.35
●IC=5.08
1
2
3
4
CC
0.5
1.0
OG
IW

LITHOLOGIC DESCRIPTION

MARLY NANNOFOSSIL OOZE

Entire core is undisturbed.

Major lithology: MARLY NANNOFOSSIL OOZE, mottled olive (5Y 4/3, 4/2) and light olive gray (5Y 5/3, 5/2) intervals of irregular thickness. Siliceous microfossils present in trace amounts.

SMEAR SLIDE SUMMARY (%):

	1, 143 D	4, 30 D
TEXTURE:		
Sand	10	5
Silt	30	30
Clay	60	65
COMPOSITION:		
Access. minerals	—	2
Clay	20	20
Diatoms	—	1
Foraminifers	—	3
Inorganic calcite	30	26
Mica	Tr	Tr
Nannofossils	40	45
Quartz	10	3
Radiolarians	—	Tr
Silicoflagellates	Tr	
Sponge spicules	—	Tr

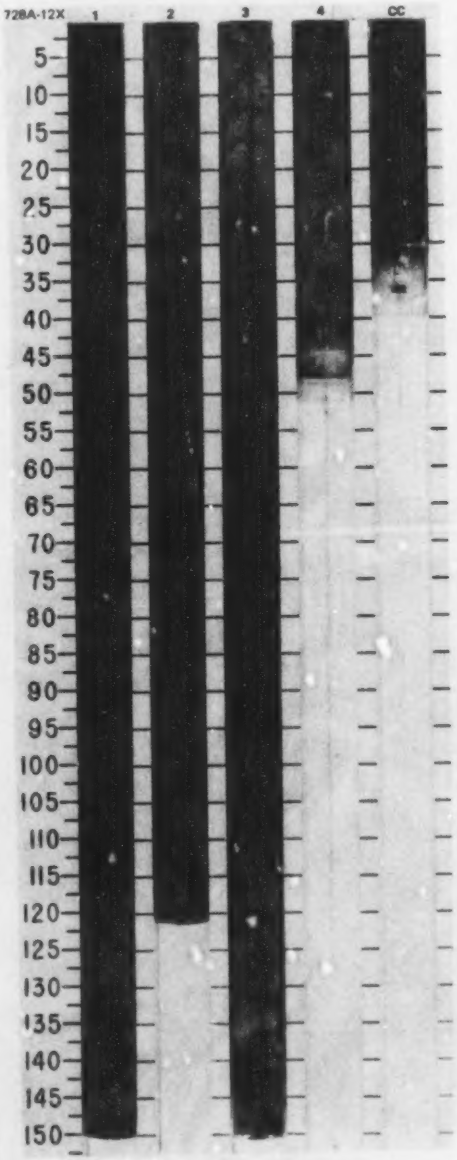
728A-12X
1
2
3
4
CC
5
10
15
20
25
30
35
40
45
50
55
60
65
70
75
80
85
90
95
100
105
110
115
120
125
130
135
140
145
150

SITE 728 HOLE A CORE 13X CORED INTERVAL 1542.3-1552.0 mbsl; 114.5-124.2 mbsf

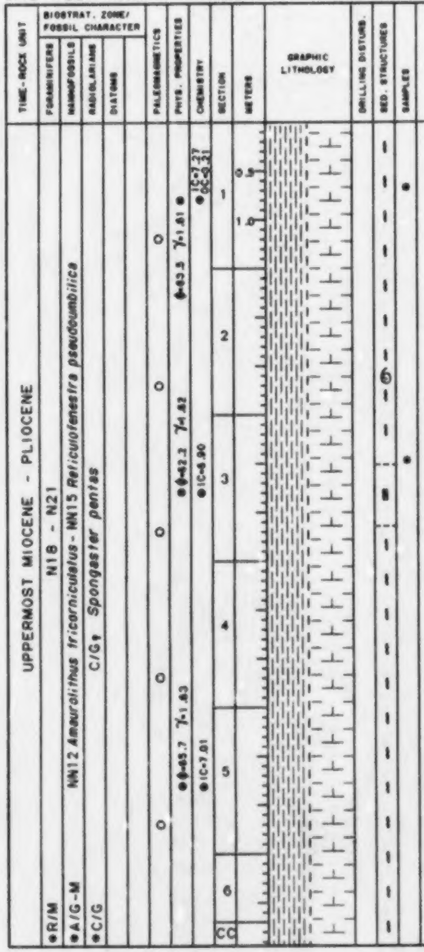
TIME-ROCK UNIT
BIOSTRAT. ZONE/ FOSSIL CHARACTER
FORAMINIFERS
NANNOFOSSILS
RADIOLARIANS
DIATOMS
PALEOMAGNETICS
PHYS. PROPERTIES
CHEMISTRY
SECTION
METERS
GRAPHIC LITHOLOGY
DRILLING DISTURB.
SED. STRUCTURES
SAMPLES
UPPERMOST MIOCENE - PLIOCENE
●R/M
N18 - N21
●A/G-M
NN12 Amaurolithus tricorniculatus - NN15 Reticulofenestra pseudoumbilica
●C/G
C/G, Spongaster pentas
φ=63.5 γ=1.81
φ=62.2 γ=1.82
φ=65.7 γ=1.83
IC=7.27 OC=0.31
IC=6.90
IC=7.01
1
2
3
4
5
6
CC
0.5
1.0

LITHOLOGIC DESCRIPTION

MARLY NANNOFOSSIL OOZE

Entire core is undisturbed.

Major lithology: MARLY NANNOFOSSIL OOZE, mottled olive (5Y 4/3) and light olive gray (5Y 5/3), homogeneous appearance. Siliceous microfossils present in trace amounts.

SMEAR SLIDE SUMMARY (%):

	1, 57 D	3, 47 D
TEXTURE:		
Sand	5	—
Silt	15	10
Clay	80	90
COMPOSITION:		
Access. minerals	1	1
Clay	30	20
Diatoms	—	Tr
Foraminifers	1	Tr
Volcanic glass	—	Tr
Inorganic calcite	15	7
Mica	1	1
Nannofossils	50	70
Phosphate	Tr	—
Quartz	2	1
Radiolarians	Tr	Tr
Silicoflagellates	—	Tr
Sponge spicules	Tr	Tr

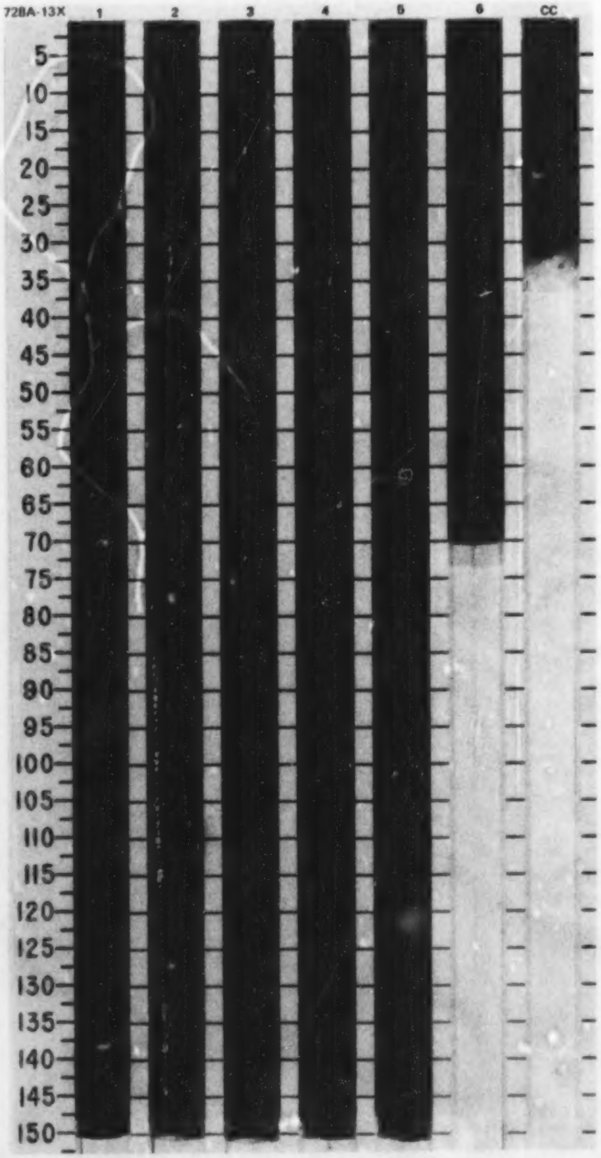
728A-13X
1
2
3
4
5
6
CC
5
10
15
20
25
30
35
40
45
50
55
60
65
70
75
80
85
90
95
100
105
110
115
120
125
130
135
140
145
150

SITE 728 HOLE A CORE 14X CORED INTERVAL 1552.0-1561.7 mbsl; 124.2-133.9 mbsf

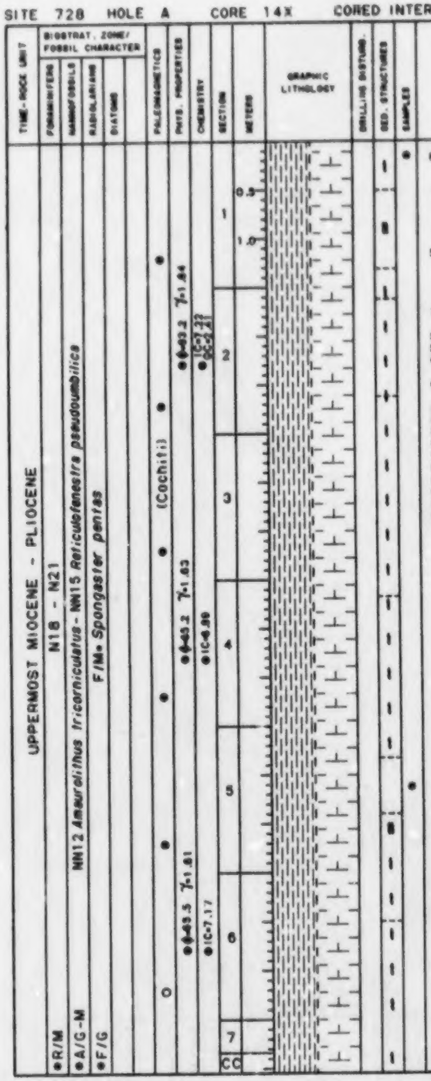
TIME-ROCK UNIT
BIOSTRAT. ZONE/ FOSSIL CHARACTER
FORAMINIFERS
NANNOFOSSILS
RADIOLARIANS
DIATOMS
PALEOMAGNETICS
PHYS. PROPERTIES
CHEMISTRY
SECTION
METERS
GRAPHIC LITHOLOGY
DRILLING DISTURB.
SED. STRUCTURES
SAMPLES
UPPERMOST MIOCENE - PLIOCENE
●R/M
N18 - N21
●A/G-M
NN12 Amaurolithus tricorniculatus - NN15 Reticulofenestra pseudoumbilica
●F/G
F/M● Spongaster pentas
(Cochiti)
●φ=63.2 γ=1.84
●φ=65.2 γ=1.83
●φ=63.5 γ=1.81
●IC=7.22 OC=2.41
●IC=6.99
●IC=7.17
0.5
1.0
1
2
3
4
5
6
7
CC

LITHOLOGIC DESCRIPTION

MARLY NANNOFOSSIL OOZE

Entire core is undisturbed.

Major lithology: MARLY NANNOFOSSIL OOZE, mottled olive (5Y 4/3, 4/2) and light olive gray (5Y 5/3) intervals of irregular thickness. Siliceous microfossils present in trace amounts.

SMEAR SLIDE SUMMARY (%):

	1, 16 D	5, 66 D
TEXTURE:		
Sand	5	—
Silt	25	20
Clay	70	80
COMPOSITION:		
Access. minerals	1	1
Clay	25	20
Diatoms	—	3
Dolomite	—	Tr
Foraminifers	5	—
Inorganic calcite	20	14
Nannofossils	45	60
Quartz	2	Tr
Radiolarians	1	Tr
Sponge spicules	1	2

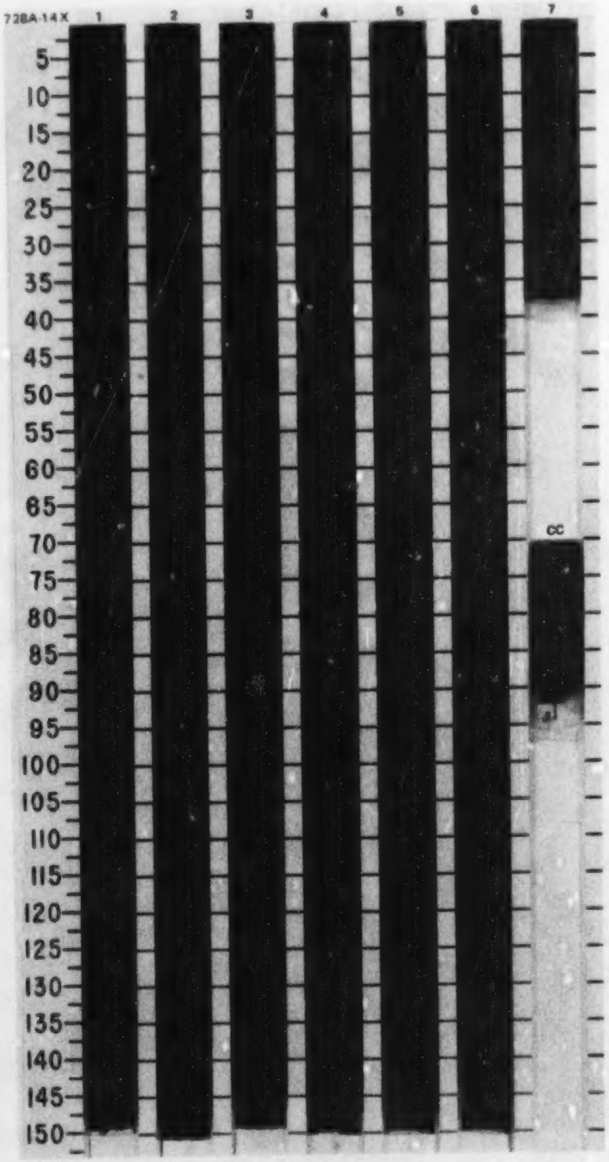
728A-14X
1
2
3
4
5
6
7
CC
5
10
15
20
25
30
35
40
45
50
55
60
65
70
75
80
85
90
95
100
105
110
115
120
125
130
135
140
145
150

SITE 728 HOLE A CORE 15X CORED INTERVAL 1561.7-1572.3 mbsl; 143.5-133.9 mbsf

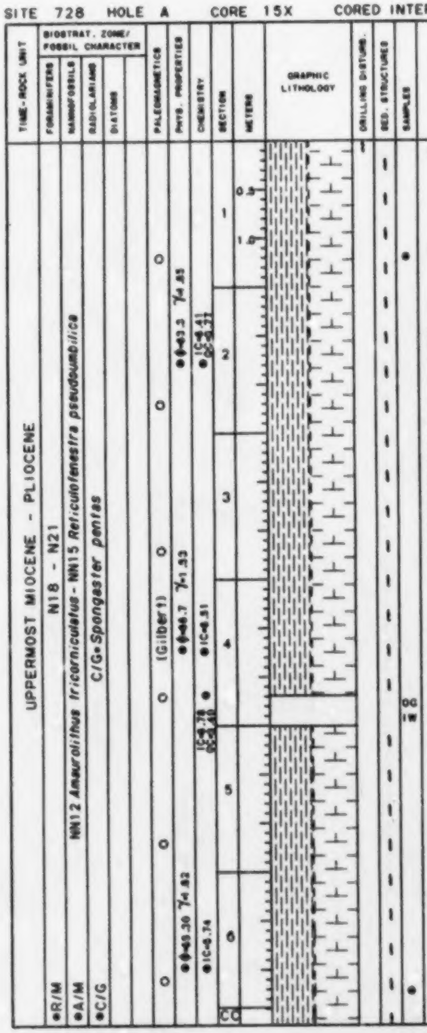
TIME-ROCK UNIT
BIOSTRAT. ZONE/ FOSSIL CHARACTER
FORAMINIFERS
NANNOFOSSILS
RADIOLARIANS
DIATOMS
PALEOMAGNETICS
PHYS. PROPERTIES
CHEMISTRY
SECTION
METERS
GRAPHIC LITHOLOGY
DRILLING DISTURB.
SED. STRUCTURES
SAMPLES
UPPERMOST MIOCENE - PLIOCENE
N18 - N21
NN12 Amaurolithus tricorniculatus - NN15 Reticulofenestra pseudoumbilica
C/G • Spongaster pentas
●R/M
●A/M
●C/G
(Gilbert)
●φ=63.3 γ=1.85
●φ=66.7 γ=1.53
●φ=63.30 γ=1.82
●IC=8.41 OC=0.37
●IC=6.51
IC=6.78 OC=0.40
●IC=6.74
0.5
1.0
1
2
3
4
5
6
CC
OG
IW

LITHOLOGIC DESCRIPTION

MARLY NANNOFOSSIL OOZE

Section 1, 0-10 cm, is slightly disturbed; remainder of core is undisturbed.

Major lithology: MARLY NANNOFOSSIL OOZE, mottled olive (5Y 4/4, 4/3), homogeneous appearance. Siliceous microfossils present, as much as 5%, in smear slides.

SMEAR SLIDE SUMMARY (%):

	1, 119 D	6, 122 D
TEXTURE:		
Sand	5	5
Silt	10	10
Clay	85	85
COMPOSITION:		
Access. minerals	1	1
Clay	25	25
Diatoms	3	3
Dolomite	Tr	—
Feldspar	—	1
Foraminifers	1	—
Inorganic calcite	6	5
Mica	1	Tr
Nannofossils	60	60
Phosphate	Tr	—
Quartz	1	3
Radiolarians	1	1
Silicoflagellates	—	Tr
Sponge spicules	1	1

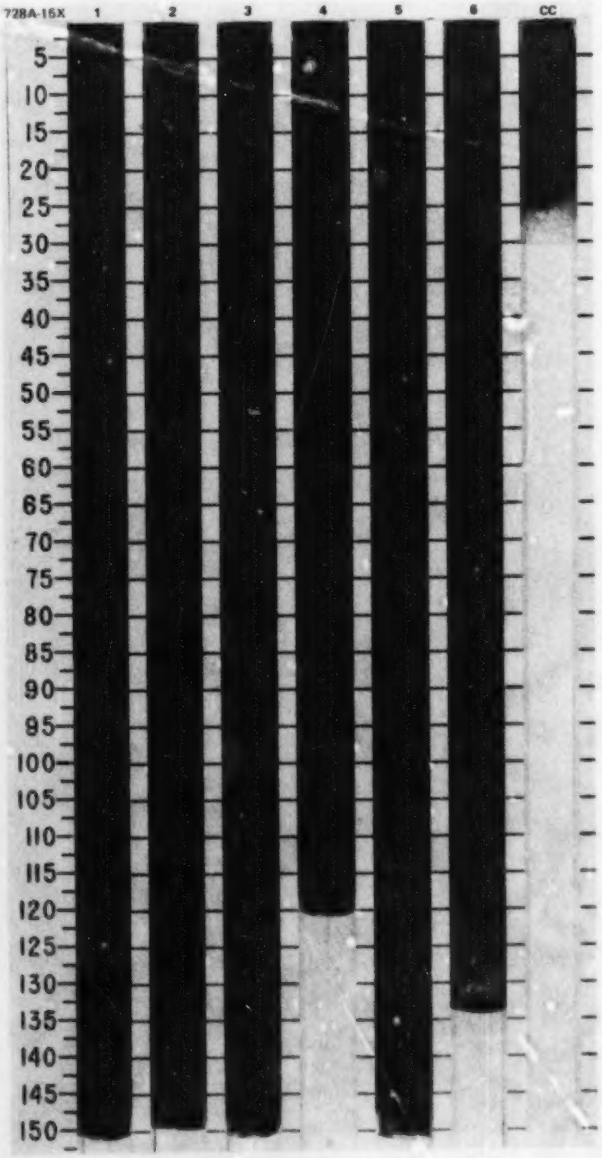
728A-15X
1
2
3
4
5
6
CC
5
10
15
20
25
30
35
40
45
50
55
60
65
70
75
80
85
90
95
100
105
110
115
120
125
130
135
140
145
150

SITE 728 HOLE A CORE 16x CORED INTERVAL571.3-1580.9 mbsl; 143.5-153.1 mbsf

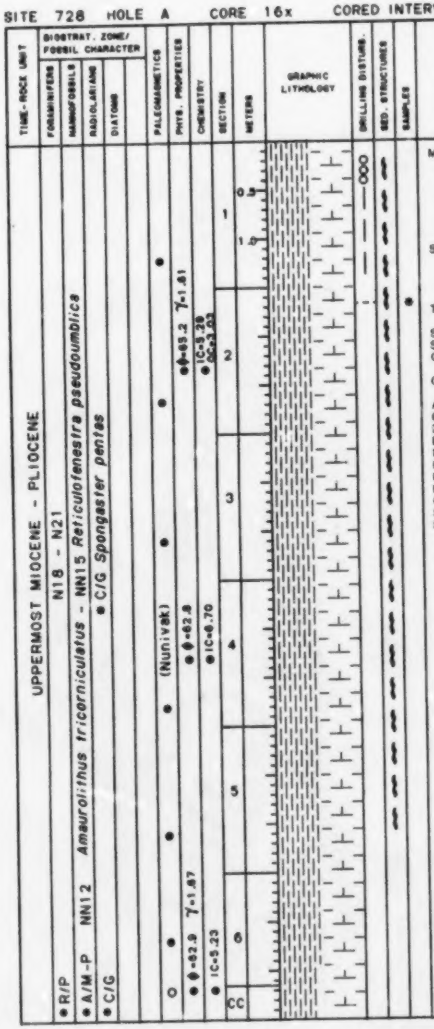
TIME-ROCK UNIT
BIOSTRAT. ZONE/ FOSSIL CHARACTER
FORAMINIFERS
NANNOFOSSILS
RADIOLARIANS
DIATOMS
PALEOMAGNETICS
PHYS. PROPERTIES
CHEMISTRY
SECTION
METERS
GRAPHIC LITHOLOGY
DRILLING DISTURB.
SED. STRUCTURES
SAMPLES
UPPERMOST MIOCENE - PLIOCENE
● R/P
N18 - N21
● A/M-P NN12 Amaurolithus tricorniculatus - NN15 Reticulofenestra pseudoumbilica
● C/G
● C/G Spongaster pentas
(Nunivak)
●φ=63.2 γ=1.81
● φ=62.8
● φ=62.9 γ=1.87
● IC=5.28 OC=3.03
● IC=6.70
● IC=5.23
1
2
3
4
5
6
CC
0.5
1.0

LITHOLOGIC DESCRIPTION

MARLY NANNOFOSSIL OOZE

Section 1, 15-30 cm, is soupy; remainder of core is undisturbed.

Major lithology: MARLY NANNOFOSSIL OOZE, mottled olive (5Y 4/3, 4/2) and light olive gray (5Y 5/3, 5/2) intervals of irregular thickness. Siliceous microfossils present in trace amounts.

SMEAR SLIDE SUMMARY (%):

	2, 18 D	4, 37 D
TEXTURE:		
Sand	10	—
Silt	30	15
Clay	60	85
COMPOSITION:		
Access. minerals	2	2
Clay	25	20
Diatoms	3	Tr
Dolomite	—	Tr
Foraminifers	1	1
Inorganic calcite	12	8
Nannofossils	45	65
Phosphate	Tr	—
Quartz	10	1
Silicoflagellates	Tr	Tr
Sponge spicules	2	3

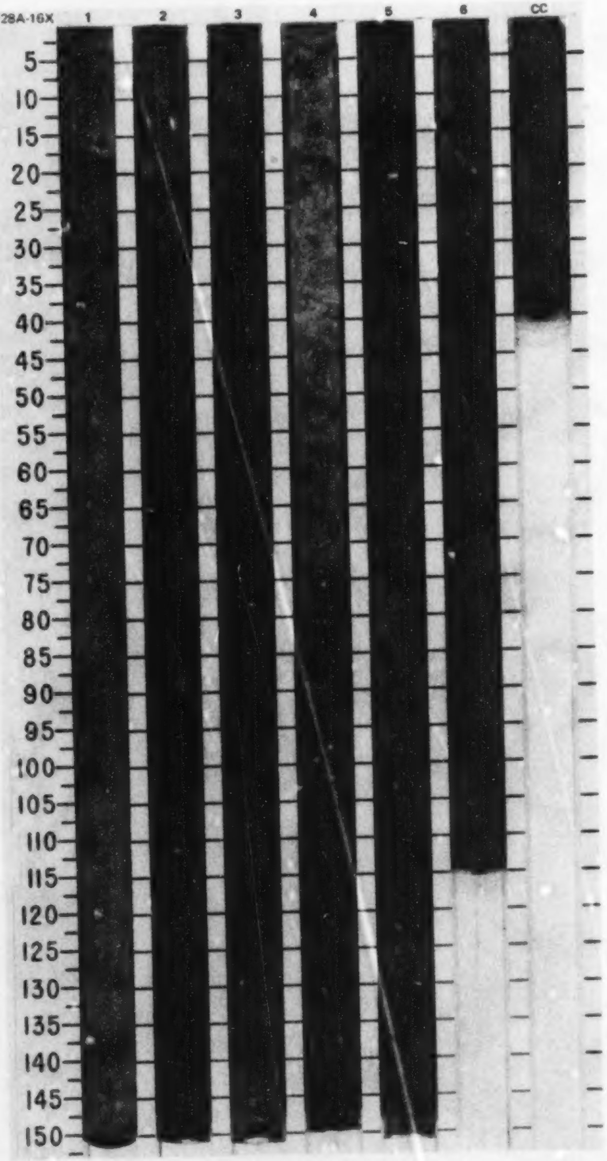
728A-16X
1
2
3
4
5
6
CC
5
10
15
20
25
30
35
40
45
50
55
60
65
70
75
80
85
90
95
100
105
110
115
120
125
130
135
140
145
150

SITE 728 HOLE A CORE 17X CORED INTERVAL 1580.9-1590.6 mbsl; 153.1-162.8 mbsf

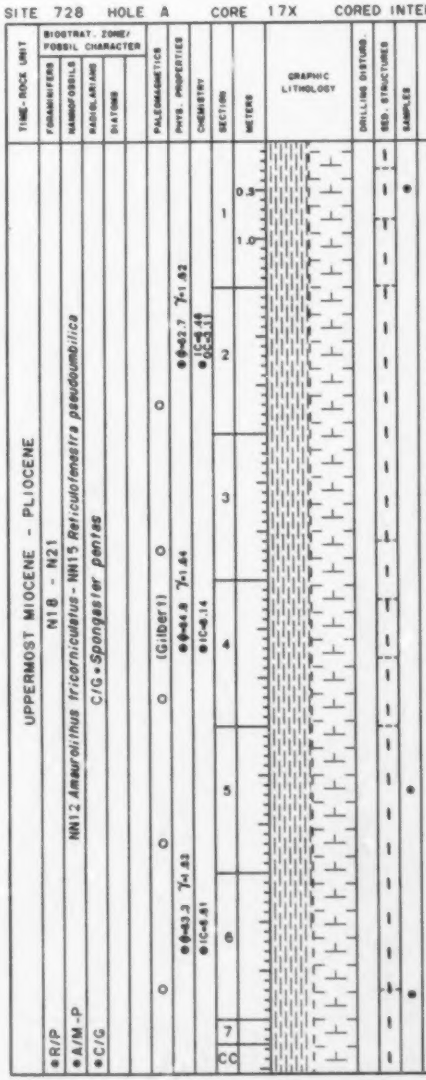

LITHOLOGIC DESCRIPTION

MARLY NANNOFOSSIL OOZE

Section 1 is slightly disturbed; remainder of core is undisturbed.

Major lithology: MARLY NANNOFOSSIL OOZE, mottled olive (5Y 4/3) and light olive gray (5Y 5/3) intervals of irregular thickness. Pyrite flecks visible in lighter layers (noted in Section 1). Siliceous microfossils present in trace amounts.

SMEAR SLIDE SUMMARY (%):

	1, 63 D	5, 64 D	6, 131 D
TEXTURE:			
Sand	3	5	5
Silt	15	10	15
Clay	82	85	80
COMPOSITION:			
Access. minerals	Tr	1	2
Clay	20	25	20
Diatoms	2	—	3
Foraminifers	3	2	4
Volcanic glass	8	—	—
Inorganic calcite	—	6	7
Nannofossils	66	60	60
Quartz	2	6	2
Radiolarians	1	—	1
Silicoflagellates	—	—	1
Sponge spicules	2	Tr	—

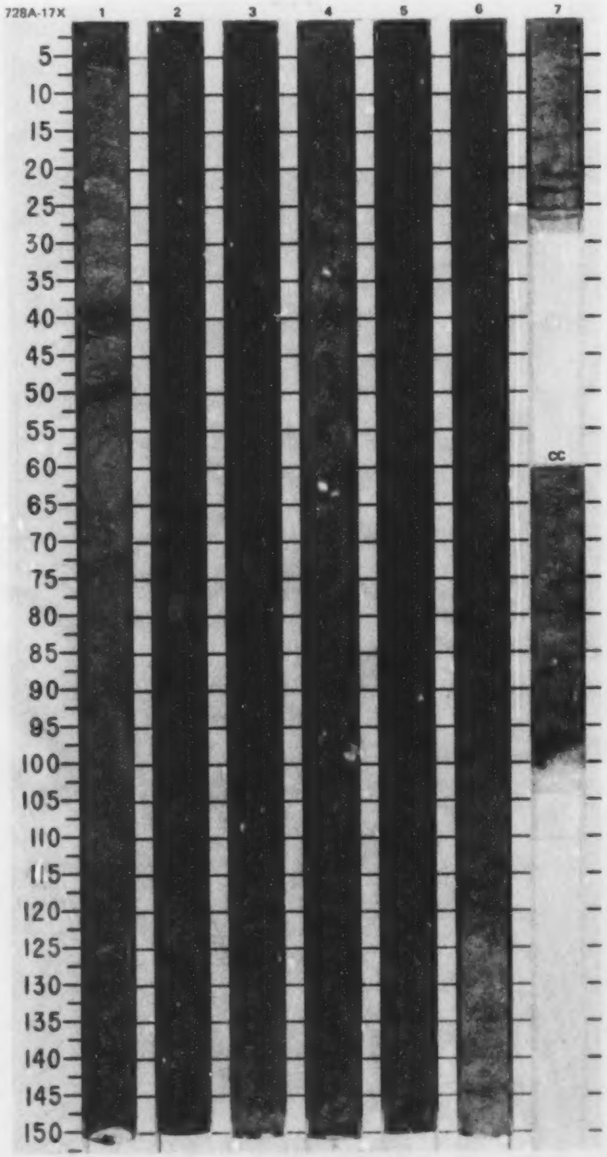
728A-17X
1
2
3
4
5
6
7
CC
5
10
15
20
25
30
35
40
45
50
55
60
65
70
75
80
85
90
95
100
105
110
115
120
125
130
135
140
145
150

SITE 728 HOLE A CORE 18X CORED INTERVAL 1590.6-1600.3 mbsl; 162.8-172.5 mbsf

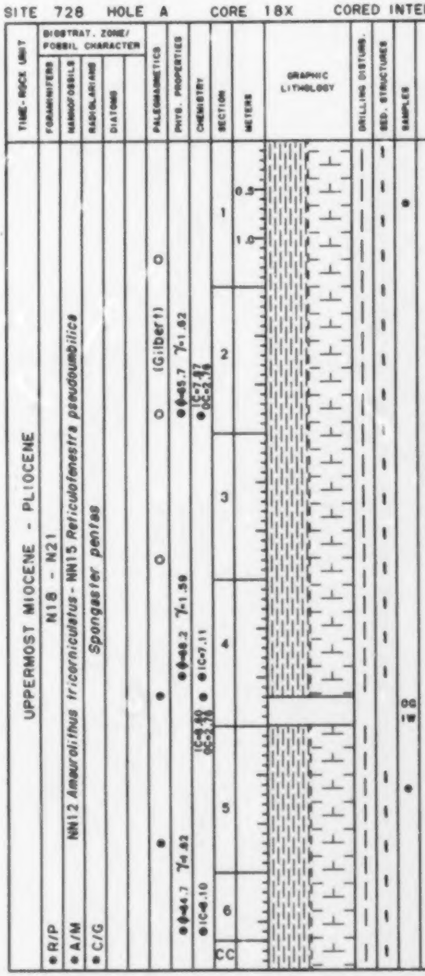
TIME-ROCK UNIT
BIOSTRAT. ZONE/FOSSIL CHARACTER
FORAMINIFERS
NANNOFOSSILS
RADIOLARIANS
DIATOMS
PALEOMAGNETICS
PHYS. PROPERTIES
CHEMISTRY
SECTION
METERS
GRAPHIC LITHOLOGY
DRILLING DISTURB.
SED. STRUCTURES
SAMPLES
UPPERMOST MIOCENE - PLIOCENE
● R/P
N18 - N21
● A/M
NN12 Amaurolithus tricorniculatus - NN15 Reticulofenestra pseudoumbilica
● C/G
Spongaster pentas
(Gilbert)
● φ=65.7 γ=1.82
● φ=60.2 γ=1.59
● φ=44.7 γ=1.82
● IC=7.87 OC=2.16
● IC=7.11
IC=8.80 OC=2.76
● IC=8.10
1
2
3
4
5
6
CC
0.5
1.0
OG
IW

LITHOLOGIC DESCRIPTION

MARLY NANNOFOSSIL OOZE and NANNOFOSSIL OOZE

Entire core is slightly disturbed.

Major lithologies: MARLY NANNOFOSSIL OOZE and NANNOFOSSIL OOZE, mottled olive gray (5Y 5/3, 5/2). Homogeneous, with little color variation. Siliceous microfossils present in trace amounts.

SMEAR SLIDE SUMMARY (%):

	1, 65 D	5, 63 D
TEXTURE:		
Sand	3	—
Silt	12	10
Clay	85	90
COMPOSITION:		
Access. minerals	2	2
Clay	20	20
Diatoms	2	—
Foraminifers	1	Tr
Inorganic calcite	7	6
Mica	—	1
Nannofossils	65	70
Quartz	1	1
Radiolarians	Tr	—
Silicoflagellates	—	1
Sponge spicules	1	Tr

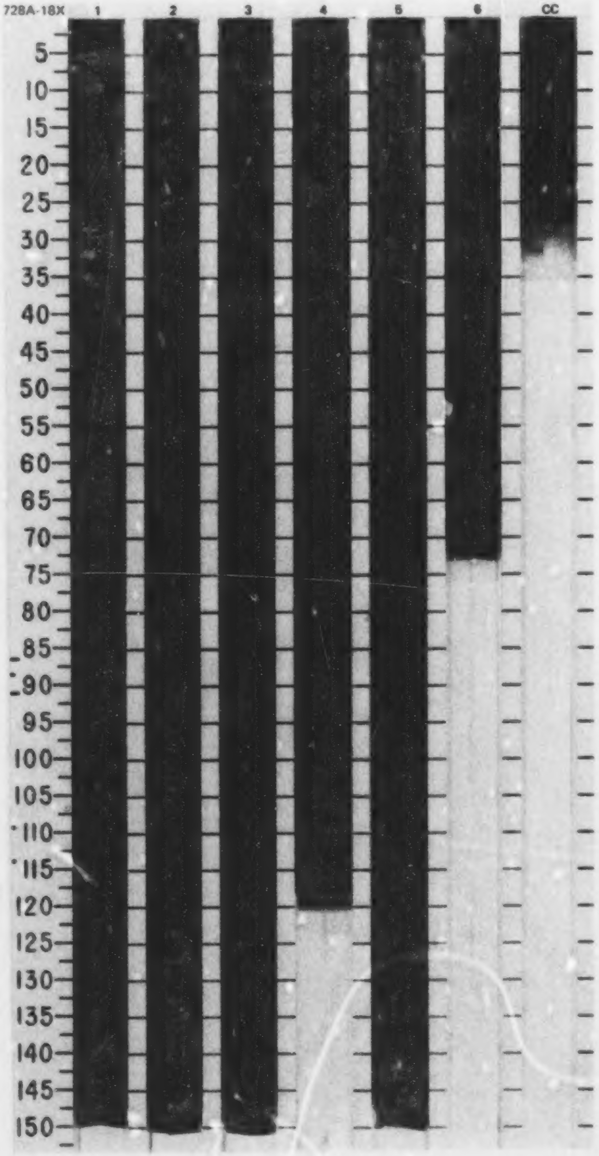
728A-18X
1
2
3
4
5
6
CC
5
10
15
20
25
30
35
40
45
50
55
60
65
70
75
80
85
90
95
100
105
110
115
120
125
130
135
140
145
150

SITE 728 HOLE A CORE 19X CORED INTERVAL 1600.3-1610.0 mbsl; 172.5-182.2 mbsf

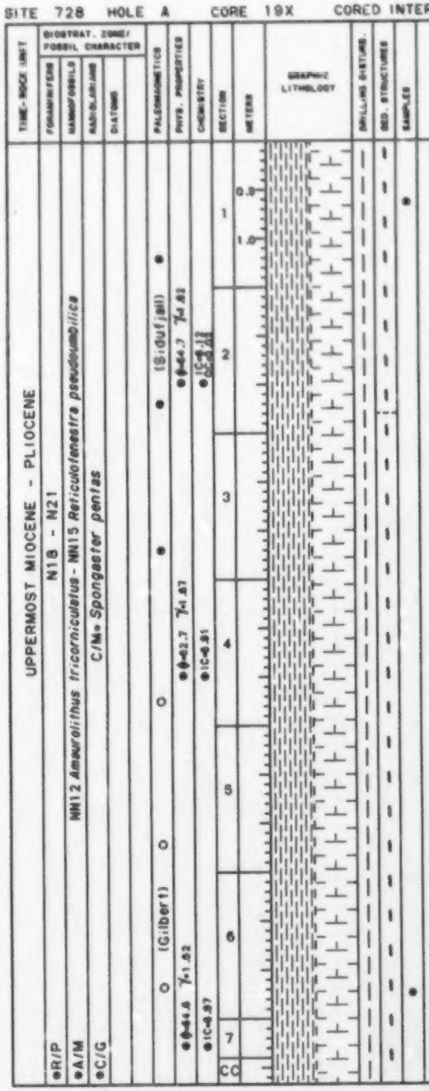
TIME-ROCK UNIT
BIOSTRAT. ZONE/ FOSSIL CHARACTER
FORAMINIFERS
NANNOFOSSILS
RADIOLARIANS
DIATOMS
PALEOMAGNETICS
PHYS. PROPERTIES
CHEMISTRY
SECTION
METERS
GRAPHIC LITHOLOGY
DRILLING DISTURB.
SED. STRUCTURES
SAMPLES
UPPERMOST MIOCENE - PLIOCENE
●R/P
N18 - N21
●A/M
NN12 Amaurolithus tricorniculatus - NN15 Reticulofenestra pseudoumbilica
●C/G
C/M= Spongaster pentas
(Sidufjall)
(Gilbert)
●ϕ=64.7 γ=1.82
●ϕ=62.7 γ=1.87
●ϕ=64.6 γ=1.82
●IC=8.91
●IC=8.97
1
2
3
4
5
6
7
CC
0.5
1.0

LITHOLOGIC DESCRIPTION

MARLY NANNOFOSSIL OOZE

Core is slightly disturbed.

Major lithology: MARLY NANNOFOSSIL OOZE, mottled olive (5Y 4/3) and light olive gray (5Y 5/3). Homogeneous, with little variation in color. Siliceous microfossils present in trace amounts.

SMEAR SLIDE SUMMARY (%):

	1, 83 D	6, 122 D
TEXTURE:		
Sand	10	10
Silt	20	35
Clay	70	55
COMPOSITION:		
Access. minerals	—	2
Clay	25	20
Diatoms	Tr	—
Dolomite	1	Tr
Foraminifers	4	1
Glauconite	Tr	Tr
Inorganic calcite	10	20
Mica	—	1
Nannofossils	50	35
Phosphate	—	Tr
Quartz	10	20
Radiolarians	Tr	1
Silicoflagellates	Tr	—
Sponge spicules	Tr	Tr

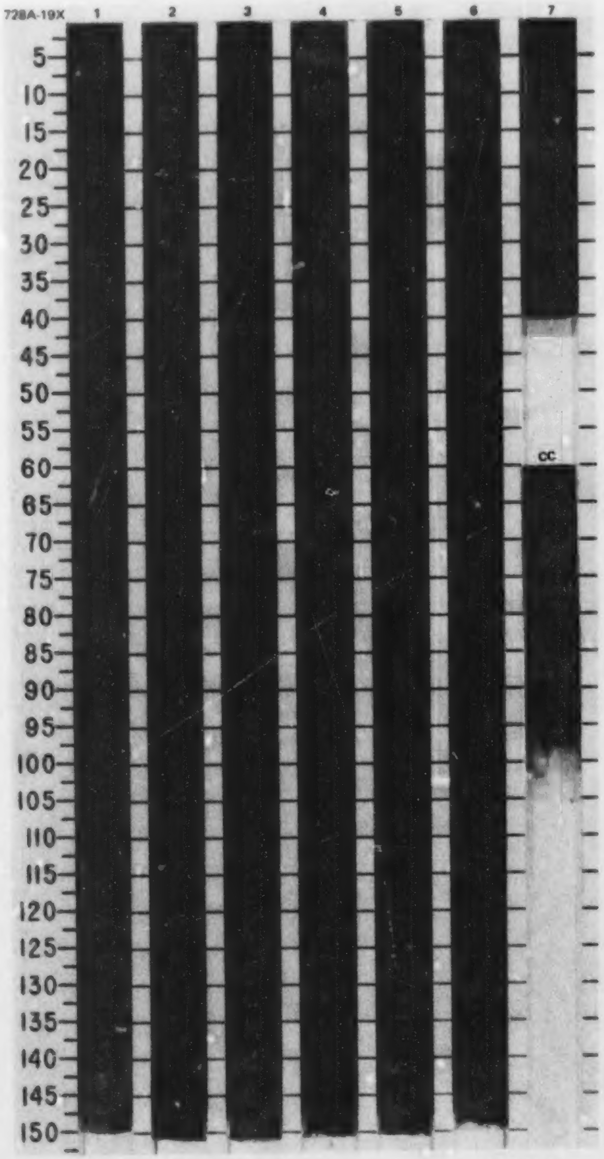
728A-19X
1
2
3
4
5
6
7
CC
5
10
15
20
25
30
35
40
45
50
55
60
65
70
75
80
85
90
95
100
105
110
115
120
125
130
135
140
145
150

SITE 728 HOLE A CORE 20X CORED INTERVAL 1610.0-1619.6 mbsl; 182.2-191.8 mbsf

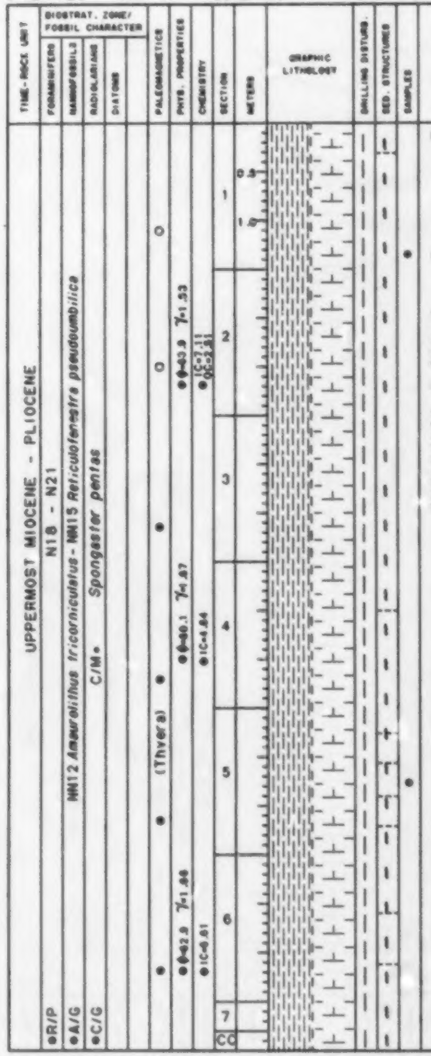
TIME-ROCK UNIT
BIOSTRAT. ZONE/ FOSSIL CHARACTER
FORAMINIFERS
NANNOFOSSILS
RADIOLARIANS
DIATOMS
PALEOMAGNETICS
PHYS. PROPERTIES
CHEMISTRY
SECTION
METERS
GRAPHIC LITHOLOGY
DRILLING DISTURB.
SED. STRUCTURES
SAMPLES
UPPERMOST MIOCENE - PLIOCENE
●R/P
N18 - N21
●A/G
NN12 Amaurolithus tricorniculatus - NN15 Reticulofenestra pseudoumbilica
●C/G
C/M●
Spongaster pentas
(Thvera)
●φ=63.9 γ=1.53
●φ=60.1 γ=1.87
●φ=62.9 γ=1.88
●IC=7.11 OC=2.81
●IC=4.84
●IC=6.61
0.5
1.0
1
2
3
4
5
6
7
CC

LITHOLOGIC DESCRIPTION

MARLY NANNOFOSSIL OOZE

Core is slightly disturbed.

Major lithology: MARLY NANNOFOSSIL OOZE, mottled olive (5Y 4/3, 4/2, 3/2) and light olive gray (5Y 5/3) intervals of irregular thickness with greater color contrast and mottling relative to cores 117-728A-18X and -19X. Siliceous microfossils present in trace amounts. Darker layers have fewer nannofossils. Calcareous silty clay indicated on one smear slide.

SMEAR SLIDE SUMMARY (%):

	1, 137 D	5, 76 D
TEXTURE:		
Sand	15	5
Silt	30	15
Clay	55	80
COMPOSITION:		
Accesn. minerals	2	1
Clay	30	25
Foraminifers	1	2
Inorganic calcite	16	15
Mica	1	—
Nannofossils	25	55
Organic debris	5	—
Quartz	20	2
Radiolarians	Tr	—

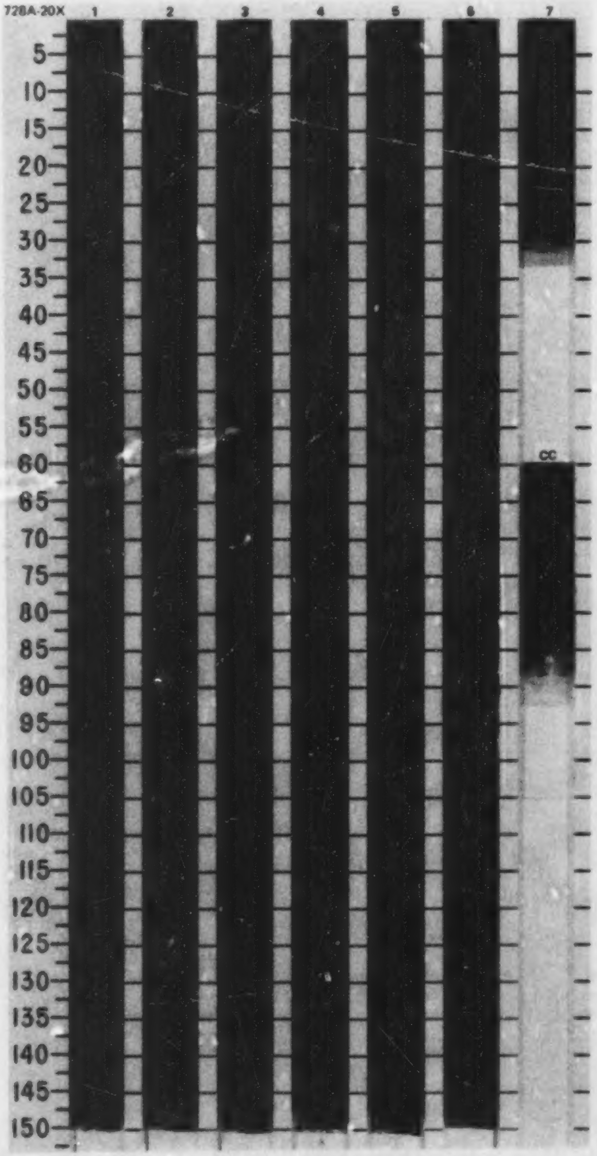
728A-20X
1
2
3
4
5
6
7
CC
5
10
15
20
25
30
35
40
45
50
55
60
65
70
75
80
85
90
95
100
105
110
115
120
125
130
135
140
145
150

SITE 728 HOLE A CORE 21X CORED INTERVAL 1619.6-1629.3 mbsl; 191.8-201.5 mbsf

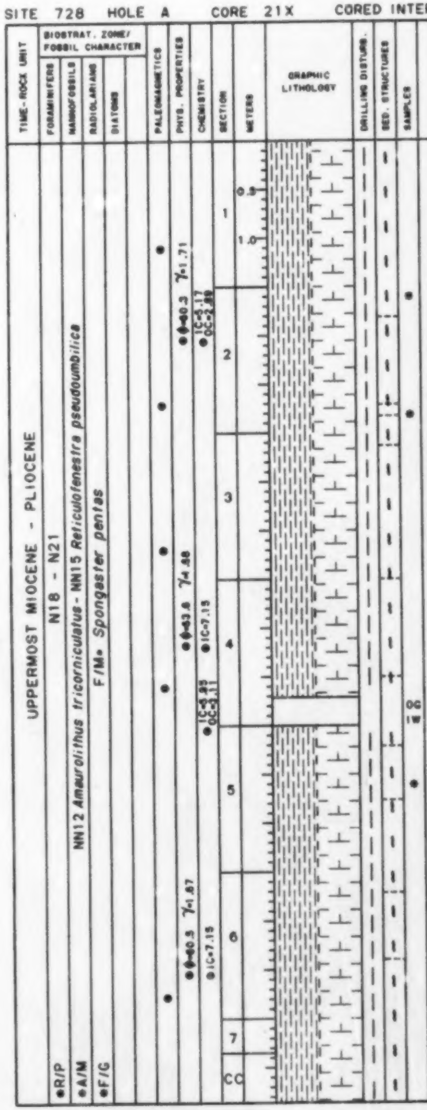
TIME-ROCK UNIT
BIOSTRAT. ZONE/ FOSSIL CHARACTER
FORAMINIFERS
NANNOFOSSILS
RADIOLARIANS
DIATOMS
PALEOMAGNETICS
PHYS. PROPERTIES
CHEMISTRY
SECTION
METERS
GRAPHIC LITHOLOGY
DRILLING DISTURB.
SED. STRUCTURES
SAMPLES
UPPERMOST MIOCENE - PLIOCENE
N18 - N21
NN12 Amaurolithus tricorniculatus - NN15 Reticulofenestra pseudoumbilica
F/M• Spongaster pentas
•R/P
•A/M
•F/G
•ϕ=60.3 γ=1.71
•ϕ=63.6 γ=1.66
•ϕ=60.5 γ=1.67
•IC=5.17 OC=2.88
•IC=7.15
•IC=5.85 OC=3.11
•IC=7.15
0.5
1.0
1
2
3
4
5
6
7
CC
OG
IW

LITHOLOGIC DESCRIPTION

MARLY NANNOFOSSIL OOZE and CALCAREOUS SILTY CLAY

Core is slightly disturbed.

Major lithologies: MARLY NANNOFOSSIL OOZE and CALCAREOUS SILTY CLAY. Dark intervals are interpreted as having less than 30% biogenic carbonate. Mottled olive (5Y 4/3) and light olive gray (5Y 5/3, 5/2) intervals of irregular thickness. Siliceous microfossils present in trace amounts.

SMEAR SLIDE SUMMARY (%):

	2, 10 D	2, 130 D	5, 59 D
TEXTURE:			
Sand	20	10	
Silt	20	15	10
Clay	60	75	90
COMPOSITION:			
Access. minerals	2	2	1
Clay	35	20	25
Dolomite	1	—	1
Foraminifers	2	1	2
Inorganic calcite	20	15	6
Nannofossils	25	55	65
Phosphate	Tr	—	Tr
Quartz	15	5	Tr
Radiolarians	Tr	—	Tr
Silicoflagellates	—	—	Tr
Sponge spicules	Tr	2	Tr

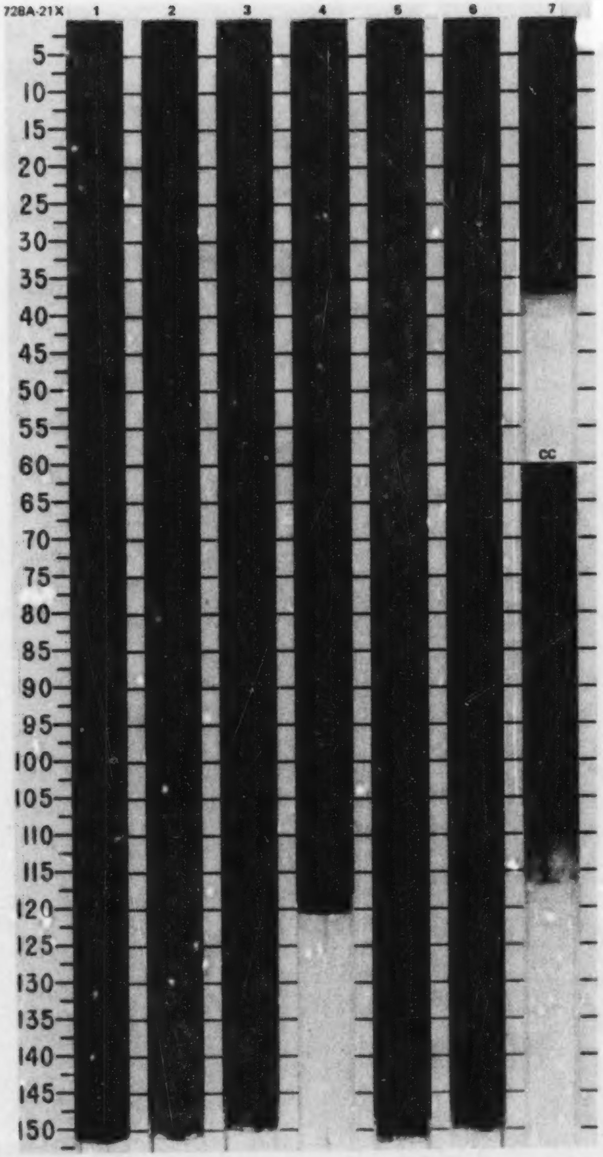
728A-21X
1
2
3
4
5
6
7
CC
5
10
15
20
25
30
35
40
45
50
55
60
65
70
75
80
85
90
95
100
105
110
115
120
125
130
135
140
145
150

SITE 728 HOLE A CORE 22X CORED INTERVAL 1629.3-1638.9 mbsl; 201.5-211.1 mbsf

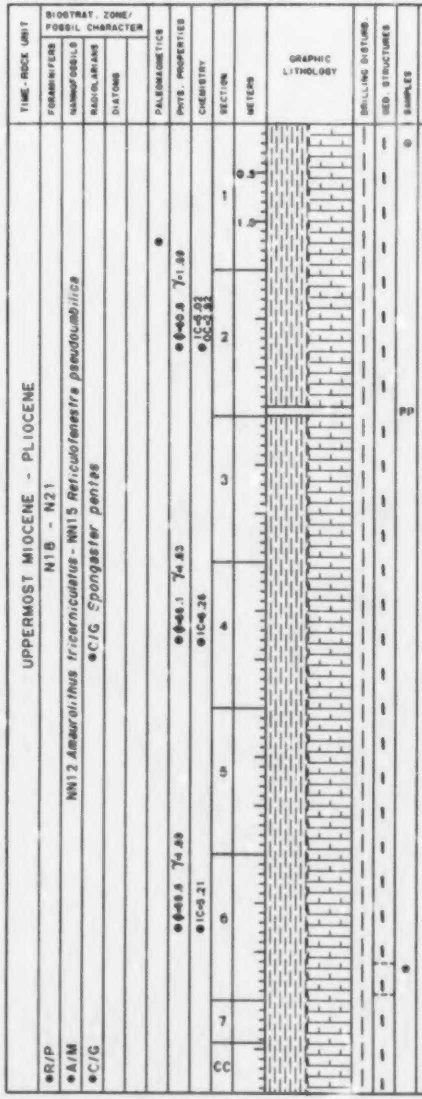
TIME-ROCK UNIT
BIOSTRAT. ZONE/ FOSSIL CHARACTER
FORAMINIFERS
NANNOFOSSILS
RADIOLARIANS
DIATOMS
PALEOMAGNETICS
PHYS. PROPERTIES
CHEMISTRY
SECTION
METERS
GRAPHIC LITHOLOGY
DRILLING DISTURB.
SED. STRUCTURES
SAMPLES
UPPERMOST MIOCENE - PLIOCENE
●R/P
N18 - N21
●A/M
NN12 Amaurolithus tricorniculatus - NN15 Reticulofenestra pseudoumbilica
●C/G
●C/G Spongaster pentas
0.5
1.0
1
2
3
4
5
6
7
CC
PP

LITHOLOGIC DESCRIPTION

NANNOFOSSIL CHALK

Core is slightly disturbed.

Major lithology: NANNOFOSSIL CHALK, mottled olive (5Y 4/3) and light olive gray (5Y 5/3) intervals of irregular thickness. Siliceous microfossils present in trace amounts. Below this level the nannofossil fraction increases and the silt-sized calcite fraction decreases.

SMEAR SLIDE SUMMARY (%):

	1, 119 D	6, 119 D
TEXTURE:		
Sand	2	—
Silt	10	10
Clay	88	90
COMPOSITION:		
Access. minerals	Tr	Tr
Clay	15	15
Dolomite	Tr	Tr
Inorganic calcite	9	7
Nannofossils	73	75
Quartz	3	3
Radiolarians	Tr	Tr
Silicoflagellates	Tr	Tr
Sponge spicules	Tr	Tr

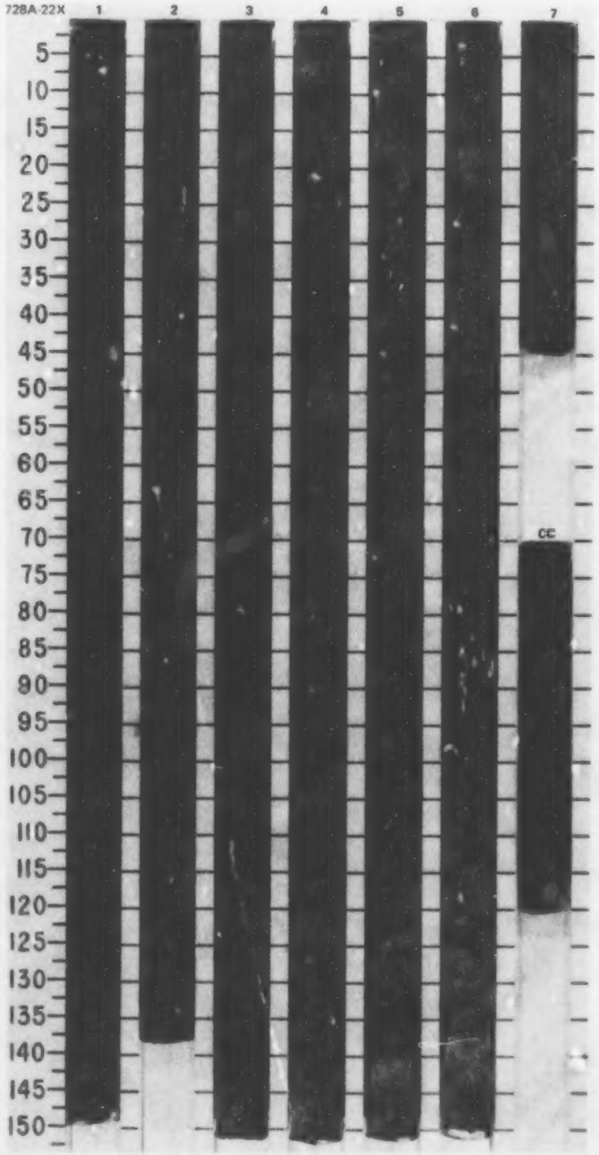
728A-22X
1
2
3
4
5
6
7
CC
5
10
15
20
25
30
35
40
45
50
55
60
65
70
75
80
85
90
95
100
105
110
115
120
125
130
135
140
145
150

SITE 728 HOLE A CORE 23X CORED INTERVAL 1628.9-1648.6 mbsl; 211.1-220.8 mbsf

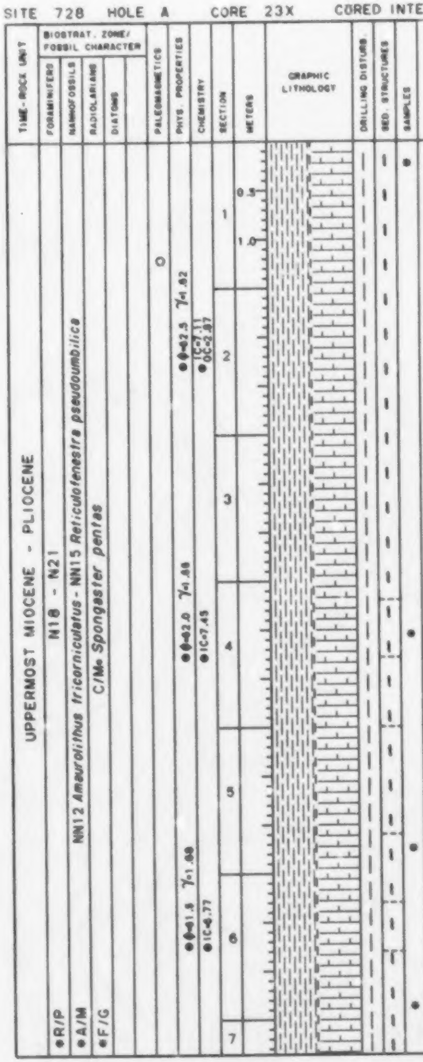
TIME-ROCK UNIT
BIOSTRAT. ZONE/ FOSSIL CHARACTER
FORAMINIFERS
NANNOFOSSILS
RADIOLARIANS
DIATOMS
PALEOMAGNETICS
PHYS. PROPERTIES
CHEMISTRY
SECTION
METERS
GRAPHIC LITHOLOGY
DRILLING DISTURB.
SED. STRUCTURES
SAMPLES
UPPERMOST MIOCENE - PLIOCENE
●R/P N18 - N21
●A/M NN12 Amaurolithus tricorniculatus - NN15 Reticulofenestra pseudoumbilica
●F/G C/M● Spongaster pentas
●ϕ=62.5 γ=1.82
●IC=7.11 OC=2.87
●ϕ=62.0 γ=1.88
●IC=7.45
●ϕ=61.8 γ=1.88
●IC=6.77
1
2
3
4
5
6
7
0.5
1.0

LITHOLOGIC DESCRIPTION

NANNOFOSSIL CHALK

Core is slightly disturbed.

Major lithology: NANNOFOSSIL CHALK, mottled olive (5Y 4/3) and light olive gray (5Y 5/3, 5/2) intervals of irregular thickness. Siliceous microfossils are present in trace amounts. Nannofossil fraction increases and silt-sized inorganic calcite fraction decreases.

SMEAR SLIDE SUMMARY (%):

	1, 21 D	4, 57 D	5, 135 D
TEXTURE:			
Sand	—	—	2
Silt	15	13	15
Clay	85	87	83
COMPOSITION:			
Access. minerals	—	Tr	Tr
Clay	15	12	23
Diatoms	—	Tr	—
Foraminifers	—	—	—
Volcanic glass	Tr	—	
Inorganic calcite	12	11	44
Nannofossils	71	75	30
Quartz	2	2	3
Radiolarians	Tr	Tr	Tr
Silicoflagellates	—	Tr	
Sponge spicules	Tr	Tr	—

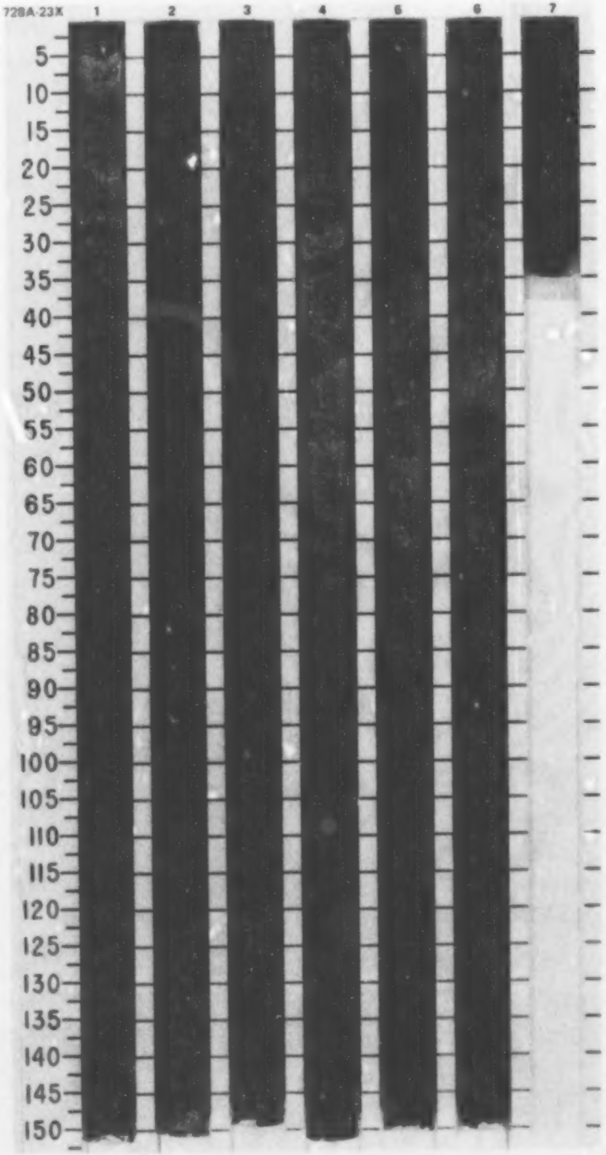
728A-23X
1
2
3
4
5
6
7
5
10
15
20
25
30
35
40
45
50
55
60
65
70
75
80
85
90
95
100
105
110
115
120
125
130
135
140
145
150

SITE 728 HOLE A CORE 24X CORED INTERVAL 1648.6-1658.3 mbsl; 220.8-230.5 mbsf

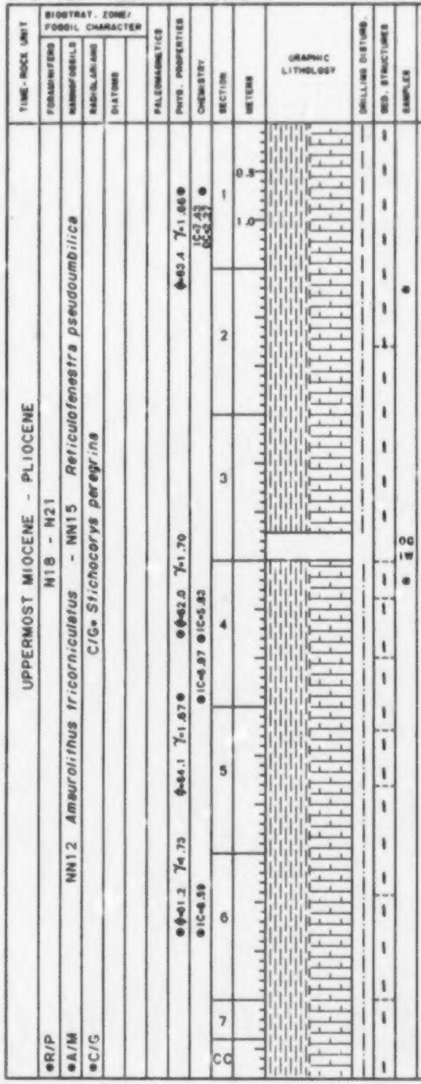
TIME-ROCK UNIT
BIOSTRAT. ZONE/ FOSSIL CHARACTER
FORAMINIFERS
NANNOFOSSILS
RADIOLARIANS
DIATOMS
PALEOMAGNETICS
PHYS. PROPERTIES
CHEMISTRY
SECTION
METERS
GRAPHIC LITHOLOGY
DRILLING DISTURB.
SED. STRUCTURES
SAMPLES
UPPERMOST MIOCENE - PLIOCENE
●R/P
N18 - N21
●A/M
NN12 Amaurolithus tricorniculatus - NN15 Reticulofenestra pseudoumbilica
●C/G
C/G= Stichocorys peregrina
●φ=63.4 γ=1.66●
IC=7.43 OC=0.27 ●
●φ=62.0 γ=1.70
●IC=6.97 ●IC=5.83
φ=64.1 γ=1.67●
●φ=61.2 γ=1.73
●IC=6.59
1
2
3
4
5
6
7
CC
0.5
1.0
OG
IW

LITHOLOGIC DESCRIPTION

NANNOFOSSIL CHALK

Core is slightly disturbed.

Major lithology: NANNOFOSSIL CHALK, mottled olive (5Y 4/3, 4/2) and light olive gray (5Y 5/3, 5/2) intervals of irregular thickness. Siliceous microfossils present in trace amounts.

SMEAR SLIDE SUMMARY (%):

	2, 20 D	4, 20 D
TEXTURE:		
Sand	10	5
Silt	20	25
Clay	70	70
COMPOSITION:		
Clay	10	20
Diatoms	—	Tr
Foraminifers	5	5
Inorganic calcite	5	15
Nannofossils	75	50
Quartz	Tr	10
Radiolarians	3	Tr
Sponge spicules	2	Tr

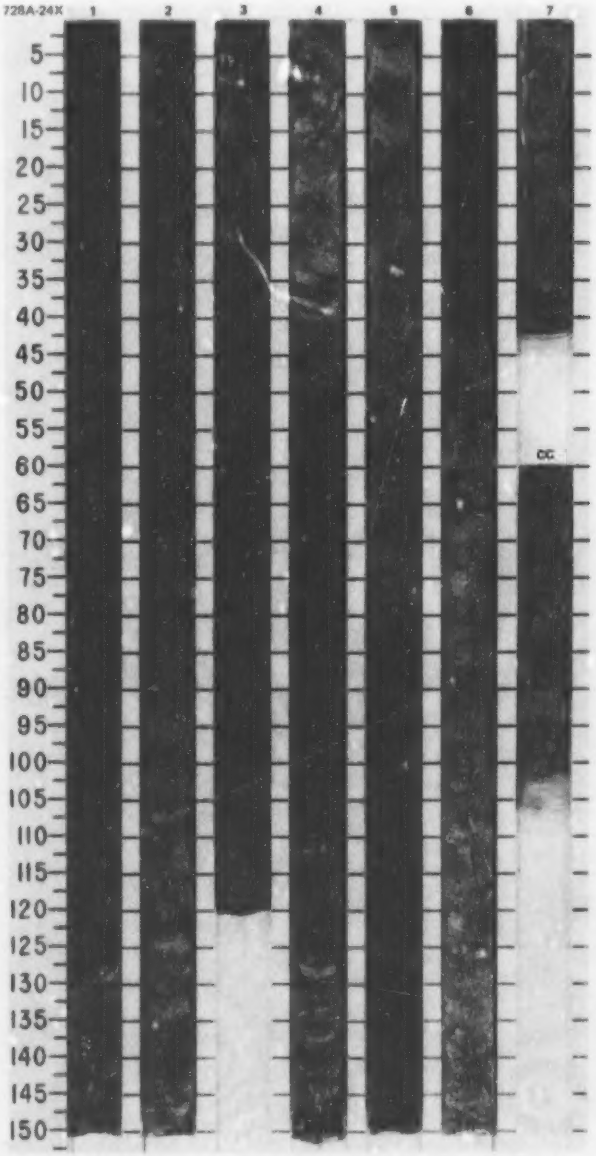
728A-24X
1
2
3
4
5
6
7
CC
5
10
15
20
25
30
35
40
45
50
55
60
65
70
75
80
85
90
95
100
105
110
115
120
125
130
135
140
145
150

SITE 728 HOLE A CORE 25X CORED INTERVAL 1656.3-1667.9 mbsl; 230.5-240.1 mbsf

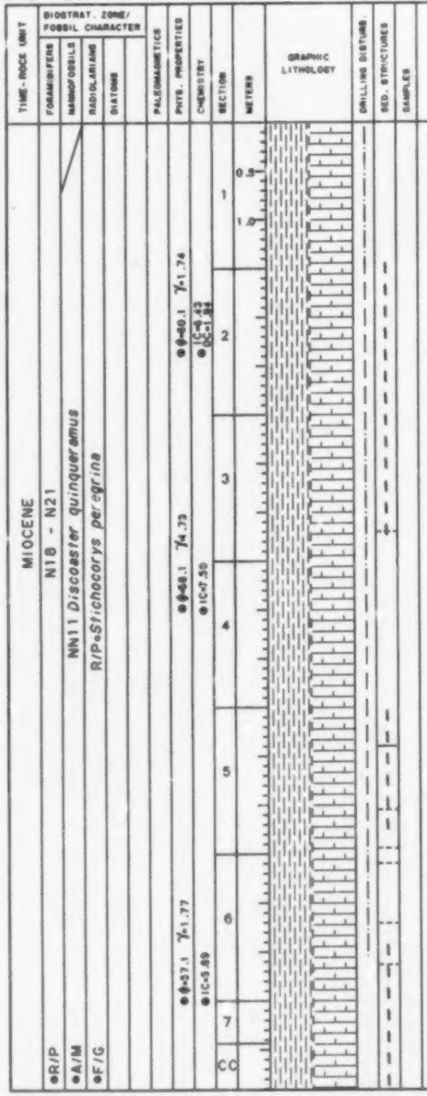
TIME-ROCK UNIT
BIOSTRAT. ZONE/ FOSSIL CHARACTER
FORAMINIFERS
NANNOFOSSILS
RADIOLARIANS
DIATOMS
PALEOMAGNETICS
PHYS. PROPERTIES
CHEMISTRY
SECTION
METERS
GRAPHIC LITHOLOGY
DRILLING DISTURB.
SED. STRUCTURES
SAMPLES
MIOCENE
N18 - N21
NN11 Discoaster quinqueramus
R/P•Stichocorys peregrina
•R/P
•A/M
•F/G
•ϕ=60.1 γ=1.74
•IC=8.43 OC=1.84
•ϕ=48.1 γ=1.73
•IC=7.30
•ϕ=57.1 γ=1.77
•IC=5.89
1
2
3
4
5
6
7
CC
0.5
1.0

LITHOLOGIC DESCRIPTION

NANNOFOSSIL CHALK

Core is slightly disturbed; some drilling biscuits formed.

Major lithology: NANNOFOSSIL CHALK, mottled olive (5Y 4/3, 4/2) and light olive gray (5Y 5/3, 5/2) intervals of irregular thickness. Siliceous microfossils present in trace amounts. Truncated burrows indicate drilling disturbance or microfaults(?).

SMEAR SLIDE SUMMARY (%):

	2, 41 D
TEXTURE:	
Sand	5
Silt	24
Clay	71
COMPOSITION:	
Clay	20
Foraminifers	5
Inorganic calcite	10
Nannofossils	60
Organic debris	3
Quartz	2

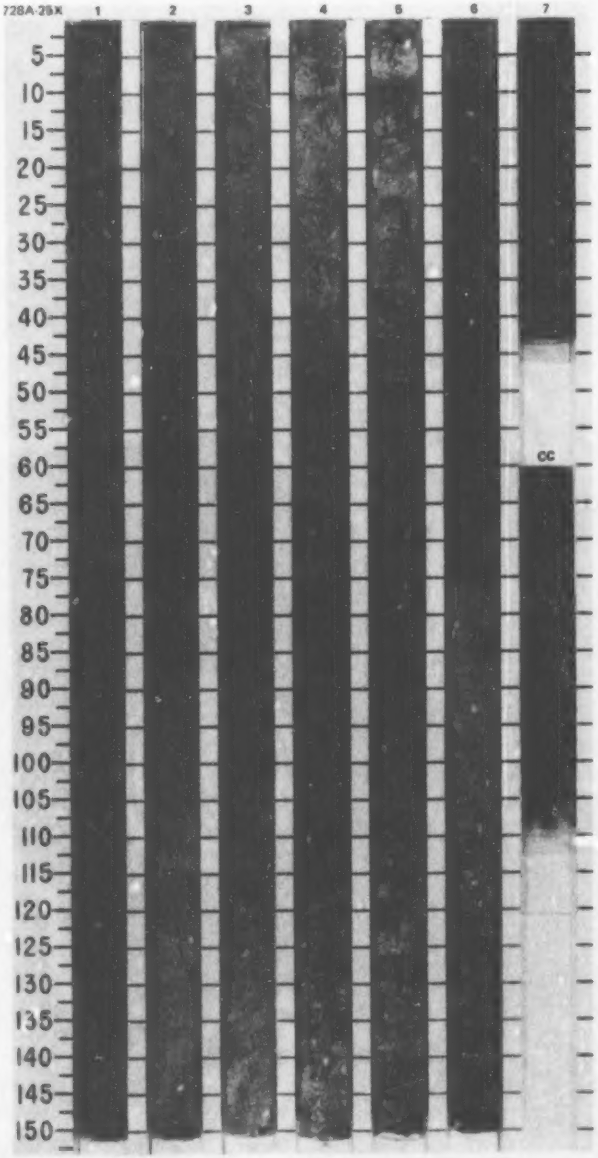
728A-25X
1
2
3
4
5
6
7
CC
5
10
15
20
25
30
35
40
45
50
55
60
65
70
75
80
85
90
95
100
105
110
115
120
125
130
135
140
145
150

SITE 728 HOLE A CORE 26X CORED INTERVAL 1667.3-1677.6 mbsl; 240.1-249.8 mbsf

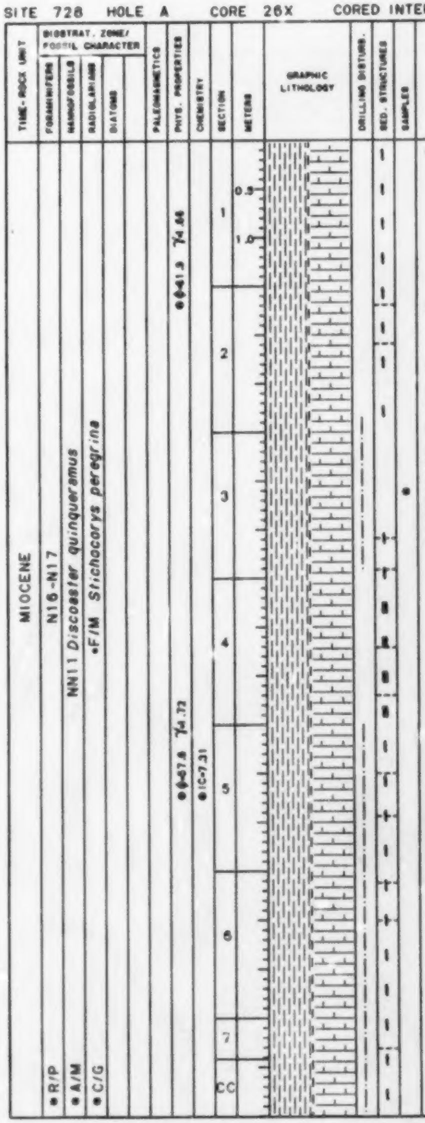

LITHOLOGIC DESCRIPTION

NANNOFOSSIL CHALK

Sections 3-6 are moderately disturbed; remainder of core is slightly disturbed. This is the first core cut with a saw. Biscuits are apparent, with flow between.

Major lithology: NANNOFOSSIL CHALK, mottled olive (5Y 4/3) and light olive gray (5Y 6/2, 5/3, 5/2) that is lighter in color than cores above, intervals of irregular thickness. Mottling is more apparent than in cores above, with *Zoophycos* burrows. Siliceous microfossils present in trace amounts; darker layers have lower nannofossil content. Shell fragments scattered throughout Section 4. Smear slide from olive layer, Section 3, 60 cm, is marly nannofossil chalk.

SMEAR SLIDE SUMMARY (%):

	3, 60 D
TEXTURE:	
Silt	40
Clay	60
COMPOSITION:	
Access. minerals	2
Clay	25
Dolomite	1
Foraminifers	3
Inorganic calcite	18
Nannofossils	30
Quartz	18
Sponge spicules	3

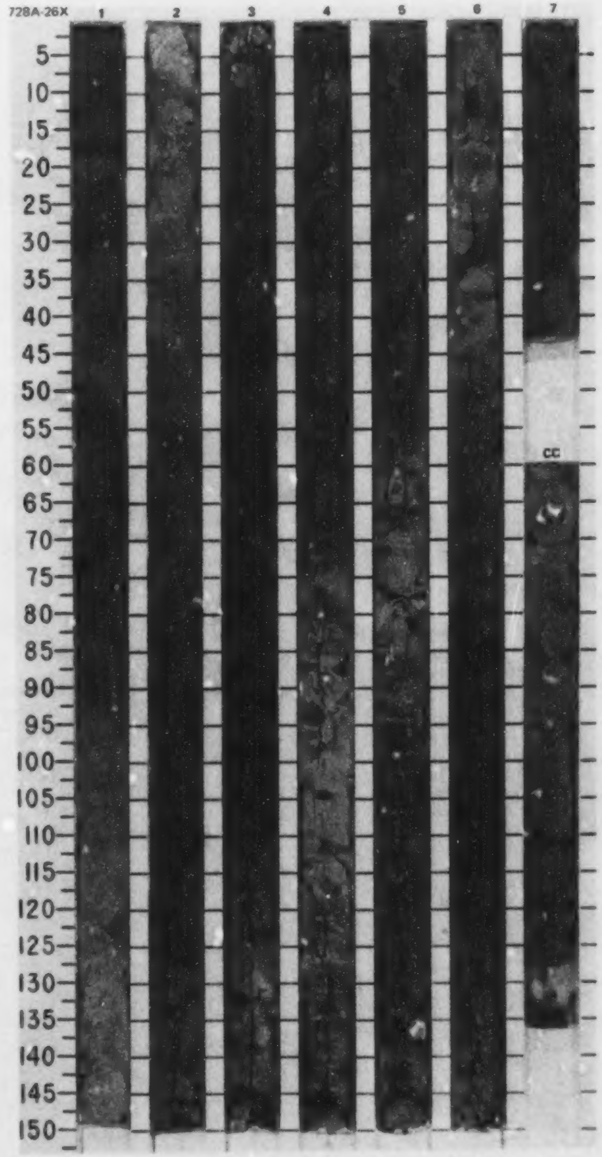
728A-26X
1
2
3
4
5
6
7
CC
5
10
15
20
25
30
35
40
45
50
55
60
65
70
75
80
85
90
95
100
105
110
115
120
125
130
135
140
145
150

SITE 728 HOLE A CORE 27X CORED INTERVAL 1677.6-1687.3 mbsl; 249.8-259.5 mbsf

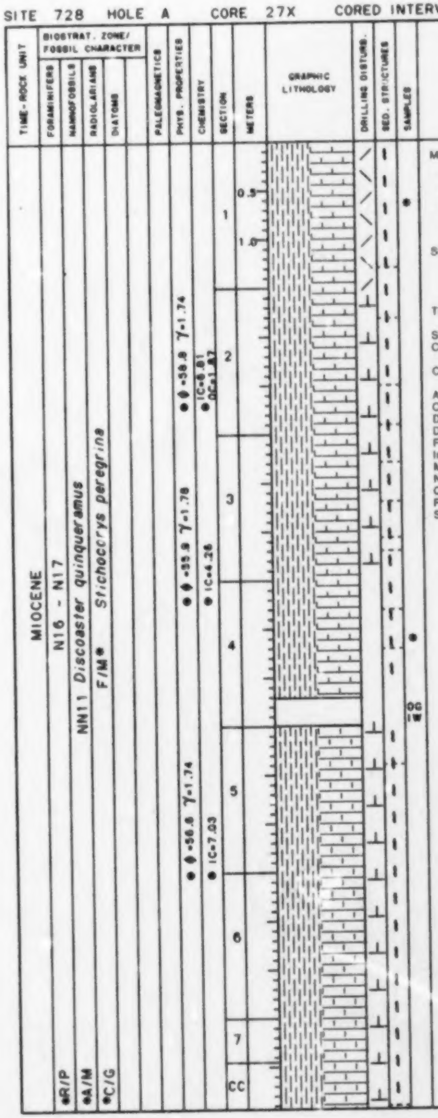
TIME-ROCK UNIT
BIOSTRAT. ZONE/ FOSSIL CHARACTER
FORAMINIFERS
NANNOFOSSILS
RADIOLARIANS
DIATOMS
PALEOMAGNETICS
PHYS. PROPERTIES
CHEMISTRY
SECTION
METERS
GRAPHIC LITHOLOGY
DRILLING DISTURB.
SED. STRUCTURES
SAMPLES
MIOCENE
N16 - N17
NN11 Discoaster quinqueramus
F/M* Stichoccrys peregrina
●R/P
●A/M
*C/G
● φ =58.8 γ=1.74
● φ =55.9 γ=1.78
● φ =56.8 γ=1.74
● IC=8.81 OC=1.87
● IC=4.26
● IC=7.03
1
2
3
4
5
6
7
CC
0.5
1.0
OG
IW

LITHOLOGIC DESCRIPTION

MARLY NANNOFOSSIL CHALK and NANNOFOSSIL CHALK

Core is slightly to moderately fractured.

Major lithologies: MARLY NANNOFOSSIL CHALK and NANNOFOSSIL CHALK, mottled olive (5Y 4/3, 4/2) and light olive gray (5Y 5/3, 5/2) intervals of irregular thickness. Siliceous microfossils present in trace amounts.

SMEAR SLIDE SUMMARY (%):

	1, 67 D	4, 60 D
TEXTURE:		
Silt	25	20
Clay	75	80
COMPOSITION:		
Access. minerals	2	—
Clay	20	19
Diatoms	Tr	—
Dolomite	1	—
Foraminifers	3	10
Inorganic calcite	7	5
Mica	1	—
Nannofossils	56	60
Quartz	7	3
Radiolarians	—	Tr
Sponge spicules	3	3

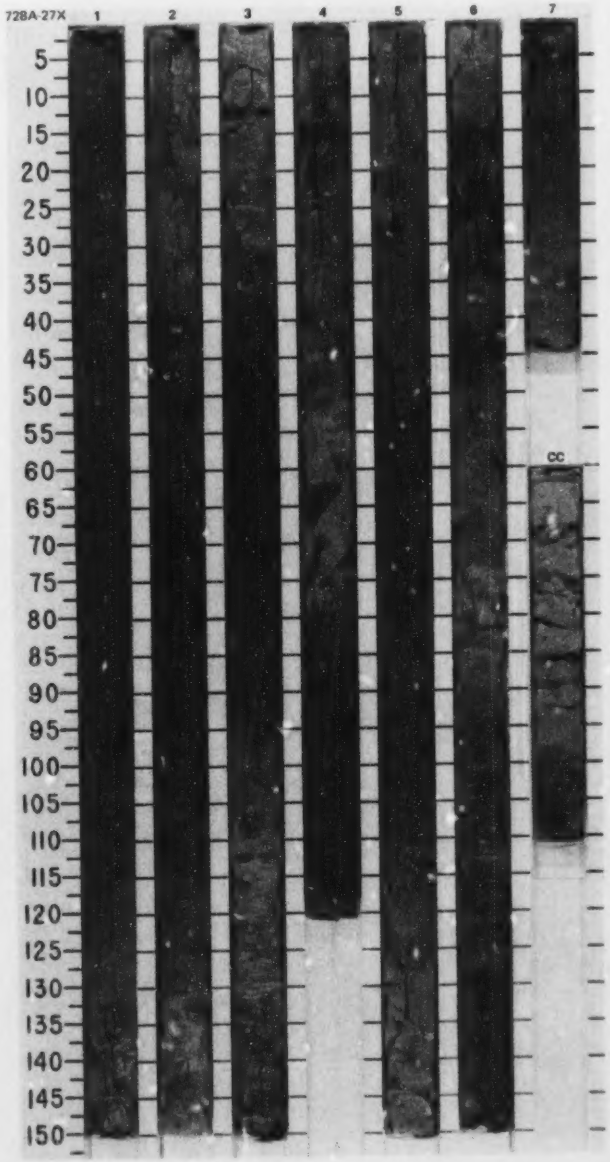
728A-27X
1
2
3
4
5
6
7
CC
5
10
15
20
25
30
35
40
45
50
55
60
65
70
75
80
85
90
95
100
105
110
115
120
125
130
135
140
145
150

SITE 728 HOLE A CORE 28X CORED INTERVAL 1687.3-1697.0 mbsl; 259.5-269.2 mbsf

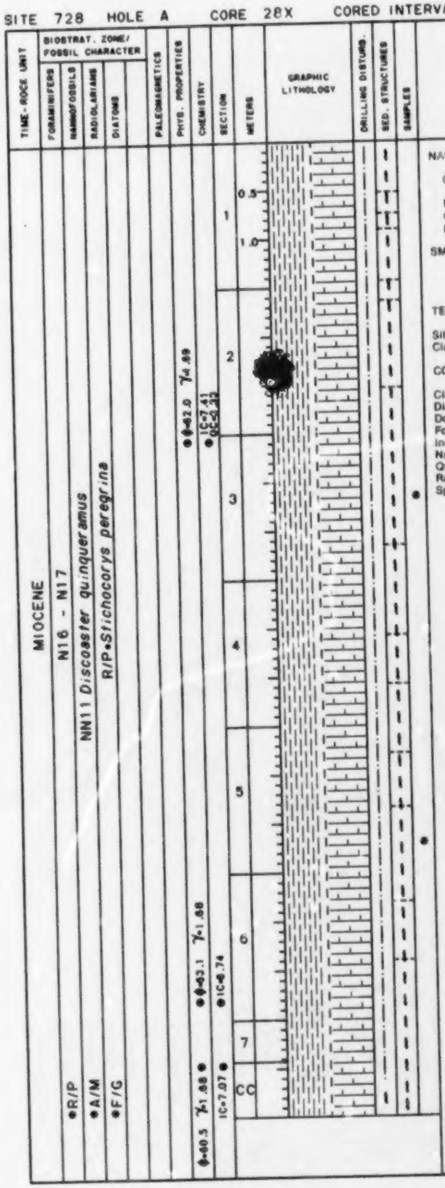
TIME-ROCK UNIT
BIOSTRAT. ZONE/ FOSSIL CHARACTER
FORAMINIFERS
NANNOFOSSILS
RADIOLARIANS
DIATOMS
PALEOMAGNETICS
PHYS. PROPERTIES
CHEMISTRY
SECTION
METERS
GRAPHIC LITHOLOGY
DRILLING DISTURB.
SED. STRUCTURES
SAMPLES
MIOCENE
N16 - N17
NN11 Discoaster quinqueramus
R/P•Stichocorys peregrina
•R/P
•A/M
•F/G
●φ=62.0 γ=1.89
●IC=7.41 OC=0.33
●φ=63.1 γ=1.88
●IC=6.74
φ=60.5 γ=1.88 ●
IC=7.07 ●
0.5
1.0
1
2
3
4
5
6
7
CC

LITHOLOGIC DESCRIPTION

NANNOFOSSIL CHALK

Core is slightly to moderately disturbed.

Major lithology: NANNOFOSSIL CHALK, mottled olive (5Y 4/3, 4/2) and light olive gray (5Y 5/3, 5/2) intervals of irregular thickness. Siliceous microfossils present in trace amounts.

SMEAR SLIDE SUMMARY (%):

	3, 65 D	5, 140 D
TEXTURE:		
Silt	10	30
Clay	90	70
COMPOSITION:		
Clay	15	20
Diatoms	2	1
Dolomite	Tr	
Foraminifers	5	2
Inorganic calcite	5	15
Nannofossils	67	55
Quartz	3	3
Radiolarians	Tr	—
Spicules	3	4

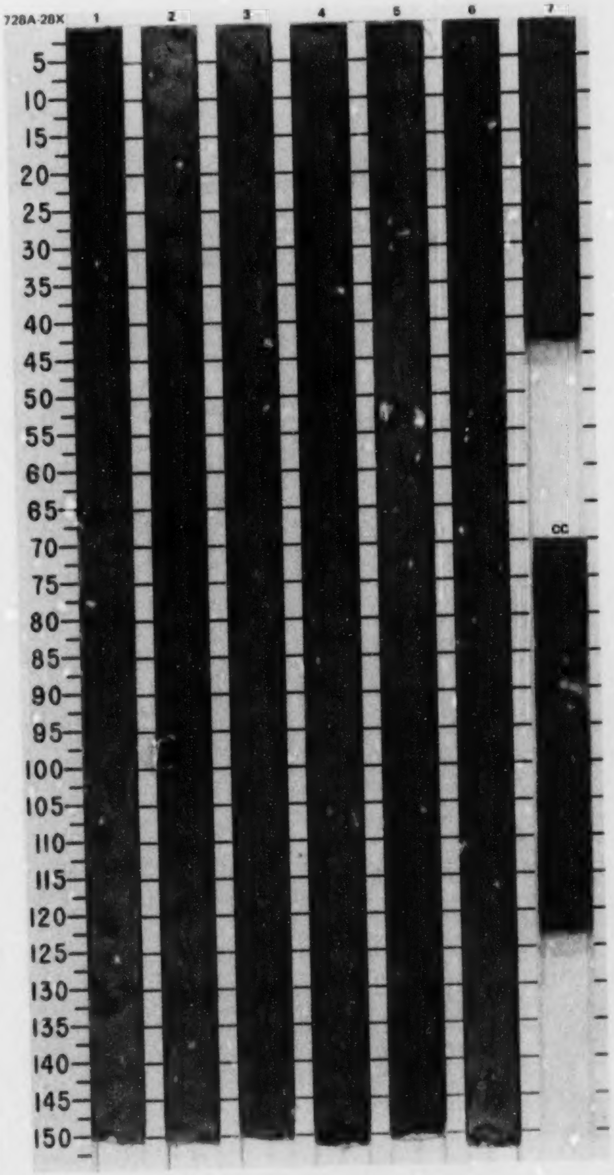
728A-28X
1
2
3
4
5
6
7
CC
5
10
15
20
25
30
35
40
45
50
55
60
65
70
75
80
85
90
95
100
105
110
115
120
125
130
135
140
145
150

SITE 728 HOLE A CORE 29X CORED INTERVAL 1697.0-1706.6 mbsl; 269.2-278.8 mbsf

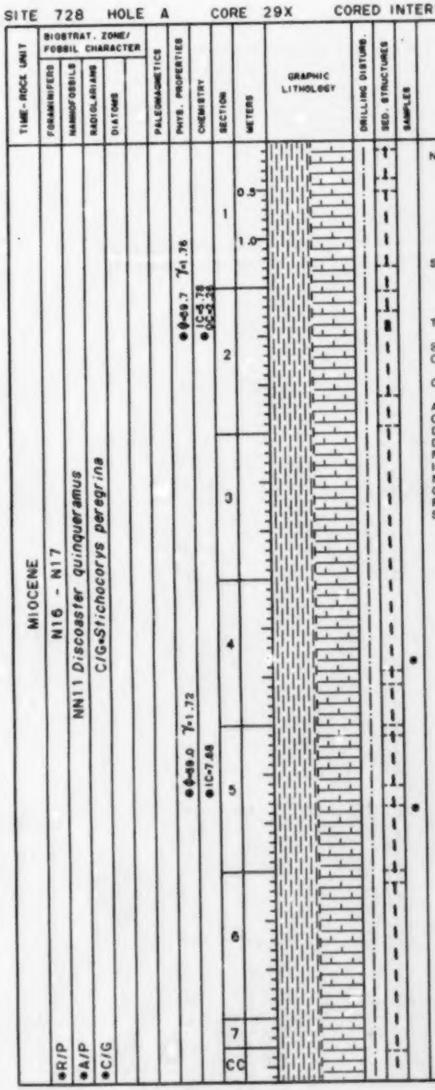
TIME-ROCK UNIT
BIOSTRAT. ZONE/ FOSSIL CHARACTER
FORAMINIFERS
NANNOFOSSILS
RADIOLARIANS
DIATOMS
PALEOMAGNETICS
PHYS. PROPERTIES
CHEMISTRY
SECTION
METERS
GRAPHIC LITHOLOGY
DRILLING DISTURB.
SED. STRUCTURES
SAMPLES
MIOCENE
N16 - N17
NN11 Discoaster quinqueramus
C/G•Stichocorys peregrina
•R/P
•A/P
•C/G
•φ=59.7 γ=1.76
•IC=6.78 OC=2.26
•φ=59.0 γ=1.72
•IC=7.88
0.5
1.0
1
2
3
4
5
6
7
CC

LITHOLOGIC DESCRIPTION

NANNOFOSSIL CHALK and MARLY NANNOFOSSIL CHALK

Core is slightly to moderately disturbed.

Major lithologies: NANNOFOSSIL CHALK and MARLY NANNOFOSSIL CHALK, mottled olive (5Y 4/3) and light olive gray (5Y 5/3, 5/2) intervals of irregular thickness. Mottling (bioturbation) is locally intense. Siliceous microfossils present in trace amounts.

SMEAR SLIDE SUMMARY (%):

	4, 85 D	5, 137 D
TEXTURE:		
Silt	25	40
Clay	75	60
COMPOSITION:		
Access. minerals	Tr	—
Clay	15	30
Diatoms	1	3
Dolomite	—	1
Foraminifers	7	3
Inorganic calcite	10	15
Nannofossils	60	36
Quartz	3	10
RadiolariansT	—	Tr
Sponge spicules	4	2

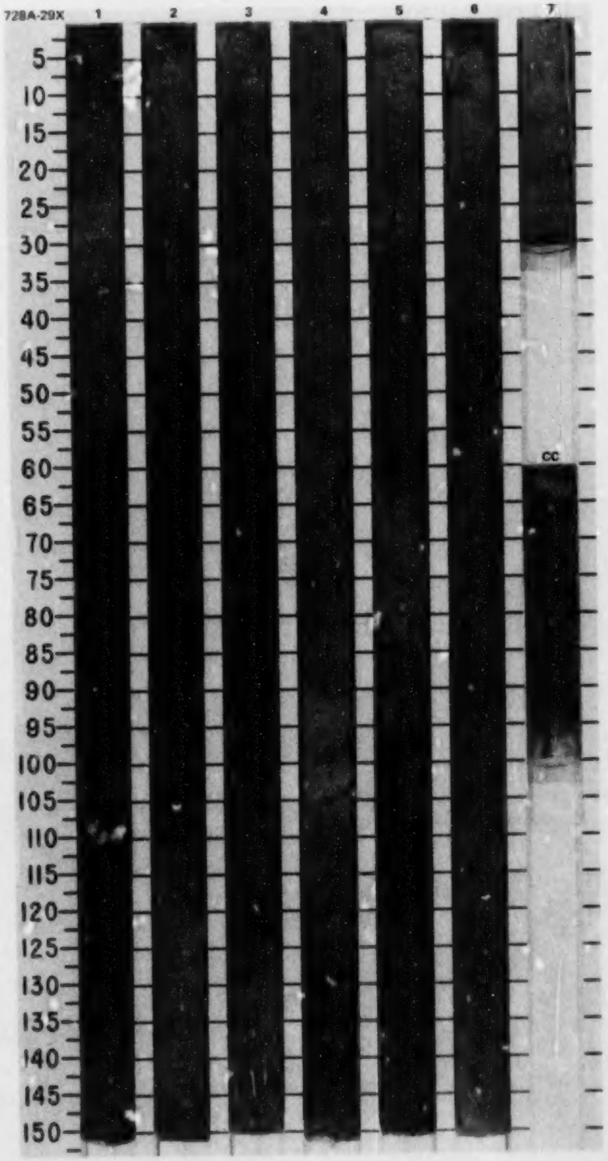
728A-29X
1
2
3
4
5
6
7
CC
5
10
15
20
25
30
35
40
45
50
55
60
65
70
75
80
85
90
95
100
105
110
115
120
125
130
135
140
145
150

SITE 728 HOLE A CORE 30X CORED INTERVAL 1706.6-1716.3 mbsl; 278.8-288.5 mbsf

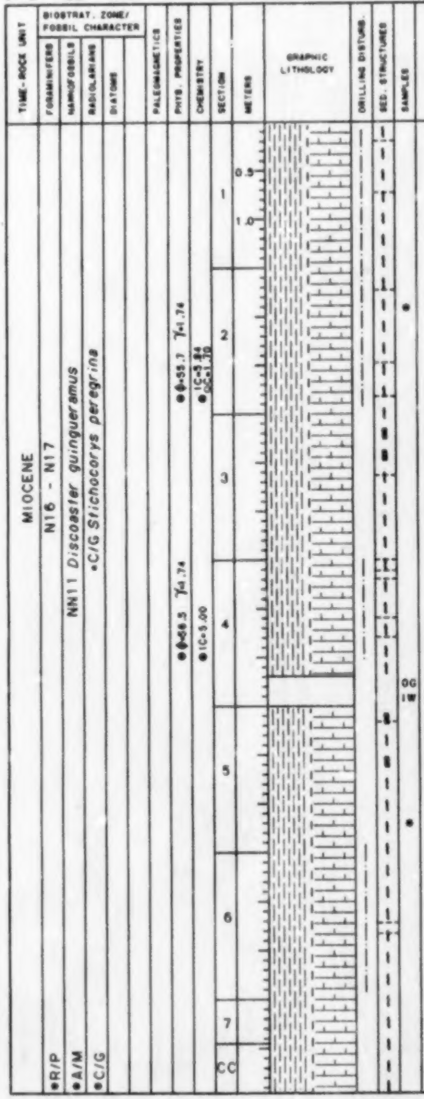
TIME-ROCK UNIT
BIOSTRAT. ZONE/ FOSSIL CHARACTER
FORAMINIFERS
NANNOFOSSILS
RADIOLARIANS
DIATOMS
PALEOMAGNETICS
PHYS. PROPERTIES
CHEMISTRY
SECTION
METERS
GRAPHIC LITHOLOGY
DRILLING DISTURB.
SED. STRUCTURES
SAMPLES
MIOCENE
N16 - N17
NN11 Discoaster quinqueramus
•C/G Stichocorys peregrina
•R/P
•A/M
•C/G
●Φ=55.7 γ=1.74
●Φ=56.5 γ=1.74
●IC=5.84 OC=1.70
●IC=5.00
1
2
3
4
5
6
7
CC
0.5
1.0
OG
IW

LITHOLOGIC DESCRIPTION

NANNOFOSSIL CHALK and MARLY NANNOFOSSIL CHALK

Core slightly to moderately disturbed.

Major lithologies: NANNOFOSSIL CHALK and MARLY NANNOFOSSIL CHALK, mottled olive (5Y 4/3) and light olive gray (5Y 5/3, 5/2) intervals of irregular thickness. Siliceous microfossils present in trace amounts.

SMEAR SLIDE SUMMARY (%):

	2, 41 D	5, 120 D
TEXTURE:		
Silt	20	40
Clay	80	60
COMPOSITION:		
Clay	20	27
Diatoms	2	—
Foraminifers	3	4
Inorganic calcite	7	15
Mica	1	—
Nannofossils	60	35
Quartz	3	15
Radiolarians	1	—
Sponge spicules	4	3

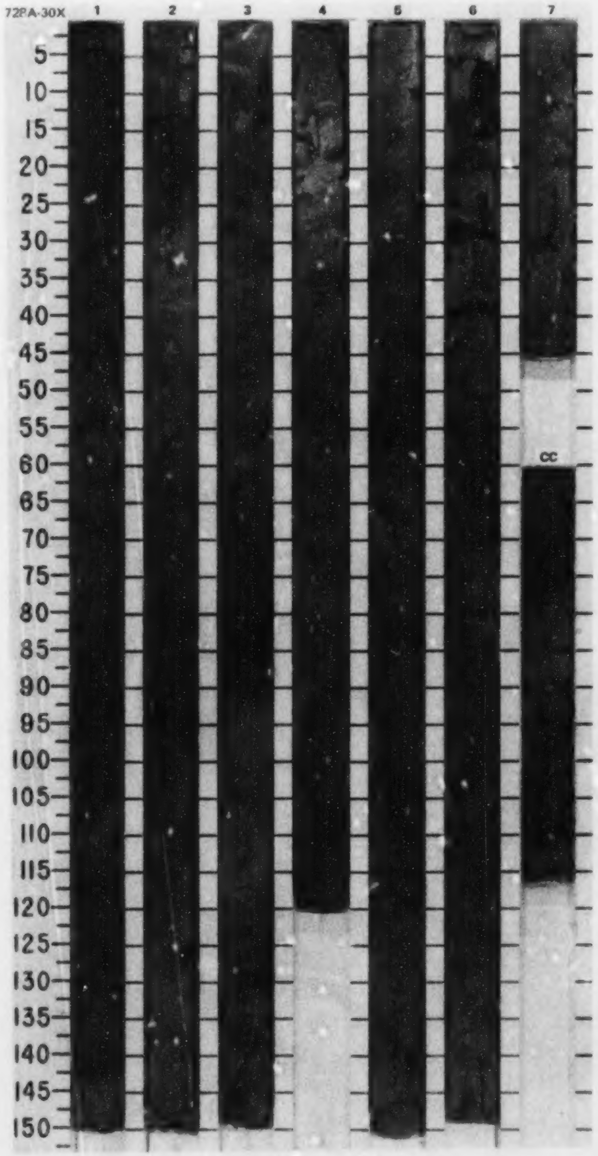
728A-30X
1
2
3
4
5
6
7
CC
5
10
15
20
25
30
35
40
45
50
55
60
65
70
75
80
85
90
95
100
105
110
115
120
125
130
135
140
145
150

SITE 728 HOLE A CORE 31X CORED INTERVAL 1716.3-1726.0 mbsl; 288.5-298.2 mbsf

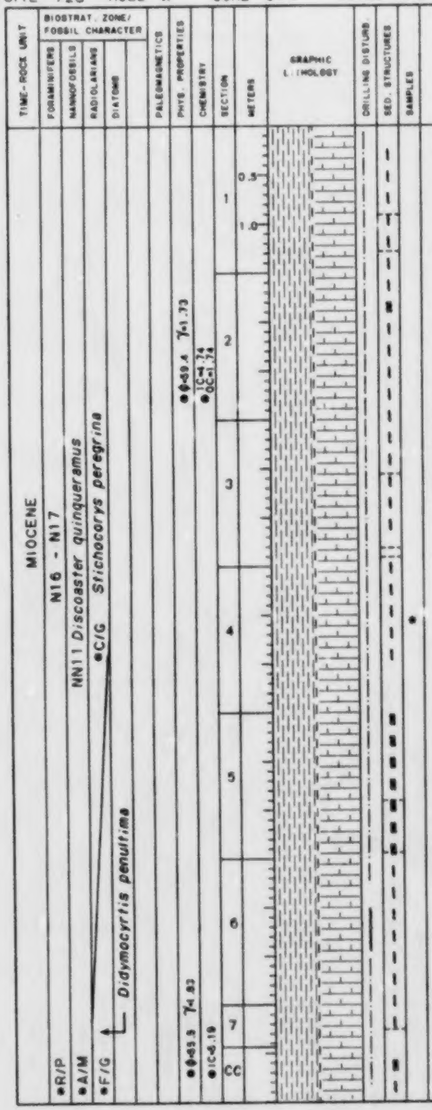
TIME-ROCK UNIT
BIOSTRAT. ZONE/ FOSSIL CHARACTER
FORAMINIFERS
NANNOFOSSILS
RADIOLARIANS
DIATOMS
PALEOMAGNETICS
PHYS. PROPERTIES
CHEMISTRY
SECTION
METERS
GRAPHIC LITHOLOGY
DRILLING DISTURB.
SED. STRUCTURES
SAMPLES
MIOCENE
N16 - N17
NN11 Discoaster quinqueramus
●C/G Stichocorys peregrina
Didymocyrtis penultima
●R/P
●A/M
●F/G
●ϕ=49.4 γ=1.73
●IC=4.74 OC=1.74
●ϕ=45.5 γ=1.83
●IC=6.19
0.5
1.0
1
2
3
4
5
6
7
CC

LITHOLOGIC DESCRIPTION

NANNOFOSSIL CHALK and MARLY NANNOFOSSIL CHALK

Core is moderately disturbed.

Major lithologies: NANNOFOSSIL CHALK and MARLY NANNOFOSSIL CHALK, mottled olive (5Y 4/3) and light olive gray (5Y 5/3, 5/2) intervals of irregular thickness. Mottling (bioturbation) locally intense. Siliceous microfossils present in trace amounts.

SMEAR SLIDE SUMMARY (%):

	4, 56 D
TEXTURE:	
Silt	30
Clay	70
COMPOSITION:	
Access. minerals	Tr
Clay	20
Diatoms	Tr
Dolomite	1
Foraminifers	3
Inorganic calcite	12
Nannofossils	56
Quartz	5
Sponge spicules	3

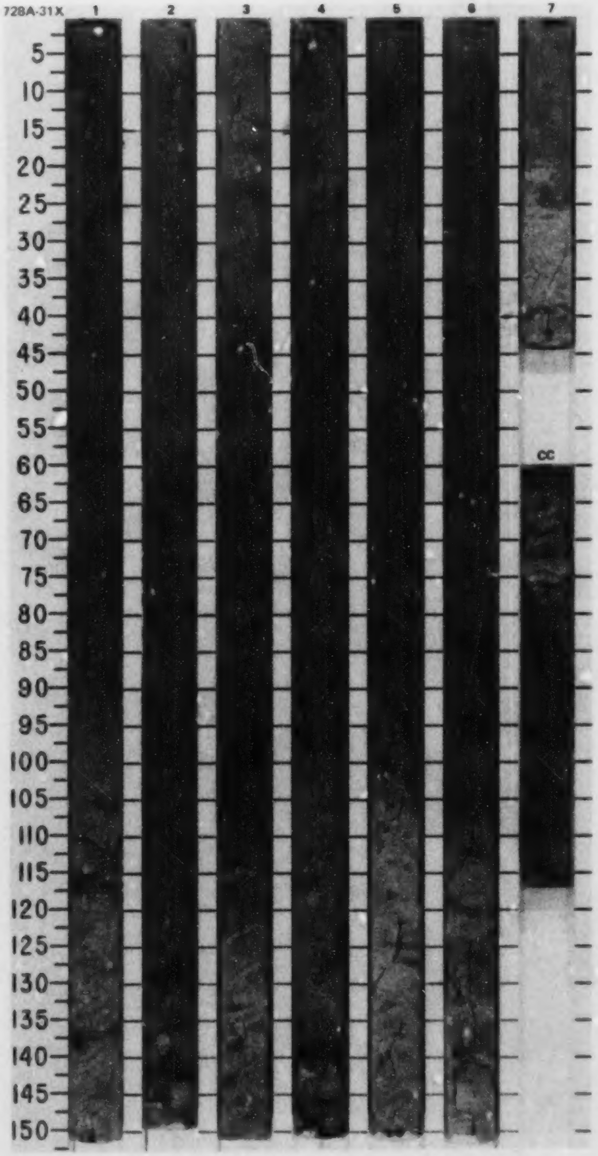
728A-31X
1
2
3
4
5
6
7
CC
5
10
15
20
25
30
35
40
45
50
55
60
65
70
75
80
85
90
95
100
105
110
115
120
125
130
135
140
145
150

SITE 728 HOLE A CORE 32X CORED INTERVAL 1726.0-1735.6 mbsl; 298.2-307.8 mbsf

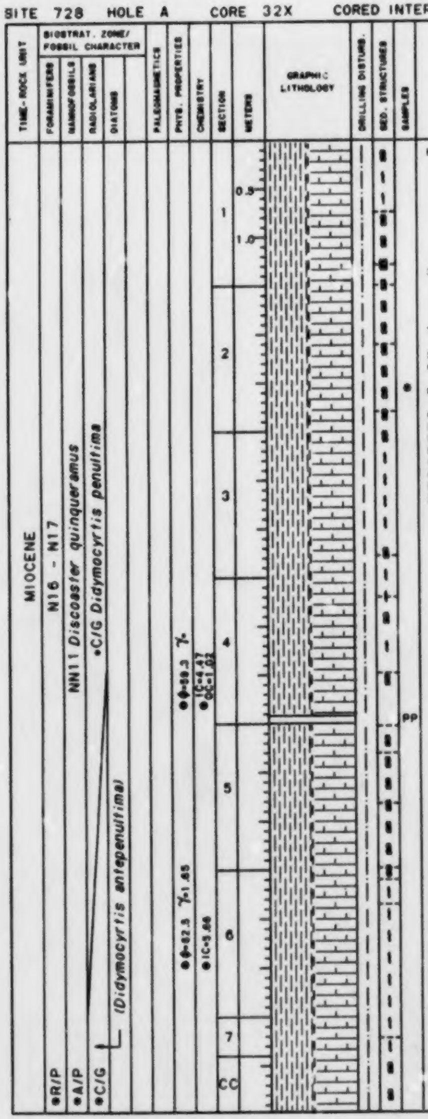
TIME-ROCK UNIT
BIOSTRAT. ZONE/ FOSSIL CHARACTER
FORAMINIFERS
NANNOFOSSILS
RADIOLARIANS
DIATOMS
PALEOMAGNETICS
PHYS. PROPERTIES
CHEMISTRY
SECTION
METERS
GRAPHIC LITHOLOGY
DRILLING DISTURB.
SED. STRUCTURES
SAMPLES
MIOCENE
N16 - N17
NN11 Discoaster quinqueramus
•C/G Didymocyrtis penultima
(Didymocyrtis antepenultima)
•R/P
•A/P
•C/G
•φ=59.3 γ=
•IC=4.47 OC=1.02
•φ=62.5 γ=1.85
•IC=3.66
1
2
3
4
5
6
7
CC
0.5
1.0
PP

LITHOLOGIC DESCRIPTION

NANNOFOSSIL CHALK and MARLY NANNOFOSSIL CHALK

Core is slightly to moderately disturbed, with evidence of drill flow between firm biscuits.

Major lithologies: NANNOFOSSIL CHALK and MARLY NANNOFOSSIL CHALK, mottled olive (5Y 4/3, 4/2) and light olive gray (5Y 6/2, 5/3, 5/2) intervals of irregular thickness. Bioturbation locally intense. Core is generally lighter in color than those above. Siliceous microfossils present in trace amounts.

SMEAR SLIDE SUMMARY (%):

	2, 106 D
TEXTURE:	
Silt	15
Clay	85
COMPOSITION:	
Clay	14
Diatoms	3
Foraminifers	5
Inorganic calcite	5
Nannofossils	70
Quartz	1
Radiolarians	Tr
Sponge spicules	2

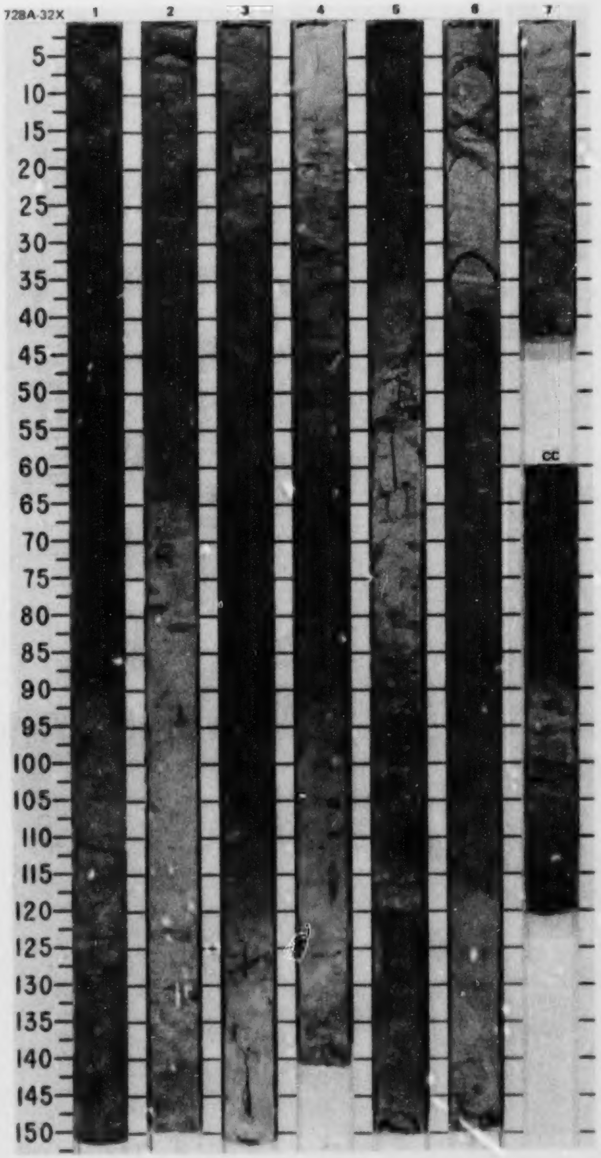
728A-32X
1
2
3
4
5
6
7
CC
5
10
15
20
25
30
35
40
45
50
55
60
65
70
75
80
85
90
95
100
105
110
115
120
125
130
135
140
145
150

SITE 728 HOLE A CORE 33X CORED INTERVAL 1735.6-1745.3 mbsl; 307.8-317.5 mbsf

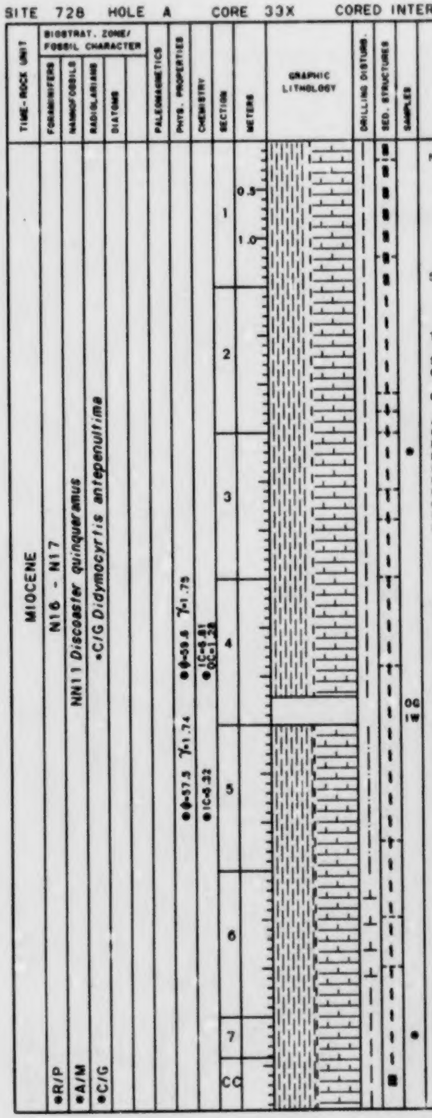
TIME-ROCK UNIT
BIOSTRAT. ZONE/ FOSSIL CHARACTER
FORAMINIFERS
NANNOFOSSILS
RADIOLARIANS
DIATOMS
PALEOMAGNETICS
PHYS. PROPERTIES
CHEMISTRY
SECTION
METERS
GRAPHIC LITHOLOGY
DRILLING DISTURB.
SED. STRUCTURES
SAMPLES
MIOCENE
N16 - N17
NN11 Discoaster quinqueramus
•C/G Didymocyrtis antepenultima
•R/P
•A/M
•C/G
•φ-59.6 γ-1.75
•φ-57.5 γ-1.74
•IC-6.81 OC-1.28
•IC-6.32
1
2
3
4
5
6
7
CC
0.5
1.0
OG
IW

LITHOLOGIC DESCRIPTION

NANNOFOSSIL CHALK and MARLY NANNOFOSSIL CHALK

Core is slightly to moderately disturbed. Lower half of Section 6 moderately fractured.

Major lithologies: NANNOFOSSIL CHALK and MARLY NANNOFOSSIL CHALK, mottled olive (5Y 4/3, 4/2) and light olive gray (5Y 6/2, 5/3, 5/2) intervals of irregular thickness. Bioturbation is locally intense, with *Chondrites* burrows in Section 7. Siliceous microfossils present in trace amounts.

SMEAR SLIDE SUMMARY (%):

	3, 20 D	7, 20 D
TEXTURE:		
Silt	20	25
Clay	80	75
COMPOSITION:		
Access. minerals	—	Tr
Clay	20	20
Diatoms	3	4
Dolomite	—	2
Foraminifers	3	4
Inorganic calcite	10	10
Nannofossils	61	51
Quartz	Tr	5
Radiolarians	Tr	Tr
Sponge spicules	3	4

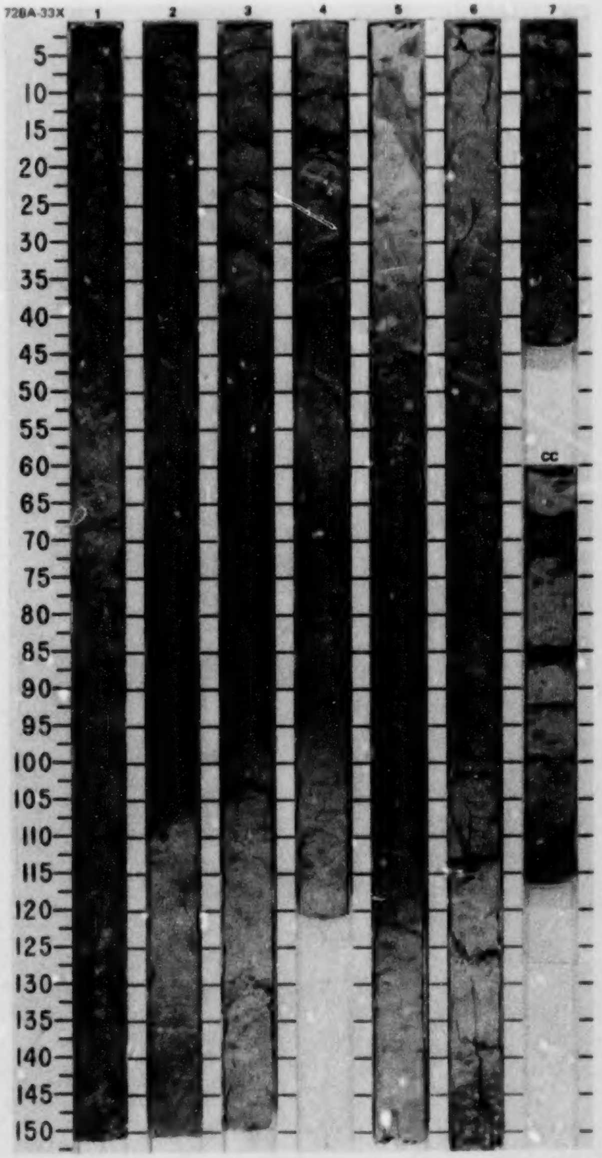
728A-33X
1
2
3
4
5
6
7
CC
5
10
15
20
25
30
35
40
45
50
55
60
65
70
75
80
85
90
95
100
105
110
115
120
125
130
135
140
145
150

SITE 728 HOLE A CORE 34X CORED INTERVAL 1745.3-1755.0 mbsl; 317.5-327.2 mbsf

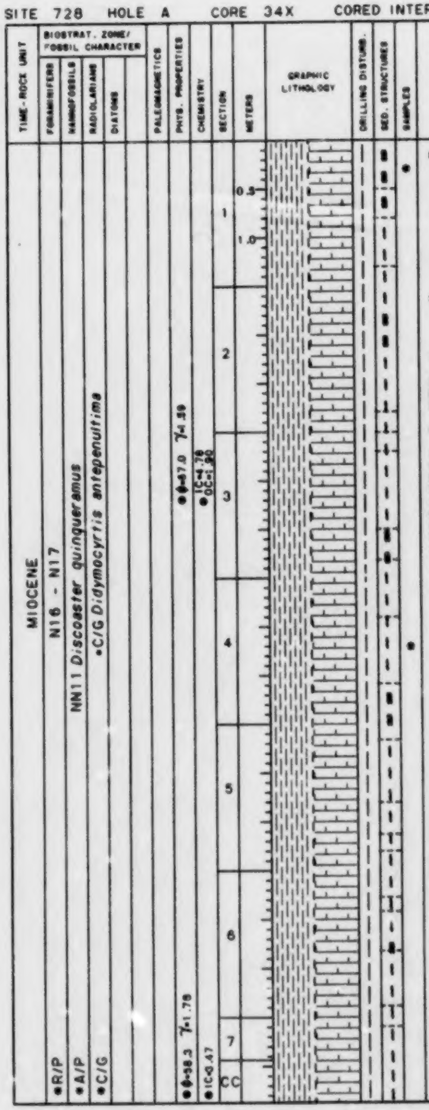
TIME-ROCK UNIT
BIOSTRAT. ZONE/ FOSSIL CHARACTER
FORAMINIFERS
NANNOFOSSILS
RADIOLARIANS
DIATOMS
PALEOMAGNETICS
PHYS. PROPERTIES
CHEMISTRY
SECTION
METERS
GRAPHIC LITHOLOGY
DRILLING DISTURB.
SED. STRUCTURES
SAMPLES
MIOCENE
N16 - N17
NN11 Discoaster quinqueramus
•C/G Didymocyrtis antepenultima
•R/P
•A/P
•C/G
•φ=47.0 γ=1.89
•IC=4.78 OC=1.90
•φ=58.3 γ=1.78
•IC=0.47
0.5
1.0
1
2
3
4
5
6
7
CC

LITHOLOGIC DESCRIPTION

NANNOFOSSIL CHALK and DIATOM-BEARING MARLY NANNOFOSSIL CHALK

Core is slightly to moderately disturbed.

Major lithologies: NANNOFOSSIL CHALK and DIATOM-BEARING MARLY NANNOFOSSIL CHALK, mottled olive (5Y 4/3, 4/2) and light olive gray (5Y 6/2, 5/3, 5/2) intervals of irregular thickness. Beds of lighter color are interpreted as having fewer nannofossils (marly). Bioturbation locally intense, with *Planolites*, *Zoophycos*, and large (greater than 2 cm diameter) burrows observed. Diatom abundance as much as 15%; other siliceous microfossils present in trace amounts.

SMEAR SLIDE SUMMARY (%):

	1, 30 D	4, 70 D
TEXTURE:		
Sand	10	5
Silt	30	5
Clay	60	90
COMPOSITION:		
Clay	10	30
Diatoms	15	—
Foraminifers	Tr	5
Inorganic calcite	5	10
Nannofossils	60	50
Quartz	5	—
Radiolarians	Tr	—
Silicoflagellates	Tr	—
Sponge spicules	5	5

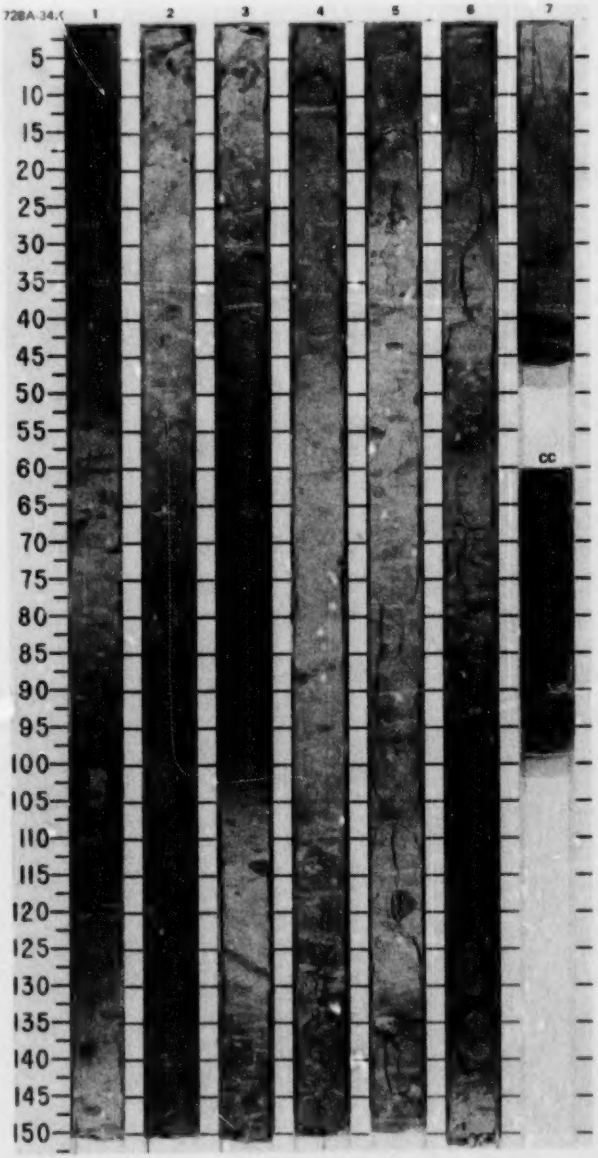
728A-34X
1
2
3
4
5
6
7
CC
5
10
15
20
25
30
35
40
45
50
55
60
65
70
75
80
85
90
95
100
105
110
115
120
125
130
135
140
145
150

SITE 728 HOLE A CORE 35X CORED INTERVAL 1755.0-1764.6 mbsl; 327.2-336.8 mbsf

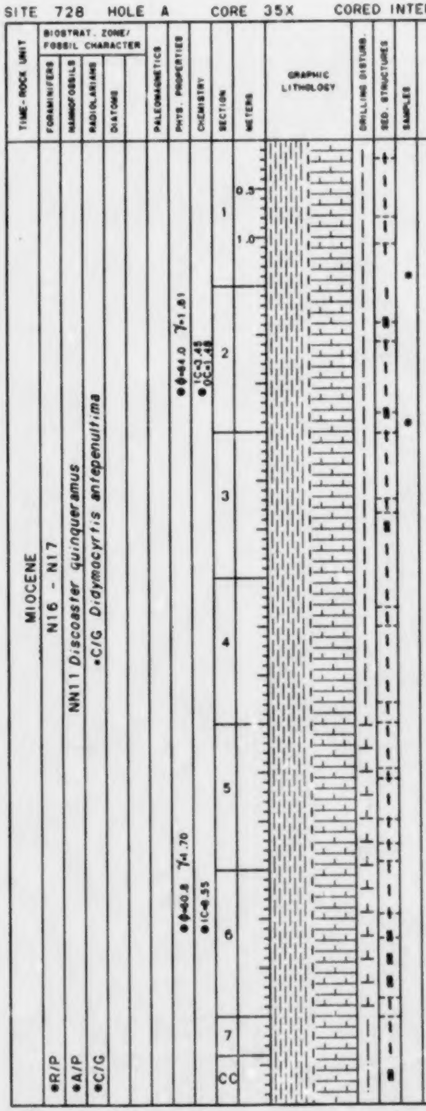

LITHOLOGIC DESCRIPTION

NANNOFOSSIL CHALK and DIATOM-BEARING MARLY NANNOFOSSIL CHALK

Core is slightly to moderately disturbed. Section 4, 0-60 cm, and Sections 5 and 6 are moderately fractured

Major lithologies: NANNOFOSSIL CHALK and DIATOM-BEARING MARLY NANNOFOSSIL CHALK, heavily mottled olive (5Y 4/3, 3/2) and light olive gray (5Y 6/2, 5/3, 5/2) intervals of irregular thickness. Darker than cores immediately above. Bioturbation locally intense; *Zoophycos* burrows transect dark beds.

Minor lithology: Clayey calcareous diatomite, occurring in dark interval at Section 1, 140 cm. Dark intervals are interpreted as less calcareous and more diatomaceous.

SMEAR SLIDE SUMMARY (%):

	1, 140 D	2, 140 D
TEXTURE:		
Silt	25	20
Clay	75	80
COMPOSITION:		
Access. minerals	1	Tr
Clay	25	17
Diatoms	40	10
Dolomite	Tr	—
Foraminifers	—	3
Inorganic calcite	7	7
Nannofossils	15	60
Quartz	10	3
Sponge spicules	2	—

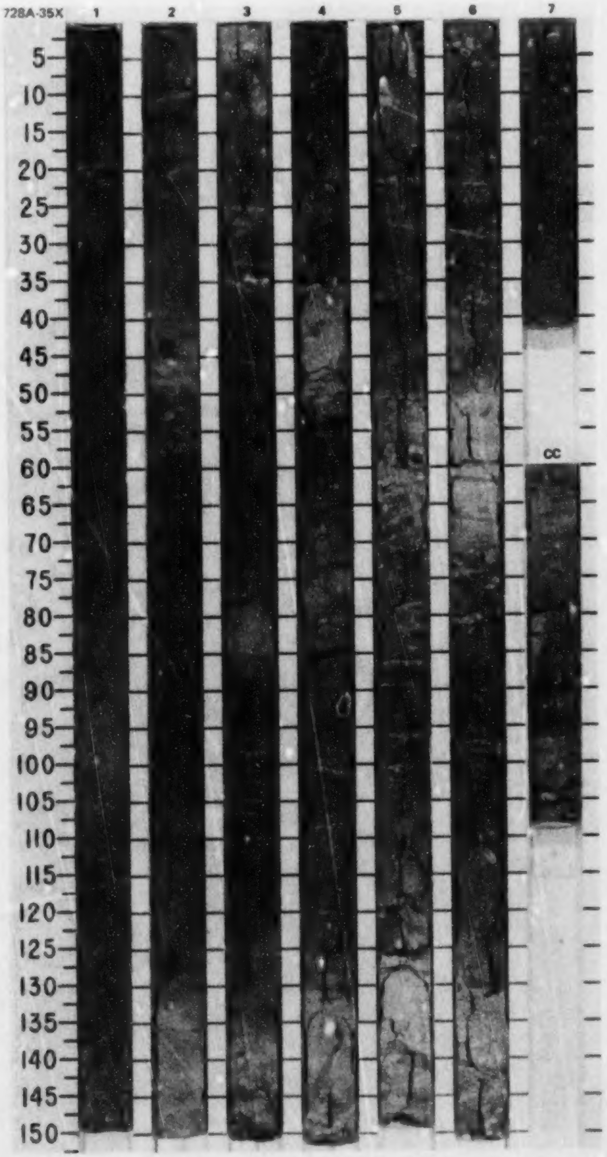

SITE 728 HOLE A CORE 36X CORED INTERVAL 1764.6-1774.2 mbsl; 336.8-346.4 mbsf

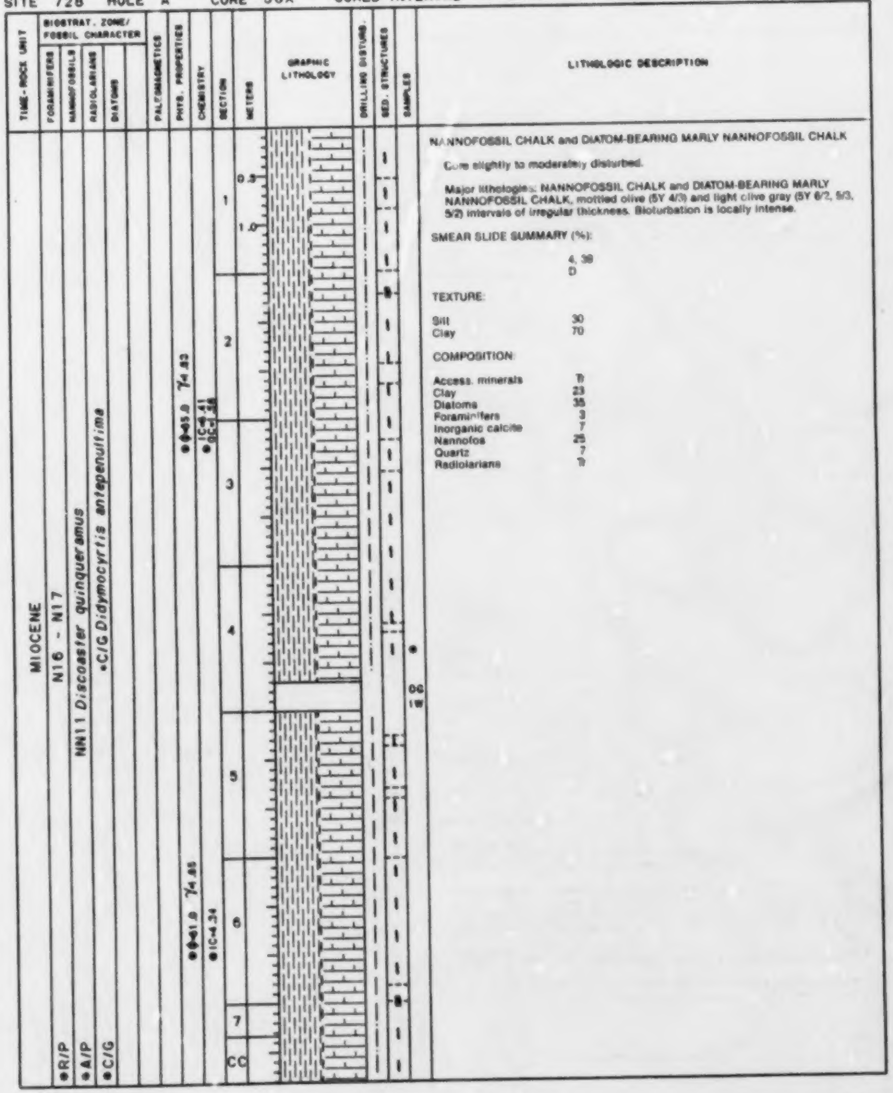
TIME-ROCK UNIT
BIOSTRAT. ZONE/ FOSSIL CHARACTER
FORAMINIFERS
NANNOFOSSILS
RADIOLARIANS
DIATOMS
PALEOMAGNETICS
PHYS. PROPERTIES
CHEMISTRY
SECTION
METERS
GRAPHIC LITHOLOGY
DRILLING DISTURB.
SED. STRUCTURES
SAMPLES
LITHOLOGIC DESCRIPTION
MIOCENE
N16 - N17
NN11 Discoaster quinqueramus
•C/G Didymocyrtis antepenultima
•R/P
•A/P
•C/G
●Φ=65.0 γ=1.83
●IC=4.41
OC=.38
●Φ=61.0 γ=1.85
●IC=4.34
0.5
1.0
1
2
3
4
5
6
7
CC
*
OG
IW

NANNOFOSSIL CHALK and DIATOM-BEARING MARLY NANNOFOSSIL CHALK

Core slightly to moderately disturbed.

Major lithologies: NANNOFOSSIL CHALK and DIATOM-BEARING MARLY NANNOFOSSIL CHALK, mottled olive (5Y 4/3) and light olive gray (5Y 6/2, 5/3, 5/2) intervals of irregular thickness. Bioturbation is locally intense.

SMEAR SLIDE SUMMARY (%):

	4, 38 D
TEXTURE:	
Silt	30
Clay	70
COMPOSITION:	
Access. minerals	Tr
Clay	23
Diatoms	35
Foraminifers	3
Inorganic calcite	7
Nannofos	25
Quartz	7
Radiolarians	Tr

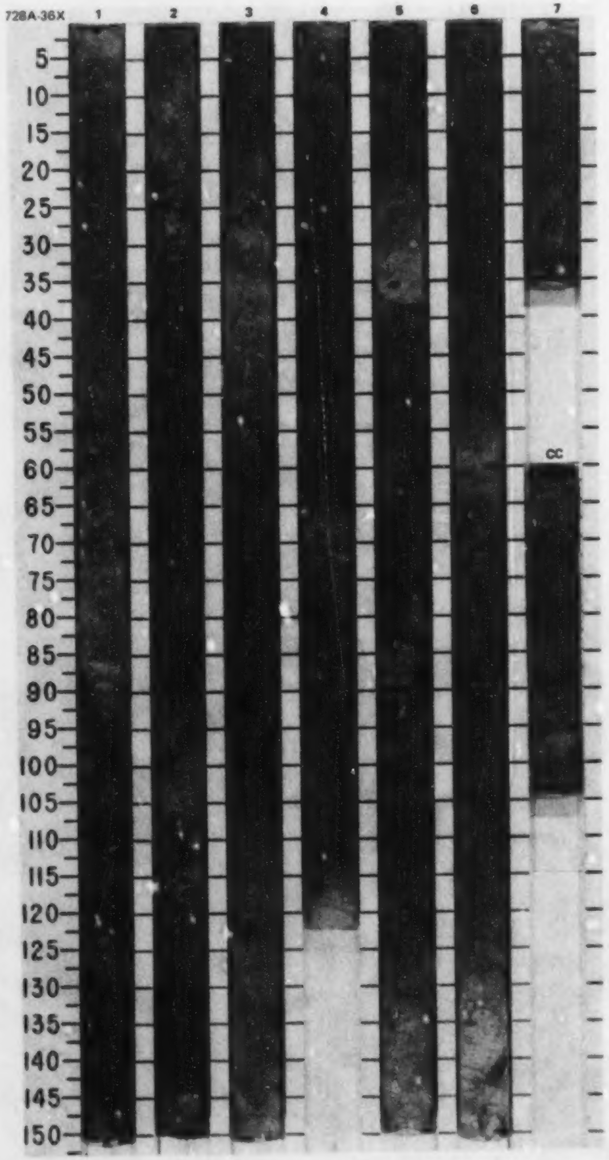
728A-36X
1
2
3
4
5
6
7
CC
5
10
15
20
25
30
35
40
45
50
55
60
65
70
75
80
85
90
95
100
105
110
115
120
125
130
135
140
145
150

SITE 728 HOLE B CORE 1H CORED INTERVAL 1427.8-1429.0 mbsl; 0.0-1.2 mbsf

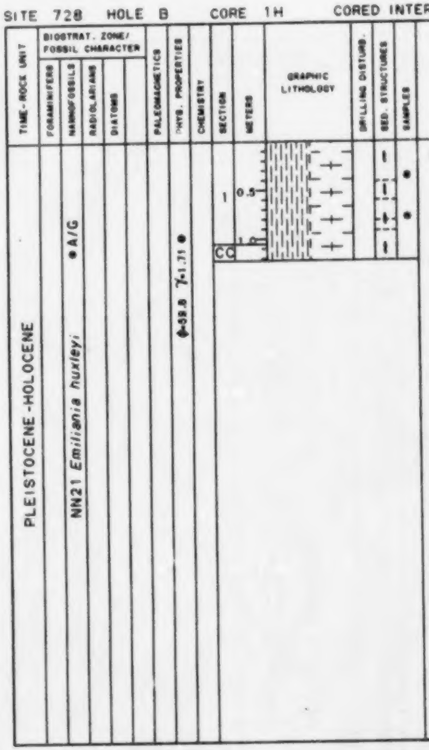
TIME-ROCK UNIT
BIOSTRAT. ZONE/ FOSSIL CHARACTER
FORAMINIFERS
NANNOFOSSILS
RADIOLARIANS
DIATOMS
PALEOMAGNETICS
PHYS. PROPERTIES
CHEMISTRY
SECTION
METERS
GRAPHIC LITHOLOGY
DRILLING DISTURB.
SED. STRUCTURES
SAMPLES
PLEISTOCENE-HOLOCENE
NN21 Emiliania huxleyi
● A/G
φ=59.8 γ=1.71 ●
1
0.5
1.0
CC

LITHOLOGIC DESCRIPTION

FORAMINIFER OOZE to MARLY FORAMINIFER-NANNOFOSSIL OOZE

Section 1, 0-9 cm, is moderately disturbed; remainder of core is undisturbed.

Major lithology: FORAMINIFER OOZE to MARLY FORAMINIFER-NANNOFOSSIL OOZE, olive (5Y 5/3, 4/4, 4/3) and olive brown (2.5Y 4/4). Slight burrow mottling throughout, *Zoophycos* burrows present. Shell debris is common on core face.

SMEAR SLIDE SUMMARY (%):

	1, 36 D	1, 78 D
TEXTURE:		
Sand	80	40
Silt	10	25
Clay	10	35
COMPOSITION:		
Access. minerals	2	2
Clay	10	15
Foraminifers	70	25
Inorganic calcite	—	25
Nannofossils	15	25
Phosphate	Tr	—
Quartz	3	8
Sponge spicules	Tr	—

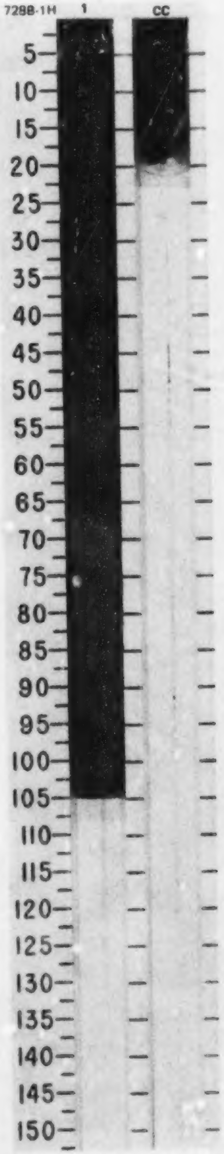
728B-1H
1
CC
5
10
15
20
25
30
35
40
45
50
55
60
65
70
75
80
85
90
95
100
105
110
115
120
125
130
135
140
145
150

SITE 728 HOLE B CORE 2H CORED INTERVAL 1429.0-1438.5 mbsl; 1.2-10.7 mbsf

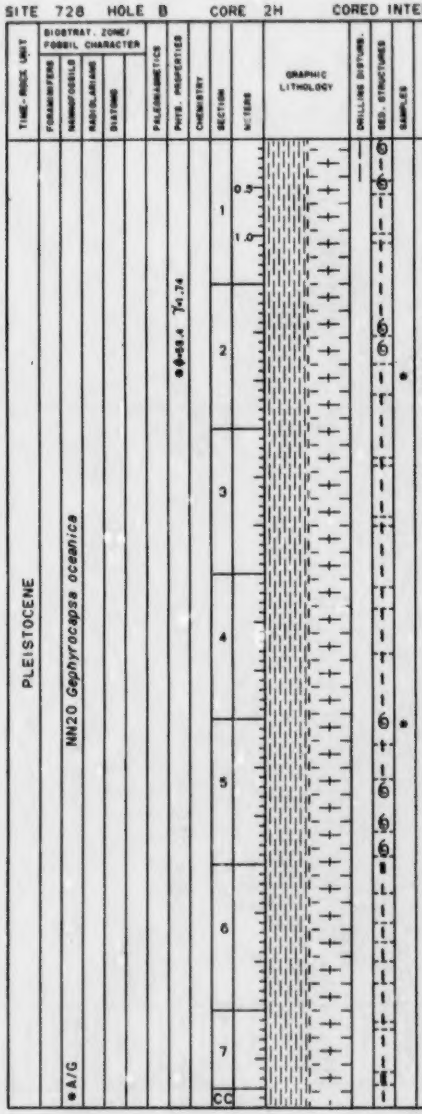
TIME-ROCK UNIT
BIOSTRAT. ZONE/ FOSSIL CHARACTER
FORAMINIFERS
NANNOFOSSILS
RADIOLARIANS
DIATOMS
PALEOMAGNETICS
PHYS. PROPERTIES
CHEMISTRY
SECTION
METERS
GRAPHIC LITHOLOGY
DRILLING DISTURB.
SED. STRUCTURES
SAMPLES
PLEISTOCENE
NN20 Gephyrocapsa oceanica
● A/G
●Φ58.4 γ1.74
0.5
1.0
1
2
3
4
5
6
7
CC

LITHOLOGIC DESCRIPTION

MARLY FORAMINIFER-NANNOFOSSIL OOZE

Section 1, 0-20 cm, is slightly disturbed. Remainder of core is undisturbed.

Major lithology: MARLY FORAMINIFER-NANNOFOSSIL OOZE, olive (5Y 4/3, 5/3) and light greenish gray (10Y 5/2). Alternation of lighter and darker layers, 20-100 cm thick. Slight burrow mottling. Shells and shell debris are present on core face.

SMEAR SLIDE SUMMARY (%):

	2, 98 D *	5, 7 D
TEXTURE:		
Sand	10	35
Silt	30	25
Clay	60	40
COMPOSITION:		
Access. minerals	2	3
Clay	15	10
Dolomite	—	1
Feldspar	Tr	—
Foraminifers	20	35
Inorganic calcite	10	11
Nannofossils	45	30
Quartz	8	10

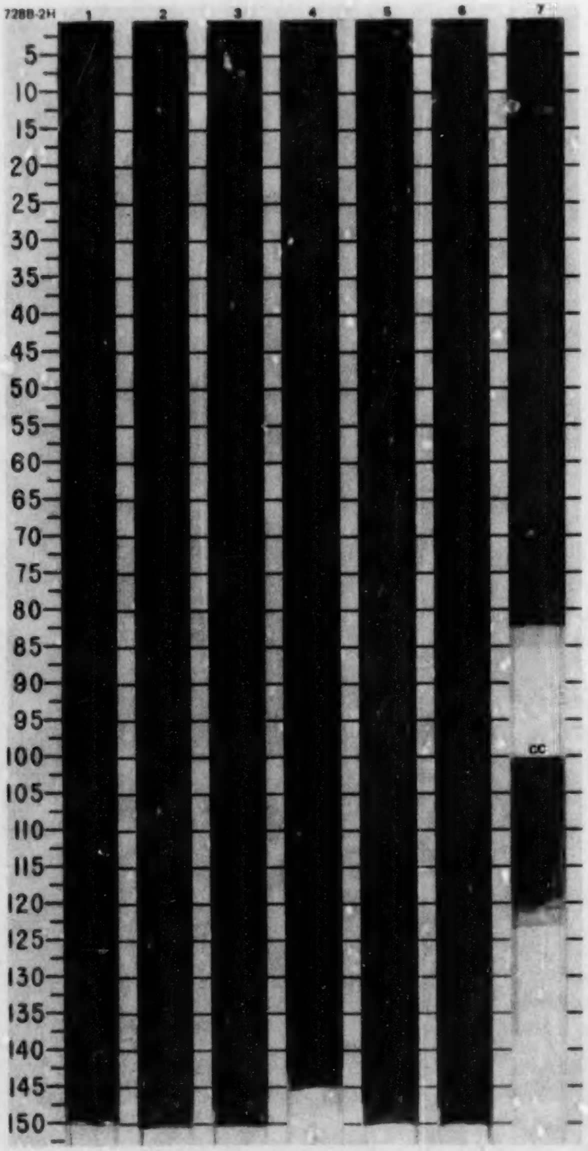
728B-2H
1
2
3
4
5
6
7
CC
5
10
15
20
25
30
35
40
45
50
55
60
65
70
75
80
85
90
95
100
105
110
115
120
125
130
135
140
145
150

SITE 728 HOLE B CORE 3H CORED INTERVAL 1438.5-1447.9 mbsl; 10.7-20.1 mbsf

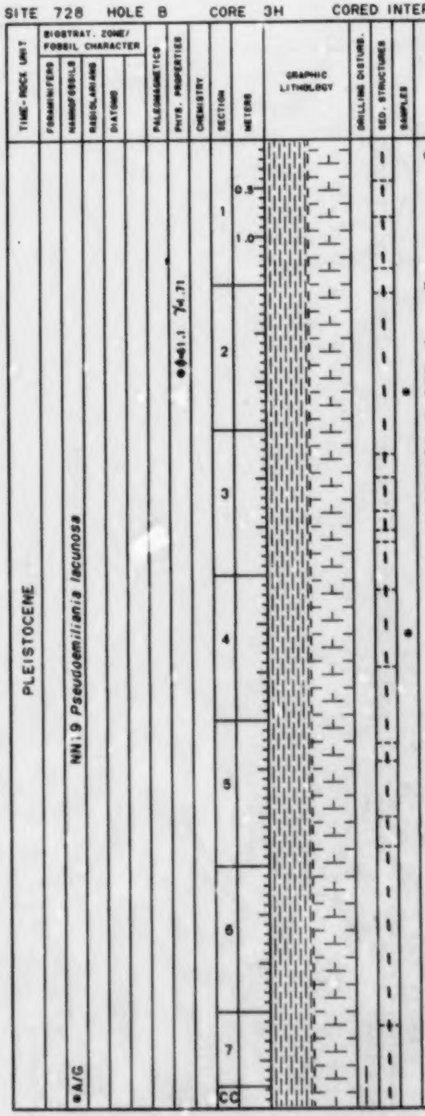

LITHOLOGIC DESCRIPTION

CALCITIC MARLY NANNOFOSSIL OOZE to NANNOFOSSIL OOZE

Section 1, 0-10 cm, is moderately disturbed. Remainder of core is undisturbed.

Major lithology: CALCITIC MARLY NANNOFOSSIL OOZE to NANNOFOSSIL OOZE, olive (5Y 4/3, 5/3), olive gray (5Y 5/2), and light greenish gray (10Y 5/2, 6/2). Alternation of lighter and darker layers, 20-100 cm thick. Dark layers have more terrigenous silty clay than lighter layers. Slight burrow mottling; large burrow from Section 3, 130 cm, to Section 4, 50 cm. Shell debris present on core face.

SMEAR SLIDE SUMMARY (%):

	2, 11 D	4, 61 D
TEXTURE:		
Sand	5	—
Silt	20	20
Clay	75	80
COMPOSITION:		
Access. minerals	2	Tr
Clay	20	10
Dolomite	Tr	Tr
Feldspar	1	—
Foraminifers	2	4
Inorganic calcite	15	15
Nannofossils	55	70
Quartz	5	1

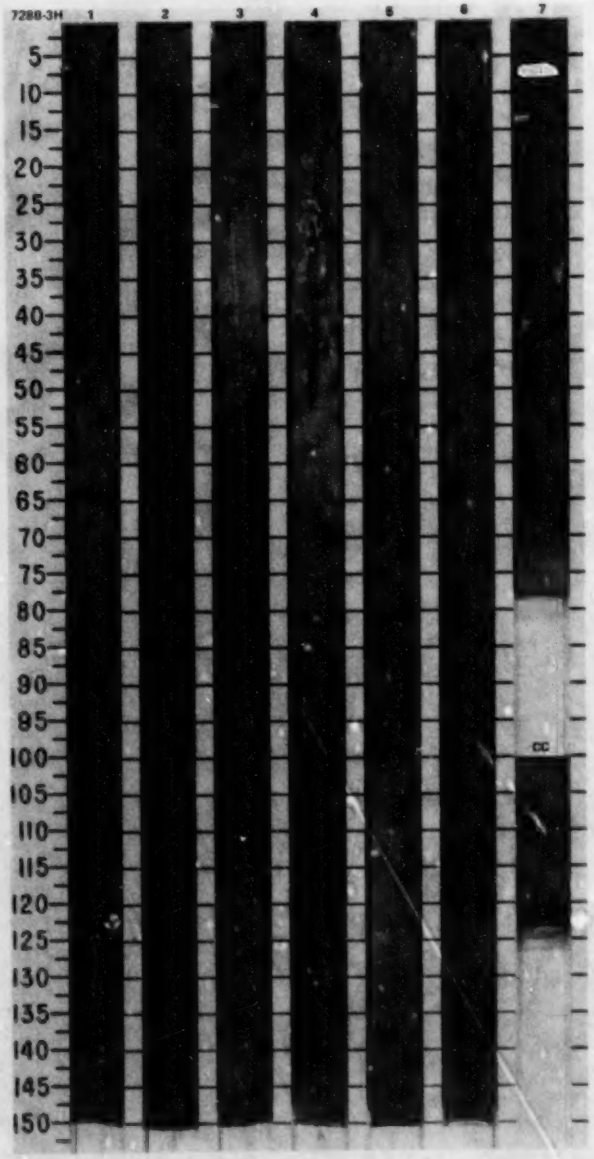
728B-3H
1
2
3
4
5
6
7
CC
5
10
15
20
25
30
35
40
45
50
55
60
65
70
75
80
85
90
95
100
105
110
115
120
125
130
135
140
145
150

SITE 728 HOLE B CORE 4H CORED INTERVAL 1447.9-1457.4 mbsl; 20.1-29.6 mbsf

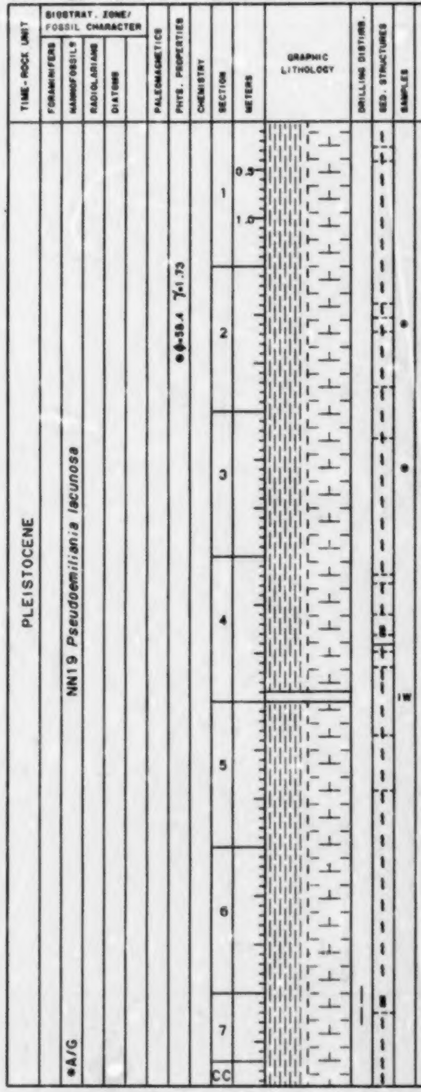
TIME-ROCK UNIT
BIOSTRAT. ZONE/ FOSSIL CHARACTER
FORAMINIFERS
NANNOFOSSILS
RADIOLARIANS
DIATOMS
PALEOMAGNETICS
PHYS. PROPERTIES
CHEMISTRY
SECTION
METERS
GRAPHIC LITHOLOGY
DRILLING DISTURB.
SED. STRUCTURES
SAMPLES
PLEISTOCENE
NN19 Pseudoemiliania lacunosa
•A/G
•ϕ=58.4 γ=1.73
0.5
1.0
1
2
3
4
5
6
7
CC
IW

LITHOLOGIC DESCRIPTION

CALCITIC MARLY CALCAREOUS OOZE to NANNOFOSSIL OOZE

Entire core is undisturbed.

Major lithology: CALCITIC MARLY CALCAREOUS OOZE to NANNOFOSSIL OOZE, olive (5Y 4/3, 5/3), light olive gray (5Y 6/2), and light greenish gray (10Y 5/2). Alternation of lighter and darker layers, 20-100 cm thick. Slight to moderate burrow mottling *Planolites* burrows common in Section 2. Shell debris present on core face in Section 6.

SMEAR SLIDE SUMMARY (%):

	2, 65 D	3, 65 D
TEXTURE:		
Sand	5	35
Silt	15	25
Clay	80	40
COMPOSITION:		
Access. minerals	22	
Clay	15	20
Dolomite	—	1
Foraminifers	5	15
Volcanic glass	Tr	—
Inorganic calcite	8	20
Nannofossils	65	20
Quartz	5	22

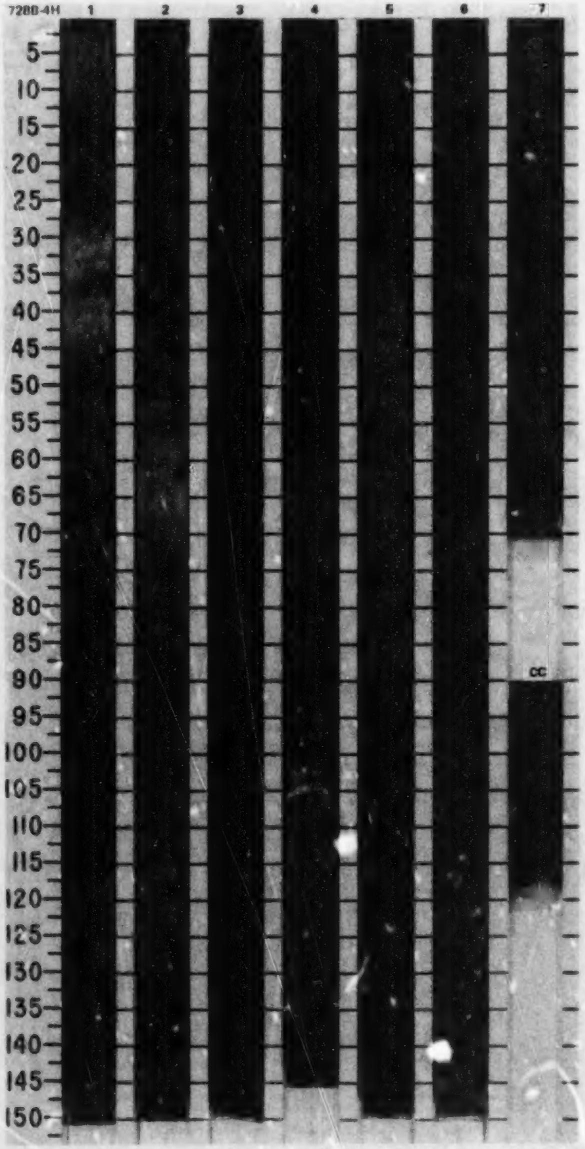
728B-4H
1
2
3
4
5
6
7
CC
5
10
15
20
25
30
35
40
45
50
55
60
65
70
75
80
85
90
95
100
105
110
115
120
125
130
135
140
145
150

SITE 728 HOLE B CORE 5H CORED INTERVAL 1457.4-1466.9 mbsl; 29.6-39.1 mbsf

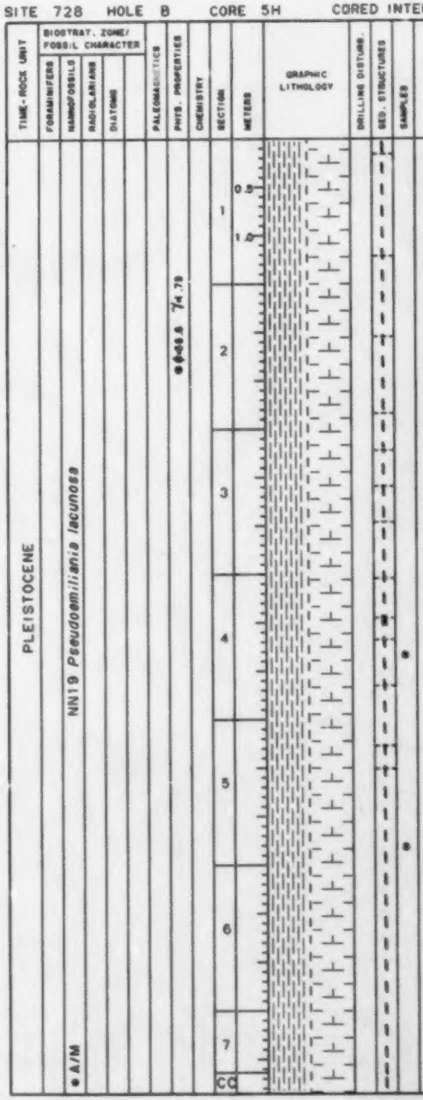
TIME-ROCK UNIT
BIOSTRAT. ZONE/ FOSSIL CHARACTER
FORAMINIFERS
NANNOFOSSILS
RADIOLARIANS
DIATOMS
PALEOMAGNETICS
PHYS. PROPERTIES
CHEMISTRY
SECTION
METERS
GRAPHIC LITHOLOGY
DRILLING DISTURB.
SED. STRUCTURES
SAMPLES
PLEISTOCENE
NN19 Pseudoemiliania lacunosa
● A/M
●φ=60.6 γ4.70
0.5
1.0
1
2
3
4
5
6
7
CC

LITHOLOGIC DESCRIPTION

CALCITIC MARLY NANNOFOSSIL OOZE

Entire core is undisturbed.

Major lithology: CALCITIC MARLY NANNOFOSSIL OOZE, olive (5Y 4/3, 5/3), olive gray (5Y 5/2), and light greenish gray (10Y 5/2). Alternation of lighter and darker layers, 20-100 cm thick. Slight to moderate burrow mottling. Shell debris present on core face.

SMEAR SLIDE SUMMARY (%):

	4, 64 D	5, 130 D
TEXTURE:		
Sand	5	15
Silt	25	15
Clay	70	70
COMPOSITION:		
Access. minerals	—	1
Clay	20	25
Dolomite	—	Tr
Foraminifers	5	2
Volcanic glass	—	Tr
Inorganic calcite	20	20
Nannofossils	50	40
Organic debris	—	Tr
Quartz	3	12

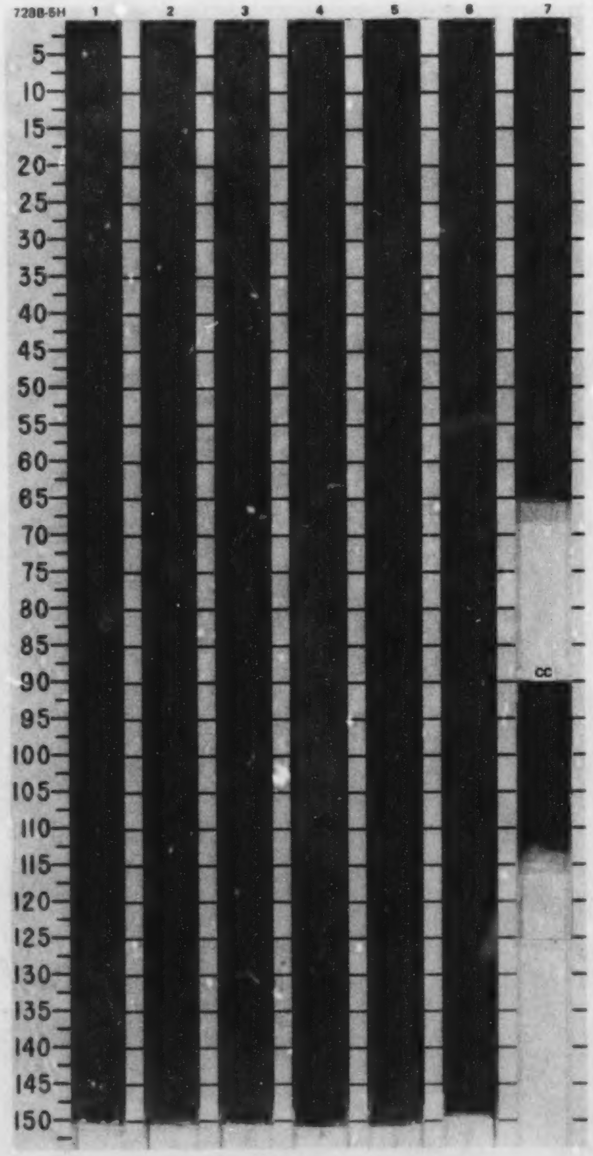
728B-5H
1
2
3
4
5
6
7
CC
5
10
15
20
25
30
35
40
45
50
55
60
65
70
75
80
85
90
95
100
105
110
115
120
125
130
135
140
145
150

SITE 728 HOLE B CORE 6H CORED INTERVAL 1466.9-1476.4 mbsl; 39.1-48.6 mbsf

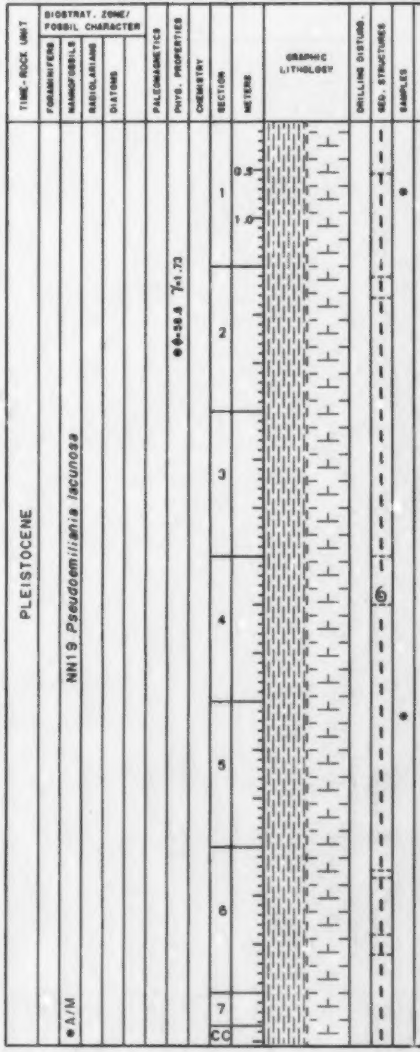
TIME-ROCK UNIT
BIOSTRAT. ZONE/ FOSSIL CHARACTER
FORAMINIFERS
NANNOFOSSILS
RADIOLARIANS
DIATOMS
PALEOMAGNETICS
PHYS. PROPERTIES
CHEMISTRY
SECTION
METERS
GRAPHIC LITHOLOGY
DRILLING DISTURB.
SED. STRUCTURES
SAMPLES
PLEISTOCENE
NN19 Pseudoemiliania lacunosa
●A/M
●Φ=58.8 γ=1.73
1
2
3
4
5
6
7
CC
0.5
1.0

LITHOLOGIC DESCRIPTION

CALCITIC MARLY NANNOFOSSIL OOZE to NANNOFOSSIL SILTY CLAY

Section 1, 0-3 cm, is soupy; remainder of core is undisturbed.

Major lithology: CALCITIC MARLY NANNOFOSSIL OOZE to NANNOFOSSIL SILTY CLAY, olive (5Y 4/3, 5/3), olive gray (5Y 4/2), and light greenish gray (10Y 5/2). Alternation of lighter and darker layers, 20-100 cm thick. Darker layers contain more terrigenous silty clay than lighter layers. Slight to moderate burrow mottling. Foraminifers common on core face and concentrated in mm-scale lenses.

SMEAR SLIDE SUMMARY (%):

	1, 71 D	5, 16 D
TEXTURE:		
Sand	20	20
Silt	25	30
Clay	55	50
COMPOSITION:		
Access. minerals	2	2
Clay	20	25
Dolomite	—	1
Foraminifers	5	4
Volcanic glass	1	—
Inorganic calcite	27	38
Nannofossils	40	25
Organic debris	Tr	—
Quartz	5	5
Shell debris	—	Tr

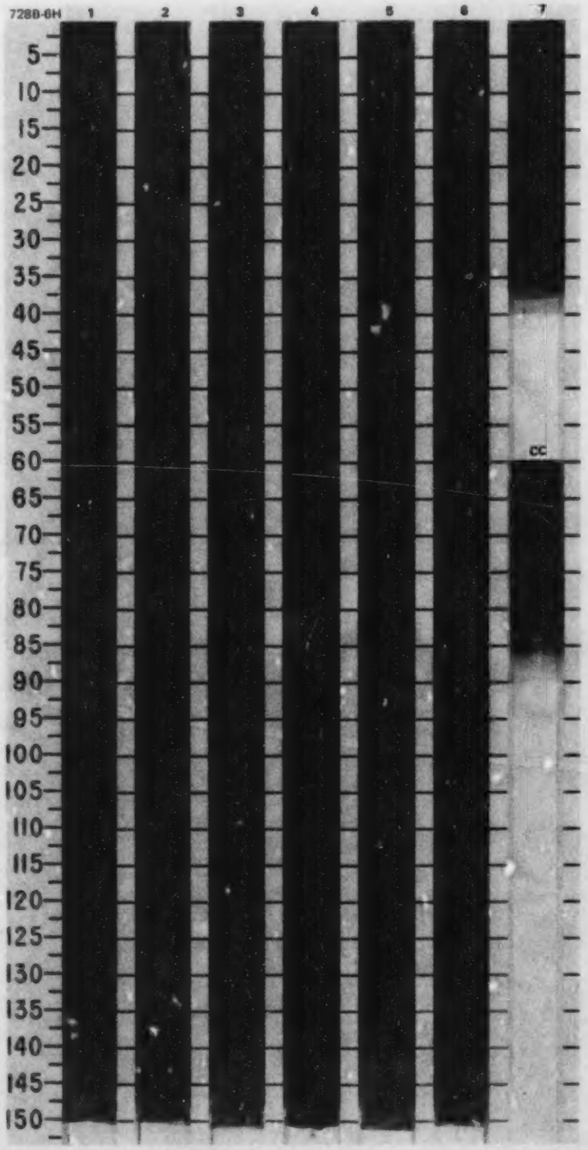
728B-6H
1
2
3
4
5
6
7
CC
5
10
15
20
25
30
35
40
45
50
55
60
65
70
75
80
85
90
95
100
105
110
115
120
125
130
135
140
145
150

SITE 728 HOLE B CORE 7H CORED INTERVAL 1467.4-1485.9 mbsl; 48.6-58.10 mbsf

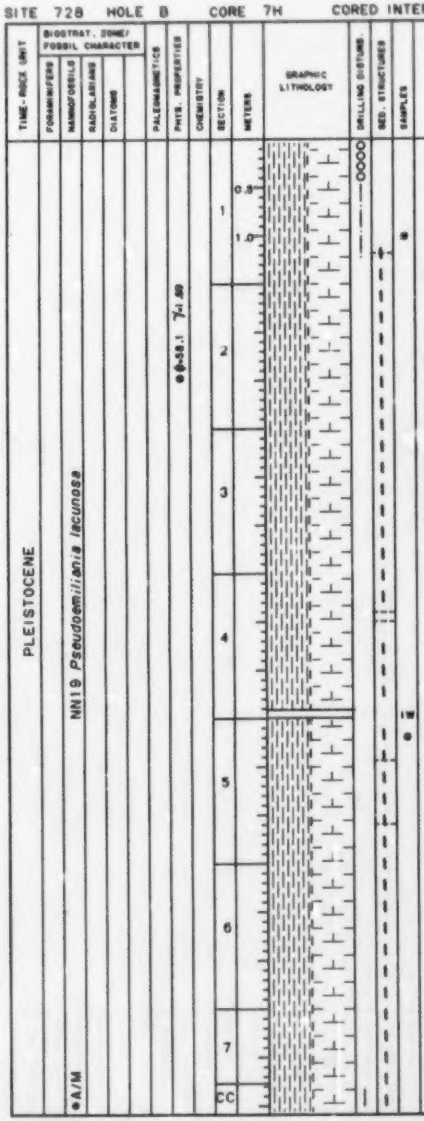
TIME-ROCK UNIT
BIOSTRAT. ZONE/ FOSSIL CHARACTER
FORAMINIFERS
NANNOFOSSILS
RADIOLARIANS
DIATOMS
PALEOMAGNETICS
PHYS. PROPERTIES
CHEMISTRY
SECTION
METERS
GRAPHIC LITHOLOGY
DRILLING DISTURB.
SED. STRUCTURES
SAMPLES
PLEISTOCENE
•A/M
NN19 Pseudoemiliania lacunosa
●ϕ=58.1 γ=1.80
0.5
1.0
1
2
3
4
5
6
7
CC

LITHOLOGIC DESCRIPTION

FORAMINIFER-BEARING CALCITIC MARLY NANNOFOSSIL OOZE

Section 1, 0-100 cm, is disturbed by pore-water sampler: 0-35 cm soupy, 35-100 cm moderate disturbance. Remainder of core is undisturbed.

Major lithology: FORAMINIFER-BEARING CALCITIC MARLY NANNOFOSSIL OOZE, olive (5Y 4/3), pale yellow (5Y 7/3), and light greenish gray (10Y 5/2). Alternation of lighter and darker layers, 20-100 cm thick. Slight to moderate burrow mottling. Shell debris present on core face.

SMEAR SLIDE SUMMARY (%):

	1, 100 D	5, 21 D
TEXTURE:		
Sand	15	20
Silt	20	30
Clay	65	50
COMPOSITION:		
Access. minerals	2	1
Clay	25	25
Dolomite	1	1
Feldspar	—	1
Foraminifers	7	12
Inorganic calcite	20	15
Mica	—	Tr
Nannofossils	40	25
Quartz	5	20

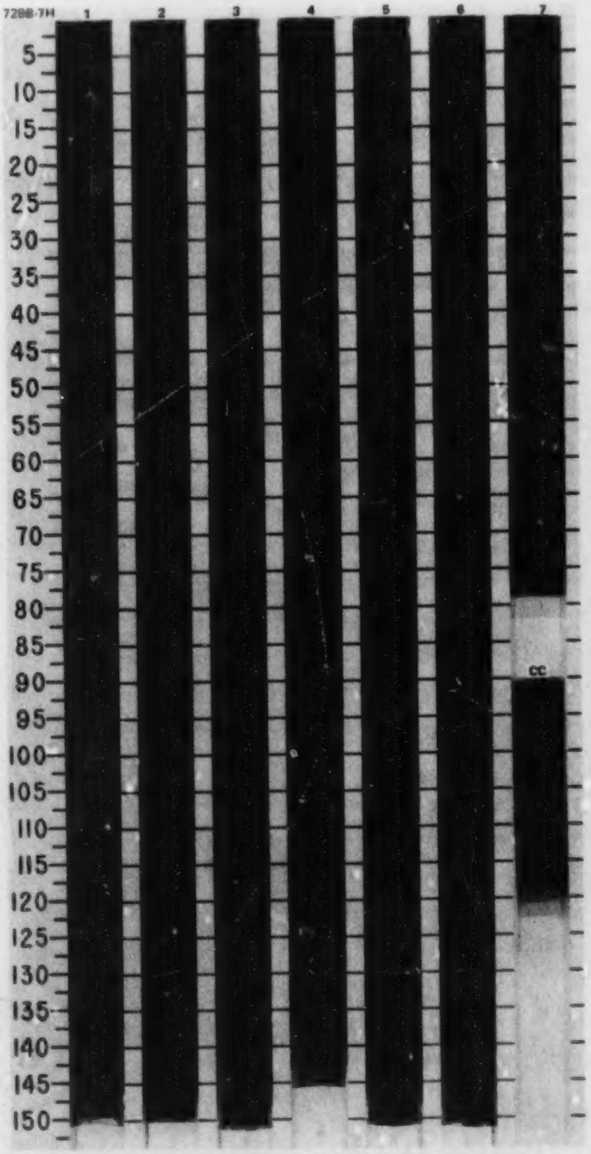
728B-7H
1
2
3
4
5
6
7
CC
5
10
15
20
25
30
35
40
45
50
55
60
65
70
75
80
85
90
95
100
105
110
115
120
125
130
135
140
145
150

SITE 728 HOLE B CORE 8H CORED INTERVAL 1485.9-1495.5 mbsl; 58.1-67.7 mbsf

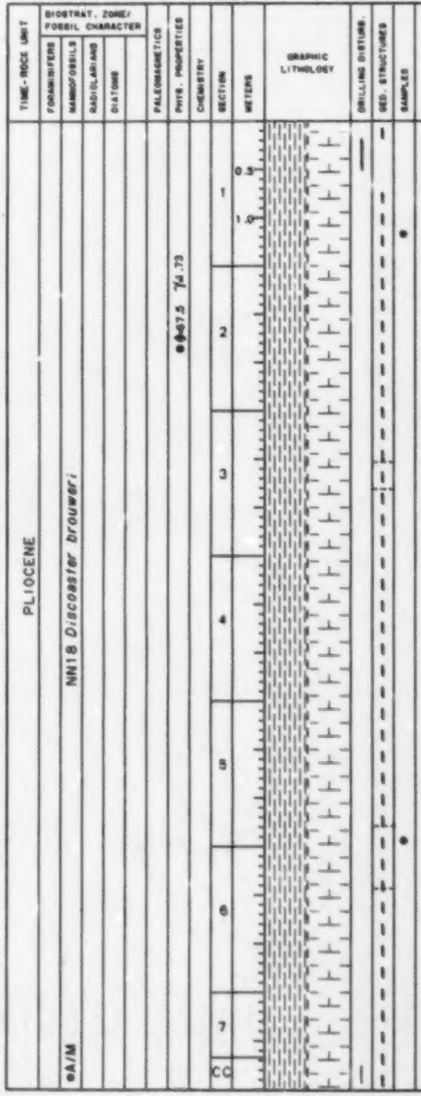
TIME-ROCK UNIT
BIOSTRAT. ZONE/ FOSSIL CHARACTER
FORAMINIFERS
NANNOFOSSILS
RADIOLARIANS
DIATOMS
PALEOMAGNETICS
PHYS. PROPERTIES
CHEMISTRY
SECTION
METERS
GRAPHIC LITHOLOGY
DRILLING DISTURB.
SED. STRUCTURES
SAMPLES
PLIOCENE
NN18 Discoaster brouweri
●A/M
●φ67.5 γ1.73
0.5
1.0
1
2
3
4
5
6
7
CC

LITHOLOGIC DESCRIPTION

FORAMINIFER-BEARING MARLY NANNOFOSSIL OOZE to CALCITIC MARLY NANNOFOSSIL OOZE

Section 1, 0-4 and 22-38 cm, is highly disturbed. Remainder of core is undisturbed.

Major lithology: FORAMINIFER-BEARING MARLY NANNOFOSSIL OOZE to CALCITIC MARLY NANNOFOSSIL OOZE, olive (5Y 4/3, 5/3, 4/4) and olive gray (5Y 4/2). Darker layers have more silty clay than lighter layers.

SMEAR SLIDE SUMMARY (%):

	1, 118 D	5, 142 D
TEXTURE:		
Sand	10	5
Silt	30	15
Clay	60	80
COMPOSITION:		
Access. minerals	1	1
Clay	25	20
Dolomite	Tr	—
Foraminifers	1	6
Inorganic calcite	17	8
Mica	1	—
Nannofossils	35	60
Quartz	20	5

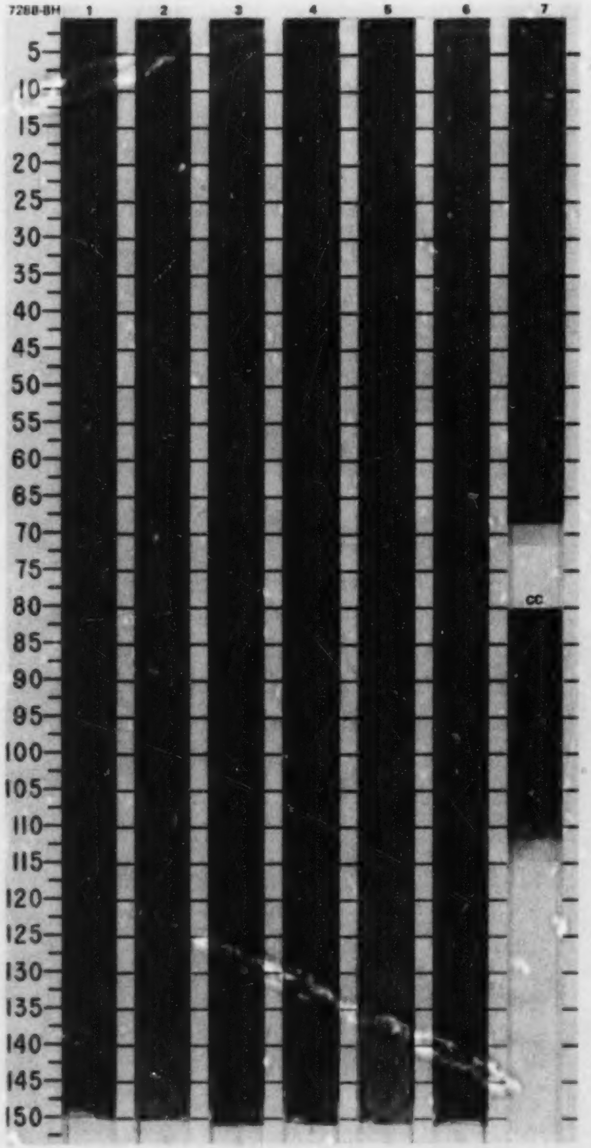
728B-8H
1
2
3
4
5
6
7
CC
5
10
15
20
25
30
35
40
45
50
55
60
65
70
75
80
85
90
95
100
105
110
115
120
125
130
135
140
145
150

SITE 728 HOLE B CORE 9H CORED INTERVAL 1495.5-1505.1 mbsl; 67.7-77.3 mbsf

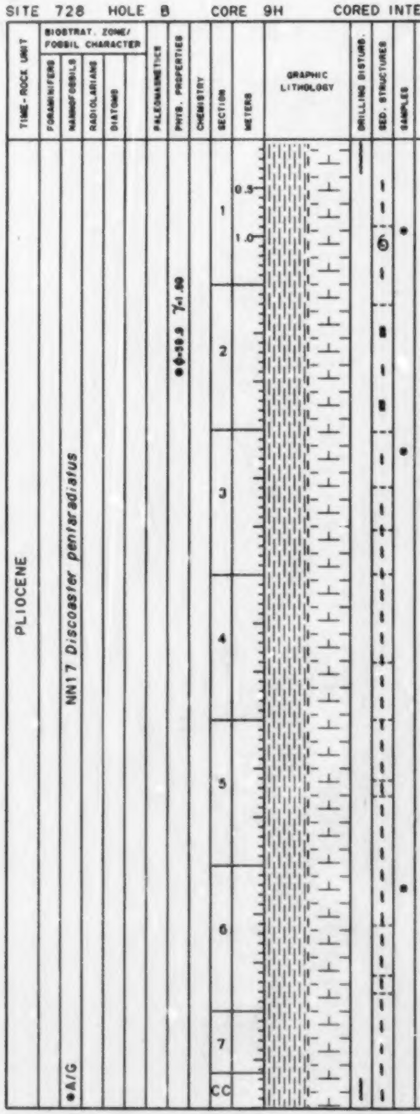
TIME-ROCK UNIT
BIOSTRAT. ZONE/ FOSSIL CHARACTER
FORAMINIFERS
NANNOFOSSILS
RADIOLARIANS
DIATOMS
PALEOMAGNETICS
PHYS. PROPERTIES
CHEMISTRY
SECTION
METERS
GRAPHIC LITHOLOGY
DRILLING DISTURB.
SED. STRUCTURES
SAMPLES
PLIOCENE
NN17 Discoaster pentaradiatus
●A/G
●ϕ=59.9 γ=1.90
0.5
1.0
1
2
3
4
5
6
7
CC

LITHOLOGIC DESCRIPTION

CALCITIC MARLY NANNOFOSSIL OOZE and NANNOFOSSIL SILTY CLAY

Section 1, 0-31 cm, is highly disturbed. Remainder of core is undisturbed.

Major lithology: CALCITIC MARLY NANNOFOSSIL OOZE, olive (5Y 4/3), alternating with a dark olive gray (5Y 3/2) nannofossil silty clay. Foraminifers common on core face. Bioturbation is minor.

SMEAR SLIDE SUMMARY (%):

	1, 93 M	3, 22 D	6, 22 D
TEXTURE:			
Sand	40	10	15
Silt	20	40	20
Clay	40	50	65
COMPOSITION:			
Access. minerals	4	2	2
Clay	40	25	20
Dolomite	Tr	1	1
Feldspar	3	1	—
Foraminifers	—	—	2
Inorganic calcite	6	45	20
Mica	—	—	2
Nannofossils	—	25	45
Organic debris	5	—	—
Quartz	40	1	10
Sponge spicules	—	—	Tr

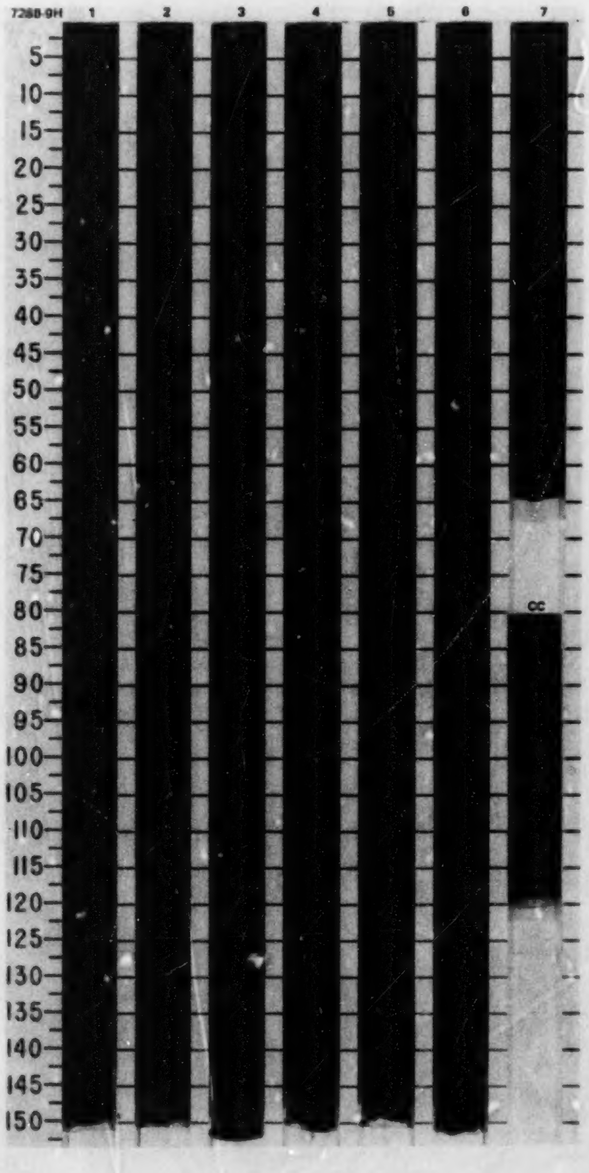
728B-9H
1
2
3
4
5
6
7
CC
5
10
15
20
25
30
35
40
45
50
55
60
65
70
75
80
85
90
95
100
105
110
115
120
125
130
135
140
145
150

SITE 728 HOLE B CORE 10X CORED INTERVAL 1505.4-1514.7 mbsl; 77.3-86.9 mbsf

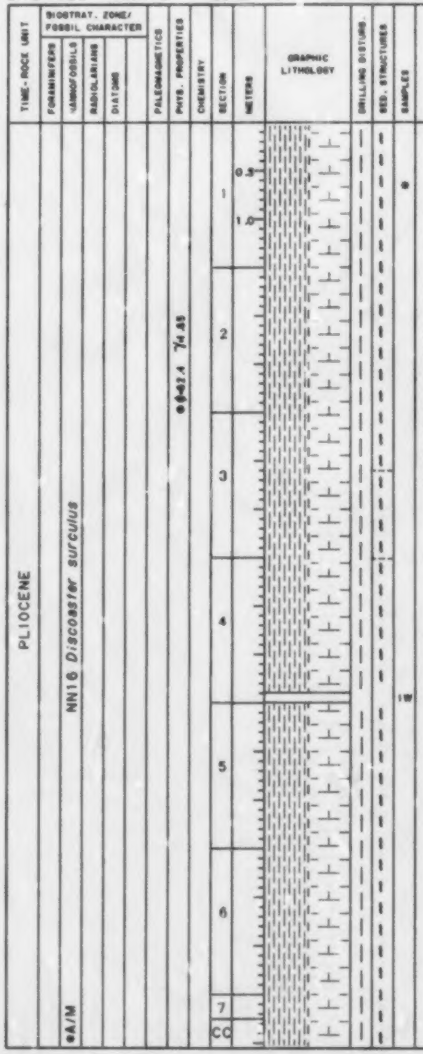
TIME-ROCK UNIT
BIOSTRAT. ZONE/ FOSSIL CHARACTER
FORAMINIFERS
NANNOFOSSILS
RADIOLARIANS
DIATOMS
PALEOMAGNETICS
PHYS. PROPERTIES
CHEMISTRY
SECTION
METERS
GRAPHIC LITHOLOGY
DRILLING DISTURB.
SED. STRUCTURES
SAMPLES
PLIOCENE
NN16 Discoaster surculus
●A/M
●Φ-62.4 γ-1.85
0.5
1.0
1
2
3
4
5
6
7
CC
*
IW

LITHOLOGIC DESCRIPTION

CALCITIC MARLY NANNOFOSSIL OOZE

Section 1, 0-8 cm, is highly disturbed. Remainder of core has minor disturbance and some biscuiting.

Major lithology: CALCITIC MARLY NANNOFOSSIL OOZE, olive (5Y 4/3) and olive gray (5Y 4/2). Foraminifers common on core face. Bioturbation is slight to moderate. Shell debris present but sparse.

SMEAR SLIDE SUMMARY (%):

	1, 84 D
TEXTURE:	
Sand	10
Silt	20
Clay	70
COMPOSITION:	
Access. minerals	2
Clay	20
Dolomite	1
Foraminifers	4
Inorganic calcite	13
Nannofossils	50
Quartz	10
Sponge spicules	Tr

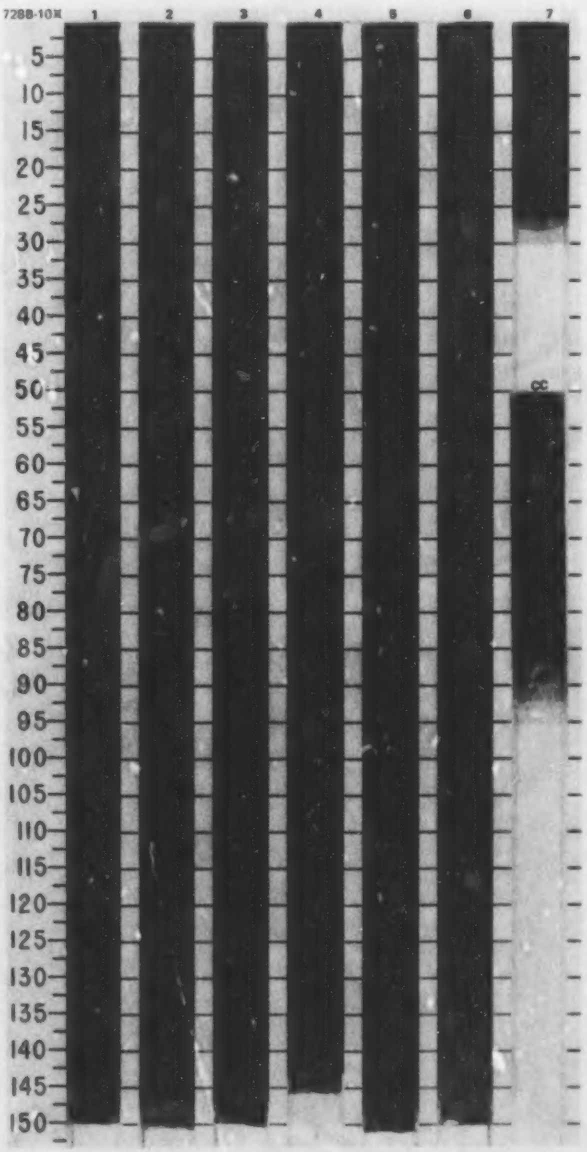
728B-10X
1
2
3
4
5
6
7
CC
5
10
15
20
25
30
35
40
45
50
55
60
65
70
75
80
85
90
95
100
105
110
115
120
125
130
135
140
145
150

SITE 728 HOLE B CORE 11X CORED INTERVAL 1514.7-1524.3 mbsl; 86.9-96.5 mbsf

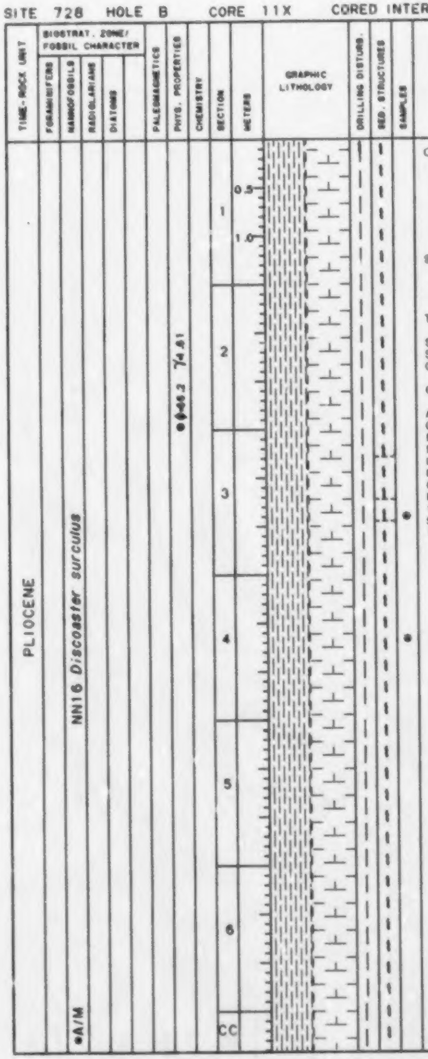
TIME-ROCK UNIT
BIOSTRAT. ZONE/ FOSSIL CHARACTER
FORAMINIFERS
NANNOFOSSILS
RADIOLARIANS
DIATOMS
PALEOMAGNETICS
PHYS. PROPERTIES
CHEMISTRY
SECTION
METERS
GRAPHIC LITHOLOGY
DRILLING DISTURB.
SED. STRUCTURES
SAMPLES
PLIOCENE
NN16 Discoaster surculus
●A/M
●ϕ66.2 γ1.81
1
2
3
4
5
6
CC
0.5
1.0

LITHOLOGIC DESCRIPTION

CALCITIC MARLY NANNOFOSSIL OOZE

Section 1, 0-10 cm, is highly disturbed. Remainder of core has minor disturbance and some biscuiting.

Major lithology: CALCITIC MARLY NANNOFOSSIL OOZE, olive (5Y 4/3, 5/3) and olive gray (5Y 4/2). Foraminifers common on core face. Bioturbation is slight to moderate. Shell debris present but sparse.

SMEAR SLIDE SUMMARY (%):

	3, 69 D	4, 67 D
TEXTURE:		
Sand	10	10
Silt	35	15
Clay	55	75
COMPOSITION:		
Access. minerals	2	2
Clay	30	25
Feldspar	3	—
Foraminifers	—	4
Inorganic calcite	20	15
Nannofossils	35	50
Quartz	20	2
Radiolarians 1	—	—
Sponge spicules 1	—	—

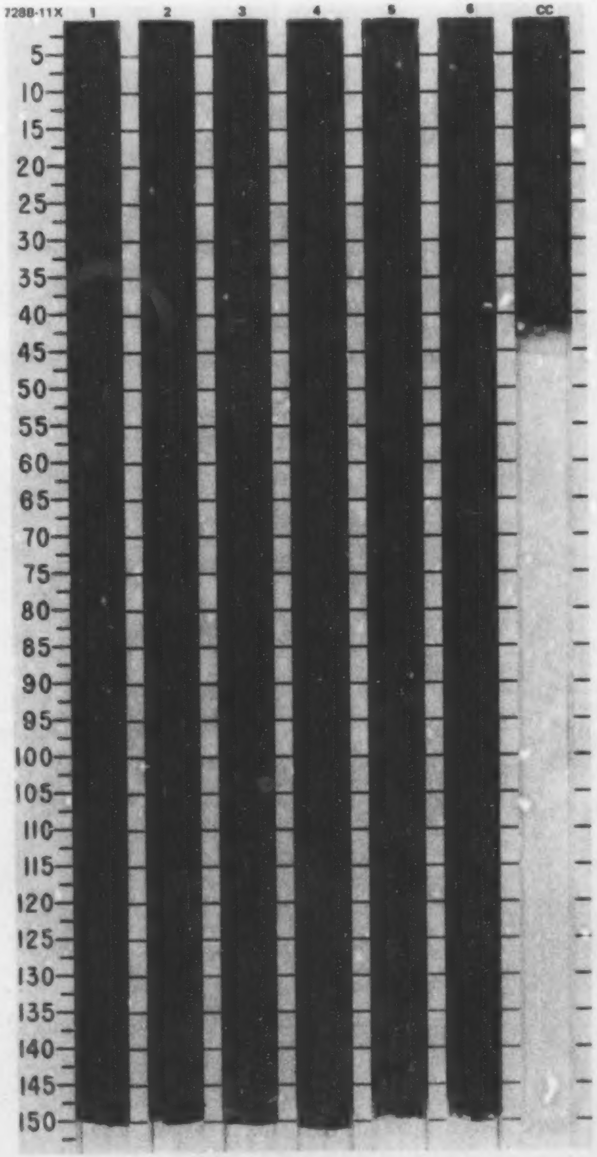
728B-11X
1
2
3
4
5
6
CC
5
10
15
20
25
30
35
40
45
50
55
60
65
70
75
80
85
90
95
100
105
110
115
120
125
130
135
140
145
150

SITE 728 HOLE B CORE 12X CORED INTERVAL 1524.3-1533.9 mbsl; 96.5-106.1 mbsf

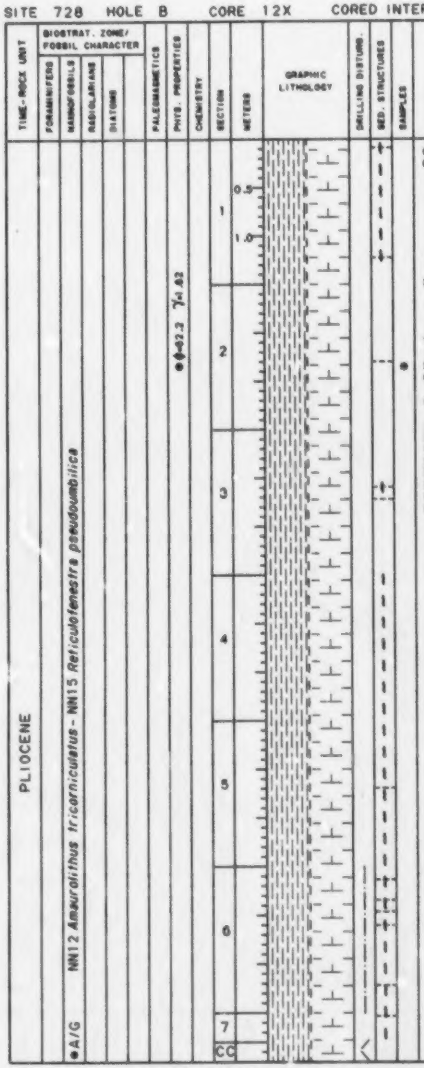
TIME-ROCK UNIT
BIOSTRAT. ZONE/ FOSSIL CHARACTER
FORAMINIFERS
NANNOFOSSILS
RADIOLARIANS
DIATOMS
PALEOMAGNETICS
PHYS. PROPERTIES
CHEMISTRY
SECTION
METERS
GRAPHIC LITHOLOGY
DRILLING DISTURB.
SED. STRUCTURES
SAMPLES
PLIOCENE
●A/G
NN12 *Amaurolithus tricorniculatus* - NN15 *Reticulofenestra pseudoumbilica*
●ϕ=62.2 γ=1.82
0.5
1.0
1
2
3
4
5
6
7
CC

LITHOLOGIC DESCRIPTION

CALCITIC MARLY NANNOFOSSIL OOZE to NANNOFOSSIL CALCITIC SILTY CLAY

Void in Section 1, 36-37 cm. Remainder of core has minor disturbance and some biscuiting.

Major lithology: CALCITIC MARLY NANNOFOSSIL OOZE to NANNOFOSSIL CALCITIC SILTY CLAY, olive (5Y 4/3) and olive gray (5Y 4/2) to dark olive gray (5Y 3/2). Dark layers have more terrigenous silty clay than the light layers. Bioturbation is slight to absent.

SMEAR SLIDE SUMMARY (%):

	2, 85 D
TEXTURE:	
Silt	40
Clay	60
COMPOSITION:	
Access. minerals	2
Dolomite	5
Foraminifers	2
Inorganic calcite	30
Mica	30
Nannofossils	20
Quartz	10
Sponge spicules	1

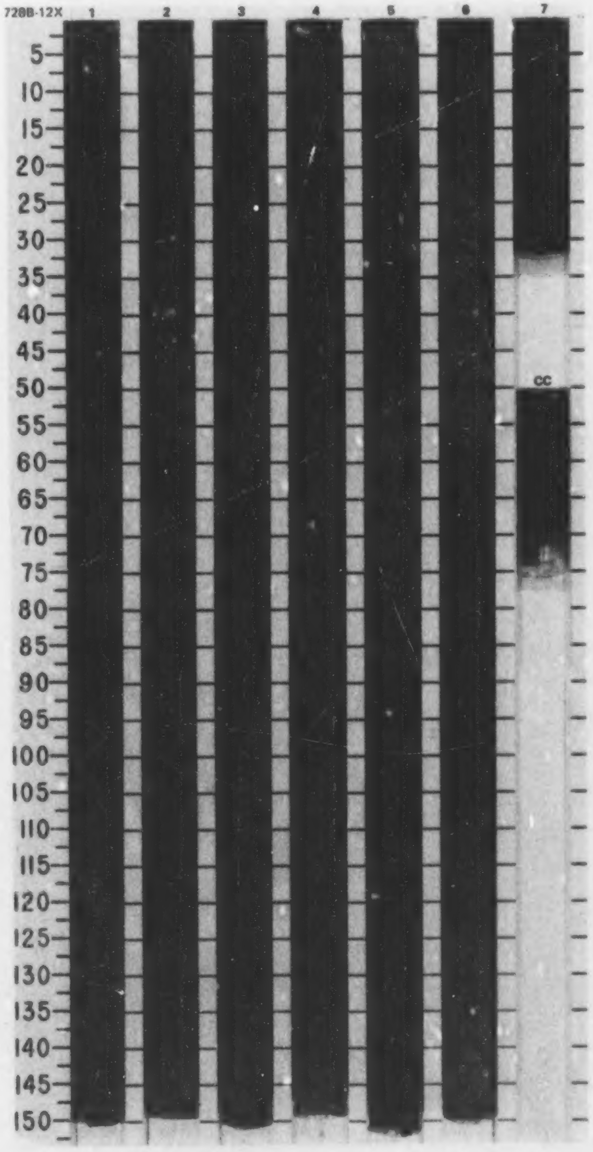
728B-12X
1
2
3
4
5
6
7
CC
5
10
15
20
25
30
35
40
45
50
55
60
65
70
75
80
85
90
95
100
105
110
115
120
125
130
135
140
145
150

SITE 728 HOLE B CORE 13X CORED INTERVAL 1533.9-1543.6 mbsl: 106.1-115.8 mbsf

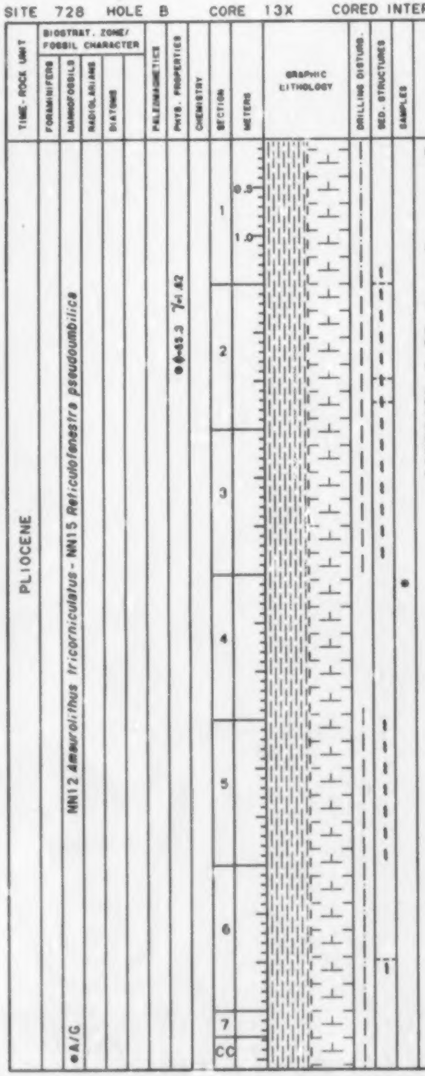
TIME-ROCK UNIT
BIOSTRAT. ZONE/ FOSSIL CHARACTER
FORAMINIFERS
NANNOFOSSILS
RADIOLARIANS
DIATOMS
PALEOMAGNETICS
PHYS. PROPERTIES
CHEMISTRY
SECTION
METERS
GRAPHIC LITHOLOGY
DRILLING DISTURB.
SED. STRUCTURES
SAMPLES
PLIOCENE
●A/G
NN12 Amaurolithus tricorniculatus - NN15 Reticulofenestra pseudoumbilica
●ϕ-63.3 γ-1.82
0.5
1.0
1
2
3
4
5
6
7
CC

LITHOLOGIC DESCRIPTION

MARLY NANNOFOSSIL OOZE

Section 1, 0-115 cm, is disturbed by *in situ* water sampler. Remainder of core has minor disturbance and some biscuiting.

Major lithology: MARLY NANNOFOSSIL OOZE, olive (5Y 4/3, 5/3) and dark olive gray (5Y 3/2). Bioturbation is slight to absent.

SMEAR SLIDE SUMMARY (%):

	4, 10 D
TEXTURE:	
Silt	30
Clay	70
COMPOSITION:	
Access. minerals	5
Clay	30
Foraminifers	Tr
Inorganic calcite	20
Mica	Tr
Nannofossils	40
Organic debris	Tr
Quartz	5

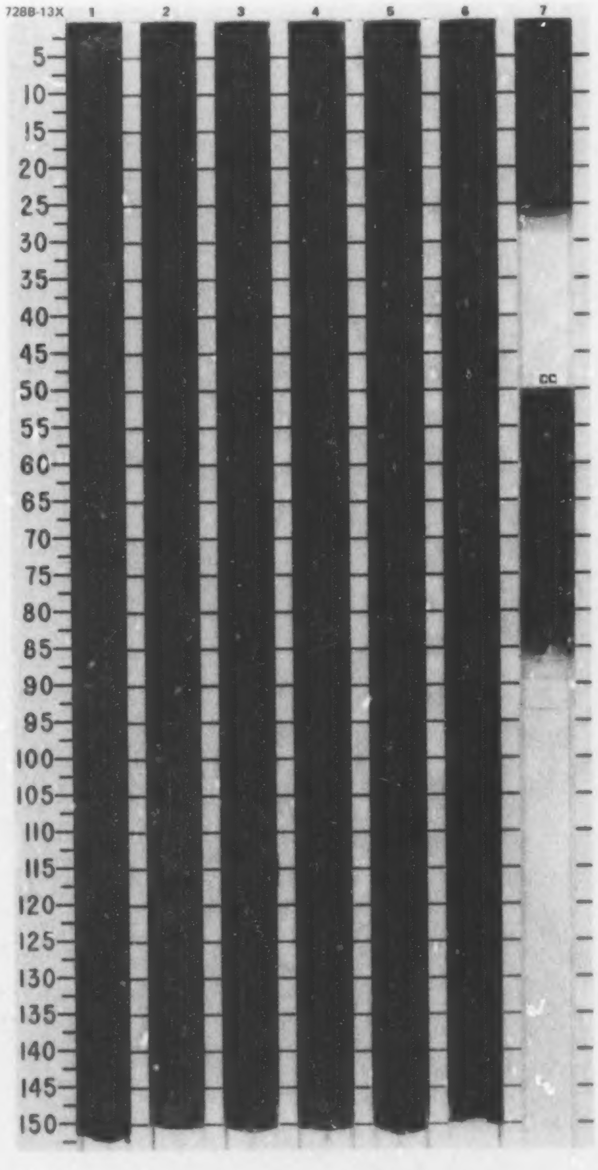
728B-13X
1
2
3
4
5
6
7
CC
5
10
15
20
25
30
35
40
45
50
55
60
65
70
75
80
85
90
95
100
105
110
115
120
125
130
135
140
145
150

SITE 728 HOLE B CORE 14X CORED INTERVAL 1543.6-1553.3 mbsl; 115.8-125.5 mbsf

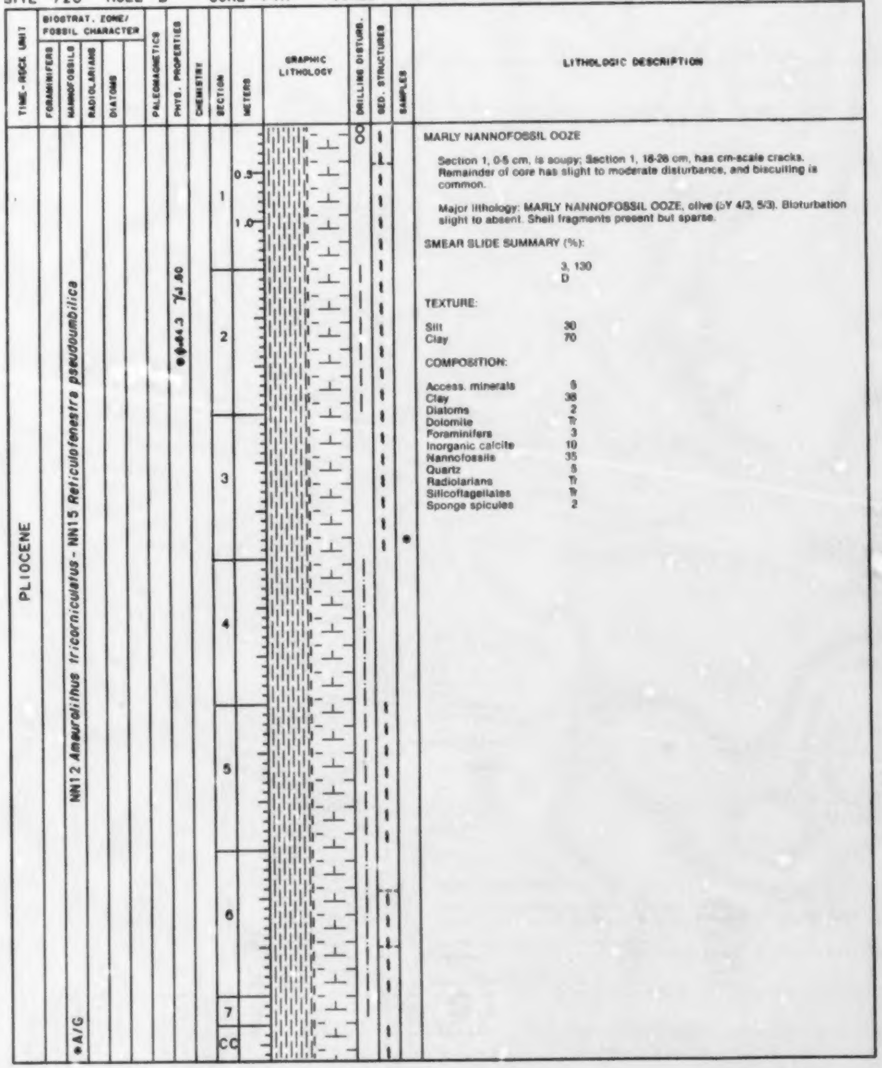
TIME-ROCK UNIT
BIOSTRAT. ZONE/ FOSSIL CHARACTER
FORAMINIFERS
NANNOFOSSILS
RADIOLARIANS
DIATOMS
PALEOMAGNETICS
PHYS. PROPERTIES
CHEMISTRY
SECTION
METERS
GRAPHIC LITHOLOGY
DRILLING DISTURB.
SED. STRUCTURES
SAMPLES
LITHOLOGIC DESCRIPTION
PLIOCENE
NN12 *Amaurolithus tricorniculatus* - NN15 *Reticulofenestra pseudoumbilica*
*A/G
●φ=64.3 γ=1.80
0.5
1.0
1
2
3
4
5
6
7
CC

MARLY NANNOFOSSIL OOZE

Section 1, 0-5 cm, is soupy; Section 1, 18-28 cm, has cm-scale cracks. Remainder of core has slight to moderate disturbance, and biscuiting is common.

Major lithology: MARLY NANNOFOSSIL OOZE, olive (5Y 4/3, 5/3). Bioturbation slight to absent. Shell fragments present but sparse.

SMEAR SLIDE SUMMARY (%):

	3, 130 D
TEXTURE:	
Silt	30
Clay	70
COMPOSITION:	
Access. minerals	5
Clay	38
Diatoms	2
Dolomite	Tr
Foraminifers	3
Inorganic calcite	10
Nannofossils	35
Quartz	5
Radiolarians	Tr
Silicoflagellates	Tr
Sponge spicules	2

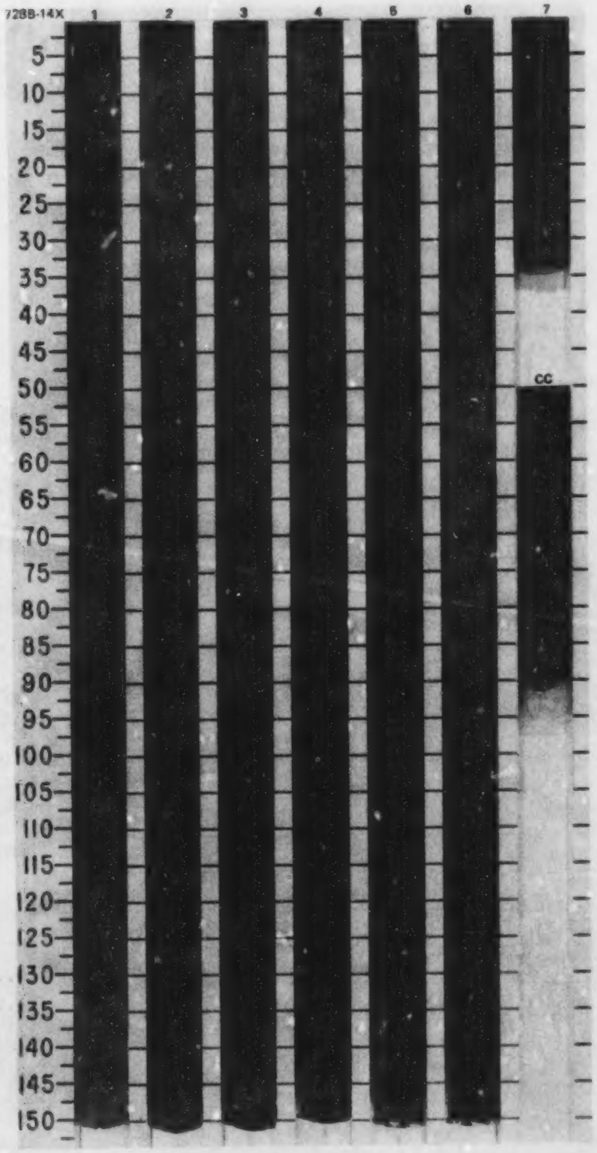
728B-14X
1
2
3
4
5
6
7
CC
5
10
15
20
25
30
35
40
45
50
55
60
65
70
75
80
85
90
95
100
105
110
115
120
125
130
135
140
145
150

SITE 728 HOLE B CORE 15X CORED INTERVAL 1553.3-1562.9 mbsl; 125.5-135.1 mbsf

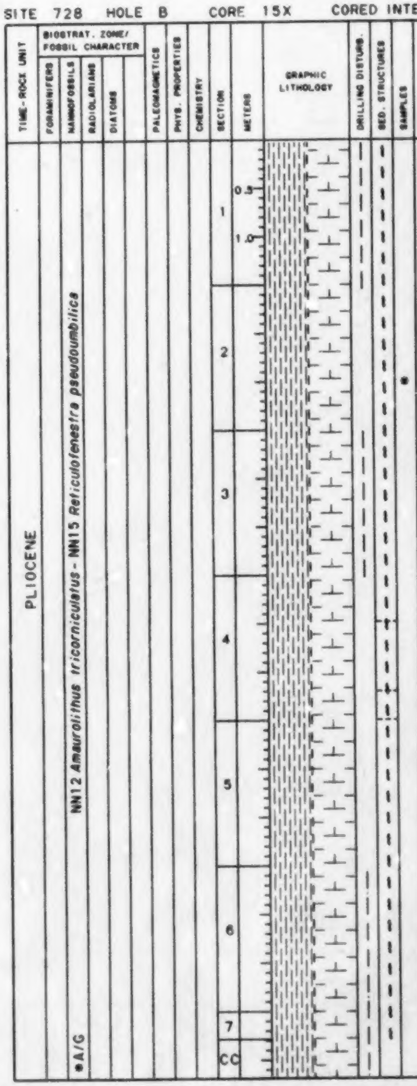
TIME-ROCK UNIT
BIOSTRAT. ZONE/ FOSSIL CHARACTER
FORAMINIFERS
NANNOFOSSILS
RADIOLARIANS
DIATOMS
PALEOMAGNETICS
PHYS. PROPERTIES
CHEMISTRY
SECTION
METERS
GRAPHIC LITHOLOGY
DRILLING DISTURB.
SED. STRUCTURES
SAMPLES
PLIOCENE
NN12 *Amaurolithus tricorniculatus* - NN15 *Reticulofenestra pseudoumbilica*
●A/G
1
2
3
4
5
6
7
CC
0.5
1.0

LITHOLOGIC DESCRIPTION

MARLY NANNOFOSSIL OOZE

Slight to moderate drilling disturbance.

Major lithology: MARLY NANNOFOSSIL OOZE, olive (5Y 4/3, 5/3). Bioturbation slight to absent. Shark's tooth found at Section 5, 69 cm.

SMEAR SLIDE SUMMARY (%):

	2, 100 D
TEXTURE:	
Silt	45
Clay	55
COMPOSITION:	
Access. minerals	5
Clay	24
Diatoms	Tr
Dolomite	1
Foraminifers	3
Inorganic calcite	15
Mica	Tr
Nannofossils	35
Organic debris	5
Quartz	10
Sponge spicules	2

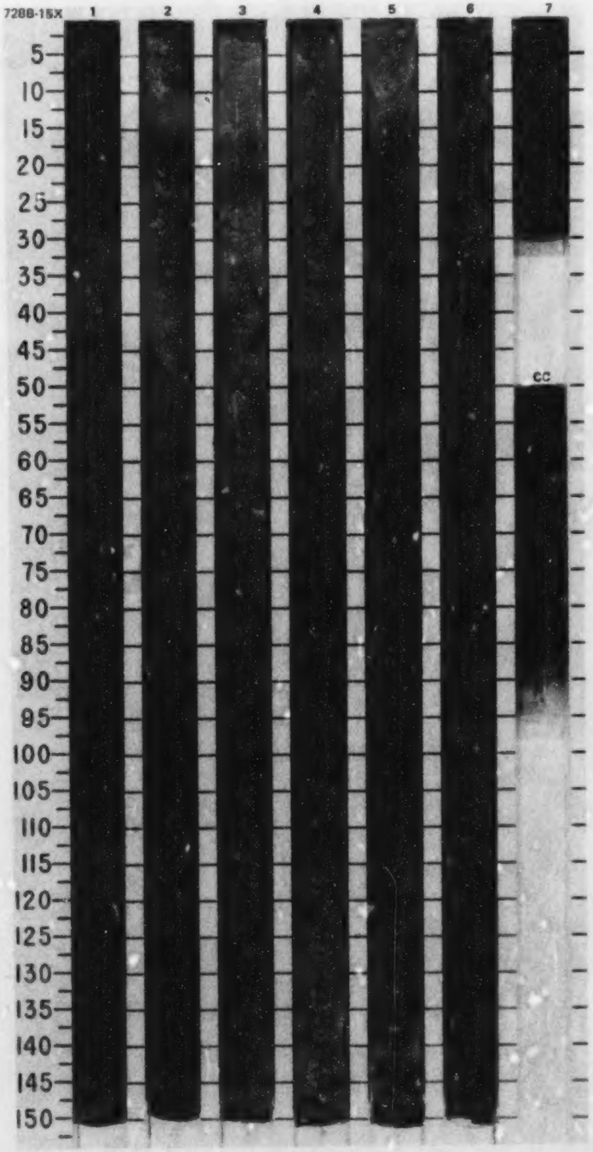
728B-15X
1
2
3
4
5
6
7
CC
5
10
15
20
25
30
35
40
45
50
55
60
65
70
75
80
85
90
95
100
105
110
115
120
125
130
135
140
145
150

SITE 728 HOLE B CORE 16X CORED INTERVAL 1562.9-1572.5 mbsl; 135.1-144.7 mbsf

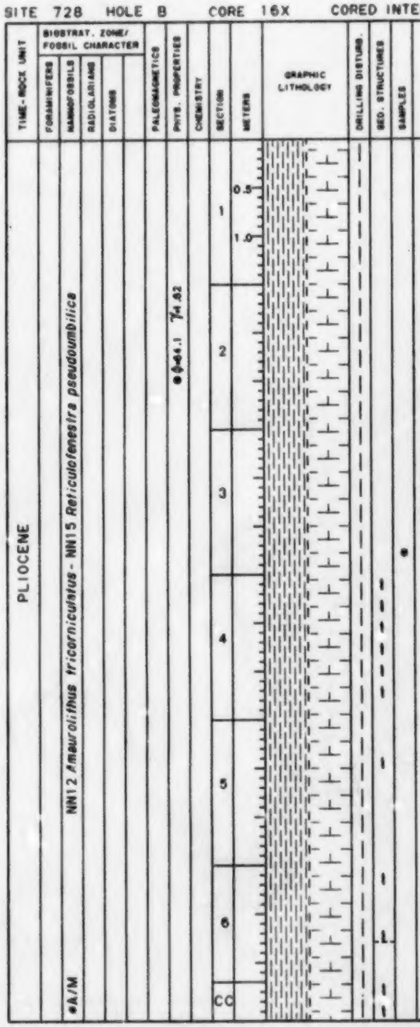
TIME-ROCK UNIT
BIOSTRAT. ZONE/ FOSSIL CHARACTER
FORAMINIFERS
NANNOFOSSILS
RADIOLARIANS
DIATOMS
PALEOMAGNETICS
PHYS. PROPERTIES
CHEMISTRY
SECTION
METERS
GRAPHIC LITHOLOGY
DRILLING DISTURB.
SED. STRUCTURES
SAMPLES
PLIOCENE
●A/M
NN12 Amaurolithus tricorniculatus - NN15 Reticulofenestra pseudoumbilica
●φ=64.1 γ1.82
1
2
3
4
5
6
CC
0.5
1.0

LITHOLOGIC DESCRIPTION

MARLY NANNOFOSSIL OOZE

Section 1 contains cm-scale cracks. Remainder of core has minor disturbance and some biscuiting.

Major lithology: MARLY NANNOFOSSIL OOZE, olive (5Y 4/3) and olive gray (5Y 5/2). Bioturbation is slight to absent.

SMEAR SLIDE SUMMARY (%):

	3, 130 D	6, 130 D
TEXTURE:		
Silt	30	
Clay	70	
COMPOSITION:		
Access. minerals	2	2
Clay	35	20
Diatoms	Tr	—
Dolomite	Tr	—
Foraminifers	2	3
Inorganic calcite	7	10
Mica	Tr	—
Nannofossils	45	60
Organic debris	Tr	—
Pyrite	5	—
Quartz	3	3
Radiolarians	Tr	1
Silicoflagellates	Tr	—
Sponge spicules	1	1

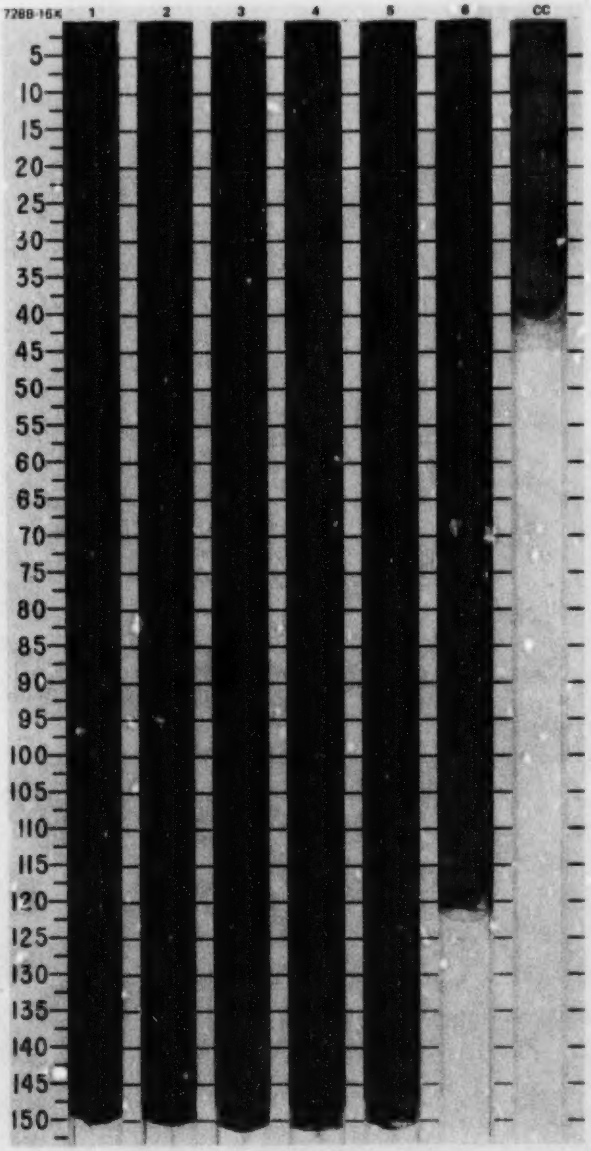
728B-16X
1
2
3
4
5
6
CC
5
10
15
20
25
30
35
40
45
50
55
60
65
70
75
80
85
90
95
100
105
110
115
120
125
130
135
140
145
150

SITE 728 HOLE B CORE 17X CORED INTERVAL 1572.5-1582.2 mbsl; 144.7-154.4 mbsf

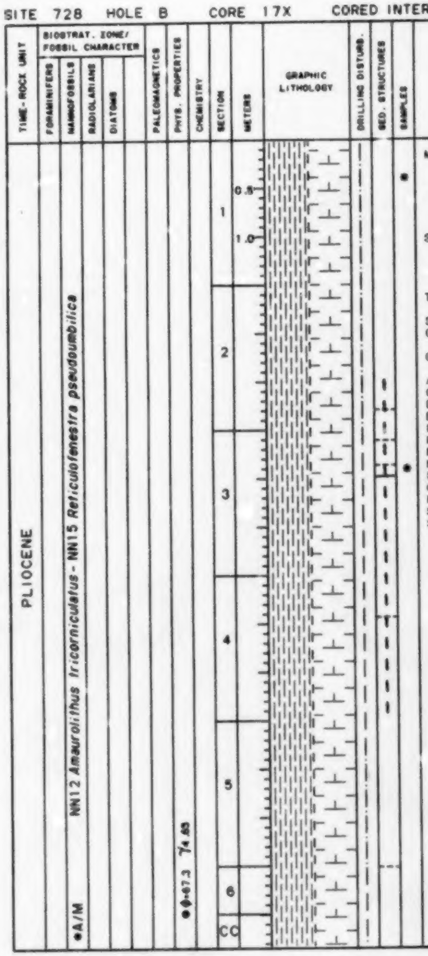
TIME-ROCK UNIT
BIOSTRAT. ZONE/ FOSSIL CHARACTER
FORAMINIFERS
NANNOFOSSILS
RADIOLARIANS
DIATOMS
PALEOMAGNETICS
PHYS. PROPERTIES
CHEMISTRY
SECTION
METERS
GRAPHIC LITHOLOGY
DRILLING DISTURB.
SED. STRUCTURES
SAMPLES
PLIOCENE
NN12 Amaurolithus tricorniculatus - NN15 Reticulofenestra pseudoumbilica
●A/M
●ϕ-67.3 γ1.65
1
2
3
4
5
6
CC
0.5
1.0

LITHOLOGIC DESCRIPTION

MARLY NANNOFOSSIL OOZE

Moderate disturbance and some biscuiting.

Major lithology: MARLY NANNOFOSSIL OOZE, olive (5Y 4/3, 5/3) and olive gray (5Y 5/2). Bioturbation is slight to absent. Rare occurrence of diatoms.

SMEAR SLIDE SUMMARY (%):

	1, 40 D	3, 40 D
TEXTURE:		
Silt	40	40
Clay	60	60
COMPOSITION:		
Access. minerals	3	5
Clay	34	19
Diatoms	5	2
Dolomite	1	1
Foraminifers	4	2
Inorganic calcite	10	15
Mica	Tr	—
Nannofossils	35	50
Pyrite	2	—
Quartz	3	3
Radiolarians	Tr	Tr
Silicoflagellates	Tr	Tr
Sponge spicules	3	3

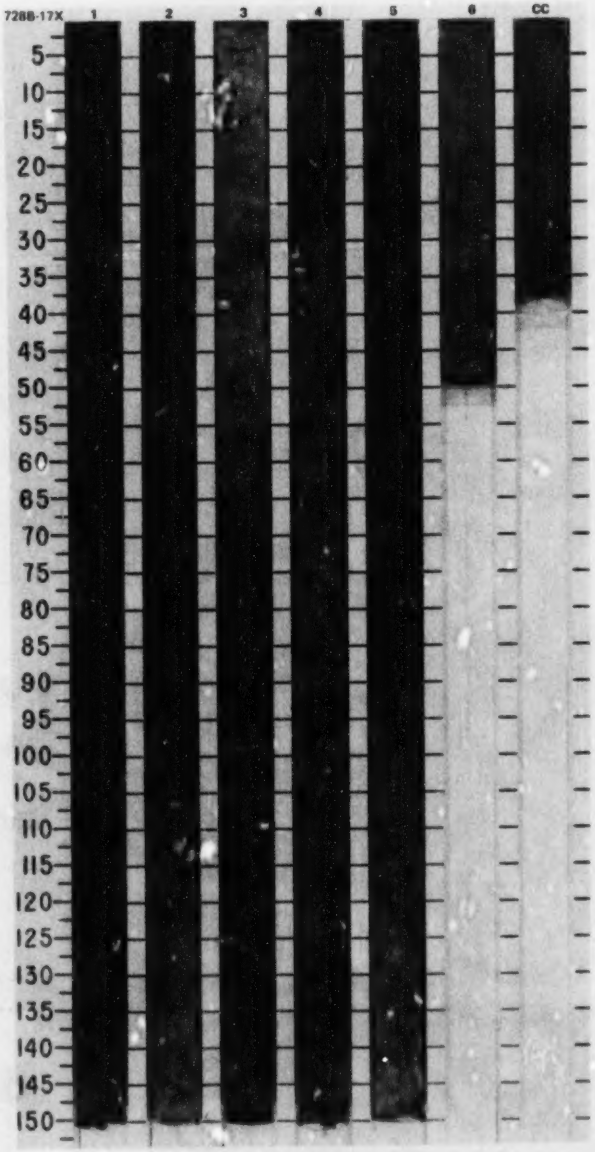
728B-17X
1
2
3
4
5
6
CC
5
10
15
20
25
30
35
40
45
50
55
60
65
70
75
80
85
90
95
100
105
110
115
120
125
130
135
140
145
150

SITE 728 HOLE B CORE 18X CORED INTERVAL 1582.2-1591.9 mbsl; 154.4-164.1 mbsf

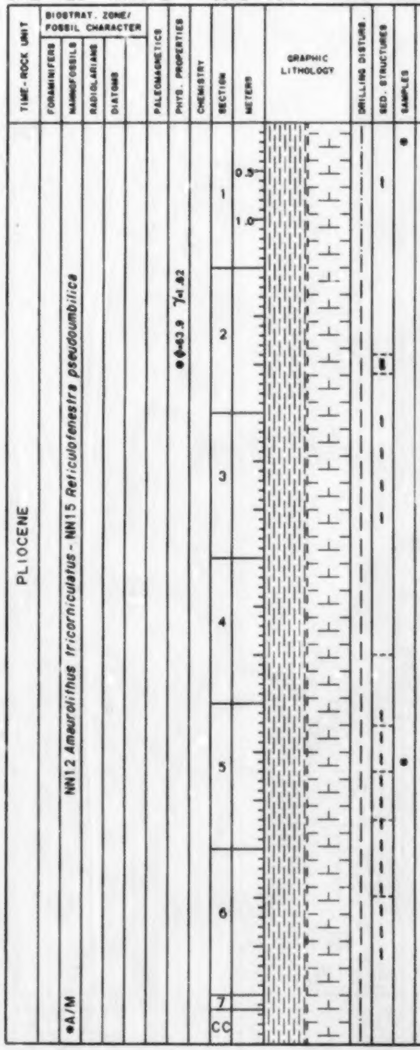
TIME-ROCK UNIT
BIOSTRAT. ZONE/ FOSSIL CHARACTER
FORAMINIFERS
NANNOFOSSILS
RADIOLARIANS
DIATOMS
PALEOMAGNETICS
PHYS. PROPERTIES
CHEMISTRY
SECTION
METERS
GRAPHIC LITHOLOGY
DRILLING DISTURB.
SED. STRUCTURES
SAMPLES
PLIOCENE
●A/M
NN12 Amaurolithus tricorniculatus - NN15 Reticulofenestra pseudoumbilica
●ϕ=63.9 γ=1.82
1
2
3
4
5
6
7
CC
0.5
1.0

LITHOLOGIC DESCRIPTION

MARLY NANNOFOSSIL OOZE

Section 1, 0-100 cm, disturbed by *in situ* water sampler. Remainder of core has minor disturbance and some biscuiting.

Major lithology: MARLY NANNOFOSSIL OOZE, olive (5Y 4/3, 5/3) and olive gray (5Y 5/2). Bioturbation is slight to absent.

SMEAR SLIDE SUMMARY (%):

	1, 20 D	5, 50 D
TEXTURE:		
Silt	30	20
Clay	70	80
COMPOSITION:		
Access. minerals	5	5
Clay	33	18
Diatoms	Tr	Tr
Dolomite	Tr	2
Foraminifers	5	2
Inorganic calcite	15	10
Mica	Tr	Tr
Nannofossils	40	60
Quartz	Tr	3
Radiolarians	Tr	—
Sponge spicules	2	Tr

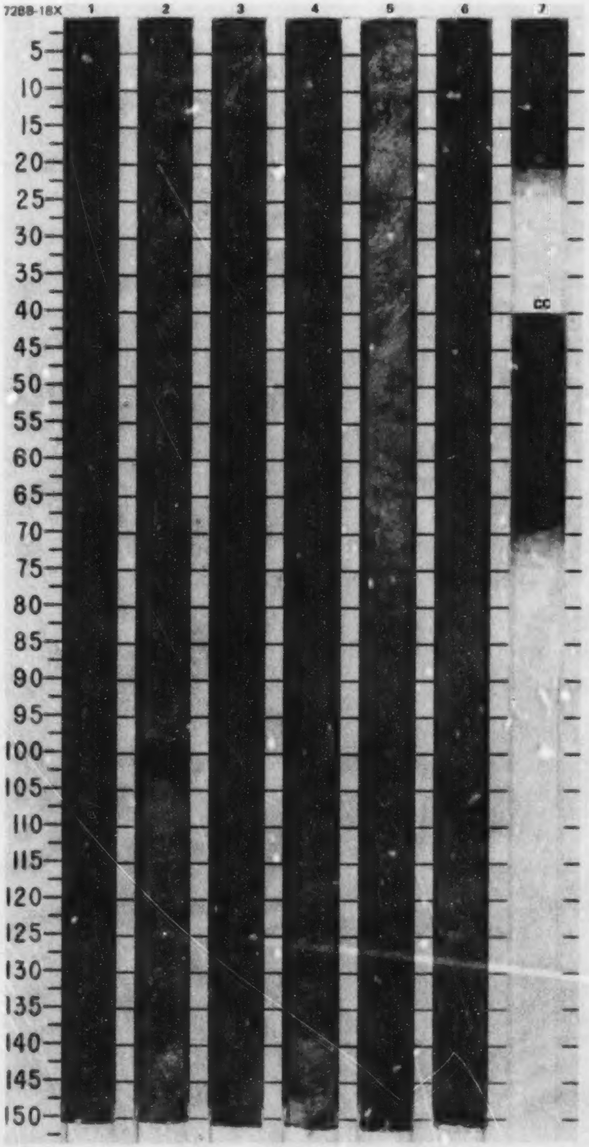
728B-18X
1
2
3
4
5
6
7
CC
5
10
15
20
25
30
35
40
45
50
55
60
65
70
75
80
85
90
95
100
105
110
115
120
125
130
135
140
145
150

SITE 728 HOLE B CORE 19X CORED INTERVAL 1591.9-1601.6 mbsl; 164.1-173.8 mbsf

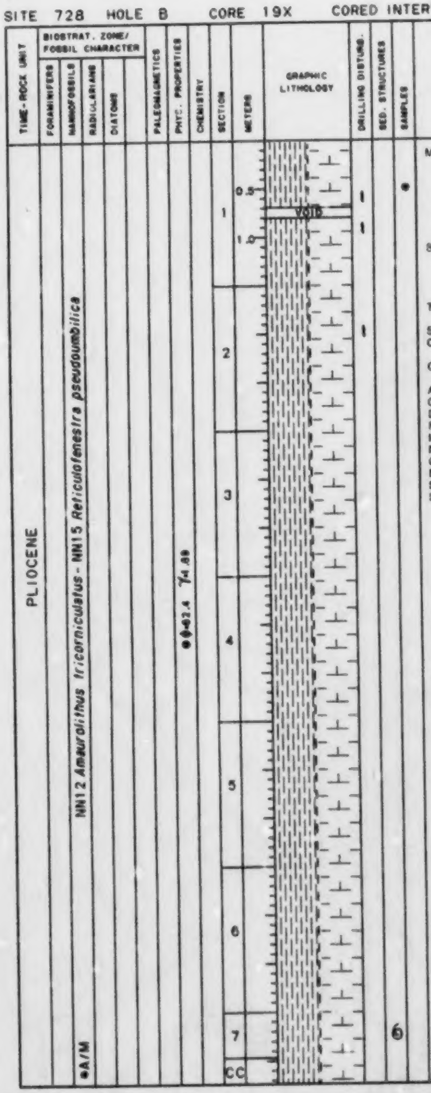
TIME-ROCK UNIT
BIOSTRAT. ZONE/ FOSSIL CHARACTER
FORAMINIFERS
NANNOFOSSILS
RADIOLARIANS
DIATOMS
PALEOMAGNETICS
PHYS. PROPERTIES
CHEMISTRY
SECTION
METERS
GRAPHIC LITHOLOGY
DRILLING DISTURB.
SED. STRUCTURES
SAMPLES
PLIOCENE
NN12 Amaurolithus tricorniculatus - NN15 Reticulofenestra pseudoumbilica
●A/M
●ϕ-62.4 γ1.89
1
2
3
4
5
6
7
CC
0.5
1.0
VOID
6

LITHOLOGIC DESCRIPTION

MARLY NANNOFOSSIL OOZE

Void at Section 1, 70-75 cm. Remainder of core has minor disturbance and some biscuiting.

Major lithology: MARLY NANNOFOSSIL OOZE, olive (5Y 4/4, 5/3). Bioturbation is slight to absent. Some layers indurated.

SMEAR SLIDE SUMMARY (%):

	1, 50 D
TEXTURE:	
Silt	25
Clay	75
COMPOSITION:	
Access. minerals	5
Clay	17
Diatoms	1
Foraminifers	5
Inorganic calcite	10
Nannofossils	60
Quartz	Tr
Radiolarians	Tr
Silicoflagellates	Tr
Sponge spicules	2

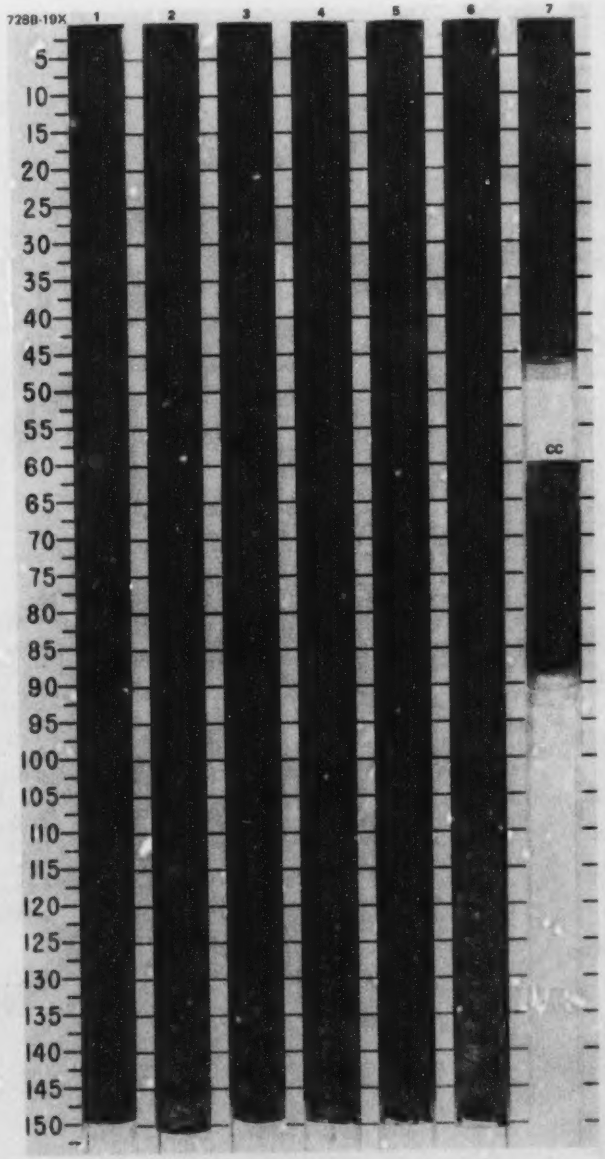
728B-19X
1
2
3
4
5
6
7
CC
5
10
15
20
25
30
35
40
45
50
55
60
65
70
75
80
85
90
95
100
105
110
115
120
125
130
135
140
145
150

SITE 728 HOLE B CORE 20X CORED INTERVAL 1601.6-1611.3 mbsl; 173.8-183.5 mbsf

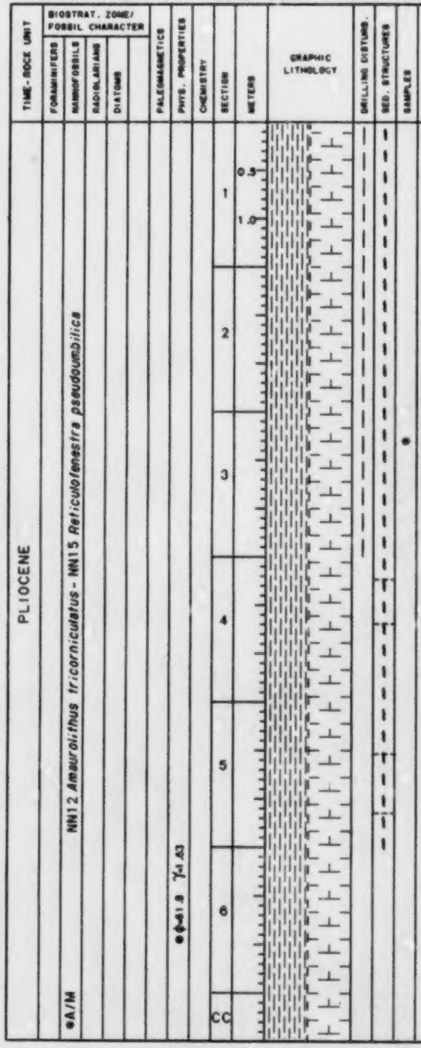
TIME-ROCK UNIT
BIOSTRAT. ZONE/ FOSSIL CHARACTER
FORAMINIFERS
NANNOFOSSILS
RADIOLARIANS
DIATOMS
PALEOMAGNETICS
PHYS. PROPERTIES
CHEMISTRY
SECTION
METERS
GRAPHIC LITHOLOGY
DRILLING DISTURB.
SED. STRUCTURES
SAMPLES
PLIOCENE
●A/M
NN12 Amaurolithus tricorniculatus - NN15 Reticulofenestra pseudoumbilica
●φ=41.8 γ=1.83
0.5
1.0
1
2
3
4
5
6
CC

LITHOLOGIC DESCRIPTION

MARLY NANNOFOSSIL OOZE

Slightly disturbed, with some biscuiting.

Major lithology: MARLY NANNOFOSSIL OOZE, olive (5Y 4/3, 5/3). Bioturbation is slight to absent. Some sections indurated.

SMEAR SLIDE SUMMARY (%):

	3, 30 D
TEXTURE:	
Silt	35
Clay	65
COMPOSITION:	
Access. minerals	5
Clay	17
Diatoms	Tr
Dolomite	Tr
Feldspar	Tr
Foraminifers	5
Inorganic calcite	15
Mica	Tr
Nannofossils	50
Quartz	5
Radiolarians	Tr
Silicoflagellates	Tr
Sponge spicules	3

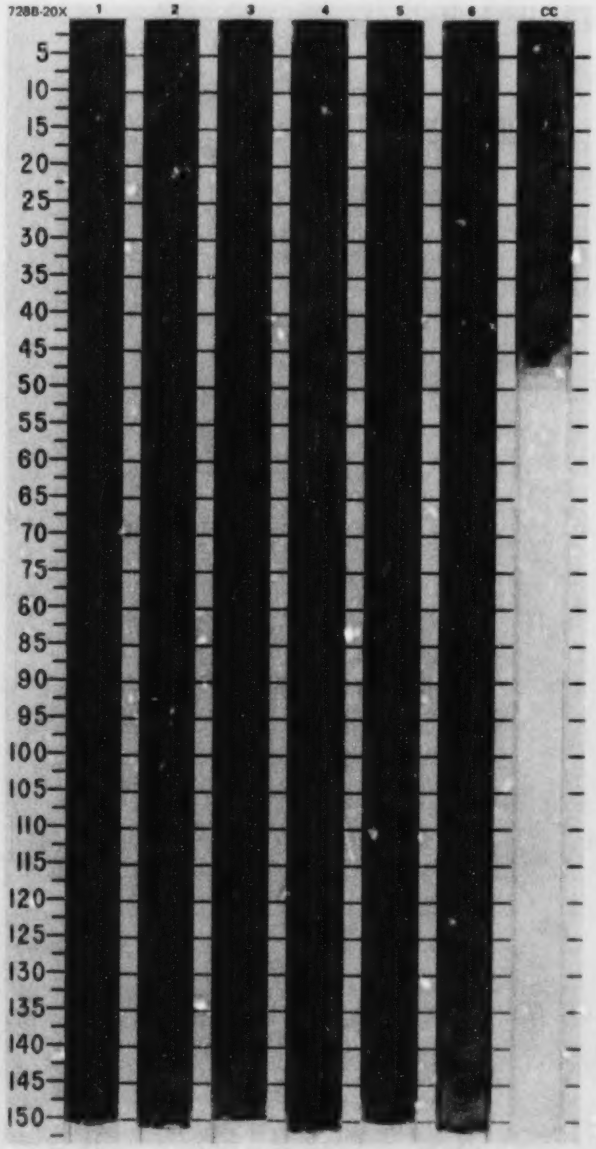
728B-20X
1
2
3
4
5
6
CC
5
10
15
20
25
30
35
40
45
50
55
60
65
70
75
80
85
90
95
100
105
110
115
120
125
130
135
140
145
150

SITE 728 HOLE B CORE 21X CORED INTERVAL 1611.3-1621.0 mbsl; 183.5-193.2 mbsf

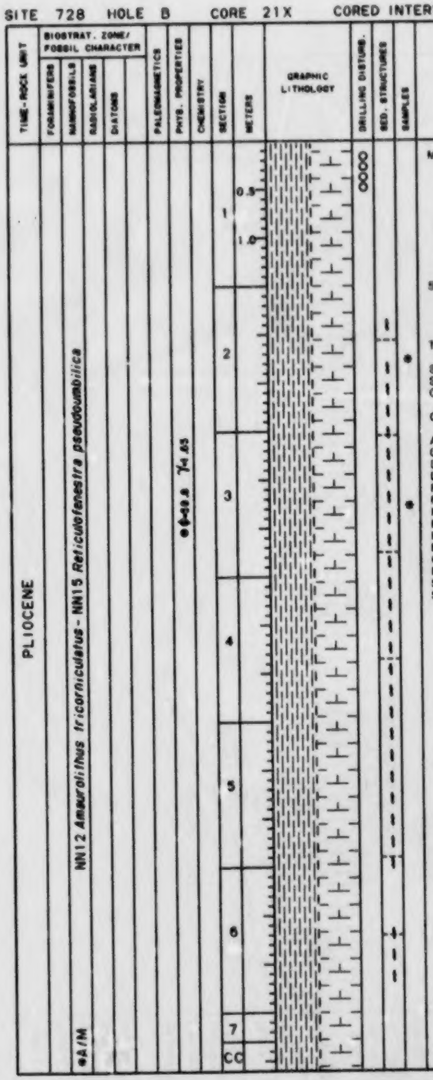
TIME-ROCK UNIT
BIOSTRAT. ZONE/ FOSSIL CHARACTER
FORAMINIFERS
NANNOFOSSILS
RADIOLARIANS
DIATOMS
PALEOMAGNETICS
PHYS. PROPERTIES
CHEMISTRY
SECTION
METERS
GRAPHIC LITHOLOGY
DRILLING DISTURB.
SED. STRUCTURES
SAMPLES
PLIOCENE
NN12 Amaurolithus tricorniculatus - NN15 Reticulofenestra pseudoumbilica
●A/M
●Φ=49.8 γ=1.83
1
2
3
4
5
6
7
CC
0.5
1.0
OOOO
*

LITHOLOGIC DESCRIPTION

MARLY NANNOFOSSIL OOZE and DIATOM-BEARING NANNOFOSSIL OOZE

Section 1, 20-45 cm, is soupy. Remainder of core has minor disturbance and biscuiting.

Major lithologies: MARLY NANNOFOSSIL OOZE and DIATOM-BEARING NANNOFOSSIL OOZE, olive (5Y 4/3, 5/3). Bioturbation slight to absent.

Minor lithology: NANNOFOSSIL CLAYEY SILT, dark olive gray (5Y 3/2). Slight to moderate bioturbation.

SMEAR SLIDE SUMMARY (%):

	2, 75 D	3, 75 M
TEXTURE:		
Sand	—	2
Silt	30	53
Clay	70	45
COMPOSITION:		
Access. minerals	5	7
Clay	13	28
Diatoms	10	—
Dolomite	Tr	Tr
Feldspar	—	2
Foraminifers	3	3
Inorganic calcite	5	20
Mica	—	Tr
Nannofossils	60	20
Pyrite	—	3
Quartz	2	15
Radiolarians	1	—
Silicoflagellates	Tr	—
Sponge spicule	1	2

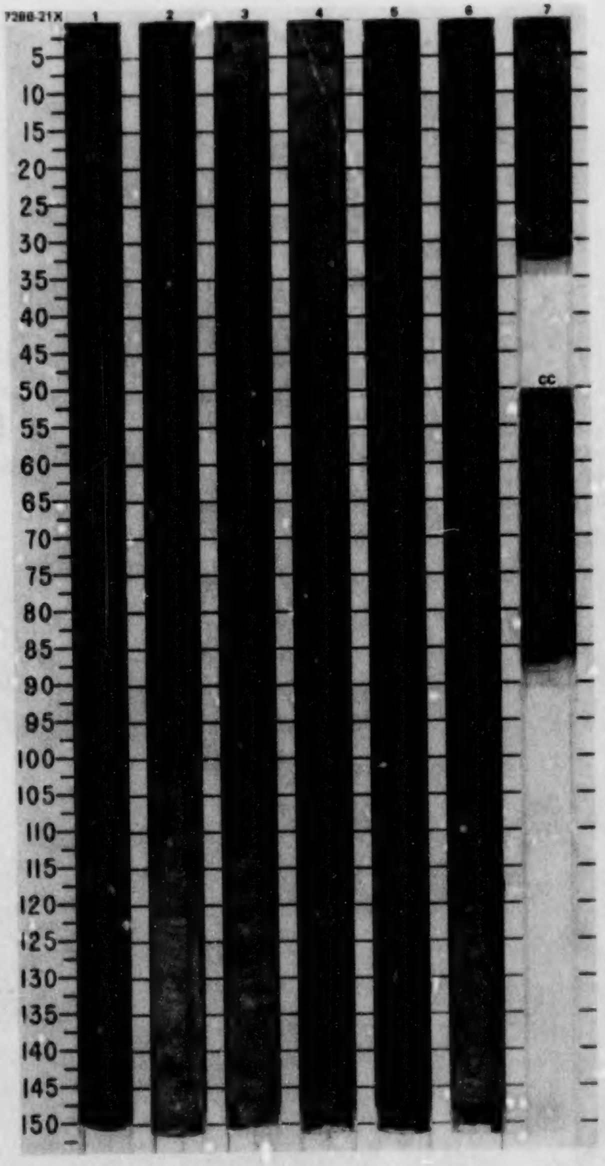
728B-21X
1
2
3
4
5
6
7
CC
5
10
15
20
25
30
35
40
45
50
55
60
65
70
75
80
85
90
95
100
105
110
115
120
125
130
135
140
145
150

SITE 728 HOLE B CORE 22X CORED INTERVAL 1621.0-1630.6 mbsl; 193.2-202.8 mbsf

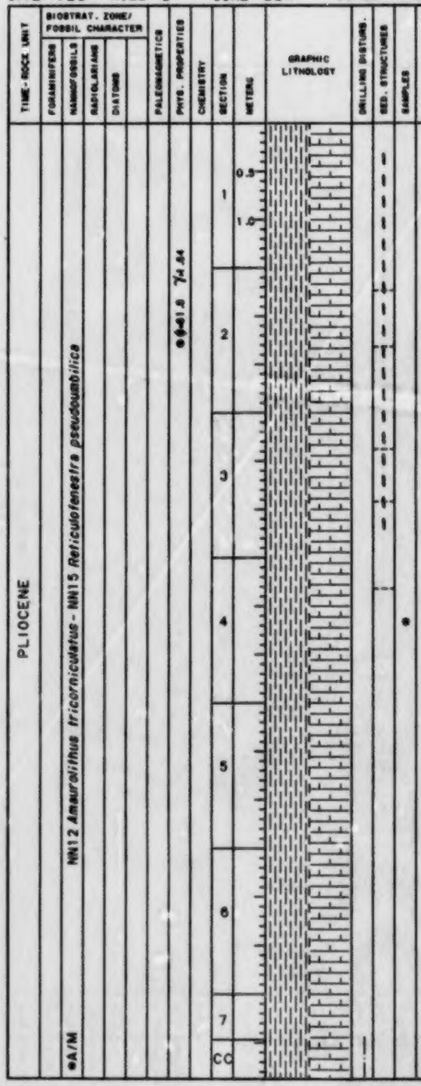
TIME-ROCK UNIT
BIOSTRAT. ZONE/ FOSSIL CHARACTER
FORAMINIFERS
NANNOFOSSILS
RADIOLARIANS
DIATOMS
PALEOMAGNETICS
PHYS. PROPERTIES
CHEMISTRY
SECTION
METERS
GRAPHIC LITHOLOGY
DRILLING DISTURB.
SED. STRUCTURES
SAMPLES
PLIOCENE
NN12 *Amaurolithus tricorniculatus* - NN15 *Reticulofenestra pseudoumbilica*
●A/M
●φ-61.8 γ1.84
0.5
1.0
1
2
3
4
5
6
7
CC

LITHOLOGIC DESCRIPTION

MARLY NANNOFOSSIL CHALK

Section 1, 0-7 cm, is disturbed. Remainder of core is slightly to moderately disturbed.

Major lithology: MARLY NANNOFOSSIL CHALK, olive (5Y 4/3, 5/3) and light olive gray (5Y 6/2). Bioturbation slight to absent; *Zoophycos* burrows present.

SMEAR SLIDE SUMMARY (%):

	4, 70 D
TEXTURE:	
Silt	15
Clay	85
COMPOSITION:	
Clay	25
Diatoms	3
Feldspar	Tr
Foraminifers	5
Inorganic calcite	8
Nannofossils	55
Quartz	2
Sponge spicules	2

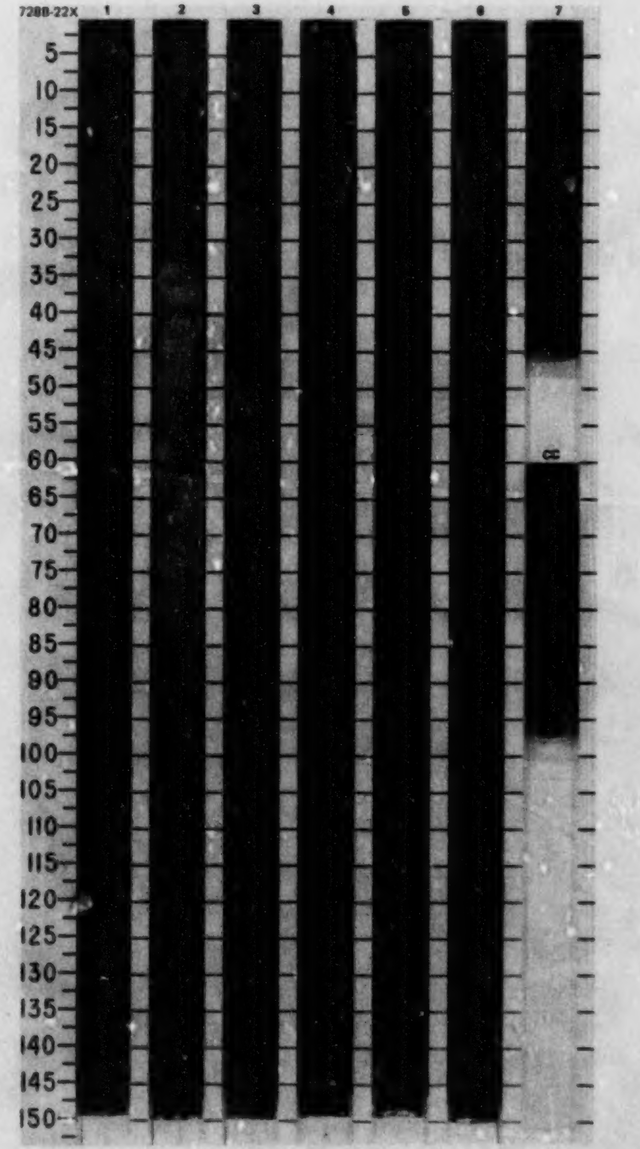
728B-22X
1
2
3
4
5
6
7
CC
5
10
15
20
25
30
35
40
45
50
55
60
65
70
75
80
85
90
95
100
105
110
115
120
125
130
135
140
145
150

SITE 728 HOLE B CORE 23X CORED INTERVAL 1630.6-1640.3 mbsl; 202.8-212.5 mbsf

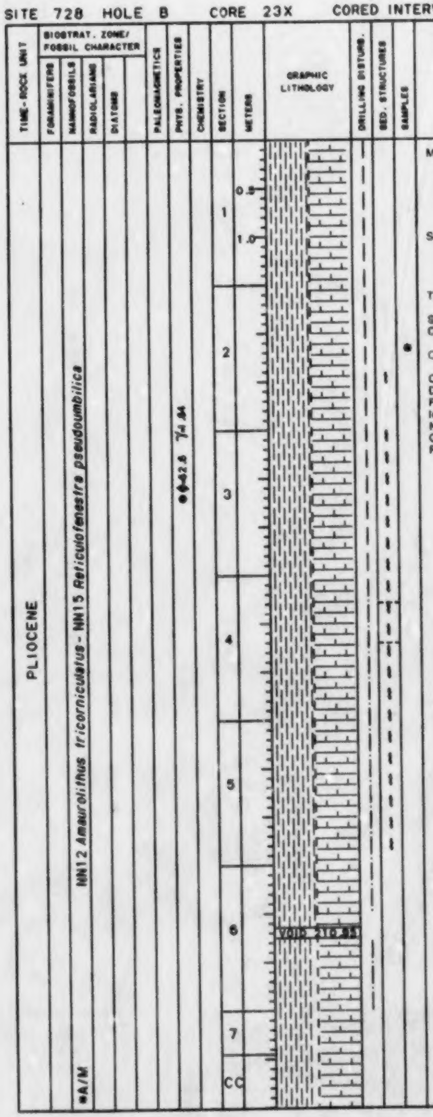
TIME-ROCK UNIT
BIOSTRAT. ZONE/ FOSSIL CHARACTER
FORAMINIFERS
NANNOFOSSILS
RADIOLARIANS
DIATOMS
PALEOMAGNETICS
PHYS. PROPERTIES
CHEMISTRY
SECTION
METERS
GRAPHIC LITHOLOGY
DRILLING DISTURB.
SED. STRUCTURES
SAMPLES
PLIOCENE
NN12 Amaurolithus tricorniculatus - NN15 Reticulofenestra pseudoumbilica
A/M
ϕ-62.6 γ-1.84
0.5
1.0
1
2
3
4
5
6
7
CC
VOID 210.85

LITHOLOGIC DESCRIPTION

MARLY NANNOFOSSIL CHALK

Slightly to moderately disturbed.

Major lithology: MARLY NANNOFOSSIL CHALK, olive (5Y 4/3). Bioturbation slight to absent.

SMEAR SLIDE SUMMARY (%):

	2, 70 D
TEXTURE:	
Silt	5
Clay	95
COMPOSITION:	
Clay	30
Diatoms	Tr
Foraminifers	3
Inorganic calcite	5
Nannofossils	60
Quartz	2
Radiolarians	Tr

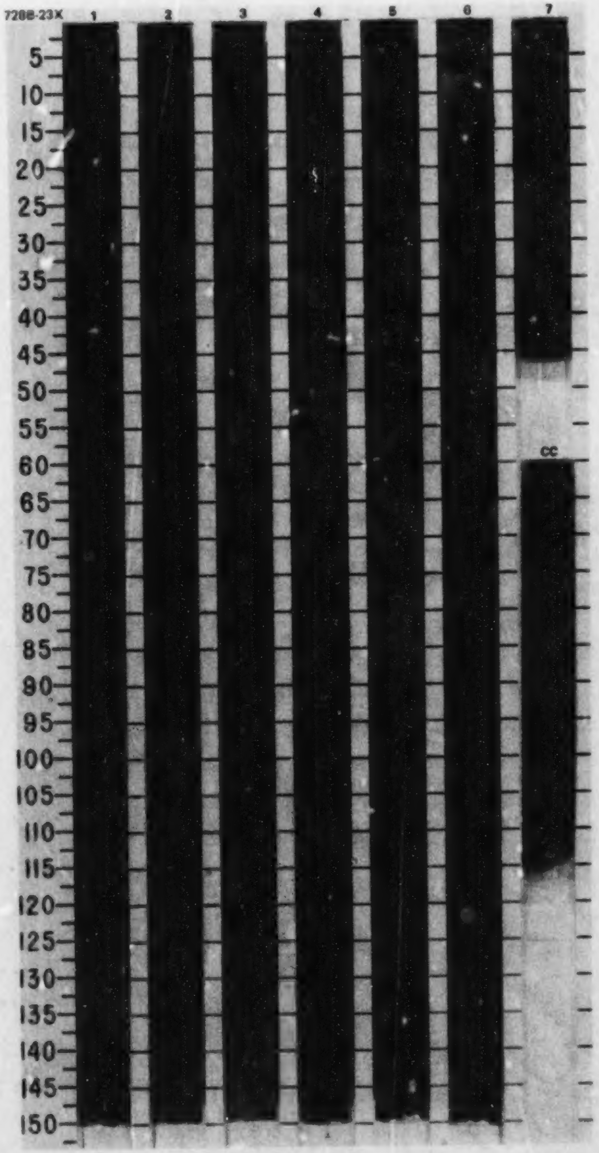
728B-23X
1
2
3
4
5
6
7
CC
5
10
15
20
25
30
35
40
45
50
55
60
65
70
75
80
85
90
95
100
105
110
115
120
125
130
135
140
145
150

SITE 728 HOLE B CORE 24X CORED INTERVAL 1640.3-1650.5 mbsl; 212.5-222.2 mbsf

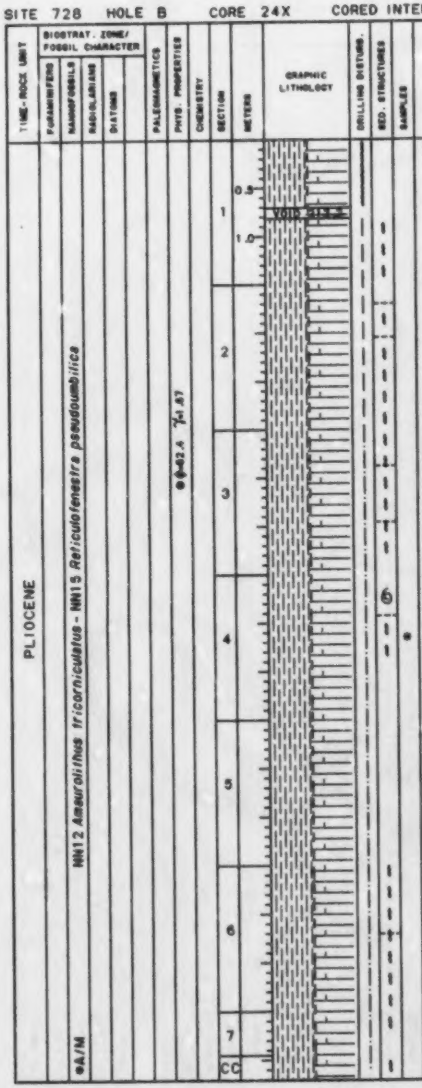
TIME-ROCK UNIT
BIOSTRAT. ZONE/ FOSSIL CHARACTER
FORAMINIFERS
NANNOFOSSILS
RADIOLARIANS
DIATOMS
PALEOMAGNETICS
PHYS. PROPERTIES
CHEMISTRY
SECTION
METERS
GRAPHIC LITHOLOGY
DRILLING DISTURB.
SED. STRUCTURES
SAMPLES
PLIOCENE
NN12 Amaurolithus tricorniculatus - NN15 Reticulofenestra pseudoumbilica
●A/M
● φ=62.4 γ=1.87
1
2
3
4
5
6
7
CC
0.5
1.0
VOID
6

LITHOLOGIC DESCRIPTION

MARLY NANNOFOSSIL CHALK

Section 1, 0-70 cm, is heavily disturbed. Void in Section 1, 70-80 cm. Remainder of core is slightly to moderately disturbed.

Major lithology: MARLY NANNOFOSSIL CHALK, olive (5Y 4/3) and olive gray (5Y 6/2). Bioturbation slight to absent.

Minor lithology: Nannofossil silty clay, dark olive gray (5Y 3/2), in Section 1, 56-150 cm.

SMEAR SLIDE SUMMARY (%):

	4, 65 D
TEXTURE:	
Silt	25
Clay	75
COMPOSITION:	
Diatoms	Tr
Foraminifers	5
Inorganic calcite	10
Mica	30
Nannofossils	48
Quartz	5
Sponge spicules	2

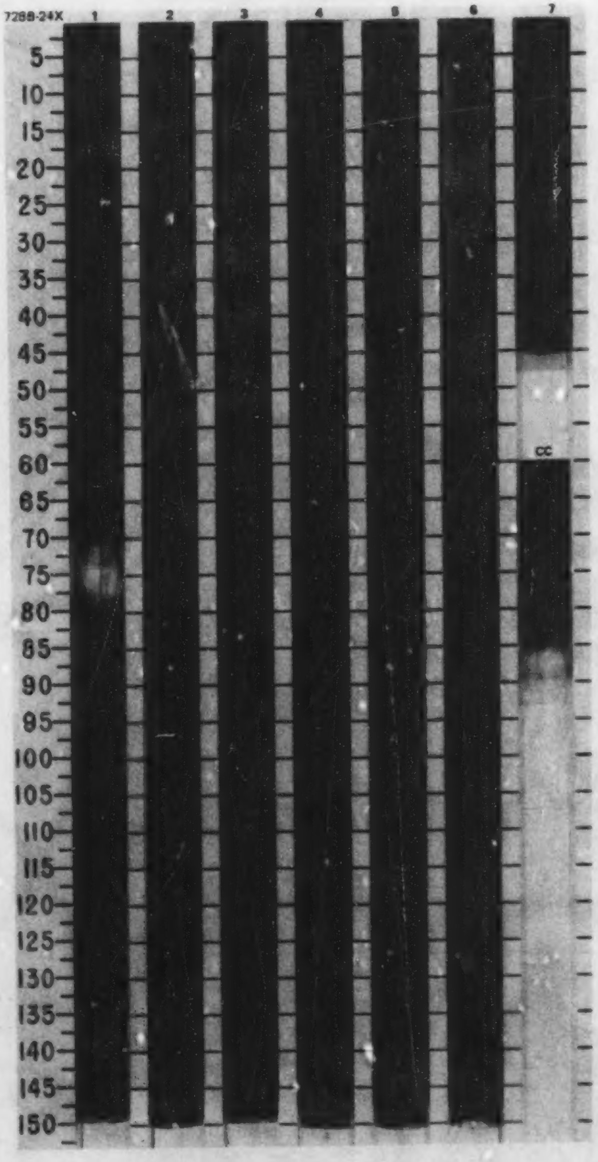
728B-24X
1
2
3
4
5
6
7
CC
5
10
15
20
25
30
35
40
45
50
55
60
65
70
75
80
85
90
95
100
105
110
115
120
125
130
135
140
145
150

SITE 728 HOLE B CORE 25X CORED INTERVAL 1650.0-1659.6 mbsl; 222.2-231.8 mbsf

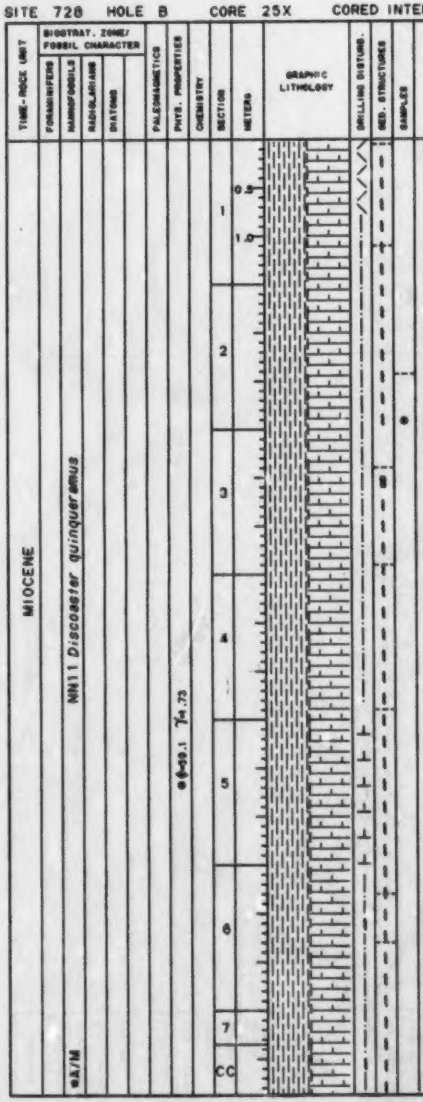
TIME-ROCK UNIT
BIOSTRAT. ZONE/ FOSSIL CHARACTER
FORAMINIFERS
NANNOFOSSILS
RADIOLARIANS
DIATOMS
PALEOMAGNETICS
PHYS. PROPERTIES
CHEMISTRY
SECTION
METERS
GRAPHIC LITHOLOGY
DRILLING DISTURB.
SED. STRUCTURES
SAMPLES
MIOCENE
NN11 Discoaster quinqueramus
AA/M
●φ-59.1 γ-1.73
1
2
3
4
5
6
7
CC
0.5
1.0

LITHOLOGIC DESCRIPTION

MARLY CALCITIC NANNOFOSSIL CHALK

Section 1, 0-75 cm, is very disturbed. Void at Section 1, 55-57 cm. Remainder of core is slightly to moderately disturbed and fractured.

Major lithology: MARLY CALCITIC NANNOFOSSIL CHALK, olive (5Y 4/3, 5/3) and olive gray (5Y 5/2). Bioturbation slight to moderate.

SMEAR SLIDE SUMMARY (%):

	2, 142 D
TEXTURE:	
Silt	35
Clay	65
COMPOSITION:	
Clay	29
Foraminifers	3
Inorganic calcite	20
Nannofossils	35
Quartz	10
Sponge spicules	1

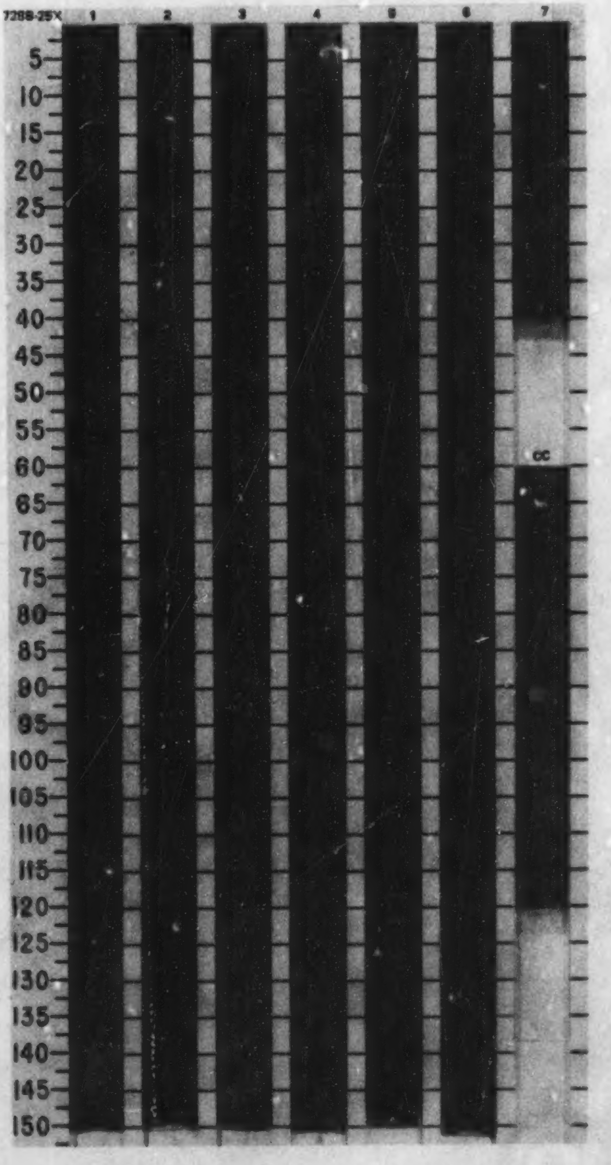
728B-25X
1
2
3
4
5
6
7
CC
5
10
15
20
25
30
35
40
45
50
55
60
65
70
75
80
85
90
95
100
105
110
115
120
125
130
135
140
145
150

SITE 728 HOLE B CORE 26X CORED INTERVAL 1659.6-1669.3 mbsl; 231.8-241.5 mbsf

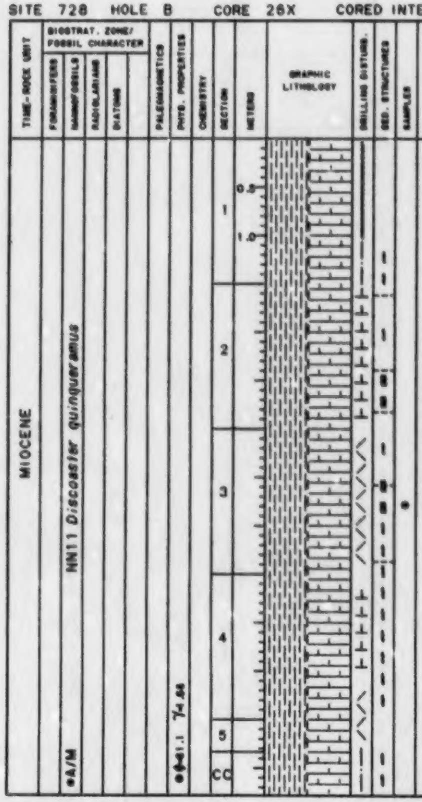
TIME-ROCK UNIT
BIOSTRAT. ZONE/ FOSSIL CHARACTER
FORAMINIFERS
NANNOFOSSILS
RADIOLARIANS
DIATOMS
PALEOMAGNETICS
PHYS. PROPERTIES
CHEMISTRY
SECTION
METERS
GRAPHIC LITHOLOGY
DRILLING DISTURB.
SED. STRUCTURES
SAMPLES
MIOCENE
NN11 Discoaster quinqueramus
●A/M
●ϕ=61.1 γ=1.94
0.5
1.0
1
2
3
4
5
CC

LITHOLOGIC DESCRIPTION

MARLY NANNOFOSSIL CHALK

Section 1, 0-110 cm, is disturbed by *in situ* water sampler. Remainder of core is moderately disturbed and fractured.

Major lithology: MARLY NANNOFOSSIL CHALK, olive (5Y 4/3, 5/3) and olive gray (5Y 5/2). Bioturbation slight to moderate.

SMEAR SLIDE SUMMARY (%):

	3, 80 D
TEXTURE:	
Silt	35
Clay	65
COMPOSITION:	
Access. minerals	5
Clay	12
Diatoms	1
Dolomite	2
Feldspar	Tr
Foraminifers	7
Inorganic calcite	15
Nannofossils	50
Quartz	6
Radiolarians	Tr
Sponge spicules	2

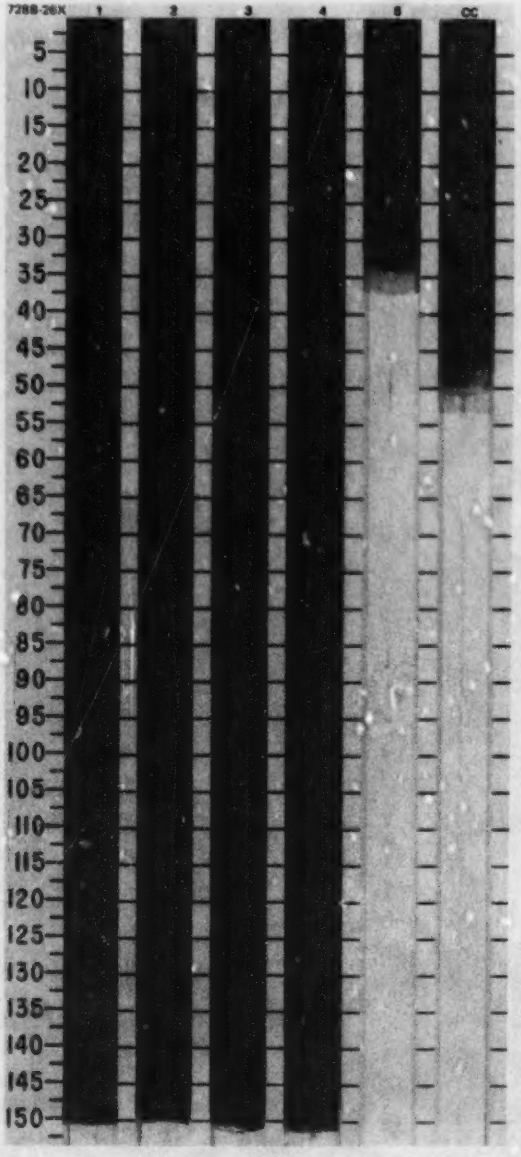
728B-26X
1
2
3
4
5
CC
5
10
15
20
25
30
35
40
45
50
55
60
65
70
75
80
85
90
95
100
105
110
115
120
125
130
135
140
145
150

SITE 728 HOLE B CORE 27X CORED INTERVAL 1669.3-1697.0 mbsl; 241.5-251.2 mbsf

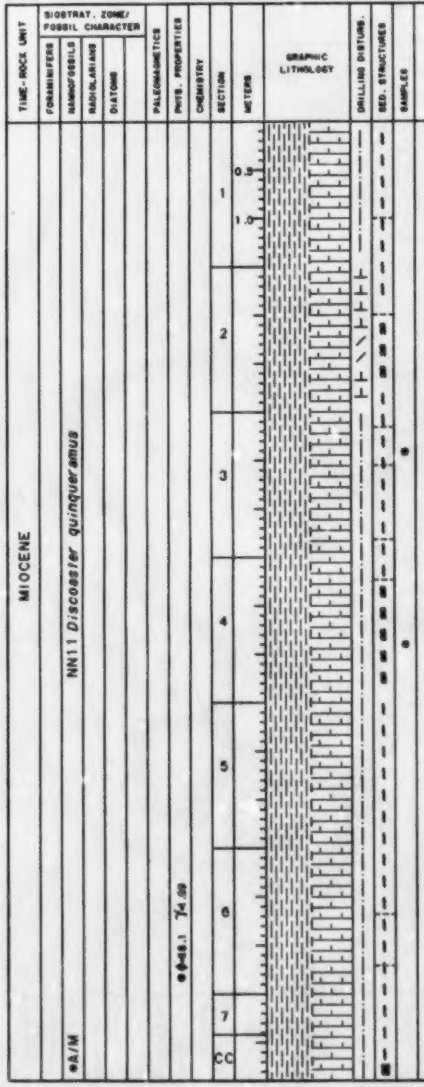
TIME-ROCK UNIT
BIOSTRAT. ZONE/ FOSSIL CHARACTER
FORAMINIFERS
NANNOFOSSILS
RADIOLARIANS
DIATOMS
PALEOMAGNETICS
PHYS. PROPERTIES
CHEMISTRY
SECTION
METERS
GRAPHIC LITHOLOGY
DRILLING DISTURB.
SED. STRUCTURES
SAMPLES
MIOCENE
NN11 Discoaster quinqueramus
A/M
●ϕ=49.1 γ=1.88
1
2
3
4
5
6
7
CC
0.5
1.0

LITHOLOGIC DESCRIPTION

MARLY NANNOFOSSIL CHALK

Section 2, 123-124 cm, is one-half filled. Remainder of core is moderately disturbed.

Major lithology: MARLY NANNOFOSSIL CHALK, olive (5Y 4/3, 5/3), light olive gray (5Y 6/2), olive gray (5Y 5/2), and dark olive gray (5Y 3/2). Alternating light and dark layers approximately 1 m thick. Bioturbation slight to moderate.

SMEAR SLIDE SUMMARY (%):

	3, 40 D	4, 90 D
TEXTURE:		
Sand	10	20
Silt	20	20
Clay	70	60
COMPOSITION:		
Access. minerals	Tr	2
Clay	30	20
Diatoms	—	Tr
Dolomite	Tr	Tr
Foraminifers	8	6
Inorganic calcite	10	20
Nannofossils	45	40
Organic debris	2	5
Quartz	5	5
Radiolarians	—	Tr
Sponge spicules	Tr	Tr

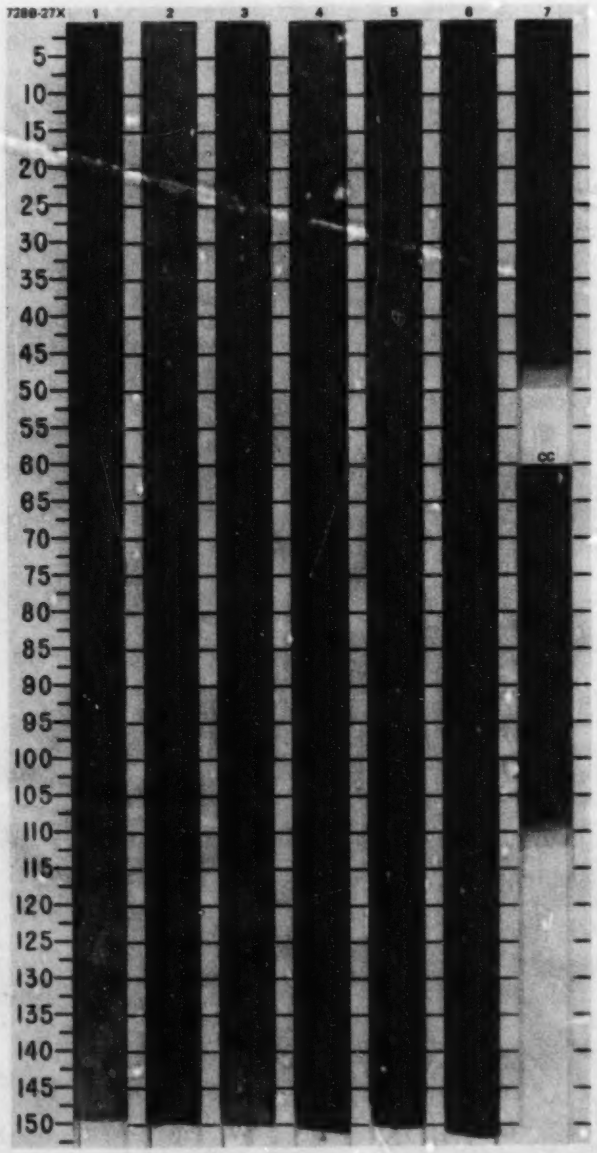
728B-27X
1
2
3
4
5
6
7
CC
5
10
15
20
25
30
35
40
45
50
55
60
65
70
75
80
85
90
95
100
105
110
115
120
125
130
135
140
145
150

SITE 728 HOLE B CORE 28X CORED INTERVAL 1679.0-1688.6 mbsl; 2512.2-260.8 mbsf

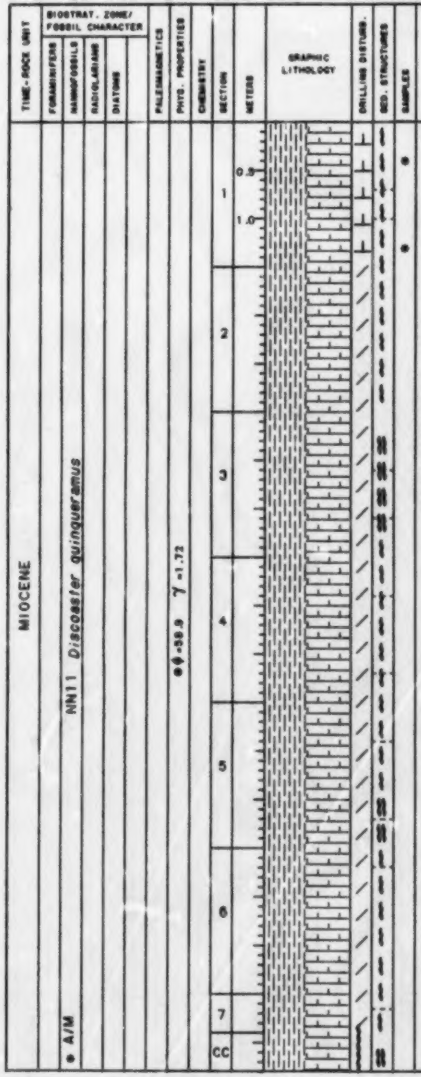
TIME-ROCK UNIT
BIOSTRAT. ZONE/ FOSSIL CHARACTER
FORAMINIFERS
NANNOFOSSILS
RADIOLARIANS
DIATOMS
PALEOMAGNETICS
PHYS. PROPERTIES
CHEMISTRY
SECTION
METERS
GRAPHIC LITHOLOGY
DRILLING DISTURB.
SED. STRUCTURES
SAMPLES
MIOCENE
● A/M
NN11 Discoaster quinqueramus
●φ=58.9 γ=1.72
1
0.5
1.0
2
3
4
5
6
7
CC

LITHOLOGIC DESCRIPTION

MARLY NANNOFOSSIL CHALK

Slight to moderate fracturing and drilling disturbance.

Major lithology: MARLY NANNOFOSSIL CHALK, olive (5Y 4/3, 5/3), olive gray (5Y 5/2, 4/2), and pale olive (5Y 6/3). Dark layers have more terrigenous silty clay than light layers. Bioturbation slight to moderate; *Zoophycos* burrows common.

SMEAR SLIDE SUMMARY (%):

	1, 43 D	1, 133 D
TEXTURE:		
Sand	—	5
Silt	10	35
Clay	90	60
COMPOSITION:		
Access. minerals	Tr	2
Clay	20	20
Dolomite	Tr	1
Feldspar	—	2
Foraminifers	2	—
Inorganic calcite	4	20
Nannofossils	70	40
Quartz	1	15
Radiolarians	1	—
Sponge spicules	2	Tr

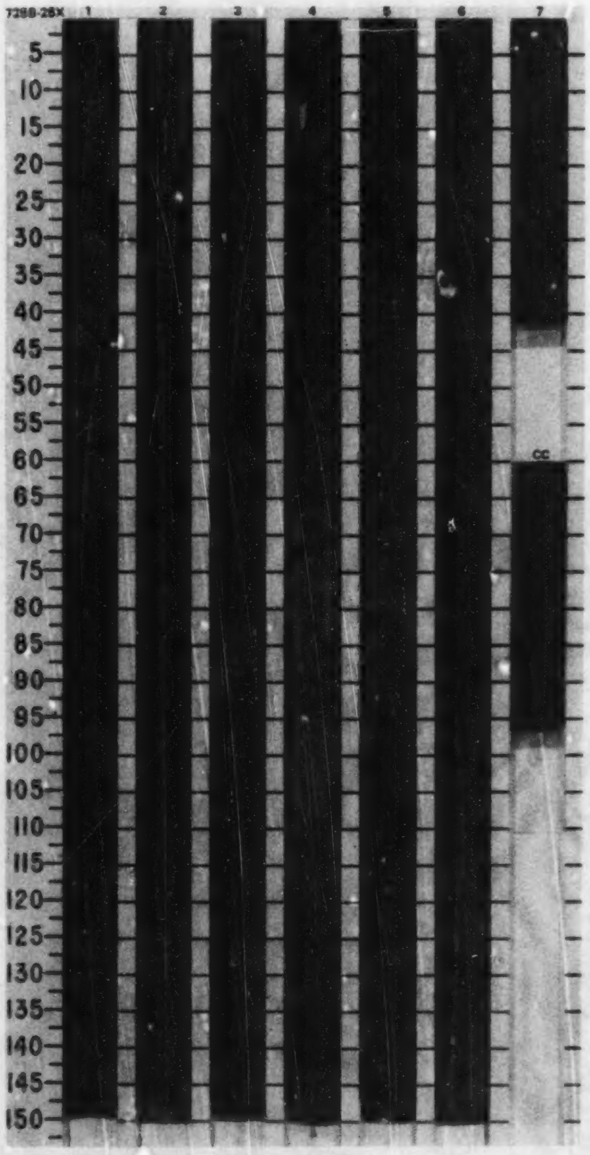
728B-28X
1
2
3
4
5
6
7
CC
5
10
15
20
25
30
35
40
45
50
55
60
65
70
75
80
85
90
95
100
105
110
115
120
125
130
135
140
145
150

SITE 728 HOLE B CORE 29X CORED INTERVAL 1688.6-1698.3 mbsl; 260.8-270.5 mbsf

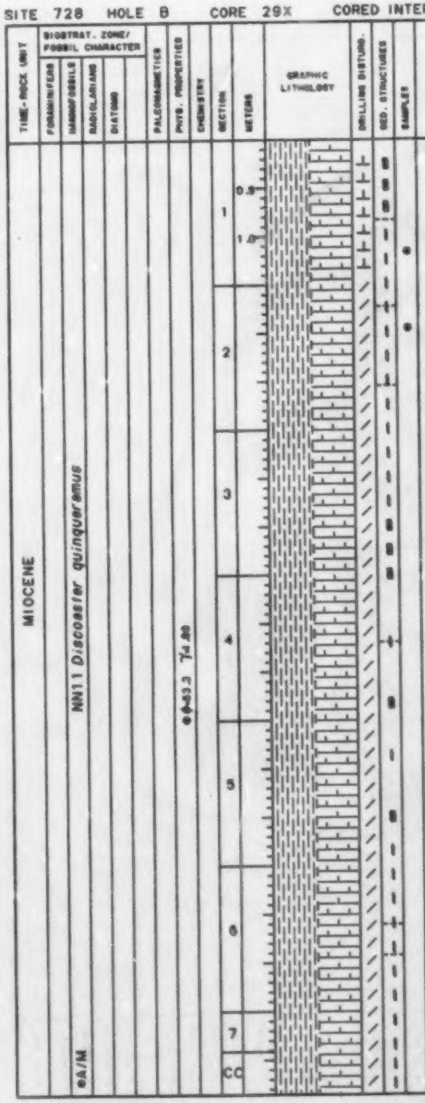
TIME-ROCK UNIT
BIOSTRAT. ZONE/ FOSSIL CHARACTER
FORAMINIFERS
NANNOFOSSILS
RADIOLARIANS
DIATOMS
PALEOMAGNETICS
PHYS. PROPERTIES
CHEMISTRY
SECTION
METERS
GRAPHIC LITHOLOGY
DRILLING DISTURB.
SED. STRUCTURES
SAMPLES
MIOCENE
NN11 Discoaster quinqueramus
●A/M
●φ=63.3 γ=1.80
0.5
1.0
1
2
3
4
5
6
7
CC

LITHOLOGIC DESCRIPTION

CALCITIC MARLY NANNOFOSSIL CHALK

Slightly to moderately disturbed and fractured.

Major lithology: CALCITIC MARLY NANNOFOSSIL CHALK, olive (5Y 4/3, 5/3) and pale olive (5Y 6/3). Bioturbation slight to moderate; *Zoophycos* and *Chondrites* burrows common.

SMEAR SLIDE SUMMARY (%):

	1, 116 D	2, 45 D
TEXTURE:		
Sand	15	20
Silt	20	30
Clay	65	50
COMPOSITION:		
Access. minerals	1	2
Clay	20	25
Dolomite	1	Tr
Feldspar	—	1
Foraminifers	—	Tr
Inorganic calcite	20	20
Mica	—	2
Nannofossils	46	35
Phosphate	Tr	Tr
Quartz	10	15
Radiolarians	Tr	Tr
Silicoflagellates	Tr	Tr
Sponge spicules	2	—

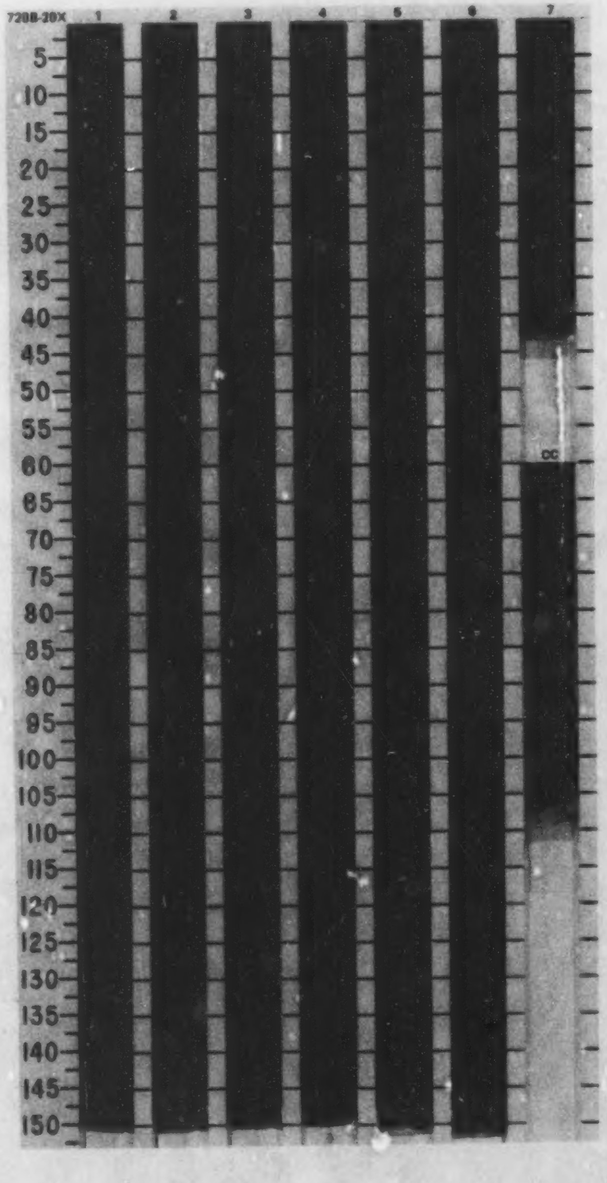
728B-29X
1
2
3
4
5
6
7
CC
5
10
15
20
25
30
35
40
45
50
55
60
65
70
75
80
85
90
95
100
105
110
115
120
125
130
135
140
145
150

SITE 728 HOLE B CORE 30X CORED INTERVAL 1698.3-1708.0 mbsl; 270.5-280.2 mbsf

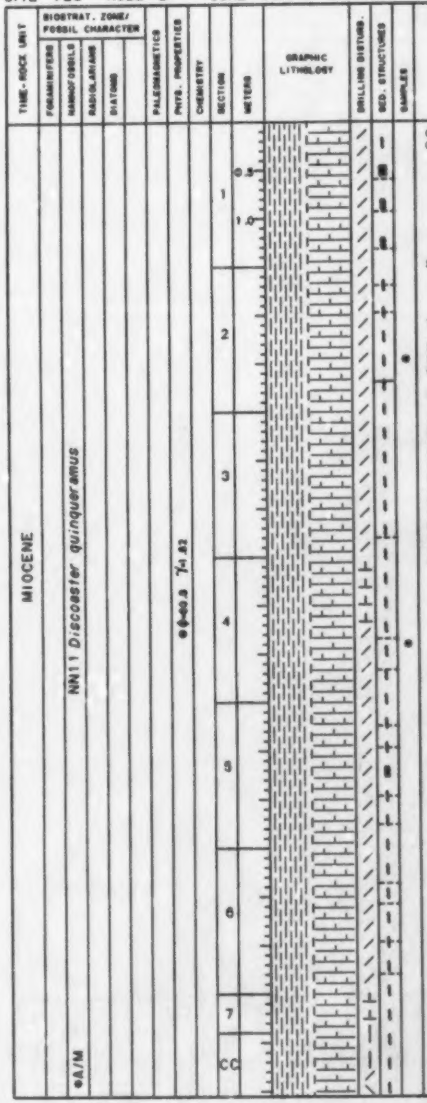
TIME-ROCK UNIT
BIOSTRAT. ZONE/ FOSSIL CHARACTER
FORAMINIFERS
NANNOFOSSILS
RADIOLARIANS
DIATOMS
PALEOMAGNETICS
PHYS. PROPERTIES
CHEMISTRY
SECTION
METERS
GRAPHIC LITHOLOGY
DRILLING DISTURB.
SED. STRUCTURES
SAMPLES
MIOCENE
NN11 Discoaster quinqueramus
●A/M
●ϕ=60.3 γ=1.82
1
2
3
4
5
6
7
CC
0.5
1.0

LITHOLOGIC DESCRIPTION

CALCITIC MARLY NANNOFOSSIL CHALK and SILICA-BEARING NANNOFOSSIL CHALK

Slightly to moderately fractured. Void at 17-24 cm in CC.

Major lithologies:
a. CALCITIC MARLY NANNOFOSSIL CHALK, olive (5Y 4/3, 5/3) and pale olive (5Y 6/3). Bioturbation slight to moderate.
b. SILICA-BEARING NANNOFOSSIL CHALK, olive gray (5Y 5/2) and light olive gray (5Y 6/2). Moderately to heavily bioturbated; *Zoophycos* burrows present.

SMEAR SLIDE SUMMARY (%):

	2, 94 D	4, 90 D
TEXTURE:		
Sand	15	5
Silt	35	15
Clay	50	80
COMPOSITION:		
Access. minerals	2	1
Clay	20	20
Diatoms	1	2
Dolomite	1	1
Feldspar	3	—
Foraminifers	Tr	2
Inorganic calcite	10	9
Mica	1	—
Nannofossils	30	60
Quartz	30	2
Radiolarians	Tr	Tr
Silicoflagellates	Tr	—
Sponge spicules	2	3

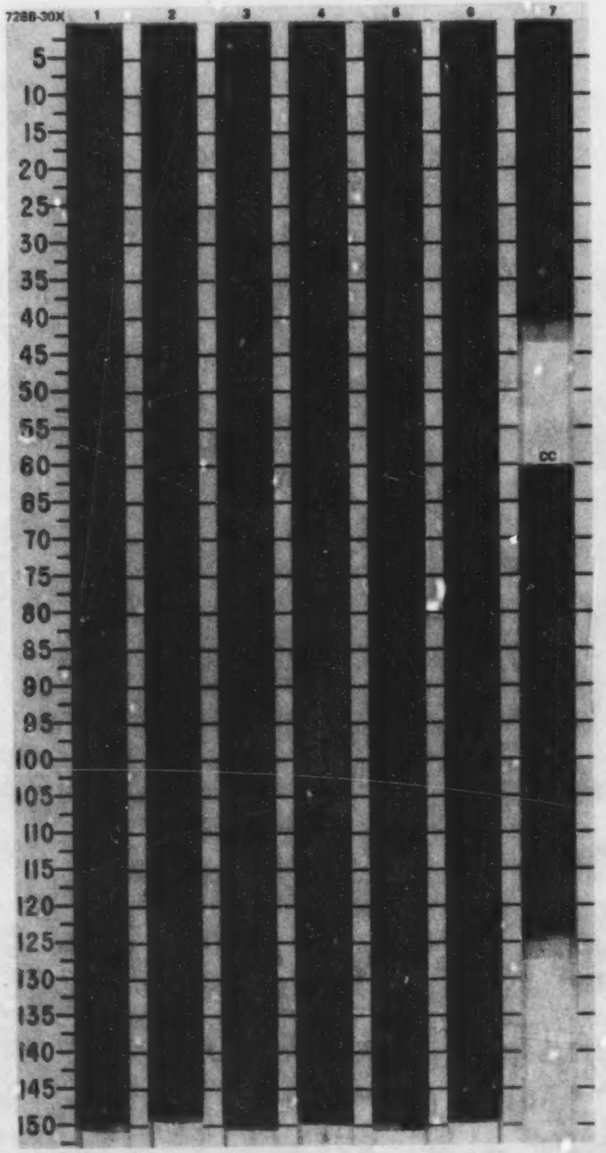
728B-30X
1
2
3
4
5
6
7
CC
5
10
15
20
25
30
35
40
45
50
55
60
65
70
75
80
85
90
95
100
105
110
115
120
125
130
135
140
145
150

SITE 728 HOLE B CORE 31X CORED INTERVAL 1708.0-1717.6 mbsl; 280.2-289.8 mbsf

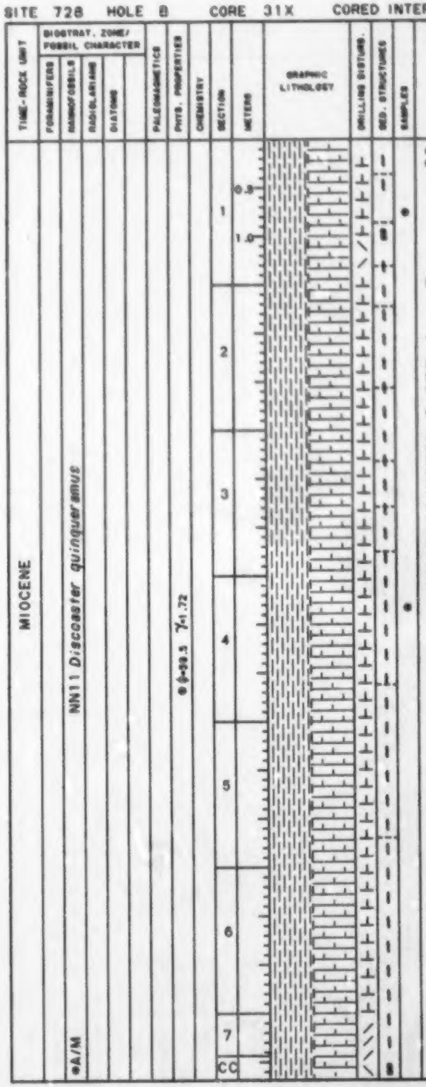
TIME-ROCK UNIT
BIOSTRAT. ZONE/ FOSSIL CHARACTER
FORAMINIFERS
NANNOFOSSILS
RADIOLARIANS
DIATOMS
PALEOMAGNETICS
PHYS. PROPERTIES
CHEMISTRY
SECTION
METERS
GRAPHIC LITHOLOGY
DRILLING DISTURB.
SED. STRUCTURES
SAMPLES
MIOCENE
NN11 Discoaster quinqueramus
●A/M
● Φ=59.5 γ=1.72
0.5
1.0
1
2
3
4
5
6
7
CC

LITHOLOGIC DESCRIPTION

CALCITIC MARLY NANNOFOSSIL CHALK and SILICA-BEARING NANNOFOSSIL CHALK

Moderately to heavily fractured.

Major lithologies:
a. CALCITIC MARLY NANNOFOSSIL CHALK, olive (5Y 4/3). Bioturbation slight to moderate.
b. SILICA-BEARING NANNOFOSSIL CHALK, olive gray (5Y 5/2) and olive (5Y 5/3). Moderately to heavily bioturbated; *Zoophycos* burrows present.

SMEAR SLIDE SUMMARY (%):

	1, 76 D	4, 32 D
TEXTURE:		
Sand	5	15
Silt	15	30
Clay	80	55
COMPOSITION:		
Access. minerals	2	2
Clay	20	20
Diatoms	—	Tr
Feldspar	—	3
Foraminifers	1	1
Volcanic glass	—	Tr
Inorganic calcite	7	17
Mica	Tr	—
Nannofossils	55	35
Quartz	10	20
Radiolarians	Tr	Tr
Silicoflagellates	1	Tr
Sponge spicules	3	2

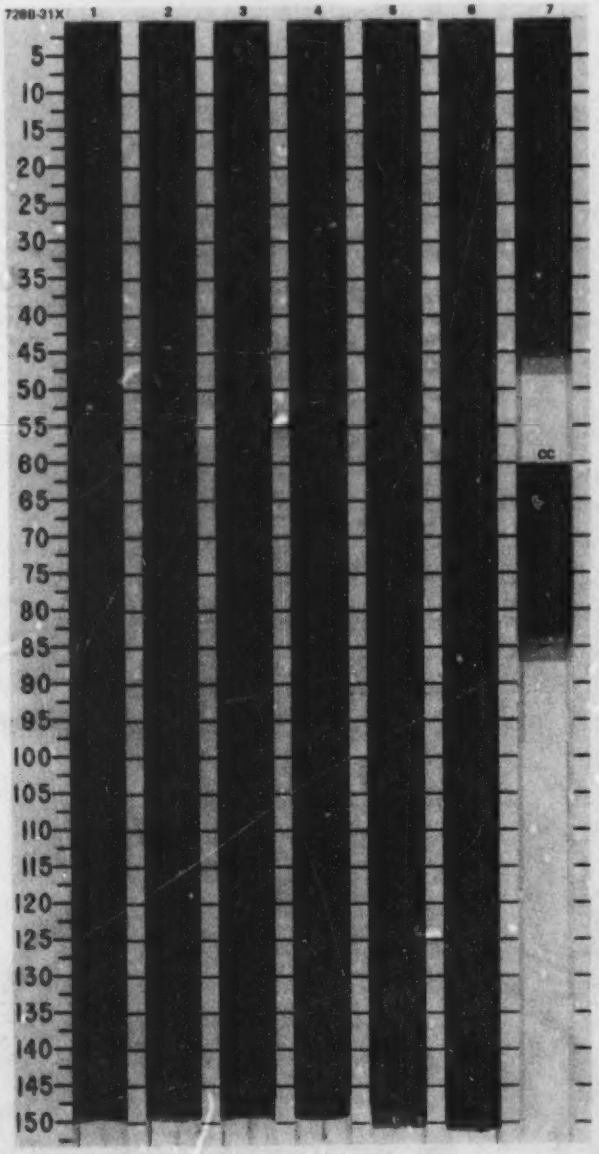
728B-31X
1
2
3
4
5
6
7
CC
5
10
15
20
25
30
35
40
45
50
55
60
65
70
75
80
85
90
95
100
105
110
115
120
125
130
135
140
145
150

SITE 728 HOLE B CORE 32X CORED INTERVAL 1717.6-1727.3 mbsl; 289.8-299.5 mbsf

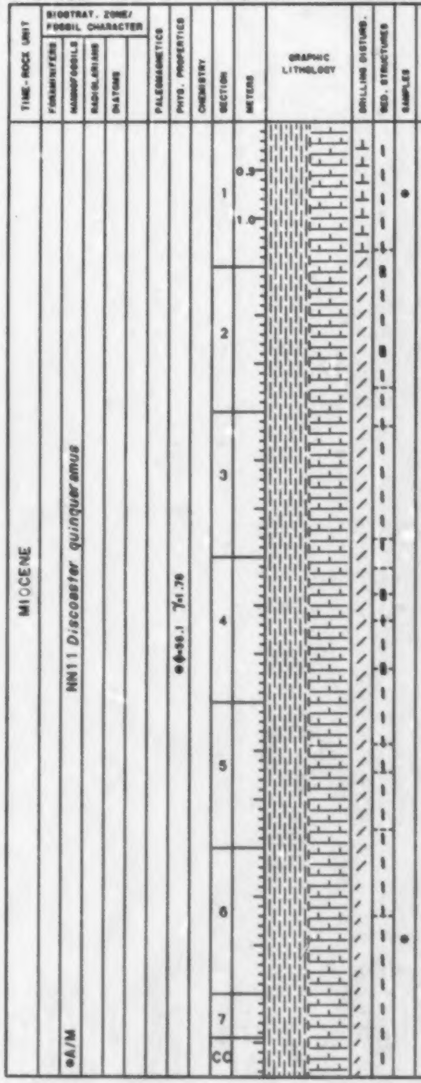
TIME-ROCK UNIT
BIOSTRAT. ZONE/ FOSSIL CHARACTER
FORAMINIFERS
NANNOFOSSILS
RADIOLARIANS
DIATOMS
PALEOMAGNETICS
PHYS. PROPERTIES
CHEMISTRY
SECTION
METERS
GRAPHIC LITHOLOGY
DRILLING DISTURB.
SED. STRUCTURES
SAMPLES
MIOCENE
NN11 Discoaster quinqueramus
●A/M
●ϕ=38.1 γ=1.76
1
2
3
4
5
6
7
CC
0.5
1.0

LITHOLOGIC DESCRIPTION

CALCITIC MARLY NANNOFOSSIL CHALK and NANNOFOSSIL CHALK

Slightly to moderately fractured.

Major lithologies:
- a. CALCITIC MARLY NANNOFOSSIL CHALK, olive (5Y 4/3, 5/3) and olive gray (5Y 5/2). Bioturbation slight to moderate; *Zoophycos* and *Chondrites* burrows common.
- b. NANNOFOSSIL CHALK, light gray (5Y 7/2) and light olive gray (5Y 6/2). Moderately bioturbated; *Planolites* burrows present.

SMEAR SLIDE SUMMARY (%):

	1, 75 D	6, 92 D
TEXTURE:		
Sand	10	—
Silt	30	10
Clay	60	90
COMPOSITION:		
Access. minerals	1	1
Carbonate	—	Tr
Clay	22	15
Diatoms	1	1
Dolomite	1	—
Foraminifers	2	—
Inorganic calcite	18	—
Nannofossils	41	80
Quartz	14	1
Radiolarians	1	1
Shell debris	Tr	—
Silicoflagellates	—	1
Sponge spicules	1	Tr

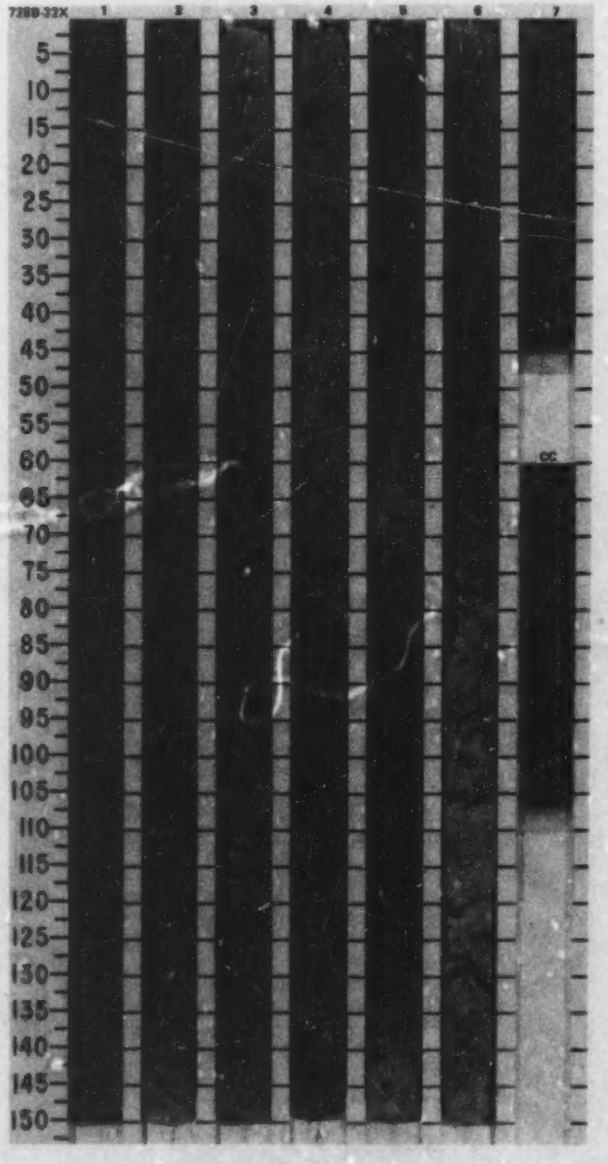
728B-32X
1
2
3
4
5
6
7
CC
5
10
15
20
25
30
35
40
45
50
55
60
65
70
75
80
85
90
95
100
105
110
115
120
125
130
135
140
145
150

SITE 728 HOLE B CORE 33X CORED INTERVAL 1727.3-1737.0 mbsl; 299.5-309.2 mbsf

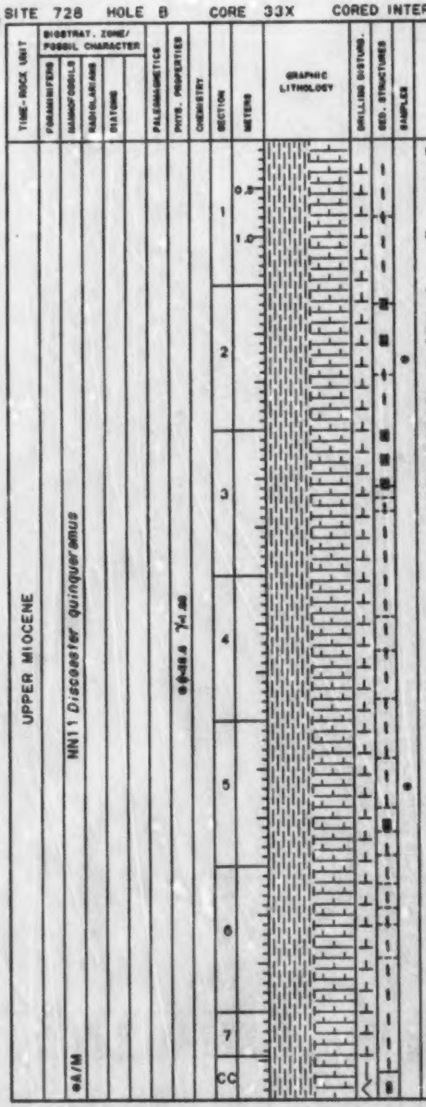
TIME-ROCK UNIT
BIOSTRAT. ZONE/ FOSSIL CHARACTER
FORAMINIFERS
NANNOFOSSILS
RADIOLARIANS
DIATOMS
PALEOMAGNETICS
PHYS. PROPERTIES
CHEMISTRY
SECTION
METERS
GRAPHIC LITHOLOGY
DRILLING DISTURB.
SED. STRUCTURES
SAMPLES
UPPER MIOCENE
NN11 Discoaster quinqueramus
●A/M
●φ=48.6 γ=1.98
0.5
1.0
1
2
3
4
5
6
7
CC

LITHOLOGIC DESCRIPTION

MARLY CALCITIC NANNOFOSSIL CHALK

Moderately to heavily fractured.

Major lithology: MARLY CALCITIC NANNOFOSSIL CHALK, olive (5Y 4/3), olive gray (5Y 5/2, 4/2), and light olive gray (5Y 6/3). Bioturbation minor.

SMEAR SLIDE SUMMARY (%):

	2, 78 D	5, 80 D
TEXTURE:		
Sand	30	—
Silt	15	10
Clay	55	90
COMPOSITION:		
Access. minerals	2	—
Clay	20	15
Diatoms	1	—
Foraminifers	—	2
Inorganic calcite	10	3
Nannofossils	35	80
Organic debris	5	—
Quartz	25	—
Radiolarians	1	Tr
Rock fragments	Tr	—
Sponge spicules	1	Tr

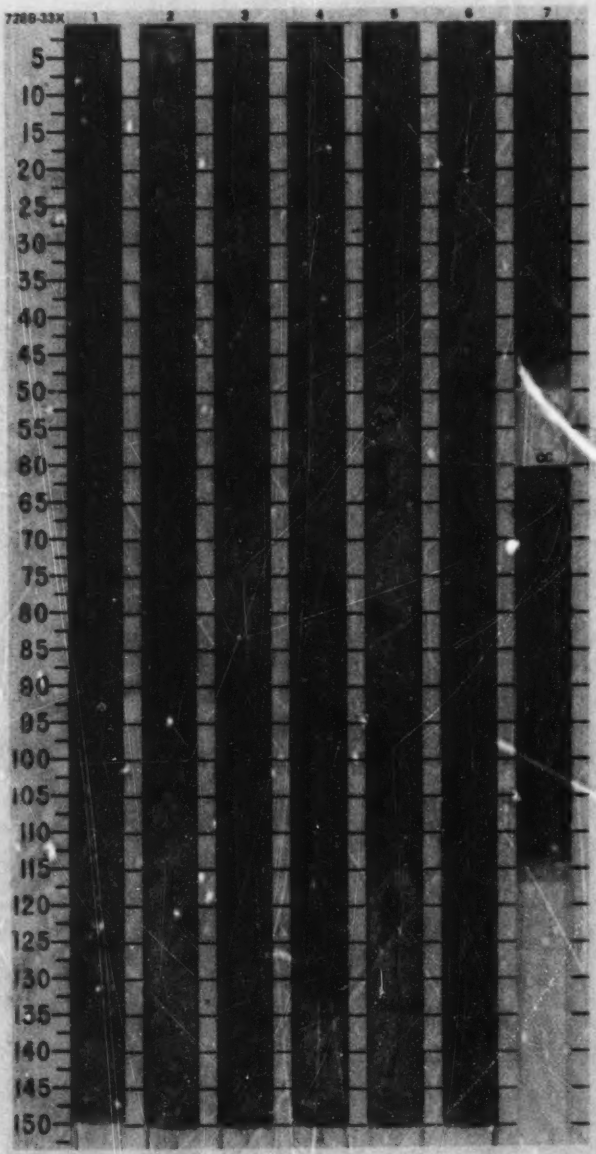
728B-33X
1
2
3
4
5
6
7
CC
5
10
15
20
25
30
35
40
45
50
55
60
65
70
75
80
85
90
95
100
105
110
115
120
125
130
135
140
145
150

SITE 728 HOLE B CORE 34X CORED INTERVAL 1737.0-1746.6 mbsl; 309.2-318.8 mbsf

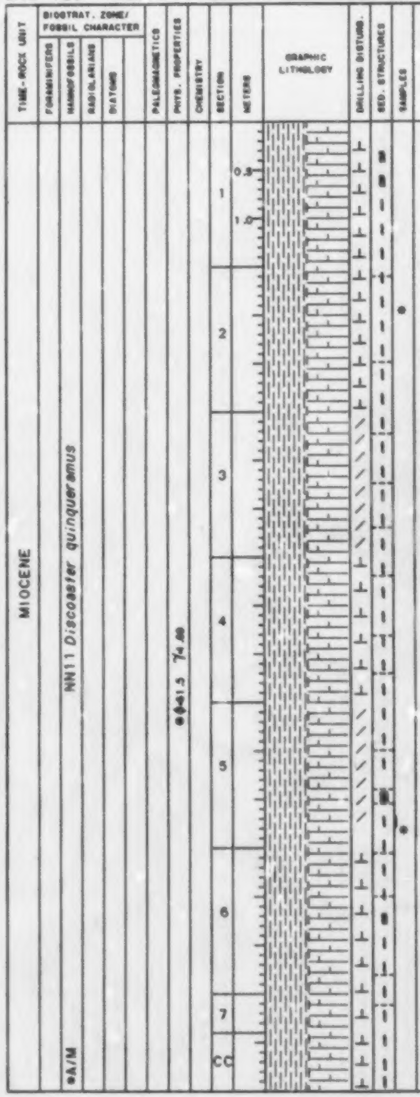
TIME-ROCK UNIT
BIOSTRAT. ZONE/ FOSSIL CHARACTER
FORAMINIFERS
NANNOFOSSILS
RADIOLARIANS
DIATOMS
PALEOMAGNETICS
PHYS. PROPERTIES
CHEMISTRY
SECTION
METERS
GRAPHIC LITHOLOGY
DRILLING DISTURB.
SED. STRUCTURES
SAMPLES
MIOCENE
NN11 Discoaster quinqueramus
●A/M
●Φ41.5 γ1.88
0.5
1.0
1
2
3
4
5
6
7
CC

LITHOLOGIC DESCRIPTION

MARLY NANNOFOSSIL CHALK and SILICA-BEARING NANNOFOSSIL CHALK

Slightly to moderately fractured.

Major lithologies:
- a. MARLY NANNOFOSSIL CHALK, olive (5Y 4/3, 5/3). Bioturbation slight to moderate.
- b. SILICA-BEARING NANNOFOSSIL CHALK, olive gray (5Y 5/2) and light olive gray (5Y 6/2). Slightly to moderately bioturbated; *Zoophycos* burrows present.

SMEAR SLIDE SUMMARY (%):

	2, 44 D	5, 134 D
TEXTURE:		
Sand	—	10
Silt	15	30
Clay	85	60
COMPOSITION:		
Access. minerals	Tr	2
Clay	20	25
Diatoms	1	1
Feldspar	—	2
Foraminifers	4	—
Inorganic calcite	5	4
Nannofossils	65	35
Organic debris	—	5
Quartz	1	25
Radiolarians	1	—
Silicoflagellates	1	—
Sponge spicules	2	1

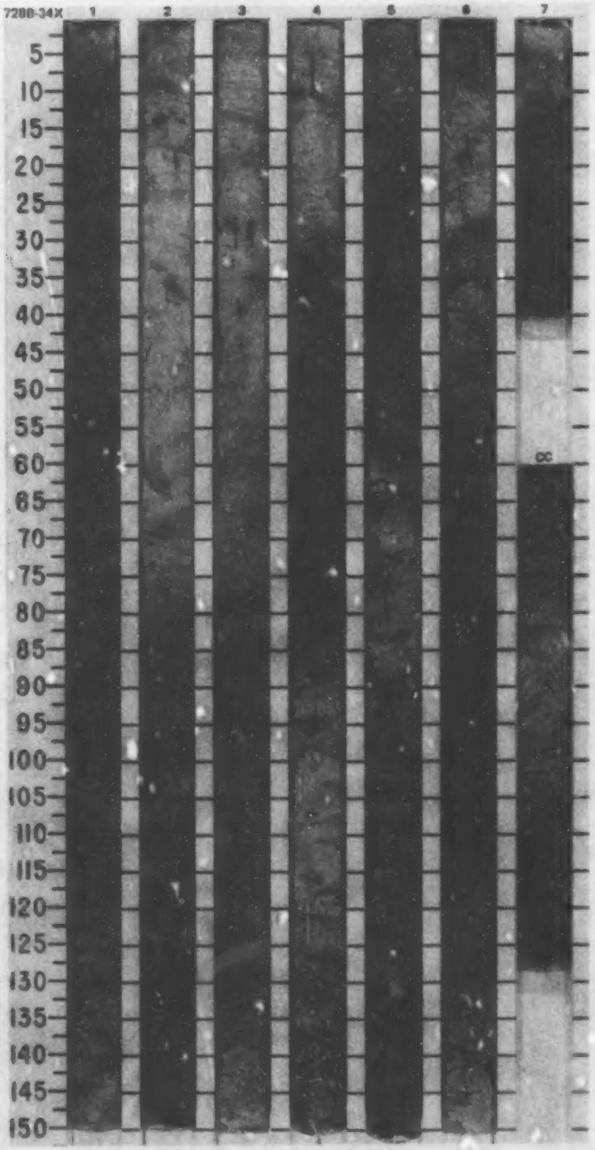
728B-34X
1
2
3
4
5
6
7
CC
5
10
15
20
25
30
35
40
45
50
55
60
65
70
75
80
85
90
95
100
105
110
115
120
125
130
135
140
145
150

SITE 728 HOLE B CORE 35X CORED INTERVAL 1746.6-1756.3 mbsl; 318.8-328.5 mbsf

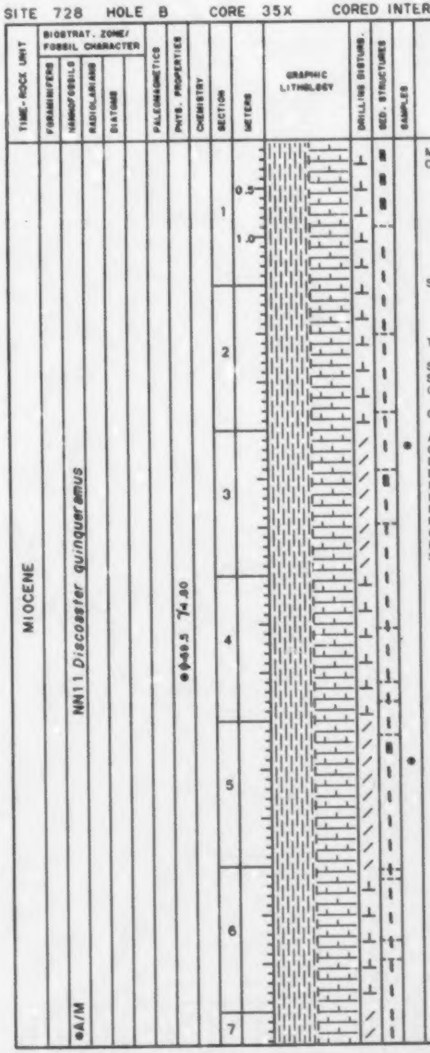
TIME-ROCK UNIT
BIOSTRAT. ZONE/ FOSSIL CHARACTER
FORAMINIFERS
NANNOFOSSILS
RADIOLARIANS
DIATOMS
PALEOMAGNETICS
PHYS. PROPERTIES
CHEMISTRY
SECTION
METERS
GRAPHIC LITHOLOGY
DRILLING DISTURB.
SED. STRUCTURES
SAMPLES
MIOCENE
NN11 Discoaster quinqueramus
●A/M
●◆60.5 γ4.80
1
2
3
4
5
6
7
0.5
1.0

LITHOLOGIC DESCRIPTION

MARLY NANNOFOSSIL CHALK and SILICA-BEARING NANNOFOSSIL SILTY CLAY

Slightly to moderately fractured.

Major lithologies:
a. MARLY NANNOFOSSIL CHALK, olive (5Y 4/3, 5/3). Bioturbation slight to moderate.
b. SILICA-BEARING NANNOFOSSIL SILTY CLAY, olive gray (5Y 5/2) and light olive gray (5Y 6/2). Bioturbation slight to moderate.

SMEAR SLIDE SUMMARY (%):

	3, 8 D	5, 41 D
TEXTURE:		
Sand	—	40
Silt	15	20
Clay	85	40
COMPOSITION:		
Access. minerals	—	4
Clay	20	20
Diatoms	Tr	3
Dolomite	Tr	—
Foraminifers	2	—
Inorganic calcite	8	14
Mica	—	3
Nannofossils	66	20
Quartz	1	35
Radiolarians	—	3
Sponge spicules	1	1

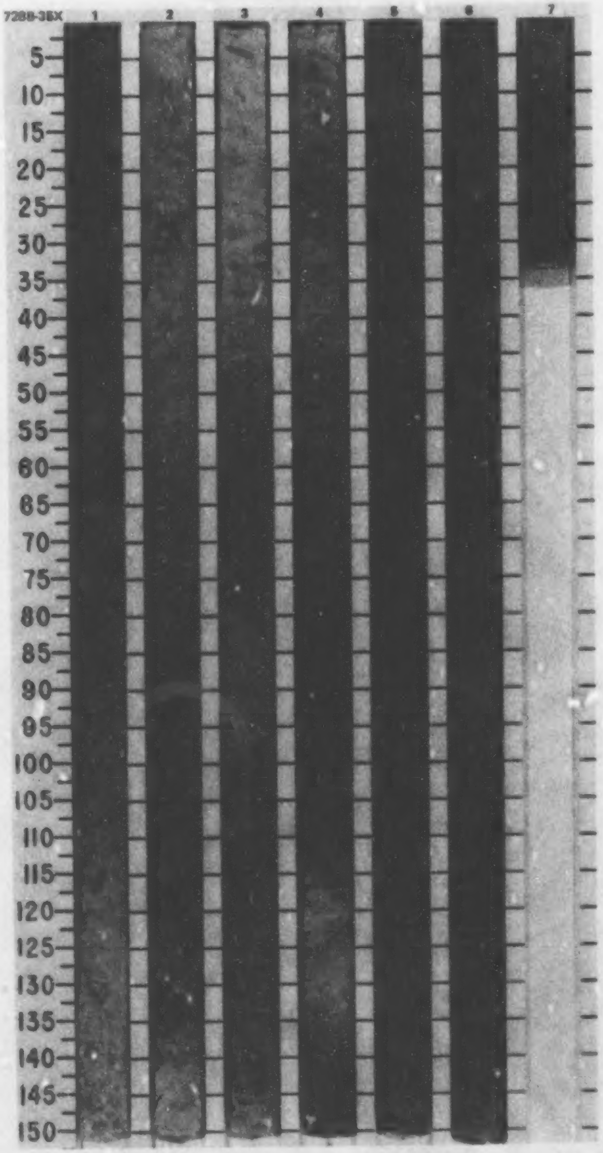
728B-35X
1
2
3
4
5
6
7
5
10
15
20
25
30
35
40
45
50
55
60
65
70
75
80
85
90
95
100
105
110
115
120
125
130
135
140
145
150

SITE 728 HOLE B CORE 36X CORED INTERVAL 1756.3-1765.9 mbsl; 328.5-338.1 mbsf

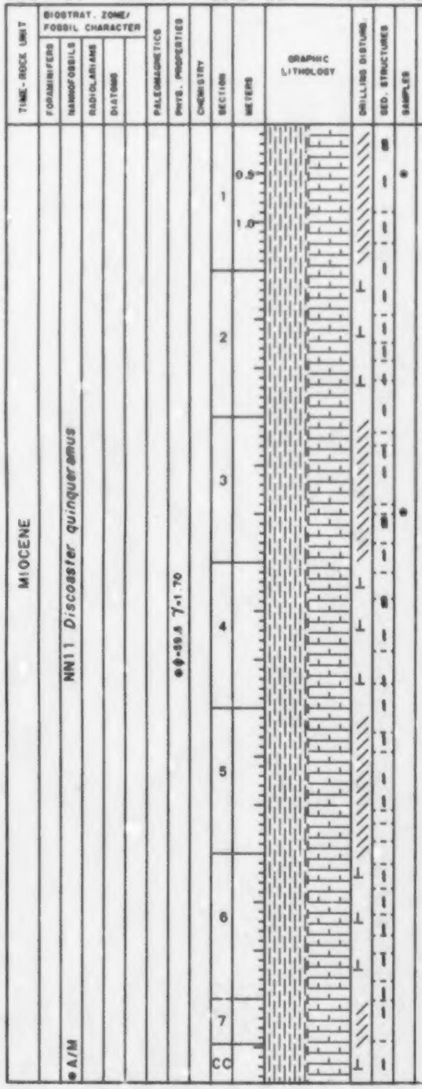
TIME-ROCK UNIT
BIOSTRAT. ZONE/ FOSSIL CHARACTER
FORAMINIFERS
NANNOFOSSILS
RADIOLARIANS
DIATOMS
PALEOMAGNETICS
PHYS. PROPERTIES
CHEMISTRY
SECTION
METERS
GRAPHIC LITHOLOGY
DRILLING DISTURB.
SED. STRUCTURES
SAMPLES
MIOCENE
NN11 Discoaster quinqueramus
●A/M
●ϕ=59.8 γ=1.70
1
2
3
4
5
6
7
CC
0.5
1.0

LITHOLOGIC DESCRIPTION

MARLY NANNOFOSSIL CHALK and DIATOMACEOUS MARLY NANNOFOSSIL CHALK

Slightly to moderately fractured.

Major lithologies:
a. MARLY NANNOFOSSIL CHALK, light olive gray (5Y 6/2) and olive gray (5Y 5/2). Bioturbation slight to moderate.
b. DIATOMACEOUS MARLY NANNOFOSSIL CHALK, olive (5Y 4/3) and olive gray (5Y 4/2). Slightly to heavily bioturbated; *Zoophycos* burrows present.

SMEAR SLIDE SUMMARY (%):

	1, 61 D	3, 98 D
TEXTURE:		
Sand	15	—
Silt	35	10
Clay	50	90
COMPOSITION:		
Access. minerals	2	—
Clay	25	20
Diatoms	10	—
Dolomite	1	—
Foraminifers	Tr	1
Inorganic calcite	10	6
Nannofossils	35	70
Quartz	15	1
Radiolarians	—	1
Silicoflagellates	1	—
Sponge spicules	1	1

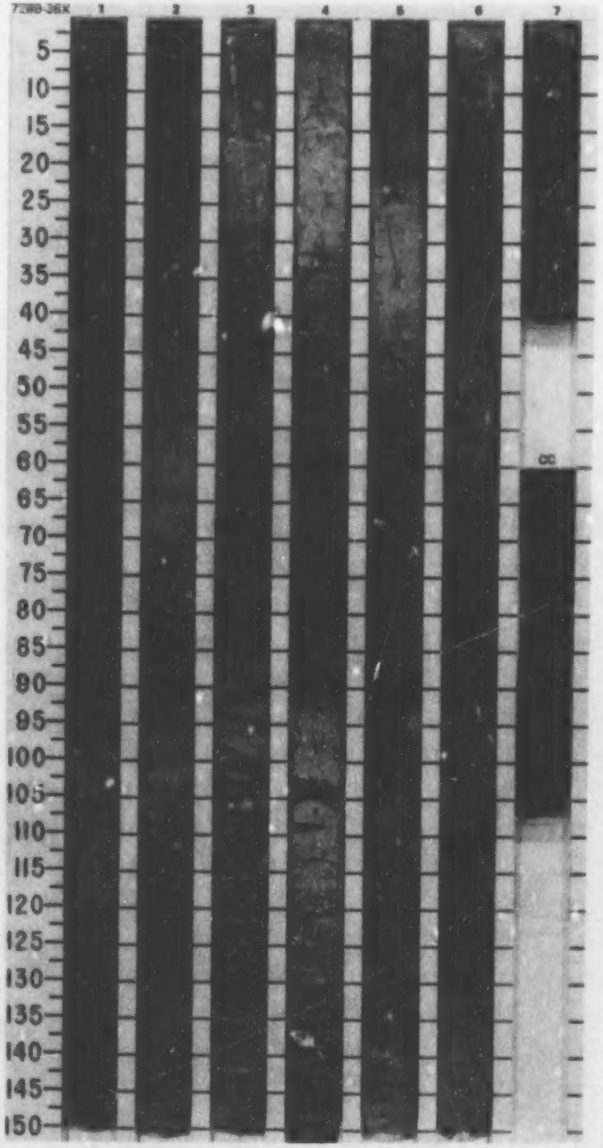
728B-36X
1
2
3
4
5
6
7
CC
5
10
15
20
25
30
35
40
45
50
55
60
65
70
75
80
85
90
95
100
105
110
115
120
125
130
135
140
145
150

SITE 728 HOLE B CORE 37X CORED INTERVAL 1765.9-1775.5 mbsl; 338.1-317.7 mbsf

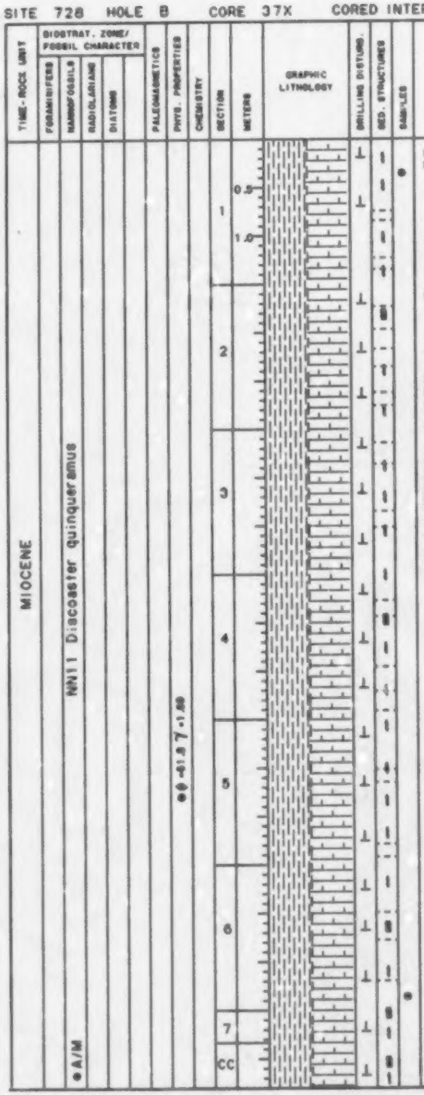
TIME-ROCK UNIT
BIOSTRAT. ZONE/ FOSSIL CHARACTER
FORAMINIFERS
NANNOFOSSILS
RADIOLARIANS
DIATOMS
PALEOMAGNETICS
PHYS. PROPERTIES
CHEMISTRY
SECTION
METERS
GRAPHIC LITHOLOGY
DRILLING DISTURB.
SED. STRUCTURES
SAMPLES
MIOCENE
NN11 Discoaster quinqueramus
● A/M
●φ-61.8 γ-1.88
1
2
3
4
5
6
7
CC
0.5
1.0

LITHOLOGIC DESCRIPTION

DIATOMACEOUS NANNOFOSSIL SILTY CLAY, alternating with MARLY NANNOFOSSIL CHALK and NANNOFOSSIL CHALK

Slightly to moderately fractured.

Major lithologies:
a. DIATOMACEOUS NANNOFOSSIL SILTY CLAY, olive (5Y 4/3, 5/3). Bioturbation slight to moderate.
b. Alternation of MARLY NANNOFOSSIL CHALK and NANNOFOSSIL CHALK, olive gray (5Y 5/2) and light olive gray (5Y 6/2) to light gray (5Y 7/2). Slightly to moderately bioturbated; Chondrites and *Planolites* burrows present.

SMEAR SLIDE SUMMARY (%):

	1, 33 D	6, 138 D
TEXTURE:		
Sand	20	—
Silt	35	10
Clay	45	90
COMPOSITION:		
Access. minerals	2	Tr
Clay	25	20
Diatoms	12	1
Dolomite	1	—
Inorganic calcite	8	8
Nannofossils	20	70
Organic debris	5	—
Quartz	25	1
Radiolarians	2	Tr
Sponge spicules	—	Tr

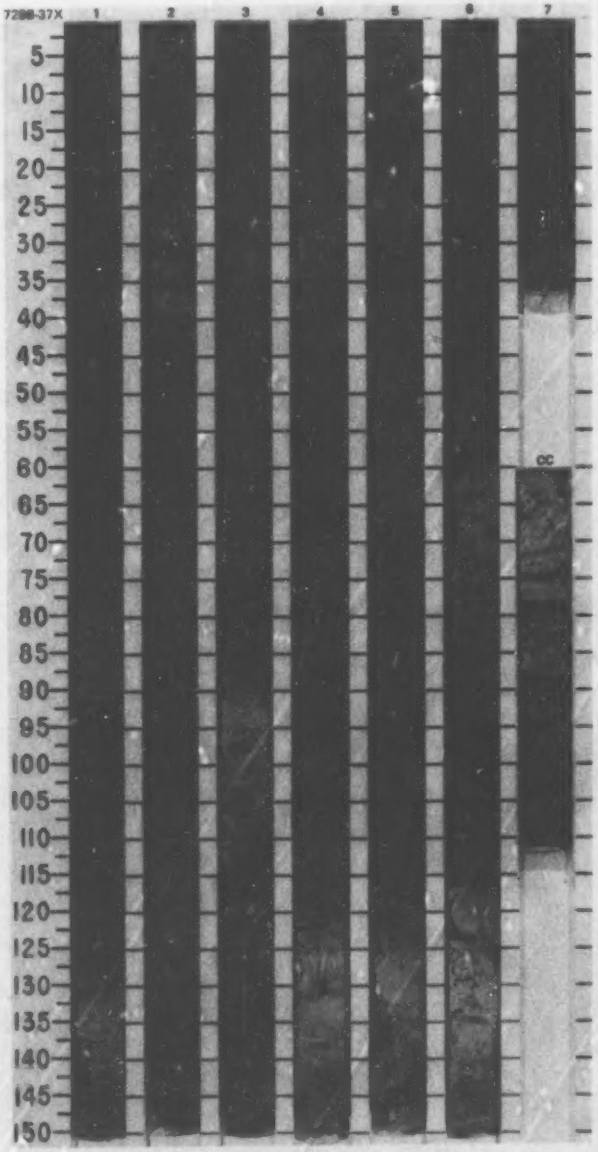
728B-37X
1
2
3
4
5
6
7
CC
5
10
15
20
25
30
35
40
45
50
55
60
65
70
75
80
85
90
95
100
105
110
115
120
125
130
135
140
145
150

SITE 729 HOLE A CORE 1R CORED INTERVAL 1398.8-1402.0 mbsl; 0.0-3.2 mbsf

TIME-ROCK UNIT	BIOSTRAT. ZONE/ FOSSIL CHARACTER: FORAMINIFERS	NANNOFOSSILS	RADIOLARIANS	DIATOMS		PALEOMAGNETICS	PHYS. PROPERTIES	CHEMISTRY	SECTION	METERS	GRAPHIC LITHOLOGY	DRILLING DISTURB.	SED. STRUCTURES	SAMPLES
PLEISTOCENE to HOLOCENE	●A/G N23	●A/G NN21 *Emiliania huxleyi*	●Barren				●ϕ=64.3 γ=1.62	●IC=8.29 OC=1.01	1 2 3 CC	0.5 1.0				● ● IW

LITHOLOGIC DESCRIPTION

MARLY FORAMINIFER-NANNOFOSSIL OOZE

Section 1, 0-75 cm, and Section 2, 25-35 cm, are soupy; remainder is very disturbed.

Major lithology: MARLY FORAMINIFER-NANNOFOSSIL OOZE, olive (5Y 5/3, 4/3). Shell fragments common.

SMEAR SLIDE SUMMARY (%):

	1, 5 D	2, 100 D
TEXTURE:		
Sand	30	10
Silt	40	20
Clay	30	70
COMPOSITION:		
Access. Minerals	1	2
Clay	30	30
Foraminifers	40	35
Inorganic Calcite	5	5
Nannofossils	24	25
Quartz	—	3

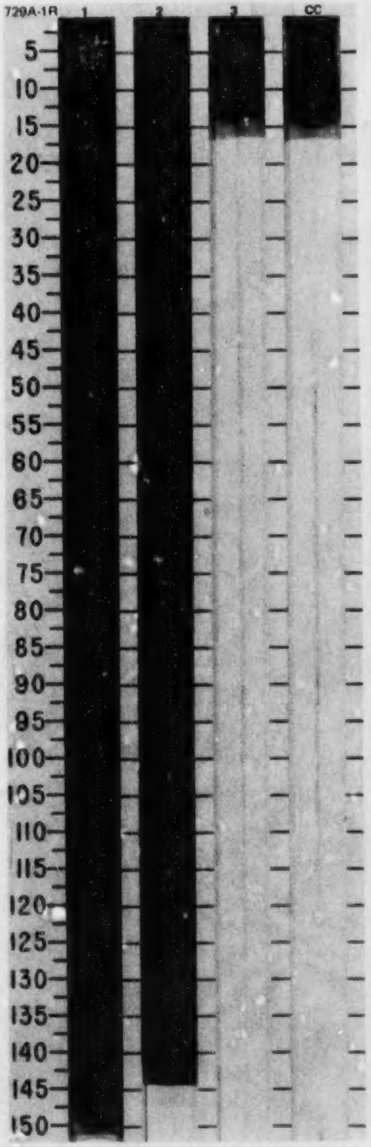
720A-1R
1
2
3
CC
5
10
15
20
25
30
35
40
45
50
55
60
65
70
75
80
85
90
95
100
105
110
115
120
125
130
135
140
145
150

SITE 729 HOLE A CORE 2R CORED INTERVAL 1402.0-1411.5 mbsl; 3.2-12.7 mbsf

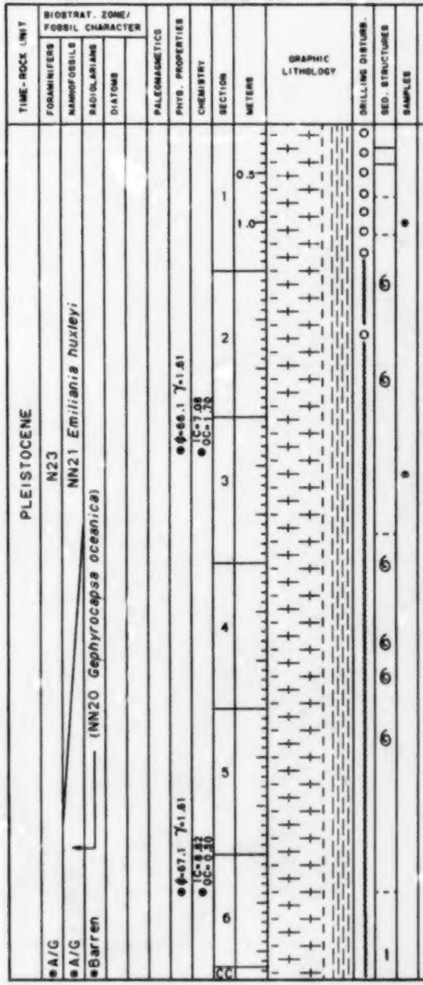
TIME-ROCK UNIT
BIOSTRAT. ZONE/ FOSSIL CHARACTER
FORAMINIFERS
NANNOFOSSILS
RADIOLARIANS
DIATOMS
PALEOMAGNETICS
PHYS. PROPERTIES
CHEMISTRY
SECTION
METERS
GRAPHIC LITHOLOGY
DRILLING DISTURB.
SED. STRUCTURES
SAMPLES
PLEISTOCENE
N23
NN21 Emiliania huxleyi
(NN20 Gephyrocapsa oceanica)
•A/G
•A/G
•Barren
•ϕ=66.1 γ=1.81
•IC=7.08 OC=1.70
•ϕ=67.1 γ=1.81
•IC=8.82 OC=0.30
1
2
3
4
5
6
CC
0.5
1.0

LITHOLOGIC DESCRIPTION

MARLY FORAMINIFER-NANNOFOSSIL OOZE

Section 1, 0-150 cm, and Section 2, 55-70 cm, are soupy; remainder is very disturbed.

Major lithology: MARLY FORAMINIFER-NANNOFOSSIL OOZE, olive gray (5Y 5/2), olive (5Y 4/3), and dark olive gray (5Y 3/2). Contacts gradational. Shell fragments common.

SMEAR SLIDE SUMMARY (%):

	1, 100 D	3, 60 D
TEXTURE:		
Sand	5	—
Silt	35	35
Clay	60	65
COMPOSITION:		
Clay	25	45
Dolomite	—	1
Feldspar	—	1
Foraminifers	30	7
Inorganic Calcite	10	17
Mica	—	1
Nannofossils	30	20
Organic Matter	—	5
Quartz	5	3

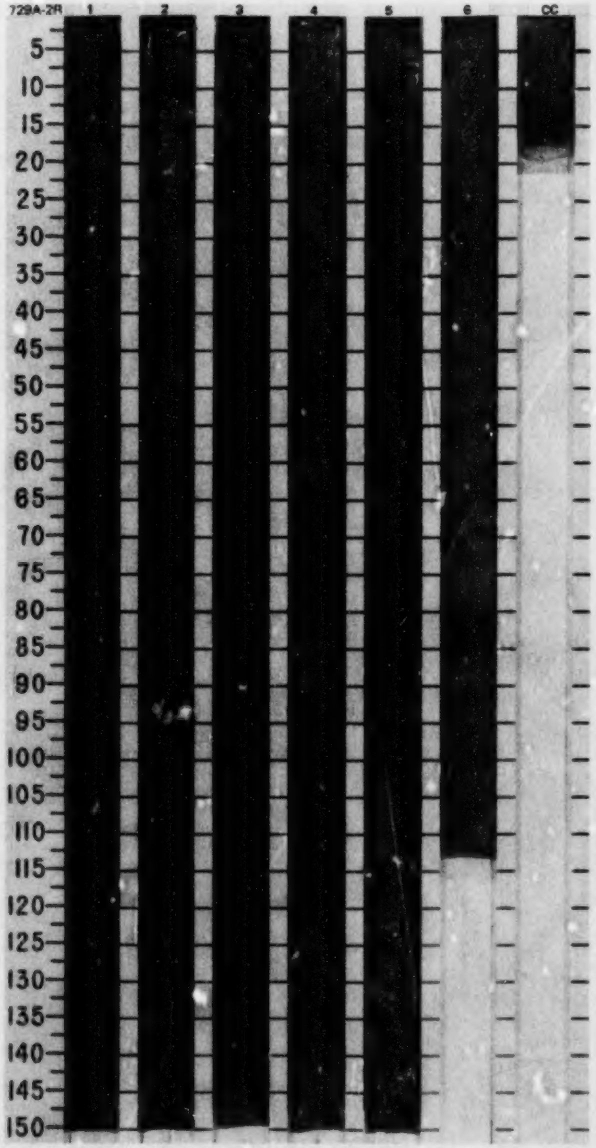
729A-2R
1
2
3
4
5
6
CC
5
10
15
20
25
30
35
40
45
50
55
60
65
70
75
80
85
90
95
100
105
110
115
120
125
130
135
140
145
150

SITE 729 HOLE A CORE 3R CORED INTERVAL 1411.5-1421.1 mbsl; 12.7-22.3 mbsf

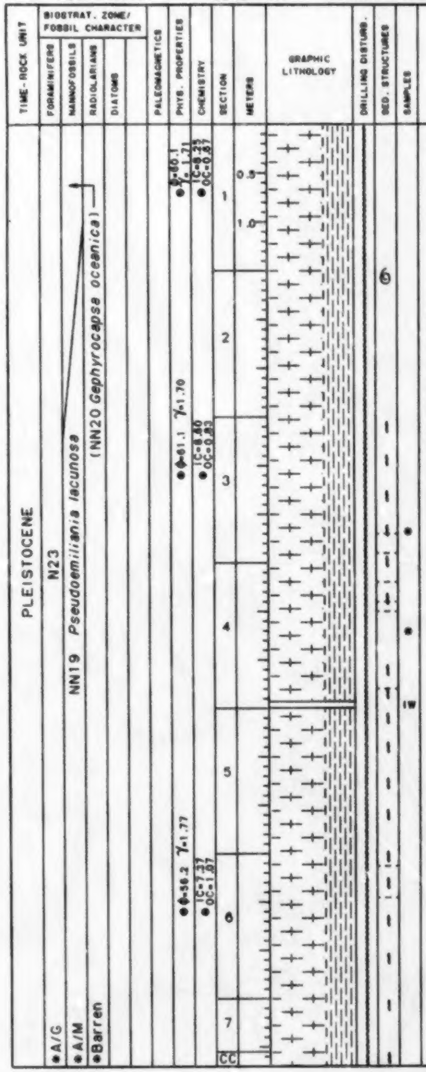
TIME-ROCK UNIT
BIOSTRAT. ZONE/ FOSSIL CHARACTER
FORAMINIFERS
NANNOFOSSILS
RADIOLARIANS
DIATOMS
PALEOMAGNETICS
PHYS. PROPERTIES
CHEMISTRY
SECTION
METERS
GRAPHIC LITHOLOGY
DRILLING DISTURB.
SED. STRUCTURES
SAMPLES
PLEISTOCENE
N23
NN19 Pseudoemiliania lacunosa
(NN20 Gephyrocapsa oceanica)
●A/G
●A/M
●Barren
●φ=60.1
●γ=1.71
●IC=8.23
OC=0.87
●φ=61.1 γ=1.70
●IC=8.60
OC=0.83
●φ=56.2 γ=1.77
●IC=7.37
OC=1.07
0.5
1.0
1
2
3
4
5
6
7
CC
IW

LITHOLOGIC DESCRIPTION

MARLY FORAMINIFER-NANNOFOSSIL OOZE

Entire core is very disturbed.

Major lithology: MARLY FORAMINIFER-NANNOFOSSIL OOZE, olive gray (5Y 5/2), olive (5Y 5/3, 4/3), and dark olive gray (5Y 3/2). Minor mottling common. Contacts gradational and mottled. Shell fragments present.

SMEAR SLIDE SUMMARY (%):

	3, 119 D	4, 72 D
TEXTURE:		
Sand	5	5
Silt	15	40
Clay	80	55
COMPOSITION:		
Clay	15	25
Dolomite	—	Tr
Foraminifers	10	10
Inorganic Calcite	10	13
Nannofossils	60	40
Quartz	5	12

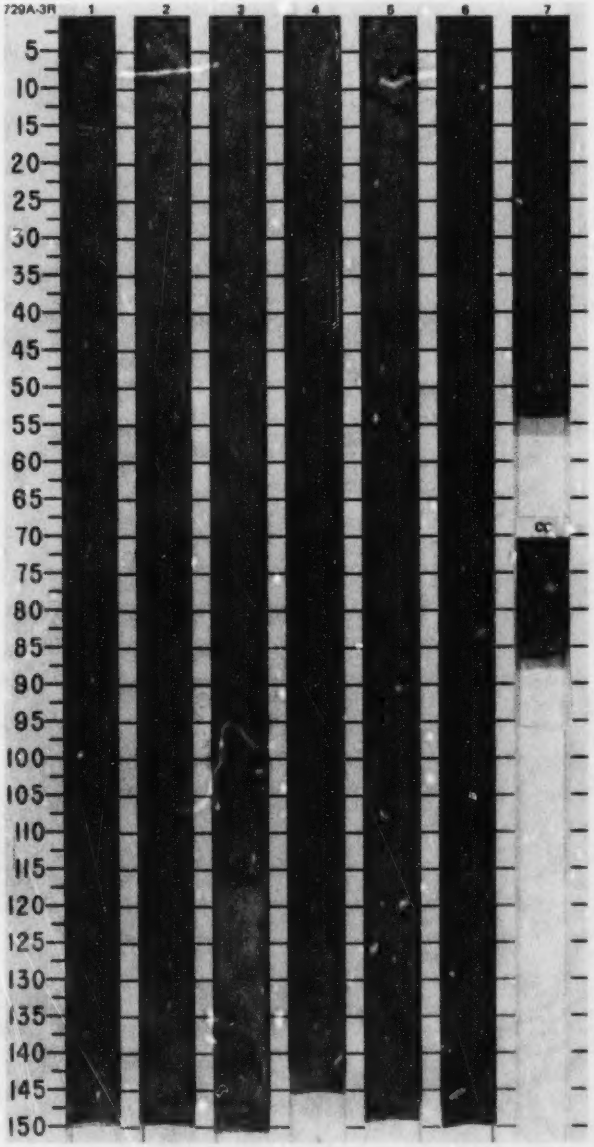
729A-3R
1
2
3
4
5
6
7
CC
5
10
15
20
25
30
35
40
45
50
55
60
65
70
75
80
85
90
95
100
105
110
115
120
125
130
135
140
145
150

SITE 729 HOLE A CORE 4R CORED INTERVAL 1421.1-1425 mbsl; 22.3-26.3 mbsf

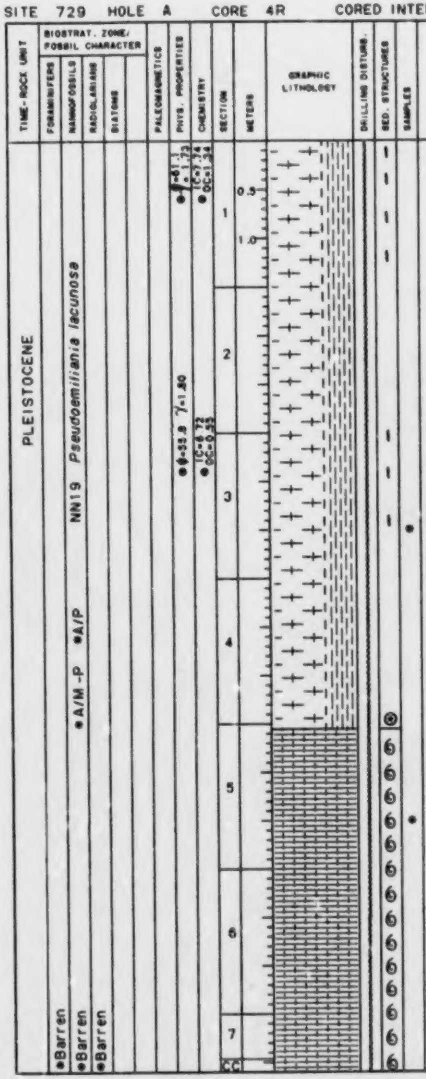
TIME-ROCK UNIT
BIOSTRAT. ZONE/ FOSSIL CHARACTER
FORAMINIFERS
NANNOFOSSILS
RADIOLARIANS
DIATOMS
PALEOMAGNETICS
PHYS. PROPERTIES
CHEMISTRY
SECTION
METERS
GRAPHIC LITHOLOGY
DRILLING DISTURB.
SED. STRUCTURES
SAMPLES
PLEISTOCENE
NN19 Pseudoemiliania lacunosa
•A/M-P •A/P
•Barren
•Barren
•Barren
φ=61.1 γ=1.73
IC=7.74 OC=1.34
φ=55.8 γ=1.80
IC=6.72 OC=0.55
0.5
1.0
1
2
3
4
5
6
7
CC

LITHOLOGIC DESCRIPTION

MARLY FORAMINIFER-NANNOFOSSIL OOZE and BENTHIC FORAMINIFER LIMESTONE

Entire core is very disturbed. Limestone is broken up by drilling, causing core to be several meters longer than core barrel was advanced.

Major lithologies:
a. MARLY FORAMINIFER-NANNOFOSSIL OOZE, olive gray (5Y 5/2), olive (5Y 5/3, 4/3), and dark olive gray (5Y 3/2). Minor mottling common. Black (5Y 2.5/1) phosphate nodule at Section 4, 145 cm.
b. BENTHIC FORAMINIFER LIMESTONE, white (5Y 8/1). Friable.

SMEAR SLIDE SUMMARY (%):

	3, 100 D	5, 100 D
TEXTURE:		
Sand	10	20
Silt	35	40
Clay	55	40
COMPOSITION:		
Access. Minerals	3	—
Bioclast	2	—
Clay	14	—
Dolomite	Tr	—
Feldspar	1	—
Foraminifers	20	30
Inorganic Calcite	15	—
Mica	Tr	—
Micrite	—	70
Nannofossils	40	—
Quartz	5	—

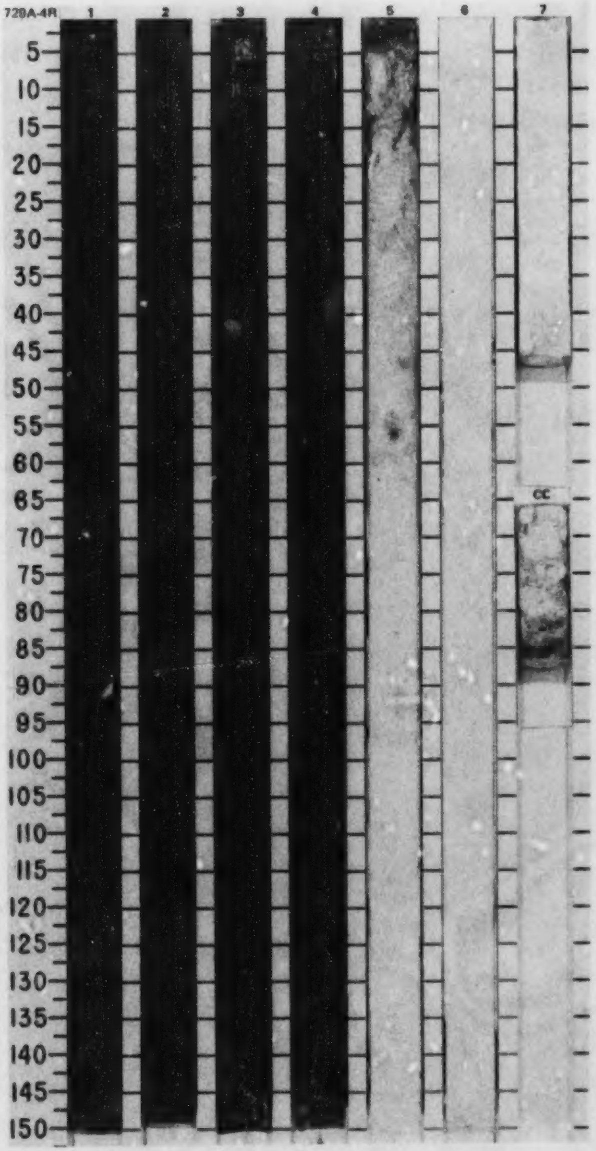
729A-4R
1
2
3
4
5
6
7
CC
5
10
15
20
25
30
35
40
45
50
55
60
65
70
75
80
85
90
95
100
105
110
115
120
125
130
135
140
145
150

CORE 117–729A–5R NO RECOVERY

CORE 117–729A–6R NO RECOVERY

CORE 117–729A–7R NO RECOVERY

CORE 117–729A–8R NO RECOVERY

CORE 117–729A–9R NO RECOVERY

SITE 729 HOLE A CORE 10R CORED INTERVAL 1469.1-1478.8 mbsl; 70.3-80.0 mbsf

TIME-ROCK UNIT	BIOSTRAT. ZONE/ FOSSIL CHARACTER				PALEOMAGNETICS	PHYS. PROPERTIES	CHEMISTRY	SECTION	METERS	GRAPHIC LITHOLOGY	DRILLING DISTURB.	SED. STRUCTURES	SAMPLES	LITHOLOGIC DESCRIPTION
	FORAMINIFERS	NANNOFOSSILS	RADIOLARIANS	DIATOMS										
?	* Barren	* Barren	* Barren					CC		▦	I	6		ONCOLITIC LIMESTONE and RED ALGAL LIMESTONE Entire core is very disturbed. Major lithology: ONCOLITIC LIMESTONE and RED ALGAL LIMESTONE, white (5Y 8/1).

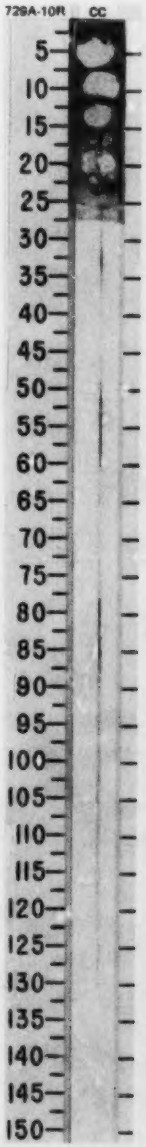
729A-10R
CC
5
10
15
20
25
30
35
40
45
50
55
60
65
70
75
80
85
90
95
100
105
110
115
120
125
130
135
140
145
150

CORE 117–729A–11R NO RECOVERY

CORE 117–729A–12R NO RECOVERY

CORE 117–729A–13R NO RECOVERY

SITE 730 HOLE A CORE 1H CORED INTERVAL 1065.8-1074.1 mbsl; 0.0-8.3 mbsf

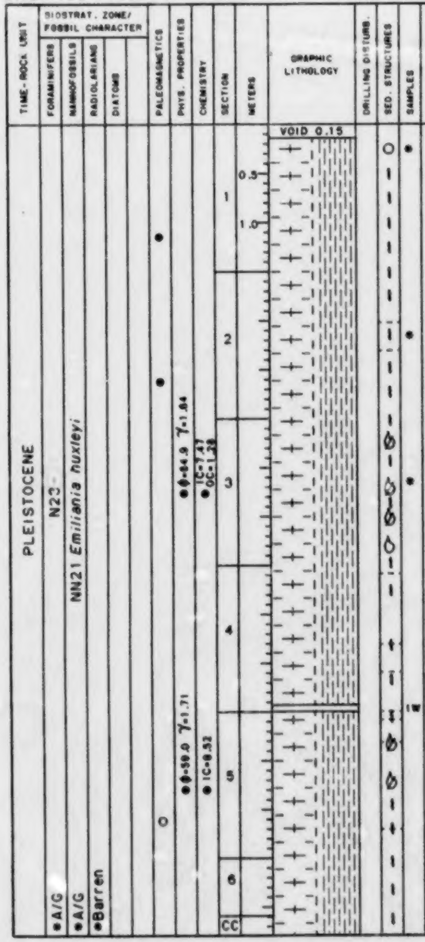
TIME-ROCK UNIT
BIOSTRAT. ZONE/ FOSSIL CHARACTER
FORAMINIFERS
NANNOFOSSILS
RADIOLARIANS
DIATOMS
PALEOMAGNETICS
PHYS. PROPERTIES
CHEMISTRY
SECTION
METERS
GRAPHIC LITHOLOGY
DRILLING DISTURB.
SED. STRUCTURES
SAMPLES
PLEISTOCENE
N23
NN21 Emiliania huxleyi
●A/G
●A/G
●Barren
●φ=64.9 γ=1.84
●φ=59.0 γ=1.71
●TC=7.47 OC=1.28
●IC=8.52
1
2
3
4
5
6
CC
0.5
1.0
VOID 0.15
IW

LITHOLOGIC DESCRIPTION

MARLY FORAMINIFER-NANNOFOSSIL OOZE

Section 1, 15-35 cm, is soupy; remainder is undisturbed.

Major lithologies: MARLY FORAMINIFER-NANNOFOSSIL OOZE, olive (5Y 5/3, 4/3) and olive gray (5Y 5/2). Minor burrow mottling throughout. Contacts gradational and mottled. Shell fragments common; echinoid spines and scaphopods visible.

SMEAR SLIDE SUMMARY (%):

	1, 27 M	2, 65 M	3, 65 D
TEXTURE:			
Sand	15	15	8
Silt	50	35	62
Clay	35	50	30
COMPOSITION:			
Access. minerals	5	2	5
Clay	15	25	15
Diatoms	Tr	—	—
Dolomite	2	Tr	3
Feldspar	—	—	1
Foraminifers	45	30	30
Inorganic calcite	10	5	20
Mica	—	3	1
Nannofossils	20	30	15
Quartz	3	5	10
Sponge spicules	Tr	Tr	

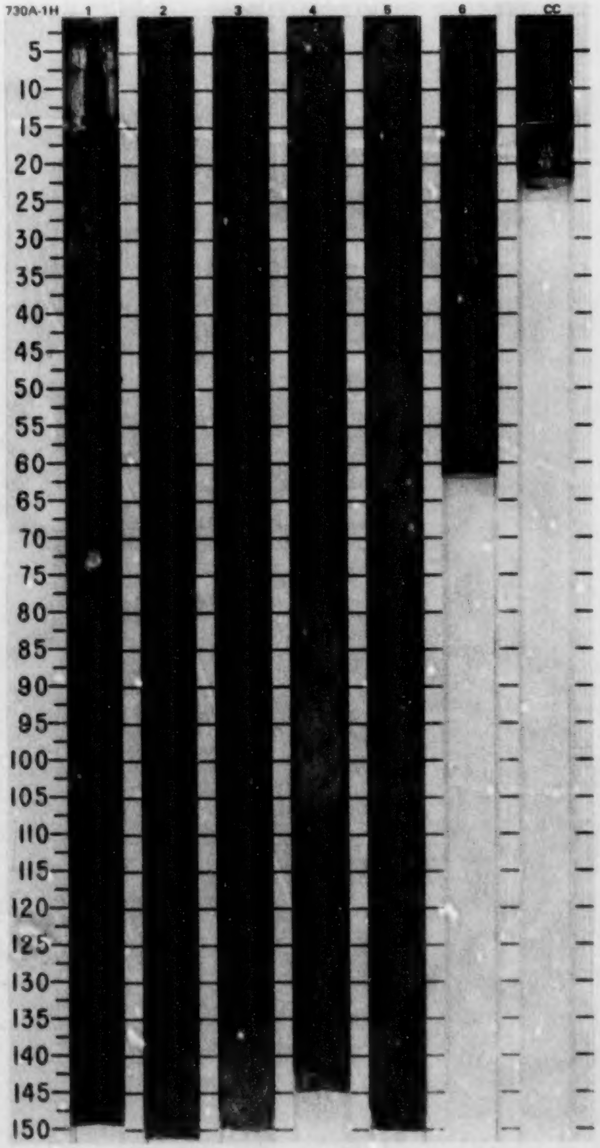
730A-1H
1
2
3
4
5
6
CC
5
10
15
20
25
30
35
40
45
50
55
60
65
70
75
80
85
90
95
100
105
110
115
120
125
130
135
140
145
150

SITE 730 HOLE A CORE 2H CORED INTERVAL 1074.1-1083.6 mbsl; 8.3-17.8 mbsf

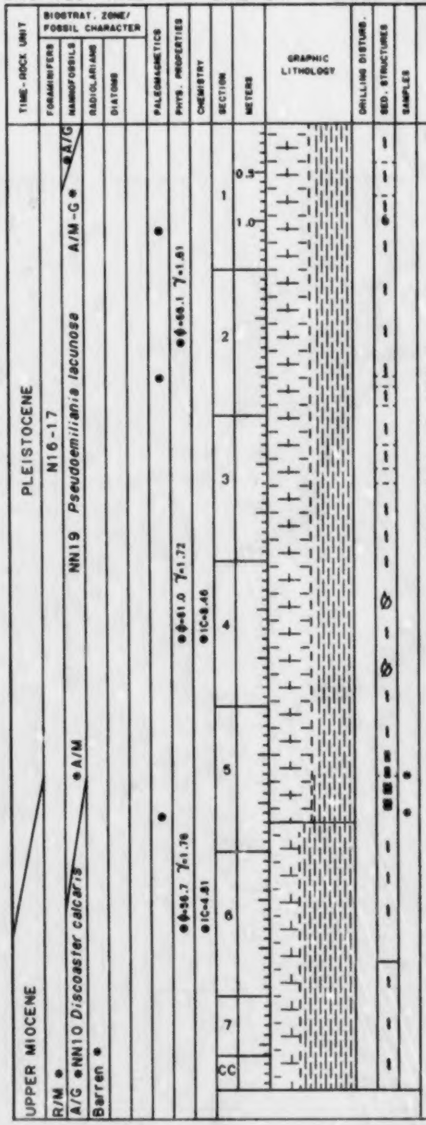
TIME-ROCK UNIT
BIOSTRAT. ZONE/ FOSSIL CHARACTER
FORAMINIFERS
NANNOFOSSILS
RADIOLARIANS
DIATOMS
PALEOMAGNETICS
PHYS. PROPERTIES
CHEMISTRY
SECTION
METERS
GRAPHIC LITHOLOGY
DRILLING DISTURB.
SED. STRUCTURES
SAMPLES
PLEISTOCENE
UPPER MIOCENE
N16-17
R/M ●
NN19 Pseudoemiliania lacunosa
A/M-G ●
●A/G
●A/M
A/G ●NN10 Discoaster calcaris
Barren ●
●φ=60.1 γ=1.81
●φ=61.0 γ=1.72
●φ=56.7 γ=1.76
●IC=8.46
●IC=4.81
0.5
1.0
1
2
3
4
5
6
7
CC

LITHOLOGIC DESCRIPTION

MARLY FORAMINIFER-NANNOFOSSIL OOZE and MARLY NANNOFOSSIL OOZE

Entire core undisturbed.

Major lithologies:

a. MARLY FORAMINIFER-NANNOFOSSIL OOZE, olive (5Y 4/3) and olive gray (5Y 5/2). Minor burrow mottling throughout. Contacts gradational and mottled. Solitary coral visible (in working half).

b. Section 5, 121 cm, to base of core: MARLY NANNOFOSSIL OOZE, olive (5Y 4/3) and olive gray (5Y 5/2). Minor burrow mottling throughout. Contacts gradational and mottled; contact between major lithologies strongly mottled.

SMEAR SLIDE SUMMARY (%):

	5, 70 D	5, 100 D
TEXTURE:		
Sand	10	—
Silt	55	40
Clay	35	60
COMPOSITION:		
Access. minerals.	5	3
Clay	16	22
Dolomite	1	Tr
Foraminifers	20	5
Inorganic calcite	20	15
Mica	3	—
Nannofossils	20	40
Pyrite	—	5
Quartz	15	10

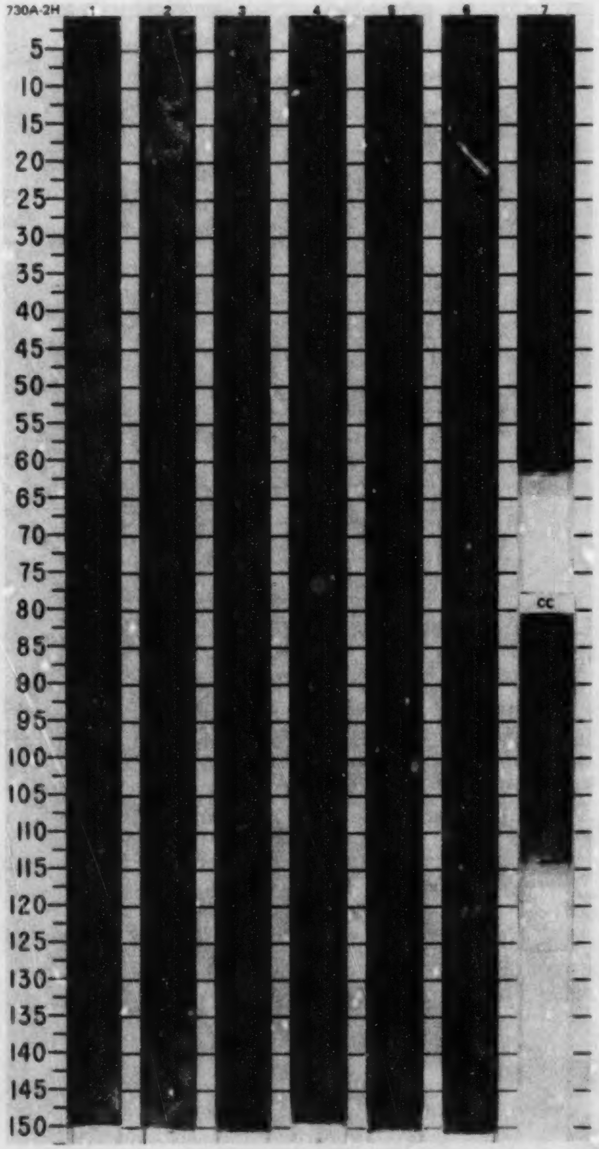
730A-2H
1
2
3
4
5
6
7
CC
5
10
15
20
25
30
35
40
45
50
55
60
65
70
75
80
85
90
95
100
105
110
115
120
125
130
135
140
145
150

SITE 730 HOLE A CORE 3H CORED INTERVAL 1083.6-1093.1 mbsl; 17.8-27.3 mbsf

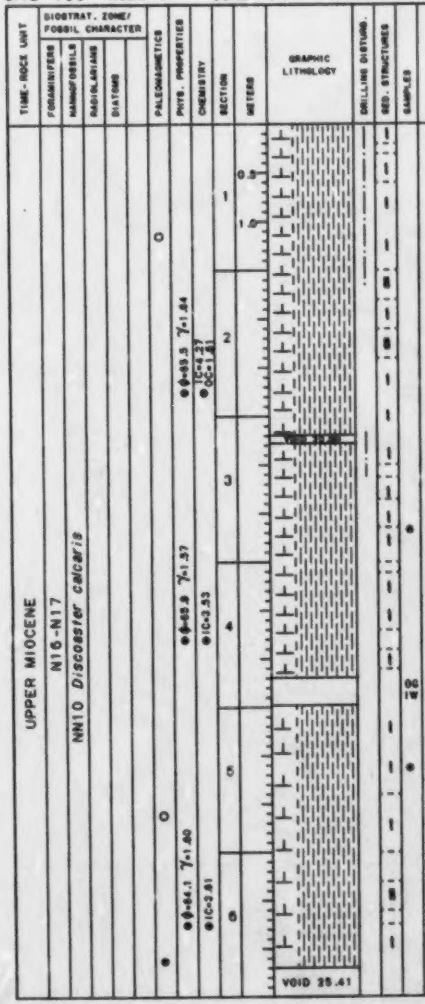
TIME-ROCK UNIT
BIOSTRAT. ZONE/ FOSSIL CHARACTER
FORAMINIFERS
NANNOFOSSILS
RADIOLARIANS
DIATOMS
PALEOMAGNETICS
PHYS. PROPERTIES
CHEMISTRY
SECTION
METERS
GRAPHIC LITHOLOGY
DRILLING DISTURB.
SED. STRUCTURES
SAMPLES
UPPER MIOCENE
N16-N17
NN10 Discoaster calcaris
●φ=65.5 γ=1.84
●φ=65.8 γ=1.57
●φ=64.1 γ=1.80
●IC=4.27 OC=1.61
●IC=3.53
●IC=3.81
1
2
3
4
5
6
0.5
1.0
OG
IW
VOID 25.41

LITHOLOGIC DESCRIPTION

MARLY NANNOFOSSIL OOZE

Section 1, 0–110 cm, and Section 3, 25–35 cm, is moderately disturbed; Section 1, 110–150 cm, is slightly disturbed; and remainder is undisturbed.

Major lithology: MARLY NANNOFOSSIL OOZE, olive (5Y 5/3, 4/3), olive gray (5Y 4/2, 5/2), and dark olive gray (5Y 3/2). Minor to moderate burrow mottling. Contacts gradational and mottled.

SMEAR SLIDE SUMMARY (%):

	3, 118 D	5, 63 D
TEXTURE:		
Silt	35	25
Clay	65	75
COMPOSITION:		
Access. minerals	—	1
Clay	40	25
Dolomite	1	1
Foraminifers	3	5
Inorganic calcite	30	18
Nannofossils	16	40
Quartz	10	10

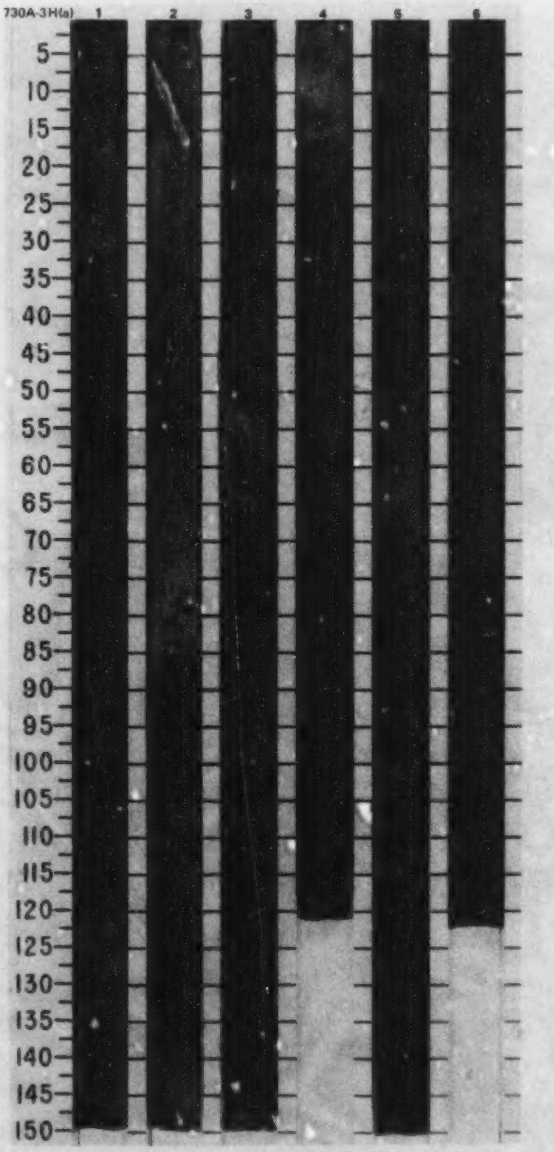
730A-3H(a)
1
2
3
4
5
6
5
10
15
20
25
30
35
40
45
50
55
60
65
70
75
80
85
90
95
100
105
110
115
120
125
130
135
140
145
150

SITE 730 HOLE A CORE 3H CORED INTERVAL 1083.6-1093.1 mbsl; 17.8-22.3 mbsf

TIME-ROCK UNIT	BIOSTRAT. ZONE/ FOSSIL CHARACTER					PALEOMAGNETICS	PHYS. PROPERTIES	CHEMISTRY	SECTION	METERS	GRAPHIC LITHOLOGY	DRILLING DISTURB.	SED. STRUCTURES	SAMPLES	LITHOLOGIC DESCRIPTION
	FORAMINIFERS	NANNOFOSSILS	RADIOLARIANS	DIATOMS											
	*R/P	*A/G	*BARREN						7		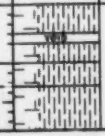				(cont.)
									8						
									CC						

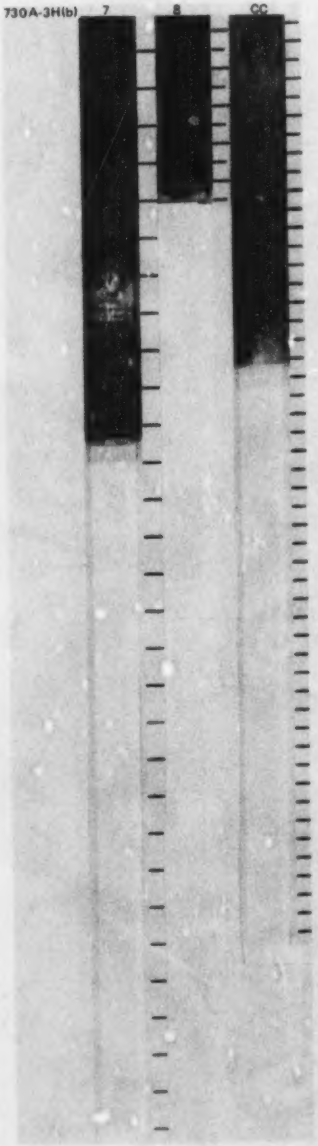

SITE 730 HOLE A CORE 4H CORED INTERVAL 1093.1-1102.6 mbsl; 27.3-36.8 mbsf

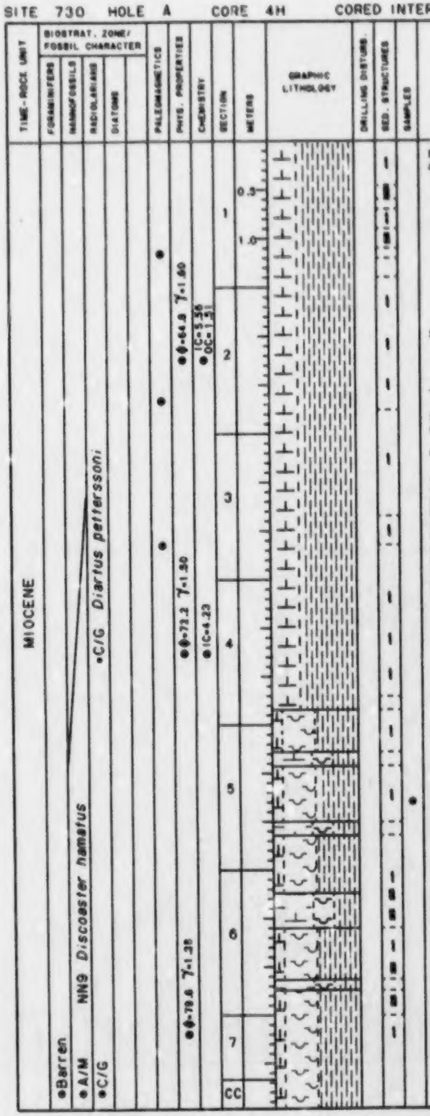
TIME-ROCK UNIT
BIOSTRAT. ZONE/ FOSSIL CHARACTER
FORAMINIFERS
NANNOFOSSILS
RADIOLARIANS
DIATOMS
PALEOMAGNETICS
PHYS. PROPERTIES
CHEMISTRY
SECTION
METERS
GRAPHIC LITHOLOGY
DRILLING DISTURB.
SED. STRUCTURES
SAMPLES
MIOCENE
•Barren
•A/M NN9 Discoaster hamatus
•C/G
•C/G Diartus petterssoni
•Φ=64.9 γ=1.80
•Φ=72.2 γ=1.90
•Φ=79.6 γ=1.38
•IC=5.56 OC=1.31
•IC=4.23
1
2
3
4
5
6
7
CC
0.5
1.0

LITHOLOGIC DESCRIPTION

MARLY NANNOFOSSIL OOZE, DIATOMACEOUS MARLY NANNOFOSSIL OOZE, and DIATOMACEOUS SILTY CLAY

Entire core is undisturbed.

Major lithologies:

a. MARLY NANNOFOSSIL OOZE, olive (5Y 5/3, 4/3), olive gray (5Y 5/2), and dark olive gray (5Y 3/2). Minor to moderate burrow mottling. Contacts gradational and mottled.

b. DIATOMACEOUS MARLY NANNOFOSSIL OOZE, olive (5Y 5/3). Minor to moderate burrow mottling. Contacts gradational and mottled.

c. DIATOMACEOUS SILTY CLAY, olive (5Y 4/3), olive gray (5Y 4/2), and dark olive gray (5Y 3/2). Minor to moderate burrow mottling. Contacts gradational and mottled.

SMEAR SLIDE SUMMARY (%):

	5, 80 D
TEXTURE:	
Silt	30
Clay	70
COMPOSITION:	
Access. minerals	2
Clay	30
Diatoms	2
Dolomite	1
Foraminifers	3
Inorganic calcite	10
Nannofossils	40
Quartz	10
Radiolarians	1
Sponge spicules	1

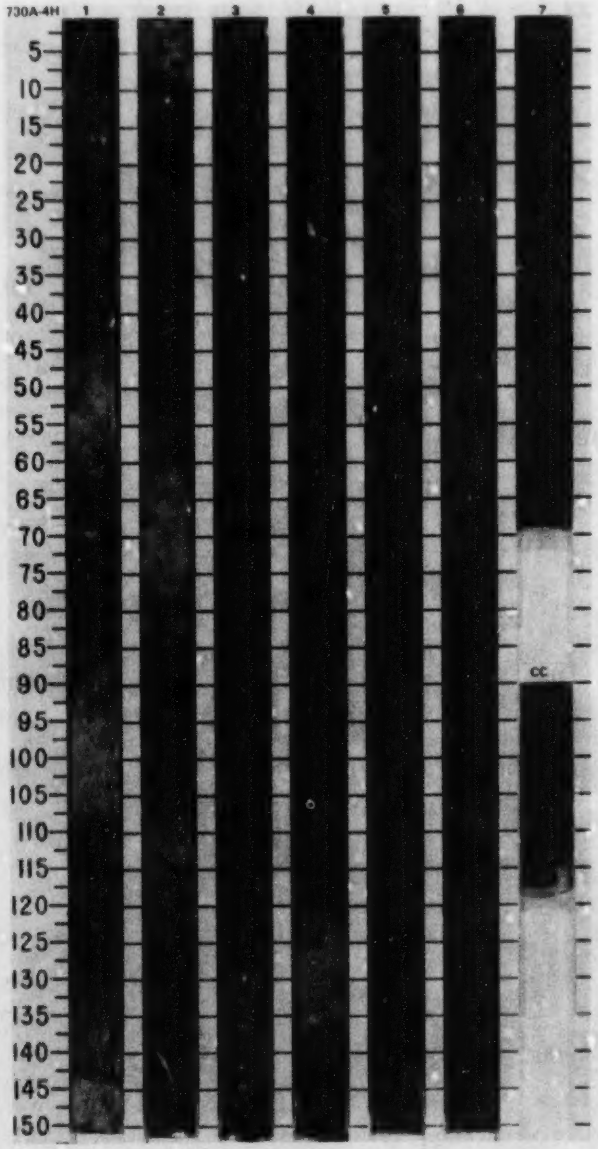
730A-4H
1
2
3
4
5
6
7
CC
5
10
15
20
25
30
35
40
45
50
55
60
65
70
75
80
85
90
95
100
105
110
115
120
125
130
135
140
145
150

SITE 730 HOLE A CORE 5H CORED INTERVAL 1102.6-1112.1 mbsl; 36.8-46.3 mbsf

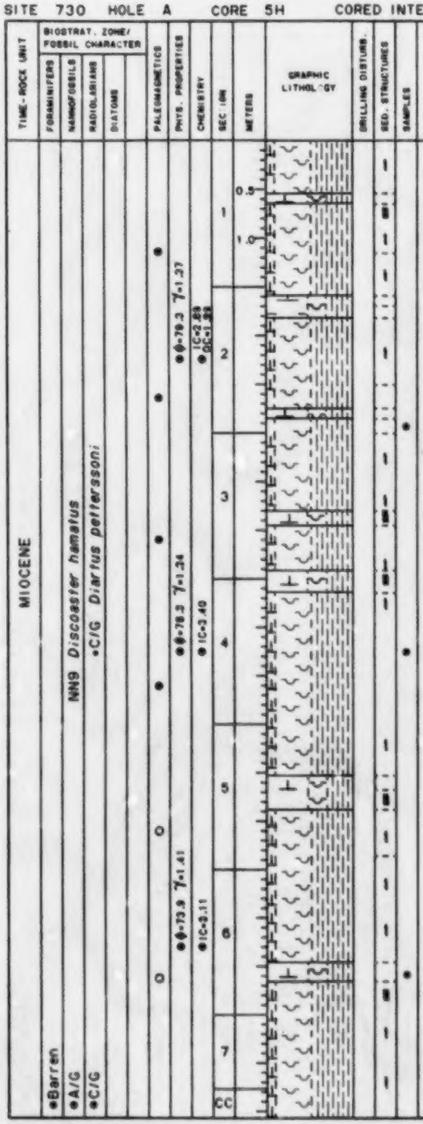
TIME-ROCK UNIT
BIOSTRAT. ZONE/ FOSSIL CHARACTER
FORAMINIFERS
NANNOFOSSILS
RADIOLARIANS
DIATOMS
PALEOMAGNETICS
PHYS. PROPERTIES
CHEMISTRY
SECTION
METERS
GRAPHIC LITHOLOGY
DRILLING DISTURB.
SED. STRUCTURES
SAMPLES
MIOCENE
●Barren
●A/G
NN9 Discoaster hamatus
●C/G
●C/G Diartus petterssoni
●Φ=79.3 γ=1.27
●Φ=78.3 γ=1.34
●Φ=73.9 γ=1.41
●IC=2.89 OC=1.29
●IC=3.40
●IC=3.11
1
2
3
4
5
6
7
CC
0.5
1.0

LITHOLOGIC DESCRIPTION

DIATOMACEOUS MARLY NANNOFOSSIL OOZE and DIATOMACEOUS SILTY CLAY

Entire core is undisturbed.

Major lithologies:

a. DIATOMACEOUS MARLY NANNOFOSSIL OOZE, olive (5Y 5/3) and olive gray (5Y 5/2). Minor burrow mottling throughout. Contacts gradational and mottled.

b. DIATOMACEOUS SILTY CLAY, olive (5Y 4/3), olive gray (5Y 4/2), and dark olive gray (5Y 3/2). Minor burrow mottling throughout. Contacts gradational and mottled.

SMEAR SLIDE SUMMARY (%):

	2, 145 M	4, 75 D	6, 110 D
TEXTURE:			
Silt	25	40	20
Clay	75	60	80
COMPOSITION:			
Clay	25	25	25
Diatoms	37	45	8
Dolomite	1	—	2
Foraminifers	3	—	3
Inorganic calcite	10	5	—
Nannofossils	15	20	55
Quartz	4	5	3
Radiolarians	5	—	—
Sponge spicules	—	—	2

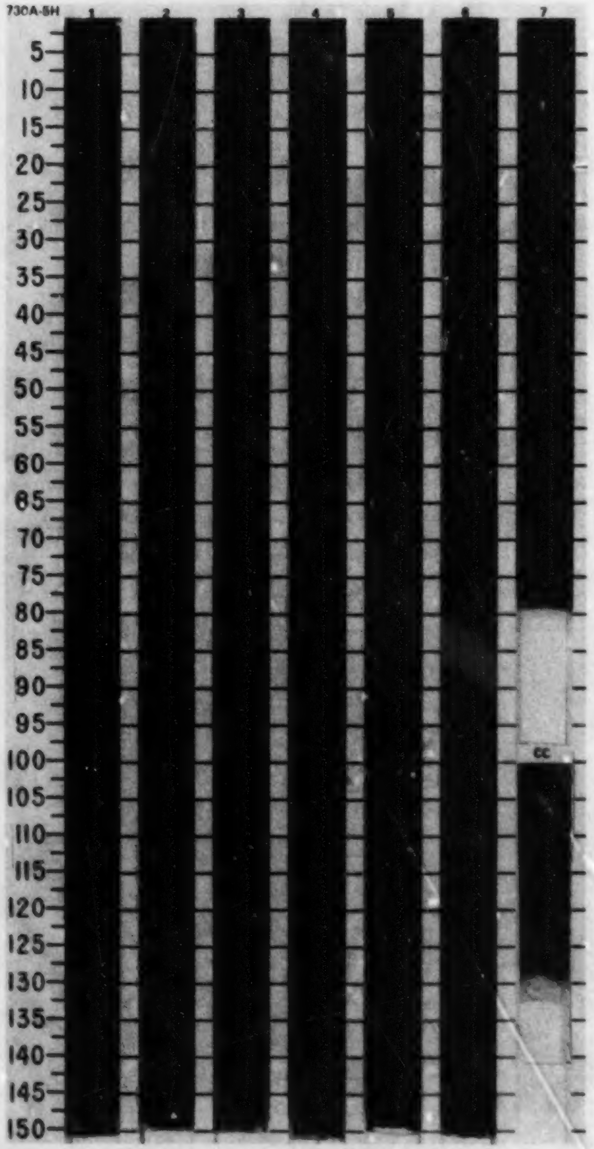
730A-5H
1
2
3
4
5
6
7
CC
5
10
15
20
25
30
35
40
45
50
55
60
65
70
75
80
85
90
95
100
105
110
115
120
125
130
135
140
145
150

SITE 730 HOLE A CORE 6X CORED INTERVAL 1112.1-1121.6 mbsl; 46.3-55.8 mbsf

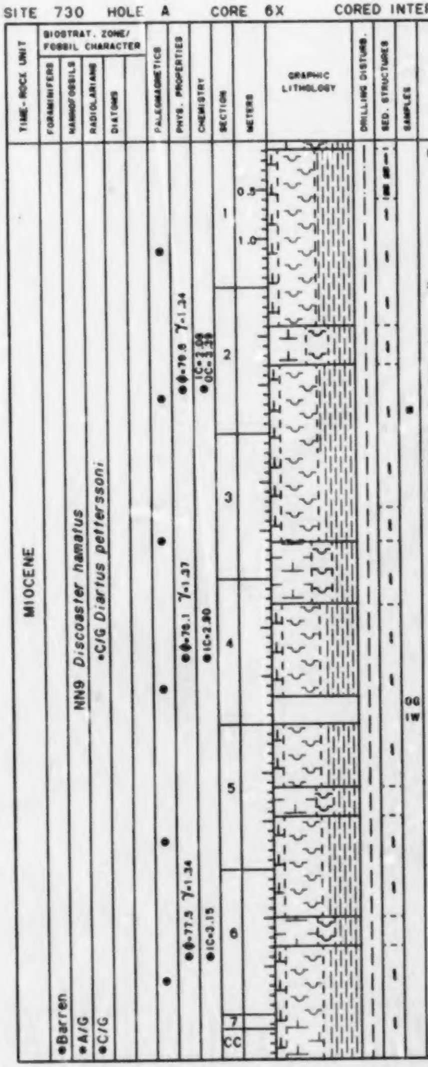
TIME-ROCK UNIT
BIOSTRAT. ZONE/ FOSSIL CHARACTER
FORAMINIFERS
NANNOFOSSILS
RADIOLARIANS
DIATOMS
PALEOMAGNETICS
PHYS. PROPERTIES
CHEMISTRY
SECTION
METERS
GRAPHIC LITHOLOGY
DRILLING DISTURB.
SED. STRUCTURES
SAMPLES
MIOCENE
•Barren
•A/G
NN9 Discoaster hamatus
•C/G
•C/G Diartus petterssoni
•φ=79.9 γ=1.34
•φ=76.1 γ=1.37
•φ=77.5 γ=1.34
•IC=1.09 OC=3.38
•IC=2.90
•IC=3.15
0.5
1.0
1
2
3
4
5
6
7
CC
OG
IW

LITHOLOGIC DESCRIPTION

DIATOMACEOUS MARLY NANNOFOSSIL OOZE and DIATOMACEOUS SILTY CLAY

Section 1, 0-50 cm, is moderately disturbed; remainder is slightly disturbed.

Major lithologies:

a. DIATOMACEOUS MARLY NANNOFOSSIL OOZE, olive (5Y 5/3) and olive gray (5Y 5/2). Minor burrow mottling throughout. Contacts gradational and mottled.

b. DIATOMACEOUS SILTY CLAY, olive (5Y 4/3) and dark olive gray (5Y 3/2). Minor burrow mottling throughout. Contacts gradational and mottled.

SMEAR SLIDE SUMMARY (%):

	2, 130 D
TEXTURE:	
Silt	25
Clay	75
COMPOSITION:	
Clay	30
Diatoms	40
Dolomite	1
Foraminifers	Tr
Inorganic calcite	7
Nannofossils	15
Quartz	7

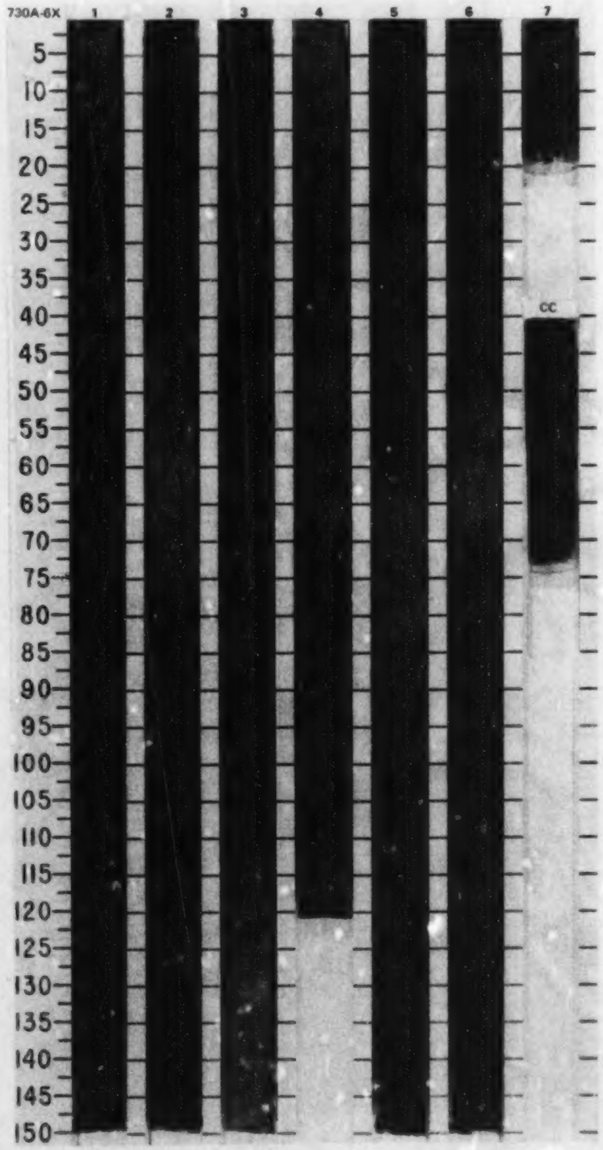
730A-6X
1
2
3
4
5
6
7
CC
5
10
15
20
25
30
35
40
45
50
55
60
65
70
75
80
85
90
95
100
105
110
115
120
125
130
135
140
145
150

SITE 730 HOLE A CORE 7X CORED INTERVAL 1121.6-1131.3 mbsl; 55.8-65.5 mbsf

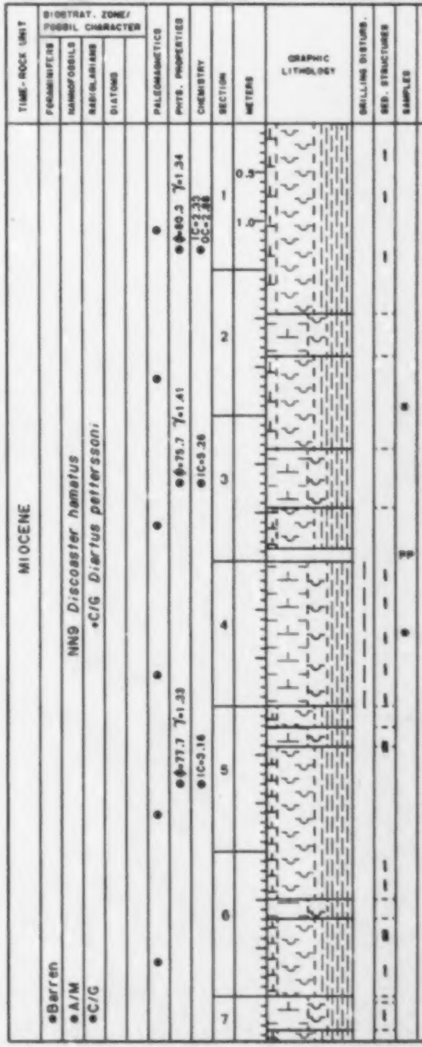
TIME-ROCK UNIT
BIOSTRAT. ZONE/ FOSSIL CHARACTER
FORAMINIFERS
NANNOFOSSILS
RADIOLARIANS
DIATOMS
PALEOMAGNETICS
PHYS. PROPERTIES
CHEMISTRY
SECTION
METERS
GRAPHIC LITHOLOGY
DRILLING DISTURB.
SED. STRUCTURES
SAMPLES
MIOCENE
●Barren
●A/M
NN9 Discoaster hamatus
●C/G
●C/G Diartus petterssoni
●ϕ=80.3 γ=1.34
●ϕ=75.7 γ=1.41
●ϕ=77.7 γ=1.33
●IC=2.33 OC=2.88
●IC=3.26
●IC=3.16
1
2
3
4
5
6
7
0.5
1.0
PP

LITHOLOGIC DESCRIPTION

DIATOMACEOUS MARLY NANNOFOSSIL OOZE and DIATOMACEOUS SILTY CLAY

Section 3, 0-35 cm, is moderately disturbed; Section 4, 0-150 cm, is slightly disturbed; and remainder is undisturbed.

Major lithologies:
a. DIATOMACEOUS MARLY NANNOFOSSIL OOZE, olive (5Y 5/3) and olive gray (5Y 5/2). Minor to moderate burrow mottling. Contacts gradational and mottled.
b. DIATOMACEOUS SILTY CLAY, olive (5Y 4/3) and dark olive gray (5Y 3/2). Minor to moderate burrow mottling. Contacts gradational and mottled.

SMEAR SLIDE SUMMARY (%):

	2, 143 D	4, 75 D
TEXTURE:		
Silt	30	10
Clay	70	90
COMPOSITION:		
Access. minerals	2	—
Clay	30	20
Diatoms	35	11
Dolomite	—	2
Foraminifers	1	—
Inorganic calcite	10	3
Mica	1	
Nannofossils	15	60
Quartz	7	2
Sponge spicules	—	1

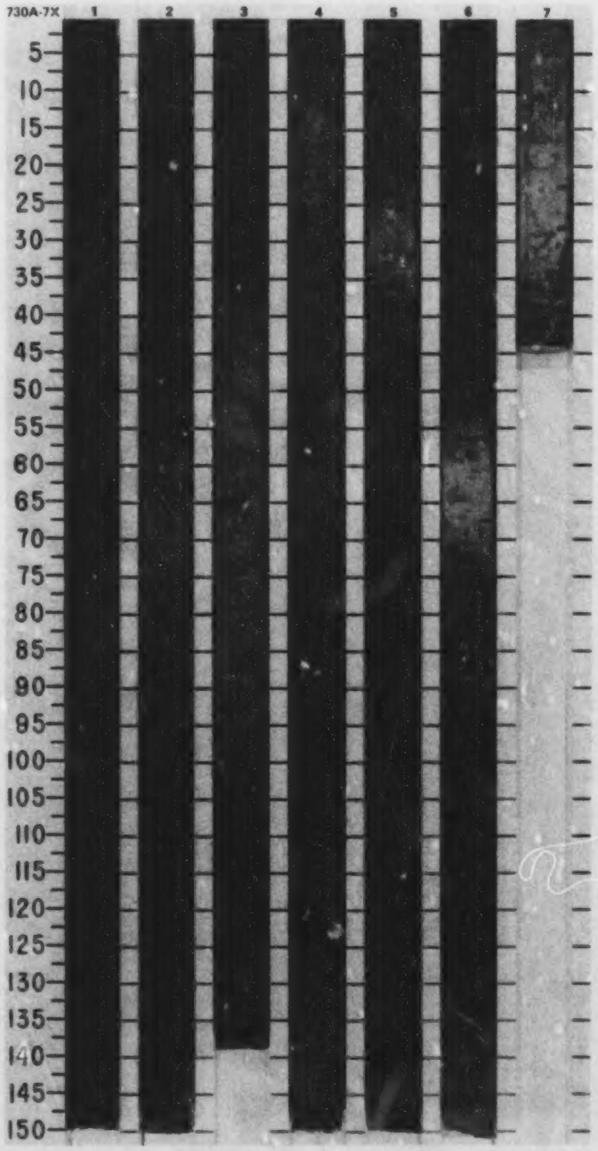
730A-7X
1
2
3
4
5
6
7
5
10
15
20
25
30
35
40
45
50
55
60
65
70
75
80
85
90
95
100
105
110
115
120
125
130
135
140
145
150

SITE 730 HOLE A CORE 8X CORED INTERVAL 1131.3-1141.0 mbsl; 65.5-75.2 mbsf

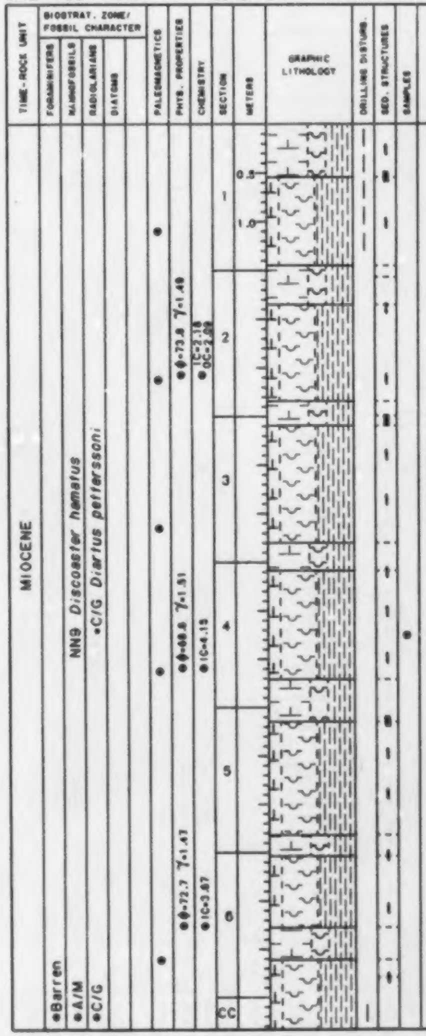
TIME-ROCK UNIT
BIOSTRAT. ZONE/ FOSSIL CHARACTER
FORAMINIFERS
NANNOFOSSILS
RADIOLARIANS
DIATOMS
PALEOMAGNETICS
PHYS. PROPERTIES
CHEMISTRY
SECTION
METERS
GRAPHIC LITHOLOGY
DRILLING DISTURB.
SED. STRUCTURES
SAMPLES
MIOCENE
NN9 Discoaster hamatus
•C/G Diartus petterssoni
•Barren
•A/M
•C/G
•ϕ=73.8 γ=1.49
•ϕ=68.6 γ=1.51
•ϕ=72.7 γ=1.47
IC=2.18
•OC=2.02
•IC=4.15
•IC=3.87
1
2
3
4
5
6
CC
0.5
1.0

LITHOLOGIC DESCRIPTION

DIATOMACEOUS MARLY NANNOFOSSIL OOZE and DIATOMACEOUS SILTY CLAY

Section 1, 0-150 cm, and CC, 0-35 cm, are slightly disturbed; remainder is undisturbed.

Major lithologies:
a. DIATOMACEOUS MARLY NANNOFOSSIL OOZE, olive (5Y 5/3) and olive gray (5Y 5/2). Minor to moderate burrow mottling. Contacts gradational and mottled.
b. DIATOMACEOUS SILTY CLAY, olive (5Y 4/3), olive gray (5Y 4/2), and dark olive gray (5Y 3/2). Minor to moderate burrow mottling. Contacts gradational and mottled.

SMEAR SLIDE SUMMARY (%):

	4, 75 D
TEXTURE:	
Silt	30
Clay	70
COMPOSITION:	
Access. minerals	1
Clay	35
Diatoms	30
Dolomite	1
Inorganic calcite	5
Nannofossils	15
Quartz	8
Radiolarians	2

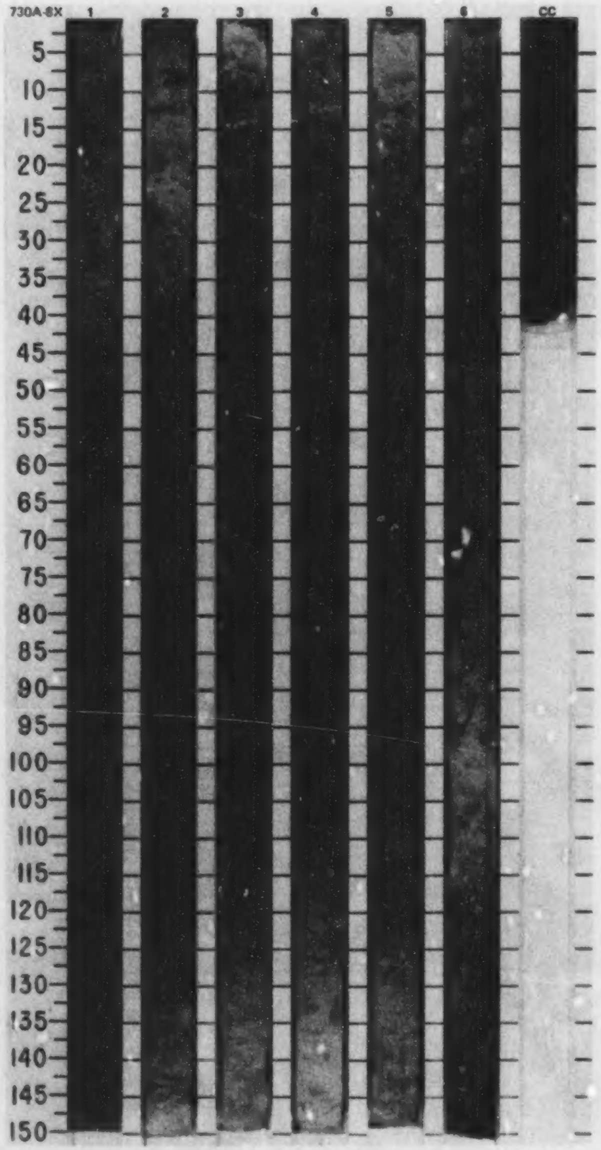
730A-8X
1
2
3
4
5
6
CC
5
10
15
20
25
30
35
40
45
50
55
60
65
70
75
80
85
90
95
100
105
110
115
120
125
130
135
140
145
150

SITE 730 HOLE A CORE 9X CORED INTERVAL 1141.0-1150.7 mbsl; 75.2-84.9 mbsf

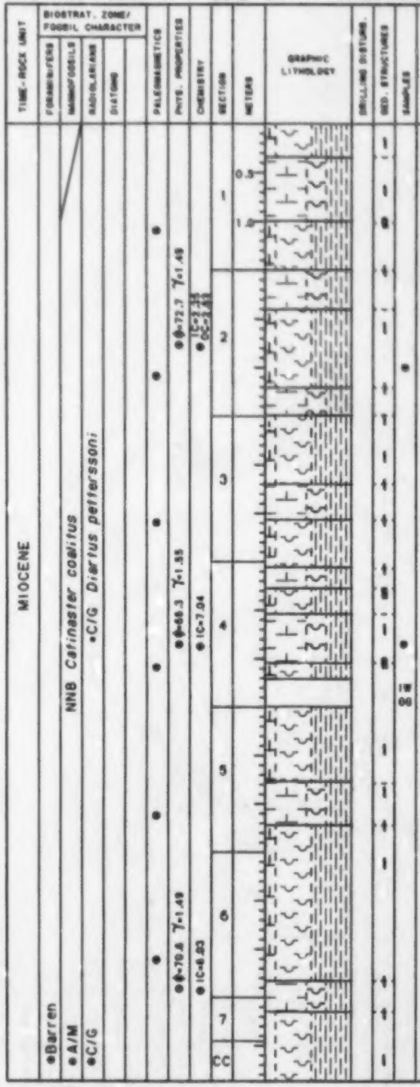
TIME-ROCK UNIT
BIOSTRAT. ZONE/ FOSSIL CHARACTER
FORAMINIFERS
NANNOFOSSILS
RADIOLARIANS
DIATOMS
PALEOMAGNETICS
PHYS. PROPERTIES
CHEMISTRY
SECTION
METERS
GRAPHIC LITHOLOGY
DRILLING DISTURB.
SED. STRUCTURES
SAMPLES
MIOCENE
●Barren
●A/M
NNB Catinaster coalitus
●C/G
●C/G Diartus petterssoni
●ϕ=72.7 γ=1.49
●ϕ=66.3 γ=1.55
●ϕ=70.6 γ=1.49
●IC=2.35 OC=2.83
●IC=7.04
●IC=6.83
1
2
3
4
5
6
7
CC
0.5
1.0
IW
OG

LITHOLOGIC DESCRIPTION

DIATOMACEOUS MARLY NANNOFOSSIL OOZE and DIATOMACEOUS SILTY CLAY

Entire core is undisturbed.

Major lithologies:
a. DIATOMACEOUS MARLY NANNOFOSSIL OOZE, olive (5Y 5/3) and olive gray (5Y 5/2). Minor to moderate burrow mottling. Contacts gradational and mottled.
b. DIATOMACEOUS SILTY CLAY, olive (5Y 4/3), olive gray (5Y 4/2), and dark olive gray (5Y 3/2). Minor to moderate burrow mottling. Contacts gradational and mottled.

SMEAR SLIDE SUMMARY (%):

	2, 100 D	4, 90 D
TEXTURE:		
Sand	5	10
Silt	20	30
Clay	75	60
COMPOSITION:		
Clay	20	20
Diatoms	20	15
Dolomite	Tr	Tr
Foraminifers	5	5
Inorganic calcite	5	10
Nannofossils	40	50
Organic debris	5	—
Quartz	5	Tr
Radiolarians	Tr	Tr
Sponge spicules	Tr	Tr

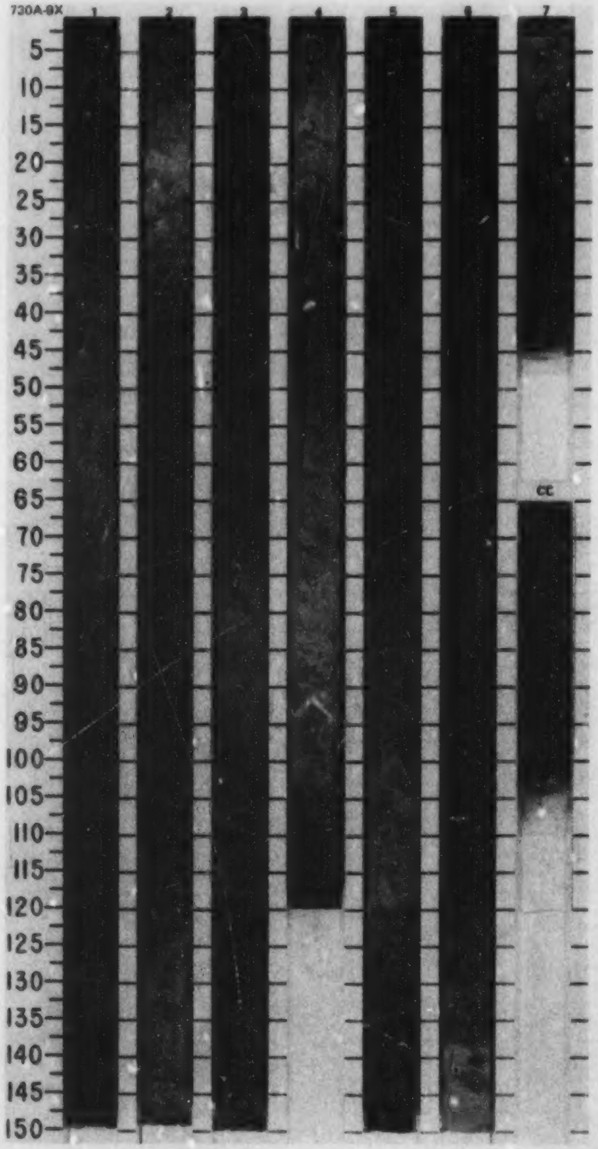
730A-9X
1
2
3
4
5
6
7
CC
5
10
15
20
25
30
35
40
45
50
55
60
65
70
75
80
85
90
95
100
105
110
115
120
125
130
135
140
145
150

SITE 730 HOLE A CORE 10X CORED INTERVAL 1150.7-1160.4 mbsl; 84.9-94.6 mbsf

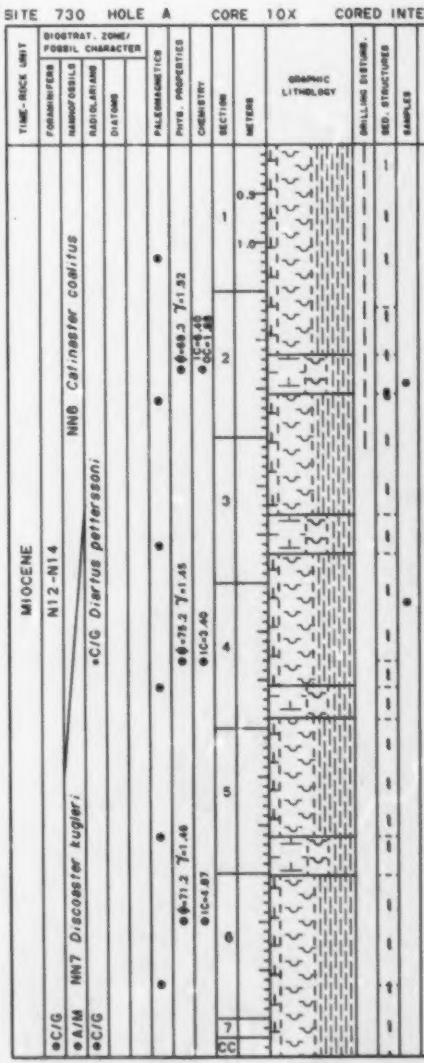
TIME-ROCK UNIT
BIOSTRAT. ZONE/ FOSSIL CHARACTER
FORAMINIFERS
NANNOFOSSILS
RADIOLARIANS
DIATOMS
PALEOMAGNETICS
PHYS. PROPERTIES
CHEMISTRY
SECTION
METERS
GRAPHIC LITHOLOGY
DRILLING DISTURB.
SED. STRUCTURES
SAMPLES
MIOCENE
N12-N14
NN8 Catinaster coalitus
NN7 Discoaster kugleri
•C/G Diartus petterssoni
•C/G
•A/M
•C/G
•φ=69.3 γ=1.52
•φ=75.2 γ=1.45
•φ=71.2 γ=1.46
•IC=6.40 OC=1.88
•IC=3.40
•IC=4.87
1
2
3
4
5
6
7
CC
0.5
1.0

LITHOLOGIC DESCRIPTION

DIATOMACEOUS MARLY NANNOFOSSIL OOZE and DIATOMACEOUS SILTY CLAY

Section 1, 0-150 cm, Section 2, 0-150 cm, and Section 5, 0-150 cm, are slightly disturbed; remainder is undisturbed.

Major lithologies:

a. DIATOMACEOUS MARLY NANNOFOSSIL OOZE, olive gray (5Y 5/2). Minor to moderate burrow mottling. Contacts gradational and mottled.

b. DIATOMACEOUS SILTY CLAY, olive (5Y 4/4, 4/3), olive gray (5Y 4/2), and dark olive gray (5Y 3/2). Minor to moderate burrow mottling. Contacts gradational and mottled.

SMEAR SLIDE SUMMARY (%):

	2, 96 D	4, 20 D
TEXTURE:		
Silt	25	60
Clay	75	40
COMPOSITION:		
Access. minerals	Tr	7
Clay	25	8
Diatoms	15	30
Dolomite	2	2
Foraminifers	3	5
Inorganic calcite	Tr	10
Nannofossils	50	30
Quartz	—	2
Radiolarians	2	3
Silicoflagellates	1	1
Sponge spicules	2	2

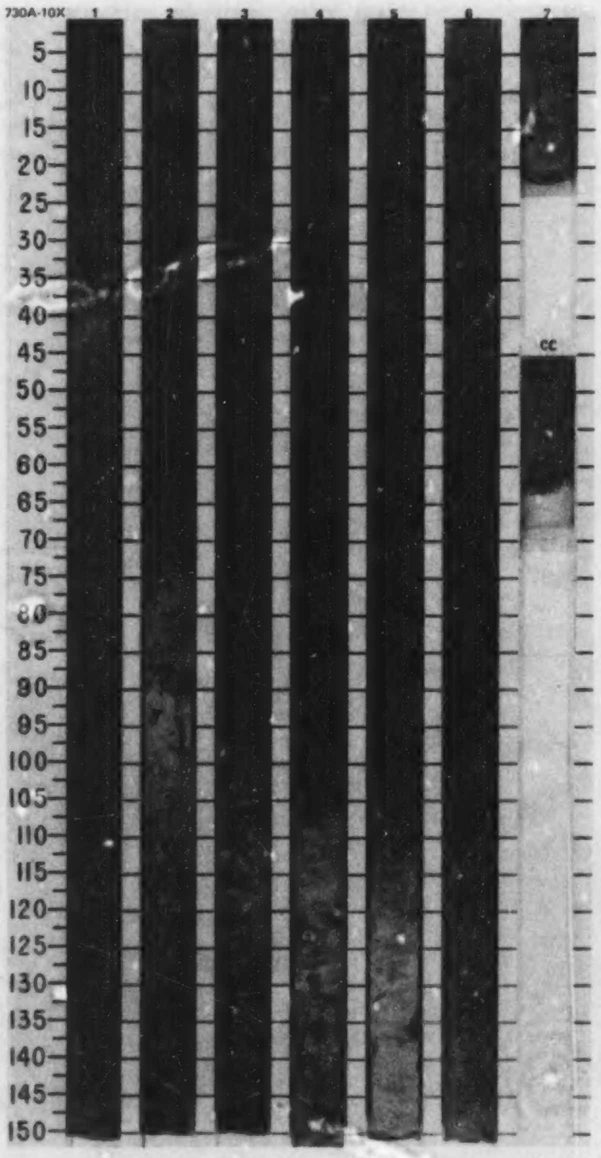
730A-10X
1
2
3
4
5
6
7
CC
5
10
15
20
25
30
35
40
45
50
55
60
65
70
75
80
85
90
95
100
105
110
115
120
125
130
135
140
145
150

SITE 730 HOLE A CORE 11X CORED INTERVAL 1160.4-1170.0 mbsl; 94.6-104.2 mbsf

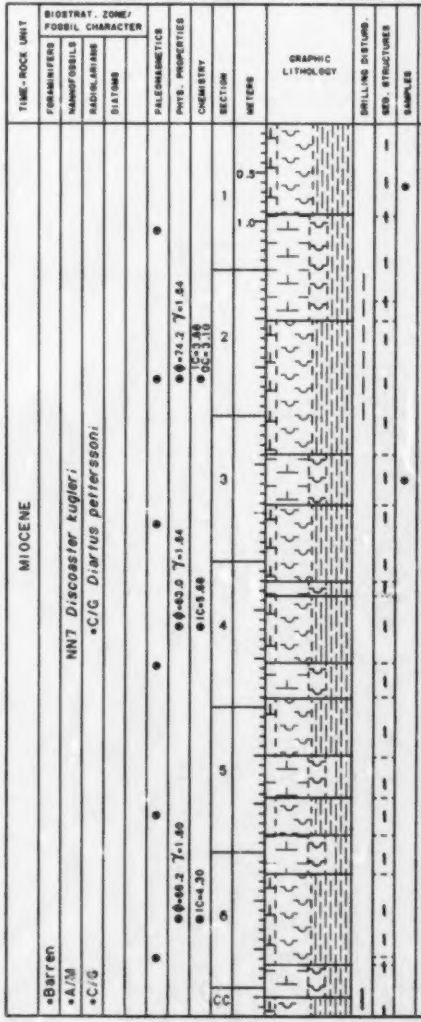
TIME-ROCK UNIT
BIOSTRAT. ZONE/ FOSSIL CHARACTER
FORAMINIFERS
NANNOFOSSILS
RADIOLARIANS
DIATOMS
PALEOMAGNETICS
PHYS. PROPERTIES
CHEMISTRY
SECTION
METERS
GRAPHIC LITHOLOGY
DRILLING DISTURB.
SED. STRUCTURES
SAMPLES
MIOCENE
•Barren
•A/M
NN7 Discoaster kugleri
•C/G
•C/G Diartus petterssoni
•φ=74.2 γ=1.84
•φ=63.0 γ=1.84
•φ=66.2 γ=1.80
•IC=3.88 OC=3.10
•IC=5.88
•IC=4.30
1
2
3
4
5
6
CC
0.5
1.0

LITHOLOGIC DESCRIPTION

DIATOMACEOUS MARLY NANNOFOSSIL OOZE and DIATOMACEOUS SILTY CLAY

CC, 0-26 cm, is very disturbed; Section 2, 0-150 cm, is slightly disturbed; and remainder is undisturbed.

Major lithologies:

a. DIATOMACEOUS MARLY NANNOFOSSIL OOZE, olive (5Y 5/3) and olive gray (5Y 5/2). Minor to moderate burrow mottling. Contacts gradational and mottled.

b. DIATOMACEOUS SILTY CLAY, olive (5Y 4/3), olive gray (5Y 4/2), and dark olive gray (5Y 3/2). Minor to moderate burrow mottling. Contacts gradational and mottled.

SMEAR SLIDE SUMMARY (%):

	1, 65 D	3, 65 D
TEXTURE:		
Silt	25	30
Clay	75	70
COMPOSITION:		
Clay	35	30
Diatoms	30	20
Dolomite	1	1
Foraminifers	3	3
Inorganic calcite	3	1
Nannofossils	25	43
Quartz	3	1
Radiolarians	—	1

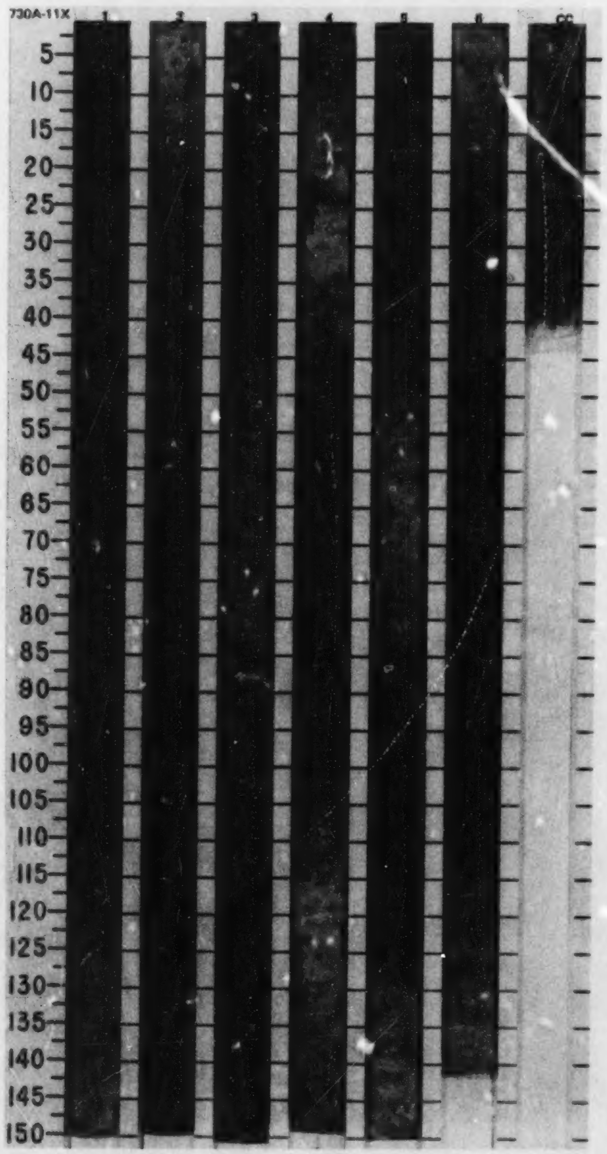
730A-11X
1
2
3
4
5
6
CC
5
10
15
20
25
30
35
40
45
50
55
60
65
70
75
80
85
90
95
100
105
110
115
120
125
130
135
140
145
150

SITE 730 HOLE A CORE 12X CORED INTERVAL 1170.0-1179.7 mbsl; 104.2-113.9 mbsf

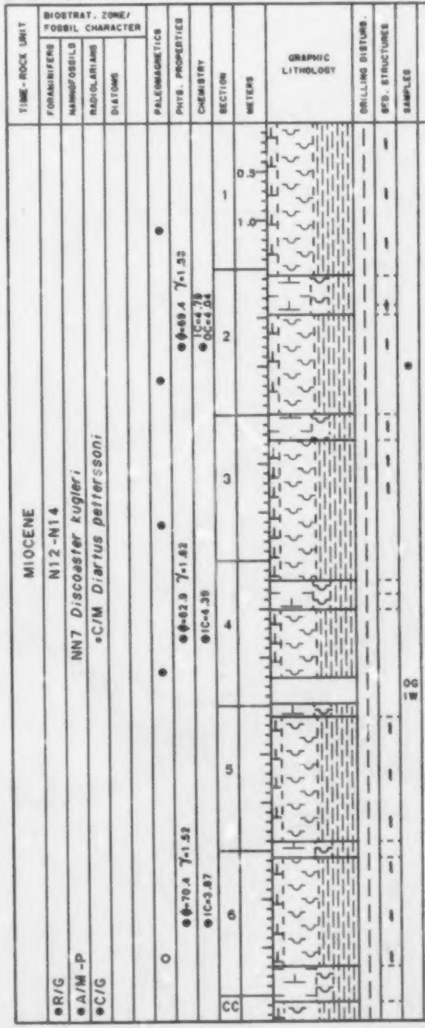
TIME-ROCK UNIT
BIOSTRAT. ZONE/ FOSSIL CHARACTER
FORAMINIFERS
NANNOFOSSILS
RADIOLARIANS
DIATOMS
PALEOMAGNETICS
PHYS. PROPERTIES
CHEMISTRY
SECTION
METERS
GRAPHIC LITHOLOGY
DRILLING DISTURB.
SED. STRUCTURES
SAMPLES
MIOCENE
N12-N14
NN7 Discoaster kugleri
•C/M Diartus petterssoni
•R/G
•A/M-P
•C/G
•φ=69.4 γ=1.33
•φ=62.9 γ=1.82
•φ=70.4 γ=1.52
IC=4.78
•OC=4.04
•IC=4.39
•IC=3.87
1
2
3
4
5
6
CC
0.5
1.0
OG
IW

LITHOLOGIC DESCRIPTION

DIATOMACEOUS MARLY NANNOFOSSIL OOZE and DIATOMACEOUS SILTY CLAY

CC, 0-28 cm, moderately disturbed; remainder is slightly disturbed.

Major lithologies:
a. DIATOMACEOUS MARLY NANNOFOSSIL OOZE, olive (5Y 5/3) and olive gray (5Y 5/2). Minor burrow mottling common. Contacts gradational and mottled.
b. DIATOMACEOUS SILTY CLAY, olive (5Y 4/3), olive gray (5Y 4/2), and dark olive gray (5Y 3/2). Minor burrow mottling common. Contacts gradational and mottled.

SMEAR SLIDE SUMMARY (%):

	2, 100 D
TEXTURE:	
Silt	20
Clay	80
COMPOSITION:	
Clay	30
Diatoms	10
Dolomite	Tr
Foraminifers	5
Inorganic calcite	10
Nannofossils	40
Organic debris	5
Quartz	Tr
Silicoflagellates	Tr
Sponge spicules	Tr

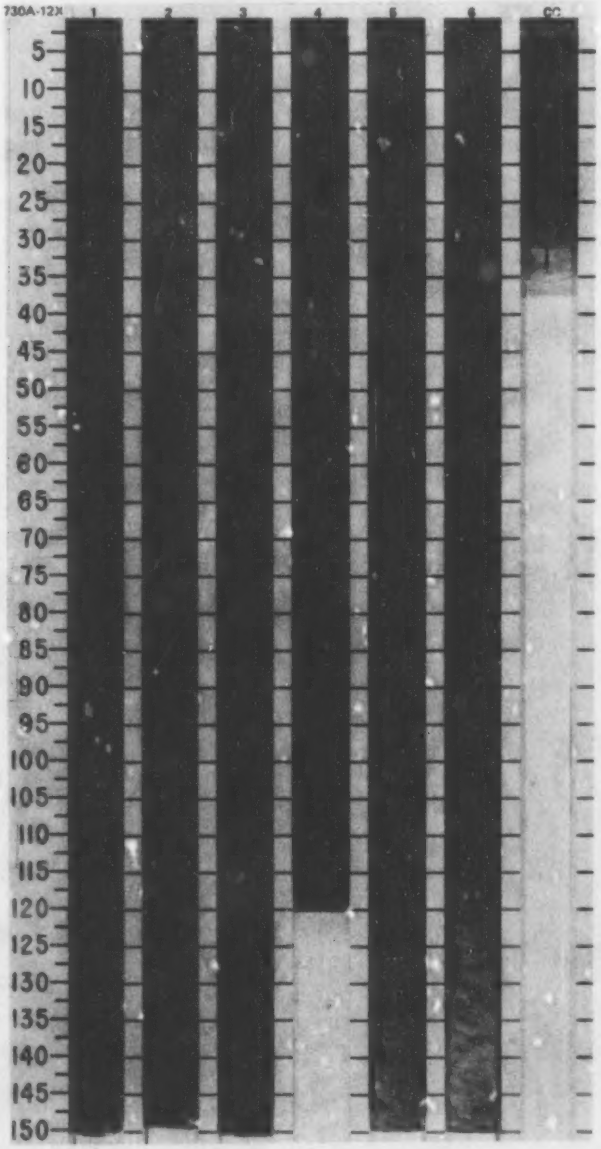
730A-12X
1
2
3
4
5
6
CC
5
10
15
20
25
30
35
40
45
50
55
60
65
70
75
80
85
90
95
100
105
110
115
120
125
130
135
140
145
150

SITE 730 HOLE A CORE 13X CORED INTERVAL 1179.7-1189.3 mbsl; 113.9-123.5 mbsf

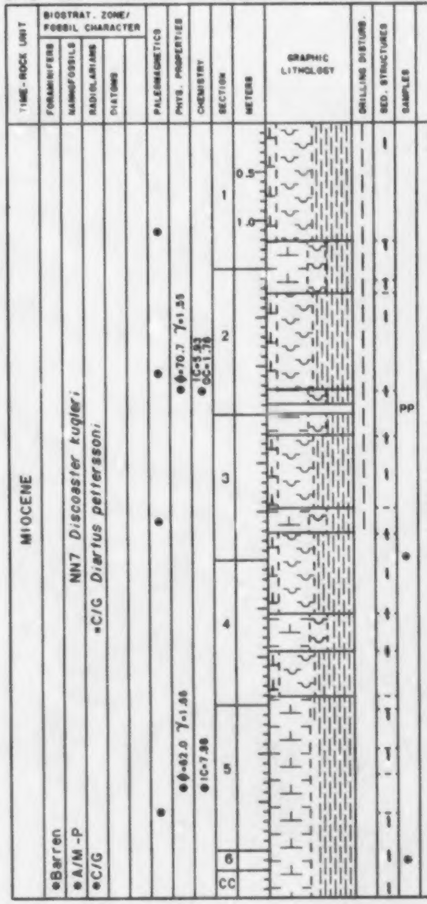
TIME-ROCK UNIT
BIOSTRAT. ZONE/ FOSSIL CHARACTER
FORAMINIFERS
NANNOFOSSILS
RADIOLARIANS
DIATOMS
PALEOMAGNETICS
PHYS. PROPERTIES
CHEMISTRY
SECTION
METERS
GRAPHIC LITHOLOGY
DRILLING DISTURB.
SED. STRUCTURES
SAMPLES
MIOCENE
●Barren
●A/M -P
NN7 Discoaster kugleri
●C/G
●C/G Diartus petterssoni
●φ=70.7 γ=1.55
●φ=62.0 γ=1.86
●IC=5.93 OC=1.76
●IC=7.88
1
2
3
4
5
6
CC
0.5
1.0
PP

LITHOLOGIC DESCRIPTION

DIATOMACEOUS MARLY NANNOFOSSIL OOZE, DIATOMACEOUS SILTY CLAY, and DIATOM-BEARING MARLY NANNOFOSSIL OOZE

Sections 1-3 and Section 6, 0-20 cm, are slightly disturbed; remainder is undisturbed.

Major lithologies:

a. DIATOMACEOUS MARLY NANNOFOSSIL OOZE, olive (5Y 5/3) and olive gray (5Y 5/2). Minor burrow mottling common. Contacts gradational and mottled.

b. DIATOMACEOUS SILTY CLAY, olive (5Y 4/3) and dark olive gray (5Y 3/2). Minor burrow mottling common. Contacts gradational and mottled.

c. Section 5 and below: DIATOM-BEARING MARLY NANNOFOSSIL OOZE, olive (5Y 5/3) and olive gray (5Y 5/2). Minor burrow mottling throughout. Contacts gradational and mottled.

SMEAR SLIDE SUMMARY (%):

	3, 147 M	6, 10 D
TEXTURE:		
Silt	30	15
Clay	70	85
COMPOSITION:		
Access. minerals	—	1
Clay	25	23
Diatoms	10	3
Dolomite	3	4
Foraminifers	2	2
Inorganic calcite	10	3
Nannofossils	40	60
Quartz	7	Tr
Radiolarians	—	1
Sponge spicules	3	3

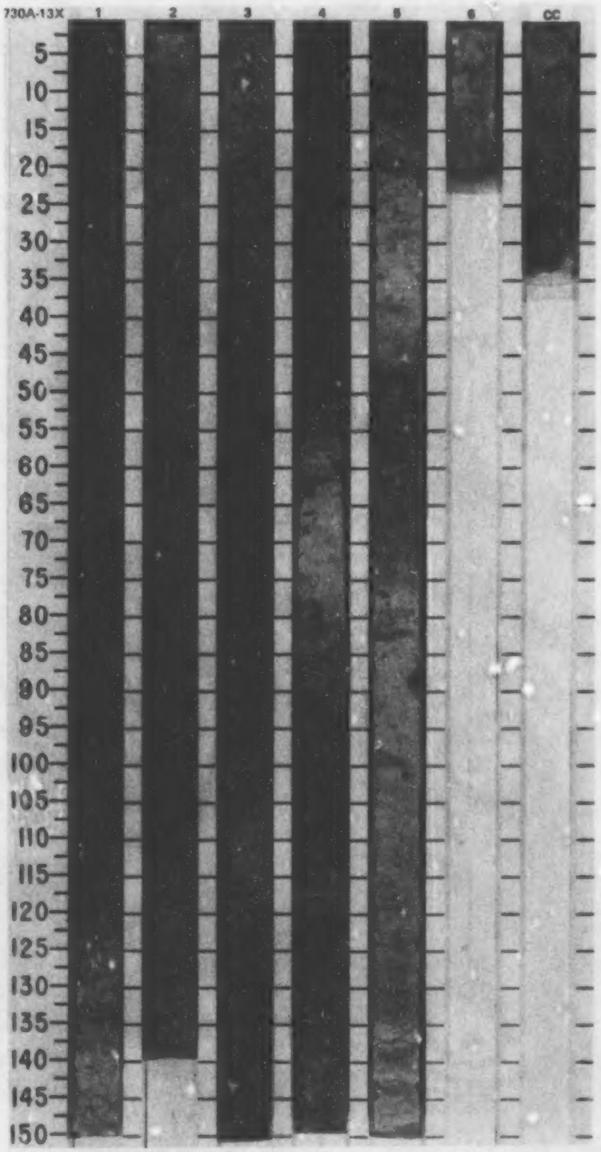
730A-13X
1
2
3
4
5
6
CC
5
10
15
20
25
30
35
40
45
50
55
60
65
70
75
80
85
90
95
100
105
110
115
120
125
130
135
140
145
150

SITE 730 HOLE A CORE 14X CORED INTERVAL 1189.3-1199.0 mbsl; 123.5-133.2 mbsf

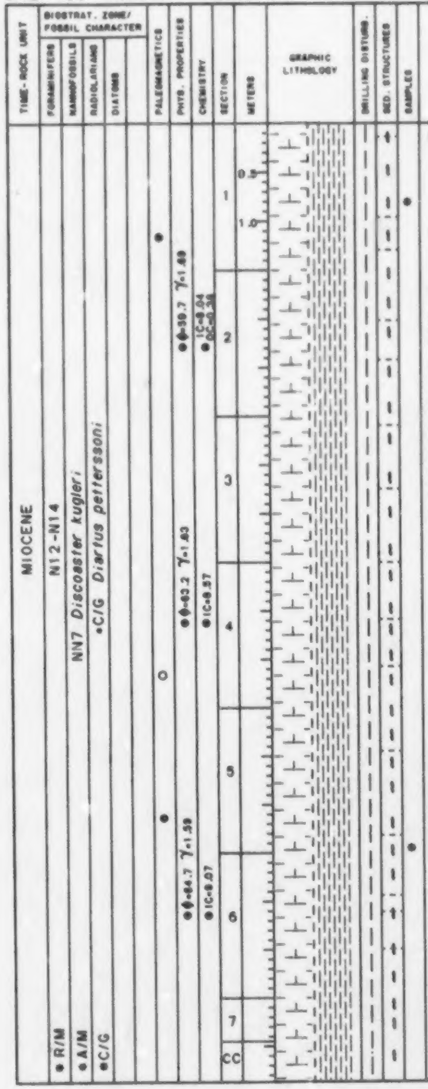

LITHOLOGIC DESCRIPTION

DIATOM-BEARING MARLY NANNOFOSSIL OOZE

CC, 0-40 cm, is moderately disturbed; remainder is slightly disturbed.

Major lithology: DIATOM-BEARING MARLY NANNOFOSSIL OOZE, olive (5Y 4/3, 5/3) and olive gray (5Y 5/2). Minor burrow mottling throughout. Contacts gradational and mottled.

SMEAR SLIDE SUMMARY (%):

	2, 80 D	5, 143 D
TEXTURE:		
Sand	—	5
Silt	20	30
Clay	80	65
COMPOSITION:		
Access. minerals	—	Tr
Clay	30	20
Diatoms	Tr	10
Dolomite	5	Tr
Foraminifers	5	5
Inorganic calcite	10	10
Nannofossils	45	45
Organic debris	—	Tr
Quartz	Tr	5
Radiolarians	Tr	Tr
Silicoflagellates	—	Tr
Sponge Spicules	5	5

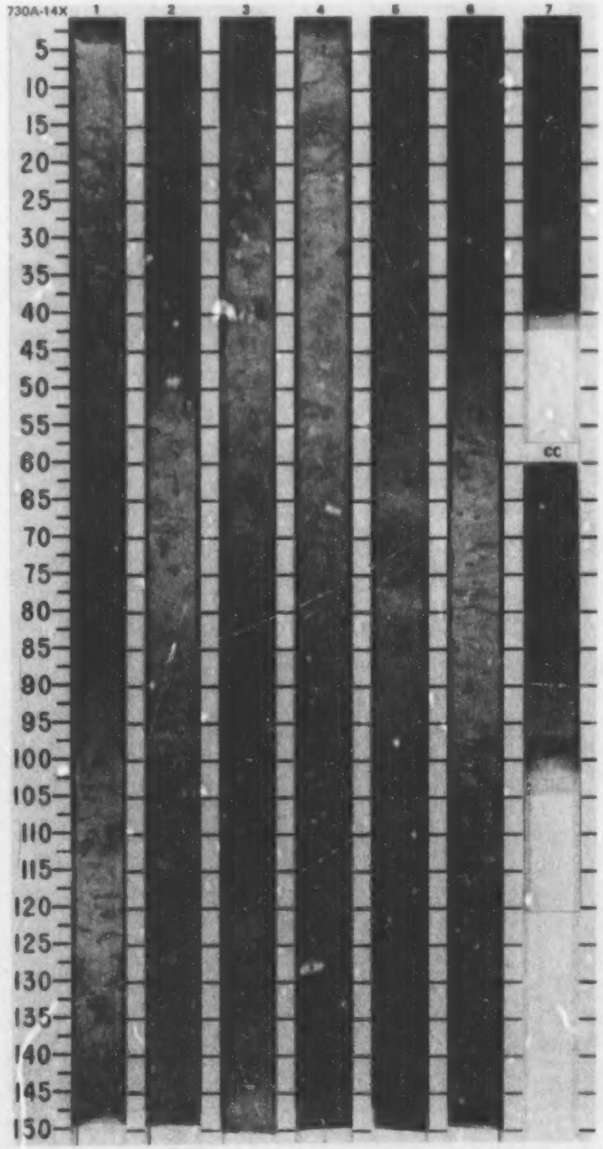
730A-14X
1
2
3
4
5
6
7
CC
5
10
15
20
25
30
35
40
45
50
55
60
65
70
75
80
85
90
95
100
105
110
115
120
125
130
135
140
145
150

SITE 730 HOLE A CORE 15X CORED INTERVAL 1199.0-1208.7 mbsl; 133.2-142.9 mbsf

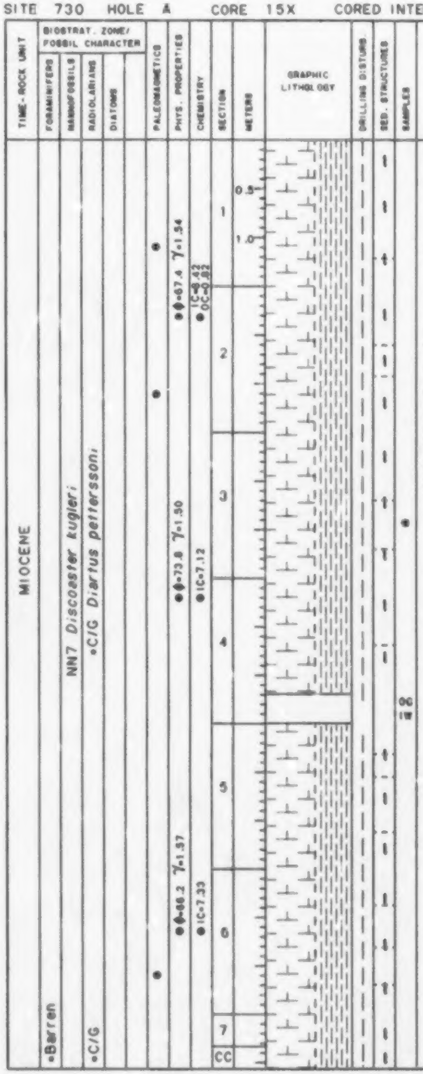
TIME-ROCK UNIT
BIOSTRAT. ZONE/ FOSSIL CHARACTER
FORAMINIFERS
NANNOFOSSILS
RADIOLARIANS
DIATOMS
PALEOMAGNETICS
PHYS. PROPERTIES
CHEMISTRY
SECTION
METERS
GRAPHIC LITHOLOGY
DRILLING DISTURB.
SED. STRUCTURES
SAMPLES
MIOCENE
•Barren
NN7 Discoaster kugleri
•C/G Diartus petterssoni
•C/G
•φ=67.4 γ=1.54
•φ=73.8 γ=1.50
•φ=66.2 γ=1.57
•IC=8.42 OC=0.82
•IC=7.12
•IC=7.33
1
2
3
4
5
6
7
CC
0.5
1.0
OG
IW

LITHOLOGIC DESCRIPTION

DIATOM-BEARING MARLY NANNOFOSSIL OOZE

CC, 0–40 cm, moderately disturbed; remainder is slightly disturbed.

Major lithology: DIATOM-BEARING MARLY NANNOFOSSIL OOZE, light gray (5Y 7/2), light olive gray (5Y 6/2), pale olive (5Y 6/3), and olive (5Y 4/3, 5/3). Minor burrow mottling throughout. Contacts gradational and mottled.

SMEAR SLIDE SUMMARY (%)

	3, 90 D
TEXTURE:	
Silt	20
Clay	80
COMPOSITION:	
Clay	25
Diatoms	5
Dolomite	Tr
Foraminifers	Tr
Inorganic calcite	5
Nannofossils	60
Radiolarians	1
Silicoflagellates	1
Sponge spicules	3

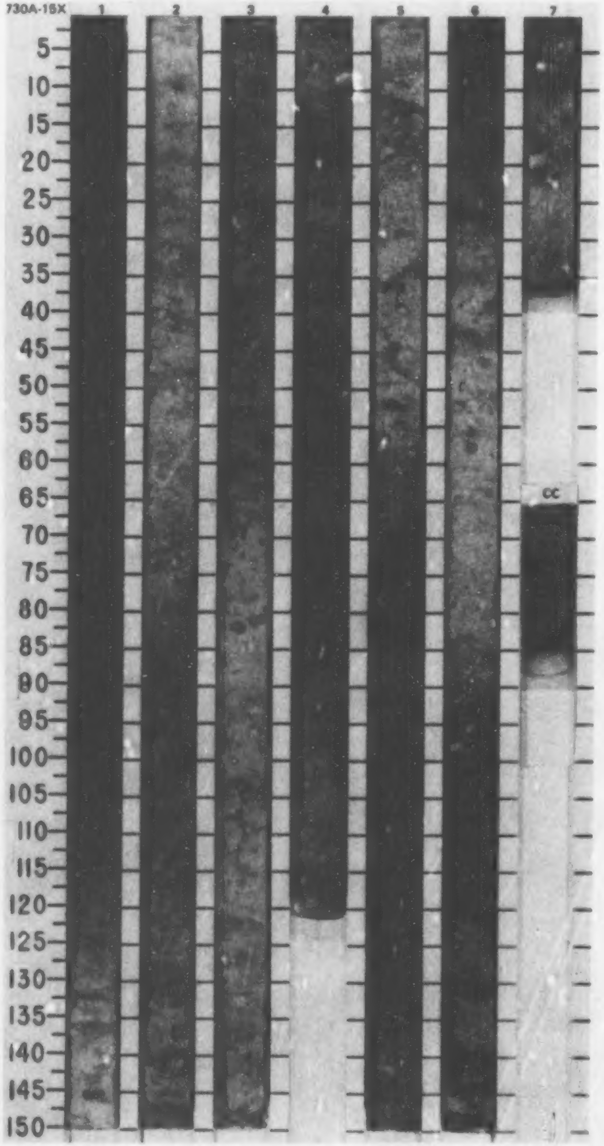
730A-15X
1
2
3
4
5
6
7
CC
5
10
15
20
25
30
35
40
45
50
55
60
65
70
75
80
85
90
95
100
105
110
115
120
125
130
135
140
145
150

SITE 730 HOLE A CORE 16X CORED INTERVAL 1208.7-1218.4 mbsl; 142.9-152.6 mbsf

TIME-ROCK UNIT	BIOSTRAT. ZONE/ FOSSIL CHARACTER: FORAMINIFERS	NANNOFOSSILS	RADIOLARIANS	DIATOMS	PALEOMAGNETICS	PHYS. PROPERTIES	CHEMISTRY	SECTION	METERS	GRAPHIC LITHOLOGY	DRILLING DISTURB.	SED. STRUCTURES	SAMPLES
MIOCENE	N12-N14 ● R/M	NN7 *Discoaster kugleri* ● A/M -P	●C/G *Diartus petterssoni* ●C/G			●ϕ=65.3 γ=1.84 ●ϕ=66.1 γ=1.84 ●ϕ=69.5 γ=1.48	● IC=6.78 OC=0.81 ● IC=6.63 ● IC=5.86	1 2 3 4 5 6 7 CC	0.5 1.0				● ●

LITHOLOGIC DESCRIPTION

DIATOM-BEARING MARLY NANNOFOSSIL OOZE and MARLY NANNOFOSSIL OOZE

Entire core is slightly disturbed.

Major lithologies:

a. DIATOM-BEARING MARLY NANNOFOSSIL OOZE, light gray (5Y 7/2), light olive gray (5Y 6/2), pale olive (5Y 6/3), olive (5Y 5/3), and olive gray (5Y 4/2, 5/2). Minor burrow mottling throughout. Contacts gradational and mottled.

b. Section 6, 5 cm, and below: MARLY NANNOFOSSIL OOZE, olive (5Y 4/3, 5/3). Minor burrow mottling throughout. Contacts gradational and mottled.

SMEAR SLIDE SUMMARY (%):

	2, 34 D	3, 128 D
TEXTURE:		
Silt	5	20
Clay	95	80
COMPOSITION:		
Access. minerals	—	2
Clay	17	25
Diatoms	—	2
Foraminifers	1	—
Volcanic glass	—	Tr
Inorganic calcite	—	2
Nannofossils	80	55
Organic debris	—	2
Quartz	—	10
Radiolarians	Tr	Tr
Silicoflagellates	Tr	—
Sponge spicules	2	2

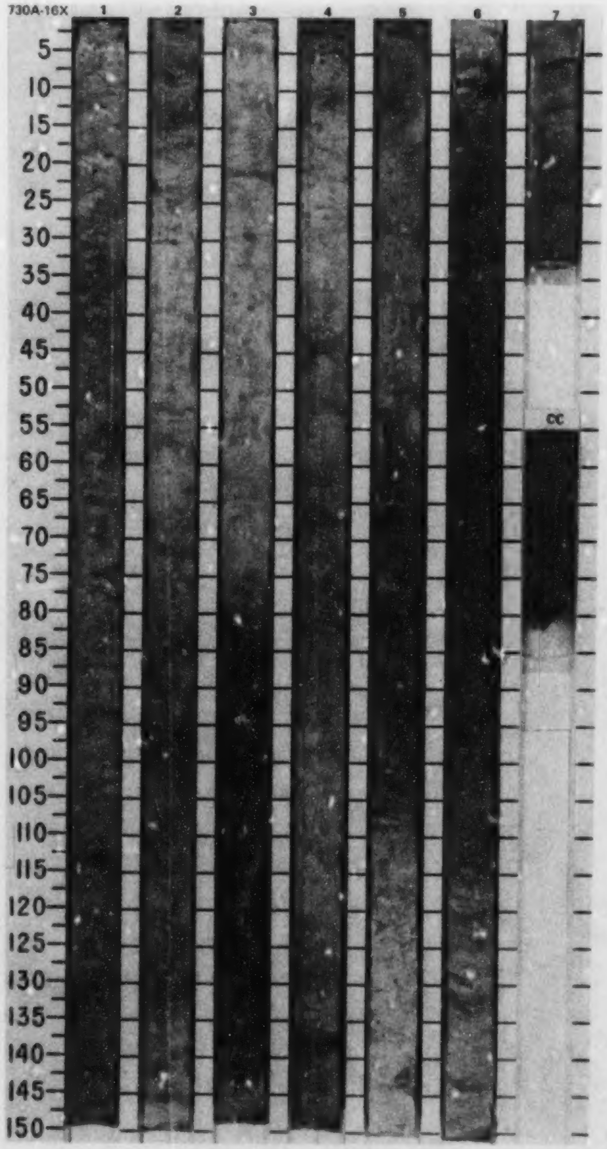

SITE 730 HOLE A CORE 17X CORED INTERVAL 1218.4-1228.0 mbsl; 152.6-162.2 mbsf

TIME-ROCK UNIT: MIOCENE

BIOSTRAT. ZONE/FOSSIL CHARACTER

- FORAMINIFERS: N12-N14; ● A/M
- NANNOFOSSILS: NN7 *Discoaster kugleri*; ● A/M
- RADIOLARIANS: ●C/G *Diartus petterssoni*; ● C/G
- DIATOMS

PALEOMAGNETICS

PHYS. PROPERTIES: ●ϕ=62.2 γ=1.87; ●ϕ=63.1 γ=1.94; ●ϕ=63.0 γ=1.85

CHEMISTRY: ● IC=4.98 OC=1.15; ● IC=4.07; ● IC=5.46

SECTION: 1, 2, 3, 4, 5, 6, CC

METERS: 0.5, 1.0

GRAPHIC LITHOLOGY

DRILLING DISTURB.

SED. STRUCTURES

SAMPLES

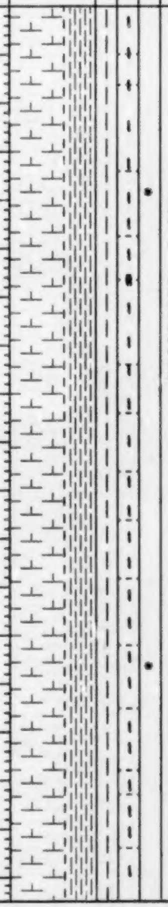

LITHOLOGIC DESCRIPTION

MARLY NANNOFOSSIL OOZE

Entire core is slightly disturbed.

Major lithology: MARLY NANNOFOSSIL OOZE, light gray (5Y 7/1), light olive gray (5Y 6/2), olive (5Y 4/3, 5/3), and olive gray (5Y 5/2). Minor burrow mottling throughout. Contacts gradational and mottled.

SMEAR SLIDE SUMMARY (%):

	2, 41 D	5, 82 D
TEXTURE:		
Sand	10	—
Silt	25	10
Clay	65	90
COMPOSITION:		
Access. minerals	2	Tr
Clay	25	10
Diatoms	1	Tr
Foraminifers	Tr	1
Inorganic calcite	10	2
Nannofossils	40	80
Organic debris	1	—
Quartz	20	—
Radiolarians	Tr	Tr
Sponge spicules	1	2

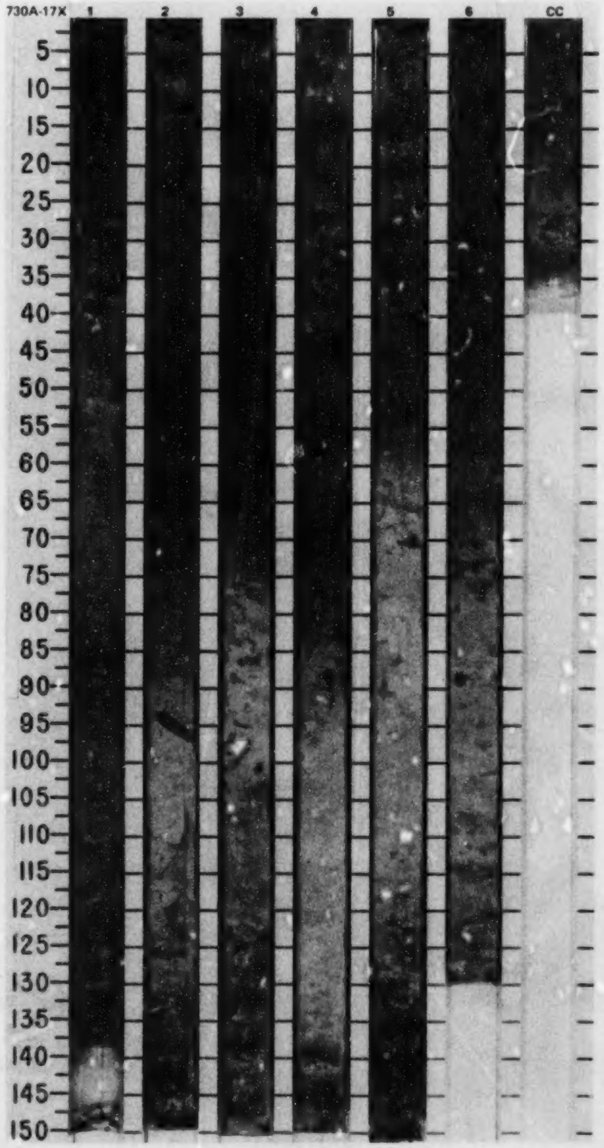

SITE 730 HOLE A CORE 18X CORED INTERVAL 1228.0-1237.7 mbsl; 162.2-171.9 mbsf

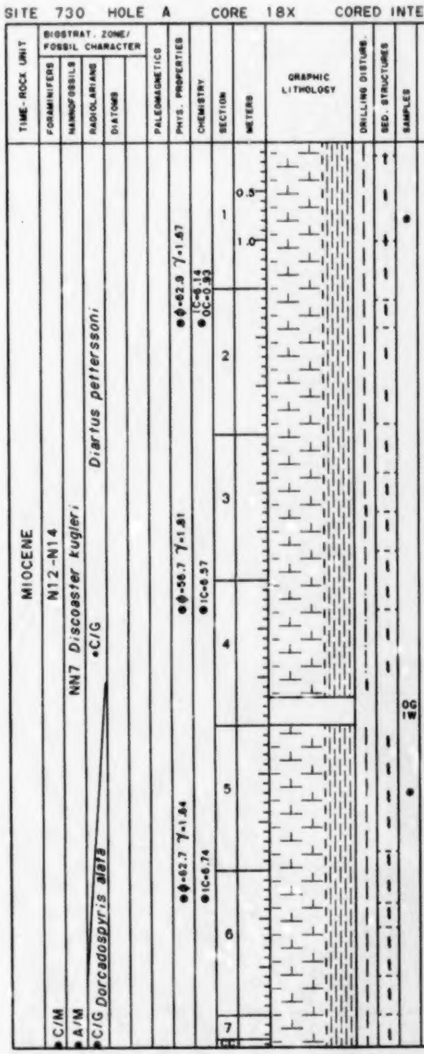
TIME-ROCK UNIT
BIOSTRAT. ZONE/ FOSSIL CHARACTER
FORAMINIFERS
NANNOFOSSILS
RADIOLARIANS
DIATOMS
PALEOMAGNETICS
PHYS. PROPERTIES
CHEMISTRY
SECTION
METERS
GRAPHIC LITHOLOGY
DRILLING DISTURB.
SED. STRUCTURES
SAMPLES
MIOCENE
N12-N14
NN7 Discoaster kugleri
Diartus petterssoni
•C/G
•C/M
•A/M
•C/G Dorcadospyris alata
•φ=62.9 γ=1.67
•IC=6.14 OC=0.93
•φ=58.7 γ=1.81
•IC=6.57
•φ=62.7 γ=1.84
•IC=6.74
1
2
3
4
5
6
7
0.5
1.0
OG
IW

LITHOLOGIC DESCRIPTION

MARLY NANNOFOSSIL OOZE

Section 3, 45-70 cm, and Section 4, 105-120 cm, are very disturbed; remainder is slightly disturbed.

Major lithology: MARLY NANNOFOSSIL OOZE, light gray (5Y 7/2), light olive gray (5Y 6/2), pale olive (5Y 6/3), olive (5Y 5/3), and olive gray (5Y 5/2). Minor burrow mottling throughout. Contacts gradational and mottled.

SMEAR SLIDE SUMMARY (%):

	1, 79 D	5, 68 D
TEXTURE:		
Sand	10	—
Silt	20	10
Clay	70	90
COMPOSITION:		
Access. minerals	Tr	Tr
Clay	25	10
Diatoms	Tr	—
Dolomite	Tr	1
Foraminifers	2	3
Inorganic calcite	17	4
Nannofossils	45	80
Quartz	10	Tr
Radiolarians	—	1
Sponge spicules	1	1

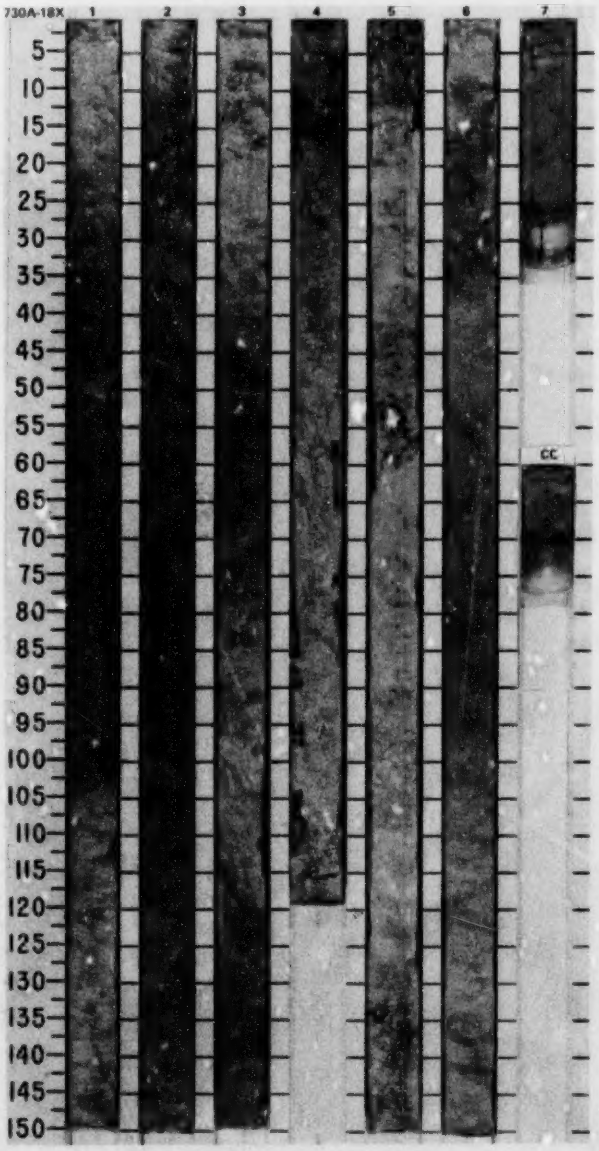
730A-18X
1
2
3
4
5
6
7
CC
5
10
15
20
25
30
35
40
45
50
55
60
65
70
75
80
85
90
95
100
105
110
115
120
125
130
135
140
145
150

SITE 730 HOLE A CORE 19X CORED INTERVAL 1237.7-1247.4 mbsl; 171.9-181.6 mbsf

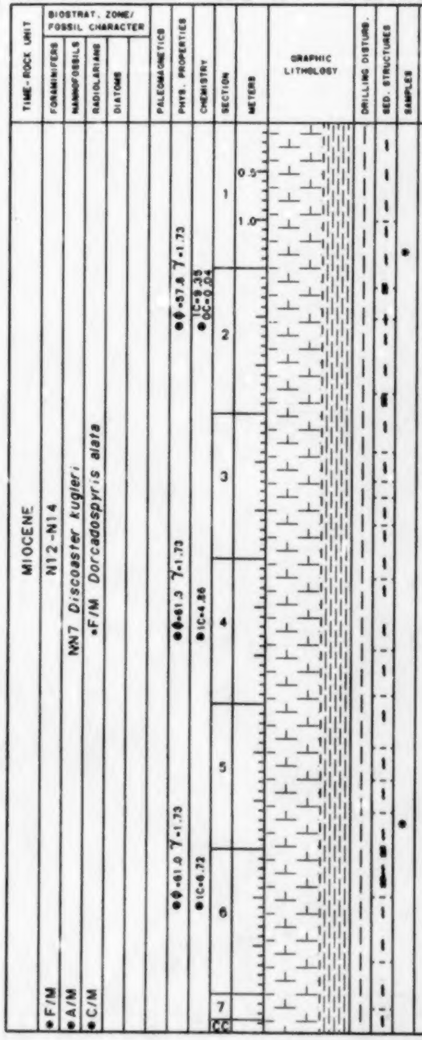
TIME-ROCK UNIT
BIOSTRAT. ZONE/ FOSSIL CHARACTER
FORAMINIFERS
NANNOFOSSILS
RADIOLARIANS
DIATOMS
PALEOMAGNETICS
PHYS. PROPERTIES
CHEMISTRY
SECTION
METERS
GRAPHIC LITHOLOGY
DRILLING DISTURB.
SED. STRUCTURES
SAMPLES
MIOCENE
N12-N14
NN7 Discoaster kugleri
•F/M Dorcadospyris alata
•F/M
•A/M
•C/M
●Φ=57.8 γ=1.73
●Φ=61.3 γ=1.73
●Φ=61.0 γ=1.73
●IC=9.35 OC=0.04
●IC=4.86
●IC=6.72
1
2
3
4
5
6
7
CC
0.5
1.0

LITHOLOGIC DESCRIPTION

MARLY NANNOFOSSIL OOZE

Entire core is slightly disturbed.

Major lithology: MARLY NANNOFOSSIL OOZE, light gray (5Y 7/1, 7/2), light olive gray (5Y 6/2), olive (5Y 5/3, 4/3), and olive gray (5Y 5/2). Minor to moderate burrow mottling. Contacts gradational and mottled.

SMEAR SLIDE SUMMARY (%):

	1, 132 D	5, 122 D
TEXTURE:		
Sand	—	10
Silt	5	25
Clay	85	65
COMPOSITION:		
Access. minerals	—	2
Clay	10	25
Diatoms	—	Tr
Dolomite	Tr	2
Foraminifers	2	2
Inorganic calcite	3	20
Nannofossils	85	40
Organic debris	—	2
Quartz	Tr	7
Sponge spicules	Tr	—

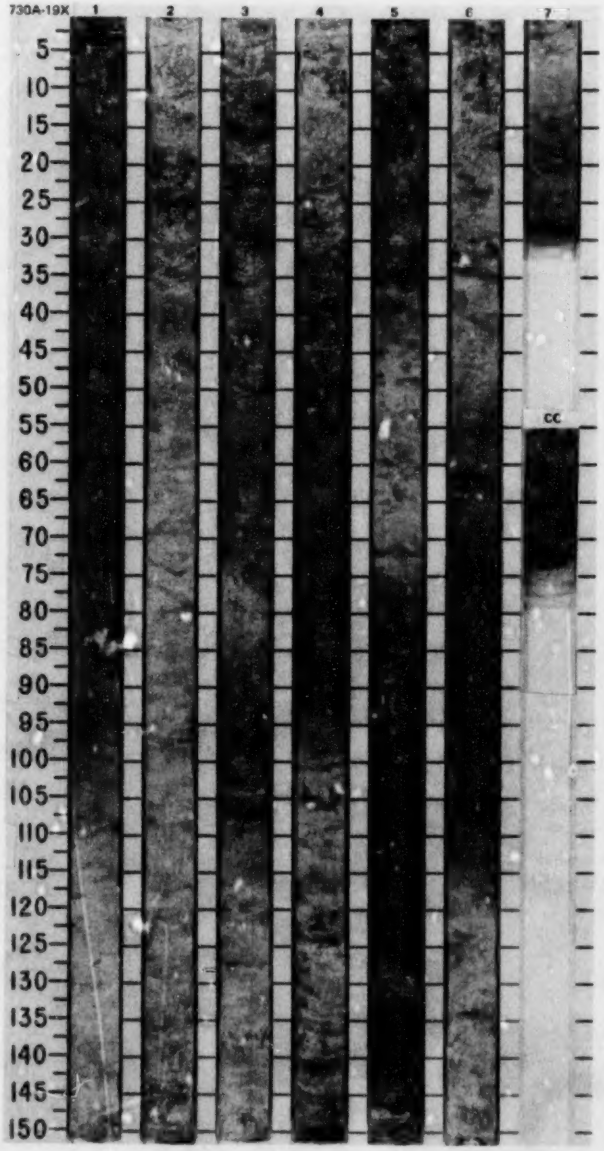
730A-19X
1
2
3
4
5
6
7
CC
5
10
15
20
25
30
35
40
45
50
55
60
65
70
75
80
85
90
95
100
105
110
115
120
125
130
135
140
145
150

SITE 730 HOLE A CORE 20X CORED INTERVAL 1247.4-1257.0 mbsl; 181.6-191.2 mbsf

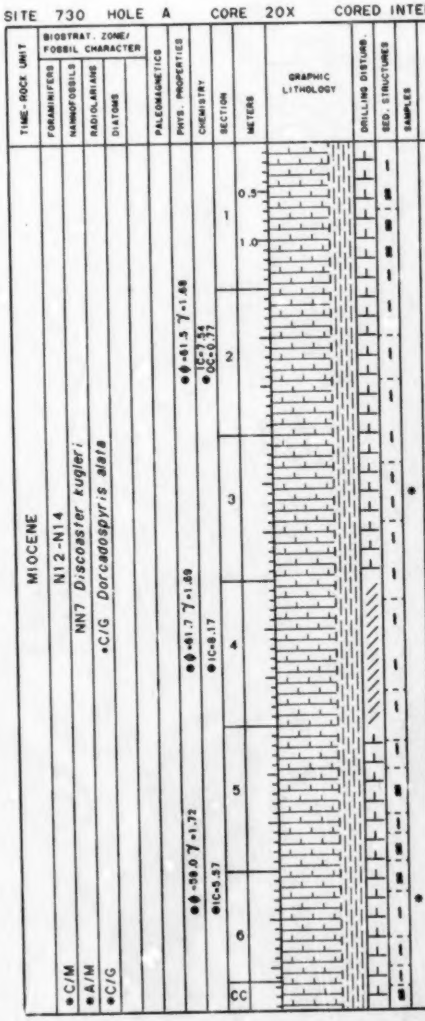
TIME-ROCK UNIT
BIOSTRAT. ZONE/ FOSSIL CHARACTER
FORAMINIFERS
NANNOFOSSILS
RADIOLARIANS
DIATOMS
PALEOMAGNETICS
PHYS. PROPERTIES
CHEMISTRY
SECTION
METERS
GRAPHIC LITHOLOGY
DRILLING DISTURB.
SED. STRUCTURES
SAMPLES
MIOCENE
N12-N14
NN7 Discoaster kugleri
•C/G Dorcadospyris alata
•C/M
•A/M
•C/G
•φ=61.5 γ=1.68
•φ=61.7 γ=1.69
•φ=59.0 γ=1.72
•IC=7.54 OC=0.77
•IC=8.17
•IC=5.57
1
2
3
4
5
6
CC
0.5
1.0

LITHOLOGIC DESCRIPTION

MARLY NANNOFOSSIL CHALK

Section 4, 0-150 cm, is slightly fractured; remainder is moderately fractured.

Major lithology: MARLY NANNOFOSSIL CHALK, light gray (5Y 7/1, 7/2), light olive gray (5Y 6/2), pale olive (5Y 6/3), olive (5Y 5/3, 4/3), and olive gray (5Y 5/2). Minor to moderate burrow mottling. Contacts gradational and mottled.

SMEAR SLIDE SUMMARY (%):

	3, 61 D	6, 34 D
TEXTURE:		
Sand	—	10
Silt	10	20
Clay	90	70
COMPOSITION:		
Access. minerals	—	1
Clay	10	25
Diatoms	—	Tr
Dolomite	—	Tr
Foraminifers	2	Tr
Volcanic glass	6	—
Inorganic calcite	1	20
Mica	—	1
Nannofossils	80	45
Organic debris	—	2
Quartz	Tr	6
Radiolarians	Tr	—
Sponge spicules	1	—

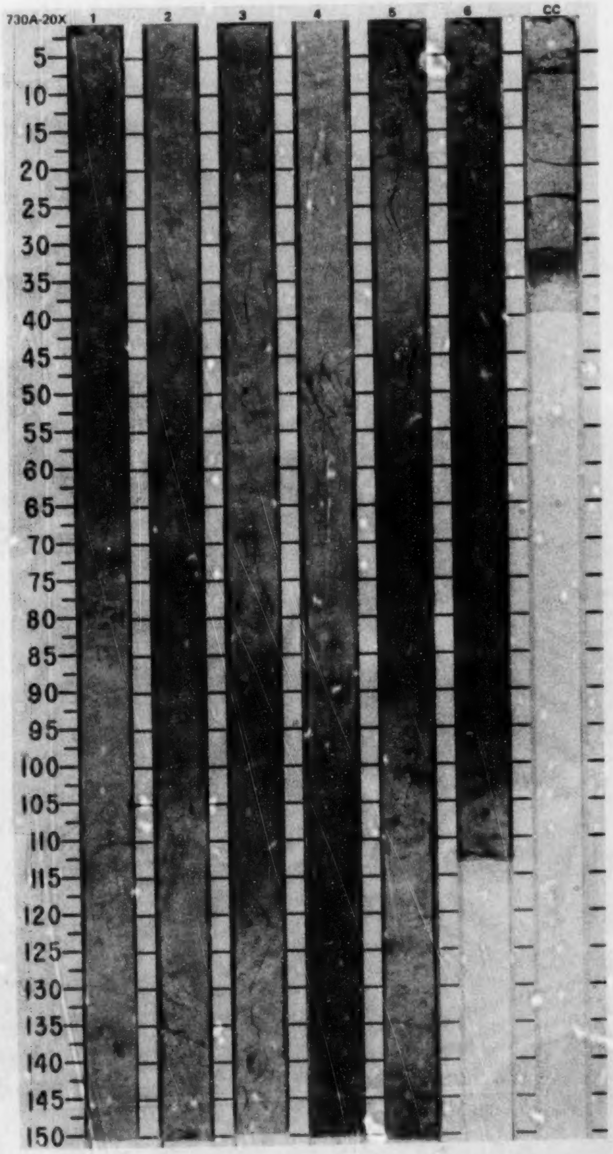
730A-20X
1
2
3
4
5
6
CC
5
10
15
20
25
30
35
40
45
50
55
60
65
70
75
80
85
90
95
100
105
110
115
120
125
130
135
140
145
150

SITE 730 HOLE A CORE 21X CORED INTERVAL 1257.0-1266.7 mbsl; 191.2-200.9 mbsf

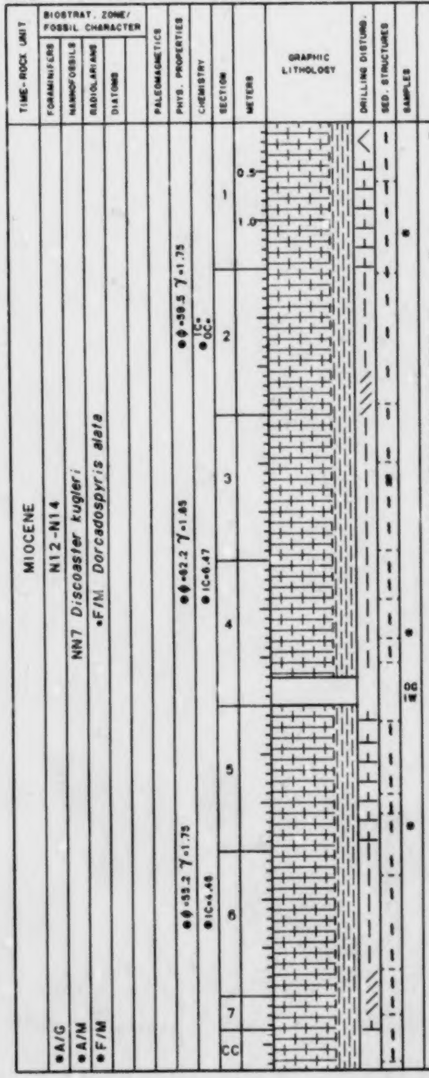
TIME-ROCK UNIT
BIOSTRAT. ZONE/ FOSSIL CHARACTER
FORAMINIFERS
NANNOFOSSILS
RADIOLARIANS
DIATOMS
PALEOMAGNETICS
PHYS. PROPERTIES
CHEMISTRY
SECTION
METERS
GRAPHIC LITHOLOGY
DRILLING DISTURB.
SED. STRUCTURES
SAMPLES
MIOCENE
N12-N14
NN7 Discoaster kugleri
•F/M Dorcadospyris alata
•A/G
•A/M
•F/M
•φ=59.5 γ=1.75
•φ=62.2 γ=1.85
•φ=55.2 γ=1.75
•IC= •OC=
•IC=6.47
•IC=4.46
1
2
3
4
5
6
7
CC
0.5
1.0
OG
IW

LITHOLOGIC DESCRIPTION

FORAMINIFER-NANNOFOSSIL CHALK

Section 1, 0-20 cm, is highly fractured; Section 2, 90-150 cm, Section 6, 120-150 cm, and Section 7, 0-115 cm, are slightly fractured; Section 4 and Section 6, 0-120 cm, are slightly disturbed; remainder is moderately fractured.

Major lithology: FORAMINIFER-NANNOFOSSIL CHALK, light gray (5Y 7/1, 7/2), light olive gray (5Y 6/2), and olive (5Y 5/3, 4/3). Minor to moderate burrow mottling. Contacts gradational and mottled.

SMEAR SLIDE SUMMARY (%):

	1, 114 D	4, 75 D	5, 129 D
TEXTURE:			
Sand	10	15	25
Silt	15	30	10
Clay	75	55	65
COMPOSITION:			
Access. minerals	Tr	2	—
Clay	15	25	10
Diatoms	1	2	—
Dolomite	1	2	—
Foraminifers	15	Tr	25
Inorganic calcite	3	25	8
Nannofossils	60	30	55
Organic debris	—	2	—
Quartz	2	10	—
Radiolarians	1	—	Tr
Silicoflagellates	Tr	—	—
Sponge spicule	2	2	2

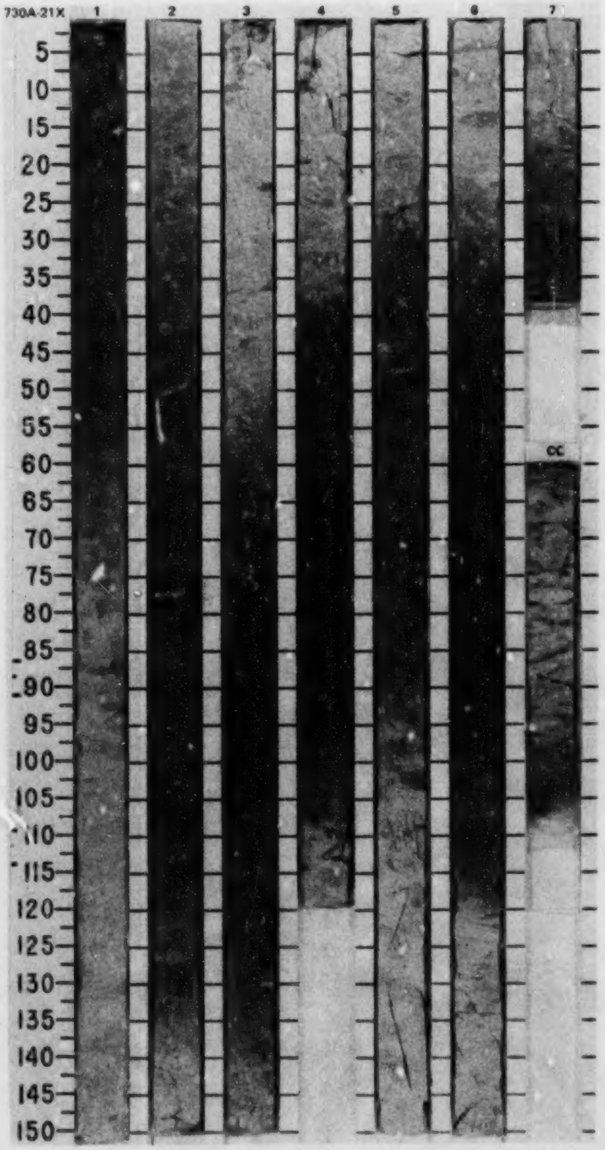
730A-21X
1
2
3
4
5
6
7
CC
5
10
15
20
25
30
35
40
45
50
55
60
65
70
75
80
85
90
95
100
105
110
115
120
125
130
135
140
145
150

SITE 730 HOLE A CORE 22X CORED INTERVAL 1266.7-1276.4 mbsl; 200.9-210.6 mbsf

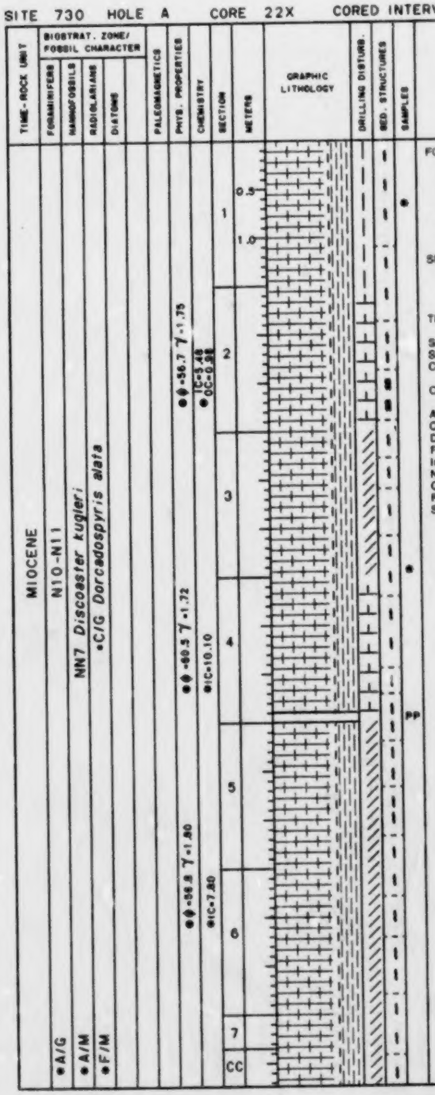
TIME-ROCK UNIT
BIOSTRAT. ZONE/ FOSSIL CHARACTER
FORAMINIFERS
NANNOFOSSILS
RADIOLARIANS
DIATOMS
PALEOMAGNETICS
PHYS. PROPERTIES
CHEMISTRY
SECTION
METERS
GRAPHIC LITHOLOGY
DRILLING DISTURB.
SED. STRUCTURES
SAMPLES
MIOCENE
N10-N11
NN7 Discoaster kugleri
•C/G Dorcadospyris alata
•A/G
•A/M
•F/M
•φ=56.7 γ=1.75
•IC=5.48 OC=0.98
•φ=60.5 γ=1.72
•IC=10.10
•φ=58.8 γ=1.80
•IC=7.80
1
2
3
4
5
6
7
CC
0.5
1.0
PP

LITHOLOGIC DESCRIPTION

FORAMINIFER-NANNOFOSSIL CHALK

Section 2, 0-150 cm, and Section 4, 0-140 cm, are moderately disturbed. Section 1, 0-150 cm, is slightly disturbed; and remainder is slightly fractured.

Major lithology: FORAMINIFER-NANNOFOSSIL CHALK, light gray (5Y 7/1, 7/2), light olive gray (5Y 6/2), and olive gray (5Y 5/2). Minor to moderate burrow mottling. Contacts gradational and mottled.

SMEAR SLIDE SUMMARY (%):

	1, 66 D	3, 146 D
TEXTURE:		
Sand	10	10
Silt	10	30
Clay	80	60
COMPOSITION:		
Access. minerals	1	1
Clay	10	25
Diatoms	—	Tr
Foraminifers	15	3
Inorganic calcite	3	10
Nannofossils	70	45
Quartz	—	15
Radiolarians	—	Tr
Sponge spicules	1	1

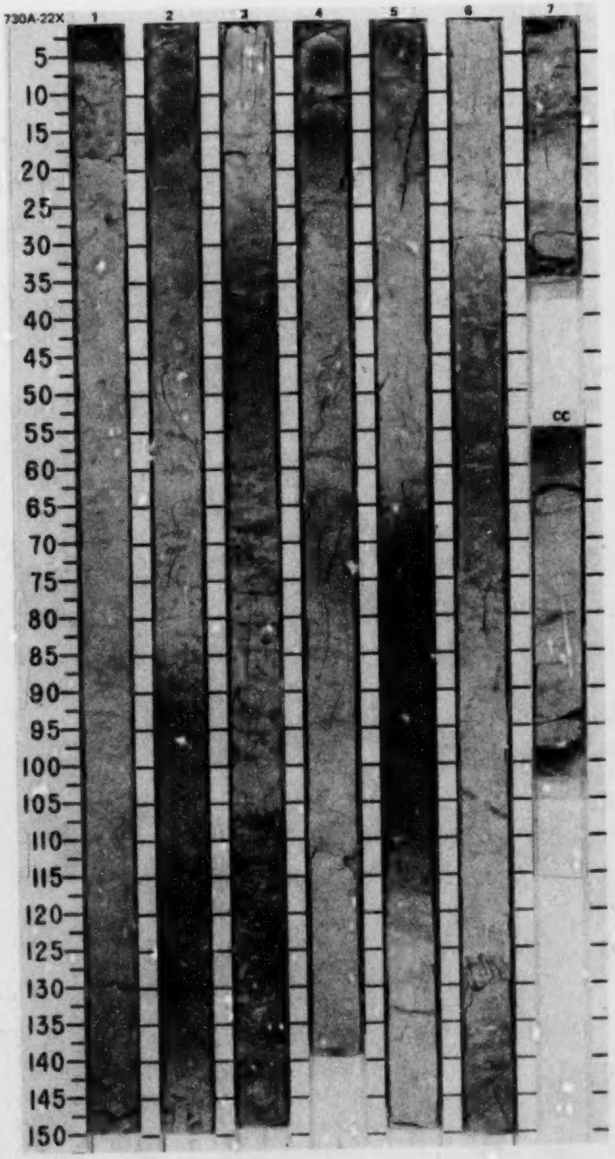
730A-22X
1
2
3
4
5
6
7
CC
5
10
15
20
25
30
35
40
45
50
55
60
65
70
75
80
85
90
95
100
105
110
115
120
125
130
135
140
145
150

SITE 730 HOLE A CORE 23X CORED INTERVAL 1276.4-1286.0 mbsl; 210.6-220.2 mbsf

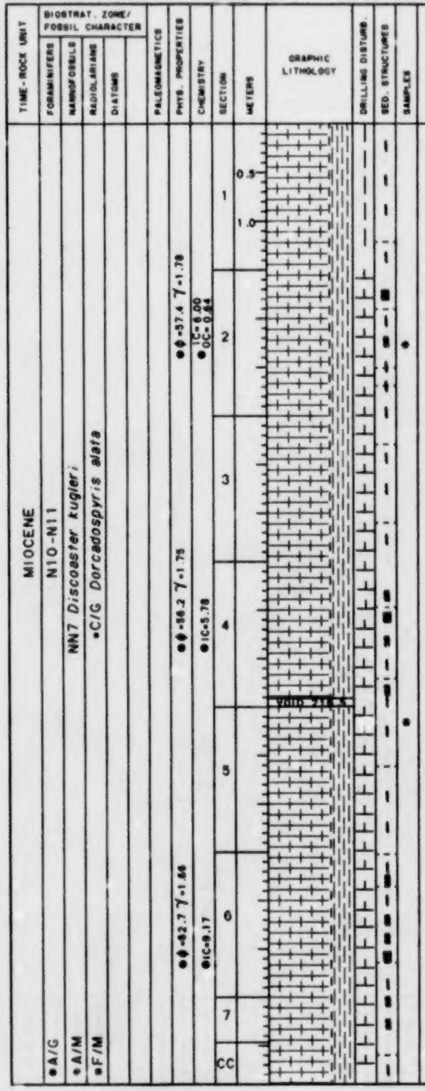
TIME-ROCK UNIT
BIOSTRAT. ZONE/ FOSSIL CHARACTER
FORAMINIFERS
NANNOFOSSILS
RADIOLARIANS
DIATOMS
PALEOMAGNETICS
PHYS. PROPERTIES
CHEMISTRY
SECTION
METERS
GRAPHIC LITHOLOGY
DRILLING DISTURB.
SED. STRUCTURES
SAMPLES
MIOCENE
N10-N11
NN7 Discoaster kugleri
•C/G Dorcadospyris alata
•A/G
•A/M
•F/M
•φ=57.4 γ=1.78
•φ=56.2 γ=1.75
•φ=62.7 γ=1.66
•IC=6.00 OC=0.64
•IC=5.78
•IC=9.17
1
2
3
4
5
6
7
CC
0.5
1.0
Void

LITHOLOGIC DESCRIPTION

FORAMINIFER-NANNOFOSSIL CHALK

Section 1, 0-150 cm, is slightly disturbed; remainder is moderately fractured.

Major lithology: FORAMINIFER-NANNOFOSSIL CHALK, light gray (5Y 7/1, 7/2), light olive gray (5Y 6/2), olive (5Y 5/3), and olive gray (5Y 5/2). Minor to strong burrow mottling. Contacts gradational and mottled.

SMEAR SLIDE SUMMARY (%):

	2, 77 D	5, 15 D
TEXTURE:		
Sand	15	20
Silt	20	5
Clay	65	75
COMPOSITION:		
Access. minerals	1	—
Clay	25	10
Diatoms	Tr	—
Dolomite	Tr	—
Foraminifers	2	20
Inorganic calcite	20	3
Nannofossils	40	65
Radiolarians	Tr	Tr
Quartz	10	—
Sponge spicules	2	2

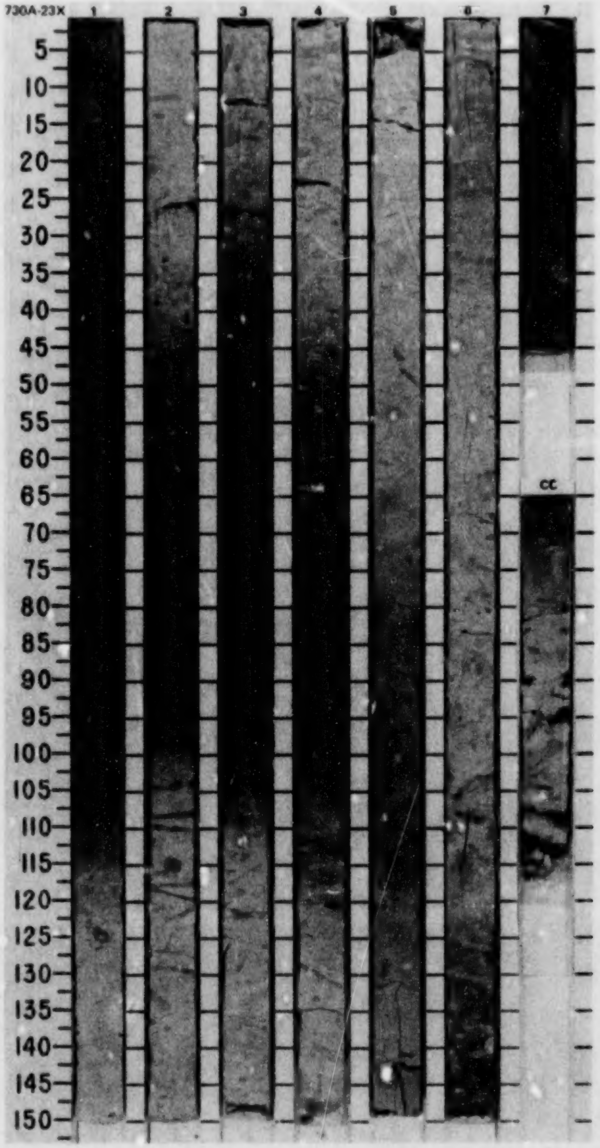
730A-23X
1
2
3
4
5
6
7
CC
5
10
15
20
25
30
35
40
45
50
55
60
65
70
75
80
85
90
95
100
105
110
115
120
125
130
135
140
145
150

SITE 730 HOLE A CORE 24X CORED INTERVAL 1286.0-1295.7 mbsl; 220.2-229.9 mbsf

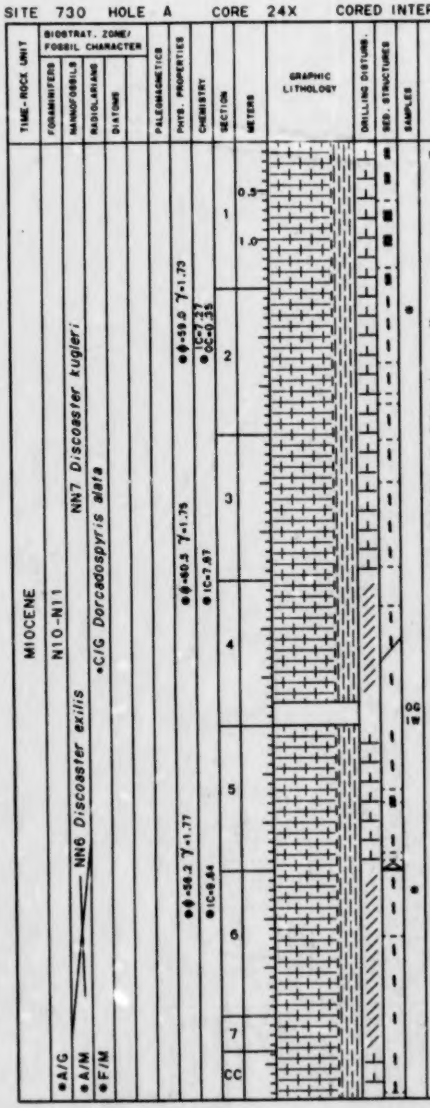
TIME-ROCK UNIT
BIOSTRAT. ZONE/ FOSSIL CHARACTER
FORAMINIFERS
NANNOFOSSILS
RADIOLARIANS
DIATOMS
PALEOMAGNETICS
PHYS. PROPERTIES
CHEMISTRY
SECTION
METERS
GRAPHIC LITHOLOGY
DRILLING DISTURB.
SED. STRUCTURES
SAMPLES
MIOCENE
N10-N11
NN7 Discoaster kugleri
NN6 Discoaster exilis
•C/G Dorcadospyris alata
•A/G
•A/M
•F/M
•φ=59.0 γ=1.73
•IC=7.27 OC=0.35
•φ=60.5 γ=1.75
•IC=7.87
•φ=58.2 γ=1.77
•IC=8.64
1
2
3
4
5
6
7
CC
0.5
1.0
OG
IW

LITHOLOGIC DESCRIPTION

FORAMINIFER-NANNOFOSSIL CHALK

Section 4, 0–123 cm, Section 6, 0–150 cm, and Section 7, 0–35 cm, are slightly fractured; remainder is moderately fractured.

Major lithology: FORAMINIFER-NANNOFOSSIL CHALK, light gray (5Y 7/1), gray (5Y 6/1), light olive gray (5Y 6/2), olive (5Y 5/3), and olive gray (5Y 5/2). Minor to strong burrow mottling. Contacts gradational and mottled. Section 3, 140–150 cm, and Section 4, 0–123 cm, has many en echelon high angle faults.

Minor lithology: Section 5, 143–146 cm, foraminifer-rich carbonate turbidite containing sand-sized clasts of black (5Y 2.5/1) shale. Sharp base and gradational top, normal grading.

SMEAR SLIDE SUMMARY (%):

	2, 23 D	6, 20 D
TEXTURE:		
Sand	15	25
Silt	20	15
Clay	65	60
COMPOSITION:		
Access. minerals	2	—
Clay	20	15
Dolomite	3	—
Foraminifers	1	25
Inorganic calcite	20	10
Mica	Tr	—
Nannofossils	40	45
Quartz	7	—
Sponge spicules	2	5

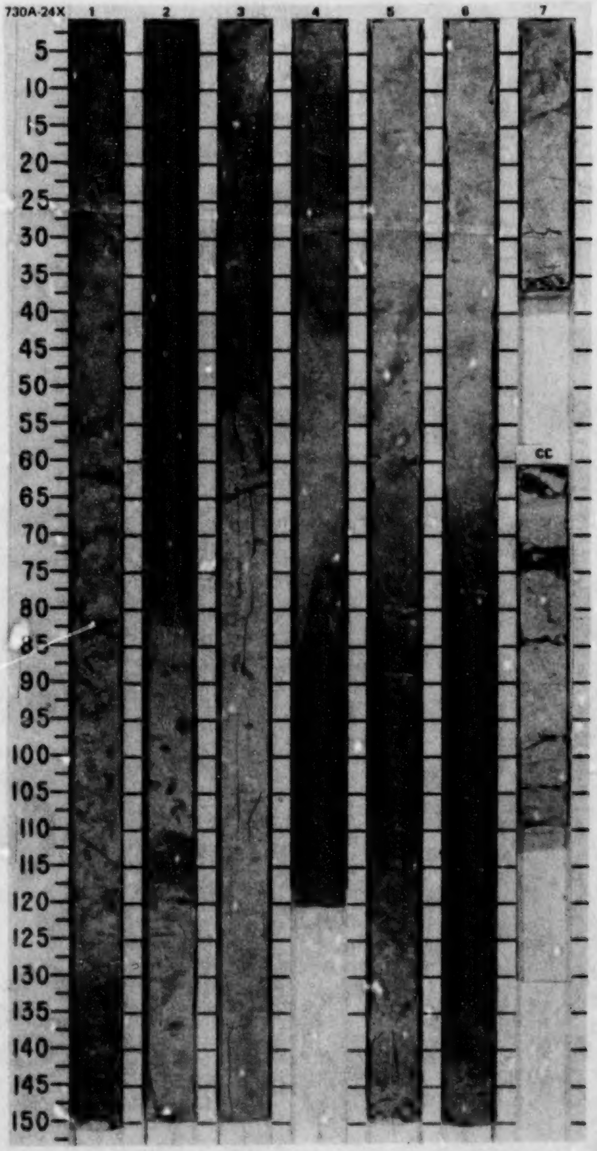
730A-24X
1
2
3
4
5
6
7
CC
5
10
15
20
25
30
35
40
45
50
55
60
65
70
75
80
85
90
95
100
105
110
115
120
125
130
135
140
145
150

SITE 730 HOLE A CORE 25X CORED INTERVAL 1295.7-1305.4 mbsl; 229.9-239.6 mbsf

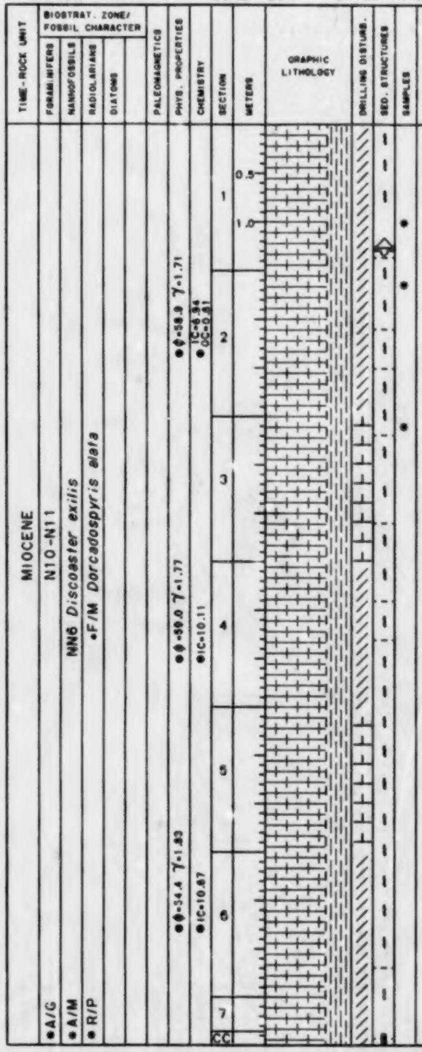
TIME-ROCK UNIT
BIOSTRAT. ZONE/ FOSSIL CHARACTER
FORAMINIFERS
NANNOFOSSILS
RADIOLARIANS
DIATOMS
PALEOMAGNETICS
PHYS. PROPERTIES
CHEMISTRY
SECTION
METERS
GRAPHIC LITHOLOGY
DRILLING DISTURB.
SED. STRUCTURES
SAMPLES
MIOCENE
N10-N11
NN6 Discoaster exilis
•F/M Dorcadospyris alata
•A/G
•A/M
•R/P
•φ=58.9 γ=1.71
•IC=6.94 OC=0.81
•φ=50.0 γ=1.77
•IC=10.11
•φ=34.4 γ=1.83
•IC=10.87
1
2
3
4
5
6
7
CC
0.5
1.0

LITHOLOGIC DESCRIPTION

FORAMINIFER-NANNOFOSSIL CHALK

Sections 3 and 5 are moderately fractured; remainder is slightly fractured.

Major lithology: FORAMINIFER-NANNOFOSSIL CHALK, white (5Y 8/1), light gray (5Y 7/1, 7/2), gray (5Y 6/1), light olive gray (5Y 6/2), olive (5Y 5/3), and olive gray (5Y 5/2). Minor burrow mottling throughout. Contacts gradational and mottled. Section 3, 140-150 cm, and Section 4, 0-123 cm, many en echelon high angle faults.

Minor lithology: Section 1, 122-125 cm, foraminifer-rich carbonate turbidite containing sand sized clasts of black (5Y 2.5/1) shale. Sharp base and gradational top.

SMEAR SLIDE SUMMARY (%):

	1, 99 D	2, 15 D	3, 11 D
TEXTURE:			
Sand	10	25	15
Silt	20	10	5
Clay	70	65	80
COMPOSITION:			
Access. minerals	2	Tr	—
Clay	25	15	10
Dolomite	1	—	—
Foraminifers	3	25	16
Inorganic calcite	20	7	3
Nannofossils	45	50	70
Quartz	2	Tr	—
Radiolarians	Tr	—	—
Sponge spicules	2	3	1

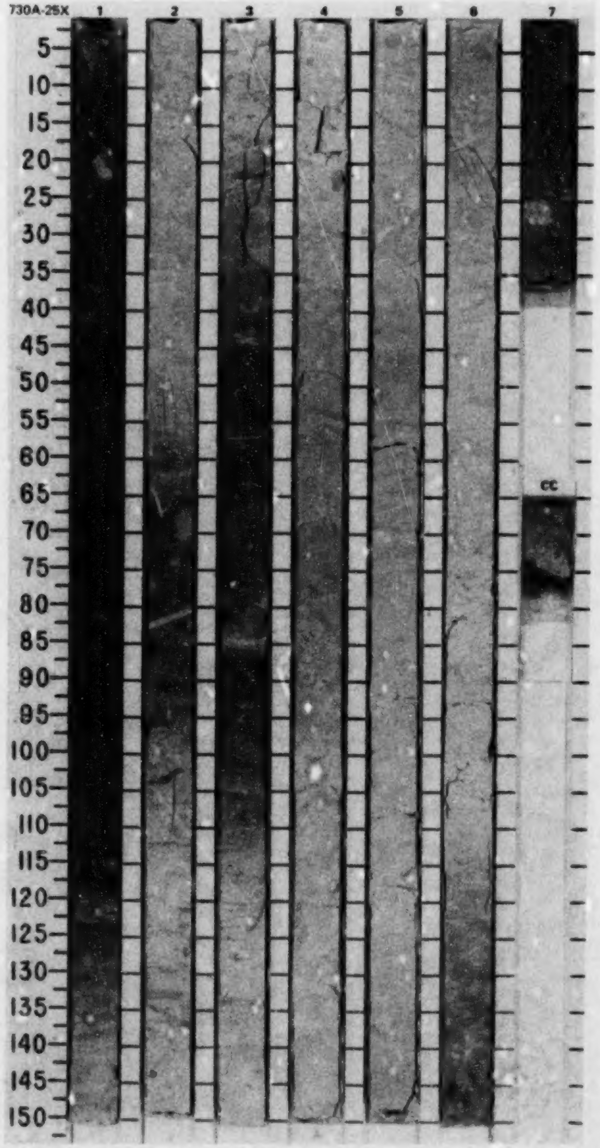
730A-25X
1
2
3
4
5
6
7
CC
5
10
15
20
25
30
35
40
45
50
55
60
65
70
75
80
85
90
95
100
105
110
115
120
125
130
135
140
145
150

SITE 730 HOLE A CORE 26X CORED INTERVAL 1305.4-1315.0 mbsl; 239.6-249.2 mbsf

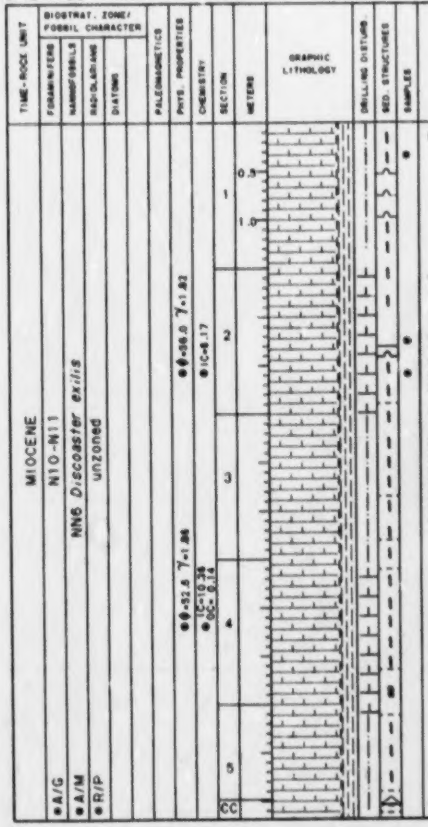
TIME-ROCK UNIT
BIOSTRAT. ZONE/ FOSSIL CHARACTER
FORAMINIFERS
NANNOFOSSILS
RADIOLARIANS
DIATOMS
PALEOMAGNETICS
PHYS. PROPERTIES
CHEMISTRY
SECTION
METERS
GRAPHIC LITHOLOGY
DRILLING DISTURB.
SED. STRUCTURES
SAMPLES
MIOCENE
●A/G N10-N11
●A/M NN6 Discoaster exilis
●R/P unzoned
●Φ=56.0 γ=1.92
●Φ=52.5 γ=1.86
●IC=8.17
●IC=10.36 OC=0.14
1
2
3
4
5
CC
0.5
1.0

LITHOLOGIC DESCRIPTION

FORAMINIFER-BEARING MARLY NANNOFOSSIL CHALK

Sections 2-4 are moderately fractured; remainder is moderately disturbed.

Major lithology: FORAMINIFER-BEARING MARLY NANNOFOSSIL CHALK, light gray (5Y 7/1), light olive gray (5Y 6/2), and olive gray (5Y 5/2). Minor burrow mottling throughout. Contacts gradational and mottled. Section 1, 55-100 cm, and Section 2, 82 cm, has slumps with recumbant folds visible.

Minor lithology: CC, 0-3 and 7-10 cm, foraminifer sand with normal grading and sand-sized shale clasts.

SMEAR SLIDE SUMMARY (%):

	1, 33 D	2, 72 D	2, 112 D
TEXTURE:			
Sand	15	5	18
Silt	10	20	14
Clay	75	75	68
COMPOSITION:			
Access. minerals	—	1	1
Clay	15	10	25
Dolomite	Tr	1	2
Foraminifers	10	6	4
Inorganic calcite	14	15	25
Nannofossils	60	65	40
Quartz	—	1	3
Sponge spicules	1	1	Tr

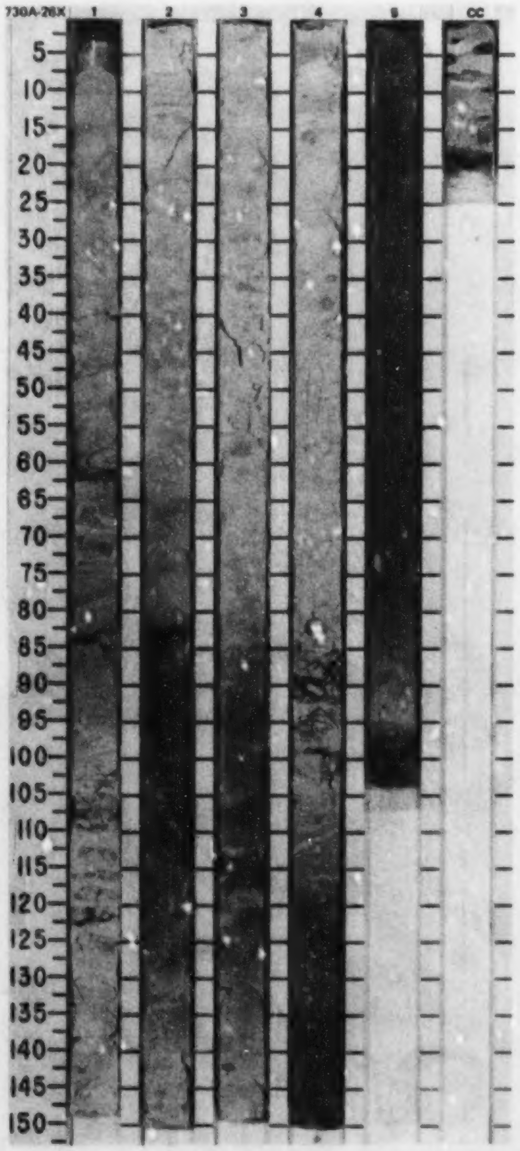
730A-26X
1
2
3
4
5
CC
5
10
15
20
25
30
35
40
45
50
55
60
65
70
75
80
85
90
95
100
105
110
115
120
125
130
135
140
145
150

SITE 730 HOLE A CORE 27X CORED INTERVAL 1315.0-1324.7 mbsl; 249.2-258.9 mbsf

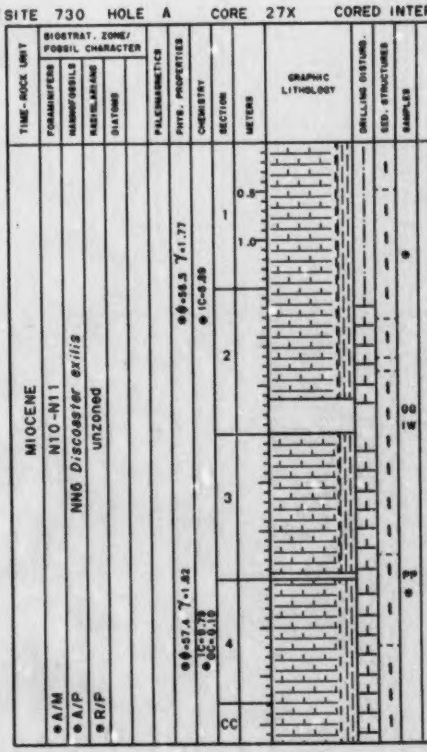
TIME-ROCK UNIT
BIOSTRAT. ZONE/ FOSSIL CHARACTER
FORAMINIFERS
NANNOFOSSILS
RADIOLARIANS
DIATOMS
PALEOMAGNETICS
PHYS. PROPERTIES
CHEMISTRY
SECTION
METERS
GRAPHIC LITHOLOGY
DRILLING DISTURB.
SED. STRUCTURES
SAMPLES
MIOCENE
N10-N11
NN6 Discoaster exilis
unzoned
● A/M
● A/P
● R/P
●Φ=58.5 γ=1.77
●Φ=57.4 γ=1.82
● IC=8.89
● IC=8.79 OC=0.10
1
2
3
4
CC
0.5
1.0
OG
IW
PP

LITHOLOGIC DESCRIPTION

FORAMINIFER-BEARING MARLY NANNOFOSSIL CHALK

[illegible]on 1, 0–150 cm, is moderately disturbed; remainder is moderately [illegible]tured.

Major lithology: FORAMINIFER-BEARING MARLY NANNOFOSSIL CHALK, white (5Y 8/1), light gray (5Y 7/1, 7/2), light olive gray (5Y 6/2), and olive (5Y 5/3). Minor burrow mottling throughout. Contacts gradational and mottled.

SMEAR SLIDE SUMMARY (%):

	1, 114 D	4, 14 D
TEXTURE:		
Sand	5	—
Silt	15	10
Clay	80	90
COMPOSITION:		
Access. minerals	2	—
Clay	25	10
Dolomite	2	1
Foraminifers	1	5
Inorganic calcite	14	4
Nannofossils	55	80
Quartz	1	—
Radiolarians	1	—

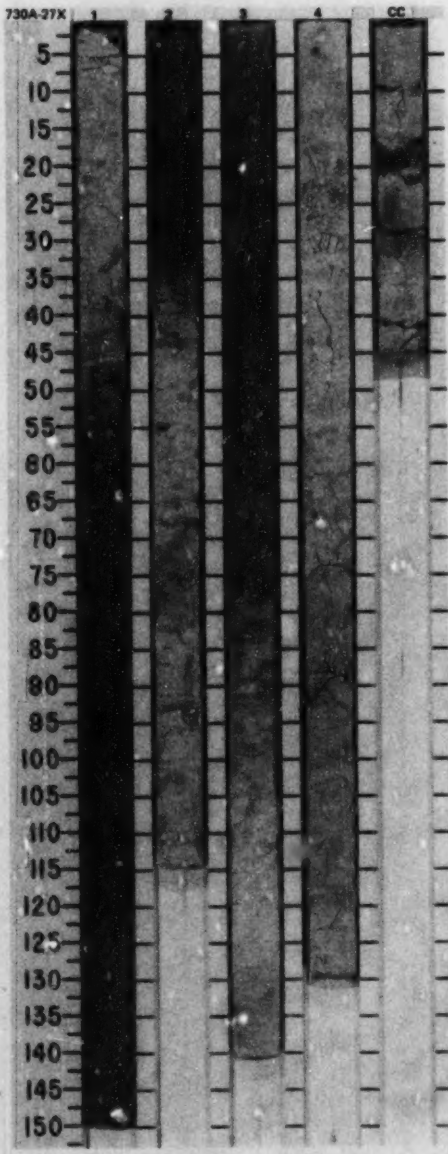
730A-27X
1
2
3
4
CC
5
10
15
20
25
30
35
40
45
50
55
60
65
70
75
80
85
90
95
100
105
110
115
120
125
130
135
140
145
150

SITE 730 HOLE A CORE 28X CORED INTERVAL 1324.7-1334.4 mbsl; 258.9-268.6 mbsf

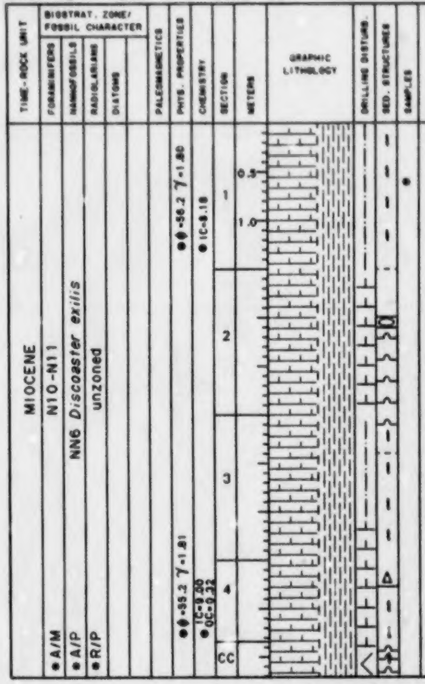
TIME-ROCK UNIT
BIOSTRAT. ZONE/ FOSSIL CHARACTER
FORAMINIFERS
NANNOFOSSILS
RADIOLARIANS
DIATOMS
PALEOMAGNETICS
PHYS. PROPERTIES
CHEMISTRY
SECTION
METERS
GRAPHIC LITHOLOGY
DRILLING DISTURB.
SED. STRUCTURES
SAMPLES
MIOCENE
N10-N11
NN6 Discoaster exilis
unzoned
● A/M
● A/P
● R/P
●φ=56.2 γ=1.80
●φ=55.2 γ=1.81
● IC=8.18
● IC=9.00 OC=0.32
1
2
3
4
CC
0.5
1.0

LITHOLOGIC DESCRIPTION

FORAMINIFER-BEARING MARLY NANNOFOSSIL CHALK

Section 1, 0-150 cm, and Section 3, 0-100 cm, are moderately disturbed; CC is heavily fractured; remainder is moderately fractured.

Major lithology: FORAMINIFER-BEARING MARLY NANNOFOSSIL CHALK, white (5Y 8/1), light gray (5Y 7/1, 7/2), and light olive gray (5Y 6/2). Minor burrow mottling common. Contacts gradational and mottled. Section 2, 56-150 cm, Section 3, 25-30 cm, and CC, 0-38 cm, slumped horizon. Section 2, 52-56 cm, dolomite clast.

Minor lithology: Section 4, 18-25 cm, foraminifer sand, normally graded with shale clasts (carbonate turbidite).

SMEAR SLIDE SUMMARY (%):

	1, 62 D
TEXTURE:	
Sand	5
Silt	15
Clay	80
COMPOSITION:	
Access. minerals	1
Clay	25
Foraminifers	2
Inorganic calcite	15
Nannofossils	55
Quartz	1
Sponge spicules	1

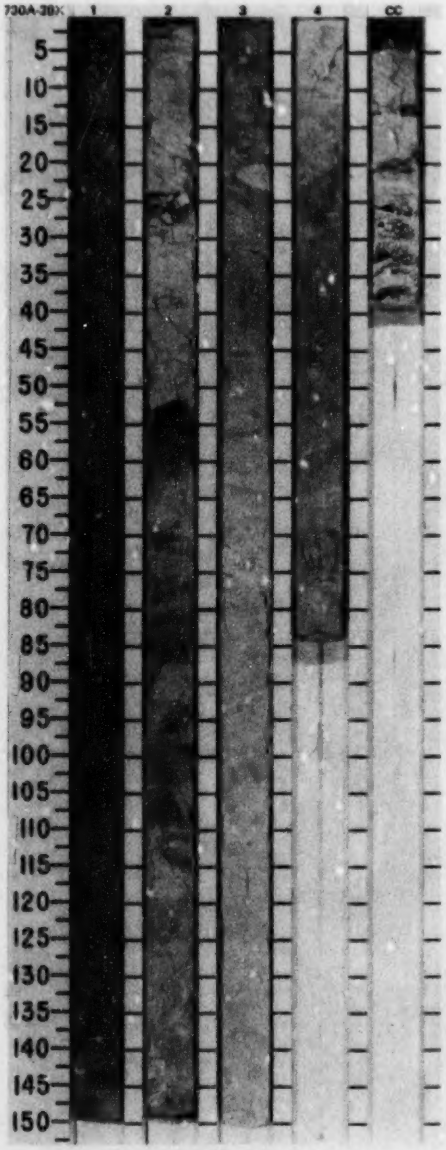
730A-28X
1
2
3
4
CC
5
10
15
20
25
30
35
40
45
50
55
60
65
70
75
80
85
90
95
100
105
110
115
120
125
130
135
140
145
150

SITE 730 HOLE A CORE 29X CORED INTERVAL 1334.4-1344.0 mbsl; 268.6-278.2 mbsf

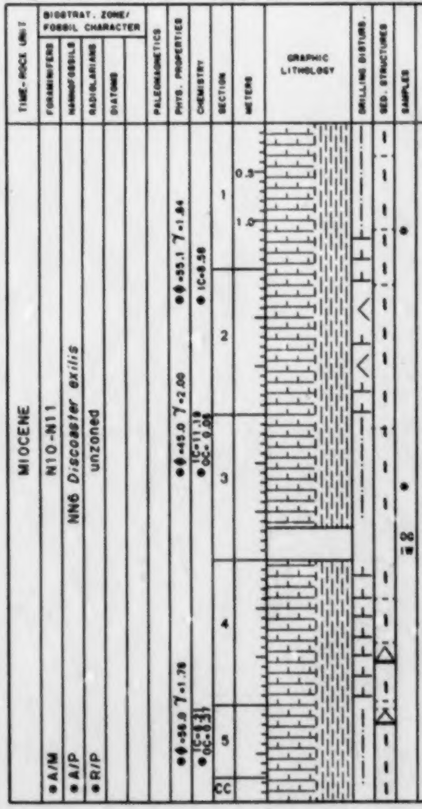
TIME-ROCK UNIT
BIOSTRAT. ZONE/ FOSSIL CHARACTER
FORAMINIFERS
NANNOFOSSILS
RADIOLARIANS
DIATOMS
PALEOMAGNETICS
PHYS. PROPERTIES
CHEMISTRY
SECTION
METERS
GRAPHIC LITHOLOGY
DRILLING DISTURB.
SED. STRUCTURES
SAMPLES
MIOCENE
N10-N11
NN6 Discoaster exilis
unzoned
●A/M
●A/P
●R/P
●ϕ=55.1 γ=1.84
●ϕ=45.0 γ=2.00
●ϕ=56.0 γ=1.78
● IC=8.58
● IC=11.19 OC=0.05
● IC=8.31 OC=0.31
1
2
3
4
5
CC
0.5
1.0
OG
IW

LITHOLOGIC DESCRIPTION

FORAMINIFER-BEARING MARLY NANNOFOSSIL CHALK

Section 2, 20-50, and 80-110 cm, are heavily fractured; Section 1, 120-150 cm, Section 2, 0-20, 50-80, and 110-150 cm, Section 4, 0-150 cm, and Section 3, 0-100 cm, are moderately fractured; and remainder is moderately disturbed.

Major lithology: FORAMINIFER-BEARING MARLY NANNOFOSSIL CHALK, white (5Y 8/1), light gray (5Y 7/2), light olive gray (5Y 6/2), and olive gray (5Y 5/2). Minor burrow mottling common. Contacts gradational and mottled.

Minor lithology: Section 4, 85-105 and 145-150 cm, and Section 5, 0-20 cm, benthic foraminifer sand to silt, normally graded with shale clasts (carbonate turbidite).

SMEAR SLIDE SUMMARY (%):

	1, 110 D	3, 73 D
TEXTURE:		
Sand	15	10
Silt	10	20
Clay	75	70
COMPOSITION:		
Access. minerals	—	1
Clay	10	20
Dolomite	—	2
Foraminifers	8	5
Inorganic calcite	15	20
Mica	—	Tr
Nannofossils	65	50
Quartz	—	1
Radiolarians	—	Tr
Sponge spicules	2	1

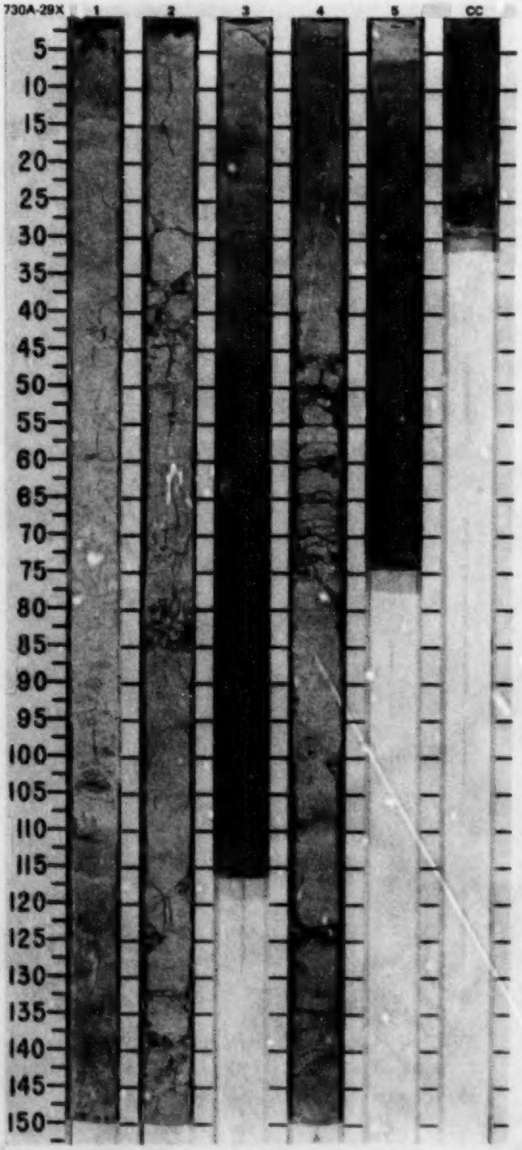
730A-29X
1
2
3
4
5
CC
5
10
15
20
25
30
35
40
45
50
55
60
65
70
75
80
85
90
95
100
105
110
115
120
125
130
135
140
145
150

SITE 730 HOLE A CORE 30X CORED INTERVAL 1344.0-1353.7 mbsl; 278.2-287.9 mbsf

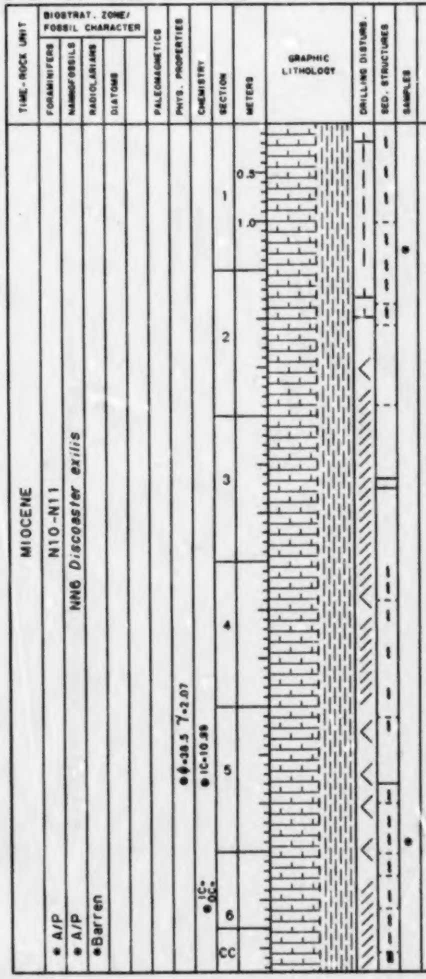
TIME-ROCK UNIT
BIOSTRAT. ZONE/ FOSSIL CHARACTER
FORAMINIFERS
NANNOFOSSILS
RADIOLARIANS
DIATOMS
PALEOMAGNETICS
PHYS. PROPERTIES
CHEMISTRY
SECTION
METERS
GRAPHIC LITHOLOGY
DRILLING DISTURB.
SED. STRUCTURES
SAMPLES
MIOCENE
N10-N11
NN6 Discoaster exilis
• A/P
• A/P
•Barren
•ϕ=38.5 γ=2.07
•IC=10.98
•IC= OC=
1
2
3
4
5
6
CC
0.5
1.0

LITHOLOGIC DESCRIPTION

FORAMINIFER-BEARING MARLY NANNOFOSSIL CHALK

Section 2, 80-110 cm, Section 3, 50-70 cm, Section 4, 20-50 cm, Section 5, 20-150 cm, and Section 6, 0-30 cm, are heavily fractured; Section 1, 0-20 cm, and Section 2, 20-50 cm, are moderately fractured; Section 1, 20-150 cm, is slightly disturbed; and remainder is slightly fractured.

Major lithology: FORAMINIFER-BEARING MARLY NANNOFOSSIL CHALK, white (5Y 8/1), light gray (5Y 7/1, 7/2), light olive gray (5Y 6/2), and olive gray (5Y 5/2). Minor burrow mottling common. Contacts gradational and mottled.

SMEAR SLIDE SUMMARY (%):

	1, 130 D	5, 140 M
TEXTURE:		
Sand	15	15
Silt	20	20
Clay	65	65
COMPOSITION:		
Cla	20	20
Dolomite	Tr	Tr
Foraminifers	20	15
Inorganic calcite	15	10
Nannofossils	45	55
Quartz	Tr	Tr

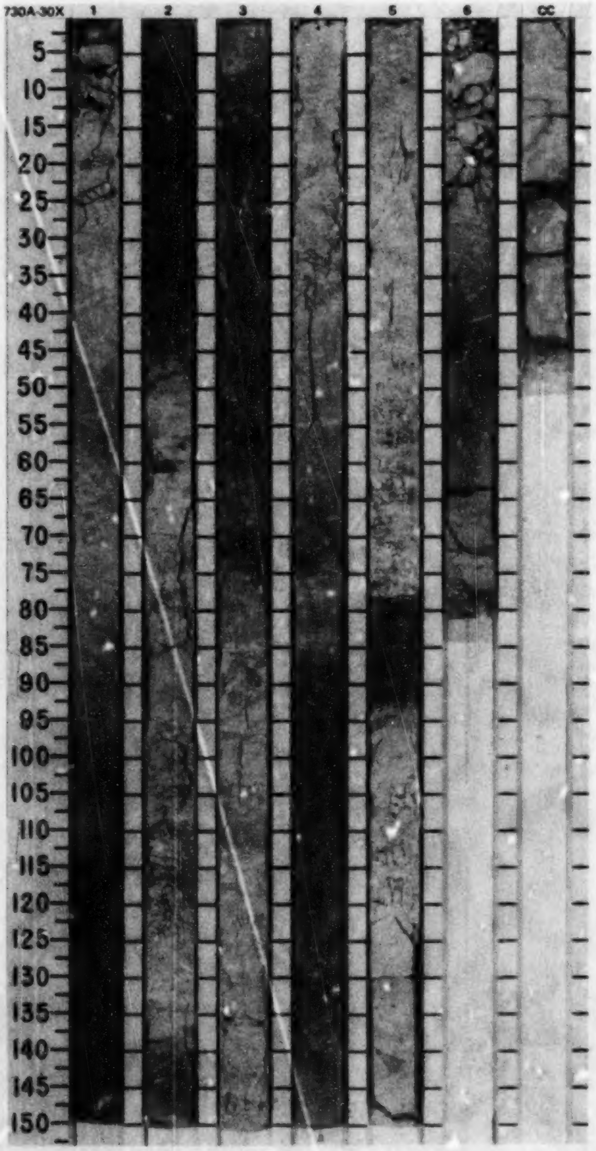
730A-30X
1
2
3
4
5
6
CC
5
10
15
20
25
30
35
40
45
50
55
60
65
70
75
80
85
90
95
100
105
110
115
120
125
130
135
140
145
150

SITE 730 HOLE A CORE 31X CORED INTERVAL 1353.7-1363.4 mbsl; 287.9-297.6 mbsf

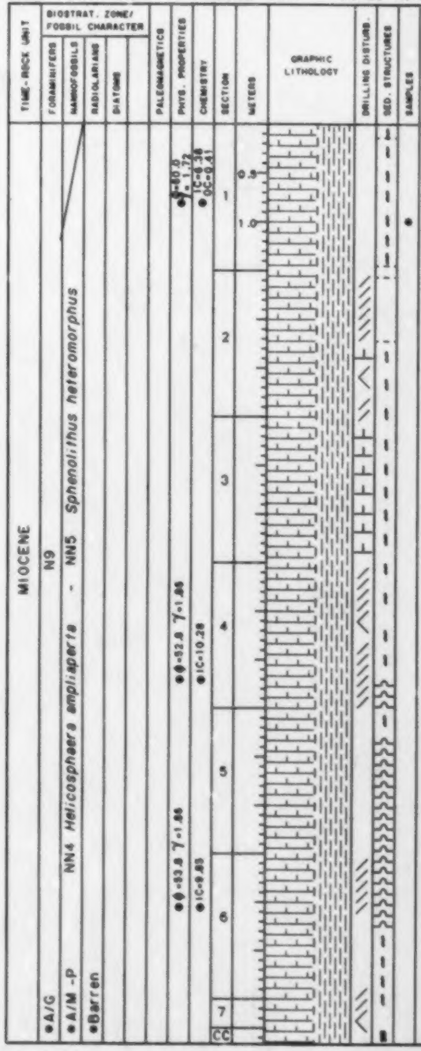
TIME-ROCK UNIT
BIOSTRAT. ZONE/ FOSSIL CHARACTER
FORAMINIFERS
NANNOFOSSILS
RADIOLARIANS
DIATOMS
PALEOMAGNETICS
PHYS. PROPERTIES
CHEMISTRY
SECTION
METERS
GRAPHIC LITHOLOGY
DRILLING DISTURB.
SED. STRUCTURES
SAMPLES
MIOCENE
N9
NN4 Helicosphaera ampliaperta - NN5 Sphenolithus heteromorphus
●A/G
●A/M -P
●Barren
●φ=60.0 γ= 1.72
●IC=6.38 OC=0.41
●φ=52.8 γ=1.86
●IC=10.28
●φ=53.8 γ=1.86
●IC=9.85
1
2
3
4
5
6
7
CC
0.5
1.0

LITHOLOGIC DESCRIPTION

FORAMINIFER-BEARING MARLY NANNOFOSSIL CHALK

Section 2, 80–110 cm, Section 4, 40–80 cm, and Section 7, 10–30 cm, are heavily fractured; Section 2, 0–60 cm, Section 3, 140–150 cm, Section 4, 0–30 and 80–150 cm, Section 6, 0–60 and 130–150 cm, and CC, 0–15 cm, are slightly fractured; and remainder is undisturbed.

Major lithology: FORAMINIFER-BEARING MARLY NANNOFOSSIL CHALK, white (5Y 8/1, 8/2), light gray (5Y 7/1), and olive gray (5Y 5/2). Minor burrow mottling common. Contacts gradational and mottled.

Minor lithology: Section 4, 135–150 cm, Section 5, 30–150 cm, and Section 6, 0–60 cm, slumped millimeter-scale laminated foraminifer-bearing nannofossil chalk.

SMEAR SLIDE SUMMARY (%):

	1, 100 D
TEXTURE:	
Silt	30
Clay	70
COMPOSITION:	
Clay	20
Dolomite	5
Foraminifers	10
Inorganic calcite	20
Nannofossils	45
Quartz	Tr

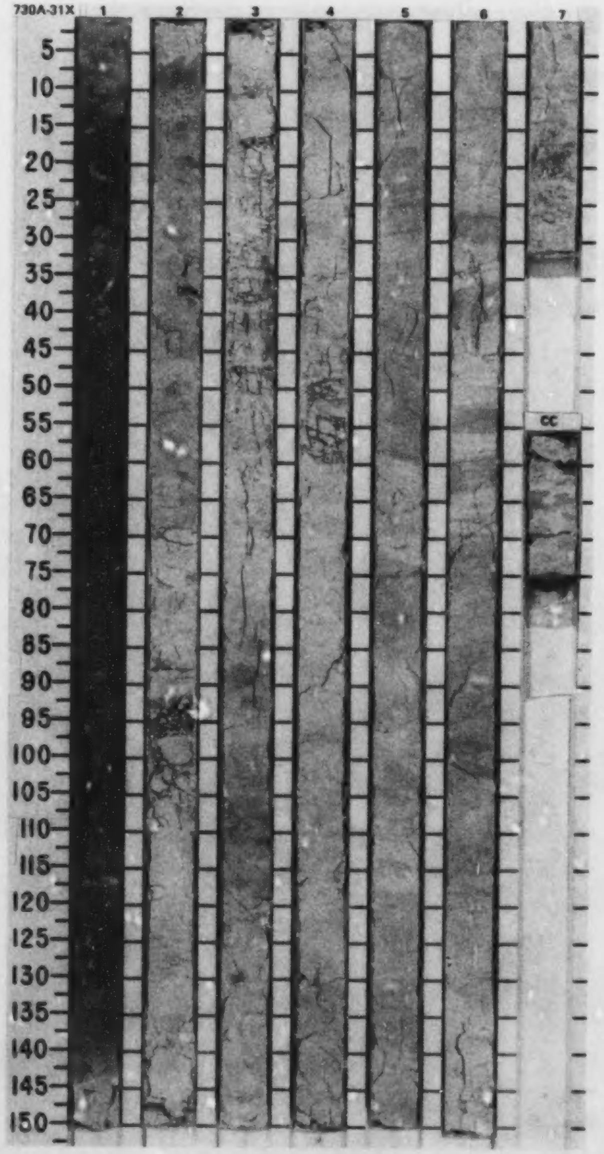
730A-31X
1
2
3
4
5
6
7
CC
5
10
15
20
25
30
35
40
45
50
55
60
65
70
75
80
85
90
95
100
105
110
115
120
125
130
135
140
145
150

SITE 730 HOLE A CORE 32X CORED INTERVAL 1363.4-1373.0 mbsl; 297.6-307.2 mbsf

TIME-ROCK UNIT	BIOSTRAT. ZONE/ FOSSIL CHARACTER FORAMINIFERS	NANNOFOSSILS	RADIOLARIANS	DIATOMS		PALEOMAGNETICS	PHYS. PROPERTIES	CHEMISTRY	SECTION	METERS	GRAPHIC LITHOLOGY	DRILLING DISTURB.	SED. STRUCTURES	SAMPLES	LITHOLOGIC DESCRIPTION
MIOCENE	N8 ●A/P	NN4 *Helicosphaera ampliaperta* - NN5 *Sphenolithus heteromorphus* ●A/P	●Barren				ϕ=48.4 γ=1.93 ●	IC=11.21 OC=0.05 ●	1 CC	0.5					NANNOFOSSIL CHALK Entire core is very disturbed. Major lithology: NANNOFOSSIL CHALK, slumped, light gray (5Y 7/1) and light olive gray (5Y 6/2). Minor lithology: Section 1, 20-32 and 50-67 cm, benthic foraminifer sand, normally graded (carbonate turbidite).

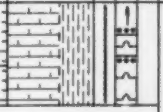

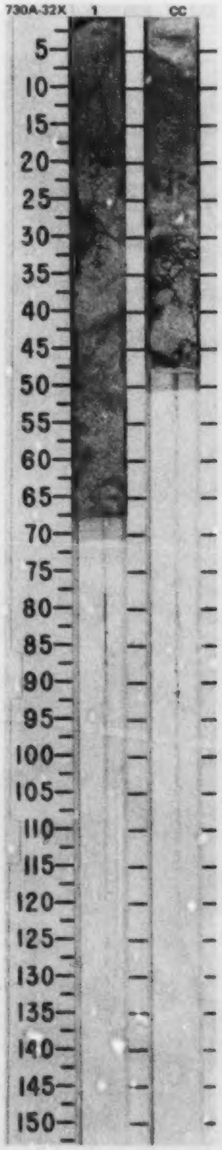
730A-32X
1
CC
5
10
15
20
25
30
35
40
45
50
55
60
65
70
75
80
85
90
95
100
105
110
115
120
125
130
135
140
145
150

SITE 730 HOLE A CORE 33X CORED INTERVAL 1373.0-1382.7 mbsl; 307.2-316.9 mbsf

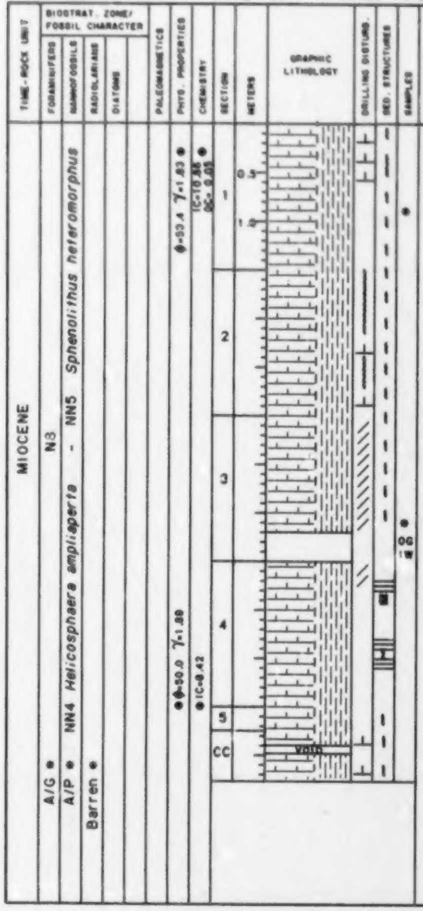
TIME-ROCK UNIT
BIOSTRAT. ZONE/ FOSSIL CHARACTER
FORAMINIFERS
NANNOFOSSILS
RADIOLARIANS
DIATOMS
PALEOMAGNETICS
PHYS. PROPERTIES
CHEMISTRY
SECTION
METERS
GRAPHIC LITHOLOGY
DRILLING DISTURB.
SED. STRUCTURES
SAMPLES
MIOCENE
N3
NN4 Helicosphaera ampliaperta - NN5 Sphenolithus heteromorphus
A/G
A/P
Barren
φ=53.4 γ=1.83
IC=10.88 OC= 0.03
φ=50.0 γ=1.89
IC=8.42
1
2
3
4
5
CC
0.5
1.0
VOID
OG
IW

LITHOLOGIC DESCRIPTION

FORAMINIFER-BEARING MARLY NANNOFOSSIL CHALK

Section 1, 0-50 cm, Section 2, 40-70 and 130-150 cm, and CC, 0-45 cm, are moderately fractured; Section 5, 0-24 cm, is moderately disturbed; Section 3, 0-130 cm, and Section 4, 0-20 cm are very disturbed; remainder is undisturbed.

Major lithology: FORAMINIFER-BEARING MARLY NANNOFOSSIL CHALK, white (5Y 8/1), light gray (5Y 7/1), light olive gray (5Y 6/2), and olive gray (5Y 5/2). Minor to strong burrow mottling. Contacts gradational and mottled.

Minor lithology: Section 4, 20-25, 80-85, and 100-105 cm, slumped(?) millimeter laminated foraminifer-bearing nannofossil chalk.

SMEAR SLIDE SUMMARY (%):

	1, 90 D	3, 109 D
TEXTURE:		
Silt	10	10
Clay	90	90
COMPOSITION:		
Clay	15	—
Dolomite	1	2
Foraminifers	5	7
Inorganic calcite	1	1
Mica	—	25
Nannofossils	75	63
Quartz	3	2

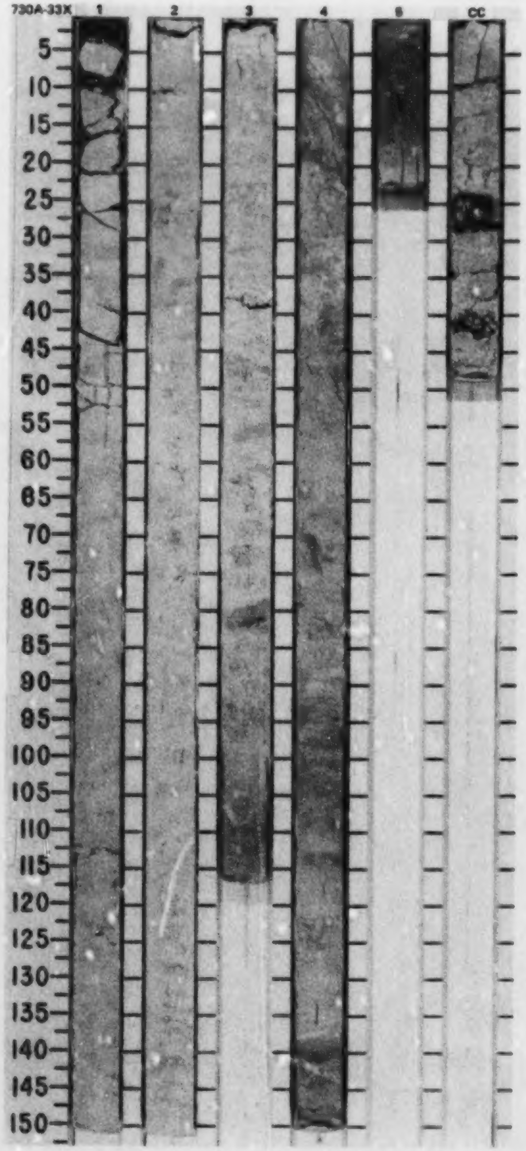
730A-33X
1
2
3
4
5
CC
5
10
15
20
25
30
35
40
45
50
55
60
65
70
75
80
85
90
95
100
105
110
115
120
125
130
135
140
145
150

SITE 730 HOLE A CORE 34X CORED INTERVAL 1382.7-1392.4 mbsl; 316.9-326.6 mbsf

TIME-ROCK UNIT	BIOSTRAT. ZONE/ FOSSIL CHARACTER: FORAMINIFERS	NANNOFOSSILS	RADIOLARIANS	DIATOMS		PALEOMAGNETICS	PHYS. PROPERTIES	CHEMISTRY	SECTION	METERS	GRAPHIC LITHOLOGY	DRILLING DISTURB.	SED. STRUCTURES	SAMPLES
MIOCENE	N8 ●C/G	NN4 *Helicosphaera ampliaperta* - NN5 *Sphenolithus heteromorphus* ●A/M	●Barren				φ=54.0 γ=1.83 ●	TC=11.30 OC=0.27 ●	1 2 CC	0.5 1.0	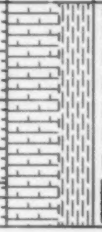			●

LITHOLOGIC DESCRIPTION

FORAMINIFER-BEARING MARLY NANNOFOSSIL CHALK

Section 1, 0–25 cm, and CC, 0–45 cm, are very disturbed; remainder is moderately disturbed.

Major lithology: FORAMINIFER-BEARING MARLY NANNOFOSSIL CHALK, white (5Y 8/1) and light gray (5Y 7/1, 7/2). Minor burrow mottling throughout. Contacts gradational and mottled.

SMEAR SLIDE SUMMARY (%):

	1, 92 M
TEXTURE:	
Sand	25
Silt	45
Clay	30
COMPOSITION:	
Access. minerals	1
Clay	15
Foraminifers	40
Inorganic calcite	4
Micrite	25
Nannofossils	15

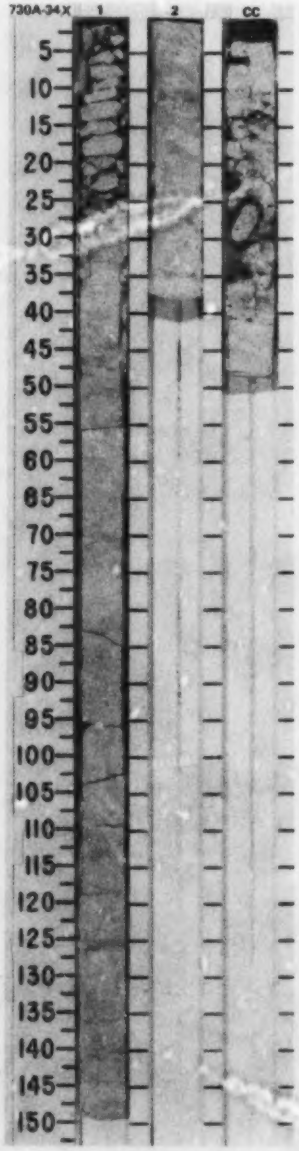

SITE 730 HOLE A CORE 35X CORED INTERVAL 1392.4-1402.0 mbsl; 326.6-336.2 mbsf

TIME-ROCK UNIT	BIOSTRAT. ZONE/ FOSSIL CHARACTER					PALEOMAGNETICS	PHYS. PROPERTIES	CHEMISTRY	SECTION	METERS
	FORAMINIFERS	NANNOFOSSILS	RADIOLARIANS	DIATOMS						
MIOCENE	N8 ●C/M	NN4 *Helicosphaera ampliaperta* - NN5 *Sphenolithus heteromorphus* ●A/P	●Barren				● ϕ=50.2 γ=1.92	● IC=11.30 OC= 0.13	1	0.5 1.0
									2	
									CC	

GRAPHIC LITHOLOGY · DRILLING DISTURB. · SED. STRUCTURES · SAMPLES

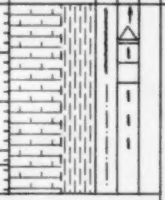

LITHOLOGIC DESCRIPTION

FORAMINIFER-BEARING MARLY NANNOFOSSIL CHALK

Section 1, 0-75 cm, very disturbed; remainder is moderately disturbed.

Major lithology: FORAMINIFER-BEARING MARLY NANNOFOSSIL CHALK, white (5Y 8/1, 8/2). Minor burrow mottling common.

Minor lithology: Section 1, 5-40 and 57-81 cm, foraminifer sands with normal grading (carbonate turbidite).

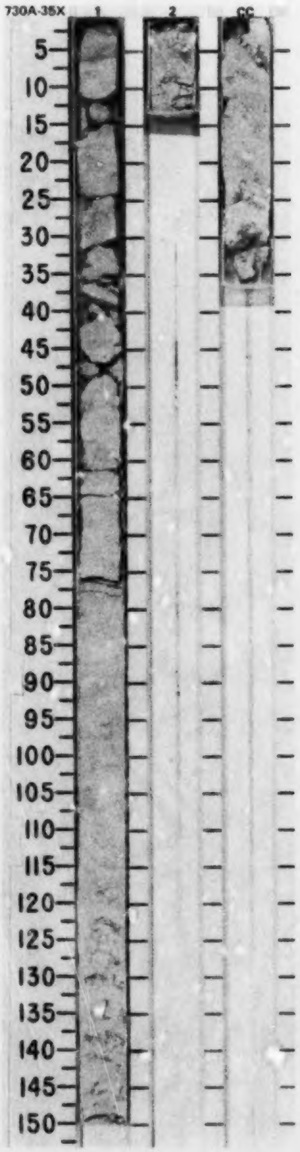
730A-35X
1
2
CC
5
10
15
20
25
30
35
40
45
50
55
60
65
70
75
80
85
90
95
100
105
110
115
120
125
130
135
140
145
150

SITE 730 HOLE A CORE 36X CORED INTERVAL 1402.0-1411.7 mbsl; 336.2-345.9 mbsf

TIME-ROCK UNIT	BIOSTRAT. ZONE/ FOSSIL CHARACTER FORAMINIFERS	NANNOFOSSILS	RADIOLARIANS	DIATOMS	PALEOMAGNETICS	PHYS. PROPERTIES	CHEMISTRY	SECTION	METERS	GRAPHIC LITHOLOGY	DRILLING DISTURB.	SED. STRUCTURES	SAMPLES	LITHOLOGIC DESCRIPTION
MIOCENE	●Barren	●A/P	●Barren					1					●	FORAMINIFER-BEARING MARLY NANNOFOSSIL CHALK
	NN4 Helicosphaera ampliaperta - NN5 Sphenolithus heteromorphus							CC						

CC, 0-50 cm, is moderately disturbed; remainder is very disturbed.

Major lithology: FORAMINIFER-BEARING MARLY NANNOFOSSIL CHALK, white (5Y 8/1) and light gray (5Y 7/1).

Minor lithology: Section 1, 0-10 cm, slumped nannofossil chalk with occasional benthic foraminifers.

SMEAR SLIDE SUMMARY (%):

	1, 8 M
TEXTURE:	
Silt	10
Clay	90
COMPOSITION:	
Cement	5
Clay	74
Dolomite	1
Nannofossils	10
Opaques	10

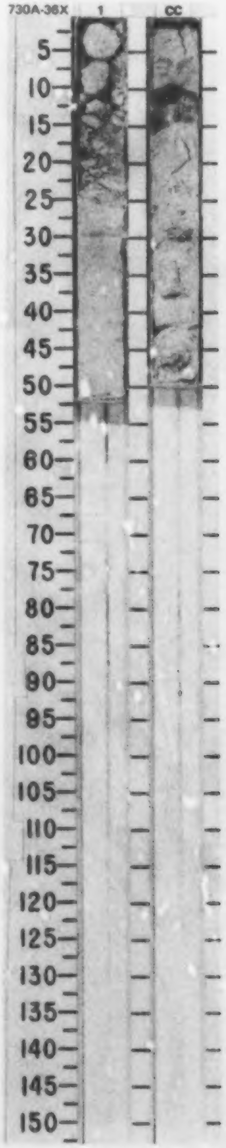
730A-36X
1
CC
5
10
15
20
25
30
35
40
45
50
55
60
65
70
75
80
85
90
95
100
105
110
115
120
125
130
135
140
145
150

SITE 730 HOLE A CORE 37X CORED INTERVAL 1411.7-1421.4 mbsl; 345.9-355.6 mbsf

TIME-ROCK UNIT: MIOCENE

BIOSTRAT. ZONE/FOSSIL CHARACTER

- FORAMINIFERS: ●A/G N8
- NANNOFOSSILS: ●A/M NN4 *Helicosphaera ampliaperta* - NN5 *Sphenolithus heteromorphus*
- RADIOLARIANS: ●Barren
- DIATOMS

PALEOMAGNETICS

PHYS. PROPERTIES: ϕ=52.1 γ=1.85 ● ; ●ϕ=52.1 γ=1.90

CHEMISTRY: IC=10.38 OC=0.19 ● ; ●IC=7.61

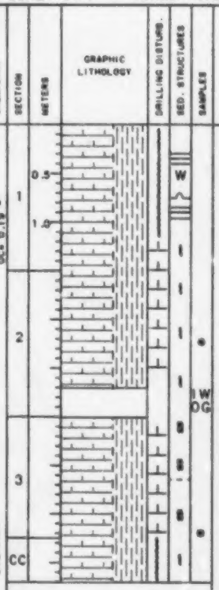
SECTION
METERS
GRAPHIC LITHOLOGY
DRILLING DISTURB.
SED. STRUCTURES
SAMPLES
1
2
3
CC
0.5
1.0
W
IW
OG

LITHOLOGIC DESCRIPTION

FORAMINIFER-BEARING MARLY NANNOFOSSIL CHALK

Section 1, 0-100 cm, and CC, 0-45 cm, are very disturbed; remainder is moderately fractured.

Major lithology: FORAMINIFER-BEARING MARLY NANNOFOSSIL CHALK, white (5Y 8/1) and light gray (5Y 7/1). Minor to moderate burrow mottling.

Minor lithology: Section 1, 30-50 and 80-90 cm, slumped nannofossil chalk with occasional benthic foraminifers.

SMEAR SLIDE SUMMARY (%):

	2, 72 D	3, 130 D
TEXTURE:		
Silt	30	20
Clay	70	80
COMPOSITION:		
Clay	15	20
Dolomite	—	Tr
Foraminifers	5	10
Inorganic calcite	Tr	10
Nannofossils	80	55
Quartz	Tr	5

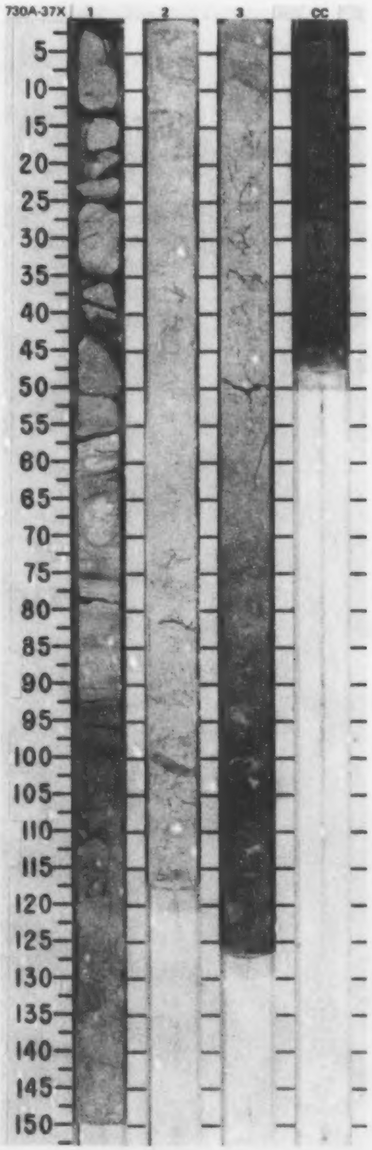
730A-37X
1
2
3
CC
5
10
15
20
25
30
35
40
45
50
55
60
65
70
75
80
85
90
95
100
105
110
115
120
125
130
135
140
145
150

SITE 730 HOLE A CORE 38X CORED INTERVAL 1421.4-1431.0 mbsl; 355.6-365.2 mbsf

TIME-ROCK UNIT	BIOSTRAT. ZONE/ FOSSIL CHARACTER: FORAMINIFERS	NANNOFOSSILS	RADIOLARIANS	DIATOMS		PALEOMAGNETICS	PHYS. PROPERTIES	CHEMISTRY	SECTION	METERS	GRAPHIC LITHOLOGY / DRILLING DISTURB. / SED. STRUCTURES	SAMPLES	LITHOLOGIC DESCRIPTION
MIOCENE	N8 ●A/G	NN4 *Helicosphaera ampliaperta* - NN5 *Sphenolithus heteromorphus* ●A/G	●Barren				●φ=52.7 γ=1.88	●IC=7.38 OC=0.27	1 2 CC	0.5 1.0	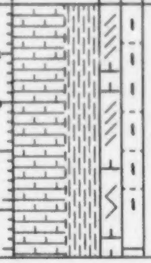		**FORAMINIFER-BEARING MARLY NANNOFOSSIL CHALK** Section 2, 30-60 cm, and Section 1, 40-80 cm, are heavily fractured; Section 1, 40-80 cm, Section 2, 0-30 cm, and CC, 0-58 cm, are moderately fractured; and remainder is slightly fractured. Major lithology: FORAMINIFER-BEARING MARLY NANNOFOSSIL CHALK, white (5Y 8/1), light olive gray (5Y 6/2), and gray (5Y 6/1). Minor burrow mottling throughout. Contacts gradational and mottled.

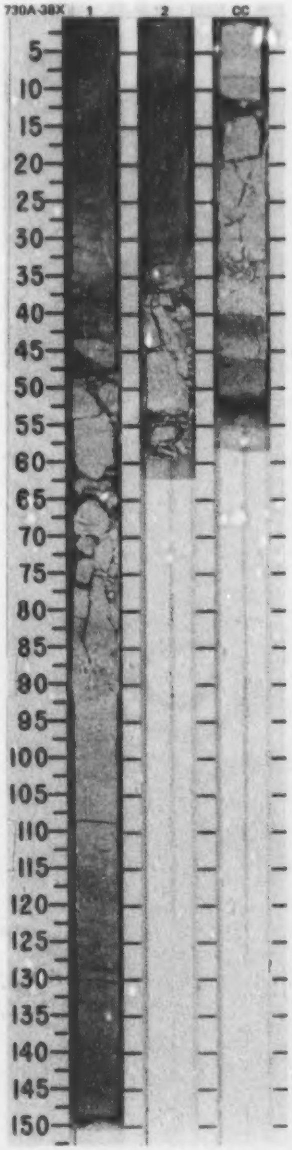
730A-38X
1
2
CC
5
10
15
20
25
30
35
40
45
50
55
60
65
70
75
80
85
90
95
100
105
110
115
120
125
130
135
140
145
150

SITE 730 HOLE A CORE 39X CORED INTERVAL 1431.0-1440.7 mbsl; 365.2-374.9 mbsf

TIME-ROCK UNIT	BIOSTRAT. ZONE/ FOSSIL CHARACTER: FORAMINIFERS	NANNOFOSSILS	RADIOLARIANS	DIATOMS	PALEOMAGNETICS	PHYS. PROPERTIES	CHEMISTRY	SECTION	METERS	SAMPLES
MIOCENE	N8 ●A/M	NN4 *Helicosphaera ampliaperta* - NN5 *Sphenolithus heteromorphus* ●A/P	●Barren		$\phi=53.2$	$\gamma=1.86$ ● $\gamma=1.88$ ●$\phi=52.1$		1 2 CC	0.5 1.0	IW

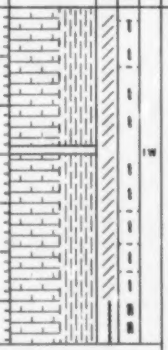
GRAPHIC LITHOLOGY
DRILLING DISTURB.
SED. STRUCTURES

LITHOLOGIC DESCRIPTION

FORAMINIFER-BEARING MARLY NANNOFOSSIL CHALK

CC, 0-45 cm, is very disturbed; remainder is slightly fractured.

Major lithology: FORAMINIFER-BEARING MARLY NANNOFOSSIL CHALK, white (5Y 8/1), light gray (5Y 7/1), gray (5Y 6/1), and olive gray (5Y 5/2). Minor burrow mottling throughout. Contacts gradational and mottled.

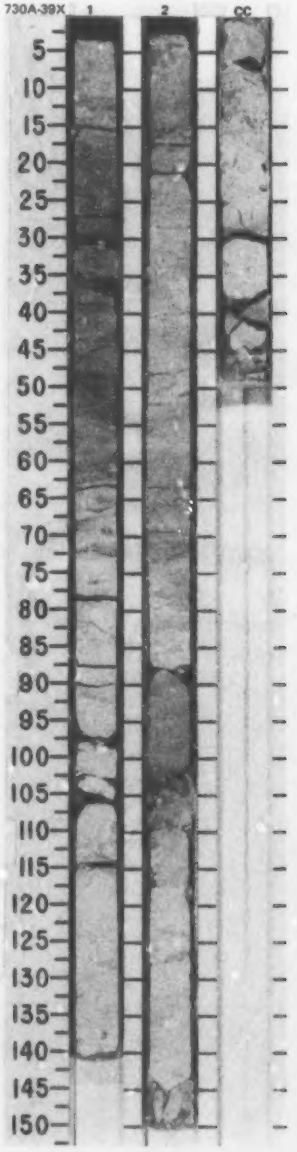
730A-39X
1
2
CC
5
10
15
20
25
30
35
40
45
50
55
60
65
70
75
80
85
90
95
100
105
110
115
120
125
130
135
140
145
150

SITE 730 HOLE A CORE 40X CORED INTERVAL 1440.7-1450.4 mbsl; 374.9-384.6 mbsf

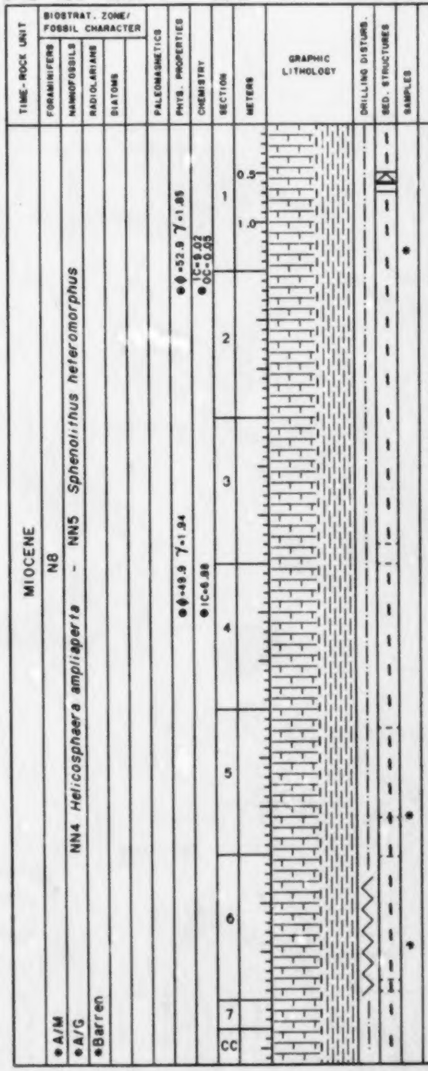
TIME-ROCK UNIT
BIOSTRAT. ZONE/ FOSSIL CHARACTER
FORAMINIFERS
NANNOFOSSILS
RADIOLARIANS
DIATOMS
PALEOMAGNETICS
PHYS. PROPERTIES
CHEMISTRY
SECTION
METERS
GRAPHIC LITHOLOGY
DRILLING DISTURB.
SED. STRUCTURES
SAMPLES
MIOCENE
N8
NN4 Helicosphaera ampliaperta - NN5 Sphenolithus heteromorphus
●A/M
●A/G
●Barren
●ϕ=52.9 γ=1.85
●ϕ=49.9 γ=1.94
●IC=9.02 OC=0.05
●IC=6.88
0.5
1.0
1
2
3
4
5
6
7
CC

LITHOLOGIC DESCRIPTION

FORAMINIFER-BEARING MARLY NANNOFOSSIL CHALK

Section 6, 0-150 cm, is heavily fractured; remainder is moderately disturbed.

Major lithology: FORAMINIFER-BEARING MARLY NANNOFOSSIL CHALK, light gray (5Y 7/1), gray (5Y 6/1), olive gray (5Y 5/2), olive (5Y 5/3), and dark gray (5Y 5/1, 4/1). Minor burrow mottling throughout. Contacts gradational and mottled.

Minor lithology: Section 1, 48-56 cm, benthic foraminifer sand with shale clasts, normally graded (carbonate turbidite).

SMEAR SLIDE SUMMARY (%):

	1, 130 D	5, 106 M	6, 94 D
TEXTURE:			
Sand	—	20	—
Silt	40	20	20
Clay	60	60	80
COMPOSITION:			
Clay	20	20	20
Dolomite	Tr	1	Tr
Foraminifers	5	30	5
Inorganic calcite	10	—	5
Micrite	—	33	—
Nannofossils	60	5	70
Opaques	—	10	—
Quartz	5	—	Tr
Sponge spicules	—	1	—

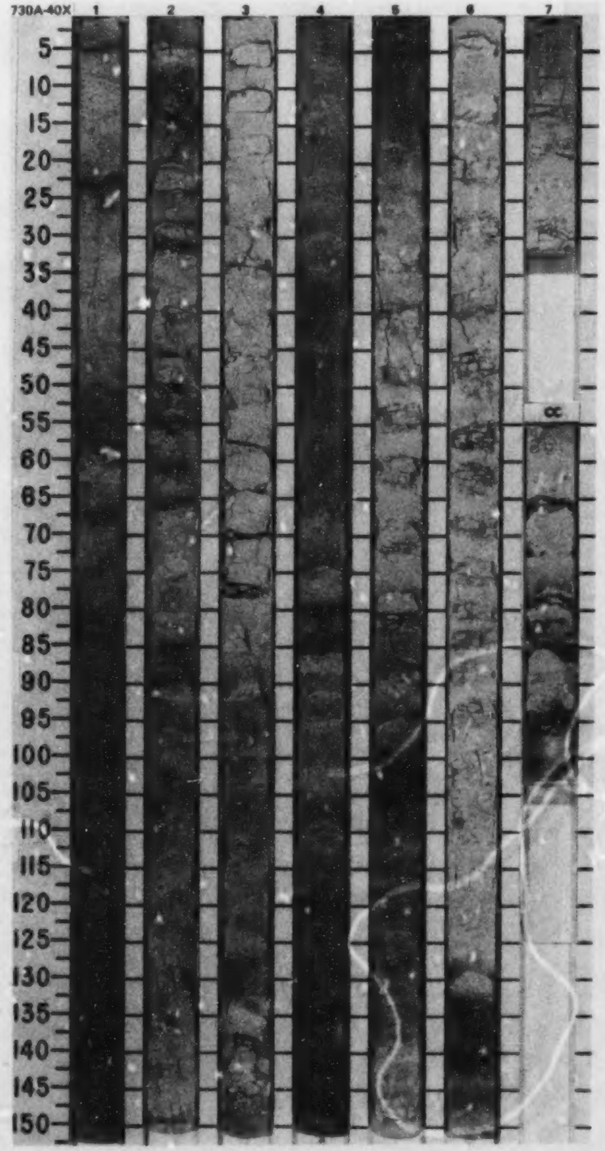
730A-40X
1
2
3
4
5
6
7
CC
5
10
15
20
25
30
35
40
45
50
55
60
65
70
75
80
85
90
95
100
105
110
115
120
125
130
135
140
145
150

SITE 730 HOLE A CORE 41X CORED INTERVAL 1450.4-1460.0 mbsl; 384.6-394.2 mbsf

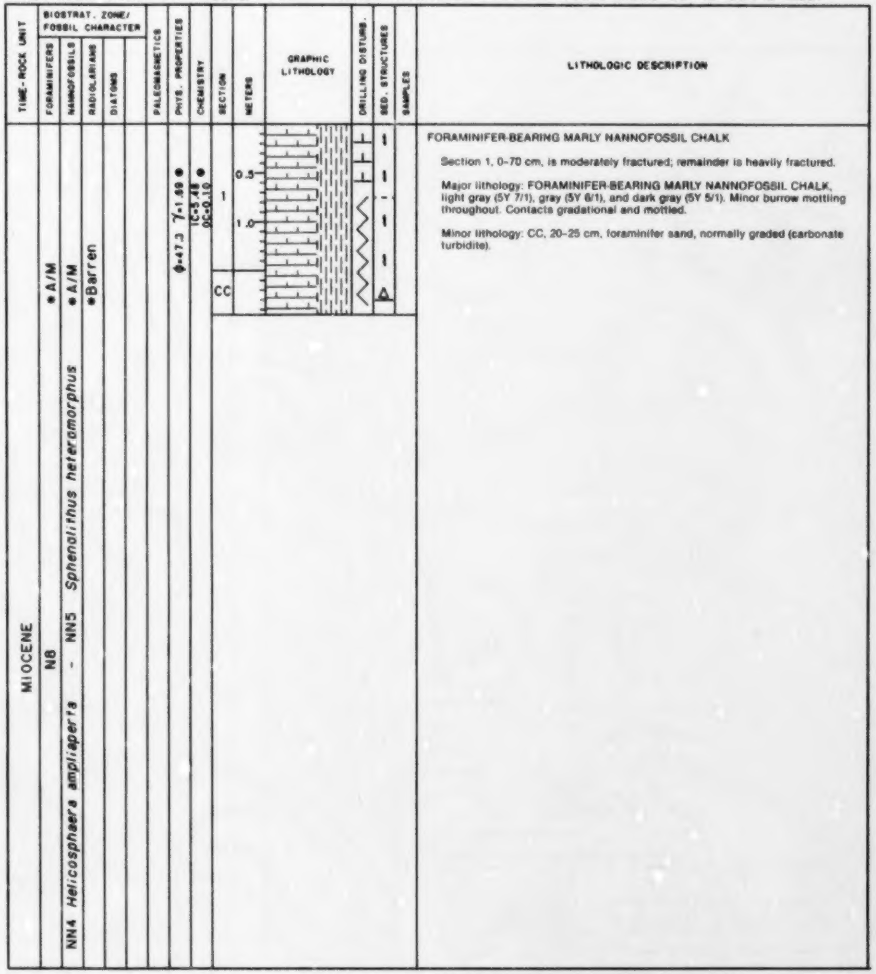
TIME-ROCK UNIT
BIOSTRAT. ZONE/ FOSSIL CHARACTER
FORAMINIFERS
NANNOFOSSILS
RADIOLARIANS
DIATOMS
PALEOMAGNETICS
PHYS. PROPERTIES
CHEMISTRY
SECTION
METERS
GRAPHIC LITHOLOGY
DRILLING DISTURB.
SED. STRUCTURES
SAMPLES
LITHOLOGIC DESCRIPTION
MIOCENE
N8
NN4 Helicosphaera ampliaperta - NN5 Sphenolithus heteromorphus
•A/M
•A/M
•Barren
ϕ=47.3 γ=1.89 •
IC=5.48 OC=0.10 •
1
CC
0.5
1.0

FORAMINIFER-BEARING MARLY NANNOFOSSIL CHALK

Section 1, 0-70 cm, is moderately fractured; remainder is heavily fractured.

Major lithology: FORAMINIFER-BEARING MARLY NANNOFOSSIL CHALK, light gray (5Y 7/1), gray (5Y 6/1), and dark gray (5Y 5/1). Minor burrow mottling throughout. Contacts gradational and mottled.

Minor lithology: CC, 20-25 cm, foraminifer sand, normally graded (carbonate turbidite).

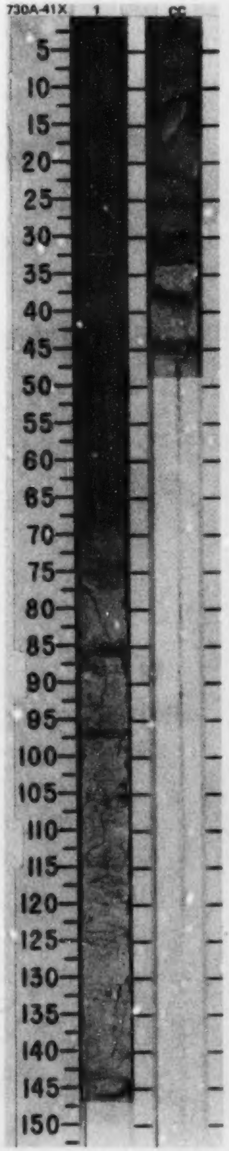
730A-41X
1
CC
5
10
15
20
25
30
35
40
45
50
55
60
65
70
75
80
85
90
95
100
105
110
115
120
125
130
135
140
145
150

SITE 730 HOLE A CORE 42X CORED INTERVAL 1460.0-1469.7 mbsl; 394.2-403.9 mbsf

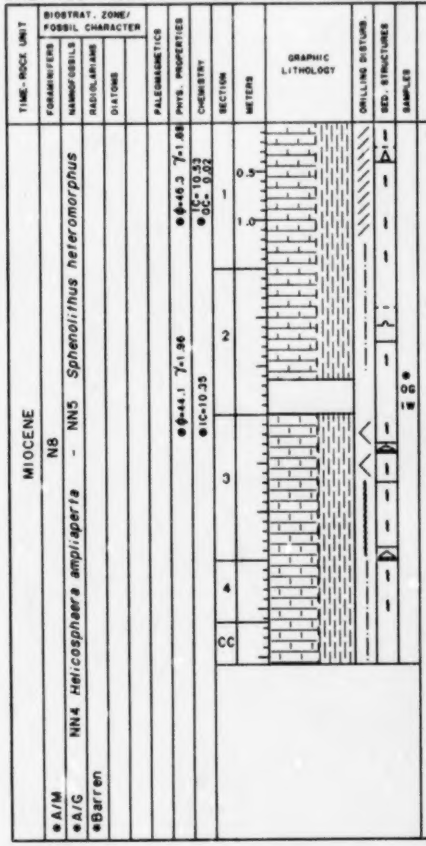
TIME-ROCK UNIT
BIOSTRAT. ZONE/ FOSSIL CHARACTER
FORAMINIFERS
NANNOFOSSILS
RADIOLARIANS
DIATOMS
PALEOMAGNETICS
PHYS. PROPERTIES
CHEMISTRY
SECTION
METERS
GRAPHIC LITHOLOGY
DRILLING DISTURB.
SED. STRUCTURES
SAMPLES
MIOCENE
N8
NN4 Helicosphaera ampliaperta - NN5 Sphenolithus heteromorphus
●A/M
●A/G
●Barren
●ϕ=46.3 γ=1.88
●ϕ=44.1 γ=1.96
●IC=10.53 OC= 0.02
●IC=10.35
1
2
3
4
CC
0.5
1.0
●
OG
IW

LITHOLOGIC DESCRIPTION

FORAMINIFER-BEARING MARLY NANNOFOSSIL CHALK

Section 3, 0-50 cm, is heavily fractured; Section 3, 50-150 cm, is very disturbed; Section 1, 0-100 cm, is slightly fractured; and remainder is moderately disturbed.

Major lithology: FORAMINIFER-BEARING MARLY NANNOFOSSIL CHALK, white (5Y 8/1), light gray (5Y 7/1), gray (5Y 6/1), dark gray (5Y 5/1), and olive (5Y 4/3). Minor burrow mottling throughout. Contacts gradational and mottled.

Minor lithology: Section 1, 30-40 cm, and Section 3, 25-30 and 135-145 cm, contains foraminifer sand, normally graded, with common sand-sized black (5Y 2.5/1) shale clasts (carbonate turbidites).

SMEAR SLIDE SUMMARY (%):

	2, 112 D
TEXTURE:	
Silt	20
Clay	80
COMPOSITION:	
Clay	18
Foraminifers	2
Inorganic calcite	10
Micrite	25
Nannofossils	45

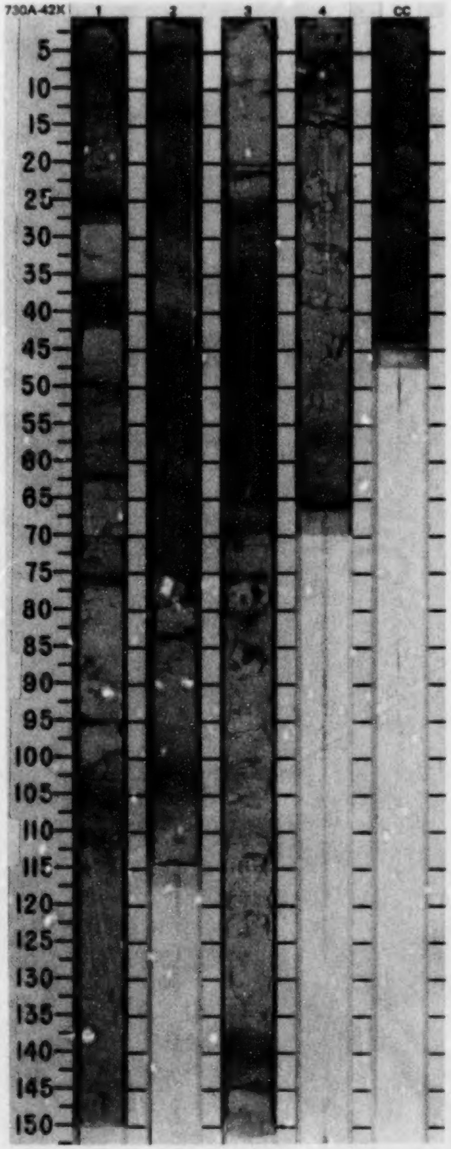
730A-42X
1
2
3
4
CC
5
10
15
20
25
30
35
40
45
50
55
60
65
70
75
80
85
90
95
100
105
110
115
120
125
130
135
140
145
150

SITE 731 HOLE A CORE 1H CORED INTERVAL 2365.8-2375.6 mbsl; 0.0-9.8 mbsf

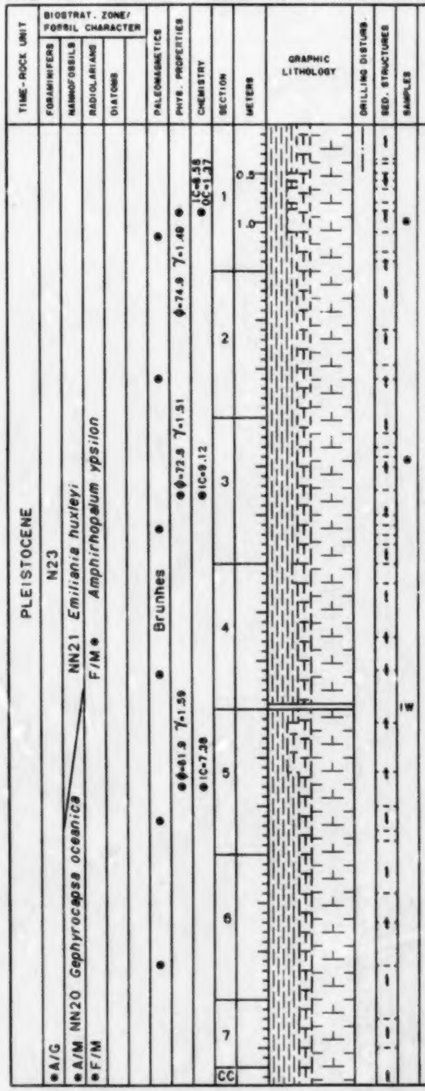
TIME-ROCK UNIT
BIOSTRAT. ZONE/ FOSSIL CHARACTER
FORAMINIFERS
NANNOFOSSILS
RADIOLARIANS
DIATOMS
PALEOMAGNETICS
PHYS. PROPERTIES
CHEMISTRY
SECTION
METERS
GRAPHIC LITHOLOGY
DRILLING DISTURB.
SED. STRUCTURES
SAMPLES
PLEISTOCENE
N23
NN21 Emiliania huxleyi
Amphirhopalum ypsilon
NN20 Gephyrocapsa oceanica
●A/G
●A/M
●F/M
F/M●
Brunhes
ϕ=74.9 γ=1.40
●ϕ=72.8 γ=1.51
●ϕ=61.9 γ=1.59
●IC=8.58 OC=1.37
●IC=9.12
●IC=7.38
1
2
3
4
5
6
7
CC
0.5
1.0
IW

LITHOLOGIC DESCRIPTION

FORAMINIFER-RICH MARLY NANNOFOSSIL OOZE to FORAMINIFER-NANNOFOSSIL OOZE

Section 1, 0–18 cm, is moderately disturbed. Remainder is undisturbed.

Major lithology: FORAMINIFER-RICH MARLY NANNOFOSSIL OOZE to FORAMINIFER-NANNOFOSSIL OOZE, light gray (5Y 7/1), light greenish gray (5GY 7/1, 10Y 6/2), light olive gray (5Y 6/2), and pale olive (5Y 6/3). Minor to moderate bioturbation and gradational color contacts throughout.

Minor lithology: Diatom-bearing foraminifer-nannofossil ooze, olive (5Y 5/3), bioturbated, and gradational with the surrounding major lithology. Section 1, 53–60, 67–77, and 84–113 cm, Section 4, 0–17 cm, and Section 5, 17–63 cm.

SMEAR SLIDE SUMMARY (%):

	1, 99 D	3, 43 D
TEXTURE:		
Sand	15	15
Silt	25	25
Clay	60	60
COMPOSITION:		
Access. minerals	2	1
Clay	20	20
Diatoms	7	1
Foraminifers	25	14
Volcanic glass	4	—
Inorganic calcite	—	14
Mica	—	Tr
Nannofossils	40	50
Quartz	2	Tr
Radiolarians	Tr	—

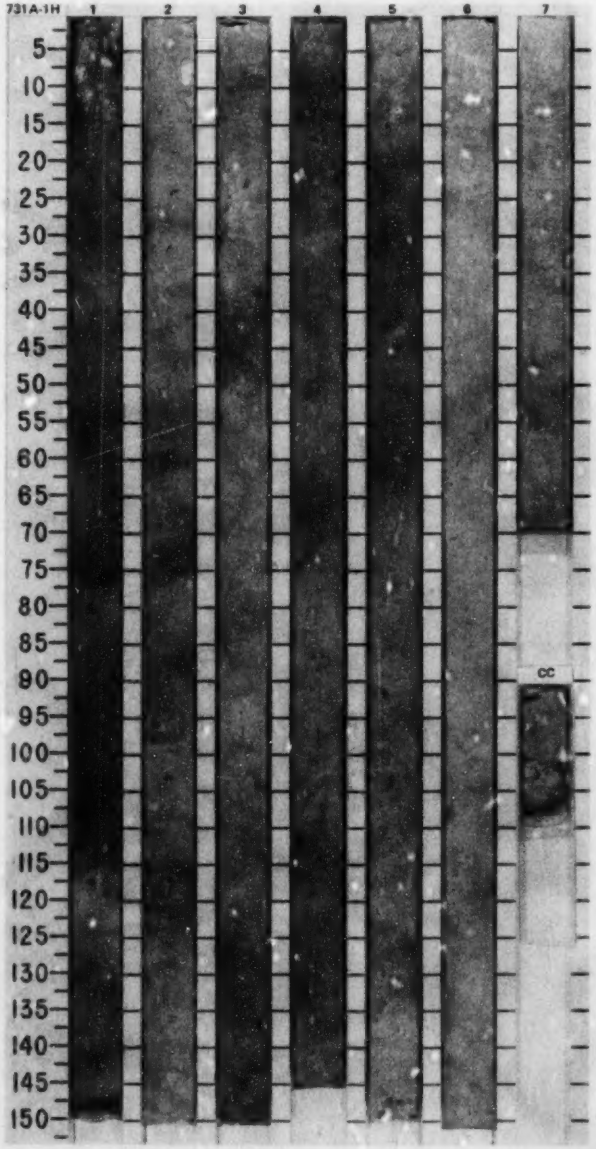
731A-1H
1
2
3
4
5
6
7
CC
5
10
15
20
25
30
35
40
45
50
55
60
65
70
75
80
85
90
95
100
105
110
115
120
125
130
135
140
145
150

SITE 731 HOLE A CORE 2H CORED INTERVAL 2375.6-2385.1 mbsl; 9.8-19.3 mbsf

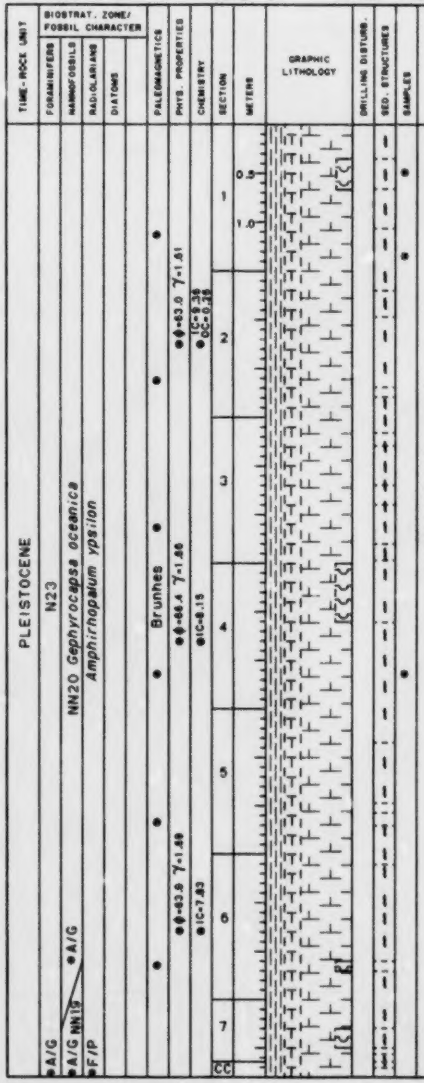

LITHOLOGIC DESCRIPTION

FORAMINIFER-NANNOFOSSIL OOZE and DIATOMACEOUS FORAMINIFER-NANNOFOSSIL OOZE

Entire core is undisturbed.

Major lithologies:
a. FORAMINIFER-NANNOFOSSIL OOZE, light gray (5Y 7/1, 7/2), light greenish gray (5GY 7/1, 10Y 6/2), and light olive gray (5Y 6/2). Gradationally interbedded, with minor to moderate bioturbation throughout.
b. DIATOMACEOUS FORAMINIFER-NANNOFOSSIL OOZE, olive (5Y 6/3), bioturbated.

SMEAR SLIDE SUMMARY (%):

	1, 50 D	1, 137 M	4, 115 D
TEXTURE:			
Sand	20	10	10
Silt	20	20	15
Clay	60	70	75
COMPOSITION:			
Access. minerals	1	1	1
Clay	20	10	15
Diatoms	15	—	Tr
Dolomite	1	—	Tr
Foraminifers	16	10	13
Volcanic glass	5	—	—
Inorganic calcite	14	10	
Mica	1	Tr	—
Nannofossils	40	60	60
Quartz	1	5	1

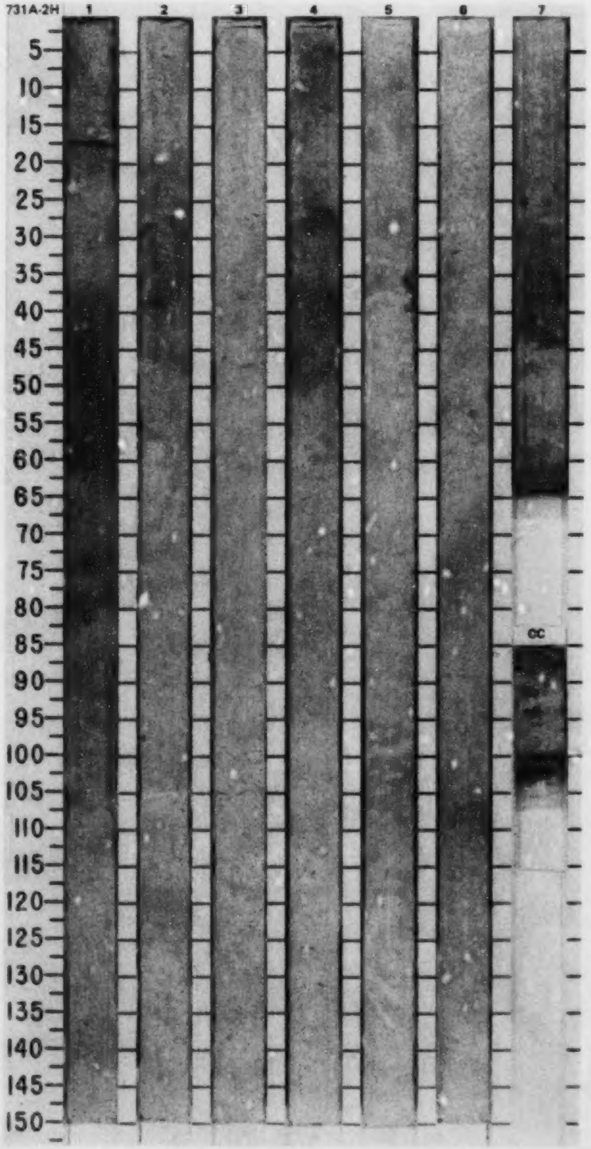
731A-2H
1
2
3
4
5
6
7
CC
5
10
15
20
25
30
35
40
45
50
55
60
65
70
75
80
85
90
95
100
105
110
115
120
125
130
135
140
145
150

SITE 731 HOLE A CORE 3H CORED INTERVAL 2385.1-2394.6 mbsl; 19.3-28.8 mbsf

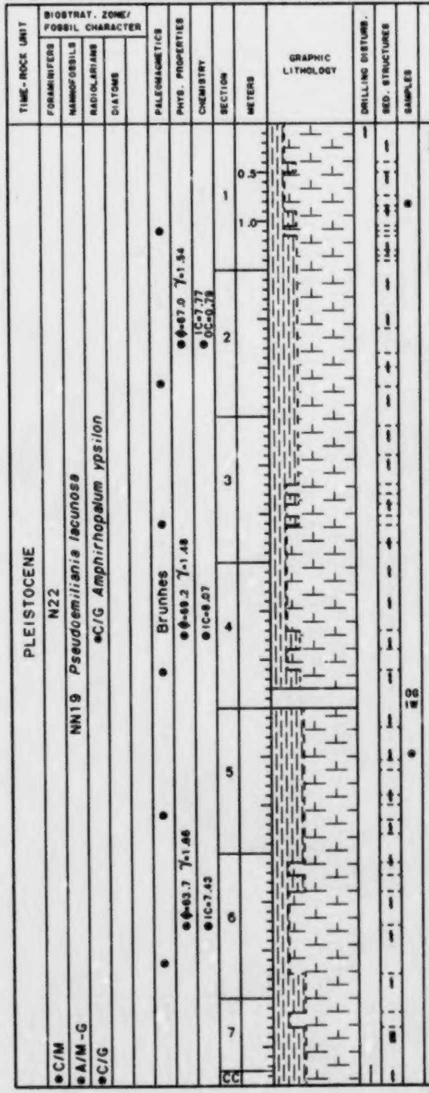
TIME-ROCK UNIT
BIOSTRAT. ZONE/ FOSSIL CHARACTER
FORAMINIFERS
NANNOFOSSILS
RADIOLARIANS
DIATOMS
PALEOMAGNETICS
PHYS. PROPERTIES
CHEMISTRY
SECTION
METERS
GRAPHIC LITHOLOGY
DRILLING DISTURB.
SED. STRUCTURES
SAMPLES
PLEISTOCENE
N22
NN19 Pseudoemiliania lacunosa
●C/G Amphirhopalum ypsilon
●C/M
●A/M-G
●C/G
Brunhes
●φ=67.0 γ=1.54
●φ=69.2 γ=1.48
●φ=63.7 γ=1.66
IC=7.77
●OC=0.79
●IC=8.07
●IC=7.43
1
2
3
4
5
6
7
CC
0.5
1.0
OG
IW

LITHOLOGIC DESCRIPTION

NANNOFOSSIL OOZE and FORAMINIFER-BEARING MARLY NANNOFOSSIL OOZE

Section 1, 0–17 cm, is highly disturbed. Remainder is undisturbed.

Major lithologies:

a. NANNOFOSSIL OOZE, light gray (5Y 7/1, 7/2) and light greenish gray (5GY 7/1, 10Y 6/2). Slight to moderate bioturbation throughout.

b. FORAMINIFER-BEARING MARLY NANNOFOSSIL OOZE, light olive gray (5Y 6/2), pale olive (5Y 6/3), and olive (5Y 5/3). Bioturbated.

SMEAR SLIDE SUMMARY (%):

	1, 83 D	5, 47 D
TEXTURE:		
Sand	5	10
Silt	10	20
Clay	85	70
COMPOSITION:		
Access. minerals	1	1
Clay	15	20
Dolomite	Tr	—
Forimiiners	4	6
Volcanic glass	Tr	—
Inorganic calcite	9	20
Nannofossils	70	50
Quartz	1	3
Sponge spicules	Tr	Tr

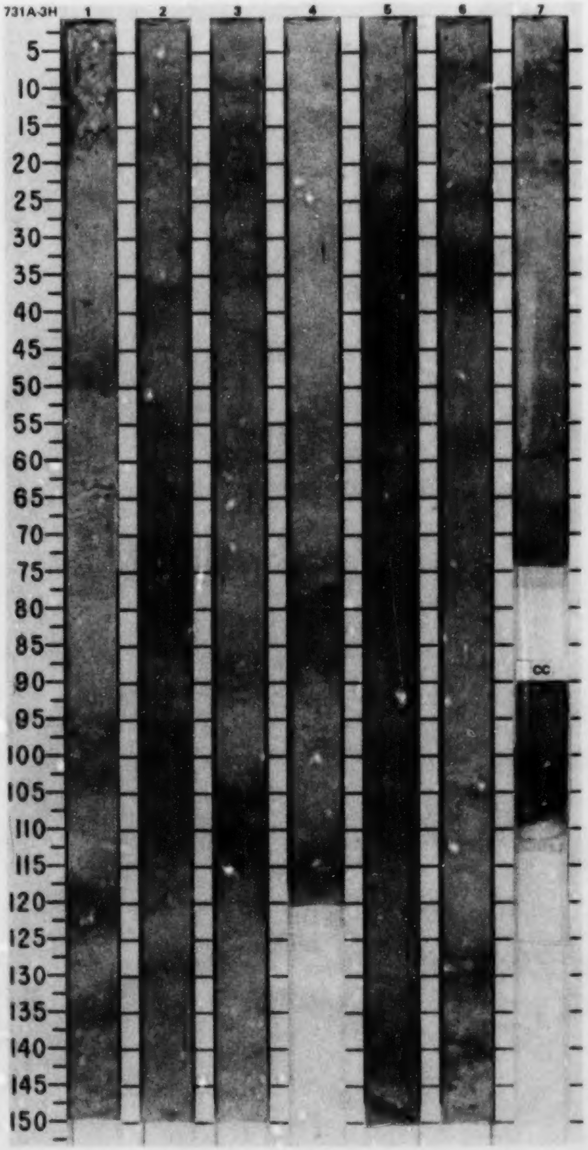
731A-3H
1
2
3
4
5
6
7
5
10
15
20
25
30
35
40
45
50
55
60
65
70
75
80
85
90
95
100
105
110
115
120
125
130
135
140
145
150
CC

SITE 731 HOLE A CORE 4H CORED INTERVAL 2394.6-2404.1 mbsl; 28.8-38.3 mbsf

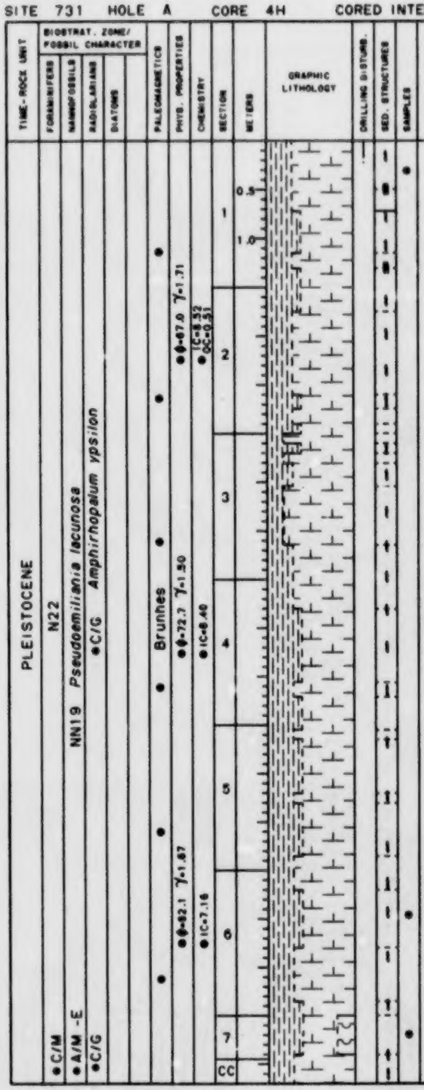
TIME-ROCK UNIT
BIOSTRAT. ZONE/ FOSSIL CHARACTER
FORAMINIFERS
NANNOFOSSILS
RADIOLARIANS
DIATOMS
PALEOMAGNETICS
PHYS. PROPERTIES
CHEMISTRY
SECTION
METERS
GRAPHIC LITHOLOGY
DRILLING DISTURB.
SED. STRUCTURES
SAMPLES
PLEISTOCENE
N22
NN19 Pseudoemiliania lacunosa
●C/G Amphirhopalum ypsilon
●C/M
●A/M -E
●C/G
Brunhes
●φ=67.0 γ=1.71
●φ=72.7 γ=1.50
●φ=62.1 γ=1.67
●IC=8.32 OC=0.51
●IC=8.40
●IC=7.16
1
2
3
4
5
6
7
CC
0.5
1.0

LITHOLOGIC DESCRIPTION

MARLY NANNOFOSSIL OOZE to FORAMINIFER-BEARING MARLY NANNOFOSSIL OOZE

Section 1, 0–10 cm, is moderately disturbed. Remainder is undisturbed.

Major lithology: MARLY NANNOFOSSIL OOZE to FORAMINIFER-BEARING MARLY NANNOFOSSIL OOZE, light greenish gray (10Y 6/2), pale olive (5Y 6/3), olive (5Y 5/3, 4/3), and light olive gray (5Y 6/2). Bioturbated and gradationally interbedded.

Minor lithologies:
a. Nannofossil ooze, light gray (5Y 7/1) and light greenish gray (5GY 7/1), bioturbated, in Section 3, 0–8, 18–28, and 56–114 cm.
b. Diatomaceous marly nannofossil ooze, olive (5Y 5/4), bioturbated, in Section 7, 0–39 cm.

SMEAR SLIDE SUMMARY (%):

	1, 31 D	6, 46 D	7, 20 D
TEXTURE:			
Sand	5	15	15
Silt	15	15	30
Clay	80	70	55
COMPOSITION:			
Access. minerals	1	1	1
Clay	15	25	20
Diatoms	—	—	20
Dolomite	—	—	1
Foraminifers	4	6	2
Glauconite	—	—	Tr
Inorganic calcite	12	20	15
Mica	—	—	2
Nannofossils	65	45	35
Organic debris	—	2	—
Quartz	3	1	2
Radiolarians	—	—	1
Silicoflagellates	—	—	1

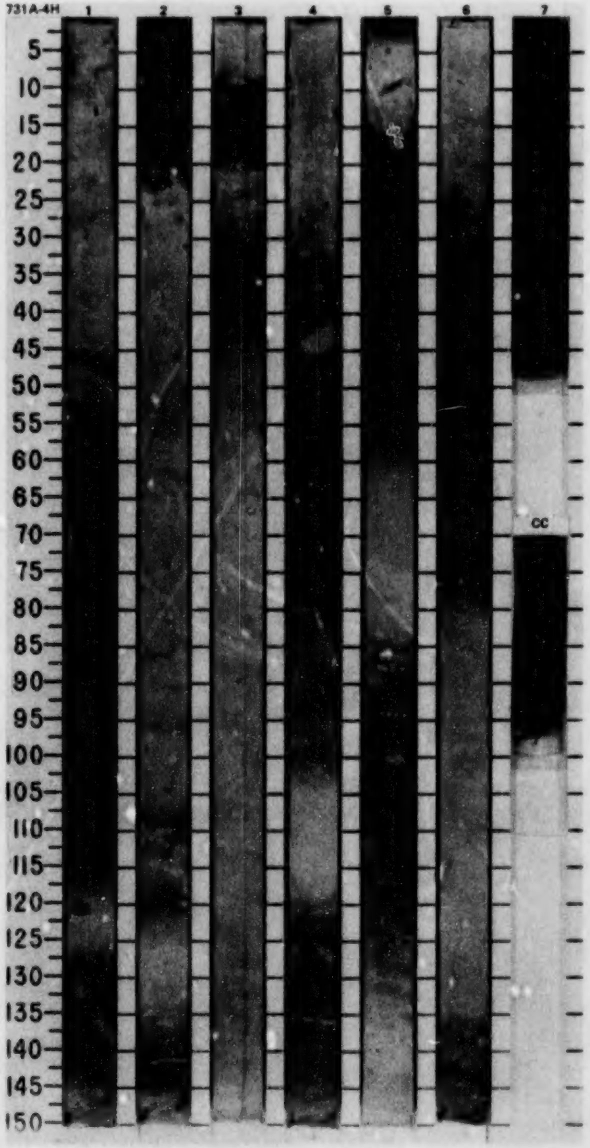
731A-4H
1
2
3
4
5
6
7
CC
5
10
15
20
25
30
35
40
45
50
55
60
65
70
75
80
85
90
95
100
105
110
115
120
125
130
135
140
145
150

SITE 731 HOLE A CORE 5H CORED INTERVAL 2404.1-2413.6 mbsl; 38.3-47.8 mbsf

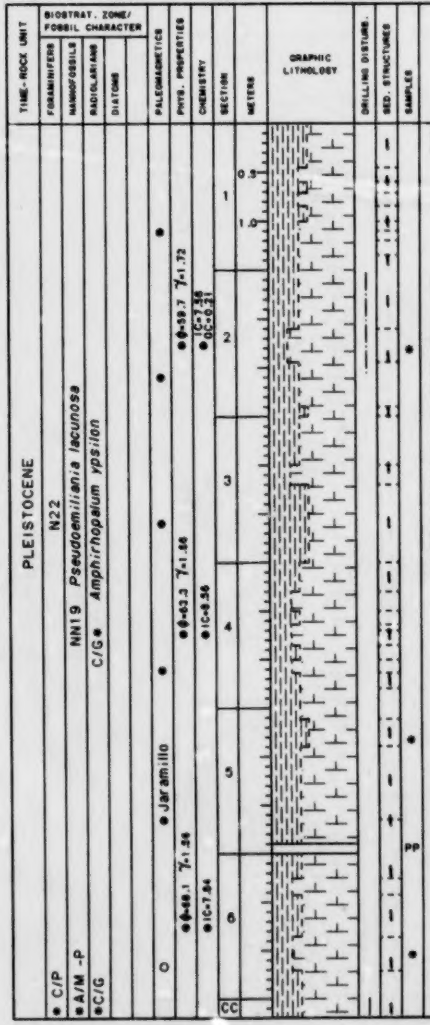
TIME-ROCK UNIT
BIOSTRAT. ZONE/ FOSSIL CHARACTER
FORAMINIFERS
NANNOFOSSILS
RADIOLARIANS
DIATOMS
PALEOMAGNETICS
PHYS. PROPERTIES
CHEMISTRY
SECTION
METERS
GRAPHIC LITHOLOGY
DRILLING DISTURB.
SED. STRUCTURES
SAMPLES
PLEISTOCENE
N22
● C/P
NN19 *Pseudoemiliania lacunosa*
●A/M -P
C/G● *Amphirhopalum ypsilon*
●C/G
● Jaramillo
○
●φ=59.7 γ=1.72
●φ=63.3 γ=1.56
●φ=66.1 γ=1.56
●IC=7.58 OC=0.21
●IC=8.56
●IC=7.84
1
2
3
4
5
6
CC
0.5
1.0
PP

LITHOLOGIC DESCRIPTION

NANNOFOSSIL OOZE and MARLY NANNOFOSSIL OOZE TO SILICEOUS-BEARING MARLY NANNOFOSSIL OOZE

Section 2, 0-76 cm, is moderately disturbed. Remainder is undisturbed.

Major lithologies:
a. NANNOFOSSIL OOZE, light gray (5Y 7/1) and light greenish gray (5GY 7/1, 10Y 7/2). Bioturbated throughout.
b. MARLY NANNOFOSSIL OOZE to SILICEOUS-BEARING MARLY NANNOFOSSIL OOZE, pale olive (5Y 6/3), light olive gray (5Y 6/2), and olive (5Y 5/4, 5/3). Bioturbated throughout.

SMEAR SLIDE SUMMARY (%):

	2, 82 D	5, 33 D	6, 105 D
TEXTURE:			
Sand	—	5	5
Silt	15	30	15
Clay	85	65	80
COMPOSITION:			
Access. minerals	Tr	1	—
Clay	10	20	10
Diatoms	3	—	
Dolomite	—	Tr	—
Foraminifers	Tr	4	6
Volcanic glass	Tr	—	—
Inorganic calcite	15	21	12
Nannofossils	75	45	70
Quartz	—	5	2
Radiolarians	—	Tr	—
Silicoflagellates	—	1	—

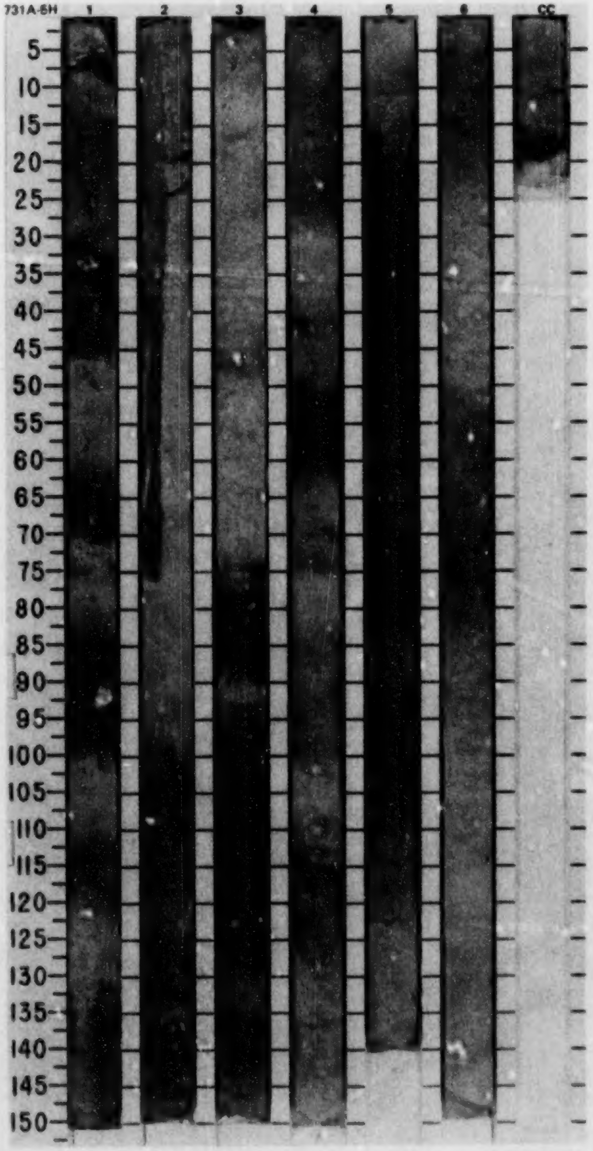
731A-5H
1
2
3
4
5
6
CC
5
10
15
20
25
30
35
40
45
50
55
60
65
70
75
80
85
90
95
100
105
110
115
120
125
130
135
140
145
150

SITE 731 HOLE A CORE 6H CORED INTERVAL 2413.6-2423.1 mbsl; 47.8-57.3 mbsf

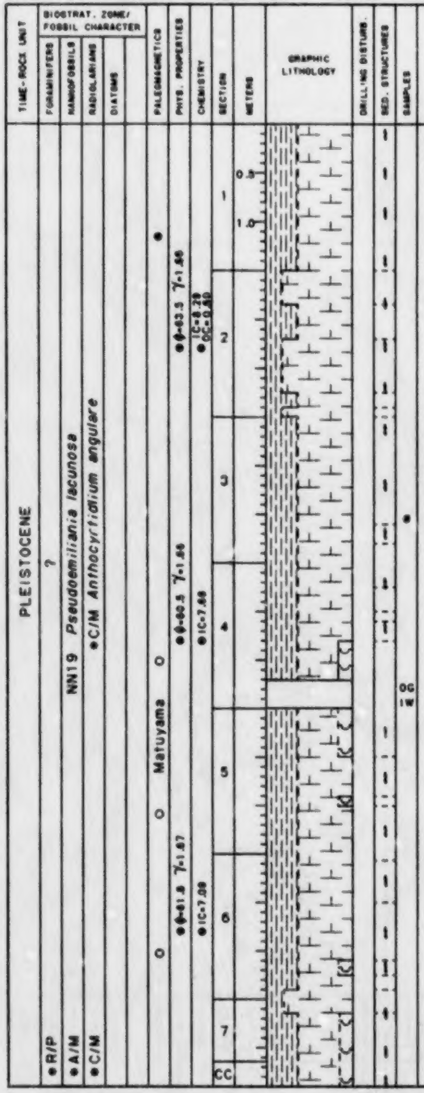
TIME-ROCK UNIT
BIOSTRAT. ZONE/FOSSIL CHARACTER
FORAMINIFERS
NANNOFOSSILS
RADIOLARIANS
DIATOMS
PALEOMAGNETICS
PHYS. PROPERTIES
CHEMISTRY
SECTION
METERS
GRAPHIC LITHOLOGY
DRILLING DISTURB.
SED. STRUCTURES
SAMPLES
PLEISTOCENE
?
NN19 Pseudoemiliania lacunosa
●C/M Anthocyrtidium angulare
●R/P
●A/M
●C/M
Matuyama
●φ=63.3 γ=1.66
●IC=8.28 OC=0.50
●φ=60.5 γ=1.66
●IC=7.66
●φ=61.8 γ=1.67
●IC=7.08
1
2
3
4
5
6
7
CC
0.5
1.0
OG
IW

LITHOLOGIC DESCRIPTION

NANNOFOSSIL OOZE, MARLY NANNOFOSSIL OOZE, and SILICEOUS MARLY NANNOFOSSIL OOZE

Entire core is undisturbed.

Major lithologies:
a. NANNOFOSSIL OOZE, light gray (5Y 7/1, 7/2) and light greenish gray (5GY 7/1, 10Y 7/2). Bioturbated throughout. Grading to minor occurrences of foraminifer- bearing nannofossil ooze.
b. MARLY NANNOFOSSIL OOZE, pale olive (5Y 6/3), light olive gray (5Y 6/2), and light greenish gray (10Y 6/2), with minor gradations to siliceous-bearing marly nannofossil ooze. Bioturbated throughout.
c. SILICEOUS MARLY NANNOFOSSIL OOZE, olive (5Y 5/3, 5/4). Bioturbated.

SMEAR SLIDE SUMMARY (%):

	3, 105 D
TEXTURE:	
Sand	5
Silt	20
Clay	75
COMPOSITION:	
Access. minerals	1
Clay	25
Diatoms	8
Dolomite	Tr
Foraminifers	4
Inorganic calcite	10
Nannofossils	50
Silicoflagellates	2

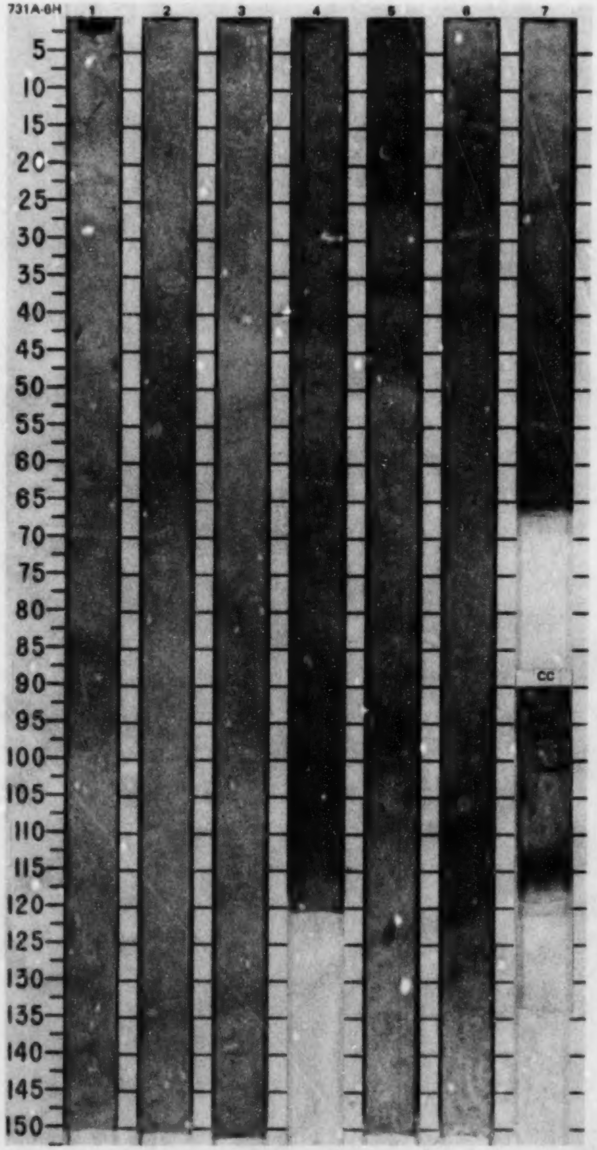
731A-6H
1
2
3
4
5
6
7
CC
5
10
15
20
25
30
35
40
45
50
55
60
65
70
75
80
85
90
95
100
105
110
115
120
125
130
135
140
145
150

SITE 731 HOLE A CORE 7H CORED INTERVAL 2423.1-2432.8 mbsl; 57.3-67.0 mbsf

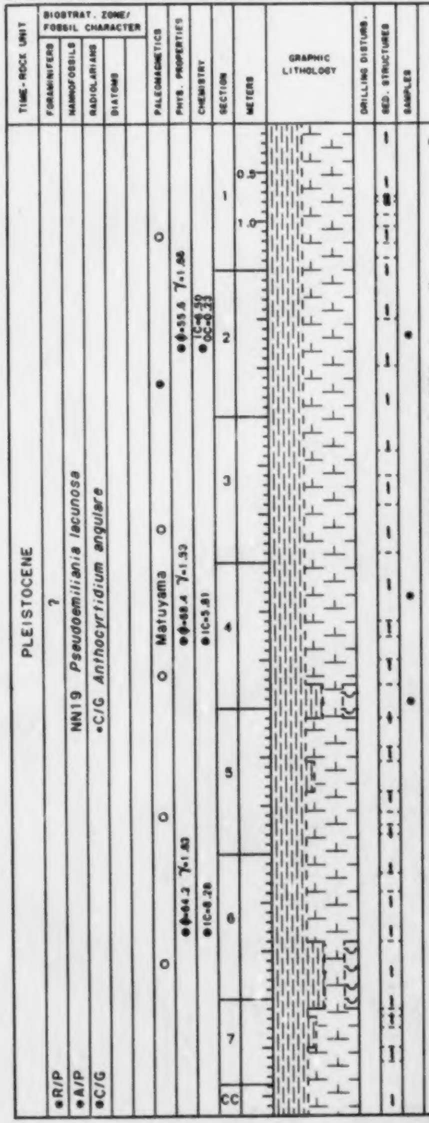
TIME-ROCK UNIT
BIOSTRAT. ZONE/ FOSSIL CHARACTER
FORAMINIFERS
NANNOFOSSILS
RADIOLARIANS
DIATOMS
PALEOMAGNETICS
PHYS. PROPERTIES
CHEMISTRY
SECTION
METERS
GRAPHIC LITHOLOGY
DRILLING DISTURB.
SED. STRUCTURES
SAMPLES
PLEISTOCENE
?
NN19 Pseudoemiliania lacunosa
•C/G Anthocyrtidium angulare
•R/P
•A/P
•C/G
Matuyama
•φ=55.6 γ=1.86
•φ=68.4 γ=1.93
•φ=64.2 γ=1.83
•IC=6.30 OC=0.23
•IC=5.81
•IC=8.28
0.5
1.0
1
2
3
4
5
6
7
CC

LITHOLOGIC DESCRIPTION

CALCITIC MARLY NANNOFOSSIL OOZE

Entire core is undisturbed.

Major lithology: CALCITIC MARLY NANNOFOSSIL OOZE, light greenish gray (10Y 6/2, 5GY 6/1), pale olive (5Y 6/3), light olive gray (5Y 6/2), and olive (5Y 5/3). Gradationally interbedded and bioturbated throughout.

Minor lithology: Diatomaceous nannofossil-rich calcitic silty clay, dark olive gray (5Y 3/2), bioturbated, in Section 4, 123 cm, to Section 5, 10 cm, and Section 6, 95 cm, to Section 7, 8 cm.

SMEAR SLIDE SUMMARY (%):

	2, 88 D	4, 35 D	4, 144 D
TEXTURE:			
Sand	10	15	15
Silt	25	20	30
Clay	65	65	55
COMPOSITION:			
Access. minerals	1	1	2
Clay	15	25	30
Diatoms	Tr	Tr	15
Dolomite	2	1	—
Foraminifers	5	3	2
Volcanic glass	Tr	—	
Inorganic calcite	25	30	20
Nannofossils	50	40	25
Organic debris	—	—	3
Quartz	2	—	2
Radiolarians	—	Tr	Tr
Sponge spicules	Tr	—	1

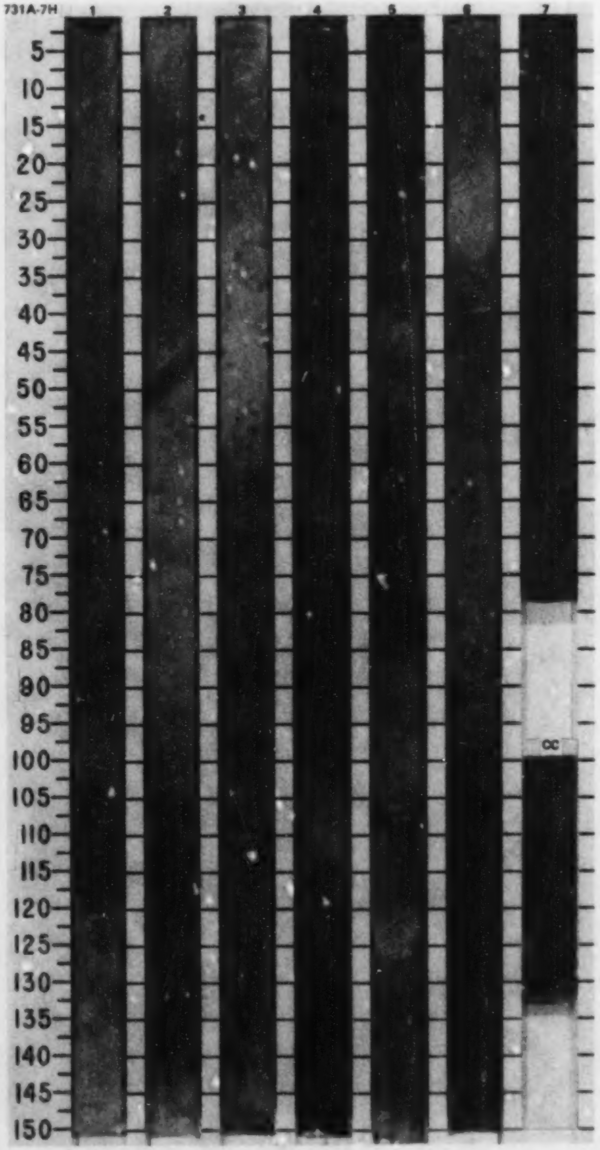
731A-7H
1
2
3
4
5
6
7
CC
5
10
15
20
25
30
35
40
45
50
55
60
65
70
75
80
85
90
95
100
105
110
115
120
125
130
135
140
145
150

SITE 731 HOLE A CORE 8X CORED INTERVAL 2432.8-2442.5 mbsl; 67.0-76.7 mbsf

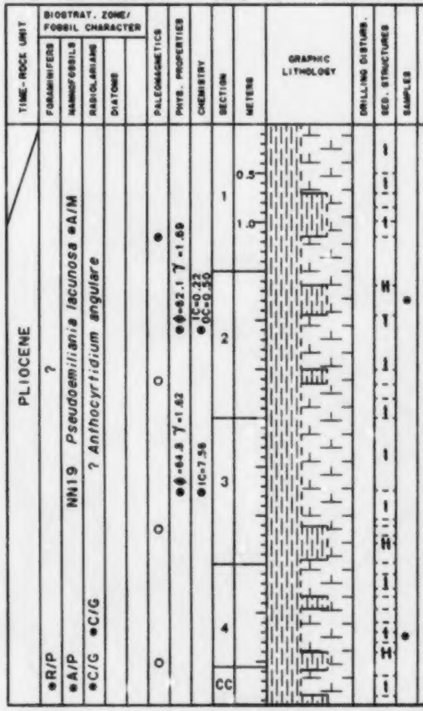
TIME-ROCK UNIT
BIOSTRAT. ZONE/ FOSSIL CHARACTER
FORAMINIFERS
NANNOFOSSILS
RADIOLARIANS
DIATOMS
PALEOMAGNETICS
PHYS. PROPERTIES
CHEMISTRY
SECTION
METERS
GRAPHIC LITHOLOGY
DRILLING DISTURB.
SED. STRUCTURES
SAMPLES
PLIOCENE
?
●R/P
NN19 Pseudoemiliania lacunosa ●A/M
●A/P
? Anthocyrtidium angulare
●C/G ●C/G
●C/G
●φ=62.1 γ=1.89
●φ=64.8 γ=1.82
●IC=0.22 OC=0.50
●IC=7.56
1
2
3
4
CC
0.5
1.0

LITHOLOGIC DESCRIPTION

FORAMINIFER-BEARING CALCITIC MARLY NANNOFOSSIL OOZE and NANNOFOSSIL-RICH CALCITIC SILTY CLAY

Section 2 is slightly disturbed. Remainder is undisturbed.

Major lithologies:

a. FORAMINIFER-BEARING CALCITIC MARLY NANNOFOSSIL OOZE, light greenish gray (5GY 7/1; 10Y 6/2, 5/2), pale olive (5Y 6/3), and olive (5Y 5/3). Gradationally interbedded and bioturbated throughout.
b. NANNOFOSSIL-RICH CALCITIC SILTY CLAY, olive (5Y 4/3) and dark olive gray (5Y 3/2). Bioturbated.

SMEAR SLIDE SUMMARY (%):

	2, 29 D	4, 72 D
TEXTURE:		
Sand	20	—
Silt	35	30
Clay	45	70
COMPOSITION:		
Access. minerals	3	1
Clay	30	15
Dolomite	—	Tr
Foraminifers	—	6
Volcanic glass	1	—
Inorganic calcite	30	20
Mica	—	Tr
Nannofossils	15	55
Organic debris	5	—
Quartz	15	2
Radiolarians	1	1
Sponge spicules	Tr	—

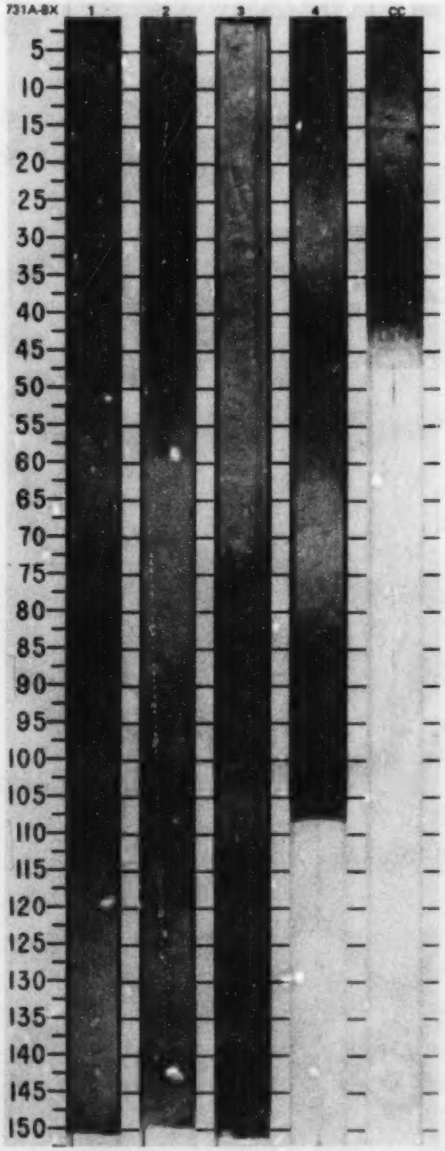
731A-8X
1
2
3
4
CC
5
10
15
20
25
30
35
40
45
50
55
60
65
70
75
80
85
90
95
100
105
110
115
120
125
130
135
140
145
150

SITE 731 HOLE A CORE 9X CORED INTERVAL 2442.5-2452.2 mbsl; 76.7-86.4 mbsf

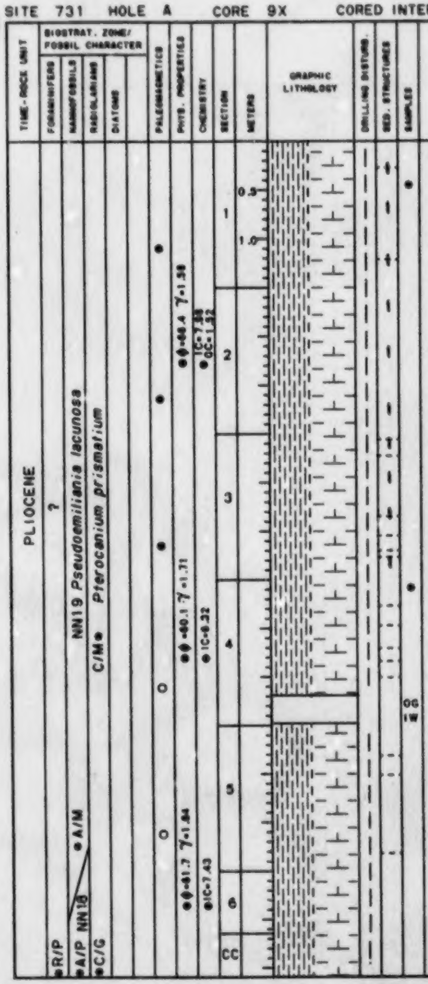
TIME-ROCK UNIT
BIOSTRAT. ZONE/ FOSSIL CHARACTER
FORAMINIFERS
NANNOFOSSILS
RADIOLARIANS
DIATOMS
PALEOMAGNETICS
PHYS. PROPERTIES
CHEMISTRY
SECTION
METERS
GRAPHIC LITHOLOGY
DRILLING DISTURB.
SED. STRUCTURES
SAMPLES
PLIOCENE
?
NN19 Pseudoemiliania lacunosa
C/M● Pterocanium prismatium
●R/P
●A/P NN18
●C/G
●A/M
●Φ=66.4 γ=1.58
●Φ=60.1 γ=1.71
●Φ=61.7 γ=1.84
●IC=7.88 OC=1.52
●IC=6.32
●IC=7.43
1
2
3
4
5
6
CC
0.5
1.0
OG
IW

LITHOLOGIC DESCRIPTION

CALCITIC MARLY NANNOFOSSIL OOZE

Entire core is slightly disturbed.

Major lithology: CALCITIC MARLY NANNOFOSSIL OOZE, light gray (5Y 7/2), light greenish gray (10Y 6/2), light olive gray (5Y 6/2), and pale olive (5Y 6/3), to olive (5Y 5/3, 4/3) and dark greenish gray (10Y 5/3). Gradationally interbedded, and bioturbated throughout. Planolites at Section 3, 125–150 cm.

SMEAR SLIDE SUMMARY (%):

	1, 48 D	4, 7 D
TEXTURE:		
Sand	10	10
Silt	25	20
Clay	65	70
COMPOSITION:		
Access. minerals	1	2
Clay	15	25
Dolomite	—	1
Foraminifers	8	1
Volcanic glass	—	1
Inorganic calcite	25	20
Nannofossils	50	45
Quartz	1	5
Radiolarians	Tr	—
Silicoflagellates	Tr	—
Sponge spicules	Tr	—

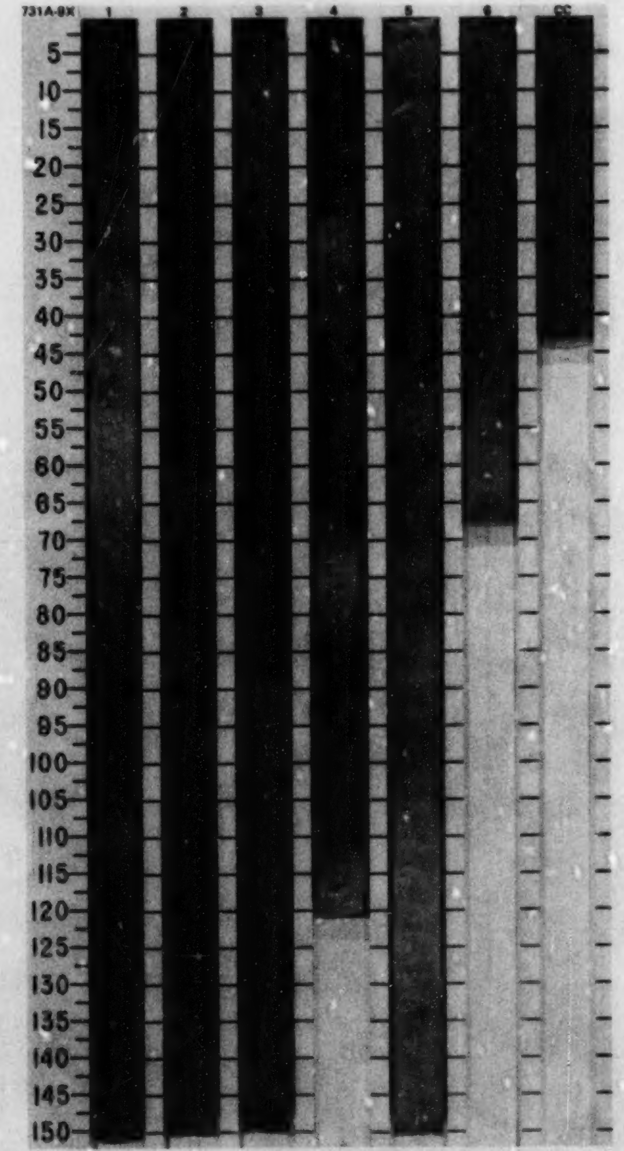
731A-9X
1
2
3
4
5
6
CC
5
10
15
20
25
30
35
40
45
50
55
60
65
70
75
80
85
90
95
100
105
110
115
120
125
130
135
140
145
150

SITE 731 HOLE A CORE 10X CORED INTERVAL 2452.2-2461.8 mbsl: 86.4-96.9 mbsf

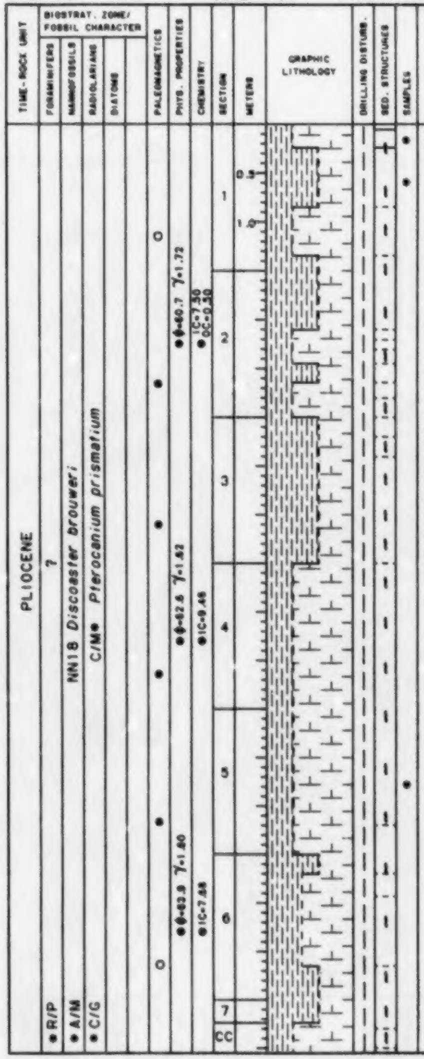
TIME-ROCK UNIT
BIOSTRAT. ZONE/ FOSSIL CHARACTER
FORAMINIFERS
NANNOFOSSILS
RADIOLARIANS
DIATOMS
PALEOMAGNETICS
PHYS. PROPERTIES
CHEMISTRY
SECTION
METERS
GRAPHIC LITHOLOGY
DRILLING DISTURB.
SED. STRUCTURES
SAMPLES
PLIOCENE
● R/P ?
● A/M NN18 Discoaster brouweri
● C/G C/M● Pterocanium prismatium
●Φ=60.7 γ=1.72
●Φ=62.6 γ=1.82
●Φ=63.9 γ=1.80
● IC=7.30 OC=0.30
●IC=9.46
●IC=7.88
1
2
3
4
5
6
7
CC
0.5
1.0

LITHOLOGIC DESCRIPTION

NANNOFOSSIL OOZE TO CALCITIC MARLY NANNOFOSSIL OOZE and CALCITIC MARLY NANNOFOSSIL OOZE

Entire core is slightly disturbed.

Major lithologies:
a. NANNOFOSSIL OOZE to CALCITIC MARLY NANNOFOSSIL OOZE, light gray (5Y 7/2, 10Y 6/2), light olive gray (5Y 6/2), and pale olive (5Y 6/3). Bioturbated.
b. CALCITIC MARLY NANNOFOSSIL OOZE, olive (5Y 5/3, 5/4, 4/3). Bioturbated.

SMEAR SLIDE SUMMARY (%):

	1, 17 D	1, 60 D	5, 70 D
TEXTURE:			
Sand	5	10	5
Silt	20	35	20
Clay	75	55	75
COMPOSITION:			
Access. minerals	—	1	—
Clay	15	20	10
Diatoms	—	Tr	Tr
Dolomite	—	1	—
Foraminifers	4	4	5
Volcanic glass	—	Tr	—
Glauconite	—	Tr	—
Inorganic calcite	20	30	20
Nannofossils	60	35	65
Quartz	1	8	—
Radiolarians	—	1	—
Silicoflagellates	—	Tr	—

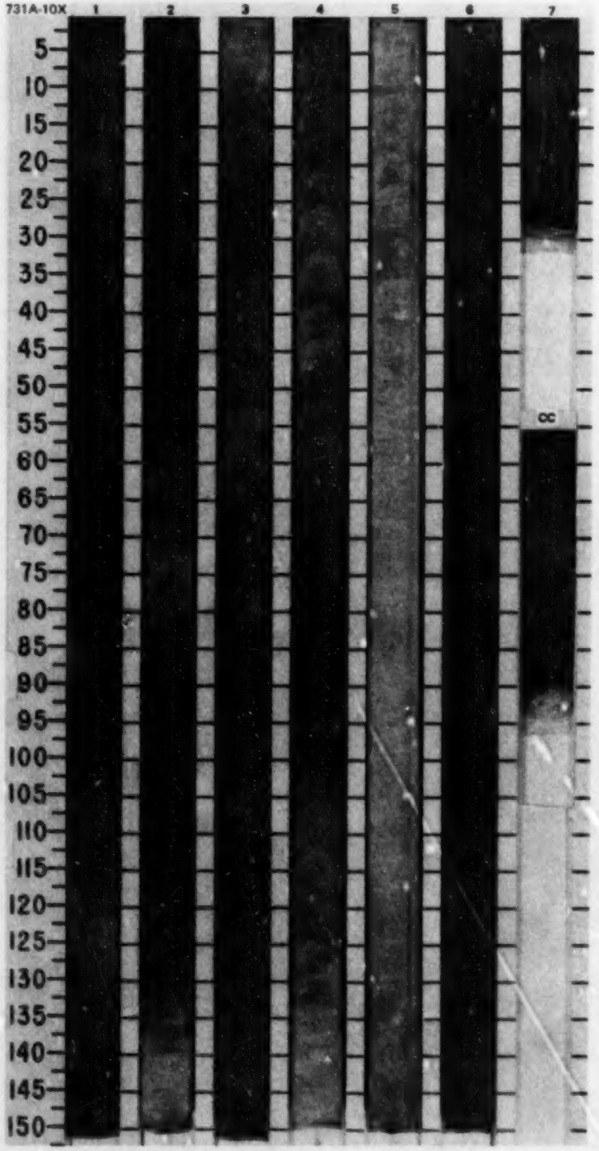
731A-10X
1
2
3
4
5
6
7
CC
5
10
15
20
25
30
35
40
45
50
55
60
65
70
75
80
85
90
95
100
105
110
115
120
125
130
135
140
145
150

SITE 731 HOLE A CORE 11X CORED INTERVAL 2461.8-2471.5 mbsl; 96.0-105.7 mbsf

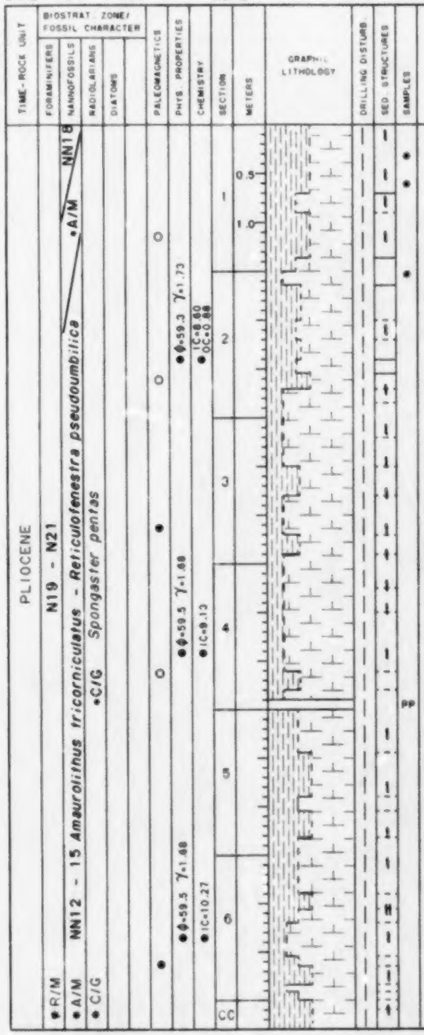
TIME-ROCK UNIT
BIOSTRAT. ZONE/ FOSSIL CHARACTER
FORAMINIFERS
NANNOFOSSILS
RADIOLARIANS
DIATOMS
PALEOMAGNETICS
PHYS. PROPERTIES
CHEMISTRY
SECTION
METERS
GRAPHIC LITHOLOGY
DRILLING DISTURB.
SED. STRUCTURES
SAMPLES
PLIOCENE
●R/M N19 - N21
●A/M NN12 - 15 Amaurolithus tricorniculatus - Reticulofenestra pseudoumbilica
●A/M
NN18
● C/G ●C/G Spongaster pentas
●Φ=59.3 γ=1.73
●Φ=59.5 γ=1.88
●Φ=59.5 γ=1.88
● IC=8.60 OC=0.88
●IC=9.13
●IC=10.27
1
2
3
4
5
6
CC
0.5
1.0
PP

LITHOLOGIC DESCRIPTION

NANNOFOSSIL OOZE and CALCITIC MARLY NANNOFOSSIL OOZE

Entire core is slightly disturbed by drilling. Section 2, 0-105 cm, contains sharp irregular contacts, which are possible slump contacts.

Major lithologies:
a. NANNOFOSSIL OOZE, light gray (5Y 7/1) and light greenish gray (10Y 7/2). Bioturbated throughout, with minor Planolites and Zoophycos.
b. CALCITIC MARLY NANNOFOSSIL OOZE, light greenish gray (10Y 6/2), light olive gray (5Y 6/2), pale olive (5Y 6/3), and olive (5Y 5/3, 5/4, 4/3). Bioturbated throughout. Minor gradations to foraminifer-bearing calcitic marly nannofossil ooze.

SMEAR SLIDE SUMMARY (%):

	1, 33 D	1, 61 M	2, 4 D
TEXTURE:			
Sand	10	10	5
Silt	25	30	15
Clay	65	60	80
COMPOSITION:			
Access. minerals	1	2	—
Clay	25	30	10
Diatoms	Tr	Tr	Tr
Foraminifers	6	1	5
Volanic glass	Tr	—	
Inorganic calcite	23	25	15
Nannofossils	40	30	70
Organic debris	—	2	—
Quartz	5	10	—
Radiolarians	Tr	Tr	Tr
Sponge spicules	—Tr	—	

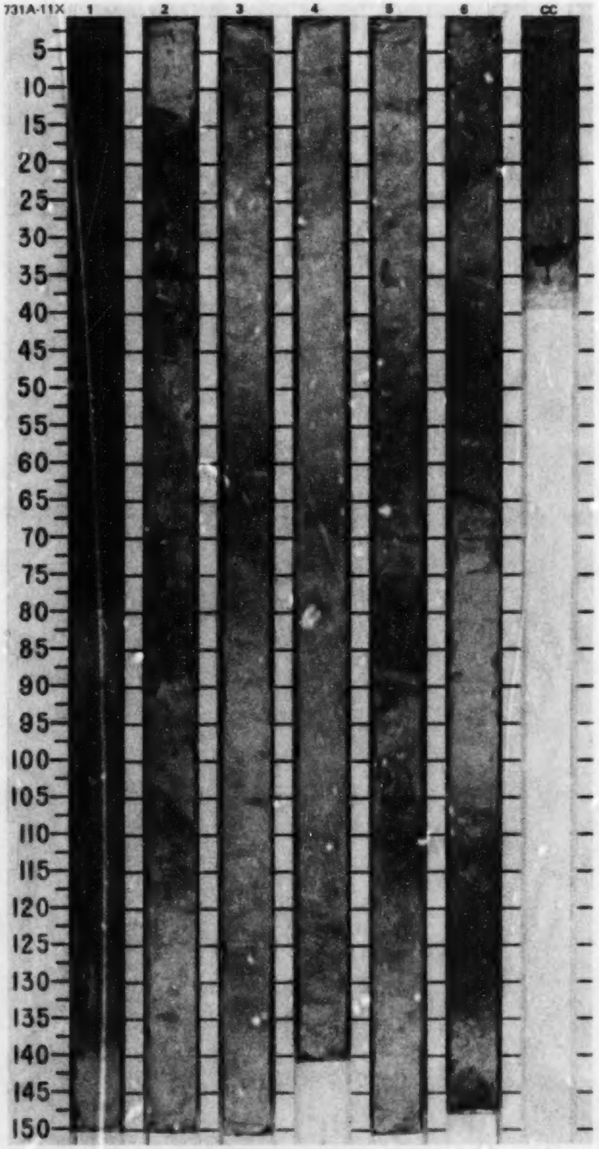
731A-11X
1
2
3
4
5
6
CC
5
10
15
20
25
30
35
40
45
50
55
60
65
70
75
80
85
90
95
100
105
110
115
120
125
130
135
140
145
150

SITE 731 HOLE A CORE 12X CORED INTERVAL 2471.5-2481.2 mbsl; 105.7-115.4 mbsf

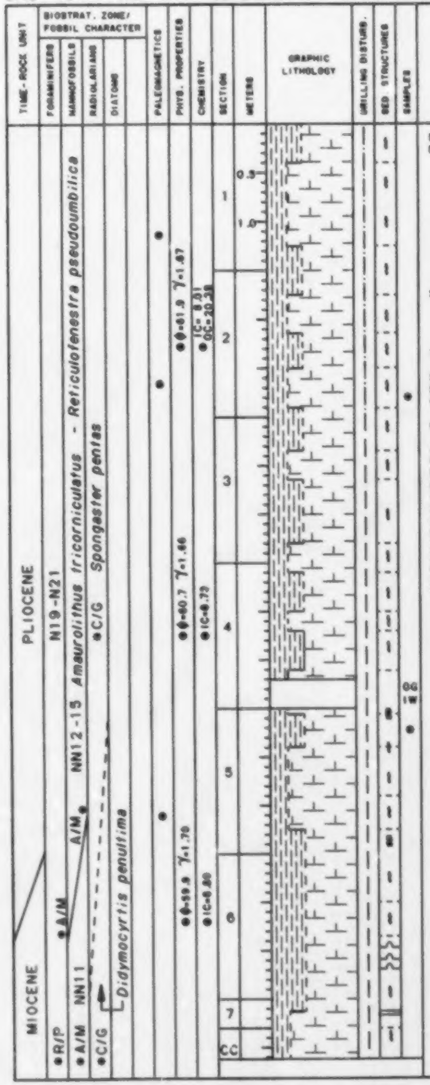
TIME-ROCK UNIT
BIOSTRAT. ZONE/ FOSSIL CHARACTER
FORAMINIFERS
NANNOFOSSILS
RADIOLARIANS
DIATOMS
PALEOMAGNETICS
PHYS. PROPERTIES
CHEMISTRY
SECTION
METERS
GRAPHIC LITHOLOGY
DRILLING DISTURB.
SED. STRUCTURES
SAMPLES
PLIOCENE
MIOCENE
N19-N21
●R/P
●A/M
NN12-15 Amaurolithus tricorniculatus - Reticulofenestra pseudoumbilica
A/M
●A/M NN11
●C/G Spongaster pentas
●C/G
Didymocyrtis penultima
●φ=61.9 γ=1.87
●φ=60.7 γ=1.86
●φ=59.9 γ=1.70
●IC= 8.01 OC=20.38
●IC=6.73
●IC=8.80
1
2
3
4
5
6
7
CC
0.5
1.0
OG
IW

LITHOLOGIC DESCRIPTION

FORAMINIFER-BEARING NANNOFOSSIL OOZE and CALCITIC MARLY NANNOFOSSIL OOZE

Entire core is slightly to moderately disturbed by drilling. Section 6, 80-120 cm, contains possible slump blocks.

Major lithologies:
a. FORAMINIFER-BEARING NANNOFOSSIL OOZE, light gray (5Y 7/1, 7/2). Minor bioturbation throughout.
b. CALCITIC MARLY NANNOFOSSIL OOZE, light greenish gray (10Y 6/2), light olive gray (5Y 6/2), pale olive (5Y 6/3), and olive (5Y 5/3, 4/3). Minor bioturbation throughout.

SMEAR SLIDE SUMMARY (%):

	2, 129 D	5, 23 D
TEXTURE:		
Sand	5	10
Silt	15	15
Clay	80	75
COMPOSITION:		
Access. minerals	1	1
Clay	15	20
Diatoms	1	2
Dolomite	—	1
Foraminifers	7	1
Volcanic glass	10	Tr
Inorganic calcite	—	15
Mica	Tr	—
Nannofossils	65	55
Phosphate	—	Tr
Quartz	—	3
Radiolarians	1	1
Sponge spicules	Tr	1

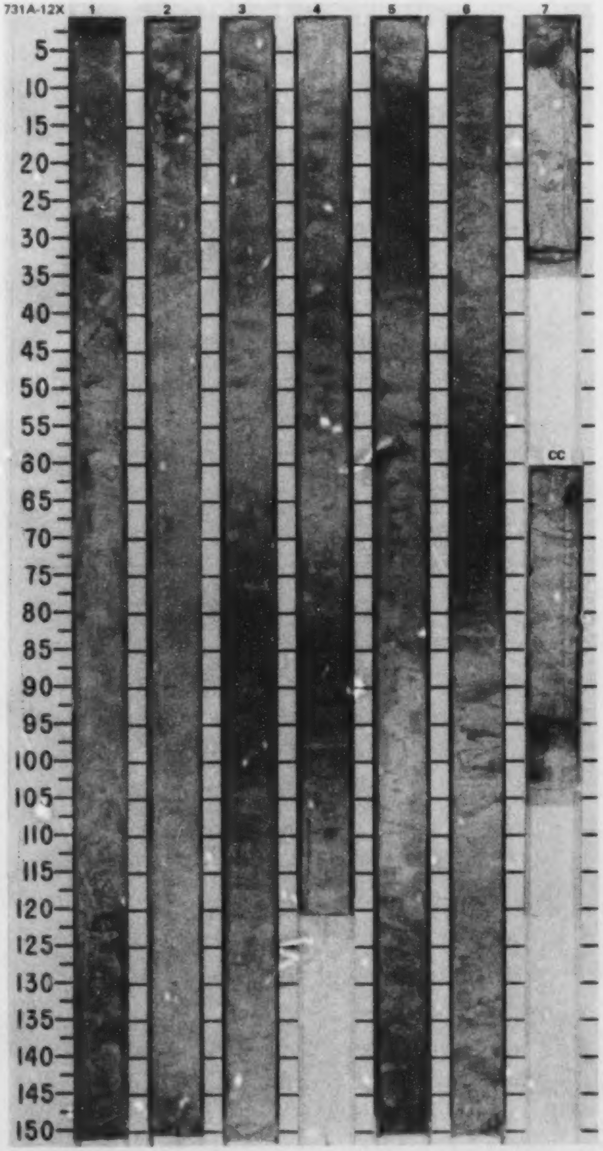
731A-12X
1
2
3
4
5
6
7
CC
5
10
15
20
25
30
35
40
45
50
55
60
65
70
75
80
85
90
95
100
105
110
115
120
125
130
135
140
145
150

SITE 731 HOLE A CORE 13X CORED INTERVAL 2481.2-2490.8 mbsl; 115.4-125.0 mbsf

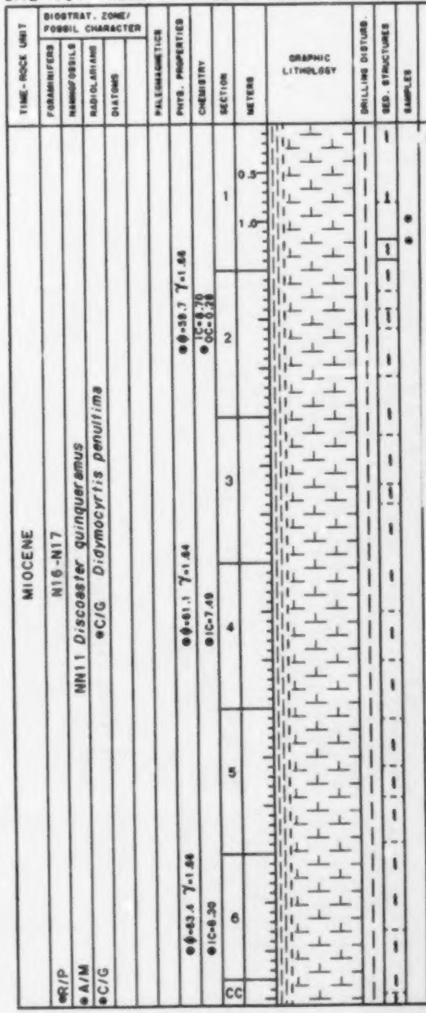
TIME-ROCK UNIT
BIOSTRAT. ZONE/ FOSSIL CHARACTER
FORAMINIFERS
NANNOFOSSILS
RADIOLARIANS
DIATOMS
PALEOMAGNETICS
PHYS. PROPERTIES
CHEMISTRY
SECTION
METERS
GRAPHIC LITHOLOGY
DRILLING DISTURB.
SED. STRUCTURES
SAMPLES
MIOCENE
N16-N17
NN11 Discoaster quinqueramus
●C/G Didymocyrtis penultima
●R/P
●A/M
●C/G
●Φ=58.7 γ=1.88
●Φ=61.1 γ=1.84
●Φ=63.4 γ=1.86
●IC=8.70 OC=0.28
●IC=7.48
●IC=8.30
1
2
3
4
5
6
CC
0.5
1.0

LITHOLOGIC DESCRIPTION

NANNOFOSSIL OOZE

Entire core is slightly disturbed.

Major lithology: NANNOFOSSIL OOZE, white (5Y 8/1), light gray (5Y 7/1, 7/2), light olive gray (5Y 6/2), and olive gray (5Y 5/2). Minor gradations to siliceous-bearing nannofossil ooze, with minor bioturbation throughout.

SMEAR SLIDE SUMMARY (%):

	1, 99 D	1, 121 D
TEXTURE:		
Silt	5	15
Clay	95	85
COMPOSITION:		
Clay	10	11
Diatoms	Tr	3
Dolomite	—	Tr
Foraminifers	2	1
Inorganic calcite	3	5
Mica	—	1
Nannofossils	85	75
Quartz	—	2
Radiolarians	Tr	—
Silicoflagellates	—	1
Sponge spicules	Tr	1

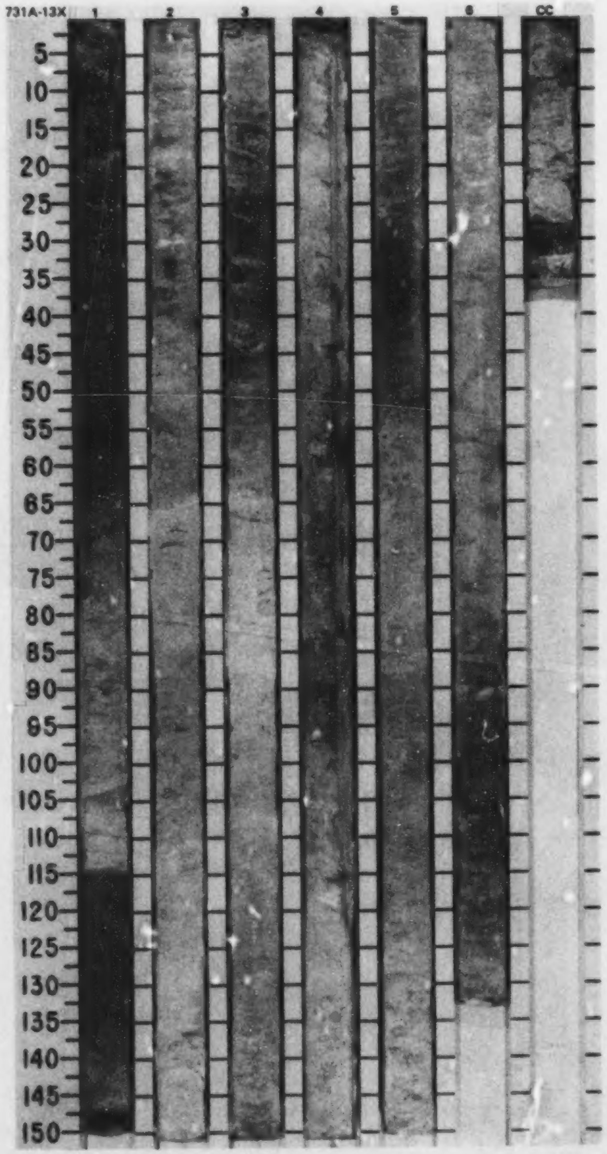
731A-13X
1
2
3
4
5
6
CC
5
10
15
20
25
30
35
40
45
50
55
60
65
70
75
80
85
90
95
100
105
110
115
120
125
130
135
140
145
150

SITE 731 HOLE A CORE 14X CORED INTERVAL 2490.8-2500.5 mbsl; 125.0-134.7 mbsf

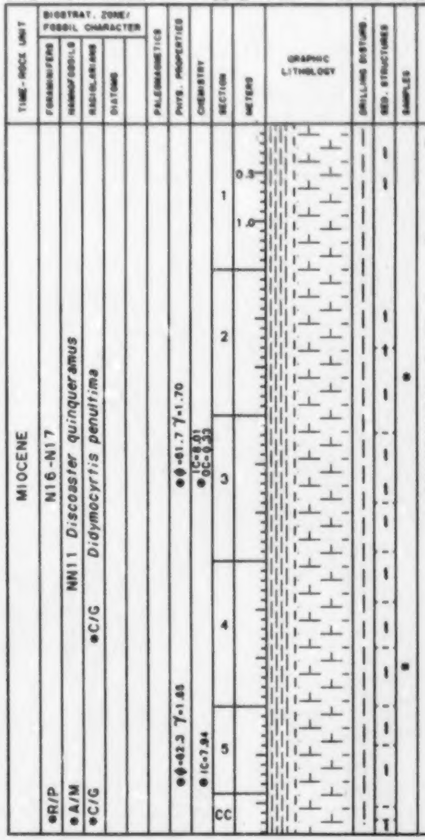
TIME-ROCK UNIT
BIOSTRAT. ZONE/ FOSSIL CHARACTER
FORAMINIFERS
NANNOFOSSILS
RADIOLARIANS
DIATOMS
PALEOMAGNETICS
PHYS. PROPERTIES
CHEMISTRY
SECTION
METERS
GRAPHIC LITHOLOGY
DRILLING DISTURB.
SED. STRUCTURES
SAMPLES
MIOCENE
N16-N17
NN11 Discoaster quinqueramus
Didymocyrtis penultima
●C/G
●R/P
●A/M
●C/G
●φ=61.7 γ=1.70
●φ=62.3 γ=1.85
● IC=8.01 OC=0.33
● IC=7.94
1
2
3
4
5
CC
0.5
1.0

LITHOLOGIC DESCRIPTION

NANNOFOSSIL OOZE to MARLY NANNOFOSSIL OOZE

Entire core is slightly disturbed.

Major lithology: NANNOFOSSIL OOZE to MARLY NANNOFOSSIL OOZE, white (5Y 8/1), light gray (5Y 7/1, 7/2), and olive gray (5Y 6/2, 5/2). Darker intervals are occasionally siliceous-bearing. Bioturbated throughout.

SMEAR SLIDE SUMMARY (%):

	2, 110 D	4, 110 D
TEXTURE:		
Silt	10	20
Clay	90	80
COMPOSITION:		
Access. minerals	—	Tr
Clay	20	15
Diatoms	—	2
Foraminifers	Tr	Tr
Inorganic calcite	10	15
Nannofossils	70	60
Quartz	—	4
Radiolarians	Tr	1
Silicoflagellates	Tr	—
Sponge spicules	Tr	3

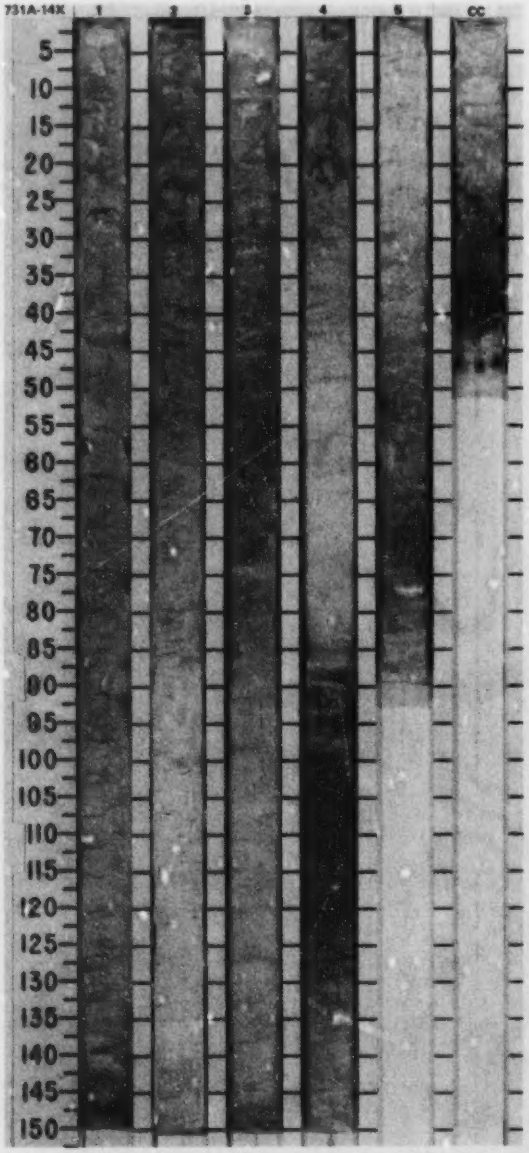
731A-14X
1
2
3
4
5
CC
5
10
15
20
25
30
35
40
45
50
55
60
65
70
75
80
85
90
95
100
105
110
115
120
125
130
135
140
145
150

SITE 731 HOLE A CORE 15X CORED INTERVAL 2500.5-2510.2 mbsl; 134.7-144.4 mbsf

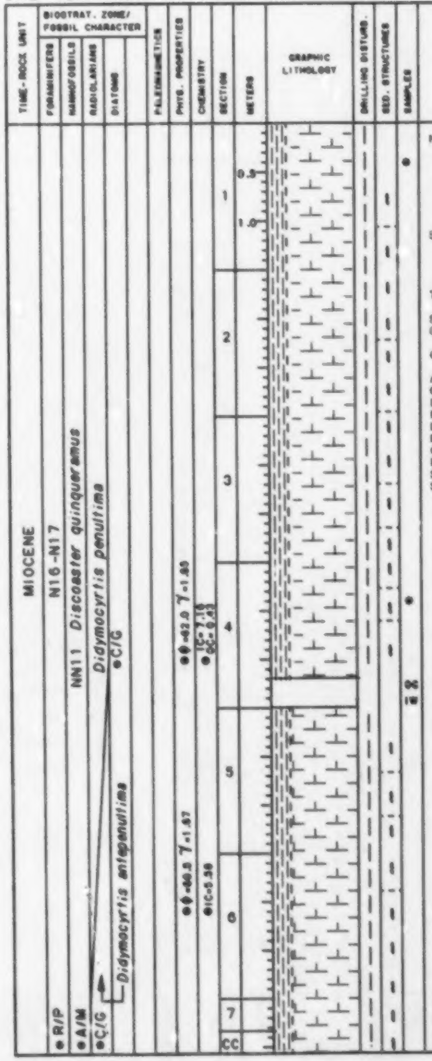
TIME-ROCK UNIT
BIOSTRAT. ZONE/ FOSSIL CHARACTER
FORAMINIFERS
NANNOFOSSILS
RADIOLARIANS
DIATOMS
PALEOMAGNETICS
PHYS. PROPERTIES
CHEMISTRY
SECTION
METERS
GRAPHIC LITHOLOGY
DRILLING DISTURB.
SED. STRUCTURES
SAMPLES
MIOCENE
N16-N17
NN11 Discoaster quinqueramus
Didymocyrtis penultima
●C/G
Didymocyrtis antepenultima
●R/P
●A/M
●C/G
●φ=62.0 γ=1.85
●φ=60.5 γ=1.87
●TC=7.16 OC=0.43
●IC=5.30
0.5
1.0
1
2
3
4
5
6
7
CC
OG
IW

LITHOLOGIC DESCRIPTION

NANNOFOSSIL OOZE to SILICEOUS-BEARING NANNOFOSSIL OOZE

Entire section is slightly disturbed.

Major lithology: NANNOFOSSIL OOZE to SILICEOUS-BEARING NANNOFOSSIL OOZE, white (5Y 8/1), light gray (5Y 7/1), and olive gray (5Y 6/2). Minor bioturbation throughout.

SMEAR SLIDE SUMMARY (%):

	1, 40 D	4, 40 D
TEXTURE:		
Silt	20	20
Clay	80	80
COMPOSITION:		
Access. minerals	1	1
Clay	22	8
Diatoms	5	1
Foraminifers	1	7
Inorganic calcite	5	5
Nannofossils	65	75
Quartz	Tr	1
Radiolarians	1	2
Silicoflagellates	Tr	Tr
Sponge spicules	Tr	Tr

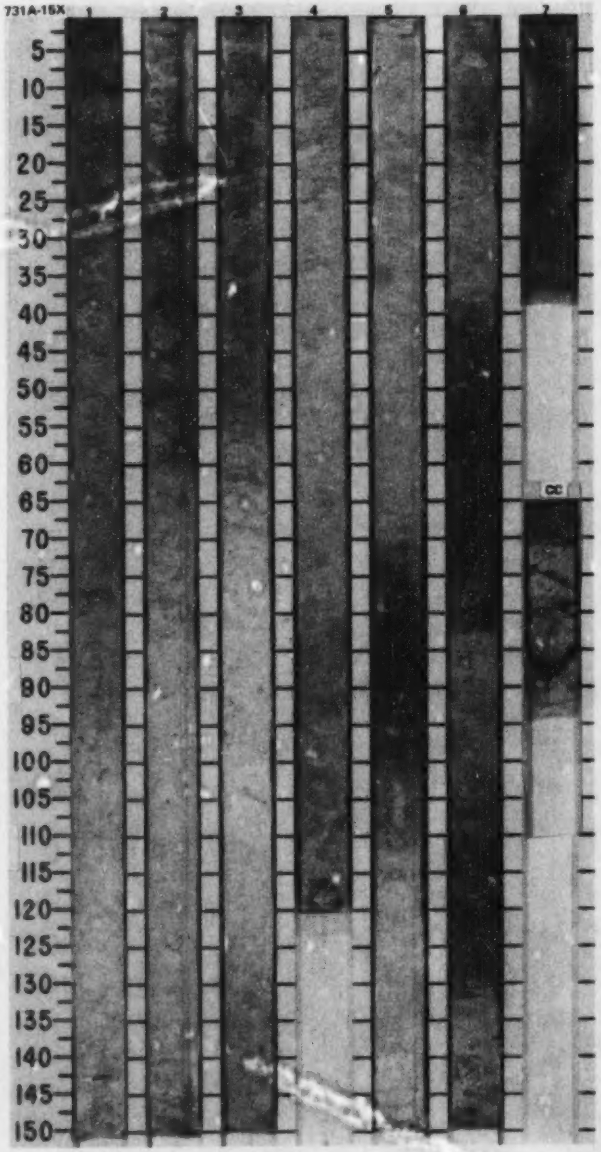
731A-15X
1
2
3
4
5
6
7
CC
5
10
15
20
25
30
35
40
45
50
55
60
65
70
75
80
85
90
95
100
105
110
115
120
125
130
135
140
145
150

SITE 731 HOLE A CORE 16X CORED INTERVAL 2510.2-2519.8 mbsl; 144.4-154.0 mbsf

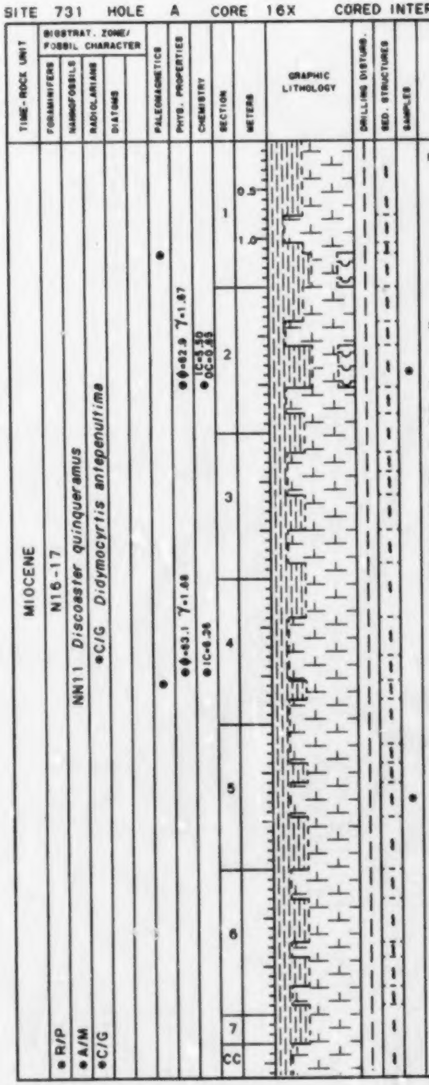
TIME-ROCK UNIT
BIOSTRAT. ZONE/ FOSSIL CHARACTER
FORAMINIFERS
NANNOFOSSILS
RADIOLARIANS
DIATOMS
PALEOMAGNETICS
PHYS. PROPERTIES
CHEMISTRY
SECTION
METERS
GRAPHIC LITHOLOGY
DRILLING DISTURB.
SED. STRUCTURES
SAMPLES
MIOCENE
N16-17
NN11 Discoaster quinqueramus
●C/G Didymocyrtis antepenultima
●R/P
●A/M
●C/G
●φ=62.9 γ=1.87
●IC=5.50 OC=0.85
●φ=63.1 γ=1.88
●IC=6.36
1
2
3
4
5
6
7
CC
0.5
1.0

LITHOLOGIC DESCRIPTION

NANNOFOSSIL OOZE and MARLY NANNOFOSSIL OOZE

Entire core is slightly disturbed.

Major lithologies:
a. NANNOFOSSIL OOZE, white (5Y 8/1) and light gray (5Y 7/1, 7/2). Bioturbated.
b. MARLY NANNOFOSSIL OOZE, light olive gray (5Y 6/2), olive gray (5Y 5/2), and olive (5Y 5/3). Bioturbated. Minor gradations to siliceous-bearing marly nannofossil ooze.

Minor lithology: Diatomaceous marly nannofossil ooze to diatomaceous nannofossil-rich silty clay, olive gray (5Y 4/2) and olive (5Y 4/3), in Section 1, 118-150 cm, and Section 2, 60-107 cm. Minor bioturbation throughout.

SMEAR SLIDE SUMMARY (%):

	2, 87 D	5, 77 D
TEXTURE:		
Silt	30	5
Clay	70	95
COMPOSITION:		
Access. minerals	2	—
Clay	33	25
Diatoms	22	—
Dolomite	1	—
Foraminifers	2	2
Inorganic calcite	20	10
Nannofossils	10	60
Quartz	10	2
Radiolarians	—	1
Silicoflagellates	—	Tr

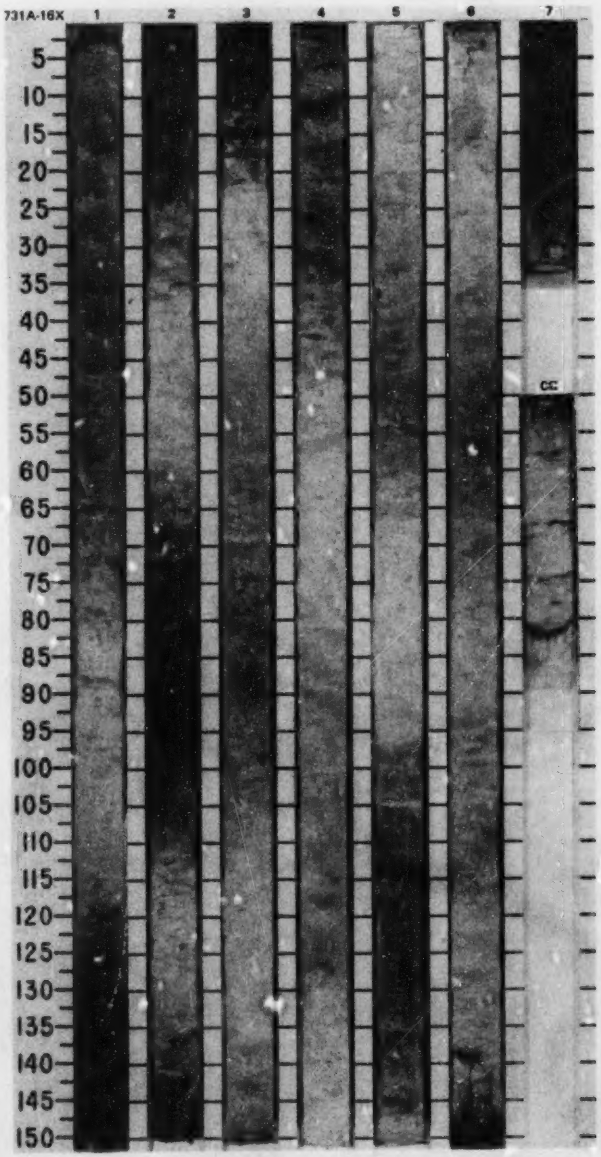
731A-16X
1
2
3
4
5
6
7
CC
5
10
15
20
25
30
35
40
45
50
55
60
65
70
75
80
85
90
95
100
105
110
115
120
125
130
135
140
145
150

SITE 731 HOLE A CORE 17X CORED INTERVAL 2519.8-2529.5 mbsl; 154.0-163.7 mbsf

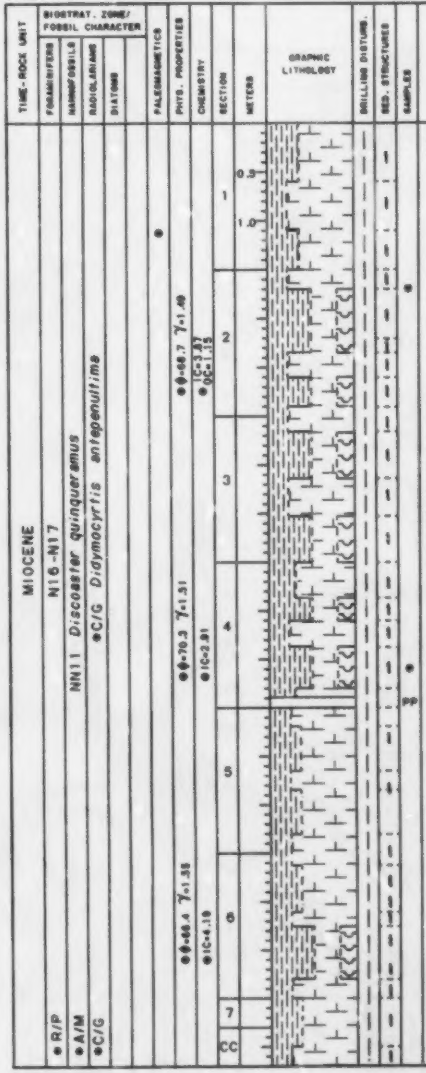
TIME-ROCK UNIT
BIOSTRAT. ZONE/ FOSSIL CHARACTER
FORAMINIFERS
NANNOFOSSILS
RADIOLARIANS
DIATOMS
PALEOMAGNETICS
PHYS. PROPERTIES
CHEMISTRY
SECTION
METERS
GRAPHIC LITHOLOGY
DRILLING DISTURB.
SED. STRUCTURES
SAMPLES
MIOCENE
N16-N17
NN11 Discoaster quinqueramus
●C/G Didymocyrtis antepenultima
●R/P
●A/M
●C/G
●φ=68.7 γ=1.49
●IC=3.87 OC=1.15
●φ=70.3 γ=1.51
●IC=2.81
●φ=68.4 γ=1.55
●IC=4.10
1
2
3
4
5
6
7
CC
0.5
1.0
PP

LITHOLOGIC DESCRIPTION

NANNOFOSSIL OOZE, MARLY NANNOFOSSIL OOZE, and DIATOMACEOUS MARLY NANNOFOSSIL OOZE

Entire core is slightly disturbed.

Major lithologies:
a. NANNOFOSSIL OOZE, light gray (5Y 7/1, 7/2). Bioturbated.
b. MARLY NANNOFOSSIL OOZE, olive gray (5Y 6/2), grading to minor occurrences of diatom-bearing marly nannofossil ooze.
c. DIATOMACEOUS MARLY NANNOFOSSIL OOZE, olive gray (5Y 5/2) and olive (5Y 5/3), grading to minor occurrences of diatomaceous nannofossil-rich silty clay.

SMEAR SLIDE SUMMARY (%):

	2, 20 D	4, 110 D
TEXTURE:		
Silt	10	15
Clay	90	85
COMPOSITION:		
Clay	20	33
Diatoms	3	23
Foraminifers	5	2
Inorganic calcite	12	22
Nannofossils	54	15
Quartz	3	3
Radiolarians	2	1
Sponge spicules	1	1

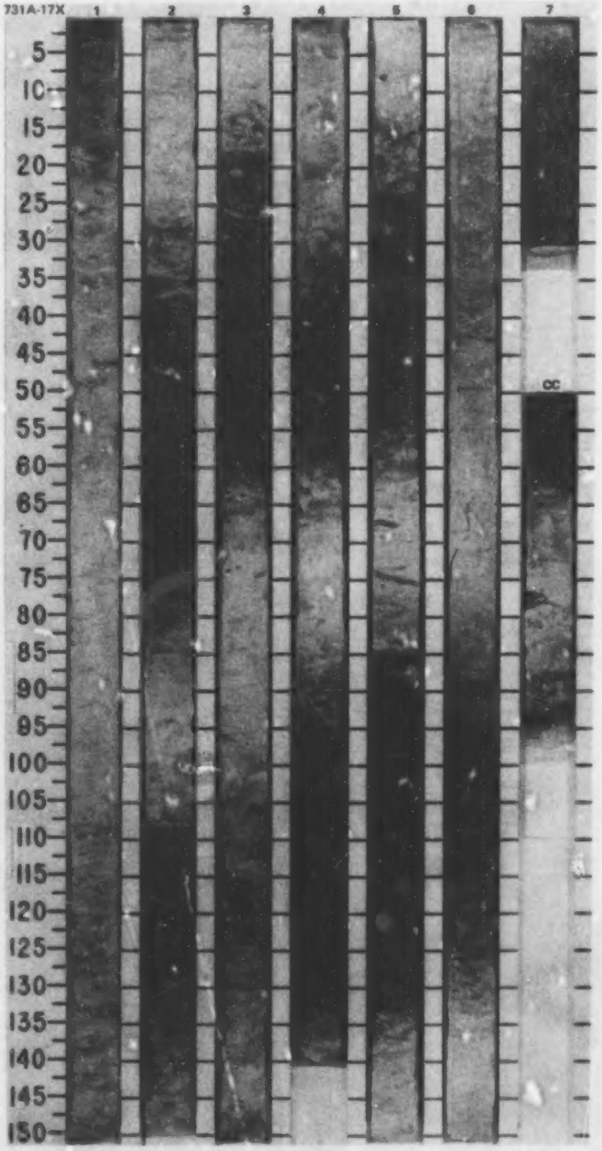
731A-17X
1
2
3
4
5
6
7
CC
5
10
15
20
25
30
35
40
45
50
55
60
65
70
75
80
85
90
95
100
105
110
115
120
125
130
135
140
145
150

SITE 731 HOLE A CORE 18X CORED INTERVAL 2529.5-2539.2 mbsl; 163.7-173.4 mbsf

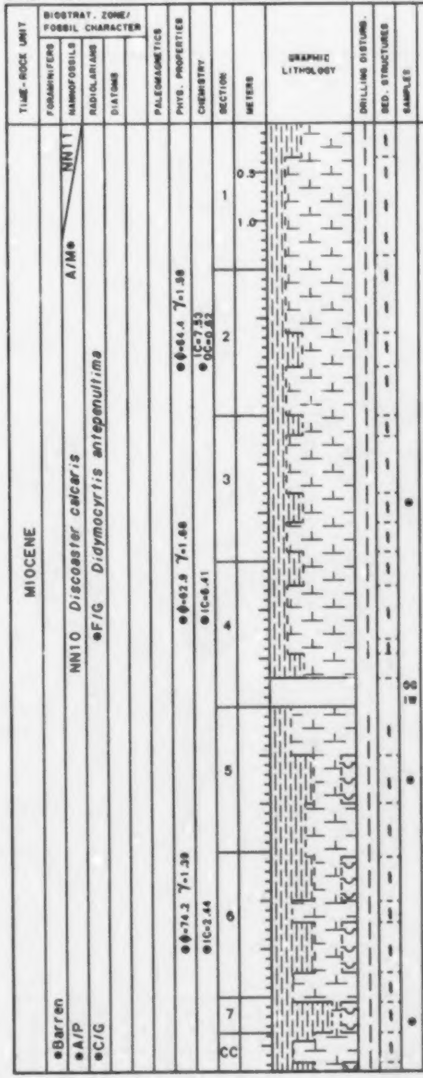

LITHOLOGIC DESCRIPTION

NANNOFOSSIL OOZE, MARLY NANNOFOSSIL OOZE, and SILICEOUS MARLY NANNOFOSSIL OOZE

Entire core is slightly disturbed.

Major lithologies:
- a. NANNOFOSSIL OOZE, light gray (5Y 7/1, 7/2). Bioturbated.
- b. MARLY NANNOFOSSIL OOZE, olive gray (5Y 6/2, 5/2) and olive (5Y 5/3). Slight bioturbation throughout, with minor gradations to siliceous-bearing marly nannofossil ooze.
- c. SILICEOUS MARLY NANNOFOSSIL OOZE, olive (5Y 4/3). Bioturbated.

Minor lithology: Siliceous clayey silt, olive (5Y 4/3), bioturbated, in Section 7, 5–35 cm.

SMEAR SLIDE SUMMARY (%):

	3, 90 D	5, 77 D	7, 28 M
TEXTURE:			
Silt	20	35	60
Clay	80	65	40
COMPOSITION:			
Access. minerals	Tr	2	5
Clay	20	40	20
Diatoms	2	10	15
Dolomite	Tr	Tr	Tr
Foraminifers	2	3	5
Inorganic calcite	3	3	15
Nannofossils	70	30	5
Organic debris	—	—	5
Quartz	1	3	15
Radiolarians	2	2	5
Silicoflagellates	—	1	—
Sponge spicules	Tr	1	—

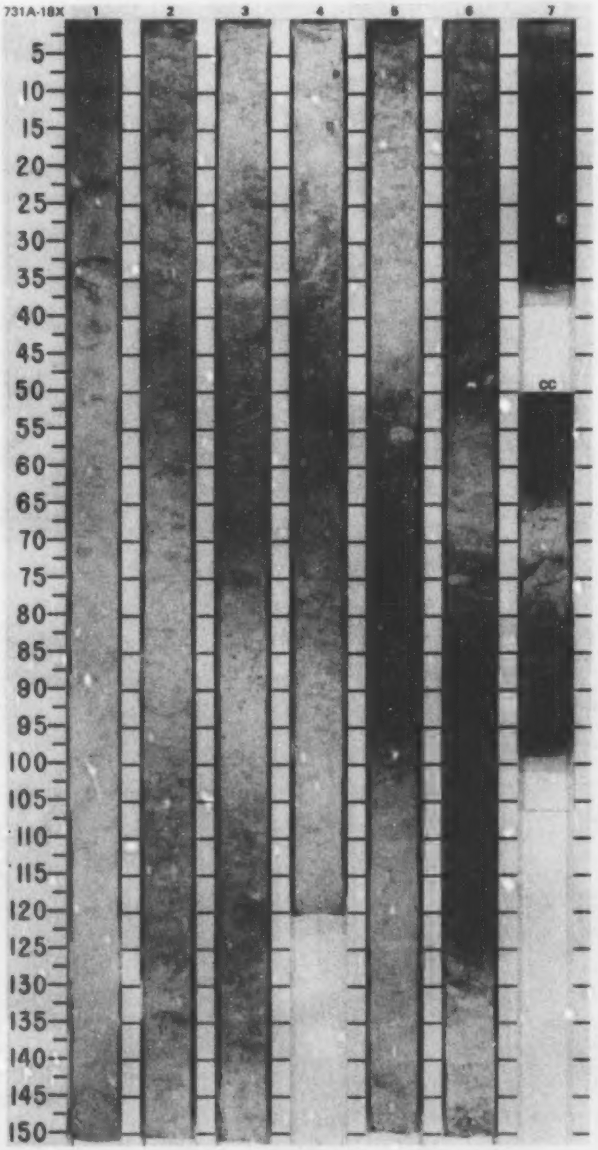
731A-18X
1
2
3
4
5
6
7
CC
5
10
15
20
25
30
35
40
45
50
55
60
65
70
75
80
85
90
95
100
105
110
115
120
125
130
135
140
145
150

SITE 731 HOLE A CORE 19X CORED INTERVAL 2539.2-2548.9 mbsl; 173.4-183.1 mbsf

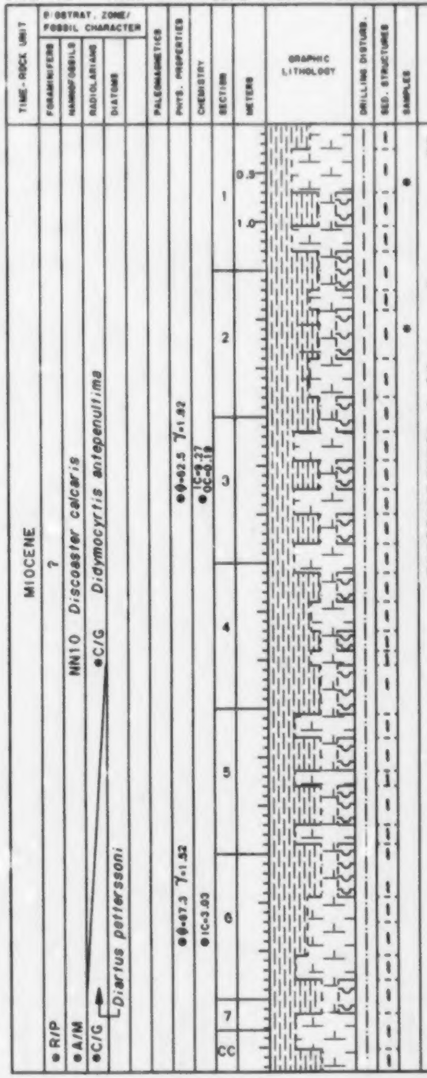
TIME-ROCK UNIT
BIOSTRAT. ZONE/ FOSSIL CHARACTER
FORAMINIFERS
NANNOFOSSILS
RADIOLARIANS
DIATOMS
PALEOMAGNETICS
PHYS. PROPERTIES
CHEMISTRY
SECTION
METERS
GRAPHIC LITHOLOGY
DRILLING DISTURB.
SED. STRUCTURES
SAMPLES
MIOCENE
?
NN10 Discoaster calcaris
●C/G Didymocyrtis antepenultima
Diartus petterssoni
● R/P
● A/M
● C/G
●Φ=62.5 γ=1.82
● IC=9.27 OC=0.19
●Φ=67.3 γ=1.52
●IC=3.03
1
2
3
4
5
6
7
CC
0.5
1.0

LITHOLOGIC DESCRIPTION

NANNOFOSSIL OOZE, MARLY NANNOFOSSIL OOZE, and DIATOMACEOUS NANNOFOSSIL-RICH CLAYEY SILT

Entire core is slightly to moderately disturbed.

Major lithologies:
a. NANNOFOSSIL OOZE, light gray (5Y 7/1, 7/2). Bioturbated.
b. MARLY NANNOFOSSIL OOZE, light olive gray (5Y 6/2) to gray (5Y 6/1) and olive gray (5Y 5/2). Minor bioturbation throughout.
c. DIATOMACEOUS NANNOFOSSIL-RICH CLAYEY SILT, olive gray (5Y 4/2) and olive (5Y 4/3). Minor bioturbation throughout.

SMEAR SLIDE SUMMARY (%):

	1, 60 D	2, 60 D
TEXTURE:		
Silt	20	60
Clay	80	40
COMPOSITION:		
Access. minerals	2	5
Clay	16	28
Diatoms	2	20
Dolomite	Tr	1
Foraminifers	3	Tr
Inorganic calcite	10	10
Mica	—	Tr
Nannofossils	65	20
Organic debris	—	3
Quartz	2	10
Radiolarians	Tr	1
Silicoflagellates	Tr	2
Sponge spicules	Tr	Tr

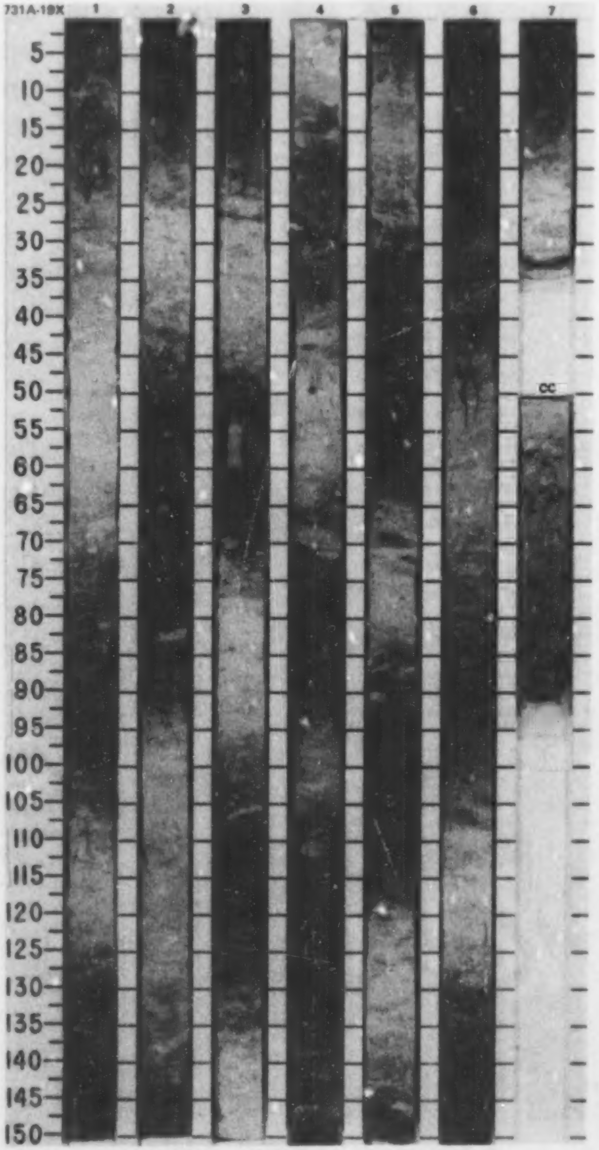
731A-19X
1
2
3
4
5
6
7
CC
5
10
15
20
25
30
35
40
45
50
55
60
65
70
75
80
85
90
95
100
105
110
115
120
125
130
135
140
145
150

SITE 731 HOLE A CORE 20X CORED INTERVAL 2548.9-2558.6 mbsl; 183.1-192.8 mbsf

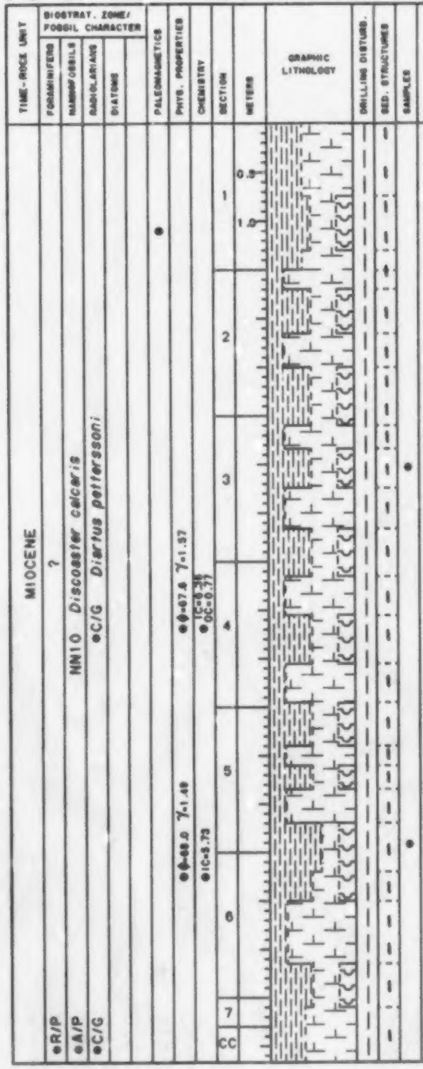
TIME-ROCK UNIT
BIOSTRAT. ZONE/ FOSSIL CHARACTER
FORAMINIFERS
NANNOFOSSILS
RADIOLARIANS
DIATOMS
PALEOMAGNETICS
PHYS. PROPERTIES
CHEMISTRY
SECTION
METERS
GRAPHIC LITHOLOGY
DRILLING DISTURB.
SED. STRUCTURES
SAMPLES
MIOCENE
?
NN10 Discoaster calcaris
●C/G Diartus petterssoni
●R/P
●A/P
●C/G
●φ=67.6 γ=1.57
●φ=68.0 γ=1.40
●IC=6.36 OC=0.77
●IC=5.73
0.5
1.0
1
2
3
4
5
6
7
CC

LITHOLOGIC DESCRIPTION

NANNOFOSSIL OOZE and SILICEOUS MARLY NANNOFOSSIL OOZE

Entire core is slightly disturbed.

Major lithologies:
a. NANNOFOSSIL OOZE, light gray (5Y 7/1). Bioturbated.
b. SILICEOUS MARLY NANNOFOSSIL OOZE, olive gray (5Y 5/2, 4/2) and olive (5Y 5/3, 4/3). Bioturbated.

Minor lithologies:
a. Marly nannofossil ooze, light gray (5Y 6/1) and light olive gray (5Y 6/2), bioturbated, in Section 1, 7-76 and 131-150 cm, Section 7, 9-30 cm, and CC.
b. Diatomaceous nannofossil-rich clay, dark olive gray (5Y 3/2) in Section 5, 122 cm, to Section 6, 22 cm.

SMEAR SLIDE SUMMARY (%):

	3, 64 D	5, 144 D
TEXTURE:		
Silt	25	10
Clay	75	90
COMPOSITION:		
Clay	20	40
Diatoms	15	20
Dolomite	2	Tr
Inorganic calcite	8	10
Mica	2	—
Nannofossils	35	20
Quartz	14	10
Radiolarians	3	—
Sponge spicules	1	—

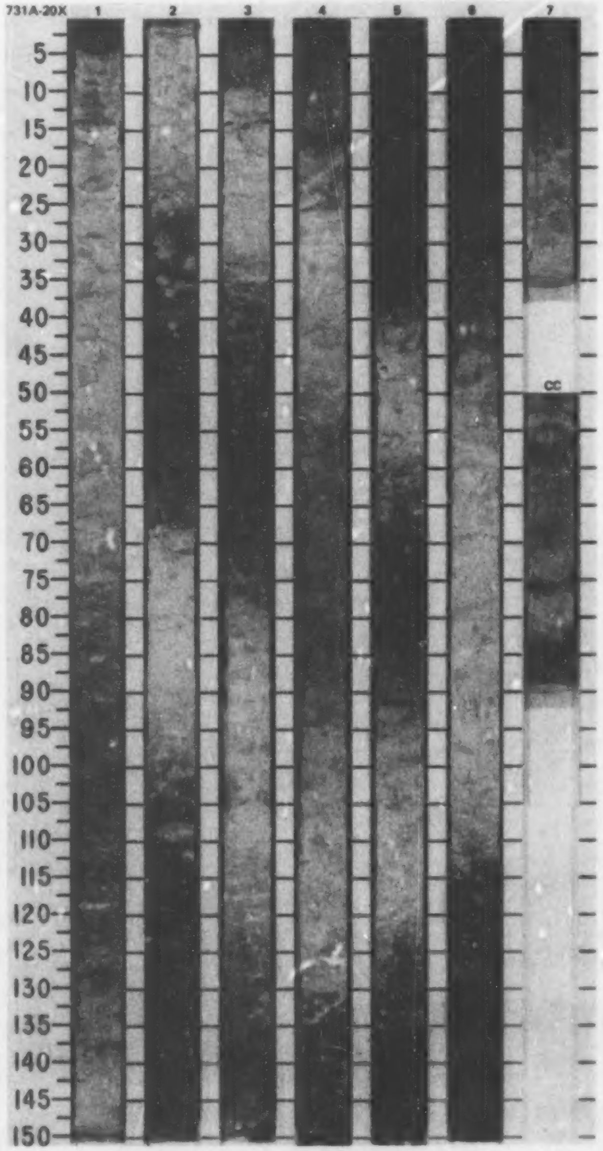
731A-20X
1
2
3
4
5
6
7
CC
5
10
15
20
25
30
35
40
45
50
55
60
65
70
75
80
85
90
95
100
105
110
115
120
125
130
135
140
145
150

SITE 731 HOLE A CORE 21X CORED INTERVAL 2558.6-2568.3 mbsl; 192.8-202.5 mbsf

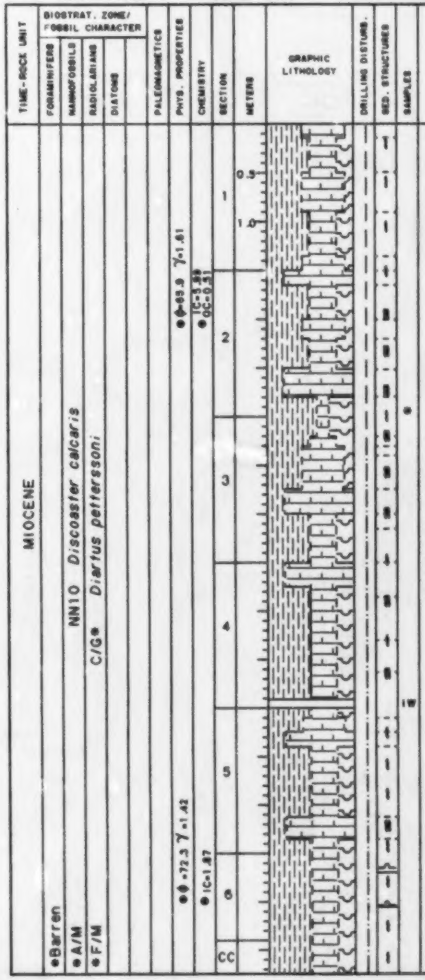
TIME-ROCK UNIT
BIOSTRAT. ZONE/ FOSSIL CHARACTER
FORAMINIFERS
NANNOFOSSILS
RADIOLARIANS
DIATOMS
PALEOMAGNETICS
PHYS. PROPERTIES
CHEMISTRY
SECTION
METERS
GRAPHIC LITHOLOGY
DRILLING DISTURB.
SED. STRUCTURES
SAMPLES
MIOCENE
●Barren
●A/M
●F/M
NN10 Discoaster calcaris
C/G● Diartus petterssoni
●ϕ=65.9 γ=1.61
●ϕ=72.3 γ=1.42
●IC=5.89 OC=0.51
●IC=1.87
1
2
3
4
5
6
CC
0.5
1.0
*
IW

LITHOLOGIC DESCRIPTION

NANNOFOSSIL CHALK and SILICEOUS MARLY NANNOFOSSIL CHALK

Entire core is slightly to moderately disturbed by drilling. Filled vertical and subvertical fractures at Section 2, 85-94 cm, and Section 3, 5-20 cm. Possible tectonic/dewatering/slump-related structures.

Major lithologies:
a. NANNOFOSSIL CHALK, light gray (5Y 7/1, 7/2). Bioturbated.
b. SILICEOUS MARLY NANNOFOSSIL CHALK, olive gray (5Y 5/2, 4/2) and olive (5Y 5/3, 4/2). Bioturbated throughout.

Minor lithologies:
a. Marly nannofossil chalk, pale olive (5Y 6/3) and light olive gray (5Y 6/2), bioturbated, in Section 1, 0-14, 54-87, and 136-150 cm, Section 2, 49-68 cm, Section 3, 24-76 cm, and Section 5, 5-23 cm.
b. Nannofossil-bearing diatomaceous mudstone, dark olive gray (5Y 3/2), in Section 2, 127 cm, to Section 3, 16 cm.

SMEAR SLIDE SUMMARY (%):

	2, 145 D
TEXTURE:	
Silt	5
Clay	95
COMPOSITION:	
Access. minerals	1
Clay	42
Diatoms	30
Dolomite	Tr
Inorganic calcite	15
Nannofossils	7
Quartz	3
Radiolarians	Tr
Sponge spicules	2

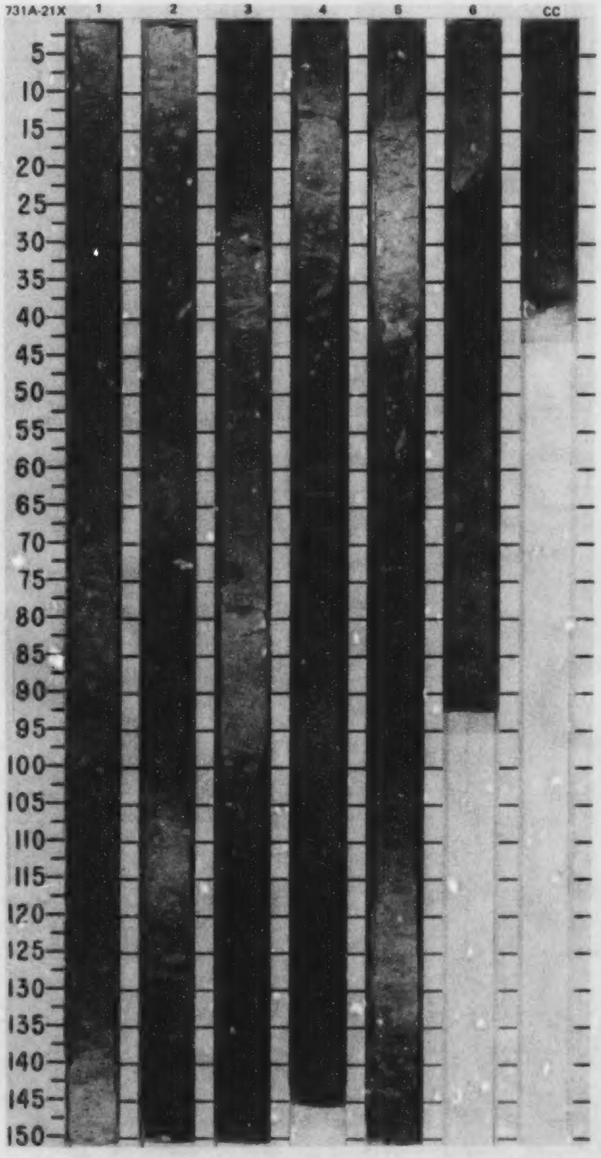
731A-21X
1
2
3
4
5
6
CC
5
10
15
20
25
30
35
40
45
50
55
60
65
70
75
80
85
90
95
100
105
110
115
120
125
130
135
140
145
150

SITE 731 HOLE A CORE 22X CORED INTERVAL 2568.3-2578.0 mbsl; 202.5-212.2 mbsf

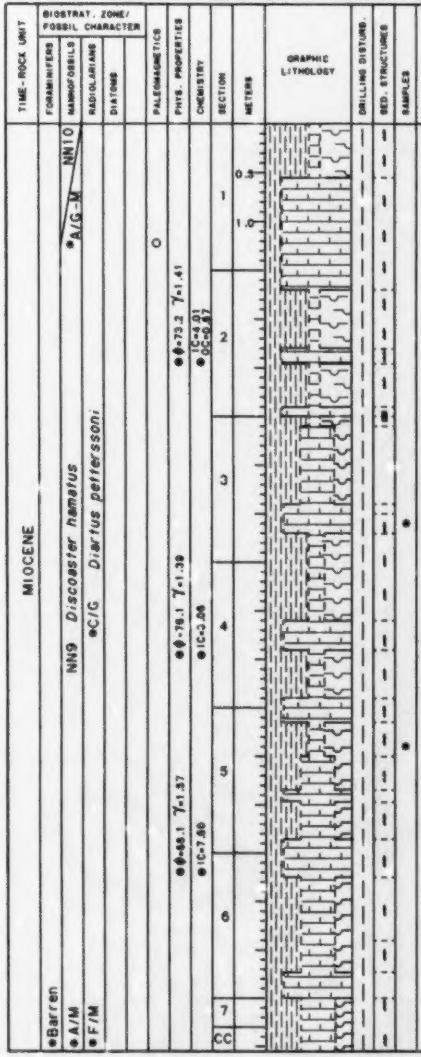
TIME-ROCK UNIT
BIOSTRAT. ZONE/ FOSSIL CHARACTER
FORAMINIFERS
NANNOFOSSILS
RADIOLARIANS
DIATOMS
PALEOMAGNETICS
PHYS. PROPERTIES
CHEMISTRY
SECTION
METERS
GRAPHIC LITHOLOGY
DRILLING DISTURB.
SED. STRUCTURES
SAMPLES
MIOCENE
NN10
A/G-M
NN9 Discoaster hamatus
C/G Diartus petterssoni
Barren
A/M
F/M
φ=73.2 γ=1.41
φ=76.1 γ=1.39
φ=65.1 γ=1.37
IC=4.01
OC=0.87
IC=3.06
IC=7.60
1
2
3
4
5
6
7
CC
0.5
1.0

LITHOLOGIC DESCRIPTION

NANNOFOSSIL CHALK, SILICEOUS MARLY NANNOFOSSIL CHALK, and NANNOFOSSIL-RICH DIATOMACEOUS MUDSTONE

Entire core is slightly to moderately disturbed.

Major lithologies:
a. NANNOFOSSIL CHALK, light gray (5Y 7/1, 7/2) and light olive gray (5Y 6/2). Bioturbated throughout.
b. SILICEOUS MARLY NANNOFOSSIL CHALK, olive gray (5Y 5/2) and olive (5Y 5/3). Bioturbated.
c. NANNOFOSSIL-RICH DIATOMACEOUS MUDSTONE, olive (5Y 4/3). Bioturbated.

SMEAR SLIDE SUMMARY (%):

	3, 110 D	5, 40 D
TEXTURE:		
Silt	2	10
Clay	98	90
COMPOSITION:		
Clay	20	33
Diatoms	3	35
Dolomite	Tr	2
Inorganic calcite	—	10
Nannofossils	75	15
Quartz	—	5
Mica	Tr	—
Radiolarians	1	—
Sponge spicules	1	—

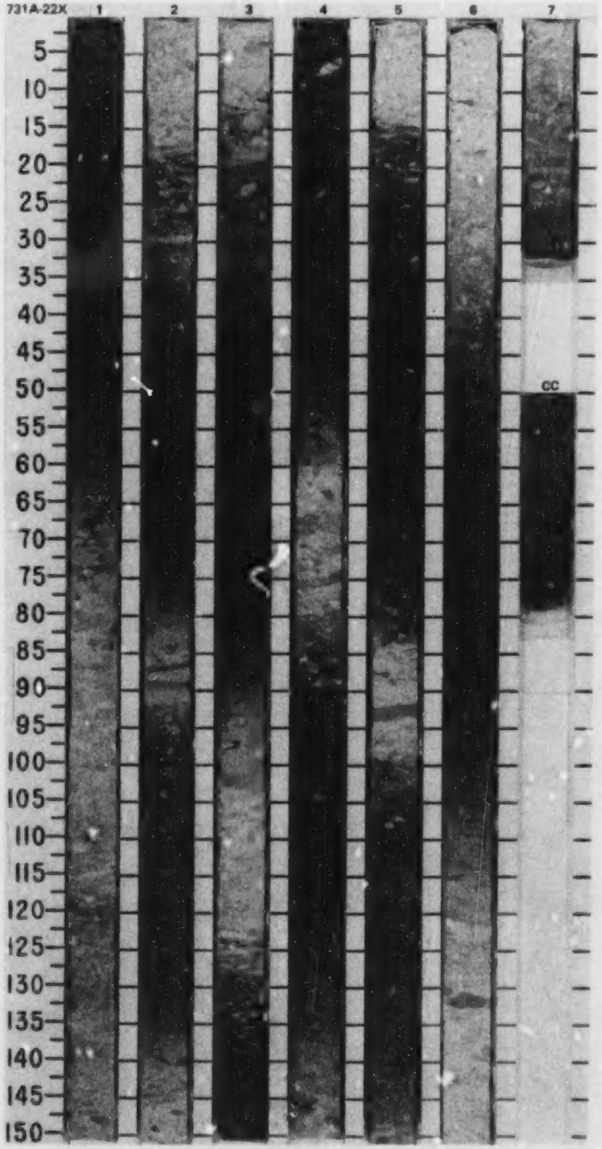
731A-22X
1
2
3
4
5
6
7
CC
5
10
15
20
25
30
35
40
45
50
55
60
65
70
75
80
85
90
95
100
105
110
115
120
125
130
135
140
145
150

SITE 731 HOLE A CORE 23X CORED INTERVAL 2578.0-2587.7 mbsl; 212.2-221.9 mbsf

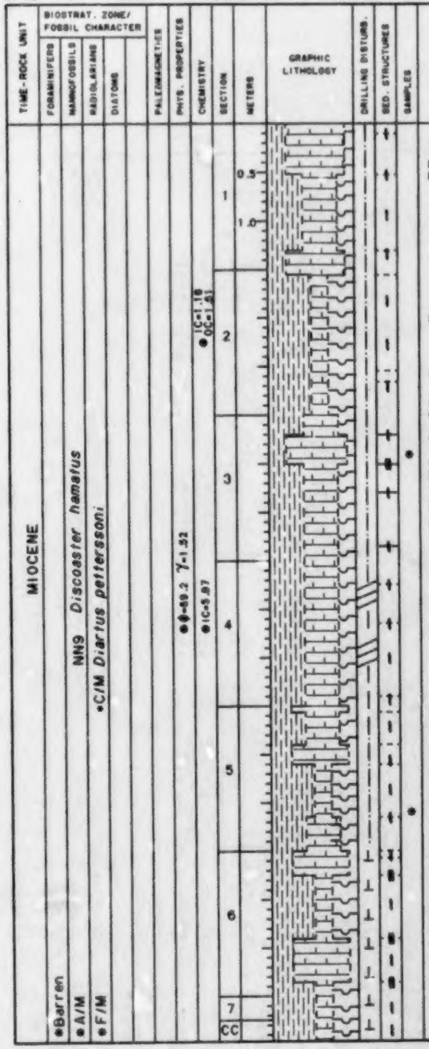
TIME-ROCK UNIT
BIOSTRAT. ZONE/ FOSSIL CHARACTER
FORAMINIFERS
NANNOFOSSILS
RADIOLARIANS
DIATOMS
PALEOMAGNETICS
PHYS. PROPERTIES
CHEMISTRY
SECTION
METERS
GRAPHIC LITHOLOGY
DRILLING DISTURB.
SED. STRUCTURES
SAMPLES
MIOCENE
●Barren
●A/M
NN9 Discoaster hamatus
●F/M
●C/M Diartus petterssoni
●ϕ=59.2 γ=1.52
●IC=1.18 OC=1.61
●IC=5.97
0.5
1.0
1
2
3
4
5
6
7
CC

LITHOLOGIC DESCRIPTION

DIATOM-BEARING NANNOFOSSIL CHALK, DIATOMACEOUS MARLY NANNOFOSSIL CHALK, and NANNOFOSSIL-RICH DIATOMACEOUS MUDSTONE

Entire core is slightly to moderately disturbed and fractured.

Major lithologies:
a. DIATOM-BEARING NANNOFOSSIL CHALK, light gray (5Y 7/1). Bioturbated.
b. DIATOMACEOUS MARLY NANNOFOSSIL CHALK, light olive gray (5Y 6/2), pale olive (5Y 6/3), and olive (5Y 5/3). Gradationally interbedded. Bioturbated.
c. NANNOFOSSIL-RICH DIATOMACEOUS MUDSTONE, olive (5Y 4/3). Moderately bioturbated, with faint mm-scale laminations at Section 2, 30-70 cm, and Section 5, 85–107 cm.

SMEAR SLIDE SUMMARY (%):

	3, 41 D	5, 107 D
TEXTURE:		
Silt	10	10
Clay	90	90
COMPOSITION:		
Clay	20	37
Diatoms	7	27
Dolomite	3	—
Inorganic calcite	2	5
Nannofossils	65	20
Quartz	2	10
Radiolarians	1	1

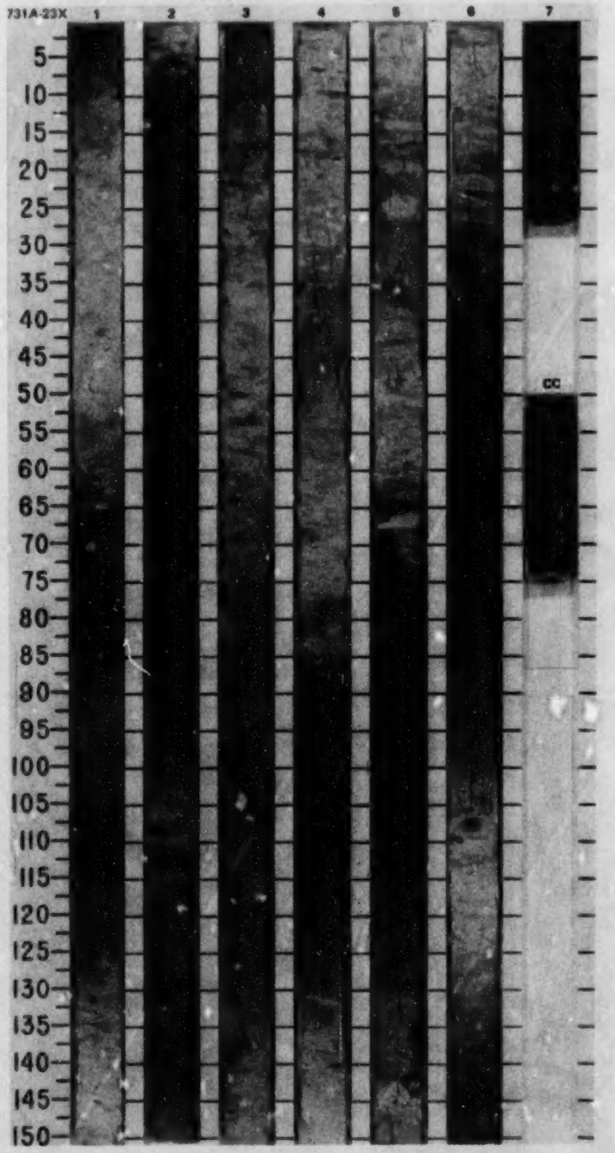
731A-23X
1
2
3
4
5
6
7
CC
5
10
15
20
25
30
35
40
45
50
55
60
65
70
75
80
85
90
95
100
105
110
115
120
125
130
135
140
145
150

SITE 731 HOLE A CORE 24X CORED INTERVAL 2587.7-2597.4 mbsl; 221.9-231.6 mbsf

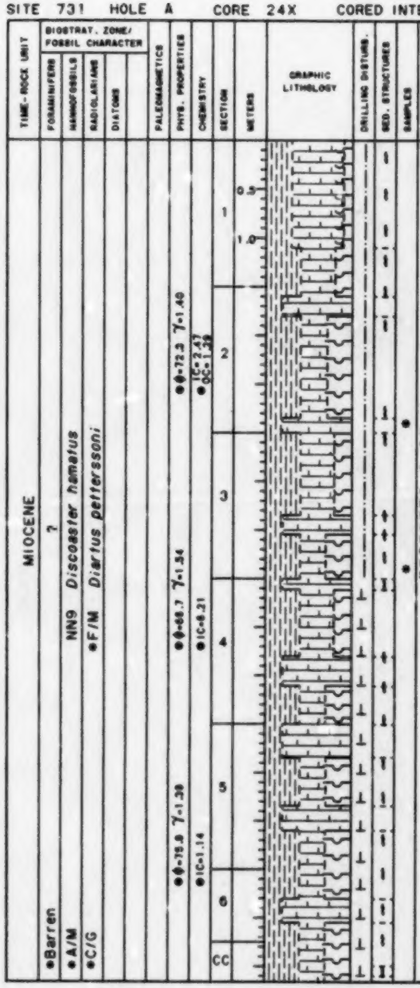
TIME-ROCK UNIT
BIOSTRAT. ZONE/ FOSSIL CHARACTER
FORAMINIFERS
NANNOFOSSILS
RADIOLARIANS
DIATOMS
PALEOMAGNETICS
PHYS. PROPERTIES
CHEMISTRY
SECTION
METERS
GRAPHIC LITHOLOGY
DRILLING DISTURB.
SED. STRUCTURES
SAMPLES
MIOCENE
?
NN9 Discoaster hamatus
●F/M Diartus petterssoni
●Barren
●A/M
●C/G
●Φ=72.3 γ=1.40
●Φ=68.7 γ=1.54
●Φ=75.9 γ=1.30
●IC=2.47 OC=1.39
●IC=8.21
●IC=1.14
1
2
3
4
5
6
CC
0.5
1.0

LITHOLOGIC DESCRIPTION

NANNOFOSSIL CHALK, DIATOMACEOUS MARLY NANNOFOSSIL CHALK, and NANNOFOSSIL-RICH DIATOMACEOUS MUDSTONE

Entire core is moderately disturbed and fractured. Filled vertical and subvertical fracture sets (mm-wide) at Section 2, 60–65 cm, and Section 5, 77–83 cm. Possible tectonic/ dewatering/slump-related structures.

Major lithologies:

a. NANNOFOSSIL CHALK, light gray (5Y 7/1). Bioturbated.
b. DIATOMACEOUS MARLY NANNOFOSSIL CHALK, pale olive (5Y 6/3) and olive (5Y 5/3).
c. NANNOFOSSIL-RICH DIATOMACEOUS MUDSTONE to DIATOMACEOUS MARLY NANNOFOSSIL CHALK, olive gray (5Y 4/2) and olive (5Y 4/3). Contains filled vertical fracture sets at Section 2, 60–65 cm, and Section 5, 77–83 cm.

SMEAR SLIDE SUMMARY (%):

	2, 140 D	3, 140 D
TEXTURE:		
Silt	50	55
Clay	50	45
COMPOSITION:		
Clay	20	15
Diatoms	5	30
Dolomite	—	Tr
Inorganic calcite	3	15
Nannofossils	70	30
Quartz	2	10
Radiolarians	Tr	Tr
Silicoflagellates	—	Tr

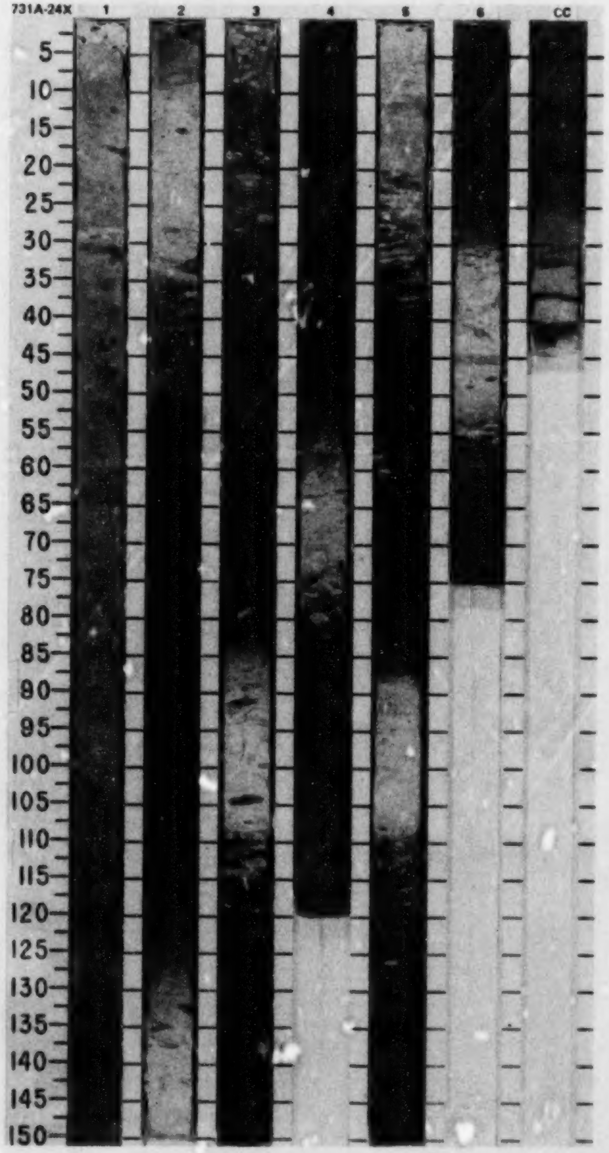
731A-24X
1
2
3
4
5
6
CC
5
10
15
20
25
30
35
40
45
50
55
60
65
70
75
80
85
90
95
100
105
110
115
120
125
130
135
140
145
150

SITE 731 HOLE A CORE 25X CORED INTERVAL 2597.4-2607.1 mbsl; 231.6-241.3 mbsf

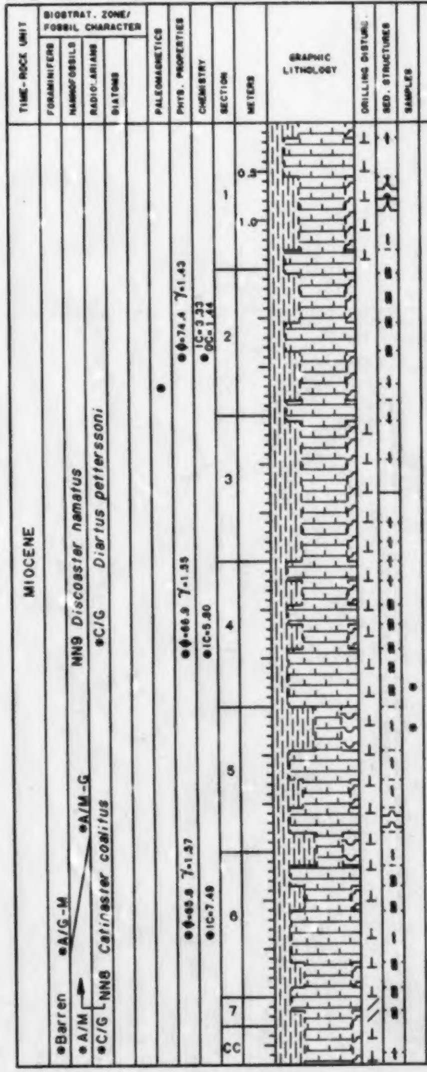
TIME-ROCK UNIT
BIOSTRAT. ZONE/ FOSSIL CHARACTER
FORAMINIFERS
NANNOFOSSILS
RADIOLARIANS
DIATOMS
PALEOMAGNETICS
PHYS. PROPERTIES
CHEMISTRY
SECTION
METERS
GRAPHIC LITHOLOGY
DRILLING DISTURB.
SED. STRUCTURES
SAMPLES
MIOCENE
●Barren ●A/G-M
●A/M NN9 Discoaster hamatus ●A/M-G
●C/G NN8 Catinaster coalitus
●C/G Diartus petterssoni
●Φ=74.4 γ=1.43
●Φ=66.9 γ=1.55
●Φ=65.8 γ=1.57
●IC=3.33 OC=1.44
●IC=5.80
●IC=7.40
1
2
3
4
5
6
7
CC
0.5
1.0

LITHOLOGIC DESCRIPTION

NANNOFOSSIL CHALK and DIATOM-BEARING MARLY NANNOFOSSIL CHALK

Entire core is moderately disturbed and fractured by drilling. Possible slump blocks at Section 1, 66–80 cm; Section 2, 75–80 cm; and Section 5, 110–128 cm.

Major lithologies:
a. NANNOFOSSIL CHALK, light gray (5Y 7/1, 7/2; N7) to light greenish gray (5GY 7/1, 10Y 7/2). Bioturbated; purple oxidation haloes are common around large burrows.
b. DIATOM-BEARING MARLY NANNOFOSSIL CHALK, light greenish gray (10Y 6/2), pale olive (5Y 6/3), and olive (5Y 5/3, 5/4). Bioturbated throughout; Planolites and Zoophycos present.

Minor lithology: Diatomaceous marly nannofossil chalk, olive (5Y 4/3), in Section 5, 0–46 cm, and Section 5, 130 cm, to Section 6, 15 cm.

SMEAR SLIDE SUMMARY (%):

	4, 131 D	5, 24 D
TEXTURE:		
Sand	—	10
Silt	10	40
Clay	90	50
COMPOSITION:		
Access. minerals	—	2
Clay	15	25
Diatoms	3	15
Foraminifers	2	Tr
Inorganic calcite	4	11
Nannofossils	75	35
Phosphate	—	Tr
Quartz	—	10
Radiolarians	1	1
Silicoflagellates	—	1
Sponge spicules	Tr	—

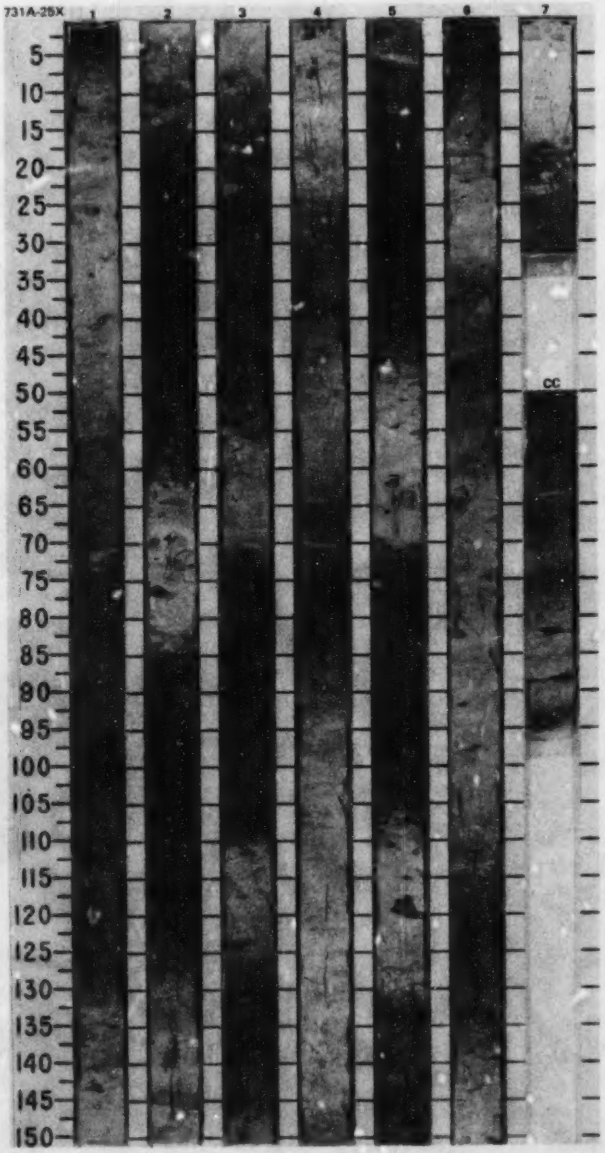
731A-25X
1
2
3
4
5
6
7
CC
5
10
15
20
25
30
35
40
45
50
55
60
65
70
75
80
85
90
95
100
105
110
115
120
125
130
135
140
145
150

SITE 731 HOLE A CORE 26X CORED INTERVAL 2607.1-2616.7 mbsl; 241.3-250.9 mbsf

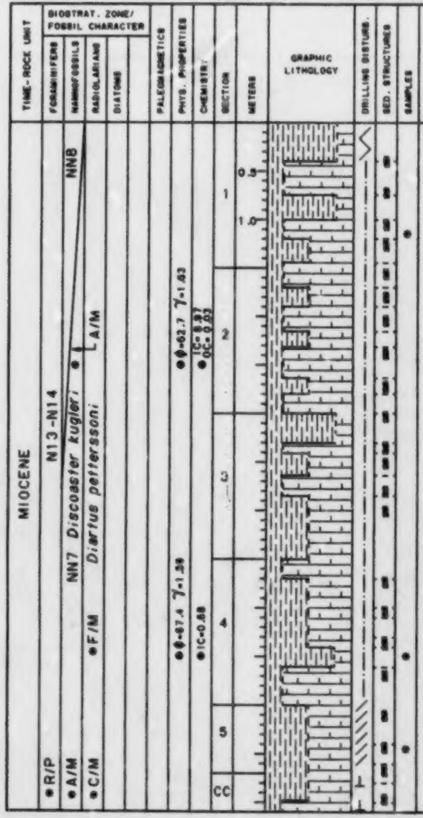
TIME-ROCK UNIT
BIOSTRAT. ZONE/ FOSSIL CHARACTER
FORAMINIFERS
NANNOFOSSILS
RADIOLARIANS
DIATOMS
PALEOMAGNETICS
PHYS. PROPERTIES
CHEMISTRY
SECTION
METERS
GRAPHIC LITHOLOGY
DRILLING DISTURB.
SED. STRUCTURES
SAMPLES
MIOCENE
N13-N14
NN8
NN7 Discoaster kugleri
A/M
Diartus petterssoni
F/M
R/P
A/M
C/M
Φ=62.7 γ=1.83
IC=8.87
OC=0.03
Φ=67.4 γ=1.38
IC=0.88
1
2
3
4
5
CC
0.5
1.0

LITHOLOGIC DESCRIPTION

NANNOFOSSIL CHALK, CALCITIC MARLY NANNOFOSSIL CHALK, and NANNOFOSSIL-RICH CALCITIC SILTY CLAYSTONE

Entire core is slightly to moderately disturbed and fractured by drilling. Vertical and subvertical sets of healed, mm-scale fractures at Section 1, 93-100 cm; Section 3, 15-20 and 89-93 cm; and Section 4, 50-55 and 95-105 cm. Possible tectonic/dewatering/slump-related structures.

Major lithologies:
a. NANNOFOSSIL CHALK, light gray (5Y 7/1) and light greenish gray (5GY 7/1, 10Y 7/1). Bioturbated. Purple oxidation haloes and laminations are common.
b. CALCITIC MARLY NANNOFOSSIL CHALK, greenish gray (10Y 6/2, 5/2; 5G 6/1), and olive (5Y 5/3, 5/4). Bioturbated throughout.
c. NANNOFOSSIL-RICH CALCITIC SILTY CLAYSTONE, olive (5Y 4/3) and dark greenish gray (10Y 4/2).

SMEAR SLIDE SUMMARY (%):

	1, 115 D	4, 100 D	5, 44 D
TEXTURE:			
Sand	—	20	15
Silt	10	35	25
Clay	90	45	60
COMPOSITION:			
Access. minerals	1	2	2
Clay	10	30	25
Diatoms	Tr	Tr	1
Dolomite	1	—	1
Feldspar	—	2	2
Fish remains	—	Tr	—
Foraminifers	2	—	—
Inorganic calcite	2	25	20
Mica	Tr	Tr	1
Nannofossils	80	15	35
Organic debris	—	5	5
Quartz	2	20	8
Radiolarians	1	1	—
Sponge spicules	1	—	—

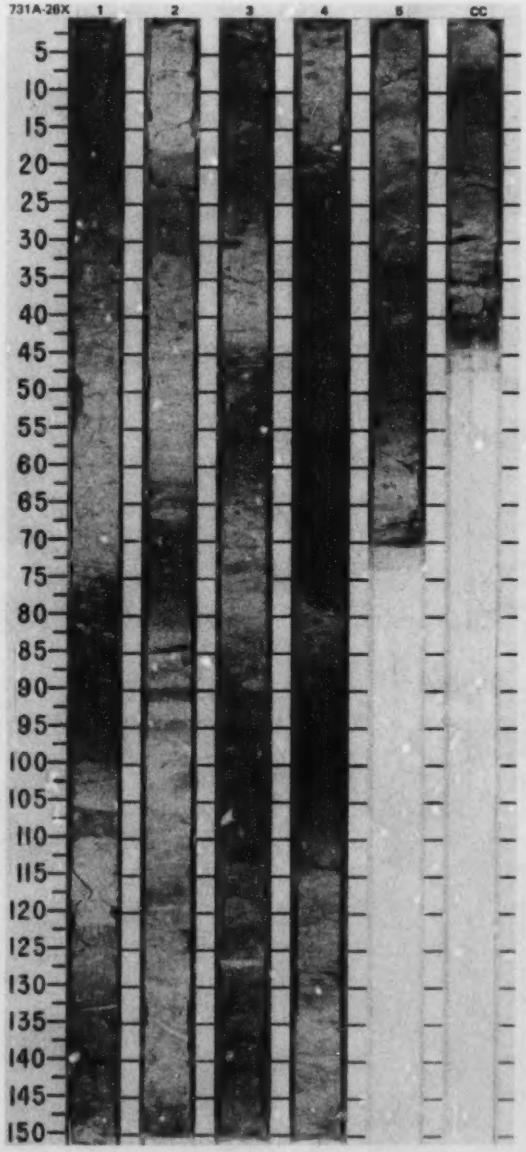
731A-26X
1
2
3
4
5
CC
5
10
15
20
25
30
35
40
45
50
55
60
65
70
75
80
85
90
95
100
105
110
115
120
125
130
135
140
145
150

SITE 731 HOLE A CORE 27X CORED INTERVAL 2616.7-2626.4 mbsl; 250.9-260.6 mbsf

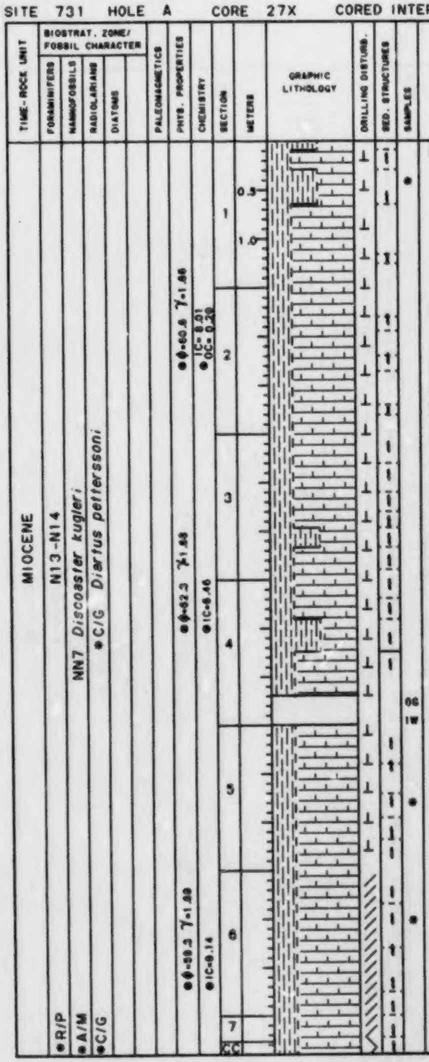
TIME-ROCK UNIT
BIOSTRAT. ZONE/ FOSSIL CHARACTER
FORAMINIFERS
NANNOFOSSILS
RADIOLARIANS
DIATOMS
PALEOMAGNETICS
PHYS. PROPERTIES
CHEMISTRY
SECTION
METERS
GRAPHIC LITHOLOGY
DRILLING DISTURB.
SED. STRUCTURES
SAMPLES
MIOCENE
N13-N14
NN7 Discoaster kugleri
●C/G Diartus petterssoni
●R/P
●A/M
●C/G
●ϕ=60.6 γ=1.86
●ϕ=62.3 γ=1.85
●ϕ=59.3 γ=1.89
●IC=8.01 OC=0.20
●IC=8.46
●IC=8.14
1
2
3
4
5
6
7
CC
0.5
1.0
OG
IW

LITHOLOGIC DESCRIPTION

NANNOFOSSIL CHALK

Entire core is slightly to moderately disturbed and fractured.

Major lithology: NANNOFOSSIL CHALK, white (5Y 8/1), light gray (5Y 7/1, 7/2), and light greenish gray (5GY 7/1, 10Y 7/2) to pale olive (5Y 6/3). Gradationally interbedded and bioturbated throughout.

Minor lithology: Marly calcitic nannofossil chalk, dark greenish gray (10Y 4/2), bioturbated. Vertical and subvertical sets of parallel, mm-scale filled fractures at Section 3, 95–113 cm, and Section 5, 25–30 cm. Possible tectonic/dewatering/slump-related structures.

SMEAR SLIDE SUMMARY (%):

	1, 41 D	5, 80 D	6, 51 D
TEXTURE:			
Sand	10	—	—
Silt	30	20	10
Clay	60	80	90
COMPOSITION:			
Access. minerals	2	Tr	Tr
Clay	25	10	10
Diatoms	Tr	—	—
Dolomite	1	1	—
Foraminifers	1	—	—
Volcanic glass	—	Tr	—
Inorganic calcite	20	15	20
Nannofossils	35	70	70
Phosphate	Tr	—	—
Quartz	15	2	—
Radiolarians	1	1	—
Sponge spicules	Tr	1	Tr

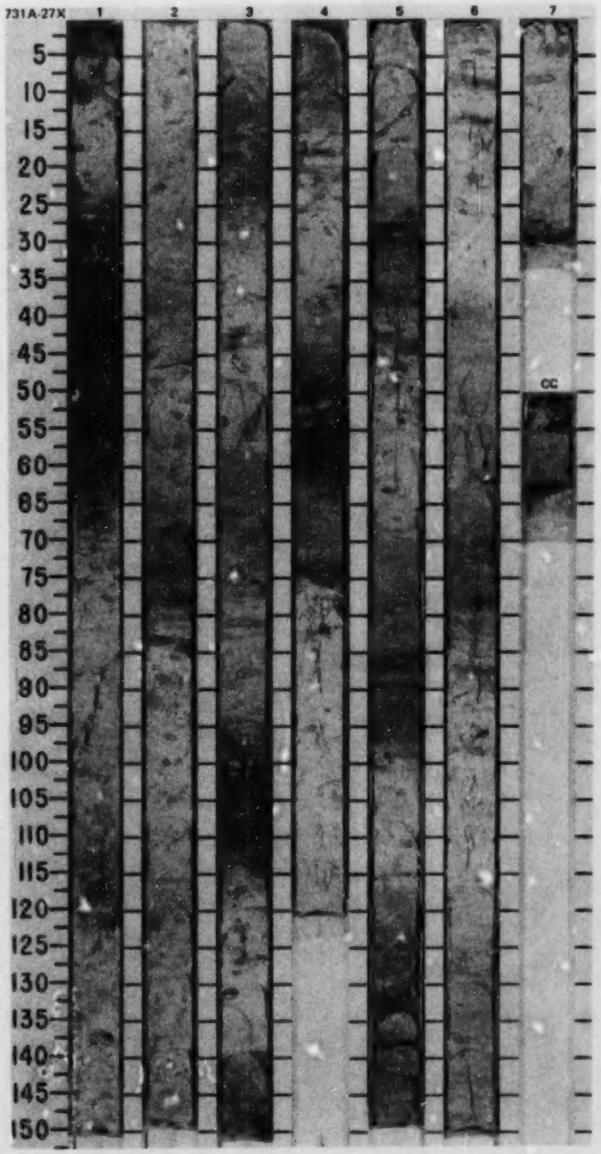
731A-27X
1
2
3
4
5
6
7
CC
5
10
15
20
25
30
35
40
45
50
55
60
65
70
75
80
85
90
95
100
105
110
115
120
125
130
135
140
145
150

SITE 731 HOLE A CORE 28X CORED INTERVAL 2626.4-2636.0 mbsl; 260.6-270.2 mbsf

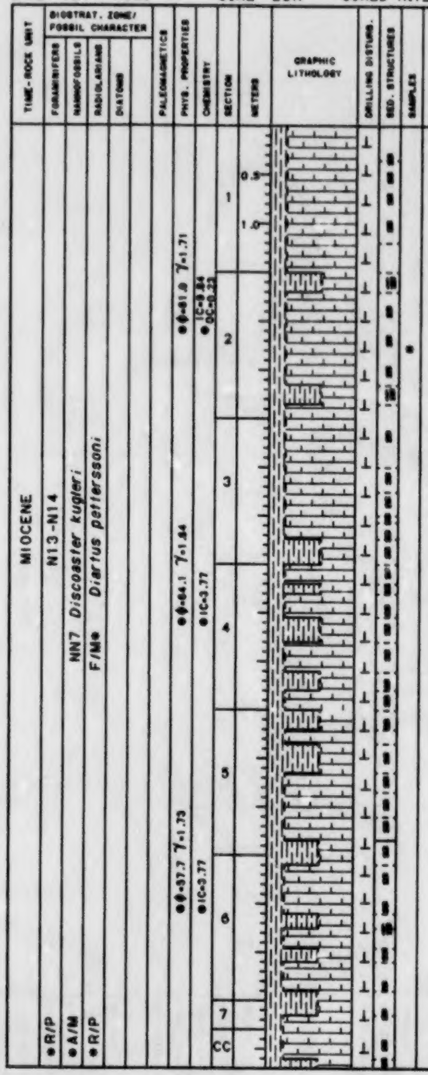
TIME-ROCK UNIT
BIOSTRAT. ZONE/FOSSIL CHARACTER
FORAMINIFERS
NANNOFOSSILS
RADIOLARIANS
DIATOMS
PALEOMAGNETICS
PHYS. PROPERTIES
CHEMISTRY
SECTION
METERS
GRAPHIC LITHOLOGY
DRILLING DISTURB.
SED. STRUCTURES
SAMPLES
MIOCENE
N13-N14
NN7 Discoaster kugleri
F/M● Diartus petterssoni
●R/P
●A/M
●R/P
●φ=61.0 γ=1.71
●φ=64.1 γ=1.84
●φ=57.7 γ=1.73
●IC=9.84 OC=0.23
●IC=3.77
●IC=3.77
1
2
3
4
5
6
7
CC
0.5
1.0

LITHOLOGIC DESCRIPTION

NANNOFOSSIL CHALK and CALCITIC MARLY NANNOFOSSIL CHALK

Entire section is moderately disturbed and fractured.

Major lithologies:
a. NANNOFOSSIL CHALK, white (5Y 8/1), light gray (5Y 7/1, N7), and light greenish gray (5GY 7/1). Moderately bioturbated throughout, with purple oxidation haloes and laminations common.
b. CALCITIC MARLY NANNOFOSSIL CHALK, light greenish gray (10Y 6/2, 6/3), greenish gray (5GY 5/1, 5G 5/1), and olive (5Y 5/3). Moderately to heavily bioturbated. Vertical/subvertical sets of filled, mm-scale parallel fractures at Section 5, 90–95 cm, and Section 6, 100–110 cm.

SMEAR SLIDE SUMMARY (%):

	2, 76 D
TEXTURE:	
Silt	20
Clay	80
COMPOSITION:	
Clay	15
Volcanic glass	Tr
Inorganic calcite	5
Nannofossils	80
Silicoflagellates	Tr

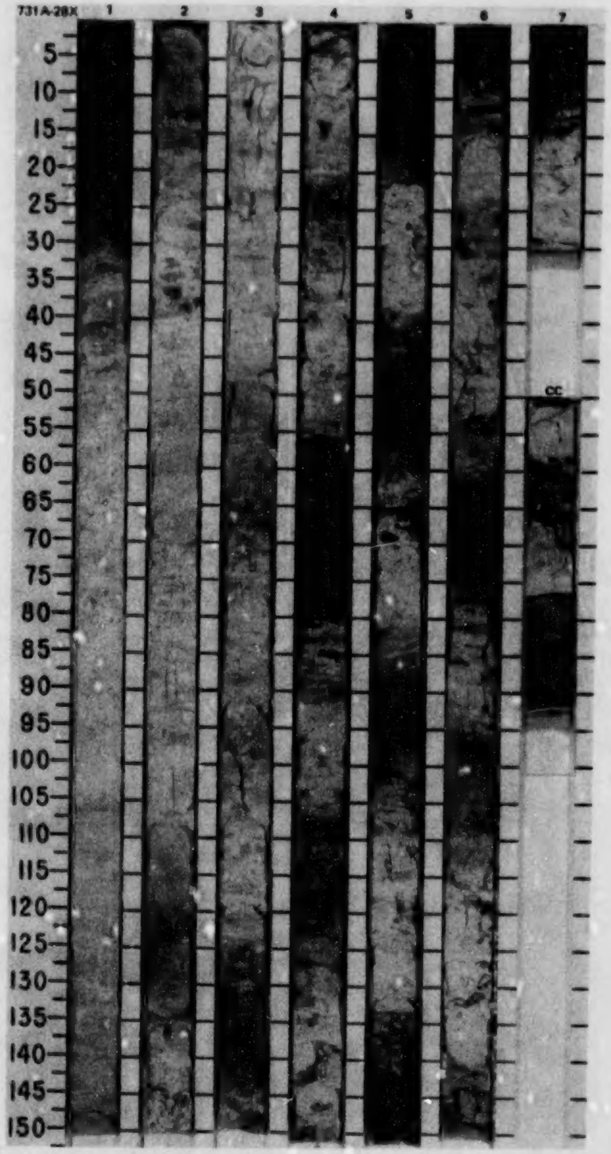
731A-28X
1
2
3
4
5
6
7
CC
5
10
15
20
25
30
35
40
45
50
55
60
65
70
75
80
85
90
95
100
105
110
115
120
125
130
135
140
145
150

SITE 731 HOLE A CORE 29X CORED INTERVAL 2636.0-2645.7 mbsl; 270.2-279.9 mbsf

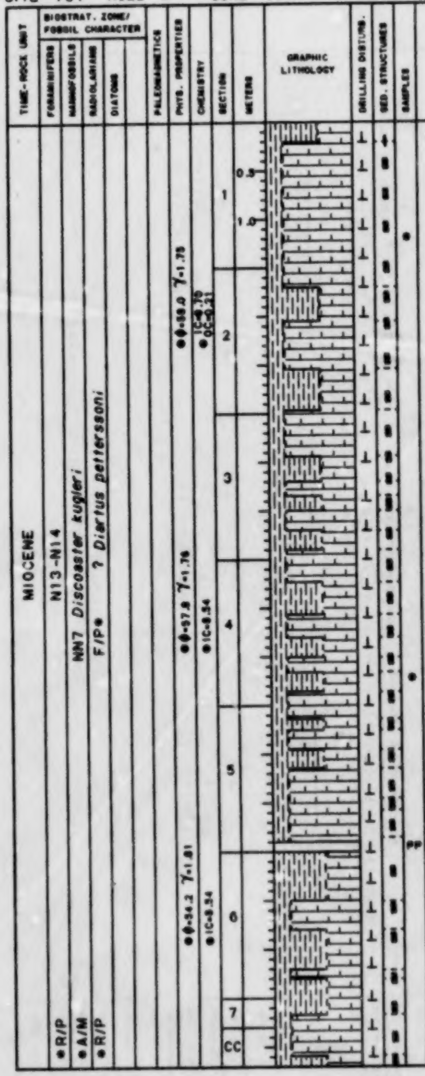
TIME-ROCK UNIT
BIOSTRAT. ZONE/ FOSSIL CHARACTER
FORAMINIFERS
NANNOFOSSILS
RADIOLARIANS
DIATOMS
PALEOMAGNETICS
PHYS. PROPERTIES
CHEMISTRY
SECTION
METERS
GRAPHIC LITHOLOGY
DRILLING DISTURB.
SED. STRUCTURES
SAMPLES
MIOCENE
N13-N14
NN7 Discoaster kugleri
F/P● ? Diartus petterssoni
●R/P
●A/M
●R/P
●ϕ=59.0 γ=1.75
●ϕ=57.8 γ=1.76
●ϕ=54.2 γ=1.81
●IC=8.70 OC=0.21
●IC=8.34
●IC=8.34
1
2
3
4
5
6
7
CC
0.5
1.0
PP

LITHOLOGIC DESCRIPTION

NANNOFOSSIL CHALK and CALCITIC MARLY NANNOFOSSIL CHALK

Entire core is moderately disturbed and fractured.

Major lithologies:
a. NANNOFOSSIL CHALK, light gray (5Y 7/1, 7/2) and light greenish gray (5GY 7/1). Moderately bioturbated throughout, with Zoophycos and purple burrow oxidation haloes and laminations.
b. CALCITIC MARLY NANNOFOSSIL CHALK, light greenish gray (10Y 6/3) and greenish gray (5GY 6/1, 5/1). Moderate bioturbation throughout. Vertical/subvertical sets of filled, mm-scale parallel fractures at Section 3, 48-51 and 83-88 cm; Section 4, 87-94 cm (show 0.5-1.0 mm vertical offset); and Section 5, 32-40 and 70-75 cm.

SMEAR SLIDE SUMMARY (%):

	1, 119 D	4, 123 D
TEXTURE:		
Sand		10
Silt	10	25
Clay	90	65
COMPOSITION:		
Access. minerals	Tr	2
Clay	15	25
Dolomite	—	1
Foraminifers	2	—
Volcanic glass	—	Tr
Inorganic calcite	3	30
Mica	Tr	—
Nannofossils	80	40
Organic debris	—	2
Quartz	Tr	—
Radiolarians	Tr	Tr
Sponge spicules	Tr	—

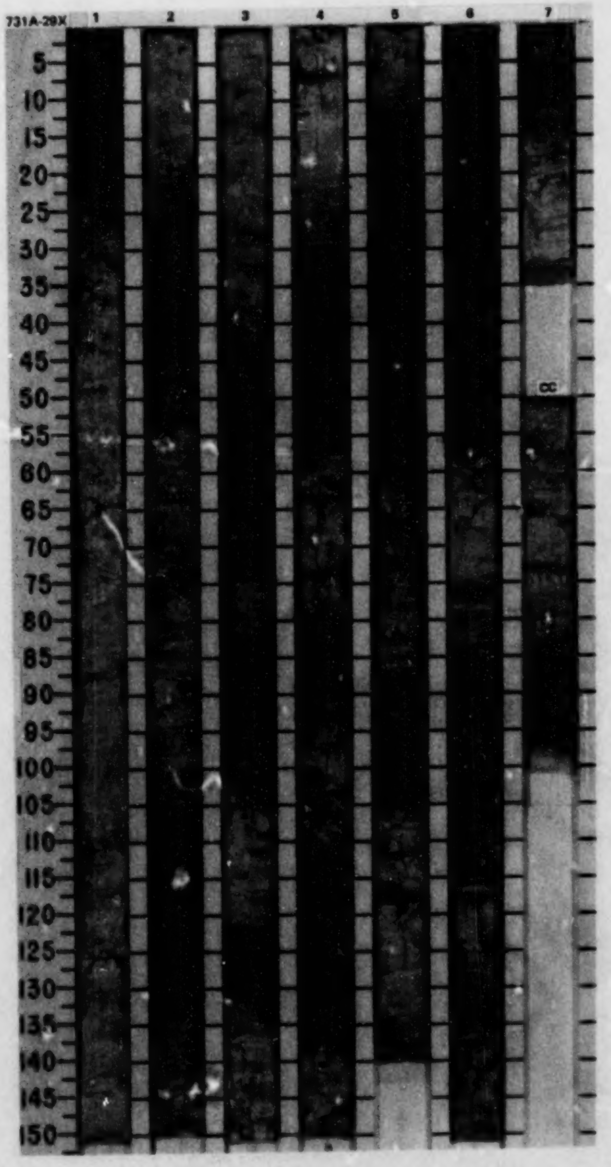
731A-29X
1
2
3
4
5
6
7
CC
5
10
15
20
25
30
35
40
45
50
55
60
65
70
75
80
85
90
95
100
105
110
115
120
125
130
135
140
145
150

SITE 731 HOLE A CORE 30X CORED INTERVAL 2645.7-2655.4 mbsl; 279.9-289.6 mbsf

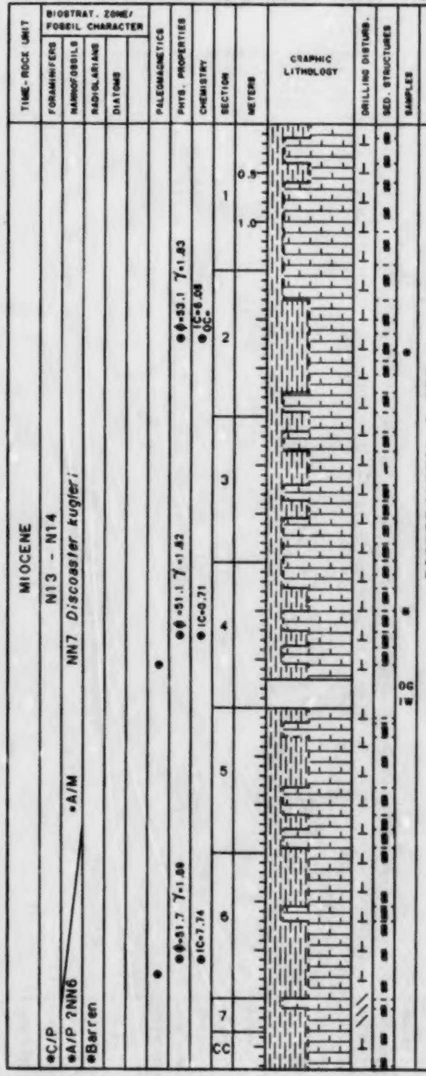
TIME-ROCK UNIT
BIOSTRAT. ZONE/ FOSSIL CHARACTER
FORAMINIFERS
NANNOFOSSILS
RADIOLARIANS
DIATOMS
PALEOMAGNETICS
PHYS. PROPERTIES
CHEMISTRY
SECTION
METERS
GRAPHIC LITHOLOGY
DRILLING DISTURB.
SED. STRUCTURES
SAMPLES
MIOCENE
N13 - N14
●C/P
NN7 Discoaster kugleri
●A/M
●A/P ?NN6
●Barren
●φ=53.1 γ=1.83
●φ=51.1 γ=1.82
●φ=51.7 γ=1.88
●IC=6.08 OC=
●IC=0.71
●IC=7.74
1
2
3
4
5
6
7
CC
0.5
1.0
OG
IW

LITHOLOGIC DESCRIPTION

NANNOFOSSIL CHALK and CALCITIC MARLY NANNOFOSSIL CHALK

Entire core is moderately disturbed and fractured.

Major lithologies:
a. NANNOFOSSIL CHALK, light gray (5Y 7/1) and light greenish gray (5GY 7/1, 5G 7/1). Moderately bioturbated, with abundant purple burrow oxidation haloes and laminations.
b. CALCITIC MARLY NANNOFOSSIL CHALK, greenish gray (5GY 6/1, 5/1; 5G 6/1) and dark greenish gray (10Y 5/2). Moderately to highly bioturbated, including Planolites.

SMEAR SLIDE SUMMARY (%):

	2, 83 D	4, 54 D
TEXTURE:		
Sand	15	—
Silt	25	5
Clay	60	95
COMPOSITION:		
Access. minerals	2	—
Clay	25	10
Dolomite	Tr	1
Feldspar	2	—
Foraminifers	—	3
Volcanic glass	1	—
Inorganic calcite	28	—
Mica	—	Tr
Nannofossils	35	85
Phosphate	Tr	—
Quartz	7	1
Radiolarians	Tr	—

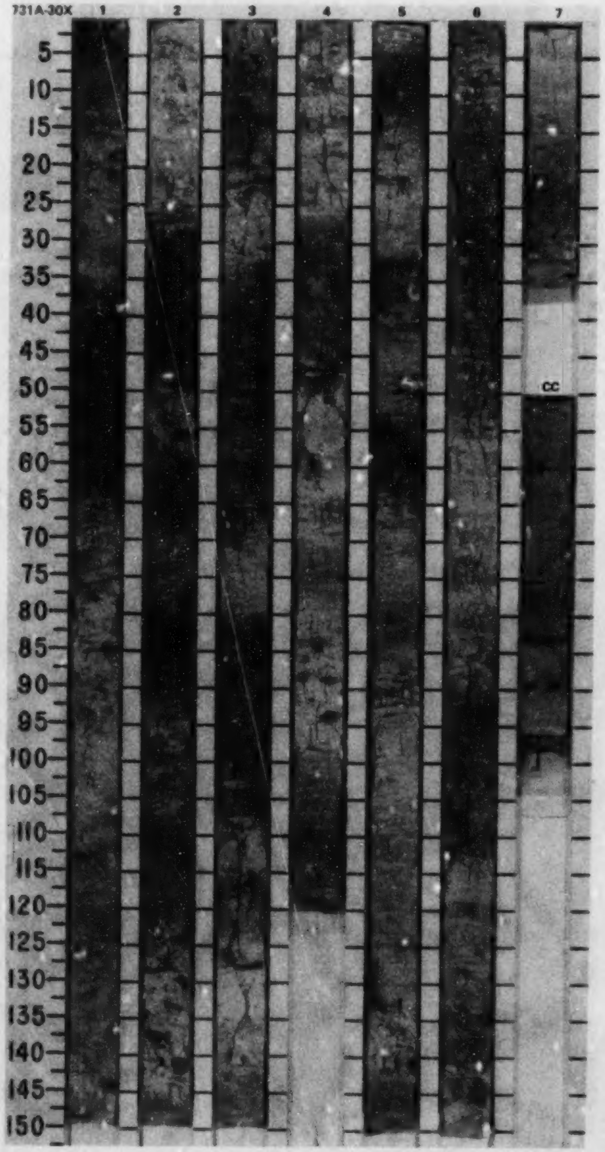
731A-30X
1
2
3
4
5
6
7
CC
5
10
15
20
25
30
35
40
45
50
55
60
65
70
75
80
85
90
95
100
105
110
115
120
125
130
135
140
145
150

SITE 731 HOLE A CORE 31X CORED INTERVAL 2655.4-2665.0 mbsl; 289.6-299.2 mbsf

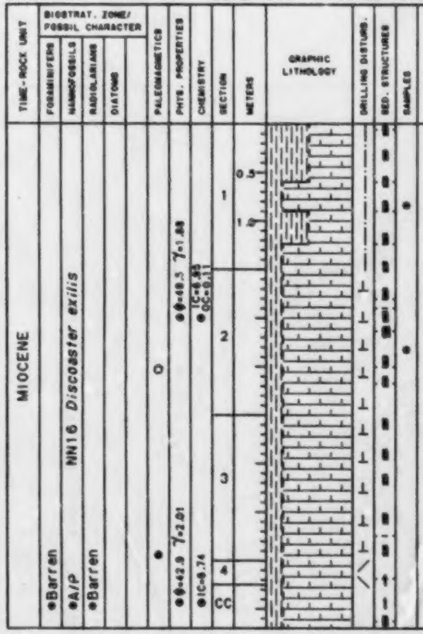
TIME-ROCK UNIT
BIOSTRAT. ZONE/ FOSSIL CHARACTER
FORAMINIFERS
NANNOFOSSILS
RADIOLARIANS
DIATOMS
PALEOMAGNETICS
PHYS. PROPERTIES
CHEMISTRY
SECTION
METERS
GRAPHIC LITHOLOGY
DRILLING DISTURB.
SED. STRUCTURES
SAMPLES
MIOCENE
●Barren
●A/P
NN16 Discoaster exilis
●Barren
●φ=48.5 γ=1.88
●φ=42.9 γ=2.01
●IC=8.85 OC=0.11
●IC=8.74
1
2
3
4
CC
0.5
1.0

LITHOLOGIC DESCRIPTION

NANNOFOSSIL CHALK and CALCITIC MARLY NANNOFOSSIL CHALK

Entire core is moderately disturbed and fractured.

Major lithologies:
a. NANNOFOSSIL CHALK, white (5Y 8/1) and light greenish gray (5GY 7/1). Moderate bioturbation throughout.
b. CALCITIC MARLY NANNOFOSSIL CHALK, greenish gray (5GY 6/1, 5G 5/1). Bioturbated.

SMEAR SLIDE SUMMARY (%):

	1, 85 D	2, 84 D
TEXTURE:		
Silt	5	5
Clay	95	95
COMPOSITION:		
Access. minerals	1	—
Clay	20	10
Dolomite	1	—
Foraminifers	1	4
Inorganic calcite	2	1
Nannofossils	75	85
Quartz	1	—

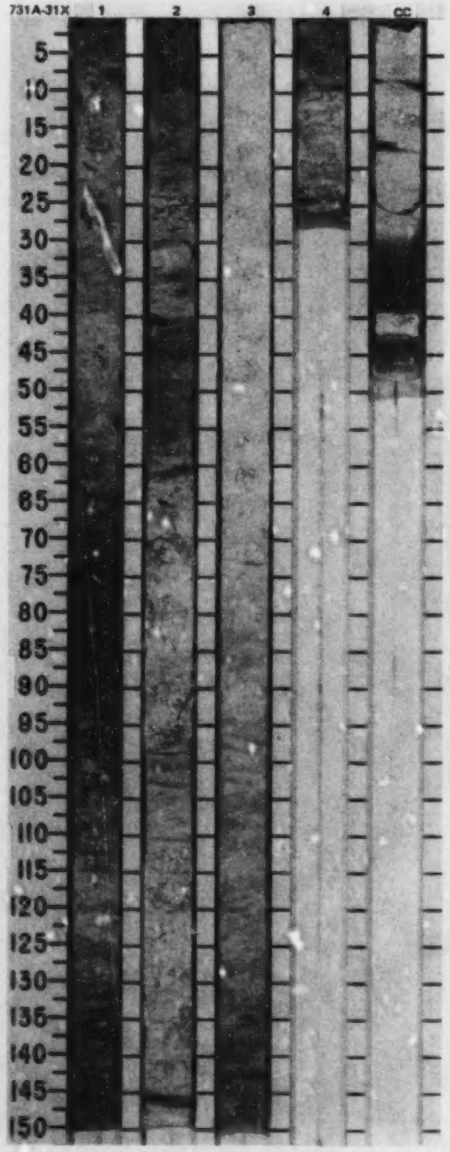
731A-31X
1
2
3
4
CC
5
10
15
20
25
30
35
40
45
50
55
60
65
70
75
80
85
90
95
100
105
110
115
120
125
130
135
140
145
150

SITE 731 HOLE A CORE 32X CORED INTERVAL 2665.0-2674.7 mbsl; 299.2-308.9 mbsf

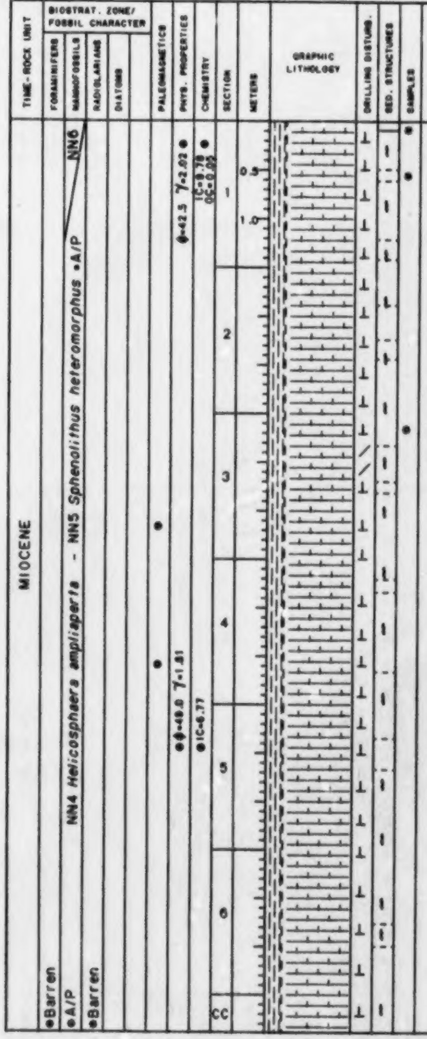
TIME-ROCK UNIT
BIOSTRAT. ZONE/ FOSSIL CHARACTER
FORAMINIFERS
NANNOFOSSILS
RADIOLARIANS
DIATOMS
PALEOMAGNETICS
PHYS. PROPERTIES
CHEMISTRY
SECTION
METERS
GRAPHIC LITHOLOGY
DRILLING DISTURB.
SED. STRUCTURES
SAMPLES
MIOCENE
•Barren
•A/P
•Barren
NN6
NN4 Helicosphaera ampliaperta - NN5 Sphenolithus heteromorphus •A/P
ϕ=42.5 γ=2.02 •
IC=8.78 •
OC=0.02
•ϕ=48.0 γ=1.81
•IC=6.77
1
2
3
4
5
6
CC
0.5
1.0

LITHOLOGIC DESCRIPTION

NANNOFOSSIL CHALK

Entire core is moderately disturbed and fractured.

Major lithology: NANNOFOSSIL CHALK, white (5Y 8/1), light gray (5Y 7/1, N7), and light greenish gray (5G 7/1), to gray (5Y 6/1) and greenish gray (5GY 6/1). Moderate bioturbation, and minor development of stylolitic bedding.

SMEAR SLIDE SUMMARY (%):

	1, 8 M	1, 57 D	3, 20 D
TEXTURE:			
Silt	5	—	5
Clay	95	100	95
COMPOSITION:			
Access. minerals	—	Tr	1
Clay	10	10	10
Dolomite	1	Tr	2
Foraminifers	1	—	—
Volcanic glass	—	Tr	Tr
Inorganic calcite	3	Tr	1
Mica	—	—	Tr
Nannofossils	85	90	85
Quartz	—	—	1

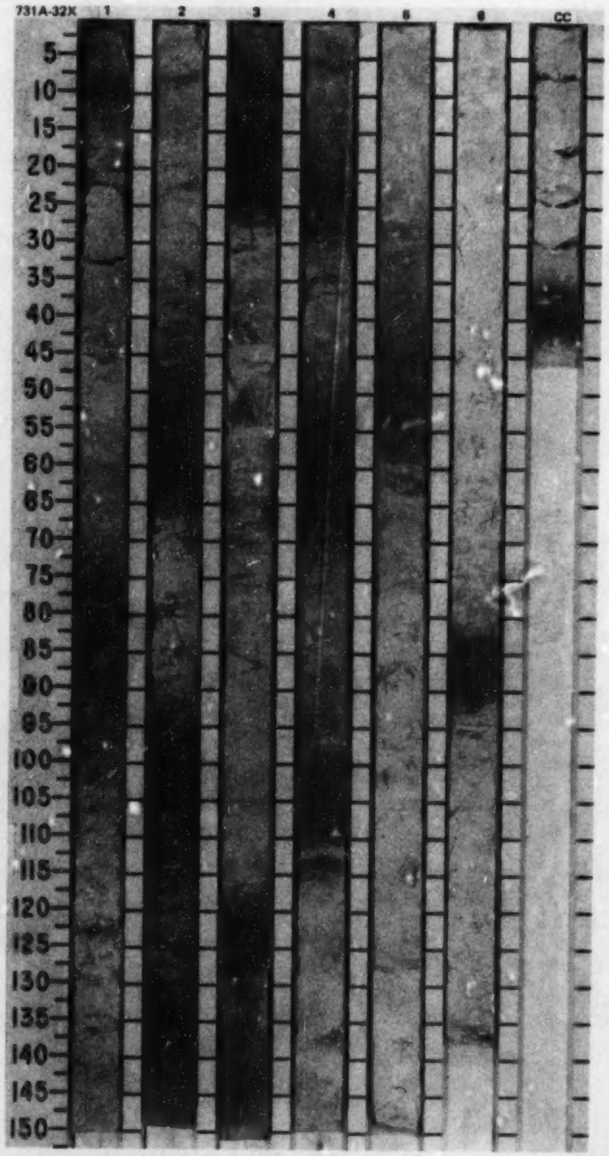
731A-32X
1
2
3
4
5
6
CC
5
10
15
20
25
30
35
40
45
50
55
60
65
70
75
80
85
90
95
100
105
110
115
120
125
130
135
140
145
150

SITE 731 HOLE A CORE 33X CORED INTERVAL 2674.7-2681.3 mbsl; 308.9-315.5 mbsf

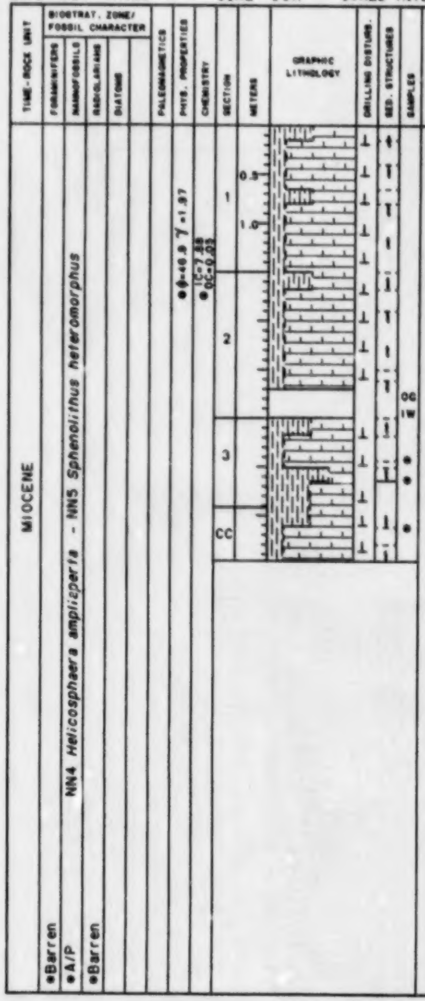
TIME-ROCK UNIT
BIOSTRAT. ZONE/ FOSSIL CHARACTER
FORAMINIFERS
NANNOFOSSILS
RADIOLARIANS
DIATOMS
PALEOMAGNETICS
PHYS. PROPERTIES
CHEMISTRY
SECTION
METERS
GRAPHIC LITHOLOGY
DRILLING DISTURB.
SED. STRUCTURES
SAMPLES
MIOCENE
●Barren
●A/P
NN4 *Helicosphaera ampliaperta* - NN5 *Sphenolithus heteromorphus*
●Barren
●ϕ=46.9 γ=1.97
●IC=7.88 OC=0.03
1
2
3
CC
0.5
1.0
OG
IW

LITHOLOGIC DESCRIPTION

NANNOFOSSIL CHALK and CALCITIC MARLY NANNOFOSSIL CHALK

Entire core is moderately disturbed and fractured.

Major lithologies:
a. NANNOFOSSIL CHALK, white (5Y 8/1) and light gray (5Y 7/1). Slight to moderate bioturbation.
b. CALCITIC MARLY NANNOFOSSIL CHALK, gray (5Y 6/1, 5/1). Slight to moderate bioturbation.

Minor lithology: Nannofossil-rich calcitic silty clay, greenish gray (5GY 5/1), in Section 3, 55-65 cm.

SMEAR SLIDE SUMMARY (%):

	3, 44 D	3, 63 M	CC, 20 D
TEXTURE:			
Silt	—	10	15
Clay	100	90	85
COMPOSITION:			
Clay	—	65	50
Fish	Tr	—	—
Inorganic calcite	—	10	15
Nannofossils	100	25	35

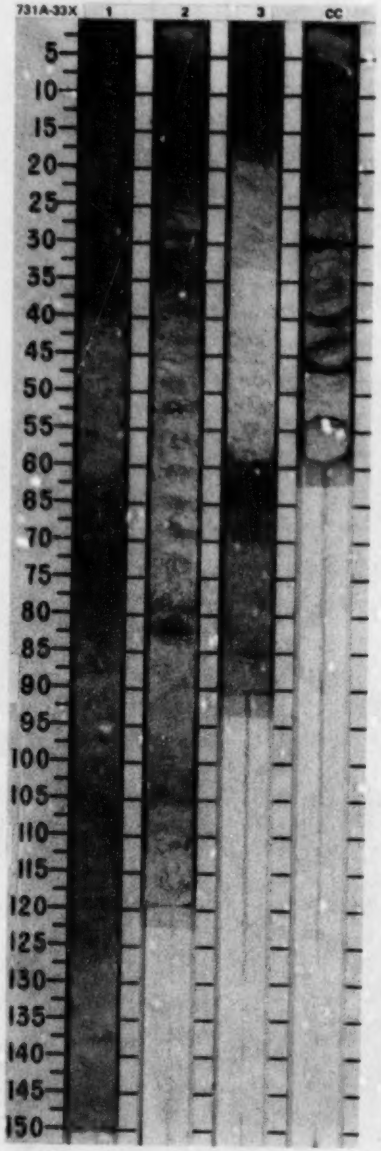
731A-33X
1
2
3
CC
5
10
15
20
25
30
35
40
45
50
55
60
65
70
75
80
85
90
95
100
105
110
115
120
125
130
135
140
145
150

SITE 731 HOLE A CORE 34X CORED INTERVAL 2681.3-2687.9 mbsl; 315.5-322.1 mbsf

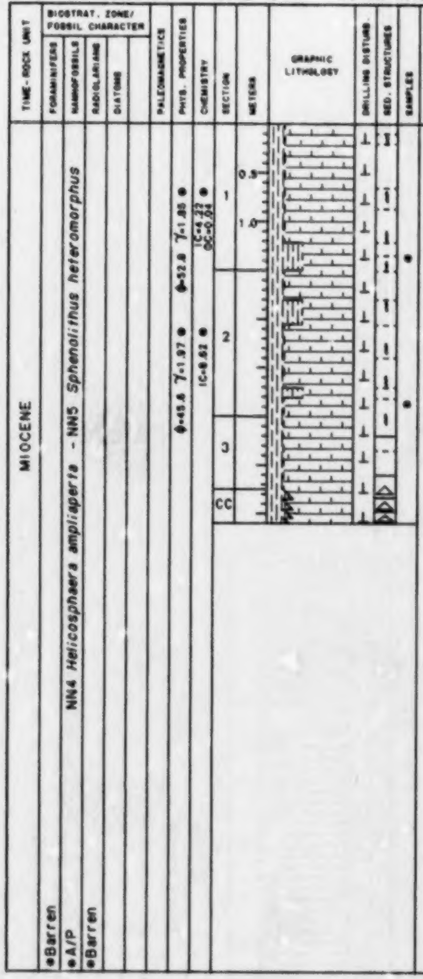
TIME-ROCK UNIT
BIOSTRAT. ZONE/ FOSSIL CHARACTER
FORAMINIFERS
NANNOFOSSILS
RADIOLARIANS
DIATOMS
PALEOMAGNETICS
PHYS. PROPERTIES
CHEMISTRY
SECTION
METERS
GRAPHIC LITHOLOGY
DRILLING DISTURB.
SED. STRUCTURES
SAMPLES
MIOCENE
●Barren
NN4 Helicosphaera ampliaperta - NN5 Sphenolithus heteromorphus
●A/P
●Barren
φ=52.8 γ=1.85 ●
φ=45.6 γ=1.97 ●
IC=4.22 OC=0.04 ●
IC=8.62 ●
1
2
3
CC
0.5
1.0

LITHOLOGIC DESCRIPTION

NANNOFOSSIL CHALK

Entire core is moderately disturbed and fractured.

Major lithology: NANNOFOSSIL CHALK, light gray (5Y 7/1, 10YR 7/1), gray (10YR 6/1, 5Y 6/1), and light brownish gray (10YR 6/2). Slight to moderate bioturbation.

Minor lithology: Calcitic marly nannofossil chalk, olive gray (5Y 5/2) and brown (10YR 5/3). Bioturbated in Section 1, 123–150 cm, and Section 2, 30–53 and 120–129 cm. Not bioturbated in the thin basal zones of upward-lightening sequences in CC.

SMEAR SLIDE SUMMARY (%):

	1, 138 D	2, 138 D
TEXTURE:		
Silt	30	10
Clay	70	90
COMPOSITION:		
Access. minerals	Tr	Tr
Clay	20	15
Dolomite	Tr	Tr
Foraminifers	Tr	—
Volcanic glass	Tr	—
Inorganic calcite	10	5
Nannofossils	65	80
Quartz	5	Tr

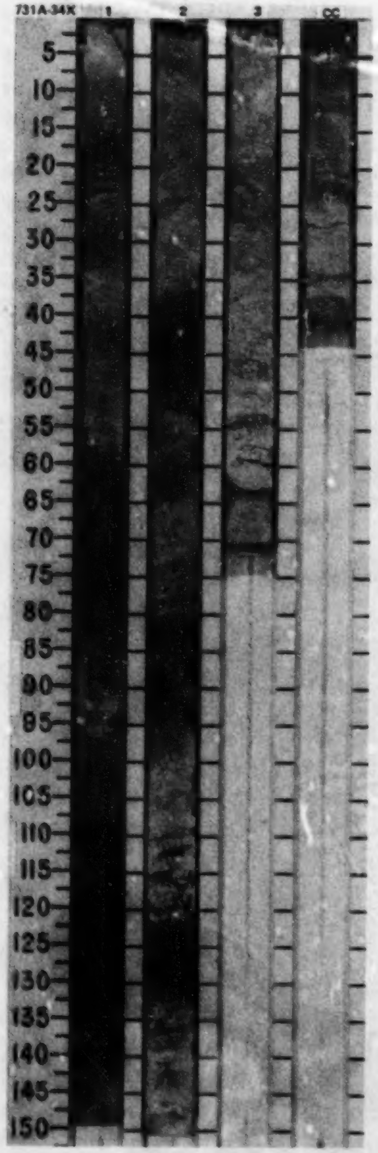
731A-34X
1
2
3
CC
5
10
15
20
25
30
35
40
45
50
55
60
65
70
75
80
85
90
95
100
105
110
115
120
125
130
135
140
145
150

SITE 731 HOLE A CORE 35X CORED INTERVAL 2687.9-2697.5 mbsl; 322.1-331.7 mbsf

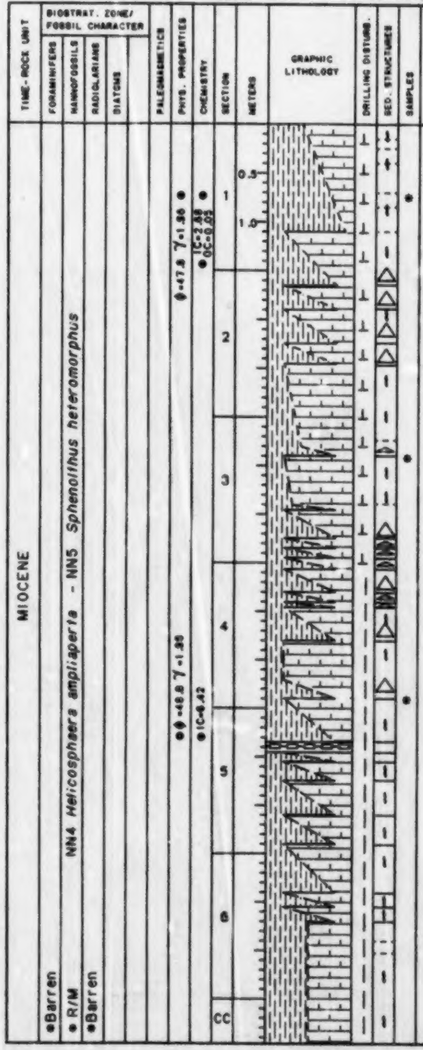

TIME-ROCK UNIT
BIOSTRAT. ZONE/ FOSSIL CHARACTER
FORAMINIFERS
NANNOFOSSILS
RADIOLARIANS
DIATOMS
PALEOMAGNETICS
PHYS. PROPERTIES
CHEMISTRY
SECTION
METERS
GRAPHIC LITHOLOGY
DRILLING DISTURB.
SED. STRUCTURES
SAMPLES
MIOCENE
●Barren
● R/M
●Barren
NN4 Helicosphaera ampliaperta - NN5 Sphenolithus heteromorphus
φ=47.8 γ=1.90
IC=2.88 OC=0.03
φ=48.8 γ=1.95
IC=6.42
1
2
3
4
5
6
CC
0.5
1.0

LITHOLOGIC DESCRIPTION

SILTY CLAYSTONE to MARLY NANNOFOSSIL CHALK

Entire core is slightly to moderately disturbed and fractured.

Major lithology: SILTY CLAYSTONE, greenish gray (5GY 5/1, 5G 6/1, 5BG 5/1), gray (5Y 5/1), and olive gray (5Y 5/2), grading upsection to MARLY NANNOFOSSIL CHALK, grayish brown (10YR 5/2), light grayish brown (10YR 6/2), and brown (10YR 5/3). Silty claystone is thin (<5 cm), with sharp bases, marly nannofossil chalk tops are bioturbated.

Minor lithology: Carbonate chalk, light gray (5Y 7/2), with sharp base. Forms an upward-fining sequence in Section 5, 34-45 cm.

SMEAR SLIDE SUMMARY (%):

	1, 77 D	3, 44 M	4, 141 M
TEXTURE:			
Silt	5	50	5
Clay	95	50	95
COMPOSITION:			
Access. minerals	1	—	—
Clay	35	50	65
Dolomite	2	Tr	—
Inorganic calcite	10	19	20
Mica	—	Tr	—
Nannofossils	50	1	5
Quartz	2	30	10

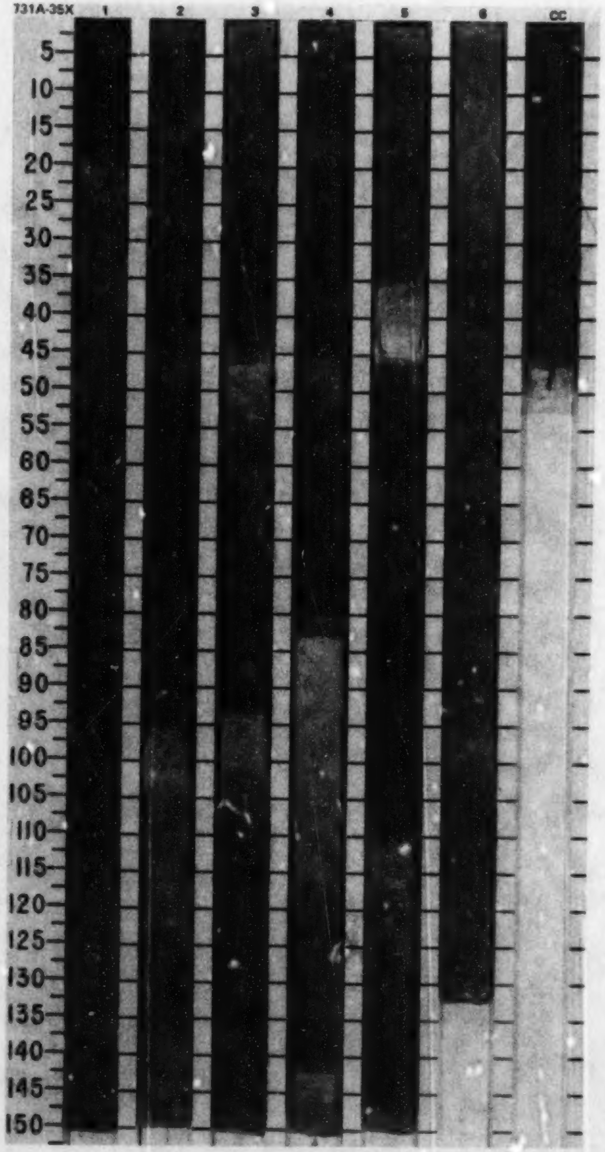

731A-35X
1
2
3
4
5
6
CC
5
10
15
20
25
30
35
40
45
50
55
60
65
70
75
80
85
90
95
100
105
110
115
120
125
130
135
140
145
150

SITE 731 HOLE A CORE 36X CORED INTERVAL 2697.5-2707.2 mbsl; 331.7-341.3 mbsf

TIME-ROCK UNIT	BIOSTRAT. ZONE/ FOSSIL CHARACTER FORAMINIFERS	NANNOFOSSILS	RADIOLARIANS	DIATOMS	PALEOMAGNETICS	PHYS. PROPERTIES	CHEMISTRY	SECTION	METERS	GRAPHIC LITHOLOGY	DRILLING DISTURB.	SED. STRUCTURES	SAMPLES	LITHOLOGIC DESCRIPTION
MIOCENE	Barren ●	NN4 *Helicosphaera ampliaperta* - NN5 *Sphenolithus heteromorphus* R/M ●	Barren ●											SILTY CLAYSTONE Entire core is moderately disturbed and fractured. Major lithology: SILTY CLAYSTONE, olive gray (5Y 4/2), with a 1-cm-thick interval of greenish gray (5BG 5/1) silty claystone.

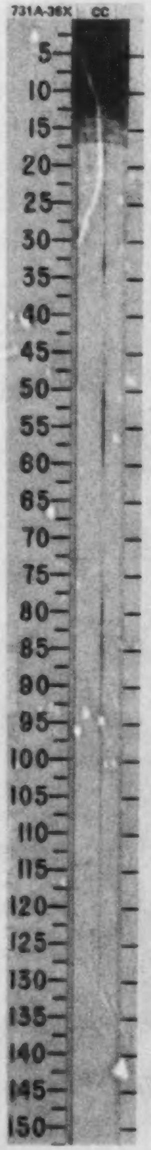
731A-36X
CC
5
10
15
20
25
30
35
40
45
50
55
60
65
70
75
80
85
90
95
100
105
110
115
120
125
130
135
140
145
150

SITE 731 HOLE A CORE 37X CORED INTERVAL 2707.1-2716.8 mbsl; 341.3-351.0 mbsf

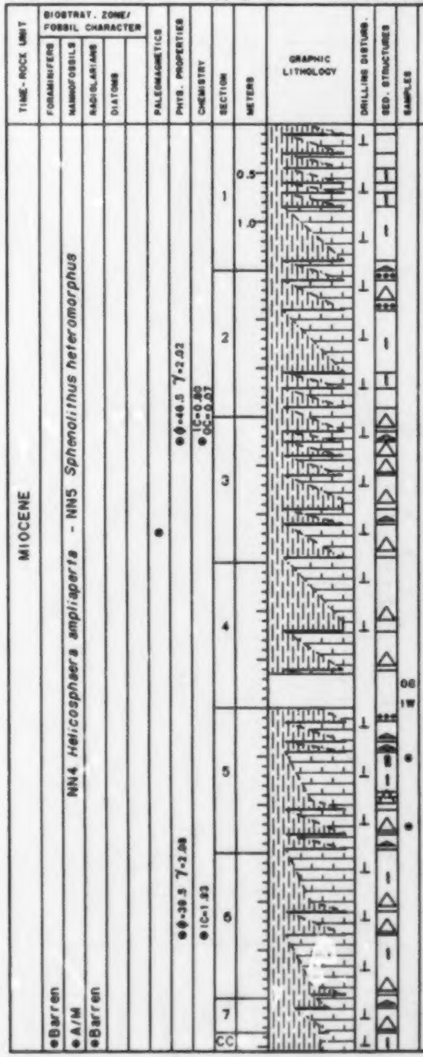
TIME-ROCK UNIT
BIOSTRAT. ZONE/ FOSSIL CHARACTER
FORAMINIFERS
NANNOFOSSILS
RADIOLARIANS
DIATOMS
PALEOMAGNETICS
PHYS. PROPERTIES
CHEMISTRY
SECTION
METERS
GRAPHIC LITHOLOGY
DRILLING DISTURB.
SED. STRUCTURES
SAMPLES
MIOCENE
NN4 Helicosphaera ampliaperta - NN5 Sphenolithus heteromorphus
●Barren
●A/M
●Barren
●Φ=46.5 γ=2.02
●Φ=38.5 γ=2.08
●IC=0.80 OC=0.07
●IC=1.93
1
2
3
4
5
6
7
CC
0.5
1.0
OG
IW

LITHOLOGIC DESCRIPTION

SILTY CLAYSTONE to NANNOFOSSIL CHALK

Entire core is moderately disturbed and fractured.

Major lithology: SILTY CLAYSTONE, greenish gray (5G 6/1, 5BG 5/1), grading upsection to NANNOFOSSIL CHALK, brown (10YR 5/3) to light brownish gray (10YR 6/2). Silty claystone is generally thin (< 10 cm), with sharp bases. Intermediate zones are olive (5Y 5/3), olive gray (5Y 5/2), and grayish brown (10YR 5/2). Nannofossil chalk is bioturbated.

SMEAR SLIDE SUMMARY (%):

	5, 52 D	5, 124 M
TEXTURE:		
Silt	—	2
Clay	100	98
COMPOSITION:		
Access. minerals	Tr	2
Clay	20	63
Inorganic calcite	Tr	15
Mica	Tr	Tr
Nannofossils	80	10
Quartz	—	10

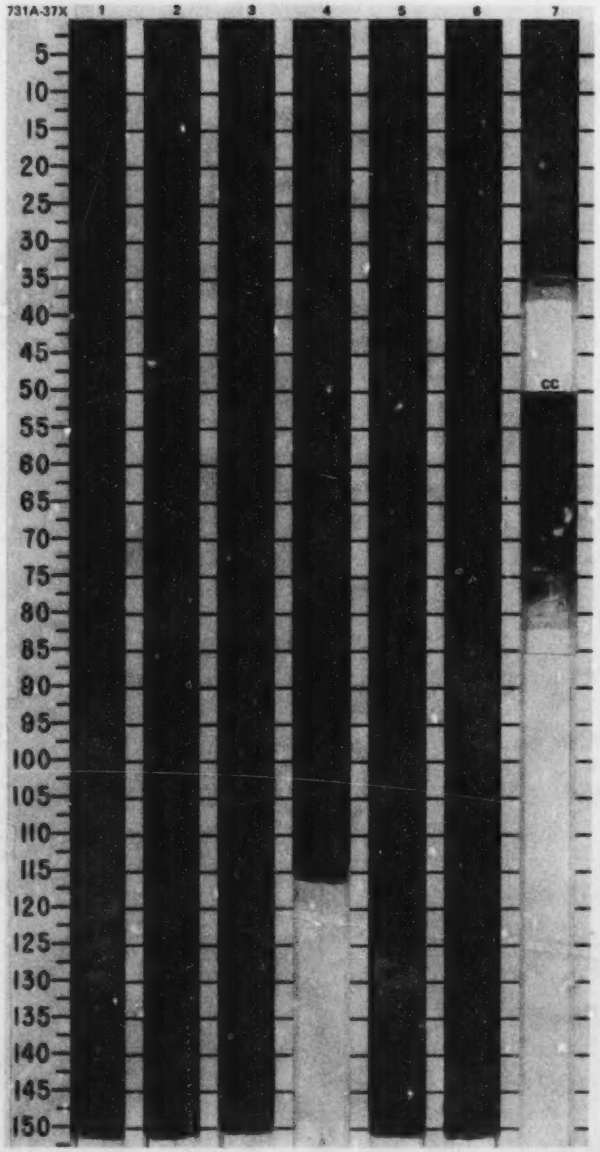
731A-37X
1
2
3
4
5
6
7
CC
5
10
15
20
25
30
35
40
45
50
55
60
65
70
75
80
85
90
95
100
105
110
115
120
125
130
135
140
145
150

SITE 731 HOLE A CORE 38X CORED INTERVAL 2716.8-2726.5 mbsl; 351.0-360.7 mbsf

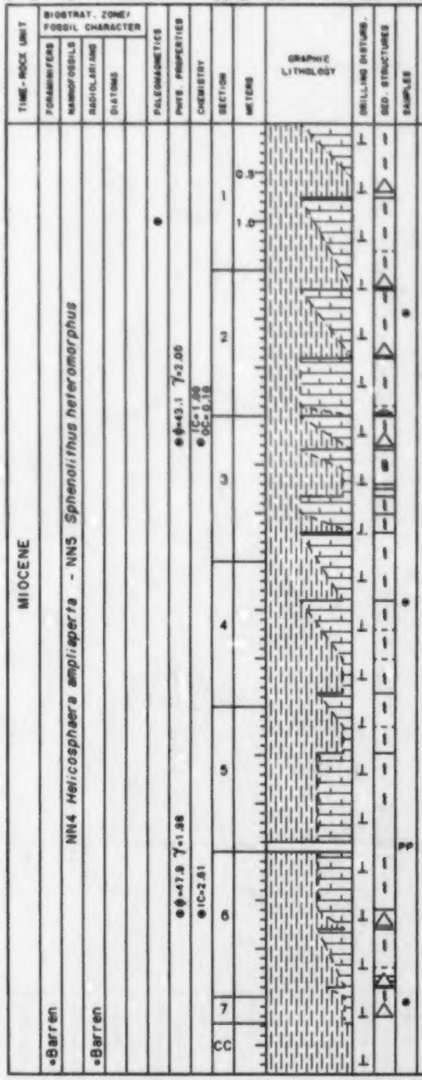
TIME-ROCK UNIT
BIOSTRAT. ZONE/ FOSSIL CHARACTER
FORAMINIFERS
NANNOFOSSILS
RADIOLARIANS
DIATOMS
PALEOMAGNETICS
PHYS. PROPERTIES
CHEMISTRY
SECTION
METERS
GRAPHIC LITHOLOGY
DRILLING DISTURB.
SED. STRUCTURES
SAMPLES
MIOCENE
•Barren
NN4 Helicosphaera ampliaperta - NN5 Sphenolithus heteromorphus
•Barren
●φ=43.1 γ=2.00
●IC=1.86 OC=0.18
●φ=47.9 γ=1.98
●IC=2.61
0.5
1.0
1
2
3
4
5
6
7
CC
PP

LITHOLOGIC DESCRIPTION

Gradationally interbedded CLAYEY SILTSTONE to MARLY NANNOFOSSIL CHALK

Entire core is moderately disturbed and fractured.

Major lithology: Gradationally interbedded CLAYEY SILTSTONE, greenish gray (5GY 5/1, 5BG 5/1), dark gray (N4), and dark greenish gray (5GY 4/1), to MARLY NANNOFOSSIL CHALK, olive gray (5Y 5/2), gray (5Y 6/1), light gray (10YR 7/1), and brown (10YR 5/3). Clayey siltstone generally has sharp bases and is not bioturbated, marly nannofossil chalk is bioturbated.

SMEAR SLIDE SUMMARY (%):

	2, 45 D	4, 42 D	7, 04 M
TEXTURE:			
Silt	40	60	10
Clay	60	40	90
COMPOSITION:			
Access. mineral	Tr	Tr	Tr
Clay	20	20	80
Dolomite	—	Tr	—
Glauconite	—	—	10
Inorganic calcite	20	30	5
Nannofossils	40	10	Tr
Quartz	20	40	5

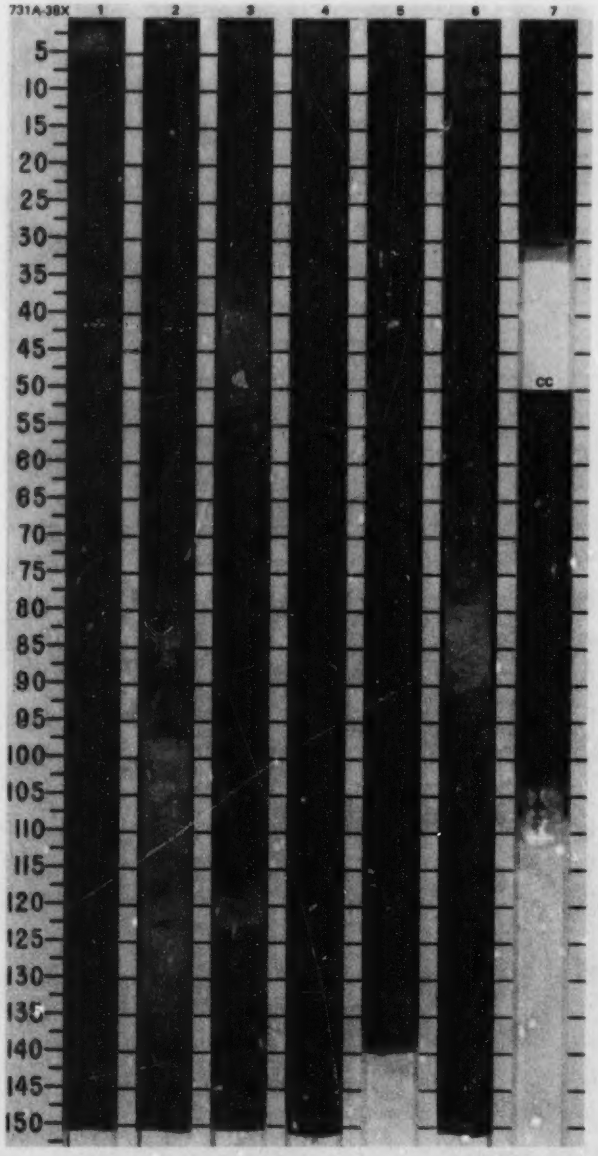
731A-38X
1
2
3
4
5
6
7
CC
5
10
15
20
25
30
35
40
45
50
55
60
65
70
75
80
85
90
95
100
105
110
115
120
125
130
135
140
145
150

SITE 731 HOLE A CORE 39X CORED INTERVAL 2726.5-2736.2 mbsl; 360.7-370.4 mbsf

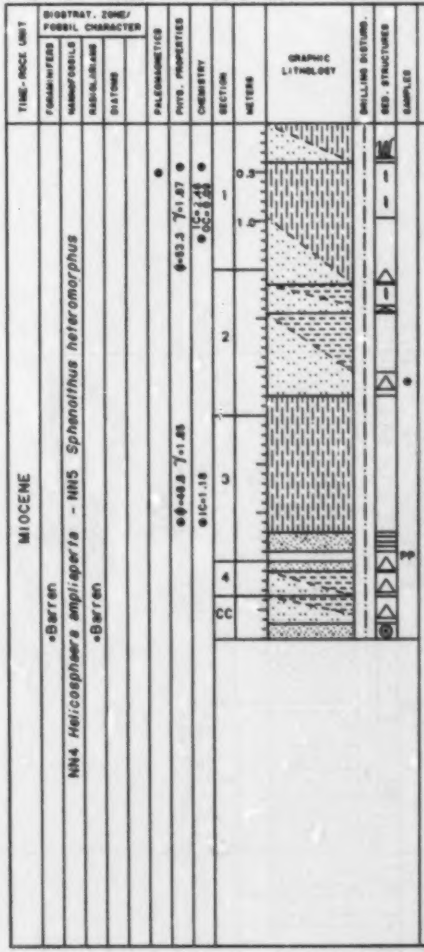
TIME-ROCK UNIT
BIOSTRAT. ZONE/ FOSSIL CHARACTER
FORAMINIFERS
NANNOFOSSILS
RADIOLARIANS
DIATOMS
PALEOMAGNETICS
PHYS. PROPERTIES
CHEMISTRY
SECTION
METERS
GRAPHIC LITHOLOGY
DRILLING DISTURB.
SED. STRUCTURES
SAMPLES
MIOCENE
•Barren
NN4 Helicosphaera ampliaperta - NN5 Sphenolithus heteromorphus
•Barren
φ=53.3 γ=1.87
φ=48.8 γ=1.85
IC=1.46 OC=0.80
IC=1.18
1
2
3
4
CC
0.5
1.0
PP

LITHOLOGIC DESCRIPTION

Gradationally interbedded SILTSTONE and SILTY CLAYSTONE, and SILTY CLAYSTONE

Entire core is moderately disturbed and fractured.

Major lithologies:
a. SILTSTONE, very dark gray (5Y 3/1), grading to overlying silty claystone, dark gray (5Y 4/1). Basal siltstone layers have sharp bases, and are commonly graded and micaceous.
b. SILTY CLAYSTONE, dark gray (5Y 4/1). Bioturbated at Section 1, 40-90 cm, and uniform from Section 2, 130 cm, to Section 3, 125 cm.

Minor lithology: Silty sand to sandy silt, very dark gray (5Y 3/1), with parallel laminations and minor grading, and Section 3, 125 cm, to Section 4, 10 cm, and CC, 36-42 cm.

SMEAR SLIDE SUMMARY (%):

	2, 128 M
TEXTURE:	
Sand	5
Silt	75
Clay	20
COMPOSITION:	
Access. minerals	2
Clay	25
Feldspar	2
Glauconite	1
Hornblende	1
Inorganic calcite	25
Mica	7
Opaques	3
Quartz	35
Rock fragment	1

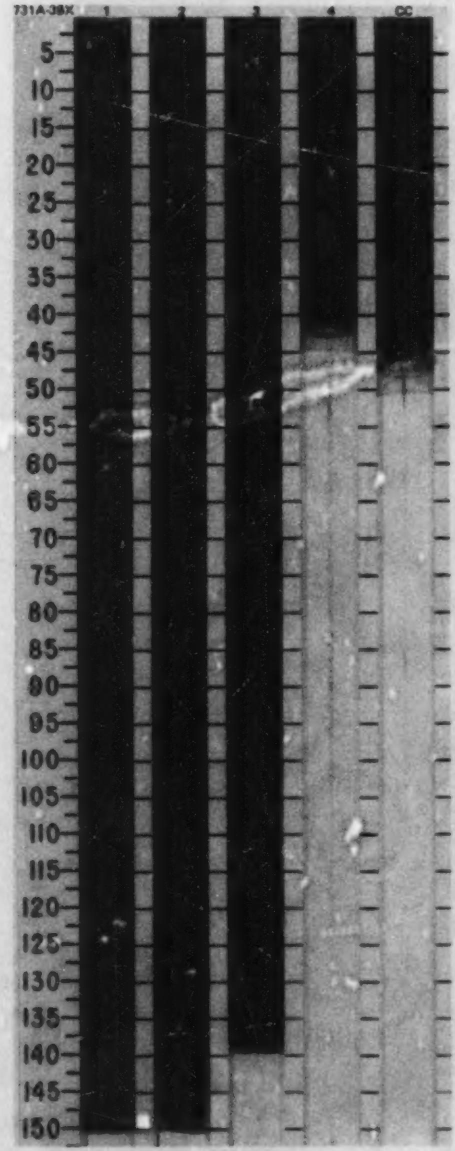
731A-39X
1
2
3
4
CC
5
10
15
20
25
30
35
40
45
50
55
60
65
70
75
80
85
90
95
100
105
110
115
120
125
130
135
140
145
150

SITE 731 HOLE A CORE 40X CORED INTERVAL 2736.2-2745.8 mbsl; 370.4-380.0 mbsf

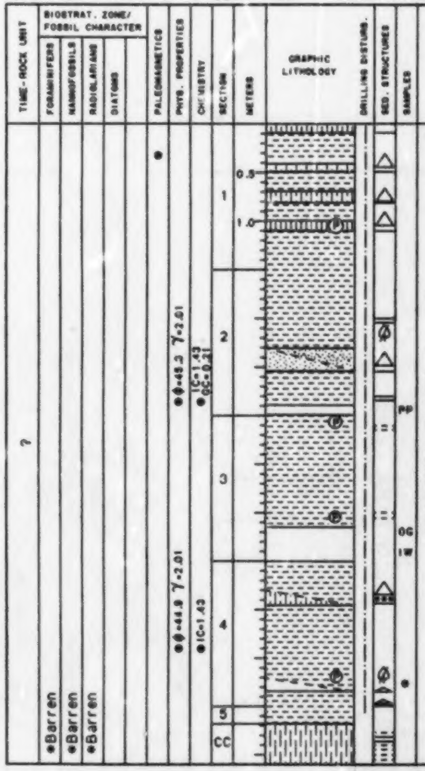
TIME-ROCK UNIT
BIOSTRAT. ZONE/ FOSSIL CHARACTER
FORAMINIFERS
NANNOFOSSILS
RADIOLARIANS
DIATOMS
PALEOMAGNETICS
PHYS. PROPERTIES
CHEMISTRY
SECTION
METERS
GRAPHIC LITHOLOGY
DRILLING DISTURB.
SED. STRUCTURES
SAMPLES
?
●Barren
●Barren
●Barren
●Φ=45.3 γ=2.01
●IC=1.43 OC=0.21
●Φ=44.9 γ=2.01
●IC=1.43
1
2
3
4
5
CC
0.5
1.0
PP
OG
IW

LITHOLOGIC DESCRIPTION

CLAYSTONE to SILTY CLAYSTONE, and SANDSTONE to SILTY SANDSTONE

Entire core is moderately disturbed and fractured.

Major lithologies:
- a. CLAYSTONE to SILTY CLAYSTONE, dark gray (5Y 4/1, 10YR 4/1) to very dark gray (5Y 3/1) and very dark grayish brown (10YR 3/2). Contains minor pyritic intervals < 1 cm thick. Upward-fining zones in Sections 1, 4, and 5. Parallel laminations at CC, 15–45 cm.
- b. SANDSTONE to SILTY SANDSTONE, very dark gray (5Y 3/1). Forms sharp-based upward-fining sequences, with abundant wood debris and charcoal, in Sections 2 and 4.

SMEAR SLIDE SUMMARY (%):

	4, 127 M
TEXTURE:	
Sand	10
Silt	70
Clay	20
COMPOSITION:	
Access. minerals	1
Clay	10
Dolomite	1
Inorganic calcite	18
Mica	5
Nannofossils	Tr
Plant debris	5
Quartz	60

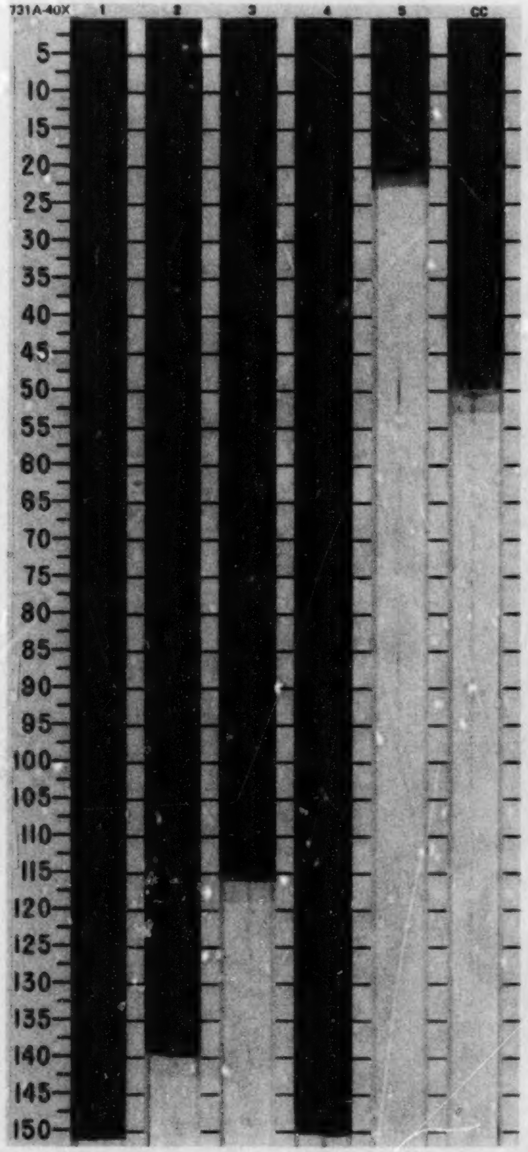
731A-40X
1
2
3
4
5
CC
5
10
15
20
25
30
35
40
45
50
55
60
65
70
75
80
85
90
95
100
105
110
115
120
125
130
135
140
145
150

SITE 731 HOLE A CORE 41X CORED INTERVAL 2745.8-2755.5 mbsl; 380.0-389.7 mbsf

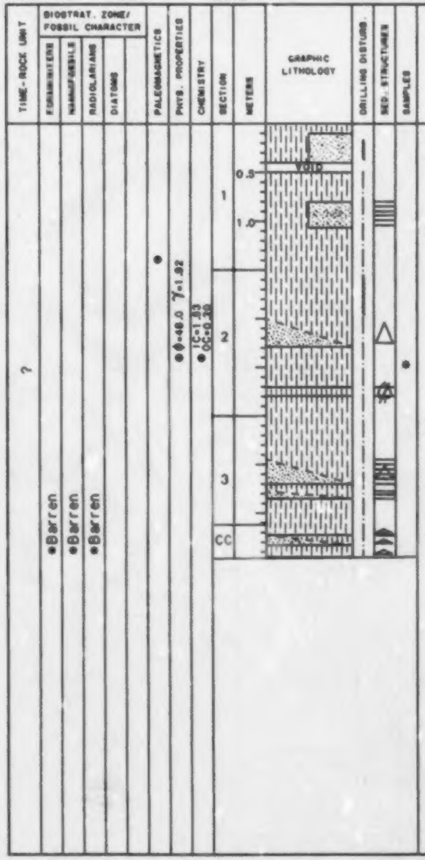
TIME-ROCK UNIT
BIOSTRAT. ZONE/ FOSSIL CHARACTER
FORAMINIFERS
NANNOFOSSILS
RADIOLARIANS
DIATOMS
PALEOMAGNETICS
PHYS. PROPERTIES
CHEMISTRY
SECTION
METERS
GRAPHIC LITHOLOGY
DRILLING DISTURB.
SED. STRUCTURES
SAMPLES
?
●Barren
●Barren
●Barren
●
●ϕ=48.0 γ=1.92
●IC=1.83 OC=0.30
1
2
3
CC
0.5
1.0
VOID

LITHOLOGIC DESCRIPTION

SILTY CLAYSTONE, interbedded SANDY SILTSTONE and SILTY CLAYSTONE, and gradationally interbedded SANDY SILTSTONE and SILTY CLAYSTONE

Entire core is moderately to highly disturbed and fractured.

Major lithologies:
a. SILTY CLAYSTONE, very dark grayish brown (10YR 3/2), uniform.
b. SANDY SILTSTONE, very dark grayish brown (10YR 3/2), and silty claystone, dark gray (10YR 4/1) to very dark grayish brown (10YR 3/2), interbedded on a scale of 0.5–2.0 cm. Section 1, 10–32 and 75–107 cm; and Section 3, 45–70 and 80–85 cm.
c. SANDY SILTSTONE, very dark grayish brown (10YR 3/2), and silty claystone, dark gray (10YR 4/1) to very dark grayish brown (10YR 3/2), gradationally interbedded to form upward-fining sequences; generally with sharp bases. Charcoal and wood debris locally common to abundant.

SMEAR SLIDE SUMMARY (%):

	2, 90 D
TEXTURE:	
Silt	25
Clay	75
COMPOSITION:	
Access. minerals	1
Clay	50
Inorganic calcite	30
Mica	2
Nannofossils	2
Quartz	15

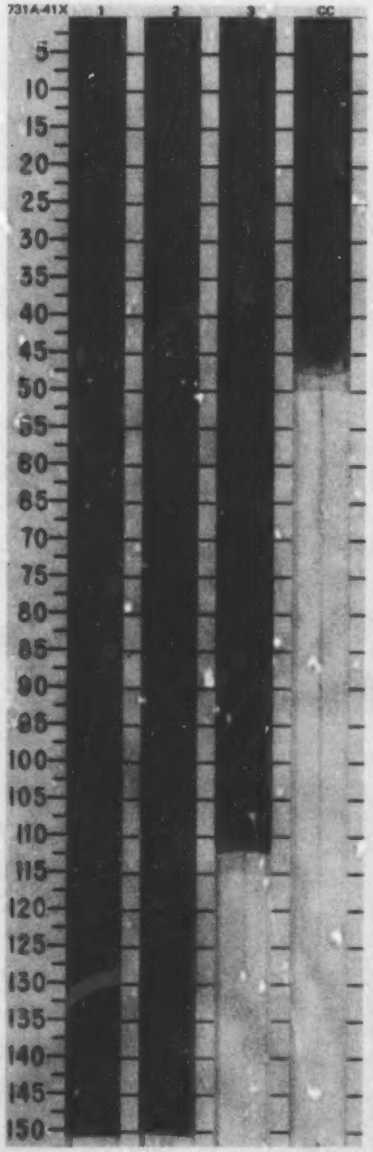
731A-41X
1
2
3
CC
5
10
15
20
25
30
35
40
45
50
55
60
65
70
75
80
85
90
95
100
105
110
115
120
125
130
135
140
145
150

SITE 731 HOLE A CORE 42X CORED INTERVAL 2755.5-2765.2 mbsl; 389.7-399.4 mbsf

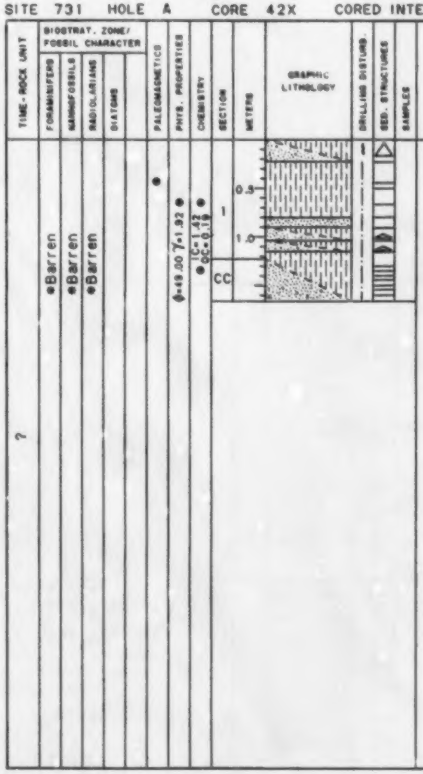
TIME-ROCK UNIT
BIOSTRAT. ZONE/FOSSIL CHARACTER
FORAMINIFERS
NANNOFOSSILS
RADIOLARIANS
DIATOMS
PALEOMAGNETICS
PHYS. PROPERTIES
CHEMISTRY
SECTION
METERS
GRAPHIC LITHOLOGY
DRILLING DISTURB.
SED. STRUCTURES
SAMPLES
?
●Barren
●Barren
●Barren
ϕ=49.00 γ=1.92 ●
● IC=1.42
OC=0.19 ●
1
CC
0.5
1.0

LITHOLOGIC DESCRIPTION

SILTY CLAYSTONE, interbedded SANDY SILTSTONE and SILTY CLAYSTONE, and gradationally interbedded SANDY SILTSTONE and SILTY CLAYSTONE

Entire core is moderately to highly disturbed and fractured.

Major lithologies:

a. SILTY CLAYSTONE, very dark grayish brown (10YR 3/2), in Section 1, 22–92 and 116–121 cm.

b. SANDY SILTSTONE, very dark gray (10YR 3/1), and SILTY CLAYSTONE, dark gray (10YR 4/1), interbedded on scale of 0.5–2.0 cm, forming an upward-fining sequence, in CC.

c. SANDY SILTSTONE and SILTY CLAYSTONE, very dark grayish brown (10YR 3/2), gradationally interbedded to form sharp-based upward-fining sequences, Section 1, 0–22, 92–106, and 106–116 cm.

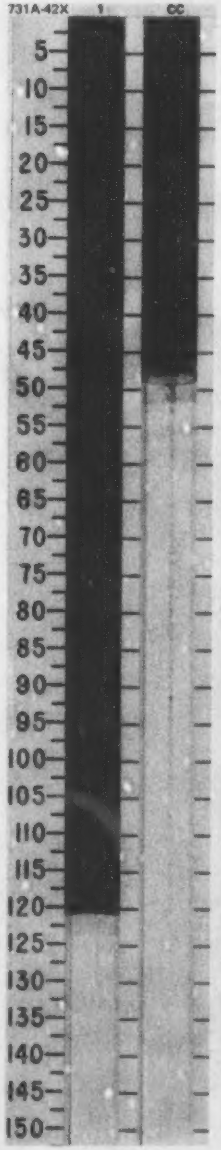
731A-42X
1
CC
5
10
15
20
25
30
35
40
45
50
55
60
65
70
75
80
85
90
95
100
105
110
115
120
125
130
135
140
145
150

SITE 731 HOLE A CORE 43X CORED INTERVAL 2765.2-2793.8 mbsl; 399.4-409.0 mbsf

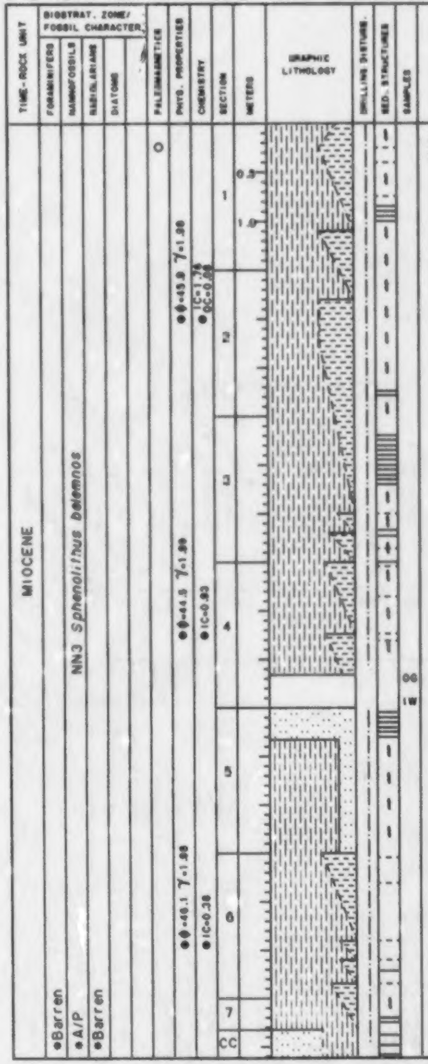
TIME-ROCK UNIT
BIOSTRAT. ZONE/ FOSSIL CHARACTER
FORAMINIFERS
NANNOFOSSILS
RADIOLARIANS
DIATOMS
PALEOMAGNETICS
PHYS. PROPERTIES
CHEMISTRY
SECTION
METERS
GRAPHIC LITHOLOGY
DRILLING DISTURB.
SED. STRUCTURES
SAMPLES
MIOCENE
NN3 Sphenolithus belemnos
●Barren
●A/P
●Barren
●φ=45.9 γ=1.90
●IC=1.76 OC=0.88
●φ=44.5 γ=1.90
●IC=0.93
●φ=40.1 γ=1.98
●IC=0.30
0.5
1.0
1
2
3
4
5
6
7
CC
OG
IW

LITHOLOGIC DESCRIPTION

Gradationally interbedded SILTSTONE to SILTY CLAYSTONE, and interbedded SILTSTONE and SILTY CLAYSTONE

Entire core is moderately disturbed and fractured.

Major lithologies:
a. SILTSTONE, greenish gray (5GY 5/1, 5G 6/1), grading upsection to silty claystone, olive gray (5Y 5/2), gray (5Y 5/1), dark gray, (10YR 4/1), and light gray (10YR 7/1). Upward-fining sequences, generally without sharp bases. Tops are bioturbated. Bases are parallel laminated at Section 1, 86-95 cm, Section 2, 22-68 cm, and Section 7, 25-31 cm.
b. SILTSTONE and SILTY CLAYSTONE, greenish gray (5G 6/1), olive (5Y 4/3), and dark grayish brown (10YR 3/2), interbedded, in Section 5 and CC.

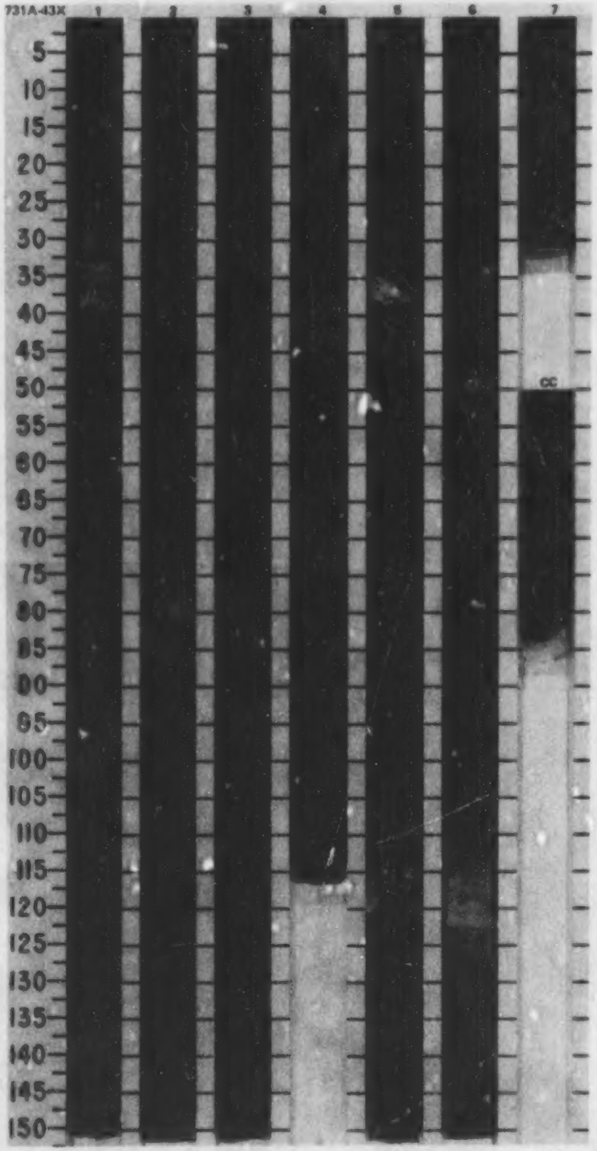
731A-43X
1
2
3
4
5
6
7
CC
5
10
15
20
25
30
35
40
45
50
55
60
65
70
75
80
85
90
95
100
105
110
115
120
125
130
135
140
145
150

SITE 731 HOLE B CORE 1X CORED INTERVAL 2774.5-2784.2 mbsl; 408.7-418.4 mbsf

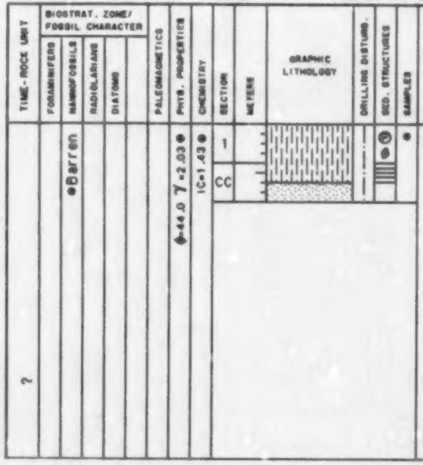
TIME-ROCK UNIT
BIOSTRAT. ZONE/ FOSSIL CHARACTER
FORAMINIFERS
NANNOFOSSILS
RADIOLARIANS
DIATOMS
PALEOMAGNETICS
PHYS. PROPERTIES
CHEMISTRY
SECTION
METERS
GRAPHIC LITHOLOGY
DRILLING DISTURB.
SED. STRUCTURES
SAMPLES
?
●Barren
ϕ=44.0 γ=2.03 ●
IC=1.43 ●
1
CC

LITHOLOGIC DESCRIPTION

CLAYEY SILTSTONE and SANDSTONE

Entire core is moderately disturbed and fractured.

Major lithologies:
- a. CLAYEY SILTSTONE, very dark grayish brown (10YR 3/2) to very dark gray (5Y 3/1). Authigenic pyrite lenses at Section 1, 25 and 28 cm. Charcoal at Section 1, 37 cm. Parallel laminated in CC, 0-20 cm.
- b. SANDSTONE, very dark gray (5Y 3/1), structureless.

SMEAR SLIDE SUMMARY

	1, 25 D
TEXTURE:	
Sand	10
Silt	50
Clay	40
COMPOSITION:	
Access. minerals	10
Clay	30
Inorganic calcite	30
Quartz	30

SITE 731 HOLE B CORE 2X CORED INTERVAL 2784.2-2793.9 mbsl; 418.4-428.1 mbsf

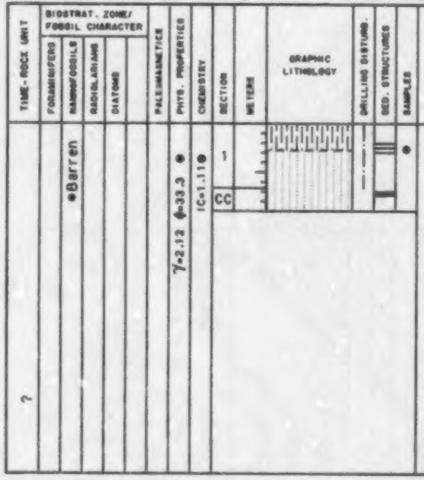
TIME-ROCK UNIT
BIOSTRAT. ZONE/ FOSSIL CHARACTER
FORAMINIFERS
NANNOFOSSILS
RADIOLARIANS
DIATOMS
PALEOMAGNETICS
PHYS. PROPERTIES
CHEMISTRY
SECTION
METERS
GRAPHIC LITHOLOGY
DRILLING DISTURB.
SED. STRUCTURES
SAMPLES
?
●Barren
γ=2.12 ϕ=33.3 ●
IC=1.11 ●
1
CC

LITHOLOGIC DESCRIPTION

CLAYEY SILTSTONE and CLAYEY SANDSTONE

Entire core is moderately disturbed and fractured.

Major lithologies:
- a. CLAYEY SILTSTONE, dark gray (5Y 4/1). Parallel laminations at Section 1, 20-27 cm, and ripple cross-laminations at CC, 5-8 cm. Section 1, 0-27 and 62-64 cm, and CC, 0-8 cm.
- b. CLAYEY SANDSTONE, dark gray (5Y 4/1). Parallel laminations at Section 1, 27-30 cm.

SMEAR SLIDE SUMMARY (%):

	1, 30 D
TEXTURE:	
Sand	60
Silt	20
Clay	20
COMPOSITION:	
Clay	20
Inorganic glass	15
Quartz	50
Feldspar	5
Accessory minerals	10

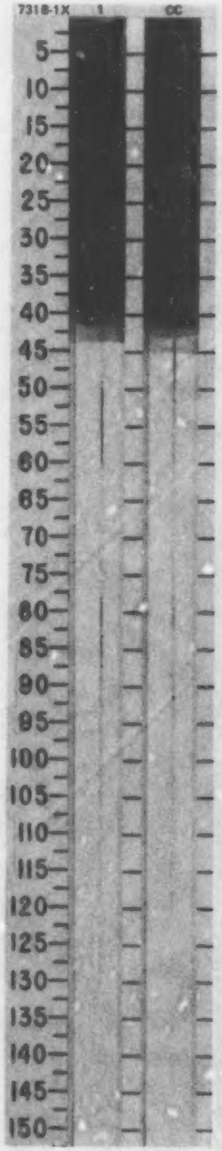
731B-1X
1
CC
5
10
15
20
25
30
35
40
45
50
55
60
65
70
75
80
85
90
95
100
105
110
115
120
125
130
135
140
145
150

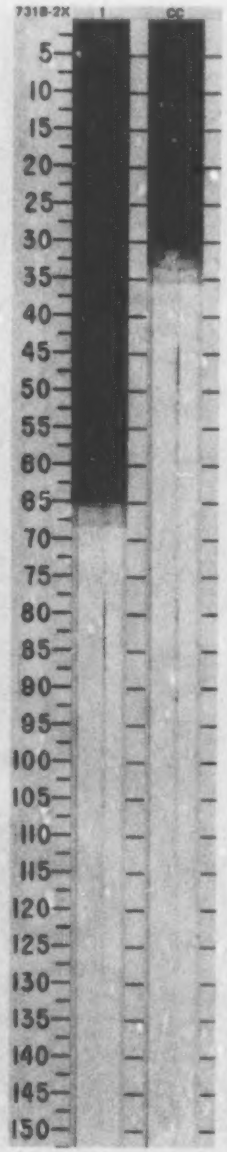
731B-2X
1
CC
5
10
15
20
25
30
35
40
45
50
55
60
65
70
75
80
85
90
95
100
105
110
115
120
125
130
135
140
145
150

SITE 731 HOLE B CORE 3X CORED INTERVAL 2793.9-2803.5 mbsl; 428.1-437.7 mbsf

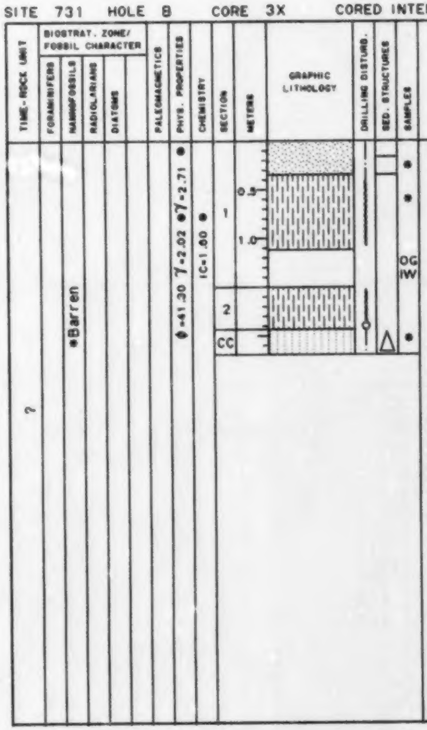
TIME-ROCK UNIT
BIOSTRAT. ZONE/ FOSSIL CHARACTER
FORAMINIFERS
NANNOFOSSILS
RADIOLARIANS
DIATOMS
PALEOMAGNETICS
PHYS. PROPERTIES
CHEMISTRY
SECTION
METERS
GRAPHIC LITHOLOGY
DRILLING DISTURB.
SED. STRUCTURES
SAMPLES
?
●Barren
ϕ=41.30 γ=2.02 ●γ=2.71 ●
IC=1.00 ●
1
2
CC
0.5
1.0
OG
IW

LITHOLOGIC DESCRIPTION

SANDSTONE, SILTY CLAYSTONE, and CLAYEY SANDSTONE

Entire core is moderately to highly disturbed and fractured.

Major lithologies:
- a. SANDSTONE, dark gray (5Y 4/1). Medium-grained and ungraded. Cemented at Section 1, 0-18 cm.
- b. SILTY CLAYSTONE, dark gray (5Y 4/1), ungraded.
- c. CLAYEY SANDSTONE, dark gray (5Y 4/1), micaceous. Forms an upward-fining sequence, in CC.

SMEAR SLIDE SUMMARY (%):

	1, 29 D	1, 60 D	CC, 10 D
TEXTURE:			
Sand	70	—	70
Silt	20	40	10
Clay	10	60	20
COMPOSITION:			
Accessory minerals	10	—	10
Quartz	60	25	60
Feldspar	5	—	5
Mica	5	—	20
Clay	10	60	20
Inorganic minerals	10	—	10

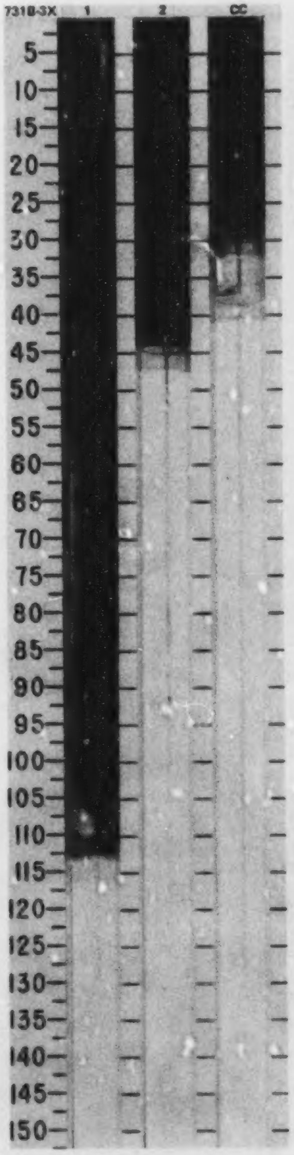
731B-3X
1
2
CC
5
10
15
20
25
30
35
40
45
50
55
60
65
70
75
80
85
90
95
100
105
110
115
120
125
130
135
140
145
150

SITE 731 HOLE B CORE 4X CORED INTERVAL 2803.5-2813.2 mbsl; 427.7-447.4 mbsf

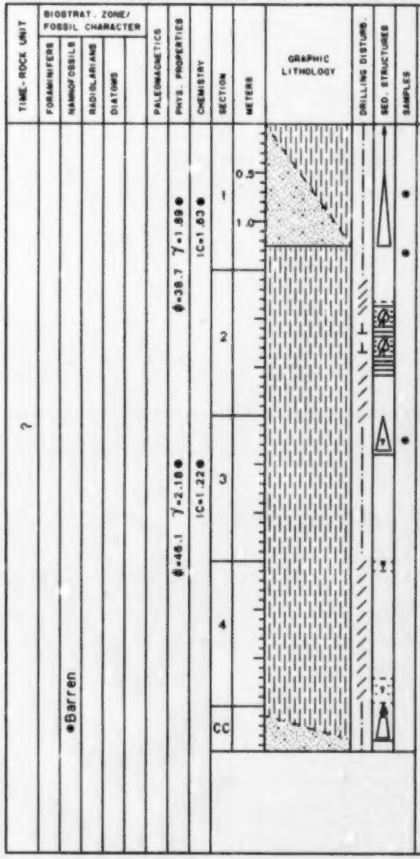
TIME-ROCK UNIT
BIOSTRAT. ZONE/ FOSSIL CHARACTER
FORAMINIFERS
NANNOFOSSILS
RADIOLARIANS
DIATOMS
PALEOMAGNETICS
PHYS. PROPERTIES
CHEMISTRY
SECTION
METERS
GRAPHIC LITHOLOGY
DRILLING DISTURB.
SED. STRUCTURES
SAMPLES
?
●Barren
φ=38.7 γ=1.89●
φ=46.1 γ=2.18●
IC=1.63●
IC=1.22●
1
2
3
4
CC
0.5
1.0

LITHOLOGIC DESCRIPTION

SILTY CLAYSTONE and CLAYEY SILTSTONE, and gradationally interbedded SILTY SANDSTONE to SILTY CLAYSTONE

Entire core is slightly to moderately disturbed and fractured.

Major lithologies:
a. SILTY CLAYSTONE and CLAYEY SILTSTONE, dark gray (5Y 4/1) to dark grayish brown (10YR 4/2). Parallel laminations at Section 2, 30-103 cm, and Section 4, 0-10 and 129-150 cm. Possible minor upward-fining interval at Section 3, 0-39 cm. Plant and charcoal debris concentrated at Section 2, 54-55 and 83 cm.
b. SILTY SANDSTONE to SILTY CLAYSTONE, dark gray (5Y 4/1), gradationally interbedded to form upward-fining sequences.

SMEAR SLIDE SUMMARY (%):

	1, 74 D	1, 140 D	3, 29 D
TEXTURE:			
Sand	30	60	5
Silt	55	25	45
Clay	15	15	45
COMPOSITION:			
Quartz	35	60	30
Feldspar	3	5	3
Mica	—	5	2
Clay	15	15	45
Inorganic glass	45	5	15
Accessory minerals	2	10	5

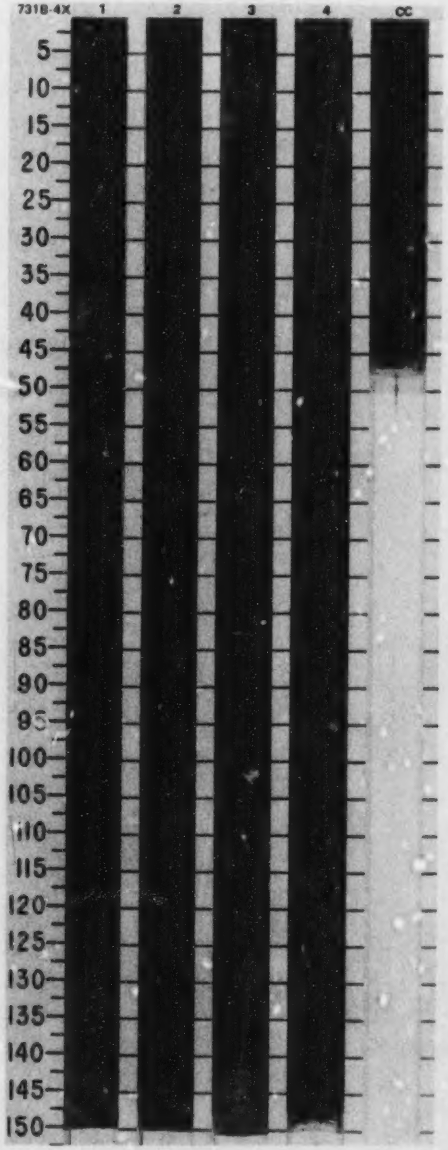
731B-4X
1
2
3
4
CC
5
10
15
20
25
30
35
40
45
50
55
60
65
70
75
80
85
90
95
100
105
110
115
120
125
130
135
140
145
150

SITE 731 HOLE B CORE 5X CORED INTERVAL 2813.2-2822.9 mbsl; 447.4-457.1 mbsf

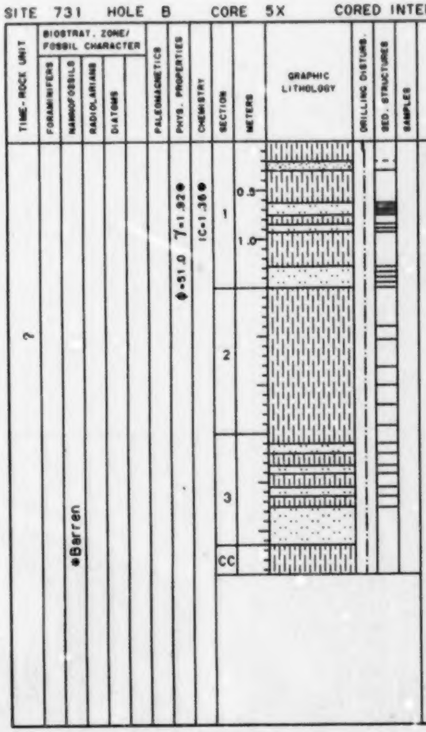
TIME-ROCK UNIT
BIOSTRAT. ZONE/ FOSSIL CHARACTER
FORAMINIFERS
NANNOFOSSILS
RADIOLARIANS
DIATOMS
PALEOMAGNETICS
PHYS. PROPERTIES
CHEMISTRY
SECTION
METERS
GRAPHIC LITHOLOGY
DRILLING DISTURB.
SED. STRUCTURES
SAMPLES
?
●Barren
φ=51.0 γ=1.92●
IC=1.36●
1
2
3
CC
0.5
1.0

LITHOLOGIC DESCRIPTION

SILTY CLAYSTONE and SILTSTONE

Entire core is moderately disturbed and fractured.

Major lithologies:
- a. SILTY CLAYSTONE, dark gray (10YR 4/1) to very dark grayish brown (10YR 3/2), and homogenous.
- b. SILTSTONE, dark gray (10YR 4/1) to very dark grayish brown (10YR 3/2), generally forming beds < 10 cm thick, with mm-scale parallel lamination.

Minor lithology: Sandstone, dark gray (10YR 4/1), with sharp base and gradational upper contact, in Section 1, 10-18 cm.

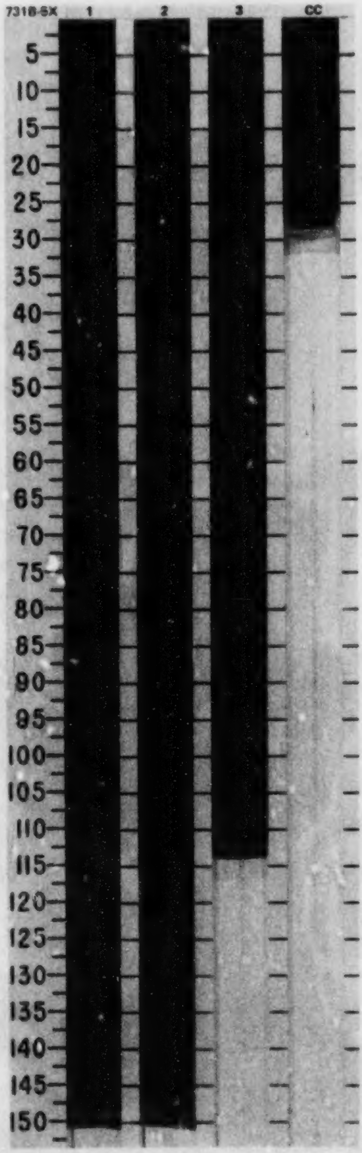
731B-5X
1
2
3
CC
5
10
15
20
25
30
35
40
45
50
55
60
65
70
75
80
85
90
95
100
105
110
115
120
125
130
135
140
145
150

SITE 731 HOLE C CORE 1W CORED INTERVAL 2717.5-2868.2 mbsl; 351.7-502.4 mbsf

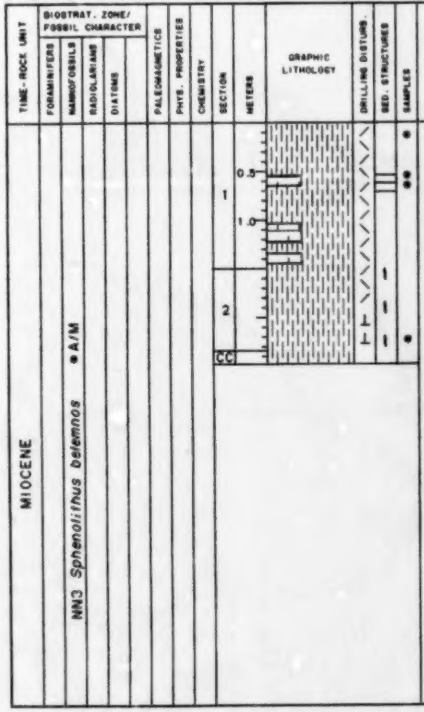
TIME-ROCK UNIT
BIOSTRAT. ZONE/ FOSSIL CHARACTER
FORAMINIFERS
NANNOFOSSILS
RADIOLARIANS
DIATOMS
PALEOMAGNETICS
PHYS. PROPERTIES
CHEMISTRY
SECTION
METERS
GRAPHIC LITHOLOGY
DRILLING DISTURB.
SED. STRUCTURES
SAMPLES
MIOCENE
NN3 Sphenolithus belemnos
● A/M
0.5
1
1.0
2
CC

LITHOLOGIC DESCRIPTION

CLAYSTONE to NANNOFOSSIL-BEARING CALCITIC SILTY CLAYSTONE

Entire core is moderately fractured and highly disturbed (wash core).

Major lithology: CLAYSTONE to NANNOFOSSIL-BEARING CALCITIC SILTY CLAYSTONE, olive (5Y 4/3, 5/3), olive gray (5Y 5/2), gray (5Y 5/1), greenish gray (5GY 5/1), dark brown (10YR 3/3), and very dark grayish brown (10YR 3/2). Uniform.

Minor lithology: Marly nannofossil chalk, gray (5Y 6/1), bioturbated. Section 1, 54-64 cm, and Section 2, 6-22 and 38-47 cm.

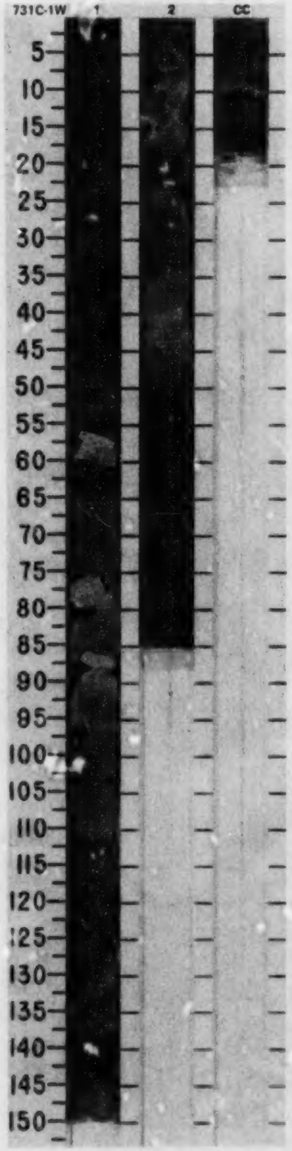
731C-1W
1
2
CC
5
10
15
20
25
30
35
40
45
50
55
60
65
70
75
80
85
90
95
100
105
110
115
120
125
130
135
140
145
150

SITE 731 HOLE C CORE 2R CORED INTERVAL 2868.2-2877.9 mbsl; 502.4-512.1 mbsf

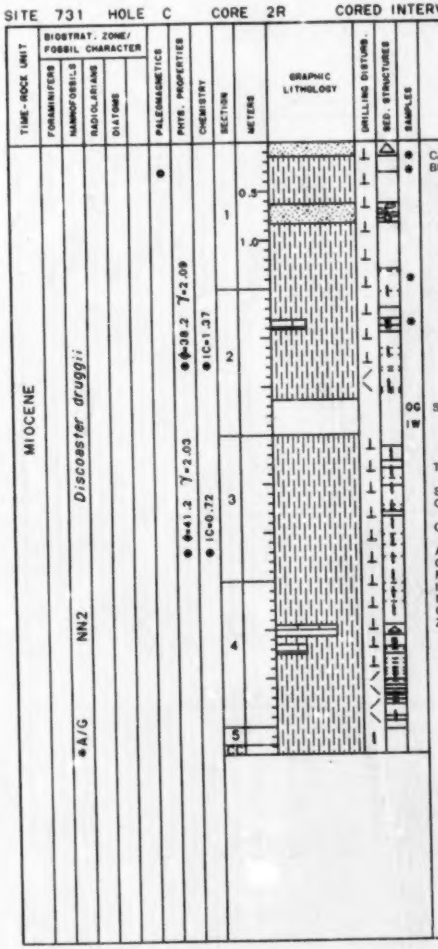
TIME-ROCK UNIT
BIOSTRAT. ZONE/ FOSSIL CHARACTER
FORAMINIFERS
NANNOFOSSILS
RADIOLARIANS
DIATOMS
PALEOMAGNETICS
PHYS. PROPERTIES
CHEMISTRY
SECTION
METERS
GRAPHIC LITHOLOGY
DRILLING DISTURB.
SED. STRUCTURES
SAMPLES
MIOCENE
Discoaster druggii
NN2
*A/G
●φ=38.2 γ=2.09
●IC=1.37
●φ=41.2 γ=2.03
●IC=0.72
1
2
3
4
5
CC
0.5
1.0
OG
IW

LITHOLOGIC DESCRIPTION

CALCITIC SILTY CLAYSTONE and CLAYEY SILTSTONE to NANNOFOSSIL-BEARING SILTY CLAYSTONE

Entire core is moderately to highly disturbed and fracturnd.

Major lithology: CALCITIC SILTY CLAYSTONE and CLAYEY SILTSTONE to NANNOFOSSIL-BEARING SILTY CLAYSTONE, gray (5YR 5/1), olive gray (5Y 4/2), and reddish gray (5YR 5/2), to dark gray (5Y 4/1), dark greenish gray (10Y 5/1, 5GY 4/1), and dark grayish brown. Clayey siltstone contains diffuse parallel laminations; silty claystone is homogenous or bioturbated.

Minor lithologies:

a. SILTY SANDSTONE to SANDY SILTSTONE, very dark gray (5Y 4/1), in Section 1, 0-16 and 65-90 cm. Forms sharp-based upward-fining sequences, with lenticular bedding at Section 1, 83-87 cm.
b. MARLY NANNOFOSSIL CHALK to NANNOFOSSIL CHALK, light gray (5Y 7/1, 6/1), light greenish gray (5G 7/1, 10Y 6/1), and greenish gray (5G 6/1). Forms two non-bioturbated, sharp-based upward-fining sequences at Section 4, 48-57 cm; other occurrences are moderately bioturbated. Section 2, 34-40 cm; and Section 4, 48-57, 68-74, 122-125, and 141-143 cm.

SMEAR SLIDE SUMMARY (%):

	1, 16 D	1, 57 D	1, 66 D	2, 76 D
TEXTURE:				
Silt	5	—	20	45
Clay	95	100	80	55
COMPOSITION:				
Access. minerals	Tr	—	1	2
Clay	90	60	74	50
Fish remains	Tr	—	—	—
Inorganic calcite	3	Tr	7	15
Nannofossils	3	40	6	3
Quartz	3	—	12	30
Zeolites	1	Tr	—	—

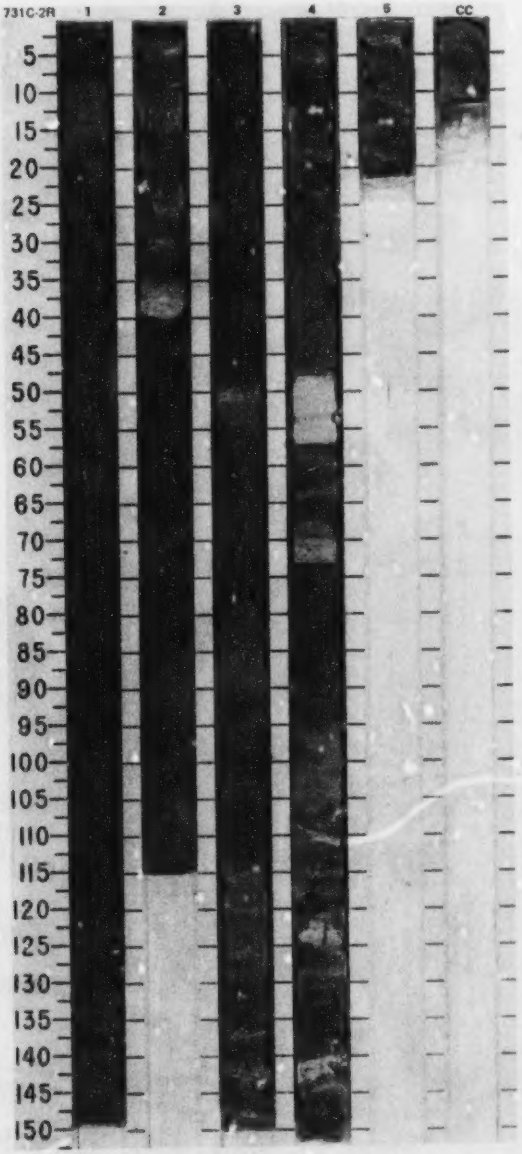
731C-2R
1
2
3
4
5
CC
5
10
15
20
25
30
35
40
45
50
55
60
65
70
75
80
85
90
95
100
105
110
115
120
125
130
135
140
145
150

SITE 731 HOLE C CORE 3W CORED INTERVAL 2877.9-2926.0 mbsl; 512.1-560.2 mbsf

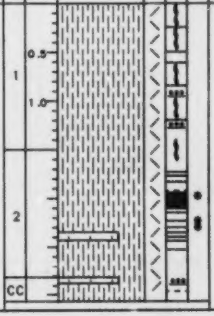

TIME-ROCK UNIT	BIOSTRAT. ZONE/ FOSSIL CHARACTER: FORAMINIFERS	NANNOFOSSILS	RADIOLARIANS	DIATOMS	PALEOMAGNETICS	PHYS. PROPERTIES	CHEMISTRY	SECTION	METERS	GRAPHIC LITHOLOGY	DRILLING DISTURB.	SED. STRUCTURES	SAMPLES	LITHOLOGIC DESCRIPTION
MIOCENE		•A/M •A/P NN2 *Dicoaster druggii*						1 2 CC	0.5 1.0					CALCITIC SILTY CLAYSTONE and CLAYEY SILTSTONE to NANNOFOSSIL-RICH CALCITIC SILTY CLAYSTONE Entire core is highly fractured and highly disturbed (wash core). Major lithology: CALCITIC SILTY CLAYSTONE and CLAYEY SILTSTONE to NANNOFOSSIL-RICH CALCITIC SILTY CLAYSTONE, olive (5Y 4/3), olive gray (5Y 5/2, 4/2), greenish gray (5G 5/1, 5BG 5/1, 5B 5/1), and reddish brown (5YR 4/3), to dark gray (5YR 4/1, 5Y 4/1), dark greenish gray (5BG 4/1), dark brown (10YR 4/3), dark grayish brown (10YR 4/2), and dark redrish brown (5YR 3/2). Predominantly homogenous, but locally bioturbated or parallel laminated. Minor lithology: Nannofossil chalk to foraminifer- nannofossil chalk, light greenish gray (5BG 7/1), greenish gray (5BG 6/1), and light olive gray (5Y 6/2). Generally forms sharp-based upward-fining sequences, in Section 1, 100 and 126 cm, Section 2, 60-64, 77-81, and 85-91 cm, and CC, 0-5 cm.

SITE 731 HOLE C CORE 4R CORED INTERVAL 2926.0-2935.7 mbsl; 560.2-569.9 mbsf

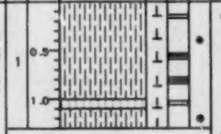

TIME-ROCK UNIT	BIOSTRAT. ZONE/ FOSSIL CHARACTER: FORAMINIFERS	NANNOFOSSILS	RADIOLARIANS	DIATOMS	PALEOMAGNETICS	PHYS. PROPERTIES	CHEMISTRY	SECTION	METERS	GRAPHIC LITHOLOGY	DRILLING DISTURB.	SED. STRUCTURES	SAMPLES	LITHOLOGIC DESCRIPTION
?		●Barren			●	ϕ=38.9 γ=2.12 ●	IC=1.36 ●	1	0.5 1.0					CALCITIC SILTY CLAYSTONE and CALCITIC CLAYEY SILTSTONE Core is moderately disturbed and fractured. Major lithology: CALCITIC SILTY CLAYSTONE and CALCITIC CLAYEY SILTSTONE, dark gray (N4, 5Y 4/1), with parallel laminations in clayey siltstone at Section 1, 15-16, 60-63, 78-82, and 127-129 cm. Homogenous elsewhere. Minor lithology: Clayey sandstone, dark gray (5Y 4/1), with charcoal.

SMEAR SLIDE SUMMARY (%):

	1, 40 D	1, 116 M
TEXTURE:		
Sand	—	50
Silt	20	20
Clay	80	30
COMPOSITION:		
Access. minerals	—	2
Clay	49	21
Feldspar	Tr	5
Inorganic calcite	30	10
Mica	—	2
Nannofossils	1	—
Quartz	20	50
Quartz	50	
Rock fragments	—	10

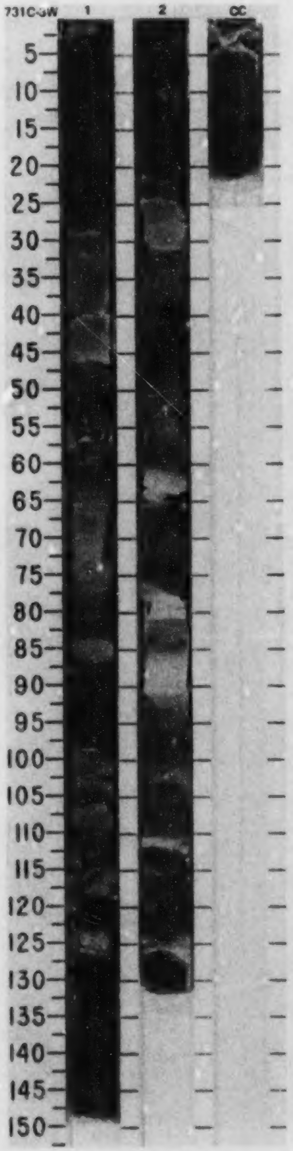

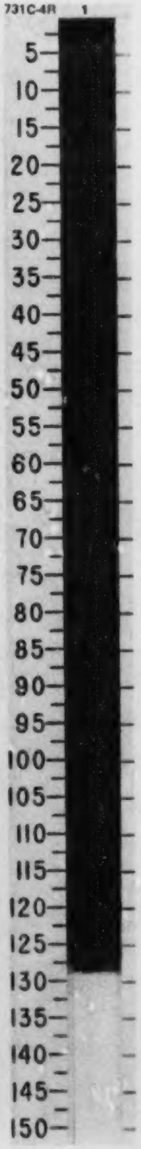

SITE 731 HOLE C CORE 5W CORED INTERVAL 2935.7-2983.9 mbsl; 569.9-618.1 mbsf

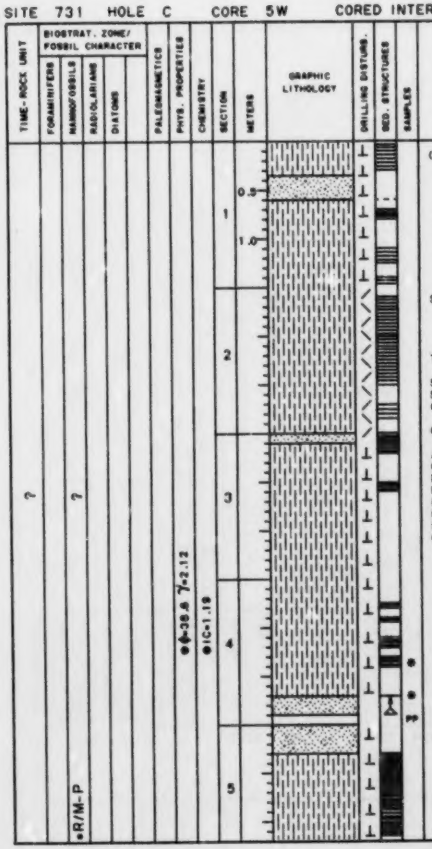
TIME-ROCK UNIT
BIOSTRAT. ZONE/ FOSSIL CHARACTER
FORAMINIFERS
NANNOFOSSILS
RADIOLARIANS
DIATOMS
PALEOMAGNETICS
PHYS. PROPERTIES
CHEMISTRY
SECTION
METERS
GRAPHIC LITHOLOGY
DRILLING DISTURB.
SED. STRUCTURES
SAMPLES
?
?
•R/M-P
•ϕ=38.6 γ=2.12
•IC=1.19
1
2
3
4
5
0.5
1.0
*
*
PP

LITHOLOGIC DESCRIPTION

CLAYSTONE to CLAYEY SILTSTONE, and SILTSTONE to SANDSTONE

Entire core is moderately fractured and highly disturbed (wash core).

Major lithologies:
- a. CLAYSTONE to CLAYEY SILTSTONE, dark gray (10YR 4/1, N4/) with interbedded homogenous (claystone to silty claystone) and parallel laminated (clayey siltstone) intervals.
- b. SILTSTONE to SANDSTONE, dark gray (10YR 4/1, 5Y 4/1) and black (10YR 2/1). Forms upward-fining sequence at Section 4, 120-140 cm. Contains charcoal at Section 1, 23-25 cm, and Section 5, 0-30 cm.

SMEAR SLIDE SUMMARY (%):

	4, 90 D	4, 126 M
TEXTURE:		
Sand	—	5
Silt	15	90
Clay	85	5
COMPOSITION:		
Access. minerals	5	7
Clay	85	5
Dolomite	—	3
Feldspar	—	5
Inorganic calcite	5	20
Mica	—	5
Nannofossils	Tr	—
Quartz	5	55

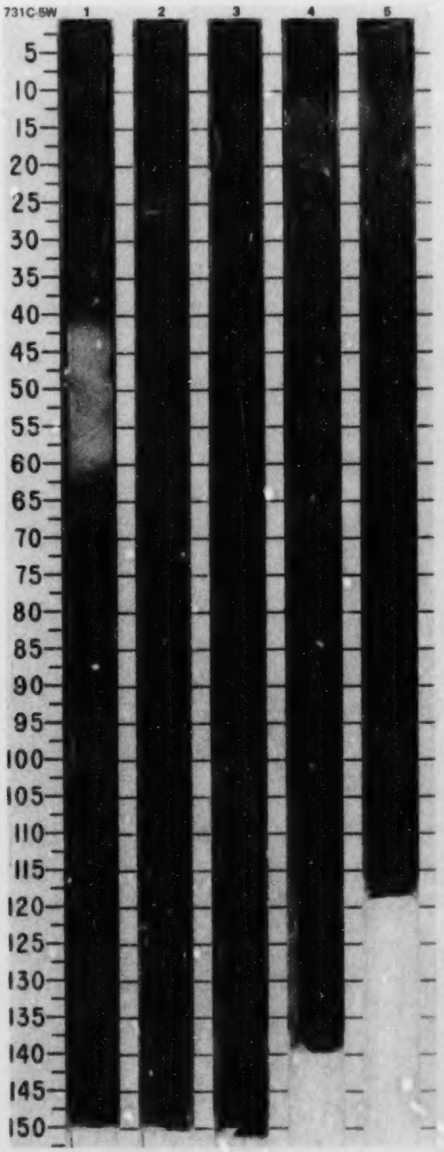
731C-5W
1
2
3
4
5
5
10
15
20
25
30
35
40
45
50
55
60
65
70
75
80
85
90
95
100
105
110
115
120
125
130
135
140
145
150

SITE 731 HOLE C CORE 6R CORED INTERVAL 2983.9-2993.6 mbsl; 618.1-627.8 mbsf

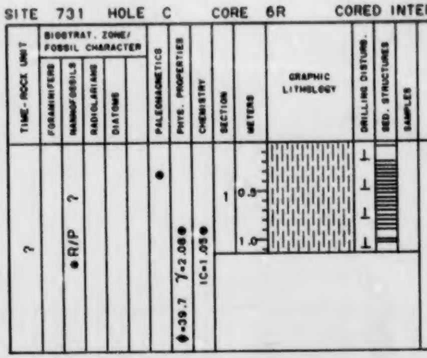
TIME-ROCK UNIT
BIOSTRAT. ZONE/ FOSSIL CHARACTER
FORAMINIFERS
NANNOFOSSILS
RADIOLARIANS
DIATOMS
PALEOMAGNETICS
PHYS. PROPERTIES
CHEMISTRY
SECTION
METERS
GRAPHIC LITHOLOGY
DRILLING DISTURB.
SED. STRUCTURES
SAMPLES
?
●R/P ?
ϕ=39.7 γ=2.08●
IC=1.05●
1
0.5
1.0

LITHOLOGIC DESCRIPTION

CLAYSTONE to CLAYEY SILTSTONE

Entire core is moderately disturbed and fractured.

Major lithology: CLAYSTONE to CLAYEY SILTSTONE, dark gray (10YR 4/1). Faint parallel laminations common.

SITE 731 HOLE C CORE 7W CORED INTERVAL 2993.6-3041.7 mbsl; 627.8-675.9 mbsf

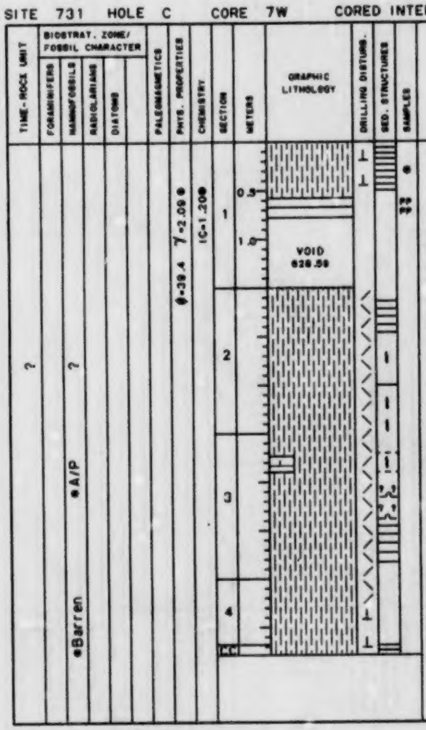
TIME-ROCK UNIT
BIOSTRAT. ZONE/ FOSSIL CHARACTER
FORAMINIFERS
NANNOFOSSILS
RADIOLARIANS
DIATOMS
PALEOMAGNETICS
PHYS. PROPERTIES
CHEMISTRY
SECTION
METERS
GRAPHIC LITHOLOGY
DRILLING DISTURB.
SED. STRUCTURES
SAMPLES
?
?
●A/P
●Barren
ϕ=39.4 γ=2.09●
IC=1.20●
1
2
3
4
CC
0.5
1.0
VOID 628.59
PP
PP

LITHOLOGIC DESCRIPTION

CLAYSTONE to CLAYEY SILTSTONE

Entire core is moderately to highly fractured and highly disturbed (wash core).

Major lithology: CLAYSTONE to CLAYEY SILTSTONE, dark gray (10YR 4/1) to dark greenish gray (5G 4/1). Claystone intervals are homogenous to bioturbated; clayey siltstone intervals contain parallel laminations. Folded 1-cm-thick sandstone laminae at Section 3, 40-75 cm, is possible slump deposit.

Minor lithology: Clayey siltstone to marly calcareous chalk, greenish gray (5G 6/1). Parallel laminations present to common, bioturbated with Zoophycos. Section 3, 25-40 cm.

SMEAR SLIDE SUMMARY (%):

	1, 30 M
TEXTURE:	
Sand	30
Silt	50
Clay	20
COMPOSITION:	
Access. minerals	10
Clay	15
Feldspar	1
Inorganic calcite	15
Mica	1
Quartz	48

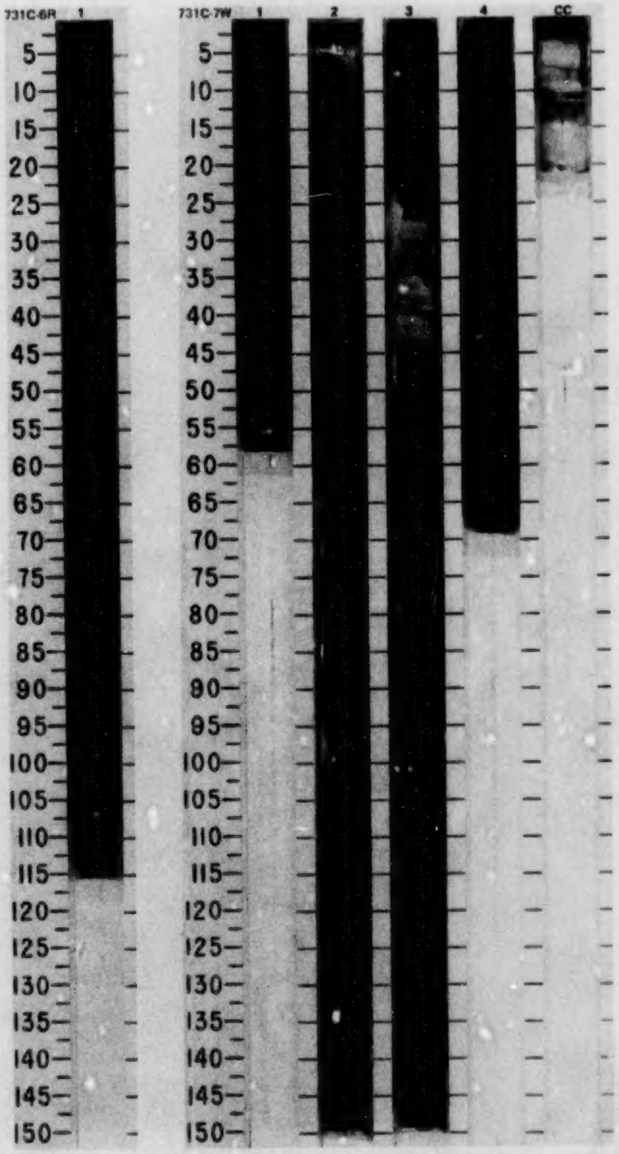
731C-6R
1
731C-7W
1
2
3
4
CC
5
10
15
20
25
30
35
40
45
50
55
60
65
70
75
80
85
90
95
100
105
110
115
120
125
130
135
140
145
150

SITE 731 HOLE C CORE 8R CORED INTERVAL 3041.7-3051.4 mbsl; 675.9-685.6 mbsf

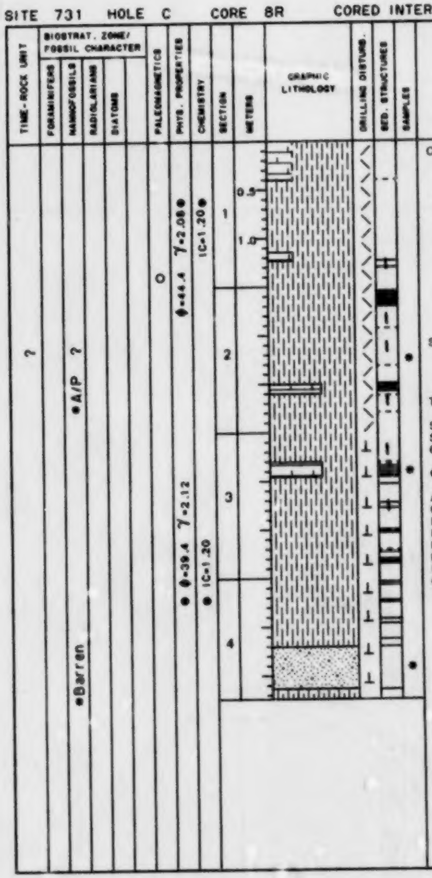
TIME-ROCK UNIT
BIOSTRAT. ZONE/ FOSSIL CHARACTER
FORAMINIFERS
NANNOFOSSILS
RADIOLARIANS
DIATOMS
PALEOMAGNETICS
PHYS. PROPERTIES
CHEMISTRY
SECTION
METERS
GRAPHIC LITHOLOGY
DRILLING DISTURB.
SED. STRUCTURES
SAMPLES
?
●A/P ?
●Barren
○
ϕ=44.4 γ=2.08●
IC=1.20●
● ϕ=39.4 γ=2.12
● IC=1.20
1
2
3
4
0.5
1.0

LITHOLOGIC DESCRIPTION

CLAYSTONE to CLAYEY SILTSTONE

Entire core is moderately to highly disturbed and fractured.

Major lithology: CLAYSTONE to SILTY CLAYSTONE, dark gray (10YR 4/1, N4), dark brown (10YR 4/3, 3/3), dark grayish brown (10YR 3/2), and dark greenish gray (5BG 4/1, 5GY 4/1, 5B 4/1). Claystone and silty claystone are homogenous or bioturbated; clayey siltstone is parallel laminated.

Minor lithologies:
a. Calcareous siltstone to marly calcareous chalk, greenish gray (5BG 5/1, 6/1; 5G 5/1). Bioturbated at Section 1, 126-133 cm, and Section 3, 32-36 cm. Parallel laminated and cross laminated at Section 2, 100-105 cm, and Section 3, 36-48 cm.
b. Sandy siltstone, dark gray (N4), in Section 4, 70-118 cm.

SMEAR SLIDE SUMMARY (%):

	2, 80 M	3, 45 M	4, 95 M
TEXTURE:			
Sand	—	—	10
Silt	2	40	30
Clay	98	60	60
COMPOSITION:			
Access. minerals	—	Tr	5
Clay	90	30	30
Dolomite	Tr	Tr	—
Foraminifers	—	15	—
Inorganic calcite	5	40	30
Mica	—	—	5
Nannofossils	—	15	—
Quartz	5	Tr	30

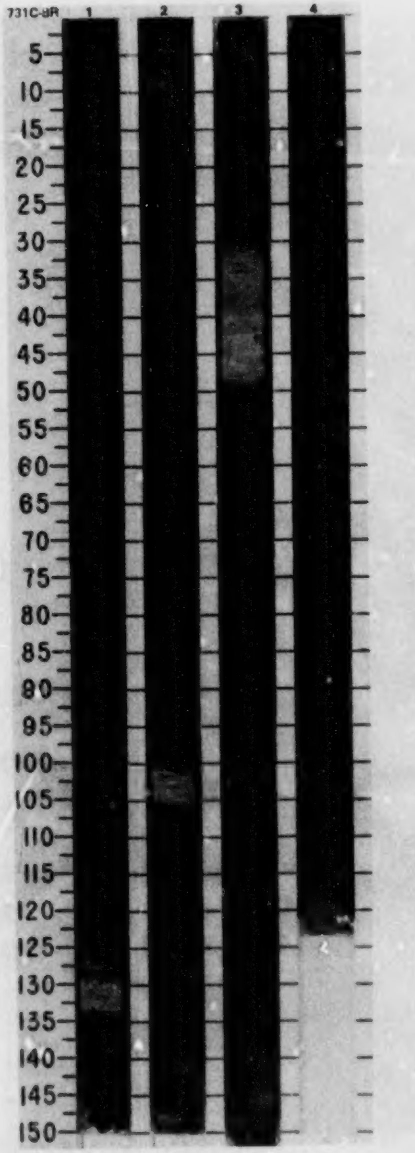
731C-8R
1
2
3
4
5
10
15
20
25
30
35
40
45
50
55
60
65
70
75
80
85
90
95
100
105
110
115
120
125
130
135
140
145
150

SITE 731 HOLE C CORE 9W CORED INTERVAL 3051.4-3099.4 mbsl; 685.6-733.6 mbsf

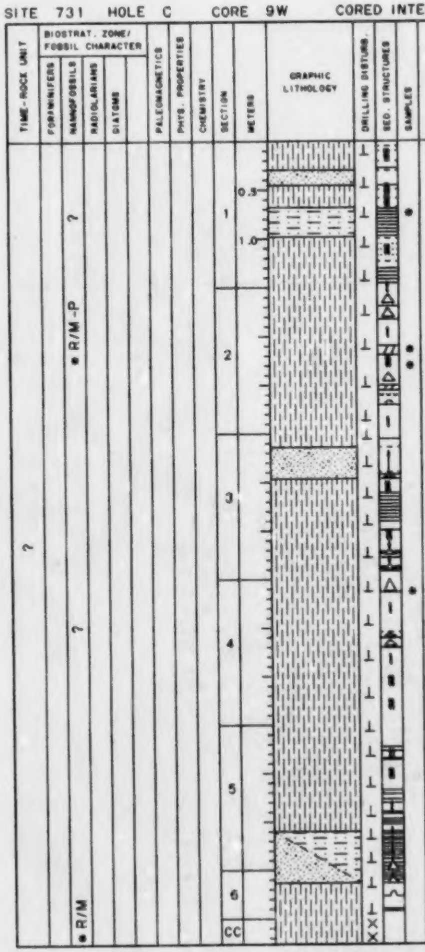
TIME-ROCK UNIT
BIOSTRAT. ZONE/ FOSSIL CHARACTER
FORAMINIFERS
NANNOFOSSILS
RADIOLARIANS
DIATOMS
PALEOMAGNETICS
PHYS. PROPERTIES
CHEMISTRY
SECTION
METERS
GRAPHIC LITHOLOGY
DRILLING DISTURB.
SED. STRUCTURES
SAMPLES
?
?
• R/M-P
?
• R/M
0.5
1.0
1
2
3
4
5
6
CC

LITHOLOGIC DESCRIPTION

CALCITIC SILTY CLAYSTONE to CLAYEY SILTSTONE, and MUDSTONE to SILTY SANDSTONE

Sections 1-6 are moderately fractured and highly disturbed (wash core). CC is drilling breccia.

Major lithologies:

a. CALCITIC SILTY CLAYSTONE to CLAYEY SILTSTONE, dark gray (N4/, 10YR 4/1). Silty claystone is homogenous or bioturbated; clayey siltstone is parallel laminated to homogenous. Generally interbedded to form upward-fining sequences 1-5 cm thick, or >10 cm thick. Ripple cross-lamination at Section 2, 66–68 and 103–105 cm; possible scour surfaces and slump folds at Section 6, 15–52 cm.

b. MUDSTONE to SILTY SANDSTONE, dark gray (N4/, 10YR 4/1). Calcite-cemented and micaceous at Section 1, 30–48 cm. Abundant charcoal and wood debris at Section 1, 68–97 cm. Upward-fining sequences, with sharp bases, at Section 3, 14–46 cm; and Section 5, 112 cm, to Section 6, 15 cm.

SMEAR SLIDE SUMMARY (%):

	1, 74 D	2, 66 D	2, 81 D	4, 13 D
TEXTURE:				
Sand	30	—	—	5
Silt	45	70	25	70
Clay	25	30	75	25
COMPOSITION:				
Access. minerals	5	—	2	3
Clay	25	30	75	25
Dolomite	—	—	—	Tr
Feldspar	5	—	—	5
Volcanic glass	5	—	—	15
Inorganic calcite	20	35	8	10
Mica	—	—	—	2
Quartz	40	35	15	40

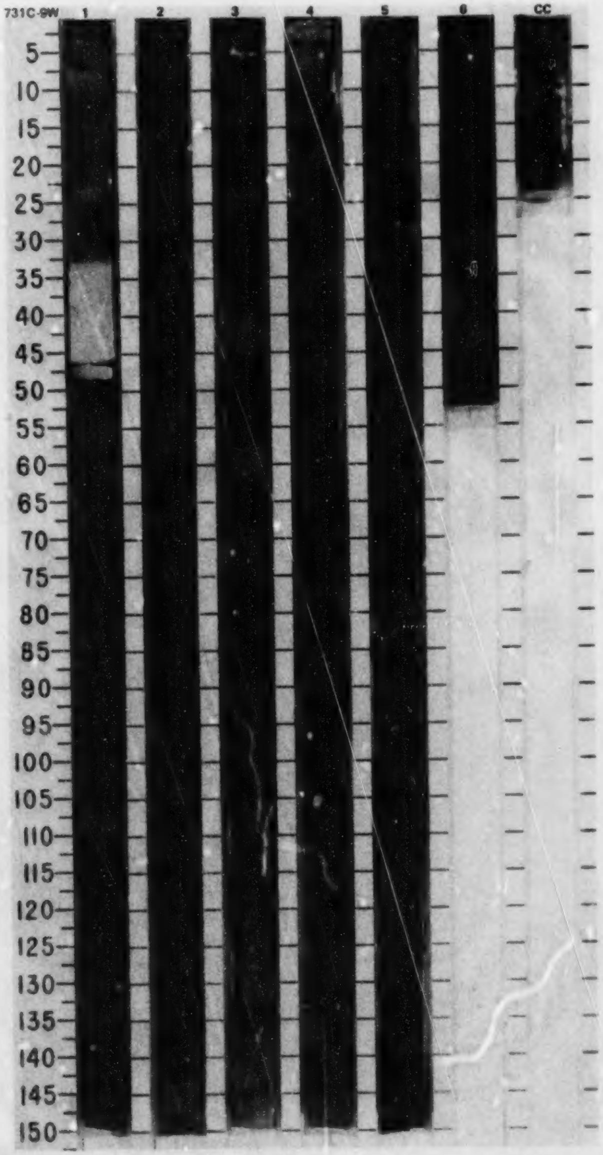
731C-9W
1
2
3
4
5
6
CC
5
10
15
20
25
30
35
40
45
50
55
60
65
70
75
80
85
90
95
100
105
110
115
120
125
130
135
140
145
150

SITE 731 HOLE C CORE 10R CORED INTERVAL 3099.4-3109.1 mbsl; 733.6-743.3 mbsf

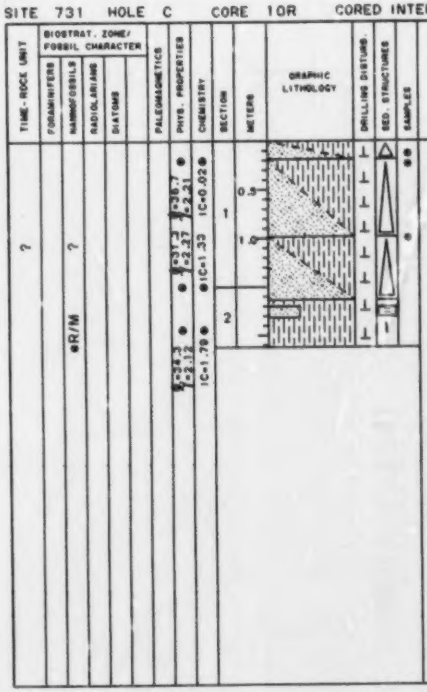
TIME-ROCK UNIT
BIOSTRAT. ZONE/ FOSSIL CHARACTER
FORAMINIFERS
NANNOFOSSILS
RADIOLARIANS
DIATOMS
PALEOMAGNETICS
PHYS. PROPERTIES
CHEMISTRY
SECTION
METERS
GRAPHIC LITHOLOGY
DRILLING DISTURB.
SED. STRUCTURES
SAMPLES
?
?
●R/M
φ=36.7
γ=2.21
φ=37.2
γ=2.27
φ=34.3
γ=2.12
IC=0.02
IC=1.33
IC=1.79
1
2
0.5
1.0

LITHOLOGIC DESCRIPTION

Gradationally interbedded SILTY SANDSTONE to SILTY CLAYSTONE

Entire core is moderately disturbed and fractured.

Major lithology: SILTY SANDSTONE to CALCITIC SILTY CLAYSTONE, dark gray (10YR 4/1), and gradationally interbedded to form upward-fining sequences 3-85 cm thick. Sharp bases, with minor parallel laminations.

Minor lithology: Silty claystone, dark gray (10YR 4/1), homogenous, in Section 2, 16-20, 23-25, and 31-62 cm.

SMEAR SLIDE SUMMARY (%):

	1, 15 D	1, 26 D	1, 100 D
TEXTURE:			
Sand	—	—	60
Silt	75	45	30
Clay	25	55	10
COMPOSITION:			
Access. minerals	5	5	5
Clay	25	55	10
Dolomite	2	—	2
Feldspar	—	—	5
Volcanic glass	3	—	8
Inorganic calcite	25	10	5
Mica	—	—	5
Quartz	40	30	60

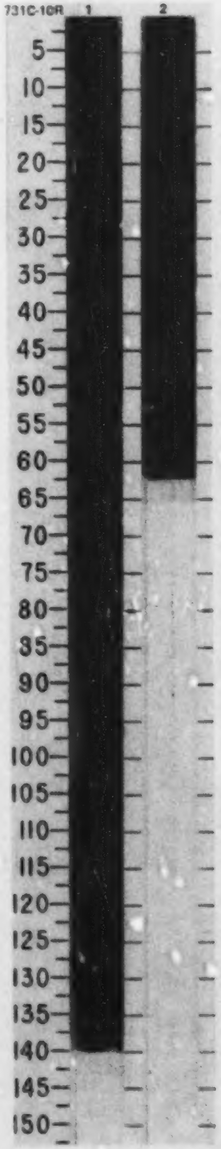
731C-10R
1
2
5
10
15
20
25
30
35
40
45
50
55
60
65
70
75
80
85
90
95
100
105
110
115
120
125
130
135
140
145
150

SITE 731 HOLE C CORE 11W CORED INTERVAL 3109.1-3157.3 mbsl; 743.3-791.5 mbsf

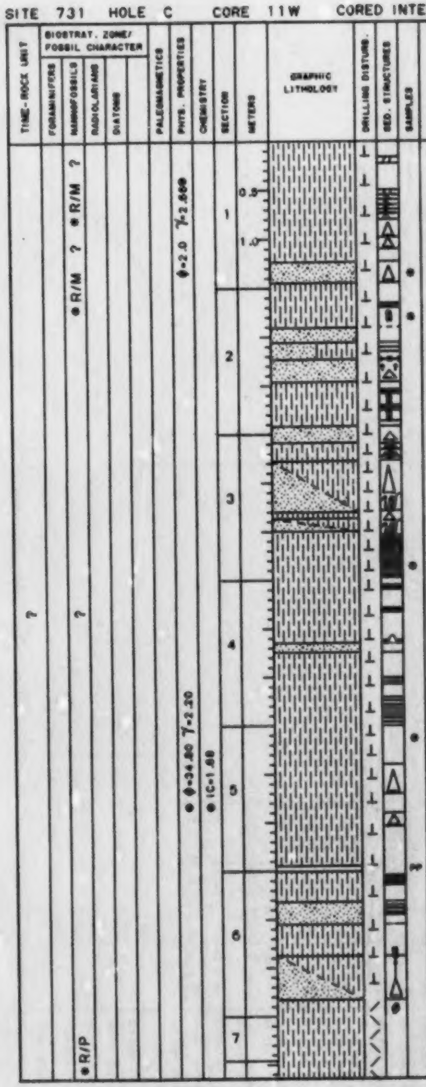
TIME-ROCK UNIT
BIOSTRAT. ZONE/ FOSSIL CHARACTER
FORAMINIFERS
NANNOFOSSILS
RADIOLARIANS
DIATOMS
PALEOMAGNETICS
PHYS. PROPERTIES
CHEMISTRY
SECTION
METERS
GRAPHIC LITHOLOGY
DRILLING DISTURB.
SED. STRUCTURES
SAMPLES
?
? ●R/M ? ●R/M ?
●R/P
ϕ=2.0 γ=2.599
● ϕ=34.80 γ=2.20
● IC=1.88
1
2
3
4
5
6
7
0.5
1.0
PP

LITHOLOGIC DESCRIPTION

CALCITIC SILTY CLAYSTONE to CLAYEY SANDSTONE, and CALCITIC SILTY SANDSTONE to SANDY/CLAYEY SILTSTONE

Entire core is moderately to highly fractured and highly disturbed (wash core).

Major lithologies:
- a. CALCITIC SILTY CLAYSTONE to CLAYEY SILTSTONE, dark gray (10YR 4/1). Silty claystone is massive or bioturbated, clayey siltstone is parallel laminated. Commonly interbedded to form repeated, sharp-based upward-fining sequences 3–7 cm thick.
- b. CALCITIC SILTY SANDSTONE to SANDY/CLAYEY SILTSTONE, dark gray (5Y 4/1), usually gradationally interbedded to form upward-fining sequences. Sharp bases, occasionally scoured. Ripple cross-laminated at Section 6, 32–47 cm.

SMEAR SLIDE SUMMARY (%):

	1, 134 D	2, 32 D	3, 139 D	5, 16 D
TEXTURE:				
Sand	50	—	35	—
Silt	30	25	45	75
Clay	20	75	20	25
COMPOSITION:				
Access. minerals	5	1	—	2
Clay	20	75	19	25
Feldspar	5	—	5	5
Volcanic glass	5	1	5	—
Inorganic calcite	10	7	10	16
Mica	5	—	1	—
Nannofossils	—	1	Tr	—
Organic debris	—	—	10	—
Quartz	50	15	50	56

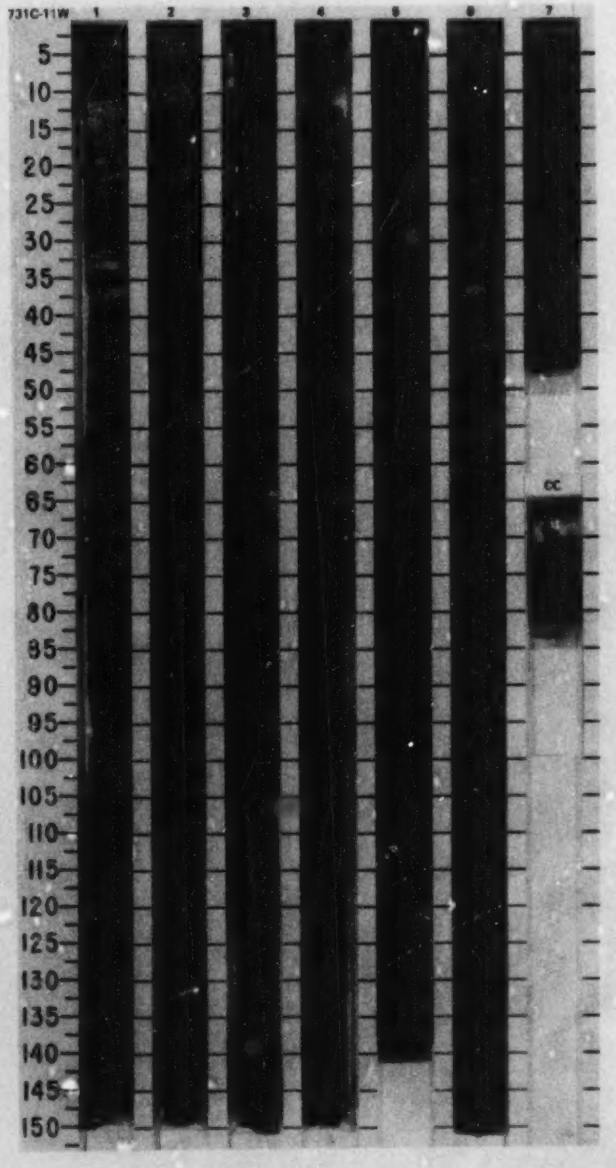
731C-11W
1
2
3
4
5
6
7
CC
5
10
15
20
25
30
35
40
45
50
55
60
65
70
75
80
85
90
95
100
105
110
115
120
125
130
135
140
145
150

SITE 731 HOLE C CORE 12R CORED INTERVAL 3157.3-3166.9 mbsl; 791.5-801.1 mbsf

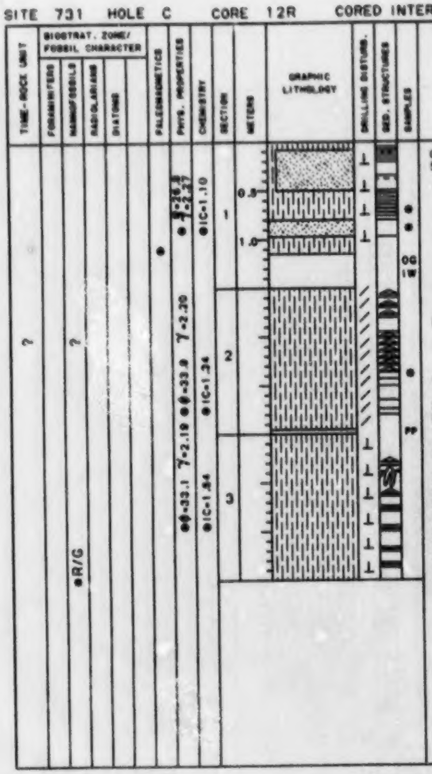
TIME-ROCK UNIT
BIOSTRAT. ZONE/ FOSSIL CHARACTER
FORAMINIFERS
NANNOFOSSILS
RADIOLARIANS
DIATOMS
PALEOMAGNETICS
PHYS. PROPERTIES
CHEMISTRY
SECTION
METERS
GRAPHIC LITHOLOGY
DRILLING DISTURB.
SED. STRUCTURES
SAMPLES
?
?
●R/G
●
● ϕ=26.8 γ=2.27
ϕ=33.1 γ=2.19 ● ϕ=33.8 γ=2.30
●IC=1.10
●IC=1.34
●IC=1.84
1
2
3
0.5
1.0
OG
IW
PP

LITHOLOGIC DESCRIPTION

CLAYEY SILTSTONE/SILTY CLAYSTONE and SILTY SANDSTONE/SANDY SILTSTONE

Entire core is slightly to moderately disturbed and fractured.

Major lithologies:
- a. CLAYEY SILTSTONE to SILTY CLAYSTONE, dark gray (10YR 4/1) to dark grayish brown (10YR 4/2). Clayey siltstone is parallel laminated, silty claystone is uniform or bioturbated. Commonly interbedded to form repeated, sharp-based upward-fining sequences 3–7 cm thick. Slump structures at Section 3, 35–39 and 50–56 cm.
- b. SILTY SANDSTONE to SANDY SILTSTONE, dark gray (10YR 4/1), without grading. Ripple cross-laminated at Section 1, 8–21 cm.

SMEAR SLIDE SUMMARY (%):

	1, 72 D	1, 89 D	2, 90 D
TEXTURE:			
Sand	5	40	—
Silt	70	35	30
Clay	25	25	70
COMPOSITION:			
Access. minerals	5	3	2
Clay	25	25	70
Dolomite	—	—	1
Feldspar	—	5	—
Volcanic glass	5	5	—
Inorganic calcite	15	5	12
Mica	—	5	—
Nannofossil	—	—	Tr
Quartz	50	50	15

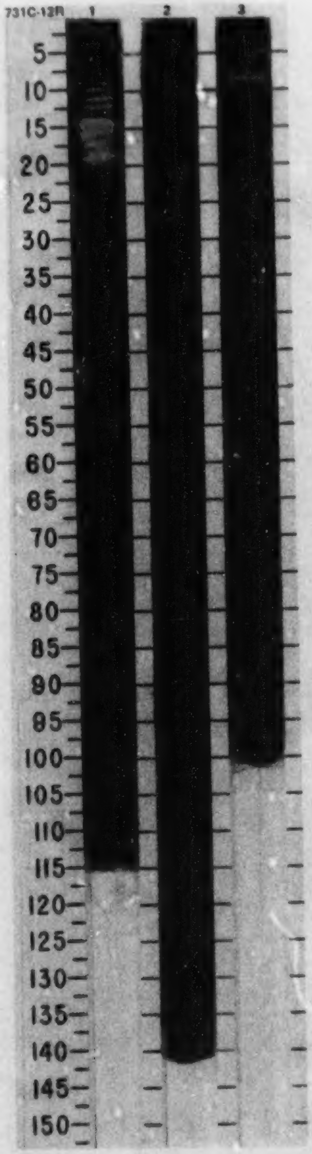
731C-12R
1
2
3
5
10
15
20
25
30
35
40
45
50
55
60
65
70
75
80
85
90
95
100
105
110
115
120
125
130
135
140
145
150

SITE 731 HOLE C CORE 13W CORED INTERVAL 3166.9-3215.2 mbsl; 801.1-849.4 mbsf

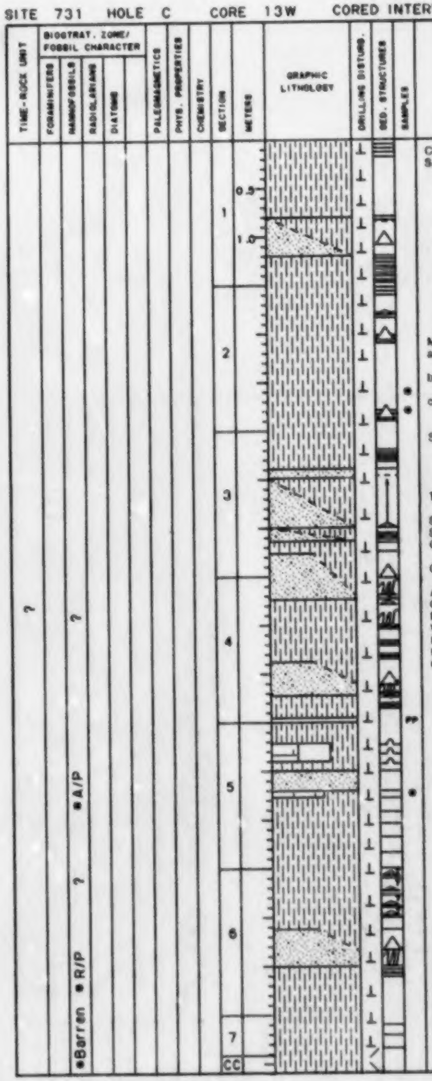
TIME-ROCK UNIT
BIOSTRAT. ZONE/ FOSSIL CHARACTER
FORAMINIFERS
NANNOFOSSILS
RADIOLARIANS
DIATOMS
PALEOMAGNETICS
PHYS. PROPERTIES
CHEMISTRY
SECTION
METERS
GRAPHIC LITHOLOGY
DRILLING DISTURB.
SED. STRUCTURES
SAMPLES
?
?
●A/P
?
●R/P
●Barren
0.5
1.0
1
2
3
4
5
6
7
CC
PP

LITHOLOGIC DESCRIPTION

CLAYEY SILTSTONE/SILTY CLAYSTONE, and gradationally interbedded SILTY SANDSTONE to CLAYEY SILTSTONE

Entire core is slightly to moderately fractured and highly disturbed (wash core).

Major lithologies:
a. CLAYEY SILTSTONE to SILTY CLAYSTONE, dark gray (10YR 4/1) to dark grayish brown (10YR 4/2). Clayey siltstone is parallel laminated; silty claystone is uniform or bioturbated. Commonly interbedded to form repeated, sharp-based upward-fining sequences 3–30 cm thick.
b. SILTY SANDSTONE to CLAYEY SILTSTONE, dark gray (10YR 4/1) to dark grayish brown (10YR 4/2), gradationally interbedded to form sharp-based upward-fining sequences 10–40 cm thick. Calcite-cemented at Section 4, 0–23 and 88–122 cm.

Minor lithologies:
a. Sandstone to silty sandstone, dark gray (10YR 4/1). Uniform, with sharp base. Section 3, 32–48 cm, and Section 5, 50–72 cm.
b. Marly nannofossil chalk, light gray (5Y 7/2) and slightly bioturbated, in Section 5, 72–76 cm.
c. Silty claystone, sandstone, and marly nannofossil chalk, dark gray (10YR 4/1) and light gray (5Y 7/2), slumped and contorted, in Section 5, 25–41 cm.

SMEAR SLIDE SUMMARY (%):

	2, 111 D	2, 132 D	5, 74 D
TEXTURE:			
Sand	5	10	—
Silt	40	70	35
Clay	55	20	65
COMPOSITION:			
Access. minerals	3	5	Tr
Clay	55	20	10
Feldspar	2	5	—
Volcanic glass	—	—	Tr
Inorganic calcite	15	15	35
Nannofossils	—	—	55
Quartz	25	55	Tr

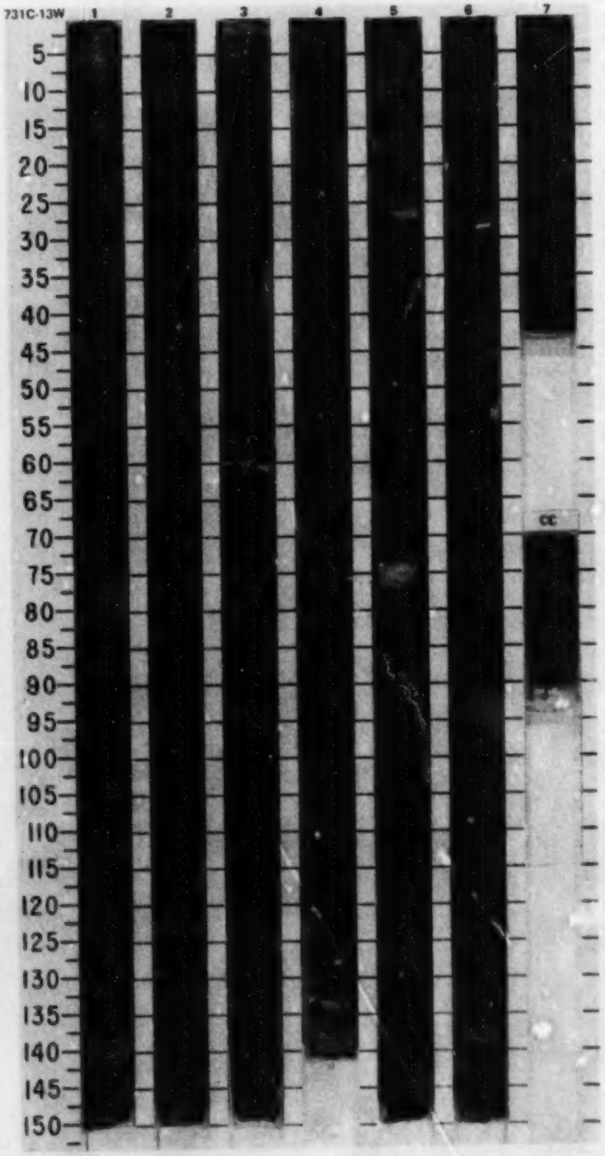
731C-13W
1
2
3
4
5
6
7
CC
5
10
15
20
25
30
35
40
45
50
55
60
65
70
75
80
85
90
95
100
105
110
115
120
125
130
135
140
145
150

SITE 731 HOLE C CORE 14R CORED INTERVAL 3215.2-3224.9 mbsl; 849.4-859.1 mbsf

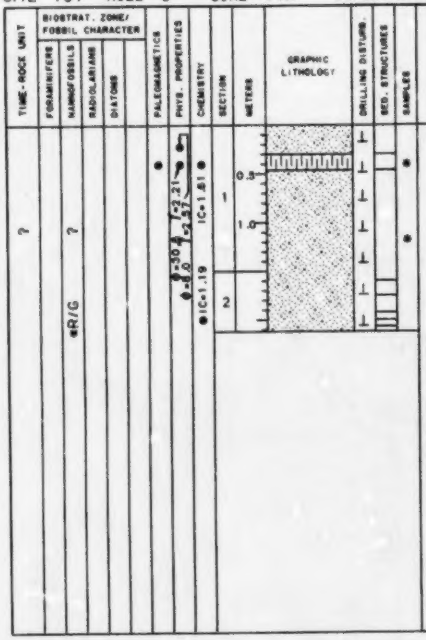
TIME-ROCK UNIT
BIOSTRAT. ZONE/ FOSSIL CHARACTER
FORAMINIFERS
NANNOFOSSILS
RADIOLARIANS
DIATOMS
PALEOMAGNETICS
PHYS. PROPERTIES
CHEMISTRY
SECTION
METERS
GRAPHIC LITHOLOGY
DRILLING DISTURB.
SED. STRUCTURES
SAMPLES
?
?
*R/G
γ=2.21
γ=2.57
φ=30.4
φ=8.0
IC=1.61
IC=1.19
1
2
0.5
1.0

LITHOLOGIC DESCRIPTION

SILTY SANDSTONE

Entire core is moderately disturbed and fractured.

Major lithology: SILTY SANDSTONE, dark gray (10YR 4/1), with minor parallel lamination. Calcite-cemented at Section 1, 0-33 cm.

Minor lithology: Calcitic clayey siltstone, dark gray (10YR 4/1) and homogenous, in Section 1, 33-48 cm.

SMEAR SLIDE SUMMARY (%):

	1, 40 D	1, 116 D
TEXTURE:		
Sand	5	45
Silt	60	35
Clay	35	20
COMPOSITION:		
Access. minerals	5	5
Clay	30	20
Feldspar	—	5
Volcanic glass	3	3
Inorganic calcite	25	10
Mica	2	2
Quartz	35	50

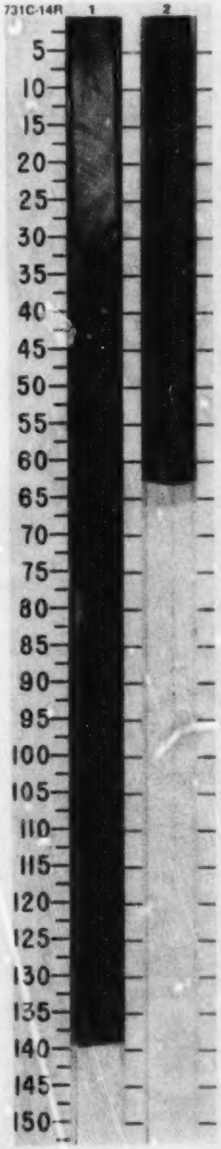
731C-14R
1
2
5
10
15
20
25
30
35
40
45
50
55
60
65
70
75
80
85
90
95
100
105
110
115
120
125
130
135
140
145
150

SITE 731 HOLE C CORE 15W CORED INTERVAL 3224.9-3273.1 mbsl; 859.1-907.3 mbsf

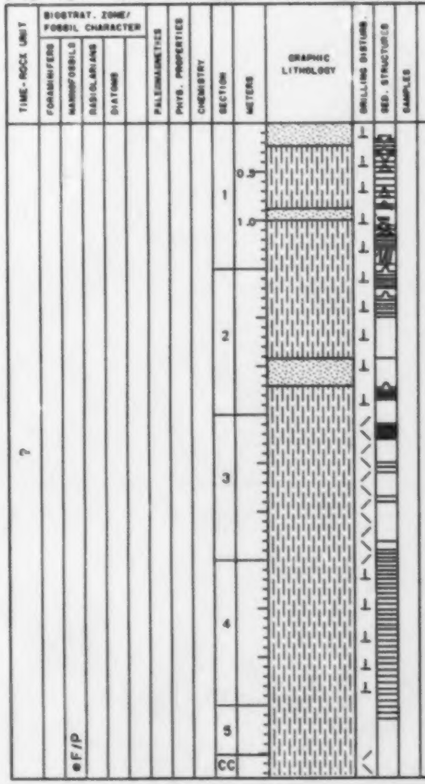
TIME-ROCK UNIT
BIOSTRAT. ZONE/FOSSIL CHARACTER
FORAMINIFERS
NANNOFOSSILS
RADIOLARIANS
DIATOMS
PALEOMAGNETICS
PHYS. PROPERTIES
CHEMISTRY
SECTION
METERS
GRAPHIC LITHOLOGY
DRILLING DISTURB.
SED. STRUCTURES
SAMPLES
?
●F/P
1
2
3
4
5
CC
0.5
1.0

LITHOLOGIC DESCRIPTION

SILTY CLAYSTONE to CLAYEY SILTSTONE

Entire core is moderately to highly fractured and highly disturbed (wash core).

Major lithology: SILTY CLAYSTONE to CLAYEY SILTSTONE, very dark gray (5Y 3/1) to very dark grayish brown (10YR 3/2). Clayey siltstone is parallel laminated, silty claystone is uniform or bioturbated. Sharp-based upward-fining sequences 5–20 cm thick are common. Small slump folds and dewatering structures common in Sections 1 and 2.

Minor lithology: Sandstone, gray (5Y 5/1) to dark gray (5Y 4/1). Inversely graded at Section 1, 0–24 cm, bioturbated or with convolute bedding at Section 1, 88–100 cm, and uniform at Section 2, 93–120 cm.

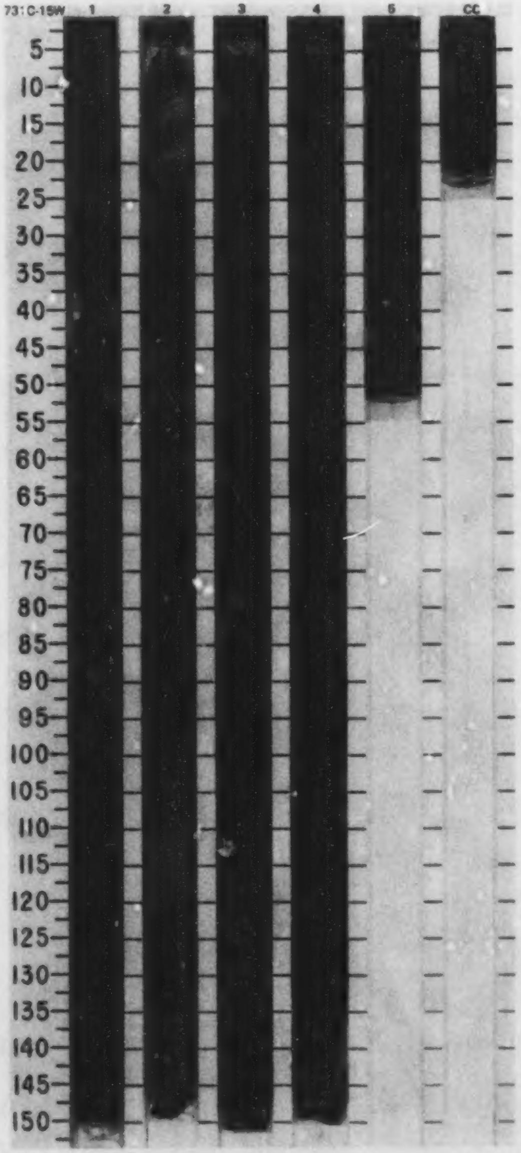
731C-15W
1
2
3
4
5
CC
5
10
15
20
25
30
35
40
45
50
55
60
65
70
75
80
85
90
95
100
105
110
115
120
125
130
135
140
145
150

SITE 731 HOLE C CORE 16R CORED INTERVAL 3273.1-3282.5 mbsl; 907.3-916.7 mbsf

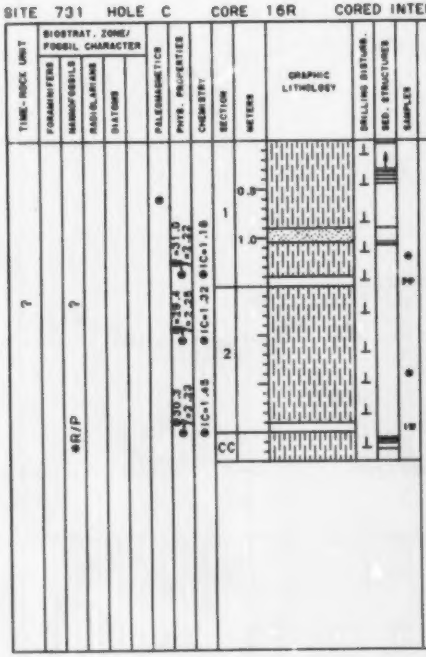
TIME-ROCK UNIT
BIOSTRAT. ZONE/FOSSIL CHARACTER
FORAMINIFERS
NANNOFOSSILS
RADIOLARIANS
DIATOMS
PALEOMAGNETICS
PHYS. PROPERTIES
CHEMISTRY
SECTION
METERS
GRAPHIC LITHOLOGY
DRILLING DISTURB.
SED. STRUCTURES
SAMPLES
?
?
●R/P
φ=31.0
γ=2.22
φ=29.4
γ=2.25
φ=30.3
γ=2.23
●IC=1.18
●IC=1.32
●IC=1.45
1
2
CC
0.5
1.0

LITHOLOGIC DESCRIPTION

SILTY CLAYSTONE to CLAYEY SILTSTONE

Entire core is moderately disturbed and fractured.

Major lithology: SILTY CLAYSTONE to CLAYEY SILTSTONE, dark gray (5Y 4/1, 5YR 4/1) to very dark gray (10YR 3/2), with abundant parallel lamination.

Minor lithology: Sandy siltstone to silty sandstone, gray (N6), homogenous, calcite-cemented, Section 1, 0-2 and 80-108 cm.

SMEAR SLIDE SUMMARY (%):

	1, 120 D	2, 90 M
TEXTURE:		
Sand	—	90
Silt	30	6
Clay	70	4
COMPOSITION:		
Access. minerals	—	15
Clay	60	—
Feldspar	—	10
Inorganic calcite	10	—
Mica	—	Tr
Quartz	30	75

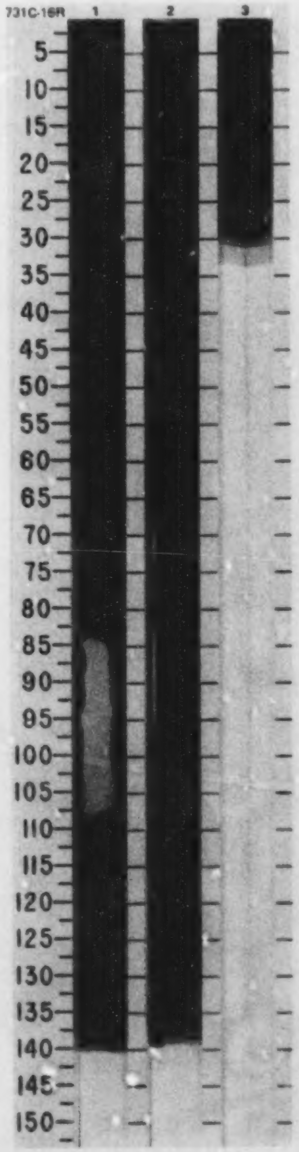
731C-16R
1
2
3
5
10
15
20
25
30
35
40
45
50
55
60
65
70
75
80
85
90
95
100
105
110
115
120
125
130
135
140
145
150

SITE 731 HOLE C CORE 17R CORED INTERVAL 3282.5-3292.2 mbsl; 916.7-926.4 mbsf

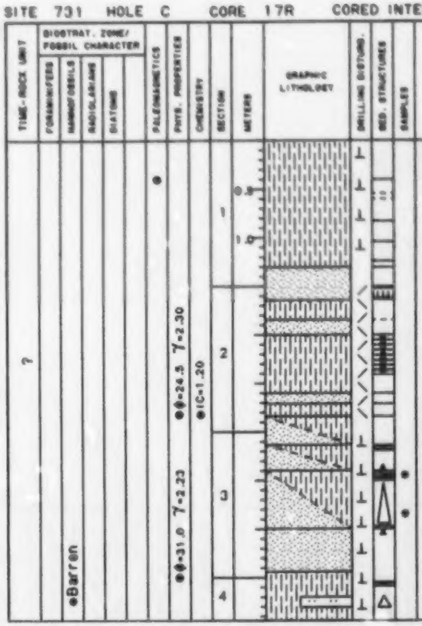
TIME-ROCK UNIT
BIOSTRAT. ZONE/ FOSSIL CHARACTER
FORAMINIFERS
NANNOFOSSILS
RADIOLARIANS
DIATOMS
PALEOMAGNETICS
PHYS. PROPERTIES
CHEMISTRY
SECTION
METERS
GRAPHIC LITHOLOGY
DRILLING DISTURB.
SED. STRUCTURES
SAMPLES
?
●Barren
●ϕ=24.5 γ=2.30
●ϕ=31.0 γ=2.23
●IC=1.20
1
2
3
4
0.5
1.0

LITHOLOGIC DESCRIPTION

SILTY CLAYSTONE to CLAYEY SILTSTONE, SANDSTONE, and gradationally interbedded SANDSTONE to SILTY CLAYSTONE

Entire core is slightly to moderately disturbed and fractured.

Major lithologies:
a. SILTY CLAYSTONE to CLAYEY SILTSTONE, dark gray (N4/) to very dark grayish brown (10YR 3/2) and very dark gray (5Y 3/1). Silty claystone is massive or bioturbated, and clayey siltstone is parallel laminated. Commonly interbedded to form sequences of repeated, sharp-based upward-fining intervals 3-10 cm thick.
b. SANDSTONE, dark gray (5Y 4/1) to very dark grayish brown (10YR 3/2) and very dark gray (5Y 3/1). Massive.
c. SANDSTONE to SILTY CLAYSTONE, dark gray (5Y 4/1) to very dark grayish brown (10YR 3/2) and very dark gray (5Y 3/1). Gradationally interbedded to form upward-fining sequences.

SMEAR SLIDE SUMMARY (%):

	3, 30 D	3, 82 D
TEXTURE:		
Sand	70	—
Silt	10	5
Clay	20	95
COMPOSITION:		
Access. minerals	5	Tr
Clay	20	90
Feldspar	5	—
Inorganic calcite	10	5
Mica	5	—
Nannofossils	Tr	3
Quartz	55	2

SITE 731 HOLE C CORE 18R CORED INTERVAL 3292.2-3301.9 mbsl; 926.4-936.1 mbsf

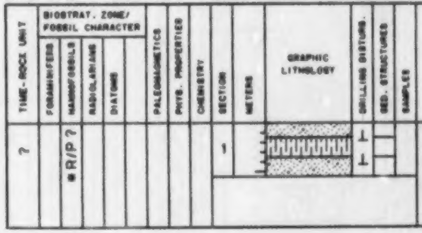
TIME-ROCK UNIT
BIOSTRAT. ZONE/ FOSSIL CHARACTER
FORAMINIFERS
NANNOFOSSILS
RADIOLARIANS
DIATOMS
PALEOMAGNETICS
PHYS. PROPERTIES
CHEMISTRY
SECTION
METERS
GRAPHIC LITHOLOGY
DRILLING DISTURB.
SED. STRUCTURES
SAMPLES
?
●R/P ?
1

LITHOLOGIC DESCRIPTION

CLAYEY SILTSTONE to SANDY SILTSTONE

Entire core is moderately disturbed and fractured.

Major lithology: CLAYEY SILTSTONE to SANDY SILTSTONE, very dark grayish brown (10YR 3/2). Clayey siltstone is parallel laminated, sandy siltstone is micaceous and contains charcoal.

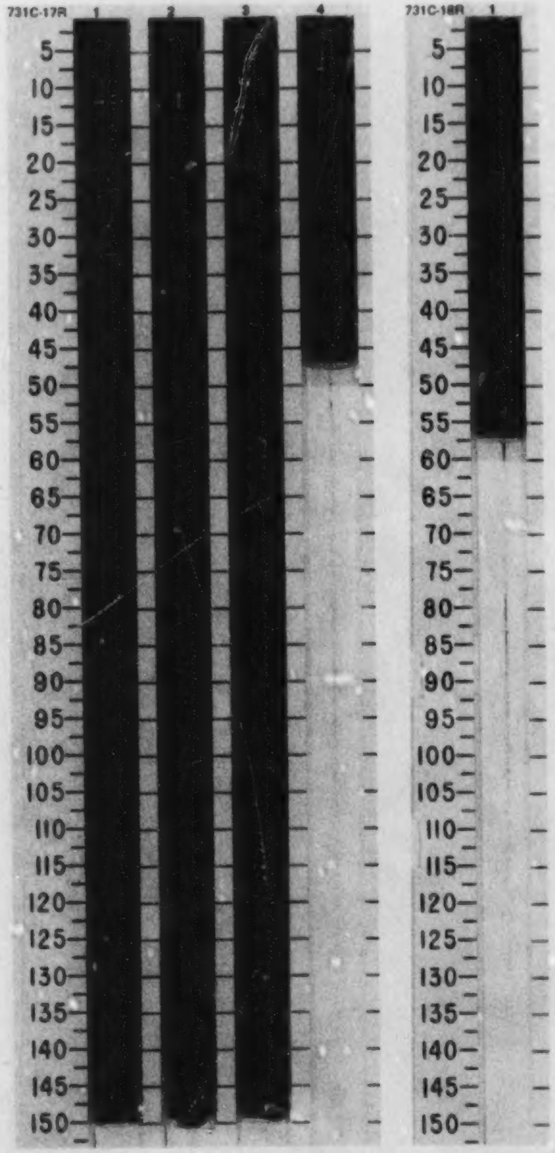
731C-17R
1
2
3
4
731C-18R
1
5
10
15
20
25
30
35
40
45
50
55
60
65
70
75
80
85
90
95
100
105
110
115
120
125
130
135
140
145
150

SITE 731 HOLE C CORE 19R CORED INTERVAL 3301.9-3311.5 mbsl; 936.1-945.7 mbsf

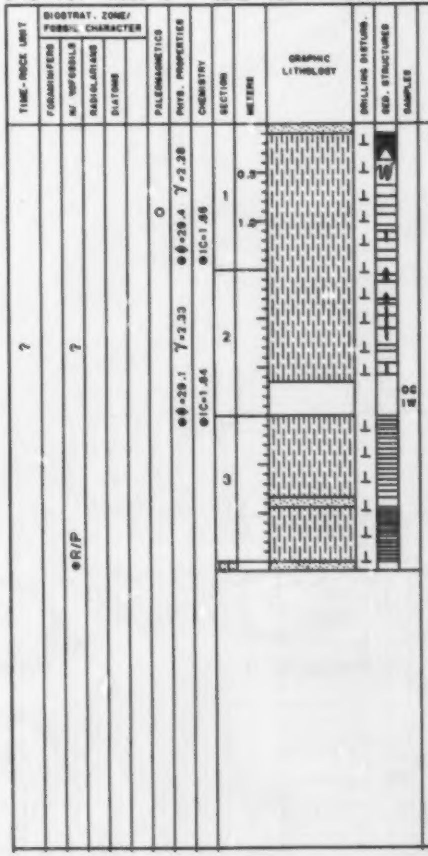
TIME-ROCK UNIT
BIOSTRAT. ZONE/ FOSSIL CHARACTER
FORAMINIFERS
N/ NOFOSSILS
RADIOLARIANS
DIATOMS
PALEOMAGNETICS
PHYS. PROPERTIES
CHEMISTRY
SECTION
METERS
GRAPHIC LITHOLOGY
DRILLING DISTURB.
SED. STRUCTURES
SAMPLES
?
?
●R/P
O
●ɸ=29.4 γ=2.28
●ɸ=29.1 γ=2.33
●IC=1.66
●IC=1.64
1
2
3
0.5
1.0
OG
IW

LITHOLOGIC DESCRIPTION

SILTY CLAYSTONE to CLAYEY SILTSTONE

Entire core is moderately disturbed and fractured.

Major lithology: SILTY CLAYSTONE to CLAYEY SILTSTONE, dark gray (5YR 4/1, 5Y 4/1) to very dark gray (5Y 3/1). Silty claystone is massive or bioturbated, and clayey siltstone is parallel laminated. Commonly interbedded to form sequences of repeated, sharp-based upward-fining intervals 3-20 cm thick.

Minor lithology: Sandstone to silty sandstone, dark gray (5YR 4/1, 5Y 4/1) to very dark gray (5Y 3/1), massive, in Section 1, 0-10 cm, Section 3, [illegible] cm, and CC.

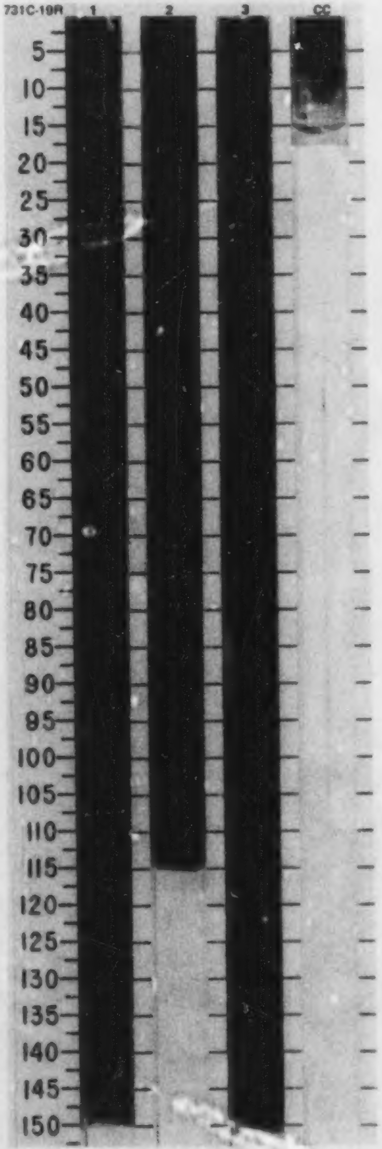
731C-19R
1
2
3
CC
5
10
15
20
25
30
35
40
45
50
55
60
65
70
75
80
85
90
95
100
105
110
115
120
125
130
135
140
145
150

SITE 731 HOLE C CORE 20R CORED INTERVAL 3311.5-3321.2 mbsl; 945.7-955.4 mbsf

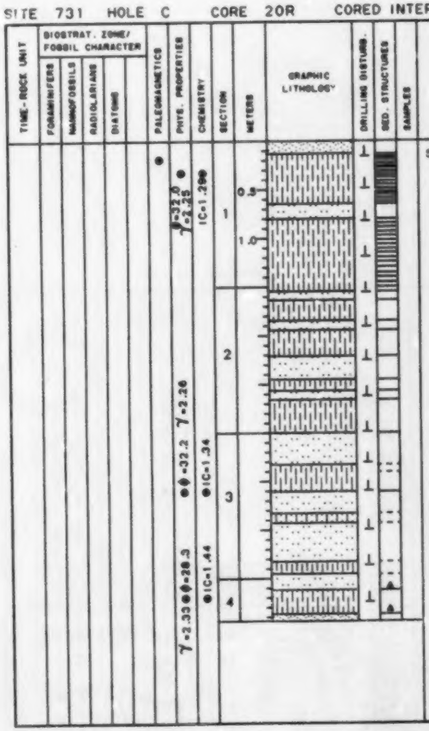
TIME-ROCK UNIT
BIOSTRAT. ZONE/ FOSSIL CHARACTER
FORAMINIFERS
NANNOFOSSILS
RADIOLARIANS
DIATOMS
PALEOMAGNETICS
PHYS. PROPERTIES
CHEMISTRY
SECTION
METERS
GRAPHIC LITHOLOGY
DRILLING DISTURB.
SED. STRUCTURES
SAMPLES
φ=32.0
γ=2.25
IC=1.29
0.5
1.0
1
2
3
4
γ=2.26
φ=32.2
IC=1.34
γ=2.33
φ=28.3
IC=1.44

LITHOLOGIC DESCRIPTION

SILTY CLAYSTONE to CLAYEY SILTSTONE and SANDSTONE to SILTSTONE

Entire core is moderately disturbed and fractured.

Major lithologies:
a. SILTY CLAYSTONE to CLAYEY SILTSTONE, dark gray (N4/) to very dark gray (5Y 3/1) and very dark grayish brown (10YR 3/2). Silty claystone is massive or bioturbated, and clayey siltstone is parallel laminated. Commonly interbedded to form sequences of repeated, sharp-based upward-fining intervals 3-10 cm thick.
b. SANDSTONE to SILTSTONE, dark gray (N4/) to very dark gray (5Y 3/1) and very dark grayish brown (10YR 3/2). Generally massive, with charcoal common and claystone lithoclasts rare. Minor upward-fining sequences in Section 4.

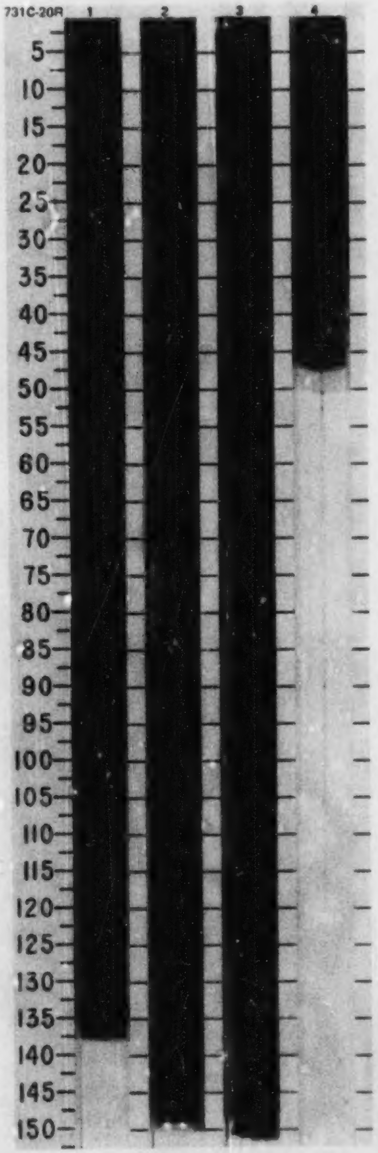
731C-20R
1
2
3
4
5
10
15
20
25
30
35
40
45
50
55
60
65
70
75
80
85
90
95
100
105
110
115
120
125
130
135
140
145
150

SITE 731 HOLE C CORE 21R CORED INTERVAL 3321.2-3330.9 mbsl; 955.4-965.1 mbsf

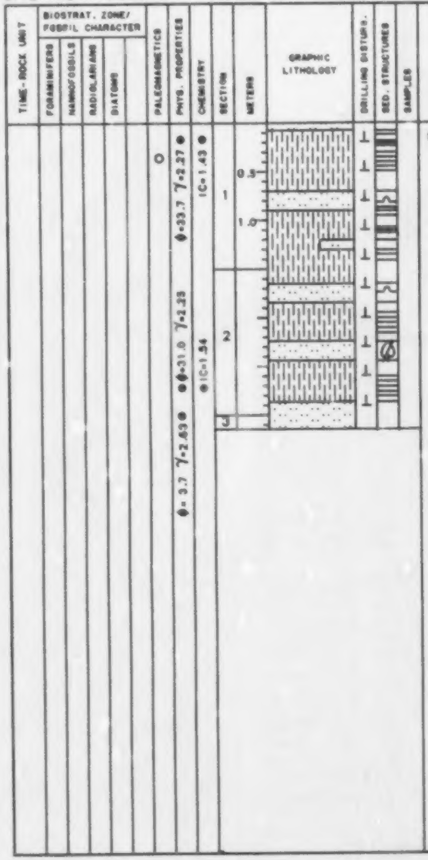
TIME-ROCK UNIT
BIOSTRAT. ZONE/ FOSSIL CHARACTER
FORAMINIFERS
NANNOFOSSILS
RADIOLARIANS
DIATOMS
PALEOMAGNETICS
PHYS. PROPERTIES
CHEMISTRY
SECTION
METERS
GRAPHIC LITHOLOGY
DRILLING DISTURB.
SED. STRUCTURES
SAMPLES
O
φ=33.7 γ=2.27 ●
●φ=31.0 γ=2.33
φ= 3.7 γ=2.63 ●
IC=1.43 ●
●IC=1.54
1
2
3
0.5
1.0

LITHOLOGIC DESCRIPTION

SILTY CLAYSTONE to CLAYEY SILTSTONE and SANDSTONE to SILTSTONE

Entire core is moderately disturbed and fractured.

Major lithologies:
a. SILTY CLAYSTONE to CLAYEY SILTSTONE, very dark grayish brown (10YR 3/2) and very dark gray (5Y 3/1). Silty claystone is massive or bioturbated, and clayey siltstone is parallel laminated. Commonly interbedded to form sequences of repeated, sharp-based upward-fining intervals 3–10 cm thick.
b. SANDSTONE to SILTSTONE, very dark gray (5Y 3/1) to very dark grayish brown (10YR 3/2). Generally massive, with charcoal common, and rare claystone lithoclasts. Slumped zones at Section 1, 70–80 cm, and Section 2, 15–35 cm. Calcite-cemented at Section 2, 136 cm, to Section 3.

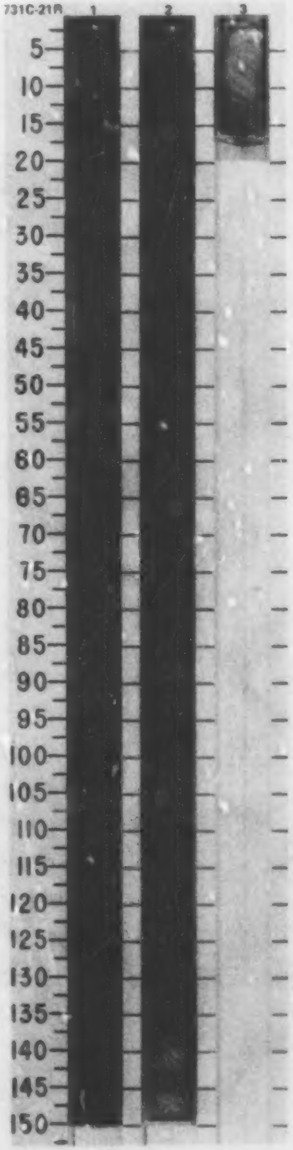
731C-21R
1
2
3
5
10
15
20
25
30
35
40
45
50
55
60
65
70
75
80
85
90
95
100
105
110
115
120
125
130
135
140
145
150

SITE 731 HOLE C CORE 22R CORED INTERVAL 3330.9-3340.6 mbsl; 965.1-974.8 mbsf

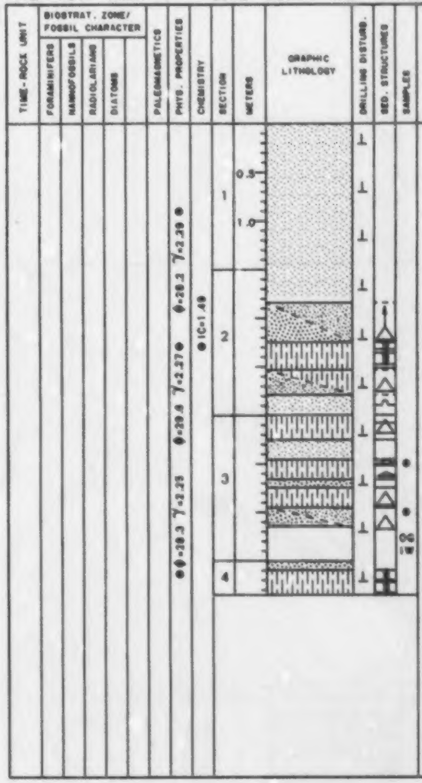
TIME-ROCK UNIT
BIOSTRAT. ZONE/ FOSSIL CHARACTER
FORAMINIFERS
NANNOFOSSILS
RADIOLARIANS
DIATOMS
PALEOMAGNETICS
PHYS. PROPERTIES
CHEMISTRY
SECTION
METERS
GRAPHIC LITHOLOGY
DRILLING DISTURB.
SED. STRUCTURES
SAMPLES
φ=28.2 γ=2.29
φ=28.9 γ=2.27
φ=28.3 γ=2.25
IC=1.48
1
2
3
4
0.5
1.0
OG
IW

LITHOLOGIC DESCRIPTION

SILTY CLAYSTONE to CLAYEY SILTSTONE, SANDSTONE to SILTSTONE, and gradationally interbedded SANDSTONE to CLAYEY SILTSTONE

Entire core is moderately to severely disturbed and fractured.

Major lithologies:

a. SILTY CLAYSTONE to CLAYEY SILTSTONE, dark gray (5Y 4/1, 10YR 4/1). Silty claystone is massive or bioturbated, and clayey siltstone is parallel laminated. Commonly interbedded to form sequences of repeated, sharp-based upward-fining intervals 3–10 cm thick.

b. SANDSTONE to SILTSTONE, dark gray (5Y 4/1, 10YR 4/1), not graded. Minor parallel fabric defined by amphiboles, pyroxene, and mica. Calcite-cemented at Section 1 and Section 3, 24–48 and 68–78 cm.

c. SANDSTONE to CLAYEY SILTSTONE, dark gray (5Y 4/1, 10YR 4/1). Gradationally interbedded to form upward-fining sequences, generally with sharp bases.

SMEAR SLIDE SUMMARY (%):

	3, 54 D	3, 108 D
TEXTURE:		
Sand	—	60
Silt	55	20
Clay	45	20
COMPOSITION:		
Access. minerals	2	5
Clay	45	20
Dolomite	—	Tr
Feldspar	5	5
Volcanic glass	—	3
Inorganic calcite	8	10
Mica	—	3
Quartz	40	55

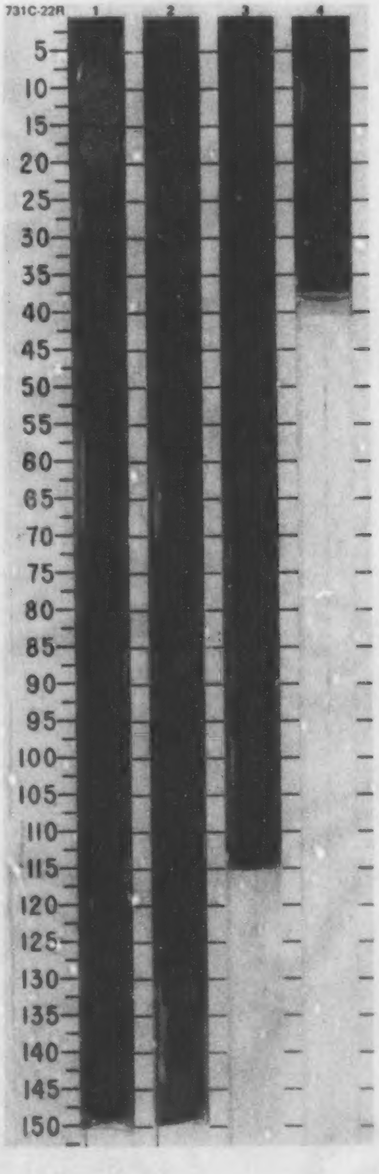
731C-22R
1
2
3
4
5
10
15
20
25
30
35
40
45
50
55
60
65
70
75
80
85
90
95
100
105
110
115
120
125
130
135
140
145
150

SITE 731 HOLE C CORE 23R CORED INTERVAL 3340.6-3350.3 mbsl; 974.8-984.5 mbsf

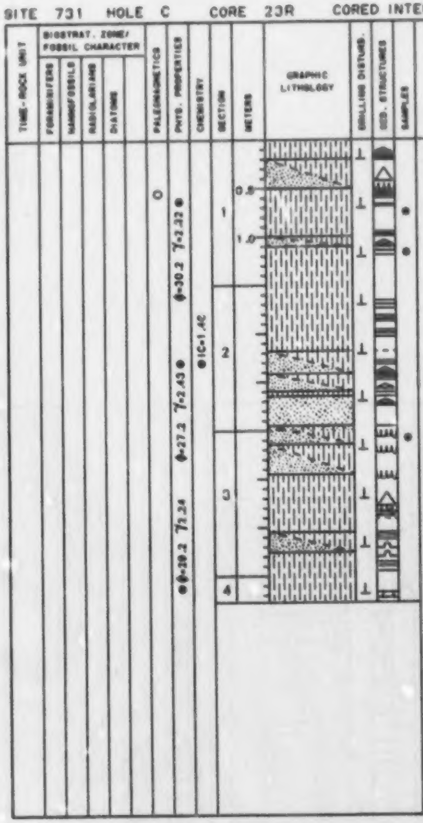
TIME-ROCK UNIT
BIOSTRAT. ZONE/ FOSSIL CHARACTER
FORAMINIFERS
NANNOFOSSILS
RADIOLARIANS
DIATOMS
PALEOMAGNETICS
PHYS. PROPERTIES
CHEMISTRY
SECTION
METERS
GRAPHIC LITHOLOGY
DRILLING DISTURB.
SED. STRUCTURES
SAMPLES
φ=30.2 γ=2.22
φ=27.2 γ=2.43
φ=29.2 γ=2.24
IC=1.42
1
2
3
4
0.5
1.0

LITHOLOGIC DESCRIPTION

SILTY CLAYSTONE to CLAYEY SILTSTONE, and gradationally interbedded SANDSTONE to SILTY CLAYSTONE

Entire core is moderately disturbed and fractured.

Major lithologies:
a. SILTY CLAYSTONE to CLAYEY SILTSTONE, dark gray (5Y 4/1, 10YR 4/1). Silty claystone is massive or bioturbated, clayey siltstone is parallel laminated. Commonly interbedded to form sequences of repeated, sharp-based upward-fining intervals 3-10 cm thick.
b. SANDSTONE to SILTY CLAYSTONE, dark gray (10YR 4/1, 5Y 4/1). Gradationally interbedded to form upward-fining sequences, generally with sharp bases.

Minor lithology: Sandstone to silty sandstone, dark gray (5Y 4/1). Uniform to slightly upward-fining sequence, in Section 2, 114-145 cm.

SMEAR SLIDE SUMMARY (%):

	1, 74 D	1, 117 D	3, 8 D
TEXTURE:			
Sand	—	5	60
Silt	45	75	30
Clay	55	20	10
COMPOSITION:			
Access. minerals	1	5	10
Clay	55	20	10
Dolomite	—	1	1
Feldspar	2	6	5
Volcanic glass	—	3	3
Inorganic calcite	7	20	10
Mica	—	1	5
Quartz	35	45	50
Rock fragment	—	—	6

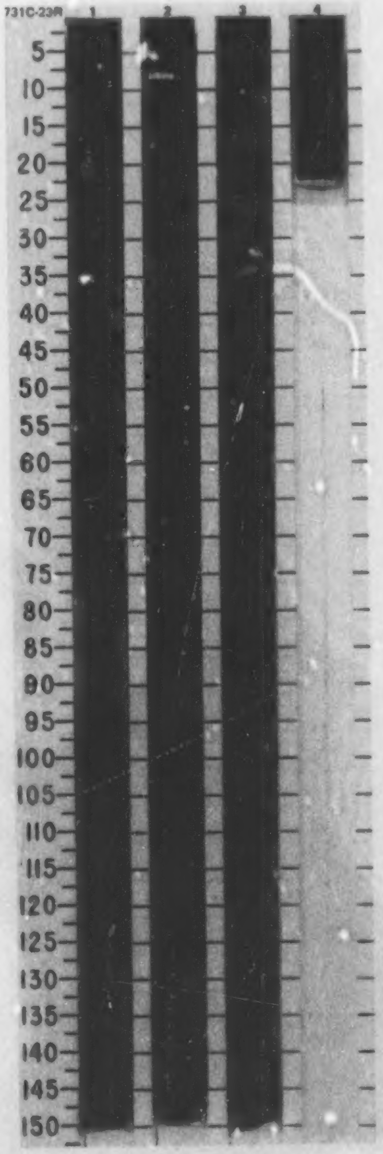
731C-23R
1
2
3
4
5
10
15
20
25
30
35
40
45
50
55
60
65
70
75
80
85
90
95
100
105
110
115
120
125
130
135
140
145
150

SITE 731 HOLE C CORE 24R CORED INTERVAL 3350.3-3360.0 mbsl; 984.5-994.2 mbsf

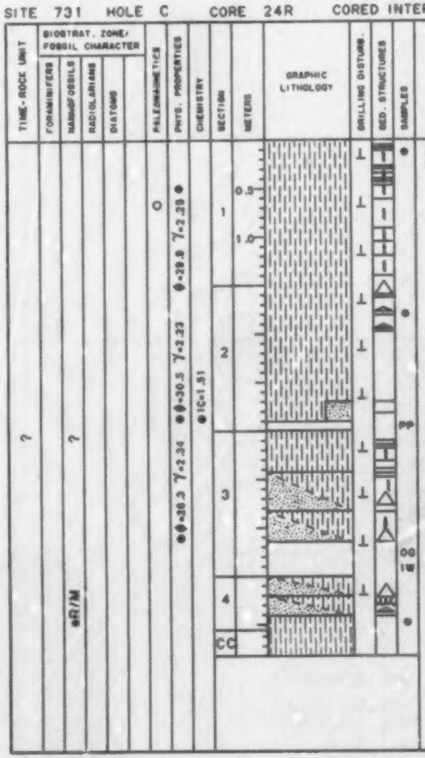
TIME-ROCK UNIT
BIOSTRAT. ZONE/ FOSSIL CHARACTER
FORAMINIFERS
NANNOFOSSILS
RADIOLARIANS
DIATOMS
PALEOMAGNETICS
PHYS. PROPERTIES
CHEMISTRY
SECTION
METERS
GRAPHIC LITHOLOGY
DRILLING DISTURB.
SED. STRUCTURES
SAMPLES
?
?
aR/M
●ϕ=26.3 γ=2.34
●ϕ=30.5 γ=2.33
ϕ=29.8 γ=2.28 ●
●IC=1.51
0.5
1.0
1
2
3
4
CC
PP
OG
IW

LITHOLOGIC DESCRIPTION

SILTY CLAYSTONE to CLAYEY SILTSTONE, and gradationally interbedded SANDSTONE TO SILTY CLAYSTONE

Entire core is moderately disturbed and fractured.

Major lithologies:
a. SILTY CLAYSTONE to CLAYEY SILTSTONE, dark gray (10YR 4/1, 5Y 4/1). Silty claystone is massive or bioturbated, and clayey siltstone is parallel laminated. Commonly interbedded to form sequences of repeated, sharp-based upward-fining intervals 3-10 cm thick.
b. SANDSTONE to SILTY CLAYSTONE, dark gray (10YR 4/1, 5Y 4/1). Gradationally interbedded to form upward-fining sequences, generally with sharp bases. Bioturbated and/or slumped at top of sequence, Section 3, 47-52 cm.

SMEAR SLIDE SUMMARY (%):

	1, 12 D	2, 30 D	4, 40 D
TEXTURE:			
Sand	5	30	—
Silt	40	45	30
55	25	70	
COMPOSITION:			
Access. minerals	2	7	—
Clay	56	25	70
Dolomite	Tr	—	—
Feldspar	3	5	3
Volcanic glass	—	5	—
Inorganic calcite	15	10	7
Mica	—	3	—
Quartz	25	45	20

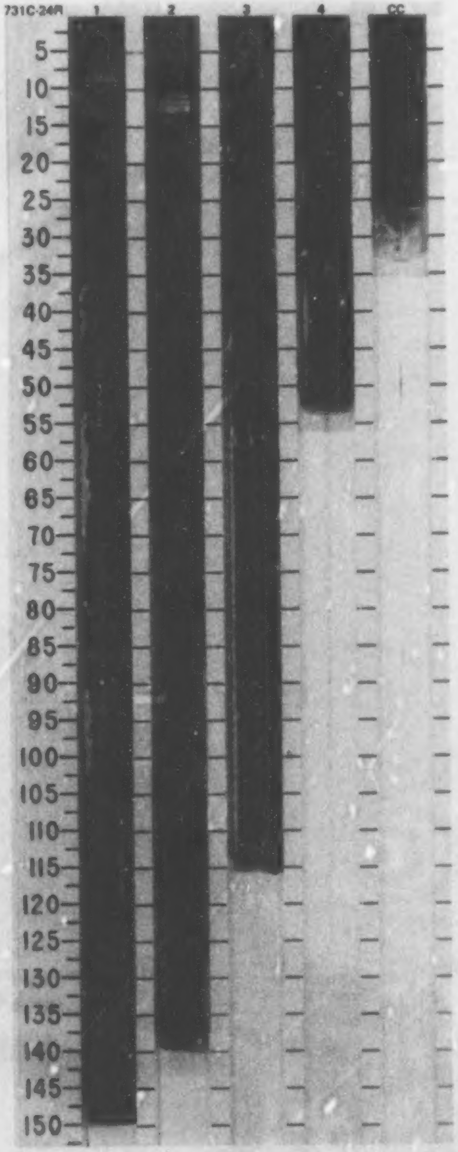
731C-24R
1
2
3
4
CC
5
10
15
20
25
30
35
40
45
50
55
60
65
70
75
80
85
90
95
100
105
110
115
120
125
130
135
140
145
150

SECTION 4: POLICY

JOIDES ADVISORY GROUPS *

Executive Committee
Douglas R. Caldwell
Oregon State University
D. James Baker, Jr. (JOI liaison)
Joint Oceanographic Institutions, Inc.
Bernard Biju-Duval
IFREMER (France)
James C. Briden
Natural Environment Research Council (U.K.)
Hans-J. Dürbaum
Bundesanstalt für Geowissenschaften und Rohstoffe
Edward A. Frieman
University of California, San Diego
C.G.A. Harrison
University of Miami
G. Ross Heath
University of Washington
Donald F. Heinrichs (NSF liaison)
National Science Foundation (U.S.)
Charles E. Helsley
University of Hawaii
Michael J. Keen
Atlantic Geoscience Centre (Canada)
John A. Knauss
University of Rhode Island
Arthur E. Maxwell
University of Texas at Austin
William J. Merrell
Texas A&M University at Galveston
Takahisa Nemoto
University of Tokyo
Nicklas G. Pisias (Planning Committee liaison)
Oregon State University
Philip D. Rabinowitz (Science Operator liaison)
Texas A&M University
Barry Raleigh
Columbia University
John Steele
Woods Hole Oceanographic Institution
Jan H. Stel
Netherlands Council for Oceanic Research

Planning Committee (PCOM)
Nicklas G. Pisias
Oregon State University
Roger N. Anderson (Wireline Logging Services Contractor liaison)
Columbia University
Garrett W. Brass
University of Miami
Jean-Paul Cadet
Université Pierre et Marie Curie
William T. Coulbourn
University of Hawaii
Olav Eldholm
University of Oslo
Timothy J. G. Francis
Institute of Oceanographic Sciences (U.K.)
Louis E. Garrison (Science Operator liaison)
Texas A&M University
Stefan Gartner
Texas A&M University
Miriam Kastner
University of California, San Diego
Marcus G. Langseth
Columbia University
Roger L. Larson
University of Rhode Island
Russell E. McDuff
University of Washington
Bruce Malfait (NSF liaison)
National Science Foundation (U.S.)
Thomas E. Pyle (JOI liaison)
Joint Oceanographic Institutions, Inc.
Paul T. Robinson
Dalhousie University
David A. Ross
Woods Hole Oceanographic Institution
Thomas H. Shipley
University of Texas at Austin
Asahiko Taira
University of Tokyo
Ulrich von Rad
Bundesanstalt für Geowissenschaften und Rohstoffe

Atlantic Regional Panel
James A. Austin, Jr.
University of Texas at Austin
Jack G. Baldauf (Texas A&M University liaison)
Texas A&M University
Jean-Paul Cadet (Planning Committee liaison)
Université Pierre et Marie Curie
Christoph Hemleben
Universität Tübingen
Lubomir F. Jansa
Atlantic Geoscience Centre (Canada)
Kim D. Klitgord
U.S. Geological Survey
Hans-Christian Larsen
Greenland Geological Survey
John Malpas (Lithospheric Panel liaison)
Memorial University
Jean Mascle
Université Pierre et Marie Curie
Philip A. Meyers (Sediments and Ocean History Panel liaison)
University of Michigan
Hisatake Okada
Yamagata University
David A. Ross (Planning Committee liaison)
Woods Hole Oceanographic Institution
Dale S. Sawyer
University of Texas at Austin
Jean-Claude Sibuet
IFREMER (France)
Robert Speed
Northwestern University
Brian E. Tucholke
Woods Hole Oceanographic Institution
Peter R. Vogt (Tectonics Panel liaison)
U.S. Naval Research Laboratory
Robert B. Whitmarsh
Institute of Oceanographic Sciences (U.K.)

Central and Eastern Pacific Regional Panel
Seymour O. Schlanger
Northwestern University
Rodey Batiza (Lithospheric Panel liaison)
Northwestern University
William T. Coulbourn (Planning Committee liaison)
University of Hawaii

---

*Membership at time of cruise.

Earl E. Davis
Pacific Geoscience Centre (Canada)
Martin F. J. Flower
University of Illinois, Chicago
Jean Francheteau
Université Pierre et Marie Curie
Hugh C. Jenkyns
Oxford University
Roger Larson (Planning Committee liaison)
University of Rhode Island
Steve Lewis (Site Survey Panel liaison)
U.S. Geological Survey
Hakuyu Okada
Shizuoka University
David K. Rea
University of Michigan, Ann Arbor
Robin P. Riddihough (Tectonics Panel liaison)
Geological Survey of Canada
Tsunemasa Saito (Sediments and Ocean History Panel liaison)
Yamagata University
Constance A. Sancetta
Columbia University
David C. Scholl
U.S. Geological Survey
Hans Joachim Schrader
University of Bergen
William V. Sliter
U.S. Geological Survey
Elliott Taylor (Texas A&M University liaison)
Texas A&M University
Ulrich von Stackelberg
Bundesanstalt für Geowissenschaften und Rohstoffe

Downhole Measurements Panel
Paul F. Worthington
British Petroleum Company, Ltd.
Roger N. Anderson (Wireline Logging Services Contractor liaison)
Columbia University
Keir Becker (Lithospheric Panel liaison)
University of Miami
Sebastian Bell
Institute of Sedimentary and Petroleum Geology (Canada)
Bobb Carson
Lehigh University
Jens M. Hovem
Institutt for Kontinentalsokkelundersokelser
Eddie P. Howell
ARCO Oil and Gas Company
Reinhard Jung
Bundesanstalt für Geowissenschaften Rohstoffe
Hajimu Kinoshita
Chiba University
Marcus Langseth (Planning Committee liaison)
Columbia University
Russell E. McDuff (Planning Committee liaison)
University of Washington
Suzanne O'Connell (Texas A&M University liaison)
Texas A&M University
Gary R. Olhoeft
U.S. Geological Survey
Robert Porter
University of Washington
J.-P. Pozzi
Ecole Normale Supirieure
Matthew H. Salisbury
Dalhousie University
Carl Sondergeld
Amoco Production Company

Ralph A. Stephen
Woods Hole Oceanographic Institution
Richard K. Traeger
Sandia National Laboratories
Roy H. Wilkens
University of Hawaii

Indian Ocean Panel
Roland Schlich
Université de Louis Pasteur
Harald Bäcker
Preussag AG, Erdöl und Erdgas
Alfonso Bosellini
Universita degli Studi di Ferrara
Bradford M. Clement (Texas A&M University liaison)
Texas A&M University
James R. Cochran
Columbia University
Thomas A. Davies
University of Texas at Austin
Robert A. Duncan
Oregon State University
David Falvey
Bureau of Mineral Resources, Geology and Geophysics (Australia)
Charles H. Langmuir (Lithospheric Panel liaison)
Columbia University
Roger Larson (Planning Committee liaison)
University of Rhode Island
John Ludden
Université de Montréal
Warren L. Prell
Brown University
Jira Segawa
University of Tokyo
Edith Vincent
Université Pierre et Marie Curie
Ulrich von Rad (Planning Committee liaison)
Bundesanstalt für Geowissenschaften und Rohstoffe
Tony Watts (Tectonics Panel liaison)
Columbia University
Robert S. White
Cambridge University

Information Handling Panel
Ted C. Moore, Jr.
Exxon Production Research Company
Cristina Broglia (Wireline Logging Service Contractor liaison)
Columbia University
Jean-Paul Cadet (Planning Committee liaison)
Université Pierre et Marie Curie
Stefan Gartner (Planning Committee liaison)
Texas A&M University
Ian Gibson
University of Waterloo (Canada)
Jan Hertogen
Katholieke Universiteit Leuven (Belgium)
Raymond V. Ingersoll
University of California, Los Angeles
Meirion T. Jones
Institute of Oceanographic Sciences (U.K.)
Michael Latremouille
International Centre for Ocean Development (Canada)
Alfred R. Loeblich, Jr.
University of California, Los Angeles
Michael S. Loughridge
National Geophysical Data Center
Russell B. Merrill (Texas A&M University liaison)
Texas A&M University

Eric Moussat
IFREMER (France)
Judit Nowak
Bundesanstalt für Geowissenschaften und Rohstoffe

Kerguelen Working Group
Warren L. Prell
Brown University
John B. Anderson
Rice University
Carl Brenner (Databank liaison)
Columbia University
Paul F. Ciesielski
University of Florida
David H. Elliot
Ohio State University
David Falvey
Bureau of Mineral Resources, Geology and Geophysics (Australia)
Louis E. Garrison (Texas A&M University liaison)
Texas A&M University
Roger Larson (Planning Committee liaison)
University of Rhode Island
John C. Mutter (Lithospheric Panel liaison)
Columbia University
Roland Schlich
Université de Louis Pasteur

Lithosphere Panel
Robert S. Detrick
University of Rhode Island
Andrew C. Adamson (Texas A&M University liaison)
Texas A&M University
Rodey Batiza
Northwestern University
Keir Becker
University of Miami
Kurt Bostrom
University of Stockholm
Lawrence M. Cathles
Cornell University
Earl E. Davis (Central and Eastern Pacific Regional Panel liaison)
Geological Survey of Canada
John R. Delaney
University of Washington
Robert A. Duncan (Indian Ocean Panel liaison)
Oregon State University
Henry Elderfield
Cambridge University
Martin R. Fisk (Southern Oceans Panel liaison)
Oregon State University
Toshitsugu Fujii
University of Tokyo
James W. Hawkins
University of California, San Diego
Miriam Kastner (Planning Committee liaison)
University of California, San Diego
Kim D. Klitgord (Atlantic Regional Panel liaison)
U.S. Geological Survey
Charles H. Langmuir
Columbia University
Marcia McNutt
Massachusetts Institute of Technology
John Malpas
Memorial University
Catherine Mevel
Université Pierre et Marie Curie
John C. Mutter
Columbia University

Julian A. Pearce
The University of Newcastle upon Tyne
Nikolai Petersen
Universität München
Paul T. Robinson (Planning Committee liaison)
Dalhousie University
Steven D. Scott (Western Pacific Regional Panel liaison)
University of Toronto
John M. Sinton
University of Hawaii

Pollution Prevention and Safety Panel
Mahlon M. Ball
U.S. Geological Survey
Carl Brenner (Databank liaison)
Columbia University
Rustum Byramjee
Total Compagnie Française des Pétroles
Graham Campbell
Department of Energy, Mines and Resources (Canada)
George E. Claypool
Mobil Oil Company
Louis E. Garrison (Texas A&M University liaison)
Texas A&M University
Arthur R. Green
Exxon Production Research Company
David B. MacKenzie
Littleton, Colorado
Nicklas G. Pisias (Planning Committee liaison)
Oregon State University
David G. Roberts
British Petroleum Company, Ltd.
Gunter Stober
Deminex
Peter A. Ziegler
Shell International Petroleum Company

Sediments and Ocean History Panel
Lawrence Mayer
Dalhousie University
Wolfgang H. Berger
University of California, San Diego
Garrett W. Brass (Planning Committee liaison)
University of Miami
Paul F. Ciesielski (Southern Oceans Panel liaison)
University of Florida
Andri W. Droxler
Rice University
Robert W. Embley
Oregon State University
Philip N. Froelich
Columbia University
Robert E. Garrison
Bureau of Mineral Resources, Geology and Geophysics (Australia)
Martin B. Goldhaber
U.S. Geological Survey
Dennis Kent
Columbia University
Philip A. Meyers
University of Michigan
William R. Normark
U.S. Geological Survey
Hisatake Okada (Atlantic Regional Panel liaison)
Yamagata University
Amanda A. Palmer (Texas A&M University liaison)
Texas A&M University
Warren L. Prell (Indian Ocean Panel liaison)
Brown University

Isabella Premoli Silva
Universita di Milano
Tsunemasa Saito
Yamagata University
Rick Sarg
Exxon Production Research Company
André Schaaf
Université de Bretagne Occidentale
Nicholas J. Shackleton
Cambridge University
William V. Sliter (Central and Eastern Pacific Regional Panel liaison)
U.S. Geological Survey
Rüdiger Stein
Universität Giessen
Ulrich von Rad (Planning Committee liaison)
Bundesanstalt für Geowissenschaften und Rohstoffe

Site Survey Panel

John W. Peirce
Petro Canada
Carl Brenner (Databank liaison)
Columbia University
Frederick K. Duennebier
University of Hawaii
Timothy J. G. Francis (Planning Committee liaison)
Institute of Oceanographic Sciences (U.K.)
Robert B. Kidd
University College of Swansea
Marcus G. Langseth (Planning Committee liaison)
Columbia University
Birger Larsen
Technical University of Denmark
Steve Lewis
U.S. Geological Survey
Alain Mauffret
Université Pierre et Marie Curie
Audrey W. Meyer (Texas A&M University liaison)
Texas A&M University
Heinrich Meyer
Bundesanstalt für Geowissenschaften und Rohstoffe
Kiyoshi Suyehiro
Chiba University

Southern Oceans Panel

Peter F. Barker
British Antarctic Survey
Brian D. Bornhold
Pacific Geoscience Centre (Canada)
Stephen C. Cande
Columbia University
Paul F. Ciesielski
University of Florida
Alan K. Cooper
U.S. Geological Survey
David DeMaster
North Carolina State University
David H. Elliot
Ohio State University
Martin R. Fisk
Oregon State University
Dieter Fuetterer
Alfred Wegener Institute for Polar Research
Louis E. Garrison (Texas A&M University liaison)
Texas A&M University
Karl Hinz (Tectonics Panel liaison)
Bundesanstalt für Geowissenschaften und Rohstoffe
Katsutada Kaminuma
National Institute of Polar Research (Japan)
James P. Kennett
University of California, Santa Barbara
Yngve Kristoffersen
Universitetet i Bergen
Lucien Leclaire
Museum National d'Histoire Naturelle
Russell E. McDuff (Planning Committee liaison)
University of Washington
John C. Mutter (Lithospheric Panel liaison)
Columbia University
Nicklas G. Pisias (Planning Committee liaison)
Oregon State University
Nicholas J. Shackleton (Southern Oceans History Panel liaison)
Cambridge University
Sherwood W. Wise, Jr.
Florida State University

Technology and Engineering Development Committee

Jean Jarry
IFREMER (France)
Martin Chenevert
University of Texas at Austin
Bert R. Dennis
Los Alamos National Laboratories
Timothy J. G. Francis (Planning Committee liaison)
Institute of Oceanographic Sciences (U.K.)
David D. Grassick
Enterprise Oil, plc.
Barry Harding (Texas A&M University liaison)
Texas A&M University
Junzo Kasahara
Nippon Schlumberger K.K.
Emilio Luna Sierra
Hispanoil
Archie R. McLerran
Solana Beach, California
Keith Manchester
Atlantic Geoscience Centre (Canada)
Claus Marx
Institut für Tiefbohrkunde und Erdölgewinnung
Keith Millheim
Amoco Production Company
Frank J. Schuh
Intertech Ops. Tech., Inc.
Charles Sparks
Institut Français du Pétrole
Paul Stanton
Exxon Production Research Company
Walter W. Svendsen
Longyear Company
Donald Wilson
Chevron Corporation

Tectonics Panel

Darrel S. Cowan
University of Washington
Christian A. Auroux (Texas A&M University liaison)
Texas A&M University
Sebastian Bell (Downhole Measurements Panel liaison)
Geological Survey of Canada
Ian W. D. Dalziel
University of Texas at Austin
Dan M. Davis
State University of New York, Stony Brook
Olav Eldholm (Planning Committee liaison)
University of Oslo
Karl Hinz
Bundesanstalt für Geowissenschaften und Rohstoffe

David G. Howell
U.S. Geological Survey
Kenneth J. Hsü
Eidgenossische Technische Hochschule
Bruce D. Marsh
Johns Hopkins University
Gregory F. Moore (Western Pacific Regional Panel liaison)
University of Tulsa
Robin P. Riddihough
Geological Survey of Canada
François Roure
Institut Français du Pétrole
David C. Scholl (Central and Eastern Pacific Regional liaison)
U.S. Geological Survey
Thomas H. Shipley (Planning Committee liaison)
University of Texas at Austin
Jean-Claude Sibuet (Atlantic Regional Panel liaison)
IFREMER (France)
Peter R. Vogt
U.S. Naval Research Laboratory
Tony Watts
Columbia University
Graham K. Westbrook
University of Birmingham

Western Pacific Panel
Brian Taylor
University of Hawaii
Michael Audley-Charles
University of London, University College
James B. Gill
University of California, Santa Cruz
James W. Hawkins (Lithospheric Panel liaison)
University of California, San Diego
Roy D. Hyndman
Pacific Geoscience Centre (Canada)
Derk Jongsma
Vrije Universiteit
H. R. Kudrass
Bundesanstalt für Geowissenschaften und Rohstoffe
Audrey W. Meyer (Texas A&M University liaison)
Texas A&M University
Gregory F. Moore
University of Tulsa
James Natland
University of California, San Diego
Nicklas G. Pisias (Planning Committee liaison)
Oregon State University
Claude Rangin
Université Pierre et Marie Curie
Jacques Recy
ORSTOM (France)
Rick Sarg (Southern Oceans History Panel liaison)
Exxon Production Research Company
Steven D. Scott
University of Toronto
Asahiko Taira (Planning Committee liaison)
University of Tokyo
Kensaku Tamaki
University of Tokyo

SAMPLE-DISTRIBUTION POLICY[1]

Distribution of Ocean Drilling Program (ODP) and Deep Sea Drilling Project (DSDP) samples is undertaken in order to (1) provide support to shipboard scientists in achieving the scientific objectives of their cruise and to support shore-based investigators who are preparing contributions to ODP reports, (2) provide individual investigators with materials to conduct detailed studies beyond the scope of ODP reports, (3) provide micropaleontological reference centers with samples for reference and comparison purposes, and (4) provide educators with samples for teaching purposes.

Funding for sample-related activities must be secured by the investigator independently of requesting the samples.

The Ocean Drilling Program Curator is responsible for distributing samples and for preserving and conserving core material. The Curator, who may accept advice from chairmen of the appropriate JOIDES advisory panels, is responsible for enforcing the provisions of this sample-distribution policy. He is responsible for maintaining a record of all samples that have been distributed, both on board ship and subsequently from the repositories, indicating the recipients and the nature of investigations proposed. This information is available to interested investigators on request.

Every sample distributed from the ship or from a repository is labeled with a standard identifier, which includes leg number, hole number, core and section numbers, and interval within the section from which the sample was removed. It is imperative that this standard identifier be associated with all data reported in the literature, and that residues of the sample remain labeled throughout their lives, so that later workers can relate the data to the cores.

Distribution of sample materials is made directly from the repositories (Lamont-Doherty Geological Observatory, Scripps Institution of Oceanography, and Texas A&M University) by the Curator or his designated representative.

1. *Distribution of Samples for Research Leading to Contributions to ODP Reports*

Any investigator who wishes to contribute to the reports of a scheduled cruise may write to the Curator, Ocean Drilling Program, 1000 Discovery Drive, College Station, Texas 77840, U.S.A., in order to request samples from that cruise. Requests for a specific cruise must be received by the Curator at least TWO MONTHS in advance of the departure of that cruise, in order to allow time for review of the request in conjunction with other requests, so that a suitable shipboard sampling program can be assembled. The request should include a statement of the nature of the proposed research, the size and approximate number of samples required to complete the study, and any particular sampling technique or equipment which may be required. Requests will be reviewed by the Staff Representative and co-chief scientists of the cruise and by the Curator. Approval/disapproval will be based on the scientific requirements of the cruise as determined by the appropriate JOIDES advisory panel(s). The scope of a request must be such that samples can be processed, that proposed research can be completed, and that the paper can be written in time for submission to the relevant ODP cruise report.

Except for rare, specific instances involving ephemeral properties, the total volume of samples removed during a cruise-related sampling program will not exceed one-quarter of the volume of core recovered, and no interval will be depleted. One-half of all recovered materials will be retained in the archives in as pristine a condition as is practicable. Investigators requesting shipboard samples of igneous materials may receive a maximum of 100 igneous samples per cruise.

Because many sample requests are received for shipboard work and because the time of the shipboard party is at a premium, co-chief scientists are strongly urged to limit shipboard sampling to the minimum necessary to accomplish the cruise objectives. Shore-based investigators whose requests for cruise-related samples are approved should expect that they will receive the samples after the cores are returned to the repository, and should schedule research activities accordingly.

Co-chief scientists may invite investigators who are not cruise participants to perform special studies of selected core samples in direct support of shipboard activities. If this occurs, the names and addresses of these investigators and details of all samples loaned or distributed to them must be forwarded to the Curator, via the ODP Staff Representative to that cruise, immediately after the cruise. These investigators are expected to contribute to the cruise reports as though they had been cruise participants. All requirements of the Sample-Distribution Policy apply.

Any publication of results other than in ODP reports within twelve (12) months of completion of the cruise must be approved and authored by the whole shipboard party and, where appropriate, shore-based investigators. After twelve (12) months, individual investigators may submit related papers for open publication, provided they have already submitted their contributions to ODP reports and had them accepted. Investigations which are not completed in time for inclusion in the ODP reports for a specific cruise may be published in a later edition of the ODP reports; however, they may not appear in another journal until the report for which they were intended has been published.

2. *Distribution of Samples for Research Leading to Publication Outside of the ODP Reports*

   A. Researchers who wish to use samples for studies beyond the scope of the ODP reports should obtain sample-request forms from the Curator, Ocean Drilling Program, 1000 Discovery Drive, College Station, Texas 77840, U.S.A. Requestors are required to specify the quantities and intervals of core required, to make a clear statement of the nature of the proposed research, to state the time which will be required to complete the work and to submit results for publication, and to specify funding status and the availability of equipment and space for the research.

   Additionally, if the requestor has received samples from ODP or from DSDP previously, he/she will be required to account for the disposition of those samples by citing published works, four (4) copies of which must be sent to the Curator. If no report has been published, this requirement can be fulfilled by sending a brief (two- or three-page) report of the status of the research.

   If the requestor has never before received samples from ODP or DSDP, he/she will be required to show that the samples will be used for responsible research. This requirement can be met by providing the Curator with a copy of the requestor's résumé and bibliography. If the requestor is a student working on a higher degree, he/she can meet this requirement by sending a copy of his/her dissertation or research proposal endorsed by the student's advisor.

   Unused and residual samples should be returned and data should be sent to the Curator if the project has terminated. Paleontological materials may be returned either to the Curator at ODP or to one of the designated micropaleontological reference centers. If material is returned to a reference center, notify the Curator when it is sent.

   Requests for samples from researchers in industrial laboratories will be honored in the same manner as those from academic organizations. Industrial investigators have the same obligations as other investigators to publish all results promptly in the open literature and to provide the Curator with copies of all reports published and of all data acquired in their research.

   In order to ensure that all requests for highly desirable but limited samples can be considered together, approval of requests and distribution of samples will be delayed until twelve (12) months after completion of the cruise or two (2) months after official publication of the core descriptions, whichever occurs earlier. The only exceptions to this policy will be made for specific requests involving ephemeral properties. Requests for samples may be based on core descriptions published in ODP reports produced by the shipboard party, copies of which are on file at various institutions throughout the world. Copies of original core logs and data are kept on open file at ODP, and at the repositories at Lamont-Doherty Geological Observatory and Scripps Institution of Oceanography.

---

[1] Revised October 1988.

B. Most investigations can be accomplished handily with sample volumes of 10 mL or less. Investigators must provide explicit justification of requests for larger sample sizes or for frequent intervals within a core. Requests which exceed reasonable size or frequency limits will require more time to process and are unlikely to be granted in their entirety.

Requests for samples from thin layers, from stratigraphically important boundaries, or from sections which are badly depleted or in unusually high demand may be delayed in order to coordinate requests from several investigators or while the Curator seeks advice from the community. Investigators who submit such requests may expect to receive suggestions for alternative sampling programs or for joining with a research consortium which will share the samples. In any event, such exceptional requests will require more time for processing than will more routine requests.

Investigators who wish to study ephemeral properties may request a waiver of the twelve-month waiting period; however, such requests will be referred automatically to the relevant co-chiefs. If such a request is approved, the investigator will join the shore-based contributors to the shipboard science effort, and will incur the obligations thereof (see section 1).

C. Samples will not be provided until the requestor assures the Curator that funding for the proposed research is available or unnecessary. If a sample request is dependent in any way on proposed funding, the Curator is prepared to provide the proposed funding organization with information on the availability (or potential availability) of suitable samples.

D. Investigators who receive samples incur the following obligations:

(1) To publish significant results promptly; however, no contribution may be submitted for publication prior to twelve (12) months following the termination of the relevant leg unless it is approved and authored by the entire shipboard party.

(2) To acknowledge in all publications that the samples were supplied through the assistance of the international Ocean Drilling Program and others as appropriate.

(3) To submit four (4) copies of reprints of all published works to the Curator, Ocean Drilling Program, 1000 Discovery Drive, College Station, Texas 77840, U.S.A. These reprints will be distributed to the repositories and to the ship. All reprints received will be logged in an on-line bibliographic data base.

(4) To submit all final analytical data obtained from the samples to the Data Librarian, Ocean Drilling Program, 1000 Discovery Drive, College Station, Texas 77840, U.S.A. Please consult announcements in the *JOIDES Journal* or call (409-845-2673) for information on acceptable data formats. Investigators should be aware that they may have other data obligations under the National Science Foundation's Ocean Science Data Policy or under relevant policies of other funding agencies which require submission of data to national data centers.

(5) To return all unused or residual samples, in good condition and with a detailed explanation of any processing they may have undergone, upon termination of the proposed research. In particular, all thin sections and smear slides manufactured on board the vessel or in the repositories are to be returned to the Curator. Paleontological materials may be returned either to the Curator at ODP or to one of the designated micropaleontological reference centers.

Failure to honor these obligations will prejudice future applications for samples.

E. Cores are available for examination by interested parties at the repositories. Investigators are welcome to visit the repositories in order to inspect cores and to specify sample locations when that is required for their research; however, time and space in the workrooms are limited, so advance appointments are required. Occasionally, the space may be fully booked several weeks in advance, so investigators are urged to call for appointments well ahead in order to avoid disappointment. Only the Curator or his delegate may actually remove samples from the cores.

F. A reference library of thin sections, smear slides, and archive photographs is maintained in the repositories for the use of visiting investigators. All thin sections and smear slides produced on board the ship or in repositories belong to this library.

3. *Distribution of Samples to Micropaleontological Reference Centers*

As a separate and special category of repository activity, selected samples are distributed to micropaleontological reference centers, where the prepared material may be studied by visitors. Foraminifers, calcareous nannofossils, and diatoms can be viewed; radiolarians will be prepared in the future. The present centers are (1) U.S. East Coast: Lamont-Doherty Geological Observatory, Palisades, NY 10964 (Ms. Rusty Lotti; telephone, 914-359-2900; telex, 7105762653 LAMONTGEO); (2) U.S. National Museum: Smithsonian Institution, Washington, D.C. 20560 (Dr. Martin Buzas; telephone, 202-357-1390; telex, 264729); (3) U.S. Gulf Coast: Texas A&M University, Department of Oceanography, College Station, TX 77843 (Dr. Stefan Gartner; telephone, 409-845-8479; telex, 792779/ODP TAMU); (4) U.S. West Coast: Scripps Institution of Oceanography, La Jolla, CA 92093 (Dr. William Riedel; telephone, 619-534-4386); telex, 910337127 IUC WWD SIOSDG); (5) Western Europe: Natural History Museum, CH-4001 Basel, Switzerland (Mr. J. B. Saunders; telephone, 061-29-55-64); (6) U.S.S.R.: Institute of the Lithosphere, Staromonet 22, Moscow 109180, U.S.S.R. (Dr. Ivan Basov; telephone, 231-48-36); (7) Japan: National Science Museum, Department of Geology, 3-23-1 Hyakunio-cho, Shinjuku-ku, Tokyo 160, Japan (Dr. Y. Tanimura; telephone, 03-364-2311; telemail, 03-364-2316); (8) New Zealand: New Zealand Geological Survey, P.O Box 30368, Lower Hutt, New Zealand (Dr. Tony Edwards; telephone, (04) 699059).

Further details concerning the micropaleontological reference centers are reported periodically in the *JOIDES Journal*.

4. *Distribution of Samples for Educational Purposes*

Samples may be available in limited quantities to college-level educators for teaching purposes. Interested educators should request application forms from the Curator, Ocean Drilling Program, 1000 Discovery Drive, College Station, Texas 77840, U.S.A. Requestors are required to specify preferred sample size and location, to make a very clear statement of the nature of the course work in which the samples will be used, to explain how the samples will be prepared and how they will be used in the classroom, to explain in detail why similar materials derived from outcrops or dredge hauls cannot be used (it is NOT acceptable to argue that it requires less effort for the requestor to obtain samples from ODP than to assemble them from other sources), and to certify that funds are available to prepare the materials for classroom use. In general, only samples of materials which are abundant in the collection and which are in little demand for research purposes should be requested for educational purposes. The Curator will not approve requests for materials which are limited in supply or for which demand (real or potential) is great, including most paleontological materials.

5. *Distribution of Data*

The Deep Sea Drilling Project and the Ocean Drilling Program have routinely captured much of the data generated on board ship and published in Program reports. Additionally, data supplied by investigators who have received samples are incorporated into the data bases, so data sets which are larger than can be published are available to investigators. Magnetic, downhole-logging, seismic-reflection, bathymetric, and other data collected by the drilling vessel become available for distribution to investigators at the same time as core samples.

Requests for ODP and DSDP data should be addressed to the Data Librarian, Ocean Drilling Program, 1000 Discovery Drive, College Station, Texas 77840, U.S.A. Many varieties of DSDP data are included in ODP data bases. Information on sources of DSDP data is available from the ODP Data Librarian.

A charge will be made to recover material expenses greater than $25.00 incurred in filling individual requests. If required, estimates of charges can be furnished before the work is performed.

May 25, 1989

Dear Friends:

The Ocean Drilling Program announces the availability of the entire collection of color core photographs from the Deep Sea Drilling Project (DSDP) and ODP through Leg 121. It consists of over 23,000 photos of cores recovered from holes drilled at more than 750 sites in the world's oceans. It will be particularly useful to scientists working on samples from the DSDP or ODP. Those considering placing requests for DSDP or ODP samples will find the photographs make it easier to select the particular interval from which they want their samples taken.

The collection comes in two formats: 35-mm slides or 12-inch video disc. Both the slides and the video disc come with an introduction booklet which contains an index and details on their use. The cost of the slide collection is US$4,500. The video disc costs US$50. To view the disc the user must have access to an NTSC standard disc player with random access capabilities and a video monitor (an example of such a player is the Sony video disc player #20002-2).

Please call or write to me if you need to place an order, or for additional information.

Sincerely,

Fabiola M. Byrne

Fabiola M. Byrne
Publications Distribution
Tel: (409)845-2016.

OCEAN DRILLING
PROGRAM

Ocean Drilling Program
Texas A&M University
ollege Station, TX 77843-3469
409) 845-2673

Drilling locations

Leg	Location	Sites
Phase 1 1968–1970		
1	North Atlantic	1–7
2	North Atlantic	8–12
3	South Atlantic	13–22
4	Central Atlantic	23–31
5	North Pacific	32–43
6	North Pacific	44–60
7	Central Pacific	61–67
8	Central Pacific	68–75
9	Central Pacific	76–84
Phase 2 1970–1972		
10	Gulf of Mexico	85–97
11	North Atlantic	98–108
Re-entry trials		109–110
12	North Atlantic	111–119
13	Mediterranean	120–134
14	Central Atlantic	135–144
15	Caribbean	146–154
16	Central Pacific	155–163
17	Central Pacific	164–171
18	North Pacific	172–182
19	North Pacific	183–193
20	North Pacific	194–202
21	Coral Sea	203–210
22	Indian Ocean	211–218
23	Arabian Sea	219–230
24	Indian Ocean	231–238
25	Indian Ocean	239–249
Phase 3 1972–1975		
26	Indian Ocean	250–258
27	Indian Ocean	259–263
28	Antarctic	264–274
29	Tasman Sea	275–284
30	South Pacific	285–289
31	North Pacific	290–302
32	North Pacific	303–313
33	North Pacific	314–318
34	South Pacific	319–321
35	South Pacific	322–325
36	South Atlantic	326–331
37	North Atlantic	332–335
38	Arctic	336–352
39	Atlantic	353–359
40	South Atlantic	360–365
41	South Atlantic	366–370
42A	Mediterranean	371–378
42B	Black Sea	379–381
43	North Atlantic	382–387
44	North Atlantic	388–392
44A	North Atlantic	393–394
IPOD 1 1975–1983		
45	North Atlantic	395–396
46	North Atlantic	396A–396B
47	North Atlantic	397–398
48	North Atlantic	399–406
49	North Atlantic	407–414
50	North Atlantic	415–416
51A	North Atlantic	417–417A
51B	North Atlantic	417B–417D
52	North Atlantic	417D–418A
53	North Atlantic	418A–418B
54	Central Pacific	419–429
55	North Pacific	430–433
56	North Pacific	434–437
57	North Pacific	438–441
58	North Pacific	442–446
59	North Pacific	447–451
60	North Pacific	452–461
61	Central Pacific	462
62	North Pacific	463–466
63	North Pacific	467–473
64	Gulf of California	474–481
65	Gulf of California	482–485
66	Central Pacific	486–493
67	Central Pacific	494–500
68	Central Pacific	502–503
69	Central Pacific	504–505, 501
70	Central Pacific	506–510, 504B
71	South Atlantic	511–514
72	South Atlantic	515–518
73	South Atlantic	519–524
74	South Atlantic	525–529
75	South Atlantic	530–532
76	North Atlantic	533–534
77	Caribbean	535–540
78	North Atlantic	541–543, 395A, B
79	North Atlantic	544–547
80	North Atlantic	548–551
81	North Atlantic	552–555
82	North Atlantic	556–564
83	Central Pacific	504B
84	Central Pacific	565–570
85	Central Pacific	571–575
86	North Pacific	576–581
87	North Pacific	582–584
88	North Pacific	581
89	Central Pacific	585–586, 462A
90	South Pacific	587–594
91	Central Pacific	595–596
92	Central Pacific	597–602, 504B
93	North Atlantic	603–605
94	North Atlantic	606–611
95	North Atlantic	612–613, 603
96	Gulf of Mexico	614–624

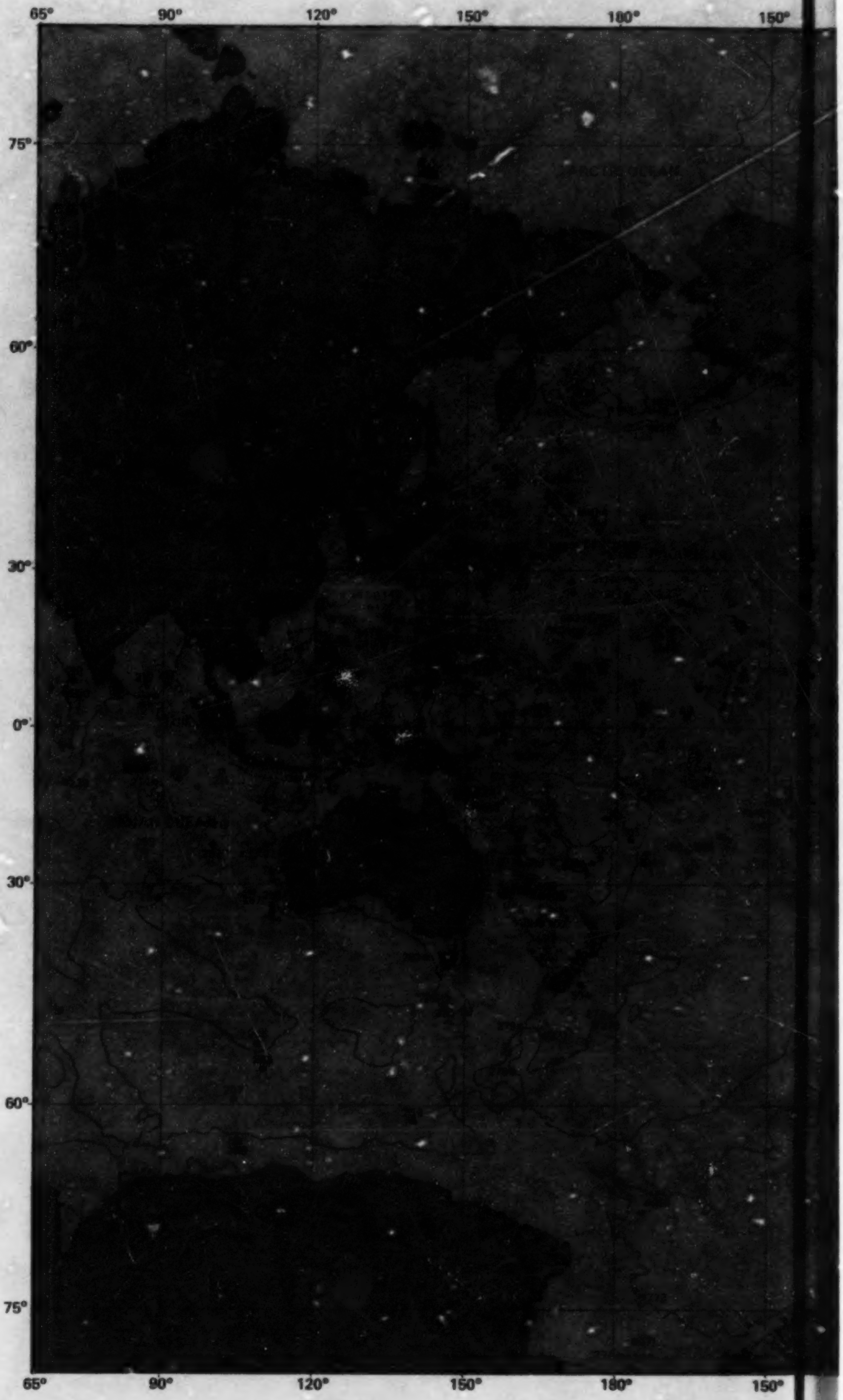

DEE SE

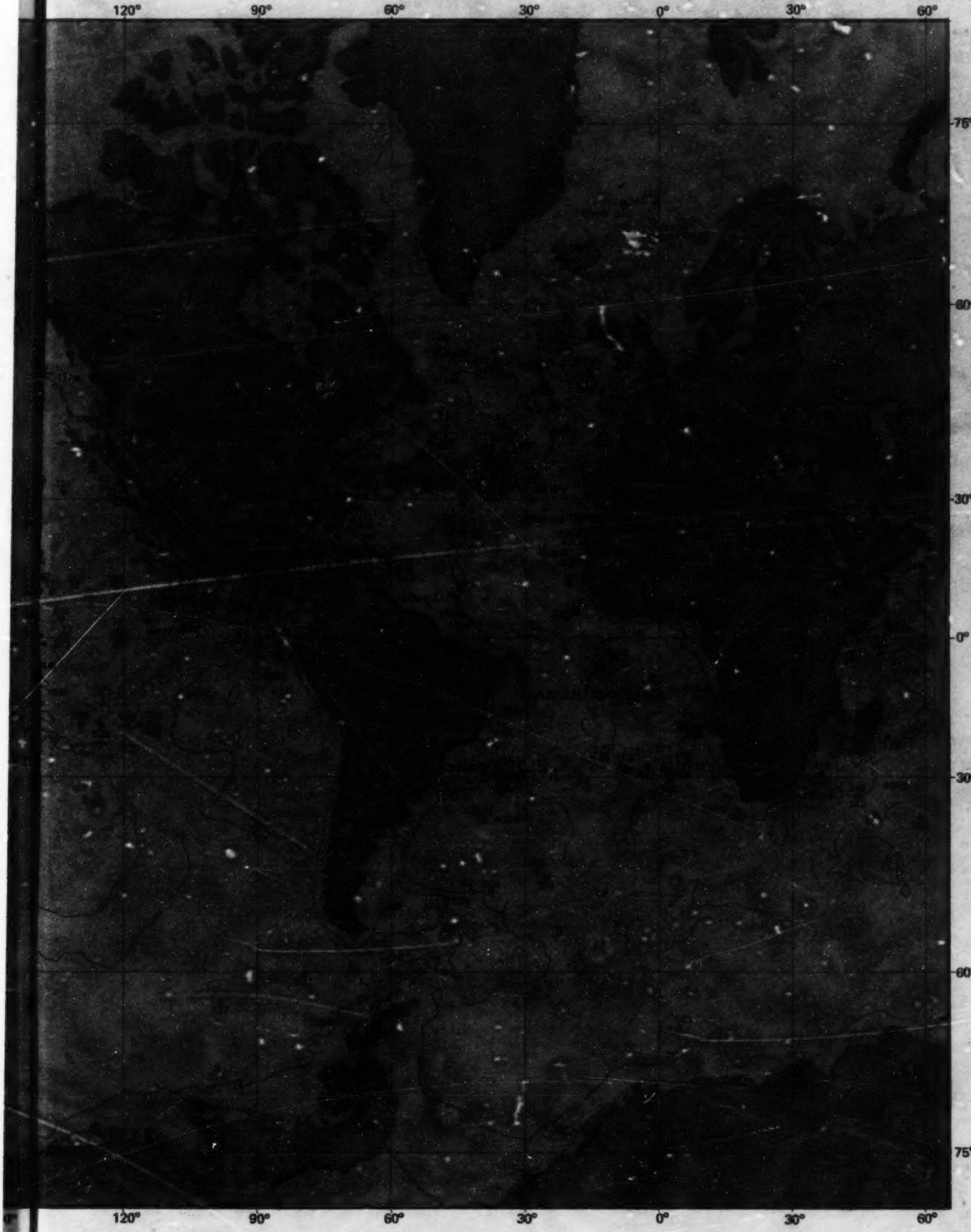
120°
90°
60°
30°
0°
30°
60°
75°
60°
30°
0°
30°
60°
75°
120°
90°
60°
30°
0°
30°
60°

EEPSEA DRILLING PROJECT

117

Initial Reports Volume 117: Chapter 17: Figure 5. A. Selected strike- and dip-line water gun reflection profiles across Owen Ridge (see inset location map.) Two reflectors highlighted by dotted lines are interpreted as (lower) a surface of regional onlap marking the earliest uplift of Owen Ridge during the late Oligocene and (upper) the diachronous (early to middle Miocene) facies change from turbidites to pelagic sediments. DSDP Site 224 was crossed on line 35; eleven cores from Pleistocene to early Eocene age were recovered at this site above volcanic basement at 787 m below the seafloor.

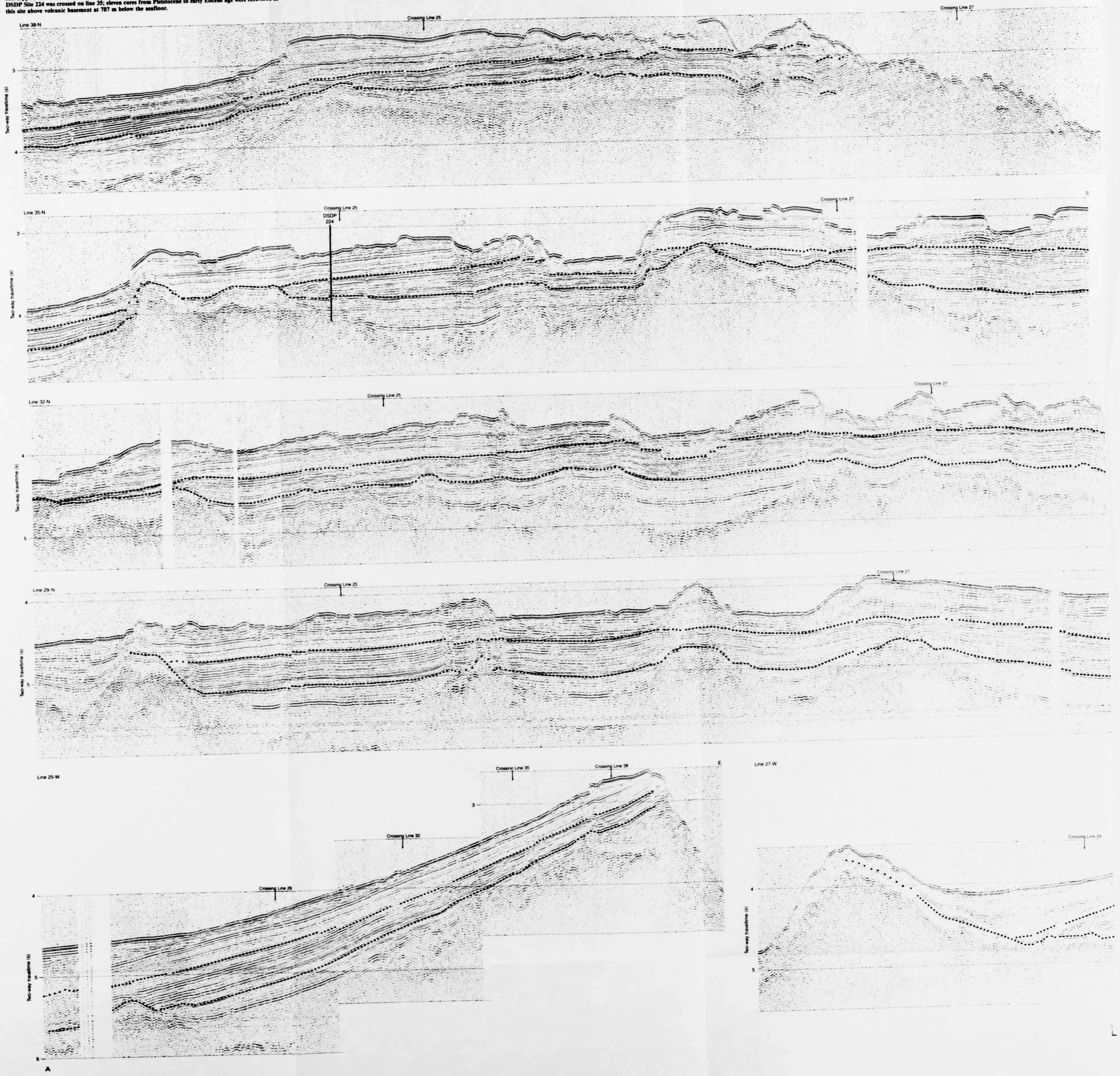

NS 1.38/2:

pro-
cted
cene
nts.
d at

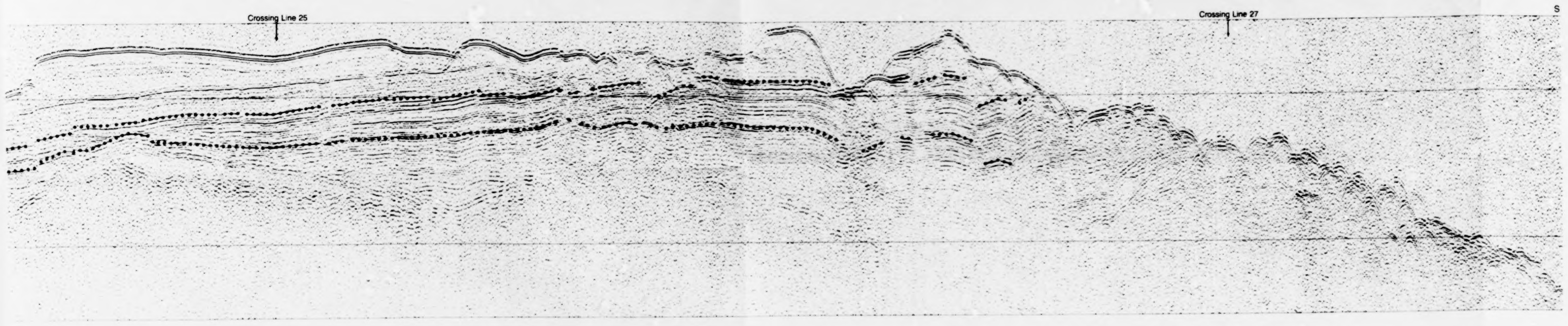

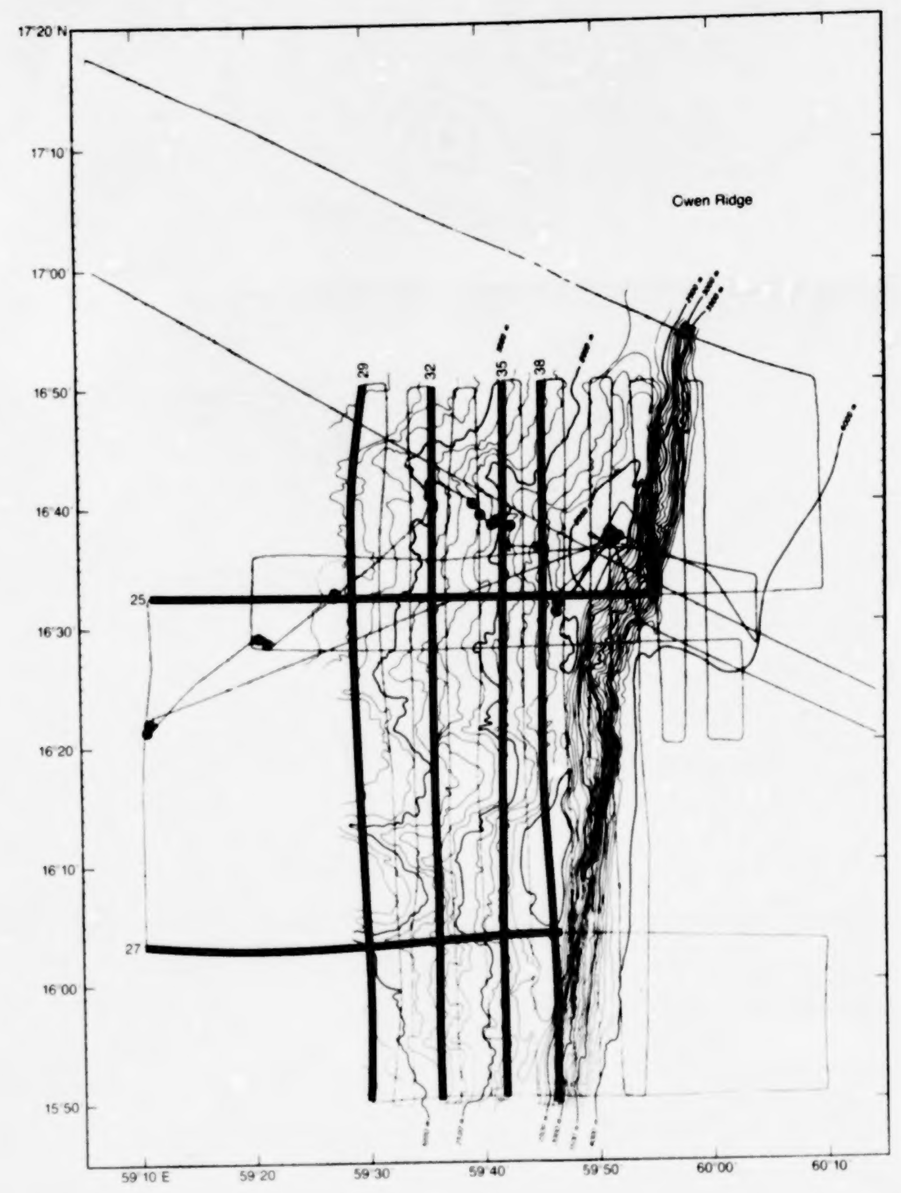
17°20' N
17°10'
17°00'
16°50'
16°40'
16°30'
16°20'
16°10'
16°00'
15°50'
59°10' E
59°20'
59°30'
59°40'
59°50'
60°00'
60°10'
Owen Ridge
29
32
35
38
25
27

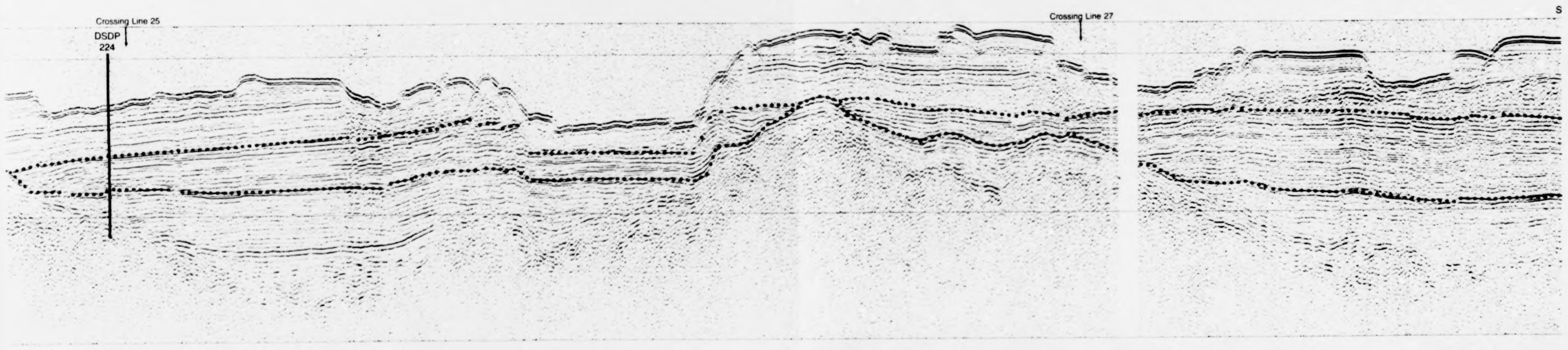

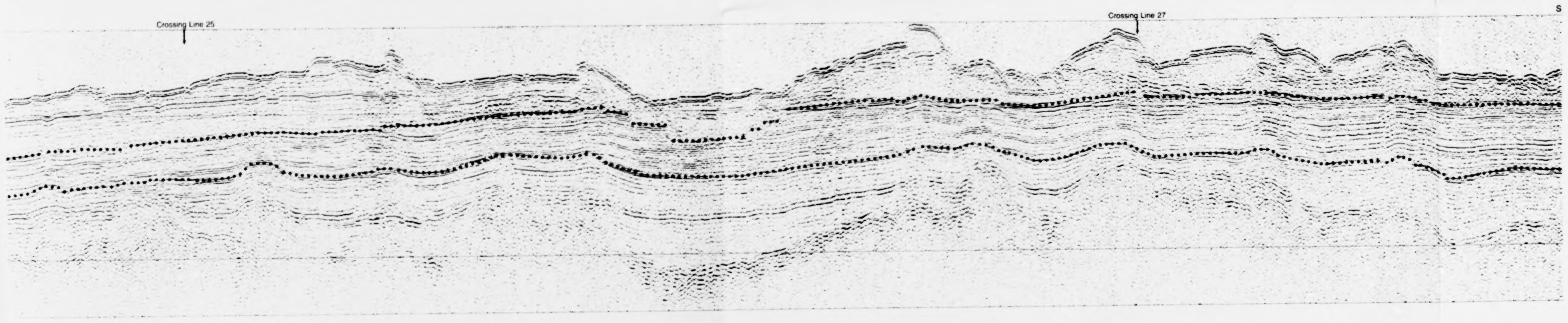

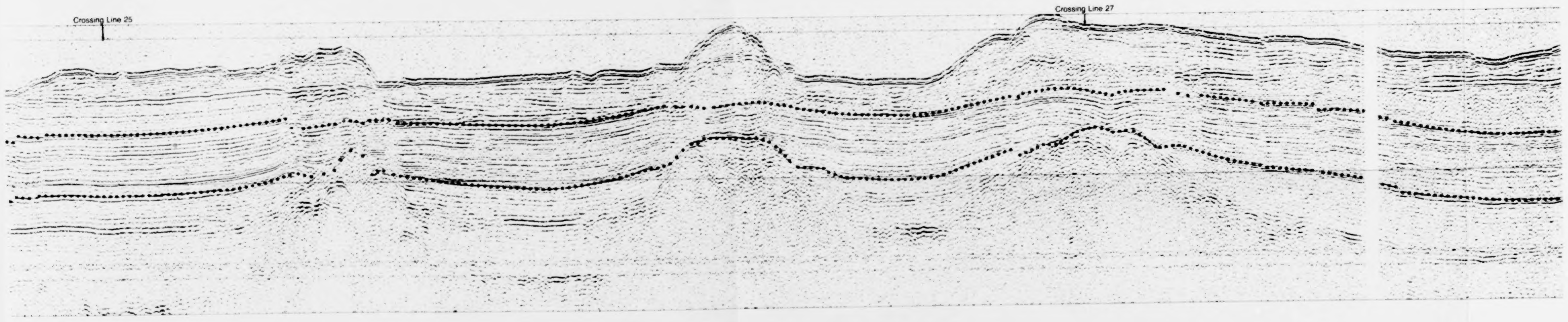

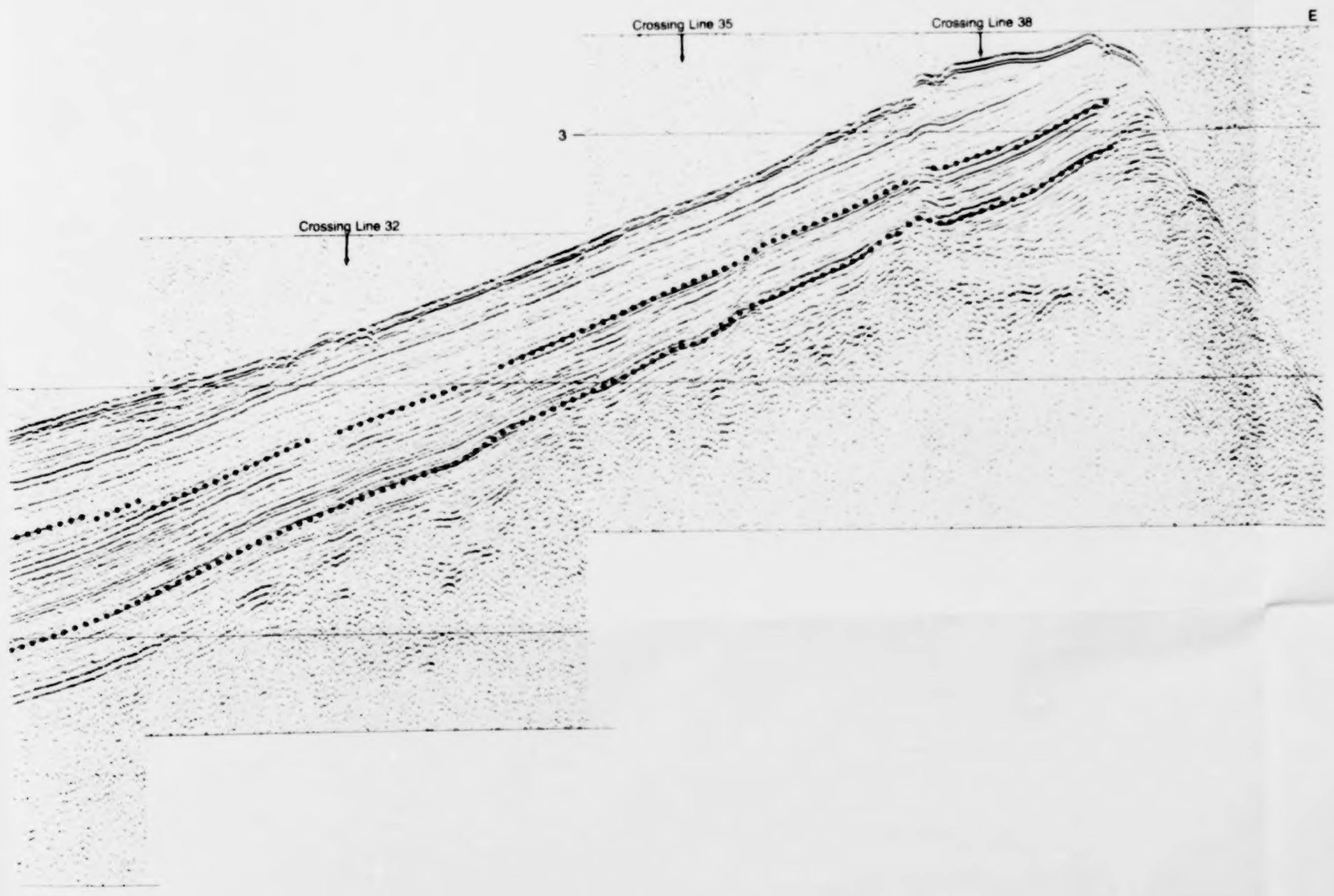

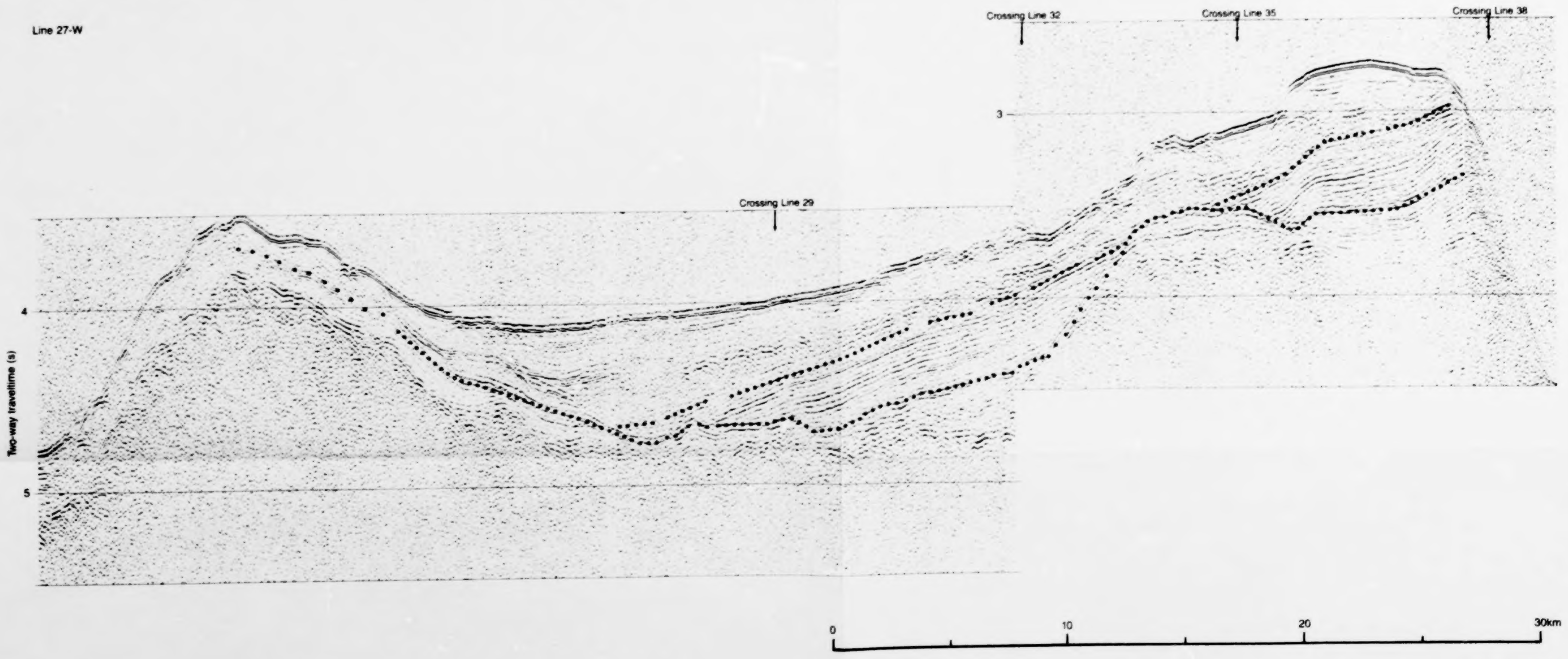

***Initial Reports* Volume 117: Chapter 17: Figure 5. B.** **Selected strike- and dip-line water gun reflection profiles across the southeast Oman margin (see inset location map.) A thick (>2 km) depocenter is between the abrupt "Siquirah Fault" and a ridge of tilted blocks so pervasively faulted and dissected by erosional canyons that they appear to be diapiric. Underlying crust throughout this survey area is interpreted as oceanic; transpressional motion between the Indian and Arabian plates produced landward thrust of Owen Basin crust against this once-passive margin.**

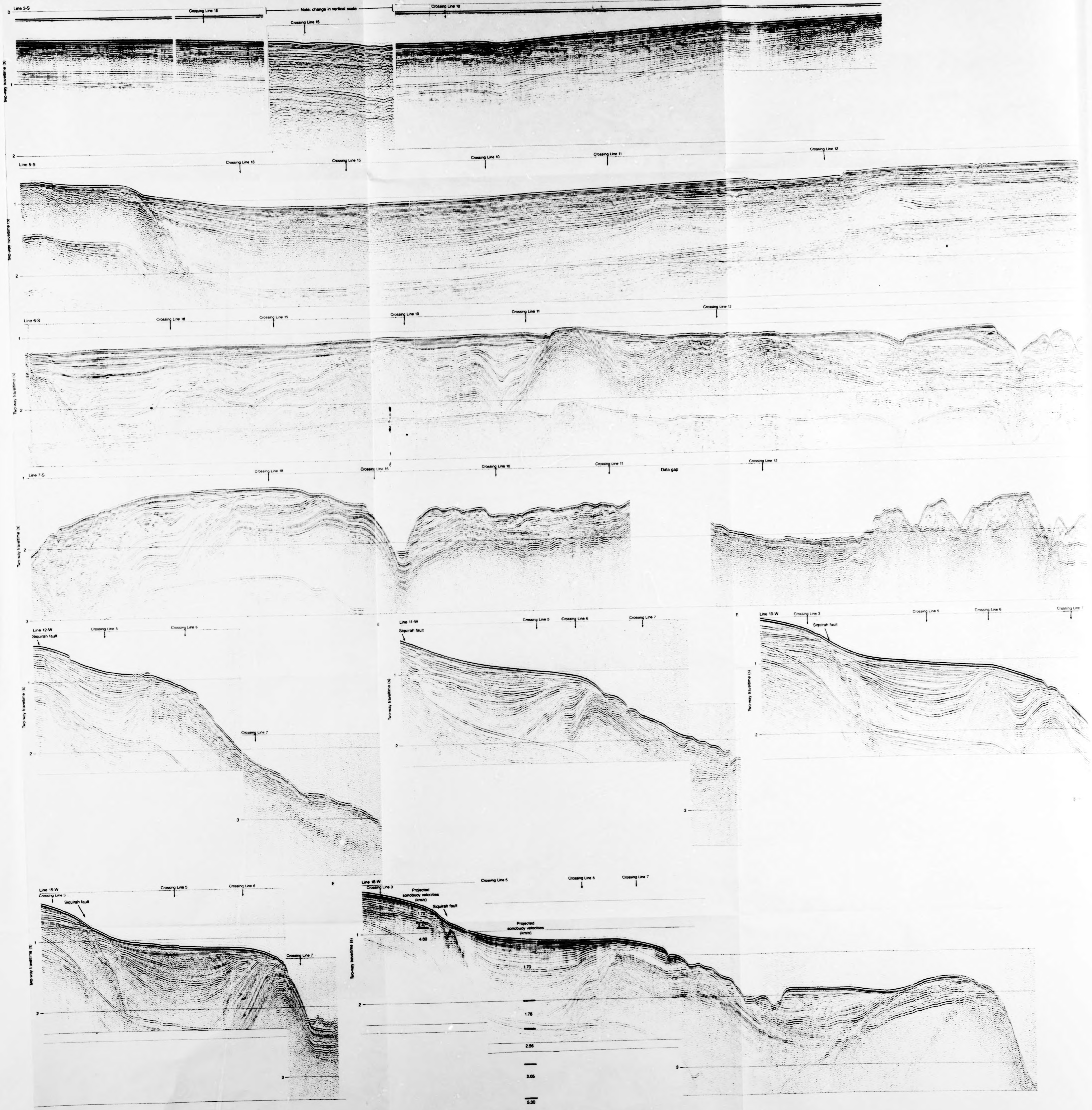

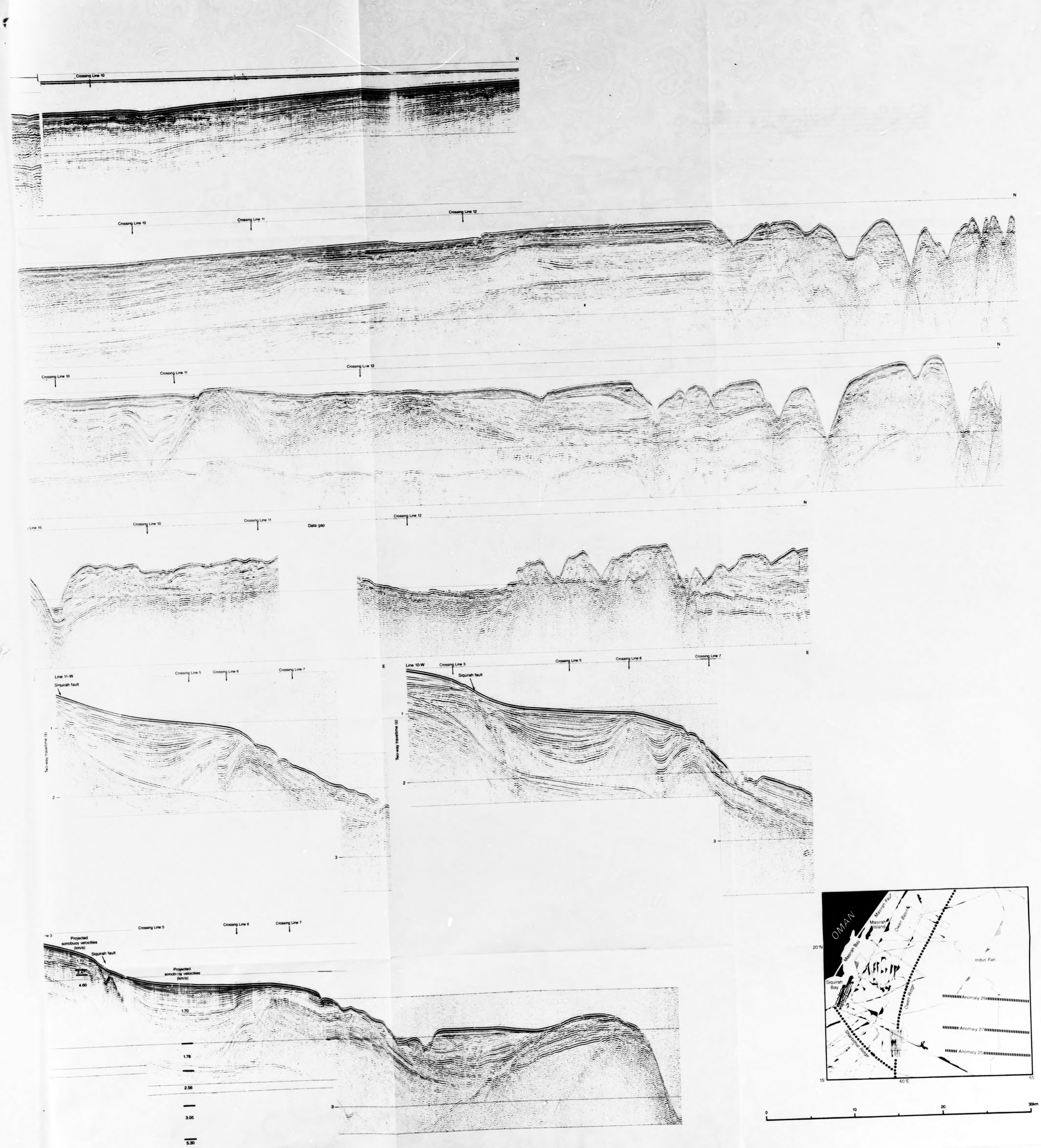
N
Crossing Line 10
N
Crossing Line 10
Crossing Line 11
Crossing Line 12
N
Crossing Line 10
Crossing Line 11
Crossing Line 12
N
Line 15
Crossing Line 10
Crossing Line 11
Data gap
Crossing Line 12
E
Line 11-W
Siquirah fault
Crossing Line 5
Crossing Line 6
Crossing Line 7
Two-way traveltime (s)
1
2
3
E
Line 10-W
Crossing Line 3
Siquirah fault
Crossing Line 5
Crossing Line 6
Crossing Line 7
Two-way traveltime (s)
1
2
3
ne 3
Projected sonobuoy velocities (km/s)
Siquirah fault
1.70
2.47
4.60
Crossing Line 5
Crossing Line 6
Crossing Line 7
Projected sonobuoy velocities (km/s)
1.70
1.78
2.56
3.05
5.30
3
OMAN
Masirah Fault
Masirah Island
Owen Basin
Masirah Bay
Siquirah Bay
Indus Fan
Owen Ridge
Sharbithat Ridge
Anomaly 29
Anomaly 27
Anomaly 25
20°N
15°
60°E
65°
0
10
20
30km